Expanding our understanding of the clinico-epidemiology, cellular biology and pathogenesis of human prion diseases.

Steven Collins MBBS (University of Melbourne), MD (University of Melbourne), FRACP

Faculty of Medicine, Dentistry and Health Sciences
School of Medicine
University of Melbourne
Parkville, Victoria, Australia

Submitted for the degree of Doctor of Medical Science, The University of Melbourne, 2021.

Table of contents

Statement

The body of work of 139 published papers contained herein, accompanied by a contextualising literature review and section preambles, constitutes a thesis submitted for the degree of Doctor of Medical Science. Included in this thesis are 78 high quality peer-reviewed principal publications presented in full, relating to clinical, epidemiological and basic scientific aspects of human prion disease for which I was first author, senior author or the leader of the Australian contribution in multi-national collaborative studies. In addition, are a further 61 publications and reports, listed by titles and publication details, dealing with human prion disease for which I was a significant contributor. A short overall review at the start of the thesis and a preamble before each of the sections dealing with my principal publications are offered to place these published studies in the context of extant clinical and scientific literature.

Abstract

This thesis is primarily constituted as a compendium of published manuscripts encapsulating a substantial volume of work relating to prion diseases, undertaken from 1999 to 2020 through the Australian National Creutzfeldt-Jakob Disease Registry based at the University of Melbourne, frequently in collaboration with pre-eminent domestic and international scholars in the field of prion diseases.

The thesis is divided into two principal parts. The larger first part comprises 78 peer-reviewed papers submitted in full, representing a diverse array of acclaimed, often landmark or pivotal, studies published in prestigious general medical and specialist journals where I have been either senior and corresponding author, primary author or leader of the Australian contribution in major multi-national projects. This body of work is divided into seven sections spanning: normal prion protein cellular biology; prion pathogenesis; human prion disease epidemiological studies; human prion disease bio-marker studies; clinical aspects of human prion disease; prion disease treatment studies; and studies of human prion-like diseases. A short review at the start of the thesis and a preamble before each of these sections dealing with my principal publications are offered to place these published studies in the context of extant clinical and scientific literature. The second part of the thesis is submitted for completeness, comprising four sub-sections encompassing 61 publications and reports, listed by title and publication details, dealing with human prion disease for which I was a significant contributor.

University of Melbourne
Faculty of Medicine, Dentistry and Health Sciences
Department of Medicine, Royal Melbourne Hospital

Declarations for this Doctor of Medical Science thesis based on compilation of published papers:

In accordance with University of Melbourne Doctorate regulations I hereby make the following general declarations:

- that this thesis comprises only my original works towards the degree of Doctor of Medical Science and it contains no material which has been accepted for the award of any other degree or diploma at any other university or equivalent institution.
- The 78 high-quality, peer-reviewed, principal publications presented in-full all relate to clinical, epidemiological and basic scientific aspects of human prion disease, work for which I was first author, senior author or the leader of the Australian contribution in multi-national collaborative studies.
- The remaining 61 papers included in this thesis are also original publications in peer reviewed journals, except the Annual ANCJDR surveillance reports, involving human prion disease. My contributions in these publications were always significant, including taking a leadership role in many studies.

Hence, this thesis contains no material previously published or written by another person, with the ideas and writing of all the papers in the thesis the principal responsibility of myself, except where acknowledgment is made within the thesis of co-authorship arrangements reflecting project leadership and cognate writing responsibilities stemming from collaborations of individual researchers directly under my supervision or between separate research teams, representing the essentially inevitable outcome of a multi-faceted, team(s)-based approach, to research.

Signed:……Date:…19/02/2021…

Acknowledgements

I would like to thank Stephen Davis for all his kind and generous support over the course of my career, including his willing acceptance of the role to act as supervisor for this thesis.

There are many people deserving of my heartfelt gratitude for achieving the body of work presented in this thesis. Firstly, I would like to thank Colin Masters, and all the members (past and present) of the Australian National Creutzfeldt-Jakob Disease Registry (ANCJDR) and my basic science research team. Some 27 years has passed since Colin offered me the opportunity to join him in establishing the ANCJDR. Colin's unstinting support, mentorship and uncompromising desire for academic excellence over this extended period were critical to the success of my work. Equally deserving of my sincere gratitude are all those members of the ANCJDR and my basic science research team who worked tirelessly and assiduously to successfully complete the various studies reported in this thesis. Spanning the spectrum from research assistants through post-graduate students to experienced post-doctoral scientists, there are too many to name individually but special thanks go to Alison Boyd, Genevieve Klug, Victoria Lewis, Shannon Sarros and Christiane Stehmann. The combined endeavours of these teams allowed me to achieve the shared vision of a world-class surveillance and epidemiology unit juxtaposed to meritorious original contributions in the realm of basic scientific discoveries in prion disease.

Next, I would like to recognize the generous and enthusiastic support of all my collaborators. Once again there are too many people to thank individually but special mention goes to a few key international collaborators such as Robert Will, Inga Zerr, Cornelia van Duijn, Paul Brown and Noriyuki Nishida. Through these collaborations many landmark studies in prion disease were made possible in the fields of epidemiology and pre-mortem diagnostic capacity. In addition, sincere gratitude is extended to my domestic collaborators Victoria Lawson, David Finkelstein and Paul Adlard within the University of Melbourne and extramurally, especially Andrew Hill and Catriona McLean.

Finally, a special thanks to my wife Gwen who was always there to support me while I endured the varying fortunes and vicissitudes that inevitably accompany a long-term career as a clinician-scientist. Always solicitous, practical and candid, it is difficult to envisage my journey as a clinician-scientist without Gwen "in my corner".

Overview of Prion Diseases

What are Prion Diseases (also known as Transmissible Spongiform Encephalopathies)?

Generically grouped nosologically as neurodegenerative disorders, prion diseases constitute a unique sub-group of such conditions due to the combination of disease transmissibility, distinctive neuropathology and affliction of both human beings and animals. Substantial evidence supports that all prion diseases are caused by accumulation in the brain of misfolded, typically protease-resistant, conformers (PrP^{Sc}) of the normal or cellular form of the prion protein (PrP^{C}), with PrP^{Sc} also constituting the transmissible agent (1, 2). In addition to immunohistochemical detection of PrP^{Sc} deposits in the brain, the other characteristic neuropathological features distinguishing prion diseases consist of vacuolation of the neuropil (spongiform change), as well as microgliosis and astrocytic gliosis (3). The spectrum of human prion diseases includes Creutzfeldt-Jakob disease (CJD), Gerstmann-Sträussler-Scheinker syndrome (GSS), Fatal Familial Insomnia (FFI) and Kuru, while animal diseases include bovine spongiform encephalopathy (BSE; “mad cow” disease) in cattle, scrapie in sheep and goats, transmissible mink encephalopathy, chronic wasting disease (CWD) in deer, moose and elk, as well as the recently recognized disorder affecting dromedary camels (2, 4). The following brief overview will almost exclusively focus on human forms of prion disease.

A (very) Potted History of Human Prion Diseases

Scrapie is the archetypal prion disease, first clearly recognized by shepherds in the 18th century, with affected sheep displaying altered gait and intense scratching, the latter leading to the colloquial descriptor “scrapie” for the illness. After approximately two centuries, indisputable evidence of transmissibility of scrapie was reported in 1936, albeit inadvertently, during attempts to vaccinate sheep against louping ill virus. The first reports of likely human prion disease were made independently by a German neuropathologist (Hans Creutzfeldt) and neurologist (Alfons Jakob) in the early 1920s although despite the eventual eponymous designation of Creutzfeldt-Jakob disease (CJD) for the conflated malady of the central nervous system, subsequent investigation makes it unlikely that the case described by Creutzfeldt and three of Jakob’s five original cases were in fact human prion disease. In the 1950s, an unusual neurological disorder

known as Kuru, predominantly manifesting as a cerebellar ataxia, was recognized as endemic amongst the Fore linguistic group in the Eastern Highlands of Papua-New Guinea, as well as neighbouring tribes with whom they inter-married (5). Shortly thereafter, the perspicacious observations of a veterinary pathologist (Dr William Hadlow) that scrapie and Kuru shared similar clinical and neuropathological features led Carleton Gajdusek and his team at the NIH in the USA to undertake transmission studies of Kuru, with Kuru reported to be transmissible to chimpanzees through intra-cerebral inoculation in 1966 (6); shortly thereafter CJD was confirmed as also transmissible in 1968 (7). Subsequent detailed epidemiological investigations concluded that Kuru had arisen and been maintained through ritualistic endo-cannibalism, practiced as part of mourning rites of the Fore (8). Further delineating the major phenotypes of human prion disease, in 1981 a landmark report suggested unification of a previously disparate group of neurodegenerative diseases under the rubric GSS through appreciation of their shared neuropathological features, with demonstration of transmissibility confirming their unified nosology as prion disease (9). Completing the major phenotypes comprising the spectrum of human prion diseases, in 1992 FFI was shown to be tightly linked to a mutation in the prion protein gene (10) with transmissibility confirmed 3 years later (11).

Elucidating the Causative Agent of Prion Diseases

Early hypotheses concerning the causative agent underlying prion diseases included a “viroid”, a “slow virus”, or an “unconventional virus”, albeit posited in parallel with mounting scientific observations making a conventional infectious agent harbouring a nucleic acid genome highly unlikely (12-14). Despite intensive efforts, there was inability to reproducibly isolate a virus or demonstrate virus sub-particles, with other experimental evidence showing the causative agent of prion diseases resisted treatments (viz, ionizing radiation and UV light) considered highly effective at destroying conventional nucleic acid-containing microbial pathogens (14), while the agent was vulnerable to methods denaturing proteins. These data culminated in the “protein-only” hypothesis for the infectious agent underpinning prion diseases, first clearly articulated in 1967 (13, 15). Indeed, a mathematician (John Griffith) was the first to offer mechanisms that might underlie how a protein could replicate and be “infectious” (16). Nevertheless, it took a further 25 years before sufficient scientific data were amassed to strongly support the "protein-only" postulate (1, 17), with Stanley Prusiner coining the term “prion” to depict a

*pro*teinaceous *in*fectious particle as the transmissible scrapie agent. Shortly thereafter, the protease-resistant component of the protein (denoted PrP27-30) that tightly correlated with prion infectivity was identified and called the “prion protein” (18) and a year later it was shown that PrP27-30 was in fact encoded by the normal mouse or host genome (19).

Rigorous confirmation of the “protein-only” hypothesis was considered to require the *de novo* or *in vitro* production of infectious prions from pure PrP^{C}. Such proof of the hypothesis took another approximately 22 years, with Stanley Prusiner and colleagues in 2004 reporting the *in vitro* production of “synthetic prions” through induction of misfolding of recombinant, truncated, mouse prion protein (MoPrP89-230) (20). Successful transmission was achieved through intracerebral inoculation of the misfolded recombinant synthetic MoPrP89-230 prions into transgenic mice carrying the same truncated prion protein gene, requiring 380-660 days after inoculation for mice to develop symptoms of a prion-like disorder. Subsequently, successful transmission into wild-type FVB mice was achieved employing the brains of sick transgenic mice initially injected with recombinant misfolded synthetic MoPrP89-230 prions. Shortly thereafter, it was demonstrated that these synthetic prions harboured strain properties akin to what is observed in “natural” prion diseases (21). Over the next six years, a number of independent research teams, utilising different experimental approaches, reported the successful *de novo* production of synthetic prions, including those able to directly induce disease in wild-type recipient mice, providing essentially indisputable collective final validation of the "protein-only" hypothesis (22-25).

Cellular Biology and Functions of the Normal Prion Protein (PrP^{C})

In homo sapiens, PrP^{C} is encoded within a single open reading frame of the single-copy housekeeping prion protein gene (*PRNP)* located on chromosome 20, while in mouse the homologous gene (*Prnp*) is located on chromosome 2. The prion protein gene is highly evolutionarily conserved across vertebrates, as is the structure of PrP^{C} in mammals (26) and lower species (27), supporting a likely critical biological function (28). PrP^{C} undergoes a biosynthetic pathway typical of secreted proteins, involving synthesis on the endoplasmic reticulum (ER) and passage through the Golgi apparatus, with packaging into endosomes for delivery to specialized detergent-resistant (cholesterol and sphingolipid-rich) microdomains (“lipid rafts”) on the external leaflet of the cell’s surface membrane (29, 30). Human PrP^{C} is

genetically coded as a 253 amino acid protein from which the first 22 residues (“signal peptide”) are co-translationally cleaved shortly after translation commences. Further post-translational processing includes addition of a C-terminal glycosylphosphatidylinositol (GPI)-anchor at serine residue 230, important for directing glycolipid linkage of PrPc into lipid rafts of the external leaflet of the cell membrane (31), while PrP^{C} can also be glycosylated, with the two potential sites for attachment of N-linked oligosaccharide chains located at residues 181 and 197. A histidine-rich, metal binding domain consisting of a nonapeptide followed by four identical octapeptide repeats (OPR) is located between residues 51 and 91.

PrP^{C} is recognized as a copper binding protein (32) with less than 0.1 nanomolar affinity and in fact the histidine residue within each OPR is capable of binding individual copper and zinc ions in a co-operative manner (33, 34), with metal binding initiating intracellular translocation of PrP^{C} via clathrin-dependent endocytosis (35). PrP^{C} also has two additional Cu^{2+} ion binding histidines located at codons 96 and 111 (36).The tertiary structure of mature, including membrane-bound PrP^{C}, displays an ordered globular C-terminus containing three alpha-helices, with helices 2 and 3 linked by a di-sulphide bridge, while the N-terminal region up to residue 120 is more flexibly unstructured (26, 37). PrP^{C} expression commences early in embryogenesis and although highest levels in the adult are found in neurons of the central nervous system (38, 39) there is almost ubiquitous cellular expression at lower levels, especially within the reticulo-endothelial system (40, 41). Codon 129 of PrP^{C} is polymorphic, containing either valine (V) or methionine (M) at this site, with polymorphic status influencing both risk of developing human prion disease (42), as well as disease phenotype (10, 43).

PrP^{C} may undergo constitutive endoproteolytic events, including alpha (at residues 111/112) and beta (“ragged”, broadly located around residue 90) (44-46), with such processing generating N1-C1 and N2-C2 cleavage pairs, respectively. In addition, PrP^{C} may be cleaved by a-disintegrin-and-metalloproteinase 10 (ADAM 10) in the region of linkage to its GPI anchor (“shedding”) liberating full-length protein or post-endproteolysis C-terminal fragments (47). Endoproteolysis appears to have importance both physiologically and pathologically, with alpha-cleavage predominant in non-disease states and protective against misfolding of full-length PrP^{C} or the C1 fragment into PrP^{Sc} (48, 49), while the C2 fragment is increased in prion disease suggesting a role for beta-cleavage in pathogenesis (45). Further circumstantially illustrating

the neuro-biological importance of alpha-cleavage, transgenic mice harbouring mutant PrP^C missing residues 105-125 (delta105-125), thereby preventing alpha-cleavage, show spontaneous neuropathological abnormalities different to those of prion disease (50).

Putative normal functions of PrP^C

Although the likely primary biological purpose of PrP^C in the peripheral nervous system appears related to maintaining myelination (51), consensus regarding the predominant role of PrP^C in the CNS remains to be achieved. Moreover, PrP^C has also been reported to have important functions outside of neurons and in fact the first functional activity reported for PrP^C was in lymphocyte activation (52). Despite the original description of *PRNP* gene-ablated (*Prn-p*$^{0/0}$) mice claiming no apparent adverse phenotypic outcome when comparing wild-type (WT) and *Prn-p*$^{0/0}$ mice (53), subsequent studies have reported a number of deficiencies in addition to peripheral nerve demyelination (51), such as hippocampal synaptic dysfunction (54) and cognate memory impairment (55), as well as diverse, more generic failures in protection against oxidative stress (56), copper and zinc binding (32, 34), membrane signal transduction (57) and synaptic function (58).

Many reports support that PrP^C may have a neuroprotective role, especially against oxidative stress (59, 60) but also other noxious insults, including the likelihood that products of PrP^C endoproteolysis may contribute to safeguarding neurons (61). These observations raise the possibility that corruption of normal PrP^C function may at least partly underscore pathogenesis in animal and human prion disease. Some reported functions of PrP^C may at least partly overlap. For example, neuroprotection against excitotoxicity may also involve a role in synaptic regulation, with PrP^C mitigating excessive activation of N-Methyl-D-aspartic acid receptors (NMDAR) and cognate calcium ion (Ca^{2+}) entry into cells induced by ischemia (62) via direct association with the NR2D subunit, favourably constraining NMDAR activity and attenuating potential excitotoxicity (63). In addition to the participation of full-length PrP^C in neuroprotective activities, the N1 fragment has also been reported to protect against staurosporine induced caspase-3 activation in rat retinal cells (64) and also bind to synaptotoxic Abeta oligomers thereby preventing Abeta peptide fibrillisation and abrogating their toxicity *in vitro* and *in vivo* (65). This type of study undertaken by Fluharty and colleagues assessing a protective role of PrP^C against Abeta peptides was prompted by a landmark report that membrane-bound PrP^C

acts as a receptor for soluble amyloid-beta (Abeta) oligomers thereby mediating their synaptotoxicity (66); however, not all studies have supported a direct role of PrP^C mediating soluble Abeta oligomer synaptotoxicity (67) (68).

Localisation of PrP^C predominantly within lipid raft domains on the plasma membrane (like other GPI-anchored proteins) supported the likelihood of participation in transmembrane signal transduction, possibly as part of a multi-molecular "scaffold". This property was first definitively demonstrated through antibody-mediated cross-linking of PrP^C in the 1C11 cell line leading to activation of the non-receptor tyrosine kinase, Fyn (57). Subsequent studies reported that antibody-induced activation of Fyn through PrP^C induced reactive oxygen species production via extracellular-regulated kinases (ERK) 1/2 and nicotinamide adenine dinucleotide phosphate (NADPH) oxidase in both neuronal and non-neuronal cells (69).

Numerous investigations support that PrP^C is involved in synaptic development and function (70-74). Early electrophysiological studies in *Prnp*$^{0/0}$ mice hippocampal slices revealed that long-term potentiation (LTP) was disrupted and receptor-associated fast inhibition involving GABA-A receptors was impaired (70), with subsequent investigation supporting that PrP^C was unlikely to have an intrinsic synaptic ion channel function but more likely acting to stabilise synapses (54). Impaired after-hyperpolarisation (through disruption of Ca^{2+}-activated K^+ currents) has been observed in *Prnp*$^{0/0}$ mice hippocampal CA1 and cerebellar Purkinje cells (75, 76). As a corollary of an important participation in synaptic function, especially in the hippocampus, several studies employing transgenic rodent models have demonstrated that PrP^C appears have a role in memory, with absence of PrP^C causing altered short-term memory (STM) formation and impairment of long-term memory (LTM) consolidation (55, 77), with apparent age-dependency of the deficits given such impairments were absent at age 3 months but present at 9 months of age (78). Memory impairments in *Prnp*$^{0/0}$ mice were rescued when PrP^C was selectively re-expressed in neurons (55).

Pathogenesis of Prion Disease

Acknowledging the fundamental role of conversion of PrP^C to PrP^{Sc} (through an auto-catalytic, template-directed process) for both successful disease transmission and subsequent pathogenesis, it is not surprising that *Prnp*$^{0/0}$ mice are completely resistant to development of prion disease (79). Moreover, conditional knock-out mice (employing the NFH-Cre/M*lox*P

system) that lose PrP^{C} expression in neurons at ~12 weeks of age are also resistant to disease when inoculated at ~4 weeks of age, with early neuropathological changes such as spongiosis reversing in these inoculated transgenic mice (80). These studies underscore the critical importance of ongoing expression of PrP^{C} serving as a substrate for conversion to PrP^{Sc} for successful disease pathogenesis.

Considerable evidence supports that small soluble oligomers of Abeta peptides in Alzheimer's disease (AD) and alpha-synuclein peptides in Parkinson's disease (PD) are primarily responsible for inducing neurotoxicity, with synaptic failure and eventual synapse loss key outcomes underpinning progressive cognitive decline in AD (81). Electrophysiological studies have demonstrated that small soluble Abeta oligomers extracted from the brains of patients with AD can potently inhibit LTP and enhance long-term depression (LTD), as well as reduce dendritic spine density, in normal rodent hippocampus (82). As described above, evidence supports that PrP^{C} can function as a high affinity receptor for soluble Abeta oligomers extracted from various sources, thereby transducing their neurotoxicity with consequent blockade of hippocampal LTP, with the latter prevented by anti-PrP antibodies (66, 83). Additional *in vivo* and i*n vitro* studies have demonstrated that soluble Abeta oligomers binding tooPrP^{C} activate Fyn causing phosphorylation of the NR2B subunit of NMDARs resulting in depletion of NMDARs and synapse loss (84).

Although there is good evidence that small oligomers of PrP^{Sc} appear to be the most efficient for prion disease transmission (85, 86) much less is known about the bio-physical properties of the neurotoxic species driving pathogenesis and their relationship to those entities sub-serving transmission. This contrasting level of understanding in prion diseases concerning the neurotoxic species and its molecular pathogenic effects stems in large part due to the relative lack of tractable, authentic models of acute prion neurotoxicity to redress such knowledge gaps. Simple *in vitro* cell culture models have demonstrated toxic effects of recombinant, soluble, oligomeric PrP enriched in beta-sheet content, as well as toxicity from purified *ex vivo* PrP^{Sc} and proteinase treated PrP^{Sc} extracted from the brains of terminally sick rodents (87-89). In addition, an *in vivo* model of acute neurotoxicity employing stereotaxic injection of recombinant, full-length, beta-sheet-rich, PrP oligomers into the hippocampal CA2 region has been reported, with

toxicity assessed morphologically at 24 hours (90). A model utilising cultured organotypic cerebellar slice explants has also been described (91) although this model relies entirely on *de novo* PrP^{Sc} propagation to generate neurotoxic species over an extended 5-7 week period, rendering it not ideal for assessing direct acute PrP^{Sc} neurotoxicity. Another recently reported model employed *ex vivo* PrP^{Sc} species, scrutinising for retraction and loss of dendritic spines in cultured hippocampal neurons following several hours of exposure to the PrP^{Sc} preparations (92); however, the reported synaptotoxicity required expression of PrP^{C} leaving uncertainty as to whether the neurotoxic PrP^{Sc} species were entirely those directly added to the culture or were species generated from host PrP^{C} through early PrP^{Sc} propagation. Nevertheless, despite considerable limitations of extant models, evidence exists in prion diseases supporting an analogous situation to AD and PD with the neurotoxic entity most likely small oligomers of PrP^{Sc} (90, 93), with synaptic failure appearing to be an important feature of pathogenesis (94-96). Moreover, studies have revealed that impairment of hippocampal LTP coincides with the earliest detection of PrP^{Sc}, slightly prior to morphological evidence of synaptic loss or neuropil vacuolation (96), supporting that impairment of hippocampal CA1 region LTP is an early, sensitive indicator of pathogenesis in prion strains that manifest prominent hippocampal damage and suggest that PrP^{Sc} is likely to be directly synaptotoxic.

Once present, however, the molecular mechanisms through which neurotoxic PrP^{Sc} species induce homeostatic failure in neurons or disrupt critical pathways necessary for cellular integrity remain incompletely resolved. Many studies aimed at elucidating prion pathogenesis have been published, with data supporting the likelihood of protean deleterious consequences from prion infection and the possibility that neurotoxic PrP^{Sc} species may simultaneously disturb more than one fundamental cellular capacity through a “toxic gain-of-function” mechanism; however, these observations do not exclude contributions to pathogenesis from corruption of normal PrP^{C} function. Arguably, the best scientific evidence supports enhanced oxidative stress (97), sustained translational repression (98), especially triggered as part of the unfolded protein response (99), disturbed synaptic calcium ion channels (100) and dysregulation of NMDA receptors causing glutamate-induced excitotoxicity (63) as key pathogenic consequences contributing to neuronal dysfunction and death. Importantly, these various deleterious consequences of neurotoxic PrP^{Sc} would initially be expressed as synaptic impairment.

Human Prion diseases

Nosologically, clinical human prion disease is primarily classified by phenotype as CJD, GSS, FFI or Kuru, with CJD by far the most common form. They can also be concurrently classified according to aetiology as sporadic (no known explanation), acquired (horizontally transmitted) or inherited (genetic). All genetic forms of prion disease are exclusively caused by various pathogenic sequence variations (missense and nonsense point changes, as well as tandem polynucleotide repeat insertions) within the open reading frame of *PRNP*.

Sporadic Creutzfeldt-Jakob disease

Sporadic CJD (sCJD) is the most common form of CJD, explaining 85-90% of all CJD cases, with genetic CJD accounting of 10-15% (101) and acquired CJD <1%. Likelihood of sCJD increases with age with an overall incidence of 1-2 cases/million per year (102). Sexes are affected approximately equally with the slight female predominance attributed to longer life expectancy. Peak occurrence is between 60 and 79 years (103). Causation is unresolved but canonically sCJD is believed to probably represent a stochastic misfolding of PrP^{C} to PrP^{Sc} in the brain, which may happen throughout life (104), with the age-associated occurrence of sporadic CJD due to accumulation of PrP^{Sc} to neurotoxic levels in the brain probably arising from age-related decline in protein quality control mechanisms. Alternatively, a spontaneous somatic mutation in *PRNP* to produce PrP^{Sc} cannot be excluded, with some recent evidence to support this from a bovine form of prion disease (105).

Characteristically, sCJD presents as a rapidly progressive dementia (RPD) accompanied by cerebellar ataxia but a diverse range of other presenting symptoms such as myoclonus and psychiatric disturbance are possible (106). Although relentless neurological deterioration is typical with median survival from first symptoms to death ~4-5 months (107), longer survival is well recognized; terminally, patients frequently develop a state of “akinetic mutism”. A definite diagnosis requires neuropathological examination, most commonly through autopsy. The phenotypic heterogeneity of sCJD appears to correlate with molecular subtype as determined by the combination of codon 129 status of *PRNP* (methionine [M] or valine [V] polymorphism) and the size of the unglycosylated, protease resistant PrP^{Sc} C-terminal fragment on western

blotting (type 1 ~21kDa, type 2 ~19 kDa), with 6 sub-types originally clearly described: MM1/MV1, VV2, MV2, MM2-cortical (MM2C), VV1 and MM2-thalamic (MM2T; sporadic fatal insomnia) (108). Illustrating the phenotypic diversity across sCJD molecular sub-types, MM1/MV1 cases are the most common (~65%) typically manifesting RPD and myoclonus with survival of <~4 months, while MV2 cases characteristically manifest ataxia with survival often longer than 24 months and have unicentric, Kuru-type (PrP^{Sc}-positive) amyloid plaques in the cerebellum; VV1 is the most uncommon (~1% of sCJD) and patients may have younger onset of clinical disease with the cognitive impairment often fronto-temporal in type, which may evolve without significant gross motor impairment. Although a competing molecular sub-typing nomenclature was developed based on refinement of the western blot mobility of the unglycosylated, protease resistant PrP^{Sc} C-terminal type 1 fragment (thereby creating 3 fragment types) the principle of phenotypic diversity correlating with molecular sub-type remained biologically valid (109). Subsequent studies have shown molecular sub-typing to be more complicated by the relatively frequent co-occurrence of type1 and type 2 fragments in the same brain if multiple cerebral hemispheric sites are sampled (110).

Further broadening the phenotypic spectrum of sCJD, in 2008 another subtype of disease known as “variably protease-sensitive prionopathy” (VPSPr) was reported with such cases thought to represent ~1-2% of all sCJD (111). In the seminal study, 11 patients with codon 129 V homozygosity were reported, and while the brain neuropathology revealed spongiform encephalopathy and positive immunohistochemistry for PrP, conventional western blotting of brain homogenates after PK digestion employing the 3F4 antibody unexpectedly showed absence of protease-resistant PrP^{Sc}. Additional immunoblot analyses using another anti-PrP antibody (1E4) did detect protease-resistant PrP but in reduced amounts and displaying an unusual laddering pattern to the banding. These patients were on average somewhat younger than usually observed for sCJD and did not show typical diagnostic features for sCJD on EEG and brain MRI, with CSF negative for 14-3-3 protein; none of the patients had parhogenic sequence variations in *PRNP*. Two years later the same group reported an elaboration of their original observations with additional VPSPr cases encompassing the codon 129 MM and MV genotypes, with all three genotypes sharing similar phenotypic and neurological profiles although VV cases harboured PrP^{Sc} with the least protease-resistance (112).

Beyond codon 129 contributing to the molecular sub-type of sCJD, homozygosity for M or V is associated with an increased risk of developing sCJD (113). While in normal Caucasian populations 52% of individuals are methionine homozygous (MM), 36% are heterozygous (MV) and 12% are V homozygous (VV) (114), homozygosity for M or V isipresent in greater than 80% of persons with sCJD. Additional *PRNP* codon influences on risk are recognised in Asian populations, with codon 219 of *PRNP* homozygous for glutamic acid (G) in >92% of Japanese, Han Chinese and Koreans, with heterozygosity with lysine (K) at this site highly protective against the development of sCJD (113).

Acquired prion disease

Acquired prion disease arises from the typically inadvertent exposure to and consequent horizontal transmission of prions to humans and accounts for <1% of human prion disease. The first report of transmission in a health care setting (iatrogenic CJD; iCJD) was in 1974 in a patient who received corneal grafts unwittingly harvested from a patient dying of CJD (115). Subsequently, iCJD has most commonly occurred through use of contaminated human cadaveric pituitary hormones as treatments for short stature (116) and infertility (117), as well as the use of dura mater grafts in neurosurgery but has also occurred secondary to contaminated neurosurgical instruments (118). Clinically, iCJD, especially if related to cadaveric pituitary hormone therapy, tends to initially manifest as a progressive cerebellar syndrome with dementia occurring late if it develops (119).

As explained previously, transmission through participation in endo-cannibalistic mourning feasts was eventually shown to be the explanation for Kuru, the unusual neurodegenerative cerebellar ataxia observed in the Fore linguistic group in the Eastern Highlands of Papua-New Guinea (8). In general, young children and women consumed more infectious tissues such as brain and internal organs, while adult men consumed less infectious skeletal muscles. The name Kuru comes from the Fore language meaning ‘to shiver’ (or ‘to be afraid’). Although highly endemic in the Fore when originally recognized and reported in the 1950s as these remote regions came under external scrutiny and control, Kuru is now essentially eradicated due to the enforced outlawing of cannibalism albeit with some most recent cases evincing incubation periods of more than 50 years since their participation in the morning feasts of relatives dying from Kuru (120). Typically, Kuru presents with impaired balance and an ataxic gait although

30% of patients report non-specific prodromal symptoms (arthralgias, headache, malaise, cough etc). With disease progression, the Kuru victim is eventually unable to ambulate and dies anywhere from 6-36 months after onset in a bed-ridden state. Neuropathologically, the brain is diffusely affected, with nosologically distinctive features being amyloid ("Kuru") plaques composed of PrP^{Sc} and spongiform degeneration with neuronal loss and astrocytic gliosis also evident. Population genetic studies support that Kuru imposed strong selection pressure on *PRNP* within the Fore, especially at codons 127 and 129, with heterozygosity at these codons offering protection against Kuru, over-represented in survivors of the sustained Kuru epidemic.

The best known form of acquired prion disease is variant CJD (vCJD), the zoonosis related to BSE, first reported in the UK in 1996 (121, 122). Strong evidence supporting the same aetiologic prion strain as BSE was provided very shortly after its recognition (122). vCJD typically presents with alterations in mood and behavior, as well as unpleasant sensory experiences, before more definite neurological symptoms ensue, and primarily occurs in young adults under age 50 years (median age at death 28 years) (121, 123). Neuropathological findings are distinctive for the presence of “florid plaques” (PrP^{Sc}-amyloid cores surrounded by vacuoles) spread across the brain, with spongiform change most pronounced in the thalamus and basal ganglia (121). In addition, vCJD is associated with more widespread distribution of PrP^{Sc} across lympho-reticular tissues such as lymph nodes, tonsil and appendix (124), which is most likely the pathophysiological explanation for the secondary transmissions of vCJD through transfusion of blood products (125, 126). Currently, 232 cases of vCJD have been recognized worldwide, spread across 12 countries, with the largest number in the UK (n=178) and the most recent case occurring in France in a person possibly contracting their illness through professional mis-adventure as a laboratory researcher (127). Until 2016 (128), all cases of vCJD had been associated with M homozygosity at codon 129.

Genetic prion disease

Inherited prion disease accounts for approximately 10-15% of all human prion disease, with essentially all genetic prion disease caused by sequence variations (mis-sense, non-sense, and octapeptide repeat insertions) in the open reading frame of the *PRNP,* which through incompletely defined mechanisms is believed to lead to PrP^{C} misfolding and most often PrP^{Sc} accumulation in the brain.

A large number of *PRNP* mis-sense sequence variations have been claimed as causal of genetic CJD (gCJD), with the most commonly reported E200K, D178N[*cis*-codon129V] and V210I (129). Carriers of E200K and D178N[cis-codon129V] display high penetrance with a nearly 100% likelihood of developing the disease during life. Genetic CJD due to the most common causal mis-sense *PRNP* mutations is usually clinically indistinguishable from sCJD and genetic analysis is required to clarify the aetiology. Shorter (2-7 in length) octapeptide repeat insertions have also been reported as a cause of gCJD and similar to mis-sense sequence variations, phenotypic variation within kindreds is well recognized (130, 131). Single octapeptide repeat insertions (129) and deletions (130) are believed to be normal polymorphisms, while a 2-octapeptide repeat deletion has been tentatively linked to CJD (132).

GSS is considered exclusively genetic in aetiology, displaying autosomal dominant inheritance, and most commonly manifesting as a chronic progressive cerebellar ataxic syndrome although phenotypic variation is recognized. Cognitive impairment usually occurs at some point in the illness, with survival often extending over many years. Neuropathologically, multi-centric amyloid plaques comprised of PrP^{Sc} are characteristic, often with a topological predilection for the cerebellum; spongiform change can vary from severe to absent. GSS has also been reported in association with a range of mis-sense *PRNP* sequence variations (such as F198S, Y218N, P105L, A117V) with P102L the first described (133) and most common (129). Other recognized *PRNP* changes include larger (8 and 9 in length) octapeptide repeat insertions (134) and non-sense mutations (135, 136).

Originally recognised in a large, mutli-generational, Italian kindred as an unusual thalamic neurodegenerative disorder of uncertain aetiology (137), similar to GSS, FFI was later revealed to be an essentially exclusively genetic disease, associated with the D178N[*cis*-codon129M] sequence variation in *PRNP* (10); three years later it was confirmed as transmissible (11) firmly establishing the malady as a prion disease. The major neuropathological findings are observed in the thalamus, especially the medial dorsal and anterior ventral nuclei, with severe neuronal loss and astrocytic gliosis but little or no spongiform degeneration although the latter can be observed to a varying extent in the cerebral cortex. FFI primarily manifests as a sleep disorder associated with dysautonomia but multifarious additional neurological features are reported. Of interest and underscoring the important potential disease-modifying influence of other single

amino acid substitutions in the primary PrP^C sequence, as described above, if the D178N *PRNP* sequence variation is in *cis* with valine at codon 129 (D178N[*cis*-codon129V]), then the clinical phenotype more often aligns to CJD rather than FFI (43). As alluded previously, the very uncommon sCJD molecular subtype MM2T (i.e. in the absence of any underlying D178N[*cis*-codon129M] sequence variation in *PRNP*) can also be associated with an illness recapitulating most of the clinical features of FFI and is known as "sporadic FFI(sFI)" (138). The most common clinical features of sFI are insomnia, ataxia and cognitive decline but motor impairments such as tremor and myoclonus can be present.

Treatments for Prion Disease

Some optimism regarding the potential for effective treatment of prion diseases is derived from the fact congenital absence of PrP^C completely prevents disease occurrence (79), while successful post-natal removal of *PRNP* with total suppression of neuronal PrP^C expression soon after disease initiation appears to completely arrest disease progression and even allow reversal of early neuropathological changes (80). Nevertheless, over many years an extremely diverse range of conventional therapies employing various models have been trialed as treatments for prion disease with limited or no meaningful success. To claim legitimacy as a treatment for sporadic human prion disease the therapy needs to offer significant disease modifying effect when commenced around the time of clinical disease onset although this imperative is not strictly applicable to genetic prion disease where pre-emptive therapeutic intervention may be possible in known mutation carriers.

Although mechanisms of action are not always clearly understood, treatment strategies have broadly tried to target one or more of a few major pathophysiological processes such as: depletion of the availability of PrP^C as substrate for conversion to PrP^{Sc} (eg RNAi); direct interference with PrP^{Sc}-templated PrP^C misfolding (eg Congo red derivatives CR-A, CR-B); and/or correction or mitigation of corrupted homeostatic mechanisms linked to pathogenesis (eg PERK inhibitor GSK2606414 to inhibit parts of the unfolded protein response). A bewildering array of therapeutics spanning small molecules, large molecules, antibodies, nucleic acids, chelators, antibiotics etc have been trialed in *in vivo* models with some prolongation of survival reported if given around the time of inoculation of animals with prions. A much smaller number of therapeutics have shown some efficacy if administered beyond 50% of the predicted

incubation period (eg chemical chaperone GN8, dimethyl sulfoxide, doxycycline etc) with the most potent treatments increasing survival compared to controls by ~170% (intra-cerebroventricular pentosan polysulphate (139)), ~140% (intra-peritoneal polyene antibiotic MS-8209 (140)); and ~23% (single stereotactic intra-hippocampal injection of RNAi (141)), with another promising treatment involving twice-weekly oral gavage of the PERK inhibitor GSK2606414 halted at the time when non-treated mice were terminally ill but treated mice appeared free of disease (142). Rarely have treatments been studied for benefit when administered around the time of clinical onset of disease.

To date, formal human trials of prion disease therapeutics are very limited with unfortunately minimal or no proven benefits demonstrated. The first controlled trial employed the non-opioid analgesic flupirtine, and while demonstrating very modest benefit in cognitive performance it showed no prolongation of survival (143). Human trials involving the ani-malarial drug quinacrine have suffered methodological flaws but no clear efficacy has been apparent (144, 145). Doxycycline was examined in a good quality, controlled trial and despite previous claims of worthwhile benefit in pre-clinical studies and through individual humane use, no efficacy was demonstrated (146). A formal review of observational compassionate use of prolonged intra-cereboventricular infusion of pentosan polysulphate in vCJD patients has suggested possible or probable prolongation of survival albeit in a vegetative state thereby questioning the meaningfulness of the therapy (147). Despite these cumulative disappointments, a cautious positive anticipation surrounds the use of an anti-sense oligonucleotide (ASO) approach, given the absolute pathogenic dependence on ongoing availability of PrP^C as substrate for conversion and the success of this technology in genetically driven diseases such as spinal muscular atrophy. The ASO is directed against the mRNA of PrP^C, promoting cell-mediated degradation prior to translation and hence substantial diminution of expression levels; hopefully human trials of this therapeutic approach will commence soon (148).

Prion-like diseases

Following Stanley Prusiner's paradigm shifting report in 1982 firmly establishing the "protein-only" hypothesis (1), the next approximately 3 decades saw prion diseases progressively construed as occupying a unique nosological category amongst neurodegenerative disorders. Over recent years, however the concept that prion diseases are biologically unique, given the

transmissible agent is constituted primarily if not exclusively by misfolded prion protein (PrP^{Sc}), has been increasingly questioned. Tentative evidence was presented many years ago suggesting the transmissibility of Abeta in animal (primate) models (149) and during the provision of human health care (150) but really gained no traction; it is only during the last approximately 5-10 years that the unparalleled biological standing of prion diseases has been seriously challenged. Although many issues in relation to this blurring of the margins between prions and other proteins underpinning non-prion neurodegenerative diseases, such as AD (Abeta and tau) and PD (alpha-synuclein) remain to be resolved, there seems little doubt that the previous neat and unassailable demarcation of prion diseases from other neurodegenerative disorders has been relegated to history. Over recent years numerous basic scientific and clinical research studies have undermined the exceptional biological standing of prion diseases. Prion-like mechanisms of propagation, inter-cellular transfer and inter-organismal spread have been reported for other proteins, especially Abeta (151, 152) and alpha-synuclein (153-156), as well as more limited data for tau (157) and huntingtin (158). This growing body of work has prompted provisional new descriptors for these transmissible non-prion proteins, including "propagons" (159) or "proteopathic seeds" (160).

Probably the most compelling evidence for inter-organismal transmissibility and propagation of non-prion proteins pertains to the use of human cadaveric pituitary hormones (161) and dura mater grafts (162) as treatments. One of the important issues to resolve is whether following transmission, the propagation and accumulation of non-prion proteins such as Abeta in a new host culminate in a disease phenotype or remain sub-clinical. Although the initial observation of transmitted Abeta being propagated and deposited in the brain as parenchymal plaques and in cerebral blood vessels as cerebral amyloid angiopathy (CAA) was in those succumbing to iCJD, subsequent reports have demonstrated these neuropathological findings in people undergoing identical treatments who did not develop iCJD (163) and also in patients receiving peripheral dura mater grafts for non-neurological reasons (164) or simply undergoing childhood neurosurgery many years previously (165). Moreover and very importantly, these very recent reports (164, 165) support the pendulum has swung towards the likely eventual development of overt disease in at least some individuals undergoing such treatments (eg dura mater grafts; neurosurgery with instruments presumably contaminated with Abeta), with the propagated Abeta

deposited as CAA causing spontaneous, often severe, intra-cranial haemorrhage in relatively young people with no genetic or other risk factors for premature CAA.

Section 1: Normal Prion Protein Cellular Biology

As outlined in the literature review, considerable progress over the last four decades has been made in understanding the cellular biology of PrP^C, such as synthetic pathways, cellular locations of the mature protein, constitutive processing events, turnover mechanisms and potential normal functions. Achieving a good understanding of the normal cellular biology of PrP^C informs fundamental issues such as likely principal function(s) in the CNS, as well as any role in the pathogenesis of prion disease; both likely to illuminate or facilitate therapeutic avenues. Despite such progress however, our understanding is far from complete and we are still without a consensus understanding of the principal biological role(s) of PrP^C in the CNS although many putative functions have been reported. Over many years I lead my research team to undertake numerous important studies, providing worthwhile new insights into the cellular biology of PrP^C and how this may relate to normal function and impact prion disease pathogenesis. These studies provided insights into the structural biology of membrane interactions and the factors influencing signal transduction of PrP^C, as well as showed that constitutive endoproteolysis, including generated fragments, are likely to have important roles in attenuating oxidative stress and mitigating conversion of PrP^C to PrP^{Sc}. Our studies also demonstrated a new type endoproteolytic ("gamma"-) cleavage, which remains incompletely defined as far as the precise site and biological significance but underscores the constitutive processing diversity open to PrP^C, as well as determined a role for PrP^C in regulating neuronal stem cells, including that mediated through beta-amyloid.

List of my publications submitted in full (in chronological order)

Haigh CL, Drew SC, Boland M, Masters CL, Barnham KJ, Lawson VA, Collins SJ. Dominant roles of the polybasic proline motif and Cu in PrP23-89 mediated stress protection response. Journal of Cell Science 2009; 122: 1518-1528.

Haigh C, Lewis V, Vella L, Masters CL, Hill AF, Lawson V, Collins SJ. PrPc related signal transduction is inter-dependently influenced by copper, membrane integrity, and the alpha cleavage site. Cell Research 2009; 19: 1062-1078.

Lewis V, Hill AF, Haigh CL, Klug GM, Masters CL, Lawson VA, Collins SJ. Increased proportions of C1 truncated prion protein protect against cellular M1000 prion infection. Journal of Neuropathology and Experimental Neurology 2009; 68: 1125-1135.

Boland MP, Hatty CR, Separovic F, Hill AF, Tew D, Barnham K, Haigh CL, James M, Masters CL, SJ Collins. Anionic phospholipid interactions of the prion protein N-terminus are

minimally perturbing and not driven solely by the octapeptide repeat domain. Journal of Biological Chemistry 2010; 285:32282-32292.

Karas JA, Boland M, Haigh C, Wall VA, Hill AF, Barnham K, Collins SJ, Scanlon D. Microwave synthesis of prion protein fragments up to 111 amino acids in length generates biologically active peptides. International Journal of Peptide Research and Therapeutics 2012; 18: 21-29.

Lewis V, Whitehouse IJ, Baybutt H, Manson JC, Collins SJ, Hooper NM. Prion protein expression is not regulated by the Alzheimer's amyloid precursor protein intracellular domain. PLoS One 2012; 7: e31754.

Johanssen VA, Johanssen T, Drew SC, Masters CL, Hill AF, Barnham KJ, Collins SJ. C-terminal peptides modelling constitutive PrPC processing demonstrate ameliorated toxicity predisposition consequent to alpha-cleavage. Biochemical Journal 2014; 459: 103-115.

LeBrun A, Haigh CL, Drew S, James M, Boland MP, Collins SJ. Neutron reflectometry studies define prion protein N-terminal peptide membrane binding. Biophysical Journal 2014; 107: 2313-2324.

Haigh CL, McGlade A, Collins SJ. MEK1 transduces the prion protein N2 fragment anti-oxidant effects. Cellular and Molecular Life Sciences 2015; 72: 1613-1629.

Collins SJ, Tumpach C, Li Q-X, Lewis V, Ryan TM, Roberts B, Drew SC, Lawson VA, Haigh CL. The prion protein regulates beta-amyloid mediated self-renewal of neural stem cells *ex-vivo.* Stem Cell Research and Therapy 2015 DOI 10.1186/s13287-015-0067-4.

Haigh CL, Tumpach C, Drew SC, Collins, SJ. The prion protein N2 fragment binds to phosphatidylserine and phosphatidic acid; relevance to stress-protection responses. PLoS One 2015: DOI:10.1371/journal.pone.0134680.

Haigh C, Collins S. Endoproteolytic cleavage as a molecular switch regulating and diversifying prion protein function. Neural Regeneration Research 2016; 11: 238-239.

Lewis V, Johannsen V, Crouch P, Klug G, Hooper N, Collins S. Prion protein "gamma-cleavage": characterizing a novel endoproteoplytic processing event. Cellular and Molecular Life Sciences 2016: 73: 667-683.

Haigh C, Tumpach C, Collins S, Drew S. A 2-substituted 8-hydroxyquinoline stimulates neural stem cell proliferation by modulating oxidase ROS signalling. Cell Biochemistry and Biophysics 2016: 74: 297-306.

Collins S, Tumpach C, Groveman B, Drew S, Haigh C. Prion protein cleavage fragments regulate adult neural stem cell quiescence through redox modulation of mitochondrial fission and SOD2 expression. Cellular and Molecular Life Sciences 2018: doi.org/10.1007/s00018-018-2790-3.

Dominant roles of the polybasic proline motif and copper in the PrP23-89-mediated stress protection response

Cathryn L. Haigh[1,2], Simon C. Drew[1,2,3,4], Martin P. Boland[1,2], Colin L. Masters[2,5], Kevin J. Barnham[1,2,3], Victoria A. Lawson[1,2] and Steven J. Collins[1,2,*]

[1]Department of Pathology, The University of Melbourne, 3010, Australia
[2]Mental Health Research Institute, The University of Melbourne, 3010, Australia
[3]Bio21 Molecular Science and Biotechnology Institute, The University of Melbourne, 3010, Australia
[4]School of Physics, Monash University, Clayton, 3800, Australia
[5]Centre for Neuroscience, The University of Melbourne, 3010, Australia
*Author for correspondence (e-mail: stevenjc@unimelb.edu.au)

Accepted 10 January 2009
Journal of Cell Science 122, 1518-1528 Published by The Company of Biologists 2009
doi:10.1242/jcs.043604

Summary

Beta-cleavage of the neurodegenerative disease-associated prion protein (PrP) protects cells from death induced by oxidative insults. The beta-cleavage event produces two fragments, designated N2 and C2. We investigated the role of the N2 fragment (residues 23-89) in cellular stress response, determining mechanisms involved and regions important for this reaction. The N2 fragment differentially modulated the reactive oxygen species (ROS) response induced by serum deprivation, with amelioration when copper bound. Amino acid residues 23-50 alone mediated a ROS reduction response. PrP23-50 ROS reduction was not due to copper binding or direct antioxidant activity, but was instead mediated through proteoglycan binding partners localised in or interacting with cholesterol-rich membrane domains. Furthermore, mutational analyses of both PrP23-50 and N2 showed that their protective capacity requires the sterically constraining double proline motif within the N-terminal polybasic region. Our findings show that N2 is a biologically active fragment that is able to modulate stress-induced intracellular ROS through interaction of its structurally defined N-terminal polybasic region with cell-surface proteoglycans.

Supplementary material available online at
http://jcs.biologists.org/cgi/content/full/122/10/1518/DC1

Key words: Prion, N-terminus, Oxidative stress, Beta-cleavage, GAG, Copper

Introduction

Prion diseases are transmissible neurodegenerative disorders causally linked to abnormal conformers (termed PrP^{Sc}) of the cellular prion protein (PrP^{C}). The role of PrP^{C} within the cell has proved difficult to resolve, with suggested functions including copper homeostasis and trafficking, signal transduction, cellular adhesion and attenuation of oxidative stress (Brown and Besinger, 1998; Brown et al., 1999; Schmitt-Ulms et al., 2001; Spielhaupter and Schätzl, 2001; Stuermer et al., 2004). Protection against oxidative stress or reactive oxygen species (ROS) has been proposed to be enzymatic, wherein PrP^{C} itself would have superoxide dismutase-like activity (Brown et al., 2001), or alternatively, mediated by signal transduction cascades, whereby the resultant reaction protects the cell (Watt et al., 2005). The regions of PrP^{C} involved in such protection have been investigated and both the C- and N-termini have been determined to be involved (Rambold et al., 2008).

The C-terminal amyloidogenic region has been more widely studied than the N-terminal region due to its propensity to misfold and so have a more prominent association with disease. However, mutations within the N-terminus are found in hereditary prion diseases, consisting of insertions or deletions within the copper-binding octameric repeat domain (Kovács et al., 2005). The N-terminal region, although not constituting part of the amyloid core of PrP^{Sc}, is thought to be biologically active, associated with clathrin-mediated internalisation and intracellular trafficking of PrP^{C} (Nunziante et al., 2003; Shyng et al., 1995; Sunyach et al., 2003), and with PrP^{C} movement at the cell surface (Taylor et al., 2005). In particular, the most N-terminal amino acids of PrP^{C} are highly conserved across mammalian species (Wopfner et al., 1999) and contain a polybasic domain (residues 23-28) shown to function as a glycosaminoglycan (GAG)-binding site (Pan et al., 2002). PrP^{C} binding to cellular receptors, including low density lipoprotein receptor-related protein 1 (Parkyn et al., 2008) and the 37 kDa/67 kDa laminin receptor (Gauczynski et al., 2001), involves the N-terminal region. Further, the latter of these PrP receptors requires heparan sulphate to mediate binding and has additionally been shown to be involved in the internalisation of PrP^{Sc} (Morel et al., 2005; Gauczynski et al., 2006).

PrP cleavage fragments, corresponding to two internal cleavage sites, can be detected in both cell culture systems and brain tissue. In non-disease states the α-cleavage fragments (N1/C1) usually have a higher prevalence than the β-cleavage fragments (N2/C2). The latter cleavage fragments are increased in the brains of Creutzfeldt-Jakob Disease (CJD) patients and mice generated as models of prion disease (Chen et al., 1995; Yadavalli et al., 2004). This increase has mainly been considered a pro-pathogenic event, but equally might represent a neuronal protective response, attempting to compensate for increased stress during disease progression. Consistent with this hypothesis, cell lines expressing mutant PrP species that do not undergo N2/C2 cleavage are rendered unable

to respond to oxidative stress insults (Watt et al., 2005). Further studies have shown that, in the context of full-length PrP, tethering the N-terminus abolishes protective responses against various cellular stressors (Dupiereux et al., 2008; Zeng et al., 2003).

The enigmatic nature of the hereditary disease-associated, highly conserved N-terminal region of PrP^C prompted us to look more closely at its function. Our specific aim was to elucidate if and how the N-terminal β-cleavage product (N2) of the prion protein modulates intracellular ROS under conditions of enhanced stress. Copper co-ordination of a representative murine N2 fragment, encompassing residues 23-89, favourably influenced intracellular ROS produced in response to serum deprivation. The most N-terminal region (23-50), independent of copper coordination, also conferred a cellular protective effect resulting in reduced intracellular ROS. This effect was shown to be dependent on cell-surface, heparan-sulphate-containing proteoglycans, which are either localised to, or require interaction with, lipid-raft domains. Furthermore, the two proline residues within the polybasic region at the N-terminus of mature PrP^C (residues 26 and 28) were found to exert a dominant effect over the cellular association of this region and the redox-protective activity of PrP23-89.

Results

N2 differentially modulates the production of intracellular ROS in response to serum deprivation depending on copper occupancy

β-Cleavage of PrP^C is reportedly ragged. Amino acid 89 was selected for the C-terminal residue, as this approximates the mid-point of the β-cleavage range (Fig. 1A) and ensures that the octapeptide repeat domain is intact, which is likely to be important for the biological functions of N2. To investigate potential protective effects, PrP23-89 was applied to CF10 cells manifesting increased intracellular ROS. CF10 cells were the primary cell line used in this study, as they represent a PrP^C-null background to avoid potentially confounding effects caused by the activity of full-length PrP, the complementary C2 fragment or endogenously produced N2. Cellular ROS insults were induced using serum deprivation to avoid the peptides contacting serum proteases that might degrade them. Intracellular ROS levels were assayed using the DCFDA assay, which detects H_2O_2 (in the presence of endogenous metal ions), $HO^{\cdot}$, $ROO^{\cdot}$, and $ONOO^-$ (Martin et al., 1998). The ROS generated and viability data in response to decreasing serum concentrations are shown in supplementary material Fig. S1. When applied in a $\log_{10}$ dilution series from 0.01-10,000 nM the N2 fragment increased the intracellular ROS in serum-deprived CF10 cells to a plateau at 1 nM peptide (Fig. 1B,C). By contrast, when 10 μM peptide was applied with equimolar followed by 2-6 molar equivalents of $CuCl_2$-6×glycine, a protective effect compared with 'no peptide', 'peptide' and 'copper alone' treatments was seen from 2-4 molar equivalents (Fig. 1B,D). One to six molar equivalents (10–60 μM) of copper alone showed progressively increasing ROS up to 5 equivalents and a lesser effect at 6 equivalents; the latter effect is most likely due to a reduction in cell viability caused by copper toxicity. A peptide corresponding to the amino acid sequence of PrP23-89 scrambled was also assayed and showed no variation from baseline ROS production in response to serum deprivation or serum deprivation with 1-6 molar equivalents of $CuCl_2$-6×glycine (supplementary material Fig. S2).

PrP23-50 attenuates the intracellular ROS response

To explore the PrP domains responsible for the activity of the N2 fragment, a peptide encompassing only the copper-binding octameric repeat domain (PrP51-89) and an N-terminal peptide lacking this domain (PrP23-50) were employed. These were applied to the CF10

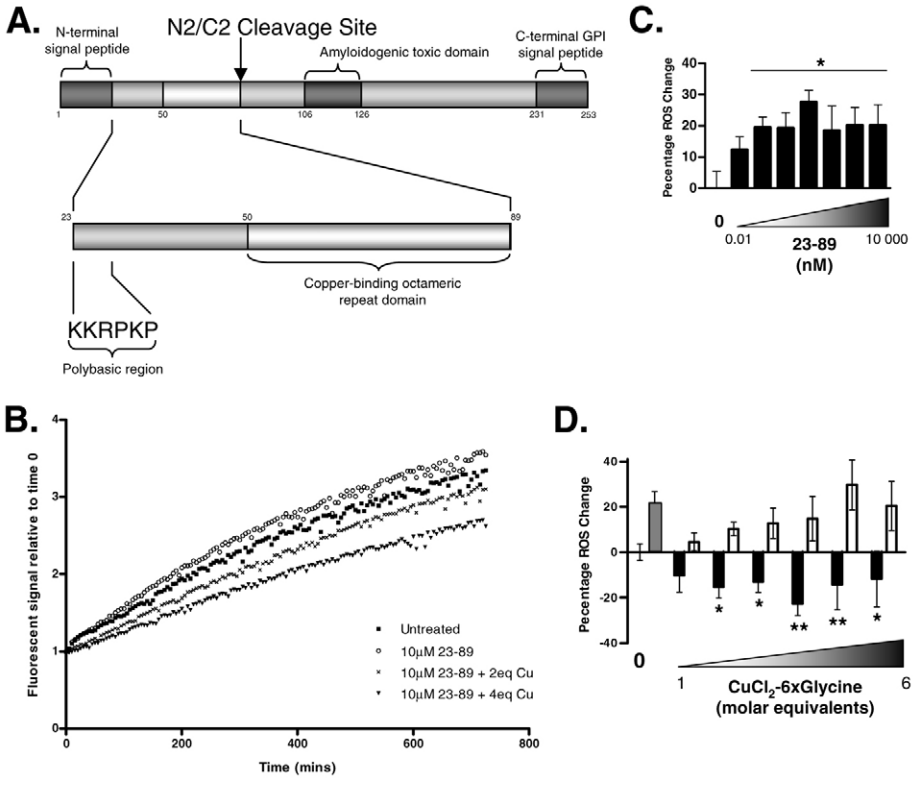

Fig. 1. PrP23-89 (N2) modulates intracellular oxidative stress conditional upon copper saturation. (A) Schematic representation showing the defined regions of PrP and the approximate internal cleavage site producing N2 and C2 fragments. (B-D) N2 reduces ROS induced by serum deprivation only when pre-loaded with copper. Synthetic N2 encompassing murine amino acids 23-89 was applied to serum-deprived CF10 cells in a $\log_{10}$ serial dilution from 0.01-10,000 nM. The 10,000 nM concentration was also applied after pre-mixing with 1-6 molar equivalents of copper; 1-6 equivalents of copper were applied without peptide for comparison. (B) Example of intracellular ROS curves obtained using the DCFDA fluorescent dye. Initial rates were calculated as the linear tangent to the curve and are shown as the percentage change from the baseline rate obtained for the serum-free environment. (C) ROS rate changes induced by the apo-PrP23-89 peptide over the dilution series. Significantly increased intracellular ROS production is seen from 0.1 nM peptide (one-way ANOVA, F=11.22, P=0.001, *P<0.01). The effect of copper-loading the PrP23-89 peptide on intracellular ROS is shown in D, with black bars indicating the copper-loaded peptide and white bars indicating the equivalent copper-alone condition. For comparison, the grey bar shows the intracellular ROS response to the peptide alone. Conditions significantly different from both the copper- and peptide-alone controls, as determined by two-way ANOVA (F=45.49, P<0.001), are indicated by *P<0.05 **P<0.01.

cells in the same $\log_{10}$ serial dilution as used for PrP23-89 and, as 51-89 is a characterised copper-binding domain, the PrP51-89 peptide was also applied with 1-6 equivalents of $CuCl_2$-6×glycine. PrP51-89 showed increased intracellular ROS at low concentrations and with 1-3 equivalents of $CuCl_2$ (Fig. 2A), whereas the PrP23-50 fragment decreased the intracellular ROS produced by serum deprivation at the lowest concentration used (0.01 nM), significant at 10 nM peptide (Fig. 2B). To check for specificity of the PrP23-50 reaction, a scrambled peptide corresponding to the amino acid composition of PrP23-50 (PrP23-50scram) was also assayed and showed no significant ability to decrease (or increase) the intracellular ROS produced by serum deprivation (Fig. 2B).

Neuro2a cells show copper-dependant PrP23-89 ROS reduction and PrP23-50 ROS reduction at higher peptide concentrations

Wild-type PrP-expressing cells are likely to be influenced by endogenous expression of full-length PrP and the N2/C2 cleavage fragments. However, to ascertain whether a response could still be elicited by increased N2 at the membrane, Neuro2a (N2a) cells were exposed to 10 μM PrP23-89 with and without 4 molar equivalents $CuCl_2$-6×glycine. Both the apo PrP23-89 and the copper-loaded peptide were able to reduce intracellular ROS in response to serum deprivation, with the copper-loaded PrP23-89 showing a lesser response than the apo PrP23-89 (Fig. 3A). The reason for such a discrepancy most likely arises from the basal copper content of the cells, as the brains of null mice have been shown to have reduced copper concentrations compared with their wild type counterparts (Brown, 2003). To confirm this we incubated the cell lines with the copper-reactive fluorescent dye Phen Green Fl, which is quenched by both Cu^+ and Cu^{2+} and also has a lesser reactivity with iron and cobalt (Chavez-Crooker et al., 2001). This confirmed greater basal metal ion concentrations in the N2a cells compared with the CF10 cells (Fig. 3B). The N2a cells showed no response to the PrP51-89 fragment (Fig. 3A); however, when PrP23-50 was assayed by dose titration, there was a specific and significant ROS reduction at 1 μM peptide (Fig. 3C). This is a higher concentration than seen for the CF10 cells and most likely indicates that the endogenous PrP is exerting an effect that mutes the reaction. As shown for the CF10 cells, the response of the N2a cells to decreasing serum concentrations and to PrP23-89scram are included in supplementary material Figs S1 and S2, respectively.

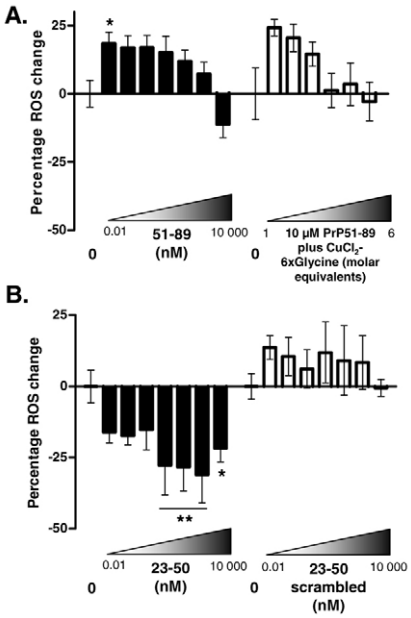

Fig. 2. Amino acids PrP23-50 alone reduce the ROS response to serum deprivation. Synthetic PrP51-89 and PrP23-50 were added to serum-deprived cells in the $\log_{10}$ serial dilution from 0.01-10,000 nM and the intracellular ROS response measured by DCFDA assay (A and B, black bars). PrP51-89 (10 μM) was also assayed with 1-6 molar equivalents $CuCl_2$-6×glycine (white bars). Changes in the rate of ROS production are represented as the percentage change from the rate induced by serum deprivation alone. PrP51-89 at 0.01 nM and when loaded with 1-2 molar equivalents $CuCl_2$-6×glycine shows no significant difference from when copper alone is applied (two-way ANOVA; F=1.225, P=0.2738). Cells treated with PrP23-50 show significantly reduced intracellular ROS in response to serum deprivation from 10-10,000 nM peptide (one-way ANOVA; F=4.774, P=0.0018, *P<0.05, **P<0.01). To eliminate the possibility of non-specific effects, a scrambled peptide (PrP23-50scram) was also assayed (B; white bars). No significant change in the rate of ROS production is seen for the PrP23-50scram peptide (one-way ANOVA, F=0.4482, P=0.8615).

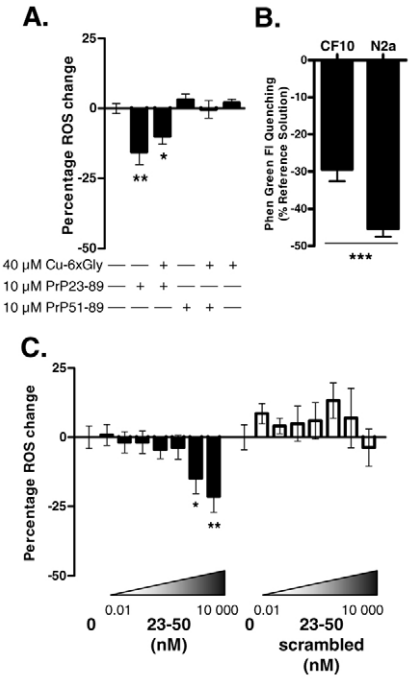

Fig. 3. Wild-type N2a cells show ROS reduction in response to PrP23-89 and PrP23-50. (A) PrP23-89 and PrP51-89 (10 μM) were added to N2a cells with and without 4 molar equivalents of $CuCl_2$-6×glycine and assayed for the ROS produced in response to serum deprivation by the DCFDA assay. Changes in the rate of ROS production are represented as the percentage change from the rate induced by serum deprivation alone. PrP23-89 both with and without copper significantly reduced the intracellular ROS induced by serum deprivation (one-way ANOVA F=6.298, P=0.0021, *P<0.05, **P<0.01). (B) Phen green quenching experiments show that N2a cells have higher basal concentrations of copper compared with CF10 cells (Student's t-test, t=4.148, **P=0.0025), possibly explaining the ROS-reducing activity of apo PrP23-89 in these cells compared to that seen in the CF10 cells. (C) PrP23-50 (black bars) and PrP23-50scram (white bars) were added to serum-deprived cells in the $\log_{10}$ serial dilution from 0.01-10,000 nM. Cells treated with PrP23-50 show significantly reduced intracellular ROS in response to serum deprivation from 1000-10,000 nM peptide (one-way ANOVA, F=4.774, P=0.0018, *P<0.05, **P<0.01). No significant change in the rate of ROS production is seen for the PrP23-50scram peptide (one-way ANOVA, F=0.4482, P=0.8615).

PrP23-50 does not mediate its protective response by copper binding or direct antioxidant activity

Although the octameric repeat copper-binding domain has been well characterised, the PrP23-50 region has been less rigorously investigated. To clarify how this fragment mediates the intracellular ROS reduction effect, we investigated its ability to coordinate copper or to directly act as an antioxidant molecule. Electron paramagnetic resonance (EPR) spectroscopy indicated that both PrP23-50 and PrP23-50scram were able to coordinate copper upon addition of 1 molar equivalent of $CuCl_2$; however, both peptides readily surrendered their copper load to 2.5 molar equivalents of the weak copper chelator glycine (Fig. 4A). This indicates that the copper binding of PrP23-50 is non-specific at pH 7.0 (K_d>1 μM) and unlikely to be biologically meaningful in the cell-protective effect. When PrP23-50 and PrP23-50scram were assayed for their ability to reduce ROS produced by the Fenton reaction, with the radicals produced detected by fluorescent spin trapping, neither peptide showed any antioxidant ability (Fig. 4B). Circular dichroism (CD) spectroscopy confirmed that PrP23-50 adopts a predominantly random coil structure, indistinguishable from that of PrP23-50scram, indicating that the assumption of altered secondary structure in the absence of the octameric repeat domain is unlikely to be relevant to the PrP23-50 ROS reduction effect (Fig. 4C).

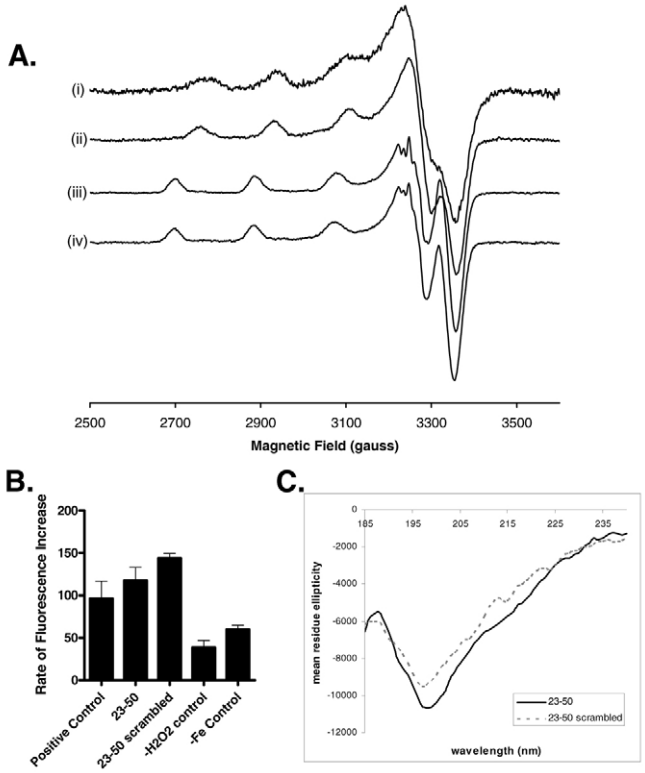

Fig. 4. The PrP23-50 region has limited copper-binding ability, is not an antioxidant and assumes no specific secondary structure. (A) EPR spectra of PrP23-50 (i,iii) and PrP23-50scram (ii,iv) with 1 molar equivalent of Cu^{2+} in the absence (i,ii) and presence (iii,iv) of 2.5 molar equivalents glycine. Both peptides readily surrender their bound copper to the low-affinity chelator glycine, indicating that PrP23-50 binds copper non-specifically like any unstructured peptide, with the N-terminal amine, backbone amide(s) and water molecules being the likely ligands. The principal $g_{||}$ and $A_{||}$ parameters characterising the spectra ($g_{||}$~2.23, $A_{||}(^{65}Cu)$~170-180×$10^{-4}cm^{-1}$) are compatible with a 3N1O or 2N2O coordination sphere of equatorial ligands. Spin quantification by double-integration of the spectra indicates that PrP23-50 and PrP23-50scram bind around 1/3 and 1/2, respectively, of the observable Cu^{2+} bound in the presence of glycine; the unbound Cu^{2+} fraction forms EPR-silent copper hydroxide at pH 7 (Drew and Barnham, 2008). (B) The ability of PrP23-50 to act as an antioxidant was assessed by response to the Fenton reaction caused by H_2O_2 and $FeSO_4$, with the fluorescent radical trap proxyl fluorescamine used to capture hydroxyl radicals produced. In comparison with the positive control, neither PrP23-50 nor PrP23-50scram showed any ability to reduce the radicals reaching the trap. Shown are the mean rates with s.e.m. for three independent experiments. (C) CD spectroscopy shows that both PrP23-50 and PrP23-50scram adopt a predominantly random coil structure.

PrP23-50 mediates its intracellular ROS-attenuating effect through a proteoglycan binding partner found within, or requiring, intact cholesterol-rich domains

In the absence of a direct biochemical explanation for the ROS reduction response of PrP23-50, cellular interactions were investigated. First trypsin was used to crudely remove all cell-surface protein and the production of intracellular ROS induced by serum deprivation monitored by the DCFDA assay as before with and without PrP23-50 applied in the log_{10} serial dilution. Trypsinising the cells did not significantly alter the rate of ROS produced in the absence of serum (Fig. 5A, left panel), but the PrP23-50 fragment no longer significantly reduced ROS levels (Fig. 5A, right panel), indicating that the PrP23-50 response most likely involves a protein-binding partner as opposed to lipid-membrane interactions. Filipin III complex, an antibiotic that binds and sequesters cholesterol, was used to disrupt cholesterol-rich lipid-raft domains within the cell membrane. Lipid-raft domains are known to be important signalling platforms, and so potential binding partners may reside in, or mediate their response through, resident proteins. Treatment with filipin III showed a trend toward a reduced ROS rate in response to serum deprivation in the absence of peptide, but this was not significant (Fig. 5B, left panel). Filipin III-treated cells showed no response to any concentration of the PrP23-50 fragment, indicating that lipid-raft domains are involved in mediating the PrP23-50 ROS reduction response (Fig. 5B, right panel). The transferrin receptor, which is excluded from lipid-raft domains, was used as a control to show preserved location of non-raft proteins (supplementary material Fig. S3).

The most N-terminal amino acids of PrP23-50 contain a polybasic GAG-binding site. Therefore to more closely examine the nature of a PrP23-50-binding partner, two GAG-catabolising enzymes were used to selectively remove cell-surface GAGs of interest from their protein cores. Cells were treated with heparin lyase III to remove heparan sulphate or chondroitinase ABC to remove chondroitin A, B and C, and were then assayed for their intracellular ROS response to serum deprivation with and without addition of the log_{10} dilution of PrP23-50. The removal of GAGs by both enzymes induced a significant increase in intracellular ROS production in response to serum deprivation (Fig. 5C,D, left panels): however, the chondroitinase ABC-treated cells were still receptive to reduction of intracellular ROS by PrP23-50 (Fig. 5D, right panel). The heparin lyase III-treated cells showed no reduction in ROS when incubated with PrP23-50 (Fig. 5C, right panel), indicating that the PrP23-50 response is dependant on proteoglycans containing heparan sulphate. The effective removal of over 40% of cellular heparan sulphate was confirmed by dot blotting, as shown in supplementary material Fig. S4.

The PrP octarepeat domain, with and without bound copper, influences N-terminal peptide cell association or internalisation and half life

The N-terminal polybasic region (amino acids 23-28) has been shown to be essential for PrP^C internalisation (Sunyach et al., 2003).

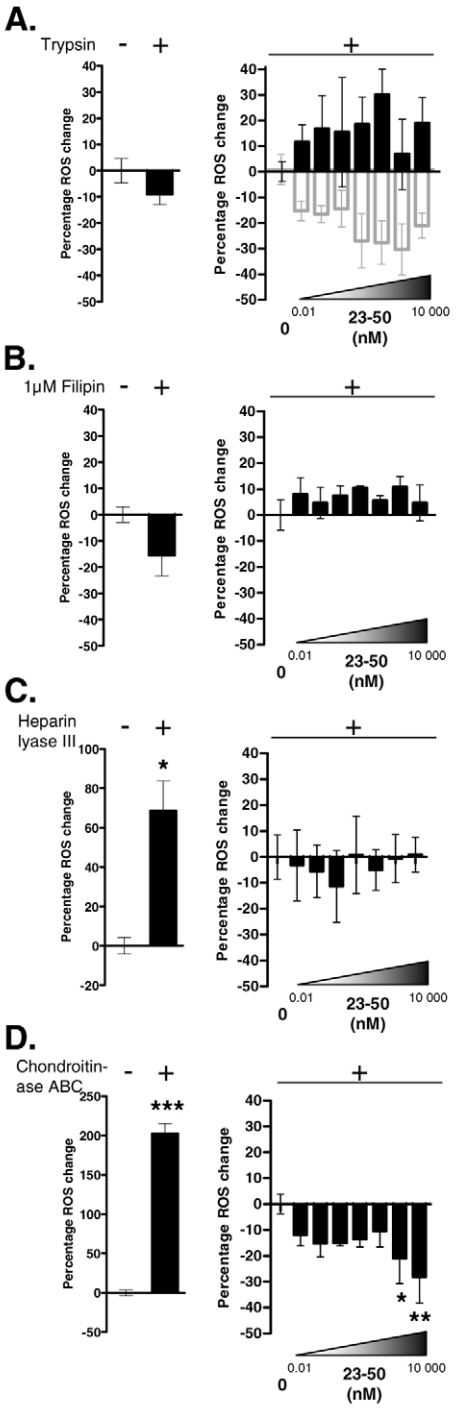

Fig. 5. Removal of cell membrane proteins or heparan sulphate, or disruption of lipid rafts, abolishes the PrP23-50-mediated intracellular ROS reduction response to serum deprivation. The effect of the cell surface environment on the protective function of PrP23-50 against intracellular ROS was assessed using the DCFDA assay. The $\log_{10}$ serial dilution of PrP23-50 was applied to the cells after treatment with (A) trypsin before the start of the assay, (B) 1 μM filipin III for the duration of the assay, (C) heparin lyase III at 10 mU/ml for 1 hour before the start then at 5 mU/ml for the duration of the assay, and (D) chondroitinase ABC as for the heparin lyase III treatment. For each condition the left panel shows the effect of the treatment on the production of intracellular ROS compared with serum-free media only, and the right panel shows the effect of the PrP23-50 peptide on the cells after they have been exposed to the treatment. Alterations in the rate of ROS production before PrP23-50 treatment have been compensated for in the analysis. The results of PrP23-50 treatment (in the absence of other treatment) are shown as empty grey bars in panel A for comparison. Significant results as determined by Student's *t*-test for changes in the rate caused by the treatment or by one-way ANOVA for changes induced by PrP23-50 are indicated by $*P<0.05$, $**P<0.01$ and $***P<0.001$.

Therefore, to address whether the PrP23-50 effect might be a result of internalisation by its protein-binding partner(s), cells were treated for 0-60 minutes with 10 μM peptide (PrP23-50 alone and PrP23-89 with/without 4 molar equivalents $CuCl_2$-6×glycine) and both cell lysates and media western blotted for the peptides. Peptide within the cell lysate fraction may be internalised or membrane-bound (referred to as 'cell-associated'). The strongest cell-associated signal was seen in cells treated with PrP23-89 without copper. Even 1 minute post-exposure the peptide can be seen clearly within this fraction and already seems to have reached its plateau (Fig. 6A,B). When PrP23-89 is applied pre-loaded with copper, the initial signal is much weaker and increases over time to an overall lower level. This indicates that in the absence of copper the octarepeats can mediate binding to the cell surface and/or internalisation, which is disconnected to protection against intracellular ROS, whereas when copper is bound the octarepeat site is less cell-accessible or binding becomes more specific. PrP23-50 shows almost no cell association, indicating that low levels of cell association are sufficient to achieve protection or that the response must be the result of a rapid, transient linkage. When the rate of disappearance of PrP23-50 from the media and the overall rate of disappearance of the fragment are considered (Fig. 6C,D), PrP23-50 is seen to disappear much faster than the PrP23-89 peptide (with or without copper), indicating that PrP23-50 is turned over much more rapidly. Rapid destruction at the membrane or within the cell may explain the lack of PrP23-50 signal within the cell-associated fraction. Copper binding to PrP23-89 appeared to slow the overall loss of this peptide, possibly as a result of more gradual binding to its cellular partners at the membrane, resulting in a slower catabolic processing.

Mutational analysis of the N-terminal polybasic region indicates that proline residues 26 and 28 are required for specific interaction and generation of the intracellular ROS protective effect

It has previously been shown that the internalisation response of PrP^C is diminished if the positively charged amino acids of the N-terminal polybasic region are mutated to more neutrally charged residues (Sunyach et al., 2003). The charge of this region, however, is not its only feature. Within the charged residues are two prolines: a motif that functionally is highly significant. Proline motifs are known to impart a degree of structure onto proteins due to the steric constraints of the rigid pyrrolidine ring (reviewed by Vanhoof et al., 1995). Proline motifs are very often found in association with positively charged amino acids, and therefore we hypothesised that these two proline residues were likely to be an essential part of the functional moiety and crucial for the biological activity of PrP23-50 and PrP23-89. To test this hypothesis, the PrP23-50 fragment was synthesised with prolines 26 and 28 mutated to alanine. Alanine was substituted for proline because of its similar size and charge properties but lack of rigid structure. The ability of PrP23-50 P26/28A to reduce the ROS induced by serum deprivation in the CF10 cells was tested using the $\log_{10}$ serial dilution of peptide. The PrP23-50 P26/28A peptide showed no ability to modulate intracellular ROS induced by serum deprivation (Fig. 7A). Furthermore, when cell lysates and media were probed to look for internalisation/cell association it was

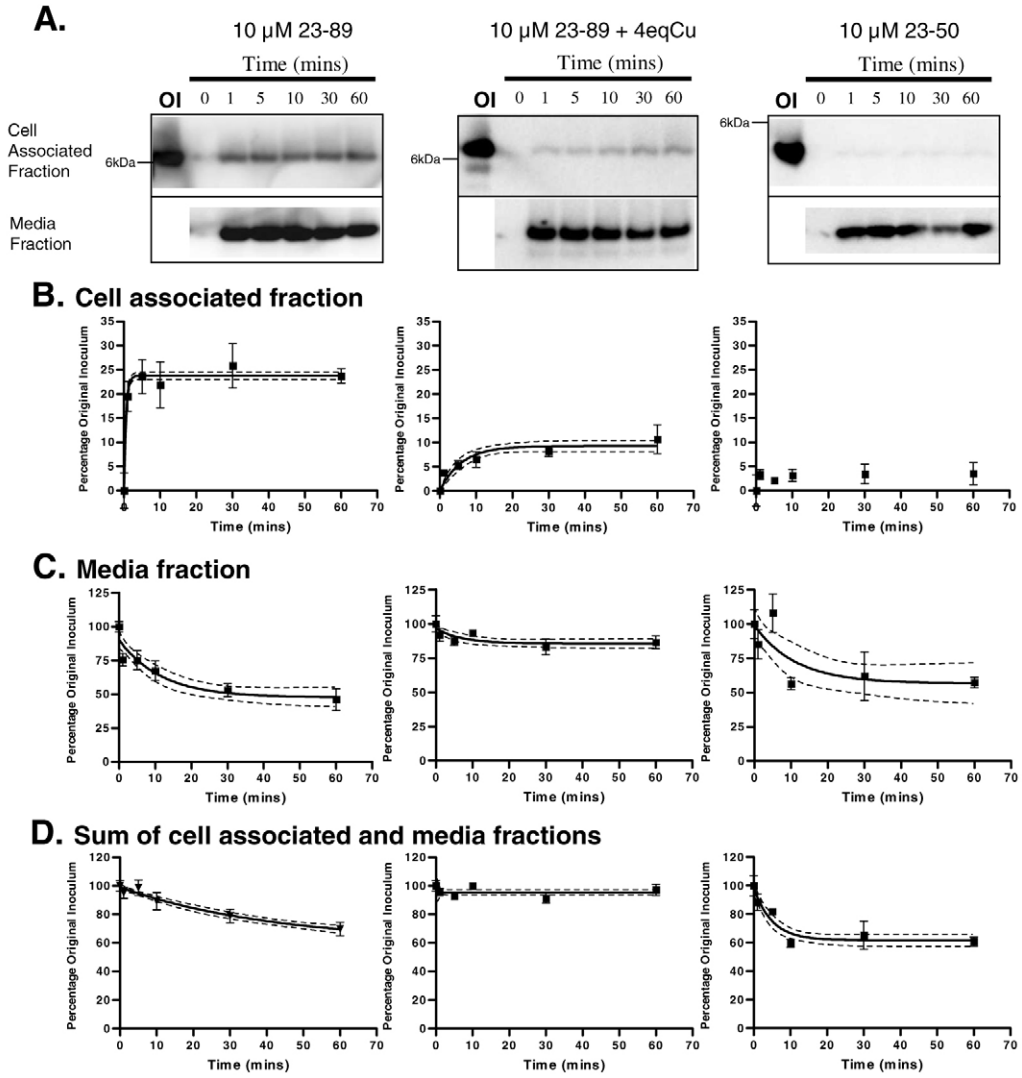

Fig. 6. The octarepeat region modulates cellular association and peptide turnover. 10 µM of the PrP23-89 fragment with and without premixing with 4 molar equivalents of $CuCl_2$-6×glycine, and the PrP23-50 fragment were added to cells at 0 (background control) to 60 minutes. After this time cell lysates and media were harvested and western blotted to detect the fragments. (A) Example blots showing the cell-associated (upper plate) and media (lower plate) fractions compared to the original inoculums (OI). Band signals were quantified densitometrically and the signal represented as a percentage of the OI signal. Graphs show the mean and s.e.m. of (B) the cell-associated fraction, (C) the media fraction and (D) the sum of both fractions as an indicator of total loss of the peptide from the system, derived from three independent experiments. Where appropriate the single exponential rate curves for association or decay are shown (unbroken line) with the 95% CI (broken lines). Copper binding reduces the rate of cellular association of the PrP23-89 fragment and the intensity once association has reached equilibrium, but also reduces its loss from the media and the overall system. The PrP23-50 fragment shows almost no cellular association but a rapid, overall greater loss from the media and the system than the PrP23-89 fragment, even when the latter is not copper-bound.

shown that this mutation enhanced signal in the cell-associated fraction (Fig. 7B,C). Complementary to the increase in cell association, a rapid decrease in the culture medium and in the overall detected peptide was observed (Fig. 7D,E). Additionally the peptide displayed altered physical properties, now showing a tendency to aggregate, with both the monomer and the aggregates showing cell association (Fig. 7B). CD spectroscopy, however, did not reveal any overt alteration in secondary structure from that of wild-type PrP23-50 (supplementary material Fig. S5).

Proline residues 26 and 28 exert a dominant influence over the properties of N2

To determine the importance of the proline residues within the polybasic region of the N2 fragment on the intracellular ROS protective activity and, further, if the polybasic region could exert a dominant effect over the octarepeat region, PrP23-89 with the P26/28A mutations was synthesised. The production of intracellular ROS in response to serum withdrawal was assessed in the presence of PrP23-89 P26/28A with and without copper as described for wild-type PrP23-89. When applied to the serum-deprived cells without pre-loading with copper, minimal variation was seen from baseline in the rate of ROS production up to 1 µM peptide, where the tendency is toward increased ROS production as seen for PrP23-89 (Fig. 8A). When PrP23-89 P26/28A was applied with equimolar, followed by 2-6 molar equivalents of $CuCl_2$-6×glycine, a pronounced difference was seen from PrP23-89 (Fig. 8B). One to three equivalents of copper induced a sizable increase in the rate of ROS production compared with copper alone or the PrP23-89

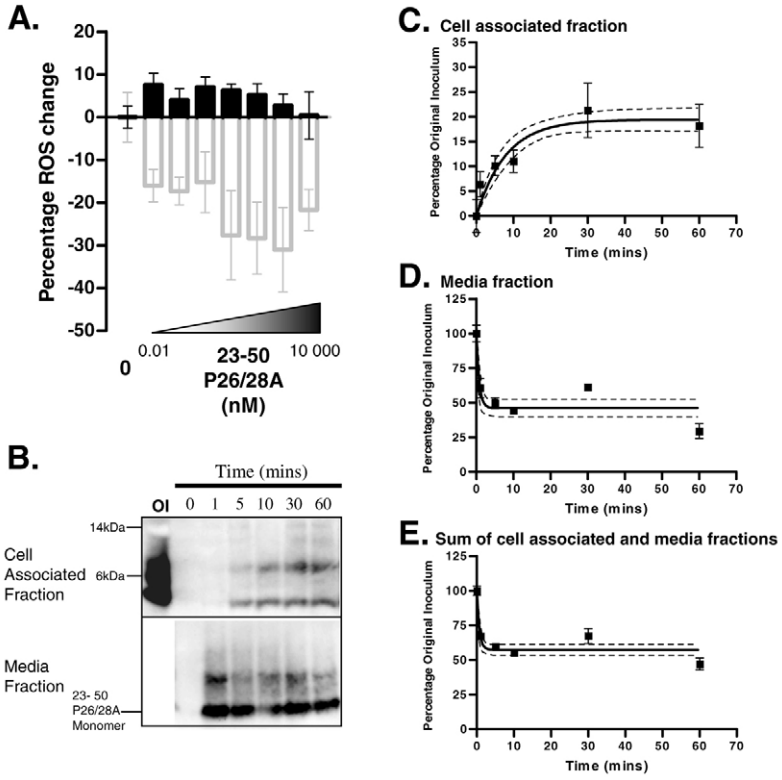

Fig. 7. Mutation of the proline residues 26 and 28 to alanine abolishes the activity of PrP23-50 and alters its cellular association. PrP23-50 was synthesised with proline residues 26 and 28 mutated to alanine. (A) Percentage changes in the rate of ROS production from the rate induced by serum deprivation alone as determined by DCFDA assay for the $\log_{10}$ serial dilution of the PrP23-50 P26/28A fragment (black bars), the PrP23-50 fragment results are shown for comparison (empty grey bars). 10 μM of the PrP23-50 P26/28A fragment was added to cells at 0 (background control) to 60 minutes. Cell lysates and media were harvested and western blotted to detect the fragment. (B) Example blots showing the cell-associated (upper plate) and media (lower plate) fractions compared to the original inoculum (OI). Band signals were quantified densitometrically and the signal represented as a percentage of the OI signal. Graphs show the single exponential rate curves for association or decay (unbroken line) with the 95% CI (broken lines) of (C) the cell-associated fraction, (D) the media fraction and (E) the sum of both fractions as an indicator of total loss of the peptide from the system, derived from three independent experiments. The PrP23-50 P26/28A fragment shows a greater propensity to associate with the cell than the PrP23-50 fragment and decays from the media and the overall system faster. Further it shows a tendency to aggregate, not seen for the PrP23-50 fragment.

copper-loaded fragment. Full saturation, at 4 equivalents of copper, was no different in ROS production from the cellular response seen for this concentration of copper alone. Five to six equivalents of copper was not significantly different from the PrP23-89 response. As the increased intracellular ROS seen at the lower equivalents of copper may have been a result of cellular toxicity by the peptide delivering copper into the cell, an MTS assay for cell viability was performed on the cells 24 hours after treatment (Fig. 8C). Significantly reduced viability was seen at the 2 equivalent copper concentration for cells treated with the PrP23-89 P26/28A fragment, but no significant difference in viability was seen at 1 equivalent, where the highest ROS were seen or at any of the higher concentrations of copper. Cells were treated for 0-60 minutes with the apo or copper-loaded PrP23-89 P26/28A and lysates and media western blotted for the presence of the fragment as described previously. Like the PrP23-50 P26/28A, the PrP23-89 P26/28A fragment showed increased tenancy to aggregate compared with the wild-type PrP23-89 (Fig. 8D,E), with two dominant oligomeric forms evident. When a 4 molar excess of copper was premixed with the PrP23-89 P26/28A fragment the oligomers were reduced, with the monomer band becoming the dominant species (Fig. 8D,F). This suggests that mutating the N-terminal prolines to less structurally constraining amino acids allows the octarepeats to associate with each other, forming aggregates sensitive to copper binding. This, however, is not the only region responsible for the aggregation, as the PrP23-50 P26/28A fragment without the octapeptide repeats aggregates and oligomeric species remain in the copper-loaded sample. The dominant aggregated species in the unloaded sample shows the greatest propensity to internalise, with the monomer showing much less cellular association; this is reversed in the cell fraction treated with the copper-loaded peptide. Cell association and rate of disappearance from the media curves are shown in supplementary material Fig. S6. Overall, the eventual cellular association concentration plateau of copper-loaded PrP23-89 P26/28A is no greater than that of copper-loaded wild-type PrP23-89. However, at 1 minute post-exposure, only approximately 4% of the copper-loaded PrP23-89 was associated with the cellular fraction, whereas approximately 15% of the copper loaded PrP23-89 P26/28A was seen in this fraction. This rate of cellular association may place cells under extra stress, resulting in the increased ROS seen in these treatments. Alternatively, the increased oxidative stress seen when cells are exposed to this fragment may be due to a mis-association of the fragment or the remaining oligomeric species. Furthermore, despite the differences in intracellular ROS production when PrP23-89 P26/28A was applied with 1 molar equivalent copper, EPR data on the binding of 1 molar equivalent copper shows there was no difference in copper coordination between the PrP23-89 and PrP23-89 P26/28A fragments, and CD spectra confirm there were no significant differences in secondary structure (Fig. 8G; Fig. 7H).

Discussion

β-Cleavage of the prion protein occurs internally around the C-terminal end of the octameric repeat domain (Chen et al., 1995) and has been shown to protect against ROS induced by copper and hydrogen peroxide (Watt et al., 2005). Our results significantly extend this knowledge by showing that the N-terminal β-cleavage product specifically modulates intracellular ROS occurring in response to cellular stress, with the protection mediated by both its copper-binding and non-copper-binding regions. Further, copper saturation facilitated the attenuation of intracellular ROS concomitant with altered cellular association properties of the N2 peptide. Hence, differences in intracellular ROS between cells treated with the apo-N2 and the copper-loaded-N2 peptide are very likely due to different interactions at the cell membrane. The PrP octameric repeat domain has been shown to bind to membranes in

model systems and the addition of copper to this region, although still allowing binding, changed the conformational arrangement (Dong et al., 2007). A change in peptide conformation, peptide-lipid orientation or peptide position in relation to the cell membrane may allow the far N-terminal residues to interact with differing binding partners, or at different locations on the cell membrane, resulting in distinct cellular responses. This is not the case for the PrP23-50 fragment, which, without the octarepeat domain, is free to interact directly with its binding partners independent of any stress-sensing or modulating role of copper binding. Proposed models of N2 interactions with itself and the lipid membrane environment are depicted schematically in Fig. 9B.

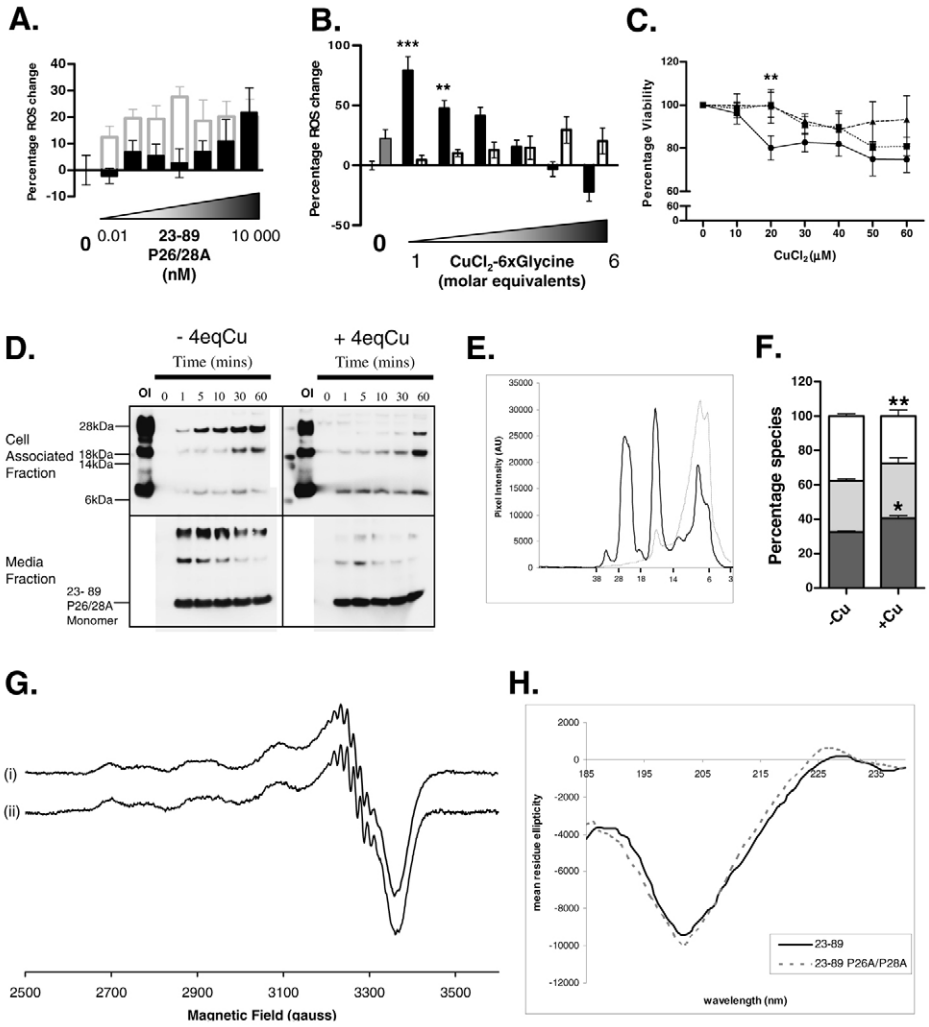

Fig. 8. Mutation of the polybasic region prolines results in altered properties of PrP23-89. The PrP23-89 fragment was synthesised with prolines 26 and 28 mutated to alanine. The ability of this peptide to modulate the ROS response to serum deprivation with and without copper loading was monitored by DCFDA assay. All plots represent the mean and s.e.m. of four independent experiments, except panel F, where n=3. (A) The apo-23-89 P26/28A fragment was applied to cells in the $\log_{10}$ serial dilution. The ROS response compared with cells not exposed to the peptide is shown (black bars) in comparison to the PrP23-89 peptide response (empty grey bars). (B) Intracellular ROS response to serum depletion when applying 10 µM peptide with 1-6 molar equivalents $CuCl_2$-6×glycine (black bars), compared with the response of the peptide alone (grey bar) and the response of $CuCl_2$-6×glycine alone (white bars). Two-way ANOVA finds that the change in ROS rate at 1 and 2 equivalents copper are significantly different from the results obtained for wild-type PrP23-89 (F=14.74, P<0.0001, **P<0.01, ***P<0.001). (C) Viability of cells treated with 10 µM PrP23-89 P26/28A peptide and increasing equivalents of copper for 24 hours (circles and solid line) expressed relative to the no-copper condition, and compared with equivalent wild-type PrP23-89 (triangles and dashed line) and copper alone (squares and dotted line). Decreased viability is seen for the PrP23-89P26/28A peptide against both PrP23-89 and copper alone at 2 equivalents copper and relative to just the PrP23-89 peptide at 5 and 6 equivalents of copper (F=4.83, P=0.0422, *P<0.05, **P<0.01). (D) Cells were treated for 0 (background control) to 60 minutes with 10 µM PrP23-89 P26/28A with and without 4 molar equivalents of $CuCl_2$-6×glycine. Cell-associated and media fractions were western blotted for the presence of the PrP23-89 P26/28A fragment compared with the original inoculum (OI). (E) Densitometric profiles measured vertically from the top to the bottom of the PrP23-89 P26/28A (solid line) and the wild-type PrP23-89 (dashed line) original inoculums. The PrP23-89 P26/28A fragment showed enhanced aggregation compared to the wild-type PrP23-89, with several dominant species appearing. (F) Densitometric quantification of the three most dominant species in the original inoculum lanes expressed as a percentage of their sum indicates copper saturation induces a shift from the dominant upper band (white bar segments) to increased dominance of the middle (pale grey bar segments) and monomeric bands (dark grey bar segments). Changes in the upper and monomeric band intensities are significant by two-way ANOVA (F=7.018, P=0.0269, *P<0.05, **P<0.01). (G) EPR spectra of (i) PrP23-89 and (ii) PrP23-89 P26/28A in the presence of 1 molar equivalent $^{65}CuCl_2$ at pH 7.0. Multiple coordination modes exist in equilibrium for PrP23-89 that are very similar to those of isolated octapeptide repeat fragments at physiological pH (Drew and Barnham, 2008). These are unchanged upon mutation of prolines 26 and 28 to alanines. The co-ordination observed in PrP23-50 (Fig. 3A) does not occur here due to the higher affinity of the octarepeat copper coordination modes. (H) CD spectra show that the mutation of the proline residues does not alter secondary structure.

The N-terminal polybasic region has previously been shown to be crucial for internalisation of PrP^C; this was dependent on its strong positive charge (Nunziante et al., 2003; Sunyach et al., 2003). In the current study the polybasic region was also involved in the ROS reduction response, requiring the proline residues 26 and 28 within this charged region. Proline residues induce small structural motifs due to the steric constraints imposed by their rigid cyclic structure. It is probable that the charge of the 23-28 polybasic region mediates N2 binding to proteoglycans and the structure imparted on the N-terminus by the double proline motif produces the selectivity of this reaction. The net result is specific recognition of target-binding partners most likely within the cholesterol-rich lipid-raft domains in which PrP^C is resident. Mutation of the prolines within the polybasic region, producing a less rigid N-terminus, permitted the N2 peptide to interact more readily with the cell while simultaneously abolishing its specific protective properties and producing potentially deleterious effects. This was exemplified by the PrP23-89 P26/28A ROS response in the presence of copper. Here, cellular association was significantly increased compared with the wild type PrP23-89 fragment, indicating that the mutant peptide probably moves copper inside the cell or to an incorrect membrane location, causing increased cellular stress at low concentrations of copper.

Among many other functions, proteoglycans can be cellular receptors and co-receptors (reviewed by Raman et al., 2005). The specific function of the proteoglycan is determined by its protein core. PrP^C has several putative GAG-binding sites that might differentially mediate binding to proteoglycans, which are located at amino acid positions PrP23-50, 53-93 and 110-128 (Warner et al., 2002). The GAGs bound by cell-free recombinant PrP include heparin, heparan sulphate, chondroitin sulphate A and B, hyaluronic acid and dextran (Andrievskaia et al., 2007; Pan et al., 2002), and cellular PrP expressed by transfection binds heparin (Pan et al., 2002). Heparan sulphate has been shown to be a cell surface receptor for PrP^{Sc} (Horonchik et al., 2005) and preincubation of infectious inoculum with heparin delays the onset of prion disease (Hijazi et al., 2005), indicating that uptake of PrP^{Sc} can be decreased by exogenous GAGs competing with endogenous GAGs. Furthermore GAGs mediate PrP^C binding to cell-surface receptors including the 37 kDa/67 kDa laminin receptor (Gauczynski et al., 2001). The regions involved in 37 kDa/67 kDa laminin receptor binding have been characterised and the N2 fragment and the octameric repeats alone, in the presence of heparan sulphate, can bind to and are outcompeted by antibodies against the laminin receptor (Hundt et al., 2001). Receptor binding such as this may transduce the ROS protective effect seen in response to the PrP N-terminus in this study; this is depicted in Fig. 9C.

Copper binding to the octameric repeat domain alters GAG binding (Andrievskaia et al., 2007; Warner et al., 2002). Increased octarepeats, as seen in some genetic prion diseases, increases the binding capacity and affinity for GAGs, and both increased repeats and increased GAG binding decrease the ability of the cell to respond to ROS (Yin et al., 2006; Yin et al., 2007). Moreover, increased GAG binding is associated with increased aggregation of full-length PrP (Yin et al., 2007), and aggregation of PrP is also associated with a decreased response to oxidative stress. These observations are consistent with those reported here, wherein altering the two N-terminal prolines resulted in enhanced cellular association and increased aggregation but with a concomitant loss of the protective response against intracellular ROS. Further, the current data support a biologically meaningful role for GAG binding in the protective function of the N-terminus, and identify the importance of structure within the polybasic region in addition to any electrostatic contributions to this interaction. By contrast, aberrant association with the cell membrane could induce an intracellular ROS insult, which might potentially contribute to the pathogenesis of prion disease.

The cellular location of the β-cleavage event has not yet been established; however the N-terminus has been shown to be important

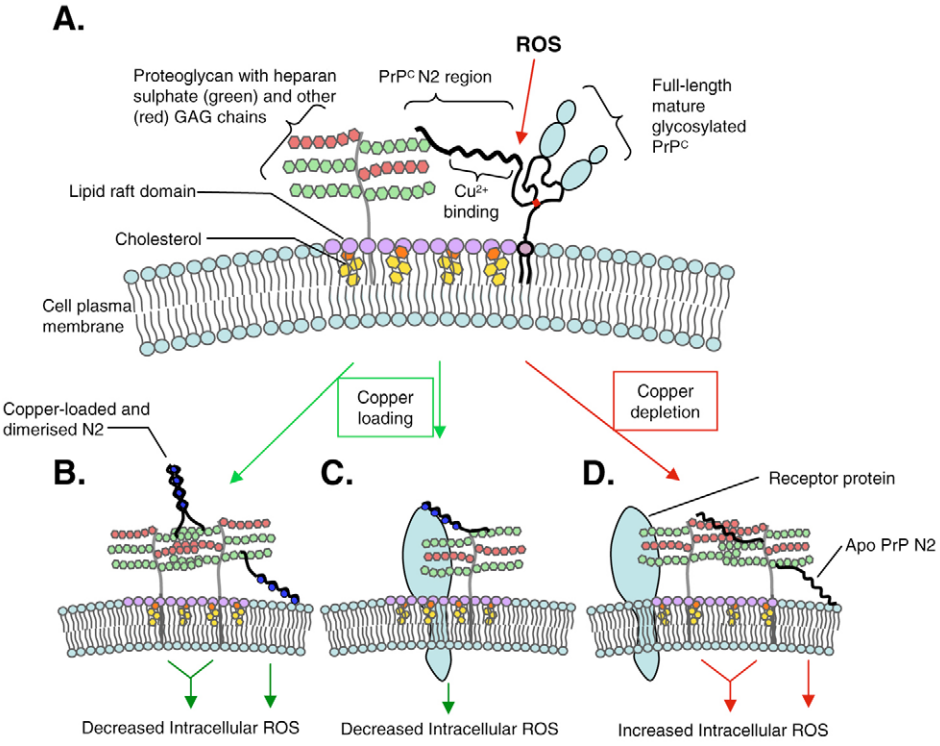

Fig. 9. Scheme depicting hypothetical modes of action of the N2 fragment. It is probable that the flexible N-terminus is bound to GAGs via the polybasic region even when resting at the cell membrane (A). Upon release of the N2 region by ROS the fragment is free to instigate further interactions. As N2/C2 cleavage most likely occurs when the octarepeats are already occupied to some extent with copper, new interactions might include metal-ion induced dimerisation of N2 fragments (B) or, as the octarepeats also bind lipids, coordination with GAGs and the lipid membrane environment, also transducing a protective effect via lipid signalling pathways. An alternative result of N2/C2 cleavage might be to deliver the N2 fragment to a cell-surface receptor such as the laminin receptor (Gauczynski et al., 2001), where binding to the receptor could initiate a protective signal transduction cascade (C). In the event the N2/C2 cleavage occurs when copper levels are depleted or if the fragment was outcompeted for copper by another protein, different interactions may occur with GAGs or with the lipid membrane environment, preventing the N2 fragment from interacting with the appropriate receptor and resulting an unrelated, possibly detrimental signal (D).

in mediating protective effects from the cell surface. Tethering of the N-terminus of full-length PrP to the membrane effectively prevented PrP-mediated protection against ROS insults induced by hydrogen peroxide (Zeng et al., 2003) and paraquat (Dupiereux et al., 2008). In the current study synthetic N-terminal fragments were added exogenously to the extracellular surface to investigate stress protection mediated from outside the cell. Given that PrP^C is an extracellular cell-surface protein and that both N-terminal (N1 and N2) cleavage fragments have been found in higher concentrations in conditioned medium than within cell lysates (Mangé et al., 2004; Vincent et al., 2001), with the N2 fragment increased especially after treatment with hydrogen peroxide and copper (McMahon et al., 2001), it is reasonable to assume that at least part of the N-terminal function is mediated from the outer leaflet of the cell membrane. Rapid degradation following internalisation of these fragments may explain their higher prevalence in the extracellular environment. This is common for peptide ligands that activate signal transduction pathways, because prolonged signalling can result in activation of detrimental cellular pathways, including apoptosis (reviewed by Junttila et al., 2008). The rapid turnover of signalling ligands probably explains the lack of PrP23-50 detected in cell lysate, as without the octarepeat region its effects are more potent than the N2 fragment, so it must be removed before its presence becomes harmful to the cell. Further experiments will reveal whether production of the N2 fragment inside the cell can initiate a differing effect from that seen when it is produced at the cell surface, or whether interaction with the complementary C2 and/or full-length PrP^C can modulate function.

β-Cleavage of PrP is increased during disease, as evidenced by increased N2/C2 cleavage products in the brains of CJD patients and in the brains of scrapie-infected mice (Chen et al., 1995; Yadavalli et al., 2004). ROS markers, such as lipid peroxidation, are also linked with early stages of prion disease (Brazier et al., 2006). The β-cleavage event is caused by ROS (McMahon et al., 2001; Watt et al., 2005), and furthermore, an inability to undergo β-cleavage renders the cell susceptible to oxidative attack (Watt et al., 2005). Impaired β-cleavage is seen for certain disease-associated PrP mutations, including expansion of the octameric repeat region (Watt et al., 2005). Cells expressing PrP mutations with increased repeats are more susceptible to oxidative-stress-induced cellular damage and death (Watt et al., 2005; Watt et al., 2007). Taken together, this indicates that the β-cleavage event is unlikely to be an irrelevant epiphenomenon of PrP^C to PrP^{Sc} conversion but, instead, part of a cellular response to stress that is compromised by certain pathogenic mutations.

Overall, the current study has shown that through binding to extracellular proteoglycans, in association with lipid-raft domains, the N-terminus of PrP^C is active in favourably modulating intracellular ROS changes caused by cellular stress. Further, we postulate that the octapeptide repeat, through variable copper binding, may function as a biosensor for activation of the protective N2 region, with the structure and charge specificity of the polybasic domain ensuring the correct transducing receptor engagement.

Materials and Methods

Cell culture

Reagents were purchased from Invitrogen (VIC, Australia) unless otherwise stated. CF10 (murine neuronal PrP knockout) cells and Neuro2a (N2a) cells were cultured in Dulbecco's modified Eagle's media supplemented with 10% (v/v) fetal bovine serum and 50 U/ml penicillin/50 µg/ml streptomycin solution (Sigma). Cells were maintained at 37°C with 5% CO_2 in a humidified incubator. For microtitre plate assays, cells were plated to be 90-95% confluent at the start of the assay.

Preparation of synthetic peptides

The following synthetic peptides based on the N-terminal sequence of murine PrP – (23)KKRPKPGGWNTGGSRYPGQGSPGGNRYP(50)PQGGTWGQPHGGGWG-QPHGGSWGQPHGGSWGQPHGGGWGQ(89) – were purchased from the peptide synthesis unit of the Bio21 Institute (Victoria, Australia), which uses microwave-assisted peptide synthesis; PrP23-89; PrP23-50; PrP23-50 P26/28A; PrP23-89 P26/28A; PrP23-50scram (GKPWSGRGTPGGRGPRKYGSNKYRNGPQ); and PrP23-89scram (KQSQYGGGPSWGNYWGWPGHGRGPGPRGQPGGTRGPGG-TQSWKPGGGHWPSGGHQGGPKHWGQNPGG). Peptides were solubilised in distilled water before addition to cell culture media with concentrations determined by UV spectroscopy.

DCFDA assay

Cells were incubated in Dulbecco's phosphate-buffered saline (dPBS) containing 5 µM 5-(and-6)-chloromethyl-2′,7′-dichlorodihydrofluorescein diacetate, acetyl ester (CM-H_2-DCFDA) at 37°C for 20 minutes, then probe solution was removed and replaced with prewarmed Opti-MEM I Reduced-Serum Medium (without phenol red) with or without test reagent added. Readings were taken every 5 minutes for 12 hours using 490 nm excitation and 520 nm emission filters in a Fluostar Optima (BMG Labtech, Victoria, Australia), and initial rates were calculated using tangents to the curve.

Phen Green Fl assay

Cells were incubated in prewarmed Opti-MEM I Reduced-Serum Medium (without phenol red) containing 10 µM Phen green FL diacetate for 20 minutes and residual cellular fluorescence compared with the cell-free control solution. Readings were taken using 490 nm excitation and 520 nm emission filters in a Fluostar Optima.

Cell viability (MTS) assay

Five µl of one solution MTS reagent per 100 µl media (Promega; VIC AUS) was added to test and medium-only background control conditions, and incubated under normal culture conditions for 90 minutes. Reaction product was quantified using absorbance at 462 nm in a Fluostar Optima.

GAG digestion

Cells were digested for 1 hour at 37°C in OptiMEM1 culture media using 10 mU/ml of heparin lyase III or chondroitinase ABC (Seikagaku, Japan) before the start of each assay. The enzyme concentration was reduced to 5 mU/ml during the assay. Negative controls were treated identically except for omission of the enzyme.

Circular dichroism

CD spectra were recorded at room temperature on a Jasco J-815 spectropolarimeter. Peptides were solubilised in distilled water to a concentration of 10 µM. Spectra were obtained in a 2 mm path length quartz cell from 190–240 nm using a 1 nm bandwidth and a scan rate of 50 nm min^{-1}. Background correction was performed by subtraction of the protein-free spectrum.

Electron paramagnetic resonance

Peptides were solubilised in distilled water at a concentration of 100 µM. A 10 mM $^{65}CuCl_2$ stock was prepared by dissolving ^{65}CuO (Cambridge Isotope Laboratories) in concentrated HCl, followed by dilution in distilled water. From this stock, 1 equivalent ^{65}Cu was added to each peptide solution. For Cu^{2+}-binding competition studies, 2.5 equivalents glycine was further added from a fresh 10 mM stock prepared in distilled water. The final pH was measured using a micro-probe (Hanna Instruments, Italy) and adjusted to pH 7.0 using concentrated NaOH. Samples were transferred to quartz EPR tubes (Wilmad) and snap-frozen in liquid nitrogen.

X-band CW-EPR was performed using a Bruker ESP380E spectrometer fitted with a rectangular TE_{102} microwave cavity and a quartz cold finger insert. Experimental conditions were: microwave frequency, 9.42 GHz; microwave power, 10 mW; modulation amplitude, 4 G; modulation frequency, 100 kHz; temperature, 77 K; sweep time, 168 seconds; time constant, 164 milliseconds; receiver gain, 10^5; 8-15 averages. Background correction was performed by subtraction of the sample-free spectrum. Displayed spectra were normalised with respect to their maximum peak-to-peak intensity.

Fluorescent spin trapping

Of each peptide, 10 µM was incubated with 10 µM proxyl fluorescamine, 10 µM H_2O_2, 5 µM $FeSO_4$ and 5% (v/v) DMSO in PBS. Reagents were added into wells of a black microplate with the $FeSO_4$ added last. Readings were begun immediately using 360 nm excitation and 480 nm emission wavelengths in a Fluostar Optima. Assays were run over a period of two hours to collect the linear rate of radical generation. Readings were taken every 30 seconds following 5 seconds mixing.

PAGE and western blotting

Media were removed from the cells and replaced with pre-warmed Opti-MEM I Reduced-Serum Medium at the beginning of the assay. At the appropriate time point, 10 µM peptide was added to the cells and at the end of the incubation media was removed and kept for analysis. Cells were lysed in RIPA buffer [50 mM Tris-HCl pH 7.4, 150 mM NaCl, 0.1% (w/v) SDS, 0.5% (w/v) sodium deoxycholate, 1% (v/v)

NP-40] supplemented with 0.5 U/ml benzonase (Sigma Aldrich), at 37°C for 20 minutes. Lysates and media were mixed with appropriate volumes of 3× LDS loading dye (containing 5% v/v beta-mercaptoethanol), denatured for 10 minutes at 80°C and electrophoresed in MES buffer using 12% NuPAGE Bis-Tris gels, at 200V for 35 minutes, with the dye front not allowed to reach the end of the gel. Protein was then transferred onto nitrocellulose membranes (BioRad, NSW AUS) using a BioRad wet blotting system for 30 minutes at 100V, and subsequently blocked in PBS containing 0.1% v/v Tween (PBS-t) and 5% non-fat milk. Synthetic PrP fragments were detected using 1 in 10,000 dilution of 8B4 monoclonal antibody (against murine amino acids 37-44; Alicon, Switzerland) in 1% milk PBS-t, anti-mouse HRP secondary antibody (GE Healthcare, NSW AUS) was used at 1 in 10,000 dilution and blots were visualised using ECL-plus detection reagent (GE Healthcare).

Densitometry and statistical analyses

Luminescent signal of the bands on the western blots was captured using a Las-3000 intelligent darkbox (FujiFilm; Berthold, VIC AUS) and the intensity quantified, after the subtraction of background, by ImageJ 1.38×. Statistical analyses were carried out using GraphPad Prism 5 statistical software. Graphs show the mean and s.e.m. of four independent experiments unless otherwise stated.

This work was supported by an NHandMRC Program Grant #400202. C.L.H. is supported by a University of Melbourne Early Career Researcher Grant, S.J.C. by an NHandMRC Practitioner Fellowship #400183, S.J.C. and V.A.L. by an NHandMRC Project Grant #454546, and V.A.L. by an NHandMRC Project Grant #400229. K.J.B. is an NHandMRC Senior Research Fellow.

References

Andrievskaia, O., Potetinova, Z., Balachandran, A. and Nielsen, K. (2007). Binding of bovine prion protein to heparin: a fluorescence polarisation study. *Arch. Biochem. Biophys.* **460**, 10-16.

Brazier, M. W., Lewis, V., Ciccotosto, G. D., Klug, G. M., Lawson, V. A., Cappai, R., Ironside, J. W., Masters, C. L., Hill, A. F., White, A. R. et al. (2006). Correlative studies support lipid peroxidation is linked to PrP^{res} propagation as an early primary pathogenic event in prion disease. *Brain Res. Bull.* **68**, 346-354.

Brown, D. R. (2003). Prion protein expression modulates neuronal copper content. *J. Neurochem.* **87**, 377-385.

Brown, D. R. and Besinger, A. (1998). Prion protein expression and superoxide dismutase activity. *Biochem. J.* **334**, 423-429.

Brown, D. R., Wong, B. S., Hafiz, F., Clive, C., Haswell, S. J. and Jones, I. M. (1999). Normal prion protein has an activity like that of superoxide dismutase. *Biochem. J.* **344**, 1-5.

Brown, D. R., Clive, C. and Haswell, S. J. (2001). Antioxidant activity related to copper binding of native prion protein. *J. Neurochem.* **76**, 69-76.

Chavez-Crooker, P., Garrido, N. and Ahearn, G. A. (2001). Copper transport by lobster hepatopancreatic epithelial cells separated by centrifugal elution: measurements with the fluorescent dye Phen Green. *J. Exp. Biol.* **204**, 1433-1444.

Chen, S. G., Teplow, D. B., Parchi, P., Teller, J. K., Gambetti, P. and Autilio-Gambetti, L. (1995). Truncated forms of the human prion protein in normal brain and in prion diseases. *J. Biol. Chem.* **270**, 19173-19180.

Dong, S. L., Cadamuro, S. A., Fiorino, F., Bertsch, U., Moroder, L. and Renner, C. (2007). Copper binding and conformation of the N-terminal octarepeats of the prion protein in the presence of DPC micelles as membrane mimetic. *Biopolymers* **88**, 840-847.

Drew, S. C. and Barnham, K. J. (2008). Biophysical investigations of the prion protein using electron paramagnetic resonance. In *Prion Protein Protocols* (*Methods in Molecular Biology)* Vol. 459 (ed. A. F. Hill). pp. 173-196. New Jersey: Humana Press.

Dupiereux, I., Falisse-Poirrier, N., Zorzi, W., Watt, N. T., Thellin, O., Zorzi, D., Pierard, O., Hooper, N. M., Heinen, E. and Elmoualij, B. (2008). Protective effect of prion protein via the N-terminal region in mediating a protective effect on paraquat-induced oxidative injury in neuronal cells. *J. Neurosci. Res.* **86**, 653-659.

Gauczynski, S., Peyrin, J. M., Haïk, S., Leucht, C., Hundt, C., Rieger, R., Krasemann, S., Deslys, J. P., Dormont, D., Lasmézas, C. I. et al. (2001). The 37kDa/67kDa laminin receptor acts as the cell-surface receptor for the cellular prion protein. *EMBO J.* **20**, 5863-5875.

Gauczynski, S., Nikles, D., El-Gogo, S., Papy-Garcia, D., Rey, C., Alban, S., Barritault, D., Lasmézas, C. I. and Weiss, S. (2006). The 37kDa/67kDa laminin receptor acts as a receptor for infectious prions and is inhibited by polysulphated glycanes. *J. Infect. Dis.* **194**, 702-709.

Hijazi, N., Kariv-Inbal, Z., Gasset, M. and Gabizon, R. (2005). PrPSc incorporation into cells requires endogenous glycosaminoglycan expression. *J. Biol. Chem.* **280**, 17057-17061.

Horonchik, L., Tzaban, S., Ben-Zaken, O., Yedidia, Y., Rouvinski, A., Papy-Garcia, D., Barritault, D., Vlodavsky, I. and Taraboulos, A. (2005). Heparan sulphate is a cellular receptor for purified infectious prions. *J. Biol. Chem.* **280**, 17062-17067.

Hundt, C., Peyrin, J. M., Haïk, S., Gauczynski, S., Leucht, C., Rieger, R., Riley, M. L., Deslys, J. P., Dormont, D., Lasmézas, C. I. et al. (2001). Identification of interaction domains of the prion protein with its 37-kDa/67-kDa laminin receptor. *EMBO J.* **20**, 5876-5886.

Junttila, M. R., Li, S. P. and Westermarck, J. (2008). Phosphatase-mediated crosstalk between the MAPK signalling pathways in the regulation of cell survival. *FASEB J.* **22**, 954-965.

Kovács, G. G., Puopolo, M., Ladogana, A., Pocchiari, M., Budka, H. van Duijn, C., Collins, S. J., Boyd, A., Giulivi, A., Coulthart, M. et al. (2005). Genetic prion disease: the EUROCJD experience. *Hum. Genet.* **118**, 166-174.

Mangé, A., Béranger, F., Peoc'h, K., Onodera, T., Frobert, Y. and Lehmann, S. (2004). Alpha- and beta-cleavages of the amino terminus of the cellular prion protein. *Biol. Cell* **96**, 125-132.

Martin, B. D., Schoenhard, J. A. and Sugden, K. D. (1998). Hypervalent chromium mimics reactive oxygen species as measured by the oxidant-sensitive dyes 2′,7′-dichlorofluorescin and dihydrorhodamine. *Chem. Res. Toxicol.* **11**, 1402-1410.

McMahon, H. E., Mangé, A., Nishida, N., Créminon, C., Casanova, D. and Lehmann, S. (2001). Cleavage of the amino terminus of the prion protein by reactive oxygen species. *J. Biol. Chem.* **276**, 2286-2291.

Morel, E. Andrieu, T., Casagrande, F., Gauczynski, S., Weiss, S., Grassi, J., Rousset, M., Dormont, D. and Chambaz, J. (2005). Bovine prion is endocytosed by human enterocytes via the 37 kDa/67 kDa laminin receptor. *Am. J. Pathol.* **167**, 1033-1042.

Nunziante, M., Gilch, S. and Schatzl, H. M. (2003). Essential role of the prion protein N terminus in subcellular trafficking and half-life of PrPc. *J. Biol. Chem.* **278**, 3726-3734.

Pan, T., Wong, B. S., Liu, T., Li, R., Petersen, R. B. and Sy, M. S. (2002). Cell-surface prion protein interacts with glycosaminoglycans. *Biochem. J.* **368**, 81-90.

Parkyn, C. J., Vermeulen, E. G. M., Mootoosamy, R. C., Sunyach, C., Jacobsen, C., Oxvig, C., Moestrup, S., Liu, Q., Bu, G., Jen, A. et al. (2008). LRP1 controls biosynthetic and endocytic trafficking of neuronal prion protein. *J. Cell Sci.* **121**, 773-783.

Raman, R., Sasisekharan, V. and Sasisekharan, R. (2005). Structural insights into biological roles of protein-glycosaminoglycan interactions. *Chem. Biol.* **12**, 267-277.

Rambold, A. S., Müller, V., Ron, U., Ben-Tal, N., Winklhofer, K. F. and Tatzelt, J. (2008). Stress-protective signalling of prion protein is corrupted by scrapie prions. *EMBO J.* **27**, 1974-1984.

Schmitt-Ulms, G., Legname, G., Baldwin, M. A., Ball, H. L., Bradon, N., Bosque, P. J., Crossin, K. L., Edelman, G. M., DeArmond, S. J., Cohen, F. E. et al. (2001). Binding of neural cell adhesion molecules (N-CAMs) to the cellular prion protein. *J. Mol. Biol.* **314**, 1209-1225.

Shyng, S. L., Moulder, K. L., Lesko, A. and Harris, D. A. (1995). The N-terminal domain of a glycolipid-anchored prion protein is essential for its endocytosis via clathrin coated pits. *J. Biol. Chem.* **270**, 14793-14800.

Spielhaupter, C. and Schätzl, H. M. (2001). PrPc directly interacts with proteins involved in signalling pathways. *J. Biol. Chem.* **276**, 44604-44612.

Stuermer, C. A., Langhorst, M. F., Wiechers, M. F., Legler, D. F. Von Hanwehr, S. H., Guse, A. H. and Plattner, H. (2004). PrPc capping in T cells promotes its association with the lipid raft proteins reggie-1 and reggie-2 and leads to signal transduction. *FASEB J.* **18**, 1731-1733.

Sunyach, C., Jen, A., Deng, J., Fitzgerald, K. T., Frobert, Y., Grassi, J., McCaffrey, M. W. and Morris, R. (2003). The mechanism of internalisation of glycosylphosphatidylinositol-anchored prion protein. *EMBO J.* **22**, 3591-3601.

Taylor, D. R., Watt, N. T., Perera, W. S. S. and Hooper, N. M. (2005). Assigning functions to distinct regions of the N-terminus of the prion protein that are involved in its copper-stimulated, clathrin-dependant endocytosis. *J. Cell Sci.* **118**, 5141-5153.

Vanhoof, G., Goossens, F., De Meester, I., Hendriks, D. and Scharpé, S. (1995). Proline motifs in peptides and their biological processing. *FASEB J.* **9**, 736-744.

Vincent, B., Paitel, E., Saftig, P., Frobert, Y., Hartmann, D., De Strooper, B., Grassi, J., Lopez-Perez, E. and Checler, F. (2001). The disintegrins ADAM10 and TACE contribute to the constitutive and phorbol ester-regulated normal cleavage of the cellular prion protein. *J. Biol. Chem.* **276**, 37743-37746.

Warner, R. G., Hundt, C., Weiss, S. and Turnbull, J. E. (2002). Identification of the heparan sulfate binding sites in the cellular prion protein. *J. Biol. Chem.* **277**, 18421-18430.

Watt, N. T., Taylor, D. R., Gillott, A., Thomas, D. A., Perera, W. S. S. and Hooper, N. M. (2005). Reactive oxygen species-mediated β-cleavage of the prion protein in the cellular response to oxidative stress. *J. Biol. Chem.* **280**, 35914-35921.

Watt, N. T., Routledge, M. N., Wild, C. P. and Hooper, N. M. (2007). Cellular prion protein protects against reactive-oxygen-species-induced DNA damage. *Free Radic. Biol. Med.* **43**, 959-967.

Wopfner, F., Weidenhöfer, G., Schneider, R. von Brunn, A., Gilch, S., Schwarz, T. F., Werner, T. and Schätzl, H. M. (1999). Analysis of 27 mammalian and 9 avian PrPs reveals high conservation of flexible regions of the prion protein. *J. Mol. Biol.* **289**, 1163-1178.

Yadavalli, R., Guttmann, R. P., Seward, T., Centers, A. P., Williamson, R. A. and Telling, G. C. (2004). Calpain-dependent endoproteolytic cleavage of PrPsc modulates scrapie prion propagation. *J. Biol. Chem.* **279**, 21948-21956.

Yin, S., Yu, S., Li, C., Wong, P., Chang, B., Xiao, F., Kang, S. C., Yan, H., Xiao, G., Grassi, J. et al. (2006). Prion proteins with insert mutations have altered N-terminal conformation and increased ligand binding and are more susceptible to oxidative attack. *J. Biol. Chem.* **281**, 10698-10705.

Yin, S., Pham, N., Yu, S., Li, C., Wong, P., Chang, B., Kang, S. C., Biasini, E., Tien, P., Harris, D. A. et al. (2007). Human prion proteins with pathogenic mutations share common conformational changes resulting in enhanced binding to glycosaminoglycans. *Proc. Natl. Acad. Sci. USA* **104**, 7546-7551.

Zeng, F., Watt, N. T., Walmsley, A. R. and Hooper, N. M. (2003). Tethering the N-terminus of the prion protein compromises the cellular response to oxidative stress. *J. Neurochem.* **84**, 480-490.

Cell Research (2009) :1-17.

www.nature.com/cr

ORIGINAL ARTICLE

PrP^C-related signal transduction is influenced by copper, membrane integrity and the alpha cleavage site

Cathryn L Haigh[1, 2], Victoria A Lewis[1, 2], Laura J Vella[1, 2, 4], Colin L Masters[2, 5], Andrew F Hill[2, 3, 4], Victoria A Lawson[1, 2], Steven J Collins[1, 2]

[1]Department of Pathology; [2]Mental Health Research Institute; [3]The Department of Biochemistry and Molecular Biology; [4]Bio21 Molecular Science and Biotechnology Institute, 30 Flemington Road; [5]Centre for Neuroscience, The University of Melbourne, Parkville, Melbourne, 3010, Australia

The copper-binding, membrane-anchored, cellular prion protein (PrP^C) has two constitutive cleavage sites producing distinct N- and C-terminal fragments (N1/C1 and N2/C2). Using RK13 cells expressing either human PrP^C, mouse PrP^C or mouse PrP^C carrying the 3F4 epitope, this study explored the influence of the PrP^C primary sequence on endoproteolytic cleavage and one putative PrP^C function, MAP kinase signal transduction, in response to exogenous copper with or without a perturbed membrane environment. PrP^C primary sequence, especially that around the N1/C1 cleavage site, appeared to influence basal levels of proteolysis at this location and extracellular signal-regulated kinase 1/2 (ERK1/2) phosphorylation, with increased processing demonstrating an inverse relationship with basal ERK1/2 activation. Human PrP^C showed increased N1/C1 cleavage in response to copper alone, accompanied by specific p38 and JNK/SAPK phosphorylation. Combined exposure to copper plus the cholesterol-sequestering antibiotic filipin resulted in a mouse PrP^C-specific substantial increase in signal protein phosphorylation, accompanied by an increase in N1/C1 cleavage. Mouse PrP^C harboring the human N1/C1 cleavage site assumed more human-like profiles basally and in response to copper and altered membrane environments. Our results demonstrate that the PrP^C primary sequence around the N1/C1 cleavage site influences endoproteolytic processing at this location, which appears linked to MAP kinase signal transduction both basally and in response to copper. Further, the primary sequence appears to confer a mutual dependence of N1/C1 cleavage and membrane integrity on the fidelity of PrP^C-related signal transduction in response to exogenous stimuli.

***Keywords*:** Prion, copper, endoproteolytic cleavage, signal transduction, lipid raft
Cell Research advance online publication 14 July 2009; doi: 10.1038/cr.2009.86

Introduction

Cumulative experimental evidence supports that abnormal isomers of the prion protein constitute the causative agent in transmissible spongiform encephalopathies (TSEs, also known as prion diseases) [1, 2], with neuronal expression and membrane anchorage of wild-type PrP being essential for efficient pathogenesis [3-9]. The disease-associated conformer, termed PrP^{Sc}, is a structurally altered form of the normal cellular protein, PrP^C. PrP^C is a glycosylphosphatidylinositol (GPI)-anchored cell surface glycoprotein, which has been shown to bind copper within an N-terminal octameric repeat region and also at one or more sites slightly more C-terminal of the repeat region [10-13].

Despite much investigation and characterization of the properties of PrP^C and PrP^{Sc}, the primary function of PrP^C and the principal pathogenic pathways of TSEs remain unresolved. One suggested role for PrP^C is the transduction of signals from the external environment into the cell interior, a function circumstantially supported by the localization of PrP^C within plasma membrane detergent-resistant microdomains (also known as lipid rafts), which are now widely recognized as membrane-signaling platforms [14]. The plasma membrane constitutes a critical site for the activation of intracellular, and transduction of extracellular, receptor-mediated signaling, and the lipid

Correspondence: Steven J Collins
Tel: +61 3 8344 1945; Fax: +61 3 9349 5105
E-mail: stevenjc@unimelb.edu.au
Received 5 November 2008; revised 10 April 2009; accepted 22 May 2009

environment itself appears to play an extensive role in modulating the activation of signaling pathways [15, 16]. PrP^C has been thought to have a role in lymphocyte signal transduction for some time [17], with suggested outcomes including T-lymphocyte activation or the initiation of a proliferation response [18, 19]. PrP^C crosslinking in lymphocytes results in mitogen-activated protein kinase (MAPK) activation and subsequent extracellular signal-regulated kinase 1/2 (ERK1/2) activation [20].

PrP^C has been shown to interact with several proteins that lead to signal transduction. Co-immunoprecipitation identifies Grb2, an adaptor protein that putatively functions to link extracellular receptors to intracellular signaling molecules, as directly interacting with PrP^C [21]. Interaction with stress-inducible protein 1 (STI-1), which occurs at the cell surface mainly on the cell body, has been shown to induce neuritogenesis and neuroprotection via the MAPK pathway [22]. Additionally, clustering of PrP^C at the cell surface activates ERK1/2 [23-25]. This may be mediated by epidermal growth factor receptor (EGFR [23]) or by the signaling molecule Fyn tyrosine kinase, recruited in turn by the interaction of caveolin-1 and PrP^C [25, 26].

PrP^C is highly conserved across mammalian species, both at the primary amino acid sequence and the tertiary folded structure levels [27]. PrP^C constitutively undergoes two well-defined endoproteolytic cleavage events. The first cleavage site, termed α-cleavage and producing fragments designated N1/C1, is at amino acids 111/112 of the human PrP^C sequence (110/111 of the mouse sequence) and is known to be a site for the enzymes A Disintegrin And Metalloprotease 10 (ADAM10) and Tumor necrosis factor α-Converting Enzyme (TACE) [28]. The second cleavage site, termed β-cleavage and producing N2/C2 fragments, is around the end of the octameric repeat region, amino acid 91 of the human sequence (residue 90 of the mouse sequence), and can be caused by reactive oxygen species (ROS) without the need for enzymes [29, 30]. Enhanced N2/C2 cleavage is associated with disease [31]. Increased prominence of the C2 fragment is found in the brains of sporadic Creutzfeldt-Jakob disease patients and progressive central nervous system accumulation of this cleavage product occurs during the incubation period of rodent disease models [32]. Given the evolutionary conservation of PrP and the apparently ubiquitous occurrence of cellular endoproteolytic processing, especially alpha cleavage in the non-diseased state, it is plausible that cleavage events may be integral to both normal PrP^C function and pathogenesis.

Mouse PrP^C is often substituted for human PrP^C in studies of prion diseases due to its ability to propagate infection within cell culture systems and the availability of a bioassay to properly confirm cell culture results. There are, however, differences in the protein sequence across the two species, notably at the N1/C1 cleavage site where the human sequence contains a methionine residue at amino acid 111 as opposed to the valine residue at the equivalent position (amino acid 110) of the mouse sequence. With the exception of human, chimpanzee, macaque and some hamster species, which have the methionine residue, all characterized mammalian species have the valine residue at the N1/C1 cleavage site [27]. Since single amino acid substitutions at certain positions within the PrP^C sequence are sufficient to cause hereditary prion disease, it seems likely that even small differences in the protein sequence homology could be highly influential in PrP^C processing, function and cellular membrane interactions.

To explore potential relationships between PrP^C endoproteolytic processing and signal transduction, we developed a model in which different primary sequences notably varying around the N1/C1 cleavage motif were expressed in the same cell line. The rabbit kidney epithelial (RK13) cell line was chosen because of the absence of detectable levels of potentially confounding endogenous PrP^C and the ability to reproducibly achieve similar expression levels upon transfection of the various PrP^C constructs. For our model, intermediates of the MAP kinase signal transduction pathway were chosen for analysis because of the specific evidence for involvement of this cascade in PrP^C-related cellular activities and the general centrality of this pathway across a range of cellular signaling events. Employing this paradigm, the specific aims of the present study were: (1) to assess basal and copper-induced PrP^C cleavage profiles, especially around the N1/C1 cleavage site, and the corresponding activation states of key MAP kinase intracellular signaling intermediates and (2) to assess the effect of perturbations to plasma membrane integrity on endogenous PrP^C cleavage and the activation of key MAP kinase-signaling intermediates in response to copper across different PrP^C primary sequences. Overall, our results demonstrated a significant influence of PrP^C primary sequence around the N1/C1 cleavage site on endoproteolytic processing at this location, which appeared linked to MAP kinase signal transduction both basally and in response to copper. Further, the primary sequence appeared to confer a mutual dependence between N1/C1 cleavage and membrane integrity on the fidelity of PrP^C-related signal transduction in response to exogenous copper.

Results

Generation of cell lines expressing human or mouse

PrP^C primary sequences

Human and mouse PrP^C share 89% (full-length sequence) or 91% (minus signal peptides) sequence identity (Supplementary information, Figure S1A). To investigate the influence of the species-specific differences in PrP^C amino acid sequence on cellular processing and signaling responses, basally and in response to membrane perturbations, human and mouse PrP^C genes were transfected into RK13 cells (referred to as huRK13 and moRK13 cells, respectively). The results presented encompass experiments using clones from three independent transfections where clones of equivalent expression levels were selected (Supplementary information, Figure S1B and S1C), and were, additionally, verified using an unselected mixed population. The RK13 cell line is a rabbit kidney epithelial line, which shows no detectable PrP^C and therefore represents a neutral or "null" background for expressing these genes. Furthermore, RK13 cells have been used as an effective host for the propagation of infection using transfected PrP^C sequences from various species [33, 34]. The empty vector was also transfected and selected to act as an appropriately treated control cell line (referred to as vecRK13). No difference in PrP^C detergent solubility or cell membrane localization/orientation (as determined by phosphatidylinositol-specific phospholipase C digestion) was seen between the huRK13 and moRK13 cell lines (data not shown); however, a slight difference in the mobility of the smaller fragments is apparent by western blot (Supplementary information, Figure S1B).

Human and mouse PrP^C show different basal C1 cleavage in RK13 cells

To look at the quantity of the C1 and C2 cleavage fragments compared to the full-length PrP^C molecule, PNGase F-digested cell lysates were analyzed by western blot. Blots and graphical results are shown in Figure 1A. The C2 fragment is not clearly seen in the example blots due to the much lower levels present. Densitometric quantification of the bands showed that basal N1/C1 cleavage of $moPrP^C$ is significantly greater than that of $huPrP^C$. This was not true for the N2/C2 cleavage, which was not significantly different across the cell lines.

Expression of human and mouse PrP^C in RK13 cells influences ERK activation

Since PrP^C cleavage may be linked to its cellular function, and one suggested function is signal transduction, the effect of expressing human and mouse PrP^C in the RK13 cell line on basal signaling protein activation was investigated. Assessment of basal levels of phosphorylation of central signaling molecules was made by western blotting lysates of the huRK13, moRK13 and vecRK13 cells with antibodies against p-ERK1/2 and ERK1/2, p-JNK/SAPK and JNK/SAPK, and p-p38 and p38. For each antibody pair, the phosphorylated form was blotted first to avoid dephosphorylation by membrane stripping. Expression of mouse PrP^C significantly reduced basal p-ERK1/2 levels compared to those of the human PrP^C and vector-only cells (Figure 1B and 1C). Only faint signal was seen for basal phosphorylation of p38 and JNK/SAPK, and no significant alterations were observed across the three RK13 cell lines (Figure 1B). Additionally, expression of human or mouse PrP^C in the RK13 cells did not alter steady state expression of any of the signaling proteins studied.

Expression of PrP^C in RK13 cells does not alter intracellular ROS levels

Since PrP^C is linked to protection against ROS insults and ROS have been shown to be involved in PrP^C cleavage, the basal levels of ROS within the RK13 cell lines were assessed by DCFDA assay. The CM-H_2-DCFDA assay detects the ROS H_2O_2 (in the presence of endogenous metal ions only), $HO^{\cdot}$, $ROO^{\cdot}$ and $ONOO^{-}$ [35]. Under basal conditions there was no difference in the intracellular ROS production between the PrP^C-expressing RK13 cells and the vector-only control (Figure 1D).

Exogenous copper and altered membrane fluidity exerts a greater influence on huRK13 N1/C1 cleavage than moRK13

Since PrP^C is a plasma membrane, lipid raft-associated protein, and its localization is considered important for normal function and pathogenesis factors that alter membrane fluidity or lipid raft integrity were deemed likely to alter PrP^C membrane position, and therefore cleavage and/or PrP^C-associated intracellular signaling events. Several well-characterized conditions for altering membrane fluidity were utilized, including 10 mM benzyl alcohol (BA), to increase membrane fluidity and lowering cell temperature to 25 ºC, with or without the stiffening agent DMSO (0.5% v/v), to decrease membrane fluidity [36-38]. In addition to these conditions, 1 μM Filipin, an antibiotic that binds and sequesters cholesterol, was employed to specifically disrupt the more densely packed cholesterol-rich lipid raft domains, with the decrease in membrane cholesterol also leading to increased membrane fluidity. To confirm that these treatments were having the expected effects, we used an ANS-based assay to verify membrane fluidity (Supplementary information, Figure S2). The huRK13 and moRK13 cells were exposed to increased exogenous copper and each of the conditions altered membrane fluidity both with and with-

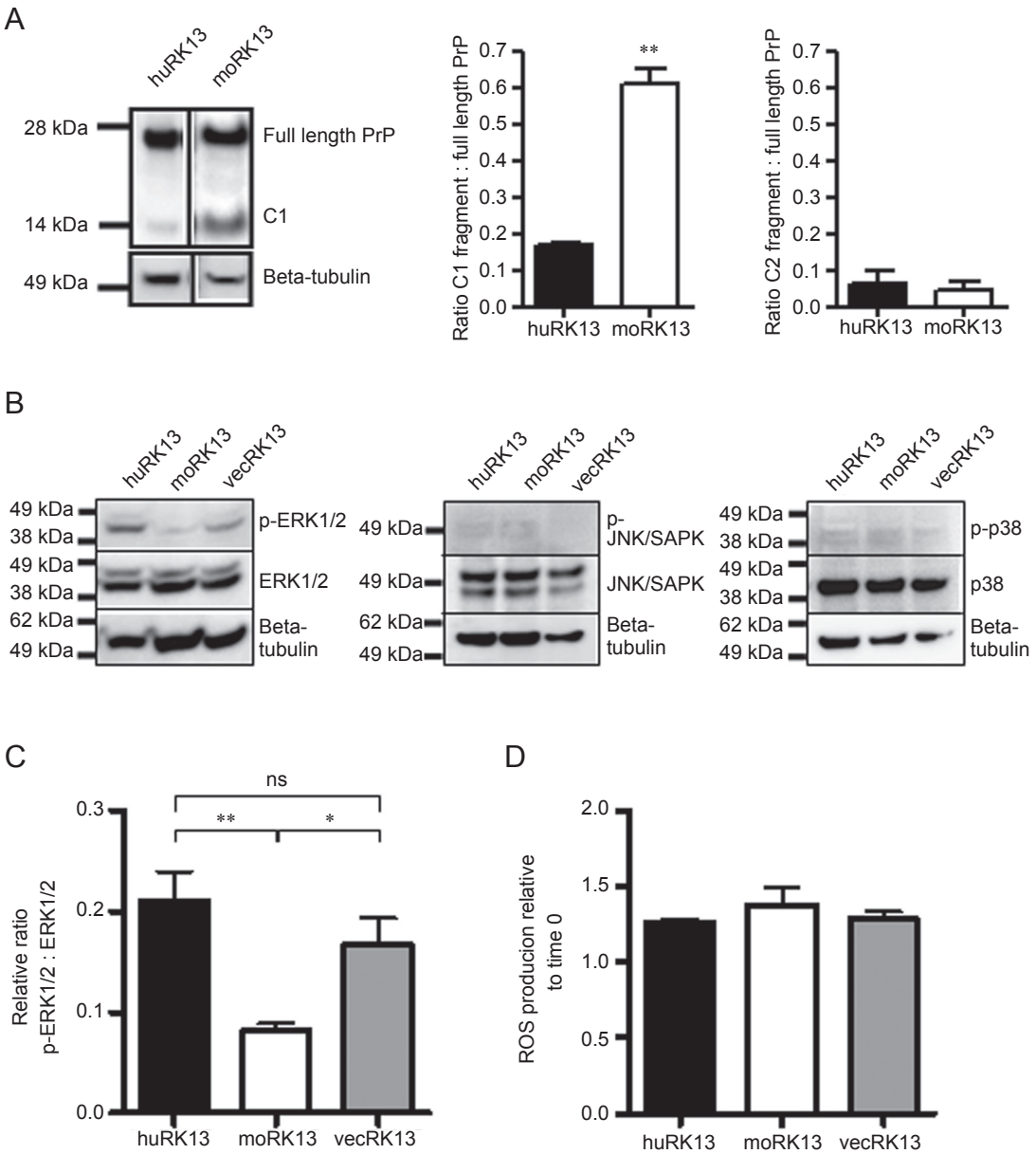

Figure 1 Basal PrP^C cleavage, MAPK activation and intracellular ROS in moRK13, huRK13 and vecRK13 cells. **(A)** Basal PrP^C cleavage of huRK13 and moRK13 cells. Lysates were PNGase F digested and western blotted with mab ICSM18 to detect the C1 fragment. β-Tubulin was blotted as a loading control. Western blots are shown on the left and densitometric quantification on the right (shown are the mean and s.e.m. of four repeats from three independently selected clones and an unselected mixed cell population). Quantification of the untreated C1 and C2 fragment band intensities is shown as a ratio to full-length PrP and reveals that moRK13 cells show significantly greater C1 cleavage compared with the huRK13 cells (t = 5.671, P = 0.0048, n = 4). No significant difference is seen between the cell lines for the C2 cleavage fragment (t = 0.368, P = 0.7328, n = 4). Western blots of basal activation of the intracellular signaling proteins ERK1/2, JNK/SAPK and p38 are shown in **(B)** and quantification of the ratio of p-ERK1/2 to ERK1/2 is shown in **(C)**. The densitometric quantification of ERK1/2 phosphorylation depicts the mean and s.e.m. of five replicates using three clones. A significant decrease in the basal level of ERK1/2 activation (phosphorylation) is observed for cells expressing $moPrP^C$ (F = 8.713, P = 0.0029, $^{**}P < 0.01$, $^{*}P < 0.05$). To assess if the expression of PrP^C within the RK13 cells alters basal ROS production, the DCFDA assay was used to quantify basal ROS **(D)**. Cells were loaded with CM-H_2-DCFDA and fluorescence was monitored at the assay start and after 30 min incubation. The plot shows the mean and s.e.m. change in fluorescence from the time 0 reading for three independently selected clones. No significant differences were seen between the cell lines by one-way ANOVA (F = 0.681, P = 0.5413). For all graphs, black, white and gray bars represent huRK13, moRK13 and vecRK13 cell line results, respectively.

out copper. PrP^C is widely accepted to be a copper-binding protein. Exposing the cell lines to copper resulted in a selective increase in N1/C1 cleavage restricted to the huRK13 cells (Figure 2A); a trend toward increased N1/C1 cleavage is seen for mouse PrP but this is not significant (Figure 2B). Using BA to non-specifically increase membrane fluidity significantly altered huRK13 PrP^C N1/C1 cleavage (Figure 2A). The huRK13 N1/C1 cleavage is also increased above untreated cells for the BA plus copper treatment; however, this increase is not significantly different to the copper-alone treatment, suggesting that there is no cumulative cleavage response. The only condition to induce a significant change in moRK13 N1/C1 cleavage was the combined copper and filipin treatment; this was also significant for the huRK13 cells. Significant N1/C1 cleavage within huRK13 was also seen at 25 ºC, and at 25 ºC with DMSO and increased exogenous copper.

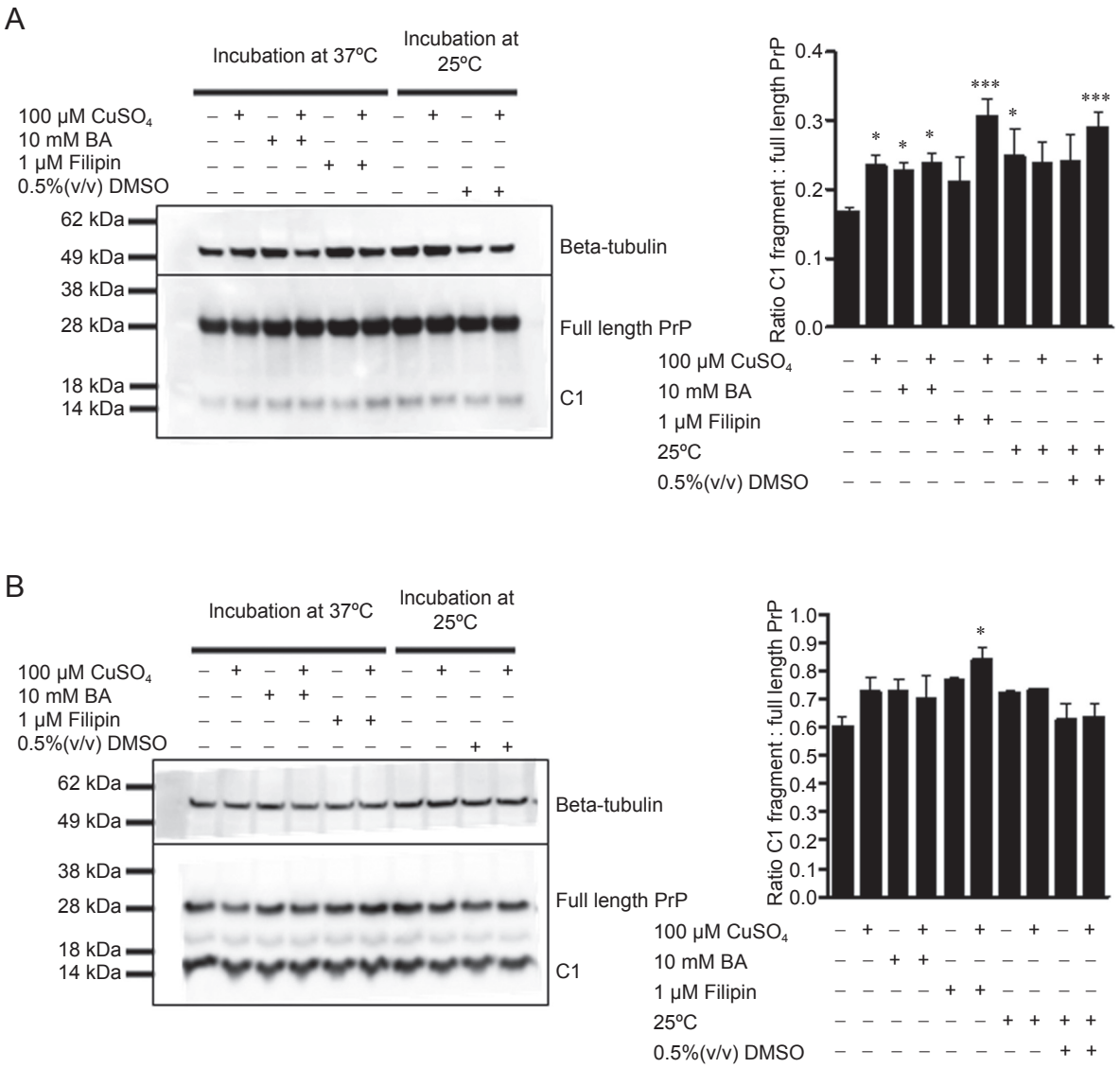

Figure 2 PrP N1/C1 cleavage profiles of the huRK13 and moRK13 cells treated with the membrane perturbing conditions with and without increased exogenous copper. HuRK13 cells **(A)** and moRK13 cells **(B)** PrP N1/C1 cleavage profile in response to treatment with each condition for 30 min before harvesting cells. Lysates were PNGase digested before electrophoresis and western blotting with mab ICSM18. Left plates show example blots and right plates show the corresponding densitometric quantification of the full-length PrP and C1 band signals with graphs representing the mean and s.e.m. of three independently selected clones. Significant differences, as determined by one-way ANOVA, are indicated by $*P < 0.05$ and $***P < 0.001$.

Increased exogenous copper activates PrP^C-specific signal transduction in huRK13 cells only

Copper treatment increased ERK1/2 phosphorylation in all of the cell lines including the vecRK13 cells, indicating that copper induces a non-specific reaction via this pathway (Supplementary information, Figure S3A and S3B). A significant huRK13-specific increase in phosphorylation was seen for JNK/SAPK and p38 (Figure 3).

Global increases or decreases in membrane fluidity reduce huRK13 signal fidelity in response to copper

Increasing membrane fluidity eliminates the fidelity of the JNK/SAPK and p38 signaling response seen in the huRK13 cells (Figure 3). The phosphorylation of these intermediates under conditions of increased fluidity is not significantly different to the vecRK13 control cells. Lowering the cellular temperature decreases membrane fluidity and the addition of DMSO allows phase transition of membranes (into the gel phase) to occur at 25 ºC, resulting in reduced mobility of membrane proteins. No clear trends in signaling were observed for the 25 ºC (without DMSO) condition across the cell lines, either with or without exogenous copper (Supplementary information, Figure S4). The addition of DMSO increased the huRK13 phosphorylation of p38 and JNK/SAPK in the presence of copper but only the p38 phosphorylation is significantly raised when compared with the vecRK13 control. Thus, under conditions of reduced protein mobility due to gel phase transition of cellular membranes, huPrP is still able to elicit a PrP^C-specific response to copper through p38 signaling (Supplementary information, Figure S4). As observed previously ERK1/2 phosphorylation appeared to be a non-specific response to gel phase promoting conditions, with the vector control cells responding equivalently to the PrP^C-expressing cells (Supplementary information, Figure S3C).

Lipid raft disruption has a pronounced effect on moPrP-induced signal transduction in the presence of copper

The filipin III complex is an antibiotic that acts by binding and sequestering cholesterol. This makes it an efficient disruptor of lipid raft (cholesterol rich) membrane domains. The filipin treatment caused a non-specific increase of signal protein phosphorylation in all of the cell lines (Figure 4A-4C). When the cells were treated with filipin and copper together, the moRK13 cells showed a dramatic and significant increase in phosphorylation of all the three signal transduction proteins.

Activation of signal transduction in response to copper and filipin is dependent on the presence of moPrP

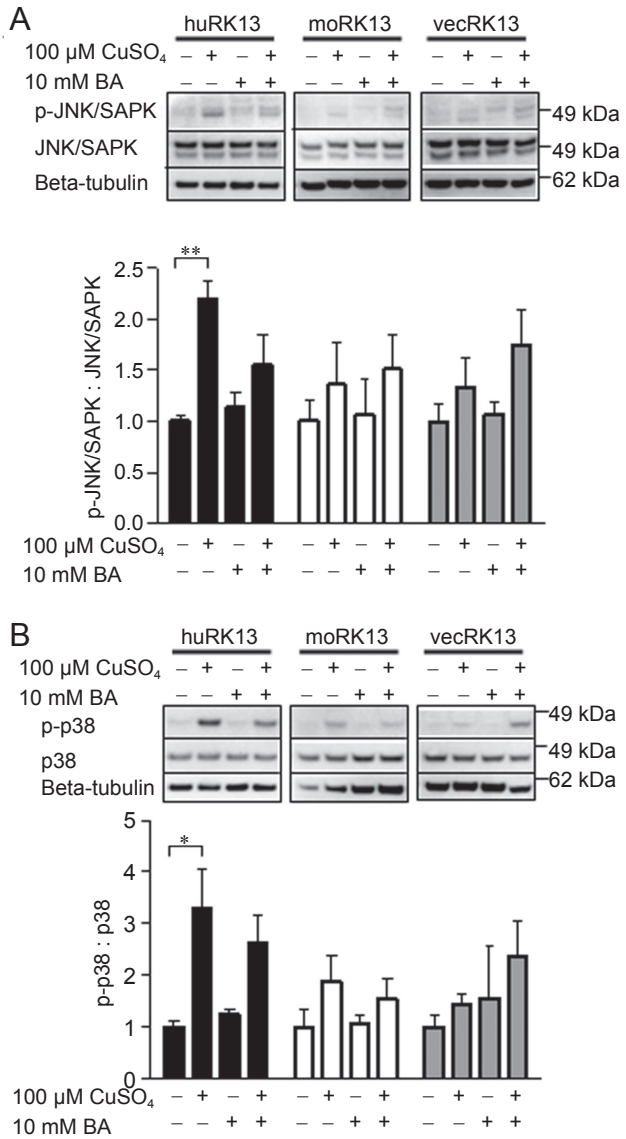

Figure 3 JNK/SAPK, and p38 activation in huRK13 and moRK13 cells exposed to increased exogenous copper and benzyl alcohol. HuRK13, moRK13 and vecRK13 cells were treated with increased exogenous copper for 30 min, both in the presence and absence of the membrane fluidizing agent benzyl alcohol. Lysates were western blotted with antibody sets against p-JNK/SAPK and JNK/SAPK **(A)**, p-p38 and p38 **(B)**. Bands were quantified densitometrically and huRK13, moRK13 and vecRK13 cells are shown as black, white and gray bars, respectively. Graphs represent the mean and s.e.m. (from four independent experiments) of the phosphorylated form to the total signaling protein ratio, and are expressed relative to the untreated cell control. Example blots are shown above the corresponding graph. Conditions that significantly changed the ratio of phospho-signaling molecule to signaling molecule, compared by one-way ANOVA within each cell line and by two-way ANOVA with the vecRK13 cell controls, are indicated by $*P < 0.05$, $**P < 0.01$ and $***P < 0.001$. Copper induces a huPrP-specific increase in JNK/SAPK and p38 phosphorylation, the specificity of which is lost when the membrane fluidity is increased.

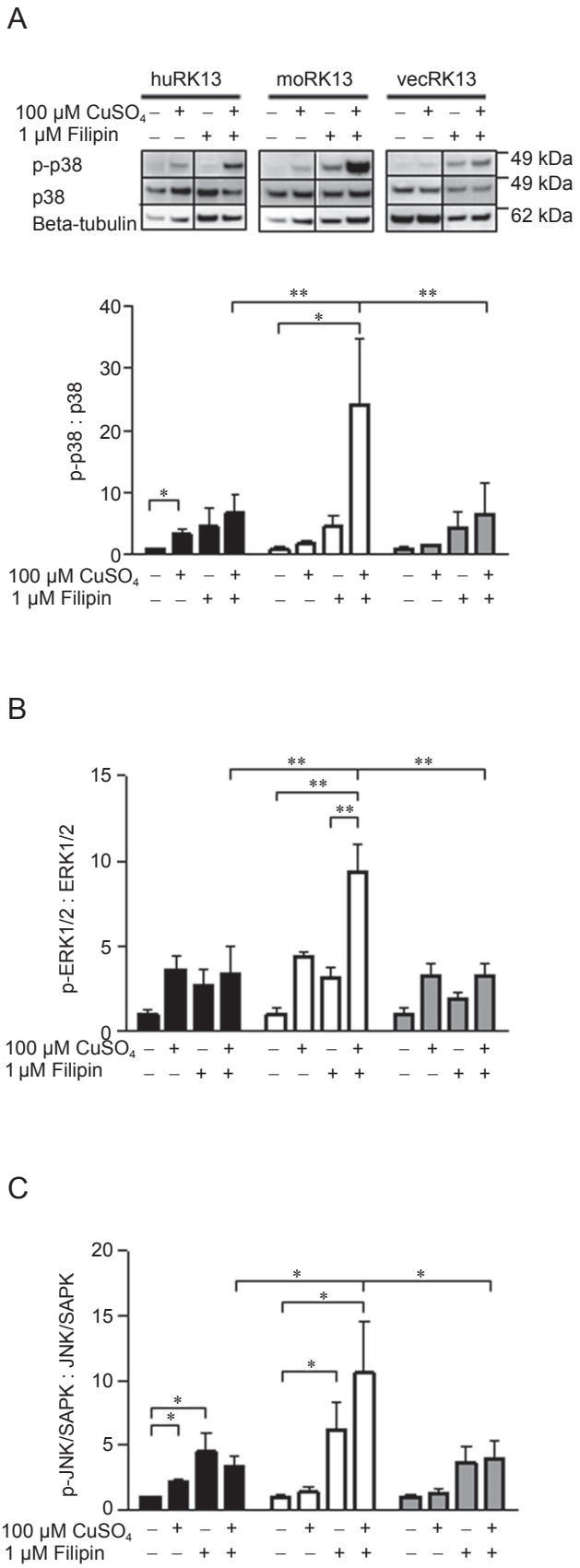

To check that the dramatic cellular signaling responses seen in response to the copper and filipin treatments were not due to clonal drift from selection pressure, the RNAi system described in Daude *et al*. [39] was employed to knock down the expression of PrP^C in the moRK13 cells, and by doing so to allow the innate responses of the cell line to be assessed in the setting of attenuated PrP^C expression. ERK1/2 signaling was assessed in the knockdown cells following treatment with copper and filipin. ERK1/2 signaling was chosen for analysis because ERK1/2 phosphorylation was altered in these cells basally and, whilst ERK1/2 responses to copper alone were non-specific, significant increases were observed in the moRK13 cells when the copper was applied with filipin. Further, Daude *et al*. [39] used ERK as a loading control, so we were confident that ERK1/2 levels would not be altered by the siRNA transfection. Since the moRK13 cells are transfected to overexpress PrP^C, a complete knockdown of PrP proved difficult; however a ~30% reduction in protein expression was reproducibly achieved (Figure 5A and 5B), and this corresponded with a ~48% decrease in ERK1/2 phosphorylation when treated with copper and filipin (Figure 5A and 5C) compared with cells expressing unaltered levels of moPrP. Therefore, it is unlikely that the cell line has suffered clonal drift that would account for the signaling responses. Instead $moPrP^C$ seems essential for these signaling responses to occur. To further ensure that the cell lines used had not drifted from the original population, the untransfected RK13 cells were treated with the copper and filipin conditions. The results obtained were not significantly different from the vecRK13 cells (Supplementary information, Figure S5).

Figure 4 Induction of signal transduction in huRK13, moRK13 and vecRK13 cells by copper when lipid rafts are disrupted. The cholesterol-sequestering antibiotic filipin was used to increase membrane fluidity by disrupting the cholesterol-rich lipid raft domains and cells were treated for 30 min with and without copper before lysis and western blotting. Example blots of p38 activation† are shown above the corresponding graphical data in **(A)** and graphical data only for ERK and JNK/SAPK are shown in **(B)** and **(C)**, respectively. Graphs represent the mean and s.e.m. of four independent experiments of huRK13 (black bars), moRK13 (white bars) and vecRK13 (gray bars) cells. MoRK13 cells show a dramatic and significant response (in contrast to hu/vecRK13 cells) of all of the signaling proteins to the filipin and copper treatment (ERK, F = 12.86, $P < 0.0001$; p38, F = 3.506, $P = 0.0494$; JNK/SAPK, F = 7.663, $P = 0.0003$; $*P < 0.05$, $**P < 0.01$, $***P < 0.001$). †These blots are separated between the filipin and non-filipin treatments, as these conditions were originally run on the same blot (for quantification purposes) with bands for other treatments between the two conditions; these have been removed to show only the relevant data here.

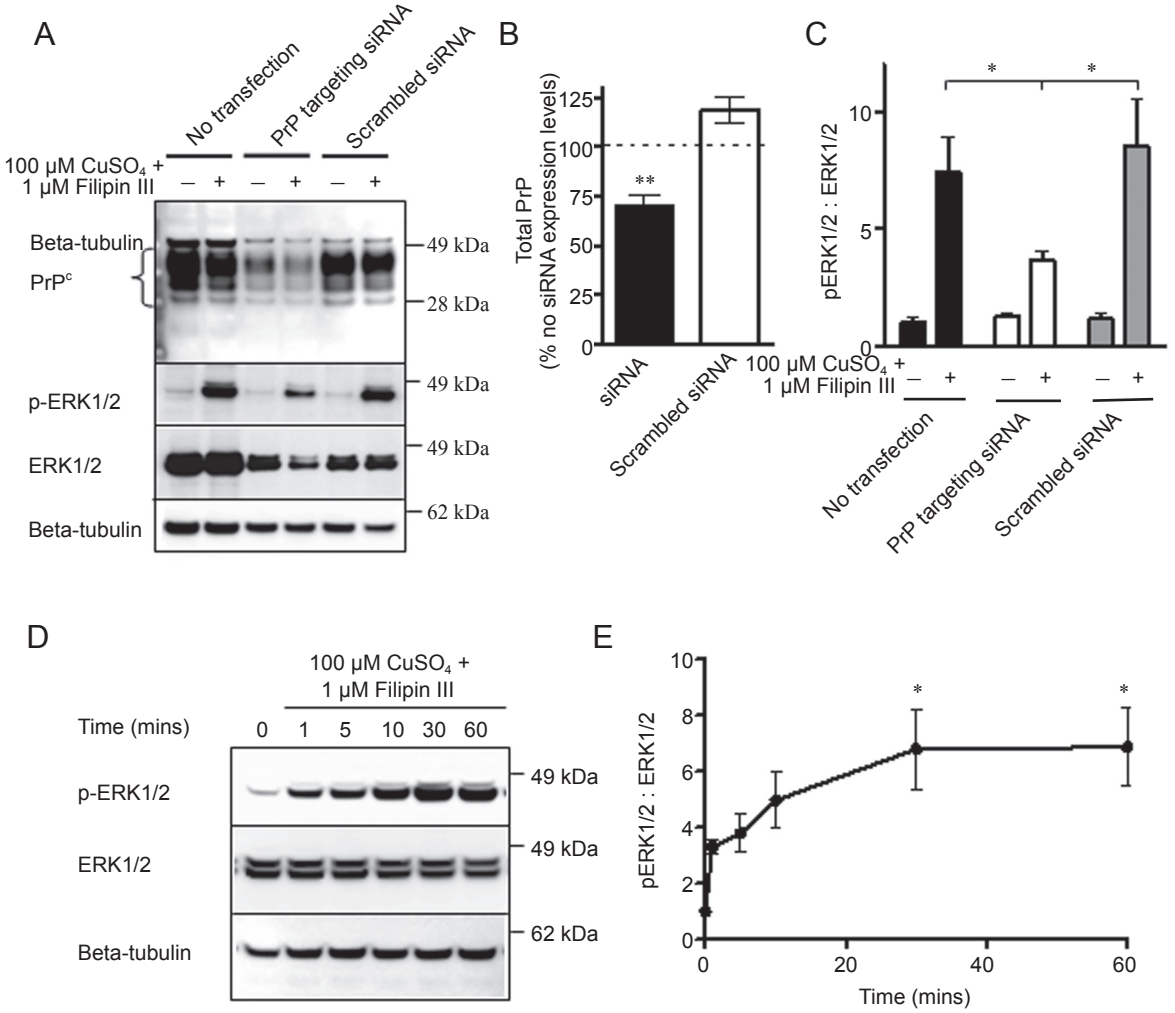

Figure 5 Dependence on moPrP^C expression and time frame of the copper- and filipin-mediated signal transduction event. **(A**-**C)** RNAi knockdown of the overexpressing moRK13 cell line was carried out using transient transfection of siRNA duplexes targeted against PrP^C or scrambled as a control for non-specific responses to transfection. **(A)** Western blots of PrP and ERK1/2 signaling in the untransfected, siRNA-transfected cells and scrambled siRNA controls, when treated with and without 100 μM copper and 1 μM filipin III. **(B)** Densitometric quantification of the PrP^C western blots. Expression of PrP^C is significantly reduced in the cells receiving the siRNA directed against PrP^C (black bar; t = 5.549, P = 0.0051, n = 3) but not in those receiving the scrambled siRNA (white bar; t = 2.81, P = 0.107, n = 3). **(C)** Induction of ERK1/2 signaling, shown as the ratio of p-ERK1/2 to total ERK1/2, by 100 μM copper and 1 μM filipin III is reduced in cells transfected with siRNA directed against PrP^C (F = 40.23, P < 0.0001, n = 3, *P < 0.05; black, white and gray bars represent no siRNA, PrP-targeting siRNA and scrambled control siRNA, respectively). **(D**, **E)** Activation of ERK1/2 when moRK13 cells were treated with 100 μM copper and 1 μM filipin III was followed over a period of 1 min to 1 h. Blots are shown in the left plate **(D)** and densitometric quantification of the p-ERK1/2 to total ERK1/2 ratio in the right panel **(E)**. Phosphorylation of ERK1/2 is seen from immediately post treatment and plateaus after 10 min of treatment. Statistical significance is achieved at 30 min and maintained until 60 min (F = 4.831, P = 0.0165, n = 4, *P < 0.05). Graphs show the mean and s.e.m..

Copper- and filipin-induced signal transduction occurs rapidly and peaks around 30 min after exposure

To make certain that the 30 min time point at which the various treatments were assessed was not limiting the responses seen, especially as many ERK1/2 signal transduction events occur within minutes of stimuli, a time course was performed on the moRK13 cells. Cells were treated with the copper and filipin treatments from 1-60 min and western blotted for ERK1/2 phosphorylation. Activation of signaling can be seen as early as 1 min post exposure to copper and filipin, and phosphorylation continues to increase until 30 min, after which it appears to start decaying (Figure 5D and 5E). Significant difference is achieved at the 30 and 60 min time points.

Cell lines endogenously expressing PrP^C show similar profiles to the transfected RK13 cell lines

Whilst PrP^C transfection into a neutral host species provides a convenient background for looking at protein sequence-specific responses, the behavior of endogenously expressed proteins may still vary. The human SH-SY5Y and mouse Neuro2a (N2a) cell lines were used to look at the responses of cells endogenously expressing PrP, and the mouse PrP-null CF10 cell line [40] was additionally considered to identify PrP-specific responses. These cell lines are derived from neuronal lineages, whereas the RK13 cells are epithelial, and would, therefore, identify distinct reactions observed due to cell origin differences. Each of the cell lines were assayed with the copper and filipin conditions as described for the RK13 cell lines and western blotted for ERK1/2 (Figure 6A), p38 (Figure 6B) and JNK/SAPK (Figure 6C), and the SH-SY5Y and N2a cells were additionally western blotted for PrP following PNGase F digesting (Figure 6D). The signaling trends seen in the RK13 cells are mostly preserved across the cell lines, with the mouse N2a cells showing significant increases in phosphorylation of all signal transduction intermediates in response to the combined copper and filipin condition. The human SH-SY5Y cells, whilst retaining the reduced phosphorylation response to copper and filipin, do not show the increase in phosphorylation of p38 and JNK/SAPK in response to copper alone that was seen for the huRK13 cells. This may indicate that the copper-induced signaling by huPrP when lipid raft integrity is preserved is influenced by cell lineage or that overexpression of huPrP in the RK13 background renders it more poised to respond to copper than when expressed at endogenous levels. The cleavage profiles are not identical to those seen in the RK13 cells, with the SH-SY5Y cells showing very limited cleavage responses but the N2a cells showing a significant increase in N1/C1 cleavage in response to combined copper and filipin treatment.

Introduction of the human N1/C1 cleavage region motif into mouse PrP^C results in mixed cleavage and signaling responses

The region encompassing the human N1/C1 cleavage site has two methionines, which are lacking in the mouse sequence (Supplementary information, Figure S1A, boxed); this is known as the 3F4 site, as this sequence is detected by the 3F4 anti-PrP antibody. To further investigate how the N1/C1 cleavage site influences the mouse PrP^C response to increased exogenous copper and the membrane-perturbing conditions, this motif was cloned into the mouse sequence and stable mixed population cell lines were selected, referred to as 3F4moRK13 cells. Basally, 3F4moRK13 cells showed less N1/C1 cleavage than moRK13 but more than huRK13 cells (Figure 7A and 7B), and N1/C1 cleavage in 3F4moRK13 cells was not significantly affected by copper and/or filipin treatment (Figure 7C). No significant difference in the basal levels of the C2 fragment was observed (data not shown). A basal difference is also apparent for ERK1/2 phosphorylation, with 3F4moRK13 showing decreased levels of phosphoERK1/2 compared to huRK13 but greater levels than moRK13 cells (Figure 7D and 7E). The N1/C1 cleavage correlates inversely with the basal phosphorylation levels ($r^2 = 0.88$, $P < 0.0001$). The 3F4moRK13 cells were treated with copper and/or filipin in parallel with the mixed population moRK13 and huRK13 cells as described previously. The PrP^C-independent response of ERK1/2 phosphorylation to copper treatment was maintained in the 3F4moRK13 cells (Figure 7D and 7F); conversely, the specific response of the moRK13 cells to the combined filipin and copper treatment was lost, with the 3F4moRK13 cells showing no significant difference from the huRK13 cell response. The huRK13-specific phosphorylation of p38 and JNK/SAPK in response to copper was also abolished (Figure 7G-7I), and all phosphorylation appeared reduced. The consistency of the cellular responses did, however, show that, although attenuated, the increase in JNK/SAPK phosphorylation that was observed for moRK13 cells after treatment with both filipin and copper was still significant for the 3F4moRK13 cells, but this was not the case for p38 phosphorylation.

Discussion

Our results suggest PrP^C alpha cleavage and PrP^C-mediated signal transduction may be linked events. Further, both events are influenced by cell membrane and particularly lipid raft integrity. In the context of the neutral RK13 cell background, the primary sequence of PrP^C, specifically the N1/C1 cleavage site, exerts a dominant influence over signal transduction through MAPK intermediates both basally and in response to membrane perturbation in the presence of copper. These effects are summarized in Figure 8.

In the current study, increased basal N1/C1 cleavage was associated with lower basal ERK phosphorylation, but increased N1/C1 cleavage in response to perturbation resulted in increased signal transduction through MAPK intermediates. This may indicate that N1/C1 processing preceded PrP^C localization at the cell surface, and that sequestration of the cleavage fragments in lipid raft domains renders them inactive. Release from the lipid raft domains by cholesterol depletion or other cellular pertur-

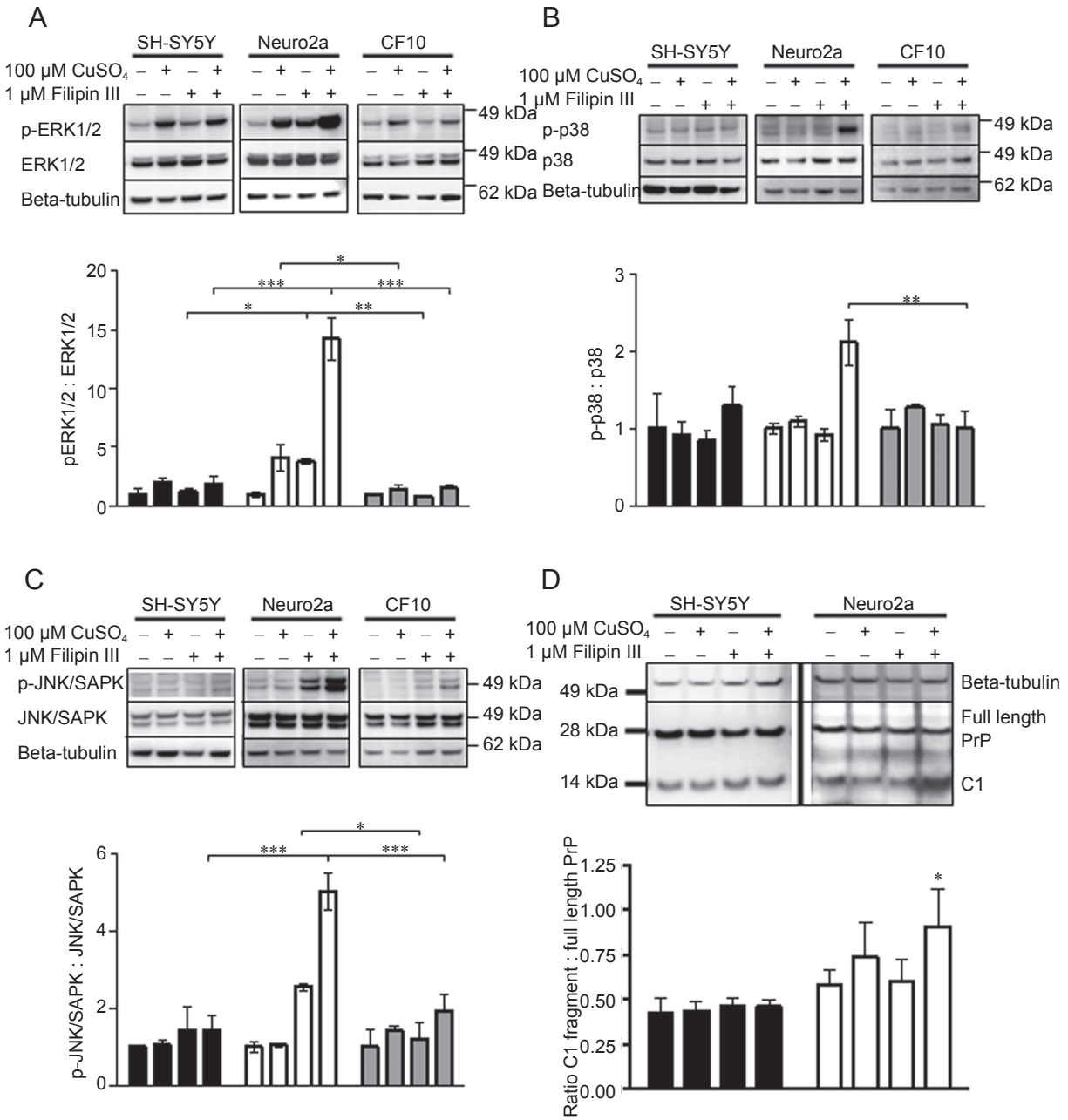

Figure 6 Human SH-SY5Y and murine Neuro2a cell responses to copper and filipin treatments. To consider how the 100 μM copper and 1 μM filipin III treatments may alter signaling and cleavage in cell lines endogenously expressing PrP^C, and, hence not subject to overexpression or selection pressure artifacts, the aforementioned treatments were carried out on SH-SY5Y and Neuro2a (N2a) cell lines as described for the RK13 cell lines. The murine neuronal PrP-null CF10 cell line was also compared to look for PrP-specific responses. **(A-C)** Western blot and densitometric quantification (mean and s.e.m.) of SH-SY5Y (black bars), N2a (white bars) and CF10 (gray bars) cells treated with copper, filipin, or copper and filipin together to disrupt lipid rafts. Shown are the changes in ERK1/2 **(A)**, p38 **(B)** and JNK/SAPK **(C)** signal transduction as ratios of the phosphorylated form of the signal protein to the total expression levels and normalized to untreated cells. Significant differences, as determined by two-way ANOVA with Bonferroni secondary testing, were seen between the N2a and both the SH-SY5Y and CF10 cell lines (ERK1/2 F = 67.39, $P < 0.0001$, $n = 4$; p38 F = 3.96, $P = 0.018$, $n = 4$; JNK/SAPK F = 12.50, $P = 0.0001$, $n = 4$; $^*P < 0.05$, $^{**}P < 0.01$, $^{***}P < 0.001$). **(D)** PrP N1/C1 cleavage of SH-SY5Y (black bars) and N2a (white bars) cells following treatment with copper, filipin, and copper with filipin. Shown are western blot of the PNGase F-treated cell lysates and densitometric quantification of band intensities. Two-way ANOVA with Bonferroni secondary testing identifies that the cell lines are significantly different from each other (F = 9.314, $P = 0.0055$, $n = 4$, $^*P < 0.05$).

bations may allow rapid activation of signal transduction pathways in response to stimuli such as copper. Raft sequestration is a known control mechanism for the activation/deactivation of certain enzymes. An example of this is TACE, where raft sequestering suppresses its catalytic activity until released [41]. Alternatively, release from rafts may allow TACE to cleave PrP at the N1/C1 site and once a threshold is reached the N1/C1 cleavage fragments produce dramatic cellular response. The former suggestion is supported by a recent study from Walmsley *et al*. [42], where alpha cleavage appears to occur along the secretory pathway, probably in the Golgi, on the way to the cell surface. The increase in PrP^C N1/C1 cleavage may, therefore, follow the signal transduction event to replenish PrP^C C1 at the cell surface. The activation of signal transduction intermediates by human PrP^C where no response was seen for mouse PrP^C, despite the higher basal levels of alpha cleavage, may reflect differing abilities of the two proteins to engage the signal transduction machinery.

The 3F4 epitope alters the structure of the alpha cleavage site as shown by the recognition specificity of the 3F4 antibody. The sulfur-containing methionines, as found in the human sequence, are substantially different from the charged histidine with its imidazole ring and the small aliphatic valine of the mouse sequence. *PRNP* point mutations within the structured C-terminal region are associated with human prion diseases, therefore supporting the likelihood that introduction of the 3F4 epitope into murine *PRNP* may have significant biological consequences. The difference in sequence may result in a different presentation of the alpha cleavage site to processing enzymes, resulting in the observed different cleavage patterns, which in turn influences PrP^C function. These potential downstream biological consequences of this sequence variation may impact on studies that use the 3F4 epitope to differentiate between human and mouse PrP^C when overexpressing one in the cellular background of the other. Researchers using these constructs in the future may wish to consider the bearing this may have on conclusions about the function of PrP^C.

N1/C1 cleavage is partially under the control of ADAM10 and TACE activities [28]. Unlike ADAM10, TACE has a very narrow substrate specificity [43]; TNFα, its preferred substrate, is cleaved between alanine and valine residues as found at the mouse N1/C1 cleavage site but not at the human. TACE may therefore have a greater role in the N1/C1 cleavage of mouse PrP^C than human, particularly under altered cellular conditions. The intermediate extent of the N1/C1 cleavage of the 3F4moRK13 cells also indicates that, whilst the N1/C1 site is clearly influencing this cleavage, further sequence differences appear to be involved, perhaps by modulating binding partner interfaces, membrane interaction or cellular trafficking.

Regardless of primary sequence, copper loading appeared to play an important role in PrP^C-mediated MAPK signal transduction. The activation of signal transduction in the moRK13 cells following lipid raft disruption was not due to the potential toxicity of copper, since a lesser reaction was observed following copper treatment alone. Copper binding has been reported to be essential for PrP^C protection against oxidative stress [44, 45], and this protection may be via activation of signal transduction pathways and the subsequent cellular response [30]. Furthermore, there is recent evidence for MAPK activation by signaling endosomes [15]. PrP^C is internalized in response to copper [46], and this reaction requires the octameric repeat domain and the palindromic sequence starting at the N1/C1 cleavage site to be intact [47, 48]. Signaling endosomes have been especially associated with clathrin and dynamin mediated internalization [15, 49, 50], and these are both pathways with which PrP^C has been shown to interact [51, 52]; hence, the role of copper in these reactions may be to promote the internalization of PrP^C to facilitate engagement with signaling intermediates. This is further supported by the findings of Caetano *et al*. [53], who show that signaling by STI-1 through ERK1/2 requires internalization of PrP^C and was inhibited by a dominant-negative mutant of dynamin.

Although multiple binding partners for PrP^C have been suggested to have a role in the activation of cellular signal transduction, including Grb2, EGFR and caveolin [21, 23, 25], the part PrP^C processing plays in relation to such events is uncertain. N1/C1 cleavage has been shown to play a role in apoptosis through modulation of caspase-3 activation. The C1 fragment is able to increase p53 transcription and induce caspase-3 activation [54]. In transgenic mice overexpressing a truncated PrP species (lacking amino acids 32-134), caspase-3 activation is via ERK1/2 and p38 activation [55]. The finding that ERK1/2 and p38 signal protein activation correlated with the changes in mouse C1 cleavage suggests that the mouse PrP^C may be able to interact more efficiently or with a greater number of intermediates involved in activating these pathways. The human PrP^C-expressing cells demonstrated more restricted associations by showing a significant linkage only between N1/C1 cleavage and p38 activation. The consistency of the PrP^C signal across the western blots also shows that the alteration in signaling is not due to significant amounts of PrP^C dissociating from the cell surface due to shedding of the GPI anchor, as has previously been reported in response to filipin and copper [56, 57]. This could be due to species or cell

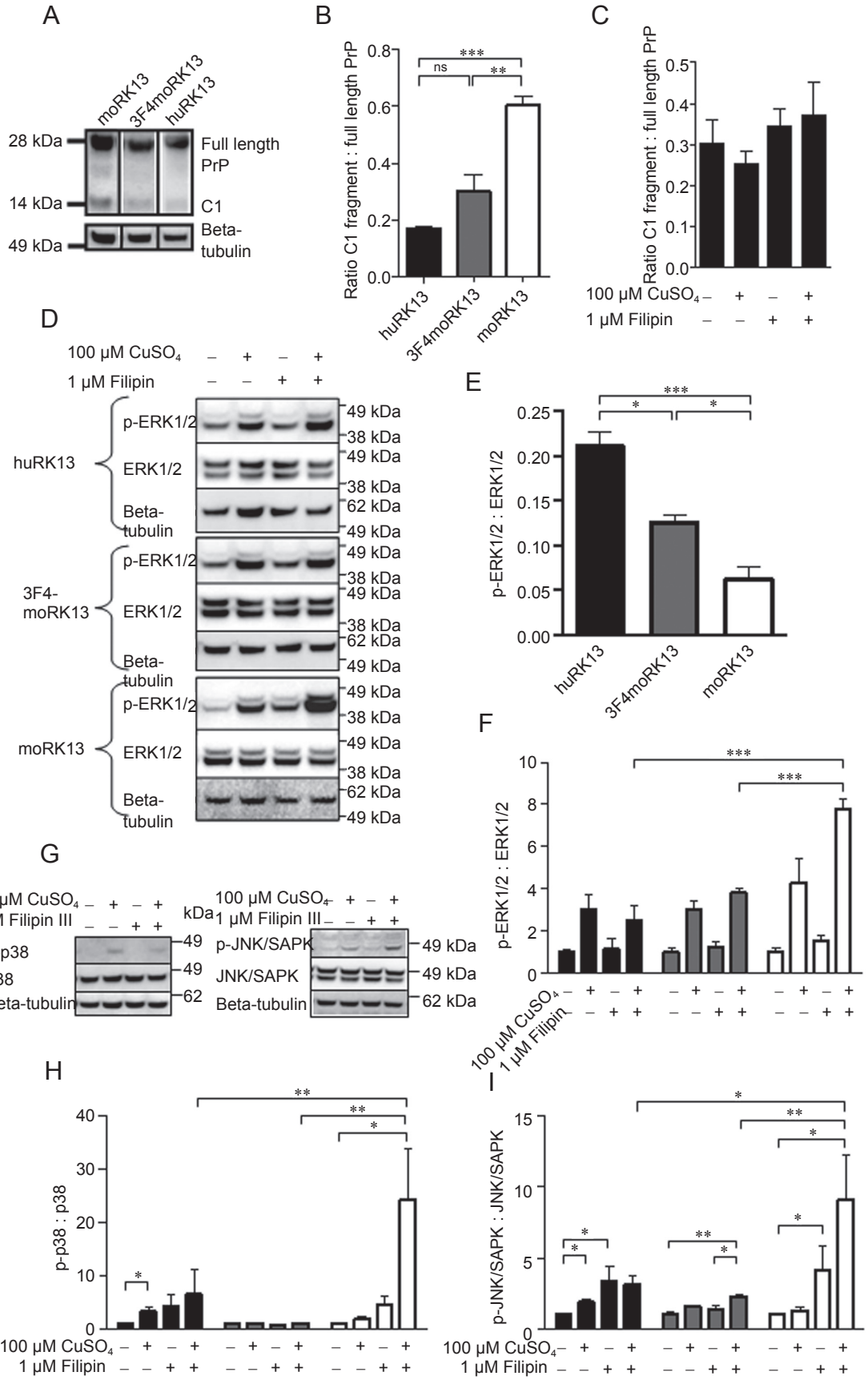
A
moRK13
3F4moRK13
huRK13
28 kDa
14 kDa
49 kDa
Full length PrP
C1
Beta-tubulin
B
Ratio C1 fragment : full length PrP
ns
**
***
huRK13
3F4moRK13
moRK13
C
Ratio C1 fragment : full length PrP
100 µM CuSO4
1 µM Filipin
D
100 µM CuSO4
1 µM Filipin
huRK13
3F4-moRK13
moRK13
p-ERK1/2
ERK1/2
Beta-tubulin
49 kDa
38 kDa
62 kDa
E
p-ERK1/2 : ERK1/2
*
***
F
p-ERK1/2 : ERK1/2
100 µM CuSO4
1 µM Filipin
G
100 µM CuSO4
1 µM Filipin III
kDa
p-p38
p38
Beta-tubulin
p-JNK/SAPK
JNK/SAPK
H
p-p38 : p38
I
p-JNK/SAPK : JNK/SAPK

Figure 7 Introduction of the 3F4 epitope into moPrP alters cleavage and signaling profiles both basally and in response to copper and filipin treatments. Example PNGase-F-digested basal PrP blots **(A)** and densitometric quantification **(B)** of huRK13, moRK13 and 3F4moRK13 cells. C1 cleavage of the 3F4moPrP falls between the levels of moPrP and huPrP, and is significantly different from moPrP. Cells were treated with copper and the lipid-raft disrupting antibiotic filipin for 30 min. Alterations in PrP N1/C1 cleavage are shown in **(C)**. Example ERK1/2 blots are shown in **(D)**. Densitometric quantification of this data show that basal ERK1/2 phosphorylation differs across the cell lines with the 3F4moRK13 levels greater than the moRK13 but lower than the huRK13 cells, and statistically different to both **(E)** ($F = 29.86$, $P = 0.0002$, $n = 4$). The ability of 3F4moRK13 cells to induce ERK1/2 signaling in response to the filipin and copper treatment is significantly reduced compared to moRK13 cells **(F)** ($F = 34.83$, $P < 0.0001$). p38 (blots are shown in **G** and quantification in **H**) and JNK/SAPK (blots are shown in **G** and quantification in **I**) signaling of the 3F4moRK13 cells are significantly different from both huRK13 and moRK13 cells(p38, $F = 3.385$, $P = 0.0284$, $n = 3$; JNK/SAPK, $F = 3.805$, $P = 0.0142$, $n = 3$), with the 3F4moRK13 cells showing a lesser ability to signal through these molecules; however, JNK/SAPK phosphorylation is still significantly increased above untreated cells in response to filipin and copper together ($F = 9.376$, $P = 0.0054$, $n = 3$; $*P < 0.05$, $**P < 0.01$, $***P < 0.001$). All plots represent the mean and s.e.m. of four independent experiments and black, grays and white bars represent the huRK13, 3F4moRK13 and moRK13 cell line results, respectively.

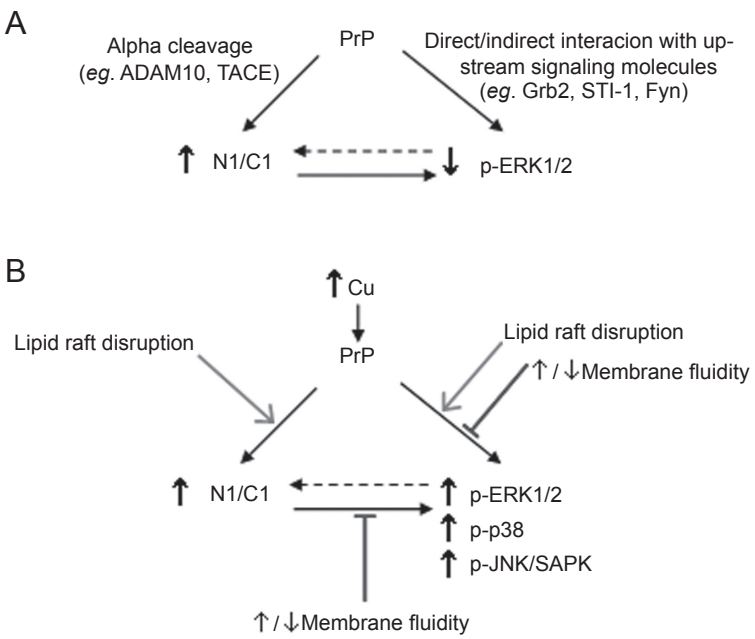

Figure 8 Schematic depiction of PrP N1/C1 cleavage and MAPK-signaling relationships. **(A)** The relationship between PrP N1/C1 cleavage and ERK1/2 phosphorylation in the RK13 cells in the unperturbed state, showing the inverse relationship. **(B)** The relationship between the PrP cleavage and intracellular signaling when an increased amount of exogenous copper is available to PrP. In the presence of copper, a direct relationship is observed between N1/C1 cleavage and signaling. Open arrowheads show how lipid raft disruption enhances these effects and blocked arrows indicate how non-specific changes in fluidity alter the specificity of the reactions.

culture model differences. Rabbit PrP^C varies from human and mouse PrP^C around the site of the GPI anchor; consequently, the rabbit host enzymes involved in cleavage at the GPI anchor may have a lower recognition for human and mouse PrP^C, resulting in less shedding within this system.

The N2/C2 cleavage event was also considered during this study (Supplementary information, Figure S6); however, alterations in N2/C2 cleavage did not correlate with any PrP-related selective change in the MAPK-signaling intermediates studied. Overall, there was no difference between moRK13, huRK13 or 3F4moRK13 basal N2/C2 processing. This is to be expected if the primary cleavage mechanism at the N2/C2 cleavage site is ROS-related, as there was no difference in intracellular ROS production between the cell lines, nor in the N2/C2 site motifs of hu-

man and mouse PrP^C. Moreover, it shows that the N1/C1 cleavage has no direct influence on the N2/C2 cleavage.

Transfecting different PrP primary sequences into identical host cells with negligible endogenous expression allowed focused research and detection of potential species-related differences in processing, particularly at the alpha site, and consequent activation of MAPK signaling. Further studies are required to confirm that the associations we found between PrP^C processing and activation of MAPK signaling are mechanistically directly linked steps in a cellular pathway, rather than simply occurring as unrelated parallel events. Further, while the RK13 cells afforded a permissive and conveniently manipulable system for the expression of PrP constructs of interest, the applicability and translation of our findings from these overexpressing cells of epithelial origin to the situation occurring in neuronal cells endogenously expressing PrP^C is supported by data with SH-SY5Y and N2a cell lines.

In conclusion, the data presented here relate PrP^C processing to signal transduction, and show the inter-dependence of the PrP^C primary sequence, particularly the N1/C1 cleavage site, and the cell membrane in these events. The PrP^C primary sequence influences the predominant type of proteolysis likely to occur in response to specific cellular perturbations, and to what extent consequent signal transduction will occur. Generally, membrane integrity appears important for the fidelity of signal transduction occurring in relation to PrP^C processing, although under certain conditions membrane disruption may allow proteolytic processing not normally accessible to the particular PrP^C primary sequence. For huRK13 cells, the selectivity of signal transduction activation due to copper treatment was often lost when membrane integrity was compromised, becoming similar to non-PrP^C-expressing cells. Independent of the overall PrP^C primary sequence, increased N1/C1 cleavage of PrP^C appears linked to the MAPK pathway, with alterations in amino acid sequence at this proteolytic site markedly influencing processing and signal transduction.

Materials and Methods

Cell culture

All cell lines were cultured in Dulbecco's Modified Eagles Media (DMEM; Gibco – Invitrogen, Victoria, Australia) supplemented with 10% fetal bovine serum (Invitrogen), 50 U/ml penicillin and 50 μg/ml streptomycin solution (Sigma-Aldrich; New South Wales, Australia). Cells were maintained at 37 ºC with 5% CO_2 in a humidified incubator. For microtitre plate assays, (used unless otherwise stated) cells were plated to be 90%-95% confluent at the start of the assay.

Constructs and transfection

pIRES-puro2 (Clontech – Scientifix, Victoria, Australia) contain the full-length human or mouse PrP^C open reading frame, as well as the vector alone was transfected into RK13 cells using FuGene 6 transfection reagent (Roche, New South Wales, Australia) as per the product protocol for a 3:1 reagent:DNA ratio. A total of 2.5 μg/ml puromycin (Sigma-Aldrich) was used for cell selection and both stable clones of equivalent expression levels and mixed populations were selected. Cells were maintained in 2.5 μg/ml puromycin during routine culture. A further mixed population cell line expressing moPrP with the 3F4 epitope (human N1/C1 cleavage site motif) was created by transfection using Lipofectamine (as per the product protocol: Invitrogen). The mixed population was selected and maintained as described above.

RNAi

The siRNA duplexes described by Daude *et al*. [39] were purchased from Sigma-Aldrich. Cells were plated 1 day prior to treatment with the siRNA at approximately 50% confluence. siRNA duplexes were delivered into the cells using FuGene HD transfection reagent in a 4:1 reagent:siRNA ratio as described in the product protocol. The final concentration of duplexes delivered to the cells was 400 nM. Cells were then incubated for 2 days under standard conditions before treatment and extraction as described below.

Western blot

Cells were treated for 30 min with appropriate test reagent before lysis in 20 μl RIPA buffer (50 mM Tris-HCl pH 7.4, 150 mM NaCl, 0.1% (w/v) SDS, 0.5% (w/v) sodium deoxycholate, 1% (v/v) NP-40) supplemented with 0.5 U/ml Benzonase (Sigma-Aldrich) for 20 min at 37 °C. Lysates were mixed with 10 μl of 3× LDS loading dye (Invitrogen) supplemented with 5% (v/v) β-mercaptoethanol (Sigma-Aldrich) and denatured gently at 80 °C for 10 min. A total of 20 μl of lysate was loaded into 15-well 12% NuPAGE Bis-Tris gels (Invitrogen). Gels were run at 200 V for 35-40 min (until the dye front reached the bottom) in the Invitrogen NuPAGE gel tank system, using MES running buffer (Invitrogen). Gels were transferred onto a nitrocellulose membrane (BioRad, New South Wales, Australia) in a Bio-Rad wet blotting system at 100V for 45 min. Membranes were blocked for 1 h in 5% (w/v) fat-free milk powder in PBS-0.1% (v/v) Tween-20 (PBS-t). For PrP^C detection, western blot incubations used a 1 in 30 000 ICSM-18 primary monoclonal antibody (mab; mouse epitope 142-152, human epitope 143-153 (DGen, London, UK)) in 1% milk PBS-t; with anti-mouse HRP secondary (GE Healthcare, New South Wales, Australia). Signaling antibodies phospho(T202/Y204)-p44/42 (p44/42 is more commonly known as ERK1/2, therefore, p-ERK1/2 is used to refer to this antibody); p44/42 (ERK1/2); phospho(T180/Y182)-p38 (p-p38); p38; phospho(T183/Y185)-JNK/SAPK (p-JNK/SAPK); and SAPK/JNK were all used at 1 in 1 000 dilution (Cell Signaling – Genesearch Pty, Queensland, Australia) in 1% (w/v) bovine serum albumin (BSA; Sigma-Aldrich) in PBS-t, with 1 in 5 000 anti-rabbit HRP secondary (Cell Signaling) in 1% (w/v) BSA in PBS-t. Anti-β-tubulin (Sigma-Aldrich) was used as a loading control and blotted using a 1 in 20 000 dilution with anti-mouse-HRP secondary used at 1 in 10 000. Membranes were stripped between probing with each antibody by incubation in low-pH stripping buffer (25 mM glycine-HCL, pH 2;

1% (w/v) SDS) for 10 min at room temperature with agitation, and then washed once in PBS-t before incubation in blocking solution for 1 h.

PNGase F digestion

Media were removed from the cells and 20 µl RIPA buffer plus 0.5 U/ml Benzonase were added per well. Plates were incubated at 37 °C for 20 min. A total of 2 µl 10× denaturation buffer (5% (w/v) SDS, 5% (v/v) β-mercaptoethanol, 50 mM EDTA, 0.02% (v/v) sodium azide in PBS, pH 8.0) was added per well and samples were heated at 80 °C for 10 min to denature. The plate was allowed to cool to room temperature, and 2.5 µl 10% (v/v) NP-40 and 5.5 µl incubation buffer (50 mM EDTA and 0.02% (v/v) sodium azide in PBS, pH8.0) plus 1 U PNGase F (Sigma-Aldrich) were added per well. Plates were incubated overnight at 37 °C in a humidified chamber. 3× NuPAGE LDS sample loading buffer supplemented with 5% (v/v) β-mercaptoethanol was added to the wells and samples were denatured at 80 °C for 10 min. A total of 20 µl of sample was loaded per well, with PrP^C detection as described above.

DCFDA assay

Media were removed and replaced with 50 µl of dPBS containing 5 µM 5-(and-6)-chloromethyl-2',7'-dichlorodihydrofluorescein diacetate, acetyl ester (CM-H_2-DCFDA, Invitrogen). Cells were incubated at 37 °C for 20 min, then the probe solution was removed and replaced with 100 µl of Opti-MEM® I Reduced-Serum Medium (without phenol red) with or without test reagent added. Readings were taken at time 0 and 30 min, using 488 nm excitation and 530 nm emission filters in a Fluostar Optima (BMG Labtech, Victoria, Australia).

Densitometry and statistical analyses

Luminescent signal of the bands on the western blots was captured using a Las-3000 intelligent darkbox (FujiFilm – Berthold, Victoria, Australia), and the intensity was quantified after the subtraction of background, by ImageJ 1.38×. Statistical analyses were carried out using GraphPad Prism 4 or Minitab15 statistical software. Two-way ANOVA with Bonferroni secondary tests was used to determine different cell line responses to the same conditions (these are tabulated in Supplementary information, Table S1) and one-way ANOVA with Tukey's secondary test was used to identify differences within a single cell line. The graphs shown throughout show the mean ± s.e.m. of all of the data; blots from replicate clone/mixed cell line data were averaged and treated as one repeat.

Acknowledgments

CF10 cells were a kind gift from Dr Suzette Priola (National Institutes of Health, USA). The authors thank Ms Robyn Sharples (The University of Melbourne, Australia) for technical assistance. This work was supported by an NH&MRC Program Grant (400202). CLH is supported by a University of Melbourne Early Career Researcher Grant; SJC by an NH&MRC Practitioner Fellowship (400183); SJC and VAL by an NH&MRC Project Grant (454546); VAL is supported by a University of Melbourne CR Roper Fellowship; VAL and AFH by an NH&MRC Project Grant (400229); and AFH by an NH&MRC Career Development Award (251745).

References

1 Prusiner SB. Novel proteinaceous infectious particles cause scrapie. *Science* 1982; **216**:136-144.
2 Legname G, Baskakov IV, Nguyen HO, *et al*. Synthetic mammalian prions. *Science* 2004; **305**:673-676.
3 Büeler H, Fischer M, Lang Y, *et al*. Normal development and behaviour of mice lacking the neuronal cell-surface PrP protein. *Nature* 1992; **356**:577-582.
4 Brandner S, Raeber A, Sailer A, *et al*. Normal host prion protein (PrP^C) is required for scrapie spread within the central nervous system. *Proc Natl Acad Sci USA* 1996; **93**:13148-13151.
5 Brown DR, Herms J, Kretzschmar HA. Mouse Cortical Cells lacking cellular PrP survive in culture with a neurotoxic PrP fragment. *Neuroreport* 1994; **5**:2057-2060.
6 Fischer M, Rulicke T, Raeber A, *et al*. Prion protein (PrP) with amino-proximal deletions restoring susceptibility of PrP knockout mice to scrapie. *EMBO J* 1996; **15**:1255-1264.
7 Chesebro B, Trifilo M, Race R, *et al*. Anchorless prion protein results in infectious amyloid disease without clinical scrapie. *Science* 2005; **308**:1435-1439.
8 Mallucci G, Dickinson A, Linehan J, Klöhn PC, Brandner S, Collinge J. Depleting neuronal PrP in prion infection prevents disease and reverses spongiosis. *Science* 2003; **302**:871-874.
9 Weissmann C, Büeler H, Fischer M, *et al*. PrP-deficient mice are resistant to scrapie. *Ann N Y Acad Sci* 1994; **724**:235-240.
10 Brown DR, Qin K, Herms JW, *et al*. The cellular prion protein binds copper *in vivo*. *Nature* 1997; **390**:684-687.
11 Hasnain SS, Murphy LM, Strange RW, *et al*. XAFS Study of the High-affinity Copper-binding Site of Human PrP^{91-231} and its Low-resolution Structure in Solution. *J Mol Biol* 2001; **311**:467-473.
12 Hornshaw MP, McDermott JR, Candy JM. Copper binding to the N-terminal tandem repeat regions of mammalian and avian prion protein. *Biochem Biophys Res Commun* 1995; **207**:621-629.
13 Jackson GS, Murray I, Hosszu LLP, *et al*. Location and properties of metal-binding sites on the human prion protein. *Proc Nat Acad Sci USA* 2001; **98**:8531-8535.
14. Allen JA, Halverson-Tamboli RA, Rasenick MM. Lipid raft microdomains and neurotransmitter signaling. *Nature Rev Neurosci* 2007; **8**:128-140.
15 Anderson DH. Role of lipids in the MAPK signaling pathway. *Prog Lipid Res* 2006; **45**:102-119.
16 Vigh L, Escribá PV, Sonnleitner A, *et al*. The significance of lipid composition for membrane activity: New concepts and ways of assessing function. *Prog Lipid Res* **44**:303-344.
17 Cashman NR, Loertscher R, Nalbantoglu J, *et al*. Cellular isoform of the scrapie agent protein participates in lymphocyte activation. *Cell* 1990; **61**:185-192.
18 Bainbridge J, Walker KB. The normal cellular form of prion protein modulates T cell responses. *Immunol Lett* 2005; **96**:147-150.
19 Li R, Liu D, Zanusso G, *et al*. The expression and potential function of cellular prion protein in human lymphocytes. *Cell Immunl*. 2001; **207**:49-58.
20 Stuermer CA, Langhorst MF, Wiechers MF, *et al*. PrP^C capping in T cells promotes its association with the lipid raft proteins reggie-1 and reggie-2 and leads to signal transduction. *FASEB J* 2004; **18**:1731-1733.

21 Spielhaupter C, Schätzl HM. PrP^C directly interacts with proteins involved in signaling pathways. *J Biol Chem* 2001; **276**:44604-44612.
22 Lopes MH, Hajj GN, Muras AG, *et al*. Interaction of cellular prion and stress-inducible protein 1 promotes neuritogenesis and neuroprotection by distinct signaling pathways. *J Neurosci* 2005; **25**:11330-11339.
23 Monnet C, Gavard J, Mège RM, Sobel A. Clustering of cellular prion protein induces ERK1/2 and stathmin phosphorylation in GT1-7 neuronal cells. *FEBS Lett* 2004; **576**:114-118.
24 Schneider B, Mutel V, Pietri M, *et al*. NADPH oxidase and extracellular regulated kinases 1/2 are targets of prion protein signaling in neuronal and non-neuronal cells. *Proc Natl Acad Sci USA* 2003; **100**:13326-13331.
25 Toni M, Spisni E, Griffoni C, *et al*. Cellular prion protein and caveolin-1 interaction in a neuronal cell line precedes Fyn/ERK 1/2 signal transduction. *J Biomed Biotech* 2006; **2006**:1-13.
26 Mouillet-Richard S, Ermonval M, Chebassier C, *et al*. Signal transduction through prion protein. *Science* 2000; **289**:1925-1928.
27 Wopfner F, Weidenhöfer G, Schneider R, *et al*. Analysis of 27 mammalian and 9 avian PrPs reveals high conservation of flexible regions of the prion protein. *J Mol Bio* 1999; **289**:1163-1178.
28 Vincent B, Paitel E, Saftig P, *et al*. The Disintegrins ADAM10 and TACE contribute to the constitutive and phorbol ester-regulated normal cleavage of the cellular prion protein. *J Biol Chem* 2001; **276**:37743-37746.
29 McMahon HE, Mangé A, Nishida N, *et al*. Cleavage of the amino terminus of the prion protein by reactive oxygen species. *J Biol Chem* 2001; **276**:2286-2291.
30 Watt NT, Taylor DR, Gillott A, *et al*. Reactive oxygen species-mediated β-cleavage of the prion protein in the cellular response to oxidative stress. *J Biol Chem* 2005; **280**:35914-35921.
31 Chen SG, Teplow DB, Parchi P, *et al*. Truncated forms of the human prion protein in normal brain and in prion diseases. *J Biol Chem* 1995; **270**:19173-19180.
32 Yadavalli R, Guttmann RP, Seward T, *et al*. Calpain-dependent endoproteolytic cleavage of prpsc modulates scrapie prion propagation. *J Biol Chem* 2004; **279**:21948-21956.
33 Courageot MP, Daude N, Nonno R, *et al*. A cell line infectable by prion strains from different species. *J Gen Virol* 2008; **89**:341-347.
34 Vella LJ, Sharples RA, Lawson VA, *et al*. Packaging of prions into exosomes is associated with a novel pathway of PrP processing. *J Pathol* 2007; **211**:582-590.
35 Martin BD, Schoenhard JA, Sugden KD. Hypervalent chromium mimics reactive oxygen species as measured by the oxidant-sensitive dyes 2',7'-dichlorofluorescin and dihydrorhodamine. *Chem Res Toxicol* 1998; **11**:1402-1410.
36 Regev R, Assaraf YD, Eytan GD. Membrane fluidization by ether, other anaesthetics, and certain agents abolishes P-glycoprotein ATPase activity and modulates efflux from multidrug resistant cells. *Eur J Biochem* 1999; **259:**18-24.
37 Sangwan V, Örvar BL, Beyerly J, Hirt H, Dhindsa RS. Opposite changes in membrane fluidity mimic cold and heat stress activation of distinct plant MAP kinase pathways. *Plant J* 2002; **31**:629-638.
38 Shigapova N, Török Z, Balogh G, *et al*. Membrane fluidization triggers membrane remodelling which affects the thermotolerance in *Escherichia coli*. *Biochem Biophys Res Commun* 2005; **328**:1216-1223.
39 Daude N, Marella M, Chabry J. Specific inhibition of pathological prion protein accumulation by small interfering RNAs. *J Cell Sci* 2003; **116**:2775-2779
40 Greil CS, Vorberg IM, Ward AE, *et al*. Acute cellular uptake of abnormal prion protein is cell type and scrapie-strain independent. *Virology* 2008; **379**:284-293
41 Tellier E, Canault M, Rebsomen L, *et al*. The shedding activity of ADAM17 is sequestered in lipid rafts. Exp *Cell Res* 2006; **312**:3969-3980.
42 Walmsley AR, Watt NT, Taylor DR, Perera WS, Hooper NM. Alpha-cleavage of the prion protein occurs in a late compartment of the secretory pathway and is independent of lipid rafts. *Mol Cell Neurosci* 2009; **40**:242-248.
43 Mohan MJ, Seaton T, Mitchell J, *et al*. The tumour necrosis factor-α converting enzyme (TACE): A unique metalloproteinase with highly defined substrate specificity. *Biochemistry* 2002; **41**:9462-9469.
44 Brown DR, Clive C, Haswell SJ. Antioxidant activity related to copper binding of native prion protein. *J Neurochem*. 2001; **76**:69-76.
45 Haigh CL, Brown DR. Prion protein reduces both oxidative and non-oxidative copper toxicity. *J Neurochem* 2006; **98**:677-689.
46 Pauly PC, Harris DA. Copper stimulates endocytosis of the prion protein. *J Biol Chem* 1998; **273**:33107-33110.
47 Haigh CL, Edwards KE, Brown DR. Copper binding is the governing determinant of prion protein turnover. *Mol Cell Neurosci* 2005; **30**:186-196.
48 Perera S, Hooper NM. Ablation of the metal ion-induced endocytosis of the prion protein by disease associated mutation of the octarepeat region. *Curr Biol* 2001; **11**:519-523.
49 Howe CL, Valletta JS, Rusnak AS, Mobley WC. NGF signaling from clathrin-coated vesicles: Evidence that signaling endosomes serve as a platform for the Ras-MAPK pathway. *Neuron* 2001; **32**:801-814.
50 Sorkin A, Zastrow M. Signal transduction and endocytosis: close encounters of many kinds. *Nature Rev Mol Cell Biol* 2002; **3**:600-614.
51 Magalhães AC, Silva JA, Lee KS, *et al*. Endocytic intermediates involved with the intracellular trafficking of a fluorescent cellular prion protein. *J Biol Chem* 2002; **277**:33311-33318.
52 Shyng SL, Heuser JE, Harris DA. A glycolipid-anchored prion protein is endocytosed via clathrin coated pits. *J Cell Biol* 1994; **125**:1239-1250.
53 Caetano FA, Lopes MH, Hajj GN, *et al*. Endocytosis of prion protein is required for ERK1/2 signaling induced by stress-inducible protein 1. *J Neurosci* 2008; **28**:6691-6702.
54 Sunyach C, Cisse MA, da Costa CA, Vincent B, Checler F. The C-terminal products of cellular prion protein processing, C1 and C2, exert distinct influence on p53-dependent staurosporine-induced caspase-3 activation. *J Biol Chem* 2007; **282**:1956-1963.
55 Nicolas O, Gavín R, Braun N, *et al*. Bcl-2 overexpression delays caspase-3 activation and rescues cerebellar degenera-

tion in prion-deficient mice that overexpress amino-terminally truncated prion. *FASEB J* 2007; **21**:3107-3117.

56 Parkin ET, Watt NT, Turner AJ, Hooper NM. Dual mechanisms for shedding of the cellular prion protein. *J Biol Chem* 2004; **279**:11170-11178.

57. Marella M, Lehmann S, Grassi J, Chabry J. Filipin prevents pathological prion protein accumulation by reducing endocytosis and inducing cellular PrP release. *J Biol Chem* 2002; **277**:25457-25464.

(**Supplementary information** is linked to the online version of the paper on the *Cell Research* website.)

J Neuropathol Exp Neurol
Vol. 68, No. 10
October 2009
pp. 1125–1135

ORIGINAL ARTICLE

Increased Proportions of C1 Truncated Prion Protein Protect Against Cellular M1000 Prion Infection

Victoria Lewis, PhD, Andrew F. Hill, PhD, Cathryn L. Haigh, PhD, Genevieve M. Klug, PGradDip(Epi.Biostats), Colin L. Masters, MD, Victoria A. Lawson, PhD, and Steven J. Collins, MD

Abstract

Prion disease pathogenesis is linked to the cell-associated propagation of misfolded protease-resistant conformers (PrP^{res}) of the normal cellular prion protein (PrP^{C}). Ongoing PrP^{C} expression is the only known absolute requirement for successful prion disease transmission and PrP^{res} propagation. Further typifying prion disease is selective neuronal dysfunction and loss, although the precise mechanisms underlying this are undefined. We utilized a single prion strain (M1000) and a range of neuronal and nonneuronal, PrP^{C} endogenously expressing and transgenically modified overexpressing cell lines, to evaluate whether PrP^{C} glycosylation patterns or constitutive N-terminal cleavage events may be determinants of sustained PrP^{res} propagation. Our data demonstrates that relative proportions of full-length and C1 truncated PrP^{C} are the most important characteristics influencing susceptibility to sustained M1000 prion infection, supporting PrP^{C} α-cleavage as a protective event, which may contribute to the selective neuronal vulnerability observed in vivo.

Key Words: Endoproteolytic cleavage, N-linked glycosylation, Prion infection, Prion protein, PrP^{C}, PrP^{res}.

INTRODUCTION

Prion diseases are fatal neurodegenerative diseases of humans and animals that are characterized by the accumulation of misfolded protease-resistant conformers (PrP^{res}) of the normal cellular prion protein (PrP^{C}) (1). PrP^{C} is a ubiquitously expressed glycoprotein (2), and like many structural and functional classes of membrane-bound proteins (3), it undergoes posttranslational proteolytic cleavage to generate distinct species. There are 2 predominant truncated PrP^{C} species, C1 and C2. PrP^{C} α-cleavage producing C1 occurs at Residues 111 or 112 (human PrP^{C} sequence nomenclature) (4); significantly, this is within a domain shown to be neurotoxic and amyloidogenic in in vitro studies of a synthetic peptide fragment (5). PrP^{C} α-cleavage is thought to be carried out at least in part by a-disintegrin-and-metalloprotease 10 (ADAM-10) and ADAM-17 (also known as tumor necrosis factor-α–converting enzyme) (6). C2 is produced from β-cleavage and is found at low levels in normal human (4, 7, 8) and cultured cells (9). β-Cleavage occurs around the C-terminus of the PrP^{C} octapeptide repeat domain (8, 9) and is mediated by reactive oxygen species (10). The functional significance of endogenous PrP^{C} cleavage is unresolved.

A defining feature of prion diseases is their transmissibility; this reached epidemic proportions in the United Kingdom during the outbreak of bovine spongiform encephalopathy (11). Ongoing expression of PrP^{C} is an absolute requirement for the successful transmission and continuing pathogenesis of prion diseases (12, 13). In animal species such as rabbits and dogs, the precise molecular determinants of their apparently very high resistance to natural and experimental prion disease are not clearly defined (14, 15), although PrP^{C} primary sequence incompatibilities have been suggested to provide protection for rabbits (16). Importantly, rabbit kidney epithelial cells that have been engineered to express exogenous PrP^{C} can be infected with cognate prion strains derived from the same foreign species, and thereafter propagate PrP^{res} and infectivity (17). These data highlight that the innate resistance of rabbits is linked specifically to endogenous rabbit PrP^{C}, as opposed to the cellular machinery required for infection or propagation.

Neuropathologic features of prion diseases include vacuolation of the neuropil, astrocytic gliosis, neuronal loss, and extracellular PrP^{res} deposits. For a single prion strain, the pattern of neuronal involvement and topographic distribution of these abnormalities can vary among host species and importantly, across different inbred host strains of the same animal species harboring the same PrP gene (*Prnp*) allele (18). These observations suggest nuances in PrP^{C} biology or intrinsic cellular factors unrelated to PrP^{C}, that

From the Departments of Pathology (VL, CLH, GMK, VAL, SJC) and Biochemistry and Molecular Biology and the Bio21 Molecular Science and Biotechnology Institute (AFH) and the Mental Health Research Institute of Victoria (VL, AFH, CLH, GMK, CLM, VAL, SJC), University of Melbourne, Parkville, Victoria, Australia.

Send correspondence and reprint requests to: Steven J. Collins, MD, Department of Pathology, University of Melbourne, Parkville, Victoria 3010, Australia; E-mail: stevenjc@unimelb.edu.au

This work was supported by an NH&MRC Program Grant No. 400202. Cathryn L. Haigh is supported by a University of Melbourne Early Career Researcher Grant; Steven J. Collins by an NH&MRC Practitioner Fellowship No. 400183; Steven J. Collins and Victoria A. Lawson by an NH&MRC Project Grant No. 454546; Victoria A. Lawson and Andrew F. Hill by an NH&MRC Project Grant No. 400229; and Andrew F. Hill by an NH&MRC Career Development Award No. 251745.

Online-only color figures are available at http://www.jneuropath.com.

TABLE 1. Summary of Reported Cellular Susceptibilities to Different Prion Strains

	Mo-Adapted Scrapie Prions						Mo-Adapted Human Prions		
Cell Line	**Chandler/RML[a]**	**22L[a]**	**139A[a]**	**ME7[a]**	**87V[b]**	**22A[b]**	**SY**	**MU-02**	**FU/M1000**
GT1-7	S (34)	S (34)	S (34)	—	R (34)	R (34)	S (32)	—	S (23, 32)
N2a[c]	S (34, 35, 51, 52)	S (34)	R (25); S(34)	R (25)	R (34)	R (34, 51)	—	—	S (52)[d]
OBL-21	R (53)	—	—	—	—	—	—	—	—
NIH/3T3	—	S (43)	—	—	—	—	—	—	—
MoRK13	S (17)	S (17)	—	R (17)	—	—	—	S (54)	S (23, 54)

References are indicated.

Mo-adapted, prion strain adapted by serial passage into mice; SY and MU-02, sporadic CJD strains; FU, Fukuoka-1 GSS strain; M1000, isolate established from FU strain; a, *Prnp*^{a} allele; b, *Prnp*^{b} allele; c, American Type Culture Collection (ATCC) parental line or derived subclones (e.g. N2a 58); d, PrP^{res} detection not attempted but positive in vivo transmission indicates successful infection; S, susceptible to prion infection; R, resistant to prion infection.

differ across neuronal populations in a manner peculiar to each host, significantly impact pathogenesis. Such phenomena exemplify selective neuronal vulnerability and focus the broader concept of innate prion disease resistance to the cellular level.

Cell lines can be persistently infected with prions and retain the biologic and biochemical features of the strain (19, 20). Analogous to observations in animal models, individual cell lines have variable susceptibilities to prion infection (Table 1). In view of the absolute requirement for PrP^C in prion disease transmission and pathogenesis, cellular PrP^C expression profiles may influence susceptibility to sustained prion infection. Here, we used cell lines, endogenously or transgenically expressing the same murine *Prnp* allele, to correlate PrP^C glycosylation patterns and constitutive endoproteolyic cleavage profiles with inherent susceptibility or resistance to a well-characterized mouse-adapted human prion strain (M1000). We found that expression of proportionately higher levels of full-length PrP^C correlated with susceptibility to sustained M1000 prion infection, while relatively higher levels of the C1 C-terminal fragment of PrP^C were associated with resistance to sustained M1000 prion infection. Overall, these results suggest that α-cleavage of PrP^C is protective against stable PrP^{res} propagation.

MATERIALS AND METHODS

Cell Lines and Culture Conditions

The following murine cell lines expressed endogenous PrP^C from the *Prnp*^{a} allele (data not shown): 2 cognate hypothalamic GT1-7 cell lines (21) obtained from the same laboratory approximately 2 years apart, designated GT1-7C and GT1-7H; uncloned N2a neuroblastoma cells (American Type Culture Collection [ATCC] CCL-131); NIH/3T3 fibroblast cells (ATCC CRL-1658); and OBL-21 olfactory bulb cells (22). MoRK13 cells, rabbit kidney–derived epithelial cells (RK13; ATCC CCL-37) stably transfected with the murine *Prnp*^{a} coding sequence as previously described (23), were also used. Cells were maintained in either Dulbecco modified Eagle medium (OBL-21, NIH/3T3, MoRK13) or OptiMEM (N2a, GT1-7) (Invitrogen, Carlsbad, CA) containing 10% (vol/vol) heat-inactivated fetal bovine serum (Thermo Fisher Scientific, Rockford, IL) and 1% (vol/vol) penicillin-streptomycin (Invitrogen), in a humidified incubator, 37°C, 5% carbon dioxide. The medium of MoRK13 cells was supplemented with a final concentration of 2.5 μg/mL puromycin dihydrochloride (Sigma-Aldrich, St Louis, MO).

Prion Strain and Cellular Prion Infection

M1000 prions from mouse brain homogenate (10% wt/vol, prepared in sterile PBS; 140 mmol/L NaCl; 2.7 mmol/L KCl; 1.8 mmol/L KH_2PO_4; 10 mmol/L Na_2HPO_4), mean lethal dose (LD_{50}) of approximately 10^9 LD_{50} per gram of tissue, as determined by end point titration in Tga20 mice (24), were used for all infections. To infect cells, subconfluent monolayers were overlaid with M1000 brain homogenate (or uninfected BALB/c brain homogenate as a negative control) diluted in media to between 0.1% and 2% (wt/vol) final dilution. After overnight incubation, the homogenates were removed, cells were then washed twice with sterile Dulbecco PBS (Invitrogen), and fresh medium was added. Cells were grown to confluence and subcultured routinely, with the first passage post–prion exposure designated Passage 1 (P1).

Cell Blot Detection of PrP^{res}

A sensitive cell blot technique was used to detect PrP^{res} in M1000–infected cell cultures, as described elsewhere (23, 25), with minor modifications. Proteinase K ([PK] Invitrogen) digestion was at a final concentration of 10 μg/mL in lysis buffer (50 mmol/L Tris-Cl pH 7.4, 150 mmol/L NaCl, 0.5% sodium deoxycholate, 0.5% Triton X-100) for 90 minutes at 37°C and was stopped by incubating for 15 minutes in 2 mmol/L phenylmethylsulfonyl fluoride (Roche Applied Science, Penzberg, Germany). Phosphate-buffered saline Tween-20 ([PBST] 140 mmol/L NaCl, 2.7 mmol/L KCl, 1.8 mmol/L KH_2PO_4, 10 mmol/L Na_2HPO_4, 0.05% Tween-20 in H_2O) was used to make the block buffer (5% [wt/vol] nonfat milk in PBST) and for all washes. A 1:10,000 dilution in block buffer of both the anti–prion protein primary antibody ICSM18 (overnight at 4°C; D-Gen, London, UK) and anti–mouse-horseradish peroxidase secondary antibody (1 hour at room temperature; GE Healthcare, Buckinghamshire, UK) was used for all cell blots.

Detection of M1000 PrP^{res}

To detect PrP^{res} in M1000 brain homogenate, samples were digested with 50 μg/mL PK for 1 hour at 37°C. The PK was stopped by the addition of Pefabloc SC (Roche Applied Science) to a final concentration of 4 mmol/L.

Cell Lysate Preparation

Confluent cell cultures were harvested, lysed, and assessed for total protein content using the Pierce BCA protein assay (Thermo Fisher Scientific), as previously described (26). Cell lysates were used directly or treated, as described later, before sodium dodecyl sulfate–polyacrylamide gel electrophoresis (SDS-PAGE) and Western blotting.

TABLE 2. Summary of Cellular Susceptibility to M1000 Prion Infection

Cell Lines Resistant to M1000 Infection	Cell Lines Susceptible to M1000 Infection
GT1-7C	GT1-7H
N2a	OBL-21
NIH/3T3	MoRK13

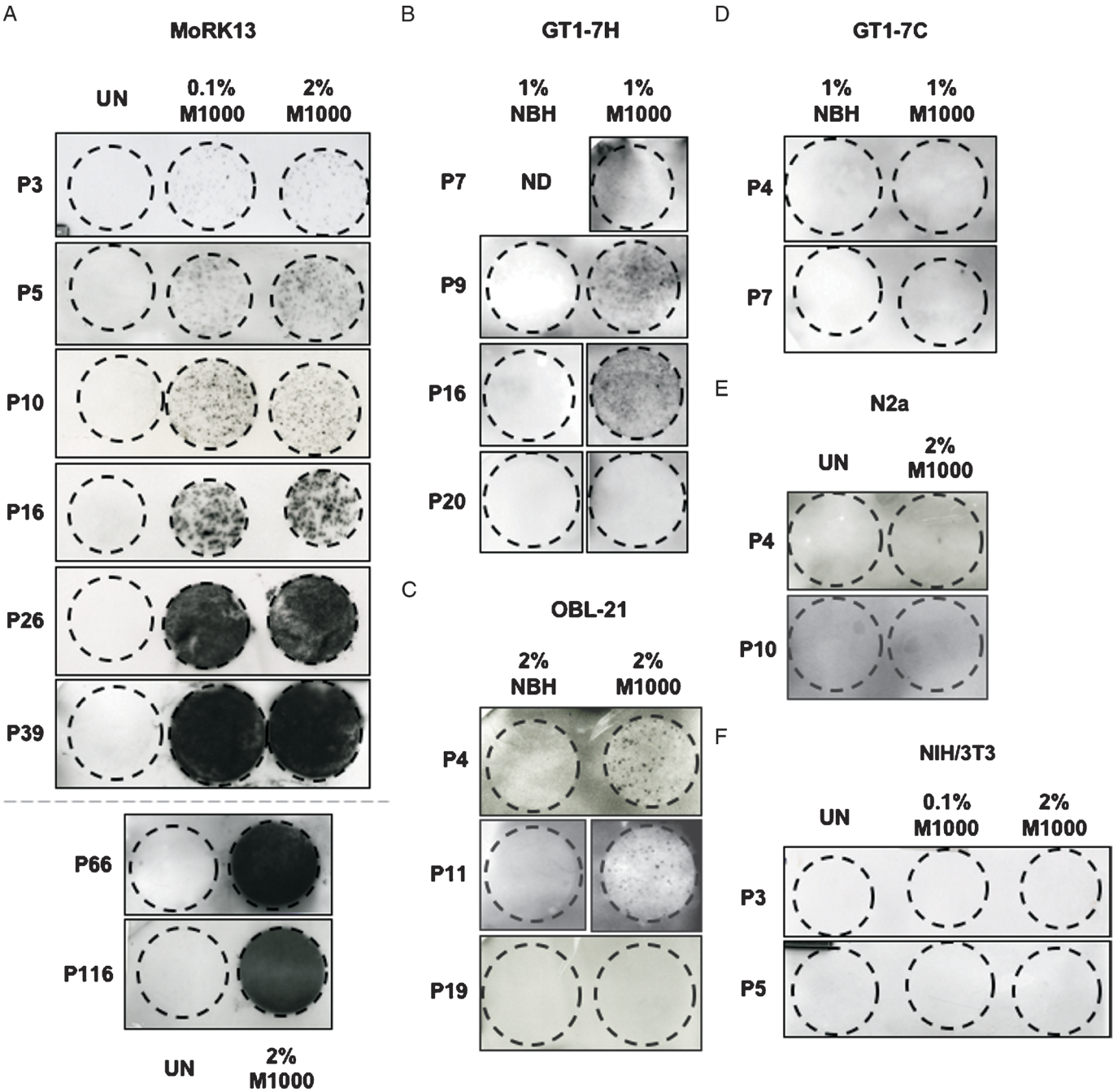

FIGURE 1. Representative cell blots of MoRK13 **(A)**, GT1-7H **(B)**, OBL-21 **(C)**, GT1-7C **(D)**, N2a **(E)**, and NIH/3T3 **(F)** exposed to the specified inoculum (M1000, Balb/c normal brain homogenate (NBH)), or left uninfected (UN). The 2 GT1-7 cell lines were exposed to lower concentrations of inocula (that is, 1% homogenate), as higher percentage homogenates were toxic to these cells. The cells were seeded onto coverslips and grown to 90% to 100% confluence before cell blotting for PrP^{res} as an indicator of successful M1000 prion infection. Passage numbers (post prion infection) are indicated.

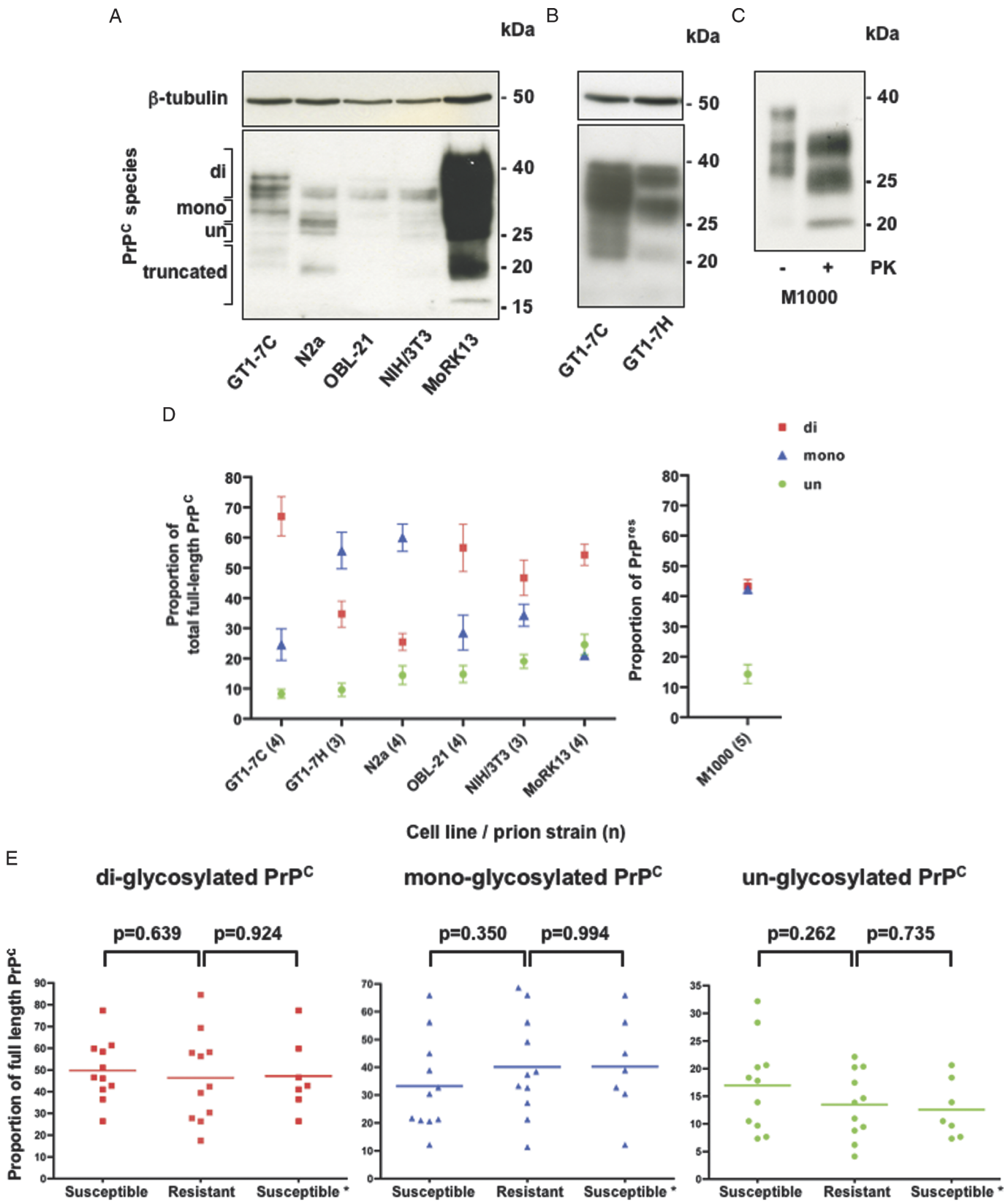

Deglycosylation of PrP^C

The glycosidase PNGaseF (Roche Applied Science) was used to remove N-linked glycans from PrP^C in cell lysates, as previously described (26).

Immunoprecipitation

Zymed rec-Protein G–Sepharose 4B conjugate (PGS) beads (Invitrogen) were equilibrated by washing with PBST. Cell lysates were precleared by diluting into 1 mL PBST and then incubating with 40 μL of prewashed beads for 1 hour with gentle mixing. Beads were collected by centrifugation (2 minutes, 336 × *g*). The supernatant was transferred to fresh tubes containing 1 μL SAF32 (Cayman Chemical, Ann Arbor, MI) and again mixed gently for 1 hour before the addition of 40 μL of fresh equilibrated beads and overnight incubation at 4°C with gentle mixing. Beads were collected as before, washed 3 times in PBST, and then used for PAGE and Western blot analysis.

PAGE and Western Immunoblotting

Untreated, PNGaseF-treated, or PK-treated samples were mixed with an appropriate volume of 4× SDS-PAGE sample buffer (170 mmol/L Tris-Cl pH 6.8, 0.5 mol/L glycine, 8% [wt/vol] SDS, 0.02% [wt/vol] bromophenol blue, 12% [vol/vol] β-mercaptoethanol), boiled (100°C) for 10 minutes, resolved by tris-glycine SDS-PAGE (percent self-made gel [26] as indicated in figure legends), and Western blotted as previously described (26). Immunoprecipitated samples on PGS beads were mixed with NuPAGE loading dye (Invitrogen), boiled (100°C) for 10 minutes, resolved on 12% Bis-tris NuPAGE gels (Invitrogen) using MES running buffer (Invitrogen), and subjected to Western blotting. The anti-PrP antibodies used were monoclonal antibodies ICSM18 (1:40,000), SAF32 (1:3000) and 8B4 (1:10,000; Alicon, Schlieren, Switzerland), and polyclonal antibody 03R19 (24) (1:5000). Anti–β-tubulin primary antibody (1:15,000; Sigma-Aldrich) and the appropriate horseradish peroxidase–conjugated secondary antibodies (i.e. anti-mouse or anti-rabbit; 1:10,000; GE Healthcare) were also used. Detection was via enhanced chemiluminescence (ECL Plus Western Blotting Detection Reagents; GE Healthcare) using Kodak Biomax film (Sigma-Aldrich) or digital capture using a Fujifilm LAS-3000 Intelligent Dark Box or Syngene GeneGnome Bioimager.

Densitometric and Statistical Analyses

Digital and scanned x-ray film images were quantitatively assessed for signal intensity using ImageJ software. Statistical analyses were carried out using GraphPad Prism v4.0a or Minitab 15 as required and as specified in the Results section.

RESULTS

Determination of Susceptibility to M1000 Prions

The abilities of each cell line to sustain M1000 prion infection and propagate PrP^{res} over multiple passages after exposure to M1000 brain homogenate were assessed. Control cells were either left uninfected or exposed to the equivalent dilution of normal BALB/c brain homogenate. Cells were tested a minimum of 3 passages post–prion exposure for de novo PrP^{res} production to indicate successful establishment of M1000 infection. As previously reported (23), MoRK13 cells were highly susceptible to M1000 prions, with increasing propagation of prions over time as seen by the increase in PrP^{res} signal with sequential passages (Fig. 1A). The GT1-7H cells and the OBL-21 cells (Figs. 1B, C, respectively) were also susceptible to M1000 prions, but they produced lower levels of PrP^{res} compared with MoRK13 cells. In both of these cell lines after an initial slight increase in PrP^{res} production, a loss of PrP^{res} propagation was observed. Importantly, this is the first report PrP^{res} propagation in an olfactory bulb cell line. PrP^{res} was never detected in the other cell lines (Figs. 1D–F). Table 2 summarizes the cellular susceptibility or resistance to M1000.

Cellular PrP^C Glycosylation Profiles Do Not Correlate With Susceptibility to M1000 Prion Infection

The prion protein has 2 conserved potential N-linked glycosylation sites (27). None, one, or both of these sites can be occupied by a polysaccharide chain of variable length, which is visualized as 3 different band sizes (i.e. unglycosylated, monoglycosylated, and diglycosylated PrP^C) on a Western blot. As shown in Figures 2A and B, the cell lines display markedly different PrP^C glycosylation profiles; this was highlighted when these patterns were quantified (Fig. 2D). Densitometric measurements were obtained by determining the intensity of the bands at the predicted molecular weights of diglycosylated, monoglycosylated, and unglycosylated PrP^C, and expressing each relative to the total PrP signal intensity. Undefined truncated PrP^C species were not included for analyses. Unexpectedly, the 2 GT1-7 cell lines had noticeably different PrP^C expression profiles (Fig. 2B). Validation of the authenticity of the common origin of GT1-7C and GT1-7H

FIGURE 2. Prion protein (PrP) expression profiles and glycoform ratios in uninfected cells (PrP^C) and M1000 brain homogenate (PrP^{res}). Representative Western blots (WB) of PrP^C expression profiles in cell lines **(A)** and specifically comparing the GT1-7C and GT1-7H cell lines **(B)**; 50 μg total protein per lane, 12% Tris-glycine sodium dodecyl sulfate–polyacrylamide gel electrophoresis, WB with ICSM18, and β-tubulin primary antibodies. **(C)** Representative WB of M1000 brain homogenate pre (−) and post (+) proteinase K digest. **(D)** Quantification (mean ± SEM) of glycoform ratios of PrP^C in the different cell lines and of M1000 PrP^{res}. Numbers of replicates for each individual cell line or homogenate (n) are indicated on x axis labels. In all cases, based on apparent molecular weight, di, diglycosylated PrP^C or PrP^{res}; mono, monoglycosylated PrP^C or PrP^{res}; un, unglycosylated PrP^C or PrP^{res}; truncated, undefined endogenously cleaved PrP^C species. **(E)** Correlative analysis of PrP^C glycosylation profiles with susceptibility to M1000 prion infection. Data points represent the replicates obtained from WB quantification of diglycosylated, monoglycosylated, and unglycosylated PrP^C as shown in **(D)**. Susceptible, evidence of PrP^{res} propagation in cell line after M1000 exposure; resistant, no evidence of de novo PrP^{res} production after M1000 exposure; susceptible*, susceptible cell lines excluding MoRK13 from analysis. Binary logistic regression (Minitab 15) was performed; no significant differences were seen.

cells (i.e. by assessing expression of SV40-T antigen and finding no glial fibrillary acidic protein expression) showed no differences between the lines, although they had slightly different morphologies; the GT1-7H cells were always stellate in appearance and predominantly grew in clusters, whereas the GT1-7C cells were fusiform single cells but became stellate when they approached confluence (not shown). Differences observed in these originally identical cells are most likely caused by clonal drift, possibly explained by the intrinsic or extrinsic models of spontaneous generation of phenotypic heterogeneity (28).

A previous study indicated that glycosylation of PrP^C might be protective by inhibiting the propensity of PrP^C to misfold and form β-sheet conformations (29). To correlate M1000 susceptibility with glycosylation pattern, the cell lines were grouped by their susceptibility or resistance (Table 2) and the proportion of each PrP^C glycoform (Fig. 2D) was separately plotted against susceptibility or resistance (Fig. 2E). To assess the effect of glycosylation in an entirely endogenous expression system, the *susceptible* group was also separated to exclude MoRK13 PrP^C overexpressing cells from the analysis. PrP^C glycosylation profiles were not a significant predictor of susceptibility or resistance to M1000 infection.

There is evidence suggesting that similarity between host PrP^C glycosylation pattern and prion strain PrP^{res} glycosylation pattern can increase the likelihood of PrP^C to PrP^{res} conversion (30). Therefore, the glycosylation pattern of M1000 PrP^{res} was quantified (Figs. 2C, D) and compared with each cell line PrP^C glycosylation profile (Table 3). Only the GT1-7H and NIH/3T3 cell lines had PrP^C glycosylation profiles that were not significantly different from M1000 PrP^{res}. Although the GT1-7H cells were susceptible to M1000 infection, the NIH/3T3 cells were not; this argues against similarities of PrP^C and PrP^{res} glycoform profiles having a dominant influence on susceptibility to infection with this prion strain.

One limitation of the glycosylation analyses is that the Western blot PrP^C glycosylation profiles were obtained using the ICSM18 antibody; the epitope for this antibody is within the C-terminus of PrP, allowing detection of N-terminally truncated PrP species as well as full-length PrP. Therefore, bands seen at the presumed relative molecular weights of diglycosylated, monoglycosylated, and unglycosylated full-length PrP^C may actually be a composite of the different glycosylated full-length and truncated species. To accurately visualize relative levels of glycosylated full-length PrP^C and assess the influence of these levels on susceptibility to M1000 infection, N-terminal antibodies were used to immunoprecipitate and then detect by Western blot exclusively full-length PrP^C species from cell lysates. The glycosylation profiles of full-length PrP^C species (Fig. 3A) are generally different from the profiles in Figure 2A, thereby further indicating that the bands in Figure 2A are most likely a composite of glycosylated full-length and truncated PrP^C. When comparing the different cell lines, the apparent sizes of the different glycosylated full-length PrP^C species are diverse; however when the proportions of each PrP^C species are quantified and graphed, they were remarkably similar (Fig. 3B). We have therefore shown that full-length PrP^C glycosylation profiles are not a significant predictor of susceptibility or resistance to M1000 infection (Fig. 3C). Furthermore, when comparing the cell line PrP^C glycosylation profiles in Figure 3 to the M1000 PrP^{res} profile (Figs. 2C, D), all of the cell lines (both susceptible and resistant) had different proportions of all their PrP^C glycoforms to M1000 PrP^{res}, with the exception of GT1-7H cells for which the relative proportion of unglycosylated PrP^C was not significantly different from the relative proportion of unglycosylated M1000 PrP^{res} (not shown). These data further argue against a predominant influence of PrP^C glycosylation in determining susceptibility to M1000 prion infection.

TABLE 3. Differences in the Relative Proportions of Each Cellular PrP^C Glycoform Compared With the M1000 PrP^{res} Glycoform Profile

	Cell Line PrP^C:M1000 PrP^{res}		
Cell Line	**Di**	**Mono**	**Un**
Resistant to M1000 infection			
GT1-7C	***	**	NS
N2a	**	**	NS
NIH/3T3	NS	NS	NS
Susceptible to M1000 infection			
GT1-7H	NS	NS	NS
OBL-21	*	*	NS
MoRK13	NS	***	NS

*$p < 0.05$; **$p < 0.01$; ***$p < 0.001$; NS, not significant.

Statistical analysis by 2-way ANOVA with Bonferroni posttests (GraphPad Prism v4.0a).

Di, diglycosylated PrP glycoform; Mono, monoglycosylated PrP glycoform; PrP, prion protein; Un, unglycosylated PrP glycoform.

Expression of Lower Proportions of Full-Length PrP^C Correlates With Resistance to M1000, Largely Influenced by Increased PrP^C α-Cleavage

PrP^C contains 2 well-characterized constitutive internal cleavage sites: around residues 111/112 (4) and at the C-terminus of the octapeptide repeat region (8, 9) (Fig. 4A). The PrP^C cleavage profile of each cell line was determined by Western blot epitope mapping of deglycosylated PrP^C (Fig. 4A). PrP^C endoproteolysis varied dramatically among the cell lines. The C1 and C2 fragments were present in all cell lines (Figs. 4B–E), however with the exception of the GT1-7C and MoRK13 cells, the lines had proportionately low C2 levels (Fig. 4F) requiring overexposure of the Western blots for detection. The OBL-21 cell line was the only line with full-length unglycosylated PrP^C (FLUG) as the clearly dominant species compared with the C1 and C2 fragments (Fig. 4F). Collectively, these data indicate that constitutive PrP^C cleavage was variable among the cell lines, but was ubiquitous, suggesting that it may have functional significance.

Similar to the PrP^C glycosylation profiles previously described, there were significantly different truncated PrP^C profiles in the 2 GT1-7 cell lines (Figs. 4E, F). Moreover, there were 2 anomalies in the GT1-7C cells. The first was an immunoreactive band detected with SAF32 at the electrophoretic mobility of the C2 fragment (Figs. 4D, E), suggesting that a proportion of β-cleavage in this line occurred slightly more N-terminally than in the other cell

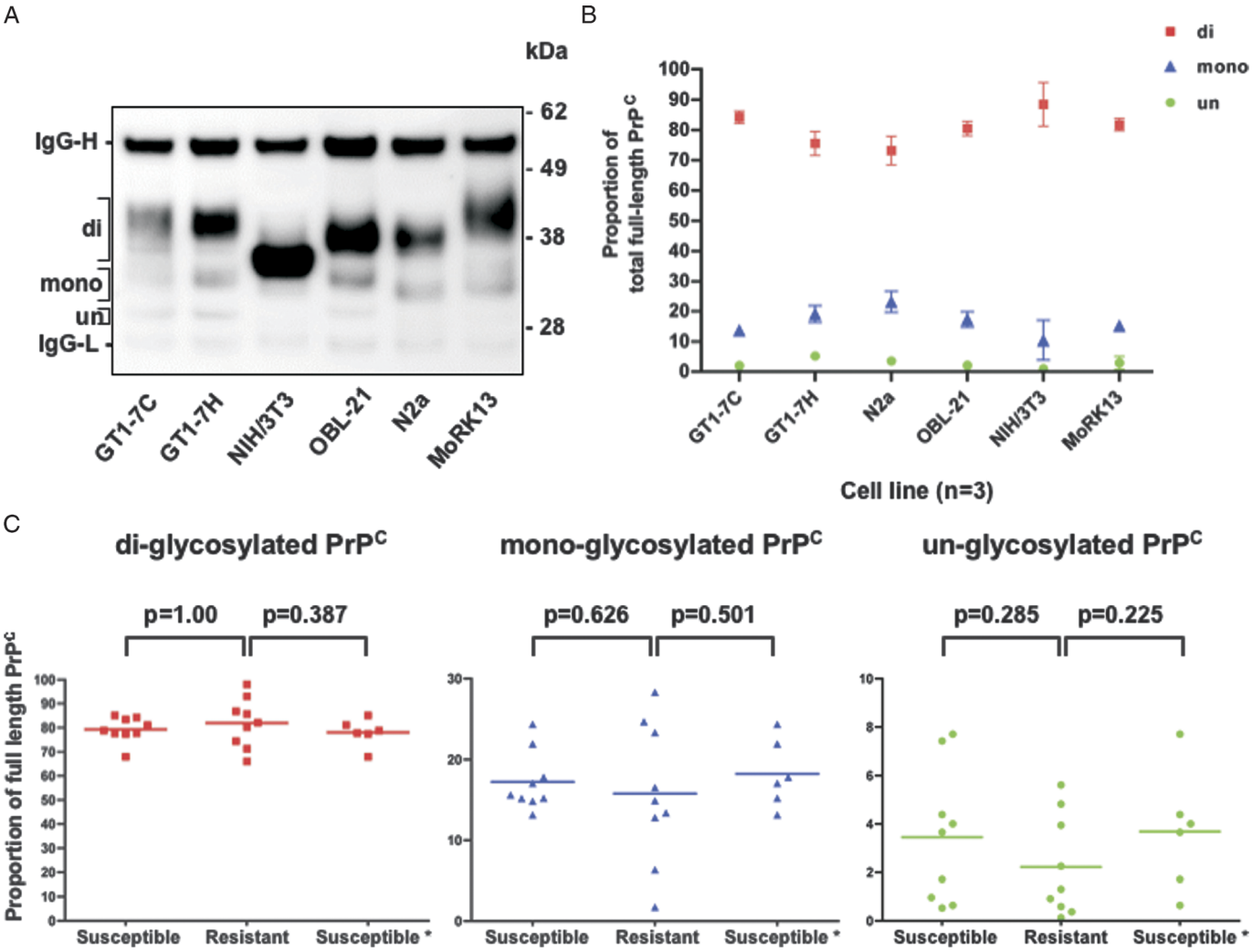

FIGURE 3. Full-length cellular prion protein (PrP^C) glycoform profiles in uninfected cells. Representative Western blot with N-terminal antibody 8B4 after immunoprecipitation with N-terminal antibody SAF32 **(A)** and quantification (mean ± SEM, n = 3) of glycoform ratios of PrP^C **(B)**. In all cases, based on apparent molecular weight, di, diglycosylated PrP^C or PrP^{res}; mono, monoglycosylated PrP^C or PrP^{res}; un, unglycosylated PrP^C or PrP^{res}. IgG heavy chain (IgG-H) and light chain (IgG-L) as indicated. **(C)** Correlative analysis of full-length PrP^C glycosylation profiles with susceptibility to M1000 prion infection. Data points represent the replicates obtained from Western blot quantification of diglycosylated, monoglycosylated, and unglycosylated PrP^C as shown in **(B)**. Susceptible, resistant, and susceptible* are as defined in Figure 2. Binary logistic regression (Minitab 15) was performed; no significant differences were seen.

lines. The second anomaly was the apparent doublet band of "FLUG" PrP^C in the GT1-7C cells (Fig. 4E). Because this faster migrating band was not detected with 8B4 (and consistent with the approximate 2- to 3-kd molecular weight difference between the 2 bands of the doublet), it likely resulted from N-terminal truncation of full-length PrP^C up to at least some point within the 37-44 8B4 epitope. A PrP^C doublet has been reported, but was not characterized (31). On close inspection of the blots, this fragment may also have been present in the N2a line (Figs. 4B, C), suggesting that it might occur in various cells but may be overlooked depending on PAGE resolution and Western blot conditions.

After characterization of PrP^C endoproteolytic cleavage profiles in each cell line, correlative analyses comparing these profiles with the innate susceptibility to M1000 prions were performed. The cells were grouped according to their susceptibility or resistance (Table 2), again including and excluding the MoRK13 cells to allow for any influence of exogenous overexpression of PrP^C. The relative proportion of each PrP^C fragment (data points obtained from quantification of FLUG, C2, and C1, as shown in Fig. 4F) was then separately plotted against susceptibility or resistance (Fig. 5). The cells that were more likely to be susceptible to M1000 infection expressed a higher proportion of full-length PrP^C, (analysis including MoRK13; $p = 0.003$; odds ratio [OR], 1.08; confidence interval [CI], 1.03–1.14; and excluding MoRK13; $p = 0.003$; OR, 1.09; CI, 1.03–1.15). Furthermore, the analyses also indicated that truncation specifically at the α-cleavage site was protective against M1000 infection, with the OR predicting decreased susceptibility with expression of

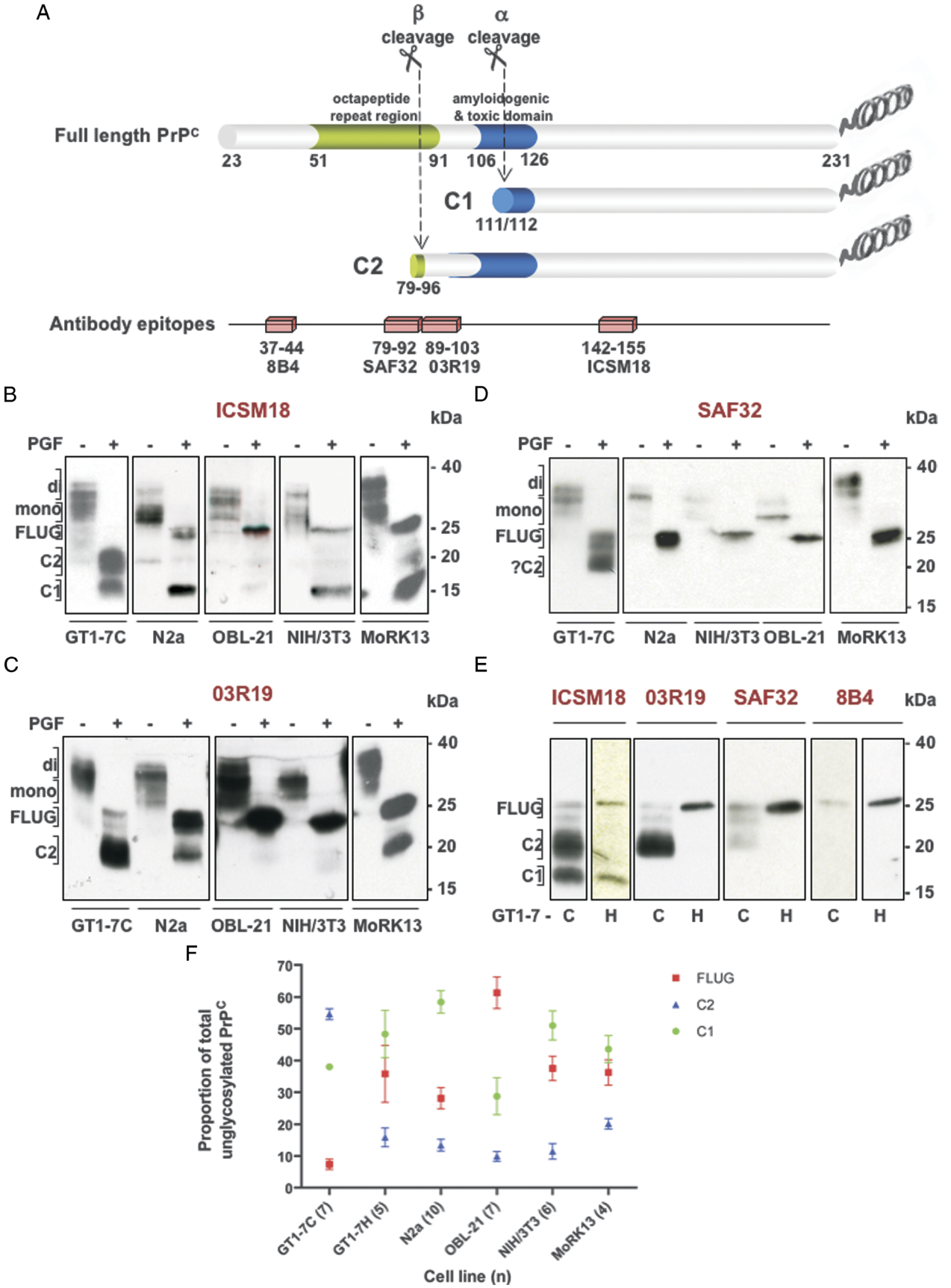

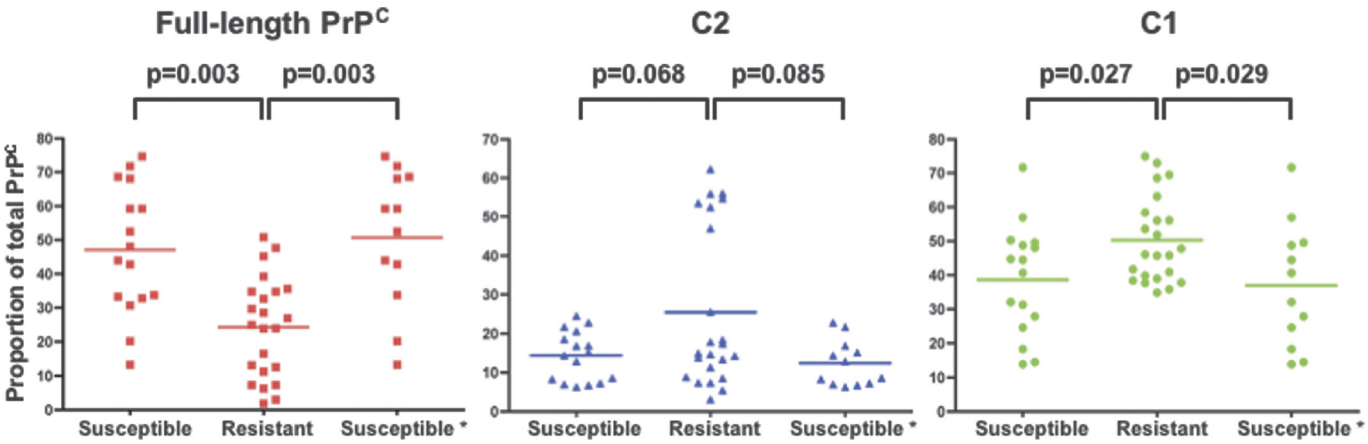

FIGURE 5. Correlative analysis of relative susceptibility to M1000 infection and constitutive cellular prion protein (PrP^C) cleavage profiles. Data points represent the replicates obtained from Western blot quantification of full-length unglycosylated PrP^C (FLUG), C2, and C1 as shown in Figure 4F. Susceptible, resistant, and susceptible* are as defined in Figure 2. Binary logistic regression was performed (Minitab 15); significant results are as indicated.

higher proportions of the C1 fragment (analysis, including MoRK13; p = 0.027; OR, 0.94; CI, 0.89–0.99; and excluding MoRK13; p = 0.029; OR, 0.94; CI, 0.88–0.99). C2 cleavage was not protective despite any bias caused by the bimodal distribution of the data (the cluster of data points with >50% C2 was exclusively from the GT1-7C cells).

DISCUSSION

Differential susceptibility of cell lines to individual prion strains is well described (Table 1), and a number of cellular properties unrelated to PrP^C may influence the intercellular variations in susceptibility and resistance to long-term propagation of PrP^{res}. The apparent subsequent loss of prion infection, shown here for the GT1-7H and OBL-21 cells, has also previously been described (32–35). The cause of this phenomenon was not specifically investigated but might represent an adaptive cellular response to the ongoing unfavorable PrP^{res} propagation. Such cellular changes may reflect diminished PrP^C/PrP^{res} interactions and conversion, and/or enhanced PrP^{res} clearance or degradation, with evidence suggesting that the steady state levels of misfolded conformers are determined by the equilibrium between their production and degradation (36). Furthermore, anecdotal evidence for a finely balanced equilibrium comes from cells that have a propensity to clear prion infection where simple changes in the batches of culture media or serum used resulting in subtle differences in serum proteins or the concentration of salts, amino acids, trace metals, or other additives, can lead to a loss in prion infection. Finally, although most prion-infected cells display no obvious detrimental phenotype, changes in iron metabolism (37), copper binding (38), synaptic functions, (39) and responses to oxidative stress (40) have all been described; loss of infection may result from effects of these subtle changes, if healthier uninfected cells outcompete or outgrow the infected cells.

The primacy of PrP^C in the transmissibility and pathogenesis of prion diseases (12, 13) supports the likelihood that subtle differences in PrP^C biology (e.g. posttranslational processing, trafficking, or specific subcellular localization) may also constitute important susceptibility determinants in addition to the presence of expression levels of PrP^C. Whilst PrP^C expression levels modulate incubation period in animal models of prion disease (41, 42), it seems that in vitro, PrP^C expression levels are less critical in influencing susceptibility to prion infection (36, 43). Therefore, we used the M1000 human-derived prion strain and a range of cell lines encompassing anticipated susceptibility or resistance to prion infection to explore PrP^C posttranslational processing as a determinant of sustained PrP^{res} propagation.

A previous study examined the heterogeneity of PrP^C glycosylation and reported that PrP^C glycoform patterns in mouse and rat brain and neuronal cell lines vary but are distinct (31). We also demonstrated diversity of PrP^C glycosylation across different cell types. Because each of the cell lines investigated has different origins, the likelihood that different glycans are available for N-linked glycosylation,

FIGURE 4. Cellular prion protein (PrP^C) cleavage profiles of cell lines determined by Western blot (WB) epitope mapping. **(A)** Schematic representation of endogenous PrP^C cleavage and alignment of antibodies used for epitope mapping. **(B–D)** Representative WB of PrP^C fragments in the different uninfected cell lines; 15% Tris-glycine sodium dodecyl sulfate–polyacrylamide gel electrophoresis (SDS-PAGE), WB with ICSM18 **(B)**, 03R19 **(C),** and SAF32 primary antibodies **(D)**. PGF, PNGaseF digested samples. **(E)** Comparison of PrP^C fragments in the 2 cognate GT1-7 cell lines (C and H); all samples were PNGaseF treated; SDS-PAGE and WB conditions were as in **(B–D)**; WB with 8B4 antibody is indicated. For all WBs, the amounts of total protein loaded in each well depended on relative PrP^C expression levels and were adjusted to enable visual identification of PrP^C truncated fragment/s. Based on apparent molecular weight and epitope mapping, diglycosylated PrP^C (di), monoglycosylated PrP^C (mono), full-length unglycosylated PrP^C (FLUG), and the C1 and C2 truncated PrP^C species are indicated. **(F)** Quantification (mean ± SEM) of relative levels of unglycosylated PrP^C species in the different cell lines, as seen in ICSM18 WB images as this is the only antibody that detects all 3 PrP^C species. The replicate numbers for each cell line (n) are indicated on x axis labels.

and varied activities of the enzymes or transferases involved in oligosaccharide processing, might explain the diversity. N-linked glycosylation sites are conserved in all mammalian prion genes (27), possibly indicating an important functional role for this posttranslational modification; however the significance of PrP glycosylation in either normal PrP^C function or in prion disease pathogenesis has not yet been determined. Nonetheless, transgenic mice that express only unglycosylated PrP^C can be infected with a mouse-adapted scrapie prion strain, propagate only unglycosylated PrP^{res}, and transmit disease to wild-type mice (44). This indicates that glycosylation of PrP^C or the infectious prion is not always essential for transmission. We also found that glycosylation profiles were not important determinants of inherent cellular susceptibility to M1000 prions and sustained PrP^{res} propagation, a finding that is broadly congruent with previous studies (45–47).

There is both in vivo (44) and in vitro (30) evidence that prion strains may preferentially convert host PrP^C with a more comparable glycosylation state. This phenomenon was not observed in the current study, suggesting that for the M1000 strain, there are alternative factors that override any influence of host PrP^C glycosylation patterns in determining susceptibility to infection. There is also a suggestion that glycosylation of PrP^C may be protective against prion infection by preventing the natural tendency of PrP^C to form a β-sheet or PrP^{Sc}-like conformation (29). Our results argue against this because all of the cell lines investigated (both susceptible and resistant) expressed higher proportions of diglycosylated PrP^C compared with the monoglycosylated and unglycosylated species.

The N-terminus of PrP^C is not required for production of PrP^{res} in cultured cells (48). Mice that express only N-terminally truncated PrP^C (lacking residues 32–80) on a *Prnp* null background generated PrP^{res} after scrapie infection and succumbed to disease after an apparently extended incubation period (41), although the significance of the longer scrapie incubation was not determined because of experimental variations in that study. In a cell-free conversion assay, progressively longer N-terminal deletion mutants (up to Residue 124) served as a template for production of PrP^{res}, with decreasing efficiency compared with full-length PrP^C, the more C-terminal the deletion (49). That purely in vitro assay, however, does not allow for possible disruption of cellular trafficking of mutant PrP^C resulting in altered conversion of PrP^C to PrP^{res}. We found that when the C1 fragment constituted a higher proportion of the total expressed PrP^C, there was reduced susceptibility to M1000 infection with sustained PrP^{res} propagation; there was increased susceptibility to infection if greater relative proportions of full-length PrP^C were expressed. Taken together, these results suggest that although truncated PrP^C can be induced to misfold, conversion and propagation of PrP^{res} are more efficient when there is a full-length PrP^C substrate. This theory also provides the most likely explanation for why the GT1-7C cells were resistant to M1000 infection because only 10% of the total PrP^C found in these cells was full-length. Furthermore, the doublet PrP^C band in the GT1-7C and possibly the N2a cell lines may represent a novel truncated PrP^C species that might also influence susceptibility to M1000 prion infection.

Endoproteolytic α- and β-cleavage of PrP^C somewhat parallels the cleavage of the Alzheimer disease–associated amyloid precursor protein (APP) (50). Alzheimer disease pathogenesis is related to aberrant endogenous proteolytic cleavage of the transmembrane glycoprotein APP and accumulation of the resultant amyloid-β peptide. Distinct from the pathogenic switch of α-secretase APP processing to predominant β-secretase APP cleavage, our results suggest that it is not a switch from 1 PrP^C processing pathway to another that is a precursor to pathogenesis, but that it is the depletion of available full-length PrP^C as the optimal substrate that is protective against prion infection. Interestingly, some of the cell lines used herein that were resistant to M1000 prions have previously shown susceptibility to other prion strains (Table 1). Therefore, analogous studies using additional prion strains would provide further insight as to whether the observations made in this study are more broadly applicable or M1000 strain specific.

Overall, the results described herein highlight the complexity of PrP^C biogenesis and how aspects of this, especially constitutive endoproteolytic cleavage of PrP^C, are important cellular characteristics that contribute to susceptibility to nontransient M1000 prion infection, with increased α-cleavage offering protection. Thorough analysis of truncated PrP^C species within different brain regions may provide insight into the selective neuronal vulnerability and topographic distribution of neuropathologic abnormalities characteristic of prion diseases.

ACKNOWLEDGMENTS

The authors thank the following researchers for kindly providing cell lines: the 2 cognate hypothalamic GT1-7 cell lines, GT1-7C and GT1-7H, were a kind gift from Professor H.M. Schätzl, Institute for Virology, Technical University Munich, to Steven J. Collins and Andrew F. Hill, respectively. The N2a neuroblastoma cells were from Dr G. Evin, Department of Pathology, the University of Melbourne. The NIH/3T3 cells were from Dr F. Sernee, formerly of the Department of Pathology, the University of Melbourne. OBL-21 cells were a gift from Dr B. Chesebro (RML, NIAID, NIH, MT) to Victoria A. Lawson. The RK13 cells were given to Victoria A. Lawson by Victorian Infectious Diseases Reference Laboratory, and the MoRK13 cells were generated by Ms R. Sharples, Department of Biochemistry and Molecular Biology, the University of Melbourne.

REFERENCES

1. Prusiner SB. Prions. Proc Natl Acad Sci U S A 1998;95:13363–83
2. Bendheim PE, Brown HR, Rudelli RD, et al. Nearly ubiquitous tissue distribution of the scrapie agent precursor protein. Neurology 1992;42: 149–56
3. Ehlers MR, Riordan JF. Membrane proteins with soluble counterparts: Role of proteolysis in the release of transmembrane proteins. Biochemistry 1991;30:10065–74
4. Chen SG, Teplow DB, Parchi P, et al. Truncated forms of the human prion protein in normal brain and in prion diseases. J Biol Chem 1995; 270:19173–80
5. Forloni G, Angeretti N, Chiesa R, et al. Neurotoxicity of a prion protein fragment. Nature 1993;362:543–46
6. Vincent B, Paitel E, Saftig P, et al. The disintegrins ADAM10 and TACE contribute to the constitutive and phorbol ester–regulated normal cleavage of the cellular prion protein. J Biol Chem 2001;276:37743–46

7. Pan T, Li R, Wong BS, et al. Heterogeneity of normal prion protein in two-dimensional immunoblot: Presence of various glycosylated and truncated forms. J Neurochem 2002;81:1092–101
8. Jimenez-Huete A, Lievens PM, Vidal R, et al. Endogenous proteolytic cleavage of normal and disease-associated isoforms of the human prion protein in neural and non-neural tissues. Am J Pathol 1998;153:1561–72
9. Mange A, Beranger F, Peoc'h K, et al. Alpha- and beta-cleavages of the amino-terminus of the cellular prion protein. Biol Cell 2004;96:125–32
10. Watt NT, Taylor DR, Gillott A, et al. Reactive oxygen species–mediated beta-cleavage of the prion protein in the cellular response to oxidative stress. J Biol Chem 2005;280:35914–21
11. Taylor DM, Woodgate SL. Bovine spongiform encephalopathy: The causal role of ruminant-derived protein in cattle diets. Rev Sci Tech 1997;16:187–98
12. Bueler H, Aguzzi A, Sailer A, et al. Mice devoid of PrP are resistant to scrapie. Cell 1993;73:1339–47
13. Mallucci G, Dickinson A, Linehan J, et al. Depleting neuronal PrP in prion infection prevents disease and reverses spongiosis. Science 2003; 302:871–74
14. Gibbs CJ Jr, Gajdusek DC. Experimental subacute spongiform virus encephalopathies in primates and other laboratory animals. Science 1973;182:67–68
15. Polymenidou M, Trusheim H, Stallmach L, et al. Canine MDCK cell lines are refractory to infection with human and mouse prions. Vaccine 2008;26:2601–14
16. Vorberg I, Groschup MH, Pfaff E, et al. Multiple amino acid residues within the rabbit prion protein inhibit formation of its abnormal isoform. J Virol 2003;77:2003–9
17. Courageot MP, Daude N, Nonno R, et al. A cell line infectible by prion strains from different species. J Gen Virol 2008;89:341–47
18. Brown DA, Bruce ME, Fraser JR. Comparison of the neuropathological characteristics of bovine spongiform encephalopathy (BSE) and variant Creutzfeldt-Jakob disease (vCJD) in mice. Neuropathol Appl Neurobiol 2003;29:262–72
19. Arima K, Nishida N, Sakaguchi S, et al. Biological and biochemical characteristics of prion strains conserved in persistently infected cell cultures. J Virol 2005;79:7104–12
20. Birkett CR, Hennion RM, Bembridge DA, et al. Scrapie strains maintain biological phenotypes on propagation in a cell line in culture. Embo J 2001;20:3351–58
21. Mellon PL, Windle JJ, Goldsmith PC, et al. Immortalization of hypothalamic GnRH neurons by genetically targeted tumorigenesis. Neuron 1990;5:1–10
22. Ryder EF, Snyder EY, Cepko CL. Establishment and characterization of multipotent neural cell lines using retrovirus vector–mediated oncogene transfer. J Neurobiol 1990;21:356–75
23. Vella LJ, Sharples RA, Lawson VA, et al. Packaging of prions into exosomes is associated with a novel pathway of PrP processing. J Pathol 2007;211:582–90
24. Lawson VA, Stewart JD, Masters CL. Enzymatic detergent treatment protocol that reduces protease-resistant prion protein load and infectivity from surgical-steel monofilaments contaminated with a human-derived prion strain. J Gen Virol 2007;88:2905–14
25. Bosque PJ, Prusiner SB. Cultured cell sublines highly susceptible to prion infection. J Virol 2000;74:4377–86
26. Lewis V, Collins SJ. Analysis of endogenous PrPC processing in neuronal and non-neuronal cell lines. In: Hill AF, ed. *Prion Protein Protocols*, Vol. 459. Totowa, NJ: Humana Press, 2008:229–39
27. Lawson VA, Collins SJ, Masters CL, et al. Prion protein glycosylation. J Neurochem 2005;93:793–801
28. Stockholm D, Benchaouir R, Picot J, et al. The origin of phenotypic heterogeneity in a clonal cell population in vitro. PLoS ONE 2007;2:e394
29. Lehmann S, Harris DA. Blockade of glycosylation promotes acquisition of scrapie-like properties by the prion protein in cultured cells. J Biol Chem 1997;272:21479–87
30. Nishina KA, Deleault NR, Mahal SP, et al. The stoichiometry of host PrPC glycoforms modulates the efficiency of PrPSc formation in vitro. Biochemistry 2006;45:14129–39
31. Monnet C, Marthiens V, Enslen H, et al. Heterogeneity and regulation of cellular prion protein glycoforms in neuronal cell lines. Eur J Neurosci 2003;18:542–48
32. Arjona A, Simarro L, Islinger F, et al. Two Creutzfeldt-Jakob disease agents reproduce prion protein–independent identities in cell cultures. Proc Natl Acad Sci U S A 2004;101:8768–73
33. Ladogana A, Liu Q, Xi YG, et al. Proteinase-resistant protein in human neuroblastoma cells infected with brain material from Creutzfeldt-Jakob patient. Lancet 1995;345:594–95
34. Nishida N, Harris DA, Vilette D, et al. Successful transmission of three mouse-adapted scrapie strains to murine neuroblastoma cell lines overexpressing wild-type mouse prion protein. J Virol 2000;74:320–25
35. Uryu M, Karino A, Kamihara Y, et al. Characterization of prion susceptibility in Neuro2a mouse neuroblastoma cell subclones. Microbiol Immunol 2007;51:661–69
36. Enari M, Flechsig E, Weissmann C. Scrapie prion protein accumulation by scrapie-infected neuroblastoma cells abrogated by exposure to a prion protein antibody. Proc Natl Acad Sci U S A 2001;98:9295–99
37. Fernaeus S, Halldin J, Bedecs K, et al. Changed iron regulation in scrapie-infected neuroblastoma cells. Brain Res Mol Brain Res 2005; 133:266–73
38. Rachidi W, Mange A, Senator A, et al. Prion infection impairs copper binding of cultured cells. J Biol Chem 2003;278:14595–98
39. Sandberg MK, Low P. Altered interaction and expression of proteins involved in neurosecretion in scrapie-infected GT1-1 cells. J Biol Chem 2005;280:1264–71
40. Milhavet O, McMahon HE, Rachidi W, et al. Prion infection impairs the cellular response to oxidative stress. Proc Natl Acad Sci U S A 2000;97: 13937–42
41. Fischer M, Rulicke T, Raeber A, et al. Prion protein (PrP) with amino-proximal deletions restoring susceptibility of PrP knockout mice to scrapie. Embo J 1996;15:1255–64
42. Manson JC, Clarke AR, McBride PA, et al. PrP gene dosage determines the timing but not the final intensity or distribution of lesions in scrapie pathology. Neurodegeneration 1994;3:331–40
43. Vorberg I, Raines A, Story B, et al. Susceptibility of common fibroblast cell lines to transmissible spongiform encephalopathy agents. J Infect Dis 2004;189:431–39
44. Tuzi NL, Cancellotti E, Baybutt H, et al. Host PrP glycosylation: A major factor determining the outcome of prion infection. PLoS Biol 2008;6:e100
45. Taraboulos A, Rogers M, Borchelt DR, et al. Acquisition of protease resistance by prion proteins in scrapie-infected cells does not require asparagine-linked glycosylation. Proc Natl Acad Sci U S A 1990;87: 8262–66
46. Korth C, Kaneko K, Prusiner SB. Expression of unglycosylated mutated prion protein facilitates PrP(Sc) formation in neuroblastoma cells infected with different prion strains. J Gen Virol 2000;81:2555–63
47. Neuendorf E, Weber A, Saalmueller A, et al. Glycosylation deficiency at either one of the two glycan attachment sites of cellular prion protein preserves susceptibility to bovine spongiform encephalopathy and scrapie infections. J Biol Chem 2004;279:53306–16
48. Rogers M, Yehiely F, Scott M, et al. Conversion of truncated and elongated prion proteins into the scrapie isoform in cultured cells. Proc Natl Acad Sci U S A 1993;90:3182–86
49. Lawson VA, Priola SA, Wehrly K, et al. N-terminal truncation of prion protein affects both formation and conformation of abnormal protease-resistant prion protein generated in vitro. J Biol Chem 2001;276: 35265–71
50. Barnham KJ, Cappai R, Beyreuther K, et al. Delineating common molecular mechanisms in Alzheimer's and prion diseases. Trends Biochem Sci 2006;31:465–72
51. Klohn PC, Stoltze L, Flechsig E, et al. A quantitative, highly sensitive cell-based infectivity assay for mouse scrapie prions. Proc Natl Acad Sci U S A 2003;100:11666–71
52. Butler DA, Scott MR, Bockman JM, et al. Scrapie-infected murine neuroblastoma cells produce protease-resistant prion proteins. J Virol 1988;62:1558–64
53. Chesebro B, Wehrly K, Caughey B, et al. Foreign PrP expression and scrapie infection in tissue culture cell lines. Dev Biol Stand 1993;80: 131–40
54. Lawson VA, Vella LJ, Stewart JD, et al. Mouse-adapted sporadic human Creutzfeldt-Jakob disease prions propagate in cell culture. Int J Biochem Cell Biol 2008;40:2793–801

THE JOURNAL OF BIOLOGICAL CHEMISTRY VOL. 285, NO. 42, pp. 32282–32292, October 15, 2010

Anionic Phospholipid Interactions of the Prion Protein N Terminus Are Minimally Perturbing and Not Driven Solely by the Octapeptide Repeat Domain*

Received for publication, March 14, 2010, and in revised form, July 22, 2010 Published, JBC Papers in Press, August 2, 2010, DOI 10.1074/jbc.M110.123398

Martin P. Boland[‡§], Claire R. Hatty[¶‖], Frances Separovic[**], Andrew F. Hill[§‡‡§§1], Deborah J. Tew[‡§‡‡], Kevin J. Barnham[‡§‡‡1], Cathryn L. Haigh[‡§], Michael James[¶¶¶], Colin L. Masters[§], and Steven J. Collins[‡§1,2]

From the [‡]Department of Pathology, [§]Mental Health Research Institute, [**]School of Chemistry, [‡‡]Bio21 Molecular Science and Biotechnology Institute, and [§§]Department of Biochemistry and Molecular Biology, University of Melbourne, Parkville 3010, the [¶]Bragg Institute, Australian Nuclear Science and Technology Organisation, Lucas Heights, New South Wales 2234, the [‖]Faculty of Health Sciences, University of Sydney, Lidcombe, New South Wales 2141, and the [¶¶]School of Chemistry, University of New South Wales, Kensington, New South Wales 2052, Australia

Although the N terminus of the prion protein (PrP^C) has been shown to directly associate with lipid membranes, the precise determinants, biophysical basis, and functional implications of such binding, particularly in relation to endogenously occurring fragments, are unresolved. To better understand these issues, we studied a range of synthetic peptides: specifically those equating to the N1 (residues 23–110) and N2 (23–89) fragments derived from constitutive processing of PrP^C and including those representing arbitrarily defined component domains of the N terminus of mouse prion protein. Utilizing more physiologically relevant large unilamellar vesicles, fluorescence studies at synaptosomal pH (7.4) showed absent binding of all peptides to lipids containing the zwitterionic headgroup phosphatidylcholine and mixtures containing the anionic headgroups phosphatidylglycerol or phosphatidylserine. At pH 5, typical of early endosomes, quartz crystal microbalance with dissipation showed the highest affinity binding occurred with N1 and N2, selective for anionic lipid species. Of particular note, the absence of binding by individual peptides representing component domains underscored the importance of the combination of the octapeptide repeat and the N-terminal polybasic regions for effective membrane interaction. In addition, using quartz crystal microbalance with dissipation and solid-state NMR, we characterized for the first time that both N1 and N2 deeply insert into the lipid bilayer with minimal disruption. Potential functional implications related to cellular stress responses are discussed.

Prion diseases (also known as transmissible spongiform encephalopathies) include a diverse group of neurodegenerative disorders that share a number of unifying features, including salient neuropathological changes and transmissibility. Creutzfeldt-Jakob disease, fatal familial insomnia, and Gerstmann-Sträussler-Scheinker syndrome constitute the more common human disorders, and scrapie in sheep and goats, bovine spongiform encephalopathy, and chronic wasting disease of mule deer, elk, and moose are the predominant animal forms of prion disease (1). A key event in prion disease pathogenesis is the misfolding of the normal form of the prion protein (PrP^C)[3] into isomeric, typically protease-resistant β-sheet rich conformers (designated PrP^{res}), with the latter also posited to predominantly, or perhaps exclusively, constitute the transmissible agent ("prion") (2). According to the protein-only hypothesis of propagation, PrP^{res} recruits and converts natively folded PrP^C into *de novo* PrP^{res} via an autocatalytic process (2).

Mature, full-length mouse PrP^C (moPrP) is a 208-residue variably *N*-linked glycosylated protein, attached to the outer membrane leaflet via a C-terminal glycosylphosphatidylinositol (GPI) anchor (3). Similar to other proteins, the GPI anchor is important for directing PrP^C to detergent-resistant microdomains (DRM; also known as lipid "rafts"), although the N terminus of PrP^C has also been shown capable of independently performing this function (4, 5). Structural analyses of unglycosylated, non-GPI-anchored mammalian PrP^C from various species, when analyzed in aqueous environments, have demonstrated a globular C-terminal region, dominated by three α-helical regions, two of which are linked through a disulfide bridge; the N-terminal region, encompassing residues 23 to ~125, appears largely unstructured (6). The N terminus of PrP^C can be construed as composed of three sequential subdomains as follows: a polybasic, charged glycosaminoglycan binding region (residues 23–50; unless otherwise stated, all references to amino acid sequences are to murine PrP) (7); an octapeptide (PHGGGWSQ) repeat domain, with hydrophobic and copper-binding properties (8); and a hydrophilic, copper binding domain (approximately residues 90–110) (9), which also

* This work was supported in part by an Australian Nuclear Science and Technology Organisation/University of Melbourne collaboration grant.
[1] Supported by National Health and Medical Research Council fellowships with further funding from National Health and Medical Research Council Program Grant 400202.
[2] To whom correspondence should be addressed. Fax: 613-9349-5105; E-mail: stevenjc@unimelb.edu.au.

[3] The abbreviations used are: PrP^C, cellular prion protein; moPrP, mouse PrP^C; LUV, large unilamellar vesicle; SUV, small unilamellar vesicle; POPC, 1-palmitoyl-2-oleoyl-*sn*-glycero-3-phosphocholine; POPG, 1-palmitoyl-2-oleoyl-*sn*-glycero-3-phospho-(1′-*rac*-glycerol); POPS, 1-palmitoyl-2-oleoyl-*sn*-glycero-3-phospho-L-serine; QCM-D, quartz crystal microbalance with dissipation; GPI, glycosylphosphatidylinositol; DRM, detergent-resistant microdomain; MLV, multilamellar vesicle; LPC, 1-(9*Z*-octadecenoyl)-*sn*-glycero-3-phosphocholine; CSA, chemical shift anisotropy; MAS, magic angle spinning; PS, phosphatidylserine; PG, phosphatidylglycerol.

appears to have some capacity to bind glycosaminoglycans albeit with lesser affinity (10).

As part of its normal cellular biology, PrP^C, upon binding Cu^{2+} (11) and/or Zn^{2+} (12), can exit DRMs and move laterally though detergent-soluble membrane zones to allow endocytosis mediated by clathrin-coated pits (13), with the polybasic region (residues 23–28) essential for this trafficking (14, 15). In addition, PrP^C can be cleaved near its C terminus or within the GPI anchor and be secreted or "shed" into the extracellular milieu (16, 17). As for the cell-associated trafficking of PrP^C, the significance of shedding is poorly understood, but it clearly liberates PrP^C to potentially participate in membrane associations not readily available to it while tethered through a GPI anchor at its C terminus.

Notably, PrP^C can undergo two constitutive cleavage events, with their true biological significance yet to be fully elucidated. Cleavage between residues 109/110 or 110/111, α-cleavage (18), gives rise to the N1 (23–110/111) and C1 (110/111–231) fragments. Alternatively, cleavage around residue 90, β-cleavage, produces the N2/C2 combination (19).

A complete understanding of the molecular basis and cellular location of PrP^C to PrP^{res} conversion remains elusive as does the normal function of PrP^C. Several biomolecules have been implicated in the structural conversion of PrP^C into its pathogenic isoform. These include RNA (20), transition metals such as copper, zinc, and manganese (21), glycosaminoglycans (22), and membrane-associated lipids, with the latter potentially serving as a platform to facilitate structural transitions (23, 24). Interactions of soluble PrP^C with the core of the lipid bilayer have also been proposed as directly contributing to prion-mediated neurotoxicity (25). In addition to these likely deleterious associations, there are less explored interactions between PrP^C and membrane lipids, which may be important for either controlling or subverting normal physiological activities. Certainly, induced membrane lipid perturbations can unfavorably influence protective properties and intracellular signaling associated with PrP^C processing or cognate peptide exposure (26, 27). Localization of proteins to the exoplasmic face of DRMs through a GPI anchor is often associated with receptor or cell-signaling properties, with evidence to support this function for PrP^C (28, 29).

Extending the lipid associating capacity of PrP^C independent of the GPI anchor, PrP(23–145) and full-length PrP^C have both been shown to also bind to model non-DRM lipid membranes, specifically to small unilamellar vesicles (SUV) containing POPS (30), with greater affinity at acidic pH. The specificity of the membrane lipid binding is of interest. No binding affinity was observed in relation to POPC, the dominant lipid in non-DRM membrane segments, with a consistent and significant pH-dependent association found with POPS. This contrasts with full-length hamster PrP, which was shown to be capable of binding to POPC at pH 5, suggesting there may be differing species affinities for specific phospholipids perhaps most easily appreciated for the restricted regions of the prion protein (31). Anionic lipids such as POPS and POPG are expressed in low quantities compared with bulk phospholipids such as POPC. However, these charged lipids have been associated with functional roles such as mediating intracellular signaling (32), promotion of phagocytosis (33), and induction of changes to the outer face of the lipid membrane (34), including those preceding the formation of endocytic pits (35). These observations are consistent with the hypothesis that it is these minor phospholipid species that determine meaningful biological activities, such as protein activation or signaling processes, within a dominant but biologically inert PC membrane scaffold (36).

Preliminary studies have suggested the N terminus of PrP^C is capable of binding to non-DRM lipid membranes. However, there remain many fundamental issues, such as the precise determinants, biophysical basis, and functional relevance, especially in relation to the constitutively produced N1 and N2 fragments. Using a range of biophysical approaches, we have been able to provide novel and important insights into these fundamental questions. Through fluorescence and QCM-D studies, we were able to demonstrate for the first time that the highest affinity binding occurred with fragments equivalent to N1 and N2, selective for anionic lipid species. Of particular note, our detailed characterization of the determinants of non-DRM lipid binding underscored the need for a combination of the octapeptide repeat region and an N-terminal polybasic domain for effective membrane interactions to occur. In addition, using QCM-D and solid-state NMR, we determined that both N1 and N2 deeply insert into the lipid bilayer but with minimal disruption. As a corollary to more clearly characterizing the determinants and biophysical underpinnings of the binding of N1 and N2 peptides to model non-DRM lipid membranes, we offer tentative insights into the possible biological relevance of such interactions.

EXPERIMENTAL PROCEDURES

Lipids and Synthetic PrP Peptides—All phospholipids were purchased from Avanti Polar Lipids, Alabaster, AL, and used without further modification. Synthetic N-terminal peptides based on the mouse PrP sequence were utilized in this study. These were synthesized by the Peptide Technology Laboratory, Research Transfer Facility, Bio21 Institute, University of Melbourne. The peptides are summarized in Fig. 1 and consisted of the following: PrP(23–50); PrP(23–89); PrP(23–110); PrP(51–89); PrP(50–110); PrP(23–110)Δ51–89 (*i.e.* 23–110 with the octapeptide repeat region deleted); and PrP(90–110). Peptide sequence and purity (>95%) were verified by HPLC and mass spectrometry. Full-length recombinant moPrP was also used in initial experiments as a positive control to assist optimizing conditions, with its production as described previously (37). Unless otherwise stated, the following buffers were used: for pH 5, 50 mM acetate, 100 mM NaF; and for pH 7.4, 20 mM phosphate, 100 mM NaCl.

Preparation of Lipid Vesicles—Large multilamellar vesicles (MLV) were produced from POPC or mixtures of POPC with either POPG or POPS in 2:1 and 4:1 molar ratios as described previously (38). Chloroform/methanol (9:1 v/v) was used to dissolve the lipids in a round bottom flask. The solvent was removed by rotational film evaporation to leave a thin film. Vesicles were formed by resuspending the lipid film with the appropriate buffer prior to 4–6 freeze-thaw cycles using liquid nitrogen and water at 37 °C.

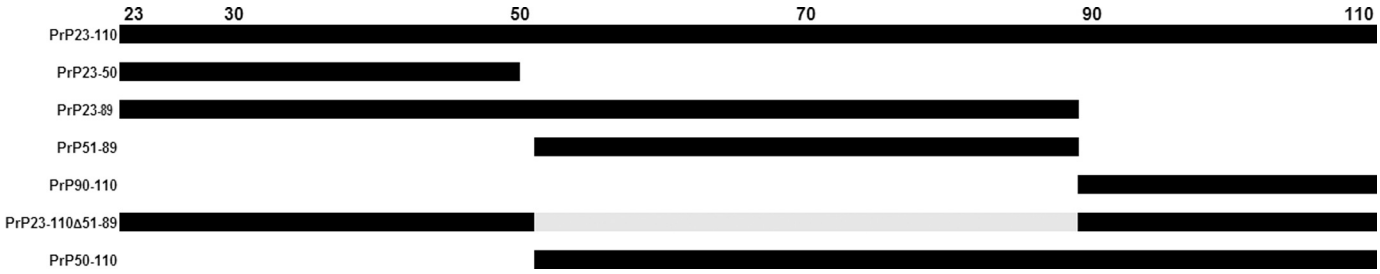

FIGURE 1. **Schematic illustration of the N-terminal region of mouse PrP encompassing residues 23–110, with the various peptides utilized in the study depicted below.** The peptides used in this work are schematically represented by the *black bars*. The *gray region* shows the residues deleted from the PrP(23–110)Δ51–89 peptide.

Large unilamellar vesicles (LUV) were produced by 11 passes of the MLV suspensions though a 0.1-μm polycarbonate membrane filter (GE Healthcare) using a manual extruder (Avestin, Ottawa, Canada). LUV were stored at room temperature and used within 24 h of preparation. Small unilamellar vesicles (SUV) were produced by the sonication method of Koenig *et al.* (39)

Fluorescence Spectroscopy—Intrinsic tryptophan fluorescence of the peptides was measured using either a Thermo-Electron Varioskan multimode plate reader equipped with onboard liquid dispenser, a Varian Eclipse spectrophotometer, or a Cary 100 fluorimeter using 1-cm path length quartz cuvettes. For plate reader experiments, initial peptide concentrations were 12.5 μM. Fluorescence was excited at 295 nm, and a spectrum was recorded between 315 and 460 nm. A point was recorded every 1 nm with an averaging time of 200 ms. Effects of dilution on the samples were accounted for in the analysis of the spectral data.

Circular Dichroism—A Jasco 810 spectropolarimeter was used to record CD spectra with wavelength analyses between 195 and 260 nm. Samples at 15 μM peptide in the appropriate buffer were contained in a 0.1-cm path length quartz cuvette, with all experiments conducted at room temperature. Background spectra (buffer or LUV solution) were subtracted from the peptide spectra.

Solid-state NMR—All solid-state NMR experiments were preformed on a Varian Inova-300 spectrometer (Palo Alto, CA) using a 5-mm Doty (Columbia, SC) magic angle spinning (MAS) probe at 30 °C. Experiments and analysis were adapted from Pukala *et al.* (40). For ^{31}P experiments, the probe was tuned to a frequency of 121.5 MHz and referenced to H_3PO_4 (0 ppm). To maximize signal/noise, ^{31}P relaxation experiments were performed under MAS conditions at a spin rate of 4 kHz. The inversion recovery pulse sequence was used to measure the longitudinal relaxation time (T_1) with internal delay times 0.01–2.0 s. Transverse relaxation times (T_2) were measured using the Hahn spin-echo experiment with internal delay times of 0.2–160 ms. ^{2}H experiments were performed at 46.1 MHz using a solid-echo sequence.

Peak intensities were measured using the integration function of the VNMR software package (Varian Inc.). Peak intensity was plotted in relation to the delay time in the inversion recovery or Hahn spin-echo pulse sequences using Prism 4 (GraphPad Software Inc.) and a single exponential curve fitted to the data. The relaxation times are presented as the average of at least two experiments, and the range between the values was calculated.

NMR samples contained a 10-mg mixture of POPC/POPS (2:1) MLV prepared as described above and suspended in 100 μl of 10 mM MES, 50 mM sodium chloride, pH 5. Peptides were added to the lipid film from stock solutions to a 20:1 lipid/peptide molar ratio prior to MLV formation.

Quartz Crystal Microbalance with Dissipation—QCM-D monitoring experiments were performed in parallel using a Q-Sense E4 quartz crystal microbalance (Q-Sense AB, Frölunda, Sweden) using methods previously published (41). Briefly, AT-cut quartz crystals with a fundamental resonance frequency of 5 MHz (Q-Sense) were used. Frequency and dissipation changes were recorded at the fundamental 1st, 3rd, 5th, 7th, 9th, 11th, and 13th harmonics. Unless stated otherwise, changes to the resonance frequency (Δf) and dissipation (ΔD) reported here are those for the 7th harmonic (or 35 MHz). Experiments were performed under temperature control at 22 °C.

The dissociation constant of the peptide-lipid complex was calculated from the kinetic binding constants extracted from the frequency curve via least squares fitting of the following Equations 1 and 2 (42),

$$\Delta f = \Delta f_0 e^{-(k_{on}(t - t_0))} \quad \text{(Eq. 1)}$$

where Δf is the frequency at time t; Δf_0 is the frequency change at time t_0, and k_{off} is the off rate;

$$\Delta f = -\frac{k_{on}[P] f_{max}}{k_{on}[P] + k_{off}}(1 - e^{-((k_{on}[P] + k_{off})(t - t_0))}) \quad \text{(Eq. 2)}$$

where k_{on} is the on rate, [P] is the concentration of the experimental peptide, and f_{max} is the resonance frequency of the crystal at maximum coverage. Data were analyzed using the Q-Tools (Q-Sense) software. Averages for each experiment were derived from a minimum of three trials.

RESULTS

The N-terminal region of PrP^C, residues 23–110, can be arbitrarily construed as composed of three relatively distinct subdomains in relation to amino acid composition, and copper and glycosaminoglycan binding capacity (8). To model the binding affinity of the three individual N-terminal subdomains, and the potential influence of interactions between certain combinations of segments in relation to synthetic membranes, the fol-

lowing peptides based on murine PrP^C were utilized: PrP(23–50), PrP(51–89), PrP(90–110), PrP(23–89) (representative of the N2 endoproteolytic fragment), PrP(23–110) (equivalent to the N1 endoproteolytic fragment), PrP(50–110), and PrP(23–110)Δ51–89; moPrP was also used as a positive control in initial synthetic membrane binding studies.

Three mono-unsaturated diacyl phospholipids were used to probe the interactions between the peptides and lipid membranes. POPC represents the bulk phospholipid of the cell membrane, with POPS and POPG anionic lipids that have functional roles in neurons. LUV and supported bilayers were chosen as model membranes, in preference to the SUV used in previous studies (30). The metastable nature of SUV and the high degree of membrane curvature they exhibit can cause anomalous lipid-peptide interactions that are not representative of the cell membranes; LUV and supported membranes do not suffer from these issues (43). All experiments were performed above the liquid lamellar (L_α) phase transition temperature of the lipid mixtures.

Intrinsic Tryptophan Fluorescence—The aromatic amino acids tyrosine and tryptophan are fluorescent, with excitation maxima around 280 nm, with tryptophan providing the stronger emission signal. Given that PrP(23–50) and PrP(90–110) each only contain single tryptophan residues, whereas PrP(51–89) contains five, peptide concentrations were optimized to obtain the best spectra from each of the peptides (43). Under fully hydrated (polar) conditions, tryptophan has an $E_{m,\max}$ ≈350 nm, although in a hydrophobic environment $E_{m,\max}$ is shifted to a shorter wavelength. In addition, the relative fluorescence intensity of tryptophan is increased in hydrophobic media when compared with the value in a polar solvent.

The $E_{m,\max}$ values observed for moPrP and all of the synthetic peptides in buffers without added lipid at both pH 5 and pH 7.4 fell within the range 346–349 nm indicating that the tryptophan residues are in a polar environment, consistent with previous observations of full-length PrP (30) and with the expectation that the peptides are unfolded in solution (6). Incubating moPrP and the various peptides with increasing concentrations of LUV composed only of the zwitterionic POPC did not induce any consistent change to $E_{m,\max}$ or relative fluorescence intensity at either pH (Fig. 2, *A* and *D*). This indicates that moPrP (especially the N-terminal region) does not interact with the bulk lipid of the cell membrane over the physiological pH range 5–7.4. At higher lipid concentrations, there was minor binding of moPrP to POPC/POPG at pH 7.4 but no observable spectral change for any of the various PrP peptides with titration of either POPC/POPG or POPC/POPS at around neutral pH (Fig. 2, *B* and *C*). The limited affinity of moPrP for anionic lipid membranes at pH 7.4 contrasts with previous studies using wild-type human PrP, where considerable binding to SUV composed of POPC/POPS (2:1) at pH 7 was observed but with decreased affinity compared with the lower pH (30). However, it is to be stressed that our experiments were conducted using LUV rather than SUV. Therefore, this discrepancy may be caused by the smaller membrane radius of the SUV allowing easier access to the hydrophobic core of the membrane resulting in less physiologically relevant binding to SUV (44). Alternatively, the sequence difference between human and mouse PrP may be sufficient to cause a difference in affinity.

At pH 5, LUV suspensions of POPC/POPG and POPC/POPS at the molar ratio 2:1, revealed a distinct blue shift of $E_{m,\max}$ and an increase of fluorescence intensity for the spectra of moPrP, PrP(23–89), and PrP(23–110), with greater changes observed for POPC/POPG LUV (Fig. 2, *E* and *F*). The fluorescence spectra of PrP(50–110) and PrP(23–110)Δ51–89 showed no change of $E_{m,\max}$ and relative fluorescence intensity at pH 5 with both POPC/POPG and POPC/POPS LUV (Fig. 2, *E* and *F*). Intrinsic fluorescence binding experiments using PrP(23–50) and PrP(90–110) did not show a change of fluorescence intensity or $E_{m,\max}$ under any experimental conditions (data not shown). The lack of change to these parameters indicates that neither of these shorter peptides has any affinity for POPC or anionic membranes irrespective of pH. Furthermore, in parallel with the above experiments, we also screened the peptides for binding to LUV containing a 4:1 ratio of zwitterionic/anionic lipids (results not shown). In these experiments, none of the peptides showed systematic changes to either $E_{m,\max}$ or fluorescence intensity, indicating that they did not bind to the lipids. Cumulatively, these findings suggest N-terminal peptide-lipid binding will only occur under relatively specific circumstances.

Given the intrinsic net charge of segments of the various peptides, for example the polybasic region 23–28, and the anionic nature of POPG and POPS, we assessed the role of electrostatic forces in the peptide-lipid interactions. Sodium chloride titration experiments (to a final concentration of 1 M) indicated electrostatic interactions did not cause the membrane binding of the peptides (results not shown).

Quartz Crystal Microbalance with Dissipation—QCM-D monitoring is a highly sensitive gravimetric technique that is able to detect changes to mass in the subnanogram range, and it has been extensively used to study the membrane binding and disruption properties of various peptides (41). Fundamentally, alterations in the resonant frequency of the QCM-D sensor (Δf) can be related to changes in the mass of the sensor consequent to the material deposited. Fig. 3 is a sensorgram of a typical QCM-D experiment, depicted from the solution-only base line to the final wash-off of the peptide.

Subsequent to the positive results of the initial fluorescence studies, we undertook detailed QCM assessment of the binding of the synthetic peptides to supported bilayers consisting of POPC/POPS or POPC/POPG at a 2:1 ratio at pH 5 (Fig. 4). Identical experiments were also conducted with pure POPC bilayers, and consistent with the fluorescence analysis, no binding of the any of the peptides was observed (data not shown). The peptides PrP(23–89), PrP(23–110), PrP(50–110), and PrP(23–110)Δ51–89 demonstrated different levels of binding to both POPC/POPG and POPC/POPS bilayers, with PrP(23–89) and PrP(23–110) showing the greatest binding. All of the binding peptides showed greater deposition on POPC/POPG membranes. Peptides PrP(23–50), PrP(51–89), and PrP90–110 did not show significant changes to Δf (Fig. 4), indicating that they do not bind to the lipids.

All experiments showed a reproducible profile, with the sensorgram trace being consistent with SUV binding to the QCM sensor before rapidly fusing to form a stable bilayer. A wash

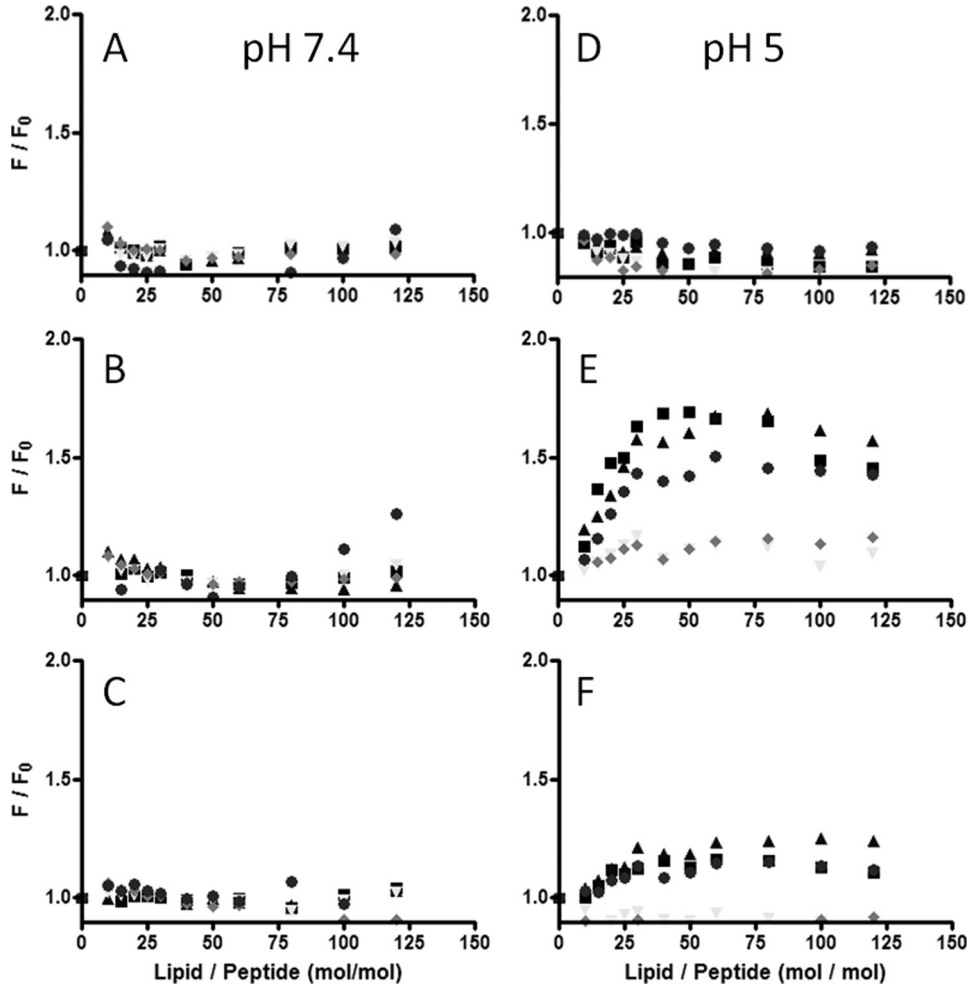

FIGURE 2. **Intrinsic tryptophan fluorescence intensity change of full-length wild type recombinant mouse PrP and various cognate N-terminal synthetic peptides in response to different LUV lipid environments.** The peptides presented are as follows: PrP(23–110) (■); PrP(23–89) (▲); PrP(50–110) (▼); PrP(23–110)Δ51–89 (♦); and recombinant moPrP (●). The panels show the results of titration as follows: *A,* POPC, pH 7.4; *B,* POPC/POPG (2:1), pH 7.4; *C,* POPC/POPS (2:1), pH 7.4; *D,* POPC, pH 5; *E,* POPC/POPG (2:1), pH 5; and *F,* POPC/POPS (2:1), pH 5. Experiments were performed at room temperature in either 50 mM sodium acetate, 100 mM NaF, pH 5, or 20 mM phosphate, 100 mM NaCl, pH 7.4. f/f_0 is the ratio of tryptophan fluorescence intensity of the peptide in the presence of LUV to the fluorescence intensity of the peptide in buffer.

with buffer caused a very small increase in Δf, indicating extraneous SUV being removed from an otherwise intact bilayer. When peptide was present, deposition was indicated by a rapid decrease in Δf before reaching a plateau. Upon starting the flow of buffer into the QCM cell, the sensorgram indicated a loss of mass from the chip. In no case was the loss of mass from the chip initiated prior to the buffer wash or was the loss greater than the increase in mass due to peptide binding. From this we suggest the loss of mass is due to the dissociation of peptide from the lipid bilayer rather than the removal of a lipid-peptide complex from the QCM sensor in a detergent-like manner.

Changes to the resonance frequency of the QCM chip at different overtones provides insight into the condition of the membrane at various distances from the chip, with higher overtones indicating activity closer to the chip surface (41). Nonetheless, in analyzing QCM-D data, it is usual to discard the first harmonic, as this senses the chip coupled molecules of the bulk solution above the chip, and thus the trace is not relevant to the behavior of the deposited lipid and peptides. In this study, we used the 3rd, 5th, 7th, 9th, 11th, and 13th overtones. All measured harmonics of the QCM chip responded in a similar way for each of the peptides for both the POPC/POPG and POPC/POPS membrane compositions. The similar effect for each overtone is consistent with the peptides inserting into the bilayer in a transmembrane manner (41). The modest difference between the 3rd and 13th harmonics for the interaction of PrP(23–110) with POPC/POPS and for each of the binding peptides with POPC/POPG suggests that a small excess of the peptide may associate with the bilayer surface only.

The amount of peptide bound to the outer leaflet of the bilayer was calculated in stoichiometric terms and expressed as the number of lipids per molecule of peptide bound (summarized in Table 1). The association rate (k_{on}) and dissociation rate (k_{off}) of the peptides can be calculated from the binding and elution phases of the QCM-D experiment (42). The calculated values of k_{on}, k_{off}, and K_d are given in Table 2.

All of the peptides that bind to the membranes have a modestly higher affinity for the POPC/POPG bilayers than for POPC/POPS and bind at a lower lipid/peptide ratio. The difference in the required number of lipid molecules was particularly noticeable for two peptides: PrP(23–110)Δ51–89, 10 for POPC/POPG compared with 20 for POPC/POPS; and PrP(50–

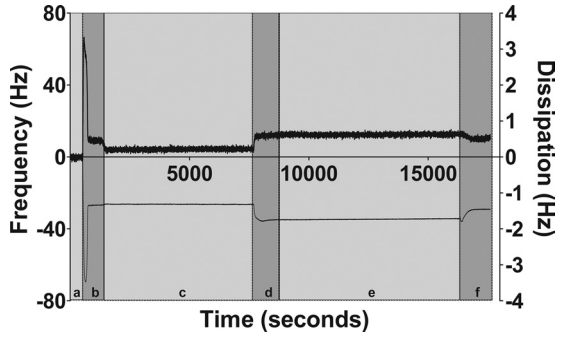

FIGURE 3. **Typical QCM-D sensorgram.** The *lower line* represents changes to the vibrational frequency of the QCM chip (Δ*f*, left-hand axis), and the *upper line* is the dissipation of energy through the adsorbed lipid (Δ*D*, right-hand axis). Progress of the experiment is delineated by alternating *light* and *dark gray shading* corresponding with the symbols *a–f*. *a,* base-line condition under acetate buffer 50 mM, pH 5, with NaCl, 100 mM; this is the condition to which changes to Δ*f* or Δ*D* are referenced. *b,* addition of lipid in the form of SUV (lipid in this example is POPC/POPS (2:1), pH 5), leading to the coating of the chip with the SUV (rapid decrease in Δ*f* to around −60 Hz) and their breaking open to form a bilayer in contact with the QCM chip (rapid increase in Δ*f* to a value around −30 Hz). *c,* wash with acetate buffer to remove extraneous SUV (slight increase in Δ*f* and decrease in Δ*D*). *d,* injection of moPrP(23–89)-peptide leading to the absorbance of the peptide to the bilayer (rapid decrease in Δ*f* to *c,* −40 Hz). *e,* incubation of peptide with bilayer with no resulting change to Δ*f* or dissipation over time, indicating that the bilayer is not disrupted by the peptide. *f,* wash with acetate buffer causing dissociation of the peptide from the lipid rapid increase in Δ*f*.

110), 20 for POPC/POPG and 80 for POPC/POPS. Each of the peptides that demonstrated binding had K_d values in the submicromolar range for membranes containing either POPS and POPG. These are composed of "on-rates" in the region of 40,000 M s^{-1} with "off-rates" around 0.004 s^{-1}. These figures would indicate that the PrP peptide-lipid complexes both associate and dissociate an order of magnitude faster than other peptides that have been studied by QCM (42).

Solid-state ^2H and ^{31}P NMR Studies—^{2}H and ^{31}P solid-state NMR of phospholipid bilayers are additional noninvasive methods to study protein-lipid interactions using deuterated phospholipids. The use of these two nuclei is complementary with ^{2}H favoring studies of the membrane hydrophobic core via the acyl chains, although ^{31}P studies probe the headgroup region of the lipids.

The NMR studies concentrated on the N-terminal peptides that show the most significant membrane binding by fluorescence and QCM-D experiments, PrP(23–89) and PrP(23–110). Furthermore, although both PrP(23–89) and PrP(23–110) bound to phosphatidylglycerol with modestly higher affinity than phosphatidylserine, we chose to undertake the NMR studies with the latter because PS is found at higher levels than PG in mammalian neural cells (45) and has been previously reported to selectively interact with other peptides such as Aβ (38, 46). Moreover, PS is found in significant amounts in the cell plasma membrane and on the surface of endosomal compartments (47), locations where PrP^C is found, whereas PG headgroups are mostly found in the mitochondrial membranes as a precursor of cardiolipin (48). Therefore, the NMR experiments were only performed with a mixture of POPC and POPS.

^{31}P Solid-state NMR—Phospholipid headgroups can be probed using ^{31}P solid-state NMR (40). In particular, the order of the headgroups can be ascertained from broad line ^{31}P NMR (49), although relaxation measurements give an insight into the

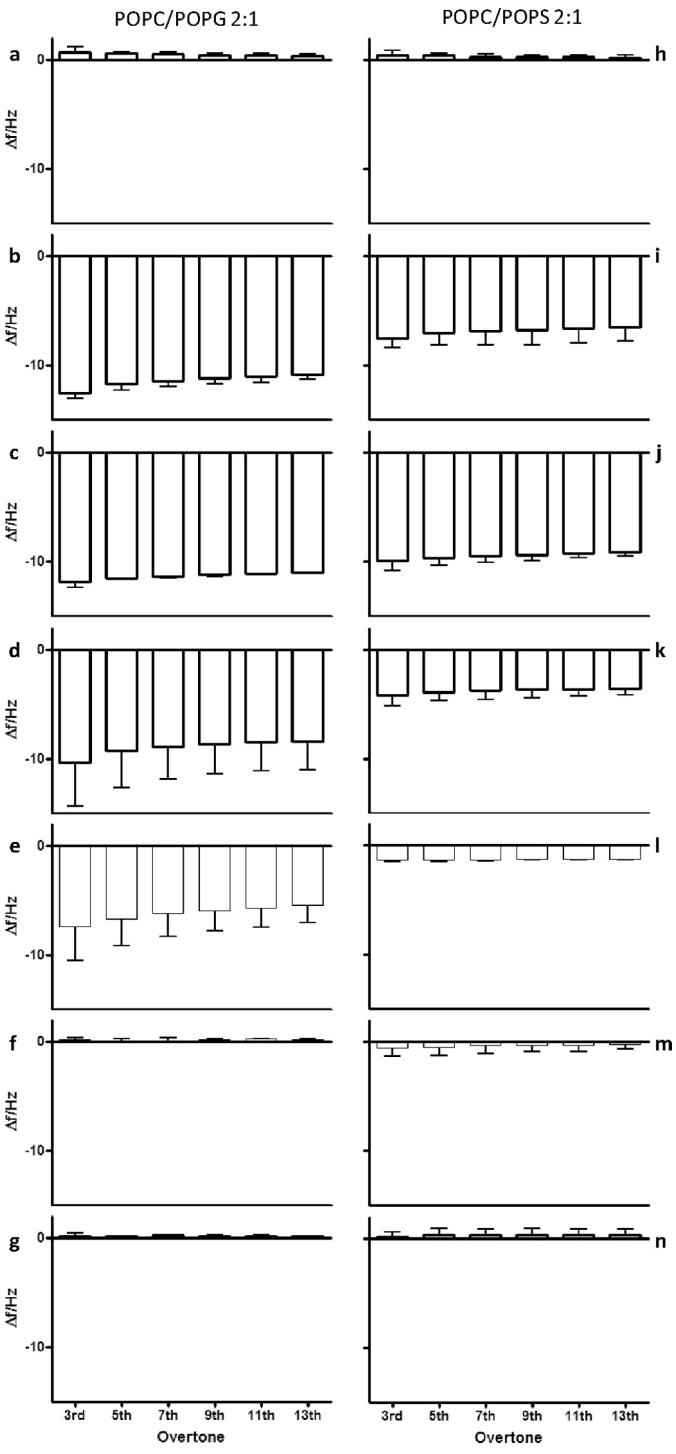

FIGURE 4. **Summary of values of Δ*f* for the 3rd, 5th, 7th, 9th, 11th, and 13th overtones derived from QCM-D measurements of supported lipid bilayers in 50 mM sodium acetate, 100 mM sodium chloride, pH 5.** The *graphs* show the change in Δ*f* induced by the addition of synthetic peptides derived from the N terminus of mouse *a* and *h,* PrP: PrP(23–50); *b* and *i,* PrP(23–89); *c* and *j,* PrP(23–110); *d* and *k,* PrP(23–110)Δ51–89; *e* and *l,* PrP(50–110); *f* and *m,* PrP(51–89); *g* and *n,* PrP(90–110) interacting with supported composite lipid bilayers consisting of (2:1) POPS/POPS (*a–g*) or POPC/POPG (*h–n*). Greater negative values indicate a larger deposit of mass to the QCM chip. Data are shown as the mean of three experiments ± S.E.

rates of motion of the headgroup (50). The width of the ^{31}P powder pattern indicates the phase of the lipids, with broader components corresponding to greater order, and narrow com-

TABLE 1

Lipid/peptide binding ratios for various synthetic peptides based on the N terminus of mouse PrP

Binding was to support composite lipid bilayers. Ratios are calculated from QCM-D measurements as the ratio between Δf upon lipid deposition and bilayer formation, to Δf associated with peptide addition. Values are the mean ± S.D. number of lipid molecules (POPC and POPG or POPS) associated with the binding of one peptide molecule. All experiments were performed in 50 mM acetate buffer, 130 mM NaCl, pH 5.

	Total lipid/peptide molar binding ratios			
	POPC/POPS, 2:1		POPC/POPG, 2:1	
PrP(23–89)	16.6	±4.0	9.8	±0.4
PrP(23–110)	15.2	±0.9	13.3	±0.3
PrP(23–110)Δ51–89	21.8	±1.9	10.7	±3.1
PrP(50–110)	79.1	±3.7	18.0	±5.6

TABLE 2

"On" (k_{on}) and "off" (k_{off}) rate constants and dissociation constants (k_d) for the association of synthetic peptides (based on the N terminus of mouse PrP) to supported composite lipid bilayers, calculated from QCM-D measurements

k_{off} was first calculated by fitting a exponential function to the dissociation phase of the QCM-D experiment. k_{on} was then calculated using the method of Christ *et al.* (42) by substituting the value of k_{off} into a binding function. Values are given as the means ± S.D. of three experiments. All experiments were performed in 50 mM acetate buffer, 130 mM NaCl, pH 5.

	Kinetic and thermodynamic lipid/peptide binding constants		
	k_{on}	k_{off}	k_d
	$M^{-1}s^{-1}$	s^{-1}	nM
POPC-POPS (2:1)			
PrP(23–89)	35,000 ± 20,000	0.005 ± 0.004	100 ± 200
PrP(23–110)	38,000 ± 23,000	0.003 ± 0.003	100 ± 140
PrP(23–110)Δ51–89	4300 ± 15,000	0.005 ± 0.001	100 ± 100
PrP(50–110)	8000 ± 10,000	0.004 ± 0.006	500 ± 600
POPC-POPG (2:1)			
PrP(23–89)	40,900 ± 21,000	0.004 ± 0.002	100 ± 70
PrP(23–110)	41,300 ± 5000	0.004 ± 0.001	100 ± 280
PrP(23–110)Δ51–89	53,000 ± 41,000	0.003 ± 0.003	100 ± 80
PrP(50–110)	54,300 ± 27,000	0.006 ± 0	120 ± 0

ponents indicate highly mobile species such as micelles undergoing isotropic motion. In contrast with the broad line ^{2}H of acyl chains, ^{31}P NMR allows differentiation between different phospholipid populations by changes in the chemical shift of the membrane components (40).

The spectra in Fig. 5 are of POPC/POPS mixtures with and without PrP(23–89) and PrP(23–110) peptides. All of the spectra have a ^{31}P powder pattern consistent with the lipids forming homogeneous lamellar bilayer vesicles. The chemical shift anisotropy (CSA) of the ^{31}P signal is related to distance between the outer edges of the powder pattern; the results are summarized in Table 3. The addition of the PrP(23–89) and PrP(23–110) peptides caused a slight increase in the ^{31}P CSA from 42.2 to 44.5 and 43.7 ppm, respectively. An increase in CSA indicates that the phospholipid headgroups undergo less extensive motions in the presence of the peptides, although the change is small, suggesting a weak interaction with the headgroup. The lack of a second CSA in the ^{31}P spectra with the peptides indicates that the peptide interaction does not cause phase separation of the POPC and anionic lipids.

^{2}H Solid-state NMR—Broad line ^{2}H NMR of chain deuterated phospholipids is a method of probing the order of the acyl chains in phospholipid bilayers. The technique probes the environment within the core of the lipid bilayer, with greater splitting between the wings of the ^{2}H spectrum correlating with greater order of the chains within the membrane. We utilized the $^2H_{31}$-palmitoyl chain of POPC to act as the probe of the bilayer. Fig. 6 shows the ^{2}H solid-state NMR spectra of MLV with and without PrP(23–89) and PrP(23–110). The spectra show that the peptides increased the outer ^{2}H splittings from 23.5 kHz for the POPC/POPS (2:1) MLV to 25.6 and 24.3 kHz with PrP(23–89) or PrP(23–110), respectively. The changes indicate an ordering of the lipid acyl chains by the peptides, with PrP(23–89) causing a greater increase than PrP(23–110). The ordering of the acyl chains is consistent with the QCM-D experiments, suggesting that the peptides insert deeply into the membrane core and may be entirely transmembrane. The more defined split-

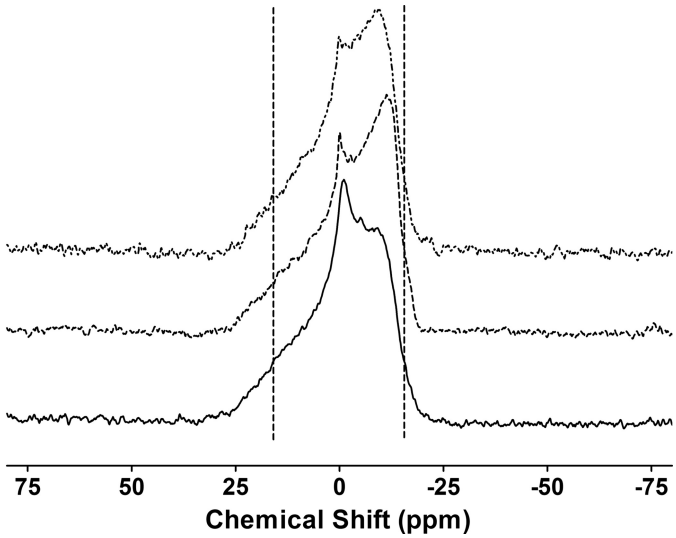

FIGURE 5. **^{31}P broad line solid-state NMR spectra of MLV composed of dPOPC/POPS (2:1) suspended in MES buffer (10 mM, pH 5) with 50 mM NaCl.** The spectra are the accumulation of 25,000 transients processed with a line broadening function of 50 Hz. *Bottom solid line* represents the lipids alone; the *middle dashed line* represents the lipids plus PrP(23–89), and the *top dot-dash line* represents the lipids plus PrP(23–110). CSA values are summarized in Table 3. The *vertical lines* are not representative and are added to aid the reader.

TABLE 3

Effect of PrP(23–89) and PrP(23–110) on the ^{2}H and ^{31}P broad line solid-state NMR spectra and ^{31}P MAS solid-state NMR experiment relaxation times of dPOPC-POPS (2:1), pH 5

CSA and quadrupolar splitting values increase when motion within the detected group decreases, in this case both the headgroups and acyl chains are only weakly affected by the presence of the peptides.

	^{31}P CSA (±1 ppm)	^{2}H CSA (±0.1 kHz)	T_1 relaxation	T_2 relaxation
			s	*ms*
POPC-POPS	−42	23.2	0.34(±0.01)	5.3(±0.1)
+PRP(23–89)	−44	25.6	0.27(±0.01)	7.5(±0.1)
+PrP(23–110)	−44	24.4	0.27(±0.01)	9.9(±0.1)

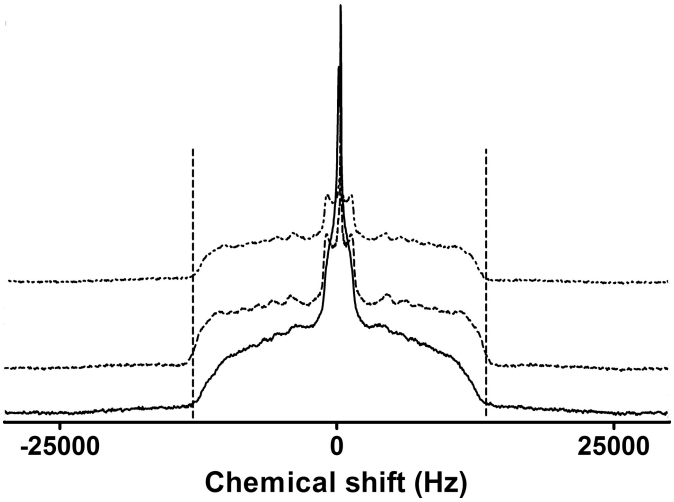

FIGURE 6. **^{2}H broad line solid-state NMR spectra of MLV composed of dPOPC/POPS (2:1) suspended in MES buffer (10 mM pH 5) with 50 mM NaCl.** The spectra are the accumulation of 250,000 transients processed with a line broadening function of 100 Hz. *Bottom solid line* represents the lipids alone; the *middle dashed line* represents the lipids plus PrP(23–89), and the *top dot-dash line* represents the lipids plus PrP(23–110). Quadrupolar splitting values are summarized in Table 3. The *vertical lines* act as an aid to the eye indicating the similarity between the outer edge of the ^{2}H spectrum with and without PrP(23–89) or PrP(23–110).

tings seen in the spectra of the MLV with peptides is due to a change in the dynamics of acyl chains, which would also suggest the peptides interact strongly with the membrane core.

^{31}P Solid-state NMR Relaxation—The ^{31}P MAS NMR longitudinal and transverse relaxation time constants (T_1 and T_2) are presented in Table 3. To determine values for T_1 and T_2, an exponential function was fitted to the intensity (integrals) of the ^{31}P NMR spectra. The spectra showed a single peak, indicating that the presence of the peptides does not lead to the formation of separate peptide bound and unbound lipid populations.

The T_1 or longitudinal ^{31}P NMR relaxation time constant for the phospholipid MLV was 338 ms. Following addition of the PrP(23–89) and PrP(23–110) peptides, the relaxation time constants decreased to 268 and 271 ms, respectively. Because T_1 reports on faster lipid headgroup motions, such as long axis rotation, the changes indicate the peptides cause the lipids to slow on the microsecond-nanosecond time scale (51). The spin-spin (T_2) NMR relaxation time constants also were determined by fitting a single exponential to the ^{31}P NMR signal. The T_2 of the MLV increased from 5.3 to 7.5 ms with PrP(23–89) and 9.9 ms with the PrP(23–110). These values are consistent with the increase in the ^{2}H order parameter and suggest that both peptides have a similar effect on rates of slower motions of the lipids, for example lateral translation.

Circular Dichroism—The peptide with the highest overall anionic membrane affinity as shown by fluorescence spectroscopy and QCM-D was studied using CD to determine whether membrane lipid binding induced changes in secondary structure. We have previously demonstrated (26) that PrP(23–89) is primarily random coil in solution at both pH 7.4 and 5. After addition of a 100-fold molar excess of the lipid mixture, 1-(9*Z*-octadecenoyl)-*sn*-glycero-3-phosphocholine (LPC) and 1-(9*Z*-octadecenoyl)-*sn*-glycero-3-phospho-L-serine (LPS) (2:1), no significant change in the CD spectrum was observed at pH 7.4 (Fig. 7*A*). However, at pH 5, the addition of LPC/LPS led to a significant change in the CD spectrum (Fig. 7*B*). The shift in negative intensity from below 200 nm to around 205 nm and increased intensity between 210 and 225 nm suggests that the presence of the lipid caused the peptide backbone to adopt a more ordered secondary structure.

DISCUSSION

Fundamental questions in relation to the normal function of PrP^{C} and the principal pathogenic pathways involved in prion disease remain unanswered, although the lipid membrane has been implicated in both roles (4). The residence of PrP^{C} within lipid rafts and the number of reported binding partners in this topographical context support the likely importance of these specialized plasmalemma microdomains in the cellular biology of the prion protein (4, 52). Much less explored has been the role of non-lipid raft domains, a consideration underscored by the endogenous trafficking and internalization route followed by PrP^{C}, especially in response to complexing of copper. Furthermore, recent studies have shown that the constitutive endoproteolytic fragments N1 and N2 both harbor intrinsic neuroprotective properties when delivered exogenously to physiologically stressed cells (26). The precise site of generation and mechanism of action of these N-terminal fragments have yet to be determined, and although intact lipid rafts appear to play at least some part in relation to the protective effects of N1/C1 cleavage (27), it is quite plausible that non-raft environments may also be important components. To further explore such possibilities, we undertook a series of experiments, with our studies providing a number of novel insights into the determinants and structural basis of the binding of PrP N-terminal peptides with non-DRM lipid membranes, especially in relation to those equivalent to the N1 and N2 fragments.

The peptides we studied were chosen to exploit the compositionally distinct regions of the N terminus, to determine the relative contribution of each in isolation, and in various combinations, to binding to synthetic non-raft membranes. Our

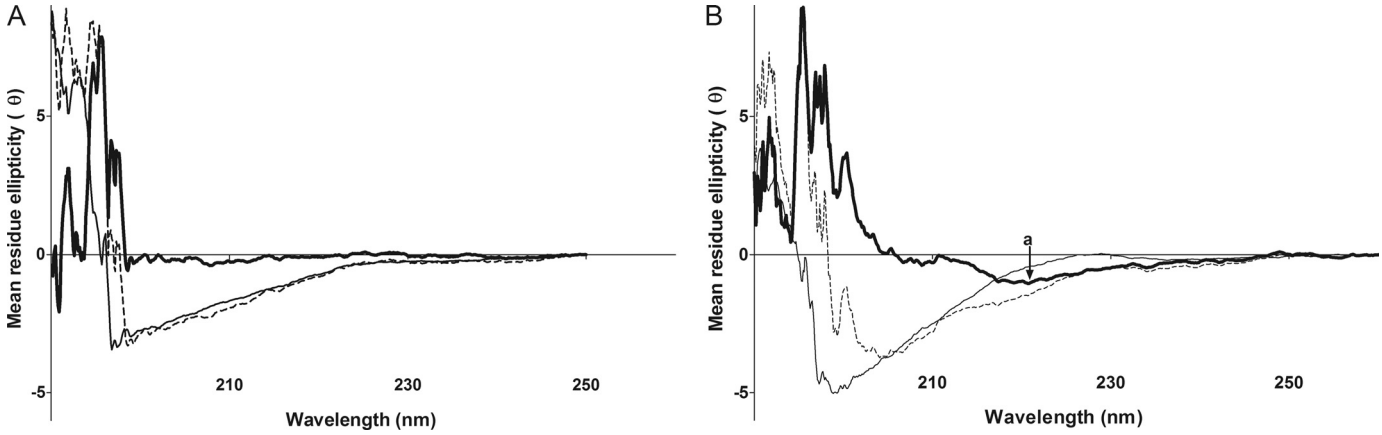

FIGURE 7. **CD spectra of PrP(23–89) in the following: *A,* in phosphate buffer, pH 7.4, without (*thin solid line*) and with (*dashed line*) LPC/LPS (2:1) with the *thick solid line* representing the difference between the two spectra; *B,* in acetate buffer, pH 5, without (*thin solid line*) and with (*dashed line*) LPC/LPS (2:1) with the *thick solid line* representing the difference between the two spectra.** The point (*a*) indicated in *B* indicates the difference in the CD spectra around 220 nm, suggesting PrP(23–89) assumes a greater proportion of β-sheet structure in the presence of lipid. The peptide/lipid molar ratio was 1:100.

QCM-D and fluorescence results were entirely congruent, with PrP(23–89) and PrP(23–110) showing the greatest binding to supported bilayers, whereas the constituent peptides (PrP(23–50), PrP(51–89), and PrP90–110) showed no binding, and PrP(50–110) and PrP(23–110)Δ51–89 displayed intermediate association. Although consistent with previous results (53), the lack of binding of the terminal region (PrP(23–50)), especially to the anionic lipids phosphatidylserine and phosphatidylglycerol, is somewhat unexpected given the high concentration of lysine residues that are positively charged at neutral pH. Our results also revealed that the octapeptide repeat region alone does not directly bind to planar lipid bilayers, indicating that a combination of the octapeptide repeat and either of the two polybasic regions (23–50 or 90–110) is needed for effective membrane interaction. These observations suggest another insight into the relevance of the evolutionary conservation of constitutive processing of PrP, which has preserved N-terminal fragments (N1 and N2) harboring at least both of these component regions.

As alluded, we believe it is noteworthy that of all the possible constituent peptide combinations assessed, the highest membrane affinity observed was for peptides equivalent to N1 and N2. Despite hypothetical considerations suggesting that each of the octapeptide repeat and polybasic regions alone could bind to anionic lipid membranes, our results suggest a synergy is required between the individual peptide segments for this to occur, which is especially prominent for the 23–50 polybasic region when combined with the octapeptide repeat domain. The precise physicochemical basis for this synergism and the structural form of the bound peptide remain to be determined. Previous work from our group has also shown the PrP(23–50) peptide to have only very limited ability to associate with lipid membranes despite mediating cytoprotective effects (26). We find the negligible membrane binding of PrP(23–50) somewhat counterintuitive given the theoretical potential for electrostatic interactions between the seven amino groups in this region to drive anionic membrane association. Nevertheless, our salt titration experiments suggest that electrostatic forces are unlikely to be operating in the membrane association of peptides containing the 23–50 segment. Regarding the octapeptide repeat domain, Raman spectroscopy studies of PrP-Cu^{II} binding suggest that at pH 5, the histidine residues of PrP will exist in a mixture of the protonated and unprotonated copper-binding states (54). As unprotonated histidine has a slight hydrophobic character, it could be speculated that the octapeptide repeat would take on this hydrophobicity because of the combination of several hydrophobic residues per repeat (proline, tryptophan, and histidine) broken only by a single hydrophilic residue (glutamine), with this characteristic serving to facilitate membrane insertion of peptides harboring this domain. Nevertheless, as for PrP(23–50), the octapeptide repeat segment alone did not bind to our synthetic membranes demonstrating that the combination of hydrophobic and polar driving forces is apparently critical to this type of lipid binding. The presence of some membrane interaction by PrP(23–110)Δ51–89 suggests that the number of repeats required to facilitate binding may be as few as one.

As described, contrary to previous claims (55), we found the octapeptide segment alone is not sufficient to drive binding to contiguous lipid membranes. Dong *et al.* (55) reported that binding of the octapeptide region to dodecylphosphocholine micelles may be driven by insertion of the tryptophan residues into the acyl chain region of the membrane. However, this region may not be as accessible in a less tightly curved membrane structure such as LUV or a cellular membrane. Furthermore, from our studies, it is clear that the N terminus does not drive binding to predominantly phosphatidylcholine membranes, as would be found in the exoplasmic face of nonstressed cellular and neuronal membranes (30). In fact, contrary to Morillas *et al.* (30), we did not observe binding at either higher pH or at lower anionic lipid ratios. Our results suggest that, even at acid pH, the N1 and N2 fragments of PrP will not directly interact with the bulk lipid of the cell membrane in the synaptic cleft without the presence of a cofactor. Conversely, the results suggest the peptides will interact directly with the cell membrane under acidic conditions similar to those found in endocytic compartments if anionic phospholipids such as phosphatidylserine are present in significant amounts (56).

In addition to facilitating a greater understanding of the determinants of non-DRM membrane binding of the N terminus of PrP, our results have also provided important new insights into the structural basis of these interactions. All peptides that bound to the lipids affected all of the QCM harmonics equally, suggesting membrane insertion rather than surface association. Furthermore, solid-state NMR of the membrane interaction of the highest affinity peptides, equivalent to the biologically relevant N1 and N2 fragments, indicated that the peptides bind by inserting into the lipid bilayer but in a minimally disruptive manner. The ^{31}P and ^{2}H solid-state NMR data indicate that the peptides insert into the membrane without strong interactions with the headgroup region, with the small increase in the order of the acyl chains showing that the presence of the peptide does not substantially perturb the freedom of motion of the palmitoyl acyl chains of POPC. Static and MAS ^{31}P experiments showed only a single peak, supporting the contention that the addition of N1 and N2 peptides did not cause a separation of the lipids into distinct micro-domains. The NMR data also showed that PrP(23–89) and PrP(23–110) have similar effects on the phospholipid membrane despite the considerably greater length of the peptide equivalent to N1. In addition, CD demonstrated a structural change in PrP(23–89) because of interaction with phosphatidylserine lipids, with a change from exclusively random coil to a significant portion of β-sheet structure.

Clearly, our results suggest that the N terminus of PrP does not interact directly with the bulk of the lipid membrane under unperturbed cell surface conditions. In contrast to previous results of wild type PrP with SUV, interactions in our studies were only seen at acidic pH, with similar pH dependence reported previously (30). Given the number of potential binding partners reported for PrP^C while in lipid rafts (7, 10, 29), the neutral pH usually present at the synaptic cleft appears to add further support for the reduced likelihood of a direct membrane interaction at this specific location. Nevertheless, as a corollary, a model is proposed to try to summarily contextualize many of our key findings, focusing on the interaction of the N terminus with membrane regions containing high concentrations of phosphatidylserine in conjunction with acidic pH. Under conditions of heightened oxidative stress, especially peroxidation of the lipid membrane as reported to occur in prion disease (57), a neuroprotective response is elicited that encompasses PrP^C while resident as a GPI-anchored protein in lipid rafts (58). As the protective response evolves, perhaps as a requisite for eliciting specific signaling cascades (59), PrP^C moves from lipid raft domains into the early endosome compartment. Simultaneously, the ATP-dependent enzyme aminophospholipid transferase, responsible for maintaining the normal membrane asymmetry of the lipid phosphatidylserine (60), is inhibited by lipid peroxidation (61), leading to increased expression of phosphatidylserine in the external leaflet of the plasmalemma, which is generally envisaged as an early marker of apoptosis (62), although other functional implications have been suggested (63, 64). Surface expression of phosphatidylserine is not in itself sufficient to inevitably cause a cell to enter apoptosis (64), and surface expression of this moiety is reversible (65) and nonhomogeneous, with regions showing disproportionately higher concentrations (47), perhaps reaching the ratios used in our study. Once trafficked, the acidic pH of the early endosome would favor the loss of any histidine-bound copper associated with PrP^C and concomitantly provide a milieu more favorable to the N-terminal binding to recently externalized phosphatidylserine, with this organelle shown to be enriched in this lipid and thereby offering a potentially important cationic protein sorting capacity (47). Endoproteolytic cleavage of PrP^C could occur at some point along this pathway and facilitate binding of liberated fragments to phosphatidylserine, but the absence of proteolysis may not preclude functionally significant binding of full-length PrP^C. Although our model is more aligned to the postulate that binding of the N terminus of PrP^C, or cognate fragments, to phosphatidylserine may serve to consolidate or promote a neuroprotective response, we cannot exclude the possibility that the loss of membrane asymmetry may serve to attenuate or abrogate PrP^C function through sequestration akin to N-terminal "tethering" (52) or perhaps indirectly such as through generic inhibition of endocytosis (67).

The peptides we studied showed a subtle but consistently higher affinity for PG- compared with PS-containing lipids. Lipids containing these headgroups have significantly different distributions within the cell with PG predominating in mitochondria. Recently, recombinant PrP has been converted into *de novo* infectious prions in association with RNA and POPG (66). Whether the differences in affinity of the N terminus of PrP for PS- and PG-containing membranes, in association with RNA, suggest a role for this region in the propagation of infection *in vivo* remains to be explored.

Acknowledgments—We thank Denis Scanlon and John Karas for their technical expertise and discussions in relation to peptide design and synthesis.

REFERENCES

1. Johnson, R. T. (2005) *Lancet Neurol.* **4,** 635–642
2. Prusiner, S. B. (1982) *Science* **216,** 136–144
3. Stahl, N., Borchelt, D. R., Hsiao, K., and Prusiner, S. B. (1987) *Cell* **51,** 229–240
4. Walmsley, A. R., Zeng, F., and Hooper, N. M. (2003) *J. Biol. Chem.* **278,** 37241–37248
5. Baron, G. S., and Caughey, B. (2003) *J. Biol. Chem.* **278,** 14883–14892
6. Hornemann, S., Korth, C., Oesch, B., Riek, R., Wider, G., Wüthrich, K., and Glockshuber, R. (1997) *FEBS Lett.* **413,** 277–281
7. Pan, T., Wong, B. S., Liu, T., Li, R., Petersen, R. B., and Sy, M. S. (2002) *Biochem. J.* **368,** 81–90
8. Viles, J. H., Cohen, F. E., Prusiner, S. B., Goodin, D. B., Wright, P. E., and Dyson, H. J. (1999) *Proc. Natl. Acad. Sci. U.S.A.* **96,** 2042–2047
9. Jones, C. E., Abdelraheim, S. R., Brown, D. R., and Viles, J. H. (2004) *J. Biol. Chem.* **279,** 32018–32027
10. Díaz-Nido, J., Wandosell, F., and Avila, J. (2002) *Peptides* **23,** 1323–1332
11. Pauly, P. C., and Harris, D. A. (1998) *J. Biol. Chem.* **273,** 33107–33110
12. Brown, L. R., and Harris, D. A. (2003) *J. Neurochem.* **87,** 353–363
13. Shyng, S. L., Heuser, J. E., and Harris, D. A. (1994) *J. Cell Biol.* **125,** 1239–1250
14. Taylor, D. R., Watt, N. T., Perera, W. S., and Hooper, N. M. (2005) *J. Cell Sci.* **118,** 5141–5153
15. Sunyach, C., Jen, A., Deng, J., Fitzgerald, K. T., Frobert, Y., Grassi, J., McCaffrey, M. W., and Morris, R. (2003) *EMBO J.* **22,** 3591–3601
16. Parkin, E. T., Watt, N. T., Turner, A. J., and Hooper, N. M. (2004) *J. Biol.*

Chem. **279,** 11170–11178
17. Caughey, B., Race, R. E., Ernst, D., Buchmeier, M. J., and Chesebro, B. (1989) *J. Virol.* **63,** 175–181
18. Harris, D. A., Huber, M. T., van Dijken, P., Shyng, S. L., Chait, B. T., and Wang, R. (1993) *Biochemistry* **32,** 1009–1016
19. Chen, S. G., Teplow, D. B., Parchi, P., Teller, J. K., Gambetti, P., and Autilio-Gambetti, L. (1995) *J. Biol. Chem.* **270,** 19173–19180
20. Deleault, N. R., Lucassen, R. W., and Supattapone, S. (2003) *Nature* **425,** 717–720
21. Wong, B. S., Chen, S. G., Colucci, M., Xie, Z., Pan, T., Liu, T., Li, R., Gambetti, P., Sy, M. S., and Brown, D. R. (2001) *J. Neurochem.* **78,** 1400–1408
22. Caughey, B., and Raymond, G. J. (1993) *J. Virol.* **67,** 643–650
23. Wang, F., Yang, F., Hu, Y., Wang, X., Wang, X., Jin, C., and Ma, J. (2007) *Biochemistry* **46,** 7045–7053
24. Kazlauskaite, J., Sanghera, N., Sylvester, I., Vénien-Bryan, C., and Pinheiro, T. J. (2003) *Biochemistry* **42,** 3295–3304
25. Wang, X., Wang, F., Arterburn, L., Wollmann, R., and Ma, J. (2006) *J. Biol. Chem.* **281,** 13559–13565
26. Haigh, C. L., Drew, S. C., Boland, M. P., Masters, C. L., Barnham, K. J., Lawson, V. A., and Collins, S. J. (2009) *J. Cell Sci.* **122,** 1518–1528
27. Haigh, C. L., Lewis, V. A., Vella, L. J., Masters, C. L., Hill, A. F., Lawson, V. A., and Collins, S. J. (2009) *Cell Res.* **19,** 1062–1078
28. Mouillet-Richard, S., Ermonval, M., Chebassier, C., Laplanche, J. L., Lehmann, S., Launay, J. M., and Kellermann, O. (2000) *Science* **289,** 1925–1928
29. Gauczynski, S., Peyrin, J. M., Haïk, S., Leucht, C., Hundt, C., Rieger, R., Krasemann, S., Deslys, J. P., Dormont, D., Lasmézas, C. I., and Weiss, S. (2001) *EMBO J.* **20,** 5863–5875
30. Morillas, M., Swietnicki, W., Gambetti, P., and Surewicz, W. K. (1999) *J. Biol. Chem.* **274,** 36859–36865
31. Re, F., Sesana, S., Barbiroli, A., Bonomi, F., Cazzaniga, E., Lonati, E., Bulbarelli, A., and Masserini, M. (2008) *FEBS Lett.* **582,** 215–220
32. Ghosh, S., Strum, J. C., Sciorra, V. A., Daniel, L., and Bell, R. M. (1996) *J. Biol. Chem.* **271,** 8472–8480
33. Fadok, V. A., Voelker, D. R., Campbell, P. A., Cohen, J. J., Bratton, D. L., and Henson, P. M. (1992) *J. Immunol.* **148,** 2207–2216
34. van den Eijnde, S. M., van den Hoff, M. J., Reutelingsperger, C. P., van Heerde, W. L., Henfling, M. E., Vermeij-Keers, C., Schutte, B., Borgers, M., and Ramaekers, F. C. (2001) *J. Cell Sci.* **114,** 3631–3642
35. Kenis, H., van Genderen, H., Bennaghmouch, A., Rinia, H. A., Frederik, P., Narula, J., Hofstra, L., and Reutelingsperger, C. P. (2004) *J. Biol. Chem.* **279,** 52623–52629
36. Farge, E., (1995) *Biophys. J.* **69,** 2501–2506
37. Coleman, B. M., Nisbet, R. M., Han, S., Cappai, R., Hatters, D. M., and Hill, A. F. (2009) *Biochem. Biophys. Res. Commun.* **380,** 564–568
38. Lau, T. L., Gehman, J. D., Wade, J. D., Perez, K., Masters, C. L., Barnham, K. J., and Separovic, F. (2007) *Biochim. Biophys. Acta* **1768,** 2400–2408
39. Koenig, B. W., Kruger, S., Orts, W. J., Majkrzak, C. F., Berk, N. F., Silverton, J. V., and Gawrisch, K. (1996) *Langmuir* **12,** 1343–1350
40. Pukala, T. L., Boland, M. P., Gehman, J. D., Kuhn-Nentwig, L., Separovic, F., and Bowie, J. H. (2007) *Biochemistry* **46,** 3576–3585
41. Mechler, A., Praporski, S., Atmuri, K., Boland, M., Separovic, F., and Martin, L. L. (2007) *Biophys. J.* **93,** 3907–3916
42. Christ, K., Al-Kaddah, S., Wiedemann, I., Rattay, B., Sahl, H. G., and Bendas, G. (2008) *J. Membr. Biol.* **226,** 9–16
43. Ladokhin, A. S., Jayasinghe, S., and White, S. H. (2000) *Anal. Biochem.* **285,** 235–245
44. Plager, D. A., and Nelsestuen, G. L. (1994) *Biochemistry* **33,** 7005–7013
45. Murphy, E. J., and Horrocks, L. A. (1993) *Lipids* **28,** 67–71
46. Lau, T. L., Ambroggio, E. E., Tew, D. J., Cappai, R., Masters, C. L., Fidelio, G. D., Barnham, K. J., and Separovic, F. (2006) *J. Mol. Biol.* **356,** 759–770
47. Yeung, T., Gilbert, G. E., Shi, J., Silvius, J., Kapus, A., and Grinstein, S. (2008) *Science* **319,** 210–213
48. Schlame, M., Brody, S., and Hostetler, K. Y. (1993) *Eur. J. Biochem.* **212,** 727–735
49. Seelig, J. (1978) *Biochim. Biophys. Acta* **515,** 105–140
50. Dufourc, E. J., Mayer, C., Stohrer, J., Althoff, G., and Kothe, G. (1992) *Biophys. J.* **61,** 42–57
51. Separovic, F., Cornell, B., and Pace, R. (2000) *Chem. Phys. Lipids* **107,** 159–167
52. Zeng, F., Watt, N. T., Walmsley, A. R., and Hooper, N. M. (2003) *J. Neurochem.* **84,** 480–490
53. Oglecka, K., Lundberg, P., Magzoub, M., Göran Eriksson, L. E., Langel, U., and Gräslund, A (2008) *Biochim. Biophys. Acta* **1778,** 206–213
54. Miura, T., Hori-i, A., Mototani, H., and Takeuchi, H. (1999) *Biochemistry* **38,** 11560–11569
55. Dong, S. L., Cadamuro, S. A., Fiorino, F., Bertsch, U., Moroder, L., and Renner, C. (2007) *Biopolymers* **88,** 840–847
56. Murphy, R. F., Powers, S., and Cantor, C. R. (1984) *J. Cell Biol.* **98,** 1757–1762
57. Brazier, M. W., Lewis, V., Ciccotosto, G. D., Klug, G. M., Lawson, V. A., Cappai, R., Ironside, J. W., Masters, C. L., Hill, A. F., White, A. R., and Collins, S. (2006) *Brain Res. Bull.* **68,** 346–354
58. Kuwahara, C., Takeuchi, A. M., Nishimura, T., Haraguchi, K., Kubosaki, A., Matsumoto, Y., Saeki, K., Matsumoto, Y., Yokoyama, T., Itohara, S., and Onodera, T. (1999) *Nature* **400,** 225–226
59. Caetano, F. A., Lopes, M. H., Hajj, G. N., Machado, C. F., Pinto, Arantes, C., Magalhães, A. C., Vieira, Mde, P, Américo, T. A., Massensini, A. R., Priola, S. A., Vorberg, I., Gomez, M. V., Linden, R., Prado, V. F., Martins, V. R., and Prado, M. A. (2008) *J. Neurosci.* **28,** 6691–6702
60. Esterbauer, H., Schaur, R. J., and Zollner, H. (1991) *Free Radic. Biol. Med.* **11,** 81–128
61. Castegna, A., Lauderback, C. M., Mohmmad-Abdul, H., and Butterfield, D. A. (2004) *Brain Res.* **1004,** 193–197
62. Rimon, G., Bazenet, C. E., Philpott, K. L., and Rubin, L. L. (1997) *J. Neurosci. Res.* **48,** 563–570
63. Smrz, D., Dráberová, L., and Dráber, P. (2007) *J. Biol. Chem.* **282,** 10487–10497
64. Stowell, S. R., Karmakar, S., Arthur, C. M., Ju, T., Rodrigues, L. C., Riul, T. B., Dias-Baruffi, M., Miner, J., McEver, R. P., and Cummings, R. D. (2009) *Mol. Biol. Cell* **20,** 1408–1418
65. Bevers, E. M., Tilly, R. H., Senden, J. M., Comfurius, P., and Zwaal, R. F. (1989) *Biochemistry* **28,** 2382–2387
66. Wang, F., Wang, X., Yuan, C. G., and Ma, J. (2010) *Science* **327,** 1132–1135
67. Farge, E., Ojcius, D. M., Subtil, A., and Dautry-Varsat, A. (1999) *Am. J. Physiol.* **276,** C725–C733

Microwave Synthesis of Prion Protein Fragments up to 111 Amino Acids in Length Generates Biologically Active Peptides

John A. Karas, Martin Boland, Cathryn Haigh, Vanessa Johanssen, Andrew Hill, Kevin Barnham, Steven Collins & Denis Scanlon

International Journal of Peptide Research and Therapeutics
formerly known as "Letters in Peptide Science"

ISSN 1573-3149
Volume 18
Number 1

Int J Pept Res Ther (2012) 18:21-29
DOI 10.1007/s10989-011-9275-7

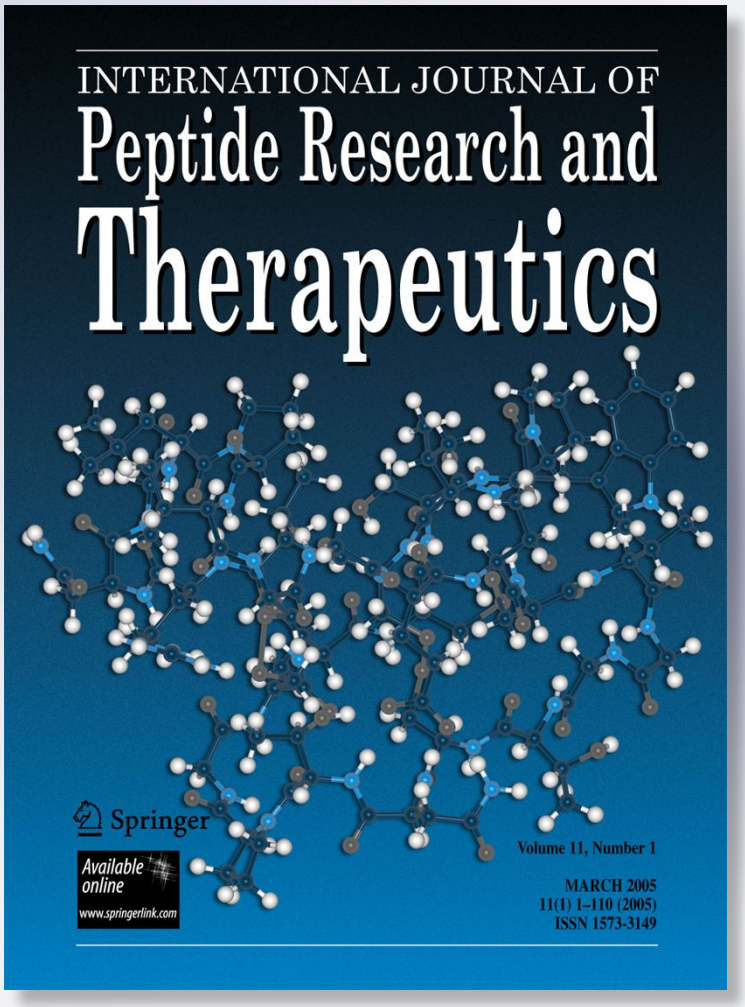

Springer

Int J Pept Res Ther (2012) 18:21–29
DOI 10.1007/s10989-011-9275-7

Microwave Synthesis of Prion Protein Fragments up to 111 Amino Acids in Length Generates Biologically Active Peptides

John A. Karas · Martin Boland · Cathryn Haigh · Vanessa Johanssen · Andrew Hill · Kevin Barnham · Steven Collins · Denis Scanlon

Accepted: 11 October 2011 / Published online: 30 October 2011

Abstract Misfolded conformers of the prion protein are aetiologically implicated in neurodegenerative conditions termed prion diseases (also known as transmissible spongiform encephalopathies). Two constitutively expressed N-terminal peptides corresponding to human residues 23–90 and 23–111 are thought to serve normal physiological roles related to neuronal protection with membrane binding possibly playing a part in their mechanism of action. These peptides, along with several derivatives up to 111 residues in length, have been produced by microwave assisted peptide synthesis. HPLC and MS characterisation showed that the peptides were manufactured in good yields at high purity. Peptides were assayed by fluorescence spectroscopy for synthetic lipid-membrane binding activity and by dichlorodihydrofluorescein diacetate assay for the amelioration of reactive oxygen species production. Results of these assays were similar to those reported for the wild type recombinant PrP, demonstrating that these synthetic peptides are useful for biological and chemical assays of PrP activity. Further, the longest peptide 1–111 was dimerised via a single internal cystine residue with good yield. The high yields and low purification burden of the microwave assisted synthesis method lends itself to the production of difficult to produce peptides for such studies.

Keywords Microwave synthesis · Prion protein · Peptide synthesis

J. A. Karas · K. Barnham
Bio21 Institute, University of Melbourne, Victoria 3010, Australia

M. Boland · C. Haigh · V. Johanssen · K. Barnham · S. Collins (✉)
Department of Pathology, University of Melbourne, Victoria 3010, Australia
e-mail: stevenjc@unimelb.edu.au

A. Hill
Bio21 Institute, Department of Biochemistry, University of Melbourne, Victoria 3010, Australia

D. Scanlon (✉)
Department of Chemistry, University of Melbourne, Victoria 3010, Australia
e-mail: deniss@unimelb.edu.au

Introduction

Diseases such as Creutzfeldt–Jakob disease (CJD) in humans, scrapie in sheep and bovine spongiform encephalopathy (BSE) in cattle are members of a family of related neurodegenerative conditions termed prion diseases. Prion diseases are aetiologically linked to changes in the conformation of a constitutively expressed protein called the prion protein (Prusiner 1982). The pathogenically defining event for the development of prion disease is believed to be the transformation of the normal cellular prion protein (PrP^{C}), into the altered pathogenic isoform, PrP^{Sc}, which is insoluble, has extensive β sheet structure, and is characteristically resistant to protease degradation. Recombinant full-length PrP^{C} NMR structures have been reported for several different species, namely human (Zahn et al. 2000), mouse (Riek et al. 1997), bovine (López Garcia et al. 2000) and Syrian hamster (Donne et al. 1997). Such studies have shown the C-terminal half of PrP^{C} to be highly ordered, containing three α-helices, and a short pleated β-sheet. Furthermore, the C terminus is GPI-anchored to the external surface of cellular membranes (see Fig. 1) (Stahl et al. 1987). The inherent physiochemical properties of PrP^{Sc}, in particular its insolubility, make its chemical synthesis and biological study difficult. Consequently, to

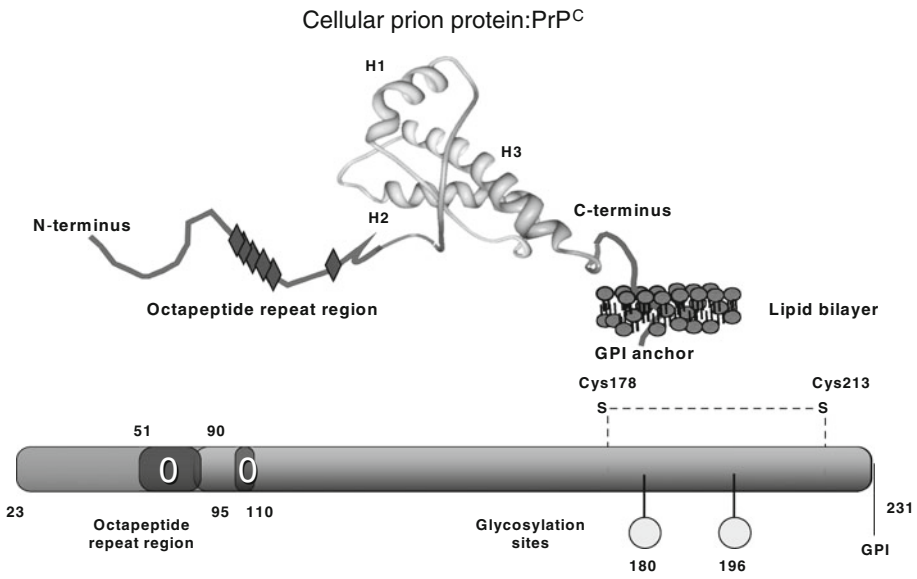

Fig. 1 Schematic of mouse prion protein. The sequence–structure relationship of the prion protein can broadly be divided into two domains: the less structured N terminus (residues 23–130) and the globular C terminus (~130–231). The former contains binding sites for an estimated six divalent metal ions (principally Cu^{2+}) while the latter can be post-translationally modified by the addition of up to two sugar chains at either or both of residues 180 and 198 and the formation of a disulphide bond between Cys178 and 218, as well as the addition of a C-terminal GPI anchor

date, the structure of PrP^{Sc} remains unsolved and there is limited tertiary or quaternary structural information available (Wille et al. 2002).

The normal function of PrP^{C} remains incompletely defined. It has been implicated in copper and zinc binding, signal transduction, reduction of oxidative stress (Brown and Besinger 1998; Milhavet and Lehmann 2002; and Stuermer et al. 2004) and most recently, maintenance of peripheral nerve myelination (Bremer et al. 2010). Protection against oxidative stress has been shown through the N-terminal region of PrP^{C} (Watt et al. 2005; Haigh et al. 2009), and the C-terminal region of PrP, via interaction with anti-apoptotic Bcl-2 (Kurschner and Morgan, 1995, 1996); however precise mechanistic details remain to be determined.

PrP amyloid deposition is found in some forms of prion disease, including a rare form of prion disease known as Gerstmann–Sträussler–Scheinker syndrome (GSS) (Collins et al. 2001). Characteristically, the amyloid fibrils and deposits are constituted by an N- and C-terminally truncated fragment of PrP comprising approximately residues 58–150 (Giaccone et al. 1992, Tagliavini et al. 1991). In part based on peptide fragments of PrP appearing associated with pathogenesis, numerous cognate peptides of PrP have been synthesised and studied (Tagliavini et al. 2001). Of these, PrP106–126 is the most studied synthetic peptide fragment of human PrP as it recapitulates some properties of PrP^{Sc}, such as amyloidogenicity (Tagliavini et al. 1993) and neurotoxicity (Forloni et al. 1993). Although these studies have provided insights into the amyloidogenic and toxic properties of PrP, the lack of an in vivo correlate leaves some uncertainty regarding pathogenic relevance.

Longer peptide sequences, especially those approximating full length PrP^{C} and the products of constitutive endoproteolytic cleavage such as the N1 (23–89) and N2 (23–110) fragments, are intuitively considered more likely to recapitulate authentic biological or biophysical properties compared to hypothetical polypeptide sequences not found in vivo. Unfortunately, generation of longer peptides in sufficient quantity and purity can be challenging. The chemical synthesis of PrP106 (or "miniprion"), a 106 amino acid peptide spanning PrP23–231 with two deletions (Δ23–88 and Δ141–176), has been reported as difficult and low yielding (Ball et al. 2001; Bonetto et al. 2002). Nevertheless, a potential advantage of chemical synthesis is that compared to recombinant peptide generation, the latter often requires demanding sequential purification strategies to achieve satisfactory purity for biological studies, often associated with substantial losses with each step.

Due to the accumulation of N-terminally truncated PrP in prion disease, the N terminus of PrP^{C} has been relatively less studied. Despite being structurally less ordered, its importance is underscored by implicated roles in the biological activity of the protein, such as neuroprotection against oxidative stress, as seen in vivo (Mitteregger et al. 2007) and in vitro (Haigh et al. 2009), and the fact that mutations in this region are found in hereditary prion disease (Mead et al. 2006). Insertion mutations of the octapeptide repeat region of PrP (51–89) are associated with the development of familial CJD (Owen et al. 1989; Gambetti et al. 2003; and Kovacs et al. 2005) and neurological illness in transgenic mice (Chiesa et al. 1998). The N terminus is highly conserved across mammalian species (Wopfner et al. 1999), and the natural absence of post-translational modifications such as *N*-linked glycosylation

and disulphide bridges (as occurs in the globular, far, C terminus), additionally renders the N-terminal peptides more likely to represent or harbour their true biological properties. Therefore, as in the case of the C-terminal PrP106 syntheses described above, long synthetic polypeptide fragments of the N terminus offer promise as desirable tools to help elucidate the biological role of PrP.

The aim of the present investigation was to synthesise a series of peptides spanning large sections of the PrP 23–111 N-terminal region and verify that such peptides would be suitable for studies of biological activity. To achieve this aim, microwave-assisted peptide synthesis was utilised. In our hands, we have found the major advantages of microwave peptide synthesis to be short cycle times and crude peptide products of reasonable purity (50–70% purity) that present few difficulties in HPLC purification. For example, we have achieved the total synthesis of Apo C I, a 57 amino acid, 6.6 kDa protein by microwave synthesis technology together with three alanine mutants of the native sequence (James et al. 2009). Synthesis and purification of the four sequences was achieved in less than 3 weeks. Microwave peptide synthesis, could potentially assemble much longer polypeptides and was therefore used to assemble PrP polypeptides ranging in length from 20 to 111 amino acids, including the N-terminal (1–111) region of PrP^{C}.

Materials and Methods

Fmoc-L-amino acids and coupling reagents *O*-(6-chlorobenzotriazol-1-yl)-*N*,*N*,*N*′,*N*′,-tetramethyluronium-hexafluorophosphate (HCTU) and *N*-hydroxy-benzotriazole (HOBt) were obtained from GLBiochem (Shanghai, China). Fmoc-Pal-PEG-PS resin was obtained from Applied Biosystems (Melbourne, Australia). Solvents dimethylformamide (DMF), dichloromethane (DCM), acetonitrile, and diethyl ether were obtained from Ajax Pty Ltd (Melbourne, Australia). Trifluoroacetic acid, 3, 6-dioxo-1,8-octanedithiol (DODT), triisopropylsilane (TIPS), piperidine, diisopropylethylamine (DIPEA), *N*-methylpyrrolidone (NMP) were obtained from Sigma Aldrich (Sydney, Australia). 1-Palmitoyl-2-oleoyl-sn-glycero-3-phosphocholine (POPC) and 1-palmitoyl-2-oleoyl-sn-glycero-3-[phospho-L-serine] (POPS) were from Avanti (AL, USA). DCFDA, Dulbecco's modified Eagle's medium, penicillin and streptomycin were from Sigma. OptiMEM was from Invitrogen (CA, USA).

Solid-Phase Peptide Synthesis

Solid phase synthesis was performed on a CEM Liberty Microwave peptide synthesizer (CEM Inc. NC, USA) on a 50 μmol scale (250 mg resin, 0.20 mmol/g) using standard CEM cycle procedures. The coupling solution was 0.5 M HCTU in DMF. The base activator was 2 M DIPEA in NMP. The Fmoc deprotection solution was 20% piperidine in DMF containing 0.1 M HOBt. Fmoc protected amino acids were made up as 0.2 M solutions in DMF and tenfold excess of activated amino acid was used in each coupling. All couplings were performed for either 5 min (standard) or 20 min (long) at 75°C and 25 W microwave power. Exceptions were Arginine couplings, which were long double couple cycles (with the microwave turned off for the first 15 min of the first coupling cycle), and cysteine and histidine couplings, which were standard double couple 50°C cycles at 25 W microwave power. In general long couplings were used after 30 cycles for all the larger fragments.

Peptide Cleavage from the Resin

The peptide was cleaved from the resin by treatment with a solution of TFA/DODT/TIPS/H_2O (92.5/2.5/2.5/2.5, 10 ml) for 2 h. The mixture was filtered and aspirated with a stream of dry nitrogen until the solution volume was reduced to 2 ml. The crude peptide was then precipitated by the addition of cold diethyl ether (40 ml). The peptide slurry was centrifuged (3,500 rpm, 3 min) and the crude material was isolated by decanting the ethereal supernatant. The peptide was then dissolved in 30% acetonitrile/water and the solution lyophilized.

Crude Peptide Analysis

Crude peptides were analysed on an Agilent 1100 HPLC system (Agilent Technologies, CA, USA) using a Gemini C18 5 μm analytical HPLC column (Phenomenex Inc, CA, USA) ((Dimension: 150 × 4.3 mm, Flow: 1.0 ml/min). Theoretical monoisotopic molecular weights were calculated with Peptide Companion software and the molecular weights confirmed on an Agilent QTOF LCMS 6200 (Agilent Technologies, CA, USA) with an electrospray source.

Peptide Purification

Crude peptides were dissolved in 30% acetonitrile/water (5–10 mg/ml) and purified sequentially in a two step HPLC protocol utilizing two reversed phase packings with different selectivities. The peptides were initially purified on a Phenomenex Hydro C18 5 μm semi-prep HPLC column (Dimension: 50 × 21.2 mm, Flow: 5 ml/min (Phenomenex Inc, CA, USA). Fractions containing the target peptide were identified by mass spectrometry and then further analysed by analytical RP-HPLC. Pure fractions were pooled, lyophilized and weighed with yields in the range of

5–50 mg depending on the length of the peptide. A second purification step was then performed on an Agilent C18 5 µm semi-prep column (Dimension: 250 × 9.4 mm, Flow: 5 ml/min (Agilent Technologies, CA, USA). Fractions were collected, analysed and lyophilized in the same manner as described above, with final yields in the range 1–20 mg.

All peptides were subjected to a final QC process in which 100–200 µg of peptide was dissolved in 30% acetonitrile/water (200 µl) and analysed by RP-HPLC and mass spectrometry in order to confirm molecular weight and quantify purity.

Dimerization of PrP1–111

PrP1–111 was dissolved in 25 mM ammonium acetate buffer pH 6.5 (2 mg, 0.5 mg/ml) and treated with half an equivalent of 2,2′-dithiodipyridine. The reaction was monitored by mass spectrometry and found to be complete within 1 h (Fig. 5e). RP-HPLC analysis of the reaction showed the dimer as the major product together with a small amount of the thiopyridyl derivative. The dimer was isolated by semi-preparative RP-HPLC , yielding the synthetic protein (0.5 mg) of molecular weight 23,292 Daltons at high purity.

Measurement of Phospholipid Binding Properties of PrP Peptides

As described previously (Boland et al. 2010), PrP peptides and the WT recombinant PrP23–231 were dissolved in acetate buffer (pH 5) with NaCl to an ionic strength of 180 mM. The solutions were excited at 295 nm and the fluorescence emission spectrum was recorded between 315 and 450 nm. The data was recorded on a Varioskan Flash (ThermoFisher Scientific, MA, USA) plate reader at room temperature.

The spectra were recorded in buffer alone and also in the presence of POPC and a 2:1 molar mixture of POPC–POPS. All lipids were freshly extruded at a concentration of 100 mM large unilamellar vesicles (LUV). The usual centre of the fluorescence emission spectrum of the aromatic amino acids is around 350 nm. Interaction of the peptide or protein with lipid causes a blueshift of the fluorescence maximum. The data-points are the mean peak centres calculated by non-linear fitting of a Lorentzian function to the fluorescence spectra. The error bars represent the standard deviation between three experiments. The fitted binding curves represent the best fit of the experimental data to either: a linear function or an exponential decay function.

Cell Culture and DCFDA Assay for Reactive Oxygen Species (ROS)

SH-SY5Y cells were routinely cultured in Dulbecco's modified Eagle's media supplemented with 10% (v/v) fetal bovine serum and 50 U/ml penicillin/50 µg/ml streptomycin solution. Cells were maintained at 37°C with 5% CO_2 in a humidified incubator. The dichlorodihydrofluorescein diacetate (DCFDA) assay for intracellular ROS has been described previously (Haigh et al. 2009). Briefly, cells were loaded in 5 µM CM-H_2-DCFDA (Invitrogen, CA, USA) in phosphate buffered saline (PBS) for 20 min under standard culture conditions. The DCFDA reagent was removed and replaced with fresh medium OptiMEM with or without serum or peptides of interest. Assays were run over 12 h with fluorescence intensity measurements made every 5 min. Rates were calculated, after correcting for equivalent "time 0" signal, using the linear tangent to the initial rate curve.

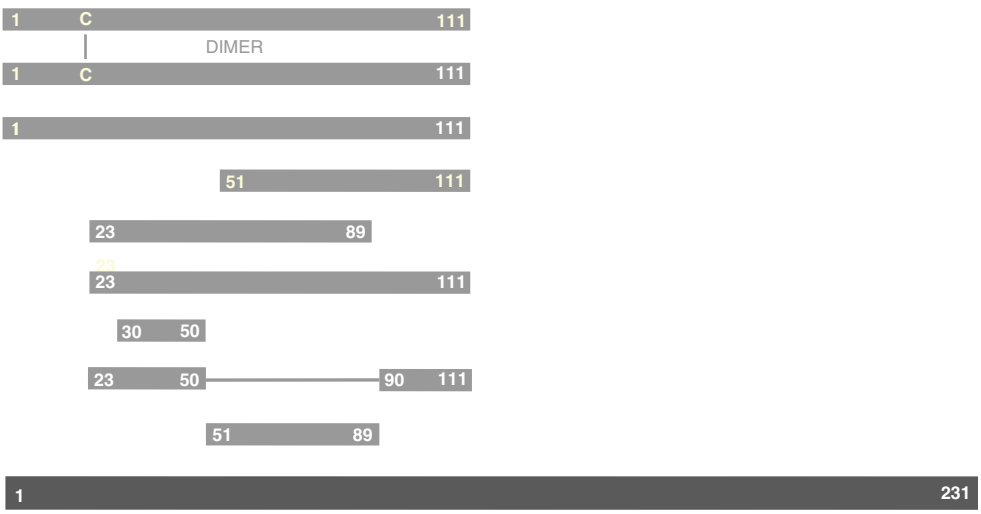

Fig. 2 PrP peptide fragments synthesised. The *black bar* represents the full length wild type prion protein, including the N-terminal ER signal recognition sequence (residues 1–22). The *grey bars* represent the peptides that were made for this project. The *C–C symbol* represents the location of the disulfide bond linking the two 1–111 peptides in the dimer. In addition to those represented above, the PrP peptides 23–50(scrambled) and 23–89(scrambled) were also produced

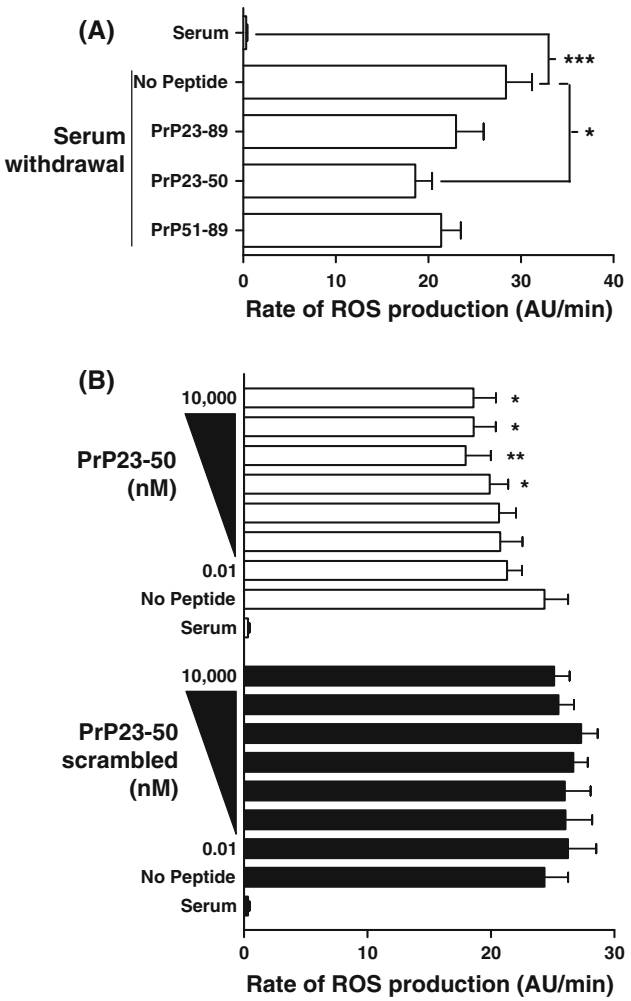

Fig. 3 Synthetic PrP23–50 significantly reduces oxidative stress in serum deprived human neuroblastoma cells. **a** Withdrawing serum from the SH-SY5Y human neuroblastoma cell line results in a highly increased rate of production of intracellular ROS. When the serum withdrawal insult is applied with synthetic PrP fragments 23–89, 23–50, and 51–89, the extent of the ROS insult was reduced, significant for the 23–50 fragment (One-way ANOVA, $F = 24.99$, $^{*}P < 0.05$, $^{***}P < 0.001$). **b** Applying the 23–50 fragment in a log10 serial dilution shows this effect is significant down to 10 nM PrP23–50 and comparison with a peptide corresponding to the amino acid composition of PrP23–50 scrambled confirms this effect is peptide specific (Two-way ANOVA, $F = 44.18$, $^{*}P < 0.05$, $^{**}P < 0.01$). Graphs show the mean and s.e.m. derived from four independent experiments

Results and Discussion

All prion protein peptides synthesized on the CEM Liberty microwave peptide synthesizer by Fmoc solid phase synthesis protocols are summarized in Fig. 2. The preferred resin used for all microwave syntheses was low loading Fmoc-Pal-PEG PS resin. Yields of crude peptide obtained on a 50 μmol scale were quantitative. For example, peptides 50 amino acids long yielded approximately 250 mg of crude peptide, ensuring that after the two step purification protocol between 5 and 20 mg pure peptide was obtained. All syntheses recorded relatively high crude purities and, even in the case of the high MW peptides, the quality and quantity of peptide isolated using these protocols was ample to perform the necessary bioassays.

N-Terminal PrP Peptides

The suite of peptides displayed in Fig. 2 was synthesised sequentially starting with the 28 residue sequence PrP23–50. Later, longer sequences were synthesised culminating in PrP1–111. The peptides were assayed for both their ability to reduce oxidative stress in human neuroblastoma cells plus their interaction with POPC and POPC/POPS phospholipids.

Synthetic PrP23–50 Reduces Oxidative Stress in Serum Deprived Human Neuroblastoma Cells

It is known that both the N- and C-terminal parts of the prion protein are implicated in the reduction of oxidative stress. Therefore, a series of synthetic N-terminal peptide fragments was tested for their ability to reduce oxidative stress in SH-SY5Y human neuroblastoma cells.

The SH-SY5Y human neuroblastoma cell line was put into oxidative stress by withdrawal of serum resulting in a highly increased rate of production of intracellular ROS (Haigh et al. 2009). The serum withdrawal insult was followed by challenge with synthetic PrP fragments PrP23–50, PrP51–89 and PrP90–111. In every case the extent of the ROS insult was reduced (Fig. 3), with the result most significant for the PrP23–50. PrP23–50 was shown by serial dilution to significantly attenuate intracellular oxidative stress down to a concentration of 10 nM. A comparison of PrP23–50 with a scrambled PrP23–50 peptide sequence, illustrated in Fig. 3, confirmed that this effect was Pr23–50 peptide specific. Analogous results have already been reported using these peptides in other cell lines (Haigh et al. 2009).

Interaction of N-Terminal PrP Peptides with POPC and POPC/POPS Phospholipids

The peptides were further screened for biophysical activity in a POPC, POPC/POPS phospholipid binding assay. Two short peptide fragments from the N-terminal region of PrP1–111, namely PrP23–50 and PrP30–50, were synthesized and tested in the assay and showed no synthetic membrane association. More regions of the N-terminal peptide sequence were synthesised including PrP51–89 (the octapeptide repeat region), PrP90–110 and PrP23–111(Δ51–89), the latter assembled without the octapeptide repeat region. Once again none of the synthetic peptides demonstrated binding activity in the phospholipid

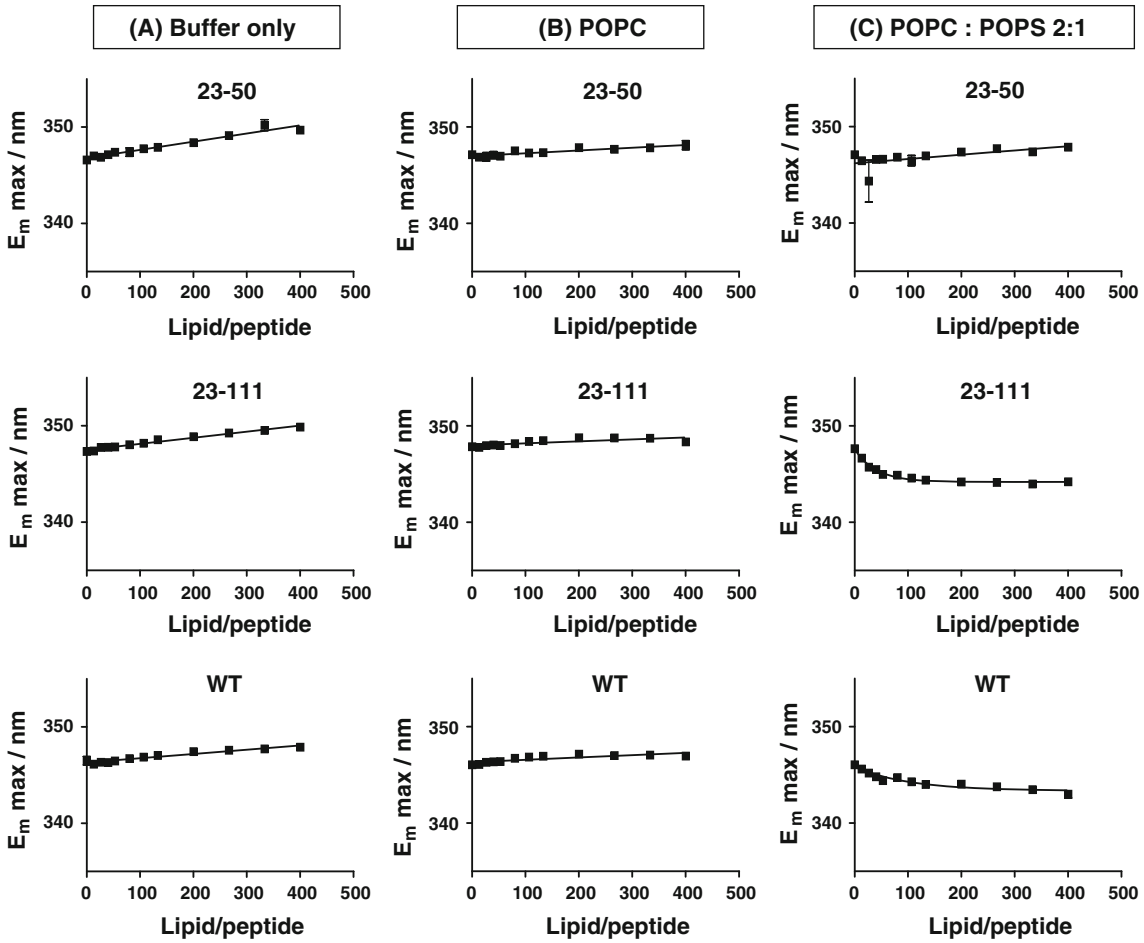

Fig. 4 Fluorescence emission wavelength changes due to membrane interaction of prion protein peptides. (**a** and **b**) Diluting the peptide (**a**) and mixing PrP23–50, PrP23–111 or wild type PrP with the zwitterionic lipid POPC (**b**) do not produce any association effects. **c** In the presence of a 2:1 molar ratio POPC/POPS mixture at pH 5, the E_{mMAX} of a 10 μM solution of 23–111 undergoes a blueshift, in common with wild type PrP. Lipid/peptide is expressed as a mol/mol ratio

binding assay. Since these peptides were synthesized in high purities and yields, up to 60 amino acids long, we therefore decided to undertake the synthesis of the complete mature N-terminal protein region, namely PrP23–111, an eighty-nine amino acid peptide. PrP51–111 was assembled on a 50 μmol scale, and half the resin was cleaved and the resulting crude peptide purified in good yield. The remaining 25 μmol of resin was extended to position 23 to isolate PrP23–111. Although all shorter peptides within the PrP23–111 region showed no binding activity in the POPC/POPS phospholipid binding assay, the full length mature fragment PrP23–111 showed similar binding to the PrP wild type recombinant protein as shown in Fig. 4. Similar results utilising analogous peptides have been previously reported (Boland et al. 2010).

Synthesis of PrP1–111 and Dimeric PrP1–111

To further test the capabilities of the Liberty microwave peptide synthesizer, the synthesis of PrP23–111 was repeated and the synthesis extended to the N terminus of nascent PrP (i.e. PrP1–111). The aim was to assess the synthetic tractability of this fragment under microwave conditions, as well as producing an even longer fragment for comparative bioassay. The progress of the synthesis was checked by cleaving a small resin sample at positions 50 and 23 and monitoring the product by analytical RP-HPLC and mass spectrometry, before extending the peptide chain to position 1. The crude analytical data for PrP1–111 (Fig. 5a, b) shows the parent sequence as the major product. The crude material was purified twice by semi-preparative RP-HPLC as described in the "Materials and Methods" section, in good yield and high purity (see Fig. 5c, d).

Position 22 in the sequence which is a cysteine residue, provided the possibility of producing a synthetic 23 kDa disulfide-bridged polypeptide dimer. It was thought that this would be an interesting addition to the suite of peptides already synthesised especially with regard to its activity in comparative bioassays.. Therefore PrP1–111 was treated

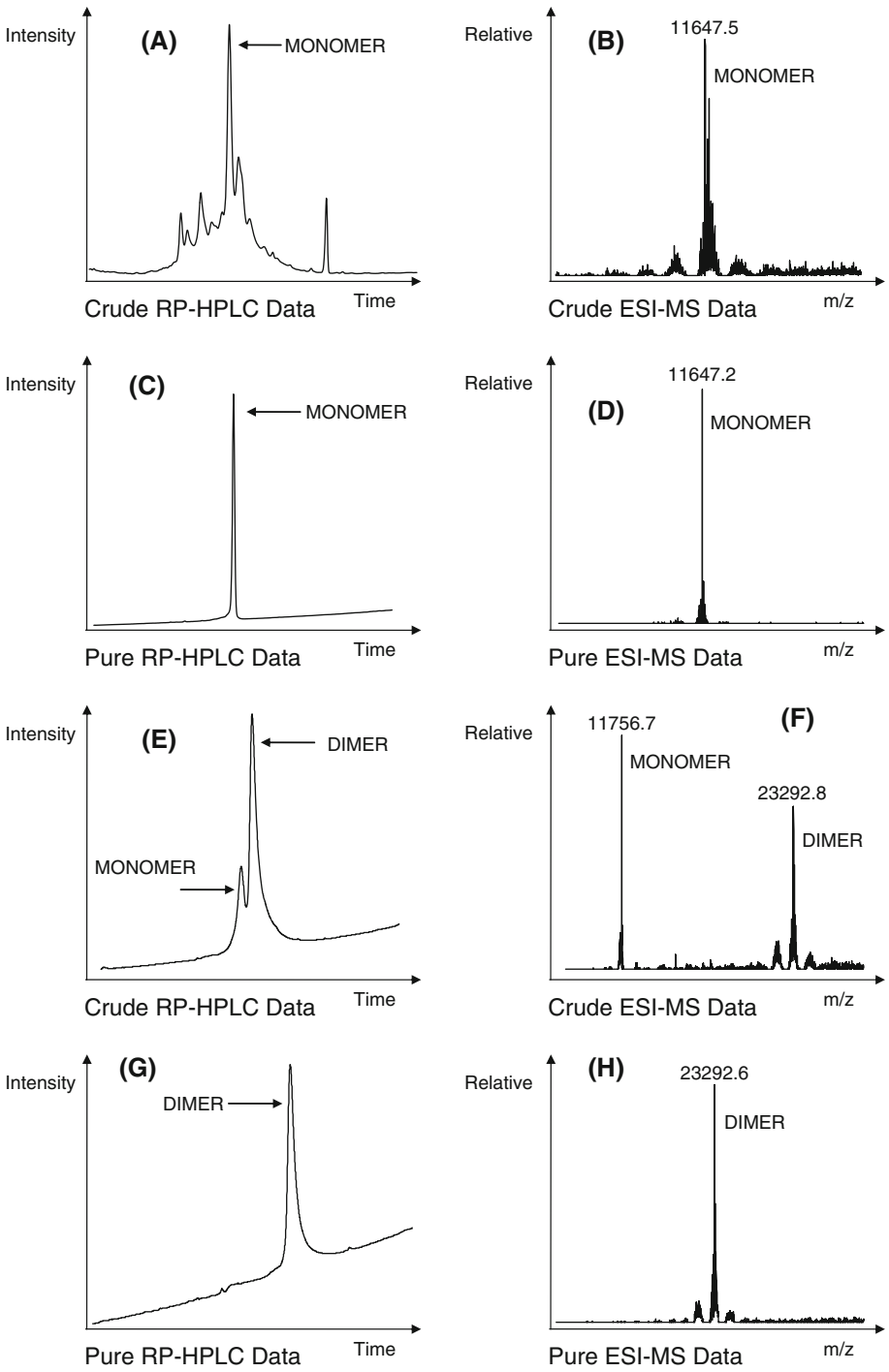

Fig. 5 HPLC and mass spectrometry data from the synthesis of PrP 1–111 and the PrP 1–111 dimer. **a** and **b**: Crude C18 RP-HPLC trace and ESI MS of PrP 1–111 monomer. **c** and **d**: Pure C18 RP-HPLC trace and ESI MS of PrP 1–111 monomer. **e** and **f**: Crude C18 RP-HPLC trace and ESI MS analysis of the reaction products from the PrP 1–111 dimerisation reaction performed in the presence of 2,2′-dithiodipyridine. The mass spectrum shows a major product with the correct dimer MW 23292.8 plus a small impurity of monomer derivatised with a pyridyl group MW 11756.7 (monomer + 109.5). **g** and **h**: C18 RP-HPLC trace and ESI MS of purified PrP 1–111 dimer

with 2;2′-dithiodipyridine in 25 mM ammonium acetate at pH6.5 which enabled the reaction monitored by mass spectrometry. Within 1 h the reaction was determined to be essentially complete (Fig. 5e, f). The dimer was isolated by semi-preparative RP-HPLC , yielding the synthetic protein product of molecular weight 23,292 Daltons at high purity (Fig. 5g, h.

The activity of these two molecules is currently being assessed in further biological studies.

Conclusions

Peptide fragments from the N-terminal region of PrP^C have been assembled in high yield and purity through the use of microwave assisted Fmoc solid phase peptide synthesis. The successful synthesis of challenging and lengthy peptide fragments such as PrP23–89, PrP23–111 and in particular PrP1–111 highlights the utility of this technology in enabling the characterization of peptides in biologically

relevant assays such as phospholipid binding activity and ROS reduction activity of the N-terminal sequence of PrP^C.

The ability of microwave technology to synthesize long and difficult polypeptide fragments, as demonstrated for PrP^C, will enable the synthesis of large discreet high purity fragments of many proteins, facilitating important insights into their protein–protein interactions and biological function.

Acknowledgments We thank Dr Sen Han for the use of the schematic PrP protein structure shown in Fig. 1. SC is supported by an NH&MRC Practitioner Fellowship #APP1005816 and Program Grant #628946.

References

Ball HL, King DS, Cohen FE, Prusiner SB, Baldwin MA (2001) Engineering the prion protein using chemical synthesis. J Pept Res 58:357–374

Boland MP, Hatty CR, Separovic F, Hill AF, Tew DJ, Barnham KJ, Haigh CL, James M, Masters CL, Collins SJ (2010) Anionic phospholipid interactions of the prion protein N terminus are minimally perturbing and not driven solely by the octapeptide repeat domain. J Biol Chem 285:32282–32292

Bonetto V, Massignan T, Chiesa R, Morbin M, Mazzoleni G, Diomede L, Angeretti N, Colombo L, Forloni G, Tagliavini F, Salmona M (2002) Synthetic miniprion PrP106. J Biol Chem 277:31327–31334

Bremer J, Baumann F, Tiberi C, Wessig C, Fischer H, Schwarz P, Steele AD, Toyka KV, Nave KA, Weis J, Aguzzi A (2010) Axonal prion protein is required for peripheral myelin maintenance. Nat Neurosci 13:310–318

Brown DR, Besinger A (1998) Prion protein expression and superoxide dismutase activity. Biochem J 334:423–429

Chiesa R, Piccardo P, Ghetti B, Harris DA (1998) Neurological illness in transgenic mice expressing a prion protein with an insertional mutation. Neuron 21:1339–1351

Collins S, McLean CA, Masters CL (2001) Gerstmann–Straussler–Scheinker syndrome, fatal familial insomnia, and kuru: a review of these less common human transmissible spongiform encephalopathies. J Clin Neurosci 8:387–397

Donne DG, Viles JH, Groth D, Mehlhorn I, James TL, Cohen FE, Prusiner SB, Wright PE, Dyson HJ (1997) Structure of the recombinant full-length hamster prion protein PrP29–231: the N terminus is highly flexible. Proc Natl Acad Sci USA 94: 13452–13457

Forloni G, Angeretti N, Chiesa R, Monzani E, Salmona M, Bugiani O, Tagliavini F (1993) Neurotoxicity of a prion protein-fragment. Nature 362:543–546

Gambetti P, Parchi P, Chen SG (2003) Hereditary Creutzfeldt–Jakob disease and fatal familial insomnia. Clin Lab Med 23:43–64

Giaccone G, Verga L, Bugiani O, Frangione B, Serban D, Pruisner SB, Farlow MR, Ghetti B, Tagliavini F (1992) Prion protein preamyloid and amyloid deposits in Gerstmann–Straussler–Scheinker disease, Indiana kindred. Proc Natl Acad Sci USA 89:9349–9353

Haigh CL, Drew SC, Boland MP, Masters CL, Barnham KJ, Collins SJ (2009) Dominant roles of the polybasic proline motif and copper in the PrP23–89 mediated stress protection response. J Cell Sci 122:1518–1528

James PF, Dogovski C, Dobson RCJ, Bailey MF, Goldie KN, Karas JA, Scanlon DB, O'Hair RAJ, Perugini MA (2009) Aromatic residues in the C-terminal helix of human apoC-I mediate phospholipid interactions and particle morphology. J Lipid Res 50:1384–1394

Kovacs GG, Puopolo M, Ladogana A, Pocchiari M, Budka, H, van Duijn C, Collins SJ, Boyd A, Giulivi A, Coulthart M, Delasnerie-Laupretre N, Brandel JP, Zerr I, Kretzschmar HA, de Pedro-Cuesta J, Calero-Lara M, Glatzel M, Aguzzi A, Bishop M, Knight R, Belay G, Will R, Mitrova E (2005) Genetic prion disease: the EUROCJD experience. Hum Genet 118:166–174

Kurschner C, Morgan JI (1995) The cellular prion protein (PrP) selectively binds to Bcl-2 in the yeast two-hybrid system. Brain Res Mol Brain Res 30:165–168

Kurschner C, Morgan JI (1996) Analysis of interaction sites in homo- and heteromeric complexes containing Bcl-2 family members and the cellular prion protein. Brain Res Mol Brain Res 37:249–258

López Garcia F, Zahn R, Riek R, Wüthrich K (2000) NMR structure of the bovine prion protein. Proc Natl Acad Sci USA 97:8334–8339

Mead S, Poulter M, Beck J, Webb TEF, Campbell TA, Linehan JM, Desbruslais M, Joiner S, Wadsworth JDF, King A, Lantos P, Collinge J (2006) Inherited prion disease with six octapeptide repeat insertional mutation – molecular analysis of phenotypic heterogeneity. Brain 129:2297–2317

Milhavet O, Lehmann S (2002) Oxidative stress and the prion protein in transmissible spongiform encephalopathies. Brain Res Rev 38:328–339

Mitteregger G, Vosko M, Krebs B, Xiang W, Kohlmannsperger V, Nolting S, Hamann GF, Kretzschmar HA (2007) The role of the octarepeat region in neuroprotective function of the cellular prion protein. Brain Path 17:174–183

Owen F, Lofthouse R, Crow TJ, Baker HF, Hsiao K, Poulter M, Collinge J, Risby D, Ridley RM, Prusiner SB (1989) Insertion in prion protein gene in familial creutzfeldt-jakob disease. Lancet 8628:51–52

Prusiner SB (1982) Novel proteinaceous particles cause scrapie. Science 216:136–144

Riek R, Hornemann S, Wider G, Glockshuber R, Wüthrich K (1997) NMR characterization of the full-length recombinant murine prion protein, *m*PrP(23–231). FEBS Lett 413:282–288

Tagliavini F, Prelli F, Ghiso J, Bugiani O, Serban D, Prusiner SB, Farlow MR, Ghetti B, Frangione B (1991) Amyloid protein of Gerstmann–Straussler–Scheinker disease (Indiana kindred) is an 11 kd fragment of prion protein with an N-terminal glycine at codon 58. EMBO J 10:513–519

Tagliavini F, Prelli F, Verga L, Gaiccone G, Sarma R, Gorevic P, Ghetti B, Passerini F, Ghibaudi E, Forloni G, Salmona M, Bugiani O, Frangione B (1993) Synthetic peptides homologous to prion protein resiudes 106–147 form amyloid-like fibrils in vitro. Proc Natl Acad Sci USA 90:9678–9682

Tagliavini F, Forloni G, D'Ursi P, Bugiani O, Salmona M (2001) Studies on peptide fragments of prion proteins. Adv Protein Chem 57:171–201

Stahl N, Borchelta DR, Hsiaoa K, Prusiner SB (1987) Scrapie prion protein contains a phosphatidylinositol glycolipid. Cell 51:229–240

Stuermer CA, Langhorst MF, Wiechers MF, Legler DF, Von Hanwehr SH, Guse AH, Plattner H (2004) PrPc capping in T cells promotes its association with the lipid raft proteins reggie-1 and reggie-2 and leads to signal transduction. FASEB J 18:1731–1733

Watt NT, Taylor DR, Gillott A, Thomas DA, Perera WSS, Hooper NM (2005) Reactive oxygen species-mediated beta-cleavage of the prion protein in the cellular response to oxidative stress. J Biol Chem 280:35914–35921

Wille H, Michelitsch MD, Guenebaut V, Supattapone S, Serban A, Cohen FE, Agard DA, Prusiner SB (2002) Structural studies of the scrapie prion protein by electron crystallography. Proc Natl Acad Sci USA 99:3563–3568

Wopfner F, Weidenhöfer G, Schneider R, von Brunn A, Gilch S, Schwarz TF, Werner T, Schätzl HM (1999) Analysis of 27 mammalian and 9 avian PrPs reveals high conservation of flexible regions of the prion protein. J Mol Biol 289:1163–1178

Zahn R, Liu A, Lührs T, Riek R, von Schroetter C, López García F, Billeter M, Calzolai L, Wider G, Wüthrich K (2000) NMR solution structure of the human prion protein. Proc Natl Acad Sci USA 97:145–150

OPEN ACCESS Freely available online

PLoS one

Cellular Prion Protein Expression Is Not Regulated by the Alzheimer's Amyloid Precursor Protein Intracellular Domain

Victoria Lewis[1,2], Isobel J. Whitehouse[1], Herbert Baybutt[3], Jean C. Manson[3], Steven J. Collins[2], Nigel M. Hooper[1]*

1 Institute of Molecular and Cellular Biology, Faculty of Biological Sciences, University of Leeds, Leeds, United Kingdom, **2** Department of Pathology, University of Melbourne, Parkville, Victoria, Australia, **3** Neuropathogenesis Unit, Roslin Institute, University of Edinburgh, Midlothian, United Kingdom

Abstract

There is increasing evidence of molecular and cellular links between Alzheimer's disease (AD) and prion diseases. The cellular prion protein, PrP^C, modulates the post-translational processing of the AD amyloid precursor protein (APP), through its inhibition of the β-secretase BACE1, and oligomers of amyloid-β bind to PrP^C which may mediate amyloid-β neurotoxicity. In addition, the APP intracellular domain (AICD), which acts as a transcriptional regulator, has been reported to control the expression of PrP^C. Through the use of transgenic mice, cell culture models and manipulation of APP expression and processing, this study aimed to clarify the role of AICD in regulating PrP^C. Over-expression of the three major isoforms of human APP (APP_{695}, APP_{751} and APP_{770}) in cultured neuronal and non-neuronal cells had no effect on the level of endogenous PrP^C. Furthermore, analysis of brain tissue from transgenic mice over-expressing either wild type or familial AD associated mutant human APP revealed unaltered PrP^C levels. Knockdown of endogenous APP expression in cells by siRNA or inhibition of γ-secretase activity also had no effect on PrP^C levels. Overall, we did not detect any significant difference in the expression of PrP^C in any of the cell or animal-based paradigms considered, indicating that the control of cellular PrP^C levels by AICD is not as straightforward as previously suggested.

Citation: Lewis V, Whitehouse IJ, Baybutt H, Manson JC, Collins SJ, et al. (2012) Cellular Prion Protein Expression Is Not Regulated by the Alzheimer's Amyloid Precursor Protein Intracellular Domain. PLoS ONE 7(2): e31754. doi:10.1371/journal.pone.0031754

Editor: Sophie Mouillet-Richard, INSERM, UMR-S747, France

Received December 6, 2011; **Accepted** January 12, 2012; **Published** February 21, 2012

Funding: The authors gratefully acknowledge the financial support of the Medical Research Council (G0802189 to NMH) and Alzheimer's Research UK (NMH and JCM). VL is supported by NHMRC (National Health and Medical Research Council) Training Fellowship (#567123). SJC is supported by NHMRC Practitioner Fellowship (#400183). The funders had no role in study design, data collection and analysis, decision to publish, or preparation of the manuscript.

Competing Interests: The authors have declared that no competing interests exist.

* E-mail: n.m.hooper@leeds.ac.uk

Introduction

Alzheimer's disease (AD) and prion diseases fall within the spectrum of neurodegenerative diseases which are causally linked to misfolded and aggregated proteins. Due to similarities in various structural elements and proteolytic processing events involving the major proteins involved in these diseases, potential links and parallels in both disease mechanisms and possible therapeutic avenues have been proposed [1,2,3,4]. Increasingly, recent studies have shown more direct molecular links between AD and prion diseases, and the proteins at the centre of these diseases; namely the amyloid precursor protein (APP) and its proteolytic cleavage product the amyloid-β (Aβ) peptide which deposits as plaques in the AD brain, and the normal cellular prion protein (PrP^C) and the disease-associated isoform PrP^{Sc}, which accumulates in prion diseases. A substantive molecular link was provided when PrP^C was shown to modulate production of Aβ from wild type APP, through an interaction with the β-secretase BACE1 [5], later demonstrated to be a mechanism for altered trafficking and localisation of BACE1 resulting in reduced Aβ production [6]. Additionally, several groups have now presented evidence that PrP^C can bind oligomeric forms of Aβ [7,8,9,10], although there is conflicting data regarding the downstream consequences of this binding. Some results suggest that Aβ oligomer synaptic toxicity is mediated through its binding to PrP^C [7,11,12], whereas others have reported that Aβ oligomer neurotoxicity is independent of PrP^C expression [8,9]. Whilst perhaps explained by methodological differences, these opposing results underscore the complexity in the possible interactions between these two key proteins and diseases.

In addition to Aβ, a number of other proteolytic fragments are generated from APP. Cleavage of the full length APP by either α-secretase or BACE1 produces large soluble N-terminal ectodomains, and C-termimal membrane-bound stubs, denoted C83 and C99, respectively. Both C83 and C99 can be cleaved by the γ-secretase complex to produce the APP intracellular domain (AICD) [13]. This latter fragment appears to act as a transcriptional regulator after forming a complex with Fe65 and Tip60 [14]. In particular AICD has been shown to regulate the expression of the Aβ degrading enzyme neprilysin [15,16]. Interestingly, it appears to be only the AICD produced from the combined action of BACE1 and γ-secretase on APP that is transcriptionally active [17,18,19].

There are three major isoforms of APP expressed in the brain, APP_{695}, APP_{751} and APP_{770}, which are produced via alternative splicing of the single mRNA [20]. Of the three, APP_{695} is the

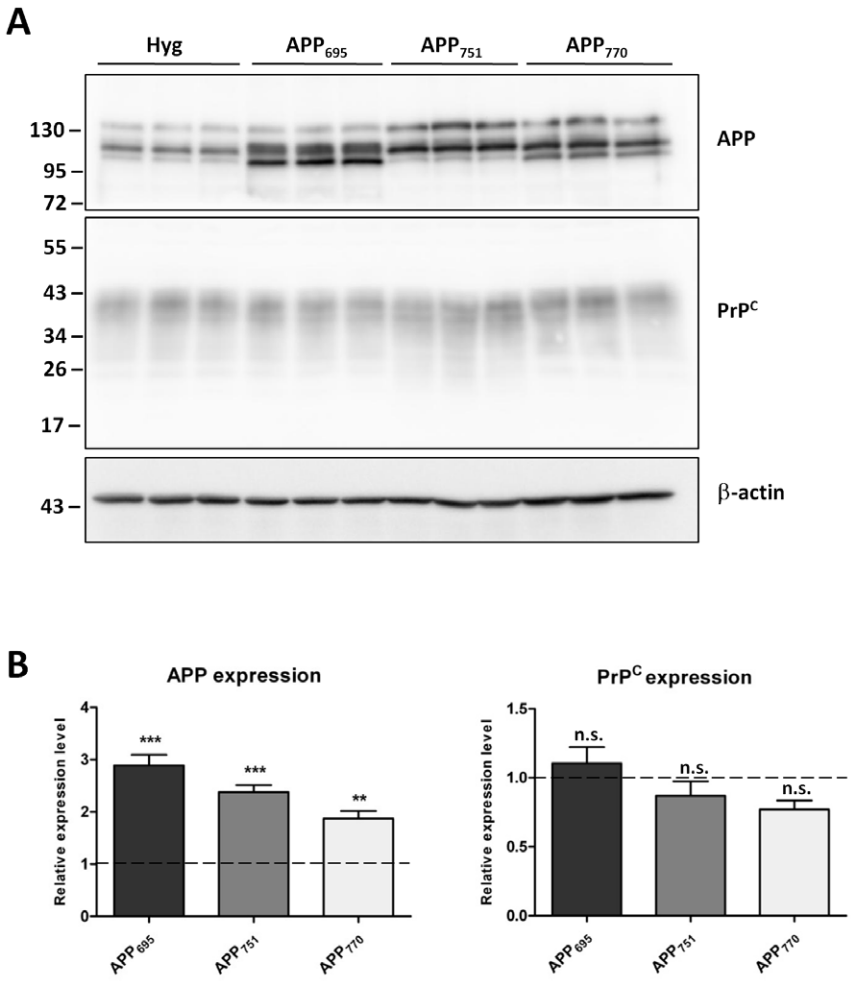

Figure 1. Over-expression of APP isoforms in HEK cells does not alter endogenous PrP^C. (A) Representative western blot of APP and PrP^C (antibody 3F4) in HEK cells stably transfected with either the vector alone (Hyg) or one of the APP isoforms (APP_{695}, APP_{751}, APP_{770}), and subsequent β-actin staining to allow adjustments for equal protein loading. Approximate molecular weights (kDa) are indicated. (B) Quantification of APP and PrP^C protein levels expressed relative to Hyg control cells (dashed line). Data from 4 independent experiments. Statistical analysis by one way ANOVA with Dunnett's post test comparison to the Hyg cells, ***$p<0.001$, **$p<0.01$, n.s. not significant.
doi:10.1371/journal.pone.0031754.g001

major neuronal splice variant. Recently, we reported that only the AICD produced from the β- and γ-secretase cleavage of APP_{695}, and not that produced from the other two isoforms, is transciptionally active as assessed by its ability to upregulate neprilysin expression [19]. This transcriptionally active AICD was only produced in neuronal (SH-SY5Y and N2a) cell lines and was not functional in non-neuronal human embryonic kidney (HEK293) cells [19]. Further, AICD produced from the familial AD associated Swedish mutant form of APP_{695}, known to be subject to increased BACE1 cleavage compared to wild type APP_{695} [21], was more transcriptionally active relative to wild type APP_{695} [19].

The molecular and cellular links between APP and PrP^C were extended recently when PrP^C expression was reported to be regulated by AICD [22]. Overexpression of APP_{751} in HEK cells triggered a significant increase in PrP^C immunoreactivity, while a reduction in PrP^C was observed in APP deficient fibroblasts. The γ-secretase inhibitor DAPT significantly reduced PrPC levels in primary neurons, implicating a role for AICD in controlling the expression of PrPC [22]. The aim of the present study was to clarify the role of AICD in the regulation of PrP^C and to specifically determine whether, similar to the control of neprilysin expression [19], there was an APP isoform effect.

Results

Over-expression of APP does not alter endogenous PrP^C protein expression

Initially we sought to replicate the findings of Vincent et al. [22] by expressing APP_{751} in HEK cells. In addition, we looked to advance this research by determining whether the control of PrP^C expression by AICD was specific to a particular APP isoform. HEK cells stably over-expressing either APP_{695}, APP_{751} or APP_{770}, alongside a vector only control were assessed for total cell associated PrP^C and APP protein levels by western blotting (Fig. 1A and B). Surprisingly, in contrast to previously published results [22], although there was a significant 2–3-fold increase in APP in the cells transfected with any of the three APP isoforms, there was no significant difference in PrP^C level in any of the APP isoform expressing cells when compared to the Hyg vector-only controls.

We have recently shown that transcriptionally active AICD is only produced by the BACE1 and γ-secretase cleavage of the

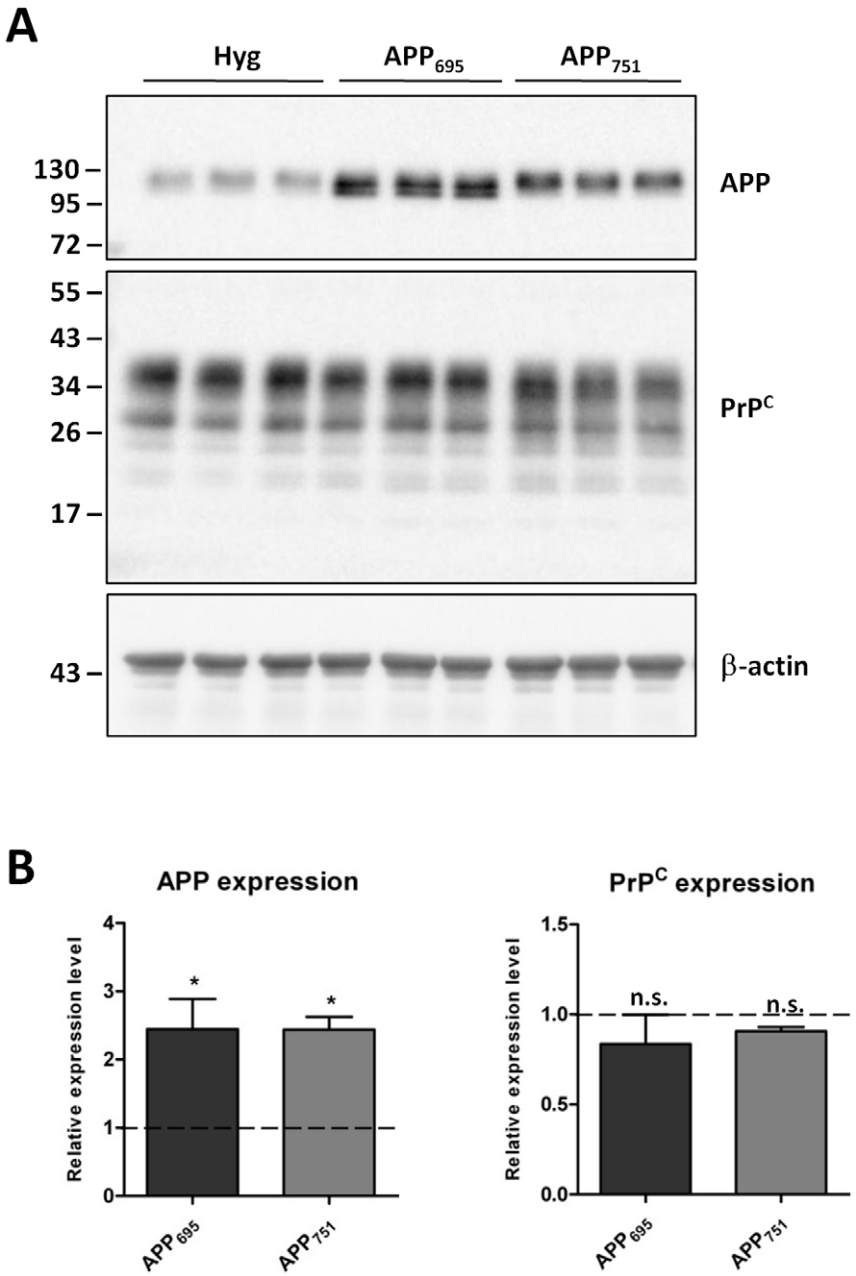

Figure 2. Over-expression of APP isoforms in N2a cells does not alter endogenous PrP^C. (A) Representative western blot of APP and PrP^C (antibody 6H4) in N2a cells stably transfected with either the vector alone (Hyg) or one of the APP isoforms (APP_{695}, APP_{751}), and subsequent β-actin staining. Approximate molecular weights (kDa) are indicated. (B) Quantification of APP and PrP^C protein levels expressed relative to Hyg control cells (dashed line). Data from 3 independent experiments. Statistical analysis by one way ANOVA with Dunnett's post test comparison to the Hyg cells, *$p<0.05$, n.s. not significant.
doi:10.1371/journal.pone.0031754.g002

APP_{695} isoform in neuronal cells [19]. In light of this, and the negative result observed in the non-neuronal HEK cells, we utilized mouse neuronal N2a cells over-expressing human APP_{695} or APP_{751} to again assess total PrP^C and APP protein levels (Fig. 2A and B). Despite a significant 2.5-fold increase in APP expression in the N2a cells transfected with the cDNAs encoding either APP_{695} or APP_{751}, there was no difference in endogenous PrP^C levels when comparing the APP over-expressing cells with each other or the vector only controls.

To further examine the effect of APP over-expression on PrP^C levels, two transgenic mouse models were investigated. PrP^C and APP protein levels were evaluated in brain homogenates from I5 mice which over-express wild type human APP, J20 mice which over-express human APP containing the Swedish/Indiana familial AD mutations [23] and non-transgenic matched genetic background control mice (Fig. 3A and B). Despite a significant 2.8 -fold increase in APP in the transgenic I5 mice, as compared to the non-transgenic mice, there was no difference in brain PrP^C levels.

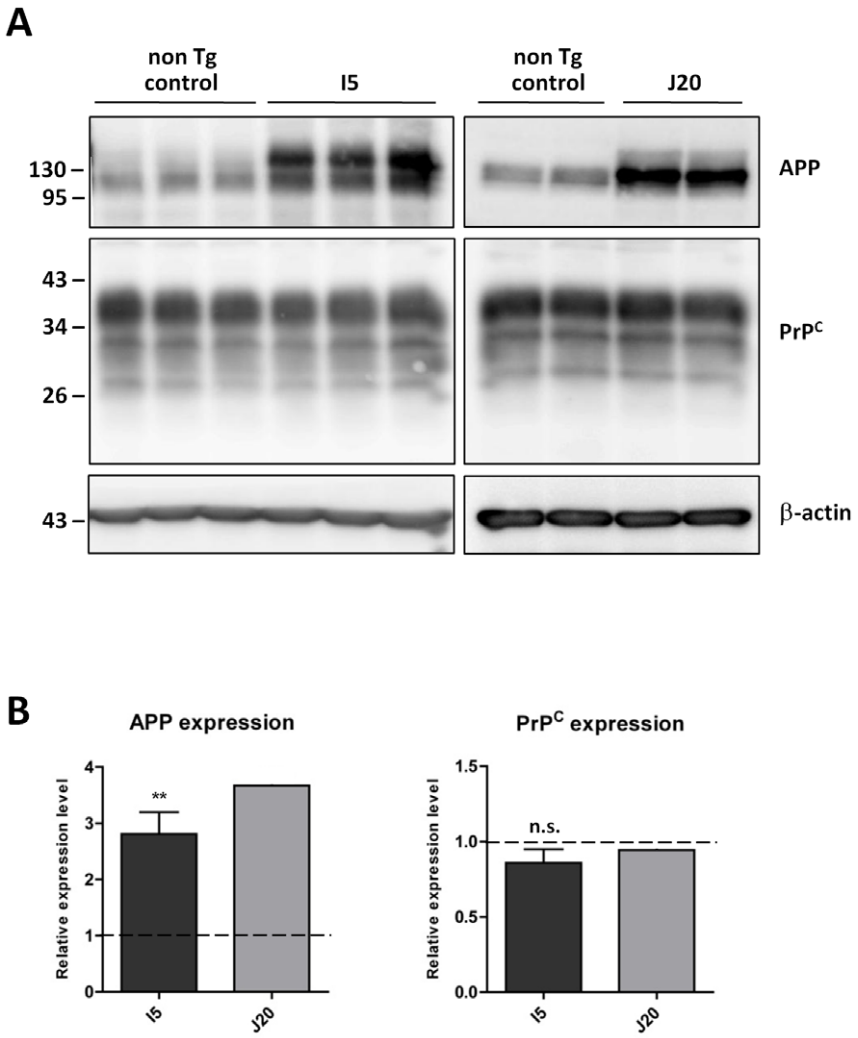

Figure 3. Unaltered PrP^C protein levels in transgenic mice over-expressing human wild type or familial AD mutant APP. (A) Western blot of APP and PrP^C (antibody 6D11) in I5 (n = 3) and J20 (n = 2) transgenic, and age-matched non-transgenic control, mouse brain homogenates, with membrane re-probing for β-actin. Approximate molecular weights (kDa) are indicated. (B) Quantification of APP and PrP^C protein levels expressed relative to the control mice (dashed line). Error bars represent ± SD. Statistical analysis by unpaired t-test, $^{**}p<0.01$, n.s. not significant.
doi:10.1371/journal.pone.0031754.g003

Analysis of the J20 mice, although only involving two animals, reinforced this conclusion. Collectively these over-expression experiments indicate that control of PrP^C expression does not appear to involve AICD in either cell-based or transgenic animal paradigms.

Reduction of AICD production through APP gene silencing or γ-secretase inhibition does not alter expression of endogenous PrP^C

In light of the above results, we considered whether the level of AICD required to regulate PrP^C expression in the cell lines or the transgenic mice were already maximal from the endogenous APP, such that the AICD produced from the over-expressed APP was not having any additional affect on PrP^C expression. Thus we sought to investigate a possible role for endogenous AICD in the control of PrP^C expression. First, to reduce endogenous APP levels and thereby remove the substrate for AICD production, N2a cells were treated with siRNA against murine APP. Cells were harvested, lysed and PrP^C and APP levels measured by western blotting (Fig. 4A and B). After directed siRNA treatment there was a significant 70% decrease in total APP levels (endogenous AICD level is below the limits of detection by immunoblot; data not shown). However, the amount of PrP^C remained unchanged following siRNA knockdown of endogenous APP.

In order to test further for a possible involvement of endogenous AICD in controlling PrP^C expression, both HEK and N2a cells were treated with DAPT, a cell permeable γ-secretase inhibitor. Again, whole cell lysates were assessed for PrP^C and APP expression, as well as the levels of C83 and C99, by western blotting (Fig. 5A and B). Although DAPT treatment inhibited γ-secretase activity, as shown by the significantly increased C83 and C99 levels (9.4-fold in the HEK cells and 17.8-fold in the N2a cells), there was no difference in endogenous PrP^C protein levels in the DAPT treated cells as compared to the untreated cells (Fig. 5C and D). Together these results indicate that in both a neuronal and a non-neuronal cell line, endogenous AICD is also not involved in the control of PrP^C protein expression.

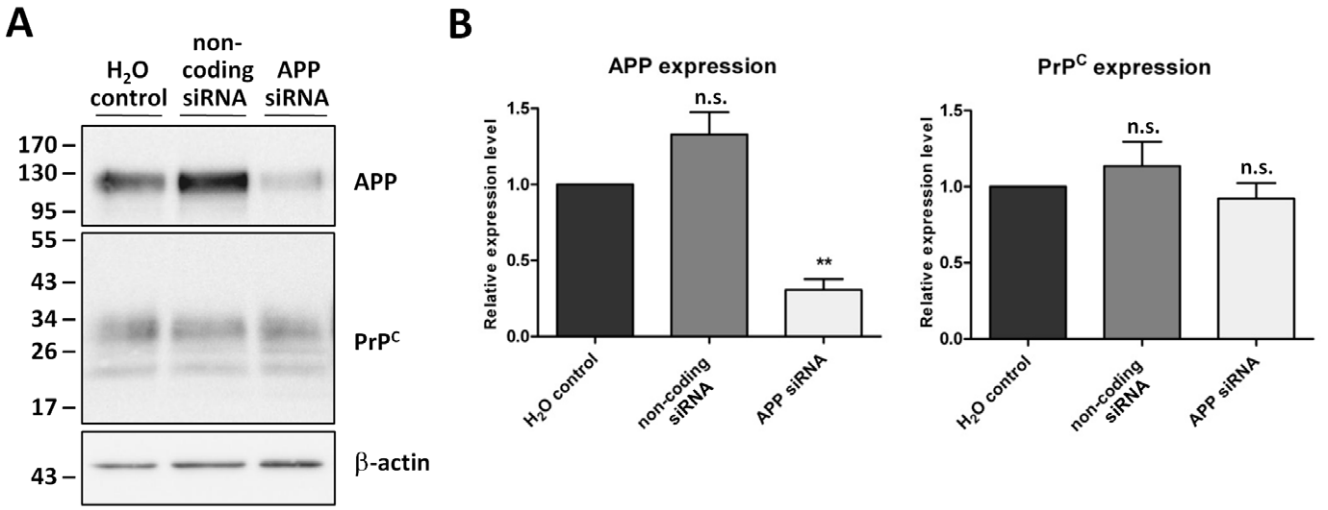

Figure 4. Knockdown of APP expression in N2a cells has no effect on PrP^C protein levels. (A) Representative western blots of APP and PrP^C (antibody 6H4) in N2a cells treated with APP directed siRNA, non-coding control siRNA, and a no RNA transfection control (H_2O control), and subsequent β-actin staining. Approximate molecular weights (kDa) are indicated. (B) Quantification of APP and PrP^C protein levels expressed relative to the H_2O control cells. Data from 3 independent experiments. Statistical analysis by one way ANOVA with Dunnett's post test comparison to the H_2O control cells, $^{**}p<0.01$, n.s. not significant.
doi:10.1371/journal.pone.0031754.g004

Discussion

Similarities in the pathogenesis of the protein-misfolding neurodegenerative illnesses, especially AD and prion diseases, and possible connections between these diseases have long been contemplated [1,2,3,4]. Elucidation of any functional links between these diseases is an important research goal, with determination of the most appropriate protein or process to target for development of therapeutics being paramount. Links in the pathologies of AD and prion diseases have been determined, with various reports of AD features in prion disease brains [24,25,26], and PrP^C localised in Aβ plaques in AD brain [27,28]. In addition, a polymorphism at codon 129 of the prion protein gene, known to influence susceptibility to sporadic and iatrogenic human prion disease [29,30], may also influence susceptibility and the pathophysiology of AD [31,32,33]. Interestingly there is some indication of a more direct interaction between Aβ and PrP^{Sc}, with the finding of an acceleration and exacerbation of both AD and prion disease pathologies in animals engineered to have both of these diseases, and enhanced protein misfolding due to cross-seeding events stimulating oligomerization *in vitro* [34]. This propensity for cross-seeding highlights the importance for a more complete understanding of interactions between these key proteins and any resultant downstream consequences.

Recent studies have provided evidence of direct interactions between the proteins central to AD and prion diseases. Various studies have determined that the cellular prion protein can act as a receptor for Aβ, with Aβ oligomers binding to PrP^C with high affinity, although there are conflicting views as to the physiological significance of this binding. Some results suggest that Aβ synaptic toxicity is mediated through its binding to PrP^C [7,11,12], which specifically impacts on spatial learning and memory *in vivo* [35], whereas others have reported that Aβ oligomer neurotoxicity occurs independently [8,9]. Confounding the relationship between these key proteins, and in apparent contrast to PrP^C mediating Aβ neurotoxicitiy, PrP^C has been shown to decrease production of Aβ from wild type APP through its interaction with the β-secretase BACE1 [5]. This interaction, mapped to the BACE1 pro-domain, leads to slowed BACE1 trafficking following exit from the ER, thereby increasing its localization in the trans-Golgi network and reducing levels at the cell surface and consequently in endosomes where APP β-cleavage occurs [6]. Importantly, these studies also ascertained links in the pathology of AD and prion diseases. It was found that human prion disease-associated mutations in PrP^C did not inhibit BACE1, and scrapie infected mice brains contained dramatically higher Aβ levels [5], suggesting a loss of PrP^C function perhaps as a result of PrP^C-PrP^{Sc} conversion during prion disease progression.

PrP^C may be a key therapeutic target for sporadic AD, and the recent report that PrP^C expression was controlled by AICD in a γ-secretase dependent manner [22] presented a potential avenue for achieving this. Further, a possible feedback model reconciling the control of APP processing and PrP^C expression in both normal conditions and in the presence of increased Aβ such as that seen in AD was proposed [36]. Therefore our study was carried out to further understand the relationship between AICD production and PrP^C expression. However, utilizing a range of experimental approaches we found no evidence for AICD involvement in PrP^C expression. This is despite using a cellular system (N2a cells expressing APP_{695}) in which we have proven that AICD is transcriptionally active [19]. If AICD is involved in regulating the transcription of PrP^C, then the mechanism underlying this is more complex than that involved in regulating the expression of neprilysin and is not readily reproduced in cultured cells or transgenic mice over-expressing human APP. Our findings have implications for the continued investigation and design of possible AD therapeutics.

Materials and Methods

Ethics statement

All experimental procedures performed on mice were approved by the Roslin Institute (University of Edinburgh) Ethical Review Process Committee and carried out under the UK Home Office License 60/3478. Human embryonic kidney (HEK) cells were obtained from the European Collection of Cell Cultures and

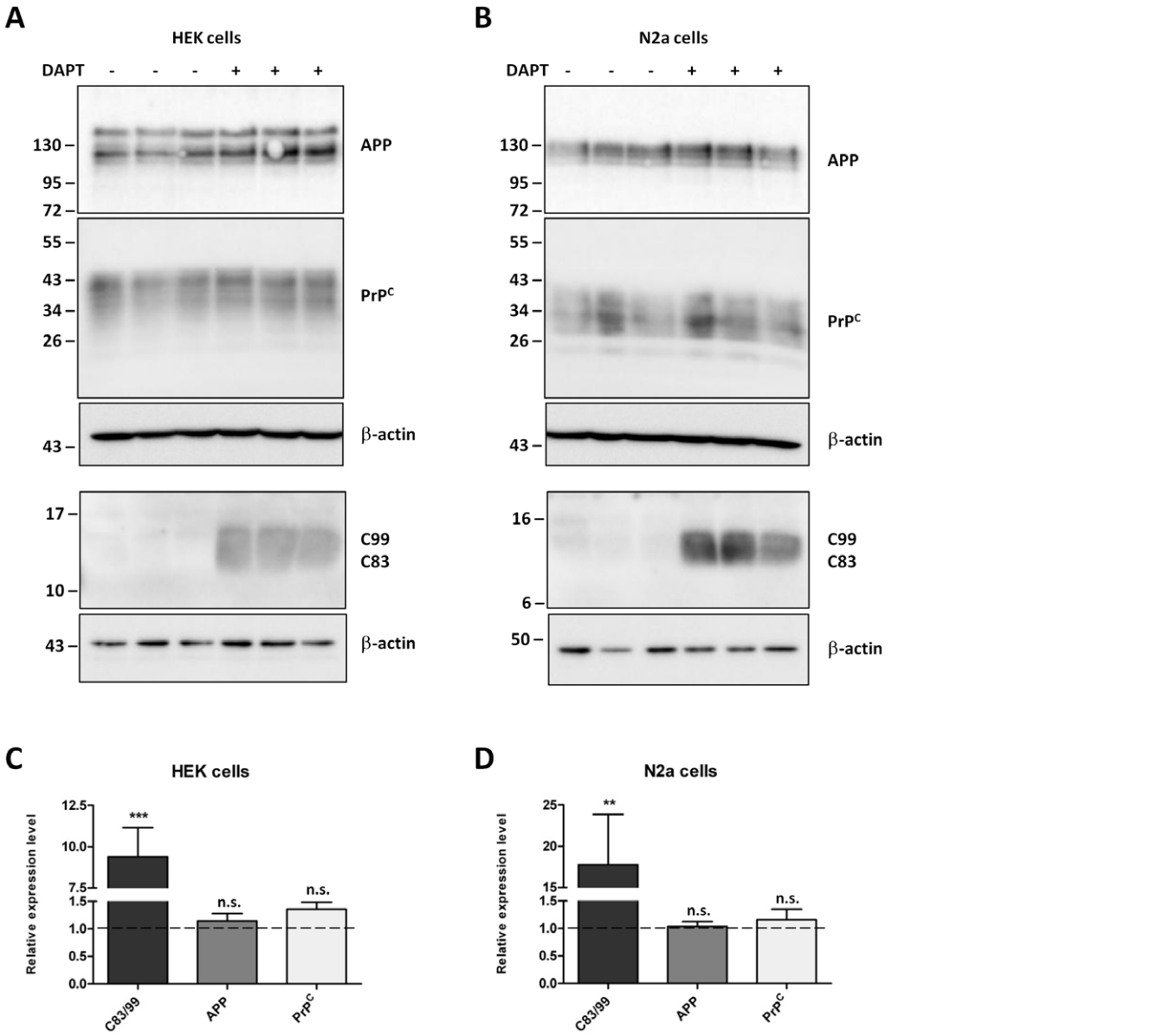

Figure 5. Inhibition of γ-secretase activity does not alter the expression of PrP^C. Representative western blots showing total cell-associated APP, PrP^C (antibody 6H4) and C-terminal APP fragments (C83/99) in control (−) and DAPT treated (+) HEK (A) and N2a (B) cells, with membrane re-probing for β-actin. Approximate molecular weights (kDa) are indicated. Quantification of C83/99, APP and PrP^C protein levels in DAPT treated HEK (C) and N2a (D) cells, expressed relative to control cells (dashed line). Data from 3 (HEK) or 4 (N2a) independent experiments. Statistical analysis by one way ANOVA with Dunnett's post test comparison to the control cells, ***$p<0.001$, **$p<0.01$, n.s. not significant.
doi:10.1371/journal.pone.0031754.g005

murine neuroblastoma (N2a) cells were obtained from Dr Lehmann, Université Montpellier, France [37].

Cell culture

HEK cells and N2a cells stably over-expressing the human APP isoforms (APP_{695}, APP_{751} and APP_{770}), alongside the vector-only (Hyg), were generated by electroporation as described previously [19]. Cells were maintained in Dulbecco's modified Eagle's medium (DMEM; Lonza, Basel, Switzerland) containing 10% (v/v) fetal bovine serum (FBS; Biosera, East Sussex, UK) and 1% penicillin/streptomycin (Lonza), in a humidified incubator at 37°C, 5% CO_2.

APP gene silencing

To ablate endogenous APP expression in the N2a cells, cells were grown to 80% confluency in growth medium prior to treatment with 50 nM final concentration of murine APP directed siRNA, non-coding siRNA or siRNA-free controls following the manufacturer's instructions (Thermo Fisher Scientific, Lafayette, CO, USA). Briefly, sub-confluent cell monolayers were washed gently with OptiMEM (GIBCO, Invitrogen, Glasgow, UK), before further incubation in OptiMEM for approximately 30 min (37°C, 5% CO_2) during siRNA preparation. A 10 μM siRNA solution in 1× siRNA buffer of either murine APP directed siRNA (ON-TARGETplus SMARTpool) or non-coding siRNA control (ON-

TARGETplus Non-targeting pool) was prepared, and diluted to 1 μM in OptiMEM. For the RNA-free control, sterile RNase-free water was diluted 1:10 in OptiMEM. DharmaFECT Transfection Reagent-1 was diluted 1:40 in OptiMEM, mixed gently and incubated for 5 min at room temperature. Equal volumes of the diluted siRNA/control and DharmaFECT solutions were then mixed and incubated for 20 min at room temperature, prior to the addition of 4× volumes of OptiMEM containing 10% (v/v) FBS. The OptiMEM was then removed from the cells, and replaced with the OptiMEM/FBS/siRNA complexes (or control) for 72 h.

Inhibition of γ-secretase

To inhibit endogenous γ-secretase activity, HEK or N2a cells were grown to 90–95% confluency prior to treatment. The cell monolayer was then washed twice with PBS prior to incubating the cells in serum-free OptiMEM containing a final concentration 10 μM N-[N-(3,5-difluorophenacetyl)-L-alanyl]-S-phenylglycine t-butyl ester (DAPT; Sigma-Aldrich, Dorset, UK), or an equal volume of dimethyl sulfoxide (DMSO, as the control) for 24 h.

Cell lysis, SDS-PAGE and immunoblotting

When confluent and/or after appropriate treatments as described above, cells were washed twice in phosphate-buffered saline (PBS with Ca^{2+} and Mg^{2+}; Lonza), harvested by scraping into PBS, and pelleted at 500× g for 3 min. Cell pellets were lysed for 30 min on ice in cold lysis buffer (25 mM Tris/HCl, pH7.5, 150 mM NaCl, 5 mM EDTA, 1% (v/v) Triton X-100) containing Complete™ protease inhibitor cocktail (Roche, West Sussex, UK), prior to centrifugation for 5 min at 1000× g. Post-nuclear supernatants were assessed for total protein content using a bicinchoninic acid protein assay (Sigma-Aldrich). Cell lysate containing 50 μg total protein was resolved on 7–17% (APP and PrP^C) or 16.5% (C83/99) polyacrylamide SDS gel, then electro-transferred to Hybond-P polyvinylidene difluoride membrane (PVDF; Amersham Life Sciences, Buckinghamshire, UK). PVDF membranes were blocked for 1–2 h at room temperature in PBS containing 0.1% Tween-20 (PBST) and 5% (w/v) skimmed milk powder, prior to incubation with primary antibody overnight at 4°C. For detection of APP the membrane was incubated with the monoclonal antibody 22C11 (Millipore, Billerica, MA, USA), and for detection of PrP^C the membrane was incubated with either the monoclonal antibody 3F4 (Covance, Princeton, NJ, USA), 6D11 (Eurogentec Ltd, Hampshire, UK) or 6H4 (Prionics, Zurich, Switzerland), as indicated in the figure legends. For detection of C83/99, a polyclonal anti-C-terminal APP antibody A8717 (Sigma-Aldrich) was used. After washing off non-specifically bound primary antibody with PBST, membranes were incubated in peroxidase-conjugated rabbit-anti-mouse or goat-anti-rabbit secondary antibodies (Sigma-Aldrich), before further washes with PBST and detection using enhanced chemiluminescence (Pierce ECL substrate; Thermo Fischer Scientific). To assess and correct for protein loading, membranes were stripped at low pH (1% (v/v) aqueous HCl) for approximately 30 min, re-blocked and probed with an anti-β-actin antibody (clone AC-15, Sigma-Aldrich) and the secondary antibody described above. All chemiluminescent images were captured by a Fujifilm LAS-3000 Intelligent Dark Box.

Transgenic mice and tissue homogenisation

Animals were obtained from The Jackson Laboratory (Bar Harbor, ME, USA), and all care was carried out in strict accordance with institutional guidelines. Transgenic I5 mice (Line B6.Cg-Tg(PDGFB-APP)5 Lms/J, stock number 004662), which over-express wild type human APP, and J20 mice (Line B6.Cg-Tg(PDGFB-APPSwInd)20 Lms/2J, stock number 006293), which over-express human APP containing the Swedish (K670N/M671L) and Indiana (V717F) familial AD mutations [23], were crossed with inbred 129P2 mice, and genotyped to confirm the *APP* gene sequence. Brain hemispheres from the I5 (8 weeks old), J20 (5–9 weeks old) and age-matched non-transgenic littermate controls were homogenized in 2% (w/v) SDS solution containing protease inhibitors, and homogenates centrifuged at 100,000× g for 1 h at 4°C. The resultant supernatant was assayed for total protein and assessed for PrP^C and APP protein by SDS-PAGE and western blotting as described above for cell lysates.

Densitometry and statistical analysis

Quantification and densitometric analyses were carried out using Image J v1.42q. Within each experiment, data was normalised to β-actin, and expressed relative to the control samples. Statistical analyses were performed in GraphPad Prism v5.03. All quantitative data are expressed as the mean ± SEM, unless stated otherwise.

Author Contributions

Conceived and designed the experiments: VL JCM SJC NMH. Performed the experiments: VL IJW HB. Analyzed the data: VL IJW HB JCM NMH. Wrote the paper: VL JCM SJC NMH.

References

1. Wisniewski T, Sigurdsson EM (2007) Therapeutic approaches for prion and Alzheimer's diseases. FEBS J 274: 3784–3798.
2. Checler F, Vincent B (2002) Alzheimer's and prion diseases: distinct pathologies, common proteolytic denominators. Trends Neurosci 25: 616–620.
3. Taylor DR, Hooper NM (2007) Role of lipid rafts in the processing of the pathogenic prion and Alzheimer's amyloid-beta proteins. Semin Cell Dev Biol 18: 638–648.
4. Barnham KJ, Cappai R, Beyreuther K, Masters CL, Hill AF (2006) Delineating common molecular mechanisms in Alzheimer's and prion diseases. Trends Biochem Sci 31: 465–472.
5. Parkin ET, Watt NT, Hussain I, Eckman EA, Eckman CB, et al. (2007) Cellular prion protein regulates beta-secretase cleavage of the Alzheimer's amyloid precursor protein. Proc Natl Acad Sci USA 104: 11062–11067.
6. Griffiths HH, Whitehouse IJ, Baybutt H, Brown D, Kellett KA, et al. (2011) Prion protein interacts with BACE1 protein and differentially regulates its activity toward wild type and Swedish mutant amyloid precursor protein. J Biol Chem 286: 33489–33500.
7. Lauren J, Gimbel DA, Nygaard HB, Gilbert JW, Strittmatter SM (2009) Cellular prion protein mediates impairment of synaptic plasticity by amyloid-beta oligomers. Nature 457: 1128–1132.
8. Balducci C, Beeg M, Stravalaci M, Bastone A, Sclip A, et al. (2010) Synthetic amyloid-beta oligomers impair long-term memory independently of cellular prion protein. Proc Natl Acad Sci USA 107: 2295–2300.
9. Calella AM, Farinelli M, Nuvolone M, Mirante O, Moos R, et al. (2010) Prion protein and Abeta-related synaptic toxicity impairment. EMBO Mol Med 2: 306–314.
10. Chen S, Yadav SP, Surewicz WK (2010) Interaction between human prion protein and amyloid-beta (Abeta) oligomers: role of N-terminal residues. J Biol Chem 285: 26377–26383.
11. Barry AE, Klyubin I, Mc Donald JM, Mably AJ, Farrell MA, et al. (2011) Alzheimer's disease brain-derived amyloid-beta-mediated inhibition of LTP in vivo is prevented by immunotargeting cellular prion protein. J Neurosci 31: 7259–7263.
12. Freir DB, Nicoll AJ, Klyubin I, Panico S, Mc Donald JM, et al. (2011) Interaction between prion protein and toxic amyloid beta assemblies can be therapeutically targeted at multiple sites. Nat Commun 2: 336.
13. Vardy ER, Catto AJ, Hooper NM (2005) Proteolytic mechanisms in amyloid-beta metabolism: therapeutic implications for Alzheimer's disease. Trends Mol Med 11: 464–472.
14. Cao X, Sudhof TC (2001) A transcriptionally active complex of APP with Fe65 and histone acetyltransferase Tip60. Science 293: 115–120.
15. Belyaev ND, Nalivaeva NN, Makova NZ, Turner AJ (2009) Neprilysin gene expression requires binding of the amyloid precursor protein intracellular domain to its promoter: implications for Alzheimer disease. EMBO Rep 10: 94–100.

16. Pardossi-Piquard R, Petit A, Kawarai T, Sunyach C, Alves da Costa C, et al. (2005) Presenilin-dependent transcriptional control of the Abeta-degrading enzyme neprilysin by intracellular domains of betaAPP and APLP. Neuron 46: 541–554.
17. Goodger ZV, Rajendran L, Trutzel A, Kohli BM, Nitsch RM, et al. (2009) Nuclear signaling by the APP intracellular domain occurs predominantly through the amyloidogenic processing pathway. J Cell Sci 122: 3703–3714.
18. Hoey SE, Williams RJ, Perkinton MS (2009) Synaptic NMDA receptor activation stimulates alpha-secretase amyloid precursor protein processing and inhibits amyloid-beta production. J Neurosci 29: 4442–4460.
19. Belyaev ND, Kellett KA, Beckett C, Makova NZ, Revett TJ, et al. (2010) The transcriptionally active amyloid precursor protein (APP) intracellular domain is preferentially produced from the 695 isoform of APP in a beta-secretase-dependent pathway. J Biol Chem 285: 41443–41454.
20. Tanaka S, Nakamura S, Ueda K, Kameyama M, Shiojiri S, et al. (1988) Three types of amyloid protein precursor mRNA in human brain: their differential expression in Alzheimer's disease. Biochem Biophys Res Commun 157: 472–479.
21. Citron M, Oltersdorf T, Haass C, McConlogue L, Hung AY, et al. (1992) Mutation of the beta-amyloid precursor protein in familial Alzheimer's disease increases beta-protein production. Nature 360: 672–674.
22. Vincent B, Sunyach C, Orzechowski HD, St George-Hyslop P, Checler F (2009) p53-Dependent transcriptional control of cellular prion by presenilins. J Neurosci 29: 6752–6760.
23. Mucke L, Masliah E, Yu GQ, Mallory M, Rockenstein EM, et al. (2000) High-level neuronal expression of abeta 1–42 in wild-type human amyloid protein precursor transgenic mice: synaptotoxicity without plaque formation. J Neurosci 20: 4050–4058.
24. Hainfellner JA, Wanschitz J, Jellinger K, Liberski PP, Gullotta F, et al. (1998) Coexistence of Alzheimer-type neuropathology in Creutzfeldt-Jakob disease. Acta Neuropathol 96: 116–122.
25. Brown P, Gibbs CJ, Jr., Rodgers-Johnson P, Asher DM, Sulima MP, et al. (1994) Human spongiform encephalopathy: the National Institutes of Health series of 300 cases of experimentally transmitted disease. Ann Neurol 35: 513–529.
26. Tsuchiya K, Yagishita S, Ikeda K, Sano M, Taki K, et al. (2004) Coexistence of CJD and Alzheimer's disease: an autopsy case showing typical clinical features of CJD. Neuropathology 24: 46–55.
27. Takahashi RH, Tobiume M, Sato Y, Sata T, Gouras GK, et al. (2010) Accumulation of cellular prion protein within dystrophic neurites of amyloid plaques in the Alzheimer's disease brain. Neuropathology 3: 2080214.
28. Voigtlander T, Kloppel S, Birner P, Jarius C, Flicker H, et al. (2001) Marked increase of neuronal prion protein immunoreactivity in Alzheimer's disease and human prion diseases. Acta neuropathologica 101: 417–423.
29. Deslys JP, Marce D, Dormont D (1994) Similar genetic susceptibility in iatrogenic and sporadic Creutzfeldt-Jakob disease. J Gen Virol 75: 23–27.
30. Windl O, Dempster M, Estibeiro JP, Lathe R, de Silva R, et al. (1996) Genetic basis of Creutzfeldt-Jakob disease in the United Kingdom: a systematic analysis of predisposing mutations and allelic variation in the PRNP gene. Hum Genet 98: 259–264.
31. Riemenschneider M, Klopp N, Xiang W, Wagenpfeil S, Vollmert C, et al. (2004) Prion protein codon 129 polymorphism and risk of Alzheimer disease. Neurology 63: 364–366.
32. Del Bo R, Scarlato M, Ghezzi S, Martinelli-Boneschi F, Fenoglio C, et al. (2006) Is M129V of PRNP gene associated with Alzheimer's disease? A case-control study and a meta-analysis. Neurobiol Aging 27: 770 e1–770 e5.
33. Gacia M, Safranow K, Styczynska M, Jakubowska K, Peplonska B, et al. (2006) Prion protein gene M129 allele is a risk factor for Alzheimer's disease. J Neural Transm 113: 1747–1751.
34. Morales R, Estrada LD, Diaz-Espinoza R, Morales-Scheihing D, Jara MC, et al. (2010) Molecular cross talk between misfolded proteins in animal models of Alzheimer's and prion diseases. J Neurosci 30: 4528–4535.
35. Gimbel DA, Nygaard HB, Coffey EE, Gunther EC, Lauren J, et al. (2010) Memory impairment in transgenic Alzheimer mice requires cellular prion protein. J Neurosci 30: 6367–6374.
36. Kellett KA, Hooper NM (2009) Prion protein and Alzheimer disease. Prion 3: 190–194.
37. Nishida N, Harris DA, Vilette D, Laude H, Frobert Y, et al. (2000) Successful transmission of three mouse-adapted scrapie strains to murine neuroblastoma cell lines overexpressing wild-type mouse prion protein. J Virol 74: 320–5.

BJ Disease

Biochem. J. (2014) **459**, 103–115 (Printed in Great Britain) doi:10.1042/BJ20131378

online data

C-terminal peptides modelling constitutive PrP^{C} processing demonstrate ameliorated toxicity predisposition consequent to α-cleavage

Vanessa A. JOHANSSEN*†‡, Timothy JOHANSSEN*‡§, Colin L. MASTERS§, Andrew F. HILL†‡§, Kevin J. BARNHAM*‡§ and Steven J. COLLINS*§[1]

*Department of Pathology, University of Melbourne, Parkville, VIC 3010, Australia
†Department of Biochemistry and Molecular Biology, University of Melbourne, Parkville, VIC 3010, Australia
‡Bio21 Molecular Science and Biotechnology Institute, University of Melbourne, Parkville, VIC 3010, Australia
§Mental Health Research Institute, University of Melbourne, Parkville, VIC 3010, Australia

Misfolding of PrP^{C} (cellular prion protein) to β-strand-rich conformations constitutes a key event in prion disease pathogenesis. PrP^{C} can undergo either of two constitutive endoproteolytic events known as α- and β-cleavage, yielding C-terminal fragments known as C1 and C2 respectively. It is unclear whether C-terminal fragments generated through α- and β-cleavage, especially C2, influence pathogenesis directly. Consequently, we compared the biophysical properties and neurotoxicity of recombinant human PrP fragments recapitulating α- and β-cleavage, namely huPrP-(112–231) (equating to C1) and huPrP-(90–231) (equating to C2). Under conditions we employed, huPrP-(112–231) could not be induced to fold into a β-stranded isoform and neurotoxicity was not a feature for monomeric or multimeric assemblies. In contrast, huPrP-(90–231) easily adopted a β-strand conformation, demonstrated considerable thermostability and was toxic to neurons. Synthetic PrP peptides modelled on α- and β-cleavage of the unique Y145STOP (Tyr^{145}→stop) mutant prion protein corroborated the differential toxicity observed for recombinant huPrP-(112–231) and huPrP-(90–231) and suggested that the persistence of soluble oligomeric β-strand-rich conformers was required for significant neurotoxicity. Our results additionally indicate that α- and β-cleavage of PrP^{C} generate biophysically and biologically non-equivalent C-terminal fragments and that C1 generated through α-cleavage appears to be pathogenesis-averse.

Key words: α-cleavage, neurotoxicity, peptide modelling, prion protein (PrP), prion protein cleavage.

INTRODUCTION

Prion diseases are neurodegenerative disorders associated with accumulation of misfolded, typically protease-resistant, prion protein conformers (PrP^{res}), generated post-translationally through conversion of the normal cellular isoform of the protein (PrP^{C}) [1,2]. PrP^{C} can undergo either of two constitutive endoproteolytic events [3,4], termed α- and β-cleavage [5] (Figure 1). PrP^{C} α-cleavage results in fragments referred to as C1 and N1 [3,5,6]. C1 is the predominant C-terminal fragment found in healthy human brains [3,5,7,8] and numerous cultured cell lines [4,5,9–11], suggesting that α-cleavage is an important, evolutionarily conserved, biological event. Indeed, evidence supports a direct link between the α-cleavage of PrP^{C} and normal function [12–14], with increased C1 expression appearing to be protective against prion transmission [9,15]. PrP (prion protein) β-cleavage, occurring around residue 90, is also evident in normal brains, albeit at lower levels, yielding fragments known as C2 and N2 [3,5]. Overall, C2 approximates the primary sequence of the PK (proteinase K)-resistant core of PrP^{res} [16,17]. In contrast with C1, the C2 fragment is prominently increased in the brains of patients with CJD (Creutzfeldt–Jakob disease) [3,7], as well as in cell lines chronically infected with prions [18], with the majority of this fragment demonstrating reduced solubility in non-denaturing detergents and/or protease-resistance similar to PrP^{res}. However, it is uncertain how much of this biochemically altered C2 occurs through direct conversion of nascent α-helical C2 or via intracellular proteolytic N-terminal trimming of pre-formed unglycosylated and glycosylated PrP^{res}. Notwithstanding this uncertainty, cell-free systems [19], infected cell lines [20] and transgenic mouse models [21] have demonstrated that C2, in contrast with C1, can still serve as an efficient substrate for conversion by PrP^{res} into conformers approximating the protease-resistant core of PrP^{res}, PrP-(27–30). Overall, these observations suggest that β-cleavage may be an unfavourable processing event, especially in the setting of prion infection. Furthermore, studies of recombinant PrP fragments equating the C2 fragment support its potential to form neurotoxic conformers [22–24].

Therefore, collectively, evidence suggests that β-cleavage of PrP may be a potentially detrimental metabolic event, whereas α-cleavage appears to be more aligned to normal function and perhaps circumvents a pathogenic isoform. To test this hypothesis, we therefore investigated the possible differential consequences of endogenous α- and β-cleavage of PrP^{C}, by directly comparing the biophysical properties and neurotoxicity of recombinant hu (human) PrP-(112–231) (C1) and huPrP-(90–231) (C2). To corroborate and extend the recombinant peptide studies, our investigations also utilized synthetic peptides modelled on α- and β-cleavage of a pathogenic mutant form of PrP^{C} [Y145STOP (Tyr^{145}→stop)] associated with GSS (Gerstmann–Sträussler–Scheinker) syndrome [25]. We found huPrP-(112–231) could not be induced to fold into a β-sheet rich isoform that was neurotoxic. In contrast, huPrP-(90–231) readily adopted β-strand conformation, with thermostability comparable with

Abbreviations: Aβ, amyloid β-peptide; AD, Alzheimer's disease; CJD, Creutzfeldt–Jakob disease; D-PBS, Dulbecco's PBS; E14, embryonic day 14; ERK, extracellular-signal-regulated kinase; GSS, Gerstmann–Sträussler–Scheinker; hu, human; MRE, mean residual ellipticity; PK, proteinase K; PrP, prion protein; PrP^{C}, cellular PrP; PrP^{res}, protease-resistant PrP; SELDI–TOF, surface-enhanced laser-desorption/ionization–time-of-flight; ThT, Thioflavin-T.

[1] To whom correspondence should be addressed (email stevenjc@unimelb.edu.au).

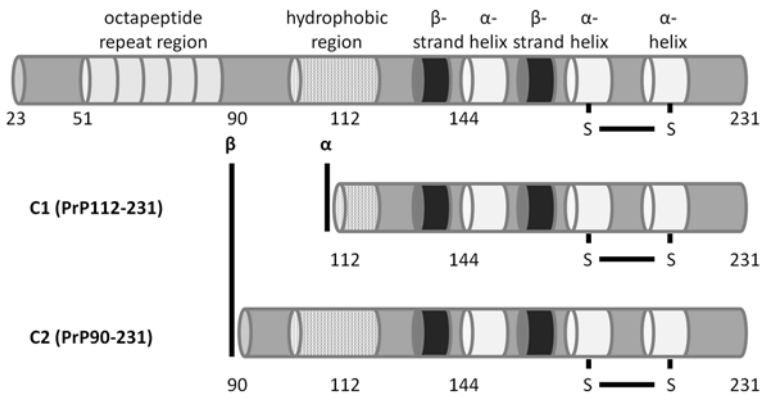

Figure 1 Schematic representation of endogenous PrP cleavage

As part of its normal metabolism, PrP undergoes proteolytic processing, described as α- and β-cleavage, resulting in characteristic N- and C-terminal fragments [5]. Depicted are the C-terminal fragments pertinent to the present study. PrP-(112–231) is equivalent to the C1 fragment following α-cleavage and PrP-(90–231) is equivalent to the C2 fragment following β-cleavage.

PrP^{res} [26], demonstrating structure-dependent neurotoxicity. Synthetic PrP peptides corroborated the differential toxicity observed for recombinant huPrP-(112–231) and huPrP-(90–231) and additionally suggested that persistence of soluble oligomeric β-sheet-rich PrP conformers was required for neurotoxicity.

EXPERIMENTAL

Recombinant PrP C1 and C2 fragments

Human C-terminal recombinant PrP peptides encompassing residues 90–231 [huPrP-(90–231)] and 112–231 [huPrP-(112–231)] were expressed and purified as described in detail previously [27]. Fresh recombinant protein working stock solutions were prepared by dissolving freeze-dried protein in ice-cold sterile Milli-Q water to 1–10 μg/μl and incubated on ice for 5 min. Unless specified otherwise, the peptide solution was then centrifuged at 13200 ***g*** for 5 min on a benchtop centrifuge (Eppendorf) at 4 °C, and the supernatant was kept on ice and used for experiments. The concentration was verified by UV absorbance spectrophotometry at 280 nm using the molar absorption coefficient values of 21890 $M^{-1} \cdot cm^{-1}$ for 90–231 and 16390 $M^{-1} \cdot cm^{-1}$ for 112–231, as calculated by ExPASY [28]. The proteins were adjusted to the desired final concentration by diluting with ice-cold Milli-Q water and 10× desired buffer.

Refolding of recombinant huPrP-(112–231) and huPrP-(90–231) into the β conformation using disulfide bond reduction and low pH

The refolding of recombinant huPrP by reduction of the disulfide bond in a low-pH acetate buffer has been described previously to yield high concentrations of a monomeric form of PrP rich in β-strand secondary structure [29]. This method was applied to HPLC-purified huPrP-(90–231) and huPrP-(112–231). The huPrP C-terminal fragment was reconstituted to 0.04 mg/ml in β-unfolding buffer (100 mM DTT, 10 mM sodium acetate, 10 mM Tris acetate and 6 M guanidinium chloride, pH 8) and incubated on a rocking platform or rotating wheel at room temperature (21 °C), unfolding overnight. The unfolded huPrP C-terminal fragment was then refolded through dialysis with β-PrP refolding buffer (1 mM DTT, 10 mM sodium acetate and 10 mM Tris acetate, pH 4). Typically, 50 ml of protein at 0.04 mg/ml was dialysed with four or five changes of refolding buffer (5 litres). The β-refolded protein was concentrated with Vivaspin® 20 spin columns, 5 kDa molecular-mass cut-off PES (polyethersulfone) (Sartorius), to 2 ml followed by centrifugation at 13200 ***g*** at 4 °C overnight in order to spin down precipitated material from soluble β-huPrP. Soluble β-huPrP was collected in the supernatant and the concentration was quantified with UV absorbance at 280 nm using the molar absorption coefficients noted above. CD spectroscopy was performed on refolded protein to verify conformation (described below).

CD spectroscopy

HuPrP peptide solutions were prepared as outlined above and diluted to 10 μM (recombinant) or 30 μM (synthetic PrP peptides) in 10 mM phosphate buffer (pH 7.4). Sample spectra were measured from 190 to 260 nm in 1 nm increments either immediately or after incubation for various times at 37 °C, employing 1-mm-pathlength quartz cuvettes (Starnez) in a Jasco J-810 spectropolarimeter. The baseline acquired in the absence of peptide was subtracted, and the resulting spectra were smoothed using a Fourier transform. The direct CD measurements (θ, in millidegrees) were converted into MRE (mean residual ellipticity), using the relationship $MRE = \theta/(10 \times c_R \times l)$, where c_R is the mean residue molar concentration and l is the pathlength.

Thermal stability experiments

Thermal stability experiments were performed at a protein concentration of 10 μM, following changes in ellipticity at 222 nm or 218 nm as a function of temperature. The heating rate was 1 °C/min. The measurements were performed using a Jasco J-810 spectropolarimeter equipped with a 1 mm water-jacketed cell and a computer-controlled water bath.

Proteinase K digestion

Samples (15 μl) of recombinant huPrP C-terminal fragment at 65 μM (146 pmol) or 13–16 μg were digested with 0.005–50 μg/ml PK (Invitrogen) for 60 min at 37 °C. The PK digest was stopped by the addition of Pefabloc SC (Roche) (final concentration of 3 mM). Samples were heated to 100 °C for 5 min in LDS (lithium dodecyl sulfate) sample buffer (Invitrogen) before electrophoresis in 12 % NuPAGE Bis-Tris gels (Invitrogen) at 200 V for 45 min (until the dye front reached the bottom) using MES running buffer (Invitrogen). Protein bands were stained using the rapid Coomassie Blue staining protocol [30].

Primary neuronal cultures

Primary cortical neuronal cultures were prepared as described previously under sterile conditions [31]. Briefly, cells from cerebral cortices of E14 (embryonic day 14) C57BL/6J×Sv129 or *Prnp*-ablated ($PrP^{-/-}$) (matched genetic background) mice were removed, dissected free of meninges and dissociated in 0.025 % trypsin (Sigma) in Krebs buffer (124 mM NaCl, 5.1 mM KCl, 1.0 mM $NaH_2PO_4 \cdot H_2O$, 14.4 mM D-glucose, 0.001 % Phenol Red, 25 mM Hepes, 0.3 % BSA and 2.6 mM $MgSO_4$, pH 7.4). Cortical neuronal cells were plated on to poly-D-lysine-coated (0.5 mg/ml) 48-well plates at a density of 150000 cells/well in plating medium. After 2 h, the plating medium was replaced with fresh Neurobasal™ medium containing B-27 supplements, gentamicin and 0.125 mM glutamine. After 6 days *in vitro*, the Neurobasal™ medium was replaced, containing B-27 minus antioxidants, gentamicin, 0.125 mM glutamine and 2.5 μg/ml cytosine arabinoside. This method resulted in cultures highly enriched for neurons (>95 % purity) with minimal astrocyte and microglial contamination [31]. All cultures were maintained in an incubator at 37 °C with 5 % CO_2. All tissue culture reagents were purchased from Invitrogen unless stated otherwise. All animal experiments were approved by the University of Melbourne Animal Ethics Committee and were in accordance with the National Health and Medical Research Council of Australia guidelines for animal experimentation.

Cell viability assays

Primary cerebral cortical neurons were allowed to mature for 6 days in culture before undergoing treatment. Freshly prepared recombinant or synthetic PrP peptide stock solutions were diluted to the final concentration in the cell culture medium. Primary neuronal cells were treated with either the recombinant or synthetic PrP peptides for 4 days. Cell survival was monitored by phase-contrast microscopy, and cell viability was quantified after 4 days using tetrazolium reduction with the Cell Counting Kit-8 (Dojindo Molecular Technologies) according to the manufacturer's instructions. Data were normalized and results are calculated as a percentage of vehicle control values. Data are shown as means ± S.E.M. Statistical comparisons between groups were performed using one-way ANOVA with Tukey's multiple comparison post-test (GraphPad Prism 4 statistical software).

Synthetic PrP peptides

Table 1 summarizes the peptides used: PrP-(111–144), PrP-(112–144) and PrP-(90–144). All peptides were chemically synthesized by the Bio21 Research Transfer Facility, Melbourne, Australia [32]. Purity and composition were verified by reverse-phase HPLC, MS and amino acid analysis. Accurate determination of amino acid content (excluding contaminating salts from synthesis) allowed the molar absorption coefficient of each peptide at 214 nm to be quantitatively determined (Table 1). All peptides studied were soluble in water and were dissolved in sterile Milli-Q water at 1 μg/μl, and then divided into suitable working aliquots followed by freeze-drying and storage at −80 °C until needed.

Preparation of PrP synthetic peptide stock solutions

Fresh synthetic peptide working stock solutions were prepared by dissolving freeze-dried peptide in ice-chilled sterile Milli-Q water to 1–10 μg/μl and sonicating in a cool water bath for 15 min. The peptide solution was then spun in a microcentrifuge for 5 min at maximum speed at 4 °C, and the supernatant was kept on ice and used in experiments. The concentration was verified by absorbance spectrophotometry at 214 nm using the molar absorption coefficient values (Table 1) determined by peptide mass and amino acid analysis (Auspep). The peptides were adjusted to the desired final concentration by diluting with ice-cold Milli-Q water and 10× D-PBS (Dulbecco's PBS) (Gibco). This method was adapted from Ciccotosto et al. [31] and is associated with increased peptide solubility and reproducibility between experiments.

Table 1 Synthetic PrP peptides used in the present study

Amino acid sequences (based on human) and molar absorption coefficients at 214 nm (see the Experimental section).

PrP peptide	Sequence	ε ($M^{-1} \cdot cm^{-1}$)
112–144	MAGAAAAGAVVGGLGGYMLGSAMSRPIIHFGSD	91400
111–144	HMAGAAAAGAVVGGLGGYMLGSAMSRPIIHFGSD	82000
90–144	GQGGGTHSQWNKPSKPKTNMKHMAGAAAAGAVVGG-LGGYMLGSAMSRPIIHFGSD	147400

Aggregation assays

Synthetic PrP peptides were prepared fresh, diluted to 30 μM in D-PBS with excess ThT (Thioflavin-T) (50 μM), and aggregation was monitored as described previously [33]. Samples were used immediately or incubated at 37 °C with agitation at 1200 rev./min until the aggregation reached a plateau. Aggregation was quantified at various time points using a PerkinElmer LS55 fluorescence spectrophotometer measuring fluorescence emission across a 1-cm-pathlength quartz cell at 480 nm when excited at 444 nm. To assay total aggregation, a discontinuous 90° light-scattering assay was used. Samples were measured in a quartz cell with a 1 cm pathlength. The ability of the solution to scatter light was quantified using a PerkinElmer LS55 fluorescence spectrophotometer employing an excitation wavelength of 300 nm and scanning the emission wavelengths from 580 to 620 nm. Maximum light scattering was observed and recorded at 600 nm.

Transmission electron microscopy

Carbon-coated grids (ProSciTech) were glow-discharged and aliquots from the end points of the aggregation assays described above were immediately spotted in the centre of the grids and incubated for 15 min. The grids were then washed twice with Milli-Q water and blotted dry to remove excess NaCl. The peptides were negatively stained with 0.5 % uranyl acetate by inverting the grid on a uranyl acetate droplet for 15 s followed by blotting off the excess. Images of the samples were taken using a Siemens ELMI-SKOP 102 electron microscope with a voltage of 60 kV (Bio21 Institute EM Facility).

SELDI–TOF-MS detection of PrP peptide oligomers

SELDI–TOF (surface-enhanced laser-desorption/ionization–time-of-flight)-MS was used to detect oligomers of synthetic PrP peptides using H50 ProteinChip arrays (Bio-Rad Laboratories), prepared as described previously [34]. In brief, arrays were washed twice with 5 μl of 10 mM phosphate buffer (pH 7.4) on a shaking table for 2 min. Phosphate buffer was then removed, and 10 μM peptide samples (prepared as described above) were

loaded on to the arrays and allowed to incubate for 5 min while shaking. Peptide samples were removed and arrays were washed twice with phosphate buffer (pH 7.4), followed by two 1 min washes with 1 mM Hepes (pH 7.2). The arrays were air-dried and 1 μl of 50 % (w/v) CHCA (α-cyano-4-hydroxycinnamic acid) matrix in 50 % (v/v) acetonitrile and 0.5 % TFA (trifluoroacetic acid) was applied twice to each array, which were air-dried between each application [35]. Arrays were then analysed by SELDI–TOF-MS, and resulting spectra were examined using ProteinChip software (version 3.2.1).

RESULTS

huPrP-(112–231) does not form a soluble β-sheet PK-resistant thermally stable isoform

We have established previously a protocol to generate huPrP of exact native sequence [27]. As reported previously, when reconstituted in phosphate buffer (pH 7.4), huPrP-(90–231) and huPrP-(112–231) adopt primarily α-helical secondary structure as determined by CD [27,29] (Figures 2A and 2E). α-Helical huPrP-(90–231) was first unfolded in a reducing buffer containing a high concentration of guanidine. Gradually, the reductant and guanidine were dialysed out, with pre-formed oligomers or aggregates removed through high-speed centrifugation overnight, yielding a soluble predominantly β-stranded secondary structure (Figure 2A) with β-huPrP-(90–231) displaying increased resistance to PK digestion (Figure 2B) and existing largely as a soluble monomer as described previously [29]. Thermal stability studies of β-huPrP-(90–231) revealed the novel finding that this recombinant isoform is very heat-stable, retaining β-strand structure at 90 °C (Figures 2C and 2D). Refolding of huPrP-(112–231) into a β-stranded structure has not been reported previously. The same protocol was applied to huPrP-(112–231), but, despite repeated attempts, notably, no soluble β-stranded isoform could be generated, with the protein predominantly remaining random coil (Figure 2E).

Structure-dependent toxicity of huPrP-(90–231)

huPrP-(90–231) and huPrP-(112–231), homologous with PrP C2 and C1 fragments respectively, in native α-helical conformation, were tested for toxicity by application to cultures of murine primary cortical neurons. Cortical neurons were prepared from E14 mice and allowed to mature for 6 days. The proteins were applied to the cultures and thereafter maintained for 4 days before cell survival was determined. Native α-helical huPrP-(112–231) and huPrP-(90–231) showed no toxicity towards cultures of cortical neurons (Figure 3A), with huPrP-(90–231) unexpectedly causing modest, but significantly increased, cell viability at 3 μM (Figure 3A). In contrast, soluble β-huPrP-(90–231) was found to be toxic to cultured cortical neurons from 1 μM (Figure 3B).

Insoluble huPrP-(112–231) and huPrP-(90–231) produced under reducing and acidic conditions are not toxic

The low-pH-reducing refolding protocol for recombinant PrP resulted in considerable loss of protein, which we estimate for huPrP-(90–231) to be approximately 80 % of the total protein forming an insoluble pellet. huPrP-(112–231) lost even more protein, which was estimated at approximately 98 % of the total protein. To assess the potential toxicity of the aggregated recombinant proteins under more physiological cellular conditions, the insoluble pellets were completely resuspended by mixing vigorously in phosphate buffer (pH 7.4). Acknowledging that PK-resistance generally correlates with β-strand structure, a change in secondary structure was investigated by determining the relative susceptibility to digestion by PK. No significant increase in PK-resistance was observed in the resuspended pellets of huPrP-(112–231) with only a modest increase observed for huPrP-(90–231) (Figure 4A) compared with soluble α-helical huPrP-(90–231) (Figure 2B). These findings suggest that resuspended insoluble huPrP-(90–231) may harbour a small amount of β-stranded structures, but resuspended insoluble huPrP-(112–231) appears unlikely to harbour any β-stranded structures, underscoring the relative resistance of huPrP-(112–231) to misfolding into soluble conformations with this secondary structure under the conditions we employed. Furthermore, insoluble huPrP-(90–231) and huPrP-(112–231), resuspended in phosphate buffer (pH 7.4), were not toxic to cultured primary neurons (Figure 4B).

Synthetic peptides based on α-and β-cleavage of PrP Y145STOP form random coil fresh in solution, but change to form β-strand secondary structure when incubated under physiological conditions

Numerous studies have been carried out employing synthetic PrP peptide segments to determine those region(s) of the protein critical for recognized biochemical and biological properties, including the neurotoxicity of misfolded disease-associated isoforms of the protein (reviewed in [36]). Arguably the most studied are peptides constituted by residues 106–126 (human sequence), with such studies demonstrating increased propensity to β-strand secondary structure, PK-resistance [37] and toxicity to PrP-expressing neuronal cultures [38,39], collectively emulating some properties of PrP^{res}.

In view of the significant insights gained from examining synthetic peptides based on human PrP, further characterization of the consequences of α- and β-cleavage of PrP^{C} were modelled using synthetic peptides based on the PrP Y145STOP mutation [25]. The peptides we studied equate to human PrP amino acid residues 112–144, 111–144 (representing α-cleavage) and 90–144 (representing β-cleavage) (Table 1). Two peptides representing α-cleavage were studied as it has been demonstrated previously from radio-sequencing that the C1 fragment N-termini begin at either His^{111} or Met^{112} [3], with His^{111} binding copper [40] and reportedly playing a role in governing structure [41,42]. Although the presence of peptides approximating PrP-(90–144) have been demonstrated previously in the presence of the Y145STOP mutation [43], to increase the relevance of our synthetic peptides, we verified the likely occurrence of α-cleavage (Supplementary Figure S1 at http://www.biochemj.org/bj/459/bj4590103add.htm).

CD spectroscopy was used to qualitatively determine secondary structure of each of the peptides. Freshly prepared peptides in phosphate buffer (pH 7.4) displayed a single minimum at ~200 nm, indicating predominantly random coil structure. Incubation of the synthetic peptides overnight at 37 °C caused a progressive change in secondary structure with a notable increase in a single minimum approximating 220 nm, suggesting an increase in β-strand structure. Incubation at 37 °C for extended periods also induced aggregation accounting for the reduced CD signal observed (Figure 5A).

Synthetic peptides based on α-and β-cleavage of PrP Y145STOP form amyloid fibrils with various kinetics

The self-aggregation capacity of the synthetic peptides was assessed by monitoring ThT fluorescence and light scattering over

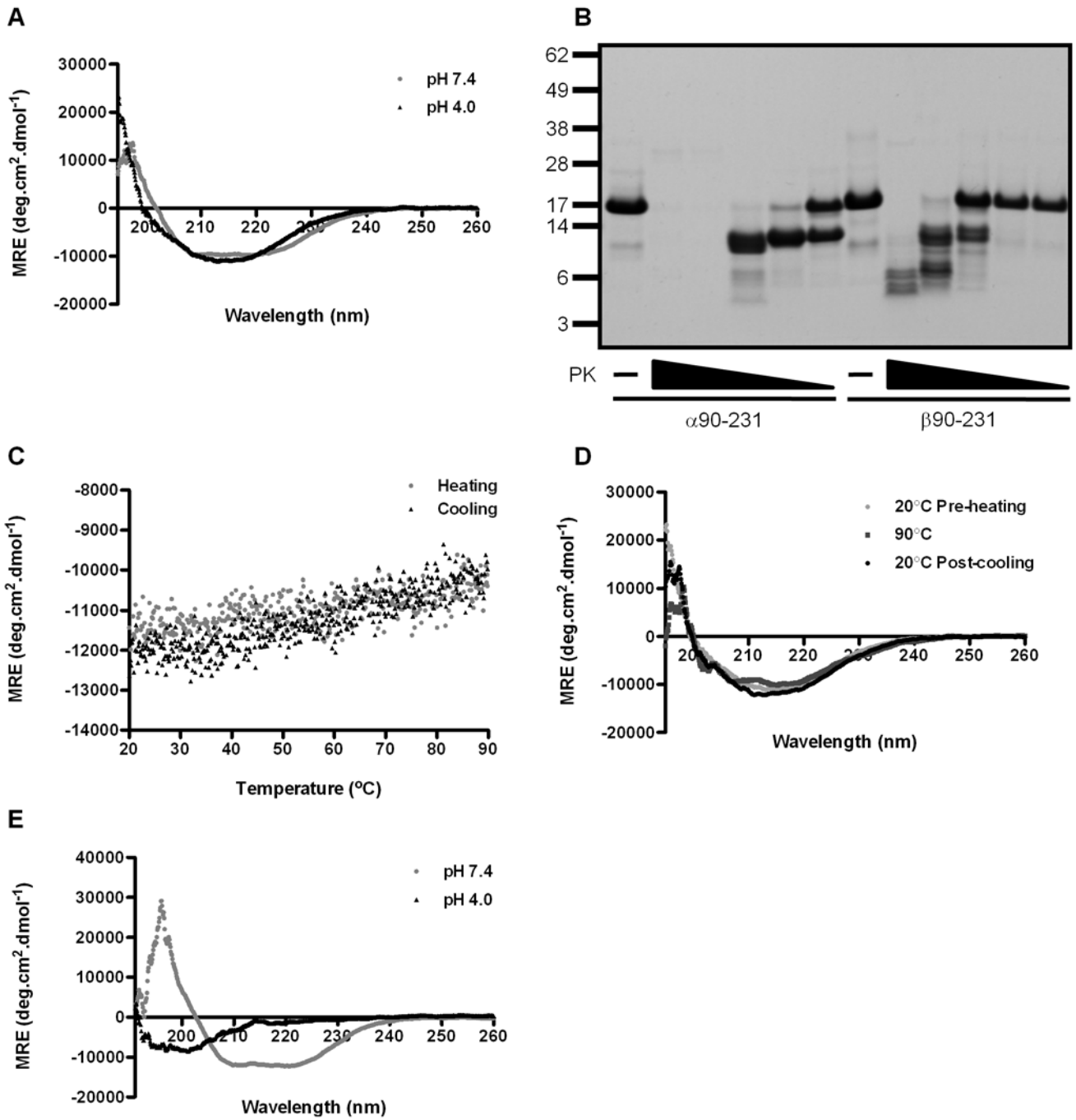

Figure 2 Biophysical properties of PrP-(90–231) and PrP-(112–231)

(**A**) Secondary structure of PrP-(90–231) in α-folded and β-folded isoforms. PrP-(90–231) (10 μM) oxidized in 10 mM phosphate buffer (pH 7.4) displays a typical predominant α-helical structure (grey). Reduced PrP-(90–231) in 1 mM DTT, 10 mM sodium acetate and 10 mM Tris acetate (pH 4) (black) displays a predominantly β-sheet structure with a single minimum at approximately 218 nm. (**B**) PK digestion of β-PrP-(90–231) and α-PrP-(90–231). Samples of 15 μg of α-PrP-(90–231) and β-PrP-(90–231) were incubated with PK at 0, 50, 5, 0.5, 0.05 or 0.005 μg/ml for 1 h at 37 °C. Digestion was halted with Pefabloc. α-PrP-(90–231) is completely digested by PK at 5 μg/ml and displays partial resistance from 0.5 μg/ml. β-PrP-(90–231) has partial PK-resistance from 50 μg/ml with most undigested at 5.0 μg/ml. Molecular masses are indicated in kDa. (**C**) Thermal stability of human recombinant β-PrP-(90–231). β-PrP-(90–231) was diluted to 10 μM. The fraction of molecules folded was determined by CD at 218 nm. The heating (grey) profile of β-PrP-(90–231) is superimposed with data for cooling (black). (**D**) Secondary structure of β-PrP-(90–231) before thermal melt at 20 °C (light grey), at 90 °C (dark grey) and post-thermal melt at 20 °C (black). Before thermal melt, at 90 °C, and after thermal melt (20 °C), β-PrP-(90–231) displays a predominantly β-sheet structure with a single minimum at approximately 218 nm. (**E**) Secondary structure of PrP-(112–231) under α-fold and β-fold buffer conditions. PrP-(112–231) oxidized in 10 mM phosphate buffer (pH 7.4) displays a typical predominant α-helical structure (grey). Reduced PrP-(112–231) in 1 mM DTT, 10 mM sodium acetate and 10 mM Tris acetate (pH 4.0) (black) displays predominantly random coil spectra, with a single minimum at approximately 195 nm.

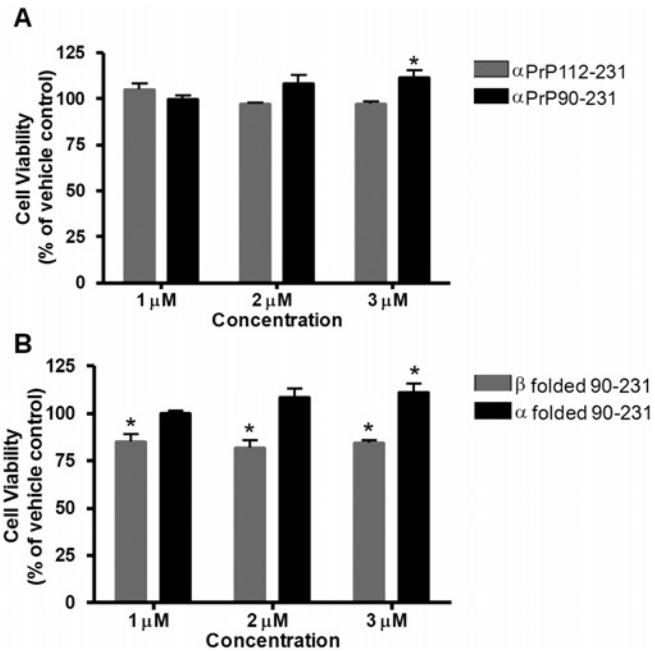

Figure 3 Effects of recombinant PrP C-terminal fragments on primary (E14) mouse cortical neuronal cultures

Cortical cells were plated in 48-well plates at a density of 1.5×10^5 cells/well and grown for 6 days before treatment. Each PrP fragment, i.e. 112–231 and 90–231 (α- or β-folded), was cleared of pre-formed aggregates, diluted to a stock solution in D-PBS and incubated directly on cell cultures for 96 h. Cell viability was determined using the Cell Counting Kit-8. (**A**) α-PrP-(112–231) and α-PrP-(90–231). (**B**) α-PrP-(90–231) and β-PrP-(90–231). Results are means $\pm$ S.E.M. ($n = 3$, in triplicate). Differences were compared with and normalized to vehicle controls. $^*P < 0.05$ compared with control group using two-way ANOVA with Bonferroni post-test correction.

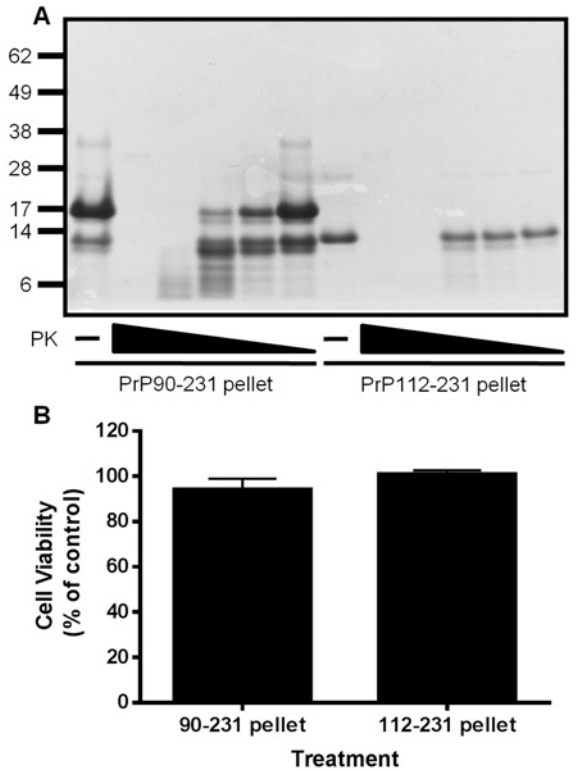

Figure 4 Insoluble huPrP-(112–231) and huPrP-(90–231) produced under reducing and acidic conditions

(**A**) Coomassie Blue-stained gels of resuspended pellets, produced under reducing low-pH refolding conditions, of PrP-(90–231) and PrP-(112–231), after digestion with PK at various concentrations. Pellets of 16 μg of PrP-(90–231) (146 pmol) and 13 μg of PrP-(112–231) (146 pmol) were incubated with PK at 0, 50, 5, 0.5, 0.05 or 0.005 μg/ml for 1 h at 37 °C. Digestion was halted with Pefabloc. Molecular masses are indicated in kDa. (**B**) Resuspended pellets generated using a reducing low-pH refolding protocol of PrP-(90–231) and PrP-(112–231) are not toxic to primary embryonic (E14) mouse cortical cultures grown for 6 days *in vitro* followed by 96 h of direct treatment. Results are means $\pm$ S.E.M. ($n = 3$, in triplicate). Differences were compared with and normalized to vehicle controls. No significant difference was found by two-way ANOVA with Bonferroni post-test correction.

time. An increase in ThT fluorescence indicates the formation of β-strand-rich amyloidogenic structures, whereas an increase in light scattering indicates the formation of macromolecular structures, either amyloid fibrils or amorphous aggregates. Each peptide was prepared fresh in D-PBS (pH 7.4), incubated with excess ThT at 37 °C and fluorescence, and light scatter were measured over time until the signal reached a plateau (Figure 5B and Supplementary Figure S2 at http://www.biochemj.org/bj/459/bj4590103add.htm). Lag times were calculated by averaging the first time point greater than 10 % normalized ThT fluorescence. The aggregation kinetics of PrP-(112–144) and PrP-(111–144) were rapid, with ThT fluorescence reaching a plateau in less than 60 and 120 min, with mean lag times of 20 and 82 min, respectively (Table 2). This was in contrast with PrP-(90–144) which, comparatively, aggregated at a significantly lower rate, reaching a fluorescence maximum within 500 min (Figure 5B) with a mean lag time of 240 min (Table 2). All experiments showed concordance between light-scatter kinetics and ThT fluorescence, indicating a low likelihood of amorphous aggregates. To confirm that the peptides were indeed forming fibrils, the aggregates were analysed further by TEM (Figure 5C). At time points when each of the peptides displayed a high ThT signal, the TEM images show that all peptides readily formed amyloid fibrils, albeit with differences in morphology observed.

Table 2 Comparison of lag times to aggregation for α-and β-cleavage PrP Y145STOP peptides

Delay times were calculated by extrapolating the aggregation curve down to zero absorbance at the first time point greater than 10 % normalized ThT fluorescence. Results are means $\pm$ S.D. ($n = 3$–5). Statistical significance was determined by ANOVA.

(a)

PrP peptide	Average lag time (min)
112–144	20 ± 7
111–144	82 ± 62
90–144	240 ± 60

(b)

Statistical comparison	*P* value
112–144 with 111–144	>0.05
112–144 with 90–144	<0.001
111–144 with 90–144	<0.01

SELDI–TOF-MS analyses of synthetic peptides based on α- and β-cleavage PrP Y145STOP

The aggregation kinetic assays combined with TEM analyses of the α- and β-cleavage of PrP Y145STOP demonstrated that PrP-(112–144) and PrP-(111–144) aggregate rapidly into amyloid fibrils, and it is plausible most of the available soluble peptides concatenate rapidly to form fibrils. PrP-(90–144), in contrast, aggregates more slowly and it is therefore reasonable to consider

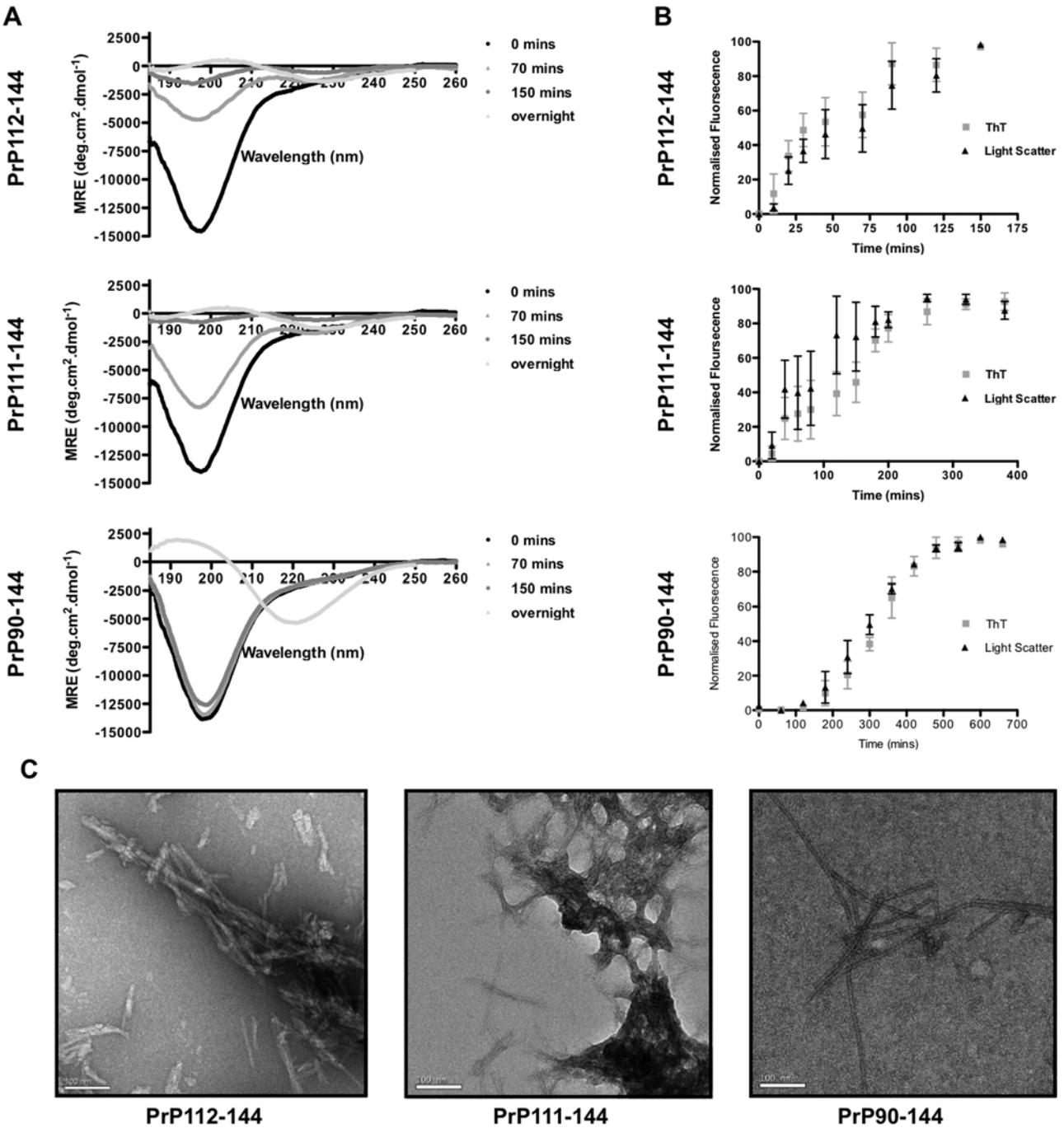

Figure 5 Biophysical properties and TEM of PrP-(112–144), PrP-(111–144) and PrP-(90–144)

(**A**) CD analysis of PrP-(112–144), PrP-(111–144) and PrP-(90–144) peptides (30 μM) in 10 mM phosphate buffer (pH 7.4) at 37 °C. Sample spectra were measured from 185 to 260 nm in 1 nm increments in 1-mm-pathlength quartz cuvettes. (**B**) Aggregation kinetics of PrP peptides (30 μM) in D-PBS and 50 μM ThT at 37 °C with agitation at 1200 rev./min. Aggregation was measured at various time points in a 1-cm-pathlength quartz cell. Results are means $\pm$ S.E.M. ($n = 3$–5). (**C**) TEM of aggregated PrP peptides (30 μM in D-PBS and 50 μM ThT) on glow-discharged carbon-coated grids. The images confirm fibril formation of PrP-(112–144), PrP-(111–144) and PrP-(90–144) peptides.

that perhaps less of the total peptide concentration is channelled directly into amyloid fibrils. To investigate this further, SELDI–TOF-MS was utilized. SELDI–TOF-MS can detect monomers and oligomers on the basis of their differential molecular masses, a technique used previously to characterize Aβ (amyloid β-peptide) glycine-substituted-to-leucine peptides [34]. As with Aβ, the α- and β-cleavage PrP Y145STOP peptides studied are hydrophobic and could therefore directly interact with the carbon molecules on the surface of an H50 Protein Chip array.

In addition to the monomer, a dimeric species was found in equal abundance in a fresh solution of PrP-(90–144), as well as comparatively smaller peaks consistent with trimers and tetramers (Figure 6). PrP-(112–144) and PrP-(111–144) also briefly displayed dimeric species, although in much lower abundance compared with their monomeric peaks. No higher-order oligomeric species were observed for PrP-(112–144) and PrP-(111–144) (Figure 6). When the peptides were incubated at 37 °C for 24 h, the relative monomeric peak of PrP-(90–144)

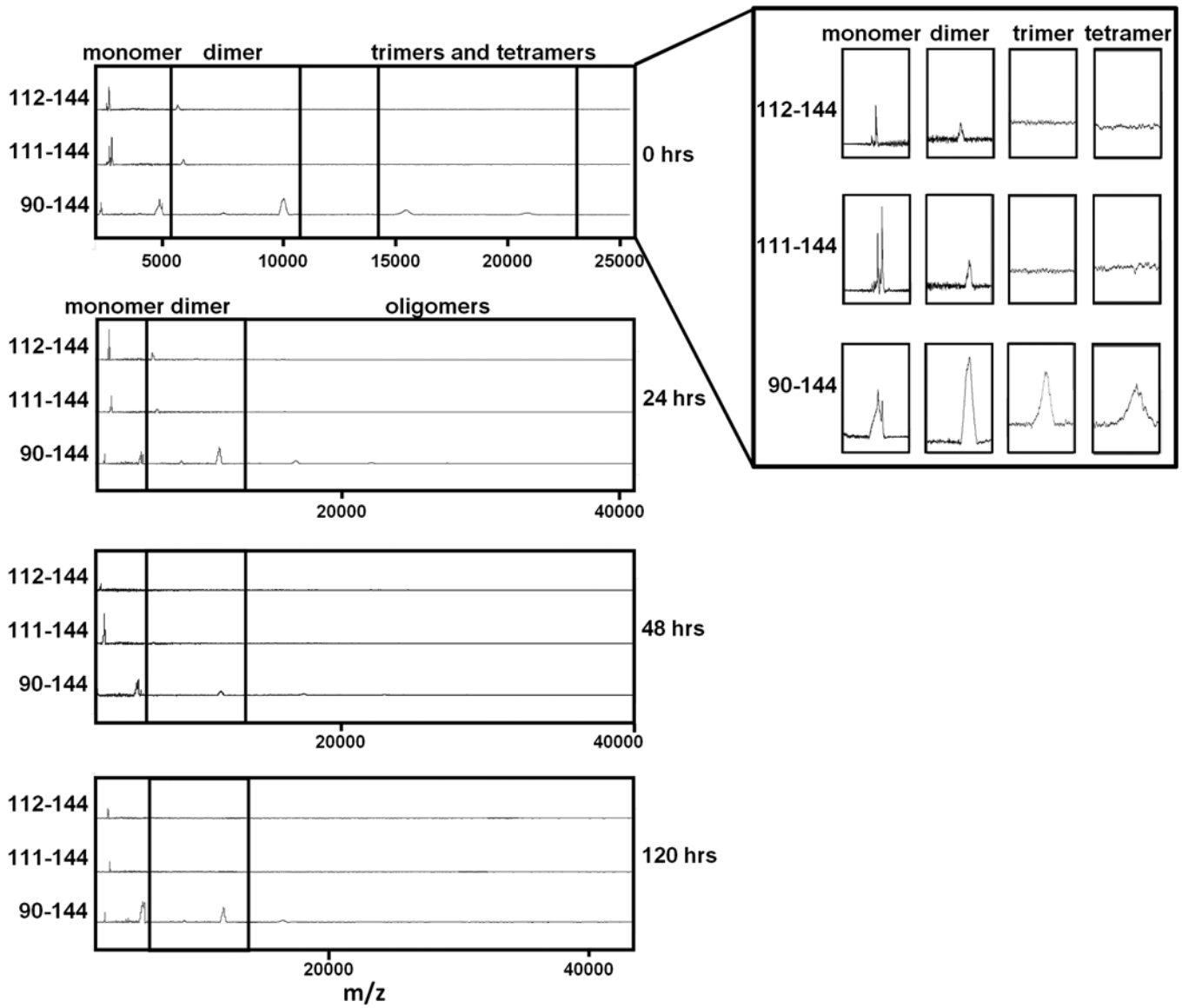

Figure 6 SELDI–TOF-MS profiles of PrP-(112–144), PrP-(111–144) and PrP-(90–144) peptides (10 μM) in 10 mM phosphate buffer on H50 arrays over time

PrP peptides were loaded on spots coated with 10 mM phosphate buffer (pH 7.4) alone and incubated for 5 min. Spots were washed to remove non-specifically bound components. CHAPS was applied to each spot and arrays were subsequently subjected to SELDI–TOF-MS. Analysis of resulting spectra revealed that all PrP peptides form dimers immediately; however, PrP-(90–144) also forms trimers and tetramers, and the oligomers remain for up to 72 h. Inset: SELDI–TOF-MS profiles of PrP peptides on H50 arrays at zero time. Spectra reveal that all PrP peptides form dimers immediately; however, PrP-(90–144) also forms trimers and tetramers.

decreased in intensity in contrast with that of the dimer. The oligomeric peaks observed when PrP-(90–144) was fresh also decreased in intensity. In contrast, no change in the MS profile was observed with PrP-(112–144) and PrP-(111–144) at 24 h. With increased time, only a monomeric species was observed in the spectra of PrP-(112–144) and PrP-(111–144). In contrast, the spectrum of PrP-(90–144) still showed an abundant dimer peak relative to the monomeric peak after 120 h, with trimer still present until 120 h, whereas tetramer was detectable for 72 h. This result, in combination with the aggregation kinetic assays and TEM data, suggest that PrP-(112–144) and PrP-(111–144) aggregate so rapidly that the relative concentrations of smaller soluble oligomers present in solution is extremely low, whereas PrP-(90–144) aggregates more slowly and consequently has a higher steady-state concentration and persistence of soluble oligomers. These oligomeric species found with PrP-(90–144) may relate directly to the consistent toxicity detected for this peptide (Figure 7C).

Synthetic peptides based on α-cleavage and β-cleavage of PrP Y145STOP demonstrate differential neurotoxicity similar to that observed for huPrP-(112–231) and huPrP-(90–231)

The biological activity of the α- and β-cleavage peptides based on the PrP Y145STOP mutant was investigated using mouse primary cortical neurons. It is noteworthy that the β-cleavage peptide PrP-(90–144) retains the entire 106–126 sequence shown previously to be neurotoxic [38,39]. Conversely, in the α-cleavage peptides PrP-(112–144) and PrP-(111–144), the 106–126 sequence is

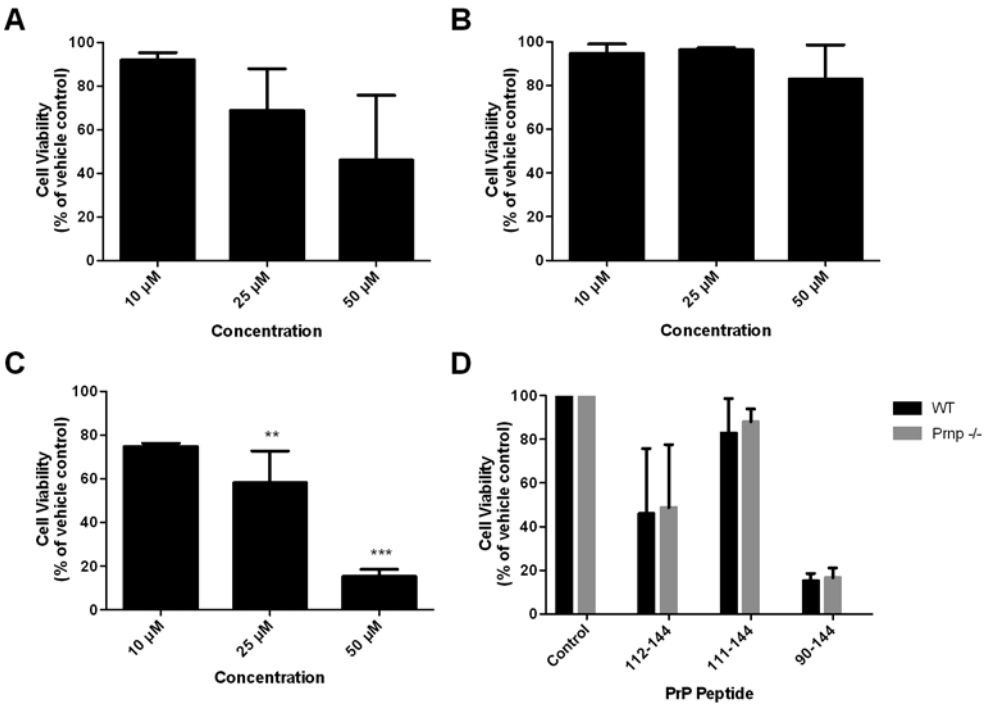

Figure 7 Effects of PrP-(112–144), PrP-(111–144) and PrP-(90–144) peptides on primary (E14) mouse cortical neuronal cultures

Cortical cells from wild-type mice (**A**–**C**) were plated in 48-well plates at a density of 1.5×10^5 cells/well and grown for 6 days before treatment. Each peptide [112–144 (**A**), 111–144 (**B**) and 90–144 (**C**)] was cleared of pre-formed aggregates, diluted to a stock solution in D-PBS and incubated directly with cell cultures for 96 h. Cell viability was determined using the Cell Counting Kit-8. Differences compared and normalized to vehicle controls. Results are means $\pm$ S.E.M. ($n=3$, in triplicate) $^{**}P<0.05$, $^{***}P<0.01$ by one-way ANOVA with Tukey's multiple comparison test; post-test for linear trend. (**D**) Effects of PrP-(112–144), PrP-(111–144) and PrP-(90–144) peptides (50 μM in D-PBS) on primary (E14) mouse cortical neuron survival from wild-type and $PrP^{-/-}$ mice. Results are means $\pm$ S.E.M. ($n=3$, in triplicate). Differences were compared between $PrP^{-/-}$ and wild-type cortical neuron viability. No significant differences were seen. Two-way ANOVA Bonferroni post-test correction.

disrupted, prompting speculation that these peptides may be less toxic. Treatment of murine E14 primary cortical neuronal cultures with PrP-(90–144) demonstrated dose-dependent neurotoxicity, significant from 25 μM (Figure 7C). Each concentration of PrP-(112–144) assessed did not show significant toxicity to cultured primary cortical neurons; however, decreasing cell viability was seen with increasing peptide concentrations. This linear trend was significant, suggesting that the peptide does have modest, less consistent, effects on cell viability in a dose-dependent manner (Figure 7A). PrP-(111–144), with an N-terminal histidine residue rather than methionine, did not demonstrate any significant compromise of cell viability, including with post-ANOVA trend analysis (Figure 7B).

The mechanism of PrP-(106–126) peptide toxicity has been reported to be dependent on PrP expression [37,38,44], but not invariably [45]. To investigate whether any biological effect exhibited by PrP-(112–144) and PrP-(90–144) also depends on PrP expression, E14 primary cortical cultures from genetically matched $PrP^{-/-}$ mouse embryos were treated with the peptides. At each concentration of PrP-(112–144), PrP-(111–144) and PrP-(90–144) tested, no significant difference was observed between treated $PrP^{-/-}$ and WT cortical neuronal viability (treatment at 50 μM shown in Figure 7D).

DISCUSSION

Determining the biological significance of constitutive endoproteolytic processing of PrP^C, especially in relation to prion disease pathogenesis, is an important goal. Investigations in the present study were on the basis of the overarching hypothesis that the two apparently mutually exclusive processing events (α- or β-cleavage) are not equivalent in their inherent pathogenic predispositions. This hypothesis was formulated from a number of observations, which include that the C1 fragment is the predominant C-terminal fragment found in healthy human brains [3,5,7,8] and numerous cultured cell lines [4,5,9–11] with the C2 fragment prominently increased in the brains of patients with CJD [3,7], as well as in cell lines chronically infected with prions [18]. We have compared directly the biophysical and neurotoxic properties of C-terminal fragments generated from alternative processing events, thereby extending the observations of previous studies and further strengthening the argument that α- and β-cleavage of PrP^C generate biophysically and biologically non-equivalent C-terminal fragments that harbour different pathogenic implications for host cells, with α-cleavage appearing more favourable and the likelihood that C2 generated through β-cleavage may contribute directly to prion pathogenesis.

We found cognate peptides of PrP, modelled on endogenous processing, have differences in their susceptibility to form neurotoxic species. This is broadly similar to what is recognized in relation to APP (amyloid precursor protein) processing in AD (Alzheimer's disease), wherein α- and β-cleavage prevents or conserves respectively the occurrence of a pathogenic peptide, Aβ, central to the pathogenesis of AD [46]. huPrP-(90–231) readily adopted a β-stranded conformation under reducing and acidic conditions, importantly displaying properties reminiscent of PrP^{res}, particularly enhanced protease-resistance as shown previously [29], and, remarkable heat-stability, further highlighting that β-folded recombinant huPrP-(90–231) correlates well with

the protease-resistant core of PrP^{res} [26]. Soluble β-huPrP-(90–231), in contrast with α-huPrP-(90–231), was toxic to cultured primary cortical neurons at very low micromolar concentrations. The low concentrations required for toxicity enhance the likely relevance of β-PrP-(90–231) to pathogenesis. We observed no dose-dependent toxicity over the narrow concentration range explored. Absence of a dose–response toxicity curve for β-PrP-(90–231) has been observed before with recombinant Syrian hamster PrP-(90–231) applied to rat PC12 cells [24]. Interestingly, in this study, higher doses restored viability [24]. The reason for our lack of dose–response toxicity is uncertain, but could relate to either a ceiling effect in relation to toxicity, which occurs at low micromolar concentrations, or existence of a substantially broader dynamic range than explored requiring much greater increments in concentration or absolute amounts of β-PrP-(90–231) to achieve commensurate increases in toxicity; examination of the latter was precluded by insolubility at higher concentrations of β-PrP-(90–231). A broader dose-dependent dynamic range for toxicity was observed with the synthetic PrP peptides studied, albeit requiring higher concentrations up to 50 μM for maximal toxicity. Other studies using synthetic PrP peptides have also reported that toxicity is only observed at higher concentrations, such as 100 μM [38,39,47], prompting concerns regarding physiological relevance.

Congruent with previous studies assessing PrP-(90–231) toxicity, the ability of PrP-(90–231) to cause cell death correlated with its secondary structure [22,23,48–50]. Distinct from huPrP-(90–231), huPrP-(112–231) could not be manipulated to adopt a soluble β-strand structure under the conditions we employed, but rather remained predominantly random coil. Discrepant with our findings, another group has reported His-tagged murine PrP-(113–231) folds into a β-stranded intermediate at pH 3.9 [51]. Different refolding methods were employed, and notably the recombinant fragment analysed was not the exact native sequence as we have studied. Predominant C1 expression has been shown to be protective against prion transmission in cell line and transgenic mouse models [9,15], with our studies reinforcing these previous observations wherein α-cleavage generates a fragment serving as a suboptimal substrate for misfolding into PrP^{res}-like neurotoxic conformers, in contrast with β-cleavage, where C2 has been demonstrated in cell-free systems [19], infected cell lines [20] and transgenic mouse models [21] to serve as a relatively efficient substrate for conversion by PrP^{res} into conformers approximating PrP-(27–30) [52].

Previous studies have reported the toxicity of thermally refolded β-PrP-(90–231), inducing SH-SY5Y cell death by promoting activation of pro-apoptotic cascades, p38 MAPK (mitogen-activated protein kinase) and caspase 3 [22,49], interestingly through the unbalancing of ERK1/2 (extracellular-signal-regulated kinase 1/2) and p38 activities [48]. PrP^{C} has a postulated neurotrophic role (reviewed in [53]). Unexpectedly, in our neurotoxicity model, we found that α-PrP-(90–231) significantly increased neuronal cell survival at low micromolar concentrations, whereas, in contrast, α-huPrP-(112–231) did not. Preliminary observations have found α-huPrP-(90–231) activates ERK (V. A. Johanssen, unpublished work) alluding to the possibility of a signalling function for the fragment and we therefore cannot exclude the possibility that β-cleavage of PrP^{C} could occur as a compensatory response to mitigate cell stress, including from prion infection [12], but the present results emphasize the need for this to be tightly constrained in the cell to forestall inadvertent misfolding into a potentially neurotoxic conformer.

A large loss of protein due to aggregation occurred using the low pH/reducing β-refolding protocol. Investigations of the insoluble pellets of both proteins, however, did not reveal a 'PrP^{res}'-like aggregate, as their PK-resistance was much the same as that of α-huPrP-(90–231) and quite different from soluble β-huPrP-(90–231). Importantly, the resuspended insoluble pellet of both protein fragments was not toxic to cultured neurons, discounting a toxic conformer of huPrP-(112–231) coming out of solution in the refolding process, and supporting further the predominant correlation of toxicity with soluble β-strand-rich conformers. The non-toxic solubilized pellets of huPrP-(90–231) and huPrP-(112–231) demonstrated that aggregates of PrP are likely to represent benign 'junk', rather than toxic species, and offer further support for the lack of toxic predisposition of α-cleaved PrP^{C}, with huPrP-(112–231) under the conditions we employed appearing to largely bypass or avoid a soluble toxic β-strand rich conformation along its aggregation pathway. To explore this hypothesis further, our additional studies utilized synthetic PrP peptides modelled on endogenous processing in the context of the nonsense Y145STOP mutation found in a single case of GSS syndrome [25]. Enhancing the relevance of our choice of synthetic peptides, parallel cell biological studies as part of our research endeavours validated that both α- and β-cleavage of Y145STOP PrP are likely to occur (Supplementary Figure S1).

In good agreement with the recombinant PrP fragment studies, PrP-(90–144) was found to be quite toxic to cultured primary neurons, notably contrasting with the toxicity observed in relation to the synthetic α-cleavage peptides. A modest concentration-dependent decline in primary neuronal viability was observed for PrP-(112–144), suggesting that His^{111}, which has been found to govern the structure of PrP-(106–126) [44], also has an impact on biological activity. Other synthetic PrP peptides similar to PrP-(112–144) and PrP-(111–144), albeit truncated at the C-terminus, for example PrP-(112–126) [resembling α-cleaved PrP-(106–126)] were found to be more toxic to cultured cerebellar neurons than PrP-(106–126) [54]. Furthermore, another peptide, PrP-(113–126) (lacking Met^{112}) was toxic to neurons although less toxic than PrP-(112–126) [54]. Although our data and those from previous reports do not provide a clear explanation, these observations collectively suggest that Met^{112} at the N-terminus as a consequence of α-like cleavage generates a peptide more likely to harbour modest neurotoxicity perhaps unrelated to soluble β-strand-rich oligomeric species.

Biophysical characterization of our synthetic peptides revealed that toxicity of PrP-(90–144) correlated with the presence of a soluble β-strand-rich structure, but, arguably more importantly, correlated with the presence of longer-lasting or stable oligomeric species, such as dimers, trimers and tetramers. These observations broadly align with previous studies of PrP, in which it has been postulated that, during the aggregation of PrP, toxic oligomers are also generated [47,55–58]. Similar evidence has been found for other peptides associated with neurodegeneration, in particular Aβ, wherein SELDI–TOF-MS and other techniques have been employed to delineate putative toxic oligomeric species [34,59–61]. In our studies, accelerated aggregation rates of the synthetic peptides corresponded with reduced detection of small oligomers, as seen with PrP-(112–144) and PrP-(111–144). The populations of PrP-(90–144) oligomers, however, appeared to be reasonably stable, present for up to 120 h when a small trimer peak was still visible. These data, along with the CD spectra and aggregation analyses, suggests that PrP-(112–144) and PrP-(111–144) form fibrils very rapidly, appearing to largely bypass sizeable pools of stable soluble β-strand-rich oligomers, which are potentially significantly neurotoxic, an observation analogous to our inability to generate toxic soluble β-strand-rich huPrP-(112–231) conformers. In contrast, PrP-(90–144), with slower aggregation kinetics, established a longer-lasting equilibrium

with various oligomeric species. Hence there appears to be a correlation between a sustained population of soluble β-strand-rich conformers, which may include small oligomeric species, and neuronal toxicity. In support of this, PrP-(106–126) and PrP-(82–146) toxicity is partially rescued when these peptides are pre-incubated with a β-strand-rich oligomer specific antibody [47,62]. Additionally, different transgenic mouse models with a fatal neurodegenerative phenotype correlate with small oligomeric species [63,64] and evidence has been provided indicating that the most infectious prions are constituted by small oligomeric PrP species [65,66]. The present study demonstrates that differential processing of the parent protein offers cognate peptides of various toxic predisposition, mainly determined by their ability to form a soluble β-strand-rich isoform.

Conclusions

Consistently employing a direct comparative approach to highlight potential differences in biophysical properties and neurotoxic predilections of C-terminal fragments consequent to α- and β-cleavage of PrP^C was an integral component of our methodology. As such, the principal aim of our experimental design has served to unify a number of previous studies assessing individual peptides broadly recapitulating either C1 or C2 [22,23,48–51,67]. In addition, acknowledging the significant influence that even a small number of additional amino acids can have on protein or peptide behaviour, such as $A\beta_{40}$ compared with $A\beta_{42}$ [68,69], another intended positive attribute of the present study was the utilization of recombinant peptides of exact primary sequence when assessing the biophysical and biological properties of C-terminal fragments modelled on α- and β-cleavage of PrP^C [27]. Future studies of interest would include investigations into what contributions there may be, if any, from other post-translational modifications of PrP C-terminal fragments such as glycosylation and the presence of a glycosylphosphatidylinositol anchor.

We have demonstrated that the C-terminal fragments generated through alternative α- and β-cleavage of PrP^C appear to harbour different pathogenic potential for host cells, particularly in the setting of prion infection. Most significantly, α-cleavage produces a C-terminal fragment that is resistant to folding into soluble β-strand-rich toxic isoforms. In contrast, β-cleavage produces a fragment with greater vulnerability to misfolding into soluble β-strand-rich toxic conformers. Consequently, the present study contributes further support for the proposition that strategies to promote α-cleavage may be a useful approach for the treatment prion disease.

AUTHOR CONTRIBUTION

Vanessa Johanssen conducted the experimental work, performed data analyses, contributed to the concepts and design of the work and wrote the paper. Timothy Johanssen contributed primary neuronal cultures and expertise. Colin Masters provided a critical revision of the paper for important intellectual content. Andrew Hill and Kevin Barnham contributed to the concepts and design of the work, equipment, materials, analysed results and provided a critical revision of the paper for important intellectual content. Steven Collins contributed the original and ongoing concepts for the design of the study, provided equipment and materials, managed the project, analysed the results and co-wrote the paper.

FUNDING

This work was supported by grants from the National Health and Medical Research Council [grant numbers 400202 and 400183] and the Bethlehem Griffiths Research Foundation [grant number 802270].

REFERENCES

1 Borchelt, D. R., Taraboulos, A. and Prusiner, S. B. (1992) Evidence for synthesis of scrapie prion proteins in the endocytic pathway. J. Biol. Chem. **267**, 16188–16199
2 Caughey, B. and Raymond, G. J. (1991) The scrapie-associated form of PrP is made from a cell surface precursor that is both protease- and phospholipase-sensitive. J. Biol. Chem. **266**, 18217–18223
3 Chen, S. G., Teplow, D. B., Parchi, P., Teller, J. K., Gambetti, P. and Autilio-Gambetti, L. (1995) Truncated forms of the human prion protein in normal brain and in prion diseases. J. Biol. Chem. **270**, 19173–19180
4 Harris, D. A., Huber, M. T., van Dijken, P., Shyng, S. L., Chait, B. T. and Wang, R. (1993) Processing of a cellular prion protein: identification of N- and C-terminal cleavage sites. Biochemistry **32**, 1009–1016
5 Mangé, A., Béranger, F., Peoc'h, K., Onodera, T., Frobert, Y. and Lehmann, S. (2004) Alpha- and beta- cleavages of the amino-terminus of the cellular prion protein. Biol. Cell **96**, 125–132
6 Vincent, B., Paitel, E., Frobert, Y., Lehmann, S., Grassi, J. and Checler, F. (2000) Phorbol ester-regulated cleavage of normal prion protein in HEK293 human cells and murine neurons. J. Biol. Chem. **275**, 35612–35616
7 Jimenez-Huete, A., Lievens, P. M. J., Vidal, R., Piccardo, P., Ghetti, B., Tagliavini, F., Frangione, B. and Prelli, F. (1998) Endogenous proteolytic cleavage of normal and disease-associated isoforms of the human prion protein in neural and non-neural tissues. Am. J. Pathol. **153**, 1561–1572
8 Laffont-Proust, I., Faucheux, B. A., Hassig, R., Sazdovitch, V., Simon, S., Grassi, J., Hauw, J. J., Moya, K. L. and Haik, S. (2005) The N-terminal cleavage of cellular prion protein in the human brain. FEBS Lett. **579**, 6333–6337
9 Lewis, V., Hill, A. F., Haigh, C. L., Klug, G. M., Masters, C. L., Lawson, V. A. and Collins, S. J. (2009) Increased proportions of C1 truncated prion protein protect against cellular M1000 prion infection. J. Neuropathol. Exp. Neurol. **68**, 1125–1135
10 Walmsley, A. R., Watt, N. T., Taylor, D. R., Perera, W. S. and Hooper, N. M. (2009) α-Cleavage of the prion protein occurs in a late compartment of the secretory pathway and is independent of lipid rafts. Mol. Cell. Neurosci. **40**, 242–248
11 Watt, N. T., Taylor, D. R., Gillott, A., Thomas, D. A., Perera, W. S. and Hooper, N. M. (2005) Reactive oxygen species-mediated β-cleavage of the prion protein in the cellular response to oxidative stress. J. Biol. Chem. **280**, 35914–35921
12 Haigh, C. L., Lewis, V. A., Vella, L. J., Masters, C. L., Hill, A. F., Lawson, V. A. and Collins, S. J. (2009) PrPC-related signal transduction is influenced by copper, membrane integrity and the α cleavage site. Cell Res. **19**, 1062–1078
13 Sunyach, C., Cisse, M. A., da Costa, C. A., Vincent, B. and Checler, F. (2007) The C-terminal products of cellular prion protein processing, C1 and C2, exert distinct influence on p53-dependent staurosporine-induced caspase-3 activation. J. Biol. Chem. **282**, 1956–1963
14 Bremer, J., Baumann, F., Tiberi, C., Wessig, C., Fischer, H., Schwarz, P., Steele, A. D., Toyka, K. V., Nave, K. A., Weis, J. and Aguzzi, A. (2010) Axonal prion protein is required for peripheral myelin maintenance. Nat. Neurosci. **13**, 310–318
15 Westergard, L., Turnbaugh, J. A. and Harris, D. A. (2011) A naturally occurring C-terminal fragment of the prion protein (PrP) delays disease and acts as a dominant-negative inhibitor of PrP^{Sc} formation. J. Biol. Chem. **286**, 44234–44242
16 Meyer, R. K., McKinley, M. P., Bowman, K. A., Braunfeld, M. B., Barry, R. A. and Prusiner, S. B. (1986) Separation and properties of cellular and scrapie prion proteins. Proc. Natl. Acad. Sci. U.S.A. **83**, 2310–2314
17 Pan, K. M., Stahl, N. and Prusiner, S. B. (1992) Purification and properties of the cellular prion protein from Syrian hamster brain. Protein Sci. **1**, 1343–1352
18 Yadavalli, R., Guttmann, R. P., Seward, T., Centers, A. P., Williamson, R. A. and Telling, G. C. (2004) Calpain-dependent endoproteolytic cleavage of PrP^{Sc} modulates scrapie prion propagation. J. Biol. Chem. **279**, 21948–21956
19 Lawson, V. A., Priola, S. A., Wehrly, K. and Chesebro, B. (2001) N-terminal truncation of prion protein affects both formation and conformation of abnormal protease-resistant prion protein generated *in vitro*. J. Biol. Chem. **276**, 35265–35271
20 Rogers, M., Yehiely, F., Scott, M. and Prusiner, S. B. (1993) Conversion of truncated and elongated prion proteins into the scrapie isoform in cultured cells. Proc. Natl. Acad. Sci. U.S.A. **90**, 3182–3186
21 Fischer, M., Rulicke, T., Raeber, A., Sailer, A., Moser, M., Oesch, B., Brandner, S., Aguzzi, A. and Weissmann, C. (1996) Prion protein (PrP) with amino-proximal deletions restoring susceptibility of PrP knockout mice to scrapie. EMBO J. **15**, 1255–1264
22 Corsaro, A., Paludi, D., Villa, V., D'Arrigo, C., Chiovitti, K., Thellung, S., Russo, C., Di Cola, D., Ballerini, P., Patrone, E. et al. (2006) Conformation dependent pro-apoptotic activity of the recombinant human prion protein fragment 90–231. Int. J. Immunopathol. Pharmacol. **19**, 339–356

23 Thellung, S., Gatta, E., Pellistri, F., Corsaro, A., Villa, V., Vassalli, M., Robello, M. and Florio, T. (2012) Excitotoxicity through NMDA receptors mediates cerebellar granule neuron apoptosis induced by prion protein 90–231 fragment. Neurotox. Res. **23**, 301–314

24 Kazlauskaite, J., Young, A., Gardner, C. E., Macpherson, J. V., Venien-Bryan, C. and Pinheiro, T. J. (2005) An unusual soluble β-turn-rich conformation of prion is involved in fibril formation and toxic to neuronal cells. Biochem. Biophys. Res. Commun. **328**, 292–305

25 Kitamoto, T., Iizuka, R. and Tateishi, J. (1993) An amber mutation of prion protein in Gerstmann–Straussler syndrome with mutant PrP plaques. Biochem. Biophys. Res. Commun. **192**, 525–531

26 Safar, J., Roller, P. P., Gajdusek, D. C. and Gibbs, Jr, C. J. (1993) Thermal stability and conformational transitions of scrapie amyloid (prion) protein correlate with infectivity. Protein Sci. **2**, 2206–2216

27 Johanssen, V. A., Barnham, K. J., Masters, C. L., Hill, A. F. and Collins, S. J. (2012) Generating recombinant C-terminal prion protein fragments of exact native sequence. Neurochem. Int. **60**, 318–326

28 Gill, S. C. and von Hippel, P. H. (1989) Calculation of protein extinction coefficients from amino acid sequence data. Anal. Biochem. **182**, 319–326

29 Jackson, G. S., Hosszu, L. L., Power, A., Hill, A. F., Kenney, J., Saibil, H., Craven, C. J., Waltho, J. P., Clarke, A. R. and Collinge, J. (1999) Reversible conversion of monomeric human prion protein between native and fibrilogenic conformations. Science **283**, 1935–1937

30 Simpson, R. J. (2010) Rapid Coomassie Blue staining of protein gels. Cold Spring Harb. Protoc. **2010**, pdb.prot5413

31 Ciccotosto, G. D., Tew, D., Curtain, C. C., Smith, D., Carrington, D., Masters, C. L., Bush, A. I., Cherny, R. A., Cappai, R. and Barnham, K. J. (2004) Enhanced toxicity and cellular binding of a modified amyloid β peptide with a methionine to valine substitution. J. Biol. Chem. **279**, 42528–42534

32 Karas, J. A., Boland, M., Haigh, C., Johanssen, V., Hill, A., Barnham, K., Collins, S. and Scanlon, D. (2012) Microwave synthesis of prion protein fragments up to 111 amino acids in length generates biologically active peptides. Int. J. Pept. Res. Ther. **18**, 21–29

33 Smith, D. P., Ciccotosto, G. D., Tew, D. J., Fodero-Tavoletti, M. T., Johanssen, T., Masters, C. L., Barnham, K. J. and Cappai, R. (2007) Concentration dependent Cu^{2+} induced aggregation and dityrosine formation of the Alzheimer's disease amyloid-β peptide. Biochemistry **46**, 2881–2891

34 Hung, L. W., Ciccotosto, G. D., Giannakis, E., Tew, D. J., Perez, K., Masters, C. L., Cappai, R., Wade, J. D. and Barnham, K. J. (2008) Amyloid-β peptide (Aβ) neurotoxicity is modulated by the rate of peptide aggregation: Aβ dimers and trimers correlate with neurotoxicity. J. Neurosci. **28**, 11950–11958

35 Guerreiro, N., Gomez-Mancilla, B. and Charmont, S. (2006) Optimization and evaluation of surface-enhanced laser-desorption/ionization time-of-flight mass spectrometry for protein profiling of cerebrospinal fluid. Proteome Sci. **4**, 7

36 Wall, V. A. and Collins, S. J. (2011) Pathogenic insights from biophysical and biological studies on cognate prion protein peptides. In The Cellular and Molecular Biology of Prion Disease (Collins, S. J. and Lawson, V. A., eds), Research Signpost, Trivandrum

37 Tagliavini, F., Prelli, F., Verga, L., Giaccone, G., Sarma, R., Gorevic, P., Ghetti, B., Passerini, F., Ghibaudi, E., Forloni, G. et al. (1993) Synthetic peptides homologous to prion protein residues 106–147 form amyloid-like fibrils *in vitro*. Proc. Natl. Acad. Sci. U.S.A. **90**, 9678–9682

38 Brown, D. R., Schmidt, B. and Kretzschmar, H. A. (1996) Role of microglia and host prion protein in neurotoxicity of a prion protein fragment. Nature **380**, 345–347

39 Forloni, G., Angeretti, N., Chiesa, R., Monzani, E., Salmona, M., Bugiani, O. and Tagliavini, F. (1993) Neurotoxicity of a prion protein fragment. Nature **362**, 543–546

40 Jackson, G. S., Murray, I., Hosszu, L. L., Gibbs, N., Waltho, J. P., Clarke, A. R. and Collinge, J. (2001) Location and properties of metal-binding sites on the human prion protein. Proc. Natl. Acad. Sci. U.S.A. **98**, 8531–8535

41 Jones, C. E., Abdelraheim, S. R., Brown, D. R. and Viles, J. H. (2004) Preferential Cu^{2+} coordination by His^{96} and His^{111} induces β-sheet formation in the unstructured amyloidogenic region of the prion protein. J. Biol. Chem. **279**, 32018–32027

42 Ragg, E., Tagliavini, F., Malesani, P., Monticelli, L., Bugiani, O., Forloni, G. and Salmona, M. (1999) Determination of solution conformations of PrP106–126, a neurotoxic fragment of prion protein, by ^{1}H NMR and restrained molecular dynamics. Eur. J. Biochem. **266**, 1192–1201

43 Ghetti, B., Piccardo, P., Spillantini, M. G., Ichimiya, Y., Porro, M., Perini, F., Kitamoto, T., Tateishi, J., Seiler, C., Frangione, B. et al. (1996) Vascular variant of prion protein cerebral amyloidosis with tau-positive neurofibrillary tangles: the phenotype of the stop codon 145 mutation in PRNP. Proc. Natl. Acad. Sci. U.S.A. **93**, 744–748

44 Jobling, M. F., Stewart, L. R., White, A. R., McLean, C., Friedhuber, A., Maher, F., Beyreuther, K., Masters, C. L., Barrow, C. J., Collins, S. J. and Cappai, R. (1999) The hydrophobic core sequence modulates the neurotoxic and secondary structure properties of the prion peptide 106–126. J. Neurochem. **73**, 1557–1565

45 Dupiereux, I., Zorzi, W., Rachidi, W., Zorzi, D., Pierard, O., Lhereux, B., Heinen, E. and Elmoualij, B. (2006) Study on the toxic mechanism of prion protein peptide 106–126 in neuronal and non neuronal cells. J. Neurosci. Res. **84**, 637–646

46 Esch, F. S., Keim, P. S., Beattie, E. C., Blacher, R. W., Culwell, A. R., Oltersdorf, T., McClure, D. and Ward, P. J. (1990) Cleavage of amyloid β peptide during constitutive processing of its precursor. Science **248**, 1122–1124

47 Fioriti, L., Angeretti, N., Colombo, L., De Luigi, A., Colombo, A., Manzoni, C., Morbin, M., Tagliavini, F., Salmona, M., Chiesa, R. and Forloni, G. (2007) Neurotoxic and gliotrophic activity of a synthetic peptide homologous to Gerstmann–Straussler–Scheinker disease amyloid protein. J. Neurosci. **27**, 1576–1583

48 Corsaro, A., Thellung, S., Chiovitti, K., Villa, V., Simi, A., Raggi, F., Paludi, D., Russo, C., Aceto, A. and Florio, T. (2009) Dual modulation of ERK1/2 and p38 MAP kinase activities induced by minocycline reverses the neurotoxic effects of the prion protein fragment 90–231. Neurotox. Res. **15**, 138–154

49 Chiovitti, K., Corsaro, A., Thellung, S., Villa, V., Paludi, D., D'Arrigo, C., Russo, C., Perico, A., Ianieri, A., Di Cola, D. et al. (2007) Intracellular accumulation of a mild-denatured monomer of the human PrP fragment 90–231, as possible mechanism of its neurotoxic effects. J. Neurochem. **103**, 2597–2609

50 Thellung, S., Corsaro, A., Villa, V., Simi, A., Vella, S., Pagano, A. and Florio, T. (2011) Human PrP90–231-induced cell death is associated with intracellular accumulation of insoluble and protease-resistant macroaggregates and lysosomal dysfunction. Cell Death Dis. **2**, e138

51 O'Sullivan, D. B., Jones, C. E., Abdelraheim, S. R., Thompsett, A. R., Brazier, M. W., Toms, H., Brown, D. R. and Viles, J. H. (2007) NMR characterization of the pH 4 β-intermediate of the prion protein: the N-terminal half of the protein remains unstructured and retains a high degree of flexibility. Biochem. J. **401**, 533–540

52 Safar, J., Roller, P. P., Gajdusek, D. C. and Gibbs, C. J., Jr. (1993) Conformational transitions, dissociation, and unfolding of scrapie amyloid (prion) protein. J. Biol. Chem. **268**, 20276–20284

53 Martins, V. R., Beraldo, F. H., Hajj, G. N., Lopes, M. H., Lee, K. S., Prado, M. M. and Linden, R. (2010) Prion protein: orchestrating neurotrophic activities. Curr. Issues Mol. Biol. **12**, 63–86

54 Brown, D. R. (2000) Prion protein peptides: optimal toxicity and peptide blockade of toxicity. Mol. Cell. Neurosci. **15**, 66–78

55 Gobbi, M., Colombo, L., Morbin, M., Mazzoleni, G., Accardo, E., Vanoni, M., Del Favero, E., Cantu, L., Kirschner, D. A., Manzoni, C. et al. (2006) Gerstmann–Straussler–Scheinker disease amyloid protein polymerizes according to the "dock-and-lock" model. J. Biol. Chem. **281**, 843–849

56 Novitskaya, V., Bocharova, O. V., Bronstein, I. and Baskakov, I. V. (2006) Amyloid fibrils of mammalian prion protein are highly toxic to cultured cells and primary neurons. J. Biol. Chem. **281**, 13828–13836

57 Rezaei, H., Eghiaian, F., Perez, J., Doublet, B., Choiset, Y., Haertle, T. and Grosclaude, J. (2005) Sequential generation of two structurally distinct ovine prion protein soluble oligomers displaying different biochemical reactivities. J. Mol. Biol. **347**, 665–679

58 Simoneau, S., Rezaei, H., Sales, N., Kaiser-Schulz, G., Lefebvre-Roque, M., Vidal, C., Fournier, J. G., Comte, J., Wopfner, F., Grosclaude, J. et al. (2007) *In vitro* and *in vivo* neurotoxicity of prion protein oligomers. PLoS Pathog. **3**, e125

59 Lesne, S., Koh, M. T., Kotilinek, L., Kayed, R., Glabe, C. G., Yang, A., Gallagher, M. and Ashe, K. H. (2006) A specific amyloid-β protein assembly in the brain impairs memory. Nature **440**, 352–357

60 Walsh, D. M., Lomakin, A., Benedek, G. B., Condron, M. M. and Teplow, D. B. (1997) Amyloid β-protein fibrillogenesis: detection of a protofibrillar intermediate. J. Biol. Chem. **272**, 22364–22372

61 Hartley, D. M., Walsh, D. M., Ye, C. P., Diehl, T., Vasquez, S., Vassilev, P. M., Teplow, D. B. and Selkoe, D. J. (1999) Protofibrillar intermediates of amyloid β-protein induce acute electrophysiological changes and progressive neurotoxicity in cortical neurons. J. Neurosci. **19**, 8876–8884

62 Kayed, R., Head, E., Thompson, J. L., McIntire, T. M., Milton, S. C., Cotman, C. W. and Glabe, C. G. (2003) Common structure of soluble amyloid oligomers implies common mechanism of pathogenesis. Science **300**, 486–489

63 Chiesa, R., Piccardo, P., Ghetti, B. and Harris, D. A. (1998) Neurological illness in transgenic mice expressing a prion protein with an insertional mutation. Neuron **21**, 1339–1351

64 Nazor, K. E., Kuhn, F., Seward, T., Green, M., Zwald, D., Purro, M., Schmid, J., Biffiger, K., Power, A. M., Oesch, B. et al. (2005) Immunodetection of disease-associated mutant PrP, which accelerates disease in GSS transgenic mice. EMBO J. **24**, 2472–2480
65 Tixador, P., Herzog, L., Reine, F., Jaumain, E., Chapuis, J., Le Dur, A., Laude, H. and Beringue, V. (2010) The physical relationship between infectivity and prion protein aggregates is strain-dependent. PLoS Pathog. **6**, e1000859
66 Silveira, J. R., Raymond, G. J., Hughson, A. G., Race, R. E., Sim, V. L., Hayes, S. F. and Caughey, B. (2005) The most infectious prion protein particles. Nature **437**, 257–261

Received 17 October 2013/23 December 2013; accepted 20 January 2014
Published as BJ Immediate Publication 20 January 2014, doi:10.1042/BJ20131378

67 Daniels, M., Cereghetti, G. M. and Brown, D. R. (2001) Toxicity of novel C-terminal prion protein fragments and peptides harbouring disease-related C-terminal mutations. Eur. J. Biochem. **268**, 6155–6164
68 Klein, A. M., Kowall, N. W. and Ferrante, R. J. (1999) Neurotoxicity and oxidative damage of β amyloid 1–42 versus β amyloid 1–40 in the mouse cerebral cortex. Ann. N.Y. Acad. Sci. **893**, 314–320
69 Shin, R. W., Ogino, K., Kondo, A., Saido, T. C., Trojanowski, J. Q., Kitamoto, T. and Tateishi, J. (1997) Amyloid β-protein (Aβ) 1–40 but not Aβ1–42 contributes to the experimental formation of Alzheimer disease amyloid fibrils in rat brain. J. Neurosci. **17**, 8187–8193

Biochem. J. (2014) **459**, 103–115 (Printed in Great Britain) doi:10.1042/BJ20131378

online data

SUPPLEMENTARY ONLINE DATA

C-terminal peptides modelling constitutive PrP^{C} processing demonstrate ameliorated toxicity predisposition consequent to α-cleavage

Vanessa A. JOHANSSEN*†‡, Timothy JOHANSSEN*‡§, Colin L. MASTERS§, Andrew F. HILL†‡§, Kevin J. BARNHAM*‡§ and Steven J. COLLINS*§[1]

*Department of Pathology, University of Melbourne, Parkville, VIC 3010, Australia
†Department of Biochemistry and Molecular Biology, University of Melbourne, Parkville, VIC 3010, Australia
‡Bio21 Molecular Science and Biotechnology Institute, University of Melbourne, Parkville, VIC 3010, Australia
§Mental Health Research Institute, University of Melbourne, Parkville, VIC 3010, Australia

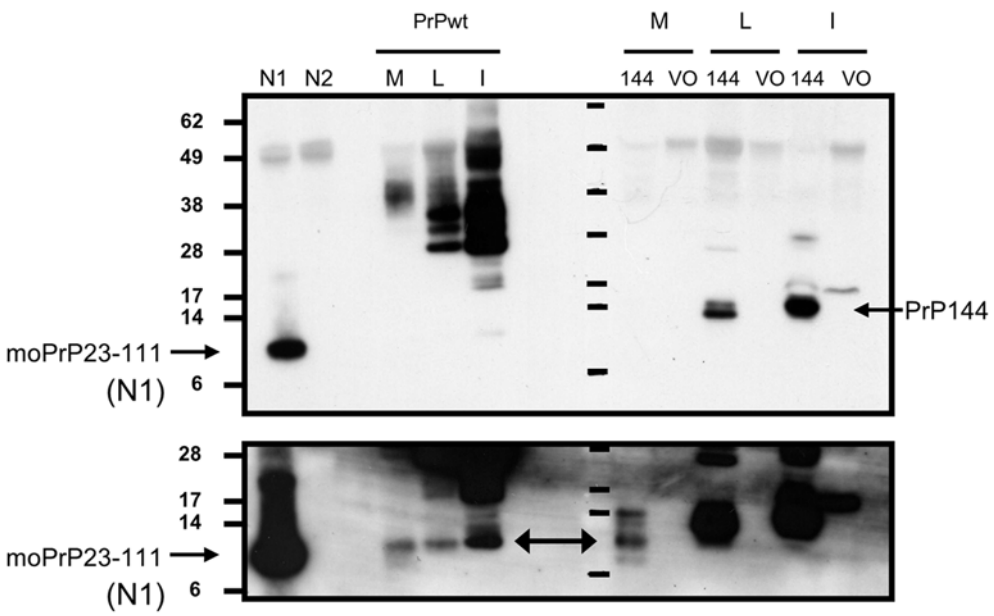

Figure S1 Immunodetection of a fragment equivalent to N1 from RK13 cells expressing mouse PrP W144STOP (Trp^{144}→stop)

To investigate the possibility of α-cleavage occurring within the mutant protein, transiently transfected wild-type mouse PrP (wt), mutant mouse PrP W144STOP (144) and vector only (VO) RK13 cells were harvested after 72 h. The conditioned media, lysate and insoluble proteins were immunoprecipitated by incubating with the polyclonal antibody, 03R19.2 [1] and Dynabeads® Protein A (Invitrogen) overnight. Dynabeads were then isolated and boiled in SDS sample buffer, and proteins were separated on a Bis-Tris NuPAGE gel followed by Western blot analysis using 03R19.2 to detect PrP protein fragments; (**A**) 10 s exposure, (**B**) 5 min exposure. The double-headed arrow in (**B**) denotes a PrP band with immunoreactivity and electrophoretic mobility indicating it to be N1, as has been characterized previously in wt PrP-expressing cells [2]. SDS/PAGE and Western blot analysis revealed low levels of a fragment from the conditioned media (M) and soluble cell lysate (L) of PrP W144STOP transiently transfected cells, which migrated at approximately 9 kDa and ran equivalent to synthetic PrP-(23–111) (used as a positive control) and a fragment observed in wt PrP cells, indicating the N1 fragment derived from α-cleavage. Molecular masses are indicated in kDa.

[1] To whom correspondence should be addressed (email stevenjc@unimelb.edu.au).

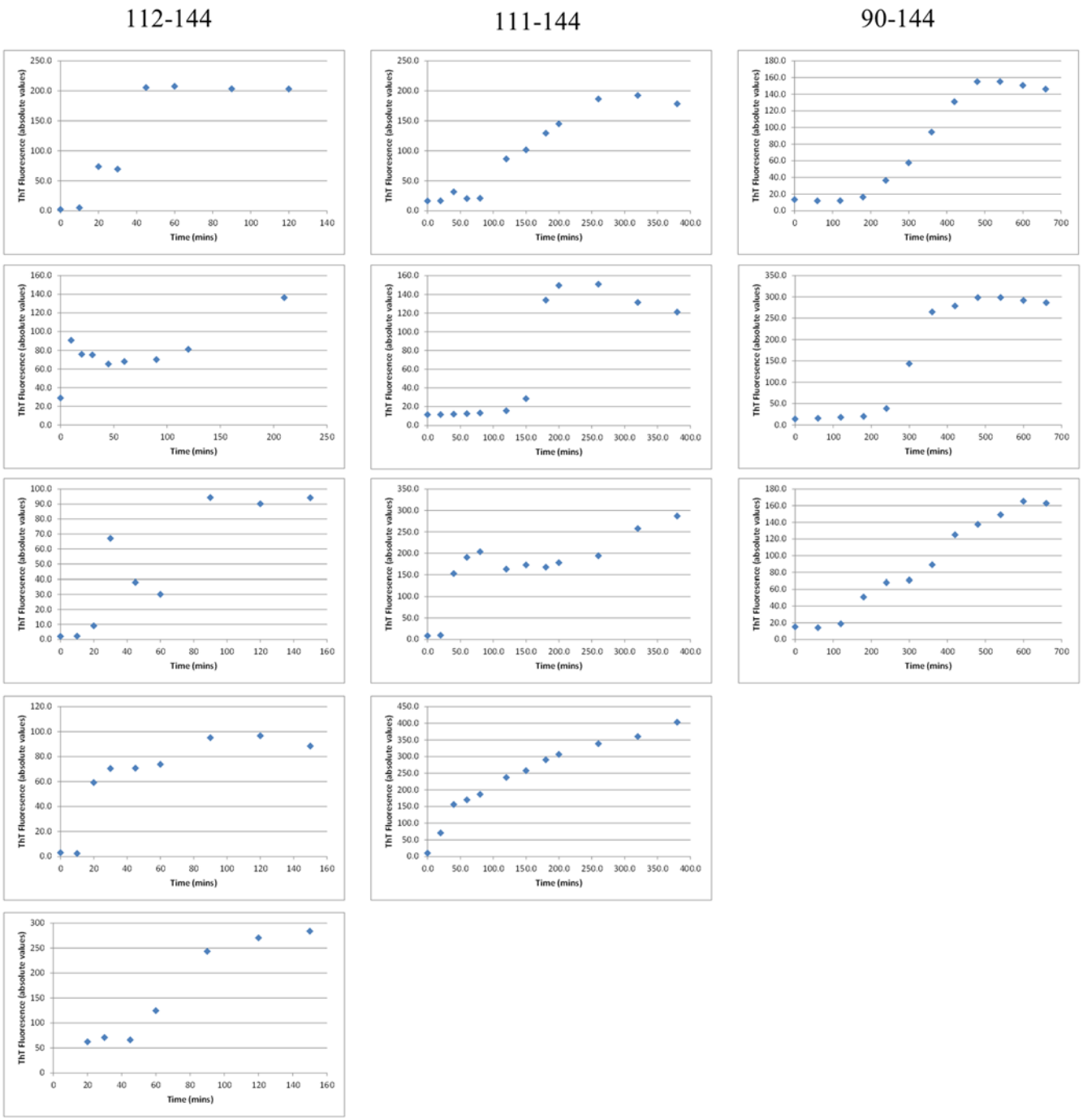

Figure S2 Aggregation kinetics of PrP peptides: individual experiments

Each peptide was cleared from pre-formed aggregates, diluted to 30 μM in D-PBS and incubated at 37 °C with constant agitation (1200 rev./min) with excess ThT (50 μM). Amyloid fibril formation was determined by ThT fluorescence (excitation at 444 nm and emission at 480 nm) in a fluorescence spectrophotometer using a 1-cm-pathlength quartz cell.

REFERENCES

1 Lawson, V. A., Vella, L. J., Stewart, J. D., Sharples, R. A., Klemm, H., Machalek, D. M., Masters, C. L., Cappai, R., Collins, S. J. and Hill, A. F. (2008) Mouse-adapted sporadic human Creutzfeldt–Jakob disease prions propagate in cell culture. Int. J. Biochem. Cell Biol. **40**, 2793–2801

2 Cisse, M. A., Sunyach, C., Lefranc-Jullien, S., Postina, R., Vincent, B. and Checler, F. (2005) The disintegrin ADAM9 indirectly contributes to the physiological processing of cellular prion by modulating ADAM10 activity. J. Biol. Chem. **280**, 40624–40631

Received 17 October 2013/23 December 2013; accepted 20 January 2014
Published as BJ Immediate Publication 20 January 2014, doi:10.1042/BJ20131378

Article

Neutron Reflectometry Studies Define Prion Protein N-terminal Peptide Membrane Binding

Anton P. Le Brun,[1] Cathryn L. Haigh,[2] Simon C. Drew,[3] Michael James,[1,4] Martin P. Boland,[2] and Steven J. Collins[2,*]

[1]Bragg Institute, Australian Nuclear Science and Technology Organisation, New Illawarra Road, Lucas Heights, New South Wales, 2234, Australia; [2]Department of Pathology, Kenneth Myer Building, The University of Melbourne, Victoria, 3010, Australia; [3]Florey Department of Neuroscience and Mental Health, The University of Melbourne, Victoria, 3010, Australia; and [4]School of Chemistry, University of New South Wales, Kensington, New South Wales, 2052, Australia

ABSTRACT The prion protein (PrP), widely recognized to misfold into the causative agent of the transmissible spongiform encephalopathies, has previously been shown to bind to lipid membranes with binding influenced by both membrane composition and pH. Aside from the misfolding events associated with prion pathogenesis, PrP can undergo various posttranslational modifications, including internal cleavage events. Alpha- and beta-cleavage of PrP produces two N-terminal fragments, N1 and N2, respectively, which interact specifically with negatively charged phospholipids at low pH. Our previous work probing N1 and N2 interactions with supported bilayers raised the possibility that the peptides could insert deeply with minimal disruption. In the current study we aimed to refine the binding parameters of these peptides with lipid bilayers. To this end, we used neutron reflectometry to define the structural details of this interaction in combination with quartz crystal microbalance interrogation. Neutron reflectometry confirmed that peptides equivalent to N1 and N2 insert into the interstitial space between the phospholipid headgroups but do not penetrate into the acyl tail region. In accord with our previous studies, interaction was stronger for the N1 fragment than for the N2, with more peptide bound per lipid. Neutron reflectometry analysis also detected lengthening of the lipid acyl tails, with a concurrent decrease in lipid area. This was most evident for the N1 peptide and suggests an induction of increased lipid order in the absence of phase transition. These observations stand in clear contrast to the findings of analogous studies of Ab and α-synuclein and thereby support the possibility of a functional role for such N-terminal fragment-membrane interactions.

INTRODUCTION

Transmissible spongiform encephalopathies (TSEs) or prion diseases are fatal neurodegenerative diseases affecting humans and animals. Misfolded conformers of the prion protein (PrP^{Sc}) are widely recognized as the causative agent of TSEs with expression of wildtype or cellular prion protein (PrP^{C}) indispensable for disease transmission and pathogenesis (1,2). During disease the predominantly alpha-helical PrP^{C} becomes misfolded into beta-sheet-rich conformers that can template further misfolding of PrP^{C} resulting in propagation of pathogenic PrP^{Sc}.

The misfolding process has been replicated in vitro utilizing recombinant PrP (rPrP), and the development of a serial protein misfolding amplification assay (PMCA) has made production of misfolded rPrP highly efficient (3). However, initial experiments with misfolded rPrP could only generate a transmissible prion species if the PMCA reaction was "seeded" with infectious PrP^{Sc} taken from a disease source (4). Such observations raised questions over the potential role for cellular cofactors in PrP^{Sc} propagation. Various anionic species have been suggested as cofactors in the production of infectious prions; these have included nucleic acids, glycosaminoglycans, and lipids (reviewed in (5,6)). In the first study to report use of the PMCA to produce genuinely infectious (transmissible in animal bioassay) rPrP species in the absence of an infectious disease-derived seed, a combination of 1-palmitoyl-2-oleoyl-*sn*-glycero-3-[phospho-*rac*-(1-glycerol)] (POPG) and nucleic acid cofactors were required (7). In addition to the inclusion of pure phospholipid species in misfolding reactions, synthetic membranes of mixed lipid composition have also been employed to mimic rPrP binding to cellular structures. These studies have demonstrated the affinity of rPrP for lipids, with binding invariably influenced by lipid composition, metal ion binding, and pH (8–10) and often resulting in structural changes to rPrP that might predispose it to or initiate misfolding (9–12).

Phospholipid-PrP binding interactions may have a wider significance beyond protein misfolding. Although a "normal" PrP^{C} function is still undetermined, suggestions

Submitted July 7, 2014, and accepted for publication September 19, 2014.

*Correspondence: stevenjc@unimelb.edu.au

Anton P. Le Brun and Cathryn L. Haigh contributed equally to this work.

Martin P. Boland's present address is School of Psychological and Clinical Sciences, Charles Darwin University, Darwin, Northern Territory, 0815, Australia.

Michael James' present address is Australian Synchrotron, 800 Blackburn Road, Clayton, Victoria, 3168, Australia.

Editor: Francesca Marassi.

0006-3495/14/11/2313/12 $2.00

http://dx.doi.org/10.1016/j.bpj.2014.09.027

have included trafficking and signal transduction (reviewed in (13)), functions intimately linked with membranes. Mature PrP^C is a glycosylphosphatidylinositol (GPI)-anchored membrane protein directed to cholesterol-rich membrane domains on the outer leaflet of the cell plasma-membrane (14). These membrane domains are often associated with cellular signaling reactions and the control of signal protein activation; such a localization may support a role for PrP^C in these functions. Part of the reason that elucidating one individual function of PrP^C has been challenging is likely to be the influence of its posttranslational modifications. Protein cleavage is a cellular mechanism of functional activation and deactivation. PrP^C is known to undergo well-characterized alpha- and beta-cleavage events as well as secretory cleavage from the cell surface (14–17). Alpha-cleavage occurs either side of residue 111 (15) producing N1 and C1 fragments and the β-cleavage site is located around residue 90 (18) producing N2 and C2 fragments. The N1 and N2 fragments contain a far N-terminal polybasic region and an octameric repeat, metal ion binding domain. The fragments differ at their C terminus by one further polybasic region containing an additional metal ion binding site that is only present in the N1 fragment. PrP^C, therefore, exists as a minimum of six different species before other posttranslational modifications (such as complex glycosylation) are considered, with the potential for differing functions of different fragments depending on cellular environment. As stated, posttranslational cleavage may be used for protein activation or deactivation and, therefore, the fragments produced by these cleavages could be functional and may alter the functional capacity of full-length PrP. Both the N1 and N2 cleavage fragments have been demonstrated to have neuroprotective functions (19,20), but the cleavage events that produce them are thought to occur at different cellular locations, with N1 produced in the Golgi (21) and N2 at the cell surface (16), indicating their production may be stimulated by different signals.

Our previous studies using synthetic N1 and N2 have shown that the peptides have a propensity to interact with anionic lipid membranes independent of the PrP globular C terminus region (22). These studies suggested that the liberated peptides could interact with the acyl chain core of the bilayer membrane without substantially disrupting the homogeneity of the lipid system and thus our previous work raised the possibility that the peptides may insert benignly through the bilayer. Our recent work aimed to expand these findings by directly probing the peptide-lipid interactions using neutron reflectometry (NR). NR directs a beam of neutrons into a sample, measuring the intensity of reflected neutrons as a function of momentum transfer. The pattern of reflection in the context of membranes provides information on the thickness and composition of the surface and from these the fluidity can be inferred by deriving the area per lipid molecule. This technique was employed specifically for its capacity to accurately probe the depth that a peptide penetrates into the bilayer, which can be measured using isotopic labeling. Furthermore, NR is nondestructive and nonperturbing, therefore giving a more valid insight into the interactions within the sample. Our findings show that both N1 and N2 interact with anionic membranes at pH 5 as originally proposed without pore-forming or lytic capacity but neither peptide penetrates deeply into the membrane.

MATERIALS AND METHODS

Vesicle and peptide preparation

1-palmitoyl-2-oleoyl-*sn*-glycero-3-phosphocholine (POPC), 1-palmitoyl-2-oleoyl-*sn*-glycero-3-[phospho-*rac*-(1-glycerol)] (POPG), 1-palmitoyl-2-oleoyl-*sn*-glycero-3-[phospho-L-serine] (POPS), 1,2-dimyristoyl-*sn*-glycero-3-phosphocholine (DMPC), 1,2-dimyristoyl-*sn*-glycero-3-[phospho-*rac*-(1-glycerol)] (DMPG), 1-palmitoyl(d31)-2-oleoyl-*sn*-glycero-3-phosphocholine (d_{31}-POPC), 1-palmitoyl(d31)-2-oleoyl-*sn*-glycero-3-[phospho-*rac*-(1-glycerol)] (d_{31}-POPG), and 1-palmitoyl(d31)-2-oleoyl-*sn*-glycero-3-[phospho-L-serine] (d_{31}-POPS) were purchased from Avanti Polar Lipids (Alabaster, AL) and used without further purification. Lipids were dissolved in chloroform/methanol (4:1 by volume) in glass vials to give POPC only, POPC/POPG (2:1 molar ratio), POPC/POPS (2:1 molar ratio), and DMPC/DMPG (2:1 molar ratio) lipid mixtures. The same lipid ratios were used for preparing vesicles with lipids containing the d_{31}-palmitoyl chain. The solvent was evaporated first by blowing nitrogen over the lipid solutions and then by storing under vacuum overnight to remove any residual solvent. The dried lipid thin films were hydrated with a buffered solution of 10 mM MOPS, 150 mM NaCl pH 7.0 (in 100% D_2O for NR experiments) with vortex mixing to a concentration of 0.5 mg/mL. The hydrated lipid solutions were incubated at 25°C for PO-containing lipids and 30°C for DM-containing lipids for 1 h before small unilamellar vesicles were prepared by sonicating the lipid solution until clear.

Fluorescent large unilamellar vesicles (LUVs) for calcein release assays were prepared as follows. Chloroform solutions (10 mg/mL) of 1-palmitoyl-2-oleoyl-*sn*-Glycero-3-phosphcholine (POPC) and 1-palmitoyl-2-oleoyl-*sn*-Glycero-3-[phospho-*rac*-(1-glycerol)] (POPG) were combined (2:1 w/w) in a round-bottom flask and the solvent removed by rotary evaporation. The lipid film was hydrated in 10 mM Tris-HCl pH 7.4 (150 mM NaCl) containing 70 mM calcein (Sigma-Aldrich Pty Ltd, Sydney, Australia) for 1 h at 40°C with gentle agitation. The multilamellar dispersion was freeze-thawed in liquid nitrogen five times, then extruded through a 100 nm polycarbonate membrane 11 times. The resultant calcein-loaded LUVs were passed through a column of Sephadex G25 resin (Sigma) preequilibrated with 50 mM Na/K acetate pH 5.2 (130 mM NaCl) to remove free calcein from the solution. Calcein-loaded LUVs were diluted to a concentration of ca. 50 μM in acetate buffer immediately before use.

The mouse PrP amino acid sequence was used to generate peptide fragments corresponding to N1 (23-111) and N2 (23-90) cleavage fragments. The Peptide Technology Laboratory (Bio21 Institute, University of Melbourne) used microwave synthesis to prepare the peptides as previously described (23). Verification of the peptide sequence and purity was performed by HPLC and mass spectrometry. Freeze-dried peptides were dissolved in buffer (17 mM sodium acetate, 150 mM NaCl pH 5.0) to a concentration of 10 μM immediately before use.

Neutron reflectometry experiments and data analysis

Polished n-type circular silicon wafers 100 mm in diam. and 10 mm thick (El-Cat Inc., Ridgefield Park, NJ) were cleaned for 1 h at 85°C in a strongly

acidic "piranha" solution of $H_2O/H_2SO_4/H_2O_2$ (4:3:1 by volume) to remove surface impurities. After cleaning in the corrosive acid solution, the silicon wafers were rinsed in Milli-Q water and dried before being UV-ozone cleaned for 20 min. A final rinse with Milli-Q water and propan-2-ol was carried out before drying under a stream of nitrogen. The silicon wafers were assembled in aluminum cells with a silicon backing plate, which had a 50 μm deep solvent reservoir and inlet and outlet tubes to allow for solvent/sample exchange.

Neutron reflectivity data were measured using the *Platypus* time-of-flight neutron reflectometer and a cold neutron spectrum (2.8 Å ≤ λ ≤ 18.0 Å) at the OPAL 20 MW research reactor (Sydney, Australia) (24,25). Neutron pulses of 20 Hz were generated using a disc chopper system (EADS Astrium GmbH, Munich, Germany) in the low resolution mode ($\Delta\lambda/\lambda = 8\%$), and recorded on a two-dimensional ^{3}He neutron detector (Denex GmbH, Lüneburg, Germany). Reflected beam spectra were collected for each of the surfaces at 0.45° for 15 min (0.72 mm slits), 1.6° for 45 min (2.56 mm slits), and 4.5° for 2 h (7.2 mm slits), respectively. Direct beam measurements were collected under the same collimation conditions for 1 h each. The data were reduced using the Slim reduction package, which stitches the three data sets together at the appropriate overlap region, re-bins the data at instrument resolution and corrects for background and detector efficiency (26). The final scaled reflectivity, R, is presented as a function of momentum transfer, Q, defined as follows:

$$Q = \frac{4\pi \sin\theta}{\lambda}$$

where θ is the angle of incidence and λ is the neutron wavelength. The reflectivity data was multiplied by Q^4 to remove the Fresnel reflectivity and thus final reflectivity data presented as RQ^4 versus Q.

Structural parameters for the native oxide layer on the silicon blocks, lipid bilayer, and peptide layers were refined using the MOTOFIT reflectivity analysis software (27). In the fitting routines, the genetic algorithm was selected to minimize χ^2 values by varying the thickness (τ), roughness (σ), and neutron scattering length density (nSLD) of each layer. Model fitting of the resulting reflectivity profiles yields information on the real space neutron scattering length density profile normal to the surface, from which the structure of a lipid bilayer may be deduced. The nSLD, ρ, can be considered as a neutron refractive index and is a function of the chemical composition of the material according to the following:

$$\rho = N_A \sum_i \frac{p_i}{A_i} b_i$$

where N_A is Avogadro's number, p_i is the mass density, A_i is the atomic mass, and b_i is the nuclear scattering length of component i. The errors generated in the analysis software are ±1 standard deviation of the parameter value from which the percentage error was calculated. The advantage of using neutrons, particularly for soft matter and biological systems, is the difference in scattering length between hydrogen ($b_H = -3.74 \times 10^{-5}$ Å) and its isotope deuterium ($b_D = +6.67 \times 10^{-5}$ Å). By selective deuteration of molecules (in this case the palmitoyl tails) different segments of the lipid bilayer can be probed by choosing a suitable solvent contrast. We used either a pure D_2O solvent contrast ($\rho = 6.35 \times 10^{-6}$ Å^{-2}) to highlight the protonated peptide or pure H_2O ($\rho = -0.56 \times 10^{-6}$ Å^{-2}) to highlight the partially deuterated lipid chains. When changing between different subphase contrasts, the physical structure of the system is assumed not to change. This means that the thickness and roughness parameters in the models are constrained to be the same between each subphase while only letting the scattering length density vary. This form of simultaneous fitting provides for a unique solution to the model. The nSLD on each component in a layer contributes to the final nSLD of the layer, ρ_{layer}, such that

$$\rho_{layer} = (\rho_{lipid}\varphi_{lipid}) + (\rho_{solvent}\varphi_{solvent}) + (\rho_{peptide}\varphi_{peptide})$$

where φ is the volume fraction of each component. Once the volume fraction has been determined the surface excess, Γ, of each component (in mol m^{-2}) can be calculated from the following:

$$\Gamma = \frac{\varphi\tau}{VN_A}$$

where V is the molecular volume. From the surface of excess the lipid to peptide ratio can be deduced.

For consideration of changes in lipid order, the area per lipid molecule, A_{lipid}, is determined from the following:

$$A_{lipid} = \frac{V}{\varphi\tau}$$

where V is the molecular volume of the lipid (1230 Å^3 for POPC/POPG bilayers and 1226 Å^3 for POPC/POPS bilayers (28–30), φ is the volume fraction, and τ is half the total bilayer thickness. The values used to calculate parameters can be found in Table S1 in the Supporting Material.

Quartz crystal microbalance (QCM) experiments and analysis

The Q-senseE4 instrument (Q-Sense, Gothenburg, Sweden) fitted with a peristaltic pump (Ismatec SA, Glattbrugg, Switzerland) used a flow rate of 100 μL min^{-1}, a constant temperature of 22°C, and silicon dioxide-coated sensor crystals (QSX-303, Q-sense). The sensor crystals were cleaned by UV-ozone for 20 min, rinsing with 2% (v/v) Hellmanex followed by copious rinsing with > 18 MΩ water and drying under nitrogen. The sensors underwent a final clean using UV-ozone for 20 min immediately before use. The piezoelectric quartz crystal was excited at its fundamental frequency (5 MHz) and the change in frequency (Δf) was observed for the third, fifth, seventh, ninth, eleventh, and thirteenth overtones. Data was collected using QSoft401 software and processed into frequency and dissipation versus time data using Q-Tools 301 v2.1. A decrease in frequency corresponds to an increased mass on the surface of the sensor. For rigid films with little water content that have minimal changes in dissipation (< 1), the Sauerbrey equation can be used to relate mass (Δm) and frequency (Δf) as follows:

$$\Delta m = -\frac{\Delta f \rho_q v_q}{2\sqrt{F}n}$$

where ρ_q is the density of quartz (2648 kg m^{-3}), v_q is the speed of sound through quartz (3340 m s^{-1}), F is the fundamental frequency (5 MHz), and n is the overtone number. For each overtone the change in dissipation (ΔD) was also measured. The dissipation is the proportion of energy dissipated during one cycle of the frequency oscillation and provides information on the viscoelastic properties of the materials deposited on the sensor surface. For films that are nonrigid and have a dissipation that is large (> 1), the Sauerbrey equation is no longer valid.

Vesicles prepared in buffer (50 mM sodium acetate/acetic acid pH 5.2, 130 mM NaCl) were deposited onto the silicon dioxide surface. Once the vesicles had ruptured and the bilayer formed, the excess lipid was removed with a buffer wash. Peptide at 10 μM prepared in the same buffer was added and incubated on the bilayer for 60 min after which the excess peptide was removed with a buffer wash.

Calcein Release Measurements

For each condition, 95 μL of calcein-loaded LUVs was added to a black 96-narrow-well plate and the initial fluorescence (f_0) monitored using a POLARstar OPTIMA microplate reader (BMG LABTECH, Ortenberg, Germany) using 480 ± 10 nm excitation and 520 ± 20 nm emission filters. Following addition of 5 μL peptide (100 μM N1, N2, or melittin

dissolved in MQ grade water), the solution briefly mixed by pipetting up and down the fluorescence signal was further monitored as a function of time. Finally, 5 μL Triton X-100 (10% v/v) was added to determine the maximum fluorescence response (f_1). The normalized fluorescence (f') was obtained from the raw fluorescence signal (f) using the following expression:

$$f'(t) = [f(t) - f_0]/[f_1 - f_0].$$

RESULTS

NR is an established technique for studying the structure of solid-supported phospholipid bilayers along the axis perpendicular to the plane of the bilayer (the z-axis) (31,32). The bilayers were generated using the vesicle deposition technique (33) onto silicon oxide surfaces typically 15 ± 1 Å thick and with an interfacial roughness of 3 Å. In these experiments we used mono-unsaturated diacyl phospholipids where the palmitoyl chain was deuterated so that there was contrast against the hydrogenous peptides. For modeling the bilayer data, the bilayers were separated into three discrete layers: headgroup one (closest to the silicon oxide surface), acyl tails, and headgroup two (closest to the bulk solvent). A 3 to 7 Å solvent layer between the silicon oxide surface and headgroup one was included in the model for each bilayer as previously described (34,35). The experiments were conducted at room temperature, which is above the phase transition temperature of POPC, POPG, and POPS (T_m of -2°C, -2°C, and 14°C, respectively) and thus the bilayers were in the fluid (L_α) phase. The thickness of the bilayers ranged from 38 ± 3 Å to 56 ± 3 Å (Table 1 and Tables S2 and S3) and the area per lipid molecule ranged from 35 to 47 Å^2 in the tail region. These observations are consistent with molecular dynamics simulation data of POPC bilayers in the fluid phase (28).

For all NR experiments a peptide concentration of 10 μM in a pH 5.0 buffer was employed, which has been previously shown to be effective for binding to anionic bilayers (18). The approach used was bilayer formation and characterization after which peptide was incubated on the surface and then the excess removed with a pH 5.0 buffer wash in either D_2O or H_2O. When both the N1 and N2 peptides were added to zwitterionic d_{31}-POPC bilayers, no change in reflectivity was observed (Fig. S1) and no presence of peptide is observed in the corresponding real space nSLD profile. This corresponds with previous data that the N1 and N2 peptides do not bind to zwitterionic bilayers (22).

When the N1 peptide was added to the negatively charged d_{31}-POPC/d_{31}-POPG (2:1 molar ratio) bilayer, a reduction in the intensity of the fringe at Q = 0.101 Å^{-1} was observed along with a slight shift in fringe position to a lower value of Q by 0.01 Å^{-1} (compare black and red reflectivity profiles in Fig. 1 *A*). These changes indicate that the N1 peptide bound to the d_{31}-POPC/d_{31}-POPG bilayer without dramatic structural changes to the bilayer. A similar effect was observed when the N1 peptide was added to a d_{31}-POPC/d_{31}-POPS (2:1 molar ratio) bilayer; however, the reduction in the intensity was less than for d_{31}-POPG-containing bilayers suggesting that less peptide was bound to the bilayer (Fig. 1 *B*). The modeling of the data to produce the real-space nSLD profiles provided more details on the membrane-bound peptide

TABLE 1 Thickness and derived properties of the lipid bilayers with and without N1 and N2 peptide bound from the fitting of the neutron reflectometry data

Layer	Thickness (no peptide) / Å	φ_{lipid} (no peptide)	Thickness (peptide bound) / Å	φ_{lipid} (peptide bound)	$\varphi_{peptide}$	Γ_{lipid} / μmol m^{-2}	$\Gamma_{peptide}$ / μmol m^{-2}
d_{31}-POPC/d_{31}-POPG (2:1) bilayer + N1 peptide							
Headgroup 1	15 ± 1	0.94 ± 0.02	18 ± 1	0.75 ± 0.01	-	7.46 ± 0.12	-
Tails	20 ± 1	1.00 ± 0.02	23 ± 1	1.00 ± 0.01	-	4.11 ± 0.01	-
Headgroup 2	10 ± 1	0.41 ± 0.02	7 ± 1	0.10 ± 0.01	0.47 ± 0.01	0.39 ± 0.01	0.07 ± 0.01
Peptide	-	-	21 ± 2	-	0.15 ± 0.01	-	0.08 ± 0.01
d_{31}-POPC/d_{31}-POPS (2:1) bilayer + N1 peptide							
Headgroup 1	7 ± 1	0.94 ± 0.06	8 ± 1	0.99 ± 0.03	-	4.58 ± 0.16	-
Tails	20 ± 1	1.00 ± 0.02	29 ± 1	0.97 ± 0.01	-	4.85 ± 0.05	-
Headgroup 2	11 ± 1	0.94 ± 0.03	9 ± 1	0.08 ± 0.01	0.47 ± 0.01	0.42 ± 0.01	0.07 ± 0.01
Peptide	-	-	21 ± 1	-	0.25 ± 0.01	-	0.08 ± 0.01
d_{31}-POPC/d_{31}-POPG (2:1) bilayer + N2 peptide							
Headgroup 1	7 ± 1	0.56 ± 0.01	7 ± 1	0.56 ± 0.02	-	2.30 ± 0.09	-
Tails	27 ± 1	1.00 ± 0.02	31 ± 1	1.00 ± 0.02	-	5.38 ± 0.12	-
Headgroup 2	11 ± 1	0.86 ± 0.03	12 ± 1	0.14 ± 0.05	0.33 ± 0.01	0.90 ± 0.03	0.08 ± 0.01
Peptide	-	-	27 ± 3	-	0.20 ± 0.03	-	0.12 ± 0.01
d_{31}-POPC/d_{31}-POPS (2:1) bilayer + N2 peptide							
Headgroup 1	13 ± 1	0.89 ± 0.02	12 ± 1	0.78 ± 0.02	-	5.44 ± 0.11	-
Tails	26 ± 1	0.98 ± 0.01	27 ± 1	0.89 ± 0.01	-	4.17 ± 0.05	-
Headgroup 2	18 ± 1	0.24 ± 0.02	16 ± 1	0.20 ± 0.01	0.53 ± 0.01	1.90 ± 0.03	0.18 ± 0.01
Peptide	-	-	20 ± 2	0	0.28 ± 0.01	-	0.12 ± 0.01

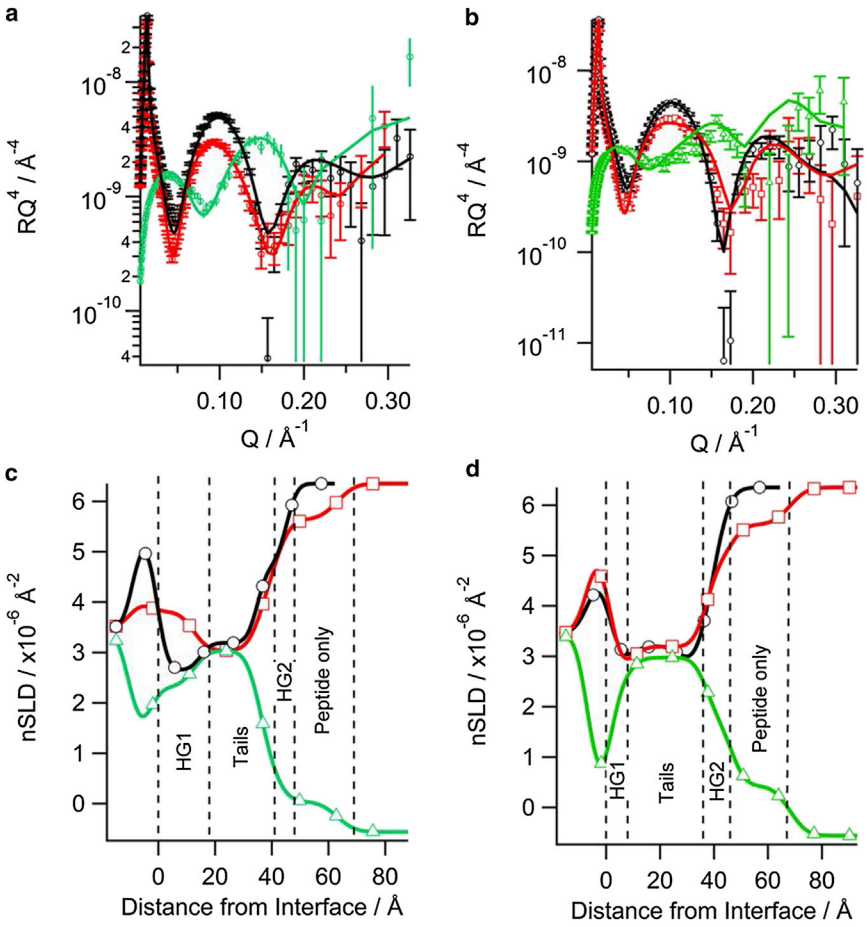

FIGURE 1 Neutron reflectometry of the N1 peptide binding to solid-supported phospholipid bilayers on silicon: (*a*) d_{31}-POPC/d_{31}-POPG (2:1) bilayer, (*b*) d_{31}-POPC/d_{31}-POPS (2:1) bilayer, the symbols with error bars are the data and the solid lines the fit. The corresponding real-space nSLD profile from the fits is also shown: (*c*) d_{31}-POPC/d_{31}-POPG (2:1) bilayer, (*d*) d_{31}-POPC/d_{31}-POPS (2:1) bilayer. The dashed vertical lines delineate the different layers in the peptide bound state. In all panels black (○) is bilayer before N1 peptide addition in D_2O, red (□) is bilayer with N1 peptide bound in D_2O, and green (△) is bilayer with peptide bound in H_2O. To see this figure in color, go online.

(Fig. 1 *C* and *D*). There was no change in the nSLD of the acyl tails region before peptide addition or when peptide was bound to both the d_{31}-POPG- and d_{31}-POPS-containing bilayers in the D_2O contrast. This shows that the N1 peptide does not penetrate into the bilayer acyl tail layer. Additionally, changing the isotopic contrast to H_2O in the presence of the N1 peptide also showed no isotopic-dependent change in the nSLD of the bilayer tails region, which further confirms the acyl tails layer is devoid of peptide and that there is no detectable pore-formation by the peptide. The calculated volume fractions of the lipid tails before and after peptide addition showed that there was no loss of lipid from the surface (Table 1), also suggesting no detectable peptide action through the membrane lysis process known as the "carpet mechanism" (36). The most profound effect that the N1 peptide had on both bilayers was in the outer headgroups of the phospholipids. The N1 peptide was present in this region along with solvent. Using the volume fractions of lipid and peptide, the surface excess and lipid-to-peptide ratio for the outer headgroup was calculated. From the lipid-to-peptide ratios in Fig. 2 it can be seen that a higher amount of peptide is bound to the d_{31}-POPG-containing bilayer than the d_{31}-POPS-containing bilayer, indicating a stronger interaction between d_{31}-POPG and the N1 peptide than for d_{31}-POPS. Both bilayers have a 21 Å layer of peptide above membrane. The peptide layer is not dense; having a peptide volume fraction of 0.15 and therefore a high solvent content (Table 1). A further observation was that the thickness of the acyl tail zone was increased on peptide binding, indicating a potential increase in lipid ordering (Table 1). This was also evident as a contraction of the area per lipid molecule of the membrane following peptide addition (Table 2), but no phase transition of the lipids was seen.

NR showed the N2 peptide displayed similar behavior to the N1 peptide when binding to negatively charged phospholipid bilayers. As with the N1 peptide, when N2 was bound to solid-supported bilayers the intensity of the fringe at Q ~ 0.1 $Å^{-1}$ decreased suggesting that the N2 peptide bound to the bilayer (Fig. 3 *A* and *B*). For the H_2O contrast in the d_{31}-POPC/d_{31}-POPS bilayer with N2 bound (Fig.3 *B*) the background of the data points did not match the fitted curve; however, the fit is still within a reasonable χ^2 value of 1.24. When the background was constrained, a poorer fit that was not biologically credible resulted. The real-space nSLD profile showed no presence of peptide in the acyl tail region for both d_{31}-POPC/d_{31}-POPG

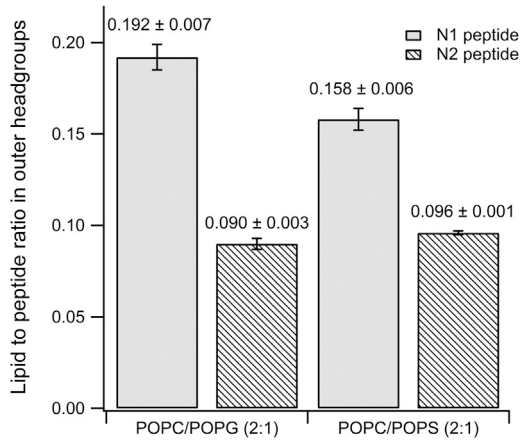

FIGURE 2 The lipid-to-peptide ratio of N1 and N2 peptides in the outer headgroups in anionic phospholipid bilayers as determined from neutron reflectometry data.

bilayer and d_{31}-POPC/d_{31}-POPS bilayers (Fig. 3 *C* and *D*). The d_{31}-POPS-containing bilayer showed an isotopic dependent change in the tail layer when changing between the D_2O and H_2O contrasts, highlighting the presence of solvent in the tail region (Fig. 3 *D*). The volume fraction of the solvent in the tail region of the d_{31}-POPC/d_{31}-POPS bilayer was 0.11 with the lipid volume fraction reducing down to 0.89 indicting some loss of lipid material from the surface. This marginal loss of lipid material over the period that the peptide was bound to the bilayer (~ 7 h) makes it unlikely that the N2 peptide has any lytic or pore-forming mechanism. The predominant binding of the N2 peptide was at the outer headgroups forming a peptide layer above the bilayer in both negatively charged membranes. The lipid-to-peptide ratio of the N2 peptide in the outer headgroup region for each bilayer was calculated. Fig. 2 shows that there was essentially no difference in the lipid-to-peptide ratio between d_{31}-POPG- or d_{31}-POPS-containing bilayers. However, the lipid-to-peptide ratio of N1 was higher than N2 in both cases indicating less N2 bound to the bilayer than N1.

The NR data clearly indicates that the N1 and N2 peptides do not insert into the hydrophobic tail region of a phospholipid bilayer. To further confirm the absence of tail insertion by the N1 and N2 peptides (and to ensure the current results were not because of batch variation in peptides), we conducted QCM-D experiments comparing the N1 and N2 fragments with melittin from bee venom, a peptide known to insert into the hydrophobic tails of anionic phospholipid bilayers (37). Fig. S2 shows that when melittin is added to a bilayer of POPC/POPG (2:1) or POPC/POPS (2:1) the dissipation increases, the overtones no longer overlap, and the Sauerbrey equation is no longer valid as is consistent with recent publications (38). This is indicative of the vibration of the bilayer no longer being in concert with the vibrations of the oscillating quartz crystal because of the increased hydration of the bilayer. Although the mass of the bound melittin cannot be determined through the use of the Sauerbrey equation, the frequency of each overtone remains more negative than the frequency of the bilayer. This shows that there is an overall mass gain suggesting the increased hydration of the bilayer rather than loss of lipid material from the surface (which would result in a less negative frequency than the initial bilayer). As can be seen, the QCM-D trace for the addition of melittin was very different from that of either the N1 or N2 peptides binding to anionic bilayers (Fig. 4). The QCM-D traces for the N1 and N2 peptides (N2 trace presented in Fig. 4 and tabulated results shown in Table S4) show an overall mass gain on the bilayer indicating no lytic action by the peptides and all the overtones overlap with a low dissipation indicating that the bilayer was intact and had not changed its hydration state. Control QCM-D experiments were also conducted with DM lipids with no differences found from the PO lipids (Table S4). By plotting Δf versus ΔD, time is excluded as a parameter and the plot shows how the lipid bilayer structure changes per unit of peptide mass added. This provides a "finger print" of the mechanistic action of peptides with lipid bilayers (39). Fig. 5 shows the Δf-ΔD plots for N1 and N2 binding to both the POPG and POPS-containing bilayers. The origin of the each graph in Fig. 5 is the point of peptide addition (the point marked PA in Fig. 4 *A*). In all cases there is a linear increase of ΔD with increasing mass (i.e., a more negative Δf) as the peptide is binding to the bilayer until the lipid bilayers are saturated with peptide and there is no further change in Δf or ΔD resulting in the large cluster of data points on the right-hand of each graph. The shape of data in Fig. 5 is indicative of peptides that have minimal structural impact on lipid bilayers and is similar to the nonlytic peptides apidaecin (40) and oncocin (41). Finally, to further ensure minimal membrane perturbation and no lytic activity of the peptides calcein release from LUVs in response to the N1 and N2 peptides was compared with the action of melittin in POPC and POPC/POPG (2:1) vesicles (Fig. 6). No change from baseline fluorescence was seen for the POPC LUVs and minimal fluctuation was measured for the POPC/POPG LUVs when exposed to the N1 and N2 peptides compared with melittin, which demonstrated rapid and almost complete release. These results further exclude pore-formation by N1 or N2 and confirm our previous findings.

TABLE 2 The change in area per lipid molecule upon binding N1 and N2 peptides

Bilayer	Peptide	A_{lipid} before peptide addition / Å^2	A_{lipid} after peptide addition / Å^2
POPC / POPG (2:1)	N1	55 ± 4	51 ± 4
POPC / POPS (2:1)	N1	65 ± 7	54 ± 4
POPC / POPG (2:1)	N2	55 ± 5	49 ± 4
POPC / POPS (2:1)	N2	44 ± 3	50 ± 3

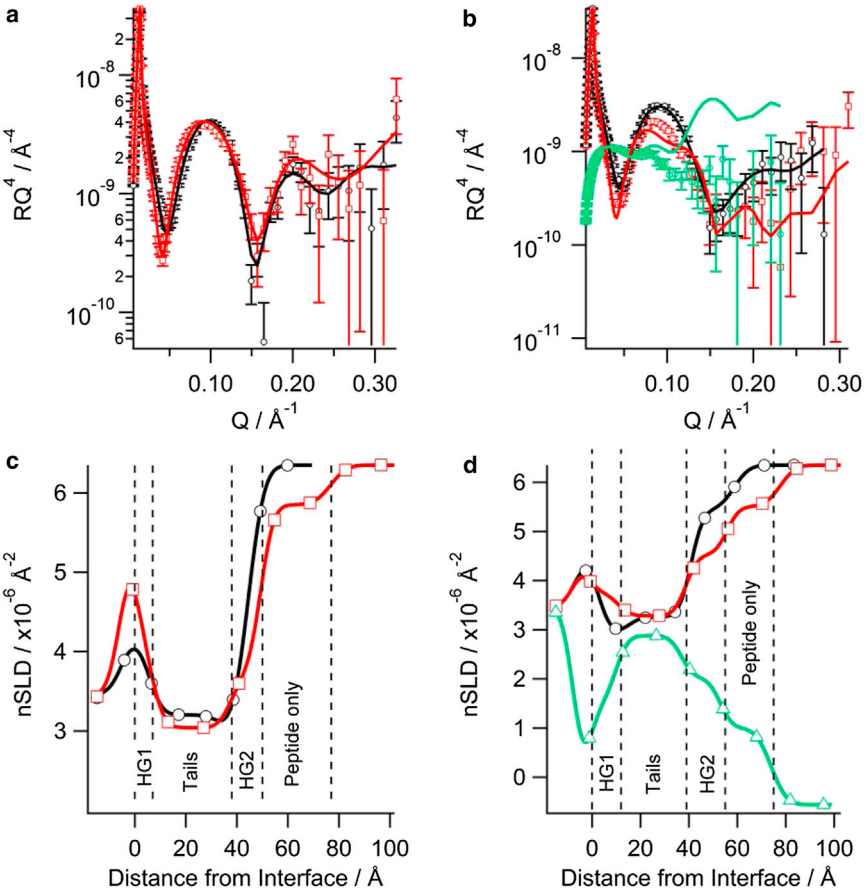

FIGURE 3 Neutron reflectometry of the N2 peptide binding to solid-supported phospholipid bilayers on silicon: (*a*) d_{31}-POPC/d_{31}-POPG (2:1) bilayer, (*b*) d_{31}-POPC/d_{31}-POPS (2:1) bilayer, the symbols with error bars are the data and the solid lines the fit. The corresponding real-space nSLD profile from the fits is also shown: (*c*) d_{31}-POPC/d_{31}-POPG (2:1) bilayer, (*d*) d_{31}-POPC/d_{31}-POPS (2:1) bilayer. The dashed vertical lines delineate the different layers in the peptide bound state. In all panels black (○) is bilayer before peptide addition in D_2O, red (□) is bilayer with N2 peptide bound in D_2O, and green (△) is bilayer with N2 peptide bound in H_2O. To see this figure in color, go online.

DISCUSSION

The NR data presented in the current study confirm the binding capabilities of the N1 and N2 endogenous cleavage fragments to phospholipid model membranes and further defines the specific engagement and changes to the lipid environment upon peptide binding. Our previous work showed interactions of the N1 and N2 peptides with anionic lipids that were consistent with either benign uniform insertion of the peptide across the bilayer or no insertion with peptide bound to the surface of the bilayer causing lipid ordering (22). Previous studies using ^{2}H-solid-state NMR with only the palmitoyl chain of the POPC lipid labeled with deuterium in a 2:1 mixture of POPC:POPS were only able to report on the ordering effect on 33% of the tails in the lipid mixture. The ^{2}H chemical shift anisotropy increased from 23.2 kHz for lipid only to 25.6 and 24.4 kHz in the presence of N1 and N2, respectively, indicating an ordering of the palmitoyl tails in POPC. This modest increase in ordering could reflect peptides inserting into the lipid tails; however, the increases did not account for a substantial perturbation in the freedom of movement of the palmitoyl tails associated with bilayer disruption and could suggest that the N1 and N2 peptides do not interact with the bulk lipid bilayer (22). In the study all parts of the lipid bilayer and the peptide were observed providing a complete picture and strong support that the latter situation is true, finding that binding was primarily in the outer headgroup region with no penetration into the acyl tails, and also confirmed that the binding affinity is greater for N1 than N2 on both the POPS/POPC and POPG/POPC bilayers, most likely because of the additional polybasic region at the C terminus of the N1 peptide (15). Therefore, these data continue to support a nonperturbing PrP N1/N2-lipid interaction and are not consistent with the peptide causing bilayer damage by other lipid disruptions such as the carpet mechanism (36).

Our findings contrast with NR studies of the neurotoxic peptide amyloid-beta (Aβ) found in Alzheimer's disease that, in combination with atomic force microscopy, shows globular aggregates of freshly prepared Aβ1-40, Aβ1-42, or both are adsorbed to the membrane and disruptively penetrate into the core increasing hydration (42). Further, once the Aβ has initially inserted into the hydrophobic core of negatively charged lipids, causing disordering of the lipids, an induction of folding and template assembly of Aβ fibrils occurs (43). As with the N1 and N2 peptides, Aβ forms a peptide layer on the surface of the lipid bilayer. However, with Aβ, a thicker (~ 40 Å), more crystalline layer is formed than observed with N1 and N2 (43). The binding parameters of the N1 and N2 peptides also differ from those of

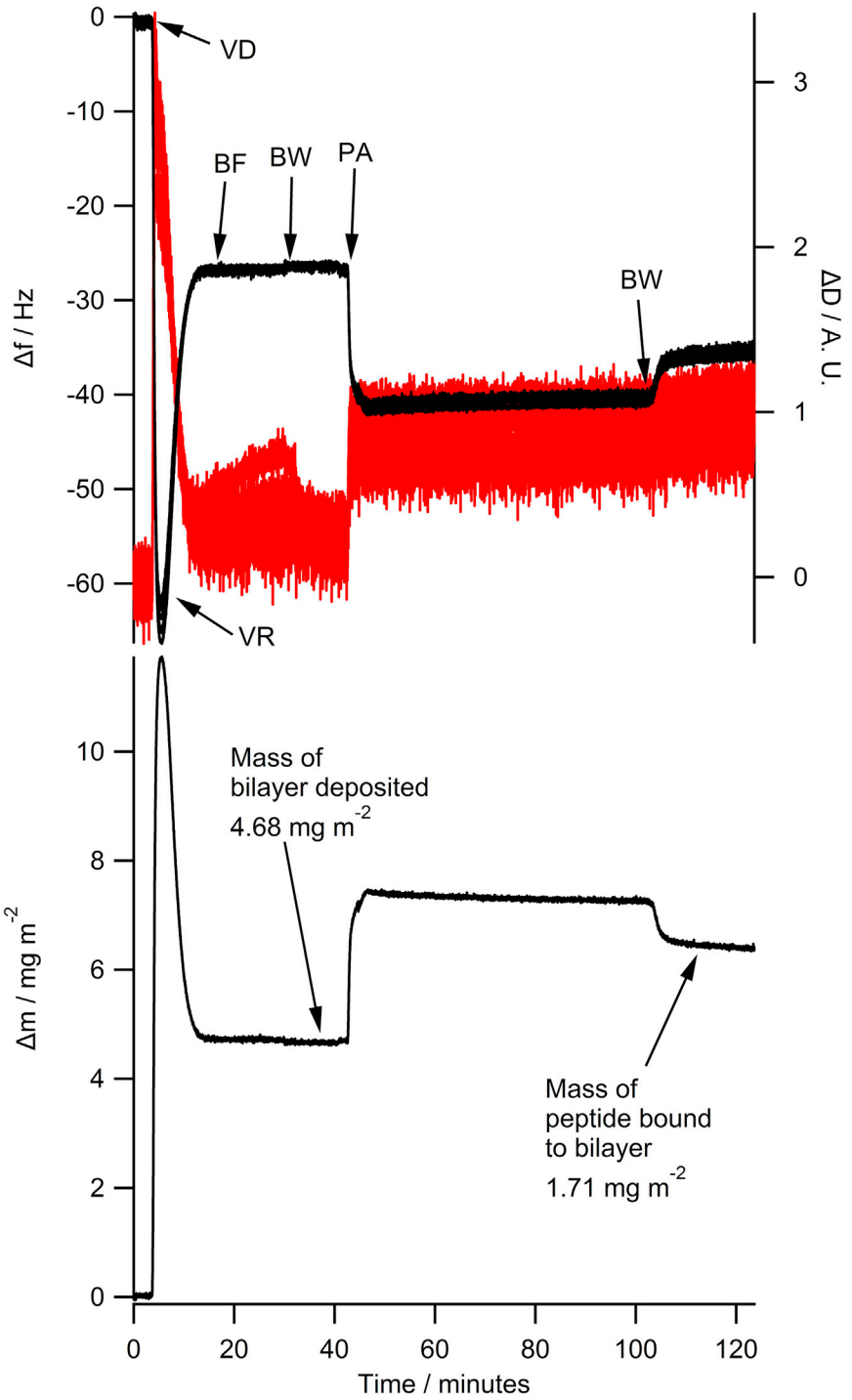

FIGURE 4 The QCM-D of 10 μM N2 peptide binding to a phospholipid bilayer of POPC/POPS (2:1). The upper panel shows the Δf trace on the left (*black trace*) and the ΔD trace is shown on the right (*red trace*). The 3rd, 5th, 7th, 9th, 11th, and 13th overtones are shown but are indistinguishable as all overtones overlap. The lower panel shows the corresponding Sauerbrey mass at each step of the measurement with final masses deposited indicated. VD—vesicle deposition, VR—vesicle rupture, BF—bilayer formation, BW—buffer wash, PA—peptide addition. To see this figure in color, go online.

α-synuclein, which forms intracellular aggregates called Lewy bodies in Parkinson's disease. Similar to N1 and N2, α-synuclein mainly embeds in the outer headgroups of mixed lipid bilayers containing anionic lipids, with a greater binding affinity seen at lower pH (44), but its membrane interaction causes thinning of the bilayer rather than the thickening effect seen for the PrP fragments. Also, binding to lipid membranes is known to induce a helical secondary structure of α-synuclein (45), although we previously observed the formation of increased beta-sheet secondary structure on binding of N2 to PC/PS (22). The structural change of α-synuclein and its lipid interactions is thought to be involved in disease pathogenesis (46). A similar situation is unlikely to be true for N1 and N2 given these fragments do not contain the amyloidogenic region of PrP and the data presented indicate that the membrane binding

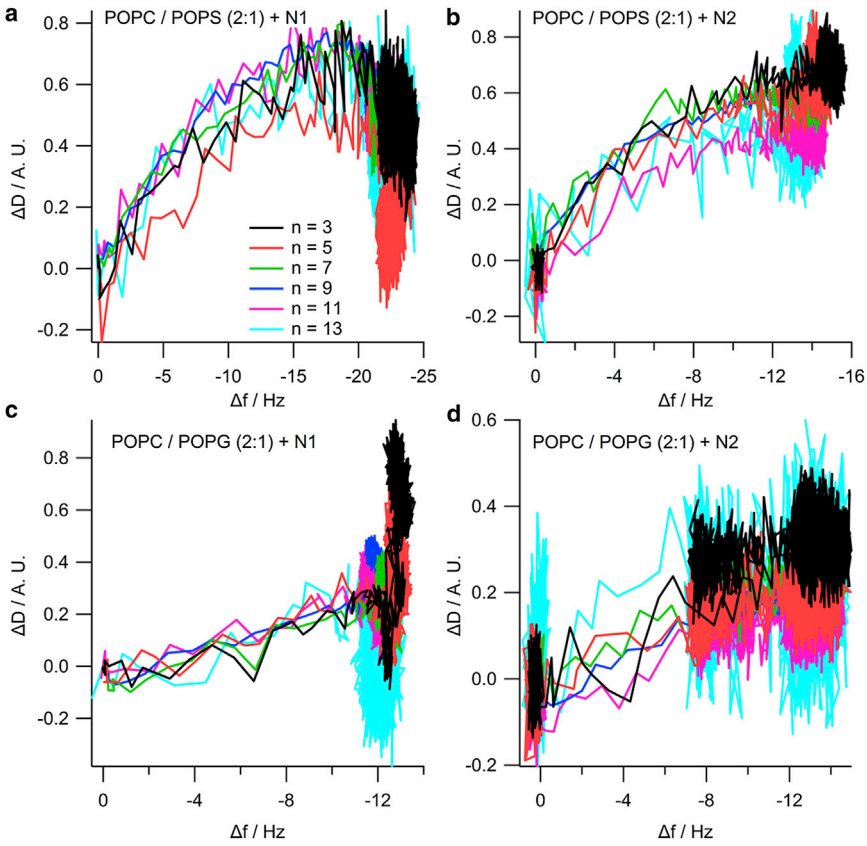

FIGURE 5 Δf-ΔD plots from the QCM-D data of (*a*) 10 μM N1 or (*b*) N2 binding to POPC/POPS (2:1) bilayers, or binding to (*c and d*) POPC/POPG (2:1) bilayers. The data shown is from the 3rd (*black*), 5th (*red*), 7th (*green*), 9th (*blue*), 11th (*magenta*), and 13th (*cyan*) overtones. To see this figure in color, go online.

events of these N-terminal fragments of PrP appear minimally perturbing and would not be expected to be directly toxic to cells. Indeed viability studies in cells have shown that these peptides do not cause lysis and are not toxic but instead demonstrate cytoprotective properties (19,20). Considering these properties, and that the N1/N2 binding events show no evidence of being acutely damaging to membranes, these interactions may be relevant to the cellular functions of these fragments and/or full-length PrP.

Analysis of the NR data of N1 and N2 peptide binding to POPG and N1 binding to POPS containing membranes showed that there was a thickening of the lipid bilayer, reducing the area per lipid. Such changes are indicative of an ordering of the lipids in the absence of a phase transition. Changes in lipid order are required for the formation of scaffolds for protein binding and the assembly of multimeric protein complexes, such as those associated with Annexin A6 (47), which through structuring membrane domains and linking with actin were found to be involved in membrane repair. Interestingly, PrP^C has been reported to bind to a number of proteins, with the N-terminal region (residues 23–32) also containing a tubulin binding site (48), indicating that full length PrP^C and the N1 and N2 fragments could link a protein scaffold to lipid membrane domains and result in membrane ordering events under specific circumstances. The membrane ordering changes were not observed for the N2 peptide with the POPS-containing membrane. This may have a technical basis, most likely because of the small loss of lipid from the bilayer over the time of the experiment. We do not believe that this necessarily represents a biologically relevant event as the NR experiments were run over a period of hours but we have previously shown that the half-life of this peptide in cell systems is very short, approximately minutes (20), and therefore it is unlikely to persist for sufficiently long times to cause such an effect in vivo.

The N-terminal domain of PrP^C has been shown to control PrP^C membrane relocalization from lipid rafts and subsequent clathrin mediated internalization (49). The formation of protein scaffolds supporting tubule formation for budding of trafficking vesicles requires organization of the lipid membrane domain to which the protein scaffold attaches. The ability to engage a lipid scaffold may be highly important for the trafficking of full-length PrP^C and potentially the N-terminal cleavage fragments. However, the absolute dependence on low pH for the observed membrane interactions suggests that any physiological role of N1 or N2 interaction with anionic lipids is likely to occur inside the cell in organelles of increased acidity. N-terminal interactions may also direct trafficking once inside the cell. A pH of 5 is representative of the pH within late endosomes, from which PrP^C might undergo retrograde transportation to the Golgi (50), be transferred to recycling endosomes or multivesicular bodies, or it may be targeted to lysosomes for

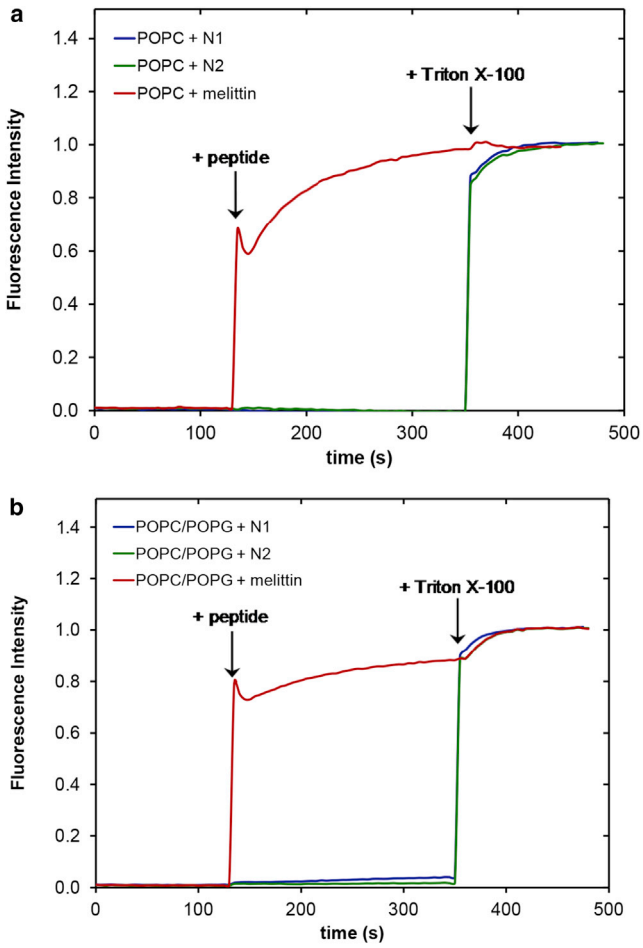

FIGURE 6 Calcein release from (*a*) POPC or (*b*) POPC/POPG (2:1) LUVs when exposed to N1 (*blue*), N2 (*green*), or melittin (*red*) peptides. Triton X-100 was added to demonstrate maximum release. To see this figure in color, go online.

destruction. N-terminal engagement with intracellular membranes may therefore be as part of an endosomal sorting signal and direct the final destination of PrP^C and/or its N-terminal cleavage fragments. A role in membrane interaction that directs intracellular trafficking might also account for intricate changes that alter exosomal membrane structure during prion disease (51). Exosomes are formed through membrane fission from multivesicular bodies (52) to which PrP^C may become directed by endosomal trafficking. Notably, N-terminal processing of PrP^C is altered in exosomes from prion-infected cells (53).

Ordering of lipids is also seen in the formation of membrane signaling complexes. An alternative hypothesis to N1 and N2 being involved in dictating intracellular trafficking is that their endocytosis is required to permit the formation of membrane signaling complexes. Endosomes are known to have a role in cellular signaling, controlling the "off" and "on" of some pathways (54). The pathways activated or deactivated are influenced by their type, maturity and cellular location (55). We have found that the protective signaling of N2 is transduced through MEK1 only after correct engagement of its internalization pathways (C. L. Haigh, unpublished observations). Therefore, endocytosis of N1 and/or N2 may instigate a lipid-protein engagement that facilitates intracellular signaling.

Although the observed membrane interactions of the N-terminal peptides did not indicate that such contact could be responsible for toxicity during disease, they may still be relevant to pathogenesis in the context of PrP misfolding. The involvement of POPG in the formation of genuinely infectious misfolded rPrP (7,56) suggests that the ability of PrP to bind these lipids as a full-length protein could be important for the generation of prions. Misfolding during prion disease is significantly more efficient if the N-terminal regions of PrP are present (57), and it has been shown that POPG binding to rPrP results in a structural change that exposes a cryptic binding site for the N-terminal polybasic region that may enhance further rPrP recruitment and templated misfolding (58). In cell cultures, high levels of PrP α-cleavage confer resistance to prion infection (59), most likely because the C1 fragment serves as a suboptimal substrate for misfolding; however, β-cleavage is seen to be increased during disease (18). In a cellular context, a greater ratio of C2 to full length PrP could result in aberrant membrane binding of C2, permitting conformational change and thus enhanced production of misfolded PrP during disease. β-cleavage leaves the core of misfolded PrP intact and C2 retains the second polybasic site that might substitute for 23-28. Studies considering rPrP fragments equivalent to the C2 region of PrP^C have shown that the ability to bind lipids and misfold is maintained (60). Additionally, the central domain has a significant role in lipid binding in full-length PrP^C and is influenced by disease-associated mutations of the proline residues at 102 and 105 (mouse sequence) to leucine residues (61). This supports that the N1 peptide should have a greater capacity to bind lipids than the N2 fragment that lacks this central domain, although disruption of lipid membranes is only observed for misfolded and aggregated rPrP, not for monomeric rPrP (60), supporting that N1 or N2 are unlikely to be membrane disruptive in vivo. When the N2 peptide was added to cells in culture at high concentrations (10 μM), a very small amount of dimer could be visualized by western blotting but no higher molecular weight oligomers, which were observed for a peptide with the prolines of the 23-28 polybasic region mutated to alanines (20). This indicates that the propensity for the N-terminal fragments to oligomerise and for any putative oligomers to cause membrane damage is also low.

Much previous work looking at PrP^C and lipid binding has focused on full-length recombinant PrP, thus remaining open to the criticism that, because rPrP is not GPI-anchored or complex glycosylated, it may not be accurately representative. The peptides used in the current study are representative of genuine cleavage fragments that occur in the brain

(18), separating the N-terminus from the structured, glycosylated, and membrane-anchored C terminus, and the data therefore present a stronger argument for how these cleavage fragments interact with cell membranes. Both N-terminal cleavage fragments have been shown to have neuroprotective functions and therefore lipid binding interactions could be crucial for these peptides to effect protection. The binding parameters of full length PrP^C, especially in the context of membrane anchoring, remain to be determined; however, the data presented herein suggest that specific lipid binding interactions could potentially be corrupted during prion disease, when the cleavage events shift toward greater β-cleavage.

CONCLUSION

The new data generated by NR support our previous findings that endogenous PrP N-terminal cleavage fragments can interact with negatively charged supported phospholipid bilayers at low physiological pH. We further show that this interaction lies predominantly at the level of the phospholipid headgroups with no clear penetration into the acyl tail plane and without damage to the structural integrity of the membrane but with induction of a domain ordering effect. These observations stand in clear contrast to the findings of analogous studies of Aβ and α-synuclein and thereby support the possibility of a functional role for such N-terminal fragment-membrane interactions.

SUPPORTING MATERIAL

Two figures and four tables are available at http://www.biophysj.org/biophysj/supplemental/S0006-3495(14)01001-7.

This work was supported by the Australian Nuclear Science and Technology Organisation (ANSTO), proposal ID2211, Australian Institute for Nuclear Science and Engineering (AINSE Ltd.) for travel support, and a National Health and Medical Research Council (NHMRC) program grant (No. 628946). S. J. C. is funded by an NHMRC Practitioner Fellowship (No. APP100581). S. C. D. is funded by an Australian Research Council Future Fellowship (FT110100199). A. P. L. B. is funded by an Australian Research Council Discovery Early Career Research Award (DE140101788). The authors declare that they have no conflicts of interest.

REFERENCES

1. Prusiner, S. B. 1982. Novel proteinaceous infectious particles cause scrapie. *Science.* 216:136–144.
2. Weissmann, C., H. Bueler, …, M. Aguet. 1994. PrP-deficient mice are resistant to scapie. *In* Slow Infections of the Central Nervous System: The Legacy of Dr Bjorn Sigurdsson. J. Bjornsson, R. I. Carp, A. Love, and H. M. Wisniewski, editors. New York Academic Sciences, New York, pp. 235–240.
3. Saborio, G. P., B. Permanne, and C. Soto. 2001. Sensitive detection of pathological prion protein by cyclic amplification of protein misfolding. *Nature.* 411:810–813.
4. Kim, J. I., I. Cali, …, W. K. Surewicz. 2010. Mammalian prions generated from bacterially expressed prion protein in the absence of any mammalian cofactors. *J. Biol. Chem.* 285:14083–14087.
5. Welton, J. M., and V. A. Lawson. 2011. The site and host dependent requirements for prion propagation. *In* The Cellular and Molecular Biology of Prion Disease. S. J. Collins and V. A. Lawson, editors. Research Signpost, Scarborough, Canada, pp. 189–206.
6. Zhou, Z., and G. Xiao. 2013. Conformational conversion of prion protein in prion diseases. *Acta Biochim. Biophys. Sin. (Shanghai).* 45:465–476.
7. Wang, F., X. Wang, …, J. Ma. 2010. Generating a prion with bacterially expressed recombinant prion protein. *Science.* 327:1132–1135.
8. Critchley, P., J. Kazlauskaite, …, T. J. T. Pinheiro. 2004. Binding of prion proteins to lipid membranes. *Biochem. Biophys. Res. Commun.* 313:559–567.
9. Re, F., S. Sesana, …, M. Masserini. 2008. Prion protein structure is affected by pH-dependent interaction with membranes: a study in a model system. *FEBS Lett.* 582:215–220.
10. Dong, S. L., S. A. Cadamuro, …, C. Renner. 2007. Copper binding and conformation of the N-terminal octarepeats of the prion protein in the presence of DPC micelles as membrane mimetic. *Biopolymers.* 88:840–847.
11. Robinson, P. J., and T. J. T. Pinheiro. 2010. Phospholipid composition of membranes directs prions down alternative aggregation pathways. *Biophys. J.* 98:1520–1528.
12. Steunou, S., J. F. Chich, …, J. Vidic. 2010. Biosensing of lipid-prion interactions: insights on charge effect, Cu(II)-ions binding and prion oligomerization. *Biosens. Bioelectron.* 26:1399–1406.
13. Haigh, C. L., S. Y. Marom, and S. J. Collins. 2010. Copper, endoproteolytic processing of the prion protein and cell signalling. *Front. Biosci.* 15:1086–1104, (Landmark ed.).
14. Borchelt, D. R., M. Rogers, …, S. B. Prusiner. 1993. Release of the cellular prion protein from cultured cells after loss of its glycoinositol phospholipid anchor. *Glycobiology.* 3:319–329.
15. Harris, D. A., M. T. Huber, …, R. Wang. 1993. Processing of a cellular prion protein: identification of N- and C-terminal cleavage sites. *Biochemistry.* 32:1009–1016.
16. McMahon, H. E. M., A. Mangé, …, S. Lehmann. 2001. Cleavage of the amino terminus of the prion protein by reactive oxygen species. *J. Biol. Chem.* 276:2286–2291.
17. Mangé, A., F. Béranger, …, S. Lehmann. 2004. Alpha- and beta-cleavages of the amino-terminus of the cellular prion protein. *Biol. Cell.* 96:125–132.
18. Chen, S. G., D. B. Teplow, …, L. Autilio-Gambetti. 1995. Truncated forms of the human prion protein in normal brain and in prion diseases. *J. Biol. Chem.* 270:19173–19180.
19. Guillot-Sestier, M. V., C. Sunyach, …, F. Checler. 2009. The alpha-secretase-derived N-terminal product of cellular prion, N1, displays neuroprotective function in vitro and in vivo. *J. Biol. Chem.* 284:35973–35986.
20. Haigh, C. L., S. C. Drew, …, S. J. Collins. 2009. Dominant roles of the polybasic proline motif and copper in the PrP23-89-mediated stress protection response. *J. Cell Sci.* 122:1518–1528.
21. Walmsley, A. R., N. T. Watt, …, N. M. Hooper. 2009. Alpha-cleavage of the prion protein occurs in a late compartment of the secretory pathway and is independent of lipid rafts. *Mol. Cell. Neurosci.* 40:242–248.
22. Boland, M. P., C. R. Hatty, …, S. J. Collins. 2010. Anionic phospholipid interactions of the prion protein N terminus are minimally perturbing and not driven solely by the octapeptide repeat domain. *J. Biol. Chem.* 285:32282–32292.
23. Karas, J. A., M. Boland, …, D. Scanlon. 2012. Microwave synthesis of prion protein fragments up to 111 amino acids in length generates biologically active peptides. *Int. J. Pept. Res. Ther.* 18:21–29.
24. James, M., A. Nelson, …, F. Klose. 2011. The multipurpose time-of-flight neutron reflectometer "Platypus" at Australia's OPAL reactor. *Nucl. Instrum. Methods Phys. Res. A.* 632:112–123.

25. Saerbeck, T., F. Klose, …, M. James. 2012. Invited article: polarization "down under": the polarized time-of-flight neutron reflectometer PLATYPUS. *Rev. Sci. Instrum.* 83:081301–081312.
26. Nelson, A. 2010. *Motofit*—integrating neutron reflectometry acquisition, reduction and analysis into one, easy to use, package. *J. Phys. Conf. Ser.* 251:012094.
27. Nelson, A. 2006. Co-refinement of multiple-contrast neutron/x-ray reflectivity data using *MOTOFIT*. *J. Appl. Crystallogr.* 39:273–276.
28. Chiu, S. W., E. Jakobsson, …, H. L. Scott. 1999. Combined Monte Carlo and molecular dynamics simulation of fully hydrated dioleyl and palmitoyl-oleyl phosphatidylcholine lipid bilayers. *Biophys. J.* 77:2462–2469.
29. Pabst, G., S. Danner, …, V. A. Raghunathan. 2007. On the propensity of phosphatidylglycerols to form interdigitated phases. *Biophys. J.* 93:513–525.
30. Petrache, H. I., S. Tristram-Nagle, …, J. F. Nagle. 2004. Structure and fluctuations of charged phosphatidylserine bilayers in the absence of salt. *Biophys. J.* 86:1574–1586.
31. Wacklin, H. P. 2010. Neutron reflection from supported lipid membranes. *Curr. Opin. Colloid Interface Sci.* 15:445–454.
32. Le Brun, A. P., T. A. Darwish, and M. James. 2013. Studies of biomimetic cellular membranes using neutron reflection. *J. Chem. Biol. Interfaces.* 1:3–24.
33. Kalb, E., S. Frey, and L. K. Tamm. 1992. Formation of supported planar bilayers by fusion of vesicles to supported phospholipid monolayers. *Biochim. Biophys. Acta—Biomembr.* 1103:307–316.
34. Johnson, S. J., T. M. Bayerl, …, E. Sackmann. 1991. Structure of an adsorbed dimyristoylphosphatidylcholine bilayer measured with specular reflection of neutrons. *Biophys. J.* 59:289–294.
35. Kiessling, V., and L. K. Tamm. 2003. Measuring distances in supported bilayers by fluorescence interference-contrast microscopy: polymer supports and SNARE proteins. *Biophys. J.* 84:408–418.
36. Fernandez, D. I., A. P. Le Brun, …, F. Separovic. 2012. The antimicrobial peptide aurein 1.2 disrupts model membranes via the carpet mechanism. *Phys. Chem. Chem. Phys.* 14:15739–15751.
37. Krueger, S., C. W. Meuse, …, A. L. Plant. 2001. Investigation of hybrid bilayer membranes with neutron reflectometry: probing the interactions of melittin. *Langmuir.* 17:511–521.
38. Lu, N. Y., K. Yang, J. L. Li, B. Yuan, and Y. Q. Ma. 2013. Vesicle deposition and subsequent membrane-melittin interactions on different substrates: a QCM-D experiment. *Biochim. Biophys. Acta—Biomembr.* 1828:1918–1925.
39. McCubbin, G. A., S. Praporski, …, L. L. Martin. 2011. QCM-D fingerprinting of membrane-active peptides. *Eur. Biophys. J.* 40:437–446.
40. Piantavigna, S., P. Czihal, …, L. L. Martin. 2009. Cell penetrating apidaecin peptide interactions with biomimetic phospholipid membranes. *Int. J. Pept. Res. Ther.* 15:139–146.
41. Knappe, D., S. Piantavigna, …, R. Hoffmann. 2010. Oncocin (VDKPPYLPRPRPPRRIYNR-NH2): a novel antibacterial peptide optimized against gram-negative human pathogens. *J. Med. Chem.* 53:5240–5247.
42. Dante, S., T. Hauss, …, N. A. Dencher. 2011. Nanoscale structural and mechanical effects of beta-amyloid (1–42) on polymer cushioned membranes: a combined study by neutron reflectometry and AFM Force Spectroscopy. *Biochim. Biophys. Acta—Biomembr.* 1808:2646–2655.
43. Chi, E. Y., C. Ege, …, K. Y. C. Lee. 2008. Lipid membrane templates the ordering and induces the fibrillogenesis of Alzheimer's disease amyloid-beta peptide. *Proteins.* 72:1–24.
44. Hellstrand, E., M. Grey, …, E. Sparr. 2013. Adsorption of α-synuclein to supported lipid bilayers: positioning and role of electrostatics. *ACS Chem. Neurosci.* 4:1339–1351.
45. Jao, C. C., B. G. Hegde, …, R. Langen. 2008. Structure of membrane-bound alpha-synuclein from site-directed spin labeling and computational refinement. *Proc. Natl. Acad. Sci. USA.* 105:19666–19671.
46. Bisaglia, M., S. Mammi, and L. Bubacco. 2009. Structural insights on physiological functions and pathological effects of alpha-synuclein. *FASEB J.* 23:329–340.
47. Cornely, R., C. Rentero, …, K. Gaus. 2011. Annexin A6 is an organizer of membrane microdomains to regulate receptor localization and signalling. *IUBMB Life.* 63:1009–1017.
48. Osiecka, K. M., H. Nieznanska, …, K. Nieznanski. 2009. Prion protein region 23-32 interacts with tubulin and inhibits microtubule assembly. *Proteins.* 77:279–296.
49. Taylor, D. R., N. T. Watt, …, N. M. Hooper. 2005. Assigning functions to distinct regions of the N-terminus of the prion protein that are involved in its copper-stimulated, clathrin-dependent endocytosis. *J. Cell Sci.* 118:5141–5153.
50. Lu, L., and W. Hong. 2014. From endosomes to the trans-Golgi network. *Semin. Cell Dev. Biol.* 31:30–39.
51. Coleman, B. M., E. Hanssen, …, A. F. Hill. 2012. Prion-infected cells regulate the release of exosomes with distinct ultrastructural features. *FASEB J.* 26:4160–4173.
52. Von Bartheld, C. S., and A. L. Altick. 2011. Multivesicular bodies in neurons: distribution, protein content, and trafficking functions. *Prog. Neurobiol.* 93:313–340.
53. Vella, L. J., R. A. Sharples, …, A. F. Hill. 2007. Packaging of prions into exosomes is associated with a novel pathway of PrP processing. *J. Pathol.* 211:582–590.
54. von Zastrow, M., and A. Sorkin. 2007. Signaling on the endocytic pathway. *Curr. Opin. Cell Biol.* 19:436–445.
55. Taub, N., D. Teis, …, L. A. Huber. 2007. Late endosomal traffic of the epidermal growth factor receptor ensures spatial and temporal fidelity of mitogen-activated protein kinase signaling. *Mol. Biol. Cell.* 18:4698–4710.
56. Zhang, Z., Y. Zhang, …, J. Ma. 2013. De novo generation of infectious prions with bacterially expressed recombinant prion protein. *FASEB J.* 27:4768–4775.
57. Lawson, V. A., S. A. Priola, …, B. Chesebro. 2004. Flexible N-terminal region of prion protein influences conformation of protease-resistant prion protein isoforms associated with cross-species scrapie infection in vivo and in vitro. *J. Biol. Chem.* 279:13689–13695.
58. Zurawel, A. A., D. J. Walsh, …, S. Supattapone. 2014. Prion nucleation site unmasked by transient interaction with phospholipid cofactor. *Biochemistry.* 53:68–76.
59. Lewis, V., A. F. Hill, …, S. J. Collins. 2009. Increased proportions of C1 truncated prion protein protect against cellular M1000 prion infection. *J. Neuropathol. Exp. Neurol.* 68:1125–1135.
60. Chich, J. F., C. Chapuis, …, S. Noinville. 2010. Vesicle permeabilization by purified soluble oligomers of prion protein: a comparative study of the interaction of oligomers and monomers with lipid membranes. *J. Mol. Biol.* 397:1017–1030.
61. Wang, F., S. Yin, …, J. Ma. 2010. Role of the highly conserved middle region of prion protein (PrP) in PrP-lipid interaction. *Biochemistry.* 49:8169–8176.

MEK1 transduces the prion protein N2 fragment antioxidant effects

C. L. Haigh, A. R. McGlade & S. J. Collins

Cellular and Molecular Life Sciences

ISSN 1420-682X
Volume 72
Number 8

Cell. Mol. Life Sci. (2015) 72:1613-1629
DOI 10.1007/s00018-014-1777-y

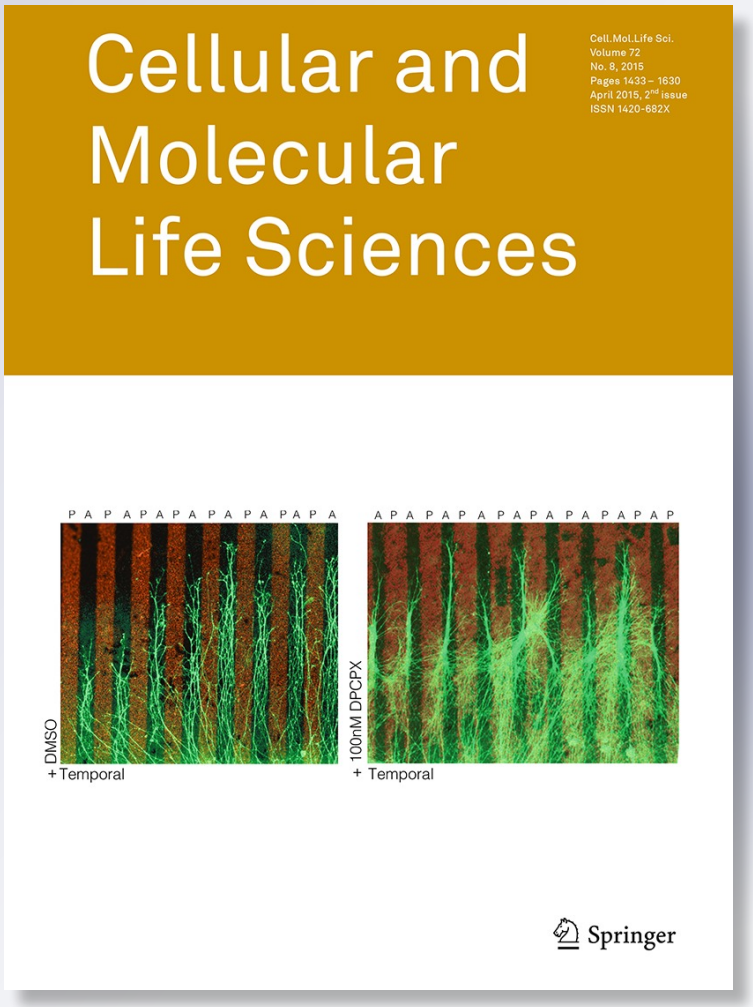

Springer

Cell. Mol. Life Sci. (2015) 72:1613–1629
DOI 10.1007/s00018-014-1777-y

Cellular and Molecular Life Sciences

RESEARCH ARTICLE

MEK1 transduces the prion protein N2 fragment antioxidant effects

C. L. Haigh · A. R. McGlade · S. J. Collins

Received: 27 June 2014 / Revised: 13 October 2014 / Accepted: 6 November 2014 / Published online: 13 November 2014

Abstract The prion protein (PrP^C) when mis-folded is causally linked with a group of fatal neurodegenerative diseases called transmissible spongiform encephalopathies or prion diseases. PrP^C normal function is still incompletely defined with such investigations complicated by PrP^C post-translational modifications, such as internal cleavage, which feasibly could change, activate, or deactivate the function of this protein. Oxidative stress induces β-cleavage and the N-terminal product of this cleavage event, N2, demonstrates a cellular protective response against oxidative stress. The mechanisms by which N2 mediates cellular antioxidant protection were investigated within an in vitro cell model. N2 protection was regulated by copper binding to the octarepeat domain, directing the route of internalisation, which stimulated MEK1 signalling. Precise membrane interactions of N2, determined by copper saturation, and involving both the copper-co-ordinating octarepeat region and the structure conferred upon the N-terminal polybasic region by the proline motif, were essential for the correct engagement of this pathway. The phenomenon of PrP^C post-translational modification, such as cleavage and copper co-ordination, as a molecular "switch" for activation or deactivation of certain functions provides new insight into the apparent multi-functionality of PrP^C.

Keywords CJD · N-terminus · PrP23-89 · Beta-cleavage · Reactive oxygen species · Signal transduction · Mitogen-activated protein kinase

Introduction

Prion diseases, fatal and transmissible neurodegenerative diseases of humans and animals, are causally linked with the prion protein (PrP). The disease-associated isoforms of the prion protein (PrP^{Sc}) are conformationally altered forms of a 'normal' cellular protein (PrP^C). The predominant central nervous system function of PrP^C is as yet undefined; however, various studies have reported a neuroprotective role [1–7]. PrP^C undergoes at least two internal cleavage events, termed α- and β-cleavage, producing N1/C1 and N2/C2 fragment pairs, respectively [8, 9]. Diversity in functionality of the different PrP fragments, may contribute to the difficulties in assigning one single function to PrP^C with each fragment potentially exerting unique effects on the cell. Hence, the possibility that PrP^C cleavage acts as a post-translational molecular "switch" has been suggested [10, 11].

The products of PrP^C β-cleavage are increased in human prion-diseased brains and mouse models of prion disease, concurrent with the appearance of PrP^{Sc}, and therefore, PrP^C β-cleavage has been mainly considered a likely pathogenic event [9, 12, 13]. However, inability to undergo β-cleavage has been shown to render cells in culture more vulnerable

Electronic supplementary material The online version of this article (doi:10.1007/s00018-014-1777-y) contains supplementary material, which is available to authorized users.

C. L. Haigh (✉) · A. R. McGlade · S. J. Collins (✉)
Department of Pathology, Melbourne Brain Centre, The University of Melbourne, Parkville, Melbourne 3010, Australia
e-mail: chaigh@unimelb.edu.au

S. J. Collins
e-mail: stevenjc@unimelb.edu.au

A. R. McGlade
Mental Health Research Institute, The University of Melbourne, Parkville, Melbourne 3010, Australia

S. J. Collins
Florey Department of Neuroscience and Mental Health, The University of Melbourne, Melbourne, VIC 3010, Australia

during times of oxidative stress, when an imbalance between reactive oxygen species (ROS) production and detoxification causes cell damage leading to death [14]. During the course of prion infection, oxidative damage occurs in the brain paralleling increased deposition of PrP^{Res} (a protease-resistant species of PrP considered a biochemical marker for PrP^{Sc}; [12]) and cellular compensation responses are essential for maintaining homoeostasis and viability in chronically infected cultured cells [15, 16]. Significantly, the β-cleavage event, itself, is caused by ROS [17] and, therefore, in contrast to being a toxic event of prion disease, this endoproteolysis may form part of a cellular protective response against heightened oxidative stress.

Recently the N-terminus of PrP has received considerable attention with diverse findings demonstrating that it is integral to PrP^{Sc}-mediated toxicity [18, 19], influences conversion of PrP^{C} to PrP^{Sc} [20–22], exerts a neuroprotective function [23, 24] and binds to soluble oligomeric amyloid-β (Aβ) peptides [25, 26] mediating the toxic signalling of oligomeric Aβ in Alzheimer's disease, unless PrP^{C} undergoes α-cleavage, whereby the N1 fragment is reported to be protective against Aβ toxicity [27, 28].

Our previous work has shown that the N-terminal β-cleavage fragment (N2) is able to reduce intra-cellular ROS induced by serum deprivation, a reaction requiring copper saturation of the eight amino acid repeat (octarepeat) domain [24]. When the regions of N2 that are important for the transduction of the protective signal were investigated, it was found that amino acid residues 23–50 alone were sufficient to initiate the reaction, indicating that the octameric repeat region (residues 51–89) played a restraining role with inhibition of signalling when present in its apo form. Transduction of the protective effect additionally required cell surface proteins, the glycosaminoglycan (GAG) heparan sulphate (HS) and intact lipid-raft domains, and was dependent upon a proline motif within the far N-terminal polybasic region. To investigate the mechanism of neuroprotective signal transduction by N2 from the exterior of the cell, this study followed N2 trafficking and assessed candidate signal transduction pathways. Our results show that MEK1 signalling is the primary mediating pathway, which is dependent upon intra-cellular trafficking, a process highly influenced by N2 copper saturation.

Materials and methods

Generation of PrP peptide sequences

The synthetic peptides derived from the mouse PrP23-89 sequence have been described previously [24] and were made as described in Karas et al. [29].

Cell culture

CF10 (PrP null, mouse neuronal; [30]), Neuro2a (N2a; mouse neuroblastoma) and OBL-21 (mouse olfactory bulb) cells were cultured in Dulbecco's Modified Eagle's Medium (DMEM; Lonza, AUS) supplemented with 10 % (v/v) foetal bovine serum (Lonza) and 50 U/ml penicillin/50 μg/ml streptomycin solution (Sigma, Melbourne, VIC, AUS). Cell cultures were maintained at 37 °C with 5 % CO_2 in a humidified incubator.

DCFDA assay

The DCFDA assay using 5 μM 5-(and-6)-chloromethyl-2′,7′-dichlorodihydro-fluorescein diacetate, acetyl ester (CM-H_2-DCFDA; Invitrogen, VIC, AUS) was performed as described previously [24, 31].

MTS viability/metabolism assay

Five microlitres of one solution MTS reagent (Promega; VIC AUS) per 100 μl media was added to test and medium-only background control conditions, and incubated under normal culture conditions for 90 min. Reaction product was quantified using absorbance at 462 nm in a Fluostar Optima (BMG Labtech, VIC, AUS).

CyQUANT DNA assay

The CyQUANT assay (Invitrogen) was carried out as per the manufacturer's product protocol for CyQUANT® NF.

Cytosolic redox potential

Cells were incubated in Opti-MEM®I reduced serum culture medium (phenol red free; Invitrogen) containing 5 μM RedoxSensor™ Red CC-1 probe (Invitrogen) and 1 μM MitoTracker® Green (Invitrogen) for 10 min. Media was removed and cells were incubated in fresh media with or without serum and test peptides.

Fluorescence and confocal microscopy

Fluorescence microscope images were visualised with a 60× oil immersion lens and captured using a Nikon Eclipse TE2000-E epi-fluorescence microscope (Nikon-Roper Scientific).

Confocal images were collected on a Leica SP8 using a 60× oil immersion lens. For quantification, all image parameters were maintained throughout an experiment, across all conditions, and the channels of probes sensitive to photo-oxidation were collected before other channels.

For imaging data, the '*n*' represents independent experiments, which each included capturing sufficient fields to analyse >50 cells per experiment. Cell intensity and co-localisation analyses were performed using Nikon NIS-elements 3.0 software with regions of interest used to gate individual cells.

Indirect immunofluorescence

Cells were grown on 13 mm glass coverslips in standard media with immunofluorescence (IF) performed when cells were 80 % confluent. Plates were incubated in the dark at all light-sensitive stages during this protocol. Cells were fixed in 4 % (v/v) paraformaldehyde/PBS for 20 min and then permeabilised in immunodiluent (ID; 1 % w/v BSA in PBS) with 0.1 % (v/v) Triton-X 100 for 5 min. Coverslips were blocked with ID containing 10 % FBS (v/v) for 30 min. Primary antibodies against PrP Saf32 (1 in 200; Cayman Chemical, Sapphire Biosciences, AUS) and 8B4 (1 in 200; Alicon Switzerland), LAMP-1 (1 in 100; Abcam, AUS), SOD2 (1 in 100; Abcam), and pMEK1 (1 in 100; Abcam) were diluted in ID and applied overnight at 4 °C. Alexafluor488/647-conjugated goat anti-rabbit/mouse secondary antibodies (Invitrogen) diluted 1 in 250 in ID were applied for 1–2 h at room temperature. Coverslips were mounted onto glass slides with mowiol or Pro-Long antifade (Invitrogen) mounting media.

Laurdan live cell imaging assay

Cells were incubated with a 5 μM solution of laurdan probe (Invitrogen) in normal media for 30 min prior to beginning the assay. At time 0, normal media was replaced with serum-free, phenol red-free OptiMEM. Peptide was added to a final concentration of 10 μM at the start of imaging and images were collected every minute for 10 min using a near UV excitation and blue emission filter set.

MitoSOX assay

Cells were labelled with 5 μM MitoSOX fluorescent indicator probe (Invitrogen) in standard media for 10 min under routine incubator conditions (as described above). Media was then replaced with fresh, phenol red-free OptiMEM for the duration of the experiment.

Pull-down assays

Dynabeads amine (Invitrogen) were resuspended by brief vortexing. Two hundred and fifty microlitres of bead suspension was transferred into microfuge tubes. Beads were washed twice, by magnetic separation, in conjugation buffer (0.1 M MES, 0.5 M NaCl, pH 6) and resuspended in 200 μl of conjugation buffer. One hundred and fifty micrograms of each peptide was resuspended in 800 μl conjugation buffer and added to the beads, with brief vortex mixing. Ten milligrams EDC and 15 mg NHS (Sigma-Aldrich) were dissolved in 1 ml cold deionised H_2O immediately prior to use and 15 μl EDC/NHS solution per reaction added with brief vortexing. Samples were incubated for 2 h at room temperature with slow tilt rotation. Hydroxylamine, to a final concentration of 10 mM, was added to quench the reaction and incubated for 15 min at room temperature with slow tilt rotation. Beads were washed three times with PBS-BSA followed by a final PBS only wash. Coated beads were resuspended in 250 μl PBS. Cells were lysed either mechanically in PBS (by freeze-fracture followed by needle aspiration) or using detergent (0.1 % Triton-X-100 in PBS). One milligram total cell lysate (protein quantification was achieved using BCA assay—Pierce) was diluted into 950 μl PBS and added to the coated beads. Lysates and beads were incubated at room temperature with slow tilting rotation for 1 h. Beads and supernatants were separated magnetically and supernatants were kept. Beads were washed three times with PBS and once in a detergent wash (0.1 % Triton-X-100 in PBS) before elution. Elutions were carried out in the order of deceasing pH followed by increasing salt and finally the beads were boiled to remove anything still bound. For each elution, 100 μl of elution buffer was added to beads, which were briefly vortexed then incubated at room temperature for 2 min of gentle mixing before collecting. The elution buffers used were 0.01 M MES, pH 6 (1.95 g/L MES, 8.75 g/L NaCl); acetate buffer pH 5 (0.6 g/L acetic acid, 8.75 g/L NaCl); acetate buffer pH 4 (0.6 g/L acetic acid, 8.75 g/L NaCl); 0.1 M citrate buffer, pH 3 (21 g/L citric acid); 300 mM NaCl; 1 M NaCl.

Dot blotting

Two microlitres per spot was dotted onto dry nitrocellulose and spots dried for 1 h at 37 °C. Membranes were then blotted as per the western blot procedures using 1 in 100,000 CTXb-HRP (Sigma-Aldrich) and 1 in 1,000 10E4 primary antibody (Jomar Bioscience, SA) with 1 in 2,000 anti-mouse-HRP secondary antibody.

Western blotting

Cells were lysed in RIPA buffer [50 mM Tris–HCl pH 7.4, 150 mM NaCl, 0.1 % (w/v) SDS, 0.5 % (w/v) sodium deoxycholate, 1 % (v/v) NP-40] with 1 in 2000 benzonase (Sigma) at 37 °C for 20 min. Samples were electrophoresed using the NuPAGE system (Invitrogen), transferred onto PVDF membranes (millipore) and blocked as

described previously [32]. Protein of interest detection was made using the following dilutions of primary antibodies; 1 in 1,000 37/67 kDa laminin receptor (Abcam), pMEK1 (Abcam), pMEK2 (Abcam), pAKT (Abcam), pERK1/2 (Cell Signalling Technologies, Genesearch, AUS), 1 in 400 p-p38 (R&D Systems, Sapphire Biosciences); and 1 in 5,000 Actin (Sigma-Aldrich) in phosphate buffered saline with 0.1 % (v/v) Tween-20 (PBS-t). Secondary antibodies (Dako, Melbourne, VIC, AUS) were used at 1 in 2,000 for the signalling proteins and 1 in 5,000 for actin. ECL-advance (GE-Healthcare) was used to visualise bands with images collected using a Las-3000 intelligent dark box (FujiFilm, Berthold, Victoria AUS). Following blotting, total protein levels on all gels were assessed to ensure even loading by Coomassie brilliant blue staining [0.1 % (w/v) Coomassie Brilliant Blue in 50 % (v/v) methanol and 7 % (v/v) acetic acid] for 2 min at room temperature with agitation. Membranes were rinsed briefly in destain [50 % (v/v) methanol and 7 % (v/v) acetic acid], then washed in de-stain for 10 min before drying for image capture.

Statistical analyses

Statistical analyses were carried out using GraphPad Prism 5 statistical software. Data are represented as mean ± -SEM. The numerical value for each independent experiment ('*n*') is the average of the technical replicates. Primary statistical tests are stated in the text and tested with 95 % confidence intervals. For ANOVA analysis Tukey's (comparisons of all conditions) or Dunnett's (comparisons with control values) secondary tests were applied.

Results

We have previously shown that a synthetic peptide equivalent to the PrP^C N2 fragment (PrP23-89 and fragments thereof, Fig. 1a) can reduce intra-cellular ROS burden in response to the stress of serum deprivation [24]. Copper coordination was important for the action of full-length PrP23-89. Serum deprivation was used as a mild insult that induces intracellular ROS and changes cellular metabolism but does not cause acute cell death (Sup Fig. 1 [24]). To extend our previous work, we performed a dose–response following the activity of copper and zinc-saturated (four molar equivalents) PrP23-89 on the intracellular ROS production in CF10 cells (*prnp* gene ablated [30]; these cells are used throughout unless otherwise stated). The response showed significant ROS reduction by the copper-saturated PrP23-89 fragment at 1 and 10 μM (Fig. 1b; One-way ANOVA, $F = 5.327$, $p = 0.019$, $n = 3$; copper-only responses are shown in Sup Fig. 2), but no significant decrease was observed when zinc loaded (One-way ANOVA, $F = 2.26$, $p = 0.07$, $n = 4$). A dose–response curve of the apo PrP23-89 ROS response has previously been published [24]. Further analysis of the metabolism of these cells showed that the ROS reduction seen when copper-bound is not due to a loss of cellular viability; however, viability is reduced when zinc-bound (Fig. 1c; 2-way ANOVA, $F = 6.833$, $p < 0.001$, $n = 3$). No zinc toxicity was observed in the absence of the N2 peptide (Sup Fig. 2).

The peptides were applied exogenously, therefore, the cell surface interactions of the apo- and copper-saturated PrP23-89 were investigated by IF localisation. Peptides were added to the serum-free media and cells incubated for 15 min before fixing. Two antibodies, 8B4 and Saf32 (recognising different epitopes, Fig. 1a) were used to probe peptide binding to the cell surface in unpermeabilised cells and throughout the cell, using Triton-X-100 permeabilisation after fixing. The cell surface (unpermeabilised) staining with the 8B4 antibody showed no difference in the pattern of staining or total intensity between the copper-loaded and apo-PrP23-89 applications (Fig. 1d). However, the PrP23-89 showed altered cell surface interactions when detection was performed with the Saf32 antibody (directed against the octameric repeat region). Here, when the copper-loaded PrP23-89 peptide was examined, slides were almost completely devoid of antibody signal (Fig. 1d; One-way ANOVA, $F = 10.27$, $p = 0.0003$). In permeabilised cells, no significant differences in the intensity of cell staining were seen across any condition (Fig. 1d; One-way ANOVA, $F = 1.391$, $p = 0.276$, $n = 3$). Control staining of permeabilised CF10 cells showed signal is specific for PrP23-89 (Fig. 1e). When cells were exposed to PrP23-89 with and without copper-loading for a longer time period, 90 min, the intra-cellular staining pattern was visibly

Fig. 1 Copper saturation of N2 influences its anti-oxidant function, cell surface interactions and trafficking. **a** Schematic of the PrP N2 cleavage fragment (residues 23–89) with antibody binding sites and the P26/28A mutation shown. The octarepeat (copper-binding) region is indicated in *blue*. **b** Log_{10} dose–response of the intracellular ROS reduction activity displayed by copper-saturated (*filled bars*) and zinc-saturated (*hollow bars*) PrP23-89 following serum deprivation. **c** Measurement of MTS metabolism 24 h after serum deprivation and peptide addition. **d** Antibody detection of the PrP23-89 fragment at the cell surface (non-permeabilised cells) and inside the cell 15 min after peptide addition with or without copper saturation. Antibody signal is shown in *green* and *blue* staining indicates DAPI within the nucleus. Graphs show quantification of the detected PrP23-89 signal with *white bars* indicating apo-PrP23-89 and *blue bars* indicating copper-saturated PrP23-89 staining. **e** Staining of CF10 cells in the absence of peptide addition to control for non-specific antibody binding. **f** Immunofluorescent detection of PrP23-89 inside of cells 90 min post-peptide addition with or without copper. **g** Immunofluorescent detection of PrP23-89P26/28A at the cell surface, with and without copper saturation, 15 min after peptide addition. *Scale bars* = 25 μm. $*p < 0.05$, $**p < 0.01$, $***p < 0.001$

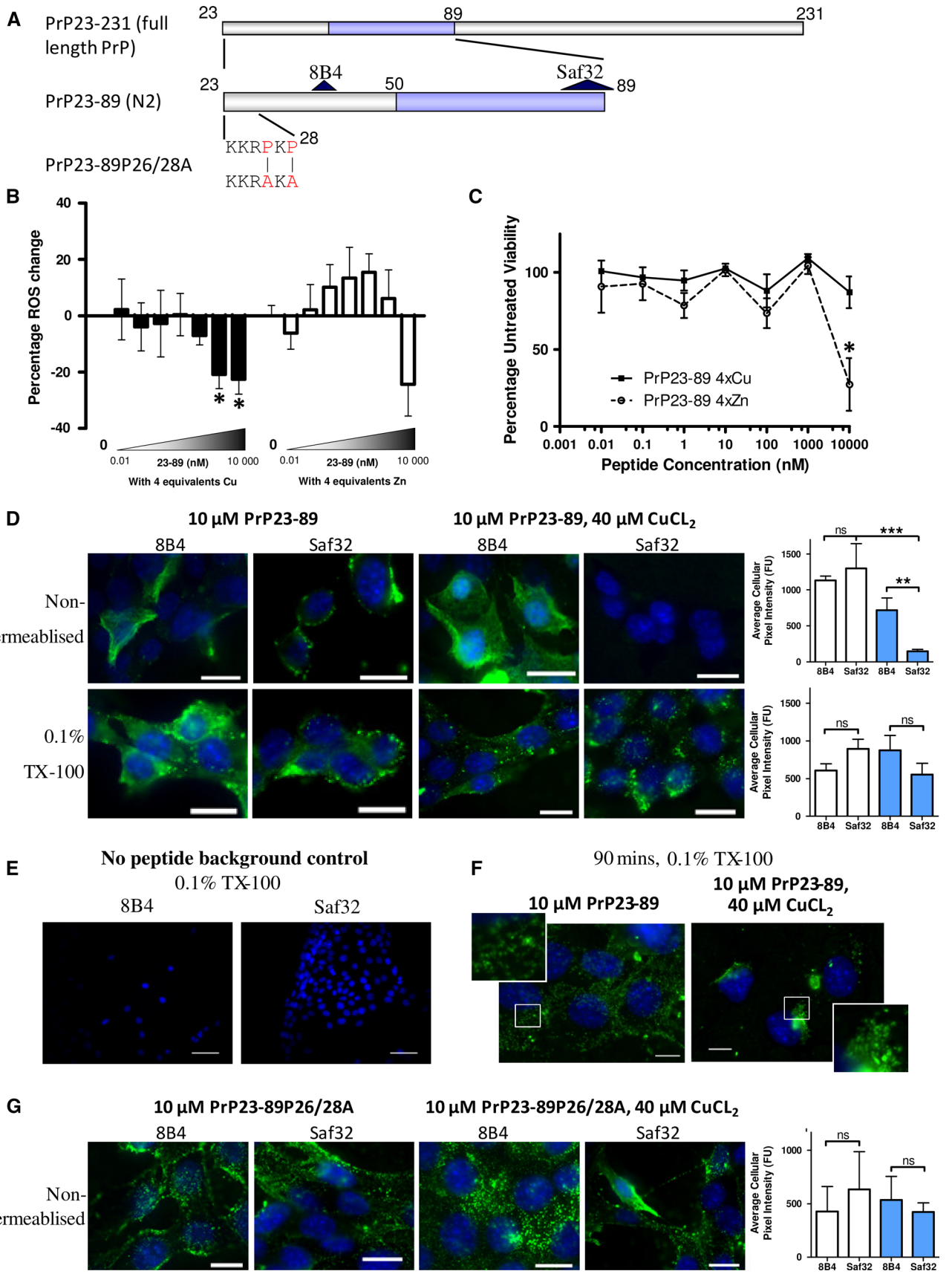

different between the two conditions; the apo-PrP23-89 appeared more diffuse with greater cell surface staining and the copper-loaded PrP23-89 showed a punctuate, vesicular, and sometimes perinuclear staining pattern (Fig. 1f).

To explore whether the lack of Saf32 immuno-reactivity with the copper-loaded PrP23-89 was due to copper co-ordination changing epitope availability, PrP23-89P26/28A, a peptide with the two proline residues at positions 26 and 28 mutated to alanine (Fig. 1a), was incubated with the CF10 cells under the same apo- and copper-saturated conditions. This mutant peptide, previously shown to co-ordinate copper in an identical way to PrP23-89 [24], was clearly detectable at the cell surface with Saf32 in both the apo- and copper-saturated states with signal no longer significantly different from 8B4 detection or the apo-peptide (Fig. 1g; One-way ANOVA, $F = 0.1595$, $p = 0.9209$, $n = 3$).

As the intracellular trafficking and sub-cellular localisation of the PrP23-89 peptide was influenced by its copper saturation, we investigated whether altering trafficking pathways would alter antioxidant activity. First, we assessed the influence of internalisation inhibition on intracellular ROS production using the DCFDA assay. The results showed that serum deprivation causes a large increase in intracellular ROS production (student's t test; $t = 12.7$, $p < 0.001$, $n = 3$; Fig. 2a; Sup Fig. 1F) and this was significantly reduced when internalisation was impeded using inhibitors of clathrin-mediated (T-A23) and dynamin-mediated (Dynasore) pathways (Fig. 2b; One-way ANOVA; $F = 52.7$, $p < 0.001$, $n = 4$). For all internalisation (and signalling) pathway inhibition studies, a dose–response curve of the inhibiting compound for both ROS production and cellular viability was tested (Sup Fig. 3) from which a concentration of compound that might influence the pathway, without causing gross cell death, was determined.

To assess the involvement of internalisation pathways in PrP N-terminally mediated intra-cellular ROS reduction response, a C-terminally truncated fragment of PrP23-89, PrP23-50, was used. The PrP23-50 fragment was previously shown to reduce intracellular ROS in the absence of the octarepeat region [24], thus not requiring copper and the use of this peptide, therefore, eliminates any confounding effects of adding redox-active copper to these reactions. Results are shown relative to the internalisation inhibitor action on serum-deprived cells; a decrease is indicative of the inhibitor and PrP23-50 effects being additive (suggesting different pathway engagement) and where no change or an attenuated response is seen the effects of the peptide may be competing with the internalisation inhibitor for engagement of the same pathway or mechanism, with overall negation of any additional effect of the PrP23-50. Inhibition of internalisation significantly reduced the ROS mitigating action of PrP23-50 with both T-A23 and dynasore-treated cells showing significantly different responses from the PrP23-50 action without inhibitors, and for the dynasore-treated cells, ROS reduction was no longer significantly different to that of the serum-deprived cells alone (Fig. 2c; One-way ANOVA; $F = 4.908$, $p = 0.0407$, $n = 3$). We have previously detected PrP23-50 in cell lysates harvested after exogenous application [24], indicating that the peptide is taken up by cells. As such we considered if cell membrane changes were occurring in real time. Laurdan fluorescent membrane probe was loaded into cells before addition of PrP23-50, or a random sequence (RS) peptide to control for random peptide uptake effects on membranes, and a time course of images to 10 min were collected. Cells exposed to PrP23-50 showed increased movement and retraction of their membranes into a smaller area, which was not seen for the RS peptide.

Elucidating the localisation of ROS production was considered important for identifying the site of PrP23-89 activity. To determine the site(s) of ROS production within the cell following serum deprivation and whether this site/these sites were the target of N2 action, intracellular ROS-localisation probes RedoxSensor Red (cytosolic and lysosomal ROS [33]) and mitoSOX (mitochondrial superoxide) were incubated within live cells throughout serum deprivation and peptide treatments. Increased ROS production upon serum deprivation was detected by RedoxSensor Red. RedoxSensor Red partitions into mitochondria if it is oxidised in the cytosol otherwise it is transported to lysosomes where it is oxidised. We analysed the contributions of cytosolic and lysosomal ROS to oxidation of this probe using co-localisation with MitoTracker [33] (Fig. 3a), which indicated the significant increase was not contributed by cytosolic ROS (Fig. 3b; One-way ANOVA; $F = 2.395$, $p = 0.0937$, $n = 4$) but instead by lysosomes (Fig. 3c; One-way ANOVA; $F = 5.31$, $p = 0.0072$, $n = 4$). Copper-loaded N2 significantly reduced the ROS produced in the lysosomes. Mitochondrial superoxide production was also significantly increased in response to serum deprivation and PrP23-89 was able to reduce superoxide production back to insignificance against that produced by cells incubated in serum-containing media both when applied apo and copper-loaded (Fig. 3d, e). The same ROS reduction response was reproduced by the PrP23-50 peptide for both the RedoxSensor Red and MitoSOX probes (Sup Fig. 6 and 7). Despite being sites of ROS production neither lysosomal nor mitochondrial function, as determined by acidity and ATP levels, respectively, were altered (Sup Fig. 4). However, incubation with the PrP23-89 peptide (either with or without copper saturation) did increase cell viability at 24 h post-exposure (Sup Fig. 5).

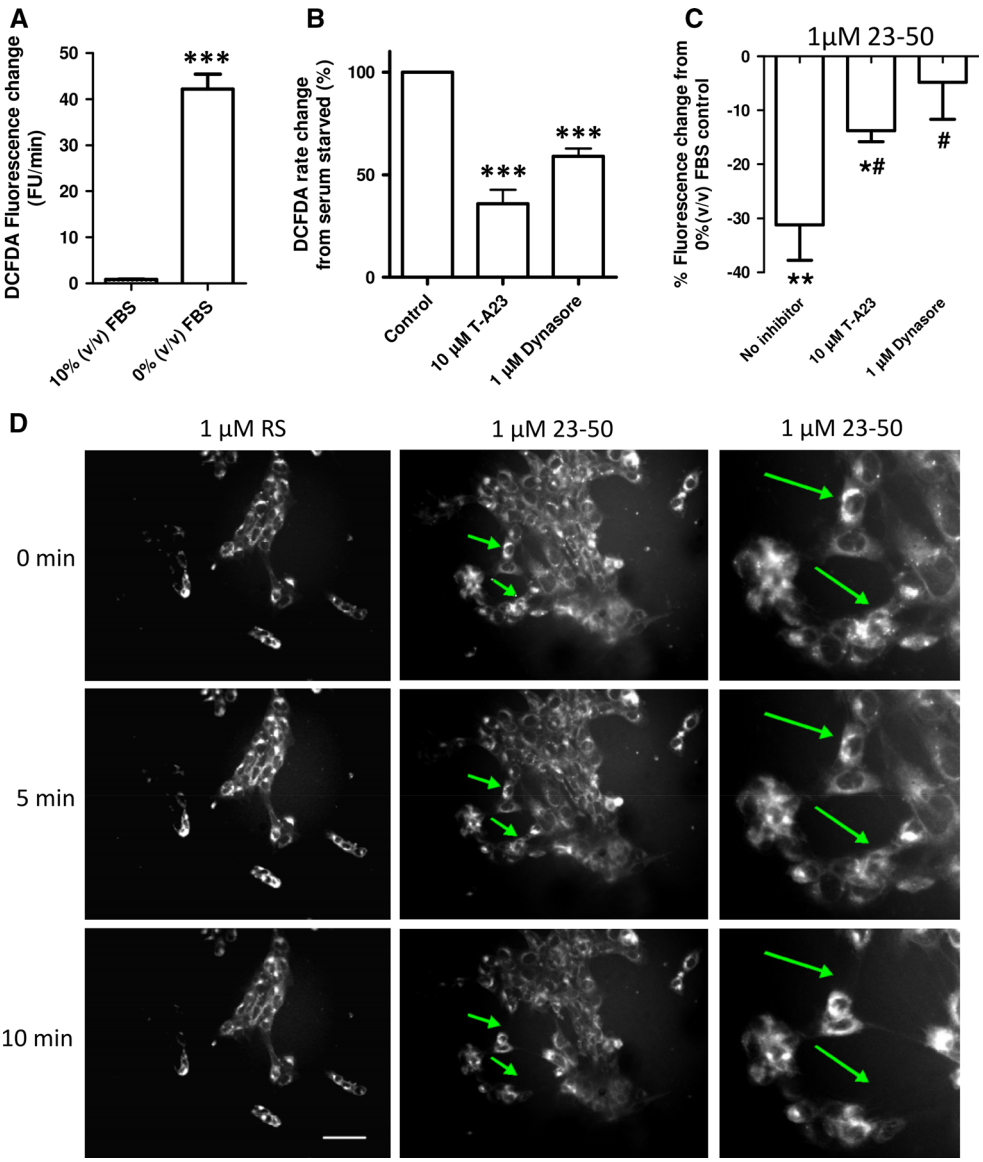

Fig. 2 Inhibition of internalisation reduces stress-induced intracellular ROS and inhibits the protective action of PrP23-50. **a** DCFDA assay for the detection of intracellular ROS produced in response to serum deprivation. **b** Cells were stressed by serum deprivation with or without the internalisation inhibitors T-A23 and Dynasore. Changes are shown normalised to 0 % (v/v) serum control values as 100 % ROS production. **c** Measurement of the percentage ROS reduction exerted by PrP23-50 with and without internalisation inhibition. Results are shown as percentage reduction from the serum-deprived ∓ inhibitor control. *Asterisks* denote significantly different from no peptide control (*$p < 0.05$, **$p < 0.01$, ***$p < 0.001$) and *hash* shows significantly different from the no inhibitor action of PrP23-50 (# < 0.05). **d** Incorporation of the lipophilic dye laurdan into cell membranes before treatment with PrP23-50 (or a RS peptide control) in serum-free media

To test if the effects on cellular ROS producing systems were directly due to the actions of the N-terminal peptides (the peptides themselves have no intrinsic anti-oxidant activity [24]), cytosolic ROS and lysosomal ROS production were investigated using inhibition of NADPH oxidase (NOX; a cytosolic signalling protein that generates superoxide to signal) and inhibitors of lysosomal acidity/acidification. The inhibitors were incubated with the serum-deprived cells and ROS production measured by DCFDA assay. No significant changes in ROS response to serum deprivation were seen with any of these inhibitors (Fig. 4a; One-way ANOVA; $F = 2.528$, $p = 0.0941$, $n = 5$). The model PrP23-50 peptide was used to look at capacity to reduce the serum deprivation-induced ROS in the presence of the NOX and lysosomal acidity/acidification inhibitors. PrP23-50 treatment of the serum-deprived cells treated with the NOX and lysosomal inhibitors showed no significant difference from the serum-deprived no inhibitor control (One-way ANOVA; $F = 2.202$, $p = 0.1453$, $n = 3$); however, the bafilomycin-treated cell response was variable and no longer significantly different from the no peptide control serum-deprived ROS production (Fig. 4b; student's t test; $t = 2.794$, $p = 0.0682$, $n = 4$). We additionally investigated the co-localisation of PrP23-89 when applied both copper-saturated and in the apo form with the lysosomal marker Lamp 1 and the mitochondrially localised superoxide dismutase (SOD)-2. The peptides were incubated with the cells for 90 min before fixing to allow significant internalisation to occur. Whilst a small amount of co-staining was seen for

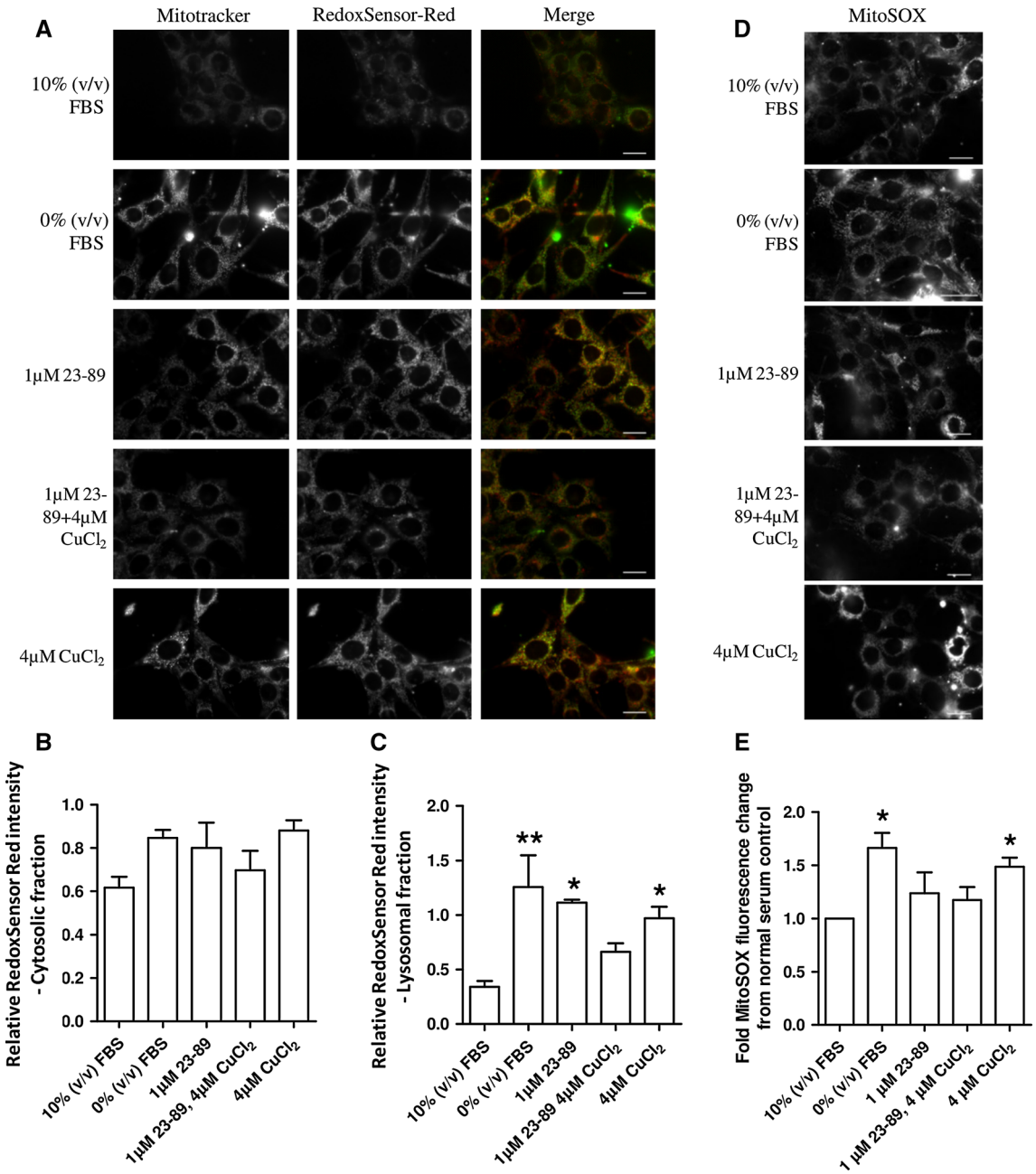

Fig. 3 Copper-saturated PrP23-89 reduces the lysosomal and mitochondrial ROS caused by serum deprivation. **a** Representative plates of RedoxSensor Red changes due to serum deprivation and as influenced by PrP23-89 with and without copper saturation. RedoxSensor Red fluorescence was co-localised with MitoTracker green to indicate compartmental partitioning. *Scale bars* = 25 μM. Quantification of the cytosolic [co-localised with MitoTracker; (**b**)] and lysosomal (**c**) ROS fractions shown relative to 10 % (v/v) serum control. **d** Representative plates of mitoSOX fluorescence production in response to serum deprivation. *Scale bars* = 25 μM. **e** Quantification of mitoSOX fluorescence intensity. $*p < 0.05$, $**p < 0.01$

copper-bound PrP23-89 with SOD2, the staining did not suggest a pronounced co-localisation of PrP23-89 with either of these organelle markers (Fig. 4c, d).

We next considered if we could detect a putative receptor for N-terminal PrP that might be involved in mediating the N2 protective signalling. To look for N-terminal binding partners, we conjugated PrP23-50, PrP30-50 (lacking the N-terminal polybasic domain), and PrP51-89 to magnetic beads. The beads were incubated with whole cell lysate prepared by mechanical disruption or detergent lysis. Lysate was separated from the beads and beads were washed four times. Elution of bound proteins was done using decreasing pH (6, 5, 4, 3), followed by two high salt washes (0.3 and 1 M NaCl—to disrupt GAG-

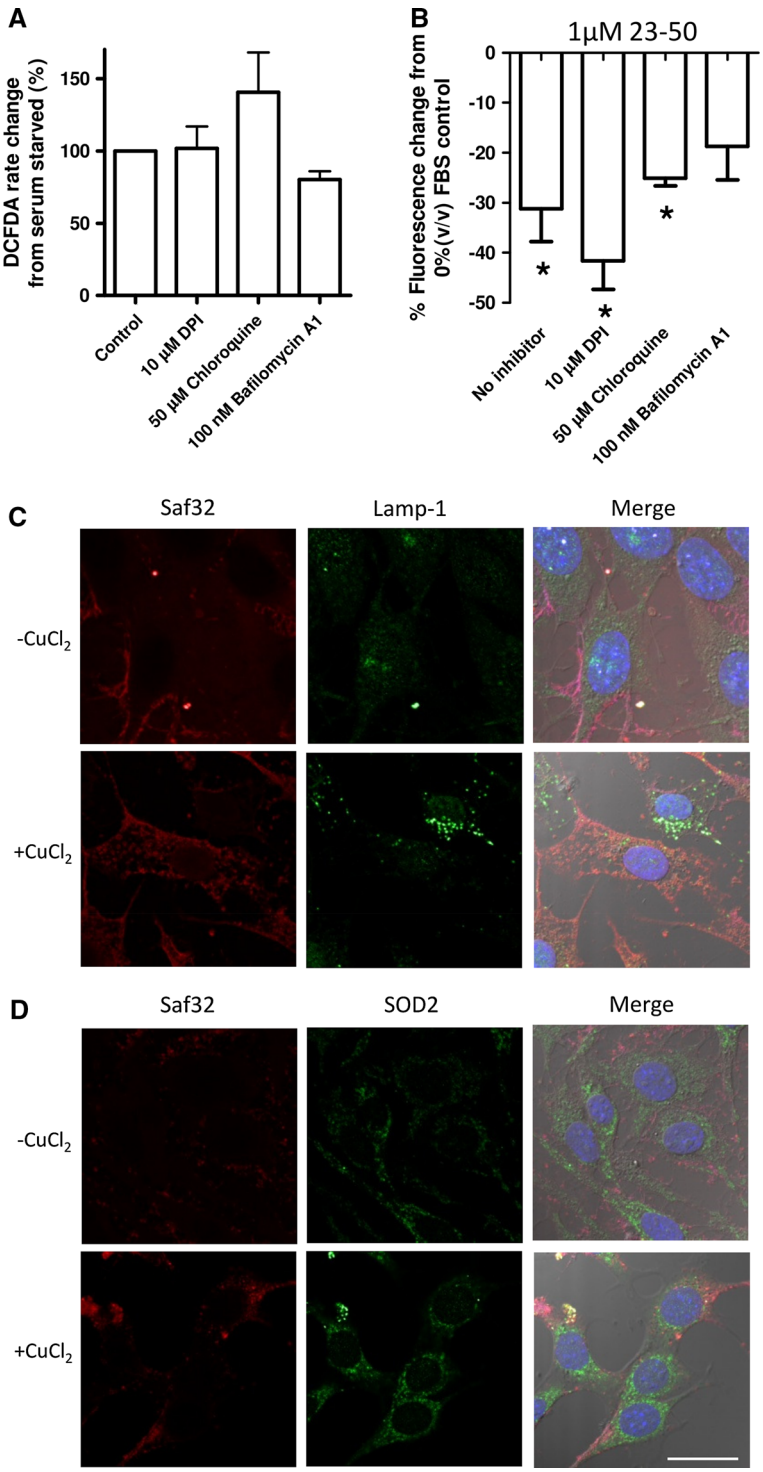

Fig. 4 Downstream targeting of lysosomes does not play a prominent role in 23–50 ROS reduction and PrP23-89 is not trafficked to this destination. **a** Effect of the inhibition of NADPH oxidase ROS signalling and lysosomal acidity on serum-deprived ROS production as assayed by DCFDA fluorescence. Data are *plotted* as a percentage of the serum-deprived control. **b** 23–50 ROS reduction response after inhibition of NADPH oxidases or lysosomal acidification. Results are shown as percentage reduction from the serum-deprived ∓ inhibitor control. $*p < 0.05$. Co-localisation of 1 μM PrP23-89 (∓ copper saturation) with lamp-1 lysosomal marker (**c**) and SOD2 mitochondrial marker (**d**). *Blue* = DAPI nuclei staining. *Scale bar* = 20 μm

binding interactions). Both HS and lipid rafts were previously identified as essential for PrP23-50 ROS reduction; therefore, we determined if either had been pulled down by spotting 2 μl of each wash and elution onto nitrocellulose and blotting for HS content (using 10E4 antibody) and for the lipid-raft marker GM1. For the mechanically disrupted cell lysates, both HS and GM1 were detected in the elutions but eluted under different conditions with HS eluting at high salt concentrations and GM1 eluting as pH dropped (Fig. 5a). No HS or GM1 pull-down was observed when lipid domains were disrupted by detergent lysis (Sup Fig. 8).

The 37/67 kDa laminin receptor has previously been shown to bind to the N-terminus of PrP in an interaction

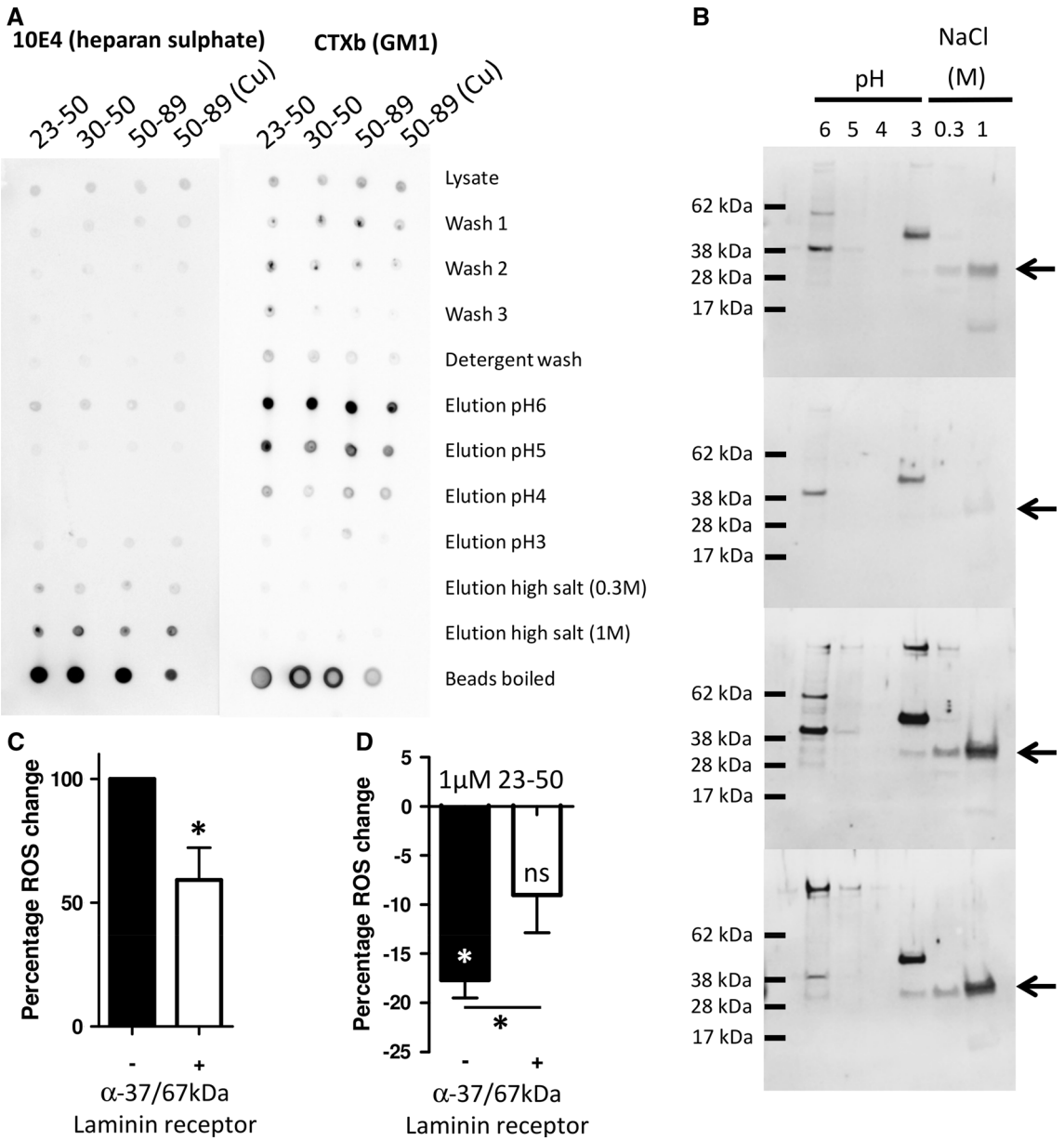

Fig. 5 The PrP N-terminus pulls down a complex containing heparan sulphate, lipid rafts and the 37/67 kDa laminin receptor. **a** *Dot blots* for HS and GM1 of pull downs from cell lysate using PrP N-terminal fragments. **b** The fractions were western blotted for the 37/67kDA laminin receptor (expected size of the 37/67 kDa laminin receptor band is indicated by *arrows*). **c** DCFDA assay of the effect of blocking the 37/67 kDa laminin receptor with antibodies on the induction of ROS during serum deprivation. **d** Assessment of the activity of PrP23-50 in reducing intracellular ROS produced in response to serum deprivation following targeting of the 37/67 kDa laminin receptor with antibodies. $^*p < 0.05$

that also requires GAGs. Therefore, samples from the elutions were electrophoresed and western blotted for the 37/67 kDa laminin receptor. This was found most strongly in the elutions from beads conjugated to PrP51-89 but was also found for PrP23-50 and very weakly for PrP30-50, which lacks the charged region thought to bind GAGs (Fig. 5b). Other bands of differing molecular weight are seen in the blots and whilst these are most likely non-specific it cannot be ruled out that they are modified species of the laminin receptor. To test if the 37/67 kDa laminin receptor might be involved in the ROS reduction action of the PrP N-terminus we used anti-37/67 kDa antibodies to sterically block interaction with the cell surface laminin receptor. Blocking the receptor reduced the ROS produced in response to serum deprivation (Fig. 5c; student's t test, $t = 4.006$, $p = 0.016$, $n = 5$) as well as reducing the efficiency of the PrP23-50 ROS reduction response (Fig. 5d; student's t test, $t = 2.953$, $p = 0.042$, $n = 5$).

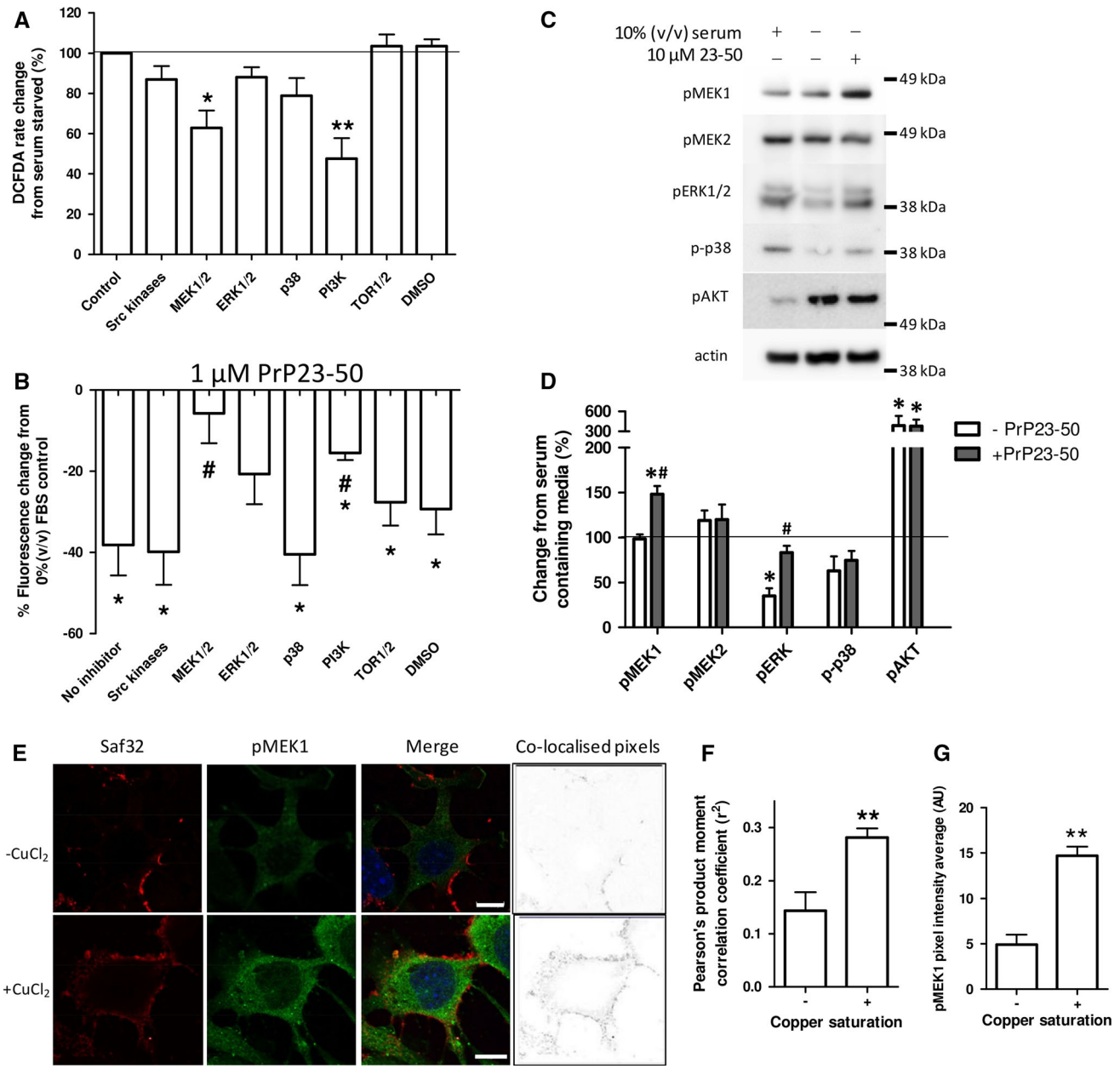

Fig. 6 PrP23-50 influences MEK-1, ERK1/2, and PI3K signalling pathways and copper-saturated N2 shows increased co-localisation with pMEK1. **a** Inhibitors of cellular signalling pathways were assayed for their ability to interfere with the ROS produced in response to serum deprivation. The inhibitors used were as follows; Src kinases—500 nM PP2; MEK—10 µM U0126; ERK—10 µM 3-(2-Aminoethyl)-5-((4-ethoxyphenyl)methylene)-2,4-thiazolidinedione hydrochloride; p38—10 µM SB203580; PI3K—1 µM wortmannin; TOR1/2—1 µM rapamycin; DMSO control—0.1 % (v/v); the target protein is indicated in the graph; DCFDA assay results are shown relative to the serum-deprived 100 % control value. **b** PrP23-50 ROS reduction was assessed by DCFDA fluorescence and shown as percentage reduction from the serum-deprived ± inhibitor control. $^{*}p < 0.05$ from the no peptide control, $^{\#}p < 0.05$ from the no inhibitor action of PrP23-50. **c** Western blots and **d** corresponding densitometry of changes in phosphorylation (activation) of central signal transduction intermediates in response to serum deprivation with and without PrP23-50. Graphical data are presented relative to serum control. **e** Co-localisation of PrP23-89 with pMEK1. PrP23-89, as detected by saf32, is shown in *red* and pMEK1 staining is shown in *green*, with DAPI staining of the nuclei in *blue*. The heat map (*right plates*) shows co-localising pixels. *Scale bars* = 10 µM. **f** Pearson's product moment correlation co-efficient analysis of the apo- and copper-saturated PrP23-89 co-localisation. $^{**}p < 0.01$. **g** Quantification of pixel intensity for the pMEK1 staining. $^{**}p < 0.01$

To investigate candidate signal transduction intermediates that might be recruited into the pathway by which copper-saturated PrP23-89 exerts its influence, we first considered the effect of signalling intermediate inhibition on the production of ROS in response to serum deprivation. Inhibitors were directed against key signalling

intermediates from well-defined pathways within the cell. Only inhibition of MEK1/2 and PI3K were observed to change the ROS produced in response to serum deprivation, with both reducing the ROS produced (Fig. 6a; One-way ANOVA; $F = 5.677$, $p < 0.001$, $n = 3$). Since these experiments were undertaken in PrP knock-out cells for the purpose of excluding confounding effects from endogenous PrP, the cellular responses may be influenced by their lack of PrP expression. Therefore, select inhibitor assays were also performed with two cell lines, N2a and OBL-21, which express detectable levels of endogenous PrP [32]. Significant differences were seen between the CF10 and N2a/OBL-21 cells in the intra-cellular ROS production upon serum starvation only when NADPH oxidases were inhibited with DPI (Sup Fig. 9). The identified candidate pathways for copper-loaded PrP23-89 function responded consistently across the cell lines regardless of PrP expression. When the ROS-reducing action of PrP23-50 was assessed in the presence of these inhibitors, MEK1/2 and PI3K inhibitors suppressed the action of PrP23-50 significantly compared with the control, no inhibitor condition, and MEK1/2 and ERK1/2 inhibition reduced the ROS reduction such that it was no longer significantly different from the control serum-deprived condition (Fig. 6b; Two-way ANOVA, $F = 18.69$, $p < 0.001$, $n = 3$).

To confirm the involvement of the identified pathways, cells were incubated with serum and without serum plus or minus PrP23-50 for 15 min, then western blotted for central signal protein phosphorylation changes. PrP23-50 inclusion in the serum-free media induced phosphorylation of MEK1 (but not MEK2) and ERK1/2. AKT showed significantly increased phosphorylation in the serum-deprived cells, but PrP23-50 did not appear to additionally influence this pathway (Fig. 6c, d). Co-localisation of the apo- or copper-loaded PrP23-89 peptides with phosphorylated MEK1 (pMEK1) were conducted. Greater co-localisation of copper-saturated PrP23-89 is seen compared with the apo-peptide (Fig. 6e, f; student's t test, $t = 3.989$, $p = 0.0013$, $n = 3$). Additionally, concordant with the PrP23-50 responses, intensity quantification of the pMEK1 IF demonstrated significantly increased staining in the cells treated with copper-loaded PrP23-89 as compared with the apo-PrP23-89 (Fig. 6g; student's t test, $t = 6.58$, $p = 0.001$, $n = 3$).

Discussion

Conditions of heightened ROS cause β-cleavage of PrP^C at the cell surface [14, 17] and the β-cleavage event and its N-terminal cleavage product, N2, have been shown to be protective against cellular stress [14, 24, 34, 35]. Herein, we have shown that the copper-saturated N2 β-cleavage product initiates a cellular protective response through binding to a lipid-raft membrane complex containing the 37/67 kDa laminin receptor, engaging its internalisation and stimulating MEK1 signal transduction pathways. The precise membrane interactions of N2, within lipid rafts and with its GAG-binding partners, and also involving both the copper-co-ordinating octarepeat region and the structure conferred upon the N-terminal polybasic region by the proline motif, were also shown essential for the correct engagement of this pathway. Figure 7 provides a schematic overview of the postulated membrane binding, internalisation mechanism and protective modulation pathway for copper-saturated N2.

A critical role for the PrP N-terminus in cellular protection is becoming well established [14, 22–24, 27, 28, 34]. The N-terminus is also required for PrP^C internalisation [36–38]. A requirement for PrP internalisation as part of ERK1/2 signalling by full-length PrP^C has previously been reported for stress signalling through STI-1 [39, 40]. Mutation of the N-terminal polybasic region, which abolishes internalisation [38], also eliminated the associated signal transduction [40]. Whilst an interaction with STI-1 is unlikely to be involved in the N2 ROS reduction pathway presented in the current study, as STI-1 binds PrP at residues 113–128 [41] beyond the N2 cleavage site, our finding that the N-terminus is able to instigate such pathways on its own suggests that PrP^C cleavage at the cell surface may be an important and deliberate event for initiating protective cellular signalling pathways. Earlier studies have also shown that copper stimulates full-length PrP^C internalisation [42, 43] and that copper-induced internalisation of full-length PrP requires the N-terminus and at least two octarepeats and is lost when the α-cleavage site is mutated [37, 44]. Copper has been linked with PrP^C α-cleavage and signal transduction in the context of an altered membrane environment [32]. Therefore, it is probable that copper-binding interactions modulate the specific function(s) of the PrP23-89 peptide.

Zinc is also known to co-ordinate to the octameric repeat domain [45] and, therefore, could have a functional influence on the N2 fragment. However, in the presented experiments we only observed heightened toxicity of zinc when bound to N2 rather than a functional outcome in the context of these experiments. During prion disease, brain metal levels are known to be altered [46, 47], and this may have significant implications for cellular functions that require copper as a molecular "switch". To the best of our knowledge, this study is the first to show that the N2 fragment intracellular ROS protection response requires copper-induced internalisation to effectively engage its downstream signalling pathways.

Whilst this study identified the 37/67 kDa laminin receptor as part of a complex that is pulled down by

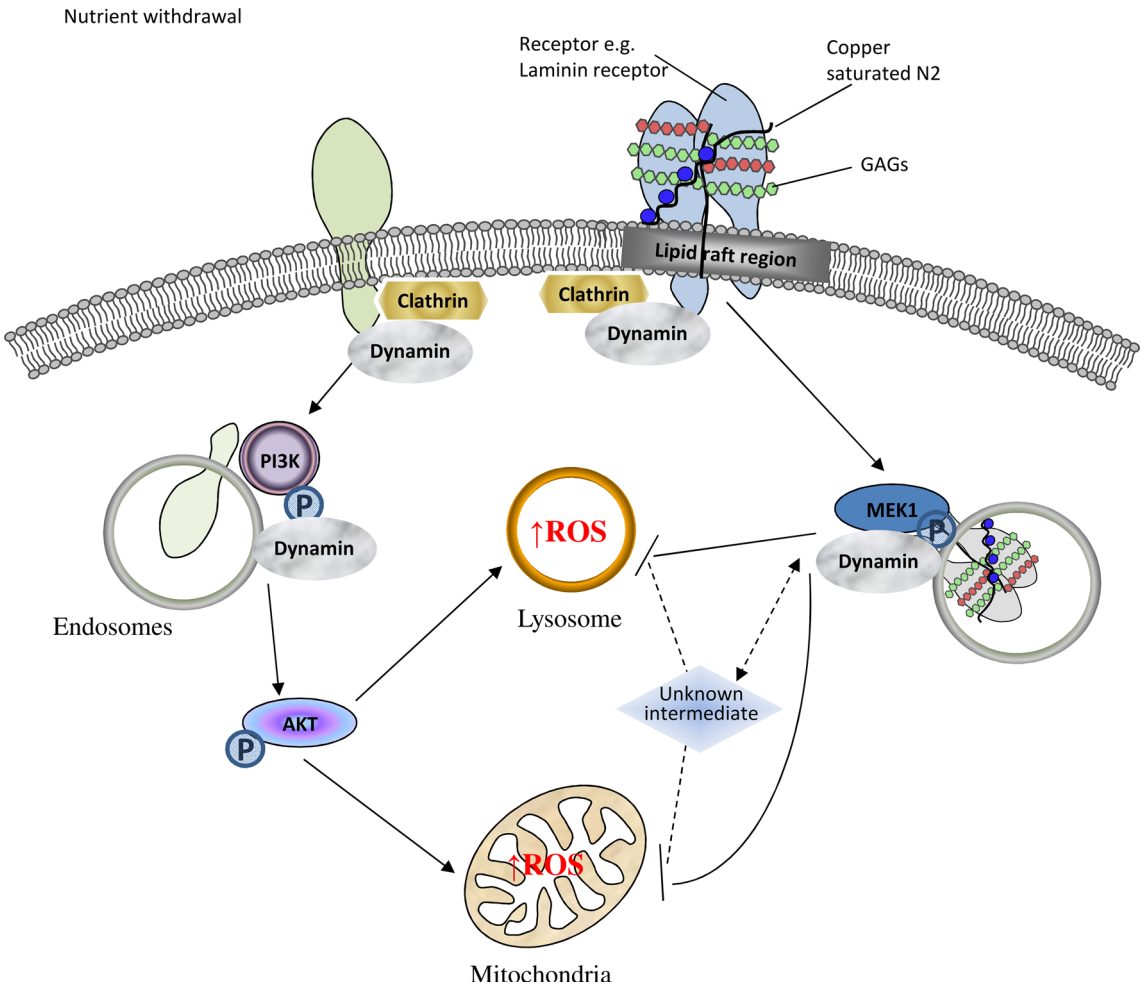

Fig. 7 Schematic representation of intracellular signalling pathways influenced by N2 during cellular protection against oxidative stress. Upon serum withdrawal, an intracellular ROS increase is stimulated within mitochondria and lysosomes. The ROS reaction is signalled through internalisation/trafficking of membrane complexes and involves central intermediates of the AKT and MAPK signal transduction pathways. Correct engagement of a lipid-raft membrane complex containing glycosaminoglycans and the 37/67 kDa laminin receptor by copper-loaded the PrP N2 fragment modulates intracellular trafficking and activates MEK1 signalling to oppose ROS production

N-terminal fragments of PrP, we hypothesise that this is one part of a much larger complex and we cannot state from the data presented herein that it is the definitive receptor for N2. However, there is significant evidence in the literature to support a functional role for the 37/67 kDa laminin receptor in the PrP N2 interaction; the 37/67 kDa laminin receptor binds to PrP^{C} through GAG interactions with the N2 region of PrP^{C} [48, 49], in a pathway that is also linked with internalisation of PrP^{Sc} during disease [50–53]. Other reported PrP receptors were not investigated in the current study but include low-density lipoprotein receptor-related protein 1, with binding in conjunction with GAGs [54], Glypican-1, an HS containing proteoglycan that co-internalises with PrP^{C} [55, 56], and α7 nicotinic receptors [57]. The latter have been shown to form a functional complex with PrP^{C} that mediates STI-1 signalling in a pathway which is known to require internalisation for signal transduction [57]. Potentially N2 may be modulating any or all of these pathways depending upon its membrane environment and copper saturation.

Our presented data indicated that peptide-partner binding interactions might be masking the octarepeat epitope at the cell surface, thus preventing antibody binding. Further, the differing binding pattern of the PrP23-89P26/28A peptide when compared with the wild-type PrP23-89 showed that the cell surface interaction of the octameric repeat domain is influenced by the proline motif within the N-terminal polybasic region. The observations might be due to interactions with the signalling complex through which the N2 fragment mediates its function or, alternatively, as the N-terminal amino-acids alone were able to instigate the same ROS reduction response to serum

deprivation, the function of this region may be orientation of the interaction within/at the cell membrane. Our previous findings have shown the importance of the octarepeat for membrane engagement under specific conditions [58], and therefore, the context of the cell membrane lipid binding interactions may also modulate correct pathway engagement for signal transduction in the present study. The rapid retraction of the cell membrane that was shown on addition of PrP23-50 could indicate that changes are occurring at the cell membrane and could have occurred due to a rapid formation of membrane domains required for internalisation. Furthermore, the PrP N-terminus has also been shown to bind to the cytoskeletal protein tubulin [59]. The observed rapid rearrangement of the cell membrane could in theory be due to cytoskeletal restructuring either through direct N2-tubulin interaction or via N2 activation of MEK1 signalling, in similarity with pathways previously reported for actin cytoskeletal rearrangements [60].

Herein, two signalling pathways were shown to be especially involved in modulating the intracellular ROS produced in response to serum deprivation, the PI3K/AKT and the MEK1/ERK1/2 pathways, with the latter influenced by PrP23-50 to act against the ROS increase. Our results showed that direct inhibition of ERK did not produce the same cellular responses as MEK1/2 inhibition and so MEK1 might be acting to stimulate further downstream targets to exert its full protective function. The vesicular internalisation pattern presented for copper-co-ordinating PrP23-89, co-localising with pMEK1, shows this peptide is found in close proximity to the signalling intermediates in the pathways with which it interacts; therefore, copper-loaded PrP23-89 may be part of an internalised complex that acts directly to influence the activity of specific signalling pathways, such as MEK1.

Whilst the ability to engage signalling pathways appears important for N2 function, the properties of this amino acid sequence also affect full-length PrP. Studies using cells expressing full-length PrP have shown that PrP expression is regulated by signalling through the MEK1 pathway [61] and PrP expression is increased in response to conditions of oxidative stress [62]. An environmental stress-induced increase in paracrine N2 signalling could be able to initiate these events even in cells with low endogenous PrP expression. β-cleavage may also prevent signalling of full-length PrP or permit signalling of the C-terminal cleavage fragments. Previous studies have found that PrP can signal through NADPH oxidase [63], which was not seen for the truncated N2 fragment in the current study, and that the C2 fragment is able to initiate signalling through p38 and ERK1/2 in astrocytes and microglia [64]. This highlights a difficulty of attributing functions to full-length PrP as many cells and tissue display more cleaved PrP than full length [65, 66], and further supports the role of cleavage as a functional event for controlling PrP activity.

Our findings are consistent with interactions at the cell surface, in the first phases of internalisation being able to influence the downstream ROS production sites, supporting the importance of correct engagement of a receptor complex at the cell surface by the N2 fragment. We showed that engagement of the N2 peptide at the cell surface was determined by the synergy between the polybasic proline motif and the copper-co-ordinating octarepeats. A predominant PrP^C function has remained elusive despite many years of intensive investigation, with many studies convincingly suggesting the likelihood of many different cellular roles. Whilst the choice of model used in each such study may lead to differing results and, therefore, add to the contention around this issue, post-translational modification to PrP^C itself is unlikely to represent an irrelevant epiphenomenon in all systems. The hypothesis that PrP^C post-translational modification occurs as a molecular switch for activation or deactivation of certain functions facilitates the beginning of our understanding of its multifunctionality. The apparent contextual dependence of the protective effects offered by the N-terminal cleavage products, as shown in our data, demonstrates the finely balanced nature of certain functions. The role of such protective functions and their potential to be corrupted during disease processes will provide new insights into both prion disease pathogenesis and other stresses deleteriously affecting the brain.

Acknowledgments The authors would like to thank Dr Victoria Lawson for her support and helpful discussions. The CF10 cells were a kind gift to Dr Victoria Lawson from Dr Suzette Priola (National Institute of Health, USA). This work was supported by an NH&MRC program grant (#628946) and SJC is supported by an NH&MRC Practitioner Fellowship (#APP100581).

References

1. Haigh CL, Brown DR (2006) Prion protein reduces both oxidative and non-oxidative copper toxicity. J Neurochem 98(3): 677–689. doi:10.1111/j.1471-4159.2006.03906.x
2. Brown DR, Schulz-Schaeffer WJ, Schmidt B, Kretzschmar HA (1997) Prion protein-deficient cells show altered response to oxidative stress due to decreased SOD-1 activity. Exp Neurol 146(1):104–112. doi:10.1006/exnr.1997.6505
3. Klamt F, Dal-Pizzol F, Conte da Frota ML Jr, Walz R, Andrades ME, da Silva EG, Brentani RR, Izquierdo I, Fonseca Moreira JC (2001) Imbalance of antioxidant defense in mice lacking cellular prion protein. Free Radic Biol Med 30(10):1137–1144
4. Rachidi W, Vilette D, Guiraud P, Arlotto M, Riondel J, Laude H, Lehmann S, Favier A (2003) Expression of prion protein increases cellular copper binding and antioxidant enzyme activities but not copper delivery. J Biol Chem 278(11):9064–9072. doi:10.1074/jbc.M211830200

5. Senator A, Rachidi W, Lehmann S, Favier A, Benboubetra M (2004) Prion protein protects against DNA damage induced by paraquat in cultured cells. Free Radic Biol Med 37(8):1224–1230. doi:10.1016/j.freeradbiomed.2004.07.006
6. Watt NT, Routledge MN, Wild CP, Hooper NM (2007) Cellular prion protein protects against reactive-oxygen-species-induced DNA damage. Free Radic Biol Med 43(6):959–967. doi:10.1016/j.freeradbiomed.2007.06.004
7. Chiarini LB, Freitas AR, Zanata SM, Brentani RR, Martins VR, Linden R (2002) Cellular prion protein transduces neuroprotective signals. EMBO J 21(13):3317–3326. doi:10.1093/emboj/cdf324
8. Harris DA, Huber MT, van Dijken P, Shyng SL, Chait BT, Wang R (1993) Processing of a cellular prion protein: identification of N- and C-terminal cleavage sites. Biochemistry 32(4):1009–1016
9. Chen SG, Teplow DB, Parchi P, Teller JK, Gambetti P, Autilio-Gambetti L (1995) Truncated forms of the human prion protein in normal brain and in prion diseases. J Biol Chem 270(32):19173–19180
10. Haigh CL, Marom SY, Collins SJ (2010) Copper, endoproteolytic processing of the prion protein and cell signalling. Front Biosci (Landmark Ed) 15:1086–1104
11. McMahon HE (2012) Prion processing: a double-edged sword? Biochem Soc Trans 40(4):735–738. doi:10.1042/bst20120031
12. Brazier MW, Lewis V, Ciccotosto GD, Klug GM, Lawson VA, Cappai R, Ironside JW, Masters CL, Hill AF, White AR, Collins S (2006) Correlative studies support lipid peroxidation is linked to PrP(res) propagation as an early primary pathogenic event in prion disease. Brain Res Bull 68(5):346–354. doi:10.1016/j.brainresbull.2005.09.010
13. Yadavalli R, Guttmann RP, Seward T, Centers AP, Williamson RA, Telling GC (2004) Calpain-dependent endoproteolytic cleavage of PrPSc modulates scrapie prion propagation. J Biol Chem 279(21):21948–21956. doi:10.1074/jbc.M400793200
14. Watt NT, Taylor DR, Gillott A, Thomas DA, Perera WS, Hooper NM (2005) Reactive oxygen species-mediated beta-cleavage of the prion protein in the cellular response to oxidative stress. J Biol Chem 280(43):35914–35921. doi:10.1074/jbc.M507327200
15. Haigh CL, McGlade AR, Lewis V, Masters CL, Lawson VA, Collins SJ (2011) Acute exposure to prion infection induces transient oxidative stress progressing to be cumulatively deleterious with chronic propagation in vitro. Free Radic Biol Med 51(3):594–608. doi:10.1016/j.freeradbiomed.2011.03.035
16. Sinclair L, Lewis V, Collins SJ, Haigh CL (2013) Cytosolic caspases mediate mislocalised SOD2 depletion in an in vitro model of chronic prion infection. Dis Model Mech 6(4):952–963. doi:10.1242/dmm.010678
17. McMahon HE, Mange A, Nishida N, Creminon C, Casanova D, Lehmann S (2001) Cleavage of the amino terminus of the prion protein by reactive oxygen species. J Biol Chem 276(3):2286–2291. doi:10.1074/jbc.M007243200
18. Westergard L, Turnbaugh JA, Harris DA (2011) A nine amino acid domain is essential for mutant prion protein toxicity. J Neurosci 31(39):14005–14017. doi:10.1523/jneurosci.1243-11.2011
19. Sonati T, Reimann RR, Falsig J, Baral PK, O'Connor T, Hornemann S, Yaganoglu S, Li B, Herrmann US, Wieland B, Swayampakula M, Rahman MH, Das D, Kav N, Riek R, Liberski PP, James MN, Aguzzi A (2013) The toxicity of antiprion antibodies is mediated by the flexible tail of the prion protein. Nature 501(7465):102–106. doi:10.1038/nature12402
20. Lawson VA, Priola SA, Meade-White K, Lawson M, Chesebro B (2004) Flexible N-terminal region of prion protein influences conformation of protease-resistant prion protein isoforms associated with cross-species scrapie infection in vivo and in vitro. J Biol Chem 279(14):13689–13695. doi:10.1074/jbc.M303697200
21. Lawson VA, Priola SA, Wehrly K, Chesebro B (2001) N-terminal truncation of prion protein affects both formation and conformation of abnormal protease-resistant prion protein generated in vitro. J Biol Chem 276(38):35265–35271. doi:10.1074/jbc.M103799200
22. Turnbaugh JA, Unterberger U, Saa P, Massignan T, Fluharty BR, Bowman FP, Miller MB, Supattapone S, Biasini E, Harris DA (2012) The N-terminal, polybasic region of PrP(C) dictates the efficiency of prion propagation by binding to PrP(Sc). J Neurosci 32(26):8817–8830. doi:10.1523/jneurosci.1103-12.2012
23. Guillot-Sestier MV, Sunyach C, Druon C, Scarzello S, Checler F (2009) The alpha-secretase-derived N-terminal product of cellular prion, N1, displays neuroprotective function in vitro and in vivo. J Biol Chem 284(51):35973–35986. doi:10.1074/jbc.M109.051086
24. Haigh CL, Drew SC, Boland MP, Masters CL, Barnham KJ, Lawson VA, Collins SJ (2009) Dominant roles of the polybasic proline motif and copper in the PrP23-89-mediated stress protection response. J Cell Sci 122(Pt 10):1518–1528. doi:10.1242/jcs.043604
25. Chen S, Yadav SP, Surewicz WK (2010) Interaction between human prion protein and amyloid-beta (Abeta) oligomers: role OF N-terminal residues. J Biol Chem 285(34):26377–26383. doi:10.1074/jbc.M110.145516
26. Younan ND, Sarell CJ, Davies P, Brown DR, Viles JH (2013) The cellular prion protein traps Alzheimer's Abeta in an oligomeric form and disassembles amyloid fibers. FASEB J 27(5):1847–1858. doi:10.1096/fj.12-222588
27. Guillot-Sestier MV, Sunyach C, Ferreira ST, Marzolo MP, Bauer C, Thevenet A, Checler F (2012) Alpha-Secretase-derived fragment of cellular prion, N1, protects against monomeric and oligomeric amyloid beta (Abeta)-associated cell death. J Biol Chem 287(7):5021–5032. doi:10.1074/jbc.M111.323626
28. Fluharty BR, Biasini E, Stravalaci M, Sclip A, Diomede L, Balducci C, La Vitola P, Messa M, Colombo L, Forloni G, Borsello T, Gobbi M, Harris DA (2013) An N-terminal fragment of the prion protein binds to amyloid-beta oligomers and inhibits their neurotoxicity in vivo. J Biol Chem 288(11):7857–7866. doi:10.1074/jbc.M112.423954
29. Karas JA, Boland M, Haigh C, Johanssen V, Hill A, Barnham K, Collins S, Scanlon D (2012) Microwave synthesis of prion protein fragments up to 111 amino acids in length generates biologically active peptides. Int J Pept Res Ther 18(1):21–29. doi:10.1007/s10989-011-9275-7
30. Greil CS, Vorberg IM, Ward AE, Meade-White KD, Harris DA, Priola SA (2008) Acute cellular uptake of abnormal prion protein is cell type and scrapie-strain independent. Virology 379(2):284–293. doi:10.1016/j.virol.2008.07.006
31. Haigh CL, Brown DR (2008) Investigation of PrPC metabolism and function in live cells : methods for studying individual cells and cell populations. Methods Mol Biol (Clifton, NJ) 459:21–34. doi:10.1007/978-1-59745-234-2_2
32. Haigh CL, Lewis VA, Vella LJ, Masters CL, Hill AF, Lawson VA, Collins SJ (2009) PrPC-related signal transduction is influenced by copper, membrane integrity and the alpha cleavage site. Cell Res 19(9):1062–1078. doi:10.1038/cr.2009.86
33. Chen CS, Gee KR (2000) Redox-dependent trafficking of 2,3,4,5,6-pentafluorodihydrotetramethylrosamine, a novel fluorogenic indicator of cellular oxidative activity. Free Radic Biol Med 28(8):1266–1278
34. Zeng F, Watt NT, Walmsley AR, Hooper NM (2003) Tethering the N-terminus of the prion protein compromises the cellular response to oxidative stress. J Neurochem 84(3):480–490

35. Dupiereux I, Falisse-Poirrier N, Zorzi W, Watt NT, Thellin O, Zorzi D, Pierard O, Hooper NM, Heinen E, Elmoualij B (2008) Protective effect of prion protein via the N-terminal region in mediating a protective effect on paraquat-induced oxidative injury in neuronal cells. J Neurosci Res 86(3):653–659. doi:10.1002/jnr.21506
36. Nunziante M, Gilch S, Schatzl HM (2003) Essential role of the prion protein N terminus in subcellular trafficking and half-life of cellular prion protein. J Biol Chem 278(6):3726–3734. doi:10.1074/jbc.M206313200
37. Taylor DR, Watt NT, Perera WS, Hooper NM (2005) Assigning functions to distinct regions of the N-terminus of the prion protein that are involved in its copper-stimulated, clathrin-dependent endocytosis. J Cell Sci 118(Pt 21):5141–5153. doi:10.1242/jcs.02627
38. Sunyach C, Jen A, Deng J, Fitzgerald KT, Frobert Y, Grassi J, McCaffrey MW, Morris R (2003) The mechanism of internalization of glycosylphosphatidylinositol-anchored prion protein. EMBO J 22(14):3591–3601. doi:10.1093/emboj/cdg344
39. Americo TA, Chiarini LB, Linden R (2007) Signaling induced by hop/STI-1 depends on endocytosis. Biochem Biophys Res Commun 358(2):620–625. doi:10.1016/j.bbrc.2007.04.202
40. Caetano FA, Lopes MH, Hajj GN, Machado CF, Pinto Arantes C, Magalhaes AC, Vieira Mde P, Americo TA, Massensini AR, Priola SA, Vorberg I, Gomez MV, Linden R, Prado VF, Martins VR, Prado MA (2008) Endocytosis of prion protein is required for ERK1/2 signaling induced by stress-inducible protein 1. J Neurosci 28(26):6691–6702. doi:10.1523/jneurosci.1701-08.2008
41. Zanata SM, Lopes MH, Mercadante AF, Hajj GN, Chiarini LB, Nomizo R, Freitas AR, Cabral AL, Lee KS, Juliano MA, de Oliveira E, Jachieri SG, Burlingame A, Huang L, Linden R, Brentani RR, Martins VR (2002) Stress-inducible protein 1 is a cell surface ligand for cellular prion that triggers neuroprotection. EMBO J 21(13):3307–3316. doi:10.1093/emboj/cdf325
42. Pauly PC, Harris DA (1998) Copper stimulates endocytosis of the prion protein. J Biol Chem 273(50):33107–33110
43. Perera WS, Hooper NM (2001) Ablation of the metal ion-induced endocytosis of the prion protein by disease-associated mutation of the octarepeat region. Curr Biol 11(7):519–523
44. Haigh CL, Edwards K, Brown DR (2005) Copper binding is the governing determinant of prion protein turnover. Mol Cell Neurosci 30(2):186–196. doi:10.1016/j.mcn.2005.07.001
45. Jackson GS, Murray I, Hosszu LL, Gibbs N, Waltho JP, Clarke AR, Collinge J (2001) Location and properties of metal-binding sites on the human prion protein. Proc Natl Acad Sci USA 98(15):8531–8535. doi:10.1073/pnas.151038498
46. Hesketh S, Sassoon J, Knight R, Brown DR (2008) Elevated manganese levels in blood and CNS in human prion disease. Mol Cell Neurosci 37(3):590–598. doi:10.1016/j.mcn.2007.12.008
47. Hesketh S, Sassoon J, Knight R, Hopkins J, Brown DR (2007) Elevated manganese levels in blood and central nervous system occur before onset of clinical signs in scrapie and bovine spongiform encephalopathy. J Anim Sci 85(6):1596–1609. doi:10.2527/jas.2006-714
48. Gauczynski S, Peyrin JM, Haik S, Leucht C, Hundt C, Rieger R, Krasemann S, Deslys JP, Dormont D, Lasmezas CI, Weiss S (2001) The 37-kDa/67-kDa laminin receptor acts as the cell-surface receptor for the cellular prion protein. EMBO J 20(21):5863–5875. doi:10.1093/emboj/20.21.5863
49. Hundt C, Peyrin JM, Haik S, Gauczynski S, Leucht C, Rieger R, Riley ML, Deslys JP, Dormont D, Lasmezas CI, Weiss S (2001) Identification of interaction domains of the prion protein with its 37-kDa/67-kDa laminin receptor. EMBO J 20(21):5876–5886. doi:10.1093/emboj/20.21.5876
50. Gauczynski S, Nikles D, El-Gogo S, Papy-Garcia D, Rey C, Alban S, Barritault D, Lasmezas CI, Weiss S (2006) The 37-kDa/67-kDa laminin receptor acts as a receptor for infectious prions and is inhibited by polysulfated glycanes. J Infect Dis 194(5):702–709. doi:10.1086/505914
51. Morel E, Andrieu T, Casagrande F, Gauczynski S, Weiss S, Grassi J, Rousset M, Dormont D, Chambaz J (2005) Bovine prion is endocytosed by human enterocytes via the 37 kDa/67 kDa laminin receptor. Am J Pathol 167(4):1033–1042. doi:10.1016/s0002-9440(10)61192-3
52. Kolodziejczak D, Da Costa Dias B, Zuber C, Jovanovic K, Omar A, Beck J, Vana K, Mbazima V, Richt J, Brenig B, Weiss SF (2010) Prion interaction with the 37-kDa/67-kDa laminin receptor on enterocytes as a cellular model for intestinal uptake of prions. J Mol Biol 402(2):293–300. doi:10.1016/j.jmb.2010.06.055
53. Pflanz H, Vana K, Mitteregger G, Renner-Muller I, Pace C, Kuchenhoff H, Kretzschmar HA, Wolf E, Weiss S (2009) Scrapie-infected transgenic mice expressing a laminin receptor decoy mutant reveal a prolonged incubation time associated with low levels of PrP^{Res}. J Mol Biol 388(4):721–729. doi:10.1016/j.jmb.2009.03.045
54. Parkyn CJ, Vermeulen EG, Mootoosamy RC, Sunyach C, Jacobsen C, Oxvig C, Moestrup S, Liu Q, Bu G, Jen A, Morris RJ (2008) LRP1 controls biosynthetic and endocytic trafficking of neuronal prion protein. J Cell Sci 121(Pt 6):773–783. doi:10.1242/jcs.021816
55. Cheng F, Lindqvist J, Haigh CL, Brown DR, Mani K (2006) Copper-dependent co-internalization of the prion protein and glypican-1. J Neurochem 98(5):1445–1457. doi:10.1111/j.1471-4159.2006.03981.x
56. Taylor DR, Whitehouse IJ, Hooper NM (2009) Glypican-1 mediates both prion protein lipid raft association and disease isoform formation. PLoS Pathog 5(11):e1000666. doi:10.1371/journal.ppat.1000666
57. Beraldo FH, Arantes CP, Santos TG, Queiroz NG, Young K, Rylett RJ, Markus RP, Prado MA, Martins VR (2010) Role of alpha7 nicotinic acetylcholine receptor in calcium signaling induced by prion protein interaction with stress-inducible protein 1. J Biol Chem 285(47):36542–36550. doi:10.1074/jbc.M110.157263
58. Boland MP, Hatty CR, Separovic F, Hill AF, Tew DJ, Barnham KJ, Haigh CL, James M, Masters CL, Collins SJ (2010) Anionic phospholipid interactions of the prion protein N terminus are minimally perturbing and not driven solely by the octapeptide repeat domain. J Biol Chem 285(42):32282–32292. doi:10.1074/jbc.M110.123398
59. Osiecka KM, Nieznanska H, Skowronek KJ, Karolczak J, Schneider G, Nieznanski K (2009) Prion protein region 23-32 interacts with tubulin and inhibits microtubule assembly. Proteins 77(2):279–296. doi:10.1002/prot.22435
60. Barros JC, Marshall CJ (2005) Activation of either ERK1/2 or ERK5 MAP kinase pathways can lead to disruption of the actin cytoskeleton. J Cell Sci 118(Pt 8):1663–1671. doi:10.1242/jcs.02308
61. Zawlik I, Witusik M, Hulas-Bigoszewska K, Piaskowski S, Szybka M, Golanska E, Liberski PP, Rieske P (2006) Regulation of PrPC expression: nerve growth factor (NGF) activates the prion gene promoter through the MEK1 pathway in PC12 cells. Neurosci Lett 400(1–2):58–62. doi:10.1016/j.neulet.2006.02.021
62. Cichon AC, Brown DR (2014) Nrf-2 regulation of prion protein expression is independent of oxidative stress. Mol Cell Neurosci 63c:31–37. doi:10.1016/j.mcn.2014.09.001
63. Schneider B, Mutel V, Pietri M, Ermonval M, Mouillet-Richard S, Kellermann O (2003) NADPH oxidase and extracellular regulated kinases 1/2 are targets of prion protein signaling in

neuronal and nonneuronal cells. Proc Natl Acad Sci USA 100(23):13326–13331. doi:10.1073/pnas.2235648100

64. Thellung S, Villa V, Corsaro A, Pellistri F, Venezia V, Russo C, Aceto A, Robello M, Florio T (2007) ERK1/2 and p38 MAP kinases control prion protein fragment 90-231-induced astrocyte proliferation and microglia activation. Glia 55(14):1469–1485. doi:10.1002/glia.20559
65. Lewis V, Haigh CL, Masters CL, Hill AF, Lawson VA, Collins SJ (2012) Prion subcellular fractionation reveals infectivity spectrum, with a high titre-low PrP^{Res} level disparity. Mol Neurodegener 7:18. doi:10.1186/1750-1326-7-18
66. Dron M, Moudjou M, Chapuis J, Salamat MK, Bernard J, Cronier S, Langevin C, Laude H (2010) Endogenous proteolytic cleavage of disease-associated prion protein to produce C2 fragments is strongly cell- and tissue-dependent. J Biol Chem 285(14): 10252–10264. doi:10.1074/jbc.M109.083857

Collins et al. Stem Cell Research & Therapy _####################_
DOI 10.1186/s13287-015-0067-4

stem cell research&therapy

SHORT REPORT Open Access

The prion protein regulates beta-amyloid-mediated self-renewal of neural stem cells *in vitro*

Steven J Collins[1,2,3*], Carolin Tumpach[3], Qiao-Xin Li[3], Victoria Lewis[1], Timothy M Ryan[3], Blaine Roberts[3], Simon C Drew[4], Victoria A Lawson[1] and Cathryn L Haigh[1*]

Abstract

The beta-amyloid (Aβ) peptide and the Aβ-oligomer receptor, prion protein (PrP), both influence neurogenesis. Using *in vitro* murine neural stem cells (NSCs), we investigated whether Aβ and PrP interact to modify neurogenesis. Aβ imparted PrP-dependent changes on NSC self-renewal, with PrP-ablated and wild-type NSCs displaying increased and decreased cell growth, respectively. In contrast, differentiation of Aβ-treated NSCs into mature cells was unaffected by PrP expression. Such marked PrP-dependent differences in NSC growth responses to Aβ provides further evidence of biologically significant interactions between these two factors and an important new insight into regulation of NSC self-renewal *in vivo*.

Findings

Introduction

Alzheimer's disease (AD) is the most common form of dementia. The core components of the senile plaques that characterise AD pathologically are beta-amyloid (Aβ) peptides cleaved from the amyloid precursor protein (APP). Various Aβ species exist as a result of differing N- and C-terminal processing sites and these species can aggregate, forming oligomers that are implicated in Aβ toxicity [1]. Most Aβ species are found in healthy brain tissue but the relative amounts shift during AD [2,3]. In health, Aβ1-40 predominates and during AD Aβ1-42, Aβ4-42 and pyroglutamated Aβ3-42 (3(pE)-42) are increased [3]. Many other species also exist with their relative amounts changing during disease.

Neurogenesis, whilst declining significantly in the adult organism, continues throughout life. Adult neural stem cells (NSCs) are confined to specific protected sites within the brain, including the sub-granular zone (SGZ) of the dentate gyrus and sub-ventricular zone of the lateral ventricle [4]. Adult NSCs can self-renew and are multipotent; they can differentiate into cells of any central nervous system lineage. In the brains of AD patients, markers of neurogenesis are increased [5,6] indicating potential neurogenic dysregulation or stimulated compensation for neuronal loss. AD pathology typically begins in the transentorhinal and entorhinal cortex. [7] This region lies adjacent to the SGZ and, therefore, NSCs in their normally protected niche environment may be exposed to hostile conditions that stimulate them to change their behaviour [4]. There is significant evidence that Aβ peptides are able to modulate neurogenesis [8-10]. Various discrepancies exist in the literature as to whether neurogenesis is enhanced or suppressed by Aβ exposure, which is most likely due to the manner in which the Aβ was prepared (that is, if monomeric, oligomeric or fibrillar Aβ species were used) and the model system for NSC study (for example, *in vivo, in vitro*, mouse strain); however, the consensus is in favour of changed NSC behaviour following exposure to Aβ species.

Neurogenesis is also modulated by another neurodegenerative disease-associated protein, the prion protein (PrP) [11,12]. Increased PrP expression is associated with increased cell cycling at the expense of differentiation [13]. Recent studies found that PrP is an essential receptor that transduces soluble Aβ1-42 oligomer signals from the plasma-membrane through the NMDA receptor via the signalling molecule fyn to tau, with this signalling thought to cause cellular toxicity [14-16]. Based on the knowledge that both Aβ and PrP can individually

* Correspondence: stevenjc@unimelb.edu.au; chaigh@unimelb.edu.au
[1]Department of Pathology, The University of Melbourne, Melbourne Brain Centre, Melbourne, VIC 3010, Australia
[3]Florey Department of Neuroscience and Mental Health, The University of Melbourne, Melbourne, VIC 3010, Australia
Full list of author information is available at the end of the article

modulate neurogenesis and that PrP is a soluble Aβ1-42 binding partner necessary for the transduction of toxic signals, we hypothesized that PrP might also transduce the Aβ peptide signals that alter neurogenesis. The present study therefore investigated the ability of various Aβ peptides to modulate *in vitro* self-renewal and differentiation of adult NSCs harvested from PrP gene-ablated (knock-out (KO)) or from wild-type (WT; normal PrP expression) mice.

Methods

Aβ-amyloid peptides (China Peptides, China) were prepared as described previously [17]. NSC harvest and routine culture was as described previously [18,19]. For

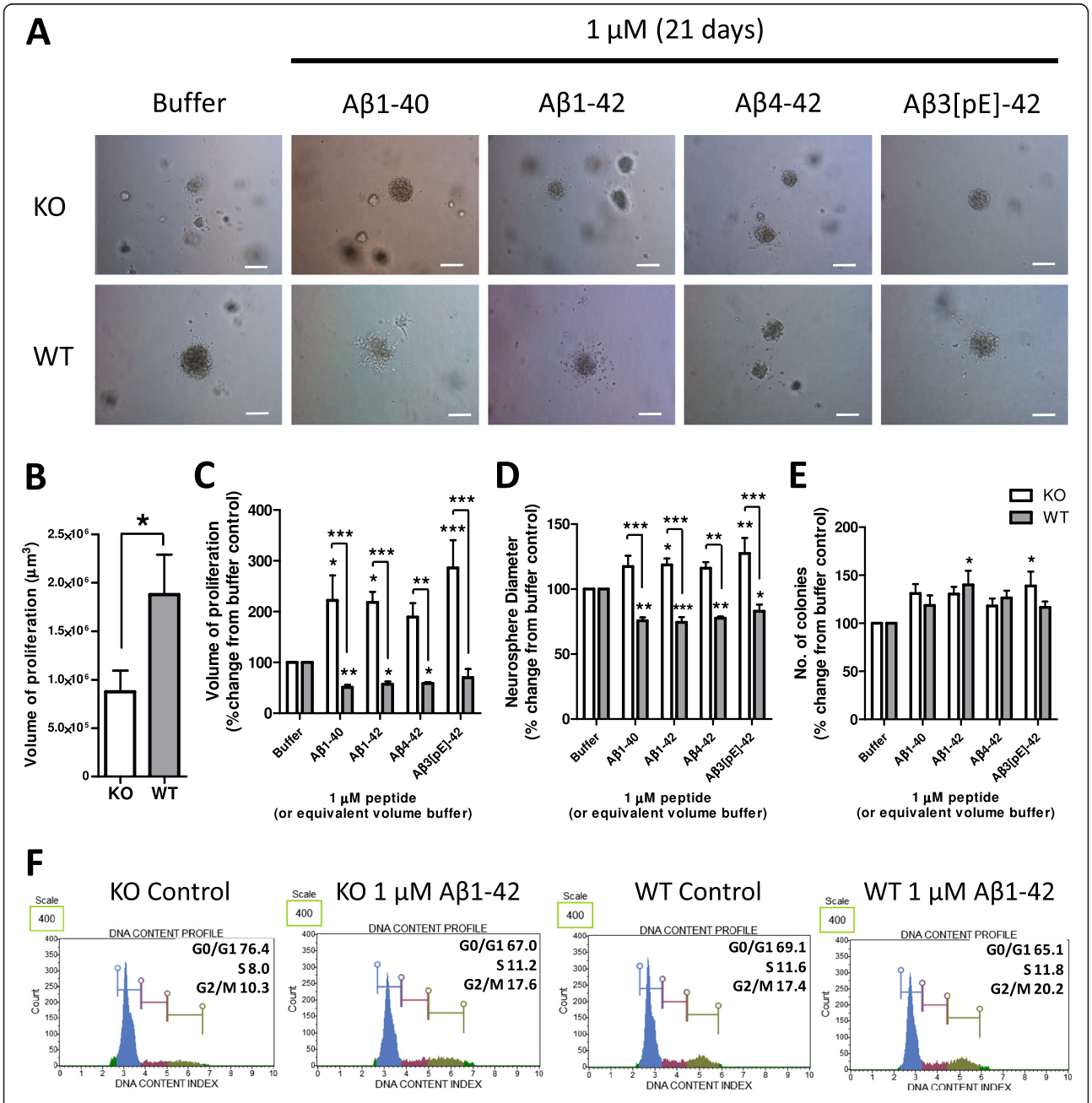

Figure 1 Beta-amyloid (Aβ) peptide modulation of neural stem cell (NSC) self-renewal is prion protein (PrP) dependent. **(A)** Representative images of NSC colonies grown in a collagen matrix with or without Aβ for 21 days. **(B)** Neurosphere volume of untreated knock-out (KO) and wild-type (WT) cells. **(C)** Neurosphere volume following Aβ treatment calculated from colony diameter **(D)** and number **(E)**. **(F)** Flow cytometry cell cycle phase analysis by DNA content; an example experiment from four repeats is shown. Scale bars = 100 μm. Data are represented as mean ± SEM. *$P < 0.05$, **$P < 0.01$, ***$P < 0.001$.

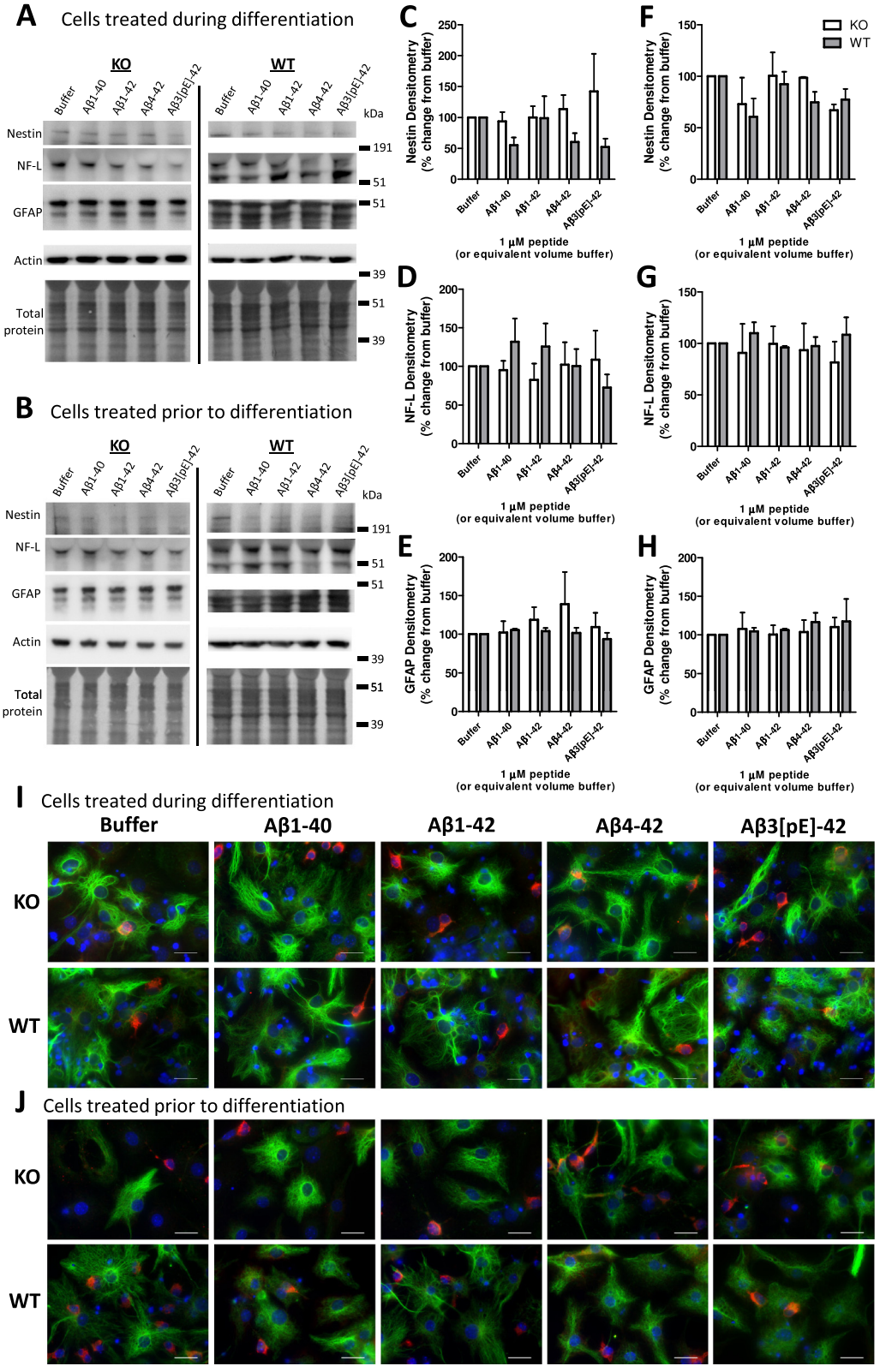

Figure 2 (See legend on next page.)

(See figure on previous page.)
Figure 2 Prion protein (PrP) expression has minimal influence on how beta-amyloid (Aβ) affects neural stem cell (NSC) differentiation. Example plates of western blots for lineage protein markers from knock-out (KO) and wild-type (WT) NSCs treated for either 7 days during differentiation **(A)** or 24 hours prior to differentiation for 7 days **(B)** with 1 μM Aβ. Quantification of the western blots (A & B) for the stem cell marker nestin **(C, F)**, mature neuronal marker, NF-L **(D, G)**, and GFAP astrocytic marker **(E, H)**. Data are represented as mean ± SEM. Example immunofluorescent images of NSCs treated with Aβ during **(I)** and before **(J)** differentiation with NF-L, GFAP and DAPI nuclear staining shown in red, green and blue respectively. Scale bars = 15 μm.

the neural colony-forming assay, cells were seeded in a semi-solid gel matrix made with a 2:1 solution of proliferation medium and collagen. After day 21, neurospheres were counted and their diameter measured using NIS-Elements (Nikon, Adelaide, Australia) software. Cell cycle analysis was performed using the Muse Cell Cycle Kit (Millipore, Bayswater, Victoria, AUS). For plate and blotting assays cells were cultured as an adherent monolayer on a 1:1 poly-D-lysine-laminin matrix. Cellular ATP content was measured using Life Sciences' ATP assay (Invitrogen, Mulgrave, Victoria, AUS). Immunodetection methods have been described previously [18-20]. Expanded methodology is provided in Additional file 1.

Results and discussion

Potential Aβ-PrP signalled changes in neurogenesis were assessed using four Aβ species; Aβ1-40, Aβ1-42, Aβ4-42 and Aβ3(pE)-42, representing those that are found 'normally' in health and those that have been linked with cellular toxicity in AD [21,22]. Previous studies have shown that fibrillar Aβ has no effect on neurogenesis [23] and soluble oligomeric Aβ42 is toxic; therefore, Aβ peptides were prepared using an established protocol for producing soluble monomeric species [17]. One μM Aβ peptide was used based on results of previous studies that demonstrated this concentration induced neurogenic effects [24]. No toxicity was observed at this concentration throughout the duration of the assays (Additional file 2).

NSCs are defined by their properties of self-renewal and differentiation into mature cells of any central nervous system lineage. First we assessed the role of PrP in modifying NSC self-renewal using a neural colony-forming assay, which considers both the number of cells able to form new clonal colonies and the size of the colonies formed as an indication of clonal growth rate. As previously reported, PrP expression positively influenced NSC self-renewal (two-way analysis of variance (ANOVA), $F = 7.84$, $P = 0.006$, $n = 4$; Figure 1A & B) [11-13]. To determine whether PrP has a role in transducing Aβ-mediated changes in NSC growth, WT and KO NSCs were incubated with the Aβ species described above. The KO cells showed a significantly greater proliferation volume when compared with the carrier buffer alone and equivalently treated WT NSCs for all Aβ species (two-way ANOVA, $F = 53.75$, $P < 0.001$, $n = 4$, see Additional file 3 for complete statistical analyses; Figure 1A & C). The difference was primarily due to increased diameter of the Aβ-treated KO colonies (Figure 1D) in contrast to a decreased diameter of the WT NSCs exposed to Aβ (two-way ANOVA, $F = 63.43$, $P < 0.001$, $n = 4$), as the number of colonies formed was not significantly different between the WT and KO NSCs (Figure 1E). Proliferation of Tga20 (PrP overexpressing) NSCs treated with Aβ showed similar changes to those observed for WT cells, with no apparent PrP dose-effect at the concentration of Aβ used (Additional file 4). The presence of PrP did not confer a greater susceptibility to any one species of Aβ, indicating that neither the N- nor C-terminal truncation of Aβ is important for induction of growth changes or interaction with PrP but that the core of the peptide appears sufficient.

To further assess differences in NSC growth, Aβ1-42 was used to assess the number of cells in each phase of the cell cycle 24 hours post-Aβ addition to liquid culture. More KO cells rested in G0/G1 basally than WT (two-way ANOVA, $F = 22.99$, $P = 0.003$, $n = 4$) but after treatment with Aβ the number of KO cells actively cycling (S, G2/M phases) was significantly increased (two-way ANOVA for S phase, $F = 39.18$, $P = 0.003$, $n = 4$; for G2/M phases, $F = 24.91$, $P = 0.003$, $n = 4$; Figure 1F). There was no significant change for the WT cells, suggesting that the changes that slow the growth and reduce the diameter of neurospheres may occur after a longer period of exposure to Aβ.

NSCs can be induced to differentiate into neurones, astrocytes and oligodendrocytes. The lineage to which an individual cell commits is influenced by its extracellular environment both before and during stimulation to differentiate. Therefore, NSCs can be manipulated to differentiate into a specific mature cell by their environment. To assess the influence of Aβ-PrP signalling on NSC differentiation, KO and WT NSCs were either exposed to the Aβ species for 7 days (one treatment only) whilst induced to differentiate or were exposed to the Aβ species for 24 hours before induction of differentiation as an Aβ-priming event. When the effect of Aβ on WT and KO cellular differentiation was considered, no significant changes were observed in lineage preference regardless of whether Aβ was present during differentiation (two-way ANOVA for nestin, $F = 4.707$, $P = 0.043$ (no individually significant condition), $n = 3$; for NF-L,

F = 1.597, $P = 0.226$, n = 3; for GFAP, F = 1.514, $P = 0.223$, n = 3; Figure 2A,C-E) or if the cells were primed by treatment before differentiation (two-way ANOVA for nestin, F = 0.616, $P = 0.442$, n = 3; for NF-L, F = 0.816, $P = 0.377$, n = 3; for GFAP, F = 0.266, $P = 0.611$, n = 3; Figure 2B,F-H; Additional file 5). However some morphological changes in WT astrocytes treated with Aβ1-42, Aβ4-42 and Aβ3(pE)-42 were observed when cells were treated during, but not when exposed before, differentiation, indicating an influence of the C-terminal two residues (Figure 2I,J).

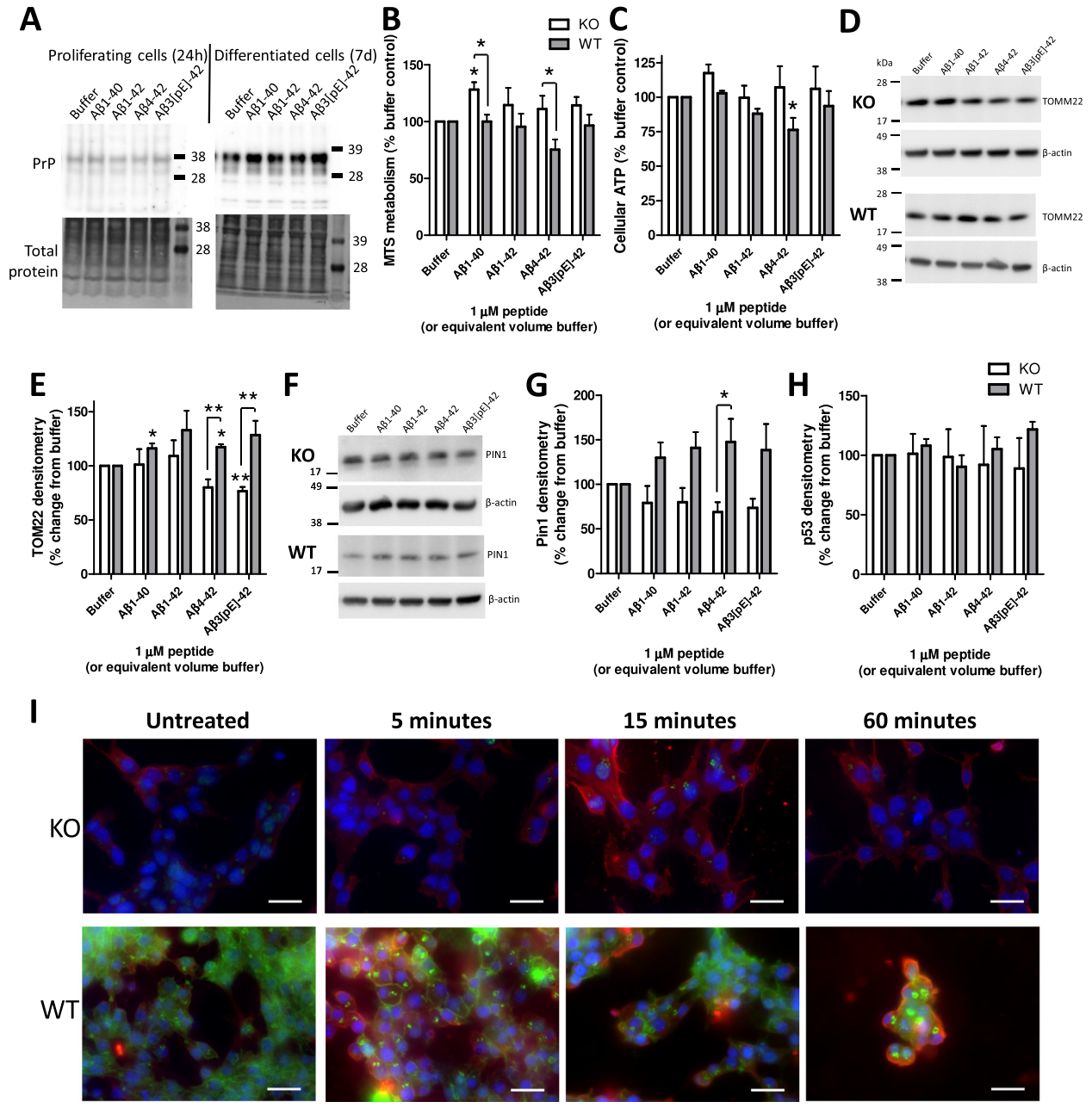

Figure 3 Beta-amyloid (Aβ) peptide influences on mitochondria and cell metabolism. **(A)** PrP expression in wild-type (WT) cells detected with Saf32 in the proliferating cells treated for 24 hours and in differentiated cells treated for 7 days. **(B-I)** Proliferating cells were treated for 24 hours with 1 μM of each of the Aβ species. **(B)** Cell metabolism as determined by MTS. **(C)** Cellular ATP content. **(D)** Western blots for the mitochondrial outer membrane translocase protein TOMM22. **(E)** Densitometry of the TOMM22 detection in Aβ-treated cells. **(F)** Western blots for the cell cycle protein Pin1. **(G)** Densitometry of Pin1 western blots. **(H)** Densitometry of p53 western blots. Data are represented as mean ± SEM. *$P < 0.05$, **$P < 0.01$. **(I)** Immunofluorescent images of Aβ1-42 (1 μM; WO2 red) and PrP (03R19 green) incubation with kock-out (KO) and WT neural stem cells for 0 to 60 minutes. Background red staining is endogenous amyloid precursor protein reactivity (endogenous Aβ cannot be detected in these cells; data not shown). DAPI nuclear staining is shown in blue, Scale bars = 25 μm.

The lack of effect on lineage but morphologic change of WT cells throughout 7 days of Aβ treatment may indicate that developing astrocytic maturity and the changes in cellular protein expression associated may be required for activation of Aβx-42 signalling pathways.

With the most striking Aβ observations relating to opposing changes in self-renewal of the KO and WT cells, it was next considered how these effects might be transduced. Contrary to previous reports [25,26], in the time frames examined no significant influences of Aβ on PrP expression levels were measurable (Figure 3A; Additional file 6). Whilst chronic exposure may reduce expression over time, in the context of the experiments performed, PrP was present to perform its function.

Changes in the rate of cell cycling are likely to require energy. Therefore, markers of cellular metabolism and mitochondrial function, as well as cell cycle, were compared in WT and KO NSCs following Aβ treatment. Formazan metabolism was significantly increased in NSC KO cells compared with the WT cells when cells were treated with Aβ1-40 and Aβ4-42 (two-way ANOVA, $F = 16.55$, $P < 0.001$, $n = 3$, see Additional file 5 for basal data and Additional file 7 for full statistical analyses; Figure 3B). Cellular ATP levels were generally unchanged between the KO and WT NSCs, only showing a decrease in WT cells treated with Aβ4-42 (two-way ANOVA, $F = 5.95$, $P = 0.021$, $n = 4$; Figure 3C). This steady-state ATP measurement does not preclude increased production balanced by increased use. Contrary to decreased growth, TOMM22, a mitochondrial outer membrane translocase, was increased in WT cells when treated with Aβ1-40, Aβ4-42, and Aβ3(pE)-42 (two-way ANOVA, $F = 16.45$, $P < 0.001$, $n = 3$; Figure 3D,E). Potentially, this might indicate that Aβ can exert an effect on mitochondria signalled through PrP that could be detrimental to their function, thus limiting growth. The cell cycle marker Pin1 has also been shown to protect against tau hyperphosphorylation and subsequent changes to the cellular cytoskeleton [27]. Pin1 was globally increased in the Aβ-treated WT compared with the KO cells, although only the Aβ4-42 condition was individually significant (two-way ANOVA, $F = 21.98$, $P < 0.001$, $n = 4$; Figure 3F,G). The overall increase in Pin1 could reflect a failed effort to increase cell cycling in these cells or might represent a cellular protective response against Aβ. p53 is linked with cell cycle and also with cell death. When activated, the half-life of this protein increases resulting in increased protein detection over time. No changes in p53 protein were observed upon treatment with Aβ in either the KO or WT NSCs (Figure 3H). We additionally considered other previously PrP-linked Aβ signalling pathways (fyn, GSK-3β and calcium) finding no changes in Aβ-induced responses that relate to PrP expression (Additional file 8).

When the localisation of Aβ added to cells was considered relative to PrP, surface staining of Aβ was observed to be more intense on the WT cells after 1 hour and PrP surface staining appeared less with greater signal inside the cells (Figure 3I). These findings are consistent with previous studies that have shown Aβ preferentially binds to cells expressing PrP causing internalisation [28] and also supports the hypothesis that Aβ stimulates different pathways in KO and WT cells.

It remains to be determined how NSCs are affected by PrP-linked Aβ signalling *in vivo*, where the context of their support cells and scaffold may lead to more diverse outcomes. However, the clear responses of the cells cultured *in vitro* indicates that sufficient cellular machinery and environmental factors to transduce PrP-Aβ signalling cascades are present. The details of these pathways will be revealed by future investigation, but it is of interest that the classical Aβ signalling pathways evaluated here were unaffected. Hypothetically, as PrP-Aβ studies to date were performed in neuronal cultures or mice, different pathways could be engaged in NSCs and post-mitotic neurones or, alternatively, differing pathways may be activated when Aβ levels reach toxic concentrations. Furthermore, during sporadic AD, brain PrP expression reduces [26], inversely correlating with Aβ burden. Reduced PrP expression (akin to KO NSCs) may

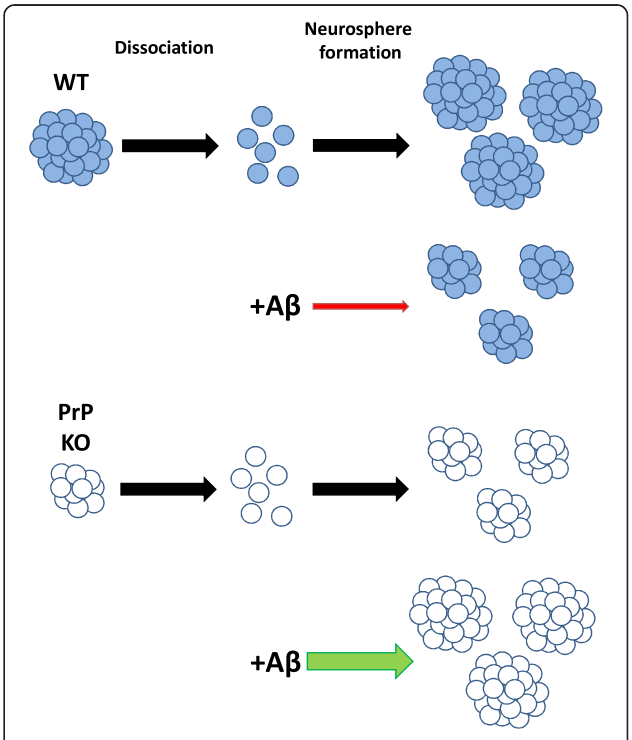

Figure 4 Schematic of beta-amyloid (Aβ) peptide influences on prion protein (PrP) knock-out (KO) and wild-type (WT) neural stem cell (NSC) growth. Representation of NSC neurosphere formation without Aβ and when Aβ is added to KO and WT NSCs.

permit Aβ stimulation of NSC proliferation, resulting in the increased neurogenic markers seen in AD brain tissue [5,6].

Conclusions

This study has validated the hypothesis that the previously observed, Aβ-signalled changes in neurogenesis can be transduced through the Aβ-oligomer receptor, PrP. In addition, we demonstrated that this signalling is more complex than PrP acting as a simple 'on' or 'off' switch for the pathway (summarised in Figure 4). Our data indicate that: i) congruous with studies using neuronal cells and mice [16,29], differing Aβ pathways are activated in the NSCs depending upon the presence and absence of PrP; ii) Aβ-PrP signalling inhibits NSC proliferation signals, although possibly monomeric forms of Aβ act in contrast to the synaptotoxic soluble oligomers; and iii) variations in the basal expression levels of PrP might also account for some of the previous variability in, and disagreements over, NSC growth responses to Aβ. This dynamic and complex interplay of key factors regulating NSC growth provides significant new insight into the control of NSC self-renewal and further evidence of biologically significant interactions between Aβ peptides and PrP.

Additional files

Additional file 1: Expanded methods.

Additional file 2: Aβ toxicity.

Additional file 3: Statistical analyses of data presented in Figure 1.

Additional file 4: NCFA results comparing Tga20 with KO and WT NSCs and baseline data.

Additional file 5: Baseline comparisons of KO and WT cells.

Additional file 6: PrP expression level changes in WT cells treated with Aβ.

Additional file 7: Statistical analyses of data presented in Figure 3.

Additional file 8: Further signalling pathways examined in cells treated with Aβ.

Abbreviations

Aβ: beta-amyloid; Aβ3(pE)-42: pyroglutamated Aβ3-42; AD: Alzheimer's disease; ANOVA: analysis of variance; KO: knock-out; NSC: neural stem cell; PrP: prion protein; SGZ: subgranular zone; WT: wild type.

Competing interests

The authors declare that they have no competing interests.

Authors' contributions

CLH, CT, QXL, TMR and BR performed experiments. CLH, SJC and CT analysed data. CLH, SJC, QXL, VL, SCD and VAL designed experiments. CLH designed the study and wrote the paper. All authors have read and approved the final version of the manuscript.

Acknowledgements

The authors would like to acknowledge Professor Colin Masters for his ongoing support and thank Dr Theo Mantamadiotis and Ms Gulay Filiz for their assistance with the cell cycle flow cytometry. This work was supported by an NHMRC program grant (#628946) and the Victorian Government's Operational Infrastructure Support program. SJC is supported by an NHMRC Practitioner Fellowship (#APP100581), SCD by an ARC Future Fellowship (FT110100199) and TMR by an Alzheimer's Australia fellowship.

Author details

[1]Department of Pathology, The University of Melbourne, Melbourne Brain Centre, Melbourne, VIC 3010, Australia. [2]Department of Medicine, Royal Melbourne Hospital, The University of Melbourne, Melbourne, VIC 3050, Australia. [3]Florey Institute of Neuroscience and Mental Health, The University of Melbourne, Melbourne, VIC 3010, Australia. [4]The Florey Department of Neuroscience and Mental Health, The University of Melbourne, Melbourne, VIC 3010, Australia.

Received: 23 October 2014 Revised: 27 January 2015
Accepted: 25 March 2015

References

1. Selkoe DJ. Soluble oligomers of the amyloid beta-protein impair synaptic plasticity and behavior. Behav Brain Res. 2008;192:106–13.
2. Portelius E, Bogdanovic N, Gustavsson MK, Volkmann I, Brinkmalm G, Zetterberg H, et al. Mass spectrometric characterization of brain amyloid beta isoform signatures in familial and sporadic Alzheimer's disease. Acta Neuropathol. 2010;120:185–93.
3. Moore BD, Chakrabarty P, Levites Y, Kukar TL, Baine AM, Moroni T, et al. Overlapping profiles of Abeta peptides in the Alzheimer's disease and pathological aging brains. Alzheimers Res Ther. 2012;4:18.
4. Lazarov O, Marr RA. Neurogenesis and Alzheimer's disease: at the crossroads. Exp Neurol. 2010;223:267–81.
5. Jin K, Peel AL, Mao XO, Xie L, Cottrell BA, Henshall DC, et al. Increased hippocampal neurogenesis in Alzheimer's disease. Proc Natl Acad Sci U S A. 2004;101:343–7.
6. Gomez-Nicola D, Suzzi S, Vargas-Caballero M, Fransen NL, Al-Malki H, Cebrian-Silla A, et al. Temporal dynamics of hippocampal neurogenesis in chronic neurodegeneration. Brain. 2014;137:2312–28.
7. Braak H, Braak E. Neuropathological staging of Alzheimer-related changes. Acta Neuropathol. 1991;82:239–59.
8. Kanemoto S, Griffin J, Markham-Coultes K, Aubert I, Tandon A, George-Hyslop PS, et al. Proliferation, differentiation and amyloid-beta production in neural progenitor cells isolated from TgCRND8 mice. Neuroscience. 2014;261:52–9.
9. Lee IS, Jung K, Kim IS, Park KI. Amyloid-beta oligomers regulate the properties of human neural stem cells through GSK-3beta signaling. Exp Mol Med. 2013;45:e60.
10. Zheng M, Liu J, Ruan Z, Tian S, Ma Y, Zhu J, et al. Intrahippocampal injection of Abeta1-42 inhibits neurogenesis and down-regulates IFN-gamma and NF-kappaB expression in hippocampus of adult mouse brain. Amyloid. 2013;20:13–20.
11. Peralta OA, Huckle WR, Eyestone WH. Expression and knockdown of cellular prion protein (PrPC) in differentiating mouse embryonic stem cells. Differentiation. 2011;81:68–77.
12. Steele AD, Emsley JG, Ozdinler PH, Lindquist S, Macklis JD. Prion protein (PrPc) positively regulates neural precursor proliferation during developmental and adult mammalian neurogenesis. Proc Natl Acad Sci U S A. 2006;103:3416–21.
13. Lee YJ, Baskakov IV. Treatment with normal prion protein delays differentiation and helps to maintain high proliferation activity in human embryonic stem cells. J Neurochem. 2010;114:362–73.
14. You H, Tsutsui S, Hameed S, Kannanayakal TJ, Chen L, Xia P, et al. Abeta neurotoxicity depends on interactions between copper ions, prion protein, and N-methyl-D-aspartate receptors. Proc Natl Acad Sci U S A. 2012;109:1737–42.
15. Larson M, Sherman MA, Amar F, Nuvolone M, Schneider JA, Bennett DA, et al. The complex PrP(c)-Fyn couples human oligomeric Abeta with pathological tau changes in Alzheimer's disease. J Neurosci. 2012;32:16857–71a.
16. Um JW, Nygaard HB, Heiss JK, Kostylev MA, Stagi M, Vortmeyer A, et al. Alzheimer amyloid-beta oligomer bound to postsynaptic prion protein activates Fyn to impair neurons. Nat Neurosci. 2012;15:1227–35.
17. McColl G, Roberts BR, Gunn AP, Perez KA, Tew DJ, Masters CL, et al. The Caenorhabditis elegans A beta 1–42 model of Alzheimer disease predominantly expresses A beta 3–42. J Biol Chem. 2009;284:22697–702.

18. Haigh CL, McGlade AR, Lewis V, Masters CL, Lawson VA, Collins SJ. Acute exposure to prion infection induces transient oxidative stress progressing to be cumulatively deleterious with chronic propagation in vitro. Free Radic Biol Med. 2011;51:594–608.
19. Sinclair L, Lewis V, Collins SJ, Haigh CL. Cytosolic caspases mediate mislocalised SOD2 depletion in an in vitro model of chronic prion infection. Dis Model Mech. 2013;6:952–63.
20. Haigh CL, Lewis VA, Vella LJ, Masters CL, Hill AF, Lawson VA, et al. PrPC-related signal transduction is influenced by copper, membrane integrity and the alpha cleavage site. Cell Res. 2009;19:1062–78.
21. Nussbaum JM, Schilling S, Cynis H, Silva A, Swanson E, Wangsanut T, et al. Prion-like behaviour and tau-dependent cytotoxicity of pyroglutamylated amyloid-beta. Nature. 2012;485:651–5.
22. Bouter Y, Dietrich K, Wittnam JL, Rezaei-Ghaleh N, Pillot T, Papot-Couturier S, et al. N-truncated amyloid beta (Abeta) 4–42 forms stable aggregates and induces acute and long-lasting behavioral deficits. Acta Neuropathol. 2013;126:189–205.
23. Heo C, Chang KA, Choi HS, Kim HS, Kim S, Liew H, et al. Effects of the monomeric, oligomeric, and fibrillar Abeta42 peptides on the proliferation and differentiation of adult neural stem cells from subventricular zone. J Neurochem. 2007;102:493–500.
24. Haughey NJ, Liu D, Nath A, Borchard AC, Mattson MP. Disruption of neurogenesis in the subventricular zone of adult mice, and in human cortical neuronal precursor cells in culture, by amyloid beta-peptide: implications for the pathogenesis of Alzheimer's disease. Neuromolecular Med. 2002;1:125–35.
25. Whitehouse IJ, Jackson C, Turner AJ, Hooper NM. Prion protein is reduced in aging and in sporadic but not in familial Alzheimer's disease. J Alzheimers Dis. 2010;22:1023–31.
26. Whitehouse IJ, Miners JS, Glennon EB, Kehoe PG, Love S, Kellett KA, et al. Prion protein is decreased in Alzheimer's brain and inversely correlates with BACE1 activity, amyloid-beta levels and Braak stage. PLoS One. 2013;8:e59554.
27. Liou YC, Sun A, Ryo A, Zhou XZ, Yu ZX, Huang HK, et al. Role of the prolyl isomerase Pin1 in protecting against age-dependent neurodegeneration. Nature. 2003;424:556–61.
28. Rushworth JV, Griffiths HH, Watt NT, Hooper NM. Prion protein-mediated toxicity of amyloid-beta oligomers requires lipid rafts and the transmembrane LRP1. J Biol Chem. 2013;288:8935–51.
29. Gimbel DA, Nygaard HB, Coffey EE, Gunther EC, Lauren J, Gimbel ZA, et al. Memory impairment in transgenic Alzheimer mice requires cellular prion protein. J Neurosci. 2010;30:6367–74.

PLOS | ONE

RESEARCH ARTICLE

The Prion Protein N1 and N2 Cleavage Fragments Bind to Phosphatidylserine and Phosphatidic Acid; Relevance to Stress-Protection Responses

Cathryn L. Haigh[1]*, Carolin Tumpach[2], Simon C. Drew[2], Steven J. Collins[1,2]*

1 Department of Medicine (Royal Melbourne Hospital), The University of Melbourne, Melbourne Brain Centre, Melbourne, VIC, AUS, 3010, **2** The Florey Department of Neuroscience and Mental Health, The University of Melbourne, Melbourne Brain Centre, Melbourne, VIC, AUS, 3010

* chaigh@unimelb.edu.au (CLH); stevenjc@unimelb.edu.au (SJC)

Citation: Haigh CL, Tumpach C, Drew SC, Collins SJ (2015) The Prion Protein N1 and N2 Cleavage Fragments Bind to Phosphatidylserine and Phosphatidic Acid; Relevance to Stress-Protection Responses. PLoS ONE 10(8): e0134680. doi:10.1371/journal.pone.0134680

Editor: Jiyan Ma, Van Andel Institute, UNITED STATES

Received: May 18, 2015

Accepted: July 13, 2015

Published: August 7, 2015

Data Availability Statement: All relevant data are within the paper and its Supporting Information files.

Funding: This work was supported by a National Health and Medical Research Council (NH&MRC; https://www.nhmrc.gov.au/) program grant (#628946) and SJC is supported by an NH&MRC Practitioner Fellowship (#APP100581). SCD is funded by an Australian Research Council Future Fellowship (FT110100199). The funders had no role in study design, data collection and analysis, decision to publish, or preparation of the manuscript.

Abstract

Internal cleavage of the cellular prion protein generates two well characterised N-terminal fragments, N1 and N2. These fragments have been shown to bind to anionic phospholipids at low pH. We sought to investigate binding with other lipid moieties and queried how such interactions could be relevant to the cellular functions of these fragments. Both N1 and N2 bound phosphatidylserine (PS), as previously reported, and a further interaction with phosphatidic acid (PA) was also identified. The specificity of this interaction required the N-terminus, especially the proline motif within the basic amino acids at the N-terminus, together with the copper-binding region (unrelated to copper saturation). Previously, the fragments have been shown to be protective against cellular stresses. In the current study, serum deprivation was used to induce changes in the cellular lipid environment, including externalisation of plasma membrane PS and increased cellular levels of PA. When copper-saturated, N2 could reverse these changes, but N1 could not, suggesting that direct binding of N2 to cellular lipids may be part of the mechanism by which this peptide signals its protective response.

Introduction

The prion protein (PrP^C) is most widely recognised for its causative association with the transmissible spongiform encephalopathies or prion diseases. During disease PrP^C becomes misfolded in a self-templating event that results in its transmissibility. PrP^C is a membrane bound (by a glycosylphosphatidylinositol [GPI] anchor), copper-co-ordinating glycoprotein [1]. Aside from GPI-anchor attachment and N-linked glycosylation, PrP^C is recognised to undergo further post-translational modifications including at least two endoproteolytic cleavage events termed alpha- and beta-cleavage that result in the formation of N-terminal (N1 and N2) and C-terminal (C1 and C2) fragments respectively [2, 3].

Competing Interests: The authors have declared that no competing interests exist.

PrP^C is localised within cholesterol-rich lipid rafts on the external leaflet of the cell membrane and its interactions with specific lipid species have been linked with both its function and mis-folding [4–9]. The lipid membrane environment is highly important for the control of cellular signal transduction [10] and association of PrP^C with lipid raft domains has been shown to be important for its signalling functions [7–9]. The N-terminus of PrP^C is known to bind to synthetic lipid membranes [11–13], to target full-length PrP to lipid rafts [14] and to control the movement of PrP^C out of lipid raft domains during its copper-induced clathrin mediated internalisation [15, 16]; therefore, the endoproteolytic cleavage events that separate the N and C-termini of PrP^C might have a significant impact on its cellular function.

Both the N1 and N2 fragments have been shown to have neuroprotective properties. N1 protects against staurosporine toxicity in cell cultures and ischemia in the rat retina via the p53 pathway [17]. N2 reduces intracellular reactive oxygen species (ROS) production in response to starvation through stimulation of MEK1 signalling in a sequence that depends upon cell surface glycosaminoglycans, intact lipid rafts and copper-dependent endocytosis [18, 19].

Our work has previously shown that synthetic N1 and N2 can bind to lipid membranes containing anionic phospholipids at low pH [12]. Binding is primarily with the lipid head group and does not extend significantly into the acyl tail region, but appears to induce a change in lipid ordering [13]. There is no evidence that these peptides insert into the membrane in such a way as to disrupt membrane integrity, therefore, the peptide-lipid interactions might represent a functional event. This study aimed to determine if N1 and N2 could bind other lipid species and in particular whether such lipid interactions might have a functional influence on the activity of these fragments under the conditions where we have previously seen a neuroprotective action of N2. We identified a previously unknown binding interaction of both N1 and N2 with PA and demonstrated that changes in the cellular lipid environment are associated with cellular stress and the protective action of N2.

Materials and Methods

Peptide synthesis

The peptides used and their synthesis have been described previously [13, 18, 20, 21]

Lipid strip western blotting

Lipid strips were purchased from Life Technologies (Invitrogen; AUS). The protocol provided by the manufacturer was used with the following modifications. Lipid strip incubations were performed in phosphate buffered saline (PBS; Gibco, Invitrogen Life Sciences AUS) at pH 7.0 or in acetate buffer (0.06 g acetic acid, 0.875 g NaCl per 100 ml dH_2O) at pH 5.0 with 0.5 μg/ml peptide. Equilibration in a sandwich/double blot of new nitrocellulose membrane and blotting paper was assembled in Tris buffer at pH 8 to ensure that if binding to the lipids was pH-dependent the peptide was not washed off the spots during antibody incubations: in this case the peptide would have transferred to the fresh membrane and been detected by blotting. To ensure any lack of detection was not because of epitope masking by the lipid-peptide interaction, western blotting was carried out with two antibodies, SAF32 (1 in 5000; SPI Bio) targeting the octarepeat region residues 79–92 and 8B4 (1 in 1000; Alicon, Switzerland) targeting the N-terminal residues 37–44. Blots and densitometry were carried out as previously [21, 22]. Shorter exposures are shown in S1 Fig to permit comparison of the intensities of the heavy signals in some spots.

Cell culture

A murine PrP-null neural cell line (CF10) was used throughout. These cells and their culture have been described in detail previously [18, 22, 23].

Generalised polarisation

Cells were labelled with 5 μM Laurdan (Invitrogen; AUS) in the dark for 30 mins under normal incubator conditions. Fluorescence emission intensity (I) was measured using excitation at 355 nm and emission at 460 and 520 nm. Generalised polarisation (GP) was calculated using the following equation; $GP = \frac{(I_{460}-I_{520})}{(I_{460}+I_{520})}$. Benzyl alcohol (Sigma-Aldrich, AUS) and filipin III (Sigma-Aldrich), agents known to perturb membranes, were used as a control for increased membrane fluidity.

NBD-PS labelling

1-oleoyl-2-{12-[(7-nitro-2-1,3-benzoxadiazol-4-yl)amino]dodecanoyl}-*sn*-glycero-3-phosphoserine (ammonium salt; 18:1–12:0 NBD-PS), referred to as NBD-PS throughout, was purchased from Avanti Polar Lipids Inc (USA) and methanol stocks made as per the manufacturer's instructions. Cells were labelled with NBD-PS to a final concentration of 20 μM in ice cold PBS (Gibco, Invitrogen, AUS) with 1 mg/ml bovine serum albumin (BSA; Sigma-Aldrich, AUS) for 2 minutes. Cells were washed once in PBS-BSA before incubation in phenol-red free OptiMEM (Gibco).

NBD-PS emission spectra

Emission spectrum scans were done following NBD-PS labelling, using 480 nm excitation and 500–600 nm emission in a Cary Eclipse spectrometer (Agilent Technologies, AUS).

NBD-PS polarisation

Anisotropy was measured following NBD-PS labelling using 470–10 nm excitation and matched 520 nm emission filters in a PolarSTAR Optima plate reader (BMG Labtech AUS).

Fluorescence microscopy

Cells were imaged as described previously [21].

Magnetic cell sorting

Cell sorting and counting were performed as previously described [24, 25]. Briefly, cells in suspension were labelled with AnnexinV (which binds with high affinity to externalised phosphatidylserine) magnetic microbeads (Miltenyi Biotech, AUS) and separation in a magnetic field performed as described in the MACS protocol (Miltenyi Biotech). Both labelled (positive) and unlabelled (negative) fractions were transferred into fresh media for counting.

DCFDA assay

Assays were performed as described previously [22].

Phospholipase D activity assay

Cells were plated, assayed and harvested in 96-well plates. Lysates were prepared using 20 μl/well 0.1% (v/v) Triton X-100 in assay buffer, followed by three freeze-thaw cycles. Lysate was

diluted in a further 30 μl of assay buffer before 1:1 addition of assay reagents as per the Amplex Red Phospholipase D Assay Kit (Invitrogen) product protocol.

Phosphatidic acid measurement

Cellular PA concentrations were measured using Total Phosphatidic Acid Fluorometric Assay Kit (Cayman Chemical, Sapphire Bioscience, AUS) as per the manufacturer's product protocol with fluorescence measured using a PolarSTAR Optima (BMG). Determination of cellular protein concentration was achieved using the BCA assay as described previously [26].

Statistical analyses

All graphs represent the mean and SEM. The numerical value for each independent experiment 'n' was the average of the technical replicates. Student's t-test was used for analysis of data with two variables and one-way ANOVA with Tukey's secondary test used for more than two variables. Confidence intervals of 95% were applied for all analyses.

Results

Our previous studies using model membranes have shown that N1 and N2 (illustrated in Fig 1A) bind anionic phospholipids at low pH [12, 13]. Such studies are relatively laborious and expensive. Hence to streamline the identification of further interactions with lipids involved in cellular signalling functions we used nitrocellulose spotted with individual lipid species (Fig 1B/2A) and incubated these with synthetically produced N1 (Fig 1) and N2 (Fig 2) at neutral (7) or low (5) pH. The membranes showed that, in accord with results obtained previously, N1 and N2 bound to anionic phosphatidylserine (PS) with limited binding to the neutral phosphatidylcholine (PC). The peptides further showed a strong affinity for phosphatidic acid (PA; Figs 1C&1D, 2B &2C, shorter exposures are shown in S1 Fig). In this assay no pH dependence or loss of peptide binding as membranes were equilibrated to neutral pH was observed (S2 Fig) and binding was identical when detection was made using the octameric repeat region targeting SAF32 antibody and the N-terminally targeted 8B4 (S3 Fig). In our prior studies, N1 bound PS with higher affinity than N2. The densitometry showed that the signal magnitude was higher for the N1 peptide than for the N2, however, the overall binding patterns did not differ (Figs 1D, 2C; plots are shown on the same axis within each peptide analysis for ease of visual comparison of absolute densitometry, for alternate scaling see S4 Fig for N1 and S5 Fig for N2). We additionally assessed the effect of copper binding on these interactions by pre-incubating the N1 and N2 peptides with four molar equivalents $CuCl_2$ before incubation with the membranes. These results indicated that copper and pH together may weakly, but not significantly, enhance binding to some lipid species but significantly decrease N2 binding to PS at pH 7.

To examine the importance of each region of the N-terminal fragments for PS and PA binding we incubated the membrane with peptides containing residues 23–50 (Fig 3A) and 51–89 octameric repeat region (Fig 3B), plus a peptide representing N1 minus the 51–89 copper-binding domain (Fig 3C) and a peptide representing N2 with the proline residues at amino acids 26 and 28 mutated to alanine (PrP23-89P26/28A; Fig 3D). The octameric repeat region alone was unable to bind to any lipid regardless of whether it was loaded with Cu^{2+} (Fig 3B/3E; a longer exposure of these strips alongside the P26/28A peptide for comparison is shown in S6 Fig and alternatively scaled axes are shown in S7 Fig). Absence of the octameric repeat region from N2, leaving only residues 23–50 (Fig 3A/3E) or deletion of the octameric repeat region from N1 (Fig 3C/3E) Fig led to a greater number of interactions with different lipids. Mutation of the two proline residues within the polybasic N-terminus (Fig 3D/3F) also resulted in a promiscuity of lipid binding with significant changes from the wild type N2 sequence seen for

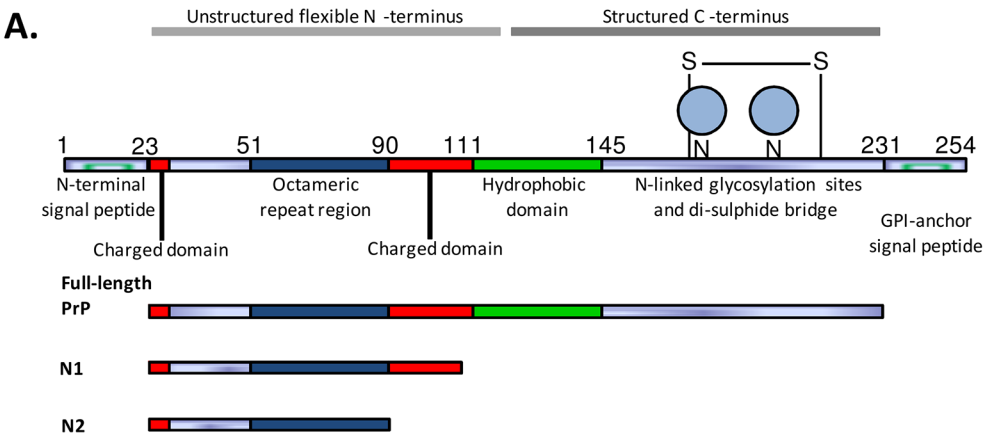
A.
Unstructured flexible N -terminus
Structured C -terminus
S
S
N
N
1
23
51
90
111
145
231
254
N-terminal signal peptide
Octameric repeat region
Hydrophobic domain
N-linked glycosylation sites and di-sulphide bridge
GPI-anchor signal peptide
Charged domain
Charged domain
Full-length PrP
N1
N2

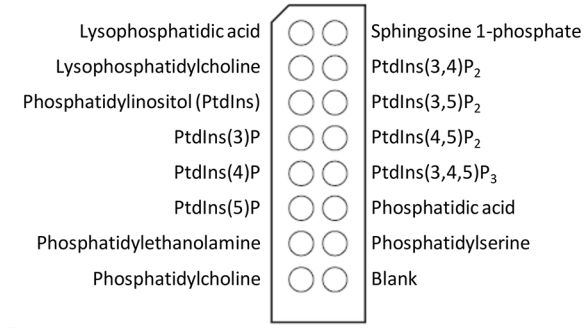
B.
Lysophosphatidic acid
Lysophosphatidylcholine
Phosphatidylinositol (PtdIns)
PtdIns(3)P
PtdIns(4)P
PtdIns(5)P
Phosphatidylethanolamine
Phosphatidylcholine
Sphingosine 1-phosphate
PtdIns(3,4)P2
PtdIns(3,5)P2
PtdIns(4,5)P2
PtdIns(3,4,5)P3
Phosphatidic acid
Phosphatidylserine
Blank

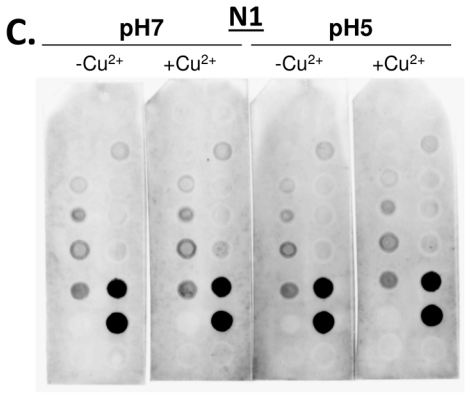
C.
N1
pH7
pH5
-Cu2+
+Cu2+
-Cu2+
+Cu2+

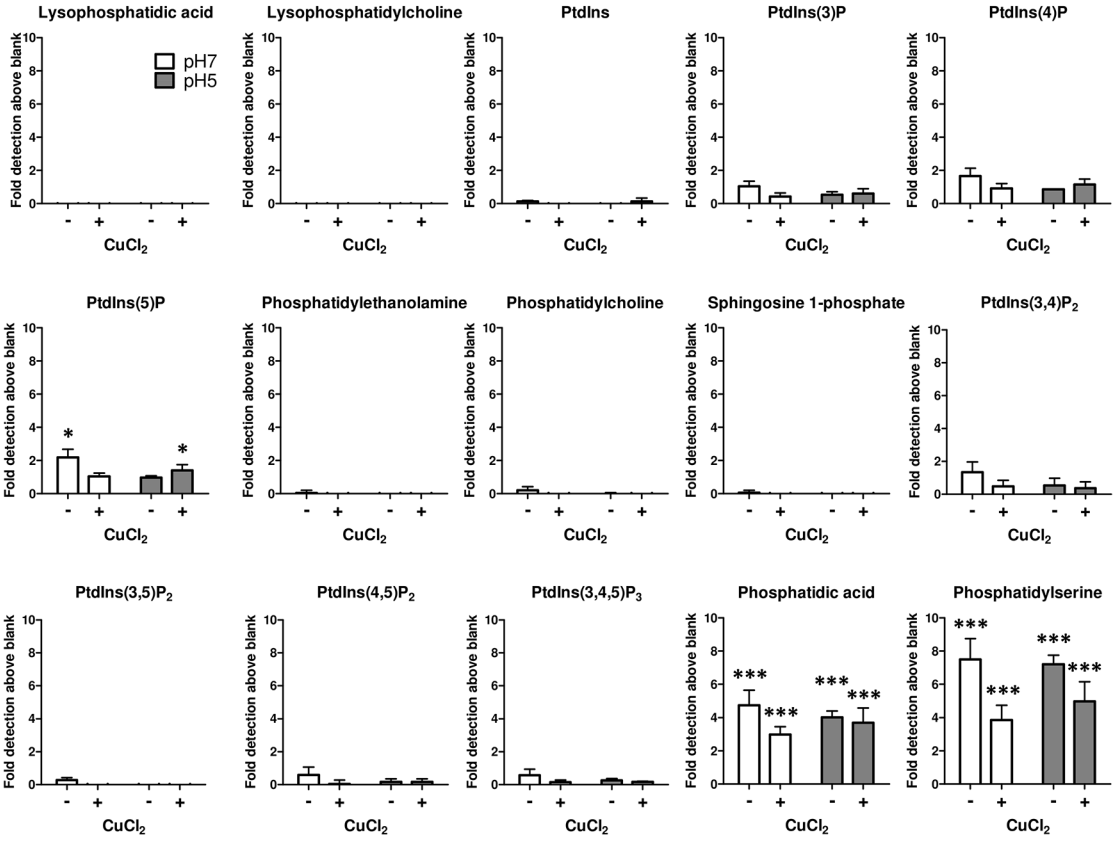
D.
Lysophosphatidic acid
Lysophosphatidylcholine
PtdIns
PtdIns(3)P
PtdIns(4)P
PtdIns(5)P
Phosphatidylethanolamine
Phosphatidylcholine
Sphingosine 1-phosphate
PtdIns(3,4)P2
PtdIns(3,5)P2
PtdIns(4,5)P2
PtdIns(3,4,5)P3
Phosphatidic acid
Phosphatidylserine
pH7
pH5
Fold detection above blank
CuCl2

Fig 1. Lipid spot blots identify N1 fragment binding to PS and PA. A. Diagram showing full length PrP and the regions comprising the N1 and N2 cleavage fragments. **B.** Schematic indicating the lipid spot arrangement on the membrane. **C.** PrP23-111 (N1) incubation with the lipid spot blots at pH 7 and pH 5 with and without pre-loading with four molar equivalents $CuCl_2$ followed by western blotting with SAF32 antibody (directed against amino acids 51–89). **D.** Densitometric quantification of spot intensity, n = 3, significance over blank control is shown as *p<0.05, ***p<0.001.

doi:10.1371/journal.pone.0134680.g001

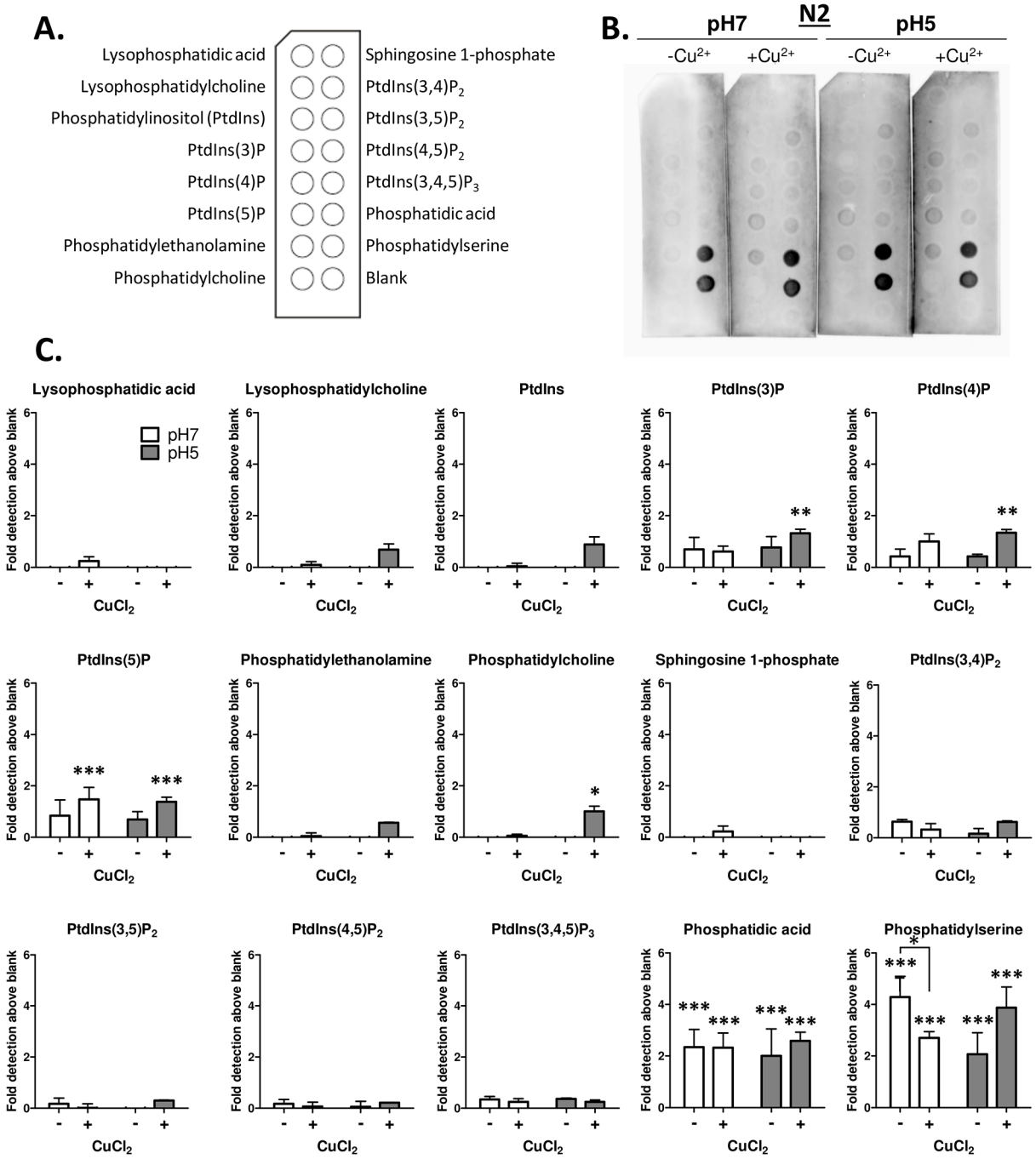

Fig 2. N2 binds PS and PA lipid spots. A. Schematic indicating the lipid spot arrangement on the membrane. **B.** PrP23-89 (N2) incubation with the lipid spot blots at pH 7 and pH 5 with and without pre-loading with four molar equivalents $CuCl_2$ followed by western blotting with SAF32 antibody (directed against amino acids 51–89). **C.** Densitometric quantification of spot intensity, n = 3, significance over blank control and between conditions is shown as *p<0.05, **p<0.01, ***p<0.001.

doi:10.1371/journal.pone.0134680.g002

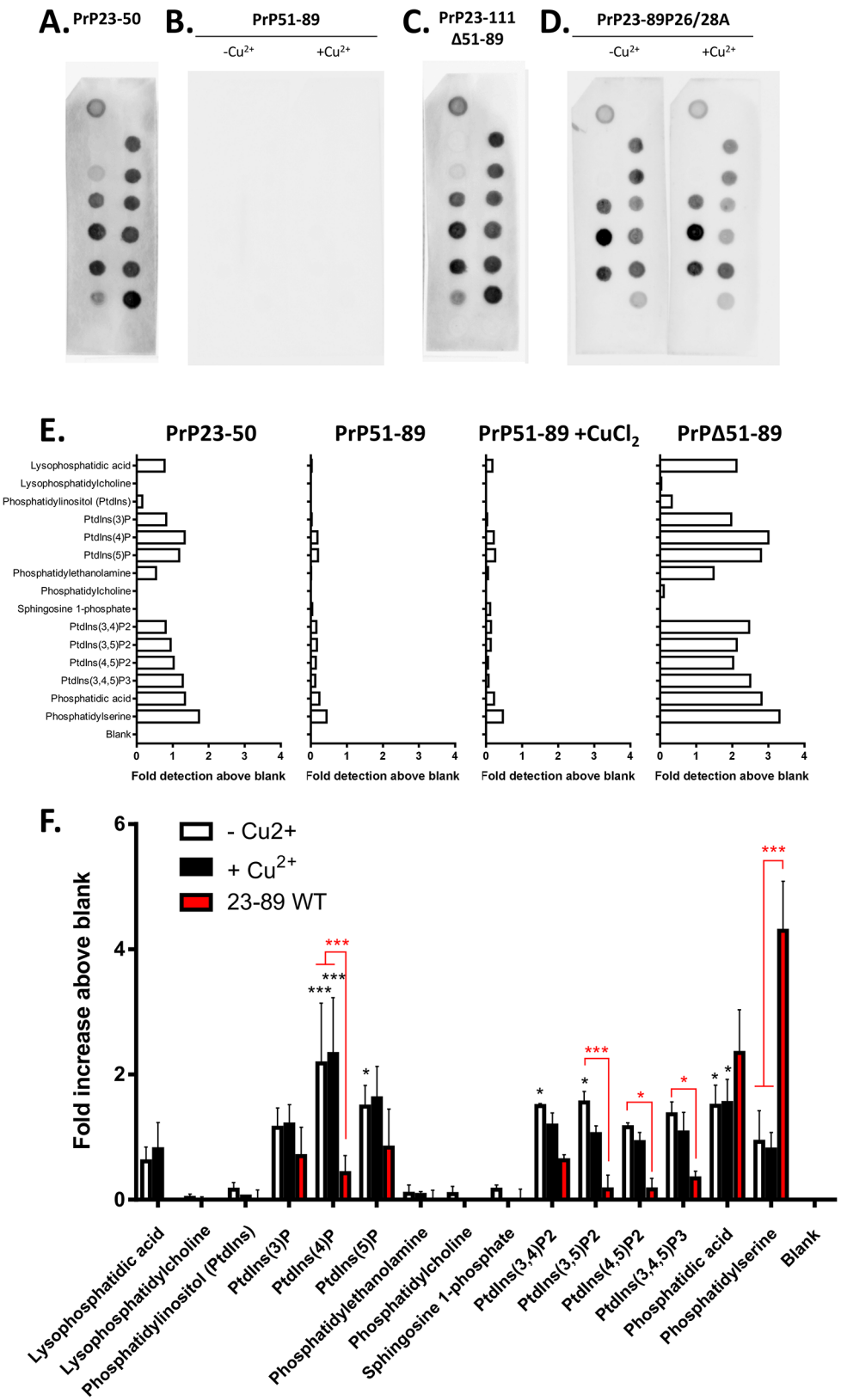

Fig 3. Lipid binding specificity is determined by regions of N1 and N2. Lipid spot blots (incubated at pH 7) of peptides corresponding to regions of N1 and N2, including residues 23–50 (**A**), residues 51–89

comprising the copper-binding region and therefore tested with and without copper saturation (**B**) and an N1 fragment lacking the residues of the copper-binding region, Δ51–89 (**C**). For 23–50 and N1Δ51–89, copper saturation was not tested as neither fragment contains the octarepeat copper-binding domain and blotting used the N-terminally targeted 8B4 antibody as SAF32 targets residues 79–92. **D.** Lipid spot blots of a mutant N2 P26/28A fragment with and without copper saturation at pH 7 detected with SAF32. **E.** Densitometric quantification of spot intensity for the domains of N1 and N2, n = 1. **F.** Densitometric quantification of spot intensity of the P26/28A mutation of N2 with and without copper saturation. Apo N2 intensities are shown for comparison of differences between the mutated and wild-type (WT) sequence, n = 3. Significance over blank control is shown in black and significant differences in detection from the wild type sequence of N2 are shown in red, *p<0.05, ***p<0.001.

doi:10.1371/journal.pone.0134680.g003

phosphatidylinositol (4)P, (3,5)P2, (4,5)P2, (3,4,5)P3 and PS. From these observations, we may conclude that the specificity of lipid binding by N1 and N2 requires the full complement of N-terminal and octarepeat residues.

Our previous studies have found that copper-bound N2 normalises cellular responses to the stress of nutrient starvation [18, 21]. To assess whether alterations in the lipid membrane environment may be involved in the cellular response to starvation, changes in the fluorescence profile of an environmentally sensitive probe, Laurdan, were assessed using generalised polarisation (GP; the principle of this assay is described in [27, 28]). The GP value upon serum deprivation showed that decreased phospholipid order within the cell membrane occurred in response to nutrient withdrawal (Fig 4A). As both peptides were shown to bind PS and PA, changes to each of these lipids were also specifically assessed. Incorporation of PS containing a NBD fluorescent label within the fatty acid chain (NBD-PS) into cultured CF10 cells and microscopic examination of the NBD-PS cells following serum withdrawal revealed a broader spatial distribution of NBD-PS fluorescence (Fig 4B). Furthermore, using this same probe it was found that upon serum withdrawal the fluorescence intensity of the probe and its anisotropy are decreased (Fig 4C & 4D). In similarity with the environmentally sensitive Laurdan probe, NBD is quenched in more aqueous environments [29], therefore, these results indicate that during serum deprivation the cell membrane is becoming less ordered and more fluid.

It is also known that an early indicator of apoptosis is loss of membrane asymmetry at the cell surface, which results in abnormal external exposure of PS and might contribute to some of the changes detected by NBD-PS. Using the affinity of Annexin-V for PS, binding of Annexin-V coated magnetic beads was employed to separate cells with exposed PS from those cells maintaining membrane asymmetry. These separations revealed a significant increase in the number of cells exposing PS in the nutrient deprived population after 15 minutes of starvation (Fig 4E).

PA is generated from catalysis of PC by phospholipase D (PLD) at the plasma membrane and acts as a second messenger in various signalling pathways [30, 31]. Therefore to look for the role of PA in signalling the cellular response to serum starvation, butan-1-ol was used to inhibit the action of this enzyme. Our previous studies have shown that serum deprivation induces a large and rapid production of reactive oxygen species (ROS) within cells [18, 21]. We confirmed this production and assessed the effect of butan-1-ol on ROS production, finding that the butan-1-ol stimulated an even greater increase in intra-cellular ROS (Fig 4F). Butan-1-ol might elicit non-specific cellular actions and therefore, to confirm whether cellular PA production was changed following serum deprivation, we examined the cellular concentration of PA thirty minutes after serum withdrawal. At this time PA concentrations in the serum deprived cells were almost double those of the cells incubated under normal conditions (Fig 4G). Measurement of PLD activity showed no significant change in enzyme activity (Fig 4H), indicating that the changed levels of PA measured might be a result of decreased degradation of PA.

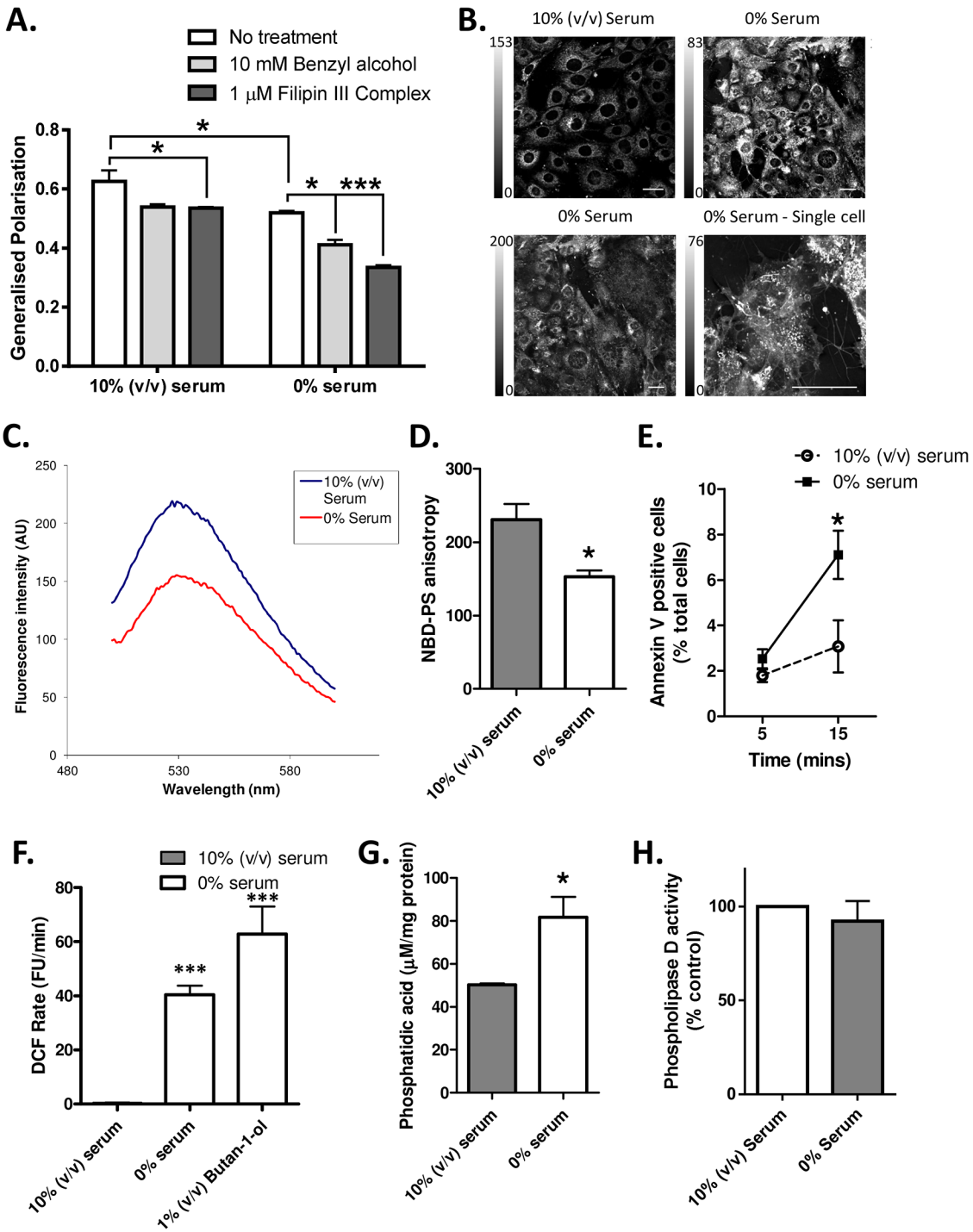

Fig 4. Serum deprivation causes changes to PS and PA in CF10 cells. A. Laurdan GP changes following serum deprivation for 30 minutes as compared with benzyl alcohol (BA) and filipin III controls. n = 3. **B.** Live cell imaging of NBD-PS labelled CF10 cells. Image intensity is thresholds have been selected to view detail in the staining pattern and do not represent a comparison of fluorescence intensity. Scale bars = 20 μm. **C.** Fluorescence emission spectra of NBD-PS labelled cells following transfer into serum-free medium, scans were taken immediately after media replacement. **D.** Anisotropy of NBD-PS in CF10 cells with and without serum present. n = 3. **E.** Counts from magnetic separation of cells that have lost membrane asymmetry allowing them to bind PS at 5 and 15 minutes post serum withdrawal. n = 4. **F.** ROS production detected by DCF fluorescence when cells are serum-starved and with exposure to butan-1-ol to inhibit PLD activity. n = 4. **G.** Measurement of cellular phosphatidic acid concentration 30 minutes after commencing serum deprivation. n = 3. **H.** Measurement of phospholipase-D activity following 15 minutes serum starvation. n = 3. For all panels, *p<0.05, ***p<0.001.

doi:10.1371/journal.pone.0134680.g004

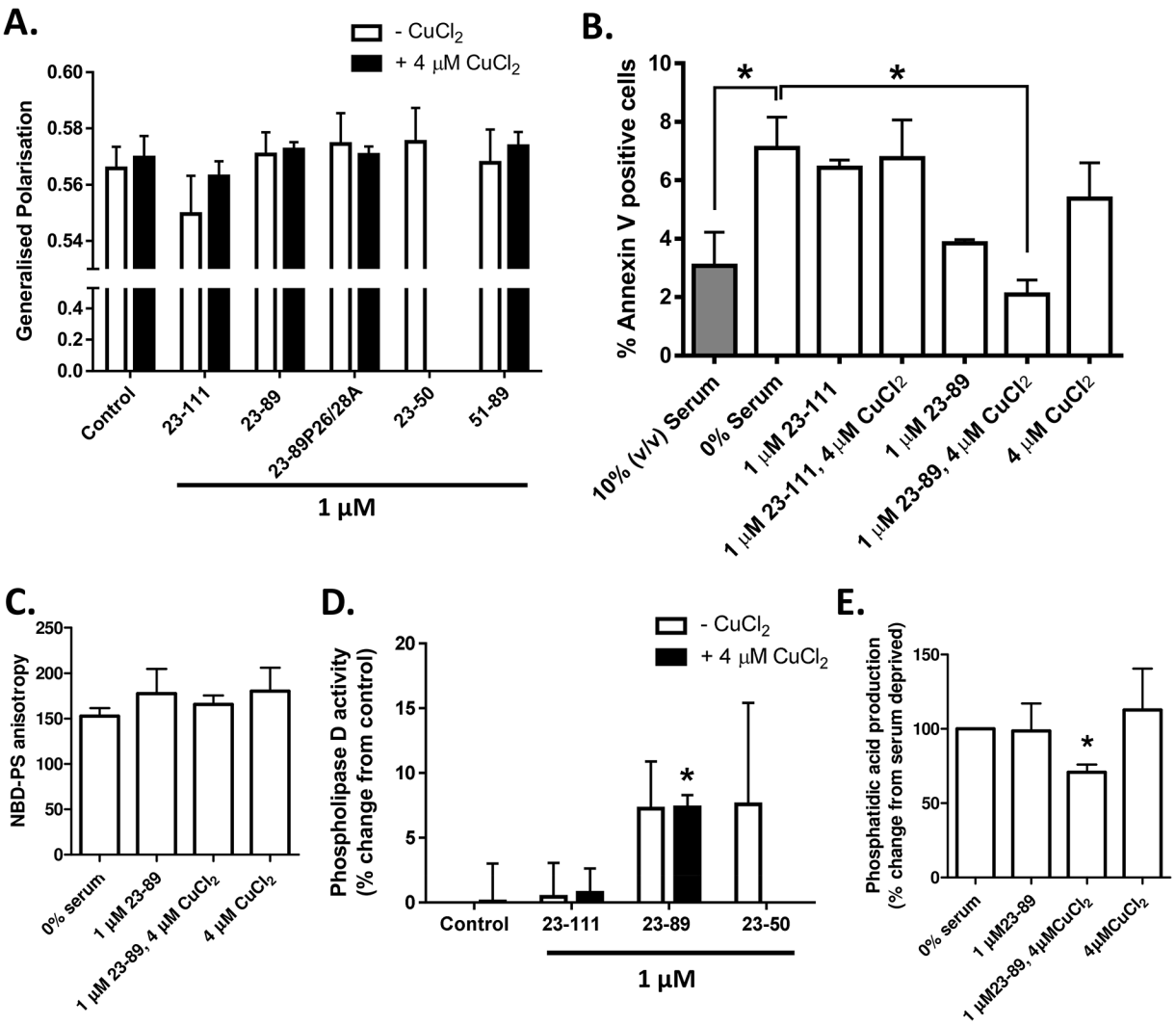

Fig 5. N2, but not N1, reverses PS externalisation and PA increase in the absence of further membrane changes. A. Laurdan GP of serum starved cells alone and when treated N2 (23–89), N1 (23–111), N2 with the two prolines within the N-terminal polybasic region mutated to alanines (23-89P26/28A, the octarepeat region (51–89), copper-saturated (four molar equivalents) N1, N2, 23-89P26/28A and 51–89, 23–50 and equivalent copper without peptide, measured under the same conditions used in Fig 4. n = 3. **B.** Annexin V magnetic separation of N1 and N2 with and without copper saturation. Filled bar indicates 10% (v/v) serum and hollow bars show conditions with 0% serum. n = 3. **C.** NBD-PS anisotropy of N2 with and without copper saturation. n = 3. **D.** Phospholipase-D activity within N1 and N2 (+/- copper), and 23–50 (no copper) serum starved cells. n = 3. **E.** Relative PA concentrations within N2 treated (+/- copper) serum starved cells. n = 3. Fig *p<0.05.

doi:10.1371/journal.pone.0134680.g005

To determine if the protective actions of copper-loaded N2 [18] or the previously observed neuroprotective actions of N1 [17] might involve or affect the membrane lipid environment, the Laurdan GP assay was repeated comparing the effects of N1 and N2 (+/- copper saturation) with the GP values of serum deprived cells alone. Neither peptide significantly influenced laurdan GP (Fig 5A), showing they are unable to influence overall membrane fluidity. To more specifically look at PS and PA we assessed the influence of serum deprivation in the presence or absence of N1 and N2 (with and without pre-loading with copper). Annexin-V separations of cells following serum deprivation showed that copper-saturated N2, but not N1, reversed the loss of asymmetry induced by serum deprivation (Fig 5B). Despite the influence of copper saturated N2 on PS externalisation, but in agreement with the results seen for laurdan generalised

polarisation, NBD-PS anisotropy was unchanged (Fig 5C). Such findings indicate that whilst the externalisation of the PS is restored in response to copper-loaded N2, the changes in fluidity caused by serum deprivation are not reversed.

In contrast with the unchanged PLD activity in response to serum deprivation, copper loaded N2 significantly increased the activity of PLD under these conditions (Fig 5D). Apo-N2 and 23–50 produced highly variable (not significant) fluctuations in PLD activity and N1 showed no change from baseline, regardless of copper saturation. To assess the consequences of the increased PLD activity stimulated by copper-saturated N2, cellular concentrations of PA were assessed. Despite the increased enzymatic activity of PLD, copper-saturated N2 counteracted increases in PA induced by serum deprivation (Fig 5E) suggesting an increased turnover of PA, which requires enzymatic compensation. An alternative interpretation of the data is that N2 binding to PA impairs its enzymatic digestion into the end products detected in the analysis, resulting in an apparently reduced PA level due to artefactual under-detection.

Discussion

Whilst the binding of the N1 and N2 fragments to PS is well established in model membrane systems [12, 13], to the best of our knowledge an interaction between any region of PrP^C and PA has never been reported. Both the 51–89 amino acid copper-binding region and the proline motif within the basic amino acids at the far N-terminus were required for the specificity of the interaction with PS and PA. This observation could be highly significant in view of the fact that the previously reported protective effect of the N2 fragment also required both of these domains [18]. Weak binding was seen for several of the other lipid species, however this is unlikely to be of relevance in a cellular context where higher affinity binding partners would be able to out-compete and dominate.

Our previous studies into N1 and N2 lipid binding found that interactions with PS-containing bilayers could only occur at low pH [12, 13], which was not the case for the lipid strip assays in the current study. A potential explanation for the discrepancy between the data lies in the methodology. The lipid strips are prepared from pure spots of a single lipid species, immobilised on a nitrocellulose membrane [32, 33]. Consequently they are intended as a screening tool and are not designed to give specific information on interactions that require free movement of lipids such as that provided by the complex biophysical techniques used in our previous studies. However, they did correctly detect the previously indentified interaction with PS and inability to bind PC; therefore, it is highly likely that the interaction with PA will occur under the right conditions. The specifics of these conditions remain to be investigated.

Assessment of the serum deprived cells showed that the lipid environment was consistently perturbed and that such changes occurred rapidly. As there is no evidence of membrane lysis during starvation (despite externalisation of PS these cells do not die [21]), such results are indicative of changed lipid order. Therefore, under conditions of nutrient withdrawal, PS externalisation may not be entirely a pro-apoptotic event but a cellular compensation to the stress of starvation and it is in this context that N1 and N2 binding could be significant. Under normal cellular conditions PS is localised to the inner leaflet of the cell membrane and PrP^C is on the outer leaflet, where the N2 cleavage is proposed to occur [34, 35]. Further, the N1 and N2 fragments are consistently found to be secreted from cells into the surrounding milieu [17, 36–39]. Therefore, the localisation of each molecule is usually so disparate that they would be unlikely to interact. However, during cellular stress, an opportunity exists for N1 and/or N2 to bind and modulate PS function.

Within the current study copper-saturated N2 reduced the percentage of cells with externalised PS. Whilst the data presented herein cannot rule out that N2 directly binds to and blocks

the annexin-V binding site, resulting in an apparently reduced detection, our data suggests that this is unlikely as the same response was not seen for N1, which has a stronger affinity for PS membranes than N2 [12, 13] and the bound N2 would have to survive trypsin digest. The difference in cellular response to N1 and N2 suggests that they mediate their protective effects by engaging different pathways or that the protective actions of each peptide are induced by different stimuli. Such differences likely stem from the additional charged domain of N1, which may increase its affinity for a non-lipid target in preference and/or addition to functionally binding the identified lipid species.

The interaction of N1 and N2 with PA is of special interest since PA is a known signalling intermediate that feeds into the ras-MEK-ERK pathway [30]. The changes in PLD activity and PA levels following treatment with the copper-saturated N2 suggest that it could be modulating this pathway through cellular PA changes. N2 stress-protective signalling has recently been shown to be transduced through MEK1 and requires copper-induced internalisation of the peptide [21]. PA production is also associated with endocytosis through its stimulation of membrane curvature, fission and fusion [40] and it has further been shown to regulate clathrin induced endocytosis [41]. Clathrin induced internalisation of full-length PrP^C is mediated by its N-terminus [15, 16], with this region being present in both the N1 and N2 fragments. Therefore, membrane association of N2 and PA could represent a genuine functional engagement activating a larger signalling complex or cascade.

Within the lipid spot binding assay copper appeared to have very subtle effects on the intensity of peptide binding. However N2 copper saturation was required for significant changes to be observed in both the annexin-V positive counts and in changes to PA production and levels. This suggests that, whilst not altering N2 affinity for lipids, acts as an essential co-factor, mediating the interactions between N2, lipids and other receptors involved in the transduction of cellular stress responses.

Conclusions

The findings of the current study showed that the N-terminal endoproteolytic cleavage products of PrP, N1 and N2, demonstrated marked binding to PS and PA and that this interaction required the full complement of N-terminal and octarepeat residues. Additionally, copper-saturated N2 demonstrated some capacity to normalise starvation-induced cellular changes to both lipids. Therefore, PS and PA feasibly represent direct targets or pathway intermediates by which N2 transduces its neuroprotective functions.

Supporting Information

S1 Fig. Lipid strip staining as revealed by shorter exposure times. A. Schematic showing the spot arrangement on the membrane. Eight second exposure of **B)** N1 membranes, **C)** N1 membranes and **D)** N1/N2 domain fragment membranes (30 second exposures are shown in the main text).
(PDF)

S2 Fig. Double blots of N2 spot blots following equilibration to neutral pH. Membranes were equilibrated in Tris buffer (pH 8) in a blotting paper—lipid spot membrane-fresh membrane—blotting paper sandwich before western blotting for N2 on both the original and new membranes with saf32 antibody. Almost no detectible transfer onto the new membrane (shown) was evident indicating the peptide remained bound to the lipid spot membrane as pH was changed.
(PDF)

S3 Fig. N1 and N2 lipid spot blots probed with 8B4 antibody. Blots were carried out exactly as for Saf32 blotting with 8B4 used as the detection antibody. The similarity in staining pattern using SAF32 (Fig 1B and 1D) and 8B4 (below) shows that detection of an interaction is not being missed by epitope masking.
(PDF)

S4 Fig. Rescaled N1 lipid spot binding plots. Plots shown in Fig 1 of the main text have been re-scaled on an axis appropriate to their signal intensity. No bars indicates no detectable signal on any repeat, n = 3.
(PDF)

S5 Fig. Rescaled N2 lipid spot binding plots. Plots shown in Fig 2 of the main text have been re-scaled on an axis appropriate to their signal intensity. No bars indicates no detectable signal on any repeat, n = 3.
(PDF)

S6 Fig. Extended exposures of lipid spot blots incubated with the PrP 51–89 peptide. All blots shown in the main text are 30 second exposures. For incubations with a peptide comprising residues 51–89 (the octarepeat copper-binding region), membranes were blank after 30 seconds so a further 5 minute exposure was done alongside the strongly labelled mutant 23-89P26/28A peptide. After the five minute exposure a small degree of labelling was evident for the 51–89 peptide was comparatively very weak against the signal seen for the 23–89 P26/28A peptide.
(PDF)

S7 Fig. Rescaled plots of N1/N2 domain fragments. Plots shown in Fig 3 of the main text have been re-scaled on an axis appropriate to their signal. No bars indicates no detectable signal, n = 1.
(PDF)

Acknowledgments

The authors would like to thank Dr. Victoria Lawson for her support and helpful discussions. The CF10 cells were a kind gift to Dr. Victoria Lawson from Dr. Suzette Priola (National Institute of Health, USA).

Author Contributions

Conceived and designed the experiments: CLH SJC. Performed the experiments: CLH CT SCD. Analyzed the data: CLH CT. Contributed reagents/materials/analysis tools: CLH CT SCD SJC. Wrote the paper: CLH CT SCD SJC.

References

1. Martins VR, Brentani RR. The biology of the cellular prion protein. Neurochemistry international. 2002; 41(5):353–5. PMID: 12176078
2. Chen SG, Teplow DB, Parchi P, Teller JK, Gambetti P, Autilio-Gambetti L. Truncated forms of the human prion protein in normal brain and in prion diseases. The Journal of biological chemistry. 1995; 270(32):19173–80. PMID: 7642585
3. Mange A, Beranger F, Peoc'h K, Onodera T, Frobert Y, Lehmann S. Alpha- and beta- cleavages of the amino-terminus of the cellular prion protein. Biology of the cell / under the auspices of the European Cell Biology Organization. 2004; 96(2):125–32. PMID: 15050367

4. Robinson PJ, Pinheiro TJ. Phospholipid composition of membranes directs prions down alternative aggregation pathways. Biophysical journal. 2010; 98(8):1520–8. doi: 10.1016/j.bpj.2009.12.4304 PMID: 20409471
5. Wang F, Yang F, Hu Y, Wang X, Wang X, Jin C, et al. Lipid interaction converts prion protein to a PrPSc-like proteinase K-resistant conformation under physiological conditions. Biochemistry. 2007; 46 (23):7045–53. PMID: 17503780
6. Miller MB, Wang DW, Wang F, Noble GP, Ma J, Woods VL Jr., et al. Cofactor molecules induce structural transformation during infectious prion formation. Structure. 2013; 21(11):2061–8. doi: 10.1016/j.str.2013.08.025 PMID: 24120764
7. Hugel B, Martinez MC, Kunzelmann C, Blattler T, Aguzzi A, Freyssinet JM. Modulation of signal transduction through the cellular prion protein is linked to its incorporation in lipid rafts. Cellular and molecular life sciences: CMLS. 2004; 61(23):2998–3007. PMID: 15583862
8. Stuermer CA, Langhorst MF, Wiechers MF, Legler DF, Von Hanwehr SH, Guse AH, et al. PrPc capping in T cells promotes its association with the lipid raft proteins reggie-1 and reggie-2 and leads to signal transduction. FASEB journal: official publication of the Federation of American Societies for Experimental Biology. 2004; 18(14):1731–3.
9. Stuermer CA, Plattner H. The 'lipid raft' microdomain proteins reggie-1 and reggie-2 (flotillins) are scaffolds for protein interaction and signalling. Biochemical Society symposium. 2005(72:):109–18. PMID: 15649135
10. Suzuki KG. Lipid rafts generate digital-like signal transduction in cell plasma membranes. Biotechnology journal. 2012; 7(6):753–61. doi: 10.1002/biot.201100360 PMID: 22488962
11. Dong SL, Cadamuro SA, Fiorino F, Bertsch U, Moroder L, Renner C. Copper binding and conformation of the N-terminal octarepeats of the prion protein in the presence of DPC micelles as membrane mimetic. Biopolymers. 2007; 88(6):840–7. PMID: 17922496
12. Boland MP, Hatty CR, Separovic F, Hill AF, Tew DJ, Barnham KJ, et al. Anionic phospholipid interactions of the prion protein N terminus are minimally perturbing and not driven solely by the octapeptide repeat domain. The Journal of biological chemistry. 2010; 285(42):32282–92. doi: 10.1074/jbc.M110.123398 PMID: 20679345
13. Le Brun AP, Haigh CL, Drew SC, James M, Boland MP, Collins SJ. Neutron Reflectometry Studies Define Prion Protein N-terminal Peptide Membrane Binding. Biophysical journal. 2014; 107(10):2313–24. doi: 10.1016/j.bpj.2014.09.027 PMID: 25418300
14. Walmsley AR, Zeng F, Hooper NM. The N-terminal region of the prion protein ectodomain contains a lipid raft targeting determinant. The Journal of biological chemistry. 2003; 278(39):37241–8. PMID: 12865430
15. Taylor DR, Watt NT, Perera WS, Hooper NM. Assigning functions to distinct regions of the N-terminus of the prion protein that are involved in its copper-stimulated, clathrin-dependent endocytosis. Journal of cell science. 2005; 118(Pt 21):5141–53. PMID: 16254249
16. Shyng SL, Moulder KL, Lesko A, Harris DA. The N-terminal domain of a glycolipid-anchored prion protein is essential for its endocytosis via clathrin-coated pits. The Journal of biological chemistry. 1995; 270(24):14793–800. PMID: 7782345
17. Guillot-Sestier MV, Sunyach C, Druon C, Scarzello S, Checler F. The alpha-secretase-derived N-terminal product of cellular prion, N1, displays neuroprotective function in vitro and in vivo. The Journal of biological chemistry. 2009; 284(51):35973–86. doi: 10.1074/jbc.M109.051086 PMID: 19850936
18. Haigh CL, Drew SC, Boland MP, Masters CL, Barnham KJ, Lawson VA, et al. Dominant roles of the polybasic proline motif and copper in the PrP23-89-mediated stress protection response. Journal of cell science. 2009; 122(Pt 10):1518–28. doi: 10.1242/jcs.043604 PMID: 19383722
19. Haigh CL, McGlade AR, Collins SJ. MEK1 transduces the prion protein N2 fragment antioxidant effects. Cellular and molecular life sciences: CMLS. 2015; 72(8):1613–29. doi: 10.1007/s00018-014-1777-y PMID: 25391659
20. Karas JA, Boland M, Haigh C, Johanssen V, Hill A, Barnham K, et al. Microwave Synthesis of Prion Protein Fragments up to 111 Amino Acids in Length Generates Biologically Active Peptides. Int J Pept Res Ther. 2012; 18(1):21–9.
21. Haigh CL, McGlade AR, Collins SJ. MEK1 transduces the prion protein N2 fragment antioxidant effects. Cellular and molecular life sciences: CMLS. 2014.
22. Haigh CL, Lewis VA, Vella LJ, Masters CL, Hill AF, Lawson VA, et al. PrPC-related signal transduction is influenced by copper, membrane integrity and the alpha cleavage site. Cell research. 2009; 19 (9):1062–78. doi: 10.1038/cr.2009.86 PMID: 19597535

23. Greil CS, Vorberg IM, Ward AE, Meade-White KD, Harris DA, Priola SA. Acute cellular uptake of abnormal prion protein is cell type and scrapie-strain independent. Virology. 2008; 379(2):284–93. doi: 10.1016/j.virol.2008.07.006 PMID: 18692214

24. Haigh CL, McGlade AR, Lewis V, Masters CL, Lawson VA, Collins SJ. Acute exposure to prion infection induces transient oxidative stress progressing to be cumulatively deleterious with chronic propagation in vitro. Free radical biology & medicine. 2011; 51(3):594–608.

25. Sinclair L, Lewis V, Collins SJ, Haigh CL. Cytosolic caspases mediate mislocalised SOD2 depletion in an in vitro model of chronic prion infection. Disease models & mechanisms. 2013; 6(4):952–63.

26. Drew SC, Haigh CL, Klemm HM, Masters CL, Collins SJ, Barnham KJ, et al. Optical imaging detects apoptosis in the brain and peripheral organs of prion-infected mice. Journal of neuropathology and experimental neurology. 2011; 70(2):143–50. doi: 10.1097/NEN.0b013e3182084a8c PMID: 21343883

27. Parasassi T, De Stasio G, d'Ubaldo A, Gratton E. Phase fluctuation in phospholipid membranes revealed by Laurdan fluorescence. Biophysical journal. 1990; 57(6):1179–86. PMID: 2393703

28. Parasassi T, Di Stefano M, Ravagnan G, Sapora O, Gratton E. Membrane aging during cell growth ascertained by Laurdan generalized polarization. Experimental cell research. 1992; 202(2):432–9. PMID: 1397095

29. Chattopadhyay A. Chemistry and biology of N-(7-nitrobenz-2-oxa-1,3-diazol-4-yl)-labeled lipids: fluorescent probes of biological and model membranes. Chemistry and physics of lipids. 1990; 53(1):1–15. PMID: 2191793

30. Andresen BT, Rizzo MA, Shome K, Romero G. The role of phosphatidic acid in the regulation of the Ras/MEK/Erk signaling cascade. FEBS letters. 2002; 531(1):65–8. PMID: 12401205

31. You JS, Lincoln HC, Kim CR, Frey JW, Goodman CA, Zhong XP, et al. The role of diacylglycerol kinase zeta and phosphatidic acid in the mechanical activation of mammalian target of rapamycin (mTOR) signaling and skeletal muscle hypertrophy. The Journal of biological chemistry. 2014; 289(3):1551–63. doi: 10.1074/jbc.M113.531392 PMID: 24302719

32. Dowler S, Currie RA, Campbell DG, Deak M, Kular G, Downes CP, et al. Identification of pleckstrin-homology-domain-containing proteins with novel phosphoinositide-binding specificities. The Biochemical journal. 2000; 351(Pt 1):19–31. PMID: 11001876

33. Dowler S, Currie RA, Downes CP, Alessi DR. DAPP1: a dual adaptor for phosphotyrosine and 3-phosphoinositides. The Biochemical journal. 1999; 342 (Pt 1):7–12. PMID: 10432293

34. McMahon HE, Mange A, Nishida N, Creminon C, Casanova D, Lehmann S. Cleavage of the amino terminus of the prion protein by reactive oxygen species. The Journal of biological chemistry. 2001; 276 (3):2286–91. PMID: 11060296

35. Watt NT, Taylor DR, Gillott A, Thomas DA, Perera WS, Hooper NM. Reactive oxygen species-mediated beta-cleavage of the prion protein in the cellular response to oxidative stress. The Journal of biological chemistry. 2005; 280(43):35914–21. PMID: 16120605

36. Cisse M, Duplan E, Guillot-Sestier MV, Rumigny J, Bauer C, Pages G, et al. The extracellular regulated kinase-1 (ERK1) controls regulated alpha-secretase-mediated processing, promoter transactivation, and mRNA levels of the cellular prion protein. The Journal of biological chemistry. 2011; 286 (33):29192–206. doi: 10.1074/jbc.M110.208249 PMID: 21586567

37. Vincent B, Paitel E, Saftig P, Frobert Y, Hartmann D, De Strooper B, et al. The disintegrins ADAM10 and TACE contribute to the constitutive and phorbol ester-regulated normal cleavage of the cellular prion protein. The Journal of biological chemistry. 2001; 276(41):37743–6. PMID: 11477090

38. Zhao H, Klingeborn M, Simonsson M, Linne T. Proteolytic cleavage and shedding of the bovine prion protein in two cell culture systems. Virus Res. 2006; 115(1):43–55. PMID: 16140411

39. Beland M, Motard J, Barbarin A, Roucou X. PrP(C) homodimerization stimulates the production of PrPC cleaved fragments PrPN1 and PrPC1. The Journal of neuroscience: the official journal of the Society for Neuroscience. 2012; 32(38):13255–63.

40. Donaldson JG. Phospholipase D in endocytosis and endosomal recycling pathways. Biochimica et biophysica acta. 2009; 1791(9):845–9. doi: 10.1016/j.bbalip.2009.05.011 PMID: 19540357

41. Antonescu CN, Danuser G, Schmid SL. Phosphatidic acid plays a regulatory role in clathrin-mediated endocytosis. Molecular biology of the cell. 2010; 21(16):2944–52. doi: 10.1091/mbc.E10-05-0421 PMID: 20573978

PERSPECTIVE

Endoproteolytic cleavage as a molecular switch regulating and diversifying prion protein function

The prion protein (PrP), through misfolding, is widely known for its causative role in prion diseases, which are transmissible neurodegenerative diseases of humans and animals. There is still no defined function assigned to PrP, especially in the central nervous system, despite many studies in this area. Proposed functions are protean and include signal transduction, neuroprotection, neurogenesis, neuritogenesis, metal-ion homeostasis, memory formation and consolidation, as well as circadian rhythms (Nicolas et al., 2009). Part of the difficulty in assigning a specific function to PrP could perhaps be that it does not have one single function. Instead it might be able to perform many functions and influence various pathways depending upon contextual post-translational modification.

PrP has been shown to undergo various post-translational modifications including glycosylphosphatidylinositol (GPI)-anchor attachment at its C-terminus, N-linked glycosylation at either or both of two locations, phosphorylation, metal ion co-ordination at no less than six sites, secretory cleavage close to the GPI-anchor and endoproteolytic cleavage at three or more sites (Haigh et al., 2010). Whilst all of these modifications may change mature PrP in ways that potentially alter its function or site of function, endoproteolytic cleavage creates new peptides with distinct features that are likely to contribute to the diversity of functions reported for this protein.

Alpha-(α-) and beta-(β-)cleavages of PrP were first characterized as constitutive processing events in both normal and diseased human brain twenty years ago (Chen et al., 1995). The cleavage sites and resultant fragments are shown schematically in **Figure 1**. The C-terminal fragments persist at detectible levels in cells post-cleavage, whereas the N-terminal fragments are likely secreted or released from cells and are detectible in the culture media. PrP cleavage differs depending upon cell type. In certain cells PrP can be over 50% α-cleaved suggesting that this processing may be part of its normal functioning (Lewis et al., 2009). The different properties and fates of the cleavage fragments further support that this cleavage is unlikely to represent a mere degradation step in the turnover of PrP but instead produces functional proteins. Indeed the different ratios across cell types may reflect the different functions of CNS cells. The β-cleavage event has traditionally been thought to be pathogenic as the relative amounts of cognate fragments are increased during prion disease (Chen et al., 1995). However, a cellular inability to undergo β-cleavage was found to result in a heightened susceptibility to cellular stress, which indicated that the produced N2/C2 fragments were also likely to be functional (Watt et al., 2005). For both α- and β-cleavages the specific site of cleavage is "ragged" with these cleavages located either side of a charged cluster domain, defining which new peptide contains this basic domain.

Recently a further cleavage event has been extensively characterized (Lewis et al., 2015). Referred to as "gamma-cleavage", this event occurs in the C-terminal structured domain and therefore produces fragments with very different features to both the α- and β-cleavages. A functional significance is yet to be assigned to this processing event but its presence in multiple cells and tissues, and in disease, suggests that the fragments produced are likely to exert cellular effects distinct to those produced by the other PrP constitutive processing events.

Our prior research has shown that the N2 fragment (and shorter fragments thereof that include the far N-terminal residues) display an anti-oxidant, neuroprotective function in response to the mild stress of serum starvation (Haigh et al., 2009a). This function required the N-terminal amino acids to be intact, including the structure conferred on the first charged cluster domain (residues 23–38) by the two proline residues at positions 26 and 28. Anti-oxidant function was further influenced by the octarepeat region and its copper-saturation, requiring a minimum of two copper molecules available for co-ordination into this site. N2 interaction with the cell surface required intact lipid rafts and heparan sulphate containing proteoglycans and if these were absent transduction of the protective effect was abolished. It was later shown that the cell surface engagement of N2 was also influenced by copper binding, directing the N2 internalisation pathway, which in turn permitted the specific activation of MEK1 in the absence of MEK2 or ERK1/2 activation (Haigh et al., 2015a). The outcome of the MEK1 activation was lower lysosomal and mitochondrial reactive oxygen species production. Therefore, two post-translational modifications of PrP, specifically β-cleavage and metal ion co-ordination, appear to co-operatively regulate and orchestrate N2 signalling, underscoring that the various permutations of post-translational modifications may determine PrP functional modulation. Further illustrating this, combinations of post-translational PrP modifications is not restricted to influencing MEK1 but has also been shown to alter other signalling pathways. For example, copper ion binding alters α-cleavage profiles as a function of membrane fluidity and lipid raft integrity and this correlates with downstream activation of the ERK1/2, p38 and JNK signalling pathways (Haigh et al., 2009b). Therefore, not only may cleavage be a function modifying event but the cellular consequences may be highly dependent upon the precise micro-environment context in which PrP exists.

Like the N2 cleavage fragment, N1 has also been shown to exert neuroprotective functions, counteracting staurosporine toxicity and hypoxia by reducing caspase-3 activation through modulating p53 protein levels and activity (Guillot-Sestier et al., 2009). Of interest, despite acting on different pathways, both N1 and N2 bind anionic synthetic lipid membranes at low pH. They integrate between the lipid head groups but do not significantly penetrate between the acyl tails and so the interactions are non-disruptive (Le Brun et al., 2014). The N1 peptide demonstrates a greater affinity for lipids than the N2. The lipid binding propensity of these peptides may function to sequester them, possibly to quench their function or alternatively to protect them from degradation and preserve their functional life-time. Additionally, lipid intercalation may serve to order membrane micro-domains for signal protein activation or to direct peptide trafficking, ensuring activation of specific signalling pathways. In anionic model membranes N1 and N2 peptide binding indeed results in alterations in lipid order (Le Brun et al., 2014). Despite N1 demonstrating a higher binding affinity for lipids, in a cellular context lipid changes appear to be influenced to a greater extent through N2 neuroprotective activity (Haigh et al., 2015b). Serum starvation of cells induces a number of changes in their lipid environment, including changes affecting phosphatidylserine and phosphatidic acid, with which both N1 and N2 interact. Through unresolved mechanisms, the N2 peptide (but not N1) was able to normalise these cellular changes during serum starvation. This could indicate that the extra poly-basic region alters engagement of membrane binding partners to such an extent that N1 and N2 exert their neuroprotective effects in different ways. A stronger binding affinity of N1 for membrane lipids may result in it being bound sufficiently tightly to prevent release for performing its function or ensure preferential binding to other partners to instigate transduction through a different signalling cascade.

Understanding the precise mechanisms underpinning the link between PrP functions and constitutive cleavage may prove valuable for understanding failing processes in disease and aging. Whilst C2 levels are increased during prion disease, possibly pathogenically (Chen et al., 1995), increased levels of C1 or PrP secretory cleavage have been shown to be protective against the uptake of prion infection (Lewis et al., 2009). The protective nature of C1 is thought to arise due to the α-cleavage site being located in the middle of a 'toxic domain' (amino acids at 106-126), which is thought to be important for efficiency of conversion into misfolded PrP. Whilst C1 may be protective in the context of prion disease, it has also been linked with signalling cellular death through p53 and caspase 3, in a pathway opposed by its counterpart N1 (Sunyach et al., 2007; Guillot-Sestier et al., 2009).

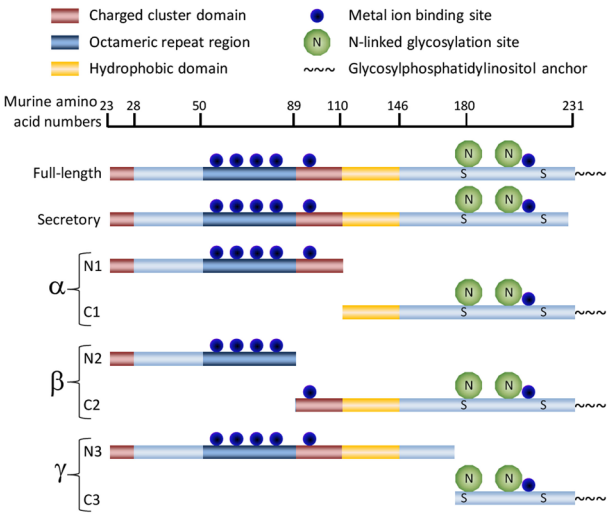

Figure 1 Schematic representation of the prion protein (PrP) cleavage sites. Linear representation of the PrP primary sequence based on murine amino acid numbering. Shown are major domains within the protein and their location following cleavage (note that cleavage events are ragged). Metal ion binding sites, potential N-linked glycosylation sites and the locations of the cysteines forming the di-sulphide bridge are also indicated (S).

No function has yet been found for C2, with an assumption that it is an inert substrate available for pathogenic misfolding during prion disease. With so many potential influences and different pathways to consider when attempting to discern functions of these fragments it could be a long time before a definitive function, or lack thereof, can be assigned to this fragment.

Beyond the causative role of PrP misfolding in prion diseases, cellular PrP has also been implicated in transducing the toxic signals that cause Alzheimer's pathology. Of special interest, the N1 fragment has been shown to bind to the soluble beta-amyloid (Aβ) peptides associated with AD pathogenesis offering neuroprotection (Guillot-Sestier et al., 2012). N1 binding to soluble Aβ oligomers is thought to block their engagement with PrP at the cell surface and thereby prevent damaging signal transduction through fyn and tau. The N1/C1 cleavage event may be doubly protective as the important Aβ binding domain is thought to fall within the amino acids between the α- and β-cleavage sites. As a result, the membrane attached C1 fragment lacks the soluble Aβ-oligomer binding domain and so should be unable to transduce any toxic signals. The C2 fragment, however, contains this amino acid region and so the β-cleavage event may still be detrimental during Alzheimer's disease, permitting toxic signalling to occur. The lack of the N-terminus when soluble Aβ oligomers bind C2 however, may also result in different cellular engagements thereby modulating signal transduction and neuronal outcome.

Understanding the influence of PrP cleavage on pathways regulating neuronal function are likely to not only provide significant information on the cellular failures that underscore or correlate with neurodegeneration but also produce insight into the role these cleavage fragments may have in the regenerative processes of the brain. Endogenous expression of PrP stimulates the activity of adult neural stem cells (Steele et al., 2006) yet the role of PrP cleavages within these cells remains to be determined. Clarifying the importance of PrP cleavage events and the resulting fragments, either as autocrine or paracrine intermediates, in neural stem cell growth and differentiation will enable us to judge whether there is potential to preserve, rescue or enhance regenerative processes by modifying PrP processing events.

In conclusion, there are many more regulatory influences both singly and in combination that must be considered before we can claim a thorough understanding of the functional roles of constitutive or inducible PrP cleavage within the cell. Nevertheless, cumulative data to date strongly suggests that constitutive PrP processing is not an irrelevant epiphenomenon of cellular turnover but regulated, precise and controlled events for specific ends. Cleavage profiles differ across different cell types (Lewis et al., 2009) and evidence so far suggests functional outcomes of cleavage are likely to differ and be context specific. The precise cellular locations of the cleavage events and of the resulting fragments, whether processing occurs at the cell surface and whether N-terminal fragments act in cis or trans, the enzymes controlling these events, the membrane micro-milieu, and dynamic rather than absolute cleavage levels may all potentially impact functional consequences. Until the various nuances of combined post-translational modifications of PrP coupled with cleavage events in different contexts and in different tissues are fully elucidated, PrP appears destined to remain an enigmatic "actor" playing in many apparent functional roles.

Cathryn L. Haigh*, Steven J. Collins*

Department of Medicine (Royal Melbourne Hospital), The University of Melbourne, Parkville, Victoria, Australia

***Correspondence to:** *Cathryn L. Haigh, Ph.D. or Steven J. Collins, Ph.D., chaigh@unimelb.edu.au or stevenjc@unimelb.edu.au.*
***Accepted:** 2015-12-21*
***orcid:** 0000-0001-7591-1149 (Cathryn L. Haigh)*
0000-0002-5245-6611 (Steven J. Collins)
***doi:** 10.4103/1673-5374.177726* ***http**://www.nrronline.org/*
***How to cite this article:** Haigh CL, Collins SJ (2016) Endoproteolytic cleavage as a molecular switch regulating and diversifying prion protein function. Neural Regen Res 11(2):238-239.*

References

Chen SG, Teplow DB, Parchi P, Teller JK, Gambetti P, Autilio-Gambetti L (1995) Truncated forms of the human prion protein in normal brain and in prion diseases. J Biol Chem 270:19173-19180.

Guillot-Sestier MV, Sunyach C, Druon C, Scarzello S, Checler F (2009) The alpha-secretase-derived N-terminal product of cellular prion, N1, displays neuroprotective function in vitro and in vivo. J Biol Chem 284:35973-35986.

Guillot-Sestier MV, Sunyach C, Ferreira ST, Marzolo MP, Bauer C, Thevenet A, Checler F (2012) alpha-Secretase-derived fragment of cellular prion, N1, protects against monomeric and oligomeric amyloid beta (Abeta)-associated cell death. J Biol Chem 287:5021-5032.

Haigh CL, Marom SY, Collins SJ (2010) Copper, endoproteolytic processing of the prion protein and cell signalling. Front Biosci 15:1086-1104.

Haigh CL, McGlade AR, Collins SJ (2015a) MEK1 transduces the prion protein N2 fragment antioxidant effects. Cell Mol Life Sci 72:1613-1629.

Haigh CL, Tumpach C, Drew SC, Collins SJ (2015b) The prion protein N1 and N2 cleavage fragments bind to phosphatidylserine and phosphatidic acid; relevance to stress-protection responses. PLoS One 10:e0134680.

Haigh CL, Drew SC, Boland MP, Masters CL, Barnham KJ, Lawson VA, Collins SJ (2009a) Dominant roles of the polybasic proline motif and copper in the PrP23-89-mediated stress protection response. J Cell Sci 122:1518-1528.

Haigh CL, Lewis VA, Vella LJ, Masters CL, Hill AF, Lawson VA, Collins SJ (2009b) PrPC-related signal transduction is influenced by copper, membrane integrity and the alpha cleavage site. Cell Res 19:1062-1078.

Le Brun AP, Haigh CL, Drew SC, James M, Boland MP, Collins SJ (2014) Neutron reflectometry studies define prion protein N-terminal peptide membrane binding. Biophys J 107:2313-2324.

Lewis V, Johanssen VA, Crouch PJ, Klug GM, Hooper NM, Collins SJ (2015) Prion protein "gamma-cleavage": characterizing a novel endoproteolytic processing event. Cell Mol Life Sci doi:10.1007/s00018-015-2022-z.

Lewis V, Hill AF, Haigh CL, Klug GM, Masters CL, Lawson VA, Collins SJ (2009) Increased proportions of C1 truncated prion protein protect against cellular M1000 prion infection. J Neuropathol Exp Neurol 68:1125-1135.

Nicolas O, Gavin R, del Rio JA (2009) New insights into cellular prion protein (PrPc) functions: the "ying and yang" of a relevant protein. Brain Res Rev 61:170-184.

Steele AD, Emsley JG, Ozdinler PH, Lindquist S, Macklis JD (2006) Prion protein (PrPc) positively regulates neural precursor proliferation during developmental and adult mammalian neurogenesis. Proc Natl Acad Sci U S A 103:3416-3421.

Sunyach C, Cisse MA, da Costa CA, Vincent B, Checler F (2007) The C-terminal products of cellular prion protein processing, C1 and C2, exert distinct influence on p53-dependent staurosporine-induced caspase-3 activation. J Biol Chem 282:1956-1963.

Watt NT, Taylor DR, Gillott A, Thomas DA, Perera WS, Hooper NM (2005) Reactive oxygen species-mediated beta-cleavage of the prion protein in the cellular response to oxidative stress. J Biol Chem 280:35914-35921.

Prion protein "gamma-cleavage": characterizing a novel endoproteolytic processing event

Victoria Lewis, Vanessa A. Johanssen, Peter J. Crouch, Genevieve M. Klug, Nigel M. Hooper & Steven J. Collins

Cellular and Molecular Life Sciences

ISSN 1420-682X
Volume 73
Number 3

Cell. Mol. Life Sci. (2016) 73:667-683
DOI 10.1007/s00018-015-2022-z

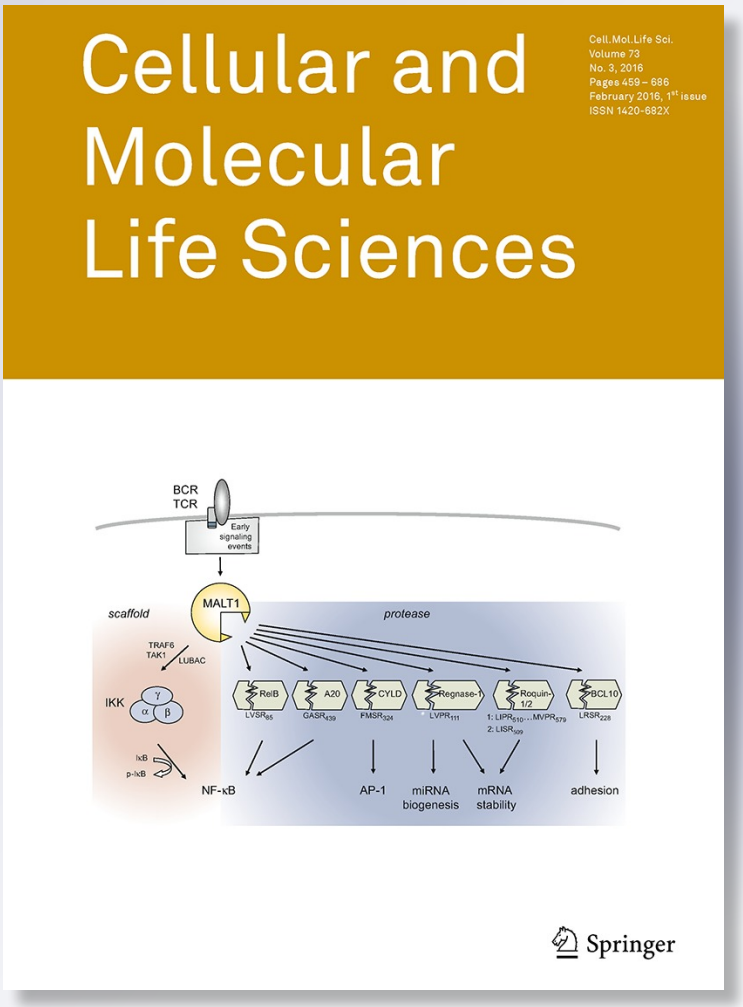

Springer

Cell. Mol. Life Sci. (2016) 73:667–683
DOI 10.1007/s00018-015-2022-z

Cellular and Molecular Life Sciences

ORIGINAL ARTICLE

Prion protein "gamma-cleavage": characterizing a novel endoproteolytic processing event

Victoria Lewis[1] · Vanessa A. Johanssen[2] · Peter J. Crouch[2] · Genevieve M. Klug[1,3] · Nigel M. Hooper[4] · Steven J. Collins[1,3]

Received: 23 March 2015 / Revised: 17 July 2015 / Accepted: 11 August 2015 / Published online: 23 August 2015

Abstract The cellular prion protein (PrP^C) is a ubiquitously expressed protein of currently unresolved but potentially diverse function. Of putative relevance to normal biological activity, PrP^C is recognized to undergo both α- and β-endoproteolysis, producing the cleavage fragment pairs N1/C1 and N2/C2, respectively. Experimental evidence suggests the likelihood that these processing events serve differing cellular needs. Through the engineering of a C-terminal c-myc tag onto murine PrP^C, as well as the selective use of a far-C-terminal anti-PrP antibody, we have identified a new PrP^C fragment, nominally 'C3', and elaborating existing nomenclature, 'γ-cleavage' as the responsible proteolysis. Our studies indicate that this novel γ-cleavage event can occur during transit through the secretory pathway after exiting the endoplasmic reticulum, and after PrP^C has reached the cell surface, by a matrix metalloprotease. We found that C3 is GPI-anchored like other C-terminal and full length PrP^C species, though it does not localize primarily at the cell surface, and is preferentially cleaved from an unglycosylated substrate. Importantly, we observed that C3 exists in diverse cell types as well as mouse and human brain tissue, and of possible pathogenic significance, γ-cleavage may increase in human prion diseases. Given the likely relevance of PrP^C processing to both its normal function, and susceptibility to prion disease, the potential importance of this previously underappreciated and overlooked cleavage event warrants further consideration.

Keywords Prion protein · Endoproteolysis · Protein processing · Protein cleavage

Introduction

The cellular prion protein, PrP^C, is a ubiquitously expressed glycosylphosphatidylinositol (GPI) anchored cell surface glycoprotein, with highest levels found in neurons and central nervous system tissues [1–4], and is causally linked to the group of fatal neurodegenerative disorders known as prion diseases. Surprisingly, engineered PrP^C gene ablated (knockout) mice were initially reported as normal with no overt phenotypic abnormalities [5], which at the time suggested the prion protein could be functionally redundant. Subsequent studies, however, demonstrated various deficits and implicated PrP^C in a diverse range of biological activities, with increasing evidence for roles in important cellular processes such as neuroprotection [6–9], cell signaling [10–13], neurological development and neuritogenesis [14, 15], and synaptic function and plasticity [16–20]. Further,

Electronic supplementary material The online version of this article (doi:10.1007/s00018-015-2022-z) contains supplementary material, which is available to authorized users.

✉ Steven J. Collins
stevenjc@unimelb.edu.au

1 Department of Medicine, RMH, The University of Melbourne, Parkville, VIC 3010, Australia

2 Department of Pathology, The University of Melbourne, Parkville, VIC 3010, Australia

3 The Australian National Creutzfeldt-Jakob Disease Registry, The University of Melbourne, Parkville, VIC 3010, Australia

4 Institute of Brain, Behaviour and Mental Health, Faculty of Medical and Human Sciences, The University of Manchester, Manchester M13 9PT, UK

prion proteins from different mammalian species show high sequence identity, especially in the far C-terminus, with several post-translational modifications and structural features conserved across species [21–25], supporting the likely significant evolutionary and biological importance of this protein.

Like many other proteins, PrP^C is subject to constitutive and selective proteolytic processing, producing several membrane-bound and soluble fragments of different sizes and features. PrP^C may be cleaved at its GPI-anchor, allowing shedding of PrP^C species from a cell by both protease and phospholipase mediated mechanisms [26–28]. PrP^C is also subject to two well-described internal cleavage events known as α- and β-cleavage [29]. The dominant PrP^C processing event, α-cleavage, occurs at the start of the hydrophobic core region (after residues 111/112, human PrP numbering) [30], producing the C-terminal C1 fragment and corresponding N-terminal N1 fragment. Adding complexity, a recent study suggests α-cleavage may actually be multifaceted, with multiple neighboring cleavage sites targeted by different proteases [31]. β-Cleavage, predominantly associated with prion disease and misfolded prion protein conformers (PrP^{Sc}) [30, 32], but also reported to befall PrP^C in uninfected cells and tissues [30, 33–36], involves 'ragged' cleavage at the end of the metal-binding octapeptide repeat region, around residue 90, producing the C2 and N2 fragments [34, 35]. The precise biological reasons for PrP^C proteolysis are not entirely elucidated, although PrP^C proteolytic fragments, especially the C-terminal fragments, are abundant in cells and tissues, and there is increasing evidence for separate roles for the different PrP molecular species [29]. In addition, the influence of PrP^C proteolytic processing on disease transmission susceptibility, pathogenesis and toxicity is recognized [33, 37, 38].

Herein we report the discovery of a novel small PrP^C C-terminal fragment, 'C3', observed in various cultured cell lines, as well as in murine and human brain extracts. Our primary aim was to characterize the basic cellular biology of this previously unrecognized PrP^C endoproteolytic event, which based on an elaboration of existing nomenclature, we have named 'γ-cleavage'. This aim was achieved through the uncovering of intrinsic C3 features, as well as identification of a time-line for γ-cleavage in relation to the normal PrP^C lifecycle within the cell and the likely cellular location of proteolysis, the approximate PrP^C γ-cleavage site, the family of proteases responsible, and potential links to human prion disease. These findings increase our understanding of PrP^C cell biology and add further complexity to the multi-faceted PrP^C proteolytic processing pathways.

Materials and methods

Animal and human tissue (ethics)

The animal brain tissue utilized herein was obtained during a previous study [39], where all animal experiments were carried out with approval from the University of Melbourne Animal Ethics Committee (AEC #04154). The detection of C3 in human brain tissue occurred during routine surveillance and classification activities carried out by the Australian National Creutzfeldt-Jakob Disease Registry (ANCJDR) [40], under contract to the Australian Government Department of Health, and with the approval of The University of Melbourne Human Research Ethics Committee (HREC #1136882.2). All human control tissue was purchased from the Victorian Brain Bank Network (VBBN), and sporadic Creutzfeldt-Jakob Disease (CJD) tissue was supplied by the ANCJDR.

Cell culture

The cell lines used in this study were mouse neuroblastoma cells, N2a (#CCL-131), human neuroblastoma cells, SHSY5Y (#CRL-2266), both purchased from the ATCC biological resource center, human embryonic kidney (HEK) cells obtained from the European Collection of Cell Cultures and the rabbit kidney epithelial cell line, RK13, a kind gift from Dr Victoria Lawson, The University of Melbourne. All cells were maintained in Dulbecco's Modified Eagle Medium (DMEM; Lonza) containing 10 % (v/v) fetal bovine serum (FBS; Bovogen), in a humidified incubator in 5 % CO_2 and at 37 °C, unless otherwise indicated.

Generation of Myc-tagged wild-type and mutant PrP constructs

To generate wild-type murine *Prnp* (WTPrnp) from a 3F4-epitope tagged murine *Prnp* (3F4Prnp) in pIRESneo template [41], primers 3F4-WT-F and 3F4-WT-R and the Quikchange® II XL Site-Directed Mutagenesis kit (Stratagene) were utilized, following the manufacturer's instructions. Insertion of the c-myc tag with repetition of murine *Prnp* codons 226–230 into WTPrnp to produce "PrP-myc", as well as EcoRI (5′) and BamHI (3′) restriction sites for ligation into the plasmid pIRESneo, was via a three-stage modified overlap extension PCR process, previously shown to be useful for generation of a chimeric gene [42]. First, WTPrnp was used in two separate PCR reactions (A) and (B), with these two PCR products purified (QIAquick PCR Purification Kit, Qiagen) to remove leftover primers from the solution. Next, a 'fusion' PCR

reaction (C) was carried out, combining PCR products (A) and (B) as template DNA and no additional primers. Lastly, the primers EcoPrPF and BamPrPR and PCR product (C) as template were utilized in a final PCR to generate the full PrP-myc open reading frame (D). PCR product (D), as well as empty pIRESneo vector, were subject to a double restriction digest with EcoRI-HF and BamHI-HF (both NEB) for 2 h at 37 °C, and the digested vector was also treated with antarctic phosphatase to prevent re-ligation of vector ends. The digested DNA was resolved on a 1 % agarose gel, purified (QIAquick Gel Extraction Kit, Qiagen) and ligated to form a circular PrP-myc in pIRESneo plasmid, which was then transformed into XL1-Gold Ultracompetent bacteria (Stratagene). Ampicillin resistant colonies were selected and myc-tag insertion was confirmed by sequencing. The above multi-step process was also carried out using 3F4Prnp as a template, to produce 3F4-myc. To generate D177NMyc, E199KMyc and V209IMyc, site-directed mutagenesis with the Quikchange® II XL Site-Directed Mutagenesis kit (Stratagene) was carried out with the appropriate primers and PrP-myc in pIRESneo as the template DNA, following the manufacturer's instructions. All primer sequences and PCR cycling conditions are listed in supplementary material (Online Resource 1 and 2, respectively). PCR reactions included a final concentration of 0.2 mM dNTP mix, 1 mM $MgSO_4$ and 1.25 Units (0.5 µl) of Platinum Pfx polymerase (all Life Technologies), except the 'fusion' PCR (C), where double the dNTPs (0.4 mM) and Platinum Pfx polymerase (2.5 Units) was added.

Transfection of mammalian cells

Transient transfections and the RK13 cells stably expressing PrP-myc (MycRK) were created using Lipofectamine 2000 (Life Technologies), following the manufacturer's instructions. Transient transfections were all approximately 72 h. All other stable cell lines were created by electroporation of appropriate cDNA as described previously [43].

Live cell treatments

Cells were treated in culture with compounds (all Sigma) or the compound diluent as controls, for the length of time and concentrations as indicated in figure legends. All treatments were carried out in OptiMEM (Life Technologies) containing 10 % FBS unless otherwise indicated. Briefly, E64d treatment was at a final concentration of 40 µg/ml for 72 h, with reagent added fresh every 24 h. Prinomastat and Brefeldin A (at indicated concentrations), and Tunicamycin (10 µg/ml final concentration) treatments were for 24 h. PIPLC treatment (0.05 U/ml final concentration) was for 1 h in serum free OptiMEM.

Temperature block experiments

MycRK cells were seeded into 12-well plates and grown to confluence. Cell monolayers were washed gently with 1X PBS, and then incubated for 4 h in 1 ml of OptiMEM with or without 10 % (v/v) FBS. All incubations were carried out in non-humidified conditions, at ambient O_2/CO_2: 37 and 15 °C incubations were constant and regulated in incubators; 20 °C incubation was at room temperature.

Cell lysate and brain homogenate preparation and treatments

Tga20 mouse brain tissue (half brain, sectioned sagittally), and approximately 50 mg of human brain tissue taken from the occipital cortex of six sporadic Creutzfeldt-Jakob disease patients and six age-matched non-neurological controls, were prepared as a 10 % (w/v) homogenate in 1X PBS as described previously [44]. Where indicated, human brain homogenates were proteinase K (PK) digested (100 µg/ml final PK concentration, 1 hour at 37 °C, as described [44]) prior to PAGE and western blot analyses. Cell monolayers were washed with 1X PBS, prior to either harvesting (scraping into PBS and pelleting at $1000\times g$ for 3 min) and lysing, or lysing directly in wells. Cells were lysed in ice-cold lysis buffer (25 mM Tris/HCl, pH 7.5, 150 mM NaCl, 5 mM EDTA, 1 % (v/v) Triton X-100) containing a final concentration of 1X Complete Ultra protease inhibitors (Roche) as described previously [45]. Post-nuclear supernatants were assessed for total protein content using a bicinchoninic acid protein assay (Pierce). Where required, cell lysates were treated for 2.5 h at 37 °C with 0.02 U final concentration PIPLC or PIPLC treated and then PNGaseF [46] digested, as described previously.

PAGE and immunoblotting

Samples were mixed with the appropriate PAGE sample buffer containing a final concentration of 3 % β-mercaptoethanol, and resolved on either 4–12 % acrylamide NuPAGE (Life Technologies) or 15.5 % acrylamide tricine SDS-PAGE gels, then electrotransferred to Hybond-P polyvinylidene difluoride membrane (PVDF). PVDF membranes were blocked for 1–2 h at room temperature in PBS containing 0.05 % Tween-20 (PBST) and either 5 % (w/v) skim milk powder, or 2 % (w/v) ECL blocking reagent, prior to incubation with the indicated primary antibody overnight at 4 °C (as indicated in figure legends). Online Resource 3 summarizes relevant antibody

information. After washing off non-specifically bound primary antibody with PBST, membranes were incubated in peroxidase-conjugated anti-mouse or anti-rabbit secondary antibodies (GE), before further washes with PBST and detection using enhanced chemiluminescence (Pierce ECL substrate; Thermo Fischer Scientific, or ECL Advance; GE Healthcare). Where necessary (i.e. when quantifying a difference in total PrP^C expression), to assess and correct for protein loading, membranes were stripped at low pH [1 % (v/v) aqueous HCl] for approximately 30 min, re-blocked and probed with an anti-β-tubulin or β-actin antibody and the secondary antibody described above, or were stained with Coomassie blue solution [50 % (v/v) methanol, 10 % (v/v) acetic acid, 0.25 % (w/v) Coomassie Brilliant Blue R-250 (BioRad)] for 1 min and de-stained [40 % (v/v) methanol, 10 % (v/v) acetic acid] for 10 min prior to quantification. All chemiluminescent and digital images were captured by a Fujifilm LAS-3000 Intelligent Dark Box.

Cell surface biotinylation and NeutrAvidin precipitation

Cell surface proteins were biotinylated for 30 min at 4 °C with the Pierce® Cell Surface Protein Isolation Kit as per the manufacturer's instructions, with all solutions and reagents utilized scaled down to suit T25 cm^2 flasks. Cells were harvested and pelleted at 500 × g for 3 min, immediately after biotinylation (T0) or were cultured for a further 6 h prior to collection of the cells (T6) and conditioned media (T6 M). Cell pellets were stored at −20 °C overnight, and media proteins were precipitated overnight at −20 °C in 4X volumes of 100 % methanol, and then pelleted at 4500×*g* max speed for 1 h at 4 °C. Cell and media pellets were lysed in 300 µl lysis buffer containing protease inhibitors as described above. Ten microlitres of lysates mixed with 10 µl of 2X NuPAGE sample buffer containing 100 mM dithiothreitol (DTT) (final DTT concentration of 50 mM) were utilized for 'input' samples in PAGE and western blotting. Lysates were diluted by mixing 150 µl of lysate with a further 150 µl of lysis buffer containing protease inhibitors, and then subjected to precipitation using 200 µl NeutrAvidin-coated agarose beads, as per the Pierce® Cell Surface Protein Isolation Kit instructions. Samples were eluted in 85 µl of 1X NuPAGE sample buffer containing 50 mM DTT for 1 h at room temperature, with 30 µl of this preparation used for PAGE and western blotting.

Density gradient ultracentrifugation

MycRK cells were harvested, lysed and subjected to Nycodenz density gradient flotation assay as described previously [39]. Fifteen microlitres of collected fractions was utilized for PAGE and western blotting as described above.

Densitometry and statistical analysis

Densitometric semi-quantitative analyses were carried out using Image J v1.42q, and routinely included background subtraction. C3 levels were always first adjusted for the total PrP^C detected within a lane/sample, and then expressed relative to control samples. When total PrP^C expression levels were compared, these were normalized to the relevant loading control (β-tubulin or Coomassie total protein, as indicated), and then expressed relative to the control samples. Statistical analyses were performed in GraphPad Prism v6.0d. All quantitative data is expressed as the mean ± SEM, with the number of independent experiment replicates (*n*) as indicated in figure legends.

Results

PrP^C is cleaved in the far C-terminus, producing a novel cleavage fragment, C3

The addition of epitope tags into proteins is a commonly utilized and relatively simple and effective way to study their cellular biology, exploiting the convenience of high affinity antibodies, or intrinsic fluorescence of the tag. The introduction of epitope tags into PrP^C which is then expressed in cells or animal tissues has been achieved several times, with different tags, and into different regions of the protein [47–51]. The nucleotide sequence encoding the 10 residue human c-myc epitope (EQKLISEEDL), along with the sequence encoding PrP^C residues 226–230 duplicated immediately after the myc-tag, was engineered into murine PRNP immediately 5′ to the GPI-anchor signal sequence, generating 'PrP-myc'. This PrP-myc construct has previously been shown to generate a PrP^C fusion protein (MycPrP) with unaltered cellular behavior or function in vivo or in vitro, including glycosylation, proteolytic processing, trafficking, localization, membrane anchoring, and incorporation into PrP^{Sc} aggregates [52]. When whole lysates from the N2a cell line, transiently transfected with the PrP-myc construct (see Fig. 1a) were analyzed by PAGE and western blotting, in addition to the expected full-length and truncated $MycPrP^C$ species, a small, less than 10 kDa, myc-immunoreactive fragment was observed (Fig. 1b). This unexpected finding indicated there may be another PrP^C endoproteolytic cleavage site towards the C-terminus, producing this small fragment, nominally 'C3'. The PrP-myc construct was stably transfected into three other routine laboratory cell lines, human embryonic

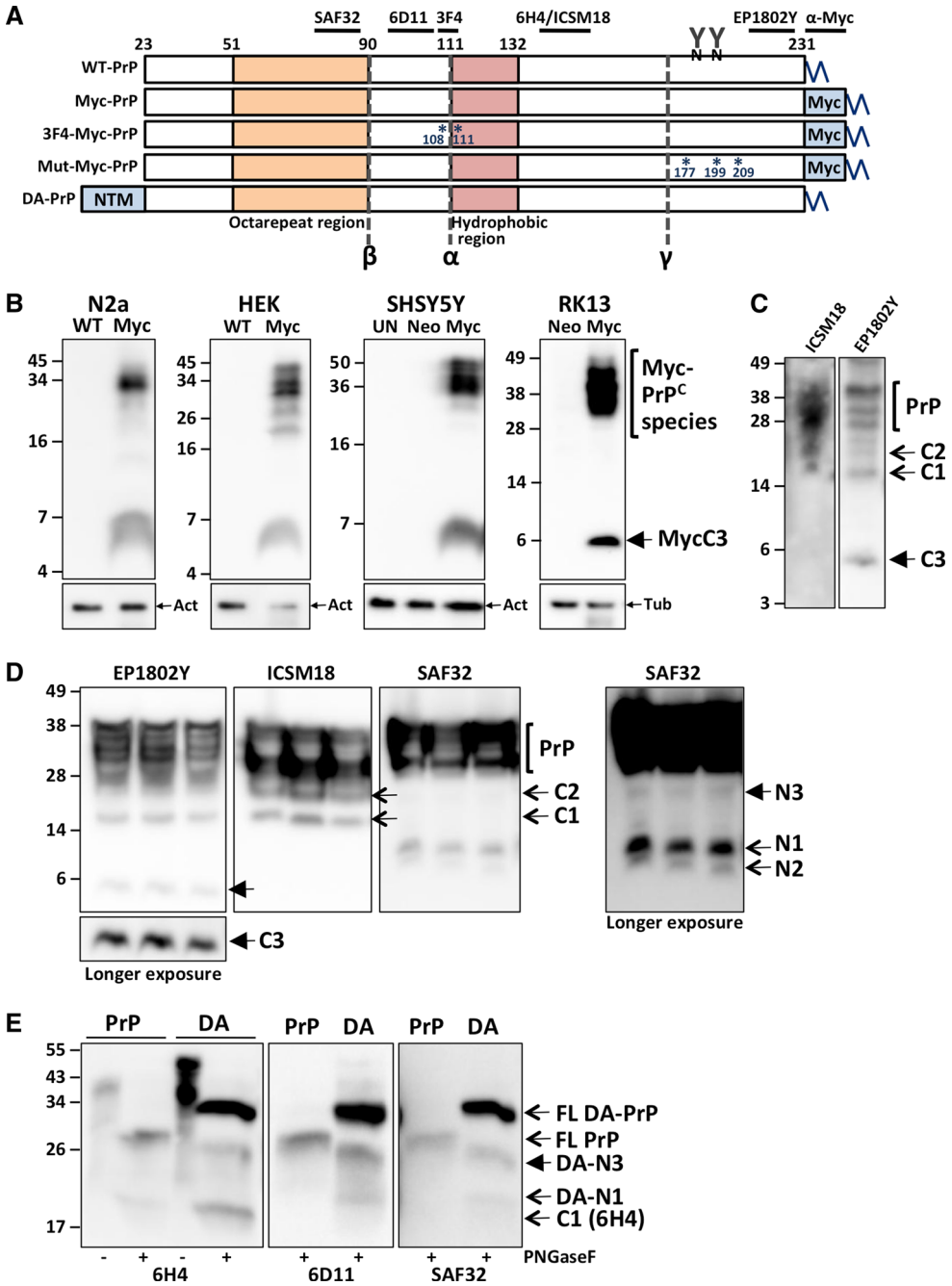

Fig. 1 A far C-terminal PrP^C fragment, C3, in cells and tissues of neuronal and non-neuronal origin. **a** Schematic representation of the constructs and alignment of the antibodies utilized in this study. Wild-type murine PrP (*WT-PrP*), containing the C-terminal Myc epitope-tag (*Myc-PrP*), the 3F4 epitope tag (*3F4-Myc-PrP*), the sites of three murine equivalents of familial CJD mutations D177N, E199K, V209I (*Mut-Myc-PrP*), the N-terminal anchor (*NTM*) in double anchored PrP (*DA-PrP*), the expected endoproteolytic cleavage sites (α, β, γ), and some key conserved features (octarepeat and hydrophobic domains, N-linked glycans, GPI-anchor), are depicted. PAGE and western blotting, with the anti-Myc (**b**) and anti-PrP (**c**–**e**) antibodies as indicated, of: **b** lysates from different cell lines (*N2a*, *HEK*, *SHSY5Y*, *RK13*) transfected with PrP-myc (*Myc*), the empty vector (*Neo*), wild-type mouse PrP (*WT*), or those left untransfected (*UN*); **c** lysate from untransfected N2a cells; **d** PBS brain homogenate from Tga20 (WT murine PrP^C over-expressing) mice; **e** PNGaseF digested (+) or undigested control (−) lysates from SHSY5Y cells expressing wild-type (*PrP*) or double-anchored (*DA*) murine PrP^C. The different full length (*FL*) and truncated PrP species are indicated, with the products of γ-cleavage highlighted with *closed arrows*, and all other cleavage events with *open arrows*. Membranes in **b** were stripped and re-probed with β-actin (*Act*) or β-tubulin (*Tub*) as indicated by the *small arrows*

kidney (HEK), human neuroblastoma (SH-SY5Y) and rabbit kidney epithelial (RK13), to determine whether this processing was restricted to the N2a cells. In all cases, MycPrP^C was also processed to C3 (Fig. 1b), indicating that cells derived from various mammalian species, and of neuronal and non-neuronal origin are capable of what we have designated PrP^C 'γ-cleavage' and C3 production.

In order to establish whether this processing was an artifact of myc tag engineering, lysates from naïve N2a cells were analyzed by PAGE and western blotting utilizing a commercially available antibody, EP1802Y, raised against the PrP far C-terminus residues 214–230 (Fig. 1a). Once again, a small approximately 6–7 kDa fragment was observed (Fig. 1c), but this fragment was not seen when utilizing an antibody (ISCM18) directed against a comparatively more N-terminal region of the protein (Fig. 1a, c). To further confirm this observation, murine brain homogenates were also analyzed by PAGE and western blotting. Tga20 mouse brains were utilized as they overexpress murine PrP^C approximately six fold, therefore increasing the likelihood of detection of what appears to be a relatively low abundance fragment. When mouse brain proteins transferred to PVDF membranes were probed with antibodies to the PrP^C N-terminus (SAF32) and mid-region (ICSM18), various PrP^C species are observed, including the α- and β-cleavage products N1 and N2 when probing with SAF32 (Fig. 1d). However, it was only probing with EP1802Y that allowed detection of an approximately 6–7 kDa C-terminal fragment in these mouse brains (Fig. 1d).

The presumed N-terminal fragment, N3, based on the apparent size of C3, is predicted to be approximately 20 kDa. In the Tga20 mouse brains there was no obvious detection of N3 using the N-terminal PrP^C antibody SAF32 with a short exposure, however upon prolonged exposure, an immunoreactive fragment of this approximate size was apparent (Fig. 1d, far right panel). Furthermore, the band attributed to C2 in the ICSM18 blot could potentially contain N3. Attempts to detect N3 in conditioned media from cultured cells were unsuccessful (data not shown). To increase the likelihood of detecting N3 in cell lysate, which may otherwise be rapidly secreted and/or degraded, we utilized SH-SY5Y cells expressing a 'double anchored' (DA) murine PrP^C [43] (Fig. 1a), and wild-type murine PrP^C expressing cells as controls. In the DA-PrP^C construct, the N-terminal PrP^C signal sequence has been replaced with the uncleaved signal sequence and transmembrane domain of murine aminopeptidase-A [43], thereby resulting in the tethering of the PrP^C N-terminus to the cell membrane. When whole cell lysates from the DA-PrP^C expressing cells were subject to PAGE and western blotting after PNGase digest to remove N-linked glycans, immunoreactive fragments consistent with N3 containing the aminopeptidase-A transmembrane domain (DA-N3), were detectable with all three anti-PrP antibodies utilized (Fig. 1a, e). N3 was not detectable in the control wild-type PrP^C expressing cells consistent with rapid degradation of this fragment.

Collectively, these results strongly support that PrP γ-cleavage is a bona fide PrP processing event, prompting us to investigate further. Note, given MycPrP has been shown to behave the same as untagged (wild-type) PrP [52], including, as shown in Fig. 1, undergoing endoproteolysis producing the various PrP fragments, for ease of C3 detection we continued to utilize cells expressing MycPrP. From this point, MycPrP and its truncated species are for simplicity referred to without the prefix 'Myc'.

PrP^C γ-cleavage occurs late in the secretory pathway, preferentially from an unglycosylated substrate

The cellular prion protein is a cell surface protein, and follows a typical pathway of trafficking and endocytosis. In order to determine at which stage during this secretory pathway γ-cleavage occurs, we first carried out temperature block experiments [53, 54], where RK13 cells stably expressing PrP-myc (MycRK) were incubated for 4 h at 15 °C [slowing protein traffic from the endoplasmic reticulum (ER)], 20 °C (slowing protein traffic from the Golgi apparatus) and 37 °C, in the presence or absence (to slow cell division and simulate oxidative stress) of serum. When compared to cells in optimal/normal conditions (37 °C + serum), cells where protein traffic was slowed through the ER showed no change in C3, while under stressed conditions, when protein traffic was held up in the Golgi network, there was a significant increase in C3 production, with a similar trend when cells were not stressed (Fig. 2a). To further investigate the cellular site of PrP^C γ-cleavage we treated MycRK cells for 24 h with Brefeldin A, a reversible inhibitor of protein translocation from the ER to the Golgi complex [55]. As predicted, given PrP^C N-linked glycosylation starts in the ER with attachment of high-mannose oligosaccharides, but continues in the Golgi with modification of these to more complex sugars [56], Brefeldin A treatment dramatically altered the glycosylation pattern of PrP^C (Fig. 2b). Importantly, we found that Brefeldin A treatment significantly reduced C3 production.

The well-described PrP^C C-terminal proteolytic fragments C1 and C2 are known to be glycosylated like the full-length protein [36]. This can make interpretation of their abundance difficult, as glycosylated but truncated PrP^C may have the approximate same molecular weight as unglycosylated full-length PrP^C. Enzymatic removal of

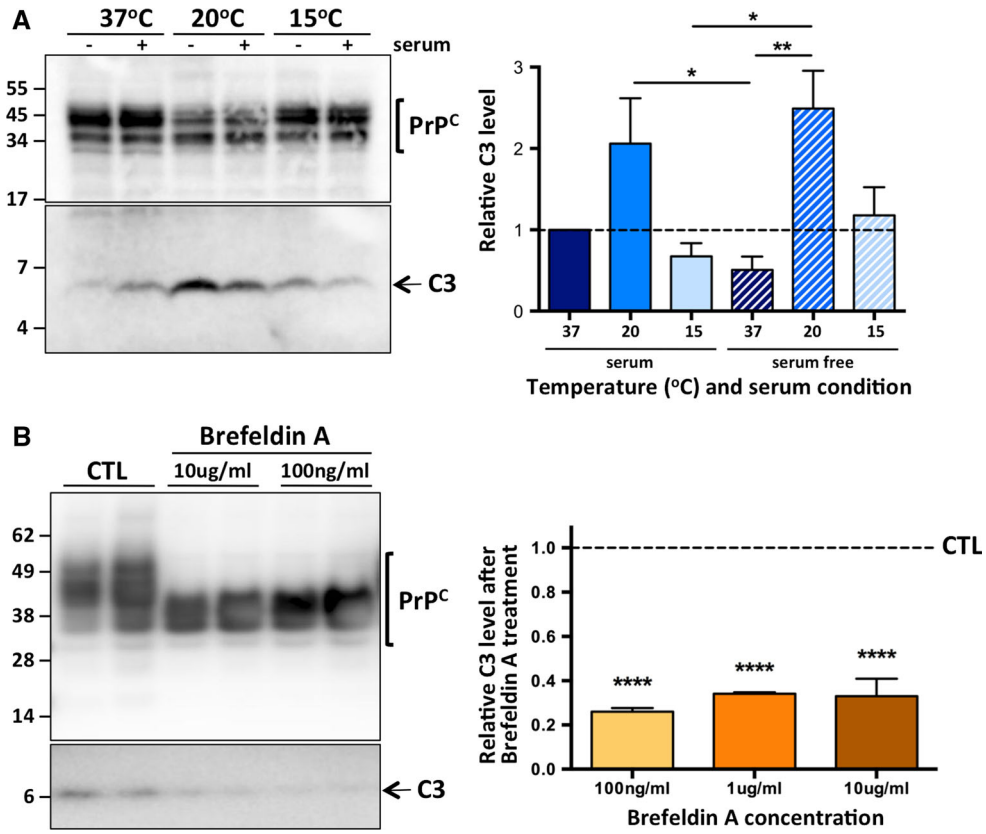

Fig. 2 γ-cleavage occurs after PrP^C has exited the ER, in the Golgi/TGN. Representative PAGE and western blot with an anti-Myc primary antibody (*left panels*) and C3 quantification (*right panels*) of cell lysates from: **a** MycRK cells incubated in the presence (+) or absence (−) of 10 % v/v fetal bovine serum for 4 h at the temperatures indicated ($n = 4$); **b** duplicate wells of MycRK cells treated with Brefeldin A, at the concentrations indicated (100 ng/ml and 10 μg/ml $n = 3$; 1 μg/ml $n = 2$), or diluent only controls (*CTL*). Statistical analyses were by one way ANOVA with **a** Tukey's multiple comparison post-test of all groups and **b** Dunnett's multiple comparison post-test of each treatment to the control. $^*p < 0.05$, $^{**}p < 0.01$, $^{****}p < 0.0001$

N-linked glycans from PrP^C, through PNGaseF treatment of cell or tissue extracts is routinely used to more clearly visualize these fragments. To this end, we used PNGaseF to visualize all C-terminal PrP^C fragments, including C3, in N2a cells transiently expressing myc-tagged wild-type murine PrP^C, or 3F4 epitope containing murine PrP^C, which is often utilized as a substitute wild-type murine sequence (Fig. 1a). It is interesting to note that in this cell line, irrespective of which construct was transfected, after PNGaseF treatment it becomes clear that there is very little full length (compared to truncated) PrP^C, which has been described previously in some cultured cells [33]. This is unlikely to be due to the cells expressing myc-tagged PrP^C, and rather reflects more the pattern of endogenous PrP^C proteolytic processing in these cells (Online Resource 4). As expected, there is an increase in detectable C1, as glycosylated species have been reduced and all of C1 now migrates as a single band (Fig. 3a). However, there is neither the appearance of a smaller than the 6–7 kDa species that would indicate C3 had (prior to PNGaseF treatment) been glycosylated and therefore was resolving slower in PAGE, nor is there an increase in intensity of the 6–7 kDa C3 band that would indicate some of the C3 present in cells is ordinarily glycosylated and upon enzymatic deglycosylation becomes visible. Also of note, after PNGaseF treatment, with prolonged exposures we can observe a previously unrecognized faster moving species below C1 (closed arrow), which we have coined C3′.

From experience, and as evident in Figs. 1, 2 and 3a, most PrP^C species in cultured cells and tissue extracts are heavily glycosylated. As C3 is not glycosylated and, similar to unglycosylated PrP^C, is in low abundance relative to other PrP^C species, we questioned whether C3 is cleaved preferentially from an unglycosylated source. When MycRK cells were treated with tunicamycin, a compound that blocks de novo N-linked glycosylation, we observed a significant increase in relative C3 levels (Fig. 3b). Interestingly, in the tunicamycin-treated cells there is again evidence of a PrP^C fragment which is a few kilodaltons smaller than C1, which we postulate is the same C3′ fragment described in Fig. 3a.

The C-terminal fragment C3 is GPI-anchored, but does not reside primarily at the cell surface

To further understand this PrP^C γ-cleavage event, we next aimed to characterize the C3 fragment itself. It is well established that GPI-anchored proteins, such as PrP^C, localize within lipid raft domains of cellular membranes [57]. In order to establish whether C3 was also GPI-anchored, we subjected lysates from MycRK cells to a floatation assay, whereby buoyant membranes (i.e. lipid

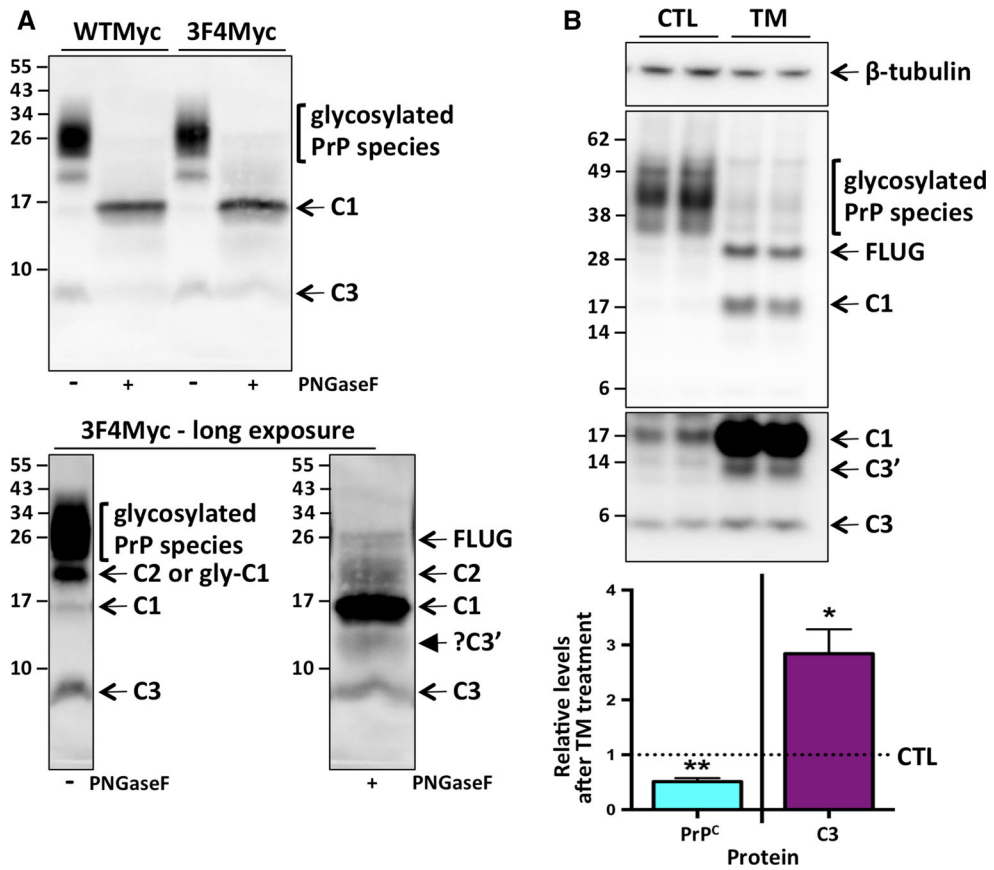

Fig. 3 C3 is not glycosylated and is preferentially cleaved from an unglycosylated substrate. **a** Lysates from N2a cells transiently transfected with wild-type or 3F4-epitope myc-tagged PrP construct as indicated, were left untreated (−) or digested with PNGaseF (+) prior to PAGE and western blotting with an anti-Myc antibody. The *bottom panel* is the same blot as the *top panel*, after a longer digital exposure time to enable visualization of additional cleavage fragments as indicated. **b** Representative PAGE and western blot with the anti-Myc antibody and re-probe with anti-β-tubulin antibody (*top panel*) and quantification (*bottom panel*, $n = 4$) of relative total PrP^C and C3 levels in duplicate wells of MycRK cells treated with tunicamycin (*TM*), compared to diluent only controls (*CTL*). The various full length unglycosylated (*FLUG*) and truncated PrP^C species are indicated. Statistical analyses by paired *t* test. $^*p < 0.05$, $^{**}p < 0.01$

raft domains) float to the top of a density gradient, following an established protocol [39]. When fractions from the MycRK cells were analyzed by PAGE and western blotting, the C3 fragment was localized predominantly in the more buoyant fractions where other PrP^C species were also enriched (Fig. 4a), consistent with C3 containing a GPI moiety. The lipid raft (Flotillin-1), ER (Bip) and mitochondria (Bcl2) marker proteins localized predominantly in the lighter/buoyant (Flot1) and denser (Bip/Bcl2) fractions as expected [39]. Next, lysates from HEK cells transiently expressing MycPrP were reacted with bacterial phosphatidylinositol-specific phospholipase C (PIPLC), an enzyme capable of catalyzing hydrolytic cleavage of the phosphoric ester bond within the GPI anchor. When the GPI anchor is enzymatically removed from a protein, empirically on PAGE separation the GPI-minus protein resolves slower than its undigested counterpart [58]. To this end, a small characteristic upward shift in PAGE mobility of the C3 fragment, as well as the other PrP^C species, was observed in the PIPLC and PNGaseF treated lysate (Fig. 4b), indicative of GPI-anchor removal.

Treating cells in culture with PIPLC induces cleavage of GPI-anchored proteins from the cell surface. When MycRK cells were treated for 1 h with PIPLC, as expected there was an increase in the detection of PrP^C in the conditioned media; however, this was not observed for the C3 fragment (Fig. 4c). Interestingly, levels of C3 in conditioned media were in fact significantly decreased. To further confirm whether C3 is localized at the cell surface, we carried out cell-surface biotinylation of MycRK cells. Using NeutrAvidin-coated agarose beads to bind and pull out all labeled cell surface proteins from whole cell lysate or conditioned media, Fig. 4d shows that whilst the cell surface transferrin receptor and many PrP^C species were biotinylated, C3 was not. Online Resource 5 shows the full biotinylation experiment result depicted in Fig. 4d,

including some relatively low level non-specific NeutrAvidin pull down of unlabelled proteins (both PrP^C and transferrin receptor), seen only on longer exposure, and no precipitation of biotinylated proteins from the conditioned media. Online Resource 5 also shows that upon longer exposure, both C3 and C3′ can be detected in the whole cell lysate (input), but not in the NeutrAvidin pull down samples.

A matrix metalloprotease is responsible for PrP^C γ-cleavage within the highly conserved C-terminus

The observations of C3 approximate molecular mass at 6–7 kDa, and the C3/N3 immuno-reactivities, suggested that the γ-cleavage site was in the far-C-terminus of PrP^C. Interestingly the C-terminus of PrP^C is highly conserved in mammals [59], with substantial sequence identity in the various species listed in the National Center for Biotechnology Information (NCBI) Conserved Domains Database [60] (Online Resource 6). In order to define the sequence identity of C3 and clarify the γ-cleavage site, several attempts, including the use of size-exclusion and immunoprecipitation techniques to increase relative detection/yield of Myc-C3 for downstream mass spectrometry or Edman degradation analyses, as well as antibody affinity based SELDI-TOF–MS, unfortunately all yielded negative or inconclusive results (data not shown). Therefore, we employed site-directed mutagenesis to potentially introduce either slight structural/steric changes or loss of a protease consensus sequence motif, in order to hinder and/or alter any interaction of PrP^C with the responsible protease, altering the efficiency of C3 production and narrowing down the putative region of the γ-cleavage site. Specifically, the murine equivalents of three inherited human prion disease mutations which are spread across the far-C-terminus of PrP^C were created, with all containing the myc tag (see Fig. 1a); MycD177N, MycE199K and MycV209I. After transient transfection into RK13 cells, we observed a significant reduction in C3 levels in cells expressing MycD177N and MycE199K compared to wild-type $MycPrP^C$ (Fig. 5a), whilst there was no significant difference seen for the MycV209I mutation.

A single previous report does identify and describe a small C-terminal PrP fragment of similar apparent molecular mass, which the authors also referred to as 'C3' and may be the same C3 described herein [50]. Taguchi and colleagues determined their fragment to result from cysteine protease cleavage, as a 72 h treatment with a pan-cysteine protease inhibitor E64 inhibited its production. In order to test whether our C3 was also generated by a cysteine protease, MycRK cells were treated for 72 h with E64d, a more membrane permeable synthetic analogue of E64. Surprisingly the MycRK cells had increased total PrP^C expression after E64d treatment, and when adjusted for the increase in PrP^C, C3 levels were also significantly increased (Fig. 5b). We considered whether the increased C3 was due to E64d increasing the proportion of a precursor fragment. Lysates from E64d treated and untreated cells were PNGaseF digested prior to PAGE and western blot analysis, in order to clearly see the relative levels of the different full-length and truncated $MycPrP^C$ species. As seen in Fig. 5c, there is no apparent change in proportion of the C1 fragment, although there is again the appearance of a faster moving $MycPrP^C$ species with E64d treatment. We believe this is consistent with C3′, observed in the various experiments described above.

Having ruled out a cysteine protease as the likely enzyme involved in PrP^C γ-cleavage, we utilized the *MEROPS* database (http://merops.sanger.ac.uk) [61] to perform low stringency searches of residues around the highly conserved residues of the PrP^C far C-terminus. Numerous proteases were identified, and of interest were several matrix metalloproteases (MMP), due to recent evidence that prion protein fragments can be digested by membrane-type MMP proteases [62]. To investigate the possibility of MMP mediated γ-cleavage of PrP^C, we treated MycRK cells for 24 h with the MMP inhibitor Prinomastat, which is selective for MMPs-2, 3, 9, 13 and 14 [63]. We observed a significant decrease in relative C3 levels for all concentrations of Prinomastat tested (Fig. 5d), suggesting an MMP is involved in PrP^C γ-cleavage.

Prion disease-associated PrP conformers are also susceptible to γ-cleavage

During a routine diagnostic characterization of PrP species detectable in a suspected Creutzfeldt-Jakob disease (CJD) patient brain for the ANCJDR, a fragment consistent with C3 was detected when utilizing the EP1802Y antibody, but not the mid-region 3F4 antibody (Fig. 6a), which indicated the human prion protein may be susceptible to γ-cleavage. In order to further characterize this, and also address whether prion disease associated PrP species are also subject to γ-cleavage, we assessed C3 production in non-neurological control and sporadic CJD patient brain tissue. While we found no clear evidence of γ-cleavage in control tissue, this was not the case in CJD brains, with detection of C3 (2/6 cases) and C3′ (6/6 cases) (Fig. 6b, top panels). Additionally, after high concentration PK treatment successfully digested away all PrP^C species, in addition to the typical profile of di-mono- and un-glycosylated partially protease-resistant (PrP^{res}) species, C3 becomes readily detectable in all the CJD brains (Fig. 6b, bottom panels). Interestingly, C3′ is also still detectable after PK digestion. Collectively this indicates that in the context of disease-associated PrP

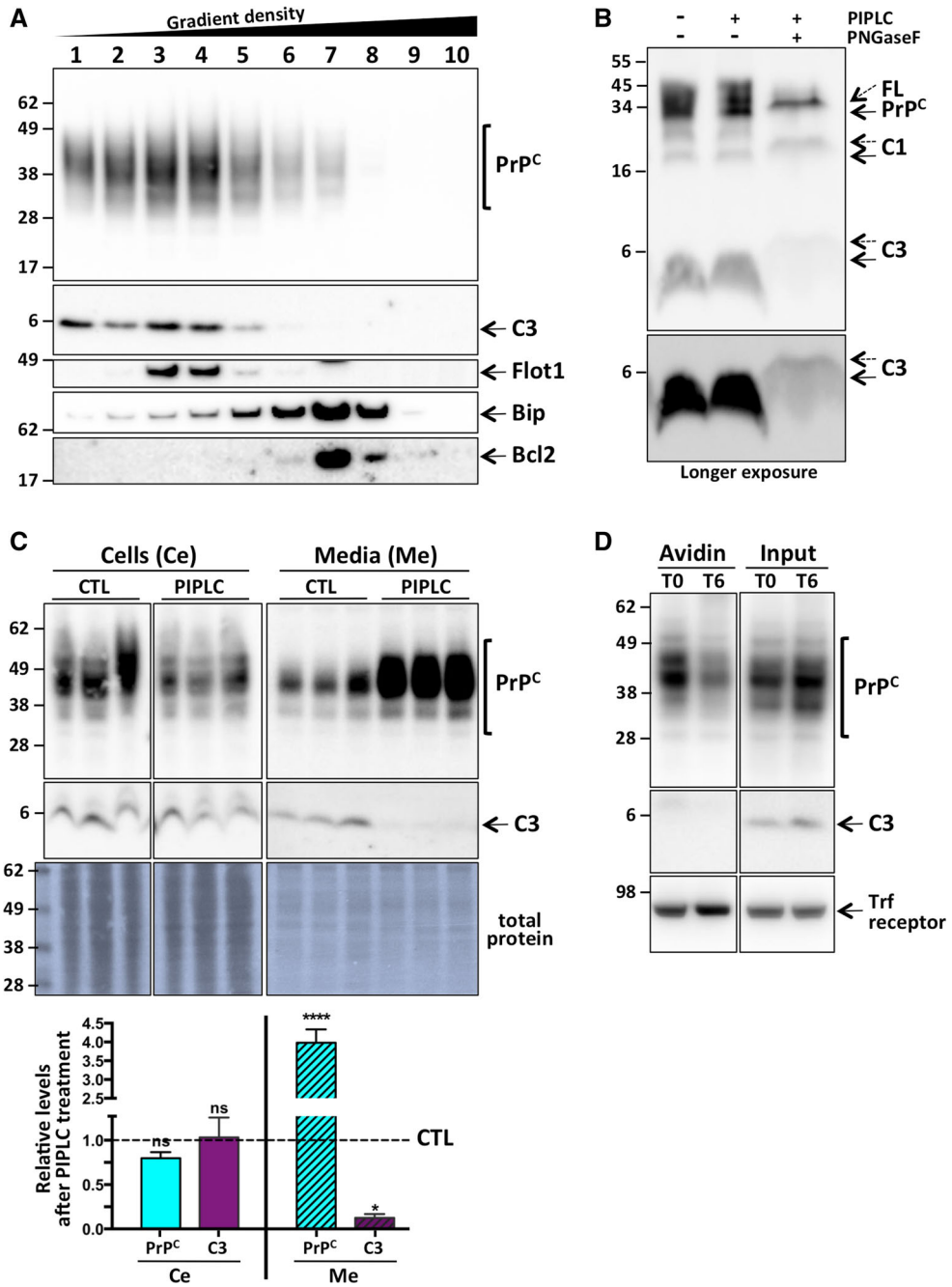

Fig. 4 C3 is GPI-anchored, and does not localize primarily at the cell surface. Representative PAGE and western blot with anti-Myc antibody of: **a** Density gradient fractionated lysate (fractions numbered 1–10) from MycRK cells, also probed with the marker protein antibodies (*Flot1*, *Bip*, *Bcl2*) as indicated; **b** lysates from HEK cells transiently expressing MycPrP, left untreated, digested with PIPLC, or PIPLC and PNGaseF. PrP^C species [full length (*FL*) and truncated] with the GPI-anchor successfully removed are indicated with the *dashed arrows*; **c** cell lysate (*Ce*) and conditioned media (*Me*) from triplicate wells of live MycRK cells exposed to PIPLC or diluent only (*CTL*), and total protein (Coomassie) stained PVDF membrane (after completed western blotting), with quantification (*bottom panel*, $n = 3$) and statistical analyses by two way ANOVA with Bonferroni's multiple comparison post-test. *ns* not significant, $*p < 0.05$, $****p < 0.0001$; **d** whole cell lysate (*Input*) or NeutrAvidin-coated agarose bead precipitated (*Avidin*) proteins from cell surface biotinylated MycRK cells, immediately (*T0*) or 6 h (*T6*) after labeling, re-probed for the cell surface transferrin (*Trf*) receptor protein

misfolding, C3 represents a highly protease-resistant unglycosylated fragment, with γ-cleavage of disease associated PrP (PrP^{Sc}) occurring, and the likelihood that the C3 seen in non-PK-treated CJD brain tissue is resultant from endoproteolysis of PrP^{Sc} rather than processing of the PrP^C present.

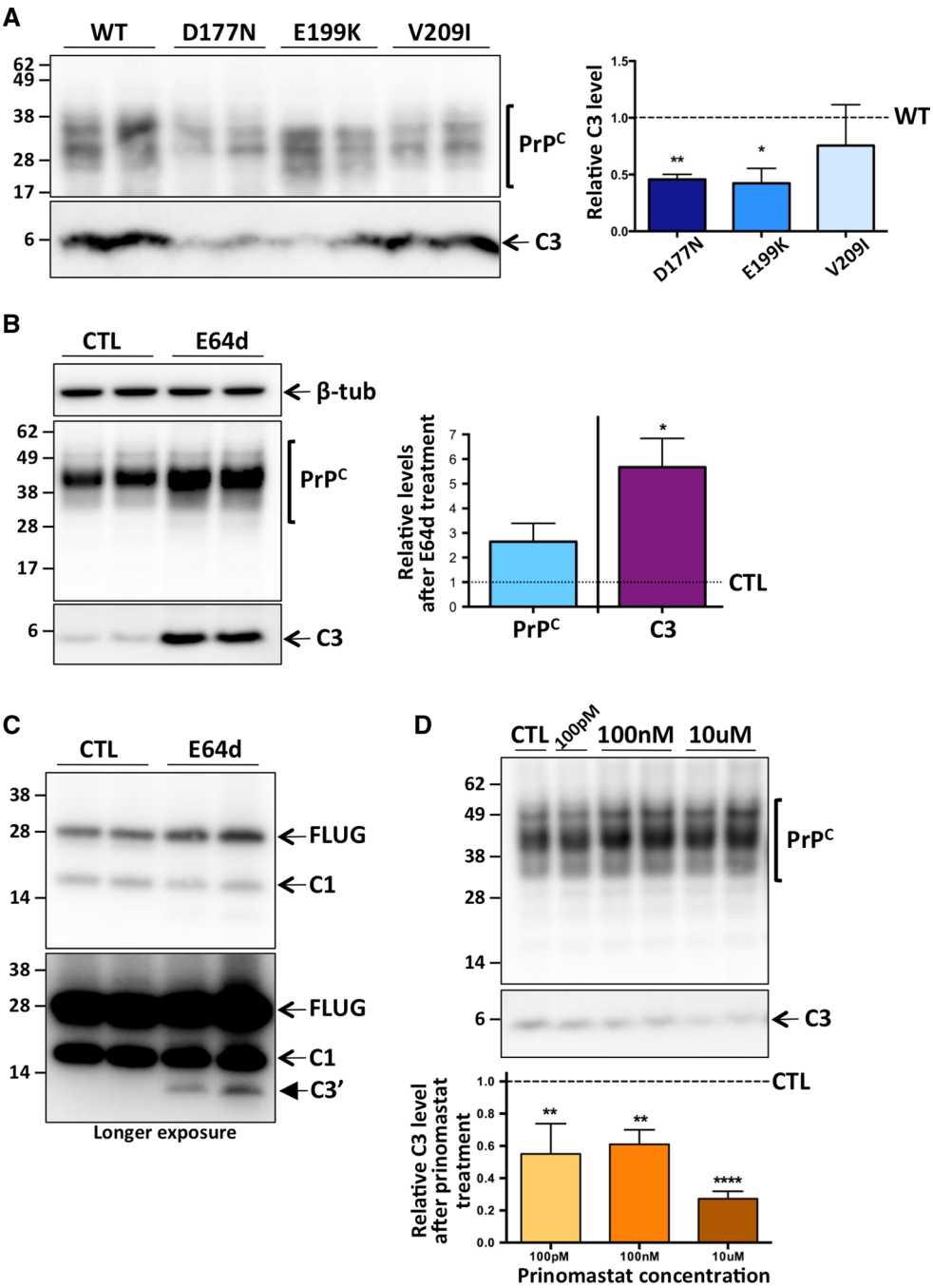

Fig. 5 An MMP not a cysteine protease is responsible for γ-cleavage within the conserved PrP^C far C-terminus. Representative PAGE and western blot with anti-Myc antibody of: **a** lysates from RK13 cells transiently expressing wild-type (*WT*) or mutated, myc-tagged PrP^C, with quantification (*right panel*, $n = 4$); **b** lysates from MycRK cells treated for 72 h with E64d or diluent only control (*CTL*), re-probed for β-tubulin detection, with quantification of total PrP^C levels and C3 levels adjusted for PrP^C (*right panel*, $n = 4$); **c** PNGaseF digested whole cell lysates from duplicate wells of E64d or diluent control (*CTL*) treated MycRK cells (as in **b**), with full length unglycosylated (*FLUG*) and truncated PrP^C species as indicated; **d** lysates from Prinomastat (concentrations as indicated, 100 pM $n = 2$, 100 nM $n = 3$, 10 μM $n = 4$) or diluent control (CTL) treated MycRK cells (in some cases in duplicate wells), with quantification (*bottom panel*). Statistical analyses in **a** and **d** were by one way ANOVA with Dunnett's multiple comparison post-test of each mutant or treatment to the control, and in **b** were by paired *t* test. $*p < 0.05$, $**p < 0.01$, $****p < 0.0001$

Discussion

Prion protein endoproteolysis, a phenomenon observed in cultured cells as well as human and various animal tissues, has been reported for many years, with a focus on α- and β-cleavage and proteolysis at the GPI anchor resulting in shedding of PrP^C from the cell surface [29]. Despite this, the biological or physiological significance of PrP^C proteolytic processing has not been entirely elucidated, with emerging, but sometimes conflicting evidence of separate functions of the full length [14, 64, 65], and different truncated PrP^C species [6, 10, 66–68]. Importantly, there are often more truncated PrP^C species than full-length PrP^C present in cells and tissues [33, 35, 69], underscoring the likely cellular requirement for these processes to occur.

Through the utilization of Myc-tagged PrP^C expressed in cells we discovered a novel, approximately 6–7 kDa, Myc-tagged 'C3' fragment, and then confirmed the presence of endogenous C3 in both human and animal brain tissue, indicating the fragment was not produced as an

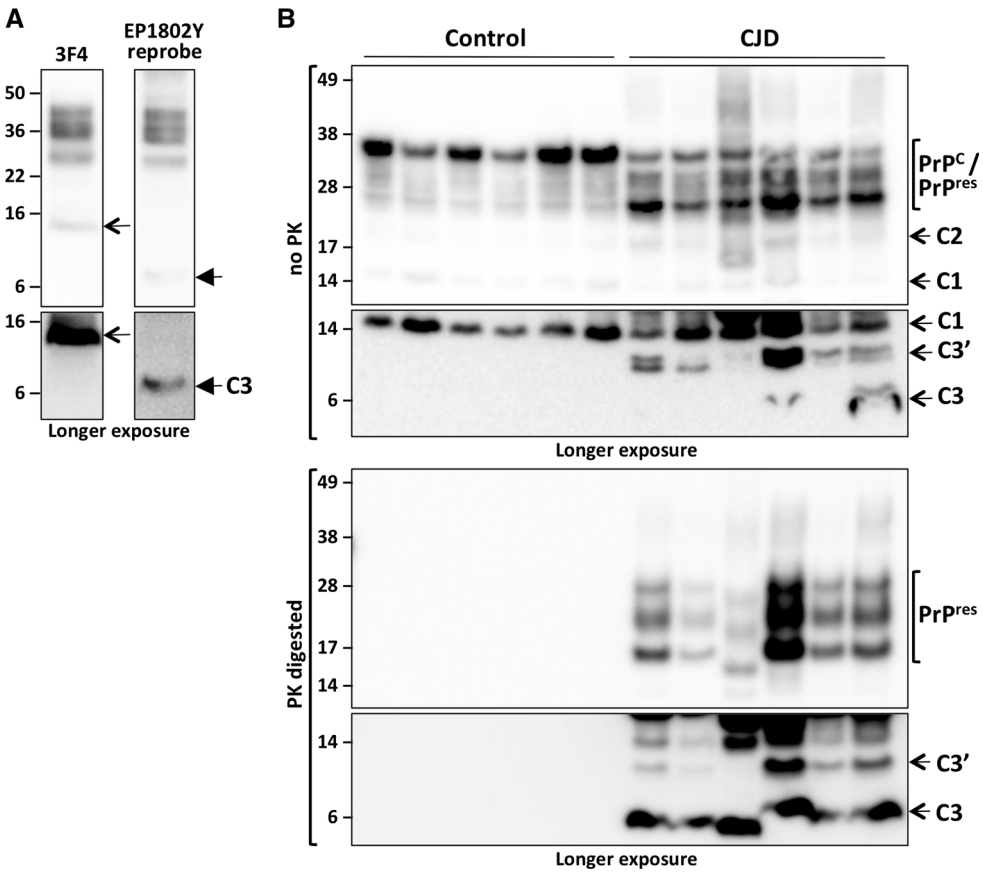

Fig. 6 C3 is present in human sporadic CJD brains. PAGE and western blot analysis of human brain tissue utilizing the anti-PrP far C-terminal EP1802Y (**a**) and (**b**) or 3F4 (**a**) antibodies as indicated. Five microliters of 10 % (w/v) CJD (**a**) and (**b**) or non-neurological control (**b**) brain homogenate was utilized untreated (**a** and **b***upper panel*), or PK digested (**b***bottom panel*), prior to analysis. The various full-length and truncated PrP species detectable (*PrP^C*, *PrP^{res}*, *C1*, *C2*, *C3*, *C3′*) are highlighted

artifact of epitope tag insertion, and thus the unequivocal existence of a PrP^C γ-cleavage event. Extensive literature searching has found that the most commonly utilized anti-PrP antibodies are directed to epitopes in the middle region of PrP^C, and unlikely to be within the C3 fragment. Furthermore, published western blot images are often trimmed, underscoring the possibility that the occurrence of PrP^C cleavage events, especially those producing small far-C-terminal fragments such as C3, may be easily overlooked. The apparent approximate molecular weight of C3 seen on PAGE and western blotting, along with the significant reduction in C3 production with the mutation of two residues within the PrP^C far C-terminus, are highly suggestive of the γ-cleavage site being within this region, potentially somewhere between residues 176 and 200. Interestingly the C-terminus of PrP^C is highly conserved in mammals [59], with 100 % amino acid sequence identity in residues 190–202 and 54 % identity in the larger region spanning residues 170–230 (human PrP numbering) in the various species listed in the National Center for Biotechnology Information (NCBI) Conserved Domains Database [60], including humans and other primates, cervids, bovids, equids, felids, cetaceans, lagomorphs and rodents, further pointing to the likely biological significance of γ-cleavage. Additionally, if our predictions of the γ-cleavage site hold true, and when direct cleavage to C3 occurs, the resulting potentially secreted N3 fragment could represent approximately 70 % of the span of previously described secreted GPI-anchorless PrP^C species, including important structural features such as the copper binding octapeptide repeat and the hydrophobic core (Fig. 1a), which may have biological/functional relevance [70–72].

After synthesis, the majority of immature PrP^C produced may undergo post-translational modifications en route to the cell surface, including addition of its GPI-anchor in the ER, and simple, followed by more complex, glycosylation of one or two asparagine (N) residues (codons 181 and 197 on human PrP^C; 180 and 196 on murine PrP^C) in the ER and Golgi, respectively [56], resulting in predominantly highly glycosylated PrP^C species. Later in the secretory pathway, after transiting the Golgi apparatus, a large proportion (in most cell types) of PrP^C is subjected to the dominant endoproteolytic processing event, α-cleavage, in the *trans*-Golgi network (TGN) [54]. Our results indicate that PrP^C also needs to exit the ER for efficient γ-cleavage, and that this endoproteolysis occurs in the Golgi complex or TGN. Furthermore, our observation of reduced cellular C3 levels in PIPLC treated cells is consistent with the phospholipase-induced loss of GPI-anchored PrP^C species from the cell surface diminishing an available substrate for

γ-cleavage. Collectively, this indicates γ-cleavage also occurs after PrP^C has transited to the cell surface, perhaps during endocytic recycling and/or retrograde transport of PrP^C to the Golgi/TGN, trafficking pathways that PrP isoforms are known to follow [73, 74]. Our data also suggest the C3 fragment itself is not glycosylated, and consistent with this, the protease responsible for γ-cleavage favors an unglycosylated substrate. Intriguingly, as the appearance of another C-terminal fragment, apparently slightly smaller than C1, sometimes coincided with increased C3 detection (for example after tunicamycin or E64d treatment), we believe γ-cleavage does not occur downstream of α-cleavage, and that C3 may not always be cleaved directly from full length PrP^C, but perhaps sometimes from an intermediary or precursor fragment, which we have coined C3′. Collectively these results may partly explain the apparently relatively low levels of the C3 fragment observed; we propose that proportionately low levels of PrP^C remain unglycosylated, and/or escape either α- or β-cleavage and remain full length, are not shed or recycled back to the cell surface, and could therefore persist long enough to be transported back to the Golgi/TGN where γ-cleavage is then able to occur. Importantly, as is the case with many other low abundance proteins, we believe the relatively low levels do not militate against the potential importance of this fragment or cleavage event.

Similar to full length PrP^C, the α- and β-cleavage C-terminal fragments C1 and C2 are known to be GPI-anchored [30]. After treatment of cells with the bacterial enzymes PIPLC and PNGaseF, a subtle size shift characteristic of GPI-anchor removal was observed in C3, along with the other PrP^C species expressed in the cells. It is unclear why PIPLC treatment alone did not result in this same discernible shift, though this may be related to the GPI-anchor attachment residues and PIPLC cleavage recognition motif being more accessible once the substrate protein has been denatured, which does occur during the conditions of PNGaseF digestion. These results, along with the detection of C3 in buoyant density gradient fractions suggest that C3 does retain its GPI-anchor. However, the lack of an observed C3 increase in conditioned media after PIPLC treatment of live cells, coupled to the lack of detection of labeled C3 after cell surface biotinylation, together indicates this fragment is unlikely to reside predominantly at the cell surface. These results are also consistent with γ-cleavage occurring after retrograde transport to the Golgi or TGN, but do not exclude contributions from nascent PrP^C coming directly from the ER. The possibility that the C3 fragment itself does not contain enough lysine residues, with amine side chains to react with the biotin, is unlikely given the predicted γ-cleavage region, although this cannot be excluded.

A single report does identify and describe a PrP^C-derived C-terminal fragment which we originally hypothesized may be the same C3 described herein [50]. The fragment described by Taguchi and colleagues was discovered during the development of a biarsenical cell surface protein labeling technique, using PrP as the model protein. This, along with our conflicting finding that γ-cleavage was not reduced by inhibition of cysteine proteases using E64d, collectively indicates the C3 fragment we have characterized is in fact not that which has been described previously, and further highlights the complexity of proteolytic processing of the prion protein far C-terminus. Whilst this study has ruled out the involvement of a cysteine protease in γ-cleavage, we have elucidated that a member/members of the matrix metalloproteinases (MMP) family of proteases are involved. Interestingly a recent report describes the proteolysis of various synthetic PrP fragments with MMP7, MMP14 (membrane-type MMP1, or MT1-MMP) and MMP16 (MT3-MMP), with some of the reported cleavage sites mapping to the far C-terminus of PrP^C between residues 169–192 [62], consistent with the region we predict to contain the γ-cleavage site. The determination of which specific MMP/s are involved is the subject of ongoing investigations.

Although prevalence of PrP^C γ-cleavage is not high, the lack of C3 seen in human control brain tissue was surprising. One explanation may be that γ-cleavage does not occur in cells of the brain region we sampled from, as cleavage profiles have been shown to vary in different tissues and regions [69]. Alternatively, C3 may be below the limits of detection by PAGE and western blotting. Whatever the explanation, our results indicate that whilst human cells are capable of accommodating γ-cleavage of murine PrP^C (e.g. the HEK and SHSY5Y cells in Fig. 1b), in vivo human PrP^C is perhaps less susceptible to this cleavage event compared to murine PrP^C. Surprisingly, PK resistant C3 and C3′ species were relatively abundant in CJD brain, indicating PrP^{Sc} may be more susceptible than PrP^C to γ-cleavage. Small, approximately 7–15 kDa, PK resistant fragments have previously been detected in human prion brain tissue (and as illustrated by Fig. 6a), particularly in the inherited Gerstmann–Sträussler–Scheinker (GSS) disease cases [75, 76], although these are typically characterized as both N- and C-terminally truncated, and are therefore not the C3 species we describe. There is published evidence of small far-C-terminal PK resistant fragments in sporadic CJD, but not control brain tissue [77], which the authors designate as PrP-CTF12/13 to reflect their approximate size. Similar to our PrP^C-derived C3, PrP-CTF12/13 are also GPI-anchored. Moreover, the N-terminus of the PrP-CTF12 fragment mapped to residues 162 and 167, which is consistent with our estimates of the γ-cleavage site, and which based on amino

acid sequence alone (i.e. codons 162–230 and 167–230) are predicted to result in C-terminal fragments of approximately 8.3 and 7.6 kDa, respectively (excluding the GPI-anchor, which when attached should actually result in slightly faster than expected resolution [58]). With PAGE protocol differences (e.g., acrylamide concentrations) and the inherent inexact nature of molecular weight standard alignment for predicting actual protein size (especially when the smallest marker is larger than the protein of interest) accounting for discrepancies, we believe these PrP-CTF12/13 species may be the same PrP^{Sc} derived PK resistant C3 and perhaps also C3′ that we have detected.

In the context of prion disease pathogenesis, experimental evidence has proven that expression of the normal cellular prion protein, PrP^{C}, is an absolute requirement [78, 79], where it aberrantly folds to the disease associated prion protein isoforms (PrP^{Sc}). Although the mechanisms underlying initiation of PrP^{C} misfolding are not understood, convention proposes the continued hetero-dimeric interaction, templating and conversion of PrP^{C} to PrP^{Sc} with eventual propagation of sufficient neurotoxic and infectious species ultimately causing cell death and neurodegeneration. Whilst it is known that the N-terminus of PrP^{C} is not required for production of PrP^{Sc} [80], we and others [33, 37, 38, 81, 82] have linked reduced susceptibility to prion infection or efficiency of conversion/misfolding, to PrP^{C} cleavage/truncation, probably due to the depletion of full-length PrP^{C} which is the optimal substrate for conversion to PrP^{Sc}. Interestingly, a recent report has also linked decreased expression and activity of MMPs 2 and 9 to increased prion propagation [83]. Given the likely involvement of MMPs in PrP^{C} γ-cleavage, it remains possible that γ-cleavage may be relevant in cellular mechanisms of susceptibility to prion propagation. Indeed, the apparent increase in γ-cleavage as indicated by the proportionally higher amounts and the PK resistance of C3 and C3′ in the brains of CJD patients may reflect increased and ultimately failed cellular attempts at managing the ongoing prion propagation through efforts to cleave and therefore degrade PrP^{Sc}.

Many areas of prion biology remain enigmatic, with considerable conflicting data published, perhaps in part due to the under-appreciation of processes such γ-cleavage. The primary objective of this study was to characterize the cellular biology of this novel PrP^{C} γ-cleavage processing, and further contribute to the understanding of currently incompletely answered questions in prion research. Whilst the exact biological and/or pathophysiological significance of γ-cleavage remain to be determined, the results we have presented herein, along with mounting evidence of the relevance of prion protein cleavage to both its normal function, and the important influence exerted in susceptibility to prion disease, underscore that this previously unappreciated cleavage event warrants further investigation.

Acknowledgments The authors thank Associate Professor Victoria Lawson for her kind gift of the RK13 cells, Professor Charles Weissmann for the Tga20 mice, and the Victorian Brain Bank Network for their assistance in human control brain tissue sampling. This work was supported by an Australian Government National Health and Medical Research Council (NHMRC) Program Grant #628946 (SJC, VL, VJ), Practitioner Fellowship #1005816 (SJC), Training Fellowship #567123 (VL), R.D. Wright Fellowship (CDF2) (PJC) and Project Grant #1061550 (PJC), a University of Melbourne Early Career Researcher Fellowship (VL), the CJD Support Group Network (VL), and the Medical Research Council of Great Britain (G0802189) (NMH).

References

1. Borchelt DR, Rogers M, Stahl N, Telling G, Prusiner SB (1993) Release of the cellular prion protein from cultured cells after loss of its glycoinositol phospholipid anchor. Glycobiology 3(4):319–329
2. Bendheim PE, Brown HR, Rudelli RD, Scala LJ, Goller NL, Wen GY, Kascsak RJ, Cashman NR, Bolton DC (1992) Nearly ubiquitous tissue distribution of the scrapie agent precursor protein. Neurology 42(1):149–156
3. Ford MJ, Burton LJ, Morris RJ, Hall SM (2002) Selective expression of prion protein in peripheral tissues of the adult mouse. Neuroscience 113(1):177–192
4. Horiuchi M, Yamazaki N, Ikeda T, Ishiguro N, Shinagawa M (1995) A cellular form of prion protein (PrPC) exists in many non-neuronal tissues of sheep. J Gen Virol 76(10):2583–2587
5. Bueler H, Fischer M, Lang Y, Bluethmann H, Lipp HP, DeArmond SJ, Prusiner SB, Aguet M, Weissmann C (1992) Normal development and behaviour of mice lacking the neuronal cell-surface PrP protein. Nature 356(6370):577–582
6. Haigh CL, Drew SC, Boland MP, Masters CL, Barnham KJ, Lawson VA, Collins SJ (2009) Dominant roles of the polybasic proline motif and copper in the PrP23-89-mediated stress protection response. J Cell Sci 122(10):1518–1528. doi:10.1242/jcs.043604
7. Brown DR, Nicholas RS, Canevari L (2002) Lack of prion protein expression results in a neuronal phenotype sensitive to stress. J Neurosci Res 67(2):211–224
8. Chiarini LB, Freitas AR, Zanata SM, Brentani RR, Martins VR, Linden R (2002) Cellular prion protein transduces neuroprotective signals. EMBO J 21(13):3317–3326
9. Klamt F, Dal-Pizzol F, Conte da Frota MJ, Walz R, Andrades ME, da Silva EG, Brentani RR, Izquierdo I, Fonseca Moreira JC (2001) Imbalance of antioxidant defense in mice lacking cellular prion protein. Free Radic Biol Med 30(10):1137–1144
10. Haigh CL, Lewis VA, Vella LJ, Masters CL, Hill AF, Lawson VA, Collins SJ (2009) PrPC-related signal transduction is influenced by copper, membrane integrity and the alpha cleavage site. Cell Res 19(9):1062–1078. doi:10.1038/cr.2009.86
11. Mouillet-Richard S, Ermonval M, Chebassier C, Laplanche JL, Lehmann S, Launay JM, Kellermann O (2000) Signal transduction through prion protein. Science 289(5486):1925–1928
12. Schneider B, Mutel V, Pietri M, Ermonval M, Mouillet-Richard S, Kellermann O (2003) NADPH oxidase and extracellular regulated kinases 1/2 are targets of prion protein signaling in neuronal and nonneuronal cells. Proc Natl Acad Sci USA 100(23):13326–13331
13. Spielhaupter C, Schatzl HM (2001) PrPC directly interacts with proteins involved in signaling pathways. J Biol Chem 276(48):44604–44612

14. Kanaani J, Prusiner SB, Diacovo J, Baekkeskov S, Legname G (2005) Recombinant prion protein induces rapid polarization and development of synapses in embryonic rat hippocampal neurons in vitro. J Neurochem 95(5):1373–1386. doi:10.1111/j.1471-4159.2005.03469.x
15. Santuccione A, Sytnyk V, Leshchyns'ka I, Schachner M (2005) Prion protein recruits its neuronal receptor NCAM to lipid rafts to activate p59fyn and to enhance neurite outgrowth. J Cell Biol 169(2):341–354
16. Colling SB, Collinge J, Jefferys JG (1996) Hippocampal slices from prion protein null mice: disrupted $Ca(2^+)$-activated K^+ currents. Neurosci Lett 209(1):49–52
17. Collinge J, Whittington MA, Sidle KC, Smith CJ, Palmer MS, Clarke AR, Jefferys JG (1994) Prion protein is necessary for normal synaptic function. Nature 370(6487):295–297
18. Herms JW, Tings T, Dunker S, Kretzschmar HA (2001) Prion protein affects Ca^{2+}-activated K^+ currents in cerebellar purkinje cells. Neurobiol Dis 8(2):324–330
19. Mallucci GR, Ratte S, Asante EA, Linehan J, Gowland I, Jefferys JG, Collinge J (2002) Post-natal knockout of prion protein alters hippocampal CA1 properties, but does not result in neurodegeneration. EMBO J 21(3):202–210
20. Powell AD, Toescu EC, Collinge J, Jefferys JG (2008) Alterations in Ca^{2+}-buffering in prion-null mice: association with reduced afterhyperpolarizations in CA1 hippocampal neurons. J Neurosci 28(15):3877–3886
21. Mastrangelo P, Westaway D (2001) Biology of the prion gene complex. Biochem Cell Biol 79(5):613–628
22. Bazan JF, Fletterick RJ, McKinley MP, Prusiner SB (1987) Predicted secondary structure and membrane topology of the scrapie prion protein. Protein Eng 1(2):125–135
23. Sulkowski E (1992) Aromatic palindrome motif in prion proteins. FASEB J 6(6):2363
24. Wopfner F, Weidenhofer G, Schneider R, von Brunn A, Gilch S, Schwarz TF, Werner T, Schatzl HM (1999) Analysis of 27 mammalian and 9 avian PrPs reveals high conservation of flexible regions of the prion protein. J Mol Biol 289(5):1163–1178. doi:10.1006/jmbi.1999.2831
25. Goldmann W (1993) PrP gene and its association with spongiform encephalopathies. Br Med Bull 49(4):839–859
26. Parkin ET, Watt NT, Turner AJ, Hooper NM (2004) Dual mechanisms for shedding of the cellular prion protein. J Biol Chem 279(12):11170–11178
27. Taylor DR, Parkin ET, Cocklin SL, Ault JR, Ashcroft AE, Turner AJ, Hooper NM (2009) Role of ADAMs in the ectodomain shedding and conformational conversion of the prion protein. J Biol Chem 284(34):22590–22600. doi:10.1074/jbc.M109.032599
28. Altmeppen HC, Prox J, Puig B, Kluth MA, Bernreuther C, Thurm D, Jorissen E, Petrowitz B, Bartsch U, De Strooper B, Saftig P, Glatzel M (2011) Lack of a-disintegrin-and-metalloproteinase ADAM10 leads to intracellular accumulation and loss of shedding of the cellular prion protein in vivo. Mol Neurodegener 6:36. doi:10.1186/1750-1326-6-36
29. Lewis V (2011) Proteolytic processing of the prion protein. In: Collins SJ, Lawson VA (eds) The cellular and molecular biology of prion disease. Research Signpost, Kerala, pp 53–71
30. Chen SG, Teplow DB, Parchi P, Teller JK, Gambetti P, Autilio-Gambetti L (1995) Truncated forms of the human prion protein in normal brain and in prion diseases. J Biol Chem 270(32):19173–19180
31. McDonald AJ, Dibble JP, Evans EG, Millhauser GL (2014) A new paradigm for enzymatic control of alpha-cleavage and beta-cleavage of the prion protein. J Biol Chem 289(2):803–813. doi:10.1074/jbc.M113.502351
32. Pan T, Wong P, Chang B, Li C, Li R, Kang SC, Wisniewski T, Sy MS (2005) Biochemical fingerprints of prion infection: accumulations of aberrant full-length and N-terminally truncated PrP species are common features in mouse prion disease. J Virol 79(2):934–943
33. Lewis V, Hill AF, Haigh CL, Klug GM, Masters CL, Lawson VA, Collins SJ (2009) Increased proportions of C1 truncated prion protein protect against cellular M1000 prion infection. J Neuropathol Exp Neurol 68(10):1125–1135. doi:10.1097/NEN.0b013e3181b96981
34. Mange A, Beranger F, Peoc'h K, Onodera T, Frobert Y, Lehmann S (2004) Alpha- and beta-cleavages of the amino-terminus of the cellular prion protein. Biol Cell 96(2):125–132
35. Jimenez-Huete A, Lievens PM, Vidal R, Piccardo P, Ghetti B, Tagliavini F, Frangione B, Prelli F (1998) Endogenous proteolytic cleavage of normal and disease-associated isoforms of the human prion protein in neural and non-neural tissues. Am J Pathol 153(5):1561–1572
36. Pan T, Li R, Wong BS, Liu T, Gambetti P, Sy MS (2002) Heterogeneity of normal prion protein in two- dimensional immunoblot: presence of various glycosylated and truncated forms. J Neurochem 81(5):1092–1101
37. Westergard L, Turnbaugh JA, Harris DA (2011) A naturally occurring C-terminal fragment of the prion protein (PrP) delays disease and acts as a dominant-negative inhibitor of PrPSc formation. J Biol Chem 286(51):44234–44242. doi:10.1074/jbc.M111.286195
38. Johanssen VA, Johanssen T, Masters CL, Hill AF, Barnham KJ, Collins SJ (2014) C-terminal peptides modelling constitutive PrPC processing demonstrate ameliorated toxicity predisposition consequent to α-cleavage. Biochem J 459(1):103–115. doi:10.1042/BJ20131378
39. Lewis V, Haigh CL, Masters CL, Hill AF, Lawson VA, Collins SJ (2012) Prion subcellular fractionation reveals infectivity spectrum, with a high titre-low PrPres level disparity. Mol Neurodegener 7:18. doi:10.1186/1750-1326-7-18
40. Klug GM, Boyd A, Zhao T, Stehmann C, Simpson M, McLean CA, Masters CL, Collins SJ (2013) Surveillance for Creutzfeldt-Jakob disease in Australia: update to December 2012. Commun Dis Intell 37(2):E115–E120
41. Perera WS, Hooper NM (1999) Proteolytic fragmentation of the murine prion protein: role of Tyr-128 and His-177. FEBS Lett 463(3):273–276
42. Wurch T, Lestienne F, Pauwels PJ (1998) A modified overlap extension PCR method to create chimeric genes in the absence of restriction enzymes. Biotechnol Tech 12(9):653–657. doi:10.1023/A:1008848517221
43. Walmsley AR, Zeng F, Hooper NM (2001) Membrane topology influences N-glycosylation of the prion protein. EMBO J 20(4):703–712
44. Lewis V, Klug GM, Hill AF, Collins SJ (2008) Molecular typing of PrPres in human sporadic CJD brain tissue. In: Hill AF (ed) Prion protein protocols, vol 459., Methods in molecular biologyHumana Press, Totowa NJ, pp 241–247
45. Lewis V, Whitehouse IJ, Baybutt H, Manson JC, Collins SJ, Hooper NM (2012) Cellular prion protein expression is not regulated by the Alzheimer's amyloid precursor protein intracellular domain. PLoS ONE 7(2):e31754. doi:10.1371/journal.pone.0031754
46. Lewis V, Collins SJ (2008) Analysis of endogenous PrPC processing in neuronal and non-neuronal cell lines. In: Hill AF (ed) Prion protein protocols, vol 459., Methods in molecular biologyHumana Press, Totowa NJ, pp 229–239
47. Barmada S, Piccardo P, Yamaguchi K, Ghetti B, Harris DA (2004) GFP-tagged prion protein is correctly localized and

functionally active in the brains of transgenic mice. Neurobiol Dis 16(3):527–537. doi:10.1016/j.nbd.2004.05.005
48. Bian J, Nazor KE, Angers R, Jernigan M, Seward T, Centers A, Green M, Telling GC (2006) GFP-tagged PrP supports compromised prion replication in transgenic mice. Biochem Biophys Res Commun 340(3):894–900. doi:10.1016/j.bbrc.2005.12.085
49. De Keukeleire B, Donadio S, Micoud J, Lechardeur D, Benharouga M (2007) Human cellular prion protein hPrPC is sorted to the apical membrane of epithelial cells. Biochem Biophys Res Commun 354(4):949–954. doi:10.1016/j.bbrc.2007.01.096
50. Taguchi Y, Shi ZD, Ruddy B, Dorward DW, Greene L, Baron GS (2009) Specific biarsenical labeling of cell surface proteins allows fluorescent- and biotin-tagging of amyloid precursor protein and prion proteins. Mol Biol Cell 20(1):233–244. doi:10.1091/mbc.E08-06-0635
51. Salamat K, Moudjou M, Chapuis J, Herzog L, Jaumain E, Beringue V, Rezaei H, Pastore A, Laude H, Dron M (2012) Integrity of helix 2-helix 3 domain of the PrP protein is not mandatory for prion replication. J Biol Chem 287(23):18953–18964. doi:10.1074/jbc.M112.341677
52. Rutishauser D, Mertz KD, Moos R, Brunner E, Rulicke T, Calella AM, Aguzzi A (2009) The comprehensive native interactome of a fully functional tagged prion protein. PLoS ONE 4(2):e4446. doi:10.1371/journal.pone.0004446
53. Saraste J, Palade GE, Farquhar MG (1986) Temperature-sensitive steps in the transport of secretory proteins through the Golgi complex in exocrine pancreatic cells. Proc Natl Acad Sci USA 83(17):6425–6429
54. Walmsley AR, Watt NT, Taylor DR, Perera WS, Hooper NM (2009) alpha-cleavage of the prion protein occurs in a late compartment of the secretory pathway and is independent of lipid rafts. Mol Cell Neurosci 40(2):242–248. doi:10.1016/j.mcn.2008.10.012
55. Fujiwara T, Oda K, Yokota S, Takatsuki A, Ikehara Y (1988) Brefeldin A causes disassembly of the Golgi complex and accumulation of secretory proteins in the endoplasmic reticulum. J Biol Chem 263(34):18545–18552
56. Lawson VA, Collins SJ, Masters CL, Hill AF (2005) Prion protein glycosylation. J Neurochem 93(4):793–801
57. Lewis V, Hooper NM (2011) The role of lipid rafts in prion protein biology. Front Biosci 16:151–168
58. Hooper NM (2001) Determination of glycosyl-phosphatidylinositol membrane protein anchorage. Proteomics 1(6):748–755
59. Pastore A, Zagari A (2007) A structural overview of the vertebrate prion proteins. Prion 1(3):185–197
60. Marchler-Bauer A, Zheng C, Chitsaz F, Derbyshire MK, Geer LY, Geer RC, Gonzales NR, Gwadz M, Hurwitz DI, Lanczycki CJ, Lu F, Lu S, Marchler GH, Song JS, Thanki N, Yamashita RA, Zhang D, Bryant SH (2013) CDD: conserved domains and protein three-dimensional structure. Nucleic Acids Res 41(Database issue):D348–D352. doi:10.1093/nar/gks1243
61. Rawlings ND, Waller M, Barrett AJ, Bateman A (2014) MEROPS: the database of proteolytic enzymes, their substrates and inhibitors. Nucleic Acids Res 42(Database issue):D503–D509. doi:10.1093/nar/gkt953
62. Kojima A, Konishi M, Akizawa T (2014) Prion fragment peptides are digested with membrane type matrix metalloproteinases and acquire enzyme resistance through Cu(2)(+)-binding. Biomolecules 4(2):510–526. doi:10.3390/biom4020510
63. Hande KR, Collier M, Paradiso L, Stuart-Smith J, Dixon M, Clendeninn N, Yeun G, Alberti D, Binger K, Wilding G (2004) Phase I and pharmacokinetic study of prinomastat, a matrix metalloprotease inhibitor. Clin Cancer Res 10(3):909–915
64. Chen S, Yadav SP, Surewicz WK (2010) Interaction between human prion protein and amyloid-beta (Abeta) oligomers: role of N-terminal residues. J Biol Chem 285(34):26377–26383. doi:10.1074/jbc.M110.145516
65. You H, Tsutsui S, Hameed S, Kannanayakal TJ, Chen L, Xia P, Engbers JD, Lipton SA, Stys PK, Zamponi GW (2012) Abeta neurotoxicity depends on interactions between copper ions, prion protein, and *N*-methyl-D-aspartate receptors. Proc Natl Acad Sci USA 109(5):1737–1742. doi:10.1073/pnas.1110789109
66. Guillot-Sestier MV, Sunyach C, Druon C, Scarzello S, Checler F (2009) The alpha-secretase-derived N-terminal product of cellular prion, N1, displays neuroprotective function in vitro and in vivo. J Biol Chem 284(51):35973–35986. doi:10.1074/jbc.M109.051086
67. Sunyach C, Cisse MA, da Costa CA, Vincent B, Checler F (2007) The C-terminal products of cellular prion protein processing, C1 and C2, exert distinct influence on p53-dependent staurosporine-induced caspase-3 activation. J Biol Chem 282(3):1956–1963
68. Shmerling D, Hegyi I, Fischer M, Blattler T, Brandner S, Gotz J, Rulicke T, Flechsig E, Cozzio A, von Mering C, Hangartner C, Aguzzi A, Weissmann C (1998) Expression of amino-terminally truncated PrP in the mouse leading to ataxia and specific cerebellar lesions. Cell 93(2):203–214
69. Kuczius T, Koch R, Keyvani K, Karch H, Grassi J, Groschup MH (2007) Regional and phenotype heterogeneity of cellular prion proteins in the human brain. Eur J Neurosci 25(9):2649–2655. doi:10.1111/j.1460-9568.2007.05518.x
70. Parizek P, Roeckl C, Weber J, Flechsig E, Aguzzi A, Raeber AJ (2001) Similar turnover and shedding of the cellular prion protein in primary lymphoid and neuronal cells. J Biol Chem 276(48):44627–44632
71. Tagliavini F, Prelli F, Porro M, Salmona M, Bugiani O, Frangione B (1992) A soluble form of prion protein in human cerebrospinal fluid: implications for prion-related encephalopathies. Biochem Biophys Res Commun 184(3):1398–1404
72. Kikuchi Y, Kakeya T, Nakajima O, Sakai A, Ikeda K, Yamaguchi N, Yamazaki T, Tanamoto K, Matsuda H, Sawada J, Takatori K (2008) Hypoxia induces expression of a GPI-anchorless splice variant of the prion protein. FEBS J 275(11):2965–2976. doi:10.1111/j.1742-4658.2008.06452.x
73. Magalhaes AC, Silva JA, Lee KS, Martins VR, Prado VF, Ferguson SS, Gomez MV, Brentani RR, Prado MA (2002) Endocytic intermediates involved with the intracellular trafficking of a fluorescent cellular prion protein. J Biol Chem 277(36):33311–33318. doi:10.1074/jbc.M203661200
74. Lee KS, Magalhaes AC, Zanata SM, Brentani RR, Martins VR, Prado MA (2001) Internalization of mammalian fluorescent cellular prion protein and N-terminal deletion mutants in living cells. J Neurochem 79(1):79–87
75. Piccardo P, Dlouhy SR, Lievens PM, Young K, Bird TD, Nochlin D, Dickson DW, Vinters HV, Zimmerman TR, Mackenzie IR, Kish SJ, Ang LC, De Carli C, Pocchiari M, Brown P, Gibbs CJ Jr, Gajdusek DC, Bugiani O, Ironside J, Tagliavini F, Ghetti B (1998) Phenotypic variability of Gerstmann-Straussler-Scheinker disease is associated with prion protein heterogeneity. J Neuropathol Exp Neurol 57(10):979–988
76. Parchi P, Chen SG, Brown P, Zou W, Capellari S, Budka H, Hainfellner J, Reyes PF, Golden GT, Hauw JJ, Gajdusek DC, Gambetti P (1998) Different patterns of truncated prion protein fragments correlate with distinct phenotypes in P102L Gerstmann-Straussler-Scheinker disease. Proc Natl Acad Sci USA 95(14):8322–8327
77. Zou WQ, Capellari S, Parchi P, Sy MS, Gambetti P, Chen SG (2003) Identification of novel proteinase K-resistant C-terminal fragments of PrP in Creutzfeldt-Jakob disease. J Biol Chem 278(42):40429–40436

78. Bueler H, Aguzzi A, Sailer A, Greiner RA, Autenried P, Aguet M, Weissmann C (1993) Mice devoid of PrP are resistant to scrapie. Cell 73(7):1339–1347
79. Mallucci G, Dickinson A, Linehan J, Klohn PC, Brandner S, Collinge J (2003) Depleting neuronal PrP in prion infection prevents disease and reverses spongiosis. Science 302(5646):871–874
80. Rogers M, Yehiely F, Scott M, Prusiner SB (1993) Conversion of truncated and elongated prion proteins into the scrapie isoform in cultured cells. Proc Natl Acad Sci USA 90(8):3182–3186
81. Fischer M, Rulicke T, Raeber A, Sailer A, Moser M, Oesch B, Brandner S, Aguzzi A, Weissmann C (1996) Prion protein (PrP) with amino-proximal deletions restoring susceptibility of PrP knockout mice to scrapie. EMBO J 15(6):1255–1264
82. Lawson VA, Priola SA, Wehrly K, Chesebro B (2001) N-terminal truncation of prion protein affects both formation and conformation of abnormal protease-resistant prion protein generated in vitro. J Biol Chem 276(38):35265–35271
83. Marbiah MM, Harvey A, West BT, Louzolo A, Banerjee P, Alden J, Grigoriadis A, Hummerich H, Kan HM, Cai Y, Bloom GS, Jat P, Collinge J, Klohn PC (2014) Identification of a gene regulatory network associated with prion replication. EMBO J 33(14):1527–1547. doi:10.15252/embj.201387150

Cell Biochem Biophys (2016) 74:297–306
DOI 10.1007/s12013-016-0747-4

ORIGINAL PAPER

A 2-Substituted 8-Hydroxyquinoline Stimulates Neural Stem Cell Proliferation by Modulating ROS Signalling

Cathryn L. Haigh[1] · **Carolin Tumpach**[2] · **Steven J. Collins**[1] · **Simon C. Drew**[2]

Received: 9 February 2016 / Accepted: 9 June 2016 / Published online: 21 June 2016

Abstract Eight-hydroxyquinolines (8HQs) are a class of compounds that have been identified as potential therapeutics for a number of neurodegenerative diseases. Understanding the influence of structural modifications to the 8HQ scaffold on cellular behaviour will aid the identification of compounds that might be effective in treating dementias. In this study, we describe the action of 2-[(dimethylamino)methyl]-8-hydroxyquinoline (DMAMQ) on adult murine neural stem cells (NSCs) cultured in vitro. Treatment of NSCs with DMAMQ resulted in enhanced self-renewal and increased neurite outgrowth. Concurrent with the positive growth effects was an increase in intracellular reactive oxygen species, with the growth being inhibited by inactivation of the NADPH oxidase (Nox) enzyme family. Our results indicate that DMAMQ can stimulate neurogenesis via the Nox signalling pathway, which may provide therapeutic benefit in treating dementias of various types by replenishing neurones using the brain's own reserves. The narrow concentration range over which these effects were observed, however, suggests that there may exist only a small therapeutic window for neuro-regenerative applications.

Keywords 8-hydroxyquinoline · Neural stem cells · Neurosphere · Proliferation · NADPH oxidase · Reactive oxygen species · 2-[(dimethylamino)methyl]-8-hydroxyquinoline · DMAMQ · PBT2

Introduction

Endogenous neural stem cells (NSCs) are an as-yet untapped resource in combatting dementia. Low levels of NSCs persist in the brain throughout adult life, maintaining the ability to self-replicate and to differentiate into mature brain cells. During dementia, neurogenesis (the ability to form new neurones) is seen to become dysregulated [1, 2]. In rodent models of Alzheimer's disease (AD), production of beta-amyloid, one hallmark of AD, changes the growth and differentiation of these cells [3–7]. Neurogenesis has been extensively linked with both learning and forgetting [8–10]; therefore, changes in these processes might contribute significantly to the cognitive changes that occur during neurodegenerative diseases, including AD. Compounds that modulate or normalise the functions of NSCs represent a prime target for alleviating the symptoms associated with, or delaying the course of, neurodegenerative diseases.

Unbiased chemical screening of substituted 8-hydroxyquinolines (8HQs) and a range of investigations in yeast, nematodes, mice and humans have highlighted the variable mechanisms by which they may act. Side-chain modifications to the 8HQ backbone may lead to functional differences in vivo, with applications of substituted 8HQs as anti-microbial agents [11, 12], anti-cancer agents [13, 14], epigenetic modulators [15, 16], dementia treatments [17–20], artificial nucleobases [21] and medical imaging agents [22, 23]. Moreover, biosynthesis of substituted

Electronic supplementary material The online version of this article (doi:10.1007/s12013-016-0747-4) contains supplementary material, which is available to authorized users.

✉ Cathryn L. Haigh
chaigh@unimelb.edu.au

✉ Simon C. Drew
sdrew@unimelb.edu.au

[1] Department of Medicine, Royal Melbourne Hospital, The University of Melbourne, Victoria 3010, Australia

[2] Florey Department of Neuroscience and Mental Health, The University of Melbourne, Victoria 3010, Australia

8HQs has been identified in mammals (e.g. xanthurenic acid [24]), bacteria (e.g. quinolobactin [25]) and insects (e.g. 2-carboxy-8HQ [26]). In dementia applications, studies utilising 5,7-dichloro-2-[(dimethylamino)methyl]-8-hydroxyquinoline reported an increased neurite number following treatment of cultured PC12 cells and a restoration of hippocampal dendritic spine density (but not number) in transgenic mouse model of AD [18].

In the current study, we sought to further understand the action of this class of 8HQ by treating adult murine NSC cultures with 2-[(dimethylamino)methyl]-8-hydroxyquinoline (DMAMQ; Fig. 1). We specifically assessed the ability of these cells to self-renew, essential for maintaining their numbers in the brain throughout life, and to differentiate into new CNS lineage cells. Our findings show that whilst neurogenesis is unchanged, NSCs treated with DMAMQ demonstrate an increase in NSC proliferation and an increased neurite outgrowth during neurogenesis that was signalled by increased production of reactive oxygen species (ROS) signalling intermediates by the NADPH oxidase (Nox) enzyme family. These effects were only observed within a narrow concentration range, suggesting a small therapeutic window for neuro-regenerative applications.

Materials and Methods

Synthesis

2-[(dimethylamino)methyl]-8-hydroxyquinoline (DMAMQ) was synthesised as described previously [27].

Cell Culture

Murine NSCs were harvested from the brains of 6–8 week-old Balb/c mice and grown without modification as neurospheres in liquid culture as described previously [28].

DMAMQ Treatments

DMAMQ was included in the culture medium at the concentrations indicated. For all assays, the compound was added as a single treatment at the start of the assay and was not replenished when the media was changed.

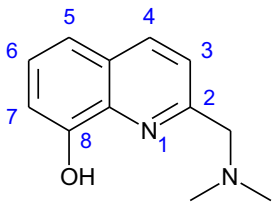

Fig. 1 Structure of DMAMQ (2-[(dimethylamino)methyl]-8-hydroxyquinoline)

Neural Colony Forming Assay (NCFA)

The NCFA has been described previously [29]. For each independent experiment over 50 colonies were measured. As stated above, DMAMQ was included in the matrix once only at the start of the incubation.

Neurite Outgrowth Assay

Neurite outgrowth was measured using a neurite outgrowth staining kit (Merck-Millipore) as per the manufacturer's instructions with the following modifications. One hundred thousand cells per condition were incubated in high FGF (20 ng/mL), no EGF, growth media before seeding 100,000 cells per well insert (1 μm pore size) in differentiation medium with or without test compound. Neurite outgrowth was permitted for 2 days before the assay.

Dichlorofluorescein (DCF) Intracellular ROS Assay

The DCF assay has been described previously [30]. Cells were seeded at a density of 3.6×10^4 cells/well 24 h before the start of the assay in poly-D lysine coated 96-well plates. Fluorescence intensity was measured every 5 min for 12 h using a FLUOstar Optima (BMG Labtech) fitted with 490 nm excitation and 520 nm emission filters, and initial rates were calculated using tangents to the curve.

MTS Metabolism Assay

Five microlitre of one solution MTS reagent (Promega) per 100 μL media was added to test and media only background control conditions, and incubated under normal culture conditions for 90 min. Reaction product was quantified using absorbance at 462 nm in a FLUOstar Optima.

β-Galactosidase Staining and Quantification

The cells were stained using a Cell Signalling Technologies' β-galactosidase staining kit as per the manufacturer's instructions. To solubilise the stain for quantitation by spectrometry, the staining solution was removed from the wells and replaced with 350 μL of DMSO. The plate was warmed with agitation at 50°C for 1 h before 100 μL of dissolved dye was transferred to three wells of a 96-well plate for triplicate reads.

Immunofluorescence Staining

The immunofluorescence staining protocol for NSC lineage has been described previously [31].

Ki67 Flow Cytometry

Ki67 expression in proliferating cells was quantified using the Muse Ki67 Proliferation Kit (Millipore) as per the manufacturer's instructions. For the final analysis, the number of unstained cells gated as positive was subtracted from the stained cells and the percentage change was calculated from the control cells.

Cell Cycle Phase Flow Cytometry

Cell cycle phase analysis by DNA content was determined using the Muse cell cycle analysis kit (Millipore) as per the manufacturer's instructions.

PAGE and Western Blotting

Polyacrylamide gel electrophoresis and western blotting were conducted as described previously [32]. Primary antibodies and concentrations were as follows; pMEK1, pMEK2 and pGSK-3β (Abcam) 1 in 1000; nestin (Sigma) 1 in 1000; GFAP (Stem Cell Technologies) 1 in 5000; and Neurofilament-L (Invitrogen) 1 in 1000. Relative densitometric comparisons were normalised for total protein loading as shown in Coomassie-stained images.

Calcium Assay

Cells were seeded in 96-well plates as mentioned above. At the beginning of the assay, 50 μL of culture media was removed from each well and replaced with calcium assay working buffer as per manufacturer's instructions (Invitrogen). Plates were incubated for 1 h under normal incubator conditions protected from light before test reagent addition. Readings were taken using 488 nm excitation and 530 nm emission filters in a FluoSTAR Optima (BMG Labtech) every 60 s for 1 h from addition.

Statistical Analyses

Statistical analyses were carried out using GraphPad Prism 5 statistical software. The relevant statistical test applied is indicated in the figure legend. Where significant differences were found, Dunnett, Bonferroni and Dunn's tests were used for multiple comparisons of one-way, two-way and non-parametric ANOVA, respectively. Graphs show the mean and standard error of the mean (SEM) of n independent experiments unless otherwise stated.

Results and Discussion

Herein we investigated the potential for DMAMQ to enhance the regenerative capacity of NSCs cultured in vitro. NSC cultures were established using cells harvested from the sub-ventricular zone of adult wild type Balb/c mice and grown in suspension culture as neurospheres. We first examined the influence of DMAMQ on proliferating neurospheres using a colony forming assay. Cells were exposed to one single treatment included in the media matrix at the start of the assay. Exposure of neurospheres to DMAMQ was observed to have a profound effect on the morphology (Fig. 2a) and volume (Fig. 2b) of the growing neurospheres. Significant toxicity of DMAMQ was only observed at the highest concentration tested (100 μM; Figure S1), whereas NSC growth was stimulated in the low μM concentration range. The observed proliferative effect was due to both the number of new neurospheres/colonies being increased (Fig. 2c) and the distribution of neurosphere sizes shifting towards larger diameters (Fig. 2d). Since the greatest proliferative effect was observed at 2.5 μM DMAMQ, this concentration was used for subsequent assays.

To investigate the increased growth further, Ki67, a marker expressed only in actively proliferating cells, was assessed by flow cytometry. An approximate 4 % increase in proliferating cells was seen after 24 h of exposure to DMAMQ in normal culture media (Fig. 3a, b). Cells that are not proliferating may be quiescent (resting in G0 until stimulated to re-enter the cell cycle) or senescent (an irrecoverable G0 state where cells are unable to re-enter the cell cycle but are not dead). β-galactosidase staining is characteristic of senescent cells. Following 3 days of DMAMQ treatment, administered as a single dose, the number of senescent cells in the culture was decreased by almost 20 % (Fig. 3c). Analysis of cell cycle phase by DNA content also showed that cells were cycling more rapidly following DMAMQ treatment, with a lower percentage of cells resting in the G0 and G1 phases of the cell cycle following 24 h DMAMQ treatment (Fig. 3d, e). These results indicate that the observed increase in NSC proliferation was due to a shift towards active proliferation coupled with protection against senescence.

In addition to heightening the ability of NSCs to proliferate in the colony forming assay, we observed a distinct pattern of outgrowth from NSCs cultured in response to DMAMQ suggesting that DMAMQ also promoted neurite outgrowth in the proliferating cultures (Fig. 2a). To determine whether this was a significant event, the number of neurospheres demonstrating this morphology were counted and showed increased frequency in the DMAMQ-treated colonies (Fig. 3f). The

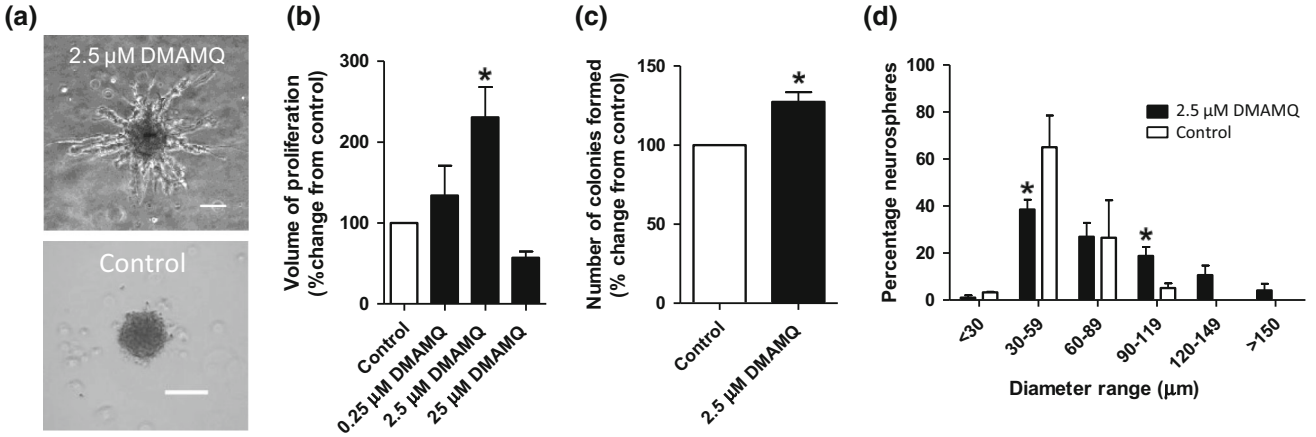

Fig. 2 DMAMQ promotes the proliferation of NSCs. **a** Representative field of view showing neurosphere morphology with and without 2.5 μm DMAMQ treatment for 21 days. *Scale bar* = 35 μm. **b** Colony volume measurement of increasing DMAMQ doses. Dissociated cells (*single cells*) were seeded at equal density with/without DMAMQ, and the growth of neurospheres present at 21 days post-plating was measured (change in volume is expressed relative to the no DMAMQ control; one-way ANOVA, $n = 3$). Neurosphere volume at 2.5 μm DMAMQ is increased both because of **c** increased colony formation (students *t* test, $n = 3$) and **d** a shift in the size of the neurospheres towards larger diameters (with significant differences being obtained for diameters in the 30–59 and 90–199 μm range; two-way ANOVA, $p < 0.001$, $n = 3$)

ability of DMAMQ to stimulate neurite outgrowth during differentiation was assessed using a colourimetric neurite staining protocol and showed that, over 2 days of differentiation, DMAMQ-treated cells displayed ca. 10 % more neurite outgrowth than was observed for control cells (Fig. 3g).

To ascertain whether enhanced neurite outgrowth could be linked with enhanced neurogenesis (the capacity to form new neurones), the influence of DMAMQ on neuronal or astrocytic lineage preference following differentiation of NSCs was considered. Lineage commitment of NSCs can be influenced by factors present both when stimulated to differentiate and before they are stimulated to differentiate. Therefore, we considered the effect of including DMAMQ in the culture media during differentiation and also before cells were differentiated as a 'priming' event. For the differentiating culture, DMAMQ was added at the induction of differentiation and remained in the media for 7 days. For the primed culture, NSCs were treated for 24 h prior to differentiation and then transferred into differentiation medium and cultured for 7 days in the absence of further exposure to DMAMQ. Subsequent immunofluorescence staining indicated that DMAMQ incubation did not alter the resulting cell lineages or overtly change the morphology of the differentiated neurones and astrocytes (Fig. 4a). In addition, western blot analysis (Fig. 4b) confirmed no changes in expression of nestin (Fig. 4c), neurofilament-L (NF-L; Fig. 4d) or GFAP (Fig. 2e) either when cells were primed or differentiated with DMAMQ. Therefore, neurogenic potential of NSCs treated with DMAMQ was neither enhanced nor compromised.

Inactivation (by phosphorylation of Ser9) or pharmacological inhibition of GSK-3 leads to both increased proliferation and enhanced neurogenesis in neural stem cell cultures [33, 34] and this phosphorylation has previously been reported in some studies using the 5,7-dichlorinated analogue of DMAMQ [18]; however, we did not observe any change in the phosphorylation status of GSK-3β following treatment with concentrations of DMAMQ that induced NSC growth (Fig. 5a). Indeed, a significant increase in phosphorylation was only observed at 100 μM DMAMQ (Figure S2), the same concentration at which DMAMQ cytotoxicity was significant (Figure S1). Therefore, signalling through GSK-3β is unlikely to be of relevance to DMAMQ-stimulated NSC growth. Additionally, no detectable changes in AKT and MEK1/2 phosphorylation were observed (Fig. 5a), indicating these redox-sensitive signalling pathways were not involved in the induction of cell growth.

Many neuronal signalling processes involve calcium flux, and stem cells utilise these pathways [35]. Changes in calcium mobilisation are also linked with redox signalling [36] and increased cytosolic Ca^{2+} can directly activate some Nox enzymes [37]. Therefore, intracellular calcium levels were measured in the NSCs. Following DMAMQ treatment, a reduction in intracellular calcium was detected (Fig. 5b).

Redox signalling pathways have been linked with NSC growth and an increased ROS burst has been linked with induction of proliferation [38–40]. A 'cellular redox cycle' has been shown to occur within the cell cycle and is thought to control cycle phase progression [41, 42]. Measurement of intracellular ROS production using the

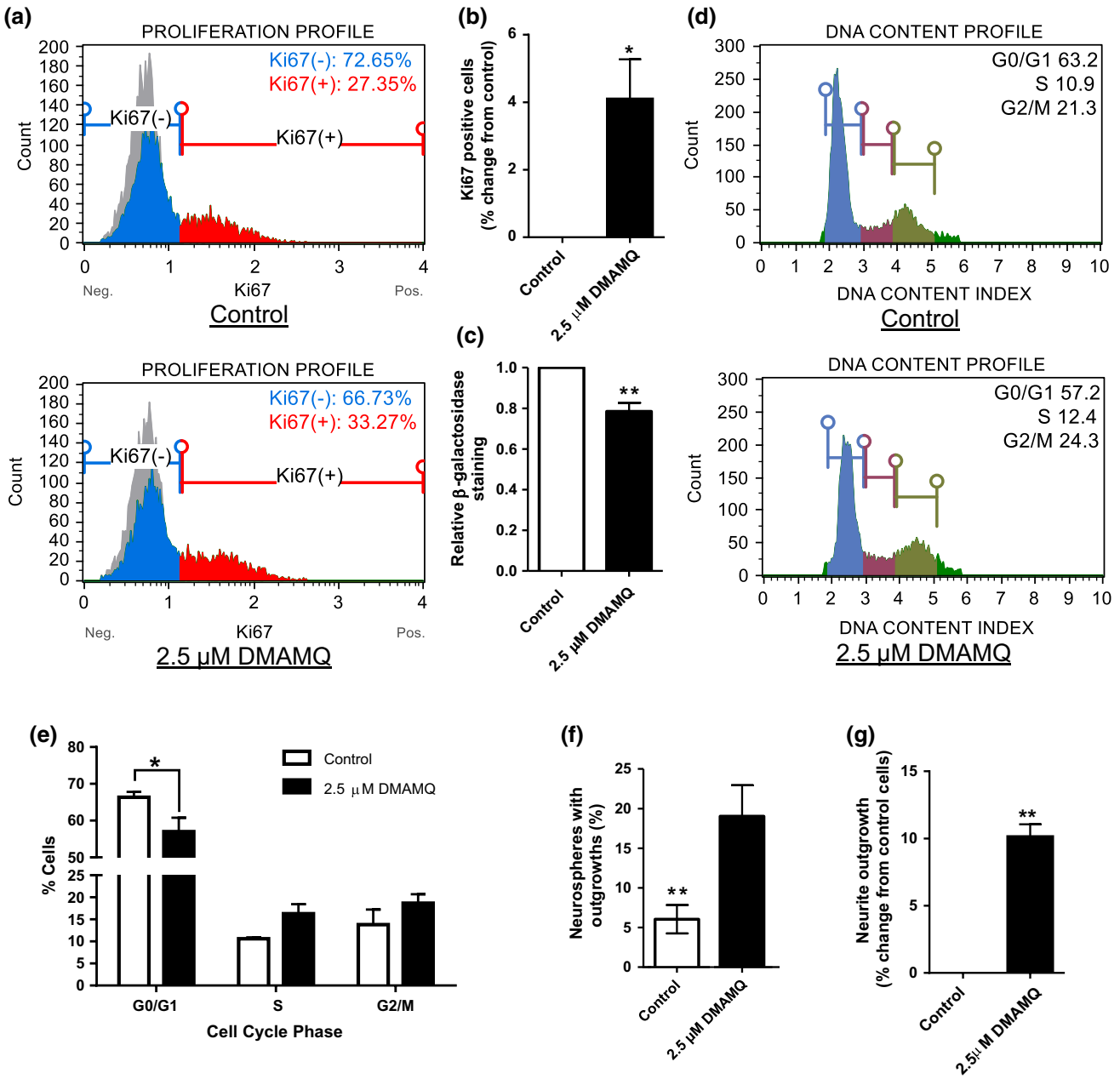

Fig. 3 DMAMQ reduces the non-proliferative population of NSCs and increases NSC growth. **a** Flow cytometry analysis of Ki67 proliferation marker expression in NSCs after 24 h treatment with 2.5 µm DMAMQ. Both populations were gated identically using the unstained background control populations shown in grey behind the Ki67 negative (*blue*) and Ki67 positive (*red*) populations. **b** Quantification of the percentage increase in Ki67 expression from the profiles in *a*; students *t* test, $p = 0.025$, $n = 4$. **c** Quantification of β-galactosidase staining following three days incubation with 2.5 µM DMAMQ, change is expressed relative to control cells; students *t* test, $n = 4$. **d** Flow cytometry profiles of DNA content as an indication of cell cycle phase after 24 h treatment with 2.5 µm DMAMQ. Control and DMAMQ samples were gated identically based on the control distribution and phases are shown as G0/G1 in *blue*, S in *red*, G2/M in *pale green* and debris in *dark green*. **e** Quantification of the percentage cells in each phase of the cell cycle from the profiles in *d*; two-way ANOVA, $p < 0.05$, $n = 4$. **f** Quantification of the number of neurospheres grown in the colony forming assay with outgrowths in response to DMAMQ; students *t* test, $n = 3$. **g** Quantification of the ability of differentiating NSCs to form neurite outgrowths in the presence of DMAMQ expressed relative to control cell outgrowths; students *t* test, $n = 6$. $^*p < 0.05$, $^{**}p < 0.01$

fluorescent probe DCFDA showed increased ROS production when NSCs were treated with DMAMQ in the micromolar range (Fig. 6a). There are various sources of intracellular ROS including the Nox family of signalling proteins. The Nox family, which generates ROS as a signalling intermediate, has been linked with stimulation of

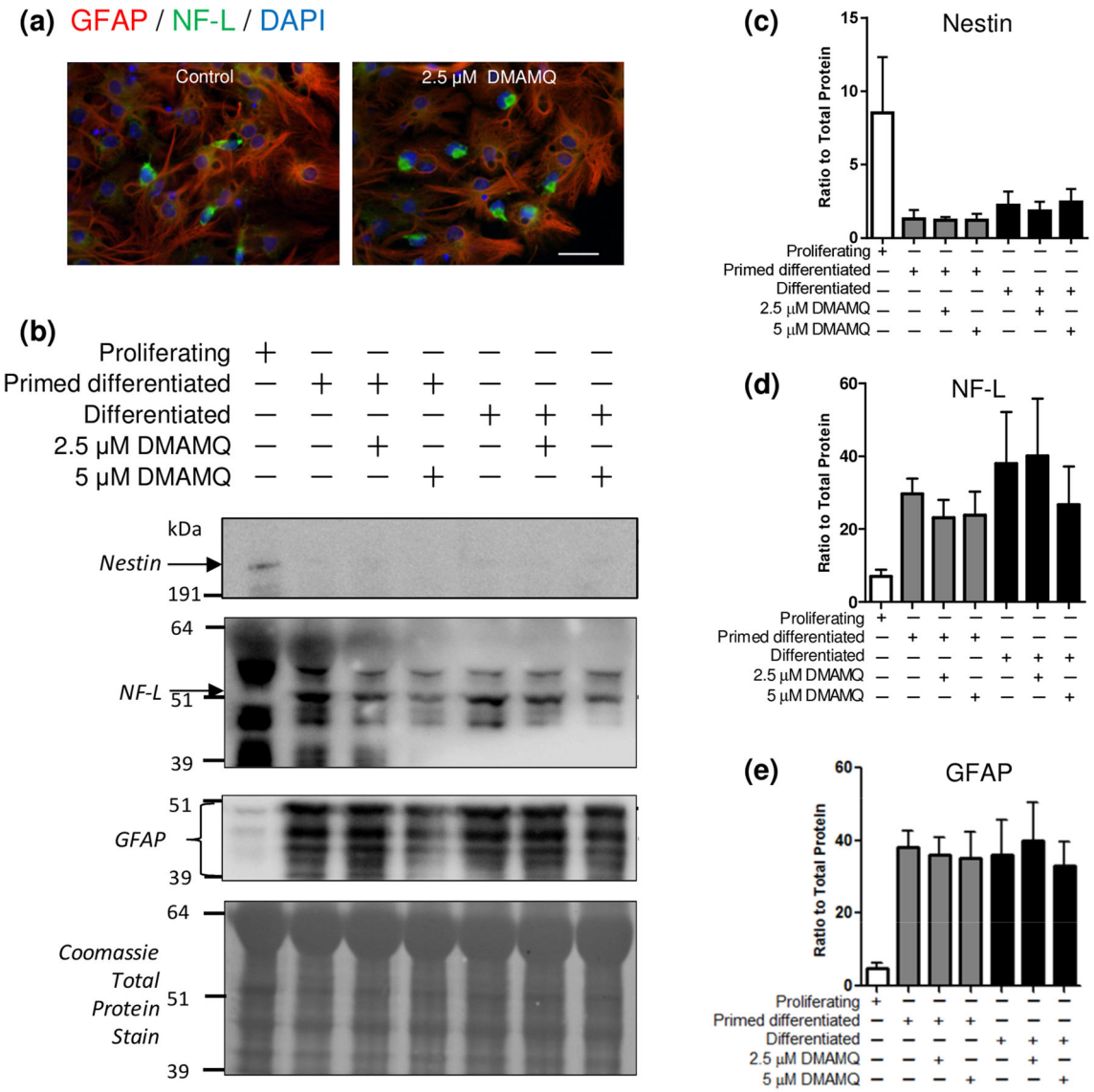

Fig. 4 Effects of DMAMQ on NSC differentiation. **a** Immunofluorescence staining demonstrates that NSCs treated with DMAMQ throughout 7 days differentiation retain their capacity to differentiate and are multipotent. *Green*, NF-L (neuronal marker); *Red*, GFAP (astrocytic marker); *Blue*, DAPI (nuclear stain); *Scale bar* = 20 μm. **b** Example western blot images of cells either differentiated after 24 h priming with DMAMQ or differentiated in the presence of DMAMQ. Densitometric quantification of western blot intensity for **c** nestin, **d** NF-L and **e** GFAP relative to the total protein (coomassie) loading control. No differences are observed in lineage preference as a result of DMAMQ exposure either before or during differentiation; one-way ANOVA $n = 5$

NSC proliferation [43–45]. To examine the role of Nox signalling in the ROS produced in response to DMAMQ, a Nox isozyme inhibitor (DPI) was co-administered with DMAMQ in the DCFDA assay. Inclusion of DPI was sufficient to block the DMAMQ-induced ROS response in the NSCs (Fig. 6b), implicating Nox in the observed intracellular ROS burst.

If the ROS produced by the addition of DMAMQ to the cells was signalling the increased growth of the cells, then inhibition of this pathway with DPI would be expected to inhibit the increased colony growth in the NCFA. DPI was included in the media matrix as a single dose at the start of the NCFA with or without NNAMQ and growth was determined as described previously. DPI alone reduced colony growth, primarily affecting the number of colonies formed (Fig. 7a–c). When DPI and DMAMQ were co-incubated in the media matrix (single treatment at the start of the assay), the growth of the spheres was stunted with fewer colonies formed (Fig. 7a–c) and decreased the diameter at the 2.5 μM treatment concentrations of DMAMQ.

Whilst our results concur with previous literature that increased ROS increases NSC growth and suggest that

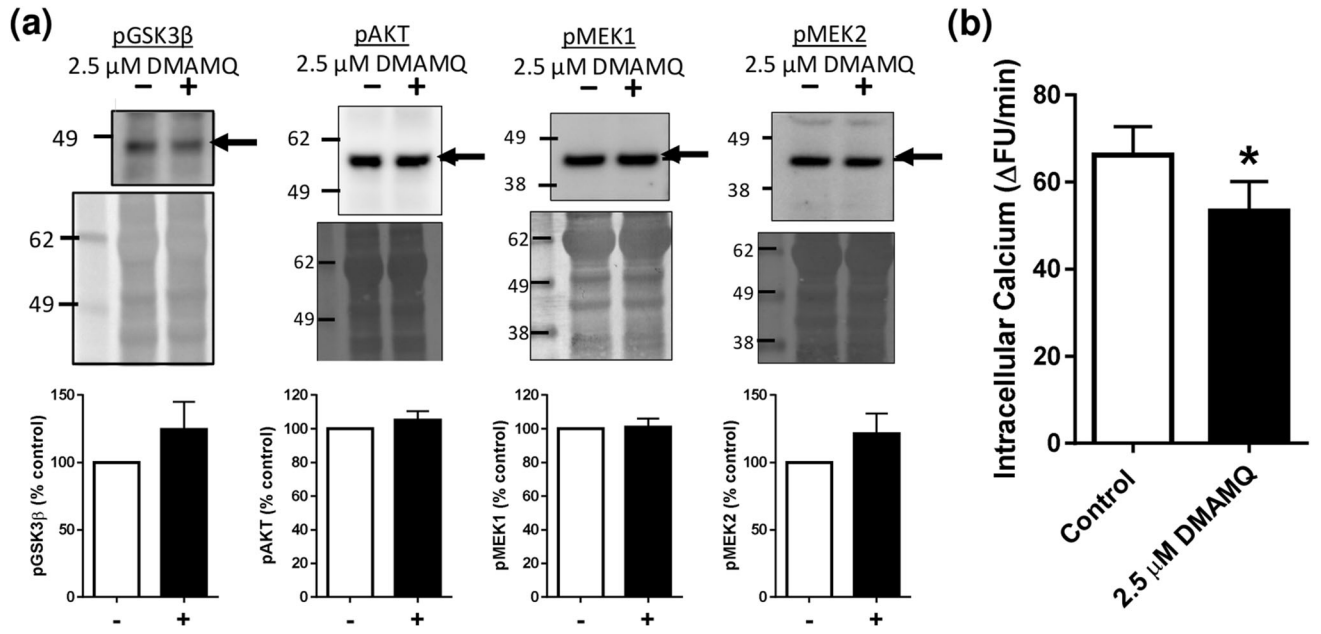

Fig. 5 DMAMQ signalling is not through GSK-3β, AKT or MEK signalling pathways. **a** NSCs were incubated for 30 min with DMAMQ and assessed for activation of signal transduction pathways by detection of changes in phosphorylation of several signalling intermediates (GSK-3β, AKT, MEK1 and MEK2). No significant differences were seen in phosphorylation; students *t* test, $n = 4$. **b** Intracellular calcium measured by fluorescence change per minute for 1 h post-DMAMQ addition. Students *t* test, $n = 4$, $^{*}p < 0.05$

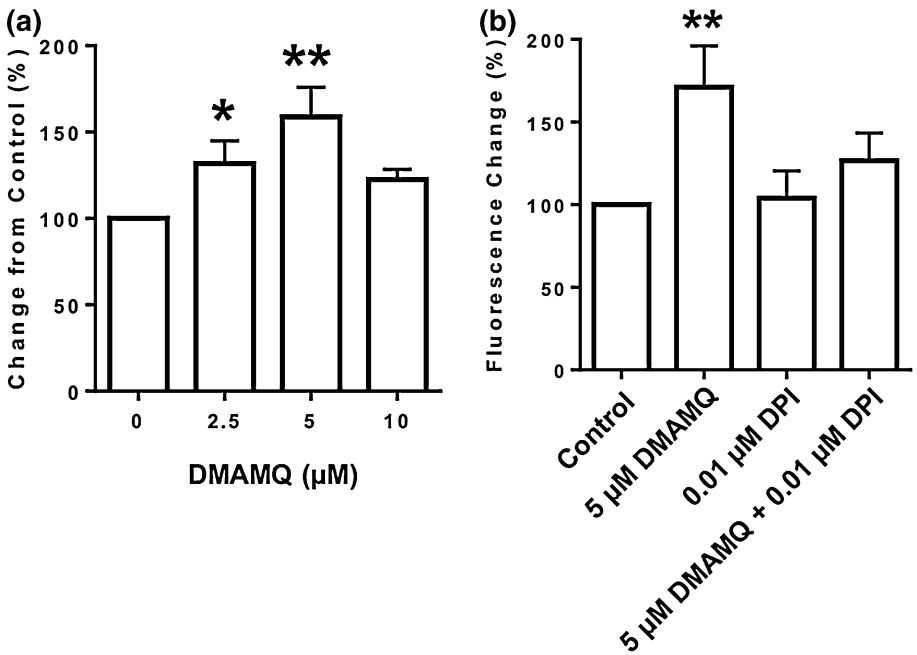

Fig. 6 DMAMQ mediates its effects through stimulation of NADPH oxidase to increase intracellular ROS production. **a** Intracellular ROS increases in response to DMAMQ treatment in proliferating NSCs treated with DMAMQ in the low μM range, as measured by DCF fluorescence. **b** Co-treatment with DMAMQ and the NOX inhibitor, DPI, prevents the DMAMQ ROS burst, suggesting the ROS increase is associated with cellular signalling involving NADPH oxidase. One-way ANOVA, $n = 4$, $^{*}p < 0.05$, $^{**}p < 0.01$ (significantly different from untreated control)

modulation of Nox to increase ROS signalling initiates such growth, the data presented cannot exclude intrinsic ROS production by DMAMQ that mimics, but does not outcompete inhibition of, this pathway. In any case, the generation of ROS in response to DMAMQ treatment contrasts with the mainstream view that 8HQs can be of therapeutic benefit by reducing aberrant metal-mediated ROS production associated with neurodegenerative disease [46].

The identification of compounds that regulate neurogenesis holds great promise for treating neurodegenerative conditions. AD-associated Aβ peptides have been shown to decrease neurogenesis using both in vivo and in vitro models, including murine NSC cultures [3, 47, 48] and

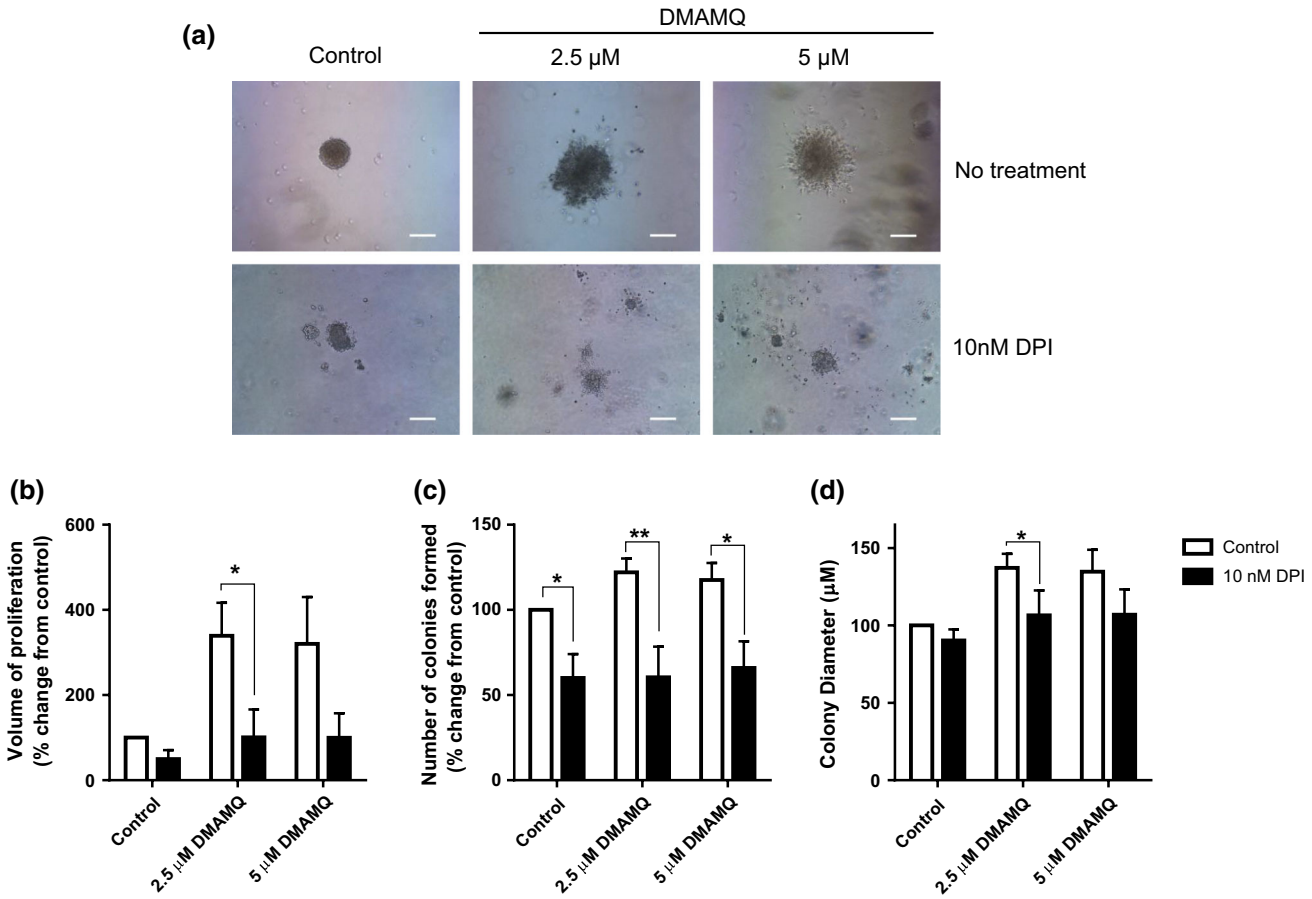

Fig. 7 Nox inhibition with DPI blocks DMAMQ-induced growth. **a** Representative colonys grown in the presence or absence of Nox family inhibitor DPI and DMAMQ. Scale bar, 100 μm. **b** Total volume of growth at 21 days calculated from the number of colonies formed **c** and the diameter of the colonies. **d**. Two-way ANOVA, $n = 3$, $^{*}p < 0.05$, $^{**}p < 0.01$

hence, restoration of NSC function by 8HQs could be of value in treating AD. The picture is far from clear, however, because markers of increased neurogenesis can be found in post-mortem analysis of AD brains [2] and also in some animal models of disease [4, 49]. Increased neurogenesis may represent a compensatory response by the NSCs within the brain to replenish lost neurones. In such a context, the current findings suggest that compounds that stimulate neurogenesis during AD may be able to augment these compensatory mechanisms. The caveat, however, is that neurogenesis has also been linked with forgetting [8]; in theory, stimulating neurogenesis may therefore inadvertently exacerbate the symptoms of memory loss. In addition to these complications, which may arise even from a targeted stimulation of neurogenesis, Nox signalling regulates diverse processes in vivo such as contractile functions of heart muscle [50, 51] and systemic immune responses [37, 52], whilst acute and chronic Nox activity is associated with neuroinflammation [53]. Moreover, substituted 8HQs can have anti-proliferative/cytotoxic properties depending on their local concentrations (Figure S1) [13–15] or have the potential to cause neuronal damage by interfering with epigenetic regulation (e.g. clioquinol [54]). Some of these considerations may explain why clioquinol and 5,7-dichoro-DMAMQ have not shown evidence of clinical benefit in treating AD [55].

Conclusions

This study demonstrates that DMAMQ modulates NSC growth and neurite outgrowth during differentiation when cultured in vitro by stimulating ROS production and Nox signalling. This suggests that DMAMQ and similar 8HQs may have neuro-regenerative potential in vivo; however, the very narrow concentration range in which DMAMQ modulates NSC growth presents some challenges for therapeutic administration. In particular, the potential benefits of replenishing damaged brain tissue must be balanced against the possibility of overstimulating neurogenesis and the propensity for undesirable "off-target" effects. A substantial increase in our understanding of the

action of substituted 8HQs in vitro and in vivo is required to determine whether this class of compound will be a viable therapeutic intervention in countering disease progression in any dementia.

Acknowledgments This work was supported by a Future Fellowship (FT110100199) administered by the Australian Research Council (S.C.D.), a Program Grant (#628946; S.J.C.) and Practitioner Fellowship (APP1005816; S.J.C.) administered by the National Health and Medical Research Council of Australia.

References

1. Gomez-Nicola, D., Suzzi, S., Vargas-Caballero, M., Fransen, N. L., Al-Malki, H., Cebrian-Silla, A., et al. (2014). Temporal dynamics of hippocampal neurogenesis in chronic neurodegeneration. *Brain, 137*, 2312–2328.
2. Jin, K., Peel, A. L., Mao, X. O., Xie, L., Cottrell, B. A., Henshall, D. C., & Greenberg, D. A. (2004). Increased hippocampal neurogenesis in Alzheimer's disease. *Proceedings of the National Academy of Sciences USA, 101*, 343–347.
3. Haughey, N. J., Nath, A., Chan, S. L., Borchard, A. C., Rao, M. S., & Mattson, M. P. (2002). Disruption of neurogenesis by amyloid beta-peptide, and perturbed neural progenitor cell homeostasis, in models of Alzheimer's disease. *Journal of Neurochemistry, 83*, 1509–1524.
4. Jin, K., Galvan, V., Xie, L., Mao, X. O., Gorostiza, O. F., Bredesen, D. E., & Greenberg, D. A. (2004). Enhanced neurogenesis in Alzheimer's disease transgenic (PDGF-APPSw, Ind) mice. *Proceedings of the National Academy of Sciences USA, 101*, 13363–13367.
5. Kanemoto, S., Griffin, J., Markham-Coultes, K., Aubert, I., Tandon, A., George-Hyslop, P. S., & Fraser, P. E. (2014). Proliferation, differentiation and amyloid-beta production in neural progenitor cells isolated from TgCRND8 mice. *Neuroscience, 261*, 52–59.
6. Karkkainen, V., Magga, J., Koistinaho, J., & Malm, T. (2012). Brain environment and Alzheimer's disease mutations affect the survival, migration and differentiation of neural progenitor cells. *Current Alzheimer Research, 9*, 1030–1042.
7. Lopez-Toledano, M. A., & Shelanski, M. L. (2007). Increased neurogenesis in young transgenic mice overexpressing human APP(Sw, Ind). *Journal of Alzheimer's Disease, 12*, 229–240.
8. Akers, K. G., Martinez-Canabal, A., Restivo, L., Yiu, A. P., De Cristofaro, A., Hsiang, H. L., et al. (2014). Hippocampal neurogenesis regulates forgetting during adulthood and infancy. *Science, 344*, 598–602.
9. Dupret, D., Revest, J. M., Koehl, M., Ichas, F., De Giorgi, F., Costet, P., et al. (2008). Spatial relational memory requires hippocampal adult neurogenesis. *Plos One, 3*, e1959.
10. Sahay, A., Scobie, K. N., Hill, A. S., O'Carroll, C. M., Kheirbek, M. A., Burghardt, N. S., et al. (2011). Increasing adult hippocampal neurogenesis is sufficient to improve pattern separation. *Nature, 472*, 466–470.
11. Leifer, W., & Steiner, K. (1949). Diodoquin as a topical therapeutic agent in cutaneous. *Journal of Investigative Dermatology, 12*, 203–204.
12. Gershon, H., Gershon, M., & Clarke, D. D. (2011). Antifungal activity of substituted 8-quinolinol-5- and 7-sulfonic acids: A mechanism of action is suggested based on intramolecular synergism. *Mycopathologia, 155*, 213–217.
13. Zhou, J., Zhang, H., Gu, P., Margolick, J. B., Yin, D., & Zhang, Y. (2009). Cancer stem/progenitor cell active compound 8-quinolinol in combination with paclitaxel achieves an improved cure of breast cancer in the mouse model. *Breast Cancer Research Treatment, 115*, 269–277.
14. Mohammed, I., Hampton, S. E., Ashall, L., Hildebrandt, E. R., Kutlik, R. A., Manandhar, S. P., et al. (2016). 8-Hydroxyquinoline-based inhibitors of the Rce1 protease disrupt Ras membrane localization in human cells. *Bioorganic and Medicinal Chemistry, 24*, 160–178.
15. Martirosyan, A., Leonard, S., Shi, X., Griffith, B., Gannett, P., & Strobl, J. (2006). Actions of a histone deacetylase inhibitor NSC3852 (5-nitroso-8-quinolinol) link reactive oxygen species to cell differentiation and apoptosis in MCF-7 human mammary tumor cells. *Journal of Pharmacology and Experimental Therapeutics, 317*, 546–552.
16. King, O. N. F., Li, X. S., Sakurai, M., Kawamura, A., Rose, N. R., Ng, S. S., et al. (2011). Quantitative high-throughput screening identifies 8-hydroxyquinolines as cell-active histone demethylase inhibitors. *Plos One, 5*, e15535.
17. Tardiff, D. F., Tucci, M. L., Caldwell, K. A., Caldwell, G. A., & Lindquist, S. (2011). Different 8-hydroxyquinolines protect models of TDP-43 protein, α-synuclein, and polyglutamine proteotoxicity through distinct mechanisms. *Journal of Biological Chemistry, 287*, 4107–4120.
18. Crouch, P. J., Savva, M. S., Hung, L. W., Donnelly, P. S., Mot, A. I., Parker, S. J., et al. (2011). The Alzheimer's therapeutic PBT2 promotes amyloid-β degradation and GSK3 phosphorylation via a metal chaperone activity. *Journal of Neurochemistry, 119*, 220–230.
19. Adlard, P. A., Bica, L., White, A. R., Nurjono, M., Filiz, G., Crouch, P. J., et al. (2011). Metal ionophore treatment restores dendritic spine density and synaptic protein levels in a mouse model of Alzheimer's disease. *Plos One, 6*, e17669.
20. Gomes, L. M., Vieira, R. P., Jones, M. R., Wang, M. C., Dyrager, C., Souza-Fagundes, E. M., et al. (2014). 8-Hydroxyquinoline Schiff-base compounds as antioxidants and modulators of copper-mediated Aβ peptide aggregation. *Journal of Inorganic Biochemistry, 139*, 106–116.
21. Mancin, F., & Chin, J. (2002). An artificial guanine that binds cytidine through the cooperative interaction of metal coordination and hydrogen bonding. *Journal of the American Chemical Society, 124*, 10946–10947.
22. Johnson, D. K., & Kline, S. J. (1991). 8-Hydroxyquinoline chelating agents. United States Patent No. 5021567 A, 4 June.
23. Rajagopalan, R., Archilefu, S. I., Bugaj, J. E., & Dorshow, R. B. (2011). Quinoline ligands and metal complexes for diagnosis and therapy. United States Patent No. 6277841 B1, Aug. 21.
24. Schwarcz, R., Bruno, J. P., Muchowski, P. J., & Wu, H. Q. (2012). Kynurenines in the mammalian brain: When physiology meets pathology. *Nature Reviews Neuroscience, 13*, 465–477.
25. Mossialos, D., Meyer, J.-M., Budzikiewicz, H., Wolff, U., Koedam, N., Baysse, C., et al. (2000). Quinolobactin, a new siderophore of *Pseudomonas fluorescens* ATCC 17400, the production of which is repressed by the cognate pyoverdine. *Applied and Environmental Microbiology, 66*, 487–492.
26. Pesek, J., Svoboda, J., Sattler, M., Bartram, S., & Boland, W. (2015). Biosynthesis of 8-hydroxyquinoline-2-carboxylic acid, an iron chelator from the gut of the lepidopteran *Spodoptera littoralis*. *Organic & Biomolecular Chemistry, 13*, 178–184.
27. Kenche, V. B., Zawisza, I., Masters, C. L., Bal, W., Barnham, K. J., & Drew, S. C. (2013). Mixed ligand Cu^{2+} complexes of a model therapeutic with Alzheimer's amyloid-β peptide and monoamine neurotransmitters. *Inorganic Chemistry, 52*, 4303–4318.

28. Haigh, C. L., McGlade, A. R., Lewis, V., Masters, C. L., Lawson, V. A., & Collins, S. J. (2011). Acute exposure to prion infection induces transient oxidative stress progressing to be cumulatively deleterious with chronic propagation in vitro. *Free Radical Biology and Medicine, 51*, 594–608.
29. Collins, S. J., Tumpach, C., Li, Q.-X., Lewis, V., Ryan, T. M., Roberts, B., et al. (2015). The prion protein regulates β-amyloid mediated self-renewal of neural stem cells. *Stem Cell Research & Therapy, 6*, 60.
30. Haigh, C. L., Drew, S. C., Boland, M., Masters, C. L., Barnham, K. J., Lawson, V. A., & Collins, S. J. (2009). Dominant roles of the polybasic proline motif and copper in PrP23–89 mediated stress protection response. *Journal of Cell Science, 122*, 1518–1528.
31. Sinclair, L., Lewis, V., Collins, S. J., & Haigh, C. L. (2013). Cytosolic caspases mediate mislocalised SOD2 depletion in an in vitro model of chronic prion infection. *Disease Models and Mechanisms, 6*, 952–963.
32. Haigh, C. L., Lewis, V. A., Vella, L. J., Masters, C. L., Hill, A. F., Lawson, V. A., & Collins, S. J. (2009). PrPC-related signal transduction is influenced by copper, membrane integrity and the alpha cleavage site. *Cell Research, 19*, 1062–1078.
33. Lang, C., Mix, E., Frahm, J., Glass, Ä., Müller, J., Schmitt, O., et al. (2011). Small molecule GSK-3 inhibitors increase neurogenesis of human neural progenitor cells. *Neuroscience Letters., 488*, 36–40.
34. Morales-Garcia, J. A., Luna-Medina, R., Alonso-Gil, S., Sanz-Sancristobal, M., Palomo, V., Gil, C., et al. (2012). Glycogen synthase kinase 3 inhibition promotes adult hippocampal neurogenesis in vitro and in vivo. *ACS Chemical Neuroscience, 3*, 963–971.
35. Tonelli, F. M., Santos, A. K., Gomes, D. A., da Silva, S. L., Gomes, K. N., Ladeira, L. O., & Resende, R. R. (2012). Stem cells and calcium signalling. *Advances in Experimental Medicine and Biology, 740*, 891–916.
36. Bogeski, I., Kappl, R., Kummerow, C., Gulaboski, R., Hoth, M., & Niemeyer, B. A. (2011). Redox regulation of calcium ion channels: Chemical and physiological aspects. *Cell Calcium, 50*, 407–423.
37. Panday, A., Sahoo, M. K., Osorio, D., & Batra, A. (2015). NADPH oxidases: An overview from structure to innate immunity-associated pathologies. *Cell & Molecluar Immunology, 12*, 5–23.
38. Le Belle, J. E., Orozco, N. M., Paucar, A. A., Saxe, J. P., Mottahedeh, J., Pyle, A. D., et al. (2011). Proliferative neural stem cells have high endogenous ROS levels that regulate self-renewal and neurogenesis in a PI3K/Akt-dependant manner. *Cell Stem Cell, 8*, 59–71.
39. Walton, N. M., Shin, R., Tajinda, K., Heusner, C. L., Kogan, J. H., Miyake, S., et al. (2012). Adult neurogenesis transiently generates oxidative stress. *Plos One, 7*, e35264.
40. Yoneyama, M., Kawada, K., Gotoh, Y., Shiba, T., & Ogita, K. (2010). Endogenous reactive oxygen species are essential for proliferation of neural stem/progenitor cells. *Neurochemistry International, 56*, 740–746.
41. Menon, S. G., & Goswami, P. C. (2007). A redox cycle within the cell cycle: Ring in the old with the new. *Oncogene, 26*, 1101–1109.
42. Sarsour, E. H., Kalen, A. L., & Goswami, P. C. (2014). Manganese superoxide dismutase regulates a redox cycle within the cell cycle. *Antioxidants & Redox Signaling, 20*, 1618–1627.
43. Lee, J. E., Cho, K. E., Lee, K. E., Kim, J., & Bae, Y. S. (2014). Nox4-mediated cell signaling regulates differentiation and survival of neural crest stem cells. *Molecules and Cells, 37*, 907–911.
44. Nayernia, Z., Jaquet, V., & Krause, K. H. (2014). New insights on NOX enzymes in the central nervous system. *Antioxidants & Redox Signaling, 20*, 2815–2837.
45. Topchiy, E., Panzhinskiy, E., Griffin, W. S., Barger, S. W., Das, M., & Zawada, W. M. (2013). Nox4-generated superoxide drives angiotensin II-induced neural stem cell proliferation. *Developmental Neuroscience, 35*, 293–305.
46. Barnham, K. J., Masters, C. L., & Bush, A. I. (2004). Neurodegenerative diseases and oxidative stress. *Nature Reviews Drug Discovery, 3*, 205–214.
47. Zheng, M., Liu, J., Ruan, Z., Tian, S., Ma, Y., Zhu, J., & Li, G. (2013). Intrahippocampal injection of Abeta1-42 inhibits neurogenesis and down-regulates IFN-gamma and NF-kappaB expression in hippocampus of adult mouse brain. *Amyloid, 20*, 13–20.
48. Haughey, N. J., Liu, D., Nath, A., Borchard, A. C., & Mattson, M. P. (2002). Disruption of neurogenesis in the subventricular zone of adult mice, and in human cortical neuronal precursor cells in culture, by amyloid β-peptide: Implications for the pathogenesis of Alzheimer's disease. *Neuromolecular Medicine, 1*, 125–135.
49. Díaz-Moreno, M., Hortigüela, R., Gonçalves, A., García-Carpio, I., Manich, G., García-Bermúdez, E., et al. (2013). Aβ increases neural stem cell activity in senescence-accelerated SAMP8 mice. *Neurobiology of Aging, 34*, 2623–2638.
50. Gonzalez, D. R., Treuer, A. V., Lamirault, G., Mayo, V., Cao, Y., Dulce, R. A., & Hare, J. M. (2014). NADPH oxidase-2 inhibition restores contractility and intracellular calcium handling and reduces arrhythmogenicity in dystrophic cardiomyopathy. *American Journal of Physiology Heart and Circulatory Physiology, 307*, H710–H721.
51. Zhang, M., Prosser, B. L., Bamboye, M. A., Gondim, A. N., Santos, C. X., Martin, D., et al. (2015). Contractile function during angiotensin-II activation: Increased Nox2 activity modulates cardiac calcium handling via phospholamban phosphorylation. *Journal of the American College of Cardiology, 66*, 261–272.
52. Rada, B., & Leto, T. L. (2008). Oxidative innate immune defenses by Nox/Duox family NADPH oxidases. *Contributions to Microbiology, 15*, 164–187.
53. Cooney, S. J., Bermudez-Sabogal, S. L., & Byrnes, K. R. (2013). Cellular and temporal expression of NADPH oxidase (NOX) isotypes after brain injury. *Journal of Neuroinflammation, 10*, 155.
54. Fukui, T., Asakura, K., Hikichi, C., Ishikawa, T., Murai, R., Hirota, S., et al. (2015). Histone deacetylase inhibitor attenuates neurotoxicity of clioquinol in PC12 cells. *Toxicology, 331*, 112–118.
55. Sampson, E. L., Jenagaratnam, L., & McShane, R. (2014). Metal protein attenuating compounds for the treatment of Alzheimer's dementia. Cochrane Database of Systematic Reviews. 2, CD005380.

Prion protein cleavage fragments regulate adult neural stem cell quiescence through redox modulation of mitochondrial fission and SOD2 expression

Steven J. Collins, Carolin Tumpach, Bradley R. Groveman, Simon C. Drew & Cathryn L. Haigh

Cellular and Molecular Life Sciences

ISSN 1420-682X

Cell. Mol. Life Sci.
DOI 10.1007/s00018-018-2790-3

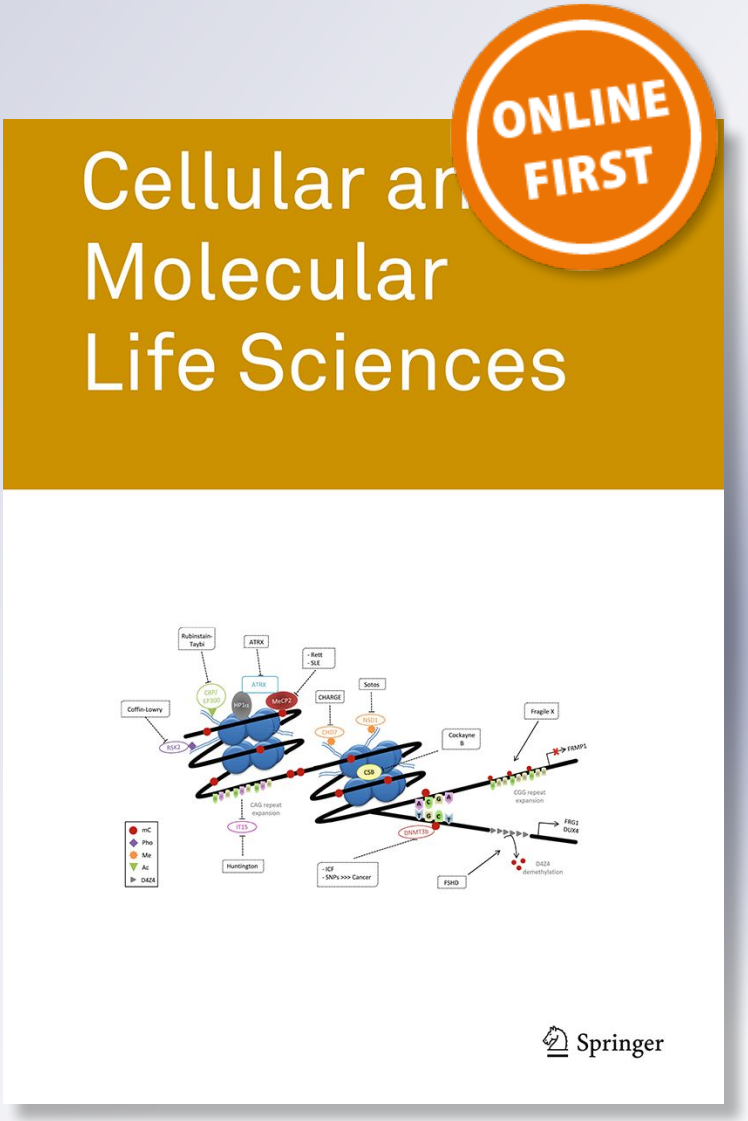

Springer

Cellular and Molecular Life Sciences
https://doi.org/10.1007/s00018-018-2790-3

ORIGINAL ARTICLE

Prion protein cleavage fragments regulate adult neural stem cell quiescence through redox modulation of mitochondrial fission and SOD2 expression

Steven J. Collins[1] · Carolin Tumpach[2] · Bradley R. Groveman[3] · Simon C. Drew[1] · Cathryn L. Haigh[1,3]

Received: 26 May 2017 / Revised: 27 February 2018 / Accepted: 5 March 2018

Abstract
Neurogenesis continues in the post-developmental brain throughout life. The ability to stimulate the production of new neurones requires both quiescent and actively proliferating pools of neural stem cells (NSCs). Actively proliferating NSCs ensure that neurogenic demand can be met, whilst the quiescent pool makes certain NSC reserves do not become depleted. The processes preserving the NSC quiescent pool are only just beginning to be defined. Herein, we identify a switch between NSC proliferation and quiescence through changing intracellular redox signalling. We show that N-terminal post-translational cleavage products of the prion protein (PrP) induce a quiescent state, halting NSC cellular growth, migration, and neurite outgrowth. Quiescence is initiated by the PrP cleavage products through reducing intracellular levels of reactive oxygen species. First, inhibition of redox signalling results in increased mitochondrial fission, which rapidly signals quiescence. Thereafter, quiescence is maintained through downstream increases in the expression and activity of superoxide dismutase-2 that reduces mitochondrial superoxide. We further observe that PrP is predominantly cleaved in quiescent NSCs indicating a homeostatic role for this cascade. Our findings provide new insight into the regulation of NSC quiescence, which potentially could influence brain health throughout adult life.

Keywords NADPH oxidase · Nox2 · DRP1 · Superoxide dismutase · SOD2 · Reactive oxygen species · Mitochondria · N1 · N2

Introduction

It is now firmly established that the adult brain contains cells that demonstrate 'stemness', i.e., are capable of self-renewal and formation of new brain cells (reviewed in [1]). Neural stem cells (NSCs) have been detected in human brain tissue from donors up to the age of 72 years [2] and markers of neurogenesis detected into the ninth decade [3], indicating the likely importance of these cells throughout adult life. The adult brain contains different populations of NSCs. Type 1 NSCs are quiescent and can be stimulated to become type 2 NSCs, which are actively replicating. Type 2 cells in turn progress to be type 3 migratory cells or neuroblasts [1, 4]. NSC growth and differentiation have been linked with hippocampal learning and memory as well as forgetting [5–9], and changes in neurogenesis correlate with various mental health issues and neurodegenerative diseases [3, 10].

Neurogenesis is modulated by several neurodegenerative disease-associated proteins or peptides including the prion protein (PrP) [11, 12], which is most widely recognised for its causative role in transmissible neurodegenerative diseases of humans and animals [13]. Research into the role of PrP in neurogenesis has found that PrP expression is linked with enhanced NSC proliferative capacity [12], associated with increased cell cycling at the expense of differentiation [14]. In addition, PrP has been shown to be part of a receptor complex for soluble neurotoxic Alzheimer's disease-associated

Electronic supplementary material The online version of this article (https://doi.org/10.1007/s00018-018-2790-3) contains supplementary material, which is available to authorized users.

✉ Cathryn L. Haigh
cathryn.haigh@nih.gov

[1] Department of Medicine (Royal Melbourne Hospital), The University of Melbourne, Melbourne, VIC 3010, Australia

[2] Doherty Institute, The University of Melbourne, Melbourne, VIC 3010, Australia

[3] Laboratory of Persistent Viral Diseases, Rocky Mountain Laboratories, NIAID, NIH, Hamilton 59840, USA

Published online: 24 March 2018

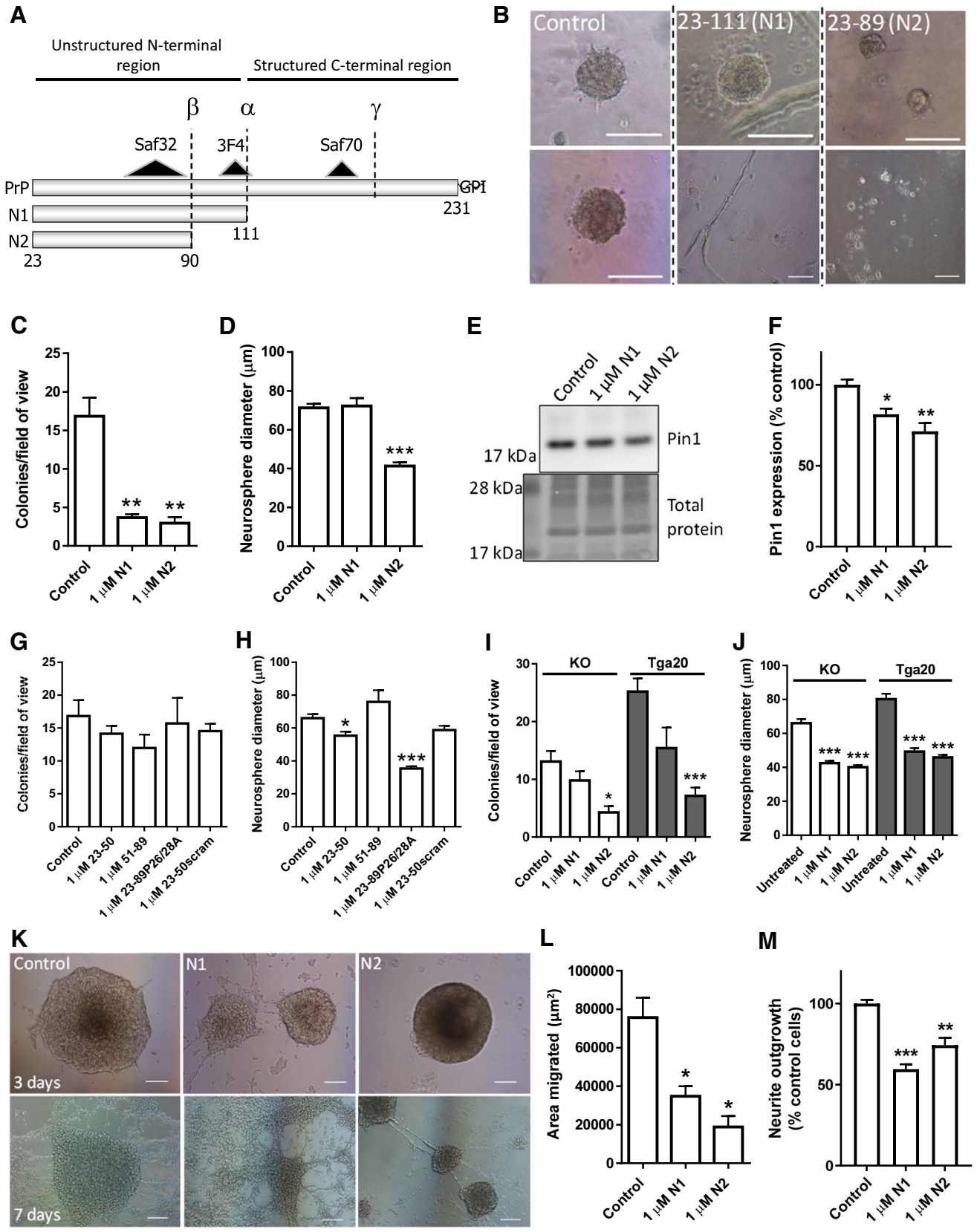
A
Unstructured N-terminal region
Structured C-terminal region
β
α
γ
Saf32
3F4
Saf70
PrP
GPI
N1
N2
111
231
23
90
B
Control
23-111 (N1)
23-89 (N2)
C
Colonies/field of view
Control
1 μM N1
1 μM N2
D
Neurosphere diameter (μm)
E
Control
1 μM N1
1 μM N2
17 kDa
28 kDa
17 kDa
Pin1
Total protein
F
Pin1 expression (% control)
G
Colonies/field of view
Control
1 μM 23-50
1 μM 51-89
1 μM 23-89P26/28A
1 μM 23-50scram
H
Neurosphere diameter (μm)
I
KO
Tga20
Colonies/field of view
J
KO
Tga20
Neurosphere diameter (μm)
Untreated
K
Control
N1
N2
3 days
7 days
L
Area migrated (μm²)
M
Neurite outgrowth (% control cells)

◂**Fig. 1** N1 and N2 change NSC growth, migration, and neurite outgrowth. **a** Schematic of PrP cleavage events, the cut positions producing the N1 and N2 fragments, and the putative site of gamma-cleavage. Also shown are the epitopes of the antibodies used to target PrP. **b** Representative images of neurosphere colony morphology in the NCFA with and without peptide treatments. Two images each are shown to illustrate the varied morphology. Scale bar = 100 µm. **c** NCFA colony counts of NSCs incubated with and without N1 and N2 included in the assay matrix. $n = 4$. **d** Diameter measurements of colonies formed in the NCFA with and without peptide incubation. $n = 4$. **e** Immunoblots for Pin1 of NSCs treated for 24 h with N1 or N2. **f** Densitometric quantification of **e**. $n = 4$. **g** NCFA colony counts of NSCs incubated with fragments corresponding to regions of N2 and an N2 peptide with the prolines of the N-terminal polybasic region mutated to alanine. $n = 3$. **h** Diameter measurements of the NCFA described in G. $n = 3$. **i** NCFA colony counts of N1 and N2 incubated with *prnp* knock-out (KO) and over-expressing (Tga20) NSCs. $n = 3$. **j** Diameter measurements of the NCFA described in I. $n = 3$. **k** Representative images of neurosphere migration as influenced by N1 and N2 taken 3 and 7 days after peptide addition. Scale bar = 100 µm. **l** Quantification of the area migrated after 3 days incubation as shown in **k**. $n = 3$. **m** Neurite outgrowth of NSCs incubated with N1 and N2 relative to control cells. $n = 3$. All data within the figure panels are presented as mean and SEM with significance indicated by $^{*}p < 0.05$, $^{**}p < 0.01$, $^{***}p < 0.001$ from control values

amyloid-beta peptides [15, 16] and the presence or absence of PrP changes NSC self-renewal in response to amyloid-beta peptides [17], thereby suggesting that a putative neurogenic function of PrP may become corrupted during neurodegenerative disease.

Despite much interest in the role of PrP during disease, there is still no defined function for this protein. However, PrP is known to be involved in cellular redox balance, both protecting against detrimental disturbance in health and causing damage during prion disease [18–27]. The cellular biology of PrP is complex; mature PrP is a glycosylphosphatidylinositol membrane-tethered glycoprotein, known to undergo various other post-translational modifications including internal cleavage at three or more sites, termed alpha-, beta- and gamma-cleavages [28–30]. The alpha- and beta-cleavage events remove the flexible, unstructured N-terminus from the structured C-terminal region, producing N1/C1 and N2/C2 fragments, respectively (Fig. 1a). Various cellular locations of cleavage have been proposed including the secretory pathway and cell surface, and the N-terminal fragments have predominantly been found as extracellular soluble peptides [31, 32]. As alluded to above, PrP is associated with cellular redox homeostasis and the N1 and N2 fragments alone have been shown to reduce intracellular reactive oxygen species (ROS) and protect against oxidative damage [32, 33].

Redox balance has a regulatory role in NSC growth and differentiation [34, 35]. Adult NSCs are not dispersed evenly through the brain but situated in specialised regions, referred to as neurogenic niches [36]. In the neurogenic niche, the environment is highly important for the preservation of the NSC populations and is maintained as a low ROS environment [37]. Increased NSC ROS are associated with stimulation of increased growth, possibly at the expense of depleting the quiescent pool in favour of the actively proliferating cells [34, 35, 38]. In neurodegenerative diseases, such as prion diseases and Alzheimer's disease, where redox balance is compromised resulting in increased ROS, increased markers of neurogenesis are detected in brain tissue [39]. We hypothesized that the ability of the N-terminal PrP peptides, N1 and N2, to modulate cellular ROS levels could exert significant regulatory effects on NSC growth and maintenance of the quiescent NSC pool.

Methods

Prion N-terminal peptides

The prion N-terminal peptides were generated by microwave synthesis and quality controlled by HPLC and mass spectrometry as previously described in Karas et al. [40]. Peptides were also purchased from China Peptides (China).

Adult neural stem cell extraction

NSCs were harvested from the brains of three 8-week-old PrP gene $(prnp)^{-/-}$ (PrP knock-out), C57/B6 wild-type, and Tga20 (PrP over-expressing by approximately eightfold) mice, and transferred into suspension culture as described previously in Haigh et al. [24]. All animal procedures were performed in accordance with University of Melbourne animal ethics committee approval (ethics ID: 1413198.1), operating under the Australian Code of Practice for the Care and Use of Animals for Scientific Purposes.

NSC culture

Routine NSC culture has been described previously [24]. In brief, cells were grown as neurospheres in complete proliferation medium (Stem Cell Technologies, VIC, AUS), supplemented with final concentrations of 10 ng/ml fibroblast growth factor (FGF) and 20 ng/ml epidermal growth factor (EGF) cytokines, and 2 µg/ml heparin (Stem Cell Technologies). Cultures were maintained in a 5% CO_2 humidified incubator.

Cell counts

Cells were mixed 1:1 (v/v) with Trypan Blue reagent (Life Technologies, VIC, AUS) and counted using a Countess cell counter (Life Technologies).

Neural colony forming assay (NCFA)

The colony forming assay is described in Collins et al. [17]. Briefly, neurospheres are dissociated into single-cell suspension and seeded in a semi-solid gel matrix made with a 2:1 solution of proliferation medium and collagen (Sigma-Aldrich, VIC, AUS) in 24-well plates at a density of 50,000 cells/ml (25,000 cells/well). Wells were supplemented with 80 µl of fresh proliferation medium every 5 days. Treatments were included at the start of the assay only. Colonies were counted and diameters measured at 21 days post the start of the assay. All colonies at all depths through the matrix were calculated and measured for a minimum of 5 fields or 50 colonies (for conditions where few colonies were found per field of view).

Migration assay

Neurospheres of 80–100 µm diameter were seeded into wells pre-coated with 5 µg/ml poly-D lysine (PDL; Sigma-Aldrich) in H_2O solution (for a minimum of 1 h at room temperature) and grown in complete proliferation medium. After 3 days, migration from the central neurosphere was calculated by application of contour ROIs around the surface area into which the cells had spread using NIS Elements 3.0 (Nikon) software package. The area covered after 7 days could not be calculated as migration had proceeded beyond the imaging area.

Neurite outgrowth assay

One hundred thousand cells/well were cultured in complete proliferation medium supplemented with 20 ng/ml FGF for 24 h before transferral into complete differentiation medium (Stem Cell Technologies). The neurite outgrowth assay (Millipore, Thermo-Fisher, VIC, AUS) was carried out as per the manufacturer's instructions. Well inserts (1 µm pore size) were coated on their under-side with 10 µg/ml laminin in H_2O solution for 2 h at 37 °C before NSCs were transferred into the insert. Cells were cultured for 2 days in differentiation medium before assaying outgrowth. To assay neurite extension onto the laminin coated under-side, well inserts were first washed in PBS, then fixed in methanol for 20 min at room temperature, washed again by transferring the insert into PBS, and then stained with neurite stain solution for 30 min. Inserts were washed again in PBS, excess dye removed from the inside of the insert, and cell somas removed by swabbing the inside of the insert. The neurites extending over the under-side of the well insert were then solubilised in extraction buffer and the absorbance read in a Spectrostar (BMG) at 562 nm. Neurite outgrowth, indicated by absorbance of the neurite stain as compared with extraction buffer alone, was calculated using MARS software (BMG).

Immunofluorescence staining

The standard immunofluorescence protocol used has been described previously [24, 41]. Briefly, cells were fixed in 4% (v/v) paraformaldehyde for 30 min, followed by permeabilization in 0.1% triton-X-100, before blocking in 10% (v/v) FBS, 0.1% (w/v) BSA in PBS for 30 min. Primary and secondary antibody incubations were carried out in 1% (v/v) FBS, 0.1% (w/v) BSA in PBS blocking buffer, with details and relevant concentrations listed in Sup Table 1.

Microscopy

Confocal images were collected using a Leica SP8 (Leica Microsystems, NSW, AUS) and wide-field fluorescence or bright-field images captured using a Nikon Eclipse TE2000-E epi-fluorescence microscope with a Roper Scientific CCD camera (Nikon, Coherent Scientific, SA, AUS). Image analysis was performed using Fiji imaging software [42] or NIS Elements 3.0 (Nikon). Mitochondrial parameters (minimum of six fields from three independent experiments) were calculated using the mito-morphology macro for image J created by Ruben K. Dagda at the University of Pittsburgh. Image enhancements, despeckling, were performed for inset digital zooms to increase picture clarity.

Pharmacological inhibition of pathway activity

Diphenyleneiodonium chloride (DPI; Sigma-Aldrich) stocks were prepared in water and stored at room temperature. N-[2-(*p*-Bromocinnamylamino)ethyl]-5-isoquinolinesulfonamide dihydrochloride (H89; Abcam, VIC, AUS) stocks were prepared in water and stored at -20°C.

Cell plating

Cells were seeded at a density of 3.6×10^4 cells/well in 5 µg/ml PDL in H_2O solution-coated 96-well plates and allowed to adhere under normal incubator conditions for 24 h before assay.

[3-(4,5-Dimethylthiazol-2-yl)-5-(3-carboxymethoxyphenyl)-2-(4-sulfophenyl)-2H-tetrazolium (MTS) metabolism assay

Five microlitres of one-solution MTS reagent (Promega, VIC, AUS) was added per 100 µl of media in each well. Plates were incubated under normal incubator conditions for the duration

of the assay. Developed colour was measured at 492 nm in a FluoSTAR/PolarSTAR Optima (BMG Labtech, VIC, AUS).

Lactate dehydrogenase (LDH) cell death assay

Cellular and extracellular LDH was measured using a Cytotoxicity Detection kit (LDH; Roche, VIC, AUS) and cytotoxicity calculated as per the manufacturer's instructions.

Caspase 3/7 assay

Caspase 3/7 staining and 7-amino-actinomycin D (7-AAD) staining were carried out and quantified using a Muse™ Caspase-3/7 Kit (Roche-Sigma, USA) and a Muse™ Cell Analyzer (Roche-Sigma) with software version 1.4. The cells were loaded as per the manufacturer's instruction with 5 µl of Caspase-3/7 working solution added to 50 µl cells (diluted to approximately 1×10^6 cells/ml). Cells were incubated for 30 min at 37 °C before addition of 150 µl of 7-ADD working solution and then analysed for apoptotic (but not dead) and dead cells.

Ki67 assay

Ki67 was assayed using the Muse® Ki67 Proliferation Kit (Roche-Sigma) and a Muse™ Cell Analyzer (Roche-Sigma). Cells were fixed and stained as per the manufacturer's instructions and the negative control staining (shown in grey shading on the plots) was used to gate the background unstained cell population for analysis using the Muse v1.4 software.

Adenosine triphosphate (ATP) assay

Cellular ATP content was measured by luminescence using Life Sciences ATP assay (Life Technologies) as per the product protocol and normalised for total protein levels determined by BCA assay (Pierce, Thermo-Fisher).

Dichlorofluorescin diacetate (DCFDA) assay

The DCFDA assay for intracellular ROS production has been described previously [33]. Briefly, cells were loaded with CM-H_2-DCFDA reagent (Invitrogen) by incubating cells with a 5 µM probe solution in PBS for 20 min at 37 °C. Basal fluorescence was then read to provide a well-background control and test conditions added to start the assay. Fluorescence intensity was monitored for 12 h.

Nicotinamide adenine dinucleotide phosphate (NADPH) consumption assay

NADPH (Arbor Assays, Bio Scientific, VIC, AUS) was diluted to 250 mM stock in sterile water, and aliquoted and stored at – 20 °C until use. At the start of the assay, 1 µM peptide was included in the culture media; then, 25 mM NADPH was added to each well and decay of the NADPH absorbance monitored at 340 nm every 60 s for 10 min and gradients calculated to show consumption of substrate.

Superoxide dismutase (SOD) activity assay

Total SOD activity of cell lysates was determined using a WST-1-based competitive inhibition assay (Abcam), as per the manufacturer's instructions, with normalisation of activity to total protein as determined by BCA assay.

Peptide:*N*-glycosidase F (PNGase-F) digests

Pre-denatured lysates were digested using 1 µl PNGase-F per 20 µl protein sample with overnight incubation at 37 °C.

Western/dot blotting

Western blotting was carried out using the Invitrogen NuPAGE/Bolt gel system (Life Technologies) with Criterion (BioRad, VIC, AUS) or iBlot (Invitrogen) transfer and developed as described previously [41, 43]. Coomassie membrane staining was performed as previously described [44]. Total protein staining was used to monitor gel loading/transfer efficiency, because the housekeeping proteins often used as loading controls are involved in the cellular processes being investigated and are, therefore, considered unreliable. Dot blotting was performed by dotting 2 µl of whole-cell lysate onto nitrocellulose membranes. Membranes were blocked and blotted as for standard western blotting procedure. Antibody information is shown in Sup Table 1. Percentage change was calculated by first normalising band signal to total protein and then applying the following equation: % change = (test band signal intensity/control band signal intensity) × 100.

Senescence staining and quantification

Senescence was determined using a β-galactosidase staining kit (Cell Signaling Technologies, Sapphire Biosciences, VIC, AUS), following the manufacturer's instructions and the blue product solubilised in DMSO by agitated heating as described in Haigh et al. [44].

Redox-sensor Red ROS assay

Redox-sensor Red (PF-H_2TMRos; Life Technologies) at a final concentration of 5 µM in Opti-MEM I reduced serum culture medium (phenol red-free; Invitrogen) was loaded into cells for 10 min and cells were imaged in fresh medium as described previously [24].

MitoSOX staining

MitoSOX fluorescent indicator probe (Life Technologies) was loaded into cells at a final concentration of 5 µM in normal media for 10 min under standard incubator conditions and imaged in fresh, phenol red-free Opti-MEM as described previously [45].

Small interfering RNA (siRNA) transfections

Pre-validated siRNA duplexes were purchased from Life Technologies. Single-cell suspensions were prepared in proliferation media and sufficient cells seeded into 1-well of a 6-well plate for all test and control assays. Transfections were achieved using Fugene HD transfection reagent (Roche) as per the manufacturer's protocol. Plates were returned to the incubator until cells were used for assay. Prior to assay, cells were re-suspended as single cells, counted and seeded into the NCFA as described previously. Pre-screening of knock-down efficiency found that knock-downs of both Nox2 and SOD2 were optimal (~ 50%) at 2 days using 30 µM siRNA for Nox2 and 50 µM for SOD2 (example western blot images of knock-downs are shown in Sup Fig 1). Therefore, all assays began 2 days post-treatment with these concentrations of siRNA and the equivalent of non-silencing control (Life Technologies). At the start of every assay, a dot blot was performed on cells from the starting culture to confirm the knock-down had been consistent. Quantifications of these quality control spots are shown in Sup Fig 1.

Statistical analysis

Statistical analyses were accomplished using GraphPad Prism 5 statistical software. Students *t* tests were used for comparison of two parameters and ANOVA or Kruskal–Wallis analyses used for > two parameters. Where significant differences were found, Dunnett, Bonferroni, or Dunn tests were used for multiple comparisons of one-way, two-way, and non-parametric ANOVA, respectively. $p < 0.05$ was used as the cutoff for significance and ≥ 95% statistical power. All stated "*n*" values indicate independent repeats.

Results

N1 and N2 alter NSC growth

To assess the ability of the soluble N-terminal fragments to influence NSC growth, adult NSCs (harvested from wild-type mice at 8 weeks of age) were incubated with 1 µM synthetically produced N1 and N2 peptides (Fig. 1a) included in the matrix of a neural colony forming assay (NCFA; Fig. 1b). The 1 µM concentration of each peptide was based upon our previous studies showing functionality at these concentrations [33, 41, 46]. Exposure of the NSCs to either the N1 or the N2 fragment resulted in decreased growth, reducing the number of colonies formed (Fig. 1c) and, for the N2 fragment, the diameter of the colonies (Fig. 1d). The N2 growth reduction was accompanied by a significant reduction in protein expression of the cell proliferation regulatory protein Pin1 (Fig. 1e, f). Using further synthetic fragments corresponding to shorter regions of the N2 fragment, and also an N2 peptide with mutated N-terminal residues, it was found that wild-type full-length N2 is the minimum needed to cause overall growth change, especially with respect to colony formation (Fig. 1g, h). A fragment representing the most N-terminal region, amino acids 23–50, could elicit a small effect on colony diameter, but, whilst this was significantly different from the untreated control, it was not statistically different from a scrambled control peptide suggesting an artefactual result (Fig. 1h). The consequence of N-terminal mutation was less clear. Whilst the effect of wild-type N2 on reducing the number of colonies formed was clearly abolished by mutation of the N-terminal proline residues to alanine (P26/28A), there was a persisting capacity to reduce colony diameter similar to that observed with un-mutated N2 fragment.

During prion disease, ongoing PrP expression is an absolute requirement for pathogenesis [47]. Therefore, we investigated whether the influence of the N1 and N2 peptides on cell growth was changed in cells of differing PrP expression levels. The effect of the fragments, especially for N2, did not depend upon the underlying expression of PrP in the NSCs, with both the *prnp* knock-out (KO) and Tga20 over-expressing cells showing reduced growth when the peptides were included in their matrix (Fig. 1i, j). However, in contrast with the wild-type cells, the KO and Tga20 cells demonstrated a changed influence of the N1 peptide, with colony diameter more influenced than the number of colonies formed.

N1 and N2 reduce migration and neurite outgrowth

Other processes that occur following division in actively replicating NSCs include migration of cells to their site of integration and the extension of neurite outgrowths, and both of these processes have been found to be influenced by cellular PrP expression levels [48, 49]. Congruent with the colony forming assay results, both migration and neurite outgrowth were reduced by the N1 and N2 peptides (Fig. 1k–m). By observing the migration of cells from the neurospheres for longer, it was apparent that the inhibitory effects of N1 and N2 were transient with migration of the N1-treated cells

indistinguishable from control cells and migration resumed, albeit at an attenuated level, for N2 by 7 days (Fig. 1k).

N1 and N2 do not cause cytotoxicity or senescence

To ascertain whether cell death was the cause of the reduced NSC growth in response to the N1 and N2 peptides, cytotoxicity and cell metabolism assays were performed (Fig. 2a, b) after 24 h, which found no discernible changes. To ensure that death was not delayed or increased over the time of the NCFA and migration assays, caspase 3 and 7 (executioner caspase) activation and cell death as indicated by uptake of 7-AAD were monitored weekly using the more potent N2 fragment. These measurements also found no significant effect on long-term viability as a result of peptide exposure (Fig. 2c, d). In addition, beta-galactosidase staining, an

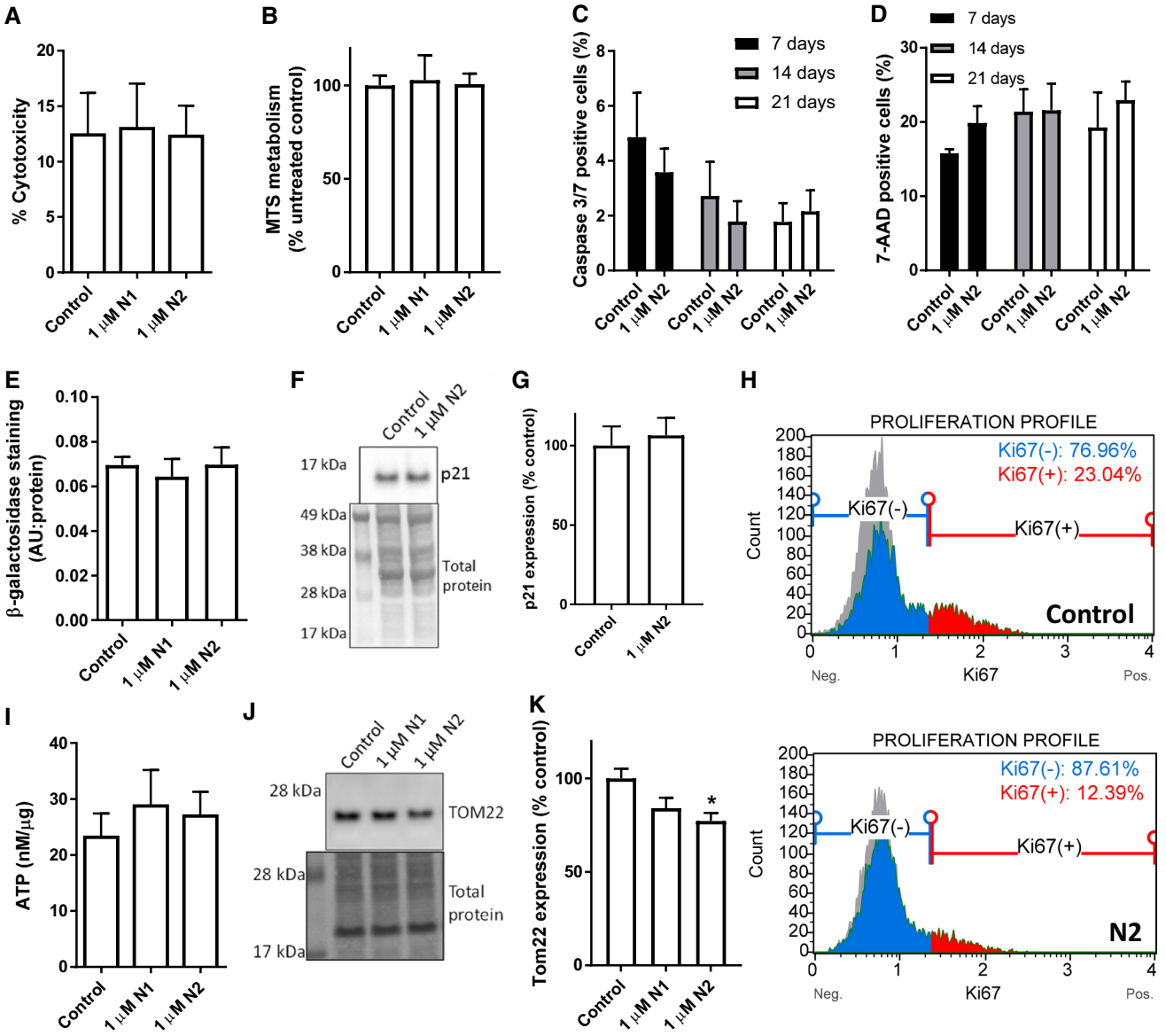

Fig. 2 Reduction in growth is not due to reduction in cell viability. **a** Cytotoxicity of N1 and N2 as measured by cellular LDH release 24 h post-exposure. $n=4$. **b** MTS measurement of cellular metabolism as an indicator of viability 24 h post-exposure to N1 or N2. $n=4$. **c** Active caspase 3/7 detection in cells cultured for 3-week post-treatment with N2. $n=3$. **d** Uptake of 7-AAD as an indicator of dead cells in the same time series as c. $n=3$. **e** Beta-galactosidase staining intensity, as an indicator of cell senescence, 3-day post-exposure to N1 or N2. $n=3$. **f** Immunoblots for the cell quiescence/senescence-associated protein p21. **g** Densitometric quantification of **f**. $n=3$. **h** Ki67 flow cytometry analysis of proliferating cells 3 days following treatment with the N2 peptide. Representative plots from $n=4$. **i** Cellular ATP concentration relative to total protein 24 h after exposure to N1 or N2. $n=4$. **j** Immunoblots for the mitochondrial transporter protein TOM22 24 h after exposure to N1 or N2. **k** Densitometric quantification of e. $n=4$. Data are presented as mean and SEM. Significance is indicated by $^*p<0.05$

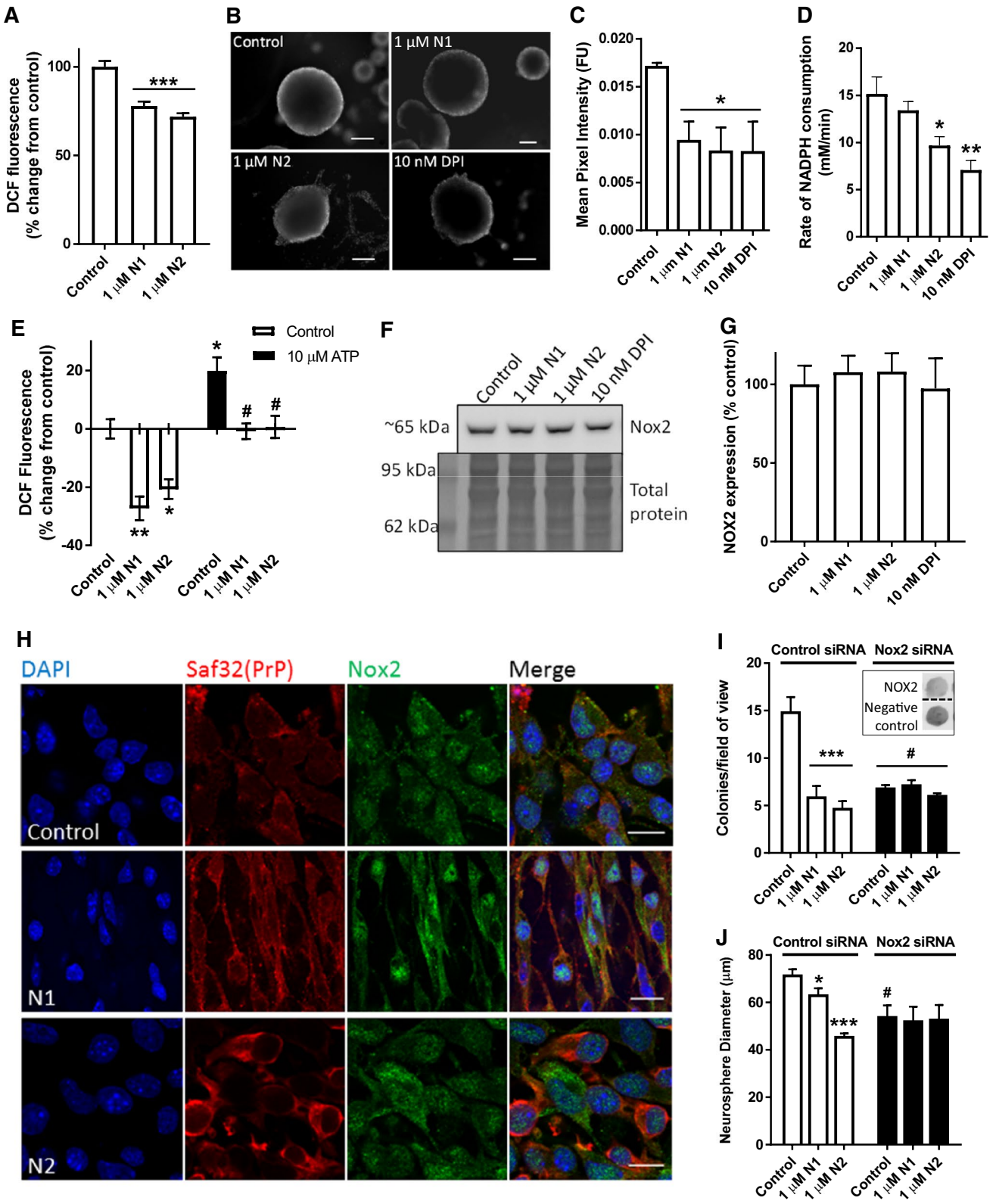

indicator of cellular senescence, was not increased in these cells (Fig. 2e). Assessment of the, quiescence/senescence-associated marker p21 showed no change in response to N2 treatment over 3 days (Fig. 2f, g); however, Ki67, a marker of cell proliferation, was reduced to half of the levels detected in control cells ($p = 0.041$, $n = 4$; Fig. 2h). A change in

◂**Fig. 3** N1 and N2 reduce intracellular redox signalling through the Nox pathway. **a** DCFDA assay detection of intracellular ROS production in NSCs treated with N1 and N2. $n=6$. **b** Representative images of Redox-Sensor Red staining of whole neurospheres 90 min after exposure to N1, N2 or the Nox inhibitor DPI. Scale bar = 50 µm. **c** Quantification of fluorescence intensity in B. $n=3$. **d** Cellular NADPH consumption rate within 20 min following exposure to the peptides. $n=3$. **e** DCFDA assay detection of intracellular ROS production in NSCs treated with N1 and N2 with or without the inclusion of ATP in the assay media. $n=4$. Hash denotes significantly different from the equivalent peptide condition without ATP. **f** Immunoblots for cellular expression of Nox2 24 h following exposure to the N1 and N2 peptides. **g** Quantification of E. $n=4$. **h** Representative confocal images of Nox2 cellular staining 90 min after peptide treatment. Scale bar = 10 µm. **i** Colony counts of the NCFA where NSCs were incubated with and without N1 and N2 and with siRNA targeting Nox2 expression or a control non-silencing siRNA (inset shows dot blots of remaining Nox2 expression in a representative experiment). $n=3$. Hash significantly different from non-silencing siRNA control, $p<0.05$. **j** Diameter measurements of colonies formed in the NCFA described in **i**. $n=3$. Hash significantly different from non-silencing siRNA control, $p<0.05$. All data within the figure are presented as mean and SEM with significance indicated by $^{*}p<0.05$, $^{**}p<0.01$, $^{***}p<0.001$ from respective control values unless otherwise stated

growth might indicate perturbed cellular energy demands; therefore, cellular ATP and mitochondrial protein expression levels were examined. Despite no changes in cellular ATP levels (Fig. 2i), a small decrease in the mitochondrial transporter TOM22 was detected following 24 h exposure to the N2 fragment (Fig. 2j, k), which indicated that mitochondrial mass was influenced by this peptide.

N1 and N2 reduce intracellular ROS production

In our previous studies, we found that the N2 fragment could protect secondary cell lines from oxidative stress and similar protective actions have been reported for the N1 fragment [32, 33, 41]. In addition, redox signalling is known to alter NSC growth [34, 35, 44]. To determine whether the influence of the N1 and N2 peptides on redox balance might underpin the NSC growth changes, we analysed the production of intracellular ROS using the DCFDA assay. The DCFDA assay is a fluorometric assay wherein cells are loaded with DCFDA; the intracellular form of DCFDA, DCF^{-}, is non-fluorescent until it is oxidised to DCF by free radicals, and therefore, an increase in fluorescence signal over the control cells indicates increased radical production and vice versa. Performing the DCFDA assay found a significant reduction of ROS production in cells incubated with either peptide (Fig. 3a). We have previously found that inhibiting NADPH oxidase (Nox) activity using the pharmacological inhibitor DPI reduces NSC growth in the NCFA [44]. Therefore, intracellular ROS levels were further considered in the NSCs using Redox-Sensor Red. Redox-Sensor Red is a partitioning probe; fluorescing when it binds ROS in the cytosol, which are primarily produced by the Nox family, or, if cytosolic ROS are not met, it then accumulates in lysosomes where its fluorescence increases as influenced by lysosomal redox balance. Redox-Sensor Red was loaded into whole neurospheres prior to addition of N1, N2, or DPI and spheres were imaged at 90 min. Fluorescence intensity showed a similar significant reduction in ROS detected for the N1-, N2-, and DPI-treated conditions (Fig. 3b, c). We next measured cellular usage of NADPH, finding that N2 and DPI showed a significant decrease in the utilisation of NADPH indicating a lesser activity of this family of enzymes (Fig. 3d). To further assess the potential for N1 and N2 to modulate Nox family function, we competed the peptides against ATP, which activates Nox signalling increasing cellular ROS production, and used the DCFDA assay to monitor changes within the cells. The peptides were overlaid on the cells first and then ATP was included in the assay media. ATP increased cellular ROS production significantly from the basal control and both peptides were able to inhibit this effect (Fig. 3e).

To directly investigate the role of Nox signalling, siRNA knock-down was used to target Nox2. Nox2 was selected as it is a central catalytic subunit of the Nox complex and known to have a role in the maintenance of NSC populations within the brain [50]. Nox2 has also previously been linked with PrP signal transduction and to prion disease pathogenesis [51–53]. Western blotting confirmed that the stem cells do express this subunit and showed no significant changes in the expression levels of Nox2 after 24 h incubation with N1, N2 or DPI (Fig. 3f, g). Confocal imaging of PrP and Nox2 showed altered cellular morphology and localisation of Nox in response to the peptides (Fig. 3h). Using siRNA to knock down the expression of Nox2, a significant decrease in cellular growth was seen in the NCFA (consistent with the previously reported effects of DPI treatment) and this completely negated the effects of both N1 and N2 (Fig. 3i, j).

Reduced redox signalling causes increased mitochondrial fission

We next wished to determine how N1/N2-redox signalling could be transduced through the cell to change cell growth. Nox signalling is linked with many of the central signal transduction pathways of the cell. We investigated several of these, including ERK1/2, AKT1, GSK-3β, and p38, but found no obvious activation or deactivation of any of those tested (Sup Fig 2). Since the central cellular signalling pathways were not seen to be influenced by the peptides, but mitochondrial involvement was indicated by TOM22 reduction in response to N2 (Fig. 2j, k), direct changes to mitochondria were considered. Mitochondrial fission and fusion are linked with cell cycle control [54]. Furthermore, in times of heighted oxidative stress, including that caused

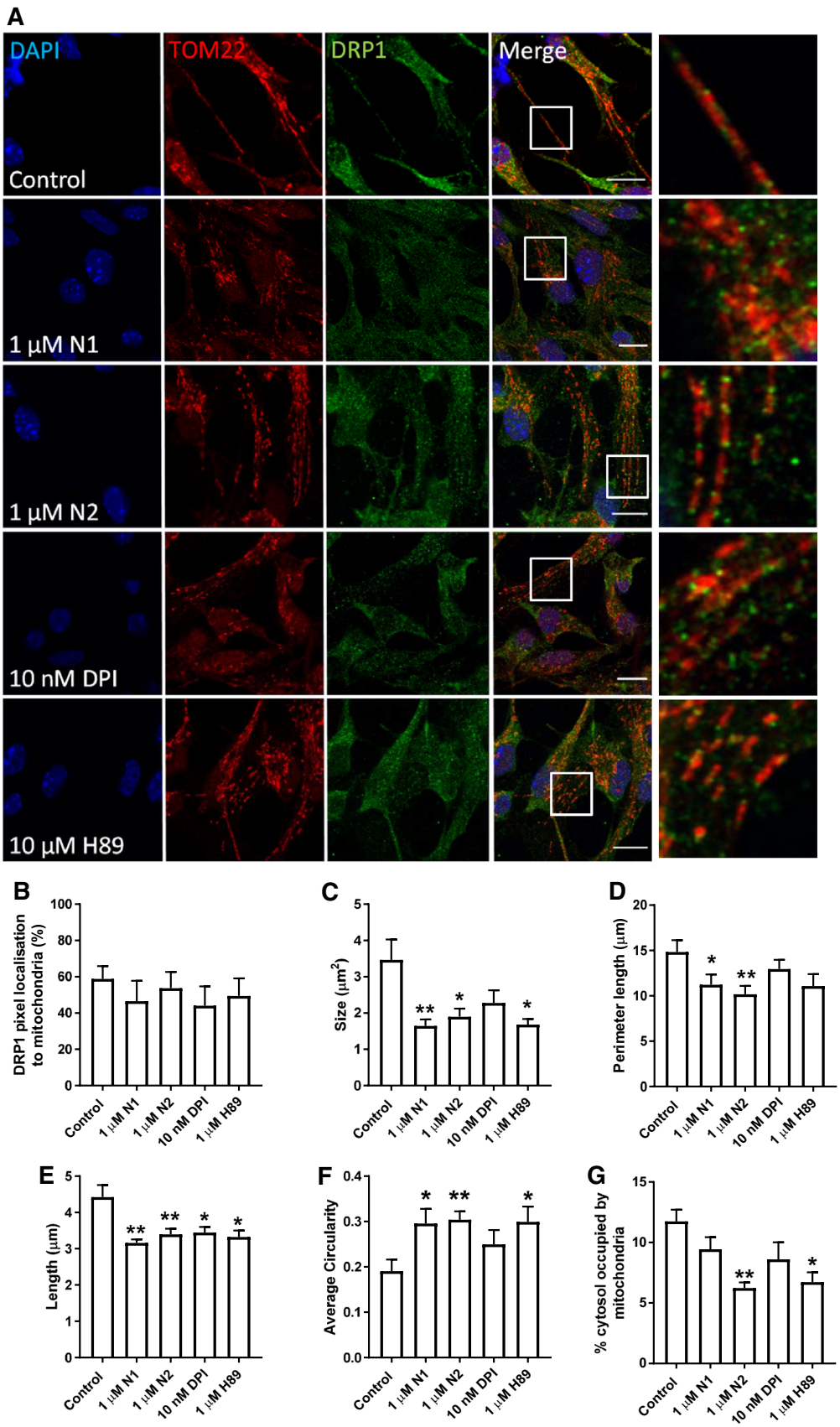
A
DAPI
TOM22
DRP1
Merge
Control
1 μM N1
1 μM N2
10 nM DPI
10 μM H89
B
DRP1 pixel localisation to mitochondria (%)
C
Size (μm²)
D
Perimeter length (μm)
E
Length (μm)
F
Average Circularity
G
% cytosol occupied by mitochondria
Control
1 μM N1
1 μM N2
10 nM DPI
1 μM H89

◂**Fig. 4** N1 and N2 increase mitochondrial fission. **a** Representative confocal images of DRP1 and mitochondrial (TOM22) morphology 90 min following addition of N1, N2, DPI, and PKA inhibitor H89 to NSCs. Scale bar = 10 µm. Boxes indicate the region shown in higher magnification on the right. **b** Measurement of percentage DRP1 stained pixels localising within mitochondria. $n = 3$. **c** Measurement of mitochondrial size under the conditions described in **a**. $n = 3$. **d** Measurement of mitochondrial perimeter length under the conditions described in **a**. $n = 3$. **e** Measurement of mitochondrial length (measurement of longest axis) under the conditions described in **a**. $n = 3$. **f**. Measurement of mitochondrial circularity under the conditions described in **a**. $n = 3$. **g** Measurement of cytosolic % occupied by mitochondria under the conditions described in **a**. $n = 3$. All data within the figure are presented as mean and SEM with significance indicated by $*p < 0.05$, $**p < 0.01$ from respective control values

by Nox and exogenous H_2O_2, mitochondria fuse to form long networks protecting themselves from autophagy [55]. H_2O_2 activates PKA, which results in inhibitory phosphorylation of dynamin-related protein-1 (DRP1), a core component of the machinery involved in mitochondrial fission and linked with dynamic control of the cell cycle by mitochondria [54, 56]. Therefore, the localisation of DRP1 in relation to mitochondrial morphology was examined by confocal microscopy. Following treatment with N1, N2, DPI, and H89 (an inhibitor of PKA and, therefore, inhibitory phosphorylation of DRP1), mitochondrial morphology appeared more punctate (Fig. 4a). Whilst no significant increase in DRP1 pixels localising to whole mitochondria was observed (Fig. 4b), DRP1 clustering at the ends of the puncta was qualitatively more apparent than seen in control cells (Fig. 4a). Measurement of mitochondrial morphology showed a significantly reduced mitochondrial size, perimeter, and length with greater mitochondrial circularity in cells treated with N1 and N2 (Fig. 4c–f). A decrease in the percentage of the cytosol occupied by mitochondria was also seen for N2 (Fig. 4g) consistent with the decrease in TOM22 previously observed following treatment (Fig. 2j, k). The increase in punctate mitochondrial morphology was also observable in live cells using Mitotracker-Green staining (Sup Fig 3). After 2 h, a small but significant decrease in detectible DRP1 was also noted for N1 and N2 (Fig. 5a, c) and this was maintained at 24 h (Fig. 5b, c). Decreased DRP1 detection might indicate that this protein is undergoing increased turnover to maintain homeostasis. No change was observed for the mitochondrial fusion protein, mitofusin-1 (MFN1), at 24 h in response to N2 or DPI (Fig. 5d, e).

N1 and N2 cause changes in SOD2 expression and SOD activity

To ascertain whether the changes in mitochondrial structure caused by the N1 and N2 peptides could also affect their redox balance, mitochondrial antioxidant defence and ROS production were evaluated. Superoxide dismutase-2 (SOD2) is the central mitochondrial antioxidant, and therefore, cellular levels of SOD2 were evaluated by western blotting. A significant increase in expression was seen following treatment with the N2 peptide and inhibition of Nox signalling with DPI (Fig. 6a, b). This was also reflected in the cellular total SOD activity, which showed significant increases in response to N1 as well as N2 and DPI (Fig. 6c). Following 24 h exposure to N1, N2, or DPI, staining of live neurospheres with MitoSOX (a mitochondrially localised fluorescent superoxide probe) showed that the production of mitochondrial superoxide is reduced throughout the sphere and in individual cells surrounding the sphere (Fig. 6d). Using siRNA to knock down SOD2 abrogated the effect of N1 and DPI on reducing colony formation in the NCFA but did not prevent N2 reducing the number of colonies formed (Fig. 6e) suggesting effects of N2 beyond SOD2. However, the size of the colonies produced when incubated with N2 was no-longer reduced (Fig. 6f).

NSCs show altered PrP N-terminal detection depending upon whether they are actively growing or quiescent

To ascertain whether endogenous cleavage of PrP correlates with NSC growth changes, we probed the profiles of N- and C-terminal PrP antibody reactivity in growing neurospheres (antibody-binding sites are shown in Fig. 1a). NSCs in the centre of a healthy neurosphere are quiescent, whereas those at the periphery are actively proliferating and this is reflected by the expression of the proliferation marker Ki67. The N-terminal fragments are rarely found in cell lysates but instead are detected as secretory fragments in conditioned media [31, 32] and, in addition, they have a predicted short cellular half life due to vulnerability to digestion. Therefore, while we cannot rule out saf32 (N-terminal) antibody reactivity due to the N-terminal fragments, the N-terminal signal in cells is more likely due to the presence of full-length, uncleaved PrP. The C-terminus of PrP has a predicted slow turnover post-cleavage and remains membrane anchored, permitting its detection in cells post-cleavage, and, therefore, saf70 (C-terminal) antibody reactivity could be due to full-length PrP, C1, or C2. N-terminal labelling of PrP was detected mostly at the periphery of the cultures, with only ~ 25% of the total signal detected in the core (Fig. 7a, b; individual channels and control nestin staining are shown in Sup Fig 4 and Sup Fig. 5, respectively). In contrast, significantly greater C-terminal labelling of PrP could be detected in the neurosphere core (Fig. 7a, c), indicating that more full-length PrP is found in cells that are actively growing and that PrP is predominantly cleaved in cells that are not growing. Cells at the periphery and within the core are shown at increased magnification in Sup Fig 6. Furthermore, when NSCs that were grown as neurospheres (where their core

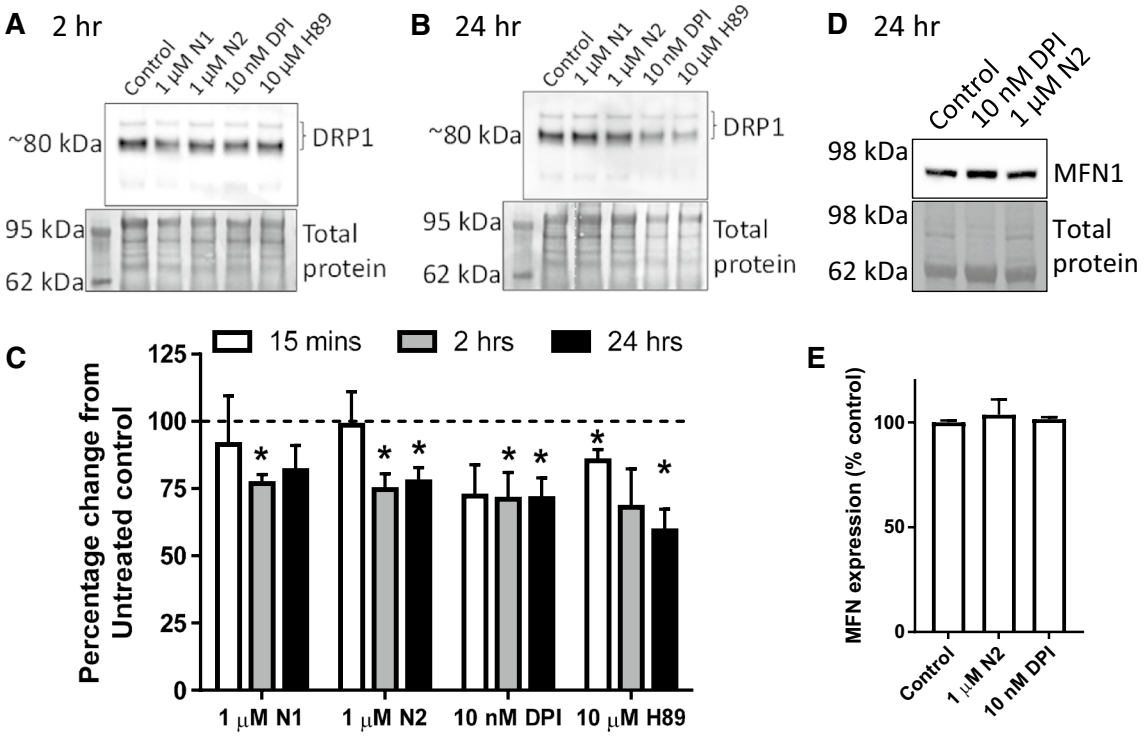

Fig. 5 N1 and N2 change DRP1 detection but not MFN1. **a** Immunoblots of DRP1 2 h following addition of N1, N2, DPI, and PKA inhibitor H89 to NSCs. **b** Immunoblots of DRP1 24 h post-treatment as described in **a**. **c** Densitometric quantification of DRP1 immunoblots at 15 min, 2 h (**a**) and 24 h (**b**). $n=4$. **d** Immunoblots of MFN1 24 h post-treatment with N2 or DPI. **e** Densitometric quantification of **d**. $n=3$. All data within the figure are presented as mean and SEM with significance indicated by $^*p<0.05$ from respective control values

is quiescent) were compared with those grown as dissociated cells in suspension (where access to the mitogens in the media stimulates their growth) for 24 h, both the C1 and C2 cleavage fragments (detected after PNGase-F digest to remove N-linked complex glycans) were increased in the neurospheres (Fig. 7d).

Discussion

Difficulty assigning a single or predominant function to PrP may have arisen, at least in part, from the numerous post-translational modifications to which it is subjected and the biochemically distinct protein/peptide species that are produced as a result. The data presented herein show that the N-terminal cleavage fragments, N1 and N2, can reduce intracellular redox signalling, with the N2 peptide directly reducing Nox catalytic activity. The reduced ROS increases the activity of DRP1, which mobilises to the mitochondria resulting in their fission within a few hours and later increasing protein levels of SOD2. The increased SOD2 levels and activity in turn maintain a low ROS environment within the mitochondria preserving cells in a quiescent state (Fig. 8).

The enzymes responsible for N1/C1 cleavage are still a matter of contention. It was first reported that A Disintegrin and metalloproteinase domain-containing protein 10 (ADAM10) was the candidate alpha-cleavage enzyme [31], although later work found that this enzyme was primarily responsible for secretory cleavage of PrP near the GPI anchor [58]. ADAM17 (alternatively known as tumour necrosis factor-α-converting enzyme [TACE]) and ADAM9 have also been implicated in N1/C1 cleavage, but a definitive identification has not yet been made; a detailed review of this work can be found in [59]. The N2/C2 cleavage event has been demonstrated to be mediated by ROS [60] and, during scrapie infection, by the calpain family [61]. Conditions that change the expression or activity of cleavage enzymes may shift the balance between full-length PrP and its cleavage fragments or shift the ratio of alpha- and beta-cleavage resulting in changed cellular outcomes. Therefore, the apparent cellular function of PrP may be as related to cellular protease expression levels as it is to total PrP levels.

The alpha-cleavage event producing N1 is generally considered constitutive, whereas the beta-cleavage event is thought to be primarily induced during disease [30] and caused by ROS. The N1 fragment, whilst demonstrating changes in each of the pathway components examined, was

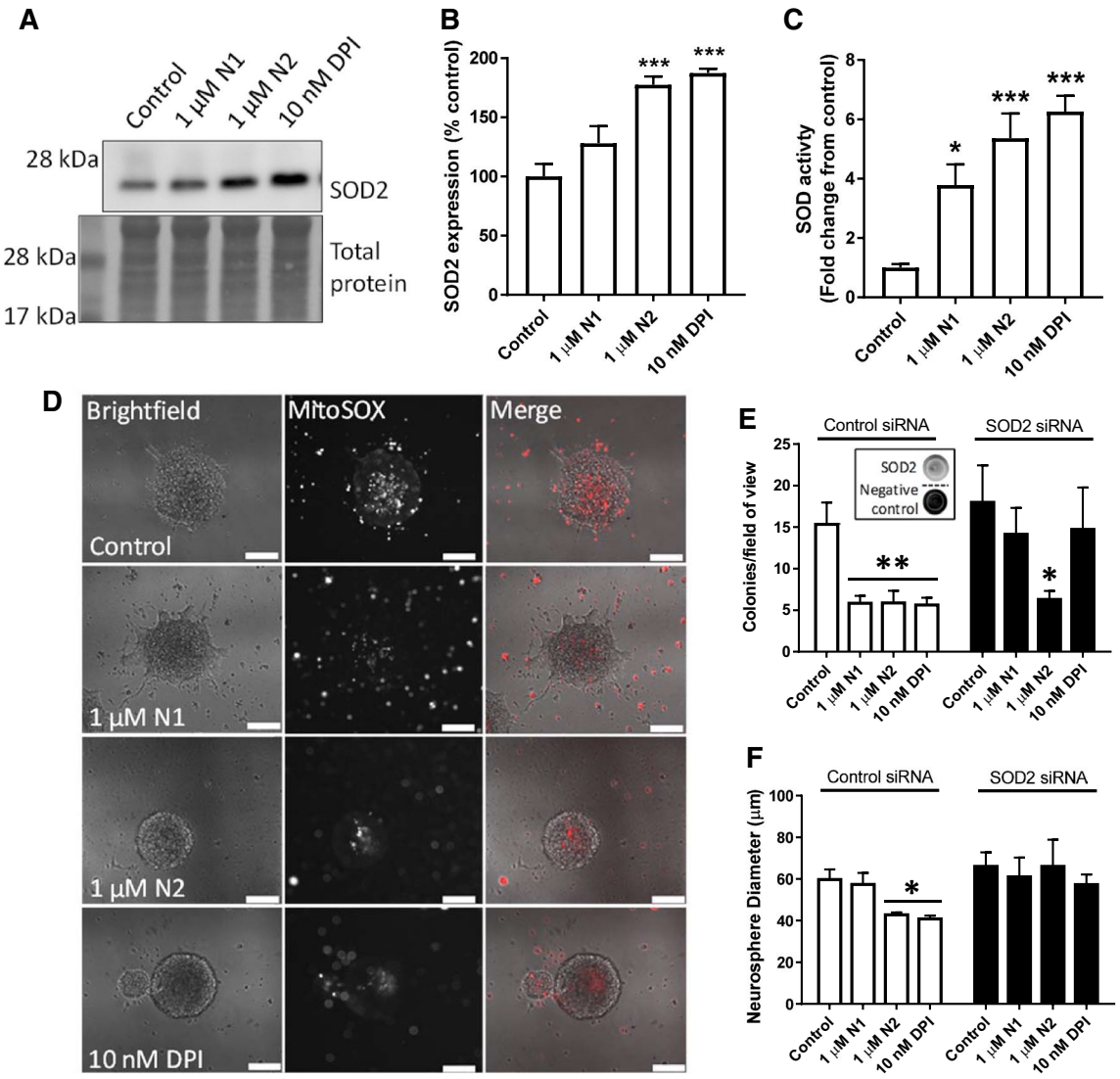

Fig. 6 Decreased growth correlates with increased SOD2 protein and activity. **a** Immunoblots for SOD2 24 h following treatment with N1, N2 or DPI. **b** Densitometric quantification of **a**. $n=4$. **c** SOD activity assay in cell lysates 24-h post-treatment with N1, N2 or DPI. $n=4$. **d** Representative images of MitoSOX staining of whole-live neurospheres 24 h following treatment with N1, N2, or DPI. Scale bars = 50 µm. **e** Colony counts of the NCFA where NSCs were incubated with and without N1 and N2 and with siRNA targeting SOD2 expression or a control non-silencing siRNA (inset shows representative dots of SOD2 detection after knock-down). $n=3$. **f** Colony diameter as measured for the NCFA described in **e**. $n=3$. All data within the figure are presented as mean and SEM with significance indicated by $^{*}p<0.05$, $^{**}p<0.01$, $^{***}p<0.001$ from respective control values

less potent in producing cellular changes than the N2 fragment and its potential to modulate Nox signalling less evident. The more aggressive action of N2 on this pathway may reflect differing functional requirements for the N1 and N2 fragments. For example, during times of stress, mitochondria fuse into tubular networks to avoid being destroyed by autophagy [55] and, in stem cells, autophagy becomes activated to prevent senescence [62]. Mitochondrial fusion is associated with G1-to-S-phase transition through the cell cycle [54], and therefore, the role of N2 in decreasing ROS signalling and maintaining a less fused mitochondrial population may function to preserve quiescence at times when the NSC pool is at risk of depletion. However, the converse could also be true that, as a result of N2 being more efficient at stimulating this pathway, such changes could be detrimental. Counteraction of mitochondrial fusion by N2 could lead to a loss of mitochondrial mass as mitochondria are engulfed by mitophagy, leaving cells struggling with energy demand. A slight decrease in mitochondria was seen for the N2 fragment, which might indicate that the fission event is causing a degree of mitochondrial loss even without the presence of damaging stress.

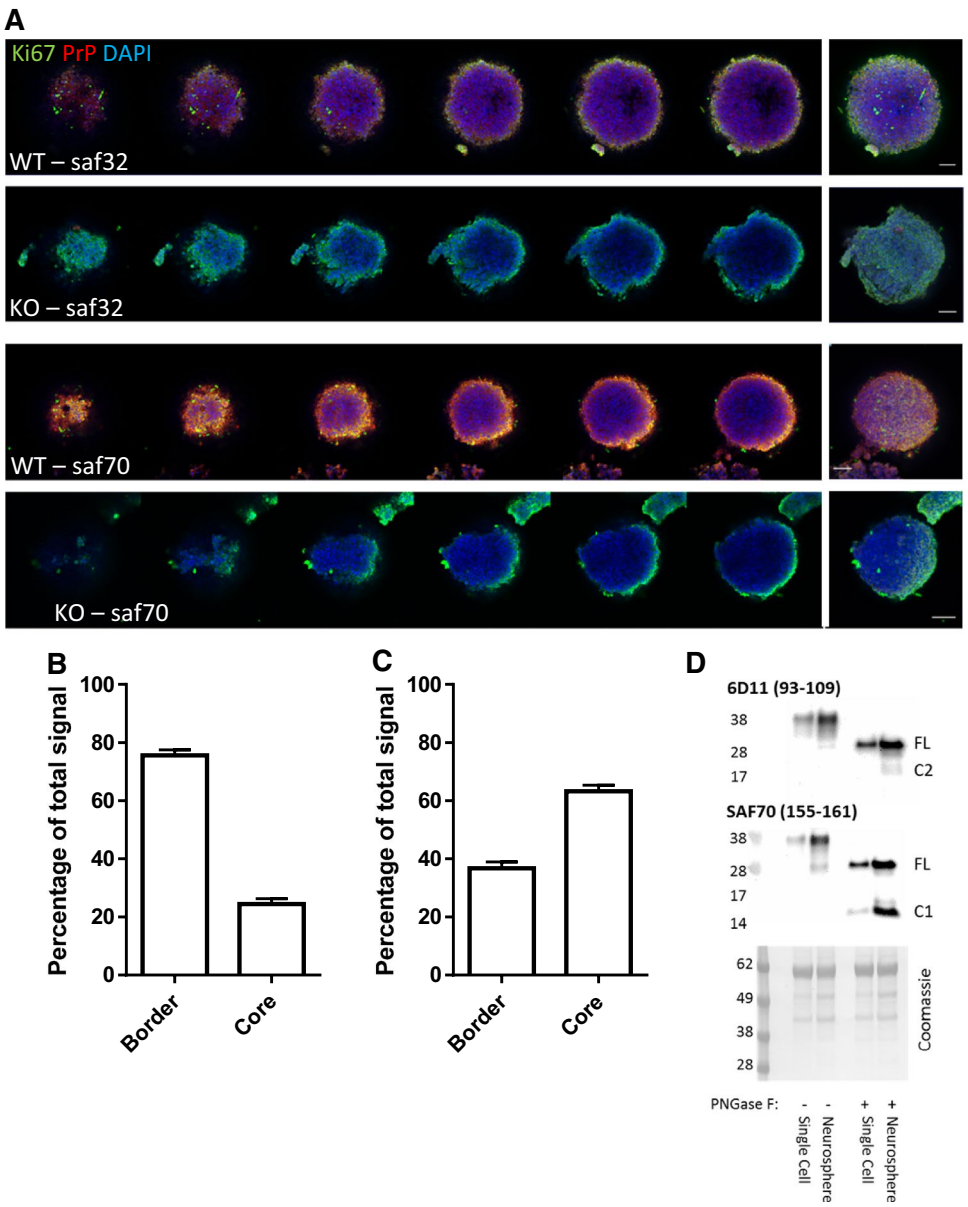

Fig. 7 Characterisation of PrP cleavage in the quiescent core of neurospheres and in human brain precursor cells. **a** Representative confocal images of serial slices through a neurosphere and merger (right) when immuno-stained with Ki67 proliferation marker and N- (Saf32) or C- (Saf90) terminal PrP antibodies. Scale bar = 20 µm. **b** Quantification of peripheral and core staining of PrP as detected by Saf32. $n = 3$ independent repeats with a minimum of 20 spheres. **c** Quantification of peripheral and core staining of PrP as detected by Saf70. $n = 3$ independent repeats with a minimum of 20 spheres. **d** PNGase-F digests and PrP immunoblots comparing NSCs grown as neurospheres and those grown in single-cell suspensions

Alternative explanations may exist for the observed differences in biological effects between the N1 and N2 fragments. The N1 fragment contains a second charged cluster domain (resulting in charged domains at both ends of the peptide); this may endow it with extra properties such as the ability to bind and engage pathways that N2 cannot. Such putative-binding capacity may result in less N1 being available for modulation of the tested pathways. We have also observed aggregation of the 23-89P26/28A mutant in the previous studies [33] and the second charged domain within N1 may facilitate greater dimerisation/oligomerisation as compared with N2 thereby rendering less N1 peptide effectively available for interactions. Furthermore, only a single peptide concentration was compared in the current study; therefore, it is possible that higher concentrations of N1 could elicit the same intensity of reaction of the tested concentrations of N2. It is also unclear from the presented data why a difference should exist in cellular responses to N1 as a result of endogenous PrP expression; this could be related to the basal levels of N1 within these cells or lack of N1 and/or the pathways compensating for changed expression levels of the full-length protein. As the knock-out and Tga20 over-expressing NSCs demonstrate changed growth properties from the wild-type, which is especially apparent for the number of colonies generated by the Tga20 cells, basally changed pathways could influence how N1 is able to interact with and modulate cellular growth pathways.

PrP has been linked with increased ROS generated by Nox in the context of prion disease [52] and oxidative damage caused by overstimulation of Nox signalling was found

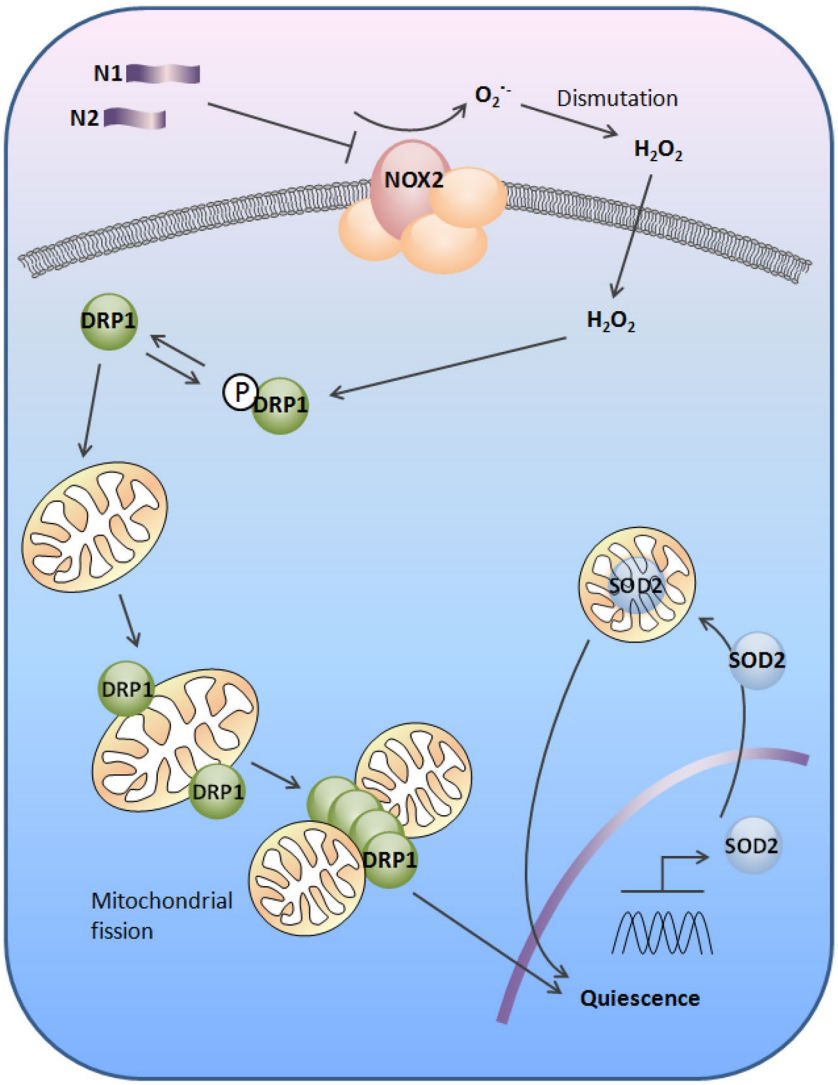

Fig. 8 Schematic illustration of the redox signal transduction by N1 and N2 to induce quiescence in neural stem cells

to be mediated by interaction of the N-terminus at the cell membrane in an antibody-stimulated model of toxicity [51]. Tethering the N-terminus of PrP to the cell membrane reduces the capacity of PrP to undergo normal N2/C2 cleavage, as well as cellular resistance to oxidative stress [63], possibly by preventing the N2 fragment from modulating Nox function. How exactly the N-terminal fragments or N-terminus of full-length PrP interact with Nox is unknown. Both our previous in vitro studies that indicated no intrinsic antioxidant activity of N2 [33] and, herein, the decreased utilisation of NADPH substrate in response to N2 argue against an indirect 'mopping up' of the superoxide radicals. Other possibilities include direct interaction with one or more of the Nox subunits or modulation of the lipid membrane environment in which the Nox complex forms. The latter is a reasonable possibility as we have shown that both of these peptides bind to lipids under specific conditions [64, 65] and changes in the lipid environment are observed during N2 protection against oxidative stress [46].

From the data presented, we cannot rule out a direct effect of the peptides on the mitochondria themselves. Whilst N1 did not significantly change Nox activity or cellular SOD2 expression it did alter mitochondrial fission and knocking down SOD2 completely counteracted the effect of this peptide on cellular growth. Of interest, it has recently been reported that a population of PrP resides in the mitochondria of normal disease-free cells and is endoproteolytically cleaved similar to total brain PrP [66]. This might offer the N-terminal peptides, especially N1 as the predominant N-terminal cleavage product, unhindered access to the mitochondria from inside the cell, directly facilitating an influence of the peptide on this organelle. Consequently, this might also have a bearing on the apparent lower efficacy of N1 in stimulating these responses. We have previously shown that N2 traffics from the cell surface to the mitochondria [41], but this has not, to our knowledge, been examined for N1. The N1 fragment may be more functionally effective in stimulating quiescence if generated at the site of action

(the mitochondria) rather than when it requires trafficking from the cell surface.

The role of SOD2 in regulating the cell cycle has become well characterised [67, 68]. Increased cellular levels of SOD2 are known to facilitate cellular transition to quiescence, whereas loss of SOD2 protein or increased superoxide signalling favours increased cellular growth [69, 70]. PrP has additionally been linked with SOD2 in the context of prion pathogenesis. During prion disease or prion infection of cells, changes of expression and activity of the SOD family of enzymes are seen, including a decrease in SOD2 protein levels [45, 71]. Correspondingly, neurogenesis during prion disease increases [39]. A further point to note when considering an influence of PrP-mediated signalling on SOD2 is that aberrations in SOD2 expression are linked with the uncontrolled cell cycling of cancer cells [68, 72]. Recently PrP expression has been linked with several cancers as well as the risk of metastases [73–75]. In addition to changes in mitochondrial SOD2, changes in mitochondrial fission and fusion have been linked with the uncontrolled cell cycling during cellular adaptation to the energy demands of cancer [76]. Regulation of SOD2 expression and mitochondrial dynamics by the N-terminal cleavage fragments of PrP or putatively the N-terminus in association with the full-length protein may explain why such disparate maladies are linked with this protein.

From our data, it would appear that detection of full-length PrP is predominantly observed in proliferating cells or cells residing alongside those that are actively proliferating, with quiescent cells staining only for C-terminal PrP. This might suggest that the signals stimulated by the N-terminal fragments can function in an autocrine or paracrine manner. Alpha-cleavage of PrP has been demonstrated to increase when PrP homodimerises at the cell membrane [77] and this may represent a mechanism for initiating intra/intercellular signalling. Questions remain as to the actions of full-length PrP, secretory (GPI-anchorless) PrP, C1, C2, or gamma cleaved PrP fragments in this pathway or cross-interactions with N1 and N2, but it seems highly likely that these proteins will be functional in their own right, bringing many more layers of complexity to the PrP function narrative.

Cross-talk between cellular redox signalling pathways and the mitochondria, and between the mitochondria and the nucleus, have been the subject of much study, but the role of the PrP N-terminal cleavage fragments as upstream modulators of these pathways has not previously been considered. As increased PrP expression levels are linked with increased growth of NSCs and herein we have linked the N-terminal cleavage fragments with reduced cell growth/increased cell quiescence, dynamic modulation of PrP cleavage may be part of an important cellular homeostatic mechanism. The modulation of redox signal transduction appears to be the first event influenced by the PrP cleavage fragments, after which the reduced intracellular ROS indicates that cells should enter a resting phase of life as modulated and maintained by their mitochondria. The diversity of the potential outcomes resulting from up-steam regulation of central redox signalling pathways in different cell types could have wide-reaching implications for many of the reported functions of PrP as this small protein begins to reveal its functional complexity.

Acknowledgements SJC is funded by an NH&MRC Practitioner Fellowship (#APP1105784). SCD is supported by a senior research fellowship administered by the faculty of Medicine, Dentistry and Health Sciences, University of Melbourne, and CLH was the recipient of a CJDSGN Rhonda McCoy memorial fellowship. This research was supported in part by the Intramural Research Program of the NIH, [NIAID].

Compliance with ethical standards

Conflict of interest The authors declare that they have no conflicts of interest.

References

1. Kempermann G (2011) Adult neurogenesis 2. Oxford University Press, Oxford
2. Eriksson PS, Perfilieva E, Bjork-Eriksson T, Alborn AM, Nordborg C, Peterson DA, Gage FH (1998) Neurogenesis in the adult human hippocampus. Nat Med 4(11):1313–1317. https://doi.org/10.1038/3305
3. Jin K, Peel AL, Mao XO, Xie L, Cottrell BA, Henshall DC, Greenberg DA (2004) Increased hippocampal neurogenesis in Alzheimer's disease. Proc Natl Acad Sci USA 101(1):343–347. https://doi.org/10.1073/pnas.2634794100
4. Wang YZ, Plane JM, Jiang P, Zhou CJ, Deng W (2011) Concise review: quiescent and active states of endogenous adult neural stem cells: identification and characterization. Stem Cells 29(6):907–912. https://doi.org/10.1002/stem.644
5. Akers KG, Martinez-Canabal A, Restivo L, Yiu AP, De Cristofaro A, Hsiang HL, Wheeler AL, Guskjolen A, Niibori Y, Shoji H, Ohira K, Richards BA, Miyakawa T, Josselyn SA, Frankland PW (2014) Hippocampal neurogenesis regulates forgetting during adulthood and infancy. Science 344(6184):598–602. https://doi.org/10.1126/science.1248903
6. Kitabatake Y, Sailor KA, Ming GL, Song H (2007) Adult neurogenesis and hippocampal memory function: new cells, more plasticity, new memories? Neurosurg Clin N Am 18 (1):105–113, x. https://doi.org/10.1016/j.nec.2006.10.008
7. Dupret D, Revest JM, Koehl M, Ichas F, De Giorgi F, Costet P, Abrous DN, Piazza PV (2008) Spatial relational memory requires hippocampal adult neurogenesis. PLoS One 3(4):e1959. https://doi.org/10.1371/journal.pone.0001959

8. Garthe A, Behr J, Kempermann G (2009) Adult-generated hippocampal neurons allow the flexible use of spatially precise learning strategies. PLoS One 4(5):e5464. https://doi.org/10.1371/journal.pone.0005464
9. Kempermann G (2008) The neurogenic reserve hypothesis: what is adult hippocampal neurogenesis good for? Trends Neurosci 31(4):163–169. https://doi.org/10.1016/j.tins.2008.01.002
10. Braun SM, Jessberger S (2014) Adult neurogenesis and its role in neuropsychiatric disease, brain repair and normal brain function. Neuropathol Appl Neurobiol 40(1):3–12. https://doi.org/10.1111/nan.12107
11. Peralta OA, Huckle WR, Eyestone WH (2011) Expression and knockdown of cellular prion protein (PrPC) in differentiating mouse embryonic stem cells. Differentiation 81(1):68–77. https://doi.org/10.1016/j.diff.2010.09.181
12. Steele AD, Emsley JG, Ozdinler PH, Lindquist S, Macklis JD (2006) Prion protein (PrPc) positively regulates neural precursor proliferation during developmental and adult mammalian neurogenesis. Proc Natl Acad Sci USA 103(9):3416–3421. https://doi.org/10.1073/pnas.0511290103
13. Prusiner SB (1982) Novel proteinaceous infectious particles cause scrapie. Science 216(4542):136–144
14. Lee YJ, Baskakov IV (2010) Treatment with normal prion protein delays differentiation and helps to maintain high proliferation activity in human embryonic stem cells. J Neurochem 114(2):362–373. https://doi.org/10.1111/j.1471-4159.2010.06601.x
15. Larson M, Sherman MA, Amar F, Nuvolone M, Schneider JA, Bennett DA, Aguzzi A, Lesne SE (2012) The complex PrP(c)-Fyn couples human oligomeric Abeta with pathological tau changes in Alzheimer's disease. J Neurosci 32(47):16857–16871a. https://doi.org/10.1523/jneurosci.1858-12.2012
16. Um JW, Strittmatter SM (2013) Amyloid-beta induced signaling by cellular prion protein and Fyn kinase in Alzheimer disease. Prion 7(1):37–41. https://doi.org/10.4161/pri.22212
17. Collins SJ, Tumpach C, Li QX, Lewis V, Ryan TM, Roberts B, Drew SC, Lawson VA, Haigh CL (2015) The prion protein regulates beta-amyloid mediated self-renewal of neural stem cells in vitro. Stem Cell Res Ther 6(1):60. https://doi.org/10.1186/s13287-015-0067-4
18. Petersen RB, Siedlak SL, Lee HG, Kim YS, Nunomura A, Tagliavini F, Ghetti B, Cras P, Moreira PI, Castellani RJ, Guentchev M, Budka H, Ironside JW, Gambetti P, Smith MA, Perry G (2005) Redox metals and oxidative abnormalities in human prion diseases. Acta Neuropathol 110(3):232–238. https://doi.org/10.1007/s00401-005-1034-4
19. Freixes M, Rodriguez A, Dalfo E, Ferrer I (2006) Oxidation, glycoxidation, lipoxidation, nitration, and responses to oxidative stress in the cerebral cortex in Creutzfeldt-Jakob disease. Neurobiol Aging 27(12):1807–1815. https://doi.org/10.1016/j.neurobiolaging.2005.10.006
20. Van Everbroeck B, Dobbeleir I, De Waele M, De Leenheir E, Lubke U, Martin JJ, Cras P (2004) Extracellular protein deposition correlates with glial activation and oxidative stress in Creutzfeldt-Jakob and Alzheimer's disease. Acta Neuropathol 108(3):194–200. https://doi.org/10.1007/s00401-004-0879-2
21. Brazier MW, Lewis V, Ciccotosto GD, Klug GM, Lawson VA, Cappai R, Ironside JW, Masters CL, Hill AF, White AR, Collins S (2006) Correlative studies support lipid peroxidation is linked to PrP(res) propagation as an early primary pathogenic event in prion disease. Brain Res Bull 68(5):346–354. https://doi.org/10.1016/j.brainresbull.2005.09.010
22. Brown DR, Nicholas RS, Canevari L (2002) Lack of prion protein expression results in a neuronal phenotype sensitive to stress. J Neurosci Res 67(2):211–224
23. Haigh CL, Brown DR (2006) Prion protein reduces both oxidative and non-oxidative copper toxicity. J Neurochem 98(3):677–689. https://doi.org/10.1111/j.1471-4159.2006.03906.x
24. Haigh CL, McGlade AR, Lewis V, Masters CL, Lawson VA, Collins SJ (2011) Acute exposure to prion infection induces transient oxidative stress progressing to be cumulatively deleterious with chronic propagation in vitro. Free Radic Biol Med 51(3):594–608. https://doi.org/10.1016/j.freeradbiomed.2011.03.035
25. Klamt F, Dal-Pizzol F, Conte da Frota ML Jr, Walz R, Andrades ME, da Silva EG, Brentani RR, Izquierdo I, Fonseca Moreira JC (2001) Imbalance of antioxidant defense in mice lacking cellular prion protein. Free Radic Biol Med 30(10):1137–1144
26. Milhavet O, McMahon HE, Rachidi W, Nishida N, Katamine S, Mange A, Arlotto M, Casanova D, Riondel J, Favier A, Lehmann S (2000) Prion infection impairs the cellular response to oxidative stress. Proc Natl Acad Sci USA 97(25):13937–13942. https://doi.org/10.1073/pnas.250289197
27. Wong BS, Liu T, Li R, Pan T, Petersen RB, Smith MA, Gambetti P, Perry G, Manson JC, Brown DR, Sy MS (2001) Increased levels of oxidative stress markers detected in the brains of mice devoid of prion protein. J Neurochem 76(2):565–572
28. Chen SG, Teplow DB, Parchi P, Teller JK, Gambetti P, Autilio-Gambetti L (1995) Truncated forms of the human prion protein in normal brain and in prion diseases. J Biol Chem 270(32):19173–19180
29. Lewis V, Johanssen VA, Crouch PJ, Klug GM, Hooper NM, Collins SJ (2016) Prion protein "gamma-cleavage": characterizing a novel endoproteolytic processing event. Cell Mol Life Sci 73(3):667–683. https://doi.org/10.1007/s00018-015-2022-z
30. Mange A, Beranger F, Peoc'h K, Onodera T, Frobert Y, Lehmann S (2004) Alpha- and beta- cleavages of the amino-terminus of the cellular prion protein. Biol Cell 96(2):125–132. https://doi.org/10.1016/j.biolcel.2003.11.007
31. Vincent B, Paitel E, Saftig P, Frobert Y, Hartmann D, De Strooper B, Grassi J, Lopez-Perez E, Checler F (2001) The disintegrins ADAM10 and TACE contribute to the constitutive and phorbol ester-regulated normal cleavage of the cellular prion protein. J Biol Chem 276(41):37743–37746. https://doi.org/10.1074/jbc.M105677200
32. Guillot-Sestier MV, Sunyach C, Druon C, Scarzello S, Checler F (2009) The alpha-secretase-derived N-terminal product of cellular prion, N1, displays neuroprotective function in vitro and in vivo. J Biol Chem 284(51):35973–35986. https://doi.org/10.1074/jbc.M109.051086
33. Haigh CL, Drew SC, Boland MP, Masters CL, Barnham KJ, Lawson VA, Collins SJ (2009) Dominant roles of the polybasic proline motif and copper in the PrP23-89-mediated stress protection response. J Cell Sci 122(Pt 10):1518–1528. https://doi.org/10.1242/jcs.043604
34. Le Belle JE, Orozco NM, Paucar AA, Saxe JP, Mottahedeh J, Pyle AD, Wu H, Kornblum HI (2011) Proliferative neural stem cells have high endogenous ROS levels that regulate self-renewal and neurogenesis in a PI3 K/Akt-dependant manner. Cell Stem Cell 8(1):59–71. https://doi.org/10.1016/j.stem.2010.11.028
35. Walton NM, Shin R, Tajinda K, Heusner CL, Kogan JH, Miyake S, Chen Q, Tamura K, Matsumoto M (2012) Adult neurogenesis transiently generates oxidative stress. PLoS One 7(4):e35264. https://doi.org/10.1371/journal.pone.0035264
36. Emsley JG, Mitchell BD, Kempermann G, Macklis JD (2005) Adult neurogenesis and repair of the adult CNS with neural progenitors, precursors, and stem cells. Prog Neurobiol 75(5):321–341. https://doi.org/10.1016/j.pneurobio.2005.04.002
37. Kokovay E, Wang Y, Kusek G, Wurster R, Lederman P, Lowry N, Shen Q, Temple S (2012) VCAM1 is essential to maintain the structure of the SVZ niche and acts as an environmental sensor to

regulate SVZ lineage progression. Cell Stem Cell 11(2):220–230. https://doi.org/10.1016/j.stem.2012.06.016
38. Yeo H, Lyssiotis CA, Zhang Y, Ying H, Asara JM, Cantley LC, Paik JH (2013) FoxO3 coordinates metabolic pathways to maintain redox balance in neural stem cells. EMBO J 32(19):2589–2602. https://doi.org/10.1038/emboj.2013.186
39. Gomez-Nicola D, Suzzi S, Vargas-Caballero M, Fransen NL, Al-Malki H, Cebrian-Silla A, Garcia-Verdugo JM, Riecken K, Fehse B, Perry VH (2014) Temporal dynamics of hippocampal neurogenesis in chronic neurodegeneration. Brain 137(Pt 8):2312–2328. https://doi.org/10.1093/brain/awu155
40. Karas JA, Boland M, Haigh C, Johanssen V, Hill A, Barnham K, Collins S, Scanlon D (2012) Microwave synthesis of prion protein fragments up to 111 amino acids in length generates biologically active peptides. Int J Pept Res Ther 18(1):21–29. https://doi.org/10.1007/s10989-011-9275-7
41. Haigh CL, McGlade AR, Collins SJ (2015) MEK1 transduces the prion protein N2 fragment antioxidant effects. Cell Mol Life Sci 72(8):1613–1629. https://doi.org/10.1007/s00018-014-1777-y
42. Schindelin J, Arganda-Carreras I, Frise E, Kaynig V, Longair M, Pietzsch T, Preibisch S, Rueden C, Saalfeld S, Schmid B, Tinevez J-Y, White DJ, Hartenstein V, Eliceiri K, Tomancak P, Cardona A (2012) Fiji: an open-source platform for biological-image analysis. Nat Meth 9(7):676–682. http://www.nature.com/nmeth/journal/v9/n7/abs/nmeth.2019.html#supplementary-information
43. Haigh CL, Lewis VA, Vella LJ, Masters CL, Hill AF, Lawson VA, Collins SJ (2009) PrPC-related signal transduction is influenced by copper, membrane integrity and the alpha cleavage site. Cell Res 19(9):1062–1078. https://doi.org/10.1038/cr.2009.86
44. Haigh CL, Tumpach C, Collins SJ, Drew SC (2016) A 2-substituted 8-hydroxyquinoline stimulates neural stem cell proliferation by modulating ROS signalling. Cell Biochem Biophys 74(3):297–306. https://doi.org/10.1007/s12013-016-0747-4
45. Sinclair L, Lewis V, Collins SJ, Haigh CL (2013) Cytosolic caspases mediate mislocalised SOD2 depletion in an in vitro model of chronic prion infection. Dis Model Mech 6(4):952–963. https://doi.org/10.1242/dmm.010678
46. Haigh CL, Tumpach C, Drew SC, Collins SJ (2015) The prion protein N1 and N2 cleavage fragments bind to phosphatidylserine and phosphatidic acid; relevance to stress-protection responses. PLoS One 10(8):e0134680. https://doi.org/10.1371/journal.pone.0134680
47. Brandner S, Isenmann S, Raeber A, Fischer M, Sailer A, Kobayashi Y, Marino S, Weissmann C, Aguzzi A (1996) Normal host prion protein necessary for scrapie-induced neurotoxicity. Nature 379(6563):339–343. https://doi.org/10.1038/379339a0
48. Graner E, Mercadante AF, Zanata SM, Forlenza OV, Cabral AL, Veiga SS, Juliano MA, Roesler R, Walz R, Minetti A, Izquierdo I, Martins VR, Brentani RR (2000) Cellular prion protein binds laminin and mediates neuritogenesis. Brain Res Mol Brain Res 76(1):85–92
49. Loubet D, Dakowski C, Pietri M, Pradines E, Bernard S, Callebert J, Ardila-Osorio H, Mouillet-Richard S, Launay JM, Kellermann O, Schneider B (2012) Neuritogenesis: the prion protein controls beta1 integrin signaling activity. FASEB J 26(2):678–690. https://doi.org/10.1096/fj.11-185579
50. Dickinson BC, Peltier J, Stone D, Schaffer DV, Chang CJ (2011) Nox2 redox signaling maintains essential cell populations in the brain. Nat Chem Biol 7(2):106–112. https://doi.org/10.1038/nchembio.497
51. Sonati T, Reimann RR, Falsig J, Baral PK, O'Connor T, Hornemann S, Yaganoglu S, Li B, Herrmann US, Wieland B, Swayampakula M, Rahman MH, Das D, Kav N, Riek R, Liberski PP, James MN, Aguzzi A (2013) The toxicity of antiprion antibodies is mediated by the flexible tail of the prion protein. Nature 501(7465):102–106. https://doi.org/10.1038/nature12402
52. Sorce S, Nuvolone M, Keller A, Falsig J, Varol A, Schwarz P, Bieri M, Budka H, Aguzzi A (2014) The role of the NADPH oxidase NOX2 in prion pathogenesis. PLoS Pathog 10(12):e1004531. https://doi.org/10.1371/journal.ppat.1004531
53. Schneider B, Mutel V, Pietri M, Ermonval M, Mouillet-Richard S, Kellermann O (2003) NADPH oxidase and extracellular regulated kinases 1/2 are targets of prion protein signaling in neuronal and nonneuronal cells. Proc Natl Acad Sci USA 100(23):13326–13331. https://doi.org/10.1073/pnas.2235648100
54. Mitra K (2013) Mitochondrial fission-fusion as an emerging key regulator of cell proliferation and differentiation. BioEssays News Rev Mol Cell Dev Biol 35(11):955–964. https://doi.org/10.1002/bies.201300011
55. Rambold AS, Kostelecky B, Elia N, Lippincott-Schwartz J (2011) Tubular network formation protects mitochondria from autophagosomal degradation during nutrient starvation. Proc Natl Acad Sci USA 108(25):10190–10195. https://doi.org/10.1073/pnas.1107402108
56. Brennan JP, Bardswell SC, Burgoyne JR, Fuller W, Schroder E, Wait R, Begum S, Kentish JC, Eaton P (2006) Oxidant-induced activation of type I protein kinase A is mediated by RI subunit interprotein disulfide bond formation. J Biol Chem 281(31):21827–21836. https://doi.org/10.1074/jbc.M603952200
57. Spalding KL, Bergmann O, Alkass K, Bernard S, Salehpour M, Huttner HB, Bostrom E, Westerlund I, Vial C, Buchholz BA, Possnert G, Mash DC, Druid H, Frisen J (2013) Dynamics of hippocampal neurogenesis in adult humans. Cell 153(6):1219–1227. https://doi.org/10.1016/j.cell.2013.05.002
58. Altmeppen HC, Prox J, Puig B, Kluth MA, Bernreuther C, Thurm D, Jorissen E, Petrowitz B, Bartsch U, De Strooper B, Saftig P, Glatzel M (2011) Lack of a-disintegrin-and-metalloproteinase ADAM10 leads to intracellular accumulation and loss of shedding of the cellular prion protein in vivo. Mol Neurodegener 6:36. https://doi.org/10.1186/1750-1326-6-36
59. Altmeppen HC, Puig B, Dohler F, Thurm DK, Falker C, Krasemann S, Glatzel M (2012) Proteolytic processing of the prion protein in health and disease. Am J Neurodegener Dis 1(1):15–31
60. McMahon HE, Mange A, Nishida N, Creminon C, Casanova D, Lehmann S (2001) Cleavage of the amino terminus of the prion protein by reactive oxygen species. J Biol Chem 276(3):2286–2291. https://doi.org/10.1074/jbc.M007243200
61. Yadavalli R, Guttmann RP, Seward T, Centers AP, Williamson RA, Telling GC (2004) Calpain-dependent endoproteolytic cleavage of PrPSc modulates scrapie prion propagation. J Biol Chem 279(21):21948–21956. https://doi.org/10.1074/jbc.M400793200
62. Garcia-Prat L, Martinez-Vicente M, Perdiguero E, Ortet L, Rodriguez-Ubreva J, Rebollo E, Ruiz-Bonilla V, Gutarra S, Ballestar E, Serrano AL, Sandri M, Munoz-Canoves P (2016) Autophagy maintains stemness by preventing senescence. Nature 529(7584):37–42. https://doi.org/10.1038/nature16187
63. Zeng F, Watt NT, Walmsley AR, Hooper NM (2003) Tethering the N-terminus of the prion protein compromises the cellular response to oxidative stress. J Neurochem 84(3):480–490
64. Boland MP, Hatty CR, Separovic F, Hill AF, Tew DJ, Barnham KJ, Haigh CL, James M, Masters CL, Collins SJ (2010) Anionic phospholipid interactions of the prion protein N terminus are minimally perturbing and not driven solely by the octapeptide repeat domain. J Biol Chem 285(42):32282–32292. https://doi.org/10.1074/jbc.M110.123398
65. Le Brun AP, Haigh CL, Drew SC, James M, Boland MP, Collins SJ (2014) Neutron reflectometry studies define prion protein N-terminal peptide membrane binding. Biophys J 107(10):2313–2324. https://doi.org/10.1016/j.bpj.2014.09.027
66. Faris R, Moore RA, Ward A, Race B, Dorward DW, Hollister JR, Fischer ER, Priola SA (2017) Cellular prion protein is present

in mitochondria of healthy mice. Sci Rep 7:41556. https://doi.org/10.1038/srep41556
67. Sarsour EH, Kalen AL, Goswami PC (2014) Manganese superoxide dismutase regulates a redox cycle within the cell cycle. Antioxid Redox Signal 20(10):1618–1627. https://doi.org/10.1089/ars.2013.5303
68. Sarsour EH, Kalen AL, Xiao Z, Veenstra TD, Chaudhuri L, Venkataraman S, Reigan P, Buettner GR, Goswami PC (2012) Manganese superoxide dismutase regulates a metabolic switch during the mammalian cell cycle. Cancer Res 72(15):3807–3816. https://doi.org/10.1158/0008-5472.can-11-1063
69. Sarsour EH, Venkataraman S, Kalen AL, Oberley LW, Goswami PC (2008) Manganese superoxide dismutase activity regulates transitions between quiescent and proliferative growth. Aging Cell 7(3):405–417. https://doi.org/10.1111/j.1474-9726.2008.00384.x
70. Zhang Y, Zhang HM, Shi Y, Lustgarten M, Li Y, Qi W, Zhang BX, Van Remmen H (2010) Loss of manganese superoxide dismutase leads to abnormal growth and signal transduction in mouse embryonic fibroblasts. Free Radic Biol Med 49(8):1255–1262. https://doi.org/10.1016/j.freeradbiomed.2010.07.006
71. Wong BS, Brown DR, Pan T, Whiteman M, Liu T, Bu X, Li R, Gambetti P, Olesik J, Rubenstein R, Sy MS (2001) Oxidative impairment in scrapie-infected mice is associated with brain metals perturbations and altered antioxidant activities. J Neurochem 79(3):689–698
72. Konzack A, Jakupovic M, Kubaichuk K, Gorlach A, Dombrowski F, Miinalainen I, Sormunen R, Kietzmann T (2015) Mitochondrial dysfunction due to lack of manganese superoxide dismutase promotes hepatocarcinogenesis. Antioxid Redox Signal 23(14):1059–1075. https://doi.org/10.1089/ars.2015.6318
73. Corsaro A, Bajetto A, Thellung S, Begani G, Villa V, Nizzari M, Pattarozzi A, Solari A, Gatti M, Pagano A, Wurth R, Daga A, Barbieri F, Florio T (2016) Cellular prion protein controls stem cell-like properties of human glioblastoma tumor-initiating cells. Oncotarget 7(25):38638–38657. https://doi.org/10.18632/oncotarget.9575
74. Liang J, Pan Y, Zhang D, Guo C, Shi Y, Wang J, Chen Y, Wang X, Liu J, Guo X, Chen Z, Qiao T, Fan D (2007) Cellular prion protein promotes proliferation and G1/S transition of human gastric cancer cells SGC7901 and AGS. FASEB J 21(9):2247–2256. https://doi.org/10.1096/fj.06-7799com
75. Martin-Lanneree S, Hirsch TZ, Hernandez-Rapp J, Halliez S, Vilotte JL, Launay JM, Mouillet-Richard S (2014) PrP(C) from stem cells to cancer. Front Cell Dev Biol 2:55. https://doi.org/10.3389/fcell.2014.00055
76. Tanwar DK, Parker DJ, Gupta P, Spurlock B, Alvarez RD, Basu MK, Mitra K (2016) Crosstalk between the mitochondrial fission protein, Drp1, and the cell cycle is identified across various cancer types and can impact survival of epithelial ovarian cancer patients. Oncotarget 7(37):60021–60037. https://doi.org/10.18632/oncotarget.11047
77. Beland M, Motard J, Barbarin A, Roucou X (2012) PrP(C) homodimerization stimulates the production of PrPC cleaved fragments PrPN1 and PrPC1. J Neurosci 32(38):13255–13263. https://doi.org/10.1523/jneurosci.2236-12.2012

Section 2: Prion Pathogenesis

Analogous to contemporary knowledge concerning the cellular biology of PrP^{C}, our understanding of the molecular factors influencing the risk of occurrence of sporadic prion disease and the primary cellular derangements or homeostatic failures that drive prion pathogenesis has advanced but remains incomplete. A more thorough understanding of these factors is an important facet of our progress in developing effective preventative and disease modifying therapies. To further assess for genetic risk factors outside of *PRNP* contributing to the occurrence of sCJD, I lead Australian collaborations in genome-wide association studies (GWAS) with the first suggesting involvement of the glutamate receptor metabotropic 8 gene while the more recent larger study implicated the syntaxin-6 and galactose-3-O-sulfotransferase-1 genes. The latter GWAS was more adequately powered through the larger number of disease and control chromosomes assessed and for the first time achieved genome-wide significance proving that loci outside of *PRNP* also influence the risk of sporadic CJD, thereby highlighting cellular pathways or processes likely to be pivotal to early pathogenesis.

For studies concerning the molecular mechanisms of pathogenesis, my research emphasized two streams: the role of prion infection in enhancing oxidative stress, with a number of original observations made; and characterization of the biophysical properties of neurotoxic PrP^{Sc}, along with the temporal occurrence of neurotoxic species during prion disease evolution, acute synaptic molecular derangements and the relationship between neurotoxic and transmitting PrP^{Sc} species. To undertake these latter studies, I designed and oversaw the development of a novel synaptic electrophysiology model that allowed these new insights regarding the biological impact and biophysical and infectious properties of neurotoxic PrP^{Sc}.

List of my publications submitted in full (in chronological order)

Collins S, Brazier M, Lewis V, Hill AF, Lawson V, Klug G, Masters CL. Extended period of asymptomatic prion disease after low dose inoculation: assessment of detection methods and implications for infection control. Neurobiology of Disease 2005; 20: 336-346.

Brazier MW, Lewis V, Ciccotosto GD, White AR, Hill AF, Cappai R, Ironside J, Lawson VA, Klug GM, Masters CL, Collins SJ. Correlative studies support lipid peroxidation is linked to

PrPres propagation as an early primary pathogenic event in prion disease. Brain Research Bulletin 2006; 68: 346-354.

Haigh CL, McGlade AJ, Lewis V, Masters CL, Lawson VA, Collins, SJ. Acute exposure to prion infection induces transient oxidative stress progressing to be cumulatively deleterious with chronic prion propagation in vitro. Free Radical Biology & Medicine 2011; 51: 594-608.

Lewis V, Klug GMA, Masters CL, Hill AF, Lawson VA, Collins SJ. Prion subcellular fractionation reveal infectivity spectrum with a high titre-low PrPSc disparity. Molecular Neurodegeneration 2012; 7: 18 (doi:10.1186/1750-1326-7-18).

Sinclair L, Lewis V, Collins SJ, Haigh CL. Cytosolic caspases mediate mislocalised SOD2 depletion in an in vitro model of chronic prion infection. Disease Models & Mechanisms 2013: 6: 952-963.

Sanchez-Juan P, Bishop M, Kovacs G, Calero M, Aulchenko Y, Ladogana A, Brandel J-P, Laplanche J, Boyd A, Lewis V, Calero O, Poleggi A, Carracedo A, van der Lee S, Rivadeneira F, Hofman A, Combarros O, Berciano J, Uitterlinden A, Haïk S, Collins S, Budka H, Pocchiari M, Zerr I, Knight R, Will R, van Duijn C. A genome wide association study links glutamate receptor pathway to Sporadic Creutzfeldt-Jakob disease risk. PLoS One 2015 DOI:10.1371/journal.pone.0123654.

Foliaki S, Lewis V, Adlard P, Finkelstein D, Coleman H, Lawson V, Collins S. Prion acute synaptotoxicity is largely driven by protease-resistant PrPSc species. PLoS Pathogens 2018 DOI: 10.1371/journal.ppat.1007214.

Foliaki S, Ellett L, Lewis V, Islam A, Senesi M, Finkelstein D, Roberts B, Lawson V, Adlard P, Collins S. Early existence and biochemical evolution characterise acutely synaptotoxic PrPSc. PLoS Pathogens: doi.org/10.1371/journal.ppat.1007712.

Ugalde C, Lewis V, Stehmann C, McClean C, Lawson V, Collins S, Hill A. Markers of A1 astrocytes stratify to molecular sub-types in sporadic Creutzfeldt-Jakob disease. Brain Communications doi:10.1093/braincomms/fcaa029.

Foliaki S, Lewis V, Islam AT, Senesi M, Finkelstein D, Ellett L, Lawson V, Adlard P, Roberts B, Collins S. PrPSc oligomerisation appears dynamic, quickly engendering inherent M1000 acute synaptotoxicity. Biophysical Journal 2020 119, 128–141.

Jones E, Hummerich H, Vire E, Uphill J, Dimitriadis A, Speedy H, Campbell T, Norsworthy P, Quinn L, Whitfield J, Linehan J, Jaunmuktane Z, Brandner S, Jat P, Nihat A, Mok T, Ahmed P, Collins S, Stehmann C, Sarros S, Kovacs G, Geschwind M, Golubjatnikov A, Budka H, Aguzzi A, Comic H, van der Lee S, Ibrahim-Verbaas C, Van Duijn C, Sikorska B, Golanska E, Liberski P, Calero M, Calero O, Sanchez Juan P, Ellacuriaga A, Martinon-torres F, Bouaziz-Amar E, Haik S, Laplanche J-L, Brandel J-P, Lambert J-C, Ladogana A, Parchi P, Bartoletti-Stella A, Capellari S, Poleggi A, Ladogana A, Pocchiari M, Aneli S, Matullo G, Knight R, Zafar S, Zerr I, Booth S, Coulthart M, Jansen G, Glisic K, Blevins J, Gambetti P, Safar J, Appleby B, Collinge J, Mead S. Genome-wide association study identifies risk variants for sporadic Creutzfeldt-Jakob disease in STX6 and GAL3ST1. Lancet Neurology 2020; 19: 840-848.

ELSEVIER

Neurobiology of Disease

www.elsevier.com/locate/ynbdi
Neurobiology of Disease 20 (2005) 336 – 346

Extended period of asymptomatic prion disease after low dose inoculation: Assessment of detection methods and implications for infection control

Steven J. Collins,[a,b,d,*] Victoria Lewis,[a,b,d] Marcus W. Brazier,[b,d] Andrew F. Hill,[b,c,d] Victoria A. Lawson,[b,d] Genevieve M. Klug,[a,b,d] and Colin L. Masters[a,b,d]

[a]*Australian National Creutzfeldt–Jakob Disease Registry, the University of Melbourne, Parkville, 3010 Victoria, Australia*
[b]*Department of Pathology, Level 5 Medical Building, the University of Melbourne, Parkville, 3010 Victoria, Australia*
[c]*Department of Biochemistry and Molecular Biology, the University of Melbourne, Parkville, 3010 Victoria, Australia*
[d]*Mental Health Research Institute of Victoria, Parkville, 3010 Victoria, Australia*

Received 2 August 2004; revised 17 March 2005; accepted 21 March 2005
Available online 27 April 2005

We used quantal dose-titration of a mouse-adapted human transmissible spongiform encephalopathy strain (M470) to compare different analytical methods for their ability to detect asymptomatic brain prion infection after low dose inoculation. At a time point approximately 2.5-fold beyond the mean incubation period of high dose inocula, asymptomatic brain infection was commonly observed using histologic examination, Western blot, and "blind" bioassay following intracerebral inoculation with low titer inocula. At this time point, when a clinical end-point titration would usually be determined, evidence of infection was seen in all healthy animals inoculated with up to 100-fold lower inoculation doses than the lowest causing consistent clinical disease. For the assessment of the presence of asymptomatic infection, we compared different Western immunoblot and histopathological methods in relation to "blind" bioassay using transgenic Tga/20 mice overexpressing mouse prion protein (PrP). Sodium phosphotungstic acid (NaPTA) precipitation of protease-resistant PrP isoforms (PrP^{res}) prior to Western blotting was found to approach the sensitivity of the Tga/20 bioassay and was superior to conventional Western blot and histopathological methods, wherein infectivity was commonly found when both of the latter were negative. Re-scaling the original titer by incorporating "blind" transmission data from surviving asymptomatic mice revises the estimate two orders of magnitude higher than the value derived using the conventional clinical disease outcome approach. We also found that the sensitivity of the NaPTA Western blot technique, if used with a diluent such as PBS compared with 10% normal brain homogenate, is adversely affected by up to around 20-fold. We postulate that infectious titer estimates based on more sensitive detection systems such as we report provide a more accurate indication of ultimate transmission risk.

Keywords: Prions; Creutzfeldt–Jakob disease; Asymptomatic infection; Preclinical infection; Subclinical infection; Transmissible spongiform encephalopathy; Detection methods

Introduction

The transmissible spongiform encephalopathies (TSEs) constitute a group of neurodegenerative disorders, which includes Creutzfeldt–Jakob disease (CJD) and its variant form (vCJD) in humans, as well as scrapie in sheep and bovine spongiform encephalopathy (BSE) (Prusiner, 1997). After the onset of clinical disease, all are invariably fatal disorders sharing neuropathological hallmarks such as spongiform change, neuronal loss, gliosis, and accumulation of abnormal isoforms of the host encoded prion protein. An underlying feature of TSEs is the conversion of the normal cellular form of the prion protein (PrP^{c}), a glycosylphosphatidylinositol-anchored cell surface protein, into a protease-resistant conformer (PrP^{res}; considered hereafter as equivalent to PrP^{sc}, the abnormal protease-resistant conformers found in scrapie), a process intimately linked to infectivity and neurodegeneration (Prusiner, 1997). Much progress in clarifying the molecular details of this conversion process has been made, but a complete and detailed understanding remains to be achieved. Notwithstanding this, the detection of abnormal isoforms of PrP serves as a very useful and reliable marker of disease and infectivity, both for diagnostic and experimental purposes in humans and animals.

CJD is the most common human TSE, but remains rare, with an incidence of only 1–1.5/million/year in comprehensive national

* Corresponding author. c/o Australian National Creutzfeldt–Jakob Disease Registry, Department of Pathology, Level 5 Medical Building, the University of Melbourne, Parkville, 3010 Victoria, Australia. Fax: +61 3 8344 4004.
E-mail address: stevenjc@unimelb.edu.au (S.J. Collins).
Available online on ScienceDirect (www.sciencedirect.com).

0969-9961/$ - see front matter © 2005 Elsevier Inc. All rights reserved.
doi:10.1016/j.nbd.2005.03.014

surveillance studies (Collins et al., 2002b). Only a small proportion (10–15%) of CJD can be accounted for by mutations in the prion protein gene (*PRNP*) or as a consequence of recognizable transmission events (1–2%), with the majority (approximately 85%) occurring without identifiable cause (sporadic). Although uncertainty persists, the prevailing concept is that sporadic CJD arises as a consequence of either rare somatic mutations in the neuronal *PRNP* pool or secondary to a spontaneous conformation change in PrP^{c} (Prusiner, 1997). An alternative hypothesis is that a proportion of apparently sporadic CJD may be due to unrecognized, low-level, contamination events. Large risk factor case-control studies lend some support to this postulate (Collins et al., 1999; Ward et al., 2002), but detailed analysis of spatiotemporal clustering of sporadic CJD has been unable to substantiate plausible transmission pathways (Collins et al., 2002a). Although convincing evidence for either of these two etiological explanations is lacking, additional circumstantial support for the covert transmission hypothesis is derived from a number of studies, including primate and mouse paradigms, showing evidence of TSE infection for lengthy periods prior to the onset of overt disease.

A common theme in murine models of prolonged asymptomatic TSE infection is that "inefficient" introduction of the infectious inoculum, by using peripheral (Collis and Kimberlin, 1985; Dickinson et al., 1975; Zlotnik, 1965) or low-titer (Thackray et al., 2002) inoculations, donor–host species barriers to the particular TSE strain (Asante et al., 2002; Hill et al., 2000; Race et al., 2001, 2002), or more resistant recipient transgenic mice (Büeler et al., 1994; Frigg et al., 1999), results in very prolonged incubation periods (preclinical infection) or complete failure to induce clinical disease during the normal lifespan of the host animal (subclinical infection). A possible additional intraspecies explanation for inefficient transmission is that despite development of TSE, the PrP^{res} produced may not be physically competent to subserve PrP^{c} conversion. Irrespective of the mechanism, for much of the extended asymptomatic phase, peripheral organs such as the spleen, as well as the brain, harbor levels of infectivity often comparable to those seen in terminally sick animals (Büeler et al., 1994; Collis and Kimberlin, 1985; Dickinson et al., 1975; Frigg et al., 1999; Thackray et al., 2002). Acknowledging that the extended incubation period may exceed the lifespan of the host (Dickinson et al., 1975), differentiation between preclinical and subclinical infection may be impossible, but does not detract from the fundamental importance of this phenomenon, especially as it relates to potential unrecognized transmission during the provision of health care. Recent reports of PrP^{res} detection in the skeletal muscles and spleens in some patients with sporadic CJD (Glatzel et al., 2003), as well as the likely secondary transmission through blood transfusion from a presymptomatic vCJD patient (Llewelyn et al., 2004), further add to the concerns generated by previous studies. Of these, the demonstration of PrP^{res} in peripheral lymphoreticular organs of living vCJD patients (Hill et al., 1999; Wadsworth et al., 2001) is of particular interest and supports the hypothesis that transmission is possible for a lengthy period before the onset of clinical disease (Hilton et al., 1998, 2002, 2004).

We undertook the present study to assess the prevalence of asymptomatic TSE infection in a model that in part simulates hypothesized neurosurgical contamination events in the health care setting, such as may occur through intracranial surgery performed unwittingly on a patient with early symptomatic sporadic CJD. Based on the premise that health care transmissions most likely involve very low infectious doses, we employed a standard quantal dose-titration paradigm using a human-derived TSE strain in non-transgenic host animals. A concomitant aim of the study was to carefully compare bioassay with the utility of standard biochemical and histopathological methods for detection of presymptomatic TSE infection, which is of relevance to screening for potential infectivity in at risk populations such as dura mater and human-derived pituitary hormone recipients. In comparative studies, we found that a high sensitivity Western blot technique utilizing a metal-enhanced (sodium phosphotungstic acid [NaPTA]) precipitation method nearly approximated the sensitivity of bioassay, as recently reported when used in a different in vitro technique (Safar et al., 2002; Wadsworth et al., 2001). Similar to others (Hill et al., 2000; Lee et al., 2000; Race et al., 2001), we determined that bioassay using highly susceptible recipient animals was clearly superior to conventional biochemical PrP^{res} detection methods and routine neuropathological examination. Finally, we also assessed factors affecting the sensitivity of the NaPTA Western blot technique as a screening method for potential asymptomatic TSE infection.

Methods

Mice and inoculations

The strain (M470) used for all experiments is a mouse-adapted form of human TSE derived from a patient dying from probable Gerstmann–Sträussler–Scheinker syndrome (GSS) (Tateishi et al., 1979). For initial calculation of infectious titer, a 10% homogenate (w/v) in phosphate-buffered saline (PBS) of pooled whole brains from mice dying from TSE was serially log diluted in PBS with concentrations spanning 10^{-1} to 10^{-9}. Prepared dilutions of inocula were immediately used for intracerebral inoculations of groups of six random outbred weanling female *Balb/c* mice (except the 10^{-9} dilution when only three mice were used). Approximately 30 μl of the appropriate dilution was injected into the left parietal region under methoxyflurane anesthesia. Unused inocula were stored at −80°C until subsequent use for Western immunoblot studies. Titer estimations were according to the method of Reed and Muench (1938).

Prior experiments employing an analogous human TSE strain (M1000) in *Balb/c* mice had demonstrated the earliest presence and highest amounts of PrP^{res} occurred in brain regions approximating the telencephalic subcortical gray nuclei and thalamus (authors' unpublished data). For bioassays assessing asymptomatic infection, 30-μl aliquots of 1% homogenates made from this brain region from individual *Balb/c* mice were inoculated intracerebrally into groups of 3–5 male and female weanling Tga/20 transgenic (PrP^{c} overexpressing) mice (Fischer et al., 1996). Brain tissues from *Balb/c* mice receiving the original 10^{-9} inoculum dilution were not subject to bioassay.

Inoculated *Balb/c* and Tga/20 mice were observed daily for signs of TSE. Animals were sacrificed under methoxyflurane anesthesia when persistent signs consistent with murine TSE were evident, such as reduced motor activity, weight loss, hunched posture, hind limb paresis, and ataxia. Mice were given food and water ad libitum, with all handling according to prescribed national guidelines, and ethical approval from the University of Melbourne Animal Ethics Committee.

Histology and immunohistochemistry

Brains were sagittally hemi-sectioned, with one-half fixed in 10% buffered formalin and the other homogenized to 10% (w/v) in PBS. Fixed brains were immersed in 99% formic acid for 1 h prior to routine processing and staining. Half-brains were paraffin embedded and 6-μm sections cut and mounted on glass slides. Sections were de-paraffinized and rehydrated through a graded ethanol series to de-ionized water, and either stained with hematoxylin and eosin or treated by hydrolytic autoclaving for 20 min at 132°C. Once cooled, autoclaved sections were washed and treated with 96% formic acid for 5 min, then exposed to 4 M guanidine thiocyanate for 2 h at 4°C. After blocking with 20% normal rabbit serum (Dako, Carpinteria, CA) for 30 min, sections were incubated with ICSM 18 anti-PrP monoclonal antibody 1:500 overnight at 4°C (White et al., 2003). Following sequential incubation in biotinylated rabbit anti-mouse secondary antibody (1:500) and HRP-conjugated streptavidin (1:1000) (Dako) for 30 min each at room temperature, diaminobenzidine (Dako) was added.

Only the more specific and reliably quantifiable neuropathological findings of spongiform change and PrP-positive plaque deposition were scored. The degree of brain vacuolation and the presence of PrP^{res} immunostaining were visually graded: 0 = normal; + = mild; ++ = moderate; +++ = severe/prominent (equivalent to what is seen in mice with terminal TSE).

Western immunoblots

Conventional Western blots were performed as described previously with minor modifications (Lewis et al., 2003). Briefly, to 50-μl aliquots of 10% brain homogenate, 0.5 μl Benzonase (25 U/μl) (Novagen, Merck, Damstadt, Germany) and 0.5 μl of 1 M $MgCl_2$ were added and incubated for 5 min at 37°C, followed by digestion with proteinase K (PK; Sigma, St Louis, MO) (final concentration 100 μg/ml) for 1 h at 37°C. Digestion was halted by adding Pefabloc (final concentration 5 mM) (Roche Diagnostics, Mannheim, Germany) and the same total volume of 2× sample buffer (containing 6% beta-mercaptoethanol) and boiling for 10 min. Samples were briefly centrifuged at low speed (1000 rpm) (Eppendorf 5415C, Hamburg, Germany) and electrophoresed on precast 12% tris-glycine gels (Invitrogen Novex, San Diego, CA). Proteins were transferred to nitrocellulose membranes (Trans-Blot; BIORAD, Hercules, CA) at 380 mA for 45 min, with the filter then blocked for 1 h at room temperature in 5% non-fat milk in PBS-T (PBS containing 0.5% Tween 20). Membranes were incubated overnight at 4°C using the anti-PrP monoclonal antibody ICSM 18 (1:25,000 in PBS-T) (White et al., 2003). Signal was detected, after incubation for 1 h at 37°C with an HRP-conjugated anti-mouse secondary antibody using ECL or ECL Plus (Amersham, Buckinghamshire, UK).

NaPTA precipitation prior to Western immunoblot was undertaken according to a previously reported method (Wadsworth et al., 2001). To 500 μl of 10% (w/v) brain tissue homogenates in PBS, an equal volume of 4% (w/v) Sarkosyl (Sigma) in PBS pH 7.4 was added, vortexed, and incubated for 10 min at 37°C with constant agitation. Benzonase (Novagen) and $MgCl_2$ were added to 50 U/ml and 1 mM, respectively, and incubated at 37°C for 30 min with vigorous agitation. To this, 81.3 μl of a pre-warmed (to 37°C) 4% (w/v) NaPTA/170 mM $MgCl_2$ solution (pH 7.4) was added, vortexed, and incubated with vigorous agitation for 30 min at 37°C. Samples were then centrifuged at 15,000 × *g* for 30 min, after which supernatants were carefully removed and the remaining pellets resuspended in 20 μl of PBS/0.1% Sarkosyl (pH 7.4), followed by PK digestion, electrophoresis using the entire sample, and Western blotting as described above, except proteins were transferred to polyvinylidine difluoride membranes (Immobilon-P; Millipore Corporation, Bedford, MA). ECL Plus was used for signal detection. Often, for individual mice, sufficient brain tissue was available to allow only a single Western blot using NaPTA precipitation. In occasional mice, less than 500 μl of 10% brain homogenate was available, prompting proportional adjustments of the various treatment steps, including the resuspension of pellets and amounts loaded onto resolving gels after the addition of sample buffer. Brain tissue spiking experiments determined reproducible lower limits of sensitivity, which were then used as an internal control for each NaPTA Western immunoassay, whereby 1 μl of a 1% whole brain homogenate from a mouse dying from TSE was always clearly detectable in a 500-μl aliquot of a 10% homogenate of normal mouse brain.

To determine levels of detection sensitivity, the brain of a *Balb/c* mouse confirmed to have died from TSE was made into a 10% homogenate (w/v) in PBS. In one experiment, a series of samples equivalent to 50, 10, 6, 3, 1, and 0.6 μg wet weight diseased brain were added to separate 500-μl aliquots of 10% brain homogenate from uninoculated mice for subsequent Western blot analysis following NaPTA precipitation. In a separate experiment, 2 μl of a 1% diseased brain homogenate was added to 500-μl aliquots of PBS, a 10% normal brain homogenate, and a 10% brain homogenate from a mouse with the *PRNP* gene ablated ($PrP^{o/o}$) (Büeler et al., 1993), with the samples subjected to NaPTA precipitation and Western blotting (as described below); half of each sample was digested with proteinase K (PK) (as described below). In addition, 1-μl aliquots of a 1% diseased brain homogenate were added to 9 μl of PBS for Western blotting both without and after digestion by PK. These were not subject to NaPTA precipitation and served as a baseline to assess the comparative efficiency of PrP^{res} retrieval from the equivalent of 1 μl of a 1% disease brain homogenate spiked into different diluents, as well as more directly assess the issue of whether an altered ratio of protease to total protein concentration was a significant factor contributing to any reduction in signal when using PBS as diluent.

Results

Titer of infectivity in Balb/c mice based on clinical disease

To facilitate a comparative assessment of markers of asymptomatic infection and to more thoroughly determine the extent and frequency of asymptomatic disease after low titer intracerebral inoculation, we generated asymptomatic infection in *Balb/c* mice using a standard quantal end-point titration assay. Based on the development of clinically apparent disease (Table 1), infectivity of M470 was calculated as 2.5×10^7 ID_{50} units/g brain. Not unexpectedly at higher dilutions, occasional *Balb/c* mice manifested TSE after extended incubation periods, including the deaths of two from the 10^{-4} inoculum dilution cohort at 391 and 399 days post-inoculation (PI). Prompted by these late deaths (approximately 21/2 times the mean incubation period for highest titer intracerebral inoculation), we considered it an appropriate time to

Table 1
Summary of quantal, end-point, dose-titration of the M470 strain in *Balb/c* mice

Inoculum dilution[a]	Clinical TSE/total inoculated[b]	Mean incubation period (days) ± SEM
10^{-1}	6/6	162 ± 3.4
10^{-2}	6/6	171 ± 4.4
10^{-3}	6/6	177 ± 5.5
10^{-4}	5/5	291 ± 38.8[c]
10^{-5}	2/6	283 ± 0.0
10^{-6}	0/6	
10^{-7}	1/6	240
10^{-8}	0/5	
10^{-9}	0/3	

SEM, standard error of the mean.
[a] Dilutions of 10% (w/v) brain homogenate.
[b] Four remaining healthy mice from each initial dilution of 10^{-5} to 10^{-8} and the three healthy mice from initial dilution 10^{-9} were sacrificed for assessment of preclinical TSE: 10^{-5} and 10^{-6} dilutions on day 401 PI, and the others on day 402 PI.
[c] Two mice developed signs of TSE and died at 391 and 399 days PI, respectively; mean incubation period (±SEM) for the other three mice was 221 (±11.8) days.

assess the prevalence of asymptomatic infection in the remaining mice. For this purpose, four healthy mice from each group inoculated with initial dilutions of 10^{-5} to 10^{-8} and the three healthy mice from the initial dilution 10^{-9} were sacrificed; mice from the 10^{-5} and 10^{-6} dilutions on day 401 PI, and the others on day 402 PI (Table 1 and Fig. 1). Two further healthy mice from the 10^{-6} dilution that were culled at day 496 PI, and one from the 10^{-7} dilution culled at day 498 PI, were inadvertently discarded and not subjected to further analysis. The last remaining mouse from the original 10^{-8} inoculation group was observed for TSE over its normal lifespan. This single mouse died suddenly without preceding illness at 740 days PI with the brain negative for PrP^{res} on Western blot (data not shown). Using a combination of PrP^{res} detection techniques, we then undertook assessment of these long surviving *Balb/c* mice for evidence of asymptomatic disease, none of which had demonstrated any definite or fluctuating clinical signs of murine TSE prior to sacrifice.

Assessment of asymptomatic infection and comparison of biochemical techniques, routine neuropathological markers, and bioassay

Tables 2 and 3 summarize the results of investigations to assess the presence of asymptomatic infection in long surviving healthy *Balb/c* mice from the original quantal end-point titration. Morphological examination of the brains of these mice showed typical spongiform change and PrP-positive plaques in three of four mice (numbers 5.1, 5.3, and 5.4) from the 10^{-5} dilution and one of four mice (number 6.4) from the 10^{-6} dilution, with remaining mice, including all those from the higher dilutions, not revealing any neuropathological abnormalities (Table 2). The neuropathological changes observed in asymptomatic mice were stereotyped and qualitatively similar but less developed than those seen in terminally sick mice (Figs. 2A, B, and E–G), although there were exceptions in which the changes approached this level of severity (compare Fig. 2C with D). Spongiform change was always first evident and most marked in the hippocampus and peri-hippocampal regions but could be widespread throughout the cerebral hemispheres and brain stem, often emphasized in the thalamus. Vacuolation and PrP-positive plaques always occurred concurrently in asymptomatically infected mice. In contrast to spongiform change, however, the plaque deposition was most prominent, and often restricted to, the thalamus. In asymptomatically infected mice, regions prone to substantial neuronal loss in this murine model (the stratum pyramidale of the hippocampus and dorsal thalamic area) showed only equivocal reductions, with this only observed in those animals with prominent vacuolation and PrP-positive plaques.

Conventional Western blots showed complete concordance with the neuropathological findings. PrP^{res} was only detected in those brains displaying typical morphological abnormalities and PrP-

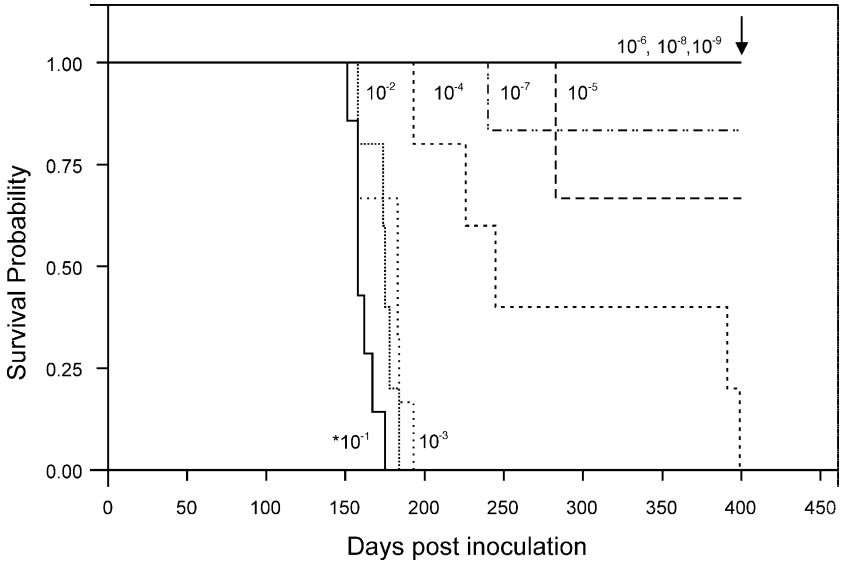

Fig. 1. Kaplan–Meier survival plots of *Balb/c* mice used for M470 titer estimation employing quantal dose-titration and clinical outcome, as well as the generation of asymptomatic infection. *Inoculum dilution cohorts ranged from 10^{-1} to 10^{-9}. The arrow depicts the time point (day 401 or 402 post-inoculation) at which remaining healthy mice were sacrificed for assessment of preclinical TSE.

Table 2
Summary of conventional and NaPTA precipitation Western blot results and morphological investigations to assess the presence of subclinical infection in surviving *Balb/c* mice inoculated with higher dilutions

Balb/c mouse no. from original inoculation cohorts	Original inoculum dilution	Conventional Western blot for brain PrP^{res}	Routine histology of brain for vacuolation[a]	Brain IHC for PrPres plaques[a]	NaPTA precipitation Western blot for brain PrP^{res}
5.1	10^{-5}	Pos	++	+	ND
5.2	10^{-5}	Neg	0	0	Neg
5.3	10^{-5}	Pos	+/++	++	ND
5.4	10^{-5}	Pos	++/+++	+/++	ND
6.1	10^{-6}	Neg	0	0	Pos
6.2	10^{-6}	Neg	0	0	Pos
6.3	10^{-6}	Neg	0	0	Pos
6.4	10^{-6}	Pos	++/+++	++	ND
7.1	10^{-7}	Neg	0	0	Neg
7.2	10^{-7}	Neg	0	0	Neg
7.3	10^{-7}	Neg	0	0	Neg
7.4	10^{-7}	Neg	0	0	Neg
8.1	10^{-8}	Neg	0	0	Neg
8.2	10^{-8}	Neg	0	0	Neg
8.3	10^{-8}	Neg	0	0	Neg
8.4	10^{-8}	Neg	0	0	Neg
9.1	10^{-9}	Neg	0	0	ND
9.2	10^{-9}	Neg	0	0	ND
9.3	10^{-9}	Neg	0	0	ND

ND, not determined; Pos, positive; Neg, negative; NaPTA, sodium phosphotungstic acid; IHC, immunohistochemistry.
[a] The degree of brain vacuolation and the presence of PrP^{res} immunostaining were visually graded: 0 = normal; + = mild; ++ = moderate; +++ = severe/prominent (the latter changes equivalent to what is seen in terminally sick mice).

positive plaques (Table 2). The estimated infectivity in these surviving mice (determined by incubation time interval assay in indicator Tga/20 mice and regression analysis using the method of least squares) was found to fall within the range of $3.2–7.0 \times 10^4$ ID_{50} units per 30 μl of inoculum (Fig. 3). Surprisingly, the infectivity in some asymptomatic M470-infected *Balb/c* mice was almost equivalent to that in terminally sick mice when a mean survival of 56 days corresponds to inoculation with 1.9×10^5 ID_{50} units.

Despite the absence of PrP^{res} by conventional Western immunoblot assay and lack of morphological evidence of preclinical infection, bioassay in Tga/20 mice confirmed infectivity in all remaining mice from the 10^{-5} and 10^{-6} dilution cohorts, and also in two mice from the 10^{-8} dilution cohort. The more sensitive Western blot method incorporating NaPTA precipitation was then used to assess the presence of PrP^{res} in those brains considered normal neuropathologically and negative for PrP^{res} by the conventional Western immunoblot. In contrast to the negative findings with the conventional Western blot, the NaPTA precipitation method was able to detect faint but definite PrP^{res} signal in all three remaining mice (numbers 6.1, 6.2, and 6.3) from the original 10^{-6} dilution cohort (Fig. 4A, lanes 6–8). We were not convinced of a definite PrP^{res} signal for the single 10^{-5} mouse (number 5.2) examined (Fig. 4A, lane 5) despite the presence of infectivity by bioassay. PrP^{res} was not detected in any of the mice from each of the 10^{-7} group and 10^{-8} groups (data not shown). These results show that in this model of preclinical disease, a conventional Western blot is able to reliably detect PrP^{res} when infectivity is $>3.2 \times 10^4$ ID_{50} units per inoculum, whereas methods employing NaPTA precipitation can often detect PrP^{res} when the infectivity is $<2.0 \times 10^2$ ID_{50} units. Hence, when working at the lower limits of infectious titers in brains harboring preclinical disease, detection of PrP^{res} by immunoblotting after NaPTA precipitation shows a much better correlation with transmissibility in a sensitive bioassay than conventional Western immunoblot and routine morphological markers, and at a practical level detects almost all brains with potential infectivity.

Western immunoblots and neuropathological examination of recipient Tga/20 mice and revised titer estimate based on asymptomatic transmissions

Deaths from murine TSE in Tga/20 mice were confirmed by Western blot detection of PrP^{res} in the brains of all mice dying beyond 100 days PI (Fig. 4B, compare lane 8 with lanes 9 and 10). Tga/20 mice dying from typical TSE less than 100 days PI were not routinely examined. Whole brain homogenates of Tga/20 mice dying from TSE displayed abundant amounts of PrP^{res} with typical banding patterns and the characteristic mobility shift following PK digestion (Fig. 4B, lanes 6, 7, and 9–11). The remaining inoculated but long-term surviving Tga/20 mice originally receiving the 10^{-6}, 10^{-7}, and 10^{-8} inocula were sacrificed at 218, 234, and 241 days PI (Table 3), and their brains assessed for evidence of murine TSE. Characteristic histological and immunohistochemical features of murine TSE were absent in these Tga/20 mice.

Supplementing the morphological exclusion of preclinical transmissions in inoculated but long-term surviving Tga/20 mice, the brains of all healthy animals at time of sacrifice were subjected to NaPTA precipitation and Western immunoblot. Unexpectedly, despite treatment with PK (100 μg/ml final concentration), two protease-resistant bands of variable intensity were often detected in the brains of these healthy Tga/20 mice (Fig. 4B, lanes 5 and 8). The two bands seen were always much less intense than those observed in mice dying from TSE (Fig. 4B, compare lane 8 with lanes 9–11). Further, the banding pattern could be clearly differentiated from that seen in terminally ill mice, with the upper

Table 3
Summary of Tga/20 bioassays to clarify the presence of asymptomatic infection in surviving *Balb/c* mice inoculated with higher dilutions

Balb/c mouse no. from original inoculation cohorts	Original inoculum dilution	NaPTA precipitation Western blot for brain PrP^{res} [a]	Tga/20 mice developing clinical TSE/total mice inoculated	Positive Western blot for PrP^{res} in brains of selected Tga/20 mice/total assessed	Mean incubation period in Tga/20 mice in days; (range)	Estimate of infectious dose inoculated (ID_{50} units)[b]
5.1	10^{-5}	ND	4/4	ND	62 (61–65)	7.0×10^4
5.2	10^{-5}	Neg	2/3[c]	2/3[c]	114 (107–120)	$<2.0 \times 10^2$
5.3	10^{-5}	ND	4/4	1/1	68 (65–72)	3.2×10^4
5.4	10^{-5}	ND	4/4	1/1	65 (63–68)	5.1×10^4
6.1	10^{-6}	Pos	3/4[d]	3/4	133 (98–202)	$<2.0 \times 10^2$
6.2	10^{-6}	Pos	3/4[d]	3/4	140 (123–154)	$<2.0 \times 10^2$
6.3	10^{-6}	Pos	4/4	2/2	83 (79–86)	3.3×10^3
6.4	10^{-6}	ND	3/3	ND	64 (62–65)	6.0×10^4
7.1	10^{-7}	Neg	0/5[e]	0/5		
7.2	10^{-7}	Neg	0/5[e]	0/5		
7.3	10^{-7}	Neg	0/5[e,f]	0/5		
7.4	10^{-7}	Neg	0/5[e]	0/5		
8.1	10^{-8}	Neg	1/5[g]	1/5	142	$<2.0 \times 10^2$
8.2	10^{-8}	Neg	0/4[g]	0/4		
8.3	10^{-8}	Neg	0/5[g]	1/5[h]		
8.4	10^{-8}	Neg	1/4[g]	1/4	129	$<2.0 \times 10^2$
9.1	10^{-9}	ND	ND	ND		
9.2	10^{-9}	ND	ND	ND		
9.3	10^{-9}	ND	ND	ND		

ND, not determined.
[a] This column of data repeated from Table 2.
[b] Based on incubation time interval assay using the linear regression equation $\log X = (Y - 135.98/-15.07)$ derived from quantal dose-titrations in Tga/20 mice using the same prion M470 strain.
[c] The third mouse was culled 214 days PI because of illness, with brain negative for PrP^{res} on Western immunoblot.
[d] Single remaining healthy mouse culled 218 days PI; brain negative for PrP^{res} on both Western immunoblot and immunohistochemistry, with no evidence of vacuolation.
[e] Remaining mice were healthy when culled 234 days PI.
[f] Single mouse found dead at 228 days PI; brain negative for PrP^{res} on Western blot.
[g] Remaining mice were healthy when culled at 241 days PI.
[h] The brain of a single healthy mouse at time of cull was positive for PrP^{res} on Western blot.

band appearing of similar mobility to non-PK-digested diglycosylated PrP, approximately 35 kDa (consistent with incomplete protease digestion), and the second band displaying a relative mobility (approximately 25–26 kDa) between those of the di- and mono-glycosylated bands seen after PK digestion in brain homogenates from terminal mice. These findings were confirmed in conventional Western blots, and also in brain homogenates from age-matched, uninoculated, and sham brain-inoculated Tga/20 mice (Fig. 4B, lane 5), and when probing with a different anti-PrP monoclonal antibody (6H4; Prionics, Switzerland) (data not shown); secondary antibody alone gave no signal (data not shown). Nevertheless, the quantitative and qualitative differences allowed confident differentiation of normal or sham brain-inoculated mice from those dying of TSE. Despite the absence of neuropathological features of murine TSE, a single healthy Tga/20 mouse culled at 241 days PI, inoculated with the brain of a mouse receiving the original 10^{-8} dilution (Table 3), was clearly positive for PrP^{res} (data not shown). Although the banding pattern was typical, the intensity was considerably less than seen in animals dying from terminal illness, consistent with incubating disease.

Based on this evidence of asymptomatic infection using more sensitive detection methods, a revised estimate of the original M470 inoculum titer in *Balb/c* mice is at least 1.3×10^9 ID_{50} units/g brain. This value is two orders of magnitude greater than the ID_{50} based solely on the development of clinical disease and is a likely underestimate because not all surviving *Balb/c* mice were subject to bioassay in Tga/20 mice.

Comparison of bioassay with biochemical indicators of potential infectivity in the original inocula and in "spiked" normal and other brain homogenates

Given the increased sensitivity using Western immunoblots after NaPTA precipitation to detect PrP^{res} at levels correlating with very low titers of infectivity in the brains of mice harboring asymptomatic prion disease, we undertook a series of additional experiments to assess the utility of this technique in other situations. The original inoculum dilution series was assayed biochemically for the presence of PrP^{res} using both Western blot methods and compared with bioassay. At best, conventional Western blot analysis showed a very faint signal at the 10^{-1} dilution (representing a 1:100 final dilution, approximating 100 μg brain loaded onto each lane of a gel) after prolonged exposure, which was more evident using enhanced chemiluminescent (ECL Plus) detection (data not shown). Using the NaPTA pre-treatment, PrP^{res} was detectable at the 10^{-2} dilution (equating 1:1000 final dilution; approximating 250 μg brain loaded onto each lane of a gel) (Fig. 5A, lane 6), but not the 10^{-3} dilution (equating 1:10,000 final dilution; approximating 25 μg brain loaded onto each lane of a gel), with further titration showing a detection limit at a final

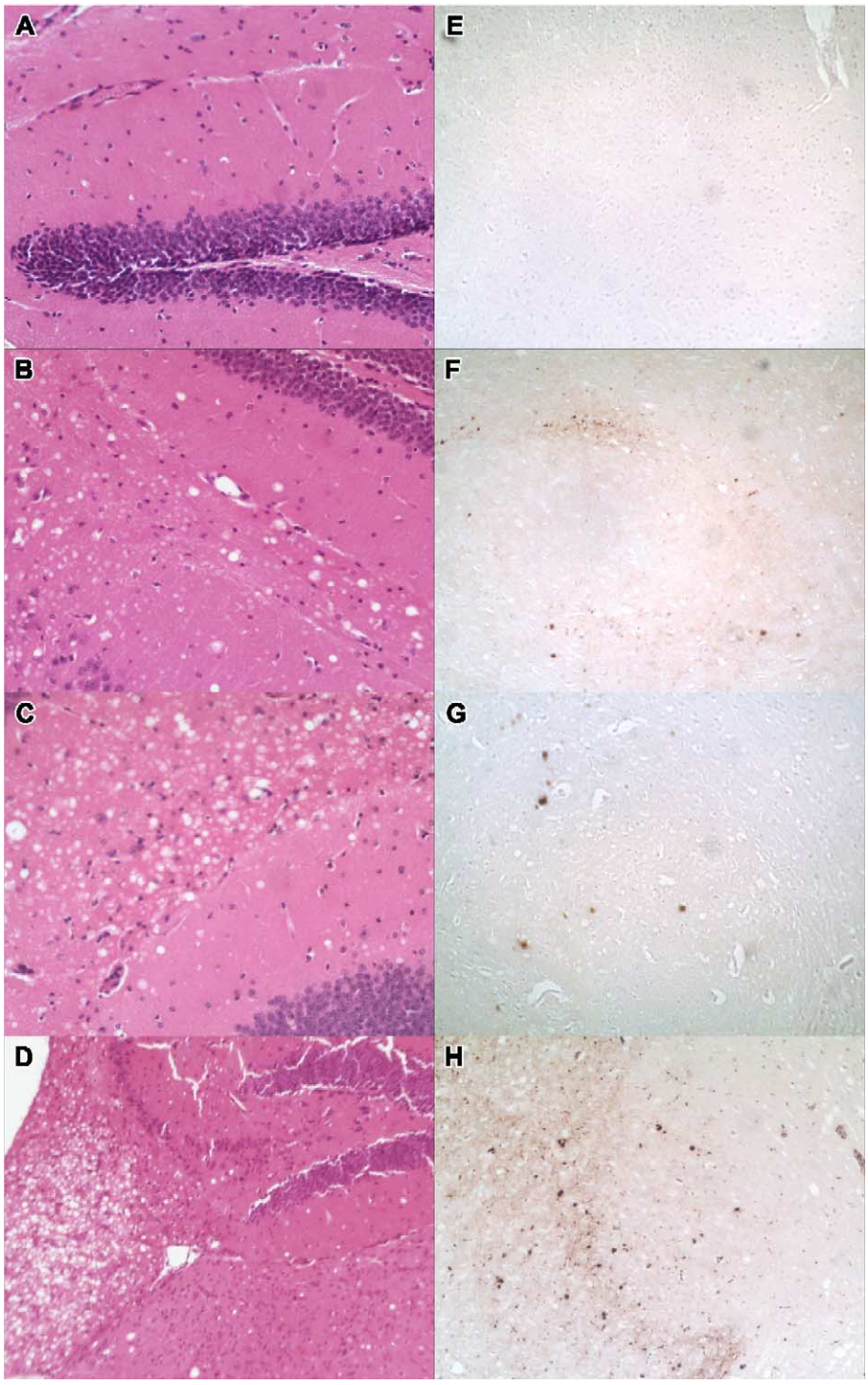

Fig. 2. (A–H) Representative photomicrographs demonstrating the range of morphological changes present in *Balb/c* mice assessed for the presence of asymptomatic infection in comparison to those seen in animals dying from terminal TSE. (A–D) Hematoxylin and eosin-stained sections of the hippocampal regions of individual mice demonstrating varying amounts of spongiform change. (E–H) Immunohistochemistry of the thalamic regions of individual mice demonstrating varying levels of PrP-positive plaque deposition using the monoclonal antibody ICSM 18 as described in Methods. Panels A and E depict mouse 6.3 from the 10^{-6} original inoculation cohort showing no evidence of spongiform change and no evidence of PrP plaques. Panels B and F depict mouse 5.3 from the 10^{-5} original inoculation cohort showing mild (+) spongiform change and mild–moderate (+ to ++) PrP-positive plaque formation. Panels C and G depict mouse 5.4 from the 10^{-5} original inoculation cohort showing moderate-to-severe (++ to +++) spongiform change and mild (+) PrP-positive plaque formation. Panels D and H depict a *Balb/c* mouse with terminal TSE showing severe (+++) spongiform change and severe (+++) PrP-positive plaque formation. Final magnifications: A–C, ×200; D–H, ×100.

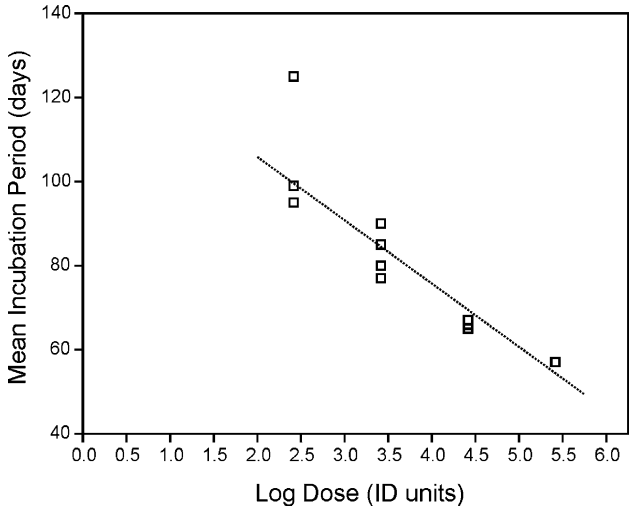

Fig. 3. Relationship between inoculation doses and incubation periods for the prion strain (M470) in Tga/20 mice. Regression analysis using the method of least squares was used to construct the fitted (dotted) line with the regression equation; $Y = 135.98 - 15.07(\log X)$, where Y equals mean incubation period (days) and X equals dose (ID_{50} units). Slope = 15.07, where $P < 0.0005$, 95% CI (−17.59 to −12.53), where the slope corresponds to a log scale estimate. The strength of the association was tested by calculating Spearman's correlation coefficient, $\rho = -0.9787$, $P < 0.0005$.

dilution of around 1:5000 of the original 10% w/v homogenate (approximating the equivalent of 50 μg wet weight diseased brain loaded per lane for immunoblotting) (Fig. 5A, lane 8). The results were replicated using an analogous fresh brain homogenate dilution series to eliminate any deleterious effects of long-term storage of the original inocula. Hence, when diseased brain is serially diluted in PBS, the NaPTA precipitation method appeared approximately twice as sensitive as the conventional technique for detecting PrP^{res}, with the advantage that the former method can load equivalent total brain weights from a substantially more dilute sample.

Our previous experiments indicated that the sensitivity of NaPTA precipitation and Western blotting approached the sensitivity of bioassay for the detection of PrP^{res} in asymptomatically infected *Balb/c* mice. However, detection of PrP^{res} diluted in PBS by the NaPTA precipitation method was 200–2000 times less sensitive than routine bioassay in *Balb/c* mice. Clinical disease invariably developed (5/5 mice) at the 10^{-4} dilution (equivalent to inoculating approximately 0.3 μg wet weight infected brain per mouse) and reproducibly occurred (2/6 mice) at the 10^{-5} dilution (equivalent to inoculating approximately 0.03 μg wet weight infected brain per animal). Acknowledging the reduced sensitivity of NaPTA precipitation for detecting potential infectivity compared to bioassay when brain tissue is progressively diluted in PBS, we assessed the influence of higher ambient mouse brain protein concentrations on PrP^{res} detection using this method. To achieve this, progressively smaller amounts of a whole brain homogenate from a *Balb/c* mouse dying from TSE (ranging from 50 μg to 0.6 μg) were spiked into 500-μl aliquots of 10% (w/v) normal mouse brain homogenates. In this situation, PrP^{res} could be detected from a spike equating to 3 μg whole brain (Fig. 5B), whereas the limit of detection of the abnormal isoform when brain was diluted in PBS occurred at around 50 μg. The former was nearly 20 times more sensitive but still around 10- to 100-fold less sensitive than bioassay.

To examine whether this effect reflected an inability of NaPTA to precipitate PrP^{res} from a low total protein concentration homogenate, 500 μl of PBS, 10% (w/v) normal brain, or $PrP^{o/o}$ brain homogenates were spiked with 2 μl of 1% terminal *Balb/c* brain homogenates and treated with NaPTA precipitation. The precipitated protein was analyzed with and without subsequent PK digestion; non-spiked 10% normal brain homogenate served as control. Facilitating comparisons of PrP^{res} retrieval as well as assessing any effect of an altered protease to total protein concentration ratio, an equivalent (1 μl) amount of 1% terminal *Balb/c* brain homogenate was added to PBS and sample buffer for direct gel loading without NaPTA precipitation. After Western blotting, we observed complete absence of PrP signal in larger-volume PBS-spiked samples, including without PK digestion, whereas abundant signal was seen in the spiked brain homogenates, including after PK digestion (data not shown). Despite digestion with the same concentration of PK, PrP banding of equivalent intensity to that observed in spiked larger volumes of brain homogenates was seen in those samples where 1 μl of a 1% terminal *Balb/c* brain homogenate was added to 9 μl of PBS. This

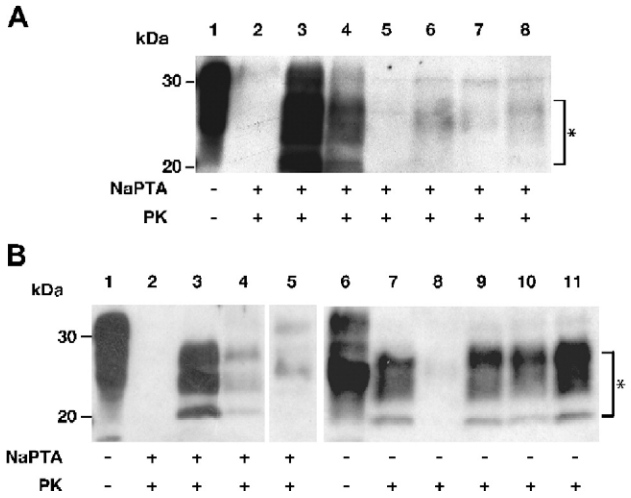

Fig. 4. (A and B) Western blots of mouse brains to assess the presence of PrP^{res} using the monoclonal antibody ICSM 18 as described in Methods. Sodium phosphotungstic acid (NaPTA) precipitation and proteinase K (PK) digestion (100 μg/ml final concentration) prior to Western blotting were performed as indicated (+). PrP^{res} is indicated by bracket marked with an asterisk. Approximate molecular weight weights (kDa) are given alongside. (A) Lanes 1 and 2, uninoculated *Balb/c* mouse; lane 3, 5 μl, and lane 4, 1 μl of a 1% brain homogenate from a terminal *Balb/c* "spiked" into 500 μl of 10% normal mouse brain homogenate; lane 5, surviving *Balb/c* mouse 5.2 from the 10^{-5} inoculation cohort culled 401 days PI, negative for PrP^{res}; lanes 6–8, surviving *Balb/c* mice 6.1, 6.2, and 6.3, respectively, from the 10^{-6} inoculation cohort culled day 401 PI, positive for PrP-res. (B) Lanes 1 and 2, uninoculated *Balb/c* mouse; lane 3, 5 μl, and lane 4, 1 μl of a 1% brain homogenate from a terminal *Balb/c* "spiked" into 500 μl of 10% normal mouse brain homogenate; lane 5, sham brain-inoculated, age-matched Tga/20 mouse; lanes 6 and 7, Tga/20 mouse culled day 74 PI with typical signs of TSE; lane 8, Tga/20 mouse dying from non-TSE intercurrent illness at day 214 PI; lane 9, Tga/20 mouse dying with typical TSE at day 154 PI; lane 10, Tga/20 dying from typical TSE at day 202 PI; lane 11, Tga/20 mouse dying from typical TSE at day 82 PI. PI, post-inoculation; TSE, transmissible spongiform encephalopathy.

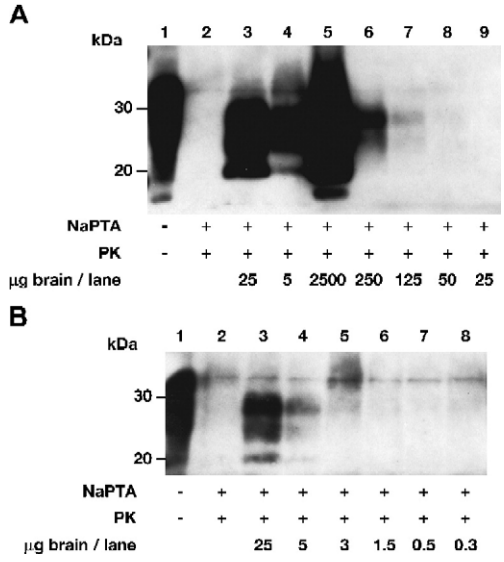

Fig. 5. (A and B) Serial dilutions of terminal mouse TSE brain homogenate aliquoted into (A) PBS and (B) 10% normal brain homogenate (w/v in PBS). Weights of diseased brain (µg) loaded into each lane from which PrP^{res} is detected are provided. Detection was by Western blot using the monoclonal antibody ICSM 18 as described in Methods. Sodium phosphotungstic acid (NaPTA) precipitation and proteinase K (PK) digestion (100 µg/ml final concentration) prior to Western blotting were performed as indicated (+). Approximate molecular weights (kDa) are given alongside. (A) Lanes 1 and 2, uninoculated *Balb/c* mouse; lane 3, 5 µl, and lane 4, 1 µl of a 1% brain homogenate from a terminal *Balb/c* "spiked" into 500 µl of 10% normal mouse brain homogenate. Lanes 5–9, serial dilutions using PBS of a 10% brain homogenate (w/v in PBS) from the terminal *Balb/c* mouse used for the original quantal, dose-titration inoculations. Final inoculum dilutions were: lane 5, 1:100; lane 6, 1:1000; lane 7, 1:2000; lane 8, 1:5000; and lane 9, 1:10,000. PrP^{res} detection limit appears at around 50 µg diseased brain per lane. (B) Lanes 1 and 2, uninoculated *Balb/c* mouse; lanes 3–8, serial dilutions of brain homogenate from a terminal *Balb/c* mouse "spiked" into 500 µl of 10% normal mouse brain homogenate (w/v in PBS). The PrP^{res} detection limit occurs at around 3 µg diseased brain per lane.

finding strongly militates against an altered PK-to-protein concentration ratio as being the predominant explanation for absence of PrP signal when PBS is used as diluent and is more in keeping with a reduced capacity of NaPTA precipitation to selectively concentrate PrP^{res} in a larger-volume, low-protein milieu.

Discussion

Our study confirmed that asymptomatic prion infection occurs commonly after low dose inoculation when using a human-derived TSE strain in non-transgenic hosts, free from a species barrier. Similar findings in previous murine scrapie (Asante et al., 2002; Büeler et al., 1994; Collis and Kimberlin, 1985; Dickinson et al., 1975; Frigg et al., 1999; Hill et al., 2000; Race and Chesebro, 1998; Race et al., 2001, 2002; Thackray et al., 2002; Zlotnik, 1965) and other models (Masters et al., 1976) reinforce the likelihood that extended periods of asymptomatic infection may be a generic property of many, possibly all, TSE strains. In the current assessment of asymptomatic infection, an incubation period of approximately 400 days was chosen because immediately prior to this there were two late deaths from TSE. We construed this as a good indication that asymptomatic infection may exist in other surviving mice, with this time point representing a more than doubling of the incubation period observed with high dose inoculations, and ensuring mice were in the latter half of their lifespan. We found asymptomatic infection to be very common, with infectivity detected in all mice receiving up to 100-fold lower inoculum doses than that which induced consistent clinical disease, and even in some mice receiving 1000-fold less infectivity. Our findings are consistent with other studies demonstrating the presence of high levels of infectivity in mice manifesting preclinical infection following inoculation with dilutions up to 100-fold higher than those causing consistent clinical disease (Dickinson et al., 1975; Thackray et al., 2002). In contrast to previous reports (Taylor et al., 2000; Thackray et al., 2002), we did not observe fluctuating or reversible signs of murine TSE in these groups of mice.

The deaths from TSE of two mice just prior to sacrificing most of the healthy survivors make it likely that clinical disease may have ensued in some mice had we allowed them to live longer. It is noteworthy that those asymptomatically infected mice displaying neuropathological abnormalities differed only in the severity of lesion burden, demonstrating a stereotyped and very similar distribution of changes, similar to that seen in mice dying with terminal disease. However, other asymptomatically infected mice did not show neuropathological abnormalities and had very low infectivity titers, and it is unclear whether these mice would have ever developed clinically overt disease. Although the very low titers of infectivity found in some of our asymptomatic mice may simply represent residual inoculum, this is not a tenable explanation in those mice harboring titers approximating those found in mice with terminal disease.

The infectious titer of our original inoculum, estimated by the development of lethal clinical disease, was 2.5×10^7 ID50 units/g of brain. A re-estimation of this titer, determined from the presence of asymptomatic infectivity using "blind" bioassay in Tga20 mice, increased this value by two orders of magnitude to 1.3×10^9 ID50 units/g brain. We believe this re-scaling offers a more genuine assessment of true overall transmission risk, which is of relevance to modeling studies such as efficacy of clearance of residual infectivity on surgical instruments. However, in order to routinely detect preclinical TSE infectivity, it would be necessary to perform second passage bioassay in sensitive indicator mice or at the very least observe mice over their entire lifespan for very late deaths. Such options would be a considerable burden and be generally considered impracticable. As an alternative approach, we undertook a detailed assessment of the utility of biochemical and histological methods to detect asymptomatic infections, thus alleviating the need for time and resource consuming animal studies.

The present study is the first to undertake a detailed comparative assessment for presymptomatic TSE infection using a number of techniques, including animal bioassay and a more sensitive Western immunoblot preceded by NaPTA precipitation of PrP^{res} (Wadsworth et al., 2001). Bioassay in appropriate host animals has previously been demonstrated to be superior to conventional Western blot detection of PrP^{res} (Hill et al., 2000; Race et al., 2001). We found conventional Western blot to be equivalent in sensitivity to histopathological markers such as spongiform change and the presence of PrP-positive plaques on immunohistochemistry, with good concordance between these techniques, but all three were clearly inferior to bioassay. NaPTA

precipitation prior to Western blotting revealed a sensitivity superior to conventional immunoblot and morphological markers, and approached that seen with bioassay. Although some caution is required in the absence of formal end-point titer estimates of asymptomatically infected *Balb/c* mice, the results from incubation time interval assays suggest that in our model of presymptomatic infection, conventional Western blot and routine histopathology are able to reliably detect PrP^{res} when infectivity is $>3.2 \times 10^4$ ID_{50} units per standard 30-μl inoculum, whereas methods employing NaPTA precipitation can detect PrP^{res} when the infectivity is $<2.0 \times 10^2$ ID_{50} units. Our ability to detect PrP^{res} in brain homogenates when infectivity is $<6.7 \times 10^3$ ID_{50} units/ml (equivalent to $<2.0 \times 10^2$ ID_{50} units per inoculum) is similar to the detection limit of approximately 3×10^3 ID_{50} units/ml found in a prior report comparing higher performance Western blots with hamster bioassay (Lee et al., 2000). There was only one mouse that did not demonstrate PrP^{res} using NaPTA precipitation when we would have expected its presence based on the titer seen with bioassay. We are uncertain of the explanation for this but suspect it represents a false-negative result stemming from technical factors. Nevertheless, given the detection of PrP^{res} in three other mice with comparable titers on bioassay, we believe the technique is clearly superior to conventional Western blot and at a practical level detects nearly all brains harboring potential transmissibility.

Our assessment of the utility of the NaPTA precipitation method for depicting potential infectivity in other situations was less favorable, appearing mainly related to lower ambient protein levels. In contrast to using PBS as sample diluent, the situation of using a 10% normal brain homogenate would be more comparable to the detection of the abnormal isoform in preclinically infected brains, as spiking experiments demonstrated a 10- to 20-fold improvement in sensitivity when using the latter to dilute aliquots compared to PBS. The influence of sample diluent on the sensitivity of Western blot detection of PrP^{res} has been reported previously and suggests benefits from inclusion of higher protein concentrations may be generic and not specific to brain-derived polypeptides (Lee et al., 2000). Precisely how a higher protein milieu assists PrP^{res} detection with NaPTA precipitation is speculative but probably relates to selectively facilitating the segregation and aggregation of the abnormal isoform. It is noteworthy that a recent report of the in vitro conformation-dependent immunoassay technique showing equivalence to bioassay using sensitive host animals also used spikes of brain homogenates from terminal mice diluted in 10% normal brain homogenates for the comparisons (Safar et al., 2002). It would be of interest to know how sensitive this detection method remains in a more dilute protein environment. Another possibility for the improved detection sensitivity of the NaPTA precipitation method in comparison to bioassay in asymptomatically infected animal brains may be a modest but critical amount of PrP^{res} propagation (of the order of 10 to 100-fold) sufficient to just allow detection, whereas only bioassay is able to detect the extreme limits of potential infectivity in our model.

In contrast to the experience of others (Thackray et al., 2002), we always found abundant PrP^{res} in whole brain homogenates from terminal Tga/20 mice using both conventional and NaPTA precipitation Western blot methods. A somewhat unexpected finding, similar to what has been reported previously in other transgenic mice over-expressing PrP^c (Telling et al., 1996), was the frequent presence of positive bands after PK digestion from brain homogenates of long-term surviving inoculated healthy Tga/20 mice. This was not observed in our wild-type (*Balb/c*) mice. The observation was confirmed in age-matched, uninoculated Tga/20 mice and Tga/20 mice inoculated with brain from healthy animals. Given the similarity of findings with two monoclonal anti-PrP antibodies, we assume the banding represents PrP^c and is related to the markedly increased expression of the protein in these transgenic mice. The banding pattern, nevertheless, was both qualitatively and quantitatively quite different to that seen in Tga/20 mice dying of TSE, always allowing confident differentiation of the two patterns.

In conclusion, the present study has demonstrated that chronic asymptomatic infection, to varying extents, is a common finding when wild-type mice are intracerebrally inoculated with low titer inocula just insufficient to induce reproducible clinical disease over extended incubation periods. Although unproven, extrapolation to a human equivalent appears likely given the very long incubation periods now recognized for kuru (Collinge, 1999) and the evidence that PrP^{res} deposition, as detected by conventional techniques, occurs in the appendixes of vCJD patients for a considerable period before the onset of symptoms (Hilton et al., 1998, 2002, 2004). The application of higher-sensitivity diagnostic methods is important to facilitate screening for potential infectivity in tissues from at risk populations such as dura mater and human-derived pituitary hormone recipients, and eventually when suitable methods are available, serum samples from all asymptomatic blood and organ donors. Comparative studies of the type described here are needed to define more accurately limitations and situations where individual tests are best applied. Further, similar to the sentiments expressed in other comparative studies (Safar et al., 2002), this knowledge coupled with other recent findings (Bosque et al., 2002; Glatzel et al., 2003) may suggest the need to re-assess the transmission risks of tissues and populations previously deemed not to harbor any infectivity.

Acknowledgments

The Australian National Creutzfeldt–Jakob Disease Registry is funded by the Commonwealth Department of Health and Ageing. This work was also funded in part by an NHMRC Program Grant #208978. AFH is an NHMRC RD Wright Fellow and VAL is supported by an NHMRC Howard Florey Fellowship. The authors wish to thank the Animal House staff for their assistance, as well as Mrs. T. Cardamone and Ms. L. Leone for performing histology and immunohistochemistry. The Tga/20 and *PRNP*-ablated mice used in the study were a generous gift from Professor Charles Weissmann. The anti-prion protein monoclonal antibody ICSM 18 was a generous gift from Professor John Collinge.

References

Asante, E.A., Linehan, J.M., Desbruslais, M., Joiner, S., Gowland, I., Wood, A.L., Welch, J., Hill, A.F., Lloyd, S.E., Wadsworth, J.D., Collinge, J., 2002. BSE prions propagate as either variant CJD-like or sporadic CJD-like prion strains in transgenic mice expressing human prion protein. EMBO J. 21, 6358–6366.

Bosque, P.J., Ryou, C., Telling, G., Peretz, D., Legname, G., DeArmond, S.J., Prusiner, S.B., 2002. Prions in skeletal muscle. Proc. Natl. Acad. Sci. U. S. A. 99, 3812–3817.

Büeler, H., Aguzzi, A., Sailer, A., Greiner, R.A., Autenreid, P., Aguet, M., Weissmann, C., 1993. Mice devoid of PrP are resistant to scrapie. Cell 73, 1339–1347.

Büeler, H., Raeber, A., Sailer, A., Fischer, M., Aguzzi, A., Weissmann, C., 1994. High prion and PrPSc levels but delayed onset of disease in scrapie-inoculated mice heterozygous for a disrupted PrP gene. Mol. Med. 1, 19–30.

Collinge, J., 1999. Variant Creutzfeldt–Jakob disease. Lancet 354, 317–323.

Collis, S.C., Kimberlin, R.H., 1985. Long-term persistence of scrapie infection in mouse spleens in the absence of clinical disease. FEMS Microbiol. Lett. 29, 111–114.

Collins, S., Law, M.G., Fletcher, A., Boyd, A., Kaldor, J., Masters, C.L., 1999. Surgical treatment and risk of sporadic Creutzfeldt–Jakob disease: a case-control study. Lancet 353, 693–697.

Collins, S., Boyd, A., Fletcher, A., Kaldor, J., Hill, A., Farish, S., McLean, C., Ansari, Z., Smith, M., Masters, C.L., 2002a. Creutzfeldt–Jakob disease cluster in an Australian rural city. Ann. Neurol. 52, 115–118.

Collins, S., Boyd, A., Lee, J.S., Lewis, V., Fletcher, A., McLean, C.A., Law, M., Kaldor, J., Smith, M.J., Masters, C.L., 2002b. Creutzfeldt–Jakob disease in Australia 1970–1999. Neurology 59, 1365–1371.

Dickinson, A.G., Fraser, H., Outram, G.W., 1975. Scrapie incubation time can exceed natural lifespan. Nature 256, 732–733.

Fischer, M., Rulicke, T., Raeber, A., Sailer, A., Moser, M., Oesch, B., Brandner, S., Aguzzi, A., Weissmann, C., 1996. Prion protein (PrP) with amino-proximal deletions restoring susceptibility of PrP knockout mice to scrapie. EMBO J. 15, 1255–1264.

Frigg, R., Klein, M.A., Hegyi, I., Zinkernagel, R.M., Aguzzi, A., 1999. Scrapie pathogenesis in subclinically infected B-cell-deficient mice. J. Virol. 73, 9584–9588.

Glatzel, M., Abela, E., Maissen, M., Aguzzi, A., 2003. Extraneural pathologic prion protein in sporadic Creutzfeldt–Jakob disease. N. Engl. J. Med. 349, 1812–1820.

Hill, A.F., Butterworth, R.J., Joiner, S., Jackson, G., Rossor, M.N., Thomas, D.J., Frosh, A., Tolley, N., Bell, J.E., Spencer, M., King, A., Al-Sarrag, S., Ironside, J.W., Lantos, P.L., Collinge, J., 1999. Investigation of variant Creutzfeldt–Jakob disease and other human prion diseases with tonsil biopsy samples. Lancet 353, 183–189.

Hill, A.F., Joiner, S., Linehan, J., Desbruslais, M., Lantos, P.L., Collinge, J., 2000. Species-barrier-independent prion replication in apparently resistant species. Proc. Natl. Acad. Sci. U. S. A. 97, 10248–10253.

Hilton, D.A., Fathers, E., Edwards, P., Ironside, J.W., Zajicek, J., 1998. Prion immunoreactivity in appendix before clinical onset of variant Creutzfeldt–Jakob disease. Lancet 352, 703–704.

Hilton, D.A., Ghani, A.C., Conyers, L., Edwards, P., McCardle, L., Penney, M., Ritchie, D., Ironside, J.W., 2002. Accumulation of prion protein in tonsil and appendix: review of tissue samples. BMJ 325, 633–634.

Hilton, D.A., Ghani, A.C., Conyers, L., Edwards, P., McCardle, L., Ritchie, D., Penney, M., Hegazy, D., Ironside, J.W., 2004. Prevalence of lymphoreticular prion protein accumulation in UK tissue samples. J. Pathol. 203, 733–739.

Lee, D.C., Stenland, C.J., Hartwell, R.C., Ford, E.K., Cai, K., Miller, J.L., Gilligan, K.J., Rubenstein, R., Fournel, M., Petteway Jr., S.R., 2000. Monitoring plasma processing steps with a sensitive Western blot assay for the detection of the prion protein. J. Virol. Methods 84, 77–89.

Lewis, V., Collins, S., Hill, A.F., Boyd, A., McLean, C.A., Smith, M., Masters, C.L., 2003. Novel prion protein insert mutation associated with prolonged neurodegenerative illness. Neurology 60, 1620–1624.

Llewelyn, C.A., Hewitt, P.E., Knight, R.S., Amar, K., Cousens, S., Mackenzie, J., Will, R.G., 2004. Possible transmission of variant Creutzfeldt–Jakob disease by blood transfusion. Lancet 363, 417–421.

Masters, C.L., Kakulas, B.A., Alpers, M.P., Gajdusek, D.C., Gibbs Jr., C.J., 1976. Preclinical lesions and their progression in the experimental spongiform encephalopathies (kuru and Creutzfeldt–Jakob disease in primates). J. Neuropathol. Exp. Neurol. 35, 593–605.

Prusiner, S.B., 1997. Prion diseases and the BSE crisis (review). Science 278, 245–251.

Race, R., Chesebro, B., 1998. Scrapie infectivity found in resistant species. Nature 392, 770.

Race, R., Raines, A., Raymond, G.J., Caughey, B., Chesebro, B., 2001. Long-term subclinical carrier state precedes scrapie replication and adaptation in a resistant species: analogies to bovine spongiform encephalopathy and variant Creutzfeldt–Jakob disease in humans. J. Virol. 75, 10106–10112.

Race, R., Meade-White, K., Raines, A., Raymond, G.J., Caughey, B., Chesebro, B., 2002. Subclinical scrapie infection in a resistant species: persistence, replication, and adaptation of infectivity during four passages. J. Infect. Dis. 186 (Suppl. 2), S166–S170.

Reed, L.J., Muench, H., 1938. A simple method of estimating fifty per cent endpoints. Am. J. Hygiene 27, 493–497.

Safar, J.G., Scott, M., Monaghan, J., Deering, C., Didorenko, S., Vergara, J., Ball, H., Legname, G., Leclerc, E., Solforosi, L., Serban, H., Groth, D., Burton, D.R., Prusiner, S.B., Williamson, R.A., 2002. Measuring prions causing bovine spongiform encephalopathy or chronic wasting disease by immunoassays and transgenic mice. Nat. Biotechnol. 20, 1147–1150.

Tateishi, J., Ohta, M., Koga, M., Sato, Y., Kuroiwa, Y., 1979. Transmission of chronic spongiform encephalopathy with kuru plaques from humans to small rodents. Ann. Neurol. 5, 581–584.

Taylor, D.M., McConnell, I., Ferguson, C.E., 2000. Closely similar values obtained when the ME7 strain of scrapie agent was titrated in parallel by two individuals in separate laboratories using two sublines of C57BL mice. J. Virol. Methods 86, 35–40.

Telling, G.C., Haga, T., Torchia, M., Tremblay, P., DeArmond, S.J., Prusiner, S.B., 1996. Interactions between wild-type and mutant prion proteins modulate neurodegeneration transgenic mice. Genes Dev. 10, 1736–1750.

Thackray, A.M., Klein, M.A., Aguzzi, A., Bujdoso, R., 2002. Chronic subclinical prion disease induced by low-dose inoculum. J. Virol. 76, 2510–2517.

Wadsworth, J.D., Joiner, S., Hill, A.F., Campbell, T.A., Desbruslais, M., Luthert, P.J., Collinge, J., 2001. Tissue distribution of protease resistant prion protein in variant Creutzfeldt–Jakob disease using a highly sensitive immunoblotting assay. Lancet 358, 171–180.

Ward, H.J., Everington, D., Croes, E.A., Alperovitch, A., Delasnerie-Lauprêtre, N., Zerr, I., Poser, S., van Duijn, C.M., 2002. Sporadic Creutzfeldt–Jakob disease and surgery: a case-control study using community controls. Neurology 59, 543–548.

White, A.R., Enever, P., Tayebi, M., Mushens, R., Linehan, J., Brandner, S., Anstee, D., Collinge, J., Hawke, S., 2003. Monoclonal antibodies inhibit prion replication and delay the development of prion disease. Nature 422, 80–83.

Zlotnik, I., 1965. Observations on the experimental transmission of scrapie of various origins to laboratory animals. In: Gajdusek, D.C., Gibbs, C.J., Alpers, M.P. (Eds.), Slow, Latent, and Temperate Virus Infections: National Institute of Neurological Diseases and Blindness, Monograph 2. Proceedings of the Workshop and Symposium on Slow, Latent, and Temperate Virus Infections, National Institute of Health, 1964 Dec 7–9, Bethesda. U.S. Government Printing Office, Washington, DC, pp. 237–248.

ELSEVIER

Brain Research Bulletin 68 (2006) 346–354

BRAIN RESEARCH BULLETIN

www.elsevier.com/locate/brainresbull

Correlative studies support lipid peroxidation is linked to PrP^{res} propagation as an early primary pathogenic event in prion disease

Marcus W. Brazier[a,b], Victoria Lewis[a,b], Giuseppe D. Ciccotosto[a,b], Genevieve M. Klug[a,b], Victoria A. Lawson[a,b], Roberto Cappai[a,b], James W. Ironside[c], Colin L. Masters[a,b], Andrew F. Hill[a,d], Anthony R. White[a,b], Steven Collins[a,b,*]

[a] *Department of Pathology, The University of Melbourne, Vic. 3010, Australia*
[b] *The Mental Health Research Institute of Victoria, Parkville, Vic. 3052, Australia*
[c] *National Creutzfeldt-Jakob Disease Surveillance Unit, Western General Hospital, University of Edinburgh, Edinburgh EH4 2XU, UK*
[d] *Department of Biochemistry and Molecular Biology, The University of Melbourne, Vic. 3010, Australia*

Received 31 March 2005; accepted 20 September 2005
Available online 5 October 2005

Abstract

To assess whether heightened oxidative stress plays an early and primary pathogenic role in transmissible spongiform encephalopathies (TSE), we undertook detailed correlative studies using a mouse-adapted model of human disease. The spatio-temporal evolution of the abnormal, protease-resistant isoform of the prion protein (PrP^{res}) and neuropathological changes were correlated with the occurrence and type of oxidative stress. Heightened oxidative stress was demonstrated, but restricted to elevated levels of free aldehydic breakdown products of lipid peroxidation, affecting all brain regions to varying extents. The increase in lipid peroxidation was highest over the mid-incubation period, with the onset showing close temporal and general topographical concordance with the first detection of PrP^{res} with both pre-empting the typical neuropathological changes of spongiform change, gliosis and neuronal loss. Further, prion propagation over the disease course was assessed using murine bioassay. This revealed that the initial rapid increase in infectivity titres was contemporaneous with the abrupt onset and maximisation of lipid peroxidation. The present results are an important extension to previous studies, showing that heightened oxidative stress in the form of lipid peroxidation is likely to constitute an early primary pathogenic event in TSE, associated temporally with the integral disease processes of prion propagation and PrP^{res} formation, and consistent with causal links between these events and subsequent typical neuropathological changes.

Keywords: Neuropathology; Oxidative stress; Prion propagation; Transmissible spongiform encephalopathy

1. Introduction

Transmissible spongiform encephalopathies (TSE; also known as prion diseases) are a group of neurodegenerative disorders, which includes Creutzfeldt–Jakob disease (CJD), Gerstmann–Sträussler–Scheinker syndrome (GSS) and fatal familial insomnia in humans, as well as scrapie and bovine spongiform encephalopathy in animals. Transmissibility is a fundamental differentiating feature from other neurodegenerative disorders such as Alzheimer's and Parkinson's diseases, that share the common feature of accumulation and aggregation of constitutively expressed cellular proteins, which are believed to be integrally related to disease pathogenesis. The conformational change of the wild type isoform of the prion protein (PrP^{C}) to the disease-associated, partially protease-resistant conformer (PrP^{res}) appears a crucial event for successful transmission and pathogenesis in TSE. PrP^{res} principally differs from PrP^{C} by containing a much greater ratio of β-sheet to α-helical content [33], contributing directly to its protease resistance and propensity for aggregation. Although PrP^{res} appears to be the main or perhaps sole constituent of the TSE infectious agent ("prion"), disease pathogenesis requires expression of PrP^{C} [2,27]. Consequently, prion protein gene (PRNP) ablated mice ($PrP^{0/0}$) are unable to be infected [8] and their neurons are resistant to the deleterious effects of direct exposure to PrP^{res} [2,27].

* Corresponding author. Tel.: +61 3 8344 1945; fax: +61 3 8344 4004.
E-mail address: stevenjc@unimelb.edu.au (S. Collins).

0361-9230/$ – see front matter © 2005 Elsevier Inc. All rights reserved.
doi:10.1016/j.brainresbull.2005.09.010

Despite the apparent primacy of PrP^C expression and PrP^{res} propagation in TSE pathogenesis, the normal function of PrP^C and the predominant mechanisms involved in pathogenesis remain uncertain. PrP^C and cognate synthetic peptides have been shown to bind Cu^{2+} ions and internalise the transition metal in a redox inactive state [4,30,32,36]. In cell culture models, neurons devoid of PrP^C expression have been shown to have an increased vulnerability to the superoxide anion [5], hydrogen peroxide [43] and Cu^{2+} ions [6] compared to controls and other models have shown that the presence of PrP^{res} appears to enhance susceptibility to pro-oxidants [29]. The brain and other tissues of $PrP^{0/0}$ mice have been shown to have decreased superoxide dismutase (SOD) activity compared to that in wild-type mice, as well as increased malondialdehyde (MDA) and 4-hydroxyalkenals (HAE), reactive aldehydic products of lipid peroxidation [22,48]. Further, a reduction of total SOD activity in brain homogenates after immuno-depletion of PrP^C has been demonstrated when compared to non-depleted homogenates, while the Cu/Zn-SOD and Mn-SOD activities remained unchanged [49]. Infected cell culture systems have revealed evidence of oxidative damage, appearing to be a consequence of unfavourable perturbations to Cu/Zn SOD and Mn-SOD, as well as to glutathione peroxidase and reductase activities [29]. Microglia may also have an effector role in the oxidative damage observed as a consequence of exposure to a toxic prion protein-derived (PrP106-126) peptide [5]. Cumulatively, this data and the ability of PrP^C to bind Cu^{2+} and demonstrate SOD-like activity [3,7] contribute to the proposition that PrP^C acts as a protective and anti-oxidant molecule, with beneficial effects probably extending beyond SOD-type catalysis [43]. In parallel with this evidence, in vivo models of TSE have demonstrated the presence of heightened oxidative stress [20] with damage to proteins [11,19] nucleic acids [18] and lipids [10,46] in terminally ill animals, and similar damage has been detected in the brains of patients dying from sporadic CJD [47].

To date, however, the mounting in vivo evidence that heightened oxidative stress may contribute to the pathogenesis of TSE has been derived primarily from studies of the terminal stages of disease. With a single exception [1], reports have failed to address the temporal development of oxidative insults and correlate them with conventional neuropathological changes or other integral features of TSE pathogenesis [10,11,19,20,46]. Data from terminal disease may not accurately represent the true pathological relevance of oxidative stress in TSE and leaves open the possibility that oxidative damage is a relatively late and non-specific contributor to the degeneration of neurons already irrevocably damaged by other primary insults. To assess whether oxidative stress constitutes a primary pathogenic mechanism in TSEs, spatio-temporal correlation of various markers of oxidative damage with classic neuropathological hallmarks, the presence of PrP^{res} and prion propagation was performed in a murine model of human disease. Our findings demonstrate that heightened oxidative stress in the form of lipid peroxidation is an early and likely primary pathogenic mechanism in TSE, with this change closely associated with PrP^{res} formation and prion propagation, consistent with causal links between these events and subsequent typical neuropathological changes.

2. Materials and methods

2.1. Mice and inoculations

The M1000 strain used represents a mouse-adapted human TSE originally isolated from a patient most likely dying from Gerstmann–Sträussler–Scheinker disease [38]. For correlative studies over the disease course, Balb/c weanling mice were intracerebrally (ic) inoculated with 30 μl of either 1% brain homogenate from a mouse dying from TSE (approximating 2.7×10^4 ID_{50} units) as previously described [12] or with 1% brain homogenate obtained from a normal animal (control mice). Unless otherwise stated, morphological and biochemical studies utilised groups of four to five diseased and four to five control mice, sacrificed at 21, 42, 64, 82, 104, 123, 137 days post-inoculation (dpi) and at the terminal stage of disease, the latter occurring at a mean incubation period of 145 dpi (±2 d). Mice generally began displaying symptoms of TSE from around 136 dpi. After this time point, mice demonstrated typical symptoms including coat ruffling, reduced spontaneous mobility, hunched posture, hind limb paresis and gait ataxia with occasional myoclonus.

Tg20 transgenic, PrP^C over-expressing mice [16] were used to assess the brain infectivity of inoculated Balb/c mice across the time-course of disease. Mice were inoculated as described above with 30 μl of 1% brain tissue homogenates (w/v in PBS) prepared from the "diencephalic" regions of previously inoculated Balb/c mice. This diencephalic region consisted of the thalamus, telencephalic deep gray nuclei, hypothalamus and brain stem, and was chosen for inoculations because preliminary studies had indicated that the highest levels of PrP^{res} and spongiform change occurred within these sites, especially the thalamus. In additional experiments, groups of Tg20 indicator mice were also inoculated with 1% diencephalic region homogenates from Balb/c mice culled at 0 and 1 h, and 1, 7 and 14 dpi. Bioassay mice were culled once signs of TSE were consistently evident, and those with lengthy incubation periods (>100 dpi) were assessed for the presence of PrP^{res}. Prior quantal dose-titrations of the M1000 strain had been performed in both Balb/c and Tg20 mice. All mice were culled by cervical dislocation, unless otherwise specified. Animal handling was in accordance with national prescribed guidelines and ethical approval for the study was granted by the University of Melbourne Animal Experimentation Ethics Committee.

2.2. Western immunoblot analysis of the spatio-temporal evolution of PrP^{res}

To demonstrate PrP^{res}, the brain regions were assayed by Western blot. Diencephalon tissue was isolated by macroscopically removing the cerebellum and the cerebral cortices and the three separate regions were homogenised to 10% in PBS. Fifty microlitre aliquots of these homogenates were treated with Benzonase (Merck, Darmstadt, Germany), 50 U/ml, in the presence of 1 mM $MgCl_2$, and incubated for 5 min at 37 °C. Proteins were digested by Proteinase K (PK; Sigma, Castle Hill, Australia) at 100 μg/ml final concentration, incubated for 1 h at 37 °C. Digestion was halted by the addition of Pefabloc (Roche, Basel, Switzerland) to 8 mM final concentration and 50 μl of 2× sample buffer containing 6% 2-mercaptoethanol (Sigma) followed by boiling for 10 min. Samples were briefly centrifuged at 5000 rpm, prior to resolving on 10% pre-cast tris/glycine gels (Novex, San Diego, California), then transferred to nitrocellulose membranes and blocked with 5% non-fat milk powder in PBS-T. Membranes were incubated at 4 °C overnight with the ICSM18 monoclonal anti-PrP antibody [44] (1:25,000 in PBS-T), with detection utilising an HRP-conjugated anti-mouse secondary antibody at 1:5000 (DAKO, Carpinteria, California), enhanced chemiluminescence (ECL; Amersham, Castle Hill, Australia) and Kodak Biomax film, developer and fixative (Sigma).

Western blot detection of PrP^{res} across the time course of disease was also undertaken using sodium phosphotungstic acid (NaPTA) precipitation of brain homogenates prior to PK digestion [41]. In summary, 500 μl of 10% diencephalon homogenates were mixed 1:1 with 4% Sarkosyl (Sigma) in PBS and incubated at 37 °C for 10 min with constant agitation. Benzonase and $MgCl_2$ were added at 50 U/ml and 1 mM final concentrations, respectively and incubated

for 30 min at 37 °C with agitation. To this, 81.3 μl of a solution containing 4% NaPTA (Sigma) and 170 mM $MgCl_2$ was added (pre-warmed to 37 °C) and the reaction mixtures vortexed then incubated for 30 min at 37 °C with agitation. The samples were then centrifuged at 15,000 × *g* for 30 min; supernatants were carefully removed and the remaining pellets resuspended in 20 μl of PBS 0.1% Sarkosyl ready for PK digestion and western blotting as described above.

2.3. Histology and immunohistochemistry

For morphological studies, mice were sacrificed by transcardial perfusion. Mice were exsanguinated with wash buffer (2000 IU/l heparin, 0.028 M sodium nitrite (Clyde Industries, Sydney, Australia) 0.005% butylated hydroxytoluene (BHT; Sigma) in PBS) followed by perfusion with 4% paraformaldehyde (ProSciTech, Kirwan, Australia) in a 0.1 M phosphate buffer for approximately 10 min. Fixed mice were then incubated at 4 °C for 30 min before brains were removed for further immersion fixation in either 10% neutral buffered formalin or methacarn [35] for 1 h at room temperature (RT); brains were stored in 70% methanol until processing. All fixed brain tissue was treated with 99% formic acid for 1 h at RT to reduce tissue infectivity. Half-brains were paraffin embedded and 6 μm sagittal sections were cut and mounted on Superfrost Plus slides (Menzel-Glaser, Braunschweig, Germany). Mounted sections from each time point were deparaffinised in Shellex and rehydrated through 100, 90 and 70% dilutions of ethanol to deionised water and stained with hematoxylin and eosin (H&E).

For immunohistochemical (IHC) assessment of neuropathological changes, adjacent serial sections from mice culled across the time course were used. After rehydration, all tissue sections were incubated in 3% hydrogen peroxide for 5 min at RT, then washed with PBS (pH 7.4). As appropriate for the subsequent secondary antibody, sections were blocked with either 20% normal swine or rabbit serum in PBS for 30 min at RT. To detect astrocytic gliosis, rabbit anti-GFAP polyclonal sera (DAKO) was applied (1:50) for 1 h at 37 °C. Detection of neurons (neuronal nuclear protein (NeuN) and neurofilament) was enhanced by boiling sections in sodium citrate buffer (pH. 6.0) for 5 min prior to application of primary antibodies. Anti-NeuN (1:500; Chemicon, Temecula, California) and anti-neurofilament (1:50; Sigma, detecting all three subunits) mouse monoclonal sera were incubated overnight at 4 °C before washing in PBS. The appropriate biotinylated secondary antibodies (swine anti-rabbit and rabbit anti-mouse (DAKO)) were applied at 1:500 dilution for 1 h at RT, then washed in PBS followed by incubation with HRP-conjugated streptavidin (DAKO) diluted 1:1000 for 30 min at RT. Visualisation utilised the diaminobenzadine (DAB+) substrate-chromagen system (DAKO). A 1 min hematoxylin counterstain was also employed.

To enhance PrP^{res} epitope detection, sections were autoclaved for 20 min at 132 °C, followed by cooling and washing twice in deionised water and then treated with 96% formic acid for 5 min [23]. After washing, sections were treated with 4 M guanidine thiocyanate for 2 h at 4 °C, then washed before blocking. PrP was detected using the monoclonal antibody ICSM18 diluted 1:500 in PBS with overnight incubation at 4 °C. Sections were then sequentially incubated with biotinylated rabbit anti-mouse IgG secondary antibody (1:500 for 30 min), HRP-conjugated streptavidin, (1:1000 for 30 min), and finally DAB+.

Heme oxygenase-1 (HO-1; StressGen, Victoria, Canada), nitrotyrosine (NT; Upstate Biotechnology, Waltham, Massachusetts) and 4-Hydroxynonenal (HNE) (Calbiochem) polyclonal antisera pre-treatments included repeated microwave boiling (up to five cycles) for 2, 3 and 4 min in 10 mM or 100 mM sodium citrate buffer (pH 6.0), as well as exposing slides to either 0.1% aqueous Trypsin, Saponin, or Triton X 100 pre-warmed to 37 °C. Trialled primary antibody concentrations varied from 1:50 to 1:400. Carrier protein concentrations for these primary antibodies were also varied, including use of 1% BSA, and 0.1, 5 and 10% fetal calf serum in PBS, and the 20% serum blocking step was extended to overnight. Positive controls for NT utilised pre-treatment of sections for 20 min at RT with peroxynitrite (Sigma), while general negative controls consisted of: (1) omitting the primary antibody; and (2) substitution of the primary antibody with pre-immune serum from the same host animal species. As further negative controls for NT immunostaining, we pre-treated tissue sections with three 20 s exposures to 100 mM sodium hydrosulphite (pH 9.0) prepared immediately prior to use in 100 mM sodium bicarbonate under anaerobic conditions, as well as pre-adsorption of the anti-NT antibody with peroxynitrite treated BSA prior to application to the tissue sections [35].

2.4. Biochemical assessment of oxidative stress

For all biochemical assessments of oxidative damage, mice were exsanguinated by transcardial perfusion as described above, with 0.005% BHT in PBS included as anti-oxidant to prevent superimposed post-mortem contributions. Mice were culled by lethal injection of Nembutal (Merial Australia, Paramatta, NSW) (200 μl intraperitoneally) and brains were macroscopically dissected as above, with each of the three principal regions (cerebral cortex, cerebellum and diencephalon) individually homogenised to 10% in PBS containing 0.005% BHT, snap frozen in liquid nitrogen and stored at −80 °C. Prior to analyses, the protein concentration of homogenates was quantified using the BCA protein assay (Pierce, Rockford, Illinois), with samples equalised for total protein content.

To assess for lipid peroxidation, the three brain regions were analysed across the time course of disease using the Bioxytech LPO586 (Oxis, Portland, Oregon) colorimetric assay. Aliquots of brain homogenates (protein concentration adjusted to 8 mg/ml) were analysed as per manufacturer's instructions and described previously [45].

Brain regions were analysed for levels of total carbonylated proteins using the OxyBlot carbonyl detection kit (Intergen, Purchase, New York). Brain homogenates (10 μg protein each) were derivatised with 10 mM 2,4-dinitrophenolhydrazine in 2 M HCl and assessed by western blot as per kit instructions.

To assess levels of inducible nitric oxide synthase (iNOS), normalised brain samples from each of the three brain regions were analysed by western blot for iNOS expression using anti-iNOS polyclonal antibody diluted 1:2000 (Affinity Bioreagents, Golden, Colorado) with mouse derived iNOS (Cayman Chemicals, Ann Arbor, Michigan) as a positive control.

2.5. Statistical analysis

Comparisons of the means of the levels of MDA/HAE at each time point for control and M1000-inoculated mice were estimated and tested for significance using two-way analysis of variance (ANOVA).

3. Results

3.1. Western immunoblot analysis of the spatio-temporal evolution of PrP^{res}

Using conventional western blots, PrP^{res} was first consistently detectable at 82 dpi in the diencephalic region of Balb/c mice, with the signal increasing thereafter. This region was occasionally weakly positive at 64 dpi. In contrast, NaPTA precipitation of the same brain region prior to electrophoresis afforded reliable detection of PrP^{res} just prior to the mid-incubation point at 64 dpi (Fig. 1), with occasional mice displaying a weakly positive signal at 42 dpi. Using NaPTA precipitation prior to western blotting, we were also able to consistently detect PrP^{res} in the homogenates of the cerebral cortex and cerebellum from 64 dpi, whereas conventional western blot only occasionally revealed weak PrP^{res} signals from these same brain regions at 64 dpi. Western blots of the diencephalic region appeared to show a plateau in PrP^{res} levels after day 104 post-inoculation (Fig. 1).

3.2. Histopathological findings through the incubation period

3.2.1. Spongiform change and astrocytic gliosis

Onset and progression of neuropathological changes were assessed over the incubation period for comparison with oxidative damage and infectivity. Spongiform change was first evident

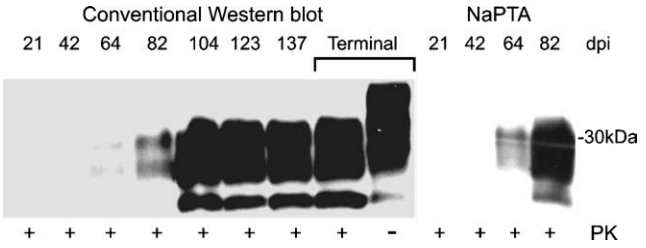

Fig. 1. Western blot detection of protease-resistant prion protein (PrP^{res}) within the diencephalic brain regions of M1000 infected Balb/c mice. The time points following intracerebral inoculation at which brains were harvested for assessment are shown as days post-inoculation (dpi) and at terminal disease (terminal). In the long exposures shown, the earliest detection of PrP^{res} was at 64 dpi, which was more clearly and consistently seen with western blotting preceded by sodium phosphotungstic acid (NaPTA) precipitation (on right). Conventional western blots (left) show that there is a rapid increase in signal from 64 to 104 dpi with plateauing thereafter. Note that in the M1000 strain, the unglycosylated (lowest) band of PrP^{res} is much less abundant than the glycosylated (upper) bands, and is only clearly seen from 104 dpi using the conventional western blots and at 82 dpi for NaPTA treated samples. Brains were treated (+) with proteinase K (PK), with the brain homogenate from a terminal animal also not treated with PK (−) to verify complete PK digestion and demonstrate overall levels of PrP^{c} and PrP^{res}. A 30 kDa molecular mass marker is provided at right.

simultaneously in the thalamus and hippocampus, immediately after the mid-incubation point, at 82 dpi (Fig. 2A and D), and this progressed to severe vacuolation at the terminal stage (Fig. 2B and E). The hippocampal microvacuolation was diffuse, evident in both the radiate and oriens strata, but accentuated in the CA2 segment. There was widespread but less severe spongiform change in the cerebral subcortical white matter from 104 dpi, with the occipital lobe usually the most affected. Brain stem spongiform change was evident from 123 dpi, sometimes becoming the most severely affected region in terminal animals. The cerebellar cortex never displayed vacuolation in any of the animals.

In control brains, modest GFAP immunoreactivity was present in the hippocampus (in the stratum lacunosum-moleculare and fimbria), corpus callosum, stria terminalis and occasionally the thalamus, which did not change throughout the time course (Fig. 2I and L). Closely paralleling the spongiform change, the hippocampus and thalamus of mice inoculated with M1000 were the first regions to demonstrate increased GFAP signal at 82 dpi (Fig. 2G and J, respectively). Gliosis was patchy but diffusely distributed in the thalamus, and in the hippocampus

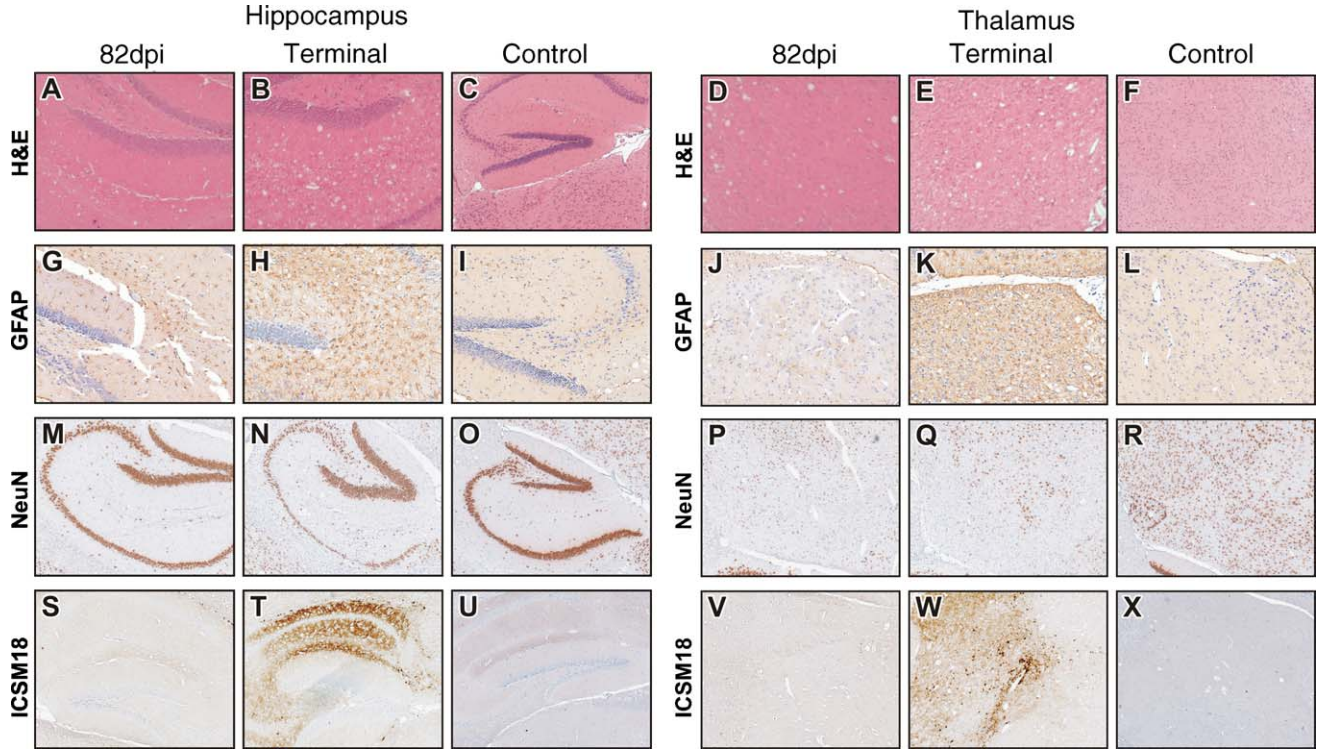

Fig. 2. Evolution of the typical neuropathological changes observed in the mouse-adapted model of TSE. Hematoxylin and eosin staining of brain sections demonstrating the earliest evidence of spongiosis occurring simultaneously in the hippocampus (A) and the thalamus (D) at 82 days post-inoculation (dpi), which progressed to severe vacuolar degeneration in these same regions in terminal animals (B and E, respectively); age-matched mice at a similar time point post-sham inoculation (controls) were free of such changes (C and F, respectively). Astrocytic gliosis demonstrated using anti-GFAP polyclonal sera was first evident simultaneously at 82 dpi in the hippocampus (G) and thalamus (J), and progressively increased so that terminal mice demonstrated dense astrocytic gliosis throughout the hippocampus (H) and thalamus (K), compared to unchanged levels in age-matched, sham-inoculated brains (I and L, respectively). Neurone loss was assessed using the neuronal marker anti-neuronal nuclear protein (NeuN) monoclonal antibody. Subtle neuronal loss was first evident simultaneously in the hippocampus (M) and thalamus (P) at 82 dpi, which progressively worsened at subsequent time points with the hippocampal CA1–CA3 (N) and dorsal thalamic (Q) regions of terminal mice showing severe depletion of neurons compared to sham-, age-matched controls (O and R, respectively). Immunohistochemical staining for PrP using the anti-PrP ICSM18 monoclonal antibody first demonstrated occasional PrP-positive plaques juxtaposed to the hippocampus (S) and within the thalamus (V) at 82 dpi, with the brains of mice with terminal disease showing very prominent plaque deposition (T and W, respectively) but absence of staining in the brains of age-matched, sham-inoculated mice (U and X, respectively). Original magnifications: (C, D–F, M–X) 200×; all others: 400×.

both the stratum oriens and stratum radiatum were affected. Thereafter, the hippocampus and thalamus progressively displayed widespread and markedly increased GFAP reactivity compared to controls, with the expansion most dramatic from 104 dpi through to the terminal stage (Fig. 2H and K). The occipital subcortical white matter was the first neocortical region to display GFAP reactivity at day 104 post inoculation at which time sparse staining was also seen in the brain stem. These areas, and the other cerebral subcortical white matter regions, progressively developed widespread but less marked increases in GFAP staining. The cerebellar cortex remained free of gliosis even in terminally ill animals.

3.2.2. Neuronal loss

Neuron-specific immunostains confirmed neuronal loss in M1000 inoculated mice relative to age matched, sham inoculated controls. Subtle thalamic neuronal loss was evident from 82 dpi (Fig. 2P) and progressively worsened thereafter, with the lateral thalamic (including pars posterior) through to the pre-tectal nuclear areas the most affected, frequently displaying complete neuronal loss in terminal mice (Fig. 2Q), when compared to controls (Fig. 2R). The CA1–CA3 pyramidal neurons of the hippocampus also displayed similar findings from day 82 post inoculation (Fig. 2M) with the loss greatly pronounced by 123 dpi. The CA1–CA3 regions of the hippocampus showed near total loss of neurons by the terminal stage (Fig. 2N) when compared to controls (Fig. 2O). The occipital cortex was seen to lose NeuN reactivity around day 104 while, in contrast but concordant with other morphological findings the cerebellum did not display any definite neuronal loss even in terminally ill animals, including Purkinje cells as demonstrated by neurofilament staining (data not shown).

3.2.3. PrP immunohistochemistry

PrP-positive plaques were occasionally detectable by IHC at 64 dpi, at the junction of the corpus callosum with the stratum oriens of the hippocampus but remained an inconstant finding at 82 dpi (Fig. 2S). At 82 dpi the thalamus often but not invariably demonstrated modest numbers of PrP-positive plaques (Fig. 2V). However, throughout the time course, the hippocampus and thalamus demonstrated the greatest degree of PrP immunostaining, which often became very prominent in terminally ill animals (Fig. 2T and W, respectively). From day 104 post-inoculation, PrP plaques were also present in the neocortical white matter, with the occipital region most affected. Even in terminal mice, the brain stem only revealed occasional plaques and the cerebellum was free of PrP deposits.

3.3. Bioassay determination of transmissibility over the incubation period

Prion propagation over the disease time course was assessed by "blind" bioassay using Tg20 mice. For each pre-scheduled cull of Balb/c mice at the various time points, incubation time interval assay estimates of infectious titres were calculated (Table 1). The diencephalic regions from mice culled 0 and 2 h post-inoculation, and 1, 7 and 14 dpi revealed transmission rates and incubation periods consistent with low titres of infectivity, which are assumed to reflect residual inoculum. The nadir of infectivity occurred at 21 dpi, suggesting maximal clearance of the inoculum, with an 80% transmission rate and mean incubation period of 118 ± 36 days. Thereafter, infectivity rapidly increased to day 42, as reflected by shorter incubation periods and 100% transmission rates, followed by a more gradual increase to reach maximal levels around 104 dpi when mean incubation periods approximated 60 days for this and subsequent time points.

Table 1
Summary of bioassay results of M1000-inoculated Balb/c mice culled at predetermined time points and at terminal illness

Balb/c mice cull times (dpi)	Number of Tg20 developing clinical disease/inoculated	Mean Tg20 incubation period ± S.E.M.	ID50 units/g brain[a]
0	10/10	82 ± 8	1.8×10^6
0.1	8/8	82 ± 6	1.8×10^6
1	14/14	81 ± 8	2.2×10^6
7	8/8	111 ± 18	4.1×10^{3b}
14	7/7	86 ± 4	7.6×10^5
21	16/20	118 ± 36	9.5×10^{2b}
42	20/20	79 ± 5	3.3×10^6
64	20/21	75 ± 6	7.6×10^6
82	17/17	68 ± 4	3.3×10^7
104	18/18	59 ± 2	2.2×10^8
123	19/19	63 ± 3	9.3×10^7
137	23/23	60 ± 2	1.8×10^8
145 ± 2	12/12	58 ± 4	2.7×10^8

S.E.M. = standard error of the mean; dpi = days post inoculation.
[a] Calculated using regression equation derived from dose titration assay of M1000 whole brain homogenates inoculated into Tg20 indicator mice: incubation period = 111.18 + (−11.02) Log dose of inoculum (Spearman coefficient $p < 0.0001$).
[b] Notional titre; incubation period fell outside interpolatable data range.

3.4. Assessment of oxidative stress through the incubation period

3.4.1. Immunohistochemistry

Immunohistochemistry employing various markers of oxidative damage was intended to provide a detailed topographical analysis over the disease course for correlation with conventional neuropathological changes. Despite varying numerous parameters of the immunohistochemical protocol, we were unable to detect consistent and convincing differences in the staining patterns of diseased and control tissue for NT modified proteins, HNE adducted proteins and HO-1. All three primary antibodies displayed widespread neuronal staining in both diseased and control brains (data not shown). The most intensely staining neurones were usually in the brain stem, a region generally showing relatively less severe conventional histopathological changes. The anti-NT antibody caused a uniform hazy staining of the neuropil, which appeared to be non-specific. Although encouraged by some of our results, such as the absence of immunostaining when omitting the primary antibodies and for NT, after pre-treatment of sections with 100 mM sodium hydrosulphite

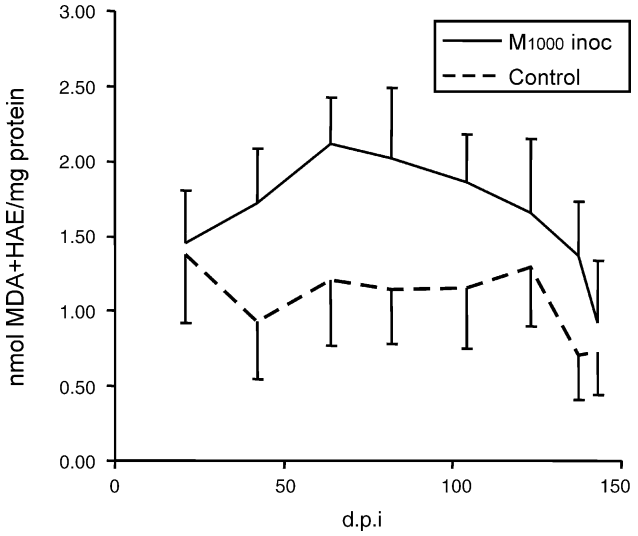

Fig. 3. Comparative assessment of brain levels (nmol/mg protein) of free HAE and MDA aldehydic breakdown products of lipid peroxidation in M1000 inoculated Balb/c mice and controls using the Bioxytech LPO586 (Oxis) colorimetric assay as described in Section 2. The diencephalic regions of the infected mice were found to contain the most significantly elevated levels of free HAE and MDA (two-way ANOVA $p = 0.0071$), increased from 42 dpi and continuing over the entire disease course but highest over the mid-incubation period. dpi = days post-inoculation.

(dithionite) under anaerobic conditions, pre-immune serum gave very similar staining patterns to that observed with polyclonal primary antisera (data not shown).

3.4.2. Biochemical assessment of lipid peroxidation

Given the limitations of immunohistochemistry to assess for a spatio-temporal pathogenic link between heightened oxidative stress, and prion propagation and the typical neuropathological changes, we undertook biochemical analyses. Free aldehydic lipid peroxidation breakdown products from the three principal brain regions were assessed across the disease course. Observed was an elevation of free MDA and HAE in all brain regions of mice inoculated with M1000 compared with controls. The most striking and significant elevation of the aldehydic breakdown products was in the diencephalon (two-way ANOVA $p = 0.0071$). MDA and HAE levels rose from background concentrations at 21 dpi to increased levels at 42 dpi, remaining elevated thereafter over the entire time course, but highest over the mid-incubation period (Fig. 3). It is notable that the onset of heightened lipid peroxidation in the diencephalic region closely correlated with both the rapid rise in prion titres as well as the earliest evidence of PrP^{res} (42 dpi), and immediately pre-empted the appearance of typical neuropathologic changes, which eventually were often most marked in this same brain region.

3.4.3. Protein carbonyl modification and inducible nitric oxide synthase (iNOS) expression

To determine if other cellular indicators of brain oxidative stress were also increased during the disease course, total protein carbonylation and levels of iNOS were assessed. The overall results for both carbonyl modification and iNOS expression were similar for the three principal brain regions analysed. Qualitative analysis did not reveal a consistent difference between M1000 and sham inoculated mice at any of the time points during the incubation period, nor in terminal mice compared to age matched controls (data not shown). Also, for total protein carbonylation there was no evidence of a trend to higher levels with time over the disease course nor with ageing in sham inoculated mice. For assessment of iNOS expression, analysis was restricted to a protein band with a relative mobility of 130 kDa (in accordance with the positive control). An additional, often more prominent band was observed at around 117 kDa with similar results in both M1000 inoculated mice and controls.

4. Discussion

The findings of the present study represent an important extension to previous in vivo studies assessing oxidative stress in animal models of TSE pathogenesis [1,10,11,19,20,46], and support a generic role for heightened oxidative damage across a range of neurodegenerative disorders [51]. Previous in vivo studies demonstrating increases in lipid peroxidation products have either been restricted to non-topographical assessments of the brains of terminally ill animals [10,11,46] or have used immunohistochemistry over a time course but only found noticeable elevations of 4-hydroxynonenal (HNE) restricted to astrocytes late in the incubation period [1]. None have correlated their findings with prion propagation. In contrast to these prior reports, the present results demonstrate that peroxidative lipid damage occurs as an early and relatively selective pathogenic event, closely linked temporally and more broadly topographically with the hallmark features of TSE pathogenesis; de novo prion propagation and the presence of PrP^{res}. The observed increase in lipid peroxidation early in disease evolution militates against the likelihood that such changes represent a less relevant epiphenomenon occurring secondarily in non-neuronal cells late in the disease course [1,11] or in neurons already compromised from other primary insults. Exemplifying our speculations regarding causality is the observation that although all brain regions were affected, the most significant peroxidative damage was seen in the diencephalic region, corresponding to where neuropathological changes were first evident and where the most severe neuropathologic findings generally eventuated (Table 2).

Support for a direct link between increased oxidative stress and spongiform neurodegeneration also comes from a transgenic mouse model in which the mitochondrial form of SOD (MnSOD) has been genetically ablated [28], as well as other animal models of TSE where mitochondrial damage has been described [10]. Precisely how PrP^{res} or the conversion process is linked to lipid peroxidation is uncertain; however evidence exists to suggest that the conformational change of PrP^{C} to PrP^{res} probably occurs within a lipid membrane environment and may involve formation of redox active, copper complexing, metastable PrP intermediates [39]. Ultrastructurally, conversion of PrP^{C} is most likely to be within detergent-resistant lipid-rafts of the plasma membrane or early endosomes [13,40], both of which are rich in easily peroxidisable arachidonic acid [34].

A detailed topographical insight into precisely which brain regions and cell types displayed oxidative damage was not

Table 2
Summary of neuropathological changes and biochemical evidence of oxidative stress in the diencephalon of M1000-inoculated Balb/c mice culled at pre-determined time points and at terminal illness

	Number of days post-intracerebral inoculation							
	21	42	64	82	104	123	137	145 ± 2
Transmissibility	+[a]	++	++	+++	++++	++++	++++	++++
Lipid peroxidation	0	++	+++	+++	++	+	+	+
PrP^{res}[b]	0	0[c]	++	+++	++++	++++	++++	++++
Vacuolation	0	0	0	++	+++	+++	++++	++++
Neuronal loss	0	0	0	+	+	++	+++	+++
GFAP	0	0	0	+	++	++	++++	++++
PrP plaques	0	0	0	+	++	++	+++	+++

[a] For illustrative comparative purposes, the various analysed features over the time course of disease were arbitrarily graded: 0 = normal/absent; + = very minor; ++ = mild; +++ = moderate; ++++ = severe or marked. Neuropathological gradings were qualitative, based on a composite average of observations from single, mid-sagittal, whole brain sections from three or four mice at each time point, using a high power field (200× original magnification) centred on the thalamus.
[b] Determined by western blot analysis of brain homogenates as described in Section 2.
[c] Occasional weak positive signal at 42 dpi.

achieved in our study. We suspect this inability may at least partly relate to a technical problem regarding tissue preparation. In contrast to previous studies reporting immunohistochemical evidence of oxidative damage or stress in animal models of prion disease [1,11,19,20], we subjected tissue sections to concentrated formic acid. Such pre-treatment may deleteriously affect the antigenic specificity of epitopes found in HNE, HO-1 and NT, and may also lead to an artefactual, diffuse increase in non-specific neuronal staining (including similarly pre-treated control tissues), overwhelming any genuine signal from oxidative damage. Consequently, we were not able to clearly reproduce the previous findings of increased HNE immuno-reactivity within astrocytes in the later incubation period [1]. Utilising a sensitive biochemical approach, however, our study did demonstrate significantly heightened lipid peroxidation in the diencephalon. The importance of the biochemical assay employed in our study is that it detects free MDA and HAE as evidence of lipid peroxidation, with these unbound aldehydes known to quickly dissipate due to very rapid reactions with other biomolecules. In contrast, immunohistochemical detection of HNE (one important HAE breakdown product) utilises antibodies that specifically recognise chemically reduced amino acid-(4)-HNE adducts, which are stable end products of reactive HNE molecules. Once formed, these would remain and accumulate in an affected tissue, allowing subsequent detection but not necessarily reflecting active lipid peroxidation at the time of detection. Hence, the presence of stable HNE adducts later in the disease is not necessarily incompatible with our finding of highest free reactive aldehyde levels earlier in the incubation period. Differing sensitivities of the two techniques may underlie a situation in which the morphological method requires greater absolute amounts of HNE before a detection threshold is reached, with progressive accumulation only achieving this by late in the incubation period [1], whereas despite lessening production of HAE and MDA their more sensitive biochemical detection is still possible even until the terminal phase of illness.

Despite inexorable progression of the disease both histopathologically and clinically, lipid peroxidation lessened in the latter stages of the incubation period but did not return to control levels. The reduction in lipid peroxidation may relate to glial proliferation, which although posited as a generic protective response [50] against many different insults including oxidative stress [14,15,37], does not impede the continuing propagation of PrP^{res}. It may be that in our in vivo model of TSEs, such a protective effect was achieved to some degree against oxidative attack on membrane lipids, but failed to mitigate the deleterious effects of additional pathogenic pathways induced as a consequence of the continued production and accumulation of PrP^{res} [50]. Additionally, certain neuronal subpopulations may have increased vulnerability to oxidative stress and are lost early, leaving surviving neurons such as seen in the cerebellum of our mice and in those infected with other prion strains [9], perhaps because of better innate anti-oxidant defences [25].

The present study found no convincing evidence of increased total protein oxidation, nor elevation of iNOS in the brains of infected mice. Our observed lack of up-regulation of iNOS accords with the findings of a recent report [42] but is discrepant with another in vivo animal study [20]. Prion strain-host animal differences are unlikely as the explanation for the discrepancy given the use of a similar combination in the two previous studies of iNOS with strikingly divergent observations. Further, although reports have described increased gene transcriptional activity and expression levels of NF-κβ, and pro-inflammatory cytokines such as TNFα and interleukins-1α and 1β in mice infected with TSE agents [21,24] (the latter most likely through reactive oxygen species inducing increased levels of NF-κβ, a major transcriptional activator regulating TNFα and interleukins-1α and 1β), this has not been an invariable finding [42]. It is possible that NF-κβ is not activated in our model of prion disease. Free HNE, likely to be considerably increased from relatively early in the incubation period in our study, has been shown to bind and inhibit the activation of NF-κβ and prevent iNOS expression in cell culture models [26,31]. Also, while the observed up-regulation of GFAP but not iNOS in our model appears contradictory, it must be noted that GFAP can be expressed in the absence of NF-κβ activation. NF-ιο and NF-κβ can differentially regulate GFAP expression in a

number of situations, including maturation and as a response to a wide variety of perturbations to the cellular environment [17].

Acknowledgements

The authors wish to thank Ashley Fletcher for assistance with statistical analysis, as well as Mrs. T. Cardamone and Ms. L. Leone for performing the histology and immunohistochemistry. Tg20 mice used in the study were a generous gift from Professor Charles Weissmann. The anti-prion protein monoclonal antibody ICSM18 was a generous gift from Professor John Collinge. S.J. Collins and A.F. Hill receive support from a National Health and Medical Research Council (NHMRC) Program Grant # 208978. A.F. Hill and A.R. White are recipients of NHMRC R. Douglas Wright Career Development Awards. V.A. Lawson is the recipient of an NHMRC Howard Florey fellowship. The Australian National CJD Registry is funded by the Commonwealth Department of Health and Ageing.

References

[1] O. Andreoletti, E. Levavasseur, E. Uro-Coste, G. Tabouret, P. Sarradin, M.B. Delisle, P. Berthon, R. Salvayre, F. Schelcher, A. Negre-Salvayre, Astrocytes accumulate 4-hydroxynonenal adducts in murine scrapie and human Creutzfeldt-Jakob disease, Neurobiol. Dis. 11 (2002) 386–393.

[2] S. Brandner, S. Isenmann, A. Raeber, M. Fischer, A. Sailer, Y. Kobayashi, S. Marino, C. Weissmann, A. Aguzzi, Normal host prion protein necessary for scrapie-induced neurotoxicity, Nature 379 (1996) 339–343.

[3] D. Brown, C. Clive, S. Haswell, Antioxidant activity related to copper binding native prion protein, J. Neurochem. 76 (2001) 69–76.

[4] D.R. Brown, K. Qin, J.W. Herms, A. Madlung, J. Manson, R. Strome, P.E. Fraser, T. Kruck, A. von Bohlen, W. Schulz-Schaeffer, A. Giese, D. Westaway, H. Kretzschmar, The cellular prion protein binds copper in vivo, Nature 390 (1997) 684–687.

[5] D.R. Brown, B. Schmidt, H.A. Kretzschmar, Role of microglia and host prion protein in neurotoxicity of a prion protein fragment, Nature 380 (1996) 345–347.

[6] D.R. Brown, B. Schmidt, H.A. Kretzschmar, Effects of copper on survival of prion protein knockout neurons and glia, J. Neurochem. 70 (1998) 1686–1693.

[7] D.R. Brown, B.S. Wong, F. Hafiz, C. Clive, S.J. Haswell, I.M. Jones, Normal prion protein has an activity like that of superoxide dismutase, Biochem. J. 344 (1999) 1–5.

[8] H. Bueler, A. Aguzzi, A. Sailer, R.A. Greiner, P. Autenried, M. Aguet, C. Weissmann, Mice devoid of PrP are resistant to scrapie, Cell 73 (1993) 1339–1347.

[9] P. Casaccia-Bonnefil, R.J. Kascsak, R. Fersko, S. Callahan, R.I. Carp, Brain regional distribution of prion protein PrP27-30 in mice stereotaxically microinjected with different strains of scrapie, J. Infect. Dis. 167 (1993) 7–12.

[10] S.I. Choi, W.K. Ju, E.K. Choi, J. Kim, H.Z. Lea, R.I. Carp, H.M. Wisniewski, Y.S. Kim, Mitochondrial dysfunction induced by oxidative stress in the brains of hamsters infected with the 263 K scrapie agent, Acta Neuropathol. (Berl.) 96 (1998) 279–286.

[11] Y.-G. Choi, J.-I. Kim, H.-P. Lee, J.-K. Jin, E.-K. Choi, R.-I. Carp, Y.-S. Kim, Induction of heme oxygenase-1 in the brains of scrapie-infected mice, Neurosci. Lett. 289 (2000) 173–176.

[12] S.J. Collins, V. Lewis, M. Brazier, A.F. Hill, A. Fletcher, C.L. Masters, Quinacrine does not prolong survival in a murine Creutzfeldt-Jakob disease model, Ann. Neurol. 52 (2002) 503–506.

[13] P. Critchley, J. Kazlauskaite, R. Eason, T.J. Pinheiro, Binding of prion proteins to lipid membranes, Biochem. Biophys. Res. Commun. 313 (2004) 559–567.

[14] S. Desagher, J. Glowinski, J. Premont, Astrocytes protect neurons from hydrogen peroxide toxicity, J. Neurosci. (1996) 2553–2562.

[15] R. Dringen, J.M. Gutterer, J. Hirrlinger, Glutathione metabolism in brain metabolic interaction between astrocytes and neurons in the defence against reactive oxygen species, Eur. J. Biochem. 267 (2000) 4912–4916.

[16] M. Fischer, T. Rulicke, A. Raeber, A. Sailer, M. Moser, B. Oesch, S. Brandner, A. Aguzzi, C. Weissmann, Prion protein (PrP) with amino-proximal deletions restoring susceptibility of PrP knockout mice to scrapie, EMBO J. 15 (1996) 1255–1264.

[17] F.C. Gomes, D. Paulin, V. Moura Neto, Glial fibrillary acidic protein (GFAP): modulation by growth factors and its implication in astrocyte differentiation, Braz. J. Med. Biol. Res. 32 (1999) 619–631.

[18] M. Guentchev, S.L. Siedlak, C. Jarius, F. Tagliavini, R.J. Castellani, G. Perry, M.A. Smith, H. Budka, Oxidative damage to nucleic acids in human prion disease, Neurobiol. Dis. 9 (2002) 275–281.

[19] M. Guentchev, T. Voigtlander, C. Haberler, M.H. Groschup, H. Budka, Evidence for oxidative stress in experimental prion disease, Neurobiol. Dis. 7 (2000) 270–273.

[20] W.K. Ju, K.J. Park, E.K. Choi, J. Kim, R.I. Carp, H.M. Wisniewski, Y.S. Kim, Expression of inducible nitric oxide synthase in the brains of scrapie-infected mice, J. Neurovirol. 4 (1998) 445–450.

[21] J.I. Kim, W.K. Ju, J.H. Choi, E. Choi, R.I. Carp, H.M. Wisniewski, Y.S. Kim, Expression of cytokine genes and increased nuclear factor-kappa B activity in the brains of scrapie-infected mice, Mol. Brain Res. 73 (1999) 17–27.

[22] F. Klamt, F. Dal-Pizzol, M.L. Conte da Frota Jr., R. Walz, M.E. Andrades, E.G. da Silva, R.R. Brentani, I. Izquierdo, J.C. Fonseca Moreira, Imbalance of antioxidant defense in mice lacking cellular prion protein, Free Radic. Biol. Med. 30 (2001) 1137–1144.

[23] R. Kordek, J.A. Hainfellner, P.P. Liberski, H. Budka, Deposition of the prion protein (PrP) during the evolution of experimental Creutzfeldt-Jakob disease, Acta Neuropathol. (Berl.) 98 (1999) 597–602.

[24] R. Kordek, V.R. Nerurkar, P.P. Liberski, S. Isaacson, R. Yanagihara, D.C. Gajdusek, Heightened expression of tumor necrosis factor alpha, interleukin 1 alpha, and glial fibrillary acidic protein in experimental Creutzfeldt-Jakob disease in mice, Proc. Natl. Acad. Sci. U.S.A. 93 (1996) 9754–9758.

[25] G.G. Kovacs, I. Kurucz, H. Budka, C. Adori, F. Muller, P. Acs, S. Kloppel, H.M. Schatzl, R.J. Mayer, L. Laszlo, Prominent stress response of Purkinje cells in Creutzfeldt-Jakob disease, Neurobiol. Dis. 8 (2001) 881–889.

[26] W. Liu, M. Kato, M. Itoigawa, H. Murakami, M. Yajima, J. Wu, N. Ishikawa, I. Nakashima, Distinct involvement of NF-kappaB and p38 mitogen-activated protein kinase pathways in serum deprivation-mediated stimulation of inducible nitric oxide synthase and its inhibition by 4-hydroxynonenal, J. Cell. Biochem. 83 (2001) 271–280.

[27] G. Mallucci, A. Dickinson, J. Linehan, P.C. Klohn, S. Brandner, J. Collinge, Depleting neuronal PrP in prion infection prevents disease and reverses spongiosis, Science 302 (2003) 871–874.

[28] S. Melov, S.R. Doctrow, J.A. Schneider, J. Haberson, M. Patel, P.E. Coskun, K. Huffman, D.C. Wallace, B. Malfroy, Lifespan extension and rescue of spongiform encephalopathy in superoxide dismutase 2 nullizygous mice treated with superoxide dismutase-catalase mimetics, J. Neurosci. 21 (2001) 8348–8353.

[29] O. Milhavet, H.E. McMahon, W. Rachidi, N. Nishida, S. Katamine, A. Mange, M. Arlotto, D. Casanova, J. Riondel, A. Favier, S. Lehmann, Prion infection impairs the cellular response to oxidative stress, Proc. Natl. Acad. Sci. U.S.A. 97 (2000) 13937–13942.

[30] T. Miura, A. Hori-i, H. Takeuchi, Metal-dependent alpha-helix formation promoted by the glycine-rich octapeptide region of prion protein, FEBS Lett. 396 (1996) 248–252.

[31] I. Nakashima, W. Liu, A.A. Akhand, K. Takeda, Y. Kawamoto, M. Kato, H. Suzuki, 4-hydroxynonenal triggers multistep signal transduction cascades for suppression of cellular functions, Mol. Aspects Med. 24 (2003) 231–238.

[32] S. Noriyuki, O. Yuriko, N. Morimitsu, The octapeptide repeat region of prion protein binds Cu(II) in the redox-inactive state, Biochem. Biophys. Res. Commun. 267 (2000) 398–402.

[33] K.M. Pan, M. Baldwin, J. Nguyen, M. Gasset, A. Serban, D. Groth, I. Mehlhorn, Z. Huang, R.J. Fletterick, F.E. Cohen, S.B. Prusiner, Conversion of alpha-helices into beta-sheets features in the formation of the scrapie prion proteins, Proc. Natl. Acad. Sci. U.S.A. 90 (1993) 10962–10966.

[34] L.J. Pike, X. Han, K.N. Chung, R.W. Gross, Lipid rafts are enriched in arachidonic acid and plasmenylethanolamine and their composition is independent of caveolin-1 expression: a quantitative electrospray ionization/mass spectrometric analysis, Biochemistry 41 (2002) 2075–2088.

[35] L.M. Sayre, G. Perry, M.A. Smith, In situ methods for detection and localization of markers of oxidative stress: application in neurodegenerative disorders, Methods Enzymol. 309 (1999) 133–152.

[36] J. Stockel, J. Safar, A.C. Wallace, F.E. Cohen, S.B. Prusiner, Prion protein selectively binds copper(II) ions, Biochemistry 37 (1998) 7185–7193.

[37] J. Tanaka, K. Toku, B. Zhang, K. Ishihara, M. Sakanaka, N. Maeda, Astrocytes prevent neuronal death induced by reactive oxygen and nitrogen species, Glia 28 (1999) 85–96.

[38] J. Tateishi, M. Ohta, M. Koga, Y. Sato, Y. Kuroiwa, Transmission of chronic spongiform encephalopathy with kuru plaques from humans to small rodents, Ann. Neurol. 5 (1979) 581–584.

[39] A.M. Thackray, R. Knight, S.J. Haswell, R. Bujdoso, D.R. Brown, Metal imbalance and compromised antioxidant function are early changes in prion disease, Biochem. J. 362 (2002) 253–258.

[40] M. Vey, S. Pilkuhn, H. Wille, R. Nixon, S.J. DeArmond, E.J. Smart, R.G. Anderson, A. Taraboulos, S.B. Prusiner, Subcellular colocalization of the cellular and scrapie prion proteins in caveolae-like membranous domains, Proc. Natl. Acad. Sci. U.S.A. 93 (1996) 14945–14949.

[41] J.D. Wadsworth, S. Joiner, A.F. Hill, T.A. Campbell, M. Desbruslais, P.J. Luthert, J. Collinge, Tissue distribution of protease resistant prion protein in variant Creutzfeldt-Jakob disease using a highly sensitive immunoblotting assay, Lancet 358 (2001) 171–180.

[42] D.T. Walsh, S. Betmouni, V.H. Perry, Absence of detectable IL-1beta production in murine prion disease: a model of chronic neurodegeneration, J. Neuropathol. Exp. Neurol. 60 (2001) 173–182.

[43] A.R. White, S.J. Collins, F. Maher, M.F. Jobling, L.R. Stewart, J.M. Thyer, K. Beyreuther, C.L. Masters, R. Cappai, Prion protein-deficient neurons reveal lower glutathione reductase activity and increased susceptibility to hydrogen peroxide toxicity, Am. J. Pathol. 155 (1999) 1723–1730.

[44] A.R. White, P. Enever, M. Tayebi, R. Mushens, J. Linehan, S. Brandner, D. Anstee, J. Collinge, S. Hawke, Monoclonal antibodies inhibit prion replication and delay the development of prion disease, Nature 422 (2003) 80–83.

[45] A.R. White, G. Multhaup, D. Galatis, W.J. McKinstry, M.W. Parker, R. Pipkorn, K. Beyreuther, C.L. Masters, R. Cappai, Contrasting, species-dependent modulation of copper-mediated neurotoxicity by the Alzheimer's disease amyloid precursor protein, J. Neurosci. 22 (2002) 365–376.

[46] B.S. Wong, D.R. Brown, T. Pan, M. Whiteman, T. Liu, X. Bu, R. Li, P. Gambetti, J. Olesik, R. Rubenstein, M.S. Sy, Oxidative impairment in scrapie-infected mice is associated with brain metals perturbations and altered antioxidant activities, J. Neurochem. 79 (2001) 689–698.

[47] B.S. Wong, S.G. Chen, M. Colucci, Z. Xie, T. Pan, T. Liu, R. Li, P. Gambetti, M.S. Sy, D.R. Brown, Aberrant metal binding by prion protein in human prion disease, J. Neurochem. 78 (2001) 1400–1408.

[48] B.S. Wong, T. Liu, R. Li, T. Pan, R.B. Petersen, M.A. Smith, P. Gambetti, G. Perry, J.C. Manson, D.R. Brown, M.S. Sy, Increased levels of oxidative stress markers detected in the brains of mice devoid of prion protein, J. Neurochem. 76 (2001) 565–572.

[49] B.S. Wong, T. Pan, T. Liu, R. Li, P. Gambetti, M.S. Sy, Differential contribution of superoxide dismutase activity by prion protein in vivo, Biochem. Biophys. Res. Commun. 273 (2000) 136–139.

[50] X. Ye, A.C. Scallet, R.J. Kascsak, R.I. Carp, Astrocytosis and amyloid deposition in scrapie-infected hamsters, Brain Res. 809 (1998) 277–287.

[51] K. Zarkovic, 4-hydroxynonenal and neurodegenerative diseases, Mol. Aspects Med. 24 (2003) 293–303.

Free Radical Biology & Medicine 51 (2011) 594–608

Contents lists available at ScienceDirect

Free Radical Biology & Medicine

journal homepage: www.elsevier.com/locate/freeradbiomed

Original Contribution

Acute exposure to prion infection induces transient oxidative stress progressing to be cumulatively deleterious with chronic propagation *in vitro*

Cathryn L. Haigh [a,b], Amelia R. McGlade [a,b], Victoria Lewis [a,b], Colin L. Masters [b,c], Victoria A. Lawson [a,b], Steven J. Collins [a,b,*]

[a] *Department of Pathology, The University of Melbourne, Parkville, 3010, Australia*
[b] *Mental Health Research Institute, The University of Melbourne, Parkville, 3010, Australia*
[c] *Centre for Neuroscience, The University of Melbourne, Parkville, 3010, Australia*

ARTICLE INFO

Article history:
Received 11 September 2010
Revised 3 March 2011
Accepted 28 March 2011
Available online 3 April 2011

Keywords:
Prion
ROS
Lysosome
Caspase
Lipid peroxidation
Free radicals

ABSTRACT

Neuronal loss is a pathological feature of prion diseases for which increased reactive oxygen species (ROS) and consequent oxidative stress is one proposed mechanism. The processes underlying ROS production in prion disease and the precise relationship to misfolding of the prion protein remain obscure. Using cell culture models of prion infection we found that cells demonstrate a rapid, prion protein (PrP) dependent, increase in intracellular ROS following exposure to infectious inoculum. ROS production correlated with internalisation and increased intracellular protease resistant PrP (PrP^{Res}). The ROS increase was predominantly lysosomal in origin but not sustained, with cells adapting within 48 hours. Overall ROS levels remained normal in the chronically prion infected cell population; however a subpopulation characterised by loss of membrane phosphatidylserine asymmetry exhibited highly peroxidised intracellular aggregates that localised with PrP and intense caspase activation. These apoptotic cells showed increased ROS closely correlating with increased PrP^{Res}. Our findings demonstrate that a PrP-dependent, transient, increase in intracellular ROS is characteristic of acute cellular prion infection, while chronic phases of prion infection *in vitro* are associated with a significant subpopulation manifesting apoptosis accompanying heightened oxidative stress and increased PrP^{Res} burden. Such observations strengthen the direct links between heightened ROS and ongoing prion propagation with eventual cellular demise.

1. Introduction

Transmissibility is a fundamental feature of prion diseases separating them from other neurodegenerative disorders such as Alzheimer's disease. Transmission and neuronal degeneration only occur when the native prion protein (PrP^{C}) is expressed, allowing ongoing formation of abnormal conformers with increased beta-sheet content [1,2]. Generally in animal models, the abnormal conformers can be detected in the brains, by means of their increased protease resistance, well before overt disease is evident. At the earliest time point when these abnormal, protease resistant conformers (referred to as PrP^{Res}) can be weakly detected there is also a significant elevation in lipid peroxidation, a marker of increased ROS [3]. This finding raises the possibility that conversion of PrP^{C} to the abnormal isoform occurs concurrently with elevated ROS production, especially before any cellular compensatory responses can be established. Recent studies have highlighted the role of methionine oxidation, caused by ROS, in destabilising PrP^{C} conformation and so indicate that oxidation of PrP^{C} itself might be part of the conversion mechanism to PrP^{Res}[4].

PrP^{C} has been linked with cellular anti-oxidant capacity. This protection may arise through an intrinsic superoxide dismutase-like activity of PrP^{C}[5,6], or through the activation of signal transduction pathways that stimulate anti-oxidant defence by other means [7]. Transgenic mice with the PrP gene ablated (*Prnp* $PrP^{o/o}$) appear to have no significant impairment of central nervous system function [1,8]; however such mice do show heightened levels of oxidative stress markers in the brain and peripheral organs [9]. Further, when challenged with large insults, such as transient cerebral ischemia, $PrP^{o/o}$ mice display much greater oxidative damage than their wild-type counterparts [9–11]. Prion diseased mice with ongoing PrP^{Res} propagation show compromised antioxidant function and, specifically, attenuated cellular superoxide dismutase activity [12,13]. The implication being that, during prion disease, a PrP^{C}-related ROS protective function is lost either as a direct or indirect result of conversion of PrP^{C} to PrP^{Res}. An alternative to such 'loss of function' theories is the possibility that PrP^{C} to PrP^{Res} conformational change brings about an innate toxic gain of function directly contributing to increased cellular oxidative stress. Increased ROS have been found due to activation of NADPH oxidase when cells are exposed to PrP^{Res} or the amyloidogenic and toxic 106–

* Corresponding author at: Department of Pathology, The University of Melbourne, Parkville, 3010, Australia. Fax: +61 3 9349 5105.
E-mail address: stevenjc@unimelb.edu.au (S.J. Collins).

0891-5849/$ – see front matter © 2011 Elsevier Inc. All rights reserved.
doi:10.1016/j.freeradbiomed.2011.03.035

126 peptide derived from the core of PrP [14]. The authors reported that exposure to the 'toxic' agent initiates deleterious signalling through PrP, fyn and NADPH oxidase thereby promoting pathogenesis.

Considerable evidence exists supporting the occurrence and likely pathogenic role of heightened oxidative stress in prion disease evolution although whether this is a primary or initiating event or a later contributor after the development of neuronal dysfunction remains to be confidently resolved. Further, the processes underlying ROS production in prion disease and the precise relationship to misfolding of the prion protein remain obscure. At the earliest time point when protease resistant conformers were detected in the brains of prion infected mice, increased lipid peroxidation was detected concurrently [3]. The purpose of the present study was therefore to better understand the associations between PrP^{Res} propagation, ROS production and toxicity at the cellular level. Accordingly this study investigated the ROS changes associated with acute and chronic phases of prion infection in cell cultures. We found that cellular adaptation quickly restores increased ROS levels following acute prion infection but appears to be progressively overwhelmed in a significant subpopulation with resultant toxicity and apoptosis during chronic propagation.

2. Materials and methods

2.1. Cell culture

Rabbit kidney epithelial (RK13) cells, transfected (using FuGene 6; Roche, AUS) with empty vector, mouse PrP or human PrP, mouse olfactory bulb (OBL-21) cells [15,16] and the GT1-7 mouse hypothalamic neuronal cell line were cultured in Dulbecco's Modified Eagle's Medium (DMEM; Invitrogen AUS) supplemented with 10% (v/v) foetal bovine serum (Lonza Australia Pty) and 50 U/ml pencillin/50 μg/ml streptomycin FBS; solution (Sigma, AUS) and maintained at 37 °C with 5% CO_2 in a humidified incubator.

2.2. Stem cell harvest and culture

The brains of three eight week-old *Prnp* wild-type and knock-out mice (C57BL/6 x SV129 background) were harvested, post-anaesthetising with methoxyfluorane and cervical dislocation, and the sub ventricular zone (SVZ) dissected from the whole brain. All procedures were approved by an animal ethics committee operating under the Australian code of practice for the care and use of animals for scientific purposes. Stem cells were harvested from the SVZ using the Neurocult enzymatic cell dissociation kit (Stem Cell Technologies - Canada), as per the product protocol. Neurospheres were expanded in complete proliferation media (Stem Cell Technologies; see the Neurocult '*In vitro* proliferation and differentiation of mouse neural stem cells' manual for more details) and used for experiments at passages three and four. Neurospheres were differentiated into neural lineage cells by transfer into differentiation media (Stem Cell Technologies). For assays cells were seeded at a concentration of 5×10^4 cells/cm^2.

2.3. Preparation of infectious lysates and cell infections

The M1000 mouse-adapted prion strain was utilised for all cell infection experiments throughout this study [3]. Infections with M1000 brain homogenate were established using a standard overlay technique described previously [17]. Cell lysates were prepared by centrifugation at 300 x g for 5 minutes, washed in Dulbecco's phosphate buffered saline (dPBS), and centrifuged again. Pellets were weighed and resuspended in dPBS to make a 10% wet-pellet-weight/volume suspension. Cells were lysed by repeated freeze-thaw cycles and vortex mixed thoroughly to ensure an even suspension before overlay techniques. *De novo* cell infections were performed by exposure of cells to cell lysates that were M1000-infected or mock-infected (cells that had been exposed to normal brain homogenate in parallel with those exposed to M1000-infected brain homogenate). Cell-to-cell contact and media exchange infections were carried out utilising M1000-infected and mock-infected cells grown on coverslips. At the start of the assay, test cells grown in 24-well culture plates were loaded with DCFDA reporter reagent (see below), with the coverslips, which fit snugly in the well, positioned over the top of the test cells either face-up (media exchange) or face-down (cell contact) and readings taken 1.5 mm from the centre of the well.

2.4. DCFDA assay

The DCFDA assay using 5 μM 5-(and-6)-chloromethyl-2',7'-dichlorodihydrofluorescein diacetate, acetyl ester (CM-H_2-DCFDA, Invitrogen) was employed as described previously [18]. Cells were loaded with CM-H_2-DCFDA ROS-activated fluorescent dye (fluorescence yield progressively increases as ROS react with the dye) and fluorescence readings recorded from the addition of inocula for 12 hours. The rate of fluorescence change, indicating increased oxidative flux and defined as the linear tangent to the initial rate curve, was quantified relative to time 0 signal.

2.5. TEMPO-9-ac assay

For plate based assays 50 μM TEMPO-9-ac (Invitrogen) was included in the cell media (media in empty wells – no cells – was used as a negative control) and fluorescence changes monitored from the addition of test lysates. The fluorescent signal initially accumulates and linear tangents to the initial rate curve were used to monitor radical detection. For microscope assays 50 μM TEMPO-9-ac was loaded onto cells in normal media for 30 minutes, prior to imaging cells after transfer into phenol-red-free media.

2.6. MTS viability assay

Five μl of one solution MTS reagent (Promega; VIC AUS) per 100 μl media was added to test and medium-only background control conditions, and incubated under normal culture conditions for 90 minutes. Reaction product was quantified using absorbance at 462 nm in a Fluostar Optima.

2.7. CyQuant viability assay

The CyQuant viability assay (based on total DNA; Invitrogen) was performed as described in the product protocol. Readings were taken using 490 nm excitation and 520 nm emission filters in a Fluostar Optima.

2.8. Bodipy staining

Stock solutions of Bodipy$^{581/591}$ C11 (Invitrogen) were made by dissolving 1 mg of probe into 50 μl chloroform. The probe-chloroform solution was then diluted into 10 ml of foetal bovine serum to produce a 0.2 mM concentration of probe. Cells were cultured in normal media containing 2 μM of Bodipy$^{581/591}$ C11 for 24 hours prior to the start of the assay. Bodipy$^{581/591}$ C11 displays red fluorescence emission until it becomes oxidised when emission shifts into the green range; therefore the ratio at time 0 was taken as the control basal levels of lipid peroxidation.

2.9. Cytosolic redox potential

Cells were incubated in Opti-MEMI reduced serum culture medium (phenol red free; Invitrogen) containing 5 μM PF-H_2TMRos (Invitrogen) probe and 1 μM mito-tracker® green (Invitrogen) for 10 minutes. Media was removed and cells were washed in fresh media then incubated in fresh media with or without test inocula.

2.10. pHrodo labelling

Fifteen mg total protein (based on determination of concentration by BCA assay) from whole cell lysates of mock or M1000 infected cells was prepared in 100 mM sodium bicarbonate buffer (pH 8.5) then incubated with 0.25 mM pHrodo dye (Invitrogen; prepared as a 10 mM solution in DMSO) for 1 hour at room temperature protected from light. Protein was separated from unbound dye by methanol precipitation and resuspended in culture media before use. Protein concentration and pH fluorescence curves were determined as quality control measures before use (Sup Fig. 3).

2.11. Immuno-depletion of PrP

After determining protein concentration in cell lysates (by BCA assay), 1 mg was diluted into 500 µl dPBS, then incubated with 1 µl Saf32 primary anti-PrP antibody (epitope: murine residues 79–89; Sapphire Biosciences, AUS) for 1 hour with 3 rpm rotational mixing at 4 °C. Twenty-five µl of protein G dynabeads (Invitrogen) was added per separation and mixing continued for a further 2 hours at 4 °C. Separations were performed using a Dynabeads magnetic separation rack (Invitrogen); the supernatant was kept as the depleted fraction. Beads were boiled in dPBS to collect the PrP enriched fraction. Depleted samples were treated identically to the enriched fraction.

2.12. Indirect immunofluorescence

Cells were grown on 13 mm glass coverslips in normal media then treated with Bodipy$^{581/591}$ C11, as described above for 24 hours at 37 °C, with immunofluorescence (IF) performed when cells were 80% confluent. Plates were protected from light at all stages during this protocol. Cells were fixed in 4% (v/v) paraformaldehyde/PBS for 20 minutes and then permeabilised either in immunodiluent (ID; 1% w/v BSA in PBS) with 0.1% (v/v) Triton-X 100 for 5 minutes or ice-cold 100% methanol for 20 minutes. Coverslips were blocked in ID with 10% FBS (v/v) for 30 minutes. Primary antibodies Saf32 and mouse monoclonal anti-vimentin (Abcam, AUS) were diluted in ID and applied for 2.5 hours at room temperature. Alexafluor350-conjugated goat anti-mouse secondary antibody (Invitrogen) also diluted in ID was applied for one hour at room temperature. Coverslips were mounted onto glass slides with mowiol mounting media.

2.13. Caspase imaging

A 600 µM stock solution of SR-VAD-FMK (Immunochemistry Technologies, USA) was prepared in sterile PBS (pH7.4; Invitrogen) containing 20% (v/v) high quality sterile-filtered DMSO (Sigma-Aldrich). Cells were plated 24 hours before the start of the assay. 0.6 µM of the SR-VAD-FMK solution was added to Opti-MEMI reduced serum, phenol red free media and cells were incubated for 30 minutes under normal growth conditions. The cells were then washed and incubated in fresh Opti-MEMI for the duration of the assay.

2.14. Phen green Fl assay

Cells were incubated in pre-warmed Opti-MEMI reduced-serum medium (without phenol red) containing 10 µM Phen green FL diacetate for 20 minutes and residual cellular fluorescence compared with the cell-free control solution. Readings were taken using 490 nm excitation and 520 nm emission filters in a Fluostar Optima.

2.15. Cell blot assay

The cell blot assay is a variation on that developed by Bosque & Prusiner [19] as described in Lewis et al [17].

2.16. Slot blotting

Slot blots were performed using a Bio-Rad Bio-Dot SF apparatus as described in the recommended product protocols using nitrocellulose membranes. Five µg of total protein (as determined by BCA assay) was loaded per sample. Membranes were dried and treated as for cell blots to detect PrP^{Res}.

2.17. MACS separation

Cells were brought into solution using trypsin and gently pipetted up and down to remove cell clumps. 10^7 cells, as determined by haemocytometer cell count, were labelled with AnnexinV microbeads (Miltenyi Biotech, AUS) and magnetic separation was performed as described in the MACS protocol (Miltenyi Biotech). Both labelled and unlabelled fractions were transferred into fresh media for use in ensuing experiments, which were carried out within 2 hours whilst the cells expressing phosphatidylserine were still viable.

2.18. PK digest and western blotting

Cell fractions from MACS separations were centrifuged at 300 x g for 10 minutes to collect the cells, followed by lysis in RIPA buffer [50 mM Tris-HCl pH 7.4, 150 mM NaCl, 0.1% (w/v) SDS, 0.5% (w/v) sodium deoxycholate, 1% (v/v) NP-40] at 37 °C for 20 minutes. Total protein concentrations were determined by BCA assay. 100 µg of total

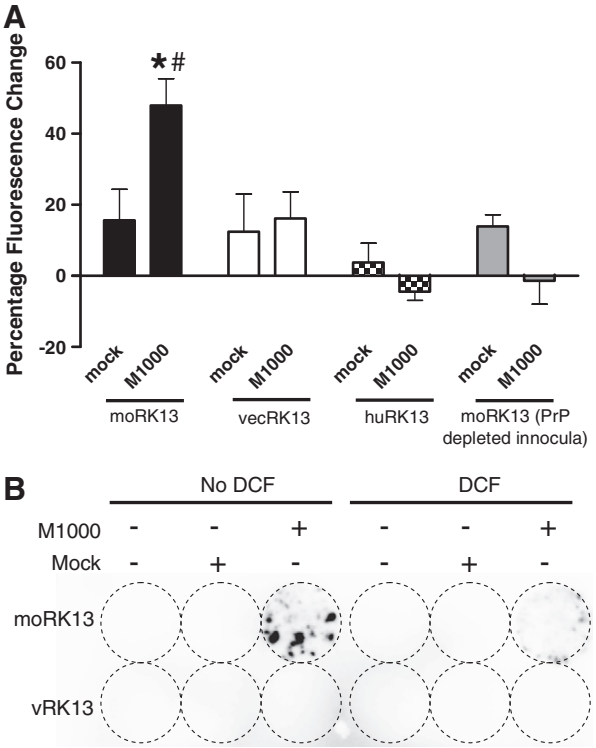

Fig. 1. Intracellular ROS increases in PrP^C-expressing cells upon exposure to infectious prions. (A) MoRK13 (black bars), vecRK13 (white bars) and huRK13 (chequered) cells were exposed to lysate derived from M1000 infected or mock infected (normal brain homogenate) moRK13 cells and intracellular ROS response determined by DCFDA assay. Shaded bars represent moRK13 cells treated as above but following immuno-depletion of PrP from the lysate inoculum. Significantly increased intracellular ROS response is seen for the moRK13 in response to the M1000 infected lysates only (2-way ANOVA $F=5.487$, $p=0.004$, $n=4$, $^*p<0.05$ significance comparing M1000 to mock lysate and $\#p<0.05$ significance comparing M1000 treatments) and this reduced to baseline when PrP is depleted from the inoculum. (B) Cell blot for infection at passage four post-treatment with infectivity. Following PK digestion, PrP^{Res} was detected by mab ICSM18. Growing the cells post DCFDA assay slowed the uptake of infection in the DCF treated cells compared to untreated counterparts (representative of $n=3$).

protein was split into two aliquots with the first incubated with 10 μg/ml proteinase K (PK) for 90 minutes. The second 50 μg of lysate was treated identically but without addition of the PK. Equal volumes of digested and undigested samples were electrophoresed using the NuPAGE system (Invitrogen), transferred onto nitrocellulose membranes and blocked as described in [20]. PrP was detected using 1 in 10,000 dilution of ICSM18 monoclonal antibody (murine epitope 142–152; D-Gen, UK) in 1% milk PBS-t. Anti-mouse HRP secondary antibody (GE Healthcare, NSW AUS) was used at 1 in 10,000 dilution and blots were visualised using ECL-plus detection reagent (GE Healthcare).

2.19. Oxyblot

Cells were lysed in RIPA buffer supplemented with 2% (v/v) β-mercaptoethanol and 20 μg derivatised as per the Oxyblot product protocol (Millipore). Two μg of each derivatisation and controls (no derivatisation negative control and derivatisation of cell lysates treated with 3% v/v H_2O_2 plus 1 mM $CuCl_4$ as a positive control) were spotted onto nitrocellulose membranes and blotting was continued as per the product protocol with visualisation using ECL-plus detection reagent (GE Healthcare).

2.20. Densitometry and statistical analyses

Luminescent signal of the bands on the western blots was captured using a LAS-3000 intelligent dark box (FujiFilm – Berthold, Victoria AUS) and the intensity quantified, after the subtraction of background, by ImageJ 1.38x. Statistical analyses were carried out using GraphPad Prism 4 or Minitab15 statistical software. Graphs represent the mean and s.e.m. of four independent experiments unless otherwise stated. Primary statistical tests are stated in the text; for ANOVA analysis Tukey's secondary test was applied. Microscope images were visualised with a 60x oil immersion lens and captured using a Nikon Eclipse TE2000-E epi-fluorescence microscope (Nikon-Roper Scientific). All image parameters were maintained throughout an experiment, across all conditions, and the channels of probes sensitive to photo-oxidation were collected before other channels. For imaging data the 'n' represents independent experiments, which each included capturing sufficient fields to analyse >50 cells per

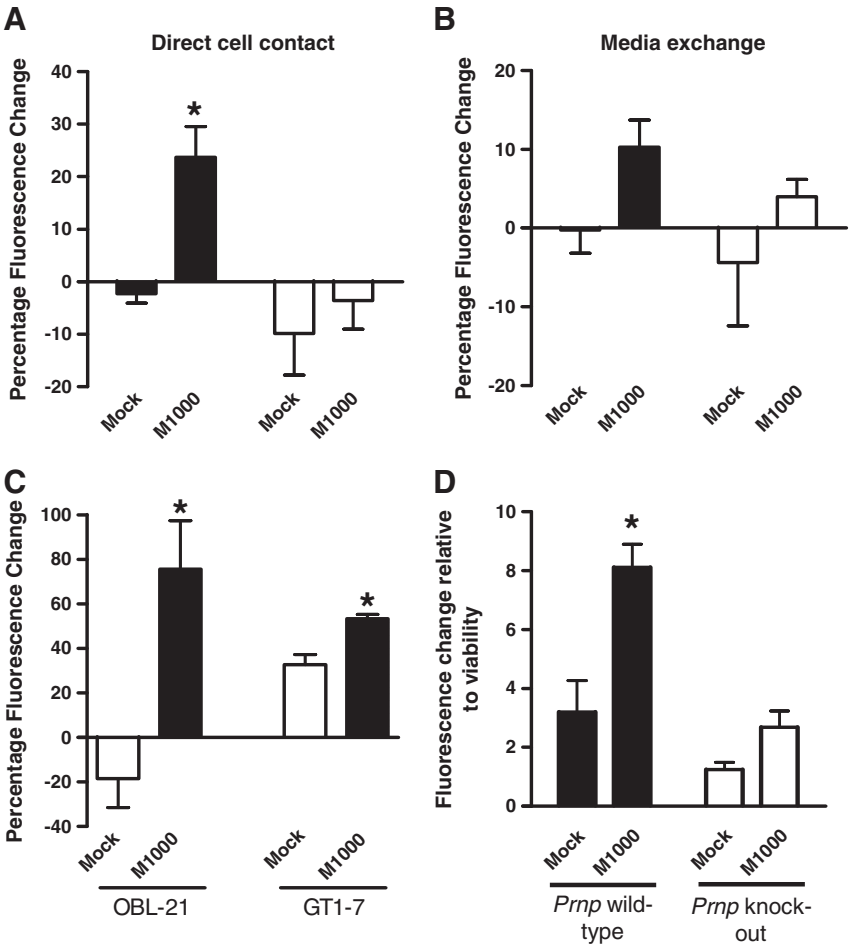

Fig. 2. Increased intracellular ROS occurs when uninfected cells directly contact infected cells and is also observed in murine neuronal cell lines and differentiated NSCs. The moRK13 (black bars) and vecRK13 (white bars) cells were incubated either in direct contact with M1000-infected or mock-infected cells (A) or allowed to exchange media with these cells (B). Significantly increased intracellular ROS as determined by the DCFDA assay is seen in moRK13 cells in direct contact with M1000 infected cells (2-way ANOVA, $F=9.409$, $p=0.0154$, $n=3$); this does not reach significance in cells allowed to media exchange (2-way ANOVA, $F=1.189$, $p=0.3072$, $n=3$). (C) OBL-21 and GT1-7 cells treated with normal mouse brain homogenate (white bars) and M1000 infected mouse brain homogenate (black bars) show increased ROS in response to the infectious inoculum (students *t*-test; OBL-21 $t=3.719$, $p=0.0338$, $n=3$; GT1-7 $t=7.106$, $p=0.0192$, $n=3$). (D) Wild-type (black bars) and *Prnp* knock-out (white bars) NSCs were differentiated for 6 days then assayed with mouse brain homogenate as described for the neuronal cell lines. The wild type cells treated with the M1000 infected homogenate showed significantly increased intracellular ROS compared with the control homogenate treated and null cells (Two-way ANOVA, $F=25.53$, $p=0.001$, $n=3$).

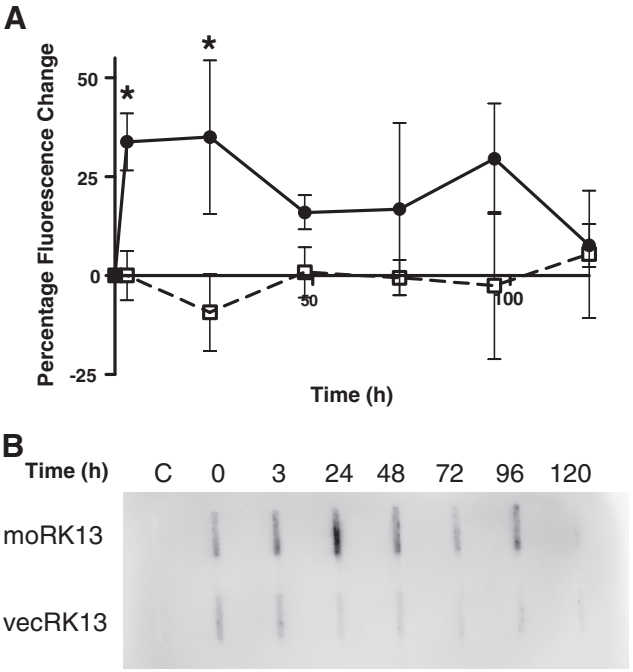

Fig. 3. ROS changes are transitory and cells compensate by 48 hours. (A) moRK13 (dots/solid line) or vecRK13 (squares/dashed line) cells were treated at various intervals up to 5 days with the M1000-infected or mock-infected lysates and intracellular ROS determined by DCFDA assay at the indicated time points up to 5 days. Significantly increased intracellular ROS in the moRK13 cells in response to the M1000 infected lysate is observed up to 24 hours post-infection after which it decreases to be non-significant (2-way ANOVA, $F=9.618$, $p=0.003$, $n=3$, $^{*}p<0.05$). (B) Slot blotting of proteinase-K treated moRK13 and vecRK13 cell lysates from the above assay shows that the quantity of PrP^{Res} increases in the moRK13 cells, plateauing at 24–56 hours (2-way ANOVA, $F=2.785$, $p=0.0298$, $n=3$) before declining to background, whereas the vecRK13 cells show a steady decrease in PrP^{Res}, which is almost undetectable by 5 days. The 0 time point represents immediate binding to the cells as soon as the infectious inoculum is added and C is the un-treated background control.

experiment. Cell intensity, intensity variation, co-localisation or ratiometric analysis (with percentage peroxidation calculated using $\% = I_{510}/(I_{510}+I_{570})$ *100) was done using Nikon NIS-elements 3.0 software with regions of interest used to gate individual cells.

3. Results

3.1. Exposure to M1000 infectious inocula induces a rapid, PrP-dependent, increase in intracellular ROS in moRK13 cells

The RK13 cell system used in this study has previously been characterised in detail [17,18]. RK13 cells transfected with mouse PrP^{C} readily propagate the M1000 mouse-adapted Gerstmann-Sträussler-Scheinker syndrome (GSS) prion strain [17,21,22]. Mixed population stable cell lines expressing mouse PrP (moRK13), human PrP (huRK13) and the empty vector control (vecRK13) were created by transfection. Infection of moRK13 cells with M1000 prions derived from the brains of mice in the end-stages of disease was established as described previously [17]. For subsequent infectivity assays, established propagating moRK13 (M1000-infected) lysates were used as the source of infectious prions, to mitigate any species barrier to prion infection, with mock-infected, equal passage moRK13 lysates used as controls.

To assess the oxidative response to infectious inocula, moRK13 and vecRK13 cells were exposed to 0.2% (wet-cell-pellet-weight/volume) M1000-infected or mock-infected lysate and subject to the DCFDA assay as outlined in the methods, whereby the ROS activated CM-H_2-DCFDA fluorescence yield progressively increases as ROS react with the dye. A significant increase in the implied intracellular ROS was seen in the moRK13 cells exposed to infectious inocula compared with the non-infectious control (Fig. 1A). An increase in ROS was not seen for the vecRK13 cells, indicating a PrP-specific effect. The difference was not due to higher basal oxidative stress levels in the vecRK13 cells restricting a potential increase, as basal ROS production is not significantly different across the cell lines [20]. The DCF responses of the moRK13 and vecRK13 cells were confirmed using a fluorescence spin-trapping assay with TEMPO-9-ac detection (Sup Fig. 1). A similar DCF response was not seen when huRK13 cells were exposed to the same treatments, indicating a species barrier to the response. Since it has not been possible to establish prion infection in the humanised RK13 cells to date [22], and prion toxicity is widely thought to be linked to converted host PrP oligomerisation, this finding was to be expected. Additionally, when PrP was immuno-depleted from the inocula and the assays repeated, no significant increase in ROS was observed for the M1000-infected compared with the mock-infected inoculum (Fig. 1A). Following the DCFDA assay, selected cells were collected and cultured until significant *de novo* propagation of infection beyond residual inoculums could be established (passage 4, approx 20 days). Control cells were equivalently treated with the exception of DCFDA loading. A cell blot assay was used to confirm prion propagation by the presence of PrP^{Res}. Loading the cells with the ROS-reactive DCFDA dye slowed, but did not prevent, the appearance of PrP^{Res} compared with the unloaded cells (Fig. 1B).

3.2. MoRK13 Intracellular ROS is increased by cell-to-cell contact with M1000 infected cells

Whilst overlaying cells with infectious brain homogenate or lysate may mimic the later stages of disease, when PrP^{Sc} deposits surround neurones, during the establishment of early disease this is unlikely; therefore to simulate an expected early *in vivo* situation, we sought to determine if either media or direct cell-to-cell contact with infected cells could produce the same effect. Using cells grown on coverslips, to allow either direct cell interfacing or indirect media exchange over the top of DCFDA-loaded test cells, the rates of ROS production in response to infected versus uninfected cell exposure were measured. ROS production was significantly increased in the moRK13 cells directly contacting infected cells but not in moRK13 cells contacting uninfected cells or in vecRK13 cells contacting M1000 infected cells, indicating that juxtaposition with cell-surface infectivity is sufficient to cause this effect in PrP expressing cells (Fig. 2A). A similar trend was observed in cells submitted to media exchange but this was not statistically significant (Fig. 2B).

Fig. 4. Increased ROS production occurs predominantly in the lysosomal compartment. (A) Fluorescence images of moRK13 cells stained with $Bodipy^{581/591}$ C11 and exposed to M1000 infectious or mock lysate for 3 hours, showing individual channels, merged channels and ratio view. Scale bar = 20 μm. (B) Ratiometric analysis of the images in A shows significantly increased lipid peroxidation in the moRK13 cells exposed to M1000-infected cell lysates compared to the mock-infected lysates (students *t*-test, $t=2.891$, $p=0.0043$, $n=4$) and (C) identifies increased numbers of peroxidised vesicular structures within the cells exposed to M1000-infected cell lysates (students *t*-test, $t=5.647$, $p=0.011$, $n=4$). (D) Fluorescence images of cells stained with PF-H_2TMRos and co-stained with mito-tracker green. Shown are split and merged images; scale bar = 20 μm. (E) Quantification of PF-H_2TMRos intensity indicates a specific increase in moRK13 cells exposed to M1000-infected cell lysates, which is significantly different from mock-infected inoculum by 1 hour and from the vecRK13 cells exposed to the M1000-infected lysates at 2 hours (2-way ANOVA, $F=15.03$, $^{***}p<0.001$, $n=4$,). (F) Using mitotracker co-localisation to quantify partitioning indicates that the increase in signal in the moRK13 cells is predominantly lysosomal (shown are data from 3 hours of treatment), with significant differences seen from both the mock treated and the vecRK13 cells treated with the infectious lysate (2-way ANOVA, $F=4.631$, $p=0.0036$, $n=4$, $^{*}p<0.05$, $^{**}p<0.01$). For graphs, grey bars and black bars show moRK13 cells and white and pale grey bars show vecRK13 cells treated with mock and infected cell lysates respectively.

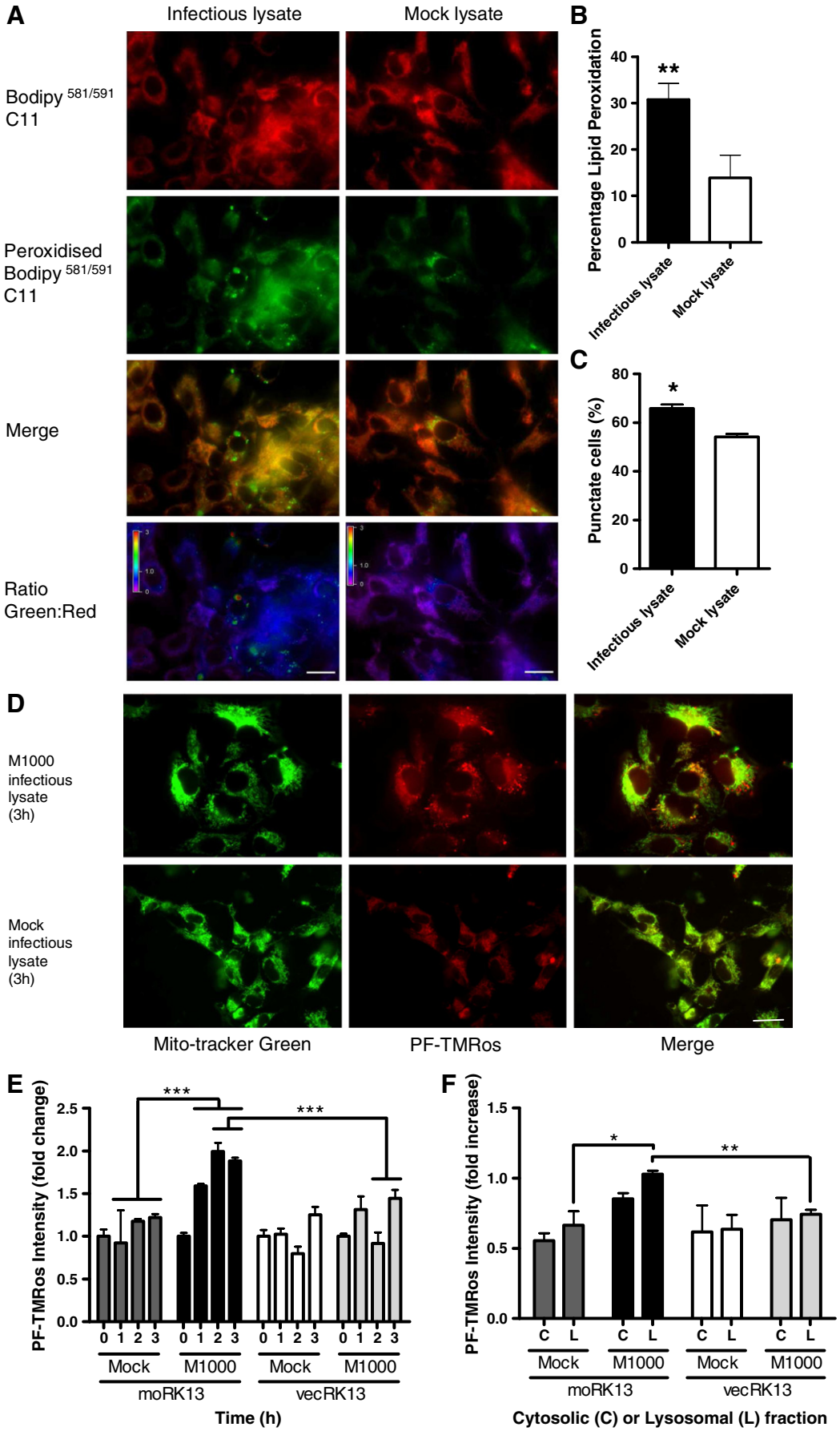

3.3. Induction of increased intracellular ROS by M1000 infectivity is also observed in murine neuronal cell lines and differentiated neural stem cells

To ensure that the ROS increase seen in the moRK13 cells exposed to the M1000 infectious lysate was not a cell line peculiarity or artefact, OBL-21 cells (a murine olfactory bulb-derived neuronal cell line) and GT1-7 cells (a murine hypothalamic neuronal cell line), which endogenously express PrP^C and were previously shown to propagate the M1000 prion strain [17], were exposed to whole brain homogenates taken from mice with terminal prion disease or their age-matched uninfected controls. Brain homogenates (0.1% brain weight/volume) rather than cell lysates were used for the OBL-21 and GT1-7 assays as there was no need to passage the brain homogenates through the cell line to avoid a species barrier. Both the OBL-21 and GT1-7 cells acutely exposed to infectious inocula also showed a heightened ROS response compared with their mock treated counterparts (Fig. 2C). To further relate this to the *in vivo* situation differentiated neural stem cells (NSCs) were also subject to the same assay. Both proliferating and differentiated NSCs have been shown to propagate prion infection *ex vivo* [23,24] and NSCs in culture differentiate into neurones, astrocytes, oligodendrocytes and neural precursor cells in mixed culture, thus mimicking the cellular constituents of the brain. NSCs were differentiated for 6 days prior to assay (See Sup Fig. 2 for images of neurosphere/differentiated cells then loaded with DCF as assayed as for the OBL-21 and GT1-7 cell lines. The neural stem cells showed a greater ROS response than the cell lines (Fig. 2D), with this change shown relative to viability as a drop in viability of approximately 40% of the NSCs was observed within the duration of the assay. Not surprisingly, this indicates that the response is more pronounced and toxic in primary cells than cell lines.

3.4. Cells exposed to M1000 inocula adapt to the intracellular ROS increase within 48 hours

Intracellular ROS rates were measured at various time points from the addition of the infectious lysate for up to five days. The significantly increased cellular ROS was no longer detected 48 hours after exposure (Fig. 3A). The highest ROS production was seen 24 hours post-exposure to the infectious inoculum. Following DCFDA assay, cells were lysed and slot blots prepared to look for PrP^{Res} levels. The 24 hour time point corresponds with the peak transient increase in detectable PrP^{Res} within the cells before it reduces to background levels prior to the establishment of persistent infection (Fig. 3B). When the ROS rates of the moRK13 cells are correlated with the corresponding PrP^{Res} densitometry, a significant non-zero correlation is seen between increased ROS and increased PrP^{Res} ($r^2 = 0.60$, $p = 0.04$). The vecRK13 cells do not show the same increase in ROS and the PrP^{Res} levels steadily decrease over time to be barely visible at 5 days post-exposure.

3.5. Acute moRK13 increased intracellular ROS is predominantly lysosomal

To identify the site of intracellular ROS production concomitant with initial exposure to M1000 prions, $Bodipy^{581/591}$ C11 fluorescently tagged lipid dye was included in cell growth media and allowed to disperse through the cell. This dye displays low toxicity, is virtually insensitive to environmental changes such as pH and exhibits red fluorescence emission until it becomes oxidised when the spectrum shifts to green emission [25]. Hence relative lipid peroxidation within a cell can be determined using ratiometric analysis. Increased lipid peroxidation was seen in cells exposed to M1000-infected lysate compared with the mock treated cells (Fig. 4A and B) and increased numbers of cells showed intracellular punctate staining that might be due to lipid containing aggregates or vesicular organelles (Fig. 4A and C). VecRK13 cells do not show the same lipid peroxidation response (Sup Fig. 3). For further characterisation, the PF-H_2TMRos fluorescent dye was loaded into the cells prior to exposure to M1000 or mock-infected lysates. This dye preferentially localises to mitochondria upon reacting with ROS in the cytosol; if ROS are not met in the cytosolic compartment the dye will accumulate in lysosomes, where fluorescence increases with increased ROS [26]. The cells were counterstained with mito-tracker green so that the partitioning could be differentiated. Cells were followed for three hours following the addition of lysates. An increase in overall fluorescence from the probe is significant from 2 hours (Fig. 4D and E) and when mito-tracker co-localisation was used to determine partitioning, the predominant increase was lysosomal (Fig. 4F). Cytosolic ROS also appeared increased; however this did not reach significance.

To confirm the lysosomal origin of the intracellular ROS increase observed with DCFDA, the DCFDA experiments were carried out in the presence of the lysosomal inhibitors NH_4Cl and chloroquine. Both inhibitors reduced the ROS increase associated with the M1000 infectious lysate in the moRK13 cells and this was significant for cells treated with chloroquine (Fig. 5A). VecRK13 control data are shown in Sup Fig. 4.

The ROS responses detected by DCFDA and PF-H_2TMRos were predominantly lysosomal, suggesting that at least some of the infectious inoculum must be directed to lysosomes; to verify this, lysates were conjugated via NHS esters to a pH sensitive rhodamine derivative (pHrodo). The pHrodo dye increases in fluorescence intensity as its environmental pH decreases; therefore as it accumulates in acidic vesicles increased fluorescence is observed. The tagged inocula (10 μg total protein as determined by BCA assay) were applied to the cells and images collected at 0, 3, 24, 48 and 72 hours. Intensity quantification indicates that lysates containing PrP^{Res} were targeted to acidic vesicles faster than mock inocula, regardless of PrP expression of the underlying cell (Fig. 5B & C, vecRK13 images can be found in Sup Fig. 5), although the signal intensity begins to decline in the vecRK13 control cells before the moRK13 cells. Fig. 3 shows that the ROS increase following exposure to infectious inocula correlates with increased cell-associated PrP^{Res}; however PrP^{Res} levels decline from 24 hours, before the pHrodo signal (which declines from 48 hours), indicating that cells begin degrading PrP^{Res} by the time the maximum inoculum uptake had been internalised to lysosomes. Confirmation that PrP can be detected in lysosomes is shown in Sup Fig. 6.

The pHrodo tagged inocula were separated, by magnetic immuno-depletion, into PrP-depleted and PrP-enriched fractions and the time course experiments repeated. The PrP-rich fractions showed much greater internalisation than the depleted fractions and, as for whole cell lysate, there was no significant difference between the PrP-null and wild-type cells. Therefore, although different rates of internalisation are not responsible for the ROS response (Fig. 5C & D), internalisation does appear to be important for the ROS responses as cellular ROS reactions are reduced in the presence of inhibitors of internalisation (Sup Fig. 7).

Previous studies have used lysosomal inhibitors to look at the role of these organelles in clearing infection with chloroquine shown to reduce prion propagation in cell culture [27]. The ability to reduce prion propagation was also seen when persistently M1000-infected cells were treated with lysosomal inhibitors although it was not sustained, with PrP^{Res} levels returning to levels seen prior to treatment by 20 days (Fig. 6A–C). Interestingly, when these chloroquine treated cells were monitored for ROS production following treatment, there was a rapid and significant reduction in intracellular ROS, which returned to baseline levels at approximately 48 hours (Fig. 6D). Therefore, it is likely that there is a very prompt reduction in PrP^{Res} propagation correlating with transiently reduced ROS levels with a brief lag period before pre-formed PrP^{Res} can be cleared by the

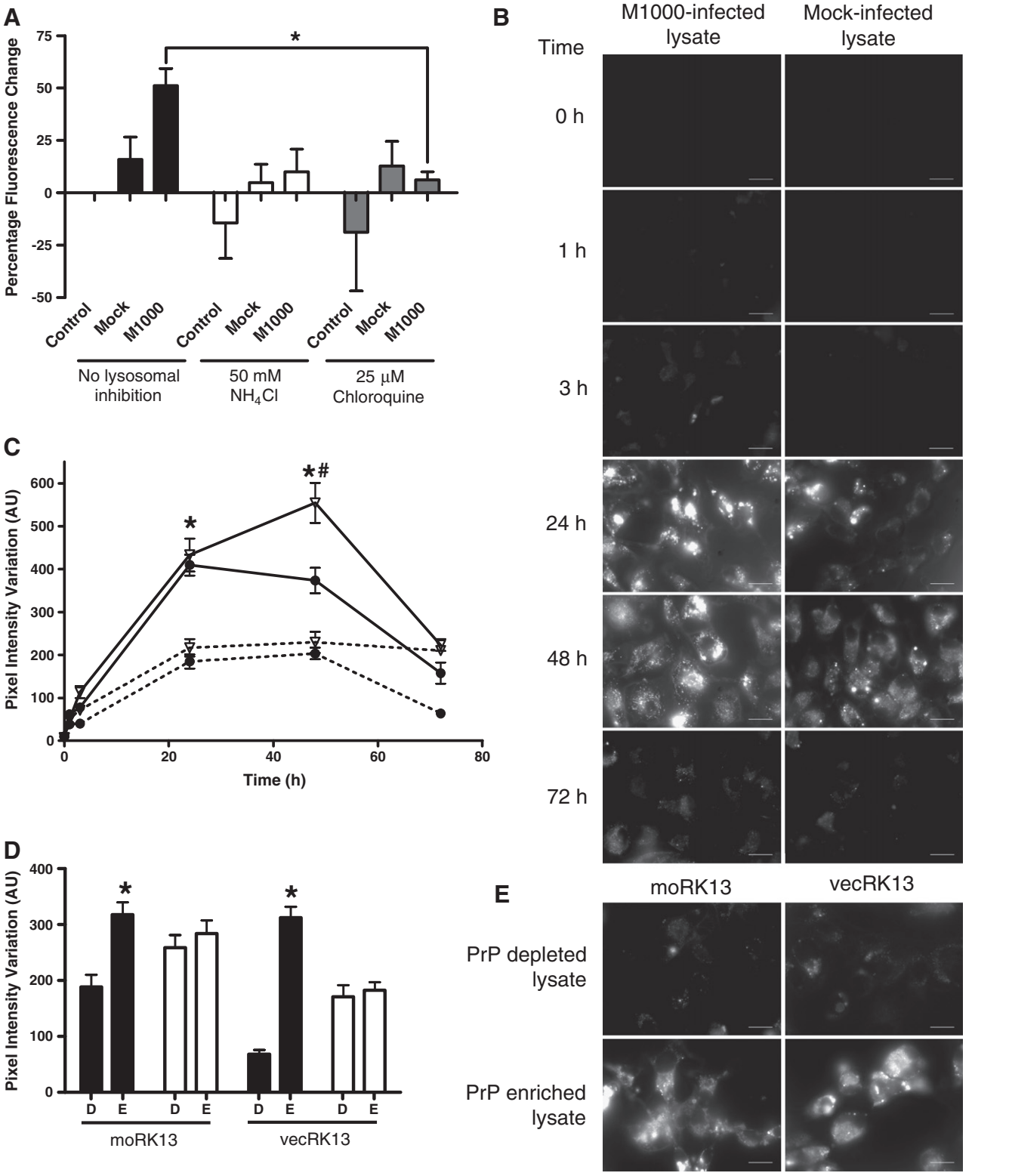

Fig. 5. Lysosomal inhibition reduces the ROS response to infected cell lysates, which are rapidly internalised into acidic compartments. (A) moRK13 cells were treated with lysosomal inhibitors and mock/M1000-infected lysate at the start of the DCFDA assay. ROS rates are expressed relative to untreated cell controls with black bars showing no lysosomal inhibition, white bars show 50 mM NH_4Cl and grey bars 25 μM chloroquine responses. Incubation with lysosomal inhibitors results in a loss of the ROS response to the infectious lysate, which is significant for the cells treated with chloroquine (2-way ANOVA, $F = 4.335$, $p = 0.0222$, $n = 4$). Mock and M1000-infected cell lysates were labelled with pHrodo, which exhibits pH dependant fluorescence with increased fluorescence at lower pH; representative images of moRK13 cells exposed to these lysates and followed for up to 72 hours are shown; scale bars represent 20 μm (B). (C) The M1000-infected cell lysate is internalised more rapidly and reaches a higher fluorescence intensity in acidic vesicles than in cells exposed to the mock-infected cell lysate (2-way ANOVA, $F = 140.1$, $p < 0.001$, $n = 4$); this is significantly different between the moRK13 and vecRK13 cells only at 48 hours when the vecRK13 intensity appears to have begun to decline before the moRK13 signal (2-way ANOVA, $F = 22.28$, $p < 0.001$, $n = 4$). (D & E) Magnetic separation of the pHrodo labelled lysates into PrP-depleted and enriched fractions shows the PrP-enriched fraction internalises and is directed to acidic vesicles more rapidly than the depleted lysate (2-way ANOVA, $F = 39.12$, $p < 0.001$, $n = 3$). Graph and sample images show the 24 hour time point (scale bar = 20 μm). (D) D – PrP-depleted inocula fraction and E – PrP enriched fraction. Internalisation into acidic vesicles is independent of PrP expression in the recipient cell with the vecRK13 cells showing no significant different to the moRK13 cells (secondary *t*-test, $t = 0.1731$, $p > 0.05$).

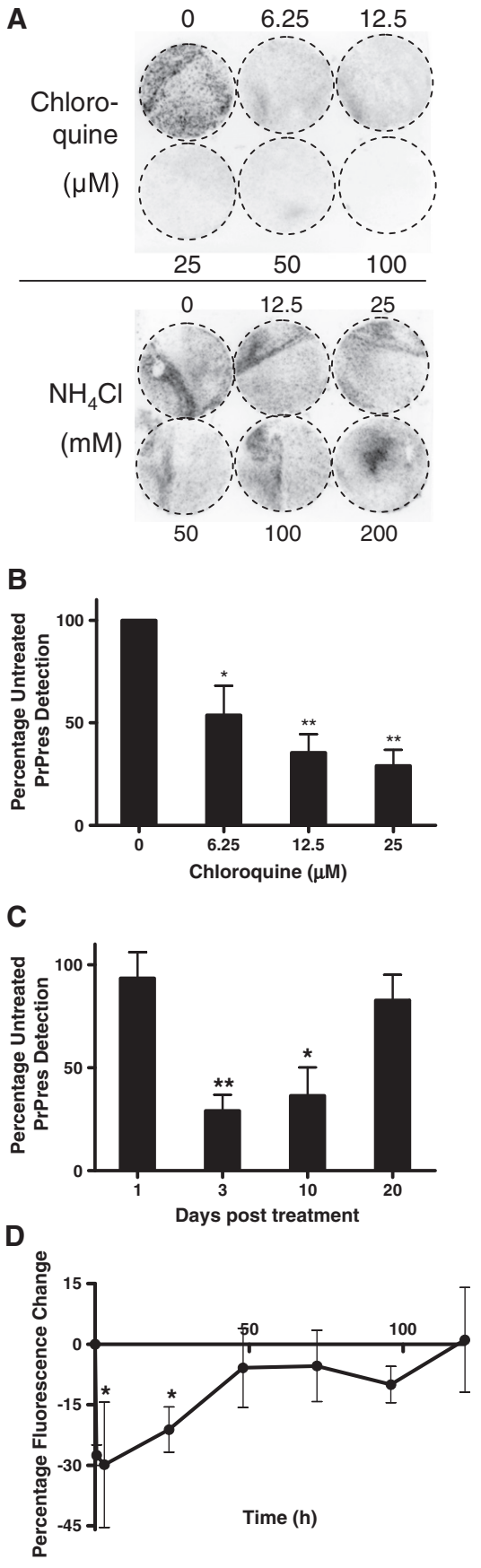

cells. The clearance of PrP^{Res} within this system is unlikely to be due to a shortened half-life of PrP^{C} through redirection to, and increased turnover of, PrP by the proteosome as total levels of cellular PrP increased upon lysosomal inhibition by chloroquine (Sup Fig. 4). Instead, it would appear that inhibiting lysosomal function renders the PrP^{C} substrate less available for conversion into PrP^{Sc} or lysosomal inhibition directly or indirectly impairs conversion.

3.6. A significant sub-population of cells stably propagating M1000 prions contain peroxidised aggregates that are not lysosomal

When assayed by DCFDA assay, the long-pass chronically infected cells (>50 passages) overall do not show increased rates of intracellular ROS production despite high levels of PrP^{Res}, indicating that the rapid adaptational responses to ROS within the general population are maintained over time (Fig. 7A); this is also true of the NSC cultures when grown in the presence of infectious inoculum (0.1% brain weight/volume) over 8 days (1 passage) before assaying (Sup Fig. 8). To ascertain whether there was evidence of ROS damage occurring in these cells, long-pass mock and M1000 infected cells were incubated with the $Bodipy^{581/591}$ C11 dye. Although lipid peroxidation was not significantly increased in cells that had been propagating infection for at least fifty passages (Fig. 7B), approximately 10% of cells (significantly more than the uninfected equivalent-pass cells) showed dense, intracellular peroxidised aggregates of larger diameter than the previously observed punctate staining patterns (Fig. 7B and C); these aggregates were also reactive with TEMPO-9-ac (Sup Fig. 9) and could be seen using phase-contrast microscopy. When equivalent experiments were performed with OBL-21 cells, increased lipid peroxidation and large peroxidised aggregates were observed in PrP^{Res} propagating cells (Sup Fig. 10). Incubating the equivalent passage mock and infected moRK13 cells with the PF-H_2TMRos dye confirms that these aggregates are not clearly lysosomal. Where the aggregates were observed, some individual lysosomes could be discerned but these were relatively scant and therefore unlikely to result in the intensity of signal seen with the $Bodipy^{581/591}$ C11 dye (Fig. 7D). These aggregates also did not co-localise with the GFP-tagged early endosome marker Rab5a and showed no convincing ThT binding by plate and microscopic analysis that would indicate they contain amyloid (data not shown).

3.7. The peroxidised intracellular aggregates observed in chronically infected cells co-localise with active caspases

To investigate whether the sub-population of cells containing peroxidised aggregates were undergoing apoptosis, the long-pass mock and infected cells were incubated with SR-VAD-FMK, a rhodamine labelled, cell permeable, pan-caspase inhibitor that irreversibly binds the active site of caspases. Caspase-positive aggregates were observed in approximately 10% of the infected cell population, similar to what was observed for the lipid peroxidation probe, and showed high intensity staining, indicating heightened

Fig. 6. Lysosomal inhibition in chronically propagating cells temporarily reduces PrP^{Res} and intracellular ROS. (A) Long-pass M1000-infected cells were treated with varying concentrations of the lysosomal inhibitors chloroquine and NH_4Cl and cell blots for PrP^{Res} performed after 1, 3, 10 and 20 days post treatment. Shown are the blots from three days post-treatment. Chloroquine reduces the detectable PrP^{Res}, however NH_4Cl has no effect on propagation. The blots from the chloroquine treated cells have been quantified densitometrically only up to the 25 μM dose as toxicity was seen at higher concentrations (Sup Fig. 1) and the PrP^{Res} dose response at three days is shown (B) along with the 25 μM dose over each of the time points (C). At three days treatment with chloroquine a significant reduction in PrP^{Res} is seen from 6.25 μM (1-way ANOVA, $F=11.82$, $p=0.0026$, $n=3$, $^{*}p<0.05$, $^{**}p<0.01$) and this is significant from 3 to 10 days (1-way ANOVA, $F=7.506$, $p=0.0136$, $n=3$, $^{*}p<0.05$, $^{**}p<0.01$). (D) DCF measurements over time from treatment with the lysosomal inhibitors shows there is an initial decrease in intracellular ROS that returns to normal levels by 48 hours (2-way ANOVA, $F=43.32$, $p<0.001$, $n=3$).

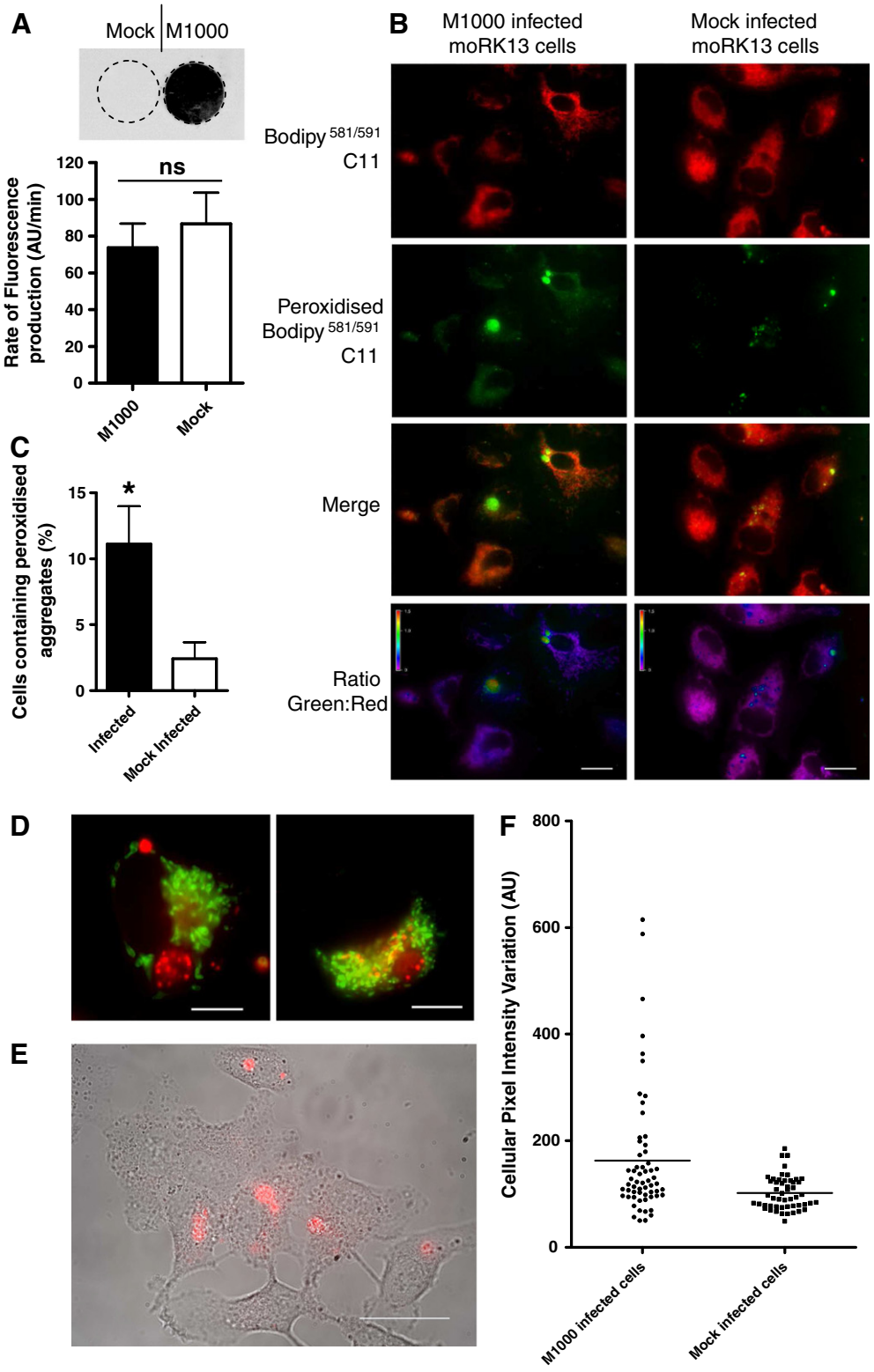

Fig. 7. Chronically M1000 infected moRK13 cells contain highly peroxidised aggregates with concentration of active caspases. (A) Late passage moRK13 cells (>50 passages) show significant production of PrP^{Res} detected by cell blot assay in M1000 infected cells, which is not seen in mock brain homogenate exposed cells, but show no significant difference in intracellular ROS production (students *t*-test, t = 0.6061, p = 0.5772, n = 4). (B) Late passage M1000 infected or mock-infected moRK13 cells were incubated with $Bodipy^{581/591}$ C11 and imaged after 24 hours (scale bar = 20 μm). Ratiometric analysis shows lipid peroxidation is not significantly increased in the infected cells compared with the uninfected controls (students *t*-test, t = 1.775, p = 0.0784, n = 4); however large peroxidised aggregates are seen in higher numbers of the infected cells than the uninfected (C; students *t*-test, t = 3.18, p = 0.0191, n = 4). (D) PF-H_2TMRos staining (red) shows that whilst some lysosomal ROS is the cause of this signal it is not dense enough to account for the whole aggregate, which also excludes mitochondria (counterstained in green). Scale bars = 10 μM. (E) Incubation with the cell-permeable, irreversible, pan-caspase inhibitor SR-VAD-FMK shows aggregates within the infected cells contain high concentrations of active caspases. (F) Quantifying this based on intensity variation, a cell size independent measure, shows a distinct population of the infected cells with high caspase activation, n = 3.

caspase activation with recruitment to these aggregates (Fig. 7E & F, Sup Fig. 11).

3.8. PrP localises to the sites of activated caspase-positive, peroxidised intracellular aggregates and deposits adjacent to vimentin

PrP has previously been shown to localise to aggresomes during chronic prion infection when proteosome function is compromised [28,29]. To determine if these peroxidised, caspase reactive aggregates localised with PrP and were classical aggresomes we fixed the Bodipy$^{581/591}$ C11 or SR-VAD-FMK labelled cells and used indirect immunofluorescence to localise PrP and vimentin. PrP surrounds both the peroxidised and caspase reactive aggregates with some co-localisation observed (Fig. 8 A & B). This halo staining may be due to dense packing of the aggregated material excluding the anti-PrP antibodies but allowing detection on the periphery or due to PrP being directed only to the exterior of the aggregates. PrP and vimentin also appear to partially co-localise and lie adjacent to each other. This suggests the formation of an aggresome-like structure with vimentin, a structural protein, forming a cage-like scaffold around peroxidised aggregates of lipid moieties.

3.9. Separation of M1000 chronically infected cells by annexinV binding shows a significantly increased subpopulation of apoptotic cells manifesting increased intracellular ROS

Increased expression of phosphatidylserine (PS) on the outer leaflet of the cell membrane occurs early in apoptosis. The recruitment of active caspases to the peroxidised aggregates suggested that this subpopulation of cells was undergoing apoptosis. Exploiting the high affinity of annexinV for PS, annexinV coated magnetic beads were used to separate the apoptotic cells with externalised PS from non-apoptotic cells. Approximately double the number of chronically M1000 infected cells were annexin-V positive (~6%) compared with the mock-infected or the vector control cells of equal passage. The background rate of annexinV reactivity is most likely due to growing cells under constant selection pressure (Fig. 9A). Loading the separated fractions with DCFDA to look at the rates of intracellular ROS production showed significantly increased ROS in the M1000-infected annexinV-positive cell fraction compared with the annexinV-negative cells and the annexinV positive fraction of mock treated cells (Fig. 9B). Proteinase-K digestion and western blot analysis of these cells showed the annexinV-positive sub-population contains more PrP^{Res} than the annexinV-negative fraction (cells were trypsinised into

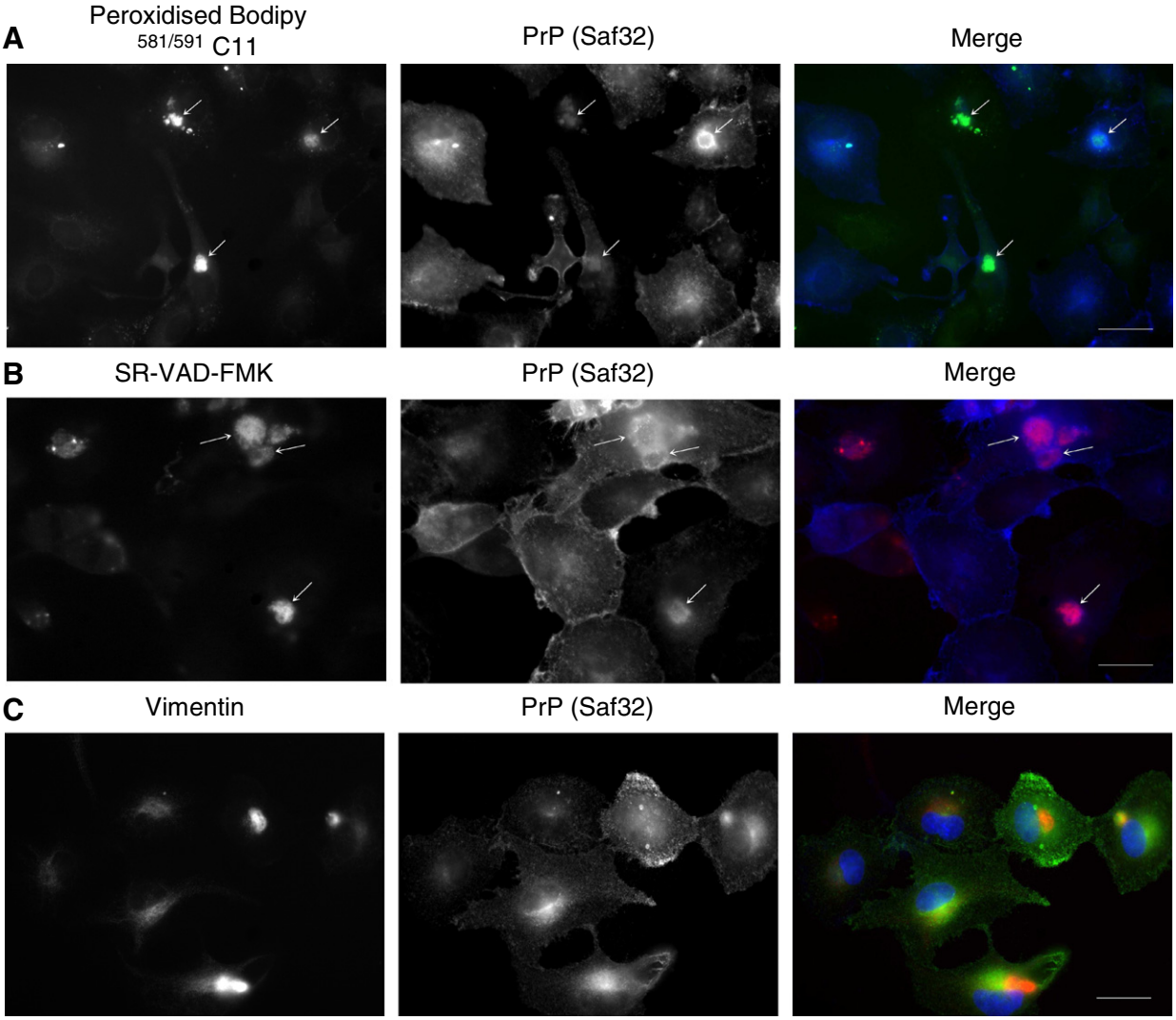

Fig. 8. In chronically infected moRK13 cells, PrP localises in and around aggregates and with or adjacent to vimentin. Indirect immunofluorescence of PrP following fixing and staining of late passage M1000 infected moRK13 cells with Bodipy$^{581/591}$ C11 (A) and SR-VAD-FMK (B). Arrows indicate areas of localisation of PrP with each probe. (C) Indirect Immunofluorescence of PrP and vimentin for aggresomal staining. PrP and vimentin are found both together and adjacent to each other. In C nuclei, stained with DAPI, are shown in blue. Images can be compared with localisation of staining in uninfected cells found in supplementary Fig. 3. Scale bar = 20 μm.

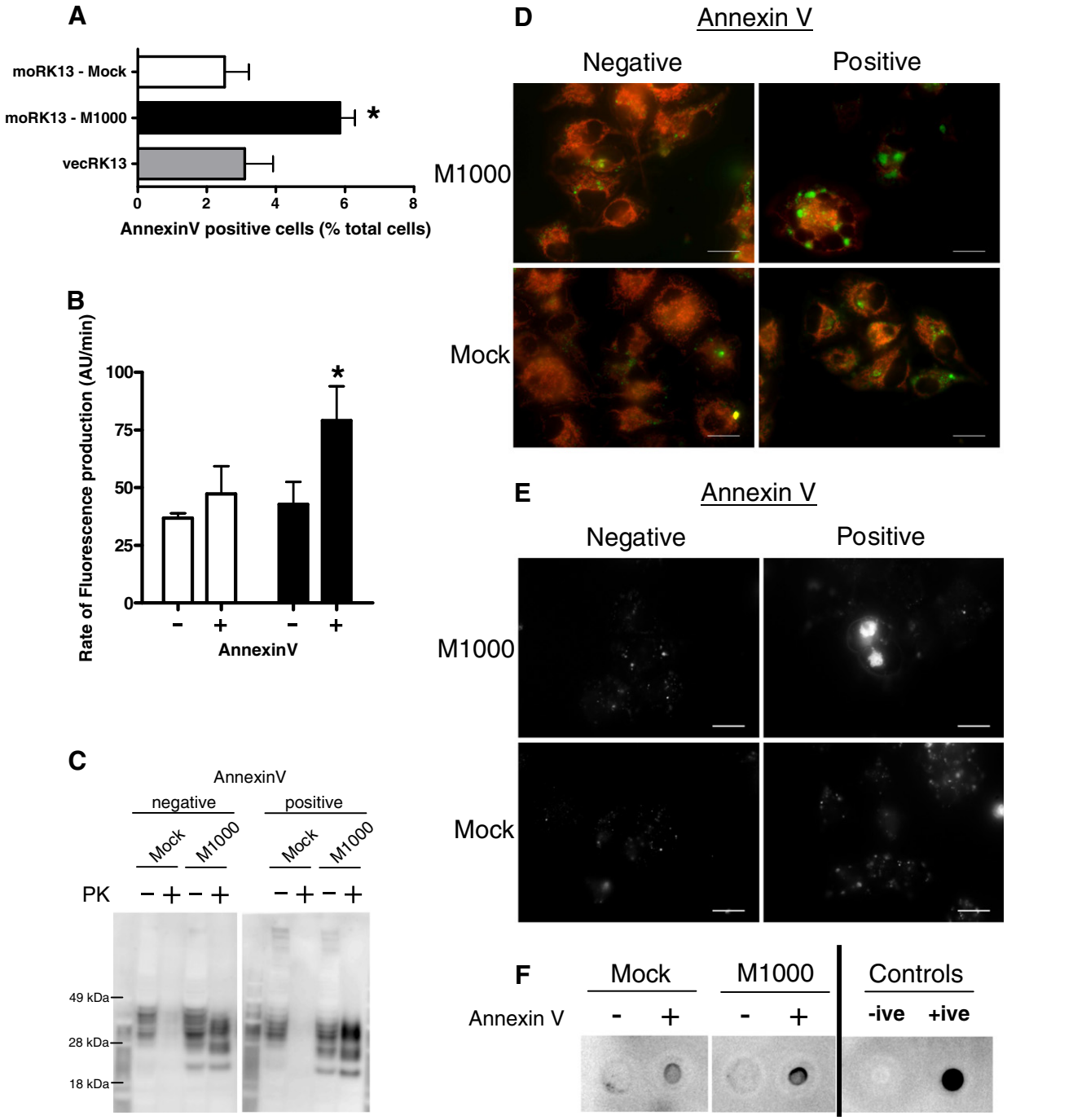

Fig. 9. AnnexinV separation yields a distinct population of M1000 infected moRK13 cells. Using annexinV conjugated magnetic microbeads to separate cells in the early phases of apoptosis from healthy cells shows a significantly increased apoptotic population in the M1000 infected cells than in uninfected or vector control cells (A; 1-way ANOVA, $F = 7.034$, $p = 0.0267$, $n = 3$). The rate of ROS production of the M1000 infected moRK13 apoptotic cells is significantly higher (adjusted for equal time 0 signal) than in the non-infected apoptotic cells (B; 2-way ANOVA, $F = 7.465$, $p = 0.0341$, $n = 3$). No significant difference is seen between the non-apoptotic cells regardless of infection. Western blot analysis using ICSM18 anti-PrP mab shows greater concentrations of PrP^{Res} in M1000 infected cells that are apoptotic compared with those that are not (C). Staining with $Bodipy^{581/591}$ C11 (D) or SR-VAD-FMK (E) prior to separation shows that the M1000 infected apoptotic cells have a greater concentration of large peroxidised/caspase reactive aggregates than the uninfected or non-apoptotic populations. Scale bars = 20 μm. (F) Oxyblot, for detection of oxidative modification of protein, was performed on dot blots of the separated samples. Whilst no difference is evident between the infected and uninfected cells that do not show PS externalisation, both cell lines showed increased protein oxidation in the apoptotic fraction and this is greater again in the M1000 infected cells.

solution and therefore most of the signal is probably from intracellular PrP and may under-estimate cellular PrP^{Res}; Fig. 9C). Incubation of these cells with $Bodipy^{581/591}$ C11 or SR-VAD-FMK prior to separation showed that lipid peroxidation and caspase activation are increased in the annexinV-positive cells with the infected cells showing high numbers of the large peroxidised aggregates and active caspase sites (Fig. 9D & E).

Preliminary experiments examining the basis of the failure in apoptotic cells found that the infected cells display reduced metal ion levels when assayed with Phen Green (a dye that has a preference for copper), which might lead to anti-oxidant enzyme dysfunction (Sup Fig. 13). Treatment with TEMPO-9-ac to scavenge the ROS being produced or with the pan-caspase inhibitor VAD-fmk for 24 hours, enhanced the viability of the cultures, although this was not specific to

infected cells (Sup Fig. 14). Further, treatment with the TEMPO-9-ac for four hours, a sufficient time to prevent the externalisation of PS, found no significant difference in the number of infected cells displaying externalised PS; however the infected cells do differ from the uninfected in that the number of uninfected cells with PS externalisation unexpectedly doubles to levels equivalent to those in infected cells when exposed to this treatment (Sup Fig. 14). We hypothesise this probably occurs due to an unintended sub-lethal disruption of normal protective cell signalling in uninfected cells, possibly suggesting extant perturbations in these pathways within infected cells, with the lack of further increase in the infected cells possibly representing a partial restoration of redox homeostasis and relative protection through the radical scavenger. Considerable further investigation is underway to clarify these points.

4. Discussion

This study has shown that intracellular ROS production changes in acute, adaptive and chronic phases of prion infection *in vitro* and further links ROS with prion propagation and cellular demise. Upon initiation of prion infection cellular adaptation to increased intracellular ROS occurs quickly within the overall cell population, a response probably essential for maintaining viability. The cells progress to a chronic phase of infection where the ROS response is kept below levels that would damage the cell. Eventually the adaptational responses fail in a significant subpopulation of chronically infected cells, with these cells showing activation of apoptosis. This progression is shown schematically in Fig. 10. As such, in addition to further strengthening the direct mechanistic and pathogenic associations between PrP^{Res} generation and heightened ROS production, these findings prompt reconsideration of the prevailing opinion that chronic PrP^{Res} propagation is a generally innocuous circumstance for host cells *in vitro*.

There is considerable evidence linking PrP and ROS *in vivo* in normal and disease states: altered metal ion and Cu/Zn superoxide dismutase activity with increased superoxide and nitric oxide in scrapie-infected mouse brain [12]; alterations in mitochondrial numbers and morphology in PrP-null mice [30]; alteration in superoxide from Complex 1 in PrP-null mice [31]; increased lipid peroxidation products correlating with the appearance of PrP^{Res} in the brains of M1000-infected mice [3]; and prolongation of survival of infected mice by an adaptive response to oxidative stressed evoked by low-dose radiation [32]. The underlying cellular pathogenic mechanisms linking PrP and ROS *in vitro* are still widely debated. The loss of PrP superoxide dismutase-like function is one possibility [6]. Another possibility is metal ion dysregulation (PrP has the capacity to bind copper and to a lesser extent several other metal ions [33,34] as a cause or result of PrP aggregation. Iron has been shown to induce the formation of protease-resistant PrP aggregates within cells [35,36] and brain levels of copper and manganese become disturbed during disease [37]; therefore metal ion imbalance may play a significant role in oxidative stress seen during prion disease, possibly by essential metal ions being sequestered from anti-oxidant enzymes into redox-active aggresomes. Observations within our model concur with this hypothesis with copper levels reduced in chronically M1000-infected cells (Sup Fig. 13), suggesting that metal ion dysregulation may play an important role in the failure of cellular oxidative stress responses.

Cell lines such as RK13 have proved invaluable for a range of studies dealing with PrP^{Res} infectivity because they will propagate infection indefinitely with apparently no adverse morphological or biochemical consequences. Our observations contradict the belief that such cells are propagating infection free of adverse effects even when they appear phenotypically normal. The results presented show

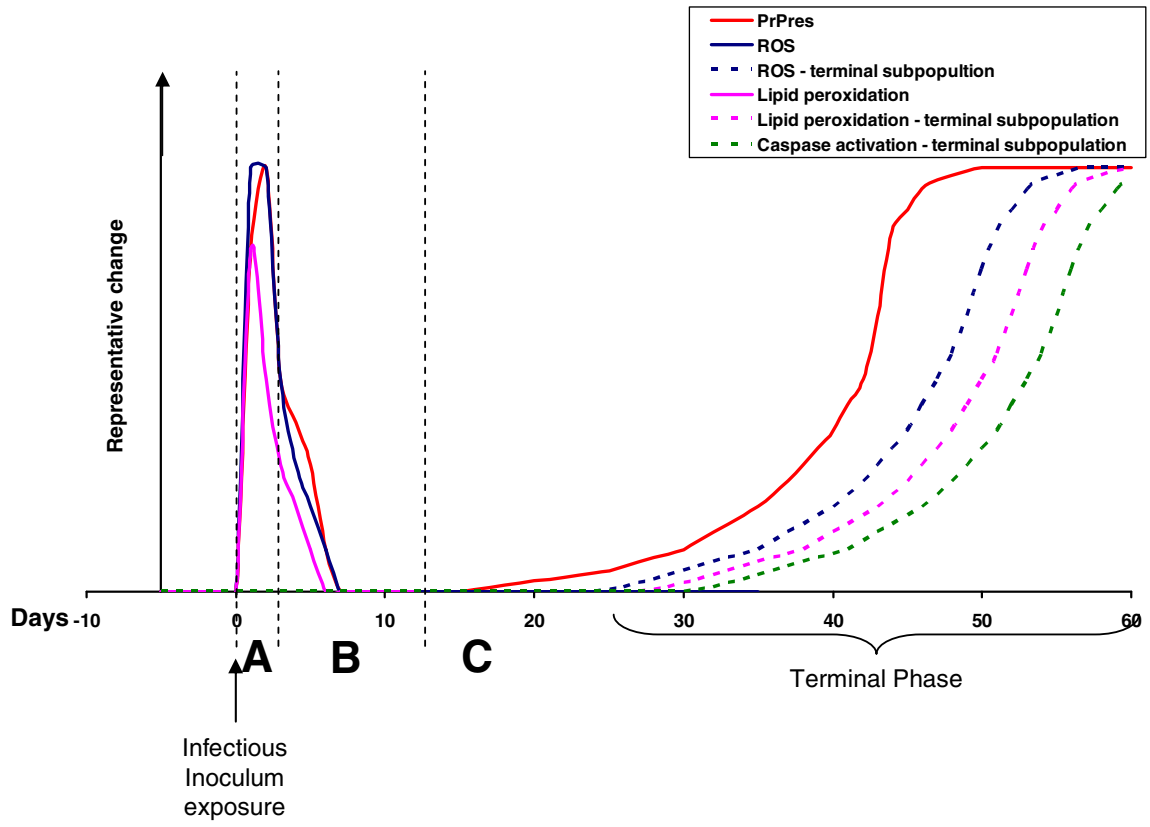

Fig. 10. Schematic of the progression of prion infection and ROS response *in vitro*. Representative increases in PrP^{Res}, ROS, oxidative damage and caspase activation are shown in both overall and terminal (annexin V positive – dashed lines) populations. A represents the acute phase of infection, B is the adaptive phase and C shows chronic infection.

interesting parallels with those reported by Schatzl et al. [38], who found that the GT1-7 cell line shows cytopathology in approximately 20% of cells chronically infected with the scrapie derived RML prion strain, with apoptosis being initiated in these cells. In combination with our findings, this raises the possibility that chronic prion infection *in vitro* is more frequently associated with low-level but ongoing cell damage and loss than currently appreciated, and may offer greater utility for studies of prion related toxicity and pathogenesis than acknowledged. In cell cultures, cytopathology in a small number of cells could be easily overlooked, especially when cells are transfected and constantly under antibiotic selection pressure. By analogy, such heightened apoptotic cells loss may not be inconsequential if it were to occur *in vivo*, where steady loss of even a small percentage of neurones over time would eventuate in devastating compromise of the function of the whole organ.

By separating the apoptotic population from the healthy (normal PS membrane asymmetry) cells, we have shown that a small but significant sub-population is manifesting heightened intracellular ROS levels and oxidative damage that cannot be detected when assessing the overall population. Furthermore, the increase in intracellular ROS in these cells is concurrent with increased PrP^{Res} and activation of caspases. The structures simultaneously showing the highest intensity of oxidative damage, activated caspases and PrP localisation appear similar to previously reported vimentin-containing aggresomes, which were shown to be temporally associated with activated caspases 3 and 8 post-exposure to PrP^{Sc} in the GT1-7 cell model following inhibition of the proteosome [29]. Lipid peroxidation is a feature of these structures, and it is known that lipid peroxidation end-products are capable of inducing apoptosis by mechanisms involving signalling through JNK and c-jun, and by impairing mitochondrial function through altering glutathione (GSH) metabolism and calcium uptake (reviewed in [39]). Therefore, adaptational failure during the ongoing intracellular ROS production related to chronic PrP^{Res} propagation could inflict oxidative damage on the interior of the cell, with subsequent recruitment and activation of caspases, which would effect the eventual demise of the cell.

Previously, it has been proposed that the 'toxic' species of PrP is able to cause oxidative injury in cells by over-stimulation of signalling pathways that generate ROS as a signalling intermediate [14]. Whilst the majority of the intracellular ROS response to M1000-infected lysates reported here was lysosomal, increased ROS from NADPH oxidase signalling is associated with phagosome production [40] and could perhaps accompany the transit of the infectious inoculum into the cell. A toxic gain of function such as this would need to be transduced through PrP^{C} signalling or initiated by the structural conversion to PrP^{Res}, as the PrP^{C}-null cells do not exhibit the same ROS responses.

The data presented do not allow discrimination between the ROS event as a cause or effect of PrP^{C} to PrP^{Res} conversion although conceivably both could occur simultaneously. Recent interest has focused on increased ROS directly causing the conformational change of PrP by modification of the protein itself. Studies of methionine oxidation have indicated that increases in cellular ROS that cause oxidation of the helix 3 methionines destabilise PrP, potentially permitting a switch of conformation that facilitates a seeding event [4,41]. This event, combined with the destabilising environment of the lysosomes, might favour conversion and a seeding event by PrP^{Res}, with sustained PrP^{Res} production thereafter. Other recent studies have identified various co-factors that are required for efficient prion conversion and infectivity including certain lipids [42] and nucleotides [43,44]; the assays used to generate these data contain sonication or rapid shaking steps, conditions that produce ROS [45] and, therefore, ROS modification of co-factors might equally contribute to the misfolding events.

In the RK13 cell system employed, lysosomes were important for the turnover of PrP, with increased total cellular PrP levels observed when lysosomal function was inhibited. This supports that, whilst total levels of PrP are clearly important for prion propagation and the evolution of prion disease *in vivo*, specific sub-cellular trafficking and the precise micro-environment of the infectious PrP species are also likely to be important for maintaining infection inside the cell. The reduction in detected PrP^{Res} is not likely to be due to the redirection of PrP^{Res} to the proteosome for degradation given the increase in PrP inside the cell population upon lysosomal inhibition and previous investigation of proteosomal involvement in this system has not shown any evidence of impairment in infected cells (Lewis et al., unpublished data).

Lysosomes have long been implicated in prion disease pathogenesis due to providing a destabilising environment that might favour unfolding of PrP^{C} allowing more efficient conversion into PrP^{Sc} [46], although quinacrine, a lysosomal inhibitor that had promising effects in cell culture, was not effective in a murine treatment paradigm [47]. Nevertheless, in support of previous postulates, lysosomes were not only involved in establishing infection but also in maintaining persistent infection. From a therapeutic perspective however, non-sustained lysosomal inhibition to slow PrP propagation has only transient and limited effects with PrP^{Res} levels returning to those observed pre-treatment very quickly once ROS levels have normalised. The increased toxicity of chloroquine to infected cells may suggest that the cells with the highest PrP^{Res} burden die rapidly as a result of inhibiting PrP turnover, producing a greater effect on overall PrP^{Res} levels with much less impact on the number of infected cells. The tendency of the cells with highest PrP^{Res} to die first is tentatively supported by the annexin V separation data which shows that the infected cells with early signs of apoptosis contain comparatively higher levels of PrP^{Res} than those that do not show signs of progression to cell death.

The observation that endosomes/lysosomes are oxidising compartments is not new. Redox-sensitive variants of the green fluorescent protein fused to endocytic proteins have shown that recycling endosomes, late endosomes and lysosomes are oxidising environments [48]. These are all organelles to which PrP is targeted during trafficking and have been suggested as sites of PrP^{C} to PrP^{Res} conversion [49,50]. Inhibition of lysosomes has also been shown to protect cells against cell death from glutamate induced ROS [51]. Here the authors proposed that lysosomal ROS had a role in regulating the later burst of mitochondrial ROS that initiates apoptosis. Aggresomal structures seen during prion infection are surrounded by mitochondria [52] and so the oxidative stress balance of the organelles caught in the aggresomes might activate apoptosis through disturbed mitochondrial function.

In conclusion, exposure of naïve PrP^{C}-expressing cells to PrP^{Res} induces a rapid lysosomal ROS response concurrent with the internalisation and accumulation of the infectious inoculum in acidic vesicles. This lysosomal ROS burst initiates or is part of an early adaptive response that quickly restores redox equilibrium despite ongoing PrP^{Res} propagation, with lysosomes appearing to play an important role in maintaining chronic PrP^{Sc} production. Eventually, failure to maintain adaptational responses occurs in a significant sub-population of chronically infected cells with consequent peroxidative damage to lipids and activation of the cellular pathways that initiate cell death. Overall, heightened oxidative stress in chronic prion disease is clearly detrimental and the formation of ROS is closely coupled to the formation of misfolded PrP. Increased ROS, possibly due to a combination of destabilising intracellular environments, aberrant signalling and even PrP itself, are all likely to contribute to damage of cellular components, with consequent activation of apoptosis effector enzymes and eventual progression to cell death.

Supplementary materials related to this article can be found online at doi:10.1016/j.freeradbiomed.2011.03.035.

Acknowledgments

The authors would like to acknowledge A/Prof AF Hill for the kind gift of the pIRES vector containing the PrP open reading frames and Dr Simon Drew for the SR-VAD-FMK reagent. The OBL-21 cell line used in this study were a kind gift of Dr Michael Oldstone, The Scripps

Research Institute, La Jolla, California, USA. This study was funded by a Brain Foundation research grant. SJC is supported by an NH&MRC Practitioner Fellowship #400183 and an NH&MRC programme grant #400202. VL is supported by an NH&MRC Training (Postdoctoral) Fellowship #567123. VAL is supported by a University of Melbourne CR Roper fellowship.

References

[1] Weissmann, C.; Büeler, H.; Fischer, M.; Sailer, A.; Aguzzi, A.; Aguet, M. PrP deficient mice are resistant to scrapie. *Ann. N.Y. Acad Sci.* **724:**235–240; 1994.
[2] Mallucci, G.; Dickinson, A.; Linehan, J.; Klöhn, P. C.; Brandner, S.; Collinge, J. Depleting neuronal PrP in prion infection prevents disease and reverses spongiosis. *Science* **302:**871–874; 2003.
[3] Brazier, M. W.; Lewis, V.; Ciccotosto, G. D.; Klug, G. M.; Lawson, V. A.; Cappai, R.; Ironside, J. W.; Masters, C. L.; Hill, A. F.; White, A. R.; Collins, S. J. Correlative studies support lipid peroxidation is linked to PrPres propagation as an early primary pathogenic event in prion disease. *Brain Res. Bull.* **68:**346–354; 2006.
[4] Wolschner, C.; Giese, A.; Kretzschmar, H. A.; Huber, R.; Moroder, L.; Budisa, N. Design of anti- and pro-aggregation variants to assess the effects of methioine oxidation in human prion protein. *Proc. Natl. Acad Sci. U.S.A.* **106** (19)**:**7756–7761; 2009.
[5] Brown, D. R.; Besinger, A. Prion protein expression and superoxide dismutase activity. *Biochem. J.* **334:**423–429; 1998.
[6] Brown, D. R.; Wong, B. S.; Hafiz, F.; Clive, C.; Haswell, S. J.; Jones, I. M. Normal prion protein has an activity like that of superoxide dismutase. *Biochem. J.* **344:**1–5; 1999.
[7] Chiarini, L. B.; Freitas, A. R. O.; Zanata, S. M.; Brentani, R. R.; Martins, V. R.; Linden, R. Cellular prion protein transduces neuroprotective signals. *EMBO J.* **21** (13)**:** 3317–3326; 2002.
[8] Büeler, H.; Fischer, M.; Lang, Y.; Bluethmann, H.; Lipp, H. P.; DeArmond, S.; Prusiner, S. B.; Aguet, M.; Weissmann, C. Normal development and behaviour of mice lacking the neuronal cell-surface PrP protein. *Nature* **356:**577–582; 1992.
[9] Klamt, F.; Dal-Pizzol, F.; Conte Da Fronta Jr., M. L.; Walz, R.; Andrades, M. E.; Da Silva, E. G.; Brentani, R. R.; Izquierdo, I.; Moreira, J. C. F. Imbalance of antioxidant defence in mice lacking cellular prion protein. *Free Radic. Biol. Med.* **30** (10)**:** 1137–1144; 2001.
[10] Brown, D. R.; Nicholas, R. S. J.; Canevari, L. Lack of Prion Protein Expression Results in a Neuronal Phenotype Sensitive to Stress. *J. Neurosci. Res.* **67:**211–224; 2002.
[11] McLennan, N. F.; Brennan, P. M.; McNeill, A.; Davies, I.; Fotheringham, A.; Rennison, K. A.; Ritchie, D.; Brannan, F.; Head, M. W.; Ironside, J. W.; Williams, A.; Bell, J. E. Prion protein accumulation and neuroprotection in hypoxic brain damage. *Am. J. Pathol.* **165** (1)**:**227–235; 2004.
[12] Wong, B. S.; Liu, T.; Li, R.; Pan, T.; Petersen, R. B.; Smith, M. A.; Gambetti, P.; Perry, G.; Manson, J. C.; Brown, D. R.; Sy, M. S. Increased levels of oxidative stress markers detected in the brains of mice devoid of prion protein. *J. Neurochem.* **76** (2)**:** 565–572; 2001.
[13] Thackray, A. M.; Knight, R.; Haswell, S. J.; Bujdoso, R.; Brown, D. R. Metal imbalance and compromised anti-oxidant function are early changes in prion disease. *Biochem. J.* **362:**253–258; 2002.
[14] Pietri, M.; Caprini, A.; Mouillet-Richard, S.; Pradines, E.; Ermonval, M.; Grassi, J.; Kellermann, O.; Schneider, B. Overstimulation of PrPC signalling pathways by prion peptide 106–126 causes oxidative injury of bioaminergic neuronal cells. *J. Biol. Chem.* **281** (38)**:**28470–28479; 2006.
[15] Chesebro, B.; Wehrly, K.; Caughey, B.; Nishio, J.; Ernst, D.; Race, R. Foreign PrP expression and scrapie infection in tissue culture cell lines. *Dev. Biol. Stand.* **80:** 131–140; 1993.
[16] Ryder, E. F.; Snyder, E. Y.; Cepko, C. L. Establishment and characterization of multipotent neural cell lines using retrovirus vector-mediated oncogene transfer. *J. Neurobiol.* **21** (2)**:**356–375; 1990.
[17] Lewis, V.; Hill, A. F.; Haigh, C. L.; Klug, G. M.; Masters, C. L.; Lawson, V. A.; Collins, S. J. Increased proportions of C1 truncated prion protein protect against cellular prion infection. *J. Neuropathol. Exp. Neurol.* **68** (10)**:**1125–1135; 2009.
[18] Haigh, C. L.; Drew, S. C.; Boland, M. P.; Masters, C. L.; Barnham, K. J.; Lawson, V. A.; Collins, S. J. Dominant roles of the polybasic proline motif and copper in PrP23-89 mediated stress protection response. *J. Cell Sci.* **122** (10)**:**1518–1528; 2009.
[19] Bosque, P. J.; Prusiner, S. B. Cultured cell sublines highly susceptible to prion infection. *J. Virol.* **74:**4377–4386; 2000.
[20] Haigh, C. L.; Lewis, V.; Vella, L. J.; Masters, C. L.; Hill, A. F.; Lawson, V. A.; Collins, S. J. PrPC related signal transduction is influenced by copper, membrane integrity and the alpha cleavage site. *Cell Res.* **19:**1062–1078; 2009.
[21] Vella, L. J.; Sharples, R. A.; Lawson, V. A.; Masters, C. L.; Cappai, R.; Hill, A. F. Packaging of prions into exosomes is associated with a novel pathway of PrP processing. *J. Pathol.* **211:**582–590; 2007.
[22] Lawson, V. A.; Vella, L. J.; Stewart, J. D.; Sharples, R. A.; Klemm, H.; Machalek, D. M.; Masters, C. L.; Cappai, R.; Collins, S. J.; Hill, A. F. Mouse-adapted sporadic human Creutzfeldt-Jakob disease prions propagate in cell culture. *Int. J. Biochem. Cell Biol.* **40** (12)**:**2793–2801; 2008.
[23] Giri, R. K.; Young, R.; Pitstick, R.; DeArmond, S. J.; Prusiner, S. B.; Carlson, G. A. Prion infection of mouse neurospheres. *Proc. Natl. Acad Sci. U.S.A.* **103** (10)**:** 3875–3880; 2006.
[24] Herva, M. E.; Relano-Ginés, A.; Villa, A.; Torres, J. M. Prion infection of differentiated neurospheres. *J. Neurosci. Methods* **188** (2)**:**270–275; 2010.
[25] Drummen, G. P. C.; Van Liebergen, L. C. M.; Op Den Kamp, J. A. F.; Post, J. A. C11-BODIPY$^{581/591}$, an oxidation-sensitive fluorescent lipid peroxidation probe: (micro)spectroscopic characterisation and validation of methodology. *Free Radic. Biol. Med.* **33** (4)**:**473–490; 2002.
[26] Chen, C. S.; Gee, K. R. Redox-dependent trafficking of 2,3,4,5, 6-pentafluorodihydrotetramethylrosamine, a novel fluorogenic indicator of cellular oxidative activity. *Free Radic. Biol. Med.* **28:**1266–1278; 2000.
[27] Doh-Ura, K.; Iwaki, T.; Caughey, B. Lysosomotropic agents and cysteine protease inhibitors inhibit scrapie-associated prion protein accumulation. *J. Virol.* **74** (10)**:** 4894–4897; 2000.
[28] Ma, J.; Lindquist, S. Wild-type PrP and a mutant associated with prion disease are subject to retrograde transport and proteasome degradation. *Proc. Natl. Acad Sci. U.S.A.* **98** (26)**:**14955–14960; 2001.
[29] Kristiansen, M.; Messenger, M. J.; Klöhn, P. C.; Brandner, S.; Wadsworth, J. D.; Collinge, J.; Tabrizi, S. J. Disease-related prion protein forms aggresomes in neuronal cells leading to caspase activation and apoptosis. *J. Biol. Chem.* **280** (46)**:** 38851–38861; 2005.
[30] Miele, G.; Jeffrey, M.; Turnbull, D.; Manson, J.; Clinton, M. Ablation of cellular prion protein expression affects mitochondrial numbers and morphology. *Biochem. Biophys. Res. Commun.* **291** (2)**:**372–377; 2002.
[31] Paterson, A. W.; Curtis, J. C.; Macleod, N. K. Complex I specific increase in superoxide formation and respiration rate by PrP-null mouse brain mitochondria. *J. Neurochem.* **105** (1)**:**177–191; 2008.
[32] Plews, M.; Simon, S. L.; Boreham, D. R., et al. A radiation induced adaptive response prolongs the survival of prion infected mice. *Free Radic. Biol. Med.*, doi:10.1016/j.freeradbiomed.2010.07.025; 2010.
[33] Brown, D. R.; Qin, K.; Herms, J. W.; Madlung, A.; Manson, J.; Strome, R.; Fraser, P. E.; Kruck, T.; von Bohlen, A.; Schulz-Schaeffer, W.; Giese, A.; Westaway, D.; Kretzschmar, H. The cellular prion protein binds copper in vivo. *Nature* **390** (6661)**:**684–687; 1997.
[34] Jackson, G. S.; Murray, I.; Hosszu, L. L.; Gibbs, N.; Waltho, J. P.; Clarke, A. R.; Collinge, J. Location and properties of metal-binding sites on the human prion protein. *Proc. Natl. Acad Sci. U.S.A.* **98** (15)**:**8531–8535; 2001.
[35] Basu, S.; Mohan, M. L.; Luo, X.; Kundu, B.; Kong, Q.; Singh, N. Modulation of proteinase K-resistant prion protein in cells and infectious brain homogenate by redox iron: implications for prion replication and disease pathogenesis. *Mol. Biol. Cell* **18** (9)**:**3302–3312; 2007.
[36] Das, D.; Luo, X.; Singh, A. Paradoxical role of prion protein aggregates in redox-iron induced toxicity. *PLoS One* **5** (7)**:**e11420; 2010.
[37] Hesketh, S.; Sassoon, J.; Knight, R.; Brown, D. R. Elevated manganese levels in blood and CNS in human prion disease. *Mol. Cell. Neurosci.* **37** (3)**:**590–598; 2008.
[38] Schätzl, H. M.; Laszlo, L.; Holtzman, D. M.; Tatzelt, J.; DeArmond, S. J.; Weiner, R. I.; Mobley, W. C.; Prusiner, S. B. A hypothalamic neuronal cell line persistently infected with scrapie prions exhibits apoptosis. *J. Virol.* **71** (11)**:**8821–8831; 1997.
[39] Negre-Salvayre, A.; Coatrieux, C.; Ingueneau, C.; Salvayre, R. Advanced lipid peroxidation end products in oxidative damage to proteins. Potential role in diseases and therapeutic prospects for the inhibitors. *Br. J. Pharmacol.* **153** (1)**:** 6–20; 2008.
[40] Chéret, C.; Gervais, A.; Lelli, A.; Colin, C.; Amar, L.; Ravassard, P.; Mallet, J.; Cumano, A.; Krause, K. H.; Mallat, M. Neurotoxic activation of microglia is promoted by a nox1-dependent NADPH oxidase. *J. Neurosci.* **28** (46)**:** 12039–12051; 2008.
[41] Colombo, G.; Meli, M.; Morra, G.; Gabizon, R.; Gasset, M. Methionine sulfoxides on prion protein Helix-3 switch on the alpha-fold destabilization required for conversion. *PLoS One* **4** (1)**:**e4296; 2009.
[42] Wang, F.; Wang, X.; Yuan, C. G.; Ma, J. Generating a prion with bacterially expressed recombinant prion protein. *Science* **327** (5969)**:**1132–1135; 2010.
[43] Geoghegan, J. C.; Valdes, P. A.; Orem, N. R.; Deleault, N. R.; Williamson, R. A.; Harris, B. T.; Supattapone, S. Selective incorporation of polyanionic molecules into hamster prions. *J. Biol. Chem.* **282** (50)**:**36341–36353; 2007.
[44] Shi, S.; Dong, C. F.; Tian, C.; Zhou, R. M.; Xu, K.; Zhang, B. Y.; Gao, C.; Han, J.; Dong, X. P. The propagation of hamster-adapted scrapie PrPSc can be enhanced by reduced pyridine nucleotide in vitro. *FEBS J.* **276** (6)**:**1536–1545; 2009.
[45] Halliwell, B., Gutteridge, J.M.C. (Eds.), 2007]. Free Radicals in Biology and Medicine, fourth edition. Oxford University Press; 2007.
[46] Laszlo, L.; Lowe, J.; Self, T.; Kenward, N.; Landon, M.; McBride, T.; Farquhar, C.; McConnell, I.; Brown, J.; Hope, J., et al. Lysosomes as key organelles in the pathogenesis of prion encephalopathies. *J. Pathol.* **166** (4)**:**333–341; 1992.
[47] Collins, S. J.; Lewis, V.; Brazier, M.; Hill, A. F.; Fletcher, A.; Masters, C. L. Quinacrine does not prolong survival in a murine Creutzfeldt-Jakob disease model. *Ann. Neurol.* **52** (4)**:**503–506; 2002.
[48] Austin, C. D.; Wen, X.; Gazzard, L.; Nelson, C.; Scheller, R. H.; Scales, S. J. Oxidizing potential of endosomes and lysosomes limits intracellular cleavage of disulfide-based antibody-drug conjugates. *Proc. Natl. Acad Sci. U.S.A.* **102** (50)**:** 17987–17992; 2005.
[49] Marijanovic, Z.; Caputo, A.; Campana, V.; Zurzolo, C. Identification of an intracellular site of prion conversion. *PLoS Pathog.* **5** (5)**:**e1000426; 2009.
[50] Veith, N. M.; Plattner, H.; Stuermer, C. A.; Schulz-Schaeffer, W. J.; Bürkle, A. Immunolocalisation of PrPSc in scrapie-infected N2a mouse neuroblastoma cells by light and electron microscopy. *Eur. J. Cell Biol.* **88** (1)**:**45–63; 2009.
[51] Kubota, C.; Torii, S.; Hou, N.; Saito, N.; Yoshimoto, Y.; Imai, H.; Takeuchi, T. Constitutive reactive oxygen species generation from autophagosome/lysosome in neuronal oxidative toxicity. *J. Biol. Chem.* **285** (1)**:**667–674; 2010.
[52] Grenier, C.; Bissonnette, C.; Volkov, L.; Roucou, X. Molecular morphology and toxicity of cytoplasmic prion protein aggregates in neuronal and non-neuronal cells. *J. Neurochem.* **97** (5)**:**1456–1466; 2006.

MOLECULAR NEURODEGENERATION

RESEARCH ARTICLE Open Access

Prion subcellular fractionation reveals infectivity spectrum, with a high titre-low PrP^{res} level disparity

Victoria Lewis[1,2], Cathryn L Haigh[1,2], Colin L Masters[2], Andrew F Hill[2,3], Victoria A Lawson[1,2] and Steven J Collins[1,2*]

Abstract

Background: Prion disease transmission and pathogenesis are linked to misfolded, typically protease resistant (PrP^{res}) conformers of the normal cellular prion protein (PrP^{C}), with the former posited to be the principal constituent of the infectious 'prion'. Unexplained discrepancies observed between detectable PrP^{res} and infectivity levels exemplify the complexity in deciphering the exact biophysical nature of prions and those host cell factors, if any, which contribute to transmission efficiency. In order to improve our understanding of these important issues, this study utilized a bioassay validated cell culture model of prion infection to investigate discordance between PrP^{res} levels and infectivity titres at a subcellular resolution.

Findings: Subcellular fractions enriched in lipid rafts or endoplasmic reticulum/mitochondrial marker proteins were equally highly efficient at prion transmission, despite lipid raft fractions containing up to eight times the levels of detectable PrP^{res}. Brain homogenate infectivity was not differentially enhanced by subcellular fraction-specific co-factors, and proteinase K pre-treatment of selected fractions modestly, but equally reduced infectivity. Only lipid raft associated infectivity was enhanced by sonication.

Conclusions: This study authenticates a subcellular disparity in PrP^{res} and infectivity levels, and eliminates simultaneous divergence of prion strains as the explanation for this phenomenon. On balance, the results align best with the concept that transmission efficiency is influenced more by intrinsic characteristics of the infectious prion, rather than cellular microenvironment conditions or absolute PrP^{res} levels.

Keywords: Prion protein, Prion infectivity, Prion disease, Protease resistance, Subcellular localisation, Fractionation

Background

Prion diseases constitute a group of unique neurodegenerative disorders, which naturally afflict a number of mammalian species including humans. Although our understanding remains incomplete, considerable evidence supports the "protein-only" hypothesis, which purports that the agent ("prion") responsible for both transmission and consequent pathogenesis is predominantly composed of misfolded conformers of the normal cellular prion protein PrP^{C} [1]. Additional discriminating features of the aberrant prion protein include increased β-sheet content [2,3], reduced solubility and increased tendency to aggregate, and typically heightened protease resistance [4-6]. Due to the characteristic protease resistant core, limited proteolysis with proteinase K (PK) truncates the N-terminus of the misfolded protein, producing PrP^{res}, whilst PrP^{C} is completely degraded, allowing a convenient biochemical differentiation of these two prion protein isoforms.

An intriguing but somewhat perplexing aspect of prion biology is the several instances in transmission studies, encompassing many prion strains, where infectivity titres and PrP^{res} levels (as detected by biochemical assessment of inocula) do not faithfully correlate. Illustrating this are pre-clinical prion infections after low dose transmissions [7], BSE infectivity in tongue and nasal mucosa [8] and slowly sedimenting high titres of infectivity separated from PrP^{res} in 'fast' prion strains [9]. Further examples

* Correspondence: stevenjc@unimelb.edu.au
[1]Department of Pathology, The University of Melbourne, Parkville, VIC 3010, Australia
Full list of author information is available at the end of the article

have occurred during cross species transmissions including intracerebral inoculation of hamster prions to mice [10], primary passage of bovine prions to rodents [11,12], scrapie prions peripherally introduced into mice [13] and transmission of three distinct prion strains (human, hamster scrapie, murine scrapie) into transgenic mice expressing the murine equivalent of a human prion protein gene mutation [14]. In addition, PrP^{res} generated through protein misfolding cyclic amplification (PMCA) evinces a longer incubation period (indicative of a lower titre) despite western blot detection levels equivalent to those observed in the original seeding inoculum [15]. This PMCA study suggests that a component within the original inoculum, which perhaps does not propagate or amplify as well as PrP^{res}, may contribute to the more efficient transmission. Although PrP^{res} is inextricably linked to prion infectivity, these numerous examples clearly illustrate the poorly understood complexities of this relationship.

The precise cellular location of PrP^{C} misfolding and conversion also remains speculative (reviewed in [16]), as does the contribution of cellular co-factors to conversion efficiency, although the participation of a species-specific protein [17-19], or negatively charged macromolecules such as nucleic acids [20-24] and glycosaminoglycans [25-29] has been posited. In contrast, evidence exists correlating the efficiency of prion propagation and transmission with the size of prion multimers serving as templates for conversion [30,31]. Acknowledging the aforementioned uncertainties, the current study investigated whether such observed disparities between infectivity titres and PrP^{res} levels could be resolved to a subcellular level and thereby provide a useful model for insights into the molecular basis of this observation. To address this aim, we utilized fractionation of MoRK13 cells infected with M1000 prions to explore the contributions of subcellular co-factors and cognate prion protein species to the efficiency of transmission.

Results

Prion protein conformers reside predominantly in lipid rafts in MoRK13 and MoRK13-inf cells

Characterisation of the MoRK13-M1000 prion infection model (MoRK13-inf) determined that per detectable 'PrP^{res} unit', MoRK13-inf cell lysate was approximately 90 times more efficient than crude M1000 brain homogenate at prion transmission to recipient MoRK13 (Additional file 1: Figure S1). This finding, perhaps an example of strain adaptation into a rabbit cell line, highlighted a discrepancy between PrP^{res} and infectivity levels, and indicated that MoRK13-inf cells may be an appropriate model to study this phenomenon. PrP isoforms have been shown to localise to various subcellular environments, including those of the secretory and endocytic pathways, and at the cell surface [32-34]. Figure 1 shows the localisation of organelle markers Bcl-2 (mitochondria; MT), Bip (endoplasmic reticulum; ER), and EEA1 (early endosome; EE) in the MoRK13 cells. As expected, the lipid raft marker Flotillin 1 was enriched within fractions at the buoyant end of the gradient, consistent with the high cholesterol:protein ratio resulting in a significantly lower density of lipid rafts compared to other solubilised membrane proteins [35]. This was confirmed by dot blot analysis of the lipid raft marker GM_1, detected by the cholera toxin subunit B (CTB). Figure 1 also indicates that the subcellular localisation of PrP^{C} in MoRK13, and total PrP (PrP^{C} and PrP^{res}, indistinguishable from each other under the conditions of these western blots) in MoRK13-inf is predominantly in the buoyant, lipid raft fractions. There were no substantial differences in organelle or membrane markers or PrP localisation when comparing the MoRK13 and MoRK13-inf cells, and also comparing vector-only transfected RK13 (vecRK13), GT1-7H and GT1-7H-inf cells (Additional file 2: Figure S2); therefore over-expression of PrP^{C}, prion infection and cell line origin (neuronal/non-neuronal/murine/rabbit) do not appear to alter localisations, or create artefacts in this system of subcellular fractionation. Previous reports indicate PrP^{res} is also localised in lipid rafts [36]. Figure 2A shows the localisation of MoRK13-inf PrP^{res} to be principally in lipid raft fractions, with a similar distribution to total PrP (Figure 1) as determined by both western blot and dot blot. Quantification of relative PrP^{res} levels (Figure 2B) highlights that the lipid raft enriched fractions contain up to eight times the detectable PrP^{res} levels than the ER/MT marker enriched fractions (eg compare fractions #3 and #8). By way of comparison to the original prion strain, Nycodenz gradient distribution of PrP isoforms and marker proteins from M1000 brain, homogenised in a comparative manner, was also similar to that observed in cell lysates (Additional file 3: Figure S3).

High levels of prion infectivity are present in lipid raft and ER/MT marker enriched fractions of MoRK13-inf cells

In order to determine whether detectable subcellular PrP^{res} levels correlate with infectivity, an *in vitro* cell culture transmission study was carried out of equivalent volumes of fractions obtained after density gradient flotation assays of MoRK13-inf cell lysate using the highly susceptible MoRK13 as recipient cells. Levels of PrP^{res} produced by recipient cells after exposure to fractions were quantified and used as a surrogate indicator of relative infectivity titres contained within the subcellular fractions. The representative cell blot and quantification (Figure 3A, B) clearly show that infectivity was contained within all fractions derived from MoRK13-inf cells, albeit to varying degrees. The EE enriched fractions (predominantly #9 and #10) contained considerably less infectivity compared with the lipid raft

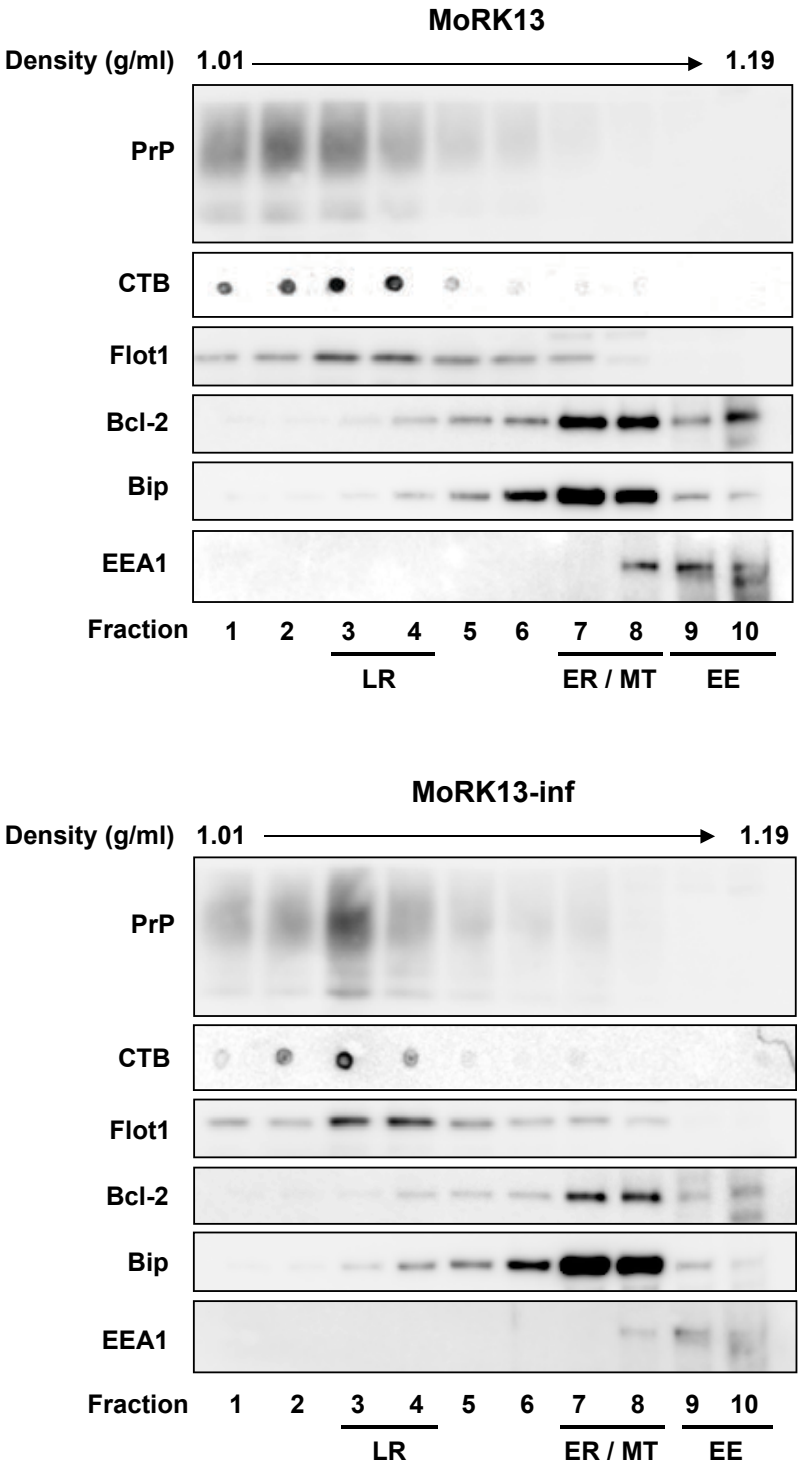

Figure 1 MoRK13 and MoRK13-inf PrP localises predominantly to lipid raft fractions. Representative immunoblots of subcellular fractions (1-10) obtained from MoRK13 and MoRK13-inf. Equivalent volumes of each fraction were resolved on gradient gels. Proteins were transferred to PVDF, which was sectioned based on the predicted molecular weight of the protein of interest, with each PVDF strip probed with the relevant antibody. CTB dot blot - 3 μl of fraction was dried onto nitrocellulose membrane, and blotted as described in the methods. LR = lipid raft; ER = endoplasmic reticulum; MT = mitochondria; EE = early endosome; CTB = cholera toxin subunit B (LR marker); Flot1 = Flotillin 1 (LR marker); Bcl-2 = anti-apoptotic MT marker protein; Bip = ER lumen chaperone protein; EEA1 = EE antigen 1.

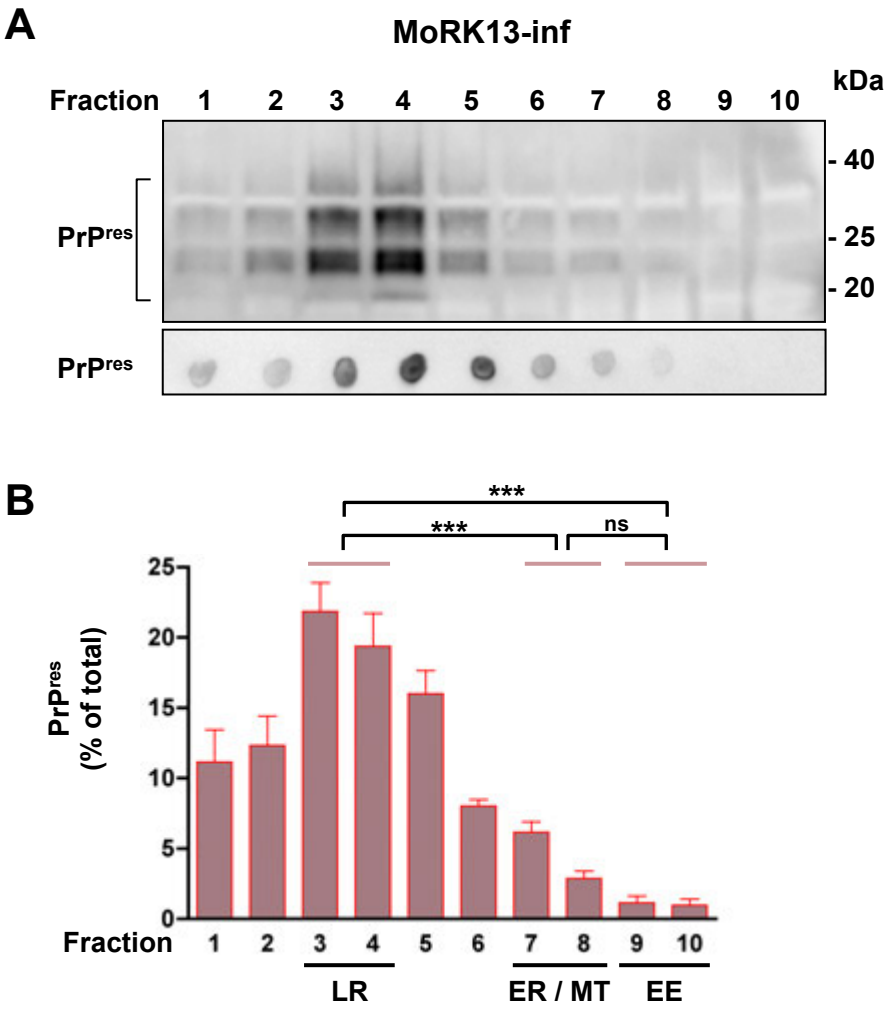

Figure 2 PrP^{res} is enriched in lipid raft fractions of MoRK13-inf cells. (A) Equivalent volumes of PK treated MoRK13-inf fractions resolved on 10-20% Tris-glycine SDS PAGE and immunoblotted (top panel), and representative fraction PrP^{res} dot blot (bottom panel). (B) Quantification of PrP^{res} from dot blots of six separate cellular fractionations. Fractions enriched in lipid raft (LR), endoplasmic reticulum (ER), mitochondrial (MT) and early endosome (EE) marker proteins are highlighted. Comparison of relative PrP^{res} levels by one way ANOVA; *** $p < 0.001$, ns = not significant.

enriched fractions (predominantly #3 and #4), and the ER and MT marker enriched fractions (predominantly #7 and #8), although the comparison of fraction #7 and fraction #9 did not reach significance. Interestingly, there was no significant difference in the amount of infectivity contained within the lipid raft enriched fractions (#3 and #4), and the ER and MT marker enriched fractions (#7 and #8). As shown in Figure 3A, fractions were also diluted in a 1/2 log series, to ensure there was no limiting sensitivity of the *in vitro* assay truncating the upper end of the dynamic range. Importantly, neat fractions that elicited the highest production of PrP^{res} by recipient MoRK13 cells (for example fractions #4 and #8), were infectious to the same dilutions (1:100), thereby validating the use of PrP^{res} produced by recipient cells as a measure of relative infectivity contained within fractions.

ER and MT marker enriched fractions show disparity between PrP^{res} levels and infectivity titres *in vitro* and *in vivo*

Correlation of the percentage of PrP^{res} present in each fraction with the level of *in vitro* infectivity produced by each fraction (Figure 4A) revealed a discrepancy in the ER/MT enriched fractions. The relative levels of PrP^{res} present in the lipid raft enriched fractions (#3 & #4) and the early endosome enriched fractions (#9 and #10) correspond with the relative levels of PrP^{res} produced by the recipient MoRK13 cells. In contrast, the ER/MT enriched fractions (#7 and #8) that display low detectable PrP^{res} levels, contained high infectivity levels similar to the lipid raft enriched fractions, with the discrepancy at fraction #8 highly significant ($p < 0.001$; two way ANOVA). Therefore, there was a reproducible and significant

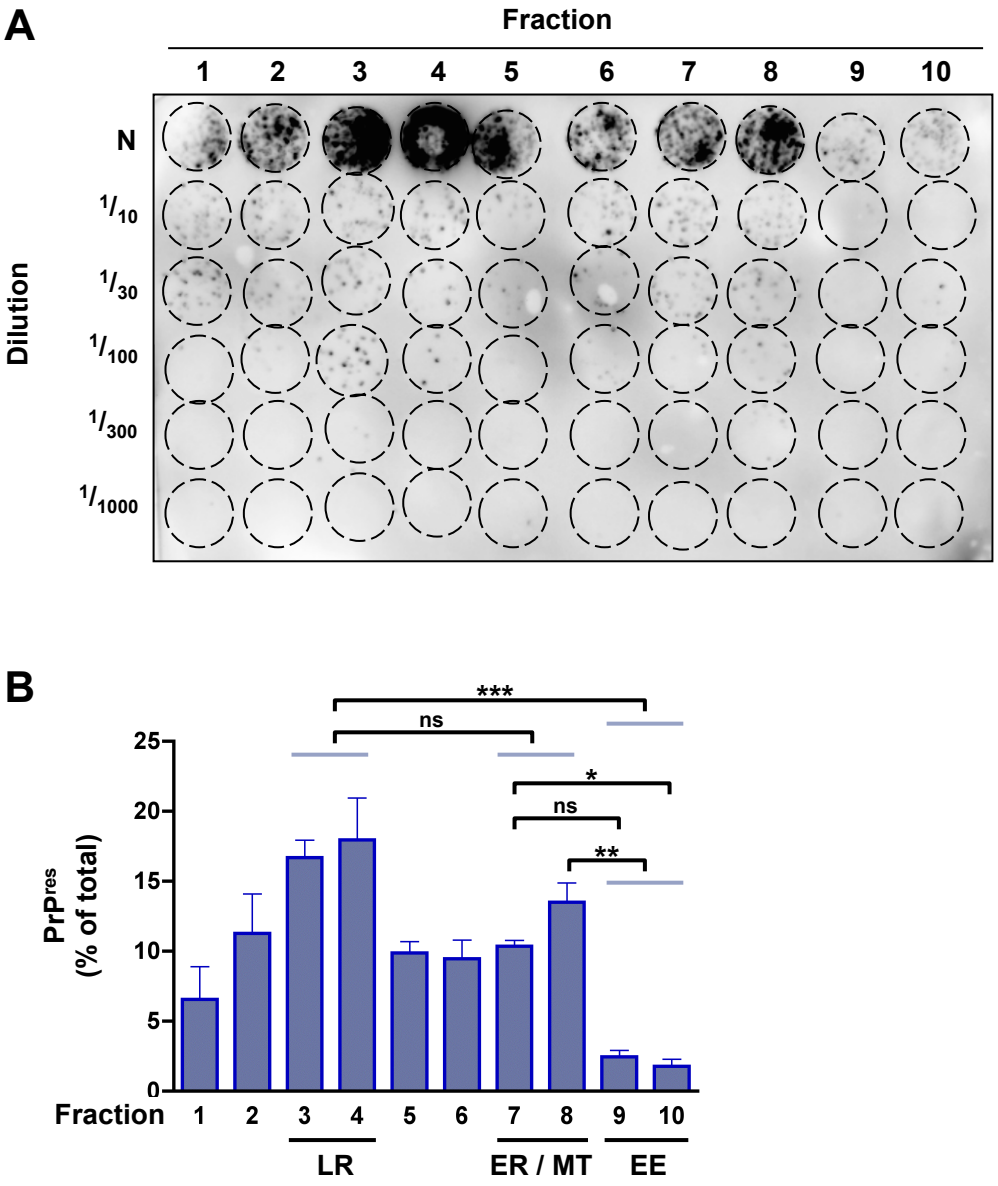

Figure 3 All MoRK13-inf fractions contain infectivity. (A) Representative cell blot showing PrP^{res} levels produced by recipient MoRK13 cells at passage 4 (P4) post-exposure to equal volumes of each fraction at the 'neat' dilution (N) or further serially diluted (1/10-1/1000). (B) Quantification of infectivity from three independent MoRK13-inf fractionations (n = 3); fractions enriched in lipid raft (LR), endoplasmic reticulum (ER), mitochondrial (MT) and early endosome (EE) marker proteins are highlighted. Statistical analysis by one way ANOVA; only the statistical findings for relevant comparisons are indicated: *** $p < 0.001$, ** $p < 0.001$, * $p < 0.05$, ns = not significant.

divergence between PrP^{res} and infectivity levels within ER/MT marker enriched fractions.

To confirm genuine prion infectivity, selected fractions were bioassayed in Tga20 PrP^{C} over-expressing mice. The fractions were chosen to provide a range of PrP^{res} and infectivity level combinations; ie high PrP^{res} and infectivity levels (fraction #4), low PrP^{res} and infectivity levels (fraction #10), and low PrP^{res} but high infectivity levels (fraction #8). Controls included inoculating mice with whole cell lysate from naive MoRK13 and MoRK13-inf cells, as well as M1000 brain homogenate, in order to make comparisons with the original prion strain. Figure 4B depicts the incubation periods for the selected fractions and control mice. Mice exposed to uninfected MoRK13 cell lysate were symptom free at 245 days post-inoculation. Mice inoculated with 0.01% M1000 brain homogenate had a significantly shorter incubation period than mice inoculated with MoRK13-inf whole cell lysate. Importantly, concordant with the *in vitro* cell culture transmissions, mice inoculated with fractions #4 and #8 had indistinguishable

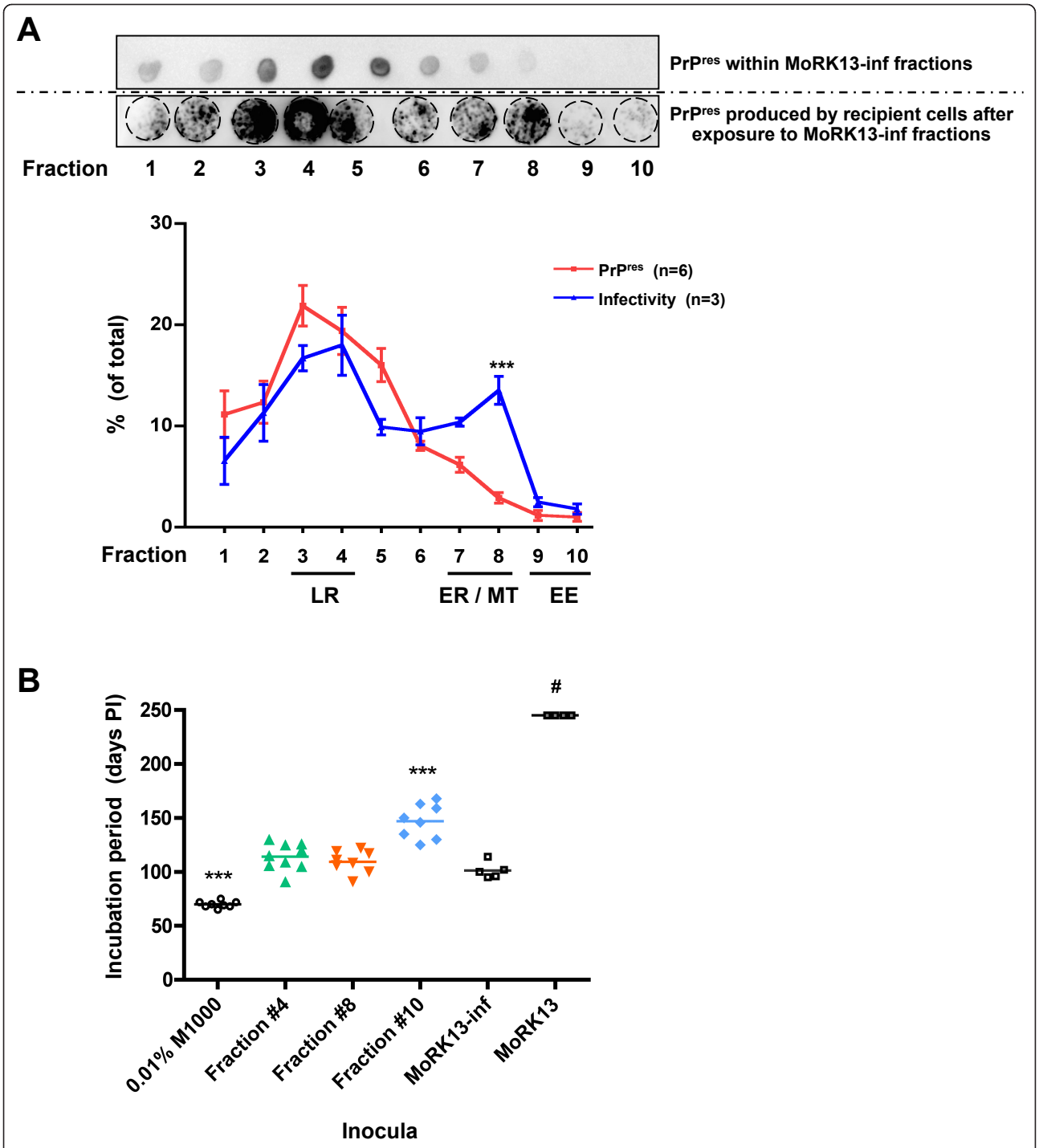

Figure 4 Disparity in subcellular fraction PrP^{res} levels and relative infectivity *in vitro* and *in vivo*. (A) Relative amounts of PrP^{res} contained within MoRK13-inf fractions (dot blot - top panel, also Figure 2; red line) plotted against relative infectivity of each fraction (PrP^{res} produced by recipient MoRK13 - bottom panel, also Figure 3; blue line). There is a highly significant separation of relative PrP^{res} and infectivity levels observed in fraction #8; statistical analysis was by two way ANOVA; *** $p < 0.001$. Fractions enriched in lipid raft (LR), endoplasmic reticulum (ER), mitochondrial (MT) and early endosome (EE) marker proteins are highlighted. (B) Mean survival (horizontal bar) of Tga20 mice inoculated with 0.01% (w/v in PBS) M1000 brain homogenate, whole cell lysate from MoRK13 and MoRK13-inf cells, and selected subcellular fractions from MoRK13-inf. Each data point represents the number of days post-inoculation (PI) that a terminally ill mouse was sacrificed, with the exception of Tga20 mice inoculated with MoRK13 cell lysate (#) which were symptom free when culled at 245 days PI. Mice inoculated with 0.01% (w/v) M1000 brain homogenate had a significantly shorter incubation period than those exposed to all other inocula. Mice inoculated with fraction #10 had a significantly longer incubation period compared to mice exposed to all other infectious inocula. Statistical analysis was by one way ANOVA; *** $p < 0.001$.

incubation periods, despite the significantly different PrP^{res} levels contained within these fractions. Mice inoculated with fraction #10 had significantly longer incubation periods than mice infected with the other two fractions, again concordant with the relative infectivity levels determined by the cell culture transmissions. For illustrative purposes, this 35 day extension in incubation period approximates a 3 log reduction of infectious titre when modelled on a time interval assay developed in Tga20 mice inoculated with M1000 brain homogenate derived prions (Additional file 4: Figure S4). In summary, the *in vivo* findings faithfully recapitulate and validate the MoRK13 *in vitro* model.

Infectious prions from different subcellular fractions do not induce unique disease *in vivo*

Neuropathologically, prion diseases are characterised by the presence of neuronal loss, spongiform change, proliferation of astrocytes and extracellular PrP deposits [37]. Further, for different prion strains the topographical distribution of neuropathological changes is distinctive, creating characteristic lesion profiles [38,39]. All diseased mice displayed symptoms typical of M1000 prion infection and brains were harvested to assess neuropathological changes. As expected, control mice inoculated with MoRK13 whole cell lysate showed no neuropathological abnormalities (Additional file 5: Figure S5). Figure 5 displays the quantification of the neuropathological features mentioned above within different brain regions, clearly indicating that each inoculum produced very similar lesion profiles (for representative photomicrographs of the histological and immunohistochemical findings see Additional file 5: Figure S5). This distribution pattern of the pathological features, with predominant involvement of the thalamus, midbrain and pons, and minimal involvement of the cerebellum is consistent with previous observations of the M1000 strain [40,41]. The only significant difference detected in lesion profiles was between MoRK13-inf whole cell lysate and fraction #10 inocula, with the former having significantly more reactive astrocytes in the occipital cortical region. The explanation for this is uncertain, but may suggest an additive effect of the individual fractions, which contribute to the whole-cell lysate profile. Different prion strains often have distinctive PrP^{res} glycoform ratios and mobilities on western blot analysis [42-46]. To further evaluate the possibility of different MoRK13-inf subcellular fractions associating with distinct prion strains, the brain PrP^{res} profiles from Tga20 mice inoculated with selected fractions were examined by western blot. Similar to the lesion profiling, there were no significant differences in PrP^{res} patterns when comparing MoRK13-inf whole cell lysate with each of the selected fractions, in keeping with them all being the same prion strain (Additional file 6: Figure S6).

The efficiency of M1000 prion transmission is not enhanced by exogenous fraction specific co-factors *in vitro* or *in vivo*

In order to explore whether subcellular fraction specific co-factors might contribute to the observed transmission efficiency spectrum, M1000 brain homogenate was spiked into fractions derived from uninfected MoRK13 or vecRK13 cells, prior to use as inocula *in vitro*. Figure 6A shows that even at the lowest dilutions of M1000 in MoRK13 fractions, PrP^{res} was produced by recipient MoRK13 cells. However, quantification (Figure 6B) shows there were no significant differences in amounts of PrP^{res} produced when comparing the various MoRK13 subcellular fraction diluents. Notably, there was a general trend for MoRK13 subcellular fractions to enhance M1000 transmission efficiency to MoRK13 cells compared to lysis buffer alone. A similar result was observed using fractions obtained from vecRK13 cells (Additional file 7: Figure S7), suggesting this trend is not PrP^{C} specific or dependent.

To further evaluate the possible contribution of cellular co-factors on the efficiency of prion infection, M1000 brain homogenate was diluted in PBS or selected subcellular fractions from uninfected MoRK13 cells (fractions #4, #8 and #10), and bioassayed in Tga20 indicator mice. M1000 was also diluted in 'empty' Nycodenz fractions (#4, #8 and #10), in order to control for any affect the Nycodenz gradient material itself may have on incubation period or the neuropathology. Neither the exogenous cellular co-factors in the selected fractions, nor Nycodenz alone, had any significant affect on the incubation time (Figure 6C) or overtly affected the neuropathology (Additional file 8: Figure S8) of M1000 in Tga20 mice.

Discrepancies between PrP^{res} and transmission efficiency are not due to protease-sensitive prions, and only in lipid raft enriched fractions is infectivity enhanced by sonication

There is experimental evidence that some disease associated [47-50], and synthetic [51] prions, may be protease sensitive. To test whether the infectious prions within the MoRK13-inf fractions may differentially contain significant amounts of protease sensitive species, selected fractions were digested mildly with PK prior to using them as a source of infectivity. There were no significant differences in PrP^{res} levels produced by MoRK13 infected with PK digested fractions #4, #8 or #10 compared to cells infected with the untreated fraction counterpart (Figure 7A, B). However there was a modest general trend towards reduced PrP^{res} production by recipient cells after PK treatment of each fraction inoculum.

Evidence suggests misfolded prion protein aggregate size correlates with efficiency of conversion or prion

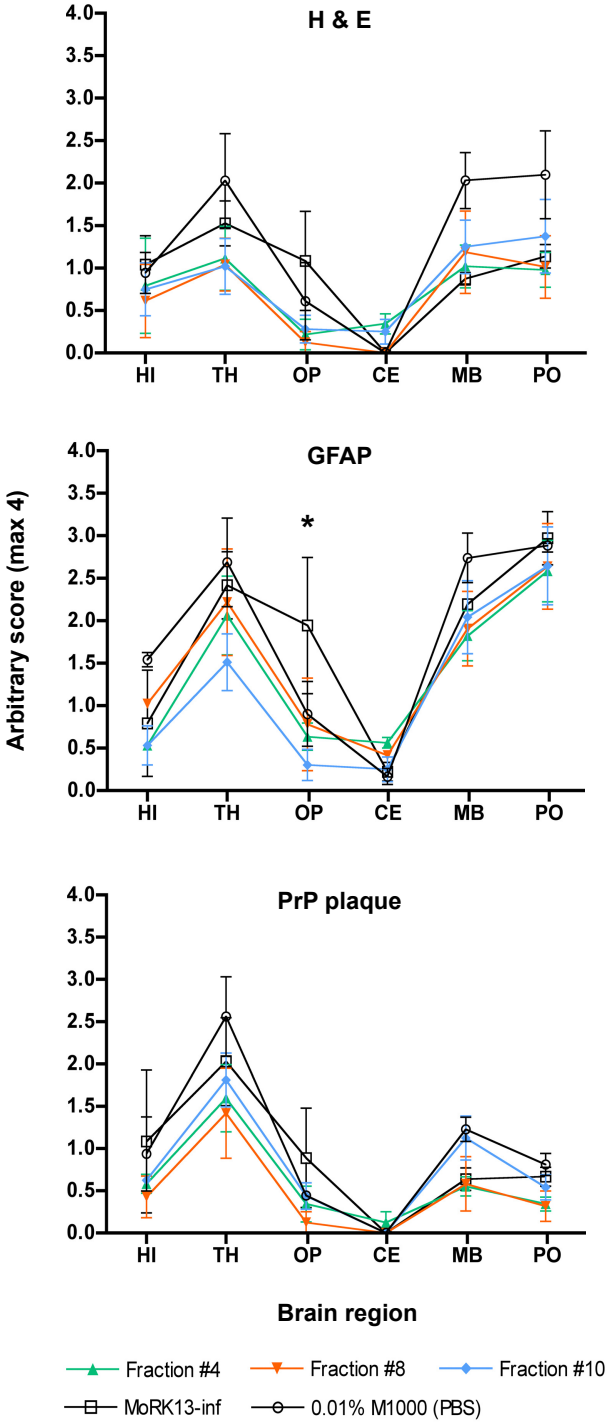

Figure 5 Lesion profiles from Tga20 mice intracerebrally inoculated with M1000, MoRK13 and MoRK13-inf whole cell lysates and selected MoRK13-inf fractions. Lesion profiles generated by quantification of the degree of vacuolation, reactive astrocytosis and PrP plaques in each brain region (HI - hippocampus, TH - thalamus, OP - occipital pole, CE - cerebellum, MB - midbrain, PO - pons) in Tga20 mice inoculated as indicated. n = 3 or 4 for all brain regions except in MoRK13-inf whole lysate HI H&E and 0.01% M1000 HI PrP plaque deposition, where n = 2. Statistical analysis comparing lesion profiles was by two way ANOVA. The only significant difference was comparing MoRK13-inf and Fraction #10 in OP region (*$p < 0.05$).

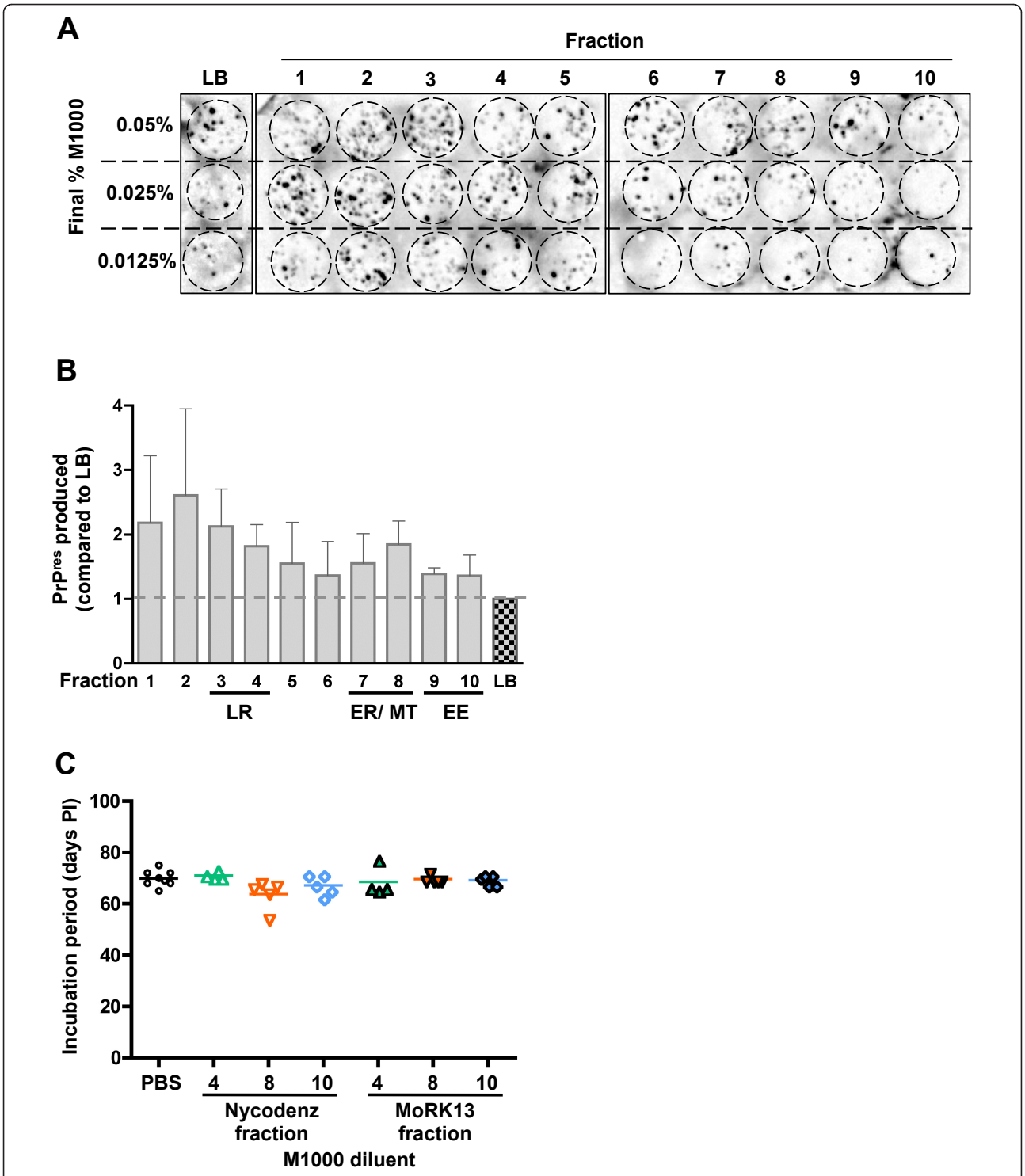

Figure 6 Exogenous cellular co-factors do not modify the efficiency of M1000 infection *in vitro* or *in vivo*. (A) Representative cell blot showing PrP^{res} levels produced by recipient MoRK13 cells exposed to M1000 brain homogenate diluted to three different final concentrations (as indicated) with either 1:4 lysis buffer (LB):medium or 1:4 MoRK13 fraction:medium mix. (B) Quantification of PrP^{res} produced by MoRK13 cells exposed to M1000 brain homogenate diluted in subcellular fraction relative to the equivalent % M1000 brain homogenate diluted in lysis buffer; data is from M1000 spiked into three independent fractionations of MoRK13. For quantification purposes, the three different % M1000 spikes into the same MoRK13 fractionated lysate were considered a triplicate of the same experiment. Fractions enriched in lipid raft (LR), endoplasmic reticulum (ER), mitochondrial (MT) and early endosome (EE) marker proteins are highlighted. Analysis of relative levels of PrP^{res} produced after infection was by one-way ANOVA with Tukey's multiple comparison test; no significant differences found comparing subcellular fractions. (C) Survival of Tga20 mice inoculated with M1000 brain homogenate diluted to 0.01% with either PBS, selected fractions from an empty Nycodenz gradient, or selected subcellular fractions from MoRK13 cells. Each data point represents the number of days post-inoculation (PI) which mice were sacrificed because of terminal prion disease. Statistical analysis was by one way ANOVA, with no significant differences in survival seen between any inocula.

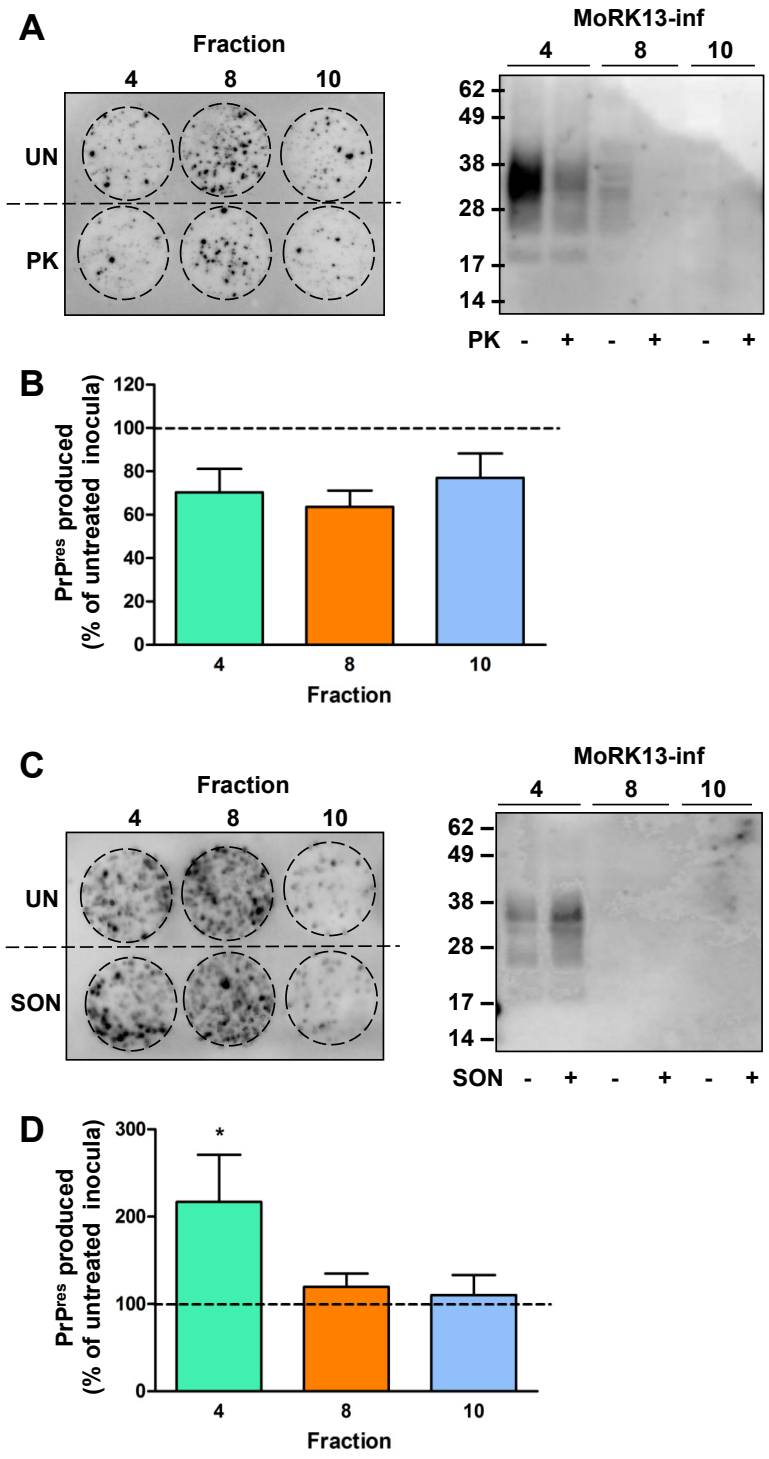

Figure 7 Sonication but not PK treatment alters efficiency of *in vitro* infection with fraction #4 only. (A) Representative cell blot (left panel) of PrP^{res} produced by MoRK13 cells exposed to selected MoRK13-inf fractions which were PK digested (PK) or left untreated (UN) and western blot (right panel) of MoRK13-inf inocula before and after PK treatment. (B) Quantification of cell blot PrP^{res} levels (n = 3 independent experiments), with PrP^{res} produced after infection with PK treated inocula expressed relative to untreated MoRK13-inf fraction inocula. (C) Representative cell blot (left panel) of PrP^{res} produced by MoRK13 cells exposed to selected MoRK13-inf fractions which were sonicated (SON) or left untreated (UN) and western blot (right panel) of MoRK13-inf fraction inocula before and after sonication. (D) Quantification of cell blot PrP^{res} levels expressed relative to untreated MoRK13-inf fraction inocula (n = 3 independent experiments). Note, levels of total PrP in fractions #8 and #10 are at or below the limits of detection by standard immunoblotting. Comparison of relative PrP^{res} levels by one way ANOVA and Dunnett's post-test for specific comparisons to a control (ie untreated fraction) found no significant differences in any PK treated inocula, and only sonicated MoRK13-inf fraction #4 was significantly different compared to its untreated control, *$p < 0.05$.

infection [30,31]. As a consequence, *in vitro* conversion assays such as PMCA may be most efficient when incorporating sonication steps [52,53]. To assess this possibility, selected fractions (#4, #8 and #10) were subjected to sonication (equivalent to one 'round' of PMCA) prior to using them as a source of infectivity in the MoRK13 cell culture model. As demonstrated by the representative cell blot in Figure 7C, quantified in Figure 7D, only subcellular fraction #4 had significantly increased levels of infectivity compared to its untreated fraction.

Discussion

The protein-only hypothesis states that misfolded conformers of the normal cellular prion protein are the principal component of the agent responsible for transmitting prion disease [1]. However, previously observed examples of high infectivity titres associated with very low or undetectable PrP^{res}, the commonly utilized surrogate prion marker, suggest a poorly understood spectrum of infectious prions. Assessing the subcellular environment of the most infectious prions may provide information about optimal pH or metal content conditions, implicate membrane domains, or subcellular co-factors involved in localisation of highly efficient prions. Investigation of the subcellular distribution of prion infectivity and corresponding PrP^{res} levels has been previously reported, albeit to a limited extent. However, absent in prior studies were attempts to explore what determines the intracellular topographical diversity of prions or the molecular basis of any observed discrepancies in PrP^{res} and infectivity levels.

The present study clearly indicates that not all prion infectivity is associated with lipid rafts, although the significance of the lipid raft microenvironment in PrP^{C} misfolding and prion conversion is yet to be resolved, with experimental evidence both for and against lipid raft localisation as an optimal site (reviewed in [16]). In complete agreement with the protein-only hypothesis, lipid raft and EE marker associated infectivity and PrP^{res} were shown to correlate in the MoRK13-inf model. In contrast however, ER/MT marker enriched fractions contained much greater infectivity when reported to relative PrP^{res} content. That lipid raft and ER/MT enriched fractions contain the same infectivity levels indicates some biological redundancy or relative inefficiency of the lipid raft localised prions, and/or higher efficiency of ER/MT localised prions, prompting further investigation.

Cell-free conversion studies have shown there is a role for cellular co-factors, such as nucleic acid or other polyanionic molecules, in the efficiency of prion conversion and propagation [21-23,29,54]. Perhaps militating against a prominent role of specific co-factors contributing to the transmission efficiency of the MoRK13-inf subcellular fractions, infectivity of brain derived M1000 prions was not significantly differentially enhanced by dilution across various subcellular fractions. However, an explanation for this result is that the transmissible prions within M1000 brain homogenate were already largely in an optimal state, pre-formed and associated with the necessary co-factors required for infection. Therefore additional exogenous co-factors supplied via the MoRK13 or vecRK13 subcellular fractions were somewhat superfluous. Alternatively, the fractionation procedure itself may have inactivated any critical co-factors, such that they were not able to significantly enhance the infectivity of M1000 brain homogenate. In fact, there was a clear trend for increased PrP^{res} propagation by recipient cells after infection with M1000 diluted in subcellular fractions compared to the lysis buffer only control, independent of whether the fractions contained PrP^{C}. This may indicate that incompletely defined but relatively ubiquitous 'cellular co-factors' contribute to the efficiency of *in vitro* prion transmission, which would be consistent with previous studies.

Numerous prion strains exist, evident in both naturally occurring human [55,56] and animal [38,57-60] prion disease, as well as those adapted to laboratory based animal models. One hypothesis for what determines different strains is the tertiary structure of the prion conformer, possibly affected by metals, co-factors or binding partners [61]. It is also believed that prions may adopt various stable tertiary conformations, and there is evidence of simultaneous propagation of more than one prion strain within the brain [55,62,63]. Furthermore, super-infection experiments indicate that the more infectious strain will predominate and determine disease expression [64-66]. Prion strains can be classified by their distinctive neuropathological lesion profiles, incubation periods, PrP^{res} glycosylation patterns and electrophoretic mobilities [39,42,43,46]. As RK13 cells are capable of supporting and maintaining propagation of many prion strains [67], and each fraction represented different subcellular localisations and potential binding partners, we explored the possibility that MoRK13-inf fractions contained structurally distinct prions of variable transmission efficiency. However histological and western blot analyses failed to detect any evidence of a subcellular divergence of prion strains, strongly militating against this as the explanation for the apparent increased relative infectivity in the ER/MT marker enriched fractions.

Previous experiments have shown that PrP^{res} aggregate size affects the efficiency of conversion and prion infection, perhaps through effects on optimising the available templating surface [30,31], with oligomers of five or fewer PrP^{res} molecules and larger fibrillar aggregates of PrP^{res} far less efficient than non-fibrillar particles of 14-28 molecules [30]. There is also experimental evidence that a proportion of disease associated prions are protease sensitive [47-49], which may form low molecular weight aggregates [47,49].

The results presented herein show that only a minor proportion of prion infectivity within MoRK13-inf fractions is protease sensitive, and is unlikely to account for the disconnect observed between PrP^{res} levels and infectivity in the ER/MT and lipid raft enriched fractions. Rather, the sonication results are in keeping with a greater proportion of multimeric assemblies, fibrils or aggregated species of prions existing in the lipid raft compared to ER/MT marker enriched fractions, with sonication increasing the number of replication-competent prion oligomeric strand ends which are then more efficient at transmission and inducing prion propagation. Recent publications provide credence to this hypothesis [68,69], with direct visualisation of the fragmentation of recombinant PrP after sonication. However, the current study does not exclude any positive effect that sonication may have had on other cellular components contained within the fraction mileu or interactions between the prion protein and other molecules. In fact another recent publication [70] found that sonication also fragments purified liver RNA, to a size that has previously been shown to stimulate prion conversion in PMCA assays. However the RNA sonication produced optimal (sized) RNA after approximately 8 cycles, whereas our sonication experiment was equivalent to one cycle, giving some support to the plausibility of our former hypothesis. Ongoing studies, including the utilisation of techniques such as the conformation dependent immunoassay (CDI) to measure prions in the fractions [71], and sophisticated size fractionation techniques, will help clarify the exact biophysical nature of the variably efficient prion species in the lipid raft and ER/MT enriched fractions.

The association of prion infectivity with MT and ER has been previously investigated with conflicting results. One study showed that purified mitochondria and mitoplast fractions from scrapie infected hamster brain contained infectivity titres equivalent to those determined for crude brain homogenate, yet mitoplast fractions were not associated with detectable levels of PrP [72], in keeping with the findings of the present study. These results, which suggested an association of high levels of scrapie infectivity with the inner mitochondrial membrane or mitochondrial matrix, are broadly consistent with the characteristics of MoRK13-inf ER/MT enriched fractions, which co-localised with the mitochondrial membrane marker Bcl-2 [73]. An integral and unique (to mitochondria) lipid component of the inner mitochondrial membrane is cardiolipin, a form of dimeric phosphatidylglycerol [74]. Interestingly, utilizing serial PMCA, researchers have recently been able to produce protease resistant, infectious prions from recombinant PrP mixed with RNA and the synthetic phosphatidylglycerol, POPG (1-palmitoyl-2-oleoylphosphatidylglycerol) [75]. The authors state that the POPG and RNA additives to their PMCA may be mimicking factors which facilitate the conversion process *in vivo*, which is entirely consistent with the results presented here implicating mitochondrial component enriched fractions as containing highly efficient infectious prions.

Somewhat incongruent with these observations, a much earlier study examined the infectivity of scrapie within membrane fractions and found that brain derived purified mitochondrial fractions were associated with very little infectivity [76]. Nevertheless, similar to our results, Millson and colleagues [76] did find both brain and spleen derived subcellular fractions containing elevated enzyme activities usually associated with the ER and plasma membrane were associated with high scrapie infectivity. Conversely, Alais and colleagues [77] found fractions enriched in the ER marker Bip harboured no infectivity, despite containing moderate levels of PrP^{res}. This result, whilst presenting another example of discrepancy between PrP^{res} levels and infectivity, clearly contrasts with what was observed in the MoRK13-inf fractions, perhaps reflecting the different methods and prion strain-cell model employed.

Conclusions

Through the use of both *in vitro* and *in vivo* transmission studies, we have corroborated previously reported discrepancies between absolute PrP^{res} levels and infectivity and provided insight into the basis of this phenomenon. Through subcellular separation of infectivity, our data indicates that a substantial amount of infectivity is contained outside of buoyant lipid raft fractions and importantly showed that the most transmission efficient prions per detectable PrP^{res} unit were associated with either ER and/or MT membranes or proteins. We established that the high transmission efficiency shown by the ER/MT containing fractions was not due to the simultaneous separation of a more potent prion strain. As critical co-factor enrichment could not be completely excluded, it remains to be determined whether cellular microenvironments directly but variably contribute to the transmission efficiency of resident prions, or only passively serve as sequestration sites for the different prion species. Overall the current study broadly aligns with the notion that rather than absolute levels of PrP^{res}, intrinsic prion properties may dictate or be dictated by the ultimate subcellular localisation of infectious prions, with transmission efficiency likely correlating best with optimal prion oligomeric state for template directed conversion. Importantly, through the development and validation of a tractable model, further detailed exploration of these fundamental aspects of prion biology, including assessment of other cell line-prion strain combinations to determine the breadth of applicability of our observations, can be undertaken.

Methods

Cell culture

Rabbit kidney epithelial cells which have no detectable endogenous PrP^C protein, were stably transfected to over-express murine PrP^C (MoRK13) or the empty vector (vecRK13) [78] and mouse hypothalamic GT1-7H cells were maintained as described previously [79], in a humidified incubator at 37°C with 5% CO_2.

Subcellular fractionation

A method of non-toxic/non-detergent cell lysis and subcellular separation was necessary to allow subsequent use of fractions for infecting recipient cells or mice. Also, due to the possible involvement of lipid rafts in prion conversion, a lysis method was chosen in order to maintain lipid raft integrity and buoyancy [35], with minor modifications. Briefly two confluent T175 cm^2 flasks (approximately 4 $x10^7$ cells) were washed twice with 20 mls ice cold lysis buffer (20 mM Tris-Cl pH 7.8, 250 mM sucrose, 1 μM $CaCl_2$, 1 μM $MgCl_2$) and harvested by scraping into a further 20 ml of lysis buffer and pelleting at 700 × g for 3 minutes. The cell pellet was re-suspended in 500 μl cold lysis buffer. Cells were lysed on ice, by passing the cell suspension through a 22 g needle exactly twenty times, and the crude lysate was centrifuged at 1000 × g, 10 minutes at 4°C. The post-nuclear supernatant was retained on ice and the extraction repeated on the pellet. The lysate was then assayed for total protein content by performing a bicinchoninic acid (BCA) assay (Pierce, Thermo Scientific, Scoresby, VIC, AUS) as per the manufacturer's instructions, and adjusted with lysis buffer to 1.8 mg/ml. The Nycodenz (HistoDenz™, Sigma-Aldrich, Castle Hill, NSW, AUS) density gradient fractionation method was adapted from a published protocol [80], to suit a Beckman Optima Max-E Benchtop Ultracentrifuge and MLS-50 rotor. Nycodenz solutions were prepared in TNE (25 mM Tris-Cl pH 7.5, 150 mM NaCl, 5 mM EDTA) and an 8-35% linear step Nycodenz gradient was poured (400 μl of each of 8%, 12%, 15%, 18%, 20%, 22.5% and 25%) with 1.1 ml of a 35% Nycodenz cushion consisting of equal parts ice cold 70% Nycodenz and cell lysate (1 mg total protein) pipetted to the bottom of the gradient. In some cases, an 'empty Nycodenz' gradient was poured, whereby the 35% Nycodenz/lysate cushion mixture was substituted for 35% Nycodenz alone. Nycodenz gradients were centrifuged at 200,000 × g (average) for 342 minutes at 4°C. Following centrifugation, 10 equal volume fractions of 390 μl were collected and stored at -80°C or kept on ice for immediate use.

Prion strain and cell infections

The M1000 prion strain used in this study was derived from a well characterised stock of pooled mouse brain homogenate [81]. Recipient MoRK13 or GT1-7H cells were infected using an overlay technique as described previously [79]. For comparisons of cell lysate and brain homogenate M1000 infectivity, cell lysates were prepared by harvesting and lysing in sterile phosphate buffered saline (PBS; Invitrogen, Mulgrave, VIC, AUS) by three cycles of freezing (10 minutes at -80°C) and thawing (3 minutes at 37°C), and centrifugation at 1000 × g for 3 minutes at 4°C to obtain a post-nuclear supernatant. The total protein content of the PBS supernatant and M1000 brain homogenate were determined by BCA assay, and the lysates and homogenate were balanced to the same protein concentration with PBS. Following this 100 μl of lysate or homogenate was mixed with 400 μl of complete medium and this was used to infect recipient cells. For fraction infections 100 μl fraction ('neat') or, where indicated, fraction which had been serially diluted in medium, was mixed with 400 μl complete medium, and used to infect recipient MoRK13 cells. For 'spiking' experiments, M1000 brain homogenate was diluted in 400 μl media and mixed with 100 μl MoRK13 or vecRK13 fraction (or as a control the lysis buffer used to prepare cells prior to fractionation) to give a final concentration of 0.05%, 0.025% and 0.0125% M1000, prior to being used to infect recipient MoRK13 cells.

Subcellular fraction pre-treatments

For PK digestion, 100 μl of a fraction was treated with a final concentration of 1 μg/ml PK for 8 hours at 37°C, conditions found to reduce PrP^C by approximately 80% when tested on control fractions (data not shown). For sonication pre-treatment, 100 μl of a fraction in a 1.5 ml microfuge tube was subjected to 60 seconds at amplitude 70 in a S4000 sonicator (Misonix, Farmingdale, NY, USA) with microplate horn adapter in 300 mL water maintained at 37°C. The PK digested or sonicated fractions (and untreated controls) were mixed with 400 μl of complete medium and used for *in vitro* infections as described above.

Immunoblotting

For determination of subcellular localisation of PrP and other proteins, fractions were mixed with 4X sample buffer and subject to PAGE (using either 4-20% or 10-20% Tris-glycine SDS or 4-12% Bis-tris NuPAGE pre-cast gels (Invitrogen), depending on the size of the proteins to be detected, and then transferred to PVDF membrane for western blotting of PrP as described previously [79] and organelle marker proteins using antibody dilutions as outlined in the manufacturer's instructions (BD Pharmingen™ Organelle Sampler Kit, BD Biosciences, North Ryde, NSW, AUS). For detection of the ganglioside GM_1 (lipid raft marker), 3 μl of each fraction was spotted onto nitrocellulose membrane, and allowed to dry for 20 minutes at

37°C. The membrane was blocked for a minimum of 1 hour in 5% skim milk powder in PBS containing 0.05% (v/v) Tween-20 (PBST) and then incubated in 1:100,000 cholera toxin B subunit (CTB)-horseradish peroxidise (HRP) conjugate (Sigma, stock concentration 0.45 mg/ml CTB and 1 mg/ml HRP in H_2O) solution in block for 1.5 hours at room temperature prior to chemiluminescent detection (ECL Plus, GE Healthcare, Rydalmere, NSW, AUS). For PrP^{res} detection, fractions, cell lysates or brain homogenate were digested with a final concentration of 50 μg/ml PK, 1 hour at 37°C before SDS-PAGE and western blotting. Dot blots of fractions were also carried out for PrP^{res} detection, whereby 5 μl of fraction was spotted onto nitrocellulose membrane, which was dried 30-60 minutes at 37°C and then treated in exactly the same manner as the cell blot assay nitrocellulose membrane. Cell blots for the detection of PrP^{res} in recipient cells, at four passages (P4) post-infection were carried out as described previously [79]. All immunoblotting (western blots and cell blots) for PrP species used the monoclonal antibody ICSM18, (D-Gen, London, UK). All chemiluminescent images were captured by a Fujifilm LAS-3000 (Berthold Australia, Bundoora, VIC, AUS).

In vivo prion transmissions

All animal experiments were carried out in strict accordance with the 'Australian Code of Practice for the Care and Use of Animals for Scientific Purposes (NHMRC)', with approval from the University of Melbourne Animal Ethics Committee (AEC #04154). Tga20 PrP^{C} overexpressing mice [82] were anesthetised using methoxyfluorane and inoculated intracerebrally with 30 μl of 0.01% M1000 brain homogenate diluted in PBS or the appropriate fractions as indicated, or with 30 μl of 'neat' fraction or whole cell PBS lysate. Mice were provided food and water *ad libitum* and housed following routine animal husbandry practices. Mice were examined daily for symptoms of prion disease. Once mice developed persisting features of advanced prion disease, including impaired righting reflexes, hunched posture and hind limb paresis, they were culled by cervical dislocation under anaesthesia and the number of days post-inoculation was recorded. Brains were removed and sagittally hemi-sectioned, with half the brain fixed and stained to allow scoring of vacuolation, astrocytic gliosis and PrP deposition as described previously [40], and the other half made to 10% (w/v) homogenates in PBS, with homogenates stored at -80°C until required. Neuropathological scoring was performed on two separate occasions, blinded as to the inoculum group, to provide a semi-quantitative comparison of lesion profiles between the groups of animals. Stained sections were visualised using a Zeiss Axioskop 50 microscope with images captured using a Zeiss AxioCam HRC camera (Carl Zeiss, North Ryde, NSW, AUS).

Densitometry and statistical analysis

All densitometric analyses used the public domain ImageJ software (National Institutes of Health, USA). For determining relative levels of PrP^{res} in fractions, each fraction PrP^{res} dot blot signal intensity was measured, with the sum of the 10 individual PrP^{res} levels providing the 'total PrP^{res}'; each individual fraction was expressed as a percentage of the total PrP^{res}. For determining relative levels of infectivity contained within MoRK13-infectious fractions, PrP^{res} produced by MoRK13 cells exposed to each 'neat' fraction was measured at passage 4 (P4) post-exposure by cell blot signal intensity, with the sum of the 10 individual PrP^{res} levels providing 'total PrP^{res}'. Once again, each individual fraction was expressed as a percentage of the calculated total PrP^{res}. All statistical analyses were performed in GraphPad Prism 4, with one way ANOVA and Tukey's multiple comparisons or two way ANOVA and Bonferonni post-tests used as indicated, unless stated otherwise.

Additional material

Additional file 1: Figure S1. Disparity in PrP^{res} levels and relative infectivity in the MoRK13-inf cell prion infection model. Representative western blot (A) and quantification (B) of PrP^{res} levels in MoRK13-inf whole cell lysates relative to M1000 brain homogenate (n = 3). Samples were balanced for total protein; 5 μg total protein was resolved in untreated (-) lanes; 50 μg total protein was proteinase K (PK) digested (+) and resolved on 4-12% Bis-tris NuPAGE gels. Very long exposures were required to visualise the PrP^{res} within cell lysates, hence the loss of distinction between M1000 PrP^{res} glycoforms. Representative cell blot (C) and quantification (D) of PrP^{res} produced by recipient MoRK13 cells infected with equivalent total protein amounts of M1000 or MoRK13-inf cell lysate (n = 3). Note infections utilised the corresponding lysate/homogenate shown in (A). NBH = Balb/c normal brain homogenate. Statistical analysis by one way ANOVA; *** $p < 0.001$, ** $p < 0.01$.

Additional file 2: Figure S2. Localisation of PrP, organelle and membrane markers in Nycodenz density gradient fractions of alternative cell lines. Representative immunoblots of subcellular fractions obtained from vector only transfected RK13 cells (vecRK13), GT1-7H and (M1000 infected) GT1-7H-inf, subject to SDS-PAGE and western blotting as described in the methods. CTB dot blot - 3 μl of fraction was dried onto nitrocellulose membrane, and blotted as described in the methods. LR = lipid raft; ER = endoplasmic reticulum; MT = mitochondria; EE = early endosome; CTB = cholera toxin subunit B; Flot1 = Flotillin 1; Bcl-2 = anti-apoptotic MT marker protein; Bip = ER lumen chaperone protein; EEA1 = EE antigen 1.

Additional file 3: Figure S3. Localisation of PrP isoforms, organelle and membrane markers in Nycodenz density gradient fractions of M1000 brain. Representative immunoblots of subcellular fractions obtained from terminal M1000 brain. Brains were homogenised in a comparative way to the detergent-free cell lysis described in the methods, and then subject to Nycodenz gradient fractionation. Briefly, whole brains (snap frozen in liquid N_2 and stored at -80°C) were homogenised in TNE buffer by passing the tissue through an 18 g and then a 20 g needle until an even homogenate was formed, followed by exactly 20 passes through a 22 g needle. The homogenate was centrifuged at 1000 × *g*, 10 minutes at 4° C, the post-nuclear supernatant was retained on ice and the extraction repeated on the pellet. The supernatant was then subject to Nycodenz gradient floatation, fractions were collected and analysed by SDS-PAGE

and western blotting as described. PrP^{res} and CTB dot blots - 3 μl of fraction was dried onto nitrocellulose membrane, and blotted as described in the methods. CTB = cholera toxin subunit B; Flot1 = Flotillin 1; Bcl-2 = anti-apoptotic mitochondrial marker protein; Bip = ER lumen chaperone protein.

Additional file 4: Figure S4. Illustration of the reduction of infectious titre in a 35-day extension of incubation period in Tga20 mice. Regression analysis (modelled on the results of an incubation time interval assay based on quantal end-point dose titration of M1000 brain homogenate in Tga20 mice) was used to plot the relationship between incubation period and titre (V.A. Lawson, unpublished data). The red and blue lines highlight an incubation period of 35 days and the corresponding titres.

Additional file 5: Figure S5. Assessment of neuropathology in the brains of Tga20 mice inoculated with 0.01% (w/v) M1000 brain homogenate, MoRK13 and MoRK13-inf whole cell lysates and selected MoRK13-inf fractions. Representative photomicrographs demonstrating the degree of (A) vacuolation in hematoxylin and eosin-stained (H & E) sections, (B) astrocytic gliosis in glial fibrillary acidic protein (GFAP) stained sections, and (C) PrP plaque deposition in ICSM18 stained sections of various brain regions as indicated. Magnification = 50 × for all sections/stains except H & E stained hippocampus and occipital pole, where magnification = 100 ×.

Additional file 6: Figure S6. PrP^{res} profiles in Tga20 mice inoculated with 0.01% (w/v) M1000 brain homogenate, MoRK13-inf and selected MoRK13-inf subcellular fractions. Representative western blot (A) and quantification (B) of PrP^{res} glycoform ratios in terminal mice brains after intracerebral inoculation as indicated. (A) 10 μl of PK digested (100 μg/ml final concentration PK, 1 hour at 37°C) 10% (w/v in PBS) homogenate was resolved on 12% Bis-tris NuPAGE and probed with ICSM18 primary antibody and (B) quantified using ImageJ. Di = di-glycosylated PrP^{res}, mono = mono-glycosylated PrP^{res}, un = unglycosylated PrP^{res}. Statistical analysis by two-way ANOVA with Bonferroni post-tests; ns = no significant differences; #M1000 in Balb/c mice was significantly different to all other inocula; ^0.01% M1000 in Tga20 mice was significantly different to all other inocula.

Additional file 7: Figure S7. Exogenous cellular co-factors from vecRK13 do not differentially increase the efficiency of M1000 infection *in vitro*. (A) Cell blot showing PrP^{res} levels produced by recipient MoRK13 cells exposed to M1000 brain homogenate diluted to three different final concentrations (as indicated) with either 1:4 lysis buffer (LB):medium or 1:4 vecRK13 fraction:medium mix. (B) Quantification of PrP^{res} produced by MoRK13 cells exposed to M1000 brain homogenate diluted in subcellular fraction relative to the equivalent % M1000 brain homogenate diluted in lysis buffer; for quantification purposes the three different % M1000 spikes into the same vecRK13 fractionated lysate were considered a triplicate of the same experiment, with the error bars representing this intra-experiment variation, and analysis of this variation (one way ANOVA) showing no significant differences. Fractions enriched in lipid raft (LR), endoplasmic reticulum (ER), mitochondrial (MT) and early endosome (EE) marker proteins are as marked.

Additional file 8: Figure S8. Lesion profiles from Tga20 mice intracerebrally inoculated with M1000 brain homogenate diluted in PBS and high density Nyocodenz with or without MoRK13 cell lysate content. Lesion profiles generated by quantification of the degree of vacuolation (H&E), reactive astrocytosis (GFAP) and PrP plaque deposition in each brain region (HI - hippocampus, TH - thalamus, OP - occipital pole, CE - cerebellum, MB - midbrain, PO - pons). n = 3 or 4 for all brain regions except in 0.01% M1000 diluted in PBS HI PrP plaque deposition, where n = 2. Statistical analysis comparing lesion profiles was by two way ANOVA. For astrocytic gliosis and PrP plaque deposition, *$p < 0.05$ comparing M1000 diluted in PBS and Nycodenz fraction #10 in TH region only. No other significant differences seen.

Abbreviations

BCA: Bicinchoninic acid; CDI: Conformation dependent immunoassay; CTB: Cholera toxin B subunit; EE: Early endosome; ER: Endoplasmic reticulum; MT: Mitochondria; PBS: Phosphate buffered saline; PK: Proteinase K; PMCA: Protein misfolding cyclic amplification; POPG: 1-palmitoyl-2-oleoylphosphatidylglycerol; PrP: Prion protein; PrP^{C}: Cellular prion protein; PrP^{res}: Protease resistant prion protein.

Acknowledgements

The authors thank Professor Charles Weissmann for the gift of the Tga20 transgenic mice, the Animal Housing Facility staff in the Faculty of Medicine, Dentistry and Health Sciences, the University of Melbourne for their assistance with animal husbandry, and Ms Laura Leone for technical assistance with preparation of the mouse brains for neuropathological assessment. This work was funded by an Australian Government National Health and Medical Research Council (NHMRC) Program Grant (#400202). VL is supported by NHMRC Training Fellowship (#567123). SJC is supported by NHMRC Practitioner Fellowship (#400183). VAL is supported by The University of Melbourne CR Roper Fellowship. AFH is supported by an Australian Research Council Future Fellowship (FT10100560).

Author details

[1]Department of Pathology, The University of Melbourne, Parkville, VIC 3010, Australia. [2]Mental Health Research Institute and the Melbourne Brain Centre, The University of Melbourne, Parkville, VIC 3010, Australia. [3]Department of Biochemistry and Molecular Biology and the Bio21 Molecular Science and Biotechnology Institute, The University of Melbourne, Parkville, VIC 3010, Australia.

Authors' contributions

VL performed all experiments. VL, CLH and SJC were involved in the acquisition of data. VL, AFH, VAL and SJC contributed to experimental conception and design. VL, CLH, CLM, AFH, VAL and SJC were involved in analysis and interpretation of data and production of this manuscript. All authors read and approved the final manuscript.

Competing interests

The authors declare that they have no competing interests.

Received: 11 November 2011 Accepted: 26 April 2012
Published: 26 April 2012

References

1. Prusiner SB: **Prions.** *Proc Natl Acad Sci USA* 1998, **95**:13363-13383.
2. Pan KM, Baldwin M, Nguyen J, Gasset M, Serban A, Groth D, Mehlhorn I, Huang Z, Fletterick RJ, Cohen FE, *et al*: **Conversion of alpha-helices into beta-sheets features in the formation of the scrapie prion proteins.** *Proc Natl Acad Sci USA* 1993, **90**:10962-10966.
3. Caughey BW, Dong A, Bhat KS, Ernst D, Hayes SF, Caughey WS: **Secondary structure analysis of the scrapie-associated protein PrP 27-30 in water by infrared spectroscopy.** *Biochemistry* 1991, **30**:7672-7680.
4. Prusiner SB, McKinley MP, Bowman KA, Bolton DC, Bendheim PE, Groth DF, Glenner GG: **Scrapie prions aggregate to form amyloid-like birefringent rods.** *Cell* 1983, **35**:349-358.
5. Prusiner SB, Bolton DC, Groth DF, Bowman KA, Cochran SP, McKinley MP: **Further purification and characterization of scrapie prions.** *Biochemistry* 1982, **21**:6942-6950.
6. McKinley MP, Bolton DC, Prusiner SB: **A protease-resistant protein is a structural component of the scrapie prion.** *Cell* 1983, **35**:57-62.
7. Collins SJ, Lewis V, Brazier MW, Hill AF, Lawson VA, Klug GM, Masters CL: **Extended period of asymptomatic prion disease after low dose inoculation: assessment of detection methods and implications for infection control.** *Neurobiol Dis* 2005, **20**:336-346.
8. Balkema-Buschmann A, Eiden M, Hoffmann C, Kaatz M, Ziegler U, Keller M, Groschup MH: **BSE infectivity in the absence of detectable PrPSc accumulation in the tongue and nasal mucosa of terminally diseased cattle.** *J Gen Virol* 2010, doi:10.1099/vir.0.025387-0.
9. Tixador P, Herzog L, Reine F, Jaumain E, Chapuis J, Le Dur A, Laude H, Beringue V: **The physical relationship between infectivity and prion protein aggregates is strain-dependent.** *PLoS Pathog* 2010, **6**: e1000859.
10. Hill AF, Joiner S, Linehan J, Desbruslais M, Lantos PL, Collinge J: **Species-barrier-independent prion replication in apparently resistant species.** *Proc Natl Acad Sci USA* 2000, **97**:10248-10253.

11. Manuelidis L, Fritch W, Xi YG: **Evolution of a strain of CJD that induces BSE-like plaques.** *Science* 1997, **277**:94-98.
12. Lasmezas CI, Deslys JP, Robain O, Jaegly A, Beringue V, Peyrin JM, Fournier JG, Hauw JJ, Rossier J, Dormont D: **Transmission of the BSE agent to mice in the absence of detectable abnormal prion protein.** *Science* 1997, **275**:402-405.
13. Czub M, Braig HR, Diringer H: **Pathogenesis of scrapie: study of the temporal development of clinical symptoms, of infectivity titres and scrapie-associated fibrils in brains of hamsters infected intraperitoneally.** *J Gen Virol* 1986, **67(Pt 9)**:2005-2009.
14. Barron RM, Campbell SL, King D, Bellon A, Chapman KE, Williamson RA, Manson JC: **High titers of transmissible spongiform encephalopathy infectivity associated with extremely low levels of PrPSc in vivo.** *J Biol Chem* 2007, **282**:35878-35886.
15. Castilla J, Saa P, Hetz C, Soto C: **In vitro generation of infectious scrapie prions.** *Cell* 2005, **121**:195-206.
16. Lewis V, Hooper NM: **The role of lipid rafts in prion protein biology.** *Front Biosci* 2011, **16**:151-168.
17. Kaneko K, Zulianello L, Scott M, Cooper CM, Wallace AC, James TL, Cohen FE, Prusiner SB: **Evidence for protein × binding to a discontinuous epitope on the cellular prion protein during scrapie prion propagation.** *Proc Natl Acad Sci USA* 1997, **94**:10069-10074.
18. Telling GC, Scott M, Mastrianni J, Gabizon R, Torchia M, Cohen FE, DeArmond SJ, Prusiner SB: **Prion propagation in mice expressing human and chimeric PrP transgenes implicates the interaction of cellular PrP with another protein.** *Cell* 1995, **83**:79-90.
19. Yehiely F, Bamborough P, Da Costa M, Perry BJ, Thinakaran G, Cohen FE, Carlson GA, Prusiner SB: **Identification of candidate proteins binding to prion protein.** *Neurobiol Dis* 1997, **3**:339-355.
20. Gomes MP, Millen TA, Ferreira PS, Cunha ESNL, Vieira TC, Almeida MS, Silva JL, Cordeiro Y: **Prion protein complexed to N2a cellular RNAs through its N-terminal domain forms aggregates and is toxic to murine neuroblastoma cells.** *J Biol Chem* 2008, **283**:19616-19625.
21. Deleault NR, Lucassen RW, Supattapone S: **RNA molecules stimulate prion protein conversion.** *Nature* 2003, **425**:717-720.
22. Adler V, Zeiler B, Kryukov V, Kascsak R, Rubenstein R, Grossman A: **Small, highly structured RNAs participate in the conversion of human recombinant PrP(Sen) to PrP(Res) in vitro.** *J Mol Biol* 2003, **332**:47-57.
23. Geoghegan JC, Valdes PA, Orem NR, Deleault NR, Williamson RA, Harris BT, Supattapone S: **Selective incorporation of polyanionic molecules into hamster prions.** *J Biol Chem* 2007, **282**:36341-36353.
24. Liu M, Yu S, Yang J, Yin X, Zhao D: **RNA and CuCl2 induced conformational changes of the recombinant ovine prion protein.** *Mol Cell Biochem* 2007, **294**:197-203.
25. Schonberger O, Horonchik L, Gabizon R, Papy-Garcia D, Barritault D, Taraboulos A: **Novel heparan mimetics potently inhibit the scrapie prion protein and its endocytosis.** *Biochem Biophys Res Commun* 2003, **312**:473-479.
26. Ben-Zaken O, Tzaban S, Tal Y, Horonchik L, Esko JD, Vlodavsky I, Taraboulos A: **Cellular heparan sulfate participates in the metabolism of prions.** *J Biol Chem* 2003, **278**:40041-40049.
27. Mayer-Sonnenfeld T, Zeigler M, Halimi M, Dayan Y, Herzog C, Lasmezas CI, Gabizon R: **The metabolism of glycosaminoglycans is impaired in prion diseases.** *Neurobiol Dis* 2005, **20**:738-743.
28. Taylor DR, Whitehouse IJ, Hooper NM: **Glypican-1 mediates both prion protein lipid raft association and disease isoform formation.** *PLoS Pathog* 2009, **5**:e1000666.
29. Lawson VA, Lumicisi B, Welton J, Machalek D, Gouramanis K, Klemm HM, Stewart JD, Masters CL, Hoke DE, Collins SJ, Hill AF: **Glycosaminoglycan sulphation affects the seeded misfolding of a mutant prion protein.** *PLoS One* 2010, **5**:e12351.
30. Silveira JR, Raymond GJ, Hughson AG, Race RE, Sim VL, Hayes SF, Caughey B: **The most infectious prion protein particles.** *Nature* 2005, **437**:257-261.
31. Weber P, Reznicek L, Mitteregger G, Kretzschmar H, Giese A: **Differential effects of prion particle size on infectivity in vivo and in vitro.** *Biochem Biophys Res Commun* 2008, **369**:924-928.
32. Borchelt DR, Scott M, Taraboulos A, Stahl N, Prusiner SB: **Scrapie and cellular prion proteins differ in their kinetics of synthesis and topology in cultured cells.** *J Cell Biol* 1990, **110**:743-752.
33. Shyng SL, Huber MT, Harris DA: **A prion protein cycles between the cell surface and an endocytic compartment in cultured neuroblastoma cells.** *J Biol Chem* 1993, **268**:15922-15928.
34. Gilch S, Winklhofer KF, Groschup MH, Nunziante M, Lucassen R, Spielhaupter C, Muranyi W, Riesner D, Tatzelt J, Schätzl HM: **Intracellular re-routing of prion protein prevents propagation of PrP^{Sc} and delays onset of prion disease.** *EMBO J* 2001, **20**:3957-3966.
35. Macdonald JL, Pike LJ: **A simplified method for the preparation of detergent-free lipid rafts.** *J Lipid Res* 2005, **46**:1061-1067.
36. Naslavsky N, Shmeeda H, Friedlander G, Yanai A, Futerman AH, Barenholz Y, Taraboulos A: **Sphingolipid depletion increases formation of the scrapie prion protein in neuroblastoma cells infected with prions.** *J Biol Chem* 1999, **274**:20763-20771.
37. Liberski PP, Ironside JW: **An outline of the neuropathology of transmissible spongiform encephalopathies (prion diseases).** *Folia Neuropathol* 2004, **42.**
38. Bruce ME, Boyle A, Cousens S, McConnell I, Foster J, Goldmann W, Fraser H: **Strain characterization of natural sheep scrapie and comparison with BSE.** *J Gen Virol* 2002, **83**:695-704.
39. Bruce ME, McConnell I, Fraser H, Dickinson AG: **The disease characteristics of different strains of scrapie in Sinc congenic mouse lines: implications for the nature of the agent and host control of pathogenesis.** *J Gen Virol* 1991, **72(Pt 3)**:595-603.
40. Brazier MW, Lewis V, Ciccotosto GD, Klug GM, Lawson VA, Cappai R, Ironside JW, Masters CL, Hill AF, White AR, Collins S: **Correlative studies support lipid peroxidation is linked to PrP(res) propagation as an early primary pathogenic event in prion disease.** *Brain Res Bull* 2006, **68**:346-354.
41. Lawson VA, Vella LJ, Stewart JD, Sharples RA, Klemm H, Machalek DM, Masters CL, Cappai R, Collins SJ, Hill AF: **Mouse-adapted sporadic human Creutzfeldt-Jakob disease prions propagate in cell culture.** *Int J Biochem Cell Biol* 2008, **40**:2793-2801.
42. Bessen RA, Marsh RF: **Distinct PrP properties suggest the molecular basis of strain variation in transmissible mink encephalopathy.** *J Virol* 1994, **68**:7859-7868.
43. Somerville RA, Chong A, Mulqueen OU, Birkett CR, Wood SC, Hope J: **Biochemical typing of scrapie strains.** *Nature* 1997, **386**:564.
44. Caughey B, Raymond GJ, Bessen RA: **Strain-dependent differences in beta-sheet conformations of abnormal prion protein.** *J Biol Chem* 1998, **273**:32230-32235.
45. Parchi P, Castellani R, Capellari S, Ghetti B, Young K, Chen SG, Farlow M, Dickson DW, Sima AA, Trojanowski JQ, *et al*: **Molecular basis of phenotypic variability in sporadic Creutzfeldt-Jakob disease.** *Ann Neurol* 1996, **39**:767-778.
46. Collinge J, Sidle KC, Meads J, Ironside J, Hill AF: **Molecular analysis of prion strain variation and the aetiology of 'new variant' CJD.** *Nature* 1996, **383**:685-690.
47. Tzaban S, Friedlander G, Schonberger O, Horonchik L, Yedidia Y, Shaked G, Gabizon R, Taraboulos A: **Protease-sensitive scrapie prion protein in aggregates of heterogeneous sizes.** *Biochemistry* 2002, **41**:12868-12875.
48. Thackray AM, Hopkins L, Bujdoso R: **Proteinase K-sensitive disease-associated ovine prion protein revealed by conformation-dependent immunoassay.** *Biochem J* 2007, **401**:475-483.
49. Pastrana MA, Sajnani G, Onisko B, Castilla J, Morales R, Soto C, Requena JR: **Isolation and characterization of a proteinase K-sensitive PrPSc fraction.** *Biochemistry* 2006, **45**:15710-15717.
50. Gambetti P, Dong Z, Yuan J, Xiao X, Zheng M, Alshekhlee A, Castellani R, Cohen M, Barria MA, Gonzalez-Romero D, *et al*: **A novel human disease with abnormal prion protein sensitive to protease.** *Ann Neurol* 2008, **63**:697-708.
51. Colby DW, Wain R, Baskakov IV, Legname G, Palmer CG, Nguyen HO, Lemus A, Cohen FE, DeArmond SJ, Prusiner SB: **Protease-sensitive synthetic prions.** *PLoS Pathog* 2010, **6**:e1000736.
52. Stathopulos PB, Scholz GA, Hwang YM, Rumfeldt JA, Lepock JR, Meiering EM: **Sonication of proteins causes formation of aggregates that resemble amyloid.** *Protein Sci* 2004, **13**:3017-3027.
53. Piening N, Weber P, Giese A, Kretzschmar H: **Breakage of PrP aggregates is essential for efficient autocatalytic propagation of misfolded prion protein.** *Biochem Biophys Res Commun* 2005, **326**:339-343.

54. Deleault NR, Harris BT, Rees JR, Supattapone S: **Formation of native prions from minimal components in vitro.** *Proc Natl Acad Sci USA* 2007, **104**:9741-9746.
55. Lewis V, Hill AF, Klug GM, Boyd A, Masters CL, Collins SJ: **Australian sporadic CJD analysis supports endogenous determinants of molecular-clinical profiles.** *Neurology* 2005, **65**:113-118.
56. Hill AF, Joiner S, Wadsworth JD, Sidle KC, Bell JE, Budka H, Ironside JW, Collinge J: **Molecular classification of sporadic Creutzfeldt-Jakob disease.** *Brain* 2003, **126**:1333-1346.
57. Biacabe AG, Laplanche JL, Ryder S, Baron T: **Distinct molecular phenotypes in bovine prion diseases.** *EMBO reports* 2004, **5**:110-115.
58. Benestad SL, Sarradin P, Thu B, Schonheit J, Tranulis MA, Bratberg B: **Cases of scrapie with unusual features in Norway and designation of a new type, Nor98.** *Vet Rec* 2003, **153**:202-208.
59. Arsac JN, Biacabe AG, Nicollo J, Bencsik A, Baron T: **Biochemical identification of bovine spongiform encephalopathies in cattle.** *Acta neuropathologica* 2007, **114**:509-516.
60. Casalone C, Zanusso G, Acutis P, Ferrari S, Capucci L, Tagliavini F, Monaco S, Caramelli M: **Identification of a second bovine amyloidotic spongiform encephalopathy: molecular similarities with sporadic Creutzfeldt-Jakob disease.** *Proc Natl Acad Sci USA* 2004, **101**:3065-3070.
61. DeMarco ML, Daggett V: **Local environmental effects on the structure of the prion protein.** *C R Biol* 2005, **328**:847-862.
62. Kimberlin RH, Walker CA: **Evidence that the transmission of one source of scrapie agent to hamsters involves separation of agent strains from a mixture.** *J Gen Virol* 1978, **39**:487-496.
63. Puoti G, Giaccone G, Rossi G, Canciani B, Bugiani O, Tagliavini F: **Sporadic Creutzfeldt-Jakob disease: co-occurrence of different types of PrP(Sc) in the same brain.** *Neurology* 1999, **53**:2173-2176.
64. Hirogari Y, Kubo M, Kimura KM, Haritani M, Yokoyama T: **Two different scrapie prions isolated in Japanese sheep flocks.** *Microbiol Immunol* 2003, **47**:871-876.
65. Hecker R, Taraboulos A, Scott M, Pan KM, Yang SL, Torchia M, Jendroska K, DeArmond SJ, Prusiner SB: **Replication of distinct scrapie prion isolates is region specific in brains of transgenic mice and hamsters.** *Genes Dev* 1992, **6**:1213-1228.
66. Bartz JC, Aiken JM, Bessen RA: **Delay in onset of prion disease for the HY strain of transmissible mink encephalopathy as a result of prior peripheral inoculation with the replication-deficient DY strain.** *J Gen Virol* 2004, **85**:265-273.
67. Courageot MP, Daude N, Nonno R, Paquet S, Di Bari MA, Le Dur A, Chapuis J, Hill AF, Agrimi U, Laude H, Vilette D: **A cell line infectible by prion strains from different species.** *J Gen Virol* 2008, **89**:341-347.
68. Gonzalez-Montalban N, Makarava N, Ostapchenko VG, Savtchenk R, Alexeeva I, Rohwer RG, Baskakov IV: **Highly efficient protein misfolding cyclic amplification.** *PLoS Pathog* 2011, **7**:e1001277.
69. Piro JR, Wang F, Walsh DJ, Rees JR, Ma J, Supattapone S: **Seeding specificity and ultrastructural characteristics of infectious recombinant prions.** *Biochemistry* 2011, **50**:7111-7116.
70. Gonzalez-Montalban N, Makarava N, Savtchenko R, Baskakov IV: **Relationship between Conformational Stability and Amplification Efficiency of Prions.** *Biochemistry* 2011, **50**:7933-7940.
71. Safar JG, Scott M, Monaghan J, Deering C, Didorenko S, Vergara J, Ball H, Legname G, Leclerc E, Solforosi L, *et al*: **Measuring prions causing bovine spongiform encephalopathy or chronic wasting disease by immunoassays and transgenic mice.** *Nat Biotechnol* 2002, **20**:1147-1150.
72. Aiken JM, Williamson JL, Marsh RF: **Evidence of mitochondrial involvement in scrapie infection.** *J Virol* 1989, **63**:1686-1694.
73. Akao Y, Otsuki Y, Kataoka S, Ito Y, Tsujimoto Y: **Multiple subcellular localization of bcl-2: detection in nuclear outer membrane, endoplasmic reticulum membrane, and mitochondrial membranes.** *Cancer Res* 1994, **54**:2468-2471.
74. Osman C, Voelker DR, Langer T: **Making heads or tails of phospholipids in mitochondria.** *J Cell Biol* 2011, **192**:7-16.
75. Wang F, Wang X, Yuan CG, Ma J: **Generating a prion with bacterially expressed recombinant prion protein.** *Science* 2010, **327**:1132-1135.
76. Millson GC, Hunter GD, Kimberlin RH: **An experimental examination of the scrapie agent in cell membrane mixtures. II. The association of scrapie activity with membrane fractions.** *Comp Pathol* 1971, **81**:255-265.
77. Alais S, Simoes S, Baas D, Lehmann S, Raposo G, Darlix JL, Leblanc P: **Mouse neuroblastoma cells release prion infectivity associated with exosomal vesicles.** *Biol Cell* 2008, **100**:603-615.
78. Vella LJ, Sharples RA, Lawson VA, Masters CL, Cappai R, Hill AF: **Packaging of prions into exosomes is associated with a novel pathway of PrP processing.** *J Pathol* 2007, **211**:582-590.
79. Lewis V, Hill AF, Haigh CL, Klug GM, Masters CL, Lawson VA, Collins SJ: **Increased Proportions of C1 Truncated Prion Protein Protect Against Cellular M1000 Prion Infection.** *J Neuropathol Exp Neurol* 2009, **68**:1125-1135.
80. Naslavsky N, Stein R, Yanai A, Friedlander G, Taraboulos A: **Characterization of detergent-insoluble complexes containing the cellular prion protein and its scrapie isoform.** *J Biol Chem* 1997, **272**:6324-6331.
81. Lawson VA, Stewart JD, Masters CL: **Enzymatic detergent treatment protocol that reduces protease-resistant prion protein load and infectivity from surgical-steel monofilaments contaminated with a human-derived prion strain.** *J Gen Virol* 2007, **88**:2905-2914.
82. Fischer M, Rulicke T, Raeber A, Sailer A, Moser M, Oesch B, Brandner S, Aguzzi A, Weissmann C: **Prion protein (PrP) with amino-proximal deletions restoring susceptibility of PrP knockout mice to scrapie.** *EMBO J* 1996, **15**:1255-1264.

doi:10.1186/1750-1326-7-18
Cite this article as: Lewis *et al.*: Prion subcellular fractionation reveals infectivity spectrum, with a high titre-low PrP^{res} level disparity. *Molecular Neurodegeneration* 2012 **7**:18.

RESEARCH ARTICLE

Disease Models & Mechanisms 6, 952-963 (2013) doi:10.1242/dmm.010678

Cytosolic caspases mediate mislocalised SOD2 depletion in an *in vitro* model of chronic prion infection

Layla Sinclair[1], Victoria Lewis[1], Steven J. Collins[1,*] and Cathryn L. Haigh[1,*]

SUMMARY

Oxidative stress as a contributor to neuronal death during prion infection is supported by the fact that various oxidative damage markers accumulate in the brain during the course of this disease. The normal cellular substrate of the causative agent, the prion protein, is also linked with protective functions against oxidative stress. Our previous work has found that, in chronic prion infection, an apoptotic subpopulation of cells exhibit oxidative stress and the accumulation of oxidised lipid and protein aggregates with caspase recruitment. Given the likely failure of antioxidant defence mechanisms within apoptotic prion-infected cells, we aimed to investigate the role of the crucial antioxidant pathway components, superoxide dismutases (SOD) 1 and 2, in an *in vitro* model of chronic prion infection. Increased total SOD activity, attributable to SOD1, was found in the overall population coincident with a decrease in SOD2 protein levels. When apoptotic cells were separated from the total population, the induction of SOD activity in the infected apoptotic cells was lost, with activity reduced back to levels seen in mock-infected control cells. In addition, mitochondrial superoxide production was increased and mitochondrial numbers decreased in the infected apoptotic subpopulation. Furthermore, a pan-caspase probe colocalised with SOD2 outside of mitochondria within cytosolic aggregates in infected cells and inhibition of caspase activity was able to restore cellular levels of SOD2 in the whole unseparated infected population to those of mock-infected control cells. Our results suggest that prion propagation exacerbates an apoptotic pathway whereby mitochondrial dysfunction follows mislocalisation of SOD2 to cytosolic caspases, permitting its degradation. Eventually, cellular capacity to maintain oxidative homeostasis is overwhelmed, thus resulting in cell death.

INTRODUCTION

The transmissible spongiform encephalopathies (TSEs; also known as prion diseases) encompass a group of fatal neurodegenerative diseases that differ from other dementias, such as Alzheimer's disease, because of their transmissible nature. The causative agent is composed wholly or largely of misfolded conformers of the prion protein (PrP) (Prusiner, 1982; Weissmann et al., 1994). These misfolded conformers (PrP^{Sc}) form a template for the cellular isoform of PrP (PrP^{C}) to misfold and in this way propagate themselves, resulting in the transmissibility of the TSEs.

Similar to other neurodegenerative diseases, prion disease in mice and humans is associated with markers of oxidative stress in the brain (Wong et al., 2001; Freixes et al., 2006), which increase concurrently with disease-associated PrP burden (Brazier et al., 2006). The oxidative stress has been attributed to an increased production of reactive oxygen species (ROS) due to metal ion dyshomeostasis and resulting redox activity (reviewed in Singh et al., 2010), changed redox signalling through NADPH oxidase (Schneider et al., 2003; Mouillet-Richard et al., 2007) and alterations in nitric oxide synthase (Park et al., 2011). PrP itself has been linked with an antioxidant function; possibly due to an inherent superoxide dismutase (SOD)-like activity (Brown et al., 1999) or by modulation of protective signal transduction pathways (Mouillet-Richard et al., 2007; Rachidi et al., 2003). Aside from a potential PrP SOD-like function, the cell has two further intracellular SODs: SOD1 (CuZnSOD) and SOD2 (MnSOD). SOD2 is localised within the mitochondria, whereas SOD1 has a more ubiquitous localisation (Kawamata and Manfredi, 2010). Reduced SOD activity is reported in prion protein knockout mice and cell cultures (Brown et al., 1997; Brown and Besinger, 1998; Klamt et al., 2001; Sakudo et al., 2005), and a loss of SOD function is one proposed mechanism of prion disease pathogenesis. Alterations in activity and redistribution to mitochondria is reported for SOD1 mutants associated with genetic amyotrophic lateral sclerosis (ALS) in humans and mice (Carrì and Cozzolino, 2011; Goldsteins et al., 2008) indicating that mislocalisation and altered activity of the SOD enzymes can have deleterious consequences for neurons.

Our previous work defined four stages of oxidative response in cultured cells exposed to infectious prions: acute, adaptive, chronic and terminal (Haigh et al., 2011). In these phases the oxidative state of the cell changes from oxidative stress to adaptational response to 'normal' oxidative capacity to loss of normal oxidative metabolism and increased ROS preceding death. The terminal subpopulation of cells accounts for ~6% of the chronically infected population and these cells show markers of apoptosis [phosphatidylserine (PS) externalisation] that correlate with detrimental oxidative stress, suggesting a possible failure of antioxidant compensatory responses. This apoptotic response is associated with the formation of aggregates of highly peroxidised lipid and activated caspases to which PrP is targeted. In this terminal phase of infection, the cells seem to be unable to maintain a defensive response to the increasing ROS burden, with a higher density of these aggregates appearing in apoptotic cells. We therefore sought to further investigate the role of the cellular

[1]Department of Pathology, Melbourne Brain Centre, The University of Melbourne, Victoria, 3010, Australia
*Authors for correspondence (stevenjc@unimelb.edu.au; chaigh@unimelb.edu.au)

Received 7 August 2012; Accepted 31 March 2013

TRANSLATIONAL IMPACT

Clinical issue

Prion diseases are aggressive, transmissible neurodegenerative disorders that often have long incubation periods. The causative agent of prion diseases, which can be transmitted through surgical procedures, blood transfusion or ingestion, is misfolded conformers of the normal cellular prion protein (PrP^{C}). These misfolded conformers (PrP^{Sc}) propagate themselves within their host by forming a template for the misfolding of PrP^{C}. The function of PrP^{C} and the mechanisms of toxicity during infection and prion propagation remain undefined, although both have been linked with cellular redox homeostasis. There is currently no effective treatment for prion diseases.

Results

Previous work by this group in a cellular model of prion infection showed distinct oxidative responses to infection that culminated in toxicity and cell death. Interestingly, in this model, despite an acute and damaging oxidative response to initial infection, prion propagation occurred in the bulk of the cellular population over a long period with only a subpopulation progressing to death, thereby emulating a long, asymptomatic incubation period. In the current study, the authors investigate the cellular response mechanisms that compensate for prion infection in their model and how these mechanisms fail in the cells that progress to death. Although the bulk population of prion-infected cells has an increased level of superoxidase dismutase (SOD; the SOD family helps to protect cells against oxidative damage) activity that is attributable to SOD1, this increased SOD activity is absent in the subpopulation of cells progressing to apoptosis. Interestingly, SOD2 (mitochondrial SOD) protein levels are reduced in the whole population as a result of mislocalisation to the cytosol and to aggregates containing caspases (enzymes involved in the execution of apoptosis) before progression to apoptosis and concomitant mitochondrial loss is observed. Notably, inhibition of caspases restores cellular levels of SOD2 in the infected cells.

Implications and future directions

These findings suggest that a failure of the cellular antioxidant response occurs during prion infection when SOD2 becomes mislocalised and available to cytosolic caspases. Although an increase in SOD1 activity can initially compensate for diminished SOD2 levels in mitochondria, subsequent failure of the SOD1 compensatory response results in mitochondrial damage, loss and ultimately cell death. These new insights into the cellular response mechanisms to prion propagation might help to explain why these diseases can have long asymptomatic incubation periods, and could also provide targets for the development of therapies for these fatal diseases.

antioxidant defence mechanisms in chronic and terminal prion infection *in vitro*. Primarily, we aimed to define the failure(s) in the adaptational response to chronic infection that result in the infected cells progressing to apoptosis. Our results suggest that chronic prion infection is associated with SOD2 mislocalisation, for which increased SOD1 activity compensates. The mislocalised SOD2 is directed to redox-active aggregates in the cytosol where it is degraded by caspases, resulting in a reduction of SOD2 protein levels. Eventually, mitochondria fail to cope with the lack of SOD2, which manifests as increased superoxide production, and ultimately mitochondrial numbers decline such that the cell can no longer maintain viability, resulting in the activation of apoptosis.

RESULTS

SOD1 activity increases in chronically infected cells and SOD2 protein levels decrease

moRK13 cells [rabbit kidney epithelial (RK13) cells expressing full-length murine PrP] readily propagate infectious prions and the line remains viable indefinitely, allowing the study of chronic cellular infection. Our previous work has shown that chronically infected cells do not show a difference in the overall production of intracellular ROS; however, increased ROS production is seen in a subpopulation of infected cells expressing apoptotic markers when separated from the predominant population (Haigh et al., 2011). To investigate the possibility that the greater population was maintaining normal ROS levels by increased antioxidant defences, we looked at intracellular total SOD activity in the infected and mock equal-passage moRK13 populations. All experimental data presented herein are generated using the moRK13 cell model unless otherwise stated. The SOD activity assay showed an increased activity in the infected cells (Fig. 1A); this activity was approximately double that seen in the mock cells. Confirming that the results were not a cell-specific effect, we also assayed differentiated murine neural stem cells (NSCs) for changes in total SOD activity after 5 days of exposure to infectious mouse brain homogenate (Fig. 1B). Increased SOD activity was found in these cultures, which displayed a PrP expression dependence. The NSCs were treated for only 5 days with infectious homogenate owing to the pronounced toxicity to these cells (Fig. 1C-E) (Haigh et al., 2011). In order to determine whether the increase in total SOD activity in the moRK13 cells was predominantly due to SOD1 or SOD2 or both, we used pharmacological intervention to inactivate each of the SODs individually. The doubled SOD activity in the infected cells is maintained when SOD2 is removed by precipitation out of the lysate but is lost when SOD1 is inactivated, indicating that SOD1 is contributing the increased SOD activity (Fig. 1F).

SOD1 and SOD2 protein levels within the mock and infected moRK13 cells were analysed by western blotting. Protein detection indicated that SOD2 levels were significantly decreased by around 50% in the infected cells (Fig. 1G), but SOD1 levels remained unchanged. When compared with the detected protein levels of each SOD, SOD2 activity was not changed relative to its expression levels. SOD1 activity was significantly increased but a concurrent increase in protein expression was not detected, indicating a possible allosteric modulation of SOD1 function (supplementary material Fig. S1).

Overall mitochondrial superoxide production is not changed in chronically infected cells

SOD2 is mitochondrially localised. With the protein levels of SOD2 decreased in the infected moRK13 cells as compared with the mock cells we sought to determine whether the mitochondria of these cells were experiencing greater oxidative stress. To measure the levels of superoxide within the mitochondria, MitoSOX fluorescent sensor probe was incubated in the live moRK13 cells and intensity levels determined. No significant difference between the mock and infected cells in mitochondrial superoxide production could be detected (Fig. 2A). This is consistent with our previously obtained results in these cells, which showed no difference in ROS production or evidence of oxidative stress between the mock and infected cells (Haigh et al., 2011). However, given the significant decrease in SOD2 protein levels, we queried whether other cellular changes might account for the apparent lack of change in mitochondrial superoxide; for example, rather than being due to maintenance of homeostasis, it might be a result of decreased numbers of

stressed mitochondria resulting in a 'normal' fluorescent signal (i.e. a lower quantity of mitochondria with a higher fluorescent signal). We therefore utilised two further mitochondrial probes: MitoTracker and Mito-RFP. The mitochondrial importation of both of these probes might be altered by the mitochondrial state of health (probe metabolism or active transport of probe), so both

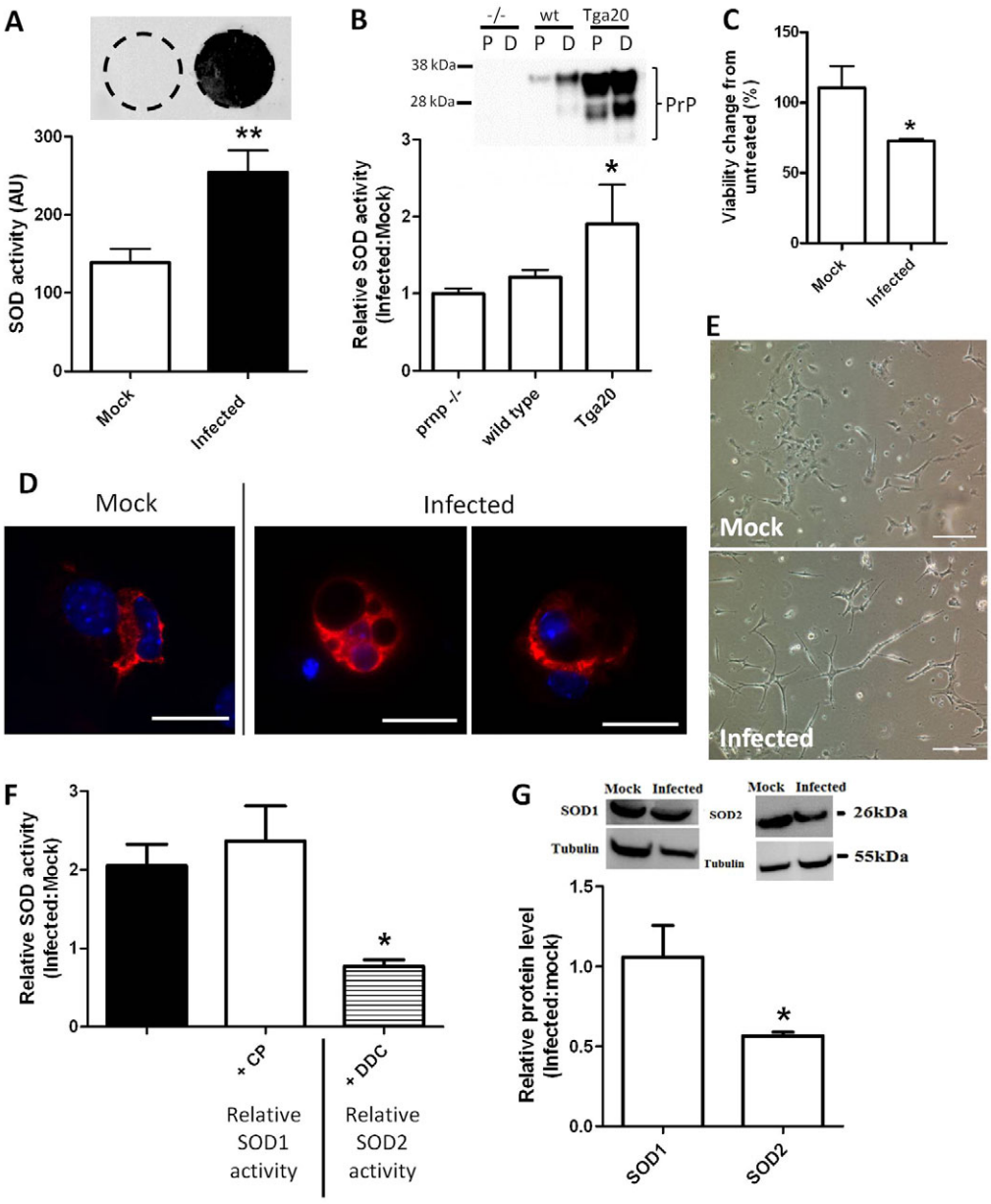

Fig. 1. Chronically infected cells demonstrate increased SOD1 activity and decreased SOD2 protein levels. (A) Chronically infected moRK13 cells show a heavy PrP^{Res} burden as detected by cell blot when compared with their mock-infected counterparts and increased total SOD activity (Student's *t*-test, t=3.46, $^{**}P$=0.0028, n=10). (B) NSCs derived from *prnp* knockout (–/–), wild-type (wt) and PrP overexpressor (Tga20) mice were differentiated into mature cultures and incubated for 5 days with mock or infectious brain homogenate. Tga20 cells exposed to infectious homogenate showed significantly increased SOD activity as compared with mock brain lysate controls (results are shown as ratios of infected to mock cell responses; Kruskal-Wallis K=6.038, $^{*}P$=0.0488, n=4). The magnitude of the SOD response correlated with PrP expression level, shown in the western blot above the SOD activity graph for comparison [duplicate lanes, proliferating cells left (P), differentiated cells right (D)]. (C) Wild-type NSCs were differentiated into mature cultures and exposed to mock or infectious inoculum for 24 hours. Cells exposed to infectious inocula demonstrate significantly reduced metabolic activity, as measured by MTS metabolism, relative to untreated or mock cells (t=2.421, $^{*}P$=0.036, n=3). (D) At 5 days post-addition of prion-infected inoculum, changes in cellular morphology were observed using fluorescence labelling of neuronal cells with antibodies targeting neurofilament-L (red); blue, DAPI. Scale bars: 25 µm. (E) Altered cellular morphology was also visible using brightfield microscopy. Scale bars: 50 µm. (F) SOD1 and SOD2 activities were differentiated using chloroform precipitation (CP) to isolate SOD1 from the lysate and addition of diethyldithiocarbamate (DDC) to inactivate SOD1. The results are shown as ratios of the infected to mock cell activities and show that SOD1 is primarily responsible for the increased activity observed (one-way ANOVA, F=5.796, $^{*}P$=0.012, n=3). (G) SOD protein levels were determined by western blotting and show SOD1 levels to be unchanged in the infected cells (Student's *t*-test, t=0.293, P=0.782, n=6) but SOD2 levels to be decreased (Student's *t*-test, t=18.67, $^{*}P$=0.0003, n=4).

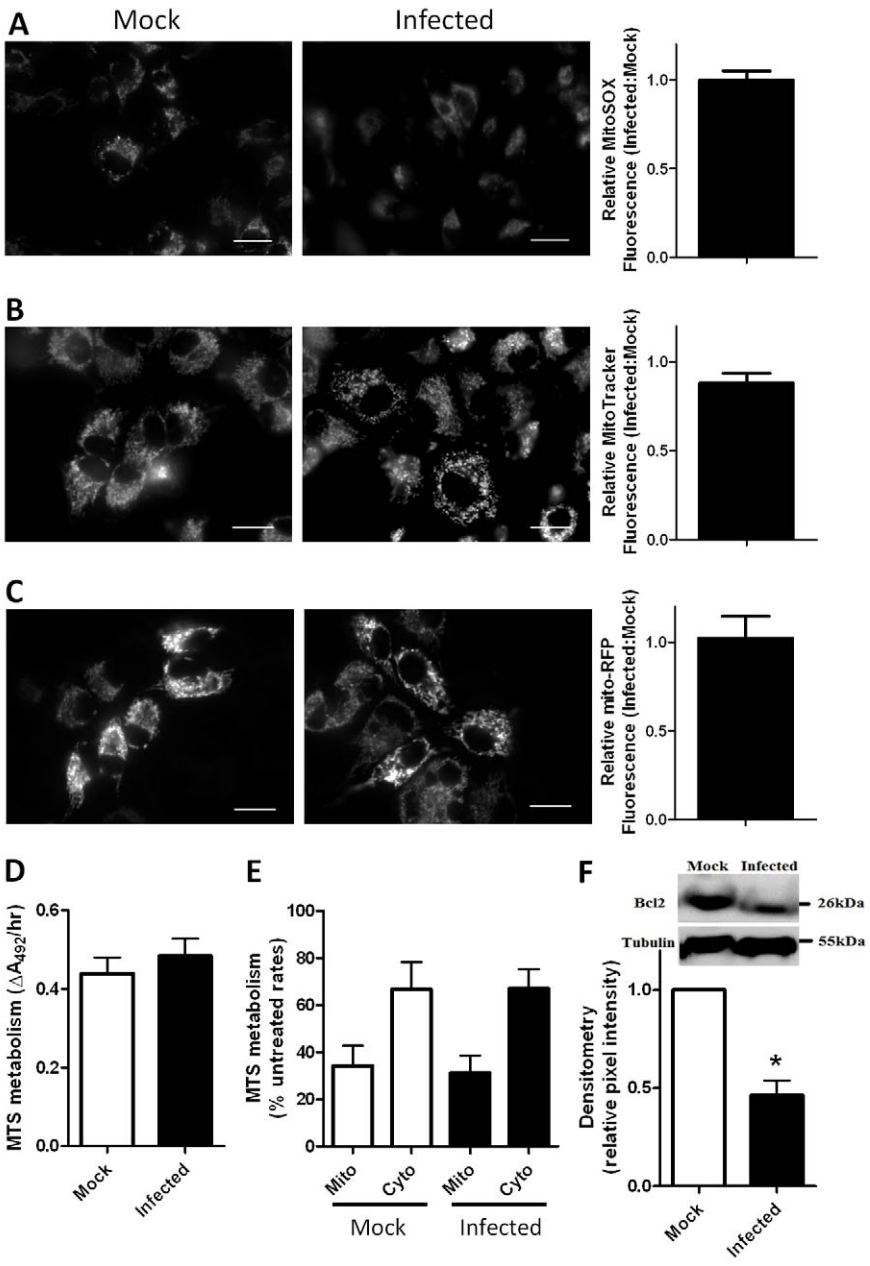

Fig. 2. Chronic prion infection does not influence mitochondrial superoxide production, numbers or metabolism but does reduce Bcl-2 protein levels. (A) MitoSOX, (B) MitoTracker and (C) Mito-RFP fluorescence (images) and intensity quantification, expressed as a ratio of infected to mock average cellular fluorescence (right of images), shows no change in mitochondrial superoxide production or mitochondrial numbers in the prion-infected cells compared with controls [Student's *t*-test; (A) t=0.027, P=0.98, n=4; (B) t=2.123, P=0.101, n=4; (C) t=0.179, P=0.869, n=4]. (D) MTS metabolism was unchanged in the prion-infected population compared with the mock control population (Student's *t*-test, t=0.749, P=0.466, n=4). (E) 1 nM rotenone and 10 μM DPI were used to inhibit mitochondrial and cytosolic metabolism, respectively. The mitochondrial (mito) and cytosolic (cyto) contributions to MTS reduction are not significantly different between the fractions (two-way ANOVA, F=0.0229, P=0.883, n=4). (F) Western blot analysis of Bcl-2 protein levels shows a reduction in prion-infected cells compared with controls (Mann-Whitney, U=0.00, *P=0.05, n=3). Black bars denote infected and white bars mock cells.

were considered together. No difference was found between the mock and infected moRK13 cells for either probe (Fig. 2B,C). As a further indication of mitochondrial stress, cellular metabolism of formazan was considered. Formazan metabolism occurs in both the mitochondria and the cytosol, so two inhibitors (rotenone, which indicates mitochondrial contribution by inhibiting NAD-linked substrate oxidation at the oxygen side of NADH dehydrogenase and DPI, an inhibitor of NADPH oxidase enzymes in the cytosol) were used to differentiate the mitochondrial contribution. Neither the cellular rate of formazan metabolism nor the mitochondrial contribution was altered in the infected moRK13 cells (Fig. 2D,E). Finally, we considered the mitochondrially localised anti-apoptotic protein Bcl-2, which has previously been linked with PrP binding and toxicity (Kurschner and Morgan, 1995; Rambold et al., 2006). This protein was decreased significantly in the infected moRK13 cells (Fig. 2F). Overall, it would seem that mitochondrial numbers, superoxide levels and function are maintained during chronic prion infection but with selective loss of SOD2 and Bcl-2.

SOD activity is increased in non-apoptotic infected cells only

In our previous study ROS levels were only found to be increased in the apoptotic subpopulation of infected moRK13 cells (Haigh et al., 2011). This population was only a small proportion of the entire culture population and changes in such a small number of cells might easily be missed; therefore, it was possible that SOD-activity was increased to compensate for the ROS insult in the dying cells only. Mock and infected moRK13 cells were separated based upon

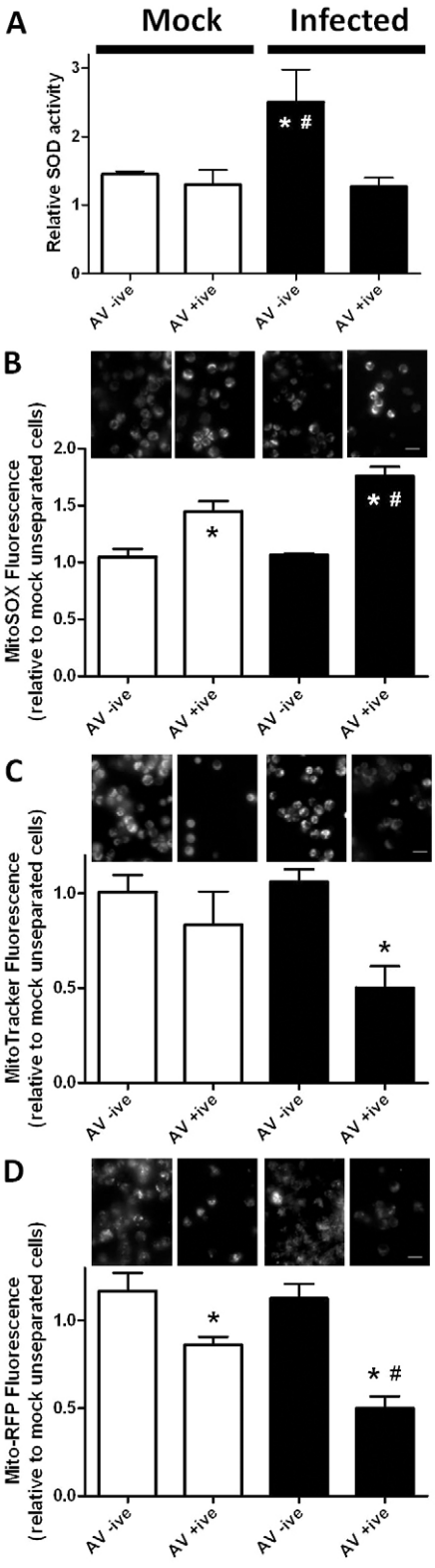

Fig. 3. An apoptotic population of prion-infected cells shows normal SOD activity but increased mitochondrial superoxide and decreased mitochondrial numbers. (A) Magnetic separation using annexin V (AV) to select the population of cells with externalised phosphatidylserine (a marker of apoptosis) showed the apoptotic fraction of prion-infected cells to have normal cellular SOD activities as compared with the mock-infected controls; the increased SOD activity was seen only in the non-apoptotic population (one-way ANOVA, F=4.402, P=0.036, n=4). (B) The apoptotic fraction of both the prion-infected and mock control cells showed increased mitochondrial superoxide over the non-apoptotic fraction and this was significantly greater in the prion-infected cells over the control cells (two-way ANOVA, F=23.56, P<0.001, n=4). (C,D) When mitochondrial numbers were considered with MitoTracker (C) and Mito-RFP (D) probes, signal was significantly reduced in the apoptotic prion-infected population (two-way ANOVA, F=4.493, P=0.025, n=4 and F=15.55, P=0.0002, n=4, respectively). * indicates significantly different to the non-apoptotic fraction, # indicates significantly different to the mock apoptotic fraction. Scale bars: 25 μm.

PS externalisation, a marker for apoptosis, and the SOD activity assays repeated. The opposite response to that hypothesised was observed, with increased SOD activity only observed in the non-apoptotic population of infected cells but not in the cells separated by their externalised PS and therefore committed to apoptotic cell death (Fig. 3A).

In the apoptotic subpopulation of infected cells, mitochondrial superoxide levels are increased and total mitochondria are decreased

Because the increased total SOD activity was not maintained in the apoptotic infected cells, it was plausible that, in the absence of appropriate antioxidant control, the mitochondrial superoxide production could be increased. Therefore, we tested the superoxide production in these cells using the MitoSOX probe. Although mitochondrial superoxide was increased in both populations of apoptotic moRK13 cells (mock and infected), the infected apoptotic cells showed significantly higher levels than the non-infected apoptotic cells (Fig. 3B). Examining these cells with the MitoTracker and Mito-RFP probes indicated that the apoptotic infected cells had lower numbers of mitochondria, as determined by lower fluorescence levels (Fig. 3C,D). Relatively, in the pro-apoptotic infected cells, fewer mitochondria were generating considerably more superoxide.

Mitochondrial SOD2 depletion is caused by SOD2 mislocalisation to the cytosol

Various pathways by which mitochondria can be lost are reported within the literature. Mitochondria can be extruded from cells by being engulfed in vesicles that are similar to autophagic vacuoles, with release into the surrounding milieu (Lyamzaev et al., 2008; Nakajima et al., 2008). To look for evidence of mitochondrial extrusion as the cause of their loss in the pro-apoptotic infected cells, conditioned media from the whole, unseparated moRK13 cell populations was western blotted for SOD2 and Bcl-2 as evidence that mitochondria were located outside of the cell. Although significant signal was seen for SOD2 in both the mock and infected conditioned media, and this was greater for the infected cells, there was no detectable Bcl-2, suggesting that mitochondria were not being extruded but SOD2 was being expelled from the cell by some other means (Fig. 4A).

Another mechanism by which mitochondria are lost in disease is through mitoptosis, considered the mitochondrial equivalent of apoptosis (Mijaljica et al., 2010; Tinari et al., 2007). In mitoptosis,

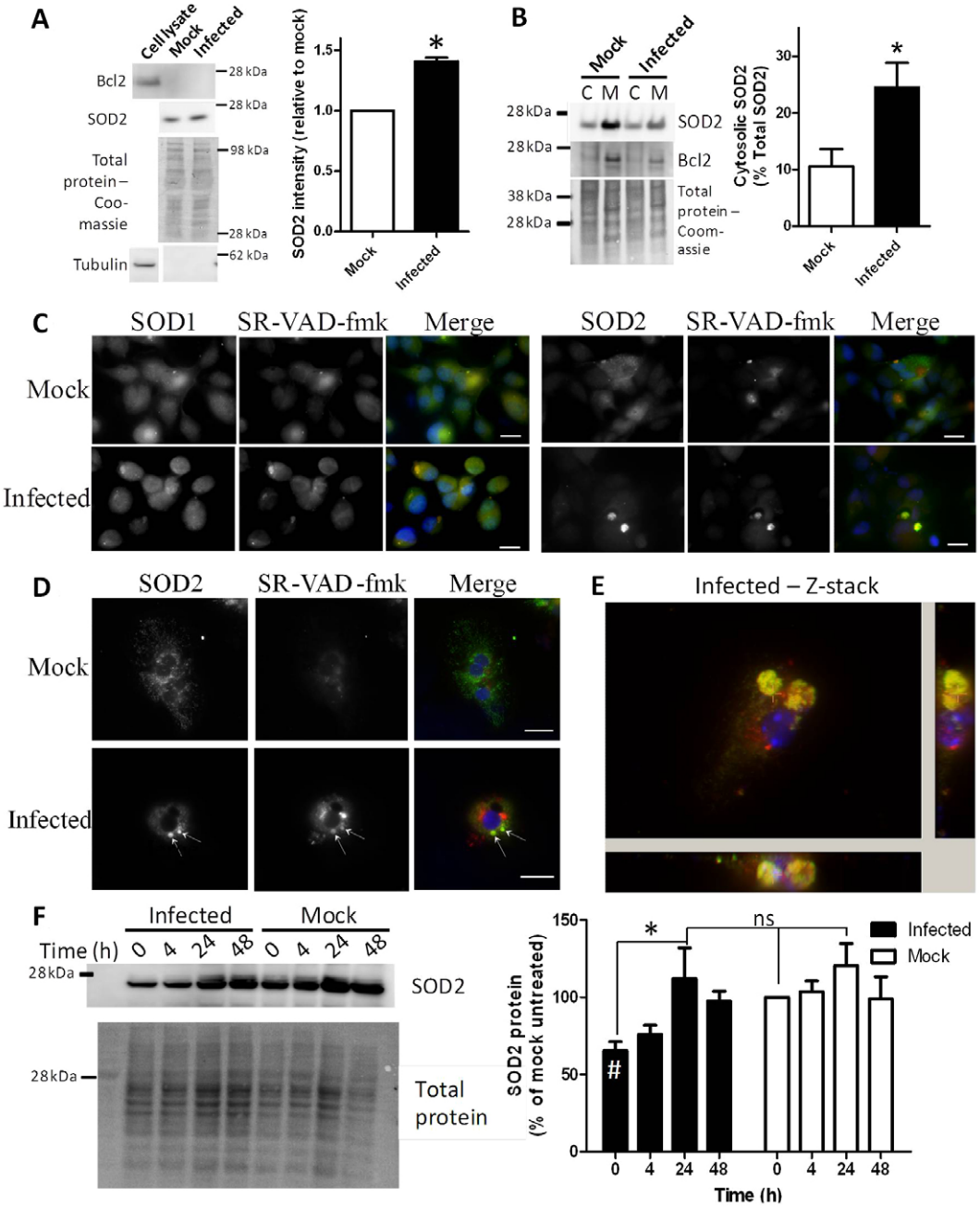

Fig. 4. SOD2 is mislocalised to the cytosol and degraded by caspases. (A) Western blotting of conditioned media shows that SOD2 is expelled from the cell in the absence of mitochondrial extrusion; this is significantly increased for the infected cells (Student's *t*-test, t=13.62, *P=0.0053, n=4). A lack of β-tubulin detection shows that conditioned media SOD2 detection is not due to cell contamination. (B) Separation of mitochondrial and cytosolic fractions demonstrates that SOD2 is found in the cytosol in relatively greater proportions in infected cells than uninfected as a result of depletion from the mitochondrial fraction (Student's *t*-test, t=2.702, *P=0.0427, n=4). Bcl-2 blotting shows that the cytosolic fraction is not highly contaminated with mitochondria. (C) Co-staining mock and infected cells with SR-VAD-FMK (pan caspase inhibitor; red in merge) and SOD1 or SOD2 (green in merge) shows SOD2 to be highly localised to caspase-reactive aggregates within the infected cells with very low detection elsewhere in the cell. Blue, DAPI. Scale bars: 25 µm. (D) Wild-type NSCs were differentiated then incubated with mock or infectious lysate for 5 days. After this time cells were incubated with SR-VAD-FMK then immunostained for SOD2. Cells exposed to infectious innocula display clumps of SOD2 colocalising with the caspase marker. Example mock and infected cell photomicrographs are shown; blue, DAPI; green, SOD2; red, SR-VAD-FMK; arrows indicate caspase-SOD2 clumps. Scale bars: 25 µm. (E) *z*-stack of a wild-type neural stem cell, exposed to infectious innoculum, containing large caspase-reactive aggregates. Colouring as for D; cross-hairs indicates sectioning. (F) Mock and infected cells were incubated with the pan-caspase inhibitor for 4, 24 or 48 hours and SOD2 protein levels determined by western blotting; left plate shows example blots and right plot shows densitometrical analysis normalised to mock time 0 expression levels. Incubation of mock and infected cells with the pan-caspase inhibitor for up to 48 hours significantly increases intracellular SOD2 at 24 hours (two-way ANOVA, F=7.78, *P=0.0038, n=4), restoring detection to that of the mock cells. $^{\#}$ indicates that SOD2 is significantly decreased in the untreated infected cell population (t=6.204, P=0.0084, n=4). Mock and infected cell responses to caspase inhibition are not significantly different to each other (ns, not significant; two-way ANOVA, F=2.194, P=0.164, n=4).

mitochondria can fragment, losing their outer membrane and releasing their contents into the cytosol, thus losing their functionality, or suffer fragmentation of the inner membrane leaving only a dysfunctional outer husk (Mijaljica et al., 2010; Tinari et al., 2007). Mitochondrial preparations of the whole, unseparated moRK13 cell populations were examined to look for evidence of SOD2 in the cytosol of infected cells as a result of leaky mitochondria. Western blotting showed that SOD2 was increased relative to total cellular SOD2 detection in the cytosol of the infected cells compared with their mock counterparts (Fig. 4B). Bcl-2 blotting confirmed minimal cross-contamination of the cytosolic fraction with the mitochondrial fraction (Fig. 4B), suggesting a selective relocalisation of SOD2.

SOD2 is degraded by caspases in the cytosol

Western blotting indicated a mislocalisation of SOD2 into the cytosol of infected cells, so immunofluorescence was used to image the location of both SOD1 and SOD2 in the cytosol of mock and infected moRK13 cells. Acknowledging that a change of location can be part of an apoptotic pathway, co-staining with a rhodamine-labelled pan-caspase inhibitor (SR-VAD-FMK) was also performed. Both SOD1 and SOD2 localise with the previously described (Haigh et al., 2011) caspase-positive aggregates within the infected cells but SOD2 shows a more pronounced colocalisation, with decreased levels of SOD2 elsewhere throughout the cell (Fig. 4C). SOD2 colocalisation with caspase-positive aggregates was also observed in cultures of differentiated wild-type NSCs exposed to infectious inoculum for 5 days (Fig. 4D,E). Immunofluorescent staining shows that cleaved (active forms of) caspases 3 and 9 localise with these aggregates but that pro-caspase 3 and caspase 6 show very little localisation (supplementary material Fig. S2). To test the hypothesis that SOD2 was being degraded by mislocalisation to the cytosolic caspase aggregates, the caspase inhibitor was used to block caspase activity for up to 48 hours. This treatment has previously been shown to increase the viability of these cells (Haigh et al., 2011). At 24 hours of caspase inhibitor treatment, the level of SOD2 protein within the cell was significantly increased (Fig. 4F), with detected levels in the infected cells restored to match those measured in the mock cells. Bcl-2 is also cleaved by caspase 3 to a Bax-like pro-apoptotic form (Cheng et al., 1997). Therefore, we also treated the mock and infected cells with the caspase inhibitor and also a radical scavenger, in case ROS production was also influencing Bcl-2 loss, at the 24-hour time point to see whether Bcl-2 also increased following treatment. No significant differences in Bcl-2 levels were observed in the treated infected cells compared with the untreated (supplementary material Fig. S3).

DISCUSSION

Previously, we have shown unchanged ROS levels in overall populations of infected cells compared with their mock counterparts during chronic prion infection; however, the cells in the acute or apoptotic terminal phase had higher ROS levels than the mock control cells (Haigh et al., 2011). Prompted by the observation that overall ROS levels were 'normal' during chronic infection but the apoptotic subpopulation showed oxidative stress, we investigated the cellular antioxidant defence pathways responsible for compensation to the chronic infection and the adaptational failure(s) associated with progression to apoptosis. Regulation of, or influence on, cellular SOD activity by PrP has been an important ongoing theme in prion infection and therefore SOD1 and SOD2 were the candidate molecules chosen for examination. SOD1 activity was increased and SOD2 protein levels decreased in chronically infected cells. SOD2 downregulation has previously been associated with prion infection *in vivo* (Choi et al., 1998; Lee et al., 1999; Park et al., 2011). Although these studies did not report an increase in SOD1 activity, regulation of SOD1 activity by PrP has also been reported (Brown et al., 1997; Sakudo et al., 2005) and SOD1 knockout has been shown to significantly reduce disease incubation time in murine models of prion disease (Akhtar et al., 2013). In the current system, the increased SOD1 activity might explain how the majority of moRK13 cells are able to remain viable in culture, despite reduced SOD2 levels, while propagating infection over long periods of time. The upregulated SOD response to infectious inoculum was also seen in the NSC cultures. The NSCs show an acute toxic response of increased ROS and decreased viability within 24 hours of exposure to infectious PrP (Fig. 1) (Haigh et al., 2011) and therefore were assayed after 5 days to allow a recovery period after the acute insult. Although it is not possible to discern whether it is *de novo* PrP^{Sc} propagation or PrP^{Sc} exposure that causes toxicity, those cells that survive to 5 days post-exposure have increased their antioxidant defences to compensate.

Given that SOD1 activity was increased in chronically infected cells, the subpopulation of apoptotic cells were separated from non-apoptotic cells to assess the activity in this apoptotic population, which has previously been shown to have increased ROS production (Haigh et al., 2011). The apoptotic population is relatively small compared with the non-apoptotic population, but still constitutes ~6% of infected cells, double the 3% of mock cells (Haigh et al., 2011), and so the responses of these cells can easily be overlooked because detection of these changes are overwhelmed by the remaining population. The total SOD activity in the infected apoptotic cells was not different from the levels seen in the mock cells (either separated or not); therefore, the overall increase in SOD1 activity must be due to the non-apoptotic population. This seems to indicate a relative decline in SOD activity in the infected apoptotic cells, thereby allowing detrimental ROS production within these cells, which contributes to their demise.

Mitochondrial respiration is one of the major cellular processes that produce ROS. Because levels of the mitochondrially localised SOD2 were decreased in chronically infected cells, mitochondrial representation within the cell was considered, but no difference was seen between the overall mock and infected populations. This lack of change is consistent with the investigations of Sisková et al., who found no prion-disease-associated changes in mitochondrial density or expression of mitochondrial proteins (Sisková et al., 2010). The same study did find changes to the mitochondrial inner membrane morphology and reduced cytochrome *c* oxidase activity, and similar observations were also made by others (Choi et al., 1998; Lee et al., 1999).

The pronounced loss of mitochondria in the pro-apoptotic prion-infected cells might indicate a primary contribution to cell death as part of the apoptotic response. Mitoptosis, the pathways of mitochondrial death, manifests in various ways (Lyamzaev et al., 2008; Nakajima et al., 2008). Although we saw evidence of SOD2 in conditioned media, there was no evidence for mitochondrial

extrusion, indicating that the cytosolic SOD2 was apparently independently being expelled from the cell. In the absence of other intracellular molecules, such as tubulin, this was probably a specific event as opposed to non-specific cell lysis or fragmentation. Colocalisation with active caspases in the previously reported oxidised aggregates (Haigh et al., 2011) indicated that SOD2 might be degraded when located outside the mitochondria. No evidence of mitochondria has ever been observed in these aggregates, additionally suggesting that the SOD2 is selectively mislocalised. Mislocalisation might be a result of mis-targeting of SOD2 to the cytosol following synthesis or could be due to loss from failing mitochondria. Furthermore, in the current study and as previously reported (Haigh et al., 2011), in cells in which the caspase reactive aggregates are observed there is no apparent depletion of mitochondria, indicating that the SOD2 relocalisation to the aggregates occurs while the mitochondria are still present and intact. Park et al. found reduced mitochondria in an *in vivo* model of prion disease, which occurred concurrently with a decrease in SOD2 (Park et al., 2011). Electron microscopy comparing infected and uninfected mouse brain tissue found evidence of loss of internal structures of the mitochondria. The authors correlated this with increased endothelial nitric oxide synthase (eNOS) and thus with increased intra-mitochondrial oxidative stress. This is consistent with our findings, but does not explain the relatively selective loss of the SOD2 protein from the mitochondria at a stage before mitochondrial function is apparently significantly compromised and the presence of this organelle depleted.

A decline in SOD2 protein level and function does not seem to be a prion-disease-specific pathway. Similar decreases are reported in other conditions of chronic oxidative stress such as heart failure, in which mRNA levels are increased but protein levels decreased (Holley et al., 2011; Sam et al., 2005), and osteoarthritis, in which SOD2 protein decreases precede erosion of cartilage (Scott et al., 2010). A paradigm attempting to recapitulate a generic model of chronic low-level oxidative stress using hydrogen peroxide exposure did not replicate a reduction in protein levels of SOD2 in the moRK13 cells (supplementary material Fig. S4), but rather an increase in SOD2 protein was instead observed. This might imply that the reduction in SOD2 protein levels in the chronic phase of prion infection requires much longer periods of time to manifest, or is caused by a specific ROS or reactive nitrogen species or localisation of these species, or that other dysfunctional pathways are also contributing to SOD2 protein level reduction. Further investigation is required to resolve these intricacies.

Caspase degradation of SOD2 has been reported as part of the extrinsic apoptotic pathways, with two caspase 3 cleavage sites identified within human SOD2 and recombinant caspase 3 shown to cleave recombinant SOD2 (Pardo et al., 2006). Activation of CD95 (also known as Fas) apoptotic pathways has been shown to redistribute PrP^{C} to mitochondria in lymphoid lineage cells (Mattei et al., 2011). Li et al. found that cytosolic PrP disrupts the proper formation of the cytoskeleton (Li et al., 2011). Together, the altered cytoskeleton and the direct PrP (or the disease-associated PrP^{Sc} isoforms) action on mitochondria might serve to mis-target SOD2 to the cytosol, permitting its incorporation into the caspase reactive aggregates and its loss into the surrounding cellular environment. Caspase 3 has also been shown to cleave Bcl-2 (Cheng et al., 1997) and could represent a common pathway, linking the decreases of SOD2 and Bcl-2. Interestingly, the resulting peptide formed by caspase 3 cleavage of Bcl-2 has Bax-like death effector function (Cheng et al., 1997) and might provide an explanation as to why prion-infected mice that overexpress Bcl-2 succumb to disease earlier than wild-type mice (Steele et al., 2007), apparently contrary to the expected anti-apoptotic function of Bcl-2. Although a pan-caspase inhibitor failed to restore Bcl-2 levels in our cell system (supplementary material Fig. S3), we cannot rule out that prion-infected cells downregulate protein expression of Bcl-2 to protect against deleterious consequences of caspase cleavage producing the pro-apoptotic form.

Evidence of caspase activation has been detected in brain tissue obtained post-mortem from human Creutzfeldt-Jakob disease (CJD) patients (Jesionek-Kupnicka et al., 1997; Puig and Ferrer, 2001) and can be observed in the brains of live mice in the pre-terminal phases of prion disease (Lawson et al., 2010), with caspase-reactive aggregates observed inside neurons using the same active caspase label as in the current study (Drew et al., 2011). Furthermore, in GT1 and N2a cell models of prion infection, aggresomes associated with increased caspases 3 and 8 activity are formed when the proteosome is inhibited (Kristiansen et al., 2005). The targeting of SOD2 to similar aggregates, with a loss of up to 50% of normal activity in the chronically infected cells, before any detectable decline in mitochondrial numbers is indicative of this event forming part of the toxic pathways that ultimately contributes to mitochondrial loss (as a result of superoxide accumulation) and cellular demise.

SOD2 knockout mice develop a neonatal lethal cardiomyopathy and metabolic acidosis within the first week of life; aside from the heart, post-mitotic tissues with high metabolic requirements including the brain are the most severely affected tissues (Lebovitz et al., 1996). Interestingly, if the mice are kept alive beyond the expected 1 week using antioxidant therapy, they develop an oxidative-stress-mediated spongiform encephalopathy (Melov et al., 1998). Complexes I-IV of the electron transport chain were found to have diminished activity and protein levels, which was pronounced for complex II, directly correlating with the dose of antioxidant used to prolong the life of the mouse (Hinerfeld et al., 2004). PrP knockout mice show increased superoxide production from complex I (Paterson et al., 2008). During prion disease, increased superoxide due to the conversion of PrP^{C} to PrP^{Sc}, coupled with a loss of SOD2 and therefore its antioxidant activity, might begin a cycle of heightened oxidative damage within mitochondria, eventuating in their loss. SOD2 mimetics have been proposed as potential therapeutics for prion disease (Fukuuchi et al., 2006). One such mimetic demonstrated an ability to extend the lifespan of prion-infected mice with reduced vacuolation within the hippocampus in early and terminal disease (Brazier et al., 2008), and therefore might indicate that a restoration of SOD2 function is crucial for cellular survival in prion disease. A schematic of potential cell death pathways enhanced by prion infection is shown in Fig. 5.

A further factor in this scenario is the heightened SOD1 activity in the non-apoptotic infected cells. As stated, this could represent a compensatory response that allows prolonged survival of cells in the same manner as using antioxidant therapy in SOD2 knockout mice. However, increased SOD1 activity might itself contribute to a loss of cellular ROS homeostasis with a potential toxic gain of

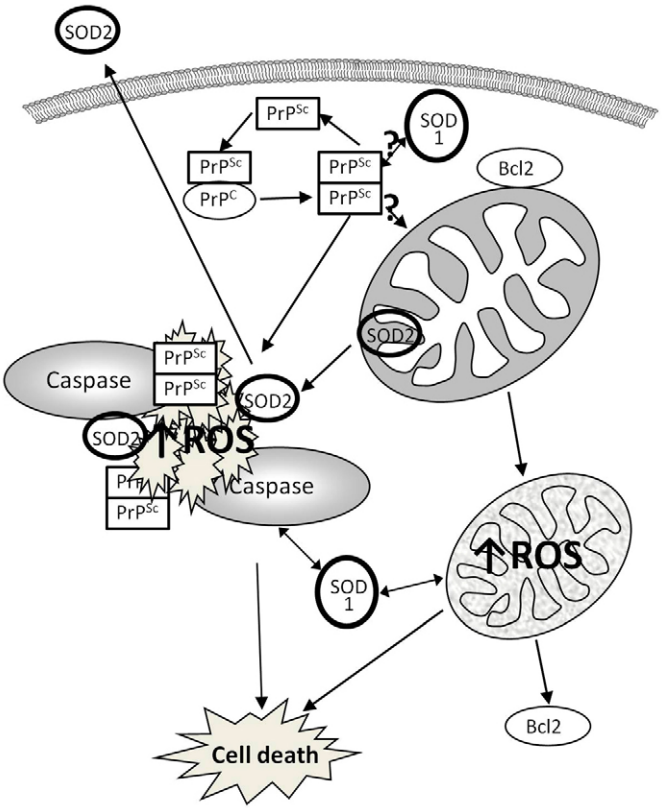

Fig. 5. Putative cell death pathway hijacked by prion infection. Schematic illustration of the potential death pathway enhanced by prion propagation.

function inadvertently contributing to cellular decline. In a murine model of ALS, in which mice express a mutant form of SOD1 displaying a toxic gain of function, the absence of PrP leads to decreased levels of Bcl-2 and vacuolation of motor neurons (Steinacker et al., 2010). These observations might indicate that an overactivity of SOD1 caused by or coinciding with a disturbance of a PrP regulatory function could be responsible for characteristic prion pathology and cellular demise. We did not observe any increased localisation of SOD1 in mitochondria of infected cells (data not shown), but cannot exclude that a gain of function is adversely affecting this organelle.

The mechanisms by which SOD2 is relocated from mitochondria and those responsible for the decline in mitochondrial numbers during terminal prion infection still remain to be revealed. The relocalisation might be a deliberate redirection by cellular targeting mechanisms to compensate for increased cytosolic oxidative flux or might be a side effect of the disease process. Overall, SOD2 mislocalisation seems to be an integral part of SOD2, mitochondria and ultimately cell loss in terminal prion infection.

In summary, elaborating on previous work, we believe that the present results support the contention that chronic prion infection is associated with relatively early loss of SOD2 from mitochondria, while organelle numbers and functionality are generally maintained. SOD2 is mislocalised to the cytosol where it is catabolised at least in part by caspases and also apparently undergoes increased selective extrusion from the cell through unclear mechanisms; overall cellular ROS homeostasis is maintained by compensatory increased SOD1 activity. Eventually, in a subset of chronically prion-infected cells, a deleterious cycle leads to initiation of apoptosis that is associated with prominent loss of mitochondria and heightened superoxide generation in the remaining dysfunctional mitochondria, culminating in the death of these cells.

MATERIALS AND METHODS

Cell culture

Rabbit kidney epithelial (RK13) cells expressing full-length murine PrP (moRK13) were generated as described previously (Haigh et al., 2009). Cells were routinely cultured in Dulbecco's modified Eagle's medium (DMEM; Invitrogen, Melbourne, VIC, Australia) supplemented with 10% (v/v) foetal bovine serum (Lonza, Australia), 50 U/ml penicillin/50 µg/ml streptomycin solution (Sigma, Melbourne, VIC, Australia) and 2.5 µg/ml puromycin (Sigma). Cell cultures were maintained at 37°C with 5% CO_2 in a humidified incubator.

Stem cell culture

Neural stem cells (NSCs) were harvested from c57BL/6×SV129 mice of *prnp*$^{-/-}$ (prion gene knockout) (Büeler et al., 1993), wild type or Tga20 (transgenic prion overexpression of approximately eightfold at the protein level) (Fischer et al., 1996) genetic background, as described in Haigh et al. (Haigh et al., 2011). NSCs were maintained in Neurocult complete proliferation medium (Stem Cell Technologies, Melbourne, VIC, Australia) at 37°C with 5% CO_2 in a humidified incubator. Differentiation was induced by transferral of cells into Neurocult complete differentiation medium (Stem Cell Technologies) and plating on a poly-D-lysine matrix (Sigma-Aldrich).

Cell infections

Cells were infected with the M1000 mouse adapted, human GSS-derived strain of prions or 'mock-infected' with normal brain homogenate (Lawson et al., 2008; Lewis et al., 2009) and permitted to propagate infection until the infected population was uniformly laden with protease-resistant PrP (PrP^{Res}; approximately >passage 50), a marker of propagating prions, as determined by cell blot assay (Fig. 1A). These cells are referred to as 'mock' or 'infected' throughout. *De novo* infections with M1000 were prepared by centrifugal collection of M1000-infected and mock-infected cells (300 ***g*** for 5 minutes), followed by washing in Dulbecco's phosphate buffered saline (dPBS; Invitrogen) and centrifugation as before. Lysate pellets were weighed and a 10% wet pellet weight/volume homogenate made in dPBS. Naïve cells were overlaid with 0.01 or 0.1% (w/v) of the mock or M1000-infected homogenised lysate. Cells were returned to the incubator until they were ready to be passaged. Long-term infection (empirically determined by cell blotting, see below) is defined as greater than passage 50. New infections were routinely established to ensure cell drift did not bias results.

SOD activity assay

Samples were prepared by washing cells in dPBS, followed by lysis with ice-cold 0.1 M Tris/HCl, pH 7.4 containing 0.5% (v/v) Triton X-100, and 0.1 mg/ml of Complete Mini, EDTA free, Protease Inhibitor Tablets (Roche, Melbourne, VIC, Australia). Cell lysates

were briefly centrifuged to separate membrane and nuclear debris and the supernatant collected for use in the assay. Determination of SOD activity was performed as described by the Superoxide Dismutase Activity Colorimetric Assay Kit protocol (Abcam, Sapphire Biosciences, Sydney, NSW, Australia).

Differentiating SOD1 and SOD2 activity

SOD1 and SOD2 activity discrimination utilised chloroform precipitation of SOD1 (SOD2 does not survive this treatment) and inclusion of diethyldithiocarbamate (DDC; Sigma) in the sample buffer to deactivate SOD1. For chloroform precipitation, 96 µl of ice-cold 37.5/62.5 (v/v) chloroform/ethanol solution was added to 60 µl of cell lysate. Samples were centrifuged for 10 minutes at 1000 ***g*** at 4°C and the aqueous phase was removed and stored at 4°C until use. SOD1 inhibition was achieved by the addition of DDC to 1 mM final concentration. Remaining SOD activity in these samples was measured as above.

Preparation of conditioned media

Cells were transferred into serum-free OptiMEM overnight (16 hours) and incubated under normal conditions. Media was collected and centrifuged at 150 ***g*** for 3 minutes to remove any cell carcasses. The media was then transferred to a fresh tube and mixed with four equivalent volumes of ice-cold methanol then stored at –20°C overnight. The precipitated protein was collected by centrifugation at 3273 ***g*** for 1 hour. Protein pellets were solubilised in 1× NuPAGE gel loading buffer (Invitrogen) with 5% (v/v) β-mercaptoethanol.

Mitochondrial preparations

Mitochondria and cysolic preparations were separated by washing cells briefly in dPBS, then collecting the cell suspension in phosphate buffered saline (PBS) by centrifugation at 335 ***g*** for 5 minutes. The cell pellet was resuspended in hypotonic buffer (10 mM NaCl, 1.5 mM $CaCl_2$, 10 mM Tris, pH 7.5) and lysed on ice by needle aspiration 20 times through an 18-gauge needle. One quarter sample volume of 5× sucrose solution (1.65 M sucrose, 30 mM EDTA, 43 mM Tris, pH 7.5) was added to the homogenate and the sample mixed. Nuclei and unbroken cells were separated by centrifugation at 600 ***g*** for 10 minutes. The supernatant was transferred to a fresh tube and centrifuged for 10 minutes at 10,000 ***g***. The supernatant (cytosolic fraction) was collected and the pellet (mitochondria) resuspended in 1× sucrose solution.

Western blotting

Cells were lysed in RIPA buffer [50 mM Tris-HCl pH 7.4, 150 mM NaCl, 0.1% (w/v) SDS, 0.5% (w/v) sodium deoxycholate, 1% (v/v) NP-40] at 37°C for 20 minutes. Samples were electrophoresed using the NuPAGE system (Invitrogen), transferred onto PVDF (Millipore) membranes and blocked as described previously (Haigh et al., 2009) with the exception of PrP blots, which used 2% (w/v) ECL Advance buffer with ECL Advance developer (GE Healthcare, Sydney, NSW, Australia). Protein of interest detection was made using the following dilutions of primary antibody: 1 in 2000 SOD1 (Abcam); 1 in 5000 SOD2 (Abcam); 1 in 1000 Bcl-2 (GE Healthcare); 1 in 5000 EP1802Y against PrP (Abcam) and 1 in 10,000 β-tubulin (Sigma-Aldrich) in PBS with 0.1% (v/v) Tween-20 (PBS-t). Secondary antibodies (Dako, Melbourne, VIC, Australia) were used at 1 in 5000 anti-rabbit (SOD1, SOD2), 1 in 10,000 anti-rabbit (PrP), 1 in 2000 anti-mouse (Bcl-2) and 1 in 10,000 anti-mouse (β-tubulin). ECL-plus (GE Healthcare) was used to visualise bands. Following blotting, total protein levels on gels were assessed by Coomassie brilliant blue staining [0.1% (w/v) Coomassie brilliant blue in 50% (v/v) methanol and 7% (v/v) acetic acid] for 2 minutes at room temperature with agitation. Membranes were rinsed briefly in destain [50% (v/v) methanol and 7% (v/v) acetic acid], then washed in destain for 10 minutes before drying and image capture.

Cell blot assay

The cell blot assay is a variation of that developed by Bosque and Prusiner (Bosque and Prusiner, 2000) as described by Lewis et al. (Lewis et al., 2009). PrP was detected using 1 in 10,000 dilution of ICSM18 monoclonal antibody (murine epitope 142-152; D-Gen, UK) in 1% milk PBS-t. Anti-mouse HRP secondary antibody (GE Healthcare) was used at 1 in 10,000 dilution and blots were visualised as above.

MitoSOX assay

Cells were labelled with 5 µM MitoSOX fluorescent indicator probe (Invitrogen) in normal media for 10 minutes under standard incubator conditions. Media was then replaced with fresh, phenol-red-free OptiMEM (Invitrogen) for the duration of the experiment.

MitoTracker staining

Labelling with MitoTracker Green (Invitrogen) was performed with 1 µl MitoTracker in normal media for 30 minutes under standard culture conditions before transfer into phenol-red-free OptiMEM.

Mito-RFP expression

CellLights BacMAM 2.0 Mito-RFP (Invitrogen) at 50 particles per cell was included in normal culture media for no less than 24 hours before cells were to be used.

MTS metabolism assay

5 µl of one-solution MTS reagent (Promega, Sydney, NSW, Australia) was added per 100 µl of culture media in a 96-well plate and absorbency change measured at 492 nm for 2 hours at 37°C. Rates of change were determined from the linear portion of the curve.

Caspase imaging

A 600 µM stock solution of SR-VAD-FMK (Immunochemistry Technologies, Sapphire Biosciences) was prepared in sterile PBS (pH 7.4; Invitrogen) containing 20% (v/v) high-quality sterile-filtered DMSO (Sigma-Aldrich). Cells were plated 24 hours before the start of the assay. 0.6 µM of the SR-VAD-FMK solution was added to Opti-MEM® reduced serum, phenol-red-free media and cells were incubated for 30 minutes under normal growth conditions. The cells were then washed and incubated in fresh Opti-MEM for the duration of the assay.

Annexin-V MACS

Cells were washed in Mg^{2+}/Ca^{2+}-free dPBS and then suspended using trypsin and gently triturated to remove cell clumps. Magnetic

separation was performed as described in the magnetic-activated cell sorting (MACS) protocol (Miltenyi Biotec, Sydney, NSW, Australia). Briefly, cells were centrifuged for 10 minutes at 300 ***g***, resuspended in 80 µl of binding buffer (Miltenyi Biotec) and 20 µl of MACS Annexin V Microbeads (Miltenyi Biotec) added. After 15 minutes incubation at 4°C, the cells were washed in 10 equivalent volumes of binding buffer, centrifuged for 10 minutes at 300 ***g*** and resuspended in 500 µl of binding buffer. MS columns (Miltenyi Biotec) were equilibrated with 500 µl of binding buffer. Labelled cells were applied to the column in a magnetic field and washed twice with 1 ml of binding buffer. The columns were removed from the magnet and cells eluted in 1 ml of binding buffer. These samples were then centrifuged for 5 minutes at 300 ***g*** and resuspended in OptiMEM media. Both annexin-V-labelled and unlabelled fractions were transferred into fresh media for use in ensuing experiments, which were carried out immediately to avoid loss of viability of the annexin-V-positive fraction.

Indirect immunofluorescence

Cells were grown in chambered coverslips (Nunc, Invitrogen) in normal media. Transfections or dye incubations were carried out before fixing. Cells were fixed in 4% (v/v) paraformaldehyde/PBS for 30 minutes and then permeabilised in PBS with 0.1% (v/v) Triton X-100 for 10 minutes. Coverslips were blocked in PBS with 10% FBS (v/v) and 1% (w/v) BSA for 30 minutes. Primary antibodies were diluted in PBS-FBS as appropriate (SOD1, 1 in 500; SOD2, 1 in 250, Abcam; neurofilament-L, 1 in 50, Stem Cell Technologies) and applied overnight at 4°C. Secondary Alexa-Fluor-488/647-conjugated antibodies (Invitrogen) were diluted 1 in 250 in PBS-FBS and were applied for 1 hour at room temperature. Coverslips were coated with Prolong-Gold mounting media (Invitrogen). Fluorophore-stained coverslips were protected from light at all times.

Densitometry and statistical analyses

Luminescent signals of bands on western blots were captured using a Las-3000 intelligent dark box (FujiFilm, Berthold, VIC, Australia) and the intensity quantified, after the subtraction of background, by ImageJ 1.38x. Statistical analyses were carried out using GraphPad Prism 4 or Minitab15 statistical software. Graphs represent the mean and standard error of the mean (s.e.m.) of four independent experiments unless otherwise stated. Primary statistical tests are stated in the text; for one-way ANOVA analysis Tukey's secondary test was applied and Bonferroni's secondary testing was used for two-way ANOVA. Microscope images were captured using a Nikon Eclipse TE2000-E epi-fluorescence microscope (Nikon-Roper Scientific, Coherent Scientific, Adelaide, SA, Australia). All image parameters were maintained throughout an experiment, across all conditions, and the channels of probes sensitive to photo-oxidation were collected before other channels. For imaging data the '*n*' represents independent experiments, which each included capturing sufficient fields to analyse >30 cells per experiment. Cell intensity analysis was done using Nikon NIS-elements 3.0 software with regions of interest used to gate individual cells.

ACKNOWLEDGEMENTS

The authors acknowledge Prof. Andrew Hill for the kind gift of the pIRES vector containing the PrP open reading frames and Dr Simon Drew for the SR-VAD-FMK reagent, and also thank Dr Victoria Lawson and Dr Marcus Brazier for helpful discussions.

COMPETING INTERESTS

The authors declare that they do not have any competing or financial interests.

AUTHOR CONTRIBUTIONS

C.L.H. and S.J.C. conceived the study and developed the experimental design. L.S., V.L. and C.L.H. carried out the experiments. C.L.H. and L.S. wrote the manuscript. S.J.C. and V.L. critically revised the manuscript.

FUNDING

This work was funded by a National Health and Medical Research Council (NH&MRC) program grant (#628946) and a Brain Foundation research grant. S.J.C. is funded by an NH&MRC Practitioner Fellowship (#APP1005816). L.S. is funded in part by a Carol Willesee Foundation Ph.D. scholarship. V.L. is supported by an NH&MRC Training Fellowship (#567123).

SUPPLEMENTARY MATERIAL

Supplementary material for this article is available at http://dmm.biologists.org/lookup/suppl/doi:10.1242/dmm.010678/-/DC1

REFERENCES

Akhtar, S., Grizenkova, J., Wenborn, A., Hummerich, H., Fernandez de Marco, M., Brandner, S., Collinge, J. and Lloyd, S. E. (2013). Sod1 deficiency reduces incubation time in mouse models of prion disease. *PLoS ONE* **8**, e54454.

Bosque, P. J. and Prusiner, S. B. (2000). Cultured cell sublines highly susceptible to prion infection. *J. Virol.* **74**, 4377-4386.

Brazier, M. W., Lewis, V., Ciccotosto, G. D., Klug, G. M., Lawson, V. A., Cappai, R., Ironside, J. W., Masters, C. L., Hill, A. F., White, A. R. et al. (2006). Correlative studies support lipid peroxidation is linked to PrP(res) propagation as an early primary pathogenic event in prion disease. *Brain Res. Bull.* **68**, 346-354.

Brazier, M. W., Doctrow, S. R., Masters, C. L. and Collins, S. J. (2008). A manganese-superoxide dismutase/catalase mimetic extends survival in a mouse model of human prion disease. *Free Radic. Biol. Med.* **45**, 184-192.

Brown, D. R. and Besinger, A. (1998). Prion protein expression and superoxide dismutase activity. *Biochem. J.* **334**, 423-429.

Brown, D. R., Schulz-Schaeffer, W. J., Schmidt, B. and Kretzschmar, H. A. (1997). Prion protein-deficient cells show altered response to oxidative stress due to decreased SOD-1 activity. *Exp. Neurol.* **146**, 104-112.

Brown, D. R., Wong, B. S., Hafiz, F., Clive, C., Haswell, S. J. and Jones, I. M. (1999). Normal prion protein has an activity like that of superoxide dismutase. *Biochem. J.* **344**, 1-5.

Büeler, H., Aguzzi, A., Sailer, A., Greiner, R. A., Autenried, P., Aguet, M. and Weissmann, C. (1993). Mice devoid of PrP are resistant to scrapie. *Cell* **73**, 1339-1347.

Carrì, M. T. and Cozzolino, M. (2011). SOD1 and mitochondria in ALS: a dangerous liaison. *J. Bioenerg. Biomembr.* **43**, 593-599.

Cheng, E. H., Kirsch, D. G., Clem, R. J., Ravi, R., Kastan, M. B., Bedi, A., Ueno, K. and Hardwick, J. M. (1997). Conversion of Bcl-2 to a Bax-like death effector by caspases. *Science* **278**, 1966-1968.

Choi, S. I., Ju, W. K., Choi, E. K., Kim, J., Lea, H. Z., Carp, R. I., Wisniewski, H. M. and Kim, Y. S. (1998). Mitochondrial dysfunction induced by oxidative stress in the brains of hamsters infected with the 263 K scrapie agent. *Acta Neuropathol.* **96**, 279-286.

Drew, S. C., Haigh, C. L., Klemm, H. M., Masters, C. L., Collins, S. J., Barnham, K. J. and Lawson, V. A. (2011). Optical imaging detects apoptosis in the brain and peripheral organs of prion-infected mice. *J. Neuropathol. Exp. Neurol.* **70**, 143-150.

Fischer, M., Rülicke, T., Raeber, A., Sailer, A., Moser, M., Oesch, B., Brandner, S., Aguzzi, A. and Weissmann, C. (1996). Prion protein (PrP) with amino-proximal deletions restoring susceptibility of PrP knockout mice to scrapie. *EMBO J.* **15**, 1255-1264.

Freixes, M., Rodríguez, A., Dalfó, E. and Ferrer, I. (2006). Oxidation, glycoxidation, lipoxidation, nitration, and responses to oxidative stress in the cerebral cortex in Creutzfeldt-Jakob disease. *Neurobiol. Aging* **27**, 1807-1815.

Fukuuchi, T., Doh-Ura, K., Yoshihara, S. and Ohta, S. (2006). Metal complexes with superoxide dismutase-like activity as candidates for anti-prion drug. *Bioorg. Med. Chem. Lett.* **16**, 5982-5987.

Goldsteins, G., Keksa-Goldsteine, V., Ahtoniemi, T., Jaronen, M., Arens, E., Akerman, K., Chan, P. H. and Koistinaho, J. (2008). Deleterious role of superoxide dismutase in the mitochondrial intermembrane space. *J. Biol. Chem.* **283**, 8446-8452.

Haigh, C. L., Lewis, V. A., Vella, L. J., Masters, C. L., Hill, A. F., Lawson, V. A. and Collins, S. J. (2009). PrPC-related signal transduction is influenced by copper, membrane integrity and the alpha cleavage site. *Cell Res.* **19**, 1062-1078.

Haigh, C. L., McGlade, A. R., Lewis, V., Masters, C. L., Lawson, V. A. and Collins, S. J. (2011). Acute exposure to prion infection induces transient oxidative stress progressing to be cumulatively deleterious with chronic propagation in vitro. *Free Radic. Biol. Med.* **51**, 594-608.

Hinerfeld, D., Traini, M. D., Weinberger, R. P., Cochran, B., Doctrow, S. R., Harry, J. and Melov, S. (2004). Endogenous mitochondrial oxidative stress: neurodegeneration,

proteomic analysis, specific respiratory chain defects, and efficacious antioxidant therapy in superoxide dismutase 2 null mice. *J. Neurochem.* **88**, 657-667.

Holley, A. K., Bakthavatchalu, V., Velez-Roman, J. M. and St Clair, D. K. (2011). Manganese superoxide dismutase: guardian of the powerhouse. *Int. J. Mol. Sci.* **12**, 7114-7162.

Jesionek-Kupnicka, D., Buczyński, J., Kordek, R., Sobów, T., Kłoszewska, I., Papierz, W. and Liberski, P. P. (1997). Programmed cell death (apoptosis) in Alzheimer's disease and Creutzfeldt-Jakob disease. *Folia Neuropathol.* **35**, 233-235.

Kawamata, H. and Manfredi, G. (2010). Import, maturation, and function of SOD1 and its copper chaperone CCS in the mitochondrial intermembrane space. *Antioxid. Redox Signal.* **13**, 1375-1384.

Klamt, F., Dal-Pizzol, F., Conte da Frota, M. L., Jr, Walz, R., Andrades, M. E., da Silva, E. G., Brentani, R. R., Izquierdo, I. and Fonseca Moreira, J. C. (2001). Imbalance of antioxidant defense in mice lacking cellular prion protein. *Free Radic. Biol. Med.* **30**, 1137-1144.

Kristiansen, M., Messenger, M. J., Klöhn, P. C., Brandner, S., Wadsworth, J. D. F., Collinge, J. and Tabrizi, S. J. (2005). Disease-related prion protein forms aggresomes in neuronal cells leading to caspase activation and apoptosis. *J. Biol. Chem.* **280**, 38851-38861.

Kurschner, C. and Morgan, J. I. (1995). The cellular prion protein (PrP) selectively binds to Bcl-2 in the yeast two-hybrid system. *Brain Res. Mol. Brain Res.* **30**, 165-168.

Lawson, V. A., Vella, L. J., Stewart, J. D., Sharples, R. A., Klemm, H., Machalek, D. M., Masters, C. L., Cappai, R., Collins, S. J. and Hill, A. F. (2008). Mouse-adapted sporadic human Creutzfeldt-Jakob disease prions propagate in cell culture. *Int. J. Biochem. Cell Biol.* **40**, 2793-2801.

Lawson, V. A., Haigh, C. L., Roberts, B., Kenche, V. B., Klemm, H. M., Masters, C. L., Collins, S. J., Barnham, K. J. and Drew, S. C. (2010). Near-infrared fluorescence imaging of apoptotic neuronal cell death in a live animal model of prion disease. *ACS Chem. Neurosci.* **1**, 720-727.

Lebovitz, R. M., Zhang, H., Vogel, H., Cartwright, J., Jr, Dionne, L., Lu, N., Huang, S. and Matzuk, M. M. (1996). Neurodegeneration, myocardial injury, and perinatal death in mitochondrial superoxide dismutase-deficient mice. *Proc. Natl. Acad. Sci. USA* **93**, 9782-9787.

Lee, D. W., Sohn, H. O., Lim, H. B., Lee, Y. G., Kim, Y. S., Carp, R. I. and Wisniewski, H. M. (1999). Alteration of free radical metabolism in the brain of mice infected with scrapie agent. *Free Radic. Res.* **30**, 499-507.

Lewis, V., Hill, A. F., Haigh, C. L., Klug, G. M., Masters, C. L., Lawson, V. A. and Collins, S. J. (2009). Increased proportions of C1 truncated prion protein protect against cellular M1000 prion infection. *J. Neuropathol. Exp. Neurol.* **68**, 1125-1135.

Li, X. L., Wang, G. R., Jing, Y. Y., Pan, M. M., Dong, C. F., Zhou, R. M., Wang, Z. Y., Shi, Q., Gao, C. and Dong, X. P. (2011). Cytosolic PrP induces apoptosis of cell by disrupting microtubule assembly. *J. Mol. Neurosci.* **43**, 316-325.

Lyamzaev, K. G., Nepryakhina, O. K., Saprunova, V. B., Bakeeva, L. E., Pletjushkina, O. Y., Chernyak, B. V. and Skulachev, V. P. (2008). Novel mechanism of elimination of malfunctioning mitochondria (mitoptosis): formation of mitoptotic bodies and extrusion of mitochondrial material from the cell. *Biochim. Biophys. Acta* **1777**, 817-825.

Mattei, V., Matarrese, P., Garofalo, T., Tinari, A., Gambardella, L., Ciarlo, L., Manganelli, V., Tasciotti, V., Misasi, R., Malorni, W. et al. (2011). Recruitment of cellular prion protein to mitochondrial raft-like microdomains contributes to apoptosis execution. *Mol. Biol. Cell* **22**, 4842-4853.

Melov, S., Schneider, J. A., Day, B. J., Hinerfeld, D., Coskun, P., Mirra, S. S., Crapo, J. D. and Wallace, D. C. (1998). A novel neurological phenotype in mice lacking mitochondrial manganese superoxide dismutase. *Nat. Genet.* **18**, 159-163.

Mijaljica, D., Prescott, M. and Devenish, R. J. (2010). Mitophagy and mitoptosis in disease processes. *Methods Mol. Biol.* **648**, 93-106.

Mouillet-Richard, S., Schneider, B., Pradines, E., Pietri, M., Ermonval, M., Grassi, J., Richards, J. G., Mutel, V., Launay, J. M. and Kellermann, O. (2007). Cellular prion protein signaling in serotonergic neuronal cells. *Ann. New York Acad. Sci.* **1096**, 106-119.

Nakajima, A., Kurihara, H., Yagita, H., Okumura, K. and Nakano, H. (2008). Mitochondrial extrusion through the cytoplasmic vacuoles during cell death. *J. Biol. Chem.* **283**, 24128-24135.

Pardo, M., Melendez, J. A. and Tirosh, O. (2006). Manganese superoxide dismutase inactivation during Fas (CD95)-mediated apoptosis in Jurkat T cells. *Free Radic. Biol. Med.* **41**, 1795-1806.

Park, J. H., Kim, B. H., Park, S. J., Jin, J. K., Jeon, Y. C., Wen, G. Y., Shin, H. Y., Carp, R. I. and Kim, Y. S. (2011). Association of endothelial nitric oxide synthase and mitochondrial dysfunction in the hippocampus of scrapie-infected mice. *Hippocampus* **21**, 319-333.

Paterson, A. W., Curtis, J. C. and Macleod, N. K. (2008). Complex I specific increase in superoxide formation and respiration rate by PrP-null mouse brain mitochondria. *J. Neurochem.* **105**, 177-191.

Prusiner, S. B. (1982). Novel proteinaceous infectious particles cause scrapie. *Science* **216**, 136-144.

Puig, B. and Ferrer, I. (2001). Cell death signaling in the cerebellum in Creutzfeldt-Jakob disease. *Acta Neuropathol.* **102**, 207-215.

Rachidi, W., Vilette, D., Guiraud, P., Arlotto, M., Riondel, J., Laude, H., Lehmann, S. and Favier, A. (2003). Expression of prion protein increases cellular copper binding and antioxidant enzyme activities but not copper delivery. *J. Biol. Chem.* **278**, 9064-9072.

Rambold, A. S., Miesbauer, M., Rapaport, D., Bartke, T., Baier, M., Winklhofer, K. F. and Tatzelt, J. (2006). Association of Bcl-2 with misfolded prion protein is linked to the toxic potential of cytosolic PrP. *Mol. Biol. Cell* **17**, 3356-3368.

Sakudo, A., Lee, D. C., Nishimura, T., Li, S., Tsuji, S., Nakamura, T., Matsumoto, Y., Saeki, K., Itohara, S., Ikuta, K. et al. (2005). Octapeptide repeat region and N-terminal half of hydrophobic region of prion protein (PrP) mediate PrP-dependent activation of superoxide dismutase. *Biochem. Biophys. Res. Commun.* **326**, 600-606.

Sam, F., Kerstetter, D. L., Pimental, D. R., Mulukutla, S., Tabaee, A., Bristow, M. R., Colucci, W. S. and Sawyer, D. B. (2005). Increased reactive oxygen species production and functional alterations in antioxidant enzymes in human failing myocardium. *J. Card. Fail.* **11**, 473-480.

Schneider, B., Mutel, V., Pietri, M., Ermonval, M., Mouillet-Richard, S. and Kellermann, O. (2003). NADPH oxidase and extracellular regulated kinases 1/2 are targets of prion protein signaling in neuronal and nonneuronal cells. *Proc. Natl. Acad. Sci. USA* **100**, 13326-13331.

Scott, J. L., Gabrielides, C., Davidson, R. K., Swingler, T. E., Clark, I. M., Wallis, G. A., Boot-Handford, R. P., Kirkwood, T. B. L., Taylor, R. W. and Young, D. A. (2010). Superoxide dismutase downregulation in osteoarthritis progression and end-stage disease. *Ann. Rheum. Dis.* **69**, 1502-1510.

Singh, N., Singh, A., Das, D. and Mohan, M. L. (2010). Redox control of prion and disease pathogenesis. *Antioxid. Redox Signal.* **12**, 1271-1294.

Sisková, Z., Mahad, D. J., Pudney, C., Campbell, G., Cadogan, M., Asuni, A., O'Connor, V. and Perry, V. H. (2010). Morphological and functional abnormalities in mitochondria associated with synaptic degeneration in prion disease. *Am. J. Pathol.* **177**, 1411-1421.

Steele, A. D., King, O. D., Jackson, W. S., Hetz, C. A., Borkowski, A. W., Thielen, P., Wollmann, R. and Lindquist, S. (2007). Diminishing apoptosis by deletion of Bax or overexpression of Bcl-2 does not protect against infectious prion toxicity in vivo. *J. Neurosci.* **27**, 13022-13027.

Steinacker, P., Hawlik, A., Lehnert, S., Jahn, O., Meier, S., Görz, E., Braunstein, K. E., Krzovska, M., Schwalenstöcker, B., Jesse, S. et al. (2010). Neuroprotective function of cellular prion protein in a mouse model of amyotrophic lateral sclerosis. *Am. J. Pathol.* **176**, 1409-1420.

Tinari, A., Garofalo, T., Sorice, M., Esposti, M. D. and Malorni, W. (2007). Mitoptosis: different pathways for mitochondrial execution. *Autophagy* **3**, 282-284.

Weissmann, C., Büeler, H., Fischer, M., Sailer, A., Aguzzi, A. and Aguet, M. (1994). PrP-deficient mice are resistant to scrapie. *Ann. New York Acad. Sci.* **724**, 235-240.

Wong, B. S., Brown, D. R., Pan, T., Whiteman, M., Liu, T., Bu, X., Li, R., Gambetti, P., Olesik, J., Rubenstein, R. et al. (2001). Oxidative impairment in scrapie-infected mice is associated with brain metals perturbations and altered antioxidant activities. *J. Neurochem.* **79**, 689-698.

PLOS | ONE

RESEARCH ARTICLE

A Genome Wide Association Study Links Glutamate Receptor Pathway to Sporadic Creutzfeldt-Jakob Disease Risk

Pascual Sanchez-Juan[1], Matthew T. Bishop[2], Gabor G. Kovacs[3], Miguel Calero[4,5], Yurii S. Aulchenko[6,7,8], Anna Ladogana[9], Alison Boyd[10], Victoria Lewis[10], Claudia Ponto[11], Olga Calero[4], Anna Poleggi[9], Ángel Carracedo[12,13], Sven J. van der Lee[6], Thomas Ströbel[3], Fernando Rivadeneira[6,14], Albert Hofman[6], Stéphane Haïk[15], Onofre Combarros[1], José Berciano[1], Andre G. Uitterlinden[6,14], Steven J. Collins[10], Herbert Budka[3], Jean-Philippe Brandel[15], Jean Louis Laplanche[16], Maurizio Pocchiari[9], Inga Zerr[11], Richard S. G. Knight[2], Robert G. Will[2], Cornelia M. van Duijn[6]*

1 Neurology Department, University Hospital "Marqués de Valdecilla". Instituto de Investigación "Marqués de Valdecilla" IDIVAL and Centro de Investigación Biomédica en Red sobre Enfermedades Neurodegenerativas (CIBERNED). Santander, Spain, **2** The National Creutzfeldt-Jakob disease Research and Surveillance Unit, University of Edinburgh, United Kingdom, **3** Institute of Neurology, Medical University Vienna, Vienna, Austria, **4** Chronic Disease Programme and CIBERNED. Carlos III Institute of Health. Madrid. Spain, **5** Alzheimer Disease Research Unit, CIEN Foundation, Carlos III Institute of Health, Alzheimer Center Reina Sofia Foundation, Madrid, Spain, **6** Department of Epidemiology, Erasmus Medical Centre, Rotterdam, the Netherlands, **7** Institute of Cytology and Genetics SB RAS, Novosibirsk, Russia, **8** Novosibirsk State University, Novosibirsk, Russia, **9** Department of Cell Biology and Neurosciences Instituto Superiore di Sanità, Roma, Italy, **10** Department of Pathology, The University of Melbourne, Parkville, 3010, Australia, **11** Department of Neurology, Clinical Dementia Centre, University Medical Center and German Center for Neurodegenerative Diseases (DZNE)—site Göttingen, Göttingen, Germany, **12** Fundación Pública Galega de Medicina Xenómica, CIBERER, Grupo de Medicina Xenómica-Universidad de Santiago de Compostela, Santiago de Compostela, Spain, **13** Center of Excellence in Genomic Medicine Research (CEGMR), King Abdulaziz University, Jeddah, KSA, **14** Department of Internal Medicine, Erasmus Medical Center, Rotterdam, the Netherlands, **15** Sorbonne Universités, UPMC Univ Paris 06 UMR S 1127, and Inserm, U 1127, and CNRS UMR 7225, and ICM, F-75013, Paris, France; AP-HP, Hôpital de la Pitié Salpêtrière, Cellule Nationale de Référence des maladies de Creutzfeldt-Jakob, F-75013, Paris, France, **16** Service de biochimie et biologie moleculaire, Laboratoire associé au CNR "ATNC", Hôpital Lariboisiére, AP-HP, Paris, France

* c.vanduijn@erasmusmc.nl

OPEN ACCESS

Citation: Sanchez-Juan P, Bishop MT, Kovacs GG, Calero M, Aulchenko YS, Ladogana A, et al. (2015) A Genome Wide Association Study Links Glutamate Receptor Pathway to Sporadic Creutzfeldt-Jakob Disease Risk. PLoS ONE 10(4): e0123654. doi:10.1371/journal.pone.0123654

Academic Editor: Gianluigi Zanusso, University of Verona, ITALY

Received: January 12, 2015

Accepted: February 23, 2015

Published: April 28, 2015

Data Availability Statement: All relevant data are within the paper and its Supporting Information files.

Funding: This study was supported by: UK: the National CJD Research and Surveillance UK Unit is funded by the Department of Health and the Scottish Government Health Department. The National CJD Research and Surveillance Unit is funded by the Policy Research Programme in the Department of Health. Germany: This work was supported by a grant from the European Commission (Protecting the food chain from prions: shaping European priorities through basic and applied research (PRIORITY, N°

Abstract

We performed a genome-wide association (GWA) study in 434 sporadic Creutzfeldt-Jakob disease (sCJD) patients and 1939 controls from the United Kingdom, Germany and The Netherlands. The findings were replicated in an independent sample of 1109 sCJD and 2264 controls provided by a multinational consortium. From the initial GWA analysis we selected 23 SNPs for further genotyping in 1109 sCJD cases from seven different countries. Five SNPs were significantly associated with sCJD after correction for multiple testing. Subsequently these five SNPs were genotyped in 2264 controls. The pooled analysis, including 1543 sCJD cases and 4203 controls, yielded two genome wide significant results: rs6107516 (p-value=$7.62x10^{-9}$) a variant tagging the prion protein gene (*PRNP*); and rs6951643 (p-value=$1.66x10^{-8}$) tagging the Glutamate Receptor Metabotropic 8 gene (*GRM8)*. Next we analysed the data stratifying by country of origin combining samples from

222887) Project number: FP7-KBBE-2007-2A). The study was performed within the recently established Clinical Dementia Center at the University Medical Center Göttingen and was partly supported by grants from the EU Joint Programme – Neurodegenerative Disease Research (JPND - DEMTEST "Biomarker based diagnosis of rapid progressive dementias-optimization of diagnostic protocols", 01ED1201A). This study was funded by the Robert Koch Institute through funds from the Federal Ministry of Health (grant no. 1369-341). Italy: The Italian Registry of CJD and related disorders is funded by the Ministry of Health, National Centre for Disease Prevention and Control, Central Actions.This work was partly supported by grant from the EU Joint Programme – Neurodegenerative Disease Research (JPND - DEMTEST "Biomarker based diagnosis of rapid progressive dementias-optimization of diagnostic protocols", 01ED1201A). The Netherlands: the generation and management of genome-wide association study (GWAS) genotype data for the Rotterdam Study is supported by the Netherlands Organization of Scientific Research NWO Investments (nr. 175.010.2005.011, 911- 03-012). This study is funded by the Research Institute for Diseases in the Elderly (014-93-015; RIDE2), the Netherlands Genomics Initiative (NGI)/Netherlands Organisation for Scientific Research (NWO) project nr. 050-060-810. The Rotterdam Study is funded by Erasmus Medical Center and Erasmus University, Rotterdam, Netherlands Organization for the Health Research and Development (ZonMw), the Research Institute for Diseases in the Elderly (RIDE), the Ministry of Education, Culture and Science, the Ministry for Health, Welfare and Sports, the European Commission (DG XII), and the Municipality of Rotterdam. YSA is supported by Russian Science Foundation (RSCF) grant 14-14-00313. Spain. PSJ was supported by a grant from FIS (PI12/02288) and JPND project DEMTEST (PI11/03028). AC is supported by PI13/01136 Acción Estratégica de Salud del Instituto de Salud Carlos III e INNOPHARMA. Australia: The Australian National Creutzfeldt-Jakob Disease Registry (ANCJDR) is funded by the Commonwealth Department of Health. SJC is supported by a NHMRC Practitioner Fellowship (#APP1005816). The funders had no role in study design, data collection and analysis, decision to publish, or preparation of the manuscript.

Competing Interests: The authors have declared that no competing interests exist.

the pooled analysis with genotypes from the *1000 Genomes Project* and imputed genotypes from the *Rotterdam Study* (Total n=12967). The meta-analysis of the results showed that rs6107516 (p-value=$3.00x10^{-8}$) and rs6951643 (p-value=$3.91x10^{-5}$) remained as the two most significantly associated SNPs. Rs6951643 is located in an intronic region of *GRM8*, a gene that was additionally tagged by a cluster of 12 SNPs within our top100 ranked results. *GRM8* encodes for mGluR8, a protein which belongs to the metabotropic glutamate receptor family, recently shown to be involved in the transduction of cellular signals triggered by the prion protein. Pathway enrichment analyses performed with both Ingenuity Pathway Analysis and ALIGATOR postulates glutamate receptor signalling as one of the main pathways associated with sCJD. In summary, we have detected GRM8 as a novel, non-PRNP, genome-wide significant marker associated with heightened disease risk, providing additional evidence supporting a role of glutamate receptors in sCJD pathogenesis.

Introduction

Sporadic Creutzfeldt-Jakob disease (sCJD), although rare, with a yearly incidence of one to two cases per million, is the most common form of human prion disease. This group of disorders is characterized by spongiform changes in the brain, as well as accumulation of misfolded, often protease-resistant, conformers (PrP^{Sc}) of the normal prion protein (PrP^{C}). The PrP^{C} gene (*PRNP*) plays a central role in prion disease susceptibility. Expression of PrP^{C} is indispensable for disease transmission [1] and the polymorphism coding for methionine (M) or valine (V) at codon 129 (*PRNP* M129V) has been linked to disease risk [2]. Homozygosity at *PRNP* M129V has been consistently associated to sCJD, being one of the strongest common genetic risk factors reported for neurodegenerative diseases. The remarkable disease-determining effect of this *PRNP* polymorphism is observed in variant CJD, a subtype acquired from dietary exposure to bovine spongiform encephalopathy [3], where all definite and probable clinical cases studied to date have been *PRNP*129MM [4].

Similar to other diseases, several genetic association studies with candidate genes have been performed on sCJD susceptibility [5]. Only one previous genome wide association study (GWAS) of sCJD risk has been published to date, showing that the *PRNP* locus was strongly associated with disease risk, specifically with rs1799990 (*PRNP* M129V) [6].

To further scrutinize genomic variations related to sCJD risk we have performed a three-stage GWAS encompassing a total of 1,543 sCJD cases and 4,203 controls, as well as a meta-analysis encompassing data from the *1000 Genomes Project* and imputations from the *Rotterdam Study*.

Results

Demographic and clinical features of the sCJD case populations are shown in S1 Table. The Q-Q plots for autosomal and X chromosome SNPs are given in S1 Fig; during discovery (stage one) the genomic inflation factor λ was 1.053 for autosomal and 1.057 for X chromosome SNPs.

S2 Table shows the top 100 SNPs associated with sCJD at discovery stage, sorted by allelic differences p-value. A total of 23 SNPs were taken forward to replication. In stage two, we successfully genotyped 22 of the 23 SNPs with the Sequenom iPLEx GOLD platform in an independent population of 1,109 samples of sCJD. Table 1 shows that five SNPs remained significant

Table 1. SNPs genotyped in stage two.

			Stage one: Discovery			Stage two: Replication in independent sCJD Cases	
SNP	**CJD risk allele in Discovery population**	**GENE tagged**	**Controls Frequencies of sCJD risk allele (n = 1939)**	**Cases Frequencies of sCJD risk allele (n = 434)**	**P1df***	**Cases Frequencies of sCJD risk allele (n = 1109)**	**P-value****
rs10061929	A	FLJ43080	0.159	0.224	4.58E-05	0.200	5.89E-05
rs10915708	T	NA	0.140	0.207	1.35E-06	0.158	0.0626
rs11075924	C	NA	0.498	0.565	5.52E-05	0.500	0.8808
rs11245373	T	NA	0.037	0.069	2.48E-05	0.049	0.0238
rs12102156	T	NA	0.863	0.912	2.00E-05	0.849	0.1457
rs12188818	C	NA	0.796	0.859	6.44E-05	0.809	0.2544
rs12419710	A	NA	0.210	0.279	2.52E-05	0.219	0.3746
rs17060736	G	NA	0.112	0.160	7.13E-05	0.121	0.3134
rs17115017	A	GRIA1	0.050	0.082	2.23E-04	0.072	5.00E-04
rs17833759	C	GRIN2B	0.085	0.140	7.74E-07	0.095	0.1955
rs196940	C	ERN1	0.758	0.818	6.19E-05	0.758	0.9631
rs2240344	G	NA	0.432	0.600	4.47E-19	0.443	0.4194
rs2627829	A	INPP4B	0.939	0.970	1.83E-04	0.931	0.2188
rs392184	T	MACROD2	0.052	0.096	2.00E-06	0.07	0.003
rs565559	T	NA	0.553	0.618	2.02E-04	0.579	0.057
rs6027482	C	LOC100131710	0.187	0.247	6.69E-05	0.181	0.5476
rs6107516	C	PRNP	0.752	0.827	6.92E-06	0.804	3.27E-06
rs6463269	G	NA	0.084	0.134	3.53E-06	GENOTYPE FAILED	-
rs6496239	T	NA	0.805	0.862	4.96E-05	0.821	0.1195
rs6820644	T	NA	0.357	0.433	3.40E-06	0.647	0.7566
rs6951643	A	GRM8	0.507	0.592	8.09E-06	0.573	6.79E-07
rs9521699	A	COL4A2	0.137	0.194	3.84E-05	0.173	2.00E-04

(*Continued*)

Table 1. (*Continued*)

			Stage one: Discovery			Stage two: Replication in independent sCJD Cases	
SNP	**CJD risk allele in Discovery population**	**GENE tagged**	**Controls Frequencies of sCJD risk allele (n = 1939)**	**Cases Frequencies of sCJD risk allele (n = 434)**	**P1df***	**Cases Frequencies of sCJD risk allele (n = 1109)**	**P-value****
rs9830696	T	NA	0.120	0.173	1.02E-05	0.104	0.0711

sCJD: Sporadic Creutzfeldt-Jakob Disease

In bold SNPs significant after Bonferroni correction (Replication P-value <0.0023)

* P-value for allellic diferences adjusted by Country of origin by PCA

**Chi Squared p-value from comparison between Allele frequencies of independent sCJD cases and stage one controls

NA: SNP in intergenic region.

doi:10.1371/journal.pone.0123654.t001

after Bonferroni correction. In stage three we genotyped those five SNPs in a population of 2,264 independent controls with Sequenom iPLEx GOLD. S2 Fig depicts neatly separated genotype clusters of the five SNPs studied in stage three. Only two SNPs were successfully replicated at stage three and reached genome wide significant p-values after meta-analysis of discovery and replication results: rs6107516 (p-value = $7.62x10^{-9}$) tagging *PRNP* and in linkage disequilibrium (LD) with *PRNP* M129V (rs1799990), and rs6951643 (p-value = $1.66x10^{-8}$) an intronic SNP within *GRM8* (Glutamate Receptor Metabotropic 8) in chromosome 7. Table 2 shows differences in allelic frequencies in the discovery, replication and pooled population sets including 1,543 sCJD cases and 4,203 controls. The A allele of rs6951643 was associated with a 1.27 fold increased risk of sCJD (95%CI = 1.17–1.38), and this effect was consistently observed across all tested populations (Table 3).

Rs6107516 (p-value = $3.00x10^{-8}$) and rs6951643 (p-value = $3.91x10^{-5}$) remained as the two most statistically significant associations in a meta-analysis of the discovery data adjusted for PCAs and analysis of replication samples stratified by country. This meta-analysis included discovery and replication samples plus data from the *1000 Genomes Project* and imputed genotypes from the *Rotterdam Study* (Total n = 12967), (Table 4). Within the top 100 SNPs, there

Table 2. SNPs studied in stage three.

			Discovery Population				Replication Population			Pooled Samples		
ID	**CJD risk allele in Discovery population**	**GENE tagged**	**Case, Control Frequencies of CJD risk allele (n = 434, n = 1939)**	**P-value**	**P-value***	**OR (95%CI)**	**Case, Control Frequencies of CJD risk allele (n = 1109, n = 2264)**	**P-value**	**OR (95%CI)**	**Case.Control Frequencies of CJD risk allele (n = 1543, n = 4203)**	**P-value**	**OR (95%CI)**
rs10061929	A	FLJ43080	0.224, 0.159	4.30E-06	4.58E-05	1.53 (1.27–1.83)	0.200, 0.196	0.6882	1.03 (0.90–1.17)	0.207, 0.179	0.0007	1.20 (1.08–1.33)
rs17115017	A	GRIA1	0.082, 0.050	3.00E-04	2.23E-04	1.69 (1.27–2.24)	0.072, 0.077	0.4434	1.08 (0.89–1.31)	0.075, 0.065	0.0597	1.17 (0.99–1.37)
rs6107516	C	PRNP	0.827, 0.752	2.07E-06	6.92E-06	1.58 (1.31–1.91)	0.804, 0.766	**5.00E-04**	1.25 (1.10–1.42)	0.811, 0.759	**7.62E-09**	1.35 (1.22–1.50)
rs6951643	A	GRM8	0.592, 0.507	6.73E-06	8.09E-06	1.41 (1.21–1.64)	0.573, 0.529	**7.00E-04**	1.19 (1.08–1.32)	0.578, 0.519	**1.66E-08**	1.27 (1.17–1.38)
rs9521699	A	COL4A2	0.194, 0.137	2.41E-05	3.84E-05	1.51 (1.25–1.83)	0.173, 0.173	0.9723	1.00 (0.88–1.15)	0.179, 0.157	0.0045	1.17 (1.05–1.31)

* Adjusted by Country of origin by PCA.

doi:10.1371/journal.pone.0123654.t002

Table 3. - rs6951643 pooled genotypes by country.

Population	GG n (%)	AG n (%)	AA n (%)	A allele n (%)	G allele n (%)
CONTOLS					
UK	364 (24.6)	741 (50.0)	377 (25.4)	1495 (50.4)	1469 (49.6)
NL	118 (22.4)	265 (50.3)	144 (27.3)	553 (52.5)	501 (47.5)
Spain	488 (22.3)	1097 (50.0)	608 (27.7)	2313 (52.7)	2073 (47.3)
CASES					
UK	28 (10.5)	155 (58.3)	83 (31.2)	321 (60.3)	211 (39.7)
NL	23 (18.1)	62 (48.8)	42 (33.1)	146 (57.5)	108 (42.5)
Germany	66 (16.7)	217 (54.8)	113 (28.5)	443 (55.9)	349 (44.1)
Italy	43 (15.0)	140 (48.8)	104 (36.2)	348 (60.6)	226 (39.4)
Australia	10 (20.8)	26 (54.2)	12 (25.0)	50 (52.1)	46 (47.9)
France	23 (15.3)	77 (51.3)	50 (33.3)	177 (59.0)	123 (41.0)
Spain	35 (17.2)	110 (54.2)	58 (28.6)	226 (55.7)	180 (44.3)
Austria	11 (20.0)	27 (49.1)	17 (30.9)	61 (55.5)	49 (44.5)
ALL CONTOLS	970 (23.1)	2103 (50.0)	1129 (26.9)	4361 (51.9)	4043 (48.1)
ALL CASES	239 (15.6)	814 (53.1)	479 (31.3)	1772 (57.8)	1292 (42.2)
HapMap Frequencies (CEU)	27 (23.9)	59 (52.2)	27 (23.9)	113 (0.50)	113 (0.50)

doi:10.1371/journal.pone.0123654.t003

were 12 tagging GRM8 (S2 Table). Pathway analysis using IPA showed that glutamate receptor signalling was the most over-represented canonical pathway within our top results (p-value = $8.01x10^{-5}$) (Fig 1). Analysis with ALIGATOR software showed (S3 Table) that the GO category glutamate receptor activity was the 4th most represented amongst our top results. Three genes from the GO category "glutamate receptor pathway" (S2 Table) were within our top 100 SNPs (*GRM8*, *GRIN2B* and *GRIA1*). Fine mapping in search for functional variants linked to rs6951643 was attempted sequencing the 11 exons of *GRM8* gene and the corresponding intronic flanking regions in 96 sCJD patients. We found 8 intronic SNPs (rs73231278, rs62468898, rs1008274, rs111546739, rs17685327, rs6951643, rs2074012, rs35648111) and one exonic non-coding SNP (rs34182595). Functional prediction analysis of these genetic variants by FuncPred or RESCUE-ESE showed no indication of regulatory implications. In the Gtex eQTL database we found no eQTL associated to any of the *GRM8* SNPs. There is no co-expression of GRM8 and *PRNP* in blood eQTLs in Genenetwork. However, based on PITA prediction we found that rs34182595, which is an insertion/deletion SNP in

Table 4. Meta-analysis by country of origin.

MarkerName	Effect estimates of discovery analysis corrected for population substructure by PCA			Meta-analysis of effect estimates of replication analysis stratified by country of origin				Meta-analysis of discovery and replication		
	β	SE	P-value	β	SE	P-value	β Direction*	β	SE	P-value
rs6107516	0.4243	0.0944	6.92E-06	0.2327	0.0637	0.000262	+++++	0.2927	0.0528	3.00E-08
rs17115017	-0.5363	0.1453	0.000223	-0.1420	0.1061	0.181	---++	-0.2792	0.0857	0.001123
rs9521699	-0.4087	0.0993	3.84E-05	-0.0233	0.0723	0.7468	+-+--	-0.157	0.0585	0.007242
rs6951643	-0.3472	0.0778	8.09E-06	-0.1033	0.0545	0.05821	-++++	-0.1837	0.0447	3.91E-05
rs10061929	-0.3737	0.0917	4.58E-05	-0.0289	0.0701	0.6801	---++	-0.1562	0.0557	0.005048

* Concordance between discovery population βs and each of the five replication populations; PCA, Principal Component Analysis; SE, standard Error.

doi:10.1371/journal.pone.0123654.t004

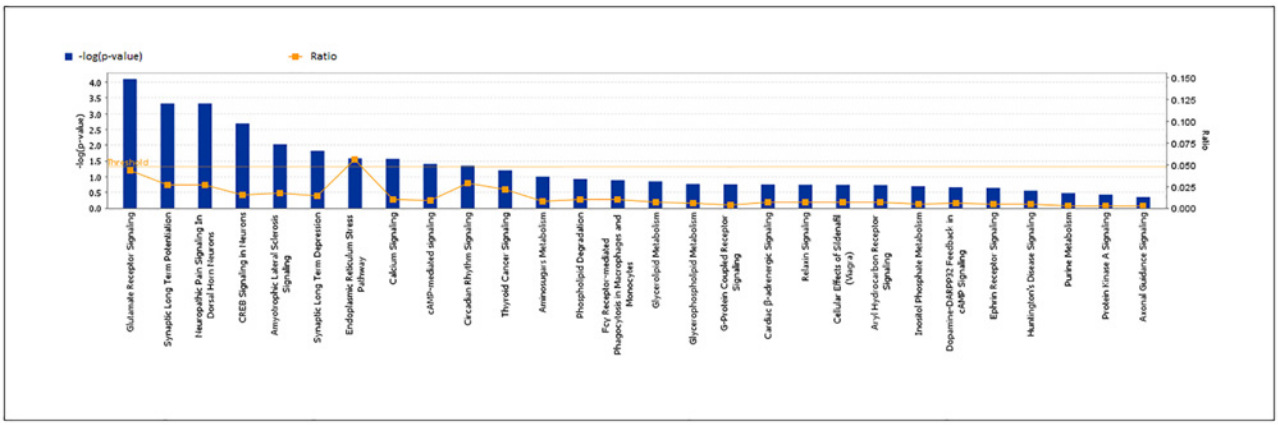

Fig 1. Canonical pathway analysis performed by IPA software including those genes tagged by SNPs with p-value <0.001 in our GWAs analysis. The horizontal axis represents the pathways identified. The ratio (vertical axis, right) is calculated by the numbers of genes in a given pathway that meet cutoff criteria, divided by total numbers of genes that make up that pathway. The orange line stands for the threshold above which there are statistically significantly (by default P<0.05). The vertical axis (left) shows the –log of the p-value calculated based on Fisher's exact test.

doi:10.1371/journal.pone.0123654.g001

exon 11 in partial LD with rs6951643 (D' = 0.41; r^2 = 0.16), is located in a target site for micro-RNAs (miR-103 and miR-107), a finding that has been previously reported [7].

We then performed an immunohistochemical study in brain samples from 48 sCJD patients. Immunoreactivity for mGluR8 was observed in neurons and microglial cells (both in the white and grey matter) While in neurons we did not observe obvious differences we found a trend towards higher combined score of mGluR8 immunoreactivity in microglia related to the A allele at rs6951643 (Fig 2); however, these differences were not statistically significant (ordinal regression A-carriers versus A-non-carriers adjusting by c129 and levels of microglia in temporal cortex; p-value = 0.093). S3 Fig shows semi-quantitative assessments of mGluR8 expression in microglia (0 to 3) in the temporal region across the three rs6951643 genotypes. We found no association between rs6951643 genotypes and patient's age of disease onset or disease duration.

Discussion

In this study we report a non-*PRNP* genetic risk variant for sCJD, *GRM8*. Moreover, building on findings from previous studies [8], pathway analyses yielded glutamate receptor signalling as one of the main pathways linked to sCJD pathogenesis.

A previous GWAS of prion diseases employed 1,259 sCJD samples, in addition to other disease subtypes and 6,015 shared controls [6]. In the sCJD sub-group and in a meta-analysis including all prion cases only variants in *PRNP* were found to be significantly associated with disease risk. Several SNPs outside *PRNP* were identified, but in contrast to our multi-national disease cohort the association with sCJD was not homogeneous across the different geographical groups. Our main novel finding (rs6951643) was not statistically significant in that analysis. One possible explanation for this discrepancy is the fact that both studies have limited power to detect small effects due to the overall restricted case numbers included for study and therefore a SNP with a relatively modest OR of 1.27 might not be detected by all analyses. The experience and insights drawn from GWAS performed in more prevalent disorders, such as Alzheimer's disease, shows that increasing sample size and performing meta-analysis might be essential in order to discover and confirm, relatively small-effect genetic risk factors. However, it is worth re-iterating that in our study, the association with rs6951643 was consistent across

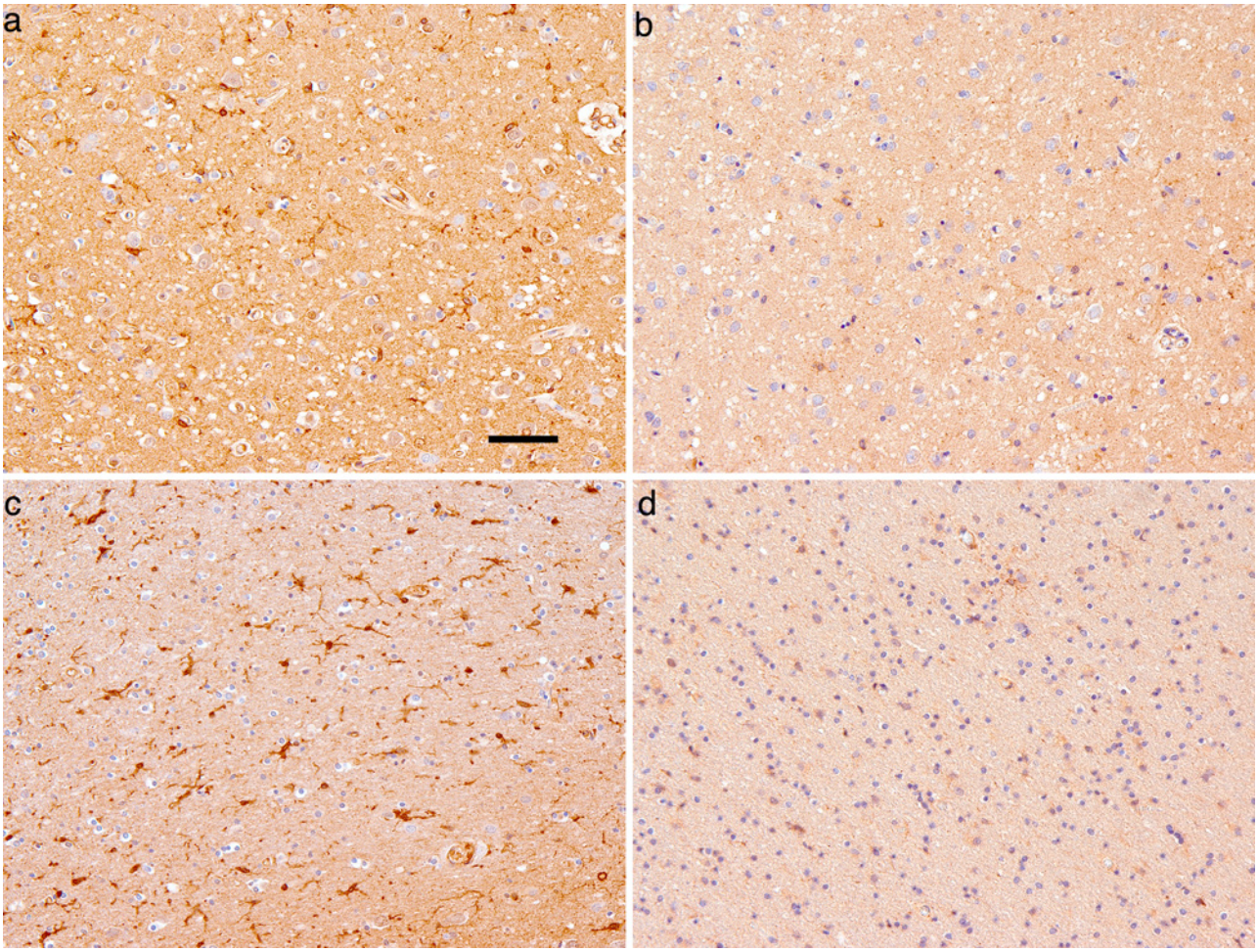

Fig 2. Representative photomicrographs of a sCJD case with AA (a, c) and a sCJD case with GG (b, d) rs6951643 genotype showing differences in mGluR8 immunostaining of microglial cells in the temporal cortex (a, b) and temporal white matter (c, d). Bar represents 50 μm for all images.

doi:10.1371/journal.pone.0123654.g002

the geographically diverse sCJD population tested, showing an over-representation of the A allele in cases, and across the different genotyping methods used.

A limitation of our primary analysis was the fact that we were not able to adjust by country of origin at the replication stage. In order to overcome this caveat we performed a meta-analysis including control data from the *1000 Genomes Project* and imputed data from the Rotterdam Study. In the meta-analysis of the stratified analysis by country of origin the association of both SNPs became less significant suggesting that some signal might be caused by population stratification. Despite the fact that both variants were nominally significant in the meta-analysis of the replication data, the *PRNP* variant was the only genome wide significantly associated to sCJD in the pooled meta-analysis. However, this meta-analysis is not perfect either, as ideally the cases and controls should originate from the same population and in our analysis we attempted to match on country of origin (see S4 Table) and this approach is statistically less powerful because of the uneven distribution of cases and controls, as might reflect the fact that the *PRNP* SNP p-value is also less significant in the meta-analysis than in the primary analysis. Still we acknowledge that the results are a call for caution and the association between *GRM8* genetic variants and sCJD should be confirmed in larger analysis with extensive control for population stratification.

GRM8 encodes for mGluR8, a protein that belongs to the metabotropic glutamate receptor family, a family that has recently been linked to the transduction of physiological and cytotoxic signals mediated by PrP^C. MGluR1 and mGluR5 have been shown to interact with PrP^C, with such associations appearing important for promoting neurite outgrowth [9, 10]. Additionally, a recent study demonstrated that mGluR5 coupled with PrP^C mediated the cellular toxicity of soluble β-amyloid oligomers [10]. Further, in the APPswe/PS1dE9 Alzheimer's disease mouse model, altered PrP^C processing and a selective increase in cortical mGluR1 expression has been reported. The authors hypothesized that complex processing of PrP^C in connection with mGluR1 over-expression is triggered by β-amyloid peptides [11]. In the setting of accumulation of PrP^{Sc}, our immunohistochemical assessment of a limited sample of sCJD patients found that carriers of the risk allele at rs6951643 tended to have higher mGluR8 expression in microglial cells compared to non-carriers. Although our functional prediction analysis for rs6951643 was uninformative, it is of interest that a nearby variant in partial LD (rs34182595) is located in a micro-RNA target site and could influence gene expression.

In conclusion, our study has detected a *GRM8* genetic variant as a suggestive marker for sCJD risk mapping outside the *PRNP* region. Our findings provide evidence supporting a role for glutamate receptor signalling pathways in sCJD susceptibility. The involvement of glutamate receptor pathway in sCJD should be addressed in future studies in order to provide new insights in its pathogenesis. Our results underscore the importance of increasing sample sizes in future studies in order to augment the likelihood of detecting additional non-*PRNP* genetic risk factors for sCJD.

Methods

Ethics statement

The present study was conducted according to the revised Declaration of Helsinki and Good Clinical Practice guidelines. A signed informed consent to participate in genetic research was obtained from all participants or patients' relatives. The study was approved by Comité de Ética de la Investigación y de Bienestar Animal (CEIyBA), National Health Institute Carlos III and Comité de Ética de Ensayos clínicos de Galicia and Comite de Ética de la Fundación Pública Gallega de Medicina Genómica (Servicio Gallego de Salud, SERGAS) (Spain); the Lothian Health Board, Lothian Research Ethics Committee (reference MCO/103/90) (UK); the Ethik-Kommission der Universitätsmedizin Göttingen (No. 9/6/0) (Germany); the Ethic Committee of the Istituto Superiore di Sanità (CE-ISS 09/266) (Italy); the Medical Ethics Committee of The Erasmus MC and the review board of The Netherlands Ministry of Health Welfare and Sports (The Netherlands); the Ethics Committee of the Medical University of Vienna (396/2011) (Austria); the Human Research Ethics Committee, based at The University of Melbourne (941450) (Australia).

Populations and study design

All patients were ascertained by National CJD Surveillance Centers. Only definite or probable sCJD cases, according to accepted classification criteria, were included [12]. Table 5 summarizes the study design and populations included after quality control. All cases and controls were of Caucasian origin. Legal representatives gave written informed consent, and all samples were taken in accordance with the Helsinki declaration.

Table 5. Study Design and populations tested.

STAGES	POPULATION EFFECTIVELY ASSESSED*	
	sCJD CASES (N)	**CONTROLS (N)**
Stage 1: Discovery	Germany (113)	
Genotyping method: Affymetrix 500k array	UK (269)	UK WTCCC controls (1482)
Number of SNPs effectively assessed 279389	Netherlands (52)	Netherlands-RS controls (457)
Number of SNPs selected for replication: 23	**TOTAL sCJD (434)**	**TOTAL controls (1939)**
Stage 2: Replication in independent sCJD Cases	Germany (284)	
Genotyping method: Sequenom iPLEX GOLD	Netherlands (76)	
Number of SNPs effectively assessed: 22	Italy (292)	
Number of SNPs replicated: 5	Australia (48)	
	France (150)	
	Spain (203)	
	Austria (56)	
	TOTAL sCJD (1109)	
Stage 3: Replication in independent Controls		Spain-USC (2193)
Genotyping method: Sequenom iPLEX GOLD		Netherlands-RS (71)
Number of SNPs effectively assessed: 5		**TOTAL controls (2264)**
Number of SNPs replicated: 2		
		TOTAL controls (4203)
POOLED ANALYSIS	**TOTAL sCJD (1543)**	
		Netherlands-RS (6192)
		British in England and Scotland-10KG (137)
Controls added in analysis stratified by country		Toscani in Italy-10KG (385)
		Iberian populations in Spain-10KG (217)
		Utah residents with Northern and Western European ancestry-10KG (290)
	TOTAL sCJD (1543)	**TOTAL controls (11424)**

*Number of samples effectively genotyped that passed quality control

sCJD, sporadic Creutzfeldt-Jakob disease; WTCCC, Welcome Trust Case Control Consortium; RS, Rotterdam Study; USC, University of Santiago de Compostela; 10KG, 1000 Genome Project.

doi:10.1371/journal.pone.0123654.t005

Genotyping and quality control

At the discovery stage (stage one) patient's samples were characterized using the Affymetrix 500k array at the USC node of the Spanish National Genotyping Center. Out of the initially available 554 sCJD samples there was not enough DNA in 61 (36 samples from the UK and 25 from Germany), leaving 493 for genotyping. Genotypes were called first by the Dynamic Model (DM) and those samples with an overall call rate >93% were subsequently called by a Bayesian Robust linear model with Mahalanobis distance (BRLMM). Samples with BRLMM call rates <95% and with call and discrimination rates of the Modified Partitioning Around Medoids algorithm (MDR-MCR) >10% were excluded (31 patient samples out of 493 did not reach these thresholds, leaving in total 462 available for the analysis). Genotype and quality control of the WTCCC controls have been described elsewhere [13]. The other set of controls (Rotterdam Study) were genotyped at the Genetic Laboratory, Department of Internal Medicine at Erasmus Medical Center (Rotterdam) also using the Afymmetrix 500K array following same protocols as those used for cases. After quality control, 28 patients and 25 controls were excluded resulting in a final discovery population of 434 sCJD patients and 1,939 controls. Replication was attempted in independent sCJD patients (n = 1,201) (stage two) and control series

(n = 2,264) (stage three) with the Sequenom iPLEx GOLD platform. SNPs for replication were selected as follows: after excluding outliers, we chose the 10 SNPs with lowest p-values (when a cluster of SNPs was in LD tagging the same gene we selected only the one with lowest p-value) and the remainder from the top 100 when a) they were in linkage disequilibrium with other top 100 SNPs or b) agreed in direction with the previous sCJD GWAS [6], or c) were connected to pathways of interest based on our previous study [14] (phosphatidylinositol) or based on the pathway analyses performed with the current data (glutamate receptors).

Statistical analysis of genetic data

The statistical analyses were conducted using GenABEL [15]. For the individual SNP analysis, we excluded those SNPs: 1) with call rates <98% within either group (n = 219,182); 2) with minor allele frequency<0.01 (n = 1); 3) with controls not in Hardy-Weinberg equilibrium (False Discovery Rate for unacceptably high individual heterozygosity<1%) (n = 1,300). The quality control further included a check of the sex chromosomes against the reported sex and unexpected sample duplicates (Identity by State, IBS>95%). All quality control was performed with the 'check.marker' function of GenABEL. After quality control, 279,389 out of 499,872 SNPs were included in the analyses. In the discovery analyses (stage one), we conducted a one degree of freedom additive score test between cases and controls coding the presence of the minor genotype 0 for non-carriers, 1 for heterozygous and 2 for homozygous carriers. We controlled subpopulation structure using principal components analysis (PCA). In brief, we selected a random set of 10,000 SNPs and calculated a genomic kinship matrix using pair wise identity by state statistic (function 'ibs'). We then performed PCA analysis (function 'cmdscale'), and adjusted our analysis by the three main IBS matrix principal components (function 'mlreg'). We calculated the genomic inflation factor lambda (λ) for both autosomal and X chromosome SNPs. In the replication phase (stages two and three), we compared allele frequencies in cases and controls by a Chi-squared test implemented in Haploview [16]. We used a Bonferroni correction to adjust for multiple testing, setting the threshold for significance to a p-value of 0.0023 (0.05/22 SNPs successfully genotyped). We combined the gene discovery and replication series of patients for all validated SNPs and used as the criterion for genome wide significance a p-value of $5x10^{-8}$. We attempted to adjust for country of origin after stage three. We analysed the data from stage two and three with genotypes of the *1000 Genomes Project* [17] and imputed genotypes from the *Rotterdam Study* [18]. We extracted the SNPs from the *1000 Genomes* reference set excluding the children and other family members (Version: phase I v3). Additionally we imputed the same SNPs from the *Rotterdam Study* (imputations of the same phase I v3of the *1000 Genomes*). Imputed genotypes had a very high quality score (R^2 > = 0.99). Next we paired our cases and controls by country of origin (S4 Table) and calculated effect estimates of the SNPs per country. The effect estimates of the SNPs from the discovery stage (adjusted by PCAs) and the effect estimates from the replication were meta-analysed using a inverse variance weighted meta-analysis(METAL version released 2011-03-25). [19]. We performed pathway analyses using ALIGATOR, a method for studying groups of genes by testing for over-representation of members of those groups within lists of genes containing significantly associated SNPs from GWA studies [20]. This analysis used 410 SNPs with a p-value for significance of <0.001 out of 115,565 within-gene SNPs from a total of 279,389 available. We found these SNPs were associated with 94 genes from a total of 13,092 genes with GO annotation covered in this study. Additionally we used Ingenuity Pathway Analysis (IPA) www.ingenuity.com) to determine the functional pathways in the genes tagged by our top ranked SNPs. We again selected those genes tagged by SNPs with p-value <0.001 and selected the canonical pathway analysis implemented in IPA software.

Sequencing

We sequenced the 11 exons and intronic flanking areas of the *GRM8* gene in 96 sCJD patients using specific primers (S5 Table). The amplification reactions were carried out with 25 ng of genomic DNA and 0.5 units of Taq DNA Polymerase in a volume of 25 μl. The final concentrations of other reactants were: 1x Taq DNA Polymerase Buffer, 0.1 mM dNTPs and 0.1 μM of each primer. The final concentration of $MgCl_2$ was 2 mM for the amplification of exons 1–7 and 10; 4 mM for exons 8 and 9a; 1.5 mM for exon 9b and 1 mM for exon 11. Additionally, the amplification reactions of exons 1 and 8 were supplied with DMSO 10% and 5%, respectively. The PCR cycling conditions were as follows: initial denaturation at 96°C for 3 min followed by 30 cycles of 96°C for 30 s, annealing temperature (see S5 Table) for 30 s and extension temperature of 72°C for 1 min with a final extension at 72°C for 10 min. A 2 μl aliquot of the amplification reaction was sequenced using 0.1μM of the above primers.

Functional prediction analysis

Functional prediction analysis of genetic variants was performed by the use of FuncPred online software (http://snpinfo.niehs.nih.gov/snpinfo/snpfunc.htm) [21]. Exonic splicing enhancers were analyzed by RESCUE-ESE Web Server (http://genes.mit.edu/burgelab/rescue-ese/) [22] and PITA online software (http://genie.weizmann.ac.il/pubs/mir07/index.html) [23] was used to assess potential micro-RNA target sites. We searched for correlations between our genetic variants and eQTL in GTEX [24] and Genenetwork (http://genenetwork.nl:8080/GeneNetwork/) [25].

Phenotypic correlations

We performed an immunohistochemical study in brain samples from 48 sCJD patients. The rs6951643 genotype distribution was as follows: 13 AA, 25 AG, and 9 GG. Sections from the hippocampal region CA1 sub-region, temporal cortex and white matter were immunostained for mGluR8. The intensity of mGluR8 (1:50; polyclonal rabbit antibody, Novus Biologicals, Cambridge, UK) immunostaining was evaluated using a scale of 0–3 (0: no; 1: weak; 2: moderate; 3: strong staining). The frequency of mGluR8 positive cells was scored semi-quantitatively using three categories: 1, <10%; 2, 10–50%; 3, >50% and was evaluated to provide information about the relative number of mGluR8 positive cells within the tissue. The product of these two values (intensity and frequency scores) was used to give the overall scores (total scores). In adjacent sections microglial activation using immunostaining for HLA-DP, DQ, DR (clone CR3/43, 1:00, monoclonal mouse), and spongiosis were also estimated semi-quantitatively. The analysis was performed (GGK) blinded to rs6951643 genotype. Ordinal regression was employed to test for association between rs6951643 genotypes and brain semi-quantitative expression of mGluR8. We adjusted by disease duration, *PRNP* M129V genotype, gliosis and spongiosis. We correlated clinical variables (age at death and patient's disease onset) with the presence of 0, 1 or 2 sCJD risk alleles. In order to assess rs6951643 influence on age at onset and disease duration we performed a time to event analysis using Cox regression adjusting by *PRNP*M129V genotype and other relevant factors like sex and country of origin.

Supporting Information

S1 Fig. Q-Q plots for autosomal and X chromosome SNPs.
(TIF)

S2 Fig. Genotype clusters of the five SNPs studied in stage three with Sequenom iPLEx GOLD.
(TIF)

S3 Fig. Semi-quantitative assessments of mGluR8 expression in microglia (0 to 3) in the temporal region across the three rs6951643 genotypes in 48 sCJD patients.
(TIF)

S1 Table. Demographic and clinical features of cases.
(DOCX)

S2 Table. Top 100 SNPs after GWA analysis.
(XLS)

S3 Table. Pathway analysis with ALIGATOR.
(XLS)

S4 Table. Meta-analysis Sample population matching.
(DOCX)

S5 Table. Pairs of primers used for sequencing of the 11 exons and intronic flanking areas of GRM8 gene.
(DOCX)

S6 Table. GWA analysis results X chromosome SNPs.
(ZIP)

S7 Table. GWA analysis results autosomic SNPs.
(ZIP)

Acknowledgments

The author thanks Simon Mead for sharing his data in order to select SNPs for replication. We also thank the Wellcome Trust Case Control Consortium (WTCCC) for the use of their control data. **UK.** The national UK CJD Surveillance Unit is grateful to clinicians, patients, and family members throughout the UK for a remarkable level of cooperation with the CJD surveillance program. **France** We thank all members of the French National Surveillance Network for Creutzfeldt-Jakob disease and all physicians for case notification. **Italy** We are very grateful to neurologists and neuropathologists, patients, and family members throughout Italy for their collaboration. **The Netherlands** We thank Pascal Arp, Mila Jhamai, Marijn Verkerk, Lizbeth Herrera, and Marjolein Peters for their help in creating the GWAS database, and Karol Estrada and Maksim V. Struchalin for their support in creation and analysis of imputed data. The authors are grateful to the study participants, the staff from the Rotterdam Study, and the participating general practitioners and pharmacists. **Spain.** The authors thank Biobanco Valdecilla and IDIVAL for its support throughout this project thanks to J.M. Polo for their critical advice, thanks to Beatriz Sobrino and María Torres (CEGEN, Spanish National Genotying Center) for all their work in the sample genotyping, and Weyma Notel for her help in editing the manuscript. **Australia.** The ANCJDR thanks all patients, families, clinicians and allied health personnel for their support and cooperation to facilitate this study.

Author Contributions

Conceived and designed the experiments: CMvD RGW RSGK MTB YSA PSJ. Performed the experiments: AC GGK MC O. Calero. Analyzed the data: PSJ YSA CMvD SJvdL. Contributed

reagents/materials/analysis tools: MTB GGK MC AL JPB JLL SJC AB VL AP AC SJvdL FR AH O. Combarros JB AGU SH HB MP IZ RSGK RGW CMvD CP TS. Wrote the paper: PSJ MTB GGK MC O. Combarros MP SJC IZ RSGK RGW CMvD.

References

1. Bueler H, Aguzzi A, Sailer A, Greiner RA, Autenried P, Aguet M, et al. Mice devoid of PrP are resistant to scrapie. Cell. 1993; 73:1339–47. PMID: 8100741
2. Alperovitch A, Zerr I, Pocchiari M, Mitrova E, de Pedro Cuesta J, Hegyi I, et al. Codon 129 prion protein genotype and sporadic Creutzfeldt-Jakob disease. Lancet. 1999; 353:1673–1674. PMID: 10335789
3. Bruce ME, Will RG, Ironside JW, McConnell I, Drummond D, Suttie A, et al. Transmissions to mice indicate that 'new variant' CJD is caused by the BSE agent. Nature. 1997; 389:498–501. PMID: 9333239
4. Bishop MT, Pennington C, Heath CA, Will RG, Knight RS. PRNP variation in UK sporadic and variant Creutzfeldt Jakob disease highlights genetic risk factors and a novel non-synonymous polymorphism. BMC Med Genet. 2009; 10:146. doi: 10.1186/1471-2350-10-146 PMID: 20035629
5. Lloyd SE, Mead S, Collinge J. Genetics of prion diseases. Curr Opin Genet Dev. 2013; 23:345–51. doi: 10.1016/j.gde.2013.02.012 PMID: 23518043
6. Mead S, Uphill J, Beck J, Poulter M, Campbell T, Lowe J, et al. Genome-wide association study in multiple human prion diseases suggests genetic risk factors additional to PRNP. Hum Mol Genet. 2012; 21:1897–906. doi: 10.1093/hmg/ddr607 PMID: 22210626
7. Duan S, Mi S, Zhang W, Dolanet ME. Comprehensive analysis of the impact of SNPs and CNVs on human microRNAs and their regulatory genes. RNA Biol. 2009; 6: 412–425. PMID: 19458495
8. Muller WE, Ushijima H, Schroder HC, Forrest JM, Schatton WF, Rytik PG, et al. Cytoprotective effect of NMDA receptor antagonists on prion protein (PrionSc)-induced toxicity in rat cortical cell cultures. Eur J Pharmacol. 1993; 15;246:261–7.
9. Beraldo FH, Arantes CP, Santos TG, Machado CF, Roffe M, Hajj GN, et al. Metabotropic glutamate receptors transduce signals for neurite outgrowth after binding of the prion protein to laminin gamma1 chain. FASEB J. 2011; 25, 265–279. doi: 10.1096/fj.10-161653 PMID: 20876210
10. Um JW, Kaufman AC, Kostylev M, Heiss JK, Stagi M, Takahashi H, et al. Metabotropic glutamate receptor 5 is a coreceptor for Alzheimer aβ oligomer bound to cellular prion protein. Neuron. 2013; 79:887–902. doi: 10.1016/j.neuron.2013.06.036 PMID: 24012003
11. Ostapchenko VG, Beraldo FH, Guimarães AL, Mishra S, Guzman M, Fan J, et al. Increased prion protein processing and expression of metabotropic glutamate receptor 1 in a mouse model of Alzheimer's disease. J Neurochem. 2013; 127:415–25. doi: 10.1111/jnc.12296 PMID: 23651058
12. WHO. Human transmissible spongiform encephalopathies. Wkly Epidemiol Rec. 1998; 47:361–365. PMID: 9844549
13. The Wellcome Trust, Case Control Consortium. Genome-wide association study of 14,000 cases of seven common diseases and 3,000 shared controls. Nature. 2007; 447: 661–678. PMID: 17554300
14. Sanchez-Juan P, Bishop MT, Aulchenko YS, Brandel JP, Rivadeneira F, Struchalin M, et al. Genome-wide study links MTMR7 gene to variant Creutzfeldt-Jakob risk. Neurobiol Aging. 2012; 33:1487. doi: 10.1016/j.neurobiolaging.2011.10.011 PMID: 22137330
15. Aulchenko YS, Ripke S, Isaacs A, van Duijn CM. GenABEL: an R library for genome-wide association analysis. Bioinformatics. 2007; 23: 1294–1296. PMID: 17384015
16. Barrett JC, Fry B, Maller J, Daly MJ. Haploview: analysis and visualization of LD and haplotype maps. Bioinformatics. 2005; 21:263–5. PMID: 15297300
17. The 1000 Genomes Project Consortium. An integrated map of genetic variation from 1,092 human genomes. Nature. 2012; 491: 56–65. doi: 10.1038/nature11632 PMID: 23128226
18. Hofman A, Darwish Murad S, van Duijn CM, Franco OH, Goedegebure A, Ikram MA. et al. The Rotterdam Study: 2014 objectives and design update. Eur J Epidemiol. 2013; 28: 889–926. doi: 10.1007/s10654-013-9866-z PMID: 24258680
19. Willer CJ, Li Y, Abecasis GR. METAL: fast and efficient meta-analysis of genomewide association scans. Bioinformatics. 2010; 26: 2190–2191. doi: 10.1093/bioinformatics/btq340 PMID: 20616382
20. Holmans P, Green EK, Pahwa JS, Ferreira MA, Purcell SM, Sklar P, et al. Gene ontology analysis of GWA study data sets provides insights into the biology of bipolar disorder. Am J Hum Genet. 2009; 85:13–24. doi: 10.1016/j.ajhg.2009.05.011 PMID: 19539887
21. Xu Z, Taylor JA. SNPinfo: integrating GWAS and candidate gene information into functional SNP selection for genetic association studies. Nucleic Acids Res. 2009; 37: W600–5. doi: 10.1093/nar/gkp290 PMID: 19417063

22. Fairbrother WG, Yeh RF, Sharp PA, Burge CB. Predictive identification of exonic splicing enhancers in human genes. Science. 2002; 297: 1007–13. PMID: 12114529

23. Kertesz M, Iovino N, Unnerstall U, Gaul U, Segal E. The role of site accessibility in microRNA target recognition. Nat Genet. 2007; 39:1278–84. PMID: 17893677

24. Lonsdale J, Thomas J, Salvatore M, Phillips R, Lo E, Shad S, et al. The genotype-tissue expression (GTEx) project. Nat Genet. 2013; 45:580–585. doi: 10.1038/ng.2653 PMID: 23715323

25. Williams RW, Mulligan MK. Genetic and molecular network analysis of behavior. Int Rev Neurobiol. 2012; 104:135–57. doi: 10.1016/B978-0-12-398323-7.00006-9 PMID: 23195314

PLOS | PATHOGENS

RESEARCH ARTICLE

Prion acute synaptotoxicity is largely driven by protease-resistant PrP^{Sc} species

Simote Totauhelotu Foliaki[1], Victoria Lewis[1], David Isaac Finkelstein[2], Victoria Lawson[3], Harold Arthur Coleman[2,4,5], Matteo Senesi[1], Abu Mohammed Taufiqual Islam[1], Feng Chen[2], Shannon Sarros[2], Blaine Roberts[2], Paul Anthony Adlard[2], Steven John Collins[1,2]*

1 Department of Medicine (Royal Melbourne Hospital), The University of Melbourne, Parkville, Victoria, Australia, **2** Florey Institute of Neuroscience and Mental Health, Parkville, Victoria, Australia, **3** Department of Pathology, The University of Melbourne, Parkville, Victoria, Australia, **4** Department of Physiology, Monash University, Clayton, Victoria, Australia, **5** Monash Biomedicine Discovery Institute, Monash University, Clayton, Victoria, Australia

* stevenjc@unimelb.edu.au

Citation: Foliaki ST, Lewis V, Finkelstein DI, Lawson V, Coleman HA, Senesi M, et al. (2018) Prion acute synaptotoxicity is largely driven by protease-resistant PrP^{Sc} species. PLoS Pathog 14(8): e1007214. https://doi.org/10.1371/journal.ppat.1007214

Editor: David Westaway, University of Alberta, CANADA

Received: February 22, 2018

Accepted: July 12, 2018

Published: August 8, 2018

Data Availability Statement: All relevant data are within the paper and its Supporting Information files.

Funding: SJC is supported in part by an NHMRC Pracititioner Fellowship (#APP1105784). BR is a NHMRC Dementia Leadership Fellow (#APP1138673) and receives partial support from the Cooperative Research Centre for Mental Health (#20100104). STF has received the following support: University of Melbourne MIR Scholarship (2014); MIFR Scholarship (2014); CJD Support

Abstract

Although misfolding of normal prion protein (PrP^{C}) into abnormal conformers (PrP^{Sc}) is critical for prion disease pathogenesis our current understanding of the underlying molecular pathophysiology is rudimentary. Exploiting an electrophysiology paradigm, herein we report that at least modestly proteinase K (PK)-resistant PrP^{Sc} (PrP^{res}) species are acutely synaptotoxic. Brief exposure to *ex vivo* PrP^{Sc} from two mouse-adapted prion strains (M1000 and MU02) prepared as crude brain homogenates (cM1000 and cMU02) and cell lysates from chronically M1000-infected RK13 cells (MoRK13-Inf) caused significant impairment of hippocampal CA1 region long-term potentiation (LTP), with the LTP disruption approximating that reported during the evolution of murine prion disease. Proof of PrP^{Sc} (especially PrP^{res}) species as the synaptotoxic agent was demonstrated by: significant rescue of LTP following selective immuno-depletion of total PrP from cM1000 (dM1000); modestly PK-treated cM1000 (PK+M1000) retaining full synaptotoxicity; and restoration of the LTP impairment when employing reconstituted, PK-eluted, immuno-precipitated M1000 preparations (PK +IP-M1000). Additional detailed electrophysiological analyses exemplified by impairment of post-tetanic potentiation (PTP) suggest possible heightened pre-synaptic vulnerability to the acute synaptotoxicity. This dysfunction correlated with cumulative insufficiency of replenishment of the readily releasable pool (RRP) of vesicles during repeated high-frequency stimulation utilised for induction of LTP. Broadly comparable results with LTP and PTP impairment were obtained utilizing hippocampal slices from PrP^{C} knockout (PrPo/o) mice, with cM1000 serial dilution assessments revealing similar sensitivity of PrPo/o and wild type (WT) slices. Size fractionation chromatography demonstrated that synaptotoxic PrP correlated with PK-resistant species >100kDa, consistent with multimeric PrP^{Sc}, with levels of these species >6 ng/ml appearing sufficient to induce synaptic dysfunction. Biochemical analyses of hippocampal slices manifesting acute synaptotoxicity demonstrated reduced levels of multiple key synaptic proteins, albeit with noteworthy differences in PrPo/o slices, while such changes were absent in hippocampi demonstrating rescued LTP through treatment with dM1000. Our findings offer important new mechanistic insights into the

Group Network (CJDSGN) Silva Coehlho Travel Grant (2016); Marek Gorcynski Top-up scholarship (2017); and Dominic Battista Memorial Grant (2018). VL has received CJDSGN Memorial grants: Stephen O'Hara, Jennifer Duckworth and others lost to CJD (2018); Sandra Kernahan, Stephen O'Hara, Catherine Heagerty, Grasso family, Victoria Larielle, Barbara Childerhouse, Marilyn Hart and Pamela Thomas (2016); and Ross Glasscock, Robert Craig, Carmelo Tripoli, Arthur Schinck and Arlene Hamilton (2015). The funders had no role in study design, data collection and analysis, decision to publish, or preparation of the manuscript.

Competing interests: The authors have declared that no competing interests exist.

synaptic impairment underlying prion disease, enhancing prospects for development of targeted effective therapies.

Author summary

Misfolding of the normal prion protein (PrP^{C}) into disease-associated conformations (PrP^{Sc}) is the critical initiating step for prion diseases. Similar to other neurodegenerative disorders, progressive failure of brain synapses is considered a primary deleterious event underpinning prion disease evolution. Our current understanding of the underlying mechanisms associated with synaptic failure is rudimentary contributing to difficulties in developing effective treatments. Herein we report the use of an electrophysiology paradigm that allowed us to demonstrate that at least modestly proteinase K (PK)-resistant PrP^{Sc} species from two mouse-adapted prion strains (M1000 and MU02) are directly synaptotoxic causing significant acute impairment of hippocampal CA1 region long-term potentiation (LTP). Of note, the LTP disruption approximated that reported in prion animal models. Additional detailed analyses provided novel pathophysiological insights suggesting possible heightened pre-synaptic vulnerability to the acute synaptotoxicity through impairment of replenishment of the readily releasable pool of neurotransmitter vesicles, while biochemical analyses demonstrated reduced levels of multiple key pre-and post-synaptic proteins. Broadly similar acute synaptic dysfunction and dose-response susceptibility were observed in slices from mice not expressing PrP^{C} albeit with minor but noteworthy differences in electrophysiological and biochemical findings. Our study offers important new mechanistic insights into the synaptic impairment underlying prion disease, enhancing prospects for development effective therapies.

Introduction

Prion diseases constitute a group of transmissible neurodegenerative disorders with the spectrum encompassing several human phenotypes, the most common being Creutzfeldt-Jakob disease (CJD), as well as a number of animal diseases including bovine spongiform encephalopathy ("mad cow" disease) and scrapie in sheep [1, 2]. Regardless of disease phenotype, misfolding of PrP^{C} into disease-associated conformers (herein collectively designated PrP^{Sc}), with their subsequent aggregation and accumulation, appears critical to pathogenesis although the precise neurotoxic species and how such species provoke neuronal dysfunction and loss leading to the onset of clinical illness remain unresolved. The precise composition of the infectious unit or "prion" also remains to be determined, although considerable evidence supports that PrP^{Sc} is the major, if not exclusive, component (the "protein only" hypothesis) [3]. Historically, PrP^{Sc} has been considered to be highly protease-resistant (designated PrP^{res} after protease treatment) but recent evidence supports the existence of a broader spectrum, including protease-sensitive conformers, which most likely contribute to pathogenesis and may comprise up to 90% of misfolded prion protein in diseased brains [4, 5].

The primary function of PrP^{C} in the central nervous system remains uncertain although a key role for this glycosylphosphatidylinositol-anchored glycoprotein in synaptic physiology and memory has been described [6]. Aligned to such functions, PrP^{C} has been reported as having a predominant synaptic localisation [7], with important influences on voltage-gated calcium (Ca^{2+}) [8] and N-methyl-D-aspartate receptor (NMDAR) ion channels [9], as well as

LTP [10]. LTP is a use-dependent neurophysiological process, enhancing the strength of synaptic connection, with hippocampal CA1 region LTP directly correlating with episodic memory acquisition [11]. Critical to LTP-type synaptic plasticity and episodic memory generated in the hippocampus are α-amino-3-hydroxy-5-methyl-4-isoxazoleproprionic acid receptor (AMPAR) and NMDAR ion channels, as well as metabotropic glutamate receptors with signal transduction mediated through pathways including calcium-regulated phosphorylated extracellular signal–regulated kinase (pERK) and phosphorylated cAMP response element binding protein (pCREB), which alter DNA transcription with consequent ultrastructural and receptor changes at synapses [12].

Our group [13] and others [14, 15] have shown in prion animal models evidence of early selective hippocampal damage, with synapses becoming significantly disrupted and retracted from the mid-incubation period [15–17]. Of particular relevance, selective and progressive impairment of LTP in the CA1 region of the hippocampal stratum radiatum has been demonstrated *in vivo* in ME7 prion infected mice from 44–70% of the incubation period [14], with early loss of hippocampal pyramidal neuronal synapses shown to correlate with first evidence of disturbances in hippocampal-dependent behaviour [15]. Additionally, studies have revealed that impairment of LTP coincides with the earliest detection of PrP^{Sc}, slightly prior to morphological evidence of synaptic loss or neuropil vacuolation [14, 18], indicating that impairment of hippocampal CA1 region LTP is a sensitive indicator of synaptic dysfunction in prion strains that cause early, prominent hippocampal damage and supporting the likelihood that PrP^{Sc} is directly synaptotoxic.

Somewhat limiting our ability to better understand prion pathogenesis is the relative paucity of tractable, authentic models of acute prion neurotoxicity. Very simple *in vitro* cell culture models have demonstrated toxic effects of recombinant, soluble, oligomeric PrP enriched in β-sheet content [19], as well as toxicity from highly "purified" PrP^{Sc} and proteinase treated PrP^{Sc} extracted from the brains of terminally sick rodents [20, 21]. An *in vivo* model of acute neurotoxicity employing stereotaxic injection of recombinant full-length ovine PrP into the hippocampal CA2 region has been reported, with assessment for acute toxicity requiring morphological analysis approximately 24 hours later [22]. In addition, a model utilizing cultured organotypic cerebellar slice explants allowing assessment of factors that interfere with PrP^{Sc} replication and abrogate cerebellar granule cell loss has been described [23], although this model relies entirely on *de novo* PrP^{Sc} propagation to generate neurotoxic species over an extended 5–7 week period. This *ex vivo* culture model is arguably therefore not ideal for assessing direct acute PrP^{Sc} neurotoxicity because PrP^{Sc} propagation can closely correlate with deleterious cellular events such as heightened oxidative stress [24] that may also contribute to pathogenesis thereby potentially confounding the delineation of a directly neurotoxic PrP^{Sc} species. Of particular interest is a recent study demonstrating that PrP^{Sc} species cause retraction and subsequent loss of dendritic spines in cultured hippocampal neurons following several hours of exposure to PrP^{Sc} preparations [25]. This study however, reported that the synaptotoxicity required expression of PrP^{C} [25] leaving some uncertainty as to whether the neurotoxic PrP^{Sc} species were entirely those directly added to the culture or were different species generated through initial PrP^{Sc} propagation from host PrP^{C}.

Electrophysiological studies employing techniques to assess LTP are an established method to explore potential acute neurotoxic effects of *ex vivo* brain material derived from neurodegenerative disorders such as Alzheimer's disease (AD) [26]. Herein we report the use of an electrophysiology paradigm to explore the acute synaptotoxicity of *ex vivo* prion preparations derived from terminal disease brains briefly superfused onto hippocampal slices. We found that PrP^{Sc} (for convenience hereafter considered as synonymous with PrP^{res} species with at least modest PK resistance) is directly deleterious to LTP in the hippocampal CA1 region, with

the degree of impairment approximating that observed during the natural evolution of prion disease in rodent models and independent of age of mice up to 11 months, with lysates from chronically M1000 prion infected cells (MoRK13-Inf) also inducing analogous acute synaptotoxicity. Additional detailed electrophysiological analyses suggested possible heightened presynaptic vulnerability to the acute synaptotoxicity, exemplified by impairment of post-tetanic potentiation (PTP) and correlating with failure of replenishment of the readily releasable pool (RRP) of vesicles during repeated high-frequency stimulation utilised for induction of LTP. Size fractionation chromatography demonstrated that synaptotoxic PrP correlated with PK-resistant species >100kDa, consistent with multimeric PrP^{Sc}, with levels of these species >0.006 μg/ml appearing sufficient to induce synaptic dysfunction. Biochemical studies confirmed that synaptotoxic PrP^{Sc} in WT slices reduces essential proteins required for the induction and maintenance of hippocampal LTP such as pERK, pCREB, synaptophysin and vesicular glutamate transporter 1 (VGLUT1), as well as the NMDAR NR2A and NR2B subunits and the GluA2 subunit of AMPAR. Importantly, the PrP^{Sc} acute impairment of LTP and PTP was largely PrP^{C} independent, albeit with some noteworthy differences in the changes in key synaptic proteins and electrophysiological findings between wild type (WT) and *Prn-p* gene-ablated (PrPo/o) hippocampal slices, supporting the likelihood of non-PrP^{C} dependent mechanistic pathways. Dose-response assessments using cM1000 revealed similar sensitivity to synaptic disruption in PrPo/o and WT hippocampal slices. Our findings offer important new pathophysiological insights into the synaptic impairment underlying prion disease, enhancing prospects for development of targeted effective therapies.

Materials and methods

Ethics statement

All animal handling was in accordance with National Health and Medical Research Council (NHMRC) guidelines. All experimental procedures were approved by The Florey Institute of Neuroscience and Mental Health Animal Ethics Committee (Ethics number: 13–048) or the Biochemistry & Molecular Biology, Dental Science, Medicine (RMH), Microbiology & Immunology, and Surgery (RMH) Animal Ethics Committee, The University of Melbourne (Ethics number: 1312997.1).

Animals

To prepare hippocampal slices for multi-electrode array (MEA) studies, 12-week-old and 11-month-old WT C57 black 6J (C57BL/6J) female mice were used (Animal Resource Centre, Western Australia), as well as 12-week-old female PrP knockout (PrPo/o) mice on a C57BL/6J background produced through 10 consecutive back-crossings of C57BL/6JX129/sv mice [27]. Mice were group caged, with 12-hour day-night light cycles and food and water provided *ad libitum*.

Brain homogenate and cell lysate preparation for electrophysiology studies. Whole brains from terminally ill mice inoculated with M1000 and MU02 prion strains [28, 29], as well as age-matched normal brain homogenate (NBH) "sham" inoculated mice, were homogenized to 20% (w/v) stocks in artificial cerebrospinal fluid (aCSF; 126mM NaCl, 2.5mM KCl, 26mM $NaHCO_3$, 1.25mM NaH_2PO_4, 10mM Glucose, 1.3mM $MgCl_2.6H_2O$, 2.4mM $CaCl_2.2H_2O$) by passing through progressively smaller gauge needles (18g, 20g, 22g, 23g, 26g), sub-aliquoted and stored at -80˚C until required. For each electrophysiology experiment, aliquots of 20% (w/v) prion-infected brain homogenate and NBH were diluted to a final concentration of 0.5% (w/v) in aCSF after pre-clearing at 100×g for one minute. These 0.5% (w/v) brain homogenates were the crude preparations (crude M1000: cM1000; crude MU02:

cMU02; crude NBH: cNBH). Rabbit kidney epithelial (RK) cells expressing murine PrP^{C} (known as mouse RK13 or MoRK13; produced by Laura Vella and Andrew Hill as described in Vella et al. [30]), either mock-infected with NBH (control) or M1000 prion infected were cultured as described previously [31]. Control and M1000 infected cells were harvested, lysed in aCSF through needles as described above for brain homogenates to a final concentration 2% (w/v) for the use in electrophysiology experiments (control or mock-infected lysate, MoRK13-Un; M1000 infected lysate, MoRK13-Inf). In addition, we performed cM1000 serial dilution experiments on both WT and PrPo/o hippocampal slices to assess the sensitivity of the slices. For these experiments we utilised cM1000 brain homogenates (w/v in aCSF) diluted to 1%, 0.5%, 0.25% and 0.1%.

Proteinase K (PK) treatment of brain homogenate preparations for electrophysiological studies. M1000 brain homogenates and NBH, diluted to 0.5% (w/v) in aCSF and pre-cleared as above were treated with a final concentration of 5μg/mL PK for one hour at 37˚C. The PK digested preparations (PK+M1000 and PK+NBH) were used immediately in electrophysiology experiments. Small aliquots of PK treated homogenates were stored at -80˚C for subsequent biochemical analyses.

PrP immuno-depletion and PK-elution of PrP species from immuno-precipitated pellets of brain homogenates. In preparation for immuno-depletion, 50% protein-G-sepharose bead slurry (PGS; Invitrogen) was pre-blocked overnight at 4˚C by incubation (with constant gentle movement) in 10% (w/v) skim milk powder in sterile phosphate buffered saline containing calcium and magnesium ($PBS^{Ca2+Mg2+}$; Life Technologies). For each PrP immuno-depletion, 03R19 anti-PrP rabbit polyclonal antibody raised against residues 89–103 [29] was coupled to pre-blocked 50% PGS at room temperature (RT) for 2 hours. Normal rabbit serum (NRS) was utilized in the same manner as 03R19 to serve as a negative control. The 03R19 (or NRS) coupled PGS were incubated with 1% (w/v in aCSF) pre-cleared M1000 brain homogenate or NBH overnight at 4˚C. PGS was pelleted by a pulse spin at 100 x g. Supernatants were collected as the PrP immuno-depleted samples and were further diluted 1:1 with aCSF to approximately a 0.5% (w/v) homogenate (PrP immuno-depleted NBH: dNBH; PrP immuno-depleted M1000: dM1000) prior to use in electrophysiology experiments. The immuno-captured PrP species bound to the pelleted PGS were resuspended in aCSF to the same starting volume of 1% (w/v) brain homogenate used for the immuno-depletion. PGS samples were then digested with a final concentration of 5μg/mL PK at 37˚C for an hour with agitation (two cycles of 20 minutes agitation at 1400 rpm followed by 10 minutes with no agitation) to prevent the PGS from settling. The PGS was again pelleted (pulse spin at 100 x g) and the supernatant containing any eluted at least modestly PK-resistant PrP^{Sc} species was collected and diluted 1:1 with aCSF for use in electrophysiology experiments (PK eluted PrP immuno-precipitated NBH, PK+IP-NBH; PK eluted PrP immuno-precipitated M1000, PK+IP-M1000). Small aliquots of PK+IP-NBH and PK+IP-M1000 were retained and stored at -80˚C for subsequent biochemical analyses.

Hippocampal slice preparation for electrophysiology studies

Mouse brains were quickly collected following decapitation while under deep anaesthesia induced by isoflurane. 300μm dorsal horizontal brain slices were prepared using a vibratome (Leica VT1200S) in ice-cold continuously carboxygenated (5% CO_2 and 95% O_2) cutting solution (3mM KCl, 25mM $NaHCO_3$, 1.25mM NaH_2PO_4, 206mM Sucrose, 10.6mM Glucose, 6 mM $MgCl_2.6H_2O$, 0.5mM $CaCl_2.2H_2O$). Approximately three optimal mid-hippocampal slices were collected from each hemisphere for electrophysiology studies. Slices were then allowed to stabilise at 32˚C by incubation for one hour in continuously carboxygenated aCSF prior to

mounting onto 60MEA200/30iR-Ti-pr-T multi-electrode arrays (MEA; Multichannel Systems; Germany) with secure placement achieved using Harp slice grids (ALA HSG-5B, Multichannel Systems; Germany) to ensure good contact of the CA1 region with the MEA (S1A(1) to S1A(3) Fig). Three slices were simultaneously mounted in separate recording chambers and were independently continuously superfused with carboxygenated aCSF (S1A(3) Fig panel i).

Electrophysiology paradigm. Hippocampal field excitatory post-synaptic potentials (fEPSP) were evoked by stimulating one of the MEA grid electrodes that was best aligned to the Schäffer collateral pathway while recording from other electrodes placed on the stratum radiatum of the CA1 region (S1A(3) Fig panel ii). The average number of electrodes recorded from and utilised for analysis in each slice was seven. The amplitude of fEPSP was recorded as the synaptic response. The basal stimulus intensity was determined by generating an input-output (I-O) curve with the intensity chosen sufficient to achieve a fEPSP of ~40% of the maximum response without causing a population spike and a baseline was recorded with stimulation every 30 secs for 30 mins. After approximately 10 mins of the 30-mins baseline, the hippocampal slice was then treated by superfusion with prion containing or control preparations for 5 mins, followed by the rest of the baseline recording in aCSF to ensure return of a stable baseline prior to trains of high frequency stimulation (HFS) (see S1A(4) Fig). The HFS trains (three 500 millisecond, 100Hz trains, 20 sec apart) were delivered (see S1A(4) Fig), followed by post-HFS stimulation every 30 sec for 30 mins, wherein the first response was the post-tetanic potentiation (PTP) and the responses recorded from five mins post-HFS considered the LTP. Immediately after the recordings, slices were snap-frozen and stored at -80˚C for future biochemical analyses. For each independent experiment (n = 5–10 for each treatment), hippocampal slices generated from the same mouse brain were simultaneously utilized for perfusion with aCSF (technical control), NBH control preparations and prion infected samples.

Several synaptic neurophysiological parameters were recorded and analysed (see S1A(4) Fig):

1. I-O curve: fEPSP responses to a series of stimuli of increasing strength from 0 mV up to a stimulus that evoked the maximum fEPSP (ie 3000 mV-5000 mV determined by plateau responses), with the I-O curve prior to treatments (I-O 1) used to determine the basal stimulus intensity, as well as measure the strength of synaptic transmission before (I-O 1) and after treatments and LTP expression (I-O 2) (S1A(4) Fig, boxes 1 & 6).
2. PTP: The first fEPSP response at 0.5 sec after the third HFS train (see S1A(4) Fig, box 4; S1B Fig).
3. LTP: Responses recorded from five minutes following HFS trains represent LTP. The last 10 mins of LTP was used for analyses (S1A(4) Fig, box 5; S1B Fig).
4. Paired pulse facilitation (PPF) ratio can be used to estimate the basal probability of neurotransmitter release, which was measured by two identical basal stimuli delivered at a 20 millisecond interval with the fEPSP amplitude of the second stimulus divided by that of the first stimulus (see S1B Fig). PPF was measured before (PPF1) exposure to prion containing or NBH control preparations, as well as after 30 minutes of LTP expression (PPF2) (see S1A (4) Fig, box 1 and box 6).
5. Readily releasable pool (RRP) depletion: For each HFS train the first 9 evoked fEPSP pulses were utilised wherein the ratio of the pulse 1 and pulse 2 fEPSP amplitude (pulse 2 divided by pulse 1) estimates the probability of transmitter release (*Pr*) in each train (see S1C Fig). The fEPSP amplitude declined after pulse 2 to the last pulse in a HFS train and the rate of decline was used to estimate the RRP decays in each train (Further explained in Data analysis section) (see S1D Fig).

6. RRP replenishment: Relative changes in RRP size were estimated by extrapolating to the Y-intercept the best-fit straight line of the last 4 pulses (pulse 6 to pulse 9) of the cumulative fEPSP amplitudes of each HFS train [32–34] (Further explained in the Data analysis section) (see S1E Fig).

7. PPF time-course: For the time-course PPF study without LTP induction, the PPF1 was measured (with basal stimulation) before (PPF1A) and immediately after (PPF1B) exposure to either cM1000 or cNBH; following PPF1B, PPF was measured every 5 minutes for one hour. The slices were stimulated with basal stimulation during the treatment and at 5-minutely intervals (see S1F Fig).

Note: the omission of specific $GABA_A$ receptor antagonists during measurements of fEPSP to calculate PPF ratios may reduce the accuracy of *Pr* estimates. Similarly, the omission of specific $GABA_A$ receptor blockade during HFS may render estimates of the RRP based on changes in fEPSP amplitudes less accurate.

Size exclusion chromatography

Prior to size exclusion chromatography, brain homogenates were solubilized in Sarkosyl (w/v in 1xPBS), dialysed and filtered. Normal brain homogenates (~10% w/v) were pelleted by 15000xg spin for 10 minutes at 4˚C. The supernatant was discarded and the pellet was reconstituted with 4% (w/v in 1xPBS) Sarkosyl, incubated at 37˚C for 30 minutes, and centrifuged at 10000xg for 10 minutes. The pellet was discarded, and the supernatant was collected and exhaustively dialysed (using 10kDa cut-off dialysis tubing) four times in 1x PBS dialysate (containing no Mg^{2+} or Ca^{2+}) that was ~166 fold greater than the sample volume with each dialysis conducted overnight at 4˚C. Parallel to these procedures, ~1% (w/v) PK+IP-M1000 was pelleted by 15000xg, and the pellet was resuspended in 4% (w/v) Sarkosyl with a volume that was 10-fold less than the initial volume to concentrate the PK+IP-M1000 into ~10% (w/v). Similar procedures were utilized to solubilize ~1% (w/v) dM1000 and concentrate to ~10% (w/v). The 10% (w/v) solubilized and dialysed preparations were filtered using a 0.22-micron filter before ~3mL was injected into a size exclusion chromatography column (HiPreP 16/60 s-100) at a flow rate of 0.5mL per min. The protein complexes were eluted in 1x PBS (containing Mg^{2+} and Ca^{2+}) at 0.5mL per min flow rate, wherein the void volume was collected at ~70 minutes after injection followed by continuous collection of 1mL fractions every two minutes for 80 minutes (~40 fractions in total). The size of proteins or protein complexes fractionated by size exclusion chromatography and eluted into each fraction was determined following size fractionation of the following size exclusion chromatography markers: bovine erythrocyte carbonic anhydrase (~29kDa), bovine serum albumin (~66kDa), yeast alcohol dehydrogenase (~150kDa), sweet potato beta-amylase (~200kDa), horse spleen apoferritin (~443kDa), and bovine thyroglobulin (~669kDa). Fractions 1 (the void volume) through 12 were enriched for proteins, protein complexes or protein oligomers and protofibrils with molecular weight above ~100kDa, whereas fractions 15 through 30 were enriched for proteins with molecular weights less than ~100kDa, including monomeric proteins such as PrP^{C}. The levels of prion proteins in each fraction were determined by western blotting, including before and after treatment with 5μg/mL PK for 60 minutes at 37˚C.

Biochemical analyses

Hippocampal slices (n = 5 for each treatment condition) were analysed after dissection of the hippocampus from surrounding tissue, homogenization in lysis buffer (50mM Tris-HCl pH 7.4, 150mM NaCl, 0.1% (w/v) SDS, 0.5% (w/v) sodium deoxycholate, 1% (v/v) NP-40) using

needles as with whole brain homogenates, methanol precipitation of proteins by adding 5× volumes of ice-cold 100% methanol and incubating at -20˚C overnight, followed by centrifugation at (20817xg) at 4˚C for one hour. Supernatants were discarded and pellets were resuspended in 50μL lysis buffer and prepared in 4x sample buffer (NuPAGE LDS, Thermo Fisher Scientific) with a final concentration of 6% beta-mercaptoethanol. As required, aliquots of 1% brain homogenates (w/v in aCSF) of M1000, MU02 and NBH were also utilised for western blot analysis, including after digestion using 5 or 50μg/ml PK for 60 minutes at 37˚C as indicated in the figure legends. The 5μg/ml PK digestion was used for all other PK treatments such as for the PrP-containing preparations used for hippocampal slice treatments (Fig 2D & 2G). In addition, for quantifying levels of PrP in brain homogenates and other preparations used in electrophysiology studies, a serial dilution of recombinant full-length mouse PrP (rPrP; made as described previously [35]) of known concentrations (prepared as described in [36]) was utilized to generate a standard curve of rPrP through probing by western blotting (using 8H4 anti-PrP antibody) and densitometric analysis, which was then used to estimate levels of PrP in the various preparations loaded onto the same gel. Proteins were analysed by PAGE and immunoblotting as described previously [37]. Briefly, samples were resolved on NuPAGE Novex 4–12% Bis-Tris gels (ThermoFisher Scientific), transferred to PVDF membrane (Millipore), blocked in either 5% (w/v) skim milk powder (SkM) or 3% (w/v) bovine serum albumin (BSA), probed with various antibodies (see S1 Table for a summary of primary and secondary antibodies utilized, their dilutions, as well as blocking conditions/antibody diluents), with protein detection using enhanced chemiluminescence (ECL Prime and Select, Invitrogen). Membranes were also stained with Coomassie blue (and de-stained) to determine relative total protein levels. All chemiluminescent and digital imaging was carried out using a Fujifilm LAS-3000 Intelligent dark box.

Statistical analyses

Statistical analyses were performed using GraphPad Prism 6 (USA). The PTP and LTP fEPSP data were exported to Excel files (by LTP Analyzer software from Multichannel Systems) where they were normalized to average fEPSP recorded over the last five minutes of baseline recording. An unpaired Student t test (parametric test with Welch's correction) was used to compare the average LTP and PTP of the treatment groups, such as NBH controls versus prion containing (or depleted) preparations. A paired Student t test (parametric test) was used to compare the average ratio of PPF1 and PPF2. I-O1 and I-O2 were compared using ANOVA with repeated measures. The fEPSP amplitudes of the HFS trains were quantified using PlotDigitizer software and normalized to the baseline fEPSP amplitude. The slope of decline of fEPSP amplitude from pulse 3 to the last pulse in each HFS train was compared between treatment groups by one phase decay exponential function in which the time constant of decay (Tau = 1/K) measures the rate of RRP decline in each train. The ratio between pulse 1 (P1) and pulse 2 (P2) of each train was compared between trains within a treatment group by paired Student t test to measure the probability of release per train. Cumulative fEPSP responses of each of the three trains were compared between treatment groups using a linear fit equation (of the last 4 cumulative fEPSPs/train) comparing Y-intercepts upon the initial stimulus after extrapolating the linear fit [32, 33]. Acute synaptotoxicity in the form of LTP and PTP change was calculated as the percentage decrease relative to their appropriate negative controls. The acute synaptotoxicity estimated in the form of PPF ratio was calculated as the percentage of PPF ratio decline in PPF2 relative to PPF1. Because the PPF ratio is inversely proportional to the *Pr*, the percentage of PPF ratio decline represents the *Pr* increase in PPF2. All data are presented as mean (m) ± standard error of mean (SEM). The western blot bands of interest were quantified by

densitometry (Image J), after correcting for total protein level and analysed by Student unpaired t test (parametric test with Welch's correction).

Results

M1000 and MU02 brain homogenates are acutely synaptotoxic to mouse hippocampal CA1 region

Brains of terminally sick prion infected mice are presumed to contain all pathogenic species responsible for the development of prion diseases. To determine if some of these species are acutely synaptotoxic, independent of *de novo* propagation of PrP^{Sc} given the very short time-frame of the experiments, crude brain homogenates were introduced onto *ex vivo* mouse hippocampal slices to determine any deleterious effects on LTP. These crude homogenates were derived from WT C57BL/6J mice intracerebrally inoculated with normal brain homogenate (cNBH) and terminally ill mice infected with either of two mouse-adapted human prion strains, M1000 (cM1000) [28] and MU02 (cMU02) [29]; Fig 1A, 1D and 1G provide examples of PrP^{res} detection by western blots of brain homogenates pre- and post-PK treatment. The hippocampal CA1 region LTP of 12-week-old WT mice was significantly reduced by 53 ± 9% (n = 6) following five-minute exposure to cM1000 (Fig 1B & 1C; see S2A Fig) and by 62 ± 19% (n = 6) following exposure to cMU02 (Fig 1E & 1F; see S2A Fig) relative to cNBH. There was no significant difference between the acute synaptotoxicity of cM1000 and cMU02 (see S2A Fig). Further, there was no significant difference in the degree of LTP disruption of cM1000 in slices generated from 11-month-old WT mice (impaired by 44 ± 7%; n = 7) compared with 12-week-old WT mice (Fig 1H & 1I; see S2A Fig). Consistent with the LTP impairment, the I-O2 curve was not significantly enhanced compared to the I-O1 curve following exposure to cM1000 (in both 12-week-old WT and 11-month-old WT mice) and cMU02 compared with cNBH (see S2E and S2F Fig). In addition, relative to aCSF technical controls, cNBH negative controls did not affect LTP (S2B & S2C Fig).

Lysates from M1000-infected MoRK13 cells are acutely synaptotoxic

Propagation of *bona fide* prions in MoRK13 cell lines that express murine PrP^{C} has been well established through studying M1000 and MU02 *ex vivo* transmission [29, 31]. PK-resistant PrP^{Sc} detected in these cells (Fig 1J) appears a valid biomarker for successful transmission of prions. To determine if these cells also propagate acutely synaptotoxic species similar to cM1000, whole cell lysates derived from MoRK13-Inf were also briefly superfused onto hippocampal slices from 11-month-old WT mice, with the amount of biochemically detectable PrP^{Sc} in MoRK13-Inf lysates balanced to equate that in cM1000. Similar concentration MoRK13-Un lysates did not affect LTP relative to aCSF controls, demonstrating no background toxicity of the uninfected cell lysates (see S2D Fig). Following brief treatment with MoRK13-Inf lysates, the LTP was significantly impaired by 40 ± 6% (n = 6) (Fig 1K & 1L), with the degree of LTP disruption similar to that obtained from cM1000 (see S2A Fig). Consistent with the LTP impairment, the I-O2 also failed to significantly increase relative to I-O1 following exposure to MoRK13-Inf compared with MoRK13-Un (see S2H Fig).

Acute synaptotoxicity of cM1000 is directly associated with PrP species

PrP^{Sc} species are readily detectable in the brains of terminal prion infected mice [38] and PrP^{Sc} species closely correlate with the disruption of neuronal structures including dendritic spines in prion disease *in vivo* mouse models [16] and a primary neuronal cell culture model [25]. To determine the relationship of PrP species to the acute disruption of LTP following

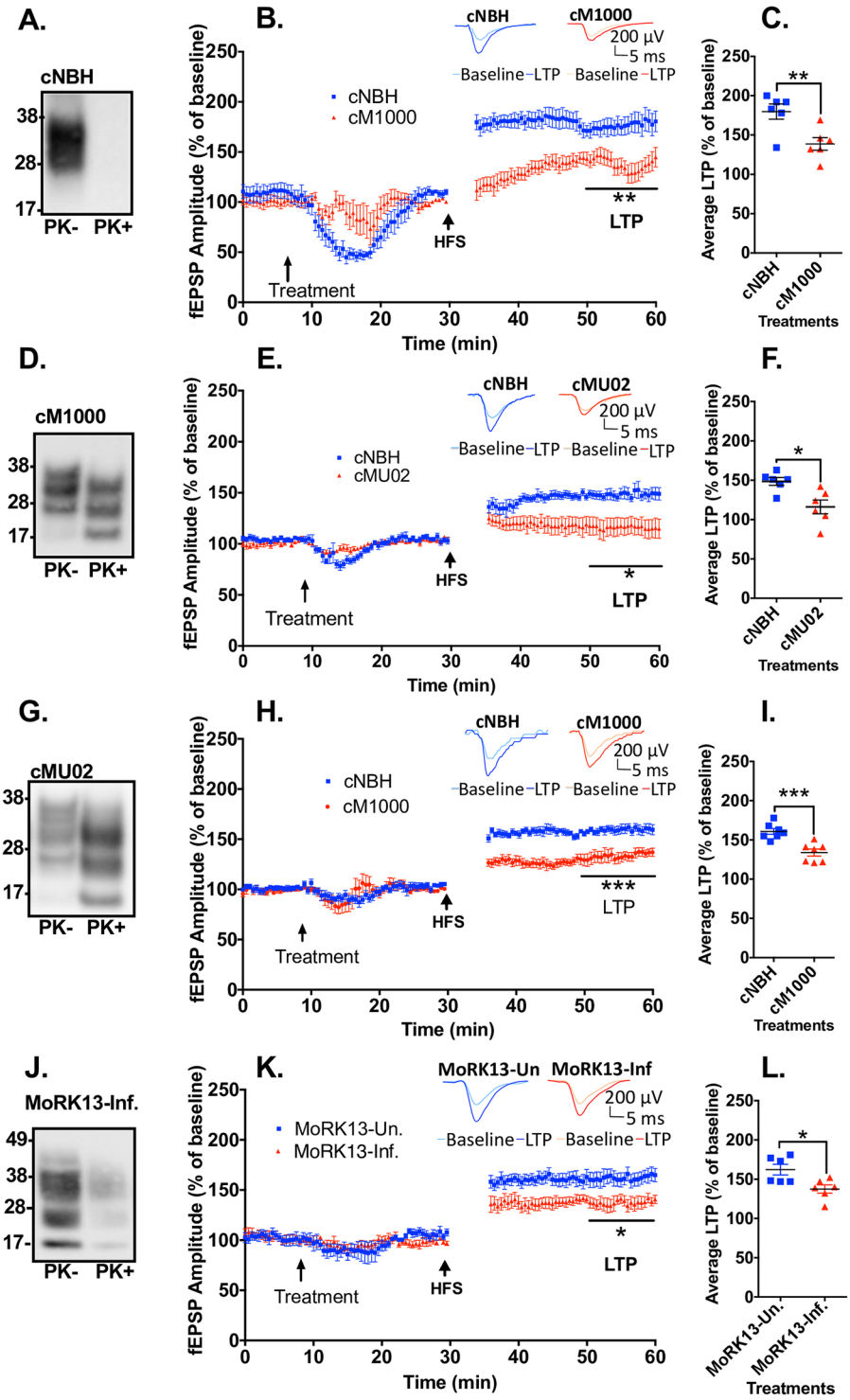

Fig 1. Crude ex vivo PrP^{Sc} containing preparations acutely impair LTP. (A) Western blot of cNBH not treated (-) or treated (+) with 50μg/ml PK. The PK- cNBH was utilised as control preparations for the treatments of WT hippocampal slices using prion-containing crude brain homogenates. (B) cM1000 superfused for 5 minutes over hippocampal slices from 12-week old WT mice approximately 20 minutes prior to HFS caused a significant impairment of LTP with (C) average LTP reduced by 53 ± 9% (n = 6) compared to cNBH. ($p = 0.0087$). (D) Western blot of cM1000 not treated (-) or treated (+) with 50μg/ml PK with PK+ proving presence of PrP^{Sc}. (E) cMU02 superfused for 5 minutes over slices from 12-week old WT mice approximately 20 minutes prior to HFS caused a significant impairment of LTP with (F) average LTP reduced by 62 ± 19% (n = 6) compared to cNBH. ($p = 0.0129$). (G)

Western blot of cMU02 not treated (-) or treated (+) with 50μg/ml with PK+ proving presence of PrP^{Sc}. (H) The PK- cM1000 was superfused for 5 minutes over slices from 11-month old WT mice approximately 20 minutes prior to HFS caused significant impairment of LTP with (I) average LTP reduced by 44 ± 7%; (n = 7) compared to cNBH. ($p = 0.0006$). (J) Western blot of MoRK13-Inf not treated (-) or treated (+) with 50μg/ml PK with PK+ proving presence of PrP^{Sc}. (K) The PK- MoRK13-Inf was superfused for 5 minutes over slices from 11-month old WT mice approximately 20 minutes prior to HFS caused significant impairment of LTP with (L) average LTP reduced by 40 ± 6% (n = 6) compared to MoRK13-Un ($p = 0.0172$). (B, E, H & K) The first five-minute fEPSP recordings following HFS trains have been removed to enhance clarity and the last 10 minutes of post-HFS recordings were used for LTP analysis. (A, D, G, J) Molecular markers are provided at left. (B, E, H, K) Examples of raw fEPSP traces are provided as insets. Data are presented as ± SEM. $^{*}p<0.05$, $^{**}p<0.01$, $^{***}p<0.001$, $^{****}p<0.0001$.

https://doi.org/10.1371/journal.ppat.1007214.g001

exposure to cM1000 in our electrophysiology assay, total PrP species were selectively immuno-depleted from both cM1000 and cNBH under native conditions using the 03R19 antibody [29] coupled to protein-G conjugated sepharose beads. As shown in Fig 2A, relative to the normal rabbit serum (NRS) control, the 03R19 immuno-depletion selectively reduced ~77 ± 12% (n = 9) of PrP^{C} from cNBH (dNBH) and ~77 ± 9% total PrP species and 96 ± 4% PrP^{res} from cM1000 (dM1000). The immuno-depletion did not introduce any synaptotoxicity, wherein dNBH did not affect LTP relative to aCSF controls (see S3B Fig). When hippocampal slices generated from 12-week-old WT mice were treated with dM1000, LTP was not significantly different to dNBH, and was therefore effectively 'rescued' by 74 ± 14% (n = 8) when compared to cM1000 (Fig 2B & 2C), clearly supporting that PrP species in cM1000 are directly responsible for the LTP disruption. In addition, I-O2 became significantly increased relative to I-O1 following exposure to the dM1000 compared with dNBH (see S3G Fig), thus verifying substantial rescue of the synaptic transmission concomitant with the recovery of LTP.

At least modestly PK-resistant PrP^{Sc} species in cM1000 are responsible for acute synaptotoxicity

Both PK-sensitive and PK-resistant species have been found capable of transmitting prion disease [39]. To determine whether any PK-resistant PrP^{Sc} species were directly responsible for the LTP disruption observed with cM1000, cM1000 was treated with PK prior to superfusion over WT hippocampal slices. The mild PK treatment (5μg/ml for one hour at 37˚C) digested ~90% of total protein from cM1000 relative to before the PK treatment but importantly a prominent amount of PK-resistant PrP^{Sc} was still evident on western blotting after the PK digestion, demonstrating that the modest PK treatment had considerably enriched for PrP^{Sc} (Fig 2D lower panel; see S3H Fig columns i-ii & S3I Fig). The mild PK treatment digested ~80% of total proteins from cNBH including all PrP^{C} relative to before the PK treatment (Fig 2D upper panel; see S3H Fig columns v-vi & S3I Fig). Importantly, this mild PK treatment and possible by-products did not cause any background synaptic impairment when comparing PK+NBH relative to the aCSF technical control (see S3C Fig). Hippocampi derived from 12-week-old WT mice exposed to PK+M1000 demonstrated significant LTP impairment of 48 ± 7% (n = 8) relative to PK+NBH (Fig 2E & 2F). Thus, the LTP disruption of the PK +M1000 was approximately equivalent to that of the cM1000 (see S2A & S3A Figs), indicating that at least modestly PK-resistant PrP^{Sc} species are most likely directly responsible for the acute synaptic disruptions caused by cM1000. This dysfunction correlated with the failure of I-O2 to significantly increase relative to I-O1 after treatment with PK+M1000 (see S3E Fig).

To further validate that PrP^{Sc} species, in particular PK resistant species, are directly responsible for the acute synaptotoxicity, the total PrP species immuno-precipitated (IP) from cM1000 (IP-M1000) and cNBH (IP-NBH) (using the method employed for PrP immuno-depletion) were eluted from the IP pellets by the same modest PK treatment (5μg/ml for one hour at 37˚C). This PK elution digested ~70% of total proteins from IP-NBH pellets including

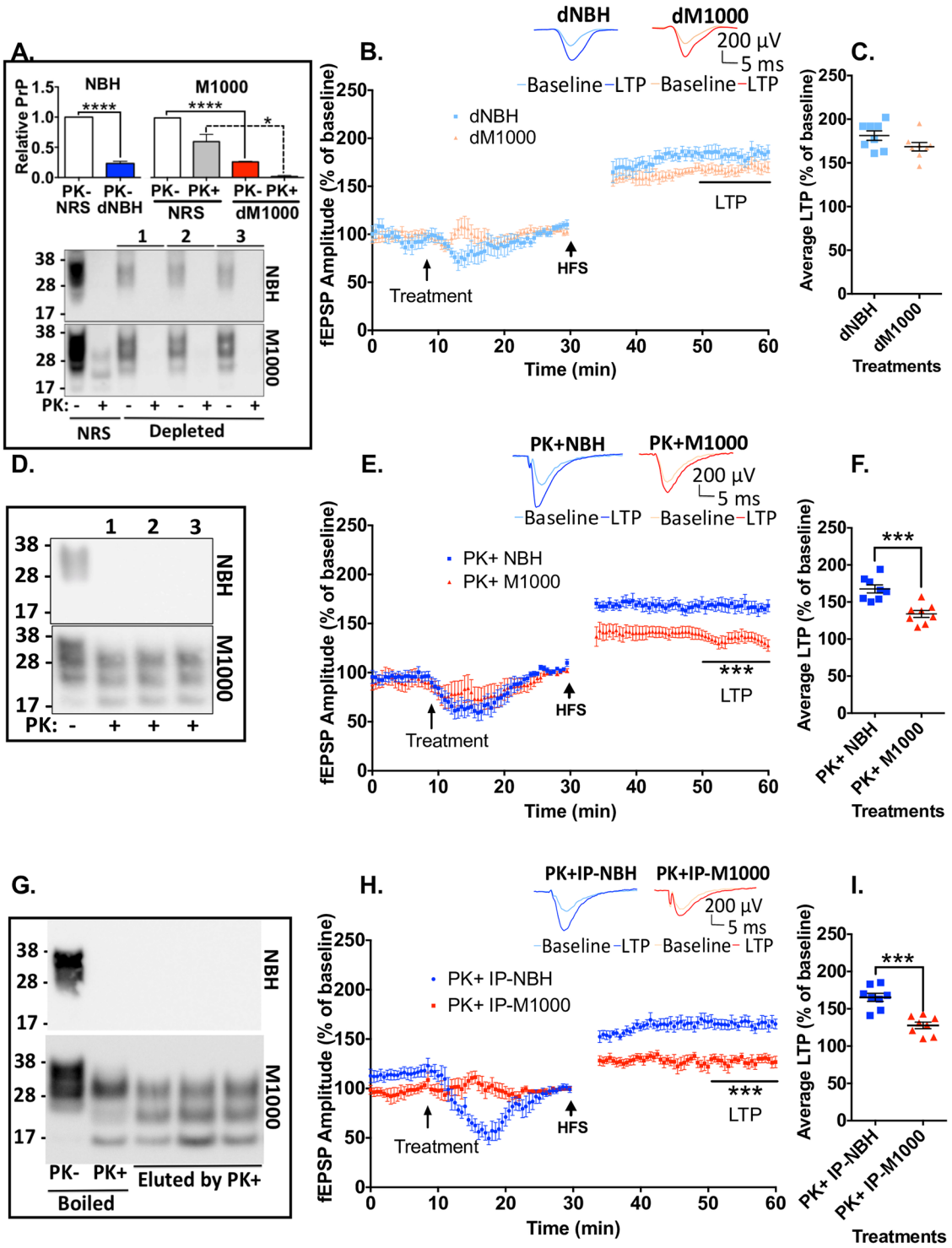

Fig 2. PK-resistant PrP species are responsible for acute synaptotoxicity. (A) PrP immuno-depletion selectively depleted ~77 ± 12% of PrP^{C} (dNBH) from cNBH and ~77 ± 9% total PrP species and 96 ± 4% of PK-resistant PrP (dM1000) from cM1000 relative to the normal rabbit serum (NRS) controls. Controls and depleted preparations were either not treated (-) or treated (+) with 50µg/ml PK to determine the level of PK-resistant PrP. (B) dM1000 superfused for 5 minutes over hippocampal slices from 12-week old WT mice approximately 20 minutes prior to HFS trains displayed significant rescue of LTP with (C) average LTP increased 74 ± 14% (n = 8), which was no longer significantly different to slices superfused with dNBH. (D) Western blot of cNBH and cM1000 treated with 5µg/mL PK (PK+NBH; PK+M1000), which was sufficient to completely degrade all PrP^{C} in cNBH. (E) PK+M1000 superfused for 5 minutes over slices from 12-week old WT mice approximately 20 minutes prior to HFS significantly impaired LTP

with (F) average LTP reduced by 48 ± 7% (n = 8) relative to PK+NBH preparations ($p = 0.003$). (G) Pellets generated through PrP immuno-precipitation (IP) of total PrP from cNBH and cM1000 were resuspended and western blotted after 5μg/mL PK digestion to specifically elute at least modestly PK resistant PrP^{Sc}, with comparison made to NBH and M1000 resuspended pellets wherein PK-resistant PrP was eluted by boiling after PK digestion with 5 μg/ml PK. (H) The resuspended, PK-eluted IP pellets from cNBH (PK +IP-NBH) or cM1000 (PK+IP-M1000) superfused for 5 minutes over slices from 12-week old WT mice approximately 20 minutes prior to HFS caused significant impairment of LTP measured during the last 10-minutes of post-HFS recording, with (I) average LTP reduced by 59 ± 5% (n = 8) relative to PK+IP-NBH preparations ($p = 0.001$). (B, E & H) The first five-minute fEPSP recordings following HFS trains have been removed to enhance clarity. (A: lower panel, D, G) Molecular markers are provided at left. (B, E, H) Examples of raw fEPSP traces are provided as insets. Data are presented as ± SEM. $^{*}p<0.05$, $^{**}p<0.01$, $^{***}p<0.001$, $^{****}p<0.0001$.

https://doi.org/10.1371/journal.ppat.1007214.g002

all PrP^{C} (Fig 2G upper panel; see S3H Fig columns vii-viii, & S3I Fig) and ~80% of total proteins from IP-M1000 pellets, leaving substantial levels of PrP^{Sc} in the preparations as revealed by western blotting (Fig 2G lower panel; see S3H Fig columns iii-iv, & S3I Fig), effectively enriching the preparations for modestly PK-resistant PrP^{Sc}. Following brief exposure of 12-week-old WT hippocampal slices to the PK-eluted IP-M1000 (PK+IP-M1000), LTP was significantly impaired by 59 ± 5% (n = 8; Fig 2H & 2I). Noteworthy is that the degree of LTP disruption caused by the PrP^{Sc} alone from IP pellets was at least as great as that obtained from cM1000 and PK+M1000 (see S2A & S3A Figs), strongly supporting that these species were responsible for the LTP disruption observed with other M1000 preparations. Consistent with the LTP dysfunction, the I-O2 was also prevented by PK+IP-M1000 from becoming significantly enhanced after LTP induction relative to I-O1 (see S3F Fig).

Multimeric PrP^{Sc} species present in M1000 preparations correlate with the acute synapototoxicity to LTP

Similar to misfolded pathogenic proteins responsible for other neurodegenerative diseases such as amyloid-beta (Aβ) in AD and alpha-synuclein in Parkinson's disease, the neurotoxic species in prion diseases is believed to be soluble multimers or oligomers [40, 41]. Considerable data supports that PrP^{Sc} species accumulate into different size multimers such as oligomers and protofibrils, correlating with the natural evolution of prion disease and the onset of clinical signs in mice [42, 43]. To determine any correlation between the presence of multimeric PrP^{Sc} species in M1000 preparations causing acute synaptic dysfunction (especially cM1000, and PK+IP-M1000), PrP^{Sc} species in these preparations underwent size exclusion chromatography and analysis by western blotting. For the negative control, PrP^{C} species in cNBH were also fractionated by size exclusion chromatography. Through the use of size exclusion markers with molecular weights of ~400kDa, ~200kDa, ~66kDa and ~29kDa, protein complexes larger than 100kDa, including PrP^{Sc} multimers, were eluted in fractions 1 through 12, whereas protein species smaller than 100kDa, including PrP^{C}, PrP^{Sc} monomers and endoproteolytic fragments were eluted in fractions 14 through 40. Relative to fractions of cNBH where most PrP^{C} species were eluted as monomers (Fig 3A and 3B), the fractions of cM1000 contained mostly multimeric PrP^{Sc} species (Fig 3C upper panel and Fig 3D) wherein significant levels were at least modestly PK-resistant (Fig 3C lower panel and Fig 3D). Interestingly, fractions of PK+IP-M1000 also contained predominantly at least modestly PK-resistant PrP^{Sc} multimers. In contrast, fractions of dM1000 contained significantly reduced levels of the multimeric PrP^{Sc} species, especially fractions 5–10, including at least modestly PK-resistant multimeric PrP^{Sc} species (Fig 3G and 3H), which were present at substantial levels in cM1000 (Fig 3C & 3D) and PK+IP-M1000 (Fig 3E & 3F). Consequently, the increased levels of multimeric PrP^{Sc} species in fractions 5–10 of cM1000 and PK+IP-M1000 which were relatively depleted in dM1000 appear most strongly correlated with the acute impairment of LTP (Fig 2).

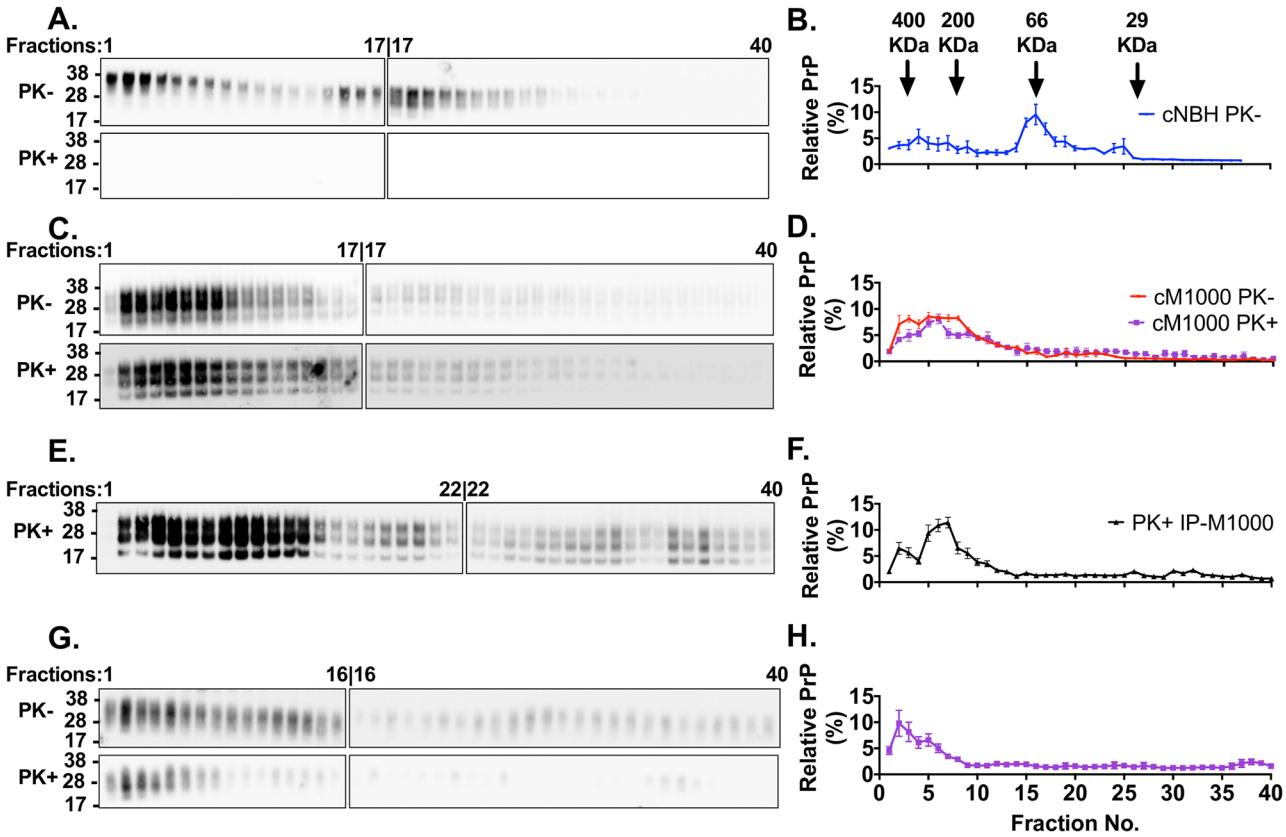

Fig 3. Prion acute synaptotoxicity is associated with increased levels of multimeric PrP^{Sc} species in *ex vivo* M1000 preparations. (A) Representative anti-PrP immunoblots of fractions collected following size exclusion chromatography of 10% (w/v) cNBH after clarifying centrifugation, solubilization in 4% (w/v) Sarkosyl and exhaustive dialysis. The fractions were immunoblotted before (-) and after (+) mild PK treatment (PK; 5μg/mL PK; incubated at 37˚C for an hour). (B) Densitometric analysis of the immunoblots of cNBH fractions (n = 3) displayed as the percentage of PrP in each fraction over the sum of PrP levels in all the fractions. (C) Representative anti-PrP immunoblots of fractions collected following size exclusion chromatography of 10% (w/v) solubilized, dialyzed, and pre-cleared cM1000. The fractions were immunoblotted before (-) and after (+) mild PK treatment as described for (A). (D) Densitometric analysis of the immunoblots of cM1000 fractions (n = 3). (E) Representative anti-PrP immunoblots of fractions collected following size exclusion chromatography of at least modestly PK-resistant PrP^{Sc}, extracted from 1% (w/v) cM1000 by immunoprecipitation (IP) and eluted by a mild PK digestion (5μg/mL PK at 37˚C for an hour) before being concentrated (10-fold to be equivalent to 10% w/v), solubilized, dialyzed, and pre-cleared for the size fractionation (PK+IP-M1000). (F) Densitometric analysis of the immunoblots of PK +IP-M1000 fractions (n = 2). (G) Representative anti-PrP immunoblots of fractions collected following size exclusion chromatography of solubilized, dialyzed, and pre-cleared 10% (w/v) M1000 brain homogenates containing only ~30% of the total PrP following selective removal of ~70% by immuno-depletion (dM1000). The fractions were immunoblotted before (-) and after (+) mild PK treatment (5μg/mL PK at 37˚C for an hour). (H) Densitometric analysis of the immunoblots of dM1000 fractions (n = 3). (D & H) The levels of fractionated PrP with and without PK treatment were overlaid for illustration purposes and cannot be compared quantitatively because they were analysed independently. The effective molecular weights of PrP species collected in fractions one through 12 were larger than 100kDa consistent with multimeric species while those collected in fractions 15 through 40 were smaller than 100kDa (Molecular weight markers are indicated as arrows above B. (A, C, E, and G) Since all 40 fractions could not be loaded onto one 26-well gel, two 26-well gels were used for immunoblotting of the fractions from one size exclusion chromatography experiment; importantly the last fraction on the first gel was also loaded as the first on the second gel, thereby allowing the levels of PrP on the second blot to be normalized to those on the first blot. The PrP species were probed by either anti-PrP 03R19 (in A, C, and G) and 8H4 (in E) antibody. (A, C, E, and G) Molecular weight markers are provided at left. (B, D, F, and H) The data are presented as mean ± SEM.

https://doi.org/10.1371/journal.ppat.1007214.g003

Detailed electrophysiological analyses suggests acute synaptotoxicity of PrP^{Sc} may be associated with heightened pre-synaptic vulnerability

PrP^{Sc} appears to reduce the probability of release (*Pr*) following expression of disrupted LTP. The paired pulse facilitation (PPF) ratio was used to determine if the *Pr* from docked neurotransmitter vesicles was disrupted and thereby contributing to the impairment of LTP in WT hippocampal slices. The PPF ratio is inversely related to the *Pr*, becoming significantly

reduced following LTP (PPF2) relative to before LTP induction (PPF1) due to an increase in the *Pr*. A normal reduction in the PPF2 ratio was demonstrated in all negative controls including cNBH similar to that obtained in aCSF technical controls (Fig 4A; see S4A & S4B Fig). Conversely, the PPF2 ratio did not significantly reduce after exposure to any prion containing preparations (cM1000, MoRK13-Inf, cMU02 and PK+IP-M1000) (Fig 4A; see S4B Fig). These data suggest there may be a significant failure of *Pr* to increase during LTP induction, thereby contributing to and correlating with the impairment of LTP. There was no difference in the degree of *Pr* impairment obtained in 12-week-old WT mice compared with 11-month-old WT mice (see S4B Fig). Importantly, the PPF ratio decline returned when slices were superfused with using dM1000, correlating with the rescued LTP (Fig 4A; see S4B Fig).

Because the impairment of PPF ratio decline in prion containing preparations had only been measured after high frequency stimulation (HFS) trains utilised to induce LTP, it remained unclear whether the PPF ratio became disrupted immediately following exposure to PrP^{Sc}. To determine if PrP^{Sc} may directly impair PPF independent of LTP expression, PPF was measured before (PPF1A) and shortly after (PPF1B) exposure to cM1000 without HFS. Baseline recordings were temporarily disrupted during the five-minute exposure to cNBH and cM1000 (maximal at ~15 minutes of recording) but quickly recovered to normal baseline levels (S4E Fig). Interestingly, the PPF ratio after exposure to cM1000 did not differ from cNBH, nor did the PPF ratio decline over the next ~ 50 minutes (Fig 4B; n = 8), suggesting that PrP^{Sc} does not appear to directly impair *Pr* and that the mechanisms underlying disruption of *Pr* by PrP^{Sc} are only manifested in the context of induction and expression of LTP.

PrP^{Sc} appears to disrupt post-tetanic potentiation in WT hippocampal slices by impairing the action potential dependent replenishment of the readily releasable pool (RRP) of vesicles during HFS trains, while *Pr* and mechanisms of neurotransmitter release remain normal. In addition to the PPF ratio, PTP was another pre-synaptic parameter assessed immediately after HFS trains. Relative to appropriate negative controls where PTP was not affected compared with aCSF controls (see S4C Fig), cM1000, cMU02, and MoRK13-Inf significantly disrupted PTP, further supporting that pre-synaptic impairment may be a key component of the acute synaptotoxicity, which was evinced by HFS (Fig 4C). Similar to the LTP impairment, the PTP disruption was age independent up to 11 months old (see S4D Fig). Further, PTP disruption was still evident when using PK+M1000 and PK+IP-M1000 (Fig 4C; S4D Fig), supporting that this PTP disruption also appears directly associated with modestly PK-resistant PrPSc. Noteworthy, however, in contrast to the significant rescue of both LTP and PPF, the PTP remained significantly impaired when exposed to dM1000 (Fig 4C; see S4D Fig), thereby further suggesting a possible enhanced pre-synaptic vulnerability to the acute synaptotoxicity possibly linked to the residual PrPSc, including some multimeric species (Fig 3G & 3H) in these preparations. PTP is strongly influenced by the *Pr*, RRP size, RRP depletion rate, and RRP replenishment rate, which are all action potential-elicited Ca2+-dependent functions in the pre-synaptic terminal during HFS trains [44]. Detailed electrophysiological analyses showed the *Pr* (Fig 4D) and RRP depletion rate (Fig 4E & 4F) appeared normal across the three HFS trains in both cM1000 and dM1000 relative to cNBH and dNBH, respectively demonstrating that mechanisms of neurotransmitter release are probably not impaired in PTP disruption; however, the size of the RRP, while normal in train 1 (T1) became progressively and significantly diminished in trains 2 (T2) and 3 (T3) in both cM1000 (n = 17) and dM1000 (n = 7) (Fig 4G & 4H) as a result of significant disruption of RRP replenishment in T2 and T3 (Fig 4I & 4J), thereby probably contributing to the disruption of PTP after exposure to both M1000 preparations.

PrP^{Sc} acute synaptotoxicity in WT hippocampi is associated with decreased expression levels of pre- and post-synaptic components crucial for LTP induction and maintenance. Altered expression levels of core synaptic components integral for maintaining normal

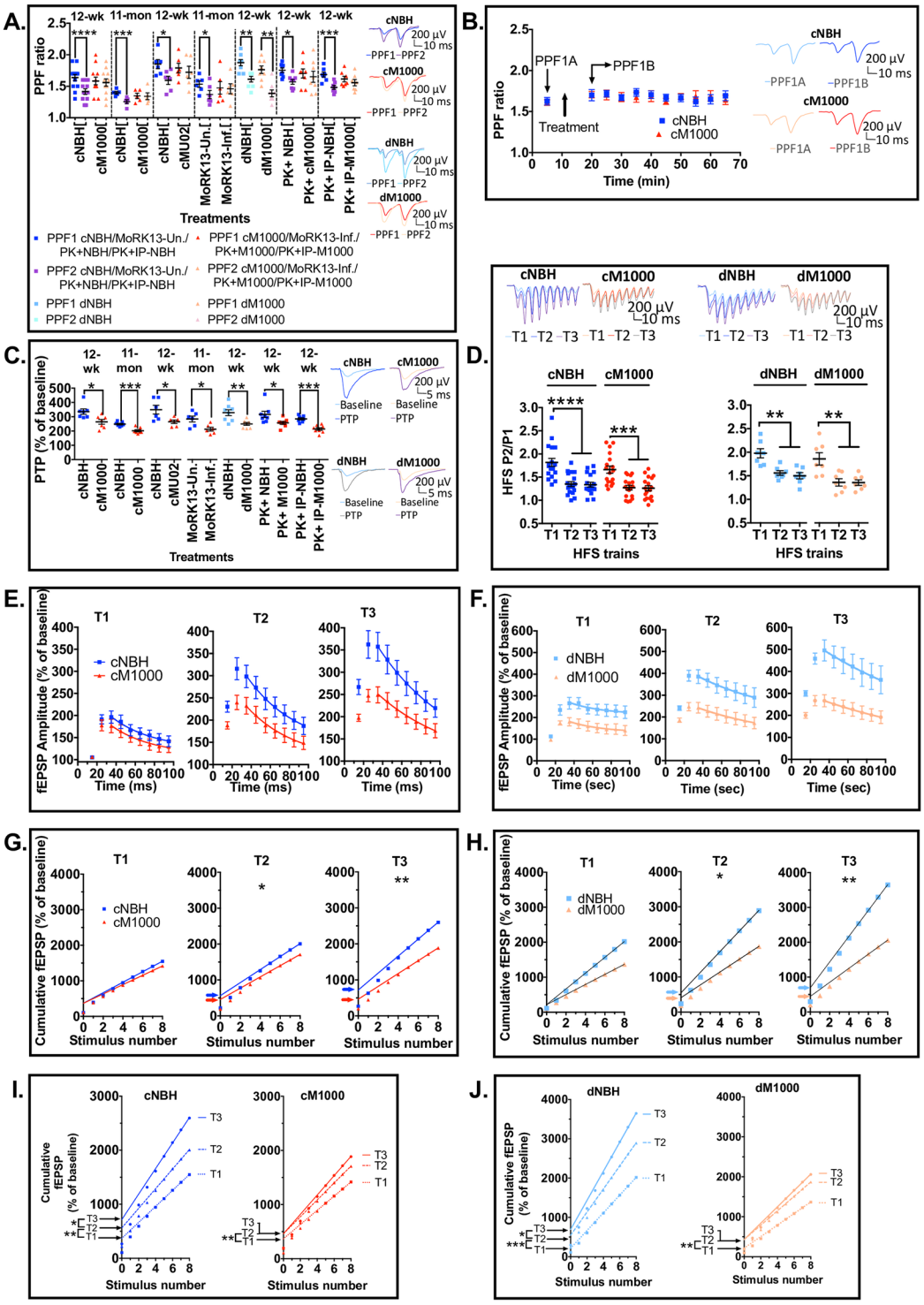

Fig 4. Prion acute synaptotoxicity demonstrates enhanced pre-synaptic vulnerability in WT hippocampal slices. (A) Normal PPF ratio reductions (the ratio becomes significantly reduced in PPF2 relative to PPF1) were obtained in slices after LTP induction and exposure to all negative controls: cNBH (for cM1000 treatments in 12-week old [$p<0001$] and 11-month old mice [$p = 0.0008$]; cMU02 treatment [$p = 0.0104$]); dNBH ($p = 0.0017$); PK+NBH ($p = 0.0182$); PK+IP-NBH ($p = 0.0002$); and MoRK13-Un ($p = 0.0170$). Conversely, PPF ratio in slices treated with cM1000 (both in 12-week and 11-month old mice), cMU02, MoRK13-Inf, PK+M1000, and PK+IP-M1000 was not reduced in PPF2 relative to PPF1, showing poor *Pr* associated with the LTP disruption. The PPF ratio was normal in dM1000 ($p = 0.0013$) concomitant with the recovery of LTP. (B) Treatment of slices with cM1000 without inducing LTP expression did not affect PPF ratios

relative to slices treated with cNBH. (C) Relative to appropriate negative controls, PTP was significantly disrupted after cM1000 treatment of slices from 12-week-old ($p = 0.0144$) and 11-month-old ($p = 0.0006$) mice. Similar PTP disruption was obtained following treatment with cMU02 ($p = 0.0391$), MoRK13-Inf ($p = 0.0172$), dM1000 ($p = 0.0062$), PK+M1000 ($p = 0.0359$), and PK+IP-M1000 ($p<0.0001$). (D) The *Pr* during the HFS trains was normal in both cM1000 and dM1000 relative to cNBH and dNBH controls, respectively where the *Pr* became significantly increased (determined by the P1 to P2 ratio in each train) in T2 and T3 relative to T1. (E & F) Consistent with the normal *Pr*, the rate of RRP depletion was normal across three HFS trains in both cM1000 (E) and dM1000 (F), where the time constant of decay between P3 and P9 in each train was not different between cNBH and cM1000, as well as between dNBH and dM1000. (G & H) The size of RRP (determined by the Y-intercepts of the linear fit of the last four pulses of HFS) became significantly diminished at T3 in cM1000 (G) and dM1000 (H) relative to cNBH (G) and dNBH (H). (I & J) This reduction in RRP size was caused by a significant impairment of the RRP replenishment (indicated by the increase in the RRP size between trains) to refill the RRP at T3 in both cM1000 (I) and dM1000 (J) compared with cNBH (I) and dNBH (J). The reduction in RRP size contributed directly to the impairment of PTP. (A-D) Examples of raw fEPSP traces are provided as insets. Data are presented as ± SEM. $^{*}p<0.05$, $^{**}p<0.01$, $^{***}p<0.001$, $^{****}p<0.0001$.

https://doi.org/10.1371/journal.ppat.1007214.g004

synaptic functions, have been frequently reported as features of Aβ42 toxicity [45]. The disruption we observed, especially the PPF ratio and PTP disruption, suggested the likelihood of perturbed expression of key pre-synaptic markers. Western blotting of WT hippocampi with impaired PPF2 ratios revealed a significant down-regulation of the synaptic vesicle proteins synaptophysin and VGLUT1, relative to hippocampi with normal PPF2 ratios (Fig 5A & 5D). It is important, however to acknowledge that because PTP reflects short-term synaptic potentiation, which lasts only a few minutes after HFS trains, and the tissues were harvested following LTP expression, these altered pre-synaptic markers represent the pre-synaptic concomitants of LTP impairment that persisted throughout the expression of LTP.

Other synaptic proteins including the NR2A- and NR2B-subunits of NMDAR and the GluA2 subunit of AMPAR, as well as pERK, pCREB (Fig 5B, 5C & 5D) were also down-regulated in WT hippocampi manifesting impaired LTP, thereby supporting that the PrP^{Sc} acute synaptotoxicity is not exclusively pre-synaptic. Although NMDAR are required for both pre- and post-synaptic functions, they are clearly most abundant post-synaptically [46]. Therefore, the reduced expression levels of NR2A and NR2B as well as GluA2 suggest post-synaptic disruptions in hippocampal glutamatergic synapses. The decreased expression levels of pERK and the transcription factor pCREB that activate pathways for production of synaptic proteins [47] further supports post-synaptic disruption. This suggests that pERK and pCREB are likely downstream effectors of PrP^{Sc} acute synaptotoxicity contributing to diminished expression of other synaptic proteins. Procaspase-3 was also down-regulated in hippocampi with impaired LTP (n = 5; Fig 5E & 5F), although the amount of active caspase 3 was normal (n = 5; Fig 5E & 5F), indicating that intracellular signalling cascades downstream of caspase-3 activation were probably normal, whereas mechanisms of generating procaspase-3 were conceivably disrupted. Importantly, expression levels of all these synaptic proteins were unaltered in hippocampal slices treated with dM1000 (Fig 5A–5F), correlating with the rescue of LTP and PPF ratio and despite persisting impairment of PTP. Moreover, post-synaptic markers such as PSD95 and Fyn remained unaltered in cM1000 (Fig 5C & 5D), suggesting that while PrP^{Sc} acutely disrupted post-synaptic function contributing to LTP impairment, it is less likely there was an acute loss of dendritic spine compartment volume over the very short time-course of our observations.

PrP^{Sc} remains acutely synaptotoxic to PTP and LTP independent of PrP^{C} expression

Ongoing PrP^{C} expression is required for the sustained propagation of transmissible and neurotoxic PrP^{Sc} to cause prion disease [27, 31]. PrP^{C} has also been described as a receptor for transducing soluble, oligomeric Aβ42 synaptotoxicity [26]. To determine if PrP^{Sc} acute

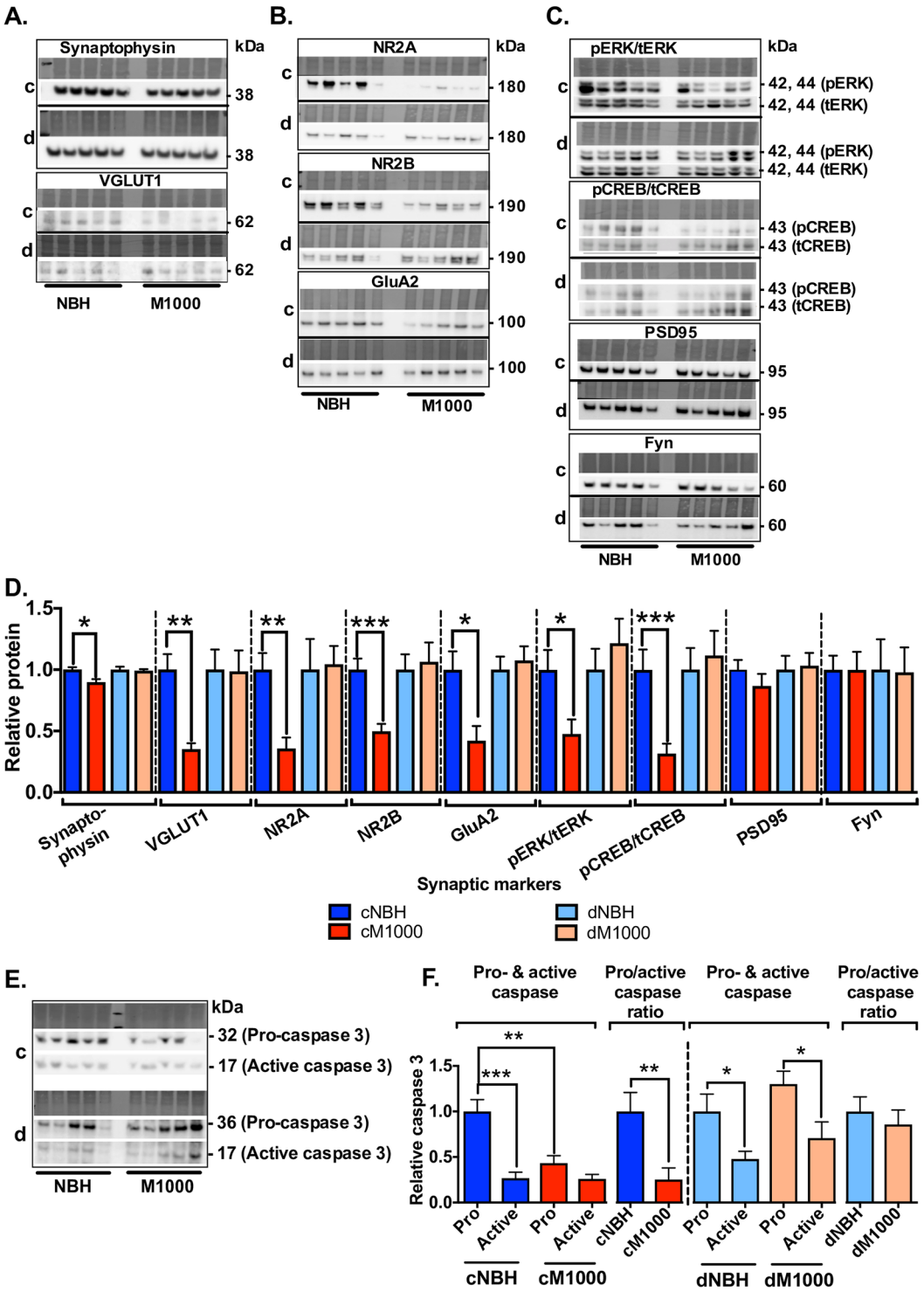

Fig 5. Altered expression levels of key pre- and post-synaptic markers correlate with synaptic dysfunction in WT hippocampi. Following induction of LTP, hippocampi were homogenized and biochemically analysed for key synaptic markers. (A & D) Hippocampi treated with cM1000 [*c*] expressed reduced levels of pre-synaptic markers, synaptophysin ($p = 0.0280$) and VGLUT1 ($p = 0.0108$), relative to those treated with cNBH [*c*]. Conversely, WT hippocampi treated with dM1000 [*d*] were associated with unaltered synaptophysin and VGLUT1 levels relative dNBH [*d*]. (B & D) NR2A/B-containing NMDAR were also reduced in hippocampi treated with cM1000 (NR2A: $p = 0.0012$; NR2B: $p = 0.0003$) relative to those treated with cNBH, with unaltered levels when employing dM1000 and dNBH. GluA2-containing AMPAR were also reduced in hippocampi treated with cM1000 relative to those treated with cNBH ($p = 0.0077$), with unaltered levels when

employing dM1000 and dNBH. (C & D) Expression levels of pERK and pCREB were reduced in slices exposed to cM1000 (pERK: $p = 0.0339$; pCREB: $p = 0.0108$) relative to cNBH but were unaltered when employing dM1000 and dNBH. PSD95 remained unaltered after exposure to both cM1000 and dM1000 supporting no loss of pre-existing synapses in prion acute synaptotoxicity. Fyn levels remained unaffected after treatment with either cM1000 or dM1000. (E & F) Relative to cNBH, cM1000 reduced expression levels of procaspase 3 ($p = 0.0028$) with unaltered production of the active form, thereby significantly reducing the pro- to active caspase 3 ratio ($p = 0.0083$). The pro-caspase 3 expression level was unaltered after treatment with dM1000 compared with dNBH with a normal pro- to active caspase 3 ratio. (A-C, E) Molecular weight markers are provided at right. Data are presented as ± SEM. $^{*}p<0.05$, $^{**}p<0.01$, $^{***}p<0.001$, $^{****}p<0.0001$.

https://doi.org/10.1371/journal.ppat.1007214.g005

hippocampal synaptic disruption requires PrP^{C} expression, the synaptotoxicity of cM1000 was assessed using slices derived from 12-week-old PrPo/o mice. The degree of LTP impairment in these PrPo/o hippocampal slices following exposure to cM1000, was less marked but broadly comparable to that observed in WT slices (Fig 6A & 6B; see S5E Fig), thereby demonstrating that PrP^{C} expression is not crucial for the acute synaptotoxic mechanisms underlying disruption of LTP by PrP^{Sc}. Notably though, in contrast to WT slices treated with cM1000 (Fig 4A), the PPF2 ratio significantly decreased following HFS trains, thereby mirroring what occurred with exposure to cNBH (Fig 6C; see S5G Fig) although PTP remained significantly impaired in PrPo/o slices following cM1000 treatment (Fig 6D; see S5F Fig). These findings suggest that any pre-synaptic dysfunction following HFS trains may also be at least partly PrP^{C} independent and that because the *Pr* was not significantly diminished during LTP expression the mechanisms of any PrP^{Sc} pre-synaptic dysfunction in PrPo/o slices are subtly but notably different compared with WT mice. Of further noteworthiness, the LTP, PTP, and PPF ratio in PrPo/o slices treated with cNBH were not affected compared with PrPo/o slices treated with aCSF (see S5 Fig), demonstrating no background synaptotoxicity from crude brain homogenates and importantly, the LTP, PTP, and PPF ratio obtained from PrPo/o and WT slices superfused with aCSF only were not different (see S5 Fig), in keeping with previous reports of no significant effect of the loss of PrP^{C} on the Schäffer collateral pathway synaptic functions in young PrPo/o mice [10].

Different mechanisms appear to underlie PrP^{Sc} acute synaptotoxicity in PrPo/o hippocampal slices relative to WT slices

Given the likely fundamental role PrP^{C} plays in synaptic functions [7, 9], it is possible that the molecular components of the pre- and post-synaptic compartments are fundamentally altered to compensate the neuro-developmental absence of PrP^{C} in an attempt to maintain normal synaptic functions, thereby perhaps supporting the possibility of different or distinct mechanisms for any PrP^{Sc} acute synaptotoxicity. The disruption of PTP and LTP in PrPo/o hippocampal slices exposed to cM1000 suggested both pre- and post-synaptic impairments, respectively. The *Pr* during T2 and T3 of the HFS trains showed a normal decline comparable to that observed for cNBH (Fig 6E) and similar to what occurred after exposure of WT slices to cM1000 (Fig 4D). Importantly however, the RRP replenishment also appeared impaired in PrPo/o slices similar to that observed in WT slices (Fig 6G) leading to a significant reduction in RRP size during T3 (n = 11; Fig 6H), thereby probably disrupting PTP (n = 11; Fig 6D). Unexpectedly, the RRP during T1 was minimally but significantly larger in the PrPo/o slices exposed to cM1000 supporting the possibility of enhanced neurodevelopmental compensation to the absence of PrP^{C} made apparent in such slices upon exposure to PrP^{Sc} (n = 11; Fig 6H) explaining why a significant impairment of RRP replenishment was not apparent until T3.

Biochemical analysis of the cM1000 treated PrPo/o hippocampi revealed significantly decreased levels of synaptophysin (Fig 6I & 6J) akin to what was observed in WT slices (Fig 5A & 5D), further supporting a pre-synaptic component to the PrP^{Sc} acute synaptotoxicity in

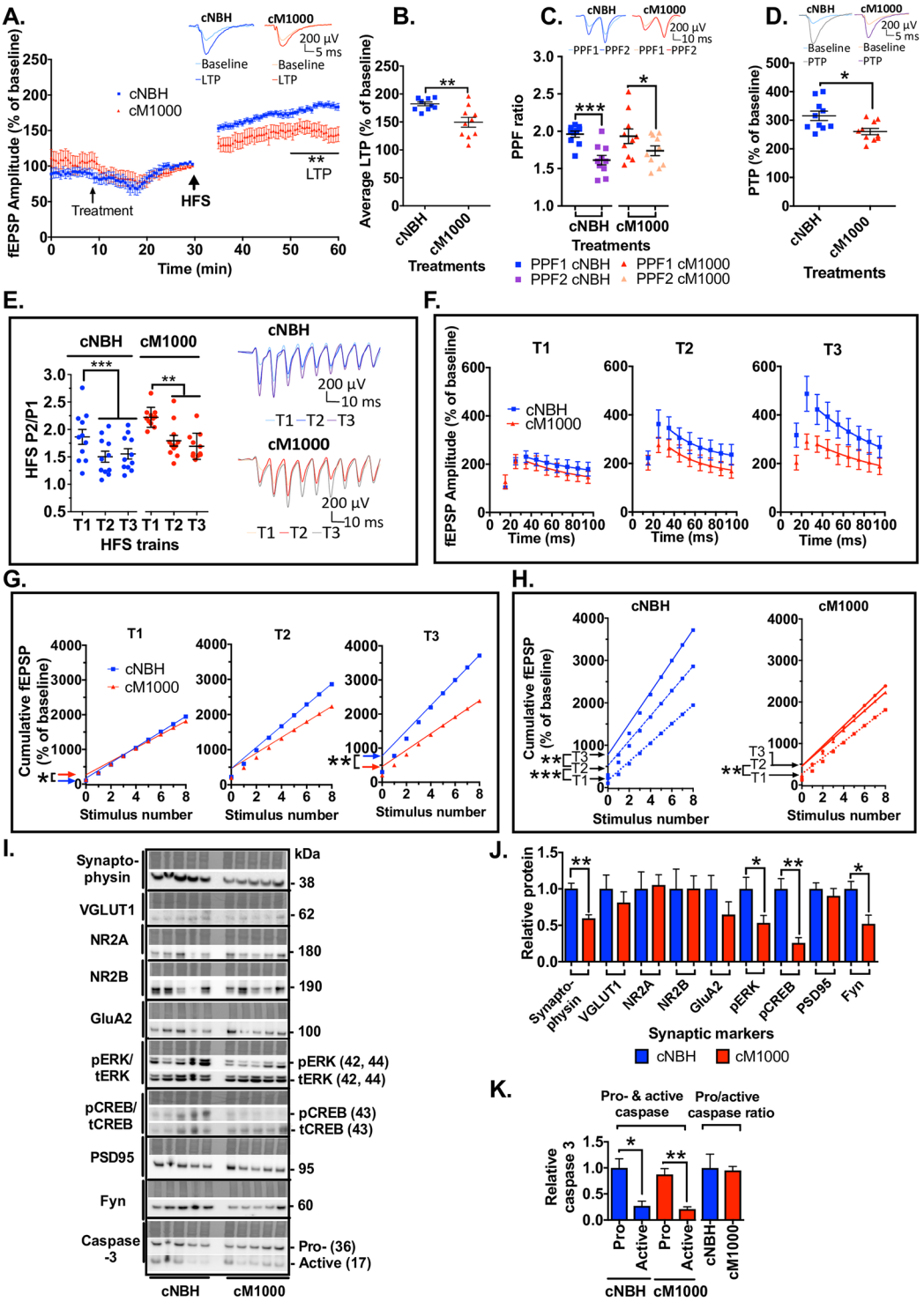

Fig 6. Acute PrP^{Sc} synaptotoxicity is largely PrP^{C} independent. Hippocampal slices derived from PrPo/o mice were used for these experiments. (A) cM1000 superfused over slices approximately 20 minutes prior to HFS trains caused significant impairment of LTP with (B) average LTP reduced by ~37 ± 12% (n = 10) compared with cNBH. (*p = 0.0046*). (C) A normal *Pr* during LTP in slices exposed to both cNBH and cM1000, where PPF2 (after treatment and LTP) became significantly reduced compared with the PPF1 (before treatment and LTP) (*p = 0.0003*). (D) PTP was significantly disrupted after exposure of slices to cM1000 relative to cNBH (*p = 0.0133*). (E) A normal increase in the *Pr* during HFS trains despite treatment with cM1000, demonstrated by a significant increase in the P1 to P2 ratio in T2 and T3 relative to T1. (F) A normal depletion rate of RRP after cM1000 exposure relative to cNBH across the three HFS trains, wherein the time

constant of decay (Tau = 1/K) between P3 and P9 in each HFS train was not different between slices treated with cNBH and cM1000. (G) The size of RRP (determined by the Y-intercepts) in slices treated with cM1000 were modestly but significantly increased in T1 relative to slices treated with cNBH (cNBH: 173 ± 16, cM1000: 269 ± 15; $p = 0.0111$), demonstrating distinctive mechanisms of the acute synaptotoxicity in PrPo/o hippocampi; however, the RRP size of slices treated with cM1000 became significantly reduced in T3 relative to cNBH. (H) The RRP refill in slices treated with cM1000 (estimated by the increase in RRP size between trains) was normal between T1 and T2 (significantly increased from 169 ± 15 in T1 to 450 ± 28 in T2; $p = 0.0048$), but failed to significantly increase between T2 (450 ± 28) and T3 (461 ± 29) (G), thereby reflecting a significantly reduced RRP size. (I & J) Western blotting of PrPo/o hippocampi treated with cM1000 revealed reduced level of synaptophysin ($p = 0.0024$), but not VGLUT1. Exposure to cM1000 significantly reduced hippocampal pERK ($p = 0.0432$) and pCREB ($p = 0.0034$) relative to hippocampi treated with cNBH. Expression levels of NR2A and NR2B-containing NMDAR, and GluA2-containing AMPAR were unaffected by cM1000 treatment. PSD95 and Fyn levels were unaltered by cM1000 ($p = 0.0168$). (I & K) Pro-caspase 3 and production of its active form were unaltered in PrPo/o hippocampi treated with cM1000 relative to cNBH. (I) Molecular weight markers are provided at right. (A, C, D, E) Examples of raw fEPSP traces are provided as insets. Data are presented as ± SEM. $^{*}p<0.05$, $^{**}p<0.01$, $^{***}p<0.001$, $^{****}p<0.0001$.

https://doi.org/10.1371/journal.ppat.1007214.g006

these slices and implying that the disruption of synaptophysin in WT hippocampal slices was probably PrP^{C} independent. In contrast, PrP^{Sc} exposure did not affect expression of VGLUT1 (Fig 6I & 6J), once again supporting that pre-synaptic functions in PrPo/o slices are probably less and differentially susceptible to PrP^{Sc} acute synaptotoxicity compared with WT slices. Additionally, expression levels of NR2A and NR2B and GluA2 remained unaffected by PrP^{Sc} in PrPo/o hippocampi, also supporting the likelihood of different post-synaptic pathophysiological mechanisms of PrP^{Sc} acute synaptotoxicity (Fig 6I & 6J) and implying that the down-regulation of VGLUT1, NR2A, NR2B, and GluA2 in WT hippocampal slices is PrP^{C} expression dependent. Nevertheless, importantly both pERK and pCREB were significantly reduced (Fig 6I & 6J) in PrPo/o slices, underscoring that although there are likely to be nuanced differences in the pathways sub-serving acute synaptic dysfunction in PrPo/o hippocampi, there appears to be overlap in the final effector pathway of post-synaptic dysfunction similar to WT hippocampi. PSD95 remained unaltered in PrPo/o hippocampi again supporting no net loss of the dendritic compartment associated with this acute synaptotoxicity over the very short timeframes of our experiments (Fig 6I & 6J). Interestingly, Fyn levels were significantly reduced in PrPo/o hippocampi after treatment with cM1000 (Fig 6I & 6J), supporting post-synaptic disruption in PrPo/o slices.

WT and PrPo/o hippocampal slices display similar sensitivity to prion acute synaptotoxicity

To determine if WT and PrPo/o hippocampal slices display similar sensitivity to prion acute synaptotoxicity, the dose-response relationships of LTP and PTP were analysed following exposure to a dilution series of cM1000 including 1% (w/v), 0.5% (w/v; as utilised previously), 0.25% (w/v) and 0.1% (w/v). In addition, the approximate level of abnormal or PK-resistant PrP^{Sc} in various preparations employed in our electrophysiological studies was determined. The 1% homogenates caused non-specific technical difficulties with electrophysiological testing precluding their use (S6A Fig). In 0.5% cM1000, there was ~0.168 ± 0.020 μg/mL total PrP including ~0.094 ± 0.020 μg/mL at least modestly PK-resistant PrP^{Sc} (n = 3; Fig 7A and 7B). In 0.25% cM1000 (n = 3), there was ~0.066 ± 0.003 μg/mL total PrP including ~0.026 ± 0.002 μg/mL at least modestly PK-resistant PrP^{Sc}, while in 0.1% cM1000 there was ~0.015 ± 0.004 μg/mL total PrP with ~0.006 ± 0.0003 μg/mL at least modestly PK-resistant PrP^{Sc} (n = 3; Fig 7A and 7B).

For WT hippocampal slices, relative to cNBH controls, the LTP was significantly disrupted in a dose-dependent manner ($p<0.0001$; One-way ANOVA with Bonferroni correction for multiple comparisons) wherein non-PK digested 0.5% (n = 6) and 0.25% (n = 5) cM1000

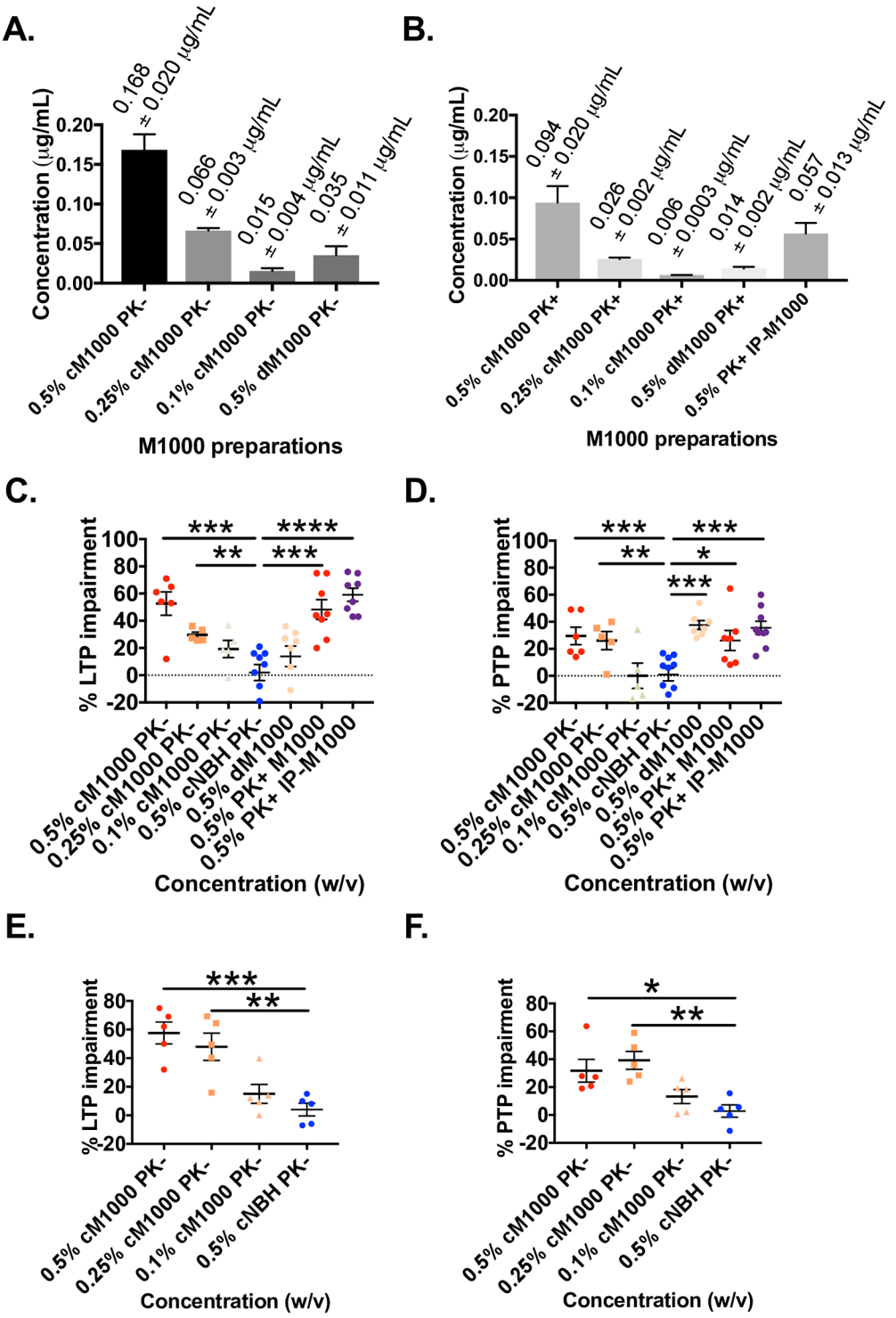

Fig 7. Crude M1000 brain homogenate acute synaptotoxicity dose-response relationships and estimation of total PrP and PK-resistant PrP^{Sc} in preparations used in electrophysiology experiments. A dilution series of recombinant full-length mouse PrP was western blotted (probed with 8H4 monoclonal antibody) and analysed with densitometry to generate a standard curve with aliquots of preparations utilised in electrophysiology experiments run on the same gel. (A) Quantification of levels of total PrP species (without PK treatment) in 0.5% (w/v), 0.25% (w/v), and 0.1% (w/v) cM1000, as well as in 0.5% dM1000 (PrP immuno-depleted cM1000). (B) Relative levels of at least modestly PK-resistant PrP^{Sc} (after treatment with 5µg/mL PK for 1 hour at 37˚C) in 0.5% (w/v), 0.25% (w/v), and 0.1% (w/v) cM1000, as well as in 0.5% (w/v) PK+M1000 and 0.5% (w/v) PK+IP-M1000. (C & D) Percentage of LTP and

PTP impairments (calculated as described in Methods) following exposure of 12-week old WT hippocampal slices to non-PK treated 0.5% (w/v), 0.25% (w/v), and 0.1% (w/v) cM1000 compared to 0.5% (w/v) cNBH controls (One-way ANOVA with Bonferroni correction for multiple comparisons [LTP: $p<0.0001$; PTP: $p<0.0001$]). In 0.5% (w/v) cM1000, LTP and PTP were significantly impaired by 53 ± 9% and 30 ± 6%, respectively. In 0.25% (w/v) cM1000, LTP and PTP were significantly impaired by 30 ± 2% and 26 ± 7%, respectively. In 0.1% (w/v) cM1000, LTP and PTP were not significantly impaired, reduced by only 19 ± 6% and 0.1 ± 9%, respectively. Percentages of LTP and PTP impairment in WT hippocampal slices following exposure to 0.5% dM1000, PK+M1000, and PK+IP-M1000 were also compared to 0.5% (w/v) cNBH controls (One-way ANOVA with Bonferroni correction for multiple comparisons [LTP: $p<0.0001$; PTP: $p<0.0039$]). In 0.5% (w/v) dM1000, the LTP was not impaired significantly (reduced by 14 ± 7%) while PTP was significantly impaired by 38 ± 3%. In 0.5% (w/v) PK+M1000, LTP and PTP were significantly impaired by 48 ± 7% and 26 ± 7%, respectively. In 0.5% (w/v) PK+IP-M1000, LTP and PTP were significantly impaired by 59 ± 5% and 36 ± 5%, respectively. (E & F) Percentage LTP and PTP impairments following exposure of 12-week old PrPo/o hippocampal slices to non-PK treated 0.5% (w/v), 0.25% (w/v), and 0.1% (w/v) cM1000 compared to 0.5% (w/v) cNBH controls (One-way ANOVA with Bonferroni correction for multiple comparisons [LTP: $p<0.0002$; PTP: $p<0.0027$]). In 0.5% (w/v) cM1000, LTP and PTP were significantly impaired by 58 ± 8% and 32 ± 8%, respectively. In 0.25% (w/v) cM1000, LTP and PTP were significantly impaired by 48 ± 10% and 39 ± 6%, respectively. In 0.1% (w/v) cM1000, LTP and PTP were not significantly impaired (reduced by only 15 ± 7% and 13 ± 5%, respectively). Data are presented as ± SEM. $^{*}p<0.05$, $^{**}p<0.01$, $^{***}p<0.001$, $^{****}p<0.0001$.

https://doi.org/10.1371/journal.ppat.1007214.g007

significantly impaired LTP (0.5% $p<0.0001$, impaired by 53 ± 9%; 0.25% $p = 0.0195$, impaired by 30 ± 2%), while it was unaffected by the 0.1% cM1000 (n = 5; Fig 7C). Similarly, PTP in WT hippocampal slices was significantly impaired in a dose-dependent manner ($p = 0.0039$; One-way ANOVA with Bonferroni correction for multiple comparisons) following treatments with the same dilutions of cM1000 wherein both 0.5% (n = 6) and 0.25% (n = 5) cM1000 were significantly toxic to PTP (0.5% $p = 0.0073$, impaired by 30 ± 6%; 0.25% $p = 0.0270$, impaired by 26 ± 7%), while 0.1% cM1000 did not adversely affect PTP (n = 5; Fig 7D). Hence, these results demonstrated a correlation between the levels of PK-resistant PrP^{Sc} and the degree of LTP and PTP dysfunction with a threshold level of at least modestly PK-resistant PrP^{Sc} > ~0.006 μg/ml being toxic to PTP and although acknowledging a probable non-uniform immuno-depletion across the spectrum of PrP species in dM1000 a level >~0.014 μg/ml was toxic to LTP. Levels of at least modestly PK-resistant PrP^{Sc} in 0.5% PK+M1000 and PK+IP-M1000 that were significantly toxic to LTP and PTP were ~0.094 ± 0.020 μg/mL (n = 3) and 0.057 ± 0.013 μg/mL (n = 3), respectively.

For PrPo/o slices relative to cNBH controls, a similar dose-dependent decline in LTP and PTP was observed (n = 5 each; $p = 0.0027$; One-way ANOVA with Bonferroni correction for multiple comparisons). The 0.5% cM1000 reduced LTP significantly by 58 ± 8% ($p = 0.0003$), while 0.25% impaired LTP by 48 ± 10% ($p = 0.0018$); however, 0.1% cM1000 did not significantly disrupt LTP (Fig 7E). Parallel dose-dependent dysfunction was observed with PTP following exposure of PrPo/o hippocampal slices to 0.5%, 0.25%, and 0.1% cM1000, respectively (n = 5 each; $p = 0.0027$; One-way ANOVA with Bonferroni correction for multiple comparisons). Compared to cNBH controls, both 0.5% and 0.25% cM1000 significantly disrupted PTP (0.5% reduced PTP by 32 ± 8%, $p = 0.0135$; 0.25% reduced PTP by 39 ± 6%, $p = 0.0023$); however, 0.1% cM1000 was not significantly toxic to PTP (Fig 7F). Overall, the results were similar to those obtained in WT hippocampal slices, thereby implying that the prion acute synaptotoxicity in PrPo/o hippocampal slices reported in this current study was not due to an altered sensitivity.

Discussion

Herein we report the acute synaptotoxicity of *ex vivo*, prion-containing preparations and provide important new molecular pathophysiological insights. Utilising a number of experimental approaches, our findings revealed that: (1) PrP^{Sc} (particularly at least modestly PK-resistant isoforms most likely as multimeric species) is directly synaptotoxic; (2) that the acute

synaptotoxicity was similar across the two prion strains examined and appears independent of tissue source of prions when balanced for PrP^{Sc} levels; (3) the acute synaptotoxicity is not reliant on hippocampal PrP^{C} expression albeit with noteworthy molecular and electrophysiological differences in the presence or absence of PrP^{C}; and (4) both pre- and post-synaptic functions are deleteriously affected, with the possibility of enhanced vulnerability of the former compartment.

Although previous studies have demonstrated clear correlations between the presence of PrP^{Sc} and the onset of neuropathological changes [38], disruption of LTP at the hippocampal CA1 region of mice inoculated with ME7 [14] and impairment of memory and learning [15], our studies offer compelling evidence for the direct synpatotoxicity of PrP^{Sc}, especially PK-resistant species derived from brains of terminally sick animals. First, we demonstrated that modest PK treatment of *ex vivo* preparations (sufficient to digest all PrP^{C}) did not attenuate the acute synaptotoxicity, with the impairment of LTP similar to that observed with cM1000. These protease digested preparations demonstrated substantial selective enrichment of PrP^{Sc} (see S3H Fig columns i & ii) analogous to that recently reported in another model assessing acute PrP^{Sc} synaptotoxicity [25]. Next, we demonstrated that immuno-depletion of PrP species from cM1000 substantially and proportionally mitigated the acute synaptotoxicity such that LTP was restored to levels not different to dNBH. Additionally, we demonstrated that the use of reconstituted, PK-eluted, immuno-precipitated PrP^{Sc} generated from crude brain preparations achieved full acute synaptotoxicity equivalent to that observed for cM1000, with additional biochemical characterisation of these preparations once again demonstrating significant selective enrichment of PrP^{Sc} (see S3H Fig columns iii & iv). Finally, size fractionation studies revealed that in addition to reducing total PrP species in dM1000, the spectrum of PK-resistant PrP^{Sc} species was altered and the levels of multimeric PrP^{Sc} species specifically decreased in dM1000 correlating with the rescue of LTP. Notably, the acute synaptotoxicity of cM1000 and PK+IP-M1000 clearly correlated with elevated levels of multimeric PK-resistant PrP^{Sc} species.

Our electrophysiology assay demonstrated that brains from terminally ill mice harbouring either M1000 or MU02 prions contain acutely synaptotoxic species. Interestingly, the degree and spectrum of synaptic dysfunction caused by these two different prion strains were indistinguishable, implying that the acute synaptotoxicity may be a generic property of PrP^{Sc} species and independent of the specific prion strain; the study of additional prion strains would confirm this speculation. Importantly, the degree of LTP impairment caused by both M1000 and MU02 strains was comparable to that recorded in the hippocampal CA1 region of ME7 scrapie-infected mice between 125 to 160 days post-inoculation [14], underscoring the biological validity of our findings. In further support of the biological relevance of our findings, the estimated level of misfolded or PK-resistant PrP^{Sc} in our 0.5% M1000 brain homogenates was ~0.094 ± 0.020 μg/mL, which despite methodological differences, falls well within the range of modestly (10 μg/ml) PK-resistant PrP^{Sc} levels determined by Mays et al. [48] in terminal whole brain homogenates of several prion animal models; however, uncertainty persists as to what precise levels would actually be found localised to synapses. Moreover, our results demonstrated a correlation between the levels of PK-resistant PrP^{Sc} and the degree of LTP and PTP dysfunction with a threshold level of at least modestly PK-resistant PrP^{Sc} > ~0.006 μg/ml appearing toxic to PTP while a level >~0.014 μg/ml appears toxic to LTP.

A recent study by Fang *et al* describes retraction and depletion of dendritic spines after 24 hours of exposure to PrP^{Sc} preparations [25]. In keeping with the importance of LTP in the generation and maintenance of dendritic spines, our observations may offer insights into the molecular pathogenesis underpinning at least some of the described dendritic spine morphological changes [12, 49, 50]. Though it is known that cellular expression is not required for uptake of PrP^{Sc} aggregates [51] and *in vivo* neurons not expressing PrP^{C} develop

morphological abnormalities typical of prion disease with continued exposure to PrP^{Sc} over many weeks [52], in noteworthy contrast to this and our electrophysiology studies, Fang *et al* reported complete dependence on neuronal PrP^{C} expression for toxicity. There are several potential explanations, which from our cM1000 serial dilution studies do not relate to an altered sensitivity of PrPo/o hippocampal slices. Firstly, our model assessed synaptic dysfunction within a period of approximately 45 minutes following exposure to PrP^{Sc} containing preparations, whereas the time-frame for assessment in the study of Fang *et al* was at approximately 24 hours. The importance of ongoing neuronal PrP^{Sc} propagation to provide continued PrP^{Sc} exposure for effective pathogenesis is exemplified by the reported rapid and complete reversal of morphological, hippocampal CA1 region neurophysiological and behavioural abnormalities shortly after neuronal PrP^{C} expression is abrogated in the setting of established prion infection [53, 54]. The prompt reversibility of synaptic spine loss has also been reported in relation to AD models employing naturally secreted Aβ oligomers if the toxic species is completely removed [55]. Such observations support that the CNS has evolved powerful compensatory and recuperative mechanisms and it is highly likely that a single brief exposure to a synaptoxin only causes transient dysfunction that probably does not inevitably lead to sustained failure and loss of the synapse, especially if the level of toxin exposure is not extreme. Therefore we speculate in the Fang *et al* model that an additional approximately 23 hours in the absence of any *de novo* PrP^{Sc} production from endogenous PrP^{C} may have allowed effective activation of neuro-protective or adaptational responses in PrPo/o tissues, including progressive clearance or degradation of exogenous PrP^{Sc}, and that persisting neuronal exposure above threshold levels is required to achieve sustained dendritic retraction and pruning when assessing synaptotoxicity over the longer 24 hour period. Secondly, other methodological differences, such as in the techniques for generating *ex vivo* PrP^{Sc} preparations (eg detergents plus serial ultracentrifugation versus IP plus PK digestion), the tissues used for toxicity studies (primary hippocampal neuronal cultures versus *ex vivo* hippocampal slices) and the primary metric for assessing toxicity (endogenous dendritic spine size/number versus induced LTP amplitudes), may collectively contribute to the observed discrepancies. Finally, and notwithstanding the aforementioned neurobiological and technical considerations, although LTP impairment was observed in PrPo/o slices, subtle but potentially important differences were observed in other facets of synaptic function, as well as in changes to key synaptic proteins. Namely, while PTP was also adversely affected by PrP^{Sc} preparations in addition to LTP in PrPo/o hippocampi, the PPF ratio showed a normal decline after LTP with VGLUT1, NR2A, NR2B, GluA2 and procaspase 3 levels unchanged. These discrepancies with WT hippocampi exposed to PrP^{Sc} suggest the possibility of PrP^{C}-independent mechanistic pathways contribute to LTP and PTP impairment, which may not have been easily discerned in the setting of PrP^{C} expression and further underscore uncertainty of how such differences may relate to the retraction and loss of dendritic spines over a longer period of 24 hours.

The possible impact of age associated with the lack of PrP^{C} expression were important considerations in our studies. Because the absence of PrP^{C} has been reported to be linked with age-dependent impairment of hippocampal synaptic function in 8–15-month old mice [10], we mitigated this potentially confounding phenomenon by only using hippocampal slices from young PrPo/o mice. Notably, our findings reproduced those previously reported in a number of studies [10, 56, 57] with young PrPo/o mice exhibiting hippocampal CA1 synaptic functions congruent with aged-matched WT mice although contrary findings have been reported [58, 59], which may partly relate to variations in electrophysiology techniques employed. Also of interest, WT C57BL/6 mice 9–12 months old have been reported to express age-dependent deficits in learning following treatment with neurotoxic $A\beta_{1-42}$ [60], thereby suggesting that older WT mice of this age may also be more susceptible to synaptic impairment

associated with prion-infected preparations. Our studies however, revealed age-independent disruption of hippocampal synaptic function by cM1000 up to 11 months of age.

Synaptic physiology is complex and multi-facted making the achievement of precise understanding of pathophysiological changes through electrophysiological interrogation a considerable challenge. As part of validating the acute synaptotoxicity of PrP^{Sc}, our detailed electrophysiological analyses suggest a possible enhanced pre-synaptic vulnerability, exemplified by the impairment of PTP, although contributions to LTP disruption from post-synaptic dysfunction seem likely as discussed below. A technical limitation of our assessments to probe pre-synaptic impairments was the lack of inclusion of specific GABA receptor antagonists. The 20 millisecond inter-stimulus intervals used to determine PPF ratios and the 10 millisecond intervals employed for HFS are very short, making contributions from $GABA_B$ receptors quite unlikely but leaves open the possibility that $GABA_A$ receptor related inhibitory post-synaptic potentials could have influenced some of the measured synaptic phenomena in ways we have not fully accounted for. Consequently, the absence of $GABA_A$ receptor blockade in our experiments utilising fEPSP amplitudes to infer pre-synaptic pathophysiology allows for some potential inaccuracy in the derived measurements of *Pr* and RRP and precludes our studies from being definitive in this regard. Nevertheless and notwithstanding such caveats, to try to offer an understanding of the basis of the impairment of PTP, our analyses are consistent with impairment of action potential-dependent mechanisms of RRP replenishment, made obvious by the physiological stress imposed by repeated HFS trains used to induce PTP whereby there appeared to be a progressive deterioration of RRP replenishment leading to a significant reduction of RRP size and consequently a reduced PTP. In addition, because the *Pr* and the depletion rate of RRP during HFS trains appeared normal these could exacerbate the dysfunction of RRP replenishment [61] and the reduction of PTP. Further, this suggestion of pre-synaptic disruption was observed in WT and PrPo/o mice, supporting that PrP^{C} expression appears irrelevant to this dysfunction. The observation that immuno-depletion of total PrP species by ~77% only rescued LTP but not PTP with the ongoing PTP impairment also appearing to be due to deficiency of RRP replenishment leading to a reduction in RRP size, suggests that the modest amount of PK-resistant PrP^{Sc}, including multimeric species, remaining after immuno-depletion appears sufficient to cause this disruption although contributions from a non-PrP^{Sc} factor cannot be completely excluded. These findings raise the possibility that the mechanisms responsible for RRP replenishment during repeated HFS trains appear highly vulnerable to PrP^{Sc} toxicity and more susceptible than LTP. The reduced PTP we observed appears discordant with results reported in a previous *in vivo* study of the ME7 prion strain in which PTP was reported as unaffected over the mid-incubation period [14]. We believe this apparent discrepancy is methodological in basis given that careful scrutiny of the relevant figure from this report reveals consistently lower amplitude initial PTPs in the prion infected mice similar to what we found. These authors measured PTP at a presumably varying time point during the first minute after HFS (with the PTP in non-prion infected mice decreasing rapidly after the first stimulation post-HFS) while we systematically utilised the first response immediately after serial HFS to estimate PTP.

The apparent disruption of the PPF ratio following HFS in WT slices is consistent with insufficient *Pr* during the maintenance of LTP suggesting pre-synaptic impairment following exposure to synaptotoxic PrP^{Sc} [62]. Additionally, expression levels of pre-synaptic markers, synaptophysin and VGLUT1, were consistently decreased in WT hippocampi manifesting disrupted LTP. Although synaptophsyin has been shown to be less important in neurotransmitter release [63], previous studies have uncovered that synaptophysin is significantly recruited for LTP expression and generally required for synaptic plasticity without involvement in *Pr* maintenance [64, 65]. Hence, this reduced level of synaptophysin is somehow directly concomitant

with the impairment of LTP, but probably not via diminishing *Pr*. Noteworthy are previous reports of significantly reduced synaptophysin expression levels in the hippocampi of WT (C57BL/6) mice inoculated with three different prion strains: ME7, 79A, and 22L [66]. VGLUT1 instead plays substantial roles in the packaging of glutamate into pre-synaptic vesicles and maintaining normal *Pr*, wherein neurons lacking VGLUT1 have reduced *Pr* [67]. Therefore, we believe that the reduced expression levels of both synaptophysin and VGLUT1 directly contributed to the disruption of LTP, whereas only the loss of VGLUT1 was probably associated with our postulated impairment of *Pr* after LTP induction. Unexpectedly, we observed decreased synaptophysin levels but preserved VGLUT1 levels in PrPo/o slices correlating with the normal *Pr* observed following LTP. This suggests that the loss of VGLUT1 in WT hippocampi was PrP^{C} dependent, whereas the loss of synaptophysin in these hippocampi is PrP^{C} independent. The preservation of the *Pr* and PPF ratio following HFS in PrPo/o slices exposed to synaptotoxic PrP^{Sc} suggests that any pre-synaptic impairment associated with disruption of PTP is a primary pathophysiologic driver of the LTP dysfunction in both WT and PrPo/o slices. Nevertheless, because HFS also cause post-synaptic changes such as receptor activation, new receptor insertion and terminal expansion, which may collectively alter post-synaptic sensitivity to released neurotransmitters [12], contributions from post-synaptic disruptions are likely in the HFS-dependent synaptic dysfunction such as the impairment of LTP.

Variable transient disruption of the baseline during treatments of the hippocampal slices was observed in our study. Although we are not able to offer a definitive explanation for this minor technical issue, possible contributing factors, which are not mutually exclusive and may have occurred in varying combinations, include: i) slight variation in the temperature of some of the treatments; ii) slight variation in the pH of some of the treatments or slight pH change during the treatment; iii) slight variation in the depth of the treatment solution in each MEA recording chamber across experiments; and iv) minor mouse cohort variation in the sensitivity of hippocampal slices to the treatments. Another issue that could also contribute to variability, particularly in association with the above first three speculations is subtle variation in positioning of the superfusing solution inflow and outflow and the associated flow of solution within the MEA recording chamber. The MEA recording chambers are circular and this shape is known to allow some variation in cross-chamber solution flow as the solution can flow around the circular walls of the chamber rather than inevitably directly across the centre of the chamber; however, despite the occasional transient baseline disruption during treatments, there is no evidence this phenomenon impacted our recordings or results as HFS for elicitation of LTP and PTP was not undertaken until fEPSPs had returned to baseline for at least 5 minutes after the treatment. In addition, the acute synaptotoxic effects of *ex vivo* PrP^{Sc} preparations reported in our study were not linked to or affected by whether the baseline recording was temporarily disrupted (such as in Fig 1B cM1000 and 2H PK+M1000) or not disrupted (such as in Figures IE cMU02; 1K MoRK13-INF, and 2H PK+IP-M1000).

Notwithstanding controversies concerning the exact mechanisms underpinning hippocampal LTP, it is clear that LTP expression involves significant modifications of post-synaptic properties, particularly activation of extant post-synaptic NMDAR and externalization of new AMPAR [12, 68]. Our study demonstrated reduced expression levels of NR2A- and NR2B-containing NMDAR and GluA2-containing AMPAR in WT hippocampi expressing impaired LTP following exposure to synaptotoxic PrP^{Sc}. Although these receptors can be expressed in both pre- and post-synaptic terminals [69, 70], their considerable numerical predominance post-synaptically supports that their overall loss was likely to be primarily post-synaptic [71]. NR2A/B-containing NMDAR are essential for hippocampal synaptic function and the expression of CA1 LTP [72]; therefore, their loss supports that the disruption of LTP in WT mice is at least partly dependent on NMDAR disruption. AMPAR also play a critical role in

maintaining basal synaptic functions and most importantly in LTP expression, where new AMPAR are inserted into the post-synaptic membrane as part of LTP induction to enhance the function of active synapses and activate silent synapses [73, 74]. Because the acute PrP^{Sc} synaptotoxicity we observed was HFS-dependent, we postulate that the loss of AMPAR was mediated predominantly through silent synapses. Of likely relevance to our findings, parallel losses of NMDAR and AMPAR have been reported in the brains of AD patients [75] directly correlating with Aβ synaptotoxicity [76]. Unlike in WT slices, NR2A/B-containing NMDAR, and GluA2-containing AMPAR remained unaltered in PrPo/o hippocampi following exposure to synpatotoxic PrP^{Sc}, implying different mechanisms are responsible for acute PrP^{Sc} synaptotoxicity in PrPo/o compared to WT slices. Importantly, this result infers that the disruptions of these receptors in WT mice are probably PrP^{C} dependent with the persistent impairment of LTP in PrPo/o hippocampi suggesting that the alterations of these glutamate receptors are not the sole determinant of PrP^{Sc} acute synaptotoxicity. This finding also suggests that PrPo/o mice may have higher innate resistance to PrP^{Sc} synaptotoxicity through mechanisms which mitigate acute synaptic dysfunction when studied over longer time frames than we allowed [77, 78].

Following exposure to PrP^{Sc} the key intracellular proteins pERK and pCREB involved in synaptic plasticity were also down-regulated in slices. Of note, both pERK and pCREB levels were significantly rescued following immuno-depletion of PrP, supporting a direct synaptotoxic effect of PrP^{Sc} on their function. Offering mechanistic pathway overlap in the disruption of LTP, these key intracellular synaptic proteins were also reduced in PrPo/o slices supporting that PrP^{C}-independent impairment through different mechanisms occurs upstream of ERK and CREB activation. The sustained expression of NR2A and NR2B subunits in PrPo/o slices, while observing persistently reduced pERK and pCREB levels, supports the notion that activation of ERK and CREB during LTP induction and maintenance is likely to be independent of NMDAR activity in hippocampi of PrPo/o mice [79]. Although the activation of NMDAR is known to mediate the influx of Ca^{2+} during LTP induction, the activation of ERK and CREB has also been demonstrated to be independent of NMDAR activity but dependent on L-type voltage-gated calcium channel (L-VGCC) activation. PrP^{C} may be either directly or indirectly involved in Ca^{2+} influx via neuronal L-VGCCs [8, 80], and interact with Fyn to mediate Ca^{2+} dependent activation of ERK and CREB [81–83]. The absence of PrP^{C} in PrPo/o slices may increase the vulnerability of L-VGCCs to PrP^{Sc} disruption compared with WT mice.

Phosphorylation of ERK is essential for many synaptic functions such as activation of transcription factor CREB to produce more synaptic proteins. This pathway has been implicated in structural plasticity by which activation mediates formation of new dendritic spines and thereby contributes to LTP expression in *ex vivo* hippocampi [84] and memory formation in *vivo* [85]. Hence, the diminished levels of these two-key intracellular post-synaptic markers suggest that the acute PrP^{Sc} synaptotoxicity is likely to be associated with impaired production of new synaptic proteins with associated difficulties maintaining some spines and/or producing new spines. Of note, inhibition of ERK activity with MAPK/ERK kinase (MEK) inhibitors prevents dendritic spine growth and acutely disrupts LTP induction [68]. Additionally, pERK is directly involved in AMPAR insertion into the post-synaptic membrane following HFS, which is required for both enlarging synapses and activating silent synapses [47, 68, 73]. Hence, the reduced activation of pERK might have contributed to the down-regulation of AMPAR in WT mice but supports others factors contributing to this change in PrPo/o slices.

Overall, our observations offer new insights into the pathophysiology underlying the acute synaptic dysfunction of prion disease, generally aligning with reported synaptic disruptions demonstrated in other neurodegenerative diseases such as Alzheimer's, Parkinson's, and Huntington's diseases, all of which consist of both pre-synaptic and post-synaptic impairments

[86–88]. Our findings suggest an enhanced vulnerability of the pre-synaptic compartment, especially replenishment of the RRP of vesicles, to PrP^{Sc} acute synaptotoxicity although post-synaptic impairment is likely to contribute to the disruption of short and/or long-term synaptic plasticity. We have demonstrated that PrP^{Sc} derived from terminal disease brains, particularly modestly PK-resistant most likely multimeric species, are important direct synaptotoxins in prion disease, with the likelihood of PrP^{C}-independent pathways contributing to acute PrP^{Sc} acute synaptotoxicity.

Supporting information

S1 Table. Primary and secondary antibodies used for immuno-blottings with their appropriate dilutions and comparable block buffer, which was either 5% Skim milk (Skm) or bovine serum albumin (BSA).
(DOCX)

S1 Fig. Methods and data analysis. (A) A schematic flow diagram of how the MEA experiment was done. (1) Mouse brain was sliced into hippocampal slices, (2) incubated at 32˚C for an hour, (3) loaded onto the MEA (i) that was set-up with a perfusion system and (ii) stimulated the Schäffer collateral pathway through one of the micro-electrodes (black dots; the best aligned one) to evoke fEPSPs at the stratum radiatum of the CA1 region, and (4) the amplitudes of the fEPSPs were recorded as input-output (IO) curves and paired pulse facilitation (PPF) before (baseline) and after repetitive high frequency simulation (HFS) and the treatment of hippocampal slices with different preparations. (B) Examples of fEPSPs during baseline recording, PTP, LTP, and PPF. The PPF ratio was measured by employing two identical basal stimuli delivered at a 20 ms interval and recording the change in the elicited field excitatory post-synaptic potential (fEPSP); PPF1 recorded during the baseline and PPF2 after HFS and induction of long-term potentiation (LTP). (C) A series of individual fEPSP responses (P1 to P9) to each train (T) of the three HFS trains, with the ratio between P1 and P2 representing the initial probability of release (*Pr*) in each HFS train. (D) The slope of the curve through which the P3 fEPSP reduces to the P9 fEPSP signifies the rate of depletion of the readily releasable pool (RRP) during a single HFS train, with the slope measured as a time constant of decay (Tau = 1/K) employing a one-phase decay exponential function. (E) The size of RRP was estimated by back-extrapolating to the Y-intercept a linear fit equation based on the last 4 cumulative fEPSPs per train. During repeated trains (T1, T2 and T3) of HFS over a short period, the increases in RRP size from T1 to T2 and T2 to T3 represent the efficiency of RRP replenishment. (F) For the time-course PPF study without LTP induction, PPF was measured with basal stimulation before (PPF1A) and immediately after (PPF1B) exposure to either prion containing or control preparations; thereafter PPF1B was measured every 5 minutes for one hour.
(TIF)

S2 Fig. Acute synaptotoxicity of crude *ex-vivo* PrP^{Sc} preparations. (A) Relative to the appropriate negative controls, there was a uniform and similar impairment of LTP (displayed as percentage change) caused by: 0.5% (w/v in aCSF) cM1000 (in both 12-week-old [related to Fig 1B & 1C] and 11-month-old hippocampal slices; [related to Fig 1G & 1H]); 0.5% (w/v in aCSF) cMU02 (in 12-week-old hippocampal slices; related to Fig 1E & 1F); and Two percent (w/v in aCSF) MoRK13-Inf (related to Fig 1K & 1L). To assess for potential non-PrP^{Sc} adverse synaptic effects in the various test preparations, LTP was compared to technical aCSF controls (aCSF only), with LTP (displayed as percentage of baseline field excitatory post-synaptic potential (fEPSP) amplitude over time [left panels] and as average LTP as a percentage of baseline [right panels]) not affected by: 0.5% (w/v in aCSF) cNBH in both (B) 12-week-old (related

to Fig 1B & 1E) and (C) 11-month-old hippocampal slices (related to Fig 1H); (D) Two percent (w/v in aCSF) MoRK13-Un in 11-month-old hippocampal slices (related to Fig 1K). (E-H: first column i.) Normal I-O curves were obtained in all aCSF-only technical controls and (A-G, middle column ii.) the relevant negative controls whereby the I-O curves after LTP (I-O2) became significantly increased relative to the I-O curves before LTP (I-O1). In contrast, the I-O2 curves failed to significantly increase after exposure to PrP^{Sc} contained in: cM1000 (E: column iii—12-week-old hippocampal slices; F: column iii—11-month old mice hippocampal slices); cMU02 (G: column iii—12-week old mice hippocampal slices); MoRK13-Inf (H: column iii—11-month old mice hippocampal slices). Scatterplot: Student's t test; I-O curves: Two-way ANOVA with repeated measures; mean ± SEM; $^{*}p<0.05$, $^{**}p<0.01$, $^{***}p<0.001$, $^{****}p<0.0001$.
(TIF)

S3 Fig. Validation of the prion acute synaptotoxicity model. (A) Relative to the appropriate negative controls, there was a uniform and similar impairment of LTP (displayed as percentage change) caused by 0.5% (w/v; in aCSF) PK-treated cM1000 (PK+M1000) (in 12-week-old hippocampal slices; related to Fig 2E & 2F); and reconstituted PK-eluted PrP immuno-precipitated 0.5% (w/v) cM1000 (PK+IP-M1000) pellets (in 12-week-old hippocampal slices; related to Fig 2H & 2I). Importantly, immuno-depletion of PrP^{Sc} in 0.5% (w/v in aCSF) PrP immuno-depleted brain homogenate from cM1000 (dM1000) significantly rescued LTP to levels not different to the NBH control (related to Fig 2B & 2C). To assess for potential non-PrP^{Sc} synaptotoxicity in the various test preparations, LTP was compared to technical aCSF controls (aCSF only), with LTP (displayed as percentage of baseline field excitatory post-synaptic potential (fEPSP) amplitude over time [left panels] and as average LTP as a percentage of baseline [right panels]) not affected by (B) 0.5% (w/v in aCSF) PrP immuno-depleted NBH (dNBH) in 12-week-old hippocampal slices (related to Fig 1B); (C) PK treated 0.5% (w/v; in aCSF; with 5μg/ml PK) cNBH (PK+NBH) in 12-week-old hippocampal slices (related to Fig 1E); and (D) reconstituted PK-eluted immuno-precipitated 0.5% NBH (PK+IP-NBH) pellets in 12-week-old hippocampal slices (related to Fig 1H). The first five-minute fEPSP recordings following HFS trains have been omitted to assist clarity. (E-G) Normal I-O curves were demonstrated in aCSF (column i.) and negative controls (column ii.) wherein I-O2 became significantly increased relative to I-O1. Conversely, PK-treated cM1000 (PK+M1000) (E: column iii—12-week old mice hippocampal slices); and reconstituted, PK-eluted immuno-precipitated cM1000 brain homogenate (PK+IP-M1000) pellets (F: column iii—12-week old mice hippocampal slices) prevented I-O2 from becoming enhanced relative to I-O1. The only exception was following immuno-depletion of PrP (dM1000) wherein the I-O2 was normal compared with the controls (G: column iii—12-week old mice hippocampal slices). (H) Level of total protein (i, iii, v, vii) and PrP (ii, iv, vi, viii) in each *ex vivo* PrP preparation detected by coomassie stain and western blotting probed with 8H4 antibody. (I) Quantification of the total protein in each *ex vivo* PrP preparation. Relative to the total protein level in 0.5% (w/v) cM1000 without PK treatment, modest PK treatment (5μg/mL PK) of the 0.5% (w/v) cM1000 and IP-M1000 significantly reduced the total protein level to only 10% and 20% respectively, while containing substantial level of modestly PK-resistant PrP^{Sc} (H column ii & iv). Similarly, total proteins in 0.5% (w/v) cNBH and IP-NBH were significantly reduced to 20% and 30% by modest PK treatment compared with those in cNBH before PK treatment. However, no PrP detected by 8H4 antibody in modestly PK-treated NBH preparations (H column vi & viii). Densitometry analysis was performed as described in [Lewis, 2015 #248] Scatterplot: Student's t test; I-O curves: Two-way ANOVA with repeated measures; mean ± SEM; $^{*}p<0.05$, $^{**}p<0.01$, $^{***}p<0.001$, $^{****}p<0.0001$.
(TIF)

S4 Fig. Presynaptic functions. (A) Relative to aCSF-only technical controls where the paired pulse facilitation (PPF) ratio after LTP induction (PPF2) was significantly reduced compared with the PPF before LTP (PPF1), similar normal PPF results were obtained in the cNBH, MoR-K13Un, dNBH, PK treated NBH, and PK-eluted IP-NBH controls (related to Fig 4A). (B) Synaptic disruption in the form of altered paired pulse facilitation (PPF) ratios (displayed as percentage change) was calculated after LTP (PPF2) relative to before LTP (PPF1). Relative to appropriate negative controls, all preparations containing PrP^{Sc} prevented reduction in the PPF ratio after LTP except dM1000, where the PPF ratio was significantly rescued (related to Fig 4A). (C) PTP displayed as a percentage of baseline fEPSP amplitude, was not affected by: Crude 0.5% (w/v in aCSF) brain homogenate from a normal brain ("sham") inoculated mouse (cNBH) in both 12-week-old and 11-month-old hippocampal slices; crude 2.0% (w/v in aCSF) NBH "sham" uninfected RK13 cells lysate (MoRK13-Un) in 11-month-old hippocampal slices; 0.5% (w/v in aCSF) PrP immuno-depleted brain homogenate from a normal brain ("sham") inoculated mouse (dNBH) in 12-week-old hippocampal slices; proteinase K (PK) treated 0.5% (w/v; in aCSF) cNBH (PK+NBH) in 12-week-old hippocampal slices; and reconstituted PK-eluted immunoprecipitated 0.5% NBH (PK+IP-NBH) pellets in 12-week-old hippocampal slices (related to Fig 4C). (D) Relative to the appropriate negative controls, all preparations containing PrP^{Sc}, including the dM1000 caused similar PTP impairment (displayed as percentage change), thereby suggesting that PTP appears more sensitive to the acute synaptotoxic effects of PrP^{Sc} than LTP (related to Fig 4C). (E) Average baseline fEPSPs at every five minutes in hippocampal slices treated with aCSF, cNBH, and cM1000 (between the 10 and 15-minute time points) recorded for ~60 minutes. Scatterplot (A-D): mean ± SEM, Student's t test; $^{*}p<0.05$, $^{**}p<0.01$, $^{***}p<0.001$, $^{****}p<0.0001$.
(TIF)

S5 Fig. Additional electrophysiology results from PrPo/o hippocampal slices (related to Fig 6). (A-D) Analogous to what was observed in WT hippocampal slices, cNBH did not harbour non-PrP^{Sc} adverse synaptic effects on LTP (displayed as percentage of baseline fEPSP amplitude over time (A) or and as average LTP as a percentage of baseline (B), PTP (C) or PPF ratios after LTP induction (PPF2; D) in 12-week-old PrPo/o mice hippocampal slices relative to aCSF-only technical controls. (E & F) In comparison to cNBH, cM1000 impaired both LTP (E) and PTP (F) in 12-week old PrPo/o hippocampal slices (displayed as percentage change), with the changes comparable in degree to the disruption of LTP and PTP observed with 12-week-old WT hippocampal slices (related to Fig 6A, 6B & 6D). (G) In contrast, cM1000 did not impair the PPF ratio of 12-week-old PrPo/o hippocampal slices (displayed as percentage change) following LTP induction, with results not significantly different to cNBH (related to Fig 6C). (H) Relative to the aCSF-only technical control, cNBH did not disrupt the I-O curve after LTP expression (I-O2) compared with the I-O curve before LTP expression (I-O1) in 12-week-old PrPo/o hippocampal slices; however, cM1000 significantly impaired the enhancement of I-O2 relative to I-O1. Scatterplot: Student t test; Two-way ANOVA with repeated measures; mean ± SEM; $^{*}p<0.05$, $^{**}p<0.01$, $^{***}p<0.001$, $^{****}p<0.0001$.
(TIF)

S6 Fig. The effects of 1% (w/v) versus 0.5% (w/v) crude normal brain homogenate (cNBH) on hippocampal synaptic functions (related to Fig 7). Relative to hippocampal slices from 12-week old wild type mice treated with aCSF, (A) slices treated with 1% (w/v) cNBH for five minutes following an eight to 10-minute stable baseline exhibited a disrupted baseline that did not recover back to normal baseline before the trains of high frequency stimulation (HFS), associated with disruption of the long-term potentiation (LTP). (B) However, hippocampal

slices treated with 0.5% (w/v) cNBH did not affect the baseline and LTP.
(TIF)

Author Contributions

Conceptualization: Simote Totauhelotu Foliaki, Steven John Collins.

Data curation: Simote Totauhelotu Foliaki, Abu Mohammed Taufiqual Islam.

Formal analysis: Simote Totauhelotu Foliaki, Harold Arthur Coleman, Blaine Roberts.

Funding acquisition: Steven John Collins.

Investigation: Simote Totauhelotu Foliaki, Steven John Collins.

Methodology: Simote Totauhelotu Foliaki, Victoria Lewis, Harold Arthur Coleman, Feng Chen, Blaine Roberts, Steven John Collins.

Project administration: Steven John Collins.

Resources: Victoria Lawson, Matteo Senesi, Shannon Sarros, Steven John Collins.

Supervision: Victoria Lewis, David Isaac Finkelstein, Blaine Roberts, Paul Anthony Adlard, Steven John Collins.

Validation: Simote Totauhelotu Foliaki, Harold Arthur Coleman, Blaine Roberts, Steven John Collins.

Visualization: Simote Totauhelotu Foliaki, Steven John Collins.

Writing – original draft: Simote Totauhelotu Foliaki.

Writing – review & editing: Simote Totauhelotu Foliaki, Victoria Lewis, Steven John Collins.

References

1. Collins SJ, Lawson VA, Masters CL. Transmissible spongiform encephalopathies. Lancet. 2004; 363 (9402):51–61. Epub 2004/01/16. https://doi.org/10.1016/S0140-6736(03)15171-9 PMID: 14723996.
2. Prusiner SB. Prion diseases and the BSE crisis. Science. 1997; 278(5336):245–51. Epub 1997/10/10. PMID: 9323196.
3. Prusiner SB, Cochran SP, Groth DF, Downey DE, Bowman KA, Martinez HM. Measurement of the scrapie agent using an incubation time interval assay. Ann Neurol. 1982; 11(4):353–8. Epub 1982/04/01. https://doi.org/10.1002/ana.410110406 PMID: 6808890.
4. Zou WQ, Puoti G, Xiao X, Yuan J, Qing L, Cali I, et al. Variably protease-sensitive prionopathy: a new sporadic disease of the prion protein. Ann Neurol. 2010; 68(2):162–72. Epub 2010/08/10. https://doi.org/10.1002/ana.22094 PMID: 20695009.
5. Kim C, Haldiman T, Cohen Y, Chen W, Blevins J, Sy MS, et al. Protease-sensitive conformers in broad spectrum of distinct PrPSc structures in sporadic Creutzfeldt-Jakob disease are indicator of progression rate. PLoS Pathog. 2011; 7(9):e1002242. Epub 2011/09/21. https://doi.org/10.1371/journal.ppat.1002242 PMID: 21931554.
6. Criado JR, Sanchez-Alavez M, Conti B, Giacchino JL, Wills DN, Henriksen SJ, et al. Mice devoid of prion protein have cognitive deficits that are rescued by reconstitution of PrP in neurons. Neurobiol Dis. 2005; 19(1–2):255–65. Epub 2005/04/20. https://doi.org/10.1016/j.nbd.2005.01.001 PMID: 15837581.
7. Herms J, Tings T, Gall S, Madlung A, Giese A, Siebert H, et al. Evidence of presynaptic location and function of the prion protein. The Journal of neuroscience: the official journal of the Society for Neuroscience. 1999; 19(20):8866–75. Epub 1999/10/12. PMID: 10516306.
8. Fuhrmann M, Bittner T, Mitteregger G, Haider N, Moosmang S, Kretzschmar H, et al. Loss of the cellular prion protein affects the Ca2+ homeostasis in hippocampal CA1 neurons. J Neurochem. 2006; 98 (6):1876–85. Epub 2006/09/02. https://doi.org/10.1111/j.1471-4159.2006.04011.x PMID: 16945105.

9. Khosravani H, Zhang Y, Tsutsui S, Hameed S, Altier C, Hamid J, et al. Prion protein attenuates excitotoxicity by inhibiting NMDA receptors. J Cell Biol. 2008; 181(3):551–65. Epub 2008/04/30. https://doi.org/10.1083/jcb.200711002 PMID: 18443219.
10. Curtis J, Errington M, Bliss T, Voss K, MacLeod N. Age-dependent loss of PTP and LTP in the hippocampus of PrP-null mice. Neurobiol Dis. 2003; 13(1):55–62. Epub 2003/05/22. https://doi.org/10.1016/s0969-9961(03)00017-2 PMID: 12758067.
11. Nabavi S, Fox R, Proulx CD, Lin JY, Tsien RY, Malinow R. Engineering a memory with LTD and LTP. Nature. 2014; 511(7509):348–52. Epub 2014/06/05. https://doi.org/10.1038/nature13294 PMID: 24896183.
12. Luscher C, Malenka RC. NMDA receptor-dependent long-term potentiation and long-term depression (LTP/LTD). Cold Spring Harb Perspect Biol. 2012; 4(6):1–15. Epub 2012/04/19. https://doi.org/10.1101/cshperspect.a005710 PMID: 22510460.
13. Brazier MW, Lewis V, Ciccotosto GD, Klug GM, Lawson VA, Cappai R, et al. Correlative studies support lipid peroxidation is linked to PrP(res) propagation as an early primary pathogenic event in prion disease. Brain Res Bull. 2006; 68(5):346–54. Epub 2005/12/27. https://doi.org/10.1016/j.brainresbull.2005.09.010 PMID: 16377442.
14. Johnston AR, Fraser JR, Jeffrey M, MacLeod N. Synaptic plasticity in the CA1 area of the hippocampus of scrapie-infected mice. Neurobiol Dis. 1998; 5(3):188–95. Epub 1998/12/16. https://doi.org/10.1006/nbdi.1998.0194 PMID: 9848090.
15. Cunningham C, Deacon R, Wells H, Boche D, Waters S, Diniz CP, et al. Synaptic changes characterize early behavioural signs in the ME7 model of murine prion disease. Eur J Neurosci. 2003; 17(10):2147–55. Epub 2003/06/06. https://doi.org/10.1046/j.1460-9568.2003.02662.x PMID: 12786981.
16. Fuhrmann M, Mitteregger G, Kretzschmar H, Herms J. Dendritic pathology in prion disease starts at the synaptic spine. The Journal of neuroscience: the official journal of the Society for Neuroscience. 2007; 27(23):6224–33. Epub 2007/06/08. https://doi.org/10.1523/JNEUROSCI.5062-06.2007 PMID: 17553995.
17. Siskova Z, Page A, O'Connor V, Perry VH. Degenerating synaptic boutons in prion disease: microglia activation without synaptic stripping. The American journal of pathology. 2009; 175(4):1610–21. Epub 2009/09/26. https://doi.org/10.2353/ajpath.2009.090372 PMID: 19779137.
18. Chiti Z, Knutsen OM, Betmouni S, Greene JR. An integrated, temporal study of the behavioural, electrophysiological and neuropathological consequences of murine prion disease. Neurobiol Dis. 2006; 22(2):363–73. Epub 2006/01/25. https://doi.org/10.1016/j.nbd.2005.12.002 PMID: 16431123.
19. Novitskaya V, Bocharova OV, Bronstein I, Baskakov IV. Amyloid fibrils of mammalian prion protein are highly toxic to cultured cells and primary neurons. The Journal of biological chemistry. 2006; 281(19):13828–36. Epub 2006/03/24. https://doi.org/10.1074/jbc.M511174200 PMID: 16554307.
20. Muller WE, Ushijima H, Schroder HC, Forrest JM, Schatton WF, Rytik PG, et al. Cytoprotective effect of NMDA receptor antagonists on prion protein (PrionSc)-induced toxicity in rat cortical cell cultures. Eur J Pharmacol. 1993; 246(3):261–7. Epub 1993/08/15. PMID: 7901042.
21. Giese A, Brown DR, Groschup MH, Feldmann C, Haist I, Kretzschmar HA. Role of microglia in neuronal cell death in prion disease. Brain Pathol. 1998; 8(3):449–57. Epub 1998/07/21. PMID: 9669696.
22. Simoneau S, Rezaei H, Sales N, Kaiser-Schulz G, Lefebvre-Roque M, Vidal C, et al. In vitro and in vivo neurotoxicity of prion protein oligomers. PLoS Pathog. 2007; 3(8):e125. Epub 2007/09/06. https://doi.org/10.1371/journal.ppat.0030125 PMID: 17784787.
23. Falsig J, Sonati T, Herrmann US, Saban D, Li B, Arroyo K, et al. Prion pathogenesis is faithfully reproduced in cerebellar organotypic slice cultures. PLoS Pathog. 2012; 8(11):e1002985. Epub 2012/11/08. https://doi.org/10.1371/journal.ppat.1002985 PMID: 23133383.
24. Haigh CL, McGlade AR, Lewis V, Masters CL, Lawson VA, Collins SJ. Acute exposure to prion infection induces transient oxidative stress progressing to be cumulatively deleterious with chronic propagation in vitro. Free radical biology & medicine. 2011; 51(3):594–608. Epub 2011/04/07. https://doi.org/10.1016/j.freeradbiomed.2011.03.035 PMID: 21466851.
25. Fang C, Imberdis T, Garza MC, Wille H, Harris DA. A Neuronal Culture System to Detect Prion Synaptotoxicity. PLoS Pathog. 2016; 12(5):e1005623. Epub 2016/05/27. https://doi.org/10.1371/journal.ppat.1005623 PMID: 27227882.
26. Lauren J, Gimbel DA, Nygaard HB, Gilbert JW, Strittmatter SM. Cellular prion protein mediates impairment of synaptic plasticity by amyloid-beta oligomers. Nature. 2009; 457(7233):1128–32. Epub 2009/02/27. https://doi.org/10.1038/nature07761 PMID: 19242475.
27. Bueler H, Fischer M, Lang Y, Bluethmann H, Lipp HP, DeArmond SJ, et al. Normal development and behaviour of mice lacking the neuronal cell-surface PrP protein. Nature. 1992; 356(6370):577–82. Epub 1992/04/16. https://doi.org/10.1038/356577a0 PMID: 1373228.

28. Tateishi J, Ohta M, Koga M, Sato Y, Kuroiwa Y. Transmission of chronic spongiform encephalopathy with kuru plaques from humans to small rodents. Ann Neurol. 1979; 5(6):581–4. Epub 1979/06/01. https://doi.org/10.1002/ana.410050616 PMID: 382976.

29. Lawson VA, Vella LJ, Stewart JD, Sharples RA, Klemm H, Machalek DM, et al. Mouse-adapted sporadic human Creutzfeldt-Jakob disease prions propagate in cell culture. Int J Biochem Cell Biol. 2008; 40(12):2793–801. Epub 2008/07/02. https://doi.org/10.1016/j.biocel.2008.05.024 PMID: 18590830.

30. Vella LJ, Sharples RA, Lawson VA, Masters CL, Cappai R, Hill AF. Packaging of prions into exosomes is associated with a novel pathway of PrP processing. J Pathol. 2007; 211(5):582–90. Epub 2007/03/06. https://doi.org/10.1002/path.2145 PMID: 17334982.

31. Lewis V, Haigh CL, Masters CL, Hill AF, Lawson VA, Collins SJ. Prion subcellular fractionation reveals infectivity spectrum, with a high titre-low PrPres level disparity. Mol Neurodegener. 2012; 7:18. Epub 2012/04/27. https://doi.org/10.1186/1750-1326-7-18 PMID: 22534096.

32. Fioravante D, Regehr WG. Short-term forms of presynaptic plasticity. Curr Opin Neurobiol. 2011; 21(2):269–74. Epub 2011/03/01. https://doi.org/10.1016/j.conb.2011.02.003 PMID: 21353526.

33. Schneggenburger R, Meyer AC, Neher E. Released Fraction and Total Size of a Pool of Immediately Available Transmitter Quanta at a Calyx Synapse. Neuron. 1999; 23(2):399–409. https://doi.org/10.1016/s0896-6273(00)80789-8 PMID: 10399944

34. Powell AD, Gill KK, Saintot PP, Jiruska P, Chelly J, Billuart P, et al. Rapid reversal of impaired inhibitory and excitatory transmission but not spine dysgenesis in a mouse model of mental retardation. J Physiol. 2012; 590(4):763–76. Epub 2011/11/30. https://doi.org/10.1113/jphysiol.2011.219907 PMID: 22124149.

35. Coleman BM, Nisbet RM, Han S, Cappai R, Hatters DM, Hill AF. Conformational detection of prion protein with biarsenical labeling and FlAsH fluorescence. Biochemical and Biophysical Research Communications. 2009; 380(3):564–8. Epub 2009/03/17. https://doi.org/10.1016/j.bbrc.2009.01.120 PMID: 19285001.

36. Cappai R, Stewart L, Jobling MF, Thyer JM, White AR, Beyreuther K, et al. Familial Prion Disease Mutation Alters the Secondary Structure of Recombinant Mouse Prion Protein- Implications for the Mechanism of Prion Formation. Biochemistry. 1999; 38:3280–4. https://doi.org/10.1021/bi982328z PMID: 10079070

37. Lewis V, Johanssen VA, Crouch PJ, Klug GM, Hooper NM, Collins SJ. Prion protein "gamma-cleavage": characterizing a novel endoproteolytic processing event. Cell Mol Life Sci. 2016; 73(3):667–83. Epub 2015/08/25. https://doi.org/10.1007/s00018-015-2022-z PMID: 26298290.

38. Sandberg MK, Al-Doujaily H, Sharps B, De Oliveira MW, Schmidt C, Richard-Londt A, et al. Prion neuropathology follows the accumulation of alternate prion protein isoforms after infective titre has peaked. Nature communications. 2014; 5(4347):4347. Epub 2014/07/10. https://doi.org/10.1038/ncomms5347 PMID: 25005024.

39. Sajnani G, Silva CJ, Ramos A, Pastrana MA, Onisko BC, Erickson ML, et al. PK-sensitive PrP is infectious and shares basic structural features with PK-resistant PrP. PLoS Pathog. 2012; 8(3):e1002547. Epub 2012/03/08. https://doi.org/10.1371/journal.ppat.1002547 PMID: 22396643.

40. Freir DB, Nicoll AJ, Klyubin I, Panico S, Mc Donald JM, Risse E, et al. Interaction between prion protein and toxic amyloid beta assemblies can be therapeutically targeted at multiple sites. Nature communications. 2011; 2:336. Epub 2011/06/10. https://doi.org/10.1038/ncomms1341 PMID: 21654636.

41. Ferreira DG, Temido-Ferreira M, Miranda HV, Batalha VL, Coelho JE, Szego EM, et al. alpha-synuclein interacts with PrPC to induce cognitive impairment through mGluR5 and NMDAR2B. Nat Neurosci. 2017; 20(11):1569–79. Epub 2017/09/26. https://doi.org/10.1038/nn.4648 PMID: 28945221.

42. Mays CE, van der Merwe J, Kim C, Haldiman T, McKenzie D, Safar JG, et al. Prion Infectivity Plateaus and Conversion to Symptomatic Disease Originate from Falling Precursor Levels and Increased Levels of Oligomeric PrPSc Species. Journal of virology. 2015; 89(24):12418–26. Epub 2015/10/02. https://doi.org/10.1128/JVI.02142-15 PMID: 26423957.

43. Sasaki K, Minaki H, Iwaki T. Development of oligomeric prion-protein aggregates in a mouse model of prion disease. J Pathol. 2009; 219(1):123–30. Epub 2009/05/30. https://doi.org/10.1002/path.2576 PMID: 19479969.

44. Lee JS, Kim MH, Ho WK, Lee SH. Presynaptic release probability and readily releasable pool size are regulated by two independent mechanisms during posttetanic potentiation at the calyx of Held synapse. The Journal of neuroscience: the official journal of the Society for Neuroscience. 2008; 28(32):7945–53. Epub 2008/08/08. https://doi.org/10.1523/JNEUROSCI.2165-08.2008 PMID: 18685020.

45. Zhang LL, Sui HJ, Liang B, Wang HM, Qu WH, Yu SX, et al. Atorvastatin prevents amyloid-beta peptide oligomer-induced synaptotoxicity and memory dysfunction in rats through a p38 MAPK-dependent pathway. Acta Pharmacol Sin. 2014; 35(6):716–26. Epub 2014/05/06. https://doi.org/10.1038/aps.2013.203 PMID: 24793311.

46. Kim MJ, Dunah AW, Wang YT, Sheng M. Differential roles of NR2A- and NR2B-containing NMDA receptors in Ras-ERK signaling and AMPA receptor trafficking. Neuron. 2005; 46(5):745–60. Epub 2005/06/01. https://doi.org/10.1016/j.neuron.2005.04.031 PMID: 15924861.

47. Thomas GM, Huganir RL. MAPK cascade signalling and synaptic plasticity. Nat Rev Neurosci. 2004; 5 (3):173–83. Epub 2004/02/21. https://doi.org/10.1038/nrn1346 PMID: 14976517.

48. Mays CE, Kim C, Haldiman T, van der Merwe J, Lau A, Yang J, et al. Prion disease tempo determined by host-dependent substrate reduction. J Clin Invest. 2014; 124(2):847–58. Epub 2014/01/17. https://doi.org/10.1172/JCI72241 PMID: 24430187.

49. Engert F, Bonhoeffer T. Dendritic spine changes associated with hippocampal long-term synaptic plasticity. Nature. 1999; 399(6731):66–70. Epub 1999/05/20. https://doi.org/10.1038/19978 PMID: 10331391.

50. Toni N, Buchs PA, Nikonenko I, Bron CR, Muller D. LTP promotes formation of multiple spine synapses between a single axon terminal and a dendrite. Nature. 1999; 402(6760):421–5. https://doi.org/10.1038/46574 PMID: 10586883

51. Greil CS, Vorberg IM, Ward AE, Meade-White KD, Harris DA, Priola SA. Acute cellular uptake of abnormal prion protein is cell type and scrapie-strain independent. Virology. 2008; 379(2):284–93. Epub 2008/08/12. https://doi.org/10.1016/j.virol.2008.07.006 PMID: 18692214.

52. Jeffrey M, Goodsir CM, Race RE, Chesebro B. Scrapie-specific neuronal lesions are independent of neuronal PrP expression. Ann Neurol. 2004; 55(6):781–92. Epub 2004/06/03. https://doi.org/10.1002/ana.20093 PMID: 15174012.

53. Mallucci GR, White MD, Farmer M, Dickinson A, Khatun H, Powell AD, et al. Targeting cellular prion protein reverses early cognitive deficits and neurophysiological dysfunction in prion-infected mice. Neuron. 2007; 53(3):325–35. Epub 2007/02/03. https://doi.org/10.1016/j.neuron.2007.01.005 PMID: 17270731.

54. Mallucci G, Dickinson A, Linehan J, Klohn PC, Brandner S, Collinge J. Depleting neuronal PrP in prion infection prevents disease and reverses spongiosis. Science. 2003; 302(5646):871–4. Epub 2003/11/01. https://doi.org/10.1126/science.1090187 PMID: 14593181.

55. Shankar GM, Bloodgood BL, Townsend M, Walsh DM, Selkoe DJ, Sabatini BL. Natural oligomers of the Alzheimer amyloid-beta protein induce reversible synapse loss by modulating an NMDA-type glutamate receptor-dependent signaling pathway. The Journal of neuroscience: the official journal of the Society for Neuroscience. 2007; 27(11):2866–75. Epub 2007/03/16. https://doi.org/10.1523/JNEUROSCI.4970-06.2007 PMID: 17360908.

56. Lledo PM, Tremblay P, DeArmond SJ, Prusiner SB, Nicoll RA. Mice deficient for prion protein exhibit normal neuronal excitability and synaptic transmission in the hippocampus. Proceedings of the National Academy of Sciences of the United States of America. 1996; 93(6):2403–7. Epub 1996/03/19. PMID: 8637886.

57. Herms JW, Kretzchmar HA, Titz S, Keller BU. Patch-clamp analysis of synaptic transmission to cerebellar purkinje cells of prion protein knockout mice. Eur J Neurosci. 1995; 7(12):2508–12. Epub 1995/12/01. PMID: 8845956.

58. Collinge J, Whittington MA, Sidle KC, Smith CJ, Palmer MS, Clarke AR, et al. Prion protein is necessary for normal synaptic function. Nature. 1994; 370(6487):295–7. Epub 1994/07/28. https://doi.org/10.1038/370295a0 PMID: 8035877.

59. Mallucci GR, Ratte S., Asante E.A., Linehan J., Gowland I., Jefferys J.G.R., et al. Post-natal knockout of prion protein alters hippocampal CA1 properties, but does not result in neurodegeneration. The EMBO journal. 2002; 21(3):202–10. https://doi.org/10.1093/emboj/21.3.202 PMID: 11823413

60. Malm T, Ort M, Tahtivaara L, Jukarainen N, Goldsteins G, Puolivali J, et al. beta-Amyloid infusion results in delayed and age-dependent learning deficits without role of inflammation or beta-amyloid deposits. Proceedings of the National Academy of Sciences of the United States of America. 2006; 103 (23):8852–7. Epub 2006/05/26. https://doi.org/10.1073/pnas.0602896103 PMID: 16723396.

61. Lou X, Fan F, Messa M, Raimondi A, Wu Y, Looger LL, et al. Reduced release probability prevents vesicle depletion and transmission failure at dynamin mutant synapses. Proceedings of the National Academy of Sciences of the United States of America. 2012; 109(8):E515–23. Epub 2012/02/07. https://doi.org/10.1073/pnas.1121626109 PMID: 22308498.

62. Schulz PE. Long-term potentiation involves increases in the probability of neurotransmitter release. Proceedings of the National Academy of Sciences of the United States of America. 1997; 94(11):5888–93. Epub 1997/05/27. PMID: 9159170.

63. Mcmahon HT, Bolshakov VY, Janz R, Hammer RE, Siegelbaum SA, Siidhof TC. Synaptophysin, a major synaptic vesicle protein, is not essential for neurotransmitter release. Proceeding of the National Academy of Sciences USA. 1996; 93:5.

64. Janz R, Sudhof TC, Hammer RE, Unni V, Siegelbaum SA, Bolshakov VY. Essential roles in synaptic plasticity for synaptogyrin I and synaptophysin I. Neuron. 1999; 24(3):687–700. Epub 1999/12/14. PMID: 10595519.

65. Jin I, Udo H, Hawkins RD. Rapid increase in clusters of synaptophysin at onset of homosynaptic potentiation in Aplysia. Proceedings of the National Academy of Sciences of the United States of America. 2011; 108(28):11656–61. Epub 2011/06/29. https://doi.org/10.1073/pnas.1102695108 PMID: 21709228.

66. Hilton KJ, Cunningham C, Reynolds RA, Perry VH. Early Hippocampal Synaptic Loss Precedes Neuronal Loss and Associates with Early Behavioural Deficits in Three Distinct Strains of Prion Disease. PloS one. 2013; 8(6):e68062. Epub 2013/07/11. https://doi.org/10.1371/journal.pone.0068062 PMID: 23840812.

67. Herman MA, Ackermann F, Trimbuch T, Rosenmund C. Vesicular glutamate transporter expression level affects synaptic vesicle release probability at hippocampal synapses in culture. The Journal of neuroscience: the official journal of the Society for Neuroscience. 2014; 34(35):11781–91. Epub 2014/08/29. https://doi.org/10.1523/JNEUROSCI.1444-14.2014 PMID: 25164673.

68. Zhu JJ, Qin Y, Zhao M, Van Aelst L, Malinow R. Ras and Rap control AMPA receptor trafficking during synaptic plasticity. Cell. 2002; 110(4):443–55. Epub 2002/08/31. PMID: 12202034.

69. Kunz PA, Roberts AC, Philpot BD. Presynaptic NMDA receptor mechanisms for enhancing spontaneous neurotransmitter release. The Journal of neuroscience: the official journal of the Society for Neuroscience. 2013; 33(18):7762–9. Epub 2013/05/03. https://doi.org/10.1523/JNEUROSCI.2482-12.2013 PMID: 23637168.

70. Rigby M, Cull-Candy SG, Farrant M. Transmembrane AMPAR regulatory protein gamma-2 is required for the modulation of GABA release by presynaptic AMPARs. The Journal of neuroscience: the official journal of the Society for Neuroscience. 2015; 35(10):4203–14. Epub 2015/03/13. https://doi.org/10.1523/JNEUROSCI.4075-14.2015 PMID: 25762667.

71. Gao C, Gill MB, Tronson NC, Guedea AL, Guzman YF, Huh KH, et al. Hippocampal NMDA receptor subunits differentially regulate fear memory formation and neuronal signal propagation. Hippocampus. 2010; 20(9):1072–82. Epub 2009/10/07. https://doi.org/10.1002/hipo.20705 PMID: 19806658.

72. Berberich S, Punnakkal P, Jensen V, Pawlak V, Seeburg PH, Hvalby O, et al. Lack of NMDA receptor subtype selectivity for hippocampal long-term potentiation. Journal of Neuroscience. 2005; 25(29):6907–10. Epub 2005/07/22. https://doi.org/10.1523/JNEUROSCI.1905-05.2005 PMID: 16033900.

73. Liao D, Scannevin RH, Huganir R. Activation of silent synapses by rapid activity-dependent synaptic recruitment of AMPA receptors. The Journal of neuroscience: the official journal of the Society for Neuroscience. 2001; 21(16):6008–17. Epub 2001/08/07. PMID: 11487624.

74. Chater TE, Goda Y. The role of AMPA receptors in postsynaptic mechanisms of synaptic plasticity. Front Cell Neurosci. 2014; 8:401. Epub 2014/12/17. https://doi.org/10.3389/fncel.2014.00401 PMID: 25505875.

75. Bi H, Sze CI. N-methyl-D-aspartate receptor subunit NR2A and NR2B messenger RNA levels are altered in the hippocampus and entorhinal cortex in Alzheimer's disease. J Neurol Sci. 2002; 200(1–2):11–8. Epub 2002/07/20. PMID: 12127670.

76. Tu S, Okamoto S, Lipton SA, Xu H. Oligomeric Abeta-induced synaptic dysfunction in Alzheimer's disease. Mol Neurodegener. 2014; 9(48):48. Epub 2014/11/15. https://doi.org/10.1186/1750-1326-9-48 PMID: 25394486.

77. Sailer A. No propagation of prions in mice devoid of PrP. Cell. 1994; 77(7):967–8. https://doi.org/10.1016/0092-8674(94)90436-7 PMID: 7912659

78. Bueler H, Aguzzi A, Sailer A, Greiner RA, Autenried P, Aguet M, et al. Mice devoid of PrP are resistant to scrapie. Cell. 1993; 73(7):1339–47. Epub 1993/07/02. PMID: 8100741.

79. Kanterewicz BI, Urban NN, McMahon DBT, Norman ED, Giffen LJ, Favata MF, et al. The Extracellular Signal-Regulated Kinase Cascade Is Required for NMDA Receptor-Independent LTP in Area CA1 But Not Area CA3 of the Hippocampus. The Journal of Neuroscience. 2000; 20(9):3057–66. PMID: 10777769

80. Herms JW, Korte S, Gall S, Schneider I, Dunker S, Kretzschmar HA. Altered Intracellular Calcium Homeostasis in Cerebellar Granule Cells of Prion Protein-Deficient Mice. Journal of Neurochemistry. 2002; 75(4):1487–92. https://doi.org/10.1046/j.1471-4159.2000.0751487.x

81. De Mario A, Castellani A, Peggion C, Massimino ML, Lim D, Hill AF, et al. The prion protein constitutively controls neuronal store-operated Ca(2+) entry through Fyn kinase. Front Cell Neurosci. 2015; 9:416. Epub 2015/11/19. https://doi.org/10.3389/fncel.2015.00416 PMID: 26578881.

82. Hernandez-Rapp J, Martin-Lanneree S, Hirsch TZ, Launay JM, Mouillet-Richard S. Hijacking PrP(c)-dependent signal transduction: when prions impair Abeta clearance. Frontiers in aging neuroscience. 2014; 6(25):25. Epub 2014/03/05. https://doi.org/10.3389/fnagi.2014.00025 PMID: 24592237.

83. Krebs B, Wiebelitz A, Balitzki-Korte B, Vassallo N, Paluch S, Mitteregger G, et al. Cellular prion protein modulates the intracellular calcium response to hydrogen peroxide. J Neurochem. 2007; 100(2):358–67. Epub 2007/01/24. https://doi.org/10.1111/j.1471-4159.2006.04256.x PMID: 17241158.

84. English JD, Sweatt JD. Activation of p42 Mitogenactivated Protein Kinase in Hippocampal Long Term Potentiation. The Journal of biological chemistry. 1996; 271(40):4.

85. Blum S, Moore AN, Adams F, Dash PK. A mitogen-activated protein kinase cascade in the CA1/CA2 subfield of the dorsal hippocampus is essential for long-term spatial memory. Journal of Neuroscience. 1999; 19(9):3535–44. PMID: 10212313

86. Palop JJ, Chin J, Mucke L. A network dysfunction perspective on neurodegenerative diseases. Nature. 2006; 443(7113):768–73. Epub 2006/10/20. https://doi.org/10.1038/nature05289 PMID: 17051202.

87. Yasuda T, Nakata Y, Choong CJ, Mochizuki H. Neurodegenerative changes initiated by presynaptic dysfunction. Transl Neurodegener. 2013; 2(1):16. Epub 2013/08/08. https://doi.org/10.1186/2047-9158-2-16 PMID: 23919415.

88. Gong Y, Lippa CF. Review: disruption of the postsynaptic density in Alzheimer's disease and other neurodegenerative dementias. Am J Alzheimers Dis Other Demen. 2010; 25(7):547–55. Epub 2010/09/23. https://doi.org/10.1177/1533317510382893 PMID: 20858652.

PLOS PATHOGENS

RESEARCH ARTICLE

Early existence and biochemical evolution characterise acutely synaptotoxic PrP^{Sc}

Simote Totauhelotu Foliaki[1], Victoria Lewis[1,2], Abu Mohammed Taufiqual Islam[1], Laura Jane Ellett[3,4], Matteo Senesi[1], David Isaac Finkelstein[2], Blaine Roberts[2], Victoria A. Lawson[3,4], Paul Anthony Adlard[2], Steven John Collins[1,2]*

1 Department of Medicine (Royal Melbourne Hospital), The University of Melbourne, Parkville, Victoria, Australia, **2** Florey Institute of Neuroscience and Mental Health, Parkville, Victoria, Australia, **3** Department of Pathology The University of Melbourne, Parkville, Victoria, Australia, **4** Department of Microbiology and Immunology, The University of Melbourne, Parkville, Victoria, Australia

* stevenjc@unimelb.edu.au

OPEN ACCESS

Citation: Foliaki ST, Lewis V, Islam AMT, Ellett LJ, Senesi M, Finkelstein DI, et al. (2019) Early existence and biochemical evolution characterise acutely synaptotoxic PrP^{Sc}. PLoS Pathog 15(4): e1007712. https://doi.org/10.1371/journal.ppat.1007712

Editor: David Westaway, University of Alberta, CANADA

Received: October 7, 2018

Accepted: March 18, 2019

Published: April 10, 2019

Data Availability Statement: All relevant data are within the manuscript and its Supporting Information files.

Funding: SJC is supported in part by an NHMRC Practitioner Fellowship (#APP1105784). BR is a NHMRC Dementia Leadership Fellow (#APP1138673) and receives partial support from the Cooperative Research Centre for Mental Health (#20100104). SF has received a University of Melbourne MIR Scholarship (2014), a MIFR Scholarship (2014), a CJD Support Group Network

Abstract

Although considerable evidence supports that misfolded prion protein (PrP^{Sc}) is the principal component of "prions", underpinning both transmissibility and neurotoxicity, clear consensus around a number of fundamental aspects of pathogenesis has not been achieved, including the time of appearance of neurotoxic species during disease evolution. Utilizing a recently reported electrophysiology paradigm, we assessed the acute synaptotoxicity of *ex vivo* PrP^{Sc} prepared as crude homogenates from brains of M1000 infected wild-type mice (cM1000) harvested at time-points representing 30%, 50%, 70% and 100% of the terminal stage of disease (TSD). Acute synaptotoxicity was assessed by measuring the capacity of cM1000 to impair hippocampal CA1 region long-term potentiation (LTP) and post-tetanic potentiation (PTP) in explant slices. Of particular note, cM1000 from 30% of the TSD was able to cause significant impairment of LTP and PTP, with the induced failure of LTP increasing over subsequent time-points while the capacity of cM1000 to induce PTP failure appeared maximal even at this early stage of disease progression. Evidence that the synaptotoxicity directly related to PrP species was demonstrated by the significant rescue of LTP dysfunction at each time-point through immuno-depletion of >50% of total PrP species from cM1000 preparations. Moreover, similar to our previous observations at the terminal stage of M1000 prion disease, size fractionation chromatography revealed that capacity for acute synpatotoxicity correlated with predominance of oligomeric PrP species in infected brains across all time points, with the profile appearing maximised by 50% of the TSD. Using enhanced sensitivity western blotting, modestly proteinase K (PK)-resistant PrP^{Sc} was detectable at very low levels in cM1000 at 30% of the TSD, becoming robustly detectable by 70% of the TSD at which time substantial levels of highly PK-resistant PrP^{Sc} was also evident. Further illustrating the biochemical evolution of acutely synaptotoxic species the synaptotoxicity of cM1000 from 30%, 50% and 70% of the TSD, but not at 100% TSD, was abolished by digestion of immuno-captured PrP species with mild PK treatment (5μg/ml for an hour at 37˚C), demonstrating that the predominant synaptotoxic PrP^{Sc} species up to and including 70% of the TSD were proteinase-sensitive. Overall, these findings in combination with our previous assessments of transmitting prions support that synaptotoxic and

(CJDSGN) Silva Coehlho Travel Grant (2016), a Marek Gorcynski Top-up scholarship (2017) and Dominic Battista Memorial Grant (2018). VL has received CJDSGN Memorial grants: Stephen O'Hara, Jennifer Duckworth and others lost to CJD (2018); Sandra Kernahan, Stephen O'Hara, Catherine Heagerty, Grasso family, Victoria Larielle, Barbara Childerhouse, Marilyn Hart and Pamela Thomas (2016); and Ross Glasscock, Robert Craig, Carmelo Tripoli, Arthur Schinck and Arlene Hamilton (2015). These indirect funders had no role in study design, data collection and analysis, decision to publish, or preparation of the manuscript.

Competing interests: The authors have declared that no competing interests exist.

infectious M1000 PrP^{Sc} species co-exist from at least 30% of the TSD, simultaneously increasing thereafter, albeit with eventual plateauing of transmitting conformers.

Author summary

Although evidence clearly supports that misfolded prion protein (PrP^{Sc}) is the principal component of "prions", underpinning both transmissibility and neurotoxicity, consensus is lacking around the time of appearance and biochemical profile of neurotoxic species during disease evolution. Employing an electrophysiology model, measuring the capacity of brain homogenates derived from across the disease time-course to impair CA1 region long-term potentiation (LTP) and post-tetanic potentiation (PTP) in hippocampal slices, we observed that synaptotoxic species were present from 30% of the terminal stage of disease (TSD). Evidence that synaptotoxicity directly related to PrP species was demonstrated by significant rescue of LTP dysfunction at each time-point through immunodepleting >~50% of total PrP species from cM1000 preparations. Moreover, size fractionation chromatography revealed that acute synpatotoxicity correlated with predominance of oligomeric PrP species in infected brains across all time points, while additional characterisation of cM1000 demonstrated that the predominant synaptotoxic PrP^{Sc} species up to and including 70% of the TSD were quite proteinase-sensitive. These findings in combination with our previous assessments of transmitting prions support that synaptotoxic and infectious M1000 PrP^{Sc} species co-exist from at least 30% of the TSD, simultaneously increasing thereafter, with biochemical transformation of synaptotoxic conformers continuing until late in disease.

Introduction

Prion diseases are transmissible neurodegenerative disorders with human phenotypes including Creutzfeldt-Jakob disease (CJD), Gerstmann-Sträussler-Scheinker syndrome (GSS) and Kuru, while the principal animal diseases comprise scrapie in sheep and goats, bovine spongiform encephalopathy ("mad cow" disease) and chronic wasting disease in deer, elk and moose [1, 2]. The key pathogenic event in all prion diseases is believed to be misfolding of the normal prion protein (PrP^{C}) into altered conformers (PrP^{Sc}) with progressive accumulation of PrP^{Sc} in the brain linked to neurotoxicity through incompletely resolved mechanisms [3–8]. PrP^{Sc}, especially that found at the terminal stage of disease (TSD: the advanced stage of disease requiring animal euthanasia) was previously construed as invariably highly protease-resistant whereas more recent evidence supports a broader spectrum encompassing a substantial proportion that are protease-sensitive [9–12], with such species evident during disease evolution [13] and terminal disease [10] most likely contributing to neurotoxicity [12].

Although experimental approaches exploiting successful rodent-adaptation of human and animal prion diseases such as CJD and scrapie have facilitated our understanding of the pathogenic evolution of these disorders [14–16], consensus around some fundamental aspects of pathogenesis has not been achieved. In contrast to various *in vivo* models consistently demonstrating rising titres of infectivity from early in disease development, well before overt clinical features [8, 12, 17] there is controversy over the time of appearance of neurotoxic PrP^{Sc} species. Reports of electrophysiological [18], morphological [19] and behavioural [20] disturbances prior to the mid-incubation point, generally coinciding with the first detection of

PrP^{Sc}, support relatively early production of neurotoxic PrP^{Sc}. Conversely, other *in vivo* and *in vitro* studies describe that predominantly transmitting PrP^{Sc} species are produced first [21, 22] with neurotoxic species only propagated later in disease evolution nearer the onset of clinical disease, appearing to correlate with the plateauing of infectivity and depletion of PrP^{C} levels [12, 13, 21, 23]. Evidence of significantly increased expression levels of GFAP and active caspase 3, as well as heightened oxidative stress from around the mid-incubation period [8, 24] further support the likely presence of neurotoxic PrP^{Sc} species extant from relatively early in disease evolution, considerably pre-empting the onset of conventional clinical signs such as weight loss, ataxia, and hind limb paresis [8, 25].

In addition to uncertainty regarding the time of occurrence and propagation sequence of neurotoxic PrP^{Sc} species across the disease incubation period, it remains unresolved whether such species are devoid of transmission capacity or harbour both pathogenic properties. Some findings support that disease transmissibility and neurotoxicity are at least partially disconnected and perhaps relate to separate PrP^{Sc} species [12, 21, 23, 26]. Part of this apparent disconnection however, may relate to the types of techniques deployed to detect neurotoxicity [27], as well as the innate neuroprotective mechanisms of the host, such as microglial activation [28, 29] and brain clearance capacity [30], which may successfully mollify neurotoxicity to sub-threshold levels thereby delaying features evincing the presence of neurotoxic PrP^{Sc} over a prolonged period. Compounding such difficulties is the current lack of detailed understanding of the biochemical and biophysical characteristics of PrP^{Sc} species directly underpinning transmissibility and neurotoxicity and whether such properties change over the course of disease evolution. Recently we reported that acutely synaptotoxic PrP^{Sc} species derived from brains at the TSD appear to be at least modestly proteinase K (PK)-resistant and oligomeric [31] while other groups utilising size fractionation and sedimentation velocity fractionation with terminal disease tissue suggest that the most efficient PrP^{Sc} species for disease transmission are small oligomers [32, 33]. The reported predominance of relatively protease-sensitive PrP^{Sc} species until late in the incubation period [12, 34], which appear to be oligomeric [34], supports that both transmitting and synaptotoxic species extant earlier in disease progression would be likely to display such characteristics. This observation broadly concurs with the limited available information suggesting that the most infectious species and conversion to overt symptomatic disease corresponds with an increasing relative presence of PrP^{Sc} conformers found in smaller, more protease-sensitive oligomers [13]. Also to be determined is whether there is a single or predominant neurotoxic PrP^{Sc} species and if so, does specific biochemical or biophysical transformation occur during disease progression or conversely does a diverse spectrum of toxic PrP^{Sc} of varied biochemical properties eventuate during disease progression.

As a part of studies comprehensively characterising a new electrophysiological paradigm, we recently demonstrated the ability to objectively and sensitively detect the presence of acutely synaptotoxic *ex vivo* PrP^{Sc} derived from brains of mice terminally ill with M1000 prion infection [31]. The current study aimed to determine whether such synaptotoxic species could be detected in the brains of mice during disease evolution following precise stereotaxic intracerebral inoculation with M1000 prions. To achieve this, we assessed the acute synaptotoxicity of *ex vivo* homogenate preparations derived from the brains of M1000 infected mice (cM1000) at 30%, 50%, 70% and 100% of the TSD, through exploring the capacity of cM1000 to impair hippocampal CA1 region long-term potentiation (LTP), paired-pulse facilitation (PPF), and post-tetanic potentiation (PTP) in explant hippocampal slices. LTP and PTP are physiological measures of synaptic plasticity correlating with memory and learning induced by repetitive high frequency stimulations wherein PTP is a short-term predominantly pre-synaptically mediated enhancement of synaptic responsiveness followed by LTP, which is expressed as a persistently enhanced post-synaptic potential generated by a combination of both pre- and post-synaptic

functions [31]. PPF is a physiological measure of the probability of neurotransmitter release (*Pr*), which is frequently used to estimate *Pr* during expression of LTP [31]. Of particular note, cM1000 from 30% of the TSD was able to cause significant impairment of LTP, PPF, and PTP. Evidence that the synaptotoxicity directly related to PrP species was demonstrated by the significant rescue of LTP dysfunction at each time-point through immuno-depletion of >50% of total PrP species from cM1000 preparations. Size fractionation chromatography revealed that capacity for acute synaptotoxicity correlated with predominance of oligomeric PrP species in infected brains across all time points, with the profile appearing maximised by 50% of the TSD. Interestingly, both pooled oligomeric and monomeric PrP^{Sc} fractions from across the time-points were acutely synaptotoxic, with the toxicity of pooled monomeric fractions appearing associated with likely rapid spontaneous oligomerization of PrP^{Sc} monomers in physiological buffer following their size fractionation. Moreover, the synaptotoxicity of cM1000 from 30%, 50% and 70% of the TSD, but not at 100% TSD, was abolished by digestion of immuno-captured PrP species with mild PK treatment (5μg/ml for an hour at 37˚C), demonstrating that the predominant synaptotoxic PrP^{Sc} species up to and including 70% of the TSD appears quite proteinase-sensitive. Overall, these findings in combination with our previous assessments of transmitting prions support that synaptotoxic and infectious M1000 PrP^{Sc} species co-exist from at least 30% of the TSD.

Materials and methods

Ethics statement

All animal handling was in accordance with National Health and Medical Research Council (NHMRC) guidelines. Animal handling and experimental procedures were approved by The Florey Institute of Neuroscience and Mental Health Animal Ethics Committee (Ethics number: 13–048) or the Biochemistry & Molecular Biology, Dental Science, Medicine (RMH), Microbiology & Immunology, and Surgery (RMH) Animal Ethics Committee, The University of Melbourne (Ethics number: 1312997.1).

Animals

The M1000 prion strain has been well described and characterised [8], and was originally adapted to mice from a person most likely dying from GSS [15]. Mice used for electrophysiological studies and to generate M1000 infected brains at varying stages of prion infection following stereotaxic intracerebral (ic) inoculation were 12-week-old wild-type (WT) female C57BL/6J mice (Animal Resource Centre, Western Australia). In addition, 12-week-old WT female Balb/c mice were used to generate M1000 infected brains through routine ic inoculation as described previously [8]. Mice used for bioassay studies were six-week old transgenic (over-expressing PrP^{C} ~10-fold; [35]) tga20 mice bred at the Florey Institute of Neuroscience and Mental Health (originally a generous gift from The Scripps Research Institute, La Jolla, California, USA).

Mice inoculations for electrophysiology experiments

To optimise precision with M1000 inoculations for producing time course *ex vivo* preparations for electrophysiology experiments, 12-week old WT C57BL/6J mice were stereotactically ic inoculated. Briefly, mice were anesthetized with an intraperitoneal cocktail injection of ketamine (100mg/kg) and xylazine (20mg/kg) and placed on a small animal stereotactic frame (Model 940, Kopf, Germany fitted with a Model 5000 microinjection unit) equipped with a 37˚C heating mat. The pedal reflex was monitored every 15–20 minutes to assess the level of

unconsciousness. A small incision along the sagittal line of the scalp allowed the identification of the bregma. A small drill fitted with a blunt burr was then used to make a hole in the skull, through which a 26-gauge needle (Model 1701, Hamilton, Switzerland) was placed. Four microlitres of 10% (w/v in sterile PBS) cM1000 was then injected (flow-rate of 0.8μl/min) just above the dorsal hippocampus (bregma coordinates: -2.5 caudally, +/- 2.5 laterally and -1.5 ventrally). The needle was then slowly retracted, placed in position above the contralateral hippocampus and the procedure repeated as above. The scalp wound was closed with Super Glue and Ilium Neocort was applied. The mice were allowed to recover for 1 hour on a 37˚C heating mat and then transferred to single-caging for 3 days. The mice were checked once daily for physiological parameters such as weight and normal motor behaviour and an intraperitoneal dose of carprofen (5mg/kg) given at 0, 24 and 48 hours after surgery to relieve pain. These M1000 inoculated mice reach the TSD (requiring euthanasia) at a mean of ~170 (±3 SD) days post-inoculation (dpi). Relative to the TSD, mice were sacrificed at 30%, 50%, 70% and at the 100% time points (ie representing ~51, ~85, ~119, and ~170 dpi, respectively), brains were collected and homogenized to 20% (w/v) in 1x PBS, and stored at -80˚C until use. As negative or sham controls, similar aged WT mice were ic inoculated as above with normal brain homogenate (NBH; 10% w/v in PBS) and brains were harvested at the same dpi as the M1000 infected mice. To further assess the presence of synaptotoxic PrP^{Sc} species at an early time point following M1000 inoculation, 12-week-old WT female Balb/c mice were routinely ic inoculated as described previously [36] with brains collected at 30% of the TSD (representing ~44 dpi).

Immuno-depletion/-precipitation of PrP

Total prion proteins were specifically immuno-depleted using 03R19 anti-PrP polyclonal antibody from 1% (w/v) cNBH and cM1000 as previously described [31] to generate depleted normal and M1000 brain homogenates (dNBH and dM1000, respectively), with specificity checked by comparison with "mock" immuno-depletion using normal rabbit serum. Additionally, the immuno-precipitated prion proteins were eluted from protein-G-sepharose pellets reconstituted to original volumes, by a mild PK treatment of 5 μg/mL at 37˚C for an hour, with two cycles of 20-minutes of agitation interspersed with 10 minutes without agitation to generate PK-eluted immuno-precipitated NBH and M1000 brain homogenates (PK+IP-NBH and PK+IP-M1000, respectively). Aliquots of the ~1% (w/v) depleted and resuspended PK-treated preparations were taken for analysis by western blotting, prior to further dilution to 0.5% (w/v) in artificial CSF (aCSF: 126mM NaCl, 2.5mM KCl, 26mM $NaHCO_3$, 1.25mM NaH_2PO_4, 10mM Glucose, 1.3mM $MgCl_2.6H_2O$ and 2.4mM $CaCl_2.2H_2O$) for use in electrophysiology studies.

Electrophysiology paradigm

Electrophysiology studies were performed as described [31] with brain homogenates for these studies pre-cleared by a one minute 100xg spin. In brief, 300μm hippocampal slices were prepared from WT mice utilizing a vibratome (Leica VT1200S) and ice cold cutting solution (3mM KCl, 25mM $NaHCO_3$, 1.25mM NaH_2PO_4, 206mM Sucrose, 10.6mM Glucose, 6 mM $MgCl_2.6H_2O$, 0.5mM $CaCl_2.2H_2O$) while continuously carboxygenating with 5% CO_2 and 95% O_2. Following an hour of incubation in carboxygenated aCSF at 32˚C, slices were mounted on to 60MEA200/30iR-Ti-pr-T multi-electrode arrays (MEA; Multichannel Systems; Germany) for recording while continuously superfused with carboxygenated aCSF. Harp slice grids (ALA HSG-5B, Multichannel Systems; Germany) were utilized to ensure optimal contact of the slices with microelectrodes. Electric stimulation (1500 to 2500 mV) was utilised to evoke

hippocampal field excitatory post-synaptic potentials (fEPSP) from the Schäffer collateral pathway while recording from the CA1 region. A 30-minute baseline was recorded at 30 second intervals using a basal stimulus determined by an input-output curve, which was obtained by stimulating the Schäffer collateral pathway with increasing stimulation intensities (at 30 second intervals) starting from 500 mV to a stimulation intensity that evoked the maximum fEPSP as indicated by plateau curve (usually between 4000–5000 mV) wherein the basal stimulus was declared as the stimulus that evoked ~40% of the maximum fEPSP. Channels of the MEA grid utilized for analysis were those best aligned to the Schäffer collateral pathway through recording from electrodes placed on the stratum radiatum of the CA1 region and selecting those demonstrating fEPSPs that manifested PPF (as described previously [31]), generated positive trend input-output curves, produced non-spiky fEPSP curves, and maintained fEPSP amplitudes above the eight standard deviation threshold of the noise levels for at least 80% of the total recording time. The average number of electrodes recorded from and utilised for analysis in each slice was seven. The treatments (the crude homogenates or other preparations) were superfused over the hippocampal slices for five minutes following 8–10 minutes of stable baseline. For tetanus, three trains of high frequency stimulation (HFS: 100Hz each) were applied (for 0.5 seconds at 20 second intervals) following the baseline recording to induce PTP and LTP. Each train of HFS evoked serial pulses of fEPSPs, wherein the first nine of those pulses were recorded to estimate presynaptic activity associated with the induction of PTP. Post-HFS recording continued for 30 minutes wherein the first response was utilised to estimate PTP and last 10-minute period taken as representing LTP. LTP and PTP were calculated as the percentage fEPSP increase after HFS relative to the last five-minute baseline of fEPSPs. PPF was evoked by basal stimuli delivered 20 ms apart as previously reported [31]. The ratio between the fEPSP amplitude of the first and the second pulse was the PPF ratio. PPF ratio was measured before treatment and induction of LTP (PPF1) and after treatments and expression of LTP (PPF2).

Incubation time interval bioassays

To assess levels of prion infectivity contained within the various *ex vivo* M1000 PrP^{Sc} preparations utilized to characterise acutely synaptotoxic species present in cM1000 derived from terminal prion disease, tga20 mice were ic inoculated with these *ex vivo* samples (30μL per mouse) as previously described [8]. In addition, 1% (w/v) cM1000 and NBH served as positive and negative controls, respectively. The tga20 mice were euthanized when they become terminally ill as indicated by features including reduced spontaneous activity, prominent ataxia and hind limb paresis. Total survival in dpi was recorded and utilized to calculate an approximate, especially relative infectivity titre for each *ex vivo* M1000 PrP^{Sc} preparation as described [8]. One-way ANOVA was used to compare the average terminal incubation period of tga20 mice, as well as average infectivity titre of inocula. The infectivity titres, ID_{50} units/g brain were converted to log ID_{50} units/μL 1% crude M1000 brain homogenate and plotted as a function of percentage of incubation period to the terminal stage.

Western blotting

PrP levels were analysed by standard PAGE and immunoblotting as described previously [37], with protease-resistant PrP also detected following the higher sensitivity method of sodium phosphotungstate (NaPTA) precipitation as previously described [36]. For non-NaPTA immunoblotting, brain homogenates (1% w/v) from all time points were either not treated or treated with 5μg/mL PK for an hour at 37˚C, while brain homogenates undergoing NaPTA

precipitation were treated with 5, 25, and 50μg/mL PK for an hour at 37˚C. Proteins were denatured in 1x sample buffer (containing 6% Beta-mercaptoethanol), resolved on NuPAGE Novex 4–12% Bis-Tris gels (ThermoFisher Scientific), transferred to PVDF membrane (Millipore; transfer buffer containing 25 mM Tris, 200 mM glycine and 20% methanol), blocked with 5% (w/v) skim milk then probed with the anti-PrP primary antibodies either 03R19[14] or 8H4 (Abcam) as indicated in the figure legends. For native western blotting, protein samples containing 2% (w/v) Sarkosyl were diluted 1:1 with 2x Novex Tris-Glycine native sample buffer, resolved on NuPAGE Novex 3% Tris-Acetate gels in 1x Novex Tris-Glycine native running buffer (at constant 160V; ThermoFisher Scientific), and transferred to PVDF membrane (at constant 70V for 3 hours) using a transfer buffer containing 25 mM Tris, 200 mM glycine and 10% methanol. A few microliters of a High Marker protein standard (Invitrogen) were resolved alongside the protein samples on native gels to estimate sizes of native proteins. The PVDF membranes of native protein samples were blocked and probed with 8H4 antibody to detect PrP species. Following the appropriate secondary antibody, protein bands were detected by chemiluminescence (ECL Prime and Select, Invitrogen) and digitized in a Fujifilm LAS-3000 Intelligent dark box. Membranes were stained with Coomassie blue to determine relative total protein levels. Protein bands of interest were quantified by densitometry (Image J) normalized for total protein level as previously described [37]. Approximate estimation of PrP quantities in preparations used for electrophysiology studies was achieved by intra-experimental comparison to a recombinant full-length mouse PrP (rPrP) standard curve, as described previously [31].

Size exclusion chromatography

As described in detail previously [31], whole brains from infected mice at each time point, as well as sham-infected control mice, were homogenized at 20% (w/v in 1x PBS), pelleted at a 15000xg spin, solubilized with 4% (w/v in 1x PBS) Sarkosyl into ~10% (w/v) final concentration, and centrifuged at 10000xg to collect the supernatants. The supernatants were then exhaustively dialyzed using 10 kDa cut-off dialysis membranes in 1x PBS dialysate (without calcium) and filtered across a 0.22-micron filter. Approximately 3 mL of each preparation was slowly injected into a sephacryl-100 column pre-equilibrated with at least 2 column volumes of 1x PBS containing calcium and magnesium. The protein complexes were eluted in 1x PBS (containing calcium and magnesium) at a flow rate of 0.5 mL per minute, wherein the void volume was collected at ~70 minutes after injection. One mL fractions were then collected every two minutes for 80 minutes (40 fractions) following collection of the void volume. The relative levels of PrP in each fraction were analysed by western blotting, including before and after digestion with PK as described [31]. The size of proteins or complexes eluted into each fraction was determined through size fractionation of size exclusion chromatography protein markers: bovine erythrocyte carbonic anhydrase (~29kDa), bovine serum albumin (~66kDa), yeast alcohol dehydrogenase (~150kDa), sweet potato beta-amylase (~200kDa), horse spleen apoferritin (~443kDa), and bovine thyroglobulin (~669kDa) [31]. Operationally, PrP species eluted into fractions with molecular weights smaller than 100kDa were considered to be mostly monomeric PrP while prion proteins eluted into fractions with molecular weights >100kDa but <500kDa were considered predominantly oligomeric PrP or large protein complexes containing PrP and although not experimentally verified PrP >500kDa was considered to represent increasingly fibrillar assemblies.

Statistical analyses

The total levels of PrP and levels of at least modestly PK resistant PrP^{Sc} were compared across time points of the disease evolution by One-way ANOVA. Levels of PK-resistant PrP^{Sc} across

the time points detected by NaPTA precipitation after digestion with each PK concentration (5, 25, and 50μg/mL) were compared by One-way ANOVA with Tukey's correction for multiple comparisons. The average LTP or PTP in slices treated with M1000 preparations from across the time points were compared with the appropriate negative controls by One-way ANOVA with Dunnett's correction for multiple comparisons (comparing mean LTP and PTP of M1000 treated slices to those of negative controls). The degree of synaptotoxicity was calculated as the percentage LTP reduction from that observed in negative controls. The average degree of synaptotoxicity as either LTP or PTP disruption in slices treated with M1000 preparations from across the time points were compared by One-way ANOVA with Tukey's correction for multiple comparisons (comparing mean degree of toxicity at each time point with that at every other time point). Unpaired Student t-test was used to compare the average PrP levels before and after the PrP-immuno-depletion. PPF was calculated as the percentage PPF ratio decrease in PPF2 relative to PPF1 and compared to that of the appropriate negative control by One-way ANOVA with Dunnett's correction for multiple comparisons. The probability of neurotransmitter release during HFS trains was calculated by dividing the second pulse by the first pulse of the first 9 pulses evoked by each train. The average probability of neurotransmitter release at the second and third train was compared to that of the first train by One-way ANOVA with Dunnett's correction for multiple comparisons. The depletion of the readily releasable pool (RRP) of neurotransmitter during each train of HFS was estimated and compared between treatment groups using a one-phase decay exponential function to determine the slope of fEPSP amplitude decline (time constant of decay) from pulse three to the last pulse as described previously [31]. The size of RRP was estimated and compared between treatment groups by a linear fit equation of cumulative fEPSP of each train (best fit of the last four cumulative fEPSP) wherein the size of RRP was the Y-intercept of the linear fit (see Methods of [31] for further details). The efficiency of RRP replenishment following each HFS train was determined by size of RRP increase at train two and three [31]. One-way ANOVA with Tukey's correction for multiple comparisons was used to compare the average incubation period of tga20 mice inoculated with different preparations from the TSD, as well as to compare the average infectivity titres of these M1000 preparations. Tukey's correction for multiple comparisons was used to compare the mean of each group to the mean of every other group (suited for time point results), whereas Dunnett's correction for multiple comparison was used to compare the mean of the control group to the mean of every other tested group.

Results

Acutely synaptotoxic PrP^{Sc} is detectable from early in M1000 prion disease development

Neuropathological features of prion disease such as microvacuolation and astrocytic gliosis are initially detected in the hippocampus and thalamus of WT Balb/c mice ic infected with M1000 prions at ~57% of the TSD (~83 dpi) [8], which suggests the presence of neurotoxic PrP^{Sc} species prior to this. To explore whether acutely synaptotoxic PrP^{Sc} species are propagated at earlier time points of M1000 prion disease pre-empting these first neuropathological changes, we used a recently developed electrophysiology paradigm to assess cM1000 prepared from WT mice at 30%, 50%, 70% and 100% of the TSD following stereotaxic ic infection with M1000 prions. To biochemically characterise the 0.5% (w/v) cM1000 from each of the time points (n = 3 for each time point) they were initially evaluated by routine western blotting before and after treatment with modest PK digestion in combination with comparative quantitative analysis based on a rPrP standard curve. A significant increase in total PrP ($p = 0.0019$), largely due to increased levels of at least modestly PK-resistant PrP^{Sc} ($p<0.0001$) at 100% of the TSD relative

to earlier time points was observed (Fig 1A & S1A Fig) with a trend towards reduced total levels at 70% of the TSD. Moreover, at least modestly PK-resistant PrP^{Sc} was not detected at 30% and 50% of the TSD, with only minimal levels evident at 70% of the TSD (~0.005 μg/mL), which were approximately 16-fold less than the robust levels observed at 100% of the TSD (~0.080 μg/mL). As expected, PK-resistant PrP was never observed in cNBH across the time course, with no difference in PrP^{C} levels across all time points (S1B Fig).

To further characterise the PrP in the 0.5% (w/v) NBH and cM1000 across the time course, western blotting following NaPTA precipitation and digestion with increasing PK concentrations was performed. In cM1000 preparations, this analysis (Fig 1B & and 1C) revealed barely detectable levels of very modestly PK-resistant PrP^{Sc} at 30% (<< 0.012μg/mL) and 50% (<<0.012 μg/mL) of the TSD, with significantly higher levels at 70% (~0.059 μg/mL) and 100% (~0.090 μg/mL) of the TSD ($p = 0.0043$; One-way ANOVA with Tukey's correction for multiple comparisons). The 25 μg/mL PK digestion completely abolished PK-resistant PrP^{Sc} species at 30% of the TSD, while minimal levels were detected at 50% (<<0.012μg/mL) of the TSD and significantly higher levels observed at 70% (~0.035 μg/mL) and 100% (~0.051 μg/mL) of the TSD ($p = 0.0045$; One-way ANOVA with Tukey's correction for multiple comparisons). The 50 μg/mL PK completely digested PK-resistant PrP^{Sc} species at 30% and 50% of the TSD, while significantly higher levels remained at 70% (~0.037 μg/mL) and 100% (~0.058 μg/mL) of the TSD ($p = 0.023$; One-way ANOVA with Tukey's correction for multiple comparisons). Of note, these data suggest that PK-resistant PrP^{Sc} species at 70% of the TSD were rendered more detectable by NaPTA precipitation compared to results of routine western blotting such that levels of PK-resistant PrP^{Sc} species (including at least modestly PK-resistant species) were no longer significantly different to those at 100% of the TSD (compare Fig 1B and 1C with S1A Fig). Given PK-resistant PrP was never observed in cNBH across the time points, only cNBH from 100% of the TSD was utilized as negative control for assessing acute synaptotoxicity.

Relative to the normal CA1 region LTP obtained in WT hippocampal slices treated with cNBH (180 ± 7%; n = 5), the CA1 LTP was significantly impaired following exposure to cM1000 prepared from the brains of C57BL/6J mice at 30% of the TSD following M1000 prion inoculation through hippocampal stereotaxic injection (154 ± 4%; $p = 0.0122$; n = 5; Fig 2B; One-way ANOVA with Dunnett's correction for multiple comparisons), which was very similar to the degree of LTP disruption obtained in WT hippocampal slices after exposure to cM1000 derived from brains of routinely ic inoculated Balb/c mice also culled at 30% of the disease progression (159 ± 5%; $p = 0.0368$; n = 5; Fig 2A; One-way ANOVA with Dunnett's correction for multiple comparisons). CA1 LTP was also significantly impaired by cM1000 derived from the brains of stereotactically infected C57BL/6J WT mice at 50% (142 ± 4%; $p = 0.0001$; n = 5), 70% (141 ± 5%; $p = 0.0001$; n = 5) and 100% (133 ± 6%; $p<0.0001$; n = 5) of the TSD (Fig 2C–2F; One-way ANOVA with Dunnett's correction for multiple comparisons). Consistently, the degree of PPF ratio decline in slices with impaired LTP were significantly lower than those in slices treated with cNBH demonstrating normal LTP, confirming significant disruption of the probability of neurotransmitter release associated with LTP dysfunction (Fig 2G; One-way ANOVA with Dunnett's correction for multiple comparisons). In addition, PTP was significantly disrupted in WT slices treated with cM1000 prepared from each time point (Balb/c at 30% of the TSD, 261 ± 25%, $p = 0.0480$; C57BL/6J at 30% of the TSD, 255 ± 24%; $p = 0.0334$; 50% of the TSD: 238 ± 14%, $p = 0.0093$; 70% of the TSD, 222 ± 19%, $p = 0.0052$; and 100% of the TSD: 261 ± 25%, $p = 0.0191$; n = 5 for each time point) relative to normal PTP generated in WT hippocampal slices treated with cNBH (344 ± 25%; n = 5; Fig 2H). Interestingly, the degree of PTP impairment did not significantly increase across the time points ($p = 0.3306$; One-way ANOVA with Tukey's correction for multiple comparisons; Fig

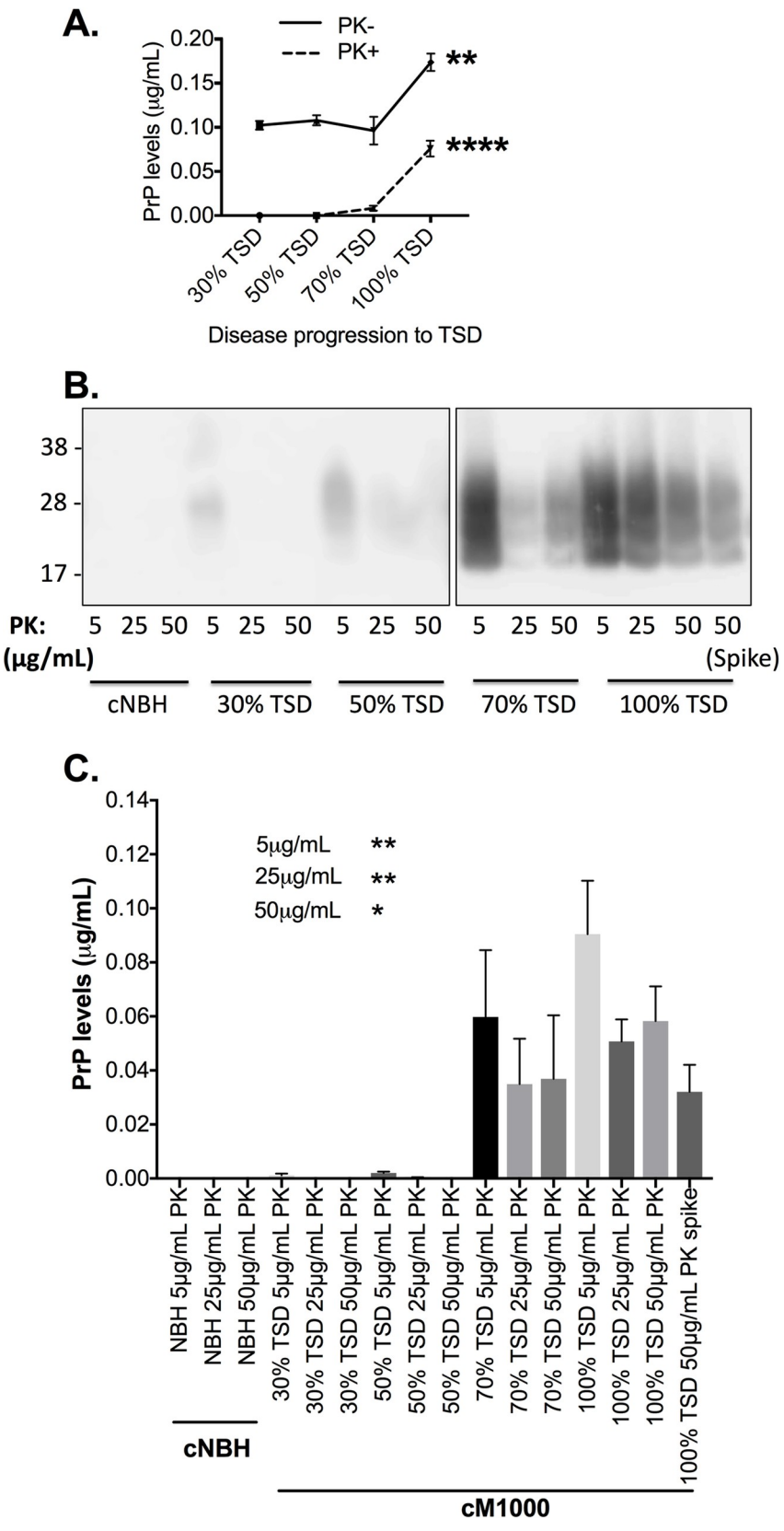
A.
PK-
PK+
**
****
PrP levels (µg/mL)
0.20
0.15
0.10
0.05
0.00
30% TSD
50% TSD
70% TSD
100% TSD
Disease progression to TSD
B.
38
28
17
PK:
5 25 50 5 25 50 5 25 50 5 25 50 5 25 50 50
(µg/mL)
(Spike)
cNBH
30% TSD
50% TSD
70% TSD
100% TSD
C.
PrP levels (µg/mL)
0.14
0.12
0.10
0.08
0.06
0.04
0.02
0.00
5µg/mL **
25µg/mL **
50µg/mL *
NBH 5µg/mL PK-
NBH 25µg/mL PK-
NBH 50µg/mL PK-
30% TSD 5µg/mL PK-
30% TSD 25µg/mL PK-
30% TSD 50µg/mL PK-
50% TSD 5µg/mL PK-
50% TSD 25µg/mL PK-
50% TSD 50µg/mL PK-
70% TSD 5µg/mL PK-
70% TSD 25µg/mL PK-
70% TSD 50µg/mL PK-
100% TSD 5µg/mL PK-
100% TSD 25µg/mL PK-
100% TSD 50µg/mL PK-
100% TSD 50µg/mL PK spike
cNBH
cM1000

Fig 1. Levels of total PrP and proteinase K (PK)-resistant PrP^{Sc} species across the natural evolution of M1000 prion disease. (A) Quantification of the immunoblots in S1A Fig with the levels of total PrP (without PK digestion: PK-) and at least modestly PK-resistant PrP^{Sc} (PK+) compared across M1000 disease evolution by One-way ANOVA with Tukey's correction for multiple comparisons. (B) Western immunoblots of cNBH and cM1000 from all the disease time points following precipitation of PrP^{Sc} species by sodium phosphotungstic acid (NaPTA) and digestion with 5, 25, and 50 μg/mL PK (at 37˚C for an hour), respectively. The "spike" represents the positive control demonstrating successful precipitation and detection of PrP^{Sc} species in 5μL of 10% (w/v) cM1000 that was spiked into 500μL of 1% (w/v) cNBH. (C) Approximate quantification of PrP levels (in μg/mL) in brain homogenates in B (n = 4). Results are presented as mean ± standard error of mean. $^{*}p<0.05$, $^{**}p<0.01$, $^{****}p<0.0001$.

https://doi.org/10.1371/journal.ppat.1007712.g001

2I upper panel), whereas the degree of LTP impairment significantly increased across the disease evolution in mice inoculated by stereotaxic injection ($p<0.0001$; One-way ANOVA with Tukey's correction for multiple comparisons; Fig 2I bottom panel). Transient depression of fEPSPs during and following the brief treatments was frequently observed, but importantly, they invariably return to baseline before instigation of HFS trains, with potential explanations for this phenomenon and the lack of implications for assessments of synaptic function discussed in detail previously [31].

Further analyses of presynaptic events during HFS trains that subsequently induced PTP were undertaken. Of note, the cNBH negative controls used in these electrophysiology studies did not affect synaptic functions as compared to the aCSF technical controls (S2A–S2G, S2K & S2L Fig). Specifically, normal RRP replenishment was exhibited by slices treated with aCSF and cNBH wherein the size of RRP significantly increased at train 2 and again at train 3 (S2K & S2L Fig); however, the RRP replenishment was impaired in slices with PTP impairment, wherein the RRP size failed to significantly increase from train 2 to train 3 across all treatments with cM1000 from the time course (S2M–S2P Fig). Although the RRP replenishment was impaired, the probability of neurotransmitter release was normal with the second and third trains evoking significantly higher neurotransmitter release than the first train (S2D Fig). The RRP rate of depletion was also normal, whereby the time-constant of decay of the third-to-ninth pulses were not different when comparing between slices treated with cNBH and those treated with cM1000 (S2H–S2J Fig).

Acute synaptotoxicity derived from earlier time points of M1000 prion disease evolution is associated with PrP species

To determine if *ex vivo* PrP species propagated at earlier time points of the disease evolution are directly associated with the acute synaptotoxicity of cM1000, we immuno-depleted total PrP species in cM1000 derived from each time point and assessed the acute synaptotoxicity of the depleted M1000 preparations using our electrophysiology paradigm. The immuno-depletion removed ~63 ± 18% of total PrP from cNBH (n = 3), ~52 ± 0.6% from cM1000 at 30% TSD (n = 5), ~60 ± 0.4% at 50% TSD (n = 5), ~58 ± 2% at 70% TSD (n = 5), and ~79 ± 7% at 100% TSD (n = 4; Fig 3A and 3B). In parallel with the ~79% total PrP depletion from cM1000 at 100% of the TSD, ~89 ± 0.3% of at least modestly PK-resistant PrP^{Sc} was also depleted (n = 2; Fig 3C). Importantly, the LTP dysfunction caused by cM1000 preparations from each time point was abolished following the depletion of PrP species (Fig 3D–3G) wherein the LTPs generated by slices treated with dM1000 from 30%, 50%, 70%, and 100% of the TSD (161 ± 7%, 157 ± 6%, 163 ± 5%, and 169 ± 5%, respectively; n = 5 for each) were no longer different from the LTP of slices treated with dNBH (163 ± 6%; n = 5) (Fig 3H). Consistent with the rescue of LTP, the degree of PPF ratio decline was no longer significantly lower in slices treated with dM1000 compared to slices treated with dNBH consistent with rescue of the impairment of the probability of neurotransmitter release during LTP through the immuno-depletion of PrP (Fig 3I). Further, the PTP was no longer disrupted following treatment with

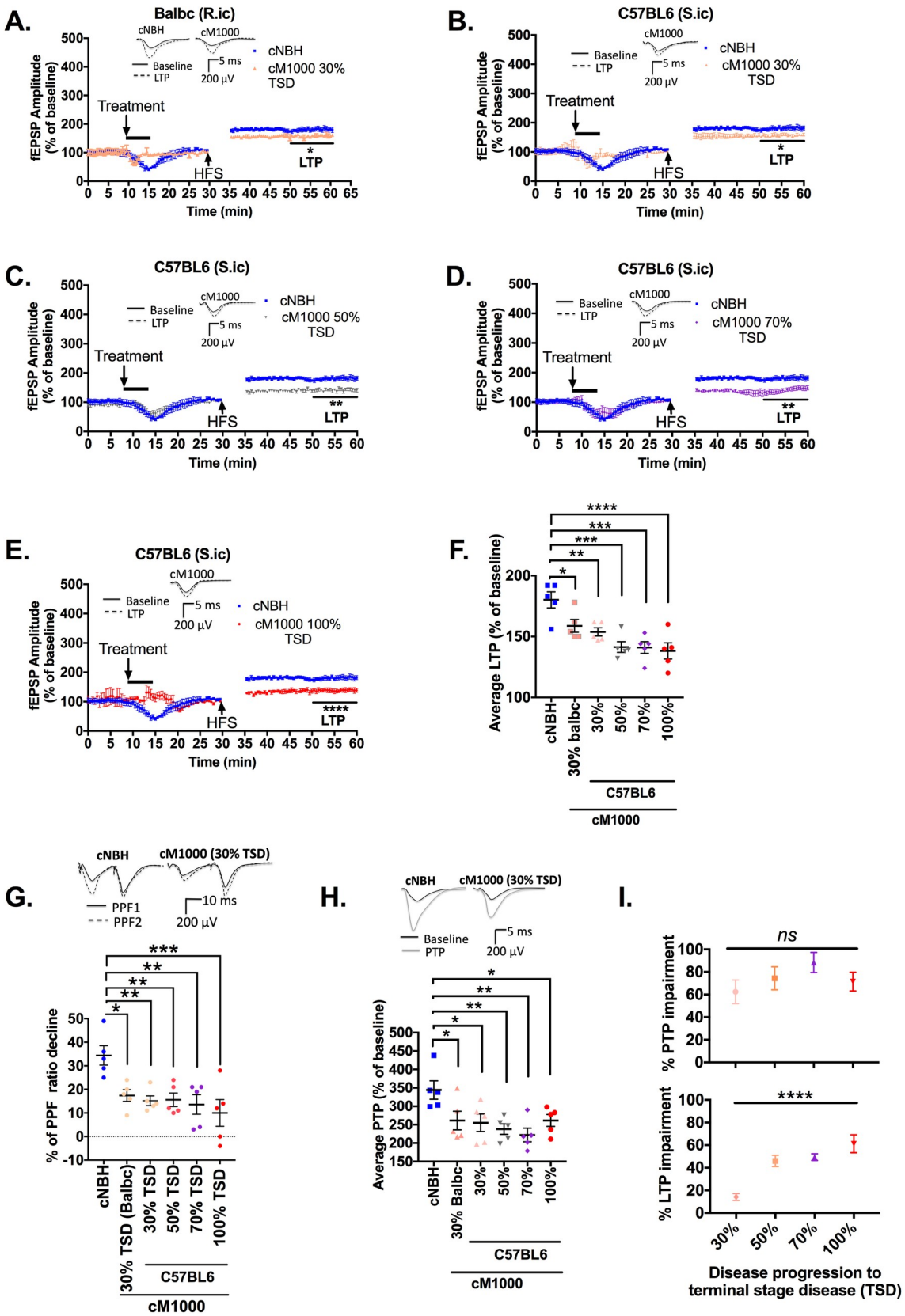
A.
Balbc (R.ic)
cNBH
cM1000
Baseline
LTP
5 ms
200 µV
cNBH
cM1000 30% TSD
Treatment
HFS
LTP
fEPSP Amplitude (% of baseline)
Time (min)
B.
C57BL6 (S.ic)
cM1000 30% TSD
C.
cM1000 50% TSD
D.
cM1000 70% TSD
E.
cM1000 100% TSD
F.
Average LTP (% of baseline)
cNBH
30% balbc
30%
50%
70%
100%
C57BL6
cM1000
G.
cNBH
cM1000 (30% TSD)
PPF1
PPF2
10 ms
200 µV
% of PPF ratio decline
30% TSD (Balbc)
30% TSD
50% TSD
70% TSD
100% TSD
H.
PTP
Average PTP (% of baseline)
I.
ns
% PTP impairment
% LTP impairment
Disease progression to terminal stage disease (TSD)

Fig 2. Synaptotoxic PrP^{Sc} species are propagated from early in the evolution of M1000 prion disease. (A) CA1 region LTP of WT mouse hippocampal slices was significantly disrupted following a five minute exposure to 0.5% (w/v; in artificial CSF) crude M1000 brain homogenates (cM1000) derived from M1000 infected WT Balb/c mice (infected through routine intracerebral injection [R.ic]) at 30% of the incubation period to the terminal stage of disease (TSD). (B to E) CA1 region LTP of WT mouse hippocampal slices was significantly disrupted following a 5 minute exposure to 0.5% (w/v; in artificial CSF) cM1000 derived from M1000 infected WT C57BL/6J mice (infected by stereotaxic intracerebral injection [S.ic]) at 30% (B), 50% (C), 70% (D) and 100% (E) of the TSD. (F) Average LTP from the last 10 minutes of recordings (fEPSP readings following high frequency stimulation, HFS) after treatments with cM1000 from 30%, 50%, 70% and 100% of the TSD compared to the negative control 0.5% (w/v) crude normal brain homogenates (cNBH) derived from sham infected mice at the equivalent of 100% of the TSD. (G) Average percentage paired pulse facilitation (PPF) ratio decline following treatments in WT mouse hippocampal slices treated with cM1000 compared with cNBH controls as described in the Methods. (H) The average PTP generated by WT mouse hippocampal slices treated with cM1000 from across the disease evolution compared to the cNBH control as described in the Methods. (I) The percentage of PTP and LTP impairments (upper and lower panel, respectively) following treatments with cM1000 from each time point of the disease progression calculated as the percentage of PTP and LTP decrease compared to the normal PTP and LTP in slices treated with cNBH controls (One-way ANOVA with Tukey's correction for multiple comparison). (A to E) The five minute treatments started after 8-to-10 minutes of stable baseline. The HFS trains were applied following 30 minutes of baseline recordings. (A, C, D) Results are presented as mean ± standard error of mean. (A-E, F, G & H) Average LTP/PTP/PPF ratio degree of decline in WT mouse hippocampal slices treated with cM1000 preparations from across the time points were compared with NBH controls by One-way ANOVA with Dunnett's correction for multiple comparisons. (A-E, G & H) Some examples of raw fEPSP traces are provided as insets. $^{*}p<0.05$, $^{**}p<0.01$, $^{***}p<0.001$, $^{****}p<0.0001$, *ns* = not statistically significant ($p>0.05$).

https://doi.org/10.1371/journal.ppat.1007712.g002

dM1000 from 30% and 50% of the TSD (n = 5 each; Fig 3J). In contrast, relative to the dNBH control, the PTP remained impaired after treatment with dM1000 from 70% ($p = 0.0221$; n = 5) and 100% ($p = 0.0009$; n = 5) of the TSD regardless of the significant rescue of LTP by the immuno-depletion of PrP species (Fig 3J). This inconsistent rescue of PTP aligned with the significant rescue of RRP replenishment after depletion of PrP when treated with dM1000 from 30% and 50% of the TSD (significant increase of RRP size at train 2 and again at train 3), while it remained impaired by dM1000 from 70% and 100% of the TSD (failure of RRP size to significantly increase from train 2 to train 3) (S3M–S3P Fig). Both the probability of release and RRP depletion during HFS trains were normal in slices treated with dM1000 similar to those treated with dNBH (S3D, S3H–S3J Fig). Importantly, dNBH negative controls did not affect synaptic functions as compared to aCSF technical controls (S3A–S3G, S3K & S3L).

Acute synaptotoxicity at earlier time points is associated with PK-sensitive PrP species

In a previous report, we described that the prion acute synaptotoxicity harboured in brains at the terminal stage of M1000 prion disease appeared directly linked to at least modestly PK-resistant PrP species [31]; however, the virtual absence of at least modestly PK-resistant PrP species at 30% and 50% of the TSD (Fig 1A–1C and S1A Fig) regardless of the link between total PrPs and acute synaptotoxicity suggests that synaptotoxic species at earlier time points probably relate to PK-sensitive PrP^{Sc}. To verify this speculation, we immuno-precipitated total PrP species from cM1000 at each time point, digested pellets with the same mild PK treatment to elute immuno-captured PrP species, and assessed their toxicity using our electrophysiology paradigm. Using routine western blotting, there was no detectable PK-resistant PrP^{Sc} in immuno-captured PrP species prepared from 30% and 50% of the TSD, while very minimal levels were detected at 70% of the TSD (<<0.012μg/mL; n = 5) and substantial amounts at 100% of the TSD (~0.057 ± 12 μg/mL; n = 4; $p<0.0001$; One-way ANOVA with Tukey's correction for multiple comparisons) (Fig 4A and 4B). Importantly, the LTP was not impaired by treatment with PK+IP-M1000 from 30%, 50% and 70% of the TSD relative to the PK+IP-NBH controls (Fig 4C–4E; n = 5 for each), while congruent with our previous observations the LTP was significantly disrupted by exposure to PK+IP-M1000 from 100% of the TSD (Fig 4F, $p = 0.0176$; n = 5 each; [31]). Overall, similar to the results in cM1000 (Fig 2I), there was a correlation between disease progression and LTP dysfunction due to the presence of at least

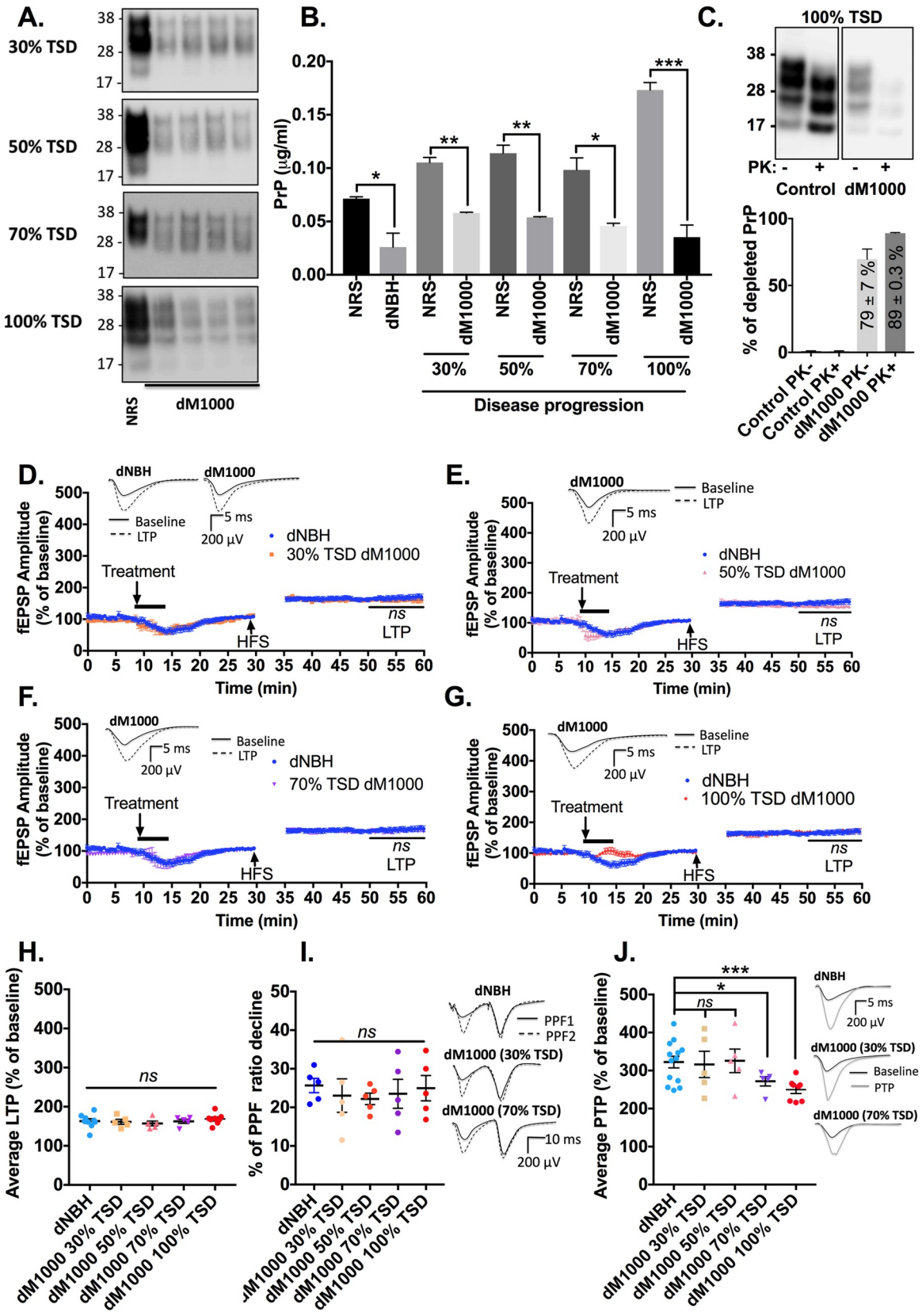
A.
30% TSD
50% TSD
70% TSD
100% TSD
38
28
17
NRS
dM1000
B.
PrP (µg/ml)
0.20
0.15
0.10
0.05
0.00
*
**
**
*
***
NRS
dNBH
NRS
dM1000
NRS
dM1000
NRS
dM1000
NRS
dM1000
30%
50%
70%
100%
Disease progression
C.
100% TSD
PK: - + - +
Control dM1000
% of depleted PrP
100
50
0
79 ± 7 %
89 ± 0.3 %
Control PK-
Control PK+
dM1000 PK-
dM1000 PK+
D.
dNBH
dM1000
Baseline
LTP
5 ms
200 µV
dNBH
30% TSD dM1000
Treatment
HFS
ns
LTP
fEPSP Amplitude (% of baseline)
Time (min)
E.
dM1000
Baseline
LTP
5 ms
200 µV
dNBH
50% TSD dM1000
Treatment
HFS
ns
LTP
fEPSP Amplitude (% of baseline)
Time (min)
F.
dM1000
Baseline
LTP
5 ms
200 µV
dNBH
70% TSD dM1000
Treatment
HFS
ns
LTP
fEPSP Amplitude (% of baseline)
Time (min)
G.
dM1000
Baseline
LTP
5 ms
200 µV
dNBH
100% TSD dM1000
Treatment
HFS
ns
LTP
fEPSP Amplitude (% of baseline)
Time (min)
H.
Average LTP (% of baseline)
ns
dNBH
dM1000 30% TSD
dM1000 50% TSD
dM1000 70% TSD
dM1000 100% TSD
I.
% of PPF ratio decline
ns
dNBH
PPF1
PPF2
dM1000 (30% TSD)
dM1000 (70% TSD)
10 ms
200 µV
dM1000 30% TSD
dM1000 50% TSD
dM1000 70% TSD
dM1000 100% TSD
J.
Average PTP (% of baseline)
***
*
ns
dNBH
5 ms
200 µV
dM1000 (30% TSD)
Baseline
PTP
dM1000 (70% TSD)
dNBH
dM1000 30% TSD
dM1000 50% TSD
dM1000 70% TSD
dM1000 100% TSD

Fig 3. Acute synaptotoxicity of cM1000 from earlier time points of M1000 prion disease is associated with prion protein species. (A) Western blotting of 20 μL 1% (w/v) crude M1000 brain homogenates (cM1000) from 30%, 50%, 70%, and 100% of M1000 prion disease progression to terminal stage disease (TSD) following mock immuno-depletion of total PrP species with normal rabbit serum (control) or immuno-depletion of total PrP species with 03R19 prion antibody (Probed with 8H4 antibody; molecular weight markers are provided at left). (B) Quantification of total PrP species in PrP immuno-depleted normal brain homogenate (dNBH) and PrP immuno-depleted cM1000 (dM1000) from across the disease progression (by densitometry analysis) compared to appropriate negative controls by Unpaired Student's t-test (mock immuno-depleted NBH or mock immuno-depleted cM1000). (C) Upper panel: A representative western blot of PrP levels in 20 μL cM1000 at 100% TSD following a mock immuno-depletion with normal rabbit serum (NRS) and an immuno-depletion with 03R19 antibody, and mild PK digestion. Lower panel: Quantification of total PrP (n = 4) and at least modestly PK-resistant PrP (n = 2) immuno-depleted from cM1000 (from 100% of the TSD) by 03R19 relative to the controls (probed with 8H4 antibody; molecular weight markers are provided at left). (D to G) LTP of WT mouse hippocampal slices following a five minute treatment with 0.5% (w/v in aCSF) dM1000 from 30% (D), 50% (E), 70% (F), and 100% of the TSD (G) compared with the LTP of slices treated with 0.5% (w/v in aCSF) dNBH controls (One-way ANOVA with Dunnett's correction for multiple comparisons). (H) The average LTPs, (I) the average percentage of PPF ratio decline, and (J) the average PTPs generated by WT mouse hippocampal slices treated with dNBH and dM1000 from across time points of the disease progression were compared by One-way ANOVA with Dunnett's correction for multiple comparisons when comparing across time points. (D to G) The five minute treatment started after 8-to-10 minutes of stable baseline. The high frequency stimulation (HFS) trains were applied following 30 minutes of baseline recordings. Results are presented as mean ± standard error of mean. (D-G, I & J) Some examples of raw fEPSP traces are provided as insets. $^{*}p<0.05$, $^{**}p<0.01$, $^{***}p<0.001$, *ns* = not statistically significant ($p>0.05$).

https://doi.org/10.1371/journal.ppat.1007712.g003

modestly PK-resistant PrP^{Sc} largely driven by the results at 100% of the TSD (Fig 4G, $p = 0.0264$; One-way ANOVA with Dunnett's correction for multiple comparisons). Additionally, relative to the normal PPF ratio decline in slices treated with PK+IP-NBH control, levels of PPF ratio decline in slices treated with PK+IP-M1000 from 30%, 50%, and 70% of the TSD also appeared normal (Fig 4H), while the degree of PPF ratio decline in slices treated with PK +IP-M1000 from 100% of the TSD was still significantly lower (Fig 4H; $p = 0.0011$: One-way ANOVA with Dunnett's correction for multiple comparisons). These PPF ratio results revealed that synaptotoxic PrP^{Sc} species responsible for the disruption of the probability of neurotransmitter release during LTP expression are highly PK-sensitive at earlier stages of the disease evolution and acquire resistance to PK as part of biochemical maturation toward the terminal stage of the disease. Parallel results were obtained with PTP dysfunction wherein only the PTP of slices treated with the PK+IP-M1000 from 100% of the TSD were impaired ($p = 0.0222$), but not with the PK+IP-M1000 from earlier time points (Fig 4I; One-way ANOVA with Dunnett's correction for multiple comparisons). The PK+IP-NBH did not cause any background disruption of LTP, PTP, and PPF ratios relative to aCSF technical controls (S4A–S4C Fig).

Propagation of oligomeric PrP^{Sc} species correlates with the detection of prion acute synaptotoxic PrP^{Sc} during the evolution of M1000 prion disease

Our previous studies demonstrated that acutely synaptotoxic species at the TSD in M1000 prion infection were strongly correlated with at least modestly PK resistant and oligomeric PrP^{Sc} [31]. To further explore the biophysical status of PK-sensitive, acutely synaptotoxic PrP^{Sc} species from earlier time points of M1000 prion disease we undertook size exclusion chromatography to fractionate *ex vivo* preparations from PrP^{Sc} from brains at 30%, 50%, and 70% of the TSD and compared them with *ex vivo* PrP^{Sc} fractions prepared from 100% of the TSD (positive control), as well as PrP^{C} fractions prepared from sham-infected NBH controls (negative control). Our results revealed that oligomeric PrP^{Sc} species were present and predominant at all the time points of the evolution of M1000 prion disease (Fig 5), which appeared directly correlated with the detection of the acutely synaptotoxic species at these earlier stages of the disease. Relative to fractions of the sham-infected NBH controls wherein PrP^{C} species were mostly monomeric (<100kDa in fractions 15 to 40; Fig 5 B), PrP^{Sc} fractions of

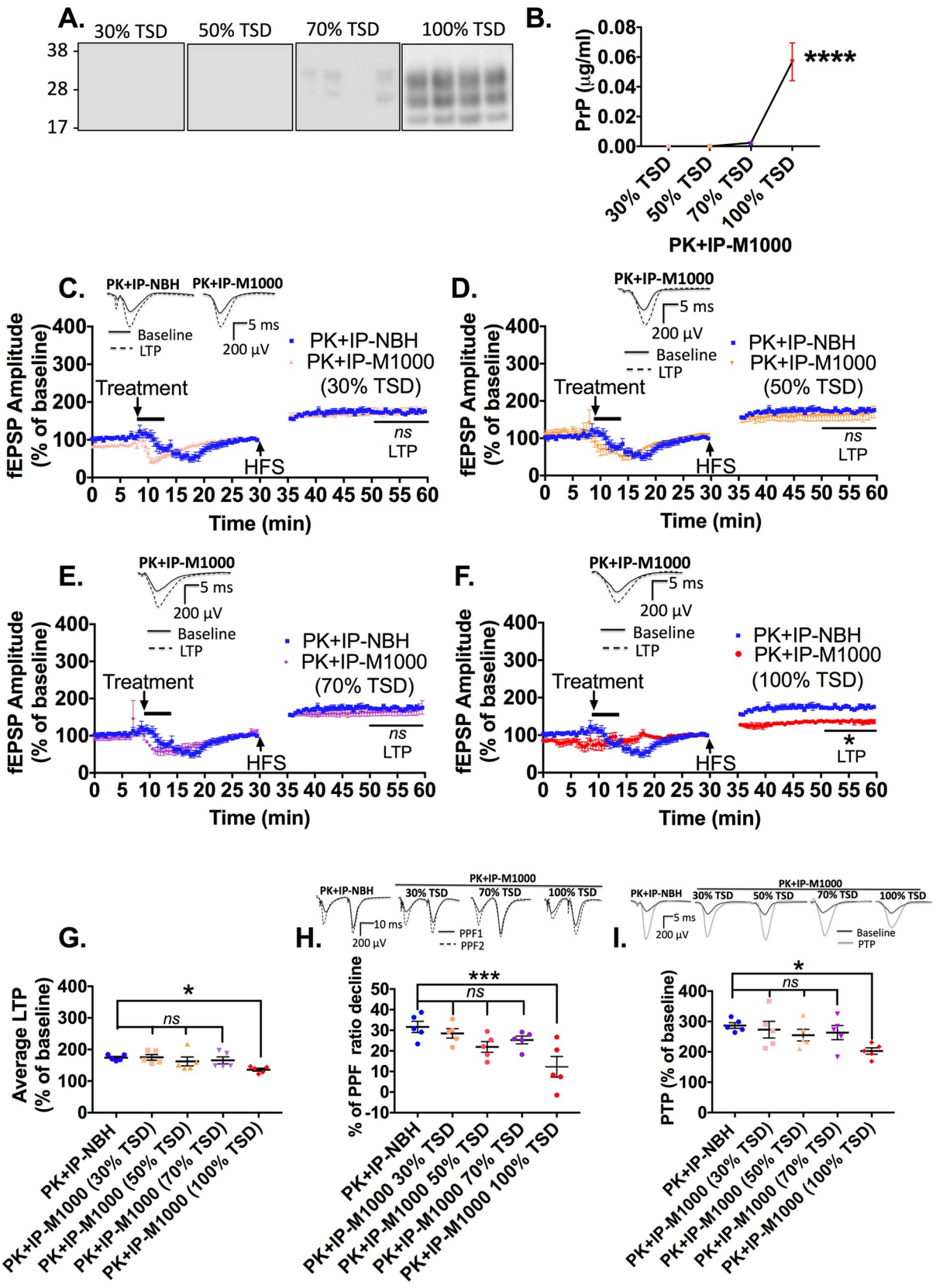
A.
30% TSD
50% TSD
70% TSD
100% TSD
38
28
17
B.
PrP (µg/ml)
0.08
0.06
0.04
0.02
0.00
****
30% TSD
50% TSD
70% TSD
100% TSD
PK+IP-M1000
C.
PK+IP-NBH
PK+IP-M1000
5 ms
200 µV
Baseline
LTP
Treatment
HFS
PK+IP-NBH
PK+IP-M1000
(30% TSD)
ns
LTP
fEPSP Amplitude
(% of baseline)
Time (min)
D.
PK+IP-M1000
5 ms
200 µV
Baseline
LTP
Treatment
HFS
PK+IP-NBH
PK+IP-M1000
(50% TSD)
ns
LTP
fEPSP Amplitude
(% of baseline)
Time (min)
E.
PK+IP-M1000
5 ms
200 µV
Baseline
LTP
Treatment
HFS
PK+IP-NBH
PK+IP-M1000
(70% TSD)
ns
LTP
fEPSP Amplitude
(% of baseline)
Time (min)
F.
PK+IP-M1000
5 ms
200 µV
Baseline
LTP
Treatment
HFS
PK+IP-NBH
PK+IP-M1000
(100% TSD)
*
LTP
fEPSP Amplitude
(% of baseline)
Time (min)
G.
Average LTP
(% of baseline)
*
ns
PK+IP-NBH
PK+IP-M1000 (30% TSD)
PK+IP-M1000 (50% TSD)
PK+IP-M1000 (70% TSD)
PK+IP-M1000 (100% TSD)
H.
PK+IP-NBH
PK+IP-M1000
30% TSD
70% TSD
100% TSD
10 ms
200 µV
PPF1
PPF2
% of PPF ratio decline
***
ns
PK+IP-NBH
PK+IP-M1000 30% TSD
PK+IP-M1000 50% TSD
PK+IP-M1000 70% TSD
PK+IP-M1000 100% TSD
I.
PK+IP-NBH
PK+IP-M1000
30% TSD
50% TSD
70% TSD
100% TSD
5 ms
200 µV
Baseline
PTP
PTP (% of baseline)
*
ns
PK+IP-NBH
PK+IP-M1000 (30% TSD)
PK+IP-M1000 (50% TSD)
PK+IP-M1000 (70% TSD)
PK+IP-M1000 (100% TSD)

Fig 4. Acute synaptotoxicity at earlier time points of M1000 prion disease is associated with PK-sensitive prion protein species. (A) Western blotting of 20μL of preparations obtained following immuno-precipitation of total PrP species from 1% (w/v) crude M1000 brain homogenates (cM1000) from 30%, 50%, 70%, and 100% of M1000 disease progression to the terminal stage of disease (TSD; in WT C57BL6J mice) and mild PK digestion (probed with 8H4; molecular weight markers are provided at left). (B) Quantification of at least modestly PK-resistant PrP species obtained in A (by densitometry analysis) with the levels of PrP in each PK-eluted immuno-precipitated M1000 preparation (PK+IP-M1000) compared across the time points (One-way ANOVA with Tukey's correction for multiple comparisons). (C to F) LTP of WT mouse hippocampal slices following a five minute treatment with 0.5% (w/v in aCSF) PK+IP-M1000 from 30% (C), 50% (D), 70% (E), and 100% (F) of the TSD compared with LTP of slices treated with 0.5% (w/v in aCSF) PK-eluted immuno-precipitated normal brain homogenate (PK+IP-NBH) controls (One-way ANOVA with Dunnett's correction for multiple comparisons). (G) The average LTPs, (H) the average percentage of PPF ratio decline, and (I) the average PTPs generated by WT mouse hippocampal slices treated with PK+IP-NBH and PK+IP-M1000 from across time points of the disease progression (compared by One-way ANOVA with Dunnett's correction for multiple comparisons). (C-F) The 5 minute treatment started after 8–to-10 minutes of stable baseline. The high frequency stimulation (HFS) trains were applied following 30 minutes of baseline recordings. Results are presented as mean ± standard error of mean. (C-F, H & I) Some examples of raw fEPSP traces are provided as insets. $^{*}p<0.05$, $^{****}p<0.0001$, *ns* = not statistically significant ($p>0.05$).

https://doi.org/10.1371/journal.ppat.1007712.g004

M1000 preparations were mostly oligomers (>100KDa) wherein most PrP^{Sc} species were eluted in fractions 1 to 10 (Fig 5B, 5D, 5F & 5H). In fact, the most noteworthy change at 30% of the TSD is the loss of predominance of monomeric PrP species, with the predominance of oligomers appearing to be maximised by 50% of the TSD (Fig 5B & 5D). No PK-resistant PrP^{Sc} was detected in the fractions from 30% to 70% of the TSD employing routine western blotting with only fractions from 100% TSD containing at least modestly PK-resistant PrP^{Sc} species (Fig 5A, 5C, 5E & 5G lower panels).

Oligomeric PrP^{Sc} species propagated during M1000 prion disease progression are acutely synaptotoxic to LTP

To assess the acute synaptotoxicity of different sized assemblies of PrP^{Sc} (predominantly monomeric versus mainly oligomeric) at different time-points of the disease progression, we pooled fractions 1 through 10 to generate oligomer enriched fractions (oM1000) and fractions 15 through 40 to create principally monomeric fractions (mM1000) and assessed their acute synaptotoxicity on WT hippocampal slices. Similar fractions of NBH pooled together as oligomeric NBH (oNBH) and monomeric NBH (mNBH) were assessed for non-specific or background toxicity of brain homogenates introduced through size exclusion chromatography. Crude M1000 brain homogenates (~0.5% w/v) from 100% of the TSD, and crude normal brain homogenates (cNBH, ~0.5% w/v), both processed as for size exclusion chromatography (i.e. Sarkosyl solubilization and exhaustive dialysis), were also used as positive and negative controls for prion acute synaptotoxicity. PBS (1x) alone served as an additional technical negative control for all fractions because it was the size exclusion chromatography buffer, as well as the diluent for PrP fractions. Importantly, cNBH was not toxic to synaptic functions relative to 1x PBS controls (S5A–S5C Fig). In addition, one-to-one dilution of oNBH and mNBH with 1xPBS did not cause any hippocampal synaptic disruption relative to 1xPBS controls (S5A–S5C Fig). In contrast, however, one-to-one dilution of oM1000 from all time points appeared to cause significant impairment of LTP (Fig 6A–6E) and PTP (Fig 6F). Unexpectedly, one-to-one dilution of mM1000 from all the time points was also significantly synaptotoxic to LTP (Fig 6A–6E) and PTP (Fig 6F) relative to 1xPBS controls (compared by One-way ANOVA with Dunnett's correction for multiple comparisons).

Given evidence that PrP^{Sc} exists in dynamic equilibria [38, 39] with the possibility that monomers separated from oligomers by size exclusion chromatography might rapidly oligomerise in a physiological buffer, we checked if the pooled monomeric fractions prepared for the toxicity assay remained monomers as assessed by native gel western blotting. We found that monomers separated by size exclusion chromatography spontaneously oligomerised (to a size approximating those observed in mM1000 pooled fractions) prior to assessing their acute

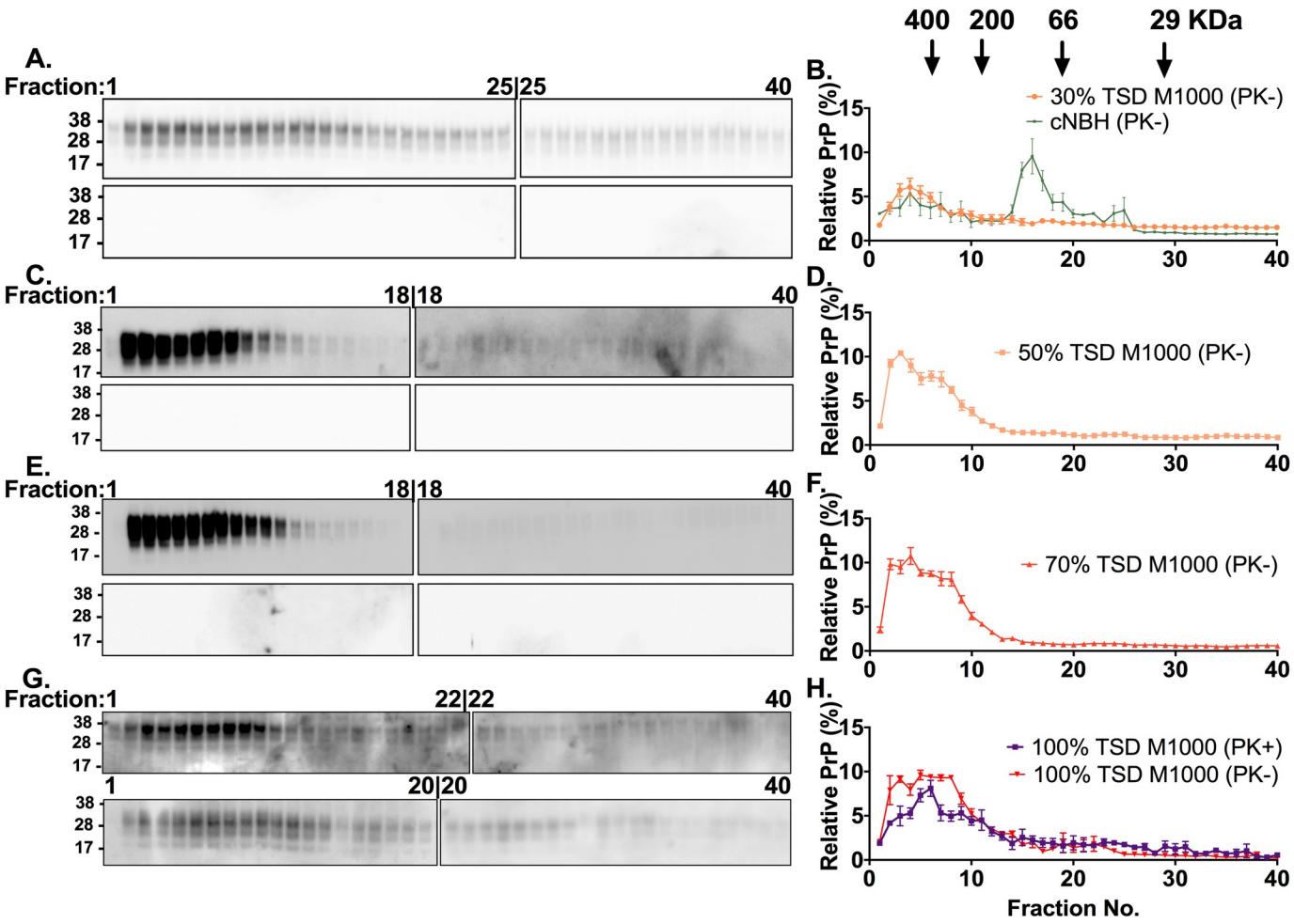

Fig 5. Size fractionation chromatography of M1000 brain homogenates prepared from different time points of the disease progression to the terminal stage. (A, C, E, G) Representative anti-PrP immunoblots of fractions collected after size exclusion chromatography and solubilization of 10% (w/v) crude M1000 brain homogenates from 30% (A), 50% (C), 70% (E), and 100% of the terminal stage of disease (G). The fractions were immunoblotted before (top panel) and after (bottom panel) mild proteinase K treatment (PK; 5μg/mL incubated at 37˚C for an hour). Since all 40 fractions could not be loaded in one 26-well gel, two 26-well gels were used for the immunoblotting of fractions from one size exclusion experiment wherein the last fraction on the first gel was also loaded as the first lane on the second gel, thereby allowing the levels of PrP on the second blot to be normalized to those on the first blot. The PrP species were probed by 03R19 antibody. Molecular weight markers are provided at left. (B, D, F) Densitometric analysis of total PrP in fractions from 30% (B; n = 3), 50% (D; n = 3), 70% (F; n = 3) of the terminal stage of disease. (H) Densitometric analysis of total PrP (PK-) and PrP^{Sc} (PK+) in fractions from the terminal stage of the disease (100%; n = 3). (B) Densitometric analysis of the immunoblots of fractions from NBH (data were extracted from our previous publication Fig 3A [31]) is superimposed over the results of M1000 fractions from 30% of the TSD to enhance comparison of PrP species in sham-inoculated mice to those at different stages of prion disease. All data are displayed as mean ± SEM.

https://doi.org/10.1371/journal.ppat.1007712.g005

synaptotoxicity (Fig 6G & 6H), providing a plausible explanation for why pooled mM1000 preparations were also acutely synaptotoxic.

Propagation of transmitting M1000 prions and acutely synaptotoxic prions display broadly similar temporal profiles

Despite evidence clearly supporting that PrP^{Sc} is responsible for disease transmission [8, 13] as well as neurotoxicity in prion disease, there has been relatively limited exploration of the propagation profiles of neurotoxic species compared with transmitting species [13, 21]. As described above, the degree of synaptotoxicity in the form of LTP dysfunction across M1000 disease evolution progressively and significantly increased (Fig 2I lower panel; One-way

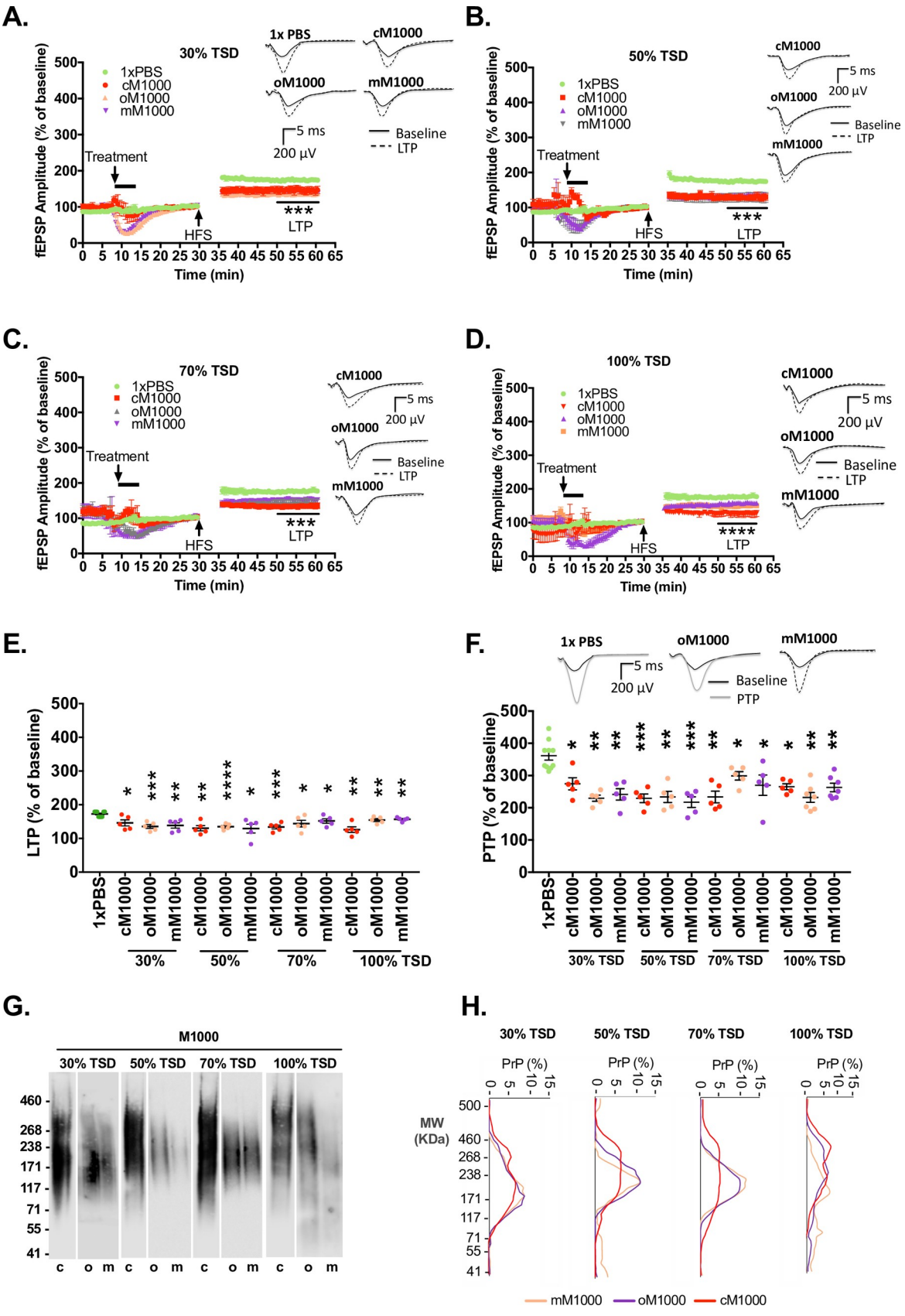
A.
30% TSD
1xPBS
cM1000
oM1000
mM1000
Treatment
HFS
LTP
***
fEPSP Amplitude (% of baseline)
Time (min)
1x PBS
cM1000
oM1000
mM1000
5 ms
200 µV
Baseline
LTP
B.
50% TSD
C.
70% TSD
D.
100% TSD
****
E.
LTP (% of baseline)
1xPBS
cM1000
oM1000
mM1000
30%
50%
70%
100% TSD
F.
PTP (% of baseline)
PTP
30% TSD
50% TSD
70% TSD
100% TSD
G.
M1000
460
268
238
171
117
71
55
41
c o m c o m c o m c o m
H.
PrP (%)
MW (KDa)
mM1000
oM1000
cM1000

Fig 6. Acute synaptotoxicity of pooled oligomeric and monomeric PrP^{Sc} species. (A-D) LTP from WT hippocampal slices induced by high frequency stimulation (HFS) following treatment for 5-minutes with 1xPBS negative control and M1000 preparations from 30% (A), 50% (B), 70% (C), and 100% (D) of the TSD. These M1000 preparations include crude M1000 brain homogenates (cM1000 positive controls) and pooled M1000 fractions containing either predominantly PrP oligomers (oM1000) or PrP monomers (mM1000). The last 10-minutes of LTP recording of slices treated with M1000 preparations were compared to the LTP of slices treated with 1xPBS (by One-way ANOVA with Dunnett's correction for multiple comparisons). (E) The average LTPs and average PTPs (F) generated by WT mouse hippocampal slices treated with cM1000, oM1000, and mM1000 from across time points of the disease progression were compared to 1x PBS controls (by One-way ANOVA with Dunnett's correction for multiple comparisons). (G) Native western blotting of M1000 preparations (20uL in 2% w/v Sarkosyl) used for treatments of WT slices in A-D revealing that monomeric PrP^{Sc} fractionated by size exclusion chromatography appeared to have spontaneously become oligomers. Molecular weight markers are provided at left. (H) Densitometry analysis of blots in G showing that most of the PrP^{Sc} species are oligomers with molecular weights (MW) of at least 150kDa. The 5-minute treatment started after 8–to-10 minutes of stable baseline. The high frequency stimulation (HFS) trains were applied following 30 minutes of baseline recordings. Results are presented as mean ± standard error of mean. (A-D & F) Some examples of raw fEPSP traces are provided as insets. $^{*}p<0.05$, $^{**}p<0.01$, $^{***}p<0.001$, $^{****}p<0.0001$, *ns* = not statistically significant ($p>0.05$).

https://doi.org/10.1371/journal.ppat.1007712.g006

ANOVA with Tukey's correction for multiple comparisons; $p<0.0001$), whereas PTP impairment did not significantly increase across the time points, which may relate to a "ceiling effect" due to the apparent heightened pre-synaptic sensitivity to prion toxicity [31] (Fig 2I upper panel; One-way ANOVA with Tukey's correction for multiple comparison; $p = 0.3306$). To qualitatively compare the propagation of acutely synaptotoxic PrP^{Sc} species to that of transmitting species, we utilised our previous study of the temporal profile of M1000 infectivity in WT mice following ic inoculation [8]. The infectivity titre (log ID_{50} units per μL of 1% [w/v] M1000 brain homogenate) progressively increased from ~6.5 at ~30% of the TSD (~42 dpi) to ~6.9 at ~44% (~64 dpi) of the TSD to plateau at ~8.3 at ~72% of the TSD (~104 dpi). Hence, when plotted for illustrative purposes (Fig 7A), there appeared to be broadly similar propagation profiles for transmitting and acutely synaptotoxic species albeit with plateauing of infectivity noteworthy from ~72% of TSD while synaptotoxic species appear to continue to modestly increase until terminal disease. Further, despite the degree of PTP impairment not being significantly increased across the disease evolution, the overall profile of PTP dysfunction (as illustrated by the best-fit curve) during the disease progression appeared similar to that of LTP dysfunction but at a higher level (Fig 7A).

Efficiently transmitting minimally synaptotoxic PrP^{Sc} species co-exist with primarily acutely synaptotoxic PrP^{Sc} species at terminal disease stage

We previously showed that cM1000 and modestly PK-treated cM1000 prepared from brains at 100% of the TSD were equivalently synaptotoxic to WT hippocampal CA1 region LTP [31]. This acute synaptotoxicity was demonstrated to be directly associated with PrP species present in cM1000 given the significant rescue of LTP impairment by selective immuno-depletion of ~79% total PrP from cM1000 (Fig 3A; including ~89% of at least modestly PK resistant PrP^{Sc} [Fig 3C] and ~96% of highly protease-resistant PrP^{Sc} (resistant to 50μg/mL for one hour at 37˚C) (refer to Fig 2A–2C in [31]) through PrP immuno-precipitation. The direct contribution of PrP^{Sc} to this acute synaptotoxicity was further supported by the return of LTP impairment following exposure of WT hippocampal slices to reconstituted, immuno-precipitated PrP^{Sc} species eluted from pellets by modest PK treatment (Fig 4F and also refer to Fig 2G–2I in [31]).

To determine the infectivity of these various M1000 preparations (cM1000, PK+M1000, dM1000 and PK+IP-M1000) at 100% of the TSD, we undertook incubation time interval bioassays employing routine ic inoculation of tga20 mice, euthanized once they reached the TSD as reflected by reduced spontaneous activity, severe ataxia and hind limb paresis. Control tga20 mice ic inoculated with cNBH did not develop features of prion disease by the time the experiment was terminated (120 dpi). In contrast, the mean time to the TSD of mice

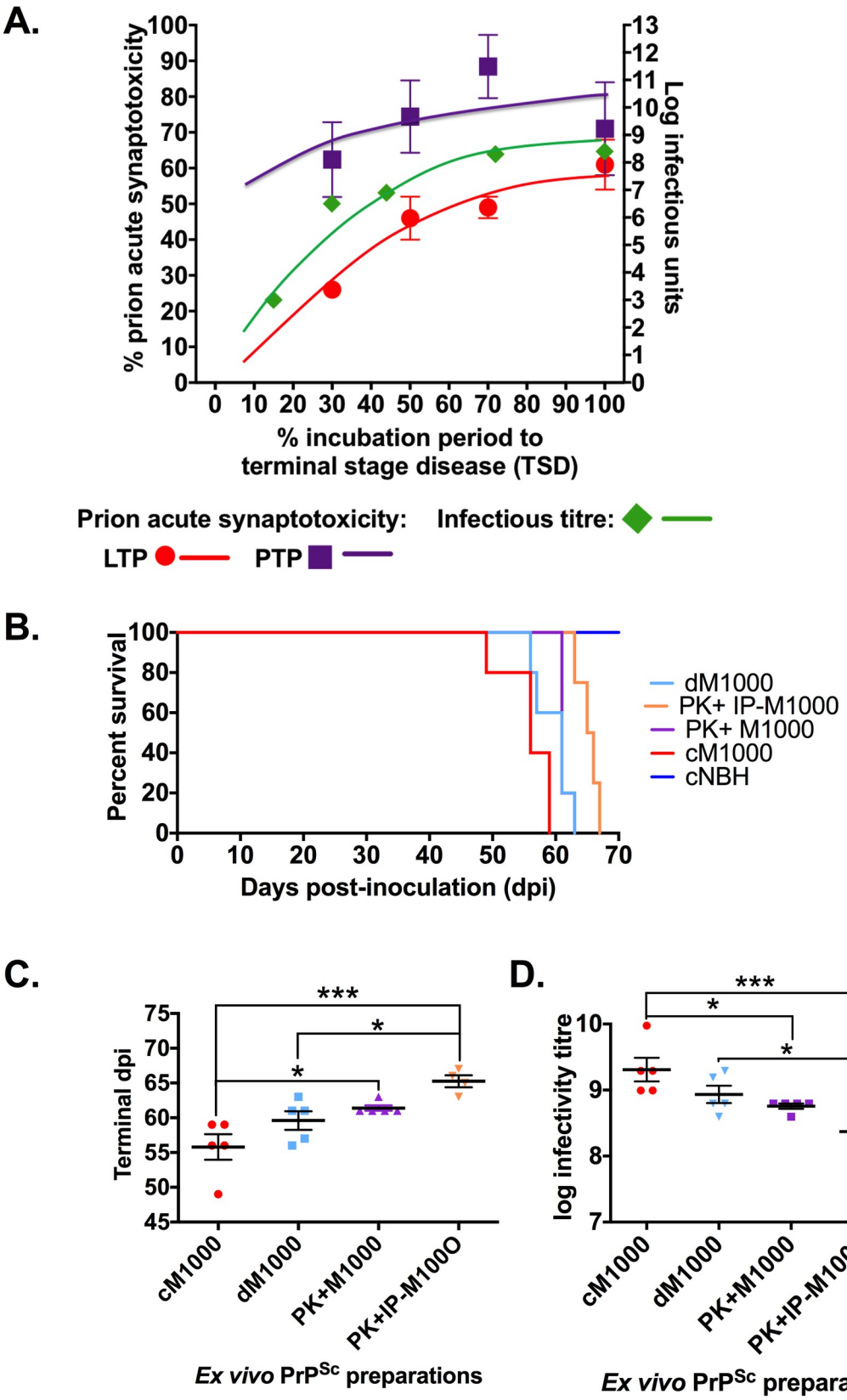
A.
% prion acute synaptotoxicity
Log infectious units
% incubation period to terminal stage disease (TSD)
Prion acute synaptotoxicity:
Infectious titre:
LTP
PTP
B.
Percent survival
Days post-inoculation (dpi)
dM1000
PK+ IP-M1000
PK+ M1000
cM1000
cNBH
C.
Terminal dpi
cM1000
dM1000
PK+M1000
PK+IP-M100O
Ex vivo PrPSc preparations
D.
log infectivity titre
cM1000
dM1000
PK+M1000
PK+IP-M1000
Ex vivo PrPSc preparations

Fig 7. Evidence for efficiently transmitting minimally synaptotoxic PrP^{Sc} species co-existing with separate primarily synaptotoxic species at terminal disease stage. (A) Concomitant representation of the degree of prion acute synaptotoxicity across the disease progression calculated as the percentage of LTP and PTP decline from normal LTP together with titre of infectivity (log ID_{50} units/g brain) across the designated time points as published previously [8]. (B) Kaplan-Meier survival curves of tga20 mice intracerebrally (ic) inoculated with various 1% (w/v) preparations generated from brains of terminally sick M1000 inoculated WT mice, including crude M1000 brain homogenates (cM1000), PrP-immuno-depleted cM1000 (dM1000), 5μg/ml proteinase-K (PK) digested cM1000 (PK+M1000), and reconstituted PK-eluted immuno-precipitated PrP (PK+IP-M1000), as well as tga20 mice sham inoculated with crude NBH (cNBH). (C) Comparison of the average survival (day post-inoculation; dpi) to the TSD in tga20 mice ic inoculated with cM1000, dM1000, PK+M1000, and PK+IP-M1000 (One-way ANOVA with Tukey's correction for multiple comparisons). (D) Comparison of the estimated mean infectivity titres (log_{10} ID_{50} units/g brain) of the cM1000, dM1000, PK+M1000, and PK+IP-M1000 preparations (One-way ANOVA with Tukey's correction for multiple comparisons). The mean time to the TSD was used to calculate the approximate infectivity titre of each M1000 preparation using a linear regression formula obtained from previous quantal dose titration of M1000 prion infectivity in tga20 mice [8]. Data are presented as mean ± standard error of mean. $^{*}p<0.05$, $^{***}p<0.001$.

https://doi.org/10.1371/journal.ppat.1007712.g007

inoculated with dM1000 (60 ± 1.7 dpi) was similar to those inoculated with cM1000 (56 ± 1.8 dpi; $p = 0.1737$), while modestly but significantly shorter than those inoculated with PK+-IP-M1000 (65 ± 1.3; $p = 0.0360$; Fig 7B & 7C). The mean time to the TSD of those mice inoculated with PK+M1000 (61 ± 0.4 dpi) was not different from those infected with dM1000 ($p = 0.7335$), as well as PK+IP-M1000 ($p = 0.2034$) but significantly albeit minimally longer than those infected with cM1000 ($p = 0.0266$; Fig 7B & 7C). The mean time to the TSD was used to calculate the approximate infectivity titre of each M1000 preparation using a linear regression formula ($y = -11.02x + 111.8$) obtained from previous quantal dose-titration of M1000 prion infectivity in tga20 mice [8]. The estimated average infectivity titre (log_{10} ID_{50} units/g brain) of dM1000 (~8.9) was not different to cM1000 (~9.2; $p = 0.1736$) and PK+M1000 (~8.8; $p = 0.7320$) but was significantly although minimally higher than the PK+-IP-M1000 (~8.4; $p = 0.0343$; Fig 7D). Further, the infectivity titre of the PK+M1000 was significantly lower than the cM1000 ($p = 0.0265$), but not significantly different from the PK+IP-M1000 ($p = 0.1961$; Fig 7D). Noteworthy from these collective observations is the substantially abrogated acute synaptotoxicity of dM1000 while retaining essentially unaltered high levels of infectivity (despite removal of ~77% of total PrP species), which stands in contrast to the prominent acute synaptotoxicity of PK+IP-M1000 with its modestly albeit significantly reduced infectivity.

Discussion

The primary purpose of this body of work was to gain insights into the time of occurrence and biophysical properties of acutely synaptotoxic PrP^{Sc}. Employing a combination of experimental approaches the current study has demonstrated some important observations, especially: that acutely synaptotoxic PrP^{Sc} species related to M1000 prions are generated from early in disease evolution generally coinciding with the propagation of transmitting species; and that acutely synaptotoxic PrP^{Sc} species most likely constitute small oligomers, appearing to undergo significant biochemical transformation relatively late in the incubation period, particularly transition from quite protease-sensitive to at least modestly protease-resistant. The early presence of synaptotoxic conformers in combination with the relative stability of their size fractionation profile and only comparatively modest increase in absolute acute synaptotoxicity from 50% of the TSD suggests that progressive failure of neuro-protective mechanisms is likely to be an important component of the eventual transition to overt prion disease.

The ability to detect the presence of acutely synaptotoxic PrP^{Sc} in the brains of M1000 infected mice at 30% of the TSD was independent of the host animal species (Balb/c or C57BL/6J mice) and method of inoculation (routine or stereotaxic ic injection). Moreover, in further contrast to the reported plateauing of the production of infectious PrP^{Sc} in the latter phase of

the disease [8, 12, 21], possibly related to declining PrP^{C} levels [13], we found propagation of synaptotoxic PrP^{Sc} appeared to increase throughout disease development although the capacity of cM1000 to induce PTP failure appeared maximal even at the earliest stage of disease progression assessed, in keeping with previous findings suggesting an enhanced pre-synaptic vulnerability [31]. The explanation for discrepancies in the reported time of occurrence of neurotoxic PrP^{Sc} conformers during disease progression is unclear. Some evidence suggests that the prion strain utilised is unlikely to be a major influence [22] underscoring that methodological factors, especially the sensitivity of techniques employed to discern neurotoxicity may be important contributors. Indeed, we have recently argued that somewhat hindering previous efforts to detect neurotoxic prion species present in *ex vivo* preparations from early time points of disease has been the relative lack of tractable, sensitive, detection paradigms [27]. Congruent with this speculation is that *in vivo* studies reporting the late, sequential propagation of neurotoxic PrP^{Sc} species have relied primarily on the occurrence of typical clinical features of murine prion disease [12, 21], while those describing findings supporting an earlier propagation of toxic conformers have utilised techniques such as serial specific electrophysiological or behavioural interrogation across the incubation period [18, 20]. Of particular note, the observation of acutely synaptotoxic PrP^{Sc} at 30% of the TSD aligns with a study reporting progressive failure of hippocampal CA1 LTP from ~44% of the incubation period during ME7 prion infection [18] and also correlates with our previous report that *in vivo* M1000 infection is associated with elevated by-products of lipid peroxidation from ~30% of the TSD with typical neuropathological changes occurring from ~57% of the TSD, well in advance of the plateauing of infectivity at ~72% of the TSD [8]. Evidence also supports that elevated free radicals in neurodegenerative diseases are neurotoxic and can impair synaptic functions [40–42]. Because the levels of free by-products of lipid peroxidation are elevated at earlier stages of M1000 prion disease [8], we cannot exclude that part of the early synaptotoxicity is due to the presence of free radicals related to propagation of PrP^{Sc}; however, the abrogation of synaptotoxicity with selective immuno-depletion of PrP coupled to the fact that levels of free lipid peroxidation by-products progressively decline from around 50% of the TSD [8] appears inconsistent with heightened oxidative stress being the primary driver of the progressive increase in the synaptotoxicity across the latter disease progression that we (in this study) and others [18] have observed.

Previously we reported that acutely synaptotoxic PrP^{Sc} at the TSD in M1000 infection were most likely constituted as small oligomers [31]. The present findings elaborate this observation and suggest that acutely synaptotoxic PrP^{Sc} species are oligomeric from inception as well as protease-sensitive, which is in broad agreement with previous suggestions regarding the biophysical nature of neurotoxic species during disease progression [13, 34]. The observed biochemical evolution of such oligomeric PrP^{Sc} relatively late in the incubation period (after 70% of the TSD) from quite protease-sensitive to at least modestly protease-resistant is consistent with a previous report using the same prion strain (Fukuoka-1) [8, 34]. Further illustrating the biochemical transformation of PrP^{Sc} in the latter part of the incubation period and similar to what was reported by Sasaki and colleagues [34] is the apparently altered solubility or interaction of misfolded PrP^{Sc} conformers in NaPTA. Notwithstanding the reduced sensitivity of routine western blot detection, we observed very little PrP^{Sc} after modest PK digestion at 70% of the TSD without NaPTA pre-treatment while substantial quantities were detectable when utilising NaPTA precipitation. Of note though, despite PK-resistant PrP^{Sc} levels being substantially increased at 70% of the TSD as determined by employing NaPTA pre-treatment of cM1000, they do not yet represent the acutely synaptotoxic PrP^{Sc} species given that modest protease treatment is able to completely attenuate the synaptotoxicity of immuno-precipitated PrP^{Sc} derived from this time point. These findings underscore a likely cumulative or step-wise

maturation of the biophysical properties of synaptotoxic oligomers with protease-resistance perhaps one of the last hallmark changes to occur.

Acknowledging the reported inherent imprecision of incubation time interval assays (±0.5 log_{10} median infective dose units) when calculating infectivity [3], we believe only estimates outside this range are reliably different. Importantly, our bioassays showed that the estimated infectivity of dM1000 was not clearly different to that of mice inoculated with cM1000, while PK+IP-M1000 was lower in infectivity with respect to cM1000 and probably significantly reduced compared to dM1000. It is noteworthy that although a ~0.8 log_{10} relative decrease in infectivity between cM1000 and PK+IP-M1000 preparations appears rather modest it equates to an absolute reduction of the order of 1,300 million ID_{50} units/g brain. It is also worth emphasising that while depletion of ~79 ± 7% of total PrP to generate dM1000 at 100% of the TSD was sufficient to significantly ameliorate synaptotoxicity, the remaining ~21% harboured infectivity that was not clearly different to that contained in cM1000 brain homogenate. Further, employing the same immuno-depletion method, including anti-PrP capture and detection antibodies, we previously showed that an essentially identical reduction in total PrP species of ~77 ± 9% from cM1000 at 100% of the TSD was associated with ~96 ± 4% reduction in highly protease-resistant PrP^{Sc} [31] in addition to the ~89% reduction of at least modestly PK-resistant species we now report, with reciprocal enrichment of PK-resistant PrP^{Sc} confirmed in PK+IP-M1000 preparations. Consequently, the unaltered infectivity in the presence of substantial depletion of PK-resistant PrP^{Sc} in dM1000 supports that the residual predominantly PK-sensitive conformers are highly infectious species.

We previously attributed the ongoing impairment of PTP by dM1000 at 100% of the TSD to an enhanced pre-synaptic vulnerability to the small residual amount of PK-resistant PrP^{Sc} [31]; however, some refinement of this simple explanation appears necessary when trying to encompass results at earlier time points. At 70% of the TSD, despite similar absolute amounts of total PrP remaining after immuno-depletion when compared to 30% and 50% of the TSD, only dM1000 from 70% caused PTP impairment, with modest PK treatment of the complementary 60% of total PrP captured in the immuno-precipitated pellets able to completely abrogate any acute synaptotoxicity. Although alternative explanations cannot be excluded, these data are compatible with a differential interaction of the immuno-capturing antibody with PK-sensitive synaptotoxic PrP^{Sc} at 70% of the TSD stemming from its evolving biochemical transformation (akin to the differential interaction of PrP^{Sc} with NaPTA at this time point), as suggested by previous results we reported (Fig 3 [31], compare panel F with panel H), such that less PTP impairing species are removed by immuno-precipitation leaving sufficient to impair this pre-synaptic function. In addition, we also reported that PK+IP-M1000 preparations at 100% of the TSD contained full acute synaptotoxicity equivalent to or even a little greater than that caused by cM1000 [31]. Collectively we construe these previous and present findings as supporting the likelihood that pathogenic PrP^{Sc} at 100% of the TSD clusters into at least two overlapping but relatively separable biophysical ensembles: one, PrP^{Sc} species that are minimally or non-synaptotoxic but highly efficient in transmission harbouring little PK-resistance; and a second group, highly synaptotoxic species replete in PK-resistant conformers that retain substantial infectivity. Given that the infectivity titres estimated by our incubation time interval approach for all preparations were within a one log_{10} of each other suggests that infectivity is perhaps an integral feature of all PrP^{Sc} species at the TSD.

The observation that acutely synaptotoxic PrP^{Sc} up to and including 70% of the TSD was highly protease-sensitive rendered our experimental approach (PrP immuno-precipitation coupled to elution through modest PK treatment of pellets) impracticable to rigorously assess whether separable pathogenic species could be verified at earlier time points; consequently we restricted these evaluations to 100% of the TSD by which stage acutely synaptotoxic

conformers are sufficiently resistant to the modest PK treatment required to elute them from immuno-precipitation pellets to allow their subsequent use in electrophysiology experiments. Also, although size exclusion chromatography profiles appeared generally similar over the disease evolution albeit with an apparent increase in predominance of higher molecular weight fractions between 30% and 50% of the TSD, we did not quantify absolute amounts of PrP^{Sc} species. Hence, this leaves unresolved whether acutely synaptotoxic PrP^{Sc} species, especially PK-sensitive species at earlier time points in disease evolution, may harbour greater synaptotoxicity per notional "toxic unit" and whether the intrinsic synaptotoxicity per "toxic unit" can change over the course of disease evolution. This concept is similar to that of a previous study of the M1000 prion strain utilising subcellular fractions containing PrP^{Sc} prepared from M1000-infected mouse RK13 cells wherein some fractions were shown to harbour equally efficient transmissibility despite much lower levels of PK-resistant PrP^{Sc} [43].

In summary, the current study is the first practical application of our recently developed electrophysiological paradigm designed to assess the presence of acutely synaptotoxic *ex vivo* PrP^{Sc}, demonstrating that synaptotoxic species related to M1000 prions are generated from early in disease evolution broadly overlapping the propagation profile of transmissible species. The very short period over which our assay is performed militates against significant propagation of *de novo* synaptotoxic PrP^{Sc} and also limits the time available for attenuating compensatory or neuroprotective mechanisms thereby enhancing the specificity and sensitivity for detecting directly synaptotoxic species. Conventional indicators of the presence of neurotoxic prion species during disease evolution such as the presence of neuropathological changes or the development of overt clinical signs [12, 27] are arguably less sensitive metrics because they only become manifest when overall or regional adaptive and/or neuroprotective CNS thresholds have been persistently exceeded by accumulating neurotoxic species [28].

Supporting information

S1 Fig. Routine western blotting of crude brain homogenates from M1000-infected mice and sham-infected mice. (A) Western immunoblots of 20 μL crude 1% (w/v) M1000 brain homogenates (cM1000) from 30%, 50%, 70% and 100% of M1000 prion disease progression to the terminal stage disease (TSD) before (-) and after (+) digestion with PK (5μg/mL) at 37˚C for an hour (Upper panel: PK-; Lower panel: PK+). PrP species were probed with 8H4 antibody. Total protein was stained with Commassie blue stain (Coom.) as a loading control. (B) Western immunoblots of 20 μL crude 1% (w/v) normal brain homogenates (cNBH) obtained from mice sham inoculated with uninfected brain homogenates and culled at time points equivalent to the 30%, 50%, 70% and 100% of the TSD of M1000 disease showed no change in total PrP or any evidence of PK-resistant PrP. PrP levels before and after PK digestion (5μg/mL at 37˚C for an hour) were probed with 03R19 antibody.
(TIF)

S2 Fig. Other electrophysiology results related to Fig 2. (A) The average LTPs, (B) the average PTP, and (C) the average percentage of PPF ratio decline generated by slices treated with cNBH compared to aCSF technical controls by unpaired Student's t-test. (D) Average probability of neurotransmitter release evoked by each of the three HFS trains (T1, T2, & T3; determined by dividing the fEPSP amplitude of pulse 2 by that of pulse 1) were compared within each treatment group by One-way ANOVA with Dunnett's correction for multiple comparisons. (E) Readily releasable pool (RRP) depletion during (E) T1, (F) T2, and (G) T3 in slices treated with cNBH compared to aCSF controls by one phase decay exponential function (comparing the time-constant of fEPSP amplitude decay from pulse 3 to pulse 9). RRP depletion during (H) T1, (I) T2, and (J) T3 in slices treated with cNBH compared to cM1000 from across

four time-points of the disease progression. Replenishment of RRP following each train of the three HFS trains was measured in slices treated with (K) aCSF controls, (L) cNBH, and cM1000 from (M) 30%, (N) 50%, (O) 70% and (P) 100% of the TSD. See Methods for how the RRP size and RRP replenishment were estimated. Results are presented as mean ± standard error of mean. $^{*}p<0.05$, $^{**}p<0.01$, $^{***}p<0.001$, *ns* = not statistically significant ($p>0.05$).
(TIF)

S3 Fig. Other electrophysiology results related to Fig 3. The average LTPs, (B) the average PTP, and (C) the average percentage of PPF ratio decline generated by slices treated with dNBH compared to aCSF technical controls by unpaired Student's t-test. (D) Average probability of neurotransmitter release evoked by each of the three HFS trains (T1, T2, & T3; determined by dividing the fEPSP amplitude of pulse 2 by that of pulse 1) were compared within each treatment group by One-way ANOVA with Dunnett's correction for multiple comparisons. (E) Readily releasable pool (RRP) depletion during (E) T1, (F) T2, and (G) T3 in slices treated with cNBH compared to aCSF controls by one phase decay exponential function (comparing the time-constant of fEPSP amplitude decay from pulse 3 to pulse 9; see Methods for details). RRP depletion during (H) T1, (I) T2, and (J) T3 in slices treated with dNBH compared to dM1000 from across four time-points of the disease progression. Replenishment of RRP following each train of the three HFS trains was measured in slices treated with (K) aCSF controls, (L) dNBH, and dM1000 from (M) 30%, (N) 50%, (O) 70% and (P) 100% of the TSD. See Methods for how the RRP size and the RRP replenishment were estimated. Results are presented as mean ± standard error of mean. $^{*}p<0.05$, $^{**}p<0.01$, $^{***}p<0.001$, *ns* = not statistically significant ($p>0.05$).
(TIF)

S4 Fig. Other electrophysiology results related to Fig 4. The average LTPs, (B) the average PTPs, and (C) the average percentages of PPF ratio decline generated by slices treated with dNBH compared to aCSF technical controls by unpaired Student's t-test. Results are presented as mean ± standard error of mean. *ns* = not statistically significant ($p>0.05$).
(TIF)

S5 Fig. Electrophysiology results related to pooled size fractionated M1000 and normal brain homogenates displayed in main Fig 6. (A) LTP of WT mouse hippocampal slices following a five-minute treatment with 1x PBS negative technical control compared to ~0.5% (w/v in 1x PBS) cNBH after processing for size exclusion chromatography, as well as pooled oligomeric and monomeric fractions of NBH after size fractionation in 1x PBS. The five-minute treatment started after eight to 10 minutes of stable baseline. The high frequency stimulation (HFS) trains were applied following 30 minutes of baseline recordings. The average LTPs (B) and average PTPs (C) of slices treated with cNBH, oNBH, and mNBH were compared to those of slices treated with 1x PBS by One-way ANOVA with Dunnett's correction for multiple comparisons. Results are presented as mean ± standard error of mean. *ns* = not statistically significant ($p>0.05$).
(TIF)

Author Contributions

Conceptualization: Simote Totauhelotu Foliaki, Steven John Collins.

Data curation: Simote Totauhelotu Foliaki.

Formal analysis: Simote Totauhelotu Foliaki.

Funding acquisition: Steven John Collins.

Investigation: Simote Totauhelotu Foliaki, Steven John Collins.

Methodology: Simote Totauhelotu Foliaki, Blaine Roberts.

Project administration: Steven John Collins.

Resources: Abu Mohammed Taufiqual Islam, Laura Jane Ellett, Matteo Senesi, Victoria A. Lawson, Steven John Collins.

Supervision: Victoria Lewis, David Isaac Finkelstein, Blaine Roberts, Paul Anthony Adlard, Steven John Collins.

Validation: Steven John Collins.

Visualization: Steven John Collins.

Writing – original draft: Simote Totauhelotu Foliaki, Steven John Collins.

Writing – review & editing: Simote Totauhelotu Foliaki, Victoria Lewis, Victoria A. Lawson, Paul Anthony Adlard, Steven John Collins.

References

1. Collins SJ, Lawson VA, Masters CL. Transmissible spongiform encephalopathies. Lancet. 2004; 363 (9402):51–61. Epub 2004/01/16. https://doi.org/10.1016/S0140-6736(03)15171-9 PMID: 14723996.
2. Prusiner SB. Prion diseases and the BSE crisis. Science. 1997; 278(5336):245–51. Epub 1997/10/10. PMID: 9323196.
3. Prusiner SB, Cochran SP, Groth DF, Downey DE, Bowman KA, Martinez HM. Measurement of the scrapie agent using an incubation time interval assay. Ann Neurol. 1982; 11(4):353–8. Epub 1982/04/01. https://doi.org/10.1002/ana.410110406 PMID: 6808890.
4. Chiesa R. The elusive role of the prion protein and the mechanism of toxicity in prion disease. PLoS Pathog. 2015; 11(5):e1004745. Epub 2015/05/08. https://doi.org/10.1371/journal.ppat.1004745 PMID: 25951168; PubMed Central PMCID: PMCPMC4423772.
5. Aguzzi A, Falsig J. Prion propagation, toxicity and degradation. Nat Neuroscience. 2012; 15(7):936–9. Epub 2012/06/28. https://doi.org/10.1038/nn.3120 PMID: 22735515.
6. Deriziotis P, Andre R, Smith DM, Goold R, Kinghorn KJ, Kristiansen M, et al. Misfolded PrP impairs the UPS by interaction with the 20S proteasome and inhibition of substrate entry. EMBO J. 2011; 30 (15):3065–77. Epub 2011/07/12. https://doi.org/10.1038/emboj.2011.224 PMID: 21743439; PubMed Central PMCID: PMCPMC3160194.
7. Iwamaru Y, Takenouchi T, Imamura M, Shimizu Y, Miyazawa K, Mohri S, et al. Prion replication elicits cytopathic changes in differentiated neurosphere cultures. J Virol. 2013; 87(15):8745–55. Epub 2013/06/07. https://doi.org/10.1128/JVI.00572-13 PMID: 23740992; PubMed Central PMCID: PMCPMC3719834.
8. Brazier MW, Lewis V, Ciccotosto GD, Klug GM, Lawson VA, Cappai R, et al. Correlative studies support lipid peroxidation is linked to PrP(res) propagation as an early primary pathogenic event in prion disease. Brain Res Bull. 2006; 68(5):346–54. Epub 2005/12/27. https://doi.org/10.1016/j.brainresbull.2005.09.010 PMID: 16377442.
9. Zou WQ, Puoti G, Xiao X, Yuan J, Qing L, Cali I, et al. Variably protease-sensitive prionopathy: a new sporadic disease of the prion protein. Ann Neurol. 2010; 68(2):162–72. Epub 2010/08/10. https://doi.org/10.1002/ana.22094 PMID: 20695009; PubMed Central PMCID: PMCPMC3032610.
10. Kim C, Haldiman T, Cohen Y, Chen W, Blevins J, Sy MS, et al. Protease-sensitive conformers in broad spectrum of distinct PrPSc structures in sporadic Creutzfeldt-Jakob disease are indicator of progression rate. PLoS Pathog. 2011; 7(9):e1002242. Epub 2011/09/21. https://doi.org/10.1371/journal.ppat.1002242 PMID: 21931554; PubMed Central PMCID: PMCPMC3169556.
11. Safar JG, Geschwind MD, Deering C, Didorenko S, Sattavat M, Sanchez H, et al. Diagnosis of human prion disease. Proceedings of the National Academy of Sciences. 2005; 102(9):3501–6.
12. Sandberg MK, Al-Doujaily H, Sharps B, De Oliveira MW, Schmidt C, Richard-Londt A, et al. Prion neuropathology follows the accumulation of alternate prion protein isoforms after infective titre has peaked.

Nat Commun. 2014; 5(4347):4347. Epub 2014/07/10. https://doi.org/10.1038/ncomms5347 PMID: 25005024; PubMed Central PMCID: PMCPMC4104459.

13. Mays CE, van der Merwe J, Kim C, Haldiman T, McKenzie D, Safar JG, et al. Prion Infectivity Plateaus and Conversion to Symptomatic Disease Originate from Falling Precursor Levels and Increased Levels of Oligomeric PrPSc Species. J Virol. 2015; 89(24):12418–26. Epub 2015/10/02. https://doi.org/10.1128/JVI.02142-15 PMID: 26423957; PubMed Central PMCID: PMCPMC4665242.
14. Lawson VA, Vella LJ, Stewart JD, Sharples RA, Klemm H, Machalek DM, et al. Mouse-adapted sporadic human Creutzfeldt-Jakob disease prions propagate in cell culture. Int J Biochem Cell Biol. 2008; 40(12):2793–801. Epub 2008/07/02. https://doi.org/10.1016/j.biocel.2008.05.024 PMID: 18590830.
15. Tateishi J, Ohta M, Koga M, Sato Y, Kuroiwa Y. Transmission of chronic spongiform encephalopathy with kuru plaques from humans to small rodents. Ann Neurol. 1979; 5(6):581–4. Epub 1979/06/01. https://doi.org/10.1002/ana.410050616 PMID: 382976.
16. Chandler RL. Encephalopathy in mice produced by inoculation with scrapie brain material. Lancet. 1961; 1(7191):1378–9. Epub 1961/06/24. PMID: 13692303.
17. Sawyer EB, Edgeworth JA, Thomas C, Collinge J, Jackson GS. Preclinical detection of infectivity and disease-specific PrP in blood throughout the incubation period of prion disease. Sci Rep. 2015; 5:17742. Epub 2015/12/04. https://doi.org/10.1038/srep17742 PMID: 26631638; PubMed Central PMCID: PMCPMC4668555.
18. Johnston AR, Fraser JR, Jeffrey M, MacLeod N. Synaptic plasticity in the CA1 area of the hippocampus of scrapie-infected mice. Neurobiol Dis. 1998; 5(3):188–95. Epub 1998/12/16. https://doi.org/10.1006/nbdi.1998.0194 PMID: 9848090.
19. Jeffrey M, Halliday WG, Bell J, Johnston AR, Macleod NK, Ingham C, et al. Synapse loss associated with abnormal PrP precedes neuronal degeneration in the scrapie-infected murine hippocampus. Neuropathology and Applied Neurobiology 2000; 26:41–54. PMID: 10736066
20. Cunningham C, Deacon R, Wells H, Boche D, Waters S, Diniz CP, et al. Synaptic changes characterize early behavioural signs in the ME7 model of murine prion disease. Eur J Neurosci. 2003; 17(10):2147–55. Epub 2003/06/06. https://doi.org/10.1046/j.1460-9568.2003.02662.x PMID: 12786981.
21. Sandberg MK, Al-Doujaily H, Sharps B, Clarke AR, Collinge J. Prion propagation and toxicity in vivo occur in two distinct mechanistic phases. Nature. 2011; 470(7335):540–2. Epub 2011/02/26. https://doi.org/10.1038/nature09768 PMID: 21350487.
22. Hannaoui S, Maatouk L, Privat N, Levavasseur E, Faucheux BA, Haik S. Prion propagation and toxicity occur in vitro with two-phase kinetics specific to strain and neuronal type. Journal of Virology. 2013; 87(5):2535–48. Epub 2012/12/21. https://doi.org/10.1128/JVI.03082-12 PMID: 23255799; PubMed Central PMCID: PMCPMC3571390.
23. Thackray AM, Klein MA, Aguzzi A, Bujdoso R. Chronic subclinical prion disease induced by low-dose inoculum. J Virol. 2002; 76(5):2510–7. Epub 2002/02/12. https://doi.org/10.1128/jvi.76.5.2510–2517.2002 PMID: 11836429; PubMed Central PMCID: PMCPMC153817.
24. Jamieson E, Jeffrey M, Ironside JW, Fraser JR. Apoptosis and dendritic dysfunction precede prion protein accumulation in 87V scrapie. Neuroreport. 2001; 12(10):2147–53. Epub 2001/07/12. PMID: 11447324.
25. Lawson VA, Haigh CL, Roberts B, Kenche VB, Klemm HM, Masters CL, et al. Near-infrared fluorescence imaging of apoptotic neuronal cell death in a live animal model of prion disease. ACS Chem Neurosci. 2010; 1(11):720–7. Epub 2010/11/17. https://doi.org/10.1021/cn100068x PMID: 22778809; PubMed Central PMCID: PMCPMC3368636.
26. Hill AF, Joiner S, Linehan J, Desbruslais M, Lantos PL, Collinge J. Species-barrier-independent prion replication in apparently resistant species. Proc Natl Acad Sci U S A. 2000; 97(18):10248–53. Epub 2000/08/30. PMID: 10963685; PubMed Central PMCID: PMCPMC27848.
27. Senesi M, Lewis V, Kim JH, Adlard PA, Finkelstein DI, Collins SJ. In vivo prion models and the disconnection between transmissibility and neurotoxicity. Ageing Res Rev. 2017; 36:156–64. Epub 2017/04/30. https://doi.org/10.1016/j.arr.2017.03.007 PMID: 28450269.
28. Zhu C, Herrmann US, Falsig J, Abakumova I, Nuvolone M, Schwarz P, et al. A neuroprotective role for microglia in prion diseases. J Exp Med. 2016; 213(6):1047–59. Epub 2016/05/18. https://doi.org/10.1084/jem.20151000 PMID: 27185853; PubMed Central PMCID: PMCPMC4886355.
29. Brown GC, Neher JJ. Microglial phagocytosis of live neurons. Nature Review Neuroscience. 2014; 15(4):209–16. Epub 2014/03/22. https://doi.org/10.1038/nrn3710 PMID: 24646669.
30. Safar JG, DeArmond SJ, Kociuba K, Deering C, Didorenko S, Bouzamondo-Bernstein E, et al. Prion clearance in bigenic mice. Journal of General Virology. 2005; 86(Pt 10):2913–23. Epub 2005/09/28. https://doi.org/10.1099/vir.0.80947-0 PMID: 16186247.

31. Foliaki ST, Lewis V, Finkelstein DI, Lawson V, Coleman HA, Senesi M, et al. Prion acute synaptotoxicity is largely driven by protease-resistant PrPSc species. PLoS Pathog. 2018; 14(8):e1007214. Epub 2018/08/09. https://doi.org/10.1371/journal.ppat.1007214 PMID: 30089152.

32. Silveira JR, Raymond GJ, Hughson AG, Race RE, Sim VL, Hayes SF, et al. The most infectious prion protein particles. Nature. 2005; 437(7056):257–61. https://doi.org/10.1038/nature03989 PMID: 16148934; PubMed Central PMCID: PMC1513539.

33. Tixador P, Herzog L, Reine F, Jaumain E, Chapuis J, Le Dur A, et al. The physical relationship between infectivity and prion protein aggregates is strain-dependent. PLoS pathogens. 2010; 6(4):e1000859. https://doi.org/10.1371/journal.ppat.1000859 PMID: 20419156; PubMed Central PMCID: PMCPMC2855332.

34. Sasaki K, Minaki H, Iwaki T. Development of oligomeric prion-protein aggregates in a mouse model of prion disease. Journal of Pathology. 2009; 219(1):123–30. Epub 2009/05/30. https://doi.org/10.1002/path.2576 PMID: 19479969.

35. Fischer M, Rulicke T, Raeber A, Sailer A, Moser M, Oesch B, et al. Prion protein (PrP) with amino-proximal deletions restoring susceptibility of PrP knockout mice to scrapie. EMBO J. 1996; 15(6):1255–64. Epub 1996/03/15. PMID: 8635458; PubMed Central PMCID: PMCPMC450028.

36. Collins SJ, Lewis V, Brazier MW, Hill AF, Lawson VA, Klug GM, et al. Extended period of asymptomatic prion disease after low dose inoculation: assessment of detection methods and implications for infection control. Neurobiol Dis. 2005; 20(2):336–46. Epub 2005/10/26. https://doi.org/10.1016/j.nbd.2005.03.014 PMID: 16242640.

37. Lewis V, Johanssen VA, Crouch PJ, Klug GM, Hooper NM, Collins SJ. Prion protein "gamma-cleavage": characterizing a novel endoproteolytic processing event. Cell Mol Life Sci. 2016; 73(3):667–83. Epub 2015/08/25. https://doi.org/10.1007/s00018-015-2022-z PMID: 26298290.

38. Larda ST, Simonetti K, Al-Abdul-Wahid MS, Sharpe S, Prosser RS. Dynamic equilibria between monomeric and oligomeric misfolded states of the mammalian prion protein measured by 19F NMR. J Am Chem Soc. 2013; 135(28):10533–41. Epub 2013/06/21. https://doi.org/10.1021/ja404584s PMID: 23781904.

39. Gerber R, Tahiri-Alaoui A, Hore PJ, James W. Oligomerization of the human prion protein proceeds via a molten globule intermediate. J Biol Chem. 2007; 282(9):6300–7. Epub 2007/01/11. https://doi.org/10.1074/jbc.M608926200 PMID: 17210575.

40. Keller JN, Mark RJ, Bruce AJ, Blanc E, Rothstein JD, Uchida K, et al. 4-Hydroxynonenal, an aldehydic product of membrane lipid peroxidation, impairs glutamate transport and mitochondrial function in synaptosomes. Neuroscience. 1997; 80(3):685–96. Epub 1997/10/01. PMID: 9276486.

41. McCracken E, Valeriani V, Simpson C, Jover T, McCulloch J, Dewar D. The lipid peroxidation by-product 4-hydroxynonenal is toxic to axons and oligodendrocytes. Journal of Cerebral Blood Flow and Metabolism. 2000; 20(11):1529–36. WOS:000165183900002. https://doi.org/10.1097/00004647-200011000-00002 PMID: 11083227

42. Perluigi M, Coccia R, Butterfield DA. 4-Hydroxy-2-nonenal, a reactive product of lipid peroxidation, and neurodegenerative diseases: a toxic combination illuminated by redox proteomics studies. Antioxid Redox Signal. 2012; 17(11):1590–609. Epub 2011/11/26. https://doi.org/10.1089/ars.2011.4406 PMID: 22114878; PubMed Central PMCID: PMCPMC3449441.

43. Lewis V, Haigh CL, Masters CL, Hill AF, Lawson VA, Collins SJ. Prion subcellular fractionation reveals infectivity spectrum, with a high titre-low PrPres level disparity. Mol Neurodegener. 2012; 7:18. Epub 2012/04/27. https://doi.org/10.1186/1750-1326-7-18 PMID: 22534096; PubMed Central PMCID: PMCPMC3355018.

doi:10.1093/braincomms/fcaa029 BRAIN COMMUNICATIONS 2020: Page 1 of 8 | 1

BRAIN COMMUNICATIONS

Markers of A1 astrocytes stratify to molecular sub-types in sporadic Creutzfeldt–Jakob disease brain

Cathryn L. Ugalde,[1] Victoria Lewis,[2] Christiane Stehmann,[2] Catriona A. McLean,[2,3] Victoria A. Lawson,[4] Steven J. Collins[2,5] and Andrew F. Hill[1]

Astrocytes are glial cells of the central nervous system that become reactive under conditions of stress. The functional properties of reactive astrocytes depend on their stimulus that induces the upregulation of specific genes. Reactive astrocytes are a neuropathological feature of prion disorders; however, their role in the disease pathogenesis is not well understood. Here, we describe our studies of one polarization state of reactive astrocytes, termed A1 astrocytes, in the frontal cortex region of 35 human sporadic Creutzfeldt–Jakob disease brains encompassing a range of molecular sub-types. Examination of two mRNA markers of A1 astrocytes, C3 and GBP2, revealed a strong linear correlation between the two following their log-normalization ($P = 0.0011$). Both markers were found upregulated in the sporadic Creutzfeldt–Jakob disease brain compared with age-matched control tissues ($P = 0.0029$ and 0.0002, for C3log and GBP2log, respectively), and stratifying samples based on codon 129 genotype revealed that C3log is highest in homozygous methionine and lowest in homozygous valine patients, which followed a linear trend ($P = 0.027$). Upon assessing other disease parameters, a significant positive correlation was found between GBP2log and disease duration ($P = 0.031$). These findings provide evidence for a divergence in the astrocytic environment amongst patients with sporadic Creutzfeldt–Jakob disease based on molecular sub-type parameters of disease. While more research will be needed to determine the global changes in the genomic profiles and resulting functional properties of reactive astrocytes in disease, considering the evidence demonstrating that A1 astrocytes harbour neurotoxic properties, the changes seen in C3log and GBP2log in the current study may reflect differences in pathogenic mechanisms amongst the sporadic Creutzfeldt–Jakob disease sub-types associated with the A1 polarization state.

1 Department of Biochemistry and Genetics, La Trobe University, Bundoora, Victoria 3082, Australia
2 Australian National CJD Registry, Florey Institute of Neuroscience & Mental Health, Parkville, Victoria 3010, Australia
3 Department of Anatomical Pathology, Alfred Health, Melbourne, Victoria 3004, Australia
4 Department of Microbiology and Immunology, University of Melbourne, Parkville, Victoria 3010, Australia
5 Department of Medicine (Royal Melbourne Hospital), The University of Melbourne, Parkville, Victoria 3010, Australia

Correspondence to: Cathryn L. Ugalde, La Trobe Institute for Molecular Science, La Trobe University, Bundoora, Victoria 3086, Australia E-mail: c.ugalde@latrobe.edu.au

Keywords: prion; astrocyte; inflammation; Creutzfeldt–Jakob disease; microglia

Abbreviations: CJD = Creutzfeldt–Jakob disease; MM = homozygous methionine; sCJD = sporadic Creutzfeldt–Jakob disease

Received November 26, 2019. Revised January 17, 2020. Accepted March 16, 2020. Advance Access publication March 17, 2020

J_ID: BRAINCOMMS Customer A_ID: FCAA029 Copyedited by: Manuscript Category: Original article Cadmus Art: OP

Graphical Abstract

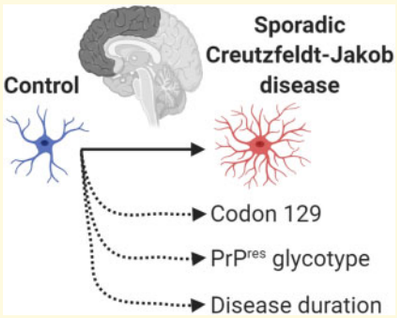

Abbreviated summary

Two RNA markers of A1 astrocytes were assessed in 35 sporadic Creutzfeldt–Jakob disease brain tissues that represented various molecular sub-type parameters. Following log-normalization, we show that the A1 astrocyte markers $C3_{log}$ and $GBP2_{log}$ stratify to disease parameters: $C3_{log}$ stratifies to codon 129 genotype and $GBP2_{log}$ positively correlates to disease duration.

Introduction

Prion disorders are a group of transmissible, incurable neurodegenerative conditions that affect humans and animals. These diseases are caused by 'prions' (Prusiner, 1982) that are composed predominantly, if not entirely of PrP^{Sc}, which is a misfolded isoform of the normal cellular prion protein, PrP^{C}. The ability of PrP^{Sc} to autocatalytically propagate, by inducing the template-driven misfolding of PrP^{C}, is the central pathogenic event in disease. Amplification of PrP^{Sc} with resultant accumulation results in neuronal loss in the CNS, as well as widespread vacuolation and reactive astrogliosis and microgliosis through unresolved mechanisms.

In humans, around 85% of Creutzfeldt–Jakob disease (CJD) cases are sporadic CJD (sCJD) with an unknown aetiology. An important genetic component in sCJD is the genotype [either valine (V) or methionine (M)] at codon 129 in the human prion protein gene with homozygous genotypes [homozygous methionine (MM) or homozygous valine] being over-represented compared with the heterogeneous methionine/valine genotype after standardization to their frequency in the normal population (Palmer *et al.*, 1991; Alperovitch *et al.*, 1999; Parchi *et al.*, 1999). Historically, sCJD-associated PrP^{Sc} was distinguished from PrP^{C} by its resistance to proteinase K digestion with different banding patterns of the glycosylated and unglycosylated isoforms of proteinase K-resistant PrP (especially mobility of the unglycosylated band) constituting identifiable 'molecular types' in the brains of such patients (Collinge *et al.*, 1996; Parchi *et al.*, 1996; Hill *et al.*, 2003). The presence of proteinase K-resistant PrP types suggests that different conformations of PrP^{Sc} exist and, in combination with codon 129 genotype, defines various molecular sub-types of sCJD correlating with features of disease including disease duration and clinical presentation (Collinge *et al.*, 1996; Parchi *et al.*, 1999; Hill *et al.*, 2003; Bishop *et al.*, 2010). The correspondence of distinct clinical features with molecular sub-types suggests that divergent pathogenic mechanisms exist, although the neurobiological mechanisms underpinning these associations are not well understood.

Astrocytes are important glial cells of the CNS that become reactive in states of stress, causing them to adopt protective or damaging properties (reviewed in Liddelow and Barres, 2017). Two states of polarization have been observed for reactive astrocytes whereby specific activators cause the upregulation of certain genes (Zamanian *et al.*, 2012), the combination of which is considered to dictate the cell's functional phenotype. This has been thoroughly characterized for one of these states, termed A1 reactive astrocytes, that harbour highly neurotoxic properties (Liddelow *et al.*, 2017). While more research is needed to determine the extent of these neurotoxic properties in disease models, the observation that A1-specific astrocyte markers C3 and GBP2 co-localize with astrocytes in the frontal cortex of sCJD brain (Hartmann *et al.*, 2019) confirms that they are present in disease; however, it is not known whether these cells preferentially occur in disease of a certain molecular sub-type.

In the current study, we measured mRNA expression of the aforementioned A1 markers in frontal cortex samples from a cohort of 35 patients with sCJD , encompassing various molecular sub-types, and eight healthy age-matched controls. In further support of C3 and GBP2 as specific markers of A1 astrocytes, we report a strong correlation between the two in human brain and confirm both are elevated in sCJD. Critically, we found that $C3_{log}$ stratified to codon 129 genotype. Moreover, we report $C3_{log}$ and $GBP2_{log}$ expression levels associated with glycotype within codon 129 groups and observed a significant positive correlation between $GBP2_{log}$ and disease duration of patients with sCJD. These differences in

J_ID: BRAINCOMMS Customer A_ID: FCAA029 Copyedited by: Manuscript Category: Original article Cadmus Art: OP

the expression of the A1 astrocyte markers suggest that the reactive astrocyte environment differs between the molecular sub-types in sCJD. While further research into the genetic and functional properties of A1 astrocytes will provide important insight into the nature of these changes, their reported neurotoxic properties (Liddelow *et al.*, 2017) suggest that their differential expression may contribute to divergences in prion disease pathogenesis amongst the molecular sub-types.

Materials and methods

Patient selection

The use of human tissue in this study was with the approval of La Trobe Human Research Ethics Committee (HEC18004), and all consent was obtained according to the Declaration of Helsinki. sCJD brain tissues were obtained from the Australian National CJD Registry, and control brain tissues were obtained from the Victorian Brain Bank. Frozen tissue was from the frontal cortex. For sCJD samples, cases for analysis were chosen from research-consented tissues after the consideration of disease duration of the patient, proteinase K-resistant PrP glycotype (Types 1–3) and codon 129 genotype, determined as described previously (Lewis *et al.*, 2005). Diagnostic tests that may indicate prion disease *ante-mortem* include the detection of 14-3-3 protein in the CSF, an abnormal electroencephalogram showing periodic sharp wave activity and brain magnetic resonance imaging showing increased T_2 signal in the basal ganglia and/or cerebral cortex. Whenever available, the following additional information was collected: age, gender, post-mortem delay, years of storage and results of *ante-mortem* clinical assessment for suspected CJD reviewed as per established diagnostic criteria (Will, 1999; Will *et al.*, 2000). The control brain tissues used in this study were chosen according to the following criteria: (i) a non-neurological cause of death as reported from the Coroner or Full Medical Cause of Death Certificate written by the donor's General Practitioner, (ii) no known neurological/psychiatric history in the donor's general medical history, obtained from their treating doctor and (iii) absence of amyloid-β and tau (proteins found aggregated in the brain in many neurodegenerative proteinopathies, including Alzheimer's disease) deposition in brain tissue sections following immunostaining to detect these proteins. The sCJD and control cohorts had an M:F gender ratio of 1:1.5 and 1:0.6, respectively.

RNA isolation from human brain

Extraction of RNA from human brain tissues was performed using the QIAzol lysis buffer and the RNeasy RNA isolation kit (Qiagen) according to the manufacturer's instructions with the following adjustments: 5PRIME phase lock gel light tubes were used for phase separation to physically separate the aqueous from the interphase and the organic phase. The isolated aqueous phase was diluted 2:1:1 with chloroform and RNA-free water in fresh phase lock tubes, vortexed and centrifuged again. This was repeated for two chloroform extractions in total. After phase separation, tubes were checked to ensure the gel separating the phases resolved below the aqueous phase. In cases where the density of the sample was greater than the gel, RNA-free water was injected under the gel to reduce the density of the aqueous phase; the sample was then vortexed and centrifuged again. RNA was isolated in 60 μl of RNA-free water and purity and concentration determined using NanoDrop.

Reverse transcriptase and real-time qualitative PCR

cDNA was produced using the high-capacity cDNA reverse transcriptase kit, gene primers and fast advanced master mix by PCR under the following conditions: 25°C for 10 min, 37°C for 120 min, 85°C for 5 min and then held at 4°C. RT-qPCR (Taqman Fast Advanced Master Mix; Applied Biosystems) was performed using the following Taqman gene expression array primers (Life Technologies): *RPLP0*: Hs00420895_gH, *C3*: Hs00163811_m1 and *GBP2*: Hs00894837_m1. Samples were processed using a ViiA7 Real-Time PCR System (Life Technologies) whereby each biological replicate was run in triplicate and normalized to the house-keeping gene *RPLP0*. Normalization of Ct values of each gene and determination of fold differences in gene expression (normalized to control samples) were calculated by the $-2^{\Delta\Delta Ct}$ method. QuantStudio™ Real-Time PCR software (Applied Biosystems) was used to analyse the data.

Statistical analysis

All data were assessed for outliers (ROUT Q = 1%) and normality (Shapiro–Wilk test). Pearson *r* correlation analysis was performed to determine the relationship between two normally distributed variables. Disease duration data was non-normally distributed and contained statistical outliers and so Spearman *r* correlation was used to assess this dataset. Statistical differences of mRNA between groups were examined using two-tailed Student's *t*-test or one-way ANOVA with a multiple comparisons test for linear trend. All statistical analyses were performed using GraphPad Prism with a statistical criterion of 0.05. AQ6

Data availability

Upon reasonable request, the data that support the findings of this study are available from the corresponding author.

J_ID: BRAINCOMMS Customer A_ID: FCAA029 Copyedited by: Manuscript Category: Original article Cadmus Art: OP

Table 1 Summary of sCJD patient information: sCJD PrP^{res} glycotype 1–3, grouped by codon 129 genotype

Codon 129 genotype	Glycotype	*n*	Sex (M, F)	Age (years), median (range)	Disease duration (months), median (range)	Typical magnetic resonance imaging[a]	Positive 14-3-3[a]	Typical electro encephalogram[a]	PMD[b] (days), median (range)	Storage (years), median (range)
MM	1	6	1, 5	72 (58–81)	2.2 (1–3)	5/5	5/5	2/5	1.5 (0–3)	11.5 (5–12)
MM	2	6	2, 4	64 (60–82)	4.6 (1.5–9.6)	5/5	6/6	4/5	2	11.5 (9–13)
MM	3	6	4, 2	56.5 (47–85)	8.4 (2–21)	4/4	3/5	1/4	1 (0–2)	11.5 (8–15)
MV	1	2	1, 1	65.5 (58–73)	1.8 (1.5–2.1)	2/2	2/2	1/2	2 (1–3)	14 (11–17)
MV	2	4	2, 2	67 (63–74)	2.7 (2–8)	4/4	3/4	0/4	3	11.5 (7–13)
MV	3	5	1, 4	67 (50–75)	11.5 (6–40.5)	4/4	3/3	1/3	2.5 (2–6)	12 (10–15)
VV	3	6	3, 3	71 (59–78)	4.5 (2–6.5)	6/6	3/3	1/5	4 (2–6)	11 (6–15)
Total		35	14, 21	67 (47–85)	3.5 (1–40.5)	30/30	25/28	10/28	2 (0–6)	12 (5–17)

Disease duration and age are represented as median (range). Wherever performed, outcome of *ante-mortem* clinical testing results suggestive of CJD are provided. Variables relating to tissue handling are included as PMD and storage time of tissues prior to experimental use.

[a]Values indicate the number of positive outcomes/total number of results available.

[b]Value indicates number reported, where information is available.

PMD, post-mortem delay; F, female; M, male; VV, homozygous valine; PrP^{res}, proteinase K-resistant PrP; MV, heterozygous methionine/valine.

Table 2 Summary of control donor information: donor information, including cause of death of control cases

Diagnosis	Sex	Age (years)	Cause of death	PMD (days)	Storage (years)
Control	M	75	Abdominal aortic aneurysm	1	12
Control	M	73	Ischaemic heart disease	0	14
Control	M	77	Acute posterolateral myocardial infarction	2	15
Control	M	48	Cardiac failure	2	13
Control	M	57	Intra-abdominal haemorrhage	0	11
Control	F	60	Pancreatic cancer	1	1
Control	F	68	Pulmonary thromboembolism	2	14
Control	F	81	Metastatic endometrial stromal sarcoma	1	6
Median (range)		70 (48–81)		1 (0–2)	12.5 (1–15)

Variables relating to tissue handling are included as PMD and storage time of tissues prior to experimental use.

PMD, post-mortem delay; F, female; M, male.

Results

Assessment of the relationship between two markers of A1 astrocytes, *C3* and *GBP2*, in human brain

Patient information and molecular sub-type analysis of the 35 pathologically confirmed subjects with sCJD used in this study are shown in Table 1. The outcome (when available) of clinical investigations indicative of CJD is also summarized here. Eight normal brains were used as controls, which were age-matched to the disease cohort (Supplementary Fig. 1). Patient information of the control cohort is shown in Table 2.

The utility of C3 and GBP2 to serve as markers of A1 astrocytes in human brain has been confirmed previously (Liddelow *et al.*, 2017; Hartmann *et al.*, 2019). The translated proteins co-localize with astrocytes in the frontal cortex of human prion-diseased brain (Hartmann *et al.*, 2019). Using fluorescence *in situ* hybridization, *C3*

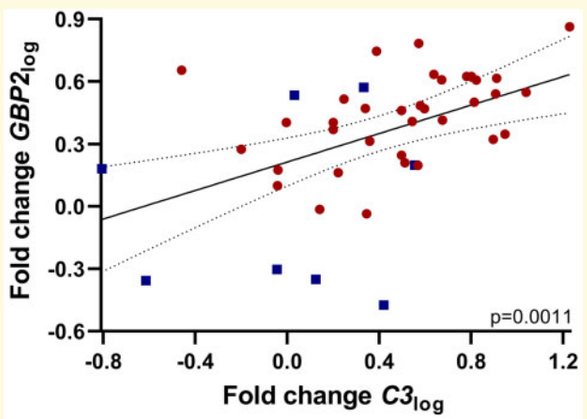

Figure 1 Correlation analysis of two mRNA markers of A1 astrocytes, *GBP2* and *C3*, following log-transformation. Symbols represent the following: ■, control; ●, sCJD frontal cortex brain tissues. $GBP2_{log}$ and $C3_{log}$ significantly correlate (Pearson *r* test, $P = 0.0011$). Graph shows line of best fit, and dotted lines show the 95% confidence interval (95% CI = 0.2111–0.6827, $r = 0.4810$); $n = 43$.

J_ID: BRAINCOMMS Customer A_ID: FCAA029 Copyedited by: Manuscript Category: Original article Cadmus Art: OP

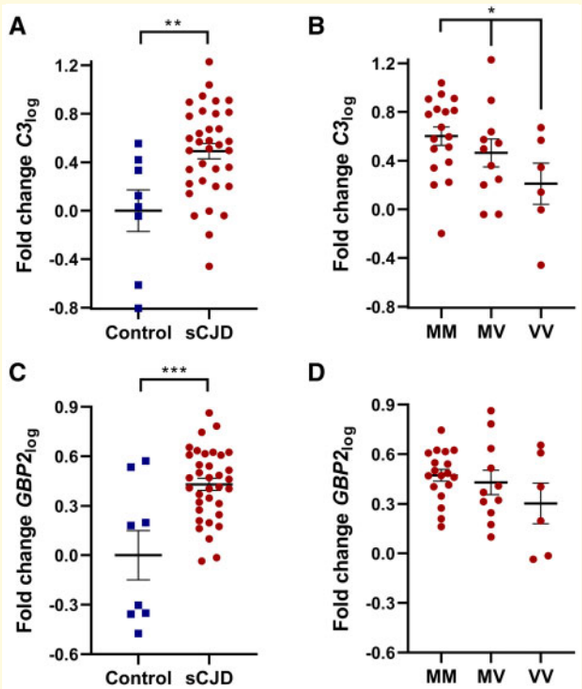

Figure 2 Expression of reactive A1 astrocyte markers in sCJD and control frontal cortex brain tissues and stratification to codon 129 genotype in sCJD. Symbols represent the following: ■, control; ●, sCJD brain tissues. (**A**) $C3_{log}$ was significantly elevated in sCJD brain tissues compared with control samples (Student's *t*-test, $n = 8,35$, $P = 0.0029$) and (**B**) in the sCJD tissues $C3_{log}$ expression stratified according to codon 129 genotype (one-way ANOVA with a multiple comparisons test for linear trend, $n = 18,11,6$, $P = 0.027$). (**C**) $GBP2_{log}$ was significantly elevated in sCJD brain tissues compared with control samples (Student's *t*-test, $n = 8,35$, $P = 0.0002$). (**D**) Stratifying $GBP2_{log}$ expression to codon 129 genotype was not statistically significant (one-way ANOVA with a multiple comparisons test for linear trend, $n = 18,11,6$).

AQ13

selectively co-localizes with astrocytes and its mRNA is elevated in a range of neurodegenerative diseases associated with A1 astrocyte reactivity (Liddelow *et al.*, 2017). As specific markers for the same cell population and given their low basal expression in the CNS under normal conditions (Fagerberg *et al.*, 2014), it is expected that *C3* and *GBP2* correlate within diseased and healthy human brain, although this has not been confirmed. Therefore, we first performed correlation analysis between *C3* and *GBP2* using all brain tissues. Data were non-normally distributed and hence log-normalization was performed for results of all samples. Assessment of the correlation between $C3_{log}$ and $GBP2_{log}$ was found to be strongly significant (Fig. 1, $n = 43$, $P = 0.0011$) suggesting that either may be used to describe the A1 phenotype but does not exclude some degree of complementarity. Accordingly, the A1 astrocyte markers were subsequently assessed in the sCJD cohort with respect to the molecular sub-types of disease.

$C3_{log}$ and $GBP2_{log}$ stratify to molecular sub-type parameters in sCJD brains

The expression of $C3_{log}$ and $GBP2_{log}$ was examined in both sCJD and control brain tissues. $C3_{log}$ was significantly elevated in sCJD brain tissues compared with control counterparts (Fig. 2A, $P = 0.0029$). Using the sCJD samples, these data were then divided into groups according to the genotype at codon 129 of the patient. Following this stratification to genotype, a significant difference was found in $C3_{log}$ expression between the groups that exhibited a linear trend whereby MM samples had the highest and homozygous valine had the lowest $C3_{log}$ expression (Fig. 2B, $P = 0.027$). Likewise, $GBP2_{log}$ was also elevated in sCJD brain compared with control tissues (Fig. 2C, $P = 0.0002$). Although a similar trend was observed, unlike $C3_{log}$, $GBP2_{log}$ stratification according to codon 129 did not reach significance (Fig. 2D). The expression of both markers in sCJD tissues was subsequently subdivided according to the proteinase K-resistant PrP glycotype and the codon 129 genotype (Fig. 3A and C). While no significant differences were identified amongst the groups, Type 3 patients of both MM and heterozygous methionine/valine genotypes exhibited the highest $C3_{log}$ and $GBP2_{log}$ mean values compared with Type 1 and Type 2 counterparts. Type 1 cases in both MM and heterozygous methionine/valine typically have shorter disease durations than Type 3 counterparts (Lewis *et al.*, 2005); hence, correlation analysis was next performed between $C3_{log}$ or $GBP2_{log}$ and disease duration (Fig. 3B and D). A significant positive correlation was found between disease duration and $GBP2_{log}$ (Fig. 3D, $P = 0.031$). No significant correlation was observed between disease duration and $C3_{log}$ (Fig. 3B). Neither $C3_{log}$ nor $GBP2_{log}$ correlated with other patient variables (gender, age, post-mortem delay or years of tissue storage) in either the control or sCJD groups (Supplementary Figs 2 and 3).

Discussion

Reactive A1 astrocytes have been reported to exhibit powerful neurotoxic properties (Liddelow *et al.*, 2017). These cells are present in sCJD brain (Hartmann *et al.*, 2019), as well as brains from a range of other neurodegenerative conditions (Liddelow *et al.*, 2017). In a transgenic rodent model of Parkinson's disease, ablating the cytokines that stimulate their production results in neuroprotection (Yun *et al.*, 2018). Likewise, an A1 profile is

J_ID: BRAINCOMMS Customer A_ID: FCAA029 Copyedited by: Manuscript Category: Original article Cadmus Art: OP

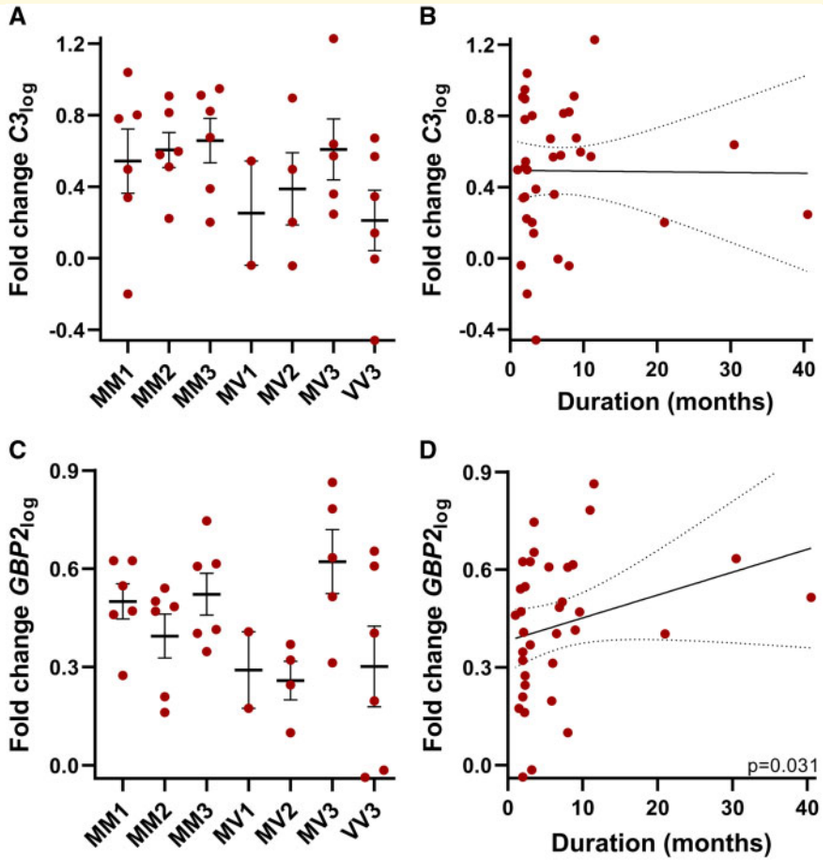

Figure 3 Expression of A1 markers in sCJD frontal cortex brain tissues based on codon 129 and PrP^{res} glycotype and correlations to disease duration. (**A**) $C3_{log}$ expression grouped by PrP^{res} glycotype and genotype at codon 129 ($n = 6,6,6,2,4,5,6$) and (**B**) $C3_{log}$ did not correlate with disease duration (Spearman r correlation, $n = 35$). Graph shows line of best fit, and dotted lines show the 95% confidence interval (95% CI=−0.2817 to −0.4002, $r = 0.06707$). (**C**) $GBP2_{log}$ expression grouped based on PrP^{res} glycotype and genotype at codon 129 ($n = 6,6,6,2,4,5,6$) and (**D**) $GBP2_{log}$ correlated with disease duration (Spearman r correlation, $n = 35$). Graph shows line of best fit, and dotted lines show the 95% confidence interval (95% CI = 0.02573–0.6286, $r = 0.3648$). PrP^{res}, proteinase K-resistant PrP.

observed in a tauopathy mouse model (Shi *et al.*, 2017). These studies have led to merited discussion on A1 astrocytes as a therapeutic target for neurodegenerative disorders that are associated with their activation [reviewed in Liddelow and Barres (2017)].

It is well established that sCJD is phenotypically highly heterogeneous, with several groups reporting clinical correlation with molecular sub-type parameters of disease (Collinge *et al.*, 1996; Parchi *et al.*, 1999; Hill *et al.*, 2003; Bishop *et al.*, 2010). It is not known whether any given sub-type is particularly vulnerable to produce an A1 environment. In this study, we confirm that two markers of A1 astrocytes are significantly elevated in sCJD brain and that they associate with disease parameters: $C3_{log}$ stratifies to codon 129 genotype while $GBP2_{log}$ positively correlates to disease duration.

In rodents, A1 astrocytes can be induced by factors released from activated microglia following exposure to the proinflammatory molecule lipopolysaccharide (Zamanian *et al.*, 2012; Liddelow *et al.*, 2017). Hence, the generation of A1 astrocytes is intimately related to inflammation. Their stratification to codon 129 status in sCJD suggests that disease associated with the 129MM genotype exhibits enhanced microglial and inflammatory responses. This is consistent with another study showing that microglial (CD11b, CD68) and proinflammatory (TNFα) markers are elevated in frontal cortex sCJD tissues of 129MM compared with 129 homozygous valine (Llorens *et al.*, 2014). However, the relevance of the codon 129 genotype to A1 astrocytes may also be related to astrocyte-specific PrP propagation. Astrocytes are amenable hosts for prion replication and astrocytes derived from human stem cells host prion replication most efficiently when the infecting inoculum (derived from human sCJD brain) has the same codon 129 genotype as the stem cells (Krejciova *et al.*, 2017). Given that the astrocyte-specific marker, GFAP, appears in concert with PrP^{Sc} deposition in human sCJD brain

tissues (Muhleisen *et al.*, 1995), this could indicate that astrocyte-specific propagation is relevant to 129MM patients. Additional assessment of these A1 astrocyte markers and PrP^{Sc} deposition across brain regions that have differential disease pathology amongst the sCJD sub-types would provide insight into these notions.

The significant positive correlation of $GBP2_{log}$ to disease duration suggests that A1 astrocytes may not solely be necessary for sCJD-associated neurotoxicity. This is consistent with a recent study that reported transgenic mice lacking the factors that activate A1 astrocytes do not exhibit neuroprotection following prion exposure (Hartmann *et al.*, 2019). Collectively, these findings support the concept that microglia are neuroprotective in disease. The role of microglia in prion disease pathogenesis has long been a point of interest, with contrasting reports of their activation as enhancing or inhibiting disease progression in various animal models of disease [reviewed in Aguzzi and Zhu (2017)]. Several comprehensive *in vivo* and *ex vivo* studies using transgenic mice show a protective role of microglia associated with prion clearance (Falsig *et al.*, 2008; Zhu *et al.*, 2016). Hence, it is possible in sCJD, A1 astrocytes may be produced from activated microglia as a by-product or result of significant and/or prolonged neuroprotective actions. The progressive accumulation of these astrocytes in patients based on the duration of illness could ultimately mean that microglia can play both protective and damaging roles in disease, whereby their initial capacity to be protective may switch to damaging neurotoxic properties over time with corresponding generation of A1 astrocytes. Such considerations prompt the need for further analysis of A1 astrocytes in larger cohorts of sCJD tissues as well as better models to determine the precise nature of their generation over disease course. This is particularly relevant given that, despite the majority of patients having short disease durations (Table 1), 5–10% of CJD cases have duration of illness ù 24 months (Brown *et al.*, 1984). Hence, comprehensive modelling of the role of A1 astrocytes and disease duration requires large patient numbers.

While there are numerous studies detailing the detrimental effects of A1 astrocytes and the utility of C3 and GBP2 to identify them, the genetic and phenotypic changes that astrocytes undergo upon activation are not well understood. Hence, there may be unknown nuances to the capacity of *C3* and *GBP2* to serve as markers for A1 astrocytes. For example, possibly, multiple polarization states exist that share a degree of overlap in genomic profiles. Alternatively, the markers themselves may undergo expression changes in other brain morbidities. Such notions may explain the variation in the abilities of the two markers to stratify to disease sub-types in the current study. However, the positive correlation between the two markers in control and sCJD brain, and their co-localization with astrocytes in sCJD brain (Hartmann *et al.*, 2019) is evidence for *C3* and *GBP2* reporting a population of astrocytes that are equivalent or highly similar. Regardless, further investigations into reactive astrocytes and their activator/s will provide important additional insight into their role in disease and markers to identify them.

The results of this study may contribute to our understanding across the range of broadly related neurodegenerative conditions. Pathogenic mechanisms are shared amongst the different proteins that aggregate in the brain causing neurodegenerative disorders, including significant heterogeneity in the clinical and biochemical features of the diseases (reviewed in Ugalde *et al.*, 2016; Walker 2016). In the context of A1 astrocytes, it is possible that their involvement in the range of neurodegenerative disorders depends on patient-specific disease parameters. Phenotyping of disease, including molecular sub-typing, could represent an important paradigm for determining the best strategies to target A1 astrocytes, with the identification of patient groups who would most benefit from therapies aimed at neurotoxic astrocytes across a range of neurodegenerative conditions.

Supplementary material

Supplementary material is available at *Brain Communications* online.

Acknowledgements

The authors wish to thank the Australian National CJD Registry, the CJD Support Group Network, the friends, families and healthcare professionals who support these organizations.

Funding

This project was funded by the CJD Support Group Network Memorial Award 2019 in memory of Catherine and Michael Heagerty (to C.L.U.) and the National Health and Medical Research Council (NHMRC; APP1132604 to A.F.H.). S.J.C. is supported in part by a National Health and Medical Research Council Practitioner Fellowship (APP1105784). Control tissues were received from the Victorian Brain Bank, supported by The Florey Institute of Neuroscience and Mental Health and The Alfred and the Victorian Forensic Institute of Medicine and funded in part by Parkinson's Victoria, MND Victoria, FightMND and Yulgilbar Foundation.

Competing interests

The authors report no competing interests.

References

Aguzzi A, Zhu C. Microglia in prion diseases. J Clin Invest 2017; 127: 3230–9.

Alperovitch A, Zerr I, Pocchiari M, Mitrova E, Cuesta JDP, Hegyi I, et al. Codon 129 prion protein genotype and sporadic Creutzfeldt-Jakob disease. Lancet 1999; 353: 1673–4.

Bishop MT, Will RG, Manson JC. Defining sporadic Creutzfeldt-Jakob disease strains and their transmission properties. Proc Natl Acad Sci USA 2010; 107: 12005–10.

Brown P, Rodgers-Johnson P, Cathala FO, Gibbs CJ, Gajdusek DC. Creutzfeldt-Jakob disease of long duration: clinicopathological characteristics, transmissibility, and differential diagnosis. Ann Neurol 1984; 16: 295–304.

Collinge J, Sidle KCL, Meads J, Ironside J, Hill AF. Molecular analysis of prion strain variation and the aetiology of 'new variant' CJD. Nature 1996; 383: 685–90.

Fagerberg L, Hallström BM, Oksvold P, Kampf C, Djureinovic D, Odeberg J, et al. Analysis of the human tissue-specific expression by genome-wide integration of transcriptomics and antibody-based proteomics. Mol Cell Proteomics 2014; 13: 397–406.,

Falsig J, Julius C, Margalith I, Schwarz P, Heppner FL, Aguzzi A, et al. A versatile prion replication assay in organotypic brain slices. Nat Neurosci 2008; 11: 109–17.

Hartmann K, Sepulveda-Falla D, Rose IVL, Madore C, Muth C, Matschke J, et al. Complement 3(+)-astrocytes are highly abundant in prion diseases, but their abolishment led to an accelerated disease course and early dysregulation of microglia. Acta Neuropathol Commun 2019; 7: 83.

Hill AF, Joiner S, Wadsworth JDF, Sidle KCL, Bell JE, Budka H, et al. Molecular classification of sporadic Creutzfeldt-Jakob disease. Brain 2003; 126: 1333–46.

Krejciova Z, Alibhai J, Zhao C, Krencik R, Rzechorzek NM, Ullian EM, et al. Human stem cell-derived astrocytes replicate human prions in a PRNP genotype-dependent manner. J Exp Med 2017; 214: 3481–95.

Lewis V, et al. Australian sporadic CJD analysis supports endogenous determinants of molecular-clinical profiles. Lippincott Williams and Wilkins; 2005. p. 113.

Liddelow SA, Barres BA. Reactive astrocytes: production, function, and therapeutic potential. Immunity 2017; 46: 957–67.

Liddelow SA, Guttenplan KA, Clarke LE, Bennett FC, Bohlen CJ, Schirmer L, et al. Neurotoxic reactive astrocytes are induced by activated microglia. Nature 2017; 541: 481–7.

Llorens F, López-González I, Thüne K, Carmona M, Zafar S, Andréoletti O, et al. Subtype and regional-specific neuroinflammation in sporadic Creutzfeldt-Jakob disease. Front Aging Neurosci 2014; 6: 198.

Muhleisen H, Gehrmann J, Meyermann R. Reactive microglia in Creutzfeldt-Jakob disease. Neuropathol Appl Neurobiol 1995; 21: 505–17.

Palmer MS, Dryden AJ, Hughes JT, Collinge J. Homozygous prion protein genotype predisposes to sporadic Creutzfeldt-Jakob disease. Nature 1991; 352: 340–2.

Parchi P, Castellani R, Capellari S, Ghetti B, Young K, Chen SG, et al. Molecular basis of phenotypic variability in sporadic Creutzfeldt-Jakob disease. Ann Neurol 1996; 39: 767–78.

Parchi P, Giese A, Capellari S, Brown P, Schulz-Schaeffer W, Windl O, et al. Classification of sporadic Creutzfeldt-Jakob disease based on molecular and phenotypic analysis of 300 subjects. Ann Neurol 1999; 46: 224–33.

Prusiner SB. Novel proteinaceous infectious particles cause scrapie. Science 1982; 216: 136–44.

Shi Y, Yamada K, Liddelow SA, Smith ST, Zhao L, Luo W, et al.; Alzheimer's Disease Neuroimaging Initiative. ApoE4 markedly exacerbates tau-mediated neurodegeneration in a mouse model of tauopathy. Nature 2017; 549: 523–7.

Ugalde CL, Finkelstein DI, Lawson VA, Hill AF. Pathogenic mechanisms of prion protein, amyloid-β and α-synuclein misfolding: the prion concept and neurotoxicity of protein oligomers. J Neurochem 2016; 139: 162–80.

Walker LC. Proteopathic strains and the heterogeneity of neurodegenerative diseases. Annu Rev Genet 2016; 50: 329–46.

Will RG. Prion related disorders. J R Coll Physicians Lond 1999; 33: 311–5.

Will RG, Zeidler M, Stewart GE, Macleod MA, Ironside JW, Cousens SN, et al. Diagnosis of new variant Creutzfeldt-Jakob disease. Ann Neurol 2000; 47: 575–82.

Yun SP, Kam T-I, Panicker N, Kim S, Oh Y, Park J-S, et al. Block of A1 astrocyte conversion by microglia is neuroprotective in models of Parkinson's disease. Nat Med 2018; 24: 931–8.

Zamanian JL, Xu L, Foo LC, Nouri N, Zhou L, Giffard RG, et al. Genomic analysis of reactive astrogliosis. J Neurosci 2012; 32: 6391–410.

Zhu C, Herrmann US, Falsig J, Abakumova I, Nuvolone M, Schwarz P, et al. A neuroprotective role for microglia in prion diseases. J Exp Med 2016; 213: 1047–59.

Biophysical Journal
Article

Biophysical Society

PrPSc Oligomerization Appears Dynamic, Quickly Engendering Inherent M1000 Acute Synaptotoxicity

Simote T. Foliaki,[1] Victoria Lewis,[1] Abu M. T. Islam,[1] Matteo Senesi,[1] David I. Finkelstein,[2] Laura J. Ellett,[3,4] Victoria A. Lawson,[3,4] Paul A. Adlard,[2] Blaine R. Roberts,[2] and Steven J. Collins[1,2,*]
[1]Department of Medicine (RMH), [2]Florey Institute of Neuroscience and Mental Health, [3]Department of Pathology, and [4]Department of Microbiology and Immunology, The University of Melbourne, Parkville, Australia

ABSTRACT Prion diseases are neurodegenerative disorders pathogenically linked to cellular prion protein (PrPC) misfolding into abnormal conformers (PrPSc), with PrPSc underpinning both transmission and synaptotoxicity. Although the biophysical features of PrPSc required to induce acute synaptic dysfunction remain incompletely defined, we recently reported that acutely synaptotoxic PrPSc appeared to be oligomeric. We herein provide further insights into the kinetic and requisite biophysical characteristics of acutely synaptotoxic ex vivo PrPSc derived from the brains of mice dying from M1000 prion disease. Pooled fractions of M1000 PrPSc located within the molecular weight range approximating monomeric PrP (mM1000) generated through size exclusion chromatography were found to harbor acute synaptotoxicity equivalent to preformed oligomeric fractions (oM1000). Subsequent investigation showed mM1000 corresponded to PrPSc rapidly concatenating in physiological buffer to exist as predominantly, closely associated, small oligomers. The oligomerization of PrP in mM1000 could be substantially mitigated by treatment with the antiaggregation compound epigallocatechin gallate, thereby maintaining the PrPSc as primarily nonoligomeric with completely abrogated acute synaptotoxicity; moreover, despite epigallocatechin gallate treatment, pooled oM1000 remained oligomeric and acutely synaptotoxic. A similar tendency to rapid formation of oligomers was observed for PrPC when monomeric fractions derived from size exclusion chromatography of normal brain homogenates (mNBH) were pooled, but neither mNBH nor preformed higher-order NBH complexes (oNBH) were acutely synaptotoxic. Oligomers formed from mNBH could be reduced to mainly monomers (<100 kDa) after enzymatic digestion of nucleic acids, whereas higher-order PrP assemblies derived from pooled mM1000, oM1000, and oNBH resisted such treatment. Collectively, these findings support that oligomerization of PrPSc into small multimeric assemblies appears to be a critical biophysical feature for engendering inherent acute synaptotoxicity, with preformed oligomers found in oM1000 appearing to be stable, tightly self-associated ensembles that coexist in dynamic equilibrium with mM1000, with the latter appearing capable of rapid aggregation, albeit initially forming smaller, weakly self-associated, acutely synaptotoxic oligomers.

SIGNIFICANCE Although PrPSc comprise the synaptotoxic species in prion diseases, their biophysical characteristics remain incompletely understood. Herein, we reaffirmed that oligomerization of M1000 PrPSc is an integral feature for acute synaptotoxicity. We found that synaptotoxic oligomers can be tightly or weakly aggregated, with size exclusion chromatography showing tightly assembled oligomers are preformed and the most abundant. Broadly consistent with monomer-oligomer equilibria, separation of preformed oligomers from PrPSc located within the range of PrP monomers caused the monomer-like PrPSc to rapidly concatenate in physiological buffer into the loosely aggregated synaptotoxic oligomers. The antiaggregation compound epigallocatechin gallate was able to disrupt the loosely assembled oligomers into nonsynaptotoxic species but was ineffective on preformed oligomers, suggesting that more potent epigallocatechin gallate analogs may have therapeutic potential.

INTRODUCTION

Prion diseases are neurodegenerative disorders with substantial evidence supporting that misfolding of normal prion protein (PrPC) into abnormal conformers (PrPSc) is central to pathogenesis, with PrPSc constituting the transmitting and synaptotoxic species associated with these disorders

Submitted January 10, 2020, and accepted for publication April 24, 2020.
*Correspondence: stevenjc@unimelb.edu.au
Editor: James Shorter.
https://doi.org/10.1016/j.bpj.2020.04.040

(1–3). Notably, prion diseases affect both humans and animals (1), with the most common human phenotype being Creutzfeldt-Jakob disease, whereas in animals, the spectrum includes bovine spongiform encephalopathies in cattle, scrapie in sheep and goats, and chronic wasting disease in deer and elk (1).

Numerous studies have attempted to determine the pathway, critical auxiliary factors, and mechanism by which PrPC is misfolded to PrPSc (4–6), with analytical techniques including the use of cell-free assays such as protein misfolding cyclic amplification (PMCA), wherein a cocktail containing abundant PrPC is seeded with ex vivo PrPSc from prion-infected tissues, facilitating propagation of de novo PrPSc species. PMCA assays have variably demonstrated the requirement for cofactors such as nucleic acids, as well as certain ionic levels, pH, and temperature conditions to successfully misfold PrPC in the presence of PrPSc (6–9). The fact that misfolding of PrPC requires a physical templating interaction with PrPSc has also promoted a potential therapeutic approach in which this close association can be disrupted by drugs that bind tightly to PrPC or PrPSc (10). In addition, given that disease pathogenesis is highly dependent on the ongoing presence of PrPC to serve as substrate for conversion (11,12), with complete resistance of mice devoid of PrPC expression to developing the disease (13), studies have reported successful delay of disease progression by depleting PrPC levels either by disrupting protein synthesis through RNA interference or through compounds that facilitate cellular PrPC removal (5,11,12). One such procatabolic compound is epigallocatechin gallate (EGCG), an antioxidant extract of green tea with known protein antiaggregation properties (14), which has also been shown to tightly bind to PrPC, preventing self-association and facilitating its intracellular degradation (15).

In the M1000 mouse model of human prion disease, PrPSc propagated during the disease incubation period has been shown to harbor infectivity and synaptotoxicity, with acutely synaptotoxic species evident from early in the natural evolution of M1000 murine prion disease, appearing coincident with the production of transmitting PrPSc species (3,16,17). Further, acutely synaptotoxic species undergo biochemical maturation during disease progression (especially the acquisition of protease resistance near the end stage of the disease (3)), whereby there appeared to be some differentiating emphasis in the biochemical features of acutely synaptotoxic versus infectious PrPSc at terminal disease, albeit with the likelihood of overlap in their biophysical features. As prion disease evolves, a considerable amount of PrPSc progressively accumulates as variably sized multimeric aggregates that appear to correlate with the development of certain pathogenic features and neuropathological changes (3,18–20). Indeed, we recently reported the likely direct relevance of oligomeric PrPSc to acute synaptotoxicity (3,16). Previous investigators have additionally shown that ex vivo small oligomers of PrPSc are easily internalized by neuronal cells regardless of PrPC expression (21), efficiently template the production of nascent PrPSc (22), and can induce intracellular neurotoxicity (23), further underscoring their pathogenic relevance. Oligomers of pathogenic proteins such as Aβ in Alzheimer's disease and α-synuclein in Parkinson's disease are also believed to represent assemblies toxic to synaptic functions (24–27). Cumulatively, experimental evidence supports that oligomeric species of PrPSc are most likely responsible for the neurotoxicity in prion diseases, with a detailed understanding of unique, as well as any shared biochemical and biophysical characteristics of acutely synaptotoxic and infectious PrPSc, especially across a range of prion strains, yet to be achieved.

In our aforementioned study assessing the temporal profile of acutely synaptotoxic PrPSc over the course of murine M1000 prion disease, we also undertook preliminary investigation of PrP species migrating in the molecular weight ranges of monomeric and oligomeric prion protein species generated through size fractionation chromatography. As hypothesized, we observed that oligomeric species were acutely synaptotoxic (3) but unexpectedly detected acute synaptotoxicity of ex vivo M1000 PrPSc fractionating as apparent monomers. Additional pilot experiments suggested that such monomeric PrPSc species may rapidly concatenate in physiological buffer, presumably forming into toxic multimeric species, thereby theoretically explaining their observed acute synaptotoxicity (3). Nevertheless, these provisional findings left some uncertainty as to whether oligomerization of PrPSc is a mandatory biophysical prerequisite for misfolded conformers to harbor acute synaptotoxicity in M1000 prion disease. Hence, this study primarily aimed to gain additional insights into critical biophysical properties underpinning acutely synaptotoxic PrPSc species found in M1000 prion disease, especially by further interrogating prion protein species (PrP) within the molecular weight ranges around the size of monomeric and oligomeric PrP generated through size fractionation chromatography.

MATERIALS AND METHODS

Ethics statement

All animal handling was in accordance with National Health and Medical Research Council guidelines. Animal handling and experimental procedures were approved by The Florey Institute of Neuroscience and Mental Health Animal Ethics Committee (Ethics# 13-048) or the Biochemistry & Molecular Biology, Dental Science, Medicine (RMH), Microbiology & Immunology, and Surgery (RMH) Animal Ethics Committee, The University of Melbourne (Ethics# 1312997.1).

Animals

Mice used for electrophysiological studies and for inoculation to generate M1000 infected brains at the terminal stage of disease after stereotaxic intracerebral inoculation were 12-week-old wild-type (WT) female C57BL/6J mice (Animal Resource Centre, Murdoch, Western Australia).

Electrophysiology

Electrophysiology studies utilizing ex vivo preparations were performed as described (3,16) with brain homogenates for these studies precleared by a 1-min 100 × *g* spin. In summary, electric stimulation (1500–2500 mV) was utilized to evoke hippocampal field excitatory postsynaptic potentials (fEPSPs) from the Schäffer collateral pathway while recording from the CA1 region. A 30-min baseline was recorded at 30 s intervals using a basal stimulus determined by an input-output curve, wherein the basal stimulus was declared as the stimulus that evoked ∼40% of the maximal fEPSP. Channels of the multi-electrode array (MEA) grid utilized for analysis were those best aligned to the Schäffer collateral pathway determined through selecting those demonstrating fEPSPs that manifested paired pulse facilitation (PPF), generated positive trend input-output curves, and maintained fEPSP amplitudes above the eight standard deviation threshold of the noise levels for at least 80% of the total recording time. The treatments (crude homogenates or other preparations) were superfused over the hippocampal slices for 5 min after 8–10 min of stable baseline. For tetanus, three trains of high-frequency stimulation (HFS: 100 Hz each) were applied (for 0.5 s at 20 s intervals) after the baseline recording to induce post-tetanic potentiation (PTP) and long-term potentiation (LTP). Post-HFS recording continued for 30 min, wherein the first response was utilized to estimate PTP and the last 10-min period taken as representing LTP. LTP and PTP were calculated as the percentage fEPSP increase after HFS relative to the last 5 min of baseline fEPSPs. PPF was evoked by basal stimuli delivered 20 ms apart. The ratio between the fEPSP amplitude of the first and the second pulse was the PPF ratio. PPF ratio was measured before treatment and induction of LTP (PPF1) and after treatments and expression of LTP (PPF2).

Size exclusion chromatography

Size exclusion chromatography (SEC) was performed as described previously, employing crude homogenates of mouse brains inoculated with M1000 prions (cM1000) or normal brain homogenate (cNBH), as well as reconstituted proteinase K (PK)-eluted supernatants of PrP-immunoprecipitated pellets generated from M1000 prion-infected brains (cPK+IP-M1000) (3,16). Briefly, 3 mL of 10% (w/v) brain homogenate preparations (cM1000, cNBH) and cPK+IP-M1000, after solubilization with 4% sarkosyl and exhaustive dialysis, were injected into a Sephacryl S-100 column (Sigma-Aldrich, St. Louis, MO) (∼47 μm particle size in 16 × 600 mm column), wherein different sizes of PrP species were eluted in 1× phosphate-buffered saline (PBS) at a flow rate of 0.5 mL per minute. One-mL fractions were collected and analyzed for PrP levels by Western blotting. The size of PrP species eluted in each fraction was approximately determined by SEC markers: bovine erythrocyte carbonic anhydrase (∼29 kDa), bovine serum albumin (∼66 kDa), yeast alcohol dehydrogenase (∼150 kDa), sweet potato beta-amylase (∼200 kDa), horse spleen apoferritin (∼443 kDa), and bovine thyroglobulin (∼669 kDa) (16). Those fractions containing PrP larger than 100 kDa were pooled as oligomeric fractions, whereas those containing PrP smaller than 100 kDa were pooled as monomeric fractions. For the refractionation of pooled fractions, 3 mL of each pooled fraction was injected into the S-100 Sephacryl column and fractionated as described above. In addition, each fraction collected from the refractionation was spiked into five volumes of ice-cold 100% methanol, incubated at −20°C for overnight and centrifuged at 24,000 × *g* for 1 h to pellet proteins. The pellets were then resuspended in 20 μL of 0.1% sarkosyl for Western blotting analysis.

EGCG treatment

EGCG (Sigma-Aldrich) was dissolved in milliQ water and added to ∼1% (w/v) ex vivo pooled PrPSc preparations (prepared in 1× PBS) to generate final concentrations of 30, 50, and 100 μM, respectively. These samples were then incubated at 37°C for 30 min with constant agitation at 1400 rpm. After the EGCG treatment, 10 μL from each sample was analyzed by Western blotting for any change in the quaternary structures of PrP. The preparations used in electrophysiology assays were treated with 50 μM EGCG and then diluted 1:1 with 1× PBS immediately before superfusion onto hippocampal slices.

Benzonase treatment

Benzonase (Millipore, Burlington, MA) was added to ∼1% (w/v) ex vivo pooled PrPSc fractions (prepared in 1× PBS containing 6 mM $MgCl_2$ and 0.5 mM $CaCl_2$) to create final sample concentrations of 10, 25, and 50 U/mL. Benzonase-treated samples were then incubated for 30 min at 37°C with constant agitation at 1400 rpm. After the benzonase treatment, 10 μL from each sample was analyzed by Western blotting for any change in the quaternary structures of PrP. Samples for electrophysiology assays were treated with 25 U/mL benzonase, then diluted 1:1 with 1× PBS immediately before being used to treat hippocampal slices.

Chemical cross-linking

Disuccinimidyl suberate (DSS) (Sigma-Aldrich) cross-linker was prepared in 100 mM dimethyl sulfoxide. Brain homogenates or pooled SEC PrP fractions were cross-linked using a 20 mM final concentration of DSS for 30 min at 37°C. After treatment, the DSS cross-linking was quenched by 100 mM final concentration of glycine, and 10 μL from each sample was analyzed by Western blotting after denaturation of proteins.

Western blotting

Western blotting and assessment of levels of PrP were by standard PAGE and immunoblotting as described previously (16,28) unless otherwise stated. DSS cross-linked samples in 1× sample buffer containing 6% (v/v) beta-mercaptoethanol were boiled at 100°C for 5 min, resolved on NuPAGE 3–8% Tris-acetate Protein Gels using 1× Tris-acetate running buffer (Thermo Fisher Scientific, Waltham, MA) transferred to polyvinylidene fluoride (Millipore) and probed for PrP with 8H4 (epitope 145–180; Abcam, Cambridge, UK)). Molecular weights were determined using SeeBlue Plus2 prestained (Invitrogen, Carlsbad, CA). Approximate sizes of PrP species in their quaternary structures were analyzed by Western blotting as described previously (3). For assessment under "native" conditions, PrP samples containing 2% (w/v) sarkosyl and 1× Novex Tris-glycine native sample buffer (Thermo Fisher Scientific) were resolved on NuPAGE Novex 3% Tris-Acetate gels in 1× Novex Tris-glycine native running buffer (at constant 160 V; Thermo Fisher Scientific) and transferred to a polyvinylidene fluoride membrane (at constant 70 V for 3 h) using a transfer buffer containing 25 mM Tris, 200 mM glycine, and 10% methanol. Molecular weights of proteins were determined using High Marker protein standard (Invitrogen). As described previously, a serial dilution of recombinant human PrP of known concentrations was immunoblotted alongside PrP fractions to estimate the approximate relative levels of PrP (16). The total protein levels were determined by BCA assay (Invitrogen).

Data analysis

Unless stated otherwise, the average LTP and PTP of hippocampal slices treated with ex vivo PrPSc preparations were compared with those treated with control preparations by one-way ANOVA with Dunnett's correction for multiple comparisons. The percentage of PrP species resolved by Western blotting according to the sizes of their quaternary structures before and after treatments with the serial concentrations of EGCG were compared by two-way ANOVA with Dunnett's correction for multiple comparisons.

RESULTS

Pooled oligomeric and monomeric M1000 fractions generated through SEC cause acute synaptotoxicity that appears independent of absolute PrP levels

We previously demonstrated that the significant disruption of hippocampal CA1 LTP correlated with abundant levels of oligomeric PrPSc species in M1000-infected preparations from the terminal stage of the disease (16). In more recent studies, however, we unexpectedly observed that both pooled oligomeric and monomeric fractions of cM1000 generated through SEC from across the disease natural evolution were toxic to hippocampal CA1 LTP, albeit with preliminary observations suggesting that pooled monomeric species most likely rapidly concatenated into multimers in physiological buffer (3).

To further investigate these preliminary observations, we first aimed to determine whether the acute synaptotoxicity of these pooled fractions generated in our previous studies (3) was influenced by the total protein concentrations or levels of PrP. This study utilized M1000-infected preparations from the terminal stage of the disease, given that the apparent degree of acute synaptotoxicity of monomeric and oligomeric M1000 was not noticeably different across the disease incubation period (3). Our most recent report demonstrated no background synaptotoxicity of ~0.5% (w/v) cNBH (after processing for SEC), 1:1 diluted pooled oligomeric NBH fractions (fractions 1–10; oNBH), and 1:1 diluted pooled monomeric NBH fractions (fractions 15–30; mNBH) (3); nonspecific background synaptotoxicity was observed with neat mNBH containing a total protein concentration of ~1688 μg/mL (i.e., without the 1:1 dilution in 1× PBS; Fig. S1). Herein, we report that ~0.5% (w/v) cNBH contained ~358 μg/mL of total protein with ~113 ng/mL PrPC. The 1:1 diluted pooled oNBH contained ~580 μg/mL total proteins with <<12 ng/mL PrPC, whereas 1:1 diluted pooled mNBH contained ~844 μg/mL total proteins with ~71 ng/mL PrPC (Fig. 1). By contrast, 0.5% (w/v) cM1000 contained ~359 μg/mL total proteins with ~187 ng/mL PrP species, whereas a 1:1 dilution of the pooled oligomeric M1000 fractions (fractions 1–10; oM1000) contained ~704 μg/mL total protein with ~81 ng/mL PrP species, and a 1:1 dilution of the pooled mM1000 fractions (fractions 15–30; mM1000) contained ~656 μg/mL total proteins with only <<12 ng/mL PrP species (Fig. 1; Table 1). These results demonstrate that the acute synaptotoxicity of oM1000 and mM1000 do not directly correlate with levels of total proteins or PrP species. The previously observed significant acute synaptotoxicity of pooled mM1000 (3), given the reduced levels of PrP species, suggests that monomeric fractions have the capacity to generate highly synaptotoxic species.

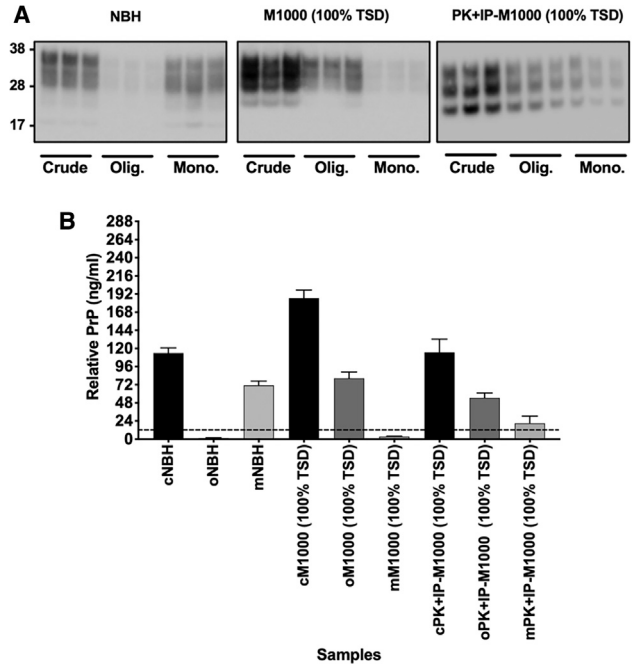

FIGURE 1 Levels of total PrP species and total proteins in ex vivo PrPC and PrPSc preparations. (*A*) Representative Western blots of 20 μL of ~0.5% (w/v) crude (c; before SEC), oligomeric (o), and monomeric (m) normal brain homogenates (NBHs; *left panel*), M1000 brain homogenates (M1000; *middle panel*), and PK-eluted immunoprecipitated M1000 brain homogenates (PK+IP-M1000; *right panel*) are shown. Molecular weight markers are at left. (*B*) Levels (ng) of PrP species in ~0.5% (w/v) cNBH, cM1000, and cPK+IP-M1000, as well as in 1:1 dilution of oNBH, mNBH, oM1000, mM1000, oPK+IP-M1000, and mPK+IP-M1000, are shown. All data are presented as standard error of mean. TSD, terminal stage disease.

Pooled oligomeric and monomeric fractions of at least modestly PK-resistant immunopurified PrPSc species exhibit acute synaptotoxicity analogous to fractions of cM1000

As part of the validation of our prion acute synaptotoxicity model, we demonstrated that cPK+IP-M1000 PrPSc species (immunocaptured by the 03R19 prion antibody from terminal cM1000 and eluted by a mild (5 μg/mL for 1 h at 37°C) PK treatment) were acutely synaptotoxic, and the

TABLE 1 Total Protein and PrP Concentrations in PrP Preparations

Samples	Total Protein Concentrations (μg/mL) (± SEM)	PrP Concentrations (ng/mL) (± SEM)
0.5% cNBH	~358 ± 78	~113 ± 7
mNBH	~844 ± 190	~71 ± 6
oNBH	~580 ± 125	<<12
0.5% cM1000	~359 ± 69	~187 ± 11
mM1000	~656 ± 27	<<12
oM1000	~704 ± 90	~81 ± 8
0.5% cPK+IP-M1000	~213 ± 64	~115 ± 18
mPK+IP-M1000	~30 ± 18	~17 ± 9
oPK+IP-M1000	~75 ± 18	~55 ± 6

size fractionation of these at least modestly PK-resistant PrPSc species by SEC revealed that they consisted of mostly PrPSc oligomers (16). In this study, we aimed to determine whether pooled monomers of at least modestly PK-resistant immunocaptured PrPSc were synaptotoxic and to provide further insights into the biophysical features of such synaptotoxic PrPSc species. Fractions of cPK+IP-M1000 from the terminal stage of the disease (16) were pooled, creating preparations mostly containing PrPSc oligomers (fractions 1–10; oPK+IP-M1000) and those predominantly containing PrPSc monomers (fractions 15–30; mPK+IP-M1000). First, we demonstrated that relative to a 1× PBS negative control, ∼0.5% (w/v) cPK+IP-M1000 remained acutely synaptotoxic after treatment with sarkosyl and exhaustive dialysis as undertaken in the preparation for SEC (Fig. 2 *A*; see *work-flow diagram summary* in Fig. S3). Relative to the normal LTP and PTP of slices treated with 1× PBS (LTP: 173 ± 3; PTP: 376 ± 25), cPK+IP-M1000 disrupted PTP and LTP by ∼30 and ∼35%, respectively (LTP: 151 ± 3; PTP: 277 ± 18; Fig. 2, *A*, *D*, and *E*). These results confirmed that synaptotoxic species of at least modestly PK-resistant immunocaptured PrPSc were among those size fractionated. Next, we assessed the pooled fractions and showed that relative to 1× PBS control, LTP and PTP were significantly disrupted by oPK+IP-M1000 (LTP: 134 ± 9; PTP: 250 ± 21) and mPK+IP-M1000 (LTP: 141 ± 10; PTP: 281 ± 8) after dilution 1:1 in 1× PBS (Fig. 2, *B*–*E*), similar to our observations with size fractionation of cM1000 brain homogenates at the terminal stage of disease (3). This finding also supports that the acutely synaptotoxic species in both oM1000 and mM1000 at terminal disease were most likely at least modestly PK-resistant ex vivo PrPSc. Additional quantitation showed that ∼0.5% (w/v) cPK+IP-M1000 contained ∼213 μg/mL total protein with ∼115 ng/mL at least modestly PK-resistant PrPSc (Fig. 1; Table 1). oPK+IP-M1000 after 1:1 dilution contained ∼75 μg/mL total protein with ∼55 ng/mL at least modestly PK-resistant PrPSc, whereas mPK+IP-M1000 after 1:1 dilution contained ∼30 μg/mL total protein with ∼17 ng/mL at least modestly PK-resistant PrPSc (Table 1). These levels of total protein were notably lower than the nontoxic levels in 0.5% (w/v) cNBH, mNBH, and oNBH, further supporting that the acute synaptotoxicity of these PK+IP-M1000 preparations was not due to nonspecific toxic effects of total protein. The acute synaptotoxicity of mPK+IP-M1000 associated with only ∼17 ng/mL of at least modestly PK-resistant PrPSc suggests that such monomeric fractions harbor potentially highly synaptotoxic PrPSc species.

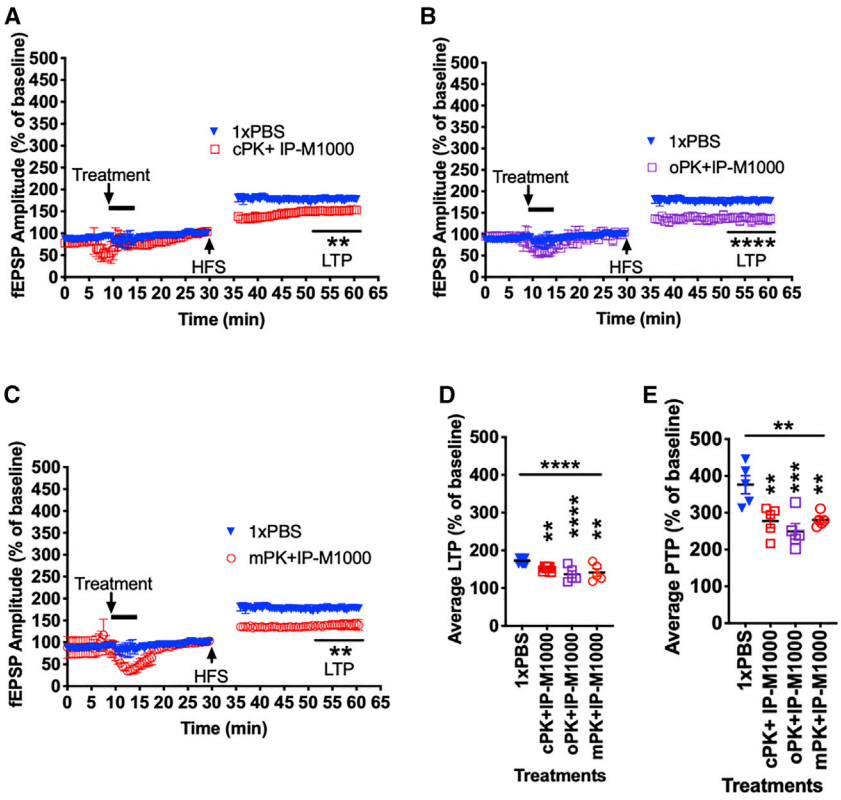

FIGURE 2 Acute synaptotoxicity of oligomeric and monomeric at least modestly PK-resistant PrPSc in M1000 preparations from the disease terminal stage. (*A*) Hippocampal CA1 LTP in WT mice after treatments with 1× PBS negative control and ∼0.5% (w/v in 1× PBS) crude PK-eluted immunoprecipitated M1000 (cPK+IP-M1000) after solubilization with sarkosyl and exhaustive dialysis in preparations for the size fractionation of PrP species by SEC is shown. The hippocampal slices were treated for 5 min (*black solid line*) started after an 8–10 min of stable baseline recording, which was ∼20 min before the induction of LTP by serial trains of HFS. (*B* and *C*) Hippocampal CA1 LTP in WT mice after treatments with oligomeric and monomeric PK+IP-M1000 (*B*: oPK+IP-M1000 and *C*: mPK+IP-M1000) relative to the 1× PBS control is shown. (*D*) The average LTPs of slices treated with cPK+IP-M1000, oPK+IP-M1000, and mPK+IP-M1000 (i.e., average of the last 10-min recording in *A*–*C*) are shown, statistically compared with the 1× PBS negative control by one-way ANOVA with Dunnett's corrections for multiple comparisons. The statistically significant difference of each treatment to the negative controls obtained by the multiple comparisons is presented at the last 10 min of the recordings in (*A*)–(*C*). (*E*) The average PTPs of slices treated with cPK+IP-M1000, oPK+IP-M1000, and mPK+IP-M1000 are shown, statistically compared with the 1× PBS negative control by one-way ANOVA with Dunnett's corrections for multiple comparisons. All data are presented as standard error of mean. $^{**}p < 0.01$, $^{***}p < 0.001$, $^{****}p < 0.0001$. To see this figure in color, go online.

Prion proteins in monomeric SEC fractions derived from both cM1000 and cNBH can rapidly concatenate to generate predominantly oligomeric species

Our recent report of acute synaptotoxicity of pooled mM1000 preparations (3) appeared to contradict a previous observation of the correlation between the abundance of PrPSc oligomers and prion acute synaptotoxicity (16). This finding also appears at odds with a previous study showing only recombinant PrP oligomers, but not monomers, were neurotoxic (29). Preliminary investigations of pooled mM1000 preparations, however, suggested that monomeric PrPSc appears to rapidly concatenate in physiological buffer, presumably forming acutely synaptotoxic oligomers (3).

To further explore this and other potential explanations for pooled monomeric SEC PrPSc fractions being acutely synaptotoxic, we first fractionated cNBH and cM1000 preparations (cNBH: Fig. 3, *A* and *D*; cM1000: Fig. 3, *E* and *H*; see *work-flow summary diagram* in Fig. S3) and then immediately refractionated pooled oNBH and mNBH preparations, as well as oM1000 and mM1000 preparations,

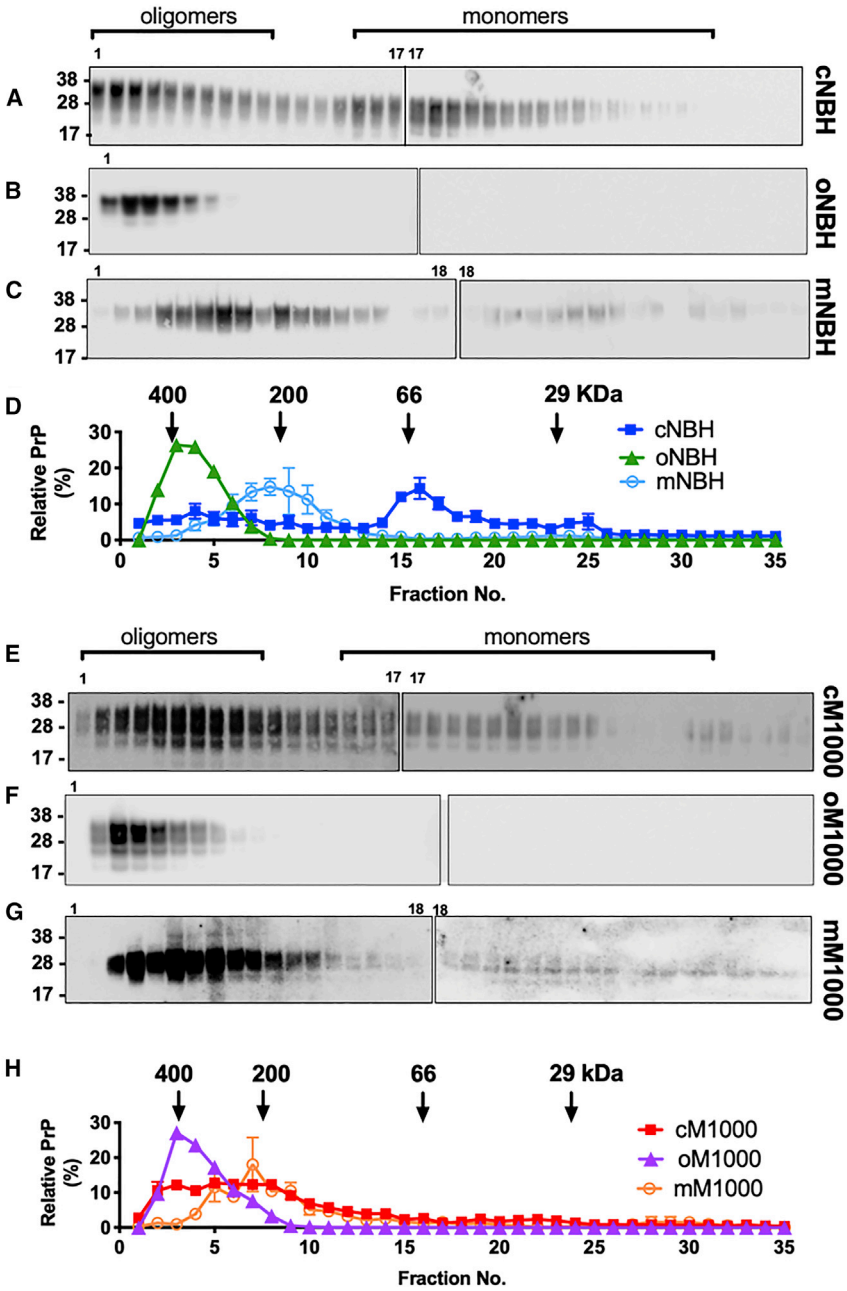

FIGURE 3 Refractionation of PrP species contained in pooled monomeric and oligomeric fractions of NBH and M1000 brain homogenates generated by SEC. (*A* and *D*) Representative Western blot (*A*) and quantification of the relative levels of PrPC (*D*) in crude NBH (cNBH) after size fractionation chromatography are shown, wherein oligomeric fractions of PrPC were eluted into fractions 1–10, and the monomeric fractions were eluted into fractions 15–30. (*B* and *D*) Representative Western blots (*B*) and quantification of the relative levels of PrPC in each fraction (*D*) after the refractionation of the pooled fractions of oligomeric NBH (oNBH) are shown. (*C* and *D*) Representative Western blots (*C*) and quantification of the relative levels of PrPC in each fraction (*D*) after the refractionation of the pooled fractions of monomeric NBH (mNBH) are shown. (*E* and *H*) Representative Western blot (*E*) and quantification of the relative levels of PrP (*H*) in crude M1000 (cM1000) after the size fractionation chromatography are shown, wherein oligomeric fractions of PrPSc were eluted into fractions 1–10, and the monomeric fractions were eluted into fractions 15–30. (*F* and *H*) Representative Western blots (*F*) and quantification of the relative levels of PrP in each fraction (*H*) after refractionation of the pooled fractions of oligomeric M1000 (oM1000) are shown. (*G* and *H*) Representative Western blots (*G*) and quantification of the relative levels of PrP species in each fraction (*H*) after refractionation of the pooled fractions of monomeric M1000 (mM1000) are shown. The approximate molecular weights of proteins eluted into each fraction are listed in (*D*) and (*H*). (*A–C*, *E*, and *F*) PrP species were probed with 8H4 antibody. To see this figure in color, go online.

using SEC as soon as practicable after the size fractionations of the crude brain homogenates. The PrPSc species in pooled oM1000 remained predominantly oligomers after the refractionation (∼400 kDa median size in fractions 1–10; Fig. 3, *F* and *H*). Interestingly, the refractionation of pooled mM1000 revealed that PrPSc species were now mainly oligomers, albeit with relatively smaller sizes (∼200 kDa median size in fractions 3–13) (Fig. 3, *G* and *H*) compared with PrPSc in oM1000, thereby providing a plausible explanation for pooled mM1000 exhibiting acute synaptotoxicity. The refractionation of oNBH revealed that the pooled PrPC species remained as higher molecular weight complexes and oligomers (∼400 kDa median size in fractions 1–8; Fig. 3, *B* and *D*). Unexpectedly, PrPC in mNBH was also detected after refractionation as predominantly oligomers with a median size of ∼200 kDa (Fig. 3, *C* and *D*). Attempts at analogous refractionation of pooled oPK+IP-M1000 and mPK+IP-M1000 were unsuccessful for unclear but likely technical reasons, with failure to detect PrP by Western blotting possibly due to the dynamic equilibrium strongly favoring production of very large PrP species (probably fibrils) too large to enter the pores of the SEC column.

To further examine the apparent rapid self-oligomerization phenomenon of PrP monomers and assess any technical limitation of SEC, we utilized a supplementary "native" Western blotting approach to resolve different sizes of PrP species in our pooled preparations while trying to maintain their quaternary structures (see *work-flow summary diagram* in Fig. S3). Size fractionation of proteins by SEC is primarily dependent on the assumption that proteins enter the pores of the matrix beads used to fill the chromatography column, whereas bigger proteins too large to enter the pores of the beads flow out of the column faster than smaller proteins. Native Western blotting, on the other hand, attempts to minimally perturb in situ proteins, including multimeric assemblies, leaving them natively folded, and assumes that the overall charges of such normally folded proteins and assemblies have been rendered negative, thus allowing electrophoresis to separate them predominantly by size and shape, thereafter detected by immunoblotting. Hence, sarkosyl (2% w/v) was used to enhance the negative charges of proteins to facilitate their resolution in Tris-acetate NuPAGE gels employing Tris-glycine running buffer. The quaternary structures of PrP species, as represented by gel mobility, were detected with 8H4 monoclonal antibody (Fig. 4). Given the possibility that some PrP species were folded or aggregated in ways by which epitopes for 8H4 were not accessible, the relative PrP levels detected by this approach could not be directly compared across PrP preparations; therefore, levels of differently sized PrP in each preparation (lane) were normalized as the percentages of total PrP for that preparation. Similar to SEC of cNBH (Fig. 3, *A* and *D*), the native Western blotting resolved PrPC in cNBH into species that were mostly monomers or very small oligomers (∼55– ∼117 kDa), albeit with

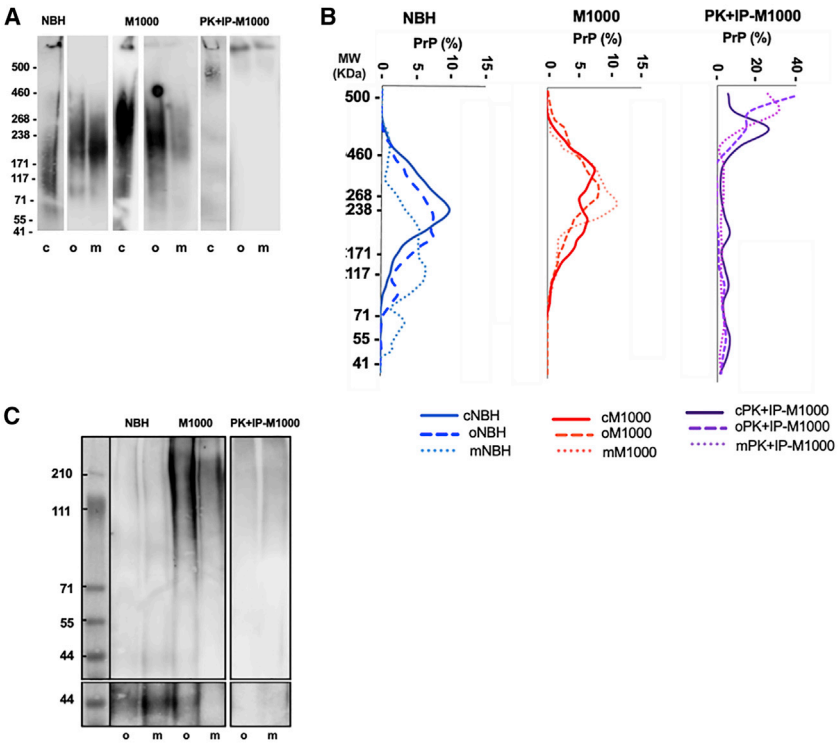

FIGURE 4 Additional evidence that monomeric PrP fractions of NBH and M1000 brain homogenates appear able to quickly self-associate to varying extents and proximity to form predominantly higher molecular weight complexes or PrP oligomers. (*A*) Western blotting after native gel electrophoresis of PrP species in 10 μL of ∼0.5% (w/v) crude (c), oligomeric (o), and monomeric (m) NBH, M1000, and PK-eluted immunoprecipitated M1000 (PK+IP-M1000) is shown. (*B*) Densitometry analyses of the sizes of PrP in each lane of the blots in (*A*) is shown. (*C*) Western blotting for denatured structures of PrP species in 20 μL of o and m NBH, M1000, and PK+IP-M1000 after a 30-min treatment with DSS cross-linker is shown. The lower panel is a longer exposure of the 44 kDa bands of PrP. Molecular weight (MW) markers are provided at left. To see this figure in color, go online.

prominent levels of higher-order oligomers or higher molecular weight complexes (~117 to ~460 kDa) (Fig. 4, *A* and *B*). Approximating the results of SEC of cM1000, the native Western blotting also resolved PrPSc in cM1000 into species that appeared to be mostly oligomers (~117 to ~460 kDa) with minimal levels of monomers or very small oligomers (~55 to ~117 kDa) (Fig. 4, *A* and *B*). Interestingly, the Western blotting of pooled oNBH and mNBH, collected as soon as possible after the SEC, revealed that PrPC species in both fractions appeared to have relatively similar sizes between ~117 and ~460 kDa with oNBH appearing relatively predominant up to ~460 kDa. The native gel Western blotting showed that PrP species in pooled oM1000 and mM1000 contained mostly oligomers (from ~171 to 460 kDa) with oM1000 appearing to contain greater amounts of larger oligomers than mM1000 (Fig. 4, *A* and *B*), which was consistent with the SEC results and our previous findings with native gel resolution and Western blotting of mice brains across the evolution of M1000 prion disease. On the other hand, PrPSc species in cPK+IP-M1000, as well as in its pooled oligomeric and monomeric fractions, were detected by native Western blotting as very high molecular weight oligomers (>460 kDa) (Fig. 4, *A* and *B*, *right panels*). It is noteworthy that the levels of PrPSc species in the PK+IP-M1000 preparations were generally quite low as compared to the amounts of PrP detected by post-denaturation Western blotting in Fig. 1 *A*. Close inspection of the Western blotting gels used for pooled fractions of PK+IP-M1000 performed under native conditions revealed substantial amounts of PrP located in the loading wells of the gel, suggesting failure to enter the resolving component of the gel, thereby offering a likely partial explanation for the apparent low levels compared to the pooled fractions of NBH and M1000. As such, this suggests that the process of probing fractions of cPK+IP-M1000 under native conditions may have allowed further concatenation of pooled oligomeric and initially monomeric PrP into higher molecular weight species larger than 500 kDa, preventing their ability to move from the loading wells. A further possible explanation for the low levels observed under native conditions was that residual PK in these PK+IP-M1000 preparations may have remained active when the temperature was between 37 and 50°C during the 3–4 h of electrophoresis and possibly digesting away more PK-sensitive PrP species with low molecular weights, thereby relatively enhancing the presence of more PK-resistant, higher-order PrP oligomers.

To additionally ensure the validity of SEC and native Western blotting results, we employed DSS lysine-to-lysine bonding to covalently cross-link proteins interacting very closely at a distance of $\leq$11.4 Å (see a *work-flow summary diagram* in Fig. S3). Samples were boiled in the presence of denaturants to denature proteins as well as disassemble protein complexes that were not covalently cross-linked, followed by resolution in low-percentage Tris-acetate NuPAGE gels probed for PrP species using 8H4 antibody. The Western blot analysis revealed that mNBH contained mostly PrPC monomers (~44 kDa), whereas oNBH contained some PrPC monomers mixed with higher molecular weight species (~111– ~210 kDa), supporting the very close interaction of the latter with other PrPC or non-PrPC protein partners (Fig. 4 *C*). Interestingly, all PrP species in mM1000 and mPK+IP-M1000 appeared to have been successfully cross-linked into substantial levels of higher molecular weight complexes with similar sizes to those in oM1000 and oPK+IP-M1000 (Fig. 4 *C*). Of note, some PrP in oM1000 was not cross-linked, suggesting that some species were not tightly self-associated, or their lysine residues were not aligned sufficiently closely to be cross-linked (Fig. 4 *C*). Moreover, the presence of some PrPSc species <460 kDa in PK+IP-M1000 preparations is consistent with digestion of more PK-sensitive PrP species with lower molecular weights, thereby leaving predominantly more PK-resistant higher-order PrP oligomers (>460 kDa) as discussed above in native Western blot experiments, although this does not exclude the partial disaggregation of larger, noncovalently linked PrPSc oligomers when boiling in denaturants.

Importantly, all methods utilized to further interrogate acutely synaptotoxic pooled mM1000 PrPSc generated through SEC collectively support that these species were not predominantly monomers, but oligomers, which may account for their acute synaptotoxicity. The detection of predominantly PrPSc oligomers in pooled mM1000 by native Western blotting performed as soon as possible after fractionation by SEC (within 1 h) suggests that the conversion of the PrPSc monomers to oligomers occurs relatively rapidly in physiological buffer.

Nucleic acids appear to facilitate the secondary oligomerization of PrP in mNBH, but not mM1000

The basis of the unanticipated, prominent association of PrPC monomers into higher molecular weight complexes in pooled mNBH similar to what occurred for PrPSc monomers in mM1000 was unclear. PrPC may self-associate as dimers as part of normal function (30), with substantial evidence supporting that PrPC to PrPSc conversion requires close physical association and can be enhanced in the presence of other cofactors, including nucleic acids (31–33). Exemplifying this, nucleic acids are known to bind PrPC (34) and have been shown to be essential components of the reaction to generate de novo PrPSc aggregates in the PMCA assay (6,33). To determine whether nucleic acids contributed to the apparent oligomerization of PrP monomers in mNBH and mM1000, we treated the pooled fractions of monomers, as well as the pooled fractions of oligomers, with serial dilutions of benzonase (10, 25, and 50 units/mL) for 30 min at 37°C with constant agitation at 1400 rpm (see *work-flow summary diagram* in Fig. S3).

Western blotting analyses of these samples for PrP species revealed that relative to fractions without the benzonase treatment, only pooled mNBH demonstrated a benzonase-dose-dependent shift in PrP sizes, whereas 25 and 50 U/mL benzonase appeared to reduce the size of PrPC complexes from ∼100 to 200 kDa to less than ∼100 kDa, respectively (Fig. 5, *A* and *B*). Interestingly, this dose-dependent reduction of the size of PrP higher molecular weight complexes was not observed in pooled mM1000 (Fig. 5, *A* and *B*) or in oNBH and oM1000 (Fig. 5, *C* and *D*). These results, in combination with previous data, support that nucleic acids were involved in the assembly of PrPC monomers into loosely associated multimeric assemblies in pooled mNBH but did not appear to play a role in the higher-order complexes found in mM1000, oNBH, and oM1000.

Any potential direct contribution of nucleic acids to prion acute synaptotoxicity was assessed on WT mice hippocampal slices after digestion of pooled mM1000, oM1000, and mNBH with 25 U/mL benzonase (see a *work-flow summary diagram* in Fig. S3). Relative to the normal LTP and PTP observed in WT hippocampal slices treated with mNBH (191 ± 9 LTP; 475 ± 47 PTP), equivalent to that observed in the 1× PBS control (Fig. S1), the PTP and LTP of slices treated with mM1000 and oM1000 were significantly disrupted (mM1000: 149 ± 12 LTP and 224 ± 7 PTP; oM1000: 158 ± 6 LTP and 196 ± 18 PTP) (Fig. 5, *E–G*). Furthermore, the degree of LTP and PTP change in slices treated with mNBH containing benzonase were not significantly different relative to slices treated with mNBH without benzonase (Fig. 5, *H* and *I*). Although not statistically significant, the degree of the LTP disruption caused by the Benzonase-treated mM1000 and oM1000 appeared to increase compared with the degree of LTP disruption caused by mM1000 and oM1000 without the benzonase treatment (Fig. 5 *H*). The degrees of PTP dysfunction caused

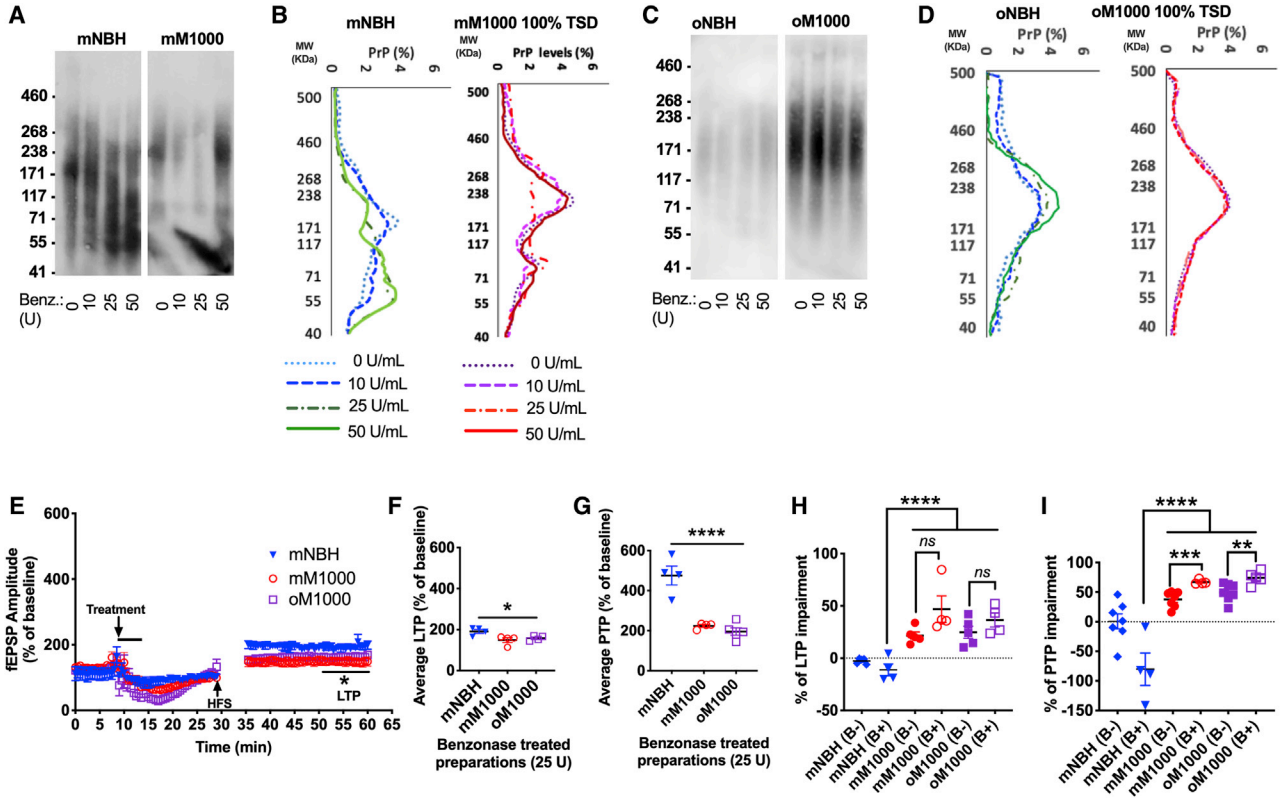

FIGURE 5 Nucleic acids were significantly involved in the self-assembly of PrP in monomeric NBH, but not in the self-assembly and acute synaptotoxicity of monomeric M1000. (*A*) Western blotting for quaternary structures of PrP in monomeric fractions of NBH and M1000 (mNBH and mM1000) before and after the treatment with 10, 25, and 50 units/mL of benzonase is shown. (*B*) Densitometry quantification of the Western blots in (*A*) is shown. (*C*) Western blotting for quaternary structures of PrP in oligomeric fractions of NBH and M1000 (oNBH and oM1000) before and after the treatment with 10, 25, and 50 units/mL of benzonase is shown. (*D*) Densitometry quantification of the Western blots in (*C*) is shown. (*E*) Hippocampal CA1 LTP in slices from WT mice after treatment with oM1000, mM1000, and mNBH treated with 25 U/mL benzonase is shown. The hippocampal slices were treated for 5 min (*black solid line*) started after an 8–10 min of stable baseline recording, which was ∼20 min before the induction of LTP by serial trains of HFS. (*F*) Average LTP recorded at the last 10 min of the recordings in (*D*) is shown. (*G*) Average PTPs recorded after the treatments listed in (*D*) are shown. (*H* and *I*) Degrees of LTP (*H*) and PTP (*I*) disruptions after treatment of WT hippocampal slices with mNBH, mM1000, and oM1000 are shown, including before (B−) and after (B+) treatments with 25 U/mL benzonase. (*F–I*) Data are analyzed by one-way ANOVA with Dunnett's correction for multiple comparisons. All data are presented as standard error of mean. *$p < 0.05$, **$p < 0.01$, ***$p < 0.001$, ****$p < 0.0001$. To see this figure in color, go online.

by mM1000 and oM1000 after digestion with benzonase were significantly increased relative to M1000 fractions without the benzonase treatment (Fig. 5 *I*). Collectively, these results suggest that nucleic acids were not directly synaptotoxic but appeared to reduce the acute synaptotoxicity of PrPSc oligomers (Fig. 5, *H* and *I*).

EGCG disrupts PrPSc oligomers in pooled mM1000 into nonsynaptotoxic species

It is known that PrPSc monomers can tightly self-associate to form oligomers (35,36). This interaction can be at least partially disturbed in some complexes by physical forces such as heating, sonication, and quaking or by chemical treatments (10,18). PrPSc monomers produced through physical forces can quickly reaggregate into fibrils (18). Chemical treatments can disrupt PrPSc oligomerization by binding individual PrP molecules, thereby interfering with monomer-oligomer equilibria (10,15). It has also been shown that PrPSc monomers initially oligomerize into small, immature or unstable, weakly self-associated complexes, which then mature into highly stable oligomers (18,37,38).

To test whether PrP oligomers formed in pooled mM1000 were unstable or mature, we treated pooled mM1000 and oM1000, as well as mNBH and oNBH, with serial dilutions of EGCG (30, 50, and 100 μM) for 30 min at 37°C with constant agitation at 1400 rpm (see *work-flow summary diagram* in Fig. S3). Through Western blotting analysis of PrP in EGCG-treated preparations, we found that relative to mM1000 not treated with EGCG, PrP oligomers in pooled mM1000 were significantly reduced by increasing EGCG concentrations ($p = 0.0004$; n = 3), whereas 50 and 100 μM EGCG prominently reduced PrP oligomers with molecular weights above ~238 kDa and coincidently emphasized species smaller than ~117 kDa (Fig. 6, *D* and *H*). We also observed a slight redistribution in sizes of PrP oligomers in pooled oM1000 after the treatment with 100 μM EGCG, but not with the 30 and 50 μM EGCG (Fig. 6, *C* and *G*). Further, absolute PrP levels appeared reduced in both mM1000 and oM1000 after the treatment with 100 μM EGCG (Fig. 6, *C*, *D*, *G*, and *H*). In contrast, EGCG treatment did not significantly alter the size of PrPC oligomers in pooled mNBH and oNBH, albeit with a slight loss of PrPC levels in oNBH after the treatment with 100 μM EGCG (Fig. 6, *A*, *B*, *E*, and *F*).

Before assessing the acute synaptotoxicity of EGCG-treated, pooled M1000 fractions, we first tested for the optimal nontoxic concentration of EGCG. We found that relative to aCSF controls, a final concentration of 50 μM EGCG prepared in 0.5% (w/v in PBS) NBH was significantly toxic to hippocampal CA1 LTP, but not a final concentration of 25 μM (Fig. S2). Hence, we used 50 μM EGCG to treat the pooled PrP fractions, whereby the subsequent 1:1 dilution in 1× PBS provided the optimal nontoxic 25 μM EGCG. Importantly, relative to normal CA1 LTP and PTP obtained in hippocampal slices exposed to EGCG-treated pooled mNBH (LTP: 180 ± 9; PTP: 285 ± 22; n = 4), EGCG-treated pooled mM1000 was no longer toxic to LTP and PTP (LTP: 178 ± 3; PTP: 309 ± 37; n = 4), whereas EGCG-treated oM1000 remained significantly acutely synaptotoxic to LTP and PTP (LTP: 151 ± 6, $p = 0.0372$; PTP: 202 ± 7, $p = 0.0224$; n = 4; Fig. 6, *I–K*). The loss of acute synaptotoxicity in pooled mM1000 treated with EGCG correlated with the significant dose-response redistribution of the size of PrP complexes with a gradual decrease of PrP oligomers at molecular weights above ~200 kDa and an increase of PrP species smaller than ~100 kDa (Fig. 6, *D* and *H*). The retained acute synaptotoxicity of EGCG-treated pooled oM1000 correlated with the inefficacy of 50 μM EGCG to disrupt PrP oligomers in oM1000 (Fig. 6, *C* and *G*). Overall, these results demonstrate that PrP oligomers in pooled mM1000 were closely associated, albeit through relatively weak interactions compared with PrP oligomers in oM1000, suggesting that the multimeric complexes in mM1000 were composed of less stable oligomers apparently rapidly forming after fractionation by SEC but that oligomerization of PrPSc closely correlates with acute synaptotoxicity.

DISCUSSION

The primary aim of this study was to provide additional insights into the biophysical requisites of acutely synaptotoxic M1000 PrPSc species, especially the role of PrPSc oligomerization, which we previously reported as appearing to clearly correlate with prion acute synaptotoxicity (3,16), as well as further explore the unexpected synaptotoxicity of pooled mM1000 preparations (3). Collectively, the findings reported herein support that 1) the acute synaptotoxicity of pooled monomeric and oligomeric PrPSc fractions we observed previously during M1000 prion disease evolution (3) was not due to nonspecific toxic effects of total protein concentration nor directly related to total concentration of PrPSc species or their resistance to PK digestion; 2) the acute synaptotoxicity of pooled mM1000 we observed previously (3) does correlate with apparent rapid concatenation of PrPSc in physiological buffers to generate mostly oligomers; 3) PrPC monomers in mNBH can form higher-order, nontoxic aggregates, with aggregation preventable by benzonase treatment; 4) PrPSc oligomerization in pooled mM1000 fractions resisted the antiaggregation effects of benzonase treatment but was vulnerable to the aggregation mitigation properties of EGCG, thereby maintaining PrPSc as mainly nonoligomeric, nonsynaptotoxic species; and 5) preformed PrPSc oligomers in pooled oM1000 fractions resist the antiaggregation effects of EGCG, suggesting these multimeric assemblies are maintained through stronger interactions than those occurring in nascent oligomers formed during pooling of mM1000 fractions.

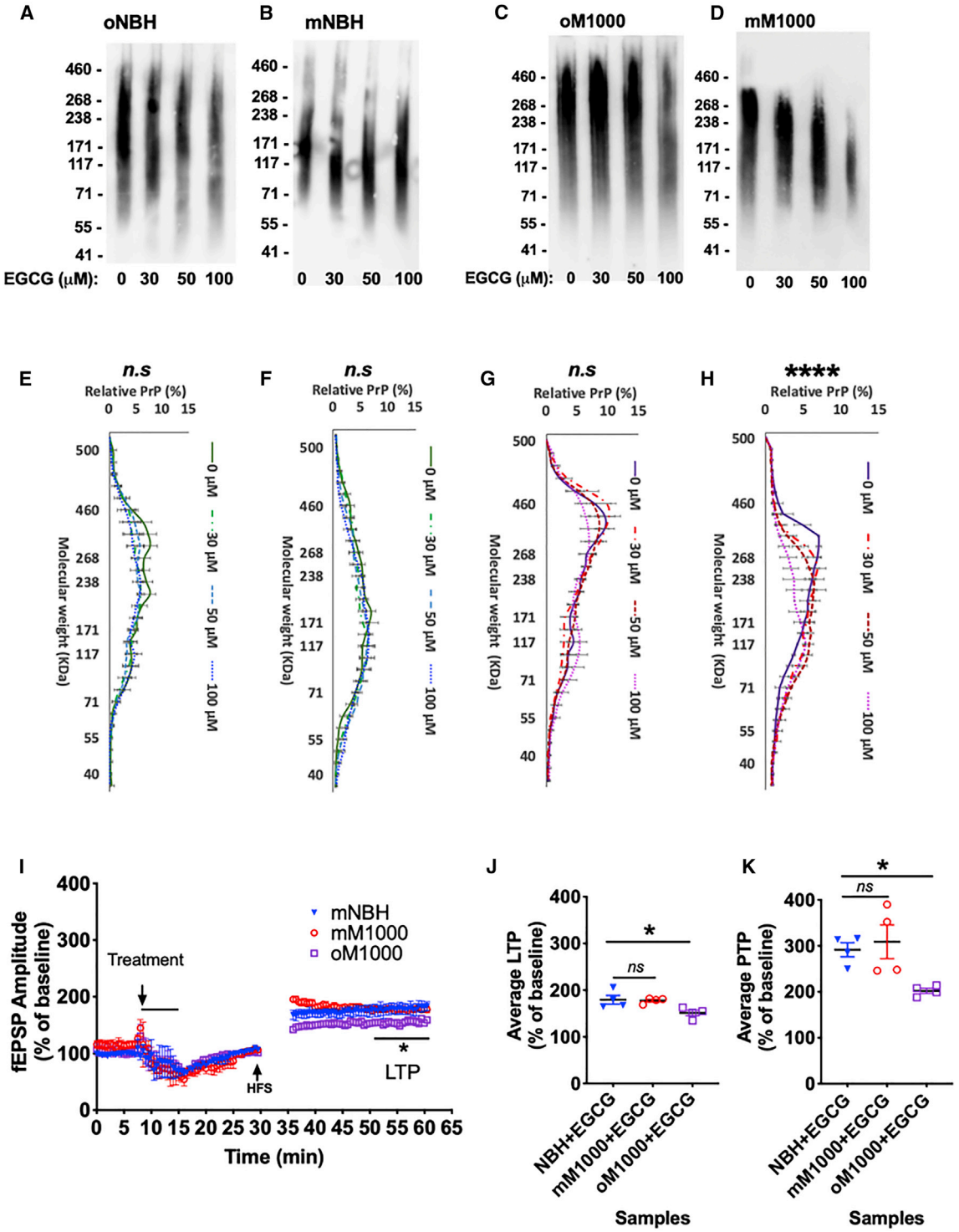

FIGURE 6 EGCG disassembled synaptotoxic PrPSc oligomers into nonsynaptotoxic species. (*A–D*) Western blotting is shown for quaternary folded PrP species in oligomeric and monomeric fractions of NBH (*A*: oNBH; *B*: mNBH) as well as M1000 (*C*: oM1000; *D*: mM1000) before and after digesting with 30, 50, and 100 μM EGCG, respectively. (*E–H*) Quantifications of PrP species as they were resolved according to their sizes by Western blotting are shown in (*A*)–(*D*); (*E*) and (*F*) are the quantifications of oNBH (n = 3) and mNBH (n = 3), and (*G*) and (*H*) are the quantifications of oM1000 (n = 3) and mM1000 (n = 3). (*I*) Hippocampal CA1 LTP in slices from WT mice after treatment with oM1000, mM1000, and mNBH treated with 50 μM EGCG is shown. The hippocampal slices were treated for 5 min (*black solid line*) started after an 8–10 min of stable baseline recording, which was ~20 min before the induction of LTP by serial trains of HFS. (*J*) Average LTPs recorded at the last 10 min of the recordings in (*I*) are shown. (*K*) Average PTPs recording after the treatments listed in (*I*) are shown. (*E–H*) Results are analyzed by two-way ANOVA with Dunnett's correction for multiple comparisons. (*J* and *K*) Results are analyzed by one-way ANOVA with Dunnett's correction for multiple comparisons. All data are presented as standard error of mean. *$p < 0.05$, ****$p < 0.0001$. To see this figure in color, go online.

The additional studies we report have verified our previous preliminary findings supporting that although the PrPSc in mM1000 fractions were initially fractionated as monomeric (as per their size exclusion behavior), they are likely to be misfolded, pathogenic species in a state of unstable equilibrium, via which they may rapidly become oligomers (19,37,39,40). The new interrogations of PrP species in pooled mM1000 in this study through tandem SEC, native Western blotting, and DSS cross-linking revealed that mM1000 appeared to quickly form closely self-associated PrPSc oligomers when pooled in a physiological buffer. Given the evidence that transition between β-PrP monomers and oligomers could occur between four to 10 s (37), it is possible that monomeric PrPSc species in the mM1000 immediately became oligomers as they were eluted from the SEC column. Importantly, given the absence of acute synaptotoxicity of multimeric complexes in mNBH and oNBH, misfolding to form PrPSc appears a fundamental but insufficient prerequisite for such toxic effects, and although biophysical differences exist between mM1000 and oM1000 oligomers, as reflected by the effects of EGCG treatment and the median size of constituent oligomers revealed by densitometry, it appears oligomerization of PrPSc engenders inherent acute synaptotoxicity not evident when PrPSc can be maintained as primarily monomeric.

Although the protection of synaptic function through EGCG treatment of pooled mM1000 fractions may suggest this as a potential therapeutic, the primary reason we used this compound was to more directly assess the role of oligomerization as a prerequisite for acute synaptotoxicity, aware of evidence that EGCG can interfere with the normal physiological roles of proteins, including PrPC (10,15). Nevertheless, our finding that EGCG can prevent acute synaptotoxicity by mitigating oligomerization of PrPSc found in pooled mM1000 verifies this as a potential therapeutic approach, albeit requiring the discovery or development of drugs analogous to EGCG but with arguably higher efficacy and acceptable "off-target" effects. We were not able to assess for any altered toxicity of "mature" oligomers in pooled oM1000 fractions after being slightly disassembled by a higher concentration of EGCG (100 μM) because of the background synaptotoxicity of such high doses of ECGC, but a safe, more potent compound with broadened antiaggregation capacity would enhance the appeal of this type of therapy.

Although a similar rapid transition to higher-order assemblies was observed in PrPC from pooled mNBH, our evidence of the reduced size of higher molecular weight complexes only in mNBH, but not in mM1000, after treatment with benzonase suggests that the intermolecular interactions of such multimeric PrP in mNBH and mM1000 were fundamentally different. Further support for such difference was the resistance of higher-order complexes containing PrP in pooled mNBH to EGCG treatment, but not those in pooled mM1000, as well as the differences revealed with DSS cross-linker studies wherein the ~11.4 Å spacer cross-linked substantial levels of PrPSc oligomers in mM1000 compared with minimal effects on PrPC within the multimeric assemblies of mNBH. These observations suggest that relative to PrP oligomers in mM1000, PrP in pooled mNBH was not aggregated at sufficiently close proximity to be cross-linked. Given the evidence that sarkosyl alters PrP conformation and promotes PrPSc aggregation (41), it is possible that the use of sarkosyl in this study contributed to the self-concatenation and conformations of PrP in mNBH and mM1000. Collectively, our findings clearly support that self-concatenation of PrP in mNBH and mM1000 preparations yielded multimeric PrP species with different molecular interactions and consequent conformations. Further studies are required to clarify whether SEC fractionation of cNBH, and consequent pooling of mNBH and oNBH, simply allows irrelevant artifactual agglomeration of PrPC through unclear mechanisms into loosely associated multimers or is truly capturing, or perhaps affording, an opportunity for PrPC to assemble into biologically meaningful homo- or heteromultimeric complexes, as suggested by the recognized large number of potential association partners (42). PrPC may only be present as oligomers or higher molecular weight complexes if they are correctly and closely partnered with other molecules, especially proteins, and the apparent self-assembly of PrPC monomers into higher-order assemblies facilitated by nucleic acids may exemplify an artifact of our SEC fractionation utilized in this study.

The molecular interactions that assembled PrPSc molecules into oligomers, as defined by the sensitivity to EGCG, appeared different and stronger in oM1000 compared to mM1000, suggesting the possibility that synaptotoxic PrPSc oligomers biophysically evolve through a maturation process from "nascent" to "mature." We speculate that "nascent" oligomers are possibly intermediates in dynamic equilibria between PrPSc monomers and "mature" oligomers, in which monomers can rapidly oligomerize, whereas oligomers, especially nascent species, can disassemble, producing monomers (37). This speculation is broadly consistent with previous reports of intermediates determined as "octamers," which were demonstrated to exhibit some toxic effects associated with prion disease (6,29,40,43). Moreover, analogous dynamic equilibria and underpinning intermolecular interactions and pathways were not observed in fractions of NBH, as indicated by the failure of the EGCG treatment to reduce the size of PrPC oligomers in both mNBH and oNBH. The molecular interactions that bound PrP multimers in mM1000, oM1000, and oNBH appeared independent of nucleic acids because benzonase treatment did not alter them. Importantly, benzonase and EGCG did not alter oNBH and oM1000, suggesting that PrP multimers in these preparations were bound by relatively strong molecular interactions

although quite possibly through different specific mechanisms given differences in DSS cross-linking studies. In addition, as opposed to the mechanisms of many antiprion therapeutic drugs (10), the mechanism by which EGCG altered the sizes of PrP multimers in this study was independent of any cellular activity because all the treatments of PrP preparations were conducted in a cell-free assay.

Our findings further support that M1000 prion acute synaptotoxicity is more dependent on the specific biophysical properties of constituent PrPSc (especially oligomerization) rather than just the absolute quantity of PrPSc. The acutely synaptotoxic level of total PrP (including PrPSc) in mM1000 was $<<12$ ng/mL despite our previous report demonstrating that $\sim$15 ng/mL total PrP in 0.1% (w/v) cM1000 and $\sim$35 ng/mL in 0.5% (w/v) PrP-depleted M1000 were not synaptotoxic to hippocampal CA1 LTP of WT mice (16). We surmise this discrepancy may be due to the different ways by which these preparations of ex vivo PrPSc were prepared, with pooling of monomeric M1000 fractions after SEC associated with production of more acutely synaptotoxic species relative to total PrP present. For example, the smaller average size mM1000 oligomers as compared with those in pooled oM1000 fractions may mean a higher effective concentration of acutely synaptotoxic entities per total PrPSc in the former. Moreover, this finding is broadly consistent with other reports of PrPSc infectivity appearing more dependent on certain species of PrPSc rather than absolute levels (18,22,44). We have not explored the infectivity of our pooled fractions, but given previous reports of significant overlap between synaptotoxic and transmitting PrPSc species at terminal disease (3), as well as the evidence that highly efficient transmissibility correlates with smaller PrPSc oligomers (18,22,44), we speculate that the smaller PrPSc oligomers in mM1000 may harbor substantial infectivity. Furthermore, given that we previously showed that prion acute synaptotoxicity appeared independent of human mouse-adapted prion strain, the results of this study are likely to be evident with other prion strains; however, additional experiments are required to confirm this.

SUPPORTING MATERIAL

Supporting Material can be found online at https://doi.org/10.1016/j.bpj.2020.04.040.

AUTHOR CONTRIBUTIONS

S.T.F., conceptualization, data curation, formal analysis, investigation, methodology, writing—original draft, writing—review and editing. V.L., supervision. A.M.T.I., resources. M.S., resources. D.I.F., supervision. L.J.E., resources. V.A.L., resources. P.A.A., supervision. B.R.R., supervision, writing—review and editing. S.J.C., conceptualization, funding acquisition, investigation, project administration, resources, supervision, validation, visualization, writing—original draft, writing—review and editing.

ACKNOWLEDGMENTS

S.J.C. is supported in part by a National Health and Medical Research Council Practitioner Fellowship (identification #APP1105784). S.T.F. was supported by a Creutzfeldt-Jakob disease Support Group Network (CJDSGN) Memorial Grant in memory of Dominic Battista.

REFERENCES

1. Collins, S. J., V. A. Lawson, and C. L. Masters. 2004. Transmissible spongiform encephalopathies. *Lancet.* 363:51–61.
2. Prusiner, S. B. 1982. Novel proteinaceous infectious particles cause scrapie. *Science.* 216:136–144.
3. Foliaki, S. T., V. Lewis, …, S. J. Collins. 2019. Early existence and biochemical evolution characterise acutely synaptotoxic PrPSc. *PLoS Pathog.* 15:e1007712.
4. Srivastava, K. R., and L. J. Lapidus. 2017. Prion protein dynamics before aggregation. *Proc. Natl. Acad. Sci. USA.* 114:3572–3577.
5. Sengupta, I., S. H. Bhate, …, J. B. Udgaonkar. 2017. Salt-mediated oligomerization of the mouse prion protein monitored by real-time NMR. *J. Mol. Biol.* 429:1852–1872.
6. Deleault, N. R., R. W. Lucassen, and S. Supattapone. 2003. RNA molecules stimulate prion protein conversion. *Nature.* 425:717–720.
7. Wang, F., X. Wang, and J. Ma. 2011. Conversion of bacterially expressed recombinant prion protein. *Methods.* 53:208–213, Published online December 19, 2010.
8. Deleault, N. R., J. R. Piro, …, S. Supattapone. 2012. Isolation of phosphatidylethanolamine as a solitary cofactor for prion formation in the absence of nucleic acids. *Proc. Natl. Acad. Sci. USA.* 109:8546–8551.
9. Miller, M. B., D. W. Wang, …, S. Supattapone. 2013. Cofactor molecules induce structural transformation during infectious prion formation. *Structure.* 21:2061–2068.
10. Barreca, M. L., N. Iraci, …, E. Biasini. 2018. Pharmacological agents targeting the cellular prion protein. *Pathogens.* 7:E27.
11. Mallucci, G. R., M. D. White, …, J. Collinge. 2007. Targeting cellular prion protein reverses early cognitive deficits and neurophysiological dysfunction in prion-infected mice. *Neuron.* 53:325–335.
12. Mallucci, G., A. Dickinson, …, J. Collinge. 2003. Depleting neuronal PrP in prion infection prevents disease and reverses spongiosis. *Science.* 302:871–874.
13. Büeler, H., A. Aguzzi, …, C. Weissmann. 1993. Mice devoid of PrP are resistant to scrapie. *Cell.* 73:1339–1347.
14. Kurnik, M., C. Sahin, …, D. E. Otzen. 2018. Potent α-synuclein aggregation inhibitors, identified by high-throughput screening, mainly target the monomeric state. *Cell Chem. Biol.* 25:1389–1402.e9.
15. Rambold, A. S., M. Miesbauer, …, J. Tatzelt. 2008. Green tea extracts interfere with the stress-protective activity of PrP and the formation of PrP. *J. Neurochem.* 107:218–229.
16. Foliaki, S. T., V. Lewis, …, S. J. Collins. 2018. Prion acute synaptotoxicity is largely driven by protease-resistant PrPSc species. *PLoS Pathog.* 14:e1007214.
17. Brazier, M. W., V. Lewis, …, S. Collins. 2006. Correlative studies support lipid peroxidation is linked to PrP(res) propagation as an early primary pathogenic event in prion disease. *Brain Res. Bull.* 68:346–354.
18. Caughey, B., G. S. Baron, …, M. Jeffrey. 2009. Getting a grip on prions: oligomers, amyloids, and pathological membrane interactions. *Annu. Rev. Biochem.* 78:177–204.
19. Mays, C. E., J. van der Merwe, …, D. Westaway. 2015. Prion infectivity plateaus and conversion to symptomatic disease originate from falling precursor levels and increased levels of oligomeric PrPSc species. *J. Virol.* 89:12418–12426.
20. Sasaki, K., H. Minaki, and T. Iwaki. 2009. Development of oligomeric prion-protein aggregates in a mouse model of prion disease. *J. Pathol.* 219:123–130.

21. Greil, C. S., I. M. Vorberg, …, S. A. Priola. 2008. Acute cellular uptake of abnormal prion protein is cell type and scrapie-strain independent. *Virology.* 379:284–293.

22. Silveira, J. R., G. J. Raymond, …, B. Caughey. 2005. The most infectious prion protein particles. *Nature.* 437:257–261.

23. Kristiansen, M., P. Deriziotis, …, S. J. Tabrizi. 2007. Disease-associated prion protein oligomers inhibit the 26S proteasome. *Mol. Cell.* 26:175–188.

24. Freir, D. B., A. J. Nicoll, …, J. Collinge. 2011. Interaction between prion protein and toxic amyloid β assemblies can be therapeutically targeted at multiple sites. *Nat. Commun.* 2:336.

25. Li, S., M. Jin, …, D. J. Selkoe. 2011. Soluble Aβ oligomers inhibit long-term potentiation through a mechanism involving excessive activation of extrasynaptic NR2B-containing NMDA receptors. *J. Neurosci.* 31:6627–6638.

26. Nakata, Y., T. Yasuda, …, H. Mochizuki. 2012. Accumulation of α-synuclein triggered by presynaptic dysfunction. *J. Neurosci.* 32:17186–17196.

27. Tu, S., S. Okamoto, …, H. Xu. 2014. Oligomeric Aβ-induced synaptic dysfunction in Alzheimer's disease. *Mol. Neurodegener.* 9:48.

28. Lewis, V., V. A. Johanssen, …, S. J. Collins. 2016. Prion protein "gamma-cleavage": characterizing a novel endoproteolytic processing event. *Cell. Mol. Life Sci.* 73:667–683.

29. Simoneau, S., H. Rezaei, …, C. I. Lasmézas. 2007. In vitro and in vivo neurotoxicity of prion protein oligomers. *PLoS Pathog.* 3:e125.

30. Knaus, K. J., M. Morillas, …, V. C. Yee. 2001. Crystal structure of the human prion protein reveals a mechanism for oligomerization. *Nat. Struct. Biol.* 8:770–774.

31. Silva, J. L., T. C. Vieira, …, Y. Cordeiro. 2011. Experimental approaches to the interaction of the prion protein with nucleic acids and glycosaminoglycans: modulators of the pathogenic conversion. *Methods.* 53:306–317.

32. Bera, A., and S. Biring. 2018. A quantitative characterization of interaction between prion protein with nucleic acids. *Biochem. Biophys. Rep.* 14:114–124.

33. Silva, J. L., and Y. Cordeiro. 2016. The "jekyll and hyde" actions of nucleic acids on the prion-like aggregation of proteins. *J. Biol. Chem.* 291:15482–15490.

34. Macedo, B., and Y. Cordeiro. 2017. Unraveling prion protein interactions with aptamers and other PrP-binding nucleic acids. *Int. J. Mol. Sci.* 18:E1023.

35. Huang, P., F. Lian, …, D. Lin. 2013. Prion protein oligomer and its neurotoxicity. *Acta Biochim. Biophys. Sin. (Shanghai).* 45:442–451.

36. Senesi, M., V. Lewis, …, S. J. Collins. 2017. In vivo prion models and the disconnection between transmissibility and neurotoxicity. *Ageing Res. Rev.* 36:156–164.

37. Larda, S. T., K. Simonetti, …, R. S. Prosser. 2013. Dynamic equilibria between monomeric and oligomeric misfolded states of the mammalian prion protein measured by 19F NMR. *J. Am. Chem. Soc.* 135:10533–10541.

38. Kim, C., T. Haldiman, …, J. G. Safar. 2012. Small protease sensitive oligomers of PrPSc in distinct human prions determine conversion rate of PrP(C). *PLoS Pathog.* 8:e1002835.

39. Gerber, R., A. Tahiri-Alaoui, …, W. James. 2007. Oligomerization of the human prion protein proceeds via a molten globule intermediate. *J. Biol. Chem.* 282:6300–6307.

40. Khan, M. Q., B. Sweeting, …, A. Chakrabartty. 2010. Prion disease susceptibility is affected by beta-structure folding propensity and local side-chain interactions in PrP. *Proc. Natl. Acad. Sci. USA.* 107:19808–19813.

41. Levine, D. J., J. Stöhr, …, J. R. Long. 2015. Mechanism of scrapie prion precipitation with phosphotungstate anions. *ACS Chem. Biol.* 10:1269–1277.

42. Zafar, S., N. von Ahsen, …, A. R. Asif. 2011. Proteomics approach to identify the interacting partners of cellular prion protein and characterization of Rab7a interaction in neuronal cells. *J. Proteome Res.* 10:3123–3135.

43. Novitskaya, V., O. V. Bocharova, …, I. V. Baskakov. 2006. Amyloid fibrils of mammalian prion protein are highly toxic to cultured cells and primary neurons. *J. Biol. Chem.* 281:13828–13836.

44. Lewis, V., C. L. Haigh, …, S. J. Collins. 2012. Prion subcellular fractionation reveals infectivity spectrum, with a high titre-low PrPres level disparity. *Mol. Neurodegener.* 7:18.

Identification of novel risk loci and causal insights for sporadic Creutzfeldt-Jakob disease: a genome-wide association study

Emma Jones, Holger Hummerich*, Emmanuelle Viré*, James Uphill, Athanasios Dimitriadis, Helen Speedy, Tracy Campbell, Penny Norsworthy, Liam Quinn, Jerome Whitfield, Jacqueline Linehan, Zane Jaunmuktane, Sebastian Brandner, Parmjit Jat, Akin Nihat, Tze How Mok, Parvin Ahmed, Steven Collins, Christiane Stehmann, Shannon Sarros, Gabor G Kovacs, Michael D Geschwind, Aili Golubjatnikov, Karl Frontzek, Herbert Budka, Adriano Aguzzi, Hata Karamujić-Čomić, Sven J van der Lee, Carla A Ibrahim-Verbaas, Cornelia M van Duijn, Beata Sikorska, Ewa Golanska, Pawel P Liberski, Miguel Calero, Olga Calero, Pascual Sanchez-Juan, Antonio Salas, Federico Martinón-Torres, Elodie Bouaziz-Amar, Stéphane Haïk, Jean-Louis Laplanche, Jean-Phillipe Brandel, Phillipe Amouyel, Jean-Charles Lambert, Piero Parchi, Anna Bartoletti-Stella, Sabina Capellari, Anna Poleggi, Anna Ladogana, Maurizio Pocchiari, Serena Aneli, Giuseppe Matullo, Richard Knight, Saima Zafar, Inga Zerr, Stephanie Booth, Michael B Coulthart, Gerard H Jansen, Katie Glisic, Janis Blevins, Pierluigi Gambetti, Jiri Safar, Brian Appleby, John Collinge, Simon Mead*

Lancet Neurol 2020; 19: 840–48

*Contributed equally

Medical Research Council Prion Unit, University College London Institute of Prion Diseases, London, UK (E Jones BSc, H Hummerich PhD, E Viré PhD, J Uphill BSc, A Dimitriadis BSc, H Speedy PhD, T Campbell BSc, P Norsworthy BSc, L Quinn PhD, J Whitfield PhD, J Linehan BSc, Prof P Jat PhD, A Nihat MBBS, T How Mok MB, P Ahmed MSc, Prof J Collinge FRS, Prof S Mead PhD)**; National Prion Clinic** (A Nihat, T How Mok, Prof J Collinge, Prof S Mead) **and Division of Neuropathology** (Z Jaunmuktane FRCPath, Prof S Brandner FRCPath), **University College London Hospitals National Health Service Foundation Trust, London, UK; Department of Clinical and Movement Neurosciences and Queen Square Brain Bank for Neurological Disorders** (Z Jaunmuktane) **and Department of Neurodegenerative Disease** (Prof S Brandner)**, University College London Queen Square Institute of Neurology, London, UK; Australian National Creutzfeldt-Jakob Disease Registry, Florey Institute of Neuroscience and Mental Health, University of Melbourne, Melbourne, VIC, Australia** (Prof S Collins MD, C Stehmann PhD, S Sarros BSc)**; Institute of Neurology, Medical University of Vienna, Vienna, Austria** (Prof G G Kovacs MD)**; Department of Laboratory Medicine and Pathobiology and Tanz Centre for Research in**

Summary

Background Human prion diseases are rare and usually rapidly fatal neurodegenerative disorders, the most common being sporadic Creutzfeldt-Jakob disease (sCJD). Variants in the *PRNP* gene that encodes prion protein are strong risk factors for sCJD but, although the condition has similar heritability to other neurodegenerative disorders, no other genetic risk loci have been confirmed. We aimed to discover new genetic risk factors for sCJD, and their causal mechanisms.

Methods We did a genome-wide association study of sCJD in European ancestry populations (patients diagnosed with probable or definite sCJD identified at national CJD referral centres) with a two-stage study design using genotyping arrays and exome sequencing. Conditional, transcriptional, and histological analyses of implicated genes and proteins in brain tissues, and tests of the effects of risk variants on clinical phenotypes, were done using deep longitudinal clinical cohort data. Control data from healthy individuals were obtained from publicly available datasets matched for country.

Findings Samples from 5208 cases were obtained between 1990 and 2014. We found 41 genome-wide significant single nucleotide polymorphisms (SNPs) and independently replicated findings at three loci associated with sCJD risk; within *PRNP* (rs1799990; additive model odds ratio [OR] 1·23 [95% CI 1·17–1·30], $p=2·68\times10^{-15}$; heterozygous model $p=1·01\times10^{-135}$), *STX6* (rs3747957; OR 1·16 [1·10–1·22], $p=9·74\times10^{-9}$), and *GAL3ST1* (rs2267161; OR 1·18 [1·12–1·25], $p=8·60\times10^{-10}$). Follow-up analyses showed that associations at *PRNP* and *GAL3ST1* are likely to be caused by common variants that alter the protein sequence, whereas risk variants in *STX6* are associated with increased expression of the major transcripts in disease-relevant brain regions.

Interpretation We present, to our knowledge, the first evidence of statistically robust genetic associations in sporadic human prion disease that implicate intracellular trafficking and sphingolipid metabolism as molecular causal mechanisms. Risk SNPs in *STX6* are shared with progressive supranuclear palsy, a neurodegenerative disease associated with misfolding of protein tau, indicating that sCJD might share the same causal mechanisms as prion-like disorders.

Funding Medical Research Council and the UK National Institute of Health Research in part through the Biomedical Research Centre at University College London Hospitals National Health Service Foundation Trust.

Introduction

Prion diseases are fatal neurodegenerative conditions in humans and animals caused by the propagation of prions: atypical infectious agents comprised solely or predominantly of host prion protein.[1] Prions are thought to propagate through a process of binding to normal prion protein, induction of conformational change by templating, and fission of the polymeric assembly. Prion diseases can be acquired from exposure to prions in the diet, or through medical or surgical procedures, which can result in public health crises. The cattle prion disease, bovine spongiform encephalopathy (BSE), which transmitted to mostly young British and other European adults as variant Creutzfeldt-Jakob disease (vCJD),[2] led to enhanced clinical surveillance for all prion diseases worldwide. Inherited prion disease, caused only by mutations of the prion protein gene (*PRNP*), causes approximately 10–15% of the annual incidence of all prion diseases in most countries.[3] The most common type of human prion disease is sporadic CJD (sCJD), a rapidly progressive dementia with a lifetime risk of approximately one in 5000, which occurs predominantly in older adults.[4,5] Other than age and

Research in context

Evidence before this study

The rarity of sporadic Creutzfeldt-Jakob disease (sCJD) has been limiting in previous genome-wide association studies (GWAS) for disease risk. We searched PubMed on April 9, 2020, with the terms ("prion" OR "creutzfeldt*") AND ("genome wide association" OR "GWAS"), without language or date restrictions, and identified four relevant publications, including two directly investigating sCJD risk through genome-wide analyses. However, the sample sizes in these studies were not sufficient to identify statistically significant associations outside of the known risk at the prion protein gene (*PRNP*). Further studies into genetic risk factors for sCJD have primarily utilised targeted replication of putative risk variants or candidate gene studies to propose association.

Added value of this study

Through international collaboration of sample resources, this study is, to our knowledge, the first GWAS to identify genetic variants associated with sCJD risk outside of *PRNP*, at genome-wide significance. Two of these variants (within *STX6* and *GAL3ST1*) were statistically robust to replication in an independent cohort, with 5208 patients with sCJD in total included in the two-stage study design. Through statistical fine-mapping and analysis of exome sequencing and gene expression data, we propose genes that are likely to be causal, and mechanisms for both novel associations. We used patient brain samples and cell-based assays to further investigate the biological implications of these associations in relevant systems. Two further loci at *PDIA4* and *BMERB1* were also associated with sCJD risk in gene-based tests.

Implications of all the available evidence

Identification of two novel non-*PRNP* loci conferring sCJD risk will provide further avenues for research, with increased evidence to support a role of modified intracellular trafficking and sphingolipid metabolism within sCJD biology, providing the potential to inform new therapeutic approaches. With the shared genetic risk of variants within *STX6* and those previously identified for the tauopathy progressive supranuclear palsy, this study also supports the notion of a common so-called prion-like causal mechanism for related neurodegenerative disorders and thus potential for shared treatments.

polymorphisms at *PRNP*, no risk factors for sCJD are known, leaving only speculative explanations for sporadic prion formation.

Polymorphisms of *PRNP* at codons 127, 129, and 219 alter amino acids and are strong genetic risk factors or modifiers of the disease phenotypes.[3] Sibling or familial concurrence of sCJD has been reported, but not to the extent that chance concurrence can be eliminated as an explanation. There are no estimates of the heritability of sCJD based on family studies.[6] Animal studies have identified acquired prion disease risk factors in *Prnp* and close by, and provided evidence for susceptible loci on other chromosomes, yet elucidating the causal genes has proven to be challenging.[3] Many other neurodegenerative diseases are thought to share fundamental mechanisms with prion diseases, including template-based protein misfolding and spreading of pathology associated with abnormally aggregated proteins in diseased brain tissue. If shared mechanisms exist, this might implicate shared genetic risk factors for these diseases.

This study follows on from previous genome-wide association studies (GWAS) in human prion diseases, which have not been powerful enough to discover non-*PRNP* risk factors.[7–10] We aimed to identify specific causal genes at risk loci, to allow molecular causal mechanisms for sCJD to be proposed.

Methods

Study design and participants

We did a GWAS using samples from patients diagnosed with probable or definite sCJD according to widely accepted criteria, which were provided by specialist or national surveillance centres in countries with populations of predominantly European ancestries (appendix pp 2, 28–32). Diagnostic criteria for probable sCJD varied over the course of sample collection for the study. Using modern diagnostic methods, including real-time quaking-induced conversion assay with CSF, a probable diagnosis refuted by post-mortem examination is extremely rare; but even more than 20 years ago, probable sCJD was a highly accurate term. Patient samples were distributed across a two-stage study design: samples were genotyped using Illumina Omniexpress arrays in the discovery stage, and additional samples were genotyped at the lead variant in each hit locus using minor groove binding probes in the replication stage. Control data from healthy individuals were obtained from publicly available datasets matched for country.

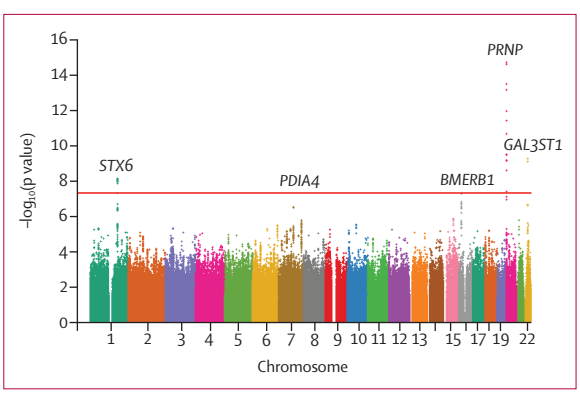

Figure 1: **Manhattan plot for significant variants**
The nearest gene to each genome-wide significant locus (significance indicated by the red horizontal line [$p<5\times10^{-8}$]) is labelled, as well as genes that were significant in gene-based tests.

Neurodegenerative Disease, University of Toronto, Toronto, ON, Canada (Prof G G Kovacs); **Laboratory Medicine Program, Krembil Brain Institute, University Health Network, Toronto, ON, Canada** (Prof G G Kovacs); **University of California San Francisco Memory and Aging Center, Department of Neurology, University of California, San Francisco, CA, USA** (Prof M D Geschwind PhD, A Golubjatnikov MS); **Institute of Neuropathology, University of Zurich, Zurich, Switzerland** (K Frontzek PhD, Prof H Budka MD, Prof A Aguzzi PhD); **Medical University Vienna, Vienna, Austria** (Prof H Budka); **Department of Epidemiology, Erasmus Medical Centre, Rotterdam, Netherlands** (H Karamujić-Čomić MD, S J van der Lee PhD, C A Ibrahim-Verbaas MD, Prof C M van Duijn FMedSci); **Nuffield Department of Population Health, University of Oxford, Oxford, UK** (Prof C M van Duijn); **Department of Molecular Pathology and Neuropathology, Medical University of Lodz, Lodz, Poland** (Prof B Sikorska MD, E Golanska PhD, Prof P P Liberski MD); **Chronic Disease Programme (UFIEC-CROSADIS) and Network Centre for Biomedical Research in Neurodegenerative Diseases (CIBERNED), and Alzheimer Disease Research Unit, CIEN Foundation, Queen Sofia Foundation Alzheimer Centre, Instituto de Salud Carlos III, Madrid, Spain** (M Calero PhD, O Calero PhD); **Neurology Service, University Hospital Marqués de Valdecilla, University of Cantabria, CIBERNED and IDIVAL, Santander, Spain** (P Sanchez-Juan PhD); **Unidade de Xenética, Instituto de Ciencias Forenses (INCIFOR), Facultade de Medicina, Universidade de Santiago de Compostela, and GenPoB Research Group, Instituto de Investigaciones Sanitarias (IDIS), Hospital Clínico Universitario de Santiago (SERGAS), Galicia, Spain** (Prof A Salas PhD); **Translational Paediatrics and Infectious Diseases, Department of Paediatrics, Hospital Clínico**

	rs1799990	rs3747957	rs2267161	rs9065	rs6498552
Nearest gene	*PRNP*	*STX6*	*GAL3ST1*	*PDIA4*	*BMERB1*
Location (in GRCh37)	20:4680251	1:180953853	22:30953295	7:148700849	16:15539901
Type of mutation	Missense exonic	Synonymous exonic	Missense exonic	3′-UTR exonic	Intronic
Risk allele	A	A	C	T	T
Minor allele	G	A	T	T	T
Discovery stage (n=4110 cases, n=13 569 controls)					
MAF cases	0·288	0·452	0·289	0·220	0·120
MAF controls	0·340	0·410	0·322	0·191	0·102
OR (95% CI)	1·23 (1·17–1·30)	1·16 (1·10–1·22)	1·18 (1·12–1·25)	1·17 (1·09–1·24)	1·27 (1·16–1·38)
p value	$2·68×10^{-15}$	$9·74×10^{-9}$	$8·60×10^{-10}$	$1·66×10^{-6}$	$5·75×10^{-8}$
Replication stage (n=1098 cases, n=498 016 controls)					
MAF cases	0·294	0·450	0·302	0·203	0·105
MAF controls	0·328	0·420	0·326	0·204	0·097
OR (95% CI)	1·15 (1·04–1·28)	1·15 (1·05–1·26)	1·11 (1·00–1·23)	1·01 (0·90–1·13)	1·11 (0·96–1·29)
p value; replication cohorts	0·0049	0·0034	0·042	0·88	0·17
p value; replication plus discovery meta-analysis	$9·61×10^{-17}$	$1·23×10^{-10}$	$1·97×10^{-10}$	$8·49×10^{-5}$	$6·45×10^{-8}$

PRNP, *STX6*, and *GAL3ST1* SNPs were successfully replicated in an independent cohort (p<0·05). OR is relative to the low-risk allele. GRCh37=Genome Reference Consortium human genome build 37. UTR=untranslated region. MAF=minor allele frequency. OR=odds ratio.

Table: **Association results of discovery and replication stages**

Universitario de Santiago de Compostela, Galicia, Spain (Prof F Martinón-Torres PhD); **Department of Biochemistry and Molecular Biology, Lariboisière Hospital, AP-HP, University of Paris, Paris, France** (E Bouaziz-Amar PhD, Prof J-L Laplanche PhD); **Sorbonne Université, INSERM U1127, CNRS UMR 7225, Institut du Cerveau et de la Moelle épinière, Paris, France** (S Haïk MD, J-P Brandel MD); **Cellule nationale de référence des maladies de Creutzfeldt-Jakob, AP-HP, University Hospital Pitié-Salpêtrière, Paris, France** (S Haïk, J-P Brandel); **INSERM, CHU Lille, Institut Pasteur de Lille, U1167-RID-AGE, Labex DISTALZ, University of Lille, Lille, France** (Prof P Amouyel PhD, J-C Lambert PhD); **IRCCS, Istituto delle Scienze Neurologiche di Bologna, Bologna, Italy** (Prof P Parchi MD, S Capellari MD, A Bartoletti-Stella PhD); **Department of Biomedical and Neuromotor Sciences** (S Capellari) **and Department of Experimental, Diagnostic, and Specialty Medicine** (Prof P Parchi),

Procedures and statistical analysis

Genotypes were imputed using the Michigan Imputation Server and standard sample and genotyping quality control measures were implemented, to generate 6 314 492 high-quality autosomal single nucleotide polymorphisms (SNPs) for subsequent analysis (appendix pp 28–32). SNPTEST version 2.5.2 was used to perform the association test using an additive logistic regression model. Association statistics for the replication stage were generated using PLINK version 1.9 in a fixed-effects meta-analysis of each cohort. The same model was used to study genetic association for kuru resistance (older asymptomatic individuals who were exposed to kuru compared to patients with young onset and those born after kuru exposure). Additional exome sequencing was performed on 501 CJD samples using the Illumina HiSeq2000 platform.

Further gene-based analysis was performed using MAGMA version 1.06 and VEGAS2 version 2.02, and SNP heritability estimates were calculated using SumHer with standard specifications. CAVIAR and PAINTOR were utilised to generate a credible causal set for SNPs surrounding each significant locus based on linkage disequilibrium and functional annotations.[11,12] eCAVIAR and eQTL colocalisation analysis was performed using 48 tissues included in the GTEx portal version 7.[13,14]

Short-hairpin RNAs targeting *Stx6* and *Prnp* were used to knockdown expression in N2aPK1/2 cells susceptible to infection with Chandler RML prions. Prion propagation was measured using the scrapie cell assay, as previously described.[15] Expression of each proposed gene was measured by RT-qPCR in cerebellum from ten patients with sCJD and ten neurologically healthy controls. Immunohistology for syntaxin-6 and protein disulfide isomerase family A, member 4 was done on formalin-fixed paraffin-embedded frontal cortex and cerebellum of 19 patients with sCJD and 15 non-neurological disease controls.

Role of the funding source

The funder of the study had no role in study design, data collection, data analysis, data interpretation, or writing of the report. The corresponding author had full access to all the data in the study and had final responsibility for the decision to submit for publication.

Results

Between 1990 and 2014, we obtained 5208 sCJD samples, of which 4110 were used in the discovery stage and 1098 were used in the replication stage.

In the discovery stage we compared genome-wide genotype data from 4110 patients with probable or definite sCJD from countries of predominantly European ancestries with 13 569 control samples from a similar range of countries (appendix pp 2–3). Imputation using the Michigan server resulted in 6 314 492 high-quality autosomal SNPs after quality control, which were used for downstream association tests in SNPTEST with ten population covariates. Genomic inflation (λ) was 1·026 (appendix p 16), indicating no significant systemic bias related to population ancestry or platforms, so no further correction was done; the threshold for genome-wide significance was $p<5×10^{-8}$. Estimated SNP heritability (LDAK model: $h^2_{SNP}=0·26$ [SD 0·014]; GCTA model: $h^2_{SNP}=0·24$ [SD 0·023]) was similar to that of common neurodegenerative diseases, in keeping with very rare reports of familial sCJD concurrence.[6,16,17]

Further to the known association at *PRNP* on chromosome 20p13, two loci achieved genome-wide significance mapping to 1q25.3 (*STX6*) and 22q12.2 (*GAL3ST1*; figure 1; table; appendix pp 17–19). Gene-based testing with VEGAS2 additionally identified *PDIA4* (p=0·040) and *BMERB1* (p=0·0014), although testing with MAGMA did not support these associations (appendix pp 20–21). No significant gene sets were found. A SNP in intron 1 of the *BMERB1* gene achieved borderline significance (rs6498552, odds ratio 1·27 [95% CI 1·16–1·38], $p=5·75×10^{-8}$, appendix p 21). Although we acknowledge that data from multiple SNPs at a locus are needed to directly replicate gene-based test results, we selected a lead SNP from the three genome-wide significant loci as well as from *PDIA4* and *BMERB1* for the replication stage.

In the replication stage we generated genotype data using minor groove binding probes from 1098 patients with probable or definite sCJD, again from multiple countries of predominantly European ancestries, and compared these with genotypes from 498 016 control samples

from the same countries (appendix pp 2–3). Association testing provided replication evidence for *PRNP* (rs1799990, heterozygous genotype and to a lesser extent the minor allele is protective), *STX6* (rs3747957, minor allele conferred risk), and *GAL3ST1* (rs2267161, minor allele was protective; table). Additionally, we explored if those loci would show an association in related prion diseases. Genotype data was generated for vCJD (acquired from exposure to BSE), iatrogenic CJD (caused by exposure to cadaveric pituitary-derived human growth hormone), or kuru (and resistance to kuru; a former epidemic of orally transmitted prion disease among people who lived in the Eastern Highlands Province of Papua New Guinea). We found no evidence for association of rs3747957 in *STX6*, or rs2267161 in *GAL3ST1* with these phenotypes ($p>0·05$), implying that these loci might confer risk specific to the sporadic form of human prion disease, although all tests were underpowered because of small sample size.[7,9]

sCJD is known to comprise a range of different clinical and pathological phenotypes, broadly correlating with prion molecular strain types, the latter including categorisation by different proportions of three glycoforms and the apparent molecular weight of abnormal prion protein by western blotting.[18] The National Prion Clinic London, UK has done longitudinal observational cohort studies of CJD involving systematic clinical assessments of patients, resulting in deep phenotype data.[19,20] We tested rs1799990, rs3747957, and rs2267161 for association with age at clinical onset, clinical duration, and the slope of decline in a functional measure of disease severity, along with 27 other phenotypic variables (appendix p 4). As expected, rs1799990 in *PRNP* showed associations with several clinical and biomarker traits (ten associations in 30 tested hypotheses). We found no evidence for epistasis between discovered loci and genotypes at rs1799990, which is known to be a major determinant of clinical phenotype.

Because association in a genomic region might not be mediated through the nearest gene, we investigated the potential mechanisms underlying associations with *PRNP*, *STX6*, and *GAL3ST1*. We used CAVIAR to fine-map the association signal at a locus through joint modelling of association statistics for all variants at a locus and estimation of a conditional posterior probability of causality while allowing for multiple plausibly functional SNPs.[12] Around *PRNP* most of the SNPs identified tagged rs1799990. Unexpectedly, a cluster of SNPs located

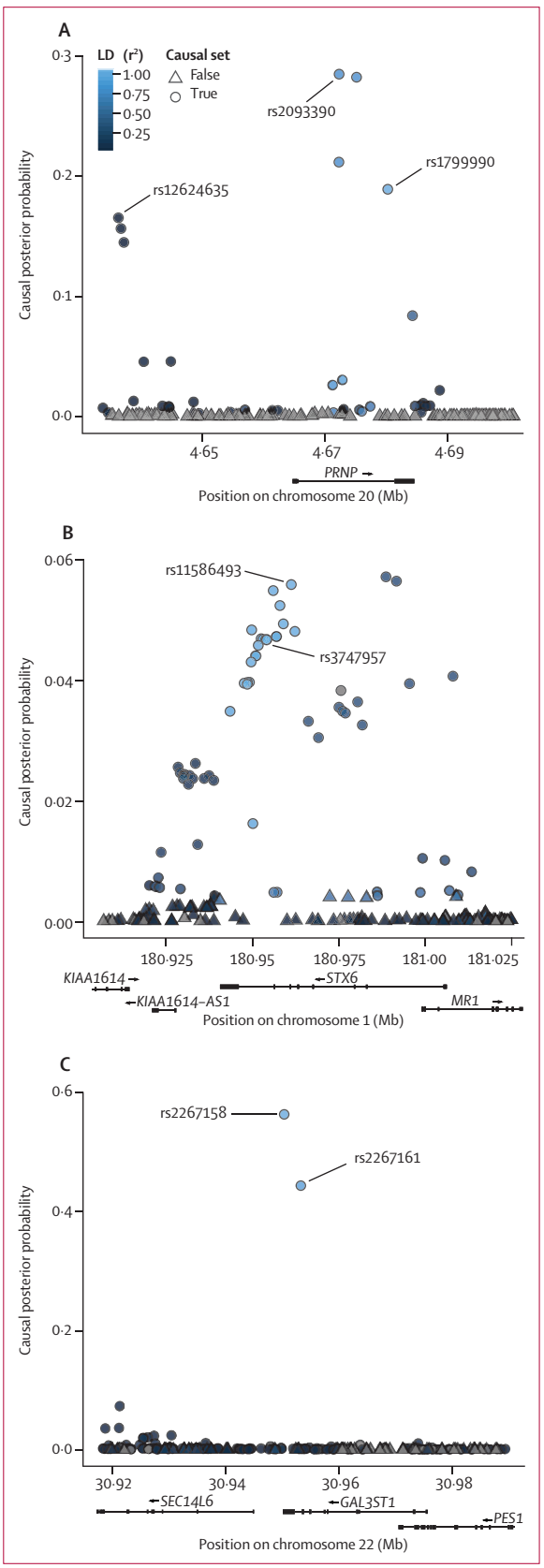

Figure 2: **Statistical fine-mapping using CAVIAR**
CAVIAR utilises summary statistics and LD structure to predict the probability of each variant being causal, producing a causal set with 95% probability of containing the causal SNP, while allowing for the possibility of multiple causal SNPs. Each locus was defined as 100 variants upstream and downstream of the top SNP. Plots show causal posterior probability of each variant at *PRNP* (A), *STX6* (B), and *GAL3ST1* (C), coloured by LD (derived from 1000 Genomes Project European populations data) with the top SNP. Circles indicate variants within the 95% causal set. Triangles highlight other SNPs not predicted to be in the causal set. Mb=megabases. LD=linkage disequilibrium. SNP=single nucleotide polymorphism.

University of Bologna, Bologna, Italy; Department of Neuroscience, Istituto Superiore di Sanità, Rome, Italy (A Poleggi PhD, A Ladogana MD, Prof M Pocchiari MD); **Department of Medical Sciences, Università degli studi di Torino, Torino, Italy** (S Aneli PhD, Prof G Matullo PhD); **National Creutzfeldt-Jakob Disease Research and Surveillance Unit, Edinburgh, UK** (Prof R Knight FRCP[E]); **Department of Neurology, Clinical Dementia Centre and National Reference Centre for Creutzfeldt-Jakob Disease Surveillance, University Medical School, Göttingen, Germany** (S Zafar PhD, Prof I Zerr MD); **German Centre for Neurodegenerative Diseases (DZNE), Göttingen, Germany** (S Zafar, Prof I Zerr); **Biomedical Engineering and Sciences Department, School of Mechanical and Manufacturing Engineering, National University of Sciences and Technology, Islamabad, Pakistan** (S Zafar); **Prion Disease Program, Public Health Agency of Canada, Winnipeg, MB, Canada** (S Booth DPhil); **Canadian Creutzfeldt-Jakob Disease Surveillance System, Public Health Agency of Canada, Ottawa, ON, Canada** (M B Coulthart PhD); **Department of Pathology and Laboratory Medicine, University of Ottawa, Ottawa, ON, Canada** (G H Jansen FRCPC); **and Departments of Pathology and Neurology** (K Glisic MA, J Blevins MA, Prof P Gambetti MD, Prof J Safar MD, B Appleby MD) **and National Prion Disease Pathology Surveillance Center** (K Glisic, J Blevins, Prof P Gambetti, Prof J Safar, B Appleby), **Case Western Reserve University, Cleveland, OH, USA**

Correspondence to:
Prof Simon Mead, Medical Research Council Prion Unit, University College London Institute of Prion Diseases, London W1W 7FF, UK
s.mead@prion.ucl.ac.uk

See **Online** for appendix

For more on **SNP heritability** see http://dougspeed.com/sumher

For more on **CAVIAR** see http://genetics.cs.ucla.edu/caviar

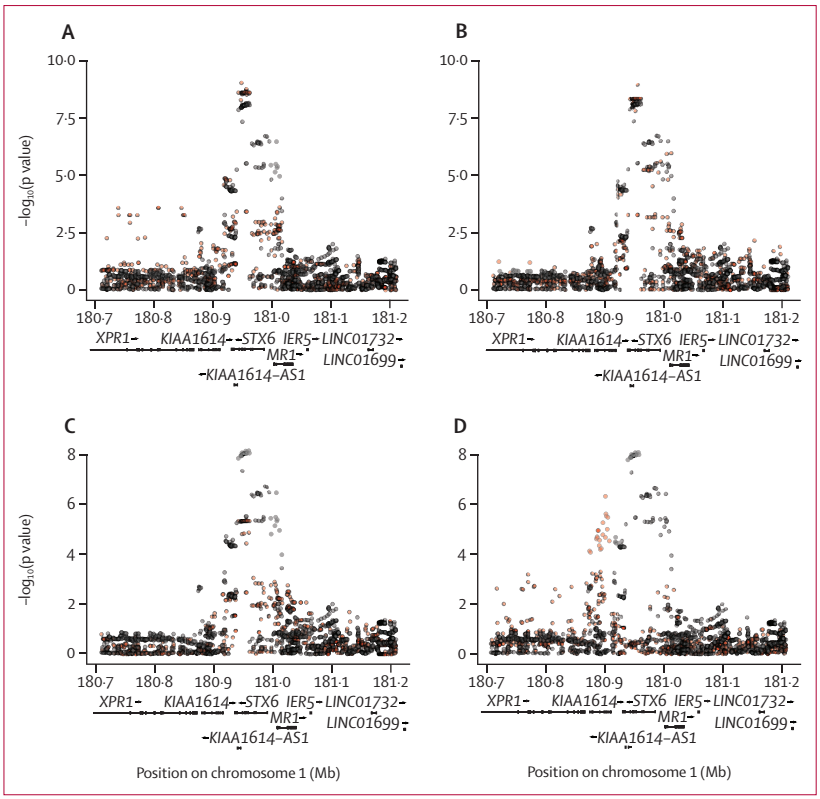

Figure 3: **Colocalisation of GWAS results at *STX6* locus with expression quantitative trait loci**
Plot of $-\log_{10}$ of p values from the GWAS analysis at the *STX6* locus (black) and the expression quantitative trait locus association analysis from the GTEx dataset (red) for: *STX6* expression in the caudate (A), *STX6* expression in the putamen (B), *STX6* expression in the hypothalamus (C), and *KIAA1614* expression in the tibial artery (D). Peaks correspond to the colocalisation posterior probability in the expression quantitative trait locus and GWAS CAVIAR analysis, with a higher degree of colocalisation with increasing colocalisation posterior probability (appendix p 12). GWAS=genome-wide association study. Mb=megabases.

For more on **PAINTOR** see https://hpc.nih.gov/apps/PAINTOR.html

5′ to those tagging rs1799990 (lead SNP rs12624635, not an eQTL) with low levels of linkage disequilibrium to rs1799990 were also putatively causal, suggesting a potential additional signal at this locus (figure 2A). Previous studies have reported that variants at the *PRNP* locus might confer an increased risk for sCJD, independently of rs1799990.[21–24] To further delineate the genetic architecture of the *PRNP* risk locus, we first performed an association analysis under a heterozygous model, which is more appropriate for the known mechanism, and confirmed rs1799990 as the lead SNP ($p=1{\cdot}01\times10^{-135}$; appendix p 22). In a conditional analysis, adjusting for heterozygosity at rs1799990, the lead SNP was rs6139515 ($p=8{\cdot}98\times10^{-4}$). This SNP, which is in low linkage disequilibrium with rs1799990 ($r^2=0{\cdot}04$), is correlated with *PRNP* transcript levels in tibial nerve in the GTEx eQTL database[14] ($p=1{\cdot}8\times10^{-6}$; appendix pp 5, 23). The conditional analysis provided no substantive evidence of an independent association signal at the CAVIAR lead SNP, rs12624635 (p=0·03; appendix pp 5, 23).

The region of high linkage disequilibrium surrounding rs3747957 in *STX6* resulted in a large causal set, making identification of a single causal variant more difficult (figure 2B). Subsequently, using eCAVIAR[13], GTEx[14], and other eQTL databases, we identified a strong correlation between sCJD risk and increased expression of *STX6* mRNA in multiple brain regions, particularly in the caudate and putamen nuclei of the brain (putamen: rs3747957, $p=2{\cdot}3\times10^{-13}$, GTEx; figure 3). Both the caudate and putamen nuclei are key regions implicated in sCJD and are the most commonly abnormal brain regions at diagnostic brain MRI.[25] Correlations between lead SNPs in *STX6*, rs11586493 and rs3747957, and other genes at the locus or within other tissues were absent or less strong (figure 3, appendix p 12). These results suggest that increased expression of *STX6* in brain regions confers an increased risk of sCJD. Using PAINTOR, a tool that integrates functional genomic annotation with association statistics, we next identified three SNPs (rs12754041, rs10797664, and rs6425657; each in strong linkage disequilibrium with lead SNP rs3747957) with high posterior probability of being causal because they were members of one of four functional annotation groups (RoadMap_Assayed_NarrowPeak; Maurano_Science2012_DHS; RoadMap_Enhancers; Roadmap_ChromeHMM_15state).[11]

As the GWAS signal is associated with only two SNPs at *GAL3ST1* (in strong linkage disequilibrium with each other but low linkage disequilibrium with all surrounding variants), these SNPs define the causal set, yet they are statistically indistinguishable from each other (figure 2C). Using GTEx, neither SNP correlated with expression of genes at the locus in brain tissues. One of the SNPs, rs2267161, is a non-synonymous variant of *GAL3ST1* p.V29M. Close to p.V29M resides p.V34M (rs55674628, allele frequency=0·02; linkage disquilibrium with rs2267161, $r^2=0{\cdot}01$, $D'=1{\cdot}00$, discovery p=0·18), the only common non-synonymous variants in European ancestries populations. These polymorphisms form three common haplotypes, rs2267161-C/rs55674628-C (CC; frequency in the combined case-control dataset of 0·667), CT (frequency of 0·018), and TC (frequency of 0·315). We found no evidence of an association driven by the rs55674628-T allele using a haplotype-based test (appendix p 13). Furthermore, analyses of 501 CJD samples by exome sequencing[26] did not identify additional rare variants in *GAL3ST1* or *STX6*.

Expression of *STX6*, *GAL3ST1*, *PDIA4*, and *BMERB1* mRNA was slightly reduced in bulk analysis of post-mortem cerebellar brain tissue from patients with sCJD, but only to a similar extent as genes that have been suggested as good comparators (appendix p 24).[27] Immunohistology of frontal cortex (in 19 patients with sCJD and 15 controls) showed that syntaxin-6 expression is restricted to neurons of different sizes, although other cell types, probably astrocytes or oligodendrocytes, were less consistently stained. In the cerebellum, syntaxin-6 staining was observed in Purkinje cells and in large neurons of the dentate nucleus, and a fine granular staining was seen in the molecular layer (appendix p 25). In all neuron populations of cerebellum and forebrain,

the staining pattern was fine granular, and was located in the cytoplasm, but did not extend into the processes. The staining pattern was compatible with the predicted target, the Golgi apparatus. The pattern for both syntaxin-6 and PDIA4 was indistinguishable between patients with CJD and controls (appendix p 26).

Based on GTEx data, we hypothesised that increased expression of *STX6* in deep brain nuclei increases risk of prion disease. To test whether this might be conferred through facilitating prion propagation in mammalian neuronal cells, we depleted prion-susceptible mouse neuroblastoma-derived cells (N2aPK1/2)[28] of *Stx6* expression using RNA interference. Using the automated scrapie cell assay we measured the impact of *Stx6* knockdown on prion propagation[15,28] using *Prnp* knockdown cells, known to inhibit prion propagation in this assay, as positive controls.[29] Figure 4 shows that *Stx6* depletion, unlike *Prnp* depletion, does not consistently reduce the ability of N2aPK1/2 cells to propagate RML prions.

Discussion

We report, to our knowledge, the first GWAS in a human prion disease powered to detect alleles with the modest effect sizes typical of complex diseases. We identified new risk factors for sCJD, including variants which appear to have pleiotropic effects in neurodegenerative diseases. Further to the known effects at *PRNP* codon 129, we report two independently replicated loci and evidence to support the conclusion that risk variants modify the primary sequence of the encoded protein (*GAL3ST1*) or increase expression in brain tissues (*STX6*). Although a multitude of potential binding partners for prion protein and mechanisms for the modification of prion infection have been proposed, GWAS discoveries have great value because risk variants identified are implicitly causal in the human disease.[30] Therapeutic targets underpinned by genetic evidence have better chances of successful drug development, further encouraging research into the mechanisms that underpin these signals.[30]

Risk variants in sCJD might act at different disease stages: increasing the chance of the spontaneous generation

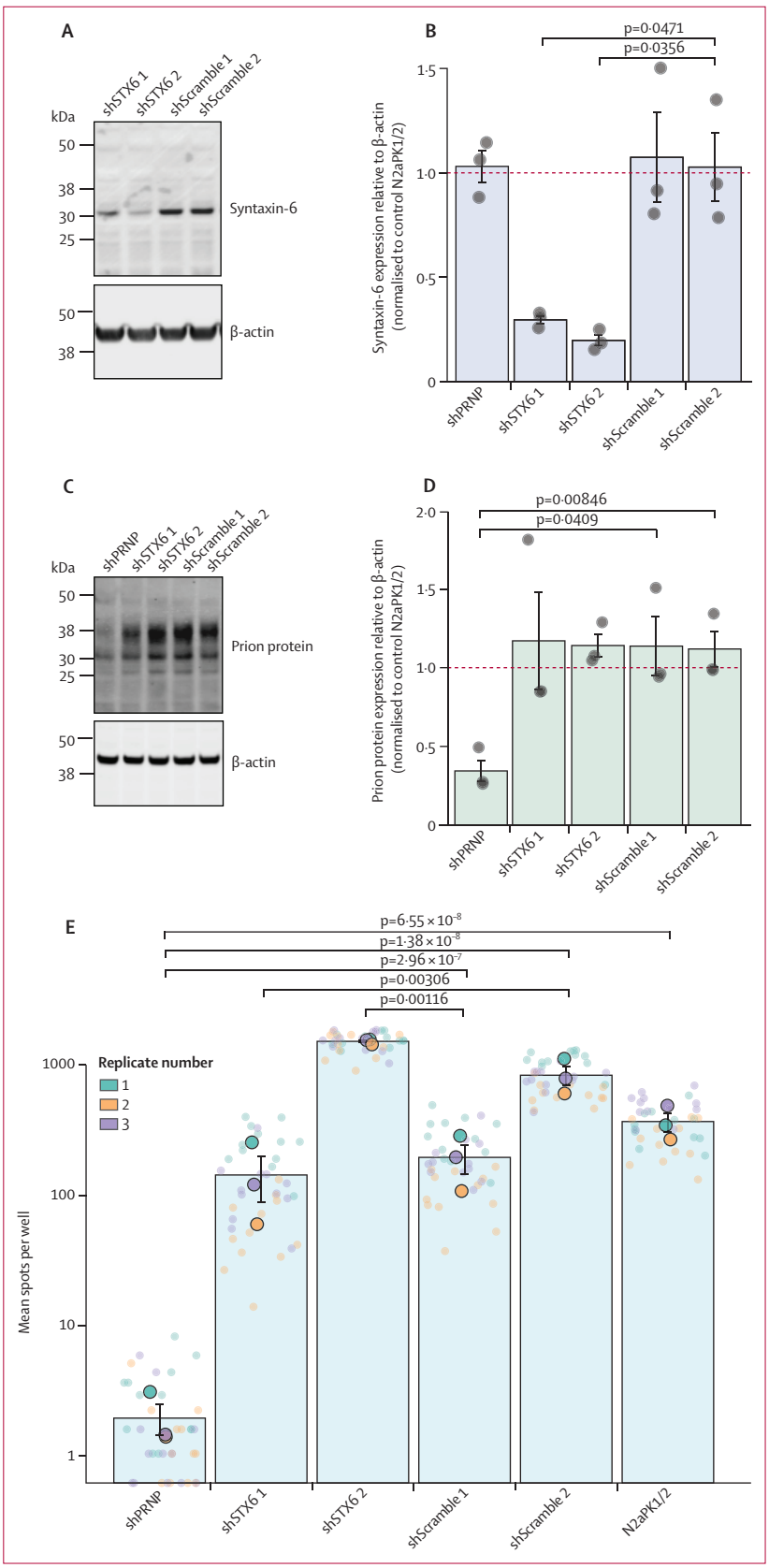

Figure 4: **Scrapie cell assay to measure prion propagation in N2aPK1/2 cells with modified *Stx6* expression**

N2aPK1/2 cells were transfected with pRetroSuper vectors containing *Stx6* (shSTX6 1, shSTX6 2) or *Prnp* (shPRNP) targeting short-hairpin RNAs or a scrambled non-silencing shRNA sequence (shScramble 1, shScramble 2) for controls. Samples were taken before scrapie cell assay for immunoblot (n=3) and expression normalised to untransfected N2aPK1/2 (indicated by dashed line). (A, B) Knockdown of syntaxin-6 protein determined by immunoblot with anti-syntaxin-6 antibody (A), with band intensity measured relative to β-actin loading control (Student's *t* test; B). (C, D) Knockdown of cellular prion protein determined by immunoblot with anti-prion-protein antibody ICSM18 (C), with band intensity measured relative to β-actin loading control (Student's *t* test; D). (E) Average spot count of infected cell number after fourth split in scrapie cell assay following infection with RML at 3×10^{-6} dilution (one-way analysis of variance with Tukey's post-hoc test on log-transformed data). Statistical associations of knockdown lines relative to controls are indicated; other results have been omitted for clarity. All error bars show mean plus and minus SEM. kDa=kilodaltons.

of prions, reducing prion clearance, enabling prion propagation throughout brain tissue, or modifying the downstream toxic effects of prion propagation on brain cells. We did not find any evidence of a role for risk variants in the modification of clinical or pathological disease phenotypes, or in modified expression of risk genes at the end stage of the disease, but it is too early to draw confident conclusions in this respect. Altering the expression of *Stx6* in a cellular model of prion infection did not modify the susceptibility of mouse cells to infection or the accumulation of abnormal forms of prion protein. Our functional data therefore point to a role early in the disease process, perhaps in altering the risk of spontaneous prion formation in the brain, but studies in other models are warranted.

STX6 encodes syntaxin-6, an eight exon, 255 amino-acid protein that localises to the trans-Golgi network, and recycling and early endosomes. Syntaxin-6 is thought to form part of the t-SNARE complex involved in the decision of a target membrane to accept the fusion of a vesicle.[31] The intracellular location of abnormal prion protein in prion-infected cells involves the plasma membrane where conversion is primarily thought to occur,[29] as well as early and recycling endosomes, late endosomes, and the perinuclear region.[32] Other studies implicate the endocytic-recycling compartment or multivesicular bodies as sites of generation of prions, and dysregulation of trafficking genes by sCJD.[33,34] Intracellular trafficking has also been implicated in the degradation of prions.[35] The modification of trafficking of normal or abnormal prion protein by syntaxin-6 might be a focus for future investigation.[36]

There has been considerable recent discussion about the extent to which neurodegenerative diseases associated with the accumulation of misfolded proteins or peptides are similar to prion diseases in their pathogenesis.[37] This concept provokes the suggestion that prion diseases and prion-like disorders might share genetic risk factors. Progressive supranuclear palsy is an uncommon neurodegenerative cognitive and movement disorder associated with the accumulation of abnormal forms of microtubule-associated protein tau with four repeats.[38,39] Variants in *STX6* are in a haplotype with SNPs previously identified as associated with progressive supranuclear palsy, with shared risk alleles (appendix p 14).[39,40] Pleiotropic effects at this locus shared between prion diseases and a tauopathy lend support to the concept of prion-like disorders and indicate the possibility of genetically inspired interventions across multiple neurodegenerative disorders.

GAL3ST1 encodes galactose-3-O-sulfotransferase 1, a 423 amino-acid protein that localises to the Golgi network in oligodendrocytes, and is the sole enzyme responsible for the sulfation of membrane sphingolipids to form sulfatides—a major brain lipid and component of the myelin sheath.[41] Degradation of sulfatides is catalysed by ARSA in the lysosome; recessive defects in this enzyme cause metachromatic leukodystrophy: a lysosomal storage disorder associated with profound central and peripheral demyelination.[42] Knockout of *Gal3st1* in mice results in a neurological phenotype associated with abnormal myelin maintenance with age, histological abnormalities at the paranodal junctions, and abnormal diffusion tensor imaging.[43] Furthermore, in a GWAS of UK Biobank participants, rs2267161 in *GAL3ST1* was significantly associated with multiple changes in white matter microstructure measured using brain diffusion tensor imaging.[44] Sphingolipid metabolism and myelin maintenance have both been previously implicated in prion protein function and prion diseases.[45,46] Multiple genes in the sphingolipid metabolic pathways are dysregulated early in the pathogenesis of mouse prion diseases, a finding consistent between inbred mouse lines and prion strains.[47] Knockout of prion protein in mice, or naturally in goats, results in a demyelinating neuropathy, which in goats is associated with abnormal sphingolipid metabolism.[36,48–50]

PDIA4 and *BMERB1* loci, identified in the discovery stage by gene-based analysis, were not replicated at their lead SNPs; however, the replication sample was necessarily limited by the rarity of the disease, and the lead SNPs had a lower allele frequency than at other risk loci. Further attempts to replicate are justified as gene-based test results are driven by multiple SNPs at each locus.

In conclusion, we present the first evidence of statistically robust genetic associations in sporadic human prion disease that implicate intracellular trafficking and sphingolipid metabolism as molecular causal mechanisms. Future work might further test the hypotheses derived from these discoveries in prion disease model systems, and examine the effects of genome-wide genetic variation on clinical, pathological, and molecular phenotypes in sporadic and inherited prion diseases.

Contributors

EJ, HH, EV, and JU did the main data collection and analysis. AD, HS, TC, PN, LQ, JW, JL, ZJ, SBr, PJ, AN, THM, and PAh contributed specific sections of data collection and analysis. SCo, CS, SS, GGK, MDG, AG, KF, HB, AA, HK-C, SJvdL, CAI-V, CMvD, BS, EG, PPL, MC, OC, PS-J, AS, FM-T, EB-A, SH, J-LL, J-PB, PAm, J-CL, PP, AB-S, SCa, AP, AL, MP, SA, GM, RK, SZ, IZ, SBo, MBC, GHJ, KG, JB, PG, JS, and BA contributed to sample collection and phenotyping. JC and SM had overall supervision of the study and obtained funding. SM and EJ drafted the text and figures for the manuscript. All authors contributed to editing of the text and figures for the manuscript.

Declaration of interests

HB reports grants from Federal Office for Health, Swiss Government, during the conduct of the study. SH reports grants from Santé Publique France, during the conduct of the study; grants from LFB Biomedicaments, Institut de Recherche Servier, and MedDay Pharmaceuticals, outside the submitted work; and has a patent method for treating prion diseases (PCT/EP2019/070457) pending. PAm reports personal fees from Fondation Alzheimer, and personal fees and other from Genoscreen, outside the submitted work. BA reports grants from Centers for Disease Control and Prevention, during the conduct of the study. KF reports grants from Ono Pharmaceuticals, outside the submitted work. SM reports grants from Medical Research Council and National Institute of Health Research's Biomedical Research Centre at University College London Hospitals NHS Foundation Trust, during the conduct of the study. GGK reports personal fees from Biogen, outside the submitted work. JC reports grants from Medical Research Council and National Institute of Health Research's Biomedical Research Centre at University College London Hospitals NHS Foundation Trust, during the conduct of

the study; and is a director and shareholder of D-Gen: an academic spinout in the field of prion disease diagnostics, decontamination, and therapeutics. MP reports personal fees from Ferring Pharmaceuticals and the Collection of National Chemical Compounds and Screening Centre, and non-financial support from Fondazione Cellule Staminali, outside the submitted work. MDG reports grants from National Institutes of Health and National Institute on Aging (R01 AG031189, R56AG055619, and R01AG062562) and Alliance Biosecure, personal fees and other from Quest Diagnostics, and other from The Michael J Homer Family Fund, during the conduct of the study, and personal fees from Blade Therapeutics and Bioscience Biopharma, and other from Grand Rounds, outside the submitted work; has consulted for 3D Communications, Adept Field Consulting, Advanced Medical, Best Doctors, Second Opinion, Gerson Lehrman Group, Guidepoint Global, InThought Consulting, Market Plus, Trinity Partners, Biohaven Pharmaceuticals, Quest Diagnostics, and various medical-legal consulting firms; has received speaking honoraria for various medical centre lectures and from Oakstone publishing; has received past research support from Alliance Biosecure, CurePSP, the Tau Consortium, and Quest Diagnostics; and serves on the board of directors for San Francisco Bay Area Physicians for Social Responsibility and on the editorial board of Dementia & Neuropsychologia. All other authors declare no competing interests.

Data sharing

Summary statistics are available through the GWAS catalog at National Human Genome Research Institute-European Bioinformatics Institute via study accession number GCST90001389. Further data are available upon request to the corresponding author.

Acknowledgments

We thank Richard Newton (University College London Institute of Prion Diseases) for support with images and University College London Genomics who did the array processing for CJD samples. This study makes use of data generated by the Wellcome Trust Case-Control Consortium. A full list of the investigators who contributed to the generation of the data is available from the Wellcome Trust Case-Control Consortium. Funding for the project was provided by the Wellcome Trust and Medical Research Council. We thank patients, their families and carers, UK neurologists and other referring physicians, co-workers at the National Prion Clinic, and our colleagues at the National Creutzfeldt-Jakob Disease Research and Surveillance Unit, Edinburgh, UK. We thank the present and previous directors and the staff of the Papua New Guinea Institute of Medical Research, especially the kuru project field team, and the communities of the kuru-affected region, for their generous support. We gratefully acknowledge the help of the late Carleton Gajdusek, the late Joseph Gibbs, and their associates from the former Laboratory of Central Nervous System Studies of the National Institutes of Health, Bethesda, MD, USA for archiving and sharing old kuru samples. The kuru studies were initially funded by a Wellcome Trust Principal Research Fellowship in the Clinical Sciences to JC, and since 2001, all other aspects of the work were funded by the Medical Research Council. Several authors at University College London and University College London Hopsitals receive funding from the Department of Health's National Institute of Health Research Biomedical Research Centres funding scheme. Some of this work was supported by the Department of Health funded National Prion Monitoring Cohort study. SCo receives a National Health and Medical Research Council Practitioner Fellowship (APP1105784). THM is supported by a Fellowship award from Alzheimer's Society, UK (341 [AS-CTF-16b-007]) and Creutzfeldt-Jakob Disease Support Network UK Research Support Grants. Many other national funders were involved in international Creutzfeldt-Jakob disease surveillance and sample collection. Funding for the collection of Polish samples for study was partially provided by the EU Joint Programme Neurodegenerative Disease Research and Medical University of Lodz. We thank Dr Maria Styczynska from Mossakowski Medical Research Centre, Polish Academy of Sciences, Warsaw, Poland, for kindly providing control DNA samples for the Polish cohort. The Italian National Surveillance of Creutzfeldt-Jakob Disease and Related Disorders is partially supported by the Ministero della Salute, Italy. The German National Reference Centre for Transmissible Spongiform Encephalopathies is funded by grants from the Robert Koch Institute. The Dutch National Prion Disease Registry is funded by the National Institute for Public Health and the Environment (Ministry for Health, Welfare, and Sports) and is conducted under the leadership of the National Coordination Infection Control (Landelijke Coördinatie Infectieziektebestrijding [LCI Landelijke coördinatie infectieziektebestrijding]). PS-J was supported by Instituto de Salud Carlos III (Fondo de Investigación Sanitaria, PI16/01652) Accion Estrategica en Salud integrated in the Spanish National I+D+i Plan and financed by Instituto de Salud Carlos III Subdireccion General de Evaluacion and the Fondo Europeo de Desarrollo Regional (FEDER "Una Manera de Hacer Europa"). We thank Inés Santiuste and the Valdecilla Biobank (PT17/0015/0019), integrated in the Spanish Biobank Network, for their support and collaboration in sample collection and management. The study on Italian controls was supported by the Ministero dell'Istruzione, dell'Università e della Ricerca MIUR project "Dipartimenti di Eccellenza 2018–2022" (D15D18000410001) to the Department of Medical Sciences, University of Torino, Torino, Italy (GM) and the Associazione Italiana per la Ricerca sul Cancro (IG 2018 Id.21390 to GM). The Three-City Study was performed as part of a collaboration between the Institut National de la Santé et de la Recherche Médicale (Inserm), the Victor Segalen Bordeaux II University, and Sanofi-Synthélabo; the Fondation pour la Recherche Médicale funded the preparation and initiation of the study. The Three-City Study was also funded by the Caisse Nationale Maladie des Travailleurs Salariés, Direction Générale de la Santé, MGEN, Institut de la Longévité, Agence Française de Sécurité Sanitaire des Produits de Santé, the Aquitaine and Bourgogne Regional Councils, and Agence Nationale de la Recherche, and ANR supported the COGINUT and COVADIS projects, Fondation de France, and the joint French Ministry of Research INSERM Cohortes et collections de données biologiques programme. Lille Génopôle received an unconditional grant from Eisai. The Three-City biological bank was developed and maintained by the laboratory for genomic analysis LAG-BRC Institut Pasteur de Lille. This work was also funded by the Pasteur Institut de Lille, the Lille Métropole Communauté Urbaine, the Haut-de France council, the European Community (FEDER), and the French Government's LABEX DISTALZ programme (development of innovative strategies for a transdisciplinary approach to Alzheimer's disease). The French National Surveillance Network for Creutzfeldt-Jakob Disease is supported by Santé Publique France. MDG would like to thank Megan Casey for her assistance with sample collection and management.

For more on the **Wellcome Trust Case-Control Consortium** see https://www.wtccc.org.uk

References

1 Collinge J. Prion diseases of humans and animals: their causes and molecular basis. *Annu Rev Neurosci* 2001; **24:** 519–50.
2 Collinge J. Variant Creutzfeldt-Jakob disease. *Lancet* 1999; **354:** 317–23.
3 Mead S, Lloyd S, Collinge J. Genetic factors in mammalian prion diseases. *Annu Rev Genet* 2019; **53:** 117–47.
4 National CJD Research and Surveillance Unit. Twenty-sixth annual report. 2017. https://www.cjd.ed.ac.uk/sites/default/files/report26.pdf (accessed June 1, 2020).
5 Maddox RA, Person MK, Blevins JE, et al. Prion disease incidence in the United States: 2003–2015. *Neurology* 2020; **94:** e153–57.
6 Webb TE, Pal S, Siddique D, et al. First report of Creutzfeldt-Jakob disease occurring in 2 siblings unexplained by *PRNP* mutation. *J Neuropathol Exp Neurol* 2008; **67:** 838–41.
7 Mead S, Uphill J, Beck J, et al. Genome-wide association study in multiple human prion diseases suggests genetic risk factors additional to *PRNP*. *Hum Mol Genet* 2012; **21:** 1897–906.
8 Sanchez-Juan P, Bishop MT, Kovacs GG, et al. A genome wide association study links glutamate receptor pathway to sporadic Creutzfeldt-Jakob disease risk. *PLoS One* 2015; **10:** e0123654.
9 Mead S, Poulter M, Uphill J, et al. Genetic risk factors for variant Creutzfeldt-Jakob disease: a genome-wide association study. *Lancet Neurol* 2009; **8:** 57–66.
10 Sanchez-Juan P, Bishop MT, Aulchenko YS, et al. Genome-wide study links *MTMR7* gene to variant Creutzfeldt-Jakob risk. *Neurobiol Aging* 2012; **33:** 1487 e21–28.
11 Kichaev G, Yang WY, Lindstrom S, et al. Integrating functional data to prioritize causal variants in statistical fine-mapping studies. *PLoS Genet* 2014; **10:** e1004722.

12 Hormozdiari F, Kostem E, Kang EY, Pasaniuc B, Eskin E. Identifying causal variants at loci with multiple signals of association. *Genetics* 2014; **198:** 497–508.

13 Hormozdiari F, van de Bunt M, Segrè AV, et al. Colocalization of GWAS and eQTL signals detects target genes. *Am J Hum Genet* 2016; **99:** 1245–60.

14 Lonsdale J, Thomas J, Salvatore M, et al. The Genotype-Tissue Expression (GTEx) project. *Nat Genet* 2013; **45:** 580–85.

15 Klöhn PC, Stoltze L, Flechsig E, Enari M, Weissmann C. A quantitative, highly sensitive cell-based infectivity assay for mouse scrapie prions. *Proc Natl Acad Sci USA* 2003; **100:** 11666–71.

16 Speed D, Balding DJ. SumHer better estimates the SNP heritability of complex traits from summary statistics. *Nat Genet* 2019; **51:** 277–84.

17 Yang J, Lee SH, Goddard ME, Visscher PM. GCTA: a tool for genome-wide complex trait analysis. *Am J Hum Genet* 2011; **88:** 76–82.

18 Collinge J, Clarke AR. A general model of prion strains and their pathogenicity. *Science* 2007; **318:** 930–36.

19 Mead S, Burnell M, Lowe J, et al. Clinical trial simulations based on genetic stratification and the natural history of a functional outcome measure in Creutzfeldt-Jakob Disease. *JAMA Neurol* 2016; **73:** 447–55.

20 Thompson AG, Lowe J, Fox Z, et al. The Medical Research Council prion disease rating scale: a new outcome measure for prion disease therapeutic trials developed and validated using systematic observational studies. *Brain* 2013; **136:** 1116–27.

21 Mead S, Mahal SP, Beck J, et al. Sporadic—but not variant—Creutzfeldt-Jakob disease is associated with polymorphisms upstream of *PRNP* exon 1. *Am J Hum Genet* 2001; **69:** 1225–35.

22 Bratosiewicz-Wąsik J, Smoleń-Dzirba J, Rozemuller AJ, et al. Association between the *PRNP* 1368 polymorphism and the occurrence of sporadic Creutzfeldt-Jakob disease. *Prion* 2012; **6:** 413–16.

23 Sanchez-Juan P, Bishop MT, Croes EA, et al. A polymorphism in the regulatory region of *PRNP* is associated with increased risk of sporadic Creutzfeldt-Jakob disease. *BMC Med Genet* 2011; **12:** 73.

24 Vollmert C, Windl O, Xiang W, et al. Significant association of a M129V independent polymorphism in the 5′ UTR of the *PRNP* gene with sporadic Creutzfeldt-Jakob disease in a large German case-control study. *J Med Genet* 2006; **43:** e53.

25 Meissner B, Kallenberg K, Sanchez-Juan P, et al. MRI and clinical syndrome in dura mater-related Creutzfeldt-Jakob disease. *J Neurol* 2009; **256:** 355–63.

26 Koriath C, Kenny J, Adamson G, et al. Predictors for a dementia gene mutation based on gene-panel next-generation sequencing of a large dementia referral series. *Mol Psychiatry* 2018; published online Oct 2. https://doi.org/10.1038/s41380-018-0224-0.

27 Rydbirk R, Folke J, Winge K, Aznar S, Pakkenberg B, Brudek T. Assessment of brain reference genes for RT-qPCR studies in neurodegenerative diseases. *Sci Rep* 2016; **6:** 37116.

28 Brown CA, Schmidt C, Poulter M, et al. In vitro screen of prion disease susceptibility genes using the scrapie cell assay. *Hum Mol Genet* 2014; **23:** 5102–08.

29 Goold R, Rabbanian S, Sutton L, et al. Rapid cell-surface prion protein conversion revealed using a novel cell system. *Nat Commun* 2011; **2:** 281.

30 Claussnitzer M, Cho JH, Collins R, et al. A brief history of human disease genetics. *Nature* 2020; **577:** 179–89.

31 Wendler F, Tooze S. Syntaxin 6: the promiscuous behaviour of a SNARE protein. *Traffic* 2001; **2:** 606–11.

32 Yamasaki T, Suzuki A, Hasebe R, Horiuchi M. Retrograde transport by clathrin-coated vesicles is involved in intracellular transport of PrP^{Sc} in persistently prion-infected cells. *Sci Rep* 2018; **8:** 12241.

33 Yim YI, Park BC, Yadavalli R, Zhao X, Eisenberg E, Greene LE. The multivesicular body is the major internal site of prion conversion. *J Cell Sci* 2015; **128:** 1434–43.

34 Bartoletti-Stella A, Corrado P, Mometto N, et al. Analysis of RNA expression profiles identifies dysregulated vesicle trafficking pathways in Creutzfeldt-Jakob disease. *Mol Neurobiol* 2019; **56:** 5009–24.

35 Goold R, McKinnon C, Tabrizi SJ. Prion degradation pathways: potential for therapeutic intervention. *Mol Cell Neurosci* 2015; **66:** 12–20.

36 Jones E, Mead S. Genetic risk factors for Creutzfeldt-Jakob disease. *Neurobiol Dis* 2020; **142:** 104973.

37 Collinge J. Mammalian prions and their wider relevance in neurodegenerative diseases. *Nature* 2016; **539:** 217–26.

38 Colin M, Dujardin S, Schraen-Maschke S, et al. From the prion-like propagation hypothesis to therapeutic strategies of anti-tau immunotherapy. *Acta Neuropathol* 2020; **139:** 3–25.

39 Chen JA, Chen Z, Won H, et al. Joint genome-wide association study of progressive supranuclear palsy identifies novel susceptibility loci and genetic correlation to neurodegenerative diseases. *Mol Neurodegener* 2018; **13:** 41.

40 Höglinger GU, Melhem NM, Dickson DW, et al. Identification of common variants influencing risk of the tauopathy progressive supranuclear palsy. *Nat Genet* 2011; **43:** 699–705.

41 Takahashi T, Suzuki T. Role of sulfatide in normal and pathological cells and tissues. *J Lipid Res* 2012; **53:** 1437–50.

42 Platt FM, d'Azzo A, Davidson BL, Neufeld EF, Tifft CJ. Lysosomal storage diseases. *Nat Rev Dis Primers* 2018; **4:** 27.

43 Honke K, Hirahara Y, Dupree J, et al. Paranodal junction formation and spermatogenesis require sulfoglycolipids. *Proc Natl Acad Sci USA* 2002; **99:** 4227–32.

44 Zhao B, Zhang J, Ibrahim JG, et al. Large-scale GWAS reveals genetic architecture of brain white matter microstructure and genetic overlap with cognitive and mental health traits (n=17706). *Mol Psychiatry* 2019; published online Oct 30. https://doi.org/10.1038/s41380-019-0569-z.

45 Klein TR, Kirsch D, Kaufmann R, Riesner D. Prion rods contain small amounts of two host sphingolipids as revealed by thin-layer chromatography and mass spectrometry. *Biol Chem* 1998; **379:** 655–66.

46 Agostini F, Dotti CG, Pérez-Cañamás A, Ledesma MD, Benetti F, Legname G. Prion protein accumulation in lipid rafts of mouse aging brain. *PLoS One* 2013; **8:** e74244.

47 Hwang D, Lee IY, Yoo H, et al. A systems approach to prion disease. *Mol Syst Biol* 2009; **5:** 252.

48 Bremer J, Baumann F, Tiberi C, et al. Axonal prion protein is required for peripheral myelin maintenance. *Nat Neurosci* 2010; **13:** 310–18.

49 Küffer A, Lakkaraju AK, Mogha A, et al. The prion protein is an agonistic ligand of the G protein-coupled receptor Adgrg6. *Nature* 2016; **536:** 464–68.

50 Skedsmo FS, Malachin G, Våge DI, et al. Demyelinating polyneuropathy in goats lacking prion protein. *FASEB J* 2020; **34:** 2359–75.

Section 3: Human Prion Disease Epidemiological Studies

The basic descriptive epidemiology of human prion diseases as rare, rapidly progressive and potentially transmissible neurodegenerative disorders was delineated more than five decades ago. In the intervening period since, incremental elaboration of the epidemiology of human prion disease has continued, especially the delineation of genetic forms of CJD in addition to GSS and FFI, as well as the recognition of various iatrogenic aetiologies such as treatments employing contaminated cadaveric pituitary hormones and dura mater grafts. Over the last approximately 20 years, I have led or led the Australian participation in large collaborative studies that have re-affirmed and further expanded our understanding of the epidemiology of human prion disease. These diverse studies have: supported the likelihood that at least some apparently sporadic CJD is likely to represent unrecognized, temporally remote, iatrogenic transmission events; determined the global experience of iatrogenic CJD; described the influence of codon 129 on the risk and phenotype of prion disease; delineated determinants of survival in prion disease; more confidently determined the incidence of prion disease and influential factors; and clarified the biological significance of spatio-temporal clusters of CJD. Information generated from these studies serves important clinical translational needs including enhanced awareness of potential iatrogenic aetiology, individual prognostication, and improved patient stratification for therapeutic trials. In addition, other studies have contributed to an enhanced understanding of the range of sequence variations in *PRNP*, their likely true biological significance and the feasibility of mounting treatment trials for persons harbouring highly penetrant disease causing *PRNP* mutations. Illustrative of the utility of these studies, for genetic counselling purposes it was found that many uncommon *PRNP* sequence variations have very low penetrance or are rare normal polymorphisms and reconfirmed that the three most common (E200K, P102 and D178N) mutations account for approximately 80-85% of all likely pathogenic sequence variations and are highly penetrant.

List of my publications submitted in full (in chronological order)

Collins S, M Law, Fletcher A, Boyd A, Kaldor J, Masters CL. Surgical treatment and risk of sporadic Creutzfeldt-Jakob disease: a case control study. Lancet 1999; 353: 693-697.

A Alperovitch, I Zerr, M Pocchiari, E Mitrova, J de Pedro Cuesta, I Hegyi, S Collins, H Kretzschmar, C van Duijn, R Will. Codon 129 prion protein genotype and sporadic Creutzfeldt-Jakob disease. Lancet 1999; 353: 1673-1674.

P Brown, M Preece, J-P Brandel, T Sato, L. McShane, I Zerr, A Fletcher, RG Will, M Pocchiari, N Cashman, JH d'Aignaux, L Cervenáková, J Fradkin, L Schonberger, SJ Collins. Iatrogenic Creutzfeldt-Jakob disease at the Millenium. Neurology 2000; 55: 1075-1081.

S Collins, A Boyd, A Fletcher, K Byron, C Harper, C McLean, CL Masters. Novel prion protein gene mutation in an octogenerian with Creutzfeldt-Jakob disease. Archives of Neurology 2000; 57: 1058-1063.

Collins S, Boyd A, Fletcher A, Hill A, Farish S, J Kaldor, Z Ansari, Smith M, Masters CL. Creutzfeldt-Jakob disease cluster in an Australian rural city. Annals of Neurology 2002; 52: 115-118.

Collins S, Boyd A, Fletcher A, V Lewis, Lee JS, Law M, Kaldor, J Masters CL. Creutzfeldt-Jakob disease in Australia, 1970 to 1999. Neurology 2002; 59: 1365-1371.

Ramasamy I, Law M, Collins S, Brooke F. Variant Creutzfeldt-Jakob disease and the potential for its accidental transmission following surgery with contaminated instruments in Australia: a quantitative transmission model. Folia Neuropathologia 2003; 41: 1-10.

Lewis V, Collins S, Hill AF, Boyd A, McLean CA, Smith M, Masters CL. Novel prion protein insert mutation associated with prolonged neurodegenerative illness. Neurology 2003; 60: 1620-1624.

Brooke FJ, Boyd A, Klug G, Masters CL and Collins SJ. Lyodura use and the risk of iatrogenic Creutzfeldt-Jakob disease in Australia. Medical Journal of Australia 2004; 180: 177-181.

Pocchiari M, Puopolo M, Croes E, Budka H, Gelpi E, Collins S, Lewis V, Sutcliffe T, Giulivi A, Delasnerie-Laupretre N, Brandel J-P, Alperovitch A, Zerr I, Poser S, Kretzschmar H, Ladogana A, Rietvald I, Mitrova E, Martinez-Martin P, de Pedro-Cuesta J, Glatzel M, Aguzzi A, Cooper S, Mackenzie J, van Duijn C, Will RG. Determinants of survival in sporadic Creuzfeldt-Jakob disease and other human transmissible spongiform encephalopathies. Brain 2004; 127: 2348-2359.

Ladogana A, Puopolo M, Croes EA, Budka H, Jarius C, Collins S, Klug GM, Sutcliffe T, Giulivi A, Alperovitch A, Delanerie-Laupretre N, Brandel J-P, Poser S, Kretzschmar H, Rietvald I, Mitrova E, de Pedro Cuesta J, Martinez-Martin P, Glatzel M, Aguzzi A, Knight R, Ward H, Pocchiari M, van Duijn C, Will RG, Zerr I. Mortality from Creutzfeldt-Jakob disease and related disorders in Europe, Australia and Canada. Neurology 2005; 64: 1586-1591.

Kovács GG, Puopolo M, Ladogana A, Pocchiari M, Budka H, van Duijn C, Collins SJ, Boyd A, Giulivi A, Delasnerie-Laupretre N, Brandel J-P, Zerr I, Kretschmar HA, Pedro de Cuesta J, Calero-Lara M, Glatzel M, Aguzzi A, Bishop M, Knight R, Belay G, Will RG, Mitrova E. Genetic prion disease: the EUROCJD experience. Human Genetics 2005; 118: 166-174.

de Pedro-Cuesta J, Glatzel M, Almazan J, Stoeck K, Mellina V, Puopolo M, Pocchiari M, Zerr I, Kretzschmar H, Brandel J-P, Delasnerie-Laupretre N, Alperovitch A, van Duijn C, Sanchez-Juan P, Collins S, Lewis V, Jansen GH, Coulthart MB, Gelpi E, Budka H, Mitrova E.

Human transmissible spongiform encephalopathies in eleven countries: diagnostic pattern across time, 1993-2002. BMC Public Health 2006; 6: 278.

Rowe DB, Lewis V, Needham M, Rodriguez M, Boyd A, McLean C, Roberts H, Masters CL, Collins SJ. Novel prion protein gene mutation presenting with subacute PSP-like syndrome. Neurology 2007; 68: 868-870.

Klug GMA, Wand H, Boyd A, Law M, Kaldor J, Masters CL, Collins SJ. Enhanced geographically-restricted surveillance simulates sporadic Creutzfeldt-Jakob disease clustering. Brain 2009; 132: 493-501.

Collins SJ, Schuur M, Boyd A, Lewis V, Klug G, McGlade A, van Oosterhout A, Breedveld G, Oostra BA, Masters CL, van Duijn CM. No evidence for prion protein gene locus multiplication in Creutzfeldt-Jakob Disease. Neuroscience Letters 2010; 472: 16-18.

Boyd A, Klug GMA, Schonberger L, McGlade A, Brandel J-P, Masters CL, Collins SJ. Iatrogenic Creutzfeldt-Jakob disease in Australia: time to amend infection control measures for pituitary hormone recipients? Medical Journal of Australia 2010; 193: 366-369.

Alcalde-Cabero E, Almazán-Isla J, Brandel JP, Breithaupt M, Catarino J, Collins S, Haybäck J, Höftberger R, Kahana E, Kovacs GG, Ladogana A, Mitrova E, Nakamura Y, Pocchiari M, Popovic M, Ruiz-Tovar M, Taratuto AL, van Duijn C, Yamada M, Zerr I, de Pedro-Cuesta. Health professions and risk of sporadic Creutzfeldt-Jakob disease. EuroSurveillance 2012; 17: pii=20144.

Klug G, Wand H, Simpson M, Boyd A, Law M, Masters C, Matej R, Howley R, Farrell M, Breithaupt M, Zerr I, van Duijn C, Ibrahim-Verbaas C, Mackenzie J, Will RG, Brandel J-P, Alperovitch A, Budka H, Kovacs GG, Jansen GH, Coulthard M, Collins S. Intensity of human prion disease surveillance predicts observed disease incidence. Journal of Neurology, Neurosurgery and Psychiatry 2013; 84: 1372-1377.

Simpson M, Johannsen V, Boyd A, Klug G, Masters CL, Pamphlett R, McLean C, Lewis V, Collins SJ. Unusual clinical and molecular-pathological profile of Gerstmann-Sträussler-Scheinker disease associated with a novel PRNP mutation (V176G). JAMA Neurology 2013; 70: 1180-1185.

Minikel E, Zerr I, Collins SJ, Ponto C, Boyd A, Klug GMA, Kenny J, Collinge J, Takada, LT, Forner S, Fong JC, Mead S, Geschwind MD. Ascertainment bias causes false signal of anticipation in genetic prion disease. American Journal of Human Genetics 2014; 95: 371-382.

Minikel E, Vallabh S, Lek M, Estrada K, Samocha K, Sathirapongsasuti J, McLean C, Tung J, Yu L, Gambetti P, Blevins J. Zhang S, Cohen Y, Chen W, Yamada M, Hamaguchi T, Sanjo N, Mizusawa H, Nakamura Y, Kitamoto T, Collins S, Boyd A, Will R, Knight R, Ponto C, Zerr I, Kraus T, Eigenbrod S, Giese A, de Pedro Cuesta J, Haïk S, Laplanche J-L, Brandel J-P, Boehnke M, Laakso M, Mohlke M, Collins F, Kähler A, Chambert K, McCarroll S, Sullivan P, Hultman C, Purcell S, Sklar P, van Duijn C, Ramirez F, Ikram A, van der Lee s, Vergeer-Drop J, Uitterlinden A, Exome Aggregation Consortium (ExAC), Daly M, MacArthur D. Quantitating

penetrance in a dominant disease gene with large population control cohorts. Science Translational Medicine 2016; 8: 322ra9.

Minikel E, Vallabh S, Orseth M, Brandel J-P, Haïk S, Laplanche J-L, Zerr I, Parchi P, Capellari S, Safar J, Kenny J, Fong J, Takada L, Ponto C, Hermann P, Knipper T, Stehmann C, Kitamoto T, Ae R, Hamaguchi T, Sanjo N, Tsukamoto T, Mizusawa H, Collins S, Chiesa R, Roiter I, de Pedro-Cuesta J, Calero M, Geschwind M, Yamada M, Nakamura Y, Mead S. Age of onset in genetic prion disease and the design of preventive clinical trials. Neurology 2019: 93: e125-e134.

Articles

Surgical treatment and risk of sporadic Creutzfeldt-Jakob disease: a case-control study

S Collins, M G Law, A Fletcher, A Boyd, J Kaldor, C L Masters

Summary

Background Apart from the small number of iatrogenic and familial cases, the cause of most cases of Creutzfeldt-Jakob disease (CJD) is not known. We aimed to identify risk factors for sporadic CJD.

Methods In a case-control study, we compared the medical history and selected demographic characteristics of 241 definite (neuropathologically confirmed) and probable (clinically likely) patients with CJD, ascertained from the Australian National Creutzfeldt-Jakob Disease Registry between Jan 1, 1970, and October 31, 1997, and of 784 controls, recruited from the community by random telephone interview in August, 1997. Standard logistic regression was used for the comparisons.

Findings Surgical procedures were significantly associated with the development of sporadic CJD. This risk progressively increased with the number of surgical treatments to a maximum for three procedures (odds ratio 2·13 [95% CI 1·34–3·41], p=0·002). There was also a significant association between risk of CJD and residence or employment on a farm (p<0·001) or market garden (p=0·002) for longer than 10 years. We found no significant risk associated with a history of blood transfusion, organ transplantation, major dental work, or occupation.

Interpretation Our findings accord with the hypothesis that a range of surgical treatments may serve as unrecognised contamination events and account for a proportion of cases of sporadic CJD. Possible biases in different methods and times for the acquisition of data on cases and controls suggest our findings need to be replicated in independent studies with community controls.

Lancet 1999; **353:** 693–97

Australian National Creutzfeldt-Jakob Disease Registry, Department of Pathology, The University of Melbourne, Parkville, Victoria, 3052 Australia (S Collins FRACP, A Fletcher BSc, A Boyd RN, Prof C L Masters FRCPA)**; and The National Centre in HIV Epidemiology and Clinical Research, University of New South Wales, St Vincent's Hospital Medical Centre, Sydney, NSW** (M G Law MSc, Prof J Kaldor PhD)

Correspondence to: Dr S Collins
(e-mail: s.collins@pathology.unimelb.edu.au)

Introduction

By contrast with iatrogenic and familial cases of Creutzfeldt-Jakob disease (CJD), the aetiology of the most common form, sporadic CJD, which constitutes 85–90% of all cases,[1,2] is unknown. One hypothesis is that sporadic disease is caused by a rare (one in a million) spontaneous somatic mutation within the cerebral neuronal pool of the prion protein (PrP).[3] An alternative is low-level contamination events.[4] The excess of homozygosity at codon 129 in iatrogenic disease[5] has also been found in sporadic CJD, and may increase the chance of normal PrP (PrP^{C}) converting to the abnormal, disease-associated isoform (PrP^{SC}) when the normal and abnormal conformers interact, as could occur after a contamination event.

Previous case-control studies have investigated possible causes or risk factors for sporadic CJD, without identifying any consistent or major influences.[7–14] In our case-control study of risk factors for sporadic CJD, we used the Australian National Creutzfeldt-Jakob Disease Registry to ascertain cases. Controls were recruited from the general community by random telephone survey, unlike most previous studies that used hospital-based controls.[9–14]

Methods

Cases

The Australian National Creutzfeldt-Jakob Disease Registry[15] collected cases retrospectively to Jan 1, 1970, and prospectively from Oct 1, 1993. 241 patients with sporadic CJD (122 men, mean age 63·1 years, 119 women, mean age 66·6 years; combined age range 25–84 years) represented all Australian cases of sporadic CJD that occurred up to Oct 31, 1997. The diagnostic subclassifications of this cohort were 151 definite (neuropathologically confirmed) and 90 probable (clinically likely) cases of CJD, according to previously published criteria.[1] For probable cases, clinical investigation excluded the possibility of an alternative explanation and triphasic periodic complexes on the electroencephalogram, the presence of 14-3-3 protein in the cerebrospinal fluid, or both were usually present. In all cases, a history of potential iatrogenic transmission in the form of dura mater and corneal grafts or exposure to human cadaveric pituitary hormones was sought and excluded.

The ascertainment methods were approved by an Ethics Committee of the University of Melbourne. The main sources of case reporting provided about 91% of the total cases and were: neurologists (32%) and neuropathologists (20%); death certificates (25%); searches of separation codes at university-affiliated hospitals with ICD-9 CM 046.1 (specific for CJD) and 290.1 (for presenile dementia), or the equivalent codes from earlier versions of the International Classification of Diseases when appropriate (12%); and similar systematic reviews of the Health Information Morbidity Data for each

	Cases (n=241)	Controls (n=784)	Odds ratio (95% CI)	p
Country of birth				
Australia	155	598	1·0	
UK	32	86	1·44 (0·92–2·23)	0·109
Other European	36	48	2·89 (1·81–4·62)	<0·001
Asia	3	19	0·61 (0·18–2·08)	0·430
Other	6	33	0·70 (0·29–1·70)	0·434
Not known	9	0	—	
Any surgery				
No	38	233	1·0	
Yes	153	550	1·71 (1·16–2·51)	0·007
Not known	50	1	—	
Any dialysis, chemotherapy, radiotherapy, or arterial embolisation				
No	171	758	1·0	
Yes	4	24	0·69 (0·23–2·01)	0·494
Not known	66	2	—	
Ever lived or worked on a farm or market garden or employed in an abattoir or as a butcher				
No	77	523	1·0	
Yes	94	261	2·61 (1·84–3·71)	<0·001
Not known	70	0	—	
Blood transfusion				
No	118	616	1·0	
Yes	27	158	0·89 (0·57–1·40)	0·621
Not known	96	10	—	
Relative with dementia				
No	156	632	1·0	
Yes	7	148	0·20 (0·09–0·43)	<0·001
Not known	78	4	—	
Close personal contact with non-relative with dementia				
No	133	695	1·0	
Yes	26	85	1·60 (0·99–2·59)	0·055
Not known	82	4	—	
Major dental work				
No	89	403	1·0	
Yes	62	375	0·75 (0·53–1·07)	0·115
Not known	90	6	—	
Transplant recipient				
No	165	780	1·0	
Yes	2	3	2·67 (0·44–16·3)	0·288
Not known	74	1	—	
Travel abroad >1 month*				
No	48	406	1·0	
Yes	29	377	0·70 (0·43–1·15)	0·157
Not known	36	1	—	
Lived in UK >1 month in 1980s*				
No	97	718	1·0	
Yes	4	65	0·46 (0·16–1·30)	0·132
Not known	12	1	—	

All factors adjusted for age, sex, and urban or rural residence. *Cases (n=113) since 1990 only.

Table 1: **Risk of CJD by medical and demographic variables**

	Cases (n=241)	Controls (n=784)	Odds ratio (95% CI)	p
Total number of surgical procedures				
0	38	233	1·0	
1	55	241	1·36 (0·86–2·14)	0·185
2	43	154	1·67 (1·03–2·71)	0·037
⩾3	55	155	2·13 (1·34–3·41)	0·002
Not known	50	1	—	
Type of surgery				
No surgery	38	233	1·0	
Skin lesions	27	141	1·17 (0·69–2·01)	0·557
Appendix	25	115	1·33 (0·77–2·31)	0·307
Tonsils	9	93	0·59 (0·28–1·28)	0·181
Heart	11	19	3·55 (1·57–8·04)	0·002
Hip/knee	5	41	0·75 (0·28–2·01)	0·565
Hysterectomy	28	58	2·96 (1·68–5·21)	<0·001
Thyroid	4	9	2·73 (0·80–9·29)	0·109
Haemorrhoids	8	11	4·46 (1·69–11·8)	0·003
Gall bladder	18	51	2·16 (1·14–4·09)	0·018
Hernia	18	46	2·40 (1·26–4·57)	0·008
Cataract/eye	24	24	6·13 (3·16–11·9)	<0·001
Ear	3	5	3·68 (0·84–16·0)	0·083
Varicose veins	10	15	4·09 (1·71–9·76)	0·002
Carpal tunnel	6	4	9·20 (2·48–34·1)	0·001
Prostate	4	16	1·53 (0·49–4·83)	0·466
Other	89	203	2·69 (1·76–4·11)	<0·001

Factors adjusted for age, sex, urban or rural residence, except reasons for surgery or treatment.

Table 2: **Risk of CJD by surgical procedures**

State and Territory (2%). The medical histories of all cases, detected through the death certificate and hospital separation coding, were reviewed and validated on-site by a field researcher. Registry staff compiled a medical and demographic profile of each case of sporadic CJD with a standard comprehensive questionnaire (72% of cases) that was completed by the spouse or a first-degree relative (92%) and occasionally in consultation with the patient's general practitioner. Questionnaires were routinely posted to the appropriate relative or spouse for completion at his or her leisure, without time constraints; a few case questionnaires were completed by telephone interview.

The retrospective retrieval of information was more difficult the longer the time since death; the datasets least likely to be complete were for cases from the 1970s.

Controls

Controls were recruited and interviewed through a random dialling telephone survey. All interviews were in English and took place over 3 days at the end of August, 1997. We developed an abridged questionnaire for controls to find out: surgical procedures; specific selected non-surgical hospital treatments (controls were asked about dialysis, chemotherapy, radiotherapy, and arterial embolisation); temporally separate episodes of blood transfusion; recipience of organ transplantation; major dental work (beyond fillings and dental hygiene); travel outside Australia for longer than 1 month (including specifically to the UK); residence or employment on a farm (of any type including a market garden); work in an abattoir or as a butcher; relative with dementia; and close personal contact with a person with dementia who was not a relative. This abridged questionnaire was specifically based on that used for cases, with the retained questions selected because of their a priori relevance to transmission of CJD. However, telephone interviews necessitate more direct questions, and the responses captured, if possible, through a restricted series of options rather than through an open-ended approach.

We intended to interview 750 controls (about three for each case of CJD), matched to the cases by age (in 5-year age groups), sex, and urban or rural residence (as defined by the Australian Bureau of Statistics[16]) and in proportion to the resident population of each State and Territory. Listed telephone numbers were called randomly and on answer we asked for the oldest man in the household to give his verbal consent to the interview. If the relevant male age stratum was already completed, or if no man was available in the household, the oldest woman was asked to give her consent. In each case, we sought the oldest person in the household because of the age distribution of CJD cases.[5] A person in an incomplete age and sex stratum who gave his or her consent was directly questioned. We did not seek independent corroboration of the volunteered information, nor verify data provided by respondents from independent sources such as general practitioners.

Statistical analysis

Cases and controls were compared by standard logistic regression techniques. All analyses were adjusted for age, sex, and urban or rural residence. Because of the incompleteness of datasets in the cases from the 1970s, we did statistical analyses for the 128 sporadic CJD cases that occurred after 1987, and all 241 cases from 1970. In view of the similar results, we mostly present findings for the entire group. However, analyses of travel abroad and residence in the UK in the 1980s were based on cases of CJD diagnosed after 1989.

	Cases (n=241)	Controls (n=784)	Odds ratio (95% CI)	p
Residence or employment				
Farm	73	205	2·59 (1·78–3·76)	<0·001
Market garden	10	21	3·43 (1·54–7·64)	0·002
Abattoir	6	23	1·87 (0·73–4·80)	0·198
Butcher	5	9	3·97 (1·28–12·3)	0·017
Not known	0	8	—	
Duration (years) lived or worked on farm or market garden				
None	77	523	1·0	
<10	12	64	1·33 (0·68–2·59)	0·404
10–19	17	46	2·71 (1·47–5·02)	0·001
⩾20	24	65	2·78 (1·60–4·81)	<0·001
Not known	20	30	—	

All factors adjusted for age, sex, and urban or rural residence.

Table 3: **Risk of CJD by residence and occupation**

	Cases (n=241)	Controls (n=784)	Odds ratio (95% CI)	p
Number of transfusions				
0	118	616	1·0	
1	20	105	0·94 (0·56–1·58)	0·804
2	4	28	0·70 (0·24–2·03)	0·506
⩾3	3	25	0·58 (0·17–1·96)	0·382
Not known	96	10	—	
Reason for transfusion				
No transfusion	118	616	1·0	
Accident	0	14	—	
Illness	1	20	0·26 (0·03–1·96)	0·192
Operation	17	109	0·81 (0·47–1·41)	0·462
Childbirth	2	15	0·70 (0·16–3·08)	0·633
Not specified	9	19	—	
Year of first transfusion				
No transfusion	118	616	1·0	
1979	11	70	0·80 (0·41–1·56)	0·510
>1980	13	74	0·81 (0·43–1·52)	0·510
Not known	3	14	—	

All factors adjusted for age, sex, and urban or rural residence.

Table 4: **Risk of CJD by blood transfusion**

Results

784 controls completed the telephone interview. 12 387 telephone calls were made, 2577 (21%) of which were number unobtainable, engaged, or no reply, and in 22 (0·2%) calls an appointment was made to ring back. In 1308 (11%) of the calls, permission for the interview was refused, and in 7349 (60%), the relevant age, sex, and urban or rural residence quota was full. Of the 1131 calls in which interviews began, 347 calls were halted—the respondent did not want to continue in 63 (6%), there were language or hearing difficulties in 158 (14%), or for other reasons in 126 (11%) calls. In 784 (69%) calls the interviews were completed.

Controls and cases were well matched for age, sex, State or Territory of residence, and urban or rural residence (data not shown). However, there was some deficit of controls from non-English speaking European countries, probably because our interviews were conducted in English.

Table 1 shows each medical and demographic variable by risk of CJD. Of the variables analysed, surgical procedures were the factor most significantly associated with risk of CJD (table 2). The risk of CJD progressively increased with the number of surgical procedures. Mean time from first surgery to death was 29 (SD=17·4) years. Assessment of separate surgical procedures indicated that the risk of CJD increased over a range of operations and was not associated with a specific anatomical site or complexity. There was no association between the risk of CJD and non-surgical hospital treatments (dialysis, chemotherapy, radiotherapy, and arterial embolisation).

Residence or employment on a farm or market garden (presence of livestock not specified), was associated with a risk for CJD, which increased with longer duration of residence or employment (table 3).

Blood transfusion was not associated with subsequent risk of developing CJD, irrespective of the total number of infusion episodes, reason for transfusion, or date of the first procedure (table 4). Other non-predisposing factors are shown in table 1 and include: major dental work; organ transplantation; close physical contact with an unrelated person with dementia and travel to the UK in the 1980s. A relative with dementia was associated with a decreased risk of CJD (table 1).

Discussion

In this case-control study, we found a range of surgical treatments were associated with an increased risk of sporadic CJD. Two previous case-control studies, also with community controls, found the risk of CJD was associated with hospital-related therapy,[8,9] but this significance was lost when the data were pooled as part of a meta-analysis.[13] The absence of this finding in a third study[12] may reflect methodological differences, since the controls were selected only from hospital populations and not from the community. One possibility is that our finding of an association between surgery and increased risk of CJD may be due to the more complete ascertainment of surgical histories in cases than controls as a result of different data-acquisition methods. The design of this study differs fundamentally from all previous case-control series.[7–14]

In accord with the report by Kondo and Kuroiwa,[8] we found that increased risk of CJD was significantly associated with various surgical procedures, but there was no consensus with regard to anatomical site, complexity, or postoperative length of stay in hospital. We also assessed progressive risk of CJD from multiple operations and found it to be cumulative, independent of the type of surgery. The mean of 29 years between first surgery and eventual death from CJD differs from the results of Kondo and Kuroiwa[8] who reported a significant association for operations performed within 5 years of symptom onset. The explanation for this difference is unknown, but our results fall within the range of reported incubation periods for iatrogenic transmission events.[17] The exception in our study was surgery involving tissue transplants, which may reflect the high level of precaution and screening in relation to graft donors. There were, however, few transplants performed among the study population.

Davanipour and colleagues[9] also reported a positive association, although the discerned surgical risk was less pervasive. The only significant associations were for procedures involving the head, face, and neck. However, hospital controls constituted about half of those recruited, and selection bias may have contributed to these more restricted findings. The possibility of similar recruitment bias was also acknowledged in the largest case-control study by van Duijn and colleagues[14] who did not find that risk of CJD was related to medical history, including the limited range of surgical procedures assessed. However, after they excluded neurological inpatient controls, the previous inverse relation for surgery of the vertebral column and other invasive investigations was lost, which lends support to

concerns about the selection of controls.[14] Differences in study design may contribute to the conflicting findings of this and previous case-control studies, particularly with regard to risk of CJD and surgical treatments.

Given the absence of any form of transmissible spongiform encephalopathy in Australian domesticated livestock,[18] the apparent association between risk of CJD and long-term agricultural residence and work is difficult to reconcile. However, the increasing risk associated with longer duration of residence or employment does lend some support to this result. Nevertheless, this finding contrasts with the more understandable absence of clear-cut risk seen for domestic butchers and abattoir workers, and the generally negative findings for various agricultural exposures, assessed by van Duijn and colleagues[14] in Europe. Our finding may stem from matching ages of controls at interview (in 1997) with ages of cases at death (1970–97). Any trends over this period toward fewer Australians living and working on farms could create an association with the risk of CJD. However, our analysis restricted to cases since 1987 gave similar results (if anything larger odds ratios). Furthermore, the persistence of increased risk of CJD in market gardeners, among whom exposure to commercial farm animals would seem to be kept to a minimum, indicates that more generic explanations may account for the increased risk with farm domicile and employment, as Cousens and co-workers[19] suggested for the increased rates for CJD in dairy farmers from countries with negligible endemic bovine spongiform encephalopathy. Given the potential for specious associations when many risk factors are analysed, circumspection is required when dealing with implausible or non-intuitive findings.

Despite anecdotal claims to the contrary,[20] the absence of detectable increased risk of CJD from blood transfusion accords with previous case-control studies.[8,9,12–14] This lack of association was maintained despite a detailed analysis that included total number of transfusion episodes, reason for the resuscitation, and date of the first infusion. Other pertinent findings were the lack of association with major dental work and contact with people with dementia. Although there was no association between risk of CJD and travel to the UK in the 1980s, there were probably too few cases to assess this risk reliably. However, to date, cases of variant CJD have not been detected in Australia.[18]

The apparent "protective" effect of a family history of dementia conflicts with previous findings.[12–14] This apparent effect probably arises from our careful exclusion of cases with any familial forms of CJD. Since classification of familial CJD is based largely on family history, the exclusion of all familial cases could have also removed some cases with a relative with some other form of dementia; the control population was not selected on this basis.

The retrospective nature of information retrieval for most of the cases led to predictable limitations of data completeness, which generally, but not exclusively, increased with the length of time since the patient's death. However, our analysis of cases after 1987, and separately of all patients, did not qualitatively affect the findings, which suggests any lack of information probably arose unsystematically. The possibility of recall bias by surrogate respondents (spouses and close relatives) who completed the medical demographic questionnaires relating to patients is unavoidable.

Other possible biases may have resulted from the way we selected and interviewed controls, as suggested by the deficiency of non-English speaking Europeans in the controls. Since controls were selected from listed telephone numbers, they may not represent an entirely random sample of the Australian population. Controls were interviewed in person which raises the possibility of different recall bias compared with cases for whom a surrogate supplied information. A similar study[14] discounted methodological discrepancies in interviewees for control data, but did not assess the potential for systematic bias relevant to our study since we used different data acquisition methods. Another potential bias is that data were ascertained in August, 1997, for controls and from 1970 to 1997 for cases, so any time trends over this period could bias results. Although the concordance of our results with previous studies in terms of absence of risk from blood transfusion[9,12–14] and dental work[8,10–14] suggest that large or pervasive biases were not introduced, our results need to be replicated in independent studies with community-based controls.

We believe our findings should reinforce the heightened vigilance about infection control at all levels of care in hospital settings, particularly given the emergence of the probable zoonotic forms of variant CJD.

Contributors

S Collins and A Boyd reviewed all cases. A Fletcher managed all data entry and manipulation. Statistical analyses were done by M Law and J Kaldor. The project design, including development of the control questionnaire, was done by S Collins, M Law, J Kaldor, and C Mastos.

Acknowledgments

This study was partly funded by grants from the Australian Commonwealth Department of Health and Family Services. We thank the referring physicians and ethics committees of tertiary hospitals for their cooperation.

References

1 Masters C, Harris J, Gajdusek D, Gibbs C, Bernoulli C, Asher D. Creutzfeldt-Jakob disease: patterns of worldwide occurrence and the significance of familial and sporadic clustering. *Ann Neurol* 1979; **5:** 177–88.

2 Brown P, Gibbs C, Rodgers-Johnson P, et al. Human spongiform encephalopathy: the National Institutes of Health series of 300 cases of experimentally transmitted disease. *Ann Neurol* 1994; **35:** 513–29.

3 Prusiner SB. Prion diseases and the BSE crisis. *Science* 1997; **278:** 245–51.

4 Bruce ME, Will RG, Ironside JW, et al. Transmissions to mice indicate that 'new variant' CJD is caused by the BSE agent. *Nature* 1997; **389:** 498–501.

5 Collinge J, Palmer M, Dryden A. Genetic predisposition to iatrogenic Creutzfeldt-Jakob disease. *Lancet* 1991; **337:** 1441–42.

6 Palmer M, Dryden A, Hughes J, Collinge J. Homozygous prion protein genotype predisposes to sporadic Creutzfeldt-Jakob disease. *Nature* 1991; **352:** 340–42.

7 Bobowick A, Brody J, Matthews M, Ross R, Gajdusek D. Creutzfeldt-Jakob disease: a case-control study. *Am J Epidemiol* 1973; **98:** 381–94.

8 Kondo K, Kuroiwa Y. A case control study of Creutzfeldt-Jakob disease: association with physical injuries. *Ann Neurol* 1982; **11:** 377–81.

9 Davanipour Z, Alter M, Sobel E, Asher D, Gajdusek D. Creutzfeldt-Jakob disease: possible medical risk factors. *Neurology* 1985; **35:** 1483–86.

10 Davanipour Z, Alter M, Sobel E, Asher D, Gajdusek D. A case-control study of Creutzfeldt-Jakob disease: dietary risk factors. *Am J Epidemiol* 1985; **122:** 443–51.

11 Davanipour Z, Alter M, Sobel E, Asher D, Gajdusek D. Transmissible virus dementia: evaluation of a zoonotic hypothesis. *Neuroepidemiology* 1986; **5:** 194–206.

12 Harries-Jones R, Knight R, Will R, Cousens S, Smith P, Matthews W. Creutzfeldt-Jakob disease in England and Wales, 1980–1984: a case-control study of potential risk factors. *J Neurol Neurosurg Psychiatry* 1988; **51:** 113–19.

13 Wientjens D, Davanipour Z, Hofman A, et al. Risk factors for Creutzfeldt-Jakob disease: a reanalysis of case-control studies. *Neurology* 1996; **46:** 1287–91.
14 van Duijn C, Delasnerie-Laupretre N, Masullo C, et al. Case-control study of risk factors of Creutzfeldt-Jakob disease in Europe during 1993–95. *Lancet* 1998; **351:** 1081–85.
15 Collins S, Fletcher A, De Luise T, Boyd A, Masters C. Creutzfeldt-Jakob disease in Australia. In: Court L, Dodet B, eds. Transmissible subacute spongiform encephaolopathies: prion diseases. Paris: Elsevier, 1996: 405–15.
16 Australian Bureau of Statistics. Statistical geography, vol 1. Canberra: Australian Government Printing Services, 1996: ABS catalogue no 1216.
17 Brown P, Preece M, Will R. "Friendly fire" in medicine: hormones, homografts, and Creutzfeldt-Jakob disease. *Lancet* 1992; **340:** 24–27.
18 Collins S, Masters C. Iatrogenic and zoonotic Creutzfeldt-Jakob disease: the Australian perspective. *Med J Aust* 1996; **164:** 598–602.
19 Cousens S, Zeidler M, Esmonde T, et al. Sporadic Creutzfeldt-Jakob disease in the United Kingdom: analysis of epidemiological surveillance data for 1970–96. *BMJ* 1997; **315:** 389–95.
20 Klein R, Dumble L. Transmission of Creutzfeldt-Jakob disease by blood transfusion. *Lancet* 1993; **341:** 768.
21 Defebvre L, Destée A, Caron J, Ruchoux M, Wurtz A, Remy J. Creutzfeldt-Jakob disease after an embolization of intercostal arteries with cadaveric dura mater suggesting a systemic transmission of the prion agent. *Neurology* 1997; **48:** 1470–71.
22 Antoine J, Michel D, Bertholon P, et al. Creutzfeldt-Jakob disease after extracranial dura mater embolization for a nasopharnygeal angiofibroma. *Neurology* 1997; **48:** 1451–53.

Comparison of three single doses of mifepristone as emergency contraception: a randomised trial

*Task Force on Postovulatory Methods of Fertility Regulation**

Summary

Background Mifepristone is a highly effective and well-tolerated emergency contraceptive when given in a dose of 600 mg within 72 h of unprotected coitus. We assessed whether the same effectiveness can be achieved with lower doses of mifepristone (50 mg and 10 mg) and a longer postcoital treatment period (120 h).

Methods We undertook a multicentre, single-masked, randomised trial in 11 family-planning clinics in Australia, China, Finland, Georgia, the UK, and the USA. 1717 healthy women with regular menstrual cycles who requested emergency contraception within 120 h of unprotected coitus were randomly assigned to three treatment groups.

Findings 32 women were lost to follow-up and one was pregnant before treatment. The 600 mg, 50 mg, and 10 mg groups did not differ in the proportions of pregnancies (seven [1·3%] of 559, six [1·1%] of 560, and seven [1·2%] of 565). Two pregnancies (both in the 50 mg group) were tubal. Among women without further acts of intercourse, treatment delay did not appear to influence the effectiveness. No major side-effects occurred, except a delay in the onset of next menses, significantly ($p<0·01$) related to the mifepristone dose.

Interpretation Lowering the dose of mifepristone sixty-fold did not decrease its effectiveness as an emergency contraceptive under typical use, though a study of this size cannot exclude differences in effectiveness up to almost three-fold. Lower doses of mifepristone were associated with less disturbance of the menstrual cycle. Thus, a dose as low as 10 mg seems preferable to the 600 mg dose.

Lancet 1999; **353:** 697–702

*Members and study organisation given at end of paper

Correspondence to: Dr Helena von Hertzen/Dr Paul F A Van Look, Special Programme of Research, Development and Research Training in Human Reproduction, World Health Organization, 1211 Geneva 27, Switzerland
(e-mail: vonhertzenh@who.ch or vanlookp@who.ch)

Introduction

Two UK randomised controlled trials of emergency contraception compared a single dose of 600 mg mifepristone with the Yuzpe regimen of oral contraceptives (ethinylestradiol 100 μg plus levonorgestrel 500 μg, repeated after 12 h) given within 72 h of unprotected coitus.[1,2] Mifepristone seemed to be a better option—three pregnancies were reported among 597 women who received mifepristone, compared with nine pregnancies among 589 women who received the Yuzpe regimen. The difference in proportions of pregnancies was not significant, but women who received mifepristone had significantly less nausea and vomiting, which are major drawbacks of the Yuzpe regimen. Women who received mifepristone were, however, more likely to have a delay in the onset of the next menses, presumably because antiprogestagen administered in the preovulatory phase of the menstrual cycle delays or blocks ovulation.[3] Such delay can worry women already fearful of an unintended pregnancy. In addition, delayed ovulation means a conception risk later in the prolonged cycle if no contraception is used. In one of the UK trials,[2] the three pregnant women were reported to have conceived 10–15 days after mifepristone treatment.

Research on the effects of mifepristone on ovarian and endometrial functions suggests that doses lower than 600 mg may confer protection against pregnancy when used for emergency contraception.[4–6] Lower doses would reduce the cost and are consistent with the principle that the lowest effective dose of a drug should be used.

This randomised controlled trial aimed to compare the effectiveness and side-effects, including the timing of the subsequent menstrual period, of single doses of 600 mg, 50 mg, and 10 mg mifepristone when the treatment was given within 120 h (5 days) of unprotected coitus.

Methods

Protocol

This trial was carried out in 11 family planning clinics in six countries on four continents. We obtained approval for the

Research letters

Codon 129 prion protein genotype and sporadic Creutzfeldt-Jakob disease

A Alperovitch, I Zerr, M Pocchiari, E Mitrova, J de Pedro Cuesta, I Hegyi, S Collins, H Kretzschmar, C van Duijn, RG Will

Methionine homozygosity at codon 129 of the prion protein (PrP) gene is a recognised risk factor for the development of sporadic Creutzfeldt-Jakob disease (CJD).[1] Between 64 and 81% of sporadic cases have this genotype,[1–3] with an overall rate, combining the data from three series, of 71%. PrP gene analysis is now available in 748 out of 1327 cases of definite or probable sporadic CJD, including data from Australia (5), France (217), Germany (239), Italy (101), the Netherlands (36), Slovakia (7), Spain (7), Switzerland (7), and the UK (129). A current issue is whether cases of variant CJD (nvCJD), might occur in individuals with a valine homozygous or heterozygous PrP genotype. To date, all 36 cases of variant CJD with available genetic analysis have been methionine homozygotes and died at an early age (mean 29 years). A small number of cases of sporadic CJD with a relatively early age at death have been identified in participating countries including Australia, France, Germany, the Netherlands, and the UK. We analysed the distribution of genotypes at codon 129 of the PrP gene by 10-year age groups in order to determine whether there is a relative excess of young valine homozygote or heterozygote cases of sporadic CJD.

The table shows data on the distribution of PrP genotypes in the normal white population, pooling data from five studies[4] (there are no data on stratification by age in these studies), and the genotype distribution in sporadic CJD, derived by pooling data from three studies (table[2]), are also shown, together with previous data from the European surveillance project.[3] The frequencies of codon 129 PrP genotypes differ significantly across the age groups (χ^2=38·2, 8 df, p<0·0001) and there is a positive linear relation between age and the frequency of the methionine homozygote genotype (p for linear trend <0·0001). The valine homozygous genotype is significantly more frequent in cases aged 49 years or less compared with those aged 50 years and over (χ^2=27·9, 2 df, p<0·0001). In some countries only limited data are available but comparisons between countries are possible for France, Germany, Italy, and the UK. Codon 129 distribution in these countries is not significantly different from previous studies of sporadic CJD, and within country comparison of cases aged less than 50 years shows a significant excess of valine homozygotes in France, Germany, and the UK, but not in Italy. There is a non-significant excess of heterozygote cases aged less than 50 years in Italy, the Netherlands, and the UK.

The relative excess of valine homozygotes in sporadic CJD aged less than 50 years is unexpected. There are a number of possible reasons. There may be a bias in the surveillance system for the identification of younger atypical cases of sporadic CJD, because of increased interest in younger suspect cases after the identification of variant CJD. Sporadic CJD with an atypical clinicopathological phenotype may occur in younger patients, particularly those with a valine homozygous genotype.[4] These cases rarely have the "typical" electroencephalogram seen in sporadic CJD and might be over-represented in systematic surveillance data because of ascertainment bias. It is also possible that CJD is underdiagnosed in older valine homozygotes because of an atypical phenotype, although the genotype distribution we have identified would necessitate underdiagnosis in the 50–59 year age group in which alternative causes of dementia are fairly uncommon. It is also difficult to understand why there should be a differential bias in the diagnosis of those aged over 50 years compared with younger cases, when suspect cases are investigated in a standard manner, independent of age, and this often includes 14-3-3 cerebrospinal fluid immunoassay and necropsy examination. The percentages of heterozygote and valine homozygote cases between the study periods 1993–95 and 1996–98 are not statistically different, and this finding does not support the hypothesis of an increase in the ascertainment of younger heterozygote or valine homozygote cases with time as a result of the identification of variant CJD in March, 1996.

It is possible that the excess of valine homozygotes in younger cases is caused by variation in the strain of infectious agent and perhaps exogenous infection, either iatrogenic or zoonotic, for example due to bovine spongiform encephalopathy (BSE). An excess of valine homozygotes has been found in growth-hormone recipients with CJD,[5] but none of the cases in our report were known to have an iatrogenic exposure. The possibility that the excess of young valine homozygote cases reflects disease caused by BSE is unlikely because there is no differential excess of valine homozygote cases in the UK, the country with the greatest potential human exposure to BSE, compared with France and Germany. Furthermore all cases of variant CJD tested to date in the UK have been methionine homozygotes and it would be surprising if cases of variant CJD with this genotype were not identified at the same time, and probably earlier, than valine homozygote BSE-related cases in other countries, should such cases actually occur. One methionine homozygote French case of variant CJD has been identified. It is of note that widespread florid plaque deposition, which is the neuropathological hallmark of variant CJD, has not been found in any of the valine homozygote cases in this series. Most of these cases have undergone necropsy and PrP glycoform analysis in a small number of cases, including three young valine homozygote cases in the UK, has not shown the PrP subtype identified in variant CJD nor the type 5 subtype

	MM	MV	VV
<49 years*	43 (23)	17 (9)	41 (22)
50–59 years	65 (97)	16 (24)	19 (28)
60–69 years	75 (227)	13 (40)	12 (36)
70–79 years	73 (148)	10 (21)	17 (35)
80+ years	84 (32)	11 (4)	5 (2)
Total	70 (527)	13 (98)	16 (123)
Previous studies†	71 (60)	17 (14)	12 (10)
European data 1993–95	74 (252)	11 (38)	15 (51)
European data 1996–98	68 (275)	15 (60)	18 (72)
Normal population	39 (156)	50 (198)	11 (44)

*The age of death of the youngest case for each genotype was 28 years for MM, 20 years for MV, and 23 years for VV. †Laplanche J-L, et al. Molecular genetics of prion diseases in France. *Neurology* 1994; **44:** 2347–51, and Salvatore M, et al. Polymorphisms of the prion protein gene in Italian patients with Creutzfeldt-Jakob disease. *Hum Genet* 1995; **94:** 375–79.

Percentage of codon 129 PRP genotypes in sporadic CJD by 10-year age groups in the European study 1993–1998 (numbers of cases in parentheses), and codon 129 distribution in the normal population and in previous studies of sporadic CJD

found in BSE transmissions to laboratory mice expressing valine at codon 129. Further analysis of temporal trends in codon 129 genotype distribution, clinicopathological features, and prion protein glycoform patterns in younger patients with CJD is being undertaken.

The data in this paper have been accumulated by many people in each participating country. J Ironside and M Head provided the data of PrP glycoform analysis in the UK. The study is funded by the European Union, contract number BMH4-CT97-2216.

1 Palmer MS, Dryden AJ, Hughes JT, Collinge J. Homozygous prion protein genotype predisposes to sporadic Creutzfeldt-Jakob disease. *Nature* 1991; **352:** 340–41.
2 Lampe J, Kitzler H, Walter MC, Lochmuller H, Reichmann H. Methionine homozygosity at prion protein gene codon 129 may predispose to sporadic inclusion-body myositis. *Lancet* 1999; **353:** 465–66.
3 Will RG, Alperovitch A, Poser S, et al. Descriptive epidemiology of Creutzfeldt-Jakob disease in six European countries, 1993–1995. *Ann Neurol* 1998; **43:** 763–67.
4 Parchi P, Castellani R, Capellari S, et al. Molecular basis of phenotypic variability in sporadic Creutzfeldt-Jakob disease. *Ann Neurol* 1996; **39:** 767–78.
5 Collinge J, Palmer MS, Dryden AJ. Genetic predisposition to iatrogenic Creutzfeldt-Jakob disease. *Lancet* 1991; **337:** 1441–442.

INSERM U.360, Hôpital La Salpêtrière 75651, Paris, cedex 13, France; Department of Neurology and Neuropathology, University of Göttingen, Göttingen, Germany; Istituto Superiore di Sanità, Laboratory of Virology, 00161 Rome, Italy; Institute of Preventive and Clinical Medicine, National Reference Centre of Slov Virus Neuroinfections, 833 01 Bratislava, Slovakia; Instituto de Salud Carlos III, Centro Nacional de Epidemiologia, Departmento de Epidemiologia Aplicada, Madrid, Spain; UniversitätsSpital Zürich, Institut für Neuropathologie, CH-8091 Zürich, Switzerland; Department of Pathology, The University of Melbourne, Vic 3052, Australia; Department of Epidemiology & Biostatistics, Erasmus University Medical School, PO Box 1738, Rotterdam, Netherlands; The National CJD Surveillance Unit, Western General Hospital, Edinburgh, EH4 2XU, UK (R Will)

Low 1-year prevalence of atopic eczema in very low birthweight infants

Christoph Bührer, Ingrid Grimmer, Bodo Niggemann, Michael Obladen

Preterm birth is associated with various diseases persisting beyond the neonatal period or becoming evident only after discharge from neonatal care units. Premature infants are potentially liable to early sensitisation to numerous antigens. Undigested proteins are poorly excluded by the mucous membranes of the gastrointestinal and respiratory system during the first weeks of life, and antigenic substances may penetrate the skin because of immaturity and invasive procedures. There has been speculation, therefore, that preterm infants are a high-risk group for asthma and eczema,[1] although population-based studies have not confirmed an association between atopy and prematurity.[2,3]

To address the frequency of atopic eczema in very immature infants who are presumably at greatest risk to early sensitisation, we investigated the 1-year prevalence of atopic eczema in a hospital-based follow-up cohort of very low birthweight (VLBW) infants. The cohort included all 315 surviving, prematurely born, infants with a birthweight below 1500 g consecutively admitted to our tertiary care referral centre between Jan 1, 1992, and Dec 31, 1996, of whom 282 infants (90%) underwent total body physical examination by a trained paediatrician at 12 months (corrected age), together with 49 VLBW infants initially cared for in two other Berlin hospitals born in the same period. At examination, the physician's diagnosis of atopic eczema was based on itchy eczema with characteristic (facial, extensor) distribution.[4] An oral history was taken from the parents or guardians at the time of the visit. In addition, parents or guardians received structured questionnaires that asked for developmental milestones, various diseases including those of the skin, and parental smoking. The same modes of data collection were applied to 137 non-VLBW infants seen in our follow-up clinic for developmental testing and 318 term healthy newborn babies who were recruited as controls.

Five (2%) of 331 former VLBW infants examined presented with atopic eczema, whereas atopic eczema was present in 18 (4%) of 455 control infants at the time of examination, and transient atopic eczema before examination was additionally reported by parents of three control infants. Both the point prevalence and the calculated 1-year lifetime prevalence of atopic eczema (1·5% *vs* 4·6%) were significantly lower in VLBW infants than in term or near-term infants (two-sided p=0·045 and p=0·016, respectively). The relative risk of developing atopic eczema until 1 year (corrected age) in VLBW infants was 0·33 (95% CI 0·13–0·86), compared with non-VLBW infants. Development of atopic eczema was not related to parental smoking or net household income.

There is no obvious explanation for the low prevalence of atopic eczema in VLBW infants. Possibly early exposure to antigen may lead to the development of tolerance rather than sensitise VLBW infants, especially after oral administration. In mice, continuous feeding with small doses of antigen has been shown to suppress antigen-specific Th2 lymphocytes and IgE production.[5] VLBW infants surviving the numerous antigens encountered during initial intensive care are apparently more resistant to atopic immune deviation than infants born close to term.

1 Lucas A, Brooke OG, Cole TJ, et al. Food and drug reactions, wheezing, and eczema in preterm infants. *Arch Dis Child* 1990; **65:** 411–15.
2 Klebanoff MA, Berendes HW. Atopic eczema and preterm birth. *Arch Dis Child* 1988; **63:** 1519–20.
3 Olesen AB, Ellingsen AR, Olesen H, et al. Atopic dermatitis and birth factors: historical follow up by record linkage. *BMJ* 1997; **314:** 1003–08.
4 Sampson HA. Pathogenesis of eczema. *Clin Exp Allergy* 1990; **20:** 459–67.
5 Wu X-M, Nakashima M, Watanabe T. Selective suppression of antigen-specific Th2 cells by continuous micro-dose oral tolerance. *Eur J Immunol* 1998; **28:** 134–42.

Department of Neonatology (C Bührer e-mail: christoph.buehrer@charite.de)**; and Department of Paediatric Pulmonology/Immunology Charité-Virchow Hospital, Humboldt University, D-13344 Berlin, Germany**

Alcohol injection: a new method of treating placental chorioangiomas

Umberto Nicolini, Guglielmo Zuliani, Elena Caravelli, Roberto Fogliani, Andres Poblete, Alistair Roberts

Placental chorioangiomas are benign vascular tumours. Complications associated with chorioangiomas larger than 4–5 cm include polyhydramnios, maternal and fetal coagulopathies, preterm delivery, pre-eclampsia, fetal heart failure, and hydrops.[1–3] Chorioangiomas probably act as peripheral arteriovenous shunts leading to progressive heart failure. Management is limited to induction of labour once fetal viability is reached. Fetal blood transfusion has been used therapeutically in infants found to be anaemic,[4] but this is at best only a temporary solution.

Two women were referred to our department with ultrasound findings of placental chorioangioma. The tumour was 6×3·5×3 cm at 25 weeks' gestation in patient 1, and 5×4·5×4 cm at 18 weeks in patient 2. Patient 1 had polyhydramnios at admission, and polyhydramnios had developed by week 22 in patient 2 (figure 1). Both fetuses

Iatrogenic Creutzfeldt–Jakob disease at the millennium

P. Brown, MD; M. Preece; J.-P. Brandel; T. Sato; L. McShane, PhD; I. Zerr; A. Fletcher; R.G. Will, FRCP; M. Pocchiari; N.R. Cashman; J.H. d'Aignaux; L. Cervenáková; J. Fradkin, MD; L.B. Schonberger, MD; and S.J. Collins

Article abstract—The causes and geographic distribution of 267 cases of iatrogenic Creutzfeldt–Jakob disease (CJD) are here updated at the millennium. Small numbers of still-occurring cases result from disease onsets after longer and longer incubation periods following infection by cadaveric human growth hormone or dura mater grafts manufactured and distributed before the mid-1980s. The proportion of recipients acquiring CJD from growth hormone varies from 0.3 to 4.4% in different countries, and acquisition from dura mater varies between 0.02 and 0.05% in Japan (where most cases occurred). Incubation periods can extend up to 30 years, and cerebellar onsets predominate in both hormone and graft recipients (in whom the site of graft placement had no effect on the clinical presentation). Homozygosity at codon 129 of the *PRNP* gene is over-represented in both forms of disease; it has no effect on the incubation period of graft recipients, but may promote shorter incubation periods in hormone cases. Knowledge about potential high-risk sources of contamination gained during the last quarter century, and the implementation of methods to circumvent them, should minimize the potential for iatrogenic contributions to the current spectrum of CJD.

NEUROLOGY 2000;55:1075–1081

Nearly 30 years have passed since the first case of iatrogenic Creutzfeldt–Jakob disease (CJD) was recognized in the recipient of a corneal graft from a donor who had died of unsuspected CJD.[1] Two further possible cases of corneal graft–related CJD have occurred in the last decade: one in a patient with verified CJD who had received a graft 16 months earlier from a donor whose cause of death was unknown,[2] and one in a patient with clinically typical CJD who had received a graft 30 years earlier from a patient with verified CJD.[3] The few cases resulting from contaminated stereotactic intracerebral EEG needles[4] or neurosurgical instruments[5] identified in the 1970s have not grown in number.

Frequency, distribution, and risk. The two most important causes of iatrogenic disease are contaminated cadaveric human growth hormone and dura mater grafts, first recognized as risks in the mid-1980s.[6,7] The original hope for a limited number of cases that would quickly diminish over time has vanished, as cases continue to occur each year, with current tallies of 139 (growth hormone) and 114 (dura mater). Table 1 summarizes cases of iatrogenic disease from all causes, and table 2 shows their international distribution. More than half of all growth hormone–related cases have occurred in France, and more than half of all dura-related cases have occurred in Japan.

The frequencies of CJD in growth hormone recipients shown in table 3 make no assumptions about risk factors other than the absence of risk in subjects treated after mid-1985 with either recombinant hormone (United States, United Kingdom, and New Zealand) or urea-treated native hormone (France), who were excluded from the treated population denominator. However, in the United States, all cases of CJD have so far occurred in individuals who began treatment before 1977, when the purification protocol was changed to include a column chromatography step. If this new purification protocol contributed to the disappearance of new cases, then a more appropriate calculation of risk in the United States would use only cases in the pre-1977 treated population, with a resulting frequency of CJD of 0.8%. Similarly, instead of the 5 cases in 184 patients treated in New

From the Laboratory of CNS Studies (Dr. Brown), NINDS, Biometric Research Branch (Dr. McShane), NCI, and Division of Diabetes, Endocrinology, and Metabolic Diseases (Dr. Fradkin), NIDDKD, NIH, Bethesda, MD; Institute of Child Health (M. Preece), University College London, UK; U 360 INSERM (J.-P. Brandel and J.H. d'Aignaux), Centre National de Référence de la Maladie de CJ, Hôpital de la Salpêtrière, Paris, France; Khonodai Hospital (T. Sato), Ichikawa, Chiba, Japan; Klinik und Poliklinik für Neurologie (I. Zerr), Georg-August-Universität Göttingen, Germany; Department of Pathology (A. Fletcher and S.J. Collins), University of Melbourne, Australia; CJD Surveillance Unit (Dr. Will), Western General Hospital, Edinburgh, UK; Istituto Superiore de Sanità (M. Pocchiari), Laboratory of Virology, Rome, Italy; Canadian CJD Surveillance System (N.R. Cashman), Ottawa, and University of Toronto, Canada; Jerome H. Holland Laboratory (L. Cervenáková), American Red Cross, Rockville, MD; and Division of Viral and Rickettsial Diseases (Dr. Schonberger), National Center for Infectious Diseases, CDC, Atlanta, GA.

Received February 21, 2000. Accepted in final form June 20, 2000.

Address correspondence and reprint requests to Dr. Paul Brown, Building 36, Room 4A-05, National Institutes of Health, 36 Convent Drive, MSC 4122, Bethesda, MD 20892; e-mail: brownp@ninds.nih.gov

Table 1 *Summary of iatrogenic cases of Creutzfeldt–Jakob disease from all causes (July 2000)*

Mode of infection	No. of patients	Agent entry into brain	Median incubation period (range)*	Clinical signs on presentation
Corneal transplant†	3	Optic nerve	16, 18, 320 mo	Dementia/cerebellar
Stereotactic EEG	2	Intracerebral	16, 20 mo	Dementia/cerebellar
Neurosurgery	5	Intracerebral	17 mo (12–28)	Visual/dementia/cerebellar
Dura mater graft	114	Cerebral surface‡	6 y (1.5–18)	Cerebellar (visual/dementia)
Growth hormone	139	Hematogenous (?)	12 y (5–30)	Cerebellar
Gonadotropin	4	Hematogenous (?)	13 y (12–16)	Cerebellar

* Calculated from the midpoint of treatment to the onset of disease.
† One definite, one probable, and one possible case.
‡ In two cases, dura was used to embolize vessels of non-CNS tissues, rather than as intracranial grafts.

Zealand with hormone prepared in the United States, the denominator would decrease to 46 individuals treated before 1977, and yield a frequency of 11%. No plausible reason has yet been advanced to explain this discrepancy between CJD incidence in United States and New Zealand hormone recipients.

In the United Kingdom, chromatography purification was inaugurated around 1980, but because of supply shortages, hormone prepared by the earlier method remained in use, and all of the CJD cases in the United Kingdom received at least some of this hormone during treatment. Thus, no limiting dates can be used for making an alternative risk calculation. In France, all cases have thus far shared a treatment period between the beginning of 1983 and mid-1985, which has been proposed as the most likely limiting period of risk.[8] Using the population under treatment during this period (1260), the calculated frequency of CJD rises to nearly 6%.

This clustering of French cases may have resulted either from a succession of several batches of independently contaminated pituitary glands or from one or two batches that cross-contaminated other batches during processing. However it happened, the contamination must have been comparatively severe, as judged by the comparatively short intervals between infection and the onset of clinical signs in most of the French cases (in experimental models of disease,

Table 2 *International distribution of iatrogenic cases of Creutzfeldt–Jakob disease (July 2000)*

	Surgical procedures				Hormone therapy	
Country	Dura mater grafts	Surgical instruments	Stereotactic EEG needles	Corneal transplants	Growth hormone	Gonadotropin
Argentina	1					
Australia	4				1	4
Austria	1					
Brazil					1	
Canada	4					
Croatia	1					
France	8	1			74	
Germany	4			1		
Holland	2				1	
Italy	4					
Japan	67			1		
New Zealand	1				5	
Spain	6					
Switzerland	1		2			
Thailand	1					
United Kingdom	6	4			35	
United States	3			1	22	
Worldwide totals	114	5	2	3	139	4

Table 3 *Frequency and median incubation periods of cases of Creutzfeldt–Jakob disease due to contaminated human cadaveric growth hormone in the four countries of maximum incidence*

Country of origin	No. of patients	Treated population*	% Frequency of CJD†	Median incubation period, y (range)‡
United States§	23	8000	0.3 (0.8)	20 (10–30)
United Kingdom	35	1880	1.9 (1.9)	16 (8–22)
New Zealand¶	5	184	2.7 (10.9)	26 (14–30)
France	74	1700	4.4 (5.9)	10 (6–16)

* Excludes patients who began treatment after mid-1985 with either recombinant hormone (United States, United Kingdom, New Zealand) or urea-treated hormone (France).
† Figures in parentheses are based on smaller denominators consequent to assumptions about "at-risk" recipient subsets (see text).
‡ Calculated from the midpoint of treatment to the onset of disease.
§ Includes one case in Brazil in a patient who received hormone processed in the United States.
¶ All patients received hormone processed in the United States, and if listed with the US cases, would increase the US case frequencies to 0.35 (1.0).

higher infectious doses generally produce shorter incubation times).

A consideration of all of this information makes it clear that no single factor can explain the different frequencies of CJD in the different countries. The introduction of a chromatography purification step in the hormone production process may have been critical in the United States, but does not appear to have played any role in the United Kingdom and France, and it is thus probable that details of chromatography purification (e.g., column matrix, fraction collection) may have been important risk determinants. It is equally clear that differences in the source of pituitary glands, and the rigor with which donor screening criteria were employed in the various hospital collection centers of each country, must also have been critical to hormone safety. No cases of CJD appear to have resulted from the administration of commercially prepared hormone, which may explain why Japan, which used commercial hormone exclusively, has had no cases among 5000 treated subjects.

Japan, however, had a different problem—that of dura mater grafts. Although nearly all contaminated dura mater grafts were produced before 1987 by a single German company, the absence of precise information about the extent of graft usage prevents reliable risk calculations. Based on a consensus estimate that in Japan about 20,000 grafts were used each year,[9] it is possible to estimate a cumulative incidence of 0.025% in neurosurgical patients receiving grafts during the 13-year period 1979 to 1991, and an incidence of 0.053% during the peak years of 1984 to 1985. The extraordinary use of dura mater grafts in Japan almost certainly exceeded its use in any other country in the world (estimated usage in the United States, for example, was fewer than 4000 grafts per year, of which less than 10% were supplied by the German company). Thus, even with a random international distribution of infected grafts, the number of cases in Japan would be expected to far exceed that in any other country.

Pathogenesis. Virtually all current pituitary hormone and dura mater cases result from infections that occurred before the mid-1980s, when native hormone was replaced by recombinant hormone, and improvements in dura mater donor screening and processing limited further risk of contamination. Thus, most of these cases have comparatively long incubation periods that are at least in part the result of a very small infecting dose (which cannot now be quantified), administered by a suboptimal route of infection.

Whereas the route of entry of the infectious agent into the CNS is obvious in cases resulting from neurosurgical interventions, the route of entry in cases resulting from peripheral infections is uncertain. Contamination from corneal grafts and intramuscular hormone administration could enter the brain either along nerves at the site of infection, or through the bloodstream, and both routes have been successful in experimental models of disease.

Contamination from dura mater grafts is unusual in that the infection is intracranial, rather than intracerebral or peripheral, and it is therefore interesting to ask whether the location of the graft influenced the clinical presentation of CJD, and by implication, the site of initial infection. Table 4 summarizes the results from dural graft recipients in 12 different countries for whom sufficient information is available to analyze the question. It is evident that graft placement had little or no effect on the clinical presentation of CJD, which in three-quarters of cases (32/44) included symptoms and signs referable to the cerebellum. Parenthetically, the presence of myoclonus among presenting symptoms in four of the cases (one in each dura placement category) is remarkable, as it is almost never seen at onset in cases of sporadic CJD.

The preponderance of cerebellar onsets and the absence of topographically distinctive features associated with different dural graft placements has been taken to indicate that cerebellar onsets are not peculiar to peripheral routes of infection.[10] Strictly speak-

Table 4 *Clinical presentation of dura mater–related cases of Creutzfeldt–Jakob disease according to location of dura mater tissue application*

Dural graft introduction	No. of cases	Clinical presentation*			
		Cerebellar	Visual	Mental	Additional symptoms
Supratentorial	20	15	4	6	Myoclonus and hemiparesis (1), drowsiness (1), headache (1)
Infratentorial	17	12	6	4	Myoclonus (1), drowsiness (1)
Infratentorial and cervical	5	3	1	2	Myoclonus and spasticity (1), stiffness and myalgia (1)
Peripheral vein embolization	2	2	1	0	Myoclonus (1), headache and drowsiness (1)
Total	44	32	12	12	

* Some patients had onsets with symptoms in more than one category.

ing, this may be true; however, it is not surprising to find brain surface infections behaving more like peripheral route infections than infections introduced directly into the substance of the brain (either via neurosurgical or stereotactic EEG instruments or via the optic nerve), because infectious material applied to the brain surface, like peripheral route infections, would be widely diffused by the CSF, whereas infections introduced directly into the cerebral cortex would be more likely to start at the site of contamination.

It might even be argued that the preferred site of replication of the infectious agent, given equal access to all regions of the brain, is the cerebellum, and that only when infection is initiated focally inside the cerebrum is mental deterioration likely to precede other signs of disease. Moreover, the clinical distinction between the usually cerebellar onset of brain surface or peripheral infections and the usually demential onset of direct intracerebral infections, together with the clinical similarity of such intracerebral infections to sporadic CJD, is consistent with the idea that sporadic CJD arises de novo within the brain itself, rather than from an external invasion.

Genetic influence. The proportion of alternative genotypes at polymorphic codon 129 of the *PRNP* gene in the normal white population is approximately 40% methionine homozygosity, 10% valine homozygosity, and 50% heterozygosity.[11] It has been known for some time that homozygotes are overrepresented in most types of CJD, and the suggestion has been made that the transition from a normal to pathologic isoform of the encoded protein may be more easily accomplished by molecules with an identical amino acid sequence, so that codon 129 homozygosity would act to predispose to disease.[12]

Table 5 compares the results gathered from published and unpublished molecular genetic studies of

Table 5 *Proportion of codon 129 genotypes in iatrogenic and other forms of Creutzfeldt–Jakob disease (CJD) compared to the general white population*

Patient category	No. of tested patients	Codon 129 genotype			Percent homozygotes
		Met/Met	Met/Val	Val/Val	
Normal white subjects*	398	156	198	44	50
Iatrogenic CJD	128	73	26	29	80
Corneal transplant	1	1	0	0	—
Stereotactic EEG	2	1	1	0	—
Dura mater graft	43	32	8	3	81
Growth hormone	82	39	17	26	78
US	9	5	2	2	78
UK	20	1	8	11	60
France	53	33	7	13	87
Sporadic CJD*	832	587	112	133	87
New variant CJD*	47	47	0	0	100

* Data cited in reference 11.

patients with iatrogenic disease to other forms of CJD: 102 (80%) of 128 iatrogenic cases were homozygous at codon 129. It is curious that whereas methionine homozygosity is the most important genotype in dura mater–related CJD (as well as in sporadic and nvCJD), valine homozygosity makes a disproportionate contribution to growth hormone–related CJD, particularly among patients in the United Kingdom. Conceivably, infected pituitaries in the United Kingdom might by chance have come mainly from valine-homozygous individuals, with a resulting predilection for similarly homozygous hormone recipients.

The possible influence of the codon 129 genotype upon incubation time was also analyzed, with the implicit assumption that the occurrence of a few additional future cases in the studied cohorts will not materially alter the conclusions. For 43 dura mater cases (from 11 different countries), the codon 129 genotype had no statistically significant effect on the length of the incubation period: the median incubation time of the eight heterozygotes was 94 months (range, 34 to 197 months), and the median for the 35 homozygotes was 108 months (range, 16 to 195 months).

Analysis of the growth hormone cohorts requires additional assumptions about both the source and time of infection, because pituitaries were processed differently at different periods and in different countries, and infection in the hormone recipients could have occurred at any point during the usual several year period of therapy. Most studies have estimated the time of infection for each case as the midpoint of the interval during which growth hormone was received.

A previously published study of the French cases observed that heterozygous cases of CJD occurred notably later than the homozygous cases.[8] Analysis of this data shows the difference to be statistically significant ($p = 0.003$), using a lognormal distribution model, and assuming the period of potential exposure was restricted to the years 1983 to 1985, as suggested by epidemiologic data. The same restriction cannot be applied to cases in the United States and United Kingdom, where random contamination occurred, and consequently, incubation times for each case had to be estimated using the midpoint of the total treatment period as the point of infection. Using this approach, no statistically significant relationship could be demonstrated between incubation time and the codon 129 genotype in either the United States or United Kingdom.

In view of the relatively small sample size in each country, and despite the different conditions of hormone preparation in each country, we attempted to increase statistical power by a stratified analysis of pooled data. If, as before, a lognormal distribution is assumed, the result is highly significant ($p = 0.0012$), and nearly identical results were found by a stratified analysis of the data as interval-censored lognormal values (which avoids having to estimate the time of infection as the treatment period midpoint). However, using Cox models that make fewer assumptions about the form of the incubation time distribution curve, none of the comparisons cited above reached statistical significance.

Probably the most serious hindrance to all of this statistical analysis is the unavoidable need to choose some point during the period of therapy as the time of infection. The most plausible choice—the midpoint of the treatment interval—could create a serious calculation artifact by hiding the possibility that the more susceptible homozygotes would be more easily infected and so contract the disease earlier in the course of treatment than would heterozygotes, thus leading to underestimates for the homozygotes and overestimates for the heterozygotes. Analysis assuming interval censoring would be subject to a similar bias. Given the inconsistency of results using these different analytic strategies, it is not possible to draw definitive conclusions about the effect of genotype on incubation time.

Glycotying has not been carried out on enough cases to know whether PrP molecular subtypes exert a further influence upon the clinical features of iatrogenic disease. Of five tested cases, two had Type 1 PrP (both homozygous for methionine at codon 129), and three had Type 2 PrP (all homozygous for valine at codon 129), and no obvious clinical distinction was apparent between the two groups.[13]

Diagnostic laboratory aids. Because many patients with iatrogenic disease are comparatively young, the clinical diagnosis of CJD may not be considered, or be considered unlikely, unless the physician is familiar with the recognized risk factors. Periodic sharp-wave complexes in the EEG and hyperlucency of the putamen in MRI are frequently found in both sporadic and iatrogenic forms of CJD, but are usually not observed early enough in the illness to help with the initial differential diagnosis.

In contrast, a test for the 14-3-3 kinase-inhibitor family of proteins in the spinal fluid has proved increasingly valuable as an aid to the diagnosis of CJD as experience with easily performed Western blot assays has been gained over the last several years. In studies of hundreds of patients with sporadic CJD (many of whom were in the early stages of illness) compared to non-CJD neurologic controls, the test has been found to have a sensitivity and specificity of 90 to 95%.[14] From both published and unpublished data, the test was positive in 33/43 (77%) cases of iatrogenic CJD, including 1/1 corneal graft, 7/8 dura mater grafts, and 25/36 growth hormone cases.

In many cases, positive test results were an important early clue to diagnosis.

Anecdotal observations. All proven or probable cases of iatrogenic CJD have resulted from the transmission of disease either from tissues or instruments contaminated by brain, or tissues proximate to the brain. Nevertheless, the literature includes a few anecdotal reports of patients with CJD in whom peripheral

tissue grafts or transplants had been performed. As examples, we briefly reiterate two published case reports and add one unpublished observation.

The first report was of a 54-year-old man who developed visual and mental abnormalities 4 years after having had a tympanic membrane repair using a pericardial graft from a patient undergoing open heart surgery, who died postoperatively.[15] The second report was of a 57-year-old woman with the onset of cerebellar symptoms 2 years after receiving a liver transplant from a 42-year-old man who died from rupture of a cerebral aneurysm.[16] The recipient of a renal transplant from the same donor remained in good health at the time of writing. During the liver transplant operation, the patient also received a small amount of albumin from a large plasma pool that included a contribution from a donor who 3 years later died of sporadic CJD. Contamination from this source can probably be excluded on the basis of experimental animal model studies showing the absence of infectivity in albumin.

The unpublished observation is of a 63-year-old man whose illness began with memory loss and nominal aphasia 4 years after receiving a bone graft from a previously healthy 46-year-old man who had died of a myocardial infarct. Bone from the same patient was used in grafts for 27 other patients, of whom 13 were reported in good health up to 6 years afterwards (14 recipients could not be reached). Both corneas were also harvested and both recipients have remained in good health.

In each of these three examples, the tissue recipients were verified by postmortem neuropathologic examination to have died of CJD, and although none of the donors was known to have a primary neurologic illness, none had undergone autopsy.

In only one of the three cases—that of the liver transplant recipient—was there a cerebellar onset of illness, which is the proportion that would be expected for sporadic CJD, but not for iatrogenic CJD contracted by peripheral route infection. Whereas it is likely that these (and other) cases represent the chance occurrence of sporadic CJD in individuals with preceding transplantation procedures, their occurrence should not be ignored, as any similar future cases will shift the balance in favor of an iatrogenic cause, just as happened after the initial case reports of CJD in recipients of growth hormone and dura mater grafts. Attention should also be given to anecdotal cases of CJD in individuals exposed to other sources of human or animal tissues, including commercial dietary supplements such as vitamin tablets compounded in tissue powders, illustrated by the following case.

A 71-year-old American woman experienced a progressive gait disorder and mental deterioration beginning in the autumn of 1989. Neurologic examination confirmed a severe ataxia with features of both cerebellar and basal ganglion dysfunction, global disorientation, and memory loss. She subsequently developed visual loss, complex involuntary movements, and myoclonus. EEG was abnormal but showed no periodic activity. Brain biopsy of the frontal cortex showed spongiform change (no plaques were seen). She died 18 months after the onset of illness, and in view of the biopsy diagnosis, no autopsy was performed. The patient's family noted that she had for many years regularly taken a megavitamin preparation that, on investigation, was found to contain large quantities of imported beef liver and bone meal. The country of origin of these imported tissues was not specified.

The millennium. For the future of iatrogenic disease in the 21st century, we are optimistic that because of an increased awareness in the scientific and medical communities of the dangers of transmitting infectious diseases from donors to recipients of tissues, tissue extracts, and fluids (such as blood and its products), together with knowledge of high-risk CJD tissue sources and methods to avoid or mitigate their infectious potential, outbreaks of iatrogenic CJD will soon fade into memory. Certainly, with disinfection techniques now well defined, there is little likelihood of iatrogenic disease resulting from contaminated instruments, although we still have not solved the problem of potential risk from instruments too delicate to withstand harsh chemicals and autoclaves, and too expensive to discard, that have contacted infectious organs in patients who only later are discovered to have been incubating CJD.

Alternatives to human tissue products, such as recombinant growth hormone and anti-hemophilic factor VIII, to name but two examples, are already in use and will become increasingly common. Where alternatives are either suboptimal or unavailable, attention to donor screening should eliminate much of the risk at its source. However, in view of the now all but certain classification of the new variant of CJD as a zoonotic disease,[17-19] we must concede the possibility that unpredictable infections of humans by analogous animal diseases could spawn donor groups whose tissues or blood would be used in complete ignorance of their potential infectivity. Until a practical diagnostic test to detect preclinical CJD becomes a reality, no method or combination of methods will guarantee risk-free conditions for recipients, and, as always, considerations of risk tolerated for benefits gained will determine the use or discontinuance of human products for therapeutic purposes.

Acknowledgment

The authors thank the Centre National de Référence de la Maladie de Creutzfeldt–Jakob Iatrogène for permission to include data on the French growth hormone and dura mater cases. They also thank the large supporting cast of individuals in North America, Europe, and Japan who in one way or another contributed to the ongoing CJD surveillance in these regions of the world.

References

1. Duffy P, Wolf J, Collins G, DeVoe AG, Streeten B, Cowen D. Possible person to person transmission of Creutzfeldt–Jakob disease. N Engl J Med 1974;290:692–693.
2. Uchiyama S, Ishida C, Yago S, Kurumaya H, Kitamoto T. An

autopsy case of Creutzfeldt–Jakob disease associated with corneal transplantation [in Japanese]. Dementia 1994;8:466–473.
3. Heckmann JG, Lang CJG, Petruch F, et al. Transmission of Creutzfeldt–Jakob disease via a corneal transplant. J Neurol Neurosurg Psychiatry 1997;63:388–390.
4. Bernoulli C, Siegfreid J, Baumgartner G, et al. Danger of accidental person-to-person transmission of Creutzfeldt–Jakob disease by surgery. Lancet 1977;i:478–479.
5. Brown P. Environmental causes of human spongiform encephalopathy. In: Baker HF, Ridley RM, eds. Methods in molecular medicine: prion diseases. Totowa, NJ: Humana Press, 1996: 139–154.
6. Koch TK, Berg BO, DeArmond SJ, Gravina RF. Creutzfeldt-Jakob disease in a young adult with idiopathic hypopituitarism. N Engl J Med 1985;313:731–733.
7. Thadani V, Penar PL, Partington J, et al. Creutzfeldt–Jakob disease probably acquired from a cadaveric dura mater graft. J Neurosurg 1988;69:766–769.
8. d'Aignaux JH, Costagliola D, Maccario J, et al. Incubation period of Creutzfeldt–Jakob disease in human growth hormone recipients in France. Neurology 1999;53:1197–1201.
9. Nakamura Y, Aso E, Yanagawa H. Relative risk of Creutzfeldt–Jakob disease with cadaveric dura transplantation in Japan. Neurology 1999;53:218–220.
10. Radbauer C, Hainfellner JA, Gaudernak T, Deecke L, Budka H. Creutzfeldt-Jakob-Krankheit bei einem Dura-Transplantat-Empfänger: Erstbeobachtung in Österrieich. Wien Klin Wochenshr 1998;110:496–500.
11. Alperovitch A, Zerr I, Pocchiari M, et al. Codon 129 prion protein genotype and sporadic Creutzfeldt-Jakob disease. Lancet 1999;353:1673–1674.
12. Palmer MS, Dryden AJ, Hughes JT, Collinge J. Homozygous prion protein genotype predisposes to sporadic Creutzfeldt–Jakob disease. Lancet 1991;352:340–342.
13. Parchi P, Zou W, Wang W, et al. Genetic influence on the structural variations of the abnormal prion protein. Proc Natl Acad Sci USA 2000;97:10168–10172.
14. Zerr I, Pocchiari M, Collins S, et al. Analysis of EEG and CSF 14-3-3 proteins as aids to the diagnosis of Creutzfeldt–Jakob disease. Neurology 2000 (in press).
15. Tange RA, Troost D, Limburg M. Progressive fatal dementia (Creutzfeldt–Jakob disease) in a patient who received homograft tissue for tympanic membrane closure. Eur Arch Otorhinolaryngol 1990;247:199–201.
16. Créange A, Gray F, Cesaro P, et al. Creutzfeldt–Jakob disease after liver transplantation. Ann Neurol 1995;38:269–272.
17. Collinge J, Sidle KCL, Heads J, Ironside J, Hill AF. Molecular analysis of prion strain variation and the aetiology of 'new variant' CJD. Nature 1996;283:685–690.
18. Bruce ME, Will RG, Ironside JW, et al. Transmissions to mice indicate that 'new variant' CJD is caused by the BSE agent. Nature 1997;389:498–501.
19. Scott MR, Will R, Ironside J, et al. Compelling transgenetic evidence for transmission of bovine spongiform encephalopathy prions to humans. Proc Natl Acad Sci USA 1999;96: 15137–15142.

OBSERVATION

Novel Prion Protein Gene Mutation in an Octogenarian With Creutzfeldt-Jakob Disease

Steven Collins, MD, FRACP; Alison Boyd, DipGenCouns; Ashley Fletcher, BSc; Keith Byron, PhD; Clive Harper, MD, FRCPA; Catriona A. McLean, MB, BS, FRCPA; Colin L. Masters, MD, FRCPA

Background: The transmissible spongiform encephalopathies constitute a fascinating and biologically unique group of invariably fatal neurodegenerative disorders that affect both animals and humans. Creutzfeldt-Jakob disease (CJD), Gerstmann-Sträussler-Scheinker syndrome, and fatal familial insomnia represent the more common human phenotypes. Excluding the small number of iatrogenically transmitted cases, approximately 85% to 90% of patients develop CJD without identifiable explanation, with an increasing number of different mutations in the prion protein gene (*PRNP*) recognized as probably causative in the remainder.

Objective: To report on an 82-year-old woman with pathologically confirmed CJD found unexpectedly to harbor a novel mutation in *PRNP*.

Methods: Routine clinical investigations were undertaken to elucidate the cause of the rapidly progressive dementia and neurological decline manifested by the patient, including magnetic resonance imaging of the brain, electroencephalography, and cerebrospinal fluid analysis for the 14-3-3 β protein. Standard postmortem neuropathological examination of the brain was performed, including immunocytochemistry of representative sections to detect the prion protein. Posthumous genetic analysis of the open reading frame of *PRNP* was performed on frozen brain tissue using polymerase chain reaction and direct sequencing.

Results: Concomitant with the exclusion of alternative diagnoses, the presence of characteristic periodic sharp-wave complexes on the electroencephalogram in combination with a positive result for 14-3-3 β protein in the cerebrospinal fluid led to a confident clinical diagnosis of CJD, confirmed at autopsy. There was no family history of dementia or similar neurological illness, but patrilineal medical information was incomplete. Unexpectedly, full sequencing of the *PRNP* open reading frame revealed a single novel mutation consisting of an adenine-to-guanine substitution at nucleotide 611, causing alanine to replace threonine at codon 188.

Conclusions: In addition to expanding the range of *PRNP* mutations associated with human prion diseases, we believe this case is important for the following reasons. First, from an epidemiological perspective, the avoidance of occasional incorrect classification of patients manifesting neurodegenerative disorders that may have a genetic basis requires systematic genotyping, particularly when there are uncertainties regarding the family history. Second, the incidence of spongiform encephalopathy in elderly patients beyond the typical age range may be underestimated and does not preclude a genetic basis. Finally, as a corollary, this case highlights problematic issues in human transmissible spongiform encephalopathies, as illustrated by disease penetrance and age of onset in genotype-phenotype correlations.

Arch Neurol. 2000;57:1058-1063

From the Department of Pathology, University of Melbourne, Parkville (Drs Collins, McLean, and Masters, Ms Boyd, and Mr Fletcher), Western Health Care Network Pathology, Royal Melbourne Hospital, Parkville (Dr Byron), and the Department of Pathology, Royal Prince Alfred Hospital, University of Sydney, Sydney (Dr Harper), Australia.

THE TRANSMISSIBLE spongiform encephalopathies (TSE; also known as *prion diseases*) are rare neurodegenerative disorders that in humans occur in 3 different epidemiological settings: sporadic, familial, and horizontally transmitted (usually iatrogenic). Creutzfeldt-Jakob disease (CJD), Gerstmann-Sträussler-Scheinker syndrome, and fatal familial insomnia constitute the most common distinguishable vertically transmitted phenotypes. These disorders follow autosomal dominant inheritance patterns and are caused by a range of mutations in the prion protein gene (*PRNP*) on chromosome 20.[1-28] Surveillance studies report the familial varieties to constitute around 10% to 15% of all human TSE,[29] but this may be an underestimate of the heredofamilial forms. Systematic *PRNP* analyses of CJD patients without a definite family history of a similar neurological disorder not infrequently disclose causal mutations, suggesting that camouflaged or unrecognized family histories may be relatively common.[3,13,15,18,27,28]

METHODS

GENETIC ANALYSIS

Two separate samples of brain tissue obtained postmortem were snap frozen and homogenized under liquid nitrogen. A portion of the resulting frozen tissue powder was added to polymerase chain reaction (PCR) buffer to which proteinase K was added. Protein digestion was allowed to proceed overnight at 56°C, after which the samples were boiled.

The open reading frame (ORF) of *PRNP* was amplified based on the method and primers previously described.[2] Five microliters of the amplified DNA was added to 1 µL of shrimp alkaline phosphatase and 1 µL of exonuclease I, then incubated at 37°C for 15 minutes followed by 80°C for 15 minutes. Direct DNA sequencing of the *PRNP* ORF was accomplished by cycle sequencing according to the manufacturer's instructions (ThermoSequenase; Amersham, Cleveland, Ohio). Deoxyribonucleic acid from 2 separate brain pieces was isolated, amplified by PCR, and sequenced on 2 separate occasions to validate findings.

The DNA sequence obtained was then compared with the *PRNP* sequence deposited in GenBank (http://www.ncbi.nlm.nih.gov; accession number M13899). The adenine-to-guanine transversion detected at nucleotide 611 in the patient was not found in 63 controls, nor was it listed in GenBank.

NEUROPATHOLOGY

Postmortem examination was limited to the brain. The brain was fixed in 15% formal saline solution for 2 weeks prior to sectioning. The brainstem and cerebellum were removed by cutting at the level of the midbrain, and the cerebral hemispheres were then sectioned in the coronal plane at 10-mm intervals. The cerebellum was sectioned in the sagittal plane, and the brainstem was sectioned at 3-mm intervals in the horizontal plane. Blocks of tissue were taken from the frontal, parietal, temporal, and occipital cortices, as well as from the thalamus, basal ganglia, midbrain, pons, medulla, cerebellar vermis, and lateral hemisphere. These samples were placed in 95% formic acid for 1 hour prior to paraffin embedding and 10-µm sectioning for routine staining.

Immunocytochemistry was performed to detect prion protein (PrP) in the representative brain regions (including occipital cortex, basal ganglia, and cerebellum) after hydrolytic autoclaving to enhance antigen retrieval.[30] The well-characterized monoclonal antibodies 3F4 (Senetek PLC, Napa, Calif) and 6H4 (Prionics AG, Zurich, Switzerland) were used, as well as a departmental polyclonal antibody (PrP-725) raised against a synthetic peptide equivalent to the amino acid sequence corresponding to codons 89 to 106 of PrP. Additional immunodetection of β-amyloid plaques (using the 1E8 antibody [departmental antibody] raised against a synthetic peptide fragment corresponding to amino acids 17 to 25 of β-amyloid), τ (Dako Corp, Carpinteria, Calif), and ubiquitin (Dako Corp) was undertaken. Relevant positive controls were routinely included for all sections, and immunoreactivity was completed using a secondary antibody conjugated to horseradish peroxidase with 3,3′-diaminobenzidine as chromagen.

WESTERN IMMUNOBLOT DETECTION OF THE 14-3-3 β PROTEIN

The method was performed as described previously[31] with the following modifications. Briefly, 50 µL of cerebrospinal fluid (CSF) was combined with 10 µL of sample buffer (final concentrations: 5% glycerol, 1% 2-mercaptoethanol, 1% sodium dodecyl sulphate, and trace bromophenol blue) and boiled for 10 minutes before separation on denaturing 15% polyacrylamide Tris hydrochloride gels with a 4% stacking component (Bio-Rad Laboratories Inc, Hercules, Calif). After resolution for approximately 40 minutes at 200 V, transfer was effected to a polyvinylidene difluoride membrane (Immobilon-P; Millipore, Bedford, Mass) using 100 V for 1 hour. Filter blocking was for 60 minutes using 0.5% Tween 20 (Sigma-Aldrich, St Louis, Mo) in a 5% (wt/vol) skim milk Tris hydrochloride buffer solution. Primary immunodetection was at room temperature for 1 hour with a 1:1000 dilution of the anti–14-3-3 β antibody (Santa Cruz Biotechnology, Santa Cruz, Calif) followed by incubation (at 1:2000) with a horseradish peroxidase–conjugated polyclonal antirabbit antibody (Amersham PLC, Buckinghamshire, England) before enhanced chemiluminescent detection (Amersham PLC) as per the manufacturer's instructions. Positive and negative controls and colored protein molecular weight markers (Rainbow; Amersham) were included to aid orientation and verify results.

In this context, we report a novel *PRNP* threonine-to-alanine codon 188 mutation in an 82-year-old woman with clinical and pathological features typical of CJD who had no known family history of neurological disease. The patient was discovered during routine monitoring activities of the Australian Creutzfeldt-Jakob Disease Case Registry. We postulate that the threonine-to-alanine substitution at codon 188 of *PRNP* is causally linked to spontaneous spongiform degeneration in humans, and we hypothesize that the mutation may have reduced penetrance or reduced pathogenetic capacity, explaining the advanced age at symptom onset, and this is perhaps why it has not been previously reported.

CASE REPORT AND RESULTS

The patient was 82 years old when admitted to the hospital with confusion following a fall at home. During the 2 years prior to admission, family members had recognized minor forgetfulness that did not compromise her ability to live alone and cope independently. There was a remote personal medical history of ischemic heart disease and osteoarthritis but no neurological or ophthalmological surgical procedures.

Preliminary inpatient investigations, including routine biochemical and hematological parameters as well as a computed tomographic head scan, did not reveal an ex-

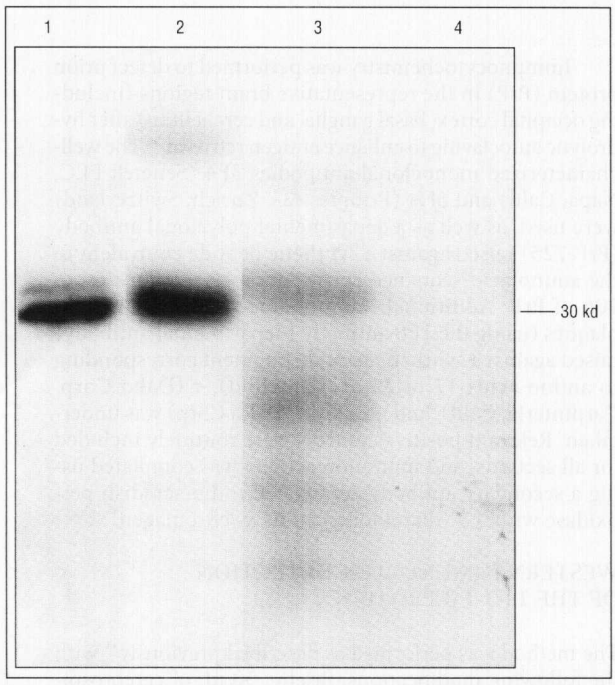

Figure 1. *Western immunoblot analysis of cerebrospinal fluid showing the presence of 14-3-3 β protein. Lane 1, positive control (pathologically confirmed case of sporadic Creutzfeldt-Jakob disease); lane 2, 82-year-old patient; lane 3, molecular weight markers with the 30-kd band indicated; and lane 4, negative control.*

planation for her confusion. During the first 2 weeks following admission, neuropsychological examinations confirmed disorientation (for day and date), dyslexia, reduced attention, dyscalculia, left-right disorientation, poor short-term memory, and visual-spatial difficulties. Cognition and mood were noted to fluctuate. The initial salient neurological findings were myoclonus affecting the left arm, generalized hyperreflexia, bilateral extensor plantar responses, and frontal release phenomena in the form of a pout reflex. An initial electroencephalogram revealed changes suggesting the possibility of nonconvulsive status epilepticus, but there was no clinical improvement with varying combinations of anticonvulsant therapy using phenytoin, gabapentin, and carbamazepine. During the ensuing weeks, the patient's neurological status progressively declined, evidenced by probable visual hallucinations, cortical blindness, reduced verbal output, and worsening generalized hypertonia. Brain imaging with 2 further computed tomographic scans and a magnetic resonance imaging scan revealed only minor cerebral atrophy consistent with the patient's age. Repeated electroencephalograms eventually showed generalized, synchronous 0.5- to 1-Hz periodic sharp-wave complexes, emphasized over the right hemisphere, typical of sporadic CJD.[32] Cerebrospinal fluid analysis revealed a very minor elevation of protein to 0.62 g/L (normal, <0.4 g/L) and minimal pleocytosis, with 10 white blood cells per microliter; using Western immunoblot analysis, the 14-3-3 β protein was detected (**Figure 1**). The patient died approximately 2 months after admission (total illness duration of approximately 4 months) with a firm clinical diagnosis of CJD.

Postmortem examination of the brain showed no macroscopic abnormalities. Microscopic assessment con-

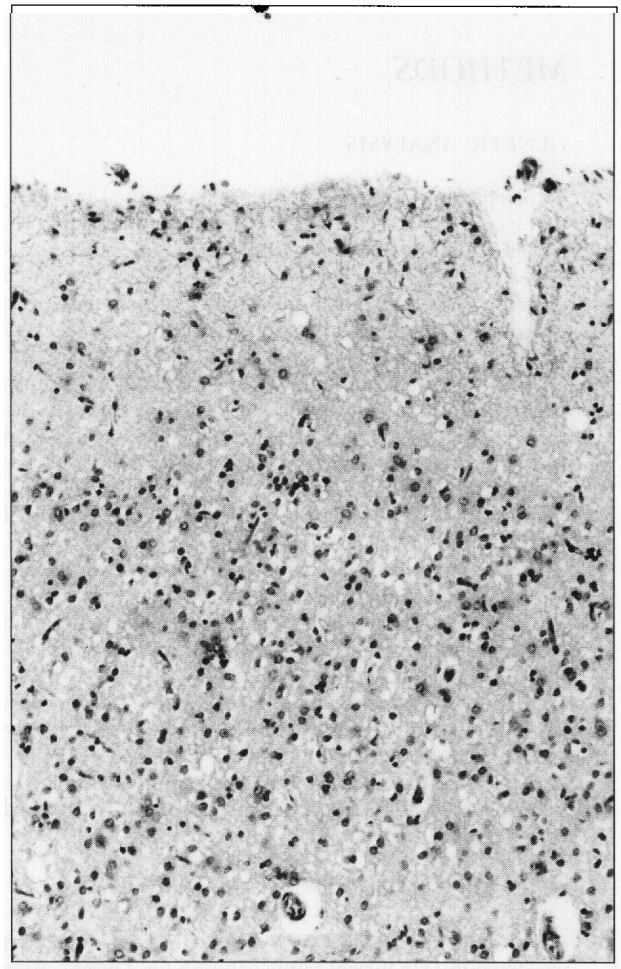

Figure 2. *Photomicrograph of representative section of occipital (striate) cortex showing prominent spongiform change with neuronal loss and gliosis (hemotoxylin-esosin, original magnification ×40).*

firmed changes typical of a spongiform encephalopathy. The changes were most severe in the occipital cortex and in particular, in the striate (visual) cortex (**Figure 2**). There were moderate neuronal loss and severe gliosis and spongiosus, mainly involving the middle and lower layers of the occipital cortex. The vacuoles were generally small (10-20 μm) but some were as large as 40 μm. The changes were reasonably uniform throughout the occipital cortex but were more focal and less severe in all other cortical regions examined. Occasional senile plaques with β-amyloid cores were noted in the cerebral cortex, but the numbers were only commensurate with age. The thalamus and basal ganglia showed mild diffuse spongiform change with relatively little gliosis or neuronal loss. The cerebellum showed only very minor spongiosis but no obvious gliosis or neuronal loss. No plaques were seen in the cerebellum. The brainstem was normal. Despite the pathognomonic histological appearance, immunohistochemical staining for PrP was repeatedly negative with the 3 different antibodies in all sections from the cerebral cortex, basal ganglia, hippocampus, and cerebellum. Western immunoblot analysis for protease-resistant PrP could not be performed because of the unavailability of fresh-frozen brain tissue. Auxiliary immunostaining showed frequent diffuse β-amyloid plaques and very occasional neuritic plaques

Table 1. Prion Protein Gene Mutations for Transmissible Spongiform Encephalopathies*

Codon	Amino Acid Change or Octapeptide Repeat	Study
	Gerstmann-Sträussler-Scheinker Syndrome	
Missense mutations		
102	Proline to leucine	Hsiao et al,[2] 1989
105	Proline to leucine	Kitamoto et al,[3] 1993
117	Alanine to valine	Doh-ura et al,[4] 1989
198	Phenylalanine to serine	Hsiao et al,[6] 1992
212	Glutamine to proline	Piccardo et al,[7] 1998
217	Glutamine to arginine	Hsiao et al,[6] 1992
Insert mutations†		
Starting at 84	8 Octapeptide repeat (192-bp) insert	Goldfarb et al,[8] 1992
Starting at 76	8 Octapeptide repeat (192-bp) insert	van Gool et al,[9] 1995
Not stated	8 Octapeptide repeat (192-bp) insert	El Hachimi et al,[10] 1998
	Creutzfeldt-Jakob Disease	
Missense mutations		
178	Aspartate to asparagine	Goldfarb et al,[12] 1991
180	Valine to isoleucine	Kitamoto et al,[3] 1993
200	Glutamate to lysine	Goldgaber et al,[13] 1989; Chapman et al,[22] 1996
208	Arginine to histidine	Mastrianni et al,[14] 1996
210	Valine to isoleucine	Pocchiari et al,[15] 1993
232	Methionine to arginine	Kitamoto et al,[3] 1993
Insert mutations		
†	1 Octapeptide repeat (24-bp) insert	Laplanche et al,[16] 1995
†	2 Octapeptide repeat (48-bp) insert	Goldfarb et al,[17] 1993
†	4 Octapeptide repeat (96-bp) insert	Campbell et al,[18] 1996
†	5 Octapeptide repeat (120-bp) insert	Goldfarb et al,[1] 1991
†	6 Octapeptide repeat (144-bp) insert‡	Collinge et al,[20] 1992
†	7 Octapeptide repeat (168-bp) insert	Goldfarb et al,[1] 1991
	Fatal Familial Insomnia Missense Mutation	
178	Aspartate to asparagine	Medori et al,[21] 1992
	Prion Protein Cerebral Amyloid Angiopathy Nonsense Mutation	
145	Tyrosine to stop	Kitamoto et al,[5] 1993; Ghetti et al,[37] 1996

*bp indicates base pair.

†All octapeptide repeat inserts and deletions (a normal polymorphism in approximately 1% of the population) occur from codons 51 to 91 of the open reading frame of the prion protein gene.

‡The 144-bp insert is associated with considerable intrafamilial clinicopathologic phenotypic variation.[20]

in areas of the cerebral cortex, basal ganglia, and hippocampus. Neurofibrillary tangles were restricted to the hippocampus, where ubiquitin was colocalized with the τ-positive neurofibrillary changes. However, because of the age of the patient, these neuropathological features were insufficient to substantiate a Consortium to Establish a Registry for Alzheimer's Disease (CERAD)[33] diagnosis of Alzheimer disease.

In the absence of any hint of familial prion disease, a son requested *PRNP* genotyping posthumously to assuage his remote concerns of this possibility. Polymerase chain reaction amplification and direct sequencing of the *PRNP* ORF revealed an adenine-to-guanine substitution at nucleotide 611, causing alanine to replace threonine at codon 188 (T188A). The patient was homozygous for methionine at codon 129.

Unfortunately, because of issues relating to the patient's illegitimate birth, no information was available concerning the medical history of the father or his family, and a protective code of secrecy was adopted by informed matrilineal relatives so that direct sourcing of information from the other surviving maternal relatives was not possible. Working within this constraint, the only history of neurological disease in the patient's mother was sudden death from a stroke at age 75 years (verified on death certificate). Among the 11 maternal half-siblings of the proband, 7 were dead, with the family's understanding of cause of death as "heart" or "stroke" in 5 (ages at death ranged from 48 to 67 years), motor neurone disease in 1 (died at age 65 years), and a motor vehicle accident in 1 (died at age 50 years). The 4 living siblings (ages ranged from 58 to 68 years) were all well. The index case had 3 children, aged 52, 60, and 65 years, who were alive and well. At the time of this report, the proband's children all declined *PRNP* genotyping, and because of the code of secrecy adopted by the informed family members, none of the other relatives was offered screening for the T188A mutation.

COMMENT

As summarized in **Table 1** and **Table 2**, to the best of our knowledge, this T188A mutation has not been described previously in association with human TSE or as a normal *PRNP* polymorphism.[1-28,34-37] We propose that this mutation is causally associated with the pathologically verified spongiform encephalopathy seen in our patient, but we await confirmation of its etiological signifi-

Table 2. Prion Protein Gene Mutations for Less Specific Phenotypes of Neurodegenerative Disorders and Normal Polymorphisms*

Codon	Amino Acid Change or Octapeptide Insert	Phenotype or Race/Ethnicity	Study
	Less Specific Phenotypes		
Missense mutations			
171	Asparagine to serine	Neuropsychiatric illness	Samaia et al,[23] 1997
183	Threonine to alanine	Presenile dementia	Nitrini et al,[24] 1997
183	Threonine to alanine	Familial "Alzheimer's" disease	Nitsch et al,[25] 1998
Insert mutation			
Not stated	9 Octapeptide repeat (216-bp) insert	Sporadic dementia	Owen et al,[26] 1991
	Normal Polymorphisms		
129	Methionine-methionine, 37%; methionine-valine, 51%; valine-valine, 12%	White	Palmer et al,[34] 1991
219	Glutamate-glutamate, 88%; lysine-glutamate, 12%	Japanese	Furukawa et al,[35] 1995
Deletion mutations			
†	Single octapeptide repeat (24-bp) deletions; 3 types	NA	Palmer et al,[36] 1993
Insert mutation			
Not stated	4 Octapeptide repeat (96-bp) insert‡	NA	Goldfarb et al,[1] 1991

*bp indicates base pair; NA, not applicable.

†All octapeptide repeat inserts and deletions (a normal polymorphism in approximately 1% of the population) occur from codons 51 to 91 of the open reading frame of the prion protein gene.

‡Found in a 63-year-old man dying of micronodular cirrhosis with no personal or family history of neurological disease.

cance with future reports. Nevertheless, the threonine normally found at codon 188 of *PRNP* is highly conserved across a broad range of mammalian species[38] (probably lying within an α helix[39]), offering further circumstantial support to the likely significance of any mutation at this site. However, the alanine substitution appears to be a relatively conservative primary sequence change, and despite its proximity, it does not appear to directly alter important native conformational determinants, such as the *N*-linked glycosylation motifs or the disulfide bridge.[39] The potentially modest structural impact of the mutation may relate to the advanced age of our patient at symptom onset, which is less typical for *PRNP* mutations.[40] This substitution may have less inherent capacity to facilitate the postulated conformational change of wild-type PrP to the relatively protease-resistant, disease-associated conformations thought to underlie the pathological etiology of *PRNP* mutations.

Camouflaged or unrecognized family histories are not unique to TSE. The range of potential explanations offered for other autosomal dominant neurodegenerative disorders is also relevant to prion diseases.[41] The most plausible explanation for our patient is probable patrilineal inheritance, with the disease unknown to the propositus and her family.

Acceptance of the pathoetiological relevance of the T188A mutation underscores potentially important epidemiological issues, especially for national TSE case registries. Using systematic genotyping, previous reports have also described the detection of recognized (V210I,[15,27] E200K,[27] and D178N[28]) and novel (V180I,[3] M232R,[3] R208H,[13] and 96–base pair insert[18,28]) *PRNP* mutations in patients manifesting CJD in the absence of any known family history of neurological disease. The large, unselected series of Windl and colleagues[28] suggests a frequency of approximately 5% (3 of 67 cases). Hence, if the optimal epidemiological classification of prion disease is to be achieved in ascertained cases (especially in cases with incomplete or uncertain family histories), ethical implications notwithstanding, the best practice would appear to necessitate universal *PRNP* genotyping.

Detection of the 14-3-3 protein in CSF by Western immunoblot analysis has proven very useful in the premortem evaluation of patients with suspected sporadic CJD.[31,42] Although a positive result in appropriately selected patients carries sensitivities and specificities of around 90%, it has proven a less reliable marker in familial prion diseases, although only small numbers of cases have been reported so far.[42,43] The likelihood of a positive result appears to depend at least partly on the specific mutation. Virtually all symptomatic patients with the E200K mutation show positive immunoreactivity for the 14-3-3 β protein in CSF, whereas positivity rates in the D178N and P102L polymorphisms range from 20% to 50%.[42,43] We believe that the 14-3-3 β protein CSF result in the patient described herein contributes to the expanding collective experience of the utility of this diagnostic test in familial TSE.

The consistently negative immunostaining results for PrP in all brain regions, despite using 3 antibodies recognizing different regions of the protein, are at variance with the usual neuropathological findings in CJD. We are unable to offer an explanation for this unexpected finding, but we are confident that it does not relate to a technical fault with tissue handling or preparation or to the antibodies used, as simultaneous control sections always stained positive with all 3 antibodies. Nevertheless, PrP immunostaining does not necessarily colocalize with routine pathological findings, and uncommonly, patients with sporadic CJD may show negative immunocytochemical results.[44] In addition, patients manifesting genetically determined spongiform encephalopathies, including fatal familial insomnia[45] and CJD[3] (due to the V180I mutation; written communication from T. Kitamoto, February 24, 1999), may show an absence of immunostaining for PrP. Although in fatal familial insomnia, the correlating absence of immunocytochemically detectable PrP and spongiform change may be due

to the relatively low intrinsic amounts of protease-resistant PrP in these negative regions[46]; this appears to be a less likely explanation in the V180I CJD case reported, which showed typical spongiform degeneration in the cerebral cortex, similar to that in our patient.

Finally, the advanced age of our patient at symptom onset is also of interest. At a practical surveillance level, it emphasizes the heightened vigilance that must be practiced to avoid missing TSE cases falling outside the typical age range,[47] especially in the elderly, for whom alternative, more common, but incorrect diagnostic explanations may be entertained. The advanced age of a patient may also militate against the rigor of diagnostic evaluation usually afforded younger patients. Consequently, underrecognition of CJD in very elderly patients remains a continuing concern, and as illustrated by the patient described herein, a genetic basis for the disease is possible.

Accepted for publication December 1, 1999.

The Australian National Creutzfeldt-Jakob Disease Registry is funded by the Commonwealth Department of Health and Aged Care.

Corresponding author: S. Collins, MD, FRACP, National Creutzfeldt-Jakob Disease Registry, Level 5, Department of Pathology, University of Melbourne, Parkville, Victoria, Australia 3052 (e-mail: s.collins@pathology.unimelb.edu.au).

REFERENCES

1. Goldfarb L, Brown P, McCombie WR, et al. Transmissible familial Creutzfeldt-Jakob disease associated with five, seven, and eight extra octapeptide coding repeats in the *PRNP* gene. *Proc Natl Acad Sci U S A.* 1991;88:10926-10930.
2. Hsiao K, Baker H, Crow T, et al. Linkage of a prion protein missense variant to Gerstmann-Sträussler syndrome. *Nature.* 1989;338:342-345.
3. Kitamoto T, Ohta M, Doh-ura K, Hitoshi S, Terao Y, Tateishi J. Novel missense variants of prion protein in Creutzfeldt-Jakob disease or Gerstmann-Sträussler syndrome. *Biochem Biophys Res Commun.* 1993;191:709-714.
4. Doh-ura K, Tateishi J, Sasaki H, Kitamoto T, Sakaki Y. Pro—leu change at position 102 of prion protein is the most common but not the sole mutation related to Gerstmann-Sträussler syndrome. *Biochem Biophys Res Commun.* 1989; 163:974-979.
5. Kitamoto T, Iizuka R, Tateishi J. An amber mutation of prion protein in Gerstmann-Sträussler syndrome with mutant PrP plaques. *Biochem Biophys Res Commun.* 1993;192:525-531.
6. Hsiao K, Dlouhy S, Farlow M, et al. Mutant prion proteins in Gerstmann-Sträussler-Scheinker disease with neurofibrillary tangles. *Nat Genet.* 1992;1:68-71.
7. Piccardo P, Young K, William A, et al. Physicochemical properties of prion protein (PrP) in Gerstmann-Sträussler-Scheinker disease (GSS) Q212P [abstract]. *Soc Neurosci Abstr.* 1998;24:1476.
8. Goldfarb L, Brown P, Vrbovská A, et al. An insert mutation in the chromosome 20 amyloid precursor gene in a Gerstmann-Sträussler-Scheinker family. *J Neurol Sci.* 1992;111:189-194.
9. van Gool W, Hensels G, Hoogerwaard E, Wiezer J, Wesseling P, Bolhuis P. Hypokinesia and presenile dementia in a Dutch family with a novel insertion in the prion protein gene. *Brain.* 1995;118:1565-1571.
10. El Hachimi K, Laplanche J, Destée A, et al. An insert mutation in the *PrP* gene in a French Gerstmann-Sträussler-Scheinker family with psychiatric features [abstract]. *Soc Neurosci Abstr.* 1998;24:1476.
11. Young K, Clark H, Piccardo P, Dlouhy SR, Ghetti B. Gerstmann-Sträussler-Scheinker disease with the *PRNP* P102L mutation and valine at codon 129. *Mol Brain Res.* 1997;44:147-150.
12. Goldfarb L, Haltia M, Brown P, et al. New mutation in scrapie amyloid precursor gene (at codon 178) in Finnish Creutzfeldt-Jakob kindred. *Lancet.* 1991;337: 425.
13. Goldgaber D, Goldfarb L, Brown P, et al. Mutations in familial Creutzfeldt-Jakob disease and Gerstmann-Sträussler-Scheinker's syndrome. *Exp Neurol.* 1989; 106:204-206.
14. Mastrianni J, Iannicola C, Myers R, DeArmond S, Prusiner S. Mutation of the prion protein gene at codon 208 in familial Creutzfeldt-Jakob disease. *Neurology.* 1996;47:1305-1312.
15. Pocchiari M, Salvatore M, Cutruzzolá F, et al. A new point mutation of the prion protein gene in Creutzfeldt-Jakob disease. *Ann Neurol.* 1993;34:802-807.
16. Laplanche JL, Delasnerie-Lauprêtre N, Brandel JP, Dussaucy M, Chatelain J, Launay JM. Two novel insertions in the prion protein gene in patients with late-onset dementia. *Hum Mol Genet.* 1995;4:1109-1111.
17. Goldfarb L, Brown P, Little BW, et al. A new (two-repeat) octapeptide coding insert mutation in Creutzfeldt-Jakob disease. *Neurology.* 1993;43:2392-2394.
18. Campbell TA, Palmer MS, Will RG, Gibb WR, Luthert PJ, Collinge J. A prion disease with a novel 96-base pair insertional mutation in the prion protein gene. *Neurology.* 1996;46:761-766.
19. Owen F, Poulter M, Lofthouse R, et al. Insertion in prion protein gene in familial Creutzfeldt-Jakob disease. *Lancet.* 1989;1:51-52.
20. Collinge J, Brown J, Hardy J, et al. Inherited prion disease with 144 base pair gene insertion: 2 clinical and pathological features. *Brain.* 1992;115:687-710.
21. Medori R, Tritschler HJ, LeBlanc A, et al. Fatal familial insomnia, a prion disease with a mutation at codon 178 of the prion protein gene. *N Engl J Med.* 1992; 326:444-449.
22. Chapman J, Arlazoroff A, Goldfarb LG, et al. Fatal insomnia in a case of familial Creutzfeldt-Jakob disease with the codon 200(lys) mutation. *Neurology.* 1996; 46:758-761.
23. Samaia HB, Mari JJ, Vallada HP, Moura RP, Simpson AJ, Brentani RR. A prion-linked psychiatric disorder [letter]. *Nature.* 1997;390:241.
24. Nitrini R, Rosemberg S, Passos-Bueno M, et al. Familial spongiform encephalopathy associated with a novel prion protein gene mutation. *Ann Neurol.* 1997; 42:138-146.
25. Nitsch R, Mann U, Finckh U, et al. A clinical syndrome similar to familial Alzheimer's disease caused by a T183A mutation of the prion protein [abstract]. *Soc Neurosci Abstr.* 1998;24:1476.
26. Owen F, Poulter M, Collinge J, et al. Insertions in the prion protein gene in atypical dementias. *Exp Neurol.* 1991;112:240-242.
27. Ripoll L, Laplanche JL, Salzmann M, et al. A new point mutation in the prion protein gene at codon 210 in Creutzfeldt-Jakob disease. *Neurology.* 1993;43:1934-1938.
28. Windl O, Dempster M, Estibeiro J, et al. Genetic basis of Creutzfeldt-Jakob disease in the United Kingdom: a systematic analysis of predisposing mutations and allelic variation in the *PRNP* gene. *Hum Genet.* 1996;98:259-264.
29. Masters CL, Harris JO, Gajdusek DC, Gibbs C, Bernoulli CJ Jr, Asher DM. Creutzfeldt-Jakob disease: patterns of worldwide occurrence and the significance of familial and sporadic clustering. *Ann Neurol.* 1979;5:177-188.
30. Haritani M, Spencer Y, Wells G. Hydrated autoclave pretreatment enhancement of prion protein immunoreactivity in formalin-fixed bovine spongiform encephalopathy-affected brain. *Acta Neuropathol.* 1994;87:86-90.
31. Hsich G, Kenney K, Gibbs C, Lee K, Harrington M. The 14-3-3 brain protein in cerebrospinal fluid as a marker for transmissible spongiform encephalopathies. *N Engl J Med.* 1996;335:924-930.
32. Bortone E, Bettoni L, Giorgi C, Terzano M, Trabattoni G, Mancia D. Reliability of EEG in the diagnosis of Creutzfeldt-Jakob disease. *Electroencephalogr Clin Neurophysiol.* 1994;90:323-330.
33. Mirra S, Heyman A, McKeel D, et al. The Consortium to Establish a Registry for Alzheimer's Disease (CERAD), part II: standardization of the neuropathologic assessment of Alzheimer's disease. *Neurology.* 1997;49:552-558.
34. Palmer M, Dryden A, Hughes J, Collinge J. Homozygous prion protein genotype predisposes to sporadic Creutzfeldt-Jakob disease. *Nature.* 1991;352:340-342.
35. Furukawa H, Kitamoto T, Tanaka Y, Tateishi J. New variant prion protein in a Japanese family with Gerstmann-Sträussler syndrome. *Mol Brain Res.* 1995;30:385-388.
36. Palmer MS, Mahal SP, Campbell TA, et al. Deletions in the prion protein gene are not associated with CJD. *Hum Mol Genet.* 1993;2:541-544.
37. Ghetti B, Piccardo P, Spillantini MG, et al. Vascular variant of prion protein cerebral amyloidosis with tau-positive neurofibrillary tangles: the phenotype of the stop codon 145 mutation in *PRNP*. *Proc Natl Acad Sci U S A.* 1996;93:744-748.
38. Billeter M, Riek R, Wider G, Hornemann S, Glockshuber R, Wüthrich K. Prion protein NMR structure and species barrier for prion diseases. *Proc Natl Acad Sci U S A.* 1997;94:7281-7285.
39. Riek R, Hornemann S, Wider G, Glockshuber R, Wüthrich K. NMR characterization of the full-length recombinant murine prion protein, mPrP(23-231). *FEBS Lett.* 1997;413:282-288.
40. Brown P. The phenotypic expression of different mutations in transmissible human spongiform encephalopathy. *Rev Neurol.* 1992;148:317-327.
41. Storey E. Dominantly inherited ataxias, part 1. *J Clin Neurosci.* 1998;5:257-264.
42. Zerr I, Bodemer M, Gefeller O, et al. Detection of 14-3-3 protein in the cerebrospinal fluid supports the diagnosis of Creutzfeldt-Jakob disease. *Ann Neurol.* 1998; 43:32-40.
43. Rosenmann H, Meiner Z, Kahana E, et al. Detection of 14-3-3 protein in the CSF of genetic Creutzfeldt-Jakob disease. *Neurology.* 1997;49:593-595.
44. Kretzschmar H, Ironside J, DeArmond S, Tateishi J. Diagnostic criteria for sporadic Creutzfeldt-Jakob disease. *Arch Neurol.* 1996;53:913-920.
45. McLean C, Storey E, Gardner R, Tannenberg A, Cervenáková L, Brown P. The D178N (cis-129M) "fatal familial insomnia" mutation associated with diverse clinicopathologic phenotypes in an Australian kindred. *Neurology.* 1997;49:552-558.
46. Parchi P, Petersen R, Chen S, et al. Molecular pathology of fatal familial insomnia. *Brain Pathol.* 1998;8:539-548.
47. Brown P, Gibbs C, Rodgers-Johnson P, et al. Human spongiform encephalopathy: the National Institutes of Health series of 300 cases of experimentally transmitted disease. *Ann Neurol.* 1994;35:513-529.

12. Sibley RK, Dahl D. Primary neuroendocrine (Merkel cell?) carcinoma of the skin. II. An immunocytochemical study of 21 cases. Am J Surg Pathol 1985;9:109–116.
13. Schmidt U, Müller U, Metz A, Leder L-D. Cytokeratin and neruofilament protein staining in Merkel cell carcinoma of the small cell type and small cell carcinoma of the lung. Am J Dermatopathol 1998;20:346–351.
14. Chan JK, Suster S, Wenig BM, et al. Cytokeratin 20 immunoreactivity distinguishes Merkel cell (primary cutaneous neuroendocrine) carcinomas and salivary gland small cell carcinomas from small cell carcinomas of various sites. Am J Surg Pathol 1997;21:226–234.
15. Gultekin SH, Rosai J, Demopoulos A, et al. Hu immunolabeling as a marker of neural and neuroendocrine differentiation in normal and neoplastic human tissues: assessment using a recombinant anti-Hu Fab fragment. Int J Surg Pathol 2000;8: 109–117.
16. Snodgrass SM, Landy H, Markoe AM, Feun L. Neurologic complications of Merkel cell carcinoma. J Neurooncol 1994;22: 231–234.
17. Cher LM, Hochberg FH, Teruya J, Nitschke M, Valenzuela RF, Schmahmann JD, et al. Therapy for paraneoplastic neurologic syndromes in six patients with protein A column immunoadsorption. Cancer 1995;75:1678–1683.
18. Eggers SZ, Salomao D, Dinapoli RP, Vernino S. Paraneoplastic and metastatic neurological complications of Merkel cell carcinoma. Mayo Clin Proc 2001;76:327–330.
19. Batchelor TT, Platten M, Hochberg FH. Immunoadsorption therapy for paraneoplastic syndromes. J Neurooncol 1998;40: 131–136.

Creutzfeldt-Jakob Disease Cluster in an Australian Rural City

Steven Collins, MD,[1,2]
Alison Boyd, Post Grad Dip Gen Coun,[1,2]
Ashley Fletcher, BSc,[1,2] John Kaldor, PhD,[3]
Andrew Hill, PhD,[2] Stephen Farish, MEd,[4]
Catriona McLean, MD,[1,2] Zahid Ansari, MPH,[5]
Margaret Smith, BSc,[2,6] and Colin L. Masters, MD[1,2]

Through the Australian National Creutzfeldt-Jakob Disease Registry, 6 pathologically confirmed sporadic cases were recognized over a 13-year period in persons who had been long-term residents of a moderate-sized rural city, whereas the expected number was 0.923. An extensive investigation could not find any point-source or case-to-case transmission links. This occurrence is highly statistically significant ($p = 0.0027$) when viewed in isolation and remains significant ($p < 0.02$) when only the cases that arose after the cluster was recognized were taken into account. However, a more conservative statistical analysis suggests that such a grouping could have arisen by chance in at least one population group of this size when the whole country is taken into consideration.

Ann Neurol 2002;52:115–118

Transmissible spongiform encephalopathies (TSEs) constitute a group of invariably fatal neurodegenerative disorders that affect both humans and animals.[1] The European epidemic of bovine spongiform encephalopathy and the more recently recognized variant Creutzfeldt-Jakob disease (CJD; first reported in the United Kingdom in 1996[2]) have drawn considerable attention to this group of diseases. In contrast with variant CJD, classic CJD typically presents as a rapidly progressive dementia in the elderly associated with ataxia and myoclonus and is the most common human TSE phenotype. Systematic

From the [1]Australian National Creutzfeldt-Jakob Disease Registry and [2]Department of Pathology, University of Melbourne, Victoria; [3]National Centre in HIV Epidemiology and Clinical Research, University of New South Wales, Sydney, New South Wales; [4]Epidemiology and Biostatistics Unit, School of Population Health, University of Melbourne, Melbourne; [5]Health Outcomes Section, Public Health Division, Department of Human Services, Melbourne; and [6]Molecular Biology Laboratory, Melbourne Health Shared Pathology Services, Royal Melbourne Hospital, Parkville, Victoria, Australia.

Received Dec 12, 2001, and in revised form Feb 13, 2002. Accepted for publication Feb 23, 2002.

Address correspondence to Dr Collins, Australian National Creutzfeldt-Jakob Disease Registry, Level 5, Department of Pathology, University of Melbourne, Parkville, Victoria, Australia 3010. E-mail: stevenjc@unimelb.edu.au

prospective genotyping detects likely causal mutations in the prion protein gene (*PRNP*) in up to 13 to 14% of CJD patients,[3] and iatrogenic transmission appears to explain only a few additional cases.[4] Recognized sources of iatrogenic transmission are diverse, including contaminated neurosurgical instruments, and long incubation periods of 15 or more years are reported.[1,4] For most cases of CJD, there is no identifiable cause. Although de novo somatic mutations in *PRNP* or spontaneous deleterious conformational changes in the normal prion protein are favored to underlie sporadic CJD,[1] other postulated mechanisms include unrecognized iatrogenic or natural transmission events.[5,6] Recent reports of spatiotemporal groupings of variant CJD have rekindled interest in undertaking detailed analyses of such occurrences, with the outcome that covert or uncertain transmission mechanisms may be elucidated.[7]

During the course of systematic Australian National Creutzfeldt-Jakob Disease Registry surveillance activities, it was observed that 7 deaths from TSE had been reported from 1988 to 2000 in persons who had been long-term residents within or immediately neighboring a single moderate-sized rural city. We present the findings of our detailed investigation.

Patients and Methods

Australian National Creutzfeldt-Jakob Disease Registry surveillance methods have been reported in detail previously.[5] In brief, ascertainment methods include reviews of morbidity separation coding data from all university-affiliated tertiary referral hospitals in Australia, as well as the centralized databases of state and territory health departments; regular national death certificate searches; and semiannual mail-out questionnaires to all neurologists and pathologists within Australia. Simultaneously with comprehensive prospective monitoring since September 1993, all Australian cases have been retrospectively sought to January 1, 1970. Through the combination of ascertainment measures, it is believed that essentially all human cases of TSE within Australia have been detected, particularly since the late 1980s.

After potential CJD cases are ascertained, a thorough medicodemographic profile is collected from medical records and family members, including the completion of a detailed questionnaire largely aimed at a priori risk factors for CJD. *PRNP* analysis (as described previously[8]) and autopsy are actively facilitated and undertaken whenever possible. Final classification is made once all data are collected and is consistent with internationally recognized diagnostic criteria, with pathological verification required for definite CJD.[9] The national CJD mortality data for 1988 to 2000 were used to obtain Australian mortality rates (adjusted for age and gender) and the expected CJD occurrence rate among residents for the rural city over this period (0.923 cases) and after the cluster was first suspected in 1996 (0.284 cases). Formal semiannual analyses are performed and reports are generated to monitor patterns and trends of CJD occurrence, including geographical ones.

The statistical significance of the cluster was assessed by estimation of relative risk through comparisons of the expected (following age and gender adjustment) and observed CJD death rates for the rural city. The comparison was made first for the entire observation period and then separately for the period from 1997 after the diagnosis of the earlier cases had given rise to the suspicion of a cluster. In addition, Poisson probabilities were used to assess the likelihood of similar clusters of CJD cases occurring in any equivalent-sized individual cohort (of approximately 73,000) with the entire Australian population divided equally into 241 groups. p values less than 0.05 were considered significant.

Results

During the course of systematic surveillance activities, it was observed that 5 deaths from pathologically confirmed TSE had been reported from 1988 to 2000 in persons who were residents of a single moderate-sized rural city (population in 1991 census, 72,976). An additional death from Gerstmann-Sträussler-Scheinker syndrome associated with the proline102valine (P102L) mutation was confirmed in a person who resided just outside the city. Further investigation, therefore, concentrated on the other five patients (Tables 1 and 2; Fig). Patients 1 to 4 were all long-term residents

Table 1. Selected Demographic Features of Sporadic Creutzfeldt-Jakob Disease Cases

Patient	Year of Death	Age at Death (yr)	Gender	Total Duration of Residence in City (yr)	Radial Distance from City Center (km)[a]	*PRNP* Mutations/codon 129[b]
1	1988	71	M	30	11.0	ND
2	1992	58	M	34	3.5	Nil/MM[c]
3	1996	58	F	40	7.5	Nil/MM
4	1996	65	F	65	10.5	Nil/MM[c]
5	2000	73	M	3.5	3.7	Nil/MM
6	1999	53	M	13[d]	3.8	Nil/MM

[a]Last city residential address.
[b]Methionine.
[c]Archival retrieval of DNA from formalin fixed brain permitted reliable nucleotide sequencing for codons 1 to 133 only in Case 2, and from 1 to 135 only in Case 4.
[d]Over 3 separate periods spanning 22 years.

ND = not determined.

Table 2. Salient Clinical Features of Sporadic Creutzfeldt-Jakob Disease Cases

Patient	Illness Duration (mo)	Family History of Similar Illness	Rapidly Progressive Dementia	Myoclonus	Typical EEG	14-3-3 CSF
1	4	No	Yes	Yes	No	ND
2	6	No	Yes	No	No	ND
3	1.5	No	Yes	Yes	No	ND
4	1	No	Yes	Yes	Yes	ND
5	1	No	Yes	Yes	No	Yes
6	2	No	Yes	Yes	No	Yes

CSF = cerebrospinal fluid; EEG = electroencephalogram; ND = not done.

of the rural city (30–65 years) and died there. The most recent case (Patient 5) was a person who lived only the last 3.5 years of his life in the rural city. In addition to these 5 deaths among residents, the Australian National Creutzfeldt-Jakob Disease Registry ascertained an additional sporadic case (Patient 6; see Tables 1 and 2; see Fig) who died while a resident of the state capital but who previously had been a long-term resident of the rural city (a total of 13 years over a span of 22 years). Patient 6 spent an additional 2 years living on a small farm 27km from the city center from which he commuted weekdays to his office located in the central city. Total residence in the rural city constituted the longest by far in any specific location over the patient's lifetime. To explore possible linkages among the cases, we included this case in the investigation. All 6 cases resided within an approximately 11km radius of the city center, with the shortest distance between any of their last residences being approximately 3.5km. A family history of similar neurodegenerative disorders was absent in all patients, and the clinical phenotype of the six patients was typical of sporadic CJD (as outlined in Table 2), with *PRNP* genotyping excluding mutations in the five patients in whom it could be undertaken. The average age at death in the six patients was 63.0 years, which is similar to the national mean of 65.2 years.

Fig. Temporal summary of rural city residence, illness onset, and death of all patients: (small vertical line) *death,* (greater than symbol) *onset,* (horizontal line) *time periods in rural city, and* (asterisk) *patient with Gerstmann-Sträussler-Scheinker syndrome.*

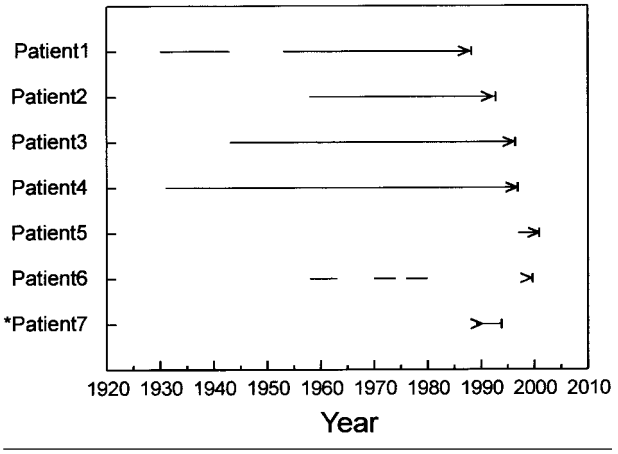

Exhaustive medicodemographic analysis, including a communal meeting with family members of 4 of the sporadic cases, could not determine any point-source or case-to-case transmission link between the 7 persons (including Patient 7 with Gerstmann-Sträussler-Scheinker syndrome). In particular, no orthodox medical, alternative medical, or dental practitioner was shared by all nor were invasive procedures or operations performed on these patients at a single institution. The only association detected was for Patients 2, 3, and 4 (see Tables 1 and 2), who shared the same ophthalmologist for 11 years, with all 3 first examined during a 7-month period commencing September 1983. Aside from a single flourescein angiogram in Patient 2, the consultations were for routine clinical assessments, which included application tonometry (Goldman) on two or three separate occasions each, with the shortest interpatient interval being approximately 9 weeks.

The simplest assessment of the statistical significance of the apparent cluster employed the hypothesis that by chance alone the number of sporadic cases observed in long-term residents from this city was greater than the number expected for this period. For the cases dying in the rural city (Patients 1–5), the relative risk was 5.4 ($p = 0.0027$). However, this approach can be questioned on the grounds that the hypothesis was generated from the data rather than being stated a priori. A more valid test of significance, therefore, applied the same method to cases arising after the cluster was suspected (represented by the third patient dying of sporadic CJD in 1996). On this basis, the observed rate of an additional 2 sporadic cases during 4 years developing in residents, compared with the expected (0.284), still represented a significant excess ($p = 0.02$).

More conservative statistical analysis, however, assessed the likelihood that somewhere in Australia, in a

population unit of the same size as this city, 5 or more cases of sporadic CJD could occur when 0.923 cases were expected. With the Australian population divided equally, there are 241 units of approximately 73,000 people. Under Poisson probability assumptions, the occurrence of a cluster of this size or greater in at least 1 of these 241 population groups quite easily could arise by chance alone ($p = 0.49$), even if the nonresident case (Patient 6) is included to make a cluster of 6 ($p = 0.124$).

Discussion

Spatiotemporal groupings of sporadic CJD have been reported previously,[10–12] including in the context of comprehensive epidemiological studies.[6,7,13] Generally, clusters detected during systematic national surveillance studies are construed as more valid for detailed analysis by obviating potential selection and detection biases that may arise when the cluster itself prompts further investigation.[13]

It is acknowledged that the relatively short duration of rural city residence of the most recent case (Patient 5) appears inconsistent with disease acquisition during this period given the incubation periods determined to date for recognized peripheral iatrogenic transmission events.[4] Nevertheless, their inclusion was determined to be important to facilitate the investigation of potentially novel transmission mechanisms. Despite the high relative risk and extensive investigation of individual cases, we were unable to identify a putative transmission pathway. Three patients infrequently attended the same ophthalmologist, but no convincing mechanism of transmission was uncovered, with the role of routine clinical tonometry being highly contentious.[14–17] Furthermore, although this cluster is apparently of high significance when viewed in isolation, more conservative statistical analysis demonstrates that such a grouping of 5 or 6 cases in at least 1 population unit the same size as the rural city within Australia would not be unexpected by chance alone over a 13-year period. Given the cumulative evidence to date, apparent clustering of CJD above background or expected average national incidence rates is not rare, and each instance requires careful epidemiological and statistical assessment to determine its true significance.

The Australian National Creutzfeldt-Jakob Disease Registry is funded by the Commonwealth Department of Health and Aging.

The authors thank Drs M. Pilbeam and G. Hunter for their generous support in facilitating the clinicopathological investigation of the patients in this study and A. Bell for his technical assistance.

References

1. Prusiner SB. Prions. Proc Natl Acad Sci U S A 1998;95:13363–13383.
2. Will RG, Ironside JW, Zeidler M, et al. A new variant of Creutzfeldt-Jakob disease. Lancet 1996;347:921–925.
3. Windl O, Dempster M, Estibeiro JP, et al. Genetic basis of Creutzfeldt-Jakob disease in the United Kingdom: a systematic analysis of predisposing mutations and allelic variations in the PRNP gene. Hum Genet 1996;98:259–264.
4. Brown P, Preece M, Brandel J-P, et al. Iatrogenic Creutzfeldt-Jakob disease at the millennium. Neurology 2000;55:1075–1081.
5. Collins S, Law M, Fletcher A, et al. Surgical treatment and risk of sporadic Creutzfeldt-Jakob disease: a case control study. Lancet 1999;353:693–697.
6. Matthews WB. Epidemiology of Creutzfeldt-Jakob disease in England and Wales. J Neurol Neurosurg Psychiatr 1975;38:210–213.
7. Cousens S, Smith PG, Ward H, et al. Geographical distribution of variant Creutzfeldt-Jakob disease in Great Britain, 1994–2000. Lancet 2001;357:1002–1007.
8. Collins S, Boyd A, Fletcher A, et al. Novel prion protein gene mutation in an octogenerian with Creutzfeldt-Jakob disease. Arch Neurol 2000;57:1058–1063.
9. Masters C, Harris J, Gajdusek D, et al. Creutzfeldt-Jakob disease: patterns of worldwide occurrence and the significance of familial and sporadic clustering. Ann Neurol 1979;5:177–188.
10. Will RG, Matthews WB. Evidence for case-to-case transmission of Creutzfeldt-Jakob disease. J Neurol Neurosurg Psychiatr 1982;45:235–238.
11. Farmer PF, Kane WC, Hollenberg-Sher J. Incidence of Creutzfeldt-Jakob disease in Brooklyn and Staten Island. N Engl J Med 1978;298:283–284.
12. Arakawa K, Nagara H, Itoyama Y, et al. Clustering of three cases of Creutzfeldt-Jakob disease near Fukuoka City, Japan. Acta Neurol Scand 1991;84:445–447.
13. Raubertas RF, Brown P, Cathala F, Brown I. The question of clustering of Creutzfeldt-Jakob disease. Am J Epidemiol 1989;129:146–154.
14. Davanipour Z, Alter M, Sobel E, et al. Creutzfeldt-Jakob disease: possible medical risk factors. Neurology 1985;35:1483–1486.
15. Alter M. How is Creutfeldt-Jakob disease acquired? Neuroepidemiology 2000;19:55–61.
16. van Duijn CM, Delasnerie-Laupretre N, Masullo C, et al. Case-control study of risk factors of Creutzfeldt-Jakob disease in Europe during 1993–1995. Lancet 1998;351:1081–1085.
17. Zerr I, Brandel J-P, Masullo C, et al. European surveillance on Creutzfeldt-Jakob disease: a case-control study for medical risk factors. J Clin Epidemiol 2000;53:747–754.

Creutzfeldt–Jakob disease in Australia 1970–1999

S. Collins, MD; A. Boyd, Dip. Gen. Coun.; J.S. Lee, BSc; V. Lewis, BSc (Hons); A. Fletcher, BSc; C.A. McLean, MD; M. Law, PhD; J. Kaldor, PhD; M.J. Smith, PhD; and C.L. Masters, MD

Abstract—*Objective*: To ascertain all persons who developed a transmissible spongiform encephalopathy (TSE) within Australia during the 30-year period 1970 to 1999 through a comprehensive national surveillance program and subject the group to detailed epidemiologic analysis. *Methods*: Cases were ascertained through reviews of morbidity separation coding data from all university-affiliated tertiary referral hospitals, as well as the centralized data bases of state and territory health departments, regular national death certificate searches, and semiannual mailout questionnaires to all neurologists and pathologists throughout Australia. Prospective monitoring commenced in September 1993. *Results*: A total of 387 patients were confirmed as having TSE during this epoch. The majority of cases were sporadic Creutzfeldt–Jakob disease (CJD) (90.7%), with 7.2% heredofamilial and 2.1% iatrogenic. Over this 30-year period, the national average annual sporadic CJD incidence rate per million progressively increased from 0.31 for the decade 1970 through 1979 to 0.77 for 1980 through 1989, reaching 1.03 for 1990 through 1999. Death certificates were found to have a false-positive rate of 11.5% and sensitivity of 83.0% for sporadic CJD. *Conclusions*: Within Australia, there has been a gradual increase in the incidence of transmissible spongiform encephalopathy over the three-decade period 1970 through 1999, peaking in 1999 at 1.4/million/year for sporadic Creutzfeldt–Jakob disease. This increase is believed secondary to improved case ascertainment. Variant Creutzfeldt–Jakob disease was not identified during this period. Age- and sex-adjusted comparisons showed a decline in incidence rates in the elderly in both sexes, usually from age 74 years. Death certificates were a useful but imperfect method of case detection.

NEUROLOGY 2002;59:1365–1371

Classic Creutzfeldt–Jakob disease (CJD) is an invariably fatal neurodegenerative disorder with a mean illness duration of 7 months and a global distribution.[1-3] The disease is recognized to occur on a genetic basis, as a result of mutations within the prion protein gene (*PRNP*) and also from rare horizontal (iatrogenic) transmission events; however, in the vast majority (85 to 90%) the occurrence is apparently sporadic.[1]

Over the years, CJD has been the subject of many systematic national and international epidemiologic surveys.[2-19] Earlier comprehensive ascertainment studies were generally undertaken to explore mechanisms of causation, including the possibility of unrecognized case-to-case transmissions and natural reservoirs of infection or to clarify the true incidence and annual death rate from this rare disease.[2-9] Recently, interest in this group of diseases has been rekindled by the bovine spongiform encephalopathy epidemic among cattle in the United Kingdom and the emergence of the zoonotically related human disorder, variant CJD (vCJD).[20,21] The outbreak of bovine spongiform encephalopathy prompted the development of a number of European national CJD surveillance registries that have undertaken large domestic and collaborative epidemiologic studies, focused primarily on detecting changes in the incidence or clinical pattern of CJD in the wake of the bovine epidemic.[18,19] It was from such efforts that the vCJD phenotype was quickly delineated, contrasted against the reaffirmed background clinicopathologic profile of classic sporadic CJD.

In Australia, a national CJD register was established in September 1993 to undertake prospective surveillance as well as retrospective ascertainment of all cases to January 1, 1970. Herein we report the results of our comprehensive national surveillance and epidemiologic investigation of CJD over the 30-year period beginning at the start of the retrospective ascertainment interval and ending in December 1999. To the best of our knowledge, this is the longest national population-based ascertainment epoch for CJD reported to date.

Methods. Surveillance procedures and all related activities of the Australian National Creutzfeldt–Jakob Disease Registry (ANCJDR) have ethical approval from the University of Melbourne and collaborating institutions as appropriate and have been described in detail previously.[22-24] There has been no statutory obligation to notify to public

From the Australian National Creutzfeldt–Jakob Disease Registry (Drs. Collins and Masters, A. Boyd, J. Lee, V. Lewis, and A. Fletcher) and Department of Pathology (Drs. Collins, McLean, Smith, and Masters, A. Boyd, J. Lee, and V. Lewis), University of Melbourne, Parkville, Victoria; National Centre in HIV Epidemiology and Clinical Research (Drs. Law and Kaldor), University of New South Wales, Sydney; and Molecular Biology Laboratory (Dr. Smith), Melbourne Health Shared Pathology Services, Royal Melbourne Hospital, Parkville, Victoria, Australia.

The ANCJDR and the National Center in HIV Epidemiology and Clinical Research are supported by the Commonwealth Department of Health and Ageing.

Received February 22, 2002. Accepted in final form July 17, 2002.

Address correspondence and reprint requests to Dr. S. Collins, Australian National CJD Registry, Department of Pathology, the University of Melbourne, Parkville, Victoria, Australia 3010; e-mail: stevenjc@unimelb.edu.au

Table 1 *Summary of all ANCJDR cases, including mean age at death and duration of illness, according to the major etiologic subtypes*

	Cases of CJD in Australia, 1970–1999, n			Average age at death, y (range)			Average duration, mo (range)		
Classification	Men	Women	Total	Men	Women	Total mean	Men	Women	Total mean
Sporadic	165	186	351	63.9 (25–84)	66.6 (33–89)	65.3 (25–89)	6.1 (1–45)	7.1 (1–60)	6.6 (1–60)
Familial	13	15	28	49.3 (20–68)	58.9 (42–82)	54.6 (20–82)	13.8 (2.3–50)	23.8 (2–156)	19.4 (2–156)
Iatrogenic	3	5	8	40.3 (27–62)	39.8 (26–50)	40.0 (26–62)	5.0 (2–10)	10.7 (3.5–25)	8.6 (2–25)

ANCJDR = Australian National Creutzfeldt–Jakob Disease Registry; CJD = Creutzfeldt–Jakob disease.

health authorities in Australia about CJD cases. National prospective surveillance began in September 1993 with the aim of identifying all persons within Australia in whom transmissible spongiform encephalopathy (TSE) had been diagnosed. In accordance with the recommendations of an independent inquiry,[25] the ANCJDR additionally sought cases retrospectively to January 1, 1970. Previous reports have summarized the outcome of evaluation of medical and other risk factors for sporadic CJD in part of this cohort and provided limited demographic details and analysis.[22,24]

At commencement of the Registry's operation in 1993, all neurologists and pathologists throughout Australia were contacted by mail and were requested to notify the ANCJDR of any patients with CJD encountered during their practice lifetime. Since then, these two specialist groups have received semiannual prompts by mail, requesting notification of recently deceased or living suspected, likely, or confirmed cases. Searches of the National Death Index, established in 1980, by the Australian Institute of Health and Welfare (AIHW) have been undertaken on an annual basis. In addition, the records of all Australian university-affiliated or tertiary referral hospitals were searched for the *International Classification of Diseases–9* CM (or equivalent earlier) separation codes 046.1 (specific for CJD) and 290.1 (presenile dementia), with the latter accepted only if it constituted the principal diagnosis. The medical files of all persons with disease ascertained in this way were reviewed and validated on-site by the ANCJDR. Annual searches for code 046.1 were also made of the centralized hospital separation morbidity databases of the health departments of each state and territory. Cases were attributed to the initial method of notification if they were identified via more than one source. Since November 1997, the ANCJDR has provided testing for the presence of 14–3–3 proteins in CSF, to facilitate notification of suspected cases and to heighten awareness of the Registry. The Registry has also offered *PRNP* genotyping to determine causative mutations and codon 129 status for selected patients. Methods used for these two investigations have been described previously.[23]

Potential case subjects underwent detailed evaluation using all available medical, demographic, and risk-related information. Data were sourced from both medical records and attending medical care providers. A history of potential iatrogenic exposure from dura mater implants, corneal grafts, or human cadaveric pituitary hormones was sought in all cases. A standardized and comprehensive questionnaire that specifically sought information on known and potential risk factors was posted to the surviving family member or relative designated as most appropriate by the treating physician. Postmortem histopathologic examination was sought for all cases but Western blot immunochemical analysis of brain was not performed as part of the study. Classification criteria for CJD cases, including vCJD, were based on previously published criteria.[3,26] Definite CJD required typical neuropathologic changes. Probable (clinically likely) sporadic CJD cases did not have pathologic confirmation but had other causes excluded by appropriate investigations and manifested the salient features of rapidly progressive dementia to death in <2 years accompanied by two of the following: myoclonus, visual or cerebellar dysfunction, pyramidal or extrapyramidal signs, or akinetic mutism. In addition, probable cases typically had characteristic periodic sharp wave complexes (PSWCs) on their EEG or the presence of 14–3–3 proteins in their CSF, or both. However, given the relative insensitivity of PSWC,[27,28] this feature was not invariably used as a criterion for classification as probable. Consequently, the possible CJD classification category was not used. All patients with suspected CJD without detectable 14–3–3 proteins in their CSF were followed up at 9 months, with death in this period prompting reevaluation.

Population denominators by age, sex, and country of birth were obtained from the Australian Bureau of Statistics.[29] Death rates in relation to sex and age for the Australian population for the years 1987 through 1998 were obtained from the AIHW. Age-adjusted rates of CJD were calculated by calendar period for Australia as a whole and for each state and territory. Time trends were assessed using Poisson regression. Country of birth was analyzed as a risk factor for CJD by comparing numbers of recorded cases with the number expected on the basis of the age and sex distribution in the population. All statistical analyses were performed using STATA (version 7; Stata Corporation, College Station, TX) and p values <0.05 were taken as significant.

Results. Out of a total of 704 suspected cases of TSE evaluated by the ANCJDR during the calendar years 1970 to 1999, 387 were found to be either definite or probable. All but 17 of these patients died during the study period. The overwhelming majority of cases were sporadic (90.7%), with 7.2% heredofamilial and 2.1% recognized to have an iatrogenic basis (table 1). Of the 351 sporadic cases, 195 were definite and 156 probable. There were no cases classified as vCJD. Specific diagnoses in excluded cases varied considerably and often a precise diagnosis could not be discerned, leaving exclusion based on a clear failure to fulfill diagnostic criteria such as recovery from a monophasic illness.

Over half the cases were reported by specialist physicians (neurologists 37.6% and neuropathologists 17.9%), either on the basis of the reminder cards or on their own initiative. National death certificate searches by the AIHW

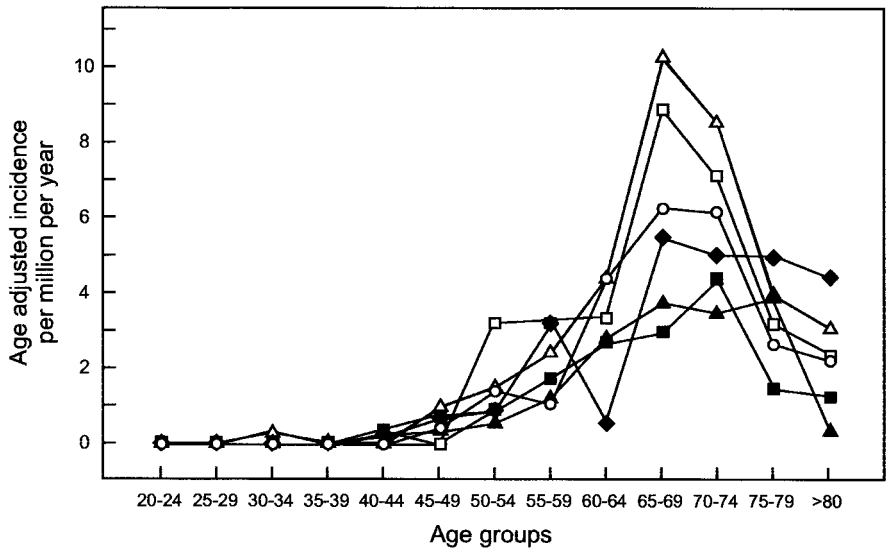

Figure 1. Age- and sex-adjusted annual incidence rates for sporadic Creutzfeldt-Jakob disease over three different time periods constituting the duration of the study. 1970 to 1989: men = ■, women = ▲; 1990 to 1994: men = ◆, women = ○; and 1995 to 1999: men = □, women = △.

yielded approximately 24.6% of the cases, and hospital medical record and state and territory morbidity separation coding searches provided an additional 8.5% of all cases. The remaining 11.4% cases came from a diversity of sources. Death certificates were available in 342 persons (97.4%) ultimately classified as having sporadic CJD, with 284 (80.9%) correctly listing the diagnosis as the cause of death (sensitivity 83.0%; false-negative rate 17.0%). Conversely, 37 patients with CJD cited as the cause of death were deemed to have died from another illness after thorough review of all available data, giving an 11.5% false-positive death certificate rate. The positive predictive value of a death certificate listing CJD as the cause of death was 88.5%.

A comparison of definite to probable sporadic CJD cases showed no differences in their sex distribution (men: definite 97/197 [49.2%] compared with probable 68/156 [43.6%]; $p = 0.25$) or mean illness duration (6.8 months for definite cases vs 6.5 for probable cases; $p = 0.76$). However, there was a significant difference in mean age at death (64.2 years for definite cases vs 66.8 for probable cases), which was restricted to men (62.2 years for definite cases vs 66.3 for probable cases: women 66.2 years vs 67.2, $p = 0.45$). Nevertheless, we considered the two groups sufficiently similar to be aggregated for subsequent statistical analysis. The overall ratio of men to women was 1:1.13, with the age-adjusted incidence for men and women very similar for the study period: men 0.662/million to women 0.661/million. The excess of women observed in those dying at age >60 years ($p = 0.004$) was not different from the predominance of women in the overall Australian population death rate in this age group ($p < 0.001$). Death occurred at a mean age of 65.3 years (men 63.9 years; women 66.6 years; range, 25 to 89 years) (see table 1). For sporadic cases, there was a significant overrepresentation of EEGs displaying PSWCs in the probable group (93 with, vs 59 without, typical EEG changes) compared with definite cases (81 positive, 88 negative), which is not unexpected given the reliance on this feature for categorization of the former group. EEGs were not performed or not available in 30 patients. About 70% of patients with sporadic CJD died within 6 months of illness onset, and 87.5% died before 12 months. The combined mean illness duration was 6.6 months (6.1 for men, 7.1 for women).

Age- and sex-adjusted death rates from sporadic CJD were assessed over three separate periods: 1970 to 1989, 1990 to 1994, and 1995 to 1999. The peak age period for death was generally 65 to 74 years in both sexes in each epoch, except for women in the 1970 to 1989 period and men in 1990 to 1994 period when the incidence did not clearly decline until after age 79 years (figure 1). A comparison of the mean age at death and age distribution of sporadic cases was made for the 1970 to 1994 and 1995 to 1999 periods. There was no difference in the average age at death in either sex (1970 to 1994: men 63.2 years compared with 65.3 for the later epoch; women 66.6 years compared with 66.8). The age distributions were also very similar, suggesting no major change in these salient demographic features over the period studied. In contrast, the 28 familial and eight iatrogenic cases were typically younger patients, with the average ages at death 54.6 years for the former group and 40.0 years for the latter, and both displayed longer mean illness durations (19.4 months for familial cases and 8.6 months for iatrogenic deaths). Patients with younger age at disease onset (<50 years) accounted for approximately 12% of the total, but of these, sporadic cases still constituted the majority (54%).

Because of the relatively recent availability of the CSF 14–3–3 protein assay, only 53 of the 387 patients underwent testing. Of the sporadic cases, 25 of 27 definite cases were positive, whereas 17 of the 18 probable patients had detectable 14–3–3 proteins. The two patients with iatrogenic (dura mater [Lyodura, B. Braun, Melsunger, Germany]–associated) disease tested both displayed immunodetectable 14–3–3 proteins in their CSF, but this was seen in only five of six patients tested with a *PRNP* mutation: 3/3 E200K; 1/1 T188A[30]; 1/1 V210I; and 0/1 P105T.[23]

Of the eight patients dying from iatrogenic CJD, four were exposed through human pituitary gonadotrophin (hGn) therapy, and four had received Lyodura implants. Incubation periods for the patients receiving hGn therapy varied from 12 to 15 years (calculated from midpoint of individual treatment courses) and from 5.5 to 17 years for the dura mater recipients (figure 2). The most recent recognized iatrogenic exposure was 1986 in relation to a dura mater implant, and the most recent death occurred in 1999.

There were 14 kindreds in which neuropathologic exam-

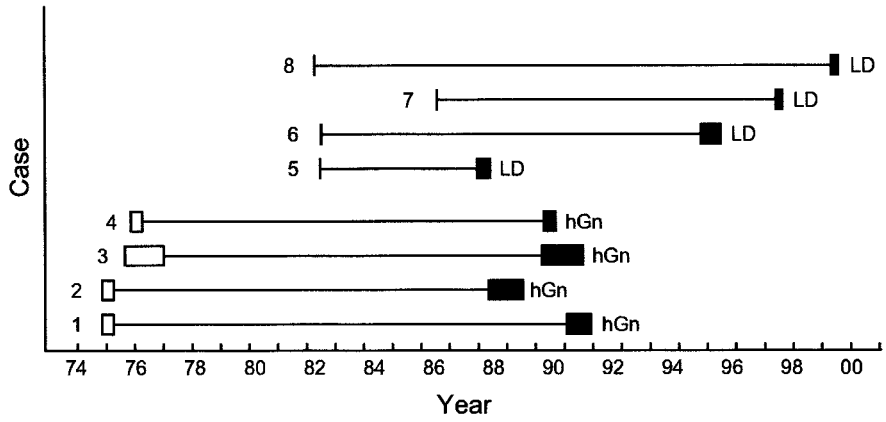

Figure 2. Australian iatrogenic Creutzfeldt–Jakob disease cases from 1970 to 1999. LD = patients who received a dura mater (Lyodura, B. Braun, Melsunger, Germany) implant. hGn = patients who were treated with human cadaveric pituitary gonadotrophins. Open boxes represent treatment and maximal possible exposure periods to contaminated batches of human cadaveric pituitary gonadotrophins. Incubation periods are calculated from the midpoint of treatment for patients treated with hGn and from day of dura mater implant for patients receiving LD. Straight lines represent incubation periods. Filled boxes represent the period of symptomatic illness.

ination (performed in 19 patients) and prion protein genotyping have been sufficient to confirm a genetic form of TSE in a total of 25 patients. The *PRNP* codon mutations included six families with E200K; two with P102L; two with D178N; and one each with V210I, T188A, and P105T. There was a single pedigree with a seven octapeptide repeat insert. A further three cases of CJD have been tentatively classified as familial awaiting genotypic confirmation in further symptomatic relatives. *PRNP* analysis was performed in 30 persons dying from sporadic CJD, confirming 24 (80%) to be homozygous at codon 129: 20 methionine/methionine, four valine/valine.

The total annual incidence of TSE within Australia has shown a steady increase over the observation period. Of the 30 cases with their onset in 1999, 27 were sporadic, two familial, and one iatrogenic, reinforcing that the increase in numbers generally conforms to the overall classification proportions for the study period. For sporadic CJD, the annual incidence peaked in 1999 at 1.4 per million (figure 3), with the provisional incidence of 0.67 per million for the year 2000, suggesting a possible plateauing of case rates. The national average annual sporadic CJD incidence rate per million for the decade 1970 to 1979 was 0.31, whereas for 1980 to 1989 the rate was 0.77 and for 1990 to 1999 it was 1.03. A single spatiotemporal cluster of six cases in a large rural city was recognized during the course of the study and is the subject of a separate report.[31] The age-adjusted incidence rate was uniform across all the states and territories of Australia (ranging from 0.92 to 1.19 cases per million per year for the period 1990 to 1999), with the exception of Tasmania, where for uncertain reasons the rate over the 30-year period (based on four cases) has been noticeably lower (0.42 cases per million per year for the period 1990 to 1999). Time trend analysis was possible for all states except Tasmania and was found to be present in all ($p < 0.001$ for Victoria, Queensland, New South Wales, and Australia as a whole; $p = 0.004$ for South Australia; $p = 0.002$ for Western Australia).

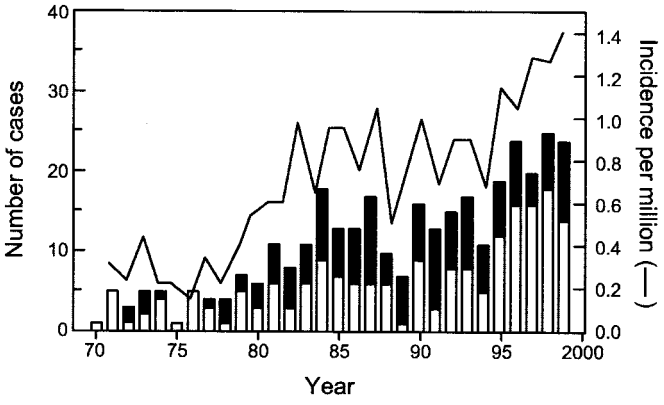

Figure 3. Annual deaths for all definite and probable sporadic Creutzfeldt–Jakob disease patients for the period 1970 to 1999 and the corresponding national annual incidence rate per million population. Open part of bar represents definite cases; filled part of bar represents probable cases.

Country of birth was recorded for all 351 sporadic cases (table 2). The proportion of patients born in Australia was 65.8%, compared with 68.3% expected after age adjustment. No country of birth was associated with a significant excess incidence of CJD. All but one of the patients recorded as born in the United Kingdom, and none of those born in continental Europe, had immigrated after 1985. Limited travel data (principally aimed at country of destination and not duration of stay) were also available on 246 of the 309 persons dying of sporadic CJD during the period 1980 to 1999. Of the 198 Australian-born patients, 64 had never left Australia whereas 22 had spent time in the United Kingdom during the 1980s and 1990s, with a further four traveling to continental Europe only. There were 46 persons born in the United Kingdom, of whom 11 returned to their country of birth for some time during this period. Another four non–Australian-born patients also traveled to the United Kingdom over the two decades specified.

Discussion. Arguably the most important finding of our study was the geographically uniform, steadily progressive increase in the recorded incidence of sporadic CJD over the three decades of ascertainment. An analogous observation has been reported from many other countries that have undertaken surveillance over extended periods, and similar to the present study these other groups have attributed the increase to enhanced case detection and reporting,[9,12,15,18] which for the ANCJDR may have become optimal in the late 1990s, with relative plateauing of

Table 2 *Comparison of country of birth for ANCJDR sporadic CJD cases and the expected percentage occurrence after age adjustment for Australian-born and immigrant subgroups based on the national population*

Country	Expected based on Australian population, %	CJD cases in register, %
Australia	68.28	65.81
United Kingdom	11.59	14.53
New Zealand	1.00	0.28
Poland	1.01	0.57
Yugoslav Republics	1.49	2.56
Greece	1.61	2.28
Asia (Vietnam, China, Phillipines, Hong Kong/Macau, India, Singapore,* Indonesia*)	1.96	1.71
Germany	1.30	1.42
Oceania and Antarctica	0.23	0.00
Lebanon	0.36	0.00
South Africa	0.26	0.28
Malta	0.51	0.57
United States and Canada	0.22	0.57
Former USSR and Baltic States	0.87	0.57
Egypt	0.40	0.85
Other countries combined	5.02	8

* Countries for which age breakdown of immigrant population is not known.

ANCJDR = Australian National Creutzfeldt–Jakob Disease Registry; CJD = Creutzfeldt–Jakob disease; USSR = Union of Soviet Socialist Republics.

incidence rates from about 1996. An increase in case rates unrelated to enhanced detection only cannot be completely excluded but is thought less likely given that our findings closely conform to what is expected when a comprehensive surveillance system is introduced for a rare disease during the latter part of an ascertainment period. Consistent with ascertainment bias in our study is the progressive lessening of retrospective incidence rates as detection becomes more temporally remote and the relative stabilizing of incidence rates within a few years of the establishment of the surveillance system. Earlier studies have reported rates as low as 0.09/million/year,[5,13] but generally the reported overall annual incidence rates have been about 0.3 to 0.7/million.[2,9,11,12,15,19] Some of these surveys noted increased rates of 0.73 to 1.2/million/year in their higher-density population centers,[2,9,12] consistent with the likelihood of better urban case detection and confirmation compared with rural areas. The strikingly higher rates seen in certain ethnic groups such Libyan Jews in Israel[4] (31.3/million) have been found to have a genetic basis.[32]

The decline in case rate we observed among very elderly persons (especially those >75 years of age) has been frequently described[2,10,11,13,18,19] and stands in clear contrast to other neurodegenerative diseases such as AD, but it raises concerns regarding suboptimal surveillance in this age group, as suggested by previous findings.[18] Increased efforts at case ascertainment in the very elderly, including the use of surveillance targeted at groups such as residents of nursing homes, would help resolve this issue. Nevertheless, although unexplained at present, the consistency of the observed decline in sporadic CJD rates in the very elderly (regardless of sex) suggests a likely further important insight into the cause and neurobiology of this disease in contrast to other neurodegenerative disorders.

The salient demographic findings of the current study are in general agreement with prior reports. Given our findings and those reported previously in relation to familial cases,[12] the aggregation of all (including familial) cases for analysis in some reports may have contributed to their overall slightly younger mean age at death[2,3,9] and longer duration of illness[2,3] in comparison with the current results when restricted to sporadic CJD. However, even for the latter group alone other authors have reported younger mean ages at death of 55.7[10] and 62.1[13] years, in contrast to the 65.3 years observed in our study. With respect to the mean duration of illness of 6.6 months observed in the present study, both longer (16.6 months[10]) and shorter (5.3 months,[13] 5.9 months[14]) have been described. Importantly, age-adjusted rates for sporadic CJD were not different for men and women over the observation period, with the slight overall excess of women (ratio 1:1.13) accounted for in our study by their longer lifespan compared with men, who on average die slightly younger from other causes. These findings are very similar to those of a previous UK study,[11] in which the excess of women was essentially restricted to those aged >60 years, with age-standardized death rates for men and women not different over the study period.

vCJD was not identified in Australia during the study period, including in persons potentially at higher risk because of travel to the United Kingdom and Europe during the 1980s and 1990s, although the travel data relating to this are limited. Our exclusion of vCJD cases relied on careful scrutiny of available clinical and neuropathologic data. It is conceded that use of auxiliary diagnostic techniques such as examination of brain prion protein glycoforms may have been of additional merit, but given the validated distinctive clinicopathologic phenotype of vCJD, we are confident that variant cases were not overlooked. Further, excluding risks from travel, only one person born in the United Kingdom dying from CJD emigrated to Australia after 1985 (and none from continental European countries with bovine spongiform encephalopathy), making it less likely that we would have seen "imported" cases of vCJD among these non–Australian born residents.

The proportion of heredofamilial cases observed in the present study (7.2%) is comparable to other large surveillance studies, which did not employ *PRNP* geno-

typing.[2,10,11] Much higher proportions (26%,[9] 44.8%,[4] and 80%[19]) have been reported from countries with recognized heightened occurrences of genetic forms of CJD,[32] but for unclear reasons some countries have reported no familial CJD.[13-15] The Australian proportion is also lower than the 13 to 14% seen in a more recent series employing systematic *PRNP* analysis of all patients in whom CJD was suspected.[33] The lower proportion of genetic cases in the present study most likely relates to the smaller overall number of cases genotyped, with consequent underdetection of *PRNP* mutations. It is very likely that with increased use of genetic screening, more PRNP mutations would have been detected by the ANCJDR, giving an improved understanding of the frequency of unrecognized genetic cases, including in people without a recognized family history of prion disease.[30]

In Australia, human cadaver pituitary hormone-related CJD has been uniquely associated with hGn treatment in contrast with growth hormone, which has been the source of contamination in all other countries.[34] The four patients with hGn-associated disease died over a 2-year period, with >10 years now elapsed since the most recent. Based on this observation, it would be reasonable to conclude that a limited number of treatment batches were contaminated over a short period. Other countries such as France continue to report a steady number of new growth hormone–associated cases, consistent with more sustained therapy-related contamination. The four cases associated with Lyodura dura mater implants had comparable incubation periods to the pituitary hormone–related cases, including one of the longest recorded anywhere in the world (17 years).

Personal communications and death certificates were the most important mechanisms of case ascertainment. Not unexpectedly, the single largest referral group was neurologists (37.6%). Despite a generally favorable ratio of this specialist physician group to the adult Australian population (1:62,000 persons aged >14 years),[35] wide differences in this ratio among European countries (varying from 1:177,000 for the United Kingdom to 1:8,117 for Italy) has not translated into noticeable differences in sporadic CJD detection rates, and of further interest the proportion of neurologist-referred suspect CJD cases in the United Kingdom is about 65% (R. Will, personal communication). Death certificates were shown to be a useful surveillance method for sporadic CJD, with a sensitivity of 83.0% and false-positive rate of 11.5%. These findings are similar to those observed previously when undertaking systematic surveillance for CJD using a combination of ascertainment methods including death certificates.[16] However, inherent slowness always caused a minimum 18- to 24-month delay before such data were available. Given the false-positive (11.5%) and false-negative (17.0%) rates we observed in relation to death certificates and sporadic CJD, additional mechanisms of surveillance and thorough review of all available patient medicodemographic information is still warranted if optimal sensitivity and specificity of case classification are to be achieved.

Note added in proof: The Swiss National Reference Centre for Prion Diseases has just reported an unexplained doubling of sporadic CJD incidence for 2001 to 2.7 deaths per million, and a rate of 3.9 for the first quarter of 2002. Such observations pose a number of questions and concerns for all national CJD surveillance programs, and further investigation and monitoring will be required to clarify the true significance of this change.[36]

Acknowledgment

The authors thank all families, medical practitioners, and associated staff for the medical and demographic information on all the patients. They also thank Dr. J. Worthington for information concerning CJD cases from New South Wales.

References

1. Prusiner SB. Prions. Proc Natl Acad Sci USA 1998;95:13363–13383.
2. Brown P, Cathala F, Raubertas RF, Gadjusek DC, Castaigne P. The epidemiology of Creutzfeldt-Jakob disease: conclusion of a 15-year investigation in France and review of the world literature. Neurology 1987;37:895–904.
3. Masters CL, Harris JO, Gajdusek DC, Gibbs CJ, Bernoulli C, Asher DM. Creutzfeldt-Jakob disease: patterns of worldwide occurrence and the significance of familial and sporadic clustering. Ann Neurol 1979;5:177–188.
4. Kahana E, Alter M, Braham J, Sofer D. Creutzfeldt-Jakob disease: focus among Libyan Jews in Israel. Science 1974;183:90–91.
5. Matthews WB. Epidemiology of Creutzfeldt-Jakob disease in England and Wales. J Neurol Neurosurg Psychiatry 1975;38:210–213.
6. Brown P, Cathala F. Creutzfeldt-Jakob disease in France: I: retrospective study of the Paris area during the ten-year period 1968–1977. Ann Neurol 1979;5:189–192.
7. Brown P, Cathala F, Gajdusek DC. Creutzfeldt-Jakob disease in France: III: epidemiological study of 170 patients dying during the decade 1968–1977. Ann Neurol 1979;6:438–446.
8. Brown P, Cathala F, Sadowsky D, Gajdusek DC. Creutzfeldt-Jakob disease in France: II: clinical characteristics of 124 consecutive verified cases during the decade 1968–1977. Ann Neurol 1979;6:430–437.
9. Galvez S, Masters CL, Gajdusek DC. Descriptive epidemiology of Creutzfeldt-Jakob disease in Chile. Arch Neurol 1980;37:11–14.
10. Tsuji S, Kuroiwa Y. Creutzfeldt-Jakob disease in Japan. Neurology 1983;33:1503–1506.
11. Will RG, Matthews WB, Smith PG, Hudson C. A retrospective study of Creutzfeldt-Jakob disease in England and Wales 1970–1979 II: epidemiology. J Neurol Neurosurg Psychiatry 1986;49:749–755.
12. Kovanen J, Haltia M. Descriptive epidemiology of Creutzfeldt-Jakob disease in Finland. Acta Neurol Scand 1988;77:474–480.
13. Masullo C, Pocchiari M, Neri G, et al. A retrospective study of Creutzfeldt-Jakob disease in Italy (1972–1986). Eur J Epidemiol 1988;4:482–487.
14. Satishchandra P, Shankar SK. Creutzfeldt-Jakob disease in India (1971–1990). Neuroepidemiology 1991;10:27–32.
15. Esmonde TF, Will RG. Creutzfeldt-Jakob disease in Scotland and Northern Ireland 1980–1989. Scot Med J 1992;37:181–184.
16. Davanipour Z, Smoak C, Bohr T, Sobel E, Liwnicz B, Chang S. Death certificates: an efficient source for ascertainment of Creutzfeldt-Jakob disease cases. Neuroepidemiology 1995;14:1–6.
17. Stratton E. Creutzfeldt-Jakob disease: the Canadian situation. Can Med Assoc J 1997;157:1405–1406.
18. Cousens S, Zeidler M, Esmonde TF, et al. Sporadic Creutzfeldt-Jakob disease in the United Kingdom: analysis of epidemiological surveillance data for 1970–1996. BMJ 1997;315:389–395.

19. Will RG, Alperovitch A, Poser S, et al. Descriptive epidemiology of Creutzfeldt-Jakob disease in six European countries, 1993–1995. Ann Neurol 1998;43:763–767.
20. Will RG, Ironside JW, Zeidler M, et al. A new variant of Creutzfeldt-Jakob disease in the UK. Lancet 1996;347:921–925.
21. Bruce ME, Will RG, Ironside JW, et al. Transmissions to mice indicate that "new variant" CJD is caused by the BSE agent. Nature 1997;389:498–501.
22. Collins S, Law MG, Fletcher A, Boyd A, Kaldor J, Masters CL. Surgical treatment and risk of sporadic Creutzfeldt-Jakob disease: a case-control study. Lancet 1999;353:693–697.
23. Collins S, Boyd A, Fletcher A, et al. Creutzfeldt-Jakob disease: diagnostic utility of 14–3-3 protein immunodetection in cerebrospinal fluid. J Clin Neurosci 2000;7:203–208.
24. Boyd A, Fletcher A, Lee JS, Lewis V, Masters CL, Collins S. Transmissible spongiform encephalopathies in Australia. Commun Dis Intell 2001;25:248–253.
25. Allars M. Report of the inquiry into the use of pituitary derived hormones in Australia and Creutzfeldt-Jakob disease. Canberra: Australian Government Publishing Service, 1994.
26. Will RG, Zeidler M, Stewart GE, et al. Diagnosis of new variant Creutzfeldt-Jakob disease. Ann Neurol 2000;47:575–582.
27. Steinhoff BF, Racher S, Herrendorf G, et al. Accuracy and reliability of periodic sharp wave complexes in Creutzfeldt-Jakob disease. Arch Neurol 1996;53:162–166.
28. Zerr I, Pocchiari M, Collins S, et al. Analysis of EEG and CSF 14–3–3 proteins as aids to the diagnosis of Creutzfeldt-Jakob disease. Neurology 2000;55:811–815.
29. Estimated resident population by country of birth, age and sex. Canberra: Australian Bureau of Statistics, 1993.
30. Collins S, Boyd A, Fletcher A, et al. Novel prion protein gene mutation in an octogenarian with Creutzfeldt-Jakob disease. Arch Neurol 2000;57:1058–1063.
31. Collins S, Boyd A, Fletcher A, et al. Creutzfeldt-Jakob disease cluster in an Australian rural city. Ann Neurol 2002;52:115–118.
32. Brown P. The phenotypic expression of different mutations in transmissible human spongiform encephalopathy. Rev Neurol 1992;148:317–327.
33. Windl O, Dempster M, Estibeiro JP, et al. Genetic basis of Creutzfeldt-Jakob disease in the United Kingdom: a systematic analysis of predisposing mutations and allelic variation in the PRNP gene. Hum Genet 1996;98:259–264.
34. Brown P, Preece M, Brandel J-P, et al. Iatrogenic Creutzfeldt-Jakob disease at the millennium. Neurology 2000;55:1075–1081.
35. Clinical Workforce in Internal Medicine and Paediatrics in Australia 2001. Clinical workforce surveys 2001. Sydney, Australia: The Royal Australasian College of Physicians.
36. Glatzel M, Rogivue C, Ghani A, Streffer JR, Amsler L, Aguzzi A. Incidence of Creutzfeldt-Jakob disease in Switzerland. Lancet 2002;360:139–141.

CME

Sleep deprivation does not affect seizure frequency during inpatient video-EEG monitoring

B.A. Malow, MD, MS; E. Passaro, MD; C. Milling, MD; D.N. Minecan, MD; and K. Levy, MD

Abstract—*Objective*: To determine whether acute sleep deprivation facilitates seizures during inpatient monitoring in a controlled protocol. *Methods*: Eighty-four patients with medically refractory partial epilepsy undergoing inpatient monitoring were assigned in consecutive blocks to either sleep deprivation every other night or to normal sleep. In both groups, subjects were requested to stay awake during the day, from 6 AM to 10 PM. In the sleep deprivation group, patients also stayed awake between 10 PM and 6 AM every other night beginning with Day 2. Patients were removed from sleep deprivation if they had two or more secondarily generalized seizures within 24 hours. Patients were removed from the normal sleep group and were sleep deprived if they did not have a complex partial or secondarily generalized seizure by Day 6 of monitoring. In these patients removed from sleep deprivation or from normal sleep, data were analyzed up to and including the day of removal from the protocol. *Results*: The sleep deprivation and normal sleep subjects did not differ in age, sex, seizure localization, or percent dosage reduction in antiepileptic drugs from baseline at days 1 to 3 of monitoring. Protocol duration was 6.5 ± 2.4 days (mean ± SD) for the sleep deprivation group and 5.8 ± 2.0 days for the normal sleep group. Seizures per day for complex partial, secondarily generalized, and combined complex partial and secondarily generalized, calculated from admission until end of protocol, did not differ significantly between the two groups. *Conclusion*: Acute sleep deprivation did not affect seizure frequency during inpatient monitoring in our patients with intractable complex partial seizures with secondary generalization.

NEUROLOGY 2002;59:1371–1374

For at least 40 years, sleep deprivation has been regarded as a precipitant of epileptic seizures.[1,2] Data from both case series[3-6] and patient surveys[7-9] have suggested that sleep deprivation has seizure-provoking effects. Acute sleep deprivation is used in some epilepsy monitoring units to facilitate seizure recordings as part of the diagnostic or presurgical evaluation for epilepsy.[10] The efficacy of acute sleep

From the Clinical Neurophysiology Section, Department of Neurology, University of Michigan Medical School, Ann Arbor.
Supported by NINDS KO2 NS02099.
Received April 2, 2002. Accepted in final form July 8, 2002.
Address correspondence and reprint requests to Dr. Beth A. Malow, Michael S. Aldrich Sleep Disorders Laboratory, UH Room 8D-8702; 1500 E. Medical Center Drive, Ann Arbor, MI, 48109-0117; e-mail: bmalow@umich.edu

Folia Neuropathologica.

Organ Distribution of Prion Proteins in variant Creutzfeldt Jakob disease

I.Ramasamy, M.Law, S.Collins, F.Brooke

Running title: Tissue distribution of prions

Author for correspondence

Dr I Ramasamy,
Communicable Diseases and Environmental Health Branch,
Population Health Division,
Department of Health,
MDP 14, PO Box 9848,
Canberra, ACT 2601
Australia

AUTHOR AFFILIATIONS

Dr. Indra Ramasamy M.Sc, Ph.D, MCB

Department of Health,

Canberra, Australia

Dr Mathew Law, Ph.D

Senior Lecturer,

National Centre for HIV Epidemiology and Clinical Research,

376 Victoria Street, Darlinghurst, NSW 2010, Australia

Dr S.Collins, MBBS, MD, FRACP,

Assoc.Prof Department of Pathology and Coordinator National CJD Registry,

Department of Pathology,

University of Melbourne,

Parkville, Victoria 3010

Australia.

Ms.F.Brooke,

Director, TSE Section,

Department of Health, Australia

Search Critera

Search strategy: Material used in this article was selected from Medline searches, references from reviews and original articles. Search items included the following words: vCJD, tissue, distribution and variant Creutzfeldt_Jakob disease. English language papers were reviewed.

ABSTRACT

In this article an overview of the Transmissible Spongiform Encephalopathies (TSEs) is given, with emphasis on the evidence for the distribution of abnormal prions in tissues. The normal prion protein is ubiquitously distributed throughout human body tissues. Endogenous expression of the normal prion protein, as well as auxiliary proteins play a role in accumulation of the abnormal prion protein. There is growing evidence that the host lymphoid system, in particular the follicular dendritic cells are involved in prion replication. The route for the disease related prion neuroinvasion is likely to involve the peripheral nervous system. An alternative route may involve blood constituents. A combination of animal studies and studies on variant Creutzfeldt_Jakob disease (vCJD) patients suggest a potential for abnormal prion distribution in several peripheral tissues other than the lymphoreticular system. In humans the abnormal prion has been reported in the brain, tonsils, spleen, lymphnode, retina and proximal optic nerve. Infectivity though present, is at lower levels than that of the central nervous system. Animal models suggest that the growth of infectivity is likely to be gradual with maximum values during the clinical phase of the disease. That tissues may harbour the abnormal prion, at different levels of infectivity, during the incubation period of the disease raises concerns of iatrogenic transmission of the disease either following surgery, blood transfusion or accidental organ transplantation from donors in the preclinical phase of the disease.

Introduction

Prion diseases also known as transmissible spongiform encephalopathies (TSE) are fatal neurodegenerative disorders of humans and other animals. Variant Creutzfeldt_Jakob disease is a transmissible form of spongiform encephalopathy, believed to have been contracted from consumption of bovine spongiform encephalopathy infected beef products. Of interest is the tissue distribution of prion protein which may lead to iatrogenic transmission of prions. The mechanism of prion invasion may indicate reservoirs where prions can multiply during the pre-clinical phase of the disease.

Background

Prion diseases: an overview.

The human prion diseases are unique in that they can have a sporadic, inherited or transmissible origin (Table 1).

Since the BSE epidemic in the UK, the unique biology of these previously obscure brain diseases has been the subject of intense research and controversy. The idea that a protein can act as an infectious pathogen and cause degeneration of the central nervous system was accepted only after a long and difficult battle.[1] Prion diseases involve the modification of the prion protein, a constituent of normal mammalian cells. The function of the normal cellular prion protein (PrP^{C}) is unknown. The disease

related isoform PrP^{Sc} is derived from the normal cellular precursor PrP^{C}, by a post-translational process that involves a conformational change. PrP^{C} is rich in α-helical structure, whereas PrP^{Sc} seems to be composed mainly of a β-pleated sheet structure. According to the protein only hypothesis, PrP^{Sc} is postulated to act as a conformational template that promotes conversion of PrP^{C} to PrP^{Sc}. PrP^{C} exists between the two different folding states, and the α (helical structure) and β (sheeted structure) forms of PrP^{C} have been shown to interconvert in suitable conditions.[2] A possible molecular mechanism for prion propagation can be that recruitment of PrP^{C} to PrP^{Sc} may be initiated by a pathogenetic mutation (resulting in PrP^{C} predisposed to form the β sheeted structure) in inherited prion diseases; by exposure to a 'seed' of PrP^{Sc} in acquired disease; or as a result of the spontaneous conversion of PrP^{C} to the β sheeted structure in sporadic prion disease.

This structural transition is accompanied by changes in the physicochemical properties. Soluble β-sheeted prion protein aggregates in physiological salt concentrations to form fibrils with morphological and biochemical characteristics similar to PrP^{Sc}. [2, 3, 4] Prion diseases of human beings and animals are associated with the accumulation in the brain of the partially protease-resistant isoform PrP^{Sc}. It now seems clear that the pathogenesis of TSE, like other neurodegenerative diseases (eg Alzheimer's disease), is a result of defective processing and accumulation of specific proteins in the central nervous system. [5]

About 10% of CJD cases have a predisposing mutation (and are considered familial). More than 20 mutations of the PrP gene are known to cause inherited human prion diseases and genetic linkage has been established for five of these mutations. [6].

Sporadic forms of prion disease constitute most cases of CJD and possibly a few cases of Gerstmann-Straussler-Scheinker Disease. In these patients mutations of the PrP gene are not found. How prions cause disease in patients with sporadic forms is unknown. Hypotheses suggest horizontal transmission of prions from humans or animals, spontaneous conversion of the normal cellular prion protein into PrP^{Sc} or somatic mutation of the PrP gene. As attempts to link sporadic CJD to previous existing disease in animals and humans have been not been successful, the chances that sporadic CJD occurs by transmission is small (Prusiner 1998). Prion strains can be distinguished by Western blot analysis with distinct cleavage sites to proteinase K and differences in glycoform ratios of the protease-digested PrP^{Sc}. Biochemical characterisation identified four main types of CJD-the sporadic and iatrogenic forms were of types 1-3, and the variant CJD was type 4. [7]

Properties of the cellular PrP.

Structure: The normal and cellular form of the prion protein is expressed in many tissues, although highest levels are found in the central nervous system in particular in association with synaptic membranes. The PrP^{C} is also found in lymphoreticular tissues. It is a glycosylated cell-surface protein held *in situ* by a glycolipid anchor. [8] The mature PrP^{C} species consists of an N-terminal region of about 100 amino acids, which is unstructured in the isolated molecule, and a C-terminal segment also around 100 amino acids in length which is folded into a largely α-helical conformation and stabilised by a single disulfide bond .[9]

Function: Mice lacking prion protein showed no gross phenotypic alterations, although they were completely resistant to prion disease following inoculation. Amongst the minor abnormalities observed were abnormalities in synaptic physiology and altered circadian rhythms. These phenomena are suggestive of certain features of TSE and suggest that loss of normal function may cause the disease. [10,11] While none of these observations define a molecular role for PrP^C, it has been argued that PrP^C may act as a receptor for as yet unidentified extracellular ligand. Newly synthesised PrP^C is transported to the cell surface and then cycles via a clathrin mediated mechanism, with a transit time of around an hour. This type of behaviour is associated with other cell-surface receptors, though a potential protein partner for PrP^C has not been identified.[12, 13] Using transfected cell lines it has been shown that PrP^C undergoes cleavage at the glycophospholipid anchor, which releases PrP^C into extracellular space.[12a] Clues to the function of PrP^C can also be given by the cell specific distribution of the prion protein.

Evidence for infectivity

Historically, the similarity between scrapie, kuru and CJD was identified because spongiform degeneration and astrocytic gliosis was found during histological examination of the CNS in all three diseases. The transmissibility of kuru and CJD was established by passaging the disease to chimpanzees by intracerebral innoculation.[14,15] The human to human transmission of prion diseases was demonstrated in the Fore people in New Guinea where Kuru was transmitted by ritualistic cannibalism.

Transgenetic mouse studies also suggest that PrP^{Sc} cause TSEs. Introduction of a mutation that causes GSS into the mouse PrP transgene, caused spontaneous CNS degeneration with vacuolation and amyloid plaques.[16] Further evidence that the prion protein plays a role in the pathogenesis of prion disease was shown when prion protein deficient mice were found to be resistant to prion infection.[17]

The passage of prions between species is almost always characterised by prolonged incubation times during first passage in the new host. Transgenetic mouse studies identified factors that contribute to the 'species barrier' as the difference in prion amino acid sequences between the prion donor and recipient and the strain of the prion. On subsequent passage in the same species the incubation time shortens. Mice constructed with Syrian hamster PrP transgene, when inoculated with Syrian hamster prions, showed abbreviated incubation times, unlike their non-transgene controls. Transgenic studies with mice expressing the Syrian hamster transgene also argue that the PrP^{Sc} acts as a template upon which PrP^{C} is refolded to form the protease resistant form. [18, 19] Thus homotypic interactions between identical PrP sequences in the PrP^{C} and PrP^{Sc} isoforms seem more favourable than the heterotypic alternatives. Further studies with transgenic mice suggest that a species specific macromolecule-protein X- participates in prion formation, and may contribute to the observed species barrier. [20]

Link between vCJD and BSE

A novel form of TSE, vCJD, was recognised in the UK in 1995. Differences were observed in the clinical presentation of the disease and classical CJD. The median age of death in these patients was generally ≈ 28 years, compared to the sporadic forms of

the disease ≈ 65 years.[21] Psychiatric and behavioural changes, involuntary movements and sensory symptoms are observed. During electroencephalography the classic periodic wave complexes of classical CJD were not observed in vCJD and MRI brain signal hyperintensities differed in frequency and distribution.[22, 23, 24]

.

Laboratory studies provide confirmatory evidence that vCJD and BSE have a common origin. Glycosylation patterns of the resistant form of the PrP from the brain tissue of patients with vCJD and animals with BSE are similar but are distinct from the sporadic and iatrogenic forms of the disease.[25] In inbred mouse strains, different strains of scrapie have distinct incubation periods and different topographic distribution of lesions. Studies show that the prions from BSE and vCJD show similarities in the incubation periods and distribution of lesions which are distinct from sporadic CJD. [26]

Genetic susceptibility

Codon 129 of the prion protein gene is the site of a common methionine (ATG)/valine (GTG) polymorphism. The polymorphism has also been shown to affect the clinical and pathological features of familial and sporadic CJD. In a study of the codon polymorphisms in the UK, there were differences in the frequency of the Met/Met homozygote (39% vs 69%) as well as in that of Val/Met heterozygote (50% vs 14%) in the general population and in people with sporadic CJD.[21, 27] All vCJD cases for which data were available were Met/Met homozygotes at codon 129 (UK CJD surveillance unit). DNA extracted from Kuru patients showed that the first population to develop the prion disease shared the common Met/Met genotype. The study also

showed that the Met/Val and Val/Val genotypes also developed the disease though with longer incubation times. [28] Recent evidence also suggests that DQ7, a gene involved in the immune response, is found in 36% of the normal population compared to 12% of the vCJD population indicating a protective effect of the gene. [29]

Other data suggest that Val/Val homozygosity increases susceptibility to iatrogenic CJD transmitted through peripheral (pituitary hormone therapy) exposure. The study also reports that Met/Met homozygosity is more frequent in centrally (dura mater) infected iatrogenic patients. A putative reason for the increased susceptibility can be that homozygous Val/Val individuals were donors of the contaminated growth hormone extracts. This conjecture is consistent with the experimental observation that amino acid sequence homology facilitates the conversion of PrP^{C} to PrP^{Sc}.[30, 31] The data suggest that depending on the prion strain given genotypes show increased susceptibility and/or reduced incubation times for developing clinical symptoms of TSE.

Developments in methodology for prion detection

Early studies used bioassays. However the cattle to mouse species barrier limited the sensitivity of the assay. Some of the published assays have been reviewed by MacGregor .[32] (Table II).

At the present time, standardisation and validation of assays are at early stages of development. A working group has recently been formed under the auspices of the

WHO for the development of reference materials. The success of the Delfia, Prionics, Enfer and CEA methodology in discriminating between BSE-infected and normal bovine tissue was evaluated in a European Commission sponsored study [33]. Both the Enfer and CEA assays and the Prionics Western blotting procedure showed 100% sensitivity and specificity suggesting that the tests had potential for the detection of BSE.

Tissue distribution:

Normal prion protein

At first the prion protein was considered to be a protein essentially found in the neuron. Subsequent observations have shown that the PrP^{C} can be expressed in relative abundance in extraneuronal tissues, some of which are given in Table III

A review of the literature suggests that a large number of cells and tissues express PrP^{C}. Endogenous expression of the prion protein is necessary for the replication of the abnormal PrP^{Sc} protein. PrP^{C} in nonneuronal cells may have important consequence for the pathogenesis of prion disease. Tissues that express PrP^{C} are most likely to support prion replication. It is also likely that the tissues which express the highest level of PrP^{C} are those most likely to accumulate abnormal prion, PrP^{Sc}, and are the most infective. Thus, the levels of normal PrP^{C} expression can be one of several factors that influence the development of prion diseases. [51, 52]. PrP was expressed under the control of various cell or tissue specific regulatory elements in PrP knockout mice. Transgenic mice expressed the PrP in high levels on B and T

lymphocytes and in low levels in the brain. Following intraperitoneal inoculation with mouse scrapie, these mice propagated prions in the spleen and thymus but infectivity was below detectability in the brain at six months post inoculation .[53]

The expression of PrP^{C} is necessary for replication of the infectious agent but may not be sufficient as only a few tissues appear to replicate the agent, namely neurons, and follicular dendritic cells. Factors other than the amount PrP^{C} expression (eg the presence of auxiliary proteins such as protein X to allow accumulation of prions) can determine the tropism of prions to certain tissues. One study showed that during human leukocyte differentiation, prion protein was expressed very early in hematopoiesis, indicated by its presence on CD34+ stem cells. Differentiation along the lymphocyte or monocyte lineages supports the expression of surface PrP^{C}, while differentiation along the granulocyte lineage results in a decrease of PrP^{C} surface protein. [54] Other studies confirm that PrP^{C} expression on human haematopoietic cells correlates with the activation of these cells. [35, 36] Thus, expression of the prion protein may also be affected by the developmental stage and physiological status (activation) and function of cells.

Abnormal prion protein:

Animal studies: The pathogenesis of natural scrapie was followed in susceptible sheep, (bred in an environment with a high incidence of scrapie), using immunohistochemistry to monitor the deposition of PrP^{Sc} in various tissues. PrP^{Sc} was present in all lymphoid tissues (spleen, tonsil and lymph node as well as Peyer's patches) at the age of 5 months and older. The authors report the appearance of the

scrapie agent at multiple sites within the enteric nervous system before appearance in the thoracic spinal cord (at the age of 10 months), and subsequently the brain, suggesting a neural spread of the agent. In this study the authors also report the presence of PrP^{Sc} in the endothelial cells of the capillaries within the thalamus, and suggest the possibility of a haematogenous spread of the prion protein as well. [55] The spread of PrP^{Sc} may depend on a chain of cells which express PrP^{C}. Since prion diseases primarily manifest as a disease of the CNS, the mechanism of prion spread/invasion from the periphery to the CNS, is of importance (i) in the understanding of peripheral pathogenesis and in (ii) assessing risks of iatrogenic transmission of vCJD from blood or tissues of preclinical cases. Prions may multiply in silent reservoirs (lymphoid tissue, peripheral nervous tissue) during the incubation period of the disease.

There is growing evidence that the host lymphoid system is involved in prion replication leading to the development of clinical symptoms.[51] Studies have reported that mice lacking B cells are resistant to PrP^{Sc} infection by the peripheral route, though later studies reported that the B cells were not the direct targets of infectious prions. However, B cells are required for the differentiation of other cell types that may be required for the propagation of PrP^{Sc}.[56, 57] Using irradiated SCID mice Brown *et al* (58) tested the potential of PrP^{Sc} replication in mice bearing $PrP^{+/+}$ or $PrP^{-/-}$ follicular dendritic cells derived from the host, along with $PrP^{+/+}$ or $PrP^{-/-}$ lymphocytes derived from bone marrow grafts. When the follicular dendritic cells from the host mice did not express PrP^{C} but the bone marrow grafted cells did, PrP^{Sc} replication did not occur in the spleen and the mice remained healthy. Thus follicular dendritic cells, that reside in the spleen and depend on B-cell signals for maturation, are required for

the replication of a mouse scrapie strain. Other studies also indicate that other dendritic cells ($CD11c^+$ dendritic cells) are also candidate cells in prion pathogenesis.[59, 60] Dendritic cells capture foreign antigens and may serve to store the infectious agent and allow it to replicate.

What then is the mechanism for transporting abnormal prions from the periphery to the CNS? Experimental evidence suggests that the transfer of infectivity from the spleen to the CNS cannot simply occur by bone marrow transfer and reconstitution of the haematopoietic system. Indirect evidence suggests that this compartment may be part of the peripheral nervous system.[61, 62]

The role of B cells in delivering prions to the spleen and follicular dendritic cells is speculative. It is possible that additional factors are involved. The finding that PrP^{Sc} binds to plasminogen may suggest a different route of prion infectivity.[63, 64] Radebold *et al.* [65] report the spread, in mice, of the FU prion strain of CJD from the brain to the gut by the vascular route, confirming the possibility of the spread of prions by blood. Other studies suggest that activation of specific complement components is involved in the initial trapping of prions in lymphoreticular organs early after infection. [66]

Western blot analysis confirmed PrP^{C} expression in both mice and cattle skeletal muscle at a level of about 5-10% of that in brain. The same study reported the presence of infectious mouse prions in the hindlimb muscle of mice following intra cerebral inoculation with mouse prions. Particular muscles eg hindlimb accumulated high levels of the prion. Infectious prion protein level in muscle was about 500 fold lower than in the brain.[49] In contrast, infectivities in heart and skeletal muscle have

been reported to be undetectable in scrapie affected sheep. [67, 68] Thus, this work may not be directly relevant to vCJD in humans.

*Subclinical infection***:** Immunodeficient mice harboring brain (prion) infectivity titers equalling terminally sick wild-type controls can be healthy on clinical grounds.[69] Hamster prions can persist and perhaps even replicate in a clinically silent fashion when transmitted to mice. [70, 70a] Similarly, there is a possibility that many humans may have developed subclinical infection rather than overt vCJD.

A summary of relevant issues:

- Animal and human studies show that PrP^{C} is ubiquitously distributed throughout several tissues, as well as in neuronal tissues;
- The levels of normal PrP^{C} expression can be one of several factors that influence the development of prion diseases;
- Other factors that influence infectious prion protein accumulation in tissues may be the presence of auxiliary proteins that participate in prion replication
- The distribution of PrP^{Sc} in non-neuronal tissues may depend on the prion strain as well as the host species;
- There is growing evidence that the initial phase of infection following peripheral transmission involves cells of the immune system in particular B-lymphocytes and follicular dendritic cells;
- The route of prion infection may indicate reservoirs of prion replication;
- Infection is characterised in its early stages by widespread colonisation of lymphoreticular organs , by a mechanism that is dependent on B lymphocytes,

follicular dendritic cells and soluble factors. The second phase requires PrP^C expression in the peripheral nervous system and results in prion dissemination in the CNS;

- A route for prion neuroinvasion, adapted from Nicotera *et al.* is given in Fig 1. [71]
- Thus the most likely organs for prion replication are Peyers patches, spleen and lymphoid organs. Neurons of the sympathetic nervous system and blood may be required for prion spreading;
- There is a theoretical risk of blood infectivity.

Human studies

Extensive studies on prion distribution in the peripheral tissues of vCJD patients have not been reported. Bruce *et al* [72] using a mouse bioassay, calculated the infectivity in the brain of a patient with vCJD as approximately $10^{5.1}$intracerebral mouse ID_{50} U/g of brain. The infectivity was lower in spleen and tonsils. For spleen the estimated titre was $10^{2.7}$ intracerebral mouse ID_{50} U/g. Because mouse bioassays cross species barriers, the assays will be relatively inefficient. Across the same species transmission may be 1000 times more efficient .[73] Table IV summarises the results from several studies.

Wadsworth *et al* [74] also report that prion concentrations in peripheral nerve, sciatic nerve, lymphocytes and monocytes, appendix, heart, lung, pancreas, kidney and skin were below the detection limit of the assay (approximately $<10^3$ ID_{50}/g tissue), in a total of 4 patients with neuropathologically confirmed vCJD. Other studies report the presence of prions in the appendix of a single patient, approximately 8 months prior to

the onset of clinical disease.[75] In a further study, all lymphoreticular tissues (tonsils spleen and lymph node) from patients (up to 10 patients), with confirmed vCJD, were positive for PrP^{Sc} by Western blotting.[76]

The following point is of relevance:

- There is evidence of extensive lymphoreticular involvement, suggesting a similar mechanism of neuroinvasion in humans and animals

Blood infectivity

Brown *et al.* [77], reviewed the published literature on attempts to detect infectivity in the blood of animals with transmissible spongiform encephalopathy. The review shows that blood from rodents experimentally infected with the agents that cause TSE, (cCJD, BSE and scrapie) show infectivity, in contrast, infectivity has never been detected in blood from animals with naturally occurring scrapie or BSE.
The review also summarises few reports of infectivity in the blood of humans with cCJD, in contrast to several reports that failed to find infectivity in human blood.
In a further article, Brown [78] challenges studies demonstrating infectivity in the blood of humans on technical grounds and the absence of reproducible results. Further, these studies were conducted on patients with cCJD and may not be applicable to vCJD.

A few studies on blood transmission are discussed in more detail below:

(i) Blood components and plasma fractions were prepared from the pooled blood of mice that had been infected with the mouse adapted strain of human GSS disease. Infectivity bioassays were conducted in healthy Swiss Webster mice. The authors report that during the preclinical phase of the disease the infectivity was present in the buffy coat at levels of 6-12 Infectious Units/mL and was either absent or present in plasma in only trace amounts. Infectivity rose following the onset of clinical signs to 100 Infectious units/mL of buffy coat and 20 Infectious units/mL of plasma. The authors also observe that 5-7 times more plasma was needed to transmit disease by the IV (intravenous) route than by the IC (intracerebral) route. [79]

(ii) The disease was produced in RIII/Fa/Dk mice by IC injection of a mouse adapted strain of vCJD. Preliminary data show that infectivity was detected in the buffy coat of mice euthanised during the incubation period. The levels of infectivity in blood components were reported as not greater than identified in (i). [80]

(iii) Diringer [81] using a hamster scrapie model and IC route of inoculation, reported that the blood infectivity during the incubation period was 5-50 infectious units/mL.

(iv) Houston *et al.*[82]demonstrated that it was possible to transmit BSE to a sheep by transfusion with whole blood taken from another sheep during the symptom free phase of an experimental BSE infection.

(v) Drohan *et al* [83] describe experiments by Rohwer *et al.*in which blood from hamsters experimentally infected with hamster scrapie contained infectivity during the pre-clinical and clinical stages of the disease, though with reduced efficiency of transmission by the IV route compared to the IC route.

Epidemiological data have not revealed cases of cCJD that could be attributed to administration of blood. [78] Explanations for this observation can be the low level of infectivity in blood and the need for 5-7 times more prion for transmission by the IV other than IC route. Tests with detection limits that are capable of detecting the low levels of prion present in blood are yet to be developed and the estimated concentration of prions in human vCJD blood have been based on animal models[84]. Comparable information on human vCJD is not available and the relevance of the animal models to vCJD infectivity in human blood is not known. Holada *et al.*[85] report on species differences (between humans, hamsters, and mice) of PrP^{C} in peripheral blood distribution. These differences need to be considered before extrapolating rodent TSE transmission studies with blood and blood components to humans.

Some assumptions can be made about blood infectivity:

- In the absence of tests with detection limits to be able to detect PrP^{Sc} in blood the level of infectivity in human vCJD blood is speculative;
- Based on animal models the infectivity is likely to be low and approximates to $\leq$200 ID_{50}/mL during the clinical phase.

Infectivity of eye tissue.

Much remains to be discovered about the relative infectivity of eye tissue in relation to CNS tissue. More is known about prion tissue distribution and infectivity in animals.

As a result, animal models are used to demonstrate whether transmission of TSE is possible through ocular pathways.

(i) Manuelidis *et al.* [86])demonstrated the infectivity of corneal tissue using a guinea pig model. Cornea from infected guinea pig was placed in the eye of 6 normal guinea pigs. Four developed clinical signs of CJD and histological examination of all six animals revealed spongiform encephalopathy.

(ii) In 1974, Marsh *et al.* [87] demonstrated the infectivity of the corneal epithelium from hamsters dying of transmissible mink encephalopathy. Infectivity was demonstrated by intracerebral innoculation of weanling hamsters. Brains of the infected animal contained the highest amount of infectivity, when compared to corneal epithelium.

(iii) In a scrapie infected hamster model, the infectivity in the optic nerve and retina were comparable to that in the brain ($\approx 10^{8-9}$ ID_{50} U/mL by intracerebral injection, using a hamster bioassay). Prion titers in the cornea and lens were lower ($\approx 10^{4-7}$ ID_{50} U/mL) than levels in the brain. In this model, infectivity was demonstrated in the brain and eye tissue before observation of neurological signs. [88]

(iv) Brown *et al.* [89] demonstrated infectivity in the eye (specimen of retina, vitreous, lens and cornea) of patients with spongiform encephalopathy. In most cases the inoculated animals were squirrel monkeys.

(v) Mice inoculated with brain and cornea samples from a patient with cCJD showed spongiform changes, glial proliferation and moderate loss of nerve cells. The authors observe that the brain samples transmitted disease more frequently with shorter incubation periods.[90]

(vi) In a single experiment, Herzberg *et al.* [91] failed to transmit CJD to two healthy capuchin monkeys, following transplantation of cornea taken from a moribund CJD infected capuchin monkey.

A further study compared the prion protein levels in single patients with neuropathologically confirmed cases of vCJD and sporadic CJD (Table V).

The authors used a sensitive Western blot method for comparative quantitation. The limitation of the method was such that PrP^{Sc} could only be detected at a sensitivity limit of 1/400 of that present in a brain homogenate. [74] The study did not discuss how levels relate to tissue infectivity.

Prion replication and disease progression:

The progression of the TSEs has been investigated in animal models.

(i) In the mouse scrapie model infectivity is observed in the spleen and lymph-nodes before the brain tissue is infected and long before the clinical stage of the disease. Infectivity was detected in the lymph-nodes at 4-8 weeks and clinical symptoms at 23 weeks after subcutaneous inoculation with the scrapie virus.[92]

(ii) Following intragastric infection in mice, scrapie was detected in Peyers patches, lymph nodes and spleen prior to replication in the spinal cord and brain.[93]

(iii) Using mouse bioassays, infectivity was demonstrated in lymphoid tissue of naturally infected scrapie sheep at 10-14 months of age (94), before it occurred in the CNS. Schreuder *et al* [95] conclude that PrP^{Sc} could be detected in the tonsils of genotype-susceptible sheep at between $1/3^{rd}$ and half the incubation period, about 18 months before clinical signs normally appear.

(iv) Injection of CJD strain into mice by the intraperitoneal route resulted in the detection of the prion protein in the lymphoreticular tissues of the GIT (28-32 days post inoculation) before the brain and spinal cord (>80 days).[65].

Some conclusions can be reached from the literature review:

- Animal and human studies suggest an approximate level of infectivity of 10^8 ID_{50}/g could be encountered in the brain. The infectivity level depends on the site at which prions are deposited, and the levels refer to material injected directly into the brain, hence they are given as intracerebral ID_{50}/g;
- Posterior eye tissue has a similar potential infectivity as CNS, though the anterior part of the eye could be considered to have a potential infectivity which is 1-2 logs less;
- Infectivity is present during the incubation period, the exact time at which infectivity becomes relevant is speculative-it is possible infectivity may be present during the last half of the incubation period. There have been few studies on eye infectivity in the pre-clinical stage of the disease. It is likely that for a peripheral route of infection, infectivity in the eye may be encountered in the latter part of the incubation period;

- It is likely that the growth of infectivity is gradual, to reach maximum values during the clinical phase of the disease.

Conclusions

This review summarises the current understanding of the biochemistry of the prion protein as it relates to the tissue distribution of abnormal prions. The variation in distribution of the abnormal prion protein in tissues may have implications for iatrogenic transmission of vCJD following surgery, blood transfusion or organ transplantation. The potential for infection arises from BSE-exposed individuals who, though asymptomatic, may be incubating the disease. It is the potential for transmission of the disease, and the appropriate implementation of procedures to prevent the risk of transmission, that pose a challenge for the infectious disease scientist.

References

1. Prusiner SB. Development of the prion concept. In Prusiner SB ed. Prion biology and diseases. Cold Spring Harbor Laboratory Press, 1999:67-112

2. Jackson GS, Hosszu LLP, Power A *et al*. Reversible conversion of monomeric human protein between native and fibrilogenic conformations. Science 1999; 283: 1935-1937

3. Pan K, Baldwin M, Nguyen J *et al.* Conversion of α-helices β-sheets features in the formation of the Scrapie Prion Proteins. PNAS 1993; 20:10962-10966

4. Meyer RK, McKinley MP, Bowman KA *et al.* Separation and properties of cellular and scrapie prion proteins. PNAS 1986; 83: 2310-2314

5. Prusiner SB. Neurodegenerative diseases and prions. NEJM 2001; 344: 1515-1526

6. Prusiner SB. Prions. PNAS 1998; 23: 13363-13383

7. Collinge J, Sidle KCL, Meads J *et al.*. Molecular analysis of prion strain variation and the aetiology of 'new variant' CJD. Nature 1996; 383: 685-690

8.Stahl N, Baldwin MA, Teplow DR *et al.* Structural studies of the scrapie prion protein using mass spectrometry and aminoacid sequencing. Biochemistry 1993; 32: 1991-2002

9. Stahl N, Borchelt DR, Hsiao K *et al.* Scrapie prion protein contains a phosphatidylinositol glycolipid. Cell 1987; 51: 229-240

10. Collinge J, Whittington MA, Sidle KC *et al.* Prion protein is necessary for normal synaptic function. Nature 1994; 370: 295-297

11. Tobler I, Gaus SE, Deboer T *et al.* Altered circadian activity rhythms and sleep in mice devoid of prion protein. Nature 1996; 380: 639-642

12. Shyng SL, Huber MT, Harris DA *et al.* A prion protein recycles between the cell surface and an endocytic compartment in cultured neuroblastoma cells. J Biol Chem 1993; 268: 15922-15928

12a. Harris D. Cellular biology of prion diseases. Clin Microbiol Rev 1999; 12: 429-444

13. Shyng SL, Borchelt DR, Harris DA. A glycolipid anchored prion protein is endocytosed via clathrin coated pits. J Cell Biol 1994; 125: 1239-1250

14, Gibbs CJ, Gajdusek DC, Asher DM *et al.* Transmission of experimental kuru to the spider monkey. Science 1968; 162: 693-694

15. Gajdusek DC, Gibbs CJ, Alpers M. Experimental transmission of a kuru like syndrome to chimpanzees. Nature 1966; 209: 794-796

16. Hsiao KK, Groth D, Scott M *et al.* Serial transmission in rodents of neurodegeneration from transgenic mice expressing mutant prion protein. PNAS 1994; 91: 9126-9130

17. Prusiner SB, Groth D, Serban A *et al.* Ablation of the prion gene in mice prevents scrapie and facilitates production of anti-PrP antibodies. PNAS 1993; 90: 10608-10612

18. Scott M, Groth D, Mirenda C *et al.* Transgenic mice expressing hamster prion protein produce species specific scrapie infection and amyloid plaques. Cell 1989; 59: 847-857

19. Prusiner SB, Scott M, Foster D *et al.* Transgenetic studies implicate interactions between homologous PrP isoforms in scrapie prion replication. Cell 1990; 63: 673-686

20. Telling GC, Scott M, Mastrianni *et al*. Prion propagation in mice expressing human and chimeric PrP transgenes implicates the interaction of cellular PrP with another protein, Cell 1995; 83: 79-90

21. Creutzfeldt-Jakob disease surveillance in the UK. The National CJD surveillance annual report 2000. www.cjd.ed.ac.uk

22. Will RG, Ironside JW, Zeidler M *et al.* A new variant of Creutzfeldt-Jakob disease in the UK. Lancet 1996; 347: 921-925

23. Zeidler M, Johnstone EC, Bamber RW *et al.* New variant Creutzfeldt-Jakob disease:psychiatric features. Lancet 1997; 350: 908-910

24. Zeidler M, Stewart GE, Barraclough CR, Bateman DE *et al.* New Variant Creutzfeldt-Jakob disease: neurological features and diagnostic tests. Lancet 1997; 350: 903-907

25. Hill AF, Desbruslais M, Joiner S *et al.* The same prion strain causes vCJD and BSE. Nature 1997; 389: 448-450

26. Bruce ME, Will RG *et al.* Transmissions to mice indicate that 'new variant' CJD is caused by the BSE agent. Nature 1997; 389: 498-501

27. Palmer MS, Dryden AJ, Hughes JT *et al.* Homozygous prion protein genotype predisposes to sporadic Creutzfeldt-Jakob disease. Nature 1991; 352: 340-342

28. Lee HS *et al.* Increased susceptibility to kuru of carriers of the PRNP 129 Met/Met genotype. J Infect Dis 2001; 183: 192-196

29. Jackson GS, Beck JA *et al.* Pathogenesis: HLA-DQ7 antigen and resistance to variant CJD. Nature 2001; 414: 269-270

30. Collinge J, Palmer MS Dryden AJ *et al.* Genetic predisposition to iatrogenic CJD. Lancet 1991; 337: 1441-1442

31. Brown P, Cervenakova L *et al.* Iatrogenic Creutzfeldt-Jakob disease: an example of the interplay between ancient genes and modern medicine. Neurology 1994; 44: 291

32. MacGregor I. Prion protein and developments in its detection. Transfusion Medicine 2001; 11: 3-14

33. Moynagh J, Schimmel H. Tests for BSE evaluated. Nature 1999; 400: 105

34. Moser M, Collelo R, Pott U *et al.* Developmental expression of the prion protein gene in glial cells. Neuron 1995; 14: 509-517

35. Cashman NR, Lortscher R, Nalbantoglu J *et al.* Cellular isoform of the scrapie agent protein particiaptes in lymphocyte activation. Cell 1990; 61: 185-192

36.. Durig J, Giese A, Schulz-Schaeffer W *et al.* Differential constitutive and activation dependent expression of prion protein in human peripheral lymphocytes. Br J Haematol 2000; 108: 488-495

37. Perini F, Frangione B, Prelli F *et al*. Prion protein released by platelets. Lancet 1996; 347: 1635-1636

38. Perini F, Vidal R, Ghetti B *et al.* PrP27-30 is a normal soluble prion protein fragment released by human platelets. BBRC 1996; 223: 572-577

39. MacGregor I, Hope J, Barnard G *et al.* Application of time resolved fluoroimmunoassay for the analysis of normal prion protein in human blood and its components. Vox sang 1999; 77: 88-96

40. Ritchie DL, Brown KL, Bruce ME. Visualisation of PrP protein and follicular dendritic cells in uninfected and scrapie infected spleen. J Cell pathology 1999; 1: 3-10

41. Brown HR, Goller N, Rudelli G *et al.* The mRNA encoding the scrapie agent protein is present in a variety of non neuronal cells. Acta Neuropath 1990; 80: 1-6

42. Brown KL, Ritchie DL, McBride PA *et al.* Detection of PrP in extraneural tissues. Micosc Res Tech 2000; 50: 40-45

43. Bendheim PE, Brown HR, Rudelli RD *et al.* Nearly ubiquitous tissue distribution of the scrapie agent precursor protein. Neurology 1992; 42: 149-156

44. Fournier JG, EscaigHaye F, Grigoriev V. Ultrastructural localisation of prion proteins: physiological and pathological implications. Mic Res & Tech 2000; 50: 76-88

45. Sy MS, Gambetti P. Prion replication-once again blaming the dendritic cell. Nat med 1999; 11: 1235-1237

46. Pammer J, Weninger W, Tschachler E. Human keratinocytes express cellular prion related protein *in vitro* and during inflammatory skin disease. Am J Pathol 1998; 153: 1353-1358

47. Askanas V, Bilak M, King E *et al.* Prion protein is strongly immunolocalised at the postsynaptic domain of human normal neuromuscular junctions. Neurosci Lett 1993; 159: 111-114

48. Horiuchi M, Yamazaki N, Ikeda T *et al.* A cellular form of prion protein exists in many non-neuronal tissues of sheep. J Gen Virol 1995; 76: 2583-2587

49. Bosque PJ, Ryou C, Telling G *et al.* Prions in skeletal muscle. PNAS 2002; 99: 3812-3817

50. Shaked Y, Rosenmann H, Talmor G *et al.* A C-terminal truncated PrP isoform is present in the mature sperm. J Biol Chem 1999; 274: 32153-32158

51. Prusiner SB, Scott MR, DeArmond SJ *et al.* Prion protein biology. Cell 1998; 93: 337-348

52. Aguzzi A, Brandner S, Fischer MB *et al.* 2001. Advances in virus research 2001; 56: 312-352

53. Raeber AJ, Sailer A, Heygi I *et al.* Ectopic expression of prion protein in T lymphocytes or hepatocytes of PrP knockout mice is insufficient to sustain prion replication. PNAS 1999; 96: 3987-3992

54. Dodelet VC, Cashman NR. Prion protein expression in human leukocyte differentiation. Blood 1998; 91: 1556-1561

55. Van Keulen LJM, Schreuder BEC, Vromans MEW *et al.* Pathogenesis of natural scrapie in sheep in Groschup MH, Kretzschmar HA. Prion diseases. 2000. Springer Life Sciences, New York

56. Klein MA *et al.* A crucial role for B cells in neuroinvasive scrapie. Nature 1997; 390: 687-690

57. Klein MA *et al.* PrP expression in B lymphocytes is not required for prion neuroinvasion. Nat Med 1998; 4: 1429-1433

58. Brown KL, Stewart K, Ritchie DL *et al.* Scrapie replication in lymphoid tissues depends on prion protein-expressing follicular dendritic cells. Nat Med 1999; 5: 1308-1312

59. Montrasio F, Frigg R, Glatzel M *et al.* Impaired prion replication in spleens of mice lacking functional follicular dendritic cells. Science 2000; 288: 1257-1259

60. Aucouturier P, Geissmann F, Damotte D *et al*. Infected splenic dendritic cells are sufficient for prion transmission to the CNS in mouse scrapie. J Clin invest 2001; 108: 703-708

61. Aguzzi A. Molecular pathology of prion diseases. Vox Sanguinis 2000; 78: Suppl 2: 25

62. Glatzel M, Heppner FL, Albers KL *et al.* Sympathetic innervation of lymphoreticular organs is rate limiting for prion neuroinvasion. Neuron 2001; 30: 25

63. Fisher MB, Roecki C, Parizek P *et al.* Binding of disease associated prion protein to plasminogen. Nature 2000 408: 479-483

64. Maissen M, Roecki C, Glatzel M *et al.* Plasminogen binds to disease-associated prion protein of multiple species. The Lancet 2001; 357: 2026-2037

65. Radebold K, Chernyak M, Martin D *et al.* Blood borne transit of CJD from brain to gut at the early stages of infection. BMC Infectious Diseases 2001; 1 :20.-24

66. Klein MA, Kaeser PS, Schwarz P *et al.* Complement facilitates early prion pathogenesis. Nat Med 2001; 7: 488-492

67. Hadlow WJ, Race RE, Kennedy RC *et al.* Natural infection of sheep with scrapie virus. In Slow Transmissible Diseases of the Nervous System. Vol2.pp3-12. Edited by SB Prusiner and WJ Hadlow. 1979. New York Academic Press.

68. Danner K. BSE-a risk for man through pharmaceutical products? Position and politics of the German pharmaceutical industry. In Transmissible Spongiform Encephalopathies-Impact on Animal and Human health. Pp 199-205. 1993. Edited by F.Brown. Basel-Karger

69. Frigg R, Klein MA, Heygi I *et al.* Scrapie pathogenesis in subclinically infected B-cell deficient mice. J of Virol 1999; 73: 9584-9588

70. Race R, Chesebro B. Long term persistence of scrapie infectivity in brain and spleen of a clinically resistant species: implications for control of BSE. Nature 1998; 392: 770

70a. Thackray AM, Klein MA, Aguzzi A *et al.* Chronic subclinical prion disease induced by low dose inoculum. J of Virol 2002; 76: 2510-2517

71. Nicotera P. A route for prion neuroinvasion. Neuron 2001; 31: 345-348

72. Bruce ME, McConnell I *et al*. Detection of variant Creutzfeldt-Jakob disease infectivity in extraneural tissues. Lancet 2001; 358: 208-209

73. Vitale K, Sahin U *et al.* The animal and human prion diseases: public health importance and risk assessment. Periodicum biologorium 2001; 103: 201-217

74. Wadsworth JDF, Joiner S *et al.* Tissue distribution protease resistant prion protein in variant Creutzfeldt-Jakob disease using a highly sensitive immunoblotting assay. The Lancet 2001: 358: 171-180

75. Hilton DA, Fathers E, Edwards P, Ironside JW, Zajicek. Prion immunoreactivity in appendix before clinical onset of variant Creutzfeldt-Jakob disease. Lancet 1998; 352: 703-704

76. Hill AF, Butterworth RJ, Joiner S *et al.* Investigation of variant Creutzfeldt-Jakob disease and tonsil biopsy samples. Lancet 1999; 353: 183-189

77. Brown P, Cerevenakova L, Diringer H. Blood infectivity and the prospects for a diagnostic screening test in Creutzfeldt-Jakob disease. J Lab Clin Med 2001; 137: 5-14

78. Brown P. The risk of blood-borne Creutzfeldt-Jakob disease. Dev Biol Stand. 1999; 102: 53-59

79. Brown P, Cerevenakova L, McShane LM *et al.* Further studies of blood infectivity in an experimental model of transmissible spongiform encephalopathy with an explanation of why blood components do not transmit Creutzfeldt-Jakob disease in humans. Transfusion 1999; 39: 1169-1178

80. L.Cerevenakova. The safety of human blood:experimental TSE/prion infectivity studies. Transfus Clin Biol 2001; 8: 260

81. Diringer H. Sustained viremia in experimental hamster scrapie. Arch of Virol 1984; 82:105-109

82. Houston F, Foster JD, Chong A *et al.* Transmission of BSE by blood transfusion in sheep. Lancet 2000; 356: 999-1000

83. Drohan WN, Cerevenakova L. Safety of blood products: are transmissible spongiform encephalopathies (prion diseases) a risk. Thromb Haemost 1999; 82: 486-493

84. Brown P. Creutzfeldt-Jakob disease:blood infectivity and screening tests. Seminars in Haematology 2001; 38: 2-6

85. Holada K, Vostal JG. Different levels of prion protein (PrPc) expression on hamster, mouse and human blood cells. Br J Haem 2000; 110: 472-480

86. Manuelidis EE, Angelo JN, Gorgacz EJ *et al.* Experimental Creutzfeldt-Jakob disease transmitted via the eye with infected cornea. N Eng J Med 1977; 296: 1334-1336

87. Marsh RF, Hanson RP. Transmissible mink encephalopathy: infectivity in corneal epithelium. Science 1974; 187: 656

88. Hogan RN, Bowman KA, Baringer JR *et al.* Replication of scrapie protein in hamster eyes precedes retinal degeneration. Opthalmic research 1986; 18: 230-235

89. Brown P, Gibbs CJ, Rodgers-Johnson P *et al.* Human spongiform encephalopathy: the National Institute of Health Series of 300 cases of experimentally transmitted disease. Ann Neurol 1994; 35: 513-529

90. Tateishi J. Transmission of Creutzfeldt-Jakob disease from human blood and urine in mice. Lancet 1985; 2: 1074

91. Herzberg L. Creutzfeldt-Jakob disease and corneal grafts. Med J Aust 1979; 1: 248.

92. Eklund CM, Kennedy RC *et al.* Pathogenesis of scrapie virus infection in the mouse. J Infect Dis 1967; 117: 15-22

93. Kimberlin RH, Walker CA. Pathogenesis of scrapie (strain 263K) in hamsters infected intracerebrally, intraperitoneally or intraocularly. J Gen Virol 1986; 67: 255-263

94. Hadlow WJ, Kennedy RC, Race RE. Natural infection of suffolk sheep with scrapie virus. J Infectious Dis 1982; 146: 657-664

95. Schreuder BEC, van Keulen LJM *et al.* Tonsillar biopsy and PrP^{Sc} detection in the preclinical diagnosis of scrapie. Vet Record 1998; 142: 564-568

Table 1. Prion diseases

Disease	**Host**	**Mechanism of pathogenesis**
Kuru	Humans	Infection through ritualistic cannibalism
Iatrogenic CJD (iCJD)	Humans	Infection from prion-contaminated hGH, dura mater grafts etc
Variant CJD (vCJD)	Humans	Infection from bovine prions
Familial CJD (fCJD)	Humans	Germ Line Mutations in PrP gene
Gerstmann-Straussler-Scheinker Disease (GSS)	Humans	Germ Line Mutations in the PrP gene
Familial Fatal Insomnia (FFI)	Humans	Germ Line mutations in PrP gene
Sporadic CJD (sCJD)	Humans	?subclinical case-to-case transmission, ?somatic mutations or spontaneous conversion of PrP^{C} to PrP^{Sc}
Scrapie	Sheep	Infection in genetically susceptible sheep
Bovine Spongiform Encephalopathy (BSE)	Cattle	Infection with prions from sheep or cattle
Transmissible Mink encephalopathy	Mink	Infections with prions from sheep or cattle
Chronic wasting disease	Mule deer, elk	Unknown
Feline Spongiform Encephalopathy	Cats	Infection with prion contaminated bovine tissues or meat and bone meal
Exotic ungulate encephalopathy	Greater kudu, nyala, oryx	Infection with prion contaminated meat and bone meal

iCJD, fCJD, sCJD are the classical forms of the disease

Table II: Tests for PrP^{Sc} detection

Assay	**Test sample**
Delfia	BSE brain homogenate
Prionics Western blotting	BSE brain homogenate
Enfer ECL ELISA	BSE brain homogenate
CEA ELISA	BSE brain homogenate
Capillary electrophoresis	Brain and blood from scrapie sheep and CWD elk.
BioRad Platelia BSE	Bovine Brain sample

Tissue	Species	Prion Strain	Detection method
Cerebral tissues			
Glial cells eg Astrocytes	Hamsters and rats	PrP^C	*In situ* hybridisation [34]
Circulating blood			
B and T Lymphocytes and monocytes	Human	PrP^C	Immunoblot and cytofluorometry [35,36]
Platelets	Human	PrP^C	Immunoblot, time resolved dissociation-enhanced immunoassay [37, 38, 39]
Lymphoreticular system			
Follicular dendritic cell	Mouse	PrP^C	Immunocytochemistry [40,41,42]
Gastrointestinal tract			
Parietal cells	Hamster	PrP^C	Immunofluorescence [43]
Mucous epithelial cells	Human	PrP^C	Anti-PrP antibodies [44]
Epithelial cells of the GIT	Human	PrP^C	Not stated [45]
Skin			
Keratinocytes in basal layer (cell culture)	Human	PrP^C	Western blot [46]
Muscle			
Neuromuscular junction	Human	PrP^C	Immunohistofluorescence [47]

Skeletal muscle	Hamster, Sheep Mice, Cattle		Western blot [43, 48, 49]
Testes			
Sperm cells	Human	PrP^C	Immunoblot detected a truncated prion protein. [50]

Table III: PrP^C distribution in tissues

Table IV: Tissue distribution PrP^{Sc} in humans

Tissue	**Prion protein concentration relative to brain**	**Approximate prion concentration ID_{50}/g tissue***	**Comments**	**Reference**
Tonsil	5-15%	10^7	Technique used:Western blotting	[74]
Spinal cord	30%	10^7	Technique used:Western blotting	"
Lymph node	0.1-1%	10^5-10^6	Technique used:Western blotting	"
Rectum, thymus and adrenal gland	1/50,000	10^3	Found in a single patient with high brain prion titres. Technique used:Western blotting	"
Spleen		10^6-10^7	Technique used:Western blotting and bioassay	[74, 72]

Based on prion concentrations in the brain of 10^8 ID_{50}/g tissue,.

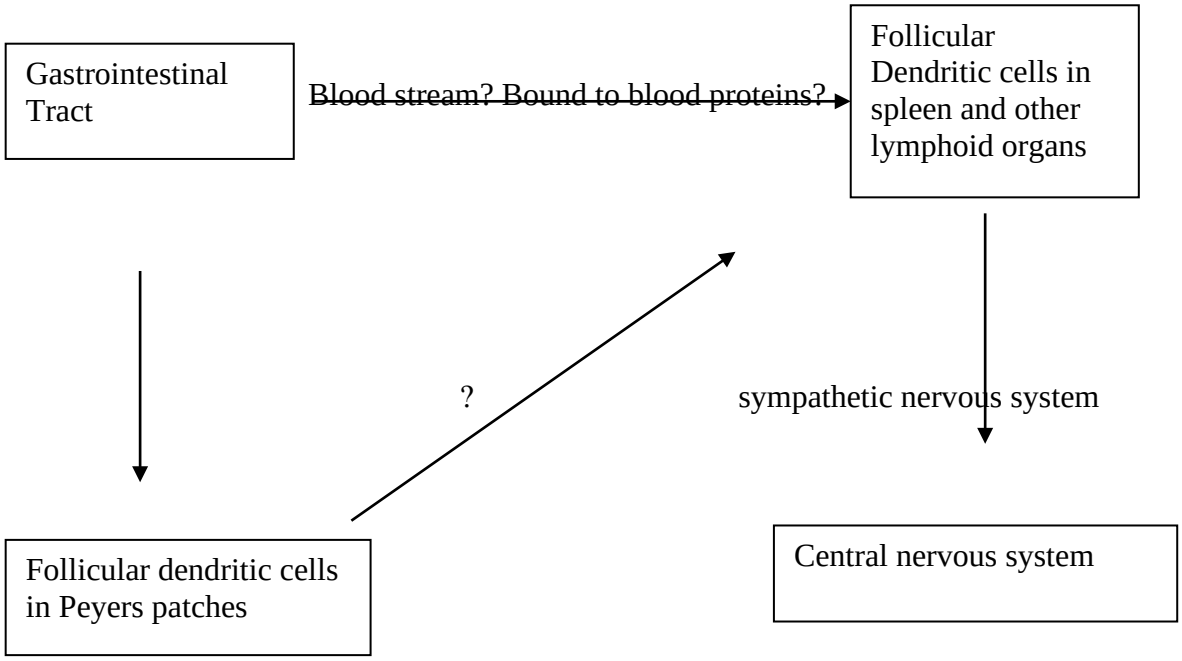

Fig 1. Possible routes for prion neuroinvasion

Table V: PrP^{Sc} distribution in eye tissues.

Eye Component	**PrP^{Sc} concentration relative to brain**	
	Sporadic CJD	**Variant CJD**
Cornea	ND	ND
Iris	ND	ND
Aqueous Humour	ND	ND
Lens	ND	ND
Vitreous humour	ND	ND
Sclera	ND	ND
Retina	ND	2.5%
Optic Nerve	ND	25%

ND=not detected

ton's disease in asymptomatic at-risk persons. Neurology 1994;44:823–828.
38. Pantoni L. Pathophysiology of age-related cerebral white matter changes. Cerebrovasc Dis 2002;13(suppl 2):7–10.
39. Sandson TA, Felician O, Edelman RR, Warach S. Diffusion-weighted magnetic resonance imaging in Alzheimer's disease. Dement Geriatr Cogn Disord 1999;10:166–171.
40. Fazekas F, Barkhof F, Wahlund LO, et al. CT and MRI rating of white matter lesions. Cerebrovasc Dis 2002;13(suppl 2):16–20.
41. Schocke MF, Seppi K, Esterhammer R, et al. Diffusion-weighted MRI differentiates the Parkinson variant of multiple system atrophy from PD. Neurology 2002;58:575–580.
42. Boone KB, Miller BL, Lesser IM, et al. Neuropsychological correlates of white-matter lesions in healthy elderly subjects. A threshold effect. Arch Neurol 1992;49:549–554.
43. Backman L, Robbins TB, Lundin A, Ginovart N, Farde L. Cognitive deficits in Huntington's disease are predicted by dopaminergic PET markers and brain volumes. Brain 1997;120:2207–2217.

Novel prion protein insert mutation associated with prolonged neurodegenerative illness

V. Lewis, BSc(Hons); S. Collins, MD; A.F. Hill, PhD; A. Boyd, Grad Dip Gen Coun; C.A. McLean, MD; M. Smith, PhD; and C.L. Masters, MD

Abstract—*Background:* Mutations in the prion protein gene (*PRNP*) are found in approximately 13 to 15% of persons classified as dying from a transmissible spongiform encephalopathy. Point and octapeptide repeat insert and deletion mutations are described in the open reading frame (ORF) of *PRNP*. The authors present a clinicopathologic study of a patient with a family history of a lengthy and progressive neurodegenerative disorder associated with a novel large octapeptide repeat insert mutation. *Methods:* Neuropathologic examination, including immunohistochemistry for the prion protein, was undertaken. The ORF of *PRNP* was amplified by PCR, cloned, and sequenced. Homogenate of cerebral tissue underwent Western blot analysis for the prion protein before and after proteinase K treatment. *Results:* The proband died after a 16-year illness commencing at age 29 years. Confident premortem clinical diagnosis was not achieved despite a brain biopsy. Autopsy examination of the brain confirmed a spongiform encephalopathy. Prion protein immunohistochemistry revealed occasional granular deposits in the cerebellar granular layer. The proband was found to harbor a novel *PRNP* 168 base pair (bp) insert mutation. *Conclusion:* The authors have identified a novel 168 bp octapeptide repeat insert mutation. Prion protein immunohistochemistry differs from previous cases harboring seven octapeptide repeat and other long insert mutations. Optimization of *PRNP* analysis, especially PCR conditions, is essential to avoid overlooking this type of mutation and delay the correct molecular genetic diagnosis.

NEUROLOGY 2003;60:1620–1624

Within the phenotypic spectrum of human transmissible spongiform encephalopathies (TSE), systematic molecular genetic analyses have confirmed various anomalies in the prion protein gene (*PRNP*) on chromosome 20 to be causally associated with 13 to 15% of cases.[1,2] Most commonly, point mutations are found in the coding region of *PRNP*, although polymorphic deletions of single repeats,[3] a pathogenic two repeat unit deletion,[4] and insertions are also recognized, with insertions the first to be described.[5] The N-terminal region from codon 51 to 91 normally codes for a nonapeptide (R1), followed by four identical octapeptide repeats (R2, R2, R3, and R4) with only minor variations at the nucleotide level (table 1). Insert mutations are postulated to arise from unequal crossover events,[6] and consequently demonstrate striking sequence similarity to the wild-type allele. With the exception of a three octapeptide repeat insert, interpolations consisting of discrete 24-base pair (bp) multiples varying in length from one (24-bp) to nine (216-bp) octapeptides have been described.[6-9,13]

Additional material related to this article can be found on the *Neurology* Web site. Go to www.neurology.org and scroll down the Table of Contents for the May 27 issue to find the title link for this article.

From the Department of Pathology (V. Lewis and A. Boyd, and Drs. Collins, Hill, McLean, Smith, and Masters) and The Australian National Creutzfeldt-Jakob Disease Registry (V. Lewis and A. Boyd, and Drs. Collins and Masters), The University of Melbourne; and Molecular Biology Laboratory (Dr. Smith), Melbourne Health Shared Pathology Services, Royal Melbourne Hospital, Parkville, Victoria, Australia.

The Australian National Creutzfeldt-Jakob Disease Registry is funded by the Commonwealth Department of Health and Ageing. S.C. receives support from a National Health and Medical Research Council Program grant (#208978) and A.F.H. received support from a Wellcome International Prize Travelling Research Fellowship.

Received June 10, 2002. Accepted in final form February 19, 2003.

Address correspondence and reprint requests to Dr. S. Collins, Australian National CJD Registry, Department of Pathology, The University of Melbourne, Victoria, Australia 3010; e-mail: stevenjc@unimelb.edu.au

Table 1 *Comparison of the proband with the normal and published codon 51–91 region of* PRNP *encompassing seven octapeptide repeat inserts*

Repeat unit sequence												Reference
R1	R2	R2	..	..	..	..	..	..	..	R3	R4	9
R1	R2	R2c	R3	R2	R3	R2	R3	R2	R3g	R3	R4	6
R1	R2	R2	R3	R2	R2	R2	R3g	R2	R2	R3	R4	9, 13
R1	R2	R2	R3	R2	R3	R2	R2	R2	R2	R3	R4	Proband; current report

Details of the octapeptide repeat insert sequence for the family reported by Dermaut et al.[12] were not cited. R1 denotes the nonapeptide PHGGGGWGQ; R2, R3, etcetera denote octapeptide repeat motifs essentially homologous to R1 but varying slightly at the nucleotide level.

A detailed clinicopathologic study of a proband harboring a novel 168-bp, representing seven repeat units, *PRNP* insert mutation is presented. This represents only the fourth family with this length octapeptide repeat insert to be reported.[6,9-13] Although the phenotype shows general conformity to previous descriptions, some deviations in the pathologic findings and the technical difficulties encountered in securing a molecular genetic diagnosis add further interest and importance to the report.

Methods. *Neuropathologic examination.* The brain was hemisectioned longitudinally with the right half frozen at −70 °C and the left half fixed in 20% formalin. Postfixation sections were taken from the frontal, parietal, temporal, and occipital cortex, basal ganglia, diencephalon, thalamus, brainstem, and cerebellum. Sections were treated with formic acid for 1 hour before normal processing. Sections were stained routinely and immunoreacted for the prion protein (PrP), using 3F4 (Signet Pathology Systems, Dedham, MA) at a concentration of 1/1,000 following the hydrated autoclaving protocol to enhance antigenicity.[14] Immunolabeling was visualized using horseradish peroxidase and diaminobenzidine (DAB Dako, Carpenteria, CA).

DNA analysis. *PRNP* analysis was undertaken posthumously on two separate occasions, with the first showing no apparent mutations. Comprehensive review of the proband's clinical details (for classification purposes) prompted repeat *PRNP* analysis. *PRNP* analyses utilized the same DNA extracted from frozen brain samples, with the initial analysis using methods described previously.[15] In the second analysis, amplification of the entire *PRNP* open reading frame (ORF) was first performed using the primer pair forward-PrP 106, reverse-PrP 46 (please see table e1 at www.neurology.org for all primer sequence details). PCR reaction conditions were optimized using FailSafe PCR 2X PreMixes (Epicentre, Madison, WI). Thereafter, PCR mixes were made according to manufacturer's instructions, using 25 μL Mix D with 1 μL DNA and 20 pM of each primer and 1 μL Taq Polymerase (Gibco, Carlsbad, CA) to a final volume of 50 μL using sterile deionized water. Cycling conditions were 94 °C for 5 minutes, followed by 35 cycles of 94 °C for 1 minute, 60 °C for 1 minute, and 72 °C for 1 minute. The final extension was at 72 °C for 10 minutes. PCR products were visualized on 1.5% agarose gels containing ethidium bromide. The insertion was confirmed again using genomic DNA and a second set of primers, which were internal to the first: forward-PrP 3F, reverse-PrP 2R. Reaction mixes contained 1 μL DNA, 5 μL 10 × dNTP mix, 20 pM of primers, 5 μL 10 × PCR buffer (Gibco), 2.5 μL DMSO, 3 μL 25 mM $MgCl_2$, and 0.5 μL Taq Polymerase (Gibco) to a final volume of 50 μL using sterile deionized water. PCR cycling conditions were as above, except during the 35 cycles, denaturation was at 94 °C for 30 seconds, while reannealing was at 60 °C for 45 seconds. Products were again visualized on 1.5% agarose gels.

Cloning. A TOPO TA Cloning kit (Invitrogen, Carlsbad, CA) was used to produce transformants from purified PCR product (Roche Diagnostics High Pure PCR Product Purification Kit; Roche, Mannheim, Germany), which were plated on LB plates containing 50 μg/mL ampicillin and Xgal/ITPG. Plates were incubated overnight at 37 °C. White colonies were picked and cultured overnight in LB containing 50 μg/mL ampicillin. Minipreps following the manufacturer's protocol (Eppendorf Perfectprep Plasmid Mini; Eppendorf, Hamburg, Germany) were performed to retrieve the plasmid, and an *Eco*RI digest was performed to confirm the presence of the inserted gene in the clone.

Sequencing. Clones were sequenced in the forward and reverse directions. Gene sequencing utilized the BigDye Terminator Cycle Sequencing Ready Reaction, DNA Sequencing Kit (Applied Biosystems, Foster City, CA), with the following modifications: 20 μL reactions were used containing 4 μL BigDye buffer, 10 pM of primer, 8 μL DNA, 2 μL dilution buffer (250 mM Tris, 10 mM $MgCl_2$), made up to 20 μL with sterile deionized water. The sequencing primers are summarized in table e1 (available at www.neurology.org): forward-M13F, PrP 5 and PrP F3, reverse-M13R, and PrP 6. Sequencing conditions were 25 cycles of 96 °C for 10 seconds, 50 °C for 5 seconds, and 60 °C for 4 minutes. DNA was further prepared using the DyeEx Spin Kit protocol for Dye-Terminator removal (Qiagen, Hilden, Germany) with automated sequencing performed on an Applied Biosystems (ABI) Prism 373XL sequencer.

Western immunoblots. Brain homogenates (10% w/v in phosphate-buffered saline) were prepared from sporadic Creutzfeldt-Jakob disease (proven not to have a *PRNP* mutation), a normal control, and the proband. Proteinase K (PK) was added to 20 μL of homogenate (final concentration 100 μg/mL) and incubated at 37 °C for 1 hour. Digestion was stopped with a final concentration of 5 mM Pefabloc (Roche) in an equal volume of sodium dodecyl sulfate sample buffer containing 6% beta-mercaptoethanol (Sigma-Aldrich, St. Louis, MO). Samples were boiled for 10 minutes before loading 5 μL of PK untreated samples and 10 μL of PK digested samples on to 12% Tris-Glycine precast gels (Novex, San Diego, CA). Samples were then transferred to nitrocellulose membrane and blocked for 45 minutes at room temperature in 5% skim milk powder/PBST. After overnight incubation at 4 °C in 3F4 (1:5,000 in phosphate buffered saline [PBS] with 0.05% (v/v) Tween 20 (Sigma-Aldrich)), the filter was incubated at room temperature in anti-mouse-horseradish peroxidase (1:10,000 in PBST). The membrane was visualized using enhanced chemiluminescence (ECL, Amersham, Buckinghamshire, UK) as per manufacturer's instructions.

Results. *Case report.* The proband's illness commenced at age 29 years, with inappropriate behavior, undue clumsiness, abnormal limb movements, and forgetfulness noted. Gradual physical and intellectual deterioration prompted hospital evaluation 6 years after symptom onset. Generalized tonic-clonic seizures had necessitated anticonvulsant therapy with phenytoin 200 mg twice daily, which was the only prescribed medication. Routine biochemical and hematologic parameters were unremarkable, including serum copper levels and Venereal Disease Research Laboratory serology. Muscle biopsy was uninformative. EEG showed a nonspecific excess of slower frequencies, whereas CT scans of the brain revealed generalized atrophy. Brain biopsy from the right frontal region was nondiagnostic. The patient was discharged with a diagnosis of degenerative brain disease.

At 10 years into the proband's illness, the combination of involuntary limb movements and cognitive decline led to diagnostic speculation of Huntington disease. Examination revealed the patient to be unable to walk or sit without assistance, with athetoid movements affecting the proximal limbs and choreiform move-

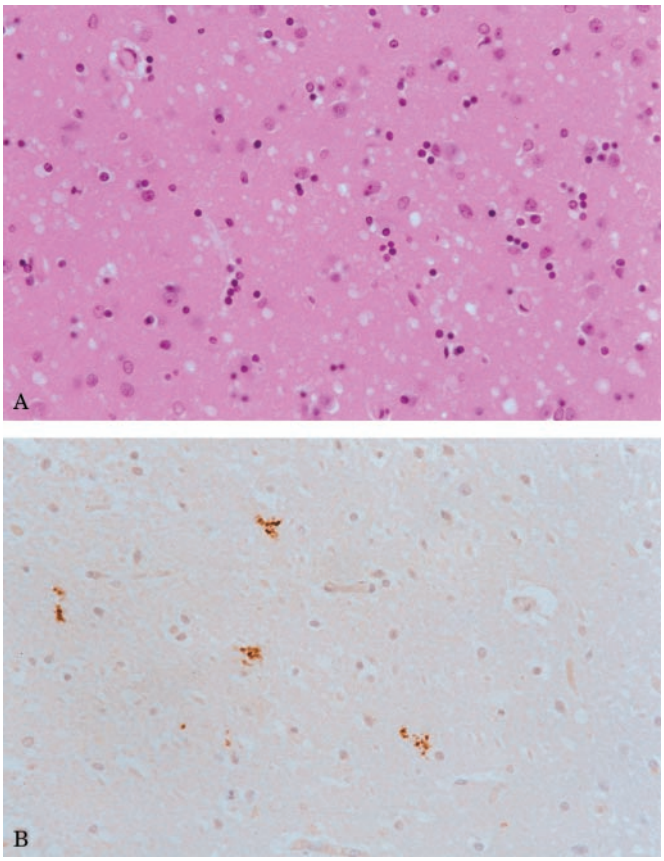

Figure 1. Photomicrographs of representative brain sections. Magnification ×400. (A) Hematoxylin and eosin–stained frontal cortex displays diffuse spongiform changes, neuronal loss, and gliosis. (B) Prion protein immunostaining of the molecular layer of the cerebellum shows occasional nonlinear granular deposits.

ments distally. Mild tetraparesis with generalized hypertonia and hyperreflexia were present but with flexor plantar responses. Limb cerebellar-type ataxia was not a feature. Frontal release signs were elicitable and there was evidence of moderately severe global cognitive impairment. Repeat EEG and CT head scan showed results similar to those previously. An MRI scan of the brain 11 years after symptom onset confirmed generalized, marked cerebral and cerebellar atrophy, with normal-appearing caudate nuclear heads. Progressive decline necessitated admission to long-term institutional care and culminated in the patient's death after an illness spanning 16 years.

A family history of similar neurodegenerative disorder was present. Clinical and investigational details were incomplete but one parent developed dementia at 32 years and died at age 39, whereas a full sibling manifested a similar illness from age 24 years and died at age 31. Both underwent postmortem neuropathologic examination in another country without a conclusive diagnosis, although frontal atrophy and gliosis with no evidence of plaques or inclusions were reported. Some sections of the lower brainstem from the propositus' sibling were obtained for review; a specific diagnosis remained unachievable. A half-sibling sharing the affected parent was reported to be alive and well 10 years ago, with further follow-up not possible since.

Neuropathologic examination. The brain (weight 990 g) showed generalized atrophy more marked in the frontal lobes with dilation of the lateral ventricles anteriorly. The caudate nuclei, basal ganglia, and cerebellar folia appeared atrophic. The cerebellum showed diffuse folial atrophy. The brainstem appeared normal.

Microscopic examination revealed prominent diffuse spongiform changes, neuronal loss, and gliosis in the cerebral cortex (most marked in the frontal [figure 1A] and temporal cortex), with

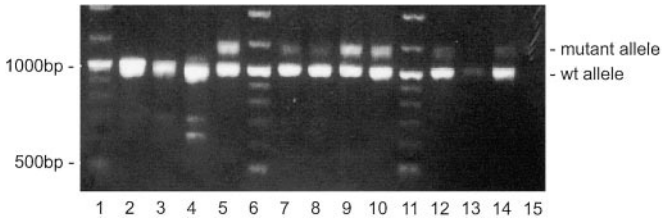

Figure 2. Optimization of PCR conditions using proband DNA with primers PrP 106 and PrP 46 and the Failsafe PCR PreMixes (Epicentre). Lanes 1, 6, and 11 are a 100 base pair DNA ladder. Lanes 2 through 5 are mixes A through D, lanes 7 through 10 are mixes E through H, and lanes 12 through 15 are mixes I through L.

similarly severe changes in the basal ganglia and diencephalon. Atrophy of the molecular and granular layers and patchy Purkinje cell loss was seen in the cerebellum. Patchy, synaptic-type PrP immunoreactivity was seen in the inferior aspects of the cerebellar folia, with occasional granular deposits (see figure 1B), and no immunostaining in the cerebral cortex and basal ganglia.

Molecular genetic studies. During the optimizing of PCR conditions, the second *PRNP* amplifications revealed an additional slower band consistent with a DNA insert of approximately 150 bp (figure 2, lanes 5, 9, and 10; figure 3, lane 4). However, absence or a very weak slower band signal in the majority of lanes is evident (see figure 2, lanes 2 through 4, 7, 8, 12, and 14). A band consistent with the wild type allele at the predicted mobility of ~1000 bp was also present. The presence of the larger DNA fragment was confirmed by a second PCR amplification using primers internal to the first (see figure 3, lane 7). Each allele was cloned and sequenced. A 168 bp insert in the 51–91 coding region of the ORF was determined in the expanded allele, equivalent to a seven octapeptide repeat. The wild type octapeptide repeat region was confirmed as R1, R2, R2, R3, R4 in cis with valine at codon 129, whereas the 168 bp insertion constituted a novel seven octapeptide repeat with methionine at codon 129 (see table 1).

Western blotting. Figure 4 shows Western blot analysis of brain tissue from a normal control, sporadic CJD, and the pro-

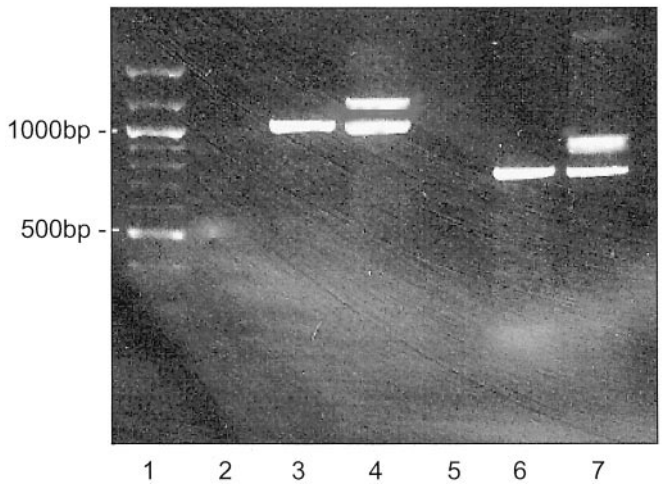

Figure 3. Ethidium bromide–stained 1.5% agarose gel shows the different-sized PCR products obtained with different primer pairs: lanes 2 through 4, PrP 106 and PrP 46; lanes 5 through 7, PrP 3F and PrP 2R. Lane 1, 100 bp molecular weight ladder; lanes 2 and 5, sterile deionized water; lanes 3 and 6, control DNA without PRNP *insert mutation; and lanes 4 and 7, our proband's DNA. Both primer pairs clearly show a second slower band consistent with an allele containing an insert mutation of approximately 150 bp.*

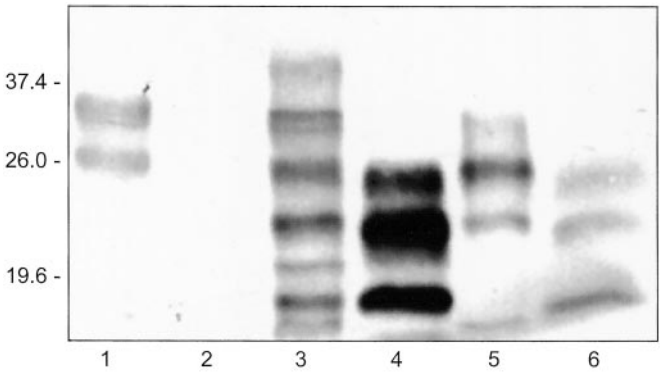

Figure 4. Western immunoblot of 10% brain homogenates before (lanes 1, 3, 5) and after (lanes 2, 4, 6) proteinase K digestion. The filter was probed with the anti-PrP monoclonal antibody 3F4. Lanes 1 and 2, non–Creutzfeldt-Jakob (CJD) disease control; lanes 3 and 4, our proband; and lanes 5 and 6, sporadic CJD. Approximate molecular weights are shown.

band, demonstrating the presence of PK resistant PrP^{Sc} in the sporadic CJD and proband samples. The PrP^{Sc} type in the proband tissue was determined as type 2 (using the classification in reference [16]), displaying a glycoform ratio similar to that observed in sporadic CJD, with an abundance of the mono-glycosylated band.[16] In the absence of PK treatment, several bands are observed in the proband sample. Higher molecular weight fragments are a direct result of the insert, and many lower molecular mass fragments result from nonspecific cleavage of the mutant allele, as these are not observed in the normal control or sporadic CJD samples.

Discussion. This family represents the fourth reported pedigree to harbor a seven octapeptide repeat insert in *PRNP* as the explanation for their spongiform encephalopathy, with the 168 bp nucleotide sequence and arrangement different from those previously described.[6,10-12] Remarkable congruity in relation to age at onset and duration of illness is apparent in comparison to previously reported families, with general similarity of other clinical features (table 2). Symptoms commenced in the current family at 24 to 32 years of age, with illness duration

Table 2 *Comparison of clinical features of illness and* PRNP *codon 129 status between the proband and other published seven octapeptide repeat cases*

		Reference 10			Reference 12			
Features/phenotype	Proband	II-3*	III-9*	III-8*	I-1*	II-2*	II-4*	Reference 13
Presenting features								
Abnormal behavior	Y		Y					
Clumsiness	Y			Y			Y	
Depression/mood change		Y	Y				Y	
Forgetful/memory problems	Y				Y			
Speech disturbances		Y	Y			Y		
Features during illness								
Akinetic mutism			Y					
Apraxia		Y					Y	
Cerebellar dysfunction		Y	Y	Y		Y		
Cognitive decline	Y	Y	Y	Y	Y	Y	Y	Y
Dysphasia		Y		Y				
Epileptic seizures	Y						Y	
Euphoria				Y				
Extrapyramidal features	Y	Y	Y	Y		Y		
Myoclonus			Y	Y		Y		
Psychosis						Y		
Pyramidal features					?Y†		Y	
Duration of illness, y	16	11	10	>13	7	11	11	7
Age at onset, y	29	31	23	28	32	24	31	
Codon 129 status								
Normal allele	Val						Met	
Mutated allele	Met	Met‡	Met‡	Met‡	Met	Met	Met	

* Individual as stated in appropriate reference.
† Described as motor problems only.
‡ Source is reference [21].

Y = feature present; blank = feature not described; Val = valine; Met = methionine.

spanning from 7 to 16 years, which is remarkably similar to the 23 to 35 years for illness onset and 7 to >13 years duration reported in the other seven octapeptide repeat cases.[6,10-12,17] Progressive cognitive deterioration was evident in the three members of the current family, as in all previous cases reported. Additional clinical features vary, but pyramidal and cerebellar dysfunction are common, and seizures[12] and involuntary movements[6,10] have been recognized, as seen in our proband. Given the long illness duration and diverse clinical features, difficulty with achieving a specific, premortem clinical diagnosis has been reported previously for this type of mutation,[12] as has the incorrect speculative diagnosis of Huntington's disease in patients with large *PRNP* octapeptide repeat insert mutations.[8]

Noteworthy in the current family was the inability to secure a correct pathologic diagnosis in the proband with brain biopsy and the two first-degree relatives despite autopsy examination. This is consistent with the significant intra- and interfamily variation in the neuropathologic findings described in patients carrying large octapeptide repeat inserts, including the 168 bp insert mutations, ranging from minimal nonspecific changes to typical spongiform encephalopathy.[6,7,10-12,17-19] The proband described in this report displayed changes similar to some members of two previously reported seven octapeptide repeat insert pedigrees, with widespread cortical atrophy, neuronal loss, spongiform change, and gliosis.[10,12] In contrast to previous cases, immunohistochemistry for PrP revealed no cerebral cortical plaques or synaptic type positivity.[11,12] The distinctive elongated cerebellar molecular layer PrP deposits perpendicularly orientated to the pial surface typically evident in previous 168 bp insert pedigrees,[11,12] and other octapeptide repeat insert families,[7,17,18] were not evident in our propositus. Pathologic phenotypic variability may relate in part to differences in the ability to clear the abnormal prion protein, with the long duration of symptoms possibly relating to neuronal dysfunction rather than morphologic change. Expression of the particular expanded mutant allele, as shown by the Western immunoblots in our proband, and the specific PrP^{Sc} type and glycoform ratio, may be germane to these issues.

Technical difficulties in achieving correct molecular genetic diagnoses have been reported with *PRNP* analysis. Polymorphisms in the intron region proximate to the 5' end of the ORF can cause problems with primer annealing,[20] and suboptimal PCR amplification of the mutant allele can occur with large octapeptide repeat insert mutations.[8] We postulate that selective amplification of the wild type allele occurred in the original *PRNP* analysis undertaken, with absence or a weak signal from the expanded *PRNP* locus (as shown in figure 2) militating against correct interpretation. In contrast to one report, we did not find that utilizing a larger candidate DNA template for PCR amplification overcame this difficulty.[8] Rather, optimizing PCR conditions, especially in relation to reaction buffers, resolved the problem. We suspect this experience may be more prevalent than appreciated, particularly in laboratories less familiar with this type of mutation analysis, and without appropriate positive controls correct diagnosis may be overlooked relatively easily. A high level of suspicion and concerted technical efforts are required to ensure this type of error is avoided.

References

1. Brown P. The phenotypic expression of different mutations in transmissible human spongiform encephalopathy. Rev Neurol 1992;148:317–327.
2. Windl O, Dempster M, Estibeiro JP, et al. Genetic basis of Creutzfeldt-Jakob disease in the United Kingdom: a systematic analysis of predisposing mutations and allelic variation in the PRNP gene. Hum Genet 1996;98:259–264.
3. Palmer MS, Mahal SP, Campbell TA, et al. Deletions in the prion protein gene are not associated with CJD. Hum Mol Genet 1993;2:541–544.
4. Beck JA, Mead S, Campbell TA, et al. Two-octapeptide repeat deletion of prion protein associated with rapidly progressive dementia. Neurology 2001;57:354–356.
5. Owen F, Poulter M, Lofthouse R, et al. Insertion in prion protein gene in familial Creutzfeldt-Jakob disease. Lancet 1989;I:51–52.
6. Goldfarb L, Brown P, McCombie R, et al. Transmissible familial Creutzfeldt-Jakob disease associated with five, seven, and eight extra octapeptide coding repeats in the PRNP gene. Proc Natl Acad Sci 1991; 88:10926–10930.
7. Vital C, Gray F, Vital A, Ferrer X, Julien J. Prion disease with octapeptide repeat insertion. Clin Exp Pathol 1999;47:153–159.
8. Moore RC, Xiang F, Monaghan J, et al. Huntington disease phenocopy is a familial prion disease. Am J Hum Genet 2001;69:1385–1388.
9. Origin of extra prion repeat units [online]. Available at: http://www.mad-cow.org/prion_repeat_insertions.html. Accessed December 2001.
10. Brown P, Goldfarb LG, McCombie WR, et al. Atypical Creutzfeldt-Jakob disease in an American family with an insert mutation in the PRNP amyloid precursor gene. Neurology 1992;42:422–427.
11. Kitamoto T, Doh-ura K, Muramoto T, Miyazono M, Tateishi J. The primary structure of the prion protein influences the distribution of abnormal prion protein in the central nervous system. Am J Pathol 1992;141:271–277.
12. Dermaut B, Cruts M, Backhovens H, et al. Familial Creutzfeldt-Jakob disease in a patient carrying both a presenilin 1 missense substitution and a prion protein gene insertion. J Neurol 2000;247:364–368.
13. Tateishi J. Recent advances in the research of Creutzfeldt-Jakob Disease (CJD) and Gerstmann-Straussler Syndrome (GSS). Rinsho Shinkeigaku 1991;31:1306–1308.
14. Kitamoto T, Shin RW, Doh-ura K, et al. Abnormal isoform of prion proteins accumulates in the synaptic structures of the central nervous system in patients with Creutzfeldt-Jakob disease. Am J Pathol 1992; 140:1285–1294.
15. Collins S, Boyd A, Fletcher A, et al. Novel prion protein gene mutation in an octogenarian with Creutzfeldt-Jakob disease. Arch Neurol 2000; 57:1058–1063.
16. Collinge J, Sidle K, Meads J, Ironside J, Hill A. Molecular analysis of prion strain variation and the aetiology of 'new variant' CJD. Nature 1996;383:685–690.
17. Oda T, Kitamoto T, Tateishi J, et al. Prion disease with 144 base pair insertion in a Japanese family line. Acta Neuropathol 1995;90:80–86.
18. Campbell TA, Palmer MS, Will RG, Gibb WRG, Luthert PJ, Collinge J. A prion disease with a novel 96-base pair insertional mutation in the prion protein gene. Neurology 1996;46:761–766.
19. Collinge J, Owen F, Poulter M, et al. Prion dementia without characteristic pathology. Lancet 1990;336:7–9.
20. Palmer MS, van Leeven RH, Mahal SP, Campbell TA, Humphreys CB, Collinge J. Sequence variation in intron of prion protein gene, crucial for complete diagnostic strategies. Hum Mutat 1996;7:280–281.
21. Gambetti P, Petersen R, Parchi P, et al. Inherited prion diseases. In: Prusiner SB, ed. Prion biology and diseases. New York: Cold Springs Harbor Laboratory Press, 1999;509–583.

Lyodura use and the risk of iatrogenic Creutzfeldt–Jakob disease in Australia

Fiona J Brooke, Alison Boyd, Genevieve M Klug, Colin L Masters and Steven J Collins

ABSTRACT

- Although infectiousness is a feature of Creutzfeldt–Jakob disease (CJD), only a small proportion of cases are linked to transmission through healthcare provision.
- As of January 2003, over 120 cases of CJD associated with use of human cadaveric dura mater had been recognised worldwide; almost all were associated with the commercial product Lyodura.
- Most cases (97) have occurred in Japan, giving an overall risk estimate of around 1 per 2268 patients treated with Lyodura (0.04%) in that country.
- In Australia, five cases of CJD have so far been linked to Lyodura, but, given the protracted tails of previous epidemics of transmissible spongiform encephalopathies, further cases are possible.
- Results of surveys of Lyodura use in Australia are incomplete, but information from the manufacturer suggests that 2208–2478 sheets of Lyodura may have been used here.
- This use translates to a relatively high incidence of Lyodura-associated CJD, with current overall rates appearing around five times higher than those reported in Japan; reasons for this difference are unclear.

eMJA Rapid online publication 14 January 2004

CREUTZFELDT–JAKOB DISEASE (CJD) is a fatal, transmissible, neurodegenerative disorder belonging to the group known as the transmissible spongiform encephalopathies (TSEs). CJD can occur without explanation (sporadic), secondary to mutations in the prion protein gene (*PRNP*), or as a complication of medical treatment using contaminated therapeutic agents or equipment (iatrogenic). Although corneal grafts and neurosurgical equipment have been associated with disease transmission, the most common causes of iatrogenic CJD have been treatments involving human-derived cadaveric pituitary hormones or dura mater.[1]

Creutzfeldt–Jakob disease and Lyodura

The first identified case of CJD in a dura mater recipient was reported in the United States in early 1987.[2] In response, the US Food and Drug Authority issued a safety alert in April 1987, seeking immediate discontinuation of use of the identified dura mater batch (Lyodura batch #2105).[3] A second patient with CJD linked to Lyodura was detected in New Zealand in 1988,[4] but the specific batch could not be identified. This has remained a frequent difficulty when tracing contamination sources.

As of January 2003, over 120 CJD cases related to dura mater use had been detected globally, with 97 in Japan.[5] These cases were predominantly associated with Lyodura, a commercial product produced since 1969 by B Braun Melsungen AG (based in Germany). Only a few reports suggest the possibility of CJD after use of dura mater from other commercial or non-commercial sources.[6-8]

Lyodura consists of lyophilised, irradiated human dura mater sourced *post mortem*. Additional processing with immersion in a solution of sodium hydroxide (1 M) was instituted in 1987, with a noticeable reduction in Lyodura-related cases thereafter.[9] Lyodura has been used in a number of countries, including Australia, Japan, Canada, the United States and the United Kingdom, mainly in neurosurgery, but also in orthopaedic, otological, dental, urological, gynaecological and cardiac procedures (Box 1) (Dr L Schonberger, Assistant Director, National Center for Infectious Diseases, Centers for Disease Control and Prevention, Atlanta, Ga, USA, personal communication).

Most cases of CJD associated with dura mater have occurred in Japan. In 1996, in response to the growing incidence, a survey was undertaken of Lyodura use in almost 3000 Japanese healthcare institutions. This estimated that up to 100 000 people received Lyodura grafts between 1983 and 1987,[9,10] and up to 220 000 between 1979 and 1991 (out of a total of 260 000 who received dura mater grafts). Use of these grafts greatly declined after 1991 but may have continued until 1997.[11,12] Assuming that all cases of CJD associated with dura mater were a consequence of Lyodura use, the overall risk of Lyodura-associated CJD in Japan is approximately 0.04%.[5]

Estimating Lyodura use and risk in Australia

Lyodura was approved by the Australian Therapeutic Goods Administration for importation and use in Australia

Communicable Diseases Branch, Department of Health and Ageing, Canberra, ACT.

Fiona J Brooke, BA(Hons), Director, Infection Management and Transmissible Spongiform Encephalopathy Section.

Australian National Creutzfeldt–Jakob Disease Registry, Department of Pathology, University of Melbourne, Melbourne, VIC.

Alison Boyd, PostGradDipGenCoun, Research Officer; **Genevieve M Klug,** BSc(Hons), PostGradDipEpiBiostat, Research Assistant; **Colin L Masters,** FRCPA, Head; **Steven J Collins,** FRACP, Co-Director.

Reprints: Ms Fiona J Brooke, Section MDP14, Communicable Diseases Branch, Department of Health and Ageing, GPO Box 9848, Canberra, ACT 2601. Fiona.Brooke@health.gov.au

Associate Professor Steven J Collins, Australian National CJD Registry, University of Melbourne, Parkville, VIC 3010. stevenjc@unimelb.edu.au

1: Non-neurosurgical uses of Lyodura in the United States*

- Development of ligaments to stabilise shoulder joints
- Replacement of the tracheal wall
- Covering pleura defects
- Securing bronchial stumps
- Repair of pericardium
- Repair of diaphragm defects (traumatic or congenital)
- Arthroplasties of the elbow
- Reinforcement of fascia in abdominal hernias
- Reinforcement of tendons or ligaments
- Plastic enlargement of the urinary bladder
- Other miscellaneous surgical uses

* Based on information from the US National Center for Infectious Diseases, Centers for Disease Control and Prevention, Atlanta, Ga.

in 1972. The product licence was withdrawn in early May 1987, shortly after recognition of the first case of CJD linked to Lyodura use.

To date, five cases of CJD have been epidemiologically linked to neurosurgical use of Lyodura in Australia. Their clinical features have already been described[13-15] and are summarised in Box 2. Patient 1 presented in 1987, about 5 years after implantation of Lyodura. The longest incubation period was in Patient 4, who presented in 1999 after an incubation period of almost 17 years.[14] The most recent (fifth) patient died in 2000. Patients 1, 2 and 4 were exposed in 1982, while Patients 3 and 5 were exposed in 1985 and 1986, respectively.

A number of studies have attempted to determine the number of people exposed to Lyodura in Australia. We collated the available information and undertook further enquiries, as a basis for estimating the risk of Lyodura-associated CJD in this country (Box 3).

Implications for Australia

Quantifying past use of Lyodura in Australia relies on data that cannot be fully confirmed. Initial estimates by the Commonwealth Department of Health and Ageing in discussion with the Therapeutic Goods Administration placed an upper limit of between 5000 and 10 000 individuals potentially exposed to Lyodura. However, from the results reported here, the true number is likely to be much smaller — probably fewer than 2500. If so, the risk of Lyodura-associated CJD is higher in Australia (0.20%–0.23%) than in other countries that have undertaken similar investigations, such as Japan.

Although the risk of Lyodura-associated CJD in Japan has appeared to fluctuate over time, two relatively stable features are a peak in contaminated grafts between 1983 and 1987, and the paucity of Lyodura-associated cases after 1987, when the manufacturer instituted effective decontamination of the tissue with a 1 M solution of sodium hydroxide.[1,5,9] Ninety-seven cases associated with dura mater had been recognised to 2003,[5] with predictions that further cases are likely until 2020, and that final numbers may reach 160.[12] Acknowledging a total of 220 000 people exposed to Lyodura, and assuming all CJD associated with dura mater was associated with Lyodura (which is reasonable based on evidence published to date),[11] then the cumulative overall risk of CJD from Lyodura in Japan is currently around 0.04% (95% CI, 0.03%–0.05%) (Box 4). Estimated risk in Australia is much higher — 0.20% to 0.23% (95% CIs, 0.06%–0.47% and 0.07%–0.53%, respectively). With the same assumptions, the risk of CJD in the higher-risk period in Japan (1983–1987) is about 0.08% (95% CI, 0.06%–0.10%), while that in Australia (1982–1986) is 0.43% (95% CI, 0.14%–0.99%). Notwithstanding the need for certain assumptions to facilitate these comparisons, the risk in Australia appears about five times greater than the analogous point estimates of risk in Japan. The reality of the differences is further supported by the lack of overlap between the confidence intervals of the calculated estimates.

Nevertheless, the risk of CJD associated with Lyodura in Australia is well below the risk associated with exposure to human-derived pituitary growth hormone (hGH) in France (Box 4). As of 1999, 55 cases of CJD had been linked to French-derived hGH, from a cohort of 1361 patients, representing an attack rate of about 1 in 25 recipients (4.0%).[17] A more recent report suggested the risk could be much higher, at 81 per 1361 (about 6.0%).[18]

The reason for the higher estimated risk of Lyodura-associated CJD in Australia compared with Japan is not

2: Features of the five Australian cases of Creutzfeldt–Jakob disease associated with Lyodura

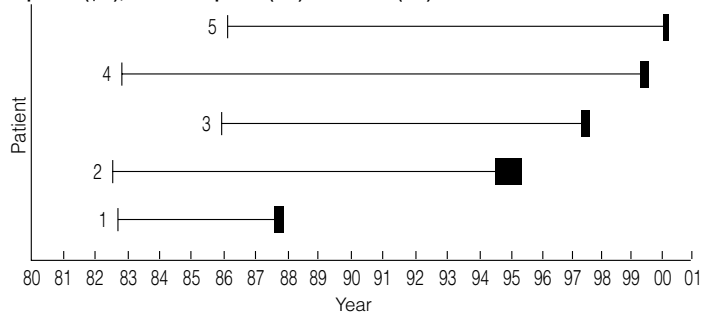

	Classification	Procedure	Presentation	Age at death (years)
5	Probable	Removal of frontal meningioma	Dementia	61
4	Definite	Removal of cerebellar astrocytoma	Cerebellar ataxia	32
3	Probable	Craniocervical decompression	Cerebellar ataxia	26
2	Probable	Removal of cerebellar astrocytoma	Non-specific dizziness, diplopia	27
1	Definite	Removal of acoustic neuroma	Speech disturbance	62

3: Studies of Lyodura use in Australia

Survey of hospitals in Victoria

In 1987, after notification of the first patient with Lyodura-associated Creutzfeldt–Jakob disease (CJD), the Victorian Department of Community Services and Health surveyed use of Lyodura in all private and public hospitals in Victoria.

Five hospitals responded, out of an uncertain total number. They reported use of 40 Lyodura grafts in 1985–1986 and 36 in 1986–1987, all in neurosurgical procedures (unpublished data).

Survey of neurosurgeons

In 1995, the Neurosurgical Society of Australasia surveyed 100 neurosurgeons (comprising all practising neurosurgeons and retired surgeons still on their register) about use of Lyodura or other dura mater during their practice lifetimes.[13] This survey was also used to assess the feasibility of tracing recipients.

Sixty-five neurosurgeons responded (response rate, 65%); 35 of these (54%) had used dura mater grafts in cranial or spinal procedures at some time, with 34 having used Lyodura. Eleven of the 34 (32%) believed that they could identify over 90% of recipients from their records, nine (27%) that they could identify 50%–90%, and 14 that they could identify fewer than 50%. The survey could not determine the precise amount of Lyodura or specific batches used, nor the number of procedures involving Lyodura. However, all three cases of Lyodura-related CJD recognised before the survey were in patients of respondents who reported using Lyodura. The remaining two confirmed cases presented after this survey.

Survey of non-neurosurgical use

In 2001, the Department of Health and Aged Care (DHAC) undertook a survey through the Royal Australasian College of Surgeons (RACS) to assess non-neurosurgical use of Lyodura. Over 5000 practising and retired surgeons across 15 surgical specialties were asked about use of dura mater grafts (and specifically Lyodura) over their practice lifetimes.

Responses were received from 172 surgeons (response rate, 3.4%). This very poor response rate precluded meaningful analysis. However, the survey confirmed that Lyodura had been used in otorhinolaryngological procedures, such as tympanoplasty, myringoplasty and mastoidectomy, with respondents reporting use of about 100 grafts in such applications. Given the poor response rate, time elapsed since the product was withdrawn, recall bias and retirement of surgeons during this time, this may be a significant underestimate of use in non-neurosurgical applications. This possibility is supported by the US Centers for Disease Control and Prevention report that up to 20% of Lyodura use in the US was in non-neurosurgical applications (Dr L Schonberger, personal communication).

Quantification study

In 2002, the Department of Health and Ageing, in conjunction with the Australian National Creutzfeldt–Jakob Disease Registry, undertook a study to quantify Lyodura use in Australia and to determine the types of procedures in which it was used, as a basis for estimating the risk of Lyodura-associated CJD.

Methods: The Registry has ethical approval for its surveillance methods and activities from the University of Melbourne Human Research Ethics Committee.

As well as collating results of previous surveys, we asked the manufacturer of Lyodura, B Braun Melsungen AG, about supplies including the Australian Therapeutic Goods Administration and the Health Insurance Commission.

Results: Braun Melsungen indicated that:

- Before 1978, about two to five packs of Lyodura per month were distributed nationally.
- Between 1978 and 1982, 600 packs were distributed in mainland Australia.
- Between 1983 and 1987, 1278 sheets were distributed for use in mainland Australia.

According to the 1985 Braun catalogue for Australia, Lyodura was available in a range of sizes, with some packs containing up to 6 pieces. The manufacturer indicated that packs sold in Australia contained either one large sheet or two smaller sheets. Its information suggests that generally the larger sheets were used for neurosurgery, and smaller sheets for other surgical applications. The single-sheet packs outsold the double-sheet packs by about three to one. Braun did not supply documentary verification of this information.

Neither the Australian Therapeutic Goods Administration nor the Health Insurance Commission could furnish further information on Lyodura use.

Based on the manufacturer's information, and assuming that all distributed product was used, then a maximum of 750 sheets may have been used in Australia between 1978 and 1982. Before 1978, assuming the same distribution of pack sizes, then 180–450 sheets may have been distributed.

These data suggest a total use in Australia of 2208 to 2478 Lyodura grafts. Assuming maximum and equal annual use, then about 1172 Lyodura grafts were used in the higher-risk period 1982–1986.

Risk estimation: Risk estimates for Lyodura-associated CJD were based on data from the manufacturer alone, as survey results were very incomplete, and Lyodura use reported in the surveys was likely to be encompassed by the manufacturer's information.

Risk estimates were calculated from the total number of individuals exposed and the number of CJD cases detected over defined periods, with 95% confidence intervals calculated using the Poisson distribution.

Based on the five Lyodura-associated CJD cases detected to 2003, the attack rate ranged from 1 in 496 patients who received Lyodura (0.20%) to 1 in 442 (0.23%) (Box 4), depending on whether a higher or lower estimate of pre-1978 use was used. In the higher-risk period (1982–1986), the attack rate may have been as high as 1 in 234 (0.43%). These calculations were based on exposure through any surgical application of Lyodura, assuming that only one sheet was used per patient and that all distributed product was used. The latter fact cannot be verified, and previous reports suggest that not all distributed Lyodura was necessarily used.[16] These attack rates are therefore likely to be underestimates.

The attack rates after neurosurgery in Australia may be even higher, depending on the proportion of Lyodura that was used in this type of surgery. Should the proportion be close to 60% of the total product used (as suggested by the manufacturer) or 80% (as found in the US), the overall neurosurgical attack rate may be as high as 1 in 397 (ie, 80% of 496) to 1 in 265 (ie, 60% of 442), or 0.25% to 0.38%.

The CJD Registry also recently reviewed all records to determine whether any patients on the CJD register might have been exposed to Lyodura through non-neurosurgical applications. No potential cases were identified.

known. Perhaps most likely is chance receipt of a relatively high percentage of contaminated batches of Lyodura and use of multiple pieces of Lyodura per patient in Australia, although the latter is contrary to anecdotal recollections of Australian neurosurgeons. Alternatively, the difference may reflect better case ascertainment in Australia, which, in contrast to Japan, had an established comprehensive, prospective, national surveillance program for CJD, with international comparisons of incidence rates for sporadic CJD attesting to the adequacy of case ascertainment.[14]

4: Risks of Creutzfeldt–Jakob disease (CJD) related to iatrogenic exposures in different countries

Country	Period	Deaths from CJD*	Recipients†	Risk (95% CI)
Lyodura				
Japan	Overall (1979–2003)	97	220 000	0.04% (0.03%–0.05%)
	Higher-risk (1983–1987)	81	100 000	0.08% (0.06%–0.10%)
Australia	Overall (pre-1978–2003)	5	2 208‡	0.23% (0.07%–0.53%)‡
			2 478‡	0.20% (0.06%–0.47%)‡
	Higher-risk (1982–1986)	5	1 172	0.43% (0.14%–0.99%)
Human growth hormone				
France	To 1999	55	1 361	4.04% (3.04%–5.26%)

* Based on cases of CJD with a history of recognised iatrogenic exposure during the defined period.
† Based on estimated total national use of Lyodura or human cadaveric pituitary growth hormone during the defined period.
‡ A range exists for the number of Australian Lyodura recipients because of uncertainty about use before 1978.

Another potential explanation is genetic difference between the populations of the two countries. For example, homozygosity for methionine at codon 129 of the *PRNP* gene appears to predispose to iatrogenic CJD.[1] However, contrary to expectations, this homozygosity appears more common in the Japanese population (about 92%) than in occidental populations (about 37%).[19]

Finally, the differences in risk may reflect greater use of Lyodura in Japanese patients with malignancies, whose survival was shorter than the lengthy incubation periods typical of TSEs, or in non-neurosurgical applications, with attendant lower transmission efficiency. Japanese studies suggest that Lyodura-related transmissions have been essentially restricted to neurosurgical procedures,[10,11]and our comparative risk analysis was predicated on the assumption that most Lyodura was used in these procedures in both countries. Although some Lyodura was most likely used in non-neurological procedures, the proportion is impossible to quantify in different countries, leaving uncertainty about our risk comparisons.

In addition to neurosurgery and the non-neurological applications identified by Australian surveys, additional uses of Lyodura have been reported in the US (Box 1). Cases of CJD have been linked epidemiologically to Lyodura used in the embolisation of the external carotid artery for treating a nasopharyngeal angiofibroma,[20] as well as dura mater used to embolise intercostal arteries before thoracic surgery.[7] This reinforces the likelihood that non-neurosurgical use of Lyodura can result in transmission.[10] Therefore, risk of Lyodura-associated CJD linked to non-neurosurgical uses appears a genuine possibility, which may be very difficult to identify epidemiologically, given the often deficient state of medical records.

The inability to clearly identify surgical uses of Lyodura, especially non-neurosurgical uses, also raises the possibility of secondary iatrogenic transmissions from Lyodura-treated patients during an extended preclinical or incubation phase. Animal models clearly support the possibility of lengthy presymptomatic periods (which may even exceed the lifespan of hosts) during which transmission is possible.[21-24] Generally, infection control and other guidelines focus on the need to limit transmission risk through identifying patients who received Lyodura during neurosurgery, and do not include guidance on risk associated with other surgical applications. This approach may need to be reconsidered based on studies such as ours.

Competing interests

None identified.

Acknowledgements

The Australian National Creutzfeldt–Jakob Disease Registry is funded by the Australian Department of Health and Ageing. The authors thank Associate Professor Peter Reilly (University of Adelaide) for many details of the Neurosurgical Society of Australasia survey of neurosurgeons, Dr L Schonberger (Centers for Disease Control and Prevention, USA) for estimated percentages for non-neurosurgical use of Lyodura, and Professor Emeritus Donald Simpson, Department of Neurosurgery, Royal Adelaide Hospital, SA, for assistance in reporting and evaluating patients with Lyodura-related CJD.

References

1. Brown P, Preece M, Brandel JP, et al. Iatrogenic Creutzfeldt-Jakob disease at the millennium. *Neurology* 2000; 55: 1075-1081.
2. Update: Creutzfeldt-Jakob disease in a patient receiving a cadaveric dura mater graft. *MMWR Morb Mortal Wkly Rep* 1987; 36: 324-325.
3. Food and Drug Administration. FDA safety alert: possibly contaminated dura mater transplant material. Rockville, Md: US Department of Health and Human Services, Public Health Service, Apr 28 1987.
4. Update: Creutzfeldt-Jakob disease in a second patient who received a cadaveric dura mater graft. *MMWR Morb Mortal Wkly Rep* 1989; 38: 37-38.
5. Nakamura Y, Watanabe M, Nagoshi K, et al. Update: Creutzfeldt-Jakob disease associated with cadaveric dura mater grafts — Japan, 1979–2003. *MMWR Morb Mortal Wkly Rep* 2003; 52: 1179-1181.
6. Hannah EL, Belay ED, Gambetti P, et al. Creutzfeldt-Jakob disease after receipt of a previously unimplicated brand of dura mater graft. *Neurology* 2001; 56: 1080-1083.
7. Defebvre L, Destee A, Caron J, et al. Creutzfeldt-Jakob disease after an embolization of intercostal arteries with cadaveric dura mater suggesting a systemic transmission of the prion agent. *Neurology* 1997; 48: 1470-1471.
8. Dobbins JG, Belay ED, Malecki J, et al. Creutzfeldt-Jakob disease in a recipient of a dura mater graft processed in the US: cause or coincidence? *Neuroepidemiology* 2000; 19: 62-66.
9. Nakamura Y, Aso E, Yanagawa H. Relative risk of Creutzfeldt-Jakob disease with cadaveric dura transplantation in Japan. *Neurology* 1999; 53: 218-220.
10. Creutzfeldt-Jakob disease associated with cadaveric dura mater grafts — Japan, January 1979–May 1996. *MMWR Morb Mortal Wkly Rep* 1997; 46: 1066-1069.

11. Hoshi K, Yoshino H, Urata J, et al. Creutzfeldt-Jakob disease associated with cadaveric dura mater grafts in Japan. *Neurology* 2000; 55: 718-721.
12. Hamada C, Sadaike T, Fukushima M. Projection of Creutzfeldt-Jakob Disease frequency based on cadaveric dura transplantation in Japan. *Neuroepidemiology* 2003; 22: 57-64.
13. Boyd A, Fletcher A, Lee JS, et al. Transmissible spongiform encephalopathies in Australia. *Commun Dis Intell* 2001; 25: 248-252.
14. Collins S, Boyd A, Lee JS, et al. Creutzfeldt-Jakob disease in Australia 1970-1999. *Neurology* 2002; 59: 1365-1371.
15. Simpson D, Masters CL, Ohlrich G, et al. Iatrogenic Creutzfeldt-Jakob disease and its neurosurgical implications. *J Clin Neurosci* 1996; 3: 118-123.
16. Newcombe RL. Neurosurgery and iatrogenic transmission of Creutzfeldt-Jakob disease. *Med J Aust* 1996; 164: 603-604.
17. Huillard d'Aignaux J, Costagliola D, et al. Incubation period of Creutzfeldt-Jakob disease in human growth hormone recipients in France. *Neurology* 1999; 53: 1197-1201.
18. Brandel J-P, Preece M, Brown P, et al. Distribution of codon 129 genotype in human growth hormone-treated CJD patients in France and the UK. *Lancet* 2003; 362: 128-130.
19. Doh-ura K, Kitamoto T, Sakaki Y, Tateishi J. CJD discrepancy. *Nature* 1991; 353: 801-802.
20. Antoine JC, Michel D, Bertholon P, et al. Creutzfeldt-Jakob disease after extracranial dura mater embolization for a nasopharyngeal angiofibroma. *Neurology* 1997; 48: 1451-1453.
21. Dickinson AG, Fraser H, Outram GW. Scrapie incubation time can exceed natural lifespan. *Nature* 1975; 256: 732-733.
22. Hill AF, Joiner S, Linehan J, et al. Species-barrier-independent prion replication in apparently resistant species. *Proc Natl Acad Sci USA* 2000; 97: 10248-10253.
23. Frigg R, Klein MA, Hegyi I, et al. Scrapie pathogenesis in subclinically infected B-cell-deficient mice. *J Virol* 1999; 73: 9584-9588.
24. Race R, Chesebro B. Scrapie infectivity found in resistant species. *Nature* 1998; 392: 770.

(Received 26 Aug 2003, accepted 11 Dec 2003) ❑

DOI: 10.1093/brain/awh249 *Brain* (2004), **127,** 2348–2359

Predictors of survival in sporadic Creutzfeldt–Jakob disease and other human transmissible spongiform encephalopathies

M. Pocchiari,[1] M. Puopolo,[1] E. A. Croes,[2] H. Budka,[3] E. Gelpi,[3] S. Collins,[4] V. Lewis,[4] T. Sutcliffe,[5] A. Guilivi,[5] N. Delasnerie-Laupretre,[6] J.-P. Brandel,[6] A. Alperovitch,[6] I. Zerr,[7] S. Poser,[7] H. A. Kretzschmar,[8] A. Ladogana,[1] I. Rietvald,[2] E. Mitrova,[9] P. Martinez-Martin,[10] J. de Pedro-Cuesta,[10] M. Glatzel,[11] A. Aguzzi,[11] S. Cooper,[12] J. Mackenzie,[12] C. M. van Duijn[2] and R. G. Will[12]

[1]*Istituto Superiore di Sanità, Department of Cell Biology and Neurosciences Rome, Italy,* [2]*Department of Epidemiology and Biostatistics, Erasmus MC, Rotterdam, The Netherlands,* [3]*Austrian Reference Centre for Human Prion Diseases (OERPE) and Institute of Neurology Department of Cell Biology and Neuro Sciences, Vienna, Austria,* [4]*Department of Pathology, The University of Melbourne, Victoria, Australia,* [5]*Blood Safety Surveillance and Health Care Acquired Infections Division, Centre for Infectious Disease Prevention and Control, LCDC Building, Ontario, Canada,* [6]*U.360 INSERM, Hôpital de la Salpetriere, Paris, France,* [7]*Department of Neurology, Georg-August-Universität Göttingen,* [8]*Institute of Neuropathology, University of Munich, Munich, Germany,* [9]*Institute of Preventative and Clinical Medicine, National Reference Centre of Slow Virus Neuroinfections, Bratislava, Slovakia,* [10]*Instituto de Salud Carlos III, Centro Nacional de Epidemiologia, Departamento de Epidemiologia Aplicada, Madrid, Spain,* [11]*Swiss National Reference Centre for Prion Diseases, University Hospital of Zurich, Zurich, Switzerland and* [12]*National CJD Surveillance Unit, Western General Hospital, Edinburgh, UK*

Correspondence to: Professor R. G. Will, National Creutzfeldt–Jakob disease Surveillance Unit, Western General Hospital, Edinburgh EH4 2XU, UK
E-mail: r.g.will@ed.ac.uk

Summary

A collaborative study of human transmissible spongiform encephalopathies has been carried out from 1993 to 2000 and includes data from 10 national registries, the majority in Western Europe. In this study, we present analyses of predictors of survival in sporadic (*n* = 2304), iatrogenic (*n* = 106) and variant Creutzfeldt–Jakob disease (*n* = 86) and in cases associated with mutations of the prion protein gene (*n* = 278), including Gerstmann–Sträussler–Scheinker syndrome (*n* = 24) and fatal familial insomnia (*n* = 41). Overall survival for each disease type was assessed by the Kaplan–Meier method and the multivariate analyses by the Cox proportional hazards model. In sporadic disease, longer survival was correlated with younger age at onset of illness, female gender, codon 129 heterozygosity, presence of CSF 14-3-3 protein and type 2a prion protein type. The ability to predict survival based on patient covariates is important for diagnosis and counselling, and the characterization of the survival distributions, in the absence of therapy, will be an important starting point for the assessment of potential therapeutic agents in the future.

Keywords: survival; sporadic CJD; variant CJD; iatrogenic CJD; genetic prion diseases

Abbreviations: CI = confidence interval; FFI = fatal familial insomnia; gCJD = genetic forms of Creutzfeldt–Jakob disease; GSS = Gerstmann–Straüssler–Scheinker disease; gTSEs = genetic transmissible spongiform encephalopathies; iCJD = iatrogenic Creutzfeldt–Jakob disease; iDM = iatrogenic Creutzfeldt–Jakob disease following dura mater implant; ihGH = iatrogenic Creutzfeldt–Jakob disease following human growth hormone therapy; MM = methionine/methionine; MV = methionine/valine;

PRNP = prion protein gene; PrP^{Sc} = protease-resistant prion protein; PSWC = periodic sharp wave complexes; RR = relative risk; sCJD = sporadic Creutzfeldt–Jakob disease; TSEs = transmissible spongiform encephalopathies; vCJD = variant Creutzfeldt–Jakob disease; VV = valine/valine.

Received February 3, 2004. Revised May 13, 2004. Accepted May 31, 2004. Advanced Access publication September 10, 2004

Introduction

Human transmissible spongiform encephalopathies (TSEs) or prion diseases comprise a number of conditions with varying aetiology and include sporadic Creutzfeldt–Jakob disease (sCJD), iatrogenic CJD (iCJD), variant CJD (vCJD) and cases associated with mutations of the prion protein gene (*PRNP*) (gTSE). Within the latter group are genetic forms of CJD (gCJD), for example cases linked to mutations at codon 200 and codon 210 of *PRNP*, Gerstmann–Sträussler–Scheinker syndrome (GSS) and fatal familial insomnia (FFI) (Pocchiari, 1994). The clinical phenotypes of the subtypes of human TSE vary, and this variation is determined in part by the polymorphism at codon 129 of *PRNP* (Collinge *et al*., 1991; Palmer *et al*., 1991; Kovacs *et al*., 2002) and the type of prion protein deposited in the brain (Parchi *et al*., 1996). One important variable is the total duration of clinical illness, also termed survival, and this parameter can be useful in clinical diagnosis of the various forms of human TSE, including sCJD (Brown *et al*., 1994). In genetic cases, iCJD cases following human growth hormone therapy (ihGH) and vCJD, survival is more prolonged than in sCJD, but considerable variation in survival is seen within all subtypes of human TSE.

Variables that are thought to influence survival are age (with a reduction in survival with increasing age in sCJD; Puopolo *et al*, 2003), the codon 129 genotype and the type of prion protein deposited in the brain. There have been suggestions of a gender effect on the incidence of sCJD (Will *et al*., 1986; Brown *et al*., 1987), but this has been inconsistent between studies (Galvez *et al*., 1980; Lundberg, 1998). The identification of significant and consistent predictors/determinants of survival is a difficult task because of the rarity of human TSEs, but establishing definitive factors that influence disease phenotype, including survival, may lead to clues to the underlying pathogenic mechanisms and to improved case recognition and clinical discrimination between the various disease subtypes.

The renewed interest in developing specific therapies for human TSEs (Brown, 2002; Korth *et al*., 2002) has highlighted the importance of clearly delineating the natural history of these disorders. Establishing the expected survival and the variables that influence survival in a cohort of untreated cases is likely to provide a crucial baseline to assessing the effectiveness of novel therapies. If, for example, age and gender are important determinants of survival, it may be crucial to include these variables in the assessment of whether or not an intervention actually prolongs survival. It is known that survival is variable in sCJD, with some cases presenting acutely (McNaughton and Will, 1994) and others surviving for many years (Brown *et al*., 1984). The aim of this paper is to define predictors of survival in all forms of human TSE and to quantify these effects as accurately as possible.

Patients and methods

Patients with all forms of human TSEs were ascertained by national surveillance centres as part of a prospective CJD surveillance programme funded by the European Union. Those patients fulfilling the validated diagnostic criteria for definite or probable TSEs were included in a common database. The database contained core medico-demographic information on all TSE cases who died between 1993 and 2000 for Australia, France, Germany, Italy, The Netherlands, Slovakia and the UK, and between 1998 and 2000 for Austria, Spain and Switzerland. Detailed descriptions of the study methodology have been published (Will *et al*., 1998a).

TSE patients were classified as sCJD, iCJD, vCJD and gTSE according to previously published diagnostic criteria. This last group includes gCJD, GSS, FFI and cases carrying an insert mutation of the *PRNP* gene (although patients with gTSEs carry a mutation of the *PRNP* gene, it is not yet clear whether the mutation is the cause of disease or a predisposing factor). Iatrogenic cases were also divided into two categories according to whether they developed the disease following therapy with native human cadaveric growth hormone (ihGH) or after human dura mater implant (iDM). The protease-resistant prion protein type (PrP^{Sc}) found in the brain was classified according to the two-type system published by Parchi *et al*. (1999). Survival was defined as the interval between disease onset and death. Dates of death were available from direct notification by clinicians, from hospital records or from death certificates. The date of onset of clinical symptoms was defined in each case after review of hospital records, clinical correspondence and/or interview with the patient's family. In the great majority of cases, there was little difficulty in defining the date of onset, but in some cases a judgement was made based on information from a range of sources. In Germany, attribution of the date of onset was dependent solely on information from relatives.

Statistical analysis

We investigated the effect on survival of the following demographic, clinical and laboratory investigation variables: sex, age at onset, polymorphism at codon 129 of the *PRNP* gene, country participating in the study, EEG pattern, presence of protein 14-3-3 in the CSF and PrP^{Sc} type.

Survival curves were estimated by the Kaplan–Meier method, both overall and by stratifying for each of the above variables.

For each form of TSE, we report as descriptive statistics the median survival times overall and stratified for each variable; the comparisons of survival curves between groups were carried out by the generalized Wilcoxon test. The Cox proportional hazards model was used to assess the independent effects of the investigated factors by a multivariate analysis. Crude relative risk (RR) and adjusted RR with 95% confidence intervals (CIs) were generated. We used the 'cluster' function on the STATA program for the categorical variable 'country'. The 'cluster' function is used to specify non-independent observations, such as all patients observed in each country, in order to allow robust calculations of standard errors.

Age (in years) at onset was analysed as a continuous variable for 10 year increments. The relative risk for codon 129 was estimated by including two dummy variables with methionine/methionine (MM) as reference.

For sCJD, the multivariate model was used first by including only the gender, the age at onset and the codon 129 polymorphism, because this set contained the largest number of data ($n = 1452$). The Cox model was then used on smaller samples with available data for EEG characteristics and presence of the 14-3-3 protein in the CSF ($n = 893$) or PrP^{Sc} type ($n = 420$). The distributions of sex, age at onset and codon 129 status in these different data sets were compared by the χ^2 test to confirm that missing values were not selected for any of the considered variable. The χ^2 test was also adopted to assess dependency between categorical variables.

The Bonferroni correction for multiple testing was adopted within the five subgroups of gTSE (E200K and V210I gCJD, GSS, FFI and insert mutations) and the two subgroups of iCJD patients. This correction was not applied for all forms of human TSEs since sCJD, iCJD, vCJD and gTSEs are distinct diseases with different aetiology. Thus, the critical level of significance for gTSE was 0.01 (five subgroups) and for iCJD 0.025 (two subgroups).

Statistical analyses were performed using BMDP and STATA.

Results

The mean and median survival times for the different forms of TSEs are summarized in Table 1. SCJD, gCJD and iDM had the shortest median survival times of <6 months; ihGH, vCJD, FFI and gTSE with insert mutations had median clinical durations of ~1 year, while that for GSS patients exceeded 3 years.

Kaplan–Meier survival curves for sCJD, iCJD and vCJD are shown in Fig. 1A, and for gTSE in Fig. 1B. One year after clinical onset, only a few patients with sCJD (15%), iDM (15%) or gCJD (8%) were still alive, while about half the patients with ihGH (54%), vCJD (55%), FFI (48%) and gTSE with insert mutations (55%) survived. About 80% of GSS patients were still alive 1 year after clinical onset.

Sporadic CJD

sCJD patients from Germany had a significantly ($P < 0.0001$) longer median duration (6 months, $n = 568$) of illness than patients from all the other countries: 5 months for Spain ($n = 123$), 4.5 months for Switzerland ($n = 43$), and 4 months for Australia ($n = 149$), Austria ($n = 29$), France ($n = 543$), Italy ($n = 379$), Slovakia ($n = 12$), The Netherlands ($n = 70$) and the UK ($n = 388$).

Univariate survival analyses of sCJD cases with available data (see Table 2) showed differences in the duration of illness by gender (Fig. 2A), age at onset (Fig. 2B) and the polymorphism at codon 129 of the *PRNP* gene (Fig. 2C). The multivariate analysis confirmed that survival is longer in females compared with males and showed that increments of 10 years in the age at onset are associated with an ~30% increase in risk of death (Table 3A). Survival was shorter in patients who were MM at codon 129 of the *PRNP* gene (Table 3A) compared with that seen in valine/valine (VV) and methionine/valine (MV) cases.

When we include a dummy variable in the Cox multivariate model indicating whether patients were from Germany or other countries, the RR for all the above parameters did not change, but the clinical duration of German sCJD patients still remained significantly longer (adjujsted RR = 0.78; CI 0.74–0.83, $P < 0.001$) than that in other countries.

Two investigational features were considered as possible predictive markers of survival: periodic sharp wave complexes (PSWC) in the EEG, the 'typical' pattern in sCJD, and the presence of the 14-3-3 protein in the CSF. In the univariate analysis, survival was significantly shorter in patients with PSWC than in patients without PSWC and in patients with a positive versus negative 14-3-3 test (Table 2). When the EEG pattern and the 14-3-3 test were included in

Table 1 *Clinical duration of disease in different forms of TSEs*

	Mean survival time months (SEM)	Median survival time months
Sporadic CJD ($n = 2304$)	7.3 (0.2)	5
Genetic TSE		
Genetic CJD ($n = 191$)	6.3 (0.5)	4
FFI ($n = 41$)	15.6 (2.2)	12
GSS ($n = 24$)	42.7 (6.1)	39
Insert ($n = 22$)	46.9 (12.8)	14
Iatrogenic CJD*		
hGH CJD ($n = 85$)	14.7 (0.9)	13
DM CJD ($n = 20$)	9.4 (2.4)	5.5
Variant CJD ($n = 86$)	15.3 (0.8)	13

FFI = fatal familial insomnia; GSS = Gerstmann Straussler–Scheinker syndrome; hGH = human growth hormone; DM = dura mater. *A single case of iatrogenic CJD following corneal transplant had a survival of 11 months.

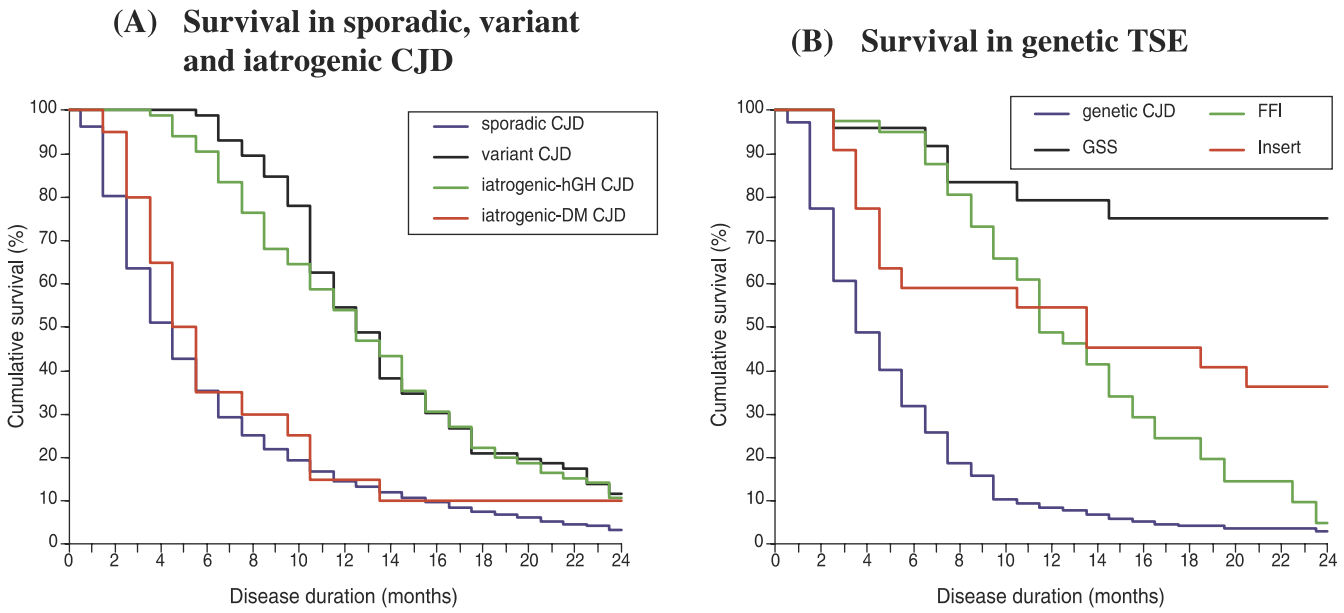

Fig. 1 Kaplan–Meier survival curves in (**A**) sporadic CJD, variant CJD, dura-mater related CJD and human growth hormone-related CJD; (**B**) genetic TSEs, including genetic CJD, GSS, FFI and insert mutations.

Table 2 *Survival time for sporadic CJD*

Features	Median (months)	*P* (generalized Wilcoxon test)
Overall (n = 2304)	5	
Gender		
Male (n = 998)	4	<0.0001
Female (n = 1304)	5	
Age at onset		
11–20 (n = 2)	54, 58*	<0.0001
21–30 (n = 6)	21	
31–40 (n = 14)	23	
41–50 (n = 95)	7	
51–60 (n = 425)	6	
61–70 (n = 937)	5	
71–80 (n = 703)	4	
81–90 (n = 120)	3	
91–100 (n = 2)	2, 3*	
Codon 129		
MM (n = 993)	4	<0.0001
MV (n = 227)	9	
VV (n = 233)	6	
EEG		
PSWC (n = 1429)	4	<0.0001
No PSWC (n = 683)	6	
14-3-3 in CSF		
Positive (n = 1254)	5	<0.0001
Negative (n = 104)	9	
PrP type		
Type 1 (n = 319)	4	<0.0001
Type 2a (n = 131)	8	

*Observed values.

the Cox regression model with sex, age at onset and codon 129 polymorphism, the 14-3-3 test, but not the EEG, retained significance in determining clinical duration of disease together with the other three parameters (Table 3A and B). The reason for the lack of significance in the multivariate analysis for the EEG variable is likely to be because a typical EEG is more frequently observed in patients with late clinical onset (78% of patients >80, 73% in age class 71–80, 69% in 61–70, 58% in 51–60 and 47% of patients ⩽50 years, $P < 0.0001$, χ^2 test), and in patients homozygous for methionine at codon 129 (80% of MM, 51% of MV and 31% of VV patients, $P < 0.0001$, χ^2 test), representing groups of patients with the shortest survival. The missing data for EEG and 14-3-3 were randomly distributed (χ^2 tests for the comparison of the distributions in the two data sets: $P = 0.97$ for gender, $P = 0.54$ for age at onset and $P = 0.66$ for codon 129).

PrP^{Sc} type analysis was available for 450 subjects. Univariate analyses (Fig. 2D) showed that patients with the PrP^{Sc} type 1 had a significantly shorter survival than PrP^{Sc} type 2a (Table 2). When PrP^{Sc} type was included with sex, age at onset and *PRNP* polymorphism at codon 129 in the Cox regression model, the genotype lost its effect on survival (Table 3A and C). This was mostly due to the concomitant fact that there was an uneven distribution of codon 129 polymorphism between PrP^{Sc} type 1 (MM = 87.9%, VV = 3.7%, MV = 8.4%) and type 2a (MM = 21.1%, VV = 47.2%, MV = 31.7%) ($P < 0.0001$, χ^2 test), and an increased proportion of MV and VV patients (with longer clinical duration) in PrP^{Sc} type 2a with respect to type 1. The missing data for PrP^{Sc} type were randomly distributed (χ^2 tests for the comparison of the distributions in the two data sets: $P = 0.23$ for gender, $P = 0.80$ for age at onset and $P = 0.97$ for codon 129).

The crude RR for gender, age at onset and codon 129 obtained in the univariate Cox regression models (Table 3) did not vary when estimated in different subgroups of patients where data on EEG and 14-3-3 test (n = 893) or on PrP^{Sc} type (n = 420) were available.

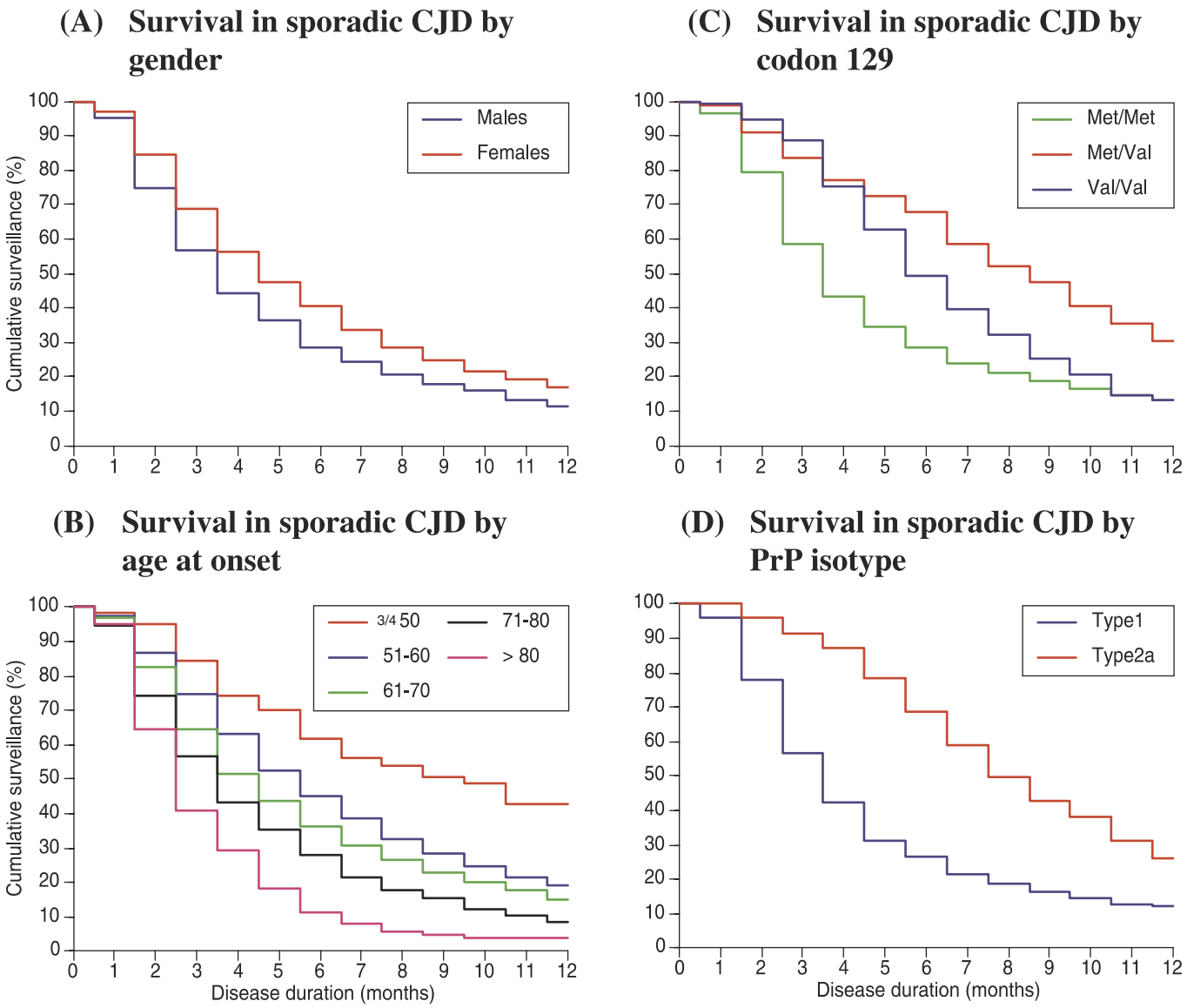

Fig. 2 Kaplan–Meier survival curves in sporadic CJD by (**A**) gender, (**B**) age at onset, (**C**) codon 129 genotype and (**D**) prion protein isotype.

Genetic TSEs

Survival in gCJD patients differed between the various mutations of the *PRNP* gene (Table 4). An analysis was only performed for the two most frequent *PRNP* mutations (i.e. E200K and V210I). Median clinical duration (Table 5) for E200Kand V210I patients was 4 months. In the univariate Cox analysis, survival of both E200K and V210I patients was shorter in males than in females. Though both mutations co-segregate with methionine at codon 129, methionine homozygosity was associated with a shorter survival in E200K patients, but a long survival in V210I patients (Table 5, Fig. 3). Survival was significantly shorter in patients with late age at onset only in V210I patients (Table 5). Multivariate analyses confirmed the significance of all variables for V210I patients (Table 5). In E200K patients, the only significant predictor of survival remained the polymorphism at codon 129. The effect of gender just missed statistical significance when correcting for multiple testing (Table 5).

In FFI (D178N) patients, only the polymorphism at codon 129 of the *PRNP* gene significantly affected survival (Table 6). MV patients showed a longer survival than MM patients.

In gTSE with insert mutations, survival was influenced by the age at onset and codon 129 polymorphism (Table 6). The multivariate analysis with age at onset and codon 129 showed that only MV patients had a significantly longer survival than MM patients (adjusted RR for age at onset = 1.88, CI 0.82–4.30, $P = 0.133$; adjusted RR for MM versus MV, 0.31, CI 0.20–0.48, $P < 0.001$; adjusted RR for MM versus VV = 0.81, CI 0.38–1.71, $P = 0.583$). We did not analyse the relationship between survival and the size of the insert because of the small numbers of cases.

Table 3 *Cox regression model for survival in sporadic CJD patients*

Features	Crude RR (95% CI)	Adjusted RR (95% CI)		
		for A (n = 1452)	for A and B (n = 893)	for A and C (n = 420)
A				
Gender				
Male	1	1	1	1
Female	0.85 (0.73–0.99)* (P = 0.045)	0.74 (0.63–0.88) (P = 0.001)	0.74 (0.67–0.82) (P < 0.001)	0.76 (0.62–0.94) (P = 0.010)
Age at onset [+]	1.34 (1.28–1.40)* (P < 0.001)	1.34 (1.28–1.40) (P < 0.001)	1.30 (1.20–1.40) (P < 0.001)	1.39 (1.34–1.44) (P < 0.001)
Codon 129				
MM	1	1	1	1
MV	0.55 (0.44–0.70)* (P < 0.001)	0.55 (0.45–0.67) (P < 0.001)	0.61 (0.46–0.80) (P < 0.001)	0.80 (0.49–1.31) (P = 0.379)
VV	0.70 (0.61–0.80)* (P < 0.001)	0.77 (0.67–0.88) (P < 0.001)	0.82 (0.71–0.94) (P = 0.005)	1.34 (0.86–2.08) (P = 0.197)
B				
EEG				
PSWC	1	–	1	–
No PSWC	0.79 (0.65–0.96) (P = 0.020)	–	1.01 (0.86–1.19) (P = 0.905)	–
14-3-3 in the CSF				–
Positive	1	–	1	
Negative	0.62 (0.43–0.88) (P = 0.007)	–	0.71 (0.52–0.96) (P = 0.027)	–
C				
PrP^{Sc} glycotype				
Type 1	1	–	–	1
Type 2a	0.54 (0.43–0.68) (P < 0.001)	–	–	0.53 (0.43–0.64) (P < 0.001)

*Crude RR did not change when estimated for A and B and A and C; [+]continuous for increment of 10 years.

Table 4 *Clinical duration of disease in genetic CJD patients carrying different point mutations of the PRNP gene*

PRNP mutations	Median (months)
D178N-129V (n = 8)	9
T188R (n = 1)	2*
E196K (n = 1)	13*
E200K (n = 123)	4
V203I (n = 2)	2, 4*
R208H (n = 1)	10*
V210I (n = 48)	4
E211Q (n = 5)	4

Observed values.

In GSS, methionine homozygous patients at codon 129 showed a median survival time 36 months longer than heterozygous patients. However, due to the small sample size and to the correction for multiple testing in the gTSE group, the difference did not reach statistical significance (Table 6).

Iatrogenic CJD

In ihGH CJD cases, a significantly lower risk was found for females compared with males and a higher risk for patients with late versus early age at onset. Survival curves were different in patients carrying distinct polymorphisms at codon 129 (Table 7, Fig. 3). However, this parameter was not significant in the univariate Cox analysis when MM patients were considered as the reference group. The multivariate Cox model with gender and age at onset confirmed these results (adjusted RR for gender = 0.75, CI 0.63–0.89, P = 0.001; adjusted RR for age at onset = 1.56, CI 1.35–1.81, P < 0.001). It is likely that the loss of significance for codon 129 was because the median survival of MM cases was between those of MV and VV cases. When we used VV cases as the reference group (those with the shortest median survival), the MV cases showed a lower risk than VV cases (crude RR = 0.41; 95% CI = 0.26–0.65, P < 0.001).

In iDM CJD cases, no significant effect of gender or age at onset was found by the Cox univariate model (Table 7). We did not analyse the effect of the codon 129 polymorphism because there were only two MV and one VV patients.

Variant CJD

Since all vCJD patients were MM, only the effect of gender and age at onset as predictors of survival was analysed. A significantly longer median illness duration was observed in females compared with males and in patients with early compared with late age at onset. These findings were confirmed by the Cox univariate and multivariate analyses (Table 8).

Table 5 *Survival times for genetic CJD (E200K and V210I)*

Features	E200K		V210I	
	Median in months	*P**	Median in months	*P**
Overall	4 (n = 123)		4 (n = 48)	
Gender				
Male	3 (n = 48)	0.020	3 (n = 22)	0.060
Female	5 (n = 75)		5 (n = 26)	
Age at onset				
31–40	14, 20$^+$ (n = 2)	0.067	5$^+$ (n = 1)	0.0047
41–50	6 (n = 20)		4 (n = 10)	
51–60	5 (n = 36)		5 (n = 14)	
61–70	3 (n = 41)		3 (n = 15)	
71–80	3 (n = 20)		2 (n = 7)	
81–90	3 (n = 4)		4y (n = 1)	
Codon 129				
MM	4 (n = 88)	0.002	5 (n = 38)	0.04
MV	8 (n = 23)		3 (n = 9)	
VV	4, 7$^+$ (n = 2)		– (n = 0)	

Cox regression model for survival in genetic E200K and V210I CJD patients

Features	E200K (n = 111)		V210I (n = 47)	
	Crude RR (95% CI)	Adjusted RR (95% CI)	Crude RR (95% CI)	Adjusted RR (95% CI)
Gender				
Male	1	1	1	1
Female	0.75 (0.60–0.92) (P = 0.007)	0.78 (0.63–0.95) (P = 0.015)	0.76 (0.64–0.90) (P = 0.002)	0.79 (0.67–0.93) (P = 0.004)
Age at onset†	1.13 (1.01–1.27) (P = 0.048)	1.13 (0.98–1.29) (P = 0.090)	1.39 (1.24–1.56) (P < 0.001)	1.51 (1.42–1.62) (P < 0.001)
Codon 129				
MM	1	1	1	1
MV	0.57 (0.50–0.65) (P < 0.001)	0.56 (0.45–0.70) (P < 0.001)	2.17 (1.51–3.11) (P < 0.001)	2.67 (2.10–3.39) (P < 0.001)

*Generalized Wilcoxon test; $^+$observed values; †continuous for increment of 10 years.

Discussion

The findings presented in this paper are generally consistent with previous studies of survival in sCJD (Wientjens, 1997; Will *et al*., 1998*a*; Parchi *et al*., 1999; Puopolo *et al*., 2003), but the large number of cases included in our analysis allows a more detailed description of predictors that influence survival in all forms of human TSE. There are a number of noteworthy and novel findings, including the influence of gender on survival in a number of subtypes of human TSE and the effect of prion protein PrP^{Sc} type on survival in sCJD. A reduction in survival with increasing age has been confirmed in sCJD, gCJD, cases with insert mutations and vCJD.

In order to allow comparability of data, it is essential to achieve consistency of data collection between countries. Details of the methodology of the study have been described previously (Will *et al*., 1998*a*). In this paper, there is a remarkable consistency in the results from country to country, for example in the median duration of illness in sCJD. The exception is a significant increase in the median survival in sCJD in Germany in comparison with the other countries (4 months in the majority compared with 6 months in Germany). The reason for this finding may be because of a systematic difference in classification of the time of disease onset. However, the analyses are not affected by this anomaly. The numbers of cases in this study are larger than any previous series, allowing firm conclusions on the major predictors of survival in sCJD. However, the numbers of cases in the subtype analyses are smaller, and this may result in insufficient power to assess some parameters properly.

Assessment of survival by disease type (Fig. 1A and B) demonstrates differences in illness duration between the various forms of human TSE. The shortest survival is in sCJD, iDM and, perhaps surprisingly, in some forms of gCJD. It is important to stress that the surveillance system depends on referral of suspect cases from neurologists, and this may result in a bias in the identification of genetic cases with a phenotype similar to sporadic cases (Will *et al*., 1998*b*). In vCJD, ihGH and FFI, a small proportion of patients survive to 24 months, which contrasts with GSS and cases associated with insert mutations in which a significant proportion survive beyond 24 months. In sCJD, about one in seven cases survives to 1 year and one in 30 to 2 years.

A reduction in survival with increasing age in sCJD is well known (Wientjens, 1997) but is not well documented. In this study, survival was found to decrease significantly with

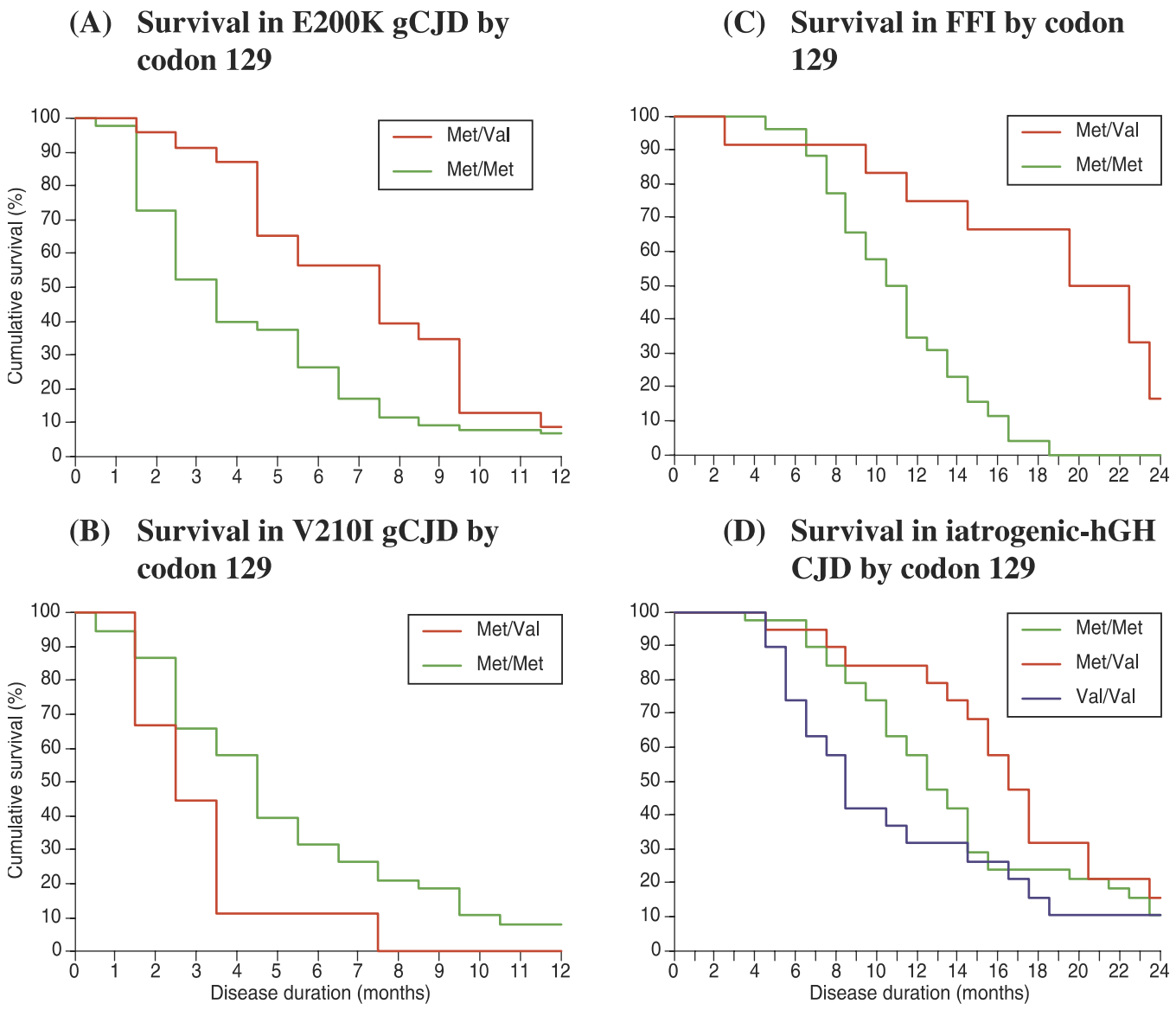

Fig. 3 Influence of codon 129 genotype on Kaplan–Meier survival curves in (**A**) E200K CJD, (**B**) V210I CJD, (**C**) FFI, (**D**) human growth hormone-related CJD.

increasing age in sCJD (Fig. 2B) with, for example, ~10% of cases aged >80 years surviving at 6 months in comparison with ~60% of cases aged <50 years. A similar age effect on survival is seen in cases associated with mutations of *PRNP* at codon 210 and in insert mutations. In ihGH, there is also a borderline relationship between prolonged survival and younger age, and there is a trend in a similar direction with vCJD. The most obvious difference between the ihGH cases and vCJD in comparison with the other subtypes is the relatively young age at death (Brown, 1988; Will *et al*., 2000). It is possible that should cases of iatrogenic or vCJD occur in the older age groups, the relationship between survival and age would become more significant as in the other forms of human TSE. The single case of vCJD in the older age group died at the age of 74 years and had one of the shortest illness durations yet seen of 7 months (Henry *et al*., 2002). The reason for the inverse relationship between age and survival in the majority of subtypes of human prion disease is unknown and, although age-related variations in care or resistance to terminal infection may play a role, there is evidence from laboratory studies of age-related effects on pathogenesis (Bruce and Fraser, 1982; Manolakou *et al*., 2001).

The overall female : male ratio in sCJD in this study, based on sex-specific mortality rates, is 1.24, representing a significant excess of female cases. A female preponderance in sCJD has been documented previously, but this finding is not consistent between studies, even in those carried out systematically (Brown, 1998). Because sCJD is predominantly a disease in the older age groups (60–79 years) and life expectancy is longer in females, population demographics may influence the overall sex distribution. However, this ratio may be affected by the uneven distribution of cases in different age classes, and a better estimate is given by the average female to male

Table 6 *Survival times for FFI, GSS and patients with insert mutations*

Features	FFI			GSS			Insert		
	Median in months	*P**	Crude RR (95% CI)	Median in months	*P**	Crude RR (95% CI)	Median in months	*P**	Crude RR (95% CI)
Overall	12.0 (n = 41)			39.0 (n = 24)			14.0 (n = 22)		
Gender									
Male	12.0 (n = 24)	0.43	1	30.5 (n = 9)	0.59	1	32.5 (n = 11)	0.53	1
Female	12.5 (n = 17)		0.92 (0.69–1.24) (P = 0.590)	39.5 (n = 15)		0.66 (0.20–2.17) (P = 0.490)	8.5 (n = 11)		1.61 (0.62–4.20) (P = 0.326)
Age at onset [+]									
21–30	–	0.65	0.82 (0.60–1.13) (P = 0.227)	7, 70[†] (n = 2)	0.52	1.19 (0.85–1.66) (P = 0.305)	–	0.018	2.00 (1.62–2.47) (P < 0.001)
31–40	11.0 (n = 6)			8, 32[†] (n = 2)			93.0 (n = 4)		
41–50	13.5 (n = 9)			46.0 (n = 9)			86.0 (n = 4)		
51–60	12.5 (n = 19)			20.0 (n = 5)			5.0 (n = 4)		
61–70	12.0 (n = 6)			29.5 (n = 3)			8.0 (n = 7)		
71–80	–			3, 67[†] (n = 2)			4, 5[†] (n = 2)		
81–90	–			–			4[†] (n = 1)		
Codon 129									
Met/Met	11.0 (n = 26)	0.0026	1	44.0 (n = 6)	0.19	1	4.0 (n = 7)	0.13	1
Met/Val	20.0 (n = 12)		0.15 (0.06–0.39) (P < 0.001)	8.0 (n = 6)		2.56 (1.03–6.39) (P = 0.044)	40.0 (n = 5)		0.28 (0.12–0.66) (P = 0.003)
Val/Val	–			–			5.0 (n = 5)		0.52 (0.16–1.71) (P = 0.280)

*Generalized Wilcoxon test; [+] continuous for increment of 10 years; [†] observed values.

Table 7 *Survival times for iatrogenic-hGH and iatrogenic-DM CJD*

Features	Iatrogenic-hGH CJD			Iatrogenic-DM CJD		
	Median in months	*P**	Crude RR (95% CI)	Median in months	*P**	Crude RR (95% CI)
Overall	13.0 (n = 85)			5.5 (n = 20)		
Gender		0.19			0.38	
Male	13.0 (n = 62)		1	5.0 (n = 12)		1
Female	14.0 (n = 23)		0.61 (0.60–0.63) (P < 0.001)	6.0 (n = 8)		0.78 (0.34–1.76) (P = 0.546)
Age at onset [+]		0.014	1.69 (1.41–2.02) (P < 0.001)		0.0008	1.17 (0.90–1.53) (P = 0.242)
10	36[†] (n = 1)			–		
11–20	25.0 (n = 8)			–		
21–30	11.5 (n = 59)			7.0 (n = 5)		
31–40	12.5 (n = 17)			4.0 (n = 3)		
41–50	–			5.0 (n = 4)		
51–60	–			4.5 (n = 5)		
61–70	–			2[†] (n = 1)		
71–80	–			3, 11[†] (n = 2)		
Codon 129		0.0065			0.70	
Met/Met	13.0 (n = 38)		1	6.0 (n = 9)		–
Met/Val	17.0 (n = 19)		0.59 (0.30–1.19) (P = 0.141)	5, 8[†] (n = 2)		–
Val/Val	9.0 (n = 19)		1.46 (0.46–4.63) (P = 0.522)	5[†] (n = 1)		–

*Generalized Wilcoxon test; [+] continuous for increment of 10 years; [†] observed values.

Table 8 *Survival times for vCJD patients*

Features	Median in months	*P**	Crude RR (95% CI)	Adjusted RR (95% CI)
Overall	13.0 (n = 86)			
Gender		0.035		
Male	12.0 (n = 45)		1	1
Female	14.0 (n = 41)		0.69 (0.61–0.79) ($P < 0.001$)	0.76 (0.68–0.85) ($P < 0.001$)
Age at onset $^{+}$		0.005	1.26 (1.25–1.28) ($P < 0.001$)	1.22 (1.18–1.26) ($P < 0.001$)
11–20	14.0 (n = 18)			
21–30	13.0 (n = 39)			
31–40	12.0 (n = 20)			
41–50	7.0 (n = 4)			
51–60	11.0 (n = 4)			
61–70	–			
71–80	7† (n = 1)			

*Generalized Wilcoxon test; $^{+}$continuous for increment of 10 years; †observed values.

ratios of each 10 year age class interval, weighting for the number of cases in each age class. The weighted female to male ratio is 1.08, but this still represents an 8% excess of female cases. The excess of female cases in sCJD does not explain the significant difference in survival in sCJD, with females surviving a median of 1 month longer than males. Similar gender effects on survival were found in cases associated with mutations of *PRNP*, with the exception of FFI, and in vCJD.

The effect of gender has been studied in mouse models, with varying results. One study has shown a major influence of gender in experimental transmission of bovine spongiform encephalopathy (BSE), with extended incubation periods in females (Abiola *et al*., 2002). In contrast, a recent study of non-*PRNP* genetic influences on incubation period showed a significant reduction in the incubation period in females (Manolakou *et al*., 2001), consistent with previous studies (Bruce and Dickinson, 1985; McLean and Bostock, 2000). The excess of female cases and the prolonged female survival in a number of types of human TSE suggest that there are sex-specific factors that influence the clinical phase of human disease. Possibilities include genetic determinants outside the *PRNP* gene, hormonal effects or neuroanatomical factors.

Prolonged survival is one of the variables that distinguish the subtypes of CJD classified according to the seminal work by Parchi and colleagues, using PrP^{Sc} type and codon 129 genotype (Parchi *et al*., 1991). The findings in our study support the hypothesis that the type of protein deposited in the brain influences the clinical phenotype. There is a clear and significant effect on survival in sCJD according to PrP^{Sc} type, with more prolonged survival in cases with the type 2a prion protein. One caveat to this conclusion is that there is evidence in some cases of sCJD of deposition of more than one PrP^{Sc} type in the brain (Puoti *et al*., 1999) and in our study there was no consistency in the brain area from which protein was extracted. Whether the PrP^{sc} type correlates with different 'strains' of infectious agent remains unproven.

There has been a recent resurgence of interest in identifying potential therapies for human TSEs, including CJD (Brown, 2002; Knight, 2002). Drug trials are likely to pose many difficulties, not least because of the rarity of CJD, and comparison of outcome, including survival, in treated cases in relation to the natural history may be an important strategy in assessing the efficacy of potential treatments. The detailed analyses in this study are likely to constitute important considerations for the assessment of treatment efficacy in human TSEs because of the identification and quantification of variables that influence survival in various TSE subtypes. This study documents the influence of a range of variables on survival in a population of cases that were not treated with any therapy known to influence the underlying disease process. A number of variables have been identified that have an influence, and often a major influence, on survival, including age, gender and codon 129 genotype. Although variables such as the PrP^{Sc} type may be of clinical use in the future by using nervous tissue taken from the biopsy of the olfactory epithelium (Zanusso *et al*, 2003), the results of investigations including the 14-3-3 CSF immunoassay correlate with survival. A 'typical' EEG is associated with shortened survival (Zerr *et al*., 2000) and a negative 14-3-3 test with relatively prolonged survival. In this study, the multivariate regression analysis has shown that only the 14-3-3 result is an independent predictor of survival, with a positive result probably reflecting rapid neuronal damage. In the univariate analysis, patients with a typical EEG had a significantly shorter survival than patients with non-specific EEG findings. This significance was lost in the multivariate analysis because the EEG pattern strongly correlates with the polymorphism at codon 129 of the *PRNP* gene. A possible explanation is that a typical EEG is likely to be related to the site of lesions in the brain, which in turn depends on the polymorphism at codon 129 (Tschampa *et al*., 2002).

This study underlines the importance of collaborative research in a rare disease. Some of the findings are novel, but attaining statistical significance has depended on the pooling of results from 10 countries carrying out national surveillance for human TSEs. The detailed analyses of factors influencing survival raise a number of scientific questions, for example the mechanism by which gender influences

disease expression, and may be critical in assessing the efficacy of novel therapeutic strategies.

Acknowledgements

This study was funded through an EU Concerted Action (BIOMED2 Contract No. BMH4-CT97-2216). Australia: the Australian National CJD Registry is funded by the Commonwealth Department of Health and Ageing. We are grateful to the following people involved in the Australian National CJD Registry: C. L. Masters, A. Boyd, G. Klug and J. Lee. Austria: the Austrian Reference Centre for Human Prion Diseases (ÖERPE, Head: Professor Herbert Budka) acknowledges the help of Drs Christa Jarius, Ellen Gelpi, Christine Haberler, Thomas Ströbel and Till Voigtländer; D. I. Dita Drobna; and Ms Helga Flicker, Brigitte Millan-Ruiz and Monika Richter. Canada: the Canadian Surveillance System is funded by Health Canada. Other collaborators on the project are Dr C. Bergeron, neuropathologist (University of Toronto), Dr M Coulthart, neuropathologist (National Laboratory for Prion Diseases, Health Canada), Dr N. Cashman, neurologist and one of the principal investigators for CJD-SS, and Dr D. Westaway, consulting scientist (University of Toronto). France: we would like to acknowledge all reporting physicians and the members of the Reseau National de surveillance de maladies de Creutzfeldt–Jakob et maladies apparentees. Germany: the German surveillance system is funded by the Federal Ministry of Health 9BMG, 325-4471-02/15). We are grateful to all reporting physicians throughout Germany who contributed to the German surveillance system and especially to Maja Schneider-Dominico for her excellent support in the coordination of surveillance. We also acknowledge the help of Drs Otto Windl and Walter Sculz-Schaeffer. Italy: we would like to acknowledge the Ministry of Health and the Istituto Superiore di Sanità for supporting the surveillance of CJD in Italy, and S. Almonti, V. Mellina and L. Ingrosso for help in collecting data and advice. The Netherlands: CJD surveillance in The Netherlands is funded by the Dutch Ministry of Health, Welfare and Sports. We acknowledge the help of colleagues at the Department of Neurology at the Academic Medical Centre, Amsterdam and the Department of Pathology at the University Medical Centre, Utrecht. Slovakia: the Slovak Surveillance System is funded by the Slovak Ministry of Health. Spain: we are grateful to all reporting physicians and to members of the Spanish TSE study group at Consejo Interterritorial and co-workers at CNE and ISCIII. Switzerland: This work was supported by the Kanton of Zurich and by grants from the European Union. The Swiss Reference Center for Prion Diseases is being funded by the Swiss Federal Office of Public Health. UK: the UK CJD Surveillance System is funded by the Department of Health and the Scottish Executive Health Department. We are grateful to all the members of staff at the National CJD Surveillance Unit and in particular to James Ironside for neuropathological expertise and to clinicians throughout the UK for their cooperation with the study.

References

Abiola OO, Iyegbe C, Lantos P, Plomin R, Anderton BH, Whatley SA. Profound sex-specific effects on incubation times for transmission of bovine spongiform encephalopathy to mice. Intervirology 2002; 45: 56–8.

Brown P. The clinical neurology and epidemiology of Creutzfeldt–Jakob disease, with special reference to iatrogenic cases. In: Bock GR, editor. Novel infectious agents and the central nervous system. Ciba Foundation symposium: 135. Chichester (UK): John Wiley; 1988. p. 3–18.

Brown P. Drug therapy in human and experimental transmissible spongiform encephalopathy. Neurology 2002; 58: 1720–5.

Brown P, Rodgers-Johnson P, Cathala F, Gibbs CJ Jr, Gajdusek DC. Creutzfeldt–Jakob disease of long duration: clinicopathological characteristics, transmissibility, and differential diagnosis. Ann Neurol 1984; 16: 295–304.

Brown P, Cathala F, Raubertas RF, Gajdusek DC, Castaigne P. The epidemiology of Creutzfeldt–Jakob disease: conclusion of a 15-year investigation in France and review of the world literature. Neurology 1987; 37: 895–904.

Brown P, Gibbs CJ Jr, Rodgers-Johnson P, Asher DM, Sulima MP, Bacote A, et al. Human spongiform encephalopathy: the National Institutes of Health series of 300 cases of experimentally transmitted disease. Ann Neurol 1994; 35: 513–29.

Bruce ME, Dickinson AG. Genetic control of amyloid plaque production and incubation period in scrapie-infected mice. J Neuropathol Exp Neurol 1985; 44: 285–94.

Bruce ME, Fraser H. Effects of age on cerebral amyloid plaques in murine scrapie. Neuropathol Appl Neurobiol 1982; 8: 71–4.

Collinge J, Palmer MS, Dryden AJ. Genetic predisposition to iatrogenic Creutzfeldt–Jakob disease. Lancet 1991; 337: 1441–2.

Galvez S, Masters C, Gajdusek DC. Descriptive epidemiology of Creutzfeldt–Jakob disease in Chile. Arch Neurol 1980; 37: 11–4.

Henry C, Lowman A, Will RG. Creutzfeldt–Jakob disease in elderly people. Age Ageing 2002; 31: 7–10.

Knight R. CJD: the promise of treatment. Br J Infect Control 2002; 3: 4.

Korth C, May BCH, Cohen FE, Prusiner SB. Acridine and phenothiazine derivatives as pharmacotherapeutics for prion disease. Proc Natl Acad Sci USA 2001; 98: 9836–41.

Kovacs GG, Trabattoni G, Hainfellner JA, Ironside JW, Knight RSG, Budka H. Mutations of the prion protein gene: phenotypic spectrum. J Neurol 2002; 249: 1567–82.

Lundberg PO. Creutzfeldt–Jakob disease in Sweden. J Neurol Neurosurg Psychiatry 1998; 65: 836–41.

Manolakou K, Beaton J, McConnell I, Farquar C, Manson J, Hastie ND, et al. Genetic and environmental factors modify bovine spongiform encephalopathy incubation period in mice. Proc Natl Acad Sci USA 2001; 98: 7402–7.

McLean AR, Bostock CJ. Scrapie infections initiated at varying doses: an analysis of 117 titration experiments. Philos Trans R Soc Lond B Biol Sci 2000; 355: 1043–50.

McNaughton H, Will R. Creutzfeldt–Jakob disease presenting as stroke: an analysis of 30 cases. Neurol Infect Epidemiol 1997; 2: 19–24

Palmer MS, Dryden AJ, Hughes JT, Collinge J. Homozygous prion protein genotype predisposes to sporadic Creutzfeldt–Jakob disease. Nature 1991; 352: 340–2.

Parchi P, Castellani R, Capellari S, Ghetti B, Young K, Chen SG, et al. Molecular basis of phenotypic variability in sporadic Creutzfeldt–Jakob disease. Ann Neurol 1996; 39: 767–78.

Parchi P, Giese A, Capellari S, Brown P, Schulz-Schaeffer W, Windl O, et al. Classification of sporadic Creutzfeldt–Jakob disease based on molecular and phenotypic analysis of 300 subjects. Ann Neurol 1999; 46: 224–33.

Pocchiari M. Prions and related neurological diseases. Mol Aspects Med 1994; 15: 195–291.

Puopolo M, Ladogana A, Almonti S, Daude N, Bevivino S, Petraroli R, et al. Mortality trend from sporadic Creutzfeldt–Jakob disease (CJD) in Italy, 1993–2000. J Clin Epidemiol 2003; 56: 494–9.

Puoti G, Giaccone G, Rossi G, Canciani B, Bugiani O, Tagliavini F. Sporadic Creutzfeldt–Jakob disease: co-occurrence of different types of PrP(Sc) in the same brain. Neurology 1999; 53: 2173–6.

Tschampa HJ, Herms JW, Schulz-Schaeffer WJ, Maruschak B, Windl O, Jastrow U, et al. Clinical findings in sporadic Creutzfeldt–Jakob disease correlate with thalamic pathology. Brain 2002; 125: 2558–66.

Wientjens DPWM. Epidemiology of Creutzfeldt–Jakob disease. Incidence, risk factors and survival in European studies [dissertation]. Rotterdam: Erasmus University; 1997.

Will RG, Matthews WB, Smith PG, Hudson C. A retrospective study of Creutzfeldt–Jakob disease in England and Wales 1970–1979. II: epidemiology. J Neurol Neurosurg Psychiatry 1986; 49: 749–55.

Will RG, Alperovitch A, Poser S, Pocchiari M, Hofman A, Mitrova E, et al. Descriptive epidemiology of Creutzfeldt–Jakob disease in six European countries, 1993–1995. Ann Neurol 1998a; 43: 763–7.

Will RG, Campbell MJ, Moss TH, Bell JE, Ironside JW. FFI cases from the United Kingdom. Brain Pathol 1998b; 8: 562–63.

Will RG, Zeidler M, Stewart GE, Macleod MA, Ironside JW, Cousens SN, et al. Diagnosis of new variant Creutzfeldt–Jakob disease. Ann Neurol 2000; 47: 575–82.

Zanusso G, Ferrari S, Cardone F, Zampieri P, Gelati M, Fiorini M, et al. Detection of pathologic prion protein in the olfactory epithelium in sporadic Creutzfeldt–Jakob disease. N Engl J Med 2003; 348: 711–9.

Zerr I, Schulz-Schaeffer W, Giese A, Bodemer M, Schroter A, Henkel K, et al. Current clinical diagnosis in Creutzfeldt–Jakob disease: identification of uncommon variants. Ann Neurol 2000; 48: 323–9.

Mortality from Creutzfeldt–Jakob disease and related disorders in Europe, Australia, and Canada

A. Ladogana, MD; M. Puopolo, DStat; E.A. Croes, MD, PhD; H. Budka, MD; C. Jarius, MD; S. Collins, MD, FRACP; G.M. Klug, BSc(Hons); T. Sutcliffe, BA; A. Giulivi, MD, FRCP; A. Alperovitch, MD; N. Delasnerie-Laupretre, MD; J.-P. Brandel, MD; S. Poser, MD; H. Kretzschmar, MD, FRCPath; I. Rietveld, MD; E. Mitrova, MD; J. de Pedro Cuesta, MD, PhD; P. Martinez-Martin, MD, PhD; M. Glatzel, MD; A. Aguzzi, MD, PhD; R. Knight, FRCP(Ed); H. Ward, MRCP, FFPH; M. Pocchiari, MD; C.M. van Duijn, PhD; R.G. Will, MD, FRCP; and I. Zerr, MD

Abstract—*Background:* An international study of the epidemiologic characteristics of Creutzfeldt–Jakob disease (CJD) was established in 1993 and included national registries in France, Germany, Italy, the Netherlands, Slovakia, and the United Kingdom. In 1997, the study was extended to Australia, Austria, Canada, Spain, and Switzerland. *Methods:* Data were pooled from all participating countries for the years 1993 to 2002 and included deaths from definite or probable CJD of all etiologic subtypes. *Results:* Four thousand four hundred forty-one cases were available for analysis and included 3,720 cases of sporadic CJD, 455 genetic cases, 138 iatrogenic cases, and 128 variant cases. The overall annual mortality rate between 1999 and 2002 was 1.67 per million for all cases and 1.39 per million for sporadic CJD. Mortality rates were similar in all countries. There was heterogeneity in the distribution of cases by etiologic subtype with an excess of genetic cases in Italy and Slovakia, of iatrogenic cases in France and the UK, and of variant CJD in the UK. *Conclusions:* This study has established overall epidemiologic characteristics for Creutzfeldt–Jakob disease (CJD) of all types in a multinational population–based study. Intercountry comparisons did not suggest any relative change in the characteristics of sporadic CJD in the United Kingdom, and the evidence in this study does not suggest the occurrence of a novel form of human bovine spongiform encephalopathy infection other than variant CJD. However, this remains a possibility, and countries currently unaffected by variant CJD may yet have cases.

NEUROLOGY 2005;64:1586–1591

Creutzfeldt–Jakob disease (CJD) is one of the transmissible spongiform encephalopathies (TSEs), or prion diseases, which include the animal diseases scrapie and bovine spongiform encephalopathy (BSE). CJD occurs in a number of distinct etiologic subtypes.[1] Sporadic CJD (sCJD) occurs worldwide and is of unknown etiology. Genetic forms of human TSE (gTSE), including genetic CJD, Gerstmann–Sträussler–Scheinker syndrome (GSS), and fatal familial insomnia (FFI), are linked to mutations of the prion protein gene (*PRNP*) (although whether the mutations are causal remains uncertain). Iatrogenic CJD (iCJD) is caused by the transmission of infection from person to person in the course of medical treatment, for example, cadaveric human pituitary growth hormone and human dura mater grafts. Vari-

Additional material related to this article can be found on the *Neurology* Web site. Go to www.neurology.org and scroll down the Table of Contents for the May 10 issue to find the title link for this article.

From the Istituto Superiore di Sanità (Drs. Ladogana, Puopolo, and Pocchiari), Department of Cell Biology and Neurosciences–ISS, Rome, Italy; Department of Epidemiology and Biostatistics (Drs. Croes, Rietveld, and van Duijn), Erasmus Medical College, Rotterdam, the Netherlands; Austrian Reference Centre for Human Prion Diseases (OERPE) and Institute of Neurology (Drs. Budka and Jarius), Vienna, Austria; Australian National CJD Registry (Dr. Collins and G.M. Klug), Department of Pathology, University of Melbourne, Victoria, Australia; Blood Safety Surveillance and Health Care Acquired Infections Division (Dr. Giulivi and T. Sutcliffe), Centre for Infectious Disease Prevention and Control, Ottawa, Ontario, Canada; U.360 INSERM (Drs. Alperovitch, Delasnerie-Laupretre, and Brandel), Hopital de la Salpetriere, Paris, France; Department of Neurology (Drs. Poser and Zerr), Georg-August-Universität Göttingen, Germany; Institute of Neuropathology (Dr. Kretzschmar), University of Munich, Germany; Institute of Preventative and Clinical Medicine (Dr. Mitrova), National Reference Centre of Slow Virus Neuroinfections, Bratislava, Slovakia; Instituto de Salud Carlos III (Drs. de Pedro Cuesta and Martinez-Martin), Departamento de Epidemiologia Aplicada, Centro Nacional de Epidemiologia, Madrid, Spain; Swiss National Reference Centre for Prion Diseases (Drs. Glatzel and Aguzzi), University Hospital of Zurich, Switzerland; and National CJD Surveillance Unit (Drs. Knight, Ward, and Will), Western General Hospital, Edinburgh, UK.

Funded through an EU Concerted Action (BIOMED2 contract no. BMH4-CT97-2216). The Australian National CJD Registry is funded by the Commonwealth Department of Health and Ageing. The Canadian Surveillance System is funded by Health Canada. The German Surveillance System is funded by the Federal Ministry of Health (BMG, 325-4471-02/15). The surveillance of CJD in Italy is funded by the Ministry of Health and the Istituto Superiore di Sanità. CJD surveillance in the Netherlands is funded by the Dutch Ministry of Health, Welfare, and Sports. The Slovak Surveillance System is funded by the Slovak Ministry of Health. The Swiss Reference Center for Prion Diseases is funded by the Swiss Federal Office of Public Health. The UK CJD Surveillance System is funded by the Department of Health and the Scottish Executive Health Department. Also supported by the Kanton of Zurich and by grants from the European Union.

Received February 27, 2004. Accepted in final form January 17, 2005.

Address correspondence and reprint requests to Dr. R.G. Will, National CJD Surveillance Unit, Western General Hospital, Edinburgh EH4 2XU, UK; e-mail: r.g.will@ed.ac.uk

ant CJD (vCJD) is a novel form of human TSE, which has been linked to transmission of BSE to the human population.[2]

The probability that vCJD represents the first zoonotic transmission of a TSE to the human population has political, economic, and social implications, not least because of the potential threat to public health in the United Kingdom and other countries. In 1993, a system was established to coordinate the epidemiologic surveillance in a number of European countries with the primary aim of identifying any change in the characteristics of CJD that might be attributable to the BSE epidemic.[3] In 1996, a new form of CJD, vCJD, was identified in the UK, and the hypothesis that this disease might be causally linked to BSE exposure has been supported by subsequent evidence.[4,5]

The occurrence of a new form of CJD in one country, the United Kingdom, and not, initially, in other countries with similar surveillance methodologies was an important component of the argument in favor of a link with BSE, and this depended on the systematic study of the incidence and case characteristics of CJD of all types in participating countries. This article reviews the data from the European, Australian, and Canadian CJD surveillance systems from 1993 to 2002 and addresses a number of important questions: What is the distribution of CJD by etiologic subtype, and does this vary by country? Is the pattern of occurrence of vCJD consistent with a link with BSE? Does analysis of the temporal trends in the characteristics of sCJD, including intercountry comparisons, suggest a change in the characteristics of sCJD that may be linked to BSE?

Methods. The European Union collaborative study of CJD was carried out from 1993 to 2002 by France, Germany, Italy, the Netherlands, Slovakia, and the United Kingdom. National Creutzfeldt–Jakob disease registry surveillance methods for these participating countries have been reported in detail previously.[3] In 1997, the study was enlarged to other European and non-European countries where similar registers and surveillance methods were set up: Australia in 1993, Austria, Spain, and Switzerland in 1996, and Canada in 1998. The aim was to monitor CJD and the occurrence of vCJD in Europe and in countries where exposure to BSE is likely to have been minimal. The annual mortality rates and the standardized mortality ratios (SMRs) were calculated using data collected from 1999 to 2002 when the surveillance system was well established in all countries.

Cases were classified according to shared diagnostic criteria[3] updated from January 1998 with the introduction of the 14-3-3 CSF test.[6] Cases classified as definite (neuropathologically confirmed) or probable that died between January 1, 1993, and December 31, 2002, have been included in the analyses. For each case, a data set including diagnostic classification, etiologic subtype, year of diagnosis, age at onset and death, results of investigations, and, when available, *PRNP* analysis and the brain prion protein type were established using standard methods.[7] The data set was checked for accuracy and consistency by all participants.

Statistical analysis. Crude and age- and sex-specific incidences or mortality rates were calculated using as denominator population data for 1998 provided from the national or federal statistics bureau of participating countries. For Canada, population data (2001) were taken from the Canadian Statistics Web site. Six age-interval classes (10 to 39, 40 to 49, 50 to 59, 60 to 69, 70 to 79, and >80) were defined for the analyses.

Differences in mortality from sCJD and gTSE among the countries were assessed by calculation of the SMR based on the overall age- and sex-specific mortality rates for the period 1999 to 2002. SMRs with 95% CIs that did not include 1.0 were considered to be significant. The CIs were calculated under the assumption that the observed number of cases followed a Poisson distribution.

Results. There were 4,441 deaths from CJD included in the study in the period 1993 to 2002. Of these 4,441 deaths, 66% of cases were classified as definite CJD and 34% as probable CJD. The overall proportion of cases classified as definite or probable did not change over time. The percentage of human TSE diseases with autopsy, EEG, measurement of 14-3-3 in the CSF, and *PRNP* analysis for the period 1999 to 2002 in each country is given in figure E-1 on the *Neurology* Web site (www.neurology.org). Postmortem examination was performed in 66% of all cases, ranging from 100% in Slovakia to 49% in Germany. In all countries, the EEG was available in the majority of patients except in Canada (7%). CSF 14-3-3 protein analysis was performed in 86% of all patients, ranging from 52% in Slovakia and Canada to 99.6% in Germany. *PRNP* analysis was carried out in 67%, ranging from 32% in Australia and the Netherlands to 97% in Slovakia.

The large number of cases collected in the database and the accuracy in terms of etiologic classification allowed analysis of incidence and mortality rates according to the classification as gTSE, sCJD, iCJD, and vCJD. Eighty-four percent of cases were classified as sporadic, 10% as genetic (including genetic CJD, FFI, and GSS), 3% as iatrogenic, and 3% as vCJD. The number of cases by country according to the etiologic subtype is shown in table 1. The highest number of deaths from sCJD was reported in Germany (n = 827), reflecting the largest population by country, whereas Slovakia reported only 18 deaths from sCJD. The number of genetic cases was highest in Italy, France, Germany, the United Kingdom, Spain, and Slovakia. The number of deaths due to iCJD varied markedly by country, with a peak of 82 cases in France and 33 in the United Kingdom related mainly to cases of CJD in human growth hormone recipients (n = 105; human dura mater recipients: n = 32; corneal graft recipient: n = 1). There were no such cases in Slovakia, Austria, or Switzerland. vCJD cases were identified during this study period (1993 to 2002) only in the UK (n = 121), France (n = 6), and Canada (n = 1). When the clinical subtypes were analyzed by year of death, apart from the yearly increase in the absolute number of deaths in each subtype related to new countries joining the study, the emergence of variant cases is the most striking feature (see table E-1).

Analysis of the age at death in each etiologic subtype confirmed previous observations on differences in the age distribution between the four subtypes: The vCJD and iCJD cases were mainly in the age class younger than 39 years, the genetic forms mostly distributed between age groups 50 to 59 and 60 to 69, and sporadic cases predominantly in age groups 60 to 69 and 70 to 79 (see figure E-2).

The overall yearly number of deaths from TSE (including all subtypes) ranged from 209 cases in 1993 to 621 in 2001 with an average yearly mortality rate of 1.67 cases per million for the period 1999 to 2002 (pooled data from all countries). The distribution of the etiologic subtypes is shown in an analysis of yearly mortality rates from CJD by European country (figure 1). The mortality rates from sCJD were relatively homogeneous, whereas high mortality rates from gTSE were reported in Austria, Italy, Slova-

Table 1 *CJD in Europe, Australia, and Canada 1993–2002: Number of cases by clinical subtype and country*

Country	Population, >10 y old	Sporadic CJD		Genetic TSE	Iatrogenic CJD	Variant CJD	Total
		Total	With *PRNP* analysis				
Australia	16,361,803	189	34	22	4	—	215
Austria*†	7,165,559	77	30	13	—	—	90
Canada‡	27,317,369	169	54	16	3	1	189
France	51,904,469	766	571	84	82	6	938
Germany	73,693,100	827	690	68	5	—	900
Italy	51,868,080	544	303	115	3	—	662
Netherlands	13,698,715	136	24	3	3	—	142
Slovakia	4,683,900	18	18	41	—	—	59
Spain*†	35,488,954	380	96	44	5	—	429
Switzerland*	6,384,109	84	45	1	—	—	85
UK	52,001,000	530	279	48	33	121	732
Total (%)	340,567,058	3,720 (83.8)	2,144 (57.6)	455 (10.2)	138 (3.1)	128 (2.9)	4,441

* Since 1996.
† Including retrospective cases from 1993.
‡ Since 1998, including retrospective cases from 1994.

CJD = Creutzfeldt–Jakob disease; TSE = transmissible spongiform encephalopathy.

kia, and Spain and from iCJD in France (0.12 case per million) and United Kingdom (0.05). Moreover, it is clear that vCJD is predominantly a disease occurring in the United Kingdom (0.38).

The distribution of genotypes at codon 129 of *PRNP* for all types of TSE is shown in table 2. Overall, about 68% of cases were methionine (M) homozygotes, with 67% of sCJD cases and 100% of vCJD cases exhibiting this genotype. In iCJD and GSS, the relative excess of methionine homozygotes was less marked, and in iCJD, the distribution of codon 129 genotypes was different between France (61% MM) and the UK (5% MM).[8] There was no significant difference in the distribution of codon 129 genotypes by country in sCJD.

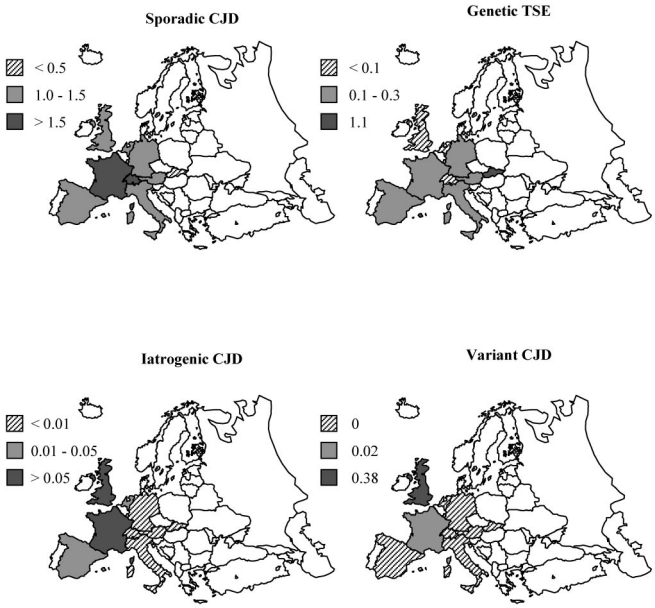

Figure 1. Yearly mortality rates from human transmissible spongiform encephalopathy (TSE) in Europe by clinical subtype (1999 to 2002). CJD = Creutzfeldt–Jakob disease.

sCJD. The SMRs and the 95% CI of SMRs for the countries in the study, for 1999 to 2002, are reported in table 3. In this period, France and Switzerland reported an observed number of deaths higher than expected (n = 397 and 57), whereas Slovakia and the UK reported an observed number of deaths lower (n = 9 and 241).

The incidence and mortality rates for sCJD are similar because of the short mean duration of disease, and data are therefore presented in terms of mortality rates. The overall annual mortality rate from sCJD in the period 1999 to 2002 is 1.39 cases per million (pooled data from all countries). The rates in individual countries range from 0.48 in Slovakia to 2.23 in Switzerland, while most of the countries showed similar rates (figure 2A).

Table 2 *Codon 129 distribution by disease type*

Human TSE	Codon 129 polymorphism, %			Total
	Met/Met	Met/Val	Val/Val	
Sporadic CJD	67.2	16.4	16.5	2,339
Genetic CJD	69.4	23.8	6.8	294
FFI	71.4	28.6	—	63
GSS	51.6	32.3	16.1	31
Iatrogenic CJD	54.0	26.5	19.5	113
Variant CJD	100	—	—	119
Total	68.1	17.3	14.6	2,959

CJD = Creutzfeldt–Jakob disease; FFI = fatal familial insomnia; GSS = Gerstmann–Sträussler–Scheinker syndrome.

Met = methionine; Val = valine.

Table 3 *SMRs and 95% CIs of sporadic Creutzfeldt–Jakob disease and genetic TSE in Europe, Australia, and Canada, 1999–2002*

	Sporadic		Genetic TSE	
Country	SMR	95% CI	SMR	95% CI
Australia	1.11	0.89–1.37	0.85	0.39–1.61
Austria	0.80	0.54–1.13	1.59	0.69–3.14
Canada	0.87	0.72–1.04	0.71	0.38–1.22
France	1.34* ↑	1.21–1.47*	1.00	0.71–1.38
Germany	0.93	0.84–1.03	0.69* ↓	0.49–0.95*
Italy	0.95	0.84–1.06	1.60* ↑	1.23–2.05*
Netherlands	0.82	0.62–1.07	0.11* ↓	0.00–0.60*
Slovakia	0.44* ↓	0.20–0.83*	6.84* ↑	4.18–10.56*
Spain	1.03	0.89–1.18	1.30	0.89–1.84
Switzerland	1.61* ↑	1.22–2.08*	0.22	0.01–1.21
UK	0.83* ↓	0.73–0.94*	0.41* ↓	0.23–0.67*

* Significant increase (↑) or decrease (↓) in mortality rates with respect to the estimates for overall Europe.

SMR = standardized mortality ratio; TSE = transmissible spongiform encephalopathy.

Data on age at death and sex were available in 3,716 patients with sCJD, and the age- and sex-specific rates are shown in figure E-3A. The distribution of the yearly age- and gender-specific mortality rates for sCJD showed a low rate in the under-50 age group, a peak in mortality in the 60 to 79 age group, and a decline in the 80 and older age group. This observation is consistent between countries. A slightly higher rate of deaths among men was observed for patients ages ≥70. The age distribution of cases was similar in all countries, with the exception of a peak mortality in the 60 to 69 age group in Slovakia.

Analysis of pooled data from Australia, Austria, France, Germany, Italy, the Netherlands, Slovakia, Spain, and the United Kingdom for the three time periods (1993 to 1995, 1996 to 1998, and 1999 to 2002) showed mortality rates from sCJD increasing with the time in all age groups, most prominently in patients over age 60 (see figure E-4).

The distribution of codon 129 genotypes in sCJD by year of death is shown in figure E-5. The distribution with time shows an overall slight decrease in the proportion of cases of sCJD with an MM genotype (χ^2 test for linear trend, $p = 0.01$). Prion protein type is available in 865 (23%) cases of sCJD. Combining the two prion protein types (type 1 or type 2A) and the three codon 129 genotypes allows cases of sCJD to be classified into six subgroups, with the MM/type 1 cases representing the majority of cases (see table E-2) of clinically "typical" sCJD. About 6% of cases have both type 1 and type 2A in the brain. Eighty-eight percent of MM cases are associated with PrP^{Sc} type 1, whereas 82% of valine/valine (VV) and 62% of MV cases are PrP^{Sc} type 2A (χ^2 test, $p < 0.0001$). Table E-3 shows the number of MM/type 1 and MV/type 2 sCJD cases in the four countries with available information. We did not observe any significant (after Bonferroni correction for multiple testing) temporal trend for patients with MM/type 1 sCJD (χ^2 test for linear trend, France, $p = 0.03$; Germany, $p = 0.12$; Italy, $p = 0.27$; UK, $p = 0.91$) or MV/type 2 (France, $p = 0.02$; Germany, $p = 0.08$; Italy, $p = 0.32$; UK, $p = 0.75$).

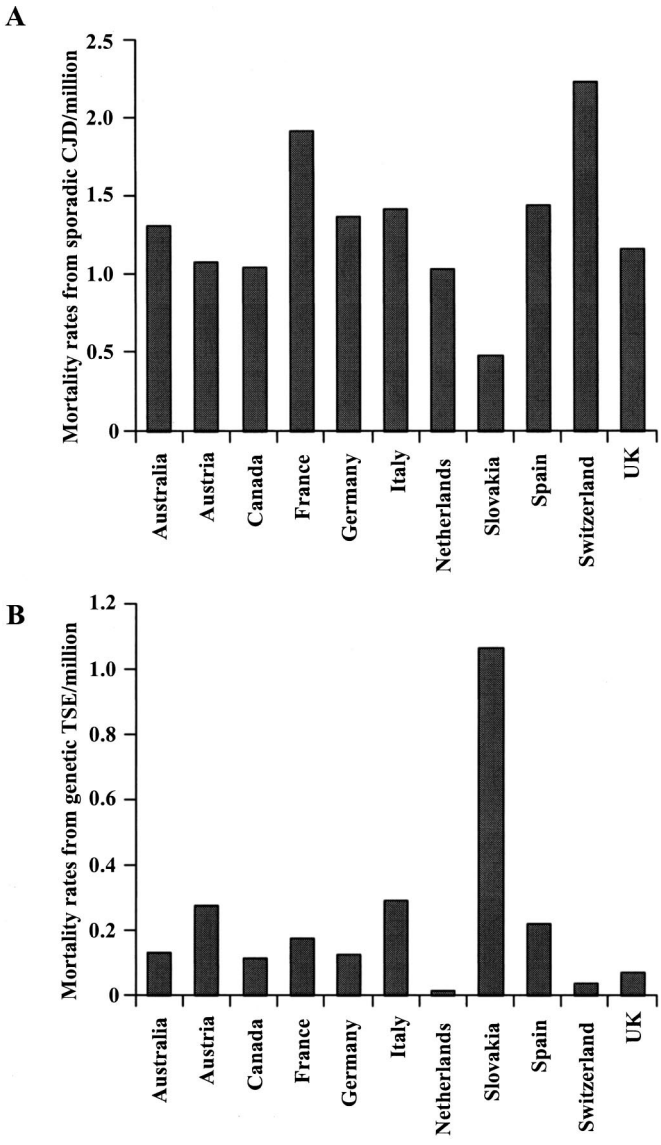

Figure 2. Yearly mortality rates from sporadic Creutzfeldt–Jakob disease (CJD) (A) and genetic transmissible spongiform encephalopathy (TSE) (B) by country (1999 to 2002).

gTSE. The SMRs and the 95% CIs of SMRs for gTSE in 1999 to 2002 are reported in table 3. In Italy (n = 62) and Slovakia (n = 20), there was a relative excess of genetic cases, whereas in Germany, the Netherlands, and the United Kingdom, there was a relatively low number.

The overall annual mortality rate in the period 1999 to 2002 for gTSE is 0.17 case per million. However, the analysis of the incidence and mortality rates for gTSE by countries showed marked differences (see figure 2B). The yearly mortality rates in individual countries ranged from 0.02 in the Netherlands (1999 to 2002) to 1.07 in Slovakia (1999 to 2002). Data on age at death and sex were available in 455 patients with gTSE, and the age- and sex-specific rates overall (pooled data from all countries) are shown in figure E-3B. The distribution of the yearly age- and gender-specific mortality rates was different from that

of sCJD cases, with higher rates in the 50 to 59 and 60 to 69 age groups and a decline in the over-70 age groups. A slightly higher rate of deaths among women was observed. There was no increase in mortality from gTSE over the 10-year period in any of the age groups under examination (data not shown).

Discussion. This is the largest systematic prospective survey of CJD ever carried out, including detailed information in >3,700 cases of sCJD and >4,400 cases in total. The proportion of cases by etiologic subtype is similar to previous studies[3,9,10] with >80% of cases classified as sporadic, but there is marked variation in the incidence of gTSE, iCJD, and vCJD between countries. Overall, there is evidence of an increase in mortality of sCJD with time, but this is not specific to any particular country or countries, and no new subtype of CJD, other than vCJD, has been identified.

Any surveillance system depends on a high-level ascertainment to allow meaningful results and for intercountry comparisons to be valid. The efficiency of case identification and data collection should be similar in all participating countries. There is variation in the provision of health care in the countries in our study, for example, in the number of neurologists per country[11] and in postmortem rates. However, there is a general consistency in the mortality rates for sCJD in this study between participating countries. Furthermore, the increasing temporal trends in mortality and the changes in the age-specific incidence rates are also very similar between countries, arguing that the efficiency of case ascertainment is similar despite the variations in health care systems and resources available to individual centers. Complete data sets were available for nearly all cases included in this study, and there was a high rate of data consistency, requiring only minor amendments to the original data set. The proportion of cases undergoing postmortem examination was high, at about two-thirds of all cases. *PRNP* analysis was available in >60% of cases; although there was variation in the proportion of tested cases ranging from 32% in Australia to 97% in Slovakia, in the majority of countries, the proportions tested were comparable (see figure E-1). Although there are uncertainties about the efficiency of case finding of CJD across time and the age range, for example, in the first years of the study and in the elderly, the data in this article suggest that surveillance for all types of CJD has been carried out efficiently and that intercountry comparisons are likely to be valid.

One notable finding is the marked variation in the incidence of etiologic subtypes by country with an excess of iatrogenic cases in France and the United Kingdom and an excess of genetic cases in Italy and Slovakia. The great majority of cases of iCJD in this study are related to human growth hormone treatment, and the reason for the excess of cases in particular countries suggests that the treated populations in these countries were exposed to a higher level of infection. It is of note that in France and the UK, human growth hormone was produced locally, whereas in other countries, commercially produced human growth hormone was mainly used.[12] Cases of gTSE were found in all participating countries, indicating that the risk of gTSE is widespread, although the excess of gTSE cases in particular countries indicates that this risk is not homogeneous. The variation in mortality rates for gTSEs by country is not directly related to differences in the proportion of cases with available *PRNP* analysis (see table 1) and is therefore likely to be a real observation. Codon 200 mutations account for about 50% of all *PRNP* mutations in this series, have been identified in all participating countries, and represent the majority of mutations found in France (55%) and Slovakia (100%) but not in Italy (32%) and Spain (33%). The worldwide dissemination of the codon 200 mutation has previously been studied, with haplotype analysis suggesting a link between the Italian and Spanish families, but no link between families in Slovakia, Germany, and Austria.[13] The possibility of genetic isolation and/or consanguinity may explain the high incidence of gTSE in Slovakia[14] and perhaps in some Italian cases.[15] Previous work from the EuroCJD Group has shown that a family history of a similar disorder is found in only about one-third of all mutation-related cases.[16] The widespread geographic occurrence of a range of *PRNP* mutations may relate to spontaneous mutations in *PRNP*, similar to those that have previously been identified in association with mutations at codon 178 of *PRNP*.[17]

Analysis of SMRs for sCJD by country indicates some variation with time (data not shown). This may represent a variation about a mean; for example, in Austria, a high SMR for sCJD in the period 1993 to 1995 (1.58) was not sustained in subsequent years. There is a possibility that the fluctuations in mortality from sCJD may explain the high incidence of sCJD identified in Switzerland,[18] but other explanations must be considered, including a locally efficient surveillance system and underreporting in other countries. This hypothesis has been judged to be implausible in view of the similarities between Switzerland and other countries such as Austria, in which there is no equivalent rise in mortality rates, despite similar population, age structure, and quality of health care. Furthermore, the proportion of cases with results of specialist investigations in Switzerland (see figure E-1) is similar to that in other countries and lower than in Austria. However, the possibility that the variation in mortality rates for sCJD between countries is related to differences in the efficiency of case identification or classification cannot be excluded.

It is clear from our study that vCJD occurs predominantly in the United Kingdom with a smaller number of cases in France during the study period, probably linked to a proportionally lower human exposure to BSE.[19] The single vCJD case in Canada most likely occurred as a consequence of exposure in the United Kingdom. The hypothesis that improved

identification of atypical cases of CJD, rather than BSE, may explain the occurrence of vCJD[20] is not supported by our data. Despite evidence of efficient surveillance for all forms of CJD in participating countries, vCJD was not identified during the study period in a population of >300 million over 4 to 7 years. Single cases of vCJD have subsequently been identified in Italy[21] and the USA,[22] but not in the other countries in the surveillance system. Furthermore, the cases in the USA and Canada had a history of extended residence in the UK during the period when human BSE exposure was maximal, a striking coincidence if these cases had been identified solely as a result of improved case identification.

Overall, there has been an increase in mortality from sCJD with time, and it is not possible to be certain whether this is related to improved efficiency of the surveillance system with time or some other cause such as a new environmental source of infection. However, the increased mortality is related mainly to increasingly mortality rates in the elderly, rather than the younger age groups, and the changes in mortality have been found in all participating countries, including Australia and Canada, in which indigenous BSE exposure is likely to have been negligible. This argues against the possibility that the rise in mortality may be related to BSE infection in humans, resulting in a phenotype indistinguishable from sCJD. Further analyses of trends in subtypes of sCJD do not support the hypothesis that BSE infection might result in an increase in the MM/type 1 subtype of sCJD[23] or an increase in the MV/type 2 subtype in relation to a novel form of BSE.[24] The proportion of all cases of sCJD with an MM genotype has decreased, if anything, during the period of the study; although data are available in only a minority of cases, there has also been a decrease overall in the proportion of cases with an MM genotype and type 1 prion protein deposition in the brain. If BSE were to result in a novel phenotype of sCJD, this is most likely to occur first and to a greater extent in the United Kingdom than in other countries. The analyses in this study do not suggest a change in the characteristics of sCJD in the United Kingdom compared with other countries. Although the phenotype of BSE infection in individuals with an MV or VV background cannot be predicted, to date there is no evidence of a novel phenotype of sCJD in Europe related to BSE infection.

Acknowledgment

The authors thank the following for their assistance and participation: in Australia, C.L. Masters, A. Boyd, V. Lewis, and J. Lee; in Austria, Drs. Christa Jarius, Ellen Gelpi, Christine Haberler, Thomas Ströbel, and Till Voigtländer, and Dita Drobna, Helga Flicker, Brigitte Millan-Ruiz, and Monika Richter; in Canada, Drs. C. Bergeron, M. Coulthart, N. Cashman, and D. Westaway; in France, reporting physicians and members of the Reseau National de surveillance de maladies de Creutzfeldt–Jakob et maladies apparentees; in Germany, reporting physicians, Maja Schneider-Dominico for help in coordination of surveillance, and Drs. Otto Windl and Walter Sculz-Schaeffer; in Italy, S. Almonti, V. Mellina, and L. Ingrosso for advice and help with data collection; in the Netherlands, **c**olleagues at the Department of Neurology at the Academic Medical Centre, Amsterdam and the Department of Pathology at the University Medical Centre, Utrecht; in Spain, reporting physicians and members of the Spanish TSE study group at Consejo Interterritorial and co-workers at CNE and ISCIII; in the UK, the staff at the National CJD Surveillance Unit, James Ironside for neuropathologic expertise, and clinicians for their cooperation with the study.

References

1. Prusiner SB. Prions. Proc Natl Acad Sci USA 1998;95:13363–13383.
2. Will RG, Ironside JW, Zeidler M, et al. A new variant of Creutzfeldt–Jakob disease in the UK. Lancet 1996;347:921–925.
3. Will RG, Alperovitch A, Poser S, et al. Descriptive epidemiology of Creutzfeldt–Jakob disease in six European countries, 1993–1995. Ann Neurol 1998;43:763–767.
4. Bruce ME, Will RG, Ironside JW, et al. Transmissions to mice indicate that "new variant" CJD is caused by the BSE agent. Nature 1997;389: 498–501.
5. Scott MR, Will RG, Ironside J, et al. Compelling transgenetic evidence for transmission of bovine spongiform encephalopathy prions to humans. Proc Natl Acad Sci USA 1999;96:15137–15142.
6. World Health Organisation. WHO manual for strengthening diagnosis and surveillance of Creutzfeldt–Jakob disease. Geneva: WHO, 1998:1–75.
7. Parchi P, Giese A, Capellari S, et al. Classification of sporadic Creutzfeldt–Jakob disease based on molecular and phenotypic analysis of 300 subjects. Ann Neurol 1999;46:224–233.
8. Brandel J-P, Preece M, Brown P, et al. A. Distribution of codon 129 genotype in human growth hormone-treated CJD patients in France and the UK. Lancet 2003;362:128–130.
9. Brown P, Cathala F, Gajdusek DC. Creutzfeldt–Jakob disease in France: III. Epidemiological study of 170 patients dying during the decade 1968–1977. Ann Neurol 1979;6:438–446.
10. Will RG, Matthews WB. A retrospective study of Creutzfeldt–Jakob disease in England and Wales 1970–79 I: clinical features. J Neurol Neurosurg Psychiatry 1984;47:134–140.
11. Kmietowicz Z. United Kingdom needs to double the number of neurologists. Br Med J 2001;322:1508.
12. Will RG, Alpers MP, Dormont D, et al. Infectious and sporadic prion diseases. In: Prusiner SB, ed. Prion biology and diseases. New York: Cold Spring Harbor Laboratory Press, 1999:465–507.
13. Lee H-S, Sambuughin N, Cervenakova L, et al. Ancestral origins and worldwide distribution of the *PRNP* 200K mutation causing familial Creutzfeldt–Jakob disease. Am J Hum Genet 1999;64:1063–1070.
14. Mitrova E, Bronis M. "Clusters" of CJD in Slovakia: the first statistically significant temporo-spatial accumulations of rural cases. Eur J Epidemiol 1991;7:450–456.
15. D'Alessandro M, Petraroli R, Ladogana A, et al. High incidence of Creutzfeldt–Jakob disease in rural Calabria, Italy. Lancet 1998;352: 1989–1990.
16. Euro-CJD Group. Genetic epidemiology of Creutzfeldt–Jakob disease in Europe. Rev Neurol (Paris) 2001;157:633–637.
17. Dagvadori A, Petersen RB, Lee H-S, et al. Spontaneous mutations in the prion protein gene causing transmissible spongiform encephalopathy. Ann Neurol 2002;53:355–359.
18. Glatzel M, Rogivue C, Ghani A, et al. Incidence of Creutzfeldt–Jakob disease in Switzerland. Lancet 2002;360:139–141.
19. Alperovitch A, Will RG. Predicting the size of the vCJD epidemic in France. CR Biol 2002;325:33–36.
20. Venters GA. New variant Creutzfeldt–Jakob disease: the epidemic that never was. Br Med J 2001;323:858–861.
21. La Bella V, Collinge J, Pocchiari M, et al. Variant Creutzfeldt–Jakob disease in an Italian woman. Lancet 2002;360:997–998.
22. Wiersma S, Cooper S, Knight R, et al. Probable variant Creutzfeldt–Jakob disease in a US resident—Florida 2002. MMWR 2002;51:927–929.
23. Asante EA, Linehan JM, Desbruslais M, et al. BSE prions propagate as either variant CJD or sporadic CJD-like prion strains in transgenic mice expressing human prion protein. EMBO J 2002;21:6358–6366.
24. Casalone C, Zanusso G, Acutis P. Identification of a second bovine amyloidotic spongiform encephalopathy: molecular similarities with sporadic Creutzfeldt–Jakob disease. Proc Natl Acad Sci USA 2004;101: 3065–3070.

Hum Genet (2005) 118: 166–174
DOI 10.1007/s00439-005-0020-1

ORIGINAL INVESTIGATION

**Gábor G. Kovács · Maria Puopolo · Anna Ladogana
Maurizio Pocchiari · Herbert Budka
Cornelia van Duijn · Steven J. Collins · Alison Boyd
Antonio Giulivi · Mike Coulthart
Nicole Delasnerie-Laupretre · Jean Philippe Brandel
Inga Zerr · Hans A. Kretzschmar
Jesus de Pedro-Cuesta · Miguel Calero-Lara
Markus Glatzel · Adriano Aguzzi · Matthew Bishop
Richard Knight · Girma Belay · Robert Will
Eva Mitrova**

Genetic prion disease: the EUROCJD experience

Received: 18 March 2005 / Accepted: 15 June 2005 / Published online: 27 September 2005

Abstract A total of 10–15% of human transmissible spongiform encephalopathies (TSEs) or prion diseases are characterised by disease-specific mutations in the prion protein gene (*PRNP*). We examined the phenotype, distribution, and frequency of genetic TSEs (gTSEs) in different countries/geographical regions. We collected standardised data on gTSEs between 1993 and 2002 in the framework of the EUROCJD collaborative

Gábor G. Kovács and Maria Propolo Contributed equally

G. G. Kovács · H. Budka
Austrian Reference Centre for Human Prion Diseases (OERPE) and Institute of Neurology, Medical University AKH 4J, Waehringer Guertel 18-20, 1097 Vienna, Austria

M. Puopolo · A. Ladogana · M. Pocchiari
Department of Cell Biology and Neurosciences, Istituto Superiore di Sanità, Viale Regina Elena 299, 00161 Rome, Italy

C. van Duijn
Department of Epidemiology and Biostatistics, Erasmus MC, PO Box 1738, 3000 DR, Rotterdam, The Netherlands

S. J. Collins · A. Boyd
Department of Pathology, The University of Melbourne, Parkville, Victoria, 3052 Australia

A. Giulivi
Blood Safety Surveillance and Health Care Acquired Infections Division, The Centre for Infectious Disease Prevention and Control, LCDC Building, PL 0601E2, Tunney's Pasture, Ottawa, ON, K1A 0L2 Canada

M. Coulthart
National Laboratory for Host Genetic and Prion Diseases, NML, PHAC, Health, Winnipeg, MB, Canada

N. Delasnerie-Laupretre · J. P. Brandel
U.360 INSERM, Hopital de la Salpetriere, 75651 Paris, Cedex 13, France

I. Zerr
Department of Neurology, Georg-August-Universität Göttingen, Robert-Koch Strasse 40, 37075 Gottingen, Germany

H. A. Kretzschmar
Institute of Neuropathology, University of Munich, Marchioninistr. 17, 81377 Munich, Germany

J. de Pedro-Cuesta
Departamento de Epidemiologia Aplicada, Instituto de Salud Carlos III, Centro Nacional de Epidemiologia, Calle Sinesio Delgado 6, 28029 Madrid, Spain

M. Calero-Lara
Centro National de Microbiologia Unidad de Encefalopatias Espongiformes, Ctra Majadakonda—Pozuelo km2, 28220 Majadakonda, Madrid, Spain

M. Glatzel · A. Aguzzi
Swiss National Reference Centre for Prion Diseases, University Hospital of Zurich, Schmelzbergstrasse 12, CH-8091 Zurich, Switzerland

M. Bishop · R. Knight
National CJD Surveillance Unit, Western General Hospital, Edinburgh, EH4 2XU UK

G. Belay · R. Will · E. Mitrova (✉)
Institute of Preventive and Clinical Medicine, Research Base of Slovak Medical University, National Reference Centre of prion Diseases, Limbova 14, 833 01 Bratislava, Slovakia
E-mail: eva.mitrova@szu.sk
Tel.: +421-2-59-36-9564
Fax: +421-2-59-36-9585

surveillance project. Our results show that clinicopathological phenotypes include genetic Creutzfeldt–Jakob disease (gCJD), fatal familial insomnia (FFI), and Gerstmann–Sträussler–Scheinker disease (GSS). Genetic TSE patients with insert mutation in the *PRNP* represent a separate group. Point and insertional mutations in the *PRNP* gene varies significantly in frequency between countries. The commonest mutation is E200K. Absence of a positive family history is noted in a significant proportion of cases in all mutation types (12–88%). FFI and GSS patients develop disease earlier than gCJD. Base pair insertions associated with the Creutzfeldt–Jakob disease (CJD) phenotype, GSS, and FFI cases have a longer duration of illness compared to cases with point mutations and gCJD. Cerebrospinal fluid 14-3-3 immunoassay, EEG, and MRI brain scan are useful in the diagnosis of CJD with point mutations, but are less sensitive in the other forms. Given the low prevalence of family history, the term "gTSE" is preferable to "familial TSE". Application of genetic screening in clinical practice has the advantage of early diagnosis and may lead to the identification of a risk of a TSE.

Keywords Prion protein gene · Creutzfeldt-Jakob disease · Fatal familial insomnia · Gerstmann-Sträussler-Scheinker disease · Point mutation · Insertional mutation

Introduction

Human transmissible spongiform encephalopathies (TSEs) or prion diseases are characterised by neurological and psychiatric symptoms and a progressive fatal course. Accumulation in the central nervous system (CNS) of the pathological prion protein (PrP^{Sc}) is a common disease marker (Prusiner 2001). The most frequent human TSE is Creutzfeldt–Jakob disease (CJD). The majority of cases (85%) present as a sporadic disorder (sCJD) without defined aetiology (Masters et al. 1979; WHO 2003). Acquired forms, including iatrogenic CJD due to transmission of infection in the course of medical or surgical treatment, and variant CJD (vCJD), which has been linked to infection with bovine spongiform encephalopathy, are less frequent (Masters et al. 1979; Prusiner 2001; WHO 2003). The familial occurrence of cases has been reported with a broad range of frequency: 6% of TSE cases in France (Brown et al. 1979), 25.5% in Israel (Kahana et al. 1974), 26% in Chile (Galvez et al. 1980), 53.6% in Slovakia (Mitrova and Belay 2002), and world-wide 15% (Masters et al. 1979).

Current clinical and neuropathological diagnostic criteria distinguish familial or genetic TSEs (gTSEs), including familial/genetic CJD (gCJD), fatal familial insomnia (FFI), and Gerstmann–Sträussler–Scheinker disease (GSS) (Budka et al. 1995; Prusiner 2001; WHO 2003). Experimental transmissibility of all the major subtypes has been established, albeit not with all mutations (Masters et al. 1981; Tateishi et al. 1979, 1995). In gTSEs, disease-specific point or insertional mutations in the prion protein gene (*PRNP*) have been demonstrated (Goldfarb et al. 1990a, b, 1992; Goldgaber et al. 1989; Haltia et al. 1991; Owen et al. 1989), with individual *PRNP* mutations showing variable geographical distribution and frequency. While certain mutations are rare (Kovacs et al. 2002), the E200K mutation has been reported not only in Europe but also in Chile, Israel, Japan, and USA (Goldfarb et al. 1990a, b; Goldgaber et al. 1989; Miyakawa et al. 1998). Geographic or ethnic clusters of cases of gTSEs have been found in Israel, Slovakia, Chile, and Italy (Chapman et al. 1994; D'Alessandro et al. 1998; Kahana et al. 1974; Mayer et al. 1977; Mitrova and Belay 2002; Mitrova and Bronis 1991).

In parallel with the increasing numbers of *PRNP* mutations, it has been recognised that, unexpectedly, not all patients with *PRNP* mutations appear to have affected family members (Chapman et al. 1994; D'Alessandro et al. 1998; EuroCJD group 2001; Goldman et al. 2004; Mitrova and Belay 2002). Therefore the terms "familial", "hereditary", or "inherited" TSE may not be appropriate in cases without a family history and the inclusive term "genetic TSE" may be preferable for cases associated with a mutation, whether or not there is a family history.

The negative family history in some gTSE cases and the identification of "healthy" carriers has drawn attention to the issue of penetrance, i.e., the proportion of carriers who will eventually develop the disease (Chapman et al. 1994; D'Alessandro et al. 1998; Goldfarb et al. 1990a, b; Mitrova and Belay 2002). Penetrance of the E200K mutation shows considerable variability. While in Israeli carriers, penetrance appears to be almost complete (89%), in Slovakian and Italian E200K carriers, penetrance is partial (54–59%) (Chapman et al. 1994; D'Alessandro et al. 1998; Goldfarb et al. 1990a, b; Mitrova and Belay 2002).

The EUROCJD project, funded by the European Commission, started in 1993 and compares data from national registries in Australia, Austria, Canada, France, Germany, Italy, The Netherlands, Slovakia, Spain, Switzerland, and the UK. The present study analyses the EUROCJD data on gTSE cases. Recently clinicopathological data of more than 500 published genetic cases of the literature has been reviewed (Kovacs et al. 2002) and some of the data on genetic epidemiology of CJD in Europe has been published (EuroCJD group 2001). The present paper includes standardised data from a large number of cases not previously reported in the context of a study carried out over a period of years in a defined population. Our aims are: (1) to describe the distribution and frequency of gTSEs, (2) to define and describe specific features of subgroups of gTSEs, (3) to contribute to a better understanding on how mutations and polymorphisms of *PRNP* influence clinical phenotypes, and (4) to assess the terms genetic and familial according to epidemiological and molecular biological data.

Patients and methods

The EUROCJD database contains data on sporadic, variant, iatrogenic, and gTSE cases collected between 1993 and 2002 (for detailed methodology see Ladogana et al. 2005a). In this paper we have analysed data of 455 gTSE cases from the following groups: gCJD cases (including patients with *PRNP* analysis and those with no available *PRNP* analysis but positive family history for TSE), FFI, GSS, and gTSE patients carrying base pair insertions (insert gTSE): referred to in previous publications as BPI (Kovacs et al. 2002) because these mutations are associated with repeat base pair insertions in the octarepeat region. No deletions in this region were identified in this study. We evaluated E200K gCJD and V210I gCJD separately as there were sufficient numbers of cases to allow statistical analyses. Cases of gCJD without either an E200K or V210I mutation are classified as "other CJD". Cases were classified either as *definite* or *probable* according to recent surveillance criteria (WHO 2003), which for the diagnosis of "familial" CJD require definite or probable CJD in the index case and a first-degree relative or a neuropsychiatric disorder in association with a *PRNP* mutation.

Statistical analysis

Differences among distinct forms of gTSE cases with respect to age at onset or clinical duration were assessed by Mann–Whitney test; variation in clinical signs by the chi-square test or the Fisher's exact probability test. The Bonferroni correction for multiple testing was adopted within the six subgroups of gTSE (E200K, V210I, and other forms of gCJD, GSS, FFI, and insert mutations) at an experimental probability type 1 error of 0.05.

Age at onset was given as mean, standard deviation (SD), and range; clinical duration as median and half interquartile range (IQR) because of highly skewed distribution of data. Box-plots were used for the graphic representations of continuous variables. Statistical analyses were performed using BMDP and STATA.

Crude and sex-specific mortality rates were calculated using as denominator populations data for 1998 provided from National or Federal Statistics Bureau of participating countries. For Canada, population data (2001) were taken from the Canadian Statistics website. The annual mortality rates were calculated using data collected from 1999–2002 when the surveillance system was well established in all countries.

Results

Distribution of cases and mutations

The distribution and frequency of *PRNP* mutations among countries participating in the study are summarised in Table. 1 and 2. The proportion of all gTSE cases with respect to the total number of TSE cases (including sporadic, iatrogenic, and variant CJD) was 10.2%, but, this varied significantly among participating countries ranging from 69.5% in Slovakia to 1.2% in Switzerland. The overall annual mortality rate of gTSE cases was 0.17 patients per million people for the period 1999–2002. It is of note that Slovakia had an overall mortality rate for gTSE diseases 3.5 times that of the second highest country (Italy). However, while the E200K mutation was the only mutation present in the Slovak population, several mutations were present in the Italian population, including the E200K and V210I gCJD, FFI, and GSS. Switzerland reported a single

Table 1 EUROCJD 1993–2002: number of reported cases in each EUROCJD country

	All genetic TSE diseases				gCJD	GSS	FFI	Insert
	n	gTSE (%)	gTSE (%) with respect to all TSE in each country	Mortality rates (million people)[a]				
Australia	22/215	4.8	10.2	0.14	14	3	4	1
Austria	13/90	2.9	14.4	0.28	9	0	3	1
Canada	16/189	3.5	8.5	0.12	7	9	0	0
France	84/938	18.5	9.0	0.18	68	5	6	5
Germany	68/900	14.9	7.6	0.13	31	8	17	12
Italy	115/662	25.3	17.4	0.30	94	8	10	3
Netherlands	3/142	0.7	2.1	0.02	1	0	0	2
Slovakia	41/59	9.0	69.5	1.07	41	0	0	0
Spain	44/429	9.7	10.3	0.23	18	0	25	1
Switzerland	1/85	0.2	1.2	0.04	1	0	0	0
UK	48/732	10.5	6.6	0.07	11	19	1	17
Total	455/4,441	–	–	0.17	295	52	66	42
% Total	–	100	10.2	–	64.9	11.4	14.5	9.2

Abbreviations: gTSE, genetic transmissible spongiform encephalopathy; gCJD, genetic Creutzfeldt–Jakob disease; FFI, fatal familial insomnia; GSS, Gerstmann–Sträussler–Scheinker disease; Insert, gTSE patients with insert mutations.
[a] For the period 1999–2002.

Table 2 EUROCJD 1993–2002: number of reported cases and distribution of *PRNP* mutations in each EUROCJD country

Country	gCJD											
	P105T-129?	N171S-129V	D178N-129V	V180I-129M	T188A-129M	E196K-129M/V	E200K-129M/V	V203I-129M	R208H-129M	V210I-129M	E211Q-129M	NS
Australia	1	–	–	–	1	–	8	–	–	2	–	2
Austria	–	–	1	–	–	1	5	–	–	1	–	1
Canada	–	–	2	–	–	–	4	1	–	–	–	–
France	–	1	8	1	–	1	46	3	–	6	2	–
Germany	–	–	–	–	2	3	15	–	1	9	1	–
Italy	–	–	–	–	–	–	35	1	1	50	1	6
Netherlands	–	–	1	–	–	–	–	–	–	–	–	–
Slovakia	–	–	–	–	–	–	40	–	–	–	–	1
Spain	–	–	4	–	–	–	14	–	–	–	–	–
Switzerland	–	–	–	–	–	–	1	–	–	–	–	–
UK	–	–	–	–	–	–	7	–	–	1	–	3
Total	1	1	16	1	3	5	175	5	2	69	4	13
% Total	0.2	0.2	3.5	0.2	0.7	1.1	38.5	1.1	0.4	15.2	0.9	2.9

Abbreviations: NS, not specified; others as in Table 1.

gTSE patient for the period 1996–2002 while the Netherlands had the lowest mortality rate for gTSE diseases. More than 90% of FFI and 75% of GSS patients underwent post-mortem examination and were classified as definite gTSE cases, while 52% of V210I gCJD patients did not undergo autopsy (see Table 3) and were classified as probable gTSE based on clinical and laboratory features. There was an excess of females in gCJD (more pronounced for E200K than V210I or "other" gCJD patients) and, to a lesser extent, in GSS or insert gTSE cases, and an excess of males in FFI cases (Table 3). Data on the polymorphic codon 129 of the *PRNP* gene were available in 87% of all cases (95% in E200K, 97% in V210I, 75% in "other" gCJD, 95% in FFI, 56% in GSS, and 79% in insert gTSE). The distribution of the polymorphic codon 129 in all forms of gTSE is shown in Table 3. Differences between codon 129 distribution in controls (39% methionine homozygous (MM), 50% heterozygous (MV), 11% valine homozygous (VV), Alperovitch et al. 1999) and in individual gTSE groups have been evaluated by chi-sqared test with the following results: E200K gCJD, V210I gCJD and FFI, $P < 0.0001$, "other" gTSE, $P = 0.0010$, Insert gTSE, $P = 0.0577$ and GSS, $P = 0.3825$. The majority of *PRNP* mutations co-segregate with methionine at the polymorphic codon 129 (see Table 2). Thus, the majority of gTSE patients overall were either MM (67.9%) or MV (25.8%) with only a few valine homozygotes (6.3%).

Family history

About 47% of all gTSE cases were reported to have no TSE or other neurological disorder in family members. Almost 90% of V210I gCJD patients had a negative family history implying that a correct classification of these cases would not have been possible without *PRNP* genetic analysis. Interestingly, a positive family history for TSE was reported in only about two-thirds of GSS patients (Table 3).

Age at onset

There were significant differences in the age at onset in gTSE forms (Fig. 1a). Patients with FFI (mean 51.2 years, SD 12.3, range 19–83) and GSS (51.6, 12.8, 26–87) developed disease significantly earlier than E200K gCJD (60.4, 10.2, 33–84, $p < 0.0001$), V210I gCJD (59.3, 9.8, 39–82, $p = 0.0001$ and 0.0009, respectively), and "other" gCJD cases (60.4, 14.7, 31–87, $p = 0.0004$, 0.0036). There was no significant difference in the age at onset between FFI and GSS patients and among distinct forms of gCJD. Age at onset in patients with insert mutations (57.2, 14.8, 32–85) did not significantly differ from that of gCJD, GSS, or from FFI ($p = 0.0193$) after Bonferroni's correction. The youngest age at onset was 19 years (FFI, MM at codon 129), while the two oldest were 87 years (gCJD with missing information on *PRNP* mutation, and A117V GSS, VV at codon 129). The age at onset was earlier in valine homozygotes in comparison to methionine homozygotes ($P = 0.0001$) and, to a lesser extent, in MV vs MM ($P = 0.0059$, not significant after Bonferroni's correction) in "other" gCJD patients. The codon 129 polymorphism did not significantly influence the age at onset in all the other forms of gTSEs (Table 4). Gender did not have any significant effect on the age at onset (data not shown).

Duration of illness

The duration of disease varied between different forms of gTSE (Fig. 1b). Clinical durations of E200K (median 5.0 months, IQR 2.5) and V210I (4.0, 1.5) gCJD patients were shorter than "other" gCJD (7.0, 7.0, $p = 0.0031$ and 0.0012, respectively), FFI (12.4, 4.2, $P < 0.0001$ and 0.0001), GSS (40.0, 25.0, $P < 0.0001$ and 0.0001) and insert gTSE (13.0, 35.5, $P = 0.0001$ and 0.0001). GSS patients had a longer survival than FFI ($P < 0.0001$) and "other" gCJD ($P < 0.0001$) patients.

GSS				FFI		Insert								
P102L-129M	A117V-129V	G131V-129M	NS	D178N-129M	NS	24-129M	48-129M	72-129?	96-129M/V	120-129M/V	144-129M	168-129M	192-129M/V	NS
1	–	1	1	3	1	–	–	–	–	–	–	1	–	–
–	–	–	–	3	–	–	–	–	–	–	1	–	–	–
1	–	–	8	–	–	–	–	–	–	–	–	–	–	–
3	2	–	–	6	–	2	–	–	1	–	1	–	1	–
3	5	–	–	17	–	1	–	1	2	8	–	–	–	–
8	–	–	–	10	–	2	–	–	1	–	–	–	–	–
–	–	–	–	–	–	1	–	–	–	–	–	–	1	–
–	–	–	–	–	–	–	–	–	–	–	–	–	–	–
–	–	–	–	24	1	–	1	–	–	–	–	–	–	–
–	–	–	–	–	–	–	–	–	–	–	–	–	–	–
8	5	–	6	1	–	–	–	–	1	4	9	1	–	2
24	12	1	15	64	2	6	1	1	5	12	11	2	2	2
5.3	2.6	0.2	3.3	14.1	0.4	1.3	0.2	0.2	1.1	2.6	2.4	0.4	0.4	0.4

The longest duration of illness was 216 months in an insert gTSE case, the group with the highest variability in clinical duration. However, in all other groups there were a few cases with an exceptional long clinical duration for their group (outliers in Fig. 1b). This included 11 cases in E200K gCJD (five MM at codon 129: 16, 19, 20 and two 24 months; 6 MV: 17, two 18, 19, and two 36 months), four cases in V210I gCJD (MM: 11, 15, 31, and 34 months), four in "other" gCJD (43 months, D178N-129VV, 46 months, V180I-129MV, 52 months, V203I-129MV, 59 months, missing mutation and codon 129), and one in FFI (MV: 97 months), and two in insert gTSE (216 months 120 bp insert-129MV, and 192 months 168 bp insert-129 MV).

Investigations

Data on CSF 14-3-3 immunoassay were available in 57% of cases (60% in E200K, 72% in V210I, 59% in "other" gCJD, 58% in FFI, 31% in GSS, and 50% in insert gTSE), EEG in 82% of cases (90% in E200K, 96% in V210I, 86% in "other" gCJD, 77% in FFI, 50% in GSS, and 67% in insert gTSE), and MRI brain scan in 43% of cases (38% in E200K, 67% in V210I, 31% in "other" gCJD, 52% in FFI, 33% in GSS, and 36% in insert gTSE). In the various forms of gTSEs, there were significant differences in the frequency in positivity of the 14-3-3 test in the CSF ($P < 0.0001$, Fisher's exact test), the EEG ($P < 0.0001$, chi-squared test) and the MRI brain scan ($P = 0.0038$, Fisher's exact test) (WHO 2003). A positive 14-3-3 test was present in the majority of gCJD patients and insert gTSE patients (Fig. 2). A typical EEG (WHO 2003) was more frequent in gCJD than in other forms of gTSE diseases. About 50% of GSS cases had a positive 14-3-3 test in the CSF, while the EEG showed typical pseudoperiodic activity in only 2 of 26 patients with available information (Fig. 2). In GSS and FFI, neither the EEG nor the 14-3-3 tests were of help in the clinical diagnosis of disease. MRI brain scan was performed in a small proportion of cases and was positive (WHO 2003) in about 50% of E200K and "other" gCJD and in about 30% of GSS and insert gTSE cases. In FFI and V210I gCJD patients, the MRI brain scan was positive in only 18 and 15%, respectively.

Classification of protease-resistant PrP

Results were available in only 43 cases. Twenty-two E200K, 6 V210I gCJD, 9 "other" gCJD, 1 FFI, 2 GSS, and 3 insert gTSE cases (Table 5). Thirty-four patients had type 1 protease-resistant prion protein (according to the system described by Parchi et al.) (Parchi et al. 1999) in brain samples, six had type 2A, and three patients had both type 1 and type 2A.

Discussion

EUROCJD has data on 23 specified *PRNP* mutations. Currently more than 30 mutations have been reported in the world literature, but many of these mutations are very rare or are restricted to specific populations (Kovacs et al. 2002). Comparison of genetic and sporadic TSEs shows striking differences in their frequency and geographic distribution. While sCJD has a similar incidence in all participating countries (Ladogana et al. 2005a), *PRNP* mutations show significant variability. Some mutations (P105L, N171S, V180I, T188A, E196K, R208H, V203I, 168 BPI) are extremely rare, while E200K is recognised in 9 out of 10 reporting countries. The high absolute and proportionate incidence of the V210I mutation in Italy is striking; most affected families lived in three adjacent areas (Ladogana et al. 2005b). It is a pertinent point that a single report on the N171S mutation suggested a psychiatric phenotype, whereas in our series this mutation was associated with CJD (Samaia et al. 1997). A high proportion of all cases in each category underwent genetic analysis. The three lowest percentages of *PRNP* tests were 42.3% (Canada), 32% (Australia) and 31.7% (Netherlands). The variability in the frequency of mutations countrywise is unexpected and is not related to variation countrywise in

Table 3 Characteristics of genetic transmissible spongiform encephalopathies

Forms of gTSE	*n*	Percentage of definite cases (*n*)	Gender			Codon 129 polymorphism			Percentage of positive family history for TSE (available data)
			F	M	F/M ratios of mortality rates[a]	MM % (*n*)	MV % (*n*)	VV % (*n*)	
E200K gCJD	175	68.0 (119)	107	68	1.69	78.3 (130)	19.9 (33)	1.8 (3)	49.1 (114)
V210I gCJD	69	47.8 (33)	39	30	1.42	73.1 (49)	26.9 (18)	–	12.3 (57)
Other gCJD	51	58.8 (30)	28	23	1.38	36.8 (14)	34.2 (13)	29.0 (11)	75.9 (29)
FFI	66	92.4 (61)	29	37	0.62	71.4 (45)	28.6 (18)	–	88.0 (50)
GSS	52	76.9 (40)	29	23	1.17	51.7 (15)	34.5 (10)	13.8 (4)	69.7 (33)
Insert gTSE	42	69.0 (29)	21	21	1.23	48.5 (16)	30.3 (10)	21.2 (7)	48.0 (25)

Abbreviations: gTSE, genetic transmissible spongiform encephalopathy; gCJD, genetic Creutzfeldt–Jakob disease; FFI, fatal familial insomnia; GSS, Gerstmann–Sträussler–Scheinker disease; Insert, gTSE patients with insert mutations.
[a] For the period 1999–2002.

the availability of genetic data. Focal accumulations of genetic patients (Mayer et al. 1977) may be due to genetic isolation but the explanation for the overall inter-country variability in this study is uncertain.

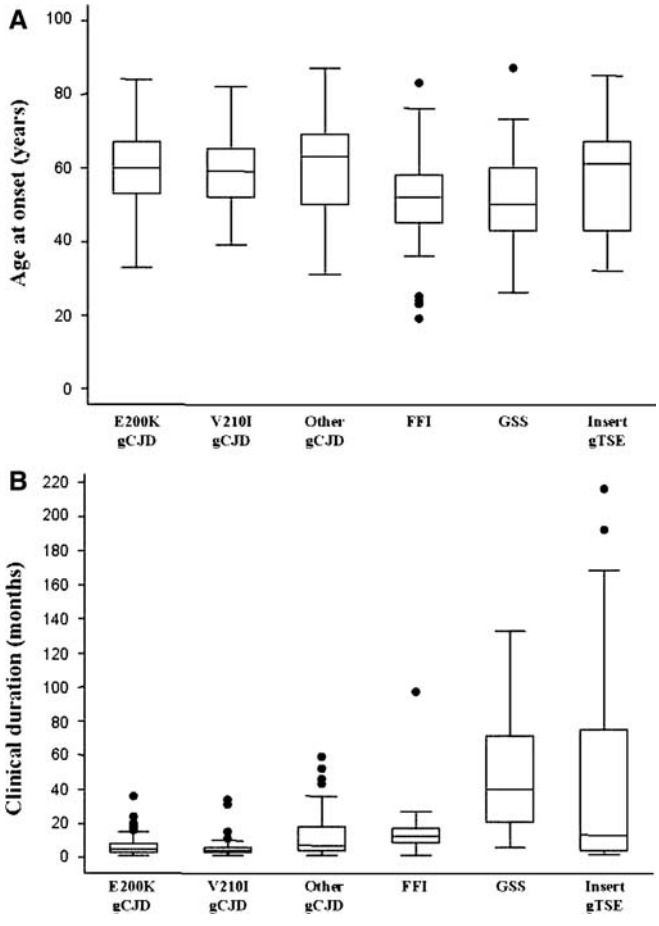

Fig. 1 *Box*- and *whisker-plots* of age at onset (**a**) and clinical duration (**b**) in different forms of genetic TSE diseases. The *line in the middle of the box* represents median. The *box* extends from the 25th percentile ($x_{[25]}$) to the 75th percentile ($x_{[75]}$), the so-called interquartile range (*2IQR*). The *lines emerging from the box* are called the *whiskers* and they extend to the upper and lower adjacent values. The upper adjacent value is defined as the largest data point less than or equal to $x_{[75]} + 1.52$IQR. The lower adjacent value is defined as the smallest data point greater than or equal to $x_{[25]} - 1.52$IQR. *Filled circles* represent values more extreme than the adjacent values (referred to as outliers)

The ratio of female to male mortality rates in Table 3 indicates that there is an excess of females in all mutations except FFI. Taking account of varying distribution by age, the weighted female to male ratio (1.59 for E200K, 1.62 for V210I, 1.90 for other gCJD, 1.43 for GSS, 1.62 for insert gTSE, and 0.62 for FFI) strongly confirms the excess of female cases in all forms of gCJD except FFI. Although consistent with similar findings in sporadic CJD (Ladogana et al. 2005a), the explanation for this gender bias in mortality is uncertain. Possible explanation include sex-linked genetic factors influencing disease expression, bias in case ascertainment linked to gender or differential susceptibility/exposure to a co-factor.

Clinical and laboratory parameters show considerable similarity between the most frequent gCJD (e.g., E200K mutation) and sCJD cases. Although gCJD cases with point mutations have an earlier mean age at death, there is no difference between gCJD cases with point mutations and sCJD in the mean duration of the disease (Alperovitch et al. 1999; Pocchiari et al. 2004). As in sCJD (Zerr et al. 2000), analysis of CSF 14-3-3 protein, EEG, and MRI is helpful in the diagnosis of gTSEs and

Table 4 Influence of codon 129 polymorphism of the *PRNP* gene in determining the age at onset

Forms of gTSE	Codon 129		
	Met/ Met mean (SD)	Met/Val mean (SD)	Val/Val mean (SD)
E200K gCJD	60.4 (10.8)	60.7 (8.6)	55.7 (9.0)
V210I gCJD	59.3 (9.7)	57.9 (9.8)	–
Other gCJD	70.9 (7.5)	56.2 (14.2)	48.1 (12.6)
FFI	50.8 (13.4)	52.5 (10.0)	–
GSS	54.0 (11.1)[a]	49.0 (12.1)	66.2 (17.9)
Insert gTSE	60.9 (14.0)[a]	56.2 (15.2)	62.7 (11.3)

Abbreviations: gTSE, genetic transmissible spongiform encephalopathy; gCJD, genetic Creutzfeldt–Jakob disease; FFI, fatal familial insomnia; GSS, Gerstmann–Sträussler–Scheinker disease; Insert, gTSE patients with insert mutations.
[a] Two patients had missing data on age at onset.

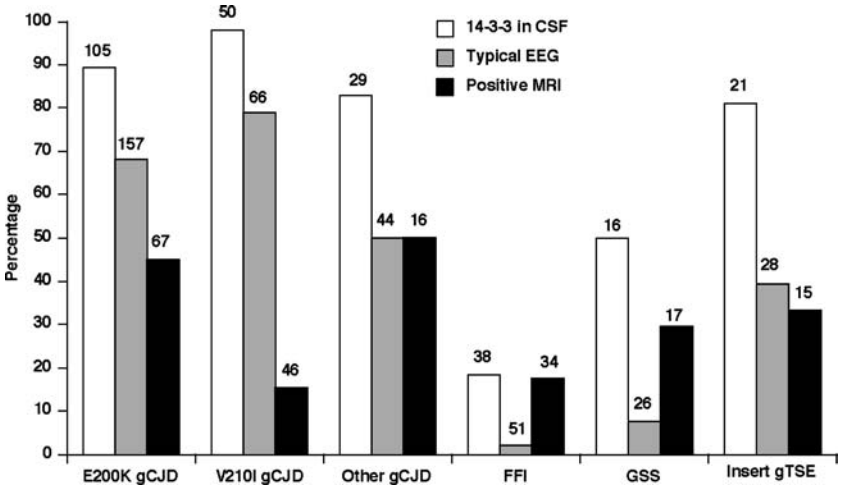

Fig. 2 Percentage of cases showing positive 14-3-3 protein in the CSF, typical EEG pattern, and positive MRI brain scan in different forms of genetic TSE disease. The number of patients with available data is shown on *top* of each column

in particular in gCJD cases with point mutations, while in other gTSE cases these laboratory examinations are less sensitive. Our data confirm previous studies that insertional mutations often present atypically with a relatively protracted duration of illness (although less protracted than a previous study which included larger numbers of cases and with a unique type of PrP immunoreactivity in the cerebellum (Kovacs et al. 2002; Vital et al. 1999).

We also demonstrate that, except for some specific mutations like D178N-129M, protease-resistant PrP may be variable within the same brain in some gTSEs as in sCJD (Puoti et al. 1999).

It is of great importance that a positive family history of a human TSE is absent in a high proportion of cases overall and with all the mutations. Although this has been reported previously by this group and others (EuroCJD group 2001; Goldman et al. 2004; Mitrova and Belay 2002), this is the first study to provide a detailed analysis of the frequency of a positive family history in a range of *PRNP* mutations. Possible explanations include lack of knowledge of the family history in the relatives of index cases, premature death in antecedents prior to the development of a TSE, and non-paternity. However, there must be some doubt that the very high frequency of a negative family history in this study can be explained by these mechanisms and there remains the possibility that a minority of mutations arise de novo (Dagvadorj et al. 2003) or that the mutations are not fully penetrant (Mitrova and Belay 2002).

As cases considered as sCJD often lack full-length *PRNP* analysis, accurate diagnosis of gTSEs may depend on more widespread genetic screening, particularly as some mutations, e.g., E200K and V210I, are associated with a phenotype indistinguishable from sCJD. The negative family history in a high proportion of cases indicates that mutations may be identified unexpectedly in cases thought to have sCJD or indeed some other neurological disorder and this may have important implications for other family members.

At present gTSEs are the only sub-group of human TSEs in which the diagnosis can be supported by genetic screening in life. There is the potential for early diagnosis and the risk of developing a TSE can be identified before the onset of disease in asymptomatic carriers. This may be an important advantage in the application of potential therapies as treatment could be instituted before severe and irreversible damage to the CNS occurs, or perhaps, as a means to prevent iatrogenic transmission of CJD from at-risk patients.

Table 5 Type of the pathological PrP in the brain of genetic TSE cases

PrP type	gCJD[a]								FFI[a]	GSS[a]	Insert[a]
	N171S	D178N	E196K	E200K	V203I	R208H	V210I	E211Q	D178N	P102L	
Type 1	–	2 VV	1 MM 1 MV	17 MM 1 MV	1 MM	1 MM	5 MM 1 MV	1 NA	–	2 MV	1 MV
Type 2A	1 VV	–	–	1 MV 1 VV	1 MV	–	–	–	–	–	1 VV
Type 1–2A	–	–	–	2 MM	–	–	–	–	–	–	1 MV
Type 2B	–	–	–	–	–	–	–	–	1 MV	–	–

Abbreviations: gTSE, genetic transmissible spongiform encephalopathy; gCJD, genetic Creutzfeldt–Jakob disease; FFI, fatal familial insomnia; GSS, Gerstmann–Sträussler–Scheinker disease; Insert, gTSE patients with insert mutations; MM, methionine homozygous; VV, valine homozygous; MV, heterozygous patients; NA, not available.

[a] Number of cases of codon 129 polymorphism.

The occurrence of asymptomatic carriers of *PRNP* mutations (Mitrova and Belay 2002) underlines the importance of genetic testing in all suspect cases of human TSEs and, in positive cases, relatives may be offered genetic testing, provided appropriate ethical protocols are followed. Although there may be incomplete penetrance and an absence of presymptomatic neuropathological changes or accumulation of disease-associated PrP (Sasaki et al. 2003), healthy carriers of *PRNP* mutations are at greater risk of developing a TSE and may be subject to restrictions, such as donating blood and tissues (e.g., cornea, dura mater), because of the risk of iatrogenic transmission.

It is not known why there is partial penetrance in some mutations, or why there is marked variability in clinical phenotype, including age at onset, both between and within pedigrees. There is a need to analyse events preceding the onset of clinical manifestation in carriers of *PRNP* mutations as possible triggering factors. In E200K, psychological stress (divorce, death of a close relative, retirement, loss of a job), complicated surgery with prolonged anaesthesia, serious accidents, or current infectious disease have been frequently noted (Brandel and Delasnerie-Laupretre 1997; Mitrova and Belay 2002).

In conclusion, the term gTSE, which includes gCJD, FFI, and GSS, is more appropriate than familial TSE for all patients with TSE-specific genetic marker, regardless of the number of affected family members, while familial TSE designates only genetic cases with other (one or more) TSE-affected relative. The distribution of gCJD is geographically heterogeneous. The codon 129 polymorphism influences phenotype. In gTSEs, *PRNP* analysis may allow early or pre-symptomatic diagnosis and this may be important if specific therapies become available. Further studies are required to identify whether *PRNP* mutations are sufficient in themselves to cause disease.

Acknowledgements This study was funded through an EU Concerted Action (BIOMED2 Contract No. BMH4-CT97-2216). *Australia*: The Australian National CJD Registry is funded by the Commonwealth Department of Health and Ageing. We are grateful to the following people involved in the Australian National CJD Registry: C.L. Masters, A. Boyd, G. Klug, and J. Lee. *Austria*: The Austrian Reference Centre for Human Prion Diseases (ÖERPE, Head: Prof. Herbert Budka) acknowledges the help of Drs Christa Jarius, Ellen Gelpi, Christine Haberler, Thomas Ströbel, and Till Voigtländer; DI Dita Drobna; and Ms. Helga Flicker, Brigitte Millan-Ruiz, and Monika Richter. *Canada*: The Canadian Surveillance System is funded by Health Canada. Other collaborators on the project are Dr C Bergeron, neuropathologist (University of Toronto), Dr N Cashman, neurologist and one of the principal investigators for CJD-SS, Dr D Westaway, consulting scientist (University of Toronto). *France*: We would like to acknowledge all reporting physicians and the members of the Reseau National de surveillance de maladies de Creutzfeldt-Jakob et maladies apparentees. *Germany*: The German surveillance system is funded by the Federal Ministry of Health 9BMG, 325-4471-02/15. We are grateful to all reporting physicians throughout Germany who contributed to the German surveillance system and especially to Maja Schneider-Dominico for her excellent support in the coordination of surveillance. We also acknowledge the help of Drs Otto Windl and Walter Sculz-Schaeffer. *Italy*: We would like to acknowledge the Ministry of Health and the Istituto Superiore di Sanità for supporting the surveillance of CJD in Italy and S. Almonti, V. Mellina, and L. Ingrosso for help in collecting data and advice. *The Netherlands*: CJD surveillance in the Netherlands is funded by the Dutch Ministry of Health, Welfare, and Sports. We acknowledge the help of colleagues at the Department of Neurology at the Academic Medical Centre, Amsterdam and the Department of Pathology at the University Medical Centre, Utrecht. *Slovakia*: The Slovak Surveillance System was supported by the Slovak Ministry of Health and by grants from the European Union. We would like to acknowledge the help of Dr. Dana Slivarichová, Dr. Vladimíra Verchovodková, all reporting physicians and collaborating pathologists. *Spain*: We are grateful to all reporting physicians and to members of the Spanish TSE study group at Consejo Interterritorial and co-workers at CNE and ISCIII and laboratories, particularly to N. Cuadrado and J.Yague. *Switzerland*: This work was supported by the Kanton of Zurich and by grants from the European Union. The Swiss Reference Center for Prion Diseases is being funded by the Swiss Federal Office of Public Health. *UK*: The UK CJD Surveillance System is funded by the Department of Health and the Scottish Executive Health Department. We are grateful to all the members of staff at the National CJD Surveillance Unit and in particular to James Ironside for neuropathological expertise and to clinicians throughout the UK for their co-operation with the study.

References

Alperovitch A, Zerr I, Pocchiari M, Mitrova E, de Pedro Cuesta J, Hegyi I, Collins S, Kretzschmar H, van Duijn C, Will RG (1999) Codon 129 prion protein genotype and sporadic Creutzfeldt–Jakob disease. Lancet 353:1673–1674

Brandel JF, Delasnerie-Laupretre N (1997) Creutzfeldt–Jakob disease and stress. J Neurol 62:541

Brown P, Cathala F, Sadowsky D, Gajdusek DC (1979) Creutzfeldt–Jakob disease in France: III. Epidemiological study of 170 patients dying during the decade 1968–1977. Ann Neurol 6:438–446

Budka H, Aguzzi A, Brown P, Brucher JM, Bugiani O, Gullotta F, Haltia M, Hauw JJ, Ironside JW, Jellinger K et al (1995) Neuropathological diagnostic criteria for Creutzfeldt–Jakob disease (CJD) and other human spongiform encephalopathies (prion diseases). Brain Pathol 5:459–466

Chapman J, Ben-Israel J, Goldhammer Y, Korczyn AD (1994) The risk of developing Creutzfeldt–Jakob disease in subjects with the PRNP gene codon 200 point mutation. Neurology 44:1683–1686

Dagvadorj A, Petersen RB, Lee HS et al (2003) Spontaneous mutations in the prion protein gene causing transmissible spongiform encephalopathy. Ann Neurol 52:355–359

D'Alessandro M, Petraroli R, Ladogana A, Pocchiari M (1998) High incidence of Creutzfeldt–Jakob disease in rural Calabria, Italy. Lancet 352:1989–1990

EuroCJD group (2001) Genetic epidemiology of Creutzfeldt–Jakob disease in Europe. Rev Neurol (Paris) 157:633–637

Galvez S, Masters C, Gajdusek C (1980) Descriptive epidemiology of Creutzfeldt–Jakob disease in Chile. Arch Neurol 37:11–14

Goldfarb LG, Korczyn AD, Brown P, Chapman J, Gajdusek DC (1990a) Mutation in codon 200 of scrapie amyloid precursor gene linked to Creutzfeldt–Jakob disease in Sephardic Jews of Libyan and non-Libyan origin. Lancet 336:637–638

Goldfarb LG, Mitrova E, Brown P, Toh BK, Gajdusek DC (1990b) Mutation in codon 200 of scrapie amyloid protein gene in two clusters of Creutzfeldt–Jakob disease in Slovakia. Lancet 336:514–515

Goldfarb LG, Petersen RB, Tabaton M, Brown P, LeBlanc AC, Montagna P, Cortelli P, Julien J, Vital C, Pendelbury WW et al (1992) Fatal familial insomnia and familial Creutzfeldt–Jakob disease: disease phenotype determined by a DNA polymorphism. Science 258:806–808

Goldgaber D, Goldfarb LG, Brown P, Asher DM, Brown WT, Lin S, Teener JW, Feinstone SM, Rubenstein R, Kascsak RJ et al (1989) Mutations in familial Creutzfeldt–Jakob disease and Gerstmann–Straussler–Scheinker's syndrome. Exp Neurol 106:204–206

Goldman JS, Miller BL, Safar J, de Tourreil S, Martindale JL, Prusiner SB, Geschwind MD (2004) When sporadic disease is not sporadic: the potential for genetic etiology. Arch Neurol 61:213–216

Haltia M, Kovanen J, Goldfarb LG, Brown P, Gajdusek DC (1991) Familial Creutzfeldt–Jakob disease in Finland: epidemiological, clinical, pathological and molecular genetic studies. Eur J Epidemiol 7:494–500

Kahana E, Alter M, Braham J, Sofer D (1974) Creutzfeldt–Jakob disease: focus among Libyan Jews in Israel. Science 183:90–91

Kovacs GG, Trabattoni G, Hainfellner JA, Ironside JW, Knight RSG, Budka H (2002) Mutations of the human prion protein gene: phenotypic spectrum. J Neurol 249:1567–1582

Ladogana A, Puopulo M, Croes EA, Budka H, Jarius C, Collins S, Masters C, Sutcliffe T, Giulivi A, Alperovitch A, Delasnerie-Laupretre N, Brandel JP, Poser S, Kretzschmar H, Rietvald I, Mitrova E, De Pedro Cuesta J, Martinez-Martin P, Glatzel M, Aguzzi A, Knight RS, Ward H, Pocchiari M, van Duijn C, Will RG, Zerr I (2005a) Mortality from Creutzfeldt–Jakob disease and related disorders in Europe, Australia and Canada. Neurology 64:1586–1591

Ladogana A, Puopulo M, Poleggi D, Almonti S, Mellina V, Equestre M, Pocchiari M (2005b) High incidence of genetic human transmissible spongiform encephalopathies in Italy. Neurology 64:1592–1597

Masters CL, Harris JO, Gajdusek DC, Gibbs CJ Jr, Bernoulli C, Asher DM (1979) Creutzfeldt–Jakob disease: patterns of worldwide occurrence and the significance of familial and sporadic clustering. Ann Neurol 5:177–188

Masters CL, Gajdusek DC, Gibbs CJ Jr (1981) Creutzfeldt–Jakob disease virus isolations from the Gerstmann–Straussler syndrome with an analysis of the various forms of amyloid plaque deposition in the virus-induced spongiform encephalopathies. Brain 104:559–588

Mayer V, Orolin D, Mitrova E (1977) Cluster of Creutzfeldt–Jakob disease and presenile dementia. Lancet 2:256

Mitrova E, Belay G (2002) Creutzfeldt–Jakob disease with E200K mutation in Slovakia: characterization and development. Acta Virol 46:31–39

Mitrova E, Bronis M (1991) "Clusters" of CJD in Slovakia: the first statistically significant temporo-spatial accumulations of rural cases. Eur J Epidemiol 7:450–456

Miyakawa T, Inoue K, Iseki E, Kawanishi C, Sugiyama N, Onishi H, Yamada Y, Suzuki K, Iwabuchi K, Kosaka K (1998) Japanese Creutzfeldt–Jakob disease patients exhibiting high incidence of the E200K PRNP mutation and located in the basin of a river. Neurol Res 20:684–688

Owen F, Poulter M, Lofthouse R, Collinge J, Crow TJ, Risby D, Baker HF, Ridley RM, Hsiao K, Prusiner SB (1989) Insertion in prion protein gene in familial Creutzfeldt–Jakob disease. Lancet 1:51–52

Parchi P, Giese A, Capellari S, Brown P, Schulz-Schaeffer W, Windl O, Zerr I, Budka H, Kopp N, Piccardo P, Poser S, Rojiani A, Streichemberger N, Julien J, Vital C, Ghetti B, Gambetti P, Kretzschmar H (1999) Classification of sporadic Creutzfeldt–Jakob disease based on molecular and phenotypic analysis of 300 subjects. Ann Neurol 46:224–233

Pocchiari M, Puopolo M, Croes EA, Budka H, Gelpi E, Collins S, Lewis V, Sutcliffe T, Guilivi A, Delasnerie-Laupretre N, Brandel JP, Alperovitch A, Zerr I, Poser S, Kretzschmar HA, Ladogana A, Rietvald I, Mitrova E, Martinez-Martin P, de Pedro-Cuesta J, Glatzel M, Aguzzi A, Cooper S, Mackenzie J, van Duijn CM, Will RG (2004) Predictors of survival in sporadic Creutzfeldt–Jakob disease and other human transmissible spongiform encephalopathies. Brain 127:2348–2359

Prusiner SB (2001) Shattuck lecture—neurodegenerative diseases and prions. N Engl J Med 344:1516–1526

Puoti G, Giaccone G, Rossi G, Canciani B, Bugiani O, Tagliavini F (1999) Sporadic Creutzfeldt–Jakob disease: co-occurrence of different types of PrP(Sc) in the same brain. Neurology 53:2173–2176

Samaia HB, Mari JJ, Vallada HP, Moura RP, Simpson AJ, Brentani RR (1997) A prion-linked psychiatric disorder. Nature 390:241

Sasaki K, Doh-Ura K, Furuta A, Nakashima S, Morisada Y, Tateishi J, Iwaki T (2003) Neuropathological features of a case with schizophrenia and prion protein gene P102L mutation before onset of Gerstmann–Straussler–Scheinker disease. Acta Neuropathol 106:92–96

Tateishi J, Ohta M, Koga M, Sato Y, Kuroiwa Y (1979) Transmission of chronic spongiform encephalopathy with kuru plaques from humans to small rodents. Ann Neurol 5:581–584

Tateishi J, Brown P, Kitamoto T, Hoque ZM, Roos R, Wollman R, Cervenakova L, Gajdusek DC (1995) First experimental transmission of fatal familial insomnia. Nature 376:434–435

Vital C, Gray F, Vital A, Ferrer X, Julien J (1999) Prion disease with octapeptide repeat insertion. Clin Exp Pathol 47:153–159

WHO (2003) WHO manual for surveillance of human transmissible spongiform encephalopathies including variant Creutzfeldt–Jakob disease

Zerr I, Pocchiari M, Collins S, Brandel JP, de Pedro Cuesta J, Knight RS, Bernheimer H, Cardone F, Delasnerie-Laupretre N, Cuadrado Corrales N, Ladogana A, Bodemer M, Fletcher A, Awan T, Ruiz Bremon A, Budka H, Laplanche JL, Will RG, Poser S (2000) Analysis of EEG and CSF 14-3-3 proteins as aids to the diagnosis of Creutzfeldt–Jakob disease. Neurology 55:811–815

BMC Public Health

Research article

Human transmissible spongiform encephalopathies in eleven countries: diagnostic pattern across time, 1993–2002

Jesús de Pedro-Cuesta*[1], Markus Glatzel[2], Javier Almazán[1], Katharina Stoeck[3], Vittorio Mellina[4], Maria Puopolo[4], Maurizio Pocchiari[4], Inga Zerr[5], Hans A Kretszchmar[6], Jean-Philippe Brandel[7], Nicole Delasnerie-Lauprêtre[7], Annick Alpérovitch[7], Cornelia Van Duijn[8], Pascual Sanchez-Juan[8], Steven Collins[9], Victoria Lewis[9], Gerard H Jansen[10], Michael B Coulthart[10], Ellen Gelpi[11], Herbert Budka[11] and Eva Mitrova[12]

Address: [1]Instituto de Salud Carlos III, Centro Nacional de Epidemiologia, Departamento de Epidemiologia Aplicada, Calle Sinesio Delgado 6, 28029, Madrid, Spain, [2]Institute of Neuropathology, University Medical Center Hamburg-Eppendorf, Martinistraße 52, D-20246 Hamburg, Germany, [3]Institute of Neuropathology, University Hospital Zurich, Switzerland, [4]Registry of Creutzfeldt-Jakob disease, -Department of Cell. Biology and Neurosciences, Istituto Superiore di Sanita, Viale Regina Elena 299, 00161 Rome, Italy, [5]Department of Neurology, Georg-August-Universität Göttingen, Robert-Koch Strasse 40, 37075 Gottingen, Germany, [6]Department. of Neuropathology, Ludwig-Maximilian University, Munich, Germany, [7]U.708 INSERM, Hopital de la Salpetriere, 75651 Paris, Cedex 13, France, [8]Department of Epidemiology and Biostatistics, Erasmus MC, PO Box 1738, 3000 DR Rotterdam, The Netherlands, [9]Australian National Creutzfeldt-Jakob disease Registry, Department of Pathology, The University of Melbourne, Parkville, Australia, [10]CJD Surveillance System, Division of Host Genetics and Prion Diseases, Public Health Agency of Canada, LCDC Building, AL 0601E2, Tunney's Pasture, Ottawa, Ontario, K1A 0L2, Canada, [11]Institute of Neurology, Medical University of Vienna, and Austrian Reference Centre for Human Prion Diseases, AKH 4J, A-1097 Vienna, Austria and [12]Research base of Slovak Medical University, Bratislava, Slovakia

Email: Jesús de Pedro-Cuesta* - jpedro@isciii.es; Markus Glatzel - m.glatzel@uke.uni-hamburg.de; Javier Almazán - jalmazan@isciii.es; Katharina Stoeck - Katarina.Stoeck@usz.ch; Vittorio Mellina - vimelli@iss.it; Maria Puopolo - mpuopolo@iss.it; Maurizio Pocchiari - pocchia@iss.it; Inga Zerr - ingazerr@med.uni-goettingen.de; Hans A Kretszchmar - hans.kretzschmar@inp.med.uni-muenchen.de; Jean-Philippe Brandel - jean-philippe.brandel@psl.ap-hop-paris.fr; Nicole Delasnerie-Lauprêtre - laupretre@chups.jussieu.fr; Annick Alpérovitch - annick.alperovitch@chups.jussieu.fr; Cornelia Van Duijn - c.vanduijn@erasmusmc.nl; Pascual Sanchez-Juan - p.sanchezjuan@erasmusmc.nl; Steven Collins - stevenjc@unimelb.edu.au; Victoria Lewis - vlewis@unimelb.edu.au; Gerard H Jansen - gerard_jansen@phac-aspc.gc.ca; Michael B Coulthart - mike_coulthart@phac-aspc.gc.ca; Ellen Gelpi - elena.gelpi-mantius@meduniwien.ac.at; Herbert Budka - herbert.budka@meduniwien.ac.at; Eva Mitrova - eva.mitrova@szu.sk

* Corresponding author

Published: 10 November 2006

BMC Public Health 2006, **6**:278 doi:10.1186/1471-2458-6-278

Received: 03 April 2006
Accepted: 10 November 2006

This article is available from: http://www.biomedcentral.com/1471-2458/6/278

Abstract

Background: The objective of this study was to describe the diagnostic panorama of human transmissible spongiform encephalopathies across 11 countries.

Methods: From data collected for surveillance purposes, we describe annual proportions of deaths due to different human transmissible spongiform encephalopathies in eleven EUROCJD-consortium countries over the period 1993–2002, as well as variations in the use of diagnostic tests. Using logistic models we quantified international differences and changes across time.

Results: In general, pre-mortem use of diagnostic investigations increased with time. International differences in pathological confirmation of sporadic Creutzfeldt-Jakob disease, stable over time, were evident. Compared to their counterparts, some countries displayed remarkable patterns, such as: 1) the high proportion, increasing with

time, of variant Creutzfeldt-Jakob disease in the United Kingdom, (OR 607.99 95%CI 84.72–4363.40), and France (OR 18.35, 95%CI 2.20–152.83); 2) high, decreasing proportions of iatrogenic Creutzfeldt-Jakob disease in France, (OR 5.81 95%CI 4.09–8.24), and the United Kingdom, (OR 1.54 95%CI 1.03–2.30); and, 3) high and stable ratios of genetic forms in Slovakia (OR 21.82 95%CI 12.42–38.33) and Italy (OR 2.12 95%CI 1.69–2.68).

Conclusion: Considerable international variation in aetiological subtypes of human transmissible spongiform encephalopathies was evident over the observation period. With the exception of variant Creutzfeldt-Jakob disease and iatrogenic Creutzfeldt-Jakob disease in France and the United Kingdom, these differences persisted across time.

Background

Human Transmissible Spongiform Encephalopathies (HTSE) constitute a group of rare, fatal central nervous system disorders [1]. A general characteristic of HTSE is deposition of a pathological isoform (termed prion protein; PrPSc) of the normal cellular prion protein (PrPC). Diverse aetiological factors and pathogenic mechanisms underlie the development of HTSE. The sporadic form of Creutzfeldt-Jakob disease (sCJD), which is of unknown aetiology, represents the most common form of HTSE, with an estimated yearly incidence of 1–1.5 per million population. An inherited form, caused by mutations in the gene encoding PrPC (*PRNP*) is known as familial or genetic Creutzfeldt-Jakob disease (gCJD), or genetic HTSE (gHTSE) when other recognized entities are included. Acquired forms of HTSE, such as iatrogenic Creutzfeldt-Jakob disease (iCJD) or variant Creutzfeldt-Jakob disease (vCJD), are caused by exposure to infectious prions, be it through contaminated medical products (iCJD) or uptake of bovine spongiform encephalopathy (BSE) prions, (vCJD) [2,4]. The period 1993–2002 witnessed an historically exceptional situation, inasmuch as eleven countries (the EUROCJD consortium) conducted co-ordinated epidemiological HTSE surveillance, using harmonised methods against a rapidly changing medical HTSE background. New entities, such as vCJD, were identified and reported in a number of countries [5]. Diagnostic tests were developed and case definitions modified [6,7] and infrequent forms of HTSE were documented [8]. The descriptive epidemiology of HTSE in these populations, plus time intervals and details about HTSE survival, iCJD and gHTSE have recently been reported [9-12].

Taking into account that individual countries are facing country-specific risk factors, the need for a comparison of national registries and temporal analysis of national surveillance data is imperative, highlighted by recent research indicating that the incidence of HTSE by aetiological subtype varies widely geographically [9,13,14]. The fact that BSE exposure may result in sCJD-like phenotypes, as suggested by experiments performed on rodents, further underlines the need for in-depth temporal analysis of HTSE [15,16]. We analysed variations in defined epidemiological parameters in the EUROCJD-consortium HTSE cohort over a ten-year period. Through this analysis we have been able to describe variations in the annual national panorama of investigations used to evaluate patients and in aetiological HTSE subtypes over a defined timeframe, both overall and by country.

Methods

Cases included in this study were those registered in the national databases of constituent countries of the European Union's and Allied countries' prospective CJD surveillance programme (EUROCJD). National registers started collecting prospective data in 1979 in Slovakia, 1990 in the UK, 1992 in France, and 1993 in Germany, Italy, The Netherlands and Australia. Spain followed in 1995, as did Austria and Switzerland in 1996, and Canada in 1997. In 1993, a standardised protocol was introduced for diagnosing cases for epidemiological surveillance purposes. After the introduction of a diagnostic test based on detection of 14.3.3 protein in cerebrospinal fluid (CSF) in 1997, this protocol was updated in 1999. Diagnostic categories were based on application of shared specific diagnostic criteria for HTSE [17,18] adapted from those originally proposed by Masters and colleagues [19], updating in 1998 for surveillance purposes diagnostic criteria for sCJD [7,9,20]. The study included all patients with a diagnosis of probable or definite sCJD, gHTSE, iCJD or vCJD, who died in the period 1993–2002 and were reported to their respective national surveillance centres. All information was centralised in Rotterdam.

The patients from each country' included in the study is summarised in Table 1. The pooled dataset comprised 4441 patients: sCJD n = 3720 (2461 definite, 1269 probable); gHTSE n = 455; iCJD n = 138; and vCJD n = 128. Iatrogenic forms were due to dura mater grafts (n = 32), growth hormone (n = 105) and corneal transplantation (n = 1).

Whenever possible, all diagnostic investigations were reviewed by a member of the surveillance system. Information on electroencephalogram (EEG) records was available in 3825 cases. Typical periodic sharp and slow wave complexes (PSWCs) were deemed to be present when periodic complexes had a bi- or triphasic morphol-

Table 1: Number of cases studied by diagnostic entity and country

	Sporadic CJD	Variant CJD	Iatrogenic CJD	Genetic TSE				All categories
				CJD	GSS	FFI	Insert	
Australia	189	-	4	14	4	3	1	215
Austria*	77	-	-	9	-	3	1	90
Canada**	169	1	3	7	9	-	-	189
France	766	6	82	68	5	6	5	938
Germany	827	-	5	31	8	17	12	900
Italy	544	-	3	94	8	10	3	662
Netherlands	136	-	3	1	-	-	2	142
Slovakia	18	-	-	41	-	-	-	59
Spain*	380	-	5	18	-	25	1	429
Switzerland	84	-	-	1	-	-	-	85
UK	530	121	33	11	19	1	17	732
All countries	3720	128	138	295	53	65	42	4441

* Since 1996, including retrospective cases from 1993. ** Since 1998, including retrospective cases from 1994

ogy, lasted 100–600 ms and were found to be synchronous, generalised or lateralised on the EEG and persist for at least 10 seconds [21]. Cerebral magnetic resonance imaging (MRI) data was available in 2013 individuals, and was considered positive for sCJD when high signal changes were present in striatum [22]. Analysis of results according to specific pulse sequences used for MRI studies (such as diffusion weighted imaging) was not undertaken. Information on 14.3.3 protein in CSF was available in 2890 cases, with 14.3.3 Western blotting was performed in single, national centres within each country with considerable expertise in the assay [4,7]. Genetic analysis was performed by sequencing the entire open reading frame of PRNP and was available for 2967 patients.

While time trends of diagnostic patterns of a group of entities may refer to a varied type of approaches, in this paper we describe distributions by year of death and proportions of aetiological HTSE type or diagnostic test used in clinical workup. Changes across time in HTSE incidence or mortality have been reported in prior papers [9,18]. Therefore, differences between individual countries and changes across time were explored here by combining national HTSE death ratios for different diagnostic categories: 1) for each aetiological subtype of disorder; 2) for sCJD, by pathological or non-diagnostic confirmation, i.e., probable/definite ratios; and, 3) for different entities by available specific diagnostic CSF or genotype information. The statistical significance of the variation in distributions was assessed using chi-square statistics. Logistic regression was used to calculate odds ratios (OR) for each country compared to the other 10, with adjustment for age at death and year of death: 1) for specific aetiological subtypes of disorder versus all remaining HTSE; and 2) for definite versus probable sCJD. For the purposes of comparability, the vCJD death ratios for the remaining 9 countries were taken as reference for France and the UK alike. OR time trends were ascertained by introducing time as a continuous independent variable in the models. In order to judge the additional contributions made by EEG patterns and presence of 14.3.3 protein in CSF to sCJD diagnosis, and by identification of mutations in PRNP to any gHTSE diagnosis, we calculated the annual proportions of positive findings in each of these auxiliary tests in cases where the corresponding findings in EEG, 14.3.3 protein test, or family history of HTSE were absence of PSWCS or negative.

The information used in the paper is grouped and mortality grouped data for each country is publicly available at the web at the CJD surveillance unit in Edinburgh. The study underwent evaluation by the Medical Committee on Ethics of the Rotterdam Academic Hospital, MEC 127.071/1993/71, and by the Carlos III Institute of Health Committee on Bioethics, report number Pub-102/06.

Results

Shown in Figure 1 are graphs depicting the population under surveillance (Figure 1-a) and annual data in the EUROCJD consortium countries for major HTSE categories in terms of number of clinical onsets (Figure 1-a), number of deaths (Figure 1-b), average age at death (Figure 1-c), as well as the proportion of HTSE deaths for which EEG, CSF 14.3.3, cerebral MRI and genotyping results were available (Figure 1-d). The most remarkable general feature was that at no period was the death or incidence rate stable from year to year. For most entities, the highest annual number of HTSE onsets occurred early in the second half of the observation period (Figure 1-a). The increase in onsets from 1993 to 1998 was mainly in evidence for vCJD (0 to 18 cases), gHTSE (22 to 47 cases) and

sCJD (216 to 426 cases). In addition, discordance between onset and death was observable for both sCJD and other entities at the end of the study period, a finding consistent with selecting cases by death up to 2002, for inclusion in a database. While a statistically significant linear trend for increased average age at death was observed for sCJD (0.30 95%CI 0.14–0.46 years per year), and iCJD (1.15 95%CI 0.26–1.95 years per year), no such trend was suggested for gHTSE or vCJD (Figure 1-c).

The use of ancillary tests, such as MRI, 14.3.3 or genetic analysis, in diagnosis of HTSE (Figure 1-d) increased with time up to 2002. Overall, the most frequently used investigation was the EEG, yet in recent years the use of the CSF 14.3.3 protein analysis increased significantly, attaining levels comparable to EEG analyses in 2000. While rising time trends were seen for 14.3.3 tests and MRI, stable values for PRNP genotyping and decreasing figures for EEG examination were in evidence.

Annual distribution by HTSE type (Figure 2) changed significantly, both overall ($p < 0.001$) and in the UK, $p < 0.001$, and France $p = 0.009$ (Pearson χ^2). Furthermore, country- specific patterns were observable, i.e., an increase in vCJD in the UK and a decrease in iCJD in France. In the comparative inter-country analysis focusing on specific diagnostic groups, remarkable differences in magnitude and linear time trends were found. Of interest were: 1) an increase over time in vCJD in the UK (OR 607.99 95%CI 84.72–4363.40; time trend OR 1.21, 95%CI 1.11–1.31), and France (OR 18.35, 95%CI 2.20–152.83; time trend OR 1.64 95%CI 1.02–2.62), as against other countries; 2) a decrease over time in iCJD in France, OR 5.81 95%CI 4.09–8.24; time trend OR 0.84, 95%CI 0.80–0.90), and in the UK, (OR 1.54 95%CI 1.03–2.30, time trend OR 0.85 95%CI 0.79–0.90); and 3) a high proportion of gHTSE in Slovakia, (OR 21.82 95%CI 12.42–38.33) and Italy, (OR 2.12 95%CI 1.69–2.68), with stable time trends in both countries, (OR 0.99 95%CI 0.95–1.03).

Annual histopathological confirmation of sCJD (definite cases) is depicted in Figure 3. There was considerable variation between individual countries, with proportions of definite sCJD varying from 100% in Slovakia to as low as 61% in France, 59% in Italy, 57% in Germany and 52% in Spain. Noteworthy was the annual variation in diagnostic confirmation of sCJD statistically significant, both overall, $p < 0.001$, and for specific countries, such as France, $p = 0.007$, Germany, $p < 0.001$, Spain $p = 0.002$, UK $p = 0.038$ and Austria (Fisher's exact test, $p = 0.019$). When comparing national, definite versus probable confirmation ratios, statistically significant low values were found for Spain (OR 0.50, 95%CI 0.41–0.62), Germany (OR 0.60 95%0.52–0.70), Italy (OR 0.68 95%CI 0.58–0.81), and France (OR 0.75 95%CI 0.65–0.88), with no differences in time trend being identified for the four countries (comparative time trend OR 1.00 95%CI 0.98–1.03).

The yearly distribution patterns of diagnostic tests -such as 14.3.3 protein detection in CSF, EEG and genetic analyses in all HTSE- are shown for all countries in Figure 4. During the study period, the proportions of definite and probable sCJD deaths with available EEG results in which PSWCS were identified were 58% and 73% respectively. The annual variations proved statistically significant, $p < 0.001$ in both cases, suggesting a rising time trend in atypical EEG patterns in sCJD since 1997. The proportions of definite and probable sCJD with 14.3.3 tests were 62% and 74% respectively for the whole period; annual variation was not statistically significant, with 88% and 95% of such tests proving positive. Genetic analyses were performed on 64% of all HTSE. Mutations could be detected in 8.5% of all HTSE (7.04% missense mutations, 1.04% insert mutations). The annual proportion of methionine homozygous cases in *PRNP* 129 codon for all genetically examined HTSE patients did not vary significantly, $p = 0.116$.

The annual proportions of probable sCJD cases having exclusively positive EEG or 14.3.3 test results, along with the proportion of gHTSE identified by genetic analysis only (without family history of prion diseases) are listed in Table 2. The annual proportion of probable sCJD solely having a positive EEG declined evenly with time, from 95% to 3% across the period. Up to 1998, few probable sCJD cases solely had a positive 14.3.3 test (diagnostic criteria changed in 1998), but in that year the annual number rose sharply, after which it fell slightly to remain at a mean proportion of 46%. The annual proportion of gHTSE identified by mutation alone was fairly stable over the study period, with a mean of 51%.

Discussion

In terms of case numbers, this study constitutes the largest-scale observation of HTSE ever conducted. Prior reports on this clinical population are sparse [10]. Taking into account that neither mortality of HTSE nor population denominators are considered in this study, the results suggest that: 1) the panorama of HTSE, as seen from deaths for all or part of the 1993–2002 period in 11 countries, varies within and between countries, sometimes exhibiting characteristic features; 2) there is an expected, overall rising time trend in annual deaths and proportions of patients studied using ancillary tests other than EEG; 3) characteristic national patterns, as seen from the magnitude of and time-trends for proportions of specific entities, were particularly relevant in the UK and France for vCJD and iCJD, and in Slovakia and Italy for gHTSE; 4) pathological confirmation of sCJD varied but international differences persisted across time; and, 5) the addi-

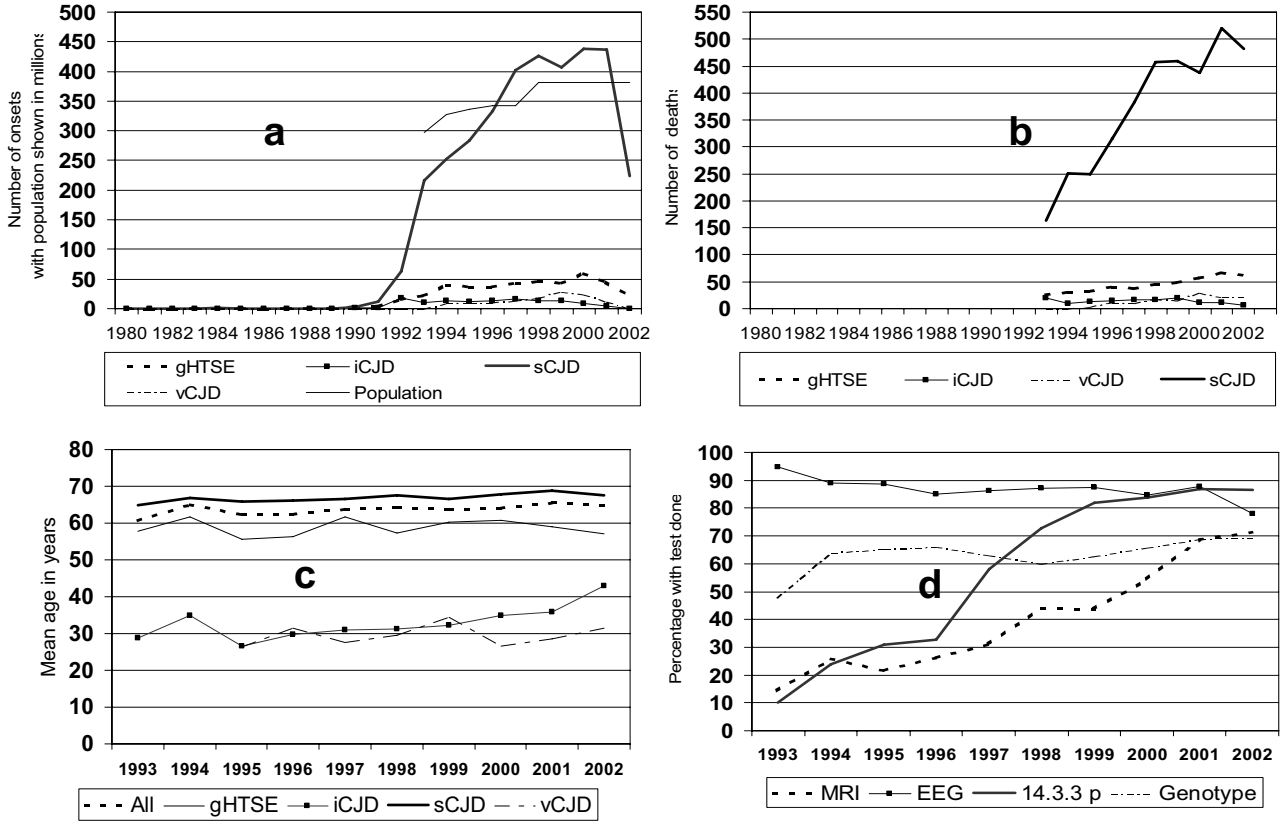

Figure 1
Variation across time for four major HTSE groups in: a) annual number of cases by year of clinical onset, with study population shown in millions; b) annual number of cases by year of death; c) annual average age at death and; d) proportion of cases, all entities, for whom diagnostic data were available in terms of EEG, 14.3.3 test in CSF, MRI and genotyping, by year of death

tional contribution of ancillary tests to sCJD diagnosis decreased to almost nil for EEG, increased to stable figures for the 14.3.3 test, and was high and stable across time for genetic assay insofar as gHTSE was concerned. The interpretation of these results is complicated by several parameters, due to the fact that use of methods for diagnosing HTSE, particularly CSF 14.3.3 test and MRI, improved significantly over the course of the study period.

The eligibility of cases for this study based on vital status after death proved most appropriate, since diagnostic criteria for probable sCJD may require measurement of disease duration, <2 years, and quality of diagnosis is frequently determined by post-mortem examination. Diagnosis classification for probable cases is therefore neither conditional to a specific disease course nor provisory. A rising time-trend in sCJD incidence or mortality has been observed over the last decade in Austria, France, Germany, Italy, Switzerland, the UK, and other countries [9,23-25] and has mainly been attributed to progressive, persistent, improvement in sCJD diagnostic ascertainment [26, 27] or has gone unexplained [9]. This large dataset makes the EUROCJD countries the most stable reference population for comparing HTSE incidence, e.g., that of sCJD in specific age-groups. Nonetheless, undercounts due to poor reporting or case ascertainment before 1998, likely due to different awareness and clinical management of dementia prior to 14.3.3 CSF test, and incomplete case-finding after 2001 by observation at death, suggest that the optimal time interval for incidence measurements using this material should be carefully selected, e.g., 2000–2001 for sCJD.

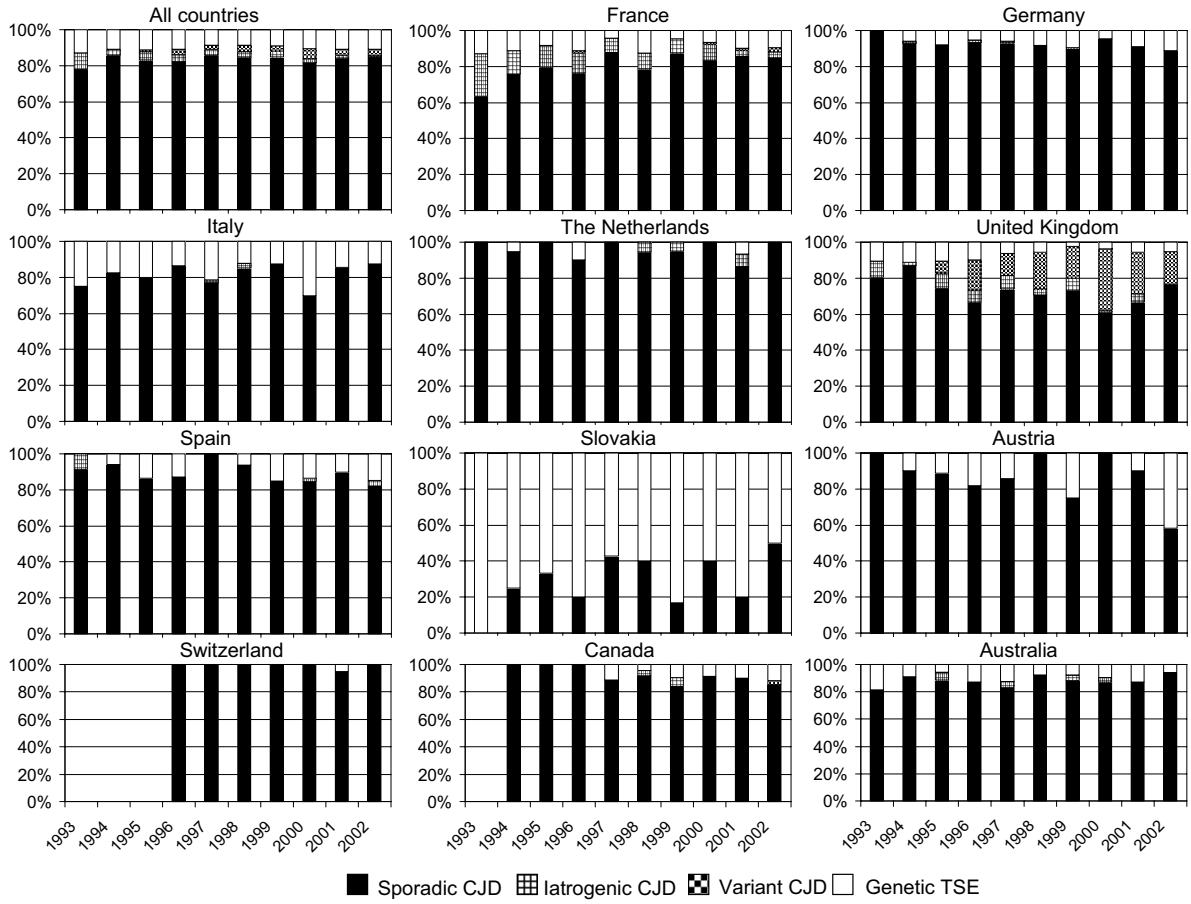

Figure 2
Annual distribution by type of HTSE in eleven countries. Different study intervals for the period, 1993–2002.

With regard to changes across time, differences due to the presence of vCJD in the UK and France are most remarkable. Abrupt changes in 1997 and 1998 for sCJD suggest a strong impact of the first vCJD report [4] on diagnostic practices and the updating of diagnostic criteria. Yet, interpretation of comparative linear time trends can sometimes prove problematic. For instance, changes in average age at death might reflect improved ascertainment for sCJD and an exposure-related cohort effect with increasing duration of incubation period for iCJD.

Changes across time reported here may, among other things, reflect clinical management and reporting, and variations in pre- and post-mortem laboratory diagnostic practices and diagnostic criteria updates. The increasing use of MRI might explain rising trends for CJD since specific patterns of abnormality on diffusion-weighted and fluid-attenuated inversion recovery images are highly sensitive and specific for CJD [28]. In EUROCJD countries, the use by clinicians of the 14.3.3 protein test in sCJD diagnosis first became significant in 1997. Accordingly, the 14.3.3 protein in CSF, identified for the not inconsiderable annual proportions of HTSE patients who died from 1993 to 1996 (Figure 1, bottom right) -with test results shown for definite and probable sCJD (Figure 4, centre) and probable sCJD (Table 2)- should have been determined post-mortem, in most cases on frozen CSF stored for research purposes. This policy might have had: a) positive effects, in terms of increasing the average amount of information per registered HTSE case, something that is particularly interesting for definite sCJD cases with date of death prior to 1998; and b) bias in research, due to inclusion of 14.3.3-test results in the database for probable sCJD being made conditional upon the presence

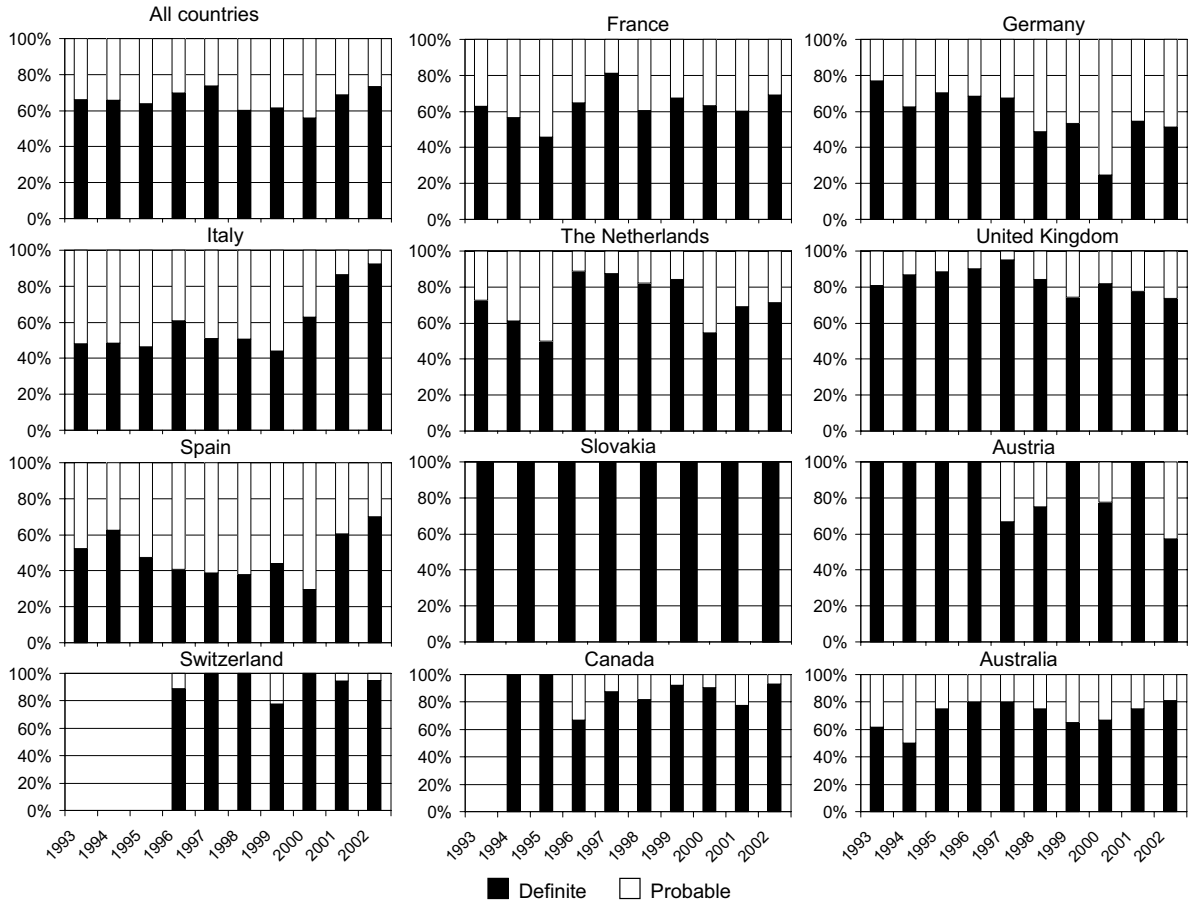

Figure 3
Annual proportion of histopathologically-confirmed, i.e. definite, sporadic CJD in EUROCJD countries.

Table 2: Additional contribution of: positive results in EEG and CSF examination (14.3.3 protein test) to diagnosis of probable sporadic CJD; and identified PrP gene mutation to diagnosis of genetic HTSE.

Year of death	Cases solely with positive EEG Number and percentage of probable sporadic CJD cases	Cases solely with positive CSF 14.3.3 test Number and percentage of probable sporadic CJD cases	Cases with mutation and negative or missing data on family history. Number and percentage of genetic TSE cases
1993	52 (95)	-	13 (48)
1994	60 (70)	7 (8)	16 (50)
1995	61 (68)	4 (4)	15 (45)
1996	62 (64)	13 (14)	23 (55)
1997	30 (30)	21 (21)	20 (53)
1998	32 (18)	65 (36)	26 (55)
1999	15 (9)	67 (38)	24 (49)
2000	11 (6)	79 (41)	23 (40)
2001	8 (5)	95 (58)	30 (44)
2002	4 (3)	69 (54)	40 (65)

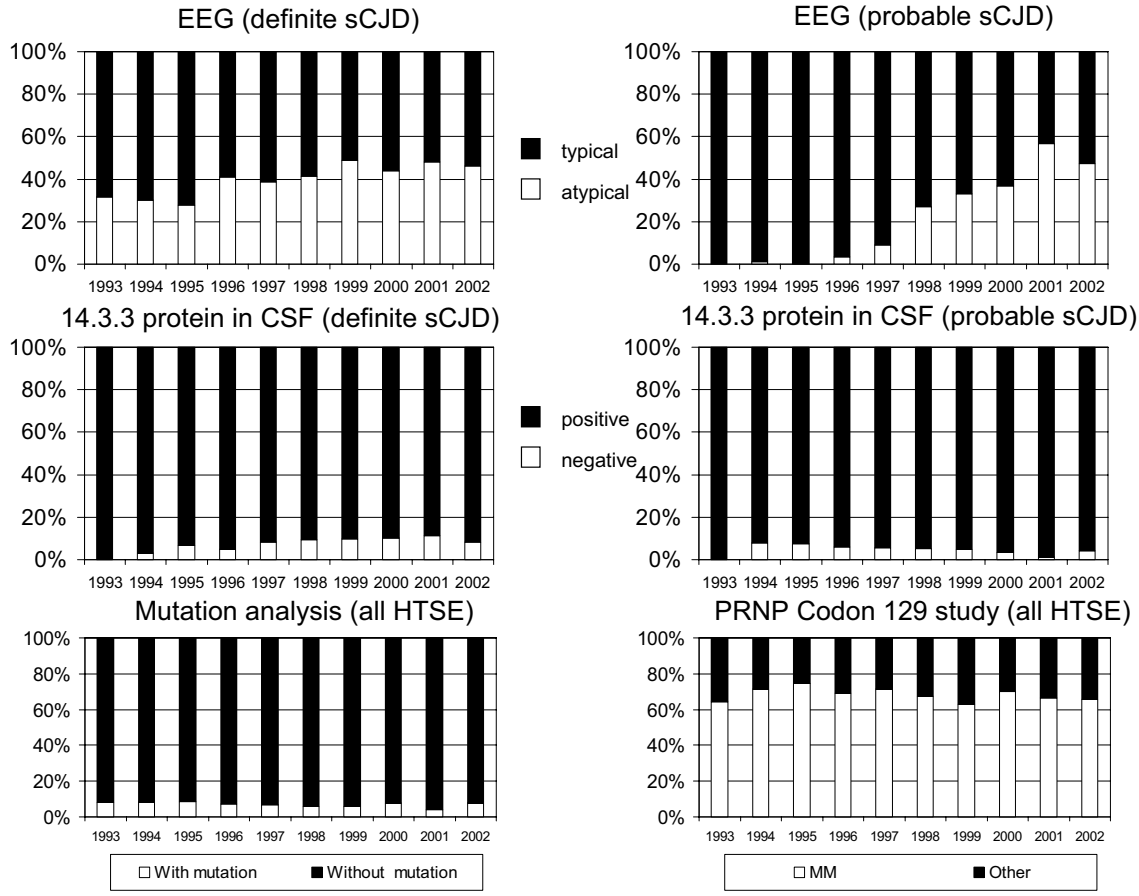

Figure 4
Annual distribution of positive results in EEG and 14.3.3 protein tests in sCJD, and for all HTSE, PRNP mutations identified (in patients who had and had not been genetically studied) and PRNP codon 129 genotype.

of PSWCs in EEG, a requisite for such diagnosis before 1998. The study of associations similar to those reported [29, 30, 31] using this large database may benefit from stratification by period of death or diagnostic criteria for probable sCJD.

Identifying a time-related increase in sCJD incidence in populations with valine in PRNP codon 129 which have been considerably exposed to BSE has been a key goal of EUROCJD-sponsored public health HTSE surveillance, reinforced by results of recent laboratory research [15,16]. The frequent lack of PRNP codon 129 data for age-specific national populations makes it impossible to calculate the incidence figures required as denominators for such analyses. Hence, a surrogate index is currently used, comparing proportions of sCJD with a valine allele in the UK versus those in other countries and their changes across time [31]. Our study results for the general population suggest that there have been no changes over time in this proportion since 1996 (Figure 4, bottom right). Due to frequent atypical clinical features [32], probable sCJD is particularly liable to being misdiagnosed in patients with valine in codon 129, and as a result expected improvement in sCJD diagnosis internationally is not reflected as a trend. Monitoring international changes across time in clinical-geno-phenotype with this extensive and unique

material might require stratification by variables potentially associated with misdiagnosis and codon 129 structure, e.g., EEG pattern.

Conclusion

This study reveals remarkable international differences in the HTSE panorama that change with time, as seen from deaths in eleven countries in the period 1993–2002. Knowledge of possible biases in the study cohort is vital for future applications of this dataset, both in clinical/epidemiological research and in public health surveillance.

Competing interests

The author(s) declare that they have no competing interests.

Authors' contributions

The EUROCJD consortium generated the EUROCJD Research Database which constituted the dataset used in this study. JP contributed with study design, design and supervision of analysis and drafted first manuscript. MG and KS reviewed and drafted biologically relevant paragraphs. JA did the statistical analysis. VM, MP and MP contributed to the data base refinement and classification of genetic forms. All other authors, particularly and repeatedly AA, CvD, SC, VL, GHJ and MC, contributed with comments to several versions and criticisms of methods and text, AA, CvD, SC, VL and figures AA, GHJ. All authors read and approved the final manuscript.

Acknowledgements

The EUROCJD consortium encompasses the national teams listed below. This study was funded through NeuroPrion, an EU Network of Excellence funded by Framework 6 Programme, Contract number: FOOD CT 2004 056579, and EUROCJD funded by DG SANCO; Contract number: 2003201.

Australia: The Australian National Creutzfeldt-Jakob Disease Registry (ANCJDR) thanks Alison Boyd, James Lee, Samantha Douglass, Genevieve Klug, Colin L Masters and Magdalena Kvasnicka for their assistance, and the families of registry patients and their medical practitioners for their cooperation. The ANCJDR is funded by the Commonwealth Department of Health and Ageing. **Austria:** The Austrian Reference Centre for Human Prion Diseases (ÖERPE, Head: Prof. Herbert Budka) acknowledges the help of Drs Christa Jarius, Ellen Gelpi, Christine Haberler, Thomas Ströbel, and Till Voigtländer; DI Dita Drobna; and Ms. Helga Flicker, Brigitte Millan-Ruiz, and Monika Richter. **Canada:** The Canadian Surveillance System is funded by Health Canada. Other collaborators on the project are Dr C Bergeron, neuropathologist (Univ. of Toronto), Dr M Coulthart, neuropathologist (National Lab. for Prion Diseases, Health Canada), Dr N Cashman, neurologist and one of the principal investigators for CJD-SS, Dr D Westaway, consulting scientist (Univ. of Toronto).**France:** We would like to acknowledge all reporting physicians and the members of the Reseau National de surveillance de maladies de Creutzfeldt-Jakob et maladies apparentées.**Germany:** The German surveillance system is funded by the Federal Ministry of Health 9BMG, 325-4471-02/15). We are grateful to all reporting physicians throughout Germany who contributed to the German surveillance system and especially to Maja Schneider-Dominico for her excellent support in the co-ordination of surveillance. We also acknowledge the help of Drs Otto Windl and Walter Schulz-Schaeffer. **Italy:** We would like to acknowledge the Ministry of Health and the Istituto Superiore di Sanità for supporting the surveillance of CJD in Italy. S. Almonti, V. Mellina and L. Ingrosso for help in collecting data and advice. **Netherlands:** CJD surveillance in the Netherlands is funded by the Dutch Ministry of Health, Welfare and Sports. We acknowledge the help of colleagues at the Department of Neurology at the Academic Medical Centre, Amsterdam and the Department of Pathology at the University Medical Centre, Utrecht. **Slovakia:** The Slovak Surveillance System was supported by the Slovak Ministry of Health and by grants from the European Union. We would like to acknowledge the help of Dr. Dana Slivarichová, Dr. Vladimíra Verchovodková, all reporting physicians and collaborating pathologists.**Spain:** We are grateful to all reporting physicians and to members of the Spanish TSE study group at Consejo Interterritorial and co-workers at CNE and ISCIII TSE Registry and Laboratories, particularly to F. Avellanal, M. Calero N. and N. Cuadrado. Supported by cooperative research networks RCESP C03-09 and CIEN C03-06. **Switzerland:** The Swiss Reference Center for Prion Diseases is funded by the Swiss Federal Office of Public Health (Bern, Switzerland). **UK:** The UK CJD Surveillance System is funded by the Department of Health and the Scottish Executive Health Department. All authors are grateful to all the members of staff at the National CJD Surveillance Unit and in particular to James Ironside for neuropathological expertise and to clinicians throughout the UK for their cooperation with the study.

References

1. Prusiner SB: **Prions.** *Proc Natl Acad Sci U S A* 1998, **95:**13363-13383.
2. Scott MR, Will R, Ironside J, Nguyen HO, Tremblay P, DeArmond SJ, Prusiner SB: **Compelling transgenetic evidence for transmission of bovine spongiform encephalopathy prions to humans.** *Proc Natl Acad Sci U S A* 1999, **96:**15137-15142.
3. Will RG, Ironside J, Zeidler M, Cousens SN, Estibeiro K, Alperovitch A, Poser S, Pocchiari M, Hofman A, Smith PG: **A new variant of Creutzfeldt-Jakob disease in the UK.** *Lancet* 1996, **347:**921-925.
4. Hsich G, Kenney K, Gibbs CJ, Lee KH, Harrington MG: **The 14-3-3 brain protein in cerebrospinal fluid as a marker for transmissible spongiform encephalopathies.** *N Engl J Med* 1996, **335:**924-930.
5. Zerr I, Pocchiari M, Collins S, Brandel JP, Pedro Cuesta J, Knight RSG, Bernheimer H, Cardone F, Delasnerie-Lauprêtre N, Cuadrado Corrales N, Ladogana A, Bodemer M, Fletcher A, Awan T, Ruiz Bremón A, Budka H, Laplanche JL, Will RG, Poser S: **Analysis of EEG and CSF 14-3-3 proteins as aids to the diagnosis of Creutzfeldt-Jakob disease.** *Neurology* 2000, **55:**811-815.
6. Zerr I, Giese A, Windl O, Kropp.S., Schulz-Schaeffer WJ, Riedemann C, Skworc F, Bodemer M, Kretzschmar HA, Poser S: **Phenotypic variability in fatal familial insomnia (D178N-129M) genotype.** *Neurology* 1998, **51:**1398-1405.
7. Ladogana A, Puopolo M, Croes E, Budka H, Jarius C, Collins S, Klug GM, Sutcliffe T, Giulivi A, Alperovitch A, Delasnerie-Lauprêtre N, Brandel JP, Poser S, Kretzschmar H, Rietveld I, de Pedro-Cuesta J, Martínez-Martín P, Glatzel M, Aguzzi A, Knight R, Ward H, Pocchiari M, van Duijn CM, Will RG, Zerr I: **Mortality from Creutzfeldt-Jakob disease and related disorders in Europe, Australia, and Canada.** *Neurology* 2005, **64:**1586-1591.
8. Pocchiari M, Puopolo M, Croes EA, Budka H, Gelpi E, Collins S, Lewis V, Sutcliffe T, Guilivi A, Delasnerie-Lauprêtre N, Brandel JP, Alperovitch A, Zerr I, Poser S, Kretzschmar HA, Ladogana A, Rietvald I, Mitrová E, Martínez-Martín J, de Pedro-Cuesta J, Glatzel M, Aguzzi A, Cooper S, Mackenzie J, van Duijn CM, Will RG: **Predictors of survival in sporadic Creutzfeldt-Jakob disease and other human transmissible spongiform encephalopathies.** *Brain* 2004, **127:**2348-2359.
9. Brandel JP, Preece M, Brown P, Croes E, Laplanche JL, Agid Y, Will R, Alperovitch A: **Distribution of codon 129 genotype in human growth hormone-treated CJD patients in France and the UK.** *Lancet* 2003, **362:**128-130.
10. Kovács GG, Puopolo M, Ladogana A, Pocchiari M, Budka H, van Duijn CM, Collins SJ, Boyd A, Guilivi A, Delasnerie-Lauprêtre N, Brandel JP,

Zerr I, Kretzschmar H, Pedro-Cuesta J, Calero M, Glatzel M, Aguzzi A, Bishop M, Knight R, Belay G, Will R, Mitrová E: **Genetic prion disease: the EUROCJD experience.** *Hum Genet* 2005, **118:**166-174.
11. Glatzel M, Rogivue C, Ghani AC, Streffer JR, Amsler L, Aguzzi A: **Incidence of Creutzfeldt-Jakob disease in Switzerland.** *Lancet* 2002, **360:**139-141 [http://www.thelancet.com].
12. Llewelyn CA, Hewitt PE, Knight RSG, Amar K, Cousens SN, Mackenzie J, Will RG: **Possible transmission of variant Creutzfeldt-Jakob disease by blood transfusion.** *Lancet* 2004, **363:**147-421.
13. Asante EA, Linehan JM, Desbruslais M, Wood AL, Welch J, Hill AF, Lloyd SE, Wadsworth JDF, Collinge J: **BSE prions propagate as either variant CJD-like or sporadic CJD-like prion strains in transgenic mice expressing human prion protein.** *EMBO J* 2002, **21:**6358-6366.
14. Budka H, Aguzzi A, Brown P, Brucher JM, Bugiani O, Collinge J, Diringer H, Gullotta F, Haltia M, Hauw JJ, Ironside JW, Kretzschmar HA, Lantos PL, Masullo C, Schlote W, Tateishi J, Weller RO: **Neuropathological diagnostic criteria for Creutzfeldt-Jakob disease (CJD) and other human spongiform encephalopathies (prion diseases).** *Brain Pathol* 1995, **5:**575-582.
15. Will RG, Zeidler M, Stewart GE, Macleod MA, Ironside JW, Cousens SN, Mackenzie J, Estibeiro K, Green AJE, Knight RSG: **Diagnosis of new variant Creutzfeldt-Jakob disease.** *Ann Neurol* 2000, **47:**575-582.
16. Steinhoff BJ, Racker S, Herrendorf G, Poser S, Grosche S, Zerr I, Kretzschmar H, Weber T: **Accuracy and reliability of periodic sharp wave complexes in Creutzfeldt-Jakob disease.** *Arch Neurol* 1996, **53:**162-166.
17. Collie DA, Sellar RJ, Zeidler M, Colchester ACF, Knight RSG, Will RG: **MRI of Creutzfeldt-Jakob disease: imaging features and recommended MRI protocol.** *Clin Radiol* 2001, **56:**726-739.
18. Radbauer C, Hainfellner JA, Jellinger K, Pilz P, Maier H, Kleinert R, Budka H: **Epidemiologie der übertragbaren spongiformen Enzephalopathien (Prion-Krankheiten)in Österreich.** *Wien Med Wochenschr* 1998, **148:**101-106.
19. Huillard d'Aignaux J, Laplanche JL, Delasnerie-Lauprêtre N, Brandel JP, Peoc'h K, Salomon D, Hauw JJ, Alperovitch A: **Trends in mortality from sporadic Creutzfeldt-Jakob disease in France 1992-7.** *J Neurol Neurosurg Psychiatry* 2000, **68:**787-789.
20. Arpino C, Conti S, Masocco M, Toccaceli V, Ladogana A, D'Alessandro M, Pocchiari M: **Creutzfeldt-Jakob disease mortality in Italy, 1982-1996.** *Neuroepidemiology* 1999, **18:**92-100.
21. Brandel JP, Delasnerie-Lauprêtre N, Laplanche JL, Hauw JJ, Alperovitch A: **Diagnosis of Creutzfeldt-Jakob disease: effect of clinical criteria on incidence estimates.** *Neurology* 2000, **54:**1095-1099.
22. Saiz A, Nos C, Yagüe J, Domínguez A, Graus F, Muñoz P: **The impact of the introduction of the 14-3-3 protein assay in the surveillance of sporadic Creutzfeldt-Jakob disease in Catalonia.** *J Neurol* 2001, **248:**592-594.
23. Parchi P, Giese A, Capellari S, Brown P, Schulz-Schaeffer WJ, Windl O, Zerr I, Budka H, Kopp N, Piccardo P, Poser S, Rojiani A, Streichenberger N, Julien J, Vital C, Ghetti B, Gambetti P, Kretzschmar HA: **Classification of sporadic Creutzfeldt-Jakob disease based on molecular and phenotypic analysis of 300 subjects.** *Ann Neurol* 1999, **46:**224-233.
24. Kovács GG, Head MW, Bunn T, László L, Will RG, Ironside JW: **Clinicopathological phenotype of codon 129 valine homozygote sporadic Creutzfeldt-Jakob disease.** *Neuropathol Appl Neurobiol* 2000, **26:**463-472.
25. Zerr I, Schulz-Schaeffer WJ, Giese A, Bodemer M, Schröter A, Henkel K, Tschampa HJ, Windl O, Pfahlberg A, Steinhoff BJ, Gefeller O, Kretzschmar HA, Poser S: **Current clinical diagnosis in Creutzfeldt-Jakob disease: identification of uncommon variants.** *Ann Neurol* 2000, **48:**323-329.
26. Alpérovitch A, Zerr I, Pocchiari M, Mitrová E, Pedro Cuesta J, Hegyi I, Collins S, Kretzschmar HA, van Duijn CM, Will RG: **Codon 129 prion protein genotype and sporadic Creutzfeldt-Jakob disease.** *Lancet* 1999, **353:**1673-1674.

Pre-publication history

The pre-publication history for this paper can be accessed here:

http://www.biomedcentral.com/1471-2458/6/278/prepub

Novel prion protein gene mutation presenting with subacute PSP-like syndrome

D.B. Rowe, PhD; V. Lewis, BSc(Hons); M. Needham, MB, BS(Hons); M. Rodriguez, MB, BS; A. Boyd, Dip Gen Coun; C. McLean, MD; H. Roberts, MB, BS; C.L. Masters, MD; and S.J. Collins, MD

Abstract—A 62-year-old Indonesian woman presenting with a progressive supranuclear palsy–like syndrome was confirmed post mortem as dying from a spongiform encephalopathy. Despite an illness duration of only 4 months, brain MRI, EEG, and CSF analysis for 14-3-3 proteins all failed to disclose changes typical of Creutzfeldt–Jakob disease. Neuropathologic examination revealed multicentric, prion protein–positive, amyloid plaques as typically seen in Gerstmann–Sträussler–Scheinker syndrome. Prion protein gene analysis revealed a previously unreported A133V mutation.

NEUROLOGY 2007;68:868–870

Genetic Creutzfeldt–Jakob disease (CJD) and other phenotypes are linked to a variety of mutations within the prion protein (PrP) gene (*PRNP*).[1] Regardless of etiology, the clinical features found in prion disease are diverse, and whereas dementia, myoclonus, and cerebellar ataxia are particularly common in CJD, additional findings may include cortical blindness, extrapyramidal dysfunction, insomnia, and psychiatric disturbances.[2] Rarely, sporadic CJD may even manifest a clinical profile, especially the presence of supranuclear vertical gaze abnormalities, prompting misdiagnosis as progressive supranuclear palsy (PSP).[3] To date, supranuclear gaze palsy has only been clearly described in two pedigrees with familial prion disease.[4,5]

We report a patient who presented with a subacute PSP-like syndrome, confirmed to be a spongiform encephalopathy at post mortem, who, despite a negative family history for CJD or other neurodegenerative disorder, revealed a hitherto unreported A133V mutation.

Methods. *DNA analysis.* Genomic DNA was extracted from a frozen (stored at −80 °C) muscle biopsy specimen. Open reading frame (ORF) sequence analysis and subsequent bacterial cloning were performed as described previously.[6] To assist the selection of clones for DNA sequencing, plasmid DNA was subjected to restriction fragment length polymorphism analysis, using the restriction enzyme *Bsp*H1, which cuts at a site just upstream of the ampicillin resistance gene on the vector (i.e., linearizing both wild-type and mutant plasmids) and additionally at the sequence introduced into *PRNP* with the A133V mutation. Three representative wild-type clones and five mutant clones were sequenced.

Neuropathology. The brain and spinal cord were examined after 17 weeks' fixation in 10% formalin. Sections taken from a number of cerebral cortical sites, as well as hippocampus, striatum, lentiform nucleus, thalamus, brain stem, cerebellum, spinal cord, and dorsal root ganglia were stained with hematoxylin and eosin (H-E) and examined. Tissues were not pretreated with formic acid. Sections of cerebellar vermis and thalamus were immunostained for PrP using the monoclonal 3F4 antibody (Signet), whereas tau immunostaining using a polyclonal rabbit anti-human antibody (DakoCytomation) and Congo red staining were performed on frontal, parietal, and occipital cortices, as well as the striatum, thalamus, and cerebellar hemisphere.

Fresh-frozen brain was not available to allow western blot analysis of PrP.

Results. *Case report.* A 62-year-old woman was admitted to hospital because of 1 month of difficulties with upper limb coordination and an unsteady gait with falls. Originally from Indonesia, the patient had resided in Australia for 16 years. There was a history of diet-controlled type 2 diabetes mellitus, hypercholesterolemia, and essential hypertension but no family history of dementia or other neurologic disorder. Neurologic examination shortly after admission was remarkable for a severe abnormality of conjugate eye movements, with no vertical saccades to command and slow, stepwise horizontal saccades. Pursuit eye movements to target were broken and incomplete. Oculocephalic reflex eye movements were normal, consistent with a predominantly supranuclear deficit of ocular movements. Cranial nerve examination was otherwise normal. Tone was normal in the limbs but increased at the neck and trunk. There was marked postural instability, with gait possible only

From the Department of Neurology (D.B.R., M.N.), Royal North Shore Hospital, St. Leonards; Australian National Creutzfeldt–Jakob Disease Registry (V.L., A.B., H.R., C.L.M., S.J.C.), Department of Pathology, University of Melbourne, Parkville; Mental Health Research Institute (V.L., A.B., C.L.M., S.J.C.), Parkville; Department of Forensic Medicine (M.R.), Sydney South West Area Health Service, New South Wales; and Department of Anatomical Pathology (C.McL.), Alfred Hospital, Prahran, Australia.

The Australian National Creutzfeldt–Jakob Disease Registry is funded by the Commonwealth Department of Health and Ageing. S.J.C. receives an NH&MRC Practitioner Fellowship (no. 400182), and both S.J.C. and C.L.M. are recipients of an NH&MRC Program Grant (no. 400202).

Disclosure: The authors report no conflicts of interest.

Received July 28, 2006. Accepted in final form November 20, 2006.

Address correspondence and reprint requests to Dr. S.J. Collins, Department of Pathology, Australian National Creutzfeldt–Jakob Disease Registry, University of Melbourne, Parkville, Australia 3010; e-mail: stevenjc@unimelb.edu.au

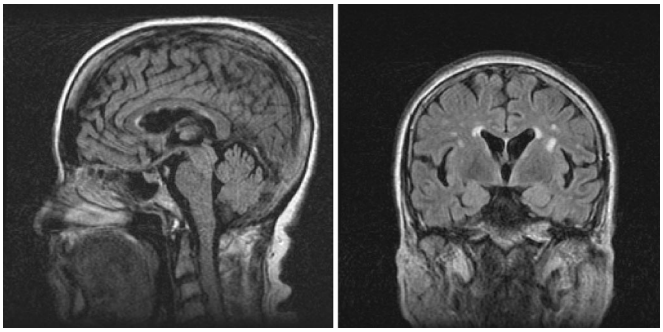

Figure 1. Representative fluid-attenuated inversion recovery sequence MRI brain scans, showing midline sagittal (A) and midhemisphere (B) coronal views. Only minor areas of increased signal are seen in the periventricular regions thought to be on the basis of coincidental, nonspecific chronic white matter ischemia.

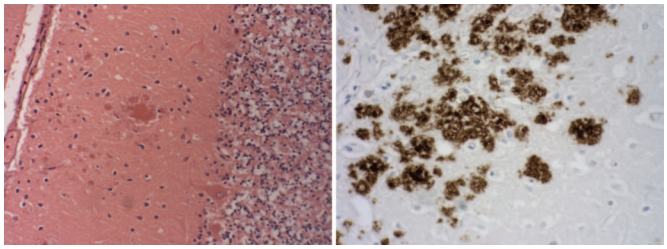

Figure 2. Photomicrographs of the cerebellar cortex showing evidence of minor microvacuolation and occasional eosinophilic, multicentric amyloid plaques confined to the molecular layer (A), with substantial numbers of prion protein (PrP)–positive plaques, also restricted to the molecular layer, confirmed on immunohistochemistry (B). Hematoxylin and eosin (A) and immunohistochemistry using the 3F4 monoclonal antibody specific for PrP (B); ×40.

with the support of two people. Repeated MRI of the brain, including diffusion-weighted imaging, fluid-attenuated inversion recovery sequences, and gadolinium enhancement, demonstrated only nonspecific periventricular white matter changes thought to be on an ischemic basis (figure 1). EEG revealed a nonspecific excess of slower frequencies but no periodic activity, and aside from a mild elevation of total protein, CSF was unremarkable, including negative for 14-3-3 proteins.

The patient progressively deteriorated over the next 4 weeks, sleeping up to 18 hours per day. Disorientation, dysarthria, dysphagia, and language difficulties became evident, but myoclonus was never observed. Truncal and nuchal rigidity became more marked. Eventually, saccadic and pursuit eye movements were lost, and oculocephalic reflexes were suppressed. There was no clinical response to trials of IV pulse methylprednisolone (1 g daily for 3 days) or levodopa/carbidopa (2 × 100/25-mg tablets three times daily). The patient died 4 months after presentation; a confident clinical diagnosis was not achieved premortem.

Neuropathology. The brain weighed 1,319 g prior to fixation. No macroscopic abnormalities were identified externally or following sectioning. Microscopic examination demonstrated widespread, multifocal, spongiform encephalopathy with neuropil vacuolation, neuronal loss, gliosis, and increased numbers of activated microglia in the cerebral cortex, basal ganglia, thalamus, brainstem, and cerebellar cortex. Findings were most severe in the thalamus and the brainstem tegmentum, with only mild focal changes in the head of the caudate nucleus and the cerebral cortex, the latter most marked in the deeper layers of the occipital cortex. Multifocal spongiform change, microglial proliferation, patchy loss of Purkinje cells and internal granular neurons with associated gliosis, and scattered small amyloid plaques, without peripheral vacuoles, were noted in the molecular layer of the cerebellar cortex (figure 2A); morphologic features of granular cell lysis and necrosis were not evident. Amyloid plaques were not identified in the cerebellar internal granular layer or anywhere else in the brain. There was no evidence of encephalitis.

3F4 immunostaining demonstrated PrP-positive plaques confined to the cerebellar molecular layer (figure 2B). Most of the deposits formed cluster or multicentric plaques. More plaques were identified with immunostaining than with H-E and Congo red. In the thalamus, there was a predominantly synaptic pattern of PrP immunoreactivity with some larger patches of immunoreactivity and occasional perineuronal granular staining but no plaque-like or definite perivacuolar staining. Tau immunostaining was negative in all brain regions.

Molecular genetic studies. DNA analysis revealed a C-to-T transition at the second nucleotide position of codon 133 of the *PRNP* ORF, resulting in a predicted amino acid change from alanine to valine. The patient was methionine homozygous at codon 129 and also carried the E219K polymorphism.[7] Sequencing of representative wild-type and mutant clones determined that the codon 133V mutation was in *cis* with the uncommon 219K allele.[7]

Discussion. In addition to expanding the spectrum of *PRNP* mutations associated with spongiform encephalopathies, our proband extends the range of specific mutations associated with supranuclear gaze palsy. Although nonspecific limitations of upward gaze have been described in Gerstmann–Sträussler–Scheinker syndrome,[8] to the best of our knowledge, this is only the third *PRNP* mutation to be clearly associated with a supranuclear gaze palsy as a salient or presenting clinical feature[4,5,8] and reaffirms the phenotypic heterogeneity that may be encountered in genetic prion disease. In contrast to affected family members harboring the S198F mutation, the vertical restriction of gaze in our patient was not just limited to supraduction and evident only in the advanced stages of long-duration illnesses[5] but was more akin to that observed in the pedigree with the E200K mutation.

Despite general similarities in the clinical findings, the rapidity of the patient's neurologic decline to death over 4 months made a diagnosis of PSP untenable,[9] and notwithstanding awareness that vertical supranuclear gaze palsy can occur uncommonly in sporadic CJD,[8] the absence of characteristic findings on EEG, CSF analysis for 14-3-3 proteins, and brain MRI militated against this diagnosis. The lack of typical clinical features such as myoclonus and the absence of periodic sharp waves on EEG have also been observed in the previous family with genetic CJD due to the E200K

mutation manifesting supranuclear gaze palsy.[10] This stands in clear contrast to most E200K patients and other *PRNP* mutations associated with genetic CJD, wherein routine investigations usually show typical findings as seen in sporadic CJD.

Although the short duration of the patient's illness was more in keeping with CJD, the combined clinical and neuropathologic findings did not clearly conform (especially for a codon 129 methionine homozygote) to a specific subtype within a recently reported classification scheme for sporadic CJD.[2] The pathologic changes observed in our patient, particularly multicentric PrP-positive plaques in the cerebellar molecular layer, are perhaps more in keeping with those observed in patients with Gerstmann–Sträussler–Scheinker syndrome, although typically in the latter disease subgroup, the PrP-positive amyloid plaques are more widespread, additionally observed in the cerebrum and diencephalon. We conjecture that our patient's phenotypic uniqueness relates specifically to the novel A133V mutation itself, but the possible disease-modifying influences of polymorphisms such as E219K should not be dismissed, as suggested for patients harboring the P102L mutation.[7]

Acknowledgment

The authors thank Dr. Andrew Hill for advice with sequencing and cloning and Ms. Denise Cappai for technical assistance.

References

1. Collins SJ, Lawson VA, Masters CL. Transmissible spongiform encephalopathies. Lancet 2004;363:51–61.
2. Parchi P, Giese A, Capellari S, et al. Classification of sporadic Creutzfeldt–Jakob disease based on molecular and phenotypic analysis of 300 subjects. Ann Neurol 1999;46:224–233.
3. Josephs KA, Dickson DW. Diagnostic accuracy of progressive supranuclear palsy in the Society for Progressive Supranuclear Palsy Brain Bank. Mov Disord 2003;18:1018–1026.
4. Bertoni JM, Brown P, Goldfarb LG, et al. Familial Creutzfeldt–Jakob disease (codon 200 mutation) with supranuclear palsy. JAMA 1992;268:2413–2415.
5. Yee RD, Farlow MR, Suzuki DA, et al. Abnormal eye movements in Gerstmann–Sträussler–Scheinker disease. Arch Ophthalmol 1992;110:68–74.
6. Lewis V, Collins S, Hill AF, et al. Novel prion protein insert mutation associated with prolonged neurodegenerative illness. Neurology 2003;60:1620–1624.
7. Furukawa H, Kitamoto T, Tanaka Y, Tateishi J. New variant prion protein in a Japanese family with Gerstmann–Sträussler syndrome. Brain Res Mol Brain Res 1995;30:385–388.
8. Lueck CJ, McIlwaine GG, Zeidler M. Creutzfeldt–Jakob disease and the eye. II. Ophthalmic and neuro-ophthalmic features. Eye 2000;14:291–301.
9. Litvan I, Agid Y, Calne D, et al. Clinical research criteria for the diagnosis of progressive supranuclear palsy (Steele–Richardson–Olszewski syndrome): report of the NINDS-SPSP International Workshop. Neurology 1996;47:1–9.
10. Tietjen GE, Drury I. Familial Creutzfeldt–Jakob disease without periodic EEG activity. Ann Neurol 1990;28:585–588.

doi:10.1093/brain/awn303 Brain 2009: 132; 493–501 | 493

BRAIN
A JOURNAL OF NEUROLOGY

Enhanced geographically restricted surveillance simulates sporadic Creutzfeldt-Jakob disease cluster

Genevieve M. Klug,[1,5,*] Handan Wand,[2,*] Alison Boyd,[1,5] Matthew Law,[2] Scott Whyte,[3,4] John Kaldor,[2] Colin L. Masters[1,5] and Steven Collins[1,5]

1 Australian National Creutzfeldt-Jakob Disease Registry, Department of Pathology, The University of Melbourne, Parkville, Victoria, Australia
2 National Centre in HIV Epidemiology and Clinical Research, The University of New South Wales, Sydney, New South Wales, Australia
3 North Sydney and Central Coast Area Health, New South Wales, Australia
4 The University of Newcastle, Newcastle, New South Wales, Australia
5 The Mental Health Research Institute of Victoria, Parkville, Victoria, Australia

*These authors contributed equally to this work.

Correspondence to: Steven J. Collins,
Department of Pathology,
The University of Melbourne,
Victoria 3010, Australia
E-mail: stevenjc@unimelb.edu.au

Spatio-temporal clustering of sporadic Creutzfeldt-Jakob disease (sCJD) has been recognized and investigated previously in various global settings including Australia. Generally, despite often extensive investigation, explanations such as point source outbreaks and plausible case-to-case transmission links have not been identified to explain the apparently higher case rates than expected. In the context of national surveillance during the period 1993–2006, an increased number of cases of sCJD were recognized in a circumscribed coastal region of eastern Australia. To assess the significance of this apparent clustering, the Spatial Scan Statistic was used to examine for geographic excess of CJD mortality at spatial and temporal combined, spatial only and temporal only levels. A significant spatial cluster was confirmed, encompassing three contiguous statistical local areas within the state of New South Wales (NSW). Detailed epidemiological analysis did not reveal a plausible cross-over or point source transmission event. Further evaluation prompted the conclusion that vigilant and motivated managing clinicians in this geographically circumscribed area of NSW evinced a sustained higher level of clinical awareness for the broad phenotypic spectrum of CJD with reliable referral of suspect cases for further investigation. In addition, these physicians established and maintained a well-coordinated and active approach to suspect CJD autopsy. This combination of factors translated into a higher intensity of surveillance at approximately twice the rate per population observed in the entire state, culminating in twice the incidence of sCJD at around 2.28 cases/million population/year. The hypothesis that intensity of surveillance for rare disorders can be objectively measured and that this can positively correlate with disease incidence deserves further exploration. It may prove to be an important insight into the varying incidence rates over periods of time within individual nations and between different countries.

Keywords: CJD; cluster analysis; epidemiology; surveillance; incidence

Abbreviations: CJD = Creutzfeldt-Jakob disease; NSW = New South Wales; *PRNP* = prion protein gene; RR_{MH} = Mantel–Haenszel rate ratio estimate; sCJD = sporadic CJD; SLA = statistical local area

Received July 29, 2008. Revised and Accepted October 20, 2008. Advance Access publication November 28, 2008

Introduction

In reported large national surveillance studies, the majority of Creutzfeldt-Jakob disease (CJD) cases are sporadic, occurring without apparent aetiology, while the remaining proportions have a genetic or iatrogenic aetiology (Masters *et al*., 1979; Brown *et al*., 1987; Ladogana *et al*., 2005). Genetic CJD is linked to various mutations in the prion protein gene (*PRNP*) (Kovacs *et al*., 2005b), while iatrogenic CJD has been recognized in association with neurosurgery, corneal transplants, dura mater grafts and human-derived pituitary hormone treatments (Brown *et al*., 2006). The origin of sporadic CJD (sCJD) remains enigmatic. Hypotheses include spontaneous conversion of the normal isoform of the prion protein to a disease-related conformer (PrPres) with progressive accumulation in the CNS thereafter, somatic *PRNP* mutations within brain neurons predisposing to misfolding to PrPres, and covert transmission events during the provision of health care (Collins *et al*., 1999; Lewis *et al*., 2002; Ward *et al*., 2002, 2008). Unidentified environmental factors and susceptibility to an environmental trigger may also be involved in disease aetiology. To date, there are very few proven risk factors for sCJD; the covariates of codon 129 methionine homozygosity, increasing age (Ladogana *et al*., 2005) and surgical history (Collins *et al*., 1999; Ward *et al*., 2002, 2008; Mahillo-Fernandez *et al*., 2008) have been shown to be associated with increased risk of disease in sporadic cases.

Long-term national surveillance units report differing annual sCJD incidence rates, ranging from 0.44 to 1.61 per million population (Ladogana *et al*., 2005), but occasionally much higher rates can occur for unclear reasons, even if only for short periods of time (Glatzel *et al*., 2002). The explanation for these differences and fluctuations in national incidence rates is uncertain although variation in case ascertainment is one potentially contributing factor. Spatio-temporal clustering of CJD has also been recognized and investigated previously in various global settings. These unusual geographical and temporal patterns of disease also tend to create public health interest and explanations are frequently sought. Attention is often directed towards potential environmental factors, and in relation to this rare, neurodegenerative disorder, this includes potential transmission events through medical interventions. However, intensive investigation of spatio-temporal clustering can lead to unexpected yet important insights, such as the delineation of the genetic basis, through inheritance of *PRNP* mutations, as the explanation for the high rates of disease in Slovakia (Mayer *et al*., 1977; Goldfarb *et al*., 1990; Kovacs *et al*., 2005b), Chile (Galvez *et al*., 1980), Israel (Kahana *et al*., 1974) and Italy (D'Alessandro *et al*., 1998). In contrast, a number of smaller sCJD clusters have been described in other countries, including Australia (Collins *et al*., 2002a), England (Matthews, 1975; Will and Matthews, 1982), Japan (Arakawa *et al*., 1991; Doi *et al*., 2008), France (D'Aignaux *et al*., 2002) and the USA (Farmer *et al*., 1978), and despite extensive evaluation, plausible explanations for the apparently higher case rates than expected have not been delineated.

In this study, formal geostatistical analysis confirmed an unusually high sCJD incidence rate in a geographically restricted coastal region of the Australian state of New South Wales (NSW). This area had been suspected to harbour an excessive number of sCJD from 1997 through local observation (Cohn *et al*., 2000), and routine national surveillance activities. Detailed epidemiological assessment did not disclose any likely horizontal transmission events but instead uncovered a heightened intensity of surveillance. This more intense level of surveillance was reflected by the significantly higher rates of referrals of suspect sCJD cases for evaluation and diagnostic testing of CSF for 14-3-3 protein detection by the Australian National CJD Registry, as well as higher neuropathological examination rates in suspect sCJD patients. We postulate this sustained, enhanced level of surveillance was due to the vigilance and motivation of local neurologists, culminating in higher CJD, and particularly sCJD, detection and consequently incidence rates. Overall, we believe this protracted period of more intense surveillance may offer a more accurate sCJD incidence rate in the Australian population rather than representing anomalous, spatial clustering of this rare, transmissible neurodegenerative disorder.

Methods

Study population

The data collected, and the analyses undertaken in this study, were subsumed under national surveillance activities of the Registry. The aims and methods of the Registry have been reported in detail previously, as has the study population in part (Collins *et al*., 2002b). In brief, ascertainment methods include: review of morbidity separation coding data from all university-affiliated tertiary referral hospitals in Australia, as well as the centralized data bases of State and Territory health departments; regular national death certificate searches; and semi-annual mail-out questionnaires to all neurologists and neuropathologists within Australia. In addition, the Registry offers a national diagnostic service, predominantly for detection of CSF 14-3-3 proteins, but also prion protein genotyping and specialized ancillary neuropathology techniques. CSF testing for 14-3-3 proteins has been available from September 1997, and has provided the overwhelming majority of annual notifications of suspected CJD since 1998. The Registry has a non-systematic approach to prion protein genotyping and this may lead to under-ascertainment of genetic CJD cases. Complementing the comprehensive prospective monitoring of human transmissible spongiform encephalopathies (TSEs) by the Registry since inception in 1993, all Australian cases have been retrospectively sought to January 1, 1970. The classification of definite and probable CJD cases by the Registry is in accordance with internationally recognized WHO diagnostic criteria (WHO, 2003). Through the combination of ascertainment measures, it was believed that the overwhelming majority of all human sporadic, genetic and iatrogenic cases of TSE within Australia were detected, particularly since 1993.

During the prospective surveillance period, restricted geographical regions of apparently higher sCJD incidence rates have been recognized, one of which has already been reported in detail (Collins *et al*., 2002a). The present cluster analysis was prompted by an ongoing seemingly disproportionate spatio-temporal grouping of sCJD in a circumscribed coastal region of NSW, Australia. As health care delivery in Australia is devolved to the State and Territory level with variations between these jurisdictions, the study was restricted to all suspect sCJD cases occurring in NSW during the period 1993–2006, as well

as all definite and probable sCJD cases whose death occurred in NSW during the same period. For the purposes of this study, 'suspect CJD' is defined as any person referred to the Registry for evaluation or on whom a CSF sample was received for 14-3-3 protein analysis. To be included, referral to the Registry of both suspect and confirmed CJD cases must have been made during the 1993–2006 epoch. This timeframe aligns with prospective ascertainment by the Registry and confidence in the surveillance of the majority of Australian CJD cases. Suspect cases that were referred or retrospectively ascertained within the designated period but died prior to or after 1993–2006, were excluded. Confirmed and suspect CJD cases must have lived within NSW with a known residential address for at least 1 year before death. This temporal criterion of one year was based on the shortest known incubation time between exposure to contaminated instruments or therapeutics and the onset of reported iatrogenic CJD (Brown *et al*., 2006). One definite CJD case was excluded from analysis on this basis.

Rates of suspect CJD referrals, and their neuropathologic examinations and CSF 14-3-3 protein testing, were determined for NSW and the area of significant geographical clustering. The rate of neuropathological examination for the NSW suspect CJD group was calculated on the basis of either a brain biopsy or post-mortem examination. For the assessment of geographical referral patterns of CSF for 14-3-3 protein analysis in NSW, all NSW-laboratory originating referrals from the commencement of the Registry's diagnostic testing in September 1997 to December 31, 2006 were included, regardless of test outcome. Geographical groupings of the referrals were based on residential address at the time of referral.

Age adjustment for rates of suspect CJD and CSF test referrals was based on notification age, except when notification occurred after death and death age was utilized. One suspect CJD case with an unknown birth date was not included in adjustment calculations. For neuropathologic examination rates in suspect CJD referrals, adjustment was based on age at death or age at notification, when death was not known to have occurred.

Estimated resident population by age group for NSW and statistical local areas (SLAs) for the period 1993–2006 was obtained from the Australian Bureau of Statistics (Australian Bureau of Statistics, 1994–1995, 1996–2006). For this period, the mean estimated resident population of NSW is 6 437 459 and from 2001, NSW consisted of 199 SLAs. The standardized mortality ratio was calculated for NSW and the specified SLAs based on all TSE deaths and separately, sporadic only CJD deaths occurring between 1993 and 2006 and with a NSW residential address at time of death. The single case that was excluded from the cluster analysis due to residential relocation to NSW less than 1 year before death was included in the CJD mortality rates calculation. The rationale for this inclusion is that the case is still attributed to NSW as a sCJD death and would have been clinically assessed and treated in the region with the possibility of posing a transmission risk.

As described previously (Collins *et al*., 2006), EEGs were considered typical for sCJD when displaying periodic sharp wave complexes. CSF 14-3-3 protein detection methods have been reported previously (Collins *et al*., 2000; Zerr *et al*., 2000). MRI brain changes considered characteristic of sCJD included increased T_2-weighted signal in the basal ganglia, thalamus and/or cerebral cortical regions, with greatest sensitivity achieved when using diffusion weighted imaging (DWI) and/or fluid attenuated inversion recovery (FLAIR) pulse sequences (Meissner *et al*., 2004; Shiga *et al*., 2004; Tschampa *et al*., 2005).

A review of employment, residential, surgical, dental, and ophthalmic procedure histories (based on medical records and a detailed questionnaire completed by relatives) was undertaken on all sCJD patients within the specified cluster SLAs, as part of routine case investigation. A questionnaire had not been completed for two cases. Data was compared for any linkage between cases.

Statistical analysis

Analysis was conducted at two levels: first, an image plot of the NSW CJD cases was created as a smooth bivariate function of the geographical data (longitude and latitude); second, statistical evidence of disease clustering was sought using a spatial, temporal and space–time scan statistic based on a Poisson model, using SaTScan software (Kulldorff, 2006). Input data on the NSW cases included geographical location, age group and sex while population data for the estimated populations at risk in NSW and the SLAs 1993–2006 was obtained from the Australia Bureau of Statistics (Australian Bureau of Statistics, 1994–1995, 1996–2006). Place of residence at death was utilized as residence history and stratified by geographical location, age groups (<65, 65–74, 75+) and gender. Geographical data coordinates of longitude and latitude for residential suburbs were obtained from the Australian Geoscience website (http://www.ga.gov.au/map/names/). Suburbs were then grouped according to SLA for analysis. Analyses were performed for the entire 1993–2006 epoch and then repeated for the 1993–1996 and 1997–2006 periods to allow comparisons to be made based on the premise that suspicions of a cluster (from 1997) had prompted enhanced surveillance thereafter.

As an initial step, we used geostatistical type models to construct an image plot over the entire NSW state by mapping the mean of a response of interest, y, based on data

$$(CJD_i, longitude_i, latitude_i),\ 1 \leq i \leq n$$

where CJD_i corresponds to sCJD cases in a particular region (image plot not shown). We applied the methodology (Kulldorff, 2002) by controlling for confounding effects of the other covariates such as age, which is known to be associated with higher CJD incidence rates regardless of other environmental exposures, and gender.

In recent years, Kulldorff's scan statistic has become the most widely used test for analysis of clustering, both because of its efficacy in detecting single 'hot spots' as well as the availability of the SaTScan software (Kulldorff, 2006) for implementing the test. The basic idea of the scan statistic is to allow circular windows of various sizes to range across the entire NSW state, centring on a large number of different locations. At each location, the rate of disease inside the window is compared to that outside the window. For an analysis of a rare disease in a case-only setting, such as CJD, we chose the Poisson probability model. A 'hot spot' is characterized by a higher localized rate of disease. For a given zone (circular window), the methodology calculates the probability of a data point being a case inside and outside the circle under evaluation. For each circle, a likelihood ratio is computed for the alternative hypothesis that there is an increased risk of disease inside the circle against the null hypothesis that the circle contains the same risk as the risk outside (Kulldorff, 2006). A 'cluster', in this context, is said to be detected within a defined geographical area during a specific time-frame if the area has a disproportionate excess in CJD mortality, when compared to the neighboring areas under study. By meeting the statistical assumptions of a set of statistical models, the unusual rise or reduction of mortality in a specific spatial and temporal window (with adjustments of age and gender) can be characterized by statistical significance. In this analysis, three options were tested; purely spatial, purely temporal and a combined spatial and temporal dimension. As a secondary analysis, any potential clusters were assessed for differences in gender proportions or age distribution using Fisher's exact test.

Table 1 Summary of SaTScan cluster analyses

Cluster analysis type		Unadjusted		Adjusted[a]	
Epoch[b]	Most likely cluster	Obs/exp cases	*P*-value	Obs/exp cases	*P*-value
Spatial only					
1993–2006	Cluster 1	14/4.46	0.012	14/5.01	0.032
1997–2006	Cluster 1	13/4.23	0.020	13/4.65	0.059
Temporal only					
1993–2006	1997–2001	47/41.19	0.142	47/41.15	0.144
1997–2006	1997–2001	47/42.04	0.325	47/42	0.338
Spatial × Temporal					
1993–2006	1997–2001 (Cluster 1)	8/2.39	0.10	8/2.64	0.156
1997–2006	1997–2001 (Cluster 1)	8/2.52	0.242	8/2.72	0.832

a Age (<65, 65–74, 75+) and gender.
b Analysis was performed on the 1993–1996 period for comparison to the 1997–2006 period. No significant clusters were identified for this epoch most likely due to the small sample size, $n = 17$, distributed into 15 SLAs.

Statistical analysis of the proportions and rates of referrals (suspect sCJD cases, CSF 14-3-3 protein analysis, and neuropathological examination) between the entire NSW study population and the specified SLAs, was performed using STATA (Intercooled Stata 7, Stata Corporation, College Station, TX). In order to adjust for potential confounding by age, rate ratios were adjusted using the Mantel–Haenszel estimate (RR_{MH}) and test for heterogeneity.

Results

For the period 1993–2006, there were 102 eligible definite and probable sCJD patients in NSW, drawn from 51 mutually exclusive geographical SLAs. SaTScan analyses performed on these 102 cases tested for spatial, spatial-temporal and temporal only clustering. Only one spatial cluster (designated 'Cluster 1'), comprising three contiguous geographical SLAs and 14 sCJD cases was found to have a significantly greater than expected number of cases (Table 1) ($P = 0.012$). Cluster 1 corresponded exactly to the geographical region previously recognized to have an apparently increased rate of sCJD during the course of routine national surveillance, which prompted the more formal cluster evaluation. Analyses for potential temporal clustering showed the most notable finding to be a non-significant grouping of cases during the 1997–2001 period (Table 1). Similarly, when combining the analysis to account for both temporal and spatial clustering, sCJD case numbers were in excess by five in Cluster 1 during the 1997–2001 period; however, this was again not significant.

The residential history of the 14 cases indicated that all had resided in the Cluster 1 area for two or more years (range, 2–43 years) and had moved to the area between the ages of 15–85 years. Four cases were long-term residents, having lived in the region for 25 or more years, while the remaining cases were either shorter-term residents ($n = 5$, 2–8 years) or medium-term ($n = 5$, 15–19 years). Ten cases moved to the area after the age of 55 and resided for an average of 11 years (range, 2–25 years).

Selected clinical features and investigation findings of the Cluster 1 cases are presented in Tables 2 and 3. The majority displayed rapidly progressive dementia (14/14) and myoclonus (12/14), and of those tested the EEG was typical in 71% and CSF positive for 14-3-3 proteins in 100%. There was a low rate of brain MRI scans reported as typical for sCJD (Table 3). However, of the 10 cases that were investigated by MRI, the type of pulse sequences were unknown for four cases but the initial radiologist reports described two patients with non-specific abnormalities only and two with normal findings. For the remaining six cases undergoing MRI, DWI and/or FLAIR sequences were performed and the images for four cases were available for independent review by two neurologists of the Registry. At review, MRIs were considered to have changes characteristic of sCJD in three cases, while the fourth was considered normal. The remaining fifth and sixth cases did not have images available for review but were officially reported as displaying features that were non-characteristic for CJD. Codon 129 genotype and/or prion protein glycotype was available for eight Cluster 1 cases with a mixture of subtypes identified (Table 3). Only 3 of the 14 cases had undergone *PRNP* genetic testing with no mutations found. In one case there was a family history of non-specific dementia in a first degree relative (parent) and in another case, non-specific psychiatric illness in a sibling. For the single case with a family history of non-specific psychiatric illness, ethnicity was linked to a European country with increased genetic human prion disease incidence (Kovacs and Majtenyi, 2005; Kovacs *et al*., 2005a) but in the absence of *PRNP* genetic analysis the case is classified as sCJD.

A comparison of the gender and age distributions of sCJD cases in Cluster 1 and the remainder of NSW (outside Cluster 1) showed a similar gender ratio but marked age differences (Table 2). In Australia, NSW and outside Cluster 1, the death age for the majority of cases was below 75 years (80%, 77% and 82%, respectively) (Table 2). Within the Cluster 1 group, however, 50% of the cases were 75 years or older, with the difference in the age distributions inside and outside Cluster 1 significant ($P = 0.0325$). Given this significantly older age of the sCJD cases in Cluster 1, and the recognition that this disease is age-related, an assessment for age biases in the Cluster 1 general population was undertaken. Between 1993 and 2006, the population in Cluster 1 was older compared to outside

Table 2 Age and gender distributions of sCJD in Cluster 1 compared with NSW and Australia

	1993–2006		Spatial - only cluster (1993–2006)		
	Australia	NSW	Inside Cluster	Outside Cluster	*P*-value*
N	300	102 (100%)	14 (14%)	88 (86%)	
Gender (% female)	165 (55%)	63 (62%)	9 (64%)	53 (60%)	0.810
Age (years)					
<65 (%)	36	33	21	35	0.0325
65–74 (%)	43	44	29	47	
⩾75 (%)	20	23	50	18	
Mean age at death (years) (SD)	66.5 ± 9.9	67.2 ± 9.8	71.8 ± 9.9	66.5 ± 9.6	
Median age at death (years) (IQR)	67 (60–73)	67 (62–73)	73 (65–79)	67 (59.5–72)	
Mean duration (months) (SD)	6.2 ± 7.0	5.5 ± 6.0	3.8 ± 2.4	5.8 ± 6.4	
Median duration (months) (IQR)	3.5 (2–7)	3.25 (2–6)	2.8 (2–4.25)	3.25 (2–7.1)	
Population over 65 years (%)[a]	12.4	13.0	16.4	12.7	<0.0001

*Inside versus outside cluster.
a Based on the average 1994–2006 estimated resident populations. (Australian Bureau of Statistics, 1994–1995, 1996–2006).

Table 3 Clinical features and investigation findings of Cluster 1 sporadic CJD cases

Case	Death Age (years)	Duration (months)	Definite/Probable CJD	RPD	Myoclonus	14-3-3 test positive	Typical MRI	Typical EEG	Codon 129	Glycotype	Past surgical history
1[a]	75	4	Probable	Y	Y	ND	ND	Y			Y
2[a]	52	2.8	Definite	Y	Y	ND	N	Y			Y
3[a]	82	2	Definite	Y	Y	ND	ND	Y			Y
4[a]	69	2	Definite	Y	Y	ND	N	N			Y
5	65	9	Definite	Y	Y	ND	Y	N	MV		Y
6	79	2.5	Definite	Y	N	Y	ND	Y			N
7	62	9	Definite	Y	Y	Y	N	N			Y
8	76	4	Definite	Y	Y	Y	N	Y	VV		Y
9	88	2.5	Definite	Y	NK	ND	N	Y	MM	2	Y
10	60	2	Definite	Y	Y	Y	N	Y	MM	2/3	Y
11	67	4.25	Definite	Y	Y	ND	ND	N	VV	3	Y
12	79	2.75	Definite	Y	Y	ND	N	Y	MM	2	Y
13	71	4.75	Definite	Y	Y	Y	Y	Y	MM	1/3	Y
14	81	2	Definite	Y	Y	Y	Y	Y	MM	1	Y

RPD = rapidly progressive dementia; NK = not known; ND = not done; MM = methionine homozygous; MV = methionine/valine heterozygous; VV = valine homozygous.
[a]Indicates cases previously published. (Cohn *et al*., 2000).

Cluster 1, particularly in the ⩾65 years age group ($P < 0.00001$). Nevertheless, even after adjustment for gender and age by stratifying definite and probable sCJD cases into <65 years, 65–74 years and ⩾75 year groups, spatial SaTScan analysis still showed a significant excess of cases in Cluster 1 ($P = 0.032$) (Table 1).

To further explore the significance of the increased number of cases in the Cluster 1 area, a review of all of definite and probable CJD cases (sporadic, familial and iatrogenic) that died in NSW between 1993 and 2006, regardless of their previous residential history was performed. Based on the total NSW and Cluster 1 cohorts, CJD mortality rates were still significantly higher in Cluster 1 compared with NSW [standardized mortality ratio (SMR) = 1.68, 95% CI = 1.04 → 2.70] (Table 4). This excess was also observed for sporadic CJD deaths (SMR = 1.68, 95% CI = 1.01 → 2.80).

Acknowledging the significant excess of sCJD in Cluster 1, we investigated potential explanations starting with possible case-to-case transmissions or point-source contamination events. An assessment of surgical (including ophthalmological) and other invasive medical procedures undertaken on the Cluster 1 cohort identified numerous interventions from 1938 to 2006 for all cases except one, where no surgical history was known. Only two possible cross-over events were recognized, although it is considered quite unlikely that any transmission would have occurred. The first episode relates to a neurosurgical procedure and a gastroscopy performed 4 days apart on two separate patients in the same institution. The second episode relates to two cases that were admitted to the same hospital within a 10-year window for minor pelvic and general surgical procedures; however specific procedure dates were unavailable to provide a meaningful insight into the possibility of a transmission event. There were a further

Table 4 Comparison of rates of CSF 14-3-3 protein testing, suspect CJD referrals, neuropathological examinations and CJD deaths in Cluster 1 and NSW

	NSW	Cluster 1 (% NSW)	Rate ratio[a] (95% CI)
NSW population 1993–2006 (%)		7.3%	
14-3-3 CSF test referrals 1997–2006			
N	576	78 (13.5%)	
Crude referral rate (ref/mil/yr)	8.76	16.19	1.59 (1.25 → 2.02)
Suspect case referrals 1993–2006			
N	648	93 (14.4%)	
Crude referral rate (ref/mil/yr)	7.20	14.20	1.68 (1.36 → 2.10)
Neuropathological examination of suspect cases 1993–2006			
N	138	28 (20.3%)	
Crude examination rate (exam/mil/yr)	1.53	4.26	2.34 (1.56 → 3.51)
Confirmed CJD[b] case deaths 1993–2006			
N	116	17 (14.6%)	
Crude mortality rate (cases/mil/yr)	1.29	2.59	
Standardized mortality ratio			1.68 (1.04 → 2.70)
Confirmed sCJD case deaths 1993–2006			
N	103	15 (14.5%)	
Crude mortality rate (cases/mil/yr)	1.14	2.28	
Standardized mortality ratio			1.68 (1.01 → 2.80)
Proportion of neurologists per capita	1 per 50000	1 per 50000	

a Age-adjusted.
b Includes sporadic, familial and iatrogenic CJD cases.

four patient pairs where admissions to hospital for acute care or non-CNS procedures (two hysterectomies, one colonoscopy and one gastroscopy, one lymph node removal/colonoscopy and one chest pain, one pan-endoscopy with gastric biopsy and one cardioversion for cardiac arrhythmia) occurred in the same year, raising the possibility of potential cross-over events; lack of information on the specific institutional locations of the care or procedures limited our ability to further evaluate and determine the significance of these potential linkages. Additional evaluation of surgical and non-surgical procedures performed on all Australian CJD cases (sporadic, genetic and iatrogenic) undertaken at institutions where Cluster 1 cases were admitted for health care, did not detect any convincing likelihood of transmission events.

Other potential linking mechanisms were examined for Cluster 1 cases but no apparent or plausible connections were found. These included: treating general practitioners; occupational history; and history of optometric assessments, dental procedures, blood donation or blood transfusion. Information pertaining to optometry was very poorly completed by family members and medical practitioners in our questionnaire; however, from the limited information available, no optometrist was found to have treated more than one patient. There was one case pair that may have attended the same ophthalmologist, however a linkage was not plausible due to a >17-year period between treatments. No overlap in general practitioners, including at disease onset, was found. Four cases were reported to have received a blood transfusion in their lifetime. In one patient where two transfusions were received, autologous blood was used for one transfusion, while the other was performed 3 days before death. In another case, a suggestion of a possible transfusion was reported by family but we were unable to confirm this through available medical records. The blood donation history of the 14 Cluster 1 cases showed that only four had donated blood. In an additional patient, it was unclear whether a donation had been made. Of the known donations, the last donation was in the 1970s.

Referral biases can lead to increased detection rates, especially when dealing with rare disorders like sCJD. Given the local recognition of an apparent increased incidence of sCJD in 1997, we considered the possibility that enhanced awareness and referral for evaluation were more likely thereafter, leading to increased incidence rates. Consequently, we performed comparative secondary SaTScan analyses for the periods 1993–1996 and 1997–2006 (Table 1). No significant clusters were identified for the earlier period but case numbers were small ($n = 17$). For the latter period, the spatial analysis identified Cluster 1 as the most likely cluster, almost achieving significance ($P = 0.059$); temporal and spatial-temporal analyses were non-significant, similar to the results for the overall period.

With the results of the secondary analyses suggesting potential detection bias, this issue was further explored. Ten neurologists were involved with one or more (eight involved with two or more) of the Cluster 1 cases and two geriatricians were involved with two or more cases. When comparing the referral patterns of the 14 sCJD cases from Cluster 1, we found that clinicians were an over-represented factor in notifying the ANCJDR of potential cases either through direct contact (six), semi-annual mailout cards to neurologists/neuropathologists (two) or through referrals for CSF 14-3-3 protein detection (six). Analysis of the proportions of neurologists per population based on 2007 estimates (MDA, 2007; Australian Bureau of Statistics, 2008) indicate that NSW and the Cluster 1 population have the equivalent proportions of neurologists (1 neurologist per 50 000 persons), which is within the range observed for other Australian States and Territories (0.6–1.05 neurologists per 50 000 persons). Excessive referrals of suspect cases in the Cluster 1 area are therefore unlikely to be related to an excessive number of neurologists servicing the population.

Further investigation of potential referral biases in Cluster 1, included examining overall suspect sCJD referrals and CSF referrals for 14-3-3 protein testing. From the CSF referrals originating

from NSW between 1997 and 2006, 13.5% were from patients that resided in the Cluster 1 geographical region at the time of referral. For the same period the referral rate for Cluster 1 was 59% greater than the NSW rate (age-adjusted RR_{MH}: 1.59, 95% CI = 1.25 → 2.02) (Table 4). In conjunction with the increased CSF referrals from the Cluster 1 region, the rate of suspect CJD case referrals from Cluster 1 was also found to be significantly higher than case referrals for NSW for the 1993–2006 epoch (age-adjusted RR_{MH}, 1.68, 95% CI = 1.36 → 2.10). The likelihood of referred suspect cases being confirmed as probable or definite CJD (all CJD types) was examined and found not to be different between the Cluster 1 area and NSW. This was also the case for sporadic CJD cases alone. Neuropathological examination of the brain was performed in a greater proportion of sCJD patients from Cluster 1 (13/14) (Table 3), compared to proportion of cases outside Cluster 1 (53/88). Of all suspect NSW case referrals, 21.3% underwent neuropathological examination, while in Cluster 1 the proportion of cases examined was 30.1%, with the difference between the rates not significant. However, when comparing the population-based rates, the rate of neuropathological examination was found to be almost two and half times greater in Cluster 1 compared with NSW (age-adjusted RR_{MH}, 2.34, 95% CI = 1.56 → 3.51).

Discussion

Despite the overall rarity of CJD, clustering of apparently sCJD has been repeatedly identified (Matthews, 1975; Farmer *et al*., 1978; Will and Matthews, 1982; Arakawa *et al*., 1991; D'Aignaux *et al*., 2002; Collins *et al*., 2002a). Given the transmission risk of these disorders, an important priority is to investigate any geographically confined excess occurrence, to identify whether transmission events or other circumstances have been extant that may pose risks to the general public. Illustrating this principle was the outcome of the detailed epidemiological investigation of a small United Kingdom cluster of the bovine spongiform encephalopathy related disorder variant CJD, wherein local butchering methods may have lead to contamination of meat products destined for human consumption (Bryant and Monk, 2001). In contrast however, such as in the present investigation, extensive analysis may highlight surveillance parameters and health care management that appear to lead to significantly improved case ascertainment.

Our analyses confirmed a disproportionate geographical grouping of 14 cases of sCJD between 1993 and 2006 in a NSW coastal area. This greater than expected number of cases was dependent on spatial dimensions, rather than temporal determinants, suggesting that the cases were evenly distributed temporally throughout the epoch. However, our secondary analyses based on dichotomizing the entire epoch around the point in time when an increased number of cases were first recognized in the region, showed that the vast majority (13/14) of Cluster 1 cases occurred in the 1997–2006 period. As a corollary, spatial analysis on this time period again yielded Cluster 1 as the most likely cluster, almost achieving significance. The increased case numbers and almost significant spatial clustering for the latter time period alone is consistent with the postulate that the sustained higher than expected incidence of sCJD in this circumscribed region of NSW, is most likely due to a more intense level of surveillance from 1997, which appeared to be directly facilitated by the local managing clinicians. This hypothesis is entirely consistent with the operation of the Registry wherein the Registry relies predominantly on the clinical perspicacity of the managing physicians to suspect CJD and then their motivation to refer these cases for diagnostic testing and clinical evaluation. The enhanced ongoing detection of cases after a few have been identified is not necessarily surprising and has been recognized previously, such that once an initial case is confirmed in a given geographical location, the potential to identify another case increases (Raubertas *et al*., 1989).

There was clear evidence to support the postulate of a physician driven enhanced surveillance. Both the rate of referral for CSF 14-3-3 protein testing and the rate of referral of suspect CJD cases per population notified to the Registry were significantly higher in the Cluster 1 area, suggesting that clinicians were more readily referring cases to the Registry compared to NSW overall, even after adjusting for age differences. The positive trend could not be explained by an elevated level of service by neurological specialists in the area as there was no difference between NSW and Cluster 1. Another measure of the interest and motivation of the region's clinicians to confirm CJD cases could be gauged by the likelihood that a given suspect CJD case would undergo neuropathological examination. Although the proportions of suspect CJD referrals that were examined neuropathologically were similar in Cluster 1 and NSW overall, when analysed as a rate per the general population, Cluster 1 had over double the rate to that of the whole state. Given that the rate of referral of suspect CJD cases and neuropathological assessments in Cluster 1 were approximately twice that of the entire state, the similar case confirmation ratios observed in the Cluster 1 area and NSW translated into approximately double the incidence of sCJD. Simply stated, double the rate of referral of suspect CJD cases combined with double the rate of neuropathological examinations equated to double the incidence of sCJD. On a national level, a greater number of ante-mortem referrals have been shown to correlate with an increased number of case confirmations (Klug *et al*., 2007). Although seeming somewhat intuitive that more intense surveillance will most likely culminate in higher ascertainment, this is the first study of sCJD to offer actual quantification of any potential correlation between the level of surveillance intensity (measured as a composite of clinical referrals and diagnostic test rates per population) and disease incidence. As such, we posit that the incidence of sCJD in Cluster 1 may be a more accurate measure of the true disease incidence in the Australian population, similar to the sCJD mortality rates of >2 cases/million population/year observed in some European countries (Glatzel *et al*., 2002; Gelpi *et al*., 2008), and contend that more intense surveillance may lead to even higher rates as already reported for brief periods by other national surveillance units (Glatzel *et al*., 2002).

A distinguishing clinical feature of the Cluster 1 cases was their older age at death, when compared to both NSW and the entire Australian cohort of sCJD. While this may have reflected the older

age population of the area, it is consistent with a greater than usual capacity to detect older age sCJD. Other European countries, including Austria where autopsy in suspect CJD cases is mandatory, have found that an increased incidence of sCJD (>2 cases/million population/year) has been associated with increased detection of older age cases (Glatzel *et al*., 2002; Ladogana *et al*., 2005; Van Everbroeck *et al*., 2006; Gelpi *et al*., 2008). This suggests that systematic under-ascertainment of sCJD in the older age population is possible in many countries due to a number of factors, including diagnostic difficulties due to the early symptomatic phase of CJD imitating other dementias and restricted medical resource allocation to the elderly.

Although our strongest suspicion is that the managing clinicians in the Cluster 1 area were well-primed to investigate and confirm CJD cases, it remains possible that other factors unrelated to enhanced surveillance may have contributed to, or explain, the increased number of sCJD in the region. It is conceivable that the cluster could have occurred by chance alone, as apparent clusters are inherent in randomness. This has been seen previously in Australia (Collins *et al*., 2002a) and with variant CJD in the United Kingdom (Cousens *et al*., 1999). In Australia, a cluster of six cases in a rural city was identified between 1988 and 2000 and was concluded to have been a chance occurrence. Since this time, no further cases have been confirmed in the area (personal communication, S. Collins) which supports the initial conclusion. In this study, our analysis of case records did not support a definite or likely instance of causal transmission linkage between any cases; however, it cannot be completely dismissed that the Registry's case record details may be incomplete or influenced by recall error from those completing case questionnaires. This leaves the possibility that some of the excess cases may have arisen through covert transmission events. A further limitation of the cluster cohort is the low proportion of cases with complete *PRNP* genetic analysis, thereby limiting our ability to rule out the possibility of an underlying genetic aetiology in some cases. Finally, a comparison of the age groups of NSW and the Cluster 1 area revealed a small but significant difference between the age structures of the areas with a trend towards an older age population in Cluster 1. Since the disease is age-dependent, it could be speculated that the higher rate simply reflected the older age population. We are confident this is not the explanation given that age-adjustment did not alter the finding that there were significantly more cases of sCJD than expected in Cluster 1.

In conclusion, we believe that vigilant and motivated managing clinicians in a geographically circumscribed area of NSW evinced a sustained higher level of clinical awareness for the broad phenotypic spectrum of CJD with reliable referral of suspect cases for further investigation. In addition, these physicians established and maintained a well coordinated and active approach to suspect CJD autopsy. The combination of these factors translated into a higher intensity of surveillance at approximately twice the rate per population observed for the entire state, culminating in twice the incidence of sCJD at around 2.28 cases/million population/year. The hypothesis that intensity of surveillance for rare disorders such as sCJD can be quantified and correlates positively with disease incidence deserves further exploration and may prove to be an important insight into the varying incidence rates over periods of time within individual nations and between different countries, particularly in light of declining variant and iatrogenic CJD case numbers and a potential waning of awareness of CJD in the years to come. This type of improved understanding could provide strategies to maintain optimal national and potentially global surveillance.

Acknowledgements

The Australian National Creutzfeldt-Jakob disease Registry is funded by the Commonwealth Department of Health and Ageing. We would like express gratitude to families for their generous support for CJD surveillance and research. The assistance of medical practitioners and health care workers who assist the Registry undertake surveillance activities in Australia is heavily relied upon and greatly appreciated. We wish to acknowledge the team at the Neuropathology Department at The University of Sydney; Prof. Clive Harper and Dr Roger Stankovic, and the Central Sydney Area Health Service, Department of Forensic Medicine. The local clinicians who have contributed significantly to the surveillance of CJD include Dr Jeff Blackie, Dr Denis Crimmins, Dr Margaret Filiptschuk, Dr David Floate, Dr Robert Heard, Dr Chris Levi, Dr Peter Lipski, Dr Mark Parsons, Dr Elizabeth Reyneke, Dr Peter Schofield, Dr Jonathan Sturm and Dr Bernard A. Walsh.

References

Arakawa K, Nagara H, Itoyama Y, Doh-ura K, Tomokane N, Tateishi J, et al. Clustering of three cases of Creutzfeldt-Jakob disease near Fukuoka City, Japan. Acta Neurol Scand 1991; 84: 445–7.

Australian Bureau of Statistics. Estimated resident population by age and sex in statistical local areas, New South Wales (Catalogue No. 3209.1, 30 June 1994, 1995). Canberra: ABS; 1994–1995.

Australian Bureau of Statistics. Population by age and sex, New South Wales (Catalogue No. 3235.1 30 June 1996, 1997, 1998, 1999, 2000, 2001, 2002, 2003, 2004, 2005, 2006). Canberra: ABS; 1996–2006.

Australian Bureau of Statistics. Regional Population Growth, Australia, 2006–07 (Catalogue No. 3218.0, 31 March 2008). Canberra: ABS; 2008.

Brown P, Brandel JP, Preece M, Sato T. Iatrogenic Creutzfeldt-Jakob disease: the waning of an era. Neurology 2006; 67: 389–93.

Brown P, Cathala F, Raubertas RF, Gajdusek DC, Castaigne P. The epidemiology of Creutzfeldt-Jakob disease: conclusion of a 15-year investigation in France and review of the world literature. Neurology 1987; 37: 895–904.

Bryant GMC, Monk PN. Final report of an investigation into the north Leicestershire cluster of variant Creutzfeldt-Jakob disease. Leicestershire Health Authority. http://www.hpa.org.uk/web/HPAwebFile/HPAweb_C/1194947321932 2001.

Cohn DA, Crimmins DS, Heard R, Rose M. Creutzfeldt-Jakob disease: the need for vigilance. J Clin Neurosci 2000; 7: 277–9.

Collins S, Boyd A, Fletcher A, Gonzales M, McLean CA, Byron K, et al. Creutzfeldt-Jakob disease: diagnostic utility of 14-3-3 protein immunodetection in cerebrospinal fluid. J Clin Neurosci 2000; 7: 203–8.

Collins S, Boyd A, Fletcher A, Kaldor J, Hill A, Farish S, et al. Creutzfeldt-Jakob disease cluster in an Australian rural city. Ann Neurol 2002a; 52: 115–8.

Collins S, Boyd A, Lee JS, Lewis V, Fletcher A, McLean CA, et al. Creutzfeldt-Jakob disease in Australia 1970-1999. Neurology 2002b; 59: 1365–71.

Collins S, Law MG, Fletcher A, Boyd A, Kaldor J, Masters CL. Surgical treatment and risk of sporadic Creutzfeldt-Jakob disease: a case-control study. Lancet 1999; 353: 693–7.

Collins SJ, Sanchez-Juan P, Masters CL, Klug GM, van Duijn C, Poleggi A, et al. Determinants of diagnostic investigation sensitivities across the clinical spectrum of sporadic Creutzfeldt-Jakob disease. Brain 2006; 129: 2278–87.

Cousens SN, Linsell L, Smith PG, Chandrakumar M, Wilesmith JW, Knight RS, et al. Geographical distribution of variant CJD in the UK (excluding Northern Ireland). Lancet 1999; 353: 18–21.

D'Aignaux JH, Cousens SN, Delasnerie-Laupretre N, Brandel JP, Salomon D, Laplanche JL, et al. Analysis of the geographical distribution of sporadic Creutzfeldt-Jakob disease in France between 1992 and 1998. Int J Epidemiol 2002; 31: 490–5.

D'Alessandro M, Petraroli R, Ladogana A, Pocchiari M. High incidence of Creutzfeldt-Jakob disease in rural Calabria, Italy. Lancet 1998; 352: 1989–90.

Doi Y, Yokoyama T, Sakai M, Nakamura Y, Tango T, Takahashi K. Spatial clusters of Creutzfeldt-Jakob disease mortality in Japan between 1995 and 2004. Neuroepidemiology 2008; 30: 222–8.

Farmer PM, Kane WC, Hollenberg-Sher J. Incidence of Creutzfeldt-Jakob disease in Brooklyn and Staten Island. N Engl J Med 1978; 298: 283–4.

Galvez S, Masters C, Gajdusek C. Descriptive epidemiology of Creutzfeldt-Jakob disease in Chile. Arch Neurol 1980; 37: 11–4.

Gelpi E, Heinzl H, Hoftberger R, Unterberger U, Strobel T, Voigtlander T, et al. Creutzfeldt-Jakob disease in Austria: an autopsy-controlled study. Neuroepidemiology 2008; 30: 215–21.

Glatzel M, Rogivue C, Ghani A, Streffer JR, Amsler L, Aguzzi A. Incidence of Creutzfeldt-Jakob disease in Switzerland. Lancet 2002; 360: 139–41.

Goldfarb LG, Mitrova E, Brown P, Toh BK, Gajdusek DC. Mutation in codon 200 of scrapie amyloid protein gene in two clusters of Creutzfeldt-Jakob disease in Slovakia. Lancet 1990; 336: 514–5.

Kahana E, Alter M, Braham J, Sofer D. Creutzfeldt-jakob disease: focus among Libyan Jews in Israel. Science 1974; 183: 90–1.

Klug GM, Boyd A, Lewis V, Douglass SL, Roberts H, Argent R, et al. Creutzfeldt-Jakob disease: Australian surveillance update to March 2007. Commun Dis Intell 2007; 31: 194–7.

Kovacs GG, Laszlo L, Bakos A, Minarovits J, Bishop MT, Strobel T, et al. Increased incidence of genetic human prion disease in Hungary. Neurology 2005a; 65: 1666–9.

Kovacs GG, Majtenyi K. Creutzfeldt-Jakob disease in Hungary. Folia Neuropathol 2005; 43: 279–85.

Kovacs GG, Puopolo M, Ladogana A, Pocchiari M, Budka H, van Duijn C, et al. Genetic prion disease: the EUROCJD experience. Hum Genet 2005b; 118: 166–74.

Kulldorff M. Geographical distribution of sporadic Creutzfeldt-Jakob disease in France. Int J Epidemiol 2002; 31: 495–6.

Kulldorff M. SaTScan^{TM} v7.0: Software for the spatial and space-time scan statistics. Information Management Services Inc., 2006.

Ladogana A, Puopolo M, Croes EA, Budka H, Jarius C, Collins S, et al. Mortality from Creutzfeldt-Jakob disease and related disorders in Europe, Australia, and Canada. Neurology 2005; 64: 1586–91.

Lewis V, Boyd A, Masters CL, Collins SJ. Apparently sporadic CJD and covert health-care transmissions. Lancet Neurol 2002; 1: 470–1.

Mahillo-Fernandez I, de Pedro-Cuesta J, Bleda MJ, Cruz M, Molbak K, Laursen H, et al. Surgery and Risk of Sporadic Creutzfeldt-Jakob Disease in Denmark and Sweden: Registry-Based Case-Control Studies. Neuroepidemiology 2008; 31: 229–40.

Masters CL, Harris JO, Gajdusek DC, Gibbs CJ Jr, Bernoulli C, Asher DM. Creutzfeldt-Jakob disease: patterns of worldwide occurrence and the significance of familial and sporadic clustering. Ann Neurol 1979; 5: 177–88.

Matthews WB. Epidemiology of Creutzfeldt-Jakob disease in England and Wales. J Neurol Neurosurg Psychiatry 1975; 38: 210–3.

Mayer V, Orolin D, Mitrova E. Cluster of Creutzfeldt-Jakob disease and presenile dementia. Lancet 1977; 2: 256.

MDA. Medical Directory of Australia. Sydney: The Australasian Medical Publishing Company Pty Ltd; 2007 (CD-ROM).

Meissner B, Kortner K, Bartl M, Jastrow U, Mollenhauer B, Schroter A, et al. Sporadic Creutzfeldt-Jakob disease: magnetic resonance imaging and clinical findings. Neurology 2004; 63: 450–6.

Raubertas RF, Brown P, Cathala F, Brown I. The question of clustering of Creutzfeldt-Jakob disease. Am J Epidemiol 1989; 129: 146–54.

Shiga Y, Miyazawa K, Sato S, Fukushima R, Shibuya S, Sato Y, et al. Diffusion-weighted MRI abnormalities as an early diagnostic marker for Creutzfeldt-Jakob disease. Neurology 2004; 63: 443–9.

Tschampa HJ, Kallenberg K, Urbach H, Meissner B, Nicolay C, Kretzschmar HA, et al. MRI in the diagnosis of sporadic Creutzfeldt-Jakob disease: a study on inter-observer agreement. Brain 2005; 128: 2026–33.

Van Everbroeck B, Michotte A, Sciot R, Godfraind C, Deprez M, Quoilin S, et al. Increased incidence of sporadic Creutzfeldt-Jakob disease in the age groups between 70 and 90 years in Belgium. Eur J Epidemiol 2006; 21: 443–7.

Ward HJ, Everington D, Cousens SN, Smith-Bathgate B, Gillies M, Murray K, et al. Risk factors for sporadic Creutzfeldt-Jakob disease. Ann Neurol 2008; 63: 347–54.

Ward HJ, Everington D, Croes EA, Alperovitch A, Delasnerie-Laupretre N, Zerr I, et al. Sporadic Creutzfeldt-Jakob disease and surgery: a case-control study using community controls. Neurology 2002; 59: 543–8.

WHO. WHO manual for surveillance of human transmissible spongiform encephalopthies including variant Creutzfeldt-Jakob disease, 2003.

Will RG, Matthews WB. Evidence for case-to-case transmission of Creutzfeldt-Jakob disease. J Neurol Neurosurg Psychiatry 1982; 45: 235–8.

Zerr I, Pocchiari M, Collins S, Brandel JP, de Pedro Cuesta J, Knight RS, et al. Analysis of EEG and CSF 14-3-3 proteins as aids to the diagnosis of Creutzfeldt-Jakob disease. Neurology 2000; 55: 811–5.

Neuroscience Letters 472 (2010) 16–18

Contents lists available at ScienceDirect

Neuroscience Letters

journal homepage: www.elsevier.com/locate/neulet

No evidence for prion protein gene locus multiplication in Creutzfeldt-Jakob disease

Steven J. Collins[a,c,*], Maaike Schuur[b,d], Alison Boyd[a,c], Victoria Lewis[a,c,1], Genevieve M. Klug[a,c], Amelia McGlade[a,c], Andrew van Oosterhout[b], Guido Breedveld[e], Ben A. Oostra[e], Colin Masters[a,c], Cornelia M. Van Duijn[b,**]

[a] Australian National CJD Registry, Department of Pathology, The University of Melbourne, Parkville 3010, Australia
[b] Department of Epidemiology, Erasmus MC University Medical Center, Rotterdam, The Netherlands
[c] Mental Health Research Institute of Victoria, The University of Melbourne, Parkville 3010, Australia
[d] Department of Neurology, Erasmus MC University Medical Center, Rotterdam, The Netherlands
[e] Department of Clinical Genetics, Erasmus MC University Medical Center, Rotterdam, The Netherlands

ARTICLE INFO

Article history:
Received 7 December 2009
Accepted 19 January 2010

Keywords:
Creutzfeldt-Jakob disease
Dementia
Prion disease
Prion protein gene multiplication

ABSTRACT

Precedent of causative multiplication of key gene loci exists in familial forms of both Alzheimer's and Parkinson's diseases. Genetic Creutzfeldt-Jakob disease (CJD) is often clinically indistinguishable from sporadic disease and inexplicably, a negative family history of a similar disorder occurs in around 50–90% of patients harboring the most common, disease-associated, prion protein gene (*PRNP*) mutations. We undertook semi-quantitative analysis of the *PRNP* copy number in 112 CJD patients using quantitative polymerase chain reaction. All included cases satisfied classification criteria for probable or definite sporadic CJD, ascertained as part of longstanding, prospective, national surveillance activities. No examples of additional copies of the *PRNP* locus as an explanation for their disease was found in any of the 112 sporadic CJD patients. Hence, contrasting with more common, age-related neurodegenerative diseases, the genetic aetiology in human prion disease continues to appear entirely restricted to small scale mutations within a single gene, with no evidence of multiplication of this validated candidate gene locus as a cause.

Creutzfeldt-Jakob disease (CJD) constitutes the most common human phenotype of the rare, transmissible neurodegenerative disorders known as prion diseases, with this disorder characterized by rapidly progressive dementia with a median survival of only 4–5 months [4]. In contrast to variant CJD, a zoonosis related to bovine spongiform encephalopathy, most CJD (approximately 85%) occurs without explanation (sporadic), with detectable mutations in the prion protein gene (*PRNP*) accounting for only 10–15% of cases (genetic) and the very small remainder due to inadvertent health care related transmissions (iatrogenic) [4]. Although unrecognized or covert horizontal transmission related to surgery or other medical procedures is presumed to explain some apparently sporadic CJD [3], this contentious mechanism is quite unlikely to be the basis for all such cases.

Analogous to the much more common neurodegenerative disorders Alzheimer's disease (AD) and Parkinson's disease (PD), which are also patho-aetiologically linked to the accumulation of neurotoxic protein species within the CNS [9,12] sporadic CJD evinces a notable increase in incidence with age [7]. Diverse evidence suggests a decline in proteasomal function occurs with advancing age [1], with the likely compromise in protein clearance thought to be one pathogenic factor contributing to the progressive build-up of certain abnormal polypeptides, such as Aβ and α-synuclein so commonly observed in the brains of older individuals. Further illustrating age-related effects on protein homeostasis and the capacity of neurons to maintain a critical balance between protein synthesis and the maintenance of quality control are examples of overexpression such as Down's syndrome due to trisomy of chromosome 21 and carriers of duplications of the Amyloid Precursor Protein (APP) gene. The presence of an extra copy of the APP gene is almost invariably associated with the early development of AD brain pathology [11,13]. Similarly, the *PARK 4* autosomal dominant form of genetic PD is explained by either duplication [5] or triplication [10] of the α-synuclein gene (*SNCA*) locus, which results in

* Corresponding author at: Australian National CJD Registry, Level 5 The Medical Building, Department of Pathology, The University of Melbourne, Parkville, Victoria 3010, Australia. Tel.: +61 3 8344 1949; fax: +61 3 9349 5105.
** Corresponding author. Tel.: +31 10 7043391; fax: +31 10 7044657.
E-mail addresses: stevenjc@unimelb.edu.au (S.J. Collins), c.vanduijn@erasmusmc.nl (C.M. Van Duijn).
[1] Present address: Institute of Molecular and Cellular Biology, Faculty of Biological Sciences, LIGHT Laboratories, Clarendon Way, University of Leeds, Leeds LS2 9JT, United Kingdom.

0304-3940/$ – see front matter © 2010 Elsevier Ireland Ltd. All rights reserved.
doi:10.1016/j.neulet.2010.01.043

Table 1
Summary of cases undergoing semi-quantitative analysis of the *PRNP* locus.

Country	Definite sCJD	Probable sCJD	Male	Female	Total	Age range, years[a] (mean)	sCJD aged <61 years
Australia	48		19	29	48		
Netherlands	41	23	26	38	64		
Combined	89	23	67	45	112	34–87 (65.4)	35

[a] Ages are at time of death.

the invariable development of disorders either recapitulating PD or dementia with Lewy bodies, with gene dosage directly correlating with younger age of onset and greater neuropathological severity.

Current diagnostic criteria for sporadic CJD require the absence of mutations in the *PRNP* or exclusion of a positive family history of prion disease in first degree relatives. Analogous to phenotypes observed in some *PARK 4* kindreds in comparison to idiopathic PD [5], genetic CJD is often clinically indistinguishable from sporadic disease. Of further importance, the penetrance of many *PRNP* mutations appears to be low, as a negative family history of a similar disorder occurs in around 50–90% of patients harboring the most common *PRNP* mutations associated with the CJD phenotype [6]. To date, only point mutations and polynucleotide insertions and deletions restricted to the open reading frame of *PRNP* are recognized as causally related to genetic CJD [4]; no gene locus multiplications have been reported, which contrasts with the findings in PD and AD. Acknowledging the aforementioned, and the fact that conventional genetic analytical techniques are insensitive for detecting disease-associated large scale chromosomal rearrangements [10], we undertook the present study to semi-quantitatively assess whether multiplication of the *PRNP* locus was an occasional explanation for disease in a cohort of classified sporadic CJD patients, especially in younger age at onset cases.

Many of the Australian and Dutch patients included in the present study have been reported on previously [2,7]. All included cases satisfied classification criteria for probable or definite sporadic CJD, ascertained as part of longstanding, prospective, national surveillance activities with case definitions and surveillance methods described previously [2,7]. In brief, definite cases were pathologically confirmed, while probable cases had alternative diagnoses excluded and manifested rapidly progressive dementia (of less than 2 years duration), accompanied by any two of myoclonus, visual or cerebellar dysfunction, extrapyramidal or pyramidal signs or akinetic mutism, with an EEG showing typical periodic discharges or the presence of 14-3-3 proteins in the CSF. Permission for inclusion in research studies was obtained for all patients.

For Dutch cases, genomic DNA was extracted from whole blood samples according to a standard non-phenol:chloroform method [8]. For Australian cases, genomic DNA was extracted using a phenol:choloroform extraction method. Briefly, approximately 50 mg frozen brain tissue was homogenised in 450 μl DNA extraction buffer (100 mM NaCl, 10 mM Tris–Cl pH 8.0, 25 mM EDTA pH 8.0, 0.5% (w/v) SDS), by passing through 18 g, then 20 g needles. Proteins were digested overnight at 37 °C by addition of proteinase K (final concentration 1 mg/ml). An equal volume of phenol:chloroform (phenol:chloroform:isoamyl alcohol, 25:24:1, Pierce) was added, samples mixed gently, and centrifuged for 5 min, maximum speed in a bench top microfuge (approximately 13,000 rpm). The aqueous (top) layer was removed to a fresh tube, and the phenol:chloroform extraction was repeated twice more, or until there was no white precipitate at the interface between the organic and aqueous layers. The extraction was then repeated, substituting the phenol:chloroform with chloroform. DNA was precipitated from the final aqueous layer by the addition of 2.5 times the volume of ice cold 100% ethanol, which was pelleted by centrifugation at maximum speed in a bench top microfuge at 4 °C. The DNA pellet was then washed with 70% ethanol, allowed to air dry, and re-suspended in an appropriate volume of sterile Milli-Q H_2O.

PRNP gene locus copy number variation was analysed by qPCR (Hydrolysis Probes). For the *PRNP* locus, we used a FAM labeled Applied Biosystems TaqMan probe (Hs01940892) located in exon 2 of the *PRNP* gene (NM_000311) and the RNase P Control Reagents Kit (VIC labeled, Applied Biosystems) as reference locus. Both probes (final concentration 1×) were tested in one single reaction, total volume 20 μl, containing 1× qPCR MasterMix Plus w/o UNG (Eurogentec) and 15 ng of genomic DNA using an Applied Biosystems 7300 Real Time PCR System. The amplification protocol was as follows: initial denaturation for 10 min at 95 °C followed by 40 cycles of denaturation at 95 °C for 15 s and annealing, extension and data collection at 60 °C for 60 s. Relative quantification was performed using the RQ-Study Application from the Sequence Detection (SDS) software V1.3.1 (Applied Biosystems). The linear amplification phase for analysis of *PRNP* was generally observed between 25 and 27 cycles.

A total of 112 sporadic CJD patients (89 definite, 23 probable) underwent *PRNP* locus quantification by qPCR; in three additional cases amplification was attempted but was unsuccessful (two due to degraded DNA; one for unclear reasons). Table 1 summarizes the demographic features of analysed cases. The ages of the 112 patients at time of death ranged from 34 to 87 years (mean 65.4 years), with 67 females (59.8%). Thirty-five individuals (31.3%) were 60 years of age or younger at their time of death, with 12 (10.7%) less than 56 years. None of the 112 successfully, semi-quantitatively, assessed sporadic CJD cases showed evidence of a definite increase in *PRNP* locus copy number with the relative quantification range 0.76–1.39 (normal: 0.7–1.3); two patients each had copy ratios just above the normal range on a single occasion, which were within the reference range on repeat testing.

Despite precedent in other age-related neurodegenerative diseases, albeit with more overt genetic associations, our study of 112 sporadic CJD patients failed to disclose any examples of additional copies of the *PRNP* locus as an explanation for their disease. Although investigation of familial CJD occurring in the absence of *PRNP* mutations would perhaps, *a priori*, be considered more likely to uncover locus copy number multiplication, such pedigrees were not available. We speculated that given the insensitivity of conventional analytical techniques to gene locus multiplication and through extrapolated analogy to the unexplained but very frequent occurrence of a negative family history despite probands harboring causative *PRNP* mutations, it was reasonable to investigate a sizeable cohort of apparently sporadic CJD patients.

Even though the number of cases included in our study is perhaps comparatively small, this finding certainly militates against undetected duplication or triplication of this genetic locus constituting a relatively common cause and possibly excludes this type of genetic basis as even a rare cause of apparently sporadic disease. From previous reports of *PARK 4* kindreds, age of disease onset correlates with gene dosage, although for *SNCA* duplications ages at onset were only modestly or equivocally reduced in comparison to idiopathic PD [5] with the most dramatic effects observed in relation to triplication of *SNCA* [10]. With nearly one third of our sporadic CJD cohort below the mean age at death reported for this disease (around 65–70 years) [2], we believe our studied group

included optimally aged patients to detect this type of underlying genetic disorder.

In conclusion, contrasting with the more common, age-related neurodegenerative diseases AD and PD, the genetic aetiology in human prion disease continues to appear entirely restricted to small scale mutations within a single gene, the *PRNP*, with no evidence of multiplication of this validated candidate gene locus as a cause.

Conflict of interest

The authors declare that they have no conflict of interest.

Acknowledgements

The Australian National Creutzfeldt-Jakob disease Registry (ANCJDR) is funded by the Commonwealth Department of Health and Ageing. This work was supported in part by an NH&MRC Program Grant (#400202). SJC is supported by an NH&MRC Practitioner Fellowship (#400183) and by an NH&MRC Project Grant (#454546). The Dutch CJD Surveillance is funded by the Dutch Ministry of Health, Welfare and Sports. The ANCJDR and the Dutch Surveillance Center thank the families of all the sporadic CJD patients and their managing clinicians for their support.

The methodology undertaken in this study complies with the ethical standards and statutes of the participating countries.

References

[1] G. Carrard, A.L. Bulteau, I. Petropoulos, B. Friguet, Impairment of proteasome structure and function in aging, The International Journal of Biochemistry & Cell Biology 34 (2002) 1461–1474.
[2] S. Collins, A. Boyd, J.S. Lee, V. Lewis, A. Fletcher, C.A. McLean, M. Law, J. Kaldor, M.J. Smith, C.L. Masters, Creutzfeldt-Jakob disease in Australia 1970–1999, Neurology 59 (2002) 1365–1371.
[3] S. Collins, M.G. Law, A. Fletcher, A. Boyd, J. Kaldor, C.L. Masters, Surgical treatment and risk of sporadic Creutzfeldt-Jakob disease: a case–control study, Lancet 353 (1999) 693–697.
[4] S.J. Collins, V.A. Lawson, C.L. Masters, Transmissible spongiform encephalopathies, Lancet 363 (2004) 51–61.
[5] P. Ibanez, A.M. Bonnet, B. Debarges, E. Lohmann, F. Tison, P. Pollak, Y. Agid, A. Durr, A. Brice, Causal relation between alpha-synuclein gene duplication and familial Parkinson's disease, Lancet 364 (2004) 1169–1171.
[6] G.G. Kovacs, M. Puopolo, A. Ladogana, M. Pocchiari, H. Budka, C. van Duijn, S.J. Collins, A. Boyd, A. Giulivi, M. Coulthart, N. Delasnerie-Laupretre, J.P. Brandel, I. Zerr, H.A. Kretzschmar, J. de Pedro-Cuesta, M. Calero-Lara, M. Glatzel, A. Aguzzi, M. Bishop, R. Knight, G. Belay, R. Will, E. Mitrova, Genetic prion disease: the EUROCJD experience, Human Genetics 118 (2005) 166–174.
[7] A. Ladogana, M. Puopolo, E.A. Croes, H. Budka, C. Jarius, S. Collins, G.M. Klug, T. Sutcliffe, A. Giulivi, A. Alperovitch, N. Delasnerie-Laupretre, J.P. Brandel, S. Poser, H. Kretzschmar, I. Rietveld, E. Mitrova, P. Cuesta Jde, P. Martinez-Martin, M. Glatzel, A. Aguzzi, R. Knight, H. Ward, M. Pocchiari, C.M. van Duijn, R.G. Will, I. Zerr, Mortality from Creutzfeldt-Jakob disease and related disorders in Europe, Australia, and Canada, Neurology 64 (2005) 1586–1591.
[8] S.A. Miller, D.D. Dykes, H.F. Polesky, A simple salting out procedure for extracting DNA from human nucleated cells, Nucleic Acids Research 16 (1988) 1215.
[9] Y. Mizuno, N. Hattori, S. Kubo, S. Sato, K. Nishioka, T. Hatano, H. Tomiyama, M. Funayama, Y. Machida, H. Mochizuki, Progress in the pathogenesis and genetics of Parkinson's disease, Philosophical Transactions of the Royal Society of London 363 (2008) 2215–2227.
[10] A.B. Singleton, M. Farrer, J. Johnson, A. Singleton, S. Hague, J. Kachergus, M. Hulihan, T. Peuralinna, A. Dutra, R. Nussbaum, S. Lincoln, A. Crawley, M. Hanson, D. Maraganore, C. Adler, M.R. Cookson, M. Muenter, M. Baptista, D. Miller, J. Blancato, J. Hardy, K. Gwinn-Hardy, alpha-Synuclein locus triplication causes Parkinson's disease, Science 302 (2003) 841.
[11] K. Sleegers, N. Brouwers, I. Gijselinck, J. Theuns, D. Goossens, J. Wauters, J. Del-Favero, M. Cruts, C.M. van Duijn, C. Van Broeckhoven, APP duplication is sufficient to cause early onset Alzheimer's dementia with cerebral amyloid angiopathy, Brain 129 (2006) 2977–2983.
[12] D.M. Walsh, I. Klyubin, J.V. Fadeeva, W.K. Cullen, R. Anwyl, M.S. Wolfe, M.J. Rowan, D.J. Selkoe, Naturally secreted oligomers of amyloid beta protein potently inhibit hippocampal long-term potentiation in vivo, Nature 416 (2002) 535–539.
[13] K.E. Wisniewski, A.J. Dalton, C. McLachlan, G.Y. Wen, H.M. Wisniewski, Alzheimer's disease in Down's syndrome: clinicopathologic studies, Neurology 35 (1985) 957–961.

Iatrogenic Creutzfeldt–Jakob disease in Australia: time to amend infection control measures for pituitary hormone recipients?

Alison Boyd, Genevieve M J A Klug, Lawrence B Schonberger, Amelia McGlade, Jean-Philippe Brandel, Colin L Masters and Steven J Collins

ABSTRACT

- From 1967, the Australian Human Pituitary Hormone Program offered treatment for short stature and infertility using human cadaver-acquired pituitary hormones (human growth hormone [hGH] and human pituitary gonadotrophin [hPG]). The program was suspended in 1985 when a growth-hormone recipient in the United States developed Creutzfeldt–Jakob disease (CJD), an incurable and rapidly progressive neurodegenerative disorder.
- Since this time, recipients have lived with the significant anxiety that they have an elevated risk of developing CJD. Furthermore, additional CJD infection control measures are required when recipients undergo some types of surgery.
- As it is 20 years since the last Australian pituitary hormone recipient developed CJD, we evaluated the risk for Australian recipients of developing iatrogenic CJD, and compared Australian data with data from New Zealand and selected other countries who had pituitary hormone programs.
- Our evaluation indicates that pituitary hormone recipients in Australia have the lowest risk of developing iatrogenic CJD, and that Australia is the only country not to have experienced ongoing CJD-related deaths. Thus, we believe that:
  - in the Australian hGH recipient cohort, the risk of developing CJD is sufficiently low for this cohort to no longer require additional infection control measures in the health care setting; and
  - in the Australian hPG recipient cohort, if another 5 years elapses with no further occurrence of CJD in this group, the hPG recipient cohort could also be considered as not requiring additional infection control measures in the health care setting.
- These recommendations should not be misunderstood as implying that there is no ongoing risk, but that the risk is acceptably low and generally in keeping with guidelines that stratify the risk.

MJA 2010; 193: 366–369

In Australia, from 1967 to mid 1985, treatment for short stature and infertility with cadaver-acquired pituitary hormones (human growth hormone [hGH] and human pituitary gonadotrophin [hPG], respectively) was provided through the Australian Human Pituitary Hormone Program (AHPHP).[1] The program was suspended in mid 1985 in response to the recognition of a link between hGH therapy and the development of Creutzfeldt–Jakob disease (CJD) in a young hormone recipient in the United States.[2] CJD is an incurable and rapidly progressive neurodegenerative disorder and one of the transmissible spongiform encephalopathies. As of mid 2010, 25 years after the moratorium on the AHPHP, and 20 years since an Australian recipient developed CJD, we present a likely, and we hope, final assessment of the Australian experience of medically transmitted CJD from human-derived pituitary hormone therapy, and compare our experience here with that in other countries.

The Australian experience

In total, four Australians have had their deaths from CJD attributed to pituitary hormone therapy, with the most recent occurring in early 1991. Unique to Australia, these four deaths were related to treatment with hPG: three had CJD confirmed at autopsy and the fourth was classified as "probable CJD" after evaluation by the Australian National Creutzfeldt–Jakob Disease Registry (ANCJDR) using World Health Organization surveillance criteria.[3]

The death of an Australian hGH recipient in 1991 is considered unlikely to be the result of CJD, as this person had numerous confounding comorbidities. However, in the absence of relevant premortem investigations and an autopsy, this case was conservatively classified as "possible CJD" and, as such, is excluded from formal epidemiological analyses and incidence data.

The Box summarises the total number of hPG and hGH recipients in Australia and in selected, larger national human pituitary hormone programs in other countries. It also shows the number of deaths from CJD among these recipients, and the relative risk of developing CJD for recipients in each country. Each national pituitary hormone treatment program has only ever confirmed iatrogenic CJD in either hPG (Australia only) or hGH recipients, never in both. This is an empirical observation, the reasons for which are not understood; however, it spans many countries and thousands of recipients over a period of 25 years.

Abbreviations

AHPHP = Australian Human Pituitary Hormone Program
ANCJDR = Australian National Creutzfeldt–Jakob Disease Registry
CJD = Creutzfeldt–Jakob disease
hGH = human growth hormone
hPG = human pituitary gonadotrophin
PRNP = prion protein gene ◆

The Australian figures are presented in two sets. The first gives the recipient numbers reported in the 1994 *Report of the inquiry into the use of pituitary derived hormones in Australia and Creutzfeldt-Jakob disease* (known as the Allars report),[1] and the second gives the recipient numbers published in 1999 by the Australian Government Department of Health and Ageing (DoHA).[4] Both sets of recipient numbers are included for transparency. Discrepancies between the sets could be attributed to early audits of program lists providing the number of patients approved for treatments, and later figures representing only those recipients confirmed by DoHA as having received treatments.

Summary of the number of recipients of cadaver-acquired human pituitary gonadotrophin (hPG) and human growth hormone (hGH) in five countries; the number of related deaths from Creutzfeldt–Jakob disease (CJD); and the relative risk of recipients in each country developing CJD using total national recipient numbers — data to December 2008

Country	No. of hPG-related deaths	No. of hPG recipents	hPG risk (%)	No. of hGH-related deaths	No. of hGH recipients	hGH risk (%)	Total risk (%) (hGH and hPG)	Year of last recipient death
Australia*	4†	1589[1]	0.25%	1‡	906[1]	0.11%‡	0.16%	1991
		1363[4]	0.29%		608[4]	0.16%‡	0.20%	
France	0	0	0	115	1700	6.76%	6.76%	2008
New Zealand	0	154§	0	6¶[5]	159**[7]	3.77%	1.92%	2004
United States	0	0	0	28	~ 7700	0.36%	0.36%	2007
United Kingdom	1†	~ 300††	0	57[6]	1849[8]	3.08%	2.65%	2008

* The two recipient totals for Australia are derived from two different reports,[1,4] and most likely represent the difference between patients approved for treatments (larger number) and those confirmed as having received treatments. Two corresponding risk calculations are given.

† One Australian hPG recipient is reported by both Australia and the UK; treatment took place in Australia, but disease onset and death occurred in the UK. This case is not included in Australian incidence figures, but for the purpose of this risk assessment, this recipient is analysed with the Australian hPG recipients only.

‡ This "possible CJD" case does not appear in Australian CJD incidence figures, and calculations of total risk exclude this case.

§ This total comprises nine hPG recipients with hormone source unknown; 37 recipients of Australian hPG; 29 recipients of US hPG; and 67 recipients of NZ hPG. A further four recipients received Australian and NZ hPG, three received Australian and US hPG, and four received US and NZ hPG. One recipient received hPG from all three sources (Medicines and Medical Devices Safety Authority [Medsafe], Ministry of Health, NZ, February 2009).

¶ These NZ recipients received US-sourced hGH (Medsafe, Ministry of Health, NZ, January 2010).

** This total comprises 34 recipients of US hGH, 15 recipients of US and Australian hGH, 94 recipients of NZ hGH, 12 recipients of Australian and NZ hGH, and four recipients of Australian- and/or Swedish-sourced hGH (Medsafe, Ministry of Health, NZ, February 2009).

†† Professor R G Will, The National CJD Surveillance Unit, Edinburgh, UK, personal communication, February 2009. ◆

The four Australian hPG recipients who developed CJD all had disease onset in the period 1987–1990, which is consistent with a single, discrete contamination event and, most likely, effective removal of prions through routine pituitary processing methods. The now 20-year interval since an Australian recipient developed CJD offers some reassurance to recipients, who have, since 1985, lived with the anxiety that they have an elevated risk of developing CJD. It is considered unlikely that national surveillance has missed identifying a further CJD illness in an Australian hGH or hPG recipient, especially given the heightened awareness of this possibility among AHPHP recipients and their families, and the significant improvements in premortem diagnostic tests since 1993, when CJD surveillance commenced in Australia. Annual incidence rates of CJD reported by the ANCJDR have increased over time,[9] in line with anticipated improvements in case ascertainment afforded by a dedicated national surveillance unit and better diagnostic tools.[10,11] Families of all patients with CJD ascertained by ANCJDR are also routinely asked for details of any past medical history, and in particular hormone-related treatments.

International comparisons

Incubation period

In Australia, there has been a 20-year interval since a pituitary hormone recipient developed CJD. This contrasts with the ongoing occurrence of CJD in hGH recipients in other countries, where, with the exception of New Zealand, hGH-related CJD cases have continued to be diagnosed and deaths reported (Box). The most recent death from CJD of an NZ recipient occurred in 2004 after an incubation period of 37 years (the incubation period is calculated from the mid-treatment point to the onset of symptoms). The most recent death from CJD of a US recipient occurred in 2007 (reported in 2008), with 30 years elapsing before the onset of symptoms — the longest US incubation period to date. In both the United Kingdom and France, there were deaths of recipients in 2008, and these cases represent the longest incubation periods reported for each country, 32 and 24 years, respectively (Professor R G Will, The National CJD Surveillance Unit, Edinburgh, UK, personal communication, February 2009). Overall, the longest incubation period is currently believed to be 38 years, occurring in a recipient in the Netherlands who received several doses of hGH for diagnostic purposes.[12] By comparison, the longest incubation period reported in an Australian recipient is 15.3 years, with incubation periods in Australia ranging from 12 to 15.3 years.

Risk in relation to pituitary hormone source country

Both the total risk (hPG and hGH) and the hGH-only risk of pituitary hormone-related CJD in NZ and the UK are similar (Box), although the hGH product used in NZ until the late 1970s was predominantly manufactured in a laboratory in the south-eastern US. Earlier reports recorded 46 of a total of 184 hGH recipients in NZ[13] as receiving hormone product processed in the US before 1977, the year when the hormone extraction method in the US was changed.[13] The total number of hGH recipients on the NZ CJD Registry (159 individuals)[7] was recently confirmed by the Medicines and Medical Devices Safety Authority (Medsafe), Ministry of Health, NZ, in February 2009. Up to the end of 2008, the six NZ hGH recipients who subsequently died of CJD all received US-sourced hormone product. The risk rate of CJD for the NZ recipients of US-sourced hGH (6/49) is 12.2%.

The explanation for the striking difference between US and NZ hGH risk rates — less than 0.5% compared with close to 4% — is

not entirely clear;[13] however, the US hormone product received by NZ patients is not thought to be identical to that received by US patients.[14] Potential differences include the final post-purification processing steps performed in the two countries; that is, the final pooling and filtering of material to eliminate bacterial contamination before placing the hormone product in sterile ampoules (Dr A Parlow, Director, National Hormone and Peptide Program, Harbor-UCLA Medical Center, Torrance, Calif, USA, personal communication, February 2009). For example, these final post-purification steps were performed manually in NZ on much smaller volumes than those used in the US.

As in Australia, in NZ, hPG was administered for infertility. There were a total of 154 NZ recipients of hPG Medsafe, Ministry of Health, NZ, January 2010). The risk analysis for these recipients can be differentiated into four groups, based on the source of the hormone administered: Australia only (37 recipients), the US only (29), NZ only (67 — from 1978),[1] and mixed sources (12). The risk for nine NZ recipients is unknown, as the hPG source was not recorded.

Recalculating the risk of developing CJD after adding the number of NZ recipients of any Australian-processed hPG to the total number of Australian hPG recipients results in no significant change in Australian risk rates; the risk of CJD in recipients of hPG processed in Australia is 0.24%–0.28%, a negligible shift of 0.01% (Box).

The risk for NZ recipients of US- and NZ-sourced hPG can be considered zero, as no CJD-related deaths have occurred in either recipient group. In contrast, combining the number of recipients of US-processed hGH in the US and NZ (7749) with the total number of CJD deaths in those countries (34) increases the US risk rate for iatrogenic CJD to 0.44%.

Risk in relation to pituitary hormone purification processes

As described by Huillard d'Aignaux[15] et al and Brown et al,[13] higher-risk periods apparently exist for recipients of hGH in France and the US. Acknowledging the unusual biophysical properties of prions, including their resistance to conventional sterilisation measures,[16,17] these higher-risk periods are considered to relate to differences in extraction and purification methods of human-derived pituitary hormones altering the infectivity of contaminated preparations.[18-20] As a potential example, through to the end of 2008, all hGH recipients who developed CJD in the US received their hGH treatment before 1977, the year a column chromatography purification processing step was introduced; this step was considered to have significantly reduced, but not necessarily eliminated, contaminating prions.[21] The risk estimate for US recipients treated before 1977 is 1%.[13] The progressively lengthening intervals of absence of iatrogenic CJD cases in US hGH recipients treated after 1977 suggest that, as in Australia, this recipient group may have a considerably lower, perhaps a negligible, risk of developing iatrogenic CJD.

The overall risk of human pituitary hormone-related CJD in France is calculated at 6.8%. The higher-risk period for French hGH recipients occurred between 1982 and mid 1985; all iatrogenic CJD cases occurred in hGH recipients treated in that period. As in the US, processing changes were implemented from mid 1985, especially universal urea-inactivation of hGH, which is believed to have significantly lowered the prion transmission risk. In this higher-risk period, Huillard d'Aignaux et al[15] reported that 1361 people were treated with hGH in France between January 1982 and July 1985, with an 8.4% risk of developing CJD, while Brown et al[13] reported 1260 individuals receiving hGH in France between January 1983 and July 1985, with a 9.1% risk.

Limitations to further refinement of the risks for Australian recipients

The information available for UK hGH recipients[8] and Australian hPG and hGH recipients does not clearly identify higher-risk periods. The UK has reported deaths from CJD in recipients treated over the entire program period — without temporal clustering. Unfortunately, the information available about the treatments administered to Australian pituitary hormone recipients is incomplete: batch numbers of hormones and the number of treatments from each batch administered are not available for all recipients. The absence of complete treatment details for all AHPHP recipients precludes further refinement of the risk for Australian recipients. In addition, the polymorphic codon 129 status of the prion protein gene (*PRNP*) is generally considered a risk factor for hGH-related iatrogenic CJD.[22] However, *PRNP* genotyping of the four Australian hPG recipients who developed CJD showed no clear association: two were homozygous for methionine, one for valine, and the fourth was heterozygous.[23] This mixed result reduces the utility of codon 129 assessment for determining the risk of developing CJD in other Australian hPG recipients. Notwithstanding such limitations, the combined total risk of iatrogenic CJD for AHPHP recipients is relatively low at 0.16%–0.20%.

Time to re-evaluate the need for infection control measures for Australian recipients?

Our assessment shows that the Australian recipient community has the lowest risk of developing iatrogenic CJD of all the countries studied, and Australia is the only country not to have experienced ongoing CJD-related deaths. This is positive news for the AHPHP recipient community. Beyond any emotional or psychological benefits stemming from the confirmed, low absolute number and low relative risks of pituitary hormone-related CJD in Australia, as well as the absence of further occurrences of CJD among the treated cohort over the past 20 years, we believe these data prompt reconsideration of the current infection control measures for the Australian recipient community.

For Australian hGH recipients: given the absence of confirmed iatrogenic CJD in hGH recipients in Australia, and the freedom from any instances of pituitary hormone-related CJD over the past 20 years, we believe that the risk of developing CJD for members of the Australian hGH recipient cohort is sufficiently low for them to no longer require additional infection control precautions in the health care setting.[24]

For Australian hPG recipients: a revision of infection control measures is less clear-cut and more contentious, principally due to the long incubation periods reported among hGH treatment cohorts in other countries where there is an established risk. Nevertheless, if another 5 years elapses[25] with no further occurrence of CJD in this Australian recipient group, we believe that an absence of iatrogenic CJD over a 25-year period would suggest that the residual risk is acceptably low, and that the Australian

hPG recipient cohort could also be considered as not requiring additional infection control measures in the health care setting.

These recommendations should not be misunderstood as implying that there is no ongoing risk, but that the risk is acceptably low and generally in keeping with guidelines that stratify the risk.[26]

Acknowledgements

The Australian National Creutzfeldt–Jakob Disease Registry is funded by the Australian Government Department of Health and Ageing. We thank the families who generously support CJD surveillance and research. The assistance of medical practitioners and health care workers in surveillance activities is also greatly appreciated. We also acknowledge the assistance of Professor Martin Pollock, Director of the New Zealand Creutzfeldt–Jakob Disease Registry, and the Medicines and Medical Devices Safety Authority (Medsafe), Ministry of Health, NZ.

Competing interests

The Australian Government Department of Health and Ageing had no involvement in study design, data collection, analysis and interpretation, nor the writing or publication of this article. Lawrence Schonberger, as an employee of the US Centers for Disease Control and Prevention responsible for prion disease-related public health issues, receives funding from the US government to investigate iatrogenic CJD.

Author details

Alison Boyd, DipAppSci(Nursing), GradDipGenCoun, Coordinator, Australian National Creutzfeldt–Jakob Disease Registry (ANCJDR)[1]
Genevieve M J A Klug, BSc(Hons), PostGradDipEpiBioStat, Research Assistant, ANCJDR[1]
Lawrence B Schonberger, MD, MPH, Assistant Director for Public Health, Division of High-Consequence Pathogens and Pathology[2]
Amelia McGlade, BSc, Research Assistant, ANCJDR[1]
Jean-Philippe Brandel, MD, Neurologist[3]
Colin L Masters, MD, Director, ANCJDR[1] and Mental Health Research Institute, Laureate Professor, Centre for Neuroscience, University of Melbourne
Steven J Collins, MD, Director, ANCJDR[1]

1 Department of Pathology, The University of Melbourne, Melbourne, VIC.
2 National Center for Emerging and Zoonotic Infectious Diseases, Centers for Disease Control and Prevention, Atlanta, Ga, USA.
3 Cellule Nationale de Référence des Maladies de Creutzfeldt–Jakob, Hospitalier Pitié-Salpêtrière, Paris, France.

Correspondence: aboyd@unimelb.edu.au; stevenjc@unimelb.edu.au

References

1 Allars M. Report of the inquiry into the use of pituitary derived hormones in Australia and Creutzfeldt-Jakob disease. Canberra: AGPS, 1994.
2 Koch TK, Berg BO, De Armond SJ, Gravina RF. Creutzfeldt-Jakob disease in a young adult with idiopathic hypopituitarism. Possible relation to the administration of cadaveric human growth hormone. *N Engl J Med* 1985; 313: 731-733.
3 World Health Organization. WHO manual for surveillance of human transmissible spongiform encephalopathies including variant Creutzfeldt-Jakob disease. Geneva: WHO, 2003. http://whqlibdoc.who.int/publications/2003/9241545887.pdf (accessed Jul 2010).
4 Australian Government Department of Health and Ageing. The use of human pituitary hormones in Australia and Creutzfeldt-Jakob disease (CJD). Key facts and figures. Canberra: DoHA, 1999.
5 The New Zealand Creutzfeldt-Jakob Disease Registry (Pollock M). Creutzfeldt-Jakob disease surveillance in New Zealand. Eighth annual report, January 2004 – December 2004. The NZ CJD Registry, 2005. (Available from the NZ CJD Registry.)
6 The National CJD Surveillance Unit. Creutzfeldt-Jakob disease surveillance in the UK. Seventeenth annual report, 2008. Edinburgh: The National CJD Surveillance Unit, 2009.
7 The New Zealand Creutzfeldt-Jakob Disease Registry (Pollock M). Creutzfeldt-Jakob disease surveillance in New Zealand. Seventh annual report, January 2003 – December 2003. The NZ CJD Registry, 2004. (Available from the NZ CJD Registry.)
8 Swerdlow AJ, Higgins CD, Adlard P, et al. Creutzfeldt-Jakob disease in United Kingdom patients treated with human pituitary growth hormone. *Neurology* 2003; 61: 783-791.
9 Klug GM, Boyd A, McGlade A, et al. Surveillance of Creutzfeldt-Jakob disease in Australia: 2010. *Commun Dis Intell* 2010; 34: 96-101.
10 Collins SJ, Sanchez-Juan P, Masters CL, et al. Determinants of diagnostic investigation sensitivities across the clinical spectrum of sporadic Creutzfeldt-Jakob disease. *Brain* 2006; 129 (Pt 9): 2278-2287.
11 Tschampa H, Zerr I, Urbach H. Radiological assessment of Creutzfeldt-Jakob disease. *Eur Radiol* 2007; 17: 1200-1211.
12 Croes E, Roks G, Jansen GH, et al. Creutzfeldt-Jakob disease 38 years after diagnostic use of human growth hormone. *J Neurol Neurosurg Psychiatry* 2002; 72: 792-793.
13 Brown P, Preece M, Brandel JP, et al. Iatrogenic Creutzfeldt-Jakob disease at the millennium. *Neurology* 2000; 55: 1075-1081.
14 National Institutes of Health. National Endocrine and Metabolic Diseases Information Service. National Hormone and Pituitary Program: information for people treated with pituitary human growth hormone (summary). http://www.endocrine.niddk.nih.gov/pubs/creutz/update.htm (accessed Jul 2010).
15 Huillard d'Aignaux J, Costagliola D, Maccario J, et al. Incubation period of Creutzfeldt-Jakob disease in human growth hormone recipients in France. *Neurology* 1999; 53: 1197-1201.
16 Brown P, Gibbs CJ Jr, Amyx HL, et al. Chemical disinfection of Creutzfeldt-Jakob disease virus. *N Engl J Med* 1982; 306: 1279-1282.
17 Taylor DM. Inactivation of transmissible degenerative encephalopathy agents: a review. *Vet J* 2000; 159: 10-17.
18 Taylor DM, Dickinson AG, Fraser H, et al. Preparation of growth-hormone free from contamination with unconventional slow viruses. *Lancet* 1985; 2: 260-262.
19 Taylor DM. Membrane filtration and the Creutzfeldt-Jakob agent. *Lancet* 1985; 2: 1430-1431.
20 Pocchiari M, Peano S, Conz A, et al. Combination ultrafiltration and 6 M urea treatment of human growth hormone effectively minimizes risk from potential Creutzfeldt-Jakob disease virus contamination. *Horm Res* 1991; 35: 161-166.
21 Fradkin JE, Schonberger L, Mills JL, et al. Creutzfeldt-Jakob disease in pituitary growth hormone recipients in the United States. *JAMA* 1991; 265: 880-884.
22 Brandel J-P, Preece M, Brown P, et al. Distribution of codon 129 in human growth hormone-treated CJD patients in France and the UK. *Lancet* 2003; 362: 128-130.
23 Cooke J. Cannibals, cows and the CJD catastrophe. Sydney: Random House, 1998: 224.
24 Australian Government Department of Health and Ageing. Infection control guidelines for the prevention of transmission of infectious diseases in the health care setting 2007. http://www.health.gov.au/internet/main/publishing.nsf/Content/icg-guidelines-index.htm (accessed Jul 2010).
25 Alpers MP. Review. The epidemiology of kuru: monitoring the epidemic from its peak to its end. *Philos Trans R Soc Lond B Biol Sci* 2008; 363: 3707-3713.
26 Health Protection Agency, Health Protection Scotland. Patients at increased risk of Creutzfeldt-Jakob disease. Actions for healthcare staff. 2009. http://www.hpa.org.uk/web/HPAwebFile/HPAweb_C/1234602045948 (accessed Jul 2010).

(Received 22 Sep 2009, accepted 15 Jun 2010) ❑

Health professions and risk of sporadic Creutzfeldt–Jakob disease, 1965 to 2010

E Alcalde-Cabero[1], J Almazán-Isla[1], J P Brandel[2], M Breithaupt[3], J Catarino[4], S Collins[5], J Haybäck[6], R Höftberger[7], E Kahana[8], G G Kovacs[7,9], A Ladogana[10], E Mitrova[11], A Molesworth[12], Y Nakamura[13], M Pocchiari[10], M Popovic[14], M Ruiz-Tovar[1], A L Taratuto[15], C van Duijn[16], M Yamada[17], R G Will[12], I Zerr[3], J de Pedro Cuesta (jpedro@isciii.es)[1]

1. National Centre of Epidemiology - Consortium for Biomedical Research in Neurodegenerative Diseases (Centro de Investigación Biomédica en Red sobre Enfermedades Neurodegenerativas – CIBERNED), Carlos III Institute of Health, Madrid, Spain
2. Institut National de la Santé et de la Recherche Médicale (INSERM) UMRS 975, National CJD Surveillance Network, Assistance publique - Hôpitaux de Paris (APHP), National Reference Centre for CJD, Pitié-Salpêtrière Hospital Group, Paris, France
3. Department of Neurology, National Reference Centre for TSE, Georg-August University, Göttingen, Germany
4. Alameda Epidemiology and Health Statistics Department, Lisbon, Portugal
5. Department of Pathology, University of Melbourne, Melbourne, Australia
6. Institute of Neuropathology, Zurich University Hospital, Zurich, Switzerland
7. Institute of Neurology, Vienna Medical University, Vienna, Austria
8. Department of Neurology, Barzilai Medical Centre, Ashkelon, Israel
9. National Reference Centre for Human Prion Diseases, Semmelweis University, Budapest, Hungary
10. Department of Cell Biology and Neurosciences, Health Institute, Rome, Italy
11. Department of Prion Diseases, Slovak Medical University Research Base, Bratislava, Slovakia
12. National CJD Research and Surveillance Unit, Western General Hospital, Edinburgh, United Kingdom
13. Department of Public Health, Jichi Medical University, Shimotsuke, Japan
14. nstitute of Pathology, Medical Faculty, University of Ljubljana, Ljubljana, Slovenia
15. Department of Neuropathology/FLENI, Referral Centre for CJD and other TSEs, Institute for Neurological Research, Buenos Aires, Argentina
16. National Surveillance of CJD, Erasmus MC, Rotterdam, The Netherlands
17. Neurology Department, Kanazawa University Hospital, Kanazawa, Japan

Citation style for this article:
Alcalde-Cabero E, Almazán-Isla J, Brandel JP, Breithaupt M, Catarino J, Collins S, Haybäck J, Höftberger R, Kahana E, Kovacs GG, Ladogana A, Mitrova E, Molesworth A, Nakamura Y, Pocchiari M, Popovic M, Ruiz-Tovar M, Taratuto AL, van Duijn C, Yamada M, Will RG, Zerr I, de Pedro Cuesta J. Health professions and risk of sporadic Creutzfeldt–Jakob disease, 1965 to 2010 . Euro Surveill. 2012;17(15):pii=20144. Available online: http://www.eurosurveillance.org/ViewArticle.aspx?ArticleId=20144

Article submitted on 4 November 2011/ published on 12 April 2012

In 2009, a pathologist with sporadic Creutzfeldt–Jakob Disease (sCJD) was reported to the Spanish registry. This case prompted a request for information on health-related occupation in sCJD cases from countries participating in the European Creutzfeldt Jakob Disease Surveillance network (EuroCJD). Responses from registries in 21 countries revealed that of 8,321 registered cases, 65 physicians or dentists, two of whom were pathologists, and another 137 healthcare workers had been identified with sCJD. Five countries reported 15 physicians and 68 other health professionals among 2,968 controls or non-cases, suggesting no relative excess of sCJD among healthcare professionals. A literature review revealed: (i) 12 case or small case-series reports of 66 health professionals with sCJD, and (ii) five analytical studies on health-related occupation and sCJD, where statistically significant findings were solely observed for persons working at physicians' offices (odds ratio: 4.6 (95 CI: 1.2–17.6)). We conclude that a wide spectrum of medical specialities and health professions are represented in sCJD cases and that the data analysed do not support any overall increased occupational risk for health professionals. Nevertheless, there may be a specific risk in some professions associated with direct contact with high human-infectivity tissue.

Introduction

Creutzfeldt–Jakob disease (CJD) is a fatal neurodegenerative disease characterised by deposition of a pathological isoform of the normal cellular prion protein (PrP^C) [1]. The annual CJD incidence worldwide is 1–2 per million population [2]. CJD exists in various forms: genetic, caused by mutations in the *PRNP* gene encoding PrP^C, acquired (variant and iatrogenic) and sporadic. Most cases have sporadic CJD (sCJD) – the cause of which is unknown. Occupational risk related to sCJD has been assessed in several case–control studies as a secondary study objective, with inconsistent results [3-7] and there have been occasional reports of health professionals with sCJD [8-12].

Occupation has not been included as a variable in all CJD surveillance protocols [13]. Nonetheless, there is concern about potential occupational excess risk of sCJD among health professions, as shown by a recent study on guidelines in European Union (EU) Member States and Norway for the prevention of CJD transmission in medical settings. This study showed that 12 of the 17 contributing countries had specific recommendations targeted at minimising occupational exposure;

eight of the 12 had systems for reporting or registering work-related incidents at hospitals or laboratories [14].

In March 2009, a CJD case was reported to the Spanish CJD registry, who was classified as having sporadic CJD. As the patient was an experienced general pathologist and neuropathologist, it was speculated that the disease might have been a result of the person's professional activities. The event was commented on in medical, scientific and mass media in Spain and elsewhere, e.g. [15]. The patient died after a four-month disease course, characterised mainly by cognitive decline, ataxia and myoclonus. The disease prion protein subtype, i.e. strain, was confirmed histochemically and biochemically as MM1, the most common subtype [2]. Risk factors for developing CJD, including blood transfusion, iatrogenic exposure (e.g. to dura mater, cadaveric pituitary-derived growth hormone) and mutations in the *PRNP* gene, were not identified. Assessment of the patient's routine hospital work indicated that the patient had had a history of minor injuries during post-mortem examinations (personal communication, E. García-Albea, April 2009).

Box

Search terms used in first step of two literature searches on sporadic Creutzfeldt–Jakob disease (sCJD) in health professionals and analytical studies on occupational risk of sCJD for health professions and selection criteria used in a second step, reported 1 January 1989–1 October 2011

MEDLINE
The search strategy was based on the following medical subject headings (MeSH) terms:

- prion diseases/prions/Creutzfeldt-Jakob syndrome; and
- health occupations/allied health occupations/ occupational groups/occupations/occupational dentistry/case control studies.

Embase
The search strategy was based on the following Emtree thesaurus terms:

- prion/prion disease/prion protein/Creutzfeldt Jakob disease/ Creutzfeldt Jakob disease agent; and
- occupation/occupation and occupation-related phenomena/ medical profession/nursing as a profession/nursing career/paramedical profession/professional development/ occupational accident/occupation and occupation-related phenomena/occupational accident/occupational disease/ occupational exposure/occupational hazard/occupational health/occupational health nursing/occupational health service/occupational medicine/occupational physician/ occupational safety/occupational therapist.

Selection criteria

Inclusion
Either specific reference to the subject (Creutzfeldt–Jakob disease and health profession) or analytical study design (either case–control or cohort), regardless of the study's stated objective.

Exclusion
Identification of the document as a letter or review, news, comment, congress abstract, when reference to health professions was not explicitly made.

Following notification of this patient, the Spanish registry circulated a request for information to each national surveillance team participating in the European Creutzfeldt Jakob Disease Surveillance Network (EuroCJD), which dates back to 1993 and currently encompasses 25 collaborating centres in EU Member States and European Free Trade Association (EFTA) countries and a further eight in countries around the world, including Australia, Canada and Japan [16]. These centres provide data from national registries either through the EuroCJD website or, as with Japanese data, at regular network meetings. The request asked for the following: (i) information on the diagnosis (year of birth and death, sex and place of residence) of reported cases of sporadic CJD among active or retired pathologists from 1996 onwards; and (ii) comments based on personal experience of occupational risk and CJD among health professionals, including technicians working at pathology laboratories.

There has been limited systematic research targeted at identifying occupational risk factors for sCJD in healthcare settings. This paper reports on the data supplied to the Spanish CJD registry in response to the request, and on the results of two literature reviews of sCJD – one on case reports involving health professionals and the other on epidemiologically assessed healthcare-related occupational risk of sCJD.

Methods

Individualised occupational data from national CJD surveillance teams

The Spanish CJD registry obtained answers in English to at least one of the requests for information from 21 national surveillance teams. The amount of information provided varied: in general, only data that had already been registered was reported; with regard to occupational history in CJD – recorded by profession or activity branch – several countries provided information on people in whom CJD had been excluded or on controls.

The data received were divided into two groups, for further analysis – one describing health professionals who were sCJD cases and the other describing health professionals among controls or non-cases. We did not attempt a formal epidemiological assessment of healthcare-related occupational risk of sCJD based on this information, for instance using a case–control design.

Case reports of sCJD among health professionals

Countries with available registry data on cases' occupations sent individualised data on physicians with neuropathologically confirmed or probable sCJD or other types of CJD [17,18]. Some countries provided such data on other health professions. In the few instances in which occupation as a pathologist was identified, professional experience or job duration at a laboratory or department was specified. The results were tabulated, using the original definitions from the countries'

reports. No standard occupational classification was used for grouping response results and each case was assigned to one occupational category. Frequently, the occupational categories corresponded to a combination of professional profiles, e.g. specialities and work types (clinical, administrative, laboratory, etc.). In such cases, the category most likely to involve direct contact with human tissue or patients was selected.

Healthcare-related occupations among controls and non-cases

Some CJD surveillance teams with a sufficient sample size provided data on occupation of people with suspected sCJD who were finally classified as not having CJD (non-cases) and also of those in control groups. Five EuroCJD countries with large populations – Germany, Italy, Japan, Spain and the United Kingdom (UK) – provided this type of data, both published and unpublished. These countries supplied data on physicians who were controls Italy and Japan also provided information on other health professionals who were non-cases. Information on different categories of health professionals was available for British controls. Occupation was usually categorised on the basis of original records at registries. In a few instances, reporting physicians or relatives were consulted about the predominant activity, e.g. general practice vs radiology, of the non-cases.

Literature reviews

The first step in the literature reviews sought to identify reports of sCJD among health professionals, whether reported as case studies or drawn from analytical studies published during 1 January 1989 to 1 October 2011. We carried out several searches in MEDLINE and Embase using the medical subject headings (MeSH) and Emtree thesaurus terms listed in the Box, to identify case studies on CJD in health professionals and

Figure 1

Literature review of case reports of sporadic Creutzfeldt–Jakob disease among health professionals, 1979–1 October 2011

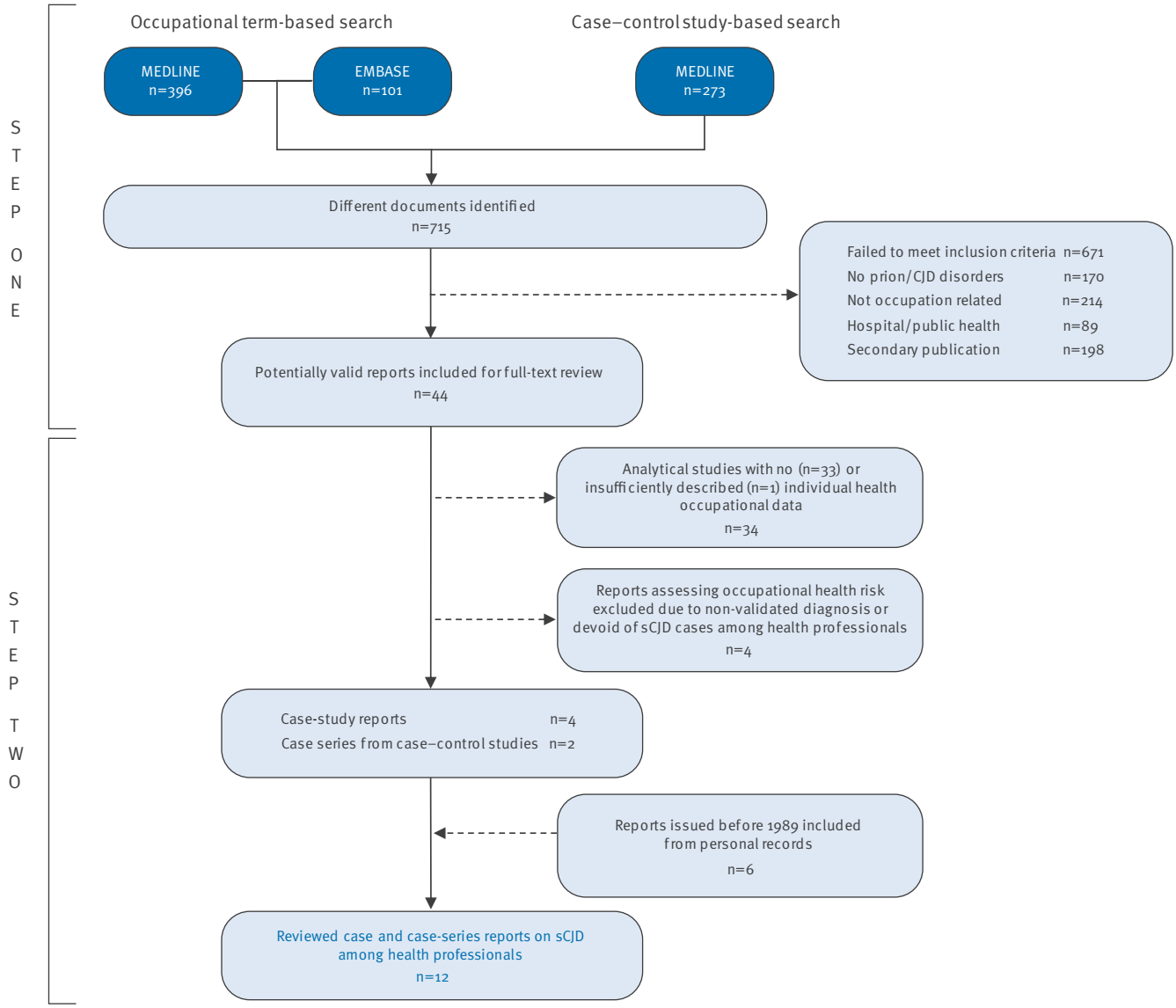

sCJD: sporadic Creutzfeldt–Jakob disease.

Figure 2

Literature review of analytical studies on occupational risk of sporadic Creutzfeldt–Jakob disease for health professionals, 1982–1 October 2011

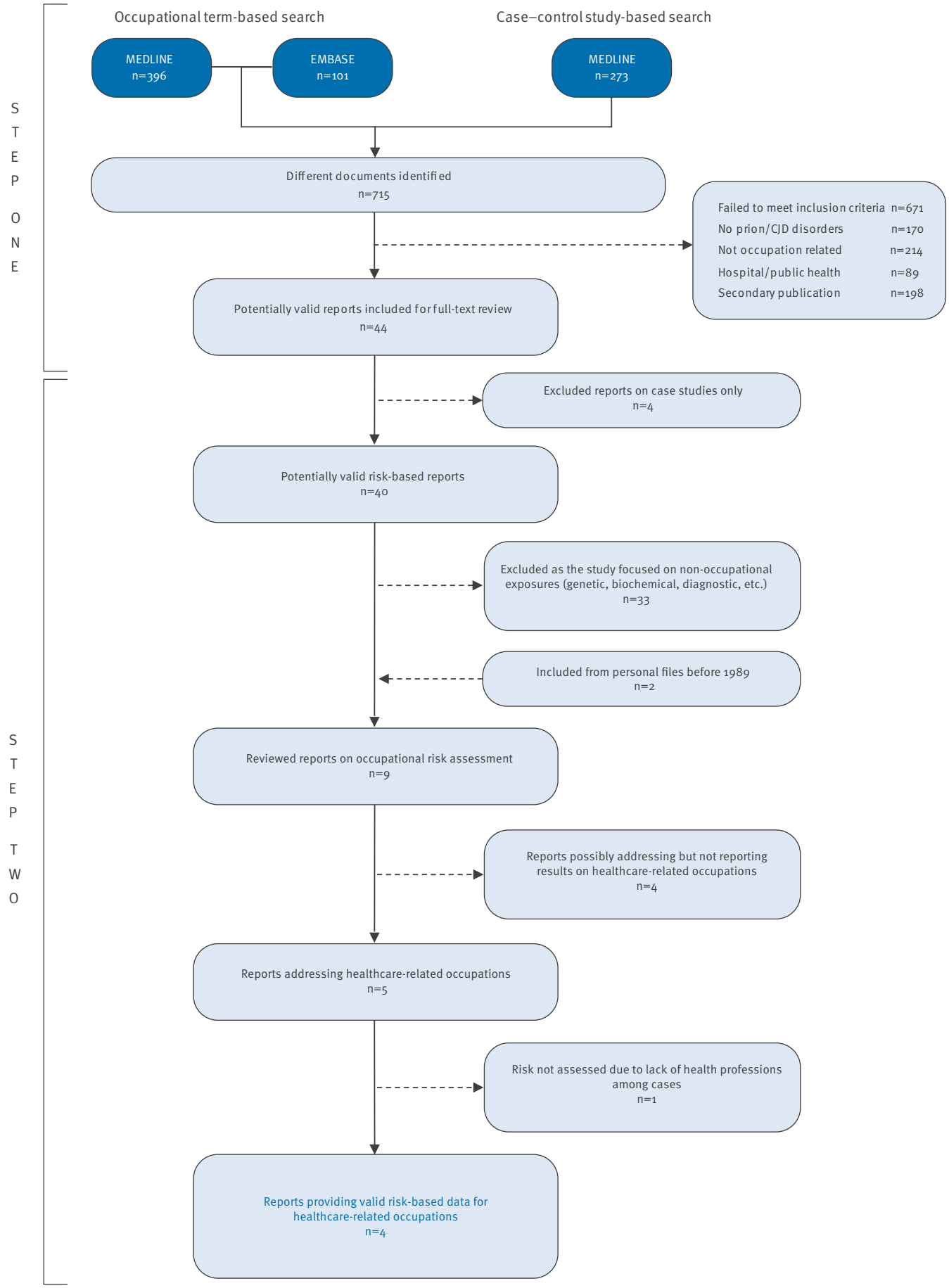

sCJD: sporadic Creutzfeldt–Jakob disease.

analytical studies on occupational risk of CJD for health professions. The initial searches yielded a total of 715 different documents.

In a second step, two independent assessors applied predefined sets of inclusion and exclusion criteria (Box) to the titles of the retrieved documents or, where available, to their abstracts.

Documents that met the inclusion criteria were processed further for full-text analysis in order to obtain the case description or to assess health-related occupational risk of sCJD.

After the selection criteria for had been independently, though not always unanimously, applied to the 715 documents by two reviewers, EAC and JPC, 671 were rejected and 44 selected for further analysis by both reviewers (Figures 1 and 2).

Case reports of sCJD among health professionals

Of the 44 documents selected for full-text review, 34 were excluded as the studies did not examine health-related occupations (Figure 1). Four studies that failed to include specific categories of health professionals with sCJD or in which the diagnosis of CJD was not validated were also excluded [3,6,7,19]. Six studies – four case reports [10-12,20] and two case–control studies, which provided information on health-related occupations in sCJD case series [5,21] – were selected for data extraction. Five case studies and one case-control study retrieved from personal records before 1989 were also included [4,8,9,17,22,23]. Thus, the final analysis of 12 reports included data on individual health professionals from case reports [8-12,17,20,22,23] and numbers of health professionals with sCJD from three reports on case–control studies [4,5,21]. These 12 reports included sCJD cases fulfilling diagnostic criteria for neuropathologically confirmed sCJD or for probable sCJD (people in the latter category were only included in case–control studies) [5,24]. Where health professions were listed in the case series of a large case–control study and numbers were not reported, only one individual, e.g. a dentist, was counted [5].

Epidemiologically assessed healthcare-related occupational risk of sCJD

Of the 44 documents selected for full-text review (the same 44 mentioned above), 40 fulfilled the inclusion criteria. After analysis of the texts, seven analytical studies on occupation and risk of sCJD remained for potential data extraction [3,5-7,19,21,25].Those excluded were multipurpose case–control investigations that made no mention of occupation in the results, occupation-unrelated meta-analyses, genetic case–control studies and public-health occupational profiles derived from empirical data. Four analytical studies reported before 1989 were reviewed: two were included [4,26] and two rejected [27,28]. Nine documents [3-7,19,21,25,26] provided data on occupational risk but only five of these addressed healthcare-related occupations [5-7,19,26]. Due to the low numbers (absence of exposed cases) in one study [26], risk-based data for health professions were only available from four case–control studies [5-7,19]. Reported associations for healthcare-related occupational risk obtained from these four epidemiological studies and raw negative findings from the above-mentioned study [26] were tabulated.

Results

Individualised occupational data from national CJD surveillance teams

Health professionals among registered sCJD cases

A total of 202 health professionals were listed among 8,321 cases of sCJD registered by 21 respondent countries participating in EuroCJD (Table 1). Of these, 65 (32%) were physicians and 137 were other healthcare workers. The highest numbers by medical speciality were general practitioners (n=9), surgeons (n=7), internists (n=7), dentists (n=4), ophthalmologists (n=3) and pathologists (n=2). The proportion of physicians or dentists among all registered sCJD cases was 65/8,321 (0.8%).

Health professionals among non-cases or controls

Table 2 shows individual data reported for health professions among non-cases or controls in five countries (Germany, Italy, Japan, Spain and the UK). Among 83 healthcare workers, 15 were physicians, six of whom had unknown specialisations, and three were surgeons. The percentage of physicians and dentists among CJD cases in Germany, Italy, Japan, Spain and the UK combined was 0.7% (34/4,949 (Table 1). This was similar to the proportion in the combined controls 0.5% (15/2,968).

Literature reviews

Reported sCJD in health professionals

Individual occupational profiles of reported health-related professionals with sCJD are outlined in Table 3. The data are derived from 12 studies, three of which were case–control studies. In these 12 studies, a total of 66 health workers with sCJD were reported, at least eight of whom were physicians [4,5,8-12,17,20-23]. One report described genetic CJD with phenotype resembling sCJD in three Slovakian health workers (two nurses and one dermatologist) with a mutation in codon 200 of the *PRNP* gene [11].

The following professions have been reported in sCJD cases: dentists (n=5), dental surgeon (n=1), neurosurgeons (n=2), pathologist (n=1), internist with training in pathology (n=1) and orthopaedic surgeon who had worked with sheep and human dura mater for industrial purposes (n=1) [12]. The majority of the remaining health professionals were nurses, two of whom had worked in neurosurgery and neurological care. Two other workers had been or were technicians at pathology laboratories.

Table 1

Occupational profile of sporadic Creutzfeldt–Jakob disease cases reported to the European Creutzfeldt Jakob Disease Surveillance Network (EuroCJD), 1965–2010 (n=8,321)

Occupation	Number of sCJD cases, by country[a], in the specified time period																					
	AR	AU	AT	BE	CA	CY	DK	FR	DE	HU	IL	IT	JP	NL	PT	SK	SL	ES	SE	CH	UK	Total
	1983–2009	1970–2008	1993–2008	1997–2009	1998–2009	1995–2009	1997–2009	1993–2008	1994–2007	1994–2009	1965–2007	1993–2008	1999–2009	1993–2008	1997–2009	1993–2010	1985–2009	1993–2009	1997–2007	1993–2009	1980–2009	
Physicians or dentists																						
Cardiovascular surgeon	0	0	0	-	-	-	-	-	0	0	0	0	1	0	0	0	0	0	-	0	0	**1**
Surgeon/urologist	1	0	0	-	-	-	-	-	1	0	0	0	0	0	0	0	0	0	-	0	0	**2**
Surgeon and neuropathologist	0	0	0	-	-	-	-	-	1	0	0	0	0	0	0	0	0	0	-	0	0	**1**
Traumatologist/surgeon	1	0	0	-	-	-	-	-	0	0	0	0	0	0	0	0	0	0	-	0	0	**1**
Ophthalmologist	0	0	0	-	-	-	-	-	0	1	0	1	0	0	0	0	0	1	-	0	0	**3**
Surgeon (not specified)	0	0	0	-	-	-	-	-	0	0	0	0	0	0	0	0	0	1	-	0	0	**1**
Pathologist	0	0	0	0	0	0	0	0	0	0	0	0	0	0	0	0	0	1	0	0	0	**1**
Neuropathologist's assistant	0	0	0	-	-	-	-	-	1	0	0	0	0	0	0	0	0	0	-	0	0	**1**
Forensic medicine	0	0	0	-	-	-	-	-	0	0	0	1	0	0	0	0	0	0	-	0	0	**1**
Dentist	1	0	1	-	-	-	-	-	0	0	2	0	0	0	0	0	0	0	-	0	0	**4**
Traumatologist	1	0	0	-	-	-	-	-	0	0	0	0	0	0	0	0	0	0	-	0	0	**1**
Plastic surgeon	0	0	0	-	-	-	-	-	0	0	0	0	0	0	0	0	0	1	-	0	0	**1**
Paediatrics/anatomy	0	0	0	-	-	-	-	-	0	0	0	0	0	0	0	0	0	0	-	0	1	**1**
Cardiologist	0	1	0	-	-	-	-	-	0	0	0	0	0	0	0	0	0	0	-	0	0	**1**
Internist	0	0	2	-	-	-	-	-	2	0	0	3	0	0	0	0	0	0	-	0	0	**7**
Clinical oncologist	1	0	0	-	-	-	-	-	0	0	0	0	0	0	0	0	0	0	-	0	0	**1**
Toxicologist	0	1	0	-	-	-	-	-	0	0	0	0	0	0	0	0	0	0	-	0	0	**1**
General practitioner	0	3	0	-	-	-	-	-	0	0	1	3	0	0	0	0	0	1	-	0	1	**9**
Psychiatrist	0	0	0	-	-	-	-	-	0	0	0	0	1	0	0	0	0	0	-	0	0	**1**
Paediatrician	1	0	0	-	-	-	-	-	0	0	0	0	0	0	0	0	0	0	-	0	0	**1**
Radiologist	0	0	0	-	-	-	-	-	0	0	0	0	0	0	0	0	0	0	-	0	1	**1**
Scientist	0	0	0	-	-	-	-	-	0	1	0	0	0	0	0	0	0	0	-	0	0	**1**
National service medical corps	0	0	0	-	-	-	-	-	0	0	0	0	0	0	0	0	0	0	-	0	1	**1**
Alternative medical practitioner	0	0	0	-	-	-	-	-	2	0	0	0	0	0	0	0	0	0	-	0	0	**2**
Epidemiologist	0	0	0	-	-	-	-	-	0	0	0	0	0	0	0	1	0	0	-	0	0	**1**
Geriatrician	0	0	0	-	-	-	-	-	0	0	1	0	0	0	0	0	0	0	-	0	0	**1**
Virologist	0	0	0	-	-	-	-	-	0	0	1	0	0	0	0	0	0	0	-	0	0	**1**
Other (specialisation not specified)	0	0	0	-	-	-	-	9	0	0	0	4	0	0	0	0	0	4	-	0	0	**17**
Number of sCJD cases among physicians or dentists	**6**	**5**	**3**	**-**	**-**	**-**	**-**	**9**	**7**	**2**	**5**	**12**	**2**	**0**	**0**	**1**	**0**	**9**	**-**	**0**	**4**	**65**
Other health professionals																						
Laboratory technician	0	-	0	-	-	-	-	-	-	0	0	1	1	1	-	0	0	-	-	-	2	**5**
Sterilisation department	0	-	0	-	-	-	-	-	-	0	0	0	0	1	-	0	0	-	-	-	0	**1**
Veterinarian	1	-	0	-	-	-	-	-	-	1[b]	0	1	0	0	-	0	0	-	-	-	0	**3**
Hospital employee	1	-	0	-	-	-	-	-	-	0	0	2	0	0	-	0	0	-	-	-	5	**8**
Other	0	-	0	-	-	-	-	-	-	1[b]	0	17	17	0	-	2	2	-	-	-	45	**84**
Number of sCJD cases among all other health professionals	**2**	**-**	**0**	**-**	**-**	**-**	**-**	**36**	**-**	**2**	**0**	**21**	**18**	**2**	**-**	**2**	**2**	**-**	**-**	**-**	**52**	**137**
Number of sCJD cases among all healthcare professionals	**8**	**5**	**3**	**-**	**-**	**-**	**-**	**45**	**7**	**4**	**5**	**33**	**20**	**2**	**-**	**3**	**2**	**9**	**-**	**-**	**56**	**202**
Total number of registered sCJD cases[c]	**206[d]**	**607**	**160[e]**	**184[f]**	**406[f]**	**9[f]**	**88[f]**	**1,462**	**1,576**	**145**	**133**	**778[d,g]**	**955**	**253[f]**	**93[f]**	**58[f]**	**38[h]**	**813[d]**	**163[f,h]**	**217[f]**	**827[g]**	**8,321[c]**

AR=Argentina, AU= Australia, AT=Austria, BE=Belgium, CA=Canada. CY=Cypus, DK=Denmark, FR=France, DE=Germany, HU=Hungary, IL=Israel, IT=Italy, JP= Japan, NL=Netherlands, PT=Portugal, SK=Slovakia,SL=Slovenia, ES=Spain, SE=Sweden, CH=Switzerland, UK=United Kingdom.

sCJD: sporadic Creutzfeldt–Jakob disease. The dashes represent years for which there are no data.

[a] There were no reports of sCJD among Polish pathologists, clinicians or medical technicians (personal communication, Dr J. Kulczycki, May 2009)./ [b] The two (non-medical) health workers were pathology assistants./ [c] Data for countries reporting presence versus absence of sCJD among pathologists (Belgium, Canada, Cyprus, Denmark and Sweden) are not included in the total number./ [d] Confirmed or probable cases./ [e] Austria reported 233 sCJD cases during 1969 to 2009 (one genetic transmissible spongiform encephalopathy excluded), including 84 cases of sCJD with occupational data (1993–2008). / [f] sCJD deaths obtained from the EuroCJD website [16].Otherwise different categories of registered sCJD on request./ [g] sCJD cases with occupational data only./ [h] Occupational data not registered.

Only one of three case–control studies [4,5,21] provided data on specialities but gave no indication of the numbers involved [5]. It is likely that most cases mentioned in the EuroCJD study by Van Duijn et al. [5] were included in country-specific occupational counts of the case set obtained from the extended EuroCJD consortium in response to the current request.

Health-related occupational risk of sCJD

The nine analytical papers on occupations and sCJD identified [3-7,19,21,25,26] tended to focus on healthcare and animal care-related occupations, with Cocco et al.'s study furnishing detailed data on other occupations [19]. This study used a large number of non-validated CJD diagnoses from death records in the United States and controls selected after exclusion of persons with neurological diseases reported as the cause of death [19]. The main findings for healthcare-related occupations from five papers are summarised in Table 4. While three of four studies on health professions did not demonstrate excess risk [5-7], statistically significant findings – for persons working at physicians' offices – were solely reported by Cocco et al. [19].

Discussion

Despite a number of case reports of sCJD in physicians and technicians, the findings of this EuroCJD survey do not suggest an increased risk of sCJD in health professionals, nor do analytical studies show a clear excess risk for health-related professions. Methodological limitations of analytical studies in which occupational data were frequently provided by informants who were probably aware of the sCJD diagnosis [3-7,26] argue in favour of a cautious interpretation of the positive association reported for persons working at physicians' offices [19]. Consequently, the main finding of this literature review and complementary EuroCJD observation is that health professionals, including medical staff, are not at greater risk of developing sCJD. However, this cannot exclude the possibility that there may be an occupational risk in specific circumstances, for example, for people in contact with high-risk central nervous system tissue, and appropriate precautions, as recommended by national authorities, should therefore be followed, particularly regarding laboratory work.

Although in some studies occupation was specifically analysed [19,25] and occupation may be the subject of specific inquiry in some surveillance systems, a limitation of some registries and scientific studies is that occupation may not have been systematically recorded. When occupation was recorded, it is unlikely that a framework for consistent occupational data collection was used, so that neither registries nor case–control studies have incorporated the classic epidemiological double approach. Recording of occupation may not identify specific chemical or biological exposures, which would require data for professions (job titles, medical specialisations) being cross-referenced with branches of activity (laboratory, administrative or clinical patient-contact work). The lack of registered surveillance data that combine profession with activity (e.g. contact with human tissue), when compared with the descriptions from previous case reports and the incident in Spain, illustrates the limits of the validity of available data for analytical purposes and precludes formal use of statistical testing. Although our study does not provide evidence of an excess risk of sCJD in health professionals, the fact that the data collected were mainly linked to medical speciality rather than actual activity might have concealed an excess risk of sCJD for some specific health professionals.

A case–control study seeking to examine the putative occupational risk posed by surgical injuries should have a biologically clear working hypothesis and a custom-tailored methodology. Matrices designed by linking medical speciality and surgical/forensic-anatomical/pathological activity, in which the health

Table 2

Occupational profile of non-cases or controls obtained through the European Creutzfeldt Jakob Disease Surveillance Network (EuroCJD), 1980–2009 (n=2,968)

Occupation	Number of professionals, by country, in the specified time period					
	DE	IT	JP	ES	UK	
	1994–2007	1993–2008	1999–2009	1993–2009	1980–2009	**Total**
Physicians						
Traumatologist/surgeon	0	1	0	0	0	**1**
Surgeon (not specified)	0	1	0	0	1	**2**
Internist	0	1	0	0	0	**1**
General practitioner	0	1	0	0	1	**2**
Psychiatrist	0	0	0	1	0	**1**
Paediatrician	1	0	0	0	0	**1**
Scientist	0	0	0	0	1	**1**
Other (specialisation not specified)	6	0	0	0	0	**6**
Number of physicians	**7**	**4**	**0**	**1**	**3**	**15**
Other health professionals						
Laboratory technician	-	2	-	-	5	**7**
Hospital employee	-	1	-	-	13	**14**
Other	-	10	-	-	34	**44**
Number of other health professionals	**-**	**13**	**3**	**-**	**52**	**68**
Number of healthcare professionals	**7**	**17**	**3**	**1**	**55**	**83**
Total number of non-cases or controls	**1,061[a]**	**656[b]**	**268**	**167**	**816[a,b]**	**2,968**

DE=Germany; IT=Italy ; JP=Japan; ES=Spain; UK=United Kingdom.
The dashes represent years for which there are no data.

[a] Controls from own case–control study.

[b] Only persons with occupational data.

professional can come into direct contact with high human-infectivity tissue by accident might not provide a sufficient background for analysis, without appropriate control being made for the influence of *PRNP* genotype, surgical or laboratory work history and long latency. Assuming that among non-cases or controls the proportion of medical specialities with potential exposure (surgeons, forensic surgeons and other surgical specialists, pathologists) may be low, i.e. approximately 1 per 1,000 (based on the figures of 3/2,968 in Table 2), the study size that would afford the necessary statistical power for a proper examination of the specific practices of health professions is higher than that provided by existing CJD registries in any one country. Since complementary analyses would be needed for professional and activity categories defined in terms of temporal references that have not been explored to date, such as 'ever employed' or 'currently employed', as well as duration of employment, requirements for study size and collaboration would be even higher.

Table 3

Health-profession-related sporadic Creutzfeldt–Jakob disease case reports from literature review, 1979–1 October 2011

Number of cases and their professions	Source
3 dentists 1 neurosurgeon 1 dental surgeon 6 nurses 1 assistant nurse	[17]
1 neurosurgeon	[23]
3 nurses 2 assistant nurses	[22]
1 histopathology technician	[8]
1 histopathology technician	[9]
1 physician 1 dentist 3 career nurses 2 people with brief nursing experience	[4][a]
1 pathologist	[20]
1 internist, formally trained in pathology 30 years previously	[10]
1 orthopaedic surgeon handling sheep and human dura mater 20–25 years before symptom onset	[12]
32 cases that included a physician; neuropathologist; nurse; laboratory technician; dentist and ambulance worker	[5][a]
1 nurse, gastrointestinal section	[21][a]
1 nurse and 1 ambulance driver without E200 mutation 2 nurses, 1 physician (dermatologist) with sporadic-like forms, carriers of E200K mutation 1 nurse (not from Slovakia. where the cases were reported), genotyping not done	[11][b]

[a] Described in case–control studies and, in general, fulfilling criteria as probable or confirmed sporadic Creutzfeldt–Jakob disease (sCJD) [17, 24].

[b] Mention of clinical features, genetic study or country of origin is frequently made in Slovakian cases given the high incidence of genetic forms and the relevance of genotyping for correct classification of CJD.

In conclusion, a wide spectrum of medical specialities and health professions are represented in sCJD registries. Although selection due to higher ascertainment may lie behind the case reports of certain professions involved in clinical management or care of patients with sCJD, the biological significance of these observations remains uncertain and available data do not indicate an increased risk of sCJD in health professionals. However, the methodological issues mentioned above indicate the need for caution in drawing conclusions from the data and large-scale studies with specific causal hypotheses are needed in order for further research to be undertaken into the potential link between health professions and sCJD

.Acknowledgments

The authors would like to thank all EuroCJD network members and officials worldwide who furnished data constituting and/or comments contributing to the basis of this study, and the following in particular: Prof. P. Cras, Belgium; Dr G. Jansen, Canada; Mrs G. Klug, Australia; Drs K. Mølbak and H. Laursen, Denmark; Dr S. Papacostas, Cyprus; Dr J. Kulczycki, Poland; Mrs F. Avellanal, Spain; Dr A. L. Hammarin and Mrs S. Ivarsson, Sweden; and Dr R. Knight, United Kingdom.

The EuroCJD network has been supported by Directorate-General for Research and Innovation (DG Research), Directorate-General for Health and Consumers (DG SANCO) and the European Centre for Disease Prevention and Control.

References

1. Prusiner SB. The prion diseases. Brain Pathol. 1998;8(3):499-513.
2. Ladogana A, Puopolo M, Croes EA, Budka H, Jarius C, Collins S, et al. Mortality from Creutzfeldt-Jakob disease and related disorders in Europe, Australia, and Canada. Neurology. 2005;64(9):1586-91.
3. Collins S, Law MG, Fletcher A, Boyd A, Kaldor J, Masters CL. Surgical treatment and risk of sporadic Creutzfeldt-Jakob disease: a case-control study. Lancet. 1999;353(9154):693-7.
4. Harries-Jones R, Knight R, Will RG, Cousens S, Smith PG, Matthews WB. Creutzfeldt-Jakob disease in England and Wales, 1980-1984: a case-control study of potential risk factors. J Neurol Neurosurg Psychiatry. 1988;51(9):1113-9.
5. van Duijn CM, Delasnerie-Laupêtre N, Masullo C, Zerr I, de Silva R, Wientjens DP, et al. Case-control study of risk factors of Creutzfeldt-Jakob disease in Europe during 1993-95. European Union (EU) Collaborative Study Group of Creutzfeldt-Jakob disease (CJD) Lancet. 1998;351(9109):1081-5.
6. Wientjens DP, Davanipour Z, Hofman A, Kondo K, Matthews WB, Will RG, et al. Risk factors for Creutzfeldt-Jakob disease: a reanalysis of case-control studies. Neurology. 1996;46(5):1287-91.
7. Ruegger J, Stoeck K, Amsler L, Blaettler T, Zwahlen M, Aguzzi A, et al. A case-control study of sporadic Creutzfeldt-Jakob disease in Switzerland: analysis of potential risk factors with regard to an increased CJD incidence in the years 2001-2004. BMC Public Health. 2009;9:18.
8. Miller DC. Creutzfeldt-Jakob disease in histopathology technicians [letter]. N Engl J Med. 1988;318(13):853-4.
9. Sitwell L, Lach B, Atack E, Atack D, Izukawa D. Creutzfeldt-Jakob disease in histopathology technicians [letter]. N Engl J Med. 1988;318(13):854.
10. Berger JR, David NJ. Creutzfeldt-Jakob disease in a physician: a review of the disorder in health care workers. Neurology. 1993;43(1):205-6.
11. Mitrová E, Belay G. Creutzfeldt-Jakob disease in health professionals in Slovakia. Eur J Epidemiol. 2000;16(4):353-5.
12. Weber T, Tumani H, Holdorff B, Collinge J, Palmer M, Kretzschmar HA, et al. Transmission of Creutzfeldt-Jakob disease by handling of dura mater. Lancet. 1993;341(8837):123-4.

Table 4

Summary of methods and main results of analytical epidemiological research into healthcare-related occupations and sporadic Creutzfeldt–Jakob disease, literature review, 1982–1 October 2011

Methods						Main occupational findings	Source
Type of study Study purpose Occupational hypotheses tested	Study population	Study period	Number of cases (number of confirmed sCJD cases)	Type of controls and controls sampling design	Occupations studied and source of information on occupational exposure	Specific occupational groups reported Odds ratio (95% CI), if calculated	
Case–control Multiple occupations. Prior health-related hypotheses were pathologists, other health professionals, work at hospitals and work at other health facilities	>6 million deaths in 24 states of the USA	1984–1995	636 cases identified as CJD diagnosis in death certificates coded as per the Nineth International Classification of Diseases (ICD9) ICD9-046.1 >25 years at death	3,180 randomly selected controls corresponding to persons whose death certificate did not contain as cause of death CJD (ICD9-046.1) or some neurological diseases (ICD9- 290.0-319.9; 320.0-349.9; 430.0-438.9; 440.0; or 780.0-781.9)	Occupational (159) and industrial (147) categories reported in death certificate, coded as per the 1980 United States Bureau of Census Classification. Age, residence, marital status at death Database publicly available	Persons working at physicians' offices OR: 4.6 (1.2–17.6) Physicians OR: 4.6 (0.7–29.0) Nursing aides, orderlies and attendants OR: 0.5 (0.1–1.6) Hospital workersOR: 1.0 (0.6–1.7) Nurses and staff of care facilities OR: 0.8 (0.2–2.6) Other health service staff OR: 1.1 (0.3–3.8)	[19]
Case–control Genetic factors Lifetime: - medical and dental history - animal exposures - diet - occupation (categories not specified)	Six European countries	1993–1995	405 (194 confirmed)	Age (5 years)- and sex-matched 405 hospital controls	Cases: proxy interview; controls: proxy interview (where possible)	Health professionals Occupations included: physician, neuropathologist, nurse, laboratory technician, dentist and ambulance worker OR: 0.92 (0.69–1.32) None of the professions studied was significantly associated with increased risk of CJD in a pooled analysis	[5]
Case–control Lifetime medical history, drug use, diet and occupation	Swiss resident population	2001–2004 during high sCJD incidence period [30]	69 cases: 61 confirmed and 8 probable. Symptom onset in 2001–2004	224 controls 69 GP-based 2004–2005 (using exclusion criteria) matched by age, sex, district and GP list 155 random digit telephone dialling in 2005; matched by age, sex, residence and language	EuroCJD questionnaire. Proxy interviews, response rate 68%.	Medical profession OR: 1.49 (0.43–5.15) Pharmaceutical laboratory OR: 3.39 (0.21–55.20) ORs adjusted for age, sex and education	[7]
Meta-analysis case–control Multipurpose in three studies For occupation, data used from two UK- and USA-based, studies [4,27-29]	Selected populations in the UK and USA	UK (England and Wales): 1980–1984 USA (Pennsylvania and other mid-Atlantic states): 1970– 1981	118 cases: UK 92 (70 confirmed) diagnosed 1980–1984 in England and Wales USA 26 (13 confirmed) diagnosed in 1970–1981 in Pennsylvania and other mid-Atlantic states	213 age- and sex-matched controls UK 184 hospital patients (1 neurological and 1 medical set) USA 40 (18 relatives, 22 hospital patients)	Not reported UK cases: proxy interview; controls: proxy interview USA mail questionnaire before interview. Cases: proxy phone interview; controls: direct phone interview	Health professionals OR: 1.5 (0.5–4.1) adjusted for age, sex and study site	[6]
Case–control Multiple, mainly non-occupational exposures	Japan, national	1975–1977	60 (37 confirmed of 75 initially recruited cases)	Age (5 years)- and sex-matched controls (n=103): 56 neighbours and 47 spouses	Occupation life history at time of onset, and 5 years and 10 years before onset. Cases: proxy interview Controls: direct interview	Health professionals No health-related professions were observed among cases A few public health workers were included among controls OR not calculated	[26][a]

CJD: Creutzfeldt–Jakob disease; EuroCJD: European Creutzfeldt Jakob Disease Surveillance Network; GP: general practitioner; OR: odds ratio
UK: United Kingdom; USA: United States of America.

[a] The information on health-related occupations from this study was not included in the meta-analysis [6].

13. Neeleman E, Molhoek R. CJD-NQUEST manual. Data entry sofware for CJD-surveillance. Rotterdam: Department of Epidemiology and Biostatistics, Erasmus University; 1998.
14. European Centre for Disease Prevention and Control (ECDC). Review of guidelines for prevention of Creutzfeldt–Jakob disease transmission in medical settings in EU Member States and Norway. Stockholm: ECDC; 2011.
15. Terry S. Singeltary Sr. Doctor Antonio Ruiz Villaespesa, pathologist and CJD researcher deceased because of Creutzfeldt-Jakob Disease SPAIN. 21 Apr 2009. [Accessed 11 Apr 2012]. In: Monitoring the occurrence of emerging forms of CJD [blog]. Available from: http://cjdusa.blogspot.com.es/2009/04/doctor-antonio-ruiz-villaespesa.html
16. The European Creutzfeldt Jakob Disease Surveillance Network. EUROCJD. [Accessed 11 Apr 2012]. Available from: http://www.eurocjd.ed.ac.uk/index.htm
17. Masters CL, Harris JO, Gajdusek DC, Gibbs CJ Jr, Bernoulli C, Asher DM. Creutzfeldt-Jakob disease: patterns of worldwide occurrence and the significance of familial and sporadic clustering. Ann Neurol. 1979;5(2):177-88.
18. Zerr I, Pocchiari M, Collins S, Brandel JP, de Pedro Cuesta J, Knight RS, et al. Analysis of EEG and CSF 14-3-3 proteins as aids to the diagnosis of Creutzfeldt-Jakob disease. Neurology. 2000;55(6):811-5.
19. Cocco PL, Caperna A, Vinci F. Occupational risk factors for the sporadic form of Creutzfeldt-Jakob disease. Med Lav. 2003;94(4):353-63.
20. Gorman DG, Benson DF, Vogel DG, Vinters HV. Creutzfeldt-Jakob disease in a pathologist. Neurology. 1992;42(2):463.
21. Nakamura Y, Oki I, Tanihara S, Ojima T, Yanagawa H, Kitamoto T, et al. A case-control study of Creutzfeldt-Jakob disease in Japan: transplantation of cadaveric dura mater was a risk factor. J Epidemiol. 2000;10(6):399-402.
22. Brown P, Cathala F, Raubertas RF, Gajdusek DC, Castaigne P. The epidemiology of Creutzfeldt-Jakob disease: conclusion of a 15-year investigation in France and review of the world literature. Neurology. 1987;37(6):895-904.
23. Schoene WC, Masters CL, Gibbs CJ Jr, Gajdusek DC, Tyler HR, Moore FD, et al. Transmissible spongiform encephalopathy (Creutzfeldt-Jakob disease). Atypical clinical and pathological findings. Arch Neurol. 1981;38(8):473-7.
24. Salazar AM, Masters CL, Gajdusek DC, Gibbs CJ Jr. Syndromes of amyotrophic lateral sclerosis and dementia: relation to transmissible Creutzfeldt-Jakob disease. Ann Neurol. 1983;14(1):17-26.
25. Cousens SN, Zeidler M, Esmonde TF, De Silva R, Wilesmith JW, Smith PG, et al. Sporadic Creutzfeldt-Jakob disease in the United Kingdom: analysis of epidemiological surveillance data for 1970-96. BMJ. 1997;315(7105):389-95.
26. Kondo K, Kuroiwa Y. A case control study of Creutzfeldt-Jakob disease: association with physical injuries. Ann Neurol. 1982;11(4):377-81.
27. Davanipour Z, Alter M, Sobel E, Asher DM, Gajdusek DC. A case-control study of Creutzfeldt-Jakob disease. Dietary risk factors. Am J Epidemiol. 1985;122(3):443-51.
28. Davanipour Z, Alter M, Sobel E, Asher D, Gajdusek DC. Creutzfeldt-Jakob disease: possible medical risk factors. Neurology. 1985;35(10):1483-6.
29. Davanipour Z, Alter M, Sobel E, Asher DM, Gajdusek DC. Transmissible virus dementia: evaluation of a zoonotic hypothesis. Neuroepidemiology. 1986;5(4):194-206.
30. Glatzel M, Rogivue C, Ghani A, Streffer JR, Amsler L, Aguzzi A. Incidence of Creutzfeldt-Jakob disease in Switzerland. Lancet. 2002;360(9327):139-41.

RESEARCH PAPER

Intensity of human prion disease surveillance predicts observed disease incidence

Genevieve M J A Klug,[1,2] Handan Wand,[3] Marion Simpson,[1] Alison Boyd,[1,2] Matthew Law,[3] Colin L Masters,[1,2] Radoslav Matěj,[4] Rachel Howley,[5] Michael Farrell,[5] Maren Breithaupt,[6] Inga Zerr,[6] Cornelia van Duijn,[7] Carla Ibrahim-Verbaas,[7,8] Jan Mackenzie,[9] Robert G Will,[9] Jean-Philippe Brandel,[10] Annick Alperovitch,[10] Herbert Budka,[11] Gabor G Kovacs,[11,12] Gerard H Jansen,[13] Michael Coulthard,[14] Steven J Collins[1,2]

▸ Additional material is published online only. To view please visit the journal online (http://dx.doi.org/10.1136/jnnp-2012-304820).

For numbered affiliations see end of article.

Correspondence to
Genevieve M Klug or Professor Steven J Collins, Australian National Creuztfeldt-Jakob Disease Registry, Department of Pathology, The University of Melbourne, Parkville 3010, Australia; gmjak@unimelb.edu.au or stevenjc@unimelb.edu.au

Received 19 December 2012
Revised 16 May 2013
Accepted 28 July 2013
Published Online First 21 August 2013

ABSTRACT

Background Prospective national screening and surveillance programmes serve a range of public health functions. Objectively determining their adequacy and impact on disease may be problematic for rare disorders. We undertook to assess whether objective measures of disease surveillance intensity could be developed for the rare disorder sporadic Creutzfeldt–Jakob disease (CJD) and whether such measures correlate with disease incidence.

Method From 10 countries with national human prion disease surveillance centres, the annual number of suspected prion disease cases notified to each national unit (n=17 610), referrals for cerebrospinal fluid (CSF) 14-3-3 protein diagnostic testing (n=28 780) and the number of suspect cases undergoing diagnostic neuropathological examination (n=4885) from 1993 to 2006 were collected. Age and survey year adjusted incidence rate ratios with 95% CIs were estimated using Poisson regression models to assess risk factors for sporadic, non-sporadic and all prion disease cases.

Results Age and survey year adjusted analysis showed all three surveillance intensity measures (suspected human prion disease notifications, 14-3-3 protein diagnostic test referrals and neuropathological examinations of suspect cases) significantly predicted the incidence of sporadic CJD, non-sporadic CJD and all prion disease.

Conclusions Routine national surveillance methods adjusted as population rates allow objective determination of surveillance intensity, which correlates positively with reported incidence for human prion disease, especially sporadic CJD, largely independent of national context. The predictive relationship between surveillance intensity and disease incidence should facilitate more rapid delineation of aberrations in disease occurrence and assessment of the adequacy of disease monitoring by national registries.

INTRODUCTION

National screening and surveillance programmes encompass a broad range of diseases, which collectively serve a diverse spectrum of important public health objectives. Examples of national screening programmes are those aimed at the early detection of cancers or precancerous states, such as in relation to cervix,[1] breast[2 3] and bowel,[4 5] while infectious or transmissible diseases like HIV,[6] hepatitis C[7 8] and Creutzfeldt–Jakob disease (CJD)[9] are a frequent focus of national surveillance centres. Evaluation of national screening and surveillance programmes, using objective measures of the adequacy of screening and the consequent impact on disease incidence, is important for measuring the utility of these public health initiatives.

In relation to national screening for certain malignancies, the 'at risk' group can often be defined by age and/or sex, with national census data delineating the size and geographical distribution of the target population. Consequently, the adequacy of screening and impact on disease incidence over time can be determined reasonably easily and accurately, including providing insights into how completeness of disease screening impacts disease incidence.[1] Objective assessment of the adequacy and consequent impact of national surveillance is arguably more difficult for rare disorders like sporadic CJD, where screening is not possible and surveillance largely based on the suspicion of disease.

CJD is the most common human phenotype of the rare, transmissible neurodegenerative disorders known as prion diseases. Over the last 15 years, there has been substantial improvement in premortem diagnostic capacity, mainly through CSF 14-3-3 protein detection and brain MRI.[10–12] With a reported sensitivity of 85%–90%,[11 13] the utilisation of the 14-3-3 protein CSF test has greatly increased since its introduction during the 1990s.[14]

Sporadic CJD incidence is frequently quoted as 1/million population/year,[15 16] implying a fixed and always maximal incidence, perhaps secondary to intrinsic biological features of the disease, yet officially reported national incidence rates vary from 0.48 to 2.23/million population/year.[9] Small populations, more vulnerable to incidence variation, may partly explain such disparities but the question remains as to why countries with inherent similarities in surveillance methodologies and population sizes have varied reported incidence rates. A recent report has suggested that surveillance intensity, measured through assessment of population interrogation rates, correlates with disease incidence.[17]

To cite: Klug GMJA, Wand H, Simpson M, *et al*. *J Neurol Neurosurg Psychiatry* 2013;**84**: 1372–1377.

This is an intuitively appealing but hitherto unsubstantiated hypothesis, particularly in a multi-national setting.

The primary aim of the current study was to examine within a multi-national context the relationship between reported disease incidence and surveillance intensity, the latter measured through adapting relatively simple monitoring methods into objective metrics.

METHODS

National surveillance centres constituting the European and Allied Countries Creutzfeldt–Jakob Disease Surveillance Consortium (EUROCJD) were invited to participate in the study. In addition, based on analogous prospective national human prion disease surveillance programmes and similar data collection mechanisms, the Czech Republic and Hungary were also included in the study. Details concerning the EUROCJD participating countries and their ascertainment and data collection methods have been published previously.[9 11] Overall, 10 countries (Australia, Austria, Canada, Czech Republic, France, Germany, Hungary, Republic of Ireland, Netherlands and the UK) provided data for the 14-year period of 1993–2006, with a key requirement being their ability to undertake detailed age-stratification of the annual national populations for each year of study data supplied. Surveillance activities in the majority of countries involved began in 1993 and the timeframe of data collected was chosen to reflect this fact and the introduction of the CSF 14-3-3 test in 1997, providing a long-term perspective of the study measures assessed. Data requested for analysis were annual counts for each category of: persons referred to national surveillance units with suspected prion disease; those referred with suspected prion disease undergoing neuropathological assessment; and persons referred for CSF 14-3-3 protein testing. For countries commencing national prospective surveillance prior to 1998, CSF 14-3-3 protein detection was available from 1997, while in countries where prospective national surveillance commenced after 1997 (Canada and Czech Republic), data were limited to the available years within the epoch (refer table 1).

Three variables were selected as potential objective predictors of disease incidence: notification of suspected prion disease to a national registry; referrals for diagnostic CSF 14-3-3 protein testing; and referrals for neuropathological examination in suspected prion disease cases. Suspected prion disease notifications included all referrals made to each national surveillance centre between 1/1/1993 and 31/12/2006, regardless of the notification source and the perceived prima facie likelihood of prion disease; the latter was to mitigate potential selection biases. Specific practices for CSF 14-3-3 protein testing varied between countries; some national surveillance centres were notified by multiple delegated diagnostic laboratories of all testing results, while in other countries only positive results were notified by external laboratories and not all samples were tested. In many countries, surveillance centres undertook all testing within their own laboratory and were therefore aware of all referrals, regardless of result. Although this variation in CSF referrals introduces a potential source of bias, it was tolerated to accommodate minor differences in national surveillance formats and to enhance the broader applicability of the study and its findings across the authentic range of national surveillance practices. Referrals for neuropathological examination included all suspected cases of prion disease referred to national surveillance centres undergoing autopsy examination of the brain or brain biopsy, offering a 'gold standard' for prion disease diagnosis.

Cases where onset and notification occurred within one country but death occurred elsewhere were excluded from the analysis, as were CSF 14-3-3 protein samples referred from outside the country in question. Within each country, data for the three predictor variables were collected as total numbers and were stratified by survey year into 5-year age groups by: year and age at notification or death (if dead at time of notification) for the suspected prion disease referral variable; year and age at CSF 14-3-3 protein sampling for CSF referrals; and year and age at notification (or death if dead at time of notification) for neuropathological examination of suspected prion disease referrals.

Three outcome variables were determined: the annual number of definite and probable cases of sporadic CJD; non-sporadic CJD (encompassing variant CJD, genetic and iatrogenic prion disease); and all prion disease cases (sporadic plus non-sporadic CJD plus other prion diseases). Human prion disease evinces a heterogeneous phenotype, such that a case may be referred as being suspected variant CJD but ultimately classified as a different form of prion disease. The national surveillance units involved in the study use the same referral systems for all types of prion disease, with final classification of definite and probable cases based on internationally recognised clinical and/or neuropathological criteria. To assess the potential influence of the numerical predominance of sporadic CJD on the all prion disease groups, non-sporadic CJD cases were analysed as a separate group.

After data auditing, the Netherlands was excluded from the modelling analyses due to incomplete data sets for the study period.

Statistical analysis

Adjustment for age structure differences in the nine countries was performed by direct age-standardisation, with data adjusted to a standard population; the Australian 2000 population was chosen due to it being the median size and midpoint of the data set collected. Crude rates of disease incidence (per million population) were initially calculated for each country. Trends in rates overall and within each country for referrals of CSF 14-3-3 protein detection, suspect CJD cases and neuropathological examinations postmortem were assessed. To investigate the predictors for sporadic, non-sporadic and all prion disease cases, incidence rate ratios (IRRs) were estimated with 95% CIs using random-effects Poisson regression methods to take into account within-country variation for repeated measures across the survey years: reported suspect cases, CSF referrals and performing neuropathology in suspected cases. The test for heterogeneity using the random-effects variance parameter estimate was significant ($p<0.01$), confirming the appropriateness and suitability of the random-effects model. Stata, V.10.0 (StataCorp, College Station, Texas, USA) statistical software was used in all analyses.

RESULTS

For the period 1993–2006, 17 610 persons with suspected prion disease were notified to national surveillance centres across the nine countries, with 28 780 CSF 14-3-3 protein referrals for diagnostic testing, and 4885 cases of suspected prion disease undergoing neuropathological assessment (table 1). For the same period, there were 4235 (definite and probable) sporadic CJD cases (approximately 84% of the total) among 5054 cases classified with any form of prion disease. Overall, 70% of the 5054 definite and probable CJD cases and 73% of all suspect prion disease referrals who underwent neuropathological examination were classified as definite cases. For the nine countries, national crude annual referral rates of suspected prion disease cases

Table 1 Summary of national data

	Time period of analysis	Suspect prion disease referrals	Diagnostic CSF 14-3-3 protein referrals	Neuropathological (NP) examination performed in suspect cases	Sporadic CJD*	All prion disease†	Definite prion cases only	Proportion of all prion cases that were classified as definite cases (%)	Proportion of suspect cases who had NP that were confirmed with CJD (%)
Australia	1993–2006	2017	1740	412	302	340	235	69	57
Austria	1996–2006	1102	1016	235	101	122	113	93	48
Canada	1998–2006	731	918	472	284	311	261	84	55
Czech Republic	2000–2006	111	154	111	55	62	62	100	56
France	1993–2006	8998	8148	1272	1177	1432	874	61	69
Germany	1993–2006	2273	15 640	1008	1366	1493	973	65	97
Hungary	1993–2006	273	83	241	115	165	162	98	67
Republic of Ireland	1993–2006	175	77	86	42	49	44	90	51
UK	1993–2006	1930	1004	1048	793	1080	825	76	79
Totals		17 610	28 780	4885	4235	5054	3549	70	73

*Includes both probable and definite (pathologically confirmed) sporadic CJD.
†Includes all forms of probable and definite prion disease: sporadic CJD, variant CJD, genetic prion disease and iatrogenic prion disease.
CJD, Creutzfeldt–Jakob disease.

ranged between 0.20 and 26.62 cases per million per year (annual average 1.55–12.32 referrals/million/year), while CSF referrals ranged from 0.20 to 29.41 per million per year (annual average 0.92–17.25 referrals/million/year) and neuropathology examination in suspect cases ranged from 0.19 to 4.84 examinations per million per year (annual average 0.88–2.64 examinations/million/year) (table 2, see online supplementary tables 1 and 2). For sporadic CJD, the crude annual incidence rates varied from 0.19 to 2.29 cases per million per year (annual average 0.77–1.42 cases/million/year) (table 3) and for all prion diseases, the crude annual incidence rates varied from 0.19 to 2.58 cases per million per year (annual average 0.87–1.73 cases/million/year) (see online supplementary table 3).

Temporal trend analysis of each age-adjusted, predictor and outcome variable over the 1993–2006 period was undertaken for the pooled national data. Overall, there was a significant increase in suspect case referrals (IRR 1.09 (95% CI 1.08 to 1.10)), diagnostic CSF 14-3-3 protein detection referrals (IRR 1.18 (95% CI 1.17 to 1.19)), sporadic CJD (IRR 1.03 (95% CI 1.01 to 1.04)) and all prion disease cases (IRR 1.02 (95% CI (1.01 to 1.03)) but no increase in neuropathological examinations of suspect cases at postmortem (IRR 1.00 (95% CI 0.99 to 1.01)) over time (see online supplementary table 4). Differences between countries in terms of the temporal trends and the correlations between surveillance intensity predictor variables and disease incidence were observed over the study period. Seven of the nine countries displayed congruence with the principle that significant increases in the average annual trend of suspect prion disease notifications combined with diagnostic CSF 14-3-3 protein detection referrals correspond with increases in disease incidence (sporadic CJD and/or all prion disease) over the study period. Increasing surveillance variables in Hungary was associated with an increase in only the 'all prion disease' category, and in one country (Czech Republic) the conformity to this principle was that no increase in surveillance intensity variables over the study period corresponded with a lack of observed increase in disease incidence. In only two countries (Australia and Republic of Ireland) was there no correspondence between a significant increase in the average annual trend in suspect prion disease notifications and diagnostic CSF 14-3-3 protein

Table 2 National crude annual suspect human prion disease referral rates (per million population)

Country	Australia	Austria	Canada	Czech Republic	France	Germany	Hungary	Ireland	UK
1993	1.25				1.10	0.36	0.68	0.30	1.35
1994	1.29				1.57	1.64	0.98	0.30	2.06
1995	2.10				1.95	1.58	1.18	0.30	1.50
1996	2.84	2.14			3.47	2.11	1.67	0.55	2.29
1997	2.86	4.39			5.12	2.18	1.78	2.46	2.78
1998	4.17	4.26	1.42		7.89	2.22	0.80	2.97	2.63
1999	5.76	7.88	2.07		10.13	1.73	1.30	3.47	2.90
2000	10.08	10.86	2.66	0.19	13.98	1.85	1.91	1.85	2.99
2001	11.23	14.55	3.24	1.08	18.61	2.10	3.09	3.64	3.03
2002	10.99	13.48	3.27	1.76	17.54	1.88	1.59	3.83	2.75
2003	11.81	14.66	2.36	2.25	18.12	2.06	1.69	1.51	2.72
2004	12.67	15.66	2.80	1.76	14.66	2.08	2.39	9.39	1.90
2005	13.14	21.01	2.96	1.95	15.24	2.35	3.17	6.77	2.03
2006	12.41	26.62	2.38	1.85	21.38	3.51	4.86	6.84	1.83
Average	7.33	12.32	2.57	1.55	10.77	1.97	1.94	3.16	2.34

Table 3 National crude annual incidence rates (per million population) for sporadic Creutzfeldt–Jakob disease for each country

Country	Australia	Austria	Canada	Czech Republic	France	Germany	Hungary	Ireland	UK
1993	0.96				0.61	0.31	0.39		0.66
1994	0.62				0.79	0.87	0.59		0.92
1995	1.05				1.03	0.93	0.49		0.60
1996	1.37	1.13			1.18	1.01	1.18	0.55	0.69
1997	1.08	0.50			1.38	1.23	1.09	0.55	1.03
1998	1.34	0.75	0.73		1.40	1.38	0.30	1.62	1.08
1999	1.32	0.88	0.85		1.58	1.20	0.50	0.27	1.06
2000	1.46	0.75	1.04	0.19	1.48	1.26	0.90	0.79	0.82
2001	1.03	1.12	0.87	0.78	1.86	1.44	1.69	1.30	0.98
2002	0.92	0.62	0.99	0.59	1.81	1.18	0.69	1.28	1.21
2003	1.11	1.85	0.85	0.78	1.80	1.28	0.80	0.50	1.33
2004	0.84	0.86	1.31	1.08	1.60	1.62	0.80	1.73	0.84
2005	1.13	1.70	1.23	0.98	1.36	1.59	0.79	1.21	1.10
2006	1.55	2.29	1.13	0.97	2.02	1.30	1.19	0.94	1.14
Average	1.13	1.13	1.00	0.77	1.42	1.19	0.81	0.98	0.96

detection referrals over the study period and increases in either sporadic CJD and/or all prion disease incidence; this lack of correlation did not clearly correspond with the magnitude of the IRRs for surveillance intensity.

The test for heterogeneity using the random-effects variance parameter was significant ($p<0.001$), indicating suitability for employing random-effects Poisson modelling. After age adjustment, the analysis showed highly significant correlations between each predictor variable and the incidence of disease (sporadic CJD, non-sporadic CJD and all prion disease groups) (table 4), with the association between the neuropathological examinations of suspect cases as predictor and disease incidence less substantial than the other two predictor variables.

By age and survey year adjusted analysis, the associations between the predictor and outcome variables (table 4) showed suspect case notifications, diagnostic CSF 14-3-3 protein detection referrals and neuropathological examination each independently predicted sporadic CJD, non-sporadic CJD and all prion disease incidence. The only exception was a modest negative association between diagnostic CSF 14-3-3 protein detection referrals and non-sporadic CJD. In comparison with the level of significance of our other analyses we believe this modest result may imply a lack of meaningful correlation. We suspect the outcomes observed for the all prion disease group most likely represent a carryover effect through the numerical predominance of sporadic CJD in this group.

COMMENT

This is the first study to directly address and verify previous suggestive findings[17] and prevailing assumptions that greater scrutiny of a population may lead to higher rates of human prion disease detection and thereby reported disease incidence. Integral to the more objective assessment approach described in our study is the adjustment of surveillance detection methods as population interrogation rates. Employing this method, we have shown that relatively simple, accessible measures (clinical case recognition with notification made to a national surveillance centre combined with a routine diagnostic test like CSF 14-3-3 protein detection and neuropathological examination) can be adjusted to generate metrics of surveillance intensity, which correlate sufficiently with sporadic CJD incidence to be predictive. The broad multinational context, very large number of cases included and the extended time period of the study all add support for the robustness of the findings. As such, our observations provide important insight into factors that contribute to variations in reported prion disease incidence, particularly for sporadic CJD.[9] Nevertheless, in the absence of universal autopsy, some uncertainty inevitably persists regarding the ascertainment of all human prion disease cases and the absolute incidence of CJD.

The observed predictive relationship between surveillance intensity and sporadic CJD incidence was present despite the recognised clinical profile variations across the sporadic CJD subtypes,[11 18] suggesting that national surveillance can be

Table 4 Overall incidence rate ratios after adjustment for age and survey years

Outcome	Predictor	Incidence rate (95% CI) ratio (age-adjusted)	p Value	Incidence rate (95% CI) ratio (age and survey year adjusted)	p Value
Sporadic cases	Suspect cases	1.007 (1.005 to 1.01)	<0.001	1.005 (1.004 to 1.006)	<0.001
	CSF referrals	1.002 (1.001 to 1.003)	<0.001	1.001 (1.0008 to 1.002)	<0.001
	Neuropathology performed in suspect cases	1.08 (1.06 to 1.09)	<0.001	1.056 (1.05 to 1.061)	<0.001
Non-sporadic cases	Suspect cases	1.007 (1.003 to 1.01)	0.003	1.004 (1.002 to 1.007)	<0.001
	CSF referrals	1.0003 (1.0002 to 1.0004)	<0.001	0.998 (0.997 to 0.999)	0.03
	Neuropathology performed in suspect cases	1.05 (1.04 to 1.07)	<0.001	1.05 (1.03 to 1.07)	<0.001
All prion disease cases	Suspect cases	1.008 (1.005 to 1.01)	<0.001	1.013 (1.012 to 1.014)	<0.001
	CSF referrals	1.002 (1.001 to 1.003)	<0.001	1.002 (1.001 to 1.003)	<0.001
	Neuropathology performed in suspect cases	1.07 (1.06 to 1.09)	0.006	1.06 (1.05 to 1.07)	<0.001

achieved for a disease through primarily relying on clinical detection even when there is a somewhat diverse phenotypic spectrum. It is also of interest that advanced age, well beyond that more typically associated with sporadic CJD, does not appear to impede clinical recognition, with previous studies suggesting that increased incidence appears to correlate with increased referrals of suspect cases in the very elderly.[17 19]

The epidemiological history of human prion diseases, especially acquired forms such as those related to the therapeutic use of cadaveric dura mater explants and pituitary hormones[20] as well as variant CJD[21] and ongoing concerns regarding transmission risks posed by routine surgery, including non-neurosurgery,[22 23] should serve as a sobering precaution against any public health complacency in relation to this group of diseases. The key objectives of prospective national surveillance programmes are to ensure adequate detection of the disease and accurate depiction of the epidemiological profile so that significant departures in disease incidence or demographic characteristics can be recognised.[24] Our findings should subserve both of these objectives. As described for variant CJD,[21] an altered phenotype can indicate important epidemiological changes with respect to disease aetiology. Notwithstanding this influence, a more accurately defined and predictive relationship between population surveillance intensity and disease recognition rates (with 95% CIs) should facilitate more rapid and confident delineation of significant deviations in national disease incidence for a given surveillance intensity and serve to prompt more detailed evaluation of why this change has occurred, possibly leading to more expeditious deployment of public health responses.

Our study revealed major variations, approximately two orders of magnitude, in annual crude notification rates of persons with suspected prion disease across the study period in the countries assessed. Although some of this variation may be a natural finding based on variable population sizes, it demonstrates the likely underappreciation of true differences when only drawing comparisons of unadjusted, average disease incidence rates from countries with varied population sizes. Over the study timeframe, CJD awareness and recognition increased markedly both nationally and globally due to factors including the bovine spongiform encephalopathy (BSE) epidemic, improved surveillance systems and advances in diagnostic capabilities, in particular the CSF 14-3-3 diagnostic test. These influences have contributed to improved notification and diagnostic assessment of suspected cases, a feature reflected in the positive temporal trends observed for suspect case and 14-3-3 CSF test referrals and, to a lesser degree, with neuropathological examination in the participant countries. Although temporal variation in predictor and outcome variables was significant between the countries over the study period, the analysis of pooled data, adjusted for time and age, demonstrated that time was independent of the association between surveillance intensity measurements and incidence, further underscoring the strength of this study.

Referrals for 14-3-3 CSF analysis in France and Germany were noticeably higher than in other countries. We surmise this may be due to subsidisation of the costs of testing and/or the strong tradition of employing CSF surrogate biomarker detection in the evaluation of dementias, including CJD. In Hungary and the Czech Republic, the lower number of referrals for 14-3-3 testing is due to the later point at which 14-3-3 testing was introduced and adopted into the criteria in comparison with France and Germany. However, despite the higher levels of CSF testing in Germany and France, incidence was not increased in comparison with other countries, suggesting that the correlation with sporadic CJD incidence also relies on referral of suspect cases to a national reference centre, as well as neuropathological examination. Furthermore, this finding argues against a potential misconception from this study that widespread 14-3-3 CSF testing is required for optimal case ascertainment. The negative association observed between CSF referrals and non-sporadic CJD cases may relate in part to modest increases in prion protein gene (*PRNP*) testing observed over the study timeframe, translating into a reduced likelihood of non-sporadic CJD cases (mainly genetic) undergoing 14-3-3 CSF testing. This is a plausible explanation, however, unverified in this study, with the negative association also possibly related to the fact that CSF 14-3-3 protein detection was primarily developed for sporadic CJD detection.

The multi-national context of the present study was an intended and important design feature by which it was ensured relatively minor but 'real life' variations in specific mechanisms of national prion disease surveillance were encompassed. Despite this, the findings clearly demonstrate overall support for a positive and predictive correlation between surveillance intensity and sporadic CJD incidence; however, we note that this predictive association was not observed in two of the nine countries. The reason for this is uncertain but may relate to unapparent variations in surveillance methods employed within these countries or a potential saturation point where no new cases are identified despite increasing surveillance intensity.

Although the public health and epidemiological context of each disease undergoing national screening or surveillance is relatively unique, and therefore of limited direct comparability, the finding that observed population diagnosis rates can be influenced by testing and resourcing issues is not unique to CJD. HIV infection diagnosis in the UK is estimated at 74% of all infections, while in Australia, the estimate is 85%–90%.[25 26] The Australian epidemic remains largely transmitted through male homosexual contact, a well-informed group with a high rate of HIV testing.[27] In contrast, the epidemic in the UK is more heterogenous and often associated with migration to the UK from high prevalence countries.[28]

So, in conclusion, our study has confirmed that routine national surveillance methods adjusted as population rates allow objective determination of surveillance intensity, which correlates positively with reported incidence for human prion disease, especially sporadic CJD, largely independent of national context. The predictive relationship between surveillance intensity and disease incidence should facilitate more rapid delineation of aberrations in disease occurrence and permit objective assessment of the adequacy of disease monitoring by national registries. Further, the approach outlined in our study could extend to other rare disorders, and should allow more objective assessment of the adequacy of population scrutiny by extant or potential members of surveillance consortia.

Author affiliations
[1]Australian National Creuztfeldt-Jakob Disease Registry, Department of Pathology, The University of Melbourne, Parkville, Australia
[2]The Mental Health Research Institute of Victoria, The University of Melbourne, Parkville, Australia
[3]The Kirby Institute (formerly National Centre in HIV Epidemiology and Clinical Research), University of New South Wales, Coogee, Australia
[4]National Reference Laboratory for Diagnostics of Human Prion Diseases, Thomayer Teaching Hospital, Prague, Czech Republic
[5]CJD Surveillance Unit, Department of Neuropathology, Beaumont Hospital, Dublin, Ireland
[6]Dementia Research Unit, Department of Neurology, National Reference Center for TSE, Georg-August University, Göttingen, Germany
[7]Dutch National Prion Disease Registry, Department of Epidemiology, Erasmus University Medical Center, Rotterdam, The Netherlands
[8]Department of Neurology, Erasmus MC University Medical Centre, Rotterdam, The Netherlands

[9]National Creutzfeldt-Jakob Disease Research and Surveillance Unit, Western General Hospital, The University of Edinburgh, Edinburgh, UK
[10]Cellule Nationale de référence des maladies de Creutzfeldt-Jakob, Groupe Hospitalier Pitié-Salpêtrière, Paris, Cedex, France
[11]Institute of Neurology, Medical University of Vienna and Austrian Reference Center for Human Prion diseases, Vienna, Austria
[12]Semmelweis University Neuropathology and Prion Disease Reference Center, Budapest, Hungary
[13]Department of Pathology and Laboratory Medicine, University of Ottawa, Ottawa, Ontario, Canada
[14]Canadian CJD Surveillance System and Prion Diseases Program, Public Health Agency of Canada, Winnipeg, Canada

Acknowledgements *Australia:* The Australian National Creutzfeldt-Jakob Disease Registry (ANCJDR) wishes to thank the families and managing physicians of patients with prion disease for their generous support. *Austria:* The Austrian Reference Center for Human Prion Diseases (ÖRPE) gratefully acknowledges the continuous support by Austrian neurologists, neuropathologists, other clinical personnel and families, without whom CJD surveillance would be impossible. *Czech Republic:* National Reference Laboratory for Diagnostics of Human Prion Diseases would like to thank the families of patients with prion disease and involved physicians for their help and support. *France:* The French National Surveillance Network for CJD wishes to thank all physicians for cases notification, biochemical laboratories for 14-3-3 protein detection and neuropathologists for pathological data. *Hungary:* The Hungarian Prion Disease Reference Center wishes to thank the families, the managing physicians of patients with prion disease and the National Center for Epidemiology (Dr Zsuzsanna Molnar) for their generous support. *Ireland:* The staff of Ireland's CJD Unit wish to acknowledge the help and cooperation of the family members of patients diagnosed with CJD in Ireland over the last 20 years. *Netherlands:* We thank all patients, families and neurologists for their participation, and our colleagues at the National Surveillance Center for Prion Disease, part of the Department of Pathology at Utrecht University Medical Center, for their close collaboration in obtaining autopsy results; and the contributions by M.Schuur to this study were greatly appreciated. *UK:* The National CJD Research and Surveillancex Unit is funded by the Policy Research Programme in the Department of Health. The views expressed in this article are not necessarily those of the Department.

Contributors SC and GK conceived the study, coordinated the data collection, analysed the data and cowrote the manuscript. MS, AB and CLM assisted with draft preparation and editing of manuscript. HW and ML performed statistical analysis and draft preparation. RM, RH, MF, MB, IZ, JMc, RW, J-PB, AA, HB, GGK, GHJ and MC collected, organised and collated case data for analysis and reviewed the manuscript. CI-V and CV reviewed and edited the manuscript. As the principal author, Professor Steven J Collins takes full responsibility for the data, analyses, interpretation and conduct of the research. Professor Collins has full access to the analysed data and has the right to publish these data.

Competing interests None.

Funding GMJAK, MS, AB, CLM: Funded by the Australian Commonwealth Department of Health and Ageing. HW, ML: The Kirby Institute is funded by the Australian Government, Department of Health and Ageing. MS: Funded by the Commonwealth Department of Health and Ageing. RM: Funded in part by IGA NT/14145/2013 grant from the Czech Ministry of Health. RH, MF: The National CJD Surveillance Unit in Ireland is funded by the Department of Health & Children. MB, IZ: Supported by grants from the Robert Koch-Institute through funds of the Federal Ministry of Health (grant no 1369-341), the European Commission (PRIORITY KBBE-2007-2-4-06 'Protecting the food chain from prions: shaping European priorities through basic and applied research', Project number: FP7-KBBE-2007-2A) and by the Verein zur Förderung der Wissenschaft und Forschung an der Neurologischen Klinik Göttingen e.V. CvD, CI-V: The Dutch National Prion Disease Registry is funded by a grant from the National Institute of Public Health and the Environment, an institute of the Ministry of Health, Welfare and Sport. JMcK, RGW: The National CJD Research and Surveillance Unit is funded by the Policy Research Programme in the Department of Health. JPB, AA: The French National Surveillance Network is funded by the Institut National de Veille Sanitaire. HB, GGK: The Austrian Reference Center for Human Prion Diseases (ÖRPE) is funded by the Austrian Federal Ministry for Health. GHJ, MC: Funding of surveillance, laboratory reference services and public health for human prion diseases in Canada is provided through the Prion Diseases Program of the Public Health Agency of Canada. SJC: Funded by the Australian Commonwealth Department of Health and Ageing and is supported in part by an NH&MRC Practitioner Fellowship #APP1005816.

Ethics approval The Australian National CJD Registry has approval for publishing de-identified epidemiological studies relating to prion disease (The University of Melbourne Human Research Ethics Committee # 941450), and as a coordinating institution for the study takes primary ethical responsibility. Other collaborating countries have given similar ethical approval.

Provenance and peer review Not commissioned; externally peer reviewed.

REFERENCES

1 Foley G, Alston R, Geraci M, *et al*. Increasing rates of cervical cancer in young women in England: an analysis of national data 1982–2006. *Br J Cancer* 2011;105:177–84.
2 Roder D, Houssami N, Farshid G, *et al*. Population screening and intensity of screening are associated with reduced breast cancer mortality: evidence of efficacy of mammography screening in Australia. *Breast Cancer Res Treat* 2008;108:409–16.
3 Gotzsche PC, Nielsen M. Screening for breast cancer with mammography. *Cochrane Database Syst Rev* 2006;(4):CD001877.
4 Hewitson P, Glasziou P, Irwig L, *et al*. Screening for colorectal cancer using the faecal occult blood test, Hemoccult. *Cochrane Database Syst Rev* 2007;(1):CD001216.
5 Hardcastle JD, Chamberlain JO, Robinson MH, *et al*. Randomised controlled trial of faecal-occult-blood screening for colorectal cancer. *Lancet* 1996;348:1472–7.
6 Mallitt K, Wilson DP, McDonald A, *et al*. HIV incidence trends vary between jurisdictions in Australia: an extended back-projection analysis of men who have sex with men. *Sex Health* 2011;9:138–43.
7 Roy KM, Hutchinson SJ, Wadd S, *et al*. Hepatitis C virus infection among injecting drug users in Scotland: a review of prevalence and incidence data and the methods used to generate them. *Epidemiol Infect* 2007;135:433–42.
8 Robotin MC, Copland J, Tallis G, *et al*. Surveillance for newly acquired hepatitis C in Australia. *J Gastroenterol Hepatol* 2004;19:283–8.
9 Ladogana A, Puopolo M, Croes EA, *et al*. Mortality from Creutzfeldt-Jakob disease and related disorders in Europe, Australia, and Canada. *Neurology* 2005;64:1586–91.
10 Zerr I, Pocchiari M, Collins S, *et al*. Analysis of EEG and CSF 14-3-3 proteins as aids to the diagnosis of Creutzfeldt-Jakob disease. *Neurology* 2000;55:811–15.
11 Collins SJ, Sanchez-Juan P, Masters CL, *et al*. Determinants of diagnostic investigation sensitivities across the clinical spectrum of sporadic Creutzfeldt-Jakob disease. *Brain* 2006;129(Pt 9):2278–87.
12 Zerr I, Kallenberg K, Summers DM, *et al*. Updated clinical diagnostic criteria for sporadic Creutzfeldt-Jakob disease. *Brain* 2009;132:2659–68.
13 Sanchez-Juan P, Sanchez-Valle R, Green A, *et al*. Influence of timing on CSF tests value for Creutzfeldt-Jakob disease diagnosis. *J Neurol* 2007;254:901–6.
14 de Pedro-Cuesta J, Glatzel M, Almazan J, *et al*. Human transmissible spongiform encephalopathies in eleven countries: diagnostic pattern across time, 1993–2002. *BMC Public Health* 2006;6:278.
15 Prusiner SB. Prions. Shattuck Lecture—neurodegenerative diseases and prions. *N Eng J Med* 2001;334:1516–26.
16 Glatzel M, Rogivue C, Ghani A, *et al*. Incidence of Creutzfeldt-Jakob disease in Switzerland. *Lancet* 2002;360:139–41.
17 Klug GM, Wand H, Boyd A, *et al*. Enhanced geographically restricted surveillance simulates sporadic Creutzfeldt-Jakob disease cluster. *Brain* 2009;132(Pt 2):493–501.
18 Parchi P, Giese A, Capellari S, *et al*. Classification of sporadic Creutzfeldt-Jakob disease based on molecular and phenotypic analysis of 300 subjects. *Ann Neurol* 1999;46:224–33.
19 Gelpi E, Heinzl H, Hoftberger R, *et al*. Creutzfeldt-Jakob disease in Austria: an autopsy-controlled study. *Neuroepidemiology* 2008;30:215–21.
20 Boyd A, Klug GMA, Schonberger L, *et al*. Iatrogenic Creutzfeldt-Jakob disease in Australia: time to amend infection control measures for pituitary hormone recipients? *Med J Aust* 2010;193:366–9.
21 Will RG, Ironside JW, Zeidler M, *et al*. A new variant of Creutzfeldt-Jakob disease in the UK. *Lancet* 1996;347:921–5.
22 Mahillo-Fernandez I, de Pedro-Cuesta J, Bleda M, *et al*. Surgery and risk of sporadic Creutzfeldt-Jakob disease in Denmark and Sweden: registry-based case-control studies. *Neuroepidemiology* 2008;31:229–40.
23 Collins S, Law M, Fletcher A, *et al*. Surgical treatment and risk of sporadic Creutzfeldt-Jakob disease: a case control study. *Lancet* 1999;353:693–7.
24 German RR, Lee LM, Horan JM, *et al*. Updated guidelines for evaluating public health surveillance systems: recommendations from the Guidelines Working Group. *MMWR Recomm Rep. CDC* 2001;50(RR-13):1–35; quiz CE31–37.
25 Wilson DP, Hoare A, Regan DG, *et al*. Importance of promoting HIV testing for preventing secondary transmissions: modelling the Australian HIV epidemic among men who have sex with men. *Sex Health* 2009;6:19–33.
26 Wand H, Yan P, Wilson D, *et al*. Increasing HIV transmission through male homosexual and heterosexual contact in Australia: results from an extended back-projection approach. *HIV Med* 2010;11:395–403.
27 Prestage G, Jin F, Zablotska IB, *et al*. Trends in HIV testing among homosexual and bisexual men in eastern Australian states. *Sex Health* 2008;5:119–23.
28 Health Protection Agency. HIV in the United Kingdom: 2010 report. Health Protection Report 2010;4 [serial online] 2010. http://www.hpa.org.uk/webc/HPAwebFile/HPAweb_C/1287145367237 (accessed 20 Jul 2012).

Case Report/Case Series

Unusual Clinical and Molecular-Pathological Profile of Gerstmann-Sträussler-Scheinker Disease Associated With a Novel *PRNP* Mutation (V176G)

Marion Simpson, MBChB; Vanessa Johanssen, PhD; Alison Boyd, DipGenCouns; Genevieve Klug, BSc; Colin L. Masters, MD; Qiao-Xin Li, PhD; Roger Pamphlett, MBChB, MD, FRCPath, FRACP; Catriona McLean, MD; Victoria Lewis, PhD; Steven J. Collins, MD

IMPORTANCE Here we describe the unusual clinical and molecular-neuropathological profile of a case of Gerstmann-Sträussler-Scheinker disease associated with a novel prion protein (*PRNP*) gene mutation.

OBSERVATIONS This case report from the Australian National Creutzfeldt-Jakob Disease Registry concerns a 61-year-old British-born woman with no history of neurodegenerative disorder in first-degree relatives. Rapidly progressive dementia, altered behavior, and cerebellar ataxia dominated the clinical picture in the period immediately following minor elective surgery, with death 1 month later in an akinetic-mute state. Brain histopathological examination revealed neuronal loss, scant foci of spongiform change, and diffuse multicentric amyloid plaques, selectively immunoreactive for prion protein, within the cerebral and cerebellar cortices and deep gray matter. Tau immune-reactive neurofibrillary tangles and neuritic threads were present in the cerebral cortex. *PRNP* sequencing demonstrated a valine to glycine mutation at codon 176, with valine homozygosity at polymorphic codon 129. Western-blot analysis of frozen brain tissue displayed a nonclassic protease-resistant prion protein banding pattern, with a prominent approximately 8-kDa protease-resistant fragment.

CONCLUSIONS AND RELEVANCE Reported is a proband with a novel *PRNP* mutation associated with neuropathologically confirmed Gerstmann-Sträussler-Scheinker disease displaying a somewhat unusual constellation of clinicopathological features, which overall subserve to further broaden an already diverse phenotypic spectrum.

JAMA Neurol. 2013;70(9):1180-1185. doi:10.1001/jamaneurol.2013.165
Published online July 15, 2013.

Author Affiliations: Department of Pathology, University of Melbourne, Victoria, Australia (Simpson, Johanssen, Boyd, Klug, Lewis, Collins); Australian National Creutzfeldt-Jakob Disease Registry, University of Melbourne, Victoria, Australia (Simpson, Boyd, Klug, Masters, Collins); Mental Health Research Institute of Victoria, University of Melbourne, Victoria, Australia (Masters, Li, Lewis, Collins); The Stacey MND Laboratory, Sydney Medical School, University of Sydney, Camperdown, Australia (Pamphlett); Department of Anatomical Pathology, Alfred Health, Commercial Road, Prahran, Australia (McLean).

Corresponding Author: Victoria Lewis, PhD, Department of Pathology, Level 4 Kenneth Myer Building, University of Melbourne, Parkville, Australia 3010 (v.lewis@unimelb.edu.au).

Gerstmann-Sträussler-Scheinker (GSS) disease is a rare, almost exclusively genetically determined prion disease, typically characterized clinically by progressive cerebellar ataxia and dementia and neuropathologically by diffuse, prion protein (PrP)-containing amyloid deposits.[1] Although the P102L mutation in the prion protein (*PRNP*) gene is the most commonly observed in GSS disease,[2] numerous insertion, missense, and point mutations, including P105L, A117V, H187R, F198S, D202N, Q212P, Q217R, and Y218N, have been detected, probably contributing to the notable clinical and pathological diversity.[2,3] Typically, GSS disease follows an autosomal-dominant inheritance pattern[4] and manifests a prolonged clinical course, with median illness duration of 39 months reported in large patient series.[5] In addition to progressive cerebellar ataxia and dementia, clinical findings in GSS disease may include myoclonus, extrapyramidal features, and evidence of pyramidal tract dysfunction.[3] Cognitive decline usually follows cerebellar ataxia as a later symptom in the clinical course, especially in P102L GSS disease,[4] and may be absent in patients with certain mutations such as Q212R[6]; however, early prominent dementia without cerebellar ataxia has been described in some less-common mutations such as G131V.[7,8] Neuropathological findings are also variable but generally there is evidence in the cerebrum and cerebellum of widespread, PrP immunopositive, unicentric and/or multicentric amyloid plaques, associated with differing degrees of spongiform change, neuronal loss, and astrocytic gliosis; tau-positive neurofibrillary tangles may also be observed.[6,9-11]

Herein, we report a patient with neuropathologically confirmed GSS disease associated with a novel *PRNP* mutation, displaying an unusual combination of clinical and molecular-pathological features, which overall subserve to further broaden an already diverse phenotypic spectrum.

Methods

The proband was a white, British-born woman whose first definite neurological symptoms occurred at age 61 years, around the time of elective surgery for removal of a dislodged breast implant. However, during a period of years prior to surgery, the patient had become increasingly estranged from all relatives. Infrequent, irregular involvement with family precluded confident delineation of any specific neurological or psychiatric symptoms and their chronological evolution but a sister maintained some contact, describing 6 months of "low mood" and possible memory problems. In addition, posthumously, the sister of the proband became aware of some apparently unusual behavior, such as buying inappropriately sized underwear and the likely hoarding of large supplies of cleaning products, although in contrast, financial affairs and housework had been maintained in good order. In the immediate postoperative period, the patient developed what was thought to be an acute confusional state with delusional ideation, for example, claiming that she had swallowed a 5-cent coin and that staff members had been forcing her to swallow jewelry. The proband's sister affirmed that the postoperative demeanor was completely uncharacteristic.

Following surgery, gait unsteadiness was also noteworthy and 2 falls occurred while she was in the hospital. Mental status assessment in the postoperative period confirmed cognitive impairment (Mini Mental State Examination score, 20 out of 30), especially defective short-term recall and mild expressive and nominal dysphasia. Neurological examination revealed cerebellar ataxia with bilateral intention tremor, generalized hyperreflexia, and myoclonus. The patient never left institutional care following her surgery, experiencing rapid, steady cognitive and gross motor decline and dying in an akinetic-mute state around 1 month following surgery.

There was no known family history of neurodegenerative disease in first-degree relatives (**Figure 1**), with the proband's mother dying aged 88 years of cancer and the father aged 92 years as a consequence of a head injury sustained from a fall. Scant, imprecise information existed for nonfirst-degree relatives, especially in the patrilineage, but there was a history of a maternal aunt dying (age unknown) in a mental hospital after an illness of only a few months' duration. The patient had migrated to Australia at the age of 37 years, around the time of onset of the United Kingdom bovine spongiform encephalopathy epidemic. There was no history of recognized risk factors for iatrogenic prion disease.

Routine blood test results were unremarkable. Cerebrospinal fluid test results were normal aside from the presence of 14-3-3 proteins. Magnetic resonance imaging of the brain showed mild generalized atrophic changes (consistent with age) and a few, nonspecific, deep white matter hyperintensities in the cerebral hemispheres, but there were no findings more typical of sporadic Creutzfeldt-Jakob disease such as areas of gray matter restricted diffusion nor increased signal on fluid-attenuated inversion recovery sequences (**Figure 2**). Electro-

Figure 1. Family Tree

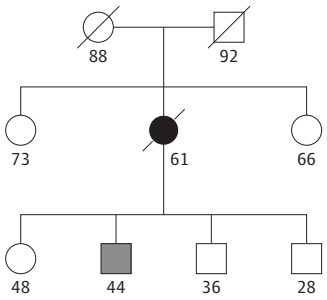

Family tree depicting the proband (solid fill) and first-degree relatives with current ages or ages at death (in years). No first-degree relative was reported to have had any neurological disease with the exception of 1 son (line fill) with schizophrenia. Circles indicate females; squares, males; strikethrough, deceased.

Figure 2. Representative Proband Brain Magnetic Resonance Images

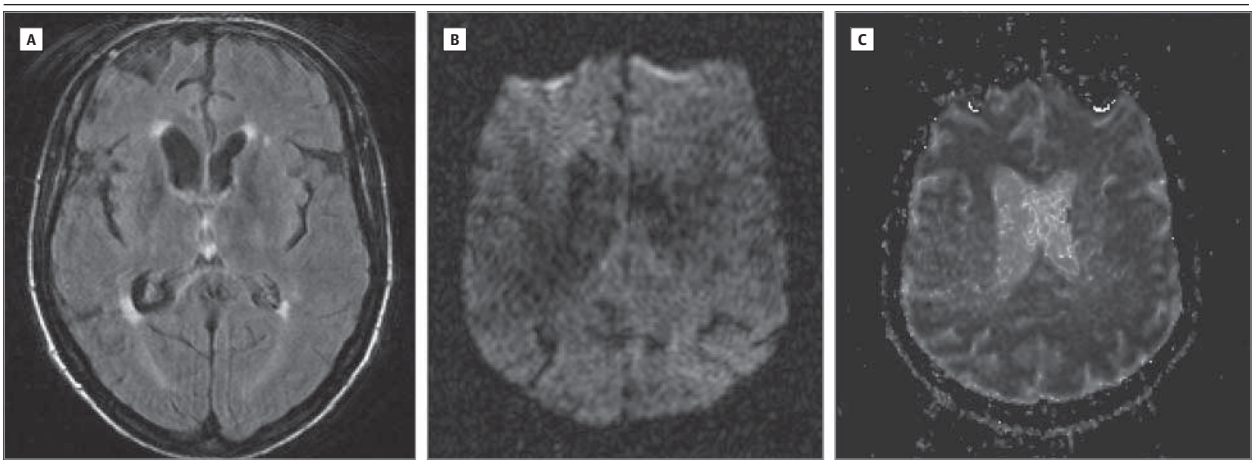

Fluid-attenuated inversion recovery (A), diffusion-weighted (B), and apparent diffusion coefficient map (C) images demonstrate mild age-appropriate cerebral atrophy, associated with some nonspecific T2 hyperintensities, but absence of changes typically found in human prion disease, especially sporadic Creutzfeldt-Jakob disease.

encephalography findings showed attenuated alpha rhythms with frequent diffuse rhythmic delta activity but no periodic complexes.

Results

Neuropathological Findings

Routine hematoxylin and eosin stains of frontal, temporal, and occipital cortical sections showed numerous (densely eosinophilic) amyloid plaques (**Figure 3**A), neuronal loss, and astrocytic gliosis. The amyloid plaques, sometimes appearing multicentric, were extensively deposited, most marked in the lower laminae, with immune-peroxidase studies showing reactivity with both 3F4 and 12F10 anti-PrP monoclonal antibodies (Figure 3B); plaques did not demonstrate amyloid-β immunoreactivity. Many of the amyloid plaques showed an associated microglial response but did not resemble florid plaques (Figure 3A). The basal ganglia showed a similar prominent deposition of closely packed, granular deposits, again immunoreactive with 3F4 and 12F10 anti-PrP monoclonal antibodies. Scant spongiform change was seen focally in the cerebral cortex, basal ganglia, and cerebellar cortex. Hippocampal sections displayed numerous tau immunoreactive neurofibrillary tangles in association with extensive neuropil thread formation and areas of neuritic plaque formation (Figure 3C). In the cerebellum, there was extensive immunopositive prion protein deposition within the molecular layer, patchy Purkinje cell loss, and a moderately intense microglial response within the cortex. This extensive PrP-positive amyloid deposition in association with prominent tau pathology was felt to be most consistent with a neuropathological diagnosis of GSS disease.

PRNP Genotyping

Appropriate consent for genetic examination was obtained. Genomic DNA was extracted from the brain, and the *PRNP* open reading frame was sequenced in the forward and reverse orientations with overlapping primers (PrP106 and PrP46 sequences described previously[12]; PrPF2 5′-CCGAGTAAGCCAAAAACCAAC-3′ and PrPR2 5′-TCACTGCCGAAATGTATGATG-3′). Sequencing revealed the patient to be homozygous for valine at the polymorphic codon 129. A guanine to adenine nucleotide substitution was found in a 5′ noncoding region, at position -21 relative to the start codon, and a synonymous adenine to guanine substitution was seen at the third position of codon 117, transitions both previously described as *PRNP* polymorphisms.[13] A thymine to guanine transversion was detected at the second position of codon 176, resulting in a predicted amino acid change from a valine to glycine. This mutation has not previously been reported. A diagrammatic representation of these sequence variations is shown in **Figure 4**A.

PrP^{res} Analysis

Frozen post mortem brain specimens from the cerebellum and occipital pole were homogenized to 10% (weight/volume) in phosphate-buffered saline. Aliquots were analyzed by Western blot with or without proteinase K (PK) digestion, as previously described.[12] Briefly, samples were digested with 100 µg/mL PK for 1 hour at 37°C, before mixing with the appropriate polyacrylamide gel electrophoresis (PAGE) sample buffer.

Figure 3. Neuropathological Findings

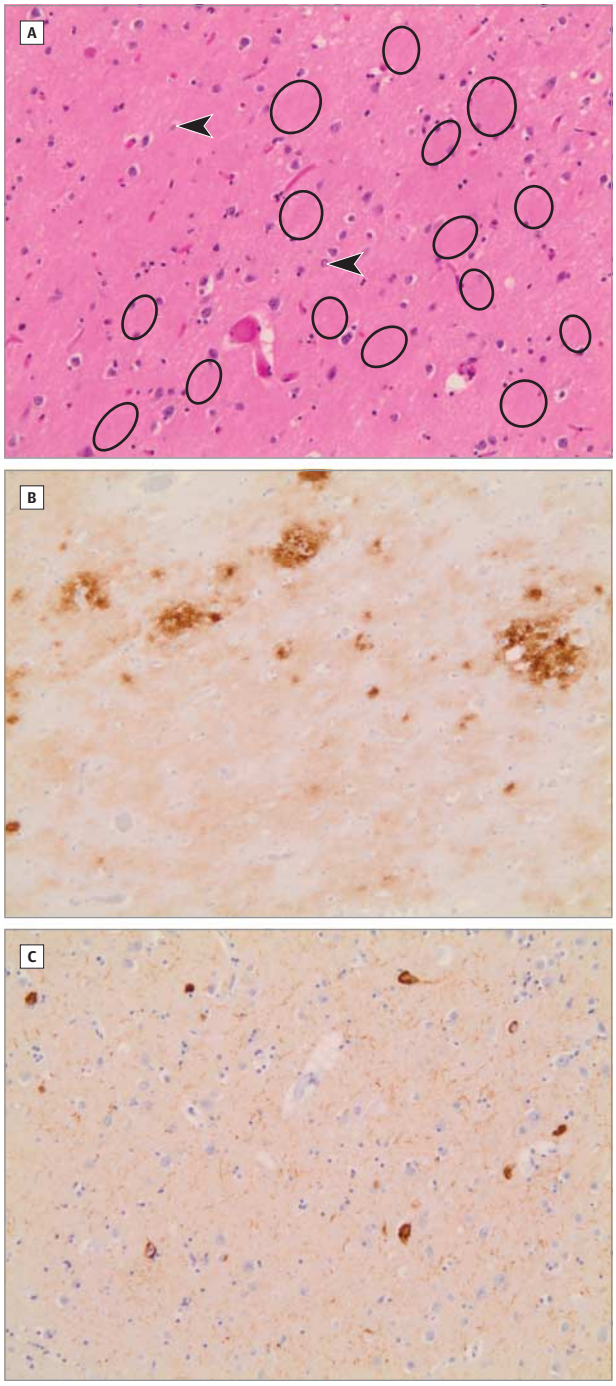

Temporal cortex showing numerous plaques (A, encircled) in combination with neuronal loss and astrocytic gliosis (A, arrowheads) (hematoxylin and eosin, original magnification x 200). The plaques are immunoreactive with the anti-PrP monoclonal antibody 12F10 (B, original magnification x 100) and associated with tau-immunoreactive neurofibrillary tangles and prominent neuropil threads (C, original magnification x 200).

Figure 4. Molecular-Genetic Characterization

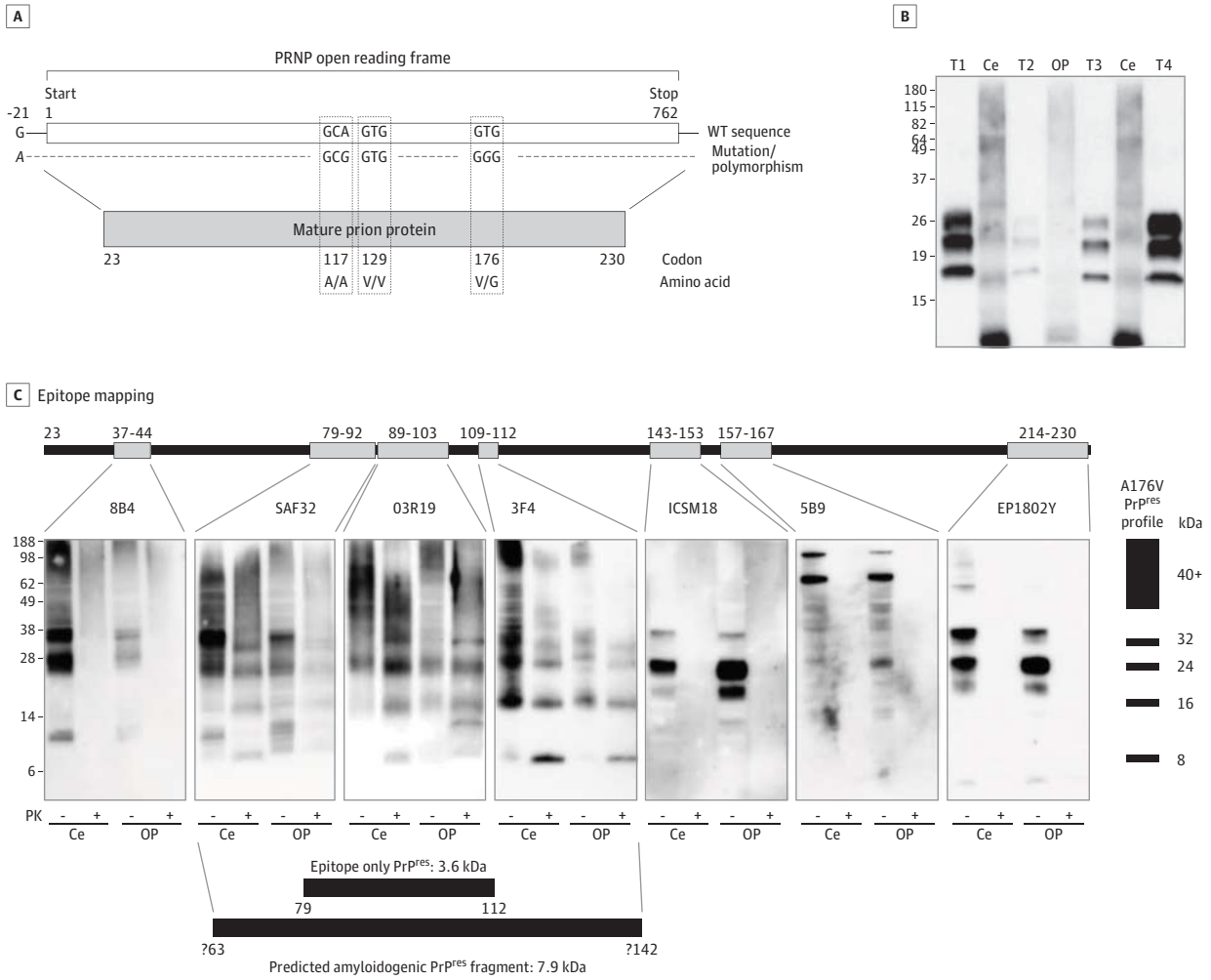

A, Schematic representation of the prion protein open reading frame and protein, with the nucleotide changes, codon positions, and resulting amino acid changes detected in the proband as indicated. B, Proteinase K (PK) digest and polyacrylamide gel electrophoresis/Western blot analysis (using 3F4 antibody) of frozen brain tissue from 2 brain regions of the proband (cerebellum [Ce] and occipital pole [OP]) compared with glycotype controls (T1, T2, T3, and T4: protease-resistant prion protein [PrP^{res}] glycotypes 1, 2, 3, and 4).[14] C, Characterization of the small amyloidogenic PrP^{res} fragment by polyacrylamide gel electrophoresis/Western blot epitope mapping, using anti-prion protein antibodies spanning the length of the protein as specified. Schematic representations of the small fragment and oligomeric species and of the potential N- and C-terminal truncation sites based on antibody epitopes are highlighted on the right and below, respectively. WT indicates wild type.

Samples (using double the volume of PK digested compared with undigested) were resolved on 16% Tris-glycine or 12% NuPAGE (Invitrogen) gels and transferred to polyvinylidene difluoride membrane (Millipore) before incubation with the appropriate primary and secondary antibody and visualization using enhanced chemiluminescence (ECL Plus; Amersham).

Initially, before *PRNP* sequencing results were known, samples were subjected to sodium dodecyl sulfate–PAGE and Western blot analyses of protease-resistant PrP (PrP^{res}) following PK digestion alongside glycotype 1-4 controls, using the commonly used 3F4 antibody as previously described.[14] As seen in Figure 4B, the characteristic di-, mono-, and unglycosylated triple banding pattern of PrP^{res} was not present in the proband. Rather, a prominent immunoreactive, PK-resistant fragment of less than 15 kDa was observed. Numerous additional minor bands, creating a ladder spanning from greater than 15 kDa to at least 50 kDa, often superimposed on subtle lane smearing, were also observed.

Epitope mapping using antibodies spanning the length of the prion protein (Figure 4C and **Table**) was carried out to further characterize the small fragment. As seen in Figure 4C, the PrP^{res} fragment, resolving at approximately 8 kDa, was not immunoreactive with antibodies to the far N-terminus (8B4) or those with epitopes beyond codon 143 (ICSM 18) toward the C-terminus of the prion protein, leading to the conclusion that the 8-kDa fragment resulted from combined N- and C-terminal truncation of PrP^{res}. Based on its apparent molecular weight and the known antibody epitopes, we predicted the 8-kDa fragment resulted from PrP cleavage around residues 60 and 140. Furthermore, the higher molecular weight bands

Table. Panel of Anti-PrP Antibodies Used for Epitope Mapping

1° Antibody	1° Dilution	2° Antibody (HRP Conjugated)	2° Dilution	Supplier
8B4 (monoclonal)	1:10 000	Anti-mouse	1:10 000	Alicon
SAF32 (monoclonal)	1:3000	Anti-mouse	1:10 000	Caymen Chemical
03R19 (polyclonal)	1:5000	Anti-rabbit	1:10 000	V Lawson[15]
3F4 (monoclonal)	1:5000	Anti-mouse	1:10 000	Covance
ICSM 18 (monoclonal)	1:40 000	Anti-mouse	1:10 000	D-Gen
5B9-biotin (monoclonal)	1:50 000	Streptavidin	1:40 000	Abcam
EP1802Y (monoclonal)	1:10 000	Anti-rabbit	1:5000	Abcam

were thought to represent aggregation of the 8-kDa fragment into highly stable, higher-order species.

Tau Analysis

Cerebrospinal fluid was examined by enzyme-linked immunosorbent assay (Innotest hTau Ag and Phospho-Tau [181P], Innogenetics NV Belgium), according to the manufacturer's instructions, and showed both total tau and tau phosphorylated at threonine 181 were elevated (total tau, 1409 [normal, <412 pg/mL], with phospho-tau, 126 [normal, <82 pg/mL]). Reference ranges were determined from 71 well-characterized, healthy elderly volunteers participating in the Australian Imaging Biomarker Lifestyle Study.[16]

The cerebellum and hippocampus were homogenized (10% [weight/volume] in phosphate-buffered saline) and analyzed by Western blotting for the different tau isoforms using 4% to 12% NuPAGE gels and probed with a rabbit anti-human tau antibody (1:3000; Dako). In the cerebellum (absence of tau pathology), there was no difference in the tau isoform profile when comparing the proband with age-matched control and Alzheimer disease brains. In the hippocampus (abundant tau pathology), the tau isoform profile of the proband did not resemble that seen in either the control or Alzheimer disease brain (data not shown).

Discussion

Characteristically, GSS disease is inherited in an autosomal-dominant manner,[4] therefore, usually occurs in the setting of a known family history of similar neurodegenerative disorder. No history of similar neurological disease was known among first-degree relatives; however, the absence of family history can occur in up to 30% of GSS disease pedigrees.[2] Awareness of a maternal aunt dying in a mental hospital from a poorly characterized illness of apparently only months in duration is of uncertain but possible relevance.

Our proband manifested rapid cognitive and gross motor decline following her minor elective surgery, dying approximately 1 month after the procedure. The proband's limited contact with her family prior to surgery rendered precise determination of presenting symptoms and their duration impossible. However, notwithstanding the long-standing estrangement from her family, the information available suggests a relatively brief duration of cognitive and behavioral changes for up to 6 months prior to hospital admission. Although limited survival after first symptoms has been reported in GSS disease, it is uncommon that durations of this length occur in patients with GSS disease.[5,6,10,11] Typically, GSS disease follows a prolonged clinical course, evincing a median duration of more than 3 years.[5] Our patient aligned more to the contrasting relatively short median survival observed in sporadic Creutzfeldt-Jakob disease.[5] In addition, molecular pathological evaluation of our propositus using the 3F4 antibody demonstrated prominent, low-molecular-weight, protease-resistant PrP^{res} bands on Western blots of the brain, a feature more usually associated with much longer survival.[6,10] Similarly, although valine homozygosity at codon 129, as seen in our patient, has been reported in GSS disease, it is most unusual; furthermore, it also appears to usually correlate with prolonged symptomatic illness.[4,6,10,11]

Predominance of shorter (<15-kDa) PK-resistant PrP^{res} fragments on Western blots has been observed in GSS disease in association with numerous mutations, including those clustered toward the C-terminus of the prion protein (H187R, F198S, D202N, Q212P, Q217R, and Y218N), as well as those situated more in the middle of the protein (P102L, P105L, A117V, G131V, and S132I).[6,10,17] It remains to be determined how PrP-containing mutations within the C-terminus, including V176G, engender processing such that the core of amyloid deposits appear to be constituted by truncated species that do not actually harbor the mutation.[10]

Aligned to previous reports for the G131V, S132I, Y160X, H187R, F198S, D202N, Q217R, Y218M, and Q227X mutations,[6,9,10,17] the presence of shorter, nonclassic PrP^{res} fragments on Western blots in our proband was associated with the neuropathological profile of high amyloid plaque burden, neurofibrillary degeneration, and relative paucity of spongiform change in the brain; however, some mutations, such as P102L, P105L, and A117V, despite the presence of shorter PrP^{res} fragments on Western blots and considerable amyloid deposition in the brain, do not consistently display neurofibrillary degeneration.[17] It is noteworthy that those patients with GSS disease displaying predominance of longer 21-kDa to 30-kDa PrP^{res} fragments on Western blots, as exemplified by some P102L carriers, generally have more prominent neuropil vacuolation, usually associated with synaptic-type PrP immunostaining rather than mainly amyloid plaque burden.[10] The presence of tau-positive neurofibrillary tangles and neuropil threads, as frequently observed in GSS disease cases including our proband, underscores the likelihood that accumula-

tion of aberrant tau in the brain may be a relatively nonspecific secondary consequence to certain primary cerebral amyloidoses, as typified by Alzheimer disease.

In summary, in addition to expanding the range of *PRNP* mutations found in neuropathologically confirmed prion disease, our case is of interest and informative through displaying a constellation of clinical, genetic, molecular, and pathological features, which although individually recognized across the spectrum of GSS disease, are unusual in their co-occurrence in a single person. Consequently, our proband serves to further broaden the already diverse genetic and phenotypic spectrum recognized for GSS disease.

ARTICLE INFORMATION

Accepted for Publication: January 21, 2013.

Published Online: July 15, 2013. doi:10.1001/jamaneurol.2013.165.

Author Contributions: All authors had full access to all of the data in the study and take full responsibility for the integrity of the data and accuracy of the data analysis.
Study concept and design: Simpson, Boyd, Lewis, Collins.
Acquisition of data: Johanssen, Boyd, Klug, Li, Pamphlett, McLean, Lewis, Collins.
Analysis and interpretation of data: Simpson, Johanssen, Boyd, Masters, Li, Pamphlett, McLean, Lewis, Collins.
Drafting of the manuscript: Simpson, Johanssen, Klug, McLean, Lewis, Collins.
Critical revision of the manuscript for important intellectual content: Boyd, Masters, Li, Pamphlett, McLean, Lewis.
Obtained funding: Masters.
Administrative, technical, and material support: All authors.
Study supervision: Masters, Lewis, Collins.

Conflict of Interest Disclosures: None reported.

Funding/Support: The Australian Creutzfeldt-Jakob Disease Registry is funded by the Commonwealth Department of Health and Ageing. Dr Lewis receives support from a National Health and Medical Research Council C. J. Martin fellowship (567123). Drs Masters and Collins receive support from a National Health and Medical Research Council program grant (628946). Dr Collins also receives support from a National Health and Medical Research Council practitioner fellowship (APP1005816).

REFERENCES

1. Gambetti P, Petersen RB, Parchi P, et al. Inherited prion diseases. In: Pruisner SB, ed. Prion Biology and Diseases. *San Francisco, CA: Cold Spring Harbor Laboratory Press; 1999:509-583.*

2. Kovács GG, Puopolo M, Ladogana A, et al; EUROCJD. Genetic prion disease: the EUROCJD experience. *Hum Genet*. 2005;118(2):166-174.

3. Collins SJ, McLean CA, Masters CL. Gerstmann-Sträussler-Scheinker syndrome, fatal familial insomnia, and kuru: a review of these less common human transmissible spongiform encephalopathies. *J Clin Neurosci*. 2001;8(5):387-397.

4. Hainfellner JA, Brantner-Inthaler S, Cervenáková L, et al. The original Gerstmann-Sträussler-Scheinker family of Austria: divergent clinicopathological phenotypes but constant PrP genotype. *Brain Pathol*. 1995;5(3):201-211.

5. Pocchiari M, Puopolo M, Croes EA, et al. Predictors of survival in sporadic Creutzfeldt-Jakob disease and other human transmissible spongiform encephalopathies. *Brain*. 2004;127(pt 10):2348-2359.

6. Piccardo P, Dlouhy SR, Lievens PM, et al. Phenotypic variability of Gerstmann-Sträussler-Scheinker disease is associated with prion protein heterogeneity. *J Neuropathol Exp Neurol*. 1998;57(10):979-988.

7. Panegyres PK, Toufexis K, Kakulas BA, et al. A new PRNP mutation (G131V) associated with Gerstmann-Sträussler-Scheinker disease. *Arch Neurol*. 2001;58(11):1899-1902.

8. Jansen C, Parchi P, Capellari S, et al. A second case of Gerstmann-Sträussler-Scheinker disease linked to the G131V mutation in the prion protein gene in a Dutch patient. *J Neuropathol Exp Neurol*. 2011;70(8):698-702.

9. Yamazaki M, Oyanagi K, Mori O, et al. Variant Gerstmann-Sträussler syndrome with the P105L prion gene mutation: an unusual case with nigral degeneration and widespread neurofibrillary tangles. *Acta Neuropathol*. 1999;98(5):506-511.

10. Parchi P, Chen SG, Brown P, et al. Different patterns of truncated prion protein fragments correlate with distinct phenotypes in P102L Gerstmann-Sträussler-Scheinker disease. *Proc Natl Acad Sci U S A*. 1998;95(14):8322-8327.

11. Webb TE, Poulter M, Beck J, et al. Phenotypic heterogeneity and genetic modification of P102L inherited prion disease in an international series. *Brain*. 2008;131(pt 10):2632-2646.

12. Lewis V, Collins S, Hill AF, et al. Novel prion protein insert mutation associated with prolonged neurodegenerative illness. *Neurology*. 2003;60(10):1620-1624.

13. Wu Y, Brown WT, Robakis NK, et al. A PvuII RFLP detected in the human prion protein (PrP) gene. *Nucleic Acids Res*. 1987;15(7):3191.

14. Lewis V, Hill AF, Klug GM, Boyd A, Masters CL, Collins SJ. Australian sporadic CJD analysis supports endogenous determinants of molecular-clinical profiles. *Neurology*. 2005;65(1):113-118.

15. Lawson VA, Vella LJ, Stewart JD, et al. Mouse-adapted sporadic human Creutzfeldt-Jakob disease prions propagate in cell culture. *Int J Biochem Cell Biol*. 2008;40(12):2793-2801.

16. Ellis KA, Bush AI, Darby D, et al; AIBL Research Group. The Australian Imaging, Biomarkers and Lifestyle (AIBL) Study of Aging: methodology and baseline characteristics of 1112 individuals recruited for a longitudinal study of Alzheimer's disease. *Int Psychogeriatr*. 2009;21(4):672-687.

17. Ghetti B, Tagliavini F, Kovacs GG, et al. Gerstmann-Sträussler-Scheinker disease. In: Dickson D, Weller R, eds. Neurodegeneration: The Molecular Pathology of Dementia and Movement Disorders. *2nd ed. Chichester, England: Wiley-Blackwell; 2011.*

Ascertainment Bias Causes False Signal of Anticipation in Genetic Prion Disease

Eric Vallabh Minikel,[1,2,3,*] Inga Zerr,[4,5] Steven J. Collins,[6] Claudia Ponto,[4] Alison Boyd,[6] Genevieve Klug,[6] André Karch,[4] Joanna Kenny,[7] John Collinge,[7] Leonel T. Takada,[8] Sven Forner,[8] Jamie C. Fong,[8] Simon Mead,[7,9] and Michael D. Geschwind[8,9]

Anticipation is the phenomenon whereby age of onset in genetic disease decreases in successive generations. Three independent reports have claimed anticipation in Creutzfeldt-Jakob disease (CJD) caused by the c.598G>A mutation in *PRNP* encoding a p.Glu200Lys (E200K) substitution in the prion protein. If confirmed, this finding would carry clear implications for genetic counseling. We analyzed pedigrees with this mutation from four prion centers worldwide (n = 217 individuals with the mutation) to analyze age of onset and death in affected and censored individuals. We show through simulation that selective ascertainment of individuals whose onset falls within the historical window since the mutation's 1989 discovery is sufficient to create robust false signals both of anticipation and of heritability of age of onset. In our data set, the number of years of anticipation observed depends upon how strictly the data are limited by the ascertainment window. Among individuals whose disease was directly observed at a study center, a 28-year difference between parent and child age of onset is observed ($p = 0.002$), but including individuals ascertained retrospectively through family history reduces this figure to 7 years ($p = 0.005$). Applying survival analysis to the most thoroughly ascertained subset of data eliminates the signal of anticipation. Moreover, even non-CJD deaths exhibit 16 years anticipation ($p = 0.002$), indicating that ascertainment bias can entirely explain observed anticipation. We suggest that reports of anticipation in genetic prion disease are driven entirely by ascertainment bias. Guidelines for future studies claiming statistical evidence for anticipation are suggested.

Introduction

Prion diseases are uniformly fatal, progressive neurodegenerative disorders caused by the conversion of the cellular prion protein, PrP^{C}, to a misfolded conformation known as the prion, or PrP^{Sc}, in which Sc stands for scrapie, the prion disease of sheep and goats.[1] In humans, prion diseases have an incidence of approximately 1 death per 1 million individuals per year,[2] and usually occur as simplex cases in individuals with two wild-type (WT) copies of the prion protein gene (*PRNP* [MIM 176640]), commonly referred to as sporadic cases. A minority of cases are genetic and, very rarely, prion disease can be environmentally acquired.[1] Creutzfeldt-Jakob disease (MIM 123400) caused by the c.598G>A (dbSNP id rs28933385) mutation, which encodes a p.Glu200Lys (E200K) substitution in PrP, is the most common genetic form of prion disease worldwide.[3] This point mutation was first identified in 1989[4] and was established as a dominant Mendelian cause of disease by 1991.[5–7] Disease penetrance in mutation heterozygotes appears to reach 80%–100% by age 80.[8,9] Reported estimates of the mean age of onset in individuals with this mutation range from 53[7] to 63,[10] and the mean survival after disease onset is 7 months.[11]

Three reports[12,13] (see also Web Resources) have claimed statistical evidence that this genetic prion disease exhibits *anticipation*, a phenomenon in which successive generations exhibit progressively earlier disease onset or more severe presentation.[14] These studies reported a 7 to 14 year younger age of onset or death among children in affected parent-child pairs, suggesting implications for genetic counseling.

The only genetic mechanisms known to cause anticipation are the germline expansion of unstable repeats in disorders such as Huntington's disease and type 1 myotonic dystrophy,[15,16] and telomere shortening in disorders such as dyskeratosis congenita and breast cancer.[17,18] Anticipation in a genetic prion disease might raise the question of whether disease in children is accelerated by exposure to infectious material during their parents' illness, however, the only known routes of human-to-human prion transmission are cannibalism[19] and iatrogenic exposure.[20,21]

Because a variety of sources of ascertainment bias are known to contribute to false statistical signals of anticipation,[14,22–25] we set out to determine whether the anticipation reported for Glu200Lys genetic prion disease could be a statistical artifact. An individual's observed age of onset cannot be greater than the age at interview or ascertainment, and previous studies have modeled the effects of this right truncation of age of onset[22] and provided methods of correction.[23–26] These methods of correction,

[1]Prion Alliance, Cambridge, MA 02139, USA; [2]Broad Institute, Cambridge, MA 02142, USA; [3]Analytical and Translational Genetics Unit, Massachusetts General Hospital, Boston, MA 02114, USA; [4]National Reference Center for TSE, Georg-August University, 37073 Goettingen, Germany; [5]German Center for Neurodegenerative Disease (DZNE), 37073 Goettingen, Germany; [6]Australian National Creutzfeldt-Jakob Disease Registry, The University of Melbourne, Parkville, Australia 3010; [7]MRC Prion Unit, Department of Neurodegenerative Disease, University College London (UCL) Institute of Neurology, and NHS National Prion Clinic, National Hospital for Neurology and Neurosurgery, UCL Hospitals NHS Trust, Queen Square, WC1N 3BG London, UK; [8]Department of Neurology, Memory and Aging Center, University of California, San Francisco, San Francisco, CA 94158, USA
[9]These authors contributed equally to this work
*Correspondence: eric.minikel@prionalliance.org
http://dx.doi.org/10.1016/j.ajhg.2014.09.003.

however, require either a consistent, known set of ascertainment criteria[23] or the use of only a subset of available data.[26] In rare diseases, data may be too sparse for subsetting, and may not represent a unified ascertainment effort, but rather consist of a mix of data points ascertained retrospectively (through family histories of varying depth and quality), directly (symptomatic individuals seen clinically), and prospectively (asymptomatic individuals with a mutation, followed for varying amounts of time). We therefore sought to model ascertainment bias due to left- and right-truncation not of the age of onset per se, but of the year of onset. Because the Glu200Lys substitution was discovered only 25 years ago and most prion surveillance programs and clinical centers have been established even more recently, we hypothesized that the selective ascertainment of parents and children whose deaths both occurred within this 25-year window could explain the reported differences in parent and child age of death.

To test this hypothesis, here we combine data from four national prion study centers to assemble the largest Glu200Lys cohort (n = 217 individuals) yet reported. We first create a simulation of the ascertainment of parent-child pairs with a mutation to identify conditions under which naive paired t tests will detect a false signal of anticipation. We explore methods for detecting and controlling for this ascertainment bias. We then apply our analytical framework to our Glu200Lys data set and successfully reproduce the anticipation reported by other groups but demonstrate that this anticipation is a false positive due to ascertainment bias.

Material and Methods

Data Collection

We combined data collected on Glu200Lys individuals and their families from four research centers with data collection practices as follows.

Australian National Creutzfeldt-Jakob Disease Registry

Details of Australian National Creutzfeldt-Jakob Disease Registry (ANCJDR) surveillance mechanisms, as well as data collection and analysis methods, have been reported previously.[27,28] In brief, prospective national surveillance of CJD has been undertaken since 1993 with CJD a Notifiable Disease throughout Australia since 2006. ANCJDR collects detailed medico-demographic information on suspect cases, including family histories, and provides diagnostic tests including *PRNP* genotyping. Year and age of death are primary variables with information on age at onset of first symptom collected if available. Informed, written consent was obtained from participants or legal next of kin. Ethical approval was obtained from the Office of Research Ethics and Integrity at The University of Melbourne.

German CJD Surveillance Unit

Details of German CJD surveillance have been reported previously.[29–31] In brief, the Surveillance Unit in Goettingen has collected data on all suspected prion disease cases in Germany since 1993. Diagnostic information is obtained from reporting hospitals and where possible, confirmation by autopsy is sought. The Surveillance Unit also accepts clinical referrals, provides diagnostic tests including *PRNP* genotyping, and, where possible, collects family history. Age of onset is defined from first symptom of a progressive neuropsychiatric disorder by interview with family members. Informed, written consent was obtained from participants or legal next of kin. Ethical approval was obtained from the Ethical Committee at the University Medical School, Georg-August University Goettingen.

MRC Prion Unit/NHS National Prion Clinic

The UK has had a centralized tertiary clinical referral service for CJD since 1991. Since 2004, all suspected CJD cases from the UK are referred to the NHS National Prion Clinic at the National Hospital for Neurology and Neurosurgery (NHNN) at University College London Hospitals NHS Trust. Age of onset was defined from first symptom of a progressive neuropsychiatric disorder and family history was obtained by interview with family members. Other details of data collection have been described previously.[32] Informed, written consent was obtained from participants or legal next of kin. Ethical approval was obtained from the NHNN/Institute of Neurology Joint Research Ethics Committee.

Memory and Aging Center, University of California San Francisco

The UCSF cohort comprises symptomatic and asymptomatic individuals from Glu200Lys families referred from the U.S. and abroad to the rapidly progressive dementia and Prion Disease research program since August 2001.[33–35] *PRNP* genotyping[36] was performed at the National Prion Disease Pathology Surveillance Center (Cleveland, OH), or by outside laboratories in some of the individuals who were tested prior to UCSF referral or lived abroad. Symptom onset was determined as previously reported.[37] A detailed, usually three generation, family pedigree was made by a neurologist and/or clinical genetic counselor for individuals participating in research. Further data were collected from medical records sent by referring physicians and/or from direct contact with family members (by email or telephone). Informed, written consent was obtained from research participants or legal next of kin. The UCSF data included in this study have been collected through UCSF Institutional Review Board-approved research protocols.

Data Annotation

Directly observed individuals were defined as those either seen clinically at one of the four centers or officially reported to one of the centers in its prion disease surveillance role. Indirectly observed individuals were those ascertained through interview with family members. Individuals were considered to have the c.598>A mutation if they (1) had either a genotyping test indicating the presence of the mutation or were related to someone with a positive test and (2) had a diagnosis of CJD or (3) were deemed to have died of CJD based on information obtained from interviewed family members. Individuals were considered to not have the mutation if they (1) had a genotyping test indicating the absence of the c.598G>A mutation or (2) were related to the family only by marriage and thus lacked a blood relationship to any affected individual. The Glu200Lys substitution causes CJD with nearly 100% penetrance,[8,9] but individuals with two WT *PRNP* alleles have a very low disease incidence of only about 1 in 1 million per year.[2] This incidence translates into a lifetime risk roughly on the order of 1 in 10,000 for a WT individual. By Bayes' rule, the high penetrance of the mutation and rarity of nongenetic CJD cases mean that any CJD case in a Glu200Lys pedigree is overwhelmingly likely to be genetic. Therefore, we assumed that all CJD cases in these pedigrees were due to the c.598G>A mutation. Data on four individuals with CJD were flagged as questionable

Table 1. Simulations of Ascertainment Bias

Simulation	Direct ascertainment window	Indirect ascertainment	Mean anticipation (years)[a]	Anticipation significant[b]	Mean additive heritability [a]	Heritability significant [b]	Mean year of birth/age of onset slope [a]	Slope significant [b]
1	1989–2013	None	16.4	100%	93%	100%	−0.67	100%
2	1950–2013	None	4.9	98%	19%	16%	−0.22	100%
3	1880–2013	None	1.6	23%	3%	5%	−0.06	100%
4	1989–2013	Declining 5%/year	10.7	100%	59%	83%	−0.55	100%
5	1950–2013	Declining 5%/year	3.4	79%	14%	11%	−0.18	100%
6	1880–2013	Declining 5%/year	1.4	18%	3%	6%	−0.05	98%
7	1989–2013	Declining 1%/year	2.0	33%	6%	5%	−0.26	100%
8	1950–2013	Declining 1%/year	0.9	12%	4%	5%	−0.12	100%
9	1880–2013	Declining 1%/year	0.4	6%	1%	4%	−0.04	85%
10	1989–2013	Exhaustive	0.2	5%	−1%	5%	−0.20	99%

Ascertaining only those individuals with disease onset within a historical window creates false signals of anticipation and heritability (Simulation 1). These false signals are reduced, but not eliminated, by expanding the ascertainment window (Simulations 2 and 3). Probabilistic retrospective ascertainment (see text) reduces these signals further (Simulations 4–9). Only when retrospective ascertainment is 100% exhaustive does anticipation become reliably nonsignificant (Simulation 10).
[a]Averages from 1,000 simulations.
[b]Percentage of 1,000 simulations in which this figure was statistically significant at $p < 0.05$.

due to uncertain diagnosis, uncertain relatedness to other individuals or uncertain age at death; none of the results reported here differed when the analysis was re-run excluding these individuals. Missing *PRNP* codon 129 information was imputed from affected family members when possible. For the purpose of assessing rates of predictive genetic testing, "at-risk" individuals were defined as those who were not symptomatic at last follow-up but who did have a parent deemed to have the mutation, per the above criteria. Recursively, individuals were also considered at-risk if they had a parent who qualified as at-risk according to the above definition.

Simulation

We hypothesized (see Introduction) that the selective ascertainment of individuals with disease onset within a specified window (for instance, 1989–2013) might explain reported anticipation in Glu200Lys prion disease. To assess whether such an "ascertainment window" was sufficient to create a false signal of anticipation, we created a simulation model in which parent and child ages of onset are drawn from the same specified distribution but ascertainment of parent-child pairs is selective based on year of onset. For each round of simulation, we generated $n = 100{,}000$ parent-child pairs. We only simulated parents and children with the causative mutation. We wished to model a situation in which individuals have been falling ill of prion disease continuously throughout history, and will continue to do so into the future, whereas our data are limited only by an artificial ascertainment window. We therefore generated parents with a year of birth uniformly distributed from 1700 to 2000, in order to ensure that (1) the density of disease onsets over our largest ascertainment window (1880 to 2013) would be uniform and that (2) observed years of onset would effectively be left-truncated only according to our ascertainment criteria and not according to the underlying simulated distribution. We set the child's birth to occur 28 ± 6 years after the parent's birth, per the actual distribution from our data. To simulate an age of onset distribution while accounting for censoring due to deaths due to other causes ("competing risks"), we first created a normally distributed 64 ± 10 year age of onset to approximate the distribution in our real data (see Results) and then randomly censored individuals according to the U.S actuarial life table for 2009 (see Web Resources). We did not model changes in the life expectancy over the time periods considered here. Further details of the specific simulations are explained in Results and in the legends of Tables 1 and 2.

Statistical Analyses

All simulations and analyses of Glu200Lys pedigree data were conducted in R 3.0.2. In order to demonstrate the effects of ascertainment bias on the evidence for anticipation reported by previous studies of genetic prion disease, we adopted methods from those studies when possible. For paired t tests, all possible parent-child pairs were generated from Glu200Lys pedigree structures using a SQL *join* operation. This results in multiple-counting parents of multiple affected children and counting both as parents and as children those individuals in the middle of pedigrees with three or more affected generations. Multiple counting means that pairs are not independent; this mirrors the methods from at least one prior study of prion disease anticipation.[13] Based on these paired lists of parents and children, differences in parent and child age of onset were assessed using two-tailed paired t tests (the R *t.test* function) for naive comparisons of observed age of onset distributions. Correlation between parent and child age of onset was assessed using linear regression (the R *lm* function). Survival analysis utilized the R *survival* package. For survival analysis, to avoid multiple-counting and ensure independence of all pairs, we randomly selected one parent-child pair from each pedigree and compared the survival curve for all parents to that of all children using a log rank test (the R *survdiff* function). Because we randomized which pairs were included, we repeated this analysis for over 1,000 iterations and have reported aggregate statistics. Source code and output are available online (see Web Resources).

Table 2. Stratification of Simulated Data

Cohort Name	Inclusion Criteria	Anticipation	p
Child early birth year	Child born < 1939	16 years	0.009
Child late birth year	Child born ≥ 1939	18 years	<0.0001
Child early death year	Child year of onset < 2000	26 years	0.0004
Child late death year	Child year of onset ≥ 2000	15 years	<0.0001
Child early death age	Child age onset < 61	21 years	<0.0001
Child late death age	Child age onset ≥ 61	11 years	0.003
Parent early death age	Parent age onset < 70	12 years	0.01
Parent late death age	Parent age onset ≥ 70	20 years	<0.0001

In n = 26 simulated parent-child pairs with independent and identically distributed ages of onset but ascertaining only those pairs whose onsets both fall within 1989–2013, all subsets of data stratified according to the variables defined in Table 3 of Pocchiari et al.[13] still show significant anticipation.

Results

Simulated Effects of Ascertainment Window

We generated 100,000 parent-child pairs with all individuals harboring a dominant genetic mutation and ages of onset for all individuals independent and identically distributed, corresponding to a scenario in which no anticipation or heritability of age of onset are present (see Material and Methods and Figure 1A). The mean age of onset without accounting for censoring was 62, whereas the median age of onset in survival analysis accounting for censoring due to intercurrent deaths was 64. When considering all simulated individuals, there was no difference in age of onset ($p = 0.91$, two-tailed paired t test), no correlation between parent and child age of onset ($p = 0.53$, linear regression), and no correlation between the year of birth and age of onset for all individuals ($p = 0.59$, linear regression).

Next we considered the effects of selectively ascertaining individuals whose disease onset occurs within an "ascertainment window," which we define as a range of years in which disease onsets can be observed. It is impossible to ascertain ages of onset after 2013, the last year in which our data were collected. Right-truncating the year of onset at 2013 and considering all affected pairs introduced only a very small difference between parent and child age of onset (0.37 years, $p < 0.0001$, two-tailed paired t test). Because we had generated parent-child pairs with years of birth as early as 1700, only a minority of pairs was affected by this right truncation. Spreading the simulated pairs out over an even greater range of years of parent birth (year 0–2000) made this anticipation cease to be significant ($p = 0.31$, two-tailed paired t test), indicating that right truncation of year of onset is not sufficient cause a false signal of anticipation. In practice, any real data set will be both left-truncated (when researchers began to study the disease) and right-truncated (at the present year or when the study stopped, whichever is earlier). For Glu200Lys CJD, we reasoned that ascertainment rates would be higher after the discovery of the disease's causal mutation in 1989,[4] so we next considered the effects of ascertaining only those individuals whose year of onset occurs between 1989 and 2013 inclusive.

When only those simulated pairs in which parent and child disease onset both occurred within this window were considered (Figure 1A), we observed 17 years of anticipation ($p < 0.0001$, two-tailed paired t test, Figure 1B). Because parents were born, on average, 28 years earlier than their children, yet the window of observation was only 25 years long, the ascertained pairs were vastly enriched for those in which the child dies at least 3 years younger than the parent. Under these conditions, we also observed an artifactual correlation between year of birth and age of onset, with slope of −0.67, ($p < 0.0001$, linear regression, Figure 1C). This relationship is intuitive because an individual born in 1970, for instance, can only be included in the data set if onset occurs by age 43 (year 2013), and an individual born in 1940 can only be included if onset occurs at age 49 or later (year 1989). Year of birth/age of onset correlation is therefore a consequence of ascertaining only individuals with the year of onset within a particular window. This problem has previously been noted in Huntington's disease pedigrees.[38] Among the ascertained pairs, parent and child age of onset were also correlated with a slope of 0.48 ($p < 0.0001$, linear regression, Figure 1D). In single parent-offspring regression, the slope can be doubled to obtain an estimate of phenotypic variance explained by additive genetic heritability plus environmental effects.[39] Applying this formula to the ascertained data would suggest that age of onset is up to 96% heritable. Because the true distributions of parent and child ages of onset in our simulation were neither different nor correlated, this shows that the year of onset "windowing" simulated here is sufficient to create false signals of both anticipation and heritability. We confirmed this finding through 1,000 iterations with the same set of simulation conditions and n = 100 ascertained pairs to simulate a realistic sample size for a rare disease (Table 1, Simulation 1).

Because we knew the anticipation and heritability identified in our above simulation to be false signals, we asked whether improved ascertainment or simple analytical methods could disprove them. We considered a two-step ascertainment model; in the first step, we ascertained all individuals with disease onset between 1989 and 2013 (simulating clinical visits), and in the second step we ascertained any and all individuals still alive and well as of 2013 who were parents or children of the individuals ascertained in step 1 (simulating genetic testing and prospective follow-up of individuals with the mutation). When we compared parent and child survival curves under this two-step ascertainment model in Kaplan-Meier survival analysis, the median age of onset of children was greater than that of parents (64 versus 62 years, $p < 0.0001$, log rank test). This counter-intuitive finding of later child

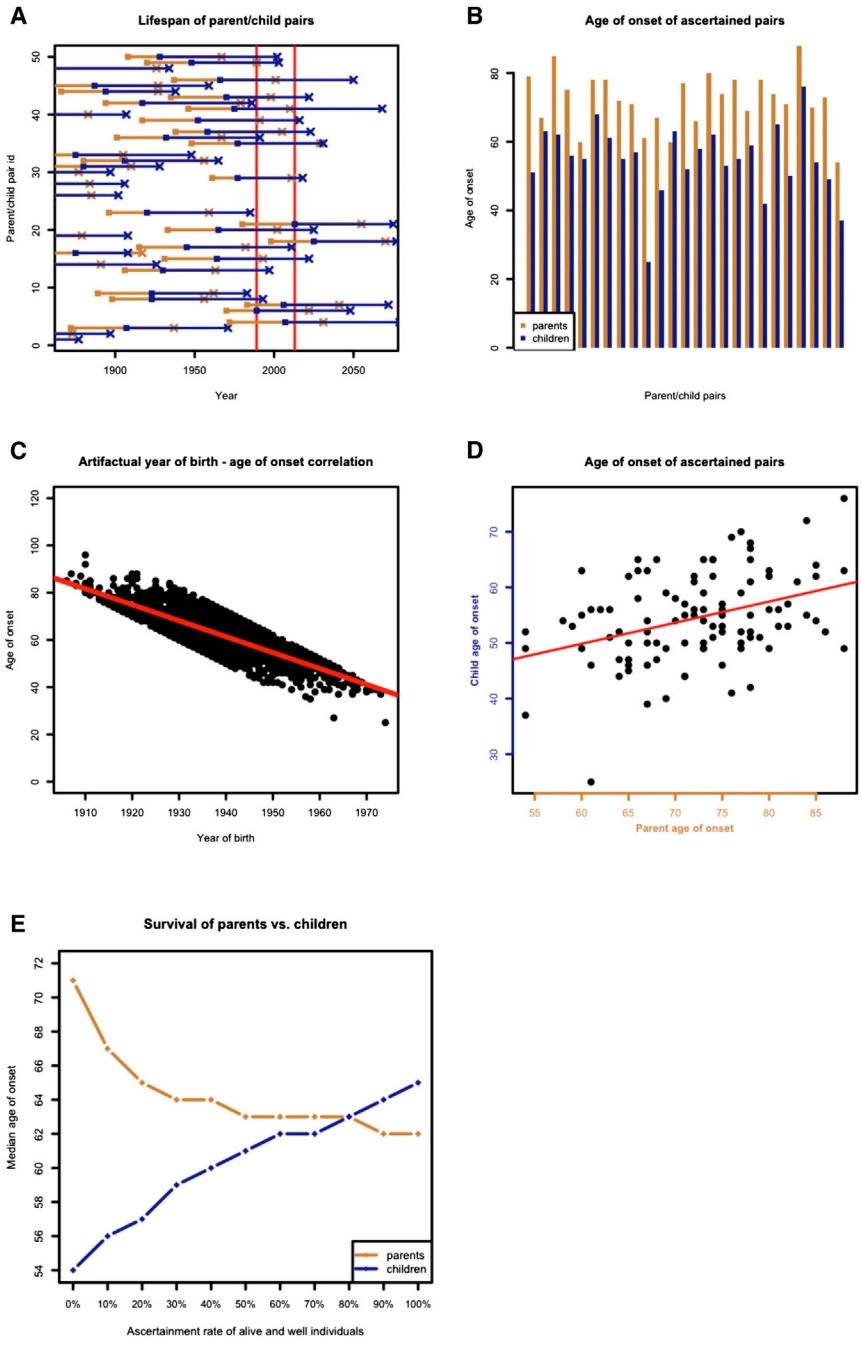

Figure 1. Simulation of Ascertainment Bias Due to Year of Onset Windowing

(A) Visual representation of a subset of simulated data. Parent-child pairs are arranged along the y axis. Parent is born on orange square and has disease onset on orange X; child is born on blue square and has disease onset on blue X. Age of onset distributions are identical, but in Simulation 1, only those pairs in which both individuals have onset between 1989 and 2013 inclusive (red vertical lines) can be ascertained. In the above example, only one pair (#49) meets these criteria.

(B) Among ascertained pairs in Simulation 1, children have almost categorically younger onset than their parents, leading to 17 years of observed anticipation ($p < 0.0001$, two-tailed paired t test). For visibility, a subset of simulated points is shown.

(C) Ascertainment windowing introduces an artifactual correlation between year of birth and age of onset, slope = −0.67 ($p < 0.0001$, linear regression).

(D) Ascertainment windowing also leads to a correlation between parent and child age of onset and thus a false signal of heritability (slope = 0.48, $p < 0.0001$, linear regression).

(E) Ascertained pairs are supplemented with those pairs where one individual's onset occurs in 1989–2013 and the other is alive and well as of 2013. The plot shows that the median survival of parents and children in Kaplan-Meier curves depends upon what proportion of alive and well individuals are included. If 0% are included, then 17 years anticipation are observed, just as in (B). As ascertainment increases, the anticipation is reduced. As inclusion of alive and well individuals approaches 100%, children have longer survival than parents. This is because more of the children are censored, so their age of onset distribution better reflects the hypothetical distribution of age of onset without the influence of competing risks.

onset can be explained as follows. Because parents are born earlier than children, pairs in this two-step ascertainment model are predominantly ones in which the parent dies of genetic prion disease between 1989 and 2013 while the child is alive and well in 2013. In such pairs, the parent's age of onset distribution is truncated by competing risks (parents who *would* have had older disease onsets were never ascertained because they died of other causes first, thus making disease onset appear younger). The child's age of onset distribution, however, is less affected by competing risks (children who would have older disease onsets are ascertained through genetic testing even if they will never develop the disease in their lifetimes).

Recall that in the two-step ascertainment model above, an affected individual is ascertained in step 1, and if that individual has a parent or child alive and well in 2013, then that parent or child is *always* ascertained. In practice, however, it is difficult to ascertain 100% of asymptomatic relatives of an affected individual. We therefore also modeled *incomplete* ascertainment of asymptomatic individuals. When we did so, we saw that the false signal of anticipation from naive t tests was not fully corrected (Figure 1E). The difference in median survival according to the log rank test was 17 years when no censored individuals were included, and this difference shrunk to 7 years when 20% of individuals alive and well in 2013 were included, and 2 years when 50% of such individuals were included. This indicates that accounting for censored

observations is not sufficient to remove false signals of anticipation unless ascertainment of censored individuals is exhaustive. In long-term studies of predictive genetic testing for neurodegenerative diseases, it has been reported that only 3% to 24% of individuals with risk of having inherited a mutation pursue predictive genetic testing.[40–45] Survival analysis including asymptomatic individuals with a mutation is therefore unlikely to mitigate false signals of anticipation and heritability in this disease setting.

We also asked whether including year of birth as a covariate could eliminate the false signal of heritability we observed in our simulation. When both parent age of onset and child year of birth were used in a linear model to explain child age of onset, only the child's year of birth proved to be correlated (slope = −0.72, $p < 0.0001$, linear regression), whereas parent age of onset was no longer significant ($p = 0.73$, linear regression). When we simulated an age of onset that truly was heritable, this method reduced, but did not eliminate, the estimate of heritability (see Table S1 available online).

Simulated Effects of Different Ascertainment Criteria

In Simulation 1 (Table 1) we assumed that it was only possible to include individuals directly ascertained within the window from 1989 to 2013. In reality, some Glu200Lys families have been followed since as early as 1963[7] and it is also possible to obtain information on deceased individuals retrospectively through interview with family members, though it can be more difficult for individuals whose year of death is long past.[46] We therefore asked whether false anticipation and heritability would still be observed with larger or more flexible ascertainment windows. In this analysis, we limited the number of ascertained pairs to 100 in order to simulate a realistic sample size for a rare disease. Expanding the size of the direct ascertainment window back to 1950 or 1880 (but still not adding indirect ascertainment) decreased the strength of the false signals quantitatively, but did not reliably eliminate them, even when the window was longer than a human lifespan (Table 1, Simulations 1–3).

Next, we considered including some indirectly ascertained individuals. To simulate retrospective ascertainment, we first directly ascertained individuals with onset within the window, then ascertained any parents or children thereof whose onset had already occurred prior to the beginning of the window. We hypothesized that it might be more difficult to ascertain individuals who died long ago, so for indirectly ascertained individuals we applied a linear reduction in ascertainment probability according to how many years prior to the beginning of the ascertainment window the individual had disease onset. In Simulation 4 (Table 1), for instance, direct ascertainment from 1989-2013 is exhaustive, but the probability of indirect ascertainment declines by 5% for each year prior to 1989 that an individual has onset so that, for instance, an individual with onset in 1988 can be retrospectively ascertained with 95% probability, in 1987 with 90% probability, and so on. Including some indirectly ascertained individuals in this manner further reduced the magnitude of anticipation but did not completely eliminate it in most scenarios tested (Simulations 4–9). The false signal of heritability was weaker than that of anticipation and could be reliably reduced to statistical insignificance in the most extreme scenarios tested (Simulations 6–9). Only when indirect ascertainment was 100% exhaustive and independent of the year of onset (Simulation 10) did a signal of anticipation cease to be detected, though a year of birth/age of onset correlation still existed.

Together, our simulations demonstrate that ascertaining individuals over a larger time window or including some indirect ascertainment (retrospective phenotyping) can quantitatively reduce the false signals of anticipation and heritability but that these false signals are still likely to be observed as statistically significant under anything other than almost complete ascertainment. Our results indicate that whenever retrospective ascertainment is less than exhaustive, there is a risk of observing false signals of anticipation and heritability of age of onset.

Stratification of Simulated Data

One recent report of anticipation in Glu200Lys genetic prion disease[13] argued that the observed anticipation must be real because anticipation was observed, using paired t tests, within every subset of 26 parent-child pairs when these were stratified by age of death, year of birth, or year of death. To determine whether such an analysis could indeed rule out a false positive due to ascertainment bias, we stratified 26 simulated parent-child pairs with onset between 1989 and 2013 in the same way described in the previous report (Table 2). In our simulation, anticipation is not real, yet a strong signal of anticipation is nevertheless observed in all eight strata. Therefore, these methods of stratification do not eliminate spurious signals of anticipation due to ascertainment bias.

Characteristics of Glu200Lys Pedigree Data

We combined data on Glu200Lys families from four independent study centers worldwide (Table 3). Each individual data set reflected a different method of ascertainment (see Material and Methods) and accordingly, the proportion of individuals ascertained indirectly or asymptomatic as of last follow-up varied considerably (Table 3).

Of individuals whose disease onset or death was directly observed by one of the study centers, 65% had no reported family history of prion disease. This figure might reflect some combination of (1) incomplete reporting of family history, (2) underdiagnosis of affected individuals in earlier generations, (3) censoring of asymptomatic individuals with the mutation upon death due to other causes, and (4) de novo mutations. Similarly, we knew the genotypes of only 22% of at-risk individuals (see Material and Methods) in our data sets. Together, these figures suggest

Table 3. Characteristics of Glu200Lys Data Sets

Study Center	In Operation Since	n c.598G>A Individuals	n c.598G>A Parent-Child Pairs	Proportion of c.598G>A Individuals Ascertained Indirectly	Proportion of c.598G>A Individuals Who Are Asymptomatic
ANCJDR	1993	24	7	42%	8%
German CJD Surveillance	1993	32	3	38%	3%
MRC Prion Unit	1991	57	29	25%	23%
UCSF	2001	104	58	73%	37%
All		**217**	**97**	**52%**	**25%**

Data from the four study centers varied in terms of the length of time for which data had been collected, the degree of indirect ascertainment, and the ascertainment of asymptomatic individuals with the mutation. See Material and Methods for details.

that neither retrospective ascertainment nor prospective following of individuals with the mutation are exhaustive in our data set.

Disease Duration and Genotypic Influence

Disease duration was defined as time from first symptom (see Data Collection in Material and Methods) to death. Disease duration followed a nonnormal distribution ($p < 0.0001$, Shapiro-Wilk normality test) with a median of 162 days ($n = 61$, interquartile range 205 days), similar to the figure reported elsewhere.[11] Disease duration did not differ by study center ($p = 0.35$, Kruskal-Wallis test, $n = 61$) or between directly and indirectly ascertained individuals ($p = 0.08$, Kruskal-Wallis test, $n = 38$ and 23 respectively). *PRNP* codon 129 information was available for a subset of individuals with known disease duration. Among individuals with a haplotype encoding Glu200Lys *cis* 129Met, disease duration was shorter for individuals with a trans allele encoding 129Met (median of 137 days, $n = 25$) than a trans allele encoding 129Val (median of 426 days, $n = 7$) and this difference was significant ($p = 0.02$, Kolmogorov-Smirnov test), consistent with previously reported data.[11] Disease duration appeared to differ between haplotypes encoding Glu200Lys *cis* 129Met ($n = 42$) and Glu200Lys *cis* 129Val ($n = 6$) proteins, with a median duration of 137 versus 331 days respectively ($p = 0.04$, Kolmogorov-Smirnov test), although trans codon 129 information was not available for all of these individuals, so it is possible that the longer duration among *cis* 129Val individuals might be due to higher rates of codon 129 heterozygosity. Because disease duration was generally a year or less and our data included age of onset for some individuals but age of death for others, we decided to consider age of onset and death interchangeably in the anticipation analysis, preferring age of death when both were available.

Age of Onset or Death and Genotypic Influence

Overall, the mean age of onset or death in affected individuals was 62 ± 10 years (±SD, $n = 158$) and was approximately normally distributed ($p = 0.36$, Shapiro-Wilk normality test; Figure 2A). The median observed age of onset or death was 63 years ($n = 158$). The median rose to 64 years when we included asymptomatic individuals with the mutation, censored at date of last follow-up or death due to other causes, and applied a survival analysis ($n = 207$). This survival analysis indicated 93% disease penetrance by age 80, within the range of previously reported estimates,[8,9] but we note that this figure is biased upward by the ascertainment of affected families and incomplete genotyping of unaffected individuals. To our knowledge, 64 years is older than any other measure of central tendency of age of onset for this mutation yet reported, probably because our use of survival analysis accounts for censoring due to competing risks, whereas other published estimates have been based simply on observed ages of onset.[3,7,10,47] Even our estimate is likely biased downward due to incomplete genotyping of unaffected individuals.

Age of onset or death did not differ by study center ($p = 0.18$, Model I ANOVA, $n = 158$), sex ($p = 0.74$, unpaired t test, $n = 132$), or mode of ascertainment (direct versus indirect, $p = 0.66$, unpaired t test, $n = 158$). Among individuals with a haplotype encoding Glu200Lys *cis* 129Met, age of onset or death did not differ between *trans* 129Met ($n = 46$) and *trans* 129Val ($n = 10$) genotypes ($p = 0.71$, two-tailed unpaired t test; $p = 0.39$, log rank test, $n = 64$ Met-Met versus 17 Met-Val including censored individuals), consistent with a previous report.[48] It was unclear whether age of onset or death might differ between individuals with haplotypes encoding Glu200Lys *cis* 129Met versus Glu200Lys *cis* 129Val, because only a weak trend could be detected whether censored individuals were included (censored median 64 versus 57 years, $p = 0.05$, log rank test, $n = 142$ Met versus 13 Val) or excluded (mean 63 versus 56 years, $p = 0.11$, two-tailed unpaired t test, $n = 105$ Met versus 10 Val). Because *trans* codon 129 did not influence age of onset or death and because a child's *cis* codon 129 is inherited from the affected parent, we deemed it unnecessary to consider codon 129 genotype in our anticipation analyses.

Ascertainment Bias in Glu200Lys Pedigree Data

Excluding asymptomatic individuals, the year of disease onset or death was known for 94% of directly ascertained individuals (68 of 72) and 55% of indirectly ascertained

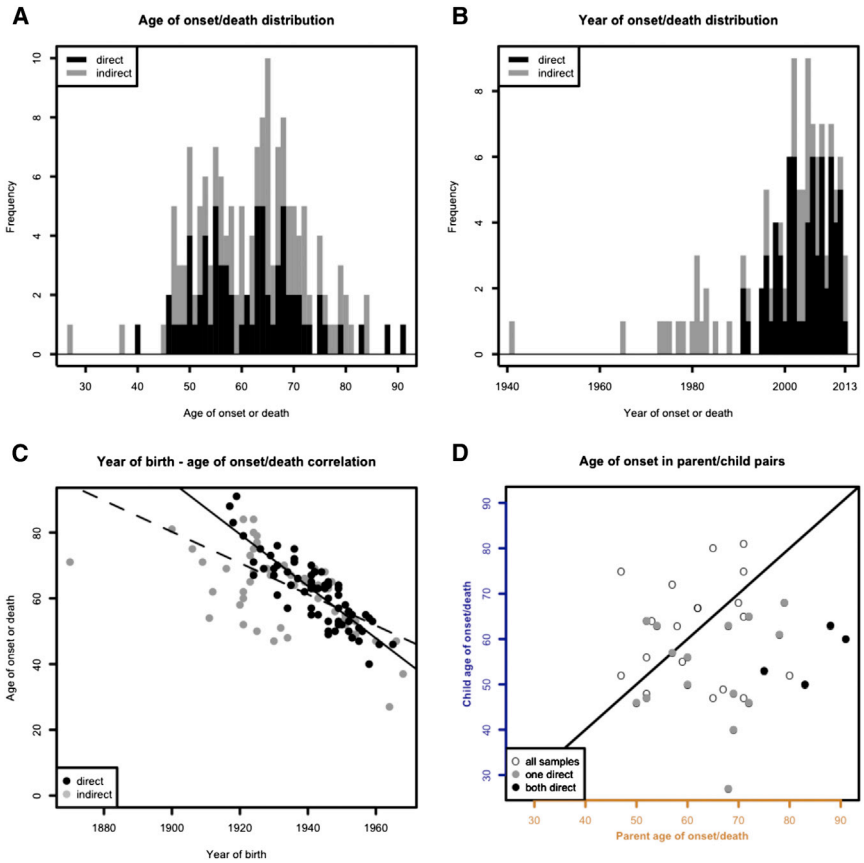

Figure 2. Ascertainment Bias and Anticipation in Glu200Lys Pedigree Data

(A) Distribution of age of onset or death by ascertainment mode.

(B) Years of onset or death, when known, occur overwhelmingly in the 25-year window since the mutation's discovery in 1989.

(C) Year of birth and age of onset are artifactually correlated. This correlation is strongest in directly ascertained individuals (black line) but remains highly significant when indirectly ascertained individuals (gray points) are included in addition (dashed black line).

(D) Parent versus child age of onset or death. Points below the diagonal line indicate pairs in which the child dies younger than the parent. Directly ascertained pairs (black points) fall categorically below the line, pairs with one directly ascertained member are largely below the line (gray points), and pairs in which both individuals are indirectly ascertained fall on both sides (white points).

individuals (50 of 91). Year of disease onset or death occurred between 1989 and 2013 in 92% of all individuals for whom this variable was known (Figure 2B). This 25-year window was shorter than the typical difference between parent and child year of birth, which was 28 ± 6 years (mean ± SD, n = 150 including unaffected individuals), thus partially limiting ascertainment to parent-child pairs in which the child died at least 3 years younger than the parent. For individuals ascertained directly, year of birth and age of onset were even more strongly correlated than in our simulation (slope = −0.79, $p < 0.0001$, linear regression, Figure 2C, black line). The correlation weakened only slightly when indirectly ascertained individuals were included as well (slope = −0.48, $p < 0.0001$, linear regression, Figure 2C, dashed line).

Our simulation (see above) indicated that ascertainment bias could introduce false signals of heritability. We did not, however, observe any correlation between parent and child age of onset ($p = 0.99$, linear regression, n = 39 pairs) nor in sibling pair ages of onset ($p = 0.63$, linear regression, n = 26 pairs). Thus we do not find any signal, whether real or artifactual, that age of onset in this disease is heritable. This is not surprising because our simulation indicated that false signals of heritability are weaker than false signals of anticipation (Table 1), and the small size of our data set might also leave us underpowered to detect any true heritability of age of onset that might exist.

Strength of Anticipation Signal Depends upon Degree of Ascertainment Bias

Because signatures of ascertainment bias were strongly evident in our data, we expected to see a difference between parent and child age of onset in observed pairs. On the basis of our simulation results (Table 1), we hypothesized that the strength of the anticipation signal from naive paired t tests would vary depending on how flexible we were able to make our ascertainment window, within the constraints of our available data. When we considered only pairs in which both parent and child were ascertained directly, we observed 28 years of anticipation ($p = 0.002$, two-sided paired t test, n = 4 pairs). When we additionally included pairs with one indirectly ascertained individual, this figure dropped to 15 years ($p = 0.0002$, two-sided paired t test, n = 20 pairs). When we also included pairs in which both individuals were ascertained indirectly, this dropped further to 7 years ($p = 0.005$, two-sided paired t test, n = 39 pairs). Thus, the number of years of anticipation observed depends upon how narrow the ascertainment window is and the mechanism of case reporting.

The strength of the anticipation signal also differed by study center according to the extent of ascertainment bias in each individual data set. The UCSF data set, which was the largest and had both the highest percentage of indirectly ascertained individuals (73%) and the least correlation between year of birth and age of onset or death (slope = −0.41), showed the least evidence of anticipation (1 year, $p = 0.68$, two-sided paired t test). The MRC Prion Unit showed a marginal paired difference (7 years, $p = 0.10$, two-sided paired t test), whereas the Australian and German cohorts showed larger differences (18 years,

$p = 0.05$ and 31 years, $p = 0.03$ respectively, two-sided paired t test).

Application of Survival Analysis to Glu200Lys Anticipation

The foregoing analysis indicated that our data exhibited a nominal signal of anticipation when analyzed with naive paired t tests. Because this signal depended upon the degree of ascertainment bias, and because our data exhibited signatures of ascertainment bias similar to what we had observed in our simulation, we suspected that the anticipation we observed was an artifact. We next set out to determine whether a survival analysis including asymptomatic individuals with the c.598G>A mutation would correct this artifact. Based on our simulation results (Figure 1E) and the fact that our ascertainment of asymptomatic individuals with the mutation was not exhaustive, we expected that survival analysis would not fully eliminate the signal of anticipation in our Glu200Lys data. For the survival analysis, we considered all parent-child pairs in which both individuals harbored the mutation, regardless of censored status. To ensure independence of tested pairs and avoid multiple counting, we randomly selected one such pair from each pedigree and compared parent and child survival curves. Across 1,000 iterations, parent and child survival curve medians differed by an average of 7 years (log rank test $p < 0.05$ in 82% of iterations). Because our simulation indicated that more thorough ascertainment of censored individuals reduces artifactual anticipation signals (Figure 1E), we repeated the same analysis on only the UCSF and MRC Prion Unit cohorts, which had the highest proportion of asymptomatic individuals with the mutation (Table 3). Within these cohorts, the median difference in parent and child survival curves was only 1 year and was usually not significant ($p < 0.05$ in only 8% of 1,000 iterations). This is consistent with the hypothesis that observed parent-child age of onset differences in Glu200Lys prion disease are due to incomplete ascertainment and not due to true anticipation.

Anticipation in Age at Death Due to Other, Non-Prion, Causes

The foregoing analyses suggested that the anticipation we observed in Glu200Lys families could be attributed entirely to ascertainment bias. We reasoned that if this were true, then anticipation in age of death might be observed in deaths attributable to other causes as well, with these unrelated deaths providing a kind of negative control. When we compared age at death for all parent-child pairs in our data set in which neither individual had CJD listed as cause of death, we observed 14 years of anticipation ($p = 0.002$, two-sided paired t test, $n = 37$ pairs). In many cases, the cause of death was not listed or was ambiguous, so we could not rule out the possibility that some of those individuals might actually have died of undiagnosed or unreported prion disease. When we therefore considered only those pairs in which each individual was known not to harbor the mutation (see Material and Methods) and/or died of a known cause clearly distinct from prion disease (cancer, heart attack, accident, etc.), the anticipation grew to 35 years ($p = 0.001$, two-sided paired t test, $n = 9$ pairs). This set included some individuals who had died much younger than the typical age of onset for Glu200Lys prion disease (Figure 2A), introducing a potential new source of ascertainment bias as individuals who die young might be counted as children but are unlikely to ever become parents.[14] When we further filtered our data to include only individuals with age at death greater than 40, 16 years of anticipation were still observed ($p = 0.002$, two-sided paired t test, $n = 5$ pairs).

Discussion

The prediction of age of onset in those carrying mutations causal of neurodegenerative diseases is important for genetic counseling, clinical trial design,[49,50] and understanding of fundamental disease mechanisms. We chose to investigate bias in a specific genetic prion disease as it has been reported[12,13] that Glu200Lys genetic prion disease exhibits anticipation, with children succumbing to disease 7 to 14 years younger than their parents on average. We approached this claim with skepticism; the causal mutation is not a repeat expansion and human prion strains are not transmitted in childbirth or through casual contact between people,[51–53] leaving no obvious mechanism for anticipation. Such a large decrease in age of onset in germline transmission ought to lead to juvenile onset cases within a few generations, as observed in repeat expansion disorders,[15] yet no such cases are observed in Glu200Lys families (Figure 2A). In the present study, we considered the possibility that reported evidence of anticipation in Glu200Lys prion disease arises instead from ascertainment bias.

We tested for anticipation in our data using naive paired t tests, and we did observe a statistically significant difference between parent and child age of onset, but four separate lines of evidence argue that this difference is artifactual rather than biological. First, 92% of known years of onset or death for CJD-affected individuals in our data set fell within the 25-year window from the mutation's discovery in 1989 to the time of our study in 2013, whereas parents were born on average 28 years earlier than their children. This enriches for pairs in which children die at least 3 years younger than their affected parent. Pairs in which children die older than their parents are much less likely to be observed during this time window. Second, we observed an artifactual correlation between year of birth and age of onset reflective of this "windowing" effect because individuals born later in time are only captured in this data set if they have earlier onset. The distribution of ages of onset is therefore shifted older for a parent's year of birth (for instance, 1920) than for their child's year of birth (for instance, 1950). Third, the strength of the

anticipation signal we observed depended upon how strictly the data were limited by the ascertainment window. When we required that both parent and child had to be directly observed as patients by the study centers contributing data, we observed 28 years of anticipation. When all indirectly ascertained individuals were also included, this figure dropped to 7 years, and when we performed survival analysis on only the data from two centers most active in performing predictive genetic testing, we saw no difference in age of onset at all. Fourth, when using naive paired t tests, we observed anticipation even among individuals in our pedigrees who did not harbor the mutation and/or died of causes unrelated to prion disease.

None of the three previous studies reporting Glu200Lys anticipation[12,13] (see also Web Resources) presented data on the distribution of year of onset, tested for correlation between year of birth and age of onset, or carried out a negative control by assessing anticipation in unrelated deaths as we have done here. One of these studies[12] found a stronger anticipation (14 years rather than 7) when only directly genotyped individuals were included, similar to our finding that the strength of anticipation depends upon the duration of the ascertainment window. We showed that the stratification analyses, as performed in one study,[13] do not remove the effects of ascertainment bias. Because anticipation was observed in certain analyses of our data as well, we consider it likely that the differences between our study and the previous studies arise from differences in methodology rather than differences in whether anticipation is truly present in the study population.

In assessing the evidence for anticipation in Glu200Lys prion disease, we have created a simulation model with relevance to other diseases as well. In contrast to previous studies of anticipation, we consider ascertainment to be limited by year of onset, not by age of onset per se. In general we find that ascertaining only those individuals with onset within a restricted time period is sufficient to create robust false signals of anticipation. This is of general concern because the genetic causes of many dominant Mendelian disorders were identified within the past 25 years, leaving a relatively narrow window for ascertainment. Our simulation shows that even high rates of retrospective ascertainment are unlikely to completely remove the resulting false signal of anticipation. Although certain statistical methods can help to correct for this bias when ascertainment criteria are consistent or data sets large enough to allow subsetting, we believe our own data may be typical of some rare diseases in representing a mixture of ascertainment modes, with both retrospective and prospective phenotyping present but nonexhaustive. For such data sets, we agree with the view[54] that statistical tests alone might be inadequate to discriminate between situations with and without anticipation. We believe that one route toward preventing spurious claims of anticipation such as seen in Glu200Lys genetic prion disease might lie not in the requirement of more rigorous statistical tests but in an expectation of thorough and transparent assessment of a data set's degree of bias. Toward that end, we propose that future studies' reporting factors that determine age of onset in adult-onset dominant conditions should be expected to provide (1) a histogram of year of onset or death, (2) a test for correlation between year of birth and age of onset, (3) descriptive statistics on the extent of retrospective ascertainment and predictive genetic testing or prospective follow-up, and (4) a test for anticipation in deaths of other causes. Our results also have implications for study design in adult-onset genetic diseases; year of birth information should be collected, asymptomatic individuals with a mutation should be tracked, and retrospective ascertainment should be as thorough as possible. These measures will make it easier to quantify and reduce ascertainment bias.

Though heritability of age of onset was not observed in our Glu200Lys data, we noticed in our simulation that windowed ascertainment can also create a false signal that age of onset is heritable. This false signal could easily be disproven by including child year of birth as a covariate in parent-offspring regression. Our result suggests that estimates of the heritability of age of onset in genetic disease made based on parent-offspring regression ought to be scrutinized carefully and accepted only if the parent-child age of onset correlation remains after controlling for year of birth.

In summary, the phenomenon of anticipation previously reported in Glu200Lys prion disease is likely an artifact. Ascertainment bias is a pervasive problem in age of onset in genetic disease but can be reduced through appropriate data collection methods and recognized with simple analytical tools.

Supplemental Data

Supplemental Data include one table and can be found with this article online at http://www.cell.com/ajhg.

Acknowledgments

We would like to thank all affected individuals and their families for contributing to this research; physicians who referred or reported cases to surveillance and provided pertinent clinical, neuroradiological, and neuropathological data; the staff of the Goettingen research unit and the Center for Neuropathology and Prion Research at the Ludwig-Maximilian University Munich; the U.S. National Prion Disease Pathology and Surveillance Center for providing genotyping services; and Michael E. Talkowski, Benjamin M. Neale, Mark J. Daly, and Daniel G. MacArthur for their contributions to this study. The Australian National Creutzfeldt-Jakob Disease Registry is funded by the Commonwealth Department of Health. German CJD Surveillance is supported by grants from the Robert Koch Institute by funds of the Federal Ministry of Health (grant no 1369-341). MRC Prion Unit is funded by Medical Research Council UK; the UK clinical studies were supported in part by the National Institute for Health Research's Biomedical Research Centre at UCLH. This work from UCSF was supported by NIH through NIH/NIA R01 AG-031189,

K23 AG021989, P50AG023501, NIH/NCRR Grant Number UL1 RR024131, NIH/NIA AG021601, NIH/NINDS Contract N01-NS-0-2328, and Michael J. Homer Family Fund. E.V.M. received no specific funding for this work and volunteers his time on behalf of Prion Alliance. The funders had no role in study design, data collection and analysis, decision to publish, or preparation of the manuscript. M.D.G. has served as a consultant for Lundbeck, MedaCorp, The Council of Advisors, and Neurophage.

Received: April 6, 2014
Accepted: September 9, 2014
Published: October 2, 2014

Web Resources

The URLs for data presented herein are as follows:

Mitrova, E. (2012). The role of anticipation in the incidence of CJD with the mutation E200K. Presented at the CJD Family Foundation Conference, Washington, D.C., July 14, 2012. Archived on August 5, 2014: http://web.archive.org/web/20140805095200/http://www.cjdfoundation.org/shared/cjdfoundation/files/webfm/admin/2012-conference/Eva-Mitrova.pdf

Online Mendelian Inheritance in Man (OMIM), http://www.omim.org/

U.S. Social Security Administration 2009 Life Tables. Archived on June 2, 2014: http://web.archive.org/web/20140602090427/http://www.ssa.gov/oact/STATS/table4c6.html

Source code and output for this study: https://github.com/ericminikel/e200k-anticipation

References

1. Prusiner, S.B. (1998). Prions. Proc. Natl. Acad. Sci. USA *95*, 13363–13383.
2. Holman, R.C., Belay, E.D., Christensen, K.Y., Maddox, R.A., Minino, A.M., Folkema, A.M., Haberling, D.L., Hammett, T.A., Kochanek, K.D., Sejvar, J.J., and Schonberger, L.B. (2010). Human prion diseases in the United States. PLoS ONE *5*, e8521.
3. Kong, Q., Surewicz, W.K., Petersen, R.B., Chen, S.G., Gambetti, P., Parchi, P., Capellari, S., Goldfarb, L., Montagna, P., Lugaresi, E., et al. (2004). Inherited Prion Diseases. In Prion Biology and Diseases (Cold Spring Harbor Laboratory Press).
4. Goldgaber, D., Goldfarb, L.G., Brown, P., Asher, D.M., Brown, W.T., Lin, S., Teener, J.W., Feinstone, S.M., Rubenstein, R., Kascsak, R.J., et al. (1989). Mutations in familial Creutzfeldt-Jakob disease and Gerstmann-Sträussler-Scheinker's syndrome. Exp. Neurol. *106*, 204–206.
5. Goldfarb, L.G., Korczyn, A.D., Brown, P., Chapman, J., and Gajdusek, D.C. (1990). Mutation in codon 200 of scrapie amyloid precursor gene linked to Creutzfeldt-Jakob disease in Sephardic Jews of Libyan and non-Libyan origin. Lancet *336*, 637–638.
6. Goldfarb, L.G., Mitrová, E., Brown, P., Toh, B.K., and Gajdusek, D.C. (1990). Mutation in codon 200 of scrapie amyloid protein gene in two clusters of Creutzfeldt-Jakob disease in Slovakia. Lancet *336*, 514–515.
7. Hsiao, K., Meiner, Z., Kahana, E., Cass, C., Kahana, I., Avrahami, D., Scarlato, G., Abramsky, O., Prusiner, S.B., and Gabizon, R. (1991). Mutation of the prion protein in Libyan Jews with Creutzfeldt-Jakob disease. N. Engl. J. Med. *324*, 1091–1097.
8. Chapman, J., Ben-Israel, J., Goldhammer, Y., and Korczyn, A.D. (1994). The risk of developing Creutzfeldt-Jakob disease in subjects with the PRNP gene codon 200 point mutation. Neurology *44*, 1683–1686.
9. Spudich, S., Mastrianni, J.A., Wrensch, M., Gabizon, R., Meiner, Z., Kahana, I., Rosenmann, H., Kahana, E., and Prusiner, S.B. (1995). Complete penetrance of Creutzfeldt-Jakob disease in Libyan Jews carrying the E200K mutation in the prion protein gene. Mol. Med. *1*, 607–613.
10. Schelzke, G., Kretzschmar, H.A., and Zerr, I. (2012). Clinical aspects of common genetic Creutzfeldt-Jakob disease. Eur. J. Epidemiol. *27*, 147–149.
11. Pocchiari, M., Puopolo, M., Croes, E.A., Budka, H., Gelpi, E., Collins, S., Lewis, V., Sutcliffe, T., Guilivi, A., Delasnerie-Laupretre, N., et al. (2004). Predictors of survival in sporadic Creutzfeldt-Jakob disease and other human transmissible spongiform encephalopathies. Brain *127*, 2348–2359.
12. Rosenmann, H., Kahana, E., Korczyn, A.D., Kahana, I., Chapman, J., and Gabizon, R. (1999). Preliminary evidence for anticipation in genetic E200K Creutzfeldt-Jakob disease. Neurology *53*, 1328–1329.
13. Pocchiari, M., Poleggi, A., Puopolo, M., D'Alessandro, M., Tiple, D., and Ladogana, A. (2013). Age at Death of Creutzfeldt-Jakob disease in subsequent family generation carrying the E200K mutation of the prion protein gene. PLoS ONE *8*, e60376.
14. Penrose, L.S. (1948). The problem of anticipation in pedigrees of dystrophia myotonica. Ann. Eugen. *14*, 125–132.
15. Orr, H.T., and Zoghbi, H.Y. (2007). Trinucleotide repeat disorders. Annu. Rev. Neurosci. *30*, 575–621.
16. La Spada, A.R., and Taylor, J.P. (2010). Repeat expansion disease: progress and puzzles in disease pathogenesis. Nat. Rev. Genet. *11*, 247–258.
17. Vulliamy, T., Marrone, A., Szydlo, R., Walne, A., Mason, P.J., and Dokal, I. (2004). Disease anticipation is associated with progressive telomere shortening in families with dyskeratosis congenita due to mutations in TERC. Nat. Genet. *36*, 447–449.
18. Martinez-Delgado, B., Yanowsky, K., Inglada-Perez, L., Domingo, S., Urioste, M., Osorio, A., and Benitez, J. (2011). Genetic anticipation is associated with telomere shortening in hereditary breast cancer. PLoS Genet. *7*, e1002182.
19. Gajdusek, D.C. (1977). Unconventional viruses and the origin and disappearance of kuru. Science *197*, 943–960.
20. Brown, P., Preece, M.A., and Will, R.G. (1992). "Friendly fire" in medicine: hormones, homografts, and Creutzfeldt-Jakob disease. Lancet *340*, 24–27.
21. Hewitt, P.E., Llewelyn, C.A., Mackenzie, J., and Will, R.G. (2006). Creutzfeldt-Jakob disease and blood transfusion: results of the UK Transfusion Medicine Epidemiological Review study. Vox Sang. *91*, 221–230.
22. Heiman, G.A., Hodge, S.E., Wickramaratne, P., and Hsu, H. (1996). Age-at-interview bias in anticipation studies: computer simulations and an example with panic disorder. Psychiatr. Genet. *6*, 61–66.
23. Vieland, V.J., and Huang, J. (1998). Statistical evaluation of age-at-onset anticipation: a new test and evaluation of its behavior in realistic applications. Am. J. Hum. Genet. *62*, 1212–1227.
24. Tsai, W.Y., Heiman, G.A., and Hodge, S.E. (2005). New simple tests for age-at-onset anticipation: application to panic disorder. Genet. Epidemiol. *28*, 256–260.

25. Boonstra, P.S., Gruber, S.B., Raymond, V.M., Huang, S.-C., Timshel, S., Nilbert, M., and Mukherjee, B. (2010). A review of statistical methods for testing genetic anticipation: looking for an answer in Lynch syndrome. Genet. Epidemiol. *34*, 756–768.
26. Rabinowitz, D., and Yang, Q. (1999). Testing for age-at-onset anticipation with affected parent-child pairs. Biometrics *55*, 834–838.
27. Collins, S., Law, M.G., Fletcher, A., Boyd, A., Kaldor, J., and Masters, C.L. (1999). Surgical treatment and risk of sporadic Creutzfeldt-Jakob disease: a case-control study. Lancet *353*, 693–697.
28. Collins, S., Boyd, A., Lee, J.S., Lewis, V., Fletcher, A., McLean, C.A., Law, M., Kaldor, J., Smith, M.J., and Masters, C.L. (2002). Creutzfeldt-Jakob disease in Australia 1970-1999. Neurology *59*, 1365–1371.
29. Windl, O., Giese, A., Schulz-Schaeffer, W., Zerr, I., Skworc, K., Arendt, S., Oberdieck, C., Bodemer, M., Poser, S., and Kretzschmar, H.A. (1999). Molecular genetics of human prion diseases in Germany. Hum. Genet. *105*, 244–252.
30. Grasbon-Frodl, E., Lorenz, H., Mann, U., Nitsch, R.M., Windl, O., and Kretzschmar, H.A. (2004). Loss of glycosylation associated with the T183A mutation in human prion disease. Acta Neuropathol. *108*, 476–484.
31. Zerr, I., Kallenberg, K., Summers, D.M., Romero, C., Taratuto, A., Heinemann, U., Breithaupt, M., Varges, D., Meissner, B., Ladogana, A., et al. (2009). Updated clinical diagnostic criteria for sporadic Creutzfeldt-Jakob disease. Brain *132*, 2659–2668.
32. Beck, J.A., Poulter, M., Campbell, T.A., Adamson, G., Uphill, J.B., Guerreiro, R., Jackson, G.S., Stevens, J.C., Manji, H., Collinge, J., and Mead, S. (2010). PRNP allelic series from 19 years of prion protein gene sequencing at the MRC Prion Unit. Hum. Mutat. *31*, E1551–E1563.
33. Geschwind, M.D., Haman, A., and Miller, B.L. (2007). Rapidly progressive dementia. Neurol. Clin. *25*, 783–807, vii.
34. Geschwind, M.D., Shu, H., Haman, A., Sejvar, J.J., and Miller, B.L. (2008). Rapidly progressive dementia. Ann. Neurol. *64*, 97–108.
35. Paterson, R.W., Torres-Chae, C.C., Kuo, A.L., Ando, T., Nguyen, E.A., Wong, K., DeArmond, S.J., Haman, A., Garcia, P., Johnson, D.Y., et al. (2012). Differential diagnosis of Jakob-Creutzfeldt disease. Arch. Neurol. *69*, 1578–1582.
36. Parchi, P., Giese, A., Capellari, S., Brown, P., Schulz-Schaeffer, W., Windl, O., Zerr, I., Budka, H., Kopp, N., Piccardo, P., et al. (1999). Classification of sporadic Creutzfeldt-Jakob disease based on molecular and phenotypic analysis of 300 subjects. Ann. Neurol. *46*, 224–233.
37. Rabinovici, G.D., Wang, P.N., Levin, J., Cook, L., Pravdin, M., Davis, J., DeArmond, S.J., Barbaro, N.M., Martindale, J., Miller, B.L., and Geschwind, M.D. (2006). First symptom in sporadic Creutzfeldt-Jakob disease. Neurology *66*, 286–287.
38. Squitieri, F., Sabbadini, G., Mandich, P., Gellera, C., Di Maria, E., Bellone, E., Castellotti, B., Nargi, E., de Grazia, U., Frontali, M., and Novelletto, A. (2000). Family and molecular data for a fine analysis of age at onset in Huntington disease. Am. J. Med. Genet. *95*, 366–373.
39. Visscher, P.M., Hill, W.G., and Wray, N.R. (2008). Heritability in the genomics era—concepts and misconceptions. Nat. Rev. Genet. *9*, 255–266.
40. Owen, J., Beck, J., Campbell, T., Adamson, G., Gorham, M., Thompson, A., Smithson, S., Rosser, E., Rudge, P., Collinge, J., et al. (2014). Predictive testing for inherited prion disease: report of 22 years experience. Eur. J. Hum. Genet. Published online April 9, 2014. http://dx.doi.org/10.1038/ejhg.2014.42.
41. Goizet, C., Lesca, G., and Dürr, A.; French Group for Presymptomatic Testing in Neurogenetic Disorders (2002). Presymptomatic testing in Huntington's disease and autosomal dominant cerebellar ataxias. Neurology *59*, 1330–1336.
42. Laccone, F., Engel, U., Holinski-Feder, E., Weigell-Weber, M., Marczinek, K., Nolte, D., Morris-Rosendahl, D.J., Zühlke, C., Fuchs, K., Weirich-Schwaiger, H., et al. (1999). DNA analysis of Huntington's disease: five years of experience in Germany, Austria, and Switzerland. Neurology *53*, 801–806.
43. Harper, P.S., Lim, C., and Craufurd, D. (2000). Ten years of presymptomatic testing for Huntington's disease: the experience of the UK Huntington's Disease Prediction Consortium. J. Med. Genet. *37*, 567–571.
44. Tassicker, R.J., Marshall, P.K., Liebeck, T.A., Keville, M.A., Singaram, B.M., and Richards, F.H. (2006). Predictive and prenatal testing for Huntington Disease in Australia: results and challenges encountered during a 10-year period (1994-2003). Clin. Genet. *70*, 480–489.
45. Morrison, P.J., Harding-Lester, S., and Bradley, A. (2011). Uptake of Huntington disease predictive testing in a complete population. Clin. Genet. *80*, 281–286.
46. Baker, H.E., Poulter, M., Crow, T.J., Frith, C.D., Lofthouse, R., and Ridley, R.M. (1991). Aminoacid polymorphism in human prion protein and age at death in inherited prion disease. Lancet *337*, 1286.
47. Kovács, G.G., Puopolo, M., Ladogana, A., Pocchiari, M., Budka, H., van Duijn, C., Collins, S.J., Boyd, A., Giulivi, A., Coulthart, M., et al.; EUROCJD (2005). Genetic prion disease: the EUROCJD experience. Hum. Genet. *118*, 166–174.
48. Gabizon, R., Rosenmann, H., Meiner, Z., Kahana, I., Kahana, E., Shugart, Y., Ott, J., and Prusiner, S.B. (1993). Mutation and polymorphism of the prion protein gene in Libyan Jews with Creutzfeldt-Jakob disease (CJD). Am. J. Hum. Genet. *53*, 828–835.
49. Ryman, D.C., Acosta-Baena, N., Aisen, P.S., Bird, T., Danek, A., Fox, N.C., Goate, A., Frommelt, P., Ghetti, B., Langbaum, J.B.S., et al.; Dominantly Inherited Alzheimer Network (2014). Symptom onset in autosomal dominant Alzheimer disease: a systematic review and meta-analysis. Neurology *83*, 253–260.
50. Bateman, R.J., Xiong, C., Benzinger, T.L.S., Fagan, A.M., Goate, A., Fox, N.C., Marcus, D.S., Cairns, N.J., Xie, X., Blazey, T.M., et al.; Dominantly Inherited Alzheimer Network (2012). Clinical and biomarker changes in dominantly inherited Alzheimer's disease. N. Engl. J. Med. *367*, 795–804.
51. Belay, E.D. (1999). Transmissible spongiform encephalopathies in humans. Annu. Rev. Microbiol. *53*, 283–314.
52. Xiao, X., Miravalle, L., Yuan, J., McGeehan, J., Dong, Z., Wyza, R., MacLennan, G.T., Golichowski, A.M., Kneale, G., King, N., et al. (2009). Failure to detect the presence of prions in the uterine and gestational tissues from a Gravida with Creutzfeldt-Jakob disease. Am. J. Pathol. *174*, 1602–1608.
53. Murray, K., Peters, J., Stellitano, L., Winstone, A.M., Verity, C., and Will, R.G. (2011). Is there evidence of vertical transmission of variant Creutzfeldt-Jakob disease? J. Neurol. Neurosurg. Psychiatry *82*, 729–731.
54. Hodge, S.E., and Wickramaratne, P. (1995). Statistical pitfalls in detecting age-of-onset anticipation: the role of correlation in studying anticipation and detecting ascertainment bias. Psychiatr. Genet. *5*, 43–47.

MEDICAL GENOMICS

Quantifying prion disease penetrance using large population control cohorts

Eric Vallabh Minikel,[1,2,3,4]* Sonia M. Vallabh,[1,3,4] Monkol Lek,[1,2] Karol Estrada,[1,2] Kaitlin E. Samocha,[1,2,3] J. Fah Sathirapongsasuti,[5] Cory Y. McLean,[5] Joyce Y. Tung,[5] Linda P. C. Yu,[5] Pierluigi Gambetti,[6] Janis Blevins,[6] Shulin Zhang,[7] Yvonne Cohen,[6] Wei Chen,[6] Masahito Yamada,[8] Tsuyoshi Hamaguchi,[8] Nobuo Sanjo,[9] Hidehiro Mizusawa,[10] Yosikazu Nakamura,[11] Tetsuyuki Kitamoto,[12] Steven J. Collins,[13] Alison Boyd,[13] Robert G. Will,[14] Richard Knight,[14] Claudia Ponto,[15] Inga Zerr,[15] Theo F. J. Kraus,[16] Sabina Eigenbrod,[16] Armin Giese,[16] Miguel Calero,[17] Jesús de Pedro-Cuesta,[17] Stéphane Haïk,[18,19] Jean-Louis Laplanche,[20] Elodie Bouaziz-Amar,[20] Jean-Philippe Brandel,[18,19] Sabina Capellari,[21,22] Piero Parchi,[21,22] Anna Poleggi,[23] Anna Ladogana,[23] Anne H. O'Donnell-Luria,[1,2,24] Konrad J. Karczewski,[1,2] Jamie L. Marshall,[1,2] Michael Boehnke,[25] Markku Laakso,[26] Karen L. Mohlke,[27] Anna Kähler,[28] Kimberly Chambert,[29] Steven McCarroll,[29] Patrick F. Sullivan,[27,28] Christina M. Hultman,[28] Shaun M. Purcell,[30] Pamela Sklar,[30] Sven J. van der Lee,[31] Annemieke Rozemuller,[32] Casper Jansen,[32] Albert Hofman,[31] Robert Kraaij,[33] Jeroen G. J. van Rooij,[33] M. Arfan Ikram,[31] André G. Uitterlinden,[31,33] Cornelia M. van Duijn,[31] Exome Aggregation Consortium (ExAC),† Mark J. Daly,[1,2] Daniel G. MacArthur[1,2]*

More than 100,000 genetic variants are reported to cause Mendelian disease in humans, but the penetrance—the probability that a carrier of the purported disease-causing genotype will indeed develop the disease—is generally unknown. We assess the impact of variants in the *prion protein* gene (*PRNP*) on the risk of prion disease by analyzing 16,025 prion disease cases, 60,706 population control exomes, and 531,575 individuals genotyped by 23andMe Inc. We show that missense variants in *PRNP* previously reported to be pathogenic are at least 30 times more common in the population than expected on the basis of genetic prion disease prevalence. Although some of this excess can be attributed to benign variants falsely assigned as pathogenic, other variants have genuine effects on disease susceptibility but confer lifetime risks ranging from <0.1 to ~100%. We also show that truncating variants in *PRNP* have position-dependent effects, with true loss-of-function alleles found in healthy older individuals, a finding that supports the safety of therapeutic suppression of prion protein expression.

INTRODUCTION

The study of pedigrees with Mendelian disease has been tremendously successful in identifying variants that contribute to severe inherited disorders (*1*–*3*). Causal variant discovery is enabled by selective ascertainment of affected individuals and especially of multiplex families. Although efficient from a gene discovery perspective, the resulting ascertainment bias confounds efforts to accurately estimate the penetrance—the probability that a carrier of the purported disease-causing genotype will indeed develop the disease—of disease-causing variants, with profound implications for genetic counseling (*4*–*7*). The development of large-scale genotyping and sequencing methods has recently made it tractable to perform unbiased assessments of penetrance in population controls. In several instances, such studies have suggested that previously reported Mendelian variants, as a class, are substantially less penetrant than had been believed (*8*–*11*). To date, however, all of these studies have been limited to relatively prevalent (>0.1%) diseases, and point estimates of the penetrance of individual variants have been limited to large copy number variations (*8*, *11*).

Here, we demonstrate the use of large-scale population data to infer the penetrance of variants in rare, dominant, monogenic disease using the example of prion diseases. These invariably fatal neurodegenerative disorders are caused by misfolding of the prion protein [PrP, the product of the *prion protein* gene (*PRNP*)] (*12*) and have an annual incidence of 1 to 2 cases per 1 million population (*13*). A small, albeit infamous, minority of cases (<1% in recent years) (*14*, *15*) are acquired through dietary or iatrogenic routes. Most of the cases (~85%) are defined as sporadic, occurring in individuals with two wild-type *PRNP* alleles and no known environmental exposures. Finally, ~15% of cases occur in individuals with rare, typically heterozygous, coding variants in *PRNP*, including missense variants, truncating variants, and octapeptide repeat insertions or deletions (table S1). Centralized ascertainment of cases by national surveillance centers (Materials and Methods) makes prion disease a good test case for using reference data sets to assess the penetrance of these variants.

PRNP was conclusively established as a dominant disease gene because a few variants exhibit clear Mendelian segregation with prion disease (*16*–*18*). Yet, ascertainment bias (*19*), low rates of predictive genetic testing (*20*), and frequent lack of family history (*21*, *22*) confound attempts to estimate penetrance by survival analysis (*19*, *23*–*26*). Meanwhile, the existence of nongenetic etiologies leaves doubt as to whether new variants are causal or coincidental.

A fully penetrant disease genotype should be no more common in the population than the disease that it causes. This observation allows us to leverage two large population control data sets to reevaluate the penetrance of reported disease variants in *PRNP*. The recently reported Exome Aggregation Consortium (ExAC) data set (*27*) contains variant calls on 60,706 unrelated individuals ascertained for case/control status

for various common diseases, without any ascertainment on neurodegenerative disease. 23andMe's database contains genotypes on 531,575 customers of its direct-to-consumer genotyping service who have opted to participate in the research, pruned to remove related individuals (first cousins or closer, Materials and Methods), preventing enrichment due to large families with prion disease.

RESULTS

Disease prevalence and variant frequency

We began by asking whether reportedly pathogenic variants are as rare as expected in these population control data sets. The proportion of people alive in the population today who harbor completely penetrant variants causal for prion disease can be approximated by the product of three numbers: the annual incidence of prion disease, the proportion of cases with such a genetic variant, and the life expectancy of individuals harboring these variants. On the basis of the upper bounds of these numbers (Fig. 1A), and assuming ascertainment is neutral with respect to neurodegenerative disease, we would expect no more than ~1.7 such individuals in the 60,706 exomes in the ExAC data set (*27*), and ~15 such individuals among the ~530,000 genotyped 23andMe customers who opted to participate in the research.

Through reviews (*28*–*30*) and PubMed searches, we identified 63 rare genetic variants reported to cause prion disease (table S2). We reviewed ExAC read-level evidence for every rare (<0.1% allele frequency) variant call in *PRNP* (Materials and Methods; tables S3 and S4) and found that 52 individuals in ExAC harbor reportedly pathogenic missense variants (Fig. 1B), at least a 30-fold excess over expectation if all such variants were fully penetrant. Similarly, in the 23andMe database, we observed a total of 141 alleles of 16 reportedly pathogenic variants genotyped on their platform (table S5).

Individuals with reportedly pathogenic *PRNP* variants did not cluster within any cohort within ExAC (table S6), arguing against enrichment resulting from comorbidity with a common disease ascertained for in exome sequencing studies. ExAC does include populations such as South Asians, in which prion disease is not closely surveilled, and we thus cannot rule out a higher incidence than that reported for developed countries, yet the individuals with reportedly pathogenic variants in either ExAC or 23andMe were of diverse inferred ancestry (tables S7 to S9). These individuals' ages were consistent with the overall ExAC age distribution (fig. S1) rather than being shifted toward younger ages, as would be expected if these individuals were depleted beyond middle age as a result of prion disease onset. We also examined ExAC genotypes at the M129V polymorphism, which affects risk, age of onset, disease duration, and phenotypic presentation in various types of prion disease (*31*–*33*). Codon 129 genotypes were consistent with population allele frequencies (table S7) rather than enriched for the lower-risk heterozygous genotype. Certain *PRNP* variants are associated with highly atypical phenotypes (*34*, *35*), which are mistakable for other dementias and might not be well ascertained by current surveillance efforts. Most of the variants found in our population control cohorts, however, have been reported in individuals with a classic, sporadic Creutzfeldt-Jakob disease phenotype (*22*, *28*, *30*, *36*–*38*), arguing that the discrepancy between observed and expected allele counts does not result primarily from an underappreciated prevalence of atypical prion disease.

Assessing penetrance

Having observed a large excess of reportedly pathogenic variants over expectation in two data sets and having excluded the most obvious confounders, we hypothesized that the unexpectedly high frequency of these variants in controls might arise from benign variants, low-risk variants, or both. We investigated which variants were responsible for the observed excess (Fig. 2). Variants with the strongest previous evidence of pathogenicity were absent from ExAC and cumulatively accounted for five or fewer alleles in 23andMe, consistent with the known rarity of genetic prion disease. Much of the excess allele frequency in population controls resulted instead from variants with very weak previous evidence of pathogenicity (Fig. 2 and Supplementary Discussion). For four variants observed in controls (V180I, R208H, V210I, and M232R), pathogenicity is controversial (*39*, *40*) or reduced penetrance has been suggested (*41*, *42*), but quantitative estimates of penetrance have never been produced, and the variants remain categorized as causes of genetic Creutzfeldt-Jakob disease (*21*, *22*). Although we cannot prove that any of the variants we observe in population controls is completely neutral, the list of reported pathogenic variants likely includes false positives. Indeed, the observation that 0.4% (236 of 60,706) of ExAC individuals harbor a rare (<0.1%) missense variant (table S4) suggests that ~4 of every 1000 sporadic prion disease cases will, by chance, harbor such a variant, which, in many cases, will be interpreted and reported as causal,

[1]Program in Medical and Population Genetics, Broad Institute of Massachusetts Institute of Technology (MIT) and Harvard, Cambridge, MA 02142, USA. [2]Analytical and Translational Genetics Unit, Massachusetts General Hospital, Boston, MA 02114, USA. [3]Program in Biological and Biomedical Sciences, Harvard Medical School, Boston, MA 02115, USA. [4]Prion Alliance, Cambridge, MA 02139, USA. [5]Research, 23andMe Inc., Mountain View, CA 94041, USA. [6]National Prion Disease Pathology Surveillance Center, Cleveland, OH 44106, USA. [7]University Hospitals Case Medical Center, Cleveland, OH 44106, USA. [8]Department of Neurology and Neurobiology of Aging, Kanazawa University Graduate School of Medical Sciences, Kanazawa 920-8640, Japan. [9]Department of Neurology and Neurological Science, Graduate School, Tokyo Medical and Dental University, Tokyo 113-8519, Japan. [10]National Center Hospital, National Center of Neurology and Psychiatry, Tokyo 187-8551, Japan. [11]Department of Public Health, Jichi Medical University, Shimotsuke 329-0498, Japan. [12]Department of Neurological Science, Tohoku University Graduate School of Medicine, Sendai 980-8575, Japan. [13]Australian National Creutzfeldt-Jakob Disease Registry, The University of Melbourne, Parkville, Victoria 3010, Australia. [14]National Creutzfeldt-Jakob Disease Research & Surveillance Unit, Western General Hospital, Edinburgh EH4 2XU, UK. [15]National Reference Center for the Surveillance of Human Transmissible Spongiform Encephalopathies, Georg-August-University, Goettingen 37073, Germany. [16]Center for Neuropathology and Prion Research (ZNP), Ludwig-Maximilians-University, Munich 81377, Germany. [17]Centro de Investigación Biomédica en Red de Enfermedades Neurodegenerativas, Instituto de Salud Carlos III, Madrid 28031, Spain. [18]INSERM U 1127, CNRS UMR 7225, Sorbonne Universités, Pierre and Marie Curie University Paris 06 UMR S 1127, Institut du Cerveau et de la Moelle Epinière, 75013 Paris, France. [19]Assistance Publique–Hôpitaux de Paris (AP-HP), Cellule Nationale de Référence des Maladies de Creutzfeldt-Jakob, Groupe Hospitalier Pitié-Salpêtrière, F-75013 Paris, France. [20]AP-HP, Service de Biochimie et Biologie Moléculaire, Hôpital Lariboisière, 75010 Paris, France. [21]Istituto di Ricovero e Cura a Carattere Scientifico, Institute of Neurological Sciences, Bologna 40123, Italy. [22]Department of Biomedical and Neuromotor Sciences, University of Bologna, Bologna 40126, Italy. [23]Department of Cell Biology and Neurosciences, Istituto Superiore di Sanità, Rome 00161, Italy. [24]Division of Genetics and Genomics, Boston Children's Hospital, Boston, MA 02115, USA. [25]Department of Biostatistics and Center for Statistical Genetics, University of Michigan School of Public Health, Ann Arbor, MI 48109, USA [26]Department of Medicine, University of Eastern Finland and Kuopio University Hospital, Kuopio 70210, Finland. [27]Department of Genetics, University of North Carolina School of Medicine, Chapel Hill, NC 27599, USA. [28]Karolinska Institutet, Stockholm SE-171 77, Sweden. [29]Stanley Center for Psychiatric Research, Broad Institute of MIT and Harvard, Cambridge, MA 02142, USA. [30]Icahn School of Medicine at Mount Sinai, New York, NY 10029, USA. [31]Department of Epidemiology, Erasmus Medical Center (MC), Rotterdam 3000 CA, Netherlands. [32]Dutch Surveillance Centre for Prion Diseases, Department of Pathology, University Medical Center, Utrecht 3584 CX, Netherlands. [33]Department of Internal Medicine, Erasmus MC, Rotterdam 3000 CA, Netherlands.
*Corresponding author. E-mail: eminikel@broadinstitute.org (E.V.M.); macarthur@atgu.mgh.harvard.edu (D.G.M.)
†A list of consortium members appears at the end of this paper.

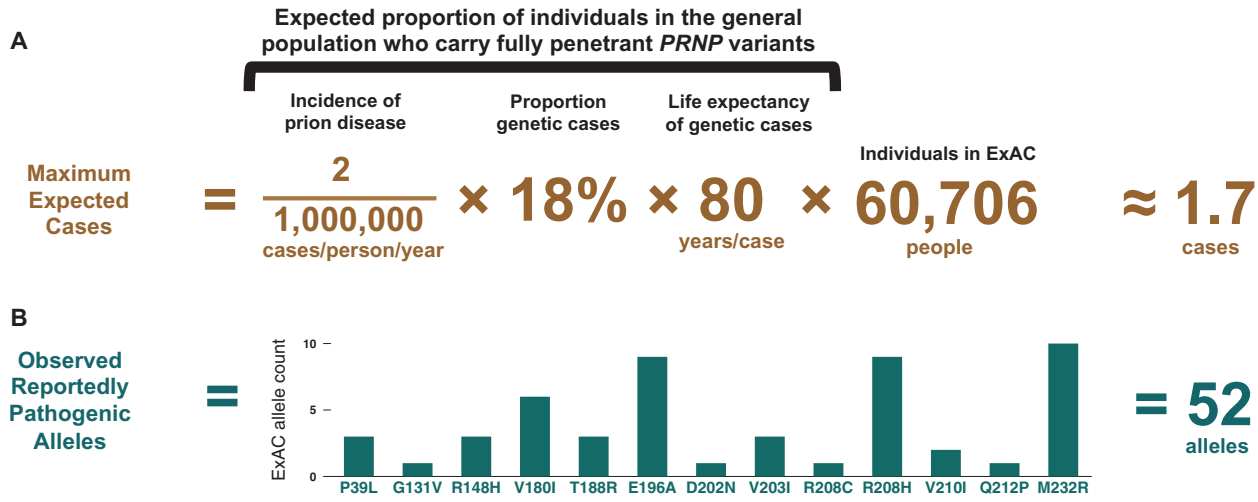

Fig. 1. Frequency of reportedly pathogenic *PRNP* variants: >30 times higher in controls than expected on the basis of disease incidence. (**A** and **B**) Reported prion disease incidence varies with the intensity of surveillance efforts (*13*), with an apparent upper bound of about two cases per million population per year (Materials and Methods). In our surveillance cohorts, 65% of cases underwent *PRNP* open reading frame sequencing, with 12% of all cases, or 18% of sequenced cases, having a rare variant (table S1), which is consistent with an oft-cited estimate that 15% of cases of Creutzfeldt-Jakob disease are familial (*43*). Genetic prion diseases typically strike in midlife, with mean age of onset for different variants ranging from 28 to 77 (table S10) (*22*, *91*); we accepted 80, a typical human life expectancy, as an upper bound for mean age of onset, and to be additionally conservative, we assumed that all individuals in the ExAC and 23andMe data sets were below any age of onset, even though both contain elderly individuals (fig. S1) (*92*). Thus, no more than ~29 people per million in the general population should harbor high-penetrance prion disease–causing variants; at most ~1.7 people in ExAC (A) and ~15 people in 23andMe would be expected to harbor such variants. Reportedly pathogenic variants were observed in 52 ExAC individuals (B) and on 141 alleles in the 23andMe database (table S5).

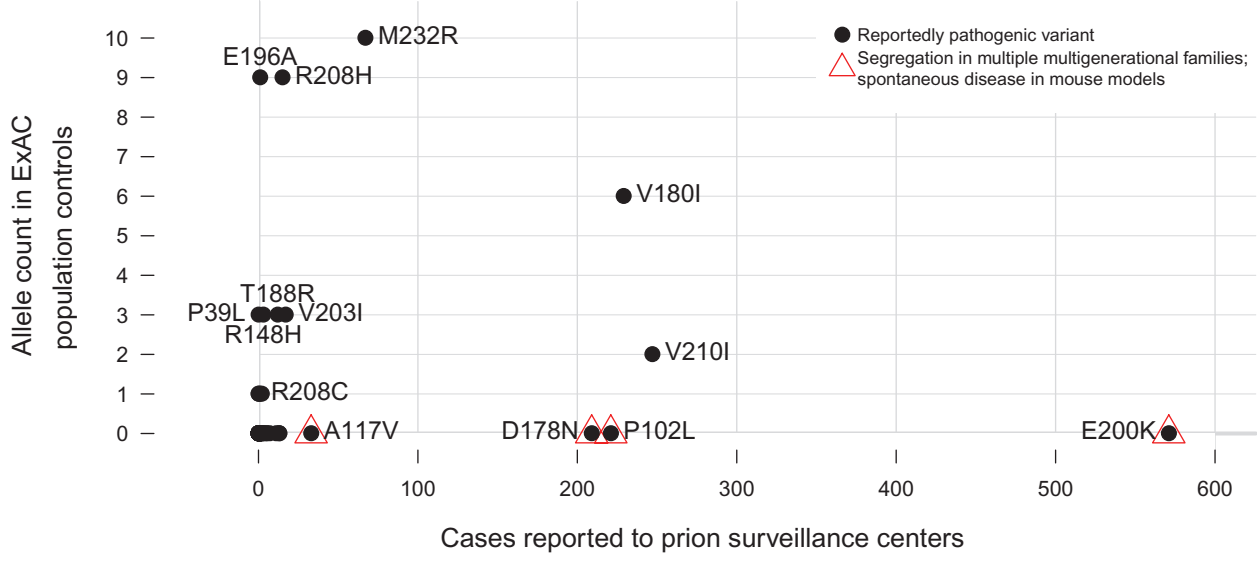

Fig. 2. Reportedly pathogenic *PRNP* variants: Mendelian, benign, and intermediate variants. Previous evidence of pathogenicity is extremely strong for four missense variants—P102L, A117V, D178N, and E200K—each of which has been observed to segregate with disease in multiple multigenerational families (*16*–*18*, *93*–*97*) and to cause spontaneous disease in mouse models (*98*–*103*). These account for >50% of genetic prion disease cases (table S1), yet are absent from ExAC (table S3) and collectively appear on five or fewer alleles in 23andMe's cohort (table S5), indicating allele frequencies sufficiently low to be consistent with the prevalence of genetic prion disease (Fig. 1). Conversely, the variants most common in controls and rare in cases had categorically weak previous evidence for pathogenicity. R208C (eight alleles in 23andMe) and P39L were observed in patients presenting clinically with other dementias, with prion disease suggested as an alternative diagnosis solely on the basis of finding a novel *PRNP* variant (*104*, *105*). E196A was originally reported in a single patient, with a sporadic Creutzfeldt-Jakob disease phenotype and no family history (*36*), and appeared in only 2 of 790 Chinese prion disease patients in a recent case series (*106*), consistent with the ~0.1% allele frequency among Chinese individuals in ExAC (tables S5 and S8). At least three variants (M232R, V180I, and V210I) occupy a space inconsistent either with neutrality or with complete penetrance (see main text and Fig. 3). R148H, T188R, V203I, R208H, and additional variants are discussed in Supplementary Discussion.

given the long-standing classification of *PRNP* as a Mendelian disease gene.

At least three variants (V180I, V210I, and M232R) failed to cluster with either the likely benign or likely Mendelian variants (Fig. 2). Because each of these three appeared primarily in one population (Japanese or Italian) in both cases and controls (tables S1, S5, S7, and S10), we compared allele frequencies in matched population groups. Each had an allele frequency in controls that was too high for a fully penetrant, dominant prion disease–causing variant and, yet, far lower than the corresponding allele frequency in prion disease cases (Fig. 3). Because we lacked genome-wide single-nucleotide polymorphism (SNP) data on cases, we were unable to directly correct for population stratification or substructure, whereby regional differences in allele frequency within Italy or Japan might affect our results. Geographical clusters of genetic prion disease have been recognized for decades (*26*, *43*, *44*). For example, nearly half of Italian prion disease cases with the V210I variant are concentrated within two regions of Italy (*45*), so any nonuniform geographic sampling in cases versus controls would add some uncertainty to our penetrance estimates.

Nonetheless, the magnitude of the enrichment of certain variants in cases over controls in our data sets makes population stratification an implausible explanation for the entire difference. For V210I to be neutral and, yet, appear with an allele frequency of 8.1% in Italian cases despite an apparent allele frequency of 0.02% in Italian controls, it would need to be fixed in a subpopulation that comprises 8% of Italy's populace. Under this scenario, the subpopulation would need to be virtually unsampled in any of our control cohorts, and the collection of V210I prion disease cases would be expected to contain many homozygotes. In reality, no cases have been reported as homozygous for this variant. Conversely, if V210I were fully penetrant, then family history would be positive in most cases, and the variant's appearance on 13 alleles in 23andMe (table S5) would indicate that this variant alone accounts for three times the known prevalence of genetic prion disease (Fig. 1A). Finally, if the low family history rate were caused by many de novo mutations, then V210I cases would be more uniformly distributed across populations (table S1). Similar arguments rule out V180I being either benign or Mendelian. M232R, though clearly not Mendelian, could still be benign because it exhibits only four- to sixfold enrichment in cases, an amount that might conceivably be explained by Japanese population substructure alone. However, because even common variants in *PRNP* affect prion disease risk with odds ratios of 3 or greater (*46*–*48*), it is plausible that M232R has a similar effect size; indeed, our data suggest that M232R having this effect on prion disease risk is a more likely scenario than M232R being neutral.

Satisfied that these three variants are likely neither benign nor Mendelian, we estimated lifetime risk in heterozygotes (Materials and Methods). The ~2 in 1 million annual incidence of prion disease translates into a baseline lifetime risk of ~1 in 5000 in the general population (Materials and Methods). Because prion diseases are so rare, even the massive enrichment of heterozygotes in cases (Fig. 3)—implying odds ratios on the order of 10 to 1000—corresponds to only low penetrance, with lifetime risks for M232R, V180I, and V210I estimated to be near 0.1, 1, and 10%, respectively. Although our estimates are imperfect because of population stratification, they accord well with family history rates (Fig. 3) and explain the unique space that these variants occupy in the plot of case versus control allele count (Fig. 2). These data indicate that *PRNP* missense variants occupy a risk continuum rather than a dichotomy of causal versus benign.

Protein-truncating variants

We asked whether the same was true of protein-truncating variants. *PRNP* has only one protein-coding exon, so premature stop codons are expected to result in truncated polypeptides rather than in nonsense-mediated decay. Prion diseases are known to arise from a gain

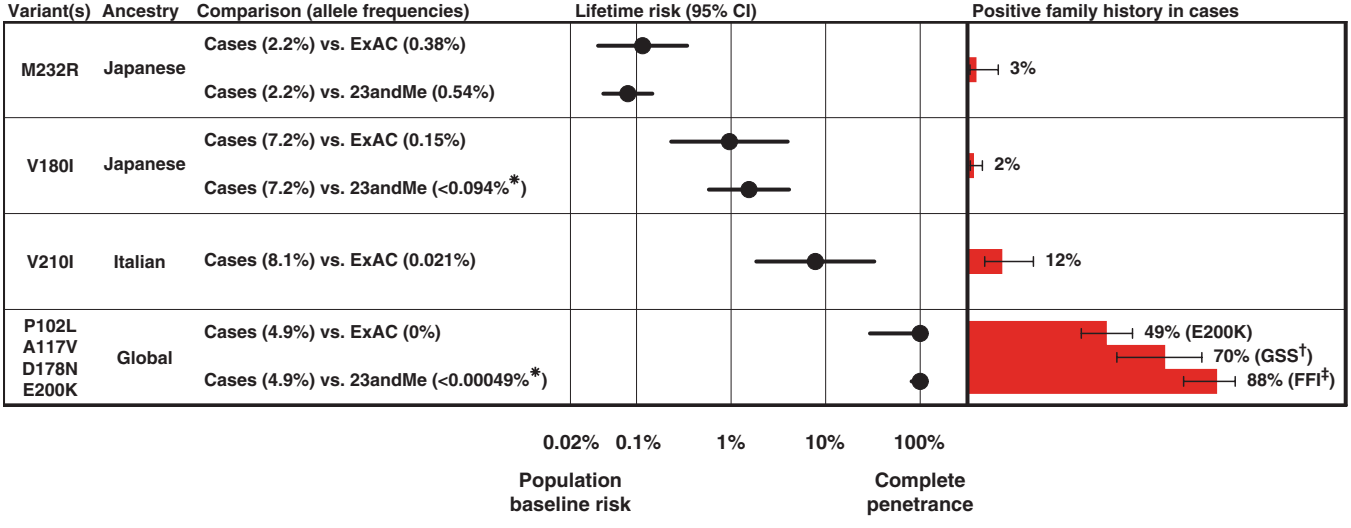

Fig. 3. Variants that confer intermediate amounts of lifetime risk. M232R, V180I, and V210I showed varying degrees of enrichment in cases over controls, indicating a weak to moderate increase in risk. Best estimates of lifetime risk in heterozygotes (Materials and Methods) range from ~0.08% for M232R to ~7.8% for V210I and correlate with the proportion of patients with a positive family history. Allele frequencies for P102L, A117V, D178N, and E200K were consistent with up to 100% penetrance, with CI including all reported estimates of E200K penetrance based on survival analysis, which range from ~60% to ~90% (*19*, *23*–*26*). Rates of family history of neurodegenerative disease in Japanese cases (table S10) and in European populations (*21*) are shown with Wilson binomial 95% CIs. *Based on allele counts rounded for privacy (Materials and Methods). †Gerstmann-Straussler-Scheinker (GSS) disease associated with variants P102L, A117V, and G131V. ‡Fatal familial insomnia (FFI) associated with a D178N (cis-129M) haplotype.

of function, because neurodegeneration is not seen in mice, cows, or goats that lack PrP (*49*–*52*), and the rate of prion disease progression is tightly correlated with PrP expression level (*53*). Yet, heterozygous C-terminal (residue ≥145) truncating variants are known to cause prion disease, sometimes with peripheral amyloidosis (*34*). Some of these patients also experience sensorimotor neuropathy phenotypically similar to that present in homozygous, but not heterozygous, PrP knockout mice (*54*); this phenotype has been attributed to amyloid infiltration of peripheral nerves, rather than loss of PrP function (*34*).

We identified heterozygous N-terminal (residue ≤131) truncating variants in four ExAC individuals and were able to obtain Sanger validation (fig. S2) and limited phenotype data (table S11) for three. These individuals were free of overt neurological disease at ages 79, 73, and 52, and report no personal or family history of neurodegeneration or peripheral neuropathy. Therefore, the pathogenicity of protein-truncating variants appears to be dictated by position within PrP's amino acid sequence (Fig. 4). Observing three *PRNP* nonsense variants in ExAC was consistent with the expected number (~3.9) based on mutation rates once we adjusted our model (*55*) to exclude codons ≥145, where truncations cause a dominant gain-of-function disease. Thus, we see no evidence that *PRNP* is constrained against truncation in its N terminus. This lack of any evidence of purifying selection against N-terminal truncating variants, combined with the lack of any obvious phenotype in individuals harboring these variants, suggests that heterozygous loss of PrP function is tolerated.

DISCUSSION

More than 100,000 genetic variants have been reported to cause Mendelian disease in humans (*56*, *57*). Many such reports do not meet current standards for assertions of pathogenicity (*58*, *59*), and if all such reports were believed, the cumulative frequency of these variants in the population would imply that most people have a genetic disease (*27*). It is generally unclear how much of the excess burden of purported disease variants in the population results from benign variants falsely associated and how much results from variants with genuine association but incomplete penetrance.

Here, we leveraged newly available large genomic reference data sets to reevaluate reported disease associations in a dominant disease gene, *PRNP*. We identify some missense variants as likely benign and show that others span a spectrum from <0.1 to ~100% penetrance. Our analyses provide quantitative estimates of lifetime risk for hundreds of asymptomatic individuals who have inherited incompletely penetrant *PRNP* variants.

Available data sets are only now approaching the size and quality required for such analyses, resulting in limitations for our study. The confidence intervals (CIs) on our lifetime risk estimates span more than an order of magnitude, and our inability to perfectly control for population stratification injects additional uncertainty. We have been unable to reclassify those *PRNP* variants that are very rare both in cases and in controls (Supplementary Discussion). We have avoided analysis of large insertions that are poorly called with short sequencing reads, although we note that existing literature on these insertions is consistent with a spectrum of penetrance similar to the spectrum that we observe for missense variants (*28*, *32*). Penetrance estimation in Mendelian disease will be improved by the collection of larger case series, particularly with genome-wide SNP data to allow more accurate population matching. This, coupled with continued large-scale population control sequencing and genotyping efforts, should reveal whether the dramatic variation in penetrance that we observe here is a more general feature of dominant disease genes.

Because PrP is required for prion pathogenesis and reduction in gene dosage slows disease progression (*53*, *60*–*62*), several groups have sought to therapeutically reduce PrP expression using RNA interference (*63*–*65*), antisense oligonucleotides (*66*), or small molecules (*67*, *68*). Our discovery of heterozygous loss-of-function variants in three healthy older humans provides the first human genetic data regarding the effects of a 50% reduction in gene dosage for *PRNP*. Both the number

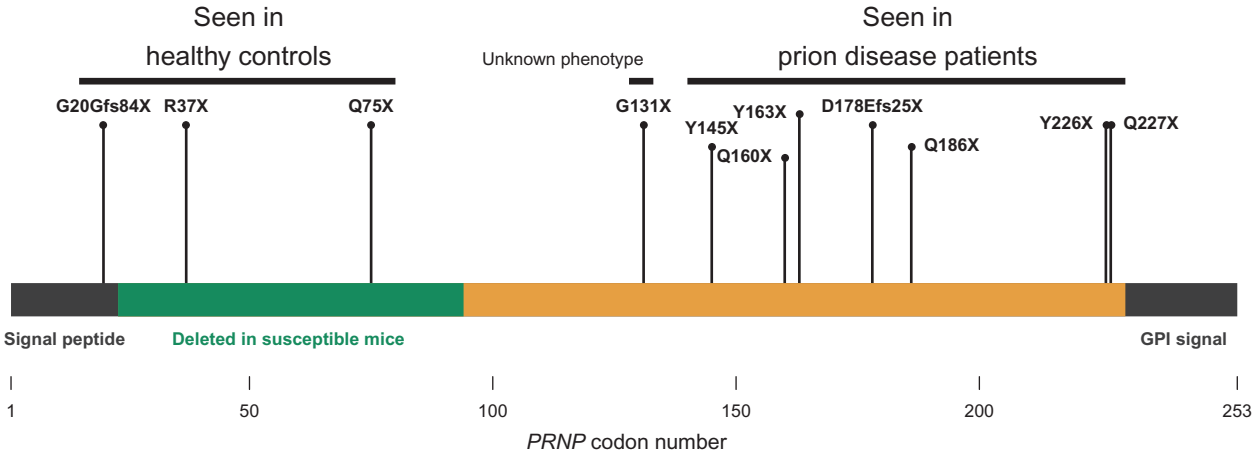

Fig. 4. Position-dependent effects of truncating variants in the human prion protein. Truncating variants reported in prion disease cases in the literature (table S2) and in our cohorts (table S1) cluster exclusively in the C-terminal region (residue ≥145), whereas truncating variants in ExAC are more N-terminal (residue ≤131). The ortholog of each residue from 23 to 94 is deleted in at least one prion-susceptible transgenic mouse line (*107*). C-terminal truncations abolish PrP's glycosylphosphatidylinositol (GPI) anchor but leave most of the protein intact, a combination that mediates gain of function through mislocalization, which causes this normally cell surface–anchored protein to be secreted. Consistent with this model of pathogenicity, mice that express full-length secreted PrP develop fatal and transmissible prion disease (*108*, *109*). By contrast, the N-terminal truncating variants that we observed retain only residues dispensable for prion propagation and are likely to cause a total loss of protein function.

of individuals and the depth of available phenotype data are limited, and lifelong heterozygous inactivation of a gene is an imperfect model of the effects of pharmacological depletion of the gene product. With those limitations, our data provide preliminary evidence that a reduction in *PRNP* dosage, if achievable in patients, is likely to be tolerated. Increasingly large control sequencing data sets will soon enable researchers to test whether the same is true of other genes currently being targeted in substrate-reduction therapeutic approaches for other protein-folding disorders. Together, our findings highlight the value of large reference data sets of human genetic variation for informing both genetic counseling and therapeutic strategy.

MATERIALS AND METHODS

Study design

We sought to estimate the penetrance of variants reported to cause genetic prion disease. We reasoned that fully penetrant variants should not be any more common in the general population than genetic prion disease is, and that by comparing allele frequencies in cases versus population controls, we could estimate penetrance for individual variants. This approach does not require controls that are certified to be free of prion disease, but instead only requires that controls not be enriched for prion disease. We carried out a retrospective analysis of existing data from three sources (prion surveillance centers, ExAC, and 23andMe research participants), which are described in detail below.

Prion disease case series

Prion disease is considered a notifiable diagnosis in most developed countries, with mandatory reporting of all suspect cases to a centralized surveillance center. Surveillance was carried out broadly according to established guidelines (*69*, *70*), with specifics as described previously for Australia (*71*), France (*72*), Germany (*73*–*75*), Italy (*76*), Japan (*22*), and the Netherlands (*77*). Sanger sequencing of the *PRNP* open reading frame was performed as described (*78*). We included only prion disease cases classified as definite (autopsy-confirmed) or probable (according to published guidelines) (*70*). Criteria for genetic testing vary between countries and over the years of data collection, with testing offered only on indication of family history in some times and places, and testing of all suspect cases with tissue available in other instances. Summary statistics on the total number and proportion of cases sequenced are presented in table S1.

Exome sequencing and analysis

The ascertainment, sequencing, and joint calling of the ExAC data set have been described previously (*27*). We extracted all rare (<0.1%) coding variant calls in *PRNP* with genotype quality (GQ) ≥10, alternate allele depth (AD) ≥3, and alternate allele balance (AB) ≥20%. Read-level evidence was visualized using Integrative Genomics Viewer (IGV) (*79*) for manual review. Because most ExAC exomes were sequenced with 76–base pair (bp) reads and the *PRNP* octapeptide repeat region (codons 50 to 90 inclusive) is 123 bp long, it was impossible to determine whether genotype calls in this region were correct, and they were not considered further. After review of IGV screenshots, 87% of genotype calls were judged to be correct and were included in table S3. Of the genotype calls judged to be correct, 99% had GQ ≥95, 99% had AB between 30 and 70%, and 97% had AD ≥10. All participants provided informed consent for exome sequencing and analysis. The ExAC's aggregation and release of exome data have been approved by the Partners Healthcare Institutional Research Board (2013P001339). ExAC data have been publicly released at http://exac.broadinstitute.org, and IGV screenshots of the rare *PRNP* variants deemed to be genuine and included in this study are available at https://github.com/ericminikel/prnp_penetrance/tree/master/supplement/igv.

23andMe research participants and genotyping

Participants were drawn from the customer base of 23andMe Inc., a personal genetics company (accessed 6 February 2015). All participants provided informed consent under a protocol approved by an external Association for the Accreditation of Human Research Protection Programs–accredited institutional review board, Ethical & Independent Review Services. DNA extraction and genotyping were performed on saliva samples by the National Genetics Institute, a Clinical Laboratory Improvement Amendments–licensed clinical laboratory and a subsidiary of Laboratory Corporation of America. Samples were genotyped on one of four Illumina platforms (V1 to V4) as described previously (*80*). Of the *PRNP* SNPs considered, 2 (P105L and E200K) were genotyped on all four platforms, whereas the other 14 were genotyped only on V3 and V4, resulting in differing numbers of total samples genotyped (table S5). Genotypes were called with Illumina GenomeStudio. A 98.5% call rate was required for all samples. As with all 23andMe research participants, individuals whose genotyping analyses failed to reach the desired call rate repeatedly were recontacted to provide additional samples. A maximal set of unrelated individuals was chosen on the basis of segmental identity-by-descent (IBD) estimation (*81*). Individuals were defined as related if they shared more than 700-centimorgan IBD (about the minimal expected sharing between first cousins). Allele counts between one and five were rounded up to five to protect individual privacy (table S5). Rounding down to one instead would raise our estimates of penetrance for V180I to 7.7% (95% CI, 1.2 to 50%) and for P102L, A117V, D178N, and E200K collectively to 100% (95% CI, 100 to 100%), but the CI would still overlap those based on ExAC allele frequencies, and the overall conclusions of our study would remain unchanged.

23andMe ancestry composition

Ancestral origins of chromosomal segments were assigned on a continental level (European, Latino, African, and East Asian) and on a country level (Japanese) as described by Durand *et al.* (*82*). Briefly, after phasing genotypes using an out-of-sample implementation of the Beagle algorithm (*83*), a string kernel support vector machine classifier assigns tentative ancestry labels to local genomic regions. Then, an autoregressive pair hidden Markov model was used to simultaneously correct phasing errors and produce reconciled local ancestry estimates and confidence scores based on the initial assignment. Finally, isotonic regression models were used to recalibrate the confidence estimates.

Europeans and East Asians were defined as individuals with more than 97% of chromosomal segments predicted as being from the respective ancestries. Because African Americans and Latinos are highly admixed, no single threshold of genome-wide ancestry is sufficient to distinguish them. However, segment length distributions of European, African, and Native American ancestries are different between African Americans and Latinos, because of the distinct admixture timing in the two ethnic groups. Thus, a logistic classifier based on segment length of European, African, and Native American ancestries was used to distinguish between African Americans and Latinos.

At the country level, individuals were classified as Japanese based on the fraction of the respective local ancestry using a threshold of 90% for classifying Japanese ancestry. This threshold is based on the average fraction of local ancestry in the reference population (23andMe research participants with all four grandparents from the reference country): 94% (5% SD, $n = 533$) for Japanese. Using the same approach, we were unable to obtain a confident set of Italian individuals for analysis of V210I because of extensive admixture. 23andMe research participants with all four grandparents from Italy only have 66% (18% SD, $n = 2090$) Italian ancestry, and only ~60 participants have >90% Italian ancestry.

ExAC ancestry inference

We computed 10 principal components based on ~5800 common SNPs as described (*27*, *84*). A centroid in eigenvalue-weighted principal component space was generated for each HapMap population based on 1000 Genomes individuals in ExAC. The remaining individuals in ExAC were assigned to the HapMap population with the nearest centroid according to eigenvalue-weighted Euclidean distance. Ancestries of all individuals, including those with reportedly pathogenic variants, are summarized in tables S7 and S8.

Prion disease incidence and baseline risk

The reported incidence of prion disease varies between countries and between years, with much of the variability explained by the intensity of surveillance, as measured by the number of cases referred to national surveillance centers (*13*). Rates of about one case per million population per year have been reported, for instance, in the United States (*85*) and in Japan (*22*); however, the countries with the most intense surveillance (greatest number of referrals per capita), such as France and Austria, observe incidence figures as high as two cases per million population per year (*13*). Only in small countries where the statistics are dominated by a particular genetic prion disease founder mutation, such as Israel and Slovakia (*23*, *26*), has an incidence higher than two per million been consistently observed (*86*). We therefore accepted two cases per million as an upper bound for the true incidence of prion disease. Assuming an all-causes death rate of ~10 per 1000 annually (*87*), this incidence corresponds to prion disease accounting for ~0.02% of all deaths, which we accepted as the baseline disease risk in the general population.

Lifetime risk estimation

By Bayes' theorem, the probability of disease given a genotype [penetrance or lifetime risk, P(D|G)] is equal to the proportion of individuals with the disease who have the genotype [genotype frequency in cases, P(G|D)] times the prevalence of the disease [baseline lifetime risk in the general population, P(D)], divided by the frequency of the genotype in the general population [here, population control allele frequency, P(G)]. The use of this formula to estimate disease risk dates back at least to Cornfield's estimation of the probability of lung cancer in smokers (*88*), with later contributions by Woolf (*89*) and a synthesis by Li (*90*) with application to genetics.

We used an allelic rather than a genotypic model, such that lifetime risk in an individual with one allele is equal to case allele frequency (based on the number of prion disease cases that underwent *PRNP* sequencing) times baseline risk divided by population control allele frequency, $P(D|A) = P(A|D) \times P(D)/P(A)$. Note that we assumed that our population control data sets include individuals who will later die of prion disease, thus enabling direct use of the ExAC and 23andMe allele frequencies as the denominator P(A). Following Kirov *et al.* (*11*), we computed Wilson 95% CI on the binomial proportions P(A|D) and P(A), and calculated the upper bound of the 95% CI for penetrance using the upper bound on case allele frequency and the lower bound on population control allele frequency, and vice versa for the lower bound on penetrance.

Statistical analysis and source code availability

Error bars in Fig. 3 are as described in the previous section. Data processing, analysis, and figure generation used custom scripts written in Python 2.7.6 and R 3.1.2. These scripts, along with vector graphics of all figures and tab-delimited text versions of all supplementary tables, are available online at https://github.com/ericminikel/prnp_penetrance and are sufficient to reproduce the figures and the analyses described in this paper.

SUPPLEMENTARY MATERIALS

www.sciencetranslationalmedicine.org/cgi/content/full/8/322/322ra9/DC1

Discussion

Table S1. Allele counts of rare *PRNP* variants in 16,025 definite and probable prion disease cases in nine countries.

Table S2. Rare *PRNP* variants reported in peer-reviewed literature to cause prion disease.

Table S3. Allele counts of rare *PRNP* variants in 60,706 individuals in ExAC.

Table S4. Summary of rare *PRNP* variants by functional class in ExAC.

Table S5. Allele counts of 16 reportedly pathogenic *PRNP* variants in >500,000 23andMe research participants.

Table S6. Phenotypes investigated in studies in which ExAC individuals with reportedly pathogenic PRNP variants were ascertained.

Table S7. Inferred ancestry and codon 129 genotypes of ExAC individuals with reportedly pathogenic variants.

Table S8. Inferred ancestry of all ExAC individuals.

Table S9. Inferred ancestry of 23andMe research participants.

Table S10. Details of Japanese prion disease cases.

Table S11. Phenotypes of individuals with N-terminal PrP-truncating variants.

Fig. S1. Age of ExAC individuals with reportedly pathogenic *PRNP* variants versus all individuals in ExAC.

Fig. S2. Sanger sequencing results for individuals with N-terminal–truncating variants.

References (*110*–*179*)

REFERENCES AND NOTES

1. L. R. Brunham, M. R. Hayden, Hunting human disease genes: Lessons from the past, challenges for the future. *Hum. Genet.* **132**, 603–617 (2013).
2. J. Amberger, C. Bocchini, A. Hamosh, A new face and new challenges for Online Mendelian Inheritance in Man (OMIM®). *Hum. Mutat.* **32**, 564–567 (2011).
3. J. X. Chong, K. J. Buckingham, S. N. Jhangiani, C. Boehm, N. Sobreira, J. D. Smith, T. M. Harrell, M. J. McMillin, W. Wiszniewski, T. Gambin, Z. H. Coban Akdemir, K. Doheny, A. F. Scott, D. Avramopoulos, A. Chakravarti, J. Hoover-Fong, D. Mathews, P. D. Witmer, H. Ling, K. Hetrick, L. Watkins, K. E. Patterson, F. Reinier, E. Blue, D. Muzny, M. Kircher, K. Bilguvar, F. López-Giráldez, V. R. Sutton, H. K. Tabor, S. M. Leal, M. Gunel, S. Mane, R. A. Gibbs, E. Boerwinkle, A. Hamosh, J. Shendure, J. R. Lupski, R. P. Lifton, D. Valle, D. A. Nickerson, Centers for Mendelian Genomics, M. J. Bamshad, The genetic basis of Mendelian phenotypes: Discoveries, challenges, and opportunities. *Am. J. Hum. Genet.* **97**, 199–215 (2015).
4. J. F. Crow, Hardy, Weinberg and language impediments. *Genetics* **152**, 821–825 (1999).
5. C. B. Begg, On the use of familial aggregation in population-based case probands for calculating penetrance. *J. Natl. Cancer Inst.* **94**, 1221–1226 (2002).
6. S. Goldwurm, M. Zini, L. Mariani, S. Tesei, R. Miceli, F. Sironi, M. Clementi, V. Bonifati, G. Pezzoli, Evaluation of *LRRK2* G2019S penetrance: Relevance for genetic counseling in Parkinson disease. *Neurology* **68**, 1141–1143 (2007).
7. D. N. Cooper, M. Krawczak, C. Polychronakos, C. Tyler-Smith, H. Kehrer-Sawatzki, Where genotype is not predictive of phenotype: Towards an understanding of the molecular basis of reduced penetrance in human inherited disease. *Hum. Genet.* **132**, 1077–1130 (2013).

8. G. M. Cooper, B. P. Coe, S. Girirajan, J. A. Rosenfeld, T. H. Vu, C. Baker, C. Williams, H. Stalker, R. Hamid, V. Hannig, H. Abdel-Hamid, P. Bader, E. McCracken, D. Niyazov, K. Leppig, H. Thiese, M. Hummel, N. Alexander, J. Gorski, J. Kussmann, V. Shashi, K. Johnson, C. Rehder, B. C. Ballif, L. G. Shaffer, E. E. Eichler, A copy number variation morbidity map of developmental delay. *Nat. Genet.* **43**, 838–846 (2011).
9. A. G. Bick, J. Flannick, K. Ito, S. Cheng, R. S. Vasan, M. G. Parfenov, D. S. Herman, S. R. DePalma, N. Gupta, S. B. Gabriel, B. H. Funke, H. L. Rehm, E. J. Benjamin, J. Aragam, H. A. Taylor Jr., E. R. Fox, C. Newton-Cheh, S. Kathiresan, C. J. O'Donnell, J. G. Wilson, D. M. Altshuler, J. N. Hirschhorn, J. G. Seidman, C. Seidman, Burden of rare sarcomere gene variants in the Framingham and Jackson Heart Study cohorts. *Am. J. Hum. Genet.* **91**, 513–519 (2012).
10. J. Flannick, N. L. Beer, A. G. Bick, V. Agarwala, J. Molnes, N. Gupta, N. P. Burtt, J. C. Florez, J. B. Meigs, H. Taylor, V. Lyssenko, H. Irgens, E. Fox, F. Burslem, S. Johansson, M. J. Brosnan, J. K. Trimmer, C. Newton-Cheh, T. Tuomi, A. Molven, J. G. Wilson, C. J. O'Donnell, S. Kathiresan, J. N. Hirschhorn, P. R. Njølstad, T. Rolph, J. G. Seidman, S. Gabriel, D. R. Cox, C. E. Seidman, L. Groop, D. Altshuler, Assessing the phenotypic effects in the general population of rare variants in genes for a dominant Mendelian form of diabetes. *Nat. Genet.* **45**, 1380–1385 (2013).
11. G. Kirov, E. Rees, J. T. R. Walters, V. Escott-Price, L. Georgieva, A. L. Richards, K. D. Chambert, G. Davies, S. E. Legge, J. L. Moran, S. A. McCarroll, M. C. O'Donovan, M. J. Owen, The penetrance of copy number variations for schizophrenia and developmental delay. *Biol. Psychiatry* **75**, 378–385 (2014).
12. S. B. Prusiner, Prions. *Proc. Natl. Acad. Sci. U.S.A.* **95**, 13363–13383 (1998).
13. G. M. J. A. Klug, H. Wand, M. Simpson, A. Boyd, M. Law, C. L. Masters, R. Matěj, R. Howley, M. Farrell, M. Breithaupt, I. Zerr, C. van Duijn, C. Ibrahim-Verbaas, J. Mackenzie, R. G. Will, J.-P. Brandel, A. Alperovitch, H. Budka, G. G. Kovacs, G. H. Jansen, M. Coulthard, S. J. Collins, Intensity of human prion disease surveillance predicts observed disease incidence. *J. Neurol. Neurosurg. Psychiatry* **84**, 1372–1377 (2013).
14. U.S. National Prion Disease Pathology Surveillance Center, Centers for Disease Control and Prevention, CJD (Creutzfeldt-Jakob Disease, Classic); http://web.archive.org/web/20150202162606/http://www.cdc.gov/ncidod/dvrd/cjd/.
15. U.K. National Creutzfeldt-Jakob Disease Research and Surveillance Unit, Creutzfeldt-Jakob disease in the UK; http://web.archive.org/web/20150330211505/http://www.cjd.ed.ac.uk/documents/figs.pdf.
16. K. Hsiao, H. F. Baker, T. J. Crow, M. Poulter, F. Owen, J. D. Terwilliger, D. Westaway, J. Ott, S. B. Prusiner, Linkage of a prion protein missense variant to Gerstmann-Sträussler syndrome. *Nature* **338**, 342–345 (1989).
17. K. Hsiao, Z. Meiner, E. Kahana, C. Cass, I. Kahana, D. Avrahami, G. Scarlato, O. Abramsky, S. B. Prusiner, R. Gabizon, Mutation of the prion protein in Libyan Jews with Creutzfeldt–Jakob disease. *N. Engl. J. Med.* **324**, 1091–1097 (1991).
18. R. Medori, H.-J. Tritschler, A. LeBlanc, F. Villare, V. Manetto, H. Y. Chen, R. Xue, S. Leal, P. Montagna, P. Cortelli, P. Tinuper, P. Avoni, M. Mochi, A. Baruzzi, J. J. Hauw, J. Ott, E. Lugaresi, L. Autilio-Gambetti, P. Gambetti, Fatal familial insomnia, a prion disease with a mutation at codon 178 of the prion protein gene. *N. Engl. J. Med.* **326**, 444–449 (1992).
19. E. V. Minikel, I. Zerr, S. J. Collins, C. Ponto, A. Boyd, G. Klug, A. Karch, J. Kenny, J. Collinge, L. T. Takada, S. Forner, J. C. Fong, S. Mead, M. D. Geschwind, Ascertainment bias causes false signal of anticipation in genetic prion disease. *Am. J. Hum. Genet.* **95**, 371–382 (2014).
20. J. Owen, J. Beck, T. Campbell, G. Adamson, M. Gorham, A. Thompson, S. Smithson, E. Rosser, P. Rudge, J. Collinge, S. Mead, Predictive testing for inherited prion disease: Report of 22 years experience. *Eur. J. Hum. Genet.* **22**, 1351–1356 (2014).
21. G. G. Kovács, M. Puopolo, A. Ladogana, M. Pocchiari, H. Budka, C. van Duijn, S. J. Collins, A. Boyd, A. Giulivi, M. Coulthart, N. Delasnerie-Laupretre, J. P. Brandel, I. Zerr, H. A. Kretzschmar, J. de Pedro-Cuesta, M. Calero-Lara, M. Glatzel, A. Aguzzi, M. Bishop, R. Knight, G. Belay, R. Will, E. Mitrova, Genetic prion disease: The EUROCJD experience. *Hum. Genet.* **118**, 166–174 (2005).
22. I. Nozaki, T. Hamaguchi, N. Sanjo, M. Noguchi-Shinohara, K. Sakai, Y. Nakamura, T. Sato, T. Kitamoto, H. Mizusawa, F. Moriwaka, Y. Shiga, Y. Kuroiwa, M. Nishizawa, S. Kuzuhara, T. Inuzuka, M. Takeda, S. Kuroda, K. Abe, H. Murai, S. Murayama, J. Tateishi, I. Takumi, S. Shirabe, M. Harada, A. Sadakane, M. Yamada, Prospective 10-year surveillance of human prion diseases in Japan. *Brain* **133**, 3043–3057 (2010).
23. J. Chapman, J. Ben-Israel, Y. Goldhammer, A. D. Korczyn, The risk of developing Creutzfeldt-Jakob disease in subjects with the PRNP gene codon 200 point mutation. *Neurology* **44**, 1683–1686 (1994).
24. S. Spudich, J. A. Mastrianni, M. Wrensch, R. Gabizon, Z. Meiner, I. Kahana, H. Rosenmann, E. Kahana, S. B. Prusiner, Complete penetrance of Creutzfeldt-Jakob disease in Libyan Jews carrying the E200K mutation in the prion protein gene. *Mol. Med.* **1**, 607–613 (1995).
25. M. D'Alessandro, R. Petraroli, A. Ladogana, M. Pocchiari, High incidence of Creutzfeldt-Jakob disease in rural Calabria, Italy. *Lancet* **352**, 1989–1990 (1998).
26. E. Mitrová, G. Belay, Creutzfeldt-Jakob disease with E200K mutation in Slovakia: Characterization and development. *Acta Virol.* **46**, 31–39 (2002).
27. Exome Aggregation Consortium, M. Lek, K. Karczewski, E. Minikel, K. Samocha, E. Banks, T. Fennell, A. O'Donnell-Luria, J. Ware, A. Hill, B. Cummings, T. Tukiainen, D. Birnbaum, J. Kosmicki, L. Duncan, K. Estrada, F. Zhao, J. Zou, E. Pierce-Hoffman, D. Cooper, M. DePristo, R. Do, J. Flannick, M. Fromer, L. Gauthier, J. Goldstein, N. Gupta, D. Howrigan, A. Kiezun, M. Kurki, A. L. Moonshine, P. Natarajan, L. Orozco, G. Peloso, R. Poplin, M. Rivas, V. Ruano-Rubio, D. Ruderfer, K. Shakir, P. Stenson, C. Stevens, B. Thomas, G. Tiao, M. Tusie-Luna, B. Weisburd, H.-H. Won, D. Yu, D. Altshuler, D. Ardissino, M. Boehnke, J. Danesh, E. Roberto, J. Florez, S. Gabriel, G. Getz, C. Hultman, S. Kathiresan, M. Laakso, S. McCarroll, M. McCarthy, D. McGovern, R. McPherson, B. Neale, A. Palotie, S. Purcell, D. Saleheen, J. Scharf, P. Sklar, S. Patrick, J. Tuomilehto, H. Watkins, J. Wilson, M. Daly, D. MacArthur, Analysis of protein-coding genetic variation in 60,706 humans. *bioRxiv* 10.1101/030338 (2015).
28. Q. Kong, W. K. Surewicz, R. B. Petersen, S. G. Chen, P. Gambetti, P. Parchi, S. Capellari, L. Goldfarb, P. Montagna, E. Lugaresi, P. Piccardo, B. Ghetti, in *Prion Biology and Diseases* (Cold Spring Harbor Laboratory Press, Cold Spring Harbor, 2004).
29. J. A. Beck, M. Poulter, T. A. Campbell, G. Adamson, J. B. Uphill, R. Guerreiro, G. S. Jackson, J. C. Stevens, H. Manji, J. Collinge, S. Mead, PRNP allelic series from 19 years of prion protein gene sequencing at the MRC prion unit. *Hum. Mutat.* **31**, E1551–E1563 (2010).
30. J. A. Mastrianni, The genetics of prion diseases. *Genet. Med.* **12**, 187–195 (2010).
31. M. S. Palmer, A. J. Dryden, J. T. Hughes, J. Collinge, Homozygous prion protein genotype predisposes to sporadic Creutzfeldt–Jakob disease. *Nature* **352**, 340–342 (1991).
32. S. Mead, Prion disease genetics. *Eur. J. Hum. Genet.* **14**, 273–281 (2006).
33. S. Capellari, R. Strammiello, D. Saverioni, H. Kretzschmar, P. Parchi, Genetic Creutzfeldt–Jakob disease and fatal familial insomnia: Insights into phenotypic variability and disease pathogenesis. *Acta Neuropathol.* **121**, 21–37 (2011).
34. S. Mead, M. M. Reilly, A new prion disease: Relationship with central and peripheral amyloidoses. *Nat. Rev. Neurol.* **11**, 90–97 (2015).
35. R. C. Moore, F. Xiang, J. Monaghan, D. Han, Z. Zhang, L. Edström, M. Anvret, S. B. Prusiner, Huntington disease phenocopy is a familial prion disease. *Am. J. Hum. Genet.* **69**, 1385–1388 (2001).
36. H. Zhang, M. Wang, L. Wu, H. Zhang, T. Jin, J. Wu, L. Sun, Novel prion protein gene mutation at codon 196 (E196A) in a septuagenarian with Creutzfeldt–Jakob disease. *J. Clin. Neurosci.* **21**, 175–178 (2014).
37. M. C. Tartaglia, J. N. Thai, T. See, A. Kuo, R. Harbaugh, B. Raudabaugh, I. Cali, M. Sattavat, H. Sanchez, S. J. DeArmond, M. D. Geschwind, Pathologic evidence that the T188R mutation in PRNP is associated with prion disease. *J. Neuropathol. Exp. Neurol.* **69**, 1220–1227 (2010).
38. K. Peoc'h, P. Manivet, P. Beaudry, F. Attane, G. Besson, D. Hannequin, N. Delasnerie-Lauprêtre, J.-L. Laplanche, Identification of three novel mutations (E196K, V203I, E211Q) in the prion protein gene (*PRNP*) in inherited prion diseases with Creutzfeldt-Jakob disease phenotype. *Hum. Mutat.* **15**, 482 (2000).
39. J. Beck, J. Collinge, S. Mead, Prion protein gene *M232R* variation is probably an uncommon polymorphism rather than a pathogenic mutation. *Brain* **135**, e209 (2012).
40. I. Nozaki, K. Sakai, T. Kitamoto, M. Yamada, Reply: Prion protein gene *M232R* variation is probably an uncommon polymorphism rather than a pathogenic mutation. *Brain* **135**, e210 (2012).
41. S. Capellari, F. Cardone, S. Notari, M. E. Schininà, B. Maras, D. Sità, A. Baruzzi, M. Pocchiari, P. Parchi, Creutzfeldt-Jakob disease associated with the R208H mutation in the prion protein gene. *Neurology* **64**, 905–907 (2005).
42. L. Ripoll, J.-L. Laplanche, M. Salzmann, A. Jouvet, B. Planques, M. Dussaucy, J. Chatelain, P. Beaudry, J.-M. Launay, A new point mutation in the prion protein gene at codon 210 in Creutzfeldt-Jakob disease. *Neurology* **43**, 1934–1938 (1993).
43. C. L. Masters, J. O. Harris, D. C. Gajdusek, C. J. Gibbs Jr., C. Bernoulli, D. M. Asher, Creutzfeldt-Jakob disease: Patterns of worldwide occurrence and the significance of familial and sporadic clustering. *Ann. Neurol.* **5**, 177–188 (1979).
44. H. S. Lee, N. Sambuughin, L. Cervenakova, J. Chapman, M. Pocchiari, S. Litvak, H. Y. Qi, H. Budka, T. del Ser, H. Furukawa, P. Brown, D. C. Gajdusek, J. C. Long, A. D. Korczyn, L. G. Goldfarb, Ancestral origins and worldwide distribution of the *PRNP* 200K mutation causing familial Creutzfeldt-Jakob disease. *Am. J. Hum. Genet.* **64**, 1063–1070 (1999).
45. A. Ladogana, M. Puopolo, A. Poleggi, S. Almonti, V. Mellina, M. Equestre, M. Pocchiari, High incidence of genetic human transmissible spongiform encephalopathies in Italy. *Neurology* **64**, 1592–1597 (2005).
46. S. Shibuya, J. Higuchi, R.-W. Shin, J. Tateishi, T. Kitamoto, Codon 219 Lys allele of PRNP is not found in sporadic Creutzfeldt-Jakob disease. *Ann. Neurol.* **43**, 826–828 (1998).
47. M. T. Bishop, C. Pennington, C. A. Heath, R. G. Will, R. S. G. Knight, *PRNP* variation in UK sporadic and variant Creutzfeldt Jakob disease highlights genetic risk factors and a novel non-synonymous polymorphism. *BMC Med. Genet.* **10**, 146 (2009).
48. S. Mead, J. Uphill, J. Beck, M. Poulter, T. Campbell, J. Lowe, G. Adamson, H. Hummerich, N. Klopp, I.-M. Rückert, H.-E. Wichmann, D. Azazi, V. Plagnol, W. H. Pako, J. Whitfield, M. P. Alpers, J. Whittaker, D. J. Balding, I. Zerr, H. Kretzschmar, J. Collinge, Genome-wide association study in multiple human prion diseases suggests genetic risk factors additional to *PRNP*. *Hum. Mol. Genet.* **21**, 1897–1906 (2012).
49. H. Büeler, M. Fischer, Y. Lang, H. Bluethmann, H.-P. Lipp, S. J. DeArmond, S. B. Prusiner, M. Aguet, C. Weissmann, Normal development and behaviour of mice lacking the neuronal cell-surface PrP protein. *Nature* **356**, 577–582 (1992).

50. J. A. Richt, P. Kasinathan, A. N. Hamir, J. Castilla, T. Sathiyaseelan, F. Vargas, J. Sathiyaseelan, H. Wu, H. Matsushita, J. Koster, S. Kato, I. Ishida, C. Soto, J. M. Robl, Y. Kuroiwa, Production of cattle lacking prion protein. *Nat. Biotechnol.* **25**, 132–138 (2007).
51. G. Yu, J. Chen, Y. Xu, C. Zhu, H. Yu, S. Liu, H. Sha, J. Chen, X. Xu, Y. Wu, A. Zhang, J. Ma, G. Cheng, Generation of goats lacking prion protein. *Mol. Reprod. Dev.* **76**, 3 (2009).
52. S. L. Benestad, L. Austbø, M. A. Tranulis, A. Espenes, I. Olsaker, Healthy goats naturally devoid of prion protein. *Vet. Res.* **43**, 87 (2012).
53. M. Fischer, T. Rülicke, A. Raeber, A. Sailer, M. Moser, B. Oesch, S. Brandner, A. Aguzzi, C. Weissmann, Prion protein (PrP) with amino-proximal deletions restoring susceptibility of PrP knockout mice to scrapie. *EMBO J.* **15**, 1255–1264 (1996).
54. J. Bremer, F. Baumann, C. Tiberi, C. Wessig, H. Fischer, P. Schwarz, A. D. Steele, K. V. Toyka, K.-A. Nave, J. Weis, A. Aguzzi, Axonal prion protein is required for peripheral myelin maintenance. *Nat. Neurosci.* **13**, 310–318 (2010).
55. K. E. Samocha, E. B. Robinson, S. J. Sanders, C. Stevens, A. Sabo, L. M. McGrath, J. A. Kosmicki, K. Rehnström, S. Mallick, A. Kirby, D. P. Wall, D. G. MacArthur, S. B. Gabriel, M. DePristo, S. M. Purcell, A. Palotie, E. Boerwinkle, J. D. Buxbaum, E. H. Cook Jr., R. A. Gibbs, G. D. Schellenberg, J. S. Sutcliffe, B. Devlin, K. Roeder, B. M. Neale, M. J. Daly, A framework for the interpretation of de novo mutation in human disease. *Nat. Genet.* **46**, 944–950 (2014).
56. M. J. Landrum, J. M. Lee, G. R. Riley, W. Jang, W. S. Rubinstein, D. M. Church, D. R. Maglott, ClinVar: Public archive of relationships among sequence variation and human phenotype. *Nucleic Acids Res.* **42**, D980–D985 (2014).
57. P. D. Stenson, M. Mort, E. V. Ball, K. Shaw, A. D. Phillips, D. N. Cooper, The human gene mutation database: Building a comprehensive mutation repository for clinical and molecular genetics, diagnostic testing and personalized genomic medicine. *Hum. Genet.* **133**, 1–9 (2014).
58. D. G. MacArthur, T. A. Manolio, D. P. Dimmock, H. L. Rehm, J. Shendure, G. R. Abecasis, D. R. Adams, R. B. Altman, S. E. Antonarakis, E. A. Ashley, J. C. Barrett, L. G. Biesecker, D. F. Conrad, G. M. Cooper, N. J. Cox, M. J. Daly, M. B. Gerstein, D. B. Goldstein, J. N. Hirschhorn, S. M. Leal, L. A. Pennacchio, J. A. Stamatoyannopoulos, S. R. Sunyaev, D. Valle, B. F. Voight, W. Winckler, C. Gunter, Guidelines for investigating causality of sequence variants in human disease. *Nature* **508**, 469–476 (2014).
59. S. Richards, N. Aziz, S. Bale, D. Bick, S. Das, J. Gastier-Foster, W. W. Grody, M. Hegde, E. Lyon, E. Spector, K. Voelkerding, H. L. Rehm, ACMG Laboratory Quality Assurance Committee, Standards and guidelines for the interpretation of sequence variants: A joint consensus recommendation of the American College of Medical Genetics and Genomics and the Association for Molecular Pathology. *Genet. Med.* **17**, 405–424 (2015).
60. H. Büeler, A. Aguzzi, A. Sailer, R.-A. Greiner, P. Autenried, M. Aguet, C. Weissmann, Mice devoid of PrP are resistant to scrapie. *Cell* **73**, 1339–1347 (1993).
61. G. Mallucci, A. Dickinson, J. Linehan, P.-C. Klöhn, S. Brandner, J. Collinge, Depleting neuronal PrP in prion infection prevents disease and reverses spongiosis. *Science* **302**, 871–874 (2003).
62. J. G. Safar, S. J. DeArmond, K. Kociuba, C. Deering, S. Didorenko, E. Bouzamondo-Bernstein, S. B. Prusiner, P. Tremblay, Prion clearance in bigenic mice. *J. Gen. Virol.* **86**, 2913–2923 (2005).
63. M. D. White, M. Farmer, I. Mirabile, S. Brandner, J. Collinge, G. R. Mallucci, Single treatment with RNAi against prion protein rescues early neuronal dysfunction and prolongs survival in mice with prion disease. *Proc. Natl. Acad. Sci. U.S.A.* **105**, 10238–10243 (2008).
64. B. Pulford, N. Reim, A. Bell, J. Veatch, G. Forster, H. Bender, C. Meyerett, S. Hafeman, B. Michel, T. Johnson, A. C. Wyckoff, G. Miele, C. Julius, J. Kranich, A. Schenkel, S. Dow, M. D. Zabel, Liposome-siRNA-peptide complexes cross the blood-brain barrier and significantly decrease PrP^{C} on neuronal cells and PrP^{RES} in infected cell cultures. *PLOS One* **5**, e11085 (2010).
65. M. Ahn, K. Bajsarowicz, A. Oehler, A. Lemus, K. Bankiewicz, S. J. DeArmond, Convection-enhanced delivery of AAV2-PrPshRNA in prion-infected mice. *PLOS One* **9**, e98496 (2014).
66. K. Nazor Friberg, G. Hung, E. Wancewicz, K. Giles, C. Black, S. Freier, F. Bennett, S. J. Dearmond, Y. Freyman, P. Lessard, S. Ghaemmaghami, S. B. Prusiner, Intracerebral infusion of antisense oligonucleotides into prion-infected mice. *Mol. Ther. Nucleic Acids* **1**, e9 (2012).
67. Y. E. Karapetyan, G. F. Sferrazza, M. Zhou, G. Ottenberg, T. Spicer, P. Chase, M. Fallahi, P. Hodder, C. Weissmann, C. I. Lasmézas, Unique drug screening approach for prion diseases identifies tacrolimus and astemizole as antiprion agents. *Proc. Natl. Acad. Sci. U.S.A.* **110**, 7044–7049 (2013).
68. B. M. Silber, J. R. Gever, S. Rao, Z. Li, A. R. Renslo, K. Widjaja, C. Wong, K. Giles, Y. Freyman, M. Elepano, J. J. Irwin, M. P. Jacobson, S. B. Prusiner, Novel compounds lowering the cellular isoform of the human prion protein in cultured human cells. *Bioorg. Med. Chem.* **22**, 1960–1972 (2014).
69. *Global Surveillance, Diagnosis and Therapy of Human Transmissible Spongiform Encephalopathies: Report of a WHO Consultation, Geneva, Switzerland, 9-11 February 1998* (World Health Organization, Geneva,1998); www.who.int/csr/resources/publications/bse/whoemczdi989.pdf.
70. *WHO Manual for Surveillance of Human Transmissible Spongiform Encephalopathies Including Variant Creutzfeldt-Jakob Disease* (World Health Organization, Geneva, 2003); www.who.int/bloodproducts/TSE-manual2003.pdf.
71. S. Collins, A. Boyd, J. S. Lee, V. Lewis, A. Fletcher, C. A. McLean, M. Law, J. Kaldor, M. J. Smith, C. L. Masters, Creutzfeldt–Jakob disease in Australia 1970–1999. *Neurology* **59**, 1365–1371 (2002).
72. J.-P. Brandel, A. Welaratne, D. Salomon, I. Capek, V. Vaillant, A. Aouba, A. Aouaba, S. Haïk, A. Alpérovitch, Can mortality data provide reliable indicators for Creutzfeldt-Jakob disease surveillance? A study in France from 2000 to 2008. *Neuroepidemiology* **37**, 188–192 (2011).
73. O. Windl, A. Giese, W. Schulz-Schaeffer, I. Zerr, K. Skworc, S. Arendt, C. Oberdieck, M. Bodemer, S. Poser, H. A. Kretzschmar, Molecular genetics of human prion diseases in Germany. *Hum. Genet.* **105**, 244–252 (1999).
74. E. Grasbon-Frodl, H. Lorenz, U. Mann, R. M. Nitsch, O. Windl, H. A. Kretzschmar, Loss of glycosylation associated with the T183A mutation in human prion disease. *Acta Neuropathol.* **108**, 476–484 (2004).
75. I. Zerr, K. Kallenberg, D. M. Summers, C. Romero, A. Taratuto, U. Heinemann, M. Breithaupt, D. Varges, B. Meissner, A. Ladogana, M. Schuur, S. Haik, S. J. Collins, G. H. Jansen, G. B. Stokin, J. Pimentel, E. Hewer, D. Collie, P. Smith, H. Roberts, J. P. Brandel, C. van Duijn, M. Pocchiari, C. Begue, P. Cras, R. G. Will, P. Sanchez-Juan, Updated clinical diagnostic criteria for sporadic Creutzfeldt-Jakob disease. *Brain* **132**, 2659–2668 (2009).
76. M. Puopolo, A. Ladogana, S. Almonti, N. Daude, S. Bevivino, R. Petraroli, A. Poleggi, L. Quanguo, M. Pocchiari, Mortality trend from sporadic Creutzfeldt-Jakob disease (CJD) in Italy, 1993–2000. *J. Clin. Epidemiol.* **56**, 494–499 (2003).
77. C. Jansen, P. Parchi, S. Capellari, C. A. Ibrahim-Verbaas, M. Schuur, R. Strammiello, P. Corrado, M. T. Bishop, W. A. van Gool, M. M. Verbeek, F. Baas, W. van Saane, W. G. M. Spliet, G. H. Jansen, C. M. van Duijn, A. J. M. Rozemuller, Human prion diseases in the Netherlands (1998–2009): Clinical, genetic and molecular aspects. *PLOS One* **7**, e36333 (2012).
78. P. Parchi, A. Giese, S. Capellari, P. Brown, W. Schulz-Schaeffer, O. Windl, I. Zerr, H. Budka, N. Kopp, P. Piccardo, S. Poser, A. Rojiani, N. Streichemberger, J. Julien, C. Vital, B. Ghetti, P. Gambetti, H. Kretzschmar, Classification of sporadic Creutzfeldt-Jakob disease based on molecular and phenotypic analysis of 300 subjects. *Ann. Neurol.* **46**, 224–233 (1999).
79. J. T. Robinson, H. Thorvaldsdóttir, W. Winckler, M. Guttman, E. S. Lander, G. Getz, J. P. Mesirov, Integrative genomics viewer. *Nat. Biotechnol.* **29**, 24–26 (2011).
80. K. Bryc, E. Y. Durand, J. M. Macpherson, D. Reich, J. L. Mountain, The genetic ancestry of African Americans, Latinos, and European Americans across the United States. *Am. J. Hum. Genet.* **96**, 37–53 (2015).
81. E. Y. Durand, N. Eriksson, C. Y. McLean, Reducing pervasive false-positive identical-by-descent segments detected by large-scale pedigree analysis. *Mol. Biol. Evol.* **31**, 2212–2222 (2014).
82. E. Y. Durand, C. B. Do, J. L. Mountain, J. M. Macpherson, Ancestry composition: A novel, efficient pipeline for ancestry deconvolution. *bioRxiv* 10.1101/010512 010512 (2014).
83. S. R. Browning, B. L. Browning, Rapid and accurate haplotype phasing and missing-data inference for whole-genome association studies by use of localized haplotype clustering. *Am. J. Hum. Genet.* **81**, 1084–1097 (2007).
84. S. M. Purcell, J. L. Moran, M. Fromer, D. Ruderfer, N. Solovieff, P. Roussos, C. O'Dushlaine, K. Chambert, S. E. Bergen, A. Kähler, L. Duncan, E. Stahl, G. Genovese, E. Fernández, M. O. Collins, N. H. Komiyama, J. S. Choudhary, P. K. E. Magnusson, E. Banks, K. Shakir, K. Garimella, T. Fennell, M. DePristo, S. G. N. Grant, S. J. Haggarty, S. Gabriel, E. M. Scolnick, E. S. Lander, C. M. Hultman, P. F. Sullivan, S. A. McCarroll, P. Sklar, A polygenic burden of rare disruptive mutations in schizophrenia. *Nature* **506**, 185–190 (2014).
85. R. C. Holman, E. D. Belay, K. Y. Christensen, R. A. Maddox, A. M. Minino, A. M. Folkema, D. L. Haberling, T. A. Hammett, K. D. Kochanek, J. J. Sejvar, L. B. Schonberger, Human prion diseases in the United States. *PLOS One* **5**, e8521 (2010).
86. Creutzfeldt-Jakob Disease International Surveillance Network; http://web.archive.org/web/20151102144718/http://www.eurocjd.ed.ac.uk/surveillance%20data%201.html.
87. United Nations Statistics Division, Demographic and Social Statistics; http://unstats.un.org/unsd/demographic/products/vitstats/.
88. J. Cornfield, A method of estimating comparative rates from clinical data: Applications to cancer of the lung, breast, and cervix. *J. Natl. Cancer Inst.* **11**, 1269–1275 (1951).
89. B. Woolf, On estimating the relation between blood group and disease. *Ann. Hum. Genet.* **19**, 251–253 (1955).
90. C. C. Li, *Human Genetics: Principles and Methods* (McGraw-Hill Book Company Inc., New York, 1961).
91. J.-L. Laplanche, K. H. E. Hachimi, I. Durieux, P. Thuillet, L. Defebvre, N. Delasnerie-Lauprêtre, K. Peoc'h, J.-F. Foncin, A. Destée, Prominent psychiatric features and early onset in an inherited prion disease with a new insertional mutation in the prion protein gene. *Brain* **122**, 2375–2386 (1999).
92. K. Servick, Can 23andMe have it all? *Science* **349**, 1472–1477 (2015).
93. L. G. Goldfarb, A. D. Korczyn, P. Brown, J. Chapman, D. C. Gajdusek, Mutation in codon 200 of scrapie amyloid precursor gene linked to Creutzfeldt-Jakob disease in Sephardic Jews of Libyan and non-Libyan origin. *Lancet* **336**, 637–638 (1990).
94. K. K. Hsiao, C. Cass, G. D. Schellenberg, T. Bird, E. Devine-Gage, H. Wisniewski, S. B. Prusiner, A prion protein variant in a family with the telencephalic form of Gerstmann-Sträussler-Scheinker syndrome. *Neurology* **41**, 681–684 (1991).

95. R. Medori, P. Montagna, H. J. Tritschler, A. LeBlanc, P. Cortelli, P. Tinuper, E. Lugaresi, P. Gambetti, Fatal familial insomnia: A second kindred with mutation of prion protein gene at codon 178. *Neurology* **42**, 669–670 (1992).
96. J. A. Mastrianni, M. T. Curtis, J. C. Oberholtzer, M. M. Da Costa, S. DeArmond, S. B. Prusiner, J. Y. Garbern, Prion disease (PrP-A117V) presenting with ataxia instead of dementia. *Neurology* **45**, 2042–2050 (1995).
97. T. E. F. Webb, M. Poulter, J. Beck, J. Uphill, G. Adamson, T. Campbell, J. Linehan, C. Powell, S. Brandner, S. Pal, D. Siddique, J. D. Wadsworth, S. Joiner, K. Alner, C. Petersen, S. Hampson, C. Rhymes, C. Treacy, E. Storey, M. D. Geschwind, A. H. Nemeth, S. Wroe, J. Collinge, S. Mead, Phenotypic heterogeneity and genetic modification of P102L inherited prion disease in an international series. *Brain* **131**, 2632–2646 (2008).
98. K. K. Hsiao, M. Scott, D. Foster, D. F. Groth, S. J. DeArmond, S. B. Prusiner, Spontaneous neurodegeneration in transgenic mice with mutant prion protein. *Science* **250**, 1587–1590 (1990).
99. W. S. Jackson, A. W. Borkowski, H. Faas, A. D. Steele, O. D. King, N. Watson, A. Jasanoff, S. Lindquist, Spontaneous generation of prion infectivity in fatal familial insomnia knockin mice. *Neuron* **63**, 438–450 (2009).
100. W. Yang, J. Cook, B. Rassbach, A. Lemus, S. J. DeArmond, J. A. Mastrianni, A new transgenic mouse model of Gerstmann–Sträussler–Scheinker syndrome caused by the A117V mutation of *PRNP*. *J. Neurosci.* **29**, 10072–10080 (2009).
101. W. S. Jackson, A. W. Borkowski, N. E. Watson, O. D. King, H. Faas, A. Jasanoff, S. Lindquist, Profoundly different prion diseases in knock-in mice carrying single PrP codon substitutions associated with human diseases. *Proc. Natl. Acad. Sci. U.S.A.* **110**, 14759–14764 (2013).
102. S. Dossena, L. Imeri, M. Mangieri, A. Garofoli, L. Ferrari, A. Senatore, E. Restelli, C. Balducci, F. Fiordaliso, M. Salio, S. Bianchi, L. Fioriti, M. Morbin, A. Pincherle, G. Marcon, F. Villani, M. Carli, F. Tagliavini, G. Forloni, R. Chiesa, Mutant prion protein expression causes motor and memory deficits and abnormal sleep patterns in a transgenic mouse model. *Neuron* **60**, 598–609 (2008).
103. I. Bouybayoune, S. Mantovani, F. Del Gallo, I. Bertani, E. Restelli, L. Comerio, L. Tapella, F. Baracchi, N. Fernández-Borges, M. Mangieri, C. Bisighini, G. V. Beznoussenko, A. Paladini, C. Balducci, E. Micotti, G. Forloni, J. Castilla, F. Fiordaliso, F. Tagliavini, L. Imeri, R. Chiesa, Transgenic fatal familial insomnia mice indicate prion infectivity-independent mechanisms of pathogenesis and phenotypic expression of disease. *PLOS Pathog.* **11**, e1004796 (2015).
104. L. Bernardi, C. Cupidi, F. Frangipane, M. Anfossi, M. Gallo, M. E. Conidi, F. Vasso, R. Colao, G. Puccio, S. A. M. Curcio, M. Mirabelli, A. Clodomiro, R. Di Lorenzo, N. Smirne, R. Maletta, A. C. Bruni, Novel N-terminal domain mutation in prion protein detected in 2 patients diagnosed with frontotemporal lobar degeneration syndrome. *Neurobiol. Aging* **35**, 2657.e7–2657.e11 (2014).
105. L. Zheng, J. Longfei, Y. Jing, Z. Xinqing, S. Haiqing, L. Haiyan, W. Fen, D. Xiumin, J. Jianping, *PRNP* mutations in a series of apparently sporadic neurodegenerative dementias in China. *Am. J. Med. Genet. Part B Neuropsychiatr. Genet.* **147B**, 938–944 (2008).
106. Q. Shi, W. Zhou, C. Chen, B.-Y. Zhang, K. Xiao, X.-C. Zhang, X.-J. Shen, Q. Li, L.-Q. Deng, J.-H. Dong, W.-Q. Lin, P. Huang, W.-J. Jiang, J. Lv, J. Han, X.-P. Dong, The features of genetic prion diseases based on Chinese surveillance program. *PLOS One* **10**, e0139552 (2015).
107. A. Aguzzi, F. Baumann, J. Bremer, The prion's elusive reason for being. *Annu. Rev. Neurosci.* **31**, 439–477 (2008).
108. B. Chesebro, B. Race, K. Meade-White, R. Lacasse, R. Race, M. Klingeborn, J. Striebel, D. Dorward, G. McGovern, M. Jeffrey, Fatal transmissible amyloid encephalopathy: A new type of prion disease associated with lack of prion protein membrane anchoring. *PLOS Pathog.* **6**, e1000800 (2010).
109. J. Stöhr, J. C. Watts, G. Legname, A. Oehler, A. Lemus, H.-O. B. Nguyen, J. Sussman, H. Wille, S. J. DeArmond, S. B. Prusiner, K. Giles, Spontaneous generation of anchorless prions in transgenic mice. *Proc. Natl. Acad. Sci. U.S.A.* **108**, 21223–21228 (2011).
110. B. Krebs, R.-M. Lederer, O. Windl, E.-M. Grasbon-Frodl, I. Zerr, H. A. Kretzschmar, Creutzfeldt-Jakob disease associated with an R148H mutation of the prion protein gene. *Neurogenetics* **6**, 97–100 (2005).
111. M. Pastore, S. S. Chin, K. L. Bell, Z. Dong, Q. Yang, L. Yang, J. Yuan, S. G. Chen, P. Gambetti, W.-Q. Zou, Creutzfeldt-Jakob disease (CJD) with a mutation at codon 148 of prion protein gene: Relationship with sporadic CJD. *Am. J. Pathol.* **167**, 1729–1738 (2005).
112. S. Roeber, E.-M. Grasbon-Frodl, O. Windl, B. Krebs, W. Xiang, C. Vollmert, T. Illig, A. Schröter, T. Arzberger, P. Weber, I. Zerr, H. A. Kretzschmar, Evidence for a pathogenic role of different mutations at codon 188 of *PRNP*. *PLOS One* **3**, e2147 (2008).
113. B.-H. Jeong, Y.-C. Jeon, Y.-J. Lee, H.-J. Cho, S.-J. Park, D.-I. Chung, J. Kim, S. H. Kim, H.-T. Kim, E.-K. Choi, K.-C. Choi, R. I. Carp, Y.-S. Kim, Creutzfeldt-Jakob disease with the V203I mutation and M129V polymorphism of the prion protein gene (*PRNP*) and a 17 kDa prion protein fragment. *Neuropathol. Appl. Neurobiol.* **36**, 558–563 (2010).
114. Q. Shi, C. Chen, X.-J. Wang, W. Zhou, J.-C. Wang, B.-Y. Zhang, C. Tian, C. Gao, J. Han, X.-P. Dong, Rare V203I mutation in the *PRNP* gene of a Chinese patient with Creutzfeldt-Jakob disease. *Prion* **7**, 259–262 (2013).
115. J. Komatsu, K. Sakai, T. Hamaguchi, Y. Sugiyama, K. Iwasa, M. Yamada, Creutzfeldt-Jakob disease associated with a V203I homozygous mutation in the prion protein gene. *Prion* **8**, 336–338 (2014).
116. J. A. Mastrianni, C. Iannicola, R. M. Myers, S. DeArmond, S. B. Prusiner, Mutation of the prion protein gene at codon 208 in familial Creutzfeldt-Jakob disease. *Neurology* **47**, 1305–1312 (1996).
117. S. Roeber, B. Krebs, M. Neumann, O. Windl, I. Zerr, E.-M. Grasbon-Frodl, H. A. Kretzschmar, Creutzfeldt-Jakob disease in a patient with an R208H mutation of the prion protein gene (*PRNP*) and a 17-kDa prion protein fragment. *Acta Neuropathol.* **109**, 443–448 (2005).
118. C. Basset-Leobon, E. Uro-Coste, K. Peoc'h, S. Haik, V. Sazdovitch, M. Rigal, O. Andreoletti, J.-J. Hauw, M.-B. Delisle, Familial Creutzfeldt-Jakob disease with an R208H-129V haplotype and Kuru plaques. *Arch. Neurol.* **63**, 449–452 (2006).
119. C. Chen, Q. Shi, C. Tian, Q. Li, W. Zhou, C. Gao, J. Han, X.-P. Dong, The first Chinese case of Creutzfeldt-Jakob disease patient with R208H mutation in *PRNP*. *Prion* **5**, 232–234 (2011).
120. R. Matěj, G. G. Kovacs, S. Johanidesová, J. Keller, M. Matějčková, J. Nováková, V. Šigut, O. Keller, R. Rusina, Genetic Creutzfeldt–Jakob disease with R208H mutation presenting as progressive supranuclear palsy. *Mov. Disord.* **27**, 476–479 (2012).
121. M. G. Vita, S. Gaudino, D. Di Giuda, D. Sauchelli, P. E. Alboini, E. Gangemi, A. Bizzarro, E. Scaricamazza, S. Capellari, P. Parchi, C. Masullo, R208H-129VV haplotype in the prion protein gene: Phenotype and neuroimaging of a patient with genetic Creutzfeldt-Jakob disease. *J. Neurol.* **260**, 2650–2652 (2013).
122. R. Nitrini, S. Rosemberg, M. R. Passos-Bueno, L. S. da Silva, P. Iughetti, M. Papadopoulos, P. M. Carrilho, P. Caramelli, S. Albrecht, M. Zatz, A. LeBlanc, Familial spongiform encephalopathy associated with a novel prion protein gene mutation. *Ann. Neurol.* **42**, 138–146 (1997).
123. K. Hsiao, S. R. Dlouhy, M. R. Farlow, C. Cass, M. Da Costa, P. M. Conneally, M. E. Hodes, B. Ghetti, S. B. Prusiner, Mutant prion proteins in Gerstmann-Sträussler-Scheinker disease with neurofibrillary tangles. *Nat. Genet.* **1**, 68–71 (1992).
124. E. S. Simon, E. Kahana, J. Chapman, T. A. Treves, R. Gabizon, H. Rosenmann, N. Zilber, A. D. Korczyn, Creutzfeldt-Jakob disease profile in patients homozygous for the PRNP E200K mutation. *Ann. Neurol.* **47**, 257–260 (2000).
125. J. A. Beck, S. Mead, T. A. Campbell, A. Dickinson, D. P. Wientjens, E. A. Croes, C. M. Van Duijn, J. Collinge, Two-octapeptide repeat deletion of prion protein associated with rapidly progressive dementia. *Neurology* **57**, 354–356 (2001).
126. S. Capellari, P. Parchi, B. D. Wolff, J. Campbell, R. Atkinson, D. M. Posey, R. B. Petersen, P. Gambetti, Creutzfeldt–Jakob disease associated with a deletion of two repeats in the prion protein gene. *Neurology* **59**, 1628–1630 (2002).
127. J. L. Laplanche, N. Delasnerie-Lauprêtre, J. P. Brandel, M. Dussaucy, J. Chatelain, J. M. Launay, Two novel insertions in the prion protein gene in patients with late-onset dementia. *Hum. Mol. Genet.* **4**, 1109–1111 (1995).
128. V. Pietrini, G. Puoti, L. Limido, G. Rossi, G. Di Fede, G. Giaccone, M. Mangieri, F. Tedeschi, A. Bondavalli, D. Mancia, O. Bugiani, F. Tagliavini, Creutzfeldt-Jakob disease with a novel extra-repeat insertional mutation in the *PRNP* gene. *Neurology* **61**, 1288–1291 (2003).
129. A. F. Hill, S. Joiner, J. A. Beck, T. A. Campbell, A. Dickinson, M. Poulter, J. D. F. Wadsworth, J. Collinge, Distinct glycoform ratios of protease resistant prion protein associated with *PRNP* point mutations. *Brain* **129**, 676–685 (2006).
130. Y. Nishida, N. Sodeyama, Y. Toru, S. Toru, T. Kitamoto, H. Mizusawa, Creutzfeldt–Jakob disease with a novel insertion and codon 219 Lys/Lys polymorphism in *PRNP*. *Neurology* **63**, 1978–1979 (2004).
131. T. A. Campbell, M. S. Palmer, R. G. Will, W. R. G. Gibb, P. J. Luthert, J. Collinge, A prion disease with a novel 96-base pair insertional mutation in the prion protein gene. *Neurology* **46**, 761–766 (1996).
132. D. N. Kaski, C. Pennington, J. Beck, M. Poulter, J. Uphill, M. T. Bishop, J. M. Linehan, C. O'Malley, J. D. F. Wadsworth, S. Joiner, R. S. G. Knight, J. W. Ironside, S. Brandner, J. Collinge, S. Mead, Inherited prion disease with 4-octapeptide repeat insertion: Disease requires the interaction of multiple genetic risk factors. *Brain* **134**, 1829–1838 (2011).
133. L. G. Goldfarb, P. Brown, W. R. McCombie, D. Goldgaber, G. D. Swergold, P. R. Wills, L. Cervenakova, H. Baron, C. J. Gibbs Jr., D. C. Gajdusek, Transmissible familial Creutzfeldt-Jakob disease associated with five, seven, and eight extra octapeptide coding repeats in the PRNP gene. *Proc. Natl. Acad. Sci. U.S.A.* **88**, 10926–10930 (1991).
134. F. Owen, M. Poulter, T. Shah, J. Collinge, R. Lofthouse, H. Baker, R. Ridley, J. McVey, T. J. Crow, An in-frame insertion in the prion protein gene in familial Creutzfeldt-Jakob disease. *Brain Res. Mol. Brain Res.* **7**, 273–276 (1990).
135. S. Mead, M. Poulter, J. Beck, T. E. F. Webb, T. A. Campbell, J. M. Linehan, M. Desbruslais, S. Joiner, J. D. F. Wadsworth, A. King, P. Lantos, J. Collinge, Inherited prion disease with six octapeptide repeat insertional mutation—Molecular analysis of phenotypic heterogeneity. *Brain* **129**, 2297–2317 (2006).
136. V. Lewis, S. Collins, A. F. Hill, A. Boyd, C. A. McLean, M. Smith, C. L. Masters, Novel prion protein insert mutation associated with prolonged neurodegenerative illness. *Neurology* **60**, 1620–1624 (2003).
137. S. Krasemann, I. Zerr, T. Weber, S. Poser, H. Kretzschmar, G. Hunsmann, W. Bodemer, Prion disease associated with a novel nine octapeptide repeat insertion in the PRNP gene. *Brain Res. Mol. Brain Res.* **34**, 173–176 (1995).
138. N. Kumar, B. F. Boeve, B. P. Boot, C. F. Orr, J. Duffy, B. K. Woodruff, A. K. Nair, J. Ellison, K. Kuntz, K. Kantarci, C. R. Jack, B. F. Westmoreland, J. A. Fields, M. Baker, R. Rademakers, J. E. Parisi,

D. W. Dickson, Clinical characterization of a kindred with a novel 12-octapeptide repeat insertion in the prion protein gene. *Arch. Neurol.* **68**, 1165–1170 (2011).
139. M. Jones, S. Odunsi, D. du Plessis, A. Vincent, M. Bishop, M. W. Head, J. W. Ironside, D. Gow, Gerstmann-Straüssler-Scheinker disease: Novel *PRNP* mutation and VGKC-complex antibodies. *Neurology* **82**, 2107–2111 (2014).
140. D. Goldgaber, L. G. Goldfarb, P. Brown, D. M. Asher, W. T. Brown, S. Lin, J. W. Teener, S. M. Feinstone, R. Rubenstein, R. J. Kascsak, Mutations in familial Creutzfeldt-Jakob disease and Gerstmann-Sträussler-Scheinker's syndrome. *Exp. Neurol.* **106**, 204–206 (1989).
141. M. Yamada, Y. Itoh, H. Fujigasaki, S. Naruse, K. Kaneko, T. Kitamoto, J. Tateishi, E. Otomo, M. Hayakawa, J. Tanaka, A missense mutation at codon 105 with codon 129 polymorphism of the prion protein gene in a new variant of Gerstmann-Sträussler-Scheinker disease. *Neurology* **43**, 2723–2724 (1993).
142. M. Yamada, Y. Itoh, A. Inaba, Y. Wada, M. Takashima, S. Satoh, T. Kamata, R. Okeda, T. Kayano, N. Suematsu, T. Kitamoto, E. Otomo, M. Matsushita, H. Mizusawa, An inherited prion disease with a PrP P105L mutation: Clinicopathologic and PrP heterogeneity. *Neurology* **53**, 181–188 (1999).
143. E. Tunnell, R. Wollman, S. Mallik, C. J. Cortes, S. J. DeArmond, J. A. Mastrianni, A novel *PRNP*-P105S mutation associated with atypical prion disease and a rare PrP^{Sc} conformation. *Neurology* **71**, 1431–1438 (2008).
144. E. Rogaeva, C. Zadikoff, J. Ponesse, G. Schmitt-Ulms, T. Kawarai, C. Sato, S. Salehi-Rad, P. St George-Hyslop, A. E. Lang, Childhood onset in familial prion disease with a novel mutation in the PRNP gene. *Arch. Neurol.* **63**, 1016–1021 (2006).
145. M. Polymenidou, S. Prokop, H. H. Jung, E. Hewer, D. Peretz, R. Moos, M. Tolnay, A. Aguzzi, Atypical prion protein conformation in familial prion disease with *PRNP* P105T mutation. *Brain Pathol.* **21**, 209–214 (2011).
146. M.-M. Rodriguez, K. Peoc'h, S. Haïk, C. Bouchet, L. Vernengo, G. Mañana, R. Salamano, L. Carrasco, M. Lenne, P. Beaudry, J.-M. Launay, J.-L. Laplanche, A novel mutation (G114V) in the prion protein gene in a family with inherited prion disease. *Neurology* **64**, 1455–1457 (2005).
147. Z. Liu, L. Jia, Y. Piao, D. Lu, F. Wang, H. Lv, Y. Lu, J. Jia, Creutzfeldt–Jakob disease with *PRNP* G114V mutation in a Chinese family. *Acta Neurol. Scand.* **121**, 377–383 (2010).
148. J. Tateishi, T. Kitamoto, K. Doh-ura, Y. Sakaki, G. Steinmetz, C. Tranchant, J. M. Warter, N. Heldt, Immunochemical, molecular genetic, and transmission studies on a case of Gerstmann-Straussler-Scheinker syndrome. *Neurology* **40**, 1578–1581 (1990).
149. C. Hinnell, M. B. Coulthart, G. H. Jansen, N. R. Cashman, J. Lauzon, A. Clark, F. Costello, C. White, R. Midha, S. Wiebe, S. Furtado, Gerstmann-Sträussler-Scheinker disease due to a novel prion protein gene mutation. *Neurology* **76**, 485–487 (2011).
150. P. K. Panegyres, K. Toufexis, B. A. Kakulas, L. Cernevakova, P. Brown, B. Ghetti, P. Piccardo, S. R. Dlouhy, A new PRNP mutation (G131V) associated with Gerstmann-Sträussler-Scheinker disease. *Arch. Neurol.* **58**, 1899–1902 (2001).
151. D. A. Hilton, M. W. Head, V. K. Singh, M. Bishop, J. W. Ironside, Familial prion disease with a novel serine to isoleucine mutation at codon 132 of prion protein gene (*PRNP*). *Neuropathol. Appl. Neurobiol.* **35**, 111–115 (2009).
152. D. B. Rowe, V. Lewis, M. Needham, M. Rodriguez, A. Boyd, C. McLean, H. Roberts, C. L. Masters, S. J. Collins, Novel prion protein gene mutation presenting with subacute PSP-like syndrome. *Neurology* **68**, 868–870 (2007).
153. T. Kitamoto, R. Iizuka, J. Tateishi, An amber mutation of prion protein in Gerstmann-Sträussler syndrome with mutant PrP plaques. *Biochem. Biophys. Res. Commun.* **192**, 525–531 (1993).
154. U. Finckh, T. Müller-Thomsen, U. Mann, C. Eggers, J. Marksteiner, W. Meins, G. Binetti, A. Alberici, C. Hock, R. M. Nitsch, A. Gal, High prevalence of pathogenic mutations in patients with early-onset dementia detected by sequence analyses of four different genes. *Am. J. Hum. Genet.* **66**, 110–117 (2000).
155. S. Jayadev, D. Nochlin, P. Poorkaj, E. J. Steinbart, J. A. Mastrianni, T. J. Montine, B. Ghetti, G. D. Schellenberg, T. D. Bird, J. B. Leverenz, Familial prion disease with Alzheimer disease-like tau pathology and clinical phenotype. *Ann. Neurol.* **69**, 712–720 (2011).
156. T. Revesz, J. L. Holton, T. Lashley, G. Plant, B. Frangione, A. Rostagno, J. Ghiso, Genetics and molecular pathogenesis of sporadic and hereditary cerebral amyloid angiopathies. *Acta Neuropathol.* **118**, 115–130 (2009).
157. S. Mead, S. Gandhi, J. Beck, D. Caine, D. Gajulapalli, C. Carswell, H. Hyare, S. Joiner, H. Ayling, T. Lashley, J. M. Linehan, H. Al-Doujaily, B. Sharps, T. Revesz, M. K. Sandberg, M. M. Reilly, M. Koltzenburg, A. Forbes, P. Rudge, S. Brandner, J. D. Warren, J. D. F. Wadsworth, N. W. Wood, J. L. Holton, J. Collinge, A novel prion disease associated with diarrhea and autonomic neuropathy. *N. Engl. J. Med.* **369**, 1904–1914 (2013).
158. M. Simpson, V. Johanssen, A. Boyd, G. Klug, C. L. Masters, Q.-X. Li, R. Pamphlett, C. McLean, V. Lewis, S. J. Collins, Unusual clinical and molecular-pathological profile of Gerstmann-Sträussler-Scheinker disease associated with a novel *PRNP* mutation (V176G). *JAMA Neurol.* **70**, 1180–1185 (2013).
159. K. Matsuzono, Y. Ikeda, W. Liu, T. Kurata, S. Deguchi, K. Deguchi, K. Abe, A novel familial prion disease causing pan-autonomic-sensory neuropathy and cognitive impairment. *Eur. J. Neurol.* **20**, e67–e69 (2013).
160. L. G. Goldfarb, M. Haltia, P. Brown, A. Nieto, J. Kovanen, W. R. McCombie, S. Trapp, D. C. Gajdusek, New mutation in scrapie amyloid precursor gene (at codon 178) in Finnish Creutzfeldt-Jakob kindred. *Lancet* **337**, 425 (1991).
161. L. G. Goldfarb, R. B. Petersen, M. Tabaton, P. Brown, A. C. LeBlanc, P. Montagna, P. Cortelli, J. Julien, C. Vital, W. W. Pendelbury, Fatal familial insomnia and familial Creutzfeldt-Jakob disease: Disease phenotype determined by a DNA polymorphism. *Science* **258**, 806–808 (1992).
162. S. Hitoshi, H. Nagura, H. Yamanouchi, T. Kitamoto, Double mutations at codon 180 and codon 232 of the PRNP gene in an apparently sporadic case of Creutzfeldt-Jakob disease. *J. Neurol. Sci.* **120**, 208–212 (1993).
163. S. Chasseigneaux, S. Haïk, I. Laffont-Proust, O. De Marco, M. Lenne, J.-P. Brandel, J.-J. Hauw, J.-L. Laplanche, K. Peoc'h, V180I mutation of the prion protein gene associated with atypical PrP^{Sc} glycosylation. *Neurosci. Lett.* **408**, 165–169 (2006).
164. C. M. Bütefisch, P. Gambetti, L. Cervenakova, K.-Y. Park, M. Hallett, L. G. Goldfarb, Inherited prion encephalopathy associated with the novel *PRNP* H187R mutation: A clinical study. *Neurology* **55**, 517–522 (2000).
165. S. Collins, A. Boyd, A. Fletcher, K. Byron, C. Harper, C. A. McLean, C. L. Masters, Novel prion protein gene mutation in an octogenarian with Creutzfeldt-Jakob disease. *Arch. Neurol.* **57**, 1058–1063 (2000).
166. K. Kotta, I. Paspaltsis, S. Bostantjopoulou, H. Latsoudis, A. Plaitakis, D. Kazis, J. Collinge, T. Sklaviadis, Novel mutation of the *PRNP* gene of a clinical CJD case. *BMC Infect. Dis.* **6**, 169 (2006).
167. M. R. Farlow, R. D. Yee, S. R. Dlouhy, P. M. Conneally, B. Azzarelli, B. Ghetti, Gerstmann-Sträussler-Scheinker disease. I. extending the clinical spectrum. *Neurology* **39**, 1446–1452 (1989).
168. M.-O. Kim, I. Cali, A. Oehler, J. C. Fong, K. Wong, T. See, J. S. Katz, P. Gambetti, B. M. Bettcher, S. J. DeArmond, M. D. Geschwind, Genetic CJD with a novel E200G mutation in the prion protein gene and comparison with E200K mutation cases. *Acta Neuropathol. Commun.* **1**, 80 (2013).
169. U. Heinemann, A. Krasnianski, B. Meissner, E. M. Grasbon-Frodl, H. A. Kretzschmar, I. Zerr, Novel PRNP mutation in a patient with a slow progressive dementia syndrome. *Med. Sci. Monit.* **14**, CS41–CS43 (2008).
170. P. Piccardo, S. R. Dlouhy, P. M. Lievens, K. D. Young, T. D. Bird, D. Nochlin, D. W. Dickson, H. V. Vinters, T. R. Zimmerman, I. R. A. Mackenzie, S. J. Kish, L.-C. Ang, C. De Carli, M. Pocchiari, P. Brown, C. J. Gibbs Jr., D. C. Gajdusek, O. Bugiani, J. Ironside, F. Tagliavini, B. Ghetti, Phenotypic variability of Gerstmann-Straussler-Scheinker disease is associated with prion protein heterogeneity. *J. Neuropathol. Exp. Neurol.* **57**, 979–988 (1998).
171. M. Pocchiari, M. Salvatore, F. Cutruzzolá, M. Genuardi, C. T. Allocatelli, C. Masullo, G. Macchi, G. Alemá, S. Galgani, Y. G. Xi, A new point mutation of the prion protein gene in Creutzfeldt-Jakob disease. *Ann. Neurol.* **34**, 802–807 (1993).
172. S. Mouillet-Richard, C. Teil, M. Lenne, S. Hugon, O. Taleb, J.-L. Laplanche, Mutation at codon 210 (V210I) of the prion protein gene in a North African patient with Creutzfeldt-Jakob disease. *J. Neurol. Sci.* **168**, 141–144 (1999).
173. K. Peoc'h, E. Levavasseur, E. Delmont, A. De Simone, I. Laffont-Proust, N. Privat, Y. Chebaro, C. Chapuis, P. Bedoucha, J.-P. Brandel, A. Laquerriere, J.-L. Kemeny, J.-J. Hauw, M. Borg, H. Rezaei, P. Derreumaux, J.-L. Laplanche, S. Haïk, Substitutions at residue 211 in the prion protein drive a switch between CJD and GSS syndrome, a new mechanism governing inherited neurodegenerative disorders. *Hum. Mol. Genet.* **21**, 5417–5428 (2012).
174. M. Muñoz-Nieto, N. Ramonet, J. I. López-Gastón, N. Cuadrado-Corrales, O. Calero, M. Díaz-Hurtado, J. R. Ipiens, S. Ramón y Cajal, J. de Pedro-Cuesta, M. Calero, A novel mutation I215V in the *PRNP* gene associated with Creutzfeldt–Jakob and Alzheimer's diseases in three patients with divergent clinical phenotypes. *J. Neurol.* **260**, 77–84 (2013).
175. A. Alzualde, B. Indakoetxea, I. Ferrer, F. Moreno, M. Barandiaran, A. Gorostidi, A. Estanga, I. Ruiz, M. Calero, F. W. van Leeuwen, B. Atares, R. Juste, A. B. Rodriguez-Martínez, A. López de Munain, A novel *PRNP Y218N* mutation in Gerstmann-Sträussler-Scheinker disease with neurofibrillary degeneration. *J. Neuropathol. Exp. Neurol.* **69**, 789–800 (2010).
176. C. Jansen, P. Parchi, S. Capellari, A. J. Vermeij, P. Corrado, F. Baas, R. Strammiello, W. A. van Gool, J. C. van Swieten, A. J. M. Rozemuller, Prion protein amyloidosis with divergent phenotype associated with two novel nonsense mutations in *PRNP*. *Acta Neuropathol.* **119**, 189–197 (2010).
177. M. Z. Hoque, T. Kitamoto, H. Furukawa, T. Muramoto, J. Tateishi, Mutation in the prion protein gene at codon 232 in Japanese patients with Creutzfeldt-Jakob disease: A clinicopathological, immunohistochemical and transmission study. *Acta Neuropathol.* **92**, 441–446 (1996).
178. J. Bratosiewicz, M. Barcikowska, L. Cervenakowa, P. Brown, D. C. Gajdusek, P. P. Liberski, A new point mutation of the PRNP gene in Gerstmann-Sträussler-Scheinker case in Poland. *Folia Neuropathol.* **38**, 164–166 (2000).
179. A. Hofman, G. G. O. Brusselle, S. Darwish Murad, C. M. van Duijn, O. H. Franco, A. Goedegebure, M. A. Ikram, C. C. W. Klaver, T. E. C. Nijsten, R. P. Peeters, B. H. C. Stricker, H. W. Tiemeier, A. G. Uitterlinden, M. W. Vernooij, The Rotterdam Study: 2016 objectives and design update. *Eur. J. Epidemiol.* **30**, 661–708 (2015).

Acknowledgments: We thank the customers of 23andMe, ExAC research participants, and prion disease patients and families who participated in this research. **Funding:** Research reported in this publication was partially supported by the National Institute of Diabetes and Digestive and Kidney Diseases and the National Institute of General Medical Sciences of the NIH (awards

U54DK105566 and R01GM104371), by Broad Institute NextGen funds, and by Prion Alliance sundry funds. S.M.V. is supported by the National Science Foundation Graduate Research Fellowship Program (grant 2015214731). U.S. prion surveillance work was conducted under Centers for Disease Control and Prevention (contract UR8/CCU515004). Japanese prion surveillance work was supported by a grant-in-aid from the Research Committee of Prion Disease and Slow Virus Infection and the Research Committee of Surveillance and Infection Control of Prion Disease of the Ministry of Health, Labour and Welfare of Japan. The French prion surveillance network is supported by the Institut National de veille Sanitaire. The German prion surveillance work was supported by Robert Koch Institute/Federal Ministry of Health (grant 1369-341). The UK National Creutzfeldt Jakob Disease Research and Surveillance Unit is supported by the Department of Health and the Scottish Executive. The Australian National Creutzfeldt-Jakob Disease Registry is funded by the Commonwealth Department of Health. S.J.C. is supported by a National Health and Medical Research Council Practitioner Fellowship (identification number APP1005816). Contributions at Erasmus Medical Center (MC) were supported by Netherlands Genomics Initiative/Netherlands Organisation for Scientific Research–sponsored Netherlands Consortium for Healthy Aging (project 050-060-810); by the Genetic Laboratory of the Department of Internal Medicine, Erasmus MC; by a Complementation Project of the Biobanking and Biomolecular Research Infrastructure Netherlands (www.bbmri.nl; project number CP2010-41); and by Erasmus MC and Erasmus University, Rotterdam, Netherlands Organisation for Health Research and Development (ZonMw Middelgroot #91111025), Netherlands Organization for the Health Research and Development, the Research Institute for Diseases in the Elderly, the Ministry of Education, Culture and Science, the Ministry for Health, Welfare and Sports, the European Commission (Directorate-General for Science, Research and Development), and the Municipality of Rotterdam. **Author contributions:** E.V.M., S.M.V., and D.G.M. conceived and designed the study. E.V.M. analyzed the data, generated figures, and wrote the manuscript. S.M.V. and E.V.M. reviewed literature and IGV screenshots. K.E.S. performed constraint analyses. M. Lek, K.E., K.E.S., K.J.K., A.H.O.-L., M.J.D., and D.G.M. consulted on data analysis and interpretation. J.F.S., C.Y.M., J.Y.T., and L.P.C.Y. prepared and consulted on analysis of 23andMe data. P.G., J.B., S.Z., Y.C., W.C., M.Y., T.H., N.S., H.M., Y.N., T.K., S.J.C., A.B., R.G.W., R. Knight, C.P., I.Z., T.F.J.K., S.E., A.G., M.C., J.d.P.-C., S.H., J.-L.L., E.B.-A., J.-P.B., S.C., P.P., A.L., A.P., R. Kraaij, J.G.J.v.R., A.R., C.J., S.J.v.d.L., and C.M.v.D. prepared and consulted on analysis of prion surveillance data. E.V.M., J.L.M., M.B., M.Laakso, K.L.M., A.K., K.C., S.M., P.S., P.F.S., C.M.H., S.M.P., C.M.v.D., A.H., M.A.I., S.J.v.d.L., and A.G.U. prepared and consulted on analysis of data regarding protein-truncating variants. ExAC provided exome sequence data. **Competing interests:** The authors declare that they have no competing interest.

Exome Aggregation Consortium collaborators: Monkol Lek, Konrad J. Karczewski, Eric V. Minikel, Kaitlin E Samocha, Eric Banks, Timothy Fennell, Anne H. O'Donnell-Luria, James S. Ware, Andrew J. Hill, Beryl B. Cummings, Taru Tukiainen, Daniel P. Birnbaum, Jack A. Kosmicki, Laramie Duncan, Karol Estrada, Fengmei Zhao, James Zou, Emma Pierce-Hoffman, Mark DePristo, Ron Do, Jason Flannick, Menachem Fromer, Laura Gauthier, Jackie Goldstein, Namrata Gupta, Daniel Howrigan, Adam Kiezun, Mitja I Kurki, Ami Levy Moonshine, Pradeep Natarajan, Lorena Orozco, Gina M. Peloso, Ryan Poplin, Manuel A Rivas, Valentin Ruano-Rubio, Douglas M. Ruderfer, Khalid Shakir, Christine Stevens, Brett P. Thomas, Grace Tiao, Maria T. Tusie-Luna, Ben Weisburd, Hong-Hee Won, Dongmei Yu, Stacey Donnelly, Andrea Saltzman, David M. Altshuler, Diego Ardissino, Michael Boehnke, John Danesh, Roberto Elosua, Jose C. Florez, Stacey B Gabriel, Gad Getz, Christina M. Hultman, Sekar Kathiresan, Markku Laakso, Steven McCarroll, Mark I. McCarthy, Dermot McGovern, Ruth McPherson, Benjamin M. Neale, Aarno Palotie, Shaun M. Purcell, Danish Saleheen, Jeremiah M. Scharf, Pamela Sklar, Patrick F. Sullivan, Jaakko Tuomilehto, Hugh C. Watkins, James G. Wilson, Mark J. Daly, Daniel G. MacArthur.

Submitted 25 September 2015
Accepted 14 December 2015
Published 20 January 2016
10.1126/scitranslmed.aad5169

Citation: E. V. Minikel, S. M. Vallabh, M. Lek, K. Estrada, K. E. Samocha, J. F. Sathirapongsasuti, C. Y. McLean, J. Y. Tung, L. P. C. Yu, P. Gambetti, J. Blevins, S. Zhang, Y. Cohen, W. Chen, M. Yamada, T. Hamaguchi, N. Sanjo, H. Mizusawa, Y. Nakamura, T. Kitamoto, S. J. Collins, A. Boyd, R. G. Will, R. Knight, C. Ponto, I. Zerr, T. F. J. Kraus, S. Eigenbrod, A. Giese, M. Calero, J. de Pedro-Cuesta, S. Haïk, J.-L. Laplanche, E. Bouaziz-Amar, J.-P. Brandel, S. Capellari, P. Parchi, A. Poleggi, A. Ladogana, A. H. O'Donnell-Luria, K. J. Karczewski, J. L. Marshall, M. Boehnke, M. Laakso, K. L. Mohlke, A. Kähler, K. Chambert, S. McCarroll, P. F. Sullivan, C. M. Hultman, S. M. Purcell, P. Sklar, S. J. van der Lee, A. Rozemuller, C. Jansen, A. Hofman, R. Kraaij, J. G. J. van Rooij, M. A. Ikram, A. G. Uitterlinden, C. M. van Duijn, Exome Aggregation Consortium, M. J. Daly, D. G. MacArthur, Quantifying prion disease penetrance using large population control cohorts. *Sci. Transl. Med.* **8**, 322ra9 (2016).

ARTICLE

Age at onset in genetic prion disease and the design of preventive clinical trials

Eric Vallabh Minikel, PhD, Sonia M. Vallabh, JD, PhD, Margaret C. Orseth, MBA, Jean-Philippe Brandel, MD, Stéphane Haïk, MD, PhD, Jean-Louis Laplanche, PhD, Inga Zerr, MD, Piero Parchi, MD, PhD, Sabina Capellari, MD, Jiri Safar, MD, Janna Kenny, MBBS, Jamie C. Fong, MS, Leonel T. Takada, MD, PhD, Claudia Ponto, MD, Peter Hermann, MD, Tobias Knipper, MD, Christiane Stehmann, PhD, Tetsuyuki Kitamoto, MD, Ryusuke Ae, MD, PhD, Tsuyoshi Hamaguchi, MD, Nobuo Sanjo, MD, PhD, Tadashi Tsukamoto, MD, Hidehiro Mizusawa, MD, PhD, Steven J. Collins, MD, Roberto Chiesa, PhD, Ignazio Roiter, MD, Jesús de Pedro-Cuesta, MD, PhD, Miguel Calero, PhD, Michael D. Geschwind, MD, PhD, Masahito Yamada, MD, PhD, Yosikazu Nakamura, MD, MPH, and Simon Mead, MD, PhD

Correspondence
Dr. E.V. Minikel
eminikel@broadinstitute.org

Neurology® 2019;93:e125-e134. doi:10.1212/WNL.0000000000007745

Abstract

Objective

To determine whether preventive trials in genetic prion disease could be designed to follow presymptomatic mutation carriers to onset of disease.

Methods

We assembled age at onset or death data from 1,094 individuals with high penetrance mutations in the prion protein gene (*PRNP*) in order to generate survival and hazard curves and test for genetic modifiers of age at onset. We used formulae and simulations to estimate statistical power for clinical trials.

Results

Genetic prion disease age at onset varies over several decades for the most common mutations and neither sex, parent's age at onset, nor *PRNP* codon 129 genotype provided additional explanatory power to stratify trials. Randomized preventive trials would require hundreds or thousands of at-risk individuals in order to be statistically powered for an endpoint of clinical onset, posing prohibitive cost and delay and likely exceeding the number of individuals available for such trials.

Conclusion

The characterization of biomarkers suitable to serve as surrogate endpoints will be essential for the prevention of genetic prion disease. Parameters such as longer trial duration, increased enrollment, and the use of historical controls in a postmarketing study could provide opportunities for subsequent determination of clinical benefit.

From Broad Institute of MIT and Harvard (E.V.M., S.M.V.), Cambridge; Analytical and Translational Genetics Unit (E.V.M.), Massachusetts General Hospital; Program in Biological and Biomedical Sciences (E.V.M., S.M.V.), Harvard Medical School, Boston; Prion Alliance (E.V.M., S.M.V.), Cambridge; Harvard Business School (M.C.O.), Boston, MA; Institut du Cerveau et de la Moelle Épinière (J.-P.B., S.H.), ICM, Inserm U 1127, CNRS UMR 7225, Sorbonne Université; Cellule Nationale de Référence des Maladies de Creutzfeldt-Jakob (J.-P.B., S.H., J.-L.P.), Assistance Publique-Hôpitaux de Paris, France; National Reference Center for TSE (I.Z., C.P., P.H., T.K.), Georg-August University, Göttingen, Germany; IRCCS–Istituto delle Scienze Neurologiche di Bologna (P.P., S.C.); Departments of Experimental, Diagnostic and Specialty Medicine (P.P.) and Biomedical and Neuromotor Sciences (S.C.), University of Bologna, Italy; National Prion Disease Pathology Surveillance Center (J.S.), Case Western Reserve University, Cleveland, OH; MRC Prion Unit at UCL (J.K., S.M.), Institute of Prion Diseases, University College London, UK; Memory and Aging Center (J.C.F., L.T.T., M.D.G.), University of California San Francisco; Australian National CJD Registry (C.S., S.J.C.), University of Melbourne, Parkville, Australia; Department of Neurological Science (T.K.), Tohoku University Graduate School of Medicine, Sendai; Department of Public Health (R.A., Y.N.), Jichi Medical University, Shimotsuke; Department of Neurology and Neurobiology of Aging (T.H., M.Y.), Kanazawa University Graduate School of Medical Sciences, Kanazawa; Department of Neurology and Neurological Science (N.S.), Tokyo Medical and Dental University; National Center of Neurology and Psychiatry (T.T., H.M.), Kodaira, Japan; Laboratory of Prion Neurobiology (R.C.), Istituto di Ricerche Farmacologiche Mario Negri IRCCS, Milan; AULSS2 Ca' Foncello Hospital (I.R.), Treviso, Italy; Spanish National Reference Center for CJD (J.d.P.-C., M.C.), Instituto de Salud Carlos III and CIBERNED, Madrid, Spain; and NHS National Prion Clinic (S.M.), National Hospital for Neurology and Neurosurgery, UCL Hospitals NHS Foundation Trust, London, WC1N 3BG, UK.

Go to Neurology.org/N for full disclosures. Funding information and disclosures deemed relevant by the authors, if any, are provided at the end of the article.

Glossary

AD = Alzheimer disease; **FDA** = Food and Drug Administration; **HR** = hazard ratio.

Regulatory agencies worldwide have created programs to support drug development in situations where requiring the gold standard—a placebo-controlled, randomized trial with a clinical endpoint (a measure of how patients feel or function)—might unduly delay patient access to potentially life-saving drugs. Under Accelerated Approval,[1] the US Food and Drug Administration (FDA) "incorporate[s] novel approaches into the review of surrogate endpoints…especially…where the low prevalence of a disease renders the existence or collection of other types of data unlikely or impractical." [2] Here we examine whether genetic prion disease meets this criterion.

Genetic prion disease (including genetic Creutzfeldt-Jakob disease, fatal familial insomnia, and Gerstmann-Sträussler-Scheinker disease) is a fatal, incurable neurodegenerative disease caused by variants in *PRNP*,[3] some of which are highly penetrant.[4] Trials in prion disease have randomized symptomatic patients, mostly with sporadic prion disease, to clinical endpoints,[5–7] but by the time of diagnosis many prion disease patients are in a state of advanced dementia, and even halting the disease process might only preserve the patient in a state with little or no quality of life.[8] Meanwhile, several therapies tested preclinically have increased survival in prion-infected mice by 2–4× when administered long before symptoms, but are less effective later on and may not be effective at all after symptom onset.[9–12] Thus, it is important to enable preventive trials in presymptomatic individuals at risk for genetic prion disease.[13]

The Alzheimer's Prevention Initiative has randomized healthy, presymptomatic *PSEN1* E280A mutation carriers to drug or placebo with a cognitive endpoint after 5 years.[14] We sought to determine whether a similar trial design would be feasible in genetic prion disease.

Methods

Standard protocol approvals, registrations, and patient consents

This study was performed under ethical approval from the Partners Healthcare Institutional Research Board (2014P000226/MGH) and the Broad Institute's Office of Research Subjects Protection (ORSP-2121 and NHSR-4190). Written consent was obtained from research participants except where waived for a subset of deceased participants due to obligatory case reporting to surveillance centers.

Literature annotation

Some *PRNP* variants can be identified as highly penetrant by their extreme enrichment in cases over population controls, but many variants are too rare in both groups for meaningful comparison.[4] We therefore reviewed primary literature for 70 reportedly pathogenic *PRNP* variants (table S1, doi.org/10.5281/zenodo.2535761) to determine which had evidence of at least one family with at least 3 affected individuals in a pattern consistent with Mendelian segregation, or had a documented case with a de novo mutation. We identified 27 such variants, deemed likely high-penetrance variants. The remainder were seen in isolated patients with a negative or unknown family history, or have population allele frequencies inconsistent with high penetrance.[4] These variants will include both benign and low-risk variants. It is possible that some genuinely high-penetrance variants may also lack literature evidence for high penetrance due to missing family history information or an unavailability of family member DNA to confirm de novo status, but this issue will only affect variants with very low case counts and thus will have minimal effect on the results reported here.

Data collection

Age at onset data were gathered from 9 study centers (table S2 and supplementary Methods, doi.org/10.5281/zenodo.2535761) and include both previously reported and newly identified families and individuals. Age at onset was based on the earliest date of symptoms, determined by the patient or witnesses, which subsequently developed into prion disease.

Estimation of the number of individuals available for trials

The National Prion Disease Pathology Surveillance Center, as the source of the majority of *PRNP* gene testing in the United States, has near exhaustive ascertainment of individuals who have chosen predictive testing for genetic prion disease in this country. It provided for this study the number of positive predictive genetic tests (n = 221) given out for *PRNP* mutations from 1996 through January 2017 to individuals not known to have developed disease as of 2017. Privacy concerns prevent publication of a breakdown of these results by age and specific *PRNP* mutation, so we multiplied the total (n = 221) by the proportion of US symptomatic prion disease cases with a rare *PRNP* variant[4] who had a mutation classified here as high penetrance (271/362 [75%]) and by the proportion of individuals in a UK predictive testing cohort[15] who were age 40 or older (37/104 [36%]). This gives a conservative estimate that 221 × 75% × 36% = ~60 individuals alive in the United States today who meet the criteria we use in our power calculations. In the supplementary Discussion (doi.org/10.5281/zenodo.2535761), we consider in detail several other approaches to estimating the number of *PRNP* mutation carriers available for trials.

Statistics, source code, and data availability

Analyses were conducted using custom R 3.5.1 scripts run in RStudio 1.1.456. We present a public GitHub repository at github.com/ericminikel/prnp_onset (including figure, tables,

Discussion, and Methods including the details of power calculations and simulations) (doi.org/10.5281/zenodo.2535761) as well source code in the R programming language and life tables for each mutation. These data and code are sufficient to reproduce most analyses and figures herein. This GitHub repository is permanently archived at doi.org/10.5281/zenodo.2535761.

Results

Age at onset in genetic prion disease

We reasoned that any preventive trial with a clinical endpoint in genetic prion disease would derive most of its statistical power from individuals with high penetrance *PRNP* variants. Literature review (see Methods) revealed 27 *PRNP* variants with evidence for high penetrance. The top 3—E200K, P102L, and D178N—collectively explain 85% of high-penetrance cases in a recent case series[4] (figure S1, doi.org/10.5281/zenodo.2535761). Each of these arises from a CpG transition (a C to T DNA change where the adjacent base is G), a type of variant that occurs by spontaneous mutation 10–100× more often than other mutation types,[16,17] explaining the recurrence of these 3 mutations on multiple *PRNP* haplotypes in families worldwide.[4,18,19] Therefore, regardless of the population studied, these 3 variants are likely to account for a large fraction of genetic prion disease cases with high-penetrance variants. We focused our analysis primarily on individuals with these 3 variants, aggregating age at onset or age at death data on 1,001 individuals from 9 study centers worldwide (tables 1 and S2 [doi.org/10.5281/zenodo.2535761]), encompassing both direct clinical reports and family histories (see Methods), and including censored individuals. Statistics on 93 individuals with the next 4 mutations most common in cases—5-OPRI (insertion of 5 extra octapeptide repeats), 6-OPRI, P105L, and A117V—are included in table S3 (doi.org/10.5281/zenodo.2535761). We used these data to compile life tables and computed the annual hazard—risk of onset in each year of life—for each mutation (supplementary life tables, doi.org/10.5281/zenodo.2535761).

We found wide variability in age at onset (table 1), consistent with previous reports.[20–22] An implication of this variability is that high lifetime risk arises not from certain onset at a specific age, but from modest risk in any given year of life, accumulated over many decades of exposure. This poses a challenge for following presymptomatic individuals to onset in a preventive clinical trial, as it is difficult to ascertain a group of individuals for whom onset is imminent. For example, even at age 57, an E200K individual has only a 5% probability of disease onset occurring in any given year. This means that 20 person-years of follow-up for E200K individuals around this age would be expected to result in only one observed disease onset. Annual hazards do rise with age, but as they reach high levels, the number of surviving individuals also dwindles (figure 1). For the 3 most common mutations, the annual hazard remains below 10% until after the majority of people have already died (figures 1 and S3 and supplementary life tables, doi.org/10.5281/zenodo.2535761).

Similarly, the median number of years until onset, conditioned on an individual's current age, remains ≥5 years until after the median age at onset has passed (supplementary life tables, doi.org/10.5281/zenodo.2535761). The next 4 most common mutations have tighter age at onset distributions, and so reach higher annual hazards sooner (figure S3, doi.org/10.5281/zenodo.2535761), but these mutations are also much rarer, accounting for only 10% of cases with a high-penetrance variant.[4]

Power for randomized preapproval trials with a clinical endpoint

Based on the age-dependent hazards calculated for each mutation, we set out to determine how many individuals would need to enroll in order to power prevention trials with an endpoint of disease onset. While younger individuals or those with a mutation of modest penetrance might seek to enroll in trials or take a preventive drug, they would not contribute much statistical power to an endpoint of clinical onset. We therefore chose to base our power calculations on individuals with the 3 most common high-penetrance mutations between age 40 and 80.

We estimated how many individuals in this age range have high-penetrance *PRNP* mutations. It is estimated based on

Table 1 Variability in age at onset in genetic prion disease

	Without censored data		Survival curve including censored data		
Mutation	**Mean ± SD**	**N**	**Median (IQR)**	**Range**	**N**
P102L	53.7 ± 10.6	193	56 (47–60)	22–75	206
D178N	51.3 ± 11.8	256	53 (46–60)	12–89[a]	289
E200K	61.3 ± 10.0	456	62 (55–68)	31–92	506

Abbreviation: IQR = interquartile range.
Censored data include individuals who were either alive and well at last follow-up or had died of an unrelated cause, and whose genetic status was known either through predictive testing or due to obligate carrier status. For D178N and E200K, because the majority of individuals have disease duration ≤1 year (figure S2, doi.org/10.5281/zenodo.2535761), age at death is used where age at onset is unavailable. For P102L, which more often has a longer disease duration, only age at onset is used. Range indicates highest and lowest observed age at onset, except where [a] the longest survival is a censored data point.

Figure 1 Hazards and survival for the most common PRNP mutations

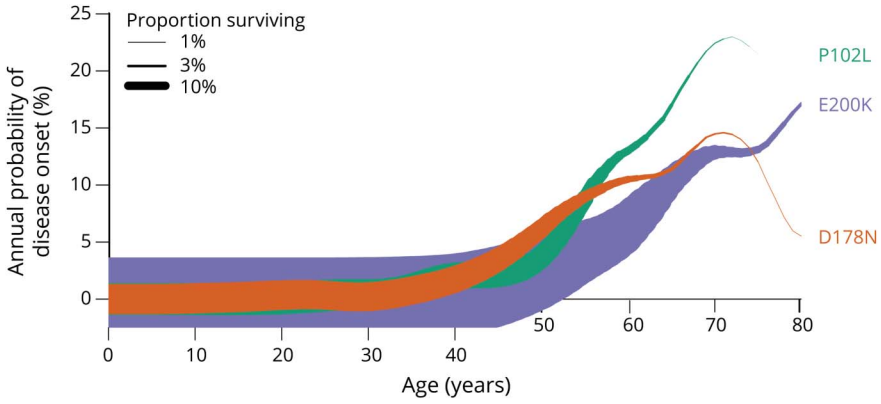

The hazard, or probability of disease onset, in each year of life (y axis) is plotted against age (x axis) with curve thickness representing the proportion of individuals still living at each age, which is the product of age-dependent survival and mutation prevalence. Supplementary mutations, and conventional survival curves and hazard plots, are included in figure S3 (doi.org/10.5281/zenodo.2535761).

disease prevalence that 1–2 people per 100,000 in the general population harbor high-penetrance *PRNP* mutations (reference 4 and supplementary Discussion, doi.org/10.5281/zenodo.2535761), but at present, many remain unaware of their risk due to underdiagnosis of affected family members,[23] and few choose predictive testing[15] as the results are currently considered medically unactionable. Based on predictive test results, we estimate there are currently ~60 people in the United States who are age 40 or older and hold a positive predictive test for a highly penetrant *PRNP* variant (see Methods).

We used published formulae[24] (see Methods) to calculate statistical power for a log-rank survival test in randomized clinical trials (table 2). Across the 3 mutations and weighted by their prevalence among cases (figure S1, doi.org/10.5281/zenodo.2535761) and number of surviving individuals at each age (figure 1), the average annual probability of onset for individuals aged 40–80 is 4.6%. With this figure as a baseline hazard, we made the following assumptions: presymptomatic individuals are randomized half to drug and half to placebo and followed for 5 years with an endpoint of clinical onset; the withdrawal rate is 15.2% annually (the median value from 8 prevention trials reviewed, table S4, doi.org/10.5281/zenodo.2535761); and the trial is designed for 80% power at the $p = 0.05$ threshold. Events in the first year are ignored as a run-in period to ensure sufficient drug exposure among individuals analyzed, because preclinical studies have suggested that drug treatment close to the symptomatic stage of disease may have diminished or no efficacy compared to earlier treatment.[9–12] We then performed power calculations for such a trial as a function of the hazard ratio—the ratio of annual risk of onset in drug-treated individuals to that in placebo-treated individuals. For context, we also determined the effect size, in median years of healthy life added, to which each hazard ratio (HR) corresponds (table 2). The calculations are sensitive to which mutations are included, the run-in period, the number of years of follow-up, and the assumed withdrawal rate, but we explored a range of different assumptions and none supports a different overall interpretation of the data (table S5, doi.org/10.5281/zenodo.2535761, and Discussion). In particular, the assumption of a 15.2% annual withdrawal rate means that only 44% of original participants remain after 5 years, but even reducing the withdrawal rate to zero only lowers the number of participants required by one-third (table S5, doi.org/10.5281/zenodo.2535761).

The above power calculations simplistically assume a uniform baseline hazard across all participants, regardless of age and

Table 2 Preventive trial requirements under survival test power calculation

Hazard ratio	Years of life added	Onsets required	Participants required
0.1	Undefined[a]	6	101
0.2	21	12	189
0.3	14	22	311
0.4	10	37	498
0.5	7	65	813
0.6	5	120	1,406
0.7	4	247	2,724
0.8	2	631	6,602
0.9	1	2,828	28,204

For example, a hazard ratio (HR) of 0.5 means that placebo-treated individuals have a 4.6% annual probability of onset, while drug-treated individuals have only a 2.3% annual probability of onset. If a population of individuals were treated from an early age with such a drug, the median age at onset would be postponed by 7 years. To have 80% power at $p = 0.05$ to detect the effect of such a drug, 65 individuals would need to become symptomatic during the trial—given the 0.5 HR, about two-thirds of these would occur in the placebo group and one-third would occur in the drug group. Observing this number of disease onsets would require randomizing 813 people for 5 years (data from the first year would be ignored, and the remaining 4 years of data would be analyzed).

[a] For a HR of 0.1, most individuals never become sick, thus, the increase in median age at onset (the age where 50% of people have had onset) is undefined.

PRNP mutation. We also used a simulation to account for the full shape of the hazard curve and diversity of genetic mutations, but the simulated power results were similar to those in table 2 (see table S6, doi.org/10.5281/zenodo.2535761). Stratification by *PRNP* mutation did not improve power in our simulations (supplementary discussion, doi.org/10.5281/zenodo.2535761), perhaps because age at onset distributions (table 1) are wide and overlapping, such that *PRNP* mutation explains only a minority of the overall variance in age at onset (adjusted $R^2 = 0.15$, linear regression, $p < 1 \times 10^{-32}$).

Statistical power might be improved by stratifying clinical trial analysis by relevant additional variables, but there are currently no variables that help to explain age at onset (supplementary Discussion, table S7, and figures S4 and S5, doi.org/10.5281/zenodo.2535761). For instance, we found no sex effect, and no evidence that parent and child age at onset are correlated after controlling for *PRNP* mutation and for child's year of birth, a variable that captures some effects of ascertainment bias[25] (table S7, doi.org/10.5281/zenodo.2535761). A common genetic variant, *PRNP* M129V, is known to affect the clinical and pathologic presentation of many forms of prion disease[26] as well as the risk of sporadic and acquired prion disease.[27] This variant has previously been reported to affect age at onset in some forms of genetic prion disease but not others.[21,25,28,29] We found no evidence that codon 129 affects age at onset for P102L or E200K individuals (table S7 and figure S4, doi.org/10.5281/zenodo.2535761). For D178N, our data are suggestive that a 129VV genotype may predispose to earlier onset than MM or MV genotypes (figure S4 and supplementary Discussion, doi.org/10.5281/zenodo.2535761), but in the overall dataset, codon 129 failed to explain additional variance in age at onset (supplementary Discussion, doi.org/10.5281/zenodo.2535761).

Based on this analysis, at present it is not possible to adequately power a randomized preapproval prevention trial with an endpoint of clinical onset in genetic prion disease. For example, for a drug that reduces annual risk by half (HR of 0.5), powering such a trial would require 813 participants age 40 or older, many times the ~60 currently estimated to exist in the United States. We next turned our attention to the possibility that a preventive drug might be developed through the Accelerated Approval pathway using a surrogate biomarker endpoint.

Power for postmarketing studies

We asked whether, if Accelerated Approval were achieved, the required postmarketing studies to confirm clinical benefit could be adequately powered by following drug-treated individuals to clinical onset and comparing their survival to that of historical controls. Such a trial design could increase power but also introduce bias; we considered each issue in turn.

We identified several factors that are likely to decrease the number of participants required to power such a study compared to its randomized preapproval equivalent: all, rather than half, of individuals are drug-treated; the number of historical controls can be large; a longer trial duration could be considered because the trial would overlap, rather than reduce, the drug's effective market exclusivity period (supplementary Discussion; doi.org/10.5281/zenodo.2535761); and a postmarketing surveillance program might allow newly drug-treated individuals to enter the program on a rolling basis, replacing any who withdraw. The effects of these assumptions (table 3) are collectively to reduce the number of individuals required to demonstrate efficacy of a drug with HR of 0.5 from 813 to 37. At the same time, the number of individuals available for a trial might increase, because an approved drug should have broader geographic reach than a preapproval trial, being limited only by the availability of medical personnel capable of prescribing and administering it rather than by a set number of trial sites; a treatment might improve awareness and diagnosis of the disease; and a treatment might stimulate more individuals to pursue predictive genetic testing. For instance, of people at 50/50 risk for a *PRNP* mutation, currently only 23% pursue predictive testing,[15] compared to 60% (2.6× higher) for

Table 3 Comparison of power calculations for preapproval and postmarketing studies

Scenario	N required	Explanation
Randomized preapproval—5-year follow-up	813	See table 2
Postmarketing with historical controls—5-year follow-up	229	Increased power because all, rather than half, of individuals are treated, and n = 1,000 historical controls are used for comparison
Postmarketing with historical controls—15- year follow-up	125	Increased power because longer trial duration may be financially tenable for postmarketing studies; power is still limited, however, by withdrawal rate, which means that few participants remain at the end of 15 years
Postmarketing with historical controls—15-year follow-up, no withdrawal	37	Increased power because the withdrawal rate is set to zero, simulating a scenario where individuals who go on drug can continuously enter the surveillance program, and the cohort being monitored can maintain its size over time

In each case, the calculation is for a hazard ratio of 0.5, the n indicated is for 80% power at the $p = 0.05$ threshold, and all assumptions other than those indicated in the table are the same as for table 2. The number of individuals required for postmarketing studies is determined by simulation (supplementary Discussion, doi.org/10.5281/zenodo.2535761).

BRCA1 or *BRCA2* mutations,[30] which are considered medically actionable.[31] Thus, a postmarketing study could be adequately powered with available numbers of individuals for a HR of 0.5 (table 3) and, over a range of assumptions, would bring power requirements into closer alignment with the number of available individuals (figure S6 and supplementary Discussion, doi.org/10.5281/zenodo.2535761).

While we conducted tests to ensure that our power simulation was not itself biased (supplementary Discussion, doi.org/10.5281/zenodo.2535761), a postmarketing study could still be biased in real life, if the historical controls used do not accurately estimate the true hazard rates facing the trial participants.[32] There are no environmental, demographic, or non-*PRNP* genetic factors known to affect prion disease risk or age at onset, although these might nonetheless exist.[33,34] Perhaps of greater concern is that most of our historical controls were collected retrospectively—individuals are only ascertained if they become sick—and may overestimate the hazard rates for individuals followed prospectively.[25] To assess this possible source of bias, we compared the survival of the limited number of individuals followed prospectively in our dataset (n = 24 individuals, with a cumulative 145 person-years of follow-up), conditioned on their ages at first ascertainment, to those of individuals with no prospective follow-up. We did not observe a significant difference in hazard (p = 0.59, Cox proportional hazards test) between these 2 groups, although this could be due to a lack of power (see Discussion).

Discussion

Both our power calculation and simulation indicate that direct demonstration of clinical benefit in a randomized preapproval prevention trial would require enrolling a number of *PRNP* mutation carriers that is not currently realistic. Achieving 80% power for a drug that reduces annual risk by half would require randomizing 813 individuals for 5 years, while we estimate only ~60 individuals in the United States fit the age and mutation criteria assumed in this calculation. Eighty percent power might be barely achievable under the most wildly optimistic assumptions of an extremely effective drug (HR of 0.1, reducing annual risk of onset by 10-fold), along with some increase in predictive testing rates and a very successful trial recruitment effort. The FDA has cautioned, however, that rare disease trials should not be designed around the hope of a huge effect size,[35] and even if a drug were so profoundly effective, it is unlikely that a sponsor would have sufficient confidence in this a priori to invest in a trial that is underpowered for more moderate effect sizes. Key assumptions underpinning this analysis may change with time: new stratifying variables could help to predict age at onset, or a first drug for prion disease could improve diagnosis and recruitment. However, the insight that randomized preapproval prevention trials with a clinical endpoint may not be feasible today motivates consideration of alternative trial designs.

At least 3 factors can explain why a randomized trial design following presymptomatic individuals to a clinical endpoint was deemed feasible for early-onset Alzheimer disease (AD), yet appears unviable for genetic prion disease. First, onset is less predictable in genetic prion disease. The standard deviation of age at onset or the 3 *PRNP* mutations we examined (±10.0 to ±11.8 years) is larger than that for *PSEN1* E280A AD (±6.4 to ±8.6 years[36,37]). In addition, an individual's age at onset in genetic AD is reported to be correlated with parental age at onset,[37] and this property has been used to attempt to enrich for high-hazard individuals in trials,[38] whereas we have found no evidence that parent and child age at onset are correlated in genetic prion disease (table S7, doi.org/10.5281/zenodo.2535761, and reference 25). Second, genetic prion disease is rarer. The *PSEN1* preventive trial recruited from a single pedigree of ~5,000 individuals[39] from which 1,065 living individuals with the mutation have been enrolled in a registry.[40] There is no known genetic prion disease family this large. Third, genetic prion disease offers more limited financial incentives for a pharmaceutical sponsor. The cost of the *PSEN1* preventive trial has been estimated at $96 million,[38,41] and while this price may be tenable for sponsors in view of potential for an expanded AD indication, no similar potential exists for prion disease. Indeed, even in AD, larger or longer primary prevention trials are likely to prove challenging for the private sector and may require public sector investment.[42]

Preclinical studies of anti-prion agents[9,10] suggest that trials in symptomatic patients could fail to show a benefit that would have been realizable in preventive treatment. Yet our results here indicate that it would be difficult or impossible to design a well-powered randomized preventive trial with a clinical endpoint in genetic prion disease. Together, these observations argue for the characterization of biomarkers suitable as endpoints in presymptomatic genetic prion disease, and for their evaluation by regulatory agencies as surrogate trial endpoints. A route to Accelerated Approval using cerebrospinal fluid prion protein as a surrogate biomarker endpoint has been proposed.[13,43]

If provisional approval could be achieved, then a postmarketing study might be required to confirm clinical benefit. We estimate that a model in which drug-treated individuals are enrolled in a surveillance program and their survival is compared to that of historical controls could reduce the number of individuals required for trials by 3- to 20-fold, compared to randomized preapproval studies. Meanwhile, conditional approval of a first prion disease drug may alter key measures such as diagnosis, recruitment, and genetic testing rates, the last of which alone could increase participant availability by more than 2-fold. Thus, while power for any trial depends upon how effective the drug is, there exists a range of assumptions under which a postmarketing study could be adequately powered. There may be various formats through which a postmarketing study could confirm clinical benefit.

Under some assumptions, a postmarketing study might last a decade or longer and would benefit from following all

mutation carriers taking the drug. With creative and careful planning, we propose that these goals could be achieved. In one model, a postmarketing study might take the form of a surveillance program, in which treated patients are followed long-term, perhaps in collaboration with existing prion specialist clinics and surveillance centers worldwide. In such a model, drug costs would be reimbursed by payors, in contrast to a more traditional sponsor-funded pivotal trial. While this model would be a departure from the more conventional design of most postmarketing studies required for recent Accelerated Approval drugs,[44] precedents exist for regulatory innovation in this area. For example, the FDA's Risk Evaluation and Mitigation Strategies program for drugs with serious safety concerns entails indefinite postmarket enrollment and monitoring of treated patients,[45] and postapproval study requirements for medical devices often include registries or surveillance efforts and are not always industry-funded.[46,47]

Our study has several limitations. First, true age at onset distributions can only be obtained prospectively,[48] whereas our data are largely retrospective. We have included asymptomatic individuals with pathogenic *PRNP* variants where possible, but our ascertainment of them is incomplete due to limited uptake of predictive testing.[15] This bias may tend to make our estimates of age at onset overly pessimistic.[25,49] To the extent that true age at onset is older, or total lifetime risk lower, than our data suggest, randomized preventive trials with a clinical endpoint would require even greater numbers of individuals, and thus further increase our caution around this study design. Second, although our dataset is, to our knowledge, the largest ever reported for genetic prion disease age at onset, our statistical power to detect genetic modifiers, which might aid in age at onset prediction, is limited. Third, although we have attempted to select a reasonable set of assumptions for modeling clinical trials, we have by no means exhaustively sampled the set of possible trial designs and measures. Fourth, powering a postmarketing study will require a good historical control dataset to compare to, and our dataset, which was collected mostly retrospectively, may or may not be adequate. We found no evidence that our dataset overestimates the hazards facing prospectively followed individuals, but this could be due to a lack of power in our analysis. Fifth, the ascertainment of genetic prion disease by prion surveillance centers may be biased towards rapidly progressive phenotypes, meaning that the prevalence of more slowly progressive forms might be underestimated.

Our findings highlight 2 priorities for the prion field. First, the discovery and characterization of biomarkers capable of serving as trial endpoints may be essential to enable near-term presymptomatic trials in genetic prion disease. Second, a postapproval surveillance mechanism for age at onset merits consideration as one option for confirmation of clinical benefit following biomarker-based provisional approval. The ability to access therapies that can prevent or delay prion disease, yet which are likely to be less effective or ineffective after symptom onset, could be greatly enhanced by success in these areas.

Acknowledgment

The authors thank the patients and families who contributed their data to this research; Javier Almazan and Dr. Maria Ruiz, CNE, Madrid, for help with data extraction at the Spanish CJD Registry; and Eric S. Lander, Michael J. Donovan, and Adam Bliss for discussions.

Study funding

E.V.M. is supported by the NIH (F31 AI122592), S.M.V. is supported by the National Science Foundation (GRFP 2015214731), and both are supported by an anonymous organization. S.H. and J.-P.B. are supported by Santé Publique France by the program "Investissement avenir" ANR-10-IAIHU-06. Work at the NHS National Prion Clinic was supported by the UK National Institute of Health Research's Biomedical Research Centre at University College London Hospitals NHS Foundation Trust. Japanese prion surveillance is funded by a grant-in-aid from the Research Committee of Prion Disease and Slow Virus Infection, the Ministry of Health, Labour and Welfare of Japan, and the Research Committee of Surveillance and Infection Control of Prion Disease, the Ministry of Health, Labour and Welfare of Japan. S.C. is supported in part by an NHMRC Practitioner Fellowship (#APP1105784) and the Australian National Creutzfeldt-Jakob Disease Registry is funded by the Commonwealth Department of Health. Data collection in Germany was supported by grant 1369-341 by Bundesministerium für Gesundheit through Robert Koch Institute. Work in Italy was partially supported by Fondazione Telethon (GGP10208). M.D.G. was supported by NIH/NIA R01 AG-031189, NIH/NIA R01 AG032289, the Michael J. Homer Family Fund, and Alliance BioSecure.

Disclosure

E. Minikel has received research support from Charles River Laboratories via charitable donations to Prion Alliance. S. Vallabh has received research support from Charles River Laboratories via charitable donations to Prion Alliance. M. Orseth is employed by Bain & Co. J. Brandel reports no disclosures relevant to the manuscript. S. Haïk has received research support from MedDay Pharmaceuticals, LFB Biomedicaments, and Institut de Recherche Servier. J. Laplanche, I. Zerr, P. Parchi, S. Capellari, J. Safar, J. Kenny, J. Fong, L. Takada, C. Ponto, P. Hermann, T. Knipper, C. Stehmann, T. Kitamoto, R. Ae, T. Hamaguchi, N. Sanjo, and T. Tsukamoto report no disclosures relevant to the manuscript. H. Mizusawa has received compensation from Eisai, EA Pharma, Novartis, Sanofi, Tenable Mitsubishi Pharma, FP Pharma, Nihon Pharma, Chugai Igaku Co., Igakushoin Co., and Nankodo Co. S. Collins, R. Chiesa, I. Roiter, and J. de Pedro-Cuesta report no disclosures relevant to the manuscript. M. Calero has received compensation from Raman Health Technologies and Springer Nature, is a shareholder of Raman Health Technologies, Biocross, and Bio Haptenyc DGR, and has received research support from AMO Pharma, Ltd. M. Geschwind has received research support from Quest Diagnostics. M. Yamada and Y. Nakamura report no disclosures relevant to the manuscript. S. Mead is a shareholder of GlaxoSmithKline and Ionis Pharmaceuticals and has received

research support from Nova Pharmaceuticals. Go to Neurology.org/N for full disclosures.

Publication history

Received by *Neurology* November 2, 2018. Accepted in final form February 21, 2019.

This manuscript was previously posted to bioRxiv (doi.org/10.1101/401406) on August 29, 2018.

Appendix Authors

Name	Location	Role	Contribution
Eric Vallabh Minikel	Broad Institute, Cambridge, MA	Author	Principally conceived and designed the study, aggregated and analyzed the data, created the figure, wrote the paper
Sonia M. Vallabh	Broad Institute, Cambridge, MA	Author	Contributed to study conception and design, assisted with data curation and figure design, revised the manuscript for intellectual content
Margaret C. Orseth	Harvard Business School, Boston, MA	Author	Contributed to study conception and design, revised the manuscript for intellectual content
Jean-Philippe Brandel	Sorbonne Université, Paris, France	Author	Major role in data collection and interpretation, revised the manuscript for intellectual content
Stéphane Haïk	Sorbonne Université, Paris, France	Author	Major role in data collection and interpretation, revised the manuscript for intellectual content
Jean-Louis Laplanche	Assistance Publique-Hôpitaux de Paris, France	Author	Major role in data collection and interpretation, revised the manuscript for intellectual content
Inga Zerr	University of Göttingen, Germany	Author	Major role in data collection and interpretation, revised the manuscript for intellectual content
Piero Parchi	University of Bologna, Italy	Author	Major role in data collection and interpretation, revised the manuscript for intellectual content
Sabina Capellari	University of Bologna, Italy	Author	Major role in data collection and interpretation, revised the manuscript for intellectual content
Jiri Safar	Case Western Reserve University, Cleveland, OH	Author	Major role in data collection and interpretation, revised the manuscript for intellectual content
Janna Kenny	MRC Prion Unit at UCL, London, UK	Author	Major role in data collection and interpretation, revised the manuscript for intellectual content
Jamie C. Fong	UCSF, San Francisco, CA	Author	Major role in data collection and interpretation, revised the manuscript for intellectual content
Leonel T. Takada	UCSF, San Francisco, CA	Author	Major role in data collection and interpretation, revised the manuscript for intellectual content
Claudia Ponto	University of Göttingen, Germany	Author	Major role in data collection and interpretation, revised the manuscript for intellectual content
Peter Hermann	University of Göttingen, Germany	Author	Major role in data collection and interpretation, revised the manuscript for intellectual content
Tobias Knipper	University of Göttingen, Germany	Author	Major role in data collection and interpretation, revised the manuscript for intellectual content
Christiane Stehmann	Australian National CJD Registry, Parkville, Australia	Author	Major role in data collection and interpretation, revised the manuscript for intellectual content
Tetsuyuki Kitamoto	Tohoku University Graduate School of Medicine, Sendai, Japan	Author	Major role in data collection and interpretation, revised the manuscript for intellectual content
Ryusuke Ae	Jichi Medical University, Shimotsuke, Japan	Author	Major role in data collection and interpretation, revised the manuscript for intellectual content
Tsuyoshi Hamaguchi	Kanazawa University Graduate School of Medical Sciences, Kanazawa, Japan	Author	Major role in data collection and interpretation, revised the manuscript for intellectual content

Appendix *(continued)*

Name	Location	Role	Contribution
Nobuo Sanjo	Tokyo Medical and Dental University, Japan	Author	Major role in data collection and interpretation, revised the manuscript for intellectual content
Tadashi Tsukamoto	National Center of Neurology and Psychiatry, Kodaira, Japan	Author	Major role in data collection and interpretation, revised the manuscript for intellectual content
Hidehiro Mizusawa	National Center of Neurology and Psychiatry, Kodaira, Japan	Author	Major role in data collection and interpretation, revised the manuscript for intellectual content
Steven J. Collins	Australian National CJD Registry, Parkville, Australia	Author	Major role in data collection and interpretation, revised the manuscript for intellectual content
Roberto Chiesa	Mario Negri Institute, Milan, Italy	Author	Major role in data collection and interpretation, revised the manuscript for intellectual content
Ignazio Roiter	AULSS2 Ca' Foncello Hospital, Treviso, Italy	Author	Major role in data collection and interpretation, revised the manuscript for intellectual content
Jesús de PedroCuesta	Spanish National Reference Center for CJD, Madrid, Spain	Author	Major role in data collection and interpretation, revised the manuscript for intellectual content
Miguel Calero	Spanish National Reference Center for CJD, Madrid, Spain	Author	Major role in data collection and interpretation, revised the manuscript for intellectual content
Michael D. Geschwind	UCSF, San Francisco, CA	Author	Major role in data collection and interpretation, revised the manuscript for intellectual content
Masahito Yamada	Kanazawa University Graduate School of Medical Sciences, Kanazawa, Japan	Author	Major role in data collection and interpretation, revised the manuscript for intellectual content
Yosikazu Nakamura	Jichi Medical University, Shimotsuke, Japan	Author	Major role in data collection and interpretation, revised the manuscript for intellectual content

Appendix *(continued)*

Name	Location	Role	Contribution
Simon Mead	MRC Prion Unit at UCL, London, UK	Author	Contributed to study conception and design, major role in data collection and interpretation, revised the manuscript for intellectual content

References

1. New drug, antibiotic, and biological drug product regulations; accelerated approval: FDA: final rule. Fed Regist 1992;57:58942–58960.
2. Food and Drug Administration Safety and Innovation Act. Public Law 112-114 Section 506(c)(3). July 9, 2012.
3. Prusiner SB. Prions. Proc Natl Acad Sci USA 1998;95:13363–13383.
4. Minikel EV, Vallabh SM, Lek M, et al. Quantifying prion disease penetrance using large population control cohorts. Sci Transl Med 2016;8:322ra9.
5. Otto M, Cepek L, Ratzka P, et al. Efficacy of flupirtine on cognitive function in patients with CJD: a double-blind study. Neurology 2004;62:714–718.
6. Geschwind MD, Kuo AL, Wong KS, et al. Quinacrine treatment trial for sporadic Creutzfeldt-Jakob disease. Neurology 2013;81:2015–2023.
7. Haïk S, Marcon G, Mallet A, et al. Doxycycline in Creutzfeldt-Jakob disease: a phase 2, randomised, double-blind, placebo-controlled trial. Lancet Neurol 2014;13:150–158.
8. Bechtel K, Geschwind MD. Ethics in prion disease. Prog Neurobiol 2013;110:29–44.
9. Doh-ura K, Ishikawa K, Murakami-Kubo I, et al. Treatment of transmissible spongiform encephalopathy by intraventricular drug infusion in animal models. J Virol 2004;78:4999–5006.
10. Giles K, Berry DB, Condello C, et al. Different 2-aminothiazole therapeutics produce distinct patterns of scrapie prion neuropathology in mouse brains. J Pharmacol Exp Ther 2015;355:2–12.
11. Kawasaki Y, Kawagoe K, Chen C, Teruya K, Sakasegawa Y, Doh-ura K. Orally administered amyloidophilic compound is effective in prolonging the incubation periods of animals cerebrally infected with prion diseases in a prion strain-dependent manner. J Virol 2007;81:12889–12898.
12. Wagner J, Ryazanov S, Leonov A, et al. Anle138b: a novel oligomer modulator for disease-modifying therapy of neurodegenerative diseases such as prion and Parkinson's disease. Acta Neuropathol 2013;125:795–813.
13. Vallabh SM. Antisense oligonucleotides for the prevention of genetic prion disease. PhD dissertation. Harvard University; 2019.
14. Tariot PN, Lopera F, Langbaum JB, et al. The Alzheimer's Prevention Initiative Autosomal Dominant Alzheimer's Disease Trial: a study of crenezumab versus placebo in preclinical PSEN1 E280A mutation carriers to evaluate efficacy and safety in the treatment of autosomal-dominant Alzheimer's disease, including a placebo-treated noncarrier cohort. 2018;4:150–160.
15. Owen J, Beck J, Campbell T, et al. Predictive testing for inherited prion disease: report of 22 years experience. Eur J Hum Genet 2014;22:1351–1356.
16. Cooper DN, Youssoufian H. The CpG dinucleotide and human genetic disease. Hum Genet 1988;78:151–155.
17. Samocha KE, Robinson EB, Sanders SJ, et al. A framework for the interpretation of de novo mutation in human disease. Nat Genet 2014;46:944–950.
18. Lee HS, Sambuughin N, Cervenakova L, et al. Ancestral origins and worldwide distribution of the PRNP 200K mutation causing familial Creutzfeldt-Jakob disease. Am J Hum Genet 1999;64:1063–1070.
19. Dagvadorj A, Petersen RB, Lee HS, et al. Spontaneous mutations in the prion protein gene causing transmissible spongiform encephalopathy. Ann Neurol 2002;52:355–359.
20. Kong Q, Surewicz WK, Petersen RB, et al. Inherited prion diseases. In: Prion Biol Dis [online]. 2nd ed. Cold Spring Harbor Laboratory Press; 2004. Available at: cshmonographs.org/index.php/monographs/article/viewArticle/4035.
21. Kovács GG, Puopolo M, Ladogana A, et al. Genetic prion disease: the EUROCJD experience. Hum Genet 2005;118:166–174.
22. Nozaki I, Hamaguchi T, Sanjo N, et al. Prospective 10-year surveillance of human prion diseases in Japan. Brain 2010;133:3043–3057.
23. Klug GMJA, Wand H, Simpson M, et al. Intensity of human prion disease surveillance predicts observed disease incidence. J Neurol Neurosurg Psychiatry 2013;84:1372–1377.
24. Schoenfeld DA. Sample-size formula for the proportional-hazards regression model. Biometrics 1983;39:499–503.
25. Minikel EV, Zerr I, Collins SJ, et al. Ascertainment bias causes false signal of anticipation in genetic prion disease. Am J Hum Genet 2014;95:371–382.
26. Capellari S, Strammiello R, Saverioni D, Kretzschmar H, Parchi P. Genetic Creutzfeldt-Jakob disease and fatal familial insomnia: insights into phenotypic variability and disease pathogenesis. Acta Neuropathol 2011;121:21–37.
27. Mead S. Prion disease genetics. Eur J Hum Genet 2006;14:273–281.

28. Mead S, Poulter M, Beck J, et al. Inherited prion disease with six octapeptide repeat insertional mutation–molecular analysis of phenotypic heterogeneity. Brain J Neurol 2006;129:2297–2317.
29. Webb TEF, Poulter M, Beck J, et al. Phenotypic heterogeneity and genetic modification of P102L inherited prion disease in an international series. Brain 2008;131: 2632–2646.
30. Lerman C, Narod S, Schulman K, et al. BRCA1 testing in families with hereditary breast-ovarian cancer: a prospective study of patient decision making and outcomes. JAMA 1996;275:1885–1892.
31. Green RC, Berg JS, Grody WW, et al. ACMG recommendations for reporting of incidental findings in clinical exome and genome sequencing. Genet Med 2013;15: 565–574.
32. US Food and Drug Administration. Rare Diseases: Common Issues in Drug Development: Draft Guidance for Industry [online]. 2015. Available at: web.archive.org/web/20190529133331/https://www.fda.gov/media/119757/download. Accessed August 22, 2018.
33. Hamasaki S, Shirabe S, Tsuda R, Yoshimura T, Nakamura T, Eguchi K. Discordant Gerstmann-Sträussler-Scheinker disease in monozygotic twins. Lancet 1998;352: 1358–1359.
34. Mead S, Uphill J, Beck J, et al. Genome-wide association study in multiple human prion diseases suggests genetic risk factors additional to PRNP. Hum Mol Genet 2012;21:1897–1906.
35. Woodcock J. Reforming clinical trials in drug development: impact of targeted therapies [online]. 2016. Available at: web.archive.org/web/20190529133445/https://www.fda.gov/media/101755/download. Accessed August 21, 2018.
36. Lopera F, Ardilla A, Martínez A, et al. Clinical features of early-onset Alzheimer disease in a large kindred with an E280A presenilin-1 mutation. JAMA 1997;277: 793–799.
37. Ryman DC, Acosta-Baena N, Aisen PS, et al. Symptom onset in autosomal dominant Alzheimer disease: a systematic review and meta-analysis. Neurology 2014;83: 253–260.
38. Mullard A. Sting of Alzheimer's failures offset by upcoming prevention trials. Nat Rev Drug Discov 2012;11:657–660.
39. Reiman EM, Langbaum JBS, Fleisher AS, et al. Alzheimer's Prevention Initiative: a plan to accelerate the evaluation of presymptomatic treatments. J Alzheimers Dis 2011;26(suppl 3):321–329.
40. The Colombian Alzheimer's Prevention Initiative (API) Registry [online]. Available at: sciencedirect.com/science/article/pii/S155252601632965X. Accessed March 22, 2017.
41. Garber K. Genentech's Alzheimer's antibody trial to study disease prevention. Nat Biotechnol 2012;30:731–732.
42. McDade E, Bateman RJ. Stop Alzheimer's before it starts. Nature 2017;547:153–155.
43. Vallabh SM, Nobuhara CK, Llorens F, et al. Prion protein quantification in human cerebrospinal fluid as a tool for prion disease drug development. Proc Natl Acad Sci. Epub 2019 Apr 1.
44. Naci H, Smalley KR, Kesselheim AS. Characteristics of preapproval and postapproval studies for drugs granted accelerated approval by the US Food and Drug Administration. JAMA 2017;318:626–636.
45. Brandenburg NA, Bwire R, Freeman J, Houn F, Sheehan P, Zeldis JB. Effectiveness of risk evaluation and mitigation strategies (REMS) for lenalidomide and thalidomide: patient comprehension and knowledge retention. Drug Saf 2017;40: 333–341.
46. Reynolds IS, Rising JP, Coukell AJ, Paulson KH, Redberg RF. Assessing the safety and effectiveness of devices after US Food and Drug Administration approval: FDA-mandated postapproval studies. JAMA Intern Med 2014;174:1773–1779.
47. Rathi VK, Krumholz HM, Masoudi FA, Ross JS. Characteristics of clinical studies conducted over the total product life cycle of high-risk therapeutic medical devices receiving FDA premarket approval in 2010 and 2011. JAMA 2015;314:604–612.
48. Langbehn DR, Hayden MR, Paulsen JS; PREDICT-HD Investigators of the Huntington Study Group. CAG-repeat length and the age of onset in Huntington disease (HD): a review and validation study of statistical approaches. Am J Med Genet B Neuropsychiatr Genet 2010;153B:397–408.
49. Langbehn DR, Brinkman RR, Falush D, Paulsen JS, Hayden MR; International Huntington's Disease Collaborative Group. A new model for prediction of the age of onset and penetrance for Huntington's disease based on CAG length. Clin Genet 2004;65:267–277.

Section 4: Human Prion Disease Biomarker Studies

Across the multifarious neurodegenerative disorders that can cause cognitive decline, when patients present with RPD accompanied by myoclonus and gross motor impairment, consideration of sCJD as a likely differential diagnostic explanation is relatively straightforward. Nonetheless, acknowledging that up to 30% of sCJD can manifest a less typical clinical profile and that co-morbidities affecting the brain commonly co-exist in the elderly, it is not infrequent that the pre-mortem diagnosis of sCJD can be more challenging. Up to the late 1990s, electroencephalography was the principal investigation available to assist with clinical evaluation, relying on the presence of generalized periodic complexes recurring at a rate of 1-2 Hz as a biomarker for sCJD. Although an EEG displaying such features in a patient with RPD remains of considerable positive predictive value, the relatively poor sensitivity of this finding across the full phenotypic spectrum of sCJD renders reliance on this single investigation unsatisfactory. Fortunately, the last 20 years has witnessed meritorious expansion of the diagnostic armamentarium for interrogating patients suspected to be manifesting sCJD. I have led the Australian participation in all landmark studies validating new biomarkers employed in the pre-mortem diagnosis of sCJD, with each of these biomarkers prompting revision of surveillance diagnostic criteria to allow their inclusion. This revolution in sCJD diagnostic biomarkers started with CSF 14-3-3 protein detection and was then followed by delineation of sensitive and specific brain MRI findings, with the most recent achievement confirmation of the utility of the protein amplification technology known as the Real-Time Quaking Induced Conversion (RT-QUIC) assay. The RT-QUIC assay has been a major advance given specificity of close to 100% and the ability to perform the test on both bio-fluids (such as CSF) and tissue samples (including from brain, olfactory epithelium and skin). The progressive translational incorporation of these diagnostic tests now means that only around 2-3% of sCJD patients do not display typical or characteristic findings with at least one of these investigations, thereby considerably enhancing our capacity to achieve an accurate clinical diagnosis pre-mortem. Despite these advances in pre-mortem diagnostic evaluation, however a diagnosis of “definite” CJD still requires neuropathological examination of the brain, preferably through autopsy to avoid potential sampling errors and transmission risks posed by brain biopsy.

List of my publications submitted in full (in chronological order)

S Collins, A Boyd, A Fletcher, M Gonzales, C McLean, K Byron, C Masters. Creutzdeldt-Jakob disease: diagnostic utility of 14-3-3 protein immunodetection in cerebrospinal fluid. Journal of Clinical Neuroscience 2000; 7: 203-208.

I Zerr, M Pocchiari, S Collins, JP Brandel, J De Pedro Cuesta, RSG Knight, H Bernheimer, F Cardone, N Delasnerie-Laupretre, N Cuadrado Corrales, A Ladogana, M Bodemer, A Fletcher, T Awan, A Ruiz, Bremon, H Budka, JL Laplanche, RG Will and S Poser. Analysis of EEG and CSF 14-3-3 proteins as aids to the diagnosis of Creutzfeldt-Jakob disease. Neurology 2000; 55: 811-815.

Collins SJ, Sanchez-Juan P, Masters CL, Klug GM, van Duijn C, Poleggi A, Pocchiari M, Almonti S, Cuadrado-Corrales N, de Pedro-Cuesta J, Budka H, Gelpi E, Glatzel M, Tolnay M, Hewer E, Zerr I, Heinemann U, Kretszchmar HA, Jansen GH, Olsen E, Mitrova E, Alpérovitch A, Brandel J-P, Mackenzie J, Murray K, Will RG. Determinants of diagnostic investigation sensitivities across the clinical spectrum of sporadic Creutzfeldt-Jakob disease. Brain 2006; 129: 2278-2287.

Holsinger RMD, Lee JS, Boyd A, Masters CL, Collins SJ. CSF BACE1 activity is increased in CJD and Alzheimer's disease compared to other dementias. Neurology 2006; 67: 710-712.

Meissner B, Kallenberg K, Sanchez-Juan P, Collie D, Summers DM, Almonti S, Collins SJ, Smith P, Cras P, Jansen GH, Brandel J-P, Coulthart MB, Roberts H, Van Everbroeck B, Galanaud D, Mellina V, Will RG, Zerr I. MRI lesion profiles in sporadic Creutzfeldt-Jakob disease. Neurology 2009; 72: 1994-2001.

Villemagne V, Reardon K, McLean C, Boyd A, Lewis V, Klug, GMA, Baxendale D, Masters CL, Rowe C, Collins SJ. Negative 11C-PiB PET in typical sporadic Creutzfeldt-Jakob Disease. Journal of Neurology, Neurosurgery and Psychiatry 2009; 80: 998-1001.

Zerr I, Kallenberg K, Summers DM, Romero C, Taratuto A, Heinemann U, Breithaupt M, Meissner B, Ladogana A, Schuur M, Galanaud D, Collins SJ, Jansen GH, Stokin GB, Pimentel J, Hewer E, Collie D, Smith P, Roberts H, Brandel J-P, van Duijn C, Pocchiari M, Begue C, Cras P, Will RG, Sanchez-Juan P. Updated clinical diagnostic criteria for sporadic CJD incorporating MRI findings. Brain 2009; 132: 2659-2668.

Collins SJ, McGlade A, Boyd A, Masters CL, Klug GMA. 14-3-3 protein detection and sporadic CJD: the status quo serves well while awaiting progress. Journal of Neurology, Neurosurgery and Psychiatry 2010; 81: 1181.

Atarashi R, Satoh K, Sano K, Fuse T, Yamaguchi N, Ishibashi D, Matsubara T, Nakagaki T, Yamada M, Yamanaka H, Shirabe S, Yamada M, Mizusawa H, Kitamoto T, Klug G,

McGlade A, Collins SJ, Nishida N. Ultrasensitive human prion detection in cerebrospinal fluids using real-time quaking-induced conversion. Nature Medicine 2011; 17: 175-178.

Schmitz M, Ebert E, Stoeck K, Karch A, Collins S, Calero M, Sklaviadis T, Laplanche J-L, Golanska E, Baldeiras I, Satoh K, Sanchez-Valle R, Ladogana A, Skinningsrud A, Hammarin A-L, Mitrova E, Kim Y-S, Green A, Zerr I. Validation of 14-3-3 protein as a marker in Creutzfeldt-Jakob disease diagnostic. Molecular Neurobiology 2016; 53:1896-1904.

McGuire L, Poleggi A, Poggiolini I, Suardi S, Grznarova K, Shi S, de Vil B, Sarros S, Satoh K, Cheng K, Cramm M, Fairfoul G, Schmitz M, Zerr I, Cras P, Equestre M, Tagliavini F, Atarashi R, Knox D, Collins S, Haïk S, Parchi P, Pocchiari M, Green A. An international study demonstrates that CSF RT-QuIC is a robust and transferable diagnostic test for sCJD. Annals of Neurology 2016; 80: 160-165.

Schmitz M, Cramm M, Llorens F, Müller-Cramm D, Collins S, Atarashi R, Satoh K, Orrù C, Groveman B, Zafar S, Schulz-Schaeffer W, Caughey B, Zerr I. The real-time quaking-induced conversion assay for detection of human prion disease and study of other protein misfolding diseases. Nature Protocols 2016: 11: 2233-2242.

Cramm M, Schmitz M, Karch A, Mitrova E, Kuhn F, Schroeder B, Raeber A, Varges D, Kim Y-S, Satoh K, Collins S, Green A, Zerr I. Stability and reproducibility underscore utility of RT-QuIC CSF analysis for diagnosis of human prion disease. Molecular Neurobiology 2015; 53: 1896-1904.

Li Q-X, Varghese S, Sarros S, Stehmann C, Doecke J, Fowler C, Masters C, Collins S. CSF Tau supplements 14-3-3 protein detection for sporadic Creutzfeldt–Jakob disease diagnosis while transitioning to next generation diagnostics. Journal of Clinical Neuroscience 2018; 50: 292-293.

Villar-Piqué A, Schmitz M, Lachmann I, Karch A, Calero O, Stehmann C, Sarros S, Ladogana A, Poleggi A, Santana I, Ferrer I, Mitrova E, Zakova D, Pocchiari M, Baldeiras I, Calero M, Collins S, Geschwind M, Sánchez-Valle R, Zerr I, Llorens F. Cerebrospinal fluid total Prion protein in the spectrum of prion diseases. Molecular Neurobiology 2018; doi.org/10.1007/s12035-018-1251-1.

Llorens F, Villar-Piqué A, Hermann P, Schmitz M, Calero O, Stehmann C, Sarros S, Moda F, Ferrer I, Poleggi A, Pocchiari M, Giaccone G, O'Regan C, Brett F, Heffernan J, Ladogana A, Collins S, Calero M, Kovacs G, Zerr I. Diagnostic accuracy of prion biomarkers in iatrogenic Creutzfeldt-Jakob disease. Biomolecules 2020, 10, 290; doi:10.3390/biom10020290.

Hermann P, Appleby B, Brandel J-P, Caughey B, Collins S, Geschwind M, Green A, Haïk S, Kovacs G, Ladogana A, Llorens F, Mead S, Nishida N, Pal S, Parchi P, Pocchiari M, Satoh K, Zanusso G, Zerr I. Biomarker-based diagnosis of sporadic Creutzfeldt-Jakob disease. In press – Lancet Neurology.

Journal of Clinical Neuroscience (2000) **7**(3), 203–208

DOI: 10.1054/ jocn.1999.0193, available online at http://www.idealibrary.com on IDEAL®

Clinical study

Creutzfeldt-Jakob disease: diagnostic utility of 14–3–3 protein immunodetection in cerebrospinal fluid

S Collins[1], A Boyd[1], A Fletcher[1], M Gonzales[2], C A McLean[1], K Byron[3], CL Masters[1]

[1]The Australian Creutzfeldt-Jakob Disease Registry, Department of Pathology, the University of Melbourne, Victoria, Australia 3010 [2]Neuropathology Laboratory, Department of Anatomical Pathology, The Royal Melbourne Hospital, Victoria, Australia 3052 [3]Molecular Pathology, North Western Health Care Network, Royal Melbourne Hospital, Victoria, Australia 3052.

Summary With the aim of improving the pre-mortem diagnostic accuracy of sporadic Creutzfeldt-Jakob disease (CJD), there has been considerable recent interest in the merit of immunodetecting 14–3–3 proteins in the cerebrospinal fluid (CSF) using Western blotting, with cumulative support for the utility of this technique. As a corollary, during a 20 month period, CSF samples from an unselected prospective series of 124 patients in whom sporadic CJD was a differential diagnostic possibility were examined by the Australian Creutzfeldt-Jakob disease Registry (ACJDR) for the presence of 14–3–3 proteins. Follow up to achieve a final diagnosis or clinical outcome was successful in 119. For definite and probable sporadic CJD combined, a positive result was 91.4% sensitive, while the sensitivity for the pathologically verified group alone was 96.0%. A negative outcome was 92.5% specific with false positive results seen in five patients with diagnoses which included inflammatory CNS disorders, cerebral ischaemia and dementia with Lewy bodies (DLB). Immunodetectable 14–3–3 proteins were present in three of four symptomatic patients with prion protein gene (PRNP) mutations. CSF samples containing significant amounts of blood were confirmed as suboptimal, with weak or qualitatively unusual positive results found in greater than 50% of such specimens, with only one of 14 such cases ultimately classified as definite or probable CJD. © 2000 Harcourt Publishers Ltd

Keywords: Creutzfeldt-Jakob disease, 14–3–3 proteins, cerebrospinal fluid, prion diseases

INTRODUCTION

Creutzfeldt-Jakob disease usually manifests as a clinically distinctive dementia because of rapid progression accompanied by cerebellar ataxia, myoclonus and typical electroencephalographic (EEG) changes, with the mean age of onset around 60 years and median survival less than 6 months.[1] However, less typical, more diagnostically challenging CJD subtypes exist, including the new variant form (vCJD) recently described in the UK, which is probably zoonotically linked to the epidemic of bovine spongiform encephalopathy.[2–4] Although a genetic basis and accidental (usually iatrogenic) horizontal transmission are both recognised causes, approximately 85% of cases occur without apparent explanation (sporadic).[5,6] Kuru, Gerstmann-Sträussler-Scheinker syndrome (GSS), and fatal familial insomnia (FFI) constitute other important but less common human transmissible spongiform encephalopathy (TSE) phenotypes.[7] All are invariably fatal neurodegenerative disorders.

Transmissibility and pathogenesis in these disorders are closely related (and probably causally linked) to an abnormal, protease-resistant, conformational isoform of the constitutively expressed prion protein (PrP).[7] Although an excellent, specific diagnostic marker of this group of disorders, at present, protease-resistant PrP (PrP^{res} or PrP^{sc}) cannot be routinely detected in blood or CSF, requiring invasive biopsy procedures to procure appropriate tissue to facilitate pre-mortem diagnosis. Immunochemical detection of the PrP^{res} isoform, in combination with standard neuropathological examination, remain necessary for definitive diagnosis,[8,9] but surgical procedures pose inherent risks for both patients and health care personnel.[10,11] Given these considerations, and the relative low sensitivity of traditional non-invasive diagnostic methods such as the presence of periodic sharp wave complexes (PSWC) in the EEG (only approximately 65% overall in sporadic CJD and never seen in certain, less common subtypes of CJD, including vCJD),[3,4,12] interest has focused on developing more sensitive, minimally invasive ante-mortem diagnostic methods.

Long repetition time magnetic resonance imaging (MRI) sequences can show distinctive heightened signal patterns in the basal ganglia of up to 80% of patients with sporadic CJD,[13] and preliminary reports suggest diffusion weighted imaging (DWI) may show even more widespread characteristic abnormalities.[14–16] Complementing this, a number of CSF proteins have been assayed as non-specific indicators of brain damage and dysfunction. Assessed for this purpose in CJD have been ubiquitin, tau, S-100, neuron-specific enolase (NSE), creatine kinase BB isoenzyme (CK-BB) and the p130/131 and 14–3–3 proteins.[17–27] Of these, the 14–3–3 proteins have undergone the greatest scrutiny and appear to be the best (albeit non-specific) premortem CSF marker of sporadic CJD.[20,25] They comprise a ubiquitous family of seven mammalian isoforms involved in a variety of important cellular functions, including signal transduction and cell cycle regulation,[28,29] and were recently shown to be synonymous with the p130 and p131 proteins described on 2-dimensional electrophoresis in 1986 as reliable and specific indicators of CJD.[18,23] In patients eventually classified as manifesting definite and probable sporadic CJD, immunodetection of 14–3–3 proteins in the CSF carried sensitivities of 90 to 96% with very good specificity.[20,23,25] However, adequate patient evaluation is important as Herpes simplex encephalitis and recent cerebral infraction are common causes of 'false' positive results[23,25,30] and there appears to be diminished likelihood of detecting 14–3–3 proteins in vCJD and genetically determined symptomatic TSEs, perhaps correlating with the specific mutation.[20,25,30–32]

Received 20 November 1999
Accepted 24 December 1999

Correspondence to: Dr S Collins, Australian Creutzfeldt-Jakob Disease Registry, Department of Pathology, The University of Melbourne, Australia 3010. Tel.: + 61 3 9344 5867; Fax: + 61 3 9344 4004; E-mail: s.collins@pathology.unimelb.edu.au

The current report details the ACJDR experience with immunodetecting 14–3–3 proteins in the CSF of 124 consecutive patients suspected to be manifesting CJD, with confirmation of the diagnostic utility of the technique. Included were four cases shown to harbour mutations in PRNP. In addition, the effects of significant blood contamination of CSF and the stability of 14–3–3 proteins over an extended time period were assessed as was the suitability of post-mortem CSF for posthumous diagnostic purposes.

METHODS

Patients and classification

Since inauguration in September 1993, the ACJDR has attempted to ascertain all domestic human TSE. Methods of case ascertainment have been described in detail previously[33] and the activities of the ACJDR have ethical approval from the University of Melbourne. In summary, the three most important methods have supplied approximately 80% of all registered cases and consist of: personal communications from medical practitioners (mainly neurologists and neuropathologists, prompted by semi-annual reply-paid mailouts); systematic searches of state and territory health department separation coding data bases; and death certificate searches by the Australian Institute of Health and Welfare. Formal collaboration with the New Zealand National Creutzfeldt-Jakob Disease Register has been ongoing since it commenced activities in July 1996, with data combined annually to generate Australasian incidence figures.

To aid surveillance and accurate classification, the ACJDR began offering CSF examination for 14–3–3 proteins using Western immunodetection from November 1997. By the end of September 1999, CSF specimens from 124 patients in which a spongiform encephalopathy was considered a differential diagnostic possibility had been analysed for the presence of 14–3–3 proteins. This included three specimens from New Zealand patients referred by the New Zealand CJD Registry. The ACJDR was never actively involved in the management of patients. Salient demographic and clinical information was requested on all patients, including the duration and type of presenting symptoms, as well as neurological examination findings. Also sought were results of pertinent investigations such as brain imaging and EEG. Correspondence and telephone follow up with the managing clinician (usually neurologist) was undertaken as necessary for all patients to achieve a final diagnosis or clinical outcome. No attempt was made to correlate 14–3–3 results with illness temporal profile.

Classification of spongifrom encephalopathies was according to previously published criteria.[9] Definite CJD required neuropathological confirmation of the typical features of spongiform change, gliosis and neuronal loss either post-mortem or by brain biopsy, supplemented by immunodetection of PrPres. Probable CJD denotes clinically likely cases based on a progressive dementia of less than 2 years' duration with an EEG showing PSWC and at least two of the following clinical features: myoclonus, visual or cerebellar signs, pyramidal or extrapyramidal signs, and/or akinetic mutism. Possible CJD patients are the same as probable cases but without PSWC on their EEG. For cases ultimately classified as not manifesting a spongiform encephalopathy, final classification was according to autopsy neuropathological findings, or the most accurate clinical diagnosis possible. The latter was based on the best consensus interpretation of all available clinical information and investigation results, and was almost invariably determined by the managing physician. In 12 14–3–3 negative patients, specific clinical diagnoses were not possible, prompting a more generic descriptive outcome as either: clinically stable, improved or illness duration greater than 2 years (11 cases); or progressive neurological illness of less than 2 years' duration. In five patients follow up was not possible.

Table 1 Final Diagnosis/Outcome in 14–3–3 Positive Cases

Creutzfeldt-Jakob Disease (CJD)	
Pathologically Confirmed	
Sporadic	20(2)
Iatrogenic (Lyodura recipient)	1
Genetic	3*
Probable CJD (includes single Lyodura recipient)	9**
Possible CJD	1
Sub-Total	34
Non-CJD	
Pathologically Examined	
Dementia with Lewy bodies	1
Final Clinical Diagnosis	
Acute Cerebral Ischaemia/infarct	2***
Non-Herpetic Encephalitis	1
Chronic Lymphocytic Meningitis with Cerebellar Ataxia	1
Overall Total	39

* Prion protein gene T188A, E200K and V210I mutations were present in three individual patients respectively. ** Includes single patient with an atypical positive result associated with a suboptimal CSF specimen. *** Includes one deceased patient.

Non-systematic genotyping of the PRNP open reading frame was undertaken (for varying reasons) on DNA extracted from the blood of 23 patients using the polymerase chain reaction as described previously.[34] Four missense mutations were found; three have been previously described (E200K, V2101 and P105T[35]) with one novel mutation (T188A).[36]

CSF studies

Routine cytological examination and total protein estimation were requested on all CSF samples prior to assessment for 14–3–3 proteins. All CSF specimens were frozen as soon as possible after lumbar puncture and transferred to the ACJDR for storage at –20°C. Macroscopically haemorrhagic specimens underwent centrifugation at 1500 rpm for 10 min prior to analysis of the supernatant. Detection of CSF 14–3–3 proteins was as described previously with some minor modifications.[23–25] Fifty microlitres of CSF was added to 10 microlitres of sample buffer (achieving final concentrations of 5% glycerol, 1% mercaptoethanol, 1% sodium dodecylsulphate and trace bromophenol blue) and boiled for 10 min before electrophoretic resolution at 200 volts on a 12% polyacrilamide gel, with 4% stacking component (Novex, San Diego, California, USA). As of mid-1998 improved proficiency allowed us to use half the volumes of CSF and sample buffer with equally reliable results. Electrophoretic transfer to polyvinylidene difluoride membranes (Immobilon-P; Millipore, Bedford, Massachusets, USA) for 1 h, was followed by overnight blocking at 4°C in Tris-buffered saline containing 0.5% Tween 20 (Sigma Chemical Company, St Louis, Missouri, USA) and 5% (w/v) skim milk powder. The primary incubation was for 3 h at room temperature (RT) using a 1:2000 dilution of rabbit polyclonal anti-14–3–3β antibody (K-19; Santa Cruz Biotechnology, Santa Cruz, California, USA). Subsequently, anti-rabbit secondary antibody conjugated with horseradish peroxidase (Amersham, Buckinghamshire, UK), was added (1:4000) for one hour at RT before detection with enhanced chemiluminescence according to the manufacturer's instructions (Amersham, Buckinghamshire, UK). Molecular weight markers (Rainbow, low molecular weight; Amersham, Buckinghamshire, UK) and a pathologically verified positive control and negative control were included in every gel. In a technically satisfactory slab gel, a typical positive result consisted of a clear discrete band at 30 kDa, although immunostaining intensities varied (Fig. 1). Weak positive results were always repeated until a preponderant outcome was achieved

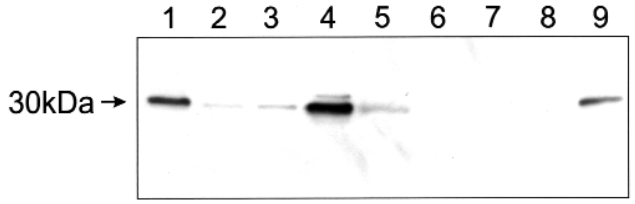

Fig. 1 Western immunodetection of 14–3–3 proteins in the cerebrospinal fluid (CSF) of patients manifesting Creutzfeldt-Jakob disease (CJD) and non-CJD neurological disorders. Lane 1, positive control (definite sporadic CJD); lane 2, patient with recent cerebral infarct; lane 3, definite CJD; lane 4, patient with probable CJD; lane 5, 30 kDa molecular weight marker; lane 6, patient thought to have corticobasal degeneration; lane 7, negative control; lane 8, patient with reversible drug related encephalopathy, lane 9, definite sporadic CJD.

(sensitivity enhancing method).[25] Weak positive and atypical results in the context of significant CSF blood contamination (arbitrarily defined as greater than 400 red blood cell/microlitre) were deemed suboptimal specimens, and these patients were not included in any statistical analyses. A repeat sample was recommended after 14 days.

For the purposes of assessing 14–3–3 protein stability, sufficient quantities of CSF testing positive and weak positive respectively, from two definite CJD patients, were thawed, with the positive specimen examined after storage at RT for 6 days and 4°C for 5 weeks, while the weak positive samples were stored at the same temperatures and assessed after 7 weeks. To explore the utility of postmortem CSF, nine specimens were obtained from the National Health and Medical Research Council sponsored Brain Bank: three samples from patients with Alzheimer's disease, one with Huntington's disease, one with alcohol related cerebral atrophy, and four patients with either no significant pathological changes or minor findings such as lipohyalinosis. The post-mortem intervals ranged from 2 to 100 h.

Statistical analyses employed the Exact method to calculate the sensitivity, specificity and predictive values with their 95% confidence intervals.

RESULTS

Of the 124 patients, 56 were females (age range 22–97 years; mean 66 years) and 68 males (age range 19–88 years; mean 60 years). A final diagnosis or generic clinical outcome was achieved in 119 patients. Mean duration of follow up (or to death) for non-pathologically examined patients was 4.8 months (range 0.3 to 15.8).

As summarised in Table 1, patients testing positive for 14–3–3 proteins totalled 39 (24 female; combined age range 26–85 years, mean 64 years), and excluding non-CJD and iatrogenic cases, the female:male ratio was 1.5:1. Of these 39 patients, one classified as probable CJD had an atypical result from a suboptimal (blood containing) CSF specimen. In the remaining 38, 24 were pathologically confirmed CJD (two after brain biopsy). One patient was considered to have contracted CJD iatrogenically through exposure to a human dura mater (Lyodura) implant, while one each of three patients had T188A, E200K and V210I mutations in PRNP respectively. There were 10 patients who fulfilled criteria for probable or possible CJD, including a further iatrogenic case related to dura mater (Lyodura) exposure.

Five patients positive for 14–3–3 proteins in the CSF had a final diagnosis that was not CJD. One with pathologically confirmed DLB had an unusually aggressive illness culminating in death after only 6 months. There was no evidence of a superimposed disorder, including a spongiform encephalopathy (negative for PrPres with both immunohistochemistry and Western blot). Three cases remain alive, with clinical diagnoses of inflammatory CNS disorders in two patients (one non-Herpetic encephalitis, the other a chronic lymphocytic meningitis with slowly progressive cerebellar ataxia) while the third suffered an episode of cerebral ischaemia. The fourth non-pathologically examined patient died after a cerebral infarct.

Of the 72 patients in which 14–3–3 proteins could not be detected, 14 underwent neuropathological examination. These results are summarised in Table 2. Diagnoses in the 13 non-CJD cases include: Alzheimer's disease (3 cases); inconclusive but no evidence of spongiform encephalopathy (3 cases); heroin leucoencephalopathy (2 cases); and single cases with amyloid angiopathy, non-specific encephalitis, hepatic encephalopathy, subacute sclerosing panencephalitis and isolated angitis of the nervous system. A further patient had CJD confirmed by brain biopsy. In addition to this patient with definite CJD, there were three patients with negative CSF who fulfilled criteria for possible or probable CJD. One of the probable CJD patients had a positive family history (first degree relative with pathologically confirmed spongiform encephalopathy), and died after an 8 month illness consisting of dementia and ataxia. A P105T mutation in PRNP was confirmed.[35]

Of the remaining 55 non-pathologically examined patients, a clinical diagnosis was achieved in 38 as summarised in Table 2.

Table 2 Final Diagnosis/Outcome in 14–3–3 Negative Cases

Creutzfeldt-Jakob disease(CJD)	
Pathologically Confirmed	1(1)
Probable (includes single patient with P105T mutation)	2
Possible	1
Pathologically Confirmed not CJD	
Alzheimer's disease	3(1)
Diagnosis unclear but not CJD	3(2)
Heroin leucoencepalopathy	2(2)
Amyloid angiopathy	1(1)
Encephalitis	1
Subacute sclerosing panencephalitis	1
Isolated angiitis of CNS	1(1)
Hepatic encepalopathy	1
Sub-total	13
Final Clinical Diagnosis	
Drug reaction or toxicity	6
Alzheimer's disease	5
Frontal lobe dementia	4
Encephalopathy	2
Corticobasal degeneration	2
Chronic, poorly controlled epilepsy	2
Paraneoplastic limbic encephalitis	2
Wernicke's encepalopathy	1
Multi-infarct dementia	1
Dementia with Lewy bodies	1
Vasculitis	1
Cerebrovascular accident	1
Normal pressure hydrocephalus	1
Acute disseminated encephalomyelitis	1
Progressive supranuclear palsy	1
Multiple system atrophy	1
Metabolic encephalopathy	1
Cryptoccocal meningitis	1
Progressive non-familial ataxia	1
Sub-cortical dementia	1
Chronic organic brain syndrome	1
Severe depression	1
Sub-total	38
Diagnosis uncertain: illness progressing and <2 years duration	1
Diagnosis uncertain: clinically stable, improved or illness of >2 years duration	11
Outcome unknown	5
Overall Total	72

Parentheses denote those patients who underwent pre-mortem brain biopsy.

The most common clinical diagnoses were drug reaction or toxicity (6 cases), Alzheimer's disease (5 cases) and frontal lobe dementia (4 cases). In a further 11 patients, a specific clinical diagnosis was not possible but the patient's clinical outcome was either stable or improved, and/or their illness duration exceeded 2 years, making CJD unlikely. There was one patient continuing to deteriorate steadily with an illness duration of less than 2 years who may be manifesting a spongiform encephalopathy, but there were insufficient details to establish an alternative clinical diagnosis or fulfil CJD classification criteria.

Using all patients with the final classification diagnosis of definite and probable CJD, a positive 14–3–3 result was 91.4% sensitive (CI 95%: 76.9–98.2). Including all cases classified as non-CJD and those with an uncertain diagnosis but unlikely to represent CJD, a negative result carried a specificity of 92.5% (CI 95%: 83.4–97.5). If analysis is confined to only definite CJD patients then the detection of 14–3–3 proteins in the CSF by Western immunoblot gives a sensitivity of 96.0% (CI 95%: 79.6–99.9). Similarly, using only pathologically examined cases, the absence of immunodetectable 14–3–3 proteins in the CSF carries a specificity of 92.9% (CI 95%: 66.1–99.8). The positive predictive value for definite and probable CJD cases was 86.5% (CI 95%: 71.2–95.5), while the negative predictive value was 95.4% (CI 95%: 87.1–99.0).

Although all CSF specimens were assessed for 14–3–3 protein content it was confirmed during the course of the study that not all samples were suitable if trying to maintain maximal diagnostic utility. Of 16 weak positive results, two showed pleocytosis (on non-Herpetic encephalitis and the other chronic lymphocytic meningitis with progressive cerebellar ataxia), while 10 of the remaining 14 contained significant amounts of blood. Three additional positive CSF specimens were heavily blood stained, from patients not considered clinically or radiologically to have suffered an intracranial haemorrhage. Although showing prominent immunostaining at 30 kDa, there was either smearing along the length of the lane (two patients) or additional prominent bands (not usually evident), rendering the result obviously different from the usual single positive band seen with definite CJD cases (Fig. 1). As already mentioned, a further patient classified as probable CJD had an atypical positive result (with additional bands present) in the context of modest blood contamination of the CSF. Hence, overall, 14 of 22 blood contaminated CSF specimens showed positivity for 14–3–3 proteins with either the qualitative appearance or the marginal nature of the immunostaining militating against the reliability of the results as far as supporting a diagnosis of spongiform encephalopathy. Illustrating this point, in one of these patients simultaneous clear and lightly blood stained CSF specimens were received, with only the latter showing a weak positive result.

Providing further support for the unreliability of weak or qualitatively different positive results from blood stained CSF specimens, 11 of these patients are still alive with clinical diagnoses that include single cases of Alzheimer's disease, paraneoplastic neurological disorder, dementia with Parkinsonism longer than 2 years duration, Wernicke's encephalopathy, lithium toxicity and frontal lobe dementia, and two patients with acute cerebral ischaemia. One patient had pathologically confirmed encephalitis. In three patients, all with a stable neurological disorder, a precise clinical diagnosis could not be achieved. Follow up was not possible in one patient. It is unclear why 8 blood stained specimens were negative with 14–3–3 testing but generally these samples contained lesser amounts of red blood cells (RBCs). The mean RBC count in these 8 specimens was 1750/μl (range 400–7750/μl), whereas in the 11 positive samples where counts were performed the mean was 19 031/μl (range 600–101,600/μl). Hence, in our experience a significantly blood stained CSF specimen carries an approximately 64% chance of a weak or atypical positive result with 14–3–3 testing, and in only one of these cases was a diagnosis of probable CJD ultimately concluded. Conversely, the four remaining (of 16) patients with weak positive results (but without significant CSF blood contamination or pleocytosis) have all died with a classification status of CJD: two probable and two pathologically confirmed (Fig. 1, lane 3).

All post-mortem CSF samples appeared strongly positive for 14–3–3 proteins (but qualitatively atypical with additional faster and slower bands), with immunostaining intensity roughly correlating with the post-mortem interval to specimen procurement. This confirmed our suspicions (based on a single previous patient) that CSF obtained after death is diagnostically unreliable, showing non-specific strong positive immunostaining.

Our results confirmed good stability of 14–3–3 proteins in CSF, with positive results not showing any significant alteration on serial assessments after storage at RT (approximately 20°C) for 6 days and 4°C for 5 weeks, while weak positive results showed only minor loss of signal intensity when tested after 7 weeks at both storage temperatures (data not shown).

DISCUSSION

The principal findings of this study show good concordance with those previously reported dealing with the diagnostic utility of detecting 14–3–3 proteins in the CSF of patients with suspected sporadic CJD. While our total number of patients is similar to the smallest of three prior series,[20] the current study had the fewest patients classified as CJD.[20,23,25]

Notwithstanding this, for definite CJD we found a sensitivity of 96.0%, which correlates well with the reported range of 88–96%, as does our sensitivity of 91.4% compared to 90–96% when both pathologically verified and probable cases are combined.[20,23,25] Our specificity of 92.5% also compares favourably with the reported range of 96–100%.

There were only five misleading positive results, giving a positive predictive value of 86.5%, which is somewhat lower than reported in previous studies (94.7%–100%).[20,25] Given the non-specific nature of the method, this may relate to the relatively higher proportion of non-CJD patients included in the current series. The diagnoses in these five patients were DLB (autopsy confirmed), a single patient dying from cerebral infarction and three patients clinically diagnosed as not-CJD. These latter three are still alive and include single patients with non-Herpetic encephalitis, chronic lymphocytic meningitis with slowly progressive cerebellar ataxia, and acute cerebral ischaemia. The patient suffering from an episode of cerebral ischaemia made an essentially complete recovery. Encephalitis (particularly of herpetic origin), chronic meningitis with concomitant parenchymal involvement (such as from malignant infiltration or bacterial invasion) and significant acute cerebral hypoxia (especially sufficient to cause obvious infarction) are all recognised 'false' positive causes of 14–3–3 protein detectability in the CSF.[23,25,27,30,31] The finding of immunodetectable 14–3–3 proteins in the CSF of patients with neurodegenerative disorders such as DLB is less typical.[20,23,27,30] However, positivity in our DLB patient may relate to their unusually rapid decline. Neurones are abundant in at least three 14–3–3 isoforms (β, γ and η) which are all detected by the commercial polyclonal antibody used for Western immunodetection. Their presence in CSF is thought to reflect acute or ongoing significant neuronal destruction from any cause with consequent non-specific release of the various 14–3–3 isoforms.[27] Hence, other uncommon but recognised causes for false positive results include subarachnoid haemorrhage, Alzheimer's disease, multiple

sclerosis, intracerebral metastases and Rett's syndrome.[23,25,27] It is the non-specificity of the 14–3–3 proteins as markers of neuronal injury or destruction that mandates adequate preliminary investigation of patients and underscores the importance of avoiding precocious use of this testing method for diagnosing CJD. This type of approach will ensure optimal utility of this valuable diagnostic technique.

As a corollary, our experience indicates that CSF specimens containing blood have a high (greater than 50%) chance of giving a (usually weak) positive result, with the likelihood appearing to correlate roughly with the amount of RBCs. Consequently, significantly blood contaminated CSF specimens should be regarded as suboptimal, with weak and atypical positive results dismissed as unreliable for diagnostic purposes. This is in accord with the refusal of some groups to examine blood containing CSF samples for 14–3–3 proteins.[27] The explanation for these apparently false positive results is unclear but may relate to the concomitant presence of platelets which are known to contain 14–3–3 isoforms important in arachidonic acid metabolism and exocytosis.[29]

The confirmatory role of detecting 14–3–3 proteins in the CSF of symptomatic patients manifesting genetic forms of prion disease is still evolving, given the comparatively small total numbers of cases studied so far. Overall, three of our four genetic cases had 14–3–3 proteins immunodetectable during their final neurological illness. Our single patient with an E200K mutation was positive which is the typical finding in symptomatic carriers of this mutation.[20,25,30]) Similarly, the patient carrying the V210I mutation tested positive, which has been reported previously in a single case,[25] whereas there is no published data concerning results with the P105T (negative in the current series) and T188A mutations.

Notwithstanding general optimal laboratory specimen handling procedures, the results of the current study have shown the 14–3–3 proteins to be quite stable in the short term when stored under different temperature conditions (RT and 4°C). This confirms and considerably extends the time period of previously reported stability assessments (from 7 and 12 days, to 7 weeks),[20,25] and additionally refutes prior claims that suboptimal thermal handling of specimens may have contributed to false negative results.[31]

To the best of our knowledge this is the first report to objectively confirm the predicted unsuitability of post-mortem CSF for 14–3–3 diagnostic testing. All nine patients examined had strongly positive but qualitatively different results, with the degree of positivity appearing to crudely correlate with the length of time between death and sample procurement. Hence, the likelihood of a positive result was independent of the neuropathological diagnosis which included Alzheimer's disease (3 patients), Huntington's disease (one patient), alcoholic dementia (1 patient), and four with unclear or no detectable abnormalities. None of these maladies are usually associated with a positive result.[20,23,25] For the purposes of diagnosis, it is regrettable that posthumous CSF sampling cannot be undertaken as a less invasive (but inferior) substitute to pathological examination when autopsy is refused. However, the findings are entirely consistent with the hypothesis that immediate, severe neuronal autolysis post-mortem would release considerable quantities of 14–3–3 and other potentially cross-reacting proteins into the CSF.[27]

In summary, the present results are in good agreement with the findings of previous studies, which have shown immunodetection of 14–3–3 proteins in the CSF to be a worthwhile, minimally invasive pre-mortem diagnostic marker for sporadic CJD, and at least some forms of symptomatic genetic prion disease. However, the non-specificity of a positive result mandates careful individual patient evaluation and optimal (non-blood containing) CSF specimens to maintain maximal diagnostic utility. Nevertheless, the considerable range of differential diagnostic possibilities which are usually negative (as outlined in Table 2) attests to the robustness and specificity of this method in the appropriate clinical setting. Given the promising recent reports of techniques likely to permit detection of PrPres in the blood of manifest TSEs,[37,38] the current high level of interest regarding less invasive diagnostic methods for sporadic CJD is likely to be maintained.

ACKNOWLEDGEMENTS

The Australian Creutzfeldt-Jakob Disease Registry is funded by the Commonwealth Department of Health and Aged Care. We are deeply indebted to all clinicians who provided CSF specimens and generously provided clinical information and follow up on the patients included in this study.

REFERENCES

1. Brown P, Gibbs C, Rodgers-Johnson P, et al. Human spongiform encephalopathy: the National Institutes of Health series of 300 cases of experimentally transmitted disease. Ann Neurol 1994; 35: 513–529.
2. Almond J, Pattison J. Human BSE. Nature 1997; 389: 437–438.
3. Will RG, Ironside JW, Zeidler M, et al. A new variant of Creutzfeldt-Jakob disease. Lancet 1996; 347: 921–925.
4. Parchi P, Giese A, Capellari S, et al. Classification of sporadic Creutzfeldt-Jakob disease based on molecular and phenotypic analysis of 300 subjects. Ann Neurol 1999; 46: 224–233.
5. Will RG, Alperovitch A, Poser S, et al. Descriptive epidemiology of Creutzfeldt-Jakob disease in six European countries, 1993–1995. Ann Neurol 1998; 43: 763–767.
6. Windl O, Dempster M, Estibeiro JP, et al. Genetic basis of Creutzfeldt-Jakob disease in the United Kingdom: a systematic analysis of predisposing mutations and allelic variation in the PRNP gene. Hum Genet 1996; 98: 259–264.
7. Prusiner S, Hsiao K. Human prion diseases. Ann Neurol 1994; 35: 385–395.
8. Kretzschmar HA, Ironside JW, DeArmond SJ, Tateishi J. Diagnostic criteria for sporadic Creutzfeldt-Jakob disease. Arch Neurol 1996; 53: 913–920.
9. Masters CL, Harris JO, Gajdusek DC, Gibbs, Bernoulli C, Asher DM. Creutzfeldt-Jakob disease: patterns of worldwide occurrence and the significance of familial and sporadic clustering. Ann Neurol 1979; 5: 177–188.
10. Collins S, Law MG, Fletcher A, Boyd A, Kaldor J, Masters CL. Surgical treatment and risk of sporadic Creutzfeldt-Jakob disease: a case-control study. Lancet 1999; 353: 693–697.
11. Zeidler M, Knight R, Stewart G, et al. Routine tonsil biopsy for diagnosis of new variant Creutzfeldt-Jkob disease is not justified. BMJ 1999; 318: 538.
12. Steinhoff BJ, Räcker S, Herrendorf G, et al. Accuracy and reliability of periodic sharp wave complexes in Creutzfeldt-Jakob disease. Arch Neurol 1996; 53: 162–166.
13. Finkenstaedt M, Szudra A, Zerr I, et al. MR imaging of Creutzfeldt-Jakob disease. Radiology 1996; 199: 793–798.
14. Bahn MM, Parchi P. Abnormal diffusion-weighted magnetic resonance images in Creutzfeldt-Jakob disease. Arch Neurol 1999; 56: 577–583.
15. Demaerel P, Heiner L, Robberecht W, Sciot R, Wilms G. Diffusion-weighted MRI in sporadic Creutzfeldt-Jakob disease. Neurology 1999; 52: 205–208.
16. Yee AS, Simon JH, Anderson CA, Sze C-I, Filley CM. Diffusion-weighted MRI of right-hemisphere dysfunction in Creutzfeldt-Jakob disease. Neurology 1999; 52: 1514–1515.
17. Zerr I, Bodemer M, Räcker S, et al. Cerebrospinal fluid concentration of neuron-specific enolase in diagnosis of Creutzfeldt-Jakob disease. Lancet 1995; 345: 1609–1610.
18. Harrington M, Merril CR, Asher DM, Gajdusek DC. Abnormal proteins in the cerebrospinal fluid of patients with Creutzfeldt-Jakob disease. N Engl J Med 1986; 315: 279–283.
19. Jimi T, Wakayama Y, Shibuya S, et al. High levels of nervous system-specific proteins in cerebrospinal fluid in patients with early stage Creutzefeldt-Jakob disease. Clinica Chimica Acta 1992; 211: 37–46.
20. Beaudry P, Cohen P, Brandel JP, et al. 14–3–3 protein, neuron-specific enolase, and S-100 protein in cerebrospinal fluid of patients with Creutzfeldt-Jakob disease. Dement Geriatr Cogn Disord 1999; 10: 40–46.
21. Otto M, Stein H, Szudra A, et al. S-100 protein concentration in the cerebrospinal fluid of patients with Creutzfeldt-Jakob disease. J Neurol 1997; 244: 566–570.
22. Otto M, Wiltfang J, Tumani H, et al. Elevated levels of tau-protein in cerebrospinal fluid of patients with Creutzfeldt-Jakob disease. Neurosci Lett 1997; 225: 210–212.
23. Hsich G, Kenney K, Gibbs Creutzfeldt-Jakob disease, Lee KH, Harrington MG. The 14–3–3 brain protein in cerebrospinal fluid as a marker for transmissible spongiform encephalopathies. N Engl J Med 1996; 335: 924–930.

24. Zerr I, Bodemer M, Weber T. The 14–3–3 brain protein and transmissible spongiform encephalopathy. N Engl J Med 1997; 336: 874 (letter).
25. Zerr I, Bodemer M, Gefeller O, et al. Detection of 14–3–3 protein in the cerebrospinal fluid supports the diagnosis of Creutzfeldt-Jakob disease. Ann Neurol 1998; 43: 32–40.
26. Manaka H, Kato T, Kurita K, et al. Marked increase in cerebrospinal fluid ubiquitin in Creutzfeldt-Jakob disease. Neurosci Lett 1992; 139: 47–49.
27. Satoh J-I, Kuohara K, Yukitake M, Kuroda Y. The 14–3–3 protein detectable in the cerebrospinal fluid of patients with prion-unrelated neurological diseases is expressed constitutively in neurons and glial cells in culture. Eur Neurol 1999; 41: 216–225.
28. Burbelo PD, Hall A. 14–3–3 proteins: hot numbers in signal transduction. Curr Biol 1995; 5: 95–96.
29. Aitken A, Collinge DB, van Heusden BPH, et al. 14–3–3 proteins: a highly conserved, widespread family of eukaryotic proteins. Trends Biochem Sci 1992; 17: 498–501.
30. Rosenmann H, Meiner Z, Kahana E, et al. Detection of 14–3–3 protein in the CSF of genetic Creutzfeldt-Jakob disease. Neurology 1997; 49: 593–595.
31. Will RG, Zeidler M, Brown P, Harrington M, LeeKH, Kenney KL. Cerebrospinal-fluid test for new-variant Creutzfeldt-Jakob disease. Lancet 1996; 348: 955.
32. Zeidler M, Stewart GE, Barraclough CR, et al. New variant Creutzfeldt-Jakob disease: neurological features and diagnostic tests. Lancet 1997; 350: 903–907.
33. Collins S, Fletcher A, de Luise T, Boyd A, Masters CL. Creutzfeldt-Jakob disease in Australia. In: Court L, Dodet B (Eds). Transmissible Subacute Spongiform Encephalopathies: Prion Diseases. Paris: Elsevier, 1996: 405–415.
34. Hsiao K, Baker H, Crow T, et al. Linkage of a prion protein missense variant to Gerstmann-Sträussler syndrome. Nature 1989; 338: 342–345.
35. Freckman ML, Masters C, Collins S, Boyd A, Byron K, Campbell R, Darveniza P. Predictive testing for Creutzfeldt-Jakob Disease (CJD) with a novel mutation in the prion protein gene. Human Genetics Society of Australasia 1998 (abstract); 11: 26.
36. Collins S, Boyd A, Fletcher A, Byron K, Harper C, McLean C, Masters C. Novel prion protein gene mutation in an octogenarian with Creutzfeldt-Jakob disease. Arch Neurol (in press).
37. Schmerr MJ, Jenny AL, Bulgin MS, et al. Use of capillary electrophoresis and fluorescent labeled peptides to detect the abnormal prion protein in the blood of animals that are infected with a transmissible spongiform encephalopathy. J Chromatogr 1999; 853: 207–214.
38. Safar J, Willie H, Itri V, et al. Eight prion strains have PrP^{sc} molecules with different conformations. Nat Med 1998; 4: 1157–1165.

Analysis of EEG and CSF 14-3-3 proteins as aids to the diagnosis of Creutzfeldt–Jakob disease

I. Zerr, MD; M. Pocchiari, MD; S. Collins, MD, FRACP; J.P. Brandel, MD; J. de Pedro Cuesta, MD; R.S.G. Knight, FRCP(E); H. Bernheimer, MD; F. Cardone, PhD; N. Delasnerie-Lauprêtre, MD; N. Cuadrado Corrales, MD; A. Ladogana, MD; M. Bodemer; A. Fletcher, BSc; T. Awan, MD; A. Ruiz Bremón, MD; H. Budka, MD; J.L. Laplanche, PhD; R.G. Will, MD; and S. Poser, MD

Article abstract—*Objective:* To improve diagnostic criteria for sporadic Creutzfeldt–Jakob disease (CJD). *Methods:* Pooled data on initial and final diagnostic classification of suspected CJD patients were accumulated, including results of investigations derived from a coordinated multinational study of CJD. Prospective analysis for a comparison of clinical and neuropathologic diagnoses and evaluation of the sensitivity and specificity of EEG and 14-3-3 CSF immunoassay were conducted. *Results:* Data on 1,003 patients with suspected CJD were collected using a standard questionnaire. After follow-up was carried out, complete clinical data and neuropathologic diagnoses were available in 805 cases. In these patients, the sensitivity of the detection of periodic sharp wave complexes in the EEG was 66%, with a specificity of 74%. The detection of 14-3-3 proteins in the CSF correlated with the clinical diagnosis in 94% (sensitivity). The specificity (84%) was higher than that of EEG. A combination of both investigations further increased the sensitivity but decreased the specificity. *Conclusions:* Incorporation of CSF 14-3-3 analysis in the diagnostic criteria for CJD significantly increases the sensitivity of case definition. Amended diagnostic criteria for CJD are proposed.

NEUROLOGY 2000;55:811–815

The initial diagnosis of Creutzfeldt–Jakob disease (CJD) is often based on clinical grounds and is usually correct in patients with a progressive dementia extant for < 2 years, with at least two of the following neurologic signs: myoclonus, visual or cerebellar signs, pyramidal or extrapyramidal signs, and akinetic mutism.[1] Investigations such as EEG,[2,3] MRI,[4,5] and detection of 14-3-3 proteins in the CSF[6,7] support or weaken the clinical suspicion of the disease, even if definite diagnosis of CJD still requires postmortem examination of the brain.[8,9] There is an urgent need for empirical data clarifying the diagnostic utility of the combined results of the 14-3-3 test in the CSF and periodic sharp and slow wave complexes (PSWC) in the EEG for confirming CJD. We analyzed the value of these two widely used diagnostic tests in CJD (i.e., EEG and CSF detection of 14-3-3 proteins) in the context of a prospective multinational study of CJD.[10] The results of these investigations were used in the classification of suspected CJD cases. Follow-up was obtained, and the accuracy of the initial clinical diagnosis based on established criteria[2] was evaluated. Finally, the sensitivity and specificity of new extended diagnostic criteria were analyzed, after inclusion of 14-3-3 CSF results.

Material and methods. *Patients.* Patients were recruited from national registries of CJD in Australia, Austria, France, Germany, Italy, Spain, and the United Kingdom.[10] They were classified as definite, probable, or possible CJD cases[2] based on available clinical and laboratory data. A standard questionnaire was used to collect data from each national center.

From the Klinik und Poliklinik für Neurologie (Drs. Zerr, Bodemer, and Poser), Georg-August-Universität, Göttingen, Germany; Laboratory of Virology (Drs. Pocchiari, Cardone, and Ladogana), Istituto Superiore di Sanità, Rome, Italy; Department of Pathology (Drs. Collins and Fletcher), University of Melbourne, Australia; U360 INSERM, Hôpital de la Salpetriere (Drs. Brandel and Delasnerie-Laupêtre), Paris, France; Department of Applied Epidemiology (Drs. de Pedro Cuesta and Ruiz Bremón), National Centre for Epidemiology, Carlos III Institute of Health, Madrid, Spain; CJD Surveillance Unit, Western General Hospital, Edinburgh, Scotland (Drs. Knight and Will); Klinisches Institut für Neurologie (Drs. Bernheimer and Budka), Universität Wien, Austria; Istituto Neurologico Nazionale C. Besta, (Dr. Awan), Milan, Italy; Department of Applied Epidemiology, National Centre for Epidemiology, Carlos III Institute of Health and Research Brain Bank (Dr. Cuadrado Corrales), Medical School, Complutensis University, Madrid, Spain; and Service de Biochimie et Biologie Moléculaire (Dr. Laplanche), Hôpital Lariboisière, Paris, France.

This research was funded through the European Commission (BMH4-98-3727). The German study was supported by a grant from the Federal Ministry of Health (Bundesministerium für Gesundheit, GZ 325-4471-02/15). The study in the United Kingdom was funded by the Department of Health and the Scottish Office Department of Health. The study in Italy was partially supported by the National Registry of Creutzfeldt–Jakob Disease, Istituto Superiore di Sanità, financed by the Italian Ministry of Health and by the Department of Social Services of the Italian Ministry of Health. The study in Spain was supported by grants 95/1835 and 99/1332 from Fondo de Inestigaciones Sanitarias. The Austrian studies on 14-3-3 proteins were supported by the Federal Ministry of Science and Traffic (project GZ 70.026/2-Pr/4/98). The Austrian Reference Centre for Human Transmissible Spongiform Encephalopathies was funded by the Federal Ministry of Labour, Health, and Social Affairs. The Australian Creutzfeldt–Jakob Disease Registry was funded by the Commonwealth Department of Health and Family Services.

Received September 7, 1999. Accepted in final form June 6, 2000.

Address correspondence and reprint requests to Dr. I. Zerr, Klinik und Poliklinik für Neurologie, Georg-August-Universität Göttingen, Robert-Koch-Str. 40, 37075 Göttingen, Germany; e-mail: 106004.1022@compuserve.com.

Diagnostic criteria for sporadic CJD. We used previously established criteria to determine the level of diagnostic accuracy in relation to sporadic CJD.[2,10] All patients with spongiform encephalopathy or immunochemical detection of PrP^{Sc} in the brain were classified as definite CJD cases. Patients were classified as probable cases if they exhibited a rapidly progressive dementia, PSWC on EEG, and two of the following: myoclonus, visual and cerebellar symptoms or both, pyramidal and extrapyramidal signs or both, or akinetic mutism. Those fulfilling the above clinical criteria but without PSWC and a duration of dementia of < 2 years were classified as "possible CJD." Cases that did not fulfill these clinical criteria were classified as "not CJD." EEG was used in the initial and follow-up classification of suspected cases. In contrast, results of 14-3-3 determination in CSF were used neither in the initial nor in the follow-up classification of the suspected cases. During follow-up, patients were regularly reviewed and reclassified according to these criteria. Cases with unambiguous clinical improvement or recovery were classified as "other" even if a definite alternative diagnosis could not be made and postmortem analysis was not undertaken.

Analysis of CSF for 14-3-3. CSF samples were obtained by lumbar puncture. CSF was analyzed for the presence of 14-3-3 proteins as previously described.[6,11] The CSF analysis was carried out in each CJD surveillance center with minor modifications. Blood-stained CSF samples were excluded from analysis because contamination of this type can lead to "false-positive" results. A blinded comparison of test results from the different centers showed good reliability and validity. (The detailed analysis of the comparison will be published elsewhere.)

Results. *Patient characteristics.* Assessment of CSF 14-3-3 proteins was performed on 1,003 patients who were referred to the national CJD registries of Australia (n = 71), Austria (n = 31), France (n = 270), Germany (n = 351), Italy (n = 79), Spain (n = 79), and the United Kingdom (n = 122). The classification of these patients is reported in table 1. CSF samples of cases classified as "not CJD" with other neurologic disorders served as controls.

The 14-3-3 proteins were detected in 91% of patients with definite or probable sporadic CJD, 45% of new variant CJD (nvCJD) and in 97% of CJD patients with a *PRNP* mutation (see table 1). The test was positive in only two of five Gerstmann–Sträussler–Scheinker (GSS) patients and was negative in all patients with fatal familial insomnia (FFI).

Among control subjects, the test was positive in only ~ 9%.

Follow-up. Complete clinical follow-up data were available in 805 cases (sporadic CJD and control subjects). In the remainder, no follow-up was possible because of study design limitations in particular countries. The mean follow-up time varied from 1.8 to 6.5 months (median) between the countries, depending on the study design (range 0.25 to 48 months).

The initial clinical classification of suspected CJD patients at the time of notification to national registries was as follows (table 2). Three hundred thirteen patients were classified as probable CJD cases; among these, 282 had detectable levels of 14-3-3 in the CSF. Two hundred eleven patients had a diagnosis of possible CJD, and CSF was posi-

Table 1 *Occurrence of 14-3-3 proteins in CSF of Creutzfeldt–Jakob disease (CJD) patients and of patients with other neurologic diseases (n = 1,003)*

Disease	14-3-3 positive
CJD	
Definite or probable CJD, n = 413	376
Possible CJD, n = 127	79
New variant CJD, n = 11	5
Iatrogenic CJD,* n = 10	6
Genetic/familial patients	
P102L,† n = 5	2
E200K, n = 13	13
V210I, n = 15	15
D178N-129M,‡ n = 15	0
Familial,§ n = 2	1
Other neurologic diseases, n = 392	34¶

* Six related to human growth hormone, three dura mater, one corneal graft.
† Gerstmann–Sträussler–Scheinker disease.
‡ Fatal familial insomnia.
§ Family history, but no genotyping available.
¶ Three AD, three encephalitis, eight vascular disorders (three anoxia, two stroke, two subarachnoid hemorrhage, one brainstem infarction), one each of multiple myeloma, metabolic encephalopathy, lymphohistiocytoma, paraneoplastic encephalopathy, malignant meningitis, and one patient with cerebral ischemia whose CSF was taken within a few days of seizures. In the remaining 14 cases, no final diagnosis could be made; most of these patients had dementia, but their clinical features did not fulfill the criteria for classification as CJD.

Table 2 *Initial and final classification in patients with suspected sporadic Creutzfeldt-Jakob disease (CJD)*

Initial classification	Probable		Possible		Not CJD	
14-3-3 in CSF	+	−	+	−	+	−
n	282	31	151	60	22	259
Follow-up						
Definite	144	8	61	6	2	1
Probable	135	15	14	—	3	1
Possible	—	—	72	26	4	—
Not CJD	3*	8†	4‡	28§	13¶	257

* One multiple myeloma, one AD, one frequent seizures.
† Three AD, five unknown.
‡ One anoxia, one stroke, one metabolic encephalopathy, and one patient with disease duration of >5 years and no final diagnosis.
§ One AD, 1 Pick's disease, 10 recovered, 15 not CJD in autopsy, and 1 patient with disease duration of >2 years and no final diagnosis.
¶ Three encephalitis, two hypoxic brain damage, one paraneoplastic, one suspected possible CJD with duration of >3 years, one probable CJD with no obvious dementia, remaining cases no outcome.

Table 3 *Comparative diagnostic value of EEG and CSF analysis in cases of Creutzfeldt–Jakob disease (CJD) initially classified as "probable" or "possible" CJD*

Characteristic	PSWC in EEG	14-3-3 in CSF	PSWC in EEG or 14-3-3 in CSF*	PSWC in EEG and 14-3-3 in CSF†
CJD	144/219	205/219	213/219	144/219
Not CJD	11/43	7/43	15/43	3/43
Sensitivity, %	66	94	97	66
Specificity, %	74	84	65	93
Positive predictive value, %	93	97	93	98
Negative predictive value, %	30	72	79	35

* Test positive: patients with either periodic sharp wave complexes (PSWC) in EEG or 14-3-3 in CSF. Test negative: patients without PSWC in EEG and without 14-3-3 in CSF.

† Test positive: only patients who had PSWC in EEG and 14-3-3 in CSF. Test negative: all other patients.

tive for 14-3-3 in 151 of them. Two hundred fifty-nine of 281 patients who did not fulfill the criteria for sporadic CJD ("not CJD") had no measurable level of 14-3-3 in the CSF.

A further analysis based on the results of follow-up investigations was carried out for each initial diagnostic classification subgroup (see below).

Follow-up on probable CJD cases. The diagnostic reliability of "probable CJD" was high. During follow-up, the diagnosis of CJD was excluded in only 11 patients; about half of the remaining were confirmed postmortem. In the remaining patients, there was no change in the diagnostic classification because either no autopsy of the brain was performed or the patients were still alive. Of the 11 patients with a false-positive EEG, 14-3-3 proteins were detectable in the CSF of 3. In one of these, however, there were high CSF protein levels and hypercalcemia, leading to a diagnosis of multiple myeloma. In four patients with AD, the diagnosis was made only after autopsy.

Follow-up on possible CJD cases. The analysis of this subgroup is of particular practical importance, as a significant proportion of sporadic CJD patients never develop typical PSWC. Ninety-three percent of patients in whom postmortem examination of the brain confirmed CJD or who developed typical PSWC during follow-up (and were therefore upgraded to "probable CJD") had detectable levels of 14-3-3 in the CSF. The 14-3-3 proteins were also detected in 73% of patients whose diagnosis of "possible CJD" did not change during the follow-up, either because autopsy was not done or because the patients were still alive. The 14-3-3 proteins were detected in only 13% of patients in whom the diagnosis of CJD was ruled out.

Follow-up on "not CJD" cases. Only a small number of patients who were initially classified as "not CJD" at the time of notification turned out to be sporadic CJD cases. Interestingly, five of seven of them had positive results for 14-3-3.

Comparative diagnostic value of EEG and CSF findings. For the calculation of sensitivity relating to EEG and 14-3-3 results or both, we used CJD patients who were clinically diagnosed as "probable" or "possible" cases and were subsequently confirmed at neuropathologic examination. Accordingly, for the evaluation of specificity, we used only "probable" or "possible" CJD patients who were ultimately neuropathologically excluded or who were clinically recovered (table 3).

A positive 14-3-3 test was more sensitive and more specific than the presence of PSWC in the EEG. The 14-3-3 test gave a false-positive result in only 7 of 43 cases (1 each of anoxia, stroke, metabolic encephalopathy, multiple myeloma, AD, cerebral ischemia with frequent seizures, and 1 patient with disease duration of > 5 years without definite diagnosis), whereas PSWC were seen in 11 of 43 "not CJD" patients (1 each of multiple myeloma and cerebral ischemia and frequent seizures, 4 patients with AD, and 5 with no definite diagnosis neuropathologically).

In patients with PSWC in the EEG and detectable 14-3-3 levels in the CSF, the clinical diagnosis of CJD was confirmed at autopsy in all but three cases. The diagnoses in these three patients were multiple myeloma, AD, and cerebral ischemia with frequent seizures. In contrast, 28 of 60 patients with a clinical diagnosis of "possible CJD" (no PSWC in the EEG), who were also negative for 14-3-3, were ultimately classified "not CJD" (table 2).

Table 4 *Modified diagnostic criteria for sporadic Creutzfeldt-Jakob disease (CJD)*

Definite CJD

- Neuropathologically confirmed and/or
- Abnormal prion protein isoform immunochemically confirmed by immunocytochemistry or western blot
- Scrapie-associated fibrils

Probable CJD

- Progressive dementia with at least two of four clinical features:
  1. Myoclonus
  2. Visual or cerebellar signs
  3. Pyramidal or extrapyramidal signs
  4. Akinetic mutism
- Periodic sharp and slow wave complexes (PSWC) in EEG
- 14-3-3 proteins in CSF and duration of <2 years

Possible CJD

- Clinical features as above
- No PSWC in EEG
- No 14-3-3 detection in CSF
- Duration of <2 years

The sensitivity of the clinical diagnosis of CJD increases from 66 to 97% with the inclusion of a positive 14-3-3 result in the diagnostic criteria (table 4). Although this procedure appears associated with decreased specificity (from 74 to 65%), it is noteworthy that the majority of false-positive results were due to the presence of PSWC in the EEG. The positive predictive value of PSWC in the EEG was comparable with the detection of 14-3-3 in CSF. The highest positive predictive value was achieved when both the EEG and the 14-3-3 proteins were positive: Ninety-eight percent of these cases were confirmed by neuropathology. The highest predictive value for the absence of CJD was achieved when both investigations were negative (negative predictive value 79%).

Discussion. The molecular basis for clinical and neuropathologic phenotypic variability in CJD has recently been described.[12] Cases of sporadic CJD with short clinical duration and typical PSWC in the EEG were identified as a distinct subgroup. However, the EEG was rarely typical in other CJD subtypes, leading to the need for improved diagnostic criteria in these forms of the disease. Detection of the pathologic isoform PrP^{Sc} outside the CNS has not yet been possible in sporadic CJD in contrast to nvCJD, in which PrP^{Sc} has been detected in lymphatic tissues.[13,14] Although the postmortem rate in CJD is relatively high, between 43 and 85%,[10] in a significant proportion of cases, the diagnosis of CJD still depends on clinical criteria. Such criteria need to have a high sensitivity and specificity to guarantee an accurate surveillance of the disease and to ensure a high level of comparability and reliability of epidemiologic data among different countries.

Several investigations have been proposed to corroborate the clinical diagnosis of CJD. In the criteria established by Masters et al.,[2] the detection of PSWC in the EEG was used to support the clinical diagnosis of CJD in patients with rapidly progressive dementia and various neurologic signs. Increased levels of neuronal or astrocytic protein have been investigated in the CSF of CJD patients, namely, 14-3-3 proteins,[6,7,11,15-17] neuron-specific enolase, and S-100.[15,18-20] Brain CT does not show specific patterns in CJD, but brain MRI may be diagnostically useful in sporadic CJD and nvCJD.[4,5,21] Other methods have been proposed, including somatosensory evoked potentials, retinography, SPECT, and PET,[22] but these methods have not been adequately evaluated in large numbers of cases.

Data on the sensitivity and specificity of PSWC in the EEG and 14-3-3 proteins in CSF have been reported in retrospective studies, but they were based on cases that fulfilled established clinical diagnostic criteria or were confirmed neuropathologically.[6,7] However, the sensitivity and specificity of a test are best evaluated in a prospective study.

The present prospective study has demonstrated that the detection of 14-3-3 proteins in the CSF is sensitive and specific for the diagnosis of sporadic CJD. In familial CJD patients bearing codon 200 or codon 210 mutations, the 14-3-3 assay had a similar diagnostic value. In contrast, 14-3-3 proteins were not detected at all in FFI and only uncommonly in GSS. Both these conditions may be difficult to diagnose clinically because of an atypical clinical picture, often with a long disease duration and absence of PSWC.[23] Nevertheless, CSF analysis for 14-3-3 proteins is not useful as a screening test in patients with dementia, as the protein is only a nonspecific marker of neuronal damage. However, in the context of suspected CJD, its presence helps to corroborate the diagnosis and to differentiate these cases from cases of AD and other conditions. False-positive findings may occur in patients with cerebral hypoxia, intracerebral hemorrhage, inflammatory CNS disorders, and blood-stained CSF samples. These conditions can and should be excluded by clinical evaluation and appropriate investigations such as CSF analysis and brain imaging.

Follow-up analysis in the "probable CJD" group demonstrated the high reliability of this clinical classification. Similar analysis of "possible CJD" cases allowed three conclusions: 1) The detection of 14-3-3 proteins strongly supports the diagnosis of CJD in this particular subgroup. 2) The elevation of 14-3-3 proteins in CSF may precede the detection of PSWC in the EEG. 3) Negative CSF 14-3-3 and no PSWC in the EEG strongly support an alternative diagnosis. The analysis in cases who do not fulfill the diagnostic criteria for CJD but who are 14-3-3 positive revealed that careful follow-up is required as this test may detect disease at a very early stage.

Overall, our results demonstrate a high accuracy of the clinical diagnosis of CJD. In our analysis, the 14-3-3 test was positive in only 34 of 392 control subjects, when trying to exclude CJD in patients with a relatively low clinical likelihood. The utility of the 14-3-3 test is further enhanced when interpreted in the clinical context, as many of these "false-positive" findings were due to diseases that do not form a differential diagnosis for CJD, such as subarachnoid hemorrhage or inflammatory disease. In the subgroup of our patients with detailed information on follow-up, 297 of 313 patients with a final diagnosis of "not CJD" were negative for 14-3-3 in the CSF, giving a high specificity of 94%.

The inclusion of a positive 14-3-3 CSF assay in the diagnostic criteria leads to a higher sensitivity. In the framework of this large surveillance study, only a few definite CJD cases did not show either a characteristic EEG or positive CSF for 14-3-3 proteins. Moreover, 14-3-3 proteins were detectable in some patients at an early stage of the disease, preceding the typical EEG changes, suggesting that they may be an earlier disease marker than the EEG. Of importance, when both the EEG and CSF were positive, the highest positive predictive value was achieved. In 98% of these cases, the clinical diagnosis was confirmed by neuropathology (positive predictive value; table 3). The highest predictive value for absence of CJD was achieved when both investi-

gations were negative (negative predictive value 79%), suggesting that in routine clinical practice, alternative diagnoses should be considered in such patients.

Although the results of this study demonstrate worthwhile diagnostic accuracy in patients with "probable" CJD using established diagnostic criteria, the sensitivity of the category "probable CJD" is increased by the inclusion of 14-3-3 assay results. Further, this study also shows that a significant proportion of cases classified as "possible CJD" according to established criteria (absence of PSWC on the EEG) do, in fact, suffer from CJD. As cases of "possible CJD" are often excluded in studies of CJD because of concerns of diagnostic validity, there is a particular need to improve the diagnostic accuracy in this subgroup of cases. It is clearly this group in which the 14-3-3 CSF test appears to be of most practical benefit in classifying patients because without autopsy, CJD may not be diagnosed in these cases. We propose new diagnostic criteria for the classification of CJD cases.

Acknowledgment

The authors thank all physicians in Germany notifying suspect cases to the German CJD surveillance unit and for their help in obtaining CSF specimens. Special thanks are given to Maja Schneider-Dominco for data management and assistance in manuscript preparation. The authors thank A. Green, E. Thompson, P. Brown, and M. Harrington of the U.K. study for carrying out the 14-3-3 analyses. They also thank Drs. S. Bevivino and Q.G. Liu for analysis of samples and Dr. P. Cortelli for CSF samples from FFI patients in the study in Italy. Also acknowledged is Ms. Clemencia Plitt for assistance at the CJD National Registry and Drs. Albert Saiz and Justo Carcia de Yebenes for support on laboratory work at Barcelona and Madrid in the study in Spain. In the Austrian study on 14-3-3 proteins, the authors thank Dr. Brigitte Gatterbauer for valuable help and DI Dita Drobna for excellent technical assistance. They are also grateful to Dr. Christa Jarius for diagnostic evaluation of the patients.

References

1. Brown P, Gibbs CJ, Jr., Rodgers-Johnson P, et al. Human spongiform encephalopathy: the National Institutes of Health series of 300 cases of experimentally transmitted disease. Ann Neurol 1994;35:513–529.
2. Masters CL, Harris JO, Gajdusek DC, Gibbs CJJ, Bernoulli C, Asher DM. Creutzfeldt–Jakob disease: patterns of worldwide occurrence and the significance of familial and sporadic clustering. Ann Neurol 1979;5:177–188.
3. Steinhoff BJ, Räcker S, Herrendorf G, et al. Accuracy and reliability of periodic sharp wave complexes in Creutzfeldt–Jakob disease. Arch Neurol 1996;53:162–166.
4. Demaerel P, Heiner L, Robberecht W, Sciot R, Wilms G. Diffusion-weighted MRI in sporadic Creutzfeldt–Jakob disease. Neurology 1999;52:205–208.
5. Finkenstaedt M, Szudra A, Zerr I, et al. MR imaging of Creutzfeldt–Jakob disease. Radiology 1996;199:793–798.
6. Hsich G, Kenney K, Gibbs CJ, Lee KH, Harrington MG. The 14-3-3 brain protein in cerebrospinal fluid as a marker for transmissible spongiform encephalopathies. N Engl J Med 1996;335:924–930.
7. Zerr I, Bodemer M, Gefeller O, et al. Detection of 14-3-3 protein in the cerebrospinal fluid supports the diagnosis of Creutzfeldt–Jakob disease. Ann Neurol 1998;43:32–40.
8. Kretzschmar HA, Ironside JW, DeArmond SJ, Tateishi J. Diagnostic criteria for sporadic Creutzfeldt–Jakob disease. Arch Neurol 1996;53:913–920.
9. Budka H, Aguzzi A, Brown P, et al. Neuropathological diagnostic criteria for Creutzfeltd–Jakob disease (CJD) and other human spongiform encephalopathies (prion diseases). Brain Pathol 1995;5:459–466.
10. Will RG, Alpérovitch A, Poser S, et al. Descriptive epidemiology of Creutzfeldt–Jakob disease in six European countries, 1993-1995. EU Collaborative Study Group for CJD. Ann Neurol 1998;43:763–767.
11. Bernheimer H, Gatterbauer B, Radbauer C, Budka H. Cerebrospinal fluid diagnosis of Creutzfeldt–Jakob disease. Wien Med Wochenschr 1998;148:96–100.
12. Parchi P, Giese A, Capellari S, et al. Classification of sporadic Creutzfeldt–Jakob disease based on molecular and phenotypic analysis of 300 subjects. Ann Neurol 1999;46:224–233.
13. Hill AF, Butterworth RJ, Joiner S, et al. Investigation of variant Creutzfeldt–Jakob disease and other human prion diseases with tonsil biopsy samples. Lancet 1999;353:183–189.
14. Kawashima T, Furukawa H, Doh-ura K, Iwaki T. Diagnosis of new variant Creutzfeldt–Jakob disease by tonsil biopsy. Lancet 1997;350:68–69.
15. Beaudry P, Cohen P, Brandel JP, et al. 14-3-3 protein, neuron-specific enolase, and S-100 protein in cerebrospinal fluid of patients with Creutzfeldt–Jakob disease. Dement Geriatr Cogn Disord 1999;10:40–46.
16. Rosenmann H, Meiner Z, Kahana E, et al. Detection of 14-3-3 protein in the CSF of genetic Creutzfeldt–Jakob disease. Neurology 1997;49:593–595.
17. Will RG, Zeidler M, Brown P, Harrington M, Lee KH, Kenney KL. Cerebrospinal fluid test for new variant Creutzfeldt–Jakob disease. Lancet 1996;348:955. Letter.
18. Jimi T, Wakayama Y, Shibuya S, et al. High levels of nervous system-specific proteins in cerebrospinal fluid in patients with early stage Creutzfeldt–Jakob disease. Clin Chim Acta 1992; 211:37–46.
19. Otto M, Stein H, Szudra A, et al. S-100 protein concentration in the cerebrospinal fluid of patients with Creutzfeldt–Jakob disease. J Neurol 1997;244:566–570.
20. Zerr I, Bodemer M, Räcker S, et al. Cerebrospinal fluid concentration of neuron-specific enolase in diagnosis of Creutzfeldt–Jakob disease. Lancet 1995;345:1609–1610.
21. Zeidler M, Stewart GE, Barraclough CR, et al. New variant Creutzfeldt–Jakob disease: neurological features and diagnostic tests. Lancet 1997;350:903–907.
22. Grünwald F, Pohl C, Bender H, et al. ^{18}F-Fluorodeoxyglucose-PET and ^{99m}Tc-bicisate-SPECT in Creutzfeldt–Jakob disease. Ann Nucl Med 1996;10:131–134.
23. Lugaresi E, Medori R, Montagna P, et al. Fatal familial insomnia and dysautonomia with selective degeneration of thalamic nuclei. N Engl J Med 1986;315:997–1003.

Brain Advance Access published July 1, 2006

doi:10.1093/brain/awl159

Determinants of diagnostic investigation sensitivities across the clinical spectrum of sporadic Creutzfeldt–Jakob disease

S. J. Collins,[1]* P. Sanchez-Juan,[2]* C. L. Masters,[1] G. M. Klug,[1] C. van Duijn,[2] A. Poleggi,[3] M. Pocchiari,[3] S. Almonti,[3] N. Cuadrado-Corrales,[4] J. de Pedro-Cuesta,[4] H. Budka,[5] E. Gelpi,[5] M. Glatzel,[6,13] M. Tolnay,[6] E. Hewer,[6] I. Zerr,[7] U. Heinemann,[7] H. A. Kretszchmar,[8] G. H. Jansen,[9] E. Olsen,[9] E. Mitrova,[10] A. Alpérovitch,[11] J.-P. Brandel,[11] J. Mackenzie,[12] K. Murray[12] and R. G. Will[12]

[1]Australian National Creutzfeldt–Jakob disease Registry, Department of Pathology, The University of Melbourne, Parkville, Vic., Australia, [2]Department of Epidemiology and Biostatistics, Erasmus MC, Rotterdam, The Netherlands, [3]National Registry of Creutzfeldt–Jakob disease, Department of Cell Biology and Neurosciences, Istituto Superiore di Sanita', Rome, Italy, [4]National HTSE Laboratory Unit at Centre of Microbiology and National HTSE Registry at Centre of Epidemiology, Instituto de Salud Carlos III, Calle Sinesio Delgado 6, Madrid, Spain, [5]Austrian Reference Centre for Human Prion Diseases, Institute of Neurology, Medical University Vienna, Wien, Austria, [6]Institute of Neuropathology and National Reference Center for Prion Diseases, University Hospital Zurich, Zurich, Switzerland, [7]Department of Neurology, Georg-August University, Göttingen, [8]Department of Neuropathology, Ludwig-Maximilian University, Munich, Germany, [9]Centre for Infectious Disease Prevention and Control, Public Health Agency of Canada, Ottawa, ON, Canada, [10]Institute of Preventive and Clinical Medicine, Research Base of Slovak Medical University, Bratislava, Slovak Republic, [11]U.708 INSERM, Hôpital de la Salpêtrière, Paris, France and [12]National CJD Surveillance Unit, Western General Hospital, Edinburgh, UK
[13]Present address: University Medical Center Hamburg-Eppendorf, Institute of Neuropathology, Hamburg, Germany

Correspondence to: S. J. Collins, Australian National CJD Registry, Department of Pathology, Level 3, Alan Gilbert Building, 161 Barry Street, Carlton South, Vic., 3053, Australia
E-mail: stevenjc@unimelb.edu.au
*These authors contributed equally to this work.

To validate the provisional findings of a number of smaller studies and explore additional determinants of characteristic diagnostic investigation results across the entire clinical spectrum of sporadic Creutzfeldt–Jakob disease (CJD), an international collaborative study was undertaken comprising 2451 pathologically confirmed (definite) patients. We assessed the influence of age at disease onset, illness duration, prion protein gene (*PRNP*) codon 129 polymorphism (either methionine or valine) and molecular sub-type on the diagnostic sensitivity of EEG, cerebral MRI and the CSF 14-3-3 immunoassay. For EEG and CSF 14-3-3 protein detection, we also assessed the influence of the time point in a patient's illness at which the investigation was performed on the likelihood of a typical or positive result. Analysis included a large subset of patients ($n = 743$) in whom molecular sub-typing had been performed using a combination of the *PRNP* codon 129 polymorphism and the form of protease resistant prion protein [type 1 or 2 according to Parchi *et al*. (Parchi P, Giese A, Capellari S, Brown P, Schulz-Schaeffer W, Windl O, Zerr I, Budka H, Kopp N, Piccardo P, Poser S, Rojiani A, Streichemberger N, Julien J, Vital C, Ghetti B, Gambetti P, Kretzschmar H. Classification of sporadic Creutzfeldt–Jakob disease based on molecular and phenotypic analysis of 300 subjects. Ann Neurol 1999; 46: 224–233.)] present in the brain. Findings for the whole group paralleled the subset with molecular sub-typing data available, showing that age at disease onset and disease duration were independent determinants of typical changes on EEG, while illness duration significantly influenced positive CSF 14-3-3 protein detection; changes on brain MRI were not influenced by either of these clinical parameters, but overall, imaging data were less complete and consequently

conclusions are more tentative. In addition to age at disease onset and illness duration, molecular sub-type was re-affirmed as an important independent determinant of investigation results. In multivariate analyses that included molecular sub-type, time point of the investigation during a patient's illness was found not to influence the occurrence of a typical or positive EEG or CSF 14-3-3 protein result. A typical EEG was most often seen in MM1 patients and was significantly less likely in the MV1, MV2 and VV2 sub-types, whereas VV2 patients had an increased likelihood of a typical brain MRI. Overall, the CSF 14-3-3 immunoassay was the most frequently positive investigation (88.1%) but performed significantly less well in the very uncommon MV2 and MM2 sub-types. Our findings confirm a number of determinants of principal investigation results in sporadic CJD and underscore the importance of recognizing these pre-test limitations before accepting the diagnosis excluded or confirmed. Combinations of investigations offer the best chance of detection, especially for the less common molecular sub-types such as MV2 and MM2.

Keywords: sporadic CJD; diagnostic investigation results; molecular sub-typing

Abbreviations: CJD = Creutzfeldt–Jakob disease; PrP^{res} = protease-resistant prion protein; PSWC = periodic sharp wave complexes

Received October 6, 2005. Revised May 9, 2006. Accepted May 16, 2006

Introduction

Pre-mortem diagnosis of the rare, transmissible neurodegenerative disorder, sporadic Creutzfeldt–Jakob disease (CJD), largely relies on an appropriate clinical profile supported by characteristic findings on routine investigations such as the EEG and CSF analysis (Collins *et al.*, 2004). Neuropathological examination of the brain remains necessary to achieve a definite diagnosis. Cerebral MRI may also demonstrate highly suggestive changes and is assuming a greater role in CJD evaluation but is not currently included in diagnostic criteria for surveillance purposes (Collie *et al.*, 2001; Meissner *et al.*, 2004; Shiga *et al.*, 2004; Tschampa *et al.*, 2005). Although the diagnostic utility of these investigations (particularly the EEG and CSF 14-3-3 protein detection) has been supported by a number of studies (Steinhoff *et al.*, 1996, 2004; Zerr *et al.*, 2000*a*), they remain imperfect surrogate markers, with apparent non-uniform sensitivity across the clinical spectrum of sporadic CJD (Parchi *et al.*, 1999).

Different clinical and pathological sub-types of sporadic CJD have been linked to polymorphism status at codon 129 of *PRNP* combined with the type (1 or 2) of protease-resistant prion protein (PrP^{res}) found in the brain, and together these probably define different human prion strains (Parchi *et al.*, 1999; Hill *et al.*, 2003; Korth *et al.*, 2003). The most widely used scheme distinguishes only two PrP^{res} types (Parchi *et al.*, 1999), while another commonly employed nomenclature delineates a greater number (Hill *et al.*, 2003). Employing this nosology to sub-type sporadic CJD, the EEG has been shown to vary widely between the specific molecular sub-types in demonstrating characteristic or typical changes (Parchi *et al.*, 1999; Zerr *et al.*, 2000*b*). Generally, the likelihood of characteristic changes on the EEG was reported to be highest in MM homozygotes, reduced in heterozygotes and lowest in VV carriers. Immunoassay for 14-3-3 proteins in CSF, increasingly utilized in the diagnostic evaluation of patients with suspect CJD (Zerr *et al.*, 2000*a*), has also been shown to vary in rates of positivity according to molecular sub-type, with the likelihood of noticeably reduced detection rates in heterozygous patients with type 2 PrP^{res} (MV2) (Zerr *et al.*, 2000*b*; Otto *et al.*, 2002; Castellani *et al.*, 2004). A notable difficulty with all previous reports assessing rates of positive diagnostic investigations in molecular sub-types of sporadic CJD is the small numbers of patients studied, especially the less common phenotypic sub-types. Such small patient numbers militate against the reliability of the observations and have precluded multivariate analyses to assess for covariates and probable confounding factors. A corollary, unexplored so far, is whether within each of the molecular subgroups and across the phenotypic spectrum of sporadic CJD there are additional independent variables influencing diagnostic test results. Consequently, there remains a need to more confidently establish the diagnostic utility of these investigations across the various molecular sub-types of sporadic CJD and define further determinants of their sensitivity and specificity across the entire clinical range. More clearly defining additional factors influencing the sensitivity and specificity of these principal investigations has important practical implications when investigating individual patients.

As part of a collaborative multi-national CJD surveillance program (EUROCJD) initiated in 1993, we assessed the effect of patient clinical features such as age at onset, illness duration and *PRNP* codon 129 polymorphism on the diagnostic sensitivity of EEG, CSF 14-3-3 immunoassay and cerebral MRI in a large, population-based sample of 2451 pathologically confirmed (definite) sporadic cases of CJD, employing harmonized case definitions and data sets. Further, similar analysis was undertaken in a subset of patients (n = 743) in whom molecular sub-typing using brain PrP^{res} isotype and codon 129 polymorphism had been determined. Inclusion of this data allowed detailed assessment of the

variation in positive test results across the molecular sub-types, as well as whether patient parameters such as age at onset, illness duration and the specific time point at which the investigation was performed during a patient's illness were additional independent determinants of investigation results.

Patients and methods

The present study was undertaken as part of the ongoing activities of the prospective CJD surveillance programme (EUROCJD) conducted by the European Union and allied countries. In 1993, national surveillance registers commenced in France, Germany, Italy, The Netherlands, Slovakia and the UK, with the aim of ascertaining all patients diagnosed with probable or definite CJD in the respective countries. The study was extended in 1997 and again in 1998 to include Australia, Austria, Canada, Spain and Switzerland. EUROCJD collaborative study methods utilizing standardized case definitions and centralized harmonized demographic data sets were as described previously (Pocchiari *et al.*, 2004; Ladogana *et al.*, 2005*a*).

The study comprised all patients ($n = 2451$) with definite sporadic CJD who died between 31 December 1992 and 31 December 2002: 136 cases from Australia, 68 from Austria, 146 from Canada, 491 from France, 450 from Germany, 342 from Italy, 100 from The Netherlands, 438 from the UK, 18 from Slovakia, 183 from Spain and 79 from Switzerland. A diagnosis of definite sporadic CJD required neuropathological confirmation most commonly through post-mortem but occasionally through brain biopsy. Analysis of the *PRNP* open reading frame was performed in the majority of patients to exclude genetic CJD, as clinical differentiation from sporadic CJD is not always possible (Collins *et al.*, 2000; Ladogana *et al.*, 2005*b*). Of the 2451 patients, 746 had their brain PrP^{res} isotype determined, which in combination with *PRNP* codon 129 genotyping allowed molecular sub-typing according to the system of Parchi *et al.*, (1999). Whenever possible, PrP^{res} typing was based on analysis of a number of brain regions, including cerebral cortex, striatum or thalamus and cerebellum, although the preferred number and precise location of sampling sites varied between participating countries.

Whenever possible, all EEGs and MRI brain scans were reviewed by a member of the surveillance system and scored for the presence or absence of typical or characteristic diagnostic features. EEG records were scored positive or characteristic when they fulfilled validated criteria (Steinhoff *et al.*, 2004): sustained periodic sharp wave complexes (PSWC) with a variability of <500 ms, with the periodic complexes (lasting 100–600 ms) demonstrating a bi- or triphasic morphology and seen in a generalized or lateralized distribution. The CSF 14-3-3 immunoassays were performed in each of the national surveillance centres using western blotting, with conformity of testing methods and results interpretation confirmed by blinded sample exchange programme. On cerebral MRI, high signal in the putamen and caudate nucleus when using long-repetition time pulse sequences was considered a positive finding for sporadic CJD (Collie *et al.*, 2001); however, there was no systematic use of particular techniques such as fluid attenuated inversion recovery (FLAIR) or diffusion weighted imaging (DWI).

For assessment of the influence of the timing of the investigation during a patient's illness on the test result, data sets were of sufficient size for EEG and CSF 14-3-3 protein detection to allow this type of analysis. Acknowledging that the median total illness duration was 5 months, we chose to divide each patient's symptomatic phase into thirds (first, middle and final) rather than into a greater number of epochs. This was to ensure avoiding the creation of illness periods of such brevity, especially at the onset of symptoms, that they would be unlikely to correspond to a clinically meaningful phase of a patient's illness during which investigations would usually be undertaken, and if undertaken because of the development of symptoms suggesting neurological dysfunction, that these features were sufficiently developed that the investigations had a reasonable likelihood of displaying abnormalities. The median times (range in months) from the onset of symptoms for the analyses of each of the first, middle and final thirds of patient's illnesses for assessing CSF 14-3-3 protein detection were 1 (0–10), 2.5 (1–17) and 4 months (1–41), respectively. With respect to EEG findings, the median times (range in months) from the onset of symptoms for the analyses of each of the first, middle and final thirds of patient's illnesses were 1 (0–18), 2 (1–42) and 4 months (1–41), respectively.

All data were centralized and analysed collaboratively.

Statistical analysis

Descriptive statistics were calculated for the whole sample and for every molecular sub-type of the disease. Fisher's exact and Mann–Whitney tests were used to assess differences between qualitative and quantitative variables, respectively. The number of positive findings (acknowledging that patients may have undergone multiple tests) over the total number of tested CJD cases for EEG, MRI and the CSF 14-3-3 immunoassay was determined for each stratum. The frequency of positive results (number of positive test results in total number of patients) was then calculated for EEG, MRI and the CSF 14-3-3 test for each stratum.

In order to analyse the independent effect of each factor on positive test results, taking into account possible confounders, we fitted two multiple logistic regression models with the test result as output. Both models included age at onset, and disease duration as predictors, and included country of origin, year of death and gender as covariates.

In the first model *PRNP* codon 129 genotype was entered as a predictor, while in the second model we used the molecular sub-type (combination of *PRNP* codon 129 genotype and PrP^{res} type). Age at onset was categorized into clinically meaningful groups, with patients younger than 50 years serving as the reference group. Disease duration was also categorized with the same criteria into three groups: duration <6, 6–12 and >12 months. *PRNP* codon 129 genotype was entered in the model using two dummy variables, with MM as the reference group; for molecular sub-types we created eight dummy variables (MM2, MM1/2, MV1, MV2, MV1/2, VV1, VV2 and VV1/2) with MM1 group as reference. Adjusted odd ratios (ORs) and 95% confidence intervals (CIs) were generated. All statistical analyses were performed using SPSS 11.0 for Windows 2000 (SPSS Inc., Chicago, IL).

Results

Table 1 summarizes the salient features of all definite sporadic CJD cases. Of the 2451 patients identified, 1329 were females (54.2%). The median age at death was 68 years (range: 20–95), while the median disease duration was 5 months (range: 1–81).

Table 1 Summary of clinical features of all patients, including the subset undergoing molecular sub-typing

Clinical feature	All patients	Patients with molecular sub-typing
Male (%)	1122 (45.8)	351 (47.2)
Female (%)	1329 (54.2)	392 (52.8)
Median age at onset (range)	67.2 (15.6–94.9)	66.2 (15.6–90.0)
Age at onset < 50 years (%)	116 (5.1)	39 (5.5)
Age at onset 50–59 years (%)	412 (18.2)	141 (19.7)
Age at onset 60–69 years (%)	867 (38.3)	286 (40.0)
Age at onset 70–79 years (%)	729 (32.2)	212 (29.7)
Age at onset > 80 years (%)	137 (6.1)	37 (5.2)
Median duration of illness in months (range)	5 (1–81)	5 (1–62)
Patients with duration < 6 months (%)	1332 (58.8)	404 (56.5)
Patients with duration 6–12 months (%)	611 (27.0)	179 (25.0)
Patients with duration > 12 months (%)	321 (14.2)	132 (18.5)
Codon 129 genotype		
Met-Met/total (%)	1061/1604 (66.1)	504/743 (67.8)
Met-Val/total (%)	272/1604 (17.0)	117/743 (15.7)
Val-Val/total (%)	271/1604 (16.9)	122/743 (16.4)
Patients with *PRNP* gene sequenced (%)	1492 (63.6)	650 (87.5)
PrP isotype		
Type 1	495/743 (66.6)	495/743 (66.6)
Type 1 and 2	44/743 (5.9)	44/743 (5.9)
Type 2	204/743 (27.5)	204/743 (27.5)
EEG		
Typical/total (%)	1216/2083 (58.4)	371/666 (55.7)
14-3-3 protein in CSF		
Positive/total (%)	1340/1521 (88.1)	486/554 (87.7)
MRI		
Characteristic findings/total (%)	405/1036 (39.1)	150/387 (38.8)

An EEG was performed on 2083 patients (85%). Of those undergoing EEG, 1216 cases showed typical PSWCs (58.4%) (Table 1). The codon 129 genotype had a significant effect on the likelihood of a positive result of the EEG in sporadic CJD patients (Table 2), which ranged from 73.2% in MM homozygotes to 21.5% in VV homozygotes. After adjusting for possible confounding variables (country, sex, year of death, age at onset and disease duration), the prevalence of PSWC on the EEG was significantly decreased in heterozygotes ($P < 0.001$) and VV homozygotes ($P < 0.001$). The median age of death of sporadic CJD patients with a typical EEG was 69.0 (range: 34–92) versus 66 years (range: 20–88) in patients with an atypical EEG ($P < 0.001$). The presence of PSWC was further analysed by age at onset and disease duration (Table 3). The likelihood of a typical EEG steadily increased with age ($P < 0.001$, adjusted for the same variables), while there was an inverse correlation with disease duration ($P = 0.001$).

CSF 14-3-3 protein analysis was performed on 1521 cases (62.1%) of sporadic CJD. Of these, 1340 cases were positive (88.1%) (Table 1). Although the frequency of a positive CSF 14-3-3 immunoassay was high for all three codon 129 genotypes, heterozygotes had a significantly lower rate (77.0%) in adjusted analyses than VV ($P < 0.001$) and MM ($P < 0.05$) (Table 2). Age at disease onset did not influence CSF 14-3-3 protein detection but as for the EEG a positive result was less likely with longer disease duration (Table 3) ($P < 0.001$).

Table 2 Summary of principal investigation findings for all patients who underwent *PRNP* codon 129 genotyping

	EEG	MRI	14-3-3 protein in CSF
	Typical/total (%)	Typical/total (%)	Positive/total (%)
PRNP genotype			
M/M	710/970 (73.2)	172/474 (36.3)	709/796 (89.1)
M/V	99/245 (40.4)	65/134 (48.5)	147/191 (77.0)
V/V	50/233 (21.5)	71/139 (51.1)	184/196 (93.9)
P-value	<0.001	0.004	0.002

Adjusted by age at onset, disease duration, sex, country of origin and year of death.

MR brain imaging was performed on 1063 patients (42.3%). Of these patients, 405 patients showed characteristic changes (39.1%) (Table 1). In contrast with the EEG, the likelihood of a positive MRI scan was higher in cases with the MV ($P < 0.05$) and VV genotypes ($P = 0.002$) in comparison to those with an MM genotype (Table 2). MRI results were not significantly associated with age at onset or disease duration (Table 3).

Table 3 Principal investigation findings for all patients according to age at disease onset and duration of illness

	EEG Typical/total (%)	MRI Typical/total (%)	14-3-3 protein in CSF Positive/total (%)
Age at onset			
Age at onset < 50 years (%)	35/104 (33.7)	18/58 (31.0)	62/77 (80.5)
Age at onset 50–59 years (%)	197/371 (53.1)	83/196 (42.3)	222/260 (85.4)
Age at onset 60–69 years (%)	457/796 (57.4)	166/415 (40.0)	472/545 (86.6)
Age at onset 70–79 years (%)	438/675 (64.9)	126/328 (38.4)	452/492 (91.9)
Age at onset > 80 years (%)	81/124 (65.3)	12/37 (32.4)	73/83 (88.0)
P for trend	<0.001	0.3	0.4
Disease duration			
Patients with duration < 6 months (%)	814/1228 (66.3)	203/587 (34.6)	779/840 (92.7)
Patients with duration 6–12 months (%)	283/558 (50.7)	125/287 (43.6)	358/408 (87.7)
Patients with duration > 12 months (%)	115/288 (39.9)	77/160 (48.1)	146/211 (69.2)
P for trend	0.001	0.4	<0.001

Adjusted by *PRNP* codon 129 genotype, sex, country of origin and year of death.

Table 4 Summary of age at disease onset and illness duration for all patients undergoing molecular sub-typing

	Sporadic CJD molecular sub-types								
	MM1	MM2	MM1/2	MV1	MV2	MV1/2	VV1	VV2	VV1/2
Total number (%)	444 (59.8)	31 (4.2)	29 (3.9)	37 (5.0)	73 (9.8)	7 (0.9)	14 (1.9)	100 (13.5)	8 (1.1)
Median age at onset (range)	67.8 (31.1–89.4)	60.3 (37.7–82.3)*	65.6 (48.9–89.9)	65.5 (15.6–84.2)	63.6 (40.8–81.1)*	66.3 (56.7–77.9)	47.2 (23.6–72.7)*	66.3 (40.2–86.3)	59.7 (18.7–72.7)
Age at onset < 50 years (%)	12 (2.8)	5 (16.7)†	1 (3.8)	1 (2.8)	2 (2.9)	0 (0.0)	7 (53.8)†	9 (9.3)†	2 (25.0)†
Age at onset 50–59 years (%)	78 (18.2)	9 (30.0)	3 (11.5)	9 (25.0)	17 (24.6)	1 (14.3)	2 (15.4)	20 (20.6)	2 (25.0)
Age at onset 60–69 years (%)	172 (40.1)	11 (36.7)	12 (46.2)	10 (27.8)	37 (53.6)†	3 (42.9)	3 (23.1)	35 (36.1)	3 (37.5)
Age at onset 70–79 years (%)	143 (33.3)	4 (13.3)*	7 (26.9)	13 (36.1)	12 (17.4)*	3 (42.9)	1 (7.7)	28 (28.9)	1 (12.5)
Age at onset > 80 years (%)	24 (5.6)	1 (3.3)	3 (11.5)	3 (8.3)	1 (1.4)	0 (0.0)	0 (0.0)	5 (5.2)	0 (0.0)
Median duration (months) (range)	4.0 (1.0–39.0)	12.5 (3.0–38.0)†	6.0 (2.0–33.0)	5.0 (1.0–54.0)†	12.0 (3.0–62.0)†	13.0 (2.0–30.0)	11.0 (2.0–29.0)†	6.0 (2.0–25.0)†	5.5 (3.0–62.0)
Duration < 6 months (%)	307 (71.6)	9 (30.0)*	11 (42.3)*	21 (58.3)	5 (7.2)*	3 (42.9)	4 (30.8)*	40 (41.2)*	4 (50.0)
Duration 6–12 months (%)	78 (18.2)	4 (13.3)	11 (42.3)†	7 (19.4)	28 (40.6)†	0 (0.0)	3 (23.0)	47 (48.5)†	1 (12.5)
Duration > 12 months (%)	44 (10.3)	17 (56.7)†	4 (15.4)	8 (22.2)†	36 (52.2)†	4 (57.1)†	6 (46.2)†	10 (10.3)	3 (37.5)†
Female (%)	239 (53.8)	15 (48.4)	14 (48.3)	18 (48.6)	35 (47.9)	5 (71.4)	5 (35.7)	56 (56.0)	5 (62.5)

*Significantly lower than MM1 ($P < 0.05$); †Significantly higher than MM1 ($P < 0.05$).

Analysis of sporadic CJD patients according to molecular sub-type

In 743 patients the codon 129 polymorphism and brain PrP^{res} isotype were determined allowing molecular phenotypic sub-stratification (Table 1) (Parchi *et al.*, 1999). In 87% of these patients the *PRNP* gene was sequenced, ruling out pathological mutations associated with genetic CJD. In comparison to the entire group, the median age at onset, median disease duration and *PRNP* codon 129 polymorphism distributions were similar, and there were no significant differences in the overall rates of positive results for each of the investigations. The most common PrP^{res} isotype was type 1 (67%); type 2 was present in 27% of the sample, and in 44 cases (6%) there was coexistence of both type 1 and 2.

The relative frequency of the various molecular sub-types is provided in Table 4. There were occasional significant differences in demographic characteristics between subgroups. MM1 patients were the oldest at disease onset (median: 67.8 years) and VV1 patients were the youngest (median: 47.2 years). The duration of the disease was significantly shorter in MM1 patients (median: 4 months) in comparison with the rest, especially the MM2 (median: 12.5 months) and MV2 (median: 12 months) subgroups, with these groups also

demonstrating a higher percentage of patients with disease lasting >1 year (57 and 52%, respectively). Of note, albeit the small patient numbers preclude statistically significant differences, patients with co-existence of PrP^{res} types 1 and 2 (MM1/2, VV1/2 and MV1/2) tended to have intermediate phenotypes but generally aligning more to the most common molecular PrP^{res} sub-type within each *PRNP* codon 129 genotype.

Overall, determinants of investigation findings in patients who underwent molecular sub-typing were the same as for the entire group. Independent of disease duration and molecular sub-type, age at disease onset correlated significantly with a positive EEG result ($P = 0.007$) (Fig. 1). Patients who developed symptoms <50 years had a lower rate of typical PSWCs (22%) than patients presenting after 60 years of age. The median age at onset of the patients with an atypical EEG was 64 years (range: 16–86), compared with 68 years (range: 31–90) in patients showing the typical findings. CSF 14-3-3 protein immunoassay and MRI results were not significantly correlated with patient's age at disease onset.

The duration of disease was independently associated with the likelihood of PSWCs. Patients with disease duration <6 months had a significantly higher rate ($P = 0.02$) of a typical EEG than patients with duration >12 months (65 versus 35%, respectively). The median disease duration of patients with an atypical EEG was 6 (range: from 1 to 62) versus 4 months (range: from 1 to 39) in patients with typical EEG. Disease duration significantly ($P = 0.004$) influenced the likelihood of a positive CSF 14-3-3 test result. Those patients with disease duration <6 months had a higher rate of positive test results than those with duration >12 months (91 versus 72%, respectively). On average, patients with 14-3-3 proteins detectable in their CSF had shorter disease durations (median: 5 months, range: 1–39) than patients with a negative test result (median: 11 months, range: 2–54). MRI results did not correlate with disease duration (Fig. 2).

Certain molecular sub-types showed significant correlations with investigation results. MM1 patients demonstrated the highest frequency of positive EEG results (73%) followed by MV1 patients (53%), although after adjusting for covariates the significance was reduced ($P = 0.01$). VV2 and MV2 patients had infrequent occurrence of a typical EEG, with a positive result only observed in 12.8 and 17.5% of the cases, respectively (Fig. 3). Of the sub-groups with coexistence of PrP^{res} types, only VV1/2 patients had a significantly lower frequency compared with the MM1 subgroup. CSF 14-3-3 immunoassay was the most frequently positive investigation, with an overall positive rate of 88%. However, there were some significant variations across molecular sub-types, with the test significantly more often positive (all *P*-values < 0.05) for MM1 and VV2 patients (91 and 95%) than for MM2 (61%) and MV2 (71%) (Fig. 3). Of the patient groups with coexistence of PrP^{res} types, only MM homozygotes had a significantly lower rate of positive results for this test (Fig. 3). For MRI, only the VV2 subgroup demonstrated a significantly increased likelihood of a typical positive result. Of note, within each molecular sub-type except VV1, occasional patients did not display typical or characteristic findings with any of the three investigations.

Assessment of the influence of the time point of the investigation during a patient's illness on the test result

For both EEG and the detection of CSF 14-3-3 proteins, sufficient data were available to analyse the influence of the time point at which the investigation was performed

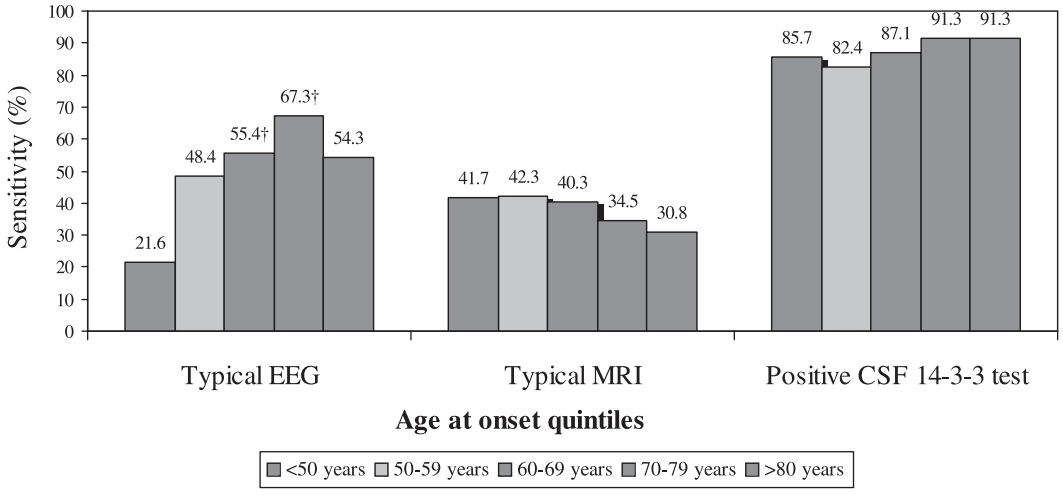

Fig. 1 The principal investigation results for EEG, brain MRI and CSF 14-3-3 protein analysis were correlated with age at disease onset in sporadic CJD for all patients undergoing molecular sub-typing. Patients were grouped by age at onset: <50, 50–59, 60–69, 70–79 and >80 years. Only the EEG showed a significant correlation with age at disease onset. †Significantly higher than in <50 years group ($P < 0.05$); adjusted by molecular sub-type, disease duration, sex, country of origin, year of death.

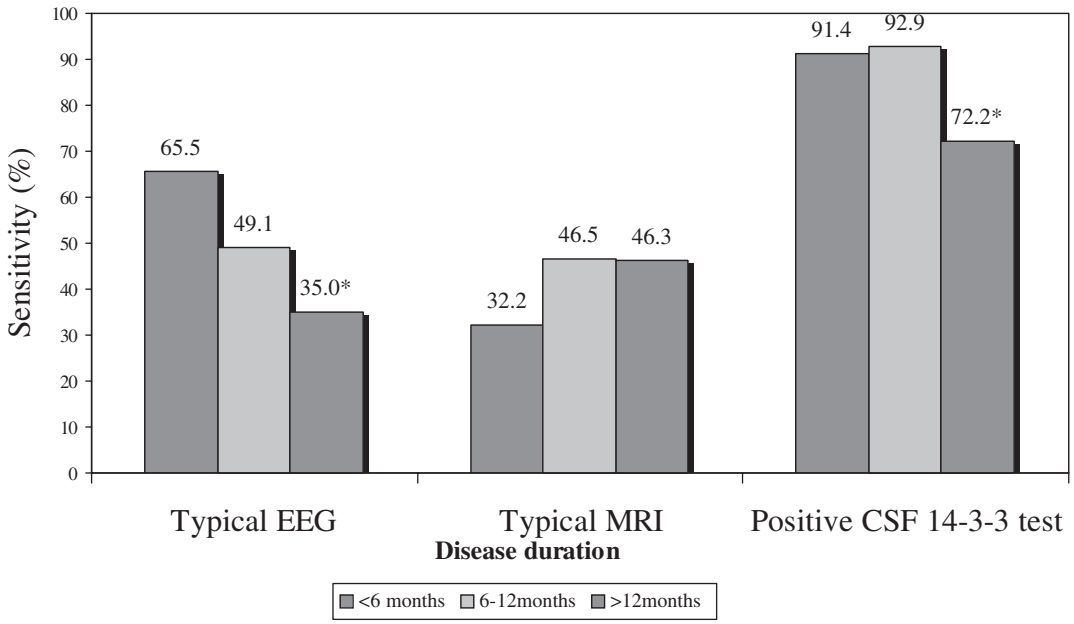

Fig. 2 The principal investigation results for EEG, brain MRI and CSF 14-3-3 protein analysis were correlated with disease duration in sporadic CJD for all patients undergoing molecular sub-typing. Disease duration was arranged as <6, 6–12 and >12 months. For both the EEG and CSF 14-3-3 protein detection there was a significant inverse correlation with disease duration >12 months. * Significantly lower than in <12-months group ($P < 0.05$); adjusted by molecular sub-type, age at onset, sex, country of origin, year of death.

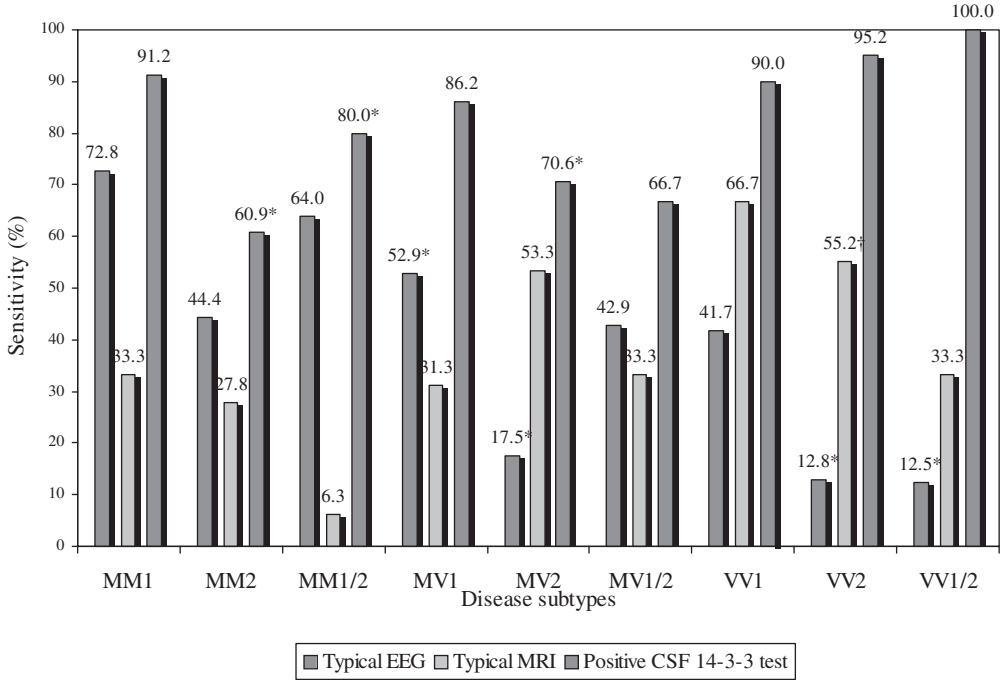

Fig. 3 The sensitivities of EEG, brain MRI and CSF 14-3-3 protein detection were assessed according to the sporadic CJD molecular sub-type: MM1, MM2, MM1/2; MV1, MV2, MV1/2; and VV1, VV2 and VV1/2. The MV1, MV2, VV2 and VV1/2 sub-types all showed a significantly reduced EEG sensitivity, while the VV2 sub-type displayed a significantly higher likelihood of a typical MRI result. The MM2, MM1/2 and MV2 sub-types all showed significantly reduced rates of CSF 14-3-3 protein positivity. * Significantly lower than MM1 ($P < 0.05$); †significantly higher than MM1 ($P < 0.05$); adjusted by age at onset, disease duration, sex, country of origin, year of death.

during the patient's illness on the likelihood of a typical or positive result. With the median duration of illness only 5 months, we chose to divide the symptomatic phase into thirds (first, middle and final) rather than into a greater number of epochs. This was undertaken to avoid the creation of illness phases of such brevity, especially at the onset of symptoms, that they would be unlikely to correspond to a clinically meaningful period of a patient's illness during which investigations would usually be undertaken and that the test would have a reasonable chance of showing typical abnormalities.

With respect to EEGs, 2425 recordings with a known time point in relation to the chronology of the patient's illness were available for analysis from 1728 cases. When analysed in isolation, the likelihood of a typical EEG was significantly less in the first third of a patient's illness compared with the last third ($P = 0.02$). Multivariate analysis (adjusted by country, gender, year of death, age at onset, disease duration and codon 129 polymorphism) also showed that a positive EEG was significantly more likely in the last third of a patient's illness compared with the first third ($P = 0.001$). When a patient's molecular sub-type was substituted for codon 129 polymorphism in the same regression model, however, a typical periodic EEG was no longer significantly more likely in any particular time period of the patient's illness. These results are consistent with the specific time point at which the diagnostic test is undertaken during the symptomatic period of a patient's illness not being independent of molecular sub-type in determining the likelihood of a positive EEG. With respect to detection of CSF 14-3-3 proteins, 1032 assays from 985 cases were available for analysis, showing no significant association between a positive result and the time point of sampling during a patient's illness, regardless of whether assessed in isolation or in analogous multivariate analyses. For each of the first, middle and final third time periods of patient's illnesses, the CSF 14-3-3 protein sensitivities were 88, 86.4 and 91.3%, respectively.

Discussion

The current study is by far the largest to date to assess the diagnostic sensitivity of investigations usually employed in the evaluation of suspected sporadic CJD. By virtue of the large number of definite sporadic CJD patients comprising our study we have been able to confidently delineate the sensitivities of the principal investigation results across the entire phenotypic spectrum, especially the less common molecular sub-types, as well as clarify and extend hitherto uncertain independent determinants of investigation results (Pocchiari *et al.*, 2004). Analysis of only neuropathologically confirmed CJD patients has allowed us to avoid the inherent difficulties that arise from analysis of investigations that also serve in case definition criteria for probable cases; however, it is noteworthy that separate analysis of all EUROCJD sporadic CJD patients from this time period, that is, inclusion of clinically probable cases, gave the same results as analysis of just definite cases (data not shown). Multivariate regression modelling demonstrated that age at disease onset and disease duration both act as independent determinants of some investigation results in sporadic CJD, in addition to the influence of molecular sub-type. Consequently, in the clinical evaluation of suspect CJD, our findings reinforce the importance of fully appreciating the limitations of specific investigations relative to these salient patient clinical features; otherwise the heightened likelihood of a negative test result may be underestimated and incorrectly interpreted as undue reassurance against the diagnosis. Specifically, the probability that an EEG will demonstrate PSWCs increases with age and conversely decreases with disease duration, especially if >12 months. Hence, in a patient <50 years it is most likely that an EEG will not show typical changes, and even in older patients, if their illness is >6 months, the probability of PSWCs is at best only ~50%. In contrast to a prior smaller study (Zerr *et al.*, 2000*b*) disease duration >12 months was also observed to significantly lessen the likelihood of a positive CSF 14-3-3 result. This underscores the importance of acknowledging illness duration when interpreting a negative result in an individual patient suspected to be manifesting sporadic CJD.

The present study re-affirmed that molecular sub-type, in addition to age at onset and illness duration, is also an important independent determinant of principal investigation results (Parchi *et al.*, 1999; Zerr *et al.*, 2000*b*; Otto *et al.*, 2002; Hill *et al.*, 2003; Castellani *et al.*, 2004; Meissner *et al.*, 2004). In contrast to the EEG, where the presence of valine alleles at codon 129 additively reduces the likelihood of PSWCs, valine homozygotes (especially VV2 patients) were significantly more likely to demonstrate a typical MRI scan than methionine homozygotes (particularly the MM1 subgroup). These data conform to a pattern whereby sub-types with 'classical' sporadic CJD and predominant cerebral cortical involvement (MM1 and MV1) are more likely to manifest PSWCs on EEG, while those with ataxia and subcortical neuropathological changes (VV2 and MV2) are more likely to demonstrate characteristic basal ganglia changes on MRI. However, in contrast to a prior report suggesting phenotypic homogeneity between the MM1 and MV1 sub-types (Parchi *et al.*, 1999), we found that the likelihood of a typical EEG was significantly lower and the average illness duration significantly longer in the MV1 patients. The most likely explanation for this difference in findings is the much larger sample of MV1 patients available for analysis in our study.

The CSF 14-3-3 protein immunoassay was the most sensitive investigation across the sporadic CJD phenotypic spectrum, but the influence of molecular sub-type was still evident. Codon 129 heterozygotes, especially the MV2 sub-group, were significantly less likely to be associated with a positive result [Zerr *et al.*, 2000*a*, *b*; Otto *et al.*, 2002; Castellani *et al.*, 2004], as were the very uncommon MM2 and MM1/2 subgroups. In comparison with the simple

demographic features of age at disease onset and illness duration, the molecular sub-typing profile is much less likely to be available pre-mortem in individual patients. Nevertheless, if this information is available, investigation results would also need to be interpreted in this specific context for the most accurate estimation of excluding or confirming the likelihood of sporadic CJD. Having recognized these overall limitations and variations across the molecular sub-types, from a practical clinical perspective it would appear prudent to utilize all three principal investigations (brain MRI, CSF 14-3-3 protein analysis and EEG), as, irrespective of molecular sub-type, only very uncommonly (except the rare MM2 sub-group) will all three investigations not show characteristic findings in an individual patient with sporadic CJD (Shiga *et al.*, 2004).

Our analyses do not suggest that the time point at which the investigation is undertaken during a patient's illness is an independent determinant of the test result. This was particularly evident for CSF 14-3-3 protein detection, for which no association between time point of sampling and a positive result was found regardless of analytical approach. For EEG, the apparent reduced likelihood of a typical or periodic recording in the first third of a patient's illness compared with the final period, when examined in isolation or with one of the multivariate regression models, was no longer evident when the regression model included molecular sub-type. Collectively, our findings are consistent with the generally dominant influence of age at onset, illness duration and molecular sub-type as the key independent determinants of investigation results compared with other demographic variables, including the time point of test sampling during a patient's illness.

Although molecular sub-typing of sporadic CJD patients has proven a useful phenotypic classification system, there are some difficulties with this approach. Not uncommonly, more than one PrP^{res} type may be present in the brain of a patient dying from sporadic CJD (Parchi *et al.*, 1999), and it is likely that the frequency of occurrence increases with the number of regions assessed (Puoti *et al.*, 1999; Head *et al.*, 2004). At present, there is no consensus on how to classify such patients and whether it is generally better to adopt a dichotomized approach based on predominance of one type when several regions are studied or accept classification based on the analysis of only one or two brain sites. In our study, patients with more than one PrP^{res} type were a small minority, but such patients were allowed status as a separate group within each *PRNP* genotype without attempting to adjust for relative abundance of the two PrP^{res} types. Regardless of *PRNP* genotype, our patients with simultaneous occurrence of both PrP^{res} types tended to present a different phenotype, sometimes intermediate between those with a single PrP^{res} isotype and the same codon 129 status, but often extending beyond the range observed. This suggests that the simultaneous presence of two PrP^{res} types may evoke a third or unique phenotype within each codon 129 genotype, although our small patient numbers militated against achieving significance with these observations. Analysis of investigation results also generally suggests that subgroups with co-existence of PrP^{res} isotypes tended to appear different although not invariably. For CSF 14-3-3 results, the MM1/2 group behaved more like MM2 patients, and for the EEG the VV1/2 group were also more like the VV2 patients. The latter is in keeping with the predominant phenotypic influence of type 2 PrP^{res} on these investigations or may simply represent a sampling bias wherein type 2 PrP^{res} was under-appreciated as the dominant protease resistant isotype across the brain.

MRI brain imaging is now very commonly employed in the diagnostic evaluation of suspected sporadic CJD but its ultimate sensitivity and specificity is still being defined (Finkenstaedt *et al.*, 1996; Collie *et al.*, 2001; Meissner *et al.*, 2004; Shiga *et al.*, 2004; Tschampa *et al.*, 2005). For a number of reasons, our overall sensitivity for typical changes on MRI scan is lower than that reported in much smaller studies (Finkenstaedt *et al.*, 1996; Schröter *et al.*, 2000; Zerr *et al.*, 2000*b*; Meissner *et al.*, 2004; Shiga *et al.*, 2004; Tschampa *et al.*, 2005). Importantly, patient MRI data collected for this study extended over a decade, during which time this imaging technique was increasingly used in the evaluation of suspect sporadic CJD, and there were concurrent improvements in the diagnostic sensitivity of pulse sequences used for this illness (Collie *et al.*, 2001; Shiga *et al.*, 2004; Tschampa *et al.*, 2005). Consequently, the overall number of patients studied with MRI was relatively low (42.3%), and the utilization of optimized MRI techniques such as DWI and FLAIR mainly occurred only in the very latter phase of our study epoch and even then was not uniformly adopted by all neuroimaging services. Further, during the study period there was progressive appreciation that increased cerebral cortical signal using the more sensitive techniques of DWI and FLAIR is probably a reasonably common feature in sporadic CJD (Shiga *et al.*, 2004; Tschampa *et al.*, 2005). Consequently, another reason for our low MRI sensitivity relates to our restrictive definition of what changes we considered characteristic of the diagnosis (i.e. signal hyperintensity limited to the basal ganglia). Overall, this combination of factors has compromised our assessment of the true diagnostic sensitivity and clinical utility of MRI in the evaluation of sporadic CJD. This sub-optimal aspect of the present study is being redressed by a further prospective EUROCJD collaborative project.

Acknowledgements

Australia: The Australian National Creutzfeldt–Jakob Disease Registry (ANCJDR) thanks Alison Boyd, James Lee, Victoria Lewis, Samantha Douglass and Magdalena Kvasnicka for their assistance, and the families of registry patients and their medical practitioners for their cooperation. The ANCJDR is funded by the Commonwealth Department of Health and Ageing. Austria: The Austrian Reference Centre for Human Prion Diseases (OeRPE, Head: Prof. Herbert Budka) acknowledges the help of Drs Christa Jarius, Ellen Gelpi,

Elisabeth Lindeck-Pozza, Thomas Ströbel and Till Voigtländer; DI Dita Drobna; and Ms Elisabeth Dirnberger, Helga Flicker, Helga Katz, and Brigitte Millan-Ruiz. Canada: The study is funded by the Public Health Agency of Canada. The authors thank all CJD Surveillance System team members and lab staff for their support, as well as all CJD suspected patients and their families. Italy: Anna Ladogana, and Vittorio Mellina for the surveillance; Maria Puopolo for maintenance of the database; Michele Equestre and Claudia Giannattasio for laboratory studies; Alessandra Garozzo and Marco Del Re for administrative support of the Italian surveillance system. This work was funded by Istituto Superiore di Sanita'. France: The authors acknowledge the members of the 'Réseau National de surveillance des maladies de Creutzfeldt-Jakob et maladies apparentées', all reporting physicians and the families of patients for their cooperation. Germany: The study was supported by the Bundesministerium für Gesundheit und Soziale Sicherung (BMGS) (GZ: 325-4471-02/15) and by the Bundesministerium für Bildung und Forschung (BMBF) (KZ: 0312720 to I.Z.). Netherlands: The Netherlands CJD surveillance is funded by the Dutch Ministry of Health, Welfare and Sports. We acknowledge the help of our colleagues Marie Josee van Rijn, Mark Houben and Mark Sie at the Erasmus University, Casper Jansen and Annemieke Rozemuller from the Department of Pathology at the University Medical Centre in Utrecht and Dr van Gool at the Academic Medical Center, University of Amsterdam. P.S.-J. was supported by the post-MIR grant Wenceslao Lopez Albo from the IFIMAV Institute of the Fundación Pública Marqués de Valdecilla. Spain: The authors acknowledge the collaboration of regional CJD surveillance coordinators, co-workers at the Registry and Laboratory Unit as well as the financial support provided by the Ministry of Health and the RCESP and CIEN Research Networks. Switzerland: The National Reference Center for Prion Diseases (Zurich, Switzerland) is funded by the Swiss Federal Office of Public Health (Berne); M.G. is supported by a career development award of the University of Zürich and by a grant from the Academic Trainee Fund Zurich. United Kingdom: The authors would like to thank the staff of the National CJD Surveillance Unit, UK, neurologists and neuropathologists throughout the UK and the families of patients. Funding to pay the Open Access publication charges for this article were provided by the ANCJDR.

References

Castellani RJ, Colucci M, Xie Z, Zou W, Li C, Parchi P, et al. Sensitivity of 14-3-3 protein test varies in subtypes of sporadic Creutzfeldt-Jakob disease. Neurology 2004; 63: 436–42.

Collie DA, Sellar RJ, Zeidler M, Colchester AC, Knight R, Will RG. MRI of Creutzfeldt-Jakob disease: imaging features and recommended MRI protocol. Clin Radiol 2001; 56: 726–39.

Collins S, Boyd A, Fletcher A, Byron K, Harper C, McLean CA, et al. Novel prion protein gene mutation in an octogenarian with Creutzfeldt-Jakob disease. Arch Neurol 2000; 57: 1058–63.

Collins SJ, Lawson VA, Masters CL. Transmissible spongiform encephalopathies. Lancet 2004; 363: 51–61.

Finkenstaedt M, Szudra A, Zerr I, Poser S, Hise JH, Stoebner JM, et al. MR imaging of Creutzfeldt-Jakob disease. Radiology 1996; 199: 793–8.

Head MW, Bunn TJ, Bishop MT, McLoughlin V, Lowrie S, McKimmie CS, et al. Prion protein heterogeneity in sporadic but not variant Creutzfeldt-Jakob disease: UK cases 1991–2002. Ann Neurol 2004; 55: 851–9.

Hill AF, Joiner S, Wadsworth JD, Sidle KC, Bell JE, Budka H, et al. Molecular classification of sporadic Creutzfeldt-Jakob disease. Brain 2003; 126: 1333–46.

Korth C, Kaneko K, Groth D, Heye N, Telling G, Mastrianni J, et al. Abbreviated incubation times for human prions in mice expressing a chimeric mouse-human prion protein transgene. Proc Natl Acad Sci USA 2003; 100: 4784–9.

Ladogana A, Puopolo M, Croes EA, Budka H, Jarius C, Collins S, et al. Mortality from Creutzfeldt-Jakob disease and related disorders in Europe, Australia, and Canada. Neurology 2005a; 64: 1586–91.

Ladogana A, Puopolo M, Poleggi A, Almonti S, Mellina V, Equestre M, et al. High incidence of genetic human transmissible spongiform encephalopathies in Italy. Neurology 2005b; 64: 1592–7.

Meissner B, Köhler K, Körtner K, Bartl M, Jastrow U, Mollenhauer B, et al. Sporadic Creutzfeldt-Jakob disease: magnetic resonance imaging and clinical findings. Neurology 2004; 63: 450–6.

Otto M, Wiltfang J, Cepek L, Neumann M, Mollenhauer B, Steinacker P, et al. Tau protein and 14-3-3 protein in the differential diagnosis of Creutzfeldt-Jakob disease. Neurology 2002; 58: 192–7.

Parchi P, Giese A, Capellari S, Brown P, Schulz-Schaeffer W, Windl O, et al. Classification of sporadic Creutzfeldt-Jakob disease based on molecular and phenotypic analysis of 300 subjects. Ann Neurol 1999; 46: 224–33.

Pocchiari M, Puopolo M, Croes EA, Budka H, Gelpi E, Collins S, et al. Predictors of survival in sporadic Creutzfeldt-Jakob disease and other human transmissible spongiform encephalopathies. Brain 2004; 127: 2348–59.

Puoti G, Giaccone G, Rossi G, Canciani B, Bugiani O, Tagliavini F. Sporadic Creutzfeldt-Jakob disease: co-occurrence of different types of PrP^{Sc} in the same brain. Neurology 1999; 53: 2173–6.

Schröter A, Zerr I, Henkel K, Tschampa HJ, Finkenstaedt M, Poser S. Magnetic resonance imaging in the clinical diagnosis of Creutzfeldt-Jakob disease. Arch Neurol 2000; 57: 1751–7.

Shiga Y, Miyazawa K, Sato S, Fukushima R, Shibuya S, Sato Y, et al. Diffusion-weighted MRI abnormalities as an early diagnostic marker for Creutzfeldt-Jakob disease. Neurology 2004; 63: 443–9.

Steinhoff BJ, Räcker S, Herrendorf G, Poser S, Grosche S, Zerr I, et al. Accuracy and reliability of periodic sharp wave complexes in Creutzfeldt-Jakob disease. Arch Neurol 1996; 53: 162–6.

Steinhoff BJ, Zerr I, Glatting M, Schulz-Schaeffer W, Poser S, Kretzschmar HA. Diagnostic value of periodic complexes in Creutzfeldt-Jakob disease. Ann Neurol 2004; 56: 702–8.

Tschampa HJ, Kallenberg K, Urbach H, Meissner B, Nicolay C, Kretzschmar HA, et al. MRI in the diagnosis of sporadic Creutzfeldt-Jakob disease: a study on inter-observer agreement. Brain 2005; 128: 2026–33.

Zerr I, Pocchiari M, Collins S, Brandel JP, de Pedro Cuesta J, Knight RS, et al. Analysis of EEG and CSF 14-3-3 proteins as aids to the diagnosis of Creutzfeldt-Jakob disease. Neurology 2000a; 55: 811–5.

Zerr I, Schulz-Schaeffer WJ, Giese A, Bodemer M, Schröter A, Henkel K, et al. Current clinical diagnosis in Creutzfeldt-Jakob disease: identification of uncommon variants. Ann Neurol 2000b; 48: 323–9.

CSF BACE1 activity is increased in CJD and Alzheimer disease versus other dementias

Abstract—To assess the diagnostic utility of CSF BACE1 activity for discriminating Alzheimer disease (AD) from other dementias, particularly Creutzfeldt–Jakob disease (CJD), the authors studied 26 patients with sporadic CJD, 21 patients with AD, and 21 patients with various non-AD, non-CJD dementias (DCs). CSF BACE1 activity was elevated in AD in comparison with DC ($p = 0.01$). Unexpectedly, CSF BACE1 activity was also increased in sporadic CJD ($p = 0.02$).

NEUROLOGY 2006;67:710–712

R.M.D. Holsinger, PhD; J.S. Lee, BSc; A. Boyd, Dip Gen Coun; C.L. Masters, MD; and S.J. Collins, MD

Alzheimer disease (AD) and Creutzfeldt–Jakob disease (CJD) can be difficult to differentiate clinically, and in both diseases, cerebral extracellular misfolded protein aggregates are a characteristic neuropathologic finding. In CJD, the plaques consist of aberrant, protease-resistant conformers (PrP^{res}) of the ubiquitously expressed prion protein (PrP^{c}), whereas in AD, the proteinaceous deposits are formed by the accumulation of β-amyloid peptide (Aβ), an amyloidogenic peptide resulting from the sequential cleavage of the amyloid precursor protein by β-secretase (BACE1) followed by γ-secretase.[1] Premortem diagnosis is based on a suggestive clinical profile supported by a variety of not entirely specific laboratory tests. BACE1 protein and catalytic activity are increased in AD brain in comparison with age-matched normal and neurologic controls, including other dementias.[2] Further studies demonstrated increased BACE1 activity in AD CSF vs normal controls.[3] Here, we compare BACE1 activity in 21 patients with AD, 26 patients with sporadic CJD, and 21 non-CJD, non-AD dementia controls (DCs).

Methods. We conducted this study with ethical approval from the Human Research Ethics Committee at the University of Melbourne. All CSF samples were from patients initially referred to the Australian National CJD Registry (ANCJDR) as suspected to have sporadic CJD. Final diagnoses were based on postmortem brain examination or made following thorough evaluation of all available clinical data. Patients included 26 sporadic CJD (23 pathologically verified, definite; 3 clinically probable), 21 AD (16 clinically probable, 5 pathologically confirmed), and 21 DC (of which 12 were pathologically confirmed) (table). CSF 14-3-3 protein detection was performed by western blot.[4] BACE1 activity was measured as an in vitro activity assay (TruPoint Assay kit; Perkin Elmer, Finland)[3] and total (nonphosphorylated and normally phosphorylated) tau protein concentration estimated by ELISA (Innotest hTAU; Innogenetics, Belgium) according to manufacturer's instructions. BACE1 activity and total tau protein concentration in CSF samples were measured in duplicate. BACE1 activity (absorbance units [AU]/μg CSF protein) was measured every 10 minutes, and data were obtained at 30 minutes as this point was in the linear phase of BACE1 activity. The median duration of symptoms at the time of lumbar puncture for sporadic CJD patients was 2 months, for patients with AD 18 months, and DC 8 months.

Levels of brain BACE1 protein were determined by western blot immunoassay.[2] BACE1 protein was extracted using Trizol, with western blot analysis performed on 20 μg of total cerebral cortical protein extract from each sample using BACE C-terminal antibody 00/6.[2] Membranes were stripped and reprobed with an antibody to β-tubulin to assess equivalence of protein loading. Densitometric comparisons, normalized to the tubulin western blot signal, were made using the NIH Image 1.60 software package. Brain samples from six age-matched normal controls were obtained from the NHMRC Tissue Resource Centre (Melbourne, Australia) and the Institute of Brain Aging and Dementia Tissue Repository (Irvine, CA). CJD brain tissue and all CSF samples were obtained from the ANCJDR (Melbourne, Australia).

Statistical analyses were performed using the SPSS 11.0 software package (SPSS, Chicago, IL).

Results. Results are summarized in the table and figure. A significant difference in both BACE1 activity and tau protein concentration was observed between the three patient groups ($p = 0.024$ and $p < 0.0001$; Kruskal–Wallis test). Mean BACE1 activity was increased in AD vs DC ($p = 0.01$; Mann–Whitney U test). Unexpectedly, mean BACE1 activity was also elevated in sporadic CJD compared with DC ($p = 0.02$; Mann–Whitney U test), with levels comparable with those observed for the AD. Two patients with sporadic CJD demonstrated coincidental AD neuropathologic changes: One had BACE1 activity lying slightly above (24,952 AU/μg CSF protein) and one slightly below (15,393 AU/μg CSF protein) the mean CJD BACE1 value (19,712 AU/μg CSF protein). The duration of symptoms at time of CSF sampling was different between the three groups ($p < 0.001$; Kruskal–Wallis test), specifically for sporadic CJD and AD ($p < 0.0005$; Mann–Whitney U test), but not between AD and DC, showing that duration of clinical illness at time of lumbar puncture did not determine BACE1 activity. In agreement with other studies, tau

From the University of Melbourne (R.M.D.H., J.S.L., A.B., C.L.M., S.J.C.), Parkville, Mental Health Research Institute of Victoria (R.M.D.H., C.L.M., S.J.C.), Parkville, and Australian National Creutzfeldt–Jakob Disease Registry (J.S.L., A.B., C.L.M., S.J.C.), Melbourne, Victoria, Australia.

The Australian National CJD Registry is funded by the Commonwealth Department of Health and Ageing. R.M.D.H. is supported by an Early Career Researcher Grant from the University of Melbourne. This work was also supported in part by an Australian NHMRC Program Grant (no. 208978).

Disclosure: C.L. Masters is executive director and chair of the Scientific Advisory Board of Prana Biotechnology Ltd., a company aimed at providing therapeutic intervention for age-related diseases. The other authors declare no conflicts of interest.

Received December 23, 2005. Accepted in final form April 20, 2006.

Address correspondence and reprint requests to Dr. R.M.D. Holsinger, School of Biomedical Sciences, University of Sydney, Lidcombe, New South Wales, 1825, Australia, e-mail: d.holsinger@fhs.usyd.edu.au; or Dr. S.J. Collins, Department of Pathology, University of Melbourne, Parkville, Victoria, 3010, Australia, e-mail: stevenjc@unimelb.edu.au

Table *Tau and 14-3-3 protein levels, as well as BACE1 activity, in the CSF of patients with sporadic Creutzfeldt–Jakob disease (CJD), Alzheimer disease (AD), and dementia control (DC)*

	CJD	AD	DC*	*p* Value
No. of subjects	26	21	21	
Gender, M/F	11/15	8/13	16/5	
Mean ± SEM age, y	65 ± 2	68 ± 3	65 ± 2	0.52‡
BACE activity,† AU/μg CSF protein	19,712	19,673	15,145	0.024‡
	(12,546–33,536)	(10,393–33,329)	(6,738–20,166)	
Tau,† pg/mL	1,751	289	249	<0.0001‡
	(228–4,162)	(95–735)	(34–1,192)	
Positive for 14-3-3 protein	22§	1	3	

* The DC group consisted of: vascular disease/multi-infarct dementia (n = 5); panencephalitis of uncertain cause (n = 1); paraneoplastic or metastatic cancer-associated neurologic disease (n = 2); thalamic dementia (n = 1); dementia with Lewy bodies (n = 7); frontotemporal dementia (n = 2); normal-pressure hydrocephalus (n = 1); idiopathic cerebrocerebellar degeneration (n = 1); and neurologic disorders where clinical improvement occurred without a precise diagnosis achieved (n = 1). The single patient with a neuropathologic diagnosis of "thalamic dementia" showed no evidence of spongiform change and was negative for PrP^{res} on western blots of the thalamic and basal ganglia regions.

† Mean value of BACE1 activity and total tau protein concentration in CSF samples (ranges in parentheses). For BACE1, two sporadic CJD patients and one AD patient had activities exceeding 40,000 absorbance units (AU)/μg CSF protein, which were considered outliers, leaving 24 sporadic CJD and 20 patients with AD who were included for statistical analysis. A single sporadic CJD tau result exceeded the upper limit of the standard curve (>4,200 pg/mL) and was excluded from data analysis.

‡ Kruskal–Wallis test.

§ One weak positive result considered nonsupportive for diagnosis of CJD was omitted.

protein levels were highest in CJD subjects vs both AD ($p < 0.0001$; Mann–Whitney *U* test) and DC ($p < 0.0001$; Mann–Whitney *U* test), whereas no difference in tau protein was observed between the AD and DC groups ($p = 0.10$; Mann–Whitney *U* test).

Receiver operating characteristic (ROC) curve analysis revealed that a BACE1 activity cut-off of 18,845 AU/μg CSF protein was optimal for differentiating AD from DC, with a sensitivity of 60% and specificity of 86%. Within the DC group, there were sufficient patients with vascular disease/multi-infarct dementia (VD/MID; n = 5) and dementia with Lewy bodies (DLB; n = 7) to allow subgroup analysis. ROC curve analysis using the same optimized cut-off (18,845 AU/μg CSF protein) revealed a sensitivity of 60% and specificity of 80% for differentiating VD/MID, with values of 60 and 86% for DLB. For both VD/MID and DLB, the CSF BACE1 activities of individual patients ranged from the lowest through to the highest observed for the entire DC group.

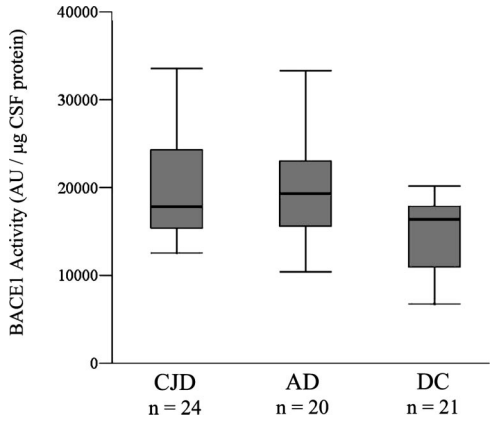

Figure. Analysis of CSF BACE1 activity in sporadic Creutzfeldt–Jakob disease (CJD), Alzheimer disease (AD), and dementia controls (DC). Box plot of CSF BACE1 activity (absorbance units [AU]/μg CSF protein) showing the median, interquartile range, and extreme cases of individual variables. A difference in CSF BACE1 activity was observed between the three patient groups ($p = 0.024$; Kruskal–Wallis test). Two sporadic CJD patients and one AD patient with BACE1 activity of approximately 40,000 AU/μg CSF protein were considered outliers and were omitted from statistical analyses.

We also measured BACE1 protein in sporadic CJD brain (n = 6) by western blot analysis[2] and compared the levels with values from age-matched normal controls (n = 6) (not shown). Densitometry failed to reveal a difference in brain BACE1 levels, normalized to tubulin western blot signal, between the two groups ($p = 0.30$; Student *t* test). Insufficient frozen brain was available from DC patients to allow meaningful comparison between the three groups, but in a limited study, patients with AD appeared to have the highest BACE1 levels (not shown).

Discussion. The reason for, and pathogenic relevance of, the increased CSF BACE1 activity in patients with sporadic CJD is uncertain and not intuitively predicted but is the subject of ongoing investigation. To date, there is no evidence that BACE1 participates in normal PrP^{c} processing or in the conversion process to PrP^{res}, and in contrast to patients with AD, BACE1 protein was not increased in the brains of a small number of sporadic CJD patients assessed. Based on brain neuropathologic examination of approximately 90% of our patients with sporadic CJD, we are confident that the observed increase in CSF BACE1 activity was not due to frequent coincidence of AD. However, previous studies have reported decreases in CSF concentrations of $A\beta_{1\text{-}42}$ in both sporadic CJD and AD when compared with other forms of dementia and nondemented controls.[5,6] In combination with our findings, these results suggest that Aβ processing is abnormal in CJD and may be similar to that observed in AD.

In keeping with recent admonitions concerning assessments of the diagnostic utility of CSF markers

for dementias,[7] we chose to maximize inclusion of patients with postmortem pathologic confirmation of their disease and selected patients manifesting dementia as the comparison groups rather than age-matched normal controls. Numerous studies have consistently confirmed the ability of CSF markers such as tau and $A\beta_{1\text{-}42}$ to discriminate AD from non-demented, age-matched controls,[8] whereas their ability to differentiate AD from dementias of other causes has proven considerably more limited.[9,10] Illustrating this difficulty, the lack of difference in CSF tau levels between our AD and DC cohorts most likely reflects the inclusion in the latter group of a number of patients with frontotemporal dementia, DLB, and dementia on a vascular basis.[9,10] Given the ongoing development of treatments with efficacy maximized for, or tailored to, specific dementias such as AD, our study was aimed at what we believe to be arguably the greater imperative, the ability to achieve the most accurate clinical diagnosis in individual patients presenting with established cognitive impairment rather than differentiation of mild dementia from age-matched normalcy.

From a diagnostic perspective, the partial overlap in the ranges of CSF BACE1 activities observed in the AD, DC, and CJD groups tends to lessen its utility when employed in isolation for individual patients. Nevertheless, an elevated CSF BACE1 activity would assist the early diagnosis of AD, with a specificity of at least 80% for differentiation from other relatively common dementias such as DLB and VD/MID. Rarely in the evaluation of suspected AD would sporadic CJD be encountered, and in patients manifesting more rapidly progressive cognitive decline, recourse to the assessment of other surrogate biomarkers such as tau or 14-3-3 protein levels would probably prove useful in helping to distinguish this type of dementia.

Acknowledgment

The authors thank all physicians who referred CSF specimens to the ANCJDR.

References

1. Selkoe DJ. Cell biology of protein misfolding: the examples of Alzheimer's and Parkinson's diseases. Nat Cell Biol 2004;6:1054–1061.
2. Holsinger RMD, Mclean CA, Beyreuther K, Masters CL, Evin G. Increased expression of the amyloid precursor β-secretase in Alzheimer's disease. Ann Neurol 2002;51:783–786.
3. Holsinger RMD, McLean CA, Collins SJ, Masters CL, Evin G. Increased β-secretase activity in cerebrospinal fluid of Alzheimer's disease subjects. Ann Neurol 2004;55:898–899.
4. Collins SJ, Boyd A, Fletcher A, et al. Novel prion protein gene mutation in an octogenarian with Creutzfeldt–Jakob disease. Arch Neurol 2000; 57:1058–1063.
5. Kapaki E, Kilidireas K, Paraskevas GP, Michalopoulou M, Patsouris E. Highly increased CSF tau protein and decreased β-amyloid (1-42) in sporadic CJD: a discrimination from Alzheimer's disease? J Neurol Neurosurg Psychiatry 2001;71:401–403.
6. Otto M, Esselmann H, Schulz-Schaeffer W, et al. Decreased β-amyloid$_{1\text{-}42}$ in cerebrospinal fluid of patients with Creutzfeldt–Jakob disease. Neurology 2000;54:1099–1102.
7. Green AJ. Cerebrospinal fluid brain-derived proteins in the diagnosis of Alzheimer's disease and Creutzfeldt–Jakob disease. Neuropathol Appl Neurobiol 2002;28:427–440.
8. Galasko D, Clark C, Chang L, et al. Assessment of CSF levels of tau protein in mildly demented patients with Alzheimer's disease. Neurology 1997;48:632–635.
9. Arai H, Morikawa Y, Higuchi M, et al. Cerebrospinal fluid tau levels in neurodegenerative diseases with distinct tau-related pathology. Biochem Biophys Res Commun 1997;236:262–264.
10. Blennow K, Wallin A, Agren H, Spenger C, Siegfried J, Vanmechelen E. Tau protein in cerebrospinal fluid: a biochemical marker for axonal degeneration in Alzheimer's disease? Mol Chem Neuropathol 1995;26: 231–245.

MRI lesion profiles in sporadic Creutzfeldt–Jakob disease

B. Meissner, MD
K. Kallenberg, MD
P. Sanchez-Juan, PhD
D. Collie, MD
D.M. Summers, MD
S. Almonti, MD
S.J. Collins, MD
P. Smith, MD
P. Cras, MD
G.H. Jansen, MD
J.P. Brandel, MD
M.B. Coulthart, PhD
H. Roberts, MD
B. Van Everbroeck, MD
D. Galanaud, MD
V. Mellina, MD
R.G. Will, MD
I. Zerr, MD

Address correspondence and reprint requests to Dr. Inga Zerr, National TSE Reference Center, Department of Neurology, Georg-August University Goettingen, Robert-Koch-Str. 40, 37075 Goettingen, Germany
epicjd@med.uni-goettingen.de

ABSTRACT

Background: With respect to sporadic Creutzfeldt–Jakob disease (sCJD), six molecular subtypes (MM1, MM2, MV1, MV2, VV1, and VV2) have been described, which vary with respect to age at disease onset, disease duration, early symptoms, and neuropathology. MRI signal alterations were reported to correlate with distinct Creutzfeldt–Jakob disease (CJD) subtypes. This multicenter, international study aimed to describe the brain MRI findings associated with each of the sCJD molecular subtypes.

Methods: Pathologically confirmed sCJD cases with codon 129 genotype (MM, MV, and VV), PrP^{Sc} type, and fluid-attenuated inversion recovery (FLAIR) or diffusion-weighted imaging (DWI) were collected in seven countries. All MRI scans were assessed for signal changes according to a standard protocol encompassing seven cortical regions, basal ganglia, thalamus, and cerebellum.

Results: MRI scans were evaluated in 211 CJD patients (98 MM1, 23 MM2, 19 MV1, 30 MV2, 9 VV1, and 32 VV2). Basal ganglia hyperintensities occurred most frequently in MV2, VV2, and MM1 subtypes (79, 77, and 70%). Wide cerebral cortical signal increase was most common in VV1, MM2, and MV1 subtypes (86, 77, and 77%). Thalamic hyperintensities occurred most often in VV2 (45%) and MV2 (43%). The most consistent finding across most subtypes was high signal in basal ganglia, with these abnormalities found in 63% (FLAIR) and 71% (DWI).

Conclusion: Cortical signal increase and hyperintensities in the basal ganglia and thalamus are detected by MRI across all molecular sporadic Creutzfeldt–Jakob disease subtypes. Our findings argue that characteristic MRI lesion patterns may occur for each molecular subtype.
Neurology® 2009;72:1994–2001

GLOSSARY

AL = anterolateral; **AUC** = area under the receiver operating characteristic curve; **BG** = basal ganglia; **CI** = confidence interval; **CJD** = Creutzfeldt–Jakob disease; **DWI** = diffusion-weighted imaging; **FLAIR** = fluid-attenuated inversion recovery; **MD** = mediodorsal; **OR** = odds ratio; **ROC** = receiver operating characteristic; **sCJD** = sporadic Creutzfeldt–Jakob disease.

MRI has played a role in the diagnosis of sporadic Creutzfeldt–Jakob disease (sCJD) for many years, and various signal abnormalities have been reported.[1-5]

Heterogeneity in sCJD correlates with the codon 129 genotype of the prion protein gene (*PRNP*) in combination with the existence either of two distinct types of pathologic prion protein (PrP^{Sc} 1 or 2). Based on these variables, six sCJD subtypes (MM1, MM2, MV1, MV2, VV1, and VV2) have been defined, and variations in the sensitivities of diagnostic tests for the different subtypes have been reported.[6-11]

Although there is now considerable experience with the use of MRI in sCJD, findings in relation to the specific subtypes are more limited.[5,9,12-15] The general conclusion from these data

Supplemental data at www.neurology.org

Authors' affiliations are listed at the end of the article.

Supported by grants from the Federal Ministry of Education and Research (BMBF 01GI0301 and KZ: 0312720), the Federal Ministry of Health (BMG Az325-4471-02/15), the Robert Koch-Institute through funds of the Federal Ministry of Health (grant 1369-341), the Department of Health (121/7369), the European Union (TSELAB QLK2-CT-2002-81523), the Department of Health and the Scottish Executive Department of Health (The UK National CJD Surveillance Unit), the National Registry of CJD and Related Disorders of the Istituto Superiore di Sanità, Rome, Italy, the Commonwealth Department of Health and Ageing, the Fonds voor Wetenschappelijk Onderzoek, and the Born Bunge Institute.

Disclosure: The authors report no disclosures.

are that characteristic MRI lesion patterns may correspond to a specific Creutzfeldt–Jakob disease (CJD) subtype.

To address this issue, we undertook a multicenter, international collaborative study to describe the MRI lesion patterns across the entire clinical spectrum of sCJD. All subjects included in the study had undergone MRI using the most sensitive pulse sequences, with systematic regional brain assessment for abnormal signal changes.

METHODS

Patients. Cases were included from seven countries (United Kingdom, France, Italy, Belgium, Germany, Canada, and Australia) according to the following criteria:

1. CJD diagnosis confirmed by brain pathology (definite cases)
2. Molecular subtype determined by codon 129 genotyping (MM, MV, or VV) and Western blot analysis of brain PrP^{Sc} type (1 or 2) (corresponding to MM1, MM2, MV1, MV2, VV1, or VV2 subtype) and[3] fluid-attenuated inversion recovery (FLAIR) or diffusion-weighted imaging (DWI) MRI of the brain available

All three criteria had to be fulfilled in each case. Genetic CJD (causal mutations found in *PRNP*), iatrogenic, and variant CJD cases were excluded.

Information on CSF (14-3-3 protein) and EEG (periodic sharp wave complex) findings was acquired and data are displayed in table e-1 on the *Neurology*® Web site at www.neurology.org. EEGs were reviewed by a member of the national surveillance and scored positive according to the criteria.[16] The CSF 14-3-3 immunoassays were performed using Western blotting (conformity of testing methods and results interpretation confirmed by blinded sample exchange program as reported previously).[17]

The study comprised 211 patients who died between March 1996 and February 2006: 92 (44%) from Germany, 38 (18%) from the United Kingdom, 34 (16%) from Italy, 17 (8%) from Australia, 15 (7%) from Belgium, 9 (4%) from Canada, and 6 (3%) from France. In 8 patients, mixed PrP^{Sc} types were detected, and they were excluded from the article. According to the study goal of characterizing the single subtypes by MRI, the inclusion of MM1 patients as most frequent molecular type was stopped toward the end of the study because of sufficient patient numbers.

Molecular subtype classification was performed as published previously,[6] determined by the combination of the codon 129 genotype of the *PRNP* (MM, MV, or VV) and the pathologic isotype of the prion protein (PrP^{Sc} 1 or 2).

The PrP^{Sc} typing was performed according to standard methods.[7] The number of examined brain regions usually included the cerebral cortex, basal ganglia or thalamus, and cerebellum.[8] Codon 129 status was determined either as part of genotyping of the entire *PRNP* open reading frame or by restriction fragment length polymorphism analysis.[8]

MRI data. The magnetic resonance images were acquired at local sites and obtained from scanners of different manufacturers and of different magnetic field strengths of 0.5 to 3 tesla (mainly 1.5 tesla).

The majority of the scans were available as hard copy. If serial MRIs were available, the first examination was used for the analysis. The scans were assessed for hyperintense signal abnormalities by neuroradiologists (K.K., P.S., and D.C.) aware of the CJD suspicion but not aware of the molecular subtype. The scans were reviewed by each radiologist individually. All scans were assessed by a neuroradiologist (K. K.) aware of the suspicion of sCJD but not aware of the diagnosis or the molecular subtype.

Two further neuroradiologists (P.S. and D.C.) assessed two separate MRI series for the estimation of the interobserver agreement. With the three raters' results, we calculated 1) the percentage of concordant results and 2) the κ statistic, which compares the agreement against that which might be expected by chance. Interobserver agreement was moderate between raters 1 and 2 (concordance 76%, $\kappa = 0.45$, $p < 0.001$) and high between raters 1 and 3 (concordance 82%, $\kappa = 0.62$, $p < 0.001$). In rare cases with discrepant findings, a consensus between three radiologists was sought. A standardized protocol including seven cerebral cortex regions (frontal, parietal, temporal, occipital, cingulate gyrus, insula, and hippocampus), basal ganglia (caudate nucleus, putamen, and globus pallidus), thalamus (anterolateral nuclei, mediodorsal nuclei, and pulvinar), and cerebellar cortex was used.[18] For the thalamus, the presence of a pulvinar sign or hockey stick sign was also rated.[19] The quality of the complete MRI examination was graded from 1 to 6 (1 = excellent, 6 = poor). Scans graded higher than 4 were excluded from the study (n = 6); no later scans were available in these patients.

Statistical analysis. To describe different sCJD MRI patterns, we aimed to select the best radiologic features for molecular subtype discrimination. We considered a brain region as affected when a high signal was found in either FLAIR or DWI MRI sequences.

General data analysis. For the radiologic features selected, we compared the proportion of patients with a high signal in each studied region against that same proportion in the rest of patients not belonging to that particular subtype, and so on for the six subtypes. Therefore, to test how well the radiologic feature discriminated each particular subtype, we used six dichotomous outputs (MM1 vs all others, MM2 vs all others, MV1 vs all others, MV2 vs all others, VV1 vs all others, and VV2 vs all others) to fit six binary logistic regression models. Odds ratios (ORs) were calculated from the logistic regression analyses. First, we performed univariate or crude analysis showing the increase or decrease in odds of the subtype-specific diagnosis when each of the radiologic signs were present. Secondly, we performed hierarchical cluster analysis to gain more insight about the relationships among the different radiologic signs. We specifically were interested to know which radiologic signs grouped together and therefore tended to appear simultaneously in the same patients. The hierarchical cluster analysis is an exploratory procedure useful for finding natural groupings and discovering hidden structures in data. The basic criterion for any clustering is distance. Objects that are near each other should belong to the same cluster, and objects that are far from each other should belong to different clusters. We performed cluster analysis using the overall sample of sCJD MRI scans. Because our main interest was to examine relationships between the different radiologic signs, the objects clustered in our analysis were the brain MRI variables (regions assessed in the MRI scans), which were all categorical (high signal [yes/no]), and the study subjects were treated as the variables of the analysis. We selected between-groups average linkage as the clustering method for our analysis, and simple matching coefficient as the measure of distance between vari-

Neurology 72 June 9, 2009

Table 1 Radiologic predictors of Creutzfeldt-Jakob disease subtypes

	Disease subtype											
	MM1		MM2		MV1		MV2		VV1		VV2	
Predictor*	OR (95% CI)	*p* Value	OR (95% CI)	*p* Value	OR (95% CI)	*p* Value	OR (95% CI)	*p* Value	OR (95% CI)	*p* Value	OR (95% CI)	*p* Value
Cortex												
Frontal	1.2 (0.6-2.4)	0.53	1.6 (0.5-4.8)	0.44	2.6 (0.6-12.0)	0.21	0.5 (0.2-1.3)	0.16	0.8 (0.1-4.4)	0.82	0.6 (0.3-1.5)	0.30
Parietal	2.1 (1.1-3.8)	0.02	2.1 (0.7-5.8)	0.17	2.0 (0.6-6.1)	0.27	0.6 (0.3-1.3)	0.22	1.4 (0.3-7.5)	0.68	0.2 (0.1-0.4)	<0.001
Temporal	1.0 (0.5-1.7)	0.90	4.1 (1.3-12.5)	0.01	2.0 (0.7-5.9)	0.21	0.5 (0.2-1.2)	0.14	2.0 (0.4-10.7)	0.41	0.4 (0.2-0.9)	0.04
Occipital	0.8 (0.4-1.6)	0.53	1.9 (0.7-4.8)	0.20	2.3 (0.8-6.4)	0.11	1.2 (0.5-3.0)	0.63	0.5 (0.1-4.2)	0.52	0.4 (0.1-1.2)	0.10
Cingulate gyrus	0.6 (0.3-1.1)	0.13	0.8 (0.3-2.0)	0.62	3.0 (0.7-13.8)	0.15	1.1 (0.5-2.9)	0.80	2.3 (0.3-19.7)	0.40	1.3 (0.5-3.3)	0.50
Insula	0.8 (0.5-1.4)	0.45	1.1 (0.4-2.6)	0.90	4.6 (1.5-14.8)	0.009	0.5 (0.2-1.3)	0.17	3.3 (0.6-17.4)	0.16	0.8 (0.3-1.7)	0.51
Hippocampus	0.3 (0.1-0.6)	<0.001	2.0 (0.8-4.6)	0.17	2.6 (0.9-7.0)	0.06	1.0 (0.4-2.3)	0.98	3.0 (0.6-13.4)	0.17	2.0 (0.9-4.2)	0.10
BG												
Putamen	0.7 (0.4-1.2)	0.22	0.5 (0.2-1.4)	0.20	1.5 (0.6-4.2)	0.41	2.5 (1.0-5.8)	0.04	0.2 (0.02-1.4)	0.10	1.5 (0.7-3.3)	0.30
Caudate	1.2 (0.7-2.3)	0.50	0.5 (0.2-1.3)	0.20	0.9 (0.3-2.5)	0.83	1.6 (0.6-3.9)	0.33	0.07 (0.01-0.6)	0.02	1.5 (0.6-3.6)	0.36
Thalamus												
AL	0.1 (0.01-0.9)	0.04	0.8 (0.1-6.9)	0.90	1.1 (0.1-9.5)	0.90	0.8 (0.1-6.9)	0.80	—	—	9.2 (2.4-34.8)	0.001
MD	0.1 (0.02-0.4)	0.002	1.3 (0.4-5.0)	0.65	1.9 (0.5-7.3)	0.35	2.9 (1.0-8.3)	0.05	—	—	3.1 (1.1-8.5)	0.03
Pulvinar	0.1 (0.06-0.4)	<0.001	2.0 (0.7-5.3)	0.16	0.8 (0.2-3.0)	0.78	3.1 (1.3-7.4)	0.009	—	—	3.7 (1.6-8.5)	0.002
Pulvinar sign	—	—	—	—	—	—	—	—	—	—	—	—
Hockey stick	—	—	—	—	11.5 (1.5-87.3)	0.02	2.2 (0.2-21.6)	0.50	—	—	1.7 (0.2-17.3)	0.63
Cerebellum	0.5 (0.3-0.8)	0.01	2.0 (0.8-4.8)	0.15	1.4 (0.5-3.9)	0.50	0.7 (0.3-1.7)	0.46	0.5 (0.1-2.6)	0.40	3.1 (1.4-7.1)	0.006

*High signal in fluid-attenuated inversion recovery or diffusion-weighted imaging sequences.
OR = odds ratio; CI = confidence interval; BG = basal ganglia; AL = anterolateral; MD = mediodorsal.

Table 2 Multivariate analysis including composite predictors

Predictor	Disease subtype											
	MM1		MM2		MV1		MV2		VV1		VV2	
	OR (95% CI)	*p* Value	OR (95% CI)	*p* Value	OR (95% CI)	*p* Value	OR (95% CI)	*p* Value	OR (95% CI)	*p* Value	OR (95% CI)	*p* Value
>3 Cortical regions	1.3 (0.6–2.6)	0.50	2.8 (0.9–8.7)	0.08	2.2 (0.6–8.0)	0.22	0.8 (0.3–2.1)	0.64	8.6 (0.8–87.6)	0.07	0.1 (0.04–0.4)	<0.001
Hippocampus affected	0.3 (0.1–0.6)	0.002	1.3 (0.5–3.6)	0.60	2.1 (0.7–6.4)	0.18	1.0 (0.3–2.9)	0.99	3.3 (0.6–18.7)	0.18	3.0 (1.0–8.5)	0.04
Any BG affected	1.9 (1.0–3.7)	0.07	0.3 (0.1–0.9)	0.03	0.7 (0.2–2.2)	0.56	1.8 (0.6–5.3)	0.31	0.05 (0.006–0.5)	0.01	1.3 (0.5–3.8)	0.57
Any thalamic nuclei affected	0.2 (0.06–0.5)	0.001	1.9 (0.6–5.9)	0.26	0.6 (0.1–2.3)	0.42	3.9 (1.2–12.1)	0.02	—	—	3.8 (1.4–10.8)	0.01
Cerebellum affected	0.7 (0.3–1.4)	0.3	1.4 (0.5–3.9)	0.47	1.3 (0.4–3.8)	0.64	0.4 (0.1–1.2)	0.09	0.4 (0.06–2.6)	0.34	3.0 (1.1–7.8)	0.02

Odds ratios (ORs) and *p* values are adjusted by all other predictors, age, sex, disease duration, and disease stage at MRI performance.
CI = confidence interval; BG = basal ganglia.

ables. The information resulting from the cluster analysis helped us to establish, independently of the molecular subtype of the patients, which signs could be pooled into composite variables; e.g., all thalamic nuclei were in the same cluster, so we subsequently used "any thalamic nuclei affected" as a new variable to test for molecular subtype discrimination (figure e-1). Clusters of variables were pooled to form composite variables when at least one of the variables included was significantly associated with subtype discrimination in the crude analysis.

We chose the following radiologic signs as sCJD subtype predictors: 1) more than three cerebral cortical regions affected, 2) hippocampus affected, 3) any basal ganglia affected, 4) any thalamic nuclei affected, and 5) cerebellum affected. Multivariate analysis including the five selected predictors was performed, for each disease subtype (yes/no) separately, to assess them independently of each other.

PrP^{Sc} type predictive model. We built a PrP^{Sc} type predictive model including, together with the MRI data, *PRNP* codon 129 genotype, and clinical information. The objective of this analysis was to assess which of these variables better predicted the type of PrP_{Sc} (1 or 2). We fitted a logistic regression model using the overall sample of sCJD MRI scans. The variable PrP^{Sc} type (1or 2) was the model's output, and the same five MRI variables plus age at onset, disease duration, CSF, and EEG results were included as predictors. We also included sex as a covariate. A second PrP^{Sc} type predictive model was fitted including codon 129 PRNP genotype information as well. The performance of both models, clinical and clinical plus genetic, were evaluated by receiver operating characteristic (ROC) curves. We calculated the area under the ROC curve by the nonparametric method implemented in SPSS version 15.0 for Windows software.

Ethics. Approvals by local ethical standard committees were obtained by each national CJD surveillance unit in participating countries.

RESULTS

Patients. Patient characteristics according to CJD subtype are shown in table e-1.

MRI findings. For all patients, MRI was performed a median of 3.1 months (range 0–55.3 months) from the onset of symptoms, corresponding to the second third of the whole disease duration in the majority of patients (table e-1). The spectrum of available sequences comprised 174 FLAIR and 113 DWI (distribution of grades given in table e-1).

Basal ganglia signal increase was found in 71% (DWI) and 63% (FLAIR) of all patients. Widespread signal increase of the cerebral cortex (more than three regions affected) was found in 66% (DWI) and 38% (FLAIR) of all patients (table e-1).

MRI findings in sCJD subtypes. DWI detected a higher percentage of signal alterations than FLAIR. The frequency of hyperintensities observed for each subtype on DWI images is given in table e-2.

For MM homozygotes, the frontal and parietal lobes signal changes were frequent, but in MM2 subjects, the signal increase was more widespread, commonly including the temporal lobes and hippocampus. In MV heterozygotes, the frontal lobes

Figure 1 Characteristic MRI findings in sporadic Creutzfeldt-Jakob disease (sCJD) subtypes

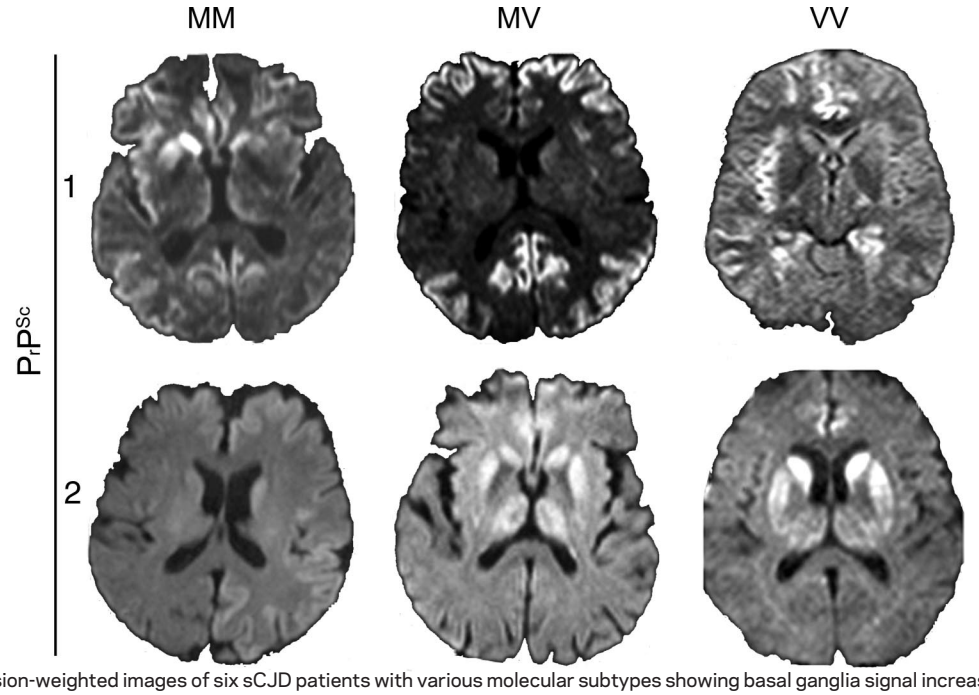

Diffusion-weighted images of six sCJD patients with various molecular subtypes showing basal ganglia signal increase and signal increase in the frontal, temporal, and insular cortex (MM1); predominant cortical signal increase in the frontal and parietal lobes (MV1); cortical hyperintensities in the cingulate gyrus, insular cortex, and hippocampus (VV1); basal ganglia and widespread cortical hyperintensities (MM2); predominant signal increase in the basal ganglia and thalamus (MV2); and predominant basal ganglia signal increase and signal increase in the cingulate gyrus (VV2). The MV1 image was published in *Am J Neuroradiol* 2008;29:1519–1524 (© 2008 American Society of Neuroradiology; reprinted with permission).[22] The VV1 image was published in *Neurology* 2005;65:1544–1550 (© 2005 AAN Enterprises, Inc.; reprinted with permission).[15] The MV2 image was published in *Am J Neuroradiol* 2006;27:1459–1462 (© 2006 American Society of Neuroradiology; reprinted with permission).[23]

and cingulate gyri were most affected. However, in the MV1 subtype, high rates of signal increase were found in the insular cortex, whereas in MV2 subjects, cerebellar signal increase was observed more frequently in DWI. The cingulate gyri were the most frequently affected cerebral cortex region in the VV2 subtype. In VV1 subjects, DWI studies were limited, but FLAIR revealed a higher frequency of hyperintensity in the parietotemporal lobes and particularly the insular cortex (71% vs 14%) compared with VV2 cases.

Crude analysis and cluster analysis of the raw data. Based on the ORs and p values obtained by crude analysis (table 1) and hierarchical cluster analysis of MRI findings across the spectrum of subtypes, five MRI criteria were selected as most suitable variables for discrimination between the subtypes:

1. Cortex: widespread involvement (including more than three cortex regions)
2. Hippocampus region affected
3. Basal ganglia affected (caudate nucleus or putamen)
4. Thalamus affected (any of the three nuclei)
5. Cerebellar cortex affected

The five selected variables were included in a logistic regression model for multivariate analysis. Table 2 shows whether the presence (OR >1.0) or absence (OR <1.0) of the MRI finding was significantly related to one of the subtypes.

Detailed analysis of individual subtypes. MRI examples showing characteristic findings of the subtypes are given in figure 1. The percentages and p values used for the characterization of the subtypes are displayed in tables 1 and 2 and figure 2.

MM1. Basal ganglia signal increase was frequent in the MM1 subtype, and cerebral cortex involvement was widespread in half the patients. The frontal lobes, parietal lobes, and cingulate gyri were most frequently affected (table e-2). The absence of hippocampal and thalamic signal increase differentiated this subtype from others.

MM2. No patient was classified as MM2-thalamic through neuropathologic examination (in 13 of the 23 MM2 patients, no thalamic and brain stem material was available). Because MM2-thalamic types have been previously described as showing no signal alterations on the MRI,[20] we examined the MM2 group for MRI negative cases: all MM2 patients were found to have signal abnormalities on all available sequences, making MM2-thalamic less likely.

Figure 2 MRI lesion patterns in MM1 and MM2, MV1 and MV2, and VV1 and VV2

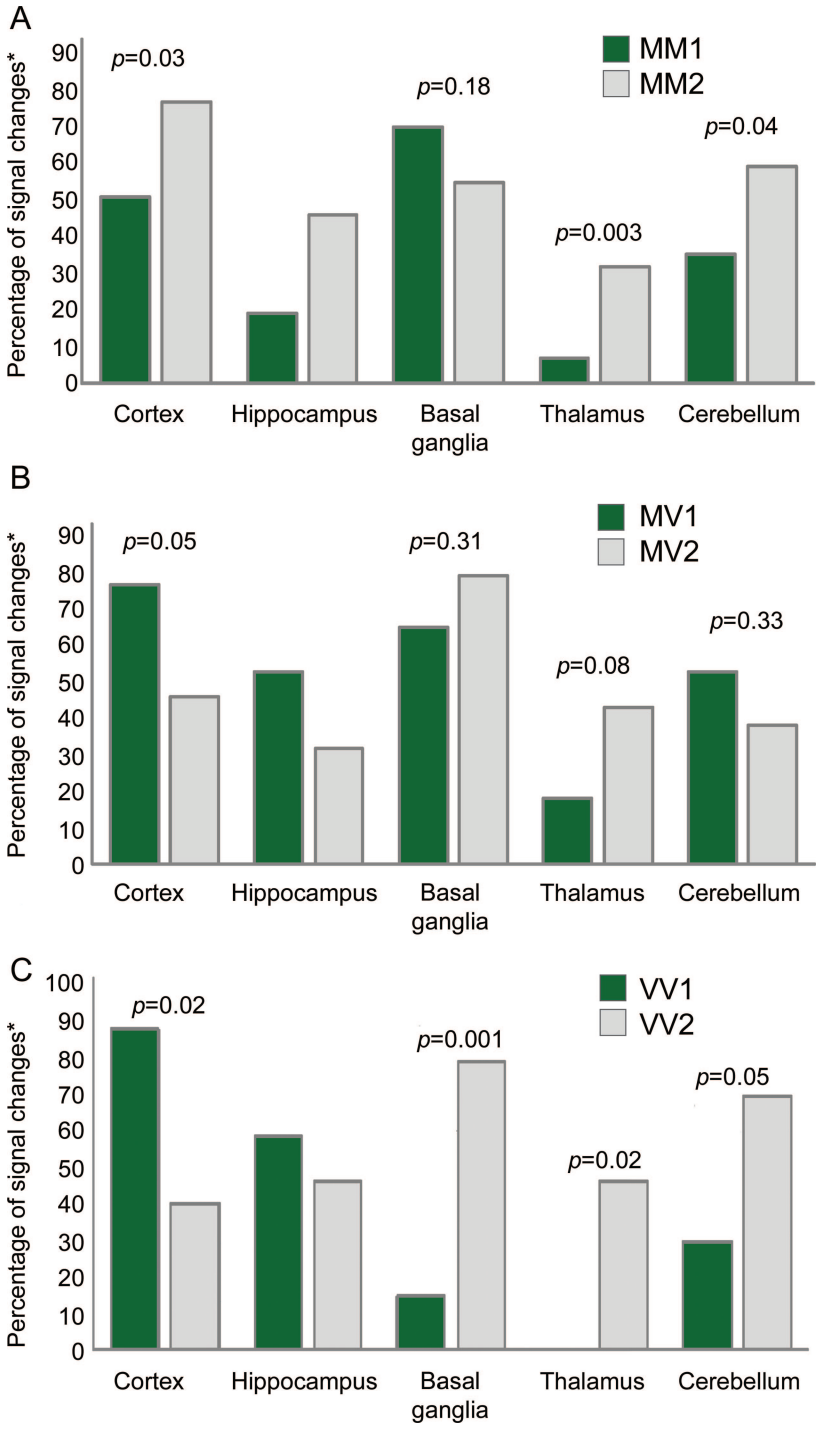

*As seen in fluid-attenuated inversion recovery or diffusion-weighted imaging.

Widespread cortical signal increase, which typically included the temporal lobes, was characteristic of this subtype. Basal ganglia involvement was rather limited, and the absence of this finding supported the diagnosis. In contrast to MM1 patients, thalamic signal increase and cerebellar signal increase occurred more frequently in MM2 types.

MV1. In MV1 patients, cerebral cortex and basal ganglia were both involved often. The cortical signal increase typically included the insula and the hippocampus.

MV2. The basal ganglia and the thalamus were characteristically affected in the MV2 subtype. Thalamic signal increase was most frequently observed in the pulvinar, followed by the mediodorsal nuclei and the anterolateral nuclei. A pulvinar sign was present in three patients, with a hockey stick sign in one. The cerebral cortex involvement was rather limited and most frequently included the frontal lobes and cingulate gyri.

VV1. The VV1 subtype showed the most frequent cerebral cortical signal changes, with the most affected cortex region being the cingulate gyri, followed by the insula and the temporal lobes (tables 1 and 2). Basal ganglia or thalamic signal increase was typically absent.

VV2. Across all molecular subtypes, VV2 patients showed the most frequent involvement of basal ganglia and thalamus. Cerebral cortical signal increase was usually restricted to less than three regions and most frequently found in the cingulate gyrus (tables 1 and 2).

Predictor analysis. Limited cerebral cortical hyperintensities and the presence of thalamic hyperintensities were significantly related to PrP^{Sc} type 2 (table 3) as well as valine homozygosity at codon 129, age at onset, and prolonged disease duration.

DISCUSSION This multicenter collaborative study has determined the brain MRI findings in a large number of cases of sCJD with defined molecular subtype according to the codon 129 genotype and PrP^{Sc} type. Although basal ganglia hyperintensities on the MRI represented a consistent finding in all subtypes except VV1, the frequency and location of cortex hyperintensities as well as the presence or absence of thalamus involvement varied between the subtypes.

The most characteristic MRI lesion patterns were found in MV2 and VV2 showing predominant involvement of thalamus and basal ganglia. Limited cortical signal increase was significantly related to PrP^{Sc} type 2. A further possible characteristic lesion pattern was found in VV1 showing widespread cortical hyperintensities and absence of basal ganglia signal alterations. In the other subtypes, there was a greater overlap between cortical and subcortical involvement.

In MV2, we found less basal ganglia and thalamic involvement than previously reported.[5] This discrepancy may be based on the use of only the first MRI study images in our study and differences in the patient case-mix. The pulvinar sign according to current criteria was identified in the MV2 subtype only.[19] Because of the generally high frequency of

Table 3 PrP type predictive model

	Model 1: Clinical and genetic		Model 2: Only clinical	
	OR (95% CI)	*p* Value	OR (95% CI)	*p* Value
PRNP codon 129 genotype				
MM	Reference		—	—
MV	7.2 (1.8–29.6)	0.006	—	—
VV	27.5 (5.9–127.5)	<0.001	—	—
Age at onset category				
<40 y	0.01 (0.001–0.3)	0.006	0.02 (0.0005–1.0)	0.05
40–59 y	0.2 (0.05–0.8)	0.02	0.3 (0.1–1.1)	0.07
60–79 y	Reference		Reference	
>80 y	8.4 (0.7–99.5)	0.09	6.5 (0.9–45.7)	0.06
Disease duration category				
Above 6.4 mo	26.3 (6.4–107.0)	<0.001	20.0 (6.6–60.9)	<0.001
Tests				
14-3-3 positive in CSF	0.06 (0.01–0.3)	<0.001	0.1 (0.03–0.5)	0.005
Typical EEG	0.1 (0.03–0.5)	0.002	0.06 (0.02–0.2)	<0.001
>3 Cortical regions affected*	0.2 (0.05–0.9)	0.03	0.2 (0.05–0.6)	0.007
Any thalamic nuclei affected*	7.4 (1.8–31.1)	0.006	6.7 (1.9–23.3)	0.003
Model performance				
AUC (95% CI)	0.95 (0.96–0.98)	<0.001	0.92 (0.88–0.96)	<0.001

OR of being type 2 vs type 1.
All OR and *p* values are adjusted by all predictors shown in the table in addition to sex, hippocampus, any basal ganglia, and cerebellum.
CI = confidence interval; OR = odds ratio; AUC = area under the receiver operating characteristic curve.

thalamic hyperintensities in MV2, this subtype is the most likely to be mistaken for variant CJD on MRI.

MRI findings in the VV2 subtype have been reported previously in three cases, demonstrating limited cerebral cortex involvement associated with strong subcortical signal increase.[14,21] Consistent with this, we found widespread thalamic involvement in our VV2 patients, with a high degree of the involvement of the mediodorsal and anterolateral thalamic nuclei.

VV1 and MM2-cortical subtypes have been previously described as atypical CJD variants because of longer disease durations with relatively slowly progressive dementia and absence of typical EEG changes. For VV1, basal ganglia hyperintensities are rare,[15] and in MM2-cortical, isolated cerebral cortex involvement with limited basal ganglia involvement is characteristic, although normal MRI scans have been reported.[12,13] In our study, 10 patients were classified as MM2-cortical, and widespread cortical signal increase represented the main characteristic.

Patients with MM1 and MM2 types, basal ganglia and widespread cortex involvement were found in at least 50% of both patient groups, leading to a high overlap. However, hippocampus involvement was more frequently found in MM2-cortical and was typically absent in MM1.

Previously, the overlap in clinical and neuropathologic findings in some studies has prompted that MM1 and MV1 patients should be combined as one phenotype,[6] although significant differences in investigation findings and clinical features have been noted between these two subtypes.[8] Our study offers additional evidence that MM1 and MV1 might be considered as separate subtypes, by showing that MRI lesion profiles differ, with MV1 showing more frequent cortical and thalamic involvement.

For the premortem diagnostic evaluation, characteristic brain MRI lesion patterns might be helpful in establishing a diagnosis of sCJD and may help to identify atypical sporadic disease forms.

Summarizing our data, basal ganglia and cortical hyperintensities (limited or widespread) represent the most frequent MRI finding in CJD and are most typically found in MM1 subjects with a rapid disease course but also in MV1 individuals. In MM2, the disease course is more prolonged and widespread cortical hyperintensity on the MRI represents the predominant finding. Finally, predominant subcortical signal increase with limited cortical hyperintensities (mainly in the cingulate gyrus) was seen in the MV2 or VV2 type of CJD.

This is the most comprehensive study on MRI findings in sCJD to date and, in combination with previous studies, provides firm evidence of the high sensitivity of brain MRI in the diagnosis of sCJD. Some hyperintensity patterns, such as involvement of more than three cortical areas and hyperintensities in the basal ganglia, should be further evaluated and discussed as potential parameters for inclusion into diagnostic clinical criteria.

Because we intended to study lesion patterns on the MRI in different disease subtypes, no control group was included. MRI changes are frequent, and knowledge about different patterns may help to recognize specifically atypical disease variants.

Nevertheless, with acknowledgment that MRI changes in sCJD differ across the subtypes and are only a surrogate disease marker, any proposed diagnostic criteria will need to be rigorously validated with respect to sensitivity and specificity in a cohort of patients presenting the differential diagnosis of rapidly progressive dementia.

AUTHORS' AFFILIATIONS

From the National TSE Reference Center (B.M., I.Z.), Department of Neurology, Georg-August University Goettingen, Germany; Department

of Neuroradiology (K.K.), Georg-August University Goettingen, Germany; Fundación "Marqués de Valdecilla" IFIMAV and Centro de Investigación Biomédica en Red sobre Enfermedades Neurodegenerativas (P.S.-J.), Santander, Spain; CJD Surveillance Unit (D.C., D.M.S., R.G.W.), Western General Hospital, Edinburgh, UK; Istituto Superiore di Sanità (S.A., V.M.), Department of Cell Biology and Neurosciences, Rome, Italy; Australian National Creutzfeldt-Jakob Disease Registry (S.J.C., H.R.), Department of Pathology, the University of Melbourne, Parkville, Australia; Mercy Private Radiology (P.S.), East Melbourne, Australia; Laboratory of Neurobiology (P.C., B.V.E.), Department of Neurology, Born Bunge Institute, University of Antwerp, Belgium; Creutzfeldt-Jakob Disease Surveillance System (G.H.J., M.B.C.), Prion Diseases Program, Public Health Agency of Canada, Ottawa, Canada; and Cellule Nationale de référence des maladies de Creutzfeldt-Jakob Groupe Hospitalier Pitié-Salpêtrière (J.P.B., D.G.), Paris, France.

ACKNOWLEDGMENT

The authors thank the physicians for case notification and provision of clinical and pathologic data and MRI scans; Dr. Piero Parchi, Prof. Salvatore Monaco, Dr. Gianluigi Zanusso, Dr. Carlo Buffa, and Dr. Bergeron for neuropathologic evaluation and PrP Western blot typing; Dr. Sabina Capellari, Dr. Daniele Imperiale, Dr. Anna Poleggi, Dr. Claudia Giannattasio, and Mr. Michele Equestre for genetic and CSF 14-3-3 analyses; Anna Ladogana and Maurizio Pocchiari for critical comments on the manuscript; and Alison Boyd, Genevieve Klug, Samantha Douglas, and Amelia McGlade for their contribution to data management. The authors also thank the Prion Diseases Program, the French National Surveillance Network for Creutzfeldt-Jakob Disease, the National TSE Surveillance Unit, Göttingen, Germany, and the families of CJD patients for their enthusiastic cooperation.

Received October 14, 2008. Accepted in final form March 12, 2009.

REFERENCES

1. Gertz HJ, Henkes H, Cervos NJ. Creutzfeldt-Jakob disease: correlation of MRI and neuropathologic findings. Neurology 1988;38:1481–1482.
2. Schröter A, Zerr I, Henkel K, Tschampa HJ, Finkenstaedt M, Poser S. Magnetic resonance imaging (MRI) in the clinical diagnosis of Creutzfeldt-Jakob disease. Arch Neurol 2000;57:1751–1757.
3. Young GS, Geschwind MD, Fischbein NJ, et al. Diffusion-weighted and fluid-attenuated inversion recovery imaging in Creutzfeldt-Jakob disease: high sensitivity and specificity for diagnosis. Am J Neuroradiol 2005;26:1551–1562.
4. Shiga Y, Miyazawa K, Sato S, et al. Diffusion-weighted MRI abnormalities as an early diagnostic marker for Creutzfeldt-Jakob disease. Neurology 2004;63:443–449.
5. Krasnianski A, Schulz-Schaeffer WJ, Kallenberg K, et al. Clinical findings and diagnostic tests in the MV-2 subtype of sporadic CJD. Brain 2006;129:2288–2296.
6. Parchi P, Giese A, Capellari S, et al. Classification of sporadic Creutzfeldt-Jakob disease based on molecular and phenotypic analysis of 300 subjects. Ann Neurol 1999;46:224–233.
7. Parchi P, Castellani R, Capellari S, et al. Molecular basis of phenotypic variability in sporadic Creutzfeldt-Jakob disease. Ann Neurol 1996;39:767–778.
8. Collins SJ, Sanchez-Juan P, Masters CL, et al. Determinants of diagnostic investigation sensitivities across the clinical spectrum of sporadic Creutzfeldt-Jakob disease. Brain 2006;129:2278–2287.
9. Zerr I, Schulz-Schaeffer WJ, Giese A, et al. Current clinical diagnosis in CJD: identification of uncommon variants. Ann Neurol 2000;48:323–329.
10. Castellani RJ, Colucci M, Xie Z, et al. Sensitivity of 14-3-3 protein test varies in subtypes of sporadic Creutzfeldt-Jakob disease. Neurology 2004;63:436–442.
11. Sanchez-Juan P, Green A, Ladogana A, et al. CSF tests in the differential diagnosis of Creutzfeldt-Jakob disease. Neurology 2006;67:637–643.
12. Krasnianski A, Meissner B, Schulz-Schaeffer W, et al. Clinical features and diagnosis of the MM2 cortical subtype of sporadic Creutzfeldt-Jakob disease. Arch Neurol 2006;63:876–880.
13. Hamaguchi T, Kitamoto T, Sato T, et al. Clinical diagnosis of MM2-type sporadic Creutzfeldt-Jakob disease. Neurology 2005;64:643–648.
14. Fukushima R, Shiga Y, Nakamura M, Fujimori J, Kitamato T, Yoshida Y. MRI characteristics of sporadic CJD with valine homozygosity at codon 129 of the prion protein gene and PrP type 2 in Japan. J Neurol Neurosurg Psychiatry 2004;75:485–487.
15. Meissner B, Westner I, Kallenberg K, et al. Sporadic Creutzfeldt-Jakob disease: clinical and diagnostic characteristics of the rare VV1 type. Neurology 2005;65:1544–1550.
16. Steinhoff BJ, Zerr I, Glatting M, Schulz-Schaeffer W, Poser S, Kretzschmar HA. Diagnostic value of periodic complexes in Creutzfeldt-Jakob disease: accuracy and reliability of periodic sharp wave complexes in Creutzfeldt-Jakob disease. Ann Neurol 2004;56:702–708.
17. Sanchez-Juan P, Green A, Ladogana A, et al. CSF tests in the differential diagnosis of Creutzfeldt-Jakob disease. Neurology 2006;67:637–643.
18. Tschampa HJ, Kallenberg K, Kretzschmar HA, et al. Pattern of cortical changes in sporadic Creutzfeldt-Jakob disease. AJNR Am J Neuroradiol 2007;28:1114–1118.
19. Collie DA, Summers DM, Sellar RJ, et al. Diagnosing variant Creutzfeldt-Jakob disease with the pulvinar sign: MR imaging findings in 86 neuropathologically confirmed cases. Am J Neuroradiol 2003;24:1560–1569.
20. Hamaguchi T, Kitamoto T, Sato T, et al. Clinical diagnosis of MM2-type sporadic Creutzfeldt-Jakob disease. Neurology 2005;64:643–648.
21. Pauri F, Amabile G, Fattapposta F, Pierallini A, Bianco F. Sporadic Creutzfeldt-Jakob disease without dementia at onset: clinical features, laboratory tests and sequential diffusion MRI (in an autopsy proven case). Neurol Sci 2004;25:234–237.
22. Meissner B, Kallenberg K, Sanchez-Juan P, et al. Isolated cortical signal increase on MR imaging as a frequent lesion pattern in sporadic Creutzfeldt-Jakob disease. AJNR Am J Neuroradiol 2008;29:1519–1524.
23. Kallenberg K, Schulz-Schaeffer WJ, Jastrow U, et al. Creutzfeldt-Jakob disease: comparative analysis of MR imaging sequences. AJNR Am J Neuroradiol 2006;27:1459–1462.

^{11}C-PiB PET studies in typical sporadic Creutzfeldt–Jakob disease

V L Villemagne,[1,2] C A McLean,[3] K Reardon,[4] A Boyd,[5] V Lewis,[5] G Klug,[5] G Jones,[1] D Baxendale,[1] C L Masters,[2,5] C C Rowe,[1] S J Collins[2,3,5]

► An additional figure is published online only at http://jnnp.bmj.com/content/vol80/issue9

[1] Department of Nuclear Medicine and Centre for PET, Austin Health, Melbourne, Australia; [2] The Mental Health Research Institute of Victoria, University of Melbourne, Melbourne, Australia; [3] Anatomical Pathology, Alfred Hospital, Melbourne, Australia; [4] Department of Clinical Neurosciences, St Vincent's Hospital, Melbourne, Australia; [5] The Australian National CJD Registry, Department of Pathology, the University of Melbourne, Parkville, Australia

Correspondence to:
Dr V L Villemagne, Department of Nuclear Medicine, Centre for PET, Austin Health, 145 Studley Road, Heidelberg, Vic. 3084, Australia; villemagne@petnm.unimelb.edu.au

Received 27 December 2008
Revised 4 March 2009
Accepted 6 March 2009
Published Online First
29 March 2009

ABSTRACT

Objective: Brain amyloid imaging using positron emission tomography (PET) is of increasing importance in the premortem evaluation of dementias, particularly in relation to Alzheimer disease (AD). The purpose of this study was to explore the premortem diagnostic utility of ^{11}C-PiB PET in sporadic Creutzfeldt–Jakob disease (CJD).

Methods: Two patients, 72 and 59 years old, underwent evaluation for rapidly progressive cognitive decline, dying after illness durations of 5 and 7 months, respectively. As part of their comprehensive assessment, ^{18}F-FDG PET and ^{11}C-PiB PET studies were performed approximately 2–4 weeks prior to death, and the brain regional distributions compared with those from cohorts of healthy controls (HC) and AD patients.

Results: Routine investigations, including brain MRI scans, revealed changes typical of sporadic CJD, with the diagnosis confirmed at autopsy in both patients. The ^{18}F-FDG PET showed global hypometabolism in one patient and thalamic and frontal hypometabolism with unexpected hypermetabolism in the dentate nuclei of the cerebellum in the other. Neither patient displayed cerebral cortical ^{11}C-PiB PET retention above the levels observed in HC.

Conclusions: No grey-matter ^{11}C-PiB retention was observed in two pathologically confirmed cases of typical sporadic CJD. We speculate that low PrP plaque density and small plaque size, as well as a relatively low affinity of the radioligand, explain the absence of ^{11}C-PiB retention. More studies to validate this hypothesis are warranted.

The spectrum of transmissible human prion disease, characterised by the presence within the CNS of conformationally altered, protease-resistant isomers (PrP^{res}) of the normal cellular form of the prion protein, PrP^{c},[1 2] encompasses Creutzfeldt–Jakob disease, the variant form (vCJD) associated with bovine spongiform encephalopathy, kuru and Gerstmann–Straussler–Scheinker syndrome (GSS).[3 4] Despite considerable improvement in diagnostic accuracy through the use of CSF biomarker assays[5] and brain MRI,[6] the search for additional diagnostic techniques continues. Neuropathological examination of brain tissue remains the only definitive method for diagnostic confirmation.

^{11}C-2-(4′-methylamino-phenyl)-6-hydroxy-benzothiazole (^{11}C-PiB) has a high affinity for Aβ fibrils, allowing in vivo quantification of amyloid deposits in the brain. There is a high correlation between ^{11}C-PiB retention and Aβ concentrations assessed at postmortem or brain biopsy.[7–9] Several commonly used neuropathological dyes have been shown to stain prion plaques. Thioflavin T (ThT), its derivative, 2-(4′-methylamino-phenyl)-benzothiazole (BTA-1),[10 11] and the Congo Red derivatives BSB[10 12] and X04[13] bind in vitro and in vivo to PrP^{res} in mouse and human prion-diseased brains. To date, however, the use of positron emission tomography (PET) in the diagnosis of sporadic CJD has been mainly centred in assessing glucose metabolism with ^{18}F-FDG.[14 15] A previous case report of two siblings with the same prion protein gene (PRNP) mutation described differential binding of two PET amyloid imaging agents (^{11}C-PiB and ^{18}F-FDDNP).[16] Acknowledging that both ThT and its derivative, BTA-1, bind to PrP plaques, we explored the diagnostic utility of ^{11}C-PiB in two patients with sporadic CJD confirmed by pathological examination.

PATIENTS AND METHODS

PET imaging studies

PET studies were approved by the Austin Health Human Research Ethics Committee. Written informed consent was obtained from the appropriate next of kin prior to the scans. A 40–70 min emission acquisition was performed after injection of 370 MBq of ^{11}C-PiB. Ten minutes after completion of the ^{11}C-PiB study, patients were injected with 185 MBq of ^{18}F-FDG. Forty minutes later, a 20 min emission scan was acquired. Standardised uptake values (SUV) were obtained from regions of interest across cortical, subcortical and cerebellar regions. Acknowledging that PrP plaques are frequently found in the cerebellar cortex,[17] ^{11}C-PiB and ^{18}F-FDG SUV ratios were determined by normalising the regional SUV to the pons ($SUVR_{pons}$). Regional distributions of each radioligand were compared against well-characterised cohorts of HC and AD patients.

Neuropathological examination and immunohistochemical detection of PrP^{res}

Brain sections were treated with formic acid prior to formalin fixation and processing. Immunostaining for Aβ was performed with the 1E8 (1:50) monoclonal antibody, and for PrP with the 3F4 (1:1000, Covance) and 12F10 (1:2000, Cayman Chemical) antiprion protein monoclonal antibodies.[18]

Determination of prion protein gene codon 129 status and PrP^{res} molecular subtype

Determination of whether the patient was methionine (M) or valine (V) homozygous or MV heterozygous at codon 129 of the prion protein gene and characterisation of the PrP^{res} molecular

subtype by western blot profile were performed as previously described.[18]

Statistical evaluations

Statistical analysis was performed through Z scores generated against ^{11}C-PiB and ^{18}F-FDG regional $SUVR_{pons}$ from cohorts of both HC and AD patients. Z scores $>\pm 2.5$ were considered significantly different.

RESULTS

Case report 1

Patient 1, a 59-year-old female, initially presented reporting 3 months of dizziness, gait unsteadiness and hearing difficulties, superimposed on a history of longstanding tinnitus and vertigo. MRI brain and ENT specialist review prior to neurological evaluation had not disclosed any abnormalities. One month later, the patient presented with increasing hearing disturbance manifesting as difficulty discerning words in conversation. Emotional lability, poor short-term memory, word-finding difficulties and prominent ataxia of gait were also evident. Brain MRI, including T1, T2-weighted, diffusion-weighted (DWI) and fast fluid-attenuated inversion recovery (FLAIR) acquisition sequences, reported non-specific small-vessel ischaemic changes. CSF examination was unremarkable aside a raised total protein, and presence of 14-3-3 protein. EEG displayed generalised slowing but no triphasic waves or periodic discharges. Six months after initial neurological evaluation, the patient was unable to hold a conversation or reliably name immediate family members, requiring assistance with feeding, standing and ambulating. There was a coarse postural tremor in the upper limbs. Repeat brain MRI revealed restricted diffusion and T2 hyperintensity in the left and right caudate nuclei and dorsomedial and pulvinar thalamic regions, with small foci of restricted diffusion in the left posterior temporal, left frontal and both occipital cortices. The patient died from respiratory difficulties approximately 7 months after initial neurological presentation. No definite myoclonus was ever observed.

Codon 129 genotyping revealed MV heterozygosity, and the PrP^{res} western blot profile was type 3 (MV3).

PET imaging studies

Visually, the ^{18}F-FDG scan showed hypometabolism of the thalami and frontal cortices, with hypermetabolism in the dentate nuclei of the cerebellum (see supplementary fig 1). There was no cerebral cortical or subcortical ^{11}C-PiB retention (table 1) with the findings indistinguishable from HC (fig 1).

Neuropathology

Macroscopic examination of the brain was unremarkable. Microscopic examination showed neuronal loss, gliosis and a spongiform encephalopathy. No Aβ plaques were observed. There was a fine ''synaptic'' pattern of PrP immunoreactivity in the corresponding areas with focal areas of granular PrP deposition (fig 1). A neuropathological diagnosis of CJD was made.

Case report 2

Patient 2, a 72-year-old female, was investigated for 4 months of progressive neurological decline. On hospital admission, dysarthria with limited speech output and reduced motor activity with shuffling gait, but no focal neurological signs nor myoclonus were observed. Brain MRI revealed increased signal in the left head of caudate nucleus on both FLAIR and DWI sequences, not present on a previous MRI 2 months earlier. CSF examination was unremarkable aside from detection of 14-3-3 proteins, while EEG demonstrated a generally slowed background with intermittent periodic sharp wave activity. The patient's neurological condition inexorably declined, developing myoclonus and fluctuating consciousness, dying in an akinetic-mute state approximately 1 month after entering hospital.

Codon 129 genotyping revealed methionine homozygosity, and the PrP^{res} western blot profile was type 2 (MM2).

PET imaging studies

Visually, the ^{18}F-FDG scan showed global hypometabolism, more marked in the left frontal and left temporal cortices (see supplementary fig 1). There was no cerebral cortical or subcortical ^{11}C-PiB retention, (table 1) with the findings indistinguishable from HC (fig 1).

Neuropathology

External examination of the brain was unremarkable. Microscopic examination showed neuronal loss, gliosis and a spongiform encephalopathy. Occasional (+) Aβ diffuse plaques were observed in the frontal section. 12F10 immunoperoxidase studies demonstrated a ''synaptic'' pattern of PrP deposition, scattered small granular concentrations of PrP in and around vacuoles in the cortex (fig 1) but no plaque deposition. 3F4 immunohistochemistry additionally showed small plaque-like PrP deposits within the underlying white matter in frontal cortical sections and small granular plaques in the thalamus. There was also quite prominent granular PrP deposition in the midbrain neuronal areas. A neuropathological diagnosis of CJD was made.

DISCUSSION

To the best of our knowledge, this is the first report of ^{11}C-PiB PET imaging in patients with confirmed sporadic CJD. Although previous studies have shown in vitro and in vivo binding of BTA-1 (the cognate parent compound of PiB) to PrP plaques, we found no significant brain retention of ^{11}C-PiB in our patients. Our observations are in broad agreement with the findings of a study assessing ^{11}C-PiB in siblings carrying a PRNP mutation.[16]

This lack of ^{11}C-PiB binding might be attributed to PrP-plaque size and density within the brain. Due to the rapid progression and relatively short duration of symptomatic illness, sporadic CJD patients do not demonstrate appreciable PrP-plaque deposition at autopsy, where a positive correlation has been reported between illness duration and PrP-plaque density.[19] Although some sporadic CJD molecular subtypes can manifest larger kuru-type plaques,[20] the most common subtype (MM2, as in Patient 2) usually demonstrates only very fine ''synaptic'' and small perivacuolar deposits.[19 20] Among the various molecular subtypes, MV3 commonly demonstrates PrP plaques, especially in the cerebellum.[20] The lack of detectable ^{11}C-PiB binding in our patients also concurs with a previous in vitro study of various forms of human prion disease, which only found BTA-1 binding to larger PrP plaques and not to smaller synaptic-type deposits.[20] It appears possible that a certain threshold of plaque size and/or density may be required before appreciable ^{11}C-PiB retention can be detected in vivo using PET. This is also highlighted by the presence of some Aβ diffuse plaques in Patient 2. While there is a positive correlation between Aβ burden as quantified by ^{11}C-PiB PET and brain Aβ at post-mortem or biopsy,[7 8] one patient with a high number of Aβ plaques presented with a ^{11}C-PiB

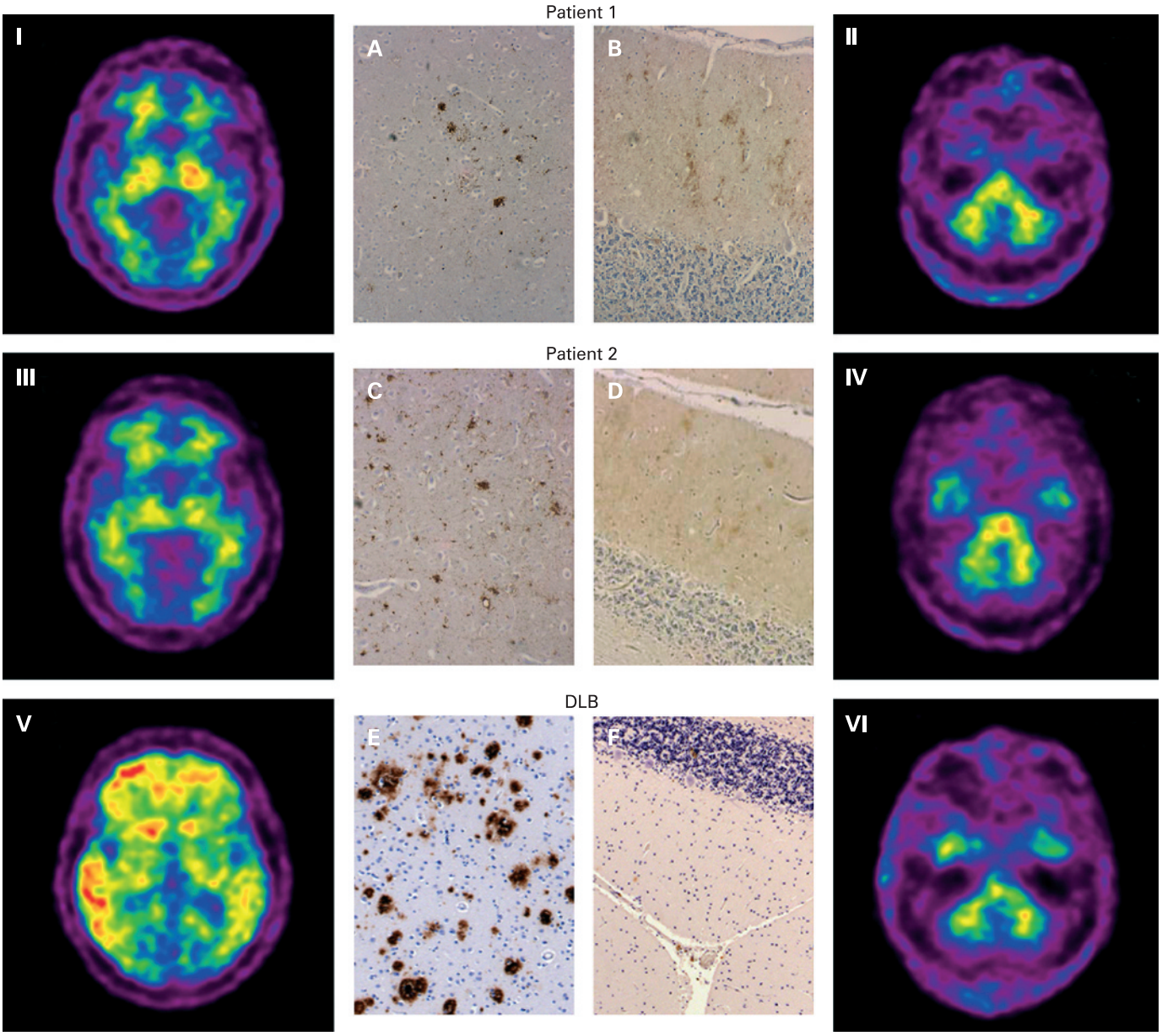

Figure 1 Immunohistochemical detection and positron emission tomography imaging of PrP deposits in sporadic CJD and Aβ plaques in Dementia with Lewy Bodies (DLB). The DLB subject was a 78-year-old man with a Mini-Mental State Examination (MMSE) 19 and Clinical Dementia Rating 2.0 who fulfilled criteria for DLB. Cerebral cortical (A and C, respectively) and cerebellar (B and D, respectively) sections from sporadic CJD Patients 1 and 2 were immunostained for PrP (3F4 antibody). Cerebral cortical (E) and cerebellar (F) sections from a patient with DLB were immunostained for Aβ (1E8 antibody). Respective ^{11}C-PiB transaxial PET images at the level of the basal ganglia (left column) and cerebellum (right column) of sporadic CJD Patient 1 (I and II, respectively), sporadic CJD Patient 2 (III and IV, respectively) and DLB patient (V and VI, respectively). There is a notable difference in the plaque size and density observed in sporadic CJD compared with DLB, which probably explains the lack of ^{11}C-PiB retention in the CJD patients. Conversely, no Aβ deposits were detected in the cerebellar cortex of the DLB patient, while PrP deposits were observed in the cerebellar cortex of both CJD patients, with absence of ^{11}C-PiB retention in the cerebellar cortex further underscoring the lack of ^{11}C-PiB binding to PrP deposits. Magnification: ×20 (A–F).

negative PET scan,[9] highlighting the possibility that there might be certain conformational types of amyloid plaques that ^{11}C-PiB does not detect in vivo.

The lack of ^{11}C-PiB retention may also relate in part to reduced blood flow or to the relative affinities of ^{11}C-PiB for the protein deposits at the concentrations achieved during PET studies. Despite almost identical PiB-negative scans, the respective ^{18}F-FDG scans were quite distinct, suggesting blood flow was unlikely to constitute a significant determinant factor in ^{11}C-PiB binding. In vitro studies demonstrating binding of BTA-1 to PrP plaques were performed using 1 μM BTA-1, while infected mice were injected with 10–30 mg/kg of BTA-1.[10] These concentrations and doses are significantly greater than the low nanomolar range achieved in the brains after 0.00006–0.00007 mg/kg is injected into humans for a ^{11}C-PiB PET study. Hence, it is likely that the relatively low affinity of ^{11}C-PiB for aggregated PrP is translated in insufficient ^{11}C-PiB concentrations to adequately label PrP plaques in vivo. This concurs with studies showing that despite their secondary β-sheet structure, ^{11}C-PiB does not bind to other misfolded proteins at the concentrations achieved during PET studies.[21 22]

Table 1 Regional $SUVR_{pons}$ for ^{11}C-PiB positron emission tomography and ^{18}F-FDG positron emission tomography studies

	^{11}C-PiB				^{18}F-FDG			
	Patient 1	Patient 2	HC (n = 60)	AD (n = 60)	Patient 1	Patient 2	HC (n = 25)	AD (n = 30)
Age/mean age, years (SD)	59	72	72 (7)	73 (10)	59	72	73 (9)	75 (9)
Region of interest								
Dorsolateral prefrontal	0.50†	0.43†	0.53 (0.07)	1.17 (0.24)	0.96	0.50*†	1.37 (0.23)	1.15 (0.17)
Ventrolateral prefrontal	0.44†	0.45†	0.58 (0.09)	1.29 (0.22)	0.97	0.44*†	1.43 (0.27)	1.21 (0.17)
Orbitofrontal	0.46†	0.45†	0.59 (0.08)	1.27 (0.21)	0.97*	0.46*†	1.42 (0.19)	1.22 (0.15)
Gyrus rectus	0.51†	0.51†	0.63 (0.09)	1.36 (0.25)	1.12	0.51*†	1.37 (0.15)	1.24 (0.12)
Somatosensory	0.51	0.46†	0.55 (0.07)	0.95 (0.19)	1.21	0.51*†	1.33 (0.18)	1.23 (0.18)
Posterior cingulate	0.53†	0.48†	0.59 (0.07)	1.35 (0.21)	1.24	0.53*†	1.61 (0.19)	1.25 (0.19)
Anterior cingulate	0.54†	0.47†	0.58 (0.08)	1.27 (0.20)	0.99	0.54*†	1.36 (0.17)	1.17 (0.14)
Parietal cortex	0.51†	0.40†	0.53 (0.07)	1.15 (0.20)	1.11	0.51*	1.36 (0.25)	1.08 (0.24)
Temporal cortex	0.50†	0.49†	0.59 (0.08)	1.20 (0.21)	1.12	0.50*†	1.37 (0.14)	1.09 (0.17)
Occipital cortex	0.53	0.43	0.65 (0.07)	0.99 (0.21)	1.13	0.53*†	1.44 (0.24)	1.23 (0.21)
Mesial temporal	0.58	0.54†	0.60 (0.07)	0.82 (0.11)	1.03	0.58*†	1.04 (0.14)	0.95 (0.11)
Caudate nucleus	0.59†	0.56†	0.62 (0.08)	1.36 (0.24)	1.32	0.59*†	1.59 (0.21)	1.47 (0.19)
Putamen	0.63†	0.56	0.62 (0.06)	1.16 (0.19)	1.31	0.63*†	1.65 (0.15)	1.57 (0.15)
Thalamus	0.74	0.60	0.66 (0.09)	0.97 (0.16)	1.03*†	0.74*†	1.68 (0.13)	1.49 (0.13)
Midbrain	0.87	0.82	0.89 (0.09)	0.94 (0.08)	1.04	0.87*	1.25 (0.13)	1.16 (0.14)
White matter	0.87	0.86	0.87 (0.09)	0.93 (0.11)	0.62	0.87†	0.62 (0.12)	0.52 (0.09)
Cerebellum	0.49	0.37†	0.48 (0.06)	0.52 (0.08)	1.23	0.49*†	1.32 (0.17)	1.26 (0.15)

*Significantly different from healthy controls (HC) (Z scores $> \pm 2.5$).
†Significantly different from Alzheimer disease (AD) (Z scores $> \pm 2.5$).

In conclusion, our observations suggest there might be a limited diagnostic role for ^{11}C-PiB PET in the clinical evaluation of sporadic CJD, but it remains possible that other forms of human prion disease, such as GSS, vCJD and some sporadic CJD subtypes with higher burdens of larger PrP plaques may demonstrate significant binding of ^{11}C-PiB. More studies to validate these hypotheses are warranted.

Funding: PET studies were supported in part by funds from the Austin Hospital Medical Research Foundation, Neurosciences Victoria and the University of Melbourne. The Australian National Creutzfeldt–Jakob disease Registry is funded by the Commonwealth Department of Health and Ageing.

Competing interests: None.

Ethics approval: Ethics approval was provided by the Austin Health Human Research Ethics Committee.

Patient consent: Obtained from the patients' families.

REFERENCES

1. **Hainfellner JA,** Wanschitz J, Jellinger K, *et al*. Coexistence of Alzheimer-type neuropathology in Creutzfeldt–Jakob disease. *Acta Neuropathol (Berl)* 1998;**96**:116–22.
2. **Budka H,** Aguzzi A, Brown P, *et al*. Neuropathological diagnostic criteria for Creutzfeldt–Jakob disease (CJD) and other human spongiform encephalopathies (prion diseases). *Brain Pathol* 1995;**5**:459–66.
3. **Knight R,** Brazier M, Collins SJ. Human prion diseases: cause, clinical and diagnostic aspects. In: Rabenau HF, Cinatl J, Doerr HW, eds. *Prions. A challenge for science, medicine and the public health system*. Basel: Karger, 2004:72–97.
4. **Collins SJ,** Lawson VA, Masters CL. Transmissible spongiform encephalopathies. *Lancet* 2004;**363**:51–61.
5. **Collins SJ,** Sanchez-Juan P, Masters CL, *et al*. Determinants of diagnostic investigation sensitivities across the clinical spectrum of sporadic Creutzfeldt–Jakob disease. *Brain* 2006;**129**:2278–87.
6. **Tschampa HJ,** Zerr I, Urbach H. Radiological assessment of Creutzfeldt–Jakob disease. *Eur Radiol* 2007;**17**:1200–11.
7. **Bacskai BJ,** Frosch MP, Freeman SH, *et al*. Molecular imaging with Pittsburgh Compound B confirmed at autopsy: a case report. *Arch Neurol* 2007;**64**:431–4.
8. **Ikonomovic MD,** Klunk WE, Abrahamson EE, *et al*. Post-mortem correlates of in vivo PiB-PET amyloid imaging in a typical case of Alzheimer's disease. *Brain* 2008;**131**:1630–45.
9. **Leinonen V,** Alafuzoff I, Aalto S, *et al*. Assessment of beta-amyloid in a frontal cortical brain biopsy specimen and by positron emission tomography with carbon 11-labeled Pittsburgh Compound B. *Arch Neurol* 2008;**65**:1304–9.
10. **Ishikawa K,** Doh-ura K, Kudo Y, *et al*. Amyloid imaging probes are useful for detection of prion plaques and treatment of transmissible spongiform encephalopathies. *J Gen Virol* 2004;**85**:1785–90.
11. **Colby DW,** Zhang Q, Wang S, *et al*. Prion detection by an amyloid seeding assay. *Proc Natl Acad Sci USA* 2007;**104**:20914–19.
12. **Hoefert VB,** Aiken JM, McKenzie D, *et al*. Labeling of the scrapie-associated prion protein in vitro and in vivo. *Neurosci Lett* 2004;**371**:176–80.
13. **Sadowski M,** Pankiewicz J, Scholtzova H, *et al*. Targeting prion amyloid deposits in vivo. *J Neuropathol Exp Neurol* 2004;**63**:775–84.
14. **Pichler R,** Ciovica I, Rachinger J, *et al*. Multitracer study in Heidenhain variant of Creutzfeldt–Jakob disease: Mismatch pattern of cerebral hypometabolism and perfusion imaging. *Neuro Endocrinol Lett* 2008;**29**:67–8.
15. **Henkel K,** Zerr I, Hertel A, *et al*. Positron emission tomography with [(18)F]FDG in the diagnosis of Creutzfeldt–Jakob disease (CJD). *J Neurol* 2002;**249**:699–705.
16. **Boxer AL,** Rabinovici GD, Kepe V, *et al*. Amyloid imaging in distinguishing atypical prion disease from Alzheimer disease. *Neurology* 2007;**69**:283–90.
17. **Vital C,** Gray F, Vital A, *et al*. Prion encephalopathy with insertion of octapeptide repeats: the number of repeats determines the type of cerebellar deposits. *Neuropathol Appl Neurobiol* 1998;**24**:125–30.
18. **Lewis V,** Collins S, Hill AF, *et al*. Novel prion protein insert mutation associated with prolonged neurodegenerative illness. *Neurology* 2003;**60**:1620–4.
19. **Liberski PP.** Amyloid plaques in transmissible spongiform encephalopathies (prion diseases). *Folia Neuropathol* 2004;**42**(Suppl B):109–19.
20. **Hill AF,** Joiner S, Wadsworth JD, *et al*. Molecular classification of sporadic Creutzfeldt–Jakob disease. *Brain* 2003;**126**:1333–46.
21. **Klunk WE,** Wang Y, Huang GF, *et al*. The binding of 2-(4′-methylaminophenyl)benzothiazole to postmortem brain homogenates is dominated by the amyloid component. *J Neurosci* 2003;**23**:2086–92.
22. **Fodero-Tavoletti MT,** Smith DP, McLean CA, *et al*. In vitro characterization of Pittsburgh compound-B binding to Lewy bodies. *J Neurosci* 2007;**27**:10365–71.

doi:10.1093/brain/awp191 Brain 2009: 132; 2659–2668 | 2659

BRAIN
A JOURNAL OF NEUROLOGY

Updated clinical diagnostic criteria for sporadic Creutzfeldt-Jakob disease

I. Zerr,[1] K. Kallenberg,[2] D. M. Summers,[3] C. Romero,[4] A. Taratuto,[4] U. Heinemann,[1] M. Breithaupt,[1] D. Varges,[1] B. Meissner,[1] A. Ladogana,[5] M. Schuur,[6] S. Haik,[7] S. J. Collins,[8] Gerard H. Jansen,[9] G. B. Stokin,[10] J. Pimentel,[11] E. Hewer,[12] D. Collie,[3] P. Smith,[13] H. Roberts,[8] J. P. Brandel,[7] C. van Duijn,[6] M. Pocchiari,[5] C. Begue,[4] P. Cras,[14] R. G. Will[3] and P. Sanchez-Juan[15]

1 National TSE Reference Center, Department of Neurology, Georg-August University Goettingen, Goettingen, Germany
2 Department of Neuroradiology, Georg-August University Goettingen, Goettingen, Germany
3 CJD Surveillance Unit, Western General Hospital, Edinburgh, UK
4 Departamento de Neuropatologia, Centro de Referencia de Encefalopatias Espongiformes Transmisibles, Instituto de Investigaciones Neurologicas/FLENI Montañeses 2325 C1428AQK, Buenos Aires, Argentina
5 Istituto Superiore di Sanità, Department of Cell Biology and Neurosciences, Roma, Italy
6 Genetic Epidemiology Unit, Department of Epidemiology, Biostatistics and Clinical Genetics, Erasmus Medical Center, Rotterdam, The Netherlands
7 INSERM UMRS 975, Hôpital de la Salpêtrière Cellule Nationale de référence des maladies de Creutzfeldt-Jakob Paris, F-75013, France
8 Australian National Creutzfeldt-Jakob Disease Registry, Department of Pathology, the University of Melbourne, Parkville, Australia 3010
9 Creutzfeldt-Jakob Disease Surveillance System, Prion Diseases Program, Public Health Agency of Canada, Ottawa, Canada
10 Division of Neurology, University Medical Center and Gerontopsychiatric Unit, University Psychiatric Hospital, SI-1000 Ljubljana, Slovenia
11 Department of Neurology, Laboratory of Neuropathology, Institute of Molecular Medicine, Hospital de Santa Maria, Lisbon Faculty of Medicine, Lisbon, Portugal
12 Institute of Neuropathology, University Hospital Zurich, Zurich, Switzerland
13 Clinic Director, Mercy Private Radiology, Grey st, East Melbourne, 3002, Australia
14 Laboratory of Neurobiology, Department of Neurology, Born Bunge Institute, University of Antwerp, Belgium
15 Fundación 'Marqués de Valdecilla' IFIMAV and Centro de Investigación Biomédica en Red sobre Enfermedades Neurodegenerativas (CIBERNED). Santander, Spain

Corresponding author: Inga Zerr, MD,
National TSE Reference Center,
Department of Neurology,
Georg-August University Goettingen,
Robert-Koch-Str. 40,
37075 Goettingen,
Germany
E-mail: epicjd@med.uni-goettingen.de

Several molecular subtypes of sporadic Creutzfeldt–Jakob disease have been identified and electroencephalogram and cerebrospinal fluid biomarkers have been reported to support clinical diagnosis but with variable utility according to subtype. In recent years, a series of publications have demonstrated a potentially important role for magnetic resonance imaging in the pre-mortem diagnosis of sporadic Creutzfeldt–Jakob disease. Magnetic resonance imaging signal alterations correlate with distinct sporadic Creutzfeldt–Jakob disease molecular subtypes and thus might contribute to the earlier identification of the whole spectrum of sporadic Creutzfeldt–Jakob disease cases. This multi-centre international study aimed to provide a rationale for the amendment of the clinical diagnostic criteria for sporadic Creutzfeldt–Jakob disease. Patients with sporadic Creutzfeldt–Jakob disease and fluid attenuated inversion recovery or diffusion-weight imaging were recruited from 12 countries. Patients

Received March 26, 2009. Revised June 12, 2009. Accepted June 14, 2009

referred as 'suspected sporadic Creutzfeldt–Jakob disease' but with an alternative diagnosis after thorough follow up, were analysed as controls. All magnetic resonance imaging scans were assessed for signal changes according to a standard protocol encompassing seven cortical regions, basal ganglia, thalamus and cerebellum. Magnetic resonance imaging scans were evaluated in 436 sporadic Creutzfeldt–Jakob disease patients and 141 controls. The pattern of high signal intensity with the best sensitivity and specificity in the differential diagnosis of sporadic Creutzfeldt–Jakob disease was identified. The optimum diagnostic accuracy in the differential diagnosis of rapid progressive dementia was obtained when either at least two cortical regions (temporal, parietal or occipital) or both caudate nucleus and putamen displayed a high signal in fluid attenuated inversion recovery or diffusion-weight imaging magnetic resonance imaging. Based on our analyses, magnetic resonance imaging was positive in 83% of cases. In all definite cases, the amended criteria would cover the vast majority of suspected cases, being positive in 98%. Cerebral cortical signal increase and high signal in caudate nucleus and putamen on fluid attenuated inversion recovery or diffusion-weight imaging magnetic resonance imaging are useful in the diagnosis of sporadic Creutzfeldt–Jakob disease. We propose an amendment to the clinical diagnostic criteria for sporadic Creutzfeldt–Jakob disease to include findings from magnetic resonance imaging scans.

Keywords: CJD; MRI; FLAIR; DWI; molecular subtypes; dementia

Abbreviations: CSF = cerebrospinal fluid; DWI = diffusion-weight imaging; EEG = electroencephalography; FLAIR = fluid attenuated inversion recovery; IgG = immunglobulin G; MRI = magnetic resonance imaging; sCJD = sporadic Creutzfeldt–Jakob disease; PRNP = prionprotein gene; PrPSc = pathogenic Prion protein; SREAT = steroid responsive encephalitis associated with autoimmune thyroiditis

Introduction

Sporadic CJD (sCJD) is a transmissible neurodegenerative disorder with a fatal outcome. Clinical diagnostic criteria for sCJD were first formulated 30 years ago, using a combination of distinctive clinical features and best available auxiliary paraclinical investigations, which at that time was electroencephalography (EEG) (Masters *et al*., 1979). In recent years, there has been progress in developing other specialist investigations, including useful surrogate biomarkers in the cerebrospinal fluid (CSF), and clinical diagnostic criteria have been amended (Zerr *et al*., 2000*a*; Collins *et al*., 2006).

A series of recent publications has dealt with the clinical and pathological phenotypes and heterogeneity in sCJD (Parchi *et al*., 1999; Gambetti *et al*., 2003; Castellani *et al*., 2004; Collins *et al*., 2006; Sanchez-Juan *et al*., 2006). It has become apparent that a multimodal approach may be necessary if detection of the entire phenotypic spectrum of sCJD is to be achieved (Zerr *et al*., 2000*b*). Whereas some classical molecular subtypes such as the MM1 subtype frequently display periodic sharp and slow wave complexes in the EEG, the other five molecular subtypes are negative with this investigation (Parchi *et al*., 1999; Castellani *et al*., 2004; Collins *et al*., 2006). Utilizing CSF 14-3-3 protein detection provides a higher sensitivity, including less typical subtypes of sCJD such as VV1 and VV2 subtypes (Collins *et al*., 2006; Sanchez-Juan *et al*., 2006; Geschwind *et al*., 2009). However, even for CSF 14-3-3 protein detection with an overall sensitivity of 85%–95%, biological variables modify the test results and cases with longer duration or younger age at onset may be missed by this investigation (Castellani *et al*., 2004; Sanchez-Juan *et al*., 2006).

Acknowledging the limitations of the clinical criteria, the search for additional sCJD diagnostic investigations has continued. Magnetic resonance imaging (MRI) has become increasingly important in the clinical diagnosis of sCJD. The use of sensitive fluid attenuated inversion recovery (FLAIR) and diffusion-weight imaging (DWI) sequences allows the detection of basal ganglia hyperintensity and signal increase in other brain regions (Satoh *et al*., 2007; Tschampa *et al*., 2007; Fujita *et al*., 2008; Galanaud *et al*., 2008; Meissner *et al*., 2008). Characteristic MRI lesion patterns corresponding to individual CJD subtypes have been reported (Meissner *et al*., 2009). As MRI findings, even from early in the illness, are proving valuable in the evaluation of suspected sCJD patients, both by excluding other disorders and by demonstrating features considered typical of human prion disease (Geschwind *et al*., 2009), we undertook a systematic multi-centre international collaborative study to analyse the value of MRI lesion patterns in comparison to CSF biomarker 14-3-3 and periodic sharp wave complexes in the EEG in terms of test sensitivity and specificity.

Material and Methods

Patients

Cases were included from twelve countries (Argentina, Australia, Belgium, Canada, France, Germany, Italy, Netherlands, Portugal, Slovenia, Switzerland and United Kingdom) according to the following criteria: (i) CJD diagnosis confirmed by brain pathology (definite cases) or fulfilling accepted case definition criteria for 'probable' sCJD (data used for a separate set of analyses); (ii) molecular subtype determined by codon 129 genotyping (MM, MV or VV) and western blot analysis of brain pathogenic prion protein (PrPSc) type (1 or 2) (corresponding to MM1, MM2, MV1, MV2, VV1 and VV2 subtype) (Parchi *et al*., 1996, 1999); and (iii) available FLAIR or DWI MRI of the brain.

Controls

Controls were included according to the following criteria: (i) cases in which the diagnosis of sCJD was suspected (patients classified at least as

probable or possible CJD) but excluded on follow up by clinical investigations (improvement or recovery, inflammatory CSF findings, other diagnosis) or at autopsy; and (ii) available FLAIR or DWI brain MRI.

Codon 129 status was determined either as part of genotyping of the entire prion protein gene (PRNP) open reading frame or by restriction fragment length polymorphism analysis (Collins *et al*., 2006). Genetic CJD (causal mutations found in prionprotein gene), iatrogenic and variant CJD cases were excluded.

EEG (periodic sharp wave complexes) findings were also ascertained. The CSF 14-3-3 immunoassays were performed using western blotting as previously reported (Zerr *et al*., 2000*a*) and the conformity of test methods and interpretation of results was confirmed by a blinded sample exchange programme between laboratories (Sanchez-Juan *et al*., 2006).

The study comprised 436 sCJD patients who died between April 1998 and March 2007, and 141 controls: 32 (5.5%) from Argentina, 15 (2.6%) from Australia, 35 (6.1%) from Belgium, 9 (1.6%) from Canada, 16 (2.8%) from France, 328 (56.8%) from Germany, 32 (5.5%) from Italy, 17 (2.9%) from Netherlands, 7 (1.2%) from Portugal, 4 (0.7%) from Slovenia, 7 (1.2%) from Switzerland and 75 (13.0%) from UK.

MRI data

The magnetic resonance images were performed as routine clinical diagnostic studies and were collected from various hospitals in the framework of epidemiological studies as reported elsewhere (Meissner *et al*., 2009).

The majority of the scans were available as hardcopy. If serial MRIs were available, the first examination was used for the analysis. All scans were assessed by at least one neuroradiologist (K.K., D.S., C.R., P.S. or D.C.) aware that sCJD was a differential diagnostic possibility but blinded to the final diagnosis. All neuroradiologists assessed a small MRI series for the estimation of the inter-observer agreement. The intra reader concordance was high: 93.3%, $\kappa = 0.64$ ($P < 0.001$). Inter-rater concordance was 89%, $\kappa = 0.61$ ($P < 0.001$) and 82%, $\kappa = 0.62$ ($P < 0.001$) (which is high agreement) or 75.4%, $\kappa = 0.50$ ($P < 0.001$) and 76%, $\kappa = 0.45$ ($P < 0.001$) (moderate agreement).

A standardized protocol was used which included seven cerebral cortex regions (specifically the cingulate gyri, insular regions and hippocampi, as well as the remaining frontal, parietal and temporal lobes and the occipital lobes), basal ganglia (caudate nucleus, putamen, globus pallidus), thalamus (anterolateral nuclei, mediodorsal nuclei, pulvinar) and cerebellar cortex. For the thalamus, the presence or absence of a 'pulvinar sign' with extension into the antero-medial thalamus underscoring the 'hockey stick sign' was also rated (hyperintensity of the pulvinar relative to the anterior putamen) (Collie *et al*., 2003). The cerebral regions were assessed as hyperintense in relation to isointense cortex areas. As most MRI data were available as hardcopy only, the grade of hyper-intensity was not quantified. For each MRI examination, T_2-weighted (T_2-w) images were evaluated first, followed by FLAIR and DWI. For further analyses, only FLAIR and DWI were considered e.g. only the most sensitive sequences, FLAIR and DWI (Kallenberg *et al*., 2006), were considered. Proton-density-weighted scans and apparent diffusion coefficient maps were less commonly used and not included in this study. Areas of hyperintensity were scored separately for each sequence. The quality of the complete MRI examination was graded from 1 to 6 (1 = excellent, 2 = good, 3 = average, 4 = sufficient, 5 = insufficient, 6 = poor). Scans graded higher than 4 were considered as non-diagnostic (mainly due to motion artefacts) and excluded from the study.

Statistical analysis

Descriptive statistics were reported for sCJD and control patients; χ^2-test and the non-parametric Mann–Whitney test were used to assess differences between categorical and continuous variables.

The goal of our study was to identify the best combination of radiological findings and MRI sequences to discriminate between sCJD and non-sCJD patients. In order to do this we compared the results of visual assessments of brain MRI scans in cases and controls. We considered a brain region as affected when a high signal was found in either FLAIR or DWI MRI sequences. We calculated sensitivity [the percentage of scans considered as characteristic (positive) of sCJD in cases] and specificity [the percentage of scans considered as not characteristic (negative) of sCJD in controls] for several criteria patterns involving different combinations of affected regions and MRI sequences. We also calculated diagnostic odds ratios—the ratio of the odds of positivity in sCJD cases relative to the odds of positivity in the controls—to assess which combinations of criteria patterns yielded better test discriminatory performance; 95% confidence intervals of the diagnostic odds ratios were estimated by the exact method.

Inter-reader agreement for brain MRI scan visual assessment (normal or affected) was calculated, using Cohen's κ coefficient and Concordance Index, for all explored areas included in the standardized protocol. Concordance Index is the percentage of agreement between readers and the κ coefficient shows the difference in agreement, from chance, between them; thus a κ-value of 0 means no different from chance and 1 is perfect agreement.

Ethics

The study was done in accordance with the current revision of the Declaration of Helsinki and the Good Clinical Practice: Consolidated Guideline approved by the International Conference on Harmonization and applicable to national and local laws and regulations. For each participating site, the study protocol and all amendments were approved by an institutional review board or independent ethics committee. All patients and their caregivers gave written informed consent.

Results

Patients

In total, MRI scans were available for 436 patients with sCJD and 141 controls.

FLAIR sequences were available in 379 cases and in 128 controls, DWI in 258 cases and 81 controls. Both sequences were available in 201 cases and 68 controls. The median time from onset to MRI was 2.7 months in sCJD cases and 6.7 months in controls. Patient characteristics are summarized in Table 1.

Definition of the criteria

In the first part of the study, we analysed which FLAIR and/or DWI MRI lesion pattern was characteristic for sCJD, regardless of molecular subtype. To achieve this, a stepwise analysis was performed: (i) selection of the cortical regions; (ii) combination cortical/subcortical areas; and (iii) definition of the best MRI sequence (FLAIR/DWI).

Table 1 Patient characteristics

	n	Autopsy (%)	Female (gender) (%)	Median age (range)	Median duration (range) (months)	Time to MRI (months)	Codon 129 MM *n* (%)	Codon 129 MV *n* (%)	Codon 129 VV *n* (%)	FLAIR MRI (*n*)	DWI MRI (*n*)
sCJD	436	60.3	55.6	64.0 (35.3–85.0)	6.4 (1.0–56.3)	2.7	195 (62.7)	58 (18.6)	58 (18.6)	379	258
controls	144	39.1	48.8	65.9 (25.9–91.5)	12.0 (0.0–104.0)	6.7	11 (44.0)	8 (32.0)	6 (24.0)	128	81
P-value			0.27	0.2	0.007						

Table 2 Selection of cortical areas

		Frontal	Cinguli	Parietal	Temporal	Occipital	Insula	Hippocampus
CJD (% positive)	FLAIR	48	52	37	32	17	24	20
Control (% negative)	FLAIR	75	71	89	82	97	89	76
CJD (% positive)	DWI	74	71	65	59	37	52	21
Control (% negative)	DWI	65	61	89	81	90	77	88
Diagnostic odds ratio (95% CI)	FLAIR	2.73 (1.52–3.94)	2.636 (1.51–3.76)	4.986 (2.03–7.94)	2.058 (1.04–3.07)	6.43 (0.2–13.06)	2.382 (0.98–3.78)	0.77 (0.4–1.15)
	DWI	5.21 (2.44–7.98)	3.667 (1.76–5.57)	14.7 (3.85–25.56)	5.92 (2.37–9.46)	5.48 (1.25–9.71)	3.58 (1.55–5.62)	1.89 (0.5–3.28)

CI = confidence interval.

Selection of cortical regions

In this part of the study, we analysed the frequency of high signal detection in each cortical region for cases and controls and stratified the data by the MRI technique used (FLAIR or DWI, Table 2). As the result of this analysis, we selected three regions with the optimum sensitivity and specificity data, irrespective of MRI technique used. The three areas with the highest values for diagnostic accuracy were the parietal, occipital and temporal cortical regions. The other cortical brain regions such as cingulate gyrus, insular cortex or hippocampus were either non-discriminatory between cases and controls, had low specificity and, in addition to this, found low inter reader agreement, as reported before (Krasnianski *et al*., 2008).

Combination of cortical and subcortical areas

Various combinations of high signal intensity were analysed in the three selected cortical (parietal, occipital and temporal) and subcortical regions. The results are given in Table 3. For FLAIR and DWI, the best results were obtained when two or more regions (either temporal, parietal, occipital) displayed a high signal in the MRI. The poorest specificity was obtained when MRI scans were considered positive when only one or more cerebral cortical region showed a high signal; therefore, those patterns were excluded for further analysis. For subcortical areas, the optimum diagnostic accuracy was obtained when a high signal increase was observed in both the caudate nucleus and putamen simultaneously. DWI was generally more sensitive than FLAIR with a similar specificity for both sequences.

Further analyses determined the best possible combination of various cerebral cortical and subcortical high signal changes. The highest diagnostic accuracy was obtained by accepting either a combination of at least two cerebral cortical regions (temporal, occipital, parietal) showing increased signal or both the putamen and the caudate nucleus showing high signal intensity (Table 4).

Definition of the MRI sequence

After choosing the combination of either at least two cerebral cortical regions or both the putamen and caudate nucleus showing high signal as the optimal radiological pattern, we analysed which MRI pulse sequence or potential combination of sequences revealed the highest sensitivity and specificity. Both sequences achieved high diagnostic accuracy (Table 5). We calculated the data for other potential combinations, such as FLAIR and DWI positive, but the sensitivity achieved was only 54%.

In order to estimate the sensitivity and specificity of the combination FLAIR or DWI, we considered that patients with both pulse sequences available were most reliable, because including patients with only one sequence would result in a predominance of the 'only FLAIR performed' and a decrease in the sensitivity (Table 5), since FLAIR is less sensitive than DWI.

False-positive findings in the MRI

According to our criteria, 19 controls had positive findings on the MRI. Most of these suffered from an infectious or inflammatory disorder of the central nervous system ($n = 9$), like lymphocytic encephalitis, progressive multifocal leucencephalopathy, steroid responsive encephalitis associated with autoimmune thyroiditis (SREAT) or encephalitis of unknown origin. In other patients with a positive MRI, autopsy confirmed Alzheimer's disease ($n = 2$), Dementia with Lewy bodies ($n = 2$), epilepsy ($n = 2$), intravascular lymphomatosis and mitochondrial cytopathy.

Table 3 Selection of cortical and subcortical areas

	FLAIR			DWI		
	Controls	Total sCJD cases	Definite CJD cases	Controls	Total sCJD cases	Definite sCJD cases
At least one cortical region[a] affected						
No (%)	94 (73.4)	190 (50.1)	111 (48.1)	60 (74.1)	57 (22.1)	29 (19.1)
Yes (%)	34 (26.6)	189 (49.9)	120 (51.9)	21 (25.9)	201 (77.9)	123 (80.9)
Diagnostic odds ratio (95% CI)	2.8 (1.5–4.0)		3.0 (1.6–4.4)	10.1 (4.3–15.9)		12.1 (4.4–19.9)
At least two cortical regions[a] affected						
No (%)	121 (94.5)	278 (73.4)	173 (74.9)	72 (88.9)	115 (44.6)	62 (40.8)
Yes (%)	7 (5.5)	101 (26.6)	58 (25.1)	9 (11.1)	143 (55.4)	90 (59.2)
Diagnostic odds ratio (95% CI)	6.3 (1.3–11.3)		5.8 (1.1–10.5)	10.0 (2.6–17.3)		11.6 (2.7–20.5)
More than three cortical regions affected						
No (%)	115 (89.8)	276 (72.8)	163 (70.6)	68 (84.0)	111 (43.0)	57 (37.5)
Yes (%)	13 (10.2)	103 (27.2)	68 (29.4)	13 (16.0)	147 (57.0)	95 (62.5)
Diagnostic odds ratio (95% CI)	3.3 (1.3–5.3)		3.7 (1.3–6.1)	6.9 (2.5–11.4)		8.7 (2.8–14.6)
Putamen or caudatum affected						
No (%)	104 (81.3)	147 (38.8)	83 (35.9)	67 (82.7)	83 (32.2)	44 (28.9)
Yes (%)	24 (18.8)	232 (61.2)	148 (64.1)	14 (17.3)	175 (67.8)	108 (71.1)
Diagnostic odds ratio (95% CI)	6.8 (3.5–10.2)		7.7 (3.7–11.7)	10.1 (3.7–16.5)		11.8 (3.8–19.7)
Both putamen and caudatum affected						
No (%)	120 (93.8)	223 (58.8)	135 (58.4)	76 (93.8)	133 (51.6)	76 (50.0)
Yes (%)	8 (6.3)	156 (41.2)	96 (41.6)	5 (6.2)	125 (48.4)	76 (50.0)
Diagnostic odds ratio (95% CI)	10.5 (2.7–18.3)	10.7 (2.5–18.8)	14.3 (0.9–27.7)	15.2 (0.6–29.8)		

a Parietal–temporal–occipital; CI = confidence interval; s = sCJD cases.

Table 4 Selection of cortical and subcortical areas best combination

	FLAIR			DWI		
	Controls	Total sCJD cases	Definite sCJD cases	Controls	Total sCJD cases	Definite sCJD cases
More than three cortical regions OR both Put. and NC affected						
No (%)	110 (85.9)	166 (43.8)	94 (40.7)	66 (81.5)	62 (24.0)	32 (21.1)
Yes (%)	18 (14.1)	213 (56.2)	137 (59.3)	15 (18.5)	196 (76.0)	120 (78.9)
Diagnostic odds ratio (95% CI)	7.8 (3.6–12.1)		8.9 (3.9–13.9)	13.9 (5.2-22.7)		16.5 (5.2-27.8)
More than three cortical regions OR Put. OR NC affected						
No (%)	99 (77.3)	113 (29.8)	60 (26.0)	61 (75.3)	41 (15.9)	19 (12.5)
Yes (%)	29 (22.7)	266 (70.2)	171 (74.0)	20 (24.7)	217 (84.1)	133 (87.5)
Diagnostic odds ratio (95% CI)	8.0 (4.3–11.8)		9.7 (4.8–14.7)	16.1 (6.4–25.9)		21.4 (6.5–36.2)
At least two cortical regions[a] affected OR both Put. and NC affected						
No (%)	116 (90.6)	162 (42.7)	97 (42.0)	70 (86.4)	63 (24.4)	33 (21.7)
Yes (%)	12 (9.4)	217 (57.3)	134 (58.0)	11 (13.6)	195 (75.6)	119 (78.3)
Diagnostic odds ratio (95% CI)	13.0 (4.8–21.1)		13.4 (4.7–22.0)	19.7 (6.0–33.4)		23.0 (5.9–40.0)
At least two cortical regions[a] affected OR Put. OR NC affected						
No (%)	103 (80.5)	106 (28.0)	58 (25.1)	62 (76.5)	42 (16.3)	21 (13.8)
Yes (%)	25 (19.5)	273 (72.0)	173 (74.9)	19 (23.5)	216 (83.7)	131 (86.2)
Diagnostic odds ratio (95% CI)	10.6 (5.4–15.8)		12.3 (5.8–18.8)	16.8 (6.5–27.0)		20.4 (6.3–34.4)

NC = nucleus caudatum; Put. = putamen.
a Parietal–temporal–occipital.

Two patients recovered and the diagnosis is not known. No distinctive MRI pattern could be detected for each disorder and the frequency of high signal abnormalities in cortical and subcortical areas was similar in all the diagnostic groups mentioned above.

Modification of clinical criteria for sCJD

Based on our results, we recommend modifying the current clinical diagnostic criteria for sCJD to include the detection of either

Table 5 Definition of MRI sequences for the pattern at least two cortical regions affected (parietal–temporal–occipital) or both putamen and nucleus caudatum affected

	Controls	Total sCJD cases	Definite sCJD cases
FLAIR AND DWI			
No (%)	64 (94.1)	92 (45.8)	55 (45.8)
Yes (%)	4 (5.9)	109 (54.2)	65 (54.2)
Total (*n*)	68	201	120
Diagnostic odds ratio (95%CI)	19.0 (0.9–38.8)		18.9 (1.4–39.2)
FLAIR OR DWI			
No (%)	122 (86.5)	133 (30.5)	75 (28.5)
Yes (%)	19 (13.5)	303 (69.5)	188 (71.5)
Total (*n*)	141	436	263
Diagnostic odds ratio (95%CI)	14.6 (7.0–22.3)		16.1 (7.2–25.0)
FLAIR OR DWI[a]			
No (%)	56 (82.3)	38 (18.9)	21 (17.5)
Yes (%)	12 (17.6)	163 (81.1)	99 (82.5)
Total (*n*)	68	201	120
Diagnostic odds ratio (95%CI)	20.0 (5.7–34.4)		22.0 (4.8–39.2)

a Only cases with both sequences available.

hyperintensity in the basal ganglia (both caudate nucleus and putamen) or in at least two cortical regions (from either the temporal, parietal or occipital cerebral cortices) (Fig. 1). This implies that the detection of the specified high signal abnormalities in FLAIR or DWI MRI will be considered at the same level of diagnostic importance as periodic sharp wave complexes on the EEG or 14-3-3 protein detection in the CSF.

Comparative analysis of the EEG, CSF and MRI

In a subgroup of 214 definite CJD patients and 77 definite non-cases, we analysed the frequency of true-positive results in cases (sensitivity) and true-negative results in controls (specificity), in relation to the detection of periodic sharp wave complexes in the EEG, elevated CSF levels of 14-3-3 protein or MRI abnormalities. Diagnostic MRI abnormalities for sCJD, as defined by our analyses, were observed in 83% of such patients with a specificity of 83%. For CSF 14-3-3 protein detection, test sensitivity was 86% but specificity was 68%. EEG had the lowest sensitivity (44%) and highest specificity (92%). Details on comparative analyses of current and amended criteria are given in Table 6. The sensitivity of current criteria is 92%, the specificity 71%. Thus, 8% of sCJD patients are not covered by the World Health

I. clinical signs:

1. dementia
2. cerebellar or visual
3. pyramidal or extrapyramidal
4. akinetic mutism

II. tests:

1. PSWCs in EEG
2. 14-3-3 detection in CSF (in patients with a disease duration of less than 2 year)
3. high signal abnormalities in caudate nucleus and putamen or at least two cortical regions (temporal-parietal-occipital) either in DWI or FLAIR

Probable CJD

two out of I and at least one out of II

Possible CJD

two out of I and duration less than 2 years

Figure 1 MRI-CJD Consortium criteria for sporadic Creutzfeldt–Jakob disease.

Table 6 Comparison of new and old criteria

	n	%	Sensitivity	Specificity
Current criteria				
Definite sporadic CJD cases with both EEG and 14-3-3 tests performed				
EEG atypical & 14-3-3 test negative	8	7.8		
EEG typical & 14-3-3 test negative	7	6.8		
EEG atypical & 14-3-3 test positive	49	47.6		
EEG typical & 14-3-3 test positive	39	37.9	92.2	
Total	103	100		
Controls with both EEG and 14-3-3 tests performed				
EEG atypical & 14-3-3 test negative	37	71.2		71.2
EEG typical & 14-3-3 test negative	1	1.9		
EEG atypical & 14-3-3 test positive	12	23.1		
EEG typical & 14-3-3 test positive	1	1.9		
Total	52	100		
New criteria				
Definite sporadic CJD cases with all three tests performed (EEG, 14-3-3 tests, and MRI FLAIR and DWI, new criteria)				
Current criteria negative & MRI negative	1	2.0		
Current criteria positive & MRI negative	7	14		
Current criteria negative & MRI positive	3	6		
Current criteria positive & MRI positive	39	78	98	
Total	50	100		
Controls with all three tests performed (EEG, 14-3-3 tests, and MRI FLAIR and DWI)				
Current criteria negative & MRI negative	17	70.8		70.8
Current criteria positive & MRI negative	5	20.8		
Current criteria negative & MRI positive	1	4.2		
Current criteria positive & MRI positive	1	4.2		
Total	24	100		

Table 7 Sensitivity of old and new criteria for each molecular disease subtype

Disease subtype	Positive MRI/total (%)	Positive 14-3-3/total (%)	Positive EEG/total (%)	New criteria positive (%)	Old criteria positive (%)
MM1	33/43 (76.7)	38/42 (90.5)	26/43 (60.5)	100	97.6
MM2	14/15 (93.3)	9/14 (64.3)	3/14 (21.4)	92.3	69.2
MV1	6/6 (100)	5/6 (83.3)	3/6 (50)	100	100
MV2	8/8 (100)	7/8 (87.5)	0/8 (0)	100	87.5
VV1	2/2 (100)	2/2 (100)	1/2 (50)	100	100
VV2	9/15(60)	14/15 (93.3)	0/15 (0)	100	93.3
All	72/89 (80.9)	75/87 (86.2)	33/88 (37.5)	98.8	91.9

Organization criteria. By inclusion of the MRI as an additional parameter for 'probable' CJD, the sensitivity of clinical criteria rises substantially to 98%, but specificity drops marginally.

Value of MRI in identification of various molecular sCJD subtypes

A comparative analysis of protein 14-3-3, EEG and MRI in a subset of CJD patients with data on pathogenic prion protein type and codon 129 genotype available is shown in Table 7. Currently used criteria improved the recognition of some of the less typical sCJD subtypes such as VV2. Amended criteria, as suggested here, are especially helpful for the rare and atypical subtypes such as MM2, MV1 and MV2. The latter may develop an atypical clinical syndrome and thus not be properly diagnosed on clinical grounds (Krasnianski *et al*., 2006*a, b*)

Discussion

This multi-centre collaborative study analysed findings from MRI scans in a large number of sCJD cases and controls; and has provided evidence that justifies the inclusion of defined MRI pattern in the clinical diagnostic criteria for sCJD. In a previous manuscript, we reported characteristic MRI patterns for each molecular CJD subtype (Meissner *et al*., 2009) and identified variables which allowed for the best discrimination between those subtypes. We chose the following radiological signs as predictors of sCJD subtypes: high signal in (i) more than three

cerebral cortical regions; (ii) hippocampus; (iii) any basal ganglia; (iv) any thalamic nuclei; and (v) cerebellum. Multivariate analysis, including the five selected regions, was performed in order to allow independent assessment of these parameters and a specific MRI lesion pattern for each molecular disease subtype was identified (Meissner *et al*., 2009). Specificity of MRI changes was not addressed. Since the information on specificity is essential for an assessment of the true utility of MRI brain scan in the diagnosis of sCJD, we performed the current study.

In order to assess the sensitivity of MRI in the diagnosis of sCJD, we developed a set of variables which allowed the optimum discrimination between CJD and controls. In this analysis, we selected anatomical regions which have been demonstrated to be frequently affected (Meissner *et al*., 2009). The characteristic MRI lesion pattern, which allowed for the best discrimination between sCJD cases and controls was found to be high signal intensity in FLAIR or DWI in at least two cortical regions, or signal increase in the caudate nucleus and putamen. Based on these findings, we propose that the clinical diagnostic criteria for sCJD are amended to include MRI signal abnormalities as defined above (Fig. 1). The MRI findings will thus be equivalent to elevated levels of 14-3-3 proteins or periodic sharp and slow wave complexes in the EEG for the clinical diagnosis of probable sCJD.

With respect to current clinical tests for sCJD, the EEG was the first *in vivo* test to be used to support the clinical diagnosis of sCJD. However, the EEG has been shown to be positive in only a subset of sCJD patients, usually MM1 or MV1 cases. Typically, periodic sharp wave complexes are detected late in the disease and the median time to positive EGG is around 12 weeks. This corresponds to the terminal stages of the illness (Poser *et al*., 1999; Zerr *et al*., 2000*a*; Collins *et al*., 2006). A number of CSF biomarkers have been reported in sCJD, including 14-3-3, tau, S100b, neuron-specific enolase, phosphorylated tau and abeta, with the majority of available data relating to 14-3-3 and tau proteins (Sanchez-Juan *et al*., 2006). Both these biomarkers support the clinical CJD diagnosis with a sensitivity of 92% and specificity of 71% (Sanchez-Juan *et al*., 2006). However, a number of publications have indicated that low levels of these biomarkers are present in the CSF in some atypical CJD variants (Castellani *et al*., 2004; Sanchez-Juan *et al*., 2006; Gmitterová *et al*., 2008). Biological variables such as long disease duration, young age at onset, type 2 pathogenic prion protein and heterozygosity at codon 129 genotype of the PrP gene are all associated with low biomarker levels (Parchi *et al*., 1999; Zerr *et al*., 2000*b*; Castellani *et al*., 2004; Sanchez-Juan *et al*., 2006). This is in contrast with the results of MRI scans in some atypical and rare variants of sCJD, such as VV1 and MV2: in VV1 patients there is high signal in the cortical areas and normal signal in the basal ganglia, while in MV2 patients characteristic abnormalities are seen in the basal ganglia, putamen and thalamus (Meissner *et al*., 2005; Krasnianski *et al*., 2006*b*, 2008). Characteristic lesion patterns have recently been reported for patients with other molecular disease subtypes (Meissner *et al*., 2009) and the question was raised whether MRI brain scan might contribute to the improved diagnosis across sCJD subtypes (Tschampa *et al*., 2005; Meissner *et al*., 2009).

Table 7 shows the data on positive tests in a subgroup of patients with known molecular type. MRI findings are positive in 81% of sCJD patients. Sensitivity of the 14-3-3 test is 86% and significantly less for the EEG. By combination of all parameters, sensitivity is 98% and specificity of the criteria is 71%. Although the frequency and location of high signal intensities vary between subtypes, by amendment of clinical criteria, most molecular disease subtypes will be covered, including rare subtypes VV1 and MV2 (Table 7).

Our results indicate a high rate of agreement between identification of cortical parietal, temporal and occipital signal and basal ganglia involvement between five raters, even in a cohort of patients where MRI scans were acquired at different centres, with some modifications. These results suggest that MRI is a robust investigation in sCJD and qualifies as a potential biomarker for CJD.

A limitation of this study is the high number of sCJD cases as compared to controls. However, the gold standard for the validation of the clinical diagnostic criteria was the analysis of the subset of sCJD cases in which the diagnosis had been confirmed by neuropathology. In controls, only data from patients in which the diagnosis of CJD had been definitely excluded by neuropathology or in which there was a definite alternative clinical diagnosis, were used. This group included cases who recovered, cases with inflammatory CSF findings indicating an alternative diagnosis or a clinical course which excluded CJD as a diagnosis (Heinemann *et al*., 2007). In the context of a multi-centre MRI study on a rare disorder, achieving a high autopsy rate in non-cases is difficult and it would take many years to obtain a representative autopsy sample of non-cases at a similar rate to the sCJD cases. Epidemiological surveillance studies on rare disorders are person and cost intensive and a study with selected MRI scans on more than 300 cases and controls on a solely autoptic sample is unlikely to be feasible in the near future. However, in this study, we have achieved neuropathology confirmation in 40% of controls and in 60% of CJD patients.

Our analysis has shown that MRI findings may lead to false positive diagnosis in a small number of cases. This is an important issue for the accurate diagnosis of sCJD. Almost 50% of false-positive findings on the MRI were associated with inflammatory conditions; the other diagnoses were Alzheimer's disease and Dementia with Lewy bodies (Haïk *et al*., 2000; Tschampa *et al*., 2001). Inflammatory conditions of the brain represent the most important differential diagnosis as there may be a possibility for treatment (Chang *et al*., 2007; Heinemann *et al*., 2007; Geschwind *et al*., 2008). In our patients, diagnoses included encephalitis of unknown origin and SREAT (Seipelt *et al*., 1999). The latter diagnosis has been described previously as an important treatable condition in the differential diagnosis of CJD. The crucial question for the clinician is how to avoid the misinterpretation of tests and how to avoid missing a treatable condition in a patient with a rapid progressive dementia and focal neurological signs (Josephs *et al*., 2009). Thorough analysis of the cerebrospinal fluid for routine parameters such as cell count, protein and oligoclonal bands (which are often positive in SREAT and other inflammatory conditions, but usually negative in CJD) may be helpful in diagnosis (Jacobi *et al*., 2005; Green *et al*., 2007). As other tests,

such as 14-3-3 and EEG, may also show 'false-positive' results in inflammatory conditions of the brain, accurate clinical diagnosis can be a major challenge. Thus, patients with 'inflammatory' abnormalities in the CSF such as pleocytosis, high elevated protein content and oligoclonal immunglobulin G should enter the diagnostic pathway for potentially treatable conditions (Vernino *et al*., 2007).

The time point at which the clinical diagnosis of sCJD is made may be very important if treatment strategies become available as any therapy will probably need to be started early if it is to be effective. The EEG has been shown to become positive usually only in the late stages of the disease. CSF biomarkers can become positive in the early disease stages, as shown in a cohort of patients with repeated lumbar punctures and multiple CSF tests (Sanchez-Juan *et al*., 2007). With MRI the question on when the typical changes appear is still unresolved because of the limited number of patients with multiple scans. However, there is a suggestion from the literature that MRI may become positive early in the disease (Young *et al*., 2005; Fujita *et al*., 2008; Galanaud *et al*., 2008; Hoshino *et al*., 2008). Further work will be needed to address this question.

In summary, our data show that basal ganglia and cortical hyperintensities represent the most frequent MRI findings in sCJD and are present in most cases. Characteristic brain MRI lesion patterns are helpful in establishing a diagnosis of sCJD and may help to identify atypical sporadic disease forms. This is the most comprehensive study on MRI findings in sCJD to date, and in combination with previous studies, provides firm evidence that brain MRI has a high sensitivity and specificity in the diagnosis of the disease.

Acknowledgements

This study was supported by grants from the German Federal Ministry of Education and Research (Brain imaging as an aid to determine molecular subtype in prion diseases, BMBF ARG07/008 and Forschungsnetz zur Verbesserung der Früh- und Differentialdiagnose der CJK und rasch progressiver Demenzen, BMBF 01 610 301 to I.Z.), by the Robert Koch-Institut through funds of the Federal Ministry of Health (grant no 1369-341), and by the Verein zur Förderung der Wissenschaft und Forschung an der Neurologischen Klinik Göttingen e.V. (to I.Z.)
Grants at national levels are reported below:

Argentina
FLENI-SECYT BID 802-OC-AR PID 98/027/BID 1728; OC-AR PID 2003/351; BMBF-MINCYT-ARG 10/008

We thank all the neurologists who contributed to CJD surveillance in Argentina and especially to Dr E.Meichtry - Moguillansky Clinic- Neuquén-Argentina for his continuous support.

Australia
The Australian National Creutzfeldt-Jakob disease Registry (ANCJDR) thanks Colin Masters, Alison Boyd, Genevieve Klug, Samantha Douglas, Christiane Stehmann and Amelia McGlade for their valuable contributions, as well as the families of CJD patients and their physicians for their generous support and assistance. The ANCJDR is funded by the Commonwealth Department of Health and Ageing.

Belgium
Fonds voor Wetenschappelijk Onderzoek; Born Bunge Institute.

Canada
The Canadian Creutzfeldt–Jakob Disease Surveillance System thanks the families of CJD patients and their physicians for participation in the study. Canadian Neuropathologists are acknowledged for their valuable contributions. All personnel of the Prion Diseases Program are thanked for their enthusiastic cooperation.

France
We thank all members of the French National Surveillance Network for Creutzfeldt–Jakob disease and all physicians for case notification and provision of clinical and pathological data and MRI scan.

Germany
This study was funded by Robert Koch-Institute through funds of the Federal Ministry of Health (grant no 1369-341).We thank physicians for case notification and provision of clinical and pathological data and MRI scans to the National TSE Surveillance Unit, Göttingen, Germany. We are grateful to Jolanthe Ehrlich for her technical assistance in the data base management.

Italy
We thank neurologists and neurodiologists for case notification and provision of clinical and MRI scans, Dr Piero Parchi, Prof. Salvatore Monaco, Dr. Gianluigi Zanusso and Dr Carlo Buffa for the neuropathological evaluation and PrP western blot typing, Dr Sabina Capellari, Dr Daniele Imperiale, Dr Anna Poleggi, Dr Claudia Giannattasio and Mr Michele Equestre for genetic and CSF 14-3-3 analyses. This work was partially supported by the National Registry of CJD and related disorders of the Istituto Superiore di Sanità, Rome, Italy.

Slovenia
We thank all members of the national CJD surveillance group as well as all physicians involved in case notification and we are especially grateful to neuroradiologists for providing us with the MRI scans.

Spain
Fondo de Investigacion Sanitaria (grant PI080139).

Switzerland
We thank all referring physicians. The national Reference Center for Prion Diseases is funded by the Swiss federal Office of Public Health.

UK
The authors are grateful to neuroradiologists from throughout the UK for access to MRI scans. In part by the Department of Health

(121/7369); European Union (Network of Excellence FOOD CT 2004 056579 and ECDC: grant number ECD 607). The UK National CJD Surveillance Unit is funded by the Department of Health and the Scottish Executive Department of Health.

References

Castellani RJ, Colucci M, Xie Z, Zou W, Li C, Parchi P, et al. Sensitivity of 14-3-3 protein test varies in subtypes of sporadic Creutzfeldt-Jakob disease. Neurology 2004; 63: 436–42.

Chang CC, Eggers SD, Johnson JK, Haman A, Miller BL, Geschwind MD. Anti-GAD antibody cerebellar ataxia mimicking Creutzfeldt-Jakob disease. Clin Neurol Neurosurg 2007; 109: 54–7.

Collie DA, Summers DM, Sellar RJ, Ironside JW, Cooper S, Zeidler M, et al. Diagnosing variant Creutzfeldt-Jakob disease with the pulvinar sign: MR imaging findings in 86 neuropathologically confirmed cases. Am J Neuroradiol 2003; 24: 1560–9.

Collins SJ, Sanchez-Juan P, Masters CL, Klug GM, van Duijn C, Poleggi A, et al. Determinants of diagnostic investigation sensitivities across the clinical spectrum of sporadic Creutzfeldt-Jakob disease. Brain 2006; 129: 2278–87.

Fujita K, Nakane S, Harada M, Izumi Y, Kaji R. Diffusion tensor imaging in patients with Creutzfeldt-Jakob disease. J Neurol Neurosurg Psychiatry 2008; 79: 1304–6.

Galanaud D, Dormont D, Haik S, Chiras J, Brandel JP, Ranjeva JP. Differences of apparent diffusion coefficient values in patients with Creutzfeldt-Jakob disease according to the codon 129 genotype. AJNR Am J Neuroradiol 2008; 29: E57.

Gambetti P, Kong Q, Zou W, Parchi P, Chen S. Sporadic and familial CJD: classification and characterisation. Br Med Bull 2003; 66: 213–39.

Geschwind MD, Potter CA, Sattavat M, Garcia PA, Rosen HJ, Miller BL, et al. Correlating DWI MRI with pathologic and other features of Jakob-Creutzfeldt disease. Alzheimer Dis Assoc Disord 2009; 23: 82.

Geschwind MD, Tan KM, Lennon VA, Barajas RFJ, Haman A, Klein CJ, et al. Voltage-gated potassium channel autoimmunity mimicking Creutzfeldt-Jakob disease. Arch Neurol 2008; 65: 1341–6.

Gmitterová K, Heinemann U, Bodemer M, Krasnianski A, Meissner B, Kretzschmar HA, et al. 14-3-3 CSF levels in sporadic Creutzfeldt-Jakob disease differ across molecular subtypes. Neurobiol Aging. epub ahead of print.

Green A, Sanchez-Juan P, Ladogana A, Cuadrado-Corrales N, Sanchez-Valle R, Mitrova E, et al. CSF analysis in patients with sporadic CJD and other transmissible spongiform encephalopathies. Eur J Neurol 2007; 14: 121–4.

HaÏk S, Brandel JP, Sazdovitch V, Delasnerie-Laupr̂tre N, Peoc'h K, Laplanche J-L, et al. Dementia with Lewy bodies in a neuropathologic series of suspected Creutzfeldt-Jakob disease. Neurology 2000; 55: 1401–4.

Heinemann U, Krasnianski A, Meissner B, Varges D, Bartl M, Stoeck K, et al. Creutzfeldt-Jakob disease in Germany: a prospective 12-year surveillance. Brain 2007; 130: 1350–9.

Hoshino A, Iwasaki Y, Izumi M, Kimura S, Ibi T, Kitamoto T, et al. MM1-type sporadic Creutzfeldt-Jakob disease with unusually prolonged disease duration presenting with panencephalopathic-type pathology. Neuropathology 2008; 28: 326–32.

Jacobi C, Arlt S, Reiber H, Westner I, Kretzschmar HA, Poser S, et al. Immunoglobulins and virus-specific antibodies in patients with Creutzfeldt-Jakob disease. Acta Neurol Scand 2005; 111: 185–90.

Josephs KA, Ahlskog E, Parisi JE, Boeve BF, Crum BA, Giannini C, et al. Rapidly progressive neurodegenerative dementias. Arch Neurol 2009; 66: 201–7.

Kallenberg K, Schulz-Schaeffer W, Jastrow U, Poser S, Meissner B, Tschampa H, et al. Creutzfeldt-Jakob disease: comparative Analysis of MR Imaging Sequences. Am J Neuroradiol 2006; 27: 1459–62.

Krasnianski A, Kallenberg K, Collie DA, Meissner B, Schulz-Schaeffer WJ, Heinemann U, et al. MRI in the classical MM1 and the atypical MV2 subtypes of sporadic CJD: an inter-observer agreement study. Eur J Neurol 2008; 15: 762–71.

Krasnianski A, Meissner B, Schulz-Schaeffer W, Kallenberg K, Bartl M, Heinemann U, et al. Clinical features and diagnosis of the MM2 cortical subtype of sporadic Creutzfeldt-Jakob disease. Arch Neurol 2006a; 63: 876–80.

Krasnianski A, Schulz-Schaeffer WJ, Kallenberg K, Meissner B, Collie DA, Roeber S, et al. Clinical findings and diagnostic tests in the MV-2 subtype of sporadic CJD. Brain 2006b; 129: 2288–96.

Masters CL, Harris JO, Gajdusek DC, Gibbs CJJ, Bernoulli C, Asher DM. Creutzfeldt-Jakob disease: patterns of worldwide occurrence and the significance of familial and sporadic clustering. Ann Neurol 1979; 5: 177–88.

Meissner B, Kallenberg K, Sanchez-Juan P, Collie DA, Summers DM, Almonti S, et al. MRI lesion profiles in sporadic Creutzfeldt-Jakob disease. Neurology 2009; 72: 1994–2001.

Meissner B, Kallenberg K, Sanchez-Juan P, Krasnianski A, Heinemann U, Varges D, et al. Isolated cortical signal increase on MR imaging as a frequent lesion pattern in sporadic Creutzfeldt-Jakob disease. Am J Neuroradiol 2008; 29: 1519–24.

Meissner B, Westner I, Kallenberg K, Krasnianski A, Bartl M, Varges D, et al. Sporadic Creutzfeldt-Jakob disease: clinical and diagnostic characteristics of the rare VV1 type. Neurology 2005; 65: 1544–50.

Parchi P, Castellani R, Capellari S, Ghetti B, Young K, Chen SG, et al. Molecular basis of phenotypic variability in sporadic Creutzfeldt-Jakob disease. Ann Neurol 1996; 39: 767–78.

Parchi P, Giese A, Capellari S, Brown P, Schulz-Schaeffer W, Windl O, et al. Classification of sporadic Creutzfeldt-Jakob disease based on molecular and phenotypic analysis of 300 subjects. Ann Neurol 1999; 46: 224–33.

Poser S, Mollenhauer B, Krauss A, Zerr I, Steinhoff BJ, Schröter A, et al. How to improve the clinical diagnosis of Creutzfeldt-Jakob disease. Brain 1999; 122: 2345–51.

Sanchez-Juan P, Green A, Ladogana A, Cuadrado-Corrales N, Sanchez-Valle R, Mitrova E, et al. CSF tests in the differential diagnosis of Creutzfeldt-Jakob disease. Neurology 2006; 67: 637–43.

Sanchez-Juan P, Sanchez-Valle R, Green A, Ladogana A, Cuadrado-Corrales N, Mitrova E, et al. Influence of timing on CSF tests value for Creutzfeldt-Jakob disease diagnosis. J Neurol 2007; 254: 901–6.

Satoh K, Shirabe S, Tsujino A, Eguchi H, Motomura M, Honda H, et al. Total tau protein in cerebrospinal fluid and diffusion-weighted MRI as an early diagnostic marker for Creutzfeldt-Jakob disease. Dement Geriatr Cogn Disord 2007; 24: 207–12.

Seipelt M, Zerr I, Nau R, Mollenhauer B, Kropp S, Steinhoff BJ, et al. Hashimoto encephalitis as a differential diagnosis of Creutzfeldt-Jakob disease. J Neurol Neurosurg Psychiatry 1999; 66: 172–6.

Tschampa HJ, Kallenberg K, Meissner B, Kretzschmar HA, Knauth M, Urbach H, et al. Pattern of cortical changes in sporadic Creutzfeldt-Jakob disease. Am J Neurorad 2007; 28: 1114–8.

Tschampa HJ, Kallenberg K, Urbach H, Meissner BC. N, Kretzschmar HA, *et al*. MRI in the diagnosis of sporadic Creutzfeldt-Jakob disease: a study on inter-observer agreement. Brain 2005; 128: 2026–33.

Tschampa HJ, Neumann M, Zerr I, Henkel K, Schröter A, Schulz-Schaeffer WJ, et al. Patients with Alzheimer's disease and dementia with Lewy bodies mistaken for Creutzfeldt-Jakob disease. J Neurol Neurosurg Psychiatry 2001; 71: 33–9.

Vernino S, Geschwind MD, Boeve B. Autoimmune encephalopathies. Neurologist 2007; 13: 140–7.

Young GS, Geschwind MD, Fischbein NJ, Martindale JL, Henry RG, Liu S, et al. Diffusion-weighted and fluid-attenuated inversion recovery imaging in Creutzfeldt-Jakob disease: high sensitivity and specificity for diagnosis. Am J Neuroradiol 2005; 26: 1551–62.

Zerr I, Pocchiari M, Collins S, Brandel JP, de Pedro Cuesta J, Knight RSG, et al. Analysis of EEG and CSF 14-3-3 proteins as aids to the diagnosis of Creutzfeldt-Jakob disease. Neurology 2000a; 55: 811–5.

Zerr I, Schulz-Schaeffer WJ, Giese A, Bodemer M, Schröter A, Henkel K, et al. Current clinical diagnosis in CJD: identification of uncommon variants. Ann Neurol 2000b; 48: 323–9.

14-3-3 protein detection and sporadic CJD: the status quo serves well while awaiting progress

Steven J Collins,[1,2] Amelia McGlade,[1,2] Alison Boyd,[1,2] C L Masters,[1,2] Genevieve M J A Klug[1,2]

Of the neurodegenerative disorders, prion diseases pose some unique challenges. The phenotypic spectrum is sufficiently diverse that this diagnosis will not infrequently intrude as a consideration, with the attendant risk of inadvertent disease transmission during healthcare provision adding concerns not extant in relation to most neurological diseases, especially disorders such as Alzheimer's disease. Prompt, accurate diagnosis can assist in pre-empting and thereby minimising transmission risk, while serving to avoid unhelpful investigations and treatments, and facilitate more informed prognostication. Notwithstanding the acknowledged need to continue searching for improvements in our diagnostic capacity, there has fortunately been major progress over the last 10–15 years in relation to the premortem diagnosis of sporadic Creutzfeldt–Jakob disease (sCJD), the most common form of human prion disease. In addition to the more recent contribution of brain MRI,[1] the recognition that 14-3-3 protein detection in the cerebrospinal fluid (CSF) constituted a robust surrogate biomarker of sCJD was a major advance in our clinical diagnostic armamentarium, far superior to that offered by EEG.[2] Although sometimes vitiated because of lower sensitivities and specificities described in smaller studies, the large, long-term study of 579 unselected patients reported by Chohan *et al* (***see page 1243***)[3] reconfirms the genuine utility of detection of CSF surrogate biomarkers, especially 14-3-3 proteins, for supporting a diagnosis of sCJD.

In their study, based at the UK national CJD surveillance centre, Chohan *et al* evaluated the sensitivity, specificity, positive and negative predictive values, and efficiency of detecting 14-3-3 proteins, τ and S100b in the CSF, either alone or in various combinations, for supporting a premortem diagnosis of sCJD. As a single biomarker, 14-3-3 protein detection was observed to have the highest overall sensitivity at 86%, remarkably similar to the findings of two previous large, collaborative studies in which 85% of 1531 (probable and definite)[4] and 88% of 1521 (definite)[5] sCJD patients returned positive results. Further, a positive 14-3-3 result was the most sensitive indicator in less typical cases, such as those less than 50 years at disease onset or those with an illness duration over 12 months, albeit with reduced sensitivities of 71% and 56%, respectively. The main limitation of 14-3-3 protein detection used in isolation was the relatively low specificity of 74%, particularly in comparison with τ (84%) and S100b (90%). Using combinations of 14-3-3 protein detection with either S100b or τ, or both, improved specificities and positive predictive values to 88–96% and 91–95%, respectively, but at the cost of diminishing sensitivities to 57–75%. Despite this reduction in sensitivity, the authors suggest that the best combination for sCJD is the use of primary 14-3-3 protein detection, followed by the S100b marker. There was no apparent demographic profile evincing a greater likelihood of a positive result with 14-3-3 protein detection in comparison with τ, thereby limiting attempts to maximise complementarity by performing both simultaneously, and as a corollary both 14-3-3 and τ displayed compromised specificity across the same range of non-CJD illnesses. Finally, and of considerable practical importance, in the absence of an autopsy the use of CSF 14-3-3 protein detection allowed at least 100 persons to be classified as sCJD over the 10-year study period, an outcome that would not have been otherwise possible given the absence of an EEG or a non-diagnostic recording in these persons.

As noted already, an unfortunate limitation of current CSF biochemical assays evaluating suspected sCJD is the non-specificity of the biomarkers, particularly in relation to the disease-associated conformations of the prion protein (PrP^{Sc}) directly linked with pathogenesis. It is anticipated that evolving diagnostic assays interrogating CSF components through methods based on the protein misfolding cyclic amplification assay[6] will have the capacity to directly detect minuscule amounts of PrP^{Sc} even when applied within a routine clinical context. Hopefully, such techniques will prove practicable as stand-alone methods while delivering optimal sensitivity and specificity but, if not, could perhaps function as reliable second-line arbiters to resolve equivocal, or suspected false-positive, 14-3-3 results.

[1]Australian National Creutzfeldt–Jakob Disease Registry, Department of Pathology, The University of Melbourne, Parkville 3010, Australia; [2]Mental Health Research Institute of Victoria, The University of Melbourne, Parkville 3010, Australia

Correspondence to Professor Steven J Collins, University of Melbourne, Australian CJD Registry, Level 3, Alan Gilbert Building, 161 Barry Street, Carlton 3053, Australia; stevenjc@unimelb.edu.au

Funding The Australian National Creutzfeldt–Jakob Disease Registry is funded by the Commonwealth Department of Health and Ageing.

Competing interests None.

Patient consent Obtained.

Provenance and peer review Commissioned; externally peer reviewed.

Received 30 July 2010
Revised 16 August 2010
Accepted 17 August 2010

J Neurol Neurosurg Psychiatry 2010;**81**:1181.
doi:10.1136/jnnp.2010.219691

REFERENCES

1. **Zerr I,** Kallenberg K, Summers DM, *et al*. Updated clinical diagnostic criteria for sporadic Creutzfeldt–Jakob disease. *Brain* 2009;**132**:2659–68.
2. **Hsich G,** Kinney K, Gibbs CJ, *et al*. The 14-3-3 brain protein in cerebrospinal fluid as a marker for transmissible spongiform encephalopathies. *N Engl J Med* 1996;**335**:924–30.
3. **Chohan G,** Pennington C, Mackenzie JM. The role of cerebrospinal fluid 14-3-3 and other proteins in the diagnosis of sporadic Creutzfeldt–Jakob disease in the United Kingdom: a 10 year review. *J Neurol Neurosurg Psychiatry* 2010;**81**:1243–8.
4. **Sanchez-Juan P,** Green A, Ladogana A, *et al*. Csf tests in the differential diagnosis of Creutzfeldt–Jakob disease. *Neurology* 2006;**67**:637–43.
5. **Collins SJ,** Sanchez-Juan P, Masters CL, *et al*. Determinants of diagnostic investigation sensitivities across the clinical spectrum of sporadic Creutzfeldt–Jakob disease. *Brain* 2006;**129**:2278–87.
6. **Atarashi R,** Wilham JM, Christensen L, *et al*. Simplified ultrasensitive prion detection by recombinant PrP conversion with shaking. *Nat Methods* 2008;**5**:211–12.

nature medicine

Ultrasensitive human prion detection in cerebrospinal fluid by real-time quaking-induced conversion

Ryuichiro Atarashi[1,2], Katsuya Satoh[1], Kazunori Sano[1,3], Takayuki Fuse[1], Naohiro Yamaguchi[1], Daisuke Ishibashi[1], Takehiro Matsubara[1], Takehiro Nakagaki[1], Hitoki Yamanaka[4], Susumu Shirabe[5], Masahito Yamada[6], Hidehiro Mizusawa[7], Tetsuyuki Kitamoto[8], Genevieve Klug[9], Amelia McGlade[9], Steven J Collins[9] & Noriyuki Nishida[1,3]

The development of technologies for the *in vitro* amplification of abnormal conformations of prion protein (PrP^{Sc}) has generated the potential for sensitive detection of prions. Here we developed a new PrP^{Sc} amplification assay, called real-time quaking-induced conversion (RT-QUIC), which allows the detection of ≥1 fg of PrPSc in diluted Creutzfeldt-Jakob disease (CJD) brain homogenate. Moreover, we assessed the technique first in a series of Japanese subjects and then in a blind study of 30 cerebrospinal fluid specimens from Australia, which achieved greater than 80% sensitivity and 100% specificity. These findings indicate the promising enhanced diagnostic capacity of RT-QUIC in the antemortem evaluation of suspected CJD.

Transmissible spongiform encephalopathies, or prion diseases, are characteristically associated with the accumulation of PrP^{Sc} in the central nervous system through autocatalytic conversion of normal cellular PrP (PrP^{c}) into replicate misfolded isomers[1,2]. Despite a few other reported markers[3,4], PrP^{Sc} remains the best characterized and most reliable marker of prion disease.

Definitive antemortem confirmation of CJD requires the detection of PrP^{Sc} in biopsy specimens, the practice of which is discouraged because it is invasive and poses risks to health care personnel. Recently, however, *in vitro* PrP^{Sc} amplification techniques, including protein misfolding cyclic amplification[5–7], the amyloid seeding assay[8] and QUIC, have been reported to enable the direct and highly sensitive detection of PrP^{Sc} in various tissues, including cerebrospinal fluid (CSF). QUIC assays involve the use of soluble recombinant PrP (rPrP-sen) as a substrate, which is seeded with PrP^{Sc} and then subjected to intermittent automated shaking. This technique can be performed more easily than the protein misfolding cyclic amplification, which requires repeated sonication. Previous studies have shown that QUIC assays correctly discriminate between normal and scrapie-infected CSF samples in both hamster and sheep prion disease models[9,10]. However, ultrasensitive PrP^{Sc} detection in CSF from subjects with CJD has not yet been accomplished. Accordingly, we further refined the QUIC assay to improve its sensitivity and practicability and then applied the technique in a blind pilot study to detect PrP^{Sc} in CJD CSF specimens.

Given that a correlation between protease-resistant rPrP aggregate (rPrP-res) abundance and thioflavin T (ThT) fluorescence had been shown previously[7], we sought to determine the relative kinetics of rPrP-res formation by monitoring levels of ThT fluorescence in the QUIC assay. This was intended to minimize the time needed to detect rPrP-res. We first tested whether PrP^{Sc}-dependent rPrP-res ($rPrP\text{-}res^{Sc}$) formation could be induced in a microplate reader with intermittent shaking. We used human rPrP-sen (rHuPrP-sen) and a 10^{-7} dilution of CJD (molecular subtype MM1) brain homogenate as the substrate and seed, respectively. We conducted QUIC reactions at various concentrations (0, 0.25, 0.5 and 1.0 M) of guanidine-HCl (GdnHCl), because it has been shown that GdnHCl greatly enhances conversion of PrP-sen to PrP-res in cell-free conversion reactions[11]. Unexpectedly, we observed positive PrP^{Sc}-dependent ThT fluorescence within 24 h, both in the presence and in the absence of GdnHCl (**Fig. 1a**). In contrast, the negative control reactions without seed and in the absence of GdnHCl resulted in no increase in ThT fluorescence over 24 h; however, *de novo* formation of rPrP-res ($rPrP\text{-}res^{spon}$) was rapidly induced in the presence of GdnHCl when shaking was added (**Fig. 1a**,**b**). These results indicate that shaking accelerates PrP^{Sc}-dependent $rPrP\text{-}res^{Sc}$ formation even without GdnHCl (**Supplementary Fig. 1**), albeit with a lower peak of fluorescence.

Shaking is thought to cause partial unfolding of a portion of rPrP-sen by increasing the air-water interface[12]. Moreover, shaking enhances the interaction between rPrP-sen and PrP^{Sc} and promotes the fragmentation of rPrP-res polymers[13]. It is generally accepted that the energetic barrier of seed-dependent fibril formation and elongation is lower than that of spontaneous fibril formation, which first requires nucleation as the rate-limiting step[14]. The partial unfolding of rPrP-sen by shaking seems to be more heterogeneous than that facilitated by a denaturant such as GdnHCl, perhaps because the air-water interfaces created by shaking are unequally distributed

[1]Department of Molecular Microbiology and Immunology, Nagasaki University Graduate School of Biomedical Sciences, Nagasaki, Japan. [2]Nagasaki University Research Centre for Genomic Instability and Carcinogenesis, Nagasaki, Japan. [3]Global Centers of Excellence Program, Nagasaki University, Nagasaki, Japan. [4]Division of Comparative Medicine, Center for Frontier Life Sciences, Nagasaki University, Nagasaki, Japan. [5]Organization of Rural Medicine and Residency Education, Nagasaki University Hospital, Nagasaki, Japan. [6]Department of Neurology and Neurobiology of Aging, Kanazawa University Graduate School of Medical Science, Kanazawa, Japan. [7]Department of Neurology and Neurological Science, Graduate School, Tokyo Medical and Dental University, Tokyo, Japan. [8]Division of Creutzfeldt-Jakob Disease Science and Technology, Department of Prion Research, Tohoku University Graduate School of Medicine, Sendai, Japan. [9]Department of Pathology, Australian National Creutzfeldt-Jakob Disease Registry, University of Melbourne, Melbourne, Australia. Correspondence should be addressed to R.A. (atarashi@nagasaki-u.ac.jp).

Received 2 July 2010; accepted 16 December 2010; published online 30 January 2011; doi:10.1038/nm.2294

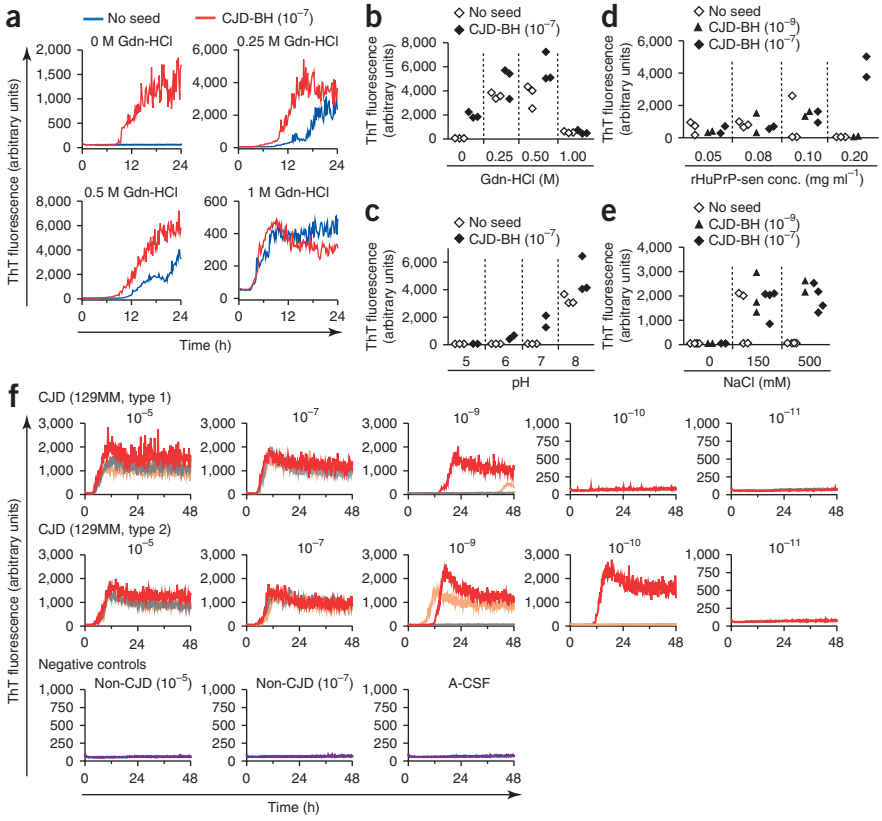

Figure 1 QUIC reactions induce PrP^{Sc}-dependent rHuPrP-res formation under GdnHCl-free conditions. (**a**,**b**) The effect of the indicated concentration of Gdn-HCl on the kinetics of rHuPrP fibril formation with or without 10^{-7} dilution of CJD brain homogenate (CJD-BH) (type 1, 129MM). The reaction buffer contained 150 mM NaCl, 50 mM PIPES, pH 7.0, 1 mM EDTA and 10 μM ThT. The concentration of rHuPrP-sen was 0.1 mg ml^{-1}. The graphs in **a** depict one representative of triplicates. The maximal fluorescence intensity of each single reaction for 24 h is plotted in **b**. (**c**–**e**) The effect of pH (**c**), the concentration of rHuPrP-sen (**d**) and the concentration of NaCl (**e**) were tested with the indicated dilutions of CJD-BH (type 1, 129MM) as seeds. Buffers used in **c** were pH 5 50 mM sodium acetate buffer, pH 6 50 mM MES, pH 7 50 mM PIPES and pH 8 50 mM HEPES. The concentration of NaCl in **c** and **d** was 150 mM, the pH of the buffer in **d** and **e** was 7.0 (50 mM PIPES) and the rHuPrP-sen concentration in **c** and **e** was 0.1 mg ml^{-1}. Each symbol represents the maximal fluorescence intensity from an individual reaction for 48 h. (**f**) Detection limit of RT-QUIC with the indicated dilutions of CJD-BH (129MM, type 1) and CJD-BH (129MM, type 2) as seeds. We used the indicated dilutions of non–CJD-BH (dissecting aneurysm) or artificial CSF (A-CSF) as negative controls. We performed the RT-QUIC reactions as described in the **Supplementary Methods**. The colored curves represent the kinetics of ThT fluorescence from an individual reaction seeded with the same dilution of BH. The graphs are representative of two independent experiments, each performed in triplicate.

in solution. We found that the addition of GdnHCl to QUIC reactions leads to an increase in the nucleation rate, and increased spontaneous fibril formation. The early appearance of rPrP-res^{spon} decreases the specificity of QUIC, because ThT fluorescence cannot distinguish between rPrP-res^{Sc} and rPrP-res^{spon}. Therefore, we chose not to use GdnHCl in subsequent analyses.

To further optimize the conditions, we examined the effects of pH, as well as of the concentrations of rHuPrP-sen and salt on QUIC reactions in GdnHCl-free conditions with shaking (**Fig. 1c–e** and **Supplementary Fig. 2**). After assessment, we successfully established a method for the real-time monitoring of the kinetics of rPrP fibril formation seeded with CJD brain homogenate (see **Supplementary Methods**), without the generation of rPrP-res^{spon} and designated the assay RT-QUIC.

To determine the minimum amount of PrP^{Sc} detectable by RT-QUIC, we diluted CJD brain homogenate (MM1 and MM2) serially with artificial CSF (A-CSF) and used these dilutions to seed the reactions. We observed increased PrP^{Sc}-dependent ThT fluorescence within 48 h in more than half the replicates of CJD brain homogenate, with dilutions ranging from 10^{-5} to 10^{-9} (**Fig. 1f** and **Supplementary Table 1**). With 10^{-10} brain homogenate dilutions, we observed a marginally lower rate of positive reactions, and 10^{-11} dilutions of the CJD-brain homogenates produced no ThT fluorescence response (**Fig. 1f** and **Supplementary Table 1**). The negative controls seeded with 10^{-5} and 10^{-7} dilutions of non-CJD brain homogenate or A-CSF alone (no seed) did not produce an increase in the fluorescence (**Fig. 1f** and **Supplementary Table 1**). The 10^{-9} dilutions of MM1 and MM2 CJD brain homogenate contained approximately 0.8 and 1.9 fg of PrP^{Sc}, respectively, according to our estimation (data not shown). Consequently, the results indicate that this assay consistently enables us to detect more than or equal to about 1 fg of PrP^{Sc} in the diluted CJD brain homogenates within 48 h. Moreover, the fact that there was no rPrP-res^{spon} formation under the conditions used implies a lower and acceptable risk of false-positive reactions. Whether the RT-QUIC has the same sensitivity to CJD brain homogenate with 129MV or 129VV as 129MM remains to be determined.

CSF is routinely used in the evaluation of central nervous system disorders and presumably contains more PrP^{Sc} and fewer impurities than blood. This prompted us to compare the RT-QUIC seeding activity in CSF samples from subjects with CJD and subjects without CJD but with other neurodegenerative diseases. For the pilot study, we initially tested CJD CSF samples from 18 definite cases of CJD in Japan (**Table 1**) and 35 non-CJD controls from subjects with other neurodegenerative diseases (**Supplementary Table 2**). We saw a minimal ThT fluorescence increase in the controls, with no false positives in the assay. In contrast, increased PrP^{Sc}-dependent fluorescence was seen in at least one of four replicates in 15/18 (83.3%) of the CJD CSF samples (**Table 1** and **Supplementary Table 3**).

To further confirm the reliability of RT-QUIC, we conducted a blind trial using 30 CSF samples from the Australian National CJD Registry and 155 CSF samples containing 25 probable cases of CJD and 130 cases of other neurological diseases obtained in Japan. In the Australian samples, we were able to detect PrP^{Sc} in 14/16 (87.5%) definite CJD CSF samples, as opposed to 0/14 of the non-CJD controls (**Table 1**, **Supplementary Fig. 3** and **Supplementary Table 3**). It should be noted that 3/4 129VV and 2/2 129MV cases were positive by RT-QUIC.

Table 1 Clinical data and RT-QUIC reactions seeded with CSF samples

CSF from 18 definite CJD samples in Japan					
Sample	Age (years)/sex	CJD type	Molecular subtype[a]	14-3-3 (γ-isoform)[b]	RT- QUIC[c]
C1	68/M	sCJD	MM 1	+	+ (3/4)
C2	66/F	sCJD	MM 1	+	+ (2/4)
C3	71/F	sCJD	MM 1	+	+ (1/4)
C4	57/F	sCJD	MM 2	+	+ (2/4)
C5	70/M	sCJD	MM 2	+	+ (2/4)
C6	66/M	sCJD	MM 2	+	+ (2/4)
C7	60/F	sCJD	MM 2	–	– (0/4)
C8	73/F	sCJD	MM 2	+	+ (4/4)
C9	74/M	sCJD	MM 2	+	– (0/4)
C10	79/F	sCJD	MM 2	–	+ (3/4)
C11	65/F	sCJD	MM 2	+	+ (4/4)
C12	69/M	sCJD	MM 2	+	– (0/4)
C13	69/F	sCJD	MM 2	+	+ (3/4)
C14	54/F	sCJD	MM 2	+	+ (3/4)
C15	76/F	sCJD	MM 2	–	+ (2/4)
C16	68/M	sCJD	MM 2	–	+ (4/4)
C17	58/F	iCJD	MM 1	+	+ (3/4)
C18	79/F	iCJD	MM 1	–	+ (3/4)

Blind trial of 30 CSF samples in Australia						
Sample	Age (years)/sex	Diagnosis[d]	Codon 129	Profile of PrP^{Sc}	14-3-3 (all isoforms)[e]	RT-QUIC[g]
A1	53/F	PN/MC			–	– (0/4)
A2	59/F	PN/ MC			–	– (0/4)
A3	85/M	AD			–	– (0/4)
A4	60/F	ICD			+	– (0/4)
A5	83/M	AD			+	– (0/4)
A6	73/M	sCJD	VV	2	+	+ (2/4)
A7	67/F	sCJD	MM	1	+	+ (4/4)
A8	82/F	sCJD	MM	1	+	+ (2/4)
A9	67/M	sCJD	MV	1	–	+ (2/4)
A10	50/M	sCJD	MM	1	+	+ (3/4)
A11	66/M	PN/MC			–	– (0/4)
A12	61/M	PN/MC			–	– (0/4)
A13	84/F	sCJD	MM	1	+	+ (3/4)
A14	76/M	sCJD	MM	1	+	+ (2/4)
A15	69/M	sCJD	MV	1	+	+ (4/4)
A16	67/M	AD			–	– (0/4)
A17	75/F	PN/MC			+	– (0/4)
A18	93/M	DLB/PD			–	– (0/4)
A19	67/F	sCJD	ND	2	+	+ (2/4)
A20	53/M	DLB/PD			–	– (0/4)
A21	71/F	sCJD	VV	2	+	– (0/4)
A22	62/F	sCJD	MM	2	–	– (0/4)
A23	90/M	sCJD	VV	ND	+	+ (1/4)
A24	61/F	DLB/PD			–	– (0/4)
A25	74/M	sCJD	MM	ND	±[f]	+ (2/4)
A26	74/F	AD			–	– (0/4)
A27	68/F	sCJD	ND	ND	+	+ (2/4)
A28	69/F	sCJD	VV	2	+	+ (1/4)
A29	82/M	DLB/PD			+	– (0/4)
A30	70/F	sCJD	ND	2	+	+ (4/4)

[a]CJD can be divided into six molecular subtypes on the basis of whether methionine (M) or valine (V) is present at codon 129 of the gene encoding prion protein combined with the profile of PrP^{Sc} (type 1 or type 2) as determined by western blotting[17]. [b]Amounts of the γ-isoform of 14-3-3 protein in CSF were determined by western blotting with a polyclonal antibody specific for the γ-isoform of the 14-3-3 protein[18] (+, positive reaction; –, negative reaction). [c]RT-QUIC was performed as described in the **Supplementary Methods**. The number of positive reactions over the number of replicates is shown in parentheses. Samples with at least one positive reaction were defined as +, representing a positive result in the RT-QUIC. [d]The final diagnosis was made by the Australian National CJD Registry. [e]Amounts of 14-3-3 protein (all isoforms) in CSF were determined by western blotting. [f]Additional atypical bands were observed. [g]Kinetics graphs are provided in **Supplementary Figure 3**. Subjects or their families agreed with the aims and role of our research and gave appropriate informed consent. The investigation protocol was approved by the Ethics Committee of Nagasaki University Hospital (ID: 10042823), and the study was registered with the University Hospital Medical Information Network (ID: UMIN000003301). sCJD, sporadic Creutzfeldt-Jakob disease; iCJD, iatrogenic Creutzfeldt-Jakob disease; PN/MC, paraneoplastic/metastatic cancer; ICD, inflammatory central nervous system disorder; DLB/PD, dementia with Lewy bodies/Parkinson's disease; AD, Alzheimer's disease; ND, not determined.

These results indicate that RT-QUIC has the ability to discriminate CJD CSF samples that include 129MM, 129MV and 129VV cases from non-CJD CSF samples. In addition, none of the 130 Japanese cases of other neurological diseases were positive, further confirming the reliability of this assay (**Supplementary Table 4**). Collectively, the RT-QUIC assays showed more than 80% sensitivity and 100% specificity. The sensitivity was equivalent to and the specificity was much higher than that achieved by 14-3-3 (refs. 14,15), a nonspecific marker of rapid neuronal damage (**Supplementary Table 3**).

Although we have never experienced a false-positive reaction among the hundreds of non-CJD neurodegenerative disease samples we have so far tested, it remains possible that certain conditions may evoke a positive reaction, and further studies will be required to eliminate this possibility. Furthermore, scrupulous attention to the conditions of the assay is essential to avoid false positives in the clinical setting. Nevertheless, we believe that the ultrasensitive detection of PrP^{Sc} in CSF by RT-QUIC represents a valuable new means for the early, rapid and specific diagnosis of CJD.

Note: Supplementary information is available on the Nature Medicine website.

ACKNOWLEDGMENTS

We thank the members of the CJD Surveillance Committee in Japan for their support of this work, K. Yamaguchi and K. Kuwata for helping with the circular dichroism analysis of rPrP-sen, M. Tsujihata (Nagasaki Kita Hospital) for providing CSF samples and information about subjects and A. Yamakawa and A. Matsuo for technical assistance. The work was supported by the Global Centers of Excellence Program (F12); a grant-in-aid for science research (B; grant no. 20390287) from the Ministry of Education, Culture, Sports, Science and Technology of Japan; a grant for bovine spongiform encephalopathy research and a grant-in-aid of the Research Committee of Prion disease and Slow Virus Infection, from the Ministry of Health, Labor and Welfare of Japan.

AUTHOR CONTRIBUTIONS

R.A. designed the project, performed experiments and wrote the manuscript. K. Satoh, K. Sano, T.F., N.Y., D.I., T.M., T.N. and H.Y. performed experiments. K. Satoh, S.S., M.Y., H.M., T.K., G.K., A.M. and S.J.C. contributed to the collection of human specimens and provided information about subjects. N.N. supervised the project. K. Satoh, K. Sano, A.M., S.J.C. and N.N. helped with the editing of the manuscript.

COMPETING FINANCIAL INTERESTS

The authors declare no competing financial interests.

Published online at http://www.nature.com/naturemedicine/.
Reprints and permissions information is available online at http://npg.nature.com/reprintsandpermissions/.

1. Prusiner, S.B. *Proc. Natl. Acad. Sci. USA* **95**, 13363–13383 (1998).
2. Aguzzi, A. & Calella, A.M. *Physiol. Rev.* **89**, 1105–1152 (2009).
3. Lasmezas, C.I. *et al. Science* **275**, 402–405 (1997).
4. Gambetti, P. *et al. Ann. Neurol.* **63**, 697–708 (2008).
5. Saborio, G.P., Permanne, B. & Soto, C. *Nature* **411**, 810–813 (2001).
6. Castilla, J. *et al. Methods Enzymol.* **412**, 3–21 (2006).
7. Atarashi, R. *et al. Nat. Methods* **4**, 645–650 (2007).
8. Colby, D.W. *et al. Proc. Natl. Acad. Sci. USA* **104**, 20914–20919 (2007).
9. Atarashi, R. *et al. Nat. Methods* **5**, 211–212 (2008).
10. Orru, C.D. *et al. Protein Eng. Des. Sel.* **22**, 515–521 (2009).
11. Kocisko, D.A. *et al. Nature* **370**, 471–474 (1994).
12. Toth, S.I., Smith, L.A. & Ahmed, S.A. *J. Pharm. Sci.* **98**, 3302–3311 (2009).
13. Collins, S.R., Douglass, A., Vale, R.D. & Weissman, J.S. *PLoS Biol.* **2**, e321 (2004).
14. Lansbury, P.T. Jr. & Caughey, B. *Chem. Biol.* **2**, 1–5 (1995).
15. Hsich, G., Kenney, K., Gibbs, C.J., Lee, K.H. & Harrington, M.G. *N. Engl. J. Med.* **335**, 924–930 (1996).
16. Zerr, I. *et al. Ann. Neurol.* **43**, 32–40 (1998).
17. Parchi, P. *et al. Ann. Neurol.* **46**, 224–233 (1999).
18. Satoh, K. *et al. Lab. Invest.* **90**, 1637–1644 (2010).

Mol Neurobiol
DOI 10.1007/s12035-015-9167-5

Validation of 14-3-3 Protein as a Marker in Sporadic Creutzfeldt-Jakob Disease Diagnostic

Matthias Schmitz[1] · Elisabeth Ebert[1] · Katharina Stoeck[1] · André Karch[1] · Steven Collins[2] · Miguel Calero[3] · Theodor Sklaviadis[4] · Jean-Louis Laplanche[5] · Ewa Golanska[6] · Ines Baldeiras[7] · Katsuya Satoh[8] · Raquel Sanchez-Valle[9] · Anna Ladogana[10] · Anders Skinningsrud[11] · Anna-Lena Hammarin[12] · Eva Mitrova[13] · Franc Llorens[1] · Yong Sun Kim[14] · Alison Green[15] · Inga Zerr[1]

Received: 12 November 2014 / Accepted: 31 March 2015

Abstract At present, the testing of 14-3-3 protein in cerebrospinal fluid (CSF) is a standard biomarker test in suspected sporadic Creutzfeldt-Jakob disease (sCJD) diagnosis. Increasing 14-3-3 test referrals in CJD reference laboratories in the last years have led to an urgent need to improve established 14-3-3 test methods. The main result of our study was the validation of a commercially available 14-3-3 ELISA next to the commonly used Western blot method as a high-throughput screening test. Hereby, 14-3-3 protein expression was quantitatively analyzed in CSF of 231 sCJD and 2035 control patients. We obtained excellent sensitivity/specificity values of 88 and 96 % that are comparable to the established Western blot method. Since standard protocols and preanalytical sample handling have become more important in routine diagnostic, we investigated in a further step the reproducibility and stability of 14-3-3 as a biomarker for human prion diseases. Ring trial data from 2009 to 2013 revealed an increase of *Fleiss' kappa* from 0.51 to 0.68 indicating an improving reliability of 14-3-3 protein detection. The stability of 14-3-3 protein under short-term and long-term storage conditions at various temperatures and after repeated freezing/thawing cycles was confirmed. Contamination of CSF samples with

Electronic supplementary material The online version of this article (doi:10.1007/s12035-015-9167-5) contains supplementary material, which is available to authorized users.

✉ Matthias Schmitz
Matthias.Schmitz@med.uni-goettingen.de

[1] Department of Neurology, University Medical Center Göttingen and German Center for Neurodegenerative Diseases (DZNE)–site Göttingen, Robert-Koch Str. 40, 37075 Göttingen, Germany

[2] Department of Pathology, The University of Melbourne, Parkville 3010, Australia

[3] Chronic Disease Programme, CIBERNED, and CIEN Foundation-Queen Sofia Foundation, Instituto de Salud Carlos III, Madrid, Spain

[4] Pharmaceutical Sciences, Laboratory of Pharmacology, Aristotle University of Thessaloniki, Thessaloniki 54124, Greece

[5] Service de Biochimie et Biologie Moléculaire, Hôpital Lariboisière, Assistance Publique - Hôpitaux de Paris, 2, rue A Paré, 75475 Paris cedex 10, France

[6] Department of Molecular Pathology and Neuropathology, Medical University of Lodz, 8/10 Czechoslowacka Str., 92-216 Lodz, Poland

[7] Center for Neuroscience and Cell Biology, Faculty of Medicine, University of Coimbra, Coimbra, Portugal

[8] Department of Molecular Microbiology and Immunology, Nagasaki University Graduate School of Biomedical Sciences, Sakamoto 1-12-4, Nagasaki, Japan

[9] Neurology Department, Hospital Clinic, IDIBAPS, Barcelona, Spain

[10] Department of Cell Biology and Neurosciences, Istituto Superiore di Sanità, Rome, Italy

[11] Department of Multidisiplinary Laboratory Medicine and Medical Biochemistry Division of Diagnostics and Technology Akerhus University Hospital 1478 Lørenskog, 1478 Lørenskog, Norway

[12] The Public Health Agency of Sweden, Unit for highly pathogenic viruses, 171 82 Solna, Sweden

[13] Department of Prion Diseases, Slovak Medical University Bratislava, Limbová 14, 833-03 Bratislava, Slovakia

[14] Ilsong Institute of Life Science, College of Medicine, Hallym University, Anyang, Republic of Korea

[15] Western General Hospital, National Creutzfeldt-Jakob Disease Surveillance Unit, Crewe Road, Edinburgh EH4 2XU, UK

Published online: 07 May 2015

blood appears likely to be an important factor at a concentration of more than 2500 erythrocytes/μL. Hemolysis of erythrocytes with significant release of 14-3-3 protein started after 2 days at room temperature. We first define clear standards for the sample handling, short- and long-term storage of CSF samples as well as the handling of blood- contaminated samples which may result in artificially elevated CSF levels of 14-3-3.

Keywords Biomarker · Cerebrospinal fluid · Creutzfeldt-Jakob disease · Pre-mortem test · 14-3-3 protein · Standardization

Introduction

14-3-3 protein belongs to a family of proteins which are conserved in eukaryotic cells with highest expression in neuronal synapses. In humans, there are seven genes that encode eight distinct 14-3-3 isoforms, alpha (α), beta (β), gamma (γ), epsilon (ε), zeta (ζ), tau (t), sigma (s), and eta (h).

14-3-3 can bind to more than 200 proteins and plays a role in cell differentiation, signal transduction and neurotransmission [1, 2]. The 14-3-3 isoforms alpha/beta and gamma have been previously reported as specific neuronal biomarkers in cerebrospinal fluid for the pre-mortem diagnosis of human prion diseases, in particular sporadic Creutzfeldt-Jakob disease (sCJD) [3–5]. In most sCJD subtypes, the levels of these isoforms are elevated compared to patients without prion disease [5, 6]; however, 14-3-3 protein levels may vary across different sCJD subtypes [7].

Detection of 14-3-3 protein is usually performed by using a 14-3-3 Western blot, which is prone to methodological and inter-rater reliability problems. Therefore, the routine use of 14-3-3 protein detection in clinical practice requires standardization of the experimental test protocol, including confinements for the sample handling.

However, there are further factors, which may influence the concentration of 14-3-3 in CSF. One of these is the contamination of CSF with 14-3-3-containing blood cells, leading to an artificial increase of 14-3-3 in CSF and to false-positive results. Another important factor is the CSF pleocytosis due to an inflammatory process of the central nervous system.

To date, there is a scarcity of studies dealing with the standardization of 14-3-3 assays as well as a lack of publications investigating the short- or long-term stability of 14-3-3 protein in human CSF.

Due to an increase in 14-3-3 test referrals in CJD reference laboratories, we analyzed a commercial 14-3-3 gamma isoform ELISA as a novel test method in sCJD diagnosis and examined potential variations in comparison to the previously established immunoblot techniques.

Ring trials were performed to estimate the reproducibility of 14-3-3 protein in prion disease diagnostic. Finally, short- and long-term stability of 14-3-3 gamma, as well as the influence of blood contamination on the 14-3-3 gamma detection levels, was examined.

Methods

Patients

The present study includes 231 sCJD patients in Germany, collected between 2009 and 2014. Thirty cases were confirmed by neuropathological examination after autopsy; the others fulfilled the diagnosis of "probable CJD" according to the WHO diagnostic criteria [5, 6, 8]. Controls were composed of patients with neurodegenerative diseases (n=150): vascular dementia (n=40), Alzheimer's disease (n=30), Parkinson's disease (n=28), patients with neuroinflammatory diseases: multiple sclerosis/encephalitis (n=29), patients with other neurological diseases: epilepsy/tumor (n=11) as well as non-neurological conditions: depression (n=8) or psychiatric diseases (n=4). The other control cohort was composed of 1885 prospectively collected samples which were enrolled from the Neurochemistry Laboratory at the Department of Neurology in the framework of quality assurance showing no symptoms for a prion disease. Gender or age-dependent effects on 14-3-3 level were not observed.

Ethics

The present study was conducted according to the revised Declaration of Helsinki and Good Clinical Practice guidelines and has been approved by the local ethics committee in Göttingen (No. 11/93).

Study Design

1. To validate a commercial 14-3-3 gamma isoform ELISA, we assessed 231 sCJD patients as well as 2035 control patients without prion disease. We calculated a cutoff level and analyzed sensitivity, specificity, and predictive value levels accordingly.
2. To compare both 14-3-3 protein detection systems, CSF samples were analyzed in parallel by Western blot (14-3-3 isoform beta) and ELISA (14-3-3 isoform gamma). Samples classified according to their Western blot signals (14-3-3 negative, trace, weak, and positive) were analyzed by ELISA for the 14-3-3 protein concentration.
3. To analyze the general reliability of CSF 14-3-3 protein detection, we conducted three ring trials. All laboratories followed a standard Western blot protocol. Samples obtained from sCJD patients and non-prion disease controls,

including samples showing atypical Western blot profiles (additional bands), as well as blood contaminated samples were examined by different laboratories using the local protocol for analysis and sample treatment. In 2009, ten CSF samples derived from one 14-3-3 positive sCJD, three 14-3-3 negative controls, one atypical positive, three with a trace of 14-3-3 and two false-positive samples due to blood contamination were analyzed by nine different laboratories. In 2011, ten CSF samples encompassing two 14-3-3 positive sCJD, four negative controls, one atypical positive, and three false-positive samples (two blood contaminated and one due to brain trauma) were analyzed by nine different laboratories. In 2013, six CSF samples encompassing one positive sCJD and five control patients were analyzed by 13 different laboratories. The control panel consisted of two samples which were 14-3-3 negative, one false-positive due to CNS inflammation, and two false-positives due to blood-contaminated CSF.

4. To determine the stability of 14-3-3 gamma isoform in sCJD CSF samples, we investigated the effect of short- and long-term storage conditions at two different temperatures.
5. To assess the impact of blood contamination of CSF samples, CSF from non-prion control donors were spiked with blood cells and analyzed by 14-3-3 ELISA.

Determination of 14-3-3 Protein Gamma in CSF by ELISA

Levels of 14-3-3 gamma protein in CSF were determined by using the *CircuLex* 14-3-3 gamma ELISA Kit (BIOZOL Diagnostica Vertrieb GmbH, Eching, Germany). We followed the manufacturer's instructions. Briefly, CSF samples were applied in a dilution of 1:5 in dilution buffer. The level of 14-3-3 gamma were measured in arbitrary units (AU) per mL (1 AU is almost equal to 1 pg). Samples were incubated for 1 h at room temperature (25 °C) for capturing. After three washing steps, 14-3-3 gamma detection antibody and later horseradish peroxidise-conjugated anti-IgG were added and incubated for 1 h at room temperature each. We measured the colorimetric reaction at 450 nm using a 1420 Multilabel Counter Victor 2 Wallac (PerkinElmer, Massachusetts, USA).

SDS-PAGE and Immunoblotting

For Western blot analysis, we followed a protocol as described previously [9, 10]. A polyclonal 14-3-3 beta antibody, obtained from Abcam (Milton, GB) diluted 1:2000, was used as primary antibody. As a secondary antibody, we used a polyclonal horseradish peroxidase-conjugated antibody (Jackson Immuno Research, Leipzig, Saxony, Germany) (diluted 1:7500).

Before being heated for 2 min at 95 C, 10 μL sample loading buffer (BioRad, München, Bavaria, Germany) were added to CSF samples (30 μL). Subsequently, the samples were separated by sodium dodecyl sulfate-polyacrylamide gel electrophoresis (SDS-PAGE) (12 % *w*/*v* polyacrylamide) and transferred to polyvinylidene difluoride (PVDF) hydrobond-P membranes (Amersham, Freiburg, Baden Württemberg, Germany) using a semidry transblot cell for 70 min at 12 V; for labeling with antibodies, PVDF-membranes were blocked with 5 % dry milk in PBS and 0.1 % Tween-20 for 1 h at room temperature, and afterward incubated with the primary antibody overnight at 4 °C. Membranes were rinsed in PBS-Tween and incubated with the corresponding horseradish peroxidise-conjugated secondary antibody for 1 h. Protein bands were visualized after immersion of the membranes in enhanced chemiluminescence (ECL) detection system solution using Chemicon system (Bio-Rad).

Statistical Analysis

In the first part of this study, inter-rater reliability within ring trials was calculated using *Fleiss' kappa* for multiple readers. In the second part, the 14-3-3 gamma isoform ELISA was evaluated as a diagnostic test by using receiver-operating characteristic (ROC) curves. Sensitivity and specificity were calculated for all potential cutoff values in a training dataset (n=103 sCJD patients, n=188 control patients) to establish the best cutoff according to the *Youden* index. An external validation of the test was performed using this cutoff in a different data set including 231 sCJD patients and 2035 control patients without prion disease. Furthermore, the proposed cutoff was also validated to an extended spectrum of control patients (including CNS inflammatory diseases and blood-stained CSF samples). When comparing 14-3-3 ELISA results with those of Western blot analysis, we used the *ANOVA* test with corresponding *Tukey* post hoc tests. For analysis of 14-3-3 gamma isoform stability and blood contamination, *Wilcoxon* rank sum tests were applied.

Results

Establishment of 14-3-3 Gamma Isoform ELISA as a Diagnostic Test for sCJD

14-3-3 protein levels in human CSF samples were measured by using the *CircuLex* 14-3-3 gamma ELISA. We aimed to establish this ELISA as a diagnostic test for CJD diagnosis. Therefore, we analyzed the diagnostic validity of the 14-3-3 gamma ELISA according to the procedure described above. Within the training dataset, the 14-3-3 gamma ELISA showed very good accuracy (AUC=0.9676).

Using a cutoff of 20,000 AU/mL (the optimum level was identified by Youden index) (Fig. 1a), a sensitivity of 93 % and a specificity of 96 % could be shown. Within the validation dataset, we could confirm a high validity of the 14-3-3 gamma ELISA (sensitivity=88 %; specificity=96 %, Fig. 1b, c). The specificity of the test decreased slightly when patients with inflammatory or blood-stained CSF were included in the analysis (sensitivity=88 %; specificity=93 %) (Fig. 1c). Predictive values were not taken directly from the study population as these values would give biased estimates due to the planned oversampling of cases. Instead, they were calculated using the *Bayes* formula assuming prevalence realistic for the application setting of the test (1.8 % prevalence of CJD in CSF samples referred to the *German National Reference Center*). The control cohort was composed of patients with neurodegenerative diseases or patients with other neurological diseases as well as non-neurological conditions. When we compared the 14-3-3 level of neurodegenerative diseases and non-neurological disorders, we obtained no significant difference (Supplement Fig. 1).

Analysis of a Combinative Effect of 14-3-3 with Tau and S100B Protein

A potential combinative effect of different biomarker proteins was examined in a patient cohort of 231 sCJD cases and 66 control donors, consisting of 15 patients with PD, 14 with AD, 29 with a non-neurodegenerative disease, 4 with encephalitis, and 4 with a tumor disease. From these patients, amounts of 14-3-3 protein, tau, and S100B were determined. Interestingly, a combination of all three biomarkers resulted in the highest specificity of 100 % and sensitivity of 94.8 %. The combination of two biomarkers 14-3-3/tau, 14-3-3/S100B, and tau/S100B showed a lower sensitivity varying between 92.2 and 93.5 % (Supplement Fig. 2).

Comparison of Western Blot and ELISA Detection of 14-3-3 Protein

To compare two different detection systems for 14-3-3 protein, we analyzed the same CSF samples from sCJD patients and control donors (randomly selected) in parallel by Western

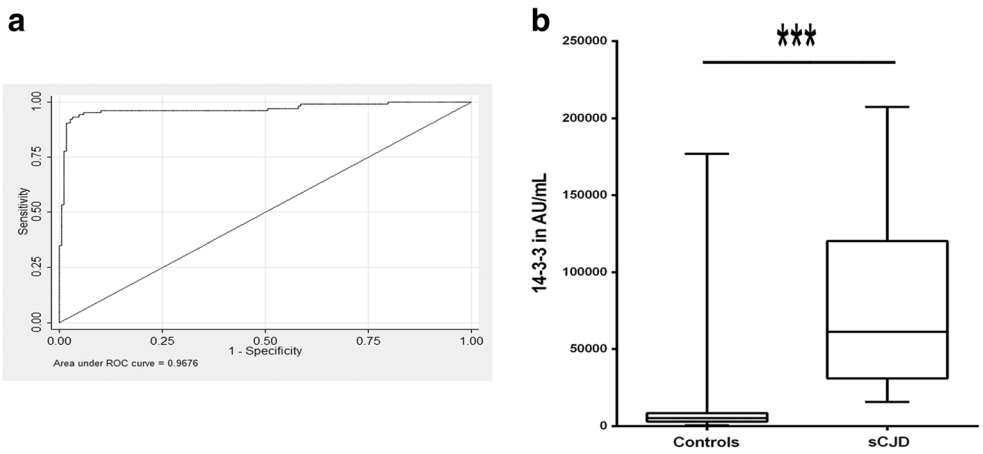

c

14-3-3 ELISA	sCJD (n=231)	Controls (n=1946)	Inflammatory or blood contaminated CSF (n=89)	Controls including inflammatory and blood contaminated CSF (n=2035)
>20,000 AU/mL	203 (87.9%) = sensitivity	71 (3.6%)	73 (82.0%)	144 (7.1%)
<20,000 AU/mL	28 (12.1%)	1875 (96.4%) = specificity 1	16 (18.0%) = specificity 2	1891 (92.9%) = specificity 3
PPV	0,34			
NPV		0,99		
Total	231 (100%)	1946 (100%)	89 (100%)	2035 (100%)

Fig. 1 Determination of sensitivity and specificity of 14-3-3 ELISA detection in CSF. A panel of CJD and non-prion control samples was analyzed for 14-3-3 gamma via ELISA. **a** ROC curve of the training dataset is shown and suggests a cutoff at 20,000 AU/mL. **b** CSF samples from sCJD contained a mean concentration of 14-3-3 of approximately 50,000 AU/mL. **c** 203 of 231 sCJD samples showed a 14-3-3 concentration higher than 20,000 AU/mL (~sensitivity of 87.9 %). From non-prion control samples, 1875 samples contained a 14-3-3 concentration lower than 20,000 AU/mL when inflammatory and blood-contaminated samples were excluded (specificity of 96.4 %). After inclusion of blood-contaminated and inflammatory samples, the specificity of the test decreases to 92.9 %. The *number of stars* indicates the significance level: *one star* (*) for $p<0.05$, *two* (**) for $p<0.01$ and *three* (***) for $p<0.001$

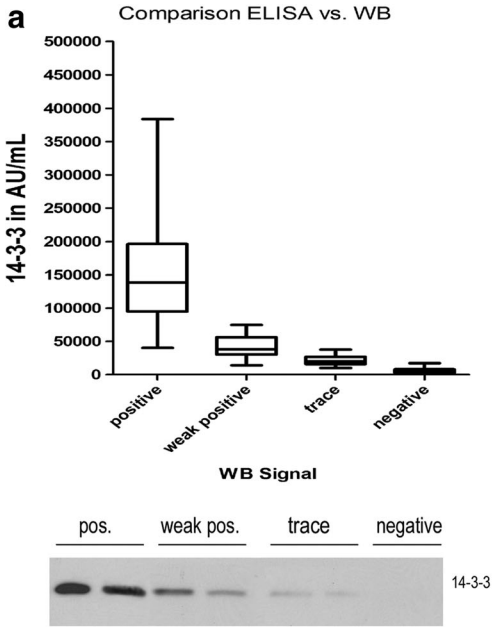

b

14-3-3 WB	14-3-3 ELISA (mean, 95% confidence interval)	P value*
negative	5773 (5268-6278) AU/mL	<0.001
trace	21322 (19015-23630) AU/mL	
weak positive	42655 (37188-48123) AU/mL	
positive	151701 (133695-169708) AU/mL	

*ANOVA with Tukey Post-hoc tests

Fig. 2 Comparison of two 14-3-3 detection systems ELISA and Western blot. CSF samples were analyzed both via Western blot for 14-3-3 beta and by 14-3-3 ELISA for 14-3-3 gamma. **a** Patients analyzed by Western blot were separated into four groups according the 14-3-3 level, which can be negative, trace positive, weak positive, and positive. The corresponding Western blot signal was shown below. **b** The average 14-3-3 concentration was calculated for each group. A strong association between 14-3-3 Western Blot results and 14-3-3 ELISA results could be confirmed when grouping Western Blot results in 4 categories (*ANOVA* with *Tukey* post hoc tests, $p<0.001$ for all pairwise comparisons)

blot and by ELISA. According to the subjectively determined signal intensities in Western blot, we divided the samples into four groups: (1) 14-3-3 negative, $n=200$; (2) 14-3-3 trace, $n=35$; (3) 14-3-3 weak positive ($n=35$); and (4) 14-3-3 positive, $n=61$ (Fig. 2a). Western blot analysis of CSF from sCJD patients usually showed either a positive or a weak positive 14-3-3 signal while controls remained negative. In trace positive classified samples, differentiation between sCJD and controls was not always possible.

Even though different 14-3-3 isoforms were detected by the Western blot and ELISA platforms, the relative amounts of 14-3-3 concurred (Fig. 2a). Samples classified by Western blot as 14-3-3 negative showed a mean level of 14-3-3 on ELISA of 5773 AU/mL; trace classified samples 21, 322 AU/mL; weak positive classified samples 42,655 AU/mL; and positive classified samples at >50,000 AU/mL ($p<0.001$, Fig. 2b). Our findings indicate that both methods deliver comparable results and are suitable for a reliable detection of 14-3-3 protein for sCJD diagnostic purposes.

Reproducibility of 14-3-3 Western Blot Analysis Across Different Laboratories

To investigate the interlaboratory reproducibility of CSF 14-3-3 protein detection, we performed three ring trials between 2009 and 2013.

The results of inter laboratory agreement were indicated by *Fleiss' kappa*, a statistical measure for assessing the reliability of agreement (Fig. 3a). Between 2009 and 2013, we observed an increase of *Fleiss' kappa* from 0.51 (indicating a moderate agreement) to 0.68, which indicates a rise in agreement in 14-3-3 protein detection from moderate to substantial (Fig. 3a, b).

In the earlier ring trials, disagreement was mainly observed in samples estimated as slightly positive (trace) or atypical profiles (multiple IgG bands, usually indicating CNS inflammation). In recent years, sample handling, terminology, and CSF testing protocols for prion diseases have become more standardized correlating with an increased reliability of 14-3-3 protein analysis.

Stability of the 14-3-3 Protein Concentration After Long- and Short-Term Storage Conditions

To evaluate the effects of storage conditions (temperature, duration of storage or freezing and thawing) on the concentration of 14-3-3 protein in CSF, we stored CSF samples from 10 sCJD patients in polypropylene tubes at room temperature and 4 °C for 8 days. In addition, CSF samples were either stored for 6 or 12 months at −80 °C or subjected to 10 repeated freezing and thawing cycles. Finally, we reanalyzed CSF samples originally classified as 14-3-3 positive and stored for 2–3, 5–6, and 8–9 years at −80 °C.

From each sample, we determined the 14-3-3 protein level via ELISA and calculated at each time point or cycle the 14-3-3 levels as percent of control (time point zero), which was defined as 100 %.

a Fleiss‘ kappa for ring trials of 14-3-3

Year (number of participants)	Fleiss' kappa (95% Confidence Interval)
2009 (n=9)	0.51 (0.41-0.61)
2011 (n=9)	0.53 (0.43-0.64)
2013 (n=13)	0.68 (0.59-0.77)

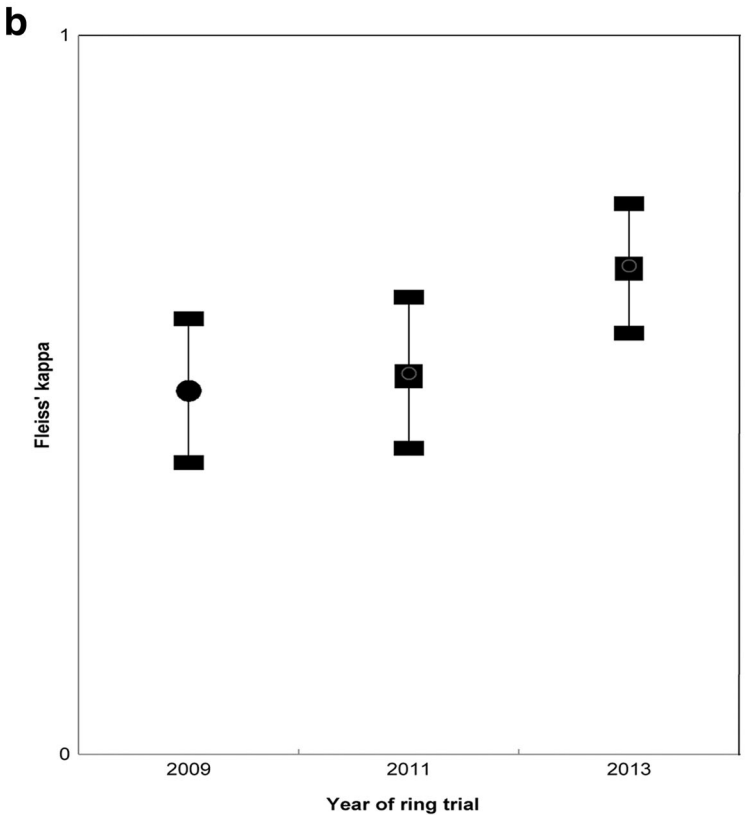

Fig. 3 Reproducibility of the 14-3-3 protein detection by Western blot. CSF from sCJD patients and control donors were analyzed by Western blotting in three different ring trials between 2009 and 2013. **a** Results of interlaboratory agreement were shown as *Fleiss' kappa*. **b** The increase of *Fleiss' kappa* from 0.51 to 0.68 in more recent years correlates with a more standardized preanalytical sample handling and testing protocols

Our obtained data indicated that the 14-3-3 proteins were less stable at higher temperatures. After short-term storage (8 days) at room temperature (~25 °C), we observed an average decrease of 14-3-3 levels (starting after 2 days) of approximately 20 % after 8 days. At lower temperatures (4 °C), the 14-3-3 concentration was more stable and remained unchanged for 2 days; afterward (starting from day 4 to day 8), we obtained a decrease between 10 and 15 % (Fig. 4a, b). Ten repeated freezing and thawing cycles did not result in a significant loss of 14-3-3 protein (Fig. 4c), while long-term storage at −80 °C reduced the level in average by 10–15 % after 6 months and by 15–20 % after 1 year (Fig. 4d). Approximately 80–85 % of the CSF samples showed elevated (>20,000 AU/mL) 14-3-3 level after 6-year storage at −80 °C. After 9 years, the number of 14-3-3 positive sCJD samples decreased to 70–75 % (Fig. 4e).

Influence of Blood Contamination on 14-3-3 Protein Levels in CSF

Since erythrocytes and platelets in human blood express 14-3-3, contamination of CSF with blood may result in false-positive 14-3-3 protein signals. To estimate the impact of blood contamination on 14-3-3 protein detection in CSF, we spiked CSF derived from a non-prion disease control exhibiting a 14-3-3 protein level below 20,000 AU/mL with blood. As controls, we used untreated and non-spiked CSF and defined the 14-3-3 protein level as 100 %. The 14-3-3 protein level of blood-spiked CSF was calculated for each sample as a percentage of control.

First, we examined whether 14-3-3 protein is measurable when erythrocytes remained intact. CSF, spiked with 50,000 erythrocytes per μL, was analyzed before and after sonication

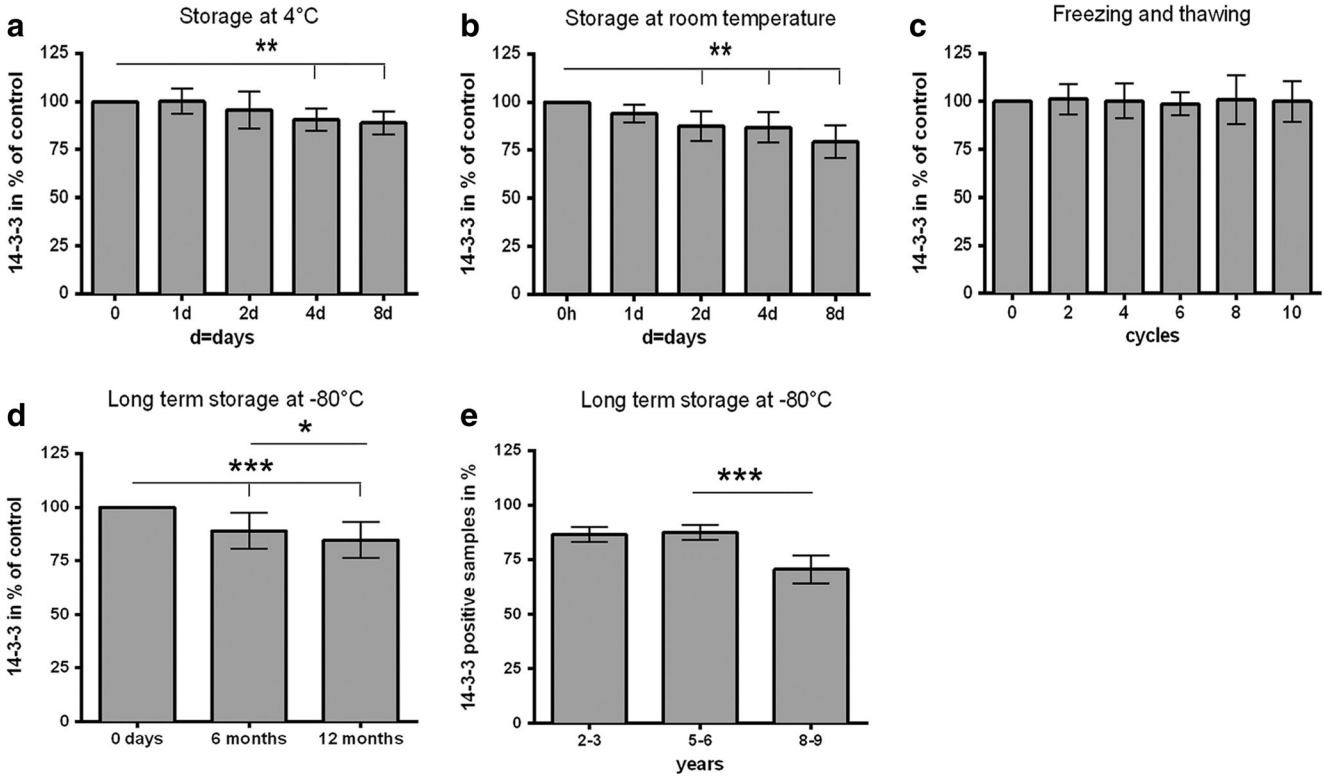

Fig. 4 Effect of short- and long-term storage on 14-3-3 concentration in human CSF of sCJD patients. We determined 14-3-3 levels by ELISA and calculated the 14-3-3 level in percent of control (time point 0) which was set as 100 %. The concentration of 14-3-3 in CSF from 10 different sCJD patients (n=10) was determined before and after **a** storage at room temperature for 8 days, **b** storage at 4 °C for 8 days, and **c** 10 repeated freezing and thawing cycles, and **d** long-term storage at −80 °C. A significant loss of 14-3-3 level could be observed in samples stored at 4 °C after 4 days and in samples stored at room temperature after 2 days. Long-term storage for the indicated times revealed a significant decrease of the number of 14-3-3 positive CSF samples after 9 years. *The number of stars* indicates the significance level: *one star* (*) for $p<0.05$, *two* (**) for $p<0.01$, and *three* (***) for $p<0.001$. *Error bars* represent standard deviations (SD). Statistics were performed by using the *Wilcoxon* rank sum tests

(5 min in a water bath) via *Circulex* ELISA for 14-3-3 gamma isoform. 14-3 3 protein level increased after spiking with blood, but the elevation was more dramatic after sonication showing that intact erythrocytes had a lower but still significant influence on 14-3-3 detection in the CSF (Fig. 5a).

CSF samples from control donors were spiked with different numbers of blood cells, sonicated (to release 14-3-3 protein), and analyzed by 14-3-3 gamma ELISA. Our results indicated that a cell number higher than 2500 cells/μL already showed a significant increase of 14-3-3 protein level, due to hemolysis of erythrocytes. A contamination of CSF samples with more than 20,000 erythrocytes/μL can even lead to a considerable false-positive 14-3-3 signal (Fig. 5b).

Hemolysis and release of 14-3-3 protein were simulated by incubating CSF samples, spiked with 50,000 erythrocytes per μL, for 16 days. A significant increase in 14-3-3 protein detection was apparently immediately and becoming marked after 2 days of incubation (Fig. 5c). For comparison, we used nonspiked CSF as a control (=100 %).

We summarized the outcome of our study and prepared a recommendation table for the preanalytical sample handling and storage in order to improve the standardization of the 14-3-3 analysis of human CSF samples from CJD patients further (Table 1).

Discussion

14-3-3 protein detection has already been established as a useful biomarker in prion disease diagnostic in various studies [3, 5, 11, 12] (Table 2). However, 14-3-3 protein had been criticized for being less reliable than other potential markers (e.g., tau protein) partly due to their usual assessment by Western blot, since Western blot assessment is less standardized and interpretation may vary in contrast to other detection assays such as ELISA. In addition to problems arising from the lack of defined standards, for example a consensus validated cutoff level for CSF 14-3-3 protein level, numerous factors can influence the concentration of 14-3-3 protein in CSF such as short- and long-term storage and the release of 14-3-3 protein from contaminating blood cells. Although recognized as potentially important contributors to suboptimal specificity, these factors have been relatively under-investigated to date. Despite these reservations, the reproducibility of

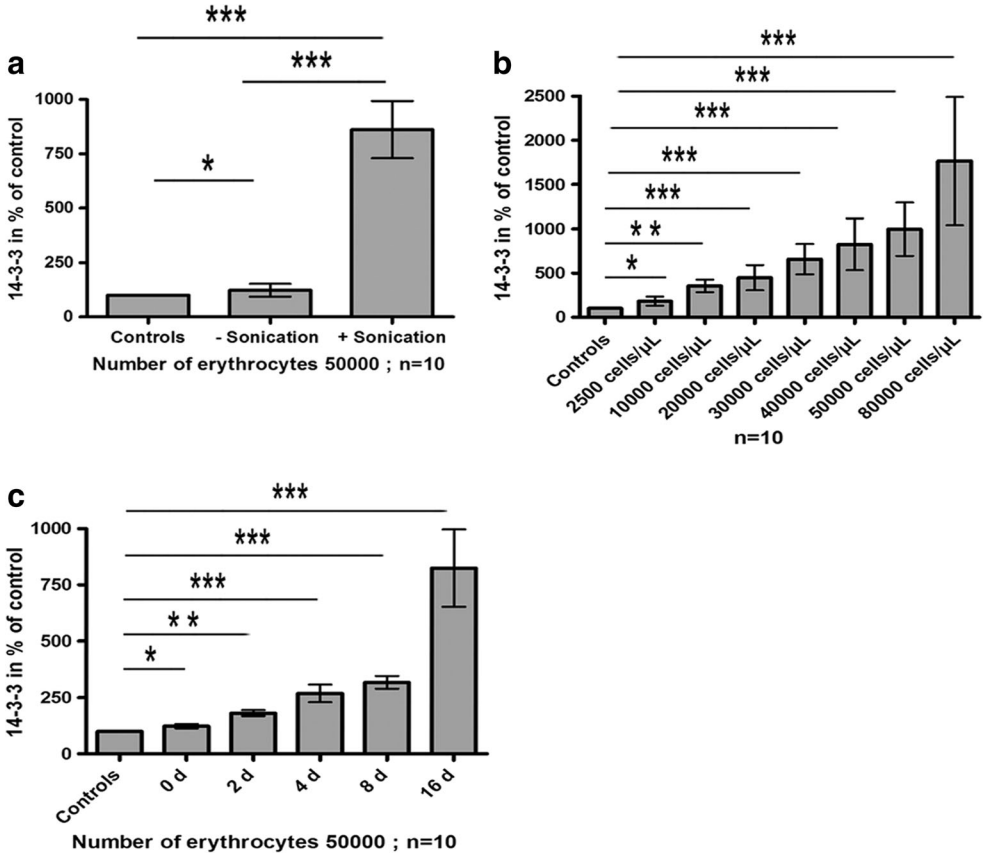

Fig. 5 Influence of blood contamination on the 14-3-3-detection. To analyze the impact of blood contamination, we spiked CSF from control donors with a defined amount of erythrocytes. The 14-3-3 level of the spiked CSF samples was calculated in percent of control (nonspiked) which was set as 100 %. **a** 14-3-3 levels in CSF, spiked with erythrocytes, were analyzed before and after sonication in comparison to nonspiked control CSF. After sonication, 14-3-3 levels were significantly increased showing that intact erythrocytes have an influence on the 14-3-3 level in CSF. **b** Sonication and spiking of CSF with different cell numbers indicated that cell numbers higher than 2500 cells/µL might give a significant false-positive 14-3-3 signal ($p<0.05$). **c** CSF was spiked with 50,000 cells/µL and incubated at room temperature without sonication for 16 days showing that a significant release of 14-3-3 via hemolysis started after 2 days. *The number of stars* indicates the significance level: *one star* (*) for $p<0.05$, *two* (**) for $p<0.01$, and *three* (***) for $p<0.001$. *Error bars* represent standard deviations of the mean (SD). Statistics were performed by using the Wilcoxon rank sum tests

14-3-3 protein in Western blot detection assay between different laboratories (center effect) was demonstrated by the results of our ring trial studies, which showed moderate agreement in the earlier trials becoming substantial in the last trial. Not surprisingly, the interlaboratory validity improved with more standardized preanalytical sample handling and testing protocols over the years in which the ring trials were conducted. Even CSF samples with a trace level of 14-3-3 protein or atypical samples (CNS inflammatory samples or those contaminated with blood cells) still revealed a moderate agreement.

Over recent years, there has been a marked increase in 14-3-3 protein test referrals for suspected sCJD cases across various laboratories [12]. Therefore, despite the utility of 14-3-3 protein detection by Western blot, a quantitative, less time-consuming, higher-throughput screening platform would appear preferable.

Determination of the Diagnostic Accuracy of the 14-3-3 Gamma Isoform Assay

We analyzed 231 sCJD and 2035 control samples without prion disease. At the cutoff at 20,000 AU/mL (as suggested from the training dataset), we obtained a specificity of 96 % and a sensitivity of 88 %.

Even though the detected isoforms are different because of technical impediments for analysis of the same isoform, Western blot and ELISA detection of 14-3-3 protein were largely congruent further underlining the validity of the assessed 14-3-3 ELIS A. In the literature, the reported sensitivities and specificities of 14-3-3 CSF testing in sCJD vary between 100 and 50 % [13, 14]; however, in most studies, specificity and sensitivity of 14-3-3 protein detection are higher than 80 % (Table 2) [3, 5, 15–19], similar to the present study.

Table 1 Recommendations for the standardization and for the preanalytical treatment of CSF samples for the 14-3-3 analysis in sCJD diagnostic

	Recommendation for a preanalytical sample treatment of CSF in sCJD diagnostic
1. Tube selection	Polypropylene tubes
2. CSF volume	0.5–1.5 mL
3. Blood contamination	Specimen macroscopically clear and <2500 erythrocytes/μL are acceptable
4. Shipping time	Up to 1 week at 4 °C is acceptable
5. After arrival	Assessment for blood contamination with visual inspection supplemented by hemasticks or routine microscopic quantification obtained from referring laboratory, centrifugation at 2000×*g* for 10 min and immediately freeze at −80 °C
6. Freeze/Thaw cycles	Stable for at least 10 cycles
7. After analysis	If 14-3-3 protein level is elevated, a confirmation by RT-QuIC assay is recommended
8. Long-term storage	After 1 year: 80–85 % and after 9 years 70–75 % of the samples are 14-3-3 positive

A more recent study, which determined 14-3-3 protein in the CSF quantitatively via ELISA, reported a specificity of 95 % and a sensitivity of 73 % [20]. The reasons for discrepancy with our findings might be (1) detection method, such as variability in the protocols in each laboratory or different cut-off points used or (2) the analyzed patient population. It has been demonstrated that the 14-3-3 protein level is influenced by the sCJD molecular subtype (variable in different countries), by the disease duration and the disease stage [7].

A recently developed diagnostic test, based on in vitro amplification of PrP^{Sc}, such as the RT-QuIC assay showed a very high specificity of almost 100 %, but the average sensitivity for diagnostics was around 80 % and comparable to 14-3-3 results [21–25].

A further possibility to increase the diagnostic accuracy of prion diseases, in particular the sensitivity, is the combination of different biomarker proteins such as 14-3-3, tau, and S100B, which has been suggested in a previous study in a Canadian sCJD population [26].

In our study, the sensitivity of sCJD diagnostic increased to 94.8 by combining all three biomarker proteins. When combining only two biomarker proteins, the combination of 14-3-3 with S100B and tau with S100B showed the highest sensitivity with 93.5 % which is line with others [27]

Short- and Long-Term Stability of 14-3-3 Protein in CSF of sCJD Patients

In the present study, we explored factors, which may influence the CSF protein levels of 14-3-3 and explain interlaboratory variations. A loss of 14-3-3 protein amount (15–20 %) was observed when samples were stored for 8 days at room temperature or 1 year at −80 °C. When we analyzed a panel of arbitrary sCJD samples which were stored between 2 and 9 years at −80 °C, approximately 70–75 % of them exhibited a 14-3-3 level higher than 20,000 rfu (after 9 years), indicating that the 14-3-3 protein level is relatively stable.

Storage conditions were reported to markedly influence the levels of brain-derived proteins in the CSF. For gamma enolase, a marked decrease has been demonstrated when samples are stored at −80 °C for months or years [28]. In case of Aβ1–42, a loss of 20 % during the first 2 days independently of whether CSF samples were stored at 4 °C or at 37 °C and a

Table 2 Comparison of the reported method, sensitivities, and specificities in different studies about 14-3-3 detection in CSF of sCJD patients

Study	Specificity (1) and sensitivity (2) in (%)	Number of patients
Zerr et al. [3, 5, 18, 19]	1) 93 2) 94	289 and 1003
Hsich et al. [33]	1) 96 2) 96	162
Beaudry et al. [13]	1) 100 2) 90	129
Lemstra et al. [34]	1) 87 2) 97	112
Kenney et al. [35]	2) 43	147
Collins et al. [36]	1) 67 2) 92	129
Green et al. [16]	1) 97 (94)** 2) 89 (82)	87
Van Everbroeck et al. [37]	1) 92 2) 100	253
Geschwind et al. [14]	2) 56 (43)*	32
Castellani et al. [38]	2) 87	90
Collins et al. [39]	2) 88	743
Sanchez-Juan et al. [27]	2) 85	227
Baldeiras et al. [40]	1) 97 2) 78	71
Matsui et al. [20]	1) 95* 2) 73	223
Begue et al. [41]	1) 92 2) 72	517
Coulthart et al. [26]	1) 88 2) 91	1000
Matsui et al. [20]	1) 95 2) 73	223
Hamlin et al. [42]	2) 68	420
Chohan et al. [43]	1) 74 2) 86	579

Other methods than Western blot are marked. In Western blot, routinely, 14-3-3 alpha/beta and in ELISA, the 14-3-3 isoform gamma was detected. Controls are usually patients with other diagnosis (a prion disease was excluded) such as other dementia, inflammatory diseases, psychiatric disorders, headache, and epilepsy

*for ELISA and **for capture assay)

low resistance to repeated freezing and thawing cycles is known [29–31]. In contrast, tau protein is considered to be relatively stable at lower temperatures (4 °C) and for at least 6 freezing and thawing cycles. However, tau level in CSF decreases when stored at higher temperature, e.g., 37 °C [30]. Here, tau may be degradated via proteases, or it may undergo conformational changes [32]. Compared to these proteins, the stability of 14-3-3 at various storage conditions can be estimated as good.

Contamination with Blood Cells Results in Elevation of 14-3-3 Levels in CSF

Lysis of blood cells, such as erythrocytes, may result in artificially elevated CSF levels of 14-3-3 protein and a false-positive signal. In routine diagnostic laboratory practice and depending on the experience of the clinicians who perform the lumbar puncture between 5 and 10 % of the CSF samples are contaminated with blood cells during the procedure. Therefore, there is a need to define clear guidelines to address this problem. Our data indicate that artificially elevated 14-3-3 protein level can be reduced when blood cells remain intact. Even though a CSF contamination with 2500 blood cells/μL already resulted in a moderate elevation of 14-3-3 protein levels, we consider a CSF contamination with more than 20, 000 cells/μL as critical for prion disease diagnosis. In CSF, samples (not older than 1 or 2 days after the lumbar puncture), a centrifugation step before freezing is recommended to remove blood cells. After 2 days, the hemolysis of blood cells was increased to such an extent that no reliable results could be obtained, and consequently, such samples should be excluded from further diagnostic procedures.

In conclusion, we standardized a commercial CSF 14-3-3 gamma isoform ELISA as a diagnostic assay for the quantification of 14-3-3 protein in sCJD and provide a recommendation for sample handling in the diagnostic workup in prion diseases.

Acknowledgments The study was performed within the recently established Clinical Dementia Center at the University Medical Center Göttingen and was supported by grants from the EU Joint Program–Neurodegenerative Disease Research [JPND-DEMTEST (Biomarker based diagnosis of rapid progressive dementias-optimization of diagnostic protocols, 01ED1201A)]. This study was also partly supported by the Robert Koch Institute through funds from the Federal Ministry of Health (grant no. 1369–341) and by a grant from the European Commission (Protecting the food chain from prions: shaping European priorities through basic and applied research (PRIORITY, No. 222887) Project number: FP7-KBBE-2007-2A). Thanks to Michele Equestre for technical assistance. The Australian National CJD Registry is funded by the Commonwealth Department of Health and S Collins is supported by a NHMRC Practitioner Fellowship (#APP1005816).

Conflict of Interests On behalf of all authors, the corresponding author states that there are no conflicts of interests.

References

1. Broadie K, Rushton E, Skoulakis E, Davis R (1997) Leonardo, a Drosophila 14-3-3 protein involved in learning, regulates presynaptic function. Neuron 2:391–402
2. van Hemert M, Steensma H, van Heusden G (2001) 14-3-3 proteins: key regulators of cell division, signalling and apoptosis. Bioessays 10:936–946
3. Zerr I, Bodemer M, Gefeller O, Otto M, Poser S, Wiltfang J, Windl O, Kretzschmar HA, Weber T (1998) Detection of 14-3-3 protein in the cerebrospinal fluid supports the diagnosis of Creutzfeldt-Jakob disease. Ann Neurol 43:32–40
4. Zerr I, Bodemer M, Weber T (1997) The 14-3-3 brain protein and transmissible spongiform encephalopathy [letter]. N Engl J Med 336:874
5. Zerr I, Pocchiari M, Collins S, Brandel JP, de Pedro CJ, Knight RSG, Bernheimer H, Cardone F, Delasnerie-Lauprêtre N, Cuadrado Corrales N, Ladogana A, Fletcher A, Bodemer M, Awan T, Ruiz Bremón A, Budka H, Laplanche JL, Will RG, Poser S (2000) Analysis of EEG and CSF 14-3-3 proteins as aids to the diagnosis of Creutzfeldt-Jakob disease. Neurology 55:811–815
6. Zerr I, Kallenberg K, Summers DM, Romero C, Taratuto A, Ladogana A, Schuur M, Haik S, Collins SJ, Jansen GH, Stokin GB, Pimentel J, Hewer E, Collie DA, Smith P, Varges D, Heinemann U, Meissner B, Roberts H, Brandel JP, Van Dujin CM, Pocchiari M, Begue P, Cras P, Will RG, Sanchez-Juan P (2009) Updated clinical diagnostic criteria for sporadic Creutzfeldt-Jakob disease. Brain 132:2659–2668
7. Gmitterová K, Heinemann U, Bodemer M, Krasnianski A, Meissner B, Kretzschmar HA, Zerr I (2008) 14-3-3 CSF levels in sporadic Creutzfeldt-Jakob disease differ across molecular subtypes. Neurobiol Aging 30:842–850
8. WHO (1998) Human transmissible spongiform encephalopathies. Wkly Epidemiol Rec 47:361–365
9. Schmitz M, Lüllmann K, Zafar S, Ebert E, Wohlhage M, Oikonomou P, Schlomm M, Mitrova E, Beekes M, Zerr I (2014) Association of prion protein genotype and scrapie prion protein type with cellular prion protein charge isoform profiles in cerebrospinal fluid of humans with sporadic of familial prion diseases. Neurobiol Aging 35:1177–1188
10. Schmitz M, Schlomm M, Hasan B, Beekes M, Mitrova E, Korth C, Brell A, Carimalo J, Gawinecka J, Varges D, Zerr I (2010) Codon 129 polymorphism and the E200K mutation do not affect the cellular prion protein isoform composition in the cerebrospinal fluid from patients with Creutzfeldt-Jakob disease. Eur J Neurosci 31: 2024–2031
11. Puoti G, Bizzi A, Forloni G, Safar JG, Tagliavini F, Gambetti P (2012) Sporadic human prion diseases: molecular insights and diagnosis. Lancet Neurol 11:618–628
12. Stoeck K, Sanchez-Juan P, Gawinecka J, Green A, Ladogana A, Pocchiari M, Sanchez-Valle R, Mitrova E, Sklaviadis T, Kulczycki J, Slivarichova D, Saiz A, Calero M, Knight R, Aguzzi A, Laplanche JL, Peoc'h K, Schelzke G, Karch A, van Duijn CM, Zerr I (2012) Cerebrospinal fluid biomarker supported diagnosis of Creutzfeldt-Jakob disease and rapid dementias: a longitudinal multicentre study over 10 years. Brain 135:3051–3061
13. Beaudry P, Cohen P, Brandel JP, Delasnerie-Laupretre N, Richard S, Launay JM, Laplanche JL (1999) 14-3-3 protein, neuron-specific enolase, and S-100 protein in cerebrospinal fluid of patients with Creutzfeldt-Jakob disease. Dement Geriatr Cogn Disord 10:40–46
14. Geschwind M, Martindale J, Miller D, De Armond SJ, Uyehara-Lock J, Gaskin D, Kramer JH, Barbaro NM, Miller BL (2003) Challenging the clinical utility of the 14-3-3 protein for the diagnosis of sporadic Creutzfeldt-Jakob disease. Arch Neurol 60:813–816

15. Cuadrado-Corrales N, Jiménez-Huete A, Albo C, Hortiguela R, Vega L, Cerrato L, Sierra-Moros M, Rábano A, de Pedro-Cuesta J, Calero M (2006) Impact of the clinical context on the 14-3-3 test for the diagnosis of sporadic CJD. BMC Neurol 6:25
16. Green AJ (2002) Use of 14-3-3 in the diagnosis of Creutzfeldt-Jakob disease. Biochem Soc Symp 30:382–386
17. Green AJ, Thompson EJ, Stewart GE, Zeidler M, McKenzie JM, MacLeod M-A, Ironside JW, Will RG, Knight RS (2001) Use of 14-3-3 and other brain-specific proteins in CSF in the diagnosis of variant Creutzfeldt-Jakob disease. J Neurol Neurosurg Psychiatry 70:744–748
18. Zerr I, Bodemer M, Räcker S, Grosche S, Poser S, Kretzschmar HA, Weber T (1995) Cerebrospinal fluid concentration of neuron-specific enolase in diagnosis of Creutzfeldt-Jakob disease. Lancet 345:1609–1610
19. Zerr I, Bodemer M, Westermann R, Schröter A, Jacobi C, Arlt S, Otto M, Poser S (2000) 14-3-3 proteins in neurological disorders. J Neurol 247(Suppl 3):III/14
20. Matsui Y, Satoh K, Miyazaki T, Shirabe S, Atarashi R, Mutsukura K, Satoh A, Kataoka Y, Nishida N (2011) High sensitivity of an ELISA kit for dedection of the gamma-isoform of 14-3-3 proteins: usefulness in laboratory diagnosis of human prion disease. BMC Neurol 11, doi:10.1186/471-2377-11-120
21. Atarashi R, Sano K,Fuse T, Yamaguchi N, Ishibashi D, Matsubara T, Nakagaki T, Yamanaka H, Shirabe S, Yamada M, Mizusawa H, Kitamoto T, Klug G, McGlade A, Collins SJ, Nishida N (2011) Ultrasensitive human prion detection in cerebrospinal fluid by real-time quaking-induced conversion.Nat Med 17:175–178
22. Cramm M, Schmitz M, Karch A, Zafar S, Varges D, Mitrova E, Schroeder B, Raeber AJ, Kuhn F, Zerr I (2015) Characteristic CSF prion-seeding efficiency in humans with prion diseases. Mol Neurobiol 51:396–405
23. Cramm M, Schmitz M, Zafar S, Karch A, Mitrova E, Schroeder B, Raeber A, Kuhn F, Satoh K, Collins S, Zerr I (2015) Stability and reproducibility underscore utility of RT-QuIC CSF analysis for diagnosis of human prion disease, in press
24. McGuire LI, Peden AH, Orrú CD, Wilham JM, Appleford NE, Mallinson G, Andrews M, Head MW, Caughey B, Will RG, Knight RS, Green AJ (2012) Real time quaking-induced conversion analysis of cerebrospinal fluid in sporadic Creutzfeldt-Jakob disease. Ann Neurol 72:278–285
25. Sano K, Satoh K, Atarashi R, Takashima H, Iwasaki Y, Yoshida M, Sanjo N, Murai H, Mizusawa H, Schmitz M, Zerr I, Kim YS, Nishida N (2013) Early detection of abnormal prion protein in genetic human prion diseases now possible using real-time QUIC assay. PLoS ONE 8:e54915
26. Coulthart MB, Jansen GH, Olsen E, Godal DL, Connolly T, Choi BC, Wang Z, Cashman NR (2011) Diagnostic accuracy of cerebrospinal fluid protein markers for sporadic Creutzfeldt-Jakob disease in Canada: a 6-year prospective study. BMC Neurol 11:133
27. Sanchez-Juan P, Green A, Ladogana A, Cuadrado-Corrales N, Sanchez-Valle R, Mitrova E, Stoeck K, Sklaviadis T, Kulczycki J, Hess K, Bodemer M, Slivarichova D, Saiz A, Calero M, Ingrosso L, Knight R, Janssens C, Van Duijn C, Zerr I (2006) CSF tests in the differential diagnosis of Creutzfeldt-Jakob disease. Neurology 67: 637–643
28. Ramont L, Thoannes H, Volondat A, Chastang F, Millet MC, Maquart FX (2005) Effects of hemolysis and storage condition on neuron-specific enolase (NSE) in cerebrospinal fluid and serum: implications in clinical practice. Clin Chem Lab Med 43:1215–1217
29. Jensen M, Hartmann T, Engvall B, Wang R, Uljon SN, Sennvik K, Näslund J, Muehlhauser F, Nordstedt C, Beyreuther K, Lannfelt L (2000) Quantification of Alzheimer amyloid beta peptides ending at residues 40 and 42 by novel ELISA systems. Mol Med 6:291–302
30. Schoonenboom NS, Mulder C, Vanderstichele H, Van Elk EJ, Kok A, Van Kamp GJ, Scheltens P, Blankenstein MA (2005) Effects of processing and storage conditions on amyloid beta (1–42) and tau concentrations in cerebrospinal fluid: implications for use in clinical practice. Clin Chem 51:189–195
31. Vanderstichele H, Van Kerschaver E, Hesse C, Davidsson P, Buyse MA, Andreasen N, Minthon L, Wallin A, Blennow K, Vanmechelen E (2000) Standardization of measurement of beta-amyloid (1–42) in cerebrospinal fluid and plasma. Amyloid 7: 245–258
32. Vandermeeren M, Mercken M, Vanmechelen E, Six J, van de Voorde A, Martin JJ, Cras P (1993) Detection of tau proteins in normal and Alzheimer's disease cerebrospinal fluid with a sensitisve sandwich enzyme-linked immunosorbent assay. J Neurochem 61:1828–1834
33. Hsich G, Kenney K, Gibbs CJ Jr, Lee KH, Harrington MG (1996) The 14-3-3 brain protein in cerebrospinal fluid as a marker for transmissible spongifrom encephalopathies. N Engl J Med 335: 924–930
34. Lemstra AW, van Meegen MT, Vreyling JP, Meijerink PH, Jansen GH, Bulk S, Baas F, van Gool WA (2000) 14-3-3 testing in diagnosing Creutzfeldt-Jakob disease: a prospective study in 112 patients. Neurology 55:514–516
35. Kenney K, Brechtel C, Takahashi H, Kurohara K, Anderson P, Gibbs CJ Jr (2000) An enzyme-linked immunosorbent assay to quantify 14-3-3 proteins in the cerebrospinal fluid of suspected Creutzfeldt-Jakob disease patients. Ann Neurol 48:395–398
36. Collins S, Boyd A, Fletcher A, Gonzales M, McLean CA, Byron K, Masters CL (2000) Creutzfeldt-Jakob disease: diagnostic utility of 14-3-3 protein immunodetection in cerebrospinal fluid. J Clin Neurosci 7:203–208
37. Van Everbroeck B, Quoilin S, Boons J, Martin JJ, Cras P (2003) A prospective study of CSF markers in 250 patients with possible Creutzfeldt-Jakob disease. J Neurol Neurosurg Psychiatry 74: 1210–1214
38. Castellani RJ, Colucci M, Xie Z, Zou W, Li C, Parchi P, Capellari S, Pastore M, Rahbar MH, Chen SG, Gambetti P (2004) Sensitivity of 14-3-3 protein test varies in subtypes of sporadic Creutzfeldt-Jakob disease. Neurology 63:436–442
39. Collins SJ, Sanchez-Juan P, Masters CL, Klug GM, van Duijn C, Poleggi A, Pocchiari M, Almonti S, Cuadrado-Corrales N, de Pedro-Cuesta J, Budka H, Gelpi E, Glatzel M, Tolnay M, Hewer E, Zerr I, Heinemann U, Kretzschmar HA, Jansen GH, Olsen E, Mitrova E, Alpérovitsch A, Brandel JP, Mackenzie J, Murray K, Will RG (2006) Determinants of diagnostic investigation sensitivities across the clinical spectrum of sporadic Creutzfeldt-Jakob disease. Brain 129:2278–2287
40. Baldeiras IE, Ribeiro MH, Pacheco P, Machado A, Santana I, Cunha L, Oliveira C (2009) Diagnostic value of CSF protein profile in a Portuguese population of sCJD patients. J Neurol 256:1540–1550
41. Begué P, Martinetto H, Schultz M, Rojas E, Romero C, D'Giano C, Sevlever G, Somoza M, Taratuto A (2011) Creutzfeldt-Jakob disease surveillance in Argentina, 1997–2008. Neuroepidemiology 37:193–202
42. Hamlin C, Puoti G, Berri S, Sting E, Harris C, Cohen M, Spear C, Bizzi A, Debanne SM, Rowland DY (2012) A comparison of tau and 14-3-3 protein in the diagnosis of Creutzfeldt-Jakob disease. Neurology 79:547–552
43. Chohan G, Pennington C, Mackenzie J, Andrews M, Everington D, Will R, Knight R, Green A (2010) The role of cerebrospinal fluid 14-3-3 and other proteins in the diagnosis of sporadic Creutzfeldt-Jakob disease in the UK: a 10-year review. J Neurol Neurosurg Psychiatry 81:1243–1248

Cerebrospinal Fluid Real-Time Quaking-Induced Conversion Is a Robust and Reliable Test for Sporadic Creutzfeldt–Jakob Disease: An International Study

Lynne I. McGuire, PhD,[1]
Anna Poleggi, PhD,[2]
Ilaria Poggiolini, PhD,[3]
Silvia Suardi, PhD,[4]
Katarina Grznarova, PhD,[5,6]
Song Shi, PhD,[7] Bart de Vil, BSc,[8]
Shannon Sarros, BSc,[9]
Katsuya Satoh, PhD,[10]
Keding Cheng, PhD,[11]
Maria Cramm, BSc,[12]
Graham Fairfoul, BSc,[1]
Matthias Schmitz, PhD,[12] Inga Zerr, MD,[12]
Patrick Cras, MD,[8]
Michele Equestre, PhD,[2]
Fabrizio Tagliavini, MD,[4]
Ryuichiro Atarashi, PhD,[10]
David Knox, PhD,[11] Steven Collins, MD,[13]
Stéphane Haïk, PhD,[5,6,14]
Piero Parchi, MD,[3,15]
Maurizio Pocchiari, MD,[2] and
Alison Green, PhD[1]

Real-time quaking-induced conversion (RT-QuIC) has been proposed as a sensitive diagnostic test for sporadic Creutzfeldt–Jakob disease; however, before this assay can be introduced into clinical practice, its reliability and reproducibility need to be demonstrated. Two international ring trials were undertaken in which a set of 25 cerebrospinal fluid samples were analyzed by a total of 11 different centers using a range of recombinant prion protein substrates and instrumentation. The results show almost complete concordance between the centers and demonstrate that RT-QuIC is a suitably reliable and robust technique for clinical practice.

ANN NEUROL 2016;80:160–165

Creutzfeldt–Jakob disease (CJD) belongs to a family of fatal neurodegenerative diseases known as transmissible spongiform encephalopathies (TSEs). TSEs are characterized by the post-translational conformational change of a normally expressed protein called prion protein (PrP) into a disease-associated form known as PrP^{Sc}. Once formed, PrP^{Sc} can induce PrP to undergo a conformational change and produce more PrP^{Sc} in a self-propagating manner. The PrP^{Sc} aggregates, becomes protease resistant, and deposits throughout the brain, leading to spongiform change and neuronal loss.

Patients with sporadic CJD (sCJD) present with a rapidly progressing dementia, and death usually occurs within 6 months. Current diagnostic criteria for sCJD rely on clinical features, the results of electroencephalography and magnetic resonance imaging, and the presence of 14-3-3 protein in the cerebrospinal fluid (CSF).[1,2] These tests are not specific for CJD, and none is able to detect all forms of CJD.[3,4]

A new approach to the premortem diagnosis of sCJD has been to exploit the ability of small amounts of CSF PrP^{Sc} to convert native PrP into PrP^{Sc} in a newly described protein aggregation assay known as real-time quaking-induced conversion (RT-QuIC). This technique uses recombinant PrP (rPrP) as a substrate, which is induced to aggregate by the addition of CSF containing

From the [1]National CJD Research & Surveillance Unit, Western General Hospital, University of Edinburgh, Edinburgh, Scotland, United Kingdom; [2]Department of Neurological Sciences, National Institute of Health, Rome, Italy; [3]Institute of Neurological Sciences, Scientific Institute for Research, Hospitalization and Health Care, Bologna, Italy; [4]Department of Neurodegenerative Diseases, Scientific Institute for Research, Hospitalization and Health Care, Carlo Besta Neurological Institute, Milan, Italy; [5]Sorbonne Universities, Pierre and Marie Curie University, Brain and Spine Institute, Paris, France; [6]National Reference Centre for Unconventional Transmissible Agents, Paris, France; [7]Center for Neuropathology and Prion Research, Ludwig Maximilian University, Munich, Germany; [8]Department of Neurology, Institute of Born Bunge, University of Antwerp, Antwerp, Belgium; [9]Florey Institute of Neuroscience and Mental Health, University of Melbourne, Melbourne, Victoria, Australia; [10]Department of Molecular Microbiology and Immunology, Nagasaki University Graduate School of Biomedical Sciences, Nagasaki, Japan; [11]Prion Laboratory Section, Public Health Agency of Canada, Winnipeg, Manitoba, Canada; [12]Department of Neurology, University Medical Center and German Center for Neurodegenerative Diseases, University of Göttingen, Göttingen, Germany; [13]Department of Medicine, University of Melbourne, Melbourne, Victoria, Australia; [14]APHP, Pitié-Salpêtrière Hospital, Paris, France; and [15]Department of Biomedical and Neuromotor Sciences, University of Bologna, Italy

Address correspondence to Dr Green, University of Edinburgh, National CJD Research & Surveillance Unit, Western General Hospital, Edinburgh, EH4 2XU Scotland, United Kingdom.
E-mail: Alison.Green@ed.ac.uk

Received Dec 22, 2015, and in revised form Apr 18, 2016. Accepted for publication Apr 19, 2016.

View this article online at wileyonlinelibrary.com. DOI: 10.1002/ana.24679

PrP^{Sc}. Thioflavin T (ThT) in the reaction binds to the aggregated PrP^{Sc}, causing a change in the ThT emission spectrum, enabling the reaction to be monitored in real time.[5,6]

CSF RT-QuIC has been shown to be an accurate diagnostic test for sCJD, with a high degree of sensitivity (85–87%) and specificity (99–100%).[7,8] An increasing number of laboratories have established RT-QuIC analysis, and more are interested in doing so. Before RT-QuIC is fully accepted into clinical practice as a reliable premortem diagnostic test, studies are required to ensure that laboratories performing this assay using different forms of recombinant PrP as a substrate and a variety of instrumentation are producing comparable results.

This study reports the findings of 2 international ring trials that were undertaken over a 2-year period. The initial ring trial comprised European participants, whereas the second ring trial was wider and included participants from Australia, Canada, and Japan.

Materials and Methods

CSF Samples

CSF samples were provided by the National CJD Research & Surveillance Unit, United Kingdom. These samples are stored at −80 °C, and consent was obtained from the next of kin for their use in research (05/MRE00/67). CSF samples were selected on the basis of having appropriate ethical consent and sufficient volume to ensure that each participant had an adequate volume of CSF for analysis. Each set of CSF samples was sent to each laboratory on dry ice and was analyzed blind to the final diagnosis. The performance of the RT-QuIC assay was evaluated in an interlaboratory ring trial, where identical CSF samples were analyzed by each of the participating laboratories. Using this approach, it may be possible to identify analytical procedures that affect overall assay performance.

Participants

A total of 11 laboratories participated in the ring trials: Department of Pathology, University of Melbourne, Melbourne, Australia (Aust); Department of Neurology, Antwerp University, Antwerp, Belgium (Bel); Prion Laboratory Section, Public Health Agency of Canada, Winnipeg, Canada (Can); Laboratory Investigations of Alzheimer's Disease and Prion Diseases, Pitié-Salpêtrière Hospital Group, Paris, France (Fra); Department of Neurology, University Medical Center and German Center for Neurodegenerative Diseases, Göttingen, Germany (Ger-Goet); Centre for Neuropathology and Prion Research, Ludwig Maximilian University, Munich, Germany (Ger-Mun); Department of Neurological Sciences, University of Bologna, Bologna, Italy (It-Bol); Department of Neurodegenerative Disease, Carlo Besta Neurological Institute, Milan, Italy (It-Mil); Department of Neurological Sciences, National Institute of Health, Rome, Italy (It-Rome); Department of Molecular Microbiology and Immunology, Nagasaki University, Nagasaki, Japan (Jpn); and National CJD Research & Surveillance Unit, University of Edinburgh, Edinburgh, UK (UK).

First Ring Trial

Seven laboratories (UK, It-Rome, It-Mil, It-Bol, Fra, Ger-Mun, Bel) participated in the first ring trial, and each received 10 CSF samples sent on dry ice. Of these, 1 was from a patient with neuropathologically confirmed sCJD, 4 were from patients with probable sCJD, diagnosed according to the World Health Organization criteria, 2 patients improved and the diagnosis of sCJD was excluded on clinical grounds, 1 patient had a steroid-responsive encephalopathy, 1 had no neuropathological evidence of CJD at postmortem, and 1 had mixed Alzheimer disease and vascular dementia at postmortem. The age of the patients ranged from 48 to 86 years and included 5 females and 5 males. The disease duration of the patients with sCJD ranged from 2 to 12 months, and the CSF samples were taken between 53% and 94% of the disease duration.

Second Ring Trial

Eleven laboratories (UK, It-Rome, It-Mil, It-Bol, Fra, Ger-Mun, Ger-Goet, Jpn, Aust, Can, and Bel) participated in the second ring trial, and each received 15 CSF samples sent on dry ice. One laboratory analyzed the CSF samples twice using a BMG LABTECH (Ortenberg, Germany) Optima and a BMG LABTECH Omega. Of the 15 CSF samples, 5 were from patients with probable sCJD, 3 were from patients with neuropathologically confirmed sCJD, 1 patient improved and the diagnosis of sCJD was excluded on clinical grounds, 1 had seizures, 1 had anti-immune encephalopathy, 1 had a psychiatric disorder, 1 had Huntington disease, 1 had a non-CJD dementia, and 1 had normal pressure hydrocephalus. The age of the patients ranged from 55 to 87 years and included 6 females and 9 males. The disease duration of the patients with sCJD ranged from 1 to 26 months and the CSF samples were taken between 57% and 90% of the disease duration.

Methodology

Each laboratory performed the RT-QuIC analysis using a standard 10mM phosphate buffer (pH 7.4), 170mM NaCl (total 400mM including phosphate buffer) containing 0.1mg/ml rPrP, 10 μM ThT, and 10 μM ethylenediaminetetraacetic acid tetrasodium salt. However, a range of instrumentations, analytical conditions, and types of rPrP were used (Table 1). Most laboratories used either a BMG LABTECH Optima or a BMG LABTECH Omega, whereas 1 laboratory used a Tecan Infinite F200PRO (Tecan Group, Männedorf, Switzerland). Nine laboratories used hamster full-length (23–231) rPrP (supplied by Bristol Institute of Blood Sciences, Bristol, UK),[8,9] 2 used human full-length (23–231) rPrP (produced in-house),[7] and 1 used a hamster–sheep chimeric rPrP (hamster 14–126 residues followed by sheep residues 141-234, produced according to previously reported conditions).[5]

TABLE 1. Instrumentation, Analytical Conditions, and Source of Recombinant PrP Used by Each of the Participating Centers

Group	Reader	Recombinant PrP	CSF Volume	Shake Conditions	Temp, °C	Criteria for Positive Result
UK Omega	Omega	Ham FL	30 µl	900rpm 90 s shake/30 s rest	42	Mean of 2 highest replicates of 4 > 24,000rfu at 90 h
UK Optima	Optima	Ham FL	30 µl	600rpm 60 s shake/60 s rest	42	Mean of 2 highest replicates of 4 > 10,000rfu at 90 h
Germany (Munich)	Optima	Ham FL	30 µl	600rpm 60 s shake/60 s rest	42	Mean of 2 highest replicates of 4 > 10,000rfu at 90 h
Germany (Göttingen)	Optima	Ham-Sh chimeric	15 µl	600rpm 60 s shake/60 s rest	42	Mean of 2 highest replicates of 4 > 10,000rfu at 80 h
Italy (Bologna)	Optima	Ham FL	15 µl	600rpm 60 s shake/60 s rest	42	Mean of 2 highest replicates of 4 > 6,000rfu at 90 h
Italy (Milan)	Optima	Ham FL	30 µl	600rpm 60 s shake/60 s rest	42	Mean of 2 highest replicates of 4 > 10,000rfu at 90 h
Italy (Rome)	Omega	Ham FL	30 µl	900rpm 90 s shake/30 s rest	42	Mean of 2 highest replicates of 4 > 32,000rfu at 90 h
France	Omega	Ham FL	30 µl	900rpm 90 s shake/30 s rest	42	Mean of 2 highest replicates of 4 > 34,345rfu at 90 h
Belgium	Omega	Ham FL	20 µl	900rpm 90 s shake/30 s rest	42	Mean of 2 highest replicates of 4 > 20,000rfu at 90 h
Canada	Omega	Ham FL	30 µl	900rpm 90 s shake/30 s rest	42	Mean of 2 highest replicates of 4 > twice baseline reading at 90 h
Japan	Tecan	Hum FL	5 µl	Max 30 s shake/30 s rest	37	At least 2 of 6 replicates > 400rfu at 90 h
Australia	Optima	Hum FL	5 µl	750rpm 30 s shake/30 s rest[a]	37	Mean of 2 highest replicates of 4 > 70% of baseline rfu reading at 90 h

[a]Shaking performed in a Thermomixer Comfort (Eppendorf, Hamburg, Germany) before being read in an Optima instrument.
CSF = cerebrospinal fluid; Ham FL = hamster full-length PrP (23–231)[8,9]; Ham-Sh chimeric = hamster residues$_{14–128}$:sheep$_{141–234}$[5]; Hum FL = human full-length (23–231)—codon 129M[6]; PrP = prion protein; rfu = relative fluorescence units.

Results

The results of the ring trials are given in Tables 2 and 3. In the first ring trial 6, of 7 laboratories obtained positive RT-QuIC responses in the CSF samples from all 5 sCJD cases; the remaining laboratory obtained positive RT-QuIC responses in the CSF of 4 of the 5 sCJD cases. A negative RT-QuIC result was obtained in the CSF of 1 sCJD case, which had a disease duration of 12 months. This laboratory was using a BMG LABTECH Optima instrument, with full-length hamster rPrP as substrate and 30 µl of CSF. These conditions were similar to other laboratories in the study that obtained positive results for this particular CSF sample. A limited volume of CSF was sent to each laboratory, and this meant that repeating the analysis of this particular CSF by the individual laboratory was not possible.

None of the laboratories obtained positive RT-QuIC responses in any of the 5 CSF samples from patients without sCJD. Four of these laboratories used a BMG LABTECH Optima, and the remaining 3 used a BMG LABTECH Omega. However, all the laboratories used the same full-length hamster rPrP.

The second ring trial included a larger number of laboratories with a wider geographical distribution and included a wider range of instrumentation and type of rPrP. Despite this, the results showed complete concordance (see Table 3). Of the 11 laboratories that participated in this ring trial, 11 obtained positive RT-QuIC

TABLE 2. Results for the First Ring Trial with 7 Participating Centers

CSF ID	Diagnosis	Gender (age, yr)	Disease Duration, mo	Timing of LP as % of Disease Duration	Laboratories Reporting Positive RT-QuIC, No.	Concordance, %
1	Patient improved	M (68)	Still alive	n/a	0/7	100
2	Steroid-responsive encephalopathy	M (69)	Still alive	n/a	0/7	100
3	Neuropathological evidence of mixed AD and vascular dementia	M (86)	3	92	0/7	100
4	Psychiatric disorder	M (63)	Still alive	n/a	0/7	100
5	Patient improved	F (74)	Still alive	n/a	0/7	100
6	Definite sCJD—codon 129 MM; PrP type: 1	F (75)	3	83	7/7	100
7	Probable sCJD	F (48)	2	77	7/7	100
8	Probable sCJD—codon 129 MM	F (64)	12	94	6/7	83
9	Probable sCJD	F (72)	4	76	7/7	100
10	Probable sCJD—codon 129 VV	M (69)	4	53	7/7	100

AD = Alzheimer disease; CSF = cerebrospinal fluid; F = female; LP = lumbar puncture; M = male; n/a = applicable; PrP = prion protein; RT-QuIC = real-time quaking-induced conversion; sCJD = sporadic Creutzfeldt–Jakob disease.

responses in all 8 CSF samples from sCJD patients. All 11 laboratories obtained a positive RT-QuIC response in the CSF from the sCJD patient, with a disease duration of 26 months. This CSF sample was taken 21 months after the onset of symptoms. The laboratory that failed to obtain a positive CSF RT-QuIC response in an sCJD case in the first ring trial correctly identified all sCJD cases in the second ring trial. None of the analytical parameters had been changed by the laboratory in question. Importantly, the laboratory that used a Tecan Infinite shaker with a human rPrP as a substrate also correctly identified all sCJD cases. One laboratory analyzed the ring trial CSF samples using both the BMG LABTECH Optima or a BMG LABTECH Omega and obtained similar results using both instruments despite having different cutoff criteria. None of the laboratories obtained positive RT-QuIC responses in CSF samples from patients with non-CJD disorders.

Discussion

In the first ring trial, 6 of 7 laboratories correctly identified all sCJD cases; however, 1 laboratory obtained a negative CSF RT-QuIC result from an sCJD patient with a disease duration of 12 months. It has been reported that CSF samples from sCJD patients with longer disease durations may have lower seeding efficiency[10]; however, this effect was not seen in the second ring trial, where the CSF from an sCJD patient with a disease duration of 26 months was identified by RT-QuIC by all laboratories. All the laboratories that participated in the first ring trial used the same source and type of rPrP and either Optima or Omega BMG LABTECH instrumentation, and demonstrated high levels of accuracy and agreement between laboratories.

The second ring trial took place 18 months later and was expanded to include other European laboratories and participants from Australia, Canada, and Japan. Some of the additional laboratories used alternative types of rPrP and other forms of instrumentation. This enabled a more rigorous assessment of the robustness and transferability of the RT-QuIC technique.

All 11 laboratories accurately identified the 8 CSF samples from sCJD patients, and none detected a positive RT-QuIC in any of the non-CJD cases. The agreement between laboratories using different rPrP as a substrate and different forms of instrumentation is encouraging. The accuracy of the results obtained was identical for each of the rPrP substrates used. From this

TABLE 3. Results from the Second Ring Trial with 11 Participating Laboratories

CSF ID	Diagnosis	Gender (age, yr)	Disease Duration, mo	Timing of LP as % of Disease Duration	Laboratories[a] Reporting Positive RT-QuIC, No.	Concordance, %
1	Patient improved	F (87)	Still alive	—	0/12	100
2	Seizures	M (56)	—	—	0/12	100
3	Autoimmune encephalitis	F (82)	Still alive	—	0/12	100
4	Psychiatric disorder	M (55)	Still alive	—	0/12	100
5	Huntington disease	F (67)	Still alive	—	0/12	100
6	Mixed vascular and Alzheimer dementia	M (80)	Still alive	—	0/12	100
7	Normal pressure hydrocephalus	M (78)	Still alive	—	0/12	100
8	Definite sCJD	F (63)	6	90	12/12	100
9	Definite sCJD—codon 129 MM; PrP^{Sc} type 1	M (73)	1	71	12/12	100
10	Definite sCJD—codon 129 MM	M (66)	5	57	12/12	100
11	Probable sCJD	M (84)	No data	—	12/12	100
12	Probable sCJD	M (66)	3	83	12/12	100
13	Probable sCJD	M (69)	3	80	12/12	100
14	Probable sCJD	F (65)	26	83	12/12	100
15	Probable sCJD	F (67)	8	88	12/12	100

[a]The UK laboratory submitted 2 sets of results using 2 sets of instruments: BMG LABTECH Omega and BMG LABTECH Optima.
CSF = cerebrospinal fluid; F = female; LP = lumbar puncture; M = male; PrP^{Sc} = disease-associated form of prion protein; RT-QuIC = real-time quaking-induced conversion; sCJD = sporadic Creutzfeldt–Jakob disease.

limited number of CSF samples, we have achieved an overall sensitivity of between 85.7% and 100% and a specificity of 100%. This compares well with a previous intralaboratory study, which had fewer participants and reported a sensitivity of 85% and a specificity of 99%.[10] The complete concordance between laboratories demonstrates that CSF RT-QuIC is adaptable to different laboratory instrumentation and different types of rPrP. The high level of accuracy and agreement between laboratories using CSF RT-QuIC is supportive of this technique being introduced into clinical practice.

Acknowledgment

This work was supported by the Joint Programming for Neurodegenerative Disease (JPND)-funded project "Optimisation, Harmonisation and Standardisation of the Analysis of Disease-Associated Prion Protein in Cerebrospinal Fluid (CSF) by Real-Time QuIC Analysis in the Diagnosis of Sporadic Creutzfeldt-Jakob Disease (sCJD)." Authors received funding from the JPND (L.I.M.) and Chief Scientific Office, Scotland (G.F.). The National CJD Research & Surveillance Unit is funded by the Department of Health and the Scottish Home Office Department of Health. The views expressed in this publication are those of the authors and not necessarily those of the Department of Health.

Author Contributions

L.I.M. organized both the ring trials, coanalyzed the data, and cowrote the manuscript; A.P., I.P., S.Su., K.G., S.Sh., B.d.V., S.Sa., K.S., K.C., M.C., G.F., and M.E. performed RT-QuIC analyses; M.S., I.Z., and P.C. developed RT-QuIC analysis; L.I.M., F.T., R.A., D.K., S.C., S.H., P.P., M.P., and A.G. participated in the design of the study; A.G. coanalyzed the data and cowrote the manuscript.

Potential Conflicts of Interest

Nothing to report.

References

1. Report of a WHO consultation on global surveillance, diagnosis and therapy of human transmissible spongiform encephalopathies. Geneva, Switzerland: World Health Organisation, 1998.
2. Zerr I, Kallenberg K, Summers DM, et al. Updated clinical diagnostic criteria for sporadic Creutzfeldt-Jakob disease. Brain 2009; 132:2659–2668.
3. Chohan G, Pennington C, Mackenzie JM, et al. The role of cerebrospinal fluid 14-3-3 and other proteins in the diagnosis of sporadic CJD in the United Kingdom: a 10 year review. J Neurol Neurosurg Psychiatry 2010;81:1243–1248.
4. Newey CR, Sarwal A, Wisco D, et al. Variability in diagnosing Creutzfeldt-Jakob disease using standard and proposed diagnostic criteria. J Neuroimaging 2013;23:58–63.
5. Wilham JM, Orrú CD, Bessen RA, et al. Rapid end-point quantitation of prion seeding activity with sensitivity comparable to bioassays. PLoS Pathog 2010;6:e1001217.
6. Atarashi R, Wilham JM, Christensen L, et al. Simplified ultrasensitive prion detection by recombinant PrP conversion with shaking. Nat Methods 2008;5:211–212.
7. Atarashi R, Satoh K, Sano K, et al. Ultrasensitive human prion detection in cerebrospinal flid by real-time quaking-induced conversion. Nat Med 2011;17:175–178.
8. McGuire L, Peden A, Orru C, et al. Prion seeding activity in cerebrospinal fluid from patients with sporadic Creutzfeldt-Jakob disease patients using real-time QuIC analysis: a potential new clinical diagnostic test with high sensitivity and specificity. Ann Neurol 2012;72:278–285.
9. Peden A, McGuire L, Appleford N, et al. Sensitive and specific detection of sporadic Creutzfeldt-Jakob disease brain prion protein using real-time quaking induced conversion. J Gen Virol 2012;93:438–449.
10. Cramm M, Schmitz M, Karch A, et al. Stability and reproducibility underscore utility of RT-QuIC for diagnosis of Creutzfeldt-Jakob disease. Mol Neurobiol 2015;51:396–405.

The real-time quaking-induced conversion assay for detection of human prion disease and study of other protein misfolding diseases

Matthias Schmitz[1,6], Maria Cramm[1,6], Franc Llorens[1], Dominik Müller-Cramm[1], Steven Collins[2], Ryuichiro Atarashi[3], Katsuya Satoh[3], Christina D Orrù[4], Bradley R Groveman[4], Saima Zafar[1], Walter J Schulz-Schaeffer[5], Byron Caughey[4] & Inga Zerr[1]

[1]Department of Neurology, University Medical Center Göttingen and German Center for Neurodegenerative Diseases (DZNE), Göttingen, Germany. [2]Department of Medicine, The University of Melbourne, Parkville, Victoria, Australia. [3]Department of Molecular Microbiology and Immunology, Nagasaki University Graduate School of Biomedical Sciences, Nagasaki, Japan. [4]Laboratory of Persistent Viral Diseases, Rocky Mountain Laboratories, National Institute of Allergy and Infectious Diseases (NIAID), National Institutes of Health (NIH), Hamilton, Montana, USA. [5]Department of Neuropathology, University Medical Center Göttingen, Georg-August University, Göttingen, Germany. [6]These authors contributed equally to this work. Correspondence should be addressed to M.S. (matthias.schmitz@med.uni-goettingen.de).

Published online 13 October 2016; doi:10.1038/nprot.2016.120

The development and adaption of *in vitro* misfolded protein amplification systems has been a major innovation in the detection of abnormally folded prion protein scrapie (PrP^{Sc}) in human brain and cerebrospinal fluid (CSF) samples. Herein, we describe a fast and efficient protein amplification technique, real-time quaking-induced conversion (RT-QuIC), for the detection of a PrP^{Sc} seed in human brain and CSF. In contrast to other *in vitro* misfolded protein amplification assays—such as protein misfolding cyclic amplification (PMCA)—which are based on sonication, the RT-QuIC technique is based on prion seed–induced misfolding and aggregation of recombinant prion protein substrate, accelerated by alternating cycles of shaking and rest in fluorescence plate readers. A single RT-QuIC assay typically analyzes up to 32 samples in triplicate, using a 96-well-plate format. From sample preparation to analysis of results, the protocol takes ~87 h to complete. In addition to diagnostics, this technique has substantial generic analytical applications, including drug screening, prion strain discrimination, biohazard screening (e.g., to reduce transmission risk related to prion diseases) and the study of protein misfolding; in addition, it can potentially be used for the investigation of other protein misfolding diseases such as Alzheimer's and Parkinson's disease.

INTRODUCTION

Transmissible spongiform encephalopathies or prion diseases, such as Creutzfeldt–Jakob disease (CJD), are fatal neurodegenerative disorders characterized by the accumulation of abnormally folded PrP^{Sc} in the brain. In humans, sporadic CJD (sCJD) is the most common prion disease, followed by genetic CJD (gCJD) and transmitted CJD (iatrogenic CJD and variant CJD). For diagnosis of sCJD, elevated levels of certain biomarkers for neurodegeneration (such as 14-3-3, total tau, calcium-binding protein B (S-100B), neuron-specific enolase, desmoplakin, and α-synuclein)[1–8], in the CSF in combination with a detailed clinical examination, magnetic resonance imaging (MRI) and electroencephalogram, are important[9,10], although currently a definite diagnosis of CJD requires confirmation at autopsy[11]. However, the development of *in vitro* prion protein conversion assays, such as RT-QuIC, to detect misfolded prion protein has, to our knowledge, for the first time led to a test with a specificity close to 100% (refs. 12–15) and with high reproducibility across different laboratories[12,16], arguably making postmortem autopsies less essential.

Development of the protocol

To date, several *in vitro* protein conversion systems, which are directly based on the conversion of cellular prion protein (PrPC) to a conformationally altered isoform, PrP scrapie (PrPSc), and aggregation of a PrP-amyloid, have been developed. These include PMCA[17], the amyloid seeding assay[18], QuIC[19] and RT-QuIC[14,19,20]. These assays are comparable to a PCR for misfolded proteins, exploiting the seeded/template-induced assembly and conversion of PrP^{C} directly to ordered PrP^{Sc} aggregates, thereby amplifying miniscule amounts of PrP^{Sc} to a detectable level[14,17,20,21]. Although initial aggregation assays used brain material as the source of PrP^{C} substrate[17], these have subsequently been improved by the use of bacterially synthesized recombinant PrP^{C} ($recPrP^{C}$) substrate[19,22].

In RT-QuIC reactions, small amounts of misfolded PrP^{Sc} act as a seed, recruiting single $recPrP^{C}$ substrate molecules and inducing their conversion by integrating them into a growing amyloid aggregate concomitant with a conformational change of the substrate to a seeding-competent state (**Fig. 1**). Atarashi *et al.*[14] were the first to use a QuIC assay to demonstrate the capacity of PrP^{Sc} from human CSF samples to seed conversion of $recPrP^{C}$. During RT-QuIC, the samples are subjected to cycles of vigorous shaking, which presumably fragment the PrP^{Sc} aggregates into additional reactive seeds for conversion. With each cycle, consisting of incubation and shaking steps, the amyloid reaction product can increase exponentially (**Fig. 1**). The PrP^{Sc}-seeded conversion reaction product is enriched in β-strand secondary structure, as seen in amyloid, which enhances the fluorescence of the thioflavin T (Th-T) dye upon binding. Hence, nascent PrP^{Sc} can be monitored in real time using a temperature-controlled shaking fluorescence plate reader. The amplitude and kinetics of fluorescence enhancement can be used to evaluate relative seeding activities in test samples. The quantitative parameters were defined as lag phase (time to reach 10,000 r.f.u. (relative fluorescence units)), area under the curve (AUC) and maximal signal intensity (**Fig. 1**). Proteinase K–resistant PrP (PrP^{res}), generated after amplification by RT-QuIC, can be detected by western blotting[13,14].

The adaptation of the RT-QuIC assay to a 96-well-plate format[14] has the advantage over previous *in vitro* amplification systems of facilitating the automation of the technical process, thus enabling the easy detection of PrP aggregates by Th-T; these aggregates are considered to be noninfectious. Analysis of multiple reactions (96-well plates) also allows the measurement of up to 32 different samples in triplicate in the same run. In our 96-well-plate-based RT-QuIC assay[12], the signal response depends in part on the amount of PrP^{Sc} seed. With the cutoff threshold set at 10,000 r.f.u., the typical detection limit for postmortem sCJD brain tissue for the assay conditions described here is a dilution of $\approx 10^{-8}$, whereas for CSF it is a dilution of $\approx 10^{-1.2}$ (**Figs. 2a–e** and **3a–e**, **Supplementary Tables 1** and **2**). Higher dilutions reveal mean positivity rates below 50%, even though a positive fluorescence signal can be still detected in some reactions (**Figs. 2e** and **3e**). Control samples (taken from patients without prion disease) show, independently of the dilution, no PrP-seeding reaction (maximal signal below cutoff) in the brain or in CSF (**Figs. 2f** and **3f**).

Applications of the method

Being able to analyze RT-QuIC reactions in 96-well plates in an automated assay permits the high-throughput analyses of samples and increases the potential for numerous other applications in scientific and industrial fields[23,24]. Moreover, RT-QuIC assays have been developed for most prion strains and many human and animal tissues and body fluids[15,20,25–28], which makes this method applicable for diagnostics, biological science, prescreening for potential therapeutics and testing of materials for contamination with infectious prions. The following paragraphs illustrate examples of the manifold applications of the RT-QuIC assays.

Human prion disease diagnostics in CSF and in nasal brushings. The RT-QuIC assay was first established as a test for human prion disease diagnostics using CSF by *Atarashi et al.*[14]. The recent experience of different groups underlines the reproducibility of RT-QuIC across various CSF storage conditions with remarkable sensitivity and specificity, indicating that RT-QuIC is a robust diagnostic method[12,13,25,29]. Currently, although the RT-QuIC assay exhibits excellent specificity, it remains contentious whether this test can be used for a 'definite' diagnosis of prion disease, for which confirmation by neuropathological examination is still generally required. Given the sensitivity of most reported RT-QuIC assays, a negative test result cannot generally be interpreted as ruling out a CJD diagnosis. Future studies need to assess the potential of the method to detect all forms of CJD, including variant, genetic and atypical cases. To minimize 'gray-zone' and/or equivocal results but maintain specificity, we recommend testing each sample at least in triplicate and defining a sample as positive when >50% of the replicate wells show a PrP seeding reaction within 80 h. The evidence for this has been published recently[12].

Another RT-QuIC application is the detection of PrP^{Sc} in the olfactory neuroepithelium of prion disease patients[15]. RT-QuIC assays seeded with dilutions of nasal brushing samples were positive in 42 of 43 sCJD patients (cumulatively from two reports) and negative in 43 of 43 control donors, indicating a sensitivity of 97% and a specificity of 100% (refs. 15,30). Testing nasal brushings elicited stronger and faster RT-QuIC responses (higher seeding signal and shorter lag phase) as compared with corresponding CSF samples from the same patients. Moreover, as compared with lumbar punctures, nasal sampling provides an alternative and less invasive tool for collecting diagnostic specimens.

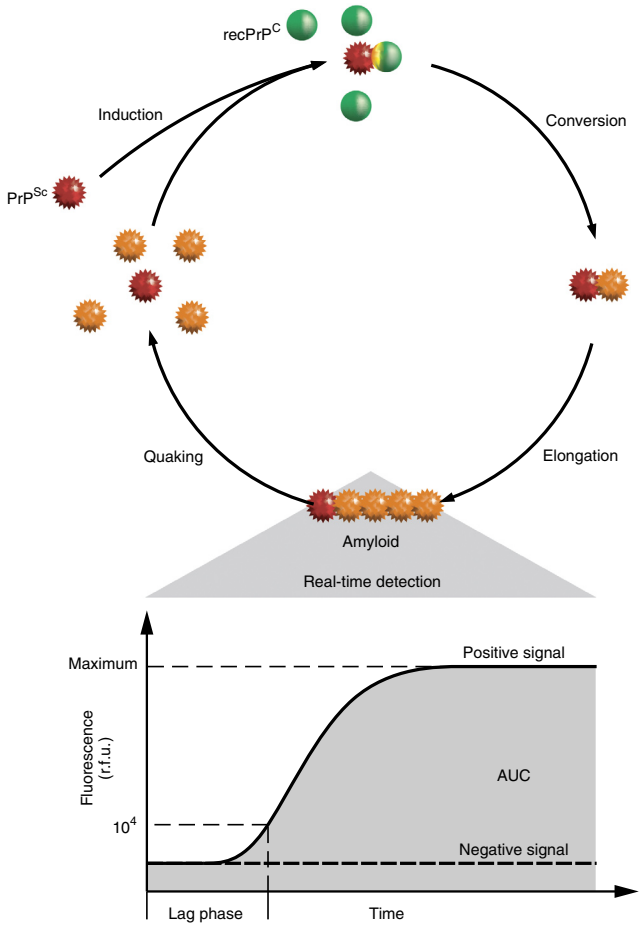

Figure 1 | Schematic diagram of PrP seed amplification by RT-QuIC assay. PrP^{Sc} seed derived from brain or CSF and $recPrP^{C}$ (substrate) is mixed and incubated, promoting the misfolding and incorporation of $recPrP^{C}$, and thus generating polymers of misfolded β strand–rich $recPrP^{C}$ as found in amyloid. The upper part shows how RT-QuIC exploits aspects of the prion replication mechanism. PrP^{Sc} is used as a seed (prickly dark red balls), which elongates through incorporation of $recPrP^{C}$ substrate (green balls). A conformational change is induced in the substrate, faithfully adopting some characteristics of the initial seed, including PK resistance, β-strand secondary structure and the ability to seed PrP amyloid formation (prickly orange balls). The growth of the generated β strand–rich PrP polymers can be detected in real time by a fluorescent dye. Through periods of shaking (quaking) and rest, these β strand–rich PrP polymers can potentially fragment, generating more seeds, in turn inducing an exponential amplification of $recPrP^{C}$ conversion. Signal quantification occurs according to the seeding parameters of interest, such as lag phase (time to reach 10,000 r.f.u.), area under the curve (AUC) and maximal signal intensity.

Prion strain typing. In sCJD, different types of PrP^{Sc} (type 1 or 2) and codon 129 genotypes of the prion protein gene (*PRNP*) determine at least six different molecular sCJD subtypes[9,31] that show distinct clinicopathological phenotypes and transmission characteristics[32]. A CSF study specifically tested the effects of molecular subtypes of prion disease on the RT-QuIC response[33] and found that the type of prion disease (sporadic or genetic), the *PRNP* mutation (E200K, D178N), codon 129 genotype and PrP^{Sc}

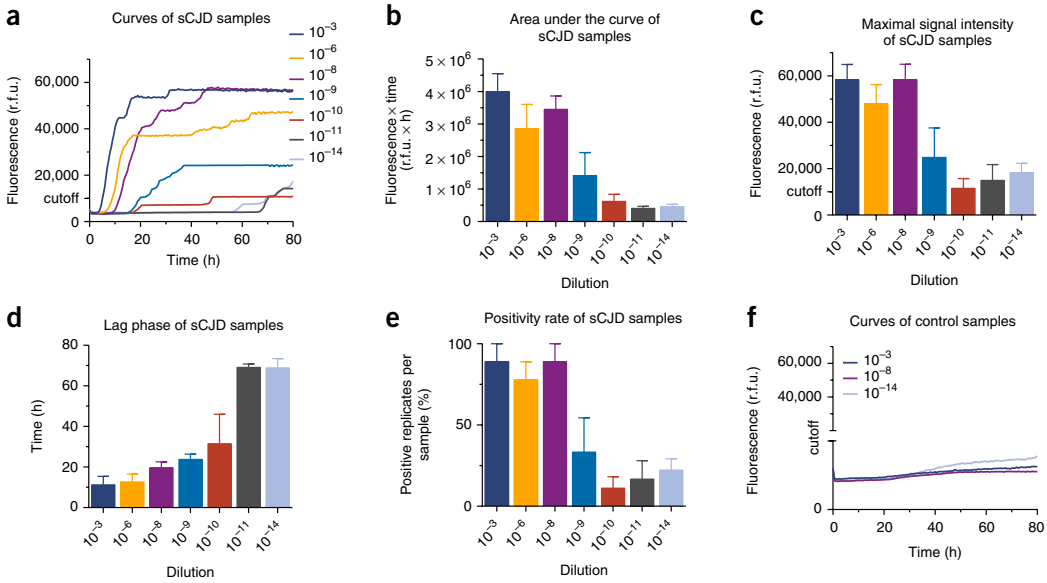

Figure 2 | Influence of serial dilution of brain homogenates on the RT-QuIC response. Serial dilution of brain homogenates, before RT-QuIC analysis, results in a decrease of the RT-QuIC response in sCJD samples. (**a**–**e**) Brain homogenates (10% (wt/vol)) from sCJD (MM1) patients ($n = 6$) and from (**f**) control patients ($n = 8$) (proven free of prion disease, such as those diagnosed with hypoxic encephalopathy, posterior infarct, cerebral amyloid angiopathy or basal ganglion infarct) were diluted in the range of 10^{-3} to 10^{-14}. Diluted samples were analyzed in triplicate by RT-QuIC. Statistical parameters quantifying the RT-QuIC response, such as AUC (**b**), maximal signal intensity (**c**) and time until the signal reached the cutoff (lag phase (**d**)), were determined per experimental group (dilution). (**a**) The curves depict the mean kinetics of the RT-QuIC response of six sCJD samples per experimental group (dilution). Fluorescence signal was measured every 30 min. Mean values were determined per sample and used to calculate total mean per experimental group (dilution) per measurement (time point). Total means were connected by linear interpolation, displaying an averaging line per experimental group (dilution). The cutoff is indicated at 10,000 r.f.u. This diagram shows aggregated data; therefore, no individual information about AUC, maximal signal intensity or lag phase can be extracted. (**b**–**d**) The RT-QuIC responses of sCJD samples were quantified by calculating statistical parameters such as area under the curve, maximal signal intensity and lag phase. Mean values were determined per sample and used to calculate total mean per experimental group (dilution) and s.e.m. Bar graphs show total mean + s.e.m. per experimental group (dilution). Cutoff is indicated at 10,000 r.f.u. (**e**) The validity of the RT-QuIC responses from sCJD samples was determined by calculating the percentage of positive replicates per sample. Mean values were determined per sample and used to calculate total mean per experimental group (dilution) and (s.e.m. Bar graphs show total mean + s.e.m. per experimental group (dilution). Samples diluted 10^{-9} to 10^{-14} showed a mean positivity rate of <50%. (**f**) The curves depict the mean kinetics of the RT-QuIC response from control samples per experimental group (dilution). Fluorescence signal was measured every 30 min. Mean values were determined per sample and used to calculate total mean per experimental group (dilution) per measurement (time point). Total means were connected by linear interpolation, displaying an averaging line per experimental group (dilution). The cutoff is indicated at 10,000 r.f.u. This diagram shows no seeding of PrP. Therefore, seeding parameters such as AUC, maximal signal intensity and lag phase were not available. The study conformed to the Code of Ethics of the World Medical Association and informed consent was given by all study participants or their legal next of kin, and the study was approved by the local ethics committee in Göttingen, Germany (no. 24/8/12). MM1, methionine/methionine 1.

type affected RT-QuIC responses; e.g., in gCJD forms, samples from E200K mutation carriers showed the strongest effect on the observed outcome variables. Recent studies by Orrú *et al.* using multiple recPrP^{C} substrates also revealed a correlation of RT-QuIC responses with different prion strains[24,28,34].

Therapeutic drug prescreening. As PrP^{Sc} is the main causative agent of prion diseases[35,36], most potentially therapeutic substances target PrP^{Sc}, the conversion process of PrP^{C} to PrP^{Sc} or PrP^{Sc} aggregation. The RT-QuIC assay can be used to compare the efficiency of antiprion compounds *in vitro* by using PrP^{Sc} from sCJD brain tissue as seed, providing a screening assay that mimics disease-relevant conditions[23]. However, unlike PMCA, RT-QuIC assays do not fully recapitulate infectious PrP^{Sc} replication[37], and thus it may be possible that some inhibitors of PrP^{Sc} formation might be missed.

However, not all substances that inhibit the conversion process of PrP in the RT-QuIC assay are potential therapeutics of prion disease; thus, we propose that substances known to interfere with Th-T, or with other chemicals from the reaction buffer, to change the reaction conditions (such as a change of the pH or digestion of the rec PrP substrate) or to show abnormal RT-QuIC seeding kinetics should be excluded[23].

In addition, the use of suitable controls without prion disease is very important in order to exclude the possibility that false-positive reactions in the RT-QuIC assay could result from the replication of a noninfectious amyloid state.

Testing of materials for contamination with infectious prions. Prions have a particularly high tolerance to inactivation and can retain infectivity even after undergoing routine sterilization processes[38,39]. Avoiding contamination of reusable surgical instruments and medical devices can therefore be challenging. The detection of prion infectivity by bioassay may take up to 2 weeks in cell-based infectivity assays[40] or even up to 20 weeks when a rapid mouse bioassay is applied[41]. In contrast, the application of an *in vitro* amplification assay (such as PMCA or RT-QuIC) for assessing prion infectivity is less time-consuming and very sensitive[20,42,43]. In this way, the efficiency of existing decontamination procedures can be estimated, and novel substances/procedures for disinfection can be developed.

Other protein misfolding diseases. A characteristic feature of the major neurodegenerative diseases is the progressive accumulation of protein aggregates in a self-propagating manner, with a topographical pattern characteristic of each disease. Although the spread of misfolded protein was initially thought to have a crucial role only in prion diseases, recent studies have identified similar characteristics for amyloid-beta, tau and α-synuclein in various other models[44–46]. The term 'prion-like' protein propagation in neurodegeneration is now widely used to address analogous mechanisms, which might have a role in Alzheimer's disease and α-synucleinopathies, such as Parkinson's disease. The RT-QuIC technique therefore also has considerable diagnostic and analytical potential with respect to other misfolded proteins (with biomarker potential), such as amyloid-beta, tau and α-synuclein[46,47].

Comparison with other methods

In comparison with the PCMA, there are technical variances between assays. PCMA is based on cyclical sonication of the reaction tube, consisting of an incubation and a sonication step at 37 °C (refs. 17,48,49). Tubes close to the horn's wall might show lower amplification efficiency compared with those in the center[50], indicating that quaking might be easier to control. There are also a few variations regarding the ingredients of the conversion/reaction buffers. The biological tissues in which human prion seeding activity has been detected by RT-QuIC include CSF, nasal fluid or brain[14,51], whereas PMCA can be used to detect PrP^{Sc} also in blood, urine, spleen, milk, oral secretions or liver[27,52–55]. A more sensitive modification of the RT-QuIC, the enhanced QuIC (eQuIC), could, however, be used to detect prion seeds in samples with a very low amount of PrP^{Sc} (e.g., urine) or in samples containing compounds inhibitory for the seeding reaction, such as blood plasma[25,27,52–55]. This includes a preanalytical immunoprecipitation step with beads coated with a PrP^{Sc}-specific antibody (e.g., 15B3).

RT-QuIC uses bacterially synthesized $recPrP^{C}$ as a substrate for the conversion and aggregation of PrP. In contrast, PMCA usually uses brain homogenate as a source of PrP^{C} substrate. In brain-homogenate-based PMCA reactions, PrP^{Sc} is faithfully replicated in the presence of necessary cofactors, giving an infectious product[56]. However, in RT-QuIC assays, the amplified $recPrP^{C}$ reaction product (PrP^{res}) is seeded by, but not conformationally identical to, PrP^{Sc} and lacks infectivity[28]. This is an advantage for prion disease diagnostics because CSF-RT-QuIC requires no high biosecurity level and has little potential for cross-contamination. A further advantage of RT-QuIC analysis compared with PMCA is the multiwell format, which enables the analysis of up to 96 samples in the same experiment and the ease of signal quantification (detection of Th-T in a fluorescence reader, whereas PMCA requires a PK digestion and semiquantitative detection of PrP^{Sc} in a western blot).

Limitations

One of the most important preanalytical issues is that contamination with blood cells, such as erythrocytes, may result in a false-negative RT-QuIC response. During the lumbar puncture, between 5 and 10% of CSF samples are contaminated with blood cells, which may disturb the PrP seeding activity. A blood cell contamination higher than 1,250 cells/μl inhibits

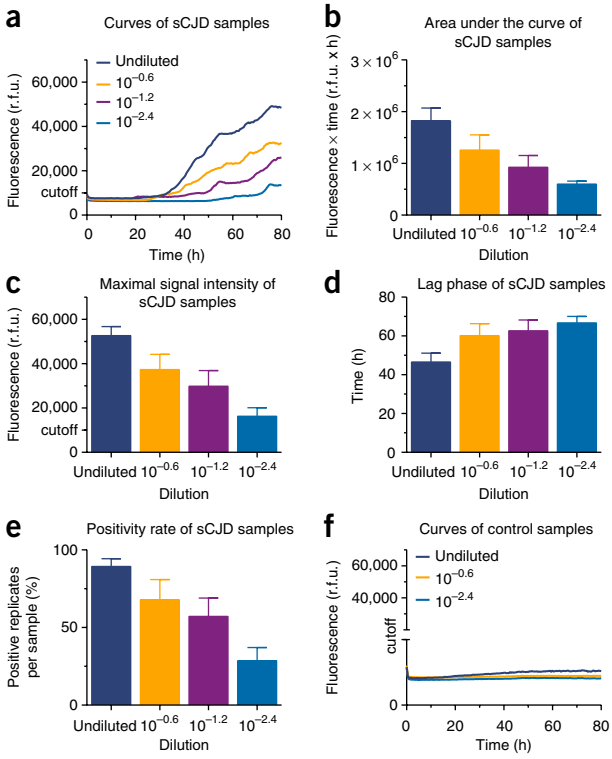

Figure 3 | Influence of serial dilution of CSF on the RT-QuIC response. Serial dilution of CSF, before RT-QuIC analysis, results in a decrease of the RT-QuIC response of sCJD samples. (**a**–**e**) CSF samples from sCJD (MM1) patients ($n = 7$) and from (**f**) control patients ($n = 8$) (without prion disease and with an alternative diagnosis such as headache, psychotic disorder, inflammation or another neurodegenerative disorder) were diluted in the range of $10^{-0.6}$ to $10^{-2.4}$. Diluted samples were analyzed in quadruplicate by RT-QuIC. Statistical parameters quantifying the RT-QuIC response, such as area under the curve (**b**), maximal signal intensity (**c**) and time until the signal reached the cutoff (lag phase (**d**)), were determined per experimental group (dilution). (**a**) The curves depict the mean kinetics of the RT-QuIC response of sCJD samples per experimental group (dilution). Fluorescence signal was measured every 30 min. Mean values were determined per sample and used to calculate total mean per experimental group (dilution) per measurement (time point). Total means were connected by linear interpolation, displaying an averaging line per experimental group (dilution). The cutoff is indicated at 10,000 r.f.u. (**b**–**d**) The RT-QuIC responses of sCJD-samples were quantified by calculating statistical parameters, such as AUC, maximal signal intensity and lag phase. Mean values were determined per sample and used to calculate total mean per experimental group (dilution) and s.e.m. Bar graphs show total mean + s.e.m. per experimental group (dilution). Cutoff is indicated at 10,000 r.f.u. (**e**) The validity of the RT-QuIC responses from sCJD samples was determined by calculating the percentage of positive replicates per sample. Mean values were determined per sample and used to calculate total mean per experimental group (dilution) and s.e.m. Bar graphs show total mean + s.e.m. per experimental group (dilution). Samples diluted $10^{-2.4}$ showed a mean positivity rate of <50%. (**f**) The curves depict the mean kinetics of the RT-QuIC response of control samples. Fluorescence signal was measured every 30 min. Mean values were determined per sample and used to calculate total mean per experimental group (dilution) per measurement (time point). Total means were connected by linear interpolation, displaying an averaging line per experimental group (dilution). The cutoff is indicated at 10,000 r.f.u. This diagram shows no seeding of PrP. Therefore, seeding parameters such as AUC, maximal signal intensity and lag phase were not available. The study conformed to the Code of Ethics of the World Medical Association, and informed consent was given by all study participants or their legal next of kin, and the study being approved by the local ethics committee in Göttingen, Germany (no. 24/8/12).

the RT-QuIC reaction markedly, when all cells are completely hemolyzed by sonication[12].

Other difficulties currently encountered when comparing results of various RT-QuIC assays from different laboratories are the variations in samples, reaction conditions and instruments, and the lack of standardized criteria for defining positive and negative responses. Such criteria will inevitably depend on the goals of the type of testing being performed (e.g., whether to minimize false positives or false negatives) and the idiosyncrasies of individual testing conditions. In the case of using RT-QuIC for human prion disease diagnosis using CSF specimens, further validation studies are required, although the RT-QuIC assay has demonstrated considerable diagnostic utility to date. For the protocol described below, a qualitative cutoff at 10,000 r.f.u. is suggested on the basis of two previous studies[12,33].

The duration of the RT-QuIC assay described below is usually 4 d. However, a recent study, which requires further validation, describes conditions, such as higher temperature (up to 55 °C) and addition of 0.002% (wt/vol) SDS and recPrP^{c} substrate (hamster 90–231), that can reduce assay times to a matter of hours and improve sensitivity[25].

Although not studied exhaustively, another limitation of RT-QuIC assays is that only very few recPrP^{c} substrates, such as bank vole recPrP^{c}, are able to amplify and to detect variant CJD prions. When using hamster 23–231 recPrP^{c}, no PrP variant CJD seeding could be obtained[28].

Experimental design

Protocol workflow. In the RT-QuIC, a PrP^{Sc} seed is incubated with a recPrP^{C} substrate (derived from several species, such as human, hamster, hamster–sheep chimera and bank vole; see further discussion below)[12,13,14,28] and a buffer to induce the conversion of the substrate and to subsequently amplify miniscule amounts of seed up to a detectable limit. Seed (derived from prion-infected human brain or CSF), substrate (recombinant hamster–sheep PrP^{C} (recHaShPrP^{C})) and buffer are prepared (Steps 4–7), combined in a 96-well plate (black 96-well, optical-bottom plates; see Steps 8–12) and incubated in a fluorescence plate reader (FLUOstar OPTIMA) at 42 °C for 80 h with intermittent shaking cycles, consisting of 1 min of double orbital shaking at the highest speed (600 r.p.m.) followed by a 1-min incubation break (Steps 13–17). Converted PrP is monitored in real time by Th-T fluorescent dye analysis. The kinetics of the aggregation process is determined by measuring the Th-T fluorescence signal (450 nm excitation and 480 nm emission) every 30 min. For data analysis, a quantification of statistical parameters, such as lag phase (time to reach the cutoff), AUC and maximal signal intensity, using common software programs is suggested (Steps 18–21).

Source of recPrP^{c}. recPrP^{c} may derive from various species—i.e., human[22], hamster[13], bank vole[24,28]—or, as in the present protocol, from a hamster–sheep chimera, which, in our experience, preferably shows less spontaneous aggregation and has been evaluated for diagnostic purposes over many years. Some evidence for comparability to other PrP substrates (e.g., human recPrP^{c}) can be derived from ring trials, in which the data suggest that various slightly modified test conditions provide similar test sensitivities and positive rates[12,16,25,29]. A recently described bank vole recPrP^{c} has been proven to support the amplification of many different PrP^{Sc} strains, different Gerstmann–Straussler–Scheinker syndrome (GSS) mutations and variant CJD, which cannot be detected with hamster recPrP^{c} (refs. 24,28). We propose that bank vole recPrP^{c} may become interesting for diagnostics in the future; however, an evaluation study on a larger patient cohort is still required.

Validation of the protocol: sensitivity and specificity. This protocol using the hamster–sheep chimera has been extensively validated through the analysis of CSF samples from different patient cohorts (within Europe and Japan) consisting of >500 patients with prion disease and >500 controls. Samples that show a seeding reaction (increase of the Th-T fluorescence signal) in 50% of the replicates are considered to be positive for a prion disease. Negative-control patients (without prion disease) show no seeding activity of PrP in the RT-QuIC assay after 80 h. A test run, in which the positive control remained negative, was considered to be a failed test. Under our conditions, we suggest a cutoff setting at 10,000 r.f.u. (cutoff may vary in different reference laboratories depending on the instrumental settings and the baseline of the reaction) to obtain a specificity of 99% and a sensitivity of 85% for the RT-QuIC assay for all prion diseases[12]. Across different prion diseases, the sensitivity varies from 100% for gCJD, 80% for sCJD and 57% for fatal familial insomnia (FFI) cases[12]. Other studies report a specificity of almost 100% and a sensitivity between 80 and 96% (refs. 13,14,25). For gCJD cases, the following sensitivities for RT-QuIC assays have been reported: FFI (100%), gCJD E200K (87%) and gCJD V210I (100%)[29]. Potential reasons for discrepancies in FFI sensitivities across studies can be sampling errors due to the low number of patients tested (7 versus 22 patients) and methodological differences (e.g., use of different PrP substrates)[12,29].

Replicates and controls. For diagnostics, each sample is generally analyzed in triplicate. A sample is considered as positive for the conversion of a competent amyloid (indicating a prion disease) if two out of three replicates show a Th-T signal higher than the cutoff (10,000 r.f.u.). As controls, samples from patients with (positive control) or without prion disease (negative control) are used. Control samples are prepared as described in the Reagent Setup.

False-positive reactions. A potential problem of *in vitro* amplification assays is the occurrence of false-positive reactions, caused by spontaneous conversion of the recPrP^{C}. Accordingly, our assay components and conditions have been carefully selected to maximize the kinetic difference between PrP^{Sc}-seeded and spontaneous, prion-independent responses. This protocol uses chimeric recPrP^{C}, composed of the Syrian hamster residues 23–137, followed by sheep residues 141–234 (of the R_{154} Q_{171} polymorphism)[26], in conjunction with reaction conditions that greatly retard the spontaneous aggregation of recPrP^{C} and thereby the occurrence of false-positive signals. A number of other combinations of recPrP^{C} substrate and reaction conditions have also been described as being suitable for the detection, and sometimes discrimination, of at least 28 different prions of humans and animals[12–14,20,24].

MATERIALS

REAGENTS

- Seed (brain homogenates or CSF samples from humans with prion diseases) ! CAUTION Informed consent must be obtained from all subjects, according to the relevant national legislation for the use of human biological samples for research. This study conformed to the Code of Ethics of the World Medical Association, and informed consent was given by all study participants or their legal next of kin, and the study was approved by the local ethics committee in Göttingen (no. 24/8/12). ! CAUTION This is a biological hazard. Biocontainment precautions need to be followed, according to the relevant national legislation for the use of biological samples from humans with prion diseases. In this study, precautions were taken related to biosafety level 3. ▲ CRITICAL Stability of the RT-QuIC seed in CSF under short- and long-term storage conditions is very high. CSF can be stored at room temperature or +4 °C for 8 d and at −80 °C for 9 years[12].
- Substrate (recombinant hamster–sheep chimeric PrP^C (recHaShPrP^C)) ▲ CRITICAL Laboratories that do not want to produce their own recHaShPrP^C (as described in **Supplementary Methods**) can request the protein from Thermo Fisher Scientific using the internal cat. no. 7700002 because it is not included in its standard catalog.
- Sodium phosphate dibasic (Sigma-Aldrich, cat. no. S7907)
- Sodium phosphate monobasic (Sigma-Aldrich, cat. no. S8282)
- NaCl (Roth, cat. no. 39571)
- Thioflavin-T (Th-T; Sigma-Aldrich, cat. no. T3516)
- SDS (Sigma-Aldrich, cat. no. L3771)
- Tris–HCl (Sigma-Aldrich, cat. no. T3253)
- 0.5 M EDTA (Fluka Analytical, cat. no. 06390)
- 5 M NaCl (SAFC Biosciences, cat. no. 59222C)
- PBS (Biochrome, cat. no. L 1825)
- 50% (wt/vol) NaOH (Roth, cat. no. 8655.1)

EQUIPMENT

- Centrifuge (Eppendorf, model no. 5415C)
- pH meter (Sartorius, model no. PP-15)
- Vortex (Scientific Industries, model no. Genie 2)
- Scale (Sartorius, model no. TE313S)
- Computer (Dell)
- Excitation filter, 450 nm for FLUOstar OPTIMA (BMG Labtech)
- Emission filter, 480 nm for FLUOstar OPTIMA (BMG Labtech)
- 96-Well Optical-Bottom Plate (Nunc, cat. no. 265301)
- Sealing tape (Nunc, cat. no. 232702)
- Syringe, 5 ml (Ecoject, cat. no. 4676651)
- Filter, Millex-GP, 0.22 µM (Merck-Millipore, cat. no. SLGP033RS)
- Microtubes, 1.5 and 2.0 ml
- Falcon tubes, 15 ml (VWR, cat. no. 734-0452)
- Falcon tubes, 50 ml (Sarstedt, cat. no. 62.547)

REAGENT SETUP

Homogenization buffer This buffer contains 0.1% (wt/vol) SDS prepared in PBS. For a 100-ml preparation, weigh 0.1 g of SDS, add 100 ml of PBS and dissolve the SDS by vortexing for 30 s, using a Vortex Genie 2 at level 10 (or an equivalent). Filter-sterilize the homogenization buffer using a 5-ml syringe and a 0.22-µM filter. Keep the buffer stock at 4 °C in 15-ml Falcon tubes, and discard after 3 months.

5× PBS, pH 6.9, buffer For a 50-ml preparation, weigh 0.67 g of sodium phosphate monobasic, 0.35 g of sodium phosphate dibasic and 1.90 g of NaCl and 48 ml of ddH_2O. Dissolve the substances by vortexing for 30 s, using a Vortex Genie 2 at level 10 (or an equivalent). Adjust the pH to 6.9, using NaOH (50% (wt/vol)) and a PP-15 pH meter (or an equivalent). Dilute 5× PBS, pH 6.9, in 50 ml of ddH_2O and mix by vortexing for 30 s, using a Vortex Genie 2 at level 10 (or an equivalent). Filter-sterilize 5× PBS, pH 6.9, using a 5-ml syringe and a 0.22-µM filter. Keep 5× PBS, pH 6.9, buffer stock at −20 °C in 15-ml Falcon tubes, and discard after 3 months.

Basis mix Prepare basis mix by mixing the following components at the ratio stated below for five reactions: 167 µl of ddH_2O, 100 µl of 5× PBS buffer, pH 6.9, 22 µl of NaCl (5 M) and 1 µl of EDTA (0.5 M). The total volume of basis mix per reaction is 57.0 µl (285 µl for five reactions). Preparing basis mix for multiple reactions in total in one tube is recommended to avoid errors in concentration by pipetting small volumes. Mix by vortexing for 30 s, using a Vortex Genie 2 at level 10 (or an equivalent). Keep the basis mix stock at −20 °C, and discard it after 3 months.

Th-T solution This solution contains 1 mM Th-T. For a 10-ml preparation of 10 mM Th-T, dissolve 0.036 g of Th-T in 10 ml of ddH_2O and vortex the mixture for 30 s, using a Vortex Genie 2 at level 10 (or an equivalent). Filter-sterilize the 10 mM Th-T solution using a 5-ml syringe and a 0.22-µM filter. Keep the 10 mM Th-T buffer stock in the dark at room temperature in a 15-ml tube, and discard it after 3 months. For a 10-ml preparation of 1 mM Th-T, dilute 1 ml of 10 mM Th-T in 9 ml of ddH_2O. Mix by vortexing for 30 s, using a Vortex Genie 2 at level 10 (or an equivalent). Keep the 1 mM Th-T buffer stock in the dark at room temperature in 2.0-ml tubes, and discard it after 3 months.

Final mix This mix contains 1× PBS, pH 6.9, 170 mM NaCl, 1 mM EDTA, 10 µM Th-T and 0.1 mg/ml recHaShPrP^C. For 1 reaction, mix 57.0 µl of basis mix, 1.0 µl of Th-T (1 mM) and 27.0 µl of recHaShPrP^C (0.37 mg/ml). Freshly prepare the final mix for each experiment, and discard it after use.

CSF sample preparation Prepare the CSF sample at room temperature (~22 °C). Centrifuge the native sample at 720*g* for 10 min to remove cell debris, using a 5415C centrifuge (or an equivalent). Remove the supernatant and discard the pellet. Transfer the supernatant to 1.5-ml tubes. Mix the supernatant for 30 s by using a Vortex Genie 2 at level 10 (or an equivalent). The supernatant can be stored at room temperature or 4 °C for up to 8 d, or at −80 °C for up to 9 years. ! CAUTION This is a biological hazard. Biocontainment precautions need to be followed according to the relevant national legislation for the use of biological samples from humans with prion diseases. In this study, precautions were performed related to biosafety level 3. ! CAUTION Informed consent must be obtained from all subjects, according to the relevant national legislation for the use of human biological samples for research. This study conformed to the Code of Ethics of the World Medical Association, and informed consent was given by all study participants or their legal next of kin, and the study was approved by the local ethics committee in Göttingen (no. 24/8/12). ▲ CRITICAL Blood contamination may cause false-negative results.

Brain sample preparation Prepare brain sample at room temperature. Weigh the native sample using a TE313S scale (or an equivalent), and add 10% (wt/vol) homogenization buffer. Homogenize the sample in homogenization buffer for 30 s, using a Polytron PT1300D (or an equivalent) at highest speed. Centrifuge the homogenized sample at 10,000*g* for 10 min to remove cell debris using a 5415C centrifuge (or an equivalent). Remove the supernatant and discard the pellet. Divide the supernatant into aliquots in 1.5-ml tubes, and vortex them for 30 s to mix adequately using a Vortex Genie 2 at level 10 (or an equivalent). The supernatant can be used immediately, or it can be stored at −80 °C. ! CAUTION Biological hazard. Biocontainment precautions need to be followed, according to the relevant national legislation for the use of biological samples from humans with prion diseases. In this study, precautions were performed related to biosafety level 3. ! CAUTION Informed consent must be obtained from all subjects, according to the relevant national legislation for the use of human biological samples for research. This study conformed to the Code of Ethics of the World Medical Association, and informed consent was given by all study participants or their legal next of kin, and the study was approved by the local ethics committee in Göttingen (no. 24/8/12).

EQUIPMENT SETUP

FLUOstar OPTIMA This RT-QuIC protocol requires the fluorescence reader FLUOstar OPTIMA, a computer and two software programs—i.e., the OPTIMA control program and the OPTIMA data analysis program. Both programs are provided by BMG Labtech. Using the FLUOStar Optima to run the RT-QuIC assay requires two protocols and one script—i.e., the Rocky Mtn Read and Rocky Mtn Shake protocols, and the Rocky Mtn Script. These can be requested from BMG Labtech. To measure the Th-T fluorescence according to this protocol, use two filters for the FLUOstar OPTIMA—i.e., an excitation filter at 450 nm and an emission filter at 480 nm. Both can be bought from the BMG Labtech Company. Enter the following settings into the Rocky Mtn Read protocol, and save the settings: microplate (Nunc 96), optic (bottom optic), excitation filter (450 nm), emission filter (480 nm) and additional shaking (no shaking). Enter the following settings into the Rocky Mtn Shake protocol, and save the settings: shaking mode (double orbital), shaking width (600 r.p.m.), additional shaking (before each cycle) and shaking time (57 s).

PROCEDURE

Operation of the fluorescence reader ● TIMING 15 min

1| Start the FLUOstar OPTIMA fluorescence reader and the computer.

2| Enter the temperature (42 °C) into the OPTIMA control program, and let the machine heat up.

3| Enter the following settings into the Rocky Mtn Script: target temperature (42 °C), cycle time (1,800 s) and total measurement time (80 h).

■ **PAUSE POINT** The fluorescence reader can wait until the start of experiment.

Preparation of recHaShPrP^C ● TIMING 1 h and 15 min

4| Thaw the recHaShPrP^C (0.6 mg/ml) at ≈4 °C.

▲ **CRITICAL STEP** Thawing at higher temperatures may induce aggregation of recHaShPrP^C.

5| Load 500 µl of recHaShPrP^C per 100-kDa filter at room temperature.

6| Centrifuge the loaded filters for 5 min at 1.310*g* at room temperature to remove possible existing aggregates, using a 5415C centrifuge (or an equivalent).

? TROUBLESHOOTING

7| Discard the filters and proceed with recHaShPrP^C filtrate at room temperature.

▲ **CRITICAL STEP** Some recHaShPrP^C is lost during the filtration process because aggregates are removed; the concentration of the filtrate should be ≈0.37 mg/ml.

■ **PAUSE POINT** Filtered recHaShPrP^C can be stored at room temperature for up to 30 min.

Unification and mixing of the sample at room temperature ● TIMING variable; ~2 h

8| Optional: thaw the frozen samples at room temperature.

9| Pipette 85 µl of final mix per well into a black 96-well optical-bottom plate.

▲ **CRITICAL STEP** Avoid creating bubbles, as they may cause variable results.

10| Vortex the sample for 30 s to mix adequately, using a Vortex Genie 2 at level 10 (or an equivalent).

11| Pipette 15 µl of sample into each well containing final mix from Step 9.

▲ **CRITICAL STEP** Avoid creating bubbles, as they may cause variable results.

12| Seal the plate with a sealing tape.

▲ **CRITICAL STEP** Make sure that the sealing tape is fixed on the plate without any air bubbles. Air bubbles may connect wells and may cause cross-contamination between different wells during the shaking process.

Running of the experiment ● TIMING 80 h and 15 min

13| Open the plate tray of the FLUOstar OPTIMA, and insert the plate from Step 12 into the plate carrier.

14| Declare used wells in the layout of the Rocky Mnt Read protocol.

15| Click the 'Start' button.

16| Wait until the temperature is at 42 °C, and confirm that the plate is inserted.

17| Run the machine for 80 h.

? TROUBLESHOOTING

■ **PAUSE POINT** After the run is completed, the fluorescence reader is ready for the taking of results; the machine stops executing the shaking and incubating cycles, but holds the temperature. To reduce the run-time of the machine, it is recommended to take the results on the day the run is completed.

Examination of results ● TIMING variable; ~2 h and 15 min

18| Open the OPTIMA data analysis program.

19| Open the latest run and verify the results. Criteria for a successful run are a complete data set (data for every well that should be measured) and valid signals from the controls.
? TROUBLESHOOTING

20| Discard the used black 96-well optical-bottom plate, or freeze it at –20 °C for further analyses of the product. Discard frozen plates after 3 months.
? TROUBLESHOOTING

21| Analyze the data using the OPTIMA data analysis program according to the manufacturer's instructions, or export the data and analyze in another program—e.g., Microsoft Office Excel or GraphPad Prism.

? TROUBLESHOOTING
Troubleshooting advice can be found in **Table 1**.

TABLE 1 | Troubleshooting table.

Step	Problem	Possible reason	Solutions
6	Loss of volume during the filtration process	~30% of the volume is usually lost during the filtration process, due to aggregation of recHaShPrP^C	Take this into account in your preparation of the final buffer mix
17	Unexpected system shutdown	Depending on the computer operating system, the system can shut down and restart for several reasons and, consequently, stop the software executing the fluorescence reader. This can be caused by, e.g., software routines aimed at saving energy or updating the system	Change the software routines to avoid this
19	Failed test (false-negative positive control)	Premature aggregation of recHaShPrP^C Aggregation of recHaShPrP^C may result in a loss of amyloid fibrillation potential	Verify storage and handling conditions RecHaShPrP^C should be stored at –80 °C. Thaw recHaShPrP^C on ice or at 4 °C and do not vortex; gently mix by swinging back and forth
	False-positive result	Bubbles may cause false-positive results	Avoid bubbles in Steps 9 and 11 while pipetting
	False-negative result	Dilution of brain sample might be too high	Choose lower dilutions of the brain sample. Dilutions from 10^{-3} to 10^{-8} usually work
		CSF sample might be contaminated with blood	Verify the absence of blood contamination. Contaminated CSF samples might be rescued by centrifugation at 720*g* for 10 min at room temperature[12]
	There are no data for some wells, and there are data for wells that should not be measured	The plate layout has been changed in the Rocky Mnt Shake protocol, instead of the Rocky Mnt Read protocol	Verify the plate layout in the Rocky Mtn Read protocol
	There are data for all wells that should be measured, but the data do not remotely correspond to anticipated results	The plate was accidently rotated by 180 °, so the original plate layout and orientation of wells no longer fit	Turn the plate layout around by 180°, and verify the position of the plate layout and anticipated results
	Fluorescence curves vary vastly between replicates	The software setting for optic is set to 'top optic'	Change the software setting from 'top optic' to 'bottom optic' in the Rocky Mnt Read protocol
		The filters have been installed in the wrong orientation	Check the orientation of the filters
20	The sealing tape is cracked	The plate is not fixed	Verify this, and if necessary, repair the machine

● TIMING

Steps 1–3, operation of the fluorescence reader: 15 min
Steps 4–7, preparation of recHaShPrP^{C}: 1 h and 15 min
Steps 8–12, unification and mixing of the sample at room temperature: variable; ~2 h to pipette a 96-well plate
Steps 13–17, running of the experiment: 80 h and 15 min
Steps 18–21, examination of results: ~2 h and 15 min; timing for analysis of the data is variable, depending on the experimental setup and analysis software: ~2 h to analyze maximal signal intensity (maximal r.f.u.), AUC and lag phase for a complete 96-well plate and compare between experimental groups

ANTICIPATED RESULTS

This protocol has been used to study the aggregation of misfolded PrP in brain tissue and CSF from prion disease patients[33]. Positive samples showed an increase of seeding activity (>cutoff) within a duration of 80 h (**Figs. 2a** and **3a**). By contrast, negative samples (those without prion disease) revealed no PrP seeding in the brain or in CSF (**Figs. 2f** and **3f**). The seeding efficiency of PrP, indicated by the Th-T signal, correlated with the dilution. Higher dilutions revealed a decrease of PrP seeding, indicated by a lower AUC, lower maximal signal intensity, longer lag phase and a lower positivity rate (**Figs. 2a–e** and **3a–e**; **Supplementary Tables 1** and **2**). In addition to prion disease diagnostics[12], this methodology can be used for a number of different approaches, such as studying protein misfolding in detail, prescreening for compounds inhibiting the PrP conversion, testing for prion contaminations or studying other protein misfolding diseases (e.g., Alzheimer's disease).

Note: Any Supplementary Information and Source Data files are available in the online version of the paper.

ACKNOWLEDGMENTS This study was performed as part of the Clinical Dementia Center at the University Medical Center Göttingen and was partly supported by grants from the EU Joint Program—Neurodegenerative Disease Research (JPND-DEMTEST (Biomarker-based diagnosis of rapid progressive dementias—optimization of diagnostic protocols, 01ED1201A) and by the Robert Koch Institute through funds from the Federal Ministry of Health (grant no. 1369-341). This work was also supported in part by the Intramural Research Program of the NIAID. S.C. is supported by a NHMRC Practitioner Fellowship (identification no. APP1005816) and by the Australian National Creutzfeldt-Jakob Disease Registry (ANCJDR), which is funded by the Commonwealth Department of Health.

AUTHOR CONTRIBUTIONS M.S. was involved in study concept and design, and validated the protocol, interpreted data and wrote the manuscript. M.C. performed experiments, analyzed and interpreted data, prepared figures and wrote the manuscript. F.L. provided samples and interpreted data.

D.M.-C. designed **Figure 1**. S.C., R.A., K.S., C.D.O., B.R.G., S.Z. and B.C. critically revised the manuscript. W.J.S.-S. provided samples. I.Z. supervised the study and critically revised the manuscript.

COMPETING FINANCIAL INTERESTS The authors declare competing financial interests: details are available in the online version of the paper.

1. Otto, M. *et al.* S-100 protein concentration in the cerebrospinal fluid of patients with Creutzfeldt-Jakob disease. *J. Neurol.* **244**, 566–570 (1997).
2. Otto, M. *et al.* Elevated levels of tau-protein in cerebrospinal fluid of patients with Creutzfeldt-Jakob disease. *Neurosci. Lett.* **225**, 210–212 (1997).
3. Zerr, I. *et al.* Detection of 14-3-3 protein in the cerebrospinal fluid supports the diagnosis of Creutzfeldt-Jakob disease. *Ann. Neurol.* **43**, 32–40 (1998).
4. Gawinecka, J. *et al.* Desmoplakin as a potential candidate for cerebrospinal fluid marker to rule out false 14-3-3 positive rates in sporadic Creutzfeldt-Jakob disease differential diagnosis. *Neurodegener. Dis.* **9**, 139–144 (2012).
5. Schmitz, M. *et al.* Validation of 14-3-3 protein as a marker in sporadic Creutzfeldt-Jakob diagnostic. *Mol. Neurobiol.* **53**, 2189–2199 (2016).
6. Llorens, F. *et al.* Quantification of CSF biomarkers using an electrochemiluminescence-based detection system in the differential diagnosis of AD and sCJD. *J. Neurol.* **262**, 2305–2311 (2015).
7. Beaudry, P. *et al.* 14-3-3 protein, neuron-specific enolase, and S-100 protein in cerebrospinal fluid of patients with Creutzfeldt-Jakob disease. *Dement. Geriatr. Cogn. Disord.* **10**, 40–46 (1999).
8. Zerr, I. *et al.* Cerebrospinal fluid concentration of neuron-specific enolase in diagnosis of Creutzfeldt-Jakob disease. *Lancet* **345**, 1609–1610 (1995).
9. Parchi, P. *et al.* Classification of sporadic Creutzfeldt-Jakob disease based on molecular and phenotypic analysis of 300 subjects. *Ann. Neurol.* **46**, 224–233 (1999).
10. Zerr, I. *et al.* Updated clinical diagnostic criteria for sporadic Creutzfeldt-Jakob disease. *Brain* **132**, 2659–2668 (2009).
11. World Health Organization. in *WHO Manual for Surveillance of Human Transmissible Spongiform Encephalopathies including variant Creutzfeldt-Jakob Disease 51-9* (World Health Organization, Geneva, 2003).
12. Cramm, M. *et al.* Stability and reproducibility underscore utility of RT-QuIC for diagnosis of Creutzfeldt-Jakob disease. *Mol. Neurobiol.* **53**, 1896–1904 (2016).
13. McGuire, L.I. *et al.* Real time quaking-induced conversion analysis of cerebrospinal fluid in sporadic Creutzfeldt-Jakob disease. *Ann. Neurol.* **72**, 278–285 (2012).
14. Atarashi, R. *et al.* Ultrasensitive human prion detection in cerebrospinal fluid by real-time quaking-induced conversion. *Nat. Med.* **17**, 175–178 (2011).
15. Orrú, C.D. *et al.* A test for Creutzfeldt-Jakob disease using nasal brushings. *N. Engl. J. Med.* **371**, 519–529 (2014).
16. McGuire, L.I. *et al.* CSF RT-QuIC is a robust and reliable test for sporadic CJD: an international study. *Ann. Neurol.* **80**, 160–165 (2016).
17. Saborio, G.P., Permanne, B. & Soto, C. Sensitive detection of pathological prion protein by cyclic amplification of protein misfolding. *Nature* **411**, 810–813 (2001).
18. Colby, D.W. *et al.* Prion detection by an amyloid seeding assay. *Proc. Natl. Acad. Sci. USA* **104**, 20914–20919 (2007).
19. Atarashi, R. *et al.* Simplified ultrasensitive prion detection by recombinant PrP conversion with shaking. *Nat. Methods* **5**, 211–212 (2008).
20. Wilham, J.M. *et al.* Rapid end-point quantitation of prion seeding activity with sensitivity comparable to bioassays. *PLoS Pathog.* **6**, e1001217 (2010).
21. Bessen, R.A. *et al.* Non-genetic propagation of strain-specific properties of scrapie prion protein. *Nature* **375**, 698–700 (1995).
22. Atarashi, R. *et al.* Ultrasensitive detection of scrapie prion protein using seeding conversion of recombinant prion protein. *Nat. Methods* **4**, 645–650 (2007).
23. Schmitz, M. *et al.* Application of an *in vitro*-amplification assay as a novel pre-screening test for compounds inhibiting the aggregation of prion protein scrapie. *Sci. Rep.* **6**, 28711 (2016).
24. Orrú, C.D. *et al.* Detection and discrimination of classical and atypical L-type bovine spongiform encephalopathy by real-time quaking-induced conversion. *J. Clin. Microbiol.* **53**, 1115–1120 (2015).

25. Orrú, C.D. *et al.* Rapid and sensitive RT-QuIC detection of human Creutzfeldt-Jakob disease using cerebrospinal fluid. *MBio* **6**, e02451–e02414 (2015).
26. Orrú, C.D. *et al.* Prion disease blood test using immunoprecipitation and improved quaking induced conversion. *MBio* **2**, e00078–e00011 (2011).
27. Orrú, C.D., Wilham, J.M., Vascellari, S., Hughson, A.G. & Caughey, B. New generation QuIC assays for prion seeding activity. *Prion* **6**, 147–152 (2012).
28. Orrú, C.D. *et al.* Bank vole prion protein as an apparently universal substrate for RT-QuIC-based detection and discrimination of prion strains. *PLoS Pathog.* **11**, e1004983 (2015).
29. Sano, K. *et al.* Early detection of abnormal prion protein in genetic human prion diseases now possible using real-time QUIC assay. *PLoS One* **8**, e54915 (2013).
30. Zanusso, G., Bongianni, M. & Caughey, B. A test for Creutzfeldt-Jakob disease using nasal brushings. *N. Engl. J. Med.* **371**, 1842–1843 (2014).
31. Cali, I. *et al.* Classification of sporadic Creutzfeldt-Jakob disease revisited. *Brain* **129**, 2266–2277 (2006).
32. Bishop, M., Will, R.G. & Manson, J.C. Defining sporadic Creutzfeldt-Jakob disease strains and their transmission properties. *Proc. Natl. Acad. Sci. USA* **107**, 12005–12010 (2010).
33. Cramm, M. *et al.* Characteristic CSF prion-seeding efficiency in humans with prion diseases. *Mol. Neurobiol.* **51**, 396–405 (2015).
34. Masujin, K. *et al.* Detection of atypical H-type bovine spongiform encephalopathy and discrimination of bovine prion strains by real-time quaking-induced conversion. *J. Clin. Microbiol.* **54**, 676–686 (2016).
35. Prusiner, S.B. Novel proteinaceous infectious particles cause scrapie. *Science* **216**, 136–144 (1982).
36. Prusiner, S.B. Prion encephalopathies of animals and humans. *Dev. Biol. Stand.* **80**, 31–44 (1993).
37. Groveman, B.R. *et al.* Charge neutralization of the central lysine cluster in prion protein (PrP) promotes PrP(Sc)-like folding of recombinant PrP amyloids. *J. Biol. Chem.* **290**, 1119–1128 (2015).
38. Johnson, C., Gilbert, P., McKenzie, D., Pedersen, J. & Aiken, J. Ultraviolet-ozone treatment reduces levels of disease-associated prion protein and prion infectivity. *BMC Res. Notes* **2**, 121–125 (2009).
39. Krasemann, S. *et al.* Preclinical deposition of pathological prion protein in muscle of experimentally infected primates. *PLoS One* **5**, e13906 (2010).
40. Kloehn, P.C., Stoltze, L., Flechsig, E., Enari, M. & Weissmann, C. A quantitative, highly sensitive cell-based infectivity assay for mouse scrapie prions. *Proc. Natl. Acad. Sci. USA* **100**, 11666–11671 (2003).
41. Fischer, M. *et al.* Prion protein (PrP) with amino-proximal deletions restoring susceptibility of PrP knockout mice to scrapie. *EMBO J.* **15**, 1255–1264 (1996).
42. Murayama, Y. *et al.* Protein misfolding cyclic amplification as a rapid test for assessment of prion inactivation. *Biochem. Biophys. Res. Commun.* **348**, 758–762 (2006).
43. Pritzkow, S. *et al.* Quantitative detections and biological propagation of scrapie seeding activity *in vitro* facilitate use of prions as moedel pathogens for disinfection. *PLoS One* **6**, e20384 (2011).
44. Eisele, Y.S. *et al.* Peripherally applied Abeta-containing inoculates induce cerebral beta-amyloidosis. *Science* **330**, 980–982 (2010).
45. Kim, J. & Holtzman, D.M. Medicine. Prion-like behavior of amyloid-beta. *Science* **330**, 918–919 (2010).
46. Meyer, V., Dinkel, P.D., Rickman Hager, E. & Margittai, M. Amplification of Tau fibrils from minute quantities of seeds. *Biochemistry* **53**, 5804–5809 (2014).
47. Salvadores, N., Shahnawaz, M., Scarpini, E., Tagliavini, F. & Soto, C. Detection of misfolded Ab oligomers for sensitive biochemical diagnosis of Alzheimer's disease. *Cell Rep.* **7**, 261–268 (2014).
48. Soto, C., Saborio, G.P. & Anderes, L. Cyclic amplification of protein misfolding: application to prion-related disorders and beyond. *Trends Neurosci.* **25**, 390–394 (2002).
49. Morales, R., Duran-Aniotz, C., Diaz-Espinoza, R., Camacho, M.V. & Soto, C. Protein misfolding cyclic amplification of infectious prions. *Nat. Protoc.* **28**, 1397–1409 (2012).
50. Gonzalez-Montalban, N. *et al.* Highly efficient protein misfolding cyclic amplification. *PLoS Pathog.* **7**, e1001277 (2011).
51. Peden, A.H. *et al.* Sensitive and specific detection of sporadic Creutzfeldt-Jakob disease brain prion protein using real-time quaking-induced conversion. *J. Gen. Virol.* **93**, 438–449 (2012).
52. Saá, P., Castilla, J. & Soto, C. Ultra-efficient replication of infectious prions by automated protein misfolding cyclic amplification. *J. Biol. Chem.* **281**, 35245–35252 (2006).
53. Maddison, B.C. *et al.* Prions are secreted into the oral cavity in sheep with preclinical scrapie. *J. Infect. Dis.* **201**, 1672–1676 (2010).
54. Chen, B., Morales, R., Barria, M.A. & Soto, C. Estimating prion concentration in fluids and tissues by quantitative PMCA. *Nat. Methods* **7**, 519–520 (2010).
55. Haley, N.J. *et al.* Detection of chronic wasting disease prions in salivary, urinary and intestinal tissues of deer: potential mechanisms of prion sheeding and transmission. *J. Virol.* **85**, 6309–6318 (2011).
56. Castilla, J. *et al.* Crossing the species barrier by PrP(Sc) replication *in vitro* generates unique infectious prions. *Cell* **134**, 757–768 (2008).

Mol Neurobiol (2016) 53:1896–1904
DOI 10.1007/s12035-015-9133-2

Stability and Reproducibility Underscore Utility of RT-QuIC for Diagnosis of Creutzfeldt-Jakob Disease

Maria Cramm · Matthias Schmitz · André Karch · Eva Mitrova · Franziska Kuhn · Bjoern Schroeder · Alex Raeber · Daniela Varges · Yong-Sun Kim · Katsuya Satoh · Steven Collins · Inga Zerr

Received: 4 December 2014 / Accepted: 22 February 2015 / Published online: 1 April 2015

Abstract Real-time quaking-induced conversion (RT-QuIC) allows the amplification of miniscule amounts of scrapie prion protein (PrP^{Sc}). Recent studies applied the RT-QuIC methodology to cerebrospinal fluid (CSF) for diagnosing human prion diseases. However, to date, there has not been a formal multicentre assessment of the reproducibility, validity and stability of RT-QuIC in this context, an indispensable step for establishment as a diagnostic test in clinical practice. In the present study, we analysed CSF from 110 prion disease patients and 400 control patients using the RT-QuIC method under various conditions. In addition, "blinded" ring trials between different participating sites were performed to estimate reproducibility. Using the previously established cut-off of 10,000 relative fluorescence units (rfu), we obtained a sensitivity of 85 % and a specificity of 99 %. The multi-centre inter-laboratory reproducibility of RT-QuIC revealed a Fleiss' kappa value of 0.83 (95 % CI: 0.40–1.00) indicating an almost perfect agreement. Moreover, we investigated the impact of short-term CSF storage at different temperatures, long-term storage, repeated freezing and thawing cycles and the contamination of CSF with blood on the RT-QuIC seeding response. Our data indicated that the PrP^{Sc} seed in CSF is stable to any type of storage condition but sensitive to contaminations with blood (>1250 erythrocytes/μL), which results in a false negative RT-QuIC response. Fresh blood-contaminated samples (3 days) can be rescued by removal of erythrocytes. The present study underlines the reproducibility and high stability of RT-QuIC across various CSF storage conditions with a remarkable sensitivity and specificity, suggesting RT-QuIC as an innovative and robust diagnostic method.

Keywords Cerebrospinal fluid · Creutzfeldt-Jakob disease · Diagnostic test · Prion protein · Real-time quaking-induced conversion

Abbreviations

CI	Confidence interval
CNS	Central nervous system
CSF	Cerebrospinal fluid
diff	Difference
FFI	Fatal familial insomnia
PrP^{C}	Cellular prion protein
PrP^{Sc}	Scrapie prion protein
PPV	Positive predictive value

Maria Cramm and Matthias Schmitz contributed equally to this work.

Electronic supplementary material The online version of this article (doi:10.1007/s12035-015-9133-2) contains supplementary material, which is available to authorized users.

M. Cramm · M. Schmitz (✉) · A. Karch · D. Varges · I. Zerr
Department of Neurology, University Medical Center Goettingen and German Center for Neurodegenerative Diseases (DZNE)—site Goettingen, Robert-Koch Str. 40, 37075 Göttingen, Germany
e-mail: matthias.schmitz@med.uni-goettingen.de

E. Mitrova
Department of Prion Diseases, Slovak Medical University Bratislava, Limbová 14, 833-03 Bratislava, Slovakia

F. Kuhn · B. Schroeder · A. Raeber
Thermo Fisher Scientific, Prionics AG, 8952 Schlieren, Switzerland

Y.-S. Kim
Ilsong Institute of Life Science, College of Medicine, Hallym University, Anyang, Republic of Korea

K. Satoh
Department of Molecular Microbiology and Immunology, Nagasaki University Graduate School of Biomedical Sciences, Sakamoto 1-12-4, Nagasaki, Japan

S. Collins
Department of Pathology, The University of Melbourne, Parkville 3010, Australia

NPV	Negative predictive value
ref	Reference
rcf	Relative centrifugal force
rel. AUC	Relative area under the curve
ROC	Receiver operating characteristic
rpm	Rounds per minute
RT-QuIC	Real-time quaking-induced conversion
rfu	Relative fluorescence units
CJD	Creutzfeldt-Jakob disease
gCJD	Genetic CJD
sCJD	Sporadic CJD
SD	Standard deviation
SEM	Standard error of the mean

Introduction

Transmissible spongiform encephalopathies or prion diseases are characterized by the aggregation and accumulation of misfolded scrapie prion protein (PrP^{Sc}) in brain tissue. They can occur spontaneously (sporadic) but also be due to familial and iatrogenic causes. Sporadic Creutzfeldt-Jakob disease (sCJD) is the most common prion disease in human, followed by genetic CJD (gCJD) and iatrogenic CJD (iCJD). Different molecular sCJD subtypes, which show unique clinicopathological phenotypes and transmission characteristics [1] and depend on the codon 129 genotype of the prion protein gene (*PRNP*) as well as the type of PrP^{Sc}, have been reported [2, 3].

The adaptation of in vitro amplification systems for the detection of PrP^{Sc} in human cerebrospinal fluid (CSF) was an innovation for the pre-mortem diagnosis. RT-QuIC analysis uses recombinant prion protein (recPrP) as a substrate to amplify very small amounts of PrP^{Sc} seed in human CSF to detectable levels. Time course of conversion can be monitored in real-time by a fluorescent dye using a fluorescent reader. Four previous studies demonstrated the diagnostic potential of RT-QuIC through amplification of PrP^{Sc} from human CSF, derived from sCJD and gCJD patients [4–7].

However, despite these initial reports, establishing RT-QuIC as a routine diagnostic test in clinical practice requires a comprehensive validation and standardization. To date, there is a lack of studies dealing with inter-laboratory reproducibility and standardization, assessment of short- and long-term stability and contamination of CSF samples with potential inhibitory blood cells of the RT-QuIC seeding response in human CSF of CJD patients. All of these parameters may lead to an artificial decrease or increase of PrP seeding activity in CSF and to false positive or negative results.

The aim of the present study was to further analyse the applicability of RT-QuIC for routine diagnostic purposes. Analysis of 110 CSF samples from prion disease patients and 400 from a control panel consisting of 200 retrospectively tested patients (diagnoses including Alzheimer's disease [AD], Parkinson's disease [PD], inflammatory [IF] and other non-prion diseases) and 200 prospectively randomly selected patients was undertaken to obtain diagnostic data more aligned to a routine clinical setting. Also, two ring trials were performed to generate data about the reproducibility of the RT-QuIC assay. Finally, the influence of different CSF storage conditions (long- and short-term storage or repeated freezing and thawing cycles) and the influence of blood contamination on the RT-QuIC seeding response were examined.

Materials and Methods

Patients

CSF samples were collected through routine activities of the German National Prion Disease Surveillance Center associated with the University Medical Center Göttingen. Samples were derived from 110 prion disease patients, consisting of 64 sCJD, 39 gCJD (33 E200K, 6 V210I mutation carriers) and 7 FFI (D178N mutation), as well as 400 control patients. Initial data on the cohort have been published elsewhere [7]. The data were used to calculate the sensitivity and specificity. All prion disease cases were neuropathologically confirmed.

The 200 retrospectively tested control patients represent those with either a clinically or pathologically defined alternative diagnosis (92 female, 108 male; aged 16–87 years; mean age 64.1±0.9 years at notification). This control group consisted of AD patients (rapid progressive and classical forms), patients with depression, Dementia with Lewy bodies, PD, psychosis, bipolar disorder, multiple sclerosis, epilepsy, schizophrenia, inflammatory CNS disease and others. The 200 prospective samples were enrolled from the Neurochemistry Laboratory at the Department of Neurology in the framework of quality assurance and were tested blinded for clinical and personal data. Gender- and age-dependent effects on the RT-QuIC seeding response were excluded before [7].

CSF Samples

CSF samples were stored at −80 °C prior to analysis. Haemorrhagic CSF samples were excluded from the study.

Ethical Statement

The study was conformed to the Code of Ethics of the World Medical Association and informed consent was given by all study participants or their legal next of kin with the study being approved by the local ethics committee in Goettingen (No. 24/8/12). All samples were analysed blinded for at least personal data.

RT-QuIC Analysis

The RT-QuIC was performed as described previously [7]. Briefly, 85 μL of reaction buffer were seeded with 15 μL of freshly thawed and neat CSF to a final volume of 100 μL, with each CSF sample generally run in triplicate. Prepared plates were sealed (VWR, Hannover, Germany) and incubated in a plate reader (FLUOStar OPTIMA, BMG Labtech, Ortenberg, Germany) at 42 °C for 80 h with intermittent shaking cycles, consisting of 1 min double orbital shaking at 600 rpm followed by a 1-min break. Beta-sheet formation kinetic was determined by measuring the thioflavin T (ThT) fluorescent signal (450 nm excitation and 480 nm emission) every 30 min in relative fluorescence units (rfu). When we obtained more than 50 % positive replicates (signal ≥10,000 rfu after 80 h), the sample was considered as positive. Controls were considered as negative when more than 50 % of the replicates revealed a RT-QuIC response after 80 h below 10,000 rfu.

Expression and Purification of Recombinant Sheep-Hamster PrP

All RT-QuIC experiments were performed using the chimeric recPrP composed of the Syrian hamster residues 14 to 128 followed by sheep residues 141 to 234 of the R_{154} Q_{171} polymorphic haplotype as described before [7, 8]. The recPrP was prepared and its functionality was verified according to the method described by Wilham et al. [9].

Study Design

The present study was performed in three stages in order to determine the reproducibility, stability and validity of RT-QuIC for use as a diagnostic test for human prion diseases:

1. To investigate the reproducibility of the RT-QuIC assay, we conducted two ring trial studies between different laboratories. Fifty-four CSF samples obtained from sCJD patients and 32 non-prion disease controls were examined in two laboratories (UMG, Thermo Fisher Scientific). In a second ring trial, one sCJD and five controls were investigated in four laboratories (UMG, Ilsong Institute of Life Science, Nagasaki University Graduate School of Biomedical Sciences, Western General Hospital, and University of Melbourne).
2. To calculate specificity, sensitivity and predictive values of the RT-QuIC assay, we analysed CSF samples from 110 prion disease patients, as well as from 400 control patients.
3. To determine the stability of RT-QuIC, sCJD CSF samples (n=12) and control samples (n=6) were incubated under short- and long-term storage conditions.
4. To assess the impact of blood contamination of CSF samples on the RT-QuIC response, we spiked CSF from sCJD (n=6–8) and control samples (n=6–8) with defined amounts of blood cells from control patients.
5. To investigate the impact of transportation on blood-contaminated samples, we spiked CSF from sCJD (n=8) and control samples (n=8) with a defined amount of blood cells from control patients and incubated the CSF samples for 0, 1, 3 and 8 days at room temperature.

Statistical Analysis

In the first part of this study, inter-rater reliability within ring trials was calculated using the Fleiss' kappa for multiple readers. A Fleiss' kappa value of >0.60 was defined as substantial agreement, Fleiss' kappa >0.80 as almost perfect agreement between raters.

To test the diagnostic validity, we established a training dataset consisting of 28 CJD patients and nine controls, which were not part of the present study. A Receiver operating characteristic (ROC) analysis was performed on this dataset, and the best cut-off value was estimated to be 10,000 rfu based on the Youden index. We thereby confirmed the analysis of McGuire et al. [4] in an independent dataset and applied the cut-off value of 10,000 rfu to this study.

For the analysis of the stability of RT-QuIC, a two-step approach was performed. First, positivity rates were calculated (defining a seeding efficiency of ≥10,000 rfu within 80 h as positive) and were compared between groups using ANOVAs. Agreement levels and Fleiss' kappas were calculated in order to investigate the stability of positivity under different circumstances. Then, measurements of seeding efficiency were calculated for each individual sample defined by relative area under the curve (rel. AUC) and maximal ThT signal (maximum), and groups were compared using paired and unpaired t tests as appropriate. For graphical illustration, time series plots are presented at each step of the analysis, displaying means of seeding activity for each point in time (each measurement) in the respective groups. Thus, these illustrations show aggregated data for each point in time, but information about means of AUCs or individual maximums cannot be read out of these plots [7].

Sensitivity, specificity and predictive values of RT-QuIC were calculated for the entire dataset as well as for distinct subgroups. All analyses were conducted using Stata 12 software (StataCorp, College Town, US) and R 2.15.3 software.

Analysis of CSF by ELISA for 14-3-3

Levels of 14-3-3 protein in CSF were determined by using the CircuLex 14-3-3 Gamma ELISA Kit (BIOZOL Diagnostica Vertrieb GmbH, Eching, Germany) according to a previously established protocol [7].

Determination of Total Tau Level

CSF levels of total tau protein were measured using a commercially available ELISA kit (INNOTEST® hTAU Ag, Innogenetics). For the determination of tau levels, we followed the manufacturer's instructions.

Results

Reliability of RT-QuIC Assay in Comparison to 14-3-3 and Tau Proteins

To investigate the reproducibility of PrP^{Sc} amplification via RT-QuIC assay, we initiated two ring trial studies and included comparison to other biomarker proteins (tau and 14-3-3). Results of inter-laboratory agreement were indicated as Fleiss' kappa, which was calculated in a first ring trial with two partners as 0.75 (95 % CI: 0.40–1.00) revealing a substantial agreement, comparable to 14-3-3 and tau proteins (Supplement 1). A second ring trial with four raters showed an almost perfect agreement (Fleiss' kappa= 0.83 (95 % CI: 0.40–1.00)), proving high reliability and reproducibility of the RT-QuIC assay (Supplement 1).

Determination of the Specificity and Sensitivity of RT-QuIC Assay

Using a cut-off at 10,000 rfu/80 h (defined by Youden index[10]), an overall sensitivity of 85 % for all prion diseases and a specificity of 99 % could be achieved (Fig. 1a–c). Genetic CJD cases showed a sensitivity of 100 %, while analysis of sCJD and FFI CSF samples revealed a sensitivity of 80 and 57 %, respectively (Fig. 1c). The control cohort consisted of

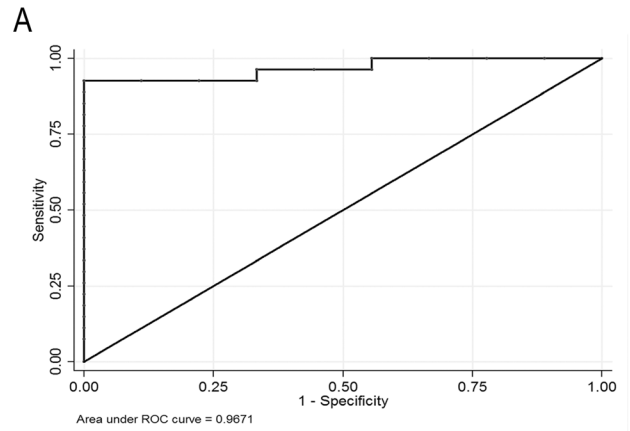

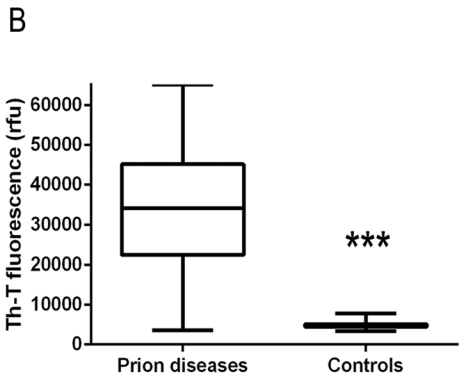

C

RT-QuIC	Prion Disease	gCJD E200K	gCJD V210I	sCJD	FFI	Controls
≥ 10,000 rfu	94 (85%) Sensitivity 1 (PPV: 61%)	33 (100%) Sensitivity 2	6 (100%) Sensitivity 3	51 (80%) Sensitivity 4	4 (57%) = Sensitivity 5	2 (1%)
< 10,000 rfu	16 (15%)	0 (0%)	0 (0%)	13 (20%)	3 (43%)	398 (99%) Specificity (NPV: 99,7%)
Total	110 (100%)	33 (100%)	6 (100%)	64 (100%)	7 (100%)	400 (100%)

D

Diagnosis	N
Vascular Dementia	40
Alzheimer's Disease	30
Inflammatory	29
Parkinson's Disease	28
non-CJD	21
Rapid Alzheimer's Disease	12
Epilepsy	11
Multiple Sclerosis	8
Depression	8
Dementia with Lewy Bodies	4
Bipolar Disorder	2
Meningitis	1
Schizophenia	1
Psychosis	1
Infarct	1
Opticus neuritis	1
Pseudotumor cerebri	1
NPH	1
Total	200

Fig. 1 Analysis of the sensitivity and specificity of the RT-QuIC assay. RT-QuIC response was measured in rfu over a period of 80 h. **a** RT-QuIC signalling response was evaluated as a diagnostic test by using receiver operating characteristic (ROC) curves. The ROC curve of the training dataset is shown suggesting a cut-off at 10,000 rfu. **b** Prion diseases exhibited a median RT-QuIC signal of 35,000 rfu, while controls remained under 10,000 rfu. **c** Considering >50 % positive RT-QuIC replicates as positive for prion disease, we obtained a specificity of 99 % and an averaged sensitivity of 85 %. **d** Two hundred CSF samples, retrospectively tested by RT-QuIC, are summarized

200 patients with different diagnoses, e.g. AD, PD, IF etc. (Fig. 1d) and 200 prospectively tested patients.

However, we obtained two false positive results with a RT-QuIC response higher than 10,000 rfu in the control samples (Supplement 2). CSF sample 1 was from a patient originally clinically diagnosed as AD, while for sample 2, the diagnosis was still outstanding at the time of RT-QuIC analysis. Sample 1 showed no abnormalities with respect to 14-3-3 and total tau protein levels, while the second patient exhibited elevated tau and 14-3-3 levels, as well as a positive MRI, in keeping with prion disease. For patient 1, autopsy was not available and the patient has been lost to follow-up.

Stability of the RT-QuIC Seeding Response with Long- and Short-Term CSF Storage Conditions

CSF samples derived from 12 sCJD and six control patients were stored in polypropylene tubes at room temperature or 4 °C for up to 8 days. To estimate the impact of long-term storage on the stability of RT-QuIC seeding response, we analysed sCJD (n=12) and control (n=6) samples, which were stored for 2–3, 5–6 or 8–9 years in a −80 °C freezer. Additionally, we subjected 12 sCJD and six control CSF samples to up to 16 repeated freezing and thawing cycles.

We calculated for each indicated condition the percent of positive replicates per sample defined as a seeding response of more than 10,000 rfu (cut-off) in 80 h (3/3=100 %, 2/3=66 %, 1/3=33 % and 0/3=0 %), which is important for CJD diagnostic. Our data indicated that the PrP^{Sc} seed in the RT-QuIC reaction remained stable under the analysed short- and long-term storage conditions and was resistant to up to 16 repeated freezing and thawing cycles (Fig. 2a–d). Under short-term storage conditions, the temperature had no significant influence on the number of positive replicates.

Subsequently, we analysed the RT-QuIC seeding efficiencies as a second parameter, which describes the intensity of the RT-QuIC signal, under the indicated storage conditions. We defined seeding efficiency as a combination of the following two parameters of interest: rel. AUC and the signal maximum of RT-QuIC response (maximum). Again, we observed that the seeding efficiency of PrP^{Sc} was not significantly influenced, neither under short-term nor under long-term storage conditions or after repeated freezing and thawing cycles of CSF samples (Fig. 3a–d).

Control samples without prion disease showed negative RT-QuIC responses (<10,000 rfu) under these conditions (data not shown).

Influence of Blood Contamination on RT-QuIC Seeding Response in CSF

Since erythrocytes and platelets in human blood contamination of CSF may influence PrP^{Sc} seeding activity in the RT-QuIC assay, we spiked CSF derived from sCJD patients (n=6–8) and non-CJD controls (n=6–8) with different amounts of

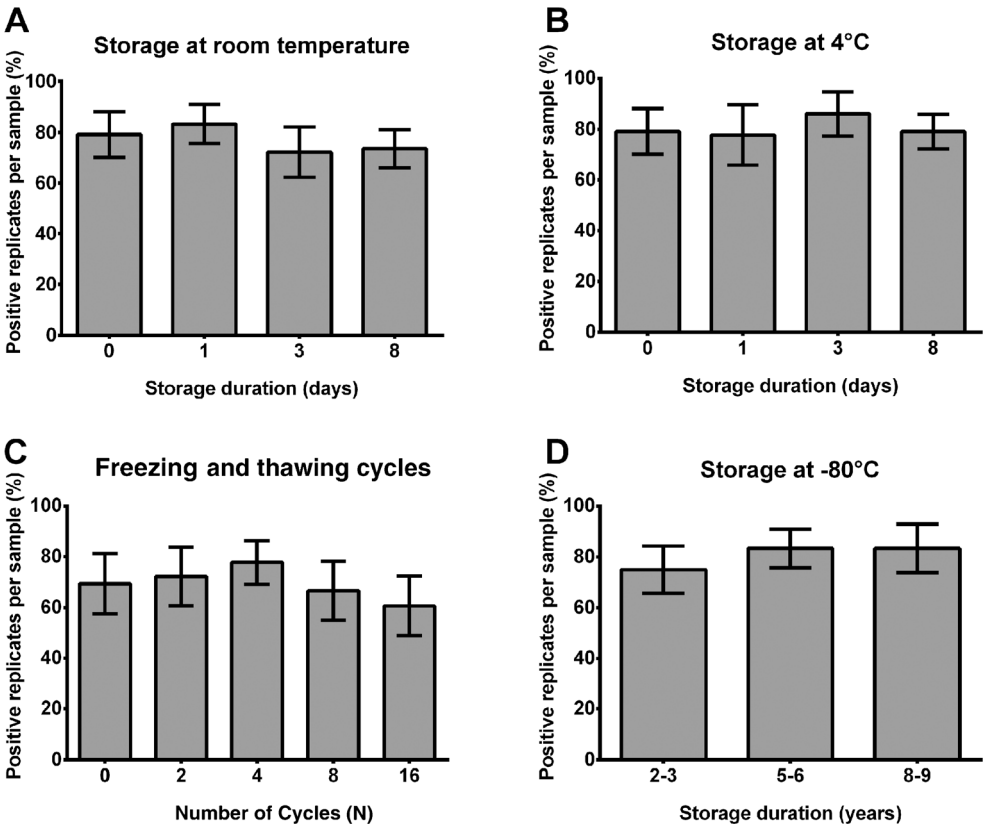

Fig. 2 Effect of various storage conditions on the RT-QuIC signal response. RT-QuIC reactions seeded with CSF from sCJD patients were analysed under short-term storage conditions (8 days) at room temperature (RT) and 4 °C (**a**, **b**), after 16 repeated freezing and thawing cycles (**c**) and after long-term storage (up to 9 years) (**d**). There was no significant trend for decreasing positivity rates over time when **a** storing at room temperature (p=0.337), **b** storing at 4 °C (p=0.713) or **c** after 16 freezing and thawing cycles (p=0.537) and **d** over several years of storage at −80 °C. Numbers of positive replicates were calculated for each sample in percent. Standard deviation of the mean from n=12 patients per group was indicated by *error bars*. For comparison between groups, we used ANOVAs

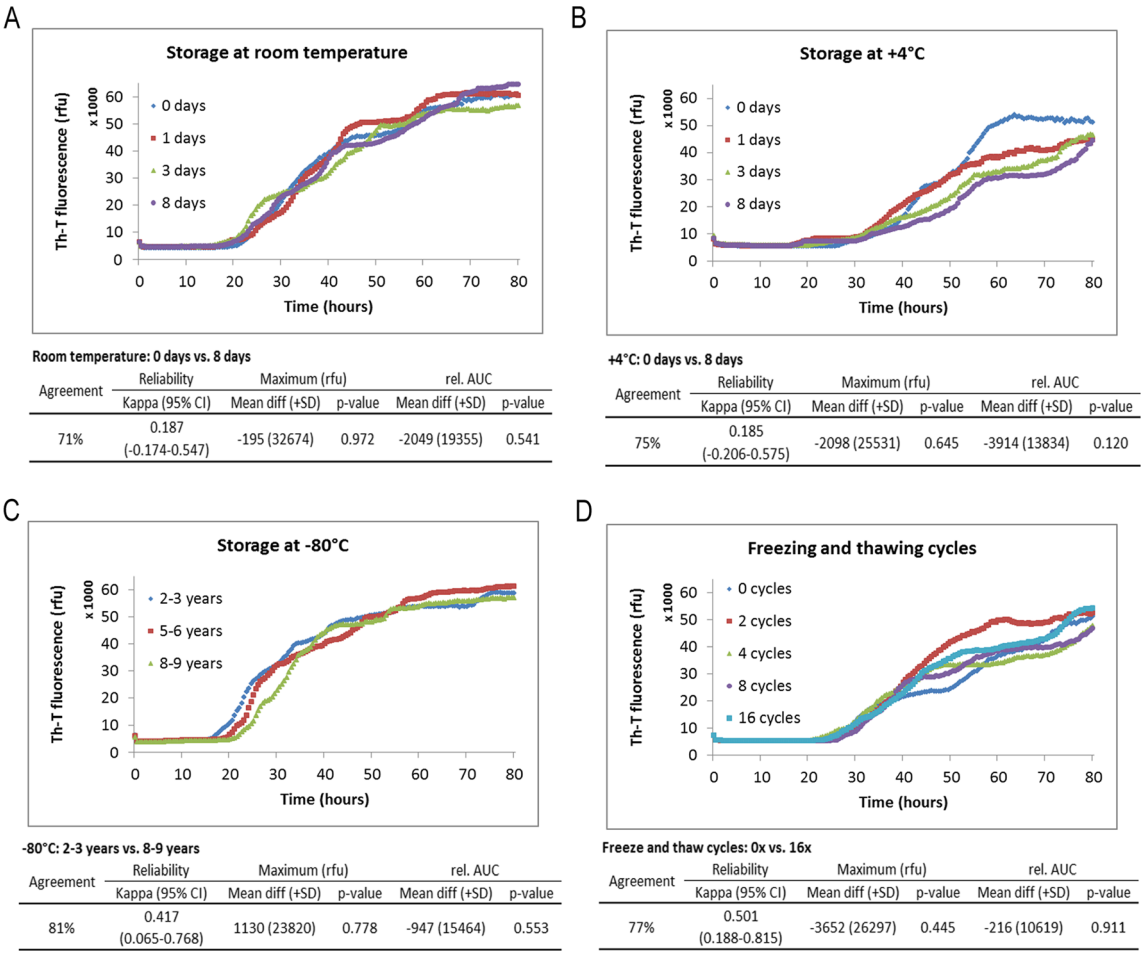

Room temperature: 0 days vs. 8 days

Agreement	Reliability	Maximum (rfu)		rel. AUC	
	Kappa (95% CI)	Mean diff (+SD)	p-value	Mean diff (+SD)	p-value
71%	0.187 (-0.174-0.547)	-195 (32674)	0.972	-2049 (19355)	0.541

+4°C: 0 days vs. 8 days

Agreement	Reliability	Maximum (rfu)		rel. AUC	
	Kappa (95% CI)	Mean diff (+SD)	p-value	Mean diff (+SD)	p-value
75%	0.185 (-0.206-0.575)	-2098 (25531)	0.645	-3914 (13834)	0.120

-80°C: 2-3 years vs. 8-9 years

Agreement	Reliability	Maximum (rfu)		rel. AUC	
	Kappa (95% CI)	Mean diff (+SD)	p-value	Mean diff (+SD)	p-value
81%	0.417 (0.065-0.768)	1130 (23820)	0.778	-947 (15464)	0.553

Freeze and thaw cycles: 0x vs. 16x

Agreement	Reliability	Maximum (rfu)		rel. AUC	
	Kappa (95% CI)	Mean diff (+SD)	p-value	Mean diff (+SD)	p-value
77%	0.501 (0.188-0.815)	-3652 (26297)	0.445	-216 (10619)	0.911

Fig. 3 Time course of prion seeding activity in the CSF of sCJD patients after defined storage conditions. RT-QuIC reactions seeded with CSF from sCJD patients were analysed under short-term storage conditions (8 days) at room temperature (RT) and 4 °C (**a**, **b**) after long-term storage (up to 9 years) (**c**) and after 16 repeated freezing and thawing cycles (**d**). The PrP^{Sc} seeding efficiency was not significantly changed under these conditions. Graphically displayed are means of all positive replicates per group at each point in time. The absolute values for rel. AUC and signal maximum were shown for each group, and the *p* values were calculated for each comparative analysis. *p* values were obtained using paired or unpaired *t* tests for comparisons of maximum values and rel. AUCs

sonicated red blood cells from control donors (78, 313, 1250, 5000 or 10,000 erythrocytes/μL).

Our results indicated that an erythrocyte concentration higher than 1250 cells/μL showed a false-negative RT-QuIC response. Blood contaminations significantly influenced the number of positive replicates (Fig. 4a) as well as the signal intensity of the RT-QuIC response (Fig. 4c).

In contrast, erythrocyte concentrations below 1250 cells/μL are tolerable for diagnostics because they did not show any significant impact on the number of positive replicates and the intensity of the RT-QuIC signal (Fig. 4a, c). CSF from non-prion controls, spiked with blood always revealed a negative RT-QuIC seeding response (data not shown).

Subsequently, we simulated the impact of transportation on blood contaminated samples by spiking CSF samples from sCJD ($n=8$) and control samples ($n=8$) with a defined amount of blood cells (5000 cells/μL) from control patients. After 0, 1, 3 and 8 days, we centrifuged the samples to remove the blood cells. The haemolysis and release of inhibitory proteins, which influence the number of positive replicates and the intensity of the RT-QuIC signal significantly, started after 3 days resulting in a false-negative RT-QuIC seeding response in sCJD patients (Fig. 4b, d). For comparison, we used non-spiked CSF from sCJD patients as a reference.

Discussion

The development of in vitro conversion assays, such as protein misfolding cyclic amplification (PMCA), enhanced quaking induced conversion (eQuIC) or RT-QuIC, exploit the self-propagating replication of the abnormally folded PrP^{Sc} to amplify miniscule amounts of PrP^{Sc} to a detectable level. Although these assays initially employed brain material, four recent studies demonstrated the capacity of RT-QuIC to replicate PrP^{Sc} from human CSF [4–7].

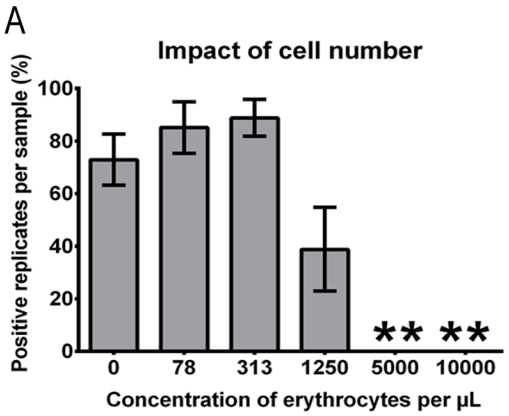

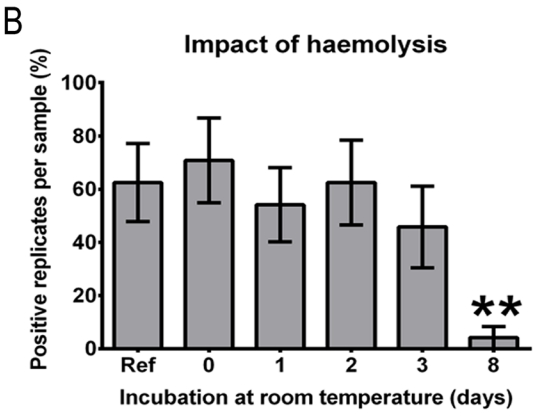

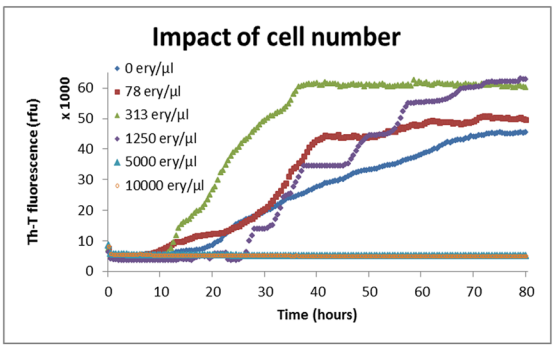

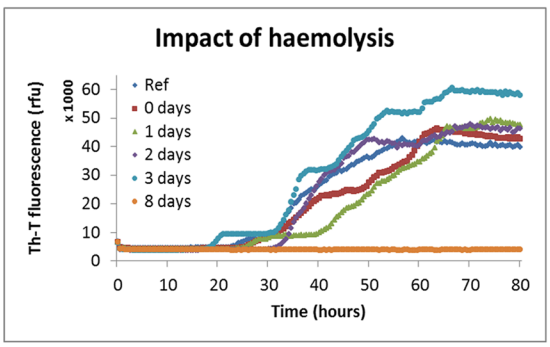

ery/µl	Agreement in positivity		Maximum (rfu)		rel. AUC	
	Agreement	Kappa (95%CI)	Difference (+SD)	p value*	Difference (+SD)	p value*
0	Reference	Reference	Reference		Reference	
78	77%	0.462 (0.167-0.756)	10203 (20639)	0.011	4758 (13959)	0.072
313	76%	0.173 (-0.279-0.625)	6289 (24396)	0.240	1570 (20385)	0.722
1250	39%	0.000 (-0.266-0.266)	-19573 (37504)	0.041	-13285 (22825)	0.024
5000	39%	0	-25837 (23446)	<0.001	-10296 (12370)	0.002
10000	39%	0	-25791 (23466)	<0.001	-10235 (12361)	0.003

*comparing the respective group (concentration of erythrocytes and type of blood in this line) with the control group (no blood)

Transport days	Agreement in positivity		Maximum (rfu)		rel.AUC	
	Agreement	Kappa (95%CI)	Difference (+SD)	p value*	Difference (+SD)	p value*
0	Reference	Reference	Reference		Reference	
0	83%	0.628 (0.303-0.953)	4979 (13361)	0.081	400 (9503)	0.838
1	88%	0.739 (0.464-1.000)	1035 (14378)	0.728	3478 (9221)	0.078
2	83%	0.644 (0.328-0.961)	3835 (20563)	0.370	274 (10281)	0.898
3	75%	0.510 (0.189-0.832)	1981 (21903)	0.662	-216 (10280)	0.981
8	42%	0.051 (-0.050-0.152)	-21151 (22612)	<0.001	-12750 (11251)	<0.001

*comparing the respective group (transport days in this line) with the control group (no transportation and no blood)

Fig. 4 Influence of blood contamination on the RT-QuIC seeding response. CSF from sCJD patients (n=6–8) was spiked with defined amounts of sonicated red blood cells. **a** The number of positive replicates was calculated and revealed that sCJD CSF samples spiked with more than 1250 cells/µL showed a false-negative RT-QuIC response. **b** CSF from sCJD (n=8) patients was spiked with 5000 cells/µL and incubated at room temperature without sonication for 8 days showing that a significant inhibition via haemolysis of the RT-QuIC response started after 3 days. **c**, **d** Graphically displayed are means of all positive replicates per group at each point in time. Absolute values for rel. AUC and signal maximum were shown for each group, and the p values were calculated for each comparative analysis. All p values <0.05 were considered as significant

The use of RT-QuIC in routine CSF diagnostics for prion diseases requires standardization of sample treatments, definitions of cut-off values by analyzing a high number of samples and assessments of reproducibility and resistance of the RT-QuIC response to short- and long-term storage conditions; until now, only scarce information on these topics is available in the literature.

Reproducibility of the RT-QuIC Assay Between Different Study Sites

To evaluate the inter-laboratory reproducibility of the RT-QuIC assay, we initiated ring trials between different laboratories. A first RT-QuIC ring trial between two different partners using a high number of samples (54 sCJD and 32 controls) indicated substantial agreement between raters (Fleiss' kappa=0.75 (95 % CI: 0.40–1.00)).

Even though the inter-laboratory agreement was relatively high, we intended to establish optimal conditions and standard operating procedures for the RT-QuIC method. The assay precision depends on various factors including (1) inter-laboratory variations in staff, protocols and substrates; (2) sensitivity of the assay to different CSF sample storage and shipping temperatures and (3) different fluorescent readers. By minimizing such variations, we achieved in a second ring trial an almost perfect agreement (Fleiss' kappa=0.83 (95 %

CI: 0.40–1.00)) showing a high reproducibility of the RT-QuIC assay with improved standardization and supporting the potential of the method for routine diagnostic purposes.

Sensitivity, Specificity and Predictive Values of the RT-QUIC Assay

We analysed CSF samples from a patient cohort consisting of 110 patients with prion disease (sCJD, gCJD and FFI) and 400 controls. When setting the cut-off at 10,000 rfu, we obtained a specificity of 99 % and a sensitivity of 85 % for all prion diseases. Among different prion diseases, the sensitivity varied from 100 % for gCJD, 80 % for sCJD and 57 % for FFI cases. Our data are in line with two previous studies, which reported a specificity of almost 100 % and a sensitivity between 80 and 90 % [4, 5]. For gCJD patients, Sano et al. reported sensitivities of RT-QUIC as follows: FFI (100 %), gCJD E200K (87 %) and gCJD V203I (100 %) [6]. Discrepancies for FFI patients may be explained by sampling errors because of the low number of specimens tested (7 versus 22 per group) and methodological differences [6, 7].

Short- and Long-Term Stability of RT-QuIC Seeding Response in CSF

A general problem of biomarker-based diagnostics is the sensitivity of biomarker proteins to storage and shipment conditions. During shipment, CSF is subjected for a defined period of time (between 1 and 8 days) to different temperatures, which are between 20 and 25 °C. After arrival, CSF is usually stored at 4 °C before analysis. Samples, which are used for research, may undergo numerous cycles of freezing and thawing or will be stored for years at −80 °C.

For simulation of these conditions, we explored the effect of short-term storage (up to 8 days at room temperature or at 4 °C), long-term storage (up to 8–9 years at −80 °C), as well as the influence of 16 repeated freezing and thawing cycles on the RT-QuIC seeding response. Our data demonstrated that the PrP^{Sc} seed in CSF of sCJD patients resisted the variations posed with across the analysed conditions, and we did not obtain any loss of sensitivity or specificity or in relation to the intensity of the RT-QuIC responses.

Compared to other biomarker proteins such as tau or Aβ42, which become degraded in particular under higher temperatures during storage [11–13], the proven stability of RT-QuIC assay is a clear advantage with respect to diagnostic purposes.

Influence of Blood Contamination on the RT-QuIC Response in CSF of sCJD Patients

Contamination with blood cells, such as erythrocytes, may influence the RT-QuIC response. In routine diagnostic laboratory practice, between 5 and 10 % of the CSF samples are contaminated with blood cells during the lumbar puncture. Therefore, there is a need to define clear guidelines for pre-analytical sample handling. Our data revealed an artificial inhibition of the PrP^{Sc} seeding activity which resulted in a false-negative RT-QuIC response in prion disease patients. Our findings may explain the variable sensitivity of the RT-QuIC assay (between 80 and 90 %) among different laboratories [4, 5]. The obtained data indicated that a blood cell contamination higher than 1250 cells/μL may inhibit the RT-QuIC reaction, when all cells were completely haemolysed by sonication. A contamination with <1250 cells/μL can be considered as unproblematic. In CSF samples (not older than 3 days after the lumbar puncture), a centrifugation step before freezing is recommended to remove blood cells. After 3 days, haemolysis of blood cells was increased to such an amount that no reliable results could be obtained. Therefore, it is strongly suggested to exclude these samples from further diagnostic analysis.

In conclusion, our data emphasize that RT-QuIC analysis of CSF is a robust and very useful tool for prion diagnosis and should become part of the clinical workup in rapidly progressive dementia cases.

Acknowledgment This work was supported by a grant from the European Commission (Protecting the food chain from prions: shaping European priorities through basic and applied research (PRIORITY, No. 222887) project number: FP7-KBBE-2007-2A). The study was performed within the recently established Clinical Dementia Center at the University Medical Hospital Göttingen and was partly supported by grants from the EU Joint Program–Neurodegenerative Disease Research (JPND—DEMTEST (Biomarker based diagnosis of rapid progressive dementias-optimization of diagnostic protocols, 01ED1201A) and by the Robert Koch-Institute through funds of the Federal Ministry of Health (grant no. 1369-341).

The authors thank Dr. Antonia Zapf (Department of Medical Statistics, University Medical Center Göttingen) for providing the R code for the bootstrap-based confidence intervals.

References

1. Gambetti P, Parchi P, Chen SG (2003) Hereditary Creutzfeldt-Jakob disease and fatal familial insomnia. Clin Lab Med 23:43–64
2. Parchi P, Giese A, Capellari S et al (1999) Classification of sporadic Creutzfeldt-Jakob disease based on molecular and phenotypic analysis of 300 subjects. Ann Neurol 46:224–233
3. Kovács GG, Puopolo M, Ladogana A et al (2005) Genetic prion disease: the EUROCJD experience. Hum Genet 118:166–174
4. McGuire LI, Peden AH, Orrú CD et al (2012) Real time quaking-induced conversion analysis of cerebrospinal fluid in sporadic Creutzfeldt-Jakob disease. Ann Neurol 72:278–285

5. Atarashi R, Satoh K, Sano K et al (2011) Ultrasensitive human prion detection in cerebrospinal fluid by real-time quaking-induced conversion. Nat Med 17:175–178
6. Sano K, Satoh K, Atarashi R et al (2013) Early detection of abnormal prion protein in genetic human prion diseases now possible using real-time QUIC assay. PLoS ONE 8:e54915
7. Cramm M, Schmitz M, Karch A et al (2015) Characteristic CSF Prion-seeding efficiency in humans with prion diseases. Mol Neurobiol 51:396–405
8. Orrú CD, Wilham JM, Raymond LD et al (2011) Prion disease blood test using immunoprecipitation and improved quaking induced conversion. MBio 2:e00078–00011
9. Wilham JM, Orrú CD, Bessen RA et al (2010) Rapid end-point quantitation of prion seeding activity with sensitivity comparable to bioassays. PLoS Pathog 6:e1001217
10. Youden WJ (1950) Index for rating diagnostic tests. Cancer 3:32–35
11. Jensen M, Hartmann T, Engvall B et al (2000) Quantification of Alzheimer amyloid beta peptides ending at residues 40 and 42 by novel ELISA systems. Mol Med 6:291–302
12. Vanderstichele H, Van Kerschaver E, Hesse C et al (2000) Standardization of measurement of beta-amyloid (1-42) in cerebrospinal fluid and plasma. Amyloid 7:245–258
13. Schoonenboom NS, Mulder C, Vanderstichele H et al (2005) Effects of processing and storage conditions on amyloid beta (1-42) and tau concentrations in cerebrospinal fluid: implications for use in clinical practice. Clin Chem 51:189–195

Journal of Clinical Neuroscience 50 (2018) 292–293

Contents lists available at ScienceDirect

Journal of Clinical Neuroscience

journal homepage: www.elsevier.com/locate/jocn

Short communication

CSF Tau supplements 14-3-3 protein detection for sporadic Creutzfeldt–Jakob disease diagnosis while transitioning to next generation diagnostics

Qiao-Xin Li [a], Shiji Varghese [a], Shannon Sarros [a,b], Christiane Stehmann [a,b], James D. Doecke [c], Christopher J. Fowler [a], Colin L. Masters [a,b], Steven J. Collins [a,b,d,*]

[a] National Dementia Diagnostics Laboratory, Florey Institute of Neuroscience and Mental Health, The University of Melbourne, Parkville 3010, Australia
[b] ANCJDR, Florey Institute of Neuroscience and Mental Health, The University of Melbourne, Parkville 3010, Australia
[c] CSIRO Health and Biosecurity, Brisbane, QLD 4029, Australia
[d] Department of Medicine (RMH), The University of Melbourne, Parkville 3010, Australia

ARTICLE INFO

Article history:
Received 29 August 2017
Accepted 18 January 2018

Keywords:
CJD
Tau
14-3-3
CSF

ABSTRACT

The pre-mortem clinical diagnosis of Creutzfeldt–Jakob disease (CJD) is supported by biomarkers, especially cerebrospinal fluid (CSF) 14-3-3 and total tau (Tau) protein levels. These CSF biomarkers have proven the most useful prior to transitioning to powerful next generation diagnostics employing protein amplification techniques such as the real time quaking-induced conversion (RT-QuIC) assay. To enhance national diagnostic capacity while transitioning to RT-QuIC assays an optimized CSF Tau cutoff was determined and shown to usefully supplement 14-3-3 protein detection.

1. Introduction

Although CJD can only be definitively confirmed neuropathologically [1] considerable advances in pre-mortem clinical diagnostic capacity have been made over the last 20 years employing brain MRI and CSF biomarkers [2,3]. Of the CSF biomarkers studied, 14-3-3 and Tau protein levels have proven the most useful prior to transitioning to powerful next generation diagnostics employing protein amplification techniques such as the RT-QuIC assay. RT-QuIC assays, which can be utilized on a range of tissues (eg brain and nasal brushings) and bodily fluids, when applied to CSF has been shown to have >80% sensitivity and approximately 100% specificity [4,5]. Consequently, contemporary diagnosis of "probable CJD" before death can be achieved by application of clinical criteria supported by typical findings on EEG or brain MRI [6,7], as well as through CSF 14-3-3 protein detection [2,3] or by positive RT-QuIC amplification of misfolded prion protein (PrP^{Sc}) in CSF or other tissues [4,5].

Similar to 14-3-3 proteins, CSF Tau levels are a non-specific marker of neuronal injury. The measurement of CSF Tau by ELISA has been standardized and extensively studied for its utility in supporting a diagnosis of Alzheimer's disease (AD) when used in conjunction with amyloid-β_{1-42} and phospho-tau [8]. In addition, CSF Tau has demonstrated meritorious sensitivity and specificity for pre-mortem diagnosis of CJD [9,10] although it is not routinely included in diagnostic criteria for "probable CJD" and no internationally agreed cutoff threshold exists. Nevertheless, to enhance national diagnostic capacity during our transition to CSF RT-QuIC assays, we have determined an optimized CSF Tau cutoff based on pathologically proven sporadic CJD and non-CJD cases, which offers worthwhile clinical utility supplementary to 14-3-3 protein detection.

2. Methods, results and discussion

We analysed CSF from 130 definite sporadic CJD cases ascertained through routine Australian National CJD Registry (ANCJDR) surveillance and 124 non-CJD controls (82 referred as "suspected CJD" to the ANCJDR with an alternative diagnosis eventually determined and 42 with abnormal amyloid-β positron emission tomographic [PET+] scans recruited through the Australian Imaging Biomarker and Lifestyle (AIBL) study, an important group given the frequency of neuropathologically confirmed AD in clinically suspected CJD cases ultimately examined at autopsy [9] (Table 1).

* Corresponding author at: Department of Medicine, The University of Melbourne, Parkville 3010, Australia.
E-mail address: stevenjc@unimelb.edu.au (S.J. Collins).

https://doi.org/10.1016/j.jocn.2018.01.064
0967-5868/

Table 1
Patient cohorts for determining CSF Tau cutoff.

Diseases	Number (post-mortem confirmed)	14-3-3 positive/ negative/TU	Tau positive/ negative
Sporadic CJD	130 (130)	109/20 (6[#])/1	111/19
Non-CJD	124 (77)	36/84 (13[#])/4	22/102
Inflammatory CNS disorder	18 (17)	8/9 (5[#])/1	8/10
Drug induced encephalopathy	7 (7)	5/2 (1[#])	2/5
AD/amnestic MCI	44[*] (2)	2/42	1/43
DLB, MND, cerebellar atrophy, hydrocephalus, alcohol encephalopathy	10 (8)	3/6 (1[#])/1	1/9
Leucoencephalopathy	10 (10)	2/8 (3[#])	3/7
Vascular disease/MID	8 (6)	4/4	3/5
Paraneoplastic/cancer	23 (23)	11/10 (2[#])/2	4/19
Disease not defined	4 (4)	1/3 (1[#])	0/4

[*] 42 were amyloid PET+.
[#] Atypical 14-3-3 positive included in the negative group; TU = technically unsuitable CSF sample and thereby excluded from sensitivity and specificity analysis.

Tau protein was measured using a commercially available assay (INNOTEST hTAU Ag, Fujirebio, Ghent, Belgium) according to the manufacturer's instructions as described previously [8]. CSF 14-3-3 protein detection was through immunoblot [11] allowing scoring as positive, atypical positive or negative relative to control CSF. The optimal cutoff level for dichotomizing CSF Tau protein values was determined using receiver operating characteristics (ROC) curve analysis, minimizing the difference between the sensitivity and specificity and maximising accuracy.

CSF Tau levels for sporadic CJD ranged between 86 and 29,484 pg/ml (median 3735 pg/ml and mean 4806 pg/ml) while non-CJD levels ranged from 22 to 9182 pg/ml (median 399 pg/ml and mean 755 pg/ml), which were significantly different ($p < 0.0001$ Mann-Whitney U test). ROC curve analysis defined an optimal cutoff as 1072 pg/ml providing 85% sensitivity and 82% specificity. For 14-3-3 protein detection, analysis based on dichotomised results gave 89% sensitivity and 66% specificity. Overall sensitivities and specificities for 14-3-3 and Tau protein detection, as well as for each of the non-CJD diagnostic groups are provided in the Table 1. Beyond the superior specificity, CSF Tau was found to be partially complementary to 14-3-3 protein detection for supporting the diagnosis of sporadic CJD, with 10 of the 21 CJD cases with either negative 14-3-3 results or technically unsuitable CSF samples revealing a Tau above 1072 pg/ml providing a combined sensitivity of 92%. Of note, sporadic CJD CSF Tau levels correlated with disease duration being significantly more likely (unpaired *t*-test with Welch's correction, $p = 0.003$) to be below our optimized cutoff of 1072 pg/ml in longer survival cases (mean 15.62 ± 3.16 months for negative Tau results) compared to those with positive Tau results (4.46 ± 0.49 months).

The CSF Tau cutoff we determined for supporting sporadic CJD is similar to that reported in previous studies, as have the modestly superior specificity [9,10] and diagnostic complementarity of CSF Tau in relation to 14-3-3 protein detection [10]. The addition of CSF Tau to 14-3-3 protein detection as a biomarker for the pre-mortem evaluation of suspected sporadic CJD offers modestly enhanced diagnostic capacity while the ANCJDR completes transition to the clearly superior RT-QuIC protein amplification technique.

Ethical information

The Human Research Ethics Committee of the University of Melbourne approved the study (#1648441).

Acknowledgement

ANCJDR is funded by the Commonwealth Department of Health – Australia. SJC is supported in part by an NHMRC Practitioner Fellowship (#APP1105784).

Disclosures

The authors declare no conflict of interests.

References

[1] Kretzschmar HA, Ironside JW, DeArmond SJ, Tateishi J. Diagnostic criteria for sporadic Creutzfeldt-Jakob disease. Arch Neurol 1996;53:913–20.
[2] Zerr I, Kallenberg K, Summers DM, Romero C, Taratuto A, Heinemann U, et al. Updated clinical diagnostic criteria for sporadic Creutzfeldt-Jakob disease. Brain 2009;132:2659–68.
[3] Stoeck K, Sanchez-Juan P, Gawinecka J, Green A, Ladogana A, Pocchiari M, et al. Cerebrospinal fluid biomarker supported diagnosis of Creutzfeldt-Jakob disease and rapid dementias: a longitudinal multicentre study over 10 years. Brain 2012;135:3051–61.
[4] Atarashi R, Satoh K, Sano K, Fuse T, Yamaguchi N, Ishibashi D, et al. Ultrasensitive human prion detection in cerebrospinal fluid by real-time quaking-induced conversion. Nat Med 2011;17:175–8.
[5] Foutz A, Appleby BS, Hamlin C, Liu X, Yang S, Cohen Y, et al. Diagnostic and prognostic value of human prion detection in cerebrospinal fluid. Ann Neurol 2017;81:79–92.
[6] Steinhoff BJ, Racker S, Herrendorf G, Poser S, Grosche S, Zerr I, et al. Accuracy and reliability of periodic sharp wave complexes in Creutzfeldt-Jakob disease. Arch Neurol 1996;53:162–6.
[7] Finkenstaedt M, Szudra A, Zerr I, Poser S, Hise JH, Stoebner JM, et al. MR imaging of Creutzfeldt-Jakob disease. Radiology 1996;199:793–8.
[8] Li QX, Villemagne VL, Doecke JD, Rembach A, Sarros S, Varghese S, et al. Alzheimer's disease normative cerebrospinal fluid biomarkers validated in PET amyloid-beta characterized subjects from the australian imaging, biomarkers and lifestyle (AIBL) study. J Alzheimer's Dis 2015;48:175–87.
[9] Hamlin C, Puoti G, Berri S, Sting E, Harris C, Cohen M, et al. A comparison of tau and 14-3-3 protein in the diagnosis of Creutzfeldt-Jakob disease. Neurology 2012;79:547–52.
[10] Otto M, Wiltfang J, Cepek L, Neumann M, Mollenhauer B, Steinacker P, et al. Tau protein and 14-3-3 protein in the differential diagnosis of Creutzfeldt-Jakob disease. Neurology 2002;58:192–7.
[11] Collins S, Boyd A, Fletcher A, Gonzales M, McLean CA, Byron K, et al. Creutzfeldt-Jakob disease: diagnostic utility of 14-3-3 protein immunodetection in cerebrospinal fluid. J Clin Neurosci 2000;7:203–8.

Molecular Neurobiology
https://doi.org/10.1007/s12035-018-1251-1

Cerebrospinal Fluid Total Prion Protein in the Spectrum of Prion Diseases

Anna Villar-Piqué[1] · Matthias Schmitz[1,2] · Ingolf Lachmann[3] · André Karch[4] · Olga Calero[5,6] · Christiane Stehmann[7] · Shannon Sarros[7] · Anna Ladogana[8] · Anna Poleggi[8] · Isabel Santana[9] · Isidre Ferrer[10,11] · Eva Mitrova[12] · Dana Žáková[12] · Maurizio Pocchiari[8] · Inês Baldeiras[9] · Miguel Calero[5,6] · Steven J. Collins[7,13] · Michael D. Geschwind[14] · Raquel Sánchez-Valle[15] · Inga Zerr[1,2] · Franc Llorens[1,11,16]

Received: 28 May 2018 / Accepted: 16 July 2018

Abstract

Cerebrospinal fluid (CSF) total prion protein (t-PrP) is decreased in sporadic Creutzfeldt-Jakob disease (sCJD). However, data on the comparative signatures of t-PrP across the spectrum of prion diseases, longitudinal changes during disease progression, and levels in pre-clinical cases are scarce. T-PrP was quantified in neurological diseases (ND, $n = 147$) and in prion diseases from different aetiologies including sporadic (sCJD, $n = 193$), iatrogenic (iCJD, $n = 12$) and genetic ($n = 209$) forms. T-PrP was also measured in serial lumbar punctures obtained from sCJD cases at different symptomatic disease stages, and in asymptomatic prion protein gene (*PRNP*) mutation carriers. Compared to ND, t-PrP concentrations were significantly decreased in sCJD, iCJD and in genetic prion diseases associated with the three most common mutations E200K, V210I (associated with genetic CJD) and D178N-129M (associated with fatal familial insomnia). In contrast, t-PrP concentrations in P102L mutants (associated with the Gerstmann-Sträussler-Scheinker syndrome) remained unaltered. In serial lumbar punctures obtained at different disease stages of sCJD patients, t-PrP concentrations inversely correlated with disease progression. Decreased mean t-PrP values were detected in asymptomatic D178-129M mutant carriers, but not in E200K and P102L carriers. The presence of low CSF t-PrP is common to all types of prion diseases regardless of their aetiology albeit with mutation-specific exceptions in a minority of genetic cases. In some genetic prion disease, decreased levels are already detected at pre-clinical stages and diminish in parallel with disease progression. Our data indicate that CSF t-PrP concentrations may have a role as a pre-clinical or early symptomatic diagnostic biomarker in prion diseases as well as in the evaluation of therapeutic interventions.

Keywords Cerebrospinal fluid · Prion protein · Sporadic Creutzfeldt-Jakob disease · Genetic prion disease · Iatrogenic prion disease

Introduction

Transmissible spongiform encephalopathies are fatal neurodegenerative disorders characterised by rapid progression and microvacuolation in the grey matter of the brain. They are also known as prion diseases relating to the causative agent, which is the abnormally folded isoform the prion protein scrapie (PrPsc) that creates insoluble aggregates and accumulate in the brain [1]. Prion diseases affecting humans include sporadic Creutzfeldt-Jakob disease (sCJD), genetic prion diseases (gPD) and acquired forms, such as iatrogenic CJD (iCJD) or variant CJD (vCJD). sCJD is the most prevalent form accounting for about 85–90% of total cases, followed by hereditary forms (~ 10%). By contrast, acquired forms only account for at most 2–5% of prion disease cases [2, 3]. Despite sharing a common pathological agent, prion diseases present a broad heterogeneity in clinical symptoms and

Anna Villar-Piqué and Matthias Schmitz contributed equally to this work.

Inga Zerr and Franc Llorens are equal senior contributors.

Electronic supplementary material The online version of this article (https://doi.org/10.1007/s12035-018-1251-1) contains supplementary material, which is available to authorized users.

✉ Anna Villar-Piqué
avillar@gwdg.de

✉ Matthias Schmitz
matthias.schmitz@med.uni-goettingen.de

✉ Franc Llorens
franc.llorens@gmail.com

Extended author information available on the last page of the article

Published online: 30 July 2018

disease manifestations. A cause of variability is the polymorphism at codon 129 of the PrP encoding gene, *PRNP*, which can be methionine (M129) or valine (V129) [4]. In combination with biochemically characterised conformational variants of PrPsc, sCJD can be stratified into at least six molecular subtypes, with MM1/MV1 and VV2 the most prevalent ones (> 80% of total sCJD cases [5]). gPD are associated with specific mutations in the *PRNP* and include familial/genetic Creutzfeldt-Jakob disease (gCJD), Gerstmann-Sträussler-Scheinker syndrome (GSS-S) and familial fatal insomnia (FFI). Several *PRNP* mutations cause gCJD and GSS-S (reviewed elsewhere [6]), with E200K and V210I the most prevalent mutations in gCJD and P102L in GSS-S. In contrast, FFI is associated with a unique haplotype, D178N-129M (D178N-M) [6, 7]. Acquired human prion diseases develop from exogenous prions and are transmitted from infected humans (iCJD) or cattle (vCJD). iCJD is caused by human-to-human transmission during medical treatments, with dura matter grafts and administration of human growth hormone the main causes of cross-contamination through surgical and medical procedures [8].

Clinical diagnosis of prion diseases is supported by cerebrospinal fluid (CSF) biomarkers. The CSF profile of prion disease patients is characterised by elevated concentrations of surrogate protein markers of the pathology such as 14-3-3, tau and alpha-synuclein [9–11], as well as by the presence of prion seeding activity [12]. By contrast, the CSF total PrP (t-PrP) concentrations are decreased in sCJD. The specificity of this decrease remains unclear as some authors reported reduced CSF t-PrP in various neurodegenerative diseases, such as Alzheimer's disease (AD), dementia with Lewy bodies and Parkinson's disease [13], while others suggested that t-PrP is specifically reduced in sCJD compared to AD, supporting its use in the differential diagnostic context [14, 15]. Among sCJD molecular subtypes, no difference was found in CSF t-PrP levels between MM1 and VV2 cases [16] and scant data exist for acquired cases. When CSF t-PrP was investigated by western blot, no variation appeared in the truncation or glycosylation state of the protein between different sCJD subtypes or in comparison with hereditary prion diseases [17–19]. To date, no further quantification of CSF t-PrP has been carried out in genetic prion diseases, including a significant number of mutation types. In addition, few data are available about the relationship of CSF t-PrP with demographic parameters, as are data on longitudinal t-PrP CSF levels in prion diseases. A preliminary exploration showed a decrease in t-PrP levels with disease progression although quantification was lacking and only six sCJD cases were studied [18].

While age does not influence t-PrP concentration in diseased individuals, low levels are associated with advanced disease stages [13]. Correlation analysis with other CSF biomarkers indicated a direct correlation between t-PrP and amyloid-beta 42 peptide in sCJD [13].

The goal of the present study was to provide complete CSF t-PrP signatures across the broad spectrum of prion diseases. Thus, we quantified the CSF t-PrP in a large number of cases that include sCJD, iCJD, various forms of gPD, and diverse neurological diseases composing our control group. In addition, we also investigated longitudinal CSF t-PrP alterations in serial lumbar punctures from sCJD cases and asymptomatic *PRNP* mutant carriers.

Methods

Patients

The study included 561 CSF samples. Samples from patients with non-primarily neurodegenerative neurological diseases (ND, $n = 147$) and sporadic Creutzfeldt-Jakob disease (sCJD, $n = 193$) were collected at the Clinical Dementia Center and the National Reference Center for CJD Surveillance at the University Medical Center of Göttingen (Germany). The ND group was composed of cases diagnosed with neurological conditions not associated with neurodegenerative pathology including the following diagnostic groups: psychosis, paranoid psychosis, bipolar disorder, schizophrenia, ischemic stroke, multiple cerebral infarcts, epilepsy, meningitis, alcohol abuse, vertigo, acute or chronic headache, pain syndromes, acute hypoxia, polyneuropathy, cerebral lymphoma, astrocytoma and paraneoplasia. ND cases were diagnosed according to acknowledged standard neurologic clinical and para-clinical findings based on the ICD 10 definitions. The presence of neurodegenerative diseases in the ND group was excluded by follow-up evaluations. All patients with sCJD were classified as probable or definite cases according to diagnostic consensus criteria [20, 21].

Iatrogenic ($n = 12$) and genetic ($n = 209$) prion diseases were collected in the following CJD reference centres: (1) Clinical Dementia Center and the National Reference Center for CJD Surveillance at the University Medical Center, Göttingen, Germany, (2) Neurochemistry Laboratory, Neurology Department of Coimbra University Hospital, Coimbra, Portugal, (3) Alzheimer's Disease and Other Cognitive Disorders Unit, Hospital Clínic, Barcelona, Spain, (4) National Centre of Microbiology-Carlos III Institute of Health, Madrid, Spain, (5) Istituto Superiore di Sanità, Rome, Italy, (6) Slovak Medical University, Bratislava, Slovakia, (7) Australian National CJD Registry, The Florey Department of Neuroscience and Mental Health, Melbourne, Australia, and (8) Department of Neurology, Memory and Aging Center, University of California, San Francisco (UCSF), USA. The diagnoses of genetic prion diseases were carried out according to surveillance criteria after prion protein gene (*PRNP*) analysis [22] and World Health Organization (WHO) criteria [23]. Iatrogenic CJD was diagnosed according to established WHO criteria [23]. Eleven iatrogenic cases were associated with dura matter grafts and one with corneal transplantation.

Table 1 Demographic and biomarkers data from our study population. Number of cases (*n*), age in years (mean values ± standard deviation), sex (female (f)/males (m)), codon 129 *PRNP* genotype and t-PrP concentrations (mean values (mean) ± standard deviation (SD) in ng/mL), and 95% CI (in ng/mL) are indicated. Mutation in the *PRNP* gene is indicated for genetic prion diseases (gPD). *gCJD* genetic Creutzfeldt-Jakob disease, *GSS-S* Gerstmann-Sträussler-Scheinker syndrome, *FFI* fatal familial insomnia, *M* methionine, *V* valine, *NA* not available. Other mutations/variants refer to cases diagnosed as prion disease with changes on the *PRNP* gene without clear evidence of being disease causative mutations

	Number of cases	Age	Sex	PRNP 129				t-PrP	
		Mean ± SD (years)	f/m	MM	MV	VV	NA	Mean ± SD (ng/mL)	95% CI (ng/mL)
Control									
ND	147	65 ± 11	78/69	0	0	0	147	230 ± 140	207–253
Sporadic prion disease									
sCJD	193	65 ± 10	114/79	74	37	45	37	120 ± 83	108–132
Aquired prion disease									
iCJD	12	48 ± 10	5/7	9	2	0	1	95 ± 71	50–140
Genetic prion disease									
Pathogenic variants associated to gCJD									
D178N-V	1	48	1/0	0	0	1	0	29	0
V180I	1	77	0/1	1	0	0	0	300	0
T188A	1	82	1/0	1	0	0	0	142	0
T188K	1	57	1/0	0	1	0	0	173	0
K194E	1	71	0/1	0	1	0	0	232	0
E196K	3	69 ± 4	2/1	1	1	1	0	69 ± 4	59–79
E200K	66	61 ± 11	39/27	45	18	2	1	98 ± 77	78–117
R208H	4	62 ± 7	2/2	3	1	0	0	243 ± 146	10–475
V210I	41	64 ± 10	24/17	31	8	2	0	161 ± 147	114–207
P238S	1	68	1/0	0	1	0	0	52	0
Pathogenic variants associated to GSS-S									
P102L	13	53 ± 11	8/4*	11	1	1	0	200 ± 148	111–289
P105T	3	36 ± 17	2/1	0	3	0	0	225 ± 168	0–642
G114V	1	20	0/1	0	1	0	0	114	0
A117V	1	47	1/0	0	0	1	0	95	0
A133V	1	62	1/0	1	0	0	0	68	0
V176G	1	61	1/0	0	0	1	0	31	0
F198S	1	51	0/1	0	1	0	0	47	0
Q217R	1	59	0/1	1	0	0	0	165	0
Y218N	1	NA	1/0	0	1	0	0	254	0
Pathogenic variants associated to FFI									
D178N-M	47	50 ± 10	16/31	31	16	0	0	119 ± 94	91–146
Insert mutations									
OPRI	14	63 ± 9	8/6	5	4	5	0	105 ± 113	40–171
Nonsense mutations									
Q160X	1	27	0/1	1	0	0	0	30	0
Other mutations/variants									
Q52P	1	80	1/0	0	1	0	0	141	0
N173K	1	73	0/1	0	1	0	0	203	0
Q212H	1	63	1/0	1	0	0	0	37	0
I215V	1	77	0/1	1	0	0	0	81	0

*Sex unknown in one case

CSF Tests

CSF t-PrP was centrally quantified (Clinical Dementia Center-Göttingen) using a commercially available enzyme-linked immunosorbent assay (ELISA) specific for human prion protein (Analytik Jena AG). Inter- and intra-assay coefficients of variation in our study were below 18 and 12%, respectively. CSF neurofilament-light (NFL) was quantified using a commercially available ELISA (Uman-Diagnostics). The analysts were masked to clinical data.

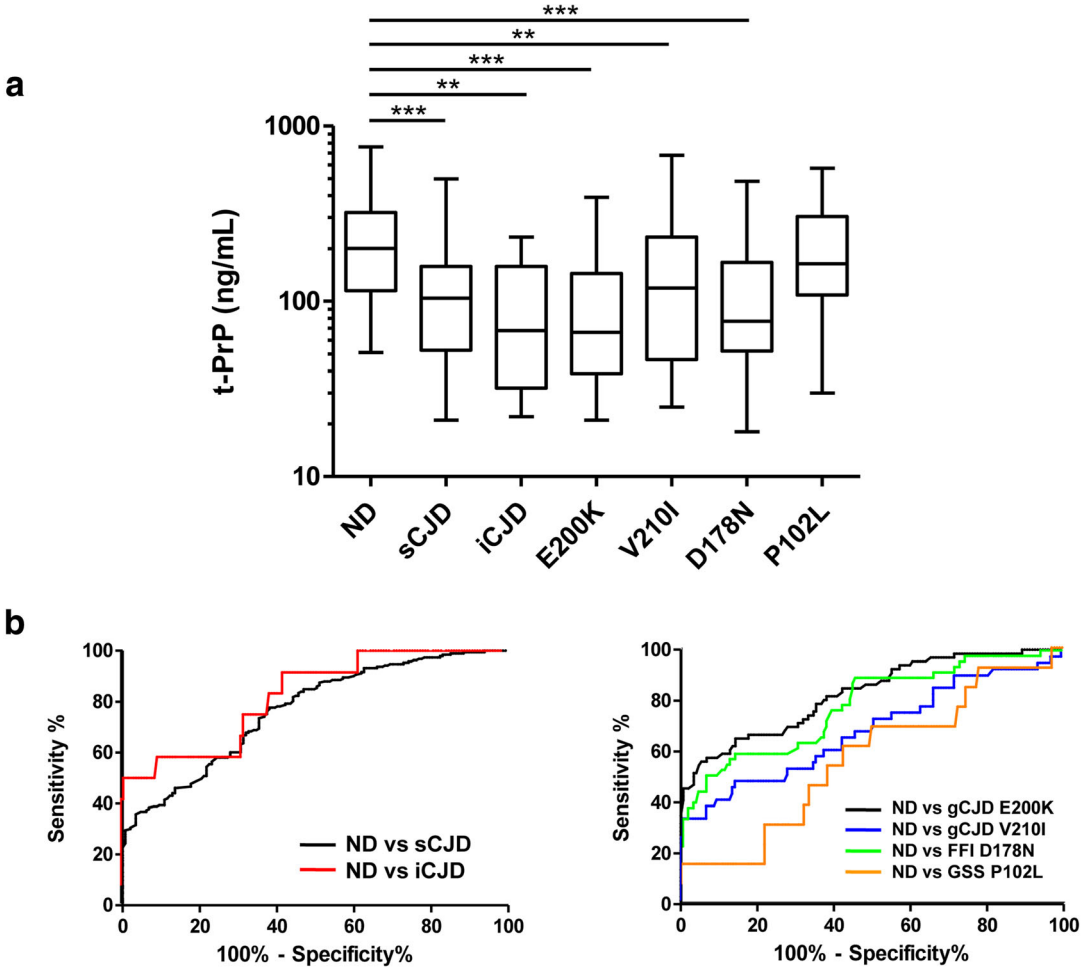

	sCJD	iCJD	gCJD E200K	gCJD V210I	FFI D178N-M	GSS P102L
Number of cases	193	12	66	41	47	13
AUC (95%CI)	0.76 (0.72-0.81)	0.82 (0.70-0.94)	0.83 (0.77-0.89)	0.69 (0.58-0.79)	0.78 (0.70-0.86)	0.57 (0.41-0.73)

Fig. 1 Analysis of CSF t-PrP concentrations in sporadic, iatrogenic and genetic prion diseases. **a** Whisker and boxplots of CSF t-PrP concentrations in non-primarily neurodegenerative neurological diseases (ND), sporadic Creutzfeldt-Jakob disease (sCJD), iatrogenic Creutzfeldt-Jakob disease (iCJD) and genetic prion diseases (gPD) associated with mutations in the *PRNP* gene E200K, V210I, D178N-M and P102L. Boxes indicate 25th to 75th percentiles and whiskers minimum to maximum values. Statistical significance was set at $*p < 0.05$, $**p < 0.01$, $***p < 0.001$. **b** Receiver operating characteristic curves for sCJD, iCJD and gPDs associated with mutations E200K, V210I, D178N-M and P102L versus the ND group are shown. Area under the curve (AUC) and 95% confidence interval (CI) are shown for t-PrP analysis

Genetic Tests

For detection of a prion disease-associated mutation and assessment of codon 129 polymorphism in *PRNP*, genetic testing was performed as described before [24].

Statistical Analysis

For two group comparisons of biomarker levels, non-parametric Mann-Whitney *U* tests were used. For comparisons between multiple groups, Kruskal-Wallis tests followed by Dunn's post hoc tests were applied. To assess the diagnostic accuracy of t-PrP, receiver operating characteristic (ROC) curve analyses were carried out and areas under the curve (AUC) with 95% confidence intervals (95% CI) were calculated. Spearman rank correlation coefficients were used to assess associations between continuous biomarker levels. Bootstrap one-tail tests for paired ROC curves based on the pROC-R package with boot replicates = 10,000 were used to assess differences in the diagnostic accuracy between biomarkers [25]. Longitudinal biomarker data were assessed using a multi-level mixed linear model. For the analysis of differences on t-PrP concentrations

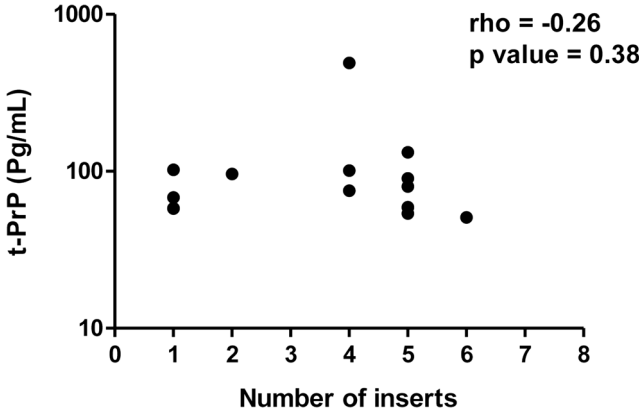

Fig. 2 Influence of the number of octapeptide repeat insertions (OPRI) in the prion protein gene (*PRNP*) on CSF t-PrP concentrations. Association analysis between t-PrP concentrations and number of OPRI in the *PRNP* gene. Spearman rank correlation coefficients were used

between different cohorts, only cohorts including enough cases to perform normality tests were used.

Data Availability The datasets used and/or analysed during the current study are available from the corresponding author on reasonable request.

Results

CSF t-PrP in Prion Disease of Different Aetiologies

CSF t-PrP concentrations were assessed in ND, sCJD, iCJD and gPD cases (Table 1). Compared to ND, mean t-PrP levels were lower in all types of prion diseases, with the exception of gPD associated with V180I, K194E and Y218N mutations (one case of each was available), and the R208H mutation (four cases available). Other mutations and variants also displayed similar concentrations to those reported in ND (P102L, P105L and N173K).

In order to assess if there were differences in t-PrP levels among diagnostic groups, t-PrP concentrations in ND, sCJD, iCJD and the four most prevalent forms of genetic prion diseases (E200K, V210I, D178N-M and P120L mutations) were further analysed in a multiple comparison test. Compared to ND, t-PrP was lower in sCJD ($p < 0.001$), iCJD ($p < 0.01$) and in gPD associated with E200K ($p < 0.001$), V210I ($p < 0.01$) and D178N-M mutations ($p < 0.001$), but not in P102L cases (Fig. 1a). Lowest t-PrP concentrations were found in iCJD (95 ± 71 ng/mL) and E200K (98 ± 77 ng/mL) (Table 1), but no statistical differences among different forms of prion diseases were detected.

AUCs for the discrimination of sCJD, iCJD and gPD E200K, V210I and D178N-M from ND ranged from 0.69 to 0.83, indicating moderate potential for a diagnostic test (Fig. 1b). In contrast, t-PrP levels showed no diagnostic value in distinguishing P102L from ND (AUC = 0.57, $p = 0.40$) (Fig. 1b).

CSF from gPD cases was obtained from different countries (see "Methods"). No differences were found when comparing t-PrP concentrations from different cohorts for the E200K, D178N-M and V210 mutations (Suppl. Fig. 1).

Established CSF prion disease biomarkers such as 14-3-3, tau [26, 27] and RT-QuIC [28] show a high diagnostic accuracy in the discrimination of non-prion disease cases from sCJD and gCJD E200K and V210I. However, they present limited value in the diagnosis of genetic prion disease associated with D178N-M. We recently reported elevated CSF NFL in D178N-M cases and showed moderate diagnostic potential for t-PrP in this analysis; therefore, we explored the ability of NFL/t-PrP ratio for improving the discrimination of D178N-M from ND. The AUC value in D178N-M cases using the NFL/t-PrP ratio (AUC = 0.97, 95% CI 0.95–0.99) was superior to that obtained by t-PrP only (AUC = 0.78, 95% CI 0.70–0.86, $p < 0.001$), but not relatively increased when compared to NFL alone (AUC = 0.96, 95% CI 0.93–0.98, $p = 0.2$).

The presence of octapeptide repeat insertions (OPRI) in the N-terminal region of the *PRNP* gene is linked with genetic prion diseases. High clinical and neuropathological heterogeneity in ORPI carriers is associated to the number of insert mutations (one to nine) [29–31] with the likelihood that low OPRI numbers are not pathogenic [32]. Mean t-PrP levels in cases with OPRI mutations were lower than in ND cases ($p = 0.003$) (Table 1). However, no association between CSF t-PrP levels and number of inserts was detected in our study population ($p = 0.38$) (Fig. 2).

Associations of Demographic and Genetic Parameters with t-PrP Concentrations

In prion diseases, CSF t-PrP levels were associated neither with age at onset ($p = 0.10$) (Fig. 3a) nor with sex ($p = 0.21$) (Fig. 3b). Lack of association with age and sex was also detected in the ND group (data not shown). CSF t-PrP concentrations were not statistically different between prion disease cases harbouring methionine/methionine [MM] (129 ± 107 ng/mL, $n = 219$), methionine/valine [MV] (114 ± 88 ng/mL, $n = 99$) and valine/valine [VV] (112 ± 85 ng/mL, $n = 59$) at codon 129 of the *PRNP* gene ($p = 0.58$) (Fig. 2c). Similarly, no differences were detected between different sCJD molecular subtypes in the subset of cases with neuropathological prion disease confirmation and available prion type (MM1/MV1 110 ± 80 pg/mL, $n = 55$; MV2 84 ± 61 pg/mL, $n = 6$; VV2 88 ± 77, $n = 16$) ($p = 0.16$) (Fig. 3d). To investigate whether t-PrP concentrations are associated with different pathological phenotypes among a mutation type, D178N-M and E200K cases were stratified according to their codon 129 *PRNP* genotype, which influences their clinico-

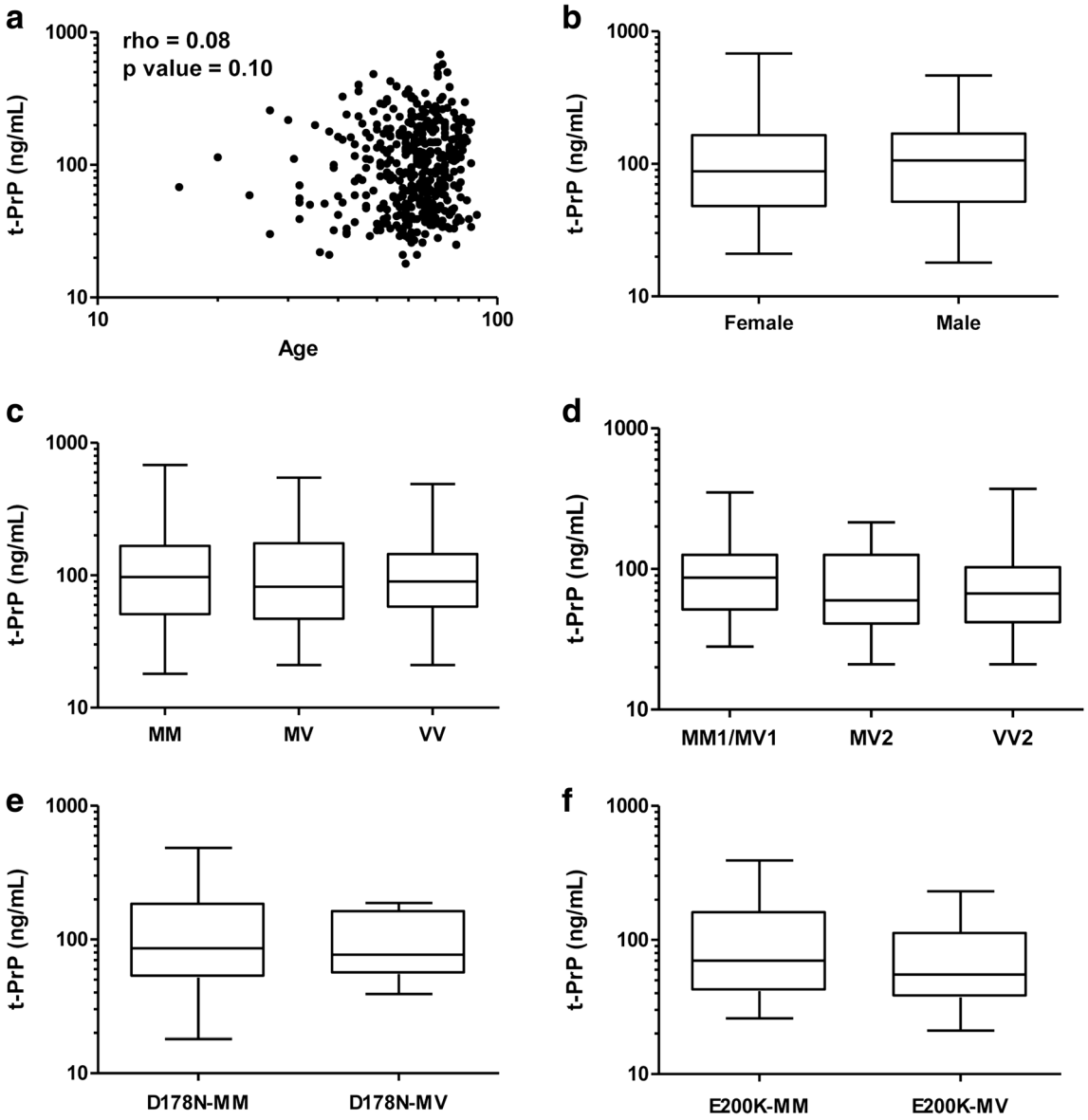

Fig. 3 Influence of demographic and PRNP codon 129 genetic factors on CSF t-PrP concentrations in prion diseases. **a** Association analysis between t-PrP concentrations and age at disease onset (in years) in all prion disease cases (sCJD, iCJD and gPD). Spearman rank correlation coefficients were used. **b** t-PrP in prion diseases stratified by sex. **c** t-PrP concentrations in prion diseases stratified by prion protein gene (*PRNP*) codon 129 polymorphism (M methionine, V valine) in probable and definite prion disease cases. **d** t-PrP concentrations in definite sCJD cases stratified by sCJD molecular subtypes. **e** t-PrP concentrations in D178-MM and MV cases. **f** t-PrP concentrations in E200K-MM and MV cases. Kruskal-Wallis test followed by Dunn's post hoc tests (correction for multiple testing) was applied for multiple comparisons and Mann-Whitney *U* test for two group comparisons

pathological features [33, 34]. t-PrP levels were neither different between D178-MM and -MV cases (Fig. 3e) nor between E200K-MM and -MV cases (Fig. 3f).

CSF t-PrP along Disease Stages

t-PrP levels were quantified in sequentially repeated lumbar punctures (LPs) obtained from 20 sCJD cases (2 LPs available in 19 cases and 3 LPs available in 1 case). To normalise time intervals between LPs, samples were grouped into three categories according to whether they underwent LP in the first (time of LP to disease onset/total duration of the disease < 0.33), second (0.33–0.66) or third (> 0.66) stage of the disease, as previously reported [35, 36]. In 15 LPs, t-PrP concentrations were lower in the follow-up LP compared to the initial estimate, while in 5 LPs, t-PrP concentrations were higher at advanced disease stages (Fig. 4). Using a multi-level mixed linear model, a decrease in t-PrP of 24.5 per unit in disease stages was calculated (95% CI 12.8–48.8, $p = 0.005$).

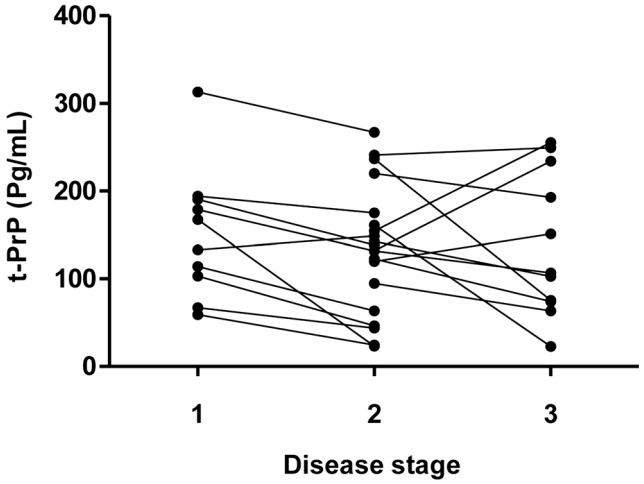

Fig. 4 Association between CSF t-PrP levels and disease duration in sCJD patients. t-PrP concentrations in serial lumbar punctures (LPs) in sCJD cases at different stages of the disease. Samples were grouped in three categories according to whether they underwent LP in the first (< 0.33), second (0.33–0.66) or third (> 0.66) stage of an individual's disease

CSF in Pre-Clinical PRNP Mutation Carriers

t-PrP concentrations were analysed in a subset of asymptomatic *PRNP* mutation carriers from the UCSF cohort and were descriptively compared with symptomatic cases from the same cohort (symptomatic, UCSF), with the whole population of cases included in the present study (symptomatic, ALL) and with the ND cases (Suppl. Fig. 2). For some cases, serial LPs from the mutation carriers were available.

In E200K, pre-symptomatic carriers (17 LPs from 14 cases) displayed t-PrP concentrations similar to ND controls (Suppl. Fig. 2) and higher than those detected in symptomatic cases in the UCSF cohort (1 case) and in the whole cohort of E200K patients (Fig. 5a). In D178N-M cases, pre-symptomatic carriers showed similar levels like symptomatic D178N-M patients from the UCSF and the whole D178N-M cohort, although only six LPs from three individuals were available (Fig. 5b), limiting any meaningful conclusions. In P102L carriers, t-PrP concentrations were similar between pre-symptomatic (two cases available) and symptomatic patients, in agreement with the absence of alterations between ND and symptomatic cases described above (Fig. 5c).

Discussion

In this study, we report the comparative signatures of CSF t-PrP concentrations across the spectrum of prion diseases. While decreased t-PrP concentrations are well-reported in sCJD cases [13–16, 18], data on genetic and iatrogenic cases have hitherto been quite limited and in most of the cases, restricted to single case reports. Our study validates previous observations of decreased CSF t-PrP in sCJD cases compared to controls and other non-neurodegenerative neurological conditions evaluated by ELISA [13–16,] and by immunoblotting techniques [18]. Additionally, although the total number of samples was relatively low, our data clearly point to the presence of reduced t-PrP concentrations in iCJD.

Low t-PrP concentrations were observed in genetic prion diseases associated with mutations E200K, D178N-M and V210I, but not in P102L cases supporting that among gCJD and GSS-S-associated mutations, t-PrP levels were not homogeneous. Genetic CJD patients with V180I, K194E and R208H mutations showed normal t-PrP concentrations, while as did GSS-S patients with P102L, P105L and Y218N mutations. The rest of the mutations displayed decreased or intermediate t-PrP levels. In this regard, well-known disease causing mutations such as A117V, P102L, E200K and D178N-M [37] showed diverse t-PrP concentrations, while some mutations with no strong evidence of increased risk for developing the disease (e.g. A133V, V176G, I215V, P238S) displayed reduced t-PrP levels. Although these results should be interpreted with caution due to the low number of cases (statistical analysis was carried out for the most prevalent forms only), our data suggest the presence of highly heterogeneous profiles, which are not associated with disease phenotype. Indeed, D178N-M cases, displaying a specific clinicopathological phenotype compared to sCJD, iCJD and gCJD E200K and V210I, presented low t-PrP concentrations. Additionally, no differences on t-PrP levels were detected between D178N-MM and -MV cases, although both groups show distinct clinical features and neuropathological profiles [33, 38]. Moreover, similar t-PrP levels were detected between E200K-MM and -MV cases, despite the presence of different types of PrP depositions in the brain tissue, with a synaptic pattern for MM subjects and granules and plaque-like structures for MV subjects [34].

Overall, the analysis of CSF signatures demonstrated high variation in t-PrP concentrations across the diagnostic groups. This, together with a moderate diagnostic accuracy in discriminating prion disease cases from ND controls (AUC of 0.76 for sCJD), argues against the use of t-PrP quantification alone as a diagnostic biomarker for prion diseases in clinical practice. However, the tentative decrease of t-PrP concentrations along disease duration observed in serial lumbar punctures from the same patients indicates that, for a given case, longitudinal alterations on t-PrP levels may have a potential role in the evaluation of disease progression, as well as in the evaluation of the efficacy of a potential therapeutic intervention. In this regard, other CSF prion biomarkers such as tau, alpha-synuclein and NFL have been able to predict disease duration [36, 39, 40], but show stable concentrations along disease progression [35, 36, 40]. These markers reflect pathological alterations associated with the neurodegeneration process such as neuro-axonal degeneration and white matter involvement. In contrast, decreased t-PrP levels may reflect primary alterations in the molecular process

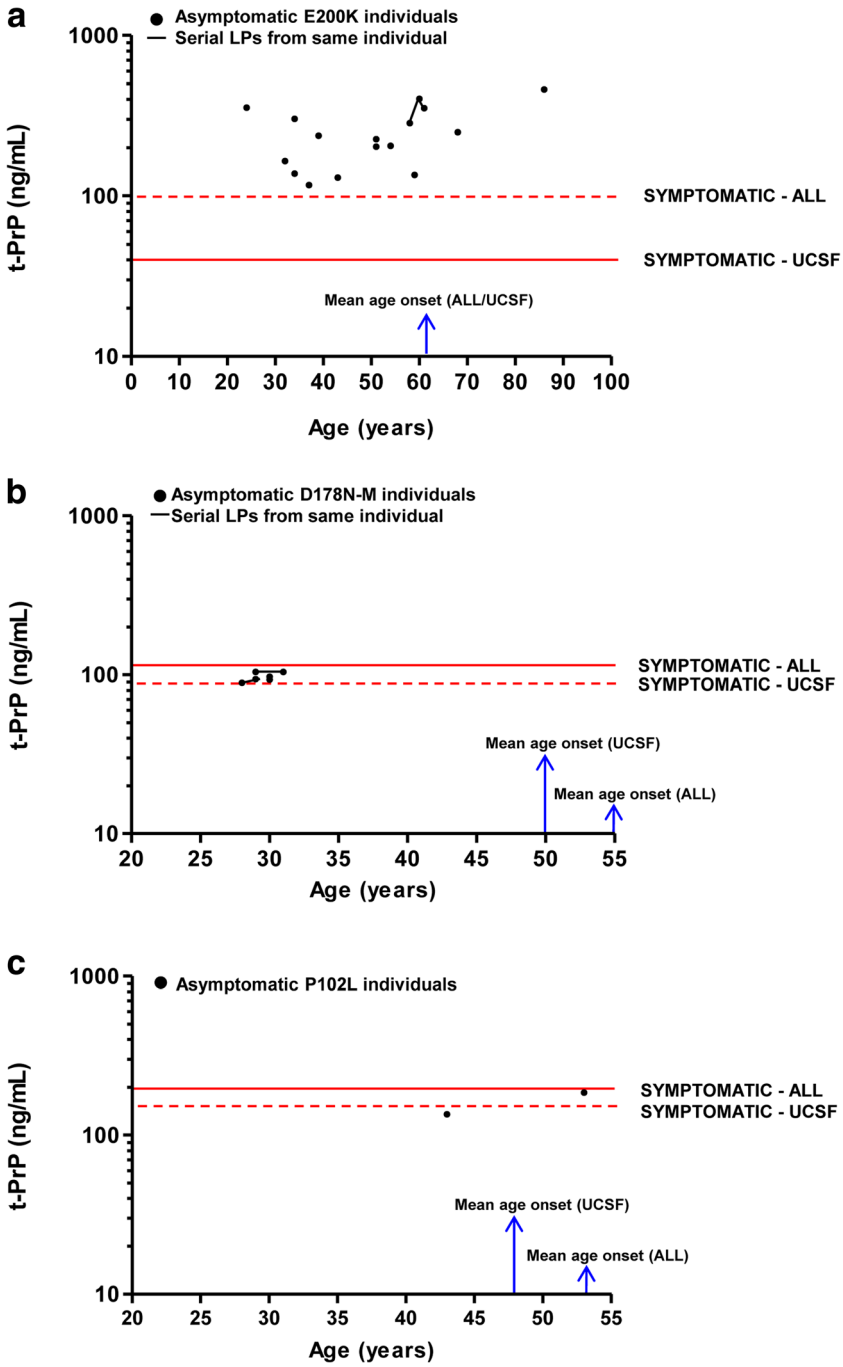

Fig. 5 CSF t-PrP concentrations in asymptomatic genetic prion diseases. CSF t-PrP concentrations and age of LP in pre-symptomatic *PRNP* mutation carries for the E200K (**a**), D178N-M (**b**) and P102L (**c**) mutations from the UCSF cohort. Black spots indicate a LP. Black spots connected with a black line indicating serial LPs from the same patient. Red lines indicate mean t-PrP concentrations for symptomatic cases from all the cases analysed in the present study (symptomatic, ALL). Dashed red lines indicate mean t-PrP concentrations for symptomatic cases from the UCSF cohort (symptomatic, UCSF). Mean age at onset from UCSF cohort and from all cases are indicated with a blue arrow

associated with the formation of prions. Broadly similar to amyloid-beta42 levels in AD, the decrease of CSF t-PrP concentrations in prion cases is speculated to be a consequence of the misfolding of the cellular prion protein (PrPc) into PrPsc with consequent "trapping" of the protein in aggregates, limiting the amount of soluble PrP filtering to the CSF. Based on this hypothesis, it could be assumed that CSF t-PrP levels would be highly dependent on prion disease aetiology and sCJD subtypes, which differ with respect to the neuropathological profiles and type of PrPsc aggregates [16, 21, 34]. For instance, in D178N-M cases, CSF t-PrP concentrations are decreased despite the reduced levels of PrPsc in the brain parenchyma, which is usually only detectable in the entorhinal cortex and in some cases with CJD-type alterations in the deep regions of the temporal cortex. Therefore, the absence of differences in CSF t-PrP concentrations between prion diseases displaying different types of PrP brain aggregates indicates that additional factors appear to explain the singular signatures of CSF t-PrP across the spectrum of prion diseases. Interestingly, decreased PrP expression was found in the two most prevalent sCJD subtypes (MM1 and VV2) [16],

as well as in the thalamus and entorhinal cortex of D178N-M cases [41] causing a reduction of PrP levels in the brain, and potentially in the CSF. Moreover, the decrease in CSF t-PrP could be associated with a decrease in proteinase-sensitive intermediate PrP isoforms not detected by the ELISA t-PrP assay.

In pre-symptomatic carriers of the D178N-M mutation, t-PrP concentrations were similar to those detected in symptomatic cases and lower than those in ND. This indicates that, at least in D178N-M, t-PrP could be a potential pre-clinical biomarker of the pathology. In contrast, pre-symptomatic E200K carriers harboured t-PrP higher than in clinical cases and similar to values measured in NDs. Although the low number of cases available impedes a statistical evaluation and, therefore, results remain descriptive, several aspects should be underlined. First, the presence of reduced t-PrP concentrations is not a general observation for all mutations. Whether these results are associated with mutation-specific disease duration, low number of cases, data dispersion and/or confounders such as heterogeneity of age at onset needs to be further explored in larger cohorts. Therefore, we cannot exclude t-PrP as a potential pre-clinical biomarker for other mutation types or prion disease types. Second, despite the absence of studies addressing the quantification of t-PrP levels in pre-symptomatic cases, we recently detected lower t-PrP concentrations in the CSF of pre-clinical and clinical naturally occurring scrapie [42], which would support the idea that reduced t-PrP concentrations may happen at pre-clinical and early prion disease stages.

Conclusions

Herein, we report the largest and most complete study of the levels of CSF t-PrP across the spectrum of prion diseases, including multiple cases of gPD associated with a broad range of *PRNP* mutations. We have confirmed previous data demonstrating reduced CSF t-PrP in sCJD.

Although the diagnostic potential of CSF t-PrP alone is perhaps limited, its combination with other biomarkers may heighten its utility. Importantly, the observed CSF t-PrP decline along disease progression in sCJD and in pre-symptomatic carriers of certain mutations such as D178N-M cases deserves further investigation towards potential translational application in clinical practice.

Acknowledgements We thank Silja Köchy for indispensable technical assistance.

Authors' Contributions AV-P, MS, IZ and FL designed the study. AV-P, MS and FL performed experiments. AV-P, MS, AK, IZ and FL analysed data and interpreted the results. IL, OC, CS, SS, AL, AP, IS, IF, EM, D.Z, MP, IB, MC, SJC, MDG, RS-V and IZ contributed to samples and/or technical expertise. FL and AV-P wrote the manuscript draft. All authors critically revised the manuscript and approved its content before submission.

Funding This study was funded by Robert Koch Institute through funds from the Federal Ministry of Health of Germany (grant no. 1369–341) to IZ, by the Spanish Ministry of Health - Instituto Carlos III/ Fondo Social Europeo (CP16/00041) to FL. This project has been funded at 65% by the Fondo Europeo de Desarrollo Regional (FEDER) through the Interreg V-A España-Francia-Andorra (POCTEFA 2014-2020) programme.

Compliance with Ethical Standards

Ethics Approval and Consent to Participate The study was conducted according to the revised Declaration of Helsinki and Good Clinical Practice guidelines, and was approved by all local Ethics committees. All study participants or their legal guardians provided written informed consent.

Consent for Publication Not applicable.

Competing Interests Dr. Lachmann reports he is a representative of AJ Roboscreen GmbH, Leipzig, Germany.

Abbreviations GSS-S, Gerstmann–Sträussler–Scheinker syndrome; ROC, Receiver operating characteristic; OPRI, Octapeptide repeat insertion; PRNP, Prion protein gene; gCJD, Genetic Creutzfeldt-Jakob disease; iCJD, Iatrogenic Creutzfeldt-Jakob disease; vCJD, Variant Creutzfeldt-Jakob disease; FFI, Fatal Familial Insomnia; NFL, Neurofilament light; PrPscz, PrPsc: Prion protein scrapie; LP, Lumbar puncture; AUC, Area under the curve; sCJD, Sporadic Creutzfeldt-Jakob disease; CSF, Cerebrospinal fluid; ELISA, Enzyme-linked immunosorbent assays; ND, Neurological diseases; t-PrP, Total prion protein

References

1. Aguzzi A, Sigurdson C, Heikenwaelder M (2008) Molecular mechanisms of prion pathogenesis. Annu Rev Pathol Mech Dis 3:11–40
2. Aguzzi A (2006) Prion diseases of humans and farm animals: epidemiology, genetics, and pathogenesis. J Neurochem 97:1726–1739
3. Chen C, Dong X-P (2016) Epidemiological characteristics of human prion diseases. Infect Dis Poverty [Internet] 5:47. Available from: http://idpjournal.biomedcentral.com/articles/10.1186/s40249-016-0143-8
4. Parchi P, Castellani R, Capellari S, Ghetti B, Young K, Chen SG et al (1996) Molecular basis of phenotypic variability in sporadic Creutzfeldt-Jakob disease. Ann Neurol [Internet] 39:767–78. Available from: http://www.ncbi.nlm.nih.gov/pubmed/8651649
5. Parchi P, Giese A, Capellari S, Brown P, Schulz-Schaeffer W, Windl O et al (1999) Classification of sporadic Creutzfeldt-Jakob disease based on molecular and phenotypic analysis of 300 subjects. Ann Neurol 46:224–233
6. Mastrianni JA (2010) The genetics of prion diseases. Genet Med 12:187–95
7. Lloyd SE, Mead S, Collinge J (2013) Genetics of prion diseases. Curr Opin Genet Dev 345–51
8. Bonda DJ, Manjila S, Mehndiratta P, Khan F, Miller BR, Onwuzulike K et al (2016) Human prion diseases: surgical lessons learned from iatrogenic prion transmission. Neurosurg Focus 41:E10
9. Zerr I, Bodemer M, Gefeller O, Otto M, Poser S, Wiltfang J, Windl O, Kretzschmar HA et al (1998) Detection of 14-3-3 protein in the cerebrospinal fluid supports the diagnosis of Creutzfeldt-Jakob disease. Ann Neurol 43:32–40
10. Otto M, Wiltfang J, Tumani H, Zerr I, Lantsch M, Kornhuber J et al (1997) Elevated levels of tau-protein in cerebrospinal fluid of patients with Creutzfeldt-Jakob disease. Neurosci Lett 225:210–212

11. Llorens F, Kruse N, Schmitz M, Gotzmann N, Golanska E, Thüne K, Zejneli O, Kanata E et al (2017) Evaluation of α-synuclein as a novel cerebrospinal fluid biomarker in different forms of prion diseases. Alzheimers Dement 13:710–719
12. Atarashi R, Satoh K, Sano K, Fuse T, Yamaguchi N, Ishibashi D, Matsubara T, Nakagaki T et al (2011) Ultrasensitive human prion detection in cerebrospinal fluid by real-time quaking-induced conversion. Nat Med 17:175–178
13. Meyne F, Gloeckner SF, Ciesielczyk B, Heinemann U, Krasnianski A, Meissner B, Zerr I (2009) Total prion protein levels in the cerebrospinal fluid are reduced in patients with various neurological disorders. J Alzheimers Dis 17:863–873
14. Dorey A, Tholance Y, Vighetto A, Perret-Liaudet A, Lachman I, Krolak-Salmon P, Wagner U, Struyfs H et al (2015) Association of cerebrospinal fluid prion protein levels and the distinction between Alzheimer disease and Creutzfeldt-Jakob disease. JAMA Neurol 72:267–275
15. Rumeileh SA, Lattanzio F, Maserati MS, Rizzi R, Capellari S, Parchi P (2016) Diagnostic accuracy of a combined analysis of cerebrospinal fluid t-PrP, t-tau, p-tau, and Aβ42 in the differential diagnosis of Creutzfeldt-Jakob disease from Alzheimer's disease with emphasis on atypical disease variants. J Alzheimers Dis 55:1–10
16. Llorens F, Ansoleaga B, Garcia-Esparcia P, Zafar S, Grau-Rivera O, López-González I, Blanco R et al (2013) PrP mRNA and protein expression in brain and PrP(c) in CSF in Creutzfeldt-Jakob disease MM1 and VV2. Prion 7:383–93
17. Schmitz M, Schlomm M, Hasan B, Beekes M, Mitrova E, Korth C, Breil A, Carimalo J et al (2010) Codon 129 polymorphism and the E200K mutation do not affect the cellular prion protein isoform composition in the cerebrospinal fluid from patients with Creutzfeldt-Jakob disease. Eur J Neurosci 31:2024–2031
18. Torres M, Cartier L, Matamala JM, Hernández N, Woehlbier U, Hetz C (2012) Altered prion protein expression pattern in CSF as a biomarker for Creutzfeldt-Jakob disease. PLoS One 7:e36159
19. Schmitz M, Lüllmann K, Zafar S, Ebert E, Wohlhage M, Oikonomou P, Schlomm M, Mitrova E et al (2014) Association of prion protein genotype and scrapie prion protein type with cellular prion protein charge isoform profiles in cerebrospinal fluid of humans with sporadic or familial prion diseases. Neurobiol Aging 35:1177–1188
20. Zerr I, Kallenberg K, Summers DM, Romero C, Taratuto A, Heinemann U, Breithaupt M, Varges D et al (2009) Updated clinical diagnostic criteria for sporadic Creutzfeldt-Jakob disease. Brain 132:2659–2668
21. Parchi P, De Boni L, Saverioni D, Cohen ML, Ferrer I, Gambetti P et al (2012) Consensus classification of human prion disease histotypes allows reliable identification of molecular subtypes: an inter-rater study among surveillance centres in Europe and USA. Acta Neuropathol 124:517–529
22. Kovács GG, Puopolo M, Ladogana A, Pocchiari M, Budka H, van Duijn C, Collins SJ, Boyd A et al (2005) Genetic prion disease: the EUROCJD experience. Hum Genet 118:166–174
23. World Health Organisation (2003) WHO manual for surveillance of human transmissible spongiform encephalopathies including variant Creutzfeldt-Jakob disease. WHO Man. Surveill. Hum. Transm. spongiform Enceph 105
24. Windl O, Giese A, Schulz-Schaeffer W, Zerr I, Skworc K, Arendt S, Oberdieck C, Bodemer M et al (1999) Molecular genetics of human prion diseases in Germany. Hum Genet 105:244–252
25. Robin X, Turck N, Hainard A, Tiberti N, Lisacek F, Sanchez JC, Müller M (2011). pROC: an open-source package for R and S+ to analyze and compare ROC curves. BMC Bioinformatics 12:77. https://doi.org/10.1186/1471-2105-12-77
26. Llorens F, Schmitz M, Karch A, Cramm M, Lange P, Gherib K, Varges D, Schmidt C et al (2016) Comparative analysis of cerebrospinal fluid biomarkers in the differential diagnosis of neurodegenerative dementia. Alzheimers Dement 12:577–589
27. Ladogana A, Sanchez-Juan P, Mitrova E, Green A, Cuadrado-Corrales N, Sanchez-Valle R et al (2009) Cerebrospinal fluid biomarkers in human genetic transmissible spongiform encephalopathies. J Neuro 256:1620–8
28. Cramm M, Schmitz M, Karch A, Mitrova E, Kuhn F, Schroeder B, Raeber A, Varges D et al (2016) Stability and reproducibility underscore utility of RT-QuIC for diagnosis of Creutzfeldt-Jakob disease. Mol Neurobiol 53:1896–1904
29. Croes EA, Theuns J, Houwing-Duistermaat JJ, Dermaut B, Sleegers K, Roks G, van den Broeck M, van Harten B et al (2004) Octapeptide repeat insertions in the prion protein gene and early onset dementia. J Neurol Neurosurg Psychiatry 75:1166–1170
30. Kovács GG, Trabattoni G, Hainfellner JA, Ironside JW, Knight RSG, Budka H (2002) Mutations of the prion protein gene: phenotypic spectrum. J Neurol 249:1567–1582
31. Schmitz M, Dittmar K, Llorens F, Gelpi E, Ferrer I, Schulz-Schaeffer WJ et al (2016) Hereditary human prion diseases: an update. Mol Neurobiol 54:4138–4149
32. Beck JA, Poulter M, Campbell TA, Adamson G, Uphill JB, Guerreiro R, Jackson GS, Stevens JC, Manji H, Collinge J, Mead S (2010) PRNP allelic series from 19 years of prion protein gene sequencing at the MRC Prion Unit. Hum Mutat 31(7):E1551–15563. https://doi.org/10.1002/humu.21281
33. Montagna P, Cortelli P, Avoni P, Tinuper P, Plazzi G, Gallassi R et al (1998) Clinical features of fatal familial insomnia: phenotypic variability in relation to a polymorphism at codon 129 of the prion protein gene. Brain Pathol [Internet] 8:515–20. Available from: http://www.ncbi.nlm.nih.gov/pubmed/9669701
34. Gambetti P, Kong Q, Zou W, Parchi P, Chen SG (2003) Sporadic and familial CJD: classification and characterisation. Br Med Bull 66:213–239
35. Sanchez-Juan P, Sánchez-Valle R, Green A, Ladogana A, Cuadrado-Corrales N, Mitrová E, Stoeck K, Sklaviadis T et al (2007) Influence of timing on CSF tests value for Creutzfeldt-Jakob disease diagnosis. J Neurol 254:901–906
36. Llorens F, Kruse N, Karch A, Schmitz M, Zafar S, Gotzmann N, Sun T, Köchy S et al (2018) Validation of α-synuclein as a CSF biomarker for sporadic Creutzfeldt-Jakob disease. Mol Neurobiol Mol Neurobiol 55:2249–2257
37. Minikel EV, Vallabh SM, Lek M, Estrada K, Samocha KE, Sathirapongsasuti JF, McLean CY, Tung JY et al (2016) Quantifying prion disease penetrance using large population control cohorts. Sci Transl Med 8:322ra9
38. Parchi P, Castellani R, Cortelli P, Montagna P, Chen SG, Petersen RB, Manetto V, Vnencak-Jones CL et al (1995) Regional distribution of protease-resistant prion protein in fatal familial insomnia. Ann Neurol 38:21–29
39. Llorens F, Karch A, Golanska E, Schmitz M, Lange P, Sikorska B et al (2017) Cerebrospinal fluid biomarker-based diagnosis of sporadic Creutzfeldt-Jakob disease: a validation study for previously established cutoffs. Dement Geriatr Cogn Disord 43:71–80
40. Zerr I, Schmitz M, Karch A, Villar-Piqué A, Kanata E, Golanska E et al (2018) Cerebrospinal fluid neurofilament light levels in neurodegenerative dementia: evaluation of diagnostic accuracy in the differential diagnosis of prion diseases. Alzheimer's Dement 14:751–763
41. Llorens F, Thüne K, Schmitz M, Ansoleaga B, Frau-Méndez MA, Cramm M et al (2016) Identification of new molecular alterations in fatal familial insomnia. Hum Mol Genet 25:2417–2436
42. Llorens F, Barrio T, Correia Â, Villar-Piqué A, Thüne K, Lange P et al (2018) Cerebrospinal fluid prion disease biomarkers in pre-clinical and clinical naturally occurring scrapie. Mol Neurobiol. https://doi.org/10.1007/s12035-018-1014-z

Affiliations

Anna Villar-Piqué[1] · Matthias Schmitz[1,2] · Ingolf Lachmann[3] · André Karch[4] · Olga Calero[5,6] · Christiane Stehmann[7] · Shannon Sarros[7] · Anna Ladogana[8] · Anna Poleggi[8] · Isabel Santana[9] · Isidre Ferrer[10,11] · Eva Mitrova[12] · Dana Žáková[12] · Maurizio Pocchiari[8] · Inês Baldeiras[9] · Miguel Calero[5,6] · Steven J. Collins[7,13] · Michael D. Geschwind[14] · Raquel Sánchez-Valle[15] · Inga Zerr[1,2] · Franc Llorens[1,11,16]

[1] Department of Neurology, University Medical School, Göttingen, Germany

[2] German Center for Neurodegenerative Diseases (DZNE), Göttingen, Germany

[3] AJ Roboscreen GmbH, Leipzig, Germany

[4] Department of Epidemiology, Helmholtz Centre for Infection Research, Braunschweig, Germany

[5] Alzheimer Disease Research Unit, CIEN Foundation, Queen Sofia Foundation Alzheimer Center, Chronic Disease Programme Carlos III Institute of Health, Madrid, Spain

[6] Network Center for Biomedical Research in Neurodegenerative Diseases (CIBERNED), Madrid, Spain

[7] Australian National Creutzfeldt-Jakob Disease Registry, Florey Institute, The University of Melbourne, Melbourne, Australia

[8] Department of Neurosciences, Istituto Superiore di Sanità, Rome, Italy

[9] Neurology Department, CHUC - Centro Hospitalar e Universitário de Coimbra, CNC- Center for Neuroscience and Cell Biology, Faculty of Medicine, University of Coimbra, Coimbra, Portugal

[10] Bellvitge University Hospital-IDIBELL, Department of Pathology and Experimental Therapeutics, Hospitalet de Llobregat, University of Barcelona, Barcelona, Spain

[11] Network Center for Biomedical Research in Neurodegenerative Diseases (CIBERNED), Barcelona, Spain

[12] Department of Prion Diseases, Slovak Medical University, Bratislava, Slovakia

[13] Department of Medicine (RMH), The University of Melbourne, Melbourne, Australia

[14] Department of Neurology, Memory and Aging Center, University of California, San Francisco, CA, USA

[15] Alzheimer's Disease and Other Cognitive Disorders Unit, Neurology Department, Institut d'Investigacions Biomediques August Pi i Sunyer (IDIBAPS), Hospital Clínic, Barcelona, Spain

[16] Bellvitge Biomedical Research Institute (IDIBELL), L'Hospitalet de Llobregat, Spain

biomolecules

MDPI

Article

Diagnostic Accuracy of Prion Disease Biomarkers in Iatrogenic Creutzfeldt-Jakob Disease

Franc Llorens [1,2,3,*], Anna Villar-Piqué [2,3,*], Peter Hermann [1], Matthias Schmitz [1,4], Olga Calero [5,6], Christiane Stehmann [7], Shannon Sarros [7], Fabio Moda [8], Isidre Ferrer [2,3,9], Anna Poleggi [10], Maurizio Pocchiari [10], Marcella Catania [8], Sigrid Klotz [11], Carl O'Regan [12], Francesca Brett [12], Josephine Heffernan [12], Anna Ladogana [10], Steven J. Collins [7,13], Miguel Calero [5,6], Gabor G. Kovacs [11,14,15] and Inga Zerr [1,4]

1 Department of Neurology, National Reference Center for CJD Surveillance, University Medical Centre Göttingen, 37075 Göttingen, Germany; peter.hermann@med.uni-goettingen.de (P.H.); matthias.schmitz@med.uni-goettingen.de (M.S.); ingazerr@med.uni-goettingen.de (I.Z.)
2 Network Center for Biomedical Research in Neurodegenerative Diseases (CIBERNED), L'Hospitalet de Llobregat, 08908 Llobregat, Spain; 8082ifa@gmail.com
3 Bellvitge Biomedical Research Institute (IDIBELL), L'Hospitalet de Llobregat, 08908 Llobregat, Spain
4 German Center for Neurodegenerative Diseases (DZNE), 37075 Göttingen, Germany
5 Chronic Disease Programme (UFIEC)-CROSADIS, Instituto de Salud Carlos III, 28029 Madrid, Spain; rueda@externos.isciii.es (O.C.); mcalero@isciii.es (M.C.)
6 Network Center for Biomedical Research in Neurodegenerative Diseases (CIBERNED), 28031 Madrid, Spain
7 Australian National Creutzfeldt-Jakob Disease Registry, Florey Institute, The University of Melbourne, Melbourne 3010, Australia; christiane.stehmann@florey.edu.au (C.S.); shannon.sarros@florey.edu.au (S.S.); s.collins@unimelb.edu.au (S.J.C.)
8 Fondazione IRCCS Istituto Neurologico Carlo Besta, Unit of Neurology 5 and Neuropathology, 20133 Milan, Italy; fabio.moda@istituto-besta.it (F.M.); Marcella.Catania@istituto-besta.it (M.C.)
9 Department of Pathology and Experimental Therapeutics, University of Barcelona, L'Hospitalet de Llobregat, 08907 Llobregat, Spain
10 Department of Neuroscience, Istituto Superiore di Sanità, 00161 Rome, Italy; anna.poleggi@iss.it (A.P.); maurizio.pocchiari@iss.it (M.P.); anna.ladogana@iss.it (A.L.)
11 Institute of Neurology, Medical University of Vienna, Vienna 1097, Austria; sigrid.klotz@meduniwien.ac.at (S.K.); Gabor.Kovacs@uhnresearch.ca (G.G.K.)
12 Department of Neuropathology, Beaumont Hospital, Dublin 9, Ireland; carloregan@hotmail.com (C.O.); francescabrett@beaumont.ie (F.B.); josephineheffernan@beaumont.ie (J.H.)
13 Department of Medicine (RMH), The University of Melbourne, Melbourne 3050, Australia
14 Department of Laboratory Medicine and Pathobiology and Tanz Centre for Research in Neurodegenerative Disease, University of Toronto, Toronto, ON M5T 0S8, Canada
15 Laboratory Medicine Program, University Health Network, Toronto, ON M5G 2C4, Canada
* Correspondence: franc.llorens@gmail.com (F.L.); avillar@idibell.cat (A.V.-P.); Tel.: +34-934-035-808 (F.L.); +34-934-035-808 (A.V.-P.)

Received: 11 December 2019; Accepted: 8 February 2020; Published: 12 February 2020

Abstract: Human prion diseases are classified into sporadic, genetic, and acquired forms. Within this last group, iatrogenic Creutzfeldt–Jakob disease (iCJD) is caused by human-to-human transmission through surgical and medical procedures. After reaching an incidence peak in the 1990s, it is believed that the iCJD historical period is probably coming to an end, thanks to lessons learnt from past infection sources that promoted new prion prevention and decontamination protocols. At this point, we sought to characterise the biomarker profile of iCJD and compare it to that of sporadic CJD (sCJD) for determining the value of available diagnostic tools in promptly recognising iCJD cases. To that end, we collected 23 iCJD samples from seven national CJD surveillance centres and analysed the electroencephalogram and neuroimaging data together with a panel of seven CSF biomarkers: 14-3-3, total tau, phosphorylated/total tau ratio, alpha-synuclein, neurofilament light, YKL-40, and real-time

quaking induced conversion of prion protein. Using the cut-off values established for sCJD, we found the sensitivities of these biomarkers for iCJD to be similar to those described for sCJD. Given the limited relevant information on this issue to date, the present study validates the use of current sCJD biomarkers for the diagnosis of future iCJD cases.

Keywords: Iatrogenic Creutzfeldt-Jakob disease; dura matter graft; corneal transplant; growth hormone; biomarker; cerebrospinal fluid; electroencephalogram; magnetic resonance imaging; RT-QuIC

1. Introduction

Prion diseases or transmissible spongiform encephalopathies (TSEs) are a family of rare neurodegenerative disorders that affect both humans and animals, caused by the conversion of the physiological cellular prion protein (PrP^{c}) into a disease-associated isoform (PrP^{Sc}). Principal prion disease neuropathological hallmarks are the presence of spongiform changes in the neuropil sometimes associated with massive neuronal loss, neuro-inflammation in the form of astrocytic gliosis and the deposition of aggregated prion protein in the brain parenchyma [1]. In humans, prion diseases can be classified according to their etiology as sporadic, genetic, and acquired [2]. The sporadic form of the disease, also known as sporadic Creutzfeldt-Jakob disease (sCJD), accounts for about 85–90% of all human cases [3]. Some 10–15% of cases are associated with autosomal dominant pathogenic sequence variations in the prion protein gene (*PRNP*), while acquired forms are rare and are caused by the transmission of infective material from human to human (Kuru and iatrogenic Creutzfeldt-Jakob disease (iCJD)) or from cattle to human (variant CJD) [4]. Iatrogenic transmission of CJD occurs through particular surgical and medical procedures. The use of contaminated growth hormone and dura mater grafts derived from human cadavers with undiagnosed sCJD are the principal sources of iCJD [5,6]. Other sources are corneal transplant, treatment with cadaveric pituitary-derived gonadotropin, and the use of CJD-contaminated electroencephalogram (EEG) depth electrodes and neurosurgical instruments. Packed red blood cells from variant CJD donors are another source of secondary infection. Iatrogenic transmission of the CJD agent has been reported in over 490 patients worldwide [7].

iCJD reached its highest incidence in the decade of the 1990s and since then the number of reported cases has drastically decreased [6]. It is not expected that new iCJD cases will arise in the coming years except for cases with very long incubation periods. However, the risk of human-to-human prion disease transmission is still present due to potential new sources of iatrogenic contamination through humans exposed to zoonotic agents or secondary transmissions [8–10]. Despite the fact that iCJD diagnosis is based on the presence of a recognized iatrogenic source, unrecognized mechanisms of human prion disease transmission may occur.

Clinical and neuropathological presentation of iCJD is related to the route of exposure to human prions, the transmitted CJD strain, and the *PRNP* genotype of the patient [5,6,11]. Thus, potential singularities in prion disease biomarkers in different iCJD types might be expected. In this regard, there is limited information about the accuracy of prion disease biomarkers, including EEG, neuroimaging, and CSF tests in iCJD. To date, available data in the literature include a limited number of iCJD cases and/or a reduced number of biomarkers employed [12–16].

In the present study, we characterised the biomarker profiles of iCJD, using a cohort generated from seven national prion disease surveillance centres and determined their clinical value in reference to established cut-off points for sCJD.

2. Materials and Methods

2.1. Patients and CSF Sampling

The study included 23 iCJD cases collected from the following CJD reference centers: 1) Clinical Dementia Center and the National Reference Center for CJD Surveillance at the University Medical Center, Göttingen, Germany (n = 11), 2) National Centre of Microbiology-Carlos III Institute of Health, Madrid, Spain (n = 2), 3) Istituto Superiore di Sanità, Rome, Italy (n = 1), 4) Australian National CJD Registry, The Florey Department of Neuroscience and Mental Health, Melbourne, Australia (n = 2), 5) Medical University of Vienna, Austria (n = 4), 6) Fondazione IRCCS Istituto Neurologico Carlo Besta, Milan, Italy (n = 1), and 7) National CJD surveillance center, Beaumont Hospital, Dublin, Ireland (n = 2). Iatrogenic CJD was diagnosed according to established World Health Organization (WHO) criteria [17]. Twenty iatrogenic cases were associated with dura matter grafts, two with human growth hormone, and one with corneal transplantation. Clinical symptoms of the 23 iCJD patients are indicated in Supplementary Table S1. CSF was collected for diagnostic purposes during regular prospective surveillance activities of the participating centers and stored in polypropylene tubes at −80 ºC at each diagnostic centre. For this study, CSF was shipped with dry ice to the University Medical Center of Göttingen to perform additional CSF biomarker tests.

2.2. CSF Analyses

The presence of 14-3-3 protein in the CSF was determined with western-blot (WB) according to established CJD diagnostic protocols [18]. Cases with inconclusive outcome (traces of 14-3-3 in the WB) were considered negative. 14-3-3 gamma was quantified using the enzyme-linked immunosorbent assay (ELISA) 14-3-3 gamma from Circulex (Nagano, Japan). Total-tau (t-tau) and phosphorylated tau T181 (p-tau) were quantified using the INNOTEST®hTAU-Ag and INNOTEST® PHOSPHO-TAU(181P) ELISA kits from Fujirebio (Ghent, Belgium), respectively. Neurofilament light (Nfl) was quantified using the Uman Diagnostics NF-light assay from Uman Diagnostics (Umeå, Sweden). Alpha-synuclein (a-syn) was quantified using the a-syn ELISA kit from EUROIMMUN as described before [19]. YKL-40 was quantified using the MicroVue YKL-40 ELISA assay from Quidel (San Diego, CA, USA). Real-time quaking-induced conversion (RT-QuIC) was performed as described before [20]. The analysts were blinded to clinical data. CSF biomarkers were centrally quantified (Clinical Dementia Center—Göttingen) at the time of the present study with the exception of WB 14-3-3, which was locally analysed in each of the participants' laboratories at the time of diagnosis.

2.3. Electroencephalogram and Magnetic Resonance Imaging

Electroencephalogram (EEG) and magnetic resonance image (MRI) tests were performed as routine clinical diagnostic studies at each prion diagnostic centre in the framework of epidemiological studies [21,22]. For the present study, biomarker outcomes were reported as "positive" or "negative" according to WHO criteria [17], which include high signal abnormalities in the caudate nucleus and/or putamen on diffusion-weighted imaging (DWI), or fluid attenuated inversion recovery (FLAIR) and the presence of generalized periodic complexes in the EEG.

2.4. Genetic Test:

Determination of codon 129 polymorphism in the prion protein gene (*PRNP*) was performed as described before [23].

2.5. Statistical Analysis

In order to determine associations between biomarkers and age at onset and sex, linear regression models (for continuous biomarkers) and logistic regression models (for categorical biomarkers) were used. Disease duration association with other variables was analysed with multivariate Cox

proportional hazards models for survival analysis. Stratification based on the source of infection was not considered in any statistical analysis due to the low number of cases in two subgroups. Pearson correlation coefficients were used to assess associations between continuous biomarkers. All statistical analyses were conducted in R, except correlations, which were performed in GraphPad Prism 5 (GraphPad Software, San Diego, CA, USA).

2.6. Ethics

The study was conducted according to the revised Declaration of Helsinki and Good Clinical Practice guidelines, and was approved by local Ethics committees.

3. Results

3.1. Study Population

Of the 23 iCJD cases included in the study, 14 were male and nine were female. Most iCJD cases (n = 20) were attributed to dura mater grafts, while two were associated with growth hormone therapy, and one was associated with corneal transplantation. Mean age at disease onset was 51.0 years old and mean disease duration was 7.9 months. Disease duration was significantly associated with age at onset and with sex ($p < 0.01$ in both). The hazard ratios were 1.0526 for the variable age and 4.2121 for the variable sex, with female patients showing increased disease duration (Figure 1). These association results with demographic parameters were not significantly altered when only dura matter grafts cases were considered.

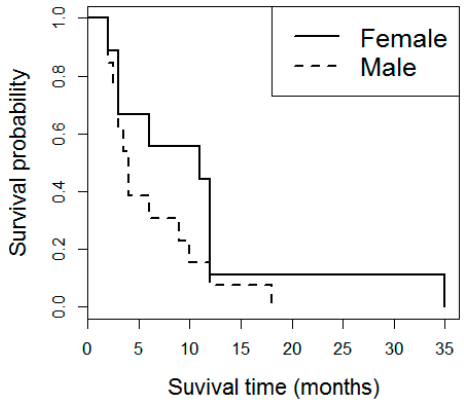

Figure 1. Disease duration in iCJD. Kaplan-Meier survival curves in iCJD stratified by sex.

Most of the cases (n = 18) were methionine/methionine (MM) homozygous at codon 129 of the *PRNP* gene, while three were methionine/valine (MV) heterozygous and one was valine/valine (VV) homozygous (Table 1).

Table 1. Demographic, genetic, and clinical data in iatrogenic CJD. Source of infection, number of cases (n), sex (female (f)/male (m)), age at onset in years (mean with standard deviation (SD) and minimum and maximum years), codon 129 genotype (methionine (M), valine (V)), and disease duration in months (mean and standard deviation (SD), with minimum and maximum months) are indicated. NA: not available. * For one case, disease duration was not available.

			Age (years)	Codon 129 *PRNP*				Disease Duration (Months)
Source of Infection	**n**	**Sex(f/m)**	**mean±SD (min-max)**	**MM**	**MV**	**VV**	**NA**	**Mean±SD (min-max)**
Dura mater grafts	20	8/12	52 ± 15 (28-76)	16	3	0	1	8.0 ± 7.9 (2-35)
Growth hormone	2	0/2	39.5 ± 0.7 (39-40)	1	0	1	0	3*
Corneal transplant	1	1/0	45	1	0	0	0	11
Total	23	9/14	51 ± 15 (28-76)	18	3	1	1	7.9 ± 7.6 (2-35)

3.2. EEG and MRI

A positive EEG was recorded in 11 out of 22 cases with available data (sensitivity 50%). MRI results were recorded in 15 cases, being positive in 10 of them (sensitivity 66.6%). The degree of agreement between EEG and MRI outcome (number of positive or negative cases in both tests) was 60% (Table 2). EEG and MRI positivity was associated neither with age at onset nor with sex ($p > 0.05$).

Table 2. Electroencephalogram and magnetic resonance imaging in iatrogenic CJD. Source of infection, electroencephalogram (EEG), and magnetic resonance imaging (MRI) outcome given as positive (Pos), negative (Neg), or not available (NA), and sensitivity of the biomarker test (%), are indicated.

	EEG				MRI			
Source of Infection	**Pos**	**Neg**	**NA**	**Sensitivity (%)**	**Pos**	**Neg**	**NA**	**Sensitivity (%)**
Dura mater grafts	9	10	1	47.4	9	4	7	69
Growth hormone	1	1	0	50	1	1	0	50
Corneal transplant	1	0	0	100	0	0	1	NA
Total	11	11	1	**50**	10	5	8	**66.6**

3.3. CSF Biomarkers

14-3-3 was measured with WB (n = 23) and ELISA (n = 21). 14-3-3 ELISA quantification out-performed WB in terms of sensitivity (95.2% vs. 87%) with only one case below the established cut-off for sCJD (20000 AU/mL, [24]) and mean values of 93,047 AU/mL. t-tau (n = 23) displayed a sensitivity of 87% based on the established sCJD cut-off of 1300 pg/mL [13], with a mean concentration of 10,915 pg/mL. The addition to p-tau in the form of p-tau/t-tau ratio (n = 19) increased the sensitivity achieved by t-tau alone up to 94.7%, with only one case below the p-tau/t-tau cut-off (<0.075, [25]). Mean p-tau/t-tau ratio was 0.018. a-syn (n = 21) displayed a sensitivity of 90.5% based on the sCJD cut-off of 3300 pg/mL [26] with a mean concentration of 13,346 pg/mL. Nfl (n = 21) displayed a sensitivity of 85.7% using a cut-off of 7000 pg/mL [27] with a mean concentration of 12,986 pg/mL. The mean YKL-40 concentration (n = 21) was 441 ng/mL with a sensitivity of 76.2% based on a sCJD cut-off of 315 ng/mL [28]. Finally, RT-QuIC positive reactions were detected in 18 out of 21 cases (sensitivity of 85.7%) based on a cut-off of 10,000 relative fluorescent units (RFU) for sCJD [20]; mean RFU was 41,129 (Table 3). None of the CSF biomarkers were associated with age at onset or sex ($p > 0.05$ in all cases). Disease duration was not associated with any biomarker after controlling for the effects of age and sex.

Table 3. Cerebrospinal fluid biomarkers in iatrogenic CJD. Cerebrospinal fluid (CSF) biomarker with cut-off point, source of infection, biomarker outcome given as positive, negative, or not available (NA), sensitivity of the biomarker test (%) with concentrations (mean with standard deviation (SD)), and minimum and maximum values are indicated. Data stratification based on infection source are only disclosed as descriptive information but no subgroup analysis was performed.

CSF Biomarker	Source of Infection	Positive	Negative	NA	Sensitivity (%)	Mean ± SD	Min-Max
14-3-3 western-blot	Dura mater grafts	17	3	0	85.0	-	-
	Growth hormone	2	0	0	100.0	-	-
	Corneal transplant	1	0	0	100.0	-	-
	Total	20	3	0	87.0	-	-
14-3-3 ELISA (>20,000 AU/mL)	Dura mater grafts	17	1	2	94.4	94,721±65,638	7677-254,152
	Growth hormone	2	0	0	100.0	56,120±36,753	36,753-75,488
	Corneal transplant	1	0	0	100.0	136,776	-
	Total	20	1	2	95.2	93,047±62,723	7677-254,152
t-tau (>1300 pg/mL)	Dura mater grafts	17	3	0	85.0	10,374±9983	510-35,280
	Growth hormone	2	0	0	100.0	19,356±22,299	3588-35124
	Corneal transplant	1	0	0	100.0	4833.0	-
	Total	20	3	0	87.0	10,915±10,822	510-35,280
p-tau/t-tau ratio (<0.075)	Dura mater grafts	16	1	3	94.1	0.018±0.025	0.002-0.094
	Growth hormone	1	0	1	100.0	0.012	-
	Corneal transplant	1	0	0	100.0	0.013	-
	Total	18	1	4	94.7	0.018±0.024	0.002-0.094
a-syn (>3300 pg/ml)	Dura mater grafts	16	2	2	88.9	11,884±13,303	2075-45,698
	Growth hormone	2	0	0	100.0	25,905±24,158	8823-42,987
	Corneal transplant	1	0	0	100.0	14,541	-
	Total	19	2	2	90.5	13,346±14,049	2075-45,698
Nfl (>7000 pg/mL)	Dura mater grafts	15	3	2	83.3	12,900±7021	5311-29,856
	Growth hormone	2	0	0	100.0	13,347±8892	7060-19,635
	Corneal transplant	1	0	0	100.0	14541	-
	Total	18	3	2	85.7	12,986±6776	5311-29,856
YKL-40 (>315 ng/mL)	Dura mater grafts	13	5	2	72.2	417±205	127-887
	Growth hormone	2	0	0	100.0	630±303	416-845
	Corneal transplant	1	0	0	100.0	495.0	-
	Total	16	5	2	76.2	441±211	127-887
RT-QuIC (>10,000 RFU)	Dura mater grafts	16	2	2	88.9	44,180±16,679	10,000-65,000
	Growth hormone	1	1	0	50.0	21,910±16,843	10,000-33,820
	Corneal transplant	1	0	0	100.0	24,651	-
	Total	18	3	2	85.7	41,129±17,594	10,000-65,000

3.4. Correlation between CSF Biomarkers

Correlations between continuous CSF biomarker data (biomarker concentrations for 14-3-3 (ELISA), t-tau, p-tau/t-tau ratio Nfl, a-syn, YKL-40, and RFU for RT-QuIC assay) were investigated. WB 14-3-3 data were not included due to the binary outcome of the assay.

Significant correlations were detected between 14-3-3 and t-tau ($\rho = 0.57$, $p = 0.0067$), 14-3-3 and p-tau/t-tau ratio ($\rho = -0.52$, $p = 0.0208$), t-tau and p-tau/t-tau ratio ($\rho = -0.56$, $p = 0.0126$), t-tau and a-syn ($\rho = 0.70$, $p < 0.001$), t-tau and Nfl ($\rho = 0.48$, $p = 0.0259$), t-tau and YKL-40 ($\rho = 0.56$, $p = 0.0079$), a-syn and Nfl ($\rho = 0.45$, $p = 0.0396$), a-syn and YKL-40 ($\rho = 0.52$, $p = 0.0148$), and Nfl and YKL-40 ($\rho = 0.80$, $p < 0.001$). RT-QuIC RFU did not correlate with any of the other biomarkers ($p > 0.05$ for all comparisons) (Table 4).

Table 4. Correlations between cerebrospinal fluid biomarkers. Cerebrospinal fluid (CSF) biomarkers correlations (biomarkers concentrations for 14-3-3 (ELISA), t-tau, p-tau/t-tau ratio Nfl, a-syn, YKL-40, and RFU for RT-QuIC assay). Pearson's correlation coefficients are shown below the diagonal line (-) and p values are shown above. Statistically significant correlations ($p < 0.05$) are shown in bold.

	14-3-3	t-tau	p-tau/t-tau ratio	a-syn	Nfl	YKL-40	RT-QuIC
14-3-3	-	**0.0067**	**0.0208**	0.1822	0.8759	0.8064	0.7713
t-tau	**0.57**	-	**0.0126**	**<0.001**	**0.0259**	**0.0079**	0.4150
p-tau/t-tau ratio	**−0.52**	**−0.56**	-	0.0822	0.1938	0.3634	0.9507
a-syn	0.30	**0.70**	−0.41	-	**0.0396**	**0.0148**	0.1822
Nfl	0.04	**0.48**	−0.31	**0.45**	-	**<0.001**	0.9358
YKL-40	0.06	**0.56**	−0.22	**0.52**	**0.80**	-	0.1920
RT-QuIC	−0.07	−0.19	0.02	−0.29	−0.02	−0.30	-

4. Discussion

The differential diagnosis of human prion diseases can be often challenging due to the phenotypic heterogeneity of the disease. Prion disease biomarker tests developed in the last two decades allow the detection of symptomatic sCJD and genetic prion disease cases, with *PRNP* sequence variations mimicking the sporadic phenotype (e.g., *PRNP*-E200K and *PRNP*-V210I) with high accuracy [27,29–33]. In contrast, very few studies have assessed the accuracy of the same biomarker tests in iCJD. Available studies described either very small numbers of cases, not necessarily representative of the overall cohort, or limited biomarker assays, mainly first-generation ones such as CSF 14-3-3 WB, EEG, or MRI [12,13,16].

Demographic and genetic characteristics of our iCJD cohort were similar to previous studies reviewing the iCJD outbreak [6]. Methionine homozygosity at codon 129 was over-represented in the present study (18 out of 22 cases), in agreement with the reported high prevalence of MM genotype in dura mater cases (80%) [6,11,16], which was indeed the source of infection most represented in our study population (87% of cases). Similar to other studies [12], mean age at onset in our iCJD cohort (51 years) was below that reported in sCJD (66 years old) [34]. Indeed, in the absence of recognized risk factors for iatrogenic transmission, iCJD may not be identified as a prion disease due to the significantly younger age at onset compared to sCJD [11]. We observed an association of disease duration with age at onset and also with sex, with female patients presenting longer survival times. This finding was previously described in sCJD and genetic prion diseases [35], as well as in iCJD [36]. Although a longer survival time in iCJD was also associated with MV heterozygosity at codon 129 and with cases caused by growth hormone treatment (compared to cases caused by dura mater implants) [36], we could not validate these findings probably due to the strong imbalance of our cohort regarding these variables.

In our biomarker panel study, we found the accuracy of EEG, MRI, and CSF 14-3-3 WB in iCJD to be broadly in line with what has been reported for sCJD. This finding is perhaps not surprising considering the similarity between the iCJD and sCJD clinical phenotypes [11]. When previously published data are simultaneously explored however, notable differences are observed between studied cohorts of iCJD. Regarding 14-3-3 detection by WB, a variety of sensitivities have been reported: 43% (n = 14, growth hormone-associated) [12], 75% (n = 20, source not indicated) [13], and 85% (n = 13, dura mater graft-associated) [16]. Other reports with one [37–39] or two iCJD cases [40] displayed 14-3-3 WB positivity in all samples. These differences may be related not to only the specific transmitted sCJD strain and the source of infection, but also to pre-analytical/analytical parameters as well as demographic/genetic characteristics of the studied cohorts. In our work, 14-3-3 WB sensitivity (87%) was at the upper range of previous iCJD studies, which is the same value as t-tau sensitivity. Importantly, 14-3-3 quantification with ELISA (sensitivity 95.2%) out-performed WB, displaying the highest sensitivity among the biomarkers herein tested. Since the development of the 14-3-3 ELISA, several studies in large cohorts of sCJD cases have demonstrated superior sensitivity compared to the WB method [24,40–42], but this is the first study to validate this observation in iCJD.

The value of EEG and MRI as diagnostic tools in iCJD was previously documented [11,14]. In a cohort of growth hormone-associated iCJD cases, EEG displayed a sensitivity of 71%, with the presence of MRI abnormalities in most of the cases [12]. CJD-associated changes on MRI were reported in two studied growth hormone-associated iCJD cases [43] and in 16 out of 22 (76%) dura matter-associated iCJD cases [16]. Case reports have also demonstrated the presence of typical abnormalities in growth hormone-related cases [44,45]. In our study, EEG and MRI displayed lower sensitivities than CSF biomarkers (50% and 66.6%, respectively) with poor agreement between both tests (60%). The low sensitivity of CJD-typical EEG findings is in line with other published data from CJD surveillance centres reporting sCJD cases [1]. In contrast, the herein reported sensitivity of MRI is lower than in sCJD cases [46–48]. On one side, this might be explained by the fact that most of the cases were reported to the reference centres before 2009, when standardized MRI criteria had not been established. On the other side, MRI data were available in only 15 out of the 23 iCJD cases; thus, caution should be taken when comparing our results with those from larger study cohorts.

Regarding next-generation CSF biomarkers, few data are available in the literature. In the present work, the addition of p-tau to t-tau quantification in the form of p-tau/t-tau ratio raised the sensitivity from 87% to 94.7%, which lies within the range of the sensitivities achieved in a large cohort of sCJD cases [29]. Interestingly, the cut-off utilised in the present study (<0.075) was generated from a cohort of sCJD and non-CJD cases wherein the control group included neurological controls and non-prion neurodegenerative diseases [25,29]. In the same cohort, exclusion of non-prion neurodegenerative diseases from the control group rendered a cut-off of <0.106 [29] that, when applied to the present iCJD study, boosts sensitivity to 100%.

Recently, CSF a-syn has been demonstrated to be a highly sensitive and specific biomarker for sCJD [26,30] and for gCJD associated with E200K and V210I mutations [30]. Herein, we also validated the value of this biomarker in the detection of iCJD cases with a sensitivity of 90.5%, which is only surpassed by the accuracies obtained for 14-3-3 ELISA and the p-tau/t-tau ratio. In contrast to surrogate markers of neuro-axonal degeneration such as tau and 14-3-3, a-syn is suggested to reflect synaptic loss, an early event in the pathology of neurodegeneration. Although synaptic and neuronal damage are common hallmarks in neurodegenerative diseases, CSF a-syn is highly specific for sCJD [30]. This is in contrast to CSF Nfl, another non-specific marker of axonal damage that is increased in several neurological conditions [49]. In our iCJD cohort, Nfl sensitivity (85.7%) was below that reported in sCJD cases [27,50,51]. YKL-40, a disease-specific marker of neuro- inflammation expressed in astrocytes, displayed the lowest sensitivity (76.2%) among CSF biomarkers herein tested. Elevated CSF YKL-40 levels are reported in sCJD, gCJD associated with E200K, and V210I mutations, and, to a lesser extent, in fatal familial insomnia [28]. CSF YKL-40 also appeared to be increased in other neurodegenerative dementias such as AD and FTD, but not in DLB [28,52,53].

The most recently updated diagnostic criteria for CJD incorporates the RT-QuIC assay as one of the CSF biomarker tests. This assay detects pathological prion protein in biofluids and has been reported to be highly sensitive and almost fully specific. We observed 85.7% sensitivity of RT-QuIC in our iCJD cohort, which is within the range of values described for sCJD [31,54]. Unfortunately, RT-QuIC results in iCJD are scarce in the literature. One study investigating iCJD reported positive RT-QuIC signal in two tested patients who received dura matter grafts [40]. Another report mentioned an RT-QuIC sensitivity of 67% in iCJD patients treated with cadaveric growth hormone although the data were not disclosed [55].

Investigation of potential associations between biomarkers in iCJD led us to the striking finding that RT-QuIC results do not correlate with any of the surrogate markers of prion pathology. While it is possible that RT-QuIC signal does not really reflect the degree of cerebral PrP pathogenesis, it may also be speculated that PrP seeding capacity for pathological conversion is not linked in a straightforward manner to neuronal damage and neuro-inflammation. By contrast, positive correlations were observed between several neuronal damage and neuro-inflammation markers, in line with those previously detected in sCJD [27,28,30,56,57]. Positive correlation between Nfl and t-tau with YKL-40 suggests

a pathogenic association between astroglial activation and axonal injury in iCJD. Interestingly, Nfl vs.YKL-40 and t-tau vs. a-syn correlations were the most significant despite the fact that each pair of biomarkers is associated with distinct prion disease pathological features. While a positive correlation between Nfl and YKL-40 was previously detected in AD [58], this has not yet been investigated in prion diseases.

Limitations of the Study

Due to the rarity of iCJD, a limited number of cases were available. Consequently, diagnostic accuracies may be partially biased due to case selection. Another important limitation is the impossibility to perform any subgroup statistical analyses based on infection source because the number of cases associated to growth hormone and corneal transplant are too low. Thus, data regarding source of infection remain purely descriptive.

5. Conclusions

In this study, we present the first simultaneous analysis of the available battery of prion disease biomarkers for iCJD. Among these, CSF biomarkers displayed greater sensitivity than EEG and MRI, with similar accuracies to those achieved in sCJD and in the most prevalent form of genetic prion disease (gCJD associated to E200K mutation) using the same cut-off points in the same ethnic populations (comparisons are summarized in Supplementary Table S2). Utilised CSF biomarkers covered the main pathological features of prion pathogenesis, including synaptic (a-syn) and neuronal damage (14-3-3, tau, Nfl), neuro-inflammation (YKL-40), and prion protein seeding and aggregation (RT-QuIC). Our study validates the use of the conventional panel of sCJD biomarkers for the diagnosis of iCJD. On one side, this would become useful in the event of the appearance of new iCJD cases (though not likely). In this regard, there is also the need to obtain data on prion biomarkers for acquired forms through blood transfusion from variant CJD donors in order to have more comprehensive information in the event of new iCJD. On the other side, the similarity between iCJD and sCJD in biomarker profiles and clinical phenotype also unveils the incapacity to distinguish sCJD from iCJD in potential situations of undiscovered sources of transmissibility, which compels the medical community to keep a strict and constant vigilance for future cases of iCJD to avoid mis-classification as sCJD.

Supplementary Materials: The following are available online at http://www.mdpi.com/2218-273X/10/2/290/s1, Table S1: CJD-typical clinical symptoms reported at the time of lumbar puncture for each iCJD case involved in this study, Table S2: Sensitivities of the studied CSF biomarkers described in the present study for iCJD compared to the sensitivities of the same biomarkers reported in previous studies for sCJD and for gCJD associated with the E200K *PRNP* mutation in the same ethnic populations.

Author Contributions: F.L. and I.Z. designed the study. F.L., A.V.-P., P.H., M.S., O.C., C.S., S.S., F.M., I.F., A.P., M.P., M.C. (Marcella Catania), S.K., C.O., F.B., J.H., A.L., S.J.C., M.C. (Miguel Calero), G.G.K. and I.Z. contributed to data acquisition, interpretation, and sampling. F.L. and A.V.-P. drafted the manuscript. All authors critically revised the manuscript and approved its contents before submission. All authors have read and agreed to the published version of the manuscript.

Funding: This research was funded by the Instituto Carlos III (grants CP/00041 and PI19/00144) and by the Fundació La Marató de TV3 (201821-30-31-32) to FL and by the Robert Koch Institute through funds from the Federal Ministry of Health (grant No, 1369-341) to IZ. This project was also funded at 65% by the Fondo Europeo de Desarrollo Regional (FEDER) through the Interreg V-A España-Francia-Andorra (POCTEFA 2014-2020) programme. SJC is funded in part by a NHMRC Practitioner Fellowship (identification #APP1105784).

Acknowledgments: We wish to acknowledge the generosity of all the patients involved and their families.

Conflicts of Interest: The authors declare no conflict of interest.

References

1. Budka, H. Neuropathology of prion diseases. *Br. Med. Bull.* **2003**, *66*, 121–130. [CrossRef]
2. Wadsworth, J.D.F.; Hill, A.F.; Beck, J.A.; Collinge, J. Molecular and clinical classification of human prion disease. *Br. Med. Bull.* **2003**, *66*, 241–254. [CrossRef]

3. Gambetti, P.; Kong, Q.; Zou, W.; Parchi, P.; Chen, S.G. Sporadic and familial CJD: Classification and characterisation. *Br. Med. Bull.* **2003**, *66*, 213–239. [CrossRef] [PubMed]
4. Will, R.G. Acquired prion disease: Iatrogenic CJD, variant CJD, kuru. *Br. Med. Bull.* **2003**, *66*, 255–265. [CrossRef] [PubMed]
5. Kobayashi, A.; Kitamoto, T.; Mizusawa, H. Iatrogenic Creutzfeldt–Jakob disease. In *Handbook of Clinical Neurology*; 2018; Volume 153, pp. 207–218.
6. Brown, P.; Brandel, J.P.; Sato, T.; Nakamura, Y.; MacKenzie, J.; Will, R.G.; Ladogana, A.; Pocchiari, M.; Leschek, E.W.; Schonberger, L.B. Iatrogenic creutzfeldt-Jakob disease, final assessment. *Emerg. Infect. Dis.* **2012**, *18*, 901–907. [CrossRef] [PubMed]
7. Bonda, D.J.; Manjila, S.; Mehndiratta, P.; Khan, F.; Miller, B.R.; Onwuzulike, K.; Puoti, G.; Cohen, M.L.; Schonberger, L.B.; Cali, I. Human prion diseases: Surgical lessons learned from iatrogenic prion transmission. *Neurosurg. Focus* **2016**, *41*. [CrossRef] [PubMed]
8. Houston, F.; Andréoletti, O. Animal prion diseases: the risks to human health. *Brain Pathol.* **2019**, *29*, 248–262. [CrossRef]
9. Torres, J.M.; Marin-Moreno, A.; Andreoletti, O.; Espinosa, J.-C.; Beringue, V.; Aguilar, P.; Fernandez-Borges, N. Prion Diseases in Animals and Zoonotic Potential. *Food Saf.* **2016**, *4*, 105–109. [CrossRef]
10. Brown, P.; Brandel, J.P.; Preese, M.; Sato, T. Iatrogenic Creutzfeldt-Jakob disease: The waning of an era. *Neurology* **2006**, *67*, 389–393. [CrossRef]
11. Brown, P.; Preece, M.; Brandel, J.P.; Sato, T.; McShane, L.; Zerr, I.; Fletcher, A.; Will, R.G.; Pocchiari, M.; Cashman, N.R.; et al. Iatrogenic Creutzfeldt-Jakob disease at the millennium. *Neurology* **2000**, *55*, 1075–1081. [CrossRef]
12. Rudge, P.; Jaunmuktane, Z.; Adlard, P.; Bjurstrom, N.; Caine, D.; Lowe, J.; Norsworthy, P.; Hummerich, H.; Druyeh, R.; Wadsworth, J.D.F.; et al. Iatrogenic CJD due to pituitary-derived growth hormone with genetically determined incubation times of up to 40 years. *Brain* **2015**, *138*, 3386–3399. [CrossRef] [PubMed]
13. Sanchez-Juan, P.; Green, A.; Ladogana, A.; Cuadrado-Corrales, N.; Sáanchez-Valle, R.; Mitrováa, E.; Stoeck, K.; Sklaviadis, T.; Kulczycki, J.; Hess, K.; et al. CSF tests in the differential diagnosis of Creutzfeldt-Jakob disease. *Neurology* **2006**, *67*, 637–643. [CrossRef] [PubMed]
14. Wieser, H.G.; Schwarz, U.; Blättler, T.; Bernoulli, C.; Sitzler, M.; Stoeck, K.; Glatzel, M. Serial EEG findings in sporadic and iatrogenic Creutzfeldt-Jakob disease. *Clin. Neurophysiol.* **2004**, *115*, 2467–2478. [CrossRef] [PubMed]
15. Meissner, B.; Kallenberg, K.; Sanchez-Juan, P.; Ramljak, S.; Krasnianski, A.; Heinemann, U.; Eigenbrod, S.; Gelpi, E.; Barsic, B.; Kretzschmar, H.A.; et al. MRI and clinical syndrome in dura materrelated Creutzfeldt-Jakob disease. *J. Neurol.* **2009**, *256*, 355–363. [CrossRef]
16. Noguchi-Shinohara, M.; Hamaguchi, T.; Kitamoto, T.; Sato, T.; Nakamura, Y.; Mizusawa, H.; Yamada, M. Clinical features and diagnosis of dura mater graft-associated Creutzfeldt-Jakob disease. *Neurology* **2007**, *69*, 360–367. [CrossRef]
17. World Health Organisation WHO manual for surveillance of human transmissible spongiform encephalopathies including variant Creutzfeldt-Jakob disease. *WHO Man. Surveill. Hum. Transm. spongiform Enceph.* **2003**, 105.
18. Zerr, I.; Bodemer, M.; Gefeller, O.; Otto, M.; Poser, S.; Wiltfang, J.; Windl, O.; Kretzschmar, H.A.; Weber, T. Detection of 14-3-3 protein in the cerebrospinal fluid supports the diagnosis of Creutzfeldt-Jakob disease. *Ann. Neurol.* **1998**, *43*, 32–40. [CrossRef]
19. Kruse, N.; Heslegrave, A.; Gupta, V.; Foiani, M.; Villar-Piqué, A.; Schmitz, M.; Lehmann, S.; Teunissen, C.; Blennow, K.; Zetterberg, H.; et al. Interlaboratory validation of cerebrospinal fluid α-synuclein quantification in the diagnosis of sporadic Creutzfeldt-Jakob disease. *Alzheimer's Dement. Diagn. Assess. Dis. Monit.* **2018**, *10*, 461–470. [CrossRef]
20. Schmitz, M.; Cramm, M.; Llorens, F.; Collins, S.; Atarashi, R.; Satoh, K.; Orr, C.D.; Groveman, B.R.; Zafar, S.; Schulz-Schaeffer, W.J.; et al. The real-time quaking-induced conversion assay for detection of human prion disease and study of other protein misfolding diseases. *Nat. Protoc.* **2016**, *11*, 2233–2242. [CrossRef]
21. Meissner, B.; Kallenberg, K.; Sanchez-Juan, P.; Collie, D.; Summers, D.M.; Almonti, S.; Collins, S.J.; Smith, P.; Cras, P.; Jansen, G.H.; et al. MRI lesion profiles in sporadic Creutzfeldt-Jakob disease. *Neurology* **2009**, *72*, 1994–2001. [CrossRef]

22. Zerr, I.; Pocchiari, M.; Collins, S.; Brandel, J.P.; de Pedro Cuesta, J.; Knight, R.S.; Bernheimer, H.; Cardone, F.; Delasnerie-Laupêtre, N.; Cuadrado Corrales, N.; et al. Analysis of EEG and CSF 14-3-3 proteins as aids to the diagnosis of Creutzfeldt-Jakob disease. *Neurology* **2000**, *55*, 811–815. [CrossRef] [PubMed]
23. Windl, O.; Giese, A.; Schulz-Schaeffer, W.; Zerr, I.; Skworc, K.; Arendt, S.; Oberdieck, C.; Bodemer, M.; Poser, S.; Kretzschmar, H.A. Molecular genetics of human prion diseases in Germany. *Hum Genet* **1999**, *105*, 244–252. [CrossRef] [PubMed]
24. Schmitz, M.; Ebert, E.; Stoeck, K.; Karch, A.; Collins, S.; Calero, M.; Sklaviadis, T.; Laplanche, J.L.; Golanska, E.; Baldeiras, I.; et al. Validation of 14-3-3 Protein as a Marker in Sporadic Creutzfeldt-Jakob Disease Diagnostic. *Mol. Neurobiol.* **2016**, *53*, 2189–2199. [CrossRef] [PubMed]
25. Llorens, F.; Karch, A.; Golanska, E.; Schmitz, M.; Lange, P.; Sikorska, B.; Liberski, P.P.; Zerr, I. Cerebrospinal Fluid Biomarker-Based Diagnosis of Sporadic Creutzfeldt-Jakob Disease: A Validation Study for Previously Established Cutoffs. *Dement. Geriatr. Cogn. Disord.* **2017**, *43*, 71–80. [CrossRef] [PubMed]
26. Schmitz, M.; Villar-Piqué, A.; Llorens, F.; Gmitterová, K.; Hermann, P.; Varges, D.; Zafar, S.; Lingor, P.; Vanderstichele, H.; Demeyer, L.; et al. Cerebrospinal Fluid Total and Phosphorylated α-Synuclein in Patients with Creutzfeldt–Jakob Disease and Synucleinopathy. *Mol. Neurobiol.* **2018**, *56*, 3476–3483. [CrossRef]
27. Zerr, I.; Schmitz, M.; Karch, A.; Villar-Piqué, A.; Kanata, E.; Golanska, E.; Díaz-Lucena, D.; Karsanidou, A.; Hermann, P.; Knipper, T.; et al. Cerebrospinal fluid neurofilament light levels in neurodegenerative dementia: Evaluation of diagnostic accuracy in the differential diagnosis of prion diseases. *Alzheimer's Dement.* **2018**, *14*, 751–763. [CrossRef]
28. Llorens, F.; Thüne, K.; Tahir, W.; Kanata, E.; Diaz-Lucena, D.; Xanthopoulos, K.; Kovatsi, E.; Pleschka, C.; Garcia-Esparcia, P.; Schmitz, M.; et al. YKL-40 in the brain and cerebrospinal fluid of neurodegenerative dementias. *Mol. Neurodegener.* **2017**, *12*, 83. [CrossRef]
29. Llorens, F.; Schmitz, M.; Karch, A.; Cramm, M.; Lange, P.; Gherib, K.; Varges, D.; Schmidt, C.; Zerr, I.; Stoeck, K. Comparative analysis of cerebrospinal fluid biomarkers in the differential diagnosis of neurodegenerative dementia. *Alzheimers. Dement.* **2015**, *12*, 577–589. [CrossRef]
30. Llorens, F.; Kruse, N.; Schmitz, M.; Gotzmann, N.; Golanska, E.; Thüne, K.; Zejneli, O.; Kanata, E.; Knipper, T.; Cramm, M.; et al. Evaluation of α-synuclein as a novel cerebrospinal fluid biomarker in different forms of prion diseases. *Alzheimer's Dement.* **2017**, *13*, 710–719. [CrossRef]
31. Cramm, M.; Schmitz, M.; Karch, A.; Mitrova, E.; Kuhn, F.; Schroeder, B.; Raeber, A.; Varges, D.; Kim, Y.S.; Satoh, K.; et al. Stability and Reproducibility Underscore Utility of RT-QuIC for Diagnosis of Creutzfeldt-Jakob Disease. *Mol. Neurobiol.* **2016**, *53*, 1896–1904. [CrossRef]
32. Gao, L.P.; Shi, Q.; Xiao, K.; Wang, J.; Zhou, W.; Chen, C.; Dong, X.P. The genetic Creutzfeldt-Jakob disease with E200K mutation: analysis of clinical, genetic and laboratory features of 30 Chinese patients. *Sci. Rep.* **2019**, *9*, 1–7. [CrossRef] [PubMed]
33. Breithaupt, M.; Romero, C.; Kallenberg, K.; Begue, C.; Sanchez-Juan, P.; Eigenbrod, S.; Kretzschmar, H.; Schelzke, G.; Meichtry, E.; Taratuto, A.; et al. Magnetic resonance imaging in E200K and V210I mutations of the prion protein gene. *Alzheimer Dis. Assoc. Disord.* **2013**, *27*, 87–90. [CrossRef] [PubMed]
34. Heinemann, U.; Krasnianski, A.; Meissner, B.; Varges, D.; Kallenberg, K.; Schulz-Schaeffer, W.J.; Steinhoff, B.J.; Grasbon-Frodl, E.M.; Kretzschmar, H.A.; Zerr, I. Creutzfeldt-Jakob disease in Germany: A prospective 12-year surveillance. *Brain* **2007**, *130*, 1350–1359. [CrossRef] [PubMed]
35. Nagoshi, K.; Sadakane, A.; Nakamura, Y.; Yamada, M.; Mizusawa, H. Duration of prion disease is longer in Japan than in other countries. *J. Epidemiol.* **2011**, *21*, 255–262. [CrossRef]
36. Pocchiari, M.; Puopolo, M.; Croes, E.A.; Budka, H.; Gelpi, E.; Collins, S.; Lewis, V.; Sutcliffe, T.; Guilivi, A.; Delasnerie-Laupretre, N.; et al. Predictors of survival in sporadic Creutzfeldt-Jakob disease and other human transmissible spongiform encephalopathies. *Brain* **2004**, *127*, 2348–2359. [CrossRef]
37. Collins, S.; Boyd, A.; Fletcher, A.; Gonzales, M.; McLean, C.A.; Byron, K.; Masters, C.L. Creutzfeldt-Jakob disease: Diagnostic utility of 14-3-3 protein immunodetection in cerebrospinal fluid. *J. Clin. Neurosci.* **2000**, *7*, 203–208. [CrossRef]
38. Ferreira Caboclo, L.O.S.; Huang, N.; Lepski, G.A.; Livramento, J.A.; Buchpiguel, C.A.; Porto, C.S.; Nitrini, R. Iatrogenic Creutzfeldt-Jakob disease following human growth hormone therapy: Case report. *Arq. Neuropsiquiatr.* **2002**, *60*, 458–461. [CrossRef]

39. Kim, H.L.; Do, J.Y.; Cho, H.J.; Jeon, Y.C.; Park, S.J.; Ma, H.I.; Song, J.H.; Lee, Y.; Choi, H.; Choi, K.C.; et al. Dura mater graft-associated creutzfeldt-jakob disease: The First case in Korea. *J. Korean Med. Sci.* **2011**, *26*, 1515–1517. [CrossRef]
40. Matsui, Y.; Satoh, K.; Miyazaki, T.; Shirabe, S.; Atarashi, R.; Mutsukura, K.; Satoh, A.; Kataoka, Y.; Nishida, N.; Hsich, G.; et al. High sensitivity of an ELISA kit for detection of the gamma-isoform of 14-3-3 proteins: usefulness in laboratory diagnosis of human prion disease. *BMC Neurol.* **2011**, *11*, 120. [CrossRef]
41. Leitão, M.J.; Baldeiras, I.; Almeida, M.R.; Ribeiro, M.H.; Santos, A.C.; Ribeiro, M.; Tomás, J.; Rocha, S.; Santana, I.; Oliveira, C.R. Sporadic Creutzfeldt-Jakob disease diagnostic accuracy is improved by a new CSF ELISA 14-3-3?? assay. *Neuroscience* **2016**, *322*, 398–407. [CrossRef]
42. Abu-Rumeileh, S.; Baiardi, S.; Polischi, B.; Mammana, A.; Franceschini, A.; Green, A.; Capellari, S.; Parchi, P. Diagnostic value of surrogate CSF biomarkers for Creutzfeldt–Jakob disease in the era of RT-QuIC. *J. Neurol.* **2019**, *266*, 3136–3143. [CrossRef]
43. Carswell, C.; Thompson, A.; Lukic, A.; Stevens, J.; Rudge, P.; Mead, S.; Collinge, J.; Hyare, H. MRI findings are often missed in the diagnosis of Creutzfeldt-Jakob disease. *BMC Neurol.* **2012**, *12*, 153. [CrossRef] [PubMed]
44. Cali, I.; Miller, C.J.; Parisi, J.E.; Geschwind, M.D.; Gambetti, P.; Schonberger, L.B. Distinct pathological phenotypes of Creutzfeldt-Jakob disease in recipients of prion-contaminated growth hormone. *Acta Neuropathol. Commun.* **2015**, *3*, 37. [CrossRef] [PubMed]
45. Lewis, A.M.; Yu, M.; DeArmond, S.J.; Dillon, W.P.; Miller, B.L.; Geschwind, M.D. Human growth hormone-related iatrogenic Creutzfeldt-Jakob disease with abnormal imaging. *Arch. Neurol.* **2006**, *63*, 288–290. [CrossRef] [PubMed]
46. Hermann, P.; Laux, M.; Glatzel, M.; Matschke, J.; Knipper, T.; Goebel, S.; Treig, J.; Schulz-Schaeffer, W.; Cramm, M.; Schmitz, M.; et al. Validation and utilization of amended diagnostic criteria in Creutzfeldt-Jakob disease surveillance. *Neurology* **2018**. [CrossRef] [PubMed]
47. Vitali, P.; MacCagnano, E.; Caverzasi, E.; Henry, R.G.; Haman, A.; Torres-Chae, C.; Johnson, D.Y.; Miller, B.L.; Geschwind, M.D. Diffusion-weighted MRI hyperintensity patterns differentiate CJD from other rapid dementias. *Neurology* **2011**, *76*, 1711–1719. [CrossRef] [PubMed]
48. Zerr, I.; Kallenberg, K.; Summers, D.M.; Romero, C.; Taratuto, A.; Heinemann, U.; Breithaupt, M.; Varges, D.; Meissner, B.; Ladogana, A.; et al. Updated clinical diagnostic criteria for sporadic Creutzfeldt-Jakob disease. *Brain* **2009**, *132*, 2659–2668. [CrossRef]
49. Bridel, C.; Van Wieringen, W.N.; Zetterberg, H.; Tijms, B.M.; Teunissen, C.E.; Alvarez-Cermeño, J.C.; Andreasson, U.; Axelsson, M.; Bäckström, D.C.; Bartos, A.; et al. Diagnostic Value of Cerebrospinal Fluid Neurofilament Light Protein in Neurology: A Systematic Review and Meta-analysis. *JAMA Neurol.* **2019**, *76*, 1035–1048. [CrossRef]
50. Steinacker, P.; Blennow, K.; Halbgebauer, S.; Shi, S.; Ruf, V.; Oeckl, P.; Giese, A.; Kuhle, J.; Slivarichova, D.; Zetterberg, H.; et al. Neurofilaments in blood and CSF for diagnosis and prediction of onset in Creutzfeldt-Jakob disease. *Sci. Rep.* **2016**, *6*, 38737. [CrossRef]
51. Kovacs, G.G.; Andreasson, U.; Liman, V.; Regelsberger, G.; Lutz, M.I.; Danics, K.; Keller, E.; Zetterberg, H.; Blennow, K. Plasma and cerebrospinal fluid tau and neurofilament concentrations in rapidly progressive neurological syndromes: a neuropathology-based cohort. *Eur. J. Neurol.* **2017**, *24*, 1326-e77. [CrossRef]
52. Wennström, M.; Surova, Y.; Hall, S.; Nilsson, C.; Minthon, L.; Hansson, O.; Nielsen, H.M. The inflammatory marker YKL-40 is elevated in cerebrospinal fluid from patients with Alzheimer's but not Parkinson's disease or dementia with Lewy bodies. *PLoS ONE* **2015**, *10*, e0135458. [CrossRef] [PubMed]
53. Janelidze, S.; Hertze, J.; Zetterberg, H.; Landqvist Waldo, M.; Santillo, A.; Blennow, K.; Hansson, O.; Landqvist Waldö, M.; Santillo, A.; Blennow, K.; et al. Cerebrospinal fluid neurogranin and YKL-40 as biomarkers of Alzheimer's disease. *Ann. Clin. Transl. Neurol.* **2015**, *3*, 12–20. [CrossRef] [PubMed]
54. Lattanzio, F.; Abu-Rumeileh, S.; Franceschini, A.; Kai, H.; Amore, G.; Poggiolini, I.; Rossi, M.; Baiardi, S.; McGuire, L.; Ladogana, A.; et al. Prion-specific and surrogate CSF biomarkers in Creutzfeldt-Jakob disease: diagnostic accuracy in relation to molecular subtypes and analysis of neuropathological correlates of p-tau and Aβ42 levels. *Acta Neuropathol.* **2017**, *133*, 559–578. [CrossRef] [PubMed]
55. Green, A.J.E.; Zanusso, G. Prion protein amplification techniques. *Handb. Clin. Neurol.* **2018**, *153*, 357–370.
56. Kanata, E.; Golanska, E.; Villar-Piqué, A.; Karsanidou, A.; Dafou, D.; Xanthopoulos, K.; Schmitz, M.; Ferrer, I.; Karch, A.; Sikorska, B.; et al. Cerebrospinal fluid neurofilament light in suspected sporadic Creutzfeldt-Jakob disease. *J. Clin. Neurosci.* **2018**, *60*, 124–127. [CrossRef]

57. Abu-Rumeileh, S.; Capellari, S.; Stanzani-Maserati, M.; Polischi, B.; Martinelli, P.; Caroppo, P.; Ladogana, A.; Parchi, P. The CSF neurofilament light signature in rapidly progressive neurodegenerative dementias. *Alzheimer's Res. Ther.* **2018**, *10*, 3. [CrossRef]
58. Melah, K.E.; Lu, S.Y.F.; Hoscheidt, S.M.; Alexander, A.L.; Adluru, N.; Destiche, D.J.; Carlsson, C.M.; Zetterberg, H.; Blennow, K.; Okonkwo, O.C.; et al. Cerebrospinal Fluid Markers of Alzheimer's Disease Pathology and Microglial Activation are Associated with Altered White Matter Microstructure in Asymptomatic Adults at Risk for Alzheimer's Disease. *J. Alzheimer's Dis.* **2016**, *50*, 873–886. [CrossRef]

Biomarkers and diagnostic guidelines for sporadic Creutzfeldt-Jakob disease

Peter Hermann, Brian Appleby, Jean-Philippe Brandel, Byron Caughey, Steven Collins, Michael D Geschwind, Alison Green, Stephane Haïk, Gabor G Kovacs, Anna Ladogana, Franc Llorens, Simon Mead, Noriyuki Nishida, Suvankar Pal, Piero Parchi, Maurizio Pocchiari, Katsuya Satoh, Gianluigi Zanusso, Inga Zerr

Sporadic Creutzfeldt-Jakob disease is a fatal neurodegenerative disease caused by misfolded prion proteins (PrP^{Sc}). Effective therapeutics are currently not available and accurate diagnosis can be challenging. Clinical diagnostic criteria use a combination of characteristic neuropsychiatric symptoms, CSF proteins 14-3-3, MRI, and EEG. Supportive biomarkers, such as high CSF total tau, could aid the diagnostic process. However, discordant studies have led to controversies about the clinical value of some established surrogate biomarkers. Development and clinical application of disease-specific protein aggregation and amplification assays, such as real-time quaking induced conversion (RT-QuIC), have constituted major breakthroughs for the confident pre-mortem diagnosis of sporadic Creutzfeldt-Jakob disease. Updated criteria for the diagnosis of sporadic Creutzfeldt-Jakob disease, including application of RT-QuIC, should improve early clinical confirmation, surveillance, assessment of PrP^{Sc} seeding activity in different tissues, and trial monitoring. Moreover, emerging blood-based, prognostic, and potentially pre-symptomatic biomarker candidates are under investigation.

Lancet Neurol 2021; 20: 235–46

This online publication has been corrected. The corrected version first appeared at thelancet.com/neurology on February 24, 2021

National Reference Center for Transmissible Spongiform Encephalopathies, Department of Neurology, University Medical Center Göttingen, Göttingen, Germany (P Hermann MD, F Llorens PhD, Prof I Zerr MD); **National Prion Disease Pathology Surveillance Center, Case Western Reserve University, Cleveland, OH, USA** (Prof B Appleby MD); **Departments of Neurology, Psychiatry, and Pathology, University Hospitals Cleveland Medical Center, Case Western Reserve University, Cleveland, OH, USA** (Prof B Appleby); **Cellule Nationale de Référence des Maladies de Creutzfeldt-Jakob, Groupe Hospitalier Pitié-Salpêtrière, Paris, France** (J-P Brandel MD, S Haïk MD); **Institut du Cerveau et de la Moelle épinière, Sorbonne Université, Paris, France** (J-P Brandel, S Haïk); **Laboratory of Persistent Viral Diseases, Rocky Mountain Laboratories, National Institute for Allergy and Infectious Diseases, National Institutes of Health, Hamilton, MT, USA** (B Caughey PhD); **Australian National Creutzfeldt-Jakob disease Registry, Florey Institute of Neuroscience and Mental Health and Department of Medicine, University of Melbourne, Parkville, VIC, Australia** (Prof S Collins MD); **Department of Neurology, University of California, San Francisco, CA, USA** (Prof M D Geschwind PhD); **National CJD Research & Surveillance Unit, Centre for Clinical Brain Sciences, University of Edinburgh, Edinburgh, UK** (A Green PhD, S Pal MD); **Tanz Centre for Research in Neurodegenerative Disease and Department of Laboratory**

Introduction

Sporadic Creutzfeldt-Jakob disease is a rapidly progressive neuropsychiatric syndrome that is fatal and characterised by aggregations of misfolded prion protein Scrapie (PrP^{Sc}) in the brain. Sporadic Creutzfeldt-Jakob disease is the most common form of human prion disease (~90% of cases) with an incidence of approximately 1·5–2·0 cases per million person-years.[1] Different phenotypes of sporadic Creutzfeldt-Jakob disease can vary in symptom evolution, biomarker profile, and neuropathological characteristics. They are defined by the polymorphism (Met and Val) at codon 129 of the prion protein gene (*PRNP*) and by the molecular mass of PrP^{Sc} (glycotype 1 and 2).[2] Definite diagnosis requires neuropathological confirmation.

The spectrum of possible symptoms is highly heterogeneous and includes rapidly progressive dementia, cerebellar ataxia, and myoclonus, which means that high-performing (ie, high sensitivity and specificity) biomarkers are important for making a confident clinical diagnosis. In 1998, WHO included a combination of particular symptoms, EEG, and detection of CSF 14-3-3 proteins in the standard diagnostic criteria.[3] Patterns of signal alteration on fluid attenuated inversion recovery (FLAIR) or diffusion weighted imaging (DWI) sequences, or both, of brain MRI were suggested in 2009.[4] Another CSF protein, total-tau (T-tau), is considered a valuable supportive biomarker.[5] Although comparative data on imaging markers for sporadic Creutzfeldt-Jakob disease are scarce, several studies have evaluated the diagnostic performance of CSF biomarkers, with occasional discrepancies leading to controversy about their clinical utility.[6,7]

Since 2011, development and clinical application of PrP^{Sc} amplification assays, such as protein misfolding cyclic amplification (PMCA) and real-time quaking induced conversion (RT-QuIC),[8] have constituted major breakthroughs as aids for an improved pre-mortem diagnosis of prion diseases. RT-QuIC has shown excellent diagnostic accuracy for sporadic Creutzfeldt-Jakob disease in retrospective studies, ring trials (consistency between laboratories),[9,10] and prospective studies,[11,12] which shows its high value for an early and accurate diagnosis. Consequently, RT-QuIC (using CSF or other tissue, such as olfactory mucosa) was included in diagnostic criteria for sporadic Creutzfeldt-Jakob disease of some surveillance centers.[12,13] However, an important discussion on its clinical utility is needed. Another unmet need is the identification of blood-based biomarkers for early diagnosis and disease progression,[14–16] particularly regarding potential new therapeutic strategies.

The aim of this Review is to provide an overview of the biomarker-based diagnosis of sporadic Creutzfeldt-Jakob disease and to suggest guidelines for clinicians to use in the differential diagnosis of rapidly progressive dementias. Advances of the past 5 years are discussed and put in the context of clinical relevance, established biomarkers, and epidemiology.

Investigating diagnostic tests

When estimates of diagnostic accuracy are being translated into clinical practice, potential selection biases of case and control groups should be considered. The selection of control groups can be particularly challenging. Healthy age-matched controls usually do not reflect the population in which a diagnostic biomarker is used. However, referral centres often use Creutzfeldt-Jakob disease mimics (eg, autoimmune encephalitis) that represent the diagnostic challenges but might not reflect the routine of a tertiary institution. An example of a biased control group was the evaluation of diagnostic criteria for sporadic Creutzfeldt-Jakob disease published in 2018.[12] The control group included many patients without Creutzfeldt-Jakob disease who had been further investigated because of positive CSF 14-3-3 tests, resulting in a weak specificity of this biomarker. In 2017, a study

Medicine and Pathobiology, University of Toronto, Toronto, ON, Canada (Prof G G Kovacs MD); **Laboratory Medicine Program, University Health Network, Toronto, ON, Canada** (Prof G G Kovacs); **Department of Neuroscience, Istituto Superiore di Sanità, Rome, Italy** (A Ladogana MD, Prof M Pocchiari MD); **Network Center For Biomedical Research Of Neurodegenerative Diseases, Institute Carlos III, L'Hospitalet de Llobregat, Barcelona, Spain** (F Llorens); **Bellvitge Biomedical Research Institute, Hospitalet de Llobregat, Barcelona, Spain** (F Llorens); **National Prion Clinic, University College London Hospitals NHS Foundation Trust, London, UK** (Prof S Mead); **Medical Research Council Prion Unit at University College London, Institute of Prion Diseases, London, UK** (Prof S Mead PhD); **Department of Molecular Microbiology and Immunology** (Prof N Nishida MD) **and Department of Locomotive Rehabilitation Science** (Prof K Satoh MD) **Nagasaki University Graduate School of Biomedical Sciences, Nagasaki, Japan; Istituto di Ricovero e Cura e Carattere Scientifico, Istituto delle Scienze Neurologiche di Bologna, Bologna, Italy** (P Parchi MD); **Department of Experimental, Diagnostic and Specialty Medicine, University of Bologna, Bologna, Italy** (P Parchi); **Department of Neurosciences, Biomedicine and Movement Sciences, University of Verona, Verona, Italy** (G Zanusso MD); **German Center for Neurodegenerative Diseases, Göttingen, Germany** (Prof I Zerr)

Correspondence to:
Dr P Hermann, National Reference Center for Transmissible Spongiform Encephalopathies Surveillance, Department of Neurology, University Medical Center Göttingen, 37075 Göttingen, Germany
peter.hermann@med.uni-goettingen.de

evaluating the use of olfactory mucosa and CSF samples in RT-QuIC[17] reported a relatively low sensitivity compared with some other studies that used RT-QuIC assays. In this study, the case group was partly selected from samples that had a previous negative first-generation RT-QuIC result, leading to a case group selection bias. Both examples highlight the importance of interpreting all biomarker test results in an adequate clinical context.

Most biomarker studies report the sensitivity and the specificity of diagnostic tests. It is debatable whether sensitivity and specificity are the most useful measures of diagnostic performance as they are not easy to interpret in a clinical setting. Predictive values might be more accurate to determine the likelihood of a disease, but they are associated with disease prevalence. To calculate predictive values, the rate of cases and controls in a study has to reflect the respective rate in the population or Bayes' rule has to be applied, which requires including disease prevalence (proportion) in the calculations.[18] In the context of an extremely rare disease, such as sporadic Creutzfeldt-Jakob disease, a sufficient number of controls cannot be obtained and applying Bayes' rule would always lead to extremely low positive and extremely high negative predictive values. Thus, predictive values are not considered in this Review. In studies of established biomarkers with defined cutoffs, we use test sensitivity and specificity as measures for diagnostic accuracy. For experimental biomarkers, we report the area under the curve (AUC) from receiver operator characteristics.

Advances in biomarker research

Neuropathological investigation and immunostaining of PrP^{Sc} allow a definite diagnosis of prion diseases.[19] For definite ante-mortem diagnosis, brain biopsy is required but is complicated by infection control concerns, the possibility of a false negative result due to sampling error in which typical pathology and PrP^{Sc} might not be present in all cortical regions (eg, sporadic or familial fatal insomnia), and issues with tissue quality. Given these considerations and the highly invasive nature of the procedure, brain biopsy is usually only considered when the diagnosis is not clear and potentially treatable conditions (eg, encephalitis or lymphoma) are under strong consideration, or a potential contamination of medical instruments requires a clear case definition. A less invasive procedure, tonsillar or adenoid biopsy, was established for the diagnosis of variant Creutzfeldt-Jakob disease (prion disease caused by consumption of beef from bovines affected by bovine spongiform encephalopathy), but is not helpful for other forms of prion disease.[20] The direct in-vivo detection of PrP^{Sc} in sporadic Creutzfeldt-Jakob disease using routinely accessible biofluids is possible but a pilot study using urine reported a poor sensitivity of 40%.[21] Given the limitations of traditional methods (eg, biopsy and direct detection) and growing clinical evidence in support of novel PrP^{Sc}-seeded assays, a shift in clinical diagnosis criteria for sporadic Creutzfeldt-Jakob disease is warranted. We describe the evidence for these novel assays and the current state of established and new diagnostic surrogate biomarkers (diagnostic tests that indirectly mark the disease process).

PrP^{Sc}-seeded aggregation assays

PMCA

In 2001, PMCA was developed to reproduce and amplify PrP^{Sc} in microtubes. Brain homogenate provided normal prion protein (PrP^{C}) substrate for the reaction and sonication fragmented growing PrP^{Sc} particles to increase their concentration.[22] Subsequently, a modified protocol introduced the use of recombinant hamster PrP^{C} as substrate to accelerate the reaction and increase its sensitivity to detect PrP^{Sc} in the CSF of scrapie-infected hamsters.[23] PMCA protocols showed excellent sensitivity for the detection of PrP^{Sc} in CSF (100%),[24] plasma (100%)[25,26] and urine (93%)[27] of patients with variant Creutzfeldt-Jakob disease but high sensitivity could not be shown in sporadic Creutzfeldt-Jakob disease or other prion diseases seen in current clinical practice.

RT-QuIC

A modified multiwell plate-based PrP^{Sc} amplification technology using quaking to energise the misfolding of prion protein coupled to a fluorescent readout was named RT-QuIC.[8,28] RT-QuIC has shown to be a potential tool not only in the diagnosis of prion diseases but also in drug screening, prion strain discrimination, and detection of other protein misfolding diseases (eg, tauopathies and synocleinopathies).[29,30] Different protocols concerning substrate (eg, recombinant hamster PrP, hamster–sheep chimeric PrP, or bank vole PrP), reaction conditions, and the definition of test positivity have been reported.[8,29,30] In general, each sample is analysed in quadruplicates[9] and positivity is confirmed when at least two of four replicates cross a fluorescence signal cutoff value; similarly, samples can be analysed as triplates[29] whereby positivity is confirmed when at least two of three replicates cross the fluorescence threshold. In 2015, the original protocol (first generation RT-QuIC) was technically modified by increasing the reaction temperature and using N-terminally truncated PrP^{Sen} (second generation RT-QuIC) to shorten the assay time and to improve the sensitivity.[31]

CSF RT-QuIC represents a disease-specific biomarker and retrospective studies have investigated its diagnostic accuracy with test specificity of 99–100%.[8–11,17,31–37] Most studies, however, did not use control groups consisting primarily of cases with rapidly progressive dementias in whom Creutzfeldt-Jakob disease was considered as a potential diagnosis during the disease course. Some false positive cases in retrospective studies were speculated to possibly represent unrecognised prion diseases.[10] Nonetheless, two cases of autopsy-verified non-Creutzfeldt-Jakob disease showing positive CSF RT-QuIC during the diagnostic process have been reported.[38,39] One of these patients had convulsions caused by steroid-responsive

	Cases		Controls		Sensitivity	Specificity	Protocol
	n	type	n	type			
Retrospective studies							
Atarashi et al (2011)*[8]	34	Definite sporadic Creutzfeldt-Jakob disease	49	Other neurological diseases	85%	100%	1st generation
McGuire et al (2012)[9]	123	Definite sporadic Creutzfeldt-Jakob disease	103	Rapidly progressive dementia	89%	99%	1st generation
Orrú et al (2014)[32]	30	Probable and definite sporadic Creutzfeldt-Jakob disease	46	Non-Creutzfeldt-Jakob disease	77%	100%	1st generation
Orrú et al (2015)[31]	48	Probable and definite sporadic Creutzfeldt-Jakob disease	39	Other neurological diseases	96%	100%	2nd generation
Cramm et al (2016)[10]	110	Definite sporadic Creutzfeldt-Jakob disease and genetic Creutzfeldt-Jakob disease	400	Other neurological diseases	85%	99%	1st generation‡
Groveman et al (2016)†[33]	113	Probable and definite sporadic Creutzfeldt-Jakob disease	64	Other neurological diseases	73%	100%	1st generation
Groveman et al (2016)†[33]	113	Probable and definite sporadic Creutzfeldt-Jakob disease	64	Other neurological diseases	94%	100%	2nd generation
Park et al (2016)[34]	81	Probable and definite sporadic Creutzfeldt-Jakob disease	100	Non-Creutzfeldt-Jakob disease	77%	100%	1st generation
Franceschini et al (2017)[35]	145	Probable and definite sporadic Creutzfeldt-Jakob disease and genetic Creutzfeldt-Jakob disease	42	Rapidly progressive dementia	97%	100%	2nd generation
Bongianni et al (2017)†[17]	49	Probable and definite sporadic Creutzfeldt-Jakob disease	71	Other neurological diseases	73%	100%	1st generation
Bongianni et al (2017)†[17]	22	Probable and definite sporadic Creutzfeldt-Jakob disease	71	Other neurological diseases	86%	100%	2nd generation
Lattanzio et al (2017)[36]	225	Definite sporadic Creutzfeldt-Jakob disease	348	Rapidly progressive dementia	84%	99%	1st generation
Foutz et al (2017)[11]	126	Definite sporadic Creutzfeldt-Jakob disease and genetic Creutzfeldt-Jakob disease	67	Rapidly progressive dementia	92%	99%	2nd generation
Rudge et al (2018)[37]	171	Definite sporadic Creutzfeldt-Jakob disease	47	Rapidly progressive dementia	89%	100%	1st generation
Prospective studies							
Foutz et al (2017)[11]	65	Definite sporadic Creutzfeldt-Jakob disease and genetic Creutzfeldt-Jakob disease	14	Rapidly progressive dementia	95%	100%	2nd generation
Hermann et al (2018)[12]	65	Definite sporadic Creutzfeldt-Jakob disease	118	Rapidly progressive dementia	89%	100%	1st generation‡
Abu-Rumeileh et al (2019)†[40]	65	Definite sporadic Creutzfeldt-Jakob disease and genetic Creutzfeldt-Jakob disease	62	Rapidly progressive dementia	82%	100%	1st generation
Abu-Rumeileh et al (2019)†[40]	65	Definite sporadic Creutzfeldt-Jakob disease and genetic Creutzfeldt-Jakob disease	62	Rapidly progressive dementia	96%	100%	2nd generation
Fiorini et al (2020)[42]	102	Probable and definite sporadic Creutzfeldt-Jakob disease	80	Rapidly progressive dementia	96%	100%	2nd generation
Mammana et al (2020)[43]	24	Probable and definite sporadic Creutzfeldt-Jakob disease	12	Rapidly progressive dementia	88%	100%	1st generation
Rhoads et al (2020)[39]	439	Definite sporadic Creutzfeldt-Jakob disease	69	Rapidly progressive dementia	93%	99%	2nd generation

Definite sporadic Creutzfeldt-Jakob disease is defined as neuropathologically confirmed diagnosis. Probable sporadic Creutzfeldt-Jakob disease is defined as clinical diagnosis based on syndrome and biomarkers.[4] Other neurological diseases include dementia syndromes. Non-Creutzfeldt-Jakob disease includes non-neurological disorders, neurological disorders, and dementia syndromes. 1st generation=first generation tests.[8] 2nd generation=second generation tests.[31] RT-QuIC=real-time quaking induced conversion. *This study investigated two different cohorts, overall sensitivity and specificity are summarised here. †These studies appplied two different protocols and used the same control group for both investigations. ‡This protocol used hamster–sheep chimeric recombinant PrP as substrate (instead of hamster PrP) and test positivity was indicated by two out of three positive replicates (instead of two of four).[29]

Table: **Diagnostic accuracy of CSF RT-QuIC in retrospective and prospective studies**

encephalitis, which is a potential clinical sporadic Creutzfeldt-Jakob disease mimic.[38] Prospective studies using rapidly progressive dementias as controls and mostly neuropathological confirmed sporadic Creutzfeldt-Jakob disease cases, were published since 2017 and the specificity was also reported as 99–100% (table).[11,12,39–42] Because of its reliability and high diagnostic accuracy, CSF RT-QuIC was incorporated in the diagnostic criteria for sporadic Creutzfeldt-Jakob disease of several surveillance centres.[13,14]

Regarding the test sensitivity, figures range from 73%[19,33] to 89%[9,12,37] using first generation RT-QuIC, and 92%[11] to 97%[35] using second generation RT-QuIC. Molecular subtypes of sporadic Creutzfeldt-Jakob disease are defined by codon 129 polymorphism (M and V) and PrP^{Sc} glycotype (1 and 2),[2] resulting in different subtypes (eg, MM1, MV1). The sensitivity is very high in MM1/MV1 and VV2 cases, the most common subtypes among sporadic Creutzfeldt-Jakob disease patients, whereas it is slightly lower in MV2 cases (75–93%).[11,35,36,39,40] Regarding rare subtypes, there are few reported cases, hampering the validity of results, but sensitivity has been reported to be substantially lower in VV1 (range 0–100%)[37–39] and MM2 cases (range 44–78%).[36,39] The MM2 subtype is further differentiated into a cortical type (MM2C) and a very rare thalamic type (MM2T) that show a distinct clinical syndrome called sporadic fatal insomnia. Only few known cases of sporadic fatal insomnia imply that classic sporadic Creutzfeldt-Jakob disease biomarkers and RT-QuIC show poor sensitivity in this condition.[39] CSF RT-QuIC showed high sensitivity for genetic prion diseases with E200K and V210I mutations but low sensitivity for fatal familial insomnia (D178N-129M).[10,11,39,40]

However, supporting data are based on small case numbers. RT-QuIC might also aid in the differentiation of distinct prion diseases such as sporadic Creutzfeldt-Jakob disease, Gerstmann-Sträussler-Scheinker syndrome, and fatal familial insomnia and sporadic Creutzfeldt-Jakob disease subtypes.[30,41]

Regarding other tissues, promising studies that applied RT-QuIC to olfactory mucosa[17,32,42] and skin biopsies[43,44] showed high sensitivities of 89% to 100%, suggesting even better diagnostic accuracy than with use of CSF. Multiple components of the eye have tested positive by RT-QuIC[45] post mortem, but the diagnostic value of analysis of routinely accessible eye tissue or fluid remains to be determined.

CSF surrogate biomarkers

14-3-3 proteins

The 14-3-3 proteins are abundantly but not solely expressed in the brain. They are located in the cytoplasm, plasma membranes, and organelles. Involvement in various functions (eg, cell signalling, growth, apoptosis) has been identified but not completely clarified.[46] Since 14-3-3 protein detection by western blot became part of commonly used clinical diagnostic criteria for sporadic Creutzfeldt-Jakob disease,[3] several studies evaluated its diagnostic performance. In 2012, a structured meta-analysis reported a sensitivity of 92% and a specificity of 80%[47] but it was reported that the test sensitivity is lower than 92% in early disease stages and differs across the spectrum of molecular subtypes. The MV2 and MM2 subtypes showed lower test sensitivities of between 60% and 70%.[48] Reported specificity ranges between 40%[49] and 92%.[50] Such discrepancies might be explained, at least partly, by different characteristics of the control groups. Over the past 5 years, several studies reported a high specificity in the discrimination of sporadic Creutzfeldt-Jakob disease and neurodegenerative diseases such as Alzheimer's disease, dementia with Lewy bodies, and fronto-temporal lobar degeneration (appendix p 1).[36,50–53] By contrast, the specificity of CSF 14-3-3 was lowered when control groups included acute neuronal injury events and inflammatory and infiltrative neoplastic CNS diseases.[36,50] Another factor possibly affecting specificity could be the execution and rating of 14-3-3 western blot. Intermediate results (ie, weak or trace readouts) can be difficult to interpret. Comparative evaluations of a new 14-3-3γ isoform ELISA assay showed a superior diagnostic performance by comparison with 14-3-3 western blot.[40,54,55] One study reported a sensitivity of 97% and a specificity of 94% with an AUC of 0·982 (optimal cutoff >14552 AU/mL),[54] whereas a larger study (including ring trials) reported a sensitivity of 88% and a specificity of 96% (cutoff >20 000 AU/mL).[55]

See Online for appendix

Tau protein

Tau, a microtubule-associated protein, is expressed in neuronal and glial cells.[56] Extremely elevated CSF T-tau was proposed as a diagnostic biomarker for sporadic Creutzfeldt-Jakob disease[5] and most studies reported good test sensitivity and specificity, each around 90%.[36,48,49,57] However, currently, CSF t-Tau is not formally accepted as part of case definition criteria.[4] Similar to 14-3-3, reduced sensitivity has been shown in MM2 and MV2 subtypes[48,58] and early disease stages.[59] Some studies reported relatively poor specificities of 67%[49] or lower than 50% at varying optimal diagnostic cut-offs.[51–53] Specificity of lower than 50% was observed when patients with atypical Alzheimer's disease were used as controls (appendix p 1). Some studies, however, have found t-Tau to be a better diagnostic marker than 14-3-3,[49,60] leading to an ongoing discussion and controversy over which biomarker should be used primarily. Besides Alzheimer's disease, inflammatory and neoplastic CNS diseases are important differential diagnoses of elevated t-Tau concentrations.[61] Unfortunately, there is no general consensus regarding the best t-Tau ELISA assay or cut-off that should be used to support sporadic Creutzfeldt-Jakob disease (eg, studies have suggested either >1072 pg/mL, >1250 pg/mL, >1300 pg/mL, or >1400 pg/mL).[5,35,62–64] CSF t-Tau can also be a predictor of survival time.[65,66] The p-Tau/t-Tau (or t-Tau/p-Tau) ratio is an important alternative biomarker for sporadic Creutzfeldt-Jakob disease.[67] It showed a very high diagnostic accuracy in the differentiation of sporadic Creutzfeldt-Jakob disease from other neurological diseases (AUC 0·98), Alzheimer's disease (AUC 0·99),[64] and rapidly progressive Alzheimer's disease (AUC 0·99).[68] Several studies that investigated large cohorts reported a superior diagnostic performance compared with t-Tau alone.[51,64,68]

Neurofilaments

Neurofilaments comprise three subunits: a light (NfL), a medium, and a heavy chain. As neuron-specific cytoskeleton proteins, their presence in body fluids represents neuroaxonal damage.[69] Several studies showed an excellent diagnostic accuracy in the discrimination of healthy individuals and patients with sporadic Creutzfeldt-Jakob disease (AUCs >0·99).[16,70,71] However, NfL might have insufficient specificity for sporadic Creutzfeldt-Jakob disease.[40] Concerning important differential diagnoses, reported AUCs were 0·95 versus patients with other neurological diseases (including dementia syndromes),[15] 0·77 versus Alzheimer's disease,[16] 0·45[16] and 0·90[70] versus other neurological diseases with dementia syndrome, 0·93 versus neurodegenerative dementias,[53] and 0·86 to 0·89 versus rapidly progressive dementia.[72] The notable differences between these studies might be explained by different group selection criteria but this requires further clarification. Additionally, different optimal cut-offs were identified (eg, >5016 pg/ml or >10 500 pg/ml).[53,70] By contrast with 14-3-3 and t-Tau, NfL was shown to be markedly elevated in MV2 and VV2 subtypes when compared with the MM1 sporadic Creutzfeldt-Jakob disease subtype.[53]

Other CSF surrogate biomarkers

Several other CSF biomarkers for sporadic Creutzfeldt-Jakob disease have been identified over the past two decades. Herein, only those that have a high amount of supported evidence are considered. CSF S100b has been widely studied, but comparative studies showed inferior diagnostic performance compared with 14-3-3 and t-Tau,[48,73] and S100b has not been widely used clinically. Total prion protein (t-PrP) is decreased in the CSF of patients with sporadic Creutzfeldt-Jakob disease, showing moderate diagnostic accuracy.[51,74] A study using targeted mass spectrometry (instead of the more routinely used ELISA) showed that all human PrP domains were reduced in the CSF of patients with sporadic Creutzfeldt-Jakob disease compared with patients with rapidly progressive dementia.[75] Additionally, it might have potential in trial monitoring[76] and constitute a valuable part of composite biomarker profiles.[51,53] α-Synuclein, a synaptic protein that aggregates in synucleinopathies, was observed to be massively increased in patients with sporadic Creutzfeldt-Jakob disease, possibly related to rapid neurodegeneration. A multicentre study showed an excellent diagnostic accuracy (AUC >0·99, 98% sensitivity, 97% specificity) in the discrimination of sporadic Creutzfeldt-Jakob disease and other neurological diseases (including dementia syndromes) at an optimal cut-off of 820 pg/mL using a commercial ELISA.[77,78] Similar results were found in an inter-laboratory validation study.[79] Advantages and disadvantages of common CSF biomarkers are summarised (appendix p 2); potential CSF biomarker candidates evaluated in the past 5 years are also noted (appendix p 3).

Blood-based biomarker candidates

Several potential roles might feasibly be fulfilled by blood-based biomarkers. Currently, there is no immediate prospect of a highly specific diagnostic blood test comparable to RT-QuIC in CSF samples. Blood assays, however, might offer an accessible triage test in primary care or first specialist assessment that flags the possibility of rapid neuronal damage, and could be useful in case prioritisation.

One potential candidate is t-Tau concentration in plasma or serum. Studies showed elevated concentrations in sporadic Creutzfeldt-Jakob disease compared with healthy controls and other neurological diseases.[15,16,80] The diagnostic accuracy ranged from an AUC of 0·94 versus healthy controls to 0·72 versus other neurological diseases that included dementia syndromes (appendix p 4). Another investigation showed that the plasma t-Tau concentration is a better predictor of survival time in sporadic Creutzfeldt-Jakob disease than CSF t-Tau concentration or other fluid biomarkers.[66] Another promising candidate for a blood-based biomarker is NfL, the most soluble subunit of neurofilament. NfL was shown to be an effective therapeutic biomarker in CNS disease during trials for multiple sclerosis.[81] NfL showed similar or even better diagnostic accuracy compared with t-Tau in the discrimination of sporadic Creutzfeldt-Jakob disease from a healthy control population.[16,80] By contrast, a study that investigated a large cohort of prion diseases and used rapidly progressive dementias as controls showed that plasma t-Tau had better diagnostic accuracy than NfL (appendix p 4). Similar to the CSF counterpart, both plasma t-Tau and NfL concentrations were significantly associated with the sporadic Creutzfeldt-Jakob disease subtype.[82]

More potential blood-based biomarkers for sporadic Creutzfeldt-Jakob disease, such as S100b and others (appendix p 4), were elevated in serum or plasma, but few available data indicate inferior diagnostic accuracy compared with t-Tau and NfL or these biomarkers still have to be validated by other groups. PrP was reported to be decreased in the CSF of sporadic Creutzfeldt-Jakob disease cases,[51,52] although it was reported in another study to be increased in plasma.[83] The explanation for this dissociation has not yet been clarified.

Imaging markers

MRI

MRI is an essential tool in the diagnosis of sporadic Creutzfeldt-Jakob disease. It allows the identification of important differential diagnoses such as ischaemia, encephalitis, and neoplasia. In Creutzfeldt-Jakob disease, typical patterns of restricted diffusion on DWI and hyperintensities in FLAIR images were suggested to be included in the WHO diagnostic criteria in 2009.[4] Another widely used protocol recommends the use of DWI and apparent diffusion coefficient (ADC) maps only.[84,85] Typical Creutzfeldt-Jakob disease MRI displays restricted diffusion in at least two cortical regions (ribboning) or restricted diffusion predominantly in the caudate nucleus, or both, followed by putamen and thalamus (figure 1). Involvement of the subcortical white matter cannot be observed in visual assessments (DWI, ADC, or FLAIR)[4,84] but was detected by quantitative diffusion tensor imaging.[86] Cortical ribboning and involvement of the caudate nucleus (of one or both hemispheres, rarely perfectly symmetrical) is typically seen in the most common MM1 subtype. Involvement of the thalamus (aside from the caudate nucleus and putamen) is more common in VV2 and MV2 subtypes.[87] High signal only on FLAIR and DWI in the posterior thalamus brighter than in anterior putamen (pulvinar sign) is a strong indicator of variant Creutzfeldt-Jakob disease.[20]

The overall diagnostic accuracy of MRI is possibly even superior to CSF 14-3-3 and t-Tau,[88,89] but extensive comparison data with CSF biomarkers is scarce. Some studies showed a sensitivity of around 80%,[12,35,40,42] others reported 92% to 98%.[37,88,89] Similarly, specificity ranges from 74%[40] to 98%.[12] In 2020, a study investigating a large cohort with 770 patients with definite sporadic Creutzfeldt-Jakob disease applied an improved diagnostic index showing 92% sensitivity and 97% specificity.[89] The discrepancies

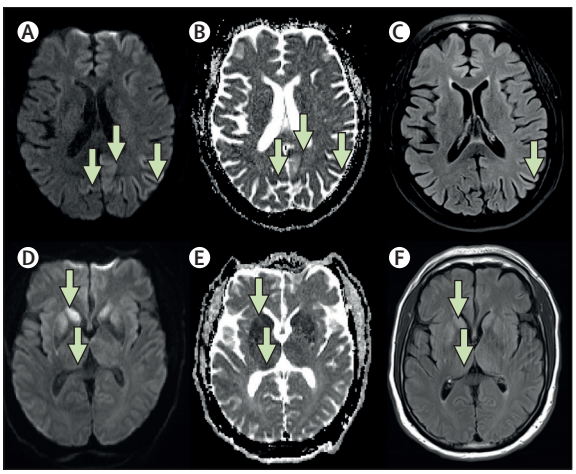

Figure 1: **Typical patterns of restricted diffusion on Creutzfeldt-Jakob disease MRI**
MRI scans were provided by the National Prion Disease Pathology Surveillance Center, Case Western Reserve University, Cleveland, OH, USA. (A–C) Brain MRI of a patient with sporadic Creutzfeldt-Jakob Disease (MM1 subtype). (A) Restricted diffusion in occipital and parietal lobes, green arrows show associated hyperintensities on DWI. (B) Hypointensities on ADC maps. (C) Less clear hyperintensities on FLAIR images than on DWI. Other patients with MM1 subtypes can present additional restricted diffusion in caudate nucleus and putamen, a similar pattern (with caudate nucleus and putamen less likely involved) can be seen in MM2 and VV1 subtypes. (D–F) Brain MRI of a patient with sporadic Creutzfeldt-Jakob Disease (VV2 subtype), restricted diffusion in caudate nucleus, putamen and thalamus, predominantly in the pulvinar (less clear than in caudate nucleus and putamen) in both hemispheres. (D) Associated hyperintensities on DWI. (E) Associated hypointensities on ADC maps. (F) Associated hyperintensities on FLAIR images. A similar pattern (with additional cortical involvement) can be seen in the MV2 subtype. ADC=apparent diffusion coefficient. DWI=diffusion weighted images. FLAIR=fluid attenuated inversion recovery.

Definite:
Progressive neuropsychiatric syndrome and neuropathological or immunocytochemical, or biochemical confirmation

Probable:
I + two of II and typical EEG*
or
I + two of II and typical brain MRI†
or
I + two of II and positive CSF 14-3-3
or
progressive neuropsychiatric syndrome and positive RT-QuIC in CSF or other tissues
+ exclusion of other causes in complete diagnostic workup

Possible:
I + two of II + duration <2 years

I
Rapidly progressive cognitive impairment

II
A. Myoclonus
B. Visual or cerebellar disturbance
C. Pyramidal or extrapyramidal signs
D. Akinetic mutism

Figure 2: **Diagnosis of sporadic Creutzfeldt-Jakob disease**
Adapted from National Creutzfeldt-Jakob Disease Research & Surveillance Unit criteria[13] that were based on the WHO criteria[3,4] and amended by including RT-QuIC as an additional biomarker. Here, imaging criteria were refined and the need for a thorough diagnostic work-up in suspected probable sporadic Creutzfeldt-Jakob disease is emphasised. *Generalised periodic sharp or wave complexes. †Restricted diffusion in caudate or caudate–putamen or caudate–putamen–thalamus, or at least two cortical regions (temporal, parietal, occipital) on MRI brain scan,[4] no subcortical white matter involvement, no isolated restricted diffusion in the thalamus. Characteristic hyperintensities can be seen on fluid attenuated inversion recovery images, but diffusion weighted sequences are required to confirm Creutzfeldt-Jakob disease-typical restricted diffusion.[84,85]
RT-QuIC=real-time quaking induced conversion.

could be caused by different scanners, imaging and rating protocols, a study focus on other biomarkers, or the individual experience of image interpreters.[90] The future possibilities of brain MRI include its application as a prognostic marker[91] and as a potential marker in trial monitoring.[92,93] Some data suggest that restricted diffusion can occur in very early disease stages. Although prospective studies are not feasible in sporadic Creutzfeldt-Jakob disease, such changes were observed more than one year before symptom onset in case reports.[94]

Positron emission tomography

Positron emission tomography using ^{18}F-fluoro-2-deoxy-d-glucose (FDG-PET) as tracer is able to detect decreased glucose metabolism in cortical regions of patients with sporadic Creutzfeldt-Jakob disease. However, the value of FDG-PET in the differential diagnosis is limited by the absence of specific patterns. FDG-PET has potential as a marker of early sporadic Creutzfeldt-Jakob disease and showed a correlation with clinical symptoms.[95] In the rare MM2T subtype (sporadic fatal insomnia), an early-reduced thalamic glucose metabolism is a distinctive feature.[96]

EEG

Periodic sharp-wave complexes (PSWCs) with a frequency of 1 Hz are considered as an EEG pattern typical of Creutzfeldt-Jakob disease and have shown a sensitivity of 64% and a specificity of 91%.[97] The non-convulsive status epilepticus is the most common clinical condition with Creutzfeldt-Jakob disease EEG.[98,99] Over the past 5 years, CSF biomarker studies reported a substantially lower sensitivity (39% to 45%) for EEG.[12,34,37,40] Most likely, the decreasing sensitivity of EEG is a result of improved early recognition of sporadic Creutzfeldt-Jakob disease cases. Typical PSWCs occur in late disease stages and are less frequent in MV2, VV2, and MM2 cases. However, the method is less invasive than CSF sampling, and non-specific periodic rhythm abnormalities[100] and quantitative analysis of frequency alterations[101] might have the potential to aid diagnosis in early stages and to predict disease progression.

Genetic markers

PRNP mutations account for 10–15% of all human prion diseases.[1] Some cause specific clinical syndromes (eg, Gerstmann–Sträussler–Scheinker syndrome or fatal familial insomnia), whereas others can mimic clinical presentation and biomarker profiles of sporadic Creutzfeldt-Jakob disease (eg, E200K).[102] Thus, the sequencing of *PRNP* is an important biomarker that should be considered in the differential diagnosis of prion diseases and is crucial in atypical cases, and in cases with positive or uninformed family history of rapidly progressive dementias. In some sporadic Creutzfeldt-Jakob disease subtypes, reduced sensitivity of surrogate biomarkers has been observed, especially in patients with the MV2 and MM2-types.[48,58]

The identification of the PrP^{Sc} type is only possible in brain tissue, but the analysis of codon 129 *PRNP* might help to interpret inconclusive biomarker results.[103]

Clinical value of RT-QuIC and CSF surrogate biomarkers

Over the past 9 years, the evidence suggesting CSF RT-QuIC as a major improvement in the clinical diagnosis of sporadic Creutzfeldt-Jakob disease has accumulated. The test sensitivity is similar to the best available surrogate biomarkers and the data display superior specificity (table). By contrast with all established biomarkers for sporadic Creutzfeldt-Jakob disease and other neurodegenerative diseases, RT-QuIC is able to detect the protein that was consensually identified to be primarily pathogenic (PrP^{Sc}). Although different protocols and definitions of test positivity have been proposed,[9,29,30] reproducibility of test results has been shown in ring trials.[10,104] However, RT-QuIC is rather expensive regarding its substrate (recombinant PrP) and, although the test is less reliant on specialised equipment when compared with MRI and PET, the method still has to be established in more centres to provide all-encompassing availability. There is an ongoing debate on infectivity of the aggregates produced by PrP^{Sc} amplification assays. Although infectivity was shown in PMCA-replicated PrP^{Sc} from patients with variant Creutzfeldt-Jakob disease,[105] mouse models could not show infectivity of the RT-QuIC product from sporadic Creutzfeldt-Jakob disease samples so far.[106]

Surrogate CSF biomarkers of sporadic Creutzfeldt-Jakob disease are reliable diagnostics but the accuracy might differ with respect to the clinical context in which these markers are used. They are not disease specific by their very nature. Thus, physicians should interpret test results with caution. CSF 14-3-3 protein is highly sensitive and well validated, but acute brain injury events might cause false positive results. CSF 14-3-3 protein is part of a widely used clinical diagnostic gold standard[3,4] and estimates of the diagnostic accuracy, especially in comparative analyses, might be influenced by verification bias.[107] A problem with the 14-3-3 western blot method is its complex interpretation and the presence of borderline results (traces). 14-3-3 ELISAs might resolve this problem but they have not been widely established. The most commonly used alternative CSF biomarker, t-Tau, showed improved (but still only moderate) specificity in the differentiation of sporadic Creutzfeldt-Jakob disease and acute brain injury events or encephalitis,[36,50] but there is some evidence that t-Tau might not have sufficient specificity in the discrimination of rapidly progressive or atypical Alzheimer's disease and sporadic Creutzfeldt-Jakob disease (appendix p 1). In a large cohort representing the full clinical spectrum of a non-specialised neurochemical laboratory, sporadic Creutzfeldt-Jakob disease accounted for only 18% of patients with highly elevated (>1200 pg/mL) CSF t-Tau concentration;[61] therefore, as with other biomarkers, it should not be used in general screening but in the proper clinical context when suspecting prion disease. Evidence-based consensus cut-offs for CSF t-Tau, at best considering different assays, differential diagnoses, and supportive information on sporadic Creutzfeldt-Jakob disease cases (eg, codon 129 *PRNP* polymorphism), would be most helpful and should be evaluated through a structured analysis. In conclusion, both markers (t-Tau and 14-3-3) share several

Panel 1: **Historical case studies from the German Creutzfeldt-Jakob Disease Surveillance Unit**

Case A (typical Creutzfeldt-Jakob disease)

A 63-year-old woman presented with language disturbance (mild amnestic aphasia) that had started 2 weeks before hospital admission.

Neurological and neuropsychiatric examination showed cognitive deficits and ataxia. The EEG showed continuous focal epileptiform patterns but enforced antiepileptic medication showed no clinical benefit. In the CSF, 14-3-3 proteins (64455 AU/mL, cutoff >20 000 AU/mL) and t-Tau (12460 pg/mL, cut-off >1300 pg/mL) were both highly increased and RT-QuIC was positive. No signs of CNS inflammation were present. MRI showed restricted diffusion in frontal, temporal, and parietal regions, and in caudate nucleus, and left putamen. The clinical condition of the patient worsened within 1 week. Clinical examination showed severe dementia, pyramidal and extrapyramidal signs, and myoclonus. Follow-up EEGs showed periodic sharp-wave complexes (PSWCs) that were typical of Creutzfeldt-Jakob disease. Prion protein (*PRNP*) sequencing showed no pathogenic mutation and homozygosity for Met at codon 129. The patient was diagnosed with probable sporadic Creutzfeldt-Jakob disease according to common criteria,[4] supported by positivity of CSF RT-QuIC.

The patient died after 2 months of disease duration. Brain autopsy showed PrP^{Sc} depositions with neuropathological characteristics of the most common MM/MV1 sporadic Creutzfeldt-Jakob disease subtype.

Case B (atypical sporadic Creutzfeldt-Jakob disease)

Family members recognised personality changes and mild cognitive deficits in a 54-year-old woman, and suspected a disorder.

After 5 months of symptom duration, a neurologist observed rapidly progressive dementia with apraxia. MRI showed restricted diffusion in parietal, occipital, and temporal regions with very subtle involvement of caudate nucleus (no other pathological findings). EEG showed sporadic triphasic complexes but no PSWCs. The Creutzfeldt-Jakob Dsease Surveillance Unit was consulted and recommended further clinical investigations, including CSF analyses. The CSF showed no evidence for inflammatory CNS diseases, positive 14-3-3 proteins at a relatively low level (21527 AU/mL, cut-off >20 000 AU/mL), and positive RT-QuIC. *PRNP* sequencing revealed no pathogenic mutation and homozygosity for Met at codon 129. Although clinical diagnostic criteria[4] for sporadic Creutzfeldt-Jakob disease were not fulfilled at that time (the patient showed only rapidly progressive dementia), the biomarker signature was highly suggestive and no alternative diagnoses were revealed.

The case was classified as probable sporadic Creutzfeldt-Jakob disease according to amended surveillance centre criteria[12] because of RT-QuIC positivity. Disease course (relatively slow progression), MRI results (predominant cortical involvement), and codon 129 were suggestive for the rare MM2C (cortical) sporadic Creutzfeldt-Jakob disease subtype. The patient died after 11 months of disease duration. Brain autopsy revealed PrP^{Sc} depositions with neuropathological characteristics of the MM/MV2C sporadic Creutzfeldt-Jakob disease subtype.

Panel 2: **Guidelines for the clinical diagnosis of sporadic Creutzfeldt-Jakob disease**

General

The clinical diagnosis of sporadic Creutzfeldt-Jakob disease requires a thorough diagnostic investigation, including blood sampling, lumbar puncture, neuroimaging (MRI), and EEG at a minimum. Further diagnostics (eg, body CT, PET, specific CSF analyses) can be necessary depending on suspected differential diagnoses.

The diagnostic criteria and its measurements

We recommend amending the established WHO criteria for the clinical diagnosis of probable sporadic Creutzfeldt-Jakob disease (figure 2). If available, RT-QuIC should be done in every case of suspected prion disease. The 14-3-3 test is the primary CSF surrogate biomarker (in some centres, CSF t-Tau is considered as primary CSF surrogate biomarker). CSF t-Tau and the p-Tau/t-tau (or t-Tau/p-Tau) ratio are valuable supportive biomarkers. All markers need be done in certified laboratories. MRI and EEG are highly specific but require experienced interpreters. MRI sequences should include T1 weighted images with contrast agent sequences (for differential diagnosis), fluid attenuated inversion recovery, and diffusion-weighted images (DWI) with apparent diffusion coefficient maps. MRI findings typical of Creutzfeldt-Jakob disease are clearly visible on DWI rather than other sequences. All mentioned biomarkers are less sensitive in early disease stage and in some molecular subtypes, follow-up investigations can be useful in case of negative results. The analysis of codon 129 (*PRNP*) polymorphism might assist in interpreting the results of other biomarker analyses. Diagnosis of possible sporadic Creutzfeldt-Jakob disease (ie, the absence of suggestive biomarkers, figure 2) should only be made if extensive diagnostics had not revealed alternative explanations for the clinical condition.

Important differential diagnoses

Genetic analyses and clinical signs of iatrogenic Creutzfeldt-Jakob disease and variant Creutzfeldt-Jakob disease should be considered in all cases with suspected prion disease. Rapidly progressive neurodegenerative diseases, (immune-mediated) encephalitis, status epilepticus, and cerebral ischaemia are frequent differential diagnoses. Among others, these diseases could mimic the clinical syndrome and most surrogate biomarkers of sporadic Creutzfeldt-Jakob disease.

Brain biopsy

Brain biopsy is an invasive procedure that can be considered when non-invasive diagnostics remain inconclusive and a potentially treatable alternative diagnosis is suspected.

characteristics, advantages, and disadvantages (appendix p 2). The clinical use must be assessed in light of suspected differential diagnoses and can be improved by stratification of demographic and genetic factors.[103]

An upcoming issue in the biomarker-based diagnosis of sporadic Creutzfeldt-Jakob disease is the use of composites. Regarding this issue, the best evidence is available for the p-Tau/t-Tau ratio, which was shown to be of superior diagnostic accuracy compared with t-Tau alone, especially in the differentiation of sporadic Creutzfeldt-Jakob disease from Alzheimer's disease.[51,64,68] Proposed ratios combining t-Tau, p-Tau, 14-3-3, S100b, t-PrP, or amyloid β showed high diagnostic accuracy,[48,52,73,108] but have not been established in the clinical setting.

Guidelines for biomarker-based diagnosis

Based on WHO criteria,[3,4] the studies presented here, and previous suggestions that include RT-QuIC,[12,13] the majority of the authors recommend amended criteria for the clinical diagnosis of sporadic Creutzfeldt-Jakob disease (figure 2). Because of the outstanding specificity of RT-QuIC, positive cases can be classified as probable sporadic Creutzfeldt-Jakob disease in early clinical stages, even when only one cardinal symptom is present, which will improve the early identification of sporadic Creutzfeldt-Jakob disease.[12,39,108]

Similar to other diagnostics, as the test becomes widely applied, even a false positive rate below 1% will lead to some incorrect diagnoses. This likelihood becomes particularly concerning if treatable conditions are missed. Ability to rely solely on RT-QuIC is further compromised by the test's inability to distinguish accurately between different forms of human prion disease and test sensitivities that vary from 73% to 97%. Additionally, RT-QuIC is mostly unavailable in countries without major surveillance programmes. Therefore, we recommend that clinicians contact national Creutzfeldt-Jakob disease surveillance units or referral centres to get information on the availability of RT-QuIC and general clinical guidance for the diagnosis and management of suspected prion disease cases (appendix p 5).

Readily available, economical, and field-tested CSF biomarkers such as 14-3-3 and t-Tau, and EEG and MRI (preferably DWI including ADC sequences) are still of major importance and should be used as routine diagnostic tests in cases of suspected sporadic Creutzfeldt-Jakob disease. These tools have been shown to be effective and accurate in the differential diagnosis of sporadic Creutzfeldt-Jakob disease, when they are applied and interpreted in a reasonable context. In case of ambiguous results or uncertain differential diagnoses, the p-Tau/t-Tau (or t-Tau/p-Tau) ratio might be considered as a supportive biomarker.[63,64,68] Genetic analysis of *PRNP* should be considered in all cases of suspected Creutzfeldt-Jakob disease to determine the codon 129 polymorphism and to exclude pathogenic mutations, which can be present in patients with a negative family history.[102] Importantly, routine blood, CSF, and imaging diagnostics should always be done to rule out the most common differential diagnoses (appendix p 8, panel 1, panel 2).

Conclusions and future directions

Despite improvements of diagnostic measures for sporadic Creutzfeldt-Jakob disease over the past 25 years, there are still plenty of challenges. The value of established and new biomarkers in the differential diagnosis of sporadic Creutzfeldt-Jakob disease subtypes and other human prion diseases (eg, iatrogenic Creutzfeldt-Jakob disease, variant Creutzfeldt-Jakob disease, and genetic Creutzfeldt-Jakob disease) has to be clarified. RT-QuIC has to be widely distributed, protocols have to be unified, past studies on peripheral tissue have to be validated with regard to important differential diagnoses, and more candidate tissues have to be evaluated. In this context, the potential infectivity of RT-QuIC positive tissues, such as olfactory mucosa,[106] might be reappraised.

Search strategy and selection criteria

We searched Google Scholar and PubMed using the terms "prion" and "Creutzfeldt-Jakob disease", each in combination with "diagnosis", "criteria", "biomarker", "imaging", "MRI", "EEG", and "RT-QuIC". We included articles published between Jan 1, 2015, and Nov 15, 2020, written in English or German, on the basis of the scientific merit and contribution to developments in biomarker research for sporadic Creutzfeldt-Jakob disease (ie, the biomarkers have shown potential for a clinical use and results were independently validated). However, comprehensive lists of articles (after 2015, not mentioned in the main text) presenting altered biomarkers in sporadic Creutzfeldt-Jakob disease were noted (appendix p 3). Older articles (ie, articles published before 2015) were selected on the basis of author expertise to substantiate basic information and evidence of biomarkers that are currently being investigated.

More potential diagnostic biomarkers are currently under investigation. We recommend that new biomarkers could be considered in future diagnostic criteria under particular conditions. Besides strong clinical evidence (ie, validation of cutoffs in independent cohorts, appropriate controls), such a biomarker should substantially improve the clinical diagnosis of sporadic Creutzfeldt-Jakob disease. This improvement can be a biomarker that shows superior diagnostic accuracy compared with established markers or equal accuracy with reduction of test invasiveness (eg, blood-based tests). Although analysis of codon 129 *PRNP* polymorphism, clinical observations, and biomarker profiles (especially MRI DWI lesion patterns[87]) already allow conclusions on the sporadic Creutzfeldt-Jakob disease subtype, new biomarkers should be able to go beyond phenotypical variability and disease stage, or at least be evaluated in this respect.

Over the past 5 years, some investigations have opened the field of prodromal, prognostic, and predictive biomarkers for sporadic Creutzfeldt-Jakob disease. One of the challenges for clinical trials in sporadic Creutzfeldt-Jakob disease is that clinical features are highly heterogeneous and it has been difficult to find a suitable single continuous measure as an outcome. Therefore, specific Creutzfeldt-Jakob disease tests, such as RT-QuIC, might be used at trial enrolment, and blood-based biomarkers might be used repeatedly during a trial to track axonal damage in the course of experimental treatment. Further work is required to establish variability of biomarkers in the natural history of Creutzfeldt-Jakob disease and if biomarkers of neurodegeneration can contribute to prognostic or trial models. Finally, blood-based biomarkers could have a role in preventive trials as a prodromal biomarker for healthy individuals who are at-risk of Creutzfeldt-Jakob disease because of iatrogenic prion exposure or *PRNP* mutation. Available published work suggests a prodromal biomarker window is small or rare in at-risk individuals with pathogenic *PRNP* mutations,[109,110] but this concept is currently the focus of many prion researchers.

Contributors

PH designed the Review outline, wrote the manuscript, did the literature search, and designed and prepared illustrations, including processing of the MRI scans. IZ designed the Review outline, did the literature search, and revised the manuscript. BA contributed to the literature search, provided the MRI scans, and revised the manuscript. All other authors contributed to the literature search and revised the manuscript.

Declaration of interests

PH reports grants from Robert Koch Institute during the conduct of the Review. BC has patent 2554996 issued (France, Germany, UK), patent 2179293 issued (Switzerland, Germany, France, UK, Ireland), and patent 8 216 788 (USA) issued. MG reports grants from US National Institutes of Health (R01-AG AG031189, R01-AG062562; R56-AG055619), grants from Michael J Homer Family Fund, and grants from Alliance Biosecure, during the conduct of the Review; personal fees from Ascel Health, LifeSci Capital, ClearView Healthcare Partners, Blade Therapeutics, Bioscience Pharma Partners, Bioscience Pharma Partners, Teledoc Health, Best Doctors, Advance Medical, Grand Rounds, and Quest Diagnostics, outside the submitted work. SH reports grants from MedDay Pharmaceuticals, grants from Institut de Recherche Servier, grants from LFB Biomedicaments, outside the submitted work, and a patent pending (PCT/EP2019/070457). MP reports personal fees from Ferring Pharmaceuticals, personal fees from Collection of National Chemical Compounds and Screening Center, non-financial support from Fondazione Cellule Staminali, outside the submitted work. IZ reports grants from Robert Koch Institute, during the conduct of the Review. All other authors declare no competing interests.

Acknowledgments

The research of IZ and PH was funded by the German Federal Ministry of Health through grants from the Robert Koch Institute (grant 139-341). BC was funded by the Intramural Research Program of the National Institute of Allergy and Infectious Diseases, National Institutes of Health. SJC is funded in part by a NHMRC Practitioner Fellowship (ID# APP1105784). FL was supported by grant from the Institute of Health Carlos III, grant PI19/00144. MG was supported by grants from the US National Institutes of Health (R01-AG AG031189, R01-AG062562, R56-AG055619) and funding from Michael J Homer Family Fund and Alliance Biosecure. KS was supported by grants for scientific research from the Ministry of Health, Labour and Welfare of Japan (KSat: 14507303), Research Committee of Prion Disease and Slow Virus Infection, Research on Policy Planning and Evaluation for Rare and Intractable Diseases, Health and Labour Sciences Research Grants, the Research Committee of Surveillance and Infection Control of Prion Disease, the Ministry of Health, Labour, and Welfare of Japan, and the Japan Agency for Medical Research and Development (grant 18ek0109362h0001). The funding sources had no role in the study design or the collection, analysis, and interpretation of data, in the writing of the report and in the decision to submit the paper for publication. PH had full access to all the data in the Review and had final responsibility for the decision to submit for publication. The authors want to thank Terri Lindsay from the European Creutzfeldt-Jakob Disease Surveillance Network, Suzanne Solvyns from the Creutzfeldt-Jakob Disease International Support Alliance, and Debbie Yobs from the Creutzfeldt-Jakob Disease Foundation for helping with information on international Creutzfeldt-Jakob Disease referral centres and family associations. PH accessed the case history information (panel 1) from the German National Reference Center for Transmissible Spongiform Encephalopathies (Göttingen, Germany).

References

1 Ladogana A, Puopolo M, Croes EA, et al. Mortality from Creutzfeldt-Jakob disease and related disorders in Europe, Australia, and Canada. *Neurology* 2005; **64:** 1586–91.

2 Parchi P, Giese A, Capellari S, et al. Classification of sporadic Creutzfeldt-Jakob disease based on molecular and phenotypic analysis of 300 subjects. *Ann Neurol* 1999; **46:** 224–33.

3 WHO. Global Surveillance, diagnosis, and therapy of human transmissible spongiform encephalopathies: report of WHO consultation, February 9-11, 1998, Geneva, Switzerland. 1998. https://www.who.int/csr/resources/publications/bse/WHO_EMC_ZDI_98_9/en/ (accessed Jan 20, 2021).

4 Zerr I, Kallenberg K, Summers DM, et al. Updated clinical diagnostic criteria for sporadic Creutzfeldt-Jakob disease. *Brain* 2009; **132:** 2659–68.

5 Otto M, Wiltfang J, Cepek L, et al. Tau protein and 14-3-3 protein in the differential diagnosis of Creutzfeldt-Jakob disease. *Neurology* 2002; **58:** 192–97.

6 Collins SJ, Sanchez-Juan P, Masters CL, et al. Determinants of diagnostic investigation sensitivities across the clinical spectrum of sporadic Creutzfeldt-Jakob disease. *Brain* 2006; **129:** 2278–87.

7 Geschwind MD, Martindale J, Miller D, et al. Challenging the clinical utility of the 14-3-3 protein for the diagnosis of sporadic Creutzfeldt-Jakob disease. *Arch Neurol* 2003; **60:** 813–16.

8 Atarashi R, Satoh K, Sano K, et al. Ultrasensitive human prion detection in cerebrospinal fluid by real-time quaking-induced conversion. *Nat Med* 2011; **17:** 175–78.

9 McGuire LI, Peden AH, Orrú CD, et al. RT-QuIC analysis of cerebrospinal fluid in sporadic Creutzfeldt-Jakob disease. *Ann Neurol* 2012; **72:** 278–85.

10 Cramm M, Schmitz M, Karch A, et al. Stability and reproducibility underscore utility of RT-QuIC for diagnosis of Creutzfeldt-Jakob disease. *Mol Neurobiol* 2016; **53:** 1896–904.

11 Foutz A, Appleby BS, Hamlin C, et al. Diagnostic and prognostic value of human prion detection in cerebrospinal fluid. *Ann Neurol* 2017; **81:** 79–92.

12 Hermann P, Laux M, Glatzel M, et al. Validation and utilisation of amended diagnostic criteria in Creutzfeldt-Jakob disease surveillance. *Neurology* 2018; **91:** e331–38.

13 National Creutzfeldt-Jakob Disease Research & Surveillance Unit. Sporadic CJS. January, 2017. https://www.cjd.ed.ac.uk/sites/default/files/criteria_0.pdf (accessed April 27, 2020).

14 Noguchi-Shinohara M, Hamaguchi T, Nozaki I, Sakai K, Yamada M. Serum tau protein as a marker for the diagnosis of Creutzfeldt-Jakob disease. *J Neurol* 2011; **258:** 1464–68.

15 Steinacker P, Blennow K, Halbgebauer S, et al. Neurofilaments in blood and CSF for diagnosis and prediction of onset in Creutzfeldt-Jakob disease. *Sci Rep* 2016; **6:** 38737.

16 Kovacs GG, Andreasson U, Liman V, et al. Plasma and cerebrospinal fluid tau and neurofilament concentrations in rapidly progressive neurological syndromes: a neuropathology-based cohort. *Eur J Neurol* 2017; **24:** 1326–e77.

17 Bongianni M, Orrù C, Groveman BR, et al. Diagnosis of human prion disease using real-time quaking-induced conversion testing of olfactory mucosa and cerebrospinal fluid samples. *JAMA Neurol* 2017; **74:** 155–62.

18 Altman DG, Bland JM. Diagnostic tests 2: predictive values. *BMJ* 1994; **309:** 102.

19 Budka H, Aguzzi A, Brown P, et al. Neuropathological diagnostic criteria for Creutzfeldt-Jakob disease (CJD) and other human spongiform encephalopathies (prion diseases). *Brain Pathol* 1995; **5:** 459–66.

20 Heath CA, Cooper SA, Murray K, et al. Validation of diagnostic criteria for variant Creutzfeldt-Jakob disease. *Ann Neurol* 2010; **67:** 761–70.

21 Luk C, Jones S, Thomas C, et al. Diagnosing sporadic Creutzfeldt-Jakob Disease by the detection of abnormal prion protein in patient urine. *JAMA Neurol* 2016; **73:** 1454–60.

22 Saborio GP, Permanne B, Soto C. Sensitive detection of pathological prion protein by cyclic amplification of protein misfolding. *Nature* 2001; **411:** 810–13.

23 Atarashi R, Moore RA, Sim VL, et al. Ultrasensitive detection of scrapie prion protein using seeded conversion of recombinant prion protein. *Nat Methods* 2007; **4:** 645–50.

24 Barria MA, Lee A, Green AJ, Knight R, Head MW. Rapid amplification of prions from variant Creutzfeldt-Jakob disease cerebrospinal fluid. *J Pathol Clin Res* 2018; **4:** 86–92.

25 Bougard D, Brandel JP, Bélondrade M, et al. Detection of prions in the plasma of presymptomatic and symptomatic patients with variant Creutzfeldt-Jakob disease. *Sci Transl Med* 2016; **8:** 370ra182.

26 Concha-Marambio L, Pritzkow S, Moda F, et al. Detection of prions in blood from patients with variant Creutzfeldt-Jakob disease. *Sci Transl Med* 2016; **8:** 370ra183.

27 Moda F, Gambetti P, Notari S, et al. Prions in the urine of patients with variant Creutzfeldt-Jakob disease. *N Engl J Med* 2014; **371:** 530–39.

28 Wilham JM, Orrú CD, Bessen RA, et al. Rapid end-point quantitation of prion seeding activity with sensitivity comparable to bioassays. *PLoS Pathog* 2010; **6:** e1001217.

29 Schmitz M, Cramm M, Llorens F, et al. The real-time quaking-induced conversion assay for detection of human prion disease and study of other protein misfolding diseases. *Nat Protoc* 2016; **11:** 2233–42.

30 Orrú CD, Groveman BR, Raymond LD, et al. Bank vole prion protein as an apparently universal substrate for RT-QuIC-based detection and discrimination of prion strains. *PLoS Pathog* 2015; **11:** e1004983.

31 Orrú CD, Groveman BR, Hughson AG, Zanusso G, Coulthart MB, Caughey B. Rapid and sensitive RT-QuIC detection of human Creutzfeldt-Jakob disease using cerebrospinal fluid. *MBio* 2015; **6:** e02451–14.

32 Orrú CD, Bongianni M, Tonoli G, et al. A test for Creutzfeldt-Jakob disease using nasal brushings. *N Engl J Med* 2014; **371:** 519–29.

33 Groveman BR, Orrú CD, Hughson AG, et al. Extended and direct evaluation of RT-QuIC assays for Creutzfeldt-Jakob disease diagnosis. *Ann Clin Transl Neurol* 2016; **4:** 139–44.

34 Park JH, Choi YG, Lee YJ, et al. Real-time quaking-induced conversion analysis for the diagnosis of sporadic Creutzfeldt-Jakob disease in Korea. *J Clin Neurol* 2016; **12:** 101–06.

35 Franceschini A, Baiardi S, Hughson AG, et al. High diagnostic value of second generation CSF RT-QuIC across the wide spectrum of CJD prions. *Sci Rep* 2017; **7:** 10655.

36 Lattanzio F, Abu-Rumeileh S, Franceschini A, et al. Prion-specific and surrogate CSF biomarkers in Creutzfeldt-Jakob disease: diagnostic accuracy in relation to molecular subtypes and analysis of neuropathological correlates of p-tau and Aβ42 levels. *Acta Neuropathol* 2017; **133:** 559–78.

37 Rudge P, Hyare H, Green A, Collinge J, Mead S. Imaging and CSF analyses effectively distinguish CJD from its mimics. *J Neurol Neurosurg Psychiatry* 2018; **89:** 461–66.

38 Hayashi Y, Iwasaki Y, Yoshikura N, et al. An autopsy-verified case of steroid-responsive encephalopathy with convulsion and a false-positive result from the real-time quaking-induced conversion assay. *Prion* 2017; **11:** 284–92.

39 Rhoads DD, Wrona A, Foutz A, et al. Diagnosis of prion diseases by RT-QuIC results in improved surveillance. *Neurology* 2020; **95:** e1017–26.

40 Abu-Rumeileh S, Baiardi S, Polischi B, et al. Diagnostic value of surrogate CSF biomarkers for Creutzfeldt-Jakob disease in the era of RT-QuIC. *J Neurol* 2019; **266:** 3136–43.

41 Zanusso G, Monaco S, Pocchiari M, Caughey B. Advanced tests for early and accurate diagnosis of Creutzfeldt-Jakob disease. *Nat Rev Neurol* 2016; **12:** 325–33.

42 Fiorini M, Iselle G, Perra D, et al. High diagnostic accuracy of RT-QuIC assay in a prospective study of patients with suspected sCJD. *Int J Mol Sci* 2020; **21:** E880.

43 Mammana A, Baiardi S, Rossi M, et al. Detection of prions in skin punch biopsies of Creutzfeldt-Jakob disease patients. *Ann Clin Transl Neurol* 2020; **7:** 559–64.

44 Orrú CD, Yuan J, Appleby BS, et al. Prion seeding activity and infectivity in skin samples from patients with sporadic Creutzfeldt-Jakob disease. *Sci Transl Med* 2017; **9:** eaam7785.

45 Orrù CD, Soldau K, Cordano C, et al. Prion seeds distribute throughout the eyes of sporadic Creutzfeldt-Jakob disease patients. *MBio* 2018; **9:** e02095–18.

46 Berg D, Holzmann C, Riess O. 14-3-3 proteins in the nervous system. *Nat Rev Neurosci* 2003; **4:** 752–62.

47 Muayqil T, Gronseth G, Camicioli R. Evidence-based guideline: diagnostic accuracy of CSF 14-3-3 protein in sporadic Creutzfeldt-Jakob disease: report of the guideline development subcommittee of the American Academy of Neurology. *Neurology* 2012; **79:** 1499–506.

48 Sanchez-Juan P, Green A, Ladogana A, et al. CSF tests in the differential diagnosis of Creutzfeldt-Jakob disease. *Neurology* 2006; **67:** 637–43.

49 Hamlin C, Puoti G, Berri S, et al. A comparison of tau and 14-3-3 protein in the diagnosis of Creutzfeldt-Jakob disease. *Neurology* 2012; **79:** 547–52.

50 Stoeck K, Sanchez-Juan P, Gawinecka J, et al. Cerebrospinal fluid biomarker supported diagnosis of Creutzfeldt-Jakob disease and rapid dementias: a longitudinal multicentre study over 10 years. *Brain* 2012; **135:** 3051–61.

51 Dorey A, Tholance Y, Vighetto A, et al. Association of cerebrospinal fluid prion protein levels and the distinction between Alzheimer disease and Creutzfeldt-Jakob disease. *JAMA Neurol* 2015; **72:** 267–75.

52 Abu Rumeileh S, Lattanzio F, Stanzani Maserati M, Rizzi R, Capellari S, Parchi P. Diagnostic accuracy of a combined analysis of cerebrospinal fluid t-PrP, t-tau, p-tau, and Aβ42 in the differential diagnosis of Creutzfeldt-Jakob disease from alzheimer's disease with emphasis on atypical disease variants. *J Alzheimers Dis* 2017; **55:** 1471–80.

53 Abu-Rumeileh S, Capellari S, Stanzani-Maserati M, et al. The CSF neurofilament light signature in rapidly progressive neurodegenerative dementias. *Alzheimers Res Ther* 2018; **10:** 3.

54 Leitão MJ, Baldeiras I, Almeida MR, et al. Sporadic Creutzfeldt-Jakob disease diagnostic accuracy is improved by a new CSF ELISA 14-3-3γ assay. *Neuroscience* 2016; **322:** 398–407.

55 Schmitz M, Ebert E, Stoeck K, et al. Validation of 14-3-3 protein as a marker in sporadic Creutzfeldt-Jakob disease diagnostic. *Mol Neurobiol* 2016; **53:** 2189–99.

56 Wang Y, Mandelkow E. Tau in physiology and pathology. *Nat Rev Neurosci* 2016; **17:** 5–21.

57 Koscova S, Zakova Slivarichova D, Tomeckova I, et al. Cerebrospinal fluid biomarkers in the diagnosis of Creutzfeldt-Jakob disease in slovak patients: over 10-year period review. *Mol Neurobiol* 2017; **54:** 5919–27.

58 Karch A, Hermann P, Ponto C, et al. Cerebrospinal fluid tau levels are a marker for molecular subtype in sporadic Creutzfeldt-Jakob disease. *Neurobiol Aging* 2015; **36:** 1964–68.

59 Cohen OS, Chapman J, Korczyn AD, et al. CSF tau correlates with CJD disease severity and cognitive decline. *Acta Neurol Scand* 2016; **133:** 119–23.

60 Coulthart MB, Jansen GH, Olsen E, et al. Diagnostic accuracy of cerebrospinal fluid protein markers for sporadic Creutzfeldt-Jakob disease in Canada: a 6-year prospective study. *BMC Neurol* 2011; **11:** 133.

61 Lehmann S, Paquet C, Malaplate-Armand C, et al. Diagnosis associated with Tau higher than 1200 pg/mL: insights from the clinical and laboratory practice. *Clin Chim Acta* 2019; **495:** 451–56.

62 Li QX, Varghese S, Sarros S, et al. CSF Tau supplements 14-3-3 protein detection for sporadic Creutzfeldt-Jakob disease diagnosis while transitioning to next generation diagnostics. *J Clin Neurosci* 2018; **50:** 292–93.

63 Llorens F, Karch A, Golanska E, et al. Cerebrospinal fluid biomarker-based diagnosis of sporadic Creutzfeldt-Jakob Disease: a validation study for previously established cutoffs. *Dement Geriatr Cogn Disord* 2017; **43:** 71–80.

64 Skillbäck T, Rosén C, Asztely F, Mattsson N, Blennow K, Zetterberg H. Diagnostic performance of cerebrospinal fluid total tau and phosphorylated tau in Creutzfeldt-Jakob disease: results from the Swedish Mortality Registry. *JAMA Neurol* 2014; **71:** 476–83.

65 Llorens F, Rübsamen N, Hermann P, et al. A prognostic model for overall survival in sporadic Creutzfeldt-Jakob disease. *Alzheimers Dement* 2020; **16:** 1438–47.

66 Staffaroni AM, Kramer AO, Casey M, et al. Association of blood and cerebrospinal fluid Tau level and other biomarkers with survival time in sporadic Creutzfeldt-Jakob disease. *JAMA Neurol* 2019; **76:** 969–77.

67 Riemenschneider M, Wagenpfeil S, Vanderstichele H, et al. Phospho-tau/total tau ratio in cerebrospinal fluid discriminates Creutzfeldt-Jakob disease from other dementias. *Mol Psychiatry* 2003; **8:** 343–47.

68 Llorens F, Schmitz M, Karch A, et al. Comparative analysis of cerebrospinal fluid biomarkers in the differential diagnosis of neurodegenerative dementia. *Alzheimers Dement* 2016; **12:** 577–89.

69 Petzold A. Neurofilament phosphoforms: surrogate markers for axonal injury, degeneration and loss. *J Neurol Sci* 2005; **233:** 183–98.

70 Zerr I, Schmitz M, Karch A, et al. Cerebrospinal fluid neurofilament light levels in neurodegenerative dementia: evaluation of diagnostic accuracy in the differential diagnosis of prion diseases. *Alzheimers Dement* 2018; **14:** 751–63.

71 Antonell A, Tort-Merino A, Ríos J, et al. Synaptic, axonal damage and inflammatory cerebrospinal fluid biomarkers in neurodegenerative dementias. *Alzheimers Dement* 2020; **16:** 262–72.

72 Kanata E, Golanska E, Villar-Piqué A, et al. Cerebrospinal fluid neurofilament light in suspected sporadic Creutzfeldt-Jakob disease. *J Clin Neurosci* 2019; **60:** 124–27.

73 Chohan G, Pennington C, Mackenzie JM, et al. The role of cerebrospinal fluid 14-3-3 and other proteins in the diagnosis of sporadic Creutzfeldt-Jakob disease in the UK: a 10-year review. *J Neurol Neurosurg Psychiatry* 2010; **81:** 1243–48.

74 Villar-Piqué A, Schmitz M, Lachmann I, et al. Cerebrospinal fluid total prion protein in the spectrum of prion diseases. *Mol Neurobiol* 2019; **56:** 2811–21.

75 Minikel EV, Kuhn E, Cocco AR, et al. Domain-specific quantification of prion protein in cerebrospinal fluid by targeted mass spectrometry. *Mol Cell Proteomics* 2019; **18:** 2388–400.

76 Vallabh SM, Nobuhara CK, Llorens F, et al. Prion protein quantification in human cerebrospinal fluid as a tool for prion disease drug development. *Proc Natl Acad Sci USA* 2019; **116:** 7793–98.

77 Llorens F, Kruse N, Schmitz M, et al. Evaluation of α-synuclein as a novel cerebrospinal fluid biomarker in different forms of prion diseases. *Alzheimers Dement* 2017; **13:** 710–19.

78 Llorens F, Kruse N, Karch A, et al. Validation of α-synuclein as a CSF biomarker for sporadic Creutzfeldt-Jakob disease. *Mol Neurobiol* 2018; **55:** 2249–57.

79 Kruse N, Heslegrave A, Gupta V, et al. Interlaboratory validation of cerebrospinal fluid α-synuclein quantification in the diagnosis of sporadic Creutzfeldt-Jakob disease. *Alzheimers Dement (Amst)* 2018; **10:** 461–70.

80 Thompson AGB, Luk C, Heslegrave AJ, et al. Neurofilament light chain and tau concentrations are markedly increased in the serum of patients with sporadic Creutzfeldt-Jakob disease, and tau correlates with rate of disease progression. *J Neurol Neurosurg Psychiatry* 2018; **89:** 955–61.

81 Piehl F, Kockum I, Khademi M, et al. Plasma neurofilament light chain levels in patients with MS switching from injectable therapies to fingolimod. *Mult Scler* 2018; **24:** 1046–54.

82 Abu-Rumeileh S, Baiardi S, Ladogana A, et al. Comparison between plasma and cerebrospinal fluid biomarkers for the early diagnosis and association with survival in prion disease. *J Neurol Neurosurg Psychiatry* 2020; **91:** 1181–88.

83 Llorens F, Villar-Piqué A, Schmitz M, et al. Plasma total prion protein as a potential biomarker for neurodegenerative dementia: diagnostic accuracy in the spectrum of prion diseases. *Neuropathol Appl Neurobiol* 2020; **46:** 240–54.

84 Vitali P, Maccagnano E, Caverzasi E, et al. Diffusion-weighted MRI hyperintensity patterns differentiate CJD from other rapid dementias. *Neurology* 2011; **76:** 1711–19.

85 Staffaroni AM, Elahi FM, McDermott D, et al. Neuroimaging in dementia. *Semin Neurol* 2017; **37:** 510–37.

86 Caverzasi E, Mandelli ML, DeArmond SJ, et al. White matter involvement in sporadic Creutzfeldt-Jakob disease. *Brain* 2014; **137:** 3339–54.

87 Pascuzzo R, Oxtoby NP, Young AL, et al. Prion propagation estimated from brain diffusion MRI is subtype dependent in sporadic Creutzfeldt-Jakob disease. *Acta Neuropathol* 2020; **140:** 169–81.

88 Forner SA, Takada LT, Bettcher BM, et al. Comparing CSF biomarkers and brain MRI in the diagnosis of sporadic Creutzfeldt-Jakob disease. *Neurol Clin Pract* 2015; **5:** 116–25.

89 Bizzi A, Pascuzzo R, Blevins J, et al. Evaluation of a new criterion for detecting prion disease with diffusion magnetic resonance imaging. *JAMA Neurol* 2020; **77:** 1141–49.

90 Carswell C, Thompson A, Lukic A, et al. MRI findings are often missed in the diagnosis of Creutzfeldt-Jakob disease. *BMC Neurol* 2012; **12:** 153.

91 Gao T, Lyu JH, Zhang JT, et al. Diffusion-weighted MRI findings and clinical correlations in sporadic Creutzfeldt-Jakob disease. *J Neurol* 2015; **262:** 1440–46.

92 Park SY, Wang MJ, Jang JW, et al. The clinical stages of sporadic Creutzfeldt-Jakob disease with Met/Met genotype in Korean patients. *Eur Neurol* 2016; **75:** 213–22.

93 Eisenmenger L, Porter MC, Carswell CJ, et al. Evolution of diffusion-weighted magnetic resonance imaging signal abnormality in sporadic Creutzfeldt-Jakob disease, with histopathological correlation. *JAMA Neurol* 2016; **73:** 76–84.

94 Zanusso G, Camporese G, Ferrari S, et al. Long-term preclinical magnetic resonance imaging alterations in sporadic Creutzfeldt-Jakob disease. *Ann Neurol* 2016; **80:** 629–32.

95 Renard D, Castelnovo G, Collombier L, Thouvenot E, Boudousq V. FDG-PET in Creutzfeldt-Jakob disease: analysis of clinical-PET correlation. *Prion* 2017; **11:** 440–53.

96 Abu-Rumeileh S, Redaelli V, Baiardi S, et al. Sporadic fatal insomnia in europe: phenotypic features and diagnostic challenges. *Ann Neurol* 2018; **84:** 347–60.

97 Steinhoff BJ, Zerr I, Glatting M, Schulz-Schaeffer W, Poser S, Kretzschmar HA. Diagnostic value of periodic complexes in Creutzfeldt-Jakob disease. *Ann Neurol* 2004; **56:** 702–08.

98 Lapergue B, Demeret S, Denys V, et al. Sporadic Creutzfeldt-Jakob disease mimicking nonconvulsive status epilepticus. *Neurology* 2010; **74:** 1995–99.

99 Marquetand J, Knake S, Strzelczyk A, et al. Periodic EEG patterns in sporadic Creutzfeldt-Jakob-disease can be benzodiazepine-responsive and be difficult to distinguish from non-convulsive status epilepticus. *Seizure* 2017; **53:** 47–50.

100 Shin JW, Yim B, Oh SH, Kim NK, Lee SK, Kim OJ. Redefining periodic patterns on electroencephalograms of patients with sporadic Creutzfeldt-Jakob disease. *Clin Neurophysiol* 2017; **128:** 756–62.

101 Franko E, Wehner T, Joly O, et al. Quantitative EEG parameters correlate with the progression of human prion diseases. *J Neurol Neurosurg Psychiatry* 2016; **87:** 1061–67.

102 Ladogana A, Kovacs GG. Genetic Creutzfeldt-Jakob disease. *Handb Clin Neurol* 2018; **153:** 219–42.

103 Karch A, Llorens F, Schmitz M, et al. Stratification by genetic and demographic characteristics improves diagnostic accuracy of cerebrospinal fluid biomarkers in rapidly progressive dementia. *J Alzheimers Dis* 2016; **54:** 1385–93.

104 McGuire LI, Poleggi A, Poggiolini I, et al. Cerebrospinal fluid real-time quaking-induced conversion is a robust and reliable test for sporadic creutzfeldt-jakob disease: an international study. *Ann Neurol* 2016; **80:** 160–65.

105 Cali I, Lavrich J, Moda F, et al. PMCA-replicated PrP^D in urine of vCJD patients maintains infectivity and strain characteristics of brain PrP^D: transmission study. *Sci Rep* 2019; **9:** 5191.

106 Raymond GJ, Race B, Orrú CD, et al. Transmission of CJD from nasal brushings but not spinal fluid or RT-QuIC product. *Ann Clin Transl Neurol* 2020; **7:** 932–44.

107 Karch A, Koch A, Zapf A, Zerr I, Karch A. Partial verification bias and incorporation bias affected accuracy estimates of diagnostic studies for biomarkers that were part of an existing composite gold standard. *J Clin Epidemiol* 2016; **78:** 73–82.

108 Peckeu L, Delasnerie-Lauprètre N, Brandel JP, et al. Accuracy of diagnosis criteria in patients with suspected diagnosis of sporadic Creutzfeldt-Jakob disease and detection of 14-3-3 protein, France, 1992 to 2009. *Euro Surveill* 2017; **22:** 16-00715.

109 Vallabh SM, Minikel EV, Williams VJ, et al. Cerebrospinal fluid and plasma biomarkers in individuals at risk for genetic prion disease. *BMC Med* 2020; **18:** 140.

110 Vallabh SM, Minikel EV, Schreiber SL, Lander ES. Towards a treatment for genetic prion disease: trials and biomarkers. *Lancet Neurol* 2020; **19:** 361–68.

Section 5: Clinical Aspects of Human Prion Disease

Although the principal phenotypes of human prion disease consisting of CJD, GSS, Kuru and FFI had been distilled by the early 1990s, the clinical spectrum of human prion disease has undergone further refinement and expansion thereafter. Arguably the most significant advance has been the delineation of the molecular-genetic sub-types of sCJD according to codon 129 and PrP^{Sc} western blot characteristics, as well as recognition of VPSPr. This improved understanding has reinforced the clinical heterogeneity of sCJD and provided a useful albeit imperfect objective biomarker framework for diagnostic and sub-type confirmation. Moreover, studies related to CJD have also seen the description of further likely forms of genetic prion disease.

Contributing to this enhanced understanding of the likely correlating determinants of human prion disease, my research has shown that the molecular-genetic sub-types of sCJD appear to occur worldwide, supporting these determinants of clinical disease are independent of environment or geographical location. Further studies have allowed: elaboration of diagnostic criteria for a less common form of sCJD presenting with Cortico-basal Syndrome; recognition of presentations with spastic paraparesis and hyperekplexia; and overlap with autoimmune encephalopathy. In addition, my studies have confirmed that sCJD occurs with a similar clinical profile and incidence rate in the Indigenous population compared to the non-indigenous population. Finally, as part of ongoing strategies to mitigate the risk of health care transmission of human prion disease I participated in the development of the current infection control guidelines, which were released and announced to the Australian medical community in 2013.

List of my publications submitted in full (in chronological order)

Lewis V, Hill AF, Klug GM, Boyd A, Masters CL, Collins SJ. Australian sporadic CJD analysis supports endogenous determinants of molecular-clinical profiles. Neurology 2005; 65: 113-118.

Chang F, Berman Y, Buckland ME, MacKinlay N, McGlade A, Collins S, Ng K. Genetic prion disease associated myelodysplasia and SIADH in siblings. European Journal of Neurology 2011; 18: e149-e150.

Lee W, Simpson M, Ling H, Mclean C, Collins S, Williams DR. Characterising the Uncommon Corticobasal Syndrome Presentation of Sporadic Creutzfeldt-Jakob Disease. Parkinsonism & Related Disorders 2013; 19: 81-85.

Koehler A, Athan E, Collins SJ. Updated Creutzfeldt-Jakob Disease Infection Control Guidelines: sifting the facts from the fiction. Medical Journal of Australia 2013; 198: 245-246.

Geevasinga N, Buckland ME, Collins SJ, Ng K. Sporadic Creutzfeldt-Jakob disease presenting as spastic paraparesis. European Journal of Neurology 2013: 20: e73-e74.

Ramanathan S, Fung V, Bielich A, Masters L, Russo R, Buckland M, Sarros S, Klug G, Collins S, Reddel S. Hyperekplexia as the initial presenting symptom of Creutzfeldt-Jakob Disease. Neurology: Clinical Practice 2015; 5: 498-501.

Kim B, Yoo P, Sutherland T, Boyd A, Stehmann C, McLean C, Collins S. LGI 1-antibody encephalopathy with faciobrachial dystonic seizures overalapping with sporadic Creutzfeldt-Jakob disease. Neurology: Neuroimmunology & Neuroinflammation 2016; 3: e248.

Panegyres P, Stehmann C, Klug G, Masters C, Collins S. Prion disease in Indigenous Australians. Internal Medicine Journal 2020 doi.org/10.1111/imj.14835.

Australian sporadic CJD analysis supports endogenous determinants of molecular-clinical profiles

V. Lewis, BSc; A.F. Hill, PhD; G.M. Klug, BSc; A. Boyd, Post Grad Dip; C.L. Masters, MD; and S.J. Collins, MD

Abstract—*Objective:* To define the protease-resistant prion protein (PrP^{res}) types and associated clinical profiles in Australian patients with sporadic Creutzfeldt–Jakob disease (CJD) to allow comparison with those reported from other continents and concomitantly reaffirm absence of variant CJD (vCJD). *Methods:* Reassessment of available clinical and neuropathologic data on patients referred to the Australian National Creutzfeldt–Jakob Disease Registry (ANCJDR) who died between January 1, 1992, and June 30, 2003, was conducted. Molecular classification of PrP^{res} was determined by immunoblot analysis of available frozen brain tissue. Brain homogenate pH and codon 129 genotype on the prion protein gene (*PRNP*) were established. *Results:* PrP^{res} patterns in 35 of 37 patients with sporadic CJD conformed to one of three common reported types. Of a range of clinical features assessed, illness duration was the only clinical feature significantly associated with PrP^{res} type. Two patients displayed coexistence of more than one PrP type, with one displaying a novel pattern of three PrP^{res} types in a single brain region. The absence of vCJD was reconfirmed, supported by the lack of the typical PrP^{res} glycoform pattern. *Conclusions:* Given Australia's geographic isolation and environmental uniqueness, the general congruity of these results with those reported from other continents suggests that endogenous factors predominantly determine sporadic Creutzfeldt–Jakob disease (CJD) phenotypic subtypes or "strains." These results support a clinicopathologic classification system whereby both PrP^{res} type and codon 129 genotype are utilized to most accurately depict phenotypic subtypes or strains of sporadic CJD.

NEUROLOGY 2005;65:113–118

In humans, the most common transmissible spongiform encephalopathy (TSE) is sporadic Creutzfeldt–Jakob disease (CJD), which occurs at a rate of approximately 1.5 per million per annum and accounts for approximately 85–90% of all human prion disorders.[1] Integral to the pathogenesis and transmissibility of TSEs is the accumulation of a protease-resistant abnormal isoform (PrP^{res}) of the host-encoded cellular prion protein, PrP^{C}.

The existence of distinct "strains" of TSE has been difficult to reconcile with the protein-only hypothesis, which states that the sole or principal component of the transmissible agent is PrP^{res}.[2] Evidence suggests that different conformers and cognate glycoforms of PrP^{res} may encode strain properties.[3-5] Experimental data support the concurrent ability of PrP^{res} to self-propagate and impart its unique strain-determining structure during a template-directed conversion of nascent PrP^{C}.[4,6] Molecular markers of TSE strains include the patterns of protease-resistant PrP^{res} visualized on western immunoblots.[6,7] A classification system has been proposed wherein both PrP^{res} type and prion protein gene (*PRNP*) codon 129 genotype are utilized to most accurately depict phenotypic subtypes or "strains" of sporadic CJD.[8] Despite competing nomenclatures relating to western blot PrP^{res} profiles[6,7] and the reported co-occurrence of different PrP^{res} types within individual brains,[8-11] the epidemiologic and diagnostic utility of PrP^{res} typing as a marker of TSE strains has been established, particularly by the maintenance of characteristic patterns following transmission across species. The latter is exemplified by bovine spongiform encephalopathy (BSE) and variant CJD (vCJD), with both sharing the same characteristic PrP^{res} (type 4 or 2B) glycoform type.[6,7,12]

Geographic isolation, environmental uniqueness, and freedom from indigenous livestock forms of TSE allow Australia to serve as an important comparison country for epidemiologic purposes. Previous reports have suggested that environmental factors such as rural residence and farm work[13,14] and transition metal concentrations in the soil[15] may influence the occurrence of sporadic CJD, whereas zoonotic transmission of BSE has been postulated to masquerade as a specific PrP^{res} subtype of sporadic human TSE.[16,17] To further

From the Australian National Creutzfeldt–Jakob Disease Registry, Department of Pathology (Drs. Masters and Collins, V. Lewis, G.M. Klug, and A. Boyd), and Department of Biochemistry and Molecular Biology (Dr. Hill), University of Melbourne, and Mental Health Research Institute of Victoria (Drs. Hill, Masters, and Collins, V. Lewis, G.M. Klug, and A. Boyd), Parkville, Victoria, Australia.

Funded in part by a National Health and Medical Research Council (NHMRC) program grant (208978). The Australian National Creutzfeldt–Jakob disease Registry is funded by the Commonwealth Department of Health and Aging. Dr. Hill receives an NHMRC RD Wright Fellowship.

Received December 30, 2004. Accepted in final form March 25, 2005.

Address correspondence and reprint requests to Dr. S.J. Collins, Australian National CJD Registry, University of Melbourne, Melbourne, Victoria, Australia, 3010; e-mail: stevenjc@unimelb.edu.au

explore the possible influence of environmental factors in determining human phenotypic subtypes or strains, we performed, where possible, PrP^{res} analysis in Australian patients with sporadic CJD with dates of death encompassing January 1, 1992, to June 30, 2003, and correlated molecular types with the clinical and investigational features to allow comparison with analogous European and North American studies.[8,9] Also, aware of strong parallels in the travel and migration patterns between Australia and other countries that have experienced the occurrence of vCJD in their citizens after residing for extended periods in the United Kingdom, all referred patients were specifically reassessed for this possibility, paying particular attention to the PrP^{res} glycoform profile distinctive for vCJD.[6] Our correlative analyses of PrP^{res} type–phenotype profiles in Australian patients with sporadic CJD support the concept that nonenvironmental factors predominate in determining phenotypic subtypes and strains. Further, our findings underscore a previously proposed clinicopathologic classification system whereby both PrP^{res} type and codon 129 genotype are needed to most accurately depict phenotypic subtypes or "strains" of sporadic CJD.

Methods. *Patient selection.* There were 365 patients referred to the Australian National Creutzfeldt–Jakob Disease Registry (ANCJDR) for evaluation, who died between January 1, 1992, and June 30, 2003. This cohort includes cases ultimately classified non-CJD and cases classified as probable or definite CJD (some of which have been reported previously).[1] Operational and surveillance methods of the ANCJDR have been described in detail,[1,13] with ethical approval from the University of Melbourne. Clinical data and available neuropathologic findings were reviewed according to published diagnostic criteria.[18,19]

Codon 129 determination. Permission to genotype the entire *PRNP* open reading frame was sought in patients with sporadic CJD. Codon 129 genotype was determined by either sequencing of the entire *PRNP* open reading frame using previously described methods[20] or, when consent was not obtainable, by *Bbr*PI (Roche, Nutley, NJ) restriction digestion.[21]

Western immunoblot analysis. Frozen brain specimens were always from the cerebral cortex, predominantly from the frontal region. Control samples for typing (representing types 1 to 4 [T1 to T4])[6,9] were supplied by the National Institute for Biological Standards and Control (NIBSC) as part of the World Health Organization Collaborative Nomenclature Study (2001 to 2002). Brain homogenates were prepared as 10% (wt/vol) homogenates in phosphate-buffered saline (pH 7.23). The pH of each homogenate was determined using a Hanna bench pH meter (U-Lab). Western immunoblots were performed as described previously[6] using a final proteinase K (PK; Gibco) concentration of 100 μg/mL. Samples were resolved alongside T1 to T3 controls on 16% Tris-glycine minigels (Novex) and transferred to nitrocellulose membrane (BioRad). In selected cases, metal-ion chelation using ethylenediaminetetra-acetate[22] (EDTA; final concentration 25 m*M*) was performed prior to, or deglycosylation with PNGaseF (Roche)[6] subsequent to, PK digestion. Membranes were incubated with the anti-PrP monoclonal antibody ICSM18 (1:25,000), which recognizes residues 146 to 159,[23,24] overnight at 4 °C and were visualized using enhanced chemiluminescence (ECL Plus; Amersham) and Biomax MR film (Kodak).

Statistical analysis. The nonparametric Mann–Whitney *U* test, based on the ranks of observations rather than actual values, was used for comparing age at onset, duration of illness, and brain homogenate pH. Comparisons of the dominant symptom at onset, EEG, and CSF test results utilized the Fisher exact test, which is suitable for small sample sizes. The Bonferroni correction method was performed to assess the significance of multiple comparisons.

Results. Of the 365 patients re-evaluated, 135 were reconfirmed as non-CJD, 69 following autopsy, and 230 were reaffirmed as having definite (n = 151) or probable (n = 79) sporadic CJD. None of the reassessed cases, including those originally excluded as manifesting a prion disease, fulfilled diagnostic criteria for possible, probable, or definite vCJD.

Forty-three patients underwent western blot analysis for the presence of PrP^{res}. Three reconfirmed non-CJD cases were negative for PrP^{res}. In three patients with definite CJD, PrP^{res} type was not determined: Two had undetectable PrP^{res} levels using conventional western blotting, with the higher sensitivity method[25] not suitable for PrP^{res} typing; in the third, technical difficulties due to suboptimal tissue storage prevented analysis. Thirty-seven patients with pathologically confirmed CJD had their PrP^{res} type determined (table), of which 35 displayed a profile consistent with previously reported T1, T2, or T3 (figure, A). These three types all displayed predominance of the monoglycosylated band and were distinguished by subtle differences in the relative mobility of their unglycosylated isomers: T1 slowest, T2 intermediate, T3 fastest. Glycoform T4 (characteristic of vCJD, with predominance of the diglycosylated band and the nonglycosylated isomer showing a similar mobility to T3) was not observed. In addition, one of the T1 patients was heterozygous (methionine/valine [MV]) at codon 129 (see table). This PrP^{res} type–genotype combination has not previously been described. Following treatment with EDTA, the unglycosylated PrP^{res} in this T1 MV patient showed the same shift in molecular mass (to a cleavage product; see figure, B) as described for T1 MM and T2 MM cases.[22] Neuropathologic examination of the brain of this patient revealed widespread spongiform degeneration, neuronal loss, and gliosis, with marked regional variation. The caudate nucleus, cerebellar molecular layer, temporal cortex, and thalamus were the most severely affected.

In the two remaining CJD patients (both MM homozygotes), there was reproducible co-occurrence of more than one PrP^{res} type in the sample of brain homogenate (see the figure, C; frozen tissue was available from only a single brain region in each patient). One of these patients revealed a novel pattern with three separate faster-migrating unglycosylated bands, in keeping with the simultaneous occurrence of T1, T2, and T3. Postmortem examination of the brain revealed widespread microvacuolation, neuronal loss, and gliosis within the basal ganglia and cerebral cortices, emphasized in the frontal lobes, with the cerebellum essentially unremarkable. The thalamus demonstrated selective, severe neuronal loss and gliosis, largely restricted to the dorsal medial and anterior nuclei. The other patient displayed banding consistent with coexistence of T1 and T3. Autopsy in this patient confirmed diffuse microvacuolation accompanied by less severe neuronal loss and gliosis throughout the cerebral cortices but most marked in the temporal lobes, along with subtle spongiform change in the molecular layer of the cerebellum and basal ganglia. Brain samples from both of these patients were subject to deglycosylation after protease digestion, revealing in both cases two broad unglycosylated full-length PrP^{res} bands (data not shown). In the patient with three PrP^{res} types evident prior to deglycosylation, we believe that the increased abundance of each of the three

Table *Analysis of clinical features* and investigation findings of Australian sporadic CJD cases, grouped by PrP^{res} type and codon 129 genotype*

PrP^{res} type	Total no. of cases (% of total)	Median (range) age at onset, y	Median (range) illness duration, mo†	Subtype (no. of cases)	Median (range) age at onset, y	Median (range) illness duration, mo‡	EEG typical (95% CI), %§	14-3-3 test positive (95% CI), %‖
1	6 (14.3)	60 (50–74)	2 (1–2.5)	T1 MM (5)	58 (50–74)	2 (1–2.5)	40 (11–79)	100** (39–100)
				T1 MV (1)	73	1.5	0 (0–97.5)	100 (2.5–100)
2	18 (51.5)	69 (55–88)	3.5 (1.5–7)	T2 MM (17)	69 (55–88)	3.5 (1.5–5.5)	75¶ (49–90)	100†† (73–100)
				T2 MV (1)	70	7	0 (0–97.5)	100 (2.5–100)
3	11 (28.6)	68 (40–76)	11 (3.5–22)	T3 MV (7)	63 (40–76)	12 (8–22)	0 (0–41)	50** (17–83)
				T3 VV (4)	71 (62–75)	4.75 (3.5–11)	25 (3.3–76)	100‡‡ (16–100)
1 and 3	1 (2.8)	64	4	—	—	—	100	0**
1, 2, 3	1 (2.8)	64	10	—	—	—	100	100
4	0	—	—	—	—	—	—	—

* Various presenting symptoms (cognitive disturbance, including memory loss, confusion, disorientation, and poor concentration; gait or limb ataxia; altered personality; visual disturbances; nonmyoclonic dyskinesia, including athetosis and tremor; dizziness, including "lightheadedness," vertigo and nonspecific disequilibrium; and insomnia) were assessed and were found not to be significantly different between the different PrP^{res} types. In addition, the majority of clinical features manifested during illness (cognitive impairment; myoclonus; cerebellar dysfunction; extrapyramidal signs, including presence of limb rigidity, dystonia, or gait apraxia; and pyramidal signs, including unequivocal upper motor neuron signs such as positive Babinski responses, limb spasticity, pathologically brisk tendon stretch reflexes) were found not to be significantly different between PrP^{res} types.

† T1 vs T2, (a) $p < 0.005$, (b) $p = 1$; T1 vs T3, (a) $p < 0.001$, (b) $p < 0.001$; T2 vs T3, (a) $p < 0.001$, (b) $p < 0.001$; a = Mann–Whitney *U* test; b = Bonferroni correction.

‡ MM vs VV, (a) $p < 0.05$, (b) $p < 0.5$; MM vs MV, (a) $p < 0.001$, (b) $p < 0.001$; T3 MV vs T3 VV, (a) $p < 0.05$, (b) $p < 0.005$; T1 MM vs T2 MM, (a) $p < 0.05$, (b) $p = 1$; homozygotes vs heterozygotes, (a) $p < 0.001$; a = Mann–Whitney *U* test; b = Bonferroni correction.

§ Typical EEG = generalized triphasic periodic complexes at approximately 1/s; T2 vs T3, $p < 0.005$; MM vs MV, $p < 0.005$; T2 MM vs T3 MV, $p < 0.005$ (Fisher exact test).

‖ T2 vs T3, $p < 0.05$; MM vs MV, $p < 0.05$; T2 MM vs T3 MV, $p < 0.05$ (Fisher exact test).

¶ One case EEG not performed

** One case 14-3-3 CSF testing not done.

†† Five cases 14-3-3 CSF testing not done.

‡‡ Two cases 14-3-3 CSF testing not done.

CJD = Creutzfeldt–Jakob disease; PrP = prion protein; T1 = type 1; T2 = type 2; T3 = type 3; M = methionine; V = valine.

cognate PrP^{res} types following deglycosylation exceeded the resolving capacity of the gel to maintain the clear separation of the subtly different mobilities of the T1 and T2 bands. This resulted in the T1 and T2 unglycosylated species appearing together as one broad band, with T3 constituting the other band.

For patients with sporadic CJD undergoing molecular PrP^{res} typing, the table summarizes their salient clinical features and diagnostic investigation results. None of the various clinical symptoms at disease onset (see asterisked footnote in the table), including cognitive disturbance, gait or limb ataxia, and visual disturbances, differed significantly between the different PrP^{res} types. Of the clinical features described over the course of illness (see the table), a significant difference between PrP^{res} types was found only for duration of illness, precluding meaningful association of any one type with a distinctive clinical profile. Despite a similar predominance of MM homozygotes in the T1 and T2 groups, T1 patients manifested the shortest median illness duration, with (see the table) and without (data not shown) inclusion of the longest-surviving T2 (MV) patient. Both T1 and T2 patients displayed significantly shorter survival than T3 patients. Codon 129 genotype also appeared to influence illness duration, most clearly seen in the T3 group, whereby MV patients displayed a significantly longer survival than VV homozygotes (see the table). Also of note, the patient with simultaneous coexistence of the three PrP^{res} types manifested an unusually long duration of illness (10 months) compared with other MM homozygotes. The two patients displaying more than one PrP^{res} type otherwise lacked clinical distinction, with both cases having cognitive impairment and myoclonus and positive diagnostic investigation results when tested.

Preliminary evaluation suggested PrP^{res} types were associated with significant differences in the EEG and 14-3-3 CSF test results (see the table). However, further analysis demonstrated that codon 129 genotype was also an important determinant of these investigation results (see the table). Regardless of PrP^{res} type, we found significantly more MM homozygotes (T1 or T2 groups) than heterozygotes (all PrP^{res} types) had an EEG described as characteristic for sporadic CJD. Greater than 70% of those MM patients tested manifested a typical EEG, whereas only 1 of the 13 patients carrying at least one valine allele was reported as having a positive study. Consistent with this observation, the proportion of characteristic EEGs in T2 patients was significantly greater when compared with T3

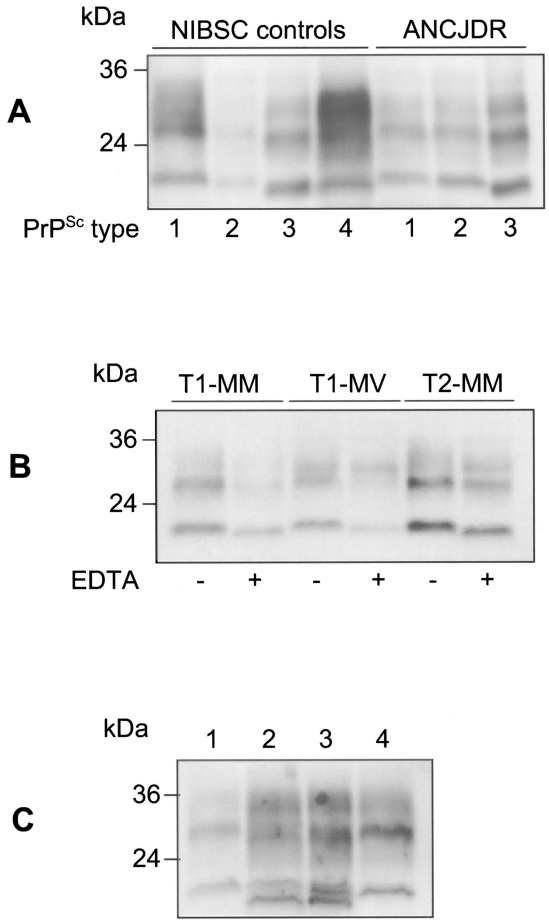

Figure. Western immunoblots of proteinase K–treated brain homogenates showing PrP^{res} patterns from representative Australian National Creutzfeldt–Jakob Disease Registry (ANCJDR) cases of sporadic CJD. Approximate molecular masses (kDa) are shown. (A) Sporadic CJD cases of known PrP^{res} types (lanes 1 to 4, controls from NIBSC) compared with ANCJDR cases (lanes 5 to 7). Subtle differences in the mobility (approximately 1 to 2 kd) of the unglycosylated isoforms of PrP^{res} differentiate the three principal types: T1 (slowest), T2 (intermediate), and T3 (fastest). T1 = lanes 1 (NIBSC) and 5 (ANCJDR); T2 = lanes 2 (NIBSC) and 6 (ANCJDR); T3 = lanes 3 (NIBSC) and 7 (ANCJDR), T4 = lanes 4 (NIBSC). (B) Effect of ethylenediaminetetra-acetate (EDTA) (final concentration 25 mM) on novel T1 MV heterozygote compared with the effect on T1 MM and T2 MM. (C) Australian sporadic CJD cases with coexistence of two (lane 2) and three (lane 3) PrP^{res} types in a single brain homogenate compared with controls, T1 (lane 1), and T2 (lane 4).

cases. Reaffirming the diagnostic utility of CSF 14-3-3 protein testing, we found the overall sensitivity to be 88.5% (n = 26), although there was noticeable variation between subgroups. Reiterating the influence of the codon 129 genotype, only 50% of results were positive in the T3 MV subtype, whereas sensitivity was 100% in those tested with all other PrP^{res}/codon 129 genotype combinations, including T3 VV.

The pH of brain homogenates was measured to assess the recent suggestion that this parameter may influence PrP^{res} isoform patterns.[26,27] Our analysis found no significant difference in the pH values of brain homogenates between any of the three principal PrP^{res} types or codon 129 genotypes, with the brain homogenates from the patients showing coexistence of multiple types also lying within the same pH range (data not shown).

Discussion. When allowing for differences in PrP^{res} typing nomenclature, the current study of Australian patients with sporadic CJD has demonstrated considerable similarity in the spectrum of PrP^{res} type–phenotype profiles to those described for analogous patients from other continents.[8,9] This overall congruity of molecular subtypes, in combination with the results of previous epidemiologic studies of Australian patients with sporadic CJD compared with patients from different countries,[1,28] suggests that environmental factors are unlikely to be a predominant determinant of the occurrence[13,14] and molecular subtypes[16,17] of sporadic human TSE. Contrasting with the considerable geographic and environmental diversity across reporting continents, the international conformity of sporadic CJD incidence rates and PrP^{res} type clinical profiles would appear more in keeping with endogenous determinants of human TSE strains and disease occurrence, such as stochastic misfolding of PrP^{C} [3] and the consequent PrP^{res} type, although environmental influences cannot be completely excluded.[15] Specifically, one minor apparent difference between the Australian and UK[9] PrP^{res} typing studies was the relatively lower number of Australian T2 patients (51.4 vs 64.7%), which is the PrP^{res} molecular subtype of sporadic CJD postulated to be possibly zoonotically linked to BSE.[16,17] This difference was due to the increased numbers of MV and VV T2 patients in the UK series. It is premature to draw any conclusions from these preliminary observations, particularly given that the presence of valine in human *PRNP* at codon 129 appears to have a considerable inhibitory effect on BSE prion transmissibility and correlates with a T5 rather than T2 PrP^{res}.[17]

Of all the clinical features we analyzed, only illness duration was distinctly and significantly associated with PrP^{res} type. Although it is generally assumed that PrP^{res} type may be a determinant of illness duration, it remains possible that the converse is true. In keeping with another study and using analogous statistical methods,[9] our T1 cases had a significantly shorter symptomatic phase than PrP^{res} types T2 and T3, despite both the T1 and the T2 cohorts being almost entirely constituted by MM homozygotes. However, when correcting for multiple comparisons, significance was lost between the T1 and T2 groups and maintained for all other analyses. We attribute this to the small T1 sample size. We are uncertain as to an explanation for the slightly shorter illness durations observed for the T1 and T2 cases compared with previous studies.[9,22] An unwitting minor selection bias related to availability of fresh brain tissue and small patient numbers within each group may be relevant, but a previous collabo-

rative study dealing with much larger patient numbers did not disclose discrepancies in the clinical profiles of Australian vs non-Australian patients with sporadic CJD.[28]

The importance of PrP^{res} type in determining sporadic CJD phenotype and investigation results was not invariable: Specifically, in accord with previous reports,[8,9] our T3 heterozygotes exhibited a significantly longer illness than VV homozygotes. As observed previously,[9] we also found a typical EEG appeared most closely linked to MM homozygosity at codon 129, and this finding was therefore underrepresented in T3 patients. However, caution should be exercised when analyzing the different PrP^{res} type–codon 129 genotype combinations, as biases may exist owing to a lack of independence between these variables. Therefore, of all our analyses, perhaps the most reliable comparisons are those within a single PrP^{res} type or codon 129 genotype. In contrast to EEG results, CSF 14-3-3 proteins were detected in all PrP^{res} types, with an overall sensitivity of nearly 90%, although, as observed in another study,[29] this sensitivity was not uniform, with our T3 MV group positive only 50% of the time.

Our study characterized a single T1 patient as heterozygous at codon 129 of *PRNP*, which has not been described previously.[9] The neuropathologic changes in this patient are different from those previously reported for T1 MM and T3 MV cases but appear to have minor overlap with those changes reported in T2 MV patients.[9] In contrast, the clinical phenotype did not differ noticeably from that of other T1 patients, aside from the short illness duration in comparison with other heterozygous patients with sporadic CJD. Collectively, our data suggest that as far as phenotype is concerned, PrP^{res} type has a relatively selective but predominant influence over codon 129 genotype in determining illness duration.

The simultaneous presence of two unglycosylated PrP^{res} bands in the one brain sample, as observed in one of our patients, has been reported previously.[8-11] The neuropathology of this patient with co-occurrence of T1 and T3 PrP^{res} appears similar to that previously reported for T1 MM.[9] Our analyses also revealed a novel pattern, wherein we observed three distinct unglycosylated bands, corresponding to T1, T2, and T3, in a single brain region. The precise frequency of the coexistence of more than one PrP^{res} type in the brains of patients with sporadic CJD is unresolved, but studies assessing multiple sites[10,11] suggest it is likely to be higher (around 33%) than reported in our study (5%) where only single brain regions were analyzed. Unavailability of additional frozen brain specimens from other cerebral cortical and subcortical sites prohibited our ability to establish the topographic extent of these co-occurrences, nor, as reported in one study,[8] could we determine whether a single type was present in subcortical regions when various types were found in the cortex. Whether our novel PrP^{res} pattern represents a new human sporadic prion strain is uncertain, but the long duration of illness for an MM homozygote is noteworthy, as are the patient's neuropathologic features that do not closely conform to any of the reported PrP^{res} subtypes.[9] Further studies, including bioassay with assessment of incubation periods and neuropathologic lesion profiles in inbred strains of mice, may resolve this issue.

Overall, our findings support a previously proposed clinicopathologic classification system whereby both PrP^{res} type and codon 129 genotype are utilized to most accurately depict phenotypic subtypes or "strains" of sporadic CJD. Nevertheless, patients such as we describe, with multiple PrP^{res} types within the brain, provoke questions regarding the relevance of this finding to ultimate determination of phenotype as well as add complexity in existing classification systems. Appreciation of these determinants is likely to be of importance in the design of emerging therapeutic trials.

Variations in the pH of brain homogenates prior to protease digestion and western blot analysis have been shown to influence the PrP^{res} glycoform pattern.[26,27] The current study, using a single physiologic buffer at constant pH, revealed overlapping variation in the actual pH of the brain homogenates but did not find significant differences between any of the PrP^{res} groups or in the two patients with intrasample coexistence of multiple types. As we describe, our PrP^{res} typing showed correlation with a single distinct clinical feature, and we did not undertake western blot analysis following deliberate alteration of brain homogenate pH to more acidic and basic values to explore whether further subtyping with apparent biologic correlates could be achieved.[26,27] Our results suggest that determinants other than brain homogenate pH promote the different PrP^{res} profiles observed in vivo and are consistent with an intrinsic, biologically relevant role in their determination of phenotype.

Acknowledgment

The authors thank Dr. Handan Wand (National Centre on HIV Epidemiology and Clinical Research at University of New South Wales) for her help with statistical analyses, Prof. John Collinge for the ICSM18 monoclonal antibody, and the families and friends of Australian CJD patients for their generous support.

References

1. Collins S, Boyd A, Lee JS, et al. Creutzfeldt–Jakob disease in Australia 1970–1999. Neurology 2002;59:1365–1371.
2. Bruce ME, McConnell I, Fraser H, Dickinson AG. The disease characteristics of different strains of scrapie in Sinc congenic mouse lines: implications for the nature of the agent and host control of pathogenesis. J Gen Virol 1991;72:595–603.
3. Prusiner SB. Prions. Proc Natl Acad Sci USA 1998;95:13363–13383.
4. Bessen RA, Kocisko DA, Raymond GJ, Nandan S, Lansbury PT, Caughey B. Non-genetic propagation of strain-specific properties of scrapie prion protein. Nature 1995;375:698–700.
5. Safar J, Wille H, Itri V, et al. Eight prion strains have PrP(Sc) molecules with different conformations. Nat Med 1998;4:1157–1165.
6. Collinge J, Sidle KC, Meads J, Ironside J, Hill AF. Molecular analysis of prion strain variation and the aetiology of "new variant" CJD. Nature 1996;383:685–690.
7. Parchi P, Castellani R, Capellari S, et al. Molecular basis of phenotypic variability in sporadic Creutzfeldt–Jakob disease. Ann Neurol 1996;39:767–778.

8. Parchi P, Giese A, Capellari S, et al. Classification of sporadic Creutzfeldt–Jakob disease based on molecular and phenotypic analysis of 300 subjects. Ann Neurol 1999;46:224–233.
9. Hill AF, Joiner S, Wadsworth JD, et al. Molecular classification of sporadic Creutzfeldt–Jakob disease. Brain 2003;126:1333–1346.
10. Puoti G, Giaccone G, Rossi G, Canciani B, Bugiani O, Tagliavini F. Sporadic Creutzfeldt–Jakob disease: co-occurrence of different types of PrP(Sc) in the same brain. Neurology 1999;53:2173–2176.
11. Head MW, Bunn TJ, Bishop MT, et al. Prion protein heterogeneity in sporadic but not variant Creutzfeldt–Jakob disease: U.K. cases 1991–2002. Ann Neurol 2004;55:851–859.
12. Hill AF, Desbruslais M, Joiner S, et al. The same prion strain causes vCJD and BSE. Nature 1997;389:448–450, 526.
13. Collins S, Law MG, Fletcher A, Boyd A, Kaldor J, Masters CL. Surgical treatment and risk of sporadic Creutzfeldt–Jakob disease: a case-control study. Lancet 1999;353:693–697.
14. Cousens SN, Zeidler M, Esmonde TF, et al. Sporadic Creutzfeldt–Jakob disease in the United Kingdom: analysis of epidemiological surveillance data for 1970–96. Br Med J 1997;315:389–395.
15. Purdey M. Ecosystems supporting clusters of sporadic TSEs demonstrate excesses of the radical-generating divalent cation manganese and deficiencies of antioxidant co factors Cu, Se, Fe, Zn. Does a foreign cation substitution at prion protein's Cu domain initiate TSE? Med Hypotheses 2000;54:278–306.
16. Asante EA, Linehan JM, Desbruslais M, et al. BSE prions propagate as either variant CJD-like or sporadic CJD-like prion strains in transgenic mice expressing human prion protein. EMBO J 2002;21:6358–6366.
17. Wadsworth JD, Asante EA, Desbruslais M, et al. Human prion protein with valine 129 prevents expression of variant CJD phenotype. Science 2004;306:1793–1796.
18. Will RG, Zeidler M, Stewart GE, et al. Diagnosis of new variant Creutzfeldt–Jakob disease. Ann Neurol 2000;47:575–582.
19. Will RG. Prion related disorders. J R Coll Physicians Lond 1999;33:311–315.
20. Lewis V, Collins S, Hill AF, et al. Novel prion protein insert mutation associated with prolonged neurodegenerative illness. Neurology 2003;60:1620–1624.
21. Zimmermann K, Turecek PL, Schwarz HP. Genotyping of the prion protein gene at codon 129. Acta Neuropathol (Berl) 1999;97:355–358.
22. Wadsworth JD, Hill AF, Joiner S, Jackson GS, Clarke AR, Collinge J. Strain-specific prion-protein conformation determined by metal ions. Nat Cell Biol 1999;1:55–59.
23. Beringue V, Mallinson G, Kaisar M, et al. Regional heterogeneity of cellular prion protein isoforms in the mouse brain. Brain 2003;126:2065–2073.
24. White AR, Enever P, Tayebi M, et al. Monoclonal antibodies inhibit prion replication and delay the development of prion disease. Nature 2003;422:80–83.
25. Wadsworth JD, Joiner S, Hill AF, et al. Tissue distribution of protease resistant prion protein in variant Creutzfeldt–Jakob disease using a highly sensitive immunoblotting assay. Lancet 2001;358:171–180.
26. Notari S, Capellari S, Giese A, et al. Effects of different experimental conditions on the PrPSc core generated by protease digestion: implications for strain typing and molecular classification of CJD. J Biol Chem 2004;279:16797–16804.
27. Zanusso G, Farinazzo A, Fiorini M, et al. pH-dependent prion protein conformation in classical Creutzfeldt–Jakob disease. J Biol Chem 2001;276:40377–40380.
28. Pocchiari M, Puopolo M, Croes EA, et al. Predictors of survival in sporadic Creutzfeldt–Jakob disease and other human transmissible spongiform encephalopathies. Brain 2004;127:2348–2359.
29. Castellani RJ, Colucci M, Xie Z, et al. Sensitivity of 14-3-3 protein test varies in subtypes of sporadic Creutzfeldt–Jakob disease. Neurology 2004;63:436–442.

LETTER TO THE EDITOR

Genetic prion disease–associated myelodysplasia and SIADH in siblings

F. C. F. Chang[a], Y. Berman[b], M. E. Buckland[c], N. MacKinlay[d], A. McGlade[e], S. Collins[e] and K. Ng[a]

[a]*Department of Neurology,* [b]*Department of Clinical Genetics, Royal North Shore Hospital and the University of Sydney, Sydney, NSW;* [c]*Department of Neuropathology, Royal Prince Alfred Hospital and the University of Sydney, Sydney, NSW;* [d]*Department of Haematology, Royal North Shore Hospital and the University of Sydney, Sydney, NSW; and* [e]*Australian National CJD Registry, Department of Pathology, The University of Melbourne, Parkville, VIC, Australia*

Correspondence: Dr Karl Ng, Department of Neurology and Clinical Neurophysiology, Royal North Shore Hospital, Pacific Hwy, St Leonards, Sydney, NSW 2065, Australia (tel.: +61299268344; fax: +61299067719; e-mail: kng@med.usyd.edu.au).

Keywords: chromosome fragility, fatal familial insomnia, inappropriate ADH syndrome, myelodysplastic syndromes, prion diseases

Received 6 May 2011
Accepted 12 July 2011

Introduction

Fatal familial insomnia (FFI) is an autosomal dominant prion disease characterized by rapidly progressive dementia, dysautonomia, myoclonus and insomnia. A mutation at position 178 in the prion protein gene can cause FFI or familial Creutzfeldt–Jacob disease (fCJD). A nonpathogenic polymorphism at codon 129 modifies the disease phenotype, with a methionine residue in *cis* resulting in an FFI phenotype and a valine residue in the fCJD phenotype [1]. We report two cases of FFI with a novel association between myelodysplasia (MDS) and syndrome of inappropriate antidiuretic hormone secretion (SIADH).

Case 1

A 60-year-old Vietnamese man presented with an 8-month history of insomnia and dementia, associated with dysautonomia manifested by hypertension and constipation. Four months later, he developed daytime hypersomnolence with oneiric behaviours, myoclonus and visual hallucinations. On examination, he was ataxic with hyper-reflexia and extensor plantar responses with intermittent generalized myoclonic jerks, not induced by auditory or tactile stimuli. The patient died 12 months later.

The cerebrospinal fluid (CSF) was acellular and 14-3-3 protein negative. Serial MRI brain showed subtle hyperintensities in the white matter. EEG did not show characteristic patterns suggestive of CJD. He had macrocytic, normochromic anaemia with normal haematinic and negative haemolysis screen. Bone marrow examination was consistent with MDS, and cytogenetic analysis revealed chromosome 20q deletion in five of 60 metaphases, with a normal cell line also present. Serum sodium, osmolality and urine osmolality were consistent with SIADH. Sequencing of the PRNP gene identified a D178N mutation and homozygous methionine variant at position 129 consistent with FFI.

His brain autopsy showed mild thalamic atrophy macroscopically. On microscopic examination, neocortical areas were unremarkable (Fig. 1a). There was severe neuronal loss with accompanying spongiform change, gliosis and microglial activation in the anterior nucleus of the thalamus (Fig. 1b) and inferior olivary nucleus (Fig. 1c, 1d). Similar, but less pronounced changes were present throughout other thalamic regions, dentate nucleus, dorsal medulla and hypothalamus, particularly the mammillary bodies, supraoptic and arcuate nuclei. No specific staining with the prion-specific antibodies 3F4 or 12F10 could be found in sections of thalamus and medulla, a finding not uncommon in FFI.

Case 2

His older sister died at the age of 65 years following 12 months of dementia associated with myoclonus, visual hallucinations and dysautonomia. She also had a profound normocytic, normochromic anaemia and hyponatraemia from SIADH. Faecal occult blood, gastroscopy and colonoscopy were normal. Brain MRI showed mild atrophy and chronic ischaemic changes in the white matter. The CSF 14-3-3 protein was negative. No prion genetic test or autopsy was performed. She had extensive other normal investigations with no explanation for SIADH other than her neurological picture.

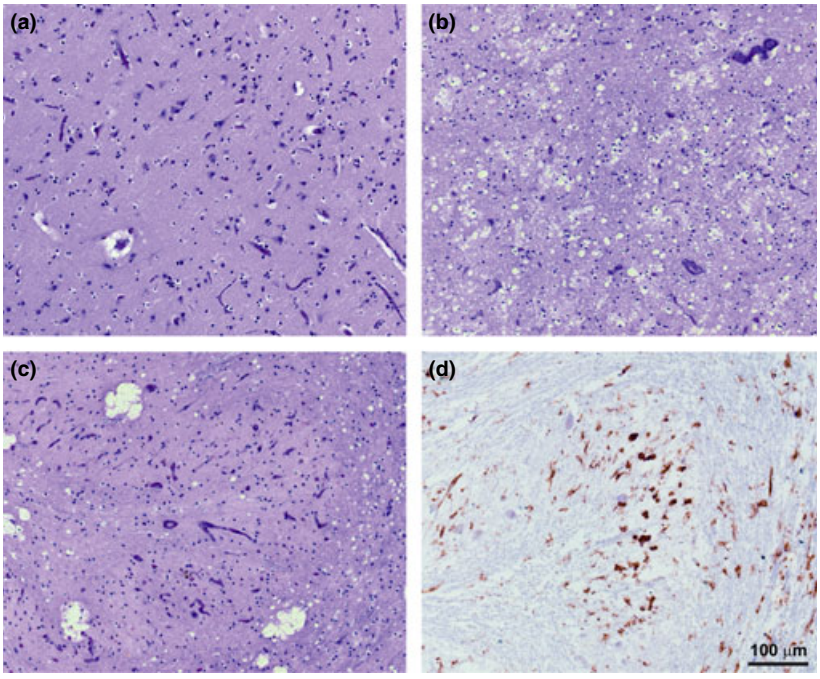

Figure 1 Histopathology. Haematoxylin and eosin–stained sections of (a) frontal cortex and other neocortical areas were unremarkable, whilst sections of anterior thalamic nucleus (b) and inferior olive (c) reveal prominent neuronal loss with some associated spongiform change, gliosis and microglial activation. (d) Microglial activation in the inferior olive is highlighted by HLA-DR immunohistochemistry. Scale bar = 100 μm (a–d).

Discussion

Phenotypic variability within this condition suggests both genetic and environmental factors are important in the expression of D178N mutation [2]. Our proband had typical clinical manifestations of FFI, and there are striking similarities with his sister's presentation.

Even though direct genetic testing was not available for proband's sister, she very likely had a methionine variant in *cis* at position 129, given a 97% homozygosity for this allele in the Han Chinese population who share a common ancestry with the Vietnamese. The anaemia in both cases appeared of recent onset and concurrent with the neurological deterioration. In our proband, the karyotypic abnormality is characteristic of MDS. The sister's anaemia was attributed to chronic disease, although a bone marrow biopsy was never performed. To date, no association or underlying mechanism between MDS and genetic prion disease has been described.

The 20q deletion associated with MDS is an acquired disorder, whereas the mutation for FFI on chromosome 20 is heritable. DNA fragmentation has been demonstrated in brains of CJD patients, perhaps leading to chromosome fragility and a susceptibility to somatic mutations [3].

Hyponatraemia because of SIADH has been reported in cases of sporadic CJD [4], but to our knowledge is a novel association with FFI. In both sporadic and genetic prion disease, it may be secondary to generalized seizures or myoclonus. Alternatively, hypothalamic involvement as shown in the proband's histology may be one possible explanation.

Further reports of FFI with anaemia and SIADH are required to clarify the strength of the association.

Acknowledgements

The authors wish to thank Dr Ron Fleischer (Department of Clinical Genetics, Royal North Shore Hospital) for pedigree analysis and Dr Roger Stankovic for technical assistance with tissue preparation and the family of the proband for assistance with genealogy and patient consent for this publication.

Conflicts of interest

The authors declare no financial or other conflict of interest.

Patient consent

Obtained.

References

1. Goldfarb LG, Petersen RB, Tabaton M, *et al*. Fatal familial insomnia and familial Creutzfeldt–Jakob disease: disease phenotype determined by a DNA polymorphism. *Science* 1992; **258:** 806–808.
2. Zerr I, Giese A, Windl O, *et al*. Phenotypic variability in fatal familial insomnia (D178N-129M) genotype. *Neurology* 1998; **51:** 1398–1405.
3. Ferrer I. Nuclear DNA fragmentation in Creutzfeldt–Jakob disease: does a mere positive in situ nuclear end-labeling indicate apoptosis? *Acta Neuropathol* 1999; **97:** 5–12.
4. Samman I, Schulz-Schaeffer WJ, Wohrle JC, *et al*. Clinical range and MRI in Creutzfeldt–Jakob disease with heterozygosity at codon 129 and prion protein type 2. *J Neurol Neurosurg Psychiatry* 1999; **67:** 678–681.

Parkinsonism and Related Disorders 19 (2013) 81–85

Contents lists available at SciVerse ScienceDirect

Parkinsonism and Related Disorders

journal homepage: www.elsevier.com/locate/parkreldis

Characterising the uncommon corticobasal syndrome presentation of sporadic Creutzfeldt-Jakob disease

Will Lee [a,e], Marion Simpson [a,b], Helen Ling [c], Catriona Mclean [d], Steven Collins [b,**], David R. Williams [a,e,*]

[a] Department of Neuroscience, The Alfred Hospital, Commercial Road, Melbourne, Victoria 3004, Australia
[b] The Australian National Creutzfeldt-Jakob Disease Registry, Department of Pathology, The University of Melbourne, Australia
[c] Queen Square Brain Bank for Neurological Disorders and Institute of Neurology, University College London, London WC1N 1PJ, UK
[d] Department of Pathology, The Alfred Hospital, Commercial Road, Melbourne, Victoria 3004, Australia
[e] Van Cleef Roet Centre for Nervous Diseases, Monash University, Melbourne, Victoria 3004, Australia

ARTICLE INFO

Article history:
Received 18 June 2012
Accepted 21 July 2012

Keywords:
Prion disease
Corticobasal
Alien limb
Dystonia
Myoclonus

ABSTRACT

Background: Corticobasal syndrome (CBS), which encompasses cortical sensory loss, alien limb, bradykinesia, rigidity, limb apraxia and dystonia, is the classic presentation of corticobasal degeneration (CBD). It may occur in other neurodegenerative disorders including sporadic Creutzfeldt-Jakob disease (sCJD). Current CBD diagnostic criteria outline features of CBS but fail to distinguish CBD from other causative pathologies.

Objectives: To characterise the CBS presentation of sCJD (sCJD-CBS) in the context of existing CBD diagnostic criteria.

Method: Data of two new cases of sCJD-CBS and seven patients identified from the Australian National Creutzfeldt-Jakob Disease Registry database was reviewed. Additional data from 11 published cases was incorporated to illustrate the natural history of sCJD-CBS. Comparison was made with pathologically diagnosed CBD cases with ante-mortem CBS presentation (CBD-CBS).

Results: sCJD-CBS accounts for 1.8% of all Australian sCJD cases. Compared to CBD-CBS, disease progression is more rapid in sCJD-CBS (median time to diagnosis 48 vs.1.5 months, $p < 0.001$; and disease duration until death 68 vs. 5 months, $p < 0.001$). Although no clinical features separate the two, alien limb and myoclonus tend to occur early in sCJD-CBS following initial 'sensory' disturbance in the affected limb. Consistent with sCJD, distinctive diffusion weighted imaging (DWI) abnormalities on magnetic resonance imaging may also occur in sCJD-CBS.

Conclusion: sCJD should be suspected in patients presenting with CBS when clinical progression is rapid and accompanied by DWI abnormalities, even without cerebrospinal fluid 14-3-3 protein detection and electroencephalographic periodic sharp wave complexes. We propose the addition of rapid (<12months) progression to akinetic-mutism or death and DWI abnormalities as exclusions in future CBD diagnostic criteria.

1. Introduction

The corticobasal syndrome (CBS) is considered the classic presentation of corticobasal degeneration (CBD), a primary neurodegenerative disease characterised by widespread neurofibrillary tau-pathology affecting the cerebral cortex and basal ganglia. A CBS presentation comprises variable combinations of limb apraxia, cortical sensory loss, limb dystonia, focal myoclonus, alien limb and rigidity and bradykinesia that do not respond to dopaminergic medications. Since the original description of CBD, it has become clear that a number of neurodegenerative diseases can present with CBS such as Alzheimer's disease (AD), Parkinson's disease (PD), progressive supranuclear palsy (PSP), dementia with Lewy bodies (DLB) and non-CBD frontotemporal dementia (FTD) pathologies including Pick's disease [1,2]. Indeed the diagnosis of CBD made on the basis of presentation with CBS will be correct in less than 25% of patients [1].

* Corresponding author. Department of Neuroscience, Alfred Hospital, Commercial Road, Melbourne, Victoria 3004, Australia. Tel.: +61 3 9076 2059; fax: +61 3 9076 5075.
** Corresponding author. The Australian National CJD Registry, Level 5, The Medical Building, Department of Pathology, Faculty of Medicine, The University of Melbourne, Grattan Street, Victoria 3010, Australia. Tel.: +61 3 8344 1949; fax: +61 3 9349 5105.
E-mail addresses: stevenjc@unimelb.edu.au (S. Collins), david.williams@monash.edu (D.R. Williams).

1353-8020/$ – see front matter © 2012 Elsevier Ltd. All rights reserved.
http://dx.doi.org/10.1016/j.parkreldis.2012.07.010

Creutzfeldt-Jakob disease (CJD) is characterised by cerebral deposition of the abnormal protease-resistant prion protein. Sporadic CJD (sCJD) accounts for the majority of CJD cases and is another condition where patients may present predominantly with CBS (sCJD-CBS). This rare clinical subtype adds to the wide clinical spectrum of sCJD that includes ataxic (Oppenheimer-Brownell), visual (Heidenhain), thalamic (sporadic fatal insomnia), dyskinetic, panencephalopathic, posterior cerebral atrophy and even PSP-like variants [3–6]. Prompted by two recent cases, we sought to better characterise sCJD-CBS and consider clues that may clinically separate it from CBD.

2. Methods

We report two new cases of sCJD-CBS and include data collected from the Australian National Creutzfeldt-Jakob Disease Registry (ANCJDR) and other published cases. For this study, CBS was defined by the presence of progressive asymmetric onset of cortical dysfunction (alien limb, apraxia, cortical sensory loss) and at least one of the following three movement disorders: akinetic-rigid syndrome, limb dystonia or myoclonus. The ANCJDR includes all pathologically diagnosed cases of CJD in Australia, prospectively collected from 1993 and retrospectively identified to 1970. The ANCJDR database was screened using the terms "corticobasal", "alien hand", "alien limb" and "extrapyramidal" and seven patients were identified and case notes were reviewed. A literature search using PubMed and keywords "Creutzfeldt-Jakob disease", "alien hand", "alien limb" and "corticobasal" in combinations identified ten English language articles describing cases of pathologically-proven sCJD-CBS [2,7–15]. From these articles, sufficient clinical data from 11 cases was available (either published or supplied by the corresponding authors). In total, we identified twenty patients with sCJD-CBS (two from our clinic, seven from the ANCJDR database and 11 from published literature).

In addition, we identified pathologically diagnosed cases of CBD presenting with CBS (CBD-CBS) from the Queen Square Brain Bank for Neurological Disorders in order to facilitate comparison with cases of sCJD-CBS. Of the 1440 cases collected over a 20-year period, 19 cases with the pathological diagnosis of CBD were found. Case notes of these 19 patients were reviewed and five were found to have initially presented with CBS. The lack of access to raw data for analysis prohibited the use of additional CBD-CBS cases from published literature.

To identify the characteristics that would be most useful in separating sCJD-CBS from CBD-CBS, we only considered the clinical features that developed in the first half of the disease course. This timeframe was chosen as the clinical characteristics of sCJD-CBS converge with those of classic sCJD as the disease progresses and it is in this early phase of disease that established sCJD diagnostic criteria are likely to be least useful. Clinical signs that were not documented were considered absent. Statistical methods including chi-square, student *t*-test, Wilcoxon Rank-sum test were applied as appropriate, to compare clinical features between these groups.

3. Results

3.1. sCJD-CBS: illustrative case

A 71-year old woman presented with two months of right hand paraesthesia and was referred for neurological consultation. On examination, she was alert and oriented and was noted to have dystonia, myoclonus, ideomotor apraxia and involuntary movements consistent with alien limb affecting her right arm. In addition, there were word-finding difficulties (Video 1). Initial magnetic resonance imaging (MRI), including diffusion weighted imaging (DWI), was normal. The patient went on to develop progressive visual blurring, dysarthria and walking difficulties over weeks, leading to hospital admission. On admission, the patient was unsteady on her feet, found it difficult to stand, was virtually anarthric and had widespread spontaneous and action myoclonus. Electroencephalogram (EEG) showed diffuse delta slowing with frequent non-periodical sharp waves. Repeat brain MRI showed DWI hyperintensities without fluid attenuation inversion recovery (FLAIR) changes, involving the right frontal parasagittal, right calcarine and bilateral insular cortices, as well as the right caudate, which appeared hypointense on the apparent diffusion coefficient (ADC) map. (Fig. 1A–C) Single-photon emission computed tomography (SPECT) demonstrated extensive asymmetrical cerebral cortical and right thalamic hypoperfusion. (Fig. 1D) Cerebrospinal fluid (CSF) 14-3-3 protein was positive. The patient died shortly afterwards, five months from disease onset.

Supplementary video related to this article can be found at doi:10.1016/j.parkreldis.2012.07.010.

Post-mortem examination confirmed CJD. No macroscopic pathology was identified. Sections of the cerebral cortex, basal ganglia, cerebellar cortex and brain stem showed similar features of neuronal loss, gliosis and a "synaptic" pattern of prion protein immunoperoxidase reactivity. (Fig. 1E–F) No cortical post-ischaemic swollen eosinophilic neurons were seen and there was no tau immunoreactivity.

3.2. All sCJD-CBS case data

We reviewed case notes of twenty patients with sCJD who presented with CBS (12 women and 8 men, Table 1A) with a mean age at disease onset of 66 years (range 50–78) and median time to present to medical attention of 1.5 months (range 0.25–10). The median time from disease onset to death was five months (range 1–48). Disease duration was less than 12 months in 80% of cases.

In sCJD-CBS, symptoms began on the non-dominant side in 55% of patients and the most common signs of cortical dysfunction were limb apraxia (14/20, 70%) and alien limb phenomena (17/20, 85%). Other features that occurred in the first half of disease included dysphasia (8/20, 40%), cortical sensory loss (8/20, 40%) and neglect (3/20, 15%). The most common movement disorders were myoclonus (16/20, 80%) and dystonia (9/20, 45%). Twelve (60%) patients had rigidity but only five (25%) were documented to have both rigidity and bradykinesia. Other common features included gait ataxia (unsteadiness while walking without other specific features) in 15 patients (75%), pyramidal disturbance (presence of hemiparesis, hyper-reflexia or positive Babinski sign) in 13 (65%) and other cognitive impairment (impairment of memory or specific cognitive domains) affecting 10 patients (50%). Early visual disturbance (25%) and cerebellar signs (20%) were uncommon. (Table 1B).

The most common symptoms reported by patients to their primary care physicians were sensory disturbances in the affected limb (10/20, 50%) and limb clumsiness (7/20, 35%). Seventeen patients (85%) developed alien limb at some stage during the course of their disease and in these patients the most common features were purposeless grasping (6/17, 35%), intermanual conflict (6/17, 35%) and limb levitation (4/17, 24%). (Table 1C and D).

EEG was documented in nineteen patients while CSF 14-3-3 protein assay result was known in seventeen. In 53% of patients (10/19), typical EEG periodic sharp wave complexes (PSWC) were seen while CSF 14-3-3 testing (generally available since 1997) was positive in 59% (10/17). MRI was performed in 17 patients and nine were documented to be normal. DWI sequence was performed (or reported) in seven patients, all showing restricted diffusion in the cerebral cortices and/or basal ganglia. SPECT or positron emission tomography (PET) was performed in six patients with the universal finding of widespread asymmetrical cortical hypoperfusion. Molecular information was unavailable for the majority of identified cases.

Of the 1440 cases in the Queen Square Brain Bank, 35 patients (2.4%) either had a final clinical diagnosis of CBS (21/1440, 1.5%) or pathological diagnosis of CBD (19/1440, 1.3%). Only five patients had CBD-CBS, therefore constituting 0.3% of all archived cases. Disease characteristics including gender, age of onset, time to diagnosis and disease duration in these five cases of CBD-CBS were compared with sCJD-CBS. (Table 2) The time from disease onset to final clinical diagnosis was significantly longer in CBD-CBS (median 48 months, range 12–66) than in sCJD-CBS (median 1.5 months, range 0.25–10, Wilcoxon Rank-sum test, $p < 0.001$). The duration from disease onset until death was significantly longer in CBD-CBS

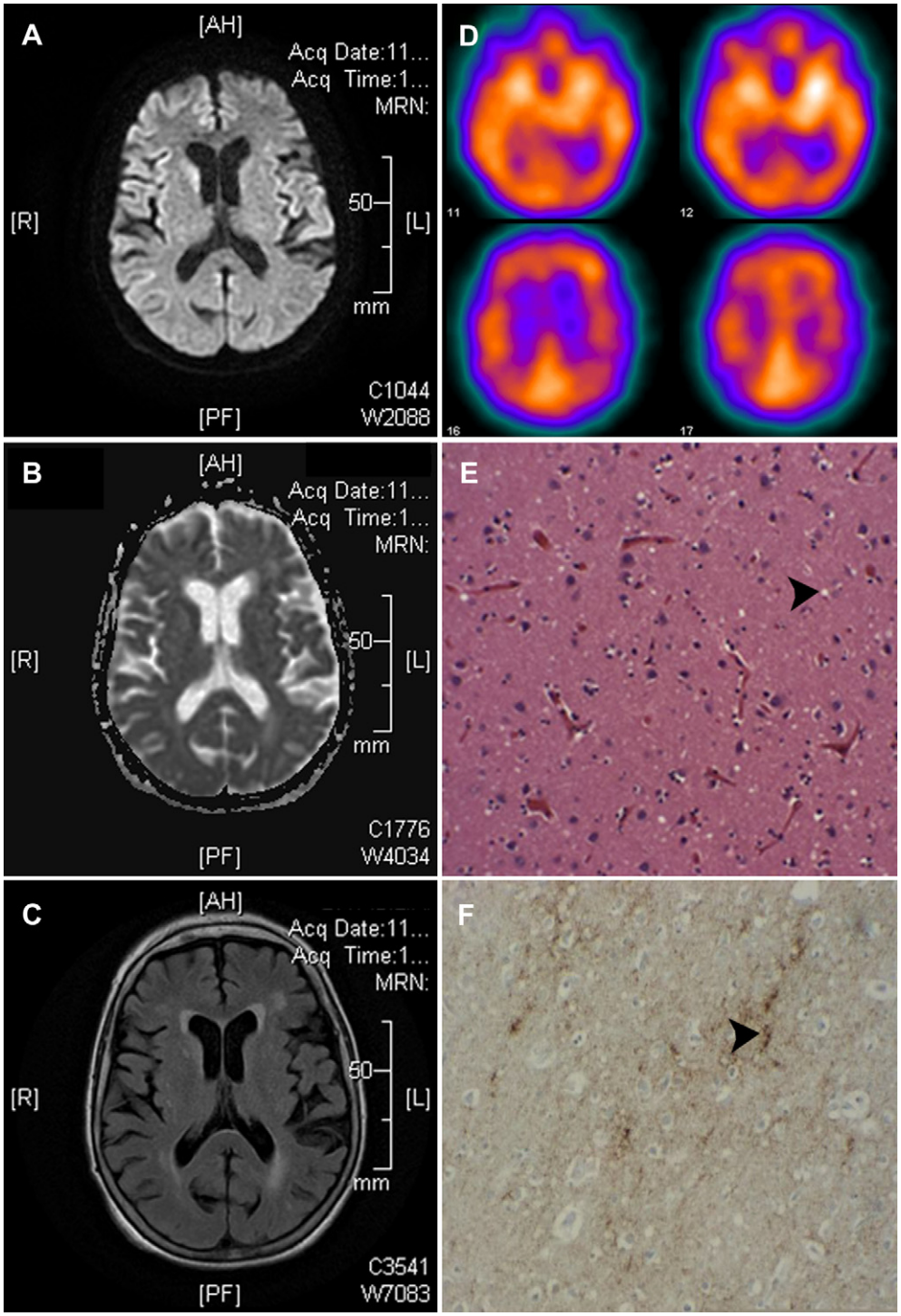

Fig. 1. A. DWI showing hyperintensities involving the right frontal parasagittal, right calcarine and bilateral insular cortices and right caudate. B. ADC map with corresponding right caudate hypointensity. C. FLAIR showing no corresponding changes. D. SPECT showing moderate left parietal and bilateral frontal and occipital cortical, as well as right thalamic hypoperfusion. E. Haematoxylin and eosin stain (×200 magnification) – Frontal cortex, showing spongiform changes (arrow), neuronal loss and gliosis. F. 12F10 PrP immunoperoxidase stain (×200 magnification) – Frontal cortex, showing synaptic pattern of prion protein deposition (arrow).

(median 68 months, range 58–106) than in sCJD-CBS (5 months, range 1–48, Wilcoxon Rank-sum test, $p < 0.001$). Core clinical features of CBS including alien limb, limb apraxia, dystonia, cortical sensory loss, myoclonus, pyramidal disturbance and extrapyramidal signs were also compared between the two groups. No single clinical feature was useful in distinguishing sCJD-CBS from CBD-CBS.

Informative epidemiological data was obtained from the ANCJDR on 387 definite sCJD cases between 1984 and 2010. Based on a median Australian population of 18 million during this period, the incidence of sCJD in Australia is in line with reported figures at 0.8 per million persons per year [16]. sCJD-CBS is exceedingly rare and accounted for 1.8% of all sCJD cases with an estimated incidence of 0.014 per million persons per year. The true incidence may in fact

Table 1
Clinical characteristics of 20 patients with sCJD-CBS. (C. Initial presenting symptoms – Some patients presented with more than one initial symptom. "Others" includes cognitive decline, gait disturbance, visual loss, limb dystonia.)

A. Disease characteristics	
Females (*n*):Males (*n*)	12:8
Age at onset in years (Mean/Range)	66 (50–78)
Time to presentation in months (Median/Range)	1.5 (0.25–10)
Disease duration in months (Median/Range)	5 (1–48)
Handedness – Right (*n*): Left (*n*): Unknown (*n*)	14:0:6
Side of onset – Dominant (*n*): Non-dominant (*n*): Unknown (*n*)	3:11:6
B. Early clinical features	
Limb apraxia (*n*/%)	14 (70%)
Alien limb (*n*/%)	17 (85%)
Dysphasia (*n*/%)	8 (40%)
Cortical sensory loss (*n*/%)	8 (40%)
Neglect (*n*/%)	3 (15%)
Myoclonus (*n*/%)	16 (80%)
Dystonia (*n*/%)	9 (45%)
Rigidity (*n*/%)	12 (60%)
Bradykinesia (*n*/%)	5 (25%)
Tremor (*n*/%)	5 (25%)
Cognitive impairment (*n*/%)	10 (50%)
Pyramidal disturbance (*n*/%)	13 (65%)
Other sensory disturbance (*n*/%)	4 (20%)
Frontal release signs (*n*/%)	3 (15%)
Cerebellar signs (*n*/%)	4 (20%)
Gait ataxia (*n*/%)	15 (75%)
Parkinsonian gait (*n*/%)	2 (10%)
Visual disturbance (*n*/%)	5 (25%)
Visual hallucinations (*n*/%)	2 (10%)
Behavioural disturbance (*n*/%)	2 (10%)
C. Initial presenting symptoms	
Hand/arm clumsiness (*n*/%)	7 (35%)
Sensory disturbance (*n*/%)	10 (50%)
Alien limb (*n*/%)	3 (15%)
Myoclonus (*n*/%)	2 (10%)
Others (*n*/%)	4 (20%)
D. Alien hand	
Hand – Non-dominant (*n*):Dominant (*n*): Unknown (*n*)	9:3:5
Intermanual conflict (*n*/%)	6 (35%)
Grasp (*n*/%)	6 (35%)
Mirror movements (*n*/%)	1 (6%)
Limb levitation (*n*/%)	4 (24%)
Purposeful movements (*n*/%)	1 (6%)
Wandering (*n*/%)	2 (12%)

Table 2
Comparing features of CBD-CBS and sCJD-CBS.

	Statistical method	CBD-CBS	sCJD-CBS	*p*-value
Sex (M:F)	Chi-square	3:2	8:12	0.42
Age of onset (years)	Student *t*-test	Mean = 69	Mean = 65.9	0.42
Time to diagnosis (months)	Wilcoxon rank-sum test	Median = 48	Median = 1.5	**<0.001**
Disease duration (months)	Wilcoxon rank-sum test	Median = 68.4	Median = 5	**<0.001**
Extrapyramidal signs (*n*/%)	Chi-square	2 (40%)	5 (25%)	0.5
Alien limb (*n*/%)	Chi-square	3 (60%)	17(85%)	0.21
Limb apraxia (*n*/%)	Chi-square	5 (100%)	14 (70%)	0.16
Dystonia (*n*/%)	Chi-square	4 (80%)	9 (45%)	0.16
Cortical sensory loss (*n*/%)	Chi-square	4 (80%)	8 (40%)	0.11
Myoclonus (*n*/%)	Chi-square	5 (100%)	16 (80%)	0.28
Pyramidal disturbance (*n*/%)	Chi-square	2 (40%)	13 (65%)	0.31

The bold text was to highlight the two items that reached statistical significance.

be higher as registry case ascertainment prior to 1993 was retrospective and most likely incomplete.

The characteristics of patients with sCJD-CBS were comparable to other sCJD patients in the ANCJDR database in age of onset (median 67.2 years), disease duration (median 5 months) and frequency of typical EEG changes (sCJD-CBS 53% vs other sCJD 58%) but not CSF 14-3-3 protein detection (sCJD-CBS 59% vs other sCJD 88%) [17].

4. Discussion

The present study constitutes the largest single reported series of sCJD patients presenting with CBS. As such, we have been able to more confidently validate previous anecdotal impressions that rapidity of disease progression is a valuable salient distinguishing feature of sCJD-CBS from other neurodegenerative causes of CBS, including CBD-CBS. Therefore, we believe the presentation of CBS in the context of sCJD should rarely be confused clinically with CBD because of the rapid disease progression, particularly when combined with characteristic MRI and EEG changes. We identified initial limb sensory disturbance that evolves rapidly to a clumsy useless arm in association with early myoclonus, as well as limb dystonia, gait ataxia, pyramidal disturbance and cognitive impairment to be the typical presentation of sCJD-CBS.

The clinical picture of sCJD-CBS can only be differentiated from CBD-CBS by the rapidity of progression, which correlates with a significantly shorter time to diagnosis and overall disease duration. While there are no predictive clinical features, the initial presenting complaint may provide clues to the diagnosis. Limb clumsiness is the most common presentation in CBD (67%) [1,18]. Other common initial symptoms in CBD include walking difficulties (28%) while isolated sensory symptoms occurred in only 8% [18]. On the contrary, limb sensory disturbance was the most common initial complaint in sCJD-CBS (50%) followed by limb clumsiness (35%) while gait disturbance was rare (5%). In CBD, myoclonus and alien hand occurred after one year from disease onset [18]. In contrast, alien limb phenomena and myoclonus often occurred early in sCJD-CBS patients and were the first symptoms in several cases. In addition to these clinical differences, MRI, particularly DWI sequences, appears to provide helpful diagnostic clues.

Epidemiological data for CBD-CBS are lacking and CBS is a rare presentation of PSP and AD, which are both more prevalent than CBD [1]. Our data suggests that sCJD-CBS is exceedingly rare with an incidence of 0.014 per million persons per year. To put this into perspective, in a metropolis of 5 million people, there will be one case of sCJD-CBS every 14 years based on our calculated incidence.

This study again reinforces the inadequacy of our current clinical diagnostic capacity and understanding of CBS and CBD. A number of diagnostic criteria for CBD have been proposed which focus on the co-occurrence of movement disorders and cortical signs [19]. These criteria are clearly not useful when applied to non-CBS presentations of CBD. Only one set of exclusion criteria had been proposed, which included early dementia, vertical gaze palsy, severe autonomic disturbance, sustained levodopa response and lesions on imaging [19]. From our findings, we propose the addition of rapid disease progression to akinetic-mutism or death in less than 12 months and brain MRI DWI abnormalities as exclusions in future CBD diagnostic criteria development.

The main limitations of our study are small patient numbers, which is not unexpected given the rarity of this form of sCJD, and the retrospective nature of the study with differing levels of detail in case note documentation.

5. Conclusion

Although sCJD-CBS is exceedingly rare, early recognition is nonetheless important due to the associated prognostic implications. sCJD should be considered in a patient presenting with CBS when progression is rapid, with initial limb sensory disturbance and early myoclonus and alien limb, particularly if asymmetrical cerebral cortical and basal ganglia DWI abnormalities are present, even without accompanying CSF 14-3-3 protein and EEG PSWC.

Financial disclosures/conflicts of interest

This study is not industry-sponsored.
Dr Lee reports no disclosures.
Dr Simpson reports no disclosures.
Dr Ling reports no disclosures.
Dr Mclean reports no disclosures.
Dr Collins is supported in part by a National Health and Medical Research Council (NHMRC) Practitioner Fellowship #APP1005816. The ANCJDR is funded by the Commonwealth Department of Health and Ageing.
Dr Williams reports no disclosures.

Acknowledgements

The authors thank Ms Genevieve Klug from the ANCDJR for assisting with data collection and Mr Eldho Paul from Monash University for performing statistical analysis of data.

References

[1] Ling H, O'Sullivan SS, Holton JL, Revesz T, Massey LA, Williams DR, et al. Does corticobasal degeneration exist? A clinicopathological re-evaluation. Brain 2010;133:2045–57.
[2] Boeve BF, Maraganore DM, Parisi JE, Ahlskog JE, Graff-Radford N, Caselli RJ, et al. Pathologic heterogeneity in clinically diagnosed corticobasal degeneration. Neurology 1999;53:795–800.
[3] Kropp S, Schulz-Schaeffer WJ, Finkenstaedt M, Riedemann C, Windl O, Steinhoff BJ, et al. The Heidenhain variant of Creutzfeldt-Jakob disease. Arch Neurol 1999;56:55–61.
[4] Appleby BS, Appleby KK, Crain BJ, Onyike CU, Wallin MT, Rabins PV. Characteristics of established and proposed sporadic Creutzfeldt-Jakob disease variants. Arch Neurol 2009;66:208–15.
[5] Gambetti P, Kong Q, Zou W, Parchi P, Chen SG. Sporadic and familial CJD: classification and characterisation. Br Med Bull 2003;66:213–39.
[6] Shimamura M, Uyama E, Hirano T, Murakami T, Mita S, Kitamoto T, et al. A unique case of sporadic Creutzfeldt-Jacob disease presenting as progressive supranuclear palsy. Intern Med 2003;42:195–8.
[7] MacGowan DJ, Delanty N, Petito F, Edgar M, Mastrianni J, DeArmond SJ. Isolated myoclonic alien hand as the sole presentation of pathologically established Creutzfeldt-Jokob disease: a report of two patients. J Neurol Neurosurg Psychiatr 1997;63:404–7.
[8] Cannard KR, Galvez-Jiminez N, Watts R. Creutzfeldt-Jakob disease presenting and evolving as rapidly progressive corticobasal degeneration. Neurology 1998;50(Suppl. 4):A95.
[9] Anschel DJ, Simon DK, Llinas R, Joseph JT. Spongiform Encephalopathy mimicking corticobasal degeneration. Mov Disord 2002;17:606–7.
[10] Kleiner-Fisman G, Bergeron C, Lang AE. Presentation of Creutzfeldt-Jakob disease as acute corticobasal degeneration syndrome. Mov Disord 2004;19: 948–9.
[11] Moreaud O, Monavon A, Brutti-Mairesse MP, Grand S, Lebas JF. Creutzfeldt-Jakob disease mimicking corticobasal degeneration: clinical and MRI data of a case. J Neurol 2005;252:1283–4.
[12] Avanzino L, Marinelli L, Buccolieri A, Trompetto C, Abbruzzese G. Creutzfeldt-Jakob disease presenting as corticobasal degeneration: a neurophysiological study. Neurol Sci 2006;27:118–21.
[13] Fogel B, Wu M, Kremen S, Murthy K, Jackson G, Vanek Z. Creutzfeldt-Jakob disease presenting with alien limb sign. Mov Disord 2006;21:1040–1.
[14] Vandenberghe W, Sciot R, Demaerel P, Van Laere K. Sparing of the substantia Nigra in sporadic Creutzfeldt-Jakob disease presenting as an acute corticobasal syndrome. Mov Disord 2007;22:1668–9.
[15] Magherini A, Pentore R, Galassi G, Stucchi CM, Capellari S, Parchi P. MV2 subtype of sporadic Creutzfeldt-Jakob disease presenting as corticobasal syndrome. Mov Disord 2007;22:898–9.
[16] World Health Organisation. WHO manual for surveillance of human transmissible spongiform encephalopathies including variant Creutzfeldt-Jakob disease. Geneva: World Health Organisation; 2003.
[17] Collins SJ, Sanchez-Juan P, Masters CL, Klug GM, van Duijn C, Poleggi A, et al. Determinants of diagnostic investigation sensitivities across the clinical spectrum of sporadic Creutzfeldt-Jakob disease. Brain 2006;129: 2278–87.
[18] Rinne JO, Lee MS, Thompson PD, Marsden CD. Corticobasal degeneration: a clinical study of 36 cases. Brain 1994;117:1183–96.
[19] Litvan I, Bhatia KP, Burn DJ. Movement disorders society scientific issues committee report: SIC task force appraisal of clinical diagnostic criteria for Parkinsonian disorders. Mov Disord 2003;18:467–86.

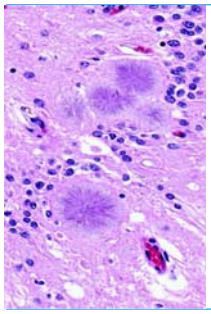

Updated Creutzfeldt–Jakob disease infection control guidelines: sifting facts from fiction

New guidelines aimed at reducing iatrogenic disease and discrimination against patients

Ann P Koehler
MB BS, FRCPA, MPH, Director[1]

Eugene Athan
MB BS, FRACP, MPH, Director[2]

Steven J Collins
MB BS, MD, FRACP, Director[3]

1 Communicable Disease Control Branch, SA Health, Adelaide, SA.

2 Department of Infectious Diseases, Barwon Health, Geelong, VIC.

3 Australian National Creutzfeldt–Jakob Disease Registry, University of Melbourne, Melbourne, VIC.

ann.koehler@health.sa.gov.au

doi: 10.5694/mja13.10114

Creutzfeldt–Jakob disease (CJD) is a rare neurodegenerative disorder which causes the death of about 25–30 Australians each year, giving an average mortality rate of 1.2 cases/million/year.[1] It is untreatable. CJD is the commonest human form of prion disease[2] and is a notifiable disease in all Australian states and territories, with notification to the relevant jurisdictional health department required for all cases in which a strong clinical suspicion for CJD exists.

CJD may be acquired through medical intervention (iatrogenic CJD), for example, from the use of cadaver-derived pituitary hormones; or it may be inherited in an autosomal dominant pattern with high penetrance (familial CJD, occurring in about 10%–15% of cases); but in at least 85% of cases it occurs sporadically (sporadic CJD),[2] with the person having no recognised cause for the disease. Variant CJD (vCJD) is the form zoonotically linked to bovine spongiform encephalopathy (mad cow disease), with a median age at death of around 28 years.[2,3]

Iatrogenic transmission is generally most likely when infectious material is placed in direct contact with the brain.[4] CJD is not transmitted through respiratory, casual or sexual contact, and bloodborne transmission has only been confirmed for vCJD.[5] Whether CJD has been transmitted through surgery not involving the central nervous system remains debatable.[6,7] Worldwide, there have been two major iatrogenic outbreaks of CJD, one caused by contaminated pituitary hormone extracts (226 cases),[8] and the other related to dura mater grafts (228 cases),[9] mostly associated with a single brand (Lyodura), when these products were derived from human cadavers with unrecognised CJD. In Australia, the most recent human-derived pituitary gonadotrophin-related CJD death occurred in 1991, and the most recent Lyodura-related CJD death occurred in 2000,[1] although new cases were reported overseas in 2011.

The Communicable Diseases Network Australia has recently completed a revision of the Australian CJD Infection Control Guidelines (CJD ICG).[10] These guidelines continue to be primarily aimed at preventing iatrogenic cases of CJD, and they differ from the previous version by being considerably more streamlined in order to enhance useability. They give up-to-date information on diagnosis (including associated genetic mutations), contain much more detail on management of surgical instruments, dealing with high- and low-risk people and procedures, and give new advice on postmortem and funeral industry practices. The updated guidelines apply a clear risk stratification approach to minimise the risk of iatrogenic disease until a blood test or other screening test for the detection of preclinical infection becomes available. vCJD has not occurred in Australia to date,[1] with most cases reported in the United Kingdom, and modelling suggesting that cases will be unlikely to occur here. Therefore vCJD is not considered in the scope of the revised guidelines.

We believe the updated CJD ICG will be of interest for two reasons. First, they serve as a reminder, that despite the relative rarity of confirmed cases, CJD is not infrequently considered in the differential diagnosis of progressive neurological disease in a variety of health care settings. Second, they contribute to equity in medical care by aiming to overcome ignorance coupled with suboptimal implementation of previous CJD ICG, which have sometimes led to discrimination, against not only sufferers of CJD, but also their family members. To illustrate these concerns: the family of one suspected CJD patient was told not to return to a particular general practice, because the general practitioner did not want "other people at the practice to become infected"; and numerous asymptomatic people at above "background" risk of CJD (due to possible iatrogenic exposure) have been refused routine endoscopies or been told they will have to pay for replacement colonoscopes, and some have been refused surgery such as hip replacement. Such occurrences lead to inordinate distress and, more insidiously, drive some patients to present to another facility where they conceal risk status in order to have a procedure performed.

We would like to highlight the information and advice in these guidelines in the hope that clinicians follow practices which are based on science and reflect the real and manageable risks surrounding CJD.

The Australian National CJD Registry (ANCJDR) has been funded by the federal government since 1993 to evaluate all suspect and proven cases of prion disease in Australia. The ANCJDR tries to follow all suspect cases until the most accurate case classification is achieved, with brain neuropathological examination being the gold standard for a definitive diagnosis. Beyond comprehensive epidemiological surveillance of all cases of prion disease in the Australian population, the ANCJDR also provides additional nationwide infection control advice, diagnostic services, and advice to families and clinicians.

Competing interests: No relevant disclosures.

Provenance: Not commissioned; externally peer reviewed.

1 Klug GM, Boyd A, McGlade A, et al. Surveillance of Creutzfeldt–Jakob disease in Australia: update to December 2011. *Comm Dis Intell* 2012; 36: E174-E179.

2 Collins SJ, Lawson VA, Masters CL. Transmissible spongiform encephalopathies. *Lancet* 2004; 363: 51-61.

3 Will RG, Ironside JW, Zeidler M, et al. A new variant of Creutzfeldt-Jakob disease in the UK. *Lancet* 1996; 347: 921-925.
4 Brown P, Preece M, Brandel JP, et al. Iatrogenic Creutzfeldt–Jakob disease at the millenium. *Neurology* 2000; 55: 1075-1081.
5 Llewelyn CA, Hewitt PE, Knight RS, et al. Possible transmission of variant Creutzfeldt–Jakob disease by blood transfusion. *Lancet* 2004; 363: 417-421.
6 Collins S, Law MG, Fletcher A, et al. Surgical treatment and risk of sporadic Creutzfeldt–Jakob disease: a case–control study. *Lancet* 1999; 353: 693-697.
7 Mahillo-Fernandez I, de Pedro-Cuesta J, Bleda M, et al. Surgery and risk of sporadic Creutzfeldt–Jakob disease in Denmark and Sweden: registry-based case–control studies. *Neuroepidemiology* 2008; 31: 229-240.
8 Koch TK, Berg BO, De Armond SJ, Gravina RF. Creutzfeldt–Jakob disease in a young adult with idiopathic hypopituitarism. Possible relation to the administration of cadaveric human growth hormone. *N Engl J Med* 1985; 313: 731-733.
9 Thadani V, Penar PL, Partington J, et al. Creutzfeldt–Jakob disease probably acquired from a cadaveric dura mater graft. *J Neurosurg* 1988; 69: 766-769.
10 Communicable Diseases Network Australia. Australian Creutzfeldt–Jakob disease infection control guidelines. Canberra: Department of Health and Ageing, 2013. http://www.health.gov.au/internet/main/publishing.nsf/Content/icg-guidelines-index.htm (accessed Feb 2013). ❑

European Journal of Neurology 2013, **20:** e73–e74 doi:10.1111/ene.12116

LETTER TO THE EDITOR

Sporadic Creutzfeldt–Jakob disease presenting as spastic paraparesis

N. Geevasinga[a], N. G. Simon[a], S. Collins[b], M. E. Buckland[c] and K. Ng[a]

[a]*Department of Neurology, Royal North Shore Hospital, The University of Sydney, Sydney, NSW;* [b]*Department of Pathology, Australian National CJD Registry, The University of Melbourne, Melbourne, NSW; and* [c]*Department of Neuropathology, Royal Prince Alfred Hospital, The University of Sydney, Sydney, NSW, Australia*

Correspondence: K. Ng, Department of Neurology and Clinical Neurophysiology, Royal North Shore Hospital, St Leonards, NSW, 2065, Australia. (tel.: +61 2 94631831; fax: +61 2 94631058; e-mail: kng@med.usyd.edu.au).

Keywords: Creutzfeldt–Jakob, prion, spastic paraparesis

Received: 11 November 2012
Accepted: 2 January 2013

Introduction

Creutzfeldt–Jakob disease (CJD) is a rare transmissible neurodegenerative disease related to cerebral accumulation of misfolded prion protein. It typically presents with a rapidly progressive dementia often associated with myoclonus and ataxia [1]. We describe an unusual presentation of sporadic CJD with spastic paraparesis, in the setting of initially preserved cognition.

Case report

A 55-year-old Asian woman presented with 3 months of progressively worsening gait disturbance, accompanied by sensory disturbance over the right leg, culminating in overt dysequilibrium. In addition, the patient reported fatigue and mild insomnia, with minor dizziness. There was no sphincter dysfunction. Past medical history included depression, but no past neurosurgical procedures or receipt of human hormone extracts or blood transfusions. On initial examination, the patient displayed evidence of gait ataxia, with lower limb upper motor signs in the form of spasticity, brisk reflexes and sustained right ankle clonus, right more than left pyramidal weakness and a right extensor plantar response. There was no objective sensory disturbance. Mood and cognition appeared normal, even to close relatives.

A right-sided spinal cord lesion was suspected, but magnetic resonance imaging (MRI) did not reveal any intra-/extra-axial spinal cord abnormality. Instead, brain MRI showed a high signal, cortical 'ribboning' pattern on diffusion-weighted sequences diffusely through the cerebrum. There were no subcortical hyperintensities. Extensive investigation for vasculitis, non-vasculitic auto-immune encephalopathies (e.g. anti-neuronal autoantibodies and antibodies to voltage-gated potassium channels and *N*-methyl-D-aspartate receptors) and viral infection were all normal. Cerebrospinal fluid (CSF) was unremarkable, and initial 14-3-3 protein was negative. Computer tomography chest/abdomen/pelvis and whole body fludeoxyglucose-positron emission tomography scan showed no neoplastic lesion.

Over the next few months, the patient continued to deteriorate, gradually developing occasional scintillation in the visual field, cognitive decline and marked

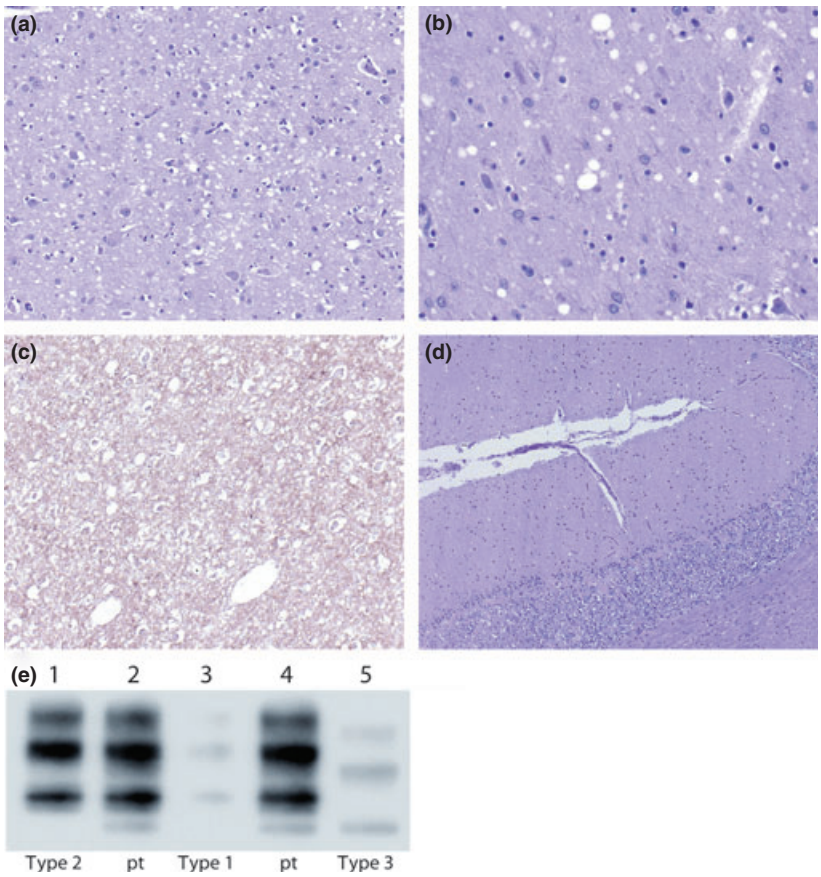

Figure 1 Histopathology. Moderate to severe mixed micro- and macrovacuolar spongiform change in the occipital, frontal (a) and entorhinal cortices, with accompanying neuronal loss and gliosis. There was no specific laminar distribution of these changes. Moderately severe spongiform change was also seen in ventrolateral and dorsomedial thalamic nuclei (b). There was severe Purkinje cell loss in the cerebellar vermis (d) and neuronal loss in the thalamus. Milder microvacuolar spongiform change was seen in other neocortical regions and deep grey nuclei, and 3F4 immunohistochemistry on the frontal cortex (c) and striatum was positive in a fine synaptic pattern. The brainstem showed mild spongiform change with some neuronal loss in superior and inferior colliculi, and inferior olives. No Kuru-type plaques were seen in any section examined. Western blot of prion protein from right frontal cortex (e). Lane 1, sporadic CJD Type 2; Lanes 2 and 4, study subject; Lane 3, sporadic CJD Type 1; Lane 5, sporadic CJD Type 3.

EUROPEAN JOURNAL OF NEUROLOGY
THE OFFICIAL JOURNAL OF THE EUROPEAN FEDERATION OF NEUROLOGICAL SOCIETIES

clumsiness of her hands. A severe truncal ataxia emerged. Neuropsychological testing at this stage revealed severe impairment in verbal learning, marked constructional apraxia and severe impairment of executive function. Electroencephalogram showed generalized nonspecific slowing. A repeat CSF 14-3-3 protein was positive. The patient continued to deteriorate, eventually dying 1 year after presentation.

A brain-only *post mortem* examination was performed. The fresh brain weight was 1308 g, and macroscopic examination revealed mild dilatation of the lateral ventricles only. The microscopic appearances are illustrated in Fig. 1. Sequencing of the *PRNP* open reading frame revealed no mutations with methionine homozygosity (MM) at codon 129. Western blot analysis of protease-resistant prion protein from a single (right frontal) cerebral cortical site revealed a mixed Type 2/3 pattern with the dominant band T2 [2].

Discussion

Although pyramidal tract degeneration may be found in the later stages of illness, presentation of sporadic CJD with spasticity restricted primarily to the lower limbs is extremely rare. There have been two reported patients with the E200K mutation who have had a similar presentation [3,4]; both were middle-aged females. Spasticity can also be an early feature in Gerstmann–Straűssler–Scheinker syndrome associated with the P102L mutation [5], and can dominate the clinical picture in patients with the P105L mutation [6]. Apparently, there was no family history in our case of any prion-like disorder, and *PRNP* analysis excluded mutations including E200K, P105L and P102L.

Co-existing, protease-resistant prion protein types are less common [2], with influence on the corresponding phenotype incompletely resolved. The Australian National CJD Registry has classified one other sporadic CJD as MM Type 2/3, with their clinical profile unremarkable, and the authors are not aware of any additional cases reported of this molecular subtype [7].

Our case reinforces the variability of presentations of sporadic CJD, and highlights that sporadic CJD can also present with a spastic gait, prior to other more characteristic features such as cognitive decline, ataxia and myoclonus.

Acknowledgements

The authors wish to acknowledge the assistance of The Australian National CJD Registry, including Genevieve Klug, BSc (Hons) for PRNP sequencing/PrPSc glycotyping. S.J.C. is supported by NHMRC Practitioner Fellowship (#AP1005816) and NHMRC Program Grant (#400202). The Australian National CJD Registry is funded by the Department of Health and Ageing.

Conflict of interest

The authors declare no financial or other conflict of interests.

Patient consent

Obtained.

References

1. Brown P, Cathala F, Castaigne P, Gajdusek DC. Creutzfeldt-Jakob disease: clinical analysis of a consecutive series of 230 neuropathologically verified cases. *Ann Neurol* 1986; **20:** 597–602.
2. Lewis V, Hill AF, Klug GM, Boyd A, Masters CL, Collins SJ. Australian sporadic CJD analysis supports endogenous determinants of molecular-clinical profiles. *Neurology* 2005; **12:** 65.
3. Mancuso M, Siciliano G, Capellari S, *et al.* Creutzfeldt-Jakob disease with E200K PRNP mutation: a case report and revision of the literature. *Neurol Sci* 2009; **30:** 417–420.
4. Masullo C, Bizzarro A, Guglielmi V, *et al.* An atypical phenotype of CJD associated with the E200K mutation in the prion protein gene. *Neurol Sci* 2010; **31:** 837–839.
5. Webb TE, Poulter M, Beck J, *et al.* Phenotypic heterogeneity and genetic modification of P102L inherited prion disease in an international series. *Brain* 2008; **131:** 2632–2646.
6. Kitamoto T,Ohta M,Doh-ura K,Hitoshi S, Terao Y,Tateishi J.Novel missense variants of prion protein in Creutzfeldt-Jakob disease or Gerstmann-Sträussler syndrome. *Biochem Biophys Res Commun* 1993; **191:** 709–714.
7. Hill AF, Joiner S, Wadsworth J, *et al.* Molecular classification of sporadic Creutzfeldt-Jakob disease. *Brain* 2003; **126:** 1333–1346.

Hyperekplexia as the presenting symptom of Creutzfeldt-Jakob disease

Sudarshini Ramanathan, FRACP
Victor S.C. Fung, FRACP, PhD
Alen Bielich, FRACGP
Lynette Masters, FRACP, FRANZCR
Robert R. Russo, FRACP
Michael E. Buckland, FRCPA, PhD
Shannon Sarros, BSc (Hons)
Genevieve M.J.A. Klug, BSc (Hons)
Steven Collins, FRACP, MD
Stephen W. Reddel, FRACP, PhD

Practical Implications

Creutzfeldt-Jakob disease should be considered in the differential diagnosis of hyperekplexia.

Video

Neurology.org/cp

We describe a patient with hyperekplexia as the initial presenting symptom in sporadic Creutzfeldt-Jakob disease (CJD). We also demonstrate the utility of the sensitive and highly specific new prion protein amplification assay, real-time quaking-induced conversion (RT-QUIC), which amplifies and detects misfolded β-sheet–rich conformers of the prion protein (PrP^{sc}), in expediting a confident clinical diagnosis of CJD in an atypical case.

Case report

A 73-year-old man presented with 4 months of an exaggerated startle response (hyperekplexia) occasionally but not exclusively associated with myoclonus and without cognitive decline at onset (video at Neurology.org/cp). The detailed case report is presented in appendix e-1.

Blood tests revealed mildly low complement and a positive lupus anticoagulant. CSF twice revealed normal biochemistry and no cells or oligoclonal bands. CSF 14-3-3 protein was not detected by Western blot. Tremor studies revealed an inconsistent order of myoclonic recruitment and entrainment of tremor to externally paced hand tapping, which alone suggested a psychogenic movement disorder. An EEG demonstrated bifrontal spikes that sometimes

Neuroimmunology Group (SR), Institute for Neuroscience and Muscle Research, The Kids Research Institute at the Children's Hospital at Westmead, Sydney Medical School, University of Sydney, Sydney, Australia; Department of Neurology (SR, VSCF), Westmead Hospital, Sydney, Australia; A.B.Surgery (AB), Kempsey, Australia; Brain and Mind Research Institution (LM, MEB), University of Sydney, Sydney, Australia; Department of Nuclear Medicine (RRR), Concord Hospital, Concord, Australia; Department of Neuropathology (MEB), Royal Prince Alfred Hospital, Camperdown, Australia; Australian National Creutzfeldt-Jakob Disease Registry (SS, GMJAK, SC), Department of Pathology, The University of Melbourne, Parkville, Australia; and Department of Neurology (SWR), Concord Repatriation General Hospital, Concord, Australia.

Funding information and disclosures are provided at the end of the article. Full disclosure form information provided by the authors is available with the **full text of this article at Neurology.org/cp**.

Correspondence to: swreddel@sydneyneurology.com.au

preceded clinical myoclonus (figure, A). SPECT imaging demonstrated widespread discrete areas of hypoperfusion involving the cerebral cortex with a focal area of right frontal hyperperfusion (figure, B and C). MRI revealed focal linear cortical T2 hyperintensities (figure, D–G). A formal cerebral angiogram was normal.

Figure **Results of EEG, radiology, and histopathologic investigations**

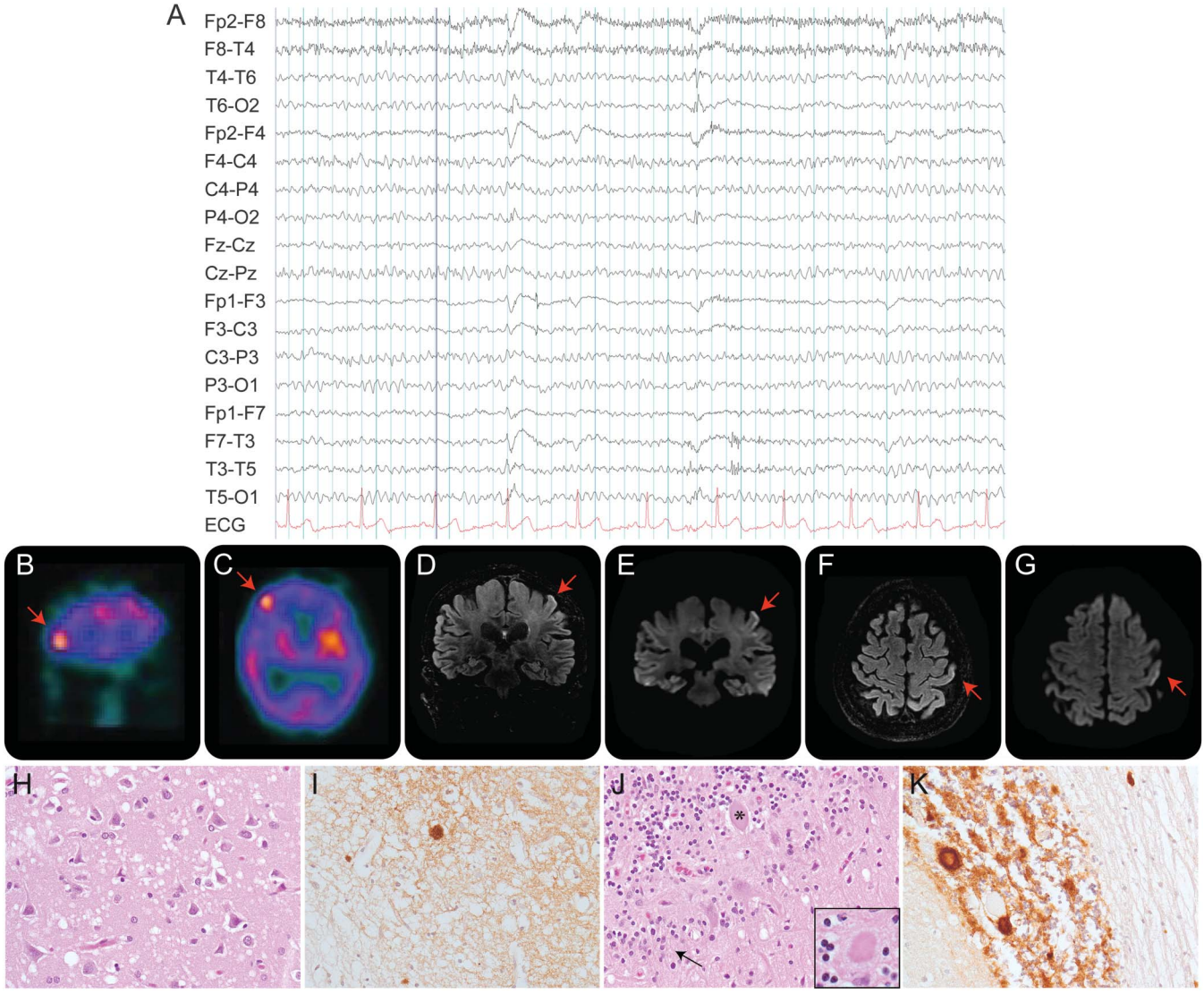

(A) EEG demonstrated intermittent bifrontal and right frontal spikes that often preceded a myoclonic jerk. There was no EEG evidence of a seizure or any periodic lateralized epileptiform discharges. (B–C) SPECT imaging demonstrated widespread discrete perfusion abnormalities involving the cerebral cortex and sparing the subcortical regions, with a focal area of increased activity in the right frontal lobe representing a region of hyperperfusion. This right frontal hot spot (arrow) is visible on both coronal (B) and axial (C) images. (D–G) 3T MRI coronal and axial reformats from a 3D fluid-attenuated inversion recovery sequence acquired in the sagittal plane revealed small focal ribbons of cortical T2 hyperintensity (coronal, D; axial, F) with associated diffusion restriction (arrow) (coronal, E; axial, G reformats from a high-resolution diffusion-weighted imaging sequence acquired in the axial plane with a slice thickness of 1.8 mm and with B0 and B1000); corresponding apparent diffusion coefficient map changes were present (data not shown). (H) Predominantly microvacuolar spongiform change was present in the cortex, including perineuronal and perivascular vacuolation, with associated mild neuronal loss and reactive gliosis (hematoxylin & eosin [H&E] stain, magnification 630×). (I) 3F4 immunohistochemistry of the cortex revealed a synaptic staining pattern with globular plaque-like immunoreactive deposits admixed (3F4 immunohistochemistry, magnification 400×). (J) The cerebellar vermis and lateral hemispheres showed mild macrovaculoar spongiform change in the molecular layer, Bergmann gliosis (arrow) with Purkinje cell drop out, numerous torpedo-like eosinophilic swellings (asterisk), and many Kuru-type plaques in the molecular and granular layers (inset) (H&E stain, magnification 630×; inset 1200×). (K) Immunostaining for prion protein in the cerebellar vermis showed intense immunoreactivity of Kuru plaques, small clusters of plaques, and fine synaptic staining mostly restricted to the granular layer, with occasional plaques seen in the white matter and molecular layer (3F4 immunohistochemistry, magnification 630×).

Differential diagnoses at this stage included CJD, cerebral vasculitis, and progressive encephalopathy with rigidity and myoclonus. Testing of CSF using the RT-QUIC assay was positive, strongly supporting a diagnosis of CJD.[1]

The patient declined, with gait and cognitive impairment plus behavioral changes, and died 13 months following symptom onset. Postmortem brain analysis confirmed CJD with histopathologic features of microvacuolation (spongiform changes) and Kuru-type plaques (figure, H–K). Sequencing of the entire PrP gene (*PRNP*) open reading frame was normal, confirming sporadic CJD with heterozygosity for methionine/valine at codon 129. Glycotyping revealed type 3 PrP^{Sc}.[2]

DISCUSSION

Sporadic CJD is a prion disease consequent to accumulation of misfolded pathogenic prion protein in the brain.[3] It typically presents with cognitive decline. Clinical heterogeneity correlates with the molecular subtype, depicted by the combination of the methionine (M) or valine (V) polymorphism at codon 129 of *PRNP* and PrP^{Sc} glycotype demonstrated though Western blot analysis of brain homogenates. Postmortem histopathology in this case was unusual in that there were Kuru-type plaques in the cerebellum, consistent with what is reported for MV3,[4] with immunostaining for PrP also showing PrP-positive plaques in the cortex and basal ganglia.

This patient's initial symptom was an exaggerated startle response (hyperekplexia). A startle reflex is a bilaterally synchronous shocklike set of movements.[5] A number of mutations in the glycine receptor gene and other postsynaptic proteins are associated with inherited hyperekplexia.[5] Acquired forms may be secondary to brainstem or extensive cerebral damage or glycine receptor antibodies.[5] Although myoclonus is an established clinical feature in CJD, hyperekplexia as the initial symptom of sporadic CJD is unique.

This case exemplifies the difficulty clinicians may face in the diagnosis of sporadic CJD. Our case was atypical for sporadic CJD because the patient presented with hyperekplexia, initially preserved cognition, a longer disease course, and the absence of CSF 14-3-3 protein.

Although CSF 14-3-3 protein detection is a useful confirmatory test for sporadic CJD, it is a nonspecific marker of neuronal damage, and both its sensitivity and specificity can be suboptimal. CSF tau levels have been shown to have a higher specificity for the diagnosis of CJD than 14-3-3[3]; however, these results were not available for our patient. In 2011, Atarashi et al.[1] described a new amplification assay, RT-QUIC, which allowed for the ultrasensitive detection of PrP^{Sc} in CSF samples with greater than 80% sensitivity and 100% specificity, thus permitting an early, rapid, and highly specific antemortem diagnostic investigation. Further independent studies have demonstrated a sensitivity of 87% or more in sporadic CJD with retained high specificity.[6] The RT-QUIC assay has also been identified as being more sensitive for the detection of genetic prion disease than biomarkers such as 14-3-3 or tau protein.[7]

This case is unique because it highlights hyperekplexia as a possible presenting symptom of sporadic CJD. It also demonstrates the utility of the highly sensitive and specific RT-QUIC assay in supporting an antemortem clinical diagnosis of CJD in a case where immunologic findings on blood tests may otherwise have suggested invasive investigation and treatment trials for possible vasculitis, a recognized differential diagnosis in CJD.

REFERENCES

1. Atarashi R, Satoh K, Sano K, et al. Ultrasensitive human prion detection in cerebrospinal fluid by real-time quaking-induced conversion. Nat Med 2011;17:175–178.
2. Collinge J, Sidle KC, Meads J, Ironside J, Hill AF. Molecular analysis of prion strain variation and the aetiology of "new variant" CJD. Nature 1996;383:685–690.

3. Puoti G, Bizzi A, Forloni G, Safar JG, Tagliavini F, Gambetti P. Sporadic human prion diseases: molecular insights and diagnosis. Lancet Neurol 2012;11:618–628.
4. Hill AF, Joiner S, Wadsworth JD, et al. Molecular classification of sporadic Creutzfeldt-Jakob disease. Brain 2003;126:1333–1346.
5. Bakker MJ, van Dijk JG, van den Maagdenberg AM, Tijssen MA. Startle syndromes. Lancet Neurol 2006;5:513–524.
6. McGuire LI, Peden AH, Orrú CD, et al. Real time quaking-induced conversion analysis of cerebrospinal fluid in sporadic Creutzfeldt-Jakob disease. Ann Neurol 2012;72:278–285.
7. Sano K, Satoh K, Atarashi R, et al. Early detection of abnormal prion protein in genetic human prion diseases now possible using real-time QUIC assay. PLoS One 2013;8:e54915.

ACKNOWLEDGMENT

The Australian National Creutzfeldt-Jakob Disease Registry is funded by the Commonwealth Department of Health. SC receives an NHMRC Practitioner Fellowship (#APP1005816).

STUDY FUNDING

No targeted funding reported.

DISCLOSURES

S. Ramanathan has received a scholarship from the National Health and Medical Research Council (Australia). V.S.C. Fung serves on scientific advisory boards for Abbott, Allergan, Boehringer-Ingelheim, Hospira, Ipsen, Lundbeck, Novartis, Solvay, and UCB; has received funding for travel or speaker honoraria from Boehringer-Ingelheim and Ipsen; serves on the editorial boards of *Movement Disorders*, *Movement Disorders Clinical Practice*, *Journal of Clinical Movement Disorders*, *Basal Ganglia*, and *F1000 Research*; and receives research support from Abbvie. A. Bielich reports no disclosures. L. Masters performs MRIs for patients with MS at Brain and Mind Research Institution. R.R. Russo has received funding for travel and speaker honoraria from Pfizer, Abbvie, UCB, and BMS. M.E. Buckland receives research support from the National Foundation for Medical Research & Innovation. S. Sarros reports no disclosures. G.M.J.A. Klug has a contractual agreement to perform surveillance and diagnostic work on behalf of the Department of Health funded by the Department of Health, Commonwealth Government via Commonwealth Grant Agreement 2010–2014. S. Collins has a contractual agreement to perform surveillance and diagnostic work on behalf of the Department of Health funded by the Department of Health, Commonwealth Government via Commonwealth Grant Agreement 2010–2014. S.W. Reddel serves on scientific advisory boards for CSL, Baxter, Genzyme, Biogen, and the National Immunoglobulin Governmental Advisory Council, Australia; has received funding for travel or speaker honoraria from CSL, Genzyme, and Biogen; receives research support from Genzyme and the Beeren Foundation; receives stock/stock options/Board of Directors compensation from Sydney Neurology and Medical Safety Systems; and has provided an expert witness affidavit in a medico-legal case. Full disclosure form information provided by the authors is available with the **full text of this article at Neurology.org/cp**.

LGI1 antibody encephalopathy overlapping with sporadic Creutzfeldt-Jakob disease

OPEN

Boaz Kim, BMedSci*
Patrick Yoo, MSc*
Tom Sutherland, MBBS, MMed
Alison Boyd, DipAppSci
Christiane Stehmann, PhD
Catriona McLean, MBBS, MD
Steven Collins, MBBS, MD

Correspondence to Dr. Collins: stevenjc@unimelb.edu.au

ABSTRACT

Objective: To report a rare case of leucine-rich, glioma inactivated 1 (LGI1) antibody–mediated autoimmune encephalopathy clinically overlapping with pathologically confirmed sporadic Creutzfeldt-Jakob disease (CJD).

Methods: The patient was investigated with repeated brain MRI, EEG, CSF examination, whole-body fluorodeoxy-glucose positron emission tomography, genetic analysis of the prion protein gene (*PRNP*), and extensive serologic screening for paraneoplastic and autoimmune encephalopathy markers. Written informed consent was obtained from the patient's next of kin for access to clinical files for research purposes and for publication.

Results: The patient was a 77-year-old man who presented with faciobrachial dystonic seizures (FBDS) secondary to LGI1 antibody–mediated autoimmune encephalopathy, with suggestive MRI findings and a complete response to treatment with combinatorial immunosuppression. Stereotactic biopsy of a nonenhancing T1 hyperintense basal ganglia lesion during the initial FBDS phase, albeit following immunosuppression, did not disclose evidence of lymphocytic inflammation. Following full remission of the FBDS, the patient manifested a rapidly progressive dementia associated with gross motor decline confirmed to be CJD at autopsy (molecular subtype VV3), with no evidence of a pathogenic *PRNP* mutation.

Conclusions: Our patient highlights that these rare diseases are not invariably mutually exclusive and underscores the benefits of comprehensive neuropathologic examination of the brain to achieve an accurate diagnosis, especially in complex cases when the clinical trajectory dramatically deviates and a concomitant disease may need to be conscientiously considered to best explain the new clinical course. ***Neurol Neuroimmunol Neuroinflamm* 2016;3:e248; doi: 10.1212/NXI.0000000000000248**

GLOSSARY

BG = basal ganglia; **CJD** = Creutzfeldt-Jakob disease; **FBDS** = faciobrachial dystonic seizures; **sCJD** = sporadic Creutzfeldt-Jakob disease; **VGKC** = voltage-gated potassium channel; **VGKCC-LE** = voltage-gated potassium channel complex limbic encephalitis.

A patient presented at age 77 years with a 1-week history of intermittent episodes of left-sided spasms involving the arm, face, shoulder, or leg, lasting 4–5 seconds, which were accompanied by recurrent falls but not associated with loss of consciousness. Medical history included type 2 diabetes mellitus managed with metformin and glimepiride; hypertension treated with atenolol and telmisartan; hypercholesterolemia controlled with simvastatin; and chronic obstructive pulmonary disease, for which salbutamol and tiotropium inhalant therapy were prescribed. There was no history of neurologic disorders. CT and MRI of the brain, as well as EEG, proved unremarkable. Neurologic examination results were normal and the patient had apparently normal cognitive

*These authors contributed equally to this work.

From the Australian National Creutzfeldt-Jakob Disease Registry, The Florey Institute of Neuroscience and Mental Health (B.K., P.Y., A.B., C.S., C.M., S.C.), and Department of Medicine, Royal Melbourne Hospital (A.B., S.C.), The University of Melbourne, Parkville; Melbourne Medical School (B.K., P.Y.), The University of Melbourne; Medical Imaging Department (T.S.), St. Vincent's Hospital Melbourne, Fitzroy; and Department of Anatomical Pathology (C.M.), Alfred Health, Prahran, Australia.

Funding information and disclosures are provided at the end of the article. Go to Neurology.org/nn for full disclosure forms. The Article Processing charge was paid by the authors.

function by informal assessment. The patient was commenced on phenytoin (300 mg daily) following a provisional diagnosis of partial epilepsy.

Approximately 1 month later, the patient was admitted to the hospital because of recurrence of the left facial and upper limb spasms of increased frequency, sometimes occurring every 8–10 minutes, with up to 30 episodes daily; minor difficulties with cognition were also apparent. During the admission, repeat MRI of the brain (figure 1A) showed T1 hyperintensity in the right basal ganglia (BG), which was nonenhancing and appeared associated with modest mass effect. Based on the new imaging findings and concerns about neoplastic infiltration, anticonvulsant therapy was changed to carbamazepine 200 mg twice daily and empirical treatment with oral dexamethasone was commenced. Shortly thereafter, the patient underwent stereotactic biopsy of the T1 hyperintense lesion, which only revealed mild, nonspecific, astrocytic gliosis but no evidence of neoplasia or inflammation. Routine investigations were unremarkable aside from a new-onset hyponatremia (122 mM; normal 135–145 mM). Investigations for an underlying neoplastic process included CT imaging of the chest-abdomen-pelvis, whole body fluorodeoxy-glucose positron emission tomography with CT correlation (FDG-PET/CT), and serum paraneoplastic antibody and tumor marker screening (including anti-Hu and anti-Yo/Purkinje cell antibodies and carcinoembryonic antigen CA 19-9), which were negative. CSF was normal and prolonged scalp EEG monitoring during episodes of spasms showed no evidence of focal epileptiform activity. An autoimmune encephalopathy screen for anti–NMDA receptor antibodies in both serum and CSF was negative but anti–voltage-gated potassium channel (VGKC) complex antibodies were positive by radioimmunoassay at 338 pM (normal <85). Posthumous retesting of the patient's serum using indirect immunofluorescence (Euroimmun, Lübeck, Germany)

Figure 1 Prebiopsy and postbiopsy MRI

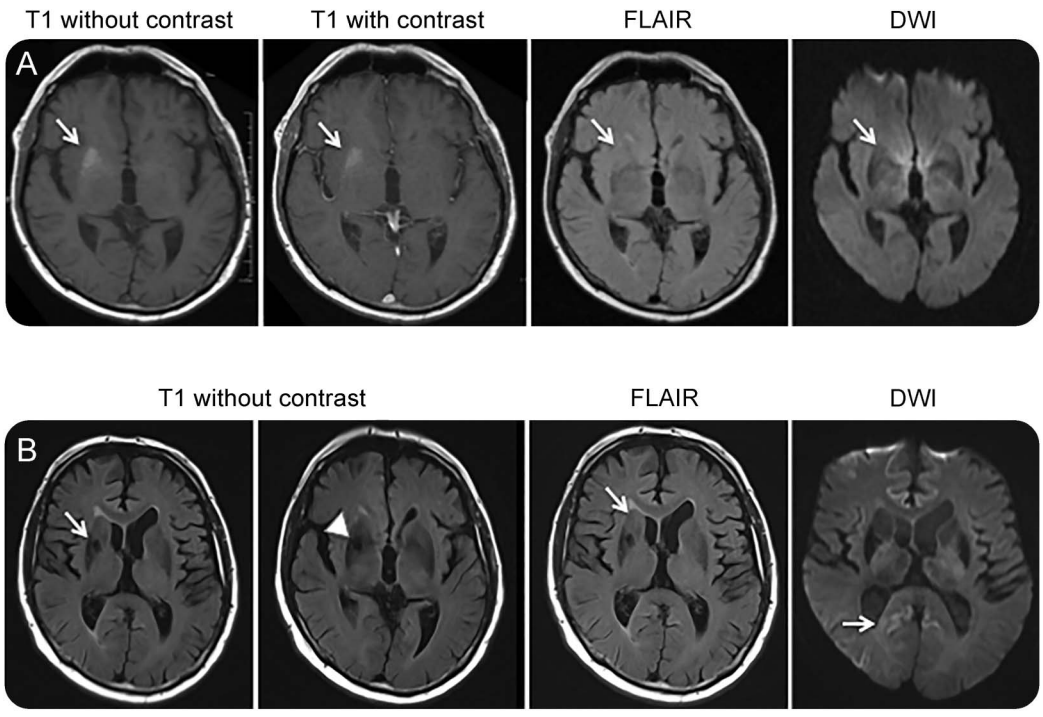

(A) Immediately prebiopsy, axial brain MRI shows a non-contrast enhancing T1 hyperintensity in the right basal ganglia juxtaposed to the external capsule (arrows) with modest mass effect; these changes were not evident in a prior MRI study. Corresponding fluid-attenuated inversion recovery (FLAIR) and diffusion-weighted imaging (DWI) sequences were essentially unremarkable. (B) Postbiopsy axial brain MRI reveals resolution of the right basal ganglia T1 hyperintensity (arrow), with biopsy artefact (arrow head), with corresponding FLAIR images remaining otherwise unremarkable aside from ongoing modest mass effect (arrow), while the DWI series displays subtle cerebral cortical signal increase in the posterior cingulate gyri (right more than left) and right posterior temporal region (arrow).

confirmed the presence of antibodies to LGI1 but not to contactin-associated protein-like 2. Based on all the available clinical information at the time of the anti-VGKC antibody result, the working diagnosis of faciobrachial dystonic seizures (FBDS) secondary to anti-VGKC encephalopathy was made. The patient was changed from dexamethasone (after approximately 1 month of treatment) to prednisolone (25 mg daily) and azathioprine (100 mg daily), with monthly IV immunoglobulin given for 4 months as combinational immunotherapy, which resulted in complete clinical remission of his FBDS and partial improvement in cognition, allowing the patient to be discharged home with gradual outpatient tapering of maintenance corticosteroid therapy.

Approximately 4 months after discharge, despite good ongoing control of the FBDS, the patient's cognition began to decline again (Mini-Mental State Examination 19/30), with minimal response to escalation of the prednisolone to 25 mg daily. Cognitive impairment at that time included amnesia, executive dysfunction, visuospatial impairment, and poor insight. Repeat brain MRI confirmed absence of the previous right BG T1 hyperintensity (with postbiopsy changes evident) and equivocal cerebral cortical signal abnormality restricted to the posterior cingulate gyri (right more than left) and posterior right temporal lobe on the diffusion-weighted series (figure 1B). Repeat EEG showed only nonspecific generalized slowing consistent with a moderate encephalopathy. The patient thereafter manifested inexorable cognitive and gross motor decline, associated with bulbar dysfunction and double incontinence, dying 6 months later, spending the final 2 months of his life in high-level care. The total illness duration from clinical presentation to death was 17 months, the first 8 months predominantly involving autoimmune FBDS and its management and the next 9 months related to a rapidly progressing dementia with profound functional decline.

A diagnosis of Creutzfeldt-Jakob disease (CJD) was confirmed at autopsy, characterized by widespread spongiform encephalopathy associated with neuronal loss and astrocytic gliosis (figure 2). There was no evidence of any lymphocytic inflammatory reaction. Genetic studies did not reveal any pathogenic variants of the prion protein gene (*PRNP*) and the patient was homozygous valine/valine (VV) at codon 129. Western blot showed evidence of protease-resistant prion protein, classified as type 3 according to the nomenclature of Collinge et al.[1] As follow-up to the brain pathologic findings at autopsy, formal re-review of the stereotactic biopsy was undertaken but did not reveal previously unappreciated spongiform changes and immunohistochemistry for abnormal prion protein deposits was negative.

DISCUSSION We propose that the 17-month illness to the time of death in our patient most likely comprised 2 overlapping neurologic illnesses: anti-LGI1 autoantibody-mediated encephalopathy predominantly

Figure 2 **Neuropathologic diagnosis of Creutzfeldt-Jakob disease (CJD) at postmortem**

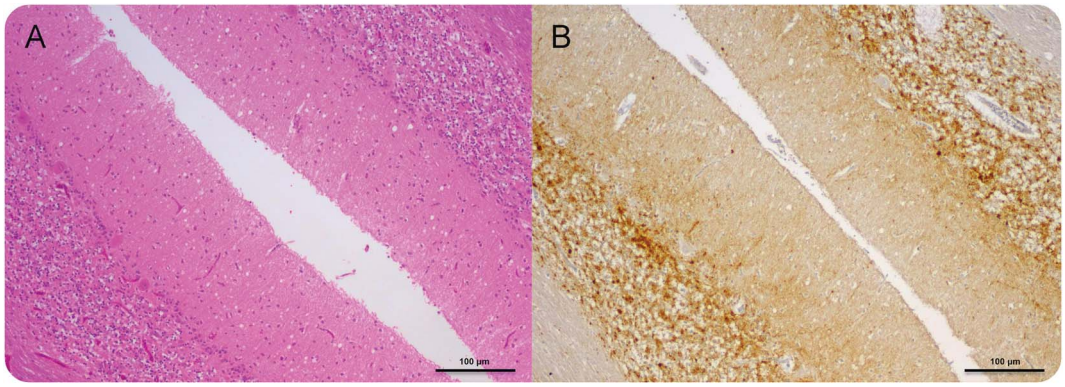

(A) Cerebellar vermis shows typical changes of CJD including spongiform encephalopathy, gliosis, and neuronal loss (hematoxylin and eosin × 100 actual magnification) and (B) synaptic pattern (PrP) immunoreactivity (12 F10 PrP antibody × 100 actual magnification). Note there is no evidence of any inflammatory cells.

manifesting as FBDS and inexorable cognitive and gross motor decline due to VV3 sporadic CJD (sCJD). While the FBDS was completely responsive to immunosuppression, the patient's early cognitive impairment was only partially responsive, and although recognized for LGI1 antibody encephalopathy raises the possibility that at least some of this impairment may have related to sCJD before more dramatic cognitive decline and accompanying features were evinced. Although we consider it unlikely, due to the response of the FBDS to immunosuppression in the setting of anti-LGI1 antibodies and typical MRI changes, we cannot exclude the possibility that the patient's illness reflected an atypical CJD phenotype from the time of first presentation with FBDS.

FBDS is a recently described immunotherapy-responsive seizure disorder characterized by highly stereotyped clinical features and the presence of autoantibodies to LGI1, a protein component of the VGKC complex.[2–4] Furthermore, FBDS is considered to be a highly specific phenotype and almost pathognomonic for LGI1 autoantibody–mediated disease.[5,6] FBDS have also been recognized as a frequent prodromal sign preceding LGI1 antibody limbic encephalitis,[5] a neuroinflammatory condition characterized by a clinical triad of FBDS, cognitive impairment, and hyponatraemia.[6] The absence of cognitive deficits at presentation with FBDS renders it more likely that our patient was in the prodromal phase prior to the onset of limbic encephalitis, which is consistent with the absence of T2/fluid-attenuated inversion recovery signal increase in the mesiotemporal lobes typically seen in limbic encephalitis.[7] In the early stage of the illness, MRI demonstrated a nonenhancing T1 hyperintensity in the right BG, typical of what is observed in a sizeable proportion of patients presenting with FBDS secondary to anti–LGI1 antibody encephalopathy. In a recent retrospective case series of 26 patients with FBDS and positive serology for LGI1 autoantibodies, 10 of these patients had the novel finding of contralateral BG T1 hyperintensity, thereby providing evidence for BG T1 hyperintensity as a useful MRI biomarker of anti-LGI1 autoimmune FBDS.[2] Our patient also developed hyponatremia (Na 122 mM), a common finding in FBDS and limbic encephalitis.[5–7]

LGI1 antibody–mediated FBDS and limbic encephalitis have been reported to show variable response rates to immunotherapy, with most cases reporting at least partial improvement of FBDS and cognitive symptoms. Moreover, early initiation of immunotherapy at the FBDS stage can prevent progression to limbic encephalitis.[8] Our patient demonstrated an initial good response of the FBDS to combination immunotherapy and anticonvulsant medication, with partial improvement in cognition, before eventually manifesting inexorable intellectual, behavioral, and gross motor decline almost certainly due to co-occurrence of sCJD.

Occasional diagnostic confusion between CJD and autoimmune encephalopathies is well-recognized. Although positive VGKC complex (and in retrospect LGI1) antibodies were present at the early stage of our patient's illness, there have been reports of elevated VGKC complex antibody levels in patients with CJD, albeit with no symptoms of FBDS or other evidence of autoimmune encephalopathy, with subsequent uncertainty about the significance of antibody levels in these clinical situations.[9] Further illustrating the diagnostic challenges that can arise in the evaluation of patients with neurologic illnesses with positive serology for autoimmune encephalopathies, previous case series have discussed autoimmune VGKC complex limbic encephalitis (VGKCC-LE) as a mimic of CJD,[10] with patients initially thought to have CJD but later confirmed to have immunotherapy-responsive VGKCC-LE, and conversely, CJD has been reported as a mimic of VGKCC-LE[11] and of Morvan syndrome associated with elevated VGKCC and glycine receptor autoantibodies.[12] Our patient was somewhat different from the usual clinical reports, manifesting a dramatic biphasic illness punctuated by a period of incomplete recovery, rather than a predominantly monophasic course, until an accurate diagnosis was achieved. Development of refractory cognitive and gross motor decline in our patient prompted some uncertainty and reconsideration of the diagnosis but was construed as probably reflecting treatment-unresponsive LGI1 antibody encephalopathy rather than representing the development of a second neurologic illness such as sCJD, especially when there was no definite objective investigational evidence to clearly support such an alternative diagnosis.

The absence of inflammation in the brain at biopsy and autopsy examinations is without definite explanation but we conjecture most likely represents the effects of immunosuppressant treatment in a patient who appeared to have at least a partially responsive anti–LGI1 antibody encephalopathy. Recent reports of anti–LGI1 antibody encephalopathy are largely devoid of neuropathologic findings.[2,3,5,6,11]

Our patient underscores the benefits of comprehensive neuropathologic examination of the brain to achieve an accurate diagnosis, especially in complex cases when the clinical trajectory dramatically deviates and vigilance for a concomitant disease is arguably the best approach to explain the new clinical course. In addition, our patient exemplifies the utility of recognizing BG T1 hyperintensity in patients with brief adventitious face and limb movements suggestive of FBDS, which should prompt investigation for VGKC complex antibodies and in particular anti-LGI1 antibodies, which may be responsive to immunosuppressive therapy.

AUTHOR CONTRIBUTIONS

B. Kim: involved in the collection of patient information and creation of figure 1 and contributed to the manuscript writing, drafting, and reviewing process. P. Yoo: involved in the collection of patient information and creation of figure 1 and contributed to the manuscript writing, drafting, and reviewing process. T. Sutherland: reviewed clinical images, assisted in the creation of figure 1, and contributed to the drafting and review of the manuscript. A. Boyd: assisted in collection of patient clinical files and in the manuscript drafting and review process. C. Stehmann: assisted in collection of patient clinical files and in the manuscript drafting and review process. C. McLean: reviewed the pathologic details of the case and contributed to the drafting and review process and creation of figure 2. S. Collins: provided overall guidance in the direction of the case report and contributed to the writing, drafting, and reviewing process.

ACKNOWLEDGMENT

The ANCJDR thanks the patient's family and associated health care personnel for their support in the preparation of the case report.

STUDY FUNDING

The Australian National Creutzfeldt-Jakob Disease Registry (ANCJDR) is funded by the Commonwealth Department of Health. S.C. was funded in part by NHMRC Practitioner Fellowship (APP1005816).

DISCLOSURE

B.S. Kim and P. Yoo report no disclosures. T. Sutherland is on the editorial board for *Insights into Imaging*. A. Boyd received research support from Australian Commonwealth Department of Health. C. Stehmann holds a patent for albumin depletion technology. C. McLean reports no disclosures. S. Collins is an associate editor for *Journal of Alzheimer Disease* and received research support from NHMRC, Rebecca Cooper Foundation, Brain Foundation, and Commonwealth Department of Health. Go to Neurology.org/nn for full disclosure forms.

Received February 25, 2016. Accepted in final form April 7, 2016.

REFERENCES

1. Collinge J, Sidle KC, Meads J, Ironside J, Hill AF. Molecular analysis of prion strain variation and the aetiology of "new variant" CJD. Nature 1996;383:685–690.
2. Flanagan EP, Kotsenas AL, Britton JW, et al. Basal ganglia T1 hyperintensity in LGI1-autoantibody faciobrachial dystonic seizures. Neurol Neuroimmunol Neuroinflamm 2015;2:e161. doi: 10.1212/NXI.0000000000000161.
3. Lai M, Huijbers MGM, Lancaster E, et al. Investigation of LGI1 as the antigen in limbic encephalitis previously attributed to potassium channels: a case series. Lancet Neurol 2010;9:776–785.
4. Irani SR, Buckley C, Vincent A, et al. Immunotherapy-responsive seizure-like episodes with potassium channel antibodies. Neurology 2008;71:1647–1648.
5. Irani SR, Michell AW, Lang B, et al. Faciobrachial dystonic seizures precede Lgi1 antibody limbic encephalitis. Ann Neurol 2011;69:892–900.
6. Casault C, Alikhani K, Pillay N, Koch M. Jerking & confused: leucine-rich glioma inactivated 1 receptor encephalitis. J Neuroimmunology 2015;289:84–86.
7. Bien CG, Elger CE. Limbic encephalitis: a cause of temporal lobe epilepsy with onset in adult life. Epilepsy Behav 2007;10:529–538.
8. Irani SR, Stagg CJ, Schott JM, et al. Faciobrachial dystonic seizures: the influence of immunotherapy on seizure control and prevention of cognitive impairment in a broadening phenotype. Brain 2013;136:3151–3162.
9. Jammoul A, Lederman RJ, Tavee J, Li Y. Presence of voltage-gated potassium channel complex antibody in a case of genetic prion disease. BMJ Case Rep 2014; 2014.
10. Geschwind MD, Tan KM, Lennon VA, et al. Voltage-gated potassium channel autoimmunity mimicking Creutzfeldt-Jakob disease. Arch Neurol 2008;65:1341–1346.
11. Newey CR, Appleby BS, Shook S, Sarwal A. Patient with voltage-gated potassium-channel (VGKC) limbic encephalitis found to have Creutzfeldt-Jakob disease (CJD) at autopsy. J Neuropsychiatry Clin Neurosci 2013;25:E05–E07.
12. Angus-Leppan H, Rudge P, Mead S, Collinge J, Vincent A. Autoantibodies in sporadic Creutzfeldt-Jakob disease. JAMA Neurology 2013;70:919–922.

Prion disease in Indigenous Australians

Peter K Panegyres MD PhD FRACP[1,2], Christiane Stehmann PhD[3], Genevieve M Klug[4], Colin L Masters MD[3], Steven Collins MD FRACP[3,4]

1. Neurodegenerative Disorders Research Pty Ltd, West Perth, Western Australia
2. The University of Western Australia, Nedlands, Western Australia
3. The Florey Institute, The University of Melbourne, Parkville, Australia
4. Department of Medicine (RMH), The University of Melbourne, Parkville, Australia

Corresponding Authors:

PK Panegyres
Neurodegenerative Disorders Research Pty Ltd
4 Lawrence Avenue, West Perth, Western Australia 6005
Email: research@ndr.org.au
Telephone: +61 8 9481 6293
Fax: +61 8 9481 6294

S Collins
Department of Medicine, The University of Melbourne
and The Florey Institute
Parkville, Australia 3010
Email: stevenjc@unimelb.edu.au
Telephone: +61 3 83441949

Keywords: Prion disease, Indigenous Australians, Creutzfeldt-Jakob disease

Funding bodies: Neurodegenerative Disorders Research (NDR) Pty Ltd, National Health and Medical Research Council (NHMRC) and Commonwealth Department of Health. Staff at NDR identified the illustrative case, analyzed data, performed statistical operations and wrote, revised and edited the manuscript. Staff at the Australian National CJD Registry at the Florey Institute, the University of Melbourne added data relating to the additional Indigenous Australian CJD cases, performed statistical and other data analyses, and revised and edited the manuscript.

Acknowledgements: We acknowledge the assistance of the nursing staff, allied health, and doctors Ference Van de Bos (Registrar) and Nidhima Puri (Resident) of Joondalup Health Campus who helped care for the patient described in the illustrative case report. We thank the physicians who referred patients to the Australian National CJD Registry. We also thank the families of the patients for their cooperation and the local medical practitioners who cared for the patients. SJC is funded in part by a NHMRC Practitioner Fellowship (ID# APP1105784).

INTRODUCTION

Creutzfeldt-Jakob disease (CJD) is a rare transmissible, neurodegenerative disorder with an annual incidence of approximately 1-2 per million population.[1–3] CJD represents the most common phenotype of human prion disease,[4] which can be sporadic (~85-90%), genetic (~10-15%) or acquired (<1%). Sporadic CJD (sCJD) typically presents as a rapidly progressive dementia associated with myoclonus and cerebellar ataxia with inexorable clinical decline resulting in death after a median survival of ~4-5 months.[2–4] In addition to sCJD, the spectrum of human prion disease includes Gerstmann-Sträussler-Scheinker syndrome and fatal familial insomnia. The detection of kuru in the 1950s established that prion diseases occur in Indigenous peoples albeit aetiologically linked to the culturally peculiar Fore practice of endocannibalism. Epidemiological studies of prion disease in specific ethnic groups are limited[5] ; however, a global epidemiological survey revealed that CJD occurs worldwide,[6] including Indigenous peoples from Oman and Papua New Guinea.[7,8] Indigenous Americans and Alaskans were later reported to also develop CJD.[5]

Encompassed in the investigation of neurodegenerative disorders occurring in Indigenous Australian (Aboriginal and Torres Strait Islander) communities, including Huntington's disease,[9] spinocerebellar ataxia[10] and early onset dementia,[11] is the study of CJD and other forms of human prion disease. Systematic epidemiological studies of neurodegenerative disorders in Indigenous Australians can be problematic for reasons that include geographical remoteness from clinical services and socio-

cultural attitudes to medical evaluation, including performance of neuropathological studies. Herein, we selectively report for the first time, all ANCJDR ascertained cases of CJD in Indigenous Australians, highlighting a Western Australian Indigenous person dying from likely prion disease. This patient illustrates some of the potential challenges faced in the diagnosis and management of prion diseases in Indigenous Australians living in remote communities. Incidence rates, indirect age-standardised mortality ratios and the clinical phenotype of sCJD in Indigenous Australians are compared to non-Indigenous Australians from the ANCJDR database.[12,13]

METHODS

The ascertainment and classification of Indigenous (Aboriginal and Torres Strait Islander) and non-Indigenous Australians with prion disease occurred as part of routine surveillance activities of the ANCJDR, employing updated case classification criteria.[13] ANCJDR data and relevant population data from the Australian Bureau of Statistics (ABS)[14,15] allowed estimation of crude annual incidence rates for specific reference years (2006, 2011 and 2016). In addition, indirect age-standardisation of all CJD to calculate the standardised mortality ratio (SMR) for the Indigenous Australian population in comparison to the all-resident Australian population was undertaken. Indirect age-standardisation was performed because case numbers for the Indigenous Australian population for the years 2006 to 2018 were small rendering age-standardised mortality rates a less robust calculation. Indirect age-standardised mortality ratios for the Indigenous population for the years 2006 to 2018 in comparison to non-Indigenous Australians represents the period during which Indigenous persons were diagnosed and classified as dying from sCJD. Due to the lack of resident Aboriginal and Torres Strait Islander population data by age group for the years 2017 and 2018, the 2016 estimate was used for these years. Indigenous ethnicity was as reported by the patient, family or caring medical practitioners.

The ANCJDR is funded by the Commonwealth Department of Health and is responsible for the national surveillance of clinically suspected and confirmed human prion disease in Australia and is based at The Florey Institute, The University of Melbourne. ANCJDR surveillance activities are approved by The University of Melbourne Human Research Ethics Committee (ID# 1341074) to collect and monitor limited personal and health information from Indigenous and non-Indigenous Australians in relation to CJD and disseminate de-identified and aggregate data for reporting and research purposes; approvals were not obtained from other sources. Written permission to release additional data for publication was obtained for the illustrative case report.

RESULTS

Illustrative case report

This patient was a 55-year-old male Indigenous Australian residing in a remote region of Western Australia at the time of illness onset. Approximately 6 weeks prior to admission, the patient developed progressive unsteadiness of gait associated with blurred vision, tinnitus, short-term memory loss and slurred speech. He was a non-smoker, did not take illicit drugs or alcohol and there was no known family history of a neurodegenerative disorder. There was no past surgical history nor any history of blood transfusions or treatment with any other medical products. Upon admission to hospital gait was impaired but he was able to walk without assistance, his Mini-Mental State Examination score was 22/30, and he was intermittently confused with disorientation to year, month and day. He had left upper limb dysmetria. Rapid decline in cognition and gross motor function continued such that by approximately ten days after admission the patient was only able to provide one or two word answers, was unable to stand independently and could not follow commands to allow a detailed neurological examination. Myoclonic jerks became evident in the upper limbs.

A MRI scan revealed increased T2 signal with restricted diffusion in the left caudate nucleus and putamen, as well as the posterior cingulate gyrus on both sides, raising the likelihood of CJD. Routine CSF parameters were unremarkable with cytology negative for malignant cells; microbiological studies were negative for bacteria, viruses and fungi; 14-3-3 protein testing was positive. EEG five days after admission showed a non-specific excess of slower frequencies consistent with an encephalopathy while a repeat study at 12 days after admission showed diffuse periodic complexes at 1 hertz, strongly increasing the likelihood of CJD.

A working diagnosis of probable sCJD and the attendant poor prognosis was explained to the family. It was the family's preference that the patient be transferred for palliative care at "home and country". The patient died with his family in his local community after an illness duration of approximately two months; the patient's family declined an autopsy.

Summary of ascertained CJD affecting Indigenous Australians

As part of comprehensive, national surveillance, eight persons identified as Indigenous Australians have been classified as dying from sCJD by the ANCJDR (Table 1). Although dealing with a small number of Indigenous Australians with sCJD, basic demographic features are similar to the broader Australian population with a median age at death of 61 years (IQR=16 years) and median disease duration of 3 months (IQR=1.6 months). Two of the patients were known to share Irish, Scandanavian and English ancestry. The patients were geographically, widely dispersed across the continent spanning from South Hedland to the eastern seaboard. Definite CJD was confirmed through post-mortem neuropathological examination in five persons, while three cases (including the illustrative case report from Western Australia) fulfilled classification criteria for probable CJD. One patient presented with prominent visual symptoms in keeping with the Heidenhain sub-type of sCJD while the others presented with typical sCJD evincing rapidly progressive dementia accompanied by myoclonus. There was no family history of similar neurological illness in any of the

eight Indigenous persons, with genetic testing performed in three patients showing codon 129 methionine homozygosity and absence of disease-associated prion protein gene (*PRNP*) mutations. CSF 14-3-3 protein was positive in six of the eight patients tested.

Using data from the ANCJDR and the ABS (populations based on three reference years 2006, 2011 and 2016), we estimated overall crude annual rates of sCJD in Indigenous Australians compared to the remainder of the Australian population (after subtracting the number of Indigenous people): 0–3.87 per million for Indigenous Australians and 0.94–1.83 per million for the remainder of the Australian population (Table 2). In addition, indirect age-standardisation was utilised to estimate a standardised mortality ratio for the Indigenous population for the years 2006 to 2018, representing the period in which Indigenous persons were diagnosed and classified as dying from sCJD. Using the ABS estimated populations for both resident Aboriginal and Torres Strait Islanders (2006-2016)[16] and all-resident Australians (2006-2018),[17] age-specific Australian mortality rates were used to calculate the number of Indigenous CJD cases expected if the Indigenous population had the same age-specific mortality rates as the entire Australian population. Compared to the eight observed Indigenous cases, the overall number of expected CJD cases was calculated to be 5.37, giving a ratio of 1.49 (95% CI, 0.75 - 2.98). Although, this suggests a 50% excess of observed cases compared to the expected number in the Indigenous Australian population, the wide confidence interval range encompassing 1.0 renders this result not statistically significant.

DISCUSSION

The present study re-confirms that CJD occurs in Indigenous populations, with the overall features of the eight Indigenous Australians in keeping with sCJD, which appears phenotypically in keeping with sCJD occurring in non-Indigenous persons with similar geographical dispersion and incidence rates. Uniformity of phenotype and rates of occurrence for sCJD is well recognised across non-Indigenous populations.[18] Our illustrative patient is the first known Indigenous Australian from that particular

remote region of Western Australia to be diagnosed with probable sCJD, dying approximately two months after the onset of symptoms with a typical clinical picture of rapidly progressive dementia, ataxia and myoclonus, positive 14-3-3 protein in the CSF and characteristic MRI and EEG findings. Although permission for post-mortem confirmation is commonly sought for persons suspected to be manifesting CJD, including in this patient, families not infrequently decline for various reasons including cultural, religious and personal preference. This rare neurodegenerative cause of death in Indigenous Australians stands in contrast with their much more common causes of death, most of which relate to ischaemic heart disease, diabetes mellitus, chronic lung diseases, lung cancer and self-harm.[19,20]

Sporadic CJD has also been reported amongst Indigenous North Americans and Alaskans with 12 CJD deaths recorded from 1981 until 2002, with an annual age-adjusted mortality rate of 0.47 per million population – possibly lower than for Caucasians but close to that reported for African Americans.[6] Potential difficulties with case ascertainment and diagnosis related to remote residence, as well as the possibility of problems obtaining autopsy because of cultural and other influences were described in relation to these Indigenous populations,[5] and these factors may have contributed to the absence of confirmed CJD in Indigenous Australians prior to 2006. This year delineates when CJD became a notifiable disease across all Australian states and territories. Presumably this or other factors mitigated any previous impediments up to around 2006 allowing detection and confirmation of CJD in Indigenous Australians at rates broadly comparable to non-Indigenous Australians. Our estimated crude incidence rates and indirect age-standardised mortality ratios for CJD in Indigenous Australians since 2006 are equivalent to rates in the non-indigenous population. Overall, and in contrast with the findings of Maddox and colleagues suggesting a lower incidence in Indigenous North Americans and Alaskans than in Caucasians,[21] it appears unlikely there are significant differences between the rates of CJD in Indigenous and non-Indigenous Australian populations.

One important limitation of this study is the small number of patients included. This renders incidence rates potentially fragile to the effects of only a small change in detected absolute case numbers. As such, although we found the rate of CJD in Indigenous Australians was not different to the non-Indigenous population, a small increase in CJD cases could engender a relatively marked effect. All Indigenous CJD patients were from regional Australia and under-recognition of Indigenous CJD cannot be excluded where it is possible some doctors might not be aware that prion disease occurs in Indigenous people and furthermore health workers might not have easy access to diagnostic tools such as MRI or CSF biomarker analysis. Of some reassurance however, five out of the eight Indigenous patients had autopsy confirmation of CJD, which approximates the proportion of definite confirmation in the non-Indigenous population and thereby militates against undue concerns regarding difficulties in achieving adequate medical evaluation of suspected CJD in Indigenous patients from remote regions. Another limitation of our study was the lack of uniformity or consensus regarding the definition of Indigenous, which was based on self, family, or practitioner reporting. Given this lack of a definition and our limited understanding of the level of awareness and the attitudes of individuals regarding identification as Indigenous or not, our study is at risk of potential under- or over-reporting of CJD in Indigenous Australians. These limitations underscore the importance of maintaining awareness of CJD amongst practitioners, especially general practitioners and general physicians servicing Indigenous Australians in remote regions, to ensure high quality national surveillance and accurate incidence rates are achieved.

In conclusion, we confirm that prion disease in the form of sCJD occurs in geographically dispersed Indigenous Australians, with the overall incidence rate and phenotype approximating that observed in non-Indigenous Australians. In combination with previous epidemiological studies, it appears likely that all human populations, regardless of genetic background and residential location, are susceptible to the pathophysiological disturbances culminating in prion disease.[22]

REFERENCES

1. Ladogana A, Puopolo M, Croes EA, Budka H, Jarius C, Collins S, et al. Mortality from Creutzfeldt-Jakob disease and related disorders in Europe, Australia, and Canada. *Neurology* 2005; **64**: 1586–1591.

2. Klug GM, Wand H, Boyd A, Law M, Whyte S, Kaldor J, et al. Enhanced geographically restricted surveillance simulates sporadic Creutzfeldt-Jakob disease cluster. *Brain* 2009; **132**: 493–501.

3. C Toms. The Department of Health, Australian Government. Communicable Diseases Intelligence 2018; **42**, PII: S2209-6051(18)00023-4) Epub 17 December 2018, available from https://www1.health.gov.au/internet/main/publishing.nsf/Content/cdi-2018-index

4. Collins SJ, Lawson VA, Masters CL. Transmissible spongiform encephalopathies. *Lancet* 2004; **363**: 51–61.

5. Maddox RA, Holman RC, Belay ED, Cheek JE, Yorita KL, Schonberger LB. Creutzfeldt-Jakob disease among American Indians and Alaskan Natives in the United States. *Neurology* 2006; **66**: 439–441.

6. Masters CL, Harris JO, Gajdusek DC, Gibbs CJ Jr, Bernoulli C, Asher DM. Creutzfeldt-Jakob disease: Patterns of worldwide occurrence and the significance of familial and sporadic clustering. *Ann Neurol* 1979; **5**: 177–188.

7. Scrimgeour EM, Chand PR, Kenny K, Brown P. Creutzfeldt-Jakob disease in Oman: report of two cases. *J Neurol Sci* 1996; **142**: 148–150.

8. Scrimgeour EM. Some recollections about kuru in a patient at Rabaul in 1978, and subsequent experiences with prion diseases. *Philos Trans R Soc Lond B Biol Sci* 2008; **363**: 3663–3665.

9. Panegyres PK, McGrath F. Huntington's disease in Indigenous Australians. *Int Med J* 2008; **38**: 130–132.

10. Burt T, Currie B, Kilburn C, Lethlean AK, Dempsey K, Blair I, et al. Machado-Joseph disease in east Arnhem Land, Australia: Chromosome 14q32.1 expanded repeat confirmed in four families. *Neurology* 1996; **46**: 11181–11122.

11. Chen HY, Panegyres PK. The role of ethnicity in Alzheimer's disease: Findings from the C-PATH online data repository. *J Alzheimer's Dis* 2016; **51**: 515-523.

12. Collins S, Boyd A, Lee JS, Lewis V, Fletcher A, McLean CA, et al. Creutzfeldt-Jakob disease in Australia 1970–1999. *Neurology* 2002; **59**: 1365–**59**1371.

13. Stehmann C, Senesi M, Lewis V, Ummi M, Simpson M, Klug G, et al. Annual report: Creutzfeldt-Jakob disease surveillance in Australia: update to 31 December 2018. *Comm Dis Intell* 2019: **43.** DOI: 10.33321/cdi.2019.43.35.

14. Australian Bureau of Statistics. 3238.0 Estimates and Projections, Aboriginal and Torres Strait Islander Australians, 2006 to 2031 (July 2019) [cited 18 August 2019], Table 9. Available from: https://www.abs.gov.au/AUSSTATS/abs@.nsf/Lookup/3238.0Main+Features12001%20to%202026).

15. Australian Bureau of Statistics. 3101.0 Australian Demographic Statistics (June 2018) [cited 17 January 2019], Table 59. Available from: https://www.abs.gov.au/AUSSTATS/abs@.nsf/DetailsPage/3101.0Jun%202018.

16. Department of Health, Australian Government. Creutzfeldt-Jakob disease surveillance in Australia: update to December 2015 (30 Sep 2016) [cited 18 August 2019]. Available from: https://www1.health.gov.au/internet/main/publishing.nsf/Content/cda-cdi4003k.htm).

17. Australian Institute of Health and Welfare, Australian Government. Australian burden of disease study: Impact and causes of illness and death in Indigenous and Torres Strait Islander people 2011 (23 Sep 2016) [cited 18 August 2019]. Available from: https://www.aihw.gov.au/reports/burden-of-disease/australian-bod-study-2011-indigenous-australians/contents/summary (accessed on 18 August 2019).

18. Ladogana A, Puopolo M, Croes EA, Budka H, Jarius C, Collins S, et al. Mortality from Creutzfeldt-Jakob disease and related disorders in Europe, Australia, and Canada. *Neurology* 2005; **64**: 1586–1591.

19. Holman RC, Belay ED, Christensen KY, Maddox RA, Minino AM, Folkema AM, et al. Human prion diseases in the United States. *PLoS ONE* 2010; **5**: e8521. DOI 10.1371/journal.pone.008521.

20. Gao C, Shi Q, Tian C, Chen C, Han J, Zhou W, et al. The epidemiological, clinical, and laboratory features of sporadic Creutzfeldt-Jakob disease patients in China: Surveillance data from 2006-2010. *PLoS One* 2011; **6**: e24231. DOI 10.1371/journal.pone.0024231.

21. Zhao W, Zhang J-T, Xing X-W, Huang DH, Tian CL, Jia WQ, et al. Chines specific characteristics of sporadic Creutzfeldt-Jakob disease: A retrospective analysis of 57 cases. *PLoS One* 2013; **8**: e58442. DOI 10.1371/journal.pone.0058442.

22. Panegyres PK. Stochastic Considerations into the Origins of Sporadic Adult Onset Neurodegenerative Disorders. *J Alzheimers Dis Parkinsonism* 2019, **9**: 1000473.

Table 1. Creutzfeldt-Jakob disease in Indigenous Australians*

Year of death	Sex	Death age (years)	Illness Duration (months)	ANCJDR Classification	CSF 14-3-3 result
2006	F	67	3	Definite	NT
2006	M	48	8	Definite	Positive
2007	F	61	6	Definite	Positive
2009	M	58	1.3	Definite	Positive
2011	F	80	3.8	Definite	Positive
2011	F	71	3.5	Probable	Positive
2015	M	61	2.3	Probable	NT
2018	M	55	2.2	Probable	Positive

NT = not tested.

* Ethics approval was granted from the NH&MRC to collect and disseminate this information.

Table 2: Crude annual rates of sporadic Creutzfeldt-Jakob diseases in Indigenous and non-Indigenous Australians.

	INDIGENOUS			NON-INDIGENOUS		
Year	**Population**	**CJD cases**	**CJD rate**	**Population**	**CJD cases**	**CJD rate**
2006	517,043	2	3.87	20,180,837	37	1.83
2007	549,234	1	1.82	20,478,698	27	1.32
2008	577,366	0	0.00	20,776,559	34	1.64
2009	605,499	1	1.65	21,074,421	30	1.42
2010	633,631	0	0.00	21,372,282	29	1.36
2011	669,881	2	2.99	21,670,143	36	1.66
2012	689,895	0	0.00	21,968,004	32	1.46
2013	718,027	0	0.00	22,265,865	25	1.12
2014	746,160	0	0.00	22,563,727	27	1.20
2015	774,292	1	1.29	22,861,588	29	1.27
2016*	798,365	0	0.00	23,392,542	22	0.94
2017	830,556	0	0.00	23,690,403		
2018	858,688	2	2.33	23,988,264		

* provisional figure
Estimated population based on three referenced years reported by ABS in 2006, 2011 and 2016.

Section 6: Prion Disease Treatment Studies

Without doubt the most important unmet need in relation to human prion diseases is the lack of an effective, disease modifying treatment. There is muted excitement in the neurological community about the emergence of efficacious therapeutics for some neurodegenerative diseases such as Spinal Muscular Atrophy (SMA), Huntington's Disease (HD) and probably Alzheimer's disease. To date, numerous potential therapeutics have been trialed in pre-clinical, including animal, models of prion disease with very limited or no efficacy demonstrated if deployed late in the incubation period or around the time of onset of clinical disease. Further, there have only been a handful of formal human clinical trials (of varying quality) reported to date, involving flupirtine, quinacrine and doxycycline with little or no meaningful benefit displayed. A *post hoc* observational report of pentosan polysulphate utilized in a very small vCJD cohort suggested possible benefit of prolonged survival (albeit in a vegetative state) but required the onerous delivery mechanism of sustained intra-cerebro-ventricular delivery. Despite this rather disappointing history of treatments for prion disease, there is a quietly renewed optimism around the prospect of application of the therapeutic approach of ASOs successfully utilized in SMA and HD being applied to prion disease, especially for genetic prion disease in the first instance.

As a corollary to the likely role of heightened oxidative stress and the possible contribution from transition metal dys-homeostasis to prion pathogenesis, in addition to further exploring the therapeutic potential of quinacrine in an *in vivo* model, my research also assessed an anti-oxidant and a chelator as candidate therapeutics in our rodent model. Disappointingly, our studies added to the literature of little or only marginal efficacy if utilized very early in the incubation period, with the latter only of potential clinical relevance therefore to genetic prion disease given the only prospect for deployment of therapies in sCJD is after the onset of clinical disease.

List of my publications submitted in full (in chronological order)

Collins S, Lewis V, Brazier M, Hill A, Fletcher A, Masters CL. Quinacrine does not prolong survival in a murine Creutzfeldt-Jakob disease model. Annals of Neurology 2002; 52: 503-506.

Brazier MW, Doctrow SR, Masters CL, Collins SJ. A manganese-superoxide dismutase/ catalase mimetic extends survival in a mouse model of human prion disease. Free Radical Biology and Medicine 2008; 45: 184-192.

Brazier MW, Volitakis I, White AR, Han S, Hill AF, Masters CL, Collins SJ. Manganese chelation therapy extends survival in a mouse model of human prion disease. Journal of Neurochemistry 2010; 114: 440-451.

Japan (11361014, M.Y.), and a Grant-in-Aid for Scientific Research on priority Area (A) from the Ministry of Education, Culture, Sports, Science and Technology, Japan (H.T.).

We thank S. Egawa, T. Hasegawa, Y. Ohta, C. Tanda, J. Takasaki, and C. Honma for their technical assistance and M. Machida, K. Abe, and T. Koike for their secretarial assistance.

References

1. Ross CA. When more is less: pathogenesis of glutamine repeat neurodegenerative diseases. Neuron 1995;15:493–496.
2. Tsuji S. Unstable expansion of triplet repeats as a new disease mechanism for neurodegenerative diseases. Jpn J Hum Genet 1996;41:279–290.
3. DiFiglia M, Sapp E, Chase KO, et al. Aggregation of huntingtin in neuronal intranuclear inclusions and dystrophic neurites in brain. Science 1997;277:1990–1993.
4. Hayashi Y, Kakita A, Yamada M, et al. Hereditary dentatorubral-pallidoluysian atrophy: detection of widespread ubiquitinated neuronal and glial intranuclear inclusions in the brain. Acta Neuropathol 1998;96:547–552.
5. Igarashi S, Koide R, Shimohata T, et al. Suppression of aggregate formation and apoptosis by transglutaminase inhibitions in cells expressing truncated DRPLA protein with an expanded polyglutamine stretch. Nat Genet 1998;18:111–117.
6. Paulson HL, Perez MK, Trottier Y, et al. Intranuclear inclusions of expanded polyglutamine protein in spinocerebellar ataxia type 3. Neuron 1997;19:333–344.
7. Ross CA Intranuclear neuronal inclusions: a common pathogenic mechanism for glutamine repeat neurodegenerative diseases? Neuron 1997;19:1147–1150.
8. Yamada M, Tsuji S, Takahashi H. Pathology of CAG repeat diseases. Neuropathology 2000;20:319–325.
9. Yamada M, Hayashi S, Tsuji S, Takahashi H. Involvement of the cerebral cortex and autonomic ganglia in Machado-Joseph disease. Acta Neuropathol 2001;101:140–144.
10. Yamada M, Wood JD, Shimohata T, et al. Widespread occurrence of intranuclear atrophin-1 accumulation in the central nervous system neurons of patients with dentatorubral-pallidoluysian atrophy. Ann Neurol 2001;49:14–23.
11. Hayashi Y, Kakita A, Yamada M, et al. Hereditary dentatorubral-pallidoluysian atrophy: ubiquitinated filamentous inclusions in the cerebellar dentate nucleus neurons. Acta Neuropathol 1998;95:479–482.
12. Yamada M, Piao YS, Toyoshima Y, et al. Ubiquitinated filamentous inclusions in cerebellar dentate nucleus neurons in dentatorubral-pallidoluysian atrophy contain expanded polyglutamine stretches. Acta Neuropathol 2000;99:615–618.
13. Yazawa I, Nakase H, Kurisaki H. Abnormal dentatorubral-pallidoluysian atrophy (DRPLA) protein complex is pathologically ubiquitinated in DRPLA brains. Biochem Biophys Res Commun 1999;260:133–138.
14. Yamada M, Sato T, Shimohata T, et al. Interaction between neuronal intranuclear inclusions and promyelocytic leukemia protein nuclear and coiled bodies in CAG repeat diseases. Am J Pathol 2001;159:1785–1795.
15. Kopito RR. Aggresomes, inclusion bodies and protein aggregation. Trends Cell Biol 2000;10:524–530.
16. Perutz MF. Glutamine repeats and neurodegenerative diseases: molecular aspects. Trends Biochem Sci 1999;24:58–63.
17. Sapp E, Schwarz C, Chase K, et al. Huntingtin localization in brains of normal and Huntington's disease patients. Ann Neurol 1997;42:604–612.

Quinacrine Does Not Prolong Survival in a Murine Creutzfeldt-Jakob Disease Model

Steven J. Collins, MD,[1] Victoria Lewis, BSc (Hons),[1] Marcus Brazier, BSc (Hons),[1] Andrew F. Hill, PhD,[1] Ashley Fletcher, BSc,[2] and Colin L. Masters, MD[1]

Paramount among issues relating to the transmissible spongiform encephalopathies (also known as prion diseases) is the absence of any effective therapy. This need has been heightened by the substantial European and emerging global problem of bovine spongiform encephalopathy and consequent variant Creutzfeldt-Jakob disease. Stimulated by the recent reports of a potent antiprion effect in cell culture–based clearance assays, we studied the utility of quinacrine in a well-characterized in vivo model of mouse-adapted transmissible spongiform encephalopathy. Our results failed to show any evidence that quinacrine is effective when using the simple but objective measure of survival prolongation.

Ann Neurol 2002;52:503–506

Creutzfeldt-Jakob disease (CJD) is the most common human phenotype of the transmissible spongiform encephalopathies (TSEs), a group of invariably fatal neurodegenerative diseases, which also affect animals.[1] CJD typically presents as a rapidly progressive dementia, often accompanied by cerebellar ataxia and myoclonus, with inexorable deterioration to death in less than 1 year. Until recently, TSEs were considered rare, with comprehensive ascertainment studies of classic CJD confirming an annual incidence of approximately one case per million population. The substantial European epidemic, and emerging global problem of bovine spongiform encephalopathy (BSE) and consequent variant CJD (vCJD), has necessitated revision of this attitude. First reported in 1996,[2] final case loads of the vCJD remain uncertain, but despite recent downward revisions based on modeling studies, total numbers are still likely to reach several hundreds to thousands over the coming years.[3,4] These developments have under-

From the [1]Department of Pathology and [2]Department of Public Health, University of Melbourne, Parkville, Victoria, Australia.

Received May 15, 2002. Accepted for publication Jun 14, 2002.

Address correspondence to Dr Collins, Australian National CJD Registry, Department of Pathology, University of Melbourne, Parkville, Victoria, Australia, 3010. E-mail: stevenjc@unimelb.edu.au

scored several exigencies in relation to prion diseases not the least of which is the complete absence of clinically appropriate, effective therapy.

A few compounds, including anthracyclines, amphotericin B, polyanions, and cyclic tetrapyrroles, have been shown in animal studies to have modest antiprion efficacy by prolonging survival, but only if delivered at approximately the time of, or exposed to the chemical from shortly after, inoculation.[5–9] Direct application of these agents to human therapy is quite limited for several reasons, including unacceptable toxicity and the limited ability of the compounds to cross the blood–brain barrier, although the latter would not preclude prophylactic use in situations relating to peripheral inoculation. Reinforcing the findings of a prior in vitro study,[10] and based on a technique previously used to examine the antiprion effects of branched polyamines[11] and sulfated polyanions,[12] interest in the acridine derivative quinacrine recently was strengthened considerably by the report that the lysosomotropic compound could rapidly eradicate production of the disease-associated, protease-resistant isoform of the prion protein (PrP^{sc}) in stably infected murine neuroblastoma (N2a) cell cultures.[13] Quinacrine, an antimalarial drug, has been used in humans for many years with known and acceptable biosafety, and the agent also has the ability to cross the blood–brain barrier.[13] Given the rapidly progressive and invariably fatal outcome of CJD, it was promptly used on compassionate grounds in two such patients with initially encouraging results in at least one patient and a large human treatment trial of these agents is planned.[14]

Prompted by these reports, we studied the efficacy of quinacrine, the most potent antiprion agent in the neuroblastoma cell culture–based PrP^{sc} clearance assays[10,13] in a well-characterized in vivo model of mouse-adapted CJD.

Materials and Methods

Animal handling and killing were in accordance with national prescribed guidelines, with ethical approval for the study granted by the University of Melbourne. Three groups of eight weanling Balb/c female mice were inoculated intracerebrally (into the left parietal region) with 30μl of a 10^{-1} dilution (final concentration in phosphate-buffered saline) of brain homogenate pooled from mice confirmed as dying from a spongiform encephalopathy. The inoculum was prepared by passing through successively higher gauge needles (to 26 gauge) and was not centrifuged before use. All mice were gavage fed 5 days per week and received routine husbandry with food and water available ad libitum. Group 1 served as controls and only received deionized water starting from day 5 postinoculation (PI). Group 2 commenced gavage feeding with quinacrine dihydrochloride (Sigma, St. Louis, MO), 10mg/kg/day in deionized water, from day 5 PI (early treatment group), whereas Group 3 received the same dose of drug from day 65 PI (late treatment group), approximating the midpoint of the incubation period. Groups 2 and 3 both received a loading dose of 20mg/kg of quinacrine on their first day of gavage feeding. The relatively high but therapeutically relevant treatment dose of 10mg/kg/day of quinacrine was chosen to allow the best opportunity to demonstrate any beneficial effects.

Mice were inspected daily for signs of TSE, which included apathy, diminished activity, hunched posture, weight loss, paretic hind legs, and loss of righting reflex and were killed when persistence and progression of these features were clearly evident (usually after a few days). Disease transmission was confirmed by the presence of proteinase K–resistant PrP in the brains of mice by Western immunoblot and evidence of typical spongiform changes in the cerebrum on routine histological examination. The log-rank test for equality of survival was used to compare treatment groups, with p value less than 0.05 considered significant.

Results

Quinacrine appeared well tolerated by the mice with the two incidental losses appearing directly related to the effects of gavage feeding, occurring in Groups 2 and 3, at days 43 and 67 PI, respectively. The brains of these mice were not examined. The mean survival of Group 1 was essentially identical to Groups 2 and 3 as summarized in the Table. The Figure presents an overview of survival, with the log-rank test for equality of survivor functions showing no significant difference between the treatment groups ($p = 0.99$). In addition, neuropathological examination and Western immunoblots for protease-resistant PrP did not show any consistent intergroup differences between the brains of the mice (data not shown).

Discussion

Our results therefore failed to show any evidence that quinacrine offers benefit when using the simple but objective measure of survival prolongation in an in vivo

Table. Comparative Summary of Survival Utilizing Quinacrine Treatment in a Murine Model of Creutzfeldt-Jakob Disease

Experimental Group	Incubation Period, Days (mean ±1 SD)	Number of mice (affected/inoculated)
Group 1/no treatment	140 ± 6.8	8/8
Group 2/early treatment	140 ± 7.3	7/7
Group 3/late treatment	140 ± 10.8	7/7

SD = standard deviation.

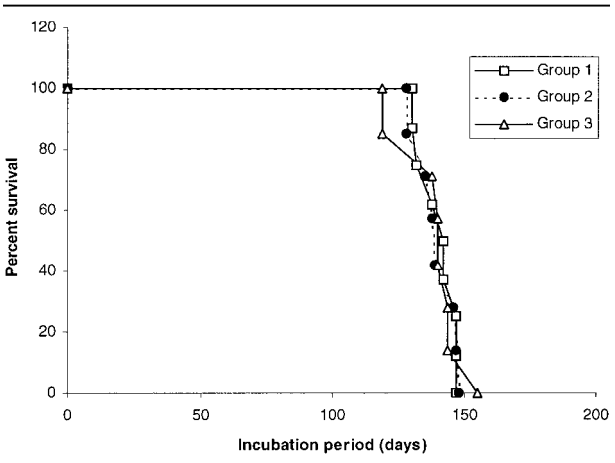

Fig 1. Comparison of the early and late quinacrine treatment groups with the untreated cohort of mice, depicted on survival curves. There was no significant difference in survival. Group 1: no treatment; Group 2: early quinacrine treatment; Group 3: late quinacrine treatment.

model of mouse-adapted CJD. This was somewhat unexpected given that previous studies of Congo Red,[15,16] selected sulfated polyanions,[12,17] and certain tetrapyrroles[5,18] have demonstrated reasonably good concordance between in vitro antiprion potency (using cell-based assays of the inhibition of PrP^{sc} production or its enhanced clearance) and their in vivo efficacy in animal studies. The reasons for such lack of correlation for quinacrine are unknown but are unlikely to relate to the inability to penetrate the blood–brain barrier, as suggested for the poor therapeutic effects of sulfated polyanions when used late in the incubation phase of rodent TSE models.[12,18] Notwithstanding the good ability of quinacrine to reach central nervous system neurons, a speculative explanation for the lack of therapeutic efficacy in our study could relate to the mode of inoculation, with the possibility that benefit may have been conferred if a peripheral transmission route were used.

Although our results do not lend any support for quinacrine antiprion efficacy in the more complex setting of in vivo treatment, they do not completely preclude the possibility of a positive effect in human trials. Variations in beneficial effects, apparently correlating with prion strains, have been reported with in vitro PrP clearance assays using the branched polyamine polypropyleneimine,[11] and also in animal studies using the polyene antibiotic amphotericin B.[7] Hamsters inoculated with the 263K strain of scrapie showed prolonged survival when treated with amphotericin B, whereas these animals and Swiss mice showed no lengthening of the incubation period if infected with the 139H strain of scrapie.

Included in our study design were early and late treatment groups, with the latter starting quinacrine 65 days after inoculation, approximating the midpoint of the incubation period and more closely simulating the authentic clinical situation in which treatment is unlikely to commence until the onset of symptomatic disease. Even those animal studies demonstrating a beneficial survival effect when compounds were used at, or from soon after, inoculation have failed to show efficacy when treatment was significantly delayed.[5] This further underscores current therapeutic limitations, because there are currently no reliable, minimally invasive, preclinical diagnostic screening tests to facilitate early treatment.

A limitation of the current study is that it did not address to any extent, potential mechanisms or pathways subserving disease pathogenesis, which could have given greater insights into the failure of quinacrine's therapeutic effect, as well as provide possible contrast with the findings of the in vitro studies. Nonetheless, correlating with the lack of efficacy seen for survival prolongation, there was no consistent difference in the cerebral neuropathological findings or brain PrP^{sc} levels between the three groups of mice, which stands in clear contrast with the potent ability of quinacrine to eradicate PrP^{sc} from stably infected mouse neuroblastoma cells. The outcome of trials of quinacrine and chlorpromazine use in human TSE is awaited with great interest.

The Australian National Creutzfeldt-Jakob Disease Registry is funded by the Commonwealth Department of Health and Ageing. This study was supported by the National Health and Medical Research Council Program (208978, S.J.C.) and by a Wellcome International Prize Travelling Research Fellowship during the study (A.F.H.).

We thank the staff of the Department of Pathology Animal House for their assistance in the execution of the study.

References

1. Prusiner SB. Prions. Proc Natl Acad Sci USA 1998;95: 13363–13383.
2. Will RG, Ironside JW, Zeidler M, et al. A new variant of Creutafeldt-Jakob disease in the UK. Lancet 1996;347: 921–925.
3. D'Aignaux J, Cousens SN, Smith P. Predictability of the UK variant Creutzfeldt-Jakob disease epidemic. Science 2001;294: 1729–1731.
4. Valleron A-J, Boelle P-Y, Will R, Cesbron J-Y. Estimation of epidemic size and incubation time based on age characteristics of vCJD in the United Kingdom. Science 2001;294: 1726–1728.
5. Priola S, Raines A, Caughey WS. Porphyrin and phthalocyanine anti-scrapie compounds. Science 2000;287:1503–1506.
6. Tagliavini F, McArthur RA, Canciani B, et al. Effectiveness of anthracycline against experimental prion disease in Syrian hamsters. Science 1997;276:1119–1122.
7. Xi YG, Ingrosso L, Ladogana A, et al. Amphotericin B treatment dissociates in vivo replication of the srcapie agent from PrP accumulation. Nature 1992;356:598–601.

8. Ehlers B, Diringer H. Dextran sulphate 500 delays and prevents mouse scrapie by impairment of agent replication in spleen. J Gen Virol 1984;65:1325–1330.
9. Kimberlin RH, Walker CA. Suppression of scrapie infection in mice by heteropolyanion 23, dextran sulfate, and some other polyanions. Antimicrob Agents Chemother 1986;30:409–413.
10. Doh-ura K, Iwaki, Caughey B. Lysosomotropic agents and cysteine protease inhibitors inhibit scrapie-associated prion protein accumulation. J Virol 2000;74:4894–4897.
11. Supattapone S, Nguyen H-O, Cohen F, et al. Elimination of prions by branched polyamines and implications for therapeutics. Proc Natl Acad Sci USA 1999;96:14529–14534.
12. Caughey B, Raymond G. Sulfated polyanion inhibition of scrapie-associated PrP accumulation in cultured cells. J Virol 1993;67:643–650.
13. Korth C, May BC, Cohen F, Prusiner SB. Acridine and phenothiazine derivatives as phamacotherapeutics for prion disease. Proc Natl Acad Sci USA 2001;98:9836–9841.
14. Love R. Old drugs to treat new variant Creutzfeldt-Jakob disease. Lancet 2001;358:563.
15. Caughey B, Race R. Potent inhibition of scrapie-associated PrP accumulation by Congo red. J Neurochem 1992;59:768–771.
16. Caughey B, Ernst D, Race R. Congo red inhibition of scrapie agent replication. J Virol 1993;67:6270–6272.
17. Diringer H, Ehlers B. Chemoprophylaxis of scrapie in mice. J Gen Virol 1991;72:457–460.
18. Caughey WS, Raymond LD, Horiuchi M, Caughey B. Inhibition of protease-resistant prion protein formation by porphyrins and phthalocyanines. Proc Natl Acad Sci USA 1998;95:12117–12122.

Cree Leukoencephalopathy and CACH/VWM Disease Are Allelic at the *EIF2B5* Locus

Anne Fogli, PhD,[1] Kondi Wong, MD,[2] Eleonore Eymard-Pierre, PhD,[1] Jack Wenger, BSc,[2] John-Paul Bouffard, MD,[2] Ehud Goldin, PhD,[3] Deborah N. Black, MD,[4] Odile Boespflug-Tanguy, MD, PhD,[1] and Raphael Schiffmann, MD[3]

Cree leukoencephalopathy is a rapidly fatal infantile autosomal recessive leukodystrophy of unknown cause observed in the native North American Cree and Chippewayan indigenous population. We found in the brain of affected individuals the typical foamy cells with the oligodendroglial phenotype described in central hypomyelination syndrome/vanishing white matter, a syndrome related to mutations in the genes encoding the five subunits of the eucaryotic translation initiation factor eIF2B. In three patients of two Cree families, we found a homozygous missense mutation resulting in a histidine substitution at arginine 195 of ε-eIF2B.

Ann Neurol 2002;52:506–510

An infantile leukoencephalopathy among the native Cree and Chippewayan indigenous population in Northern Quebec and Manitoba was first described in 1988.[1] The onset of Cree leukoencephalopathy (CLE) is between 3 and 9 months of age with death in 100% by 21 months of age. Hypotonia often is noted in early infancy followed by relatively sudden onset of seizures, spasticity, hyperventilation, vomiting, and diarrhea, often in the setting of a febrile illness. Onset is followed by developmental regression, lethargy, blindness, and cessation of head growth seen as flattening of the head circumference curve.[1] Computerized tomography of

From the [1]Institut National de la Santé et de la Recherche Médicale UMR 384, Facultéde Médecine, Clermont-Ferrand, France; [2]Department of Neuropathology at the Armed Forces Institute of Pathology, Washington, DC; [3]Developmental and Metabolic Neurology Branch, National Institutes of Health, Bethesda, MD; and [4]Department of Psychiatry, Université de Montréal, Montréal, Quebec, Canada.

Received Apr 24, 2002, and in revised form Jun 13. Accepted for publication Jun 14, 2002.

Address correspondence to Dr Boespflug-Tanguy, INSERM UMR 384, Faculté de Médecine, 28, place Henri Dunant BP 38, 63001 Clermont-Ferrand Cedex, France. E-mail: odile.boespflug@inserm.u-clermont1.fr

Free Radical Biology & Medicine 45 (2008) 184–192

Contents lists available at ScienceDirect

Free Radical Biology & Medicine

journal homepage: www.elsevier.com/locate/freeradbiomed

Original Contribution

A manganese-superoxide dismutase/catalase mimetic extends survival in a mouse model of human prion disease

Marcus W. Brazier [a,b], Susan R. Doctrow [c], Colin L. Masters [a,b], Steven J. Collins [a,b,*]

[a] Department of Pathology, The University of Melbourne, Victoria 3010, Australia
[b] The Mental Health Research Institute of Victoria, Parkville, Victoria 3052, Australia
[c] Proteome Systems, Inc., 6 Gill Street, Suite H, Woburn, MA, USA

ARTICLE INFO

Article history:
Received 8 February 2008
Revised 31 March 2008
Accepted 2 April 2008
Available online 16 April 2008

Keywords:
Antioxidants
Free radicals
Manganese
Prion diseases
Superoxide dismutase
Therapy
Transmissible spongiform encephalopathy

ABSTRACT

Animal models, and human postmortem studies, of prion disease have demonstrated the presence of heightened oxidative stress in the brain, with additional findings supporting the likelihood that the normal isoform of prion protein directly contributes to neuronal antioxidant defences. Although such data are consistent with the postulate that oxidative stress plays a salient pathogenic role in prion disease, it remains possible that oxidative damage represents a secondary or relatively less important phenomenon in neurons already rendered dysfunctional from other primary insults. To provide further insights into the relative pathogenic importance of oxidative stress, we employed a potent manganese-superoxide dismutase/catalase mimetic, EUK-189, as a therapeutic in our mouse model of human prion disease. A significant but relatively modest prolongation of survival in EUK-189-treated mice was observed, which correlated with reductions in oxidative, especially nitrative, damage to proteins when compared to untreated disease controls. Lesion profiling also revealed reductions in spongiform change in specific brain regions of terminally sick EUK-189-treated mice. Our results are consistent with heightened oxidative stress playing a pathogenic role in prion disease but underscore the need for more biologically potent and, most likely, broader spectrum antioxidant treatments if more successful amelioration is to be achieved.

Introduction

Transmissible spongiform encephalopathies (TSE), also known as prion diseases, are a group of neurodegenerative disorders that affect humans and animals. Human forms of TSE include Creutzfeldt-Jakob disease (CJD), Gerstmann-Sträussler-Scheinker syndrome (GSS), and fatal familial insomnia while scrapie of sheep and goats, bovine spongiform encephalopathy and chronic wasting disease of deer, elk, and moose constitute the main animal forms of the disease. A central event in the pathogenesis is conversion of the normal or cellular form of the prion protein (PrPc), a glycosylphosphatidylinositol-membrane-anchored glycoprotein, into a β-sheet rich, protease-resistant isoform, termed PrPres. Typical neuropathological features of TSE consist of vacuolation of the neuropil, astrocytic gliosis, neuronal loss, and extracellular deposition of PrPres in the form of plaques (reviewed in [1]).

Recent data from different laboratories suggest that PrPc may be a component of cellular antioxidant defence systems, although contradictory findings have been reported [2]. Wong et al. [3] detected a reduction of total superoxide dismutase (SOD) activity in normal brain homogenates after immuno-depletion of PrPc while Cu/Zn-SOD and Mn-SOD activities remained unchanged when compared to nondepleted homogenates. Similarly, brain homogenates from prion protein knockout (PrP%) mice have been shown to have lower total SOD activity, although greater Mn-SOD activity when compared to wild-type mice [4]. In cell culture models, neurons devoid of PrPc expression have been shown to have an increased sensitivity to superoxide anions [5], hydrogen peroxide [6] and manganese [7] and copper toxicities [8] when compared to controls. Wong et al. [9] also compared immunopurified total PrP from terminal scrapie-infected mouse brains to controls and found that PrP preparations from controls possessed 10 times the total SOD activity compared with those isolated from diseased brains. This finding is consistent with PrPc having a SOD-like function and that the disease-associated conformational change of PrPc to the PrPres isoform results in the loss of this function, or that PrPres and/or other cellular changes during infection inhibit the SOD-like activity of PrPc [10]. At neutral pH, within Cu/Zn-SOD enzymes,

Abbreviations: CJD, Creutzfeldt-Jakob disease; CNS, central nervous system; dpi, days *post*inoculation; GSS, Gerstmann-Sträussler-Scheinker syndrome; H&E, hematoxylin and eosin; ic, intracerebral; ip, intraperitoneal; Mn-SOD%, Mn-SOD knockout; Mn-TBAP, manganese 5,10,15,20-tetrakis; pCO, protein carbonylation; PK, proteinase K; NT, nitrotyrosine; PrPc, cellular isoform of prion protein; PrPres, protease resistant disease-associated isoform of PrPc; PrP%, PrPc knockout; SOD, superoxide dismutase; TSE, *t*ransmissible spongiform encephalopathy.

* Corresponding author. Steven Collins c/o Australian National CJD Registry, Department of Pathology, The University of Melbourne, Parkville, Victoria 3010, Australia. Fax: +61 3 8344 4004.
E-mail address: stevenjc@unimelb.edu.au (S.J. Collins).

0891-5849/$ – see front matter © 2008 Elsevier Inc. All rights reserved.
doi:10.1016/j.freeradbiomed.2008.04.006

copper can oscillate between the +1 and +2 valence states which is an important component of the catalytic activity during the dismutation of superoxide molecules. Similarly, the SOD-like activity of recombinant PrPc has been reported to depend on copper [11] and it is noteworthy that the putative dismutase activity of PrPc has been shown to decrease contemporaneously with the release of bound copper during the progress of experimental mouse models of prion disease [12].

Recent studies also suggest that PrPc may influence normal mitochondrial, particularly antioxidant, function. Using PrP% mice, Miele et al. [13] demonstrated diminished brain mitochondria with abnormal morphology and the mitochondria of these mice were shown to contain elevated, possibly compensational, levels of Mn-SOD protein and enzymatic activity. Further, mitochondrial preparations from transgenic PrPc-overexpressing mice have been demonstrated to contain decreased Mn-SOD activity [14] supporting the notion that PrPc may be involved in reciprocal mitochondrial antioxidant activities. The authors also showed that, as the PrPc-overexpressing mice age, they develop a spontaneous neurological dysfunction concomitant with an abnormal mitochondrial localization of PrPc when compared to wild-type controls. The precise relevance and relative importance of all these observations to in vivo TSE pathogenesis is incompletely resolved but as a corollary there is considerable evidence for heightened oxidative stress during the course of prion disease [9,15–21].

Arguably the most consistent alterations observed in rodent models of prion disease directly assessing oxidative stress are diminished SOD (Cu/Zn-SOD or Mn-SOD) or SOD-like activity [9,12,18,21] and heightened lipid peroxidation [9,15,16,18,21]. Similar changes have been detected in the brains of patients dying from sporadic CJD [22]. Additional direct support for a relative or absolute insufficiency of SOD activity in prion disease was shown in the study of Lee et al. [18], with brains of mice infected with 87V scrapie prions showing a doubling of the production rate of the superoxide radical compared to control mice. Although various biochemical mechanisms of lipid peroxidation are recognised, the presence of this form of oxidative stress suggests the likelihood of hydroxyl radical generation, and possibly the direct involvement of transition metal complexes causing decomposition of preformed lipid hydroperoxides [23]. Less frequently described types of brain damage in in vivo models and studies of human prion disease include oxidation of proteins [9,19,22], and nucleic acids [20,24], as well as changes supporting increased nitrative damage [9,17,19]. The role of hydrogen peroxide in the oxidative stress of TSE is unclear as production rates have not been directly assessed; unfavourable changes in central nervous system (CNS) catalase activity have not been described [18,21], while brain glutathione peroxidase activity has been reported to be increased [21], decreased [9], or unchanged [18]. Collectively, the aforementioned data are consistent with the principle that increased reactive oxygen and nitrogen species occur in TSE, probably accompanied by a decrease in antioxidant defences (including mitochondrial), causing heightened oxidative damage to the brain, and thereby are a major or significant contributor to pathogenesis in both prion-infected experimental animals and human patients.

Eukarion salen-manganese complexes, such as EUK-8, EUK-134, and EUK-189, have been shown to act as SOD and catalase mimetics, demonstrating activity against both oxidative and nitrative stresses [25] with varying levels of antioxidant capacity [26–28]. In addition to their ability to extend the life span of *Caenorhabditis elegans* [29], this group of synthetic catalytic antioxidants has been shown to be protective in a wide variety of in vitro [30,31] and in vivo models manifesting heightened oxidative stress [32–40]. Animal models of multiple sclerosis [32], amyotrophic lateral sclerosis [33], ischemic brain injury [34], excitotoxic neuronal damage [36], ataxia telangiectasia [37], Parkinson's disease [38], and age-associated cognitive impairment [39] have all shown benefit from therapeutic administration of Eukarion SOD/catalase mimetics, specifically showing reduction in protein oxidation [33,39], lipid oxidation [33,37,39], protein nitration damage [33,36], and oxidative change in nucleic acids [39]. More recently, EUK-189 was shown to reduce cataract incidence in aging Tg2576 mice which model Alzheimer's disease [40]. Of particular interest was a study using EUK-189, in which the development of brain vacuolation was prevented in a Mn-SOD knockout (Mn-SOD%) mouse model [28]. When Mn-SOD% mice (a lethal phenotype) were treated with a peripherally acting SOD mimetic, manganese 5,10,15,20-tetrakis (Mn-TBAP), they survived beyond 2 weeks of age but developed a free radical-mediated spongiform encephalopathy [41] reminiscent of the neuropathological changes observed in TSE. Treatment with EUK-189 from 3 days of age significantly extended the life span of Mn-TBAP-treated Mn-SOD% mice and was shown to completely prevent the development of spongiform change. In all animal models where the therapeutic activity of EUK antioxidants takes place within the CNS [32–40], it is to be stressed that the drugs were always administered peripherally attesting to their ability to effectively cross the blood–brain barrier.

Acknowledging the reported deficiency of SOD and SOD-like activity in prion disease, as well as the considerable overlap in the type of oxidative damage observed in TSE and that which is effectively ameliorated by the Eukarion salen–manganese complexes in other models, we undertook a study of the therapeutic efficacy of EUK-189 in our well characterised mouse model of human prion disease [15]. To the best of our knowledge, the present study is the first trial of a primarily antioxidant compound as therapy in an animal model of prion disease. Daily intraperitoneal (ip) administration of EUK-189 was found to significantly extend the incubation period, reduce nitrative and oxidative damage to proteins, and selectively reduce the brain vacuolar lesion burden in treated mice compared to untreated disease controls.

Materials and methods

Mice and inoculations

Animal handling and sacrifice were in accordance with national prescribed guidelines with ethical approval for the study granted by the University of Melbourne Animal Ethics Committee. Thirty-five female weanling Balb/c mice were inoculated with M1000 prions, a mouse-adapted strain originally isolated from a patient most likely dying from GSS [42]. Each mouse was inoculated intracerebrally (ic), as previously described [15,43], with 30 μl of a 0.0001% (w/v in PBS) diseased mouse brain homogenate (8.9×10^7 ID_{50} units/g brain). Twenty mice were treated with EUK-189 (Proteome Systems, MA) and 15 served as untreated disease controls. Five EUK-189-treated and five disease controls were euthanised at 100 days postinoculation (dpi) to comparatively assess early neuropathological changes, PrPres levels, and oxidative damage. Remaining mice were euthanised after displaying persistent symptoms of prion disease, including hind limb

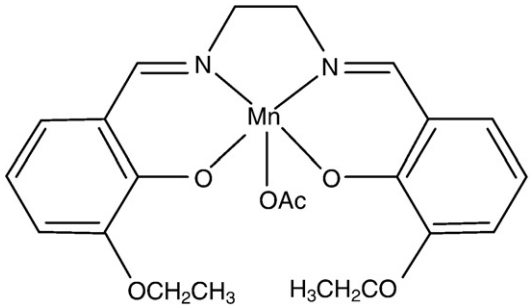

Fig. 1. Chemical structure of manganese (III)-*N*,*N*′ ethylenebis-(2-ethoxysalicylideneimine) acetate (EUK-189). EUK-189 contains ethoxy groups at the 3,3′ positions of its salen rings making it considerably more lipophilic than precursor analogs.

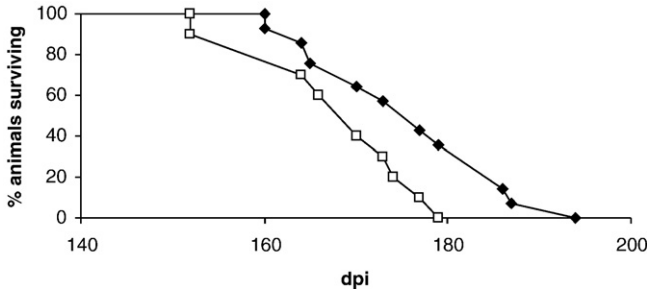

Fig. 2. Survival curves comparing M1000-infected mice treated with EUK-189 to untreated disease controls. At each time point when mice were euthanised, the percentage of mice surviving in that group is plotted against days postinoculation (dpi). The mean survival period of the EUK-189-treated group was significantly longer than the untreated control group (log-rank test $P=0.032$; t test $P=0.046$). □, untreated disease controls; ♦, EUK-189-treated group.

paresis and loss of righting reflexes. For biochemical assessments of brain oxidative damage, 8 additional age/sex-matched noninoculated Balb/c mice, 4 for each time point, were also included, serving as naïve controls. All mice were culled by cervical dislocation under deep anesthesia.

Drug treatment

Manganese (III)-*N*,*N*′ ethylenebis-(2-ethoxysalicylideneimine) acetate (EUK-189) (Fig. 1), synthesized as described previously [35], was stored in a desiccation chamber as a dry powder and solubilised in deionised water once a week to make a weekly working stock of 6 mM solution, which was stored at 4°C. Mice were administered 200 μl, equating to 30 mg/kg [28], by ip injection 7 days per week beginning at 7 dpi.

Biochemical assessments of oxidative damage

For biochemical assays, brain tissue from each of four mice in the untreated disease control and EUK-189 treatment groups at both 100 dpi and terminal disease, as well as the appropriate age/sex-matched naïve controls, was individually homogenised to 10% (w/v) in cold PBS containing 5 mM BHT, and stored at −80°C prior to analysis.

Lipid peroxidation

Aliquots were analysed in duplicate for free malondialdehyde (MDA) and hydroxyalkenals (HAE), aldehydic breakdown products of lipid peroxidation, using the Bioxytech LPO_{586} (Oxis, OR) colorimetric assay as per the manufacturer's instructions and described previously [15].

Protein nitration

Aliquots of BHT-containing brain homogenates were analysed in duplicate for protein nitration using the Bioxytech enzyme immunoassay for nitrotyrosine (NT) (Oxis). Briefly, antigens were captured using anti-NT monoclonal antibody-coated 96-well plates and detected with biotin-labeled polyclonal anti-NT sera and streptavidin-conjugated peroxidase. Tetramethylbenzidine was employed as a chromogen whose yellow activated product was detected by measuring absorbance at 450 nm.

Protein carbonylation

Protein carbonylation (pCO) was assessed using the OxyBlot protein oxidation detection kit (Chemicon International, CA). Duplicate aliquots of brain homogenate were denatured in 12% SDS and then protein carbonyl groups were derivatised with 2,4-dinitrophenylhydrazine to generate 2,4-dinitrophenylhydrazone (DNP) moities. Homogenates were then subjected to Western immunoblot and DNP moities were detected with anti-DNP primary antibody and HRP-conjugated secondary antibody. Densitometric quantification of Western blots was performed using a LAS-3000 (Fujifilm, Tokyo, Japan) and Multi Gauge software (Fujifilm). To enable comparison of the treatment group and controls between separate blots, all bands were normalised to an internal BSA standard with attached DNP residues.

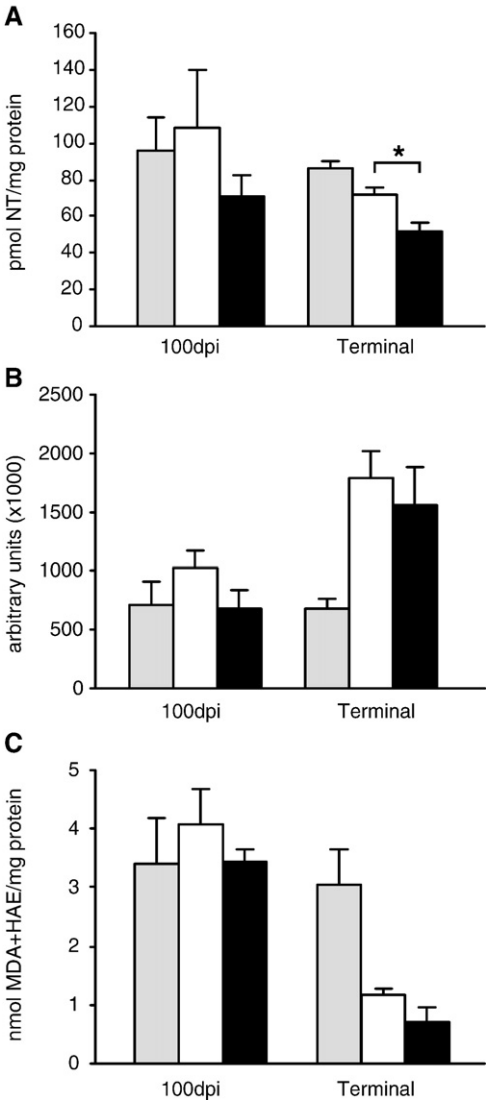

Fig. 3. Biochemical assays performed to determine the oxidative status of brains of EUK-189-treated compared to both untreated M1000-inoculated mice at 100 days postinoculation (dpi) and at the terminal stage of disease, as well as age/sex-matched uninoculated controls. At 100 dpi, brains from the treated group were demonstrated to contain nonsignificant reductions in nitrated protein tyrosine (NT) residues (A), protein carbonyl (pCO) moities (B; expressed as relative arbitrary densitometric units of protein carbonylation), and aldehydic lipid breakdown products (C) in comparison with the untreated disease group. For NT (A), levels at the terminal stage of disease in untreated disease controls were similar to the amounts observed in uninoculated naïve controls and to those recorded in untreated disease controls at 100 dpi, with this form of oxidative damage significantly reduced in EUK-189-treated mice at completion of the experiment in comparison with both untreated disease (*$P=0.019$) and naive controls. Total pCO (B) was not significantly different between treated and untreated inoculated mice at the terminal stage of disease, with total pCO in treated mice remaining significantly above that found in naive controls; however, compared to the total pCO levels observed in untreated diseased mice at 100 dpi, pCO levels in untreated diseased animals became significantly higher ($P=0.03$) by the completion of the experiment, while total pCO in EUK-189-treated animals did not show a significant further increase. Free MDA/HAE (C) was not different between disease controls and EUK-189-treated mice at the terminal stage, with levels similarly reduced in both groups when compared to those found in mice culled around the mid-incubation point, as well as in comparison to the naïve group. ▒, naïve controls; □, untreated disease controls; ■, EUK-189-treated group.

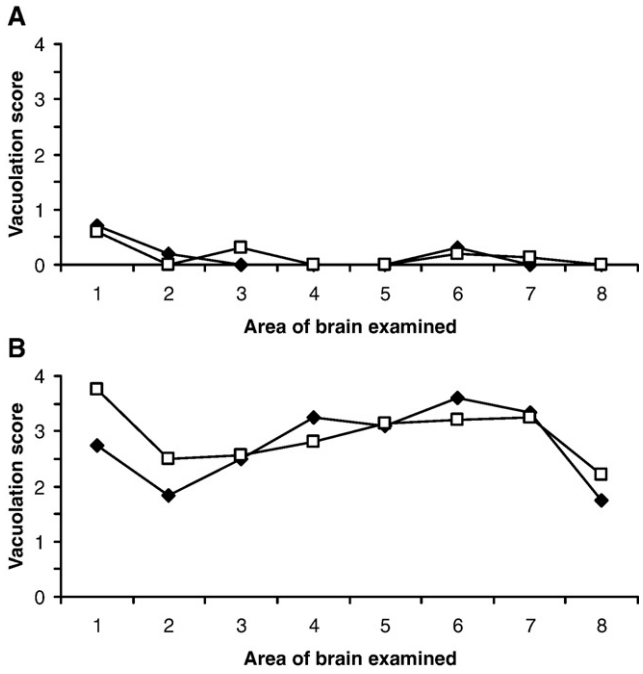

Fig. 4. Lesion profiles of brain vacuolation in M1000-infected mice treated with EUK-189 compared to untreated disease controls at 100 days postinoculation (dpi; A) and at the terminal stage of disease (B). Hematoxylin and eosin-stained sagittal sections of half-brains were visually graded for the severity of spongiform change (vacuolation) in 8 brain regions: (1) hippocampus, (2) thalamus, (3) occipital lobe, (4) parietal lobe, (5) frontal lobe, (6) cerebellum, (7) basis pontis, and (8) caudate/putamen. Lesion severity was scored using a 9-point grading system ranging from 0 to 4 and the means of each group plotted for each region. At 100 dpi there were minimal pathological changes and no difference between EUK-189-treated mice and untreated controls, whereas a significant reduction in the hippocampus was observed in treated mice at the terminal stage of disease (P=0.0051). □, untreated disease controls; ◆, EUK-189-treated group.

Histology and immunohistochemistry

Brains were quickly removed and sagittally hemisectioned with one half-brain from each untreated disease control or EUK-189-treated mouse immersion fixed in 10% neutral buffered formalin. Fixed tissue was treated with 99% formic acid for 1 h at room temperature to reduce tissue infectivity before paraffin embedding. Mounted brain sections from all groups were stained with hematoxylin and eosin (H&E) for histological analyses with adjacent serial sections utilised for immunohistochemical detection of PrPres plaque burden and astrocytic gliosis as previously described [15]. The anti-PrP monoclonal antibody, ICSM18 (generous gift from Prof J. Collinge), was applied at a dilution of 1:500 and anti-GFAP polyclonal sera (DAKO) was applied at 1:50.

Lesion profiles

To generate lesion profiles [44], sagittal sections of half-brains from untreated disease control and EUK-189-treated mice were visually graded for the severity of the various pathological changes including vacuolation, astrocytic gliosis, and PrPres plaques over eight brain regions: (1) hippocampus, (2) thalamus, (3) occipital lobe, (4) parietal lobe, (5) frontal lobe, (6) cerebellum, (7) basis pontis, and (8) caudate/putamen. Grading of EUK-189-treated (n=6) and untreated disease control (n=8) tissue sections were performed blinded to the treatment status of the mice, with reproducibility of scoring confirmed by a second blinded scoring examination. Lesion severity was scored using a 9-point grading system ranging from 0 to 4, the latter representing the most severe extent of lesion incidence that could be observed at the terminal stage of disease.

Western immunoblot analysis

For Western immunoblot analysis, half-brains from untreated disease control and EUK-189-treated mice were quickly frozen and then stored at -70°C until use. Western immunoblotting for PrPres was performed as previously described [15] using ICSM-18 monoclonal antibody at a 1:25,000 dilution. To assess equivalence of protein loading across the gel, undigested aliquots of the same brain homogenates were Western-immunoblotted utilizing anti-β-tubulin monoclonal antibody (Sigma, Castle Hill, Australia) at a 1:15,000 dilution. Horseradish peroxidase-labeled band quantification was performed as described above, using a LAS-3000 and Multi Gauge software. PrPres levels in the two groups (n=3 in each group) were

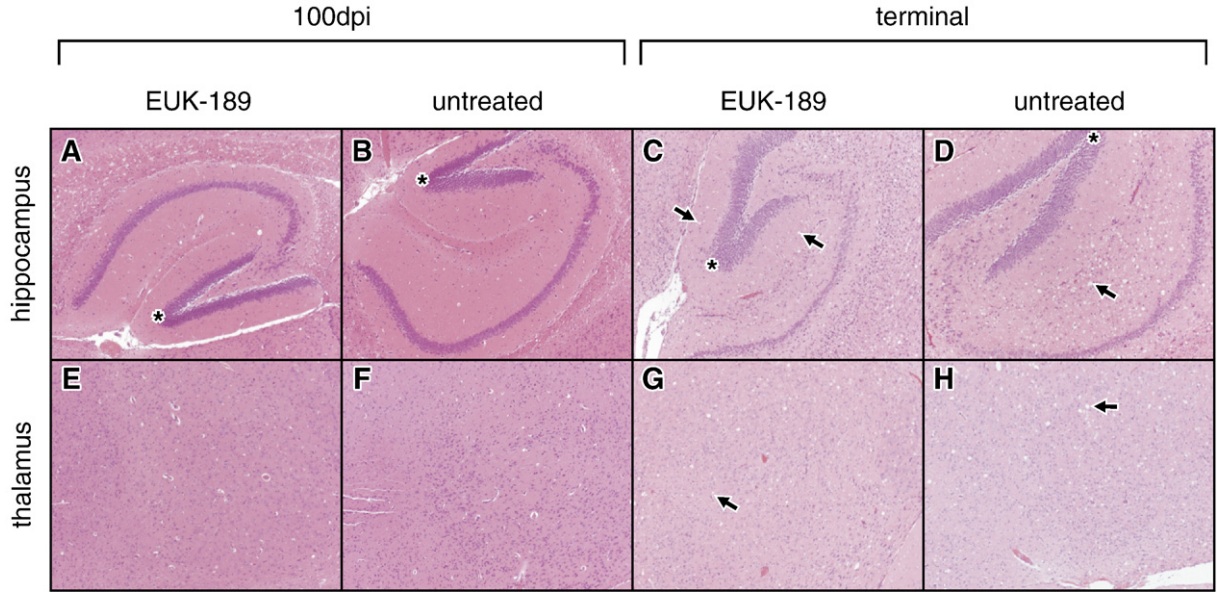

Fig. 5. Photomicrographs displaying spongiform change in the brains of EUK-189-treated and untreated disease mice. Sagittal brain sections were stained with hematoxylin and eosin for morphological examination. In M1000-inoculated mice that were euthanised at 100 days postinoculation (dpi), there was only minimal spongiform change regardless of treatment (A,B,E,F). Mice treated with EUK-189 had significantly less vacuolation in the hippocampus (C) and a clear trend to reduced spongiform change in the thalamus (G) at the terminal stage of disease when compared to untreated controls (D and H, respectively). Original magnification 200×, arrows highlight vacuoles; asterisks highlight the dentate gyrus.

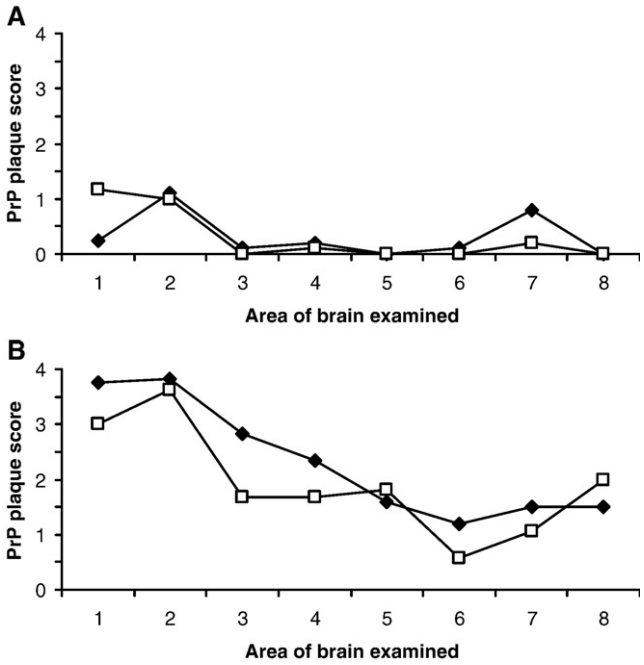

Fig. 6. Brain lesion profiles based on immunohistochemical detection of PrP in M1000-infected mice treated with EUK-189 compared to untreated disease controls at 100 days postinoculation (dpi; A) and at the terminal stage of disease (B). Sagittal sections of half-brains were immunohistochemically stained as described under Materials and methods and then visually graded for the degree of PrP positivity in 8 brain regions: (1) hippocampus, (2) thalamus, (3) occipital lobe, (4) parietal lobe, (5) frontal lobe, (6) cerebellum, (7) basis pontis, and (8) caudate/putamen. Immuno-positivity was scored using a 9-point grading system ranging from 0 to 4 and the means of each group plotted for each region. At 100 dpi there were minimal pathological changes and no difference between EUK-189-treated mice and untreated controls, whereas significant differences were observed at the terminal stage of disease in the occipital lobe ($P=0.0024$), hippocampus ($P=0.027$), and the parietal lobe ($P=0.036$). □, untreated disease controls; ♦, EUK-189-treated group.

compared at both 100 dpi and at terminal disease after adjustment for protein loading, using separate but duplicated immunoblots.

Statistical analysis

Incubation period data were analysed for statistical significance by Student *t* test and log-rank test using GraphPad Prism software (GraphPad Software CA). Intergroup comparisons of oxidative damage assay data were made utilizing the Student *t* test while comparisons of histopathological lesion profiles utilized a Mann-Whitney *U* test for nonpaired variants. In all cases the level of significance was set at $P<0.05$.

Results

Diseased control mice survived an average of 169 dpi (SE +/– 3) while EUK-189-treated mice survived significantly longer, living to a mean of 177 dpi (SE +/– 3), (*t* test and log-rank test $P=0.046$ and 0.032, respectively). One treated mouse died 97 dpi without displaying any symptoms of disease and was subsequently omitted from data analyses; otherwise daily ip administration of EUK-189 was well tolerated. Fig. 2 depicts the survival curves of both groups of inoculated mice where, at each time point when mice were euthanised, the percentage of mice surviving in that group is plotted against dpi. All mice succumbed to disease and displayed identical late-stage symptoms of reduced activity, hunched posture, weight loss, hind-limb paresis and the loss of righting reflexes.

To assess the specific type and extent of any attenuation in oxidative stress in our EUK-189-treated mice, and correlate this to the positive effects on survival, various markers of oxidative damage were assessed biochemically, including lipid peroxidation (specifically the free aldehydic breakdown products MDA and HAEs), protein carbonylation, and tyrosine nitration. Trends toward reduced oxidative damage were seen for all markers at 100 dpi in EUK-189-treated mice compared to untreated disease controls, with average levels equivalent to or below

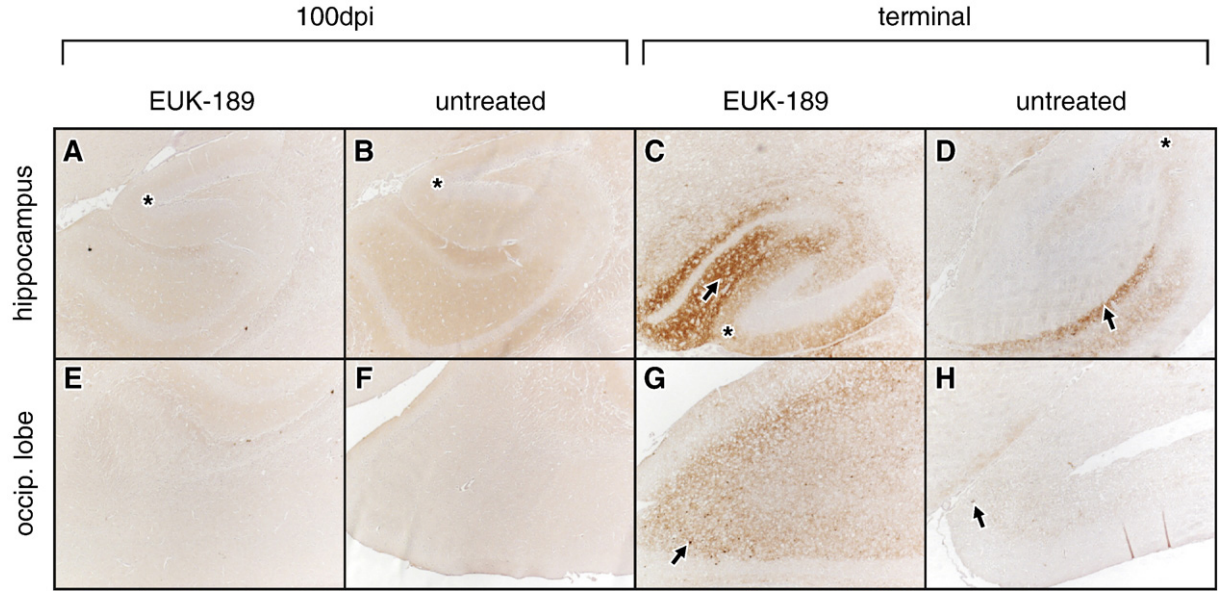

Fig. 7. Photomicrographs showing the degree of brain immunohistochemical PrP positivity in M1000-infected mice treated with EUK-189 compared to untreated disease controls. Sagittal brain sections were probed with the anti-PrP antibody, ICSM-18, to detect PrP deposits. Overall, minimal PrP positivity was evident in the brains of M1000-inoculated mice that were euthanised at 100 days postinoculation (dpi), regardless of treatment (A,B,E,F). At the terminal stage of disease, mice treated with EUK-189 had a greater plaque burden in the hippocampus (C), the occipital lobe (G), and the parietal region (data not shown) when compared to the same regions in untreated controls (hippocampus:D; occipital lobe:H). Original magnification 200×, arrows highlight PrP deposits; asterisks highlight the dentate gyrus.

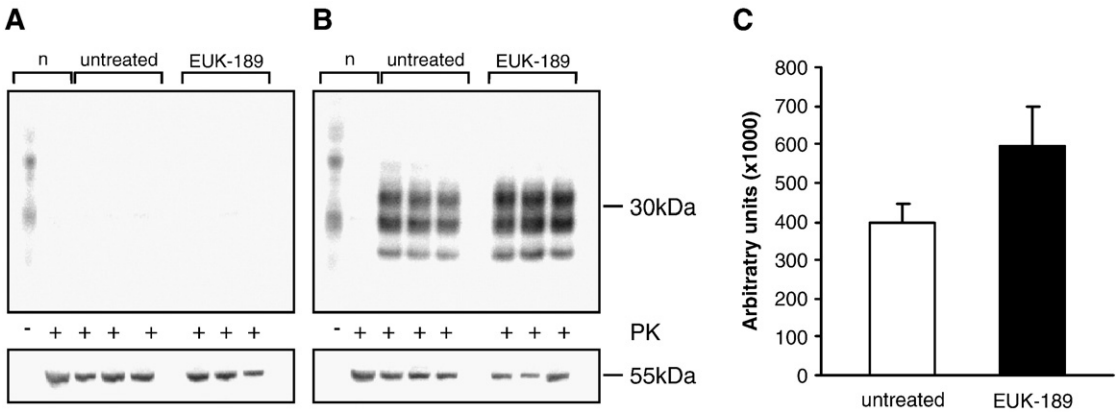

Fig. 8. Comparative Western immunoblot analysis of brain PrPres levels in EUK-189-treated and untreated M1000-inoculated mice at 100 days postinoculation (dpi) (A) and at the terminal stage of disease (B). Negligible levels of PrPres were observed at 100 dpi in both EUK-189-treated and untreated disease mice (A; upper image). Although there was some intragroup variation in brain PrPres levels at the terminal stage of disease (B; upper image), there was no significant difference in the brain PrPres burdens of EUK-189-treated mice and untreated controls when assessed densitometrically and corrected for protein loading (C; □, untreated disease controls; ■, EUK-189-treated group). Equivalence of protein loading was assessed by probing for β-tubulin (A and B; lower images) in undigested aliquots of the same brain homogenates. n, normal mouse; PK, proteinase K digestion. Molecular weight markers are indicated on the right.

those observed in naive age/sex-matched controls (Fig. 3). For NT, levels of protein nitration at the terminal stage of disease in untreated disease controls were similar to the amounts observed in uninoculated naïve controls and indistinguishable from those recorded in untreated disease controls at 100 dpi. This form of oxidative damage was significantly reduced in EUK-189-treated mice at completion of the experiment in comparison to both untreated disease ($P=0.019$) and naive controls ($P=0.004$; Fig. 3A). In contrast, total pCO was not significantly different between treated and untreated inoculated mice at the terminal stage of disease and, although levels were relatively decreased in EUK-189-treated versus untreated diseased animals, total pCO in treated mice remained just significantly above that found in naive age/sex-matched controls ($P=0.043$; Fig. 3B). However, compared to the total pCO levels observed in untreated diseased mice at 100 dpi, we found pCO levels in untreated diseased animals became significantly higher ($P=0.03$) by the completion of the experiment, while total pCO in EUK-189-treated animals did not show a further significant increase at the terminal stage of disease. This is consistent with partial protection against this form of oxidative stress in EUK-189-treated mice. Free MDA/HAE was not different between disease controls and EUK-189-treated mice at the terminal stage (Fig. 3C) with levels similarly reduced in both groups when compared to those found in mice culled around the mid-incubation point, as well as in comparison to the naïve group that were age-matched to the terminal stage of disease.

The temporal evolution and topographical distribution of neuropathological changes are generally characteristic of particular prion strain–host combinations. Indeed, the pattern of pathological abnormalities across various brain regions is sufficiently stereotyped to define a "lesion profile," which is used as one criterion for prion strain typing [45]. In our mouse model, the hippocampus and thalamus are the first areas to show vacuolation and abnormal prion protein deposition from around the mid-incubation period, although at terminal disease these changes are widespread, albeit with differential emphasis including complete sparing of the cerebellum [15].

When the brains of mice were examined at 100 dpi, there were only minor neuropathological changes evident (Figs. 4A and 6A), with no difference in vacuolation (Fig. 5), PrP-immunostaining (Fig. 7), or astrocytic gliosis (data not shown) between EUK-189-treated and untreated disease controls. At the terminal stage of disease, however, histological examination of H&E-stained brain sections from mice treated with EUK-189 revealed that the thalamus and hippocampus were relatively spared of vacuolar lesions when compared to the untreated control group (Figs. 4B and 5), with the hippocampus showing a statistically significant difference ($P=0.0051$). Scores for the hippocampus were very consistent but there was greater variation in the thalamus, with one treated mouse almost devoid of vacuoles. All other brain regions examined showed considerable abnormalities but no discernable differences between groups.

In contrast to the regional ameliorating effects observed in relation to spongiform change, comparative immunohistochemical analyses showed that the EUK-189-treated group had significantly elevated PrP positivity in several brain regions (hippocampus $P=0.027$; parietal lobe $P=0.036$) with the most pronounced difference occurring in the occipital lobe ($P=0.0024$; Figs. 6B and 7). Western immunoblots of brain homogenates comparing the amount of PrPres in EUK-189-treated and untreated diseased animals showed negligible levels at 100 dpi in both groups (Fig. 8A). At the terminal stage of disease, however, densitometric analysis revealed a trend toward elevated brain PrPres in the EUK-189-treated group (Figs. 8B and C). Astrocytic gliosis was not different between EUK-189-treated and untreated disease controls in any of the brain regions examined at 100 dpi and terminal disease (data not shown).

Discussion

Irrespective of whether PrPc harbours SOD-like catalytic activity, numerous reports have documented the presence of oxidative damage within the CNS in prion disease, suggesting that heightened oxidative stress may play an important causal role in TSE pathogenesis. Based on this hypothesis, and in accord with the approach of a number of previous in vivo paradigms wherein oxidative stress has been implicated as an integral component of pathogenesis [28,33–40], our study offers "proof of principle" support by demonstrating a significant beneficial treatment effect via use of a manganese-SOD/catalase mimetic, EUK-189. Through this proof of principle approach, our findings validate and extend the pathogenetic relevance of previous studies demonstrating evidence of increased CNS oxidative stress in TSE.

Directly correlating with the prolongation of survival in the EUK-189-treated mice, we observed significant but selective reduction in the CNS oxidative damage profile in these mice compared to untreated animals. The salient finding in the brains of antioxidant-treated mice was a reduction in NT levels at the terminal stage of disease, with levels significantly reduced below those observed in uninoculated age/sex-matched mice. Evidence for increased reactive nitrogen species, and specifically NT levels, has been reported in TSE models [9,19], as has a reduction in this type of damage, to levels found in unchallenged control animals, when manganese-SOD/catalase mimetics were employed in

other in vivo paradigms [33,36]. NT is generated by the covalent substitution of a NO_2 moiety at either ortho positioned carbon in the phenolic ring of tyrosine residues, and although some nonspecificity exists, it is widely used as a marker of peroxynitrite (OONO-) production. This type of protein nitration can lead to deleterious effects on normal function such as attenuation of inherent catalytic activity or interference in cellular signaling. Reactive nitrogen species such as nitrogen dioxide and OONO- are also capable of performing such substitution reactions within the phenolic rings of other aromatic amino acids such as tryptophan and phenylalanine. Most commonly, OONO- is formed from the combination of superoxide and nitric oxide radicals. Under normal physiological conditions SOD concentrations are around 100-fold greater than nitric oxide, allowing SOD to outcompete nitric oxide in reactions with superoxide [46]. Rodent TSE models directly assessing oxidative stress have revealed diminished SOD (Cu/Zn-SOD or Mn-SOD) or SOD-like activity [9,12,18,21]. Hence, our findings support the postulate that increases in reactive nitrogen species (particularly OONO-) play a direct pathogenic role in TSEs and are a priori in keeping with EUK-189 enhancing SOD-like activity in the brains of treated mice, thereby reducing OONO- and consequently the potentially damaging effects of elevated protein nitration.

In contrast to what was found with total protein carbonylation in untreated diseased mice, levels of NT did not increase further from those observed at 100 dpi. As outlined, under pathological conditions in which concentrations of SOD and SOD-like activity are diminished, superoxide in such circumstances could potentially be allowed to bind to the nitric oxide radical to form reactive OONO-, one of the key generators of NT. The explanation for the lack of a continuing increase in NT levels in our untreated diseased mice is unclear but may relate to the development of a new compensatory steady-state equilibrium from around the mid-incubation period, albeit at a deleteriously higher level, with ongoing degradation and removal from detection of modified proteins within neurons containing the highest amounts of NT [47].

Although perturbations to cellular SOD activities are commonly reported in TSE, there is considerable variation and greater complexity in the findings. In a previous report assessing SOD and SOD-like activity over the time course of disease evolution [12], Cu/Zn-SOD and SOD-like activity decreased from around the mid-incubation period, while Mn-SOD activity increased. Other reports have described reduced Mn-SOD activity at terminal disease, either unchanged or increased Cu/Zn-SOD activity [18,21], or reductions in all three of Cu/Zn-SOD, Mn-SOD, and SOD-like activities [9]. These divergent changes may relate to different experimental methodologies, including the precise prion strain-host combination utilised, but underscore the likelihood of a mechanistically complex situation wherein it is not easy to accurately anticipate consequences. The precise cellular site of increased superoxide radical generation, shown to occur in TSE models [18], and the degree and specific location of any protective cytogenic responses are likely to be among a number of important factors influencing the ultimate phenotypic outcome.

Protection against other forms of oxidative stress, such as protein carbonylation and lipid peroxidation, was much less successful. As similarly reported previously in a TSE mouse model [9], we found increased levels of total pCO in untreated diseased mice at the terminal stage of disease. We found some restriction in this form of oxidative damage in our EUK-189-treated mice, but not the level of efficacy described in prior experiments employing manganese-SOD/catalase mimetics in other animal disease models [33,39]. The superior efficacy (with complete attenuation of age-related increases in brain total pCO) found in one study may relate to enhanced drug bioavailability and, therefore, potency through use of continuous delivery osmotic infusion pumps [39]. In support of this possibility, sustained release delivery of EUK-189 has been shown to be effective in rodent models at doses 10- to 100-fold lower than those given by injection [37–39]. However, drug pharmacokinetics do not appear to be the obvious explanation in relation to the report of Jung and co-workers [33]. This group studied a mouse model of genetic motor neurone disease in which manganese-SOD/catalase mimetics were delivered three times weekly by ip injection, with the total weekly SOD units dose given less than half the amount given by the same route in our study. This outcome also makes it unlikely that the limited efficacy with EUK-189 in our study is simply due to poor access to the CNS. In models requiring access beyond the blood–brain barrier for treatment effect, EUK-189 has been found to be more biologically potent than EUK-134 and other derivatives of at least equal catalytic activity [28,31]. As a corollary, this particular SOD/catalase mimetic contains ethoxy groups at the 3,3′ positions of its salen rings (Fig. 1) making it more lipophilic than other EUK compounds.

No therapeutic effect was observed in relation to lipid peroxidation. Congruous with what we reported previously in our in vivo model [15], levels of free aldehydic breakdown products were reduced at terminal disease compared to around the mid-incubation period, but with similar levels in both EUK-189-treated and untreated diseased animals. Unexpectedly, however, free MDA/HAE levels were well below those observed in age/sex-matched naïve mice, with the explanation for this counterintuitive finding unclear. The biochemical technique employed measures ongoing lipid peroxidation not cumulative damage. Part of the explanation may therefore relate to the extended time period of disease and the inefficacy of this antioxidant, with the progressive loss of a large number of neurons most susceptible to this form of oxidative damage, such that by the terminal stage of disease only the relatively resistant neurons remain. Irrespective of this, the lack of any discernible therapeutic benefit in our study stands in clear contrast to what has been described in other reports utilizing the same and other analogous manganese-SOD/catalase mimetics. Once again, although superior drug delivery through use of continuous osmotic infusion pumps may explain some of this difference [37,39], pharmacokinetic factors are unlikely to be the entire explanation. In the study already cited employing the most comparable model to the one we utilized (with respect to disease type and treatment method), akin to the beneficial effects described for pCO these authors found significant attenuation of lipid peroxidation using less than half the SOD units dose per week through ip injection [33].

The aforementioned considerations raise the likelihood that TSE pathogenesis could be consequent to more aggressive oxidative stress or associated with less successful cellular compensatory responses. Equally, TSE pathogenesis may involve mechanisms which generate reactive oxygen and nitrogen species different than those occurring in other in vivo disease models whereby manganese-SOD/catalase mimetics are much less efficacious. This latter possibility is particularly relevant to lipid peroxidation, wherein the number of potentially contributing redox reactions appear much more diverse in comparison to those generating OONO- and NT. The more biochemically restricted pathways leading to OONO- production, particularly the more direct linkage to superoxide radicals, could offer more tractability in relation to treatment interventions if protein nitration is predominant in pathogenesis [23]. Additionally, it is possible that relatively subtle, localized amelioration of oxidative stress occurs in the TSE model, and that such differences are masked when utilizing total brain preparations. Supporting this contention, Jung et al. [33] and Rong et al. [36] showed suppression of localized neuronal staining for NT by EUK-134 treatment, while Liu et al. [39] showed suppression of localized staining for oxidized nucleic acids in the brain. Analysis of total brain homogenates might not have revealed such differences. Overall, to address the limitations of the current study, future in vivo assessments of antioxidants in TSE should consider methodologies that ensure optimal drug delivery to the target organ; employ single agents or antioxidant combinations attenuating a broader range of reactive oxygen and nitrogen species; and offer brain regional assessments of oxidative stress. Further, it is recognized that different host–prion strain combinations can show diversity in pathologic profiles [44] and in their response to specific therapeutic interventions [48], suggesting

the likelihood of variability in pathogenesis. We have only investigated the efficacy of EUK-189 in one model [15,42], and although we believe it is valid and appropriate for studies of human prion disease, accept that our findings may not fully represent the entire spectrum of antioxidant efficacy in prion disease.

Notwithstanding that we observed a significant prolongation of survival in our study, in parallel with the comparatively limited attenuation in CNS oxidative damage [33,37,39], the magnitude of the life-span increase also appears relatively modest. The 4.7% average increase in survival observed in our study approaches but is clearly less than the 7.7 and 10.4% mean extensions reported in the most comparable in vivo study of analogous manganese-SOD/catalase mimetic antioxidants employed in a neurodegenerative disease model [33]. As already stated in relation to the reductions in oxidative damage reported in this study, the superior prolongation of life span was achieved delivering less than half the amount of SOD unit doses to the mice per week [33]. Of greater contrast, are treatment studies utilising rodent TSE models involving compounds not primarily considered antioxidants, but also delivered from early after ic inoculation. Efficacy in such studies has ranged from showing no benefit, such as with quinacrine [43,49], to dramatically prolonging incubation periods by up to 160% as observed when using amphotericin B or pentosan polysulfate [49,50].

The precise molecular pathological mechanisms underlying the process of vacuolation observed in the neuropil and some neuronal soma in prion disease are incompletely understood. We observed topographically restricted reductions in spongiform change, confined to the hippocampus and thalamus of terminal EUK-189-treated mice, but not the complete prevention reported in Mn-SOD% mice treated with the same SOD/catalase mimetic [28]. This observation supports the likelihood that the vacuolation in Mn-SOD% mice, evidently arising from splitting of the myelin lamellae of medium sized axons [41], is probably a direct consequence of heightened oxidative stress, particularly within mitochondria, whereas other contributing pathogenic factors may be operating in prion disease. Immunohistochemical analysis revealed a variably higher amount of PrP positivity in EUK-189-treated mice, emphasised in the hippocampus, occipital lobe, and parietal lobe, while Western blots of brain homogenates from treated and untreated animals demonstrated nonsignificant differences in amounts of PrPres. Although the increase in immunohistochemical PrP positivity in the EUK-189-treated mice may relate to their modestly longer survival providing a slightly longer period for tissue deposition of abnormal PrP, the reason for the disparity in levels of the abnormal isoform of PrP as detected immunohistochemically in comparison to levels determined by Western blot is not entirely clear. Analogous discrepancies in the detection of PrPres across the two techniques have been reported previously [51–53]. As already discussed in relation to the results from our biochemical assays, relatively subtle regional differences observed using immunohistochemistry are likely to be lost through tissue homogenisation.

Acknowledgments

S.J.C. and C.L.M. are supported by an NH&MRC Program Grant (identification No. 400202). S.J.C. is also supported by an NH&MRC Practitioner Fellowship (identification No. 400183); NH&MRC Project Grant (identification No. 454546); and Bethlehem Griffiths Research Foundation, Research Project Grant. The authors thank Ms. L. Leone for technical assistance. The anti-prion protein monoclonal antibody was a generous gift from Professor John Collinge.

References

[1] Knight, R.; Brazier, M.; Collins, S. J. Human prion diseases: cause, clinical and diagnostic aspects. In: Rabenau, H.F., Cinati, J., Doerr, H.W. (Eds.), Prions: a challenge for science, medicine and the public health system. Contrib. Microbiol. Karger, Basel,pp. 72–97; 2004.

[2] Hutter, G.; Heppner, F. L.; Aguzzi, A. No superoxide dismutase activity of cellular prion protein in vivo. *Biol. Chem.* **384** (9)**:**1279–1285; 2003.

[3] Wong, B. S.; Pan, T.; Liu, T.; Li, R.; Gambetti, P.; Sy, M. S. Differential contribution of superoxide dismutase activity by prion protein in vivo. *Biochem. Biophys. Res. Commun.* **273** (1)**:**136–139; 2000.

[4] Brown, D. R.; Schulz-Schaeffer, W. J.; Schmidt, B.; Kretzschmar, H. A. Prion-protein deficient cells show altered response to oxidative stress. *Exp. Neurol.* **146** (1)**:**104–112; 1997.

[5] Brown, D. R.; Schmidt, B.; Kretzschmar, H. A. Role of microglia and host prion protein in neurotoxicity of a prion protein fragment. *Nature* **380:**345–347; 1996.

[6] White, A. R.; Collins, S. J.; Maher, F.; Jobling, M. F.; Stewart, L. R.; Thyer, J. M.; Beyreuther, K.; Masters, C. L.; Cappai, R. Prion protein-deficient neurons reveal lower glutathione reductase activity and increased susceptibility to hydrogen peroxide toxicity. *Am. J. Pathol.* **155** (5)**:**1723–1730; 1999.

[7] Choi, C. J.; Anantharam, V.; Saetveit, N. J.; Houk, R.; Kanthasamy, A.; Kanthasamy, A. G. Normal cellular prion protein protects against manganese-induced oxidative stress and apoptotic cell death. *Toxicol. Sci.* **98** (2)**:**495–509; 2007.

[8] Brown, D. R.; Schmidt, B.; Kretzschmar, H. A. Effects of copper on survival of prion protein knockout neurons and glia. *J. Neurochem.* **70:**1686–1693; 1998.

[9] Wong, B. S.; Brown, D. R.; Pan, T.; Whiteman, M.; Liu, T.; Bu, X.; Li, R.; Gambetti, P.; Olesik, J.; Rubenstein, R.; Sy, M. S. Oxidative impairment in scrapie-infected mice is associated with brain metals perturbations and altered antioxidant activities. *J. Neurochem.* **79** (3)**:**689–698; 2001.

[10] Brown, D. R. Neurodegeneration and oxidative stress: prion disease results from loss of antioxidant defence. *Folia Neuropathol.* **43** (4)**:**229–243; 2005.

[11] Brown, D.; Clive, C.; Haswell, S. Antioxidant activity related to copper binding native prion protein. *J. Neurochem.* **76:**69–76; 2001.

[12] Thackray, A. M.; Knight, R.; Haswell, S. J.; Bujdoso, R.; Brown, D. R. Metal imbalance and compromised antioxidant function are early changes in prion disease. *Biochem. J.* **362** (Pt 1)**:**253–258; 2002.

[13] Miele, G.; Jeffrey, M.; Turnbull, D.; Manson, J.; Clinton, M. Ablation of cellular prion protein expression affects mitochondrial numbers and morphology. *Biochem. Biophys. Res. Commun.* **291** (2)**:**372–377; 2002.

[14] Hachiya, N. S.; Yamada, M.; Watanabe, K.; Jozuka, A.; Ohkubo, T.; Sano, K.; Takeuchi, Y.; Kozuka, Y.; Sakasegawa, Y.; Kaneko, K. Mitochondrial localization of cellular prion protein (PrPC) invokes neuronal apoptosis in aged transgenic mice overexpressing PrPC. *Neurosci. Lett.* **374** (2)**:**98–103; 2005.

[15] Brazier, M. W.; Lewis, V.; Ciccotosto, G. D.; Klug, G. M.; Lawson, V. A.; Cappai, R.; Ironside, J. W.; Masters, C. L.; Hill, A. F.; White, A. R.; Collins, S. Correlative studies support lipid peroxidation is linked to PrP(res) propagation as an early primary pathogenic event in prion disease. *Brain Res. Bull.* **68** (5)**:**346–354; 2006.

[16] Andreoletti, O.; Levavasseur, E.; Uro-Coste, E.; Tabouret, G.; Sarradin, P.; Delisle, M. B.; Berthon, P.; Salvayre, R.; Schelcher, F.; Negre-Salvayre, A. Astrocytes accumulate 4-hydroxynonenal adducts in murine scrapie and human Creutzfeldt-Jakob disease. *Neurobiol. Dis.* **11** (3)**:**386–393; 2002.

[17] Ju, W. K.; Park, K. J.; Choi, E. K.; Kim, J.; Carp, R. I.; Wisniewski, H. M.; Kim, Y. S. Expression of inducible nitric oxide synthase in the brains of scrapie-infected mice. *J. Neurovirol.* **4** (4)**:**445–450; 1998.

[18] Lee, D. W.; Sohn, H. O.; Lim, H. B.; Lee, Y. G.; Kim, Y. S.; Carp, R. I.; Wisniewski, H. M. Alteration of free radical metabolism in the brain of mice infected with scrapie agent. *Free Radic. Res.* **30** (6)**:**499–507; 1999.

[19] Guentchev, M.; Voigtlander, T.; Haberler, C.; Groschup, M. H.; Budka, H. Evidence for oxidative stress in experimental prion disease. *Neurobiol. Dis.* **7** (4)**:**270–273; 2000.

[20] Guentchev, M.; Siedlak, S. L.; Jarius, C.; Tagliavini, F.; Castellani, R. J.; Perry, G.; Smith, M. A.; Budka, H. Oxidative damage to nucleic acids in human prion disease. *Neurobiol. Dis.* **9** (3)**:**275–281; 2002.

[21] Choi, S. I.; Ju, W. K.; Choi, E. K.; Kim, J.; Lea, H. Z.; Carp I, R.; Wisniewski, H. M.; Kim, Y. S. Mitochondrial dysfunction induced by oxidative stress in the brains of hamsters infected with the 263 K scrapie agent. *Acta Neuropathol. (Berl.)* **96** (3)**:**279–286; 1998.

[22] Wong, B. S.; Chen, S. G.; Colucci, M.; Xie, Z.; Pan, T.; Liu, T.; Li, R.; Gambetti, P.; Sy, M. S.; Brown, D. R. Aberrant metal binding by prion protein in human prion disease. *J. Neurochem.* **78** (6)**:**1400–1408; 2001.

[23] Halliwell, B., Gutteridge, J.B. (Eds.), 2007. Free radicals in biology and medicine, fourth edition. Oxford, Oxford; 2007.

[24] Petersen, R. B.; Siedlak, S. L.; Lee, H. G.; Kim, Y. S.; Nunomura, A.; Tagliavini, F.; Ghetti, B.; Cras, P.; Moreira, P. I.; Castellani, R. J.; Guentchev, M.; Budka, H.; Ironside, J. W.; Gambetti, P.; Smith, M. A.; Perry, G. Redox metals and oxidative abnormalities in human prion diseases. *Acta Neuropathol. (Berl.)* **110** (3)**:**232–238; 2005.

[25] Sharpe, M. A.; Ollosson, R.; Stewart, V. C.; Clark, J. B. Oxidation of nitric oxide by oxomanganese-salen complexes: a new mechanism for cellular protection by superoxide dismutase/catalase mimetics. *Biochem. J.* **366:**97–107; 2002.

[26] Baudry, M.; Etienne, S.; Bruce, A.; Palucki, M.; Jacobsen, E.; Malfroy, B. Salen-manganese complexes are superoxide dismutase-mimics. *Biochem. Biophys. Res. Commun.* **192** (2)**:**964–968; 1993.

[27] Gonzalez, P. K.; Zhuang, J.; Doctrow, S. R.; Malfroy, B.; Benson, P. F.; Menconi, M. J.; Fink, M. P. EUK-8, a synthetic superoxide dismutase and catalase mimetic, ameliorates acute lung injury in endotoxemic swine. *J. Pharmacol. Exp. Ther.* **275** (2)**:**798–806; 1995.

[28] Melov, S.; Doctrow, S. R.; Schneider, J. A.; Haberson, J.; Patel, M.; Coskun, P. E.; Huffman, K.; Wallace, D. C.; Malfroy, B. Lifespan extension and rescue of spongiform encephalopathy in superoxide dismutase 2 nullizygous mice treated with superoxide dismutase-catalase mimetics. *J. Neurosci.* **21** (21)**:**8348–8353; 2001.

[29] Melov, S.; Ravenscroft, J.; Malik, S.; Gill, M. S.; Walker, D. W.; Clayton, P. E.; Wallace, D. C.; Malfroy, B.; Doctrow, S. R.; Lithgow, G. J. Extension of life-span with superoxide dismutase/catalase mimetics. *Science* **289** (5484)**:**1567–1569; 2000.

[30] Bruce, A. J.; Malfroy, B.; Baudry, M. beta-Amyloid toxicity in organotypic hippocampal cultures: protection by EUK-8, a synthetic catalytic free radical scavenger. *Proc. Natl. Acad. Sci. U. S. A.* **93** (6)**:**2312–2316; 1996.
[31] Pong, K.; Doctrow, S. R.; Huffman, K.; Adinolfi, C. A.; Baudry, M. Attenuation of staurosporine-induced apoptosis, oxidative stress, and mitochondrial dysfunction by synthetic superoxide dismutase and catalase mimetics, in cultured cortical neurons. *Exp. Neurol.* **171** (1)**:**84–97; 2001.
[32] Malfroy, B.; Doctrow, S. R.; Orr, P. L.; Tocco, G.; Fedoseyeva, E. V.; Benichou, G. Prevention and suppression of autoimmune encephalomyelitis by EUK-8, a synthetic catalytic scavenger of oxygen-reactive metabolites. *Cell. Immunol.* **177** (1)**:**62–68; 1997.
[33] Jung, C.; Rong, Y.; Doctrow, S.; Baudry, M.; Malfroy, B.; Xu, Z. Synthetic superoxide dismutase/catalase mimetics reduce oxidative stress and prolong survival in a mouse amyotrophic lateral sclerosis model. *Neurosci. Lett.* **304** (3)**:**157–160; 2001.
[34] Baker, K.; Marcus, C. B.; Huffman, K.; Kruk, H.; Malfroy, B.; Doctrow, S. R. Synthetic combined superoxide dismutase/catalase mimetics are protective as a delayed treatment in a rat stroke model: a key role for reactive oxygen species in ischemic brain injury. *J. Pharmacol. Exp. Ther.* **284** (1)**:**215–221; 1998.
[35] Doctrow, S. R.; Huffman, K.; Marcus, C. B.; Tocco, G.; Malfroy, E.; Adinolfi, C. A.; Kruk, H.; Baker, K.; Lazarowych, N.; Mascarenhas, J.; Malfroy, B. Salen manganese complexes as catalytic scavengers of hydrogen peroxide and cytoprotective agents: structure-activity relationship studies. *J. Med. Chem.* **45:**4549–4558; 2002.
[36] Rong, Y.; Doctrow, S. R.; Tocco, G.; Baudry, M. EUK-134, a synthetic superoxide dismutase and catalase mimetic, prevents oxidative stress and attenuates kainate-induced neuropathology. *Proc. Natl. Acad. Sci. U. S. A.* **96** (17)**:**9897–9902; 1999.
[37] Browne, S. E.; Roberts II, L. J.; Dennery, P. A.; Doctrow, S. R.; Beal, M. F.; Barlow, C.; Levine, R. L. Treatment with a catalytic antioxidant corrects the neurobehavioral defect in ataxia-telangiectasia mice. *Free Radic. Biol. Med.* **36:**938–942; 2004.
[38] Peng, J.; Stevenson, F. F.; Doctrow, S. R.; Andersen, J. K. Superoxide dismutase/catalase mimetics are neuroprotective against selective paraquat-mediated dopaminergic neuron death in the substantia nigra. Implications for Parkinson Disease. *J. Biol. Chem.* **280:**29194–29198; 2005.
[39] Liu, R.; Liu, I. Y.; Bi, X.; Thompson, R. F.; Doctrow, S. R.; Malfroy, B.; Baudry, M. Reversal of age-related learning deficits and brain oxidative stress in mice with superoxide dismutase/catalase mimetics. *Proc. Natl. Acad. Sci. U. S. A.* **100:**8526–8531; 2003.
[40] Melov, S.; Wolf, N.; Strozyk, D.; Doctrow, S. R.; Bush, A. I. Mice transgenic for Alzheimer disease beta-amyloid develop lens cataracts that are rescued by antioxidant treatment. *Free Radic. Biol. Med.* **38** (2)**:**258–261; 2005.
[41] Melov, S.; Schneider, J. A.; Day, B. J.; Hinerfeld, D.; Coskun, P.; Mirra, S. S.; Crapo, J. D.; Wallace, D. C. A novel neurological phenotype in mice lacking mitochondrial manganese superoxide dismutase. *Nat. Genet.* **18** (2)**:**159–163; 1998.
[42] Tateishi, J.; Ohta, M.; Koga, M.; Sato, Y.; Kuroiwa, Y. Transmission of chronic spongiform encephalopathy with kuru plaques from humans to small rodents. *Ann. Neurol.* **5** (6)**:**581–584; 1979.
[43] Collins, S. J.; Lewis, V.; Brazier, M.; Hill, A. F.; Fletcher, A.; Masters, C. L. Quinacrine does not prolong survival in a murine Creutzfeldt-Jakob disease model. *Ann. Neurol.* **52** (4)**:**503–506; 2002.
[44] Masters, C. L.; Rohwer, R. G.; Franko, M. C.; Brown, P.; Gajdusek, D. C. The sequential development of spongiform change and gliosis of scrapie in the golden Syrian hamster. *J. Neuropathol. Exp. Neurol.* **43** (3)**:**242–252; 1984.
[45] Ligios, C.; Jeffrey, M.; Ryder, S. J.; Bellworthy, S. J.; Simmons, M. M. Distinction of scrapie phenotypes in sheep by lesion profiling. *J. Comp. Pathol.* **127** (1)**:**45–57; 2002.
[46] Cha, C. I.; Chung, Y. H.; Shin, C. M.; Shin, D. H.; Kim, Y. S.; Gurney, M. E.; Lee, K. W. Immunocytochemical study on the distribution of nitrotyrosine in the brain of the transgenic mice expressing a human Cu/Zn SOD mutation. *Brain Res.* **853** (1)**:**156–161; 2000.
[47] Gow, A. J.; Duran, D.; Malcolm, S.; Ischiropoulos, H. Effects of peroxynitrite-induced protein modifications on tyrosine phosphorylation and degradation. *FEBS Lett.* **385** (1-2)**:**63–66; 1996.
[48] Ishikawa, K.; Doh-ura, K.; Kudo, Y.; Nishida, N.; Murakami-Kubo, I.; Ando, Y.; Sawada, T.; Iwaki, T. Amyloid imaging probes are useful for detection of prion plaques and treatment of transmissible spongiform encephalopathies. *J. Gen. Virol.* **85** (Pt 6)**:**1785–1790; 2004.
[49] Doh-ura, K.; Ishikawa, K.; Murakami-Kubo, I.; Sasaki, K.; Mohri, S.; Race, R.; Iwaki, T. Treatment of transmissible spongiform encephalopathy by intraventricular drug infusion in animal models. *J. Virol.* **78** (10)**:**4999–5006; 2004.
[50] Pocchiari, M.; Schmittinger, S.; Masullo, C. Amphotericin B delays the incubation period of scrapie in intracerebrally inoculated hamsters. *J. Gen. Virol.* **68** (Pt 1)**:**219–223; 1987.
[51] Flechsig, E.; Shmerling, D.; Hegyi, I.; Raeber, A. J.; Fischer, M.; Cozzio, A.; von Mering, C.; Aguzzi, A.; Weissmann, C. Prion protein devoid of the octapeptide repeat region restores susceptibility to scrapie in PrP knockout mice. *Neuron* **27** (2)**:**399–408; 2000.
[52] Supattapone, S.; Muramoto, T.; Legname, G.; Mehlhorn, I.; Cohen, F. E.; DeArmond, S. J.; Prusiner, S. B.; Scott, M. R. Identification of two prion protein regions that modify scrapie incubation time. *J. Virol.* **75** (3)**:**1408–1413; 2001.
[53] Piccardo, P.; Manson, J. C.; King, D.; Ghetti, B.; Barron, R. M. Accumulation of prion protein in the brain that is not associated with transmissible disease. *Proc. Natl. Acad. Sci. U. S. A.* **104** (11)**:**4712–4717; 2007.

Journal of Neurochemistry

JOURNAL OF NEUROCHEMISTRY | 2010 | 114 | 440–451 doi: 10.1111/j.1471-4159.2010.06771.x

Manganese chelation therapy extends survival in a mouse model of M1000 prion disease

Marcus W. Brazier,*,† Irene Volitakis,*,† Magda Kvasnicka,† Anthony R. White,*,† John R. Underwood,* Jason E. Green,‡ Sen Han,§ Andrew F. Hill,†,§ Colin L. Masters*,†,¶ and Steven J. Collins*,†,¶

*Department of Pathology, The University of Melbourne, Victoria, Australia 3010

†Mental Health Research Institute, Parkville, Victoria, Australia 3010

‡Centre for Drug Candidate Optimisation, Monash Institute of Pharmaceutical Sciences, Monash University, Parkville, Victoria, Australia

§Department of Biochemistry and Molecular Biology and the Bio21 Molecular Science and Biotechnology Institute, University of Melbourne, Parkville, Australia 3010

¶Australian National Creutzfeldt-Jakob Disease Registry, University of Melbourne, Victoria, Australia 3010

Abstract

Previous *in vitro* and *in vivo* investigations have suggested manganese (Mn^{2+}) may play a role in pathogenesis through facilitating refolding of the normal cellular form of the prion protein into protease resistant, pathogenic isoforms (PrP^{Sc}), as well as the subsequent promotion of higher order aggregation of these abnormal conformers. To further explore the role of Mn^{2+} in pathogenesis, we undertook a number of studies, including an assessment of the disease modifying effects of chelation therapy in a well-characterized mouse model of prion disease. The di-sodium, calcium derivative of the chelator, cyclohexanediaminetetraacetic acid ($Na_2CaCDTA$), was administered intraperitoneally to mice inoculated intra-cerebrally with either high or low-dose inocula, with treatment beginning early (shortly after inoculation) or late (at the usual mid-survival point of untreated mice). Analyses by inductively coupled plasma-mass spectrometry demonstrated brain Mn^{2+} levels were selectively reduced by up to 50% in treated mice compared with untreated controls, with copper, iron, zinc and cobalt levels unchanged. In mice administered high-dose inocula, none of the treatment groups displayed an increase in survival although western blot analyses of early intensively treated mice showed reduced brain PrP^{Sc} levels; mice infected using low-dose inocula however, showed a significant prolongation of survival ($p = 0.002$). Although our findings support a role for Mn^{2+} in prion disease, further studies are required to more precisely delineate the extent of pathogenic involvement.

Keywords: chelation therapy, cyclohexanediaminetetraacetic acid, manganese, neurodegeneration, prion disease, transmissible spongiform encephalopathy.

J. Neurochem. (2010) **114**, 440–451.

Prion diseases are transmissible neurodegenerative disorders, which include Creutzfeldt-Jakob disease and kuru in humans, as well as scrapie and bovine spongiform encephalopathy in animals. In common with Alzheimer's and Parkinson's Diseases, prion diseases are associated with the accumulation of aberrant conformers of a constitutively expressed cellular protein; more specifically, in prion disease, pathogenesis appears linked to the conversion of the normal cellular form of the prion protein (PrP^{C}) to misfolded, relatively protease-resistant isoforms (PrP^{Sc}), which also appears to constitute the basic infectious unit (Cohen and Prusiner 1998). Despite equivalence in primary structure, PrP^{Sc} typically exhibits a number of bio-physical differences in comparison to PrP^{C}

Received February 22, 2010; revised manuscript received April 6, 2010; accepted April 15, 2010.

Address correspondence and reprint requests to Steven J. Collins, Australian National Creutzfeldt-Jakob Disease Registry, The University of Melbourne, Victoria, Australia 3010.
E-mail: stevenjc@unimelb.edu.au

Abbreviations used: CDTA, cyclohexanediaminetetraacetic acid; ic, intracerebral inoculation; ip, intra-peritoneally; LD_{50}, lethal dose for 50% animals; PAGE, polyacrylamide gel electrophoresis; PBS, phosphate buffered saline; PBS-T, PBS-0.05% Tween 20; PK, proteinase K; PrP^{C}, prion protein; PrP^{Sc}, scrapie isoform of PrP^{C}; SOD, superoxide dismutase.

with PrP^{Sc} being relatively rich in β-sheet content, more protease resistant and less soluble in detergents than PrP^{C}.

Prion protein has been shown to bind copper (Cu^{2+}) ions (Brown *et al.* 1997; Jackson *et al.* 2001; Jobling *et al.* 2001; Burns *et al.* 2003; Gaggelli *et al.* 2005; Thompsett *et al.* 2005) with a putative role in copper homeostasis suggested by the rapid endocytosis of PrP^{C} after binding the transition metal (Pauly and Harris 1998). In addition, PrP^{C} complexed with Cu^{2+} has been reported to exhibit superoxide dismutase (SOD) activity, with this posited function diminished in the presence of Cu^{2+} chelators (Brown *et al.* 1999). Furthermore, the SOD activity of recombinant PrP is diminished or nullified when the protein is refolded in the presence of other transition metals instead of Cu^{2+} (Brown *et al.* 2000), additionally supporting an important role for copper in this catalytic activity. The reduced catalytic activity in the presence of manganese may relate in part to conformational differences, supported by the differential affinities that monoclonal antibodies have for the two metallated forms (Thackray *et al.* 2003).

Transition metals such as iron and copper are typically associated with aggregated protein deposits and plaques in neurodegenerative disorders (Allsop *et al.* 2008), including Alzheimer's disease (Barnham *et al.* 2006) and are likely to contribute to pathogenesis through the generation of free radicals and oxidative insults to CNS neurons via mechanisms such as Fenton and Haber–Weiss chemistry (reviewed in Gaeta and Hider 2005; Lan and Jiang 1997). Several reports have also shown altered brain transition metal homeostasis in prion disease, with particular support for a possible direct pathogenic role for Mn^{2+}. In a mouse model, by about a third of the way through the incubation period (and concomitant with the first appearance of PrP^{Sc}), immunopurified PrP was found to be considerably less associated with Cu^{2+} while becoming increasingly associated with Mn^{2+} (Thackray *et al.* 2002). The brains of scrapie infected hamsters have also been shown to harbor increased Mn^{2+} levels compared with controls (Kim *et al.* 2005). Of direct relevance to human prion disease, Wong *et al.* (2001) have shown that the brains of sporadic Creutzfeldt-Jakob disease patients contain only half the Cu^{2+} content of age-matched controls but up to ten-fold the Mn^{2+} content. From a molecular mechanistic perspective, Mn^{2+} is thought to contribute to pathogenesis through promoting the conformational transformation of PrP^{C} to PrP^{Sc} (Brown *et al.* 2000; Treiber *et al.* 2006; Brazier *et al.* 2008) and perhaps by facilitating the formation of large, multimeric complexes of PrP^{Sc} (Thackray *et al.* 2002; Giese *et al.* 2004; Tsenkova *et al.* 2004; Levin *et al.* 2005). Contributions from enhanced oxidative stress through non-homeostatic Mn^{2+} redox activity are also likely (Tsenkova *et al.* 2004). *In vitro* studies of recombinant PrP support a direct pro-aggregatory role for Mn^{2+}, which is inhibited by copper when present prior to oligomerisation (Giese *et al.* 2004; Levin *et al.* 2005; Brazier *et al.* 2008), with experimental evidence supporting differences in the binding mechanisms of Cu^{2+} and Mn^{2+} to the prion protein and cognate peptide fragments (Tsenkova *et al.* 2004; Gaggelli *et al.* 2005; Levin *et al.* 2005). Further supporting an important pathogenic contribution, using cell culture assays, Davies and Brown (2009) recently demonstrated that the infectivity of an infectious cell lysate was enhanced around 100-fold when recipient cells were cultured in the presence of Mn^{2+} and it has been shown (Uppington and Brown 2008) that recombinant PrP refolded in the presence of Mn^{2+} was significantly more toxic to primary neuronal cultures than the holo-form of the protein.

In response to the increasing recognition of derangements in brain transition metal content and their likely pathogenic role in various neurodegenerative disorders, chelators have been utilized as a therapeutic strategy in experimental animal models and human trials (Cherny *et al.* 2001; Youdim *et al.* 2004; Lannfelt *et al.* 2008). Indeed, Sigurdsson *et al.* (2003) demonstrated that treating prion inoculated mice with the copper chelator D-penicillamine (D-PEN) prolonged survival by extending the disease incubation period.

Given the recent data suggesting a pathogenic role for Mn^{2+} in prion disease, we undertook a trial of chelation therapy in our well characterized mouse model of prion pathogenesis (Brazier *et al.* 2006). The polyaminocarboxylic acid, cyclohexanediaminetetraacetic acid (CDTA; Fig. 1), was chosen as chelator because of its proven efficacy to bind and remove Mn^{2+} from the brains of experimental animals (Tandon and Singh 1975; Tandon 1978) with subsequent urinary excretion of stable complexes (Khandelwal *et al.* 1980; Tandon and Khandelwal 1982; Wieczorek and Oberdorster 1989; Sanchez *et al.* 1995). The di-sodium, calcium salt of CDTA ($Na_2CaCDTA$), employed because it has a higher LD_{50} [5396 mg/kg (Sanchez *et al.* 1995)] than CDTA [413 mg/kg (Srivastava *et al.* 1986)], was administered intraperitoneally (ip) to mice inoculated intra-cerebrally (ic) with either high- ($\sim 2 \times 10^5$ ID_{50} units) or low-dose inocula ($\sim$ 20 ID_{50} units), with treatment beginning early (shortly after inoculation) or late (around the usual mid-survival point of untreated mice). Analyses by inductively coupled plasma-mass spectrometry demonstrated brain Mn^{2+} levels were selectively reduced by 34–50% in treated mice (depending on the intensity of chelation therapy) compared with untreated controls, with copper, iron, zinc and cobalt levels

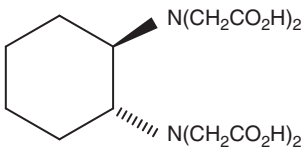

Fig. 1 Chemical structure of cyclohexanediaminetetraacetic acid. Cyclohexanediaminetetraacetic acid binds manganese via its carboxyl groups with a log stability constant of 17.4 (Dawson *et al.* 1986).

unchanged. In mice administered high-dose inocula, none of the treatment groups displayed an increase in survival although brain PrP^{Sc} levels were shown to be substantially reduced by western blot in the most intensively early treated mice. In contrast, possibly because of the extended period of pathogenesis, mice infected using low-dose inocula showed a significant prolongation of survival ($p = 0.002$) compared with non-treated controls but no reduction in brain PrP^{Sc} levels.

Methods

Production of the manganese chelator

To reduce the biotoxicity of the chelator, sodium hydroxide (Sigma, St Louis, MO, USA), calcium hydroxide (Sigma) and CDTA (Avocado, Ward Hill, MA, USA) were reacted for 2 h at ~22°C at molar equivalents of 2 : 1 : 1, respectively in 0.9% saline (Sanchez *et al.* 1995) to generate a 0.2 M stock solution of the disodium calcium salt $Na_2CaCDTA$. The pH of this solution was adjusted to 7.0 before use and aliquots were stored at −20°C.

Mouse inoculations and handling

Mouse inoculations and all animal handling procedures such as culling were performed in accordance with national prescribed guidelines and ethical approval for the study granted by the University of Melbourne Animal Experimentation Ethics Committee. Balb/c weanling mice were ic inoculated with either 1% normal brain homogenate (sham inoculated controls) or M1000 prions under methoxyfluorane anaesthesia as previously described (Collins *et al.* 2002; Brazier *et al.* 2006). For M1000 inoculations, mice were inoculated with 30 μL of a diluted brain homogenate [w/v in phosphate buffered saline (PBS)] made from a terminally ill mouse, equivalent to a dose of either $\sim 2 \times 10^5$ ID_{50} units (high dose inoculum) or ~ 20 ID_{50} units (low dose inoculum). All groups of mice used in the course of these studies are summarized in Table 1; mice were housed with food and water available *ad libitum*. Upon manifesting persisting definite features of prion disease, these mice and as appropriate, age-matched sham inoculated controls, were culled by a lethal dose of anaesthetic (200 μL Nembutal ip; Merial), with selected mice exsanguinated by transcardial perfusion with PBS containing 2000 IU/L heparin and 0.028 M sodium nitrite (Clyde Industries, Sydney, Australia) at 100 mmHg pressure.

In vivo manganese chelation treatment

For a preliminary assessment of brain transition metal changes occurring as a consequence of prion disease, Balb/c weanling mice inoculated with high doses ($\sim 2 \times 10^5$ ID_{50} units) of M1000 prions (Group 1; $n = 7$) were compared with mice receiving normal brain homogenate (sham inoculated controls; Group 2; $n = 4$). To assess the potential therapeutic effect of $Na_2CaCDTA$, mice were inoculated with either high doses ($\sim 2 \times 10^5$ ID_{50} units) or low doses (~ 20 ID_{50} units) of M1000 prions as outlined in Table 1. The high dose-inoculated mice were divided into four groups: Group 3 ($n = 7$), treated ip twice weekly with 200 μL 0.2 M $Na_2CaCDTA$ commencing day 7 post-inoculation; Group 4 ($n = 7$), treated ip four times weekly with 200 μL 0.2 M $Na_2CaCDTA$ commencing day 7 post-inoculation; Group 5 ($n = 7$), treated ip four times weekly with 200 μL 0.2 M $Na_2CaCDTA$ commencing 75 days post-inoculation (time chosen to approximate usual mid-survival point of untreated mice); and an untreated control group (Group 6; $n = 6$). Low dose-inoculated mice formed two groups, one treated thrice weekly with 200 μL 0.2 M $Na_2CaCDTA$ commencing day 7 post-inoculation (Group 7; $n = 8$) and the other untreated serving as controls (Group 8; $n = 10$). The amount of $Na_2CaCDTA$ (200 μL 0.2 M) given each treatment equates to 1/8 the LD_{50} for a single dose through this administration route (Sanchez *et al.* 1995) and was arbitrarily chosen to maximize any therapeutic potential without posing undue toxicity. Treatment with $Na_2CaCDTA$ continued until mice manifested persisting, definite features of prion disease at which point they were culled.

Transition metal analyses

Estimations of brain transition metal content were performed using inductively coupled plasma-mass spectrometry (Varian, Palo Alto, CA, USA). Following transcardial perfusion, brains from M1000 inoculated terminally sick mice and sham inoculated, age matched controls were immediately removed, with some sagittally

Table 1. Summary of the groups of mice, the inoculation doses used and treatment regimens employed for the study of transition metal changes in prion disease. Groups 1 and 2 were utilized in the preliminary assessment of transition metal dyshomeostasis in terminal prion disease and groups 3–8 were employed in the study of manganese (Mn2+) chelation as a therapeutic strategy. Groups 7 and 8 were inoculated with a low dose (~ 20 ID_{50} units) of M1000 prions while groups 1 and 3–6 received high dose inoculation ($\sim 2 \times 10^5$ ID_{50} units).

	n	Mouse strain	Inoculum	Treatment start	Frequency
Group 1	7	Balb/c	High dose M1000	n/a	
Group 2	4	Balb/c	NBH	n/a	
Group 3	7	Balb/c	High dose M1000	Early	2 × weekly
Group 4	7	Balb/c	High dose M1000	Early	4 × weekly
Group 5	7	Balb/c	High dose M1000	Late	4 × weekly
Group 6	6	Balb/c	High dose M1000	Untreated controls	
Group 7	8	Balb/c	Low dose M1000	Early	3 × weekly
Group 8	10	Balb/c	Low dose M1000	Untreated controls	

NBH, normal brain homogenate; n/a, not applied.

hemisectioned, before prompt snap freezing in liquid nitrogen and storage at −80°C until assessment for Cu^{2+}, Mn^{2+}, Co^{2+}, Zn^{2+} and $Fe^{2+/3+}$ content. Samples of brain tissue were weighed (approximate wet weight) and placed in acid-leached polypropylene tubes. Tissue samples were hydrolyzed with 700 μL of 70% nitric acid (BDH Aristar, West Chester, PA, USA) for 46 h before being heated to 80°C for 30 min. The acid treated samples were then treated with 600 μL hydrogen peroxide and heated at 70°C for 15 min. All samples were diluted in 1%HNO_3 before being assayed. Standards included multi-element solutions containing 10, 50 and 100 ppb of the relevant transition metals and National Institute of Standards and Technology bovine liver (standard reference material 1557B). Each sample was analyzed in triplicate with the results expressed as μg metal/g brain wet weight.

Western blot analyses

Brains from mice undergoing high dose inoculation and early $Na_2CaCDTA$ treatment (Groups 3 and 4) or late $Na_2CaCDTA$ treatment (Group 5), as well as untreated mice (Group 6) were assessed for PrP^{Sc} levels by western blotting as described previously (Brazier *et al.* 2006). In brief, after thawing, brain samples were homogenized to 10% (w/v) in PBS and then incubated with 50 U/mL benzonase nuclease (Merck, VIC, Australia EC number 3.1.30.2) in the presence of 1 mM $MgCl_2$ for 5 min at 37°C. Protease treatment consisted of 100 μg/mL proteinase K (PK; Sigma; EC number 3.4.21.64) for 1 h at 37°C, with the reaction halted by the addition of an equal volume of 2 × sample buffer (including 6% β-mercaptoethanol), Pefabloc (8 mM final concentration) and boiling for 10 min. Samples were then briefly centrifuged at 7500 *g* prior to loading onto 10% pre-cast tris/glycine gels (Invitrogen, Carlsbad, CA, USA). Proteins were resolved at 200 V for 60 min, then electroblot transferred to a nitrocellulose membrane (Bio-Rad Laboratories, Hercules, CA, USA) followed by blocking for 1 h at ∼22°C in PBS-0.05% Tween 20 (Sigma; PBS-T) containing 5% non-fat milk powder. Membranes were probed with either ICSM18 monoclonal anti-PrP antibody (White *et al.* 2003), diluted 1 : 25 000 in PBS-T, or the R-30 polyclonal anti-PrP antibody (gift of Bruce Chesebro [Caughey *et al.* 1991]) to control for epitope alteration as a result of chelation treatment. The ICSM18 epitope is amino acids 143–155, while the R30 polyclonal anti-PrP antibody is directed against the 89–103 sequence. After extensive washing with PBS-T, bound antibody was detected using a horseradish peroxidase-conjugated anti-mouse or anti-rabbit secondary antibody at 1 : 5000 (Dako, Carpinteria, CA, USA) as appropriate. Visualization was achieved using enhanced chemiluminescence reagent (ECL; GE Healthcare, Cardiff, UK) and Kodak Bio-max film, developer and fixative (Sigma), according to manufacturers' instructions. Densitometric evaluation for comparison of signal intensities was performed using Image J software (National Institutes of Health, USA).

In vitro manganese chelation assay

Ten percent brain homogenates (w/v in PBS) were prepared from non-$Na_2CaCDTA$ treated, terminally sick (Group 1) mice ($n = 7$) ic inoculated with a high dose of M1000 prions, by progressive passage through 18, 21 and finally 26 gauge needles. To assess whether $Na_2CaCDTA$ could alter the protease resistance of pre-formed PrP^{Sc} present in terminal brains, an equal volume of various $Na_2CaCDTA$ concentrations (0.2 M, 0.1 M, 0.05 M or 0.025 M) or H_2O (untreated control) was added to 50 μL aliquots of the terminal 10% brain homogenate prior to PK digestion. The reaction mixtures were incubated for either 30 min or 3 h at 37°C, with constant agitation at 450 *g* on a platform shaker, to assess the effect of different chelation treatment times. The effect of chelation treatments on protease-resistance of PrP^{Sc} was then assessed by digestion with 100 μg/mL PK (Sigma), with subsequent western blotting as described above, except that nitrocellulose filters were digitally imaged the Gene Gnome (Syngene, Cambridge, UK) to facilitate subsequent assessment of residual levels of PrP^{Sc}. Densitometric analyses of digital images provided relative comparisons of the effects of the various $Na_2CaCDTA$ treatments on each individual terminal brain homogenate compared with its untreated control (adjusted to 100%); relative changes for each $Na_2CaCDTA$ treatment concentration were then pooled from at least five separate experiments. Pefabloc (Roche Molecular Biochemicals, Indianapolis, IN, USA) was added (to 8 mM final concentration) to some aliquots prior to chelation treatment to determine the level of endogenous non-specific serine protease activity during the chelation incubation.

Statistical methods

A log rank test was employed for comparison of mouse survival periods and Mann–Whitney U-tests were performed on data pertaining to mouse brain metal content using GraphPad Prism software (GraphPad Software Inc., San Diego, CA, USA). Other data comparisons utilized the Student's *t*-test. In each case the level of significance was set at $p < 0.05$.

Results

Changes in brain transition metal content as a consequence of M1000 prion infection

Preliminary experiments showed that compared with age-matched, sham inoculated controls (Group 2), the brains of terminally sick M1000-inoculated mice (Group 1) showed a non-significant trend toward less Cu^{2+} (Fig. 2a and Table S1). The brains of M1000-inoculated mice (Group 1) were shown to have significantly higher levels of Mn^{2+} ($p = 0.01$) than controls with a mean concentration of 0.390 (± 0.012 SEM) μg Mn^{2+}/g brain wet weight compared with 0.323 (± 0.009 SEM) μg Mn^{2+}/g brain wet weight in controls (Fig. 2b and Table S1). There was no difference in brain Co^{2+} and $Fe^{2+/3+}$ content between terminally sick M1000-inoculated mice and sham-inoculated age matched controls, but Zn^{2+} was also significantly higher in terminally sick M1000-inoculated mice (Table S1).

Effect of *in vivo* $Na_2CaCDTA$ chelation treatment on survival

At the doses used for the period of time given, the chelation therapy appeared well tolerated with no deleterious effects. Our initial treatment trial utilized high dose (∼ 2×10^5 ID_{50} units)-inoculated mice and there was no significant difference

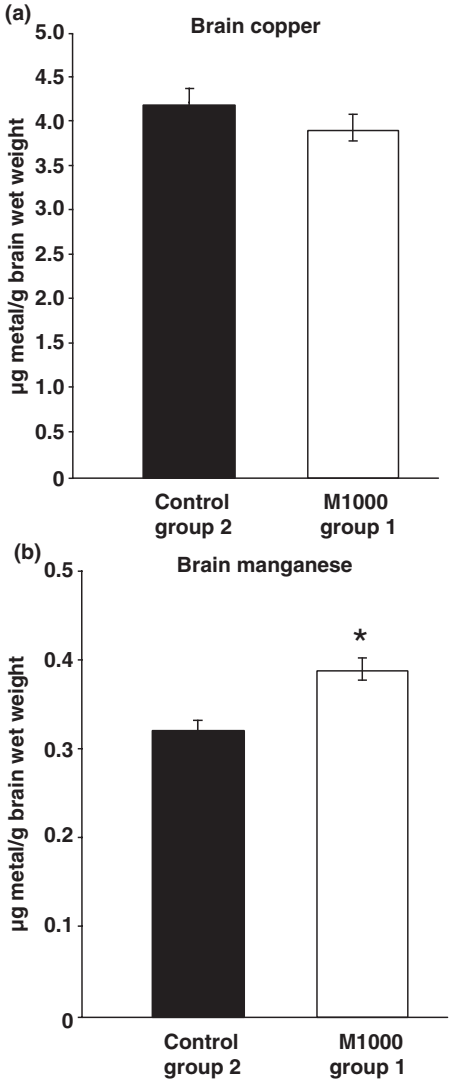

Fig. 2 Inductively coupled plasma-mass spectrometry analysis of brain transition metals in prion infected mice. There is a non-significant decrease in Cu^{2+} concentration (a) and a significant increase in Mn^{2+} concentration (b) in terminally diseased mice brains (Group 1, $n = 4$) when compared with age-matched sham inoculated control mice (Group 2, $n = 4$; $^*p < 0.01$).

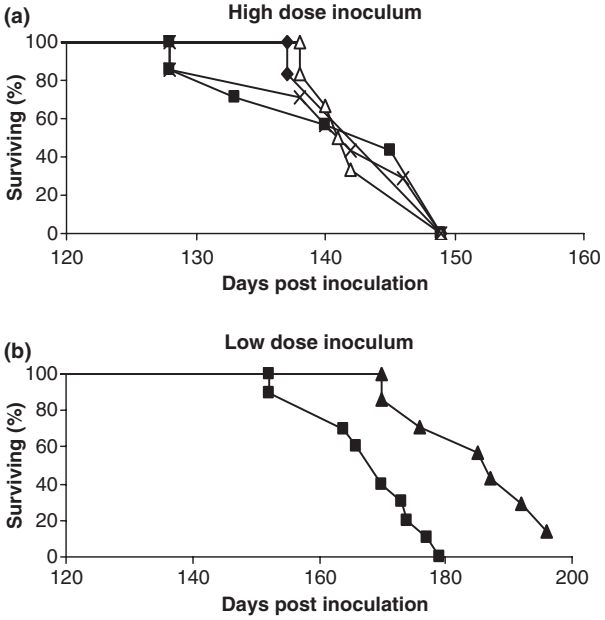

Fig. 3 Survival curves of $Na_2CaCDTA$ treated mice. There was no difference between $Na_2CaCDTA$ treatment groups compared with untreated controls when mice were inoculated with a high dose ($\sim 2 \times 10^5$ ID_{50} units) inoculum (a; △ = Group 3, $n = 7$, ◆ = Group 4, $n = 7$, × = Group 5, $n = 7$, ■ = Group 6, $n = 6$) whereas there was an approximately 10% extension to survival because of treatment after a low dose (~ 20 ID_{50} units) inoculum (b; ▲ = Group 7, $n = 8$, ■ = Group 8, $n = 10$).

in survival between the early (Groups 3 and 4) and late $Na_2CaCDTA$ treated (Group 5) and untreated (Group 6) control mice, with average incubation periods (± SD) of 147 (± 4.5) days for group 6, 142 (± 8.5) days for group 3, 143 (± 4.7) days for the group 4, and 142 (± 7.4) days for group 5 (Fig. 3a). To further assess therapeutic efficacy we undertook a second study employing low dose (~ 20 ID_{50} units)-inoculated mice, and found a significant increase in the survival period of the $Na_2CaCDTA$ treated mice (Group 7). Control mice (Group 8) survived, on average, 169 (± 2.5) days whereas the $Na_2CaCDTA$ treated group (Group 7) survived 189 (± 3.8), an approximately 20 day (11.8%) extension of the control survival period (Fig. 3b). Overall, two mice died as a direct complication of ip injection and one $Na_2CaCDTA$ treated mouse failed to develop symptoms of disease after 300 days post-inoculation, which was considered to be a technical failure with respect to inoculation. These mice were excluded from data analyses.

$Na_2CaCDTA$ chelation treatment selectively reduced brain manganese levels

Untreated control mice (Groups 6 and 8) displayed a mean concentration of brain Mn^{2+} similar to that found in previously analyzed, terminally sick, M1000-inoculated (group 1) mice (approximately 0.390 µg Mn^{2+}/g brain wet weight; Table S1). Given the failure to observe a benefit from chelation therapy in any of our initially treated, high-dose inoculated mice, only the brains from groups 4, 5 and 6 mice were analyzed for transition metal content. In these mice inoculated with high dose inocula, the chelator $Na_2CaCDTA$ significantly reduced brain manganese levels by around 50% (to approximately 0.2 µg Mn^{2+}/g brain wet weight) regardless of whether chelation treatment was commenced early or late (Mann–Whitney U-test $p < 0.05$ for both treatment groups 4 and 5) (Table S1 and Fig. 4). The level observed after $Na_2CaCDTA$ treatment was well below the average

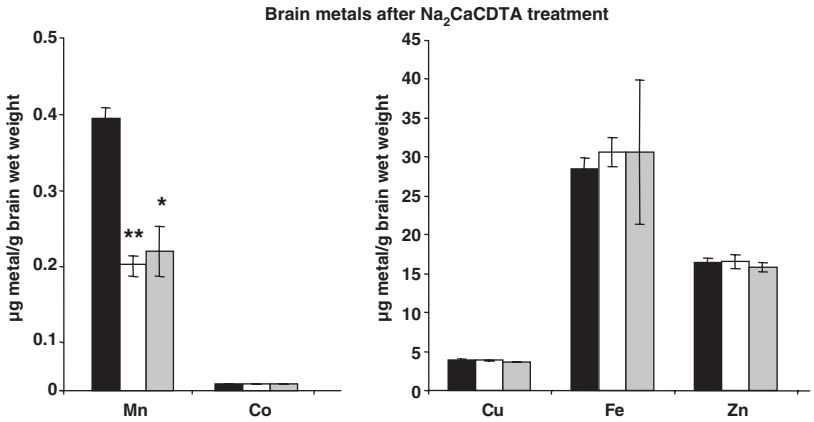

Fig. 4 Brain transition metal concentrations of $Na_2CaCDTA$ treated mice (high dose inoculum). Mean manganese concentrations are significantly decreased in the brains of $Na_2CaCDTA$ treated M1000 infected mice inoculated with $\sim 2 \times 10^5$ ID_{50} units. Metal concentrations in the brains of *in vivo* $Na_2CaCDTA$ treated mice, treated from 7 (early) and 75 days post-inoculation (late) and untreated controls were determined by inductively coupled plasma-mass spectrometry. There was a highly significant reduction (**$p < 0.005$, *$p < 0.05$) of manganese in $Na_2CaCDTA$ treatment groups whereas the concentrations of other metals Co^{2+}, Cu^{2+}, $Fe^{2+/3+}$ and Zn^{2+} were unaltered by the chelator. □ = Group 4, $n = 3$, ▒ = Group 5, $n = 3$, ■ = Group 6, $n = 3$.

Mn^{2+} levels observed in sham-inoculated, age matched controls (Group 2) (0.323 µg Mn^{2+}/g brain wet weight) (Table S1; also compare Fig. 2b with Fig. 4). The Cu^{2+}, Co^{2+}, Zn^{2+} and $Fe^{2+/3+}$ concentrations were not different across the three groups (Table S1 and Fig. 4). Overall, we observed similar results in our subsequent chelation treatment trial using low dose-inoculated mice (Fig. 5), with the Mn^{2+} levels selectively and significantly reduced approximately 34% (to 0.23 µg Mn^{2+}/g brain wet weight) in Group 7 mice compared with untreated control mice (Group 8). We attributed this modestly increased mean brain Mn^{2+} level to the slightly less intense chelation treatment protocol we employed in the second trial (because of resource constraints) wherein Group 7 mice received $Na_2CaCDTA$ three times per week rather four times weekly as undertaken in Groups 4 and 5 mice. Cobalt levels fell below that necessary for meaningful results in low dose-inoculated Groups 7 and 8 mice and could not be determined.

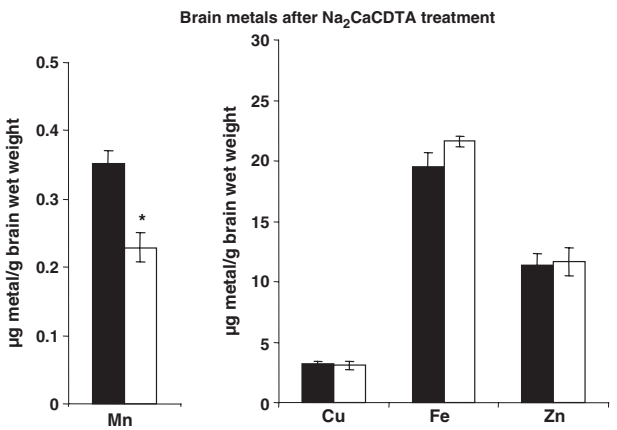

Fig. 5 Brain metal concentrations of $Na_2CaCDTA$ treated mice (low dose inoculum). Manganese concentrations are significantly decreased in the brains of $Na_2CaCDTA$ treated M1000 infected mice inoculated with ~ 20 ID_{50} units. Metal concentrations in the brains of untreated and $Na_2CaCDTA$ -treated mice were determined by inductively coupled plasma-mass spectrometry (IC-PMS). There was a highly significant reduction (*$p < 0.05$) of manganese in the $Na_2CaCDTA$ treatment group whereas the concentrations of other metals Cu^{2+}, $Fe^{2+/3+}$ and Zn^{2+} were unaltered (cobalt was below the detection limit). □ = Group 7, $n = 3$, ■ = Group 8, $n = 4$).

Assessment of brain PrP^{Sc} levels by western blot in high and low dose M1000 inoculated $Na_2CaCDTA$ treated mice

To demonstrate that there were equal amounts of total PrP in the various early and late treated brains when compared with the untreated control brain homogenates prior to PK digestion, aliquots of undigested homogenates were run parallel to their respective PK-digested samples (Fig. 6a). In high dose inoculated mice, western blots revealed that compared with the untreated (Group 6 $n = 5$) mice, the brains of early $Na_2CaCDTA$ treated (Groups 3 and 4) mice appeared to display less PrP^{Sc} after PK digestion, which was borderline significant ($p = 0.052$) for Group 3 ($n = 3$) but highly significant ($p < 0.0005$) for Group 4 ($n = 3$) in comparison to late treated Group 5 ($n = 5$) mice; group 5 brain PrP^{Sc} levels appeared similar to the group 6 controls (Fig. 6a and b). The same results were also obtained when probing with the R30 polyclonal antibody, showing that the observed difference in PrP^{Sc} signal was not because of an alteration of antibody epitope (data not shown). In contrast, there was no significant difference in brain PrP^{Sc} levels between the low-dose inoculation $Na_2CaCDTA$ treated Group 7 ($n = 3$) and untreated Group 8 ($n = 3$) mice (Fig. 6c).

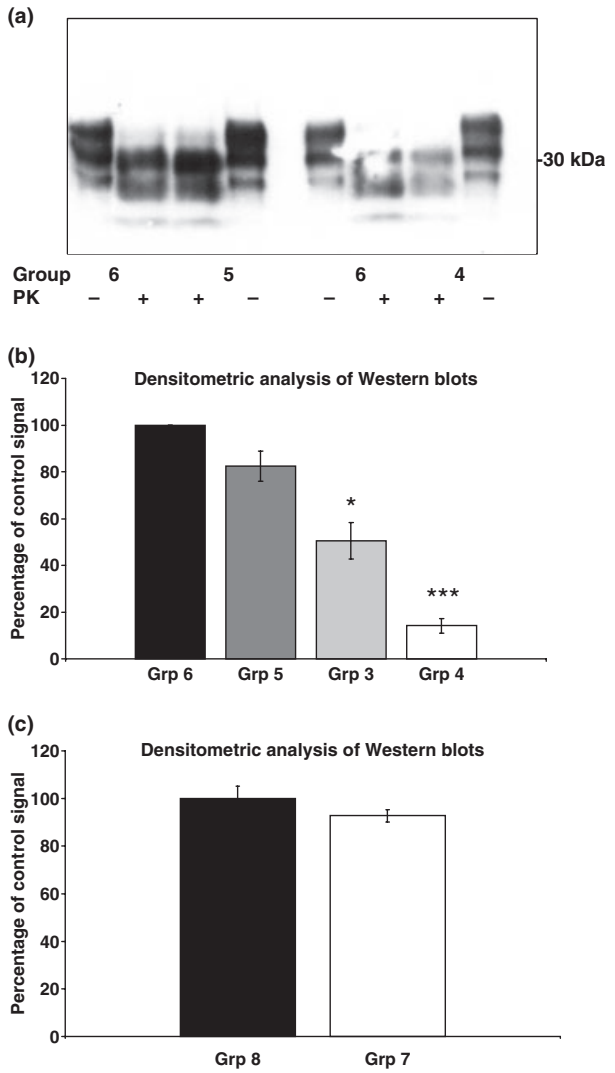

Fig. 6 Western blot analyses of the brain scrapie isoform of the prion protein (PrP^{Sc}) in $Na_2CaCDTA$ treated mice. Fig. 6a demonstrates diminished PrP^{Sc} signal in the brains of the early intensively $Na_2CaCDTA$ treated (Group 4) mice whereas the brains of the late treatment (Group 5) mice had a similar level to the untreated (Group 6) mice. The western blot in Fig. 6a demonstrates that there is similar total PrP signal in all groups before proteinase K (PK) digestion but there is a reduced signal in the early treatment (Group 4) mice after PK digestion (when detected using ICSM-18), and this reduction in signal was also evident when probing with R30 polyclonal antibody (data not shown) suggesting that the reduction of signal is not because of an alteration of epitopes for ICSM-18 monoclonal antibody. Fig. 6b summarizes densitometric comparisons of western blots of brain PrP^{Sc} from the high dose inoculation treatment groups compared with the untreated control group. In Fig. 6b, signal from Group 6 mice was set as 100% (□ = Group 4, $n = 3$; ■ = Group 6, $n = 5$; ▫ = Group 3, $n = 3$; ▪ = Group 5, $n = 5$). There was a significant reduction (***$p < 0.0005$) in PrP^{Sc} signal in the early intensively treated Group 4 mice compared with late treated Group 5 mice, with borderline significance (* $p = 0.05$) for the Group 3 mice. Fig. 6c summarizes densitometric comparisons of western blots of brain PrP^{Sc} from low dose inoculation mice with the treatment Group 7 not significantly different to the untreated control group 8 (□ = Group 7, $n = 3$; ■ = Group 8, $n = 3$).

In vitro assessment of $Na_2CaCDTA$ does not support induction of enhanced protease sensitivity of pre-formed PrP^{Sc}

Based on the finding that western blots revealed reduced PrP^{Sc} levels in the brains of early $Na_2CaCDTA$ treated mice, we assessed the *in vitro* effect of $Na_2CaCDTA$ on pre-formed PrP^{Sc} found in the brains of non-treated (Group 1) mice with terminal prion disease. Aliquots of 10% brain homogenate from these mice ($n = 7$) were reacted with differing concentrations of $Na_2CaCDTA$ for 30 min or 3 h to assess whether chelation treatment could alter the proteinase resistance of pre-formed PrP^{Sc}. Regardless of the duration of chelation treatment and $Na_2CaCDTA$ concentration employed, there was no observed alteration in the levels of PrP^{Sc} compared with untreated brain samples (data not shown). Overall, these results suggest that the reduced PrP^{Sc} levels observed in the brains of early $Na_2CaCDTA$ treated mice are more likely to be on the basis of diminished production rather than increased PK-sensitivity of mature PrP^{Sc}.

Discussion

Conversion of PrP^{C} to PrP^{Sc} is considered the principal event in the pathogenesis of prion disease, although precisely how this conversion is linked to neurotoxicity is unresolved. Stimulated by recent data suggesting a possible direct role for Mn^{2+} in prion disease, as exemplified by progressive Mn^{2+} accumulation in the brain as the disease evolves (Wong *et al.* 2001; Thackray *et al.* 2002; Kim *et al.* 2005) and the apparent facilitation by Mn^{2+} of the conversion of PrP^{C} to a protease resistant isoform (Brown *et al.* 2000; Kim *et al.* 2005; Treiber *et al.* 2006), we undertook the present study to try more accurately to define the pathogenic relevance of Mn^{2+} and as a corollary, assess manganese chelation as a potential therapeutic strategy using our mouse model of prion disease.

In accordance with previous investigations (Tandon and Singh 1975; Tandon 1978; Wieczorek and Oberdorster 1989; Sanchez *et al.* 1995), we found that $Na_2CaCDTA$ is an effective and relatively selective chelator for the removal of Mn^{2+} from the brain. Depending on the intensity of chelation therapy applied, mice treated for the whole incubation period and those from approximately the mid-survival point had approximately 34–50% of their brain Mn^{2+} removed compared with terminal disease controls, ultimately achieving levels well below those observed in age-matched, sham-inoculated animals; the level of other metals assessed were unchanged. Hence, although *in vitro* CDTA has high log stability constants for most transition metals (Dawson *et al.* 1986; Table S2), the disodium calcium salt of CDTA appears

highly specific for Mn^{2+} *in vivo*. The explanation for this empirical observation most likely relates to pharmacokinetic factors and the accessibility of the different metals *in vivo* during prion disease. Copper, for example, is highly toxic to neurons and must therefore be tightly sequestered by other molecules (Levenson 1998) leaving it much less available to a chelator, whereas the non-physiological accumulation of Mn^{2+} probably occurs mainly in relation to abundant PrP^{Sc} deposits, not primarily for the purpose of sequestration, to which it is comparatively weakly bound (Brazier *et al.* 2008). Nevertheless, despite the significant changes in brain Mn^{2+} levels we achieved, cognate mice that had been infected with high dose inocula showed no benefit in terms of prolongation of their survival, while mice infected using low dose inocula showed a modest but significant prolongation, equivalent to approximately 12% of the non-treated, control survival period.

The explanation for the limited therapeutic efficacy of Mn^{2+} chelation despite impressive removal of this transition metal from the brain, especially as observed in our high dose inoculated mice, is unclear but a few observations may be relevant. In *in vitro* conversion systems, non-manganese factors have been shown to promote production of abnormal protease-resistant conformations, with the facilitatory co-factors including detergents, other transition metals (Kim *et al.* 2005; Treiber *et al.* 2006), non-nucleic acid polyanions such as heparin sulphate (Deleault *et al.* 2007), and RNA (Deleault *et al.* 2003). The lack of reduction in levels of other transition metals examined in the brains of our early and late treated mice may be pertinent. It is possible that inoculation dose may influence whether Mn^{2+} plays a greater but non-exclusive role in the early incubation period, with other auxiliary factors for PrP^{C} conversion becoming dominant later, particularly after a sizeable or pathogenic 'threshold' amount of PrP^{Sc} has been formed. Given the lack of survival benefit in high dose inoculated mice despite early intensive $Na_2CaCDTA$ treatment, it appears likely that although PrP^{Sc} levels were reduced, sufficient conversion, perhaps mainly non-manganese associated, achieves adequate misfolded conformers for efficient pathogenesis. In the converse outcome for low dose inoculated mice, Mn^{2+}-related conversion may be predominant and rate limiting early, but the overall prolongation of pathogenesis eventually allows considerable production of PrP^{Sc} through non-Mn^{2+} related mechanisms ultimately achieving levels equivalent to those found in non-treated mice. Detailed, correlative, incubation period time course studies may provide better insight into what appears to be an imprecise correlation between overall survival and brain Mn^{2+} and PrP^{Sc} levels found at terminal disease.

In addition to the aforementioned, it is possible that in spite of the impressive reductions in the total brain Mn^{2+} levels achieved through $Na_2CaCDTA$ treatment specific removal of Mn^{2+} from PrP conformers poised for conversion was relatively suboptimal, or that enough Mn^{2+} still remained in the CNS to generate PrP^{Sc} levels above the threshold required to enable typical pathogenesis. Further, it is also possible that the most toxic or pathogenically important conformers of PrP^{Sc} are not Mn^{2+}-dependent, which may be particularly relevant in the setting of high dose inoculation of prions. The relevance of Mn^{2+} to putative non-fibrillar or soluble toxic oligomers of PrP^{Sc} thought to be most critical (Silveira *et al.* 2005), especially by analogy to other neurodegenerative disorders such as Alzheimer's disease (McLean *et al.* 1999; Walsh *et al.* 2002), is largely unexplored, as is the relevance of Mn^{2+} to prion disease with minimal or absence of PrP^{Sc} (Lasmézas *et al.* 1997).

Hypothetically, the reduced brain PrP^{Sc} levels depicted by western blot after early *in vivo* $Na_2CaCDTA$ treatment may occur through either reducing the production of PrP^{Sc} or by increasing the protease sensitivity of extant misfolded PrP conformers. *In vitro* assays have shown D-PEN could prevent the development of heightened PK-resistance induced by exogenous copper but could not alter the intrinsic protease-resistance of pre-formed PrP^{Sc} (Sigurdsson *et al.* 2003). This is similar to the report by Treiber *et al.* (2006) demonstrating that copper and manganese-induced protease resistant PrP was stable in the presence of EDTA, although more selective Cu^{1+} chelators could reverse the protease resistance induced by exogenous copper alone. Even though CDTA has a much higher affinity for Mn^{2+} than EDTA (refer Table 3; Dawson *et al.* 1986), we also found that mature PrP^{Sc}, made openly accessible through vigorous homogenization, was not rendered more protease sensitive by $Na_2CaCDTA$ exposure *in vitro*. Hence, our *in vitro* and *in vivo* data are concordant with previous experimental data contending that Mn^{2+} promotes misfolding of PrP^{C} to isoforms with higher β-sheet content (Brazier *et al.* 2008), albeit with an optimal time period exemplified by the first half of the incubation period. A prominent increase in the protease sensitivity of pre-formed PrP^{Sc} in our *in vitro* assay without observing reductions in late $Na_2CaCDTA$ treated mice would have evoked concerns such as whether ineffective chelator concentrations had been achieved in the brains of treated mice or possibly poor *in situ* accessibility to misfolded PrP. Instead, previous reports and our current data argue that the most efficient inhibition of PrP^{Sc} formation appears to require the presence of the chelator prior to, or at least concomitant with, the conversion of PrP^{C} (Sigurdsson *et al.* 2003; Kim *et al.* 2005; Treiber *et al.* 2006) and this, coupled to the likelihood that alternative co-factors offer parallel conversion pathways, may also partly explain why late treated mice had no discernible reduction in PrP^{Sc} levels despite comparable reductions in brain Mn^{2+}. However, our results do not completely resolve the mechanism by which PrP^{Sc} levels are reduced in the brains of early $Na_2CaCDTA$ treated mice but, through the paradigms employed, suggest

the explanation is less likely to be a simple biochemical enhancement of PrP^{Sc} protease sensitivity.

Although we achieved a statistically significant extension to survival of approximately 12% through $Na_2CaCDTA$ treatment of low-dose inoculated mice, this is a relatively modest outcome compared with other reported treatments (Kocisko *et al.* 2006; Doh-ura *et al.* 2004; Sethi *et al.* 2002; Priola *et al.* 2000; reviewed in Brazier *et al.* 2009), especially given our treatment commenced shortly after inoculation. The M1000 strain is of human origin, and while the lesion profile (with emphasis of spongiform change in the hippocampus and thalamus) and the incubation period (Brazier *et al.* 2006) are similar to that of scrapie strains, such as Me7 used in reported animal treatment models of prion disease showing greater efficacy (Toupet *et al.* 2008), it remains to be explored whether inferior or superior efficacy may occur against other prion strains or perhaps against the same strain in different hosts. Further supporting the possibility of strain influences on pathogenesis and treatment response, for unclear reasons, in contrast to studies utilizing other prion strains such as scrapie Rocky Mountain Laboratory (RML), we did not find that Cu^{2+} content was significantly reduced in the brains of our untreated diseased mice (Thackray *et al.* 2002; Mitteregger *et al.* 2009). Of interest, two of the most potent anti-prion compounds were reported using Tg7 mice inoculated with 263 K scrapie prions (Doh-ura *et al.* 2004; Kocisko *et al.* 2006) suggesting that particular strain/host combinations may be more inherently amenable to therapy. There is also great interest in the use of genetic models of prion disease, for example the A117V mouse model of GSS (Wenbin *et al.* 2009), in the study of anti-prion therapeutics.

We have previously found that ~ 20 ID_{50} units is the lowest dose of M1000 prions to result in a 100% attack rate (Collins *et al.* 2005). In keeping with previous studies investigating the therapeutic efficacy of D-PEN (Sigurdsson *et al.* 2003) and simvastatin (Mok *et al.* 2006), an extension of survival from $Na_2CaCDTA$ treatment was achieved only in mice inoculated with a lower dose of M1000 prions whereas, for poorly defined reasons, the treatment had no effect after inoculation with a high dose. As Mn^{2+} has been shown to stabilize and increase the survival of infectious prions (Davies and Brown 2009), it appears possible that our chelator, at the dose administered, only possessed activity capable of destabilizing the level of infectivity generated by a low dose inoculum. Hence, while many drugs have been shown to have a potent anti-prion effect in mice after high dose inoculation (Priola *et al.* 2000; Sethi *et al.* 2002; Doh-ura *et al.* 2004; Kocisko *et al.* 2006), it appears that high dose inoculation may initiate transmission and pathogenesis on too large a scale for less potent drugs such as simvastatin, D-PEN and $Na_2CaCDTA$ to provide benefit. A more biologically potent manganese chelator may provide superior

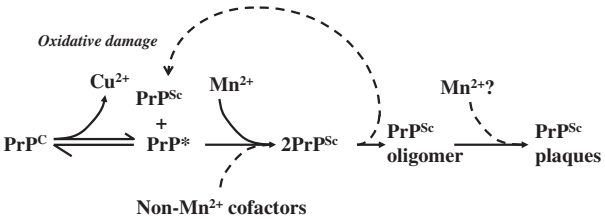

Fig. 7 Proposed mechanism for the involvement of manganese in prion pathogenesis. As part of normal protein turnover or the template-driven conformational change, prion protein (PrP^C) loses affinity for Cu^{2+} generating an infectious toxic intermediate PrP*. This alteration of PrP^C conformation to PrP* then allows Mn^{2+} (or other cofactors) to become associated, facilitating the stabilizing conversion to PrP^{Sc} with subsequent aggregation of oligomers and protofibrils into PrP plaques (Thackray *et al.* 2002; Giese *et al.* 2004; Tsenkova *et al.* 2004; Levin *et al.* 2005). Dotted lines represent associated reactions.

hindrance to the production of PrP^{Sc}, although as alluded above, it is conceded that the precise 'toxic species' in prion disease and its relationship to Mn^{2+} remains uncertain and a greater reduction in brain Mn^{2+} increases the potential for deleterious side effects.

Cumulatively, our findings raise the possibility that Mn^{2+} may facilitate conversion to PrP^{Sc} through pathways that are largely irrelevant to pathogenesis or that the contribution of Mn^{2+} to PrP^{Sc} production is dispensable or relatively superfluous in comparison to the small amount required for efficient pathogenesis. The progressive and considerable Mn^{2+} accumulation in the brain during the incubation period may therefore possibly represent more of an epiphenomenon or be simply a consequence of pathogenesis. Our results, in conjunction with previous related reports (Brown *et al.* 2000; Treiber *et al.* 2006; Brazier *et al.* 2008), allow us to propose a mechanism for the involvement of manganese in prion pathogenesis as follows (Fig. 7). Copper has a stabilizing effect, with PrP^C more readily undergoing conformational change to a pliable pathological intermediate, perhaps as part of normal turnover, as it loses bound copper ions. Manganese may then associate with the metastable intermediate and non-exclusively facilitate conversion and the acquisition of proteinase resistance, as well as promote higher order aggregation of PrP (Thackray *et al.* 2002; Giese *et al.* 2004; Tsenkova *et al.* 2004; Levin *et al.* 2005) with eventual deposition as plaques. Copper released from PrP^C or a metastable intermediate conformation of PrP, or Mn^{2+} bound to the conformationally altered PrP, may also be able to participate in oxidative reactions contributing to pathogenesis through cellular damage and neuronal loss. Hence, to reconcile the observation that large quantities of Mn^{2+} accumulate in the brain during the course of prion disease with our findings, we postulate that Mn^{2+} is likely to be only one factor involved in the conformational change of PrP^C to isoforms reminiscent of PrP^{Sc}.

Recent studies utilizing dietary modulation of copper and manganese during the incubation period of prion disease lend support for our proposed model of manganese involvement in PrP^{Sc} propagation although some apparent inconsistencies remain. Kralovicova *et al.* (2009) have demonstrated that reduced dietary copper causes decreased *in vivo* expression of the neuronal prion protein, considered to be a protective strategy against infection (Brazier *et al.* 2009), although mice fed a low-copper diet prior to and during scrapie incubation displayed a significantly shortened survival time (Mitteregger *et al.* 2009). Also, an elevated dietary copper intake has been shown to delay the onset of symptoms (Hijazi *et al.* 2003) and the terminal stage of scrapie-infection in mice when compared with controls fed a standard diet (Mitteregger *et al.* 2009). Studies of the influence that copper and manganese have on the aggregation of recombinant PrP suggest that, although copper is able to induce PrP to adopt a PrP^{Sc}-like conformation, this transition metal renders the protein less prone to aggregation (Giese *et al.* 2004; Levin *et al.* 2005; Brazier *et al.* 2008). A study by Hortells *et al.* (2009) has demonstrated that mice fed on a copper-depleted diet during scrapie infection displayed significantly more vacuolar lesions and activated astrocytes in selected regions of the brain. These pathologic changes are likely because of heightened oxidative stress resulting from a reduction of SOD activity.

Kralovicova *et al.* (2009) also demonstrated that elevated dietary manganese increases PrP^{C} expression in mice. Scrapie prion-inoculated mice fed a manganese-enhanced diet during the incubation period were found to have suffered more severe neuronal loss and their brains contained significantly more PrP-containing plaques when compared with controls (Hortells *et al.* 2009) although this diet had no influence on the animals' incubation periods (Mitteregger *et al.* 2009). In accord, our high dose inoculated mice treated for the entire incubation period with intensive $Na_2CaCDTA$, which was shown to specifically and significantly remove brain manganese during the incubation period, displayed significantly less protease resistant PrP^{Sc} when compared with late-treated and untreated controls. Nevertheless, as already stated, while Mn^{2+} is likely to facilitate the conformational change of PrP^{C} to PrP^{Sc} (Giese *et al.* 2004; Levin *et al.* 2005; Brazier *et al.* 2008), it is conceivable that the major role for manganese in prion disease is through a late downstream effect, simply facilitating higher orders of PrP^{Sc} aggregation and perhaps plaque formation (Fig. 7) which, while serving as a useful disease marker, is mechanistically largely unimportant for pathogenesis.

Acknowledgements

The authors thank the Animal Housing Facility staff in the Faculty of Medicine, Dentistry and Health Sciences, the University of Melbourne for their assistance with animal husbandry.

SJ Collins, AR White, AF Hill and CL Masters receive support from a National Health and Medical Research Council (NHMRC) Program Grant # 400202. SJ Collins is a recipient of an NHMRC Practitioner Fellowship # 400183. AF Hill is the recipient of an NHMRC RD Wright Career Development Award. The Australian National CJD Registry is funded by the Commonwealth Department of Health and Ageing. The anti-prion protein monoclonal antibody ICSM18 was a generous gift from Professor John Collinge.

Supporting Information

Additional Supporting Information may be found in the online version of this article:

Table S1. Brain transition metal analyses.

Table S2. Metal affinity of chelators.

As a service to our authors and readers, this journal provides supporting information supplied by the authors. Such materials are peer-reviewed and may be re-organized for online delivery, but are not copy-edited or typeset. Technical support issues arising from supporting information (other than missing files) should be addressed to the authors.

References

Allsop D., Mayes J., Moore S. *et al.* (2008) Metal-dependent generation of reactive oxygen species from amyloid proteins implicated in neurodegenerative disease. *Biochem. Soc. Trans.* **36**, 1293–1298.

Barnham K. J., Cappai R., Beyreuther K. *et al.* (2006) Delineating common molecular mechanisms in Alzheimer's and prion diseases. *Trends Biochem. Sci.* **31**, 465–472.

Brazier M. W., Lewis V., Ciccotosto G. D. *et al.* (2006) Correlative studies support lipid peroxidation is linked to PrP(res) propagation as an early primary pathogenic event in prion disease. *Brain Res. Bull.* **68**, 346–354.

Brazier M. W., Davies P., Player E. *et al.* (2008) Manganese binding to the prion protein. *J. Biol. Chem.* **283**, 12831–12839.

Brazier M. W., Wall V. A., Brazier B. W. *et al.* (2009) Therapeutic interventions ameliorating prion disease. *Expert Rev. Anti Infect. Ther.* **7**, 83–105.

Brown D. R., Qin K., Herms J. W. *et al.* (1997) The cellular prion protein binds copper *in vivo*. *Nature* **390**, 684–687.

Brown D. R., Wong B. S., Hafiz F. *et al.* (1999) Normal prion protein has an activity like that of superoxide dismutase. *Biochem. J.* **344**, 1–5.

Brown D. R., Hafiz F., Glasssmith L. L. *et al.* (2000) Consequences of manganese replacement of copper for prion protein function and proteinase resistance. *EMBO J.* **19**, 1180–1186.

Burns C. S., Aronoff-Spencer E., Legname G. *et al.* (2003) Copper coordination in the full-length, recombinant prion protein. *Biochemistry* **42**, 6794–6803.

Caughey B., Raymond G. J., Ernst D. *et al.* (1991) N-terminal truncation of the scrapie-associated form of PrP by lysosomal protease(s): implications regarding the site of conversion of PrP to the protease-resistant state. *J. Virol.* **65**, 6597–6603.

Cherny R. A., Atwood C. S., Xilinas M. E. *et al.* (2001) Treatment with a copper-zinc chelator markedly and rapidly inhibits beta-amyloid accumulation in Alzheimer's disease transgenic mice. *Neuron* **30**, 665–676.

Cohen F. E. and Prusiner S. B. (1998) Pathologic conformations of prion proteins. *Annu. Rev. Biochem.* **67**, 793–819.

Collins S. J., Lewis V., Brazier M. *et al.* (2002) Quinacrine does not prolong survival in a murine Creutzfeldt-Jakob disease model. *Ann. Neurol.* **52**, 503–506.

Collins S. J., Lewis V., Brazier M. W. *et al.* (2005) Extended period of asymptomatic prion disease after low dose inoculation: assessment of detection methods and implications for infection control. *Neurobiol. Dis.* **20**, 336–346.

Davies P. and Brown D. R. (2009) Manganese enhances prion protein survival in model soils and increases prion infectivity to cells. *PLoS ONE* **4**, e7518.

Dawson R. M. C., Elliot D. C., Elliot D. H. *et al.* (1986) *Data for Biochemical Research*. Oxford University Press, Oxford.

Deleault N. R., Lucassen R. W. and Supattapone S. (2003) RNA molecules stimulate prion protein conversion. *Nature* **425**, 717–720.

Deleault N. R., Harris B. T., Rees J. R. *et al.* (2007) Formation of native prions from minimal components in vitro. *Proc. Natl Acad. Sci. USA* **104**, 9741–9746.

Doh-ura K., Ishikawa K., Murakami-Kubo I. *et al.* (2004) Treatment of transmissible spongiform encephalopathy by intraventricular drug infusion in animal models. *J. Virol.* **78**, 4999–5006.

Gaeta A. and Hider R. C. (2005) The crucial role of metal ions in neurodegeneration: the basis for a promising therapeutic strategy. *Br. J. Pharmacol.* **146**(8), 1041–1059.

Gaggelli E., Bernardi F., Molteni E. *et al.* (2005) Interaction of the human prion PrP(106-126) sequence with copper(II), manganese(II), and zinc(II): NMR and EPR studies. *J. Am. Chem. Soc.* **127**, 996–1006.

Giese A., Levin J., Bertsch U. *et al.* (2004) Effect of metal ions on de novo aggregation of full-length prion protein. *Biochem. Biophys. Res. Commun.* **320**, 1240–1246.

Hijazi N., Shaked Y., Rosenmann H. *et al.* (2003) Copper binding to PrPC may inhibit prion disease propagation. *Brain Res.* **993**, 192–200.

Hortells P., Monleo′n E., Acı′n C. *et al.* (2009) The effect of metal imbalances on scrapie neurodegeneration. *Zoonoses Public Health* doi: 10.1111/j.1863-2378.2009.01230.x

Jackson G. S., Murray I., Hosszu L. L. *et al.* (2001) Location and properties of metal-binding sites on the human prion protein. *Proc. Natl Acad. Sci. USA* **98**, 8531–8535.

Jobling M. F., Huang X., Stewart L. R. *et al.* (2001) Copper and zinc binding modulates the aggregation and neurotoxic properties of the prion peptide PrP106-126. *Biochemistry* **40**, 8073–8084.

Khandelwal S., Kachru D. N. and Tandon S. K. (1980) Chelation in metal intoxication. IX. Influence of amino and thiol chelators on excretion of manganese in poisoned rabbits. *Toxicol. Lett.* **6**, 131–135.

Kim N. H., Choi J. K., Jeong B. H. *et al.* (2005) Effect of transition metals (Mn, Cu, Fe) and deoxycholic acid (DA) on the conversion of PrPC to PrPres. *FASEB J.* **19**, 783–785.

Kocisko D. A., Vaillant A., Lee K. S. *et al.* (2006) Potent antiscrapie activities of degenerate phosphorothioate oligonucleotides. *Antimicrob. Agents Chemother.* **50**, 1034–1044.

Kralovicova S., Fontaine S. N., Alderton A. *et al.* (2009) The effects of prion protein expression on metal metabolism. *Mol. Cell. Neurosci.* **41**, 135–147.

Lan J. and Jiang D. H. (1997) Desferrioxamine and vitamin E protect against iron and MPTP-induced neurodegeneration in mice. *J. Neural. Transm.* **104**, 469–481.

Lannfelt L., Blennow K., Zetterberg H. *et al.* (2008) Safety, effi cacy, and biomarker findings of PBT2 in targeting Aβ as a modifying therapy for Alzheimer's disease: a phase IIa, double-blind, randomised, placebo-controlled trial. *Lancet Neurol.* **7**, 779–786.

Lasmézas C. I., Deslys J. P., Robain O. *et al.* (1997) Transmission of the BSE agent to mice in the absence of detectable abnormal prion protein. *Science* **275**, 402–405.

Levenson C. W. (1998) Mechanisms of copper conservation in organs. *Am. J. Clin. Nutr.* **67**(5 Suppl), 978S–981S.

Levin J., Bertsch U., Kretzschmar H. *et al.* (2005) Single particle analysis of manganese-induced prion protein aggregates. *Biochem. Biophys. Res. Commun.* **329**, 1200–1207.

McLean C. A., Cherny R. A., Fraser F. W. *et al.* (1999) Soluble pool of Abeta amyloid as a determinant of severity of neurodegeneration in Alzheimer's disease. *Ann. Neurol.* **46**, 860–866.

Mitteregger G., Korte S., Shakarami M. *et al.* (2009) Role of copper and manganese in prion disease progression. *Brain Res.* **1292**, 155–164.

Mok S. W., Thelen K. M., Riemer C. *et al.* (2006) Simvastatin prolongs survival times in prion infections of the central nervous system. *Biochem. Biophys. Res. Commun.* **348**, 697–702.

Pauly P. C. and Harris D. A. (1998) Copper stimulates endocytosis of the prion protein. *J. Biol. Chem.* **273**, 33107–33110.

Priola S. A., Raines A. and Caughey W. S. (2000) Porphyrin and phthalocyanine antiscrapie compounds. *Science* **287**, 1503–1506.

Sanchez D. J., Gomez M., Domingo J. L. *et al.* (1995) Relative efficacy of chelating agents on excretion and tissue distribution of manganese in mice. *J. Appl. Toxicol.* **15**, 285–288.

Sethi S., Lipford G., Wagner H. *et al.* (2002) Postexposure prophylaxis against prion disease with a stimulator of innate immunity. *Lancet* **360**, 229–230.

Sigurdsson E. M., Brown D. R., Alim M. A. *et al.* (2003) Copper chelation delays the onset of prion disease. *J. Biol. Chem.* **278**, 46199–46202.

Silveira J. R., Raymond G. J., Hughson A. G. *et al.* (2005) The most infectious prion protein particles. *Nature* **437**, 257–261.

Srivastava R. C., Dwivedi P. P., Behari J. R. *et al.* (1986) Evaluation of LD50 of some polyaminocarboxylic acids used as chelating drugs in metal intoxication. *Toxicol. Lett.* **32**, 37–40.

Tandon S. K. (1978) Chelation in metal intoxication. VI. Influence of PAS and CDTA on the excretion of manganese in rabbits given MnO2. *Toxicology* **9**, 379–385.

Tandon S. K. and Khandelwal S. (1982) Chelation in metal intoxication X: influence of different polyaminocarboxylic acids and thiol chelators in the excretion and tissue distribution of 54Mn in rat. *Res. Commun. Chem. Pathol. Pharmacol.* **36**, 337–340.

Tandon S. K. and Singh J. (1975) Removal of manganese by chelating agents from brain and liver of manganese treated rats: as *in vitro* and an *in vivo* study. *Toxicology* **5**, 237–241.

Thackray A. M., Knight R., Haswell S. J. *et al.* (2002) Metal imbalance and compromised antioxidant function are early changes in prion disease. *Biochem. J.* **362**, 253–258

Thackray A. M., Madec J. Y., Wong E. *et al.* (2003) Detection of bovine spongiform encephalopathy, ovine scrapie prion-related protein (PrPSc) and normal PrPc by monoclonal antibodies raised to copper-refolded prion protein. *Biochem. J.* **370**, 81–90.

Thompsett A. R., Abdelraheim S. R., Daniels M. *et al.* (2005) High affinity binding between copper and full-length prion protein identified by two different techniques. *J. Biol. Chem.* **280**, 42750–42758.

Toupet K., Compan V., Crozet C. *et al.* (2008) Effective gene therapy in a mouse model of prion diseases. *PLoS ONE* **3**, e2773.

Treiber C., Simons A. and Multhaup G. (2006) Effect of copper and manganese on the de novo generation of protease-resistant prion protein in yeast cells. *Biochemistry* **45**, 6674–6680.

Tsenkova R. N., Iordanova I. K., Toyoda K. *et al.* (2004) Prion protein fate governed by metal binding. *Biochem. Biophys. Res. Commun.* **325**, 1005–1012.

Uppington K. M. and Brown D. R. (2008) Resistance of cell lines to prion toxicity aided by phosphor-ERK expression. *J. Neurochem.* **105**, 842–852.

Walsh D. M., Klyubin I., Fadeeva J. V. *et al.* (2002) Naturally secreted oligomers of amyloid beta protein potently inhibit hippocampal long-term potentiation *in vivo*. *Nature* **416**, 535–539.

Wenbin Y., Cook J., Rassbach B. *et al.* (2009) A new transgenic mouse model of Gerstmann-Straussler-Scheinker syndrome caused by the A117V mutation of PRNP. *Neurobiol. Dis.* **29**, 10072–10080.

White A. R., Enever P., Tayebi M. *et al.* (2003) Monoclonal antibodies inhibit prion replication and delay the development of prion disease. *Nature* **422**, 80–83.

Wieczorek H. and Oberdorster G. (1989) Effects of selected chelating agents on organ distribution and excretion of manganese after inhalation exposure to 54MnCl2. I. Injection of chelating agents. *Pol. J. Occup. Med.* **2**, 261–267.

Wong B. S., Chen S. G., Colucci M. *et al.* (2001) Aberrant metal binding by prion protein in human prion disease. *J. Neurochem.* **78**, 1400–1408.

Youdim M. B., Stephenson G. and Ben Shachar D. (2004) Ironing iron out in Parkinson's disease and other neurodegenerative diseases with iron chelators: a lesson from 6-hydroxydopamine and iron chelators, desferal and VK-28. *Ann. NY Acad. Sci.* **1012**, 306–325.

Section 7: Studies of Human Prion-like Diseases

Until recently, prion diseases had been construed as biologically unique neurodegenerative disorders given a transmissible agent constituted primarily, if not exclusively, by misfolded prion protein (PrP^{Sc}) free of nucleic acids. Over the last approximately 5-10 years however, numerous studies have challenged this unique standing of prion diseases with other misfolded proteins such as Abeta, alpha-synuclein and tau appearing to behave in a prion-like manner as far as mechanisms of propagation, along with inter-cellular transfer and inter-organismal transmissibility. Although many issues remain to be resolved in relation to this blurring of the margins between prions and other proteins underscoring non-prion neurodegenerative diseases, such as AD (Abeta and tau) and PDD (alpha-synuclein), there seems little doubt that the previous neat biological demarcation of prion diseases from other neurodegenerative disorders will stay relegated to history. One of the important issues to resolve is whether subsequent to transmission, the propagation and accumulation of non-prion proteins such as Abeta in a new host culminate in a disease phenotype or remain sub-clinical. Very recent work suggests the pendulum is swinging towards the likelihood of eventual overt expression of disease in at least some individuals, with the propagated Abeta deposited in cerebral blood vessels as CAA likely to be causally associated with spontaneous intra-cranial haemorrhage in relatively young people who have undergone treatments (eg dura mater grafts) associated with the deposition of Abeta proteopathic seeds in or around their brains in early childhood.

My research further supports this revision of the clear-cut demarcation between prion diseases and other neurodegenerative disorders. A large multi-national collaborative study that included Australian patients reported a disproportionately high prevalence of Abeta deposited in the brains (as both CAA and parenchymal plaques) in persons who developed iatrogenic CJD many years following cadaveric pituitary hormone treatments and Lyodura (dura mater) grafts, almost certainly due to the concomitant tainting of these therapeutics with both PrP^{Sc} and Abeta. Moreover, I very recently reported a significant increase of deaths from spontaneous intra-cerebral haemorrhage amongst Australian recipients of cadaveric pituitary hormones, consistent with the hypothesis that such treatments were contaminated by Abeta leading to CAA in the absence of PrP^{Sc}.

List of my publications submitted in full (in chronological order)

Cali I, Cohen M, Haik S, Parchi P, Giaccone G, Collins S, Kofskey D, McLean C, Brandel J-P, Duyckaerts S, Kitamoto T, Belay E, Maddox R, Tagliavini F, Pocchiari M, Leschek E, Safar J, Appleby B, Schonberger L, Gambetti P. Amyloid-beta pathology iniiatrogenic Creutzfeldt-Jakob disease: an international study. Acta Neuropathologica Communications 2018; 6: 5.

Alnakhli S, Wand H, Law M, Sarros S, Stehmann C, Senesi M, Klug G, Simpson M, Lewis V, Masters C, Collins S. Intra-cerebral haemorrhage but not neurodegenerative disease appears over-represented in deaths of Australian cadaveric pituitary hormone recipients.Journal of Clinical Neuroscience 2020; 81: 78-82.

Cali et al. Acta Neuropathologica Communications (2018) 6:5
DOI 10.1186/s40478-017-0503-z

Acta Neuropathologica Communications

RESEARCH Open Access

Iatrogenic Creutzfeldt-Jakob disease with Amyloid-β pathology: an international study

Ignazio Cali[1,20*], Mark L. Cohen[1,4], Stéphane Haïk[5,6,7], Piero Parchi[8,9], Giorgio Giaccone[10], Steven J. Collins[11], Diane Kofskey[1,4], Han Wang[12], Catriona A. McLean[13,14], Jean-Philippe Brandel[5,6], Nicolas Privat[5], Véronique Sazdovitch[5,7], Charles Duyckaerts[5,7], Tetsuyuki Kitamoto[15], Ermias D. Belay[16], Ryan A. Maddox[16], Fabrizio Tagliavini[10], Maurizio Pocchiari[17], Ellen Leschek[18], Brian S. Appleby[2,3,4], Jiri G. Safar[1,2,4], Lawrence B. Schonberger[16] and Pierluigi Gambetti[1,19*]

Abstract

The presence of pathology related to the deposition of amyloid-β (Aβ) has been recently reported in iatrogenic Creutzfeldt-Jakob disease (iCJD) acquired from inoculation of growth hormone (GH) extracted from human cadaveric pituitary gland or use of cadaveric dura mater (DM) grafts.

To investigate this phenomenon further, a cohort of 27 iCJD cases – 21 with adequate number of histopathological sections – originating from Australia, France, Italy, and the Unites States, were examined by immunohistochemistry, amyloid staining, and Western blot analysis of the scrapie prion protein (PrP^{Sc}), and compared with age-group matched cases of sporadic CJD (sCJD), Alzheimer disease (AD) or free of neurodegenerative diseases (non-ND). Cases of iCJD and sCJD shared similar profiles of proteinase K-resistant PrP^{Sc} with the exception of iCJD harboring the "MMi" phenotype. Cerebral amyloid angiopathy (CAA), either associated with, or free of, Thioflavin S-positive amyloid core plaques (CP), was observed in 52% of 21 cases of iCJD, which comprised 37.5% and 61.5% of the cases of GH- and DM-iCJD, respectively. If only cases younger than 54 years were considered, Aβ pathology affected 41%, 2% and 0% of iCJD, sCJD and non-ND, respectively. Despite the patients' younger age CAA was more severe in iCJD than sCJD, while Aβ diffuse plaques, in absence of Aβ CP, populated one third of sCJD. Aβ pathology was by far most severe in AD. Tau pathology was scanty in iCJD and sCJD.

In conclusion, (i) despite the divergences in the use of cadaveric GH and DM products, our cases combined with previous studies showed remarkably similar iCJD and Aβ phenotypes indicating that the occurrence of Aβ pathology in iCJD is a widespread phenomenon, (ii) CAA emerges as the hallmark of the Aβ phenotype in iCJD since it is observed in nearly 90% of all iCJD with Aβ pathology reported to date including ours, and it is shared by GH- and DM-iCJD, (iii) although the contributions to Aβ pathology of other factors, including GH deficiency, cannot be discounted, our findings increase the mounting evidence that this pathology is acquired by a mechanism resembling that of prion diseases.

Keywords: Amyloid-β, Pathology, iCJD, Cerebral amyloid angiopathy, Thioflavin S

* Correspondence: ixc20@case.edu; pxg13@case.edu
[1]Departments of Pathology, Case Western Reserve University, School of Medicine, Cleveland, OH 44106, USA
Full list of author information is available at the end of the article

Introduction

The key pathogenic event of all prion diseases is the conversion of a normal or cellular prion protein (PrP^{c}) into a misfolded and disease-associated isoform commonly identified as scrapie prion protein (PrP^{Sc}) or prion. Newly converted PrP^{Sc} then propagates and accumulates preferentially in the central nervous system (CNS) typically accompanied by spongiform degeneration, gliosis and neuronal cell death. These pathogenetic features apply especially to Creutzfeldt-Jakob disease (CJD), by far the most common human prion disease. The pathogenic mechanism based on the conformational conversion of PrP^{C} into PrP^{Sc}, which then acts as a seed, can conceptually accommodate not only PrP^{Sc} accumulation and propagation in the affected subject, but also the potential transmission of the process from affected to non-affected subjects. Although the sporadic and inherited forms account for the majority of human prion diseases [24], less than 1% of the prion diseases is acquired from animals or humans via an infectious mechanism [7]. Within this group, iatrogenic CJD (iCJD) is of particular interest. More than 492 cases of iCJD have been reported worldwide [4]. Most cases have been associated with the administration of growth hormone (GH) extracted from cadaveric pituitary glands and the application of cadaveric dura mater (DM) grafts [7]. The existence of iCJD and experimental evidence have firmly established the infectious property of prion diseases [18, 26, 27].

The central pathogenic event in Alzheimer's disease (AD), the most common cause of dementia, is the deposition of amyloid β (Aβ), a truncated fragment of the amyloid precursor protein (*APP*), which leads to the formation of extracellular Aβ plaques [22, 30]. Deposition of highly phosphorylated, microtubule-associated tau protein (p-tau) also occurs [57] and, is believed to be a downstream event [33]. Most evidence indicates that deposition of Aβ and p-tau in the affected brain is stereotypical and hierarchical [5, 63]. More recently, it has been pointed out that Aβ and p-tau mimic several major characteristics of PrP^{Sc} including mechanisms of accumulation and propagation and formation of distinct Aβ and p-tau species that fulfill some of the characteristics of strains [16, 28, 56, 67, 68]. Like PrP^{Sc}, Aβ has been detected in tissues other than CNS parenchyma including dura mater and pituitary glands [35, 43]. Furthermore, Aβ and p-tau pathologies (but not fully developed AD) have been replicated following Aβ or p-tau intracerebral or peripheral inoculations to transgenic mice that express human *APP* harboring AD pathogenic mutations as well as wild type human *APP*, indicating that Aβ pathology is transmissible [11, 20, 47, 48, 70]. In contrast to prion diseases, there is no evidence that AD and/or tauopathy (e.g., frontotemporal lobar degeneration) transmit from human-to-human.

Five recent studies have independently reported the presence of significant Aβ pathology in 4 of 8, 18 of 33, and 1 of 24 cases of iCJD from the United Kingdom (UK) and France, linked to injections of cadaveric GH (GH-iCJD) [19, 37, 53], and in 5 of 7 Swiss and Austrian iCJD and 13 of 16 Japanese iCJD cases who had received DM grafts (DM-iCJD) [23, 31]. In the most severely affected cases, Aβ amorphous aggregates were also detected in the pituitary gland and DM [37, 43]. The concomitant presence of Aβ and PrP^{Sc} deposits resulting in mixed AD and CJD phenotypes has been reported [8, 25, 50, 65]. However, while the AD-CJD mixed phenotype has been observed in older CJD-affected individuals [29, 64], most of the 28 iCJD cases harboring significant Aβ pathology were under 55 years of age [19, 23, 37, 53]. A possible explanation for the higher prevalence of Aβ pathology at a relatively young age in iCJD-affected subjects is that both Aβ and PrP^{Sc} seeds are transmitted during the iatrogenic procedures and then accumulate and propagate concurrently. However, Ritchie and coworkers have also observed brain Aβ pathology in absence of PrP^{Sc} deposition in recipients of cadaveric GH [53]. This important finding strongly argues for human-to-human transmission of an Aβ-related condition independently from the PrP^{Sc} seeding process. Nonetheless, whether the neuroendocrine deficiency may favor the Aβ pathology in some cases is still unknown [21].

To further investigate the iatrogenic seeding of Aβ pathology, we examined whether this condition occurs not only with UK and French GH as previously described but with receipt of GH produced before 1977 in the United States (US) as well. All US GH-iCJD patients to date received GH made before 1977, when a GH purification procedure was adopted that reduced or eliminated prion contamination. We also wanted to further examine the phenotypes of the DM-iCJD linked to the use of the Lyodura® brand. Out of 27 cases of definite iCJD, we selected 21 which were suitable for detailed histopathological examination and were provided by national prion surveillance centers of Australia, France, Italy, and the US. Cases of sporadic CJD (sCJD), non-neurodegenerative disorders (non-ND), and AD were used as comparison groups. Two autopsied cases who underwent GH treatment but did not develop iCJD were also examined. We report that (i) over 50% of iCJD cases harbored significant Aβ pathology, which included cerebral amyloid angiopathy (CAA) in all cases; (ii) the prevalence of the Aβ-positive iCJD subset was significantly higher than that of Aβ-positive sCJD cases, which were on average 17 years older; (iii) p-tau pathology was present but did not distinguish Aβ-positive iCJD cases from the sCJD controls, and seemed to be age-related; (iv) the phenotypic characteristics of the Aβ pathology in iCJD were distinct from those of typical AD.

Materials and methods

Reagents and antibodies

Dulbecco's Phosphate Buffered Saline (DPBS), NaCl, Nonidet P-40, Sodium deoxycholate, Tris–HCl, Phenylmethanesulfonyl fluoride (PMSF), proteinase K (PK), Thioflavin S, and Kodak Biomax MR and XAR films were from Sigma-Aldrich (St. Louis, MO, USA). Tween 20, β–mercaptoethanol, Tris buffered saline (TBS), 2X Laemmli sample buffer, non-fat dry milk, 15% Criterion Tris–HCl polyacrylamide precast gels, 30% Acrylamide/Bis solution, tetramethylethylenediamine (TEMED), 10% sodium dodecyl sulfate (SDS) and ammonium persulphate (APS) were from Bio-Rad Laboratories (Hercules, CA, USA). Odyssey Blocking Buffer was from LI-COR Biosciences (Lincoln, NE, USA); polyvinylidene difluoride (PVDF) membrane (Immobilon-FL and Immobilon-P) was from EMD Millipore (Billerica, MA, USA). The primary antibodies (Abs) included the AT8 (to human phospho-tau residues Ser202 and Thr205) from Thermo Fisher Scientific Inc. (Waltham, MA, USA), 4G8 (to human Aβ residues 17–24), and 3F4 (to human PrP residues 106–110) [38, 71] from Richard Kascsak at the N.Y.S. Institute for Basic Research; 12B2 (to human PrP residues 89–93) [45] was from the Wageningen University & Research (Lelystad, Netherlands), whereas Tohoku-2 (to human PrP residues 97–103) [42] was kindly provided by Dr. Tetsuyuki Kitamoto. Secondary Abs were the sheep anti-mouse IgG from Life Sciences (Piscataway, NJ, USA), IRDye 800CW goat anti-mouse IgG (1 mg/ml) and IRDye 680RD goat anti-rabbit IgG (1 mg/ml) from LI-COR Biosciences (Lincoln, NE, USA). Reagents ECL and ECL plus were from GE Healthcare, Life Sciences (Piscataway, NJ, USA); Envision Flex Peroxidase Blocking Reagent, Envision Flex/HRP and Envision Flex DAB were from Dako (Dako North America Inc., Carpinteria, USA); the Vectashield mounting medium for fluorescence was from Vector Laboratories Inc. (Burlingame, CA, USA).

Patients

Brain tissue from 27 confirmed iCJD patients was collected in this study. Thirteen of these cases were associated with cadaveric GH extracted from pituitary glands, whereas the other 14 cases were associated with cadaveric DM graft (Table 1 and Additional file 1: Table S1). All GH-iCJD were from the US and were treated with GH under the US National Hormone and Pituitary Program and started their treatment between 1969 and 1974. Tissue from 12 of the 13 US GH-iCJD was obtained at autopsy and one at biopsy. Two DM-iCJD were US cases, but only one -a 26 years old man -had received the Lyodura® brand dura (B. Braun Melsungen AG, Melsungen, Germany) (DM_L-iCJD) whereas the other case -a 39 years old woman -had received the Tutoplast® brand dura (Pfrimmer-Viggo GmbH + Co, Erlangen, Germany) (DM_T-iCJD). An important difference between these brands of dural graft is that unlike Tutoplast, Lyodura brand dural grafts were intermingled with many other dural grafts during the manufacturing procedure, thereby increasing the risk of cross-contamination. Other DM-iCJD cases included 1) two cases from the Australian National CJD Registry (Melbourne, Australia), 2) six cases from the Réseau National de Référence de maladies de Creutzfeldt-Jakob and Centre National de Référence des agents transmissibles non conventionnels (Paris, France), and 3) four cases from the Istituto Superiore di Sanita' (Rome, Italy). With the exception of one French DM-iCJD case, for which the medical product Lyodura® brand could not be confirmed, all cases were DM_L-iCJD. The histopathology and/or clinical and molecular features have been published for two US DM-iCJD (cases 1 and 2, Table 1) [3, 10, 32], three US GH-iCJD (cases 6, 9 and 10, Table 1) [10], and one Australian DM_L-iCJD (case 17, Table 1) [58]. The five distinct comparison groups included 1) two US non-CJD patients who received the GH between years 1973–1977 (50 years) or between years 1977–1981 (46 years). The latter case may not have received any of the pre-1977 produced higher risk US GH material because 1977 was the transition year when a new purification procedure of GH extraction was started [1]; 2) 67 confirmed sCJD cases from Australia ($N = 4$), France ($N = 11$), Italy ($N = 8$) and US ($N = 44$) (Additional file 1: Tables S1 and S2); 3) 11 US autopsied cases of non-ND with age at death of 40 ± 12 years (range, 25–59 years) following diagnosis of blood cancer ($N = 3$; 25, 27 and 41 years), intracranial tumors ($N = 2$; 35 and 44 years), hemoglobin sickle cell disease (28 years), scrotal abscess and pulmonary embolus (31 years), type II diabetes mellitus (47 years), gastrointestinal hemorrhage (50 years), systemic lupus erythematosus (56 years), end stage renal disease and cardiac arrest (59 years); 4) seven US cases of AD with age at death of 64 ± 8 years, and disease duration of 75 ± 39 months [12]. Disease duration was not available in one AD case. All sporadic and iatrogenic CJD cases were classified according to Parchi and collaborators (1999). Since all Aβ-positive cases had multiple cortical sections not all of which were positive, we excluded from the study six Aβ-negative cases with only one section available.

All of the US iCJD and the two CJD-free recipients of GH were collected at the National Prion Disease Pathology Surveillance Center (NPDPSC) in Cleveland (OH) in collaboration with the National Institute of Diabetes, Digestive and Kidney Diseases, NIH, (Bethesda, MD) and Division of High Consequence Pathogens and Pathology, CDC, (Atlanta, GA) and Westat Agency (Rockville, MD). The AD and US sCJD controls were

Table 1 All examined cases of iCJD from countries of treatment with clinical, molecular and histopathological features

Case number	Iatrogenic exposure	Country	Sex	Age at death (years)	Disease duration (months)	Mean incubation period[a] (years)	Codon 129 genotype	PrP^{Sc} type	Histopath. phenotype	Two or more histological sections
1[b,c]	DM_L	United States	M	26	5	19	na	na	MM(MV)1	yes
2[d,e]	DM_T		F	39	4	6	MM	1	MM(MV)1	yes
3	GH		M	33	6	23	VV	na	VV2	yes
4	GH		M	39	17	24	MV	na	MV2K	yes
5	GH		M	39	7	27	MM	2	Atypical	yes
6[e]	GH		F	41	2	26	MM	1	MM(MV)1	yes
7	GH		M	43	26	23	MV	i+2	MV2K	yes
8	GH		M	44	18	32.5	MV	i+2	MV2K	yes
9[e]	GH		M	51	14	38	MM	i	MMi	yes
10[e]	GH		M	54	2	41.5	MM	1	MM(MV)1	yes
11	GH		M	23	19	10	na	na	MV2K or MMi	no
12	GH		M	34	18	23	na	na	MV2K or MMi	no
13	GH		M	37	3	21	na	na	MM(MV)1	no
14	GH		M	42	5	>28[f]	MM	na	Undetermined[g]	no
15[h]	GH		M	52	4	43	na	na	MM(MV)1	no
mean±SD[i]				41±8.5	11±8	28±9.5[j]				
16	DM_L	Australia	M	32	3.5	16.5	MV	na	MM(MV)1	yes
17[k]	DM_L		M	62	2	5	na	na	MM(MV)1	yes
mean±SD				47±21	3±1	11±8				
18	DM_L	France	M	25	8	8	MV	na	MM(MV)1	yes
19	DM_{Unk}		M	29	6	25	MV	1	MM(MV)1	yes
20	DM_L		M	42	5	6	VV	na	VV2	yes
21	DM_L		F	50	14	11	MM	na	MMi	yes
22	DM_L		F	62	4	4	VV	na	VV2	yes
23	DM_L		F	71	4	4	MV	na	MV2K	yes
mean±SD				46.5±18	7±4	10±8				
24	DM_L	Italy	F	23	27	21	VV	2	VV2	yes
25	DM_L		F	26	6	12	MM	na	MM(MV)1	no
26	DM_L		M	42	3.5	18	MM	1+2	MM1+2	yes
27	DM_L		M	75	3	18	VV	2	VV2	yes
mean±SD				41.5±24	10±11.5	17±4				

[a]The mean incubation period was measured from the mid-point of GH therapy or date of receipt of the dura graft to the clinical onset of the disease; [b][3]; [c]Numbers in bold indicate iCJD cases with Aβ-positive pathology; [d][32]; [e] [10]; [f]Unknown starting date for GH treatment (incubation period thought to be greater than 28 years); [g]Associated with severe spongiosis and gliosis; [h]Biopsy; [i]Mean±SD of the US iCJD cases does not include DM_L (case 1) and DM_T (case 2); [j]It does not include case 14; [k][58]; Histopath. histopathological, DM_{Unk} dura mater of an unknown (Unk) brand,
na not available *SD* standard deviation

from the NPDPSC whereas the 11 non-ND cases were collected in the repository of the Department of Pathology at Case Western Reserve University. The neuropathological study was carried out either in our laboratory or in the laboratories of the participating countries. Neuropathology was reviewed by IC and MC. Western blot (WB) examination of iCJD cases was performed in our laboratory in Cleveland (cases 2, 6–10, 24, 26 and 27, Table 1), at University of California, San Francisco (UCSF) (case 5) as well as in France (case 19, Table 1) and Italy (cases 24, 26 and 27, Table 1).

Histology and immunohistochemistry

Formalin-fixed brain tissue was treated as previously described [9]. Briefly, sections were deparaffinized and rehydrated, immersed in 1X Tris buffered saline-Tween 20 (TBS-T), and endogenous peroxidase blocked after incubation with the Envision Flex Peroxidase Blocking Reagent for 10 minutes (min). Sections were washed, immersed in 1.5 mmol/L hydrochloric acid, microwaved for 15 min and probed with Abs 3F4 (1:1000), 4G8 (1:3000), and AT8 (1:200) for 1 hour (h). After washing and incubation with Envision Flex/HRP polymer for 30 min, sections were treated with Envision Flex DAB to show the immunostaining.

Thioflavin S staining

After deparaffinization, formalin-fixed sections were stained in Thioflavin S for 7 min, washed three times in 80% alcohol, dehydrated in ethanol, cleared in xylene, and cover slipped with Vectashield mounting medium for fluorescence. Sections were kept in the dark at 4 °C for 30 min before being viewed under the fluorescence microscope (Olympus IX71).

Evaluation of the histopathological changes associated with Alzheimer's disease and Prion disease

Histopathological evaluation was performed in 10 or more anatomical regions in most cases. Standard brain locations included the frontal, temporal, parietal, occipital and entorhinal cortices, hippocampus, striatum, thalamus, midbrain and cerebellar hemispheres and/or vermis. Histopathological evaluation included 1) Hematoxylin-eosin (HE) staining, to assess the presence of spongiform degeneration, gliosis, and amyloid Aβ cores; 2) Immunostaining with Abs 4G8, AT8 and 3F4 to Aβ, p-tau and PrP, respectively; 3) Staging of Aβ plaques using monoclonal Ab 4G8 and Thioflavin S, according to Thal et al. [63]. This method identifies five major stages or phases of Aβ plaques deposition affecting the neocortex, including frontal, temporal, parietal and occipital cortices (Phase 1), hippocampus and entorhinal cortex (Phase 2), striatum thalamus and midbrain (Phase 3–4), and cerebellum (Phase 5); 4) Description of the morphology of the Aβ plaques, including a) diffuse plaques, b) core plaques (CP) (i.e., a plaque with a dense core surrounded by a halo and a corona of lightly stained Aβ), c) neuritc plaques (i.e., a core plaque surrounded by p-tau dystrophic neurites); 5) Staging of Aβ CAA, according to previous procedures [61] with recognition of three major phases: CAA affecting the neocortex (Phase 1), hippocampus, entorhinal cortex, cerebellum and midbrain (Phase 2), striatum and thalamus (Phase 3); 6) Typing of CAA, identified as CAA type 1 or type 2 depending on the presence or absence of Aβ deposits in the cortical capillaries [60]. The criteria for the identification of CAA type 1 were i) diameter of the vessels ≤ 10 μm, and ii) deposition of Aβ in the outer basement membrane; 7) Severity of CAA, based on a modified protocol by Vonsattel and coworkers that uses 4G8-stained sections (with the addition of Thioflavin S in some cases) instead of Congo red [66]; 8) Brain distribution of neurofibrillary tangles (NFT) and neocortical distribution of dystrophic neurites (DN); 9) Severity of NFT and DN expressed as NFT or DN density in one microscopic field (area: 1.3×1.0 mm^2, using a 10X objective) harboring the highest density of NFT or DNs in one or more brain regions; severity was scored as mild (≤ 10 NFT or DN), moderate (> 10 to < 30 NFT or DN) and severe (≥ 30 NFT or DN); 10) Automated image acquisition and morphometric analysis to assess density (expressed as the percentage of the area of the cerebral cortex occupied by plaques) and size (diameter) of Thioflavin S-positive Aβ core plaques as well as size (perimeter) of the blood vessel; 11) Semiquantitative analysis of the percentage of 4G8-positive Aβ deposits along the wall of blood vessels; and 12) Double immunostaining with 4G8 and 3F4 to rule out the co-localization of PrP and Aβ [25].

Image acquisition and statistical analysis

Image acquisition was carried out with a Leica DFC 425 digital camera mounted on a Leica DM 2000 microscope. Images were analyzed by the software Image-Pro Plus 7.0 (Media Cybernetics, Inc.). Cumulative survival curves were generated by the Kaplan–Meier analysis. Statistical significance between the survival curves of the individual groups were determined by the log rank (Mantel-Cox) test. When comparing different patient groups, *P*-values were calculated with Chi-square test, Fisher's exact test, Student's t-test (two-tailed). All the statistical analyses were performed using GraphPad Prism 6.0.

Preparation of brain homogenates, proteinase K digestion and Western blot analysis

10% (wt/vol) brain homogenates (BH) prepared in 1X LB100 buffer (100 mM NaCl, 0.5% Nonidet P-40, 0.5% sodium deoxycholate, 10 mM EDTA, 100 mM Tris–HCl,

pH 6.9 at 37 °C), were centrifuged at 1000 x g for 5 min at 4 °C, pellets discarded and supernatants (S1) collected. S1 aliquots were incubated with 100 U/ml PK at 37 °C for 1 h [PK specific activity was 48 U/mg at 37 °C, with 1 U/ml equal to 20.8 μg/ml PK]. The enzymatic digestion was stopped with PMSF (3 mM final concentration). Each sample was diluted with an equal volume of 2X Laemmli sample buffer (6% SDS, 20% glycerol, 4 mM EDTA, 5% β −mercaptoethanol, 125 mM Tris–HCl, pH 6.8) and denatured at 100 °C for 10 min. Proteins were separated on 15% Criterion™ Tris–HCl Precast Gels (W x L: 13.3 cm × 8.7 cm) at 120 Volts (V) for 20 min followed by 150 V for 1 h 45 min, or using 15% Tris–HCl SDS–polyacrylamide gels (W x L: 20 cm × 20 cm) at 25 mA/gel for 1 h 45 min followed by 35 mA/gel for 6 h 30 min (Bio-Rad PROTEAN® II xi cell system). For near-infrared WB analysis, proteins were blotted onto the Immobilon-FL PVDF membrane for 2 h, blocked with the Blocking Buffer Odyssey for 45 min and incubated with Abs 3F4 (1:20,000), 12B2 (200 ng/ml) or Tohoku-2 (1:10,000) for 2 h. Membranes were then washed with 1X DPBS containing 0.1% of Tween 20 (1X DPBS-T) and incubated with Abs IRDye 800CW goat anti-mouse IgG (1:15,000) or IRDye 680RD goat anti-rabbit IgG (1:15,000) for 1 h. After washing in 1X DPBS-T, membranes were developed with the Odyssey infrared imaging system (LI-COR Biosciences) as described by the manufacturer. For chemiluminescence, proteins were blotted onto the Immobilon-P PVDF membrane, blocked with 5% non-fat dry milk in 0.1% Tween 20-1X TBS (blocking buffer), and incubated with primary Abs and horseradish peroxidase-conjugated goat anti-mouse secondary Ab (1:3000). Membranes were developed by the enhanced chemiluminesce reaction using ECL and ECL plus reagents, and signal captured on MR and XAR films.

Clinical evaluation

Medical records were reviewed by a clinician (BSA) and data were collected on demographics (age at death, gender, and race/ethnicity). Disease onset was defined as the time at which the first persistent and consistent symptom of prion disease was observed. Data on family history of dementia as well as past medical and surgical history were also collected. The mean incubation period in iCJD was measured from the mid-point of GH therapy or date of receipt of the DM graft to the clinical onset of the disease.

Genetic analysis

DNA was extracted from frozen brain tissues and *APP*, presenilin 1 (*PSEN1*), presenilin 2 (*PSEN2*), and *PRNP* gene analysis was performed as previously described using Illumina and Sanger Sequencing for exons 4 and 5 in *PSEN1* [12]. Sequencing analysis was performed using Mutation Surveyor Version 4.0.7 (Softgenetics, State College, PA). Genotyping of Apolipoprotein E (*ApoE*) single-nucleotide polymorphisms was performed by Sanger sequencing (Center for Human Genetics, Cleveland, OH).

Results

Demographics, molecular features and histopathological phenotype of iCJD and controls including sCJD

We examined 27 cases of iCJD linked to cadaveric DM graft ($N = 14$) or GH ($N = 13$), who received the iatrogenic treatment in Australia, France, Italy and the US (Table 1). Sixty-seven cases of sCJD obtained from the same countries as the iCJD cases were used as controls (Additional file 1: Table S2). The sCJD case population was selected to be as similar to the age of the iCJD case population as possible. As expected, the iCJD cases had a higher percentage of premorbid neurological conditions (including intracranial tumors and head trauma) and neurosurgery given that these conditions often led to treatment with GH and/or DM grafts. No statistical correlations were found when intracranial tumor or head trauma were tested against either Aβ or tau pathologies in the iCJD and sCJD populations (Additional file 1: Table S3). Both iCJD and sCJD cohorts were compared to a seven case group with typical AD (Tables 2 and 3, and Additional file 2: Table S6). The iCJD cases were stratified by country of origin, age at death, disease durations and incubation period (Table 1). The data stratified according to diagnosis, i.e. all-iCJD, GH-iCJD, DM-iCJD and sCJD, as well as according to the age at death, i.e. ≤ 54 years ("young") and > 54 years ("old") are shown in Additional file 1: Table S1 and Additional file 3: Figure S1. For all the cases combined, the three iCJD diagnostic groups revealed no significant difference in mean age at death, disease duration and median survival, while the incubation period was significantly shorter in DM-iCJD than in GH-iCJD ($P < 0.0001$) (Additional file 1: Table S1 and Additional file 3: Figure S1). Separation of cases into young and old subsets underscored the younger age of the GH-iCJD cases, which exclusively populated the young group, and the wide age range of DM-iCJD (Additional file 1: Table S1). In the young group, the incubation period again was significantly shorter in DM-iCJD than GH-iCJD ($P < 0.002$). Overall, disease duration and incubation period were significantly shorter in the older group ($P < 0.0008$ and $P < 0.03$, respectively) (Additional file 1: Table S1). The sCJD control population was 8 years older at death than the iCJD population while disease duration was comparable in the two conditions. Sporadic CJD young cases had a mean age at death comparable to that of GH-iCJD while disease duration in old cases matched that of DM-iCJD (Additional file 1: Table S1).

Table 2 Staging and amyloid presence in Aβ CP from iCJD associated with Aβ pathology along with cases of sCJD and AD used as controls

Case number	Age (y)	Disease durat. (mo)	Codon 129 genotype	PrP^{Sc} type	Phase 1		Phase 2		Phase 3-4		Phase 5	
					Neocortex	ThioFl	Hippoc.	ThioFl	Subcortical	ThioFl	Cerebellum	ThioFl
iCJD												
1 (1)[a]	26	5	na	na	+++[b,c]	+[d]	++	-	+[e]	-	+	-
2 (19)	29	6	MV	1	+++[f]	+	+	+	-	nt	-	nt
3 (8)	44	18	MV	i+2	++++	+	++	-	+++	-	-	-
4 (9)	51	14	MM	i	-	-	-	-	-	nt	+	+
5 (17)	62	2	na	na	++++	+[g]	na	na	na	na	-	-
mean±SD	42±15	9±7			78%[h]		62.5%		40%		40%	
sCJD												
1 (57)[i]	63	3	MV	1	+++[f]	+	++	+	++	nt	-	nt
2 (59)	71	9	MV	2	+[f]	+	-	-	-	nt	-	nt
3 (65)	71	10	VV	2	+	+	-	nt	-	nt	-	nt
4 (67)	79	6	VV	2	+++	+	-	nt	-	nt	-	nt
mean±SD	71±6.5	7±3			57%		25%		17%		0%	
P value[j]					NS		NS		NS		NS	
AD												
1	56	60	na	na	++++	+	++	+	+++	+	+	+
2	56	60	na	na	++++	+	++	+	+++	+	+	+
3	59	na	na	na	++++	+	++	+	+++	+	+	+
4	60	130	na	na	++++	+	++	+	+++	+	+	-
5	70	66	na	na	++++	+	++	+	+++	+	+	+
6	72	111	na	na	++++	+	++	+	+++	-	+	+
7	74	22	na	na	++++	+	++	+	+++	+	+	+
mean±SD	64±8	75±39			100%		100%		100%		100%	
P value[k]					< 0.02		< 0.04		< 0.0004		< 0.05	

Phases 1 to 5 refer to Aβ plaques deposition in various brain regions reflecting disease progression according to Thal et al [63]; [a,i]Numbers in parenthesis in the first column refer to numerals used in [a]Table 1 and [i]Additional file 1: Table S2; [b]Minus and plus signs indicate absence (-) or presence (+) of Aβ pathology affecting one (+), two (++), three (+++) or four (++++) of the brain regions that characterize each phase; Phase 1: frontal, temporal, parietal and occipital cortical regions; Phase 2: hippocampus and entorhinal cortex; Phase 3-4: striatum, thalamus and midbrain; Phase 5: cerebellum; [c,e]Refers to one iCJD with one or two missing sections from the [c]neocortex or [e]subcortical regions; [d]The (+) sign under ThioFl (Thioflavin S) indicates presence of amyloid plaques in at least one brain region; the (-) sign indicates that all regions tested had Thioflavin S negative staining; [f]Refers to one iCJD and two sCJD cases with missing parietal cortex; [g]Positive staining with Congo red [58]; [h]Percentage of brain regions with CP; [j,k]Fisher's exact test comparing iCJD to [j]sCJD or [k]AD; *Hippoc.* hippocampal formation (hippocampus and entorhinal cortex), *y* years, *durat.* duration, *mo* months, *na* not available, *nt* not tested, *NS* not significant, *SD* standard deviation

With regard to the molecular features, the percent distribution of the three genotypes (MM, MV, VV) at codon 129 of the PrP gene in the iCJD population (MM 43%, MV 33%, VV 24%) significantly differed from that of the sCJD controls (MM 65%, MV 18%, VV 17%) as well as those reported for unselected sCJD populations (MM 71%, MV 12%, VV 17%) [15] pointing to an increased relative prevalence of the MV and VV genotypes at the expense of the MM genotype in our iCJD cohort (Fig. 1). The iCJD genotype distribution also differed from those of Western European, Australian and the North American general populations (MM 37%, MV 51%, VV 12%) [14]. Keeping in mind the limited number of cases for some of these analyses, 129 genotype distribution also diverged in the GH-iCJD and DM-iCJD subsets: while the relative representation of the MV genotype was increased in both subsets, the DM-iCJD showed a three times higher representation of the VV genotype (33% vs. 11%) (Fig. 1). Analyses of the PK-resistant PrP^{Sc} ($resPrP^{Sc}$) type distribution showed that in iCJD the combined representation of types 2 (with unglycosylated $resPrP^{Sc}$ of ~19 kDa), "intermediate" (i; ~20 kDa), i + 2 (~20 + 19 kDa), and 1 + 2 (~21 + 19 kDa) (63%) was much higher than the representation of combined type 2 and i + 2 (28%) in sCJD unselected populations [15, 49], as well as in our sCJD controls, a finding consistent with the combined prevalence of the MV and VV genotypes which often are paired with type 2 and i + 2 (Fig. 1). Next, we compared phenotypic characteristics, such as disease duration and histopathological features in age-

Table 3 Staging of Aβ CAA in iCJD and control cases of sCJD and AD

Case number	Age (y)	Disease duration (mo)	Codon 129 genotype	PrP^{Sc} type	Phase 1		Phase 2					Phase 3		Vstl.[a] score	CAA[b] type
					Neocortex	ThioFl	Hippoc.	ThioFl	Crbl	ThioFl	Midb.	Subcort.	ThioFl		
iCJD															
1 (1)[c]	26	5	na	na	+++[d,e]	+[f]	++	+	+	+	na	-[e]	-	3	1
2 (19)	29	6	MV	1	+++[g]	+	+	+	+	nt	+	+	nt	2	2
3 (16)	32	3.5	MV	na	+[h]	na	-	na	-	na	-	-	na	1	2
4 (8)	44	18	MV	i+2	++++	+	++	-	+	+	-	-	-	3	2
5 (21)	50	14	MM	na	+++[g]	+	-	nt	-	nt	+	+	nt	1	2
6 (9)	51	14	MM	i	++	+	-	-	+	+	-	-	-	2	2
7 (10)	54	2	MM	1	+	+	-	-	-	-	-	-	nt	1	2
8 (17)	62	2	na	na	++++	+[i]	na	na	+	+[i]	na	na	na	na	na
9 (22)	62	4	VV	na	++[g]	-	-	nt	+	-	+	+	nt	1	2
10 (23)	71	4	MV	na	-	nt	+	-	+	-	-	-	nt	1	2
11 (27)	75	3	VV	2	++++	-	+	-	+	-	-	-	nt	1	2
mean±SD	50.5±17	7±6			69%[j]		35%		73%		33%	16%			
sCJD															
1 (55)[k]	49	4	MM	1	+[g]	-	-	-	-	nt	-	-	nt	1	2
2 (56)	63	4	MM	1	+[g]	-	++	-	+	-	+	++	nt	1	2
3 (57)	63	3	MV	1	-	-	-	-	+	nt	-	+	nt	1	2
4 (44)	64	1	MM	1	++	+	-	-	-	nt	-	-	-	1	2
5 (58)	71	8	VV	2	+++[g]	-	++	-	+	-	-	-	nt	1	2
6 (66)	74	4.5	VV	2	+	-	-	nt	-	nt	-	-	nt	1	2
mean±SD	64±9	4±2			38%		33%		50%		17%	25%			
P value[l]					< 0.03		NS		NS		NS	NS		= 0.05*	NS*
AD															
1	56	60	na	na	++++	+	-	-	+	+	+	+	-	2	2
2	56	60	na	na	++++	+	-	-	+	+	-	-	-	3	2
3	59	na	na	na	++++	-	-	-	+	+	-	-	-	3	2
4	60	130	na	na	++++	-	-[n]	-	+	-	-	+	+	2	2
5	70	66	na	na	++++	+	+	-	+	+	-	-	-	2	2
6	72	111	na	na	++++	+	+	+	+	+	+	+	+	3	1
7	74	22	na	na	+++	-	-	-	+	+	-	+	-	3	2
mean±SD	64±8	75±39			96%		15%		100%		29%	29%			
P value[m]					< 0.006		NS		NS		NS	NS		< 0.02*	NS*

Phases 1 to 3 refer to Aβ CAA deposition in various brain regions, reflecting disease progression according to Thal et al [61]; [a]Vonsattel (Vstl) 0-3 score of Aβ CAA severity to the highest score in one or more brain locations [66]; [b]Presence (type 1) or absence (type 2) of Aβ deposits in the cortical capillaries [60]; [c,k]Numbers in parenthesis in the first column refer to numerals used in [c]Table 1 and [k]Additional file 1: Table S2; [d]Minus and plus signs indicate absence (-) or presence (+) of Aβ CAA affecting one (+), two (++), three (+++) or four (++++) brain regions in each phase; Phase 1: frontal, temporal, parietal and occipital cortical regions; Phase 2: hippocampus, entorhinal cortex, cerebellum and midbrain; Phase 3: striatum, thalamus; [e]Refers to one iCJD patient with one missing section from neocortex and subcortical regions; [f]The (+) sign under ThioFl (Thioflavin S) indicates presence of positive staining of at least one brain region; the (-) sign indicates that all regions examined had Thioflavin S negative staining; [g]Refers to 3 iCJD and 3 sCJD cases with missing parietal cortex; [h]Refers to one iCJD with missing frontal cortex; [i]Positive staining with Congo red [58]; [j]Percentage of brain regions with Aβ CAA; [l,m]Fisher's exact test comparing iCJD to [l]sCJD or [m]AD; [n]Refers to one AD patient with missing entorhinal cortex; *y* years, *mo* months *Hippoc.* hippocampal formation (hippocampus and entorhinal cortex), *Crbl* cerebellum, *Midb.* midbrain, *Subcort.* subcortical regions (striatum and thalamus), *na* not available, *nt* not tested, *NS* not significant, *SD* standard deviation; *Student's t-test

group matched cases of iCJD and sCJD controls which shared both 129 genotype and PrP^{Sc} type. Iatrogenic CJD with genotypes 129MM coupled with PrP^{Sc} type 1 (iCJDMM1), the only subset with a significant number of age-group matched cases, showed shorter mean disease duration than sCJDMM1 (2.7 vs. 5.6 months; $P > 0.05$). As for the histopathological features, when histopathological phenotypes associated with the same pairing of the 129 genotype and $resPrP^{Sc}$ type were compared, all iCJD phenotypes were found to match

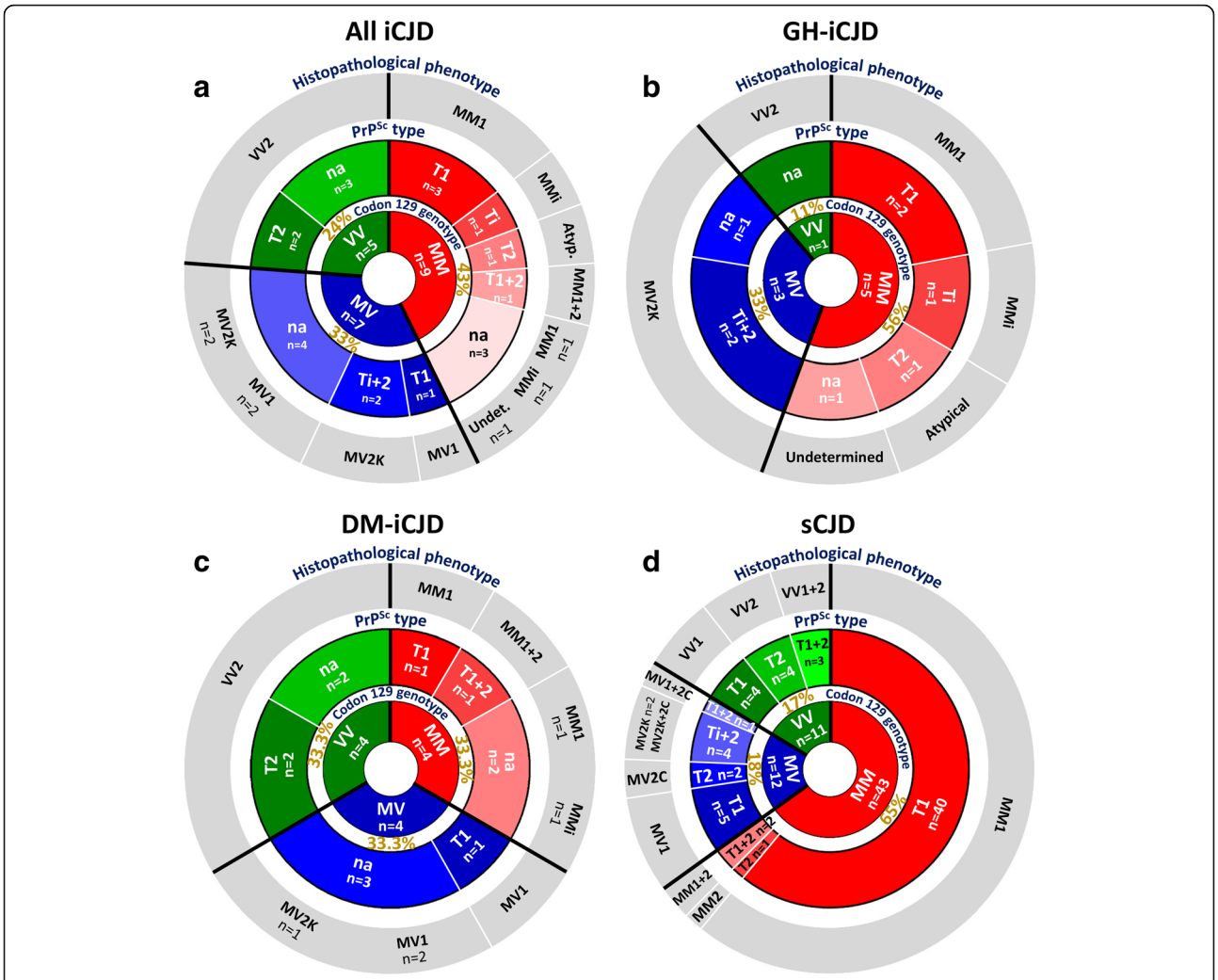

Fig. 1 Ring doughnut charts visualizing distributions of codon 129 genotypes, resPrP^{Sc} types and disease phenotypes among iCJD and sCJD cases examined. **a** whole iCJD cohort; inner circle: percent distribution of codon 129 genotype (MM, MV, VV); intermediate circle: distribution of resPrP^{Sc} types (T1, T2, Ti, Ti ± 2, T1 + 2); outer circle: distribution of histopathological phenotype. **b** GH-iCJD, legend as **a**; **c** DM-iCJD, legend as **a**; **d** sCJD. T1: type 1; Ti: type intermediate; T2: type 2; Ti + 2: type i + 2; T1 + 2: type 1 + 2; n: number of cases; na: not available; Atyp.: atypical; Undet.: undetermined. Percentages refer to the distribution of codon 129 genotype

the phenotypes of the corresponding sCJD, except for three cases. Two of these cases (GH-iCJD case 9 and DM-iCJD case 21), both harboring the 129MM genotype, had a phenotype characterized by the presence of kuru plaques resembling sCJDMV2K phenotype, which is typically not seen in sCJDMM associated either type 1 or 2 (Table 1). However, both these cases matched the previously described iCJDMMi phenotype [10, 39–41, 54]. The phenotype of the third case (GH-iCJD, case 5), which was associated with the 129MM genotype and resPrP^{Sc} type 2, differed in several features from typical phenotype of sCJDMM2. While spongiform degeneration type mimicked that of sCJDMM2, it was limited to the first cortical layers, rather than being widespread in the cerebral cortex, and it was accompanied by severe neuronal loss and astrogliosis while kuru plaques were lacking; furthermore, PrP immunostaining was punctate rather than forming coarse granular deposits (Additional file 4: Figure S2).

Western blot profiles of the resPrP^{Sc} in iCJD and matching sCJD controls

The profiles of resPrP^{Sc} from 10 iCJD suitable cases (2, 6–10, 19, 24, 26 and 27, Table 1) were compared with those of sCJD cases harboring the same 129 genotype and resPrP^{Sc} type (Fig. 2). This comparative study revealed that resPrP^{Sc} profiles from nine of the 10 iCJD cases matched those of the corresponding sCJD subtypes (Fig. 2). Thus, probing with 3F4, all CJDVV2 cases showed an unglycosylated resPrP^{Sc} fragment of ~19 kDa, which typically identifies type 2, whereas CJDMVi + 2

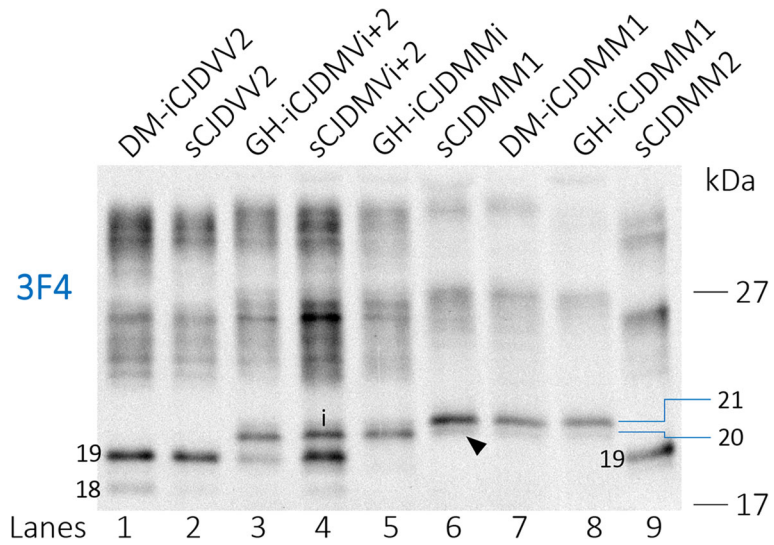

Fig. 2 WB profile of resPrP^{Sc} from iCJD and sCJD controls using high resolution gel electrophoresis. BHs from the frontal cortex (lanes 8 and 9) and cerebellum (lanes 1–7) treated with 100 U/ml PK (~2000 μg/ml) were probed with 3F4. PrP bands were resolved in a 15% Tris–HCl, 20 cm-long gel, and visualized with the near-infrared LI-COR system. The resPrP^{Sc} profiles from iCJD (lanes 1, 3, 5, 7 and 8) and matching sCJD subtypes (lanes 2, 4 and 6) are similar as shown by the co-migration of the unglycosylated resPrP^{Sc} type 2 (19) (lanes 1–4) and type 1 (21) (lanes 6–8). The different thickness of the type 2 (19) band is within the variability range for this subtype. The unglycosylated resPrP^{Sc} band of ~20 kDa, also identified as type i (i), is visible in GH-iCJDMVi + 2 (lane 3), sCJDMVi + 2 (lane 4) and GH-iCJDMMi case (lane 5); a thin band of ~20 kDa (arrowhead) is also present in CJDMM1. An ~18 kDa fragment (18) is also present in CJDVV2 and CJDMVi + 2

cases showed the type i ~20 kDa fragment in addition to the unglycosylated resPrP^{Sc} of ~19 kDa. In both iCJDMM1 and sCJDMM1, resPrP^{Sc} was characterized by the type 1 (~21 kDa) fragment as well as a faint band of ~20 kDa (Fig. 2 and Additional file 5: Figure S3). Conversely, iCJDMMi (case 9, Table 1) showed a prominent fragment matching type i and a faint band of ~21 kDa possibly representing type 1 (Fig. 2 and Additional file 5: Figure S3). These findings confirm the presence of type i in iCJDMMi and CJDMVi + 2 [39, 54], and indicate that in small amounts, a ~20 kDa fragment matching type i in mobility may be present also in iCJDMM1 and sCJDMM1 while type 1 may be present in iCJDMMi (Fig. 2 and Additional file 5: Figure S3). Tissue was not available for a detailed profile determination of resPrP^{Sc} from iCJDMM case 5 (Table 1), but it was reported to be matching resPrP^{Sc} type 2.

Aβ in iCJD, sCJD, prion disease free GH recipients and non-ND: Prevalence, clinical molecular and phenotype features

The presence of Aβ pathology was searched for in all of the 27 iCJD and 67 sCJD cases. Cases were considered positive when at least one Aβ CP containing amyloid (Thioflavin S or Congo red positive) and/or one blood vessel harboring Aβ deposits consistent with CAA were identified in at least one histology section of a minimum of two (Table 1, Fig. 3 and Materials and Methods). Eleven of 21 iCJD cases (52%) fulfilled these selection criteria. They comprised three of the eight cases of GH-iCJD, eight of the 13 cases of DM-iCJD including the two cases of iCJDMMi (cases 9 and 21 of Table 1, Fig. 4 and Additional file 2: Table S4). Despite the relatively small size of the Aβ-positive iCJD subset, a trend could be detected when basic clinical and molecular features as well as the histopathological phenotypes were comparatively analyzed in Aβ-affected and -unaffected groups and their subsets. Subjects harboring Aβ pathology were older in each iCJD subset. Age differentials varied from ~14 to 17 years, while the incubation period was ~13 years longer in Aβ-positive GH-iCJD cases (Fig. 5). Regarding the 129 genotype, the prevalence of the MV and VV genotypes over the MM genotype observed in all iCJD cohort was slightly increased in Aβ-positive iCJD cases (57% vs. 66%) ($P > 0.05$) (Figs. 1 and 5). Furthermore, histopathological phenotypes were similarly distributed in the two iCJD groups. In Aβ-positive iCJD cases (8, 9, 10 and 27 of Table 1) with available frozen tissue the Illumina and Sanger sequencing of *APP*, *PSEN1*, and *PSEN2* genes identified no novel rare variants nor known mutations. Furthermore, *ApoE* genotyping available in Aβ-positive iCJD (8, 9, 10 and 27 of Table 1) and sCJD (65, 66 and 67 of Additional file 1: Table S2) cases underlined the lack of *ApoE-ε4/4*, and the presence of *ApoE-ε3/3* in all CJD cases with the exception of one iCJD (case 8) that had genotype *ApoE-ε2/3*.

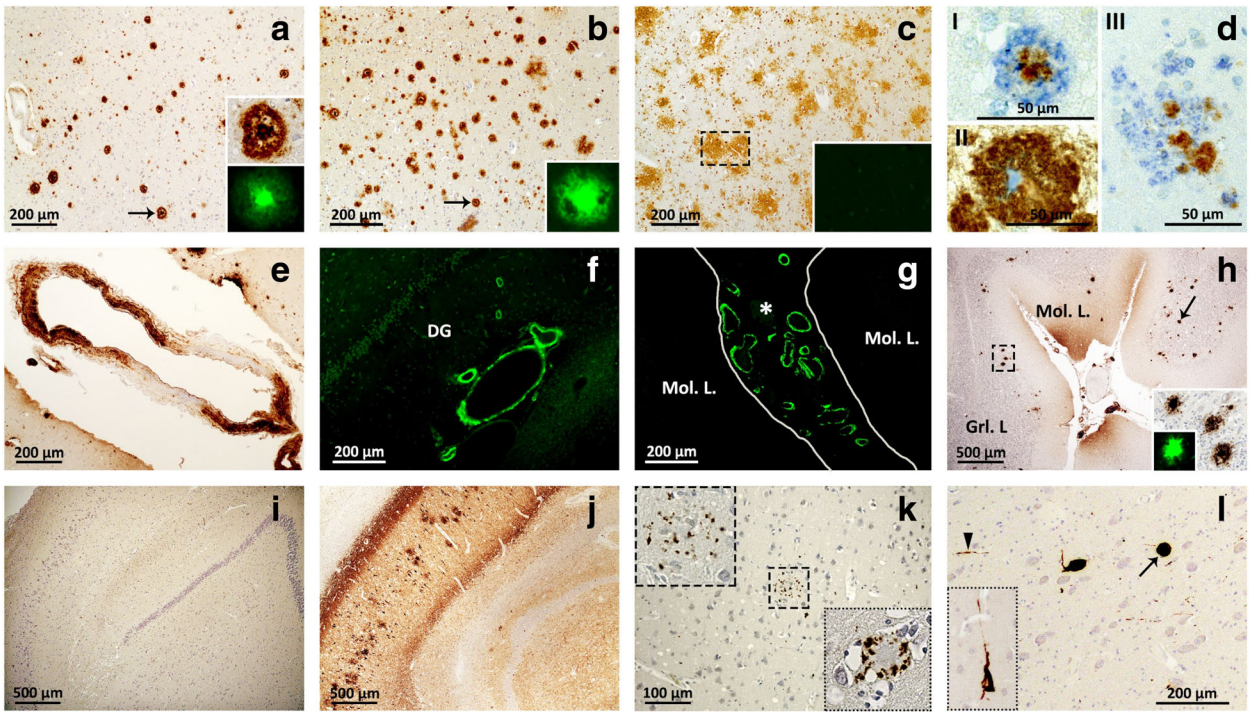

Fig. 3 Aβ and tau pathology of iCJD, sCJD and AD. **a** and **b** typical Aβ CP (arrows) from the frontal cortex of iCJD (**a**) and AD (**b**); inset **a**: Aβ CP at higher magnification immunoprobed for Aβ (top) or stained with Thioflavin S (bottom); inset **b**: Thioflavin S-positive Aβ CP. **c** diffuse plaques from the frontal cortex of a case of sCJD; inset: Thioflavin S-negative staining of plaques (dashed rectangle). **d** co-localization of Aβ (cyan dye) and PrP (brown dye) immunoreactivity in the same plaque from cerebral (I and III) and cerebellar (II) cortices of iCJD. I: plaque exhibiting a PrP-positive core surrounded by an Aβ immunoreactive crown; II-III: plaques showing either the immunostaining opposite to that of I, with Aβ-positive core and a PrP immunoreactive crown (II), or random distribution of PrP- and Aβ-reactive aggregates (III). **e**-**g** Aβ deposits (**e**) and Thioflavin S-positive staining (**f** and **g**) of vessels in frontal cortex (**e**), hippocampus (**f**) and cerebellum (**g**) in iCJD; **f**: DG, Dentate gyrus; **g**: asterisk, Aβ CAA in the subarachnoid space between two cerebellar folia. **h** Aβ CP predominantly affecting the granular layer (Grl. L) and Purkinje layer of the cerebellum in iCJD (case 9, Table 1); arrow indicates Aβ CP; large and small insets: enlargements of Aβ CP identified by the dashed rectangle in the main figure and a Thioflavin S-positive Aβ CP, respectively. **i**-**j** hippocampus free of tau pathology in iCJD (**i**) but severely affected in AD (**j**). **k** Tau-positive DN associated with an Aβ CP in frontal cortex of iCJD (case 8, Table 1) (dashed square); top inset: enlargement of tau reactive DN identified in dashed square; bottom inset: DN associated with a PrP kuru plaque in iCJD (occipital cortex, case 9, Table 1). **l** globose NFT (arrow) and neuropil threads (arrowhead) in the nucleus basalis of Meynert of iCJD (case 6, Table 1); inset: flame-shaped NFT in the temporal neocortex of the same iCJD case. Abs: 3F4 (**d**), 4G8 (**a**-**e**, **h**) and AT8 (**i**-**l**) to PrP, Aβ and phosphorylated tau, respectively; Thioflavin S to Aβ (**a**-**c**, **f**-**h**)

No Aβ pathology was detected in the two GH recipients, 46 and 50 years old, free of prion disease. However, the 50-year old case may not have received the higher risk US GH produced prior 1977.

Similar Aβ pathology was also present in nine of the 67 (13%) sCJD controls (Fig. 4 and Additional file 2: Table S4). The Aβ-positive cases were on average 20 years older than the negative cases ($P < 0.0001$) and had about half the disease duration (5.5 vs. 10.4 months) ($P = 0.029$). As for 129 genotype and PrP^{Sc} type, Aβ-positive sCJD showed a higher relative representation of the MV and VV genotypes and PrP^{Sc} type 2 than the negative cases, a trend resembling that of iCJD. However, contrary to iCJD, the MV2K phenotype was not observed but the VV2 phenotype was better represented in sCJD Aβ-positive cases. Aβ pathology was also searched for in 11 non-ND cases (age 40 ± 12 years, range 25–59 years). The two oldest cases (56- and 59-year-old) were Aβ-positive harboring CP one and CAA the other (Fig. 4).

Aβ in iCJD, sCJD and AD: Histopathological phenotype, severity and staging

All Aβ-positive iCJD cases harbored CAA. However, in about half of these subjects, CAA was accompanied by CP (CAA + CP) consistent with the presence of two phenotypes: CAA alone and CAA + CP (Additional file 2: Table S4). The mean age of the subjects harboring CAA + CP was about 15 years younger than that of the subjects with CAA alone (Tables 2 and 3). Although not statistically significant, this finding suggests that CP presence is not age-related, but more consistent with the existence of two phenotypes. In the sCJD cohort, the presence of CP alone was observed in three of the nine Aβ-positive cases along with five cases

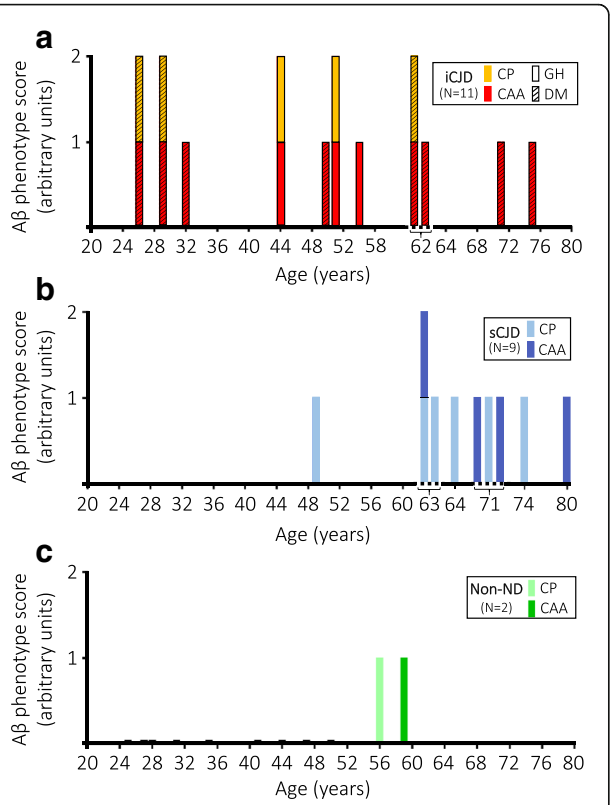

Fig. 4 Aβ phenotype and age distribution in Aβ-positive iCJD and control cases. **a**: iCJD ($N = 11$); **b**: sCJD ($N = 9$); **c**: non-ND ($N = 2$). Scores for the Aβ phenotype is relative to the presence of either Aβ CP or CAA (score 1), or combinations of both (score 2). Brackets below dotted line in the X-axis underline cases of the same age; GH: growth hormone; DM: dura mater

harboring CAA and one CAA + CP (Additional file 2: Table S4). Contrary to iCJD, sCJD cases harboring CP were older than those CP-free (71 vs. 64 years), possibly pointing to a relation to aging. Subpial Aβ deposition was observed in two DM- and one GH-iCJD young cases (≤ 54 years; cases 1, 8 and 16, Table 1) and in two old sCJD (> 54 years; cases 65 and 67, Additional file 1: Table S2).

As for the structural characteristics, most of the iCJD CP appeared to contain only Aβ as the only or dominant component since they reacted exclusively with Abs to Aβ; occasionally, however, they definitely also contained PrP either displaying an Aβ immunoreactive core with PrP reactive crown or the reverse or random mixtures of Aβ and PrP (Fig. 3). No significant difference was detected in the presence and brain distribution of Aβ diffuse (Thioflavin S-negative) plaques between iCJD ($N = 4$) and sCJD ($N = 21$) age-matched cases (Fig. 3 and Additional file 2: Table S5).

Staging of the Aβ pathology, a measure of disease progression, was carried out in 10 Aβ-positive cases of iCJD (Tables 2 and 3). Both CAA occurring alone and CAA + CP had a widespread distribution reaching at least phase 2 in the majority of the cases (82%). The CAA severity score (0–3) ranged from 1 to 3 with a mean of 1.6, and with the exception of one case (case 1, Table 3) CAA was of type 2 (capillaries unaffected) (Table 3 and Fig. 6). As expected according to the selection criteria, amyloid was demonstrated in the CP of all five CP-harboring cases, and in the vascular Aβ deposits of seven of the 10 (70%) CAA cases examined (Tables 2 and 3, and Fig. 3). In two cases, CP were present in the cerebellum (exclusively or along with other regions) mostly populating the granule cell layer (Fig. 3). The comparative study of disease staging in iCJD with those in sCJD and AD revealed that in the sCJD cohort, only in one third of the cases Aβ pathology reached phase 2; none harbored CP in the cerebellum (Tables 2 and 3). The CAA score was 1, 62% lower than that in iCJD, but the type was exclusively 2 as in most cases of iCJD (Table 3). Amyloid was demonstrated in one of six (17%) of the CAA-affected sCJD cases. Contrary to sCJD, Aβ pathology in AD surpassed in severity the Aβ pathology observed in iCJD (Tables 2 and 3). This especially applied to CP distribution that reached phase 5 in all cases, a level of disease progression reached only by half of the cases in iCJD. Furthermore, amyloid-positive CAA was observed in all cases. As for CAA, although the difference in distribution was less striking, the mean CAA score was 2.57, about 1.6 times greater than in iCJD, but CAA was almost exclusively type 2, as in iCJD.

Morphometric characteristics of amyloid-positive CP and of blood vessels carrying Aβ deposits in CAA were compared in iCJD and AD (Additional file 6: Figure S4 and Additional file 7: Figure S5). In iCJD cerebral cortex, the CP burden was over 4 times lower ($P < 0.004$) and CP about 17% smaller than in AD ($P < 0.0001$). A small population of large CP in AD were not detected in the iCJD cohort (Additional file 6: Figure S4). In iCJD CAA-affected vessels the Aβ deposits occupied a relatively larger portion of the vessel wall than in AD ($P < 0.0001$) (Additional file 7: Figure S5).

Tau pathology in iCJD, sCJD and AD: Lesion type, prevalence, staging and severity

NFT and DN, two prototypical lesions of tau pathology associated with typical AD, were found in 48% and 14%, respectively, of all iCJD cases (Additional file 2: Table S4). The NFT were found regardless of the presence of Aβ pathology while the DN were present in 3 cases, all harboring CP (Figs. 3 and 5). Although the NFT-positive iCJD subset was 8 years older than the NFT-free, the difference was not significant. Furthermore, the NFT prevalence in the entire iCJD cohort did not seem to change significantly as a function of age also when young (≤ 54 years) and old (> 54 years) NFT-positive iCJD subsets were assessed (47%

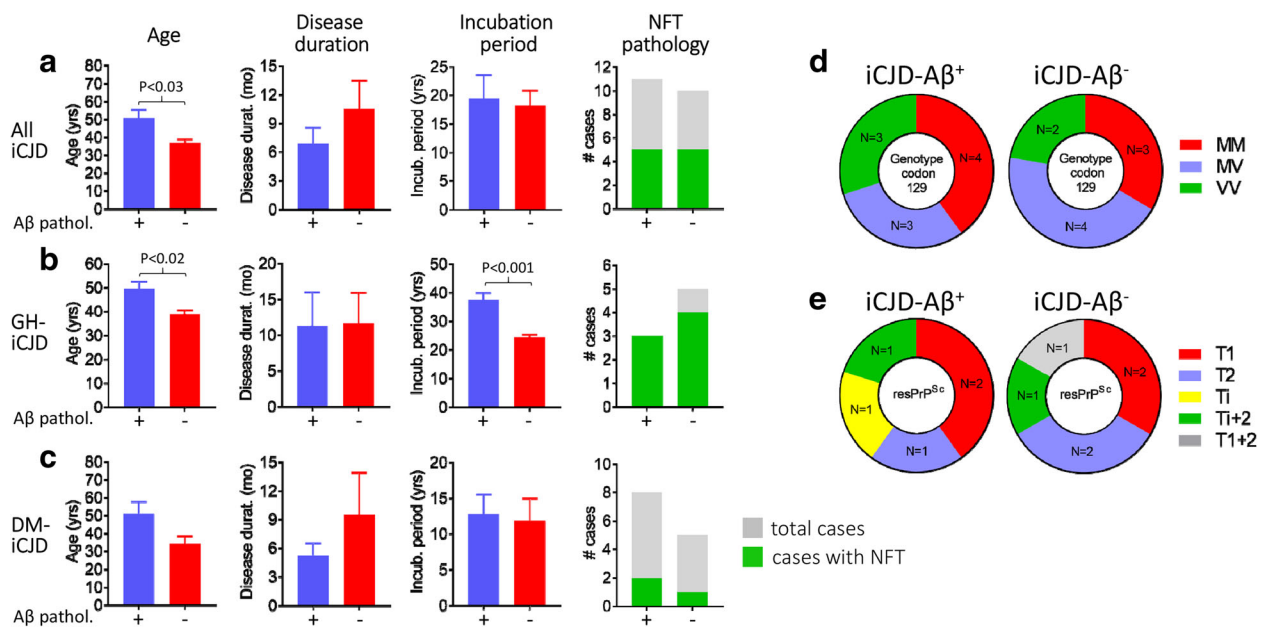

Fig. 5 Graphic representation of demographic data, NFT pathology, codon 129 genotype and resPrP^{Sc} type in iCJD with (+) and without (–) Aβ pathology. **a**-**c** age, disease duration, incubation period, and NFT pathology relative to All iCJD (**a**), GH-iCJD (**b**) and DM-iCJD (**c**); yrs.: years; mo: months. **d** and **e** ring doughnut charts visualizing genotype frequency at codon 129 (**d**) and resPrP^{Sc} type distribution (**e**) in iCJD with (iCJD-Aβ^{+}) and without (iCJD-Aβ^{-}) Aβ pathology; M: methionine; V: valine; T1: type 1; T2: type 2; Ti: type intermediate; Ti + 2: types intermediate +2; T1 + 2: types 1 + 2

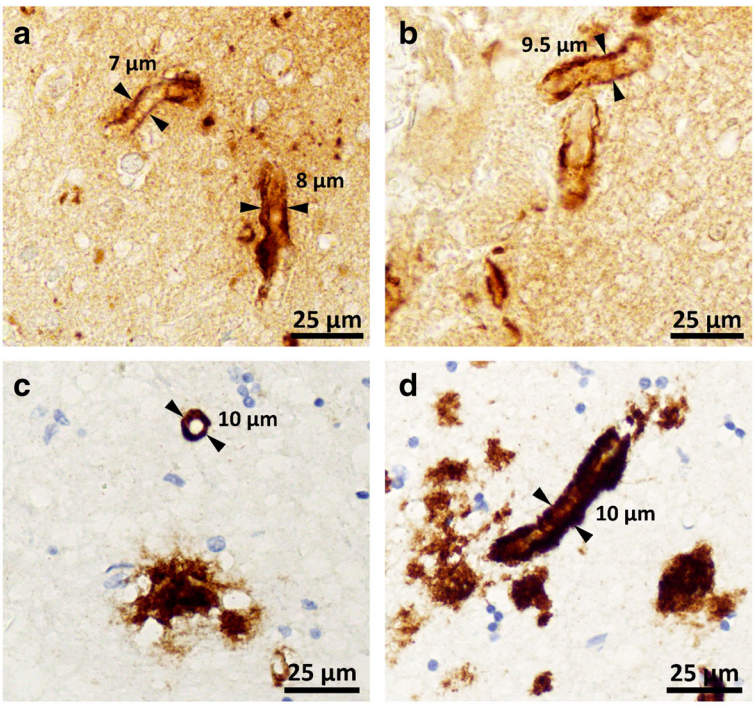

Fig. 6 Type 1 or capillary CAA in one iCJD (**a** and **b**) and one AD (**c** and **d**). **a**-**d** Aβ deposits along the basement membrane of capillaries in the parahippocampal gyrus (**a**), molecular layer of the cerebellum (**b**) and hippocampus (**c** and **d**). The mean diameter of capillaries in longitudinal sections resulted from three (**a** and **b**) and six (**d**) measurements along the capillary whereas the diameter of the capillary in cross-section in **c** is the mean diameter calculated by the software (Image-Pro Plus)

vs. 50%). In the Aβ-positive iCJD subset, NFT and DN were found in 5/11 and 3/11 cases, respectively. The similar NFT prevalence in the Aβ-positive iCJD population when compared with that of the general iCJD population (45.5% vs. 48%) [23] suggests that the presence of Aβ pathology does not influence the prevalence of NFT.

In sCJD, prevalences of NFT and DN were 53% and 1.5% respectively, comparable to the 48% prevalence of NFT in the iCJD cohort, while the DN prevalence in sCJD compared to iCJD was much lower (Additional file 2: Table S4). The NFT prevalence appeared to be age-related given the NFT presence in 41% and 80% of the younger and older cases, respectively, and the ~ 9.5 years older age of the NFT-positive compared to the negative cases ($P < 0.0006$). Distribution and severity of NFT also were comparable to those of the corresponding iCJD cohort and so was the age relation (Additional file 2: Table S6). Much higher burdens of both NFT and DN with no evidence of age effect were observed in all AD cases. However, brain distribution was comparable to that of iCJD.

Discussion

We report on 21 cases of iCJD including GH-iCJD and DM-iCJD subsets collected in Australia, France, Italy and the US, 11 (52%) of which harbored significant Aβ pathology. Despite the diversity of their geographic origin, our iCJD cases were remarkably similar concerning the 129 genotype and CJD histopathological phenotype distributions, and the features of the associated Aβ pathology.

For DM-iCJD, the similarities may reflect the use of the same Lyodura product in all these countries. In contrast, the cases of GH-iCJD were all from the US and can only be compared with the similar cohorts studied in the UK and France, where methods of GH production differed from those in the US (SH and JPB, personal communication).

Genotype and phenotype distribution in our iCJD cohort showed a relatively high prevalence of MV and VV over MM codon 129 genotypes when compared to sCJD as also observed in previous studies [54, 55]. Furthermore, we observed two iCJD with the MMi phenotype that has been shown to originate from adaptation of sCJDVV2 or sCJDMV2K to the 129MM background of the recipient [39, 42, 54, 59]. The finding that this event, initially described in Japanese DM-iCJD, is also observed in our international iCJD cohort as well as the UK cohort, and thus is widespread, suggests that 129VV and 129MV individuals may have been preferentially selected as donors in several countries. Alternatively, subjects with 129MV and 129VV genotypes might be more susceptible to acquire CJD than the carriers of the 129MM genotype, in whom the sCJDMM1 phenotype might be difficult to reproduce requiring strain adaptation [13, 46, 69]. The ~2 times longer incubation period in GH-iCJD than DM-iCJD cases resembles the longer incubation period associated with the peripheral (e.g., in the peritoneal cavity) vs. central (e.g., intracerebral) inoculations of prions or Aβ seeds in Tg mouse models for these proteinopathies [20, 36]. Concerning the Aβ pathology, iCJD-affected subjects had CAA accompanied by parenchymal Aβ CP in five cases and subpial deposits in three. The Aβ-positive iCJD subset also had a relatively young age (mean 50.5 years, range 26–75 years) along with the relative severity and widespread distribution of CAA [66]. Furthermore, with only one exception, CAA was type 2, i.e. did not affect cerebral capillaries unlike type 1 [66]. Since CAA type 1 has been directly associated with AD severity, including tau pathology, age, and with *ApoE-ε4* allele frequency, the predominance of type 2 CAA in iCJD is not surprising given the relatively younger age and short duration of this condition [52, 62].

Aβ pathology was examined in age-group matched cohorts of sCJD and of non-ND used as controls to rule out the possibility that Aβ deposition in iCJD was either related to aging or resulted from the concomitant aggregation of prion or prion-like proteins by a cross-seeding mechanism. Furthermore, type and severity of the iCJD Aβ pathology was compared with that of AD. The 13% prevalence of Aβ pathology in the sCJD cohort (mean age 50 years, range 24–79 years) was 4 times lower than that in iCJD (52%) even though the Aβ-positive sCJD subset was 17 years older. In the non-ND cohort (age 40 ± 12 years, range 25–59 years), the 2 (18%) Aβ-positive cases were 56 and 59 years of age and the oldest of this cohort. When all Aβ-positive subsets were considered in the 20–54 years range, the prevalence of Aβ pathology in iCJD, sCJD and non-ND populations was 41%, 2% and 0%, respectively. Furthermore, the Aβ pathology in iCJD cases was more severe than sCJD, and showed a significantly more widespread CP and CAA distribution and a trend toward a significantly higher CAA severity score. On the contrary, Aβ pathology in AD was dramatically more severe than in Aβ-positive iCJD with regard to number, size and distribution of CP as well as of CAA in neocortical regions, even though the AD cohort used as control had a relatively young age (64 ± 8 years). These features clearly distinguish the Aβ pathology of iCJD from typical AD. Although we cannot rule out that the Aβ pathology might have evolved toward an AD phenotype had the Aβ positive iCJD patients lived longer and not died of CJD this possibility is unlikely since no significant differences were found between the UK GH-iCJD and hGH recipients free of CJD. Even though we used a different criterion for Aβ plaque selection, our findings on Aβ pathology do not significantly differ from those reported in five previous studies [19, 23, 31, 37, 53], which collectively examined 95 cases of iCJD, including 67 GH-iCJD and 28 DM-iCJD.

However, the 54% prevalence of the Aβ pathology in UK GH-iCJD is higher than the 37.5% we observed. Similarly, the 18 year mean incubation period of UK GH-iCJD is significantly shorter than that of US cases (28 years) ($P < 0.004$). These differences may relate to the relatively high prevalence of UK GH-iCJD cases (~4.2%) compared to the 1.2% prevalence among US recipients of pre-1977 produced human GH (hGH) as well as to variations in selecting pituitary donors and in protocols of GH purification [2, 4, 7, 54]. Regardless of the causes, the higher prevalence of the Aβ pathology, the significantly lower mean incubation period and the more than a decade younger age differential of UK Aβ-positive GH-iCJD cases, suggest that GH used in UK had a higher infectious dose not only of PrP^{Sc} but also of Aβ seeds. Remarkably, despite these differences, the Aβ phenotype in US and UK was similarly characterized by CAA alone or co-existing with CP. The small subset of Aβ-positive GH-iCJD cases harboring parenchymal Aβ deposits reported by Ritchie and co-workers (2017a) presumably included diffuse plaques, which may also account for the higher prevalence of positive Aβ pathology in UK GH-iCJD. Furthermore, CAA reached similar severity scores in US (1.6) and UK (2) and type 2 CAA markedly predominated in both countries [37, 53]. The very low prevalence of the Aβ pathology (4%) in French GH-iCJD cases compared to the US and UK GH-iCJD cases has been explained possibly by the few years shorter incubation period in French GH-iCJD and to differences in GH preparations [19]. The prevalence of the Aβ pathology in DM-iCJD reported here (61.5%) is similar to that of the previous studies combined (69%) but differs from the 81% prevalence reported by Hamaguchi et al. (2016). This difference may depend on the older age of the Japanese cohort compared to those examined by us and Frontzek et al. (2016) (10 and 16 years, respectively). The co-occurrence of CAA and Aβ parenchymal deposits was observed in all the cases of Frontzek and co-workers (2016) but in only half of ours (CAA occurred alone in the others). This discrepancy along with the aforementioned discrepancy of UK GH-iCJD cases are likely due to our different criteria of Aβ plaque validation. Unlike the five previous studies that also accepted diffuse plaques, we validated only CP (i.e. Aβ plaques that contained amyloid) to better distinguish Aβ pathology associated with iCJD from that related to aging [19, 23, 31, 37, 53]. The exclusion of the plaque amyloid requirement would have increased the the Aβ-positive iCJD cases from 11 to 13 and increased by 9 the number of Aβ-positive sCJD cases (Additional file 2: Table S5 and data not shown). The CP requirement in the Aβ pathology of iCJD might establish a qualitative difference in the Aβ phenotype between iCJD and sCJD in younger populations. Nonetheless, this and previous studies show that CAA, with or without CP, is the distinctive histopathological phenotype of Aβ deposition in iCJD [19, 23, 31, 37, 53]. Our study taking advantage of the direct comparison, also shows that the Aβ phenotype is similar in GH- and DM-iCJD.

Because tau pathology is considered a consistent but secondary feature of AD, we also searched for the presence of the two most common tau related lesions, NFT and DN [33, 34, 57]. NFT were present in Aβ-negative and Aβ-positive iCJD, as well as in sCJD controls with similar prevalences (45–53%), and they were age-related. Occurrence of NFT in absence of Aβ plaques was previously shown in sCJD and was considered as "primary age-related tauopathy" in the elderly [17, 44, 51]. Overall, the NFT prevalence in cases with less than 52 years were similar in iCJD (44%) and sCJD (40%) cases, and did not differ from that reported in a large population of unselected individuals of similar age (41%) [6]. Neocortical DN were observed in only three iCJD cases and one case of sCJD where they were occasionally associated with CP, as previously reported [53]. In contrast, NFT and DN were consistently present in the AD cohort. These findings indicate that tau pathology is (i) a non-obligatory component of iCJD Aβ phenotype, (ii) likely develops independently from the Aβ pathology in iCJD, and (iii) further distinguishes iCJD Aβ pathology from AD.

Further important questions raised by our and previous studies are the origin of Aβ seeding, how Aβ seed reaches the brain, and whether Aβ-seeded diseases are contagious.

In hGH recipients, Ritchie and colleagues [53] convincingly showed that Aβ deposition occurs in the absence of prion pathology and the phenotype associated with the Aβ deposition remains similar to that of Aβ-positive iCJD cases, suggesting that Aβ deposition is a primary co-pathology in GH-iCJD and that Aβ and PrP^{Sc} seeding processes occur independently.

Although we occasionally have observed Aβ-PrP mixed plaques supporting the possibility of co-seeding, the brunt of the two pathologies were anatomically segregated: Aβ deposition affected mostly vessel walls while PrP^{Sc} affected exclusively the brain parenchyma. Moreover, the fact that Aβ-positive iCJD is associated with different CJD subtypes argues against cross-seeding of Aβ by a specific prion strain. Additional support to the independent seeding of Aβ in DM-iCJD comes from two other observations. First, Aβ deposits occurred in the dura graft but not in the patient's original dura [43], secondly, the distribution of Aβ deposits is consistent with the propagation through the brain of Aβ pathology originating from the dura graft while the distribution of PrP^{Sc} pathology is uniform [31, 43]. These findings point to the dura graft as the source of the Aβ seed and to a different tempo of Aβ and PrP^{Sc} propagation further strengthening the notion that in iCJD PrP^{Sc} and Aβ are

independent pathologies. In GH-iCJD, the Aβ seed is likely to propagate from the site of cutaneous injection to the brain. Experimental data have definitely provided the proof of principle that human Aβ seed may reach the brain causing Aβ amyloidosis following systemic inoculation [20]. Remarkably, a predominantly vascular distribution of the Aβ deposits consistent with Aβ-CAA was noted in these experiments [20].

Conclusions

Although our and previous studies do not rule out important roles for other factors contributing to Aβ pathology in iCJD such as hGH deficiency or the DM-associated neurosurgical procedures, they point to human-to-human transmission of Aβ with mechanisms similar to those of PrP^{Sc} [19, 23, 31, 37, 53].

Additional files

Additional file 1: Table S1. Age, disease duration and incubation period in iCJD and sCJD divided into three groups according to age at death. **Table S2.** Demographic data and molecular subtypes of 67 sCJD cases from the countries providing iCJD cases used as age-group matched controls in assessing prevalence of Aβ and tau pathologies. **Table S3.** Demographic and medical data on iCJD and sCJD used as controls. (DOCX 37 kb)

Additional file 2: Table S4. Prevalence of Aβ and tau pathologies in iCJD and sCJD used as controls. **Table S5.** Aβ diffuse plaque staging in cases of iCJD and sCJD not associated with Aβ CP pathology. **Table S6.** Brain distribution and severity of NFT and DN in iCJD and control cases of sCJD and AD. (DOCX 49 kb)

Additional file 3: Figure S1. Kaplan–Meier estimates of iCJD and sCJD controls. **A:** survival graphs representing whole iCJD cohort and its GH- and DM-iCJD subsets as well as sCJD cases. **B**: survival graphs of 21 iCJD and all sCJD divided into two groups according to age: 54 years or younger (≤54y), and older than 54 years (> 54y). Median survivals are indicated on the X-axis in **A** and **B** (arrowheads). Significant differences in median survivals, determined by the log rank (Mantel-Cox), were found between GH-iCJD and sCJD (P=0.0017) (**A**) or DM-iCJD ≤ 54y and sCJD ≤ 54y (P=0.0027) (**B**). (PDF 2348 kb)

Additional file 4: Figure S2. Histopathology of an atypical US iCJD (case 5, Table 1). **A**-**C**: HE staining. **D** and **E**: PrP immunohistochemistry. **A**: spongiform degeneration (SD) with large and confluent vacuoles typical of the sCJDMM2 subtype, but limited to layer II of the frontal cortex, and severe neuronal loss and gliosis affecting all layers. **B**: high magnification of the area highlighted in **A** showing SD with large vacuoles. **C**: severe loss of granule cells and gliosis of the cerebellum; Grl. L: granular layer; Mol. L: molecular layer. **D** and **E**: diffuse or "synaptic" PrP immunostaining in the frontal cortex (**D**), and molecular and granular layers of the cerebellum (**E**); **A**-**C**: HE staining. **D** and **E**: PrP immunohistochemistry with Ab 3F4. (PDF 30981 kb)

Additional file 5: Figure S3. WB profile of $resPrP^{Sc}$ from iCJD and sCJD controls using different WB systems for PrP detection. BHs from the frontal cortex (lanes 8-10) and cerebellum (lanes 1-7) treated with 100 U/ml PK (~2000 μg/ml) were probed with indicated Abs. PrP bands were resolved in 15% Tris-HCl, 8.7 cm-long (**A**-**C** and **E**) and 20 cm-long (**D**) gels, and visualized with near-infrared LI-COR system (**A**-**D** and **E**(**i**)) or chemiluminescence (**E**(**ii**) and **E**(**iii**)). **A**: profiles of $resPrP^{Sc}$ from CJD obtained with an 8.7 cm-long gel are similar to those obtained with the 20 cm-long gels in Fig. 2. The unglycosylated $resPrP^{Sc}$ ~21 kDa of type 1 (21), ~20 kDa of type i (i), ~19 kDa of type 2 (2) and ~18 kDa (18) are indicated. **B**: the ~20 kDa of type i (i) and ~21 kDa of type 1 (21) (lanes 3-8), but not the ~19 kDa band of type 2, immunoreact with Ab 12B2. Profile of $resPrP^{Sc}$ from iCJDMMi (lane 5) is indistinguishable from that of CJDMVi+2 (lanes 3 and 4), but differs from those of iCJDMM1 and sCJDMM1 (lanes 6-8), as the ~21 kDa band predominates in these three conditions. **C**: only ~19 kDa (type 2), but not ~21 kDa (type 1) and ~20 kDa (type i) immunoreacted with Tohoku-2 (To-2). An ~18 kDa (18) band in CJDW2 and CJDMVi+2, and an unidentified lower size fragment (large arrow) in all cases harboring type 2 were also detected. A non-specific band (indicated by three asterisks) was present in all tested samples. **D**: high resolution gel electrophoresis in 20-cm long gel revealing ~21 kDa (21) and the ~20 kDa band (i and arrowhead). **E**(**i**): enhanced image of dashed area in **A** showing the bands ~21 kDa (21), ~20 kDa (i and arrowhead), and ~19 kDa (19; lane 4). The detection of the $resPrP^{Sc}$ ~20 kDa band in addition to the prominent ~21 kDa fragment in CJDMM1 is most likely due to our use of a high resolution electrophoretic systems. **E**(**ii**): profiles of unglycosylated $resPrP^{Sc}$ from the same cases in **E**(**i**) visualized on film by chemiluminescence**.** Note that the three CJDMM1 (lanes 6-8) show only ~21 kDa bands. **E**(**iii**): the ~20 kDa and ~21 kDa bands visible in **B** (lanes 3-5) resolve as a single band of ~21 kDa (lanes 4 and 5) when visualized on film by chemiluminescence. (PDF 6122 kb)

Additional file 6: Figure S4. Quantitative estimates of Thioflavin S-positive Aβ CP affecting the cerebral cortex in subjects with iCJD and sporadic AD (sAD). **A**: the density of Aβ CP, expressed as the percentage of cerebral cortex area occupied, was 5 times greater in subjects with sAD than in iCJD. **B**: size of Aβ CP (N=500), expressed as diameter, was greater in patients with sAD than in those with iCJD. **C** and **D**: representative microscopic fields showing fewer and smaller CP (arrows) in iCJD (**C**) than sAD (**D**) where cluster of very large CP (dashed square) could be detected. Bar graphs are expressed as mean ± standard error of the mean (SEM) in **A** or as mean ± standard deviation in **B**. Student's t-test (two-tailed). (PDF 3338 kb)

Additional file 7: Figure S5. Size of blood vessels examined and semiquantitative evaluation of the percentage of the vessel wall perimeters occupied by Aβ deposits in subjects with iCJD and sporadic AD (sAD). **A**: scatter plot showing the similar sizes of the blood vessels from the subarachnoid spaces of frontal, occipital and cerebellar regions examined for the semiquantitative determinations made in **B**; size of individual vessels is measured as perimeter. **B**: the percentage of the blood vessel wall occupied by Aβ was significantly greater in iCJD than sAD. Bar graphs are expressed as mean±SEM. Student's t-test (two-tailed). (PDF 228 kb)

Abbreviations

Aβ: amyloid β; AD: Alzheimer's disease; *APP*: amyloid precursor protein; *PSEN1*: presenilin 1; *PSEN2*: presenilin 2; *ApoE*: Apolipoprotein E; Ab: antibody; GH: growth hormone; hGH: human GH; DM: dura mater; DM_L: Lyodura® brand DM; DM_T: Tutoplast® brand DM; CJD: Creutzfeldt-Jakob disease; sCJD: sporadic CJD; iCJD: iatrogenic CJD; GH-iCJD: GH-associated iCJD; DM-iCJD: DM-associated iCJD; p-tau: highly phosphorylated tau; PrP^{C}: normal or cellular prion protein (PrP); PrP^{Sc}: scrapie PrP; $resPrP^{Sc}$: proteinase K-resistant PrP^{Sc}; PK: proteinase K; BH: brain homogenate; WB: Western blot; M: methionine; V: valine; T1: type 1; T2: type 2; T1+2: type 1+2; Ti: type intermediate; Ti+2: type intermediate+2; CAA: cerebral amyloid angiopathy; CP: core plaques; NFT: neurofibrillary tangles; DN: dystrophic neurites; HE: hematoxylin-eosin; Non-ND: non-neurodegenerative disorders; NPDPSC: National Prion Disease Pathology Surveillance Center

Acknowledgements

We thank all the clinicians and administrative personnel for referring patients to the partecipating National Prion Diseases Surveillance Centers. We gratefully acknowledge Dr. Marta Couce, Alison Boyd, Dr. Christiane Stehmann, Dr. Colin L. Masters, Dr. Anna Ladogana, Yvonne Cohen, Dr. Laura Cracco, Dr. Wenquan Zou, Dr. Lan Zhou, James Metcalf, Miriam Warren, Katie Eppic, and Janis Blevins for their assistance and advices.

Funding

This work was supported by: CDC 000309CK14 to J.G. Safar; NIH P01AI106705, NIH 5R01NS083687 and Charles S. Britton Fund. to P. Gambetti; The Réseau National de Référence de maladies de Creutzfeldt-Jakob and the "Centre National de Référence des agents transmissibles non conventionnels" (Paris, France) are supported by Santé Publique France; Inserm 1127 has received funding from the program "Investissements 276 d'avenir" ANR-10-IAIHU-06;

Italian Ministry of Health funding to F. Tagliavini; Stivison Fund for CJD Research to B.S. Appleby; The Australian National Creutzfeldt-Jakob Disease Registry is funded by the Commonwealth Department of Health and S. Collins is funded in part by a NHMRC Practitioner Fellowship (#APP1105784); Grant-in-Aid for Scientific Research on Innovative Areas (Brain Protein Aging and Dementia Control) from MEXT to T. Kitamoto.

Authors' contributions

IC contributed to study design, conducted the experiments, analyzed the data, generated the figures, wrote the manuscript; MLC, SH, PP, GG, SJC, CAM, JPB, EL, FT, MP, JGS acquired and analyzed demographic, clinical and/or pathological data, edited the manuscript; NP, VS, DK, HW acquired clinical and/or pathological data; TK, RAM, EDB, CD edited the manuscript; BSA analyzed and wrote the clinical data, edited the manuscript; LBS: initiated the collaboration, aquired demographic data and edited the manuscript; PG designed and supervised the study, analyzed the data, wrote the manuscript. All authors read and approved the final manuscript.

Ethics approval and consent to participate

All patient protocols were approved by the Institutional Review Boards of the University Hospitals Case Medical Center of Cleveland (# 05–14-09). The Australian National CJD Registry has ethical approval for its surveillance operations from The University of Melbourne Human Research Ethics Committee (#1341074.4). In all cases, according to the French regulation, the next of kin provided informed, signed consent in the name of the patient to permit an autopsy and neuropathological investigation. The national computerized registry of objection to autopsy was systematically consulted. *PRNP* had been analyzed pre-mortem with the signed consent of the France patient's family. Data collection of clinically suspected cases is an integral part of the National CJD surveillance study, which was approved by the Ethic Committee of the Istituto Superiore di Sanità (CE-ISS 09/266 on 29 may 2009).

Consent for publication

Not applicable.

Competing interests

The authors declare that they have no competing interests.

Publisher's Note

Author details

[1]Departments of Pathology, Case Western Reserve University, School of Medicine, Cleveland, OH 44106, USA. [2]Departments of Neurology, Case Western Reserve University, School of Medicine, Cleveland, OH 44106, USA. [3]Departments of Psychiatry, Case Western Reserve University, School of Medicine, Cleveland, OH 44106, USA. [4]National Prion Disease Pathology Surveillance Center, Case Western Reserve University, School of Medicine, Cleveland, OH 44106, USA. [5]Inserm U1127, CNRS UMR 7225, Sorbonne Universités, UPMC Univ Paris VI UMR S 1127, Institut du Cerveau et de la Moelle épinière, Paris, France. [6]AP-HP, Cellule Nationale de Référence des maladies de Creutzfeldt-Jakob, Groupe Hospitalier Pitié-Salpêtrière, Paris, France. [7]AP-HP, Laboratoire de Neuropathologie R Escourolle, Groupe Hospitalier Pitié-Salpêtrière, Paris, France. [8]Department of Experimental, Diagnostic and Specialty Medicine, University of Bologna, Bologna, Italy. [9]IRCCS, Institute of Neurological Sciences, Bologna, Italy. [10]Fondazione IRCCS, Istituto Neurologico Carlo Besta, Milan, Italy. [11]Australian National Creutzfeldt-Jakob Disease Registry, Department of Medicine, and The Florey Institute of Neuroscience and Mental Health, The University of Melbourne, Parkville 3010, Australia. [12]Department of Neurology, University Hospitals Cleveland Medical Center, Cleveland, OH 44106, USA. [13]Department of Anatomical Pathology, Alfred Health, Melbourne 3181, Australia. [14]Victorian Brain Bank, the Florey institute of Neuroscience and Mental Health, The University of Melbourne, Parkville 3010, Australia. [15]Department of Neurological Science, Tohoku University Graduate School of Medicine, Sendai, Japan. [16]Division of High-Consequence Pathogens and Pathology, National Center for Emerging and Zoonotic Infectious Diseases, Centers for Disease Control and Prevention, Atlanta, GA, USA. [17]Department of Neurosciences, Istituto Superiore di Sanità, Rome, Italy. [18]National Institute of Diabetes and Digestive and Kidney Diseases, National Institutes of Health, Department of Health and Human Services, Bethesda, MD, USA. [19]Department of Pathology, 4th floor, room 419, Case Western Reserve University, 2085 Adelbert Road, Cleveland, OH 44106, USA. [20]Department of Pathology, 4th floor, room 402C, Case Western Reserve University, 2085 Adelbert Road, Cleveland, OH 44106, USA.

Received: 5 December 2017 Accepted: 13 December 2017
Published online: 08 January 2018

References

1. Abrams JY, Schonberger LB, Belay ED, Maddox RA, Leschek EW, Mills JL, Wysowski DK, Fradkin JE (2011) Lower risk of Creutzfeldt-Jakob disease in pituitary growth hormone recipients initiating treatment after 1977. J Clin Endocrinol Metab 96:E1666–E1669. https://doi.org/10.1210/jc.2011-1357
2. Belay ED, Schonberger LB (2005) The public health impact of prion diseases. Annu Rev Public Health 26:191–212. https://doi.org/10.1146/annurev.publhealth.26.021304.144536
3. Blossom DB, Maddox RA, Beavers SF, Church KA, Thoroughman DA, Schonberger LB, Belay ED (2007) A case of Creutzfeldt-Jakob disease associated with a dura mater graft in the United States. Infect Control Hosp Epidemiol 28:1396–1397. https://doi.org/10.1086/523862
4. Bonda DJ, Manjila S, Mehndiratta P, Khan F, Miller BR, Onwuzulike K, Puoti G, Cohen ML, Schonberger LB, Cali I (2016) Human prion diseases: surgical lessons learned from iatrogenic prion transmission. Neurosurg Focus 41:E10. https://doi.org/10.3171/2016.5.FOCUS15126
5. Braak H, Braak E (1995) Staging of Alzheimer's disease-related neurofibrillary changes. Neurobiol Aging 16:271–278 discussion 278–284
6. Braak H, Thal DR, Ghebremedhin E, Del Tredici K (2011) Stages of the pathologic process in Alzheimer disease: age categories from 1 to 100 years. J Neuropathol Exp Neurol 70:960–969. https://doi.org/10.1097/NEN.0b013e318232a379
7. Brown P, Brandel J-P, Sato T, Nakamura Y, MacKenzie J, Will RG, Ladogana A, Pocchiari M, Leschek EW, Schonberger LB (2012) Iatrogenic Creutzfeldt-Jakob disease, final assessment. Emerg Infect Dis 18:901–907. https://doi.org/10.3201/eid1806.120116
8. Bugiani O, Giaccone G, Verga L, Pollo B, Frangione B, Farlow MR, Tagliavini F, Ghetti B (1993) Beta PP participates in PrP-amyloid plaques of Gerstmann-Sträussler-Scheinker disease, Indiana kindred. J Neuropathol Exp Neurol 52:64–70
9. Cali I, Castellani R, Yuan J, Al-Shekhlee A, Cohen ML, Xiao X, Moleres FJ, Parchi P, Zou W-Q, Gambetti P (2006) Classification of sporadic Creutzfeldt-Jakob disease revisited. Brain J Neurol 129:2266–2277. https://doi.org/10.1093/brain/awl224
10. Cali I, Miller CJ, Parisi JE, Geschwind MD, Gambetti P, Schonberger LB (2015) Distinct pathological phenotypes of Creutzfeldt-Jakob disease in recipients of prion-contaminated growth hormone. Acta Neuropathol Commun 3:37. https://doi.org/10.1186/s40478-015-0214-2
11. Clavaguera F, Bolmont T, Crowther RA, Abramowski D, Frank S, Probst A, Fraser G, Stalder AK, Beibel M, Staufenbiel M, Jucker M, Goedert M, Tolnay M (2009) Transmission and spreading of tauopathy in transgenic mouse brain. Nat Cell Biol 11:909–913. https://doi.org/10.1038/ncb1901
12. Cohen ML, Kim C, Haldiman T, ElHag M, Mehndiratta P, Pichet T, Lissemore F, Shea M, Cohen Y, Chen W, Blevins J, Appleby BS, Surewicz K, Surewicz WK, Sajatovic M, Tatsuoka C, Zhang S, Mayo P, Butkiewicz M, Haines JL, Lerner AJ, Safar JG (2015) Rapidly progressive Alzheimer's disease features distinct structures of amyloid-β. Brain J Neurol 138:1009–1022. https://doi.org/10.1093/brain/awv006
13. Collinge J (2010) Medicine. Prion strain mutation and selection Science 328:1111–1112. https://doi.org/10.1126/science.1190815
14. Collinge J, Palmer MS, Dryden AJ (1991) Genetic predisposition to iatrogenic Creutzfeldt-Jakob disease. Lancet Lond Engl 337:1441–1442
15. Collins SJ, Sanchez-Juan P, Masters CL, Klug GM, van Duijn C, Poleggi A, Pocchiari M, Almonti S, Cuadrado-Corrales N, de Pedro-Cuesta J, Budka H, Gelpi E, Glatzel M, Tolnay M, Hewer E, Zerr I, Heinemann U, Kretszchmar HA, Jansen GH, Olsen E, Mitrova E, Alpérovitch A, Brandel J-P, Mackenzie J, Murray K, Will RG (2006) Determinants of diagnostic investigation sensitivities across the clinical spectrum of sporadic Creutzfeldt-Jakob disease. Brain J Neurol 129:2278–2287. https://doi.org/10.1093/brain/awl159
16. Condello C, Stöhr J (2017) Aβ propagation and strains: implications for the phenotypic diversity in Alzheimer's disease. Neurobiol Dis. https://doi.org/10.1016/j.nbd.2017.03.014

17. Crary JF, Trojanowski JQ, Schneider JA, Abisambra JF, Abner EL, Alafuzoff I, Arnold SE, Attems J, Beach TG, Bigio EH, Cairns NJ, Dickson DW, Gearing M, Grinberg LT, Hof PR, Hyman BT, Jellinger K, Jicha GA, Kovacs GG, Knopman DS, Kofler J, Kukull WA, Mackenzie IR, Masliah E, McKee A, Montine TJ, Murray ME, Neltner JH, Santa-Maria I, Seeley WW, Serrano-Pozo A, Shelanski ML, Stein T, Takao M, Thal DR, Toledo JB, Troncoso JC, Vonsattel JP, White CL, Wisniewski T, Woltjer RL, Yamada M, Nelson PT (2014) Primary age-related tauopathy (PART): a common pathology associated with human aging. Acta Neuropathol (Berl) 128:755–766. https://doi.org/10.1007/s00401-014-1349-0
18. Duffy P, Wolf J, Collins G, DeVoe AG, Streeten B, Cowen D (1974) Letter: possible person-to-person transmission of Creutzfeldt-Jakob disease. N Engl J Med 290:692–693
19. Duyckaerts C, Sazdovitch V, Ando K, Seilhean D, Privat N, Yilmaz Z, Peckeu L, Amar E, Comoy E, Maceski A, Lehmann S, Brion J-P, Brandel J-P, Haïk S (2017) Neuropathology of iatrogenic Creutzfeldt-Jakob disease and immunoassay of French cadaver-sourced growth hormone batches suggest possible transmission of tauopathy and long incubation periods for the transmission of Abeta pathology. Acta Neuropathol (Berl). https://doi.org/10.1007/s00401-017-1791-x
20. Eisele YS, Obermüller U, Heilbronner G, Baumann F, Kaeser SA, Wolburg H, Walker LC, Staufenbiel M, Heikenwalder M, Jucker M (2010) Peripherally applied Abeta-containing inoculates induce cerebral beta-amyloidosis. Science 330:980–982. https://doi.org/10.1126/science.1194516
21. Feeney C, Scott GP, Cole JH, Sastre M, Goldstone AP, Leech R (2016) Seeds of neuroendocrine doubt. Nature 535:E1–E2. https://doi.org/10.1038/nature18602
22. Friedrich RP, Tepper K, Rönicke R, Soom M, Westermann M, Reymann K, Kaether C, Fändrich M (2010) Mechanism of amyloid plaque formation suggests an intracellular basis of Abeta pathogenicity. Proc Natl Acad Sci U S A 107:1942–1947. https://doi.org/10.1073/pnas.0904532106
23. Frontzek K, Lutz MI, Aguzzi A, Kovacs GG, Budka H (2016) Amyloid-β pathology and cerebral amyloid angiopathy are frequent in iatrogenic Creutzfeldt-Jakob disease after dural grafting. Swiss Med Wkly 146:w14287. https://doi.org/10.4414/smw.2016.14287
24. Gambetti P, Notari S (2013) Human sporadic Prion diseases. In: Gambetti P (ed) Zou W-Q. Prions and Diseases, Springer New York, pp 59–72
25. Ghoshal N, Cali I, Perrin RJ, Josephson SA, Sun N, Gambetti P, Morris JC (2009) Codistribution of amyloid beta plaques and spongiform degeneration in familial Creutzfeldt-Jakob disease with the E200K-129M haplotype. Arch Neurol 66:1240–1246. https://doi.org/10.1001/archneurol.2009.224
26. Gibbs CJ, Asher DM, Brown PW, Fradkin JE, Gajdusek DC (1993) Creutzfeldt-Jakob disease infectivity of growth hormone derived from human pituitary glands. N Engl J Med 328:358–359. https://doi.org/10.1056/NEJM199302043280520
27. Gibbs CJ, Asher DM, Kobrine A, Amyx HL, Sulima MP, Gajdusek DC (1994) Transmission of Creutzfeldt-Jakob disease to a chimpanzee by electrodes contaminated during neurosurgery. J Neurol Neurosurg Psychiatry 57:757–758
28. Goedert M, Masuda-Suzukake M, Falcon B (2017) Like prions: the propagation of aggregated tau and α-synuclein in neurodegeneration. Brain J Neurol 140:266–278. https://doi.org/10.1093/brain/aww230
29. Hainfellner JA, Wanschitz J, Jellinger K, Liberski PP, Gullotta F, Budka H (1998) Coexistence of Alzheimer-type neuropathology in Creutzfeldt-Jakob disease. Acta Neuropathol (Berl) 96:116–122
30. Hamaguchi T, Eisele YS, Varvel NH, Lamb BT, Walker LC, Jucker M (2012) The presence of Aβ seeds, and not age per se, is critical to the initiation of Aβ deposition in the brain. Acta Neuropathol (Berl) 123:31–37. https://doi.org/10.1007/s00401-011-0912-1
31. Hamaguchi T, Taniguchi Y, Sakai K, Kitamoto T, Takao M, Murayama S, Iwasaki Y, Yoshida M, Shimizu H, Kakita A, Takahashi H, Suzuki H, Naiki H, Sanjo N, Mizusawa H, Yamada M (2016) Significant association of cadaveric dura mater grafting with subpial Aβ deposition and meningeal amyloid angiopathy. Acta Neuropathol (Berl) 132:313–315. https://doi.org/10.1007/s00401-016-1588-3
32. Hannah EL, Belay ED, Gambetti P, Krause G, Parchi P, Capellari S, Hoffman RE, Schonberger LB (2001) Creutzfeldt-Jakob disease after receipt of a previously unimplicated brand of dura mater graft. Neurology 56:1080–1083
33. Hardy JA, Higgins GA (1992) Alzheimer's disease: the amyloid cascade hypothesis. Science 256:184–185
34. Hawkes CA, Carare RO, Weller RO (2014) Amyloid and tau in the brain in sporadic Alzheimer's disease: defining the chicken and the egg. Acta Neuropathol (Berl) 127:617–618. https://doi.org/10.1007/s00401-014-1243-9
35. Irwin DJ, Abrams JY, Schonberger LB, Leschek EW, Mills JL, Lee VM-Y, Trojanowski JQ (2013) Evaluation of potential infectivity of Alzheimer and Parkinson disease proteins in recipients of cadaver-derived human growth hormone. JAMA Neurol 70:462–468. https://doi.org/10.1001/jamaneurol.2013.1933
36. Jacquemot C, Cuche C, Dormont D, Lazarini F (2005) High incidence of scrapie induced by repeated injections of subinfectious prion doses. J Virol 79:8904–8908. https://doi.org/10.1128/JVI.79.14.8904-8908.2005
37. Jaunmuktane Z, Mead S, Ellis M, Wadsworth JDF, Nicoll AJ, Kenny J, Launchbury F, Linehan J, Richard-Loendt A, Walker AS, Rudge P, Collinge J, Brandner S (2015) Evidence for human transmission of amyloid-β pathology and cerebral amyloid angiopathy. Nature 525:247–250. https://doi.org/10.1038/nature15369
38. Kascsak RJ, Rubenstein R, Merz PA, Tonna-DeMasi M, Fersko R, Carp RI, Wisniewski HM, Diringer H (1987) Mouse polyclonal and monoclonal antibody to scrapie-associated fibril proteins. J Virol 61:3688–3693
39. Kobayashi A, Matsuura Y, Mohri S, Kitamoto T (2014) Distinct origins of dura mater graft-associated Creutzfeldt-Jakob disease: past and future problems. Acta Neuropathol Commun 2:32. https://doi.org/10.1186/2051-5960-2-32
40. Kobayashi A, Parchi P, Yamada M, Brown P, Saverioni D, Matsuura Y, Takeuchi A, Mohri S, Kitamoto T (2015) Transmission properties of atypical Creutzfeldt-Jakob disease: a clue to disease etiology? J Virol 89:3939–3946. https://doi.org/10.1128/JVI.03183-14
41. Kobayashi A, Parchi P, Yamada M, Mohri S, Kitamoto T (2016) Neuropathological and biochemical criteria to identify acquired Creutzfeldt-Jakob disease among presumed sporadic cases. Neuropathol Off J Jpn Soc Neuropathol 36:305–310. https://doi.org/10.1111/neup.12270
42. Kobayashi A, Sakuma N, Matsuura Y, Mohri S, Aguzzi A, Kitamoto T (2010) Experimental verification of a traceback phenomenon in prion infection. J Virol 84:3230–3238. https://doi.org/10.1128/JVI.02387-09
43. Kovacs GG, Lutz MI, Ricken G, Ströbel T, Höftberger R, Preusser M, Regelsberger G, Hönigschnabl S, Reiner A, Fischer P, Budka H, Hainfellner JA (2016) Dura mater is a potential source of Aβ seeds. Acta Neuropathol (Berl) 131:911–923. https://doi.org/10.1007/s00401-016-1565-x
44. Kovacs GG, Rahimi J, Ströbel T, Lutz MI, Regelsberger G, Streichenberger N, Perret-Liaudet A, Höftberger R, Liberski PP, Budka H, Sikorska B (2017) Tau pathology in Creutzfeldt-Jakob disease revisited. Brain Pathol Zurich Switz 27:332–344. https://doi.org/10.1111/bpa.12411
45. Langeveld JPM, Jacobs JG, Erkens JHF, Bossers A, van Zijderveld FG, van Keulen LJM (2006) Rapid and discriminatory diagnosis of scrapie and BSE in retro-pharyngeal lymph nodes of sheep. BMC Vet Res 2:19. https://doi.org/10.1186/1746-6148-2-19
46. Makarava N, Savtchenko R, Alexeeva I, Rohwer RG, Baskakov IV (2016) New molecular insight into mechanism of evolution of mammalian synthetic Prions. Am J Pathol 186:1006–1014. https://doi.org/10.1016/j.ajpath.2015.11.013
47. Meyer-Luehmann M, Coomaraswamy J, Bolmont T, Kaeser S, Schaefer C, Kilger E, Neuenschwander A, Abramowski D, Frey P, Jaton AL, Vigouret J-M, Paganetti P, Walsh DM, Mathews PM, Ghiso J, Staufenbiel M, Walker LC, Jucker M (2006) Exogenous induction of cerebral beta-amyloidogenesis is governed by agent and host. Science 313:1781–1784. https://doi.org/10.1126/science.1131864
48. Morales R, Duran-Aniotz C, Castilla J, Estrada LD, Soto C (2012) De novo induction of amyloid-β deposition in vivo. Mol Psychiatry 17:1347–1353. https://doi.org/10.1038/mp.2011.120
49. Parchi P, Giese A, Capellari S, Brown P, Schulz-Schaeffer W, Windl O, Zerr I, Budka H, Kopp N, Piccardo P, Poser S, Rojiani A, Streichemberger N, Julien J, Vital C, Ghetti B, Gambetti P, Kretzschmar H (1999) Classification of sporadic Creutzfeldt-Jakob disease based on molecular and phenotypic analysis of 300 subjects. Ann Neurol 46:224–233
50. Preusser M, Ströbel T, Gelpi E, Eiler M, Broessner G, Schmutzhard E, Budka H (2006) Alzheimer-type neuropathology in a 28 year old patient with iatrogenic Creutzfeldt-Jakob disease after dural grafting. J Neurol Neurosurg Psychiatry 77:413–416. https://doi.org/10.1136/jnnp.2005.070805
51. Reiniger L, Lukic A, Linehan J, Rudge P, Collinge J, Mead S, Brandner S (2011) Tau, prions and Aβ: the triad of neurodegeneration. Acta Neuropathol (Berl) 121:5–20. https://doi.org/10.1007/s00401-010-0691-0
52. Richard E, Carrano A, Hoozemans JJ, van Horssen J, van Haastert ES, Eurelings LS, de Vries HE, Thal DR, Eikelenboom P, van Gool WA, Rozemuller AJM (2010) Characteristics of dyshoric capillary cerebral amyloid angiopathy. J Neuropathol Exp Neurol 69:1158–1167. https://doi.org/10.1097/NEN.0b013e3181fab558
53. Ritchie DL, Adlard P, Peden AH, Lowrie S, Le Grice M, Burns K, Jackson RJ, Yull H, Keogh MJ, Wei W, Chinnery PF, Head MW, Ironside JW (2017) Amyloid-β accumulation in the CNS in human growth hormone recipients in the UK. Acta Neuropathol (Berl). https://doi.org/10.1007/s00401-017-1703-0

54. Ritchie DL, Barria MA, Peden AH, Yull HM, Kirkpatrick J, Adlard P, Ironside JW, Head MW (2017) UK iatrogenic Creutzfeldt-Jakob disease: investigating human prion transmission across genotypic barriers using human tissue-based and molecular approaches. Acta Neuropathol (Berl) 133:579–595. https://doi.org/10.1007/s00401-016-1638-x
55. Rudge P, Jaunmuktane Z, Adlard P, Bjurstrom N, Caine D, Lowe J, Norsworthy P, Hummerich H, Druyeh R, Wadsworth JDF, Brandner S, Hyare H, Mead S, Collinge J (2015) Iatrogenic CJD due to pituitary-derived growth hormone with genetically determined incubation times of up to 40 years. Brain J Neurol 138:3386–3399. https://doi.org/10.1093/brain/awv235
56. Russo C, Schettini G, Saido TC, Hulette C, Lippa C, Lannfelt L, Ghetti B, Gambetti P, Tabaton M, Teller JK (2000) Presenilin-1 mutations in Alzheimer's disease. Nature 405:531–532. https://doi.org/10.1038/35014735
57. Serrano-Pozo A, Frosch MP, Masliah E, Hyman BT (2011) Neuropathological alterations in Alzheimer disease. Cold Spring Harb Perspect Med 1:a006189. https://doi.org/10.1101/cshperspect.a006189
58. Simpson DA, Masters CL, Ohlrich G, Purdie G, Stuart G, Tannenberg AE (1996) Iatrogenic Creutzfeldt-Jakob disease and its neurosurgical implications. J Clin Neurosci Off J Neurosurg Soc Australas 3:118–123
59. Takeuchi A, Kobayashi A, Parchi P, Yamada M, Morita M, Uno S, Kitamoto T (2016) Distinctive properties of plaque-type dura mater graft-associated Creutzfeldt-Jakob disease in cell-protein misfolding cyclic amplification. Lab Investig J Tech Methods Pathol 96:581–587. https://doi.org/10.1038/labinvest.2016.27
60. Thal DR, Ghebremedhin E, Rüb U, Yamaguchi H, Del Tredici K, Braak H (2002) Two types of sporadic cerebral amyloid angiopathy. J Neuropathol Exp Neurol 61:282–293
61. Thal DR, Griffin WST, de Vos RAI, Ghebremedhin E (2008) Cerebral amyloid angiopathy and its relationship to Alzheimer's disease. Acta Neuropathol (Berl) 115:599–609. https://doi.org/10.1007/s00401-008-0366-2
62. Thal DR, Papassotiropoulos A, Saido TC, Griffin WST, Mrak RE, Kölsch H, Del Tredici K, Attems J, Ghebremedhin E (2010) Capillary cerebral amyloid angiopathy identifies a distinct APOE epsilon4-associated subtype of sporadic Alzheimer's disease. Acta Neuropathol (Berl) 120:169–183. https://doi.org/10.1007/s00401-010-0707-9
63. Thal DR, Rüb U, Orantes M, Braak H (2002) Phases of a beta-deposition in the human brain and its relevance for the development of AD. Neurology 58:1791–1800
64. Tousseyn T, Bajsarowicz K, Sánchez H, Gheyara A, Oehler A, Geschwind M, DeArmond B, DeArmond SJ (2015) Prion disease induces Alzheimer disease-like Neuropathologic changes. J Neuropathol Exp Neurol 74:873–888. https://doi.org/10.1097/NEN.0000000000000228
65. Vital A, Canron M-H, Gil R, Hauw J-J, Vital C (2007) A sporadic case of Creutzfeldt-Jakob disease with beta-amyloid deposits and alpha-synuclein inclusions. Neuropathol Off J Jpn Soc Neuropathol 27:273–277
66. Vonsattel JP, Myers RH, Hedley-Whyte ET, Ropper AH, Bird ED, Richardson EP (1991) Cerebral amyloid angiopathy without and with cerebral hemorrhages: a comparative histological study. Ann Neurol 30:637–649. https://doi.org/10.1002/ana.410300503
67. Walker LC, Jucker M (2015) Neurodegenerative diseases: expanding the prion concept. Annu Rev Neurosci 38:87–103. https://doi.org/10.1146/annurev-neuro-071714-033828
68. Watts JC, Condello C, Stöhr J, Oehler A, Lee J, DeArmond SJ, Lannfelt L, Ingelsson M, Giles K, Prusiner SB (2014) Serial propagation of distinct strains of Aβ prions from Alzheimer's disease patients. Proc Natl Acad Sci U S A 111:10323–10328. https://doi.org/10.1073/pnas.1408900111
69. Weissmann C, Li J, Mahal SP, Browning S (2011) Prions on the move. EMBO Rep 12:1109–1117. https://doi.org/10.1038/embor.2011.192
70. Ye L, Fritschi SK, Schelle J, Obermüller U, Degenhardt K, Kaeser SA, Eisele YS, Walker LC, Baumann F, Staufenbiel M, Jucker M (2015) Persistence of Aβ seeds in APP null mouse brain. Nat Neurosci 18:1559–1561. https://doi.org/10.1038/nn.4117
71. Zou W-Q, Langeveld J, Xiao X, Chen S, McGeer PL, Yuan J, Payne MC, Kang H-E, McGeehan J, Sy M-S, Greenspan NS, Kaplan D, Wang G-X, Parchi P, Hoover E, Kneale G, Telling G, Surewicz WK, Kong Q, Guo J-P (2010) PrP conformational transitions alter species preference of a PrP-specific antibody. J Biol Chem 285:13874–13884. https://doi.org/10.1074/jbc.M109.088831

Journal of Clinical Neuroscience 81 (2020) 78–82

Contents lists available at ScienceDirect

Journal of Clinical Neuroscience

journal homepage: www.elsevier.com/locate/jocn

Short communication

Intra-cerebral haemorrhage but not neurodegenerative disease appears over-represented in deaths of Australian cadaveric pituitary hormone recipients

Sultan H. Alnakhli [a], Handan Wand [b], Matthew Law [b], Shannon Sarros [a], Christiane Stehmann [a], Matteo Senesi [a,c], Genevieve M. Klug [a], Marion Simpson [a], Victoria Lewis [a,c], Colin L. Masters [a], Steven J. Collins [a,c,*]

[a] Australian National Creutzfeldt-Jakob Disease Registry (ANCJDR), The Florey Institute of Neuroscience and Mental Health, The University of Melbourne, Parkville 3010, Australia
[b] The Kirby Institute (formerly National Centre in HIV Epidemiology and Clinical Research), University of New South Wales, Coogee 2034, Australia
[c] Department of Medicine, Royal Melbourne Hospital, The University of Melbourne, Parkville 3010, Australia

ARTICLE INFO

Article history:
Received 28 April 2020
Accepted 6 September 2020

Keywords:
Alzheimer's disease
Cadaveric pituitary hormones
Dementia
Infectious diseases
Intracerebral haemorrhage
Neurodegeneration
Neuroepidemiology
Non-prion disease transmission
Stroke

ABSTRACT

Background and purpose: Recent scientific reports and epidemiological studies have engendered mounting concerns regarding the potential human-to-human transmissibility of non-prion neurodegenerative and related diseases. This study investigated whether recipients of cadaveric pituitary hormone treatments are at increased risk of death from non-prion neurodegenerative and related diseases.
Methods: A retrospective national cohort study based on death certificates of recipients of the cadaveric pituitary hormone treatments (n = 184) as part of the Australian Human Pituitary Hormone Program (AHPHP; n = 2940) 1967–1985. Standardised mortality ratios (SMR) from non-prion neurodegenerative and other diseases were estimated based on the Australian population.
Results: Allowing for potential diagnostic mis-attributions, there was no significant increase in the SMR from non-prion central nervous system (CNS) neurodegenerative disease, especially dementia and/or Alzheimer's disease (0.47; [95% CI: 0.19, 1.12] $P = 0.081$). The SMR for intra-cerebral haemorrhage, potentially related to cerebral amyloid angiopathy (CAA), was increased (2.77; [95% CI: 1.12–5.75] $P = 0.009$), although accommodation of possible mis-diagnosis through conflation of this category with other stroke causes of death emphasising likely intra-cranial haemorrhage showed no persisting significant increase in mortality in cadaveric pituitary hormone recipients, including all deaths recorded as due to intracranial haemorrhage (1.72; [95% CI: 0.80, 3.26] $P = 0.123$).
Conclusion: In the setting of recent evidence strongly supporting the likelihood of brain-to-brain horizontal transmission and subsequent propagation and deposition of abnormally folded proteins associated with non-prion neurodegenerative and related disorders, this study offers further tentative support for deaths directly stemming from transmission of non-prion disease related to cadaveric pituitary hormone treatment. Acknowledging the limitations of the present study, however, ongoing detailed assessments of this potential risk are necessary.

1. Introduction

The transmission of human prion disease through various health care interventions (iatrogenic Creutzfeldt-Jakob disease [iCJD]), especially treatments involving prion-contaminated cadaveric pituitary hormones, is well recognised [1]. Numerous scientific studies support prion-like mechanisms of template-directed protein propagation, as well as inter-cellular spread, for misfolded isoforms associated with non-prion neurodegenerative diseases, including α-synuclein (related to Parkinson's disease [PD] and Diffuse Lewy body disease [DLBD]) and amyloid-beta (Aβ) and tau (related to Alzheimer's disease [AD]) [2–4], including the possibility that the precise conformation of aberrant proteins may subserve "strains" determining phenotypic expression and the level of transmissibility [5]. Initial circumstantial support for potential human-

* Corresponding author at: Department of Medicine, Royal Melbourne Hospital and Australian National Creutzfeldt-Jakob Disease Registry (ANCJDR), The Florey Institute of Neuroscience and Mental Health, The University of Melbourne, Royal Parade, 30 (Kenneth Myer Building), Parkvill Victoria, 3010, Australia.
E-mail address: stevenjc@unimelb.edu.au (S.J. Collins).

https://doi.org/10.1016/j.jocn.2020.09.021
0967-5868/

to-human transmission of Aβ from cadaveric adeno/neurohypophysis to hormone recipients was the immuno-histochemical detection of Aβ (as well as tau and α-synuclein) in the pituitary glands of donors with non-prion neurodegenerative disease and healthy persons [6]. This observation was soon followed by case series cogently supporting the likelihood of human transmission of Aβ causing parenchymal plaques and CAA in the brains of recipients of cadaveric human pituitary hormones [7–9], including in people who did not develop iCJD [8], with analogous findings in persons undergoing neurosurgical procedures that utilised cadaveric dura mater grafts [9]. Importantly, are recent descriptions of symptomatic intracranial haemorrhage secondary to Aβ-related CAA in younger adults decades after childhood procedures that employed use of cadaveric dura mater [10], as well as speculation of neurosurgical transmission of Aβ through contaminated instruments causing temporally remote CAA-related intracranial haemorrhage [10]. These cumulative observations underscore the possibility that misfolded proteins like Aβ, especially when derived from cadaveric dura mater, can be horizontally transmitted and act as prion-like proteopathic seeds eventually inducing cognate clinical disease such as CAA-related intra-cranial haemorrhage.

To further assess the potential for inadvertent transmission of misfolded proteins associated with non-prion neurodegeneration to induce overt related clinical disease, we assessed specific causes of death and mortality rates in recipients of cadaveric human pituitary hormones treated under the AHPHP with specific interest in deaths from dementia, AD, PD, motor neuron disease (MND) and intracranial haemorrhage (possibly related to CAA). The AHPHP operated from 1967 to 1985 and analogous to other countries utilised pooled cadaveric pituitary glands to extract growth hormone (GH) and gonadotrophins (GT) for treatment of short stature and infertility, respectively. The AHPHP was terminated in 1985 after the recognition of cases of iCJD in the USA caused by prion contaminated GH [11] by which time nearly 3000 Australian patients had been registered for treatment. To date, four Australians have been recognised to have most likely died from iCJD related to cadaveric pituitary hormones [12].

2. Materials and methods

The study was undertaken by the Australian National Creutzfeldt-Jakob Disease Registry (ANCJDR) as part of longstanding national surveillance activities as described previously [13]. Ethical approval for this project was granted by The University of Melbourne Human Research Ethics Committee (ID#1340151.3), restricted to anonymised death certificate data only. AHPHP recipient data is held by the Commonwealth Department of Health and was cross-referenced with death certificate records held on the Australian Institute of Health and Welfare (AIHW) data base [14]. The AHPHP recipient cohort consisted of 2940 patients with 232 deaths verified by the AIHW up to the end of 2015 and therefore included for the analysis. Anonymised death certificate data were reviewed by the ANCJDR with specific interest in listings of dementia, AD, PD, MND and intracranial haemorrhage (possibly related to CAA) as causes of death.

SMR comparative analysis was utilised as most appropriate when dealing with groups that contain small numbers, i.e. < 20 observations [15]. The Australian population of 2001 was used as the reference standard (as recommended by the Australian Bureau of Statistics [ABS] [16]) because it contains a similar population of men and women among all age groups and therefore it is more likely to provide consistent standardised rates [17]. Stata version 15.1 [18] was employed for analyses. stset and stsplit commands were utilised to declare the dataset for the survival analysis and to calculate the follow-up time by person-years. The latter was multiplied by the age-specific mortality rates of the reference standard population to estimate the expected number of deaths. SMR was then calculated for each category by dividing the observed by the expected number of deaths. Openepi.com [19], which is a freely available online software, was used to generate the corresponding 95% confidence intervals (CI) and the p-values.

To align with ABS data, SMRs were computed based only on the primary listed cause of death for stroke subtypes, neurodegenerative diseases and two groups of non-neurodegenerative causes of death. Notably, listings of intra-cerebral haemorrhage as a secondary cause of death always occurred in association with a primary cause likely to be an explanation (e.g. acute myeloid leukaemia). Two non-neurodegenerative causes of death (external causes of mortality and breast cancer) were arbitrarily chosen to more fully characterise the causes of death in pituitary hormone recipients and additionally assess the level of comparability of this group in relation to the Australian population. The stroke subtypes we compared emphasised likely or possible intracranial haemorrhage including "subarachnoid haemorrhage" (I60), "intracerebral haemorrhage" (I61), "other non-traumatic intracranial haemorrhage" (I62) and "stroke not specified as haemorrhage or infarction" (I64), with this last group representing approximately 60% of all deaths recorded from stroke. Therefore, in addition to the individual stroke subtypes, we obtained SMRs for three groups of combined stroke subtypes to allow for the uncertainty in the ABS data. "Cerebral infarction" (I63) was excluded from the analysis as it was deemed less relevant.

3. Results

Details concerning the year(s) of pituitary hormone treatment for individual recipients were not available; however, the median year of death for recipients was 2003, approximately 27 years from the mid-point of the period in which the AHPHP operated (1976) with a potential duration from treatment extending up to approximately 48 years (1967–2015). Of the 2940 persons registered with the AHPHP, 232 had died up to the end of 2015. Of those decedents, 184 were reported as undergoing cadaveric pituitary hormone treatment, of whom 65 (35%) were males, with a median age and standard deviation (SD) of recipient's deaths 49 (±18) years. Median ages (±SD) for the various categories of death in addition to the demographic characteristics of the overall cohort are summarised in Table 1.

Unexpectedly, the overall mortality rate was significantly lower in treated pituitary hormone recipients compared to the standard population (SMR: 0.81; [95% CI: 0.70, 0.93] $P = 0.004$). Illustrative of this, the mortality rates of "external causes of death" and "breast cancer" were inexplicably significantly lower than expected compared to the standard population (Table 2). With respect to neurodegenerative diseases, there were no specific listings for deaths from AD, PD or MND in recipients. To maximise the sensitivity of our study and ensure potentially mis-attributed deaths from neurodegenerative dementia, especially AD, were not overlooked we allowed under this rubric, deaths listed as occurring from "unspecified dementia", "unspecified degenerative CNS disease" and "unspecified brain or CNS disorder" although there were no primary listings in the last category. The mortality rate from these combined causes of death in persons who received cadaveric pituitary hormones was a non-significant 53% lower than expected compared to "dementia and AD" in the Australian reference population (SMR: 0.47; [95% CI: 0.19, 1.12] $P = 0.081$).

Acknowledging the apparent predisposition for transmitted Aβ associated with cadaveric pituitary hormone treatment to cause CAA within the cerebro-vasculature (with or without associated CJD) and the recent suggestion that even neurosurgical instru-

Table 1
Demographic characteristics of the AHPHP cohort.

	Category (N)	Age (years)	Year of Death	Gender (%)		Treated
		M, (SD), [R]	M, (SD)	Male	Female	n(%)
Death	Overall deaths (232)	48, (18), [3–95]	2003, (9)	88(38)	144(62)	184(79)
	Treated only (184)	49, (18), [3–87]	2004, (9)	65(35)	119(65)	184(100)
	External causes of morbidity and mortality (15)	40, (14), [22–76]	2004, (5)	10(67)	5(33)	12(80)
	Breast cancer (11)	58, (10), [41–68]	2003, (6)	0(0)	11(100)	8(73)
	Dementia & AD (5)	42, (23), [26–87]	1998, (9)	2(40)	3(60)	5(100)
	Intracerebral Haemorrhage (6)	60, (18), [32–75]	2002, (10)	2(33)	4(67)	6(100)
	All Stroke (9)	59, (17), [32–75]	2002, (9)	3(33)	6(67)	9(100)
Treatment	**Location**					
	ACT (13)	47, (12), [27–77]	1993, (-)	10(77)	3(23)	8(62)
	NSW (941)	62, (12), [5–95]	2004, (10)	273(29)	668(71)	722(77)
	NT (2)	44, (5), [41–48]	–	1(50)	1(50)	2(100)
	QLD (300)	57, (12), [13–80]	1999, (8)	120(40)	180(60)	219(73)
	SA (300)	63, (12), [16–93]	1999, (9)	77(26)	223(74)	260(87)
	TAS (129)	64, (10), [33–86]	2004, (6)	23(18)	106(82)	102(79)
	VIC (792)	63, (12), [3–88]	2005, (10)	233(29)	559(71)	652(82)
	WA (176)	60, (12), [23–87]	2009, (10)	54(31)	122(69)	136(77)
	Missing (63)	58, (11), [36–68]	2008, (4)	5(8)	58(92)	62(98)
	Type					
	hGH (688)	48, (10), [3–87]	2000, (10)	482(70)	206(30)	688(100)
	hGH_hPG (2)	63, (2), [61–64]	–	2(100)	0(0)	2(100)
	hPG (1473)	66, (7), [32–93]	2008, (9)	58(4)	1415(96)	1473(100)

M = Mean; SD = Standard deviation; R = Range; Treated = Received a cadaveric pituitary GH treatment.

Table 2
Standardised Mortality Ratios (SMR) for cadaveric pituitary hormone treated patients by cause of death groups.

Cause of Death◇	[ICD-10 codes]	Observed cases	Expected cases	SMR	[95% CI]	P-value
All Causes of Death	–	184	227	0.81	[0.70, 0.93]	0.004
Dementia & AD	[F01, F03, G30]	5	11	0.47	[0.19, 1.12]	0.081
Stroke						
Subarachnoid haemorrhage	[I60]	1	2	0.49	[0.02, 2.44]	0.473
Intracerebral haemorrhage	[I61]	6	2	2.77	[1.12, 5.75]	0.009
Other nontraumatic intracranial haemorrhage	[I62]	1	0	2.10	[0.10, 10.33]	0.449
Stroke, not specified as haemorrhage or infarction	[I64]	1	4	0.28	[0.01, 1.39]	0.176
Combined Stroke Group 1	[I60-I61-I62]	8	5	1.72	[0.80, 3.26]	0.123
Combined Stroke Group 2	[I60-I61-I64]	8	8	1.03	[0.48, 1.96]	0.925
Overall Stroke	[I60-I61-I62-I64]	9	8	1.10	[0.53, 2.01]	0.784
Other Causes of Death						
External causes of morbidity and mortality	[V01–Y98]	12	31	0.38	[0.22, 0.67]	<0.001
Breast cancer	[C50]	8	18	0.43	[0.22, 0.87]	0.015

Follow-up time = 101456.1 person-years.
◇ Primary cause of death. M = Mean; SD = Standard deviation; CI = Confidence intervals; ICD-10 = The International Statistical Classification of Diseases and Related Health Problems, (version-10).

ments presumably contaminated with Aβ may lead to CAA and premature symptomatic intra-cranial haemorrhage [10], the mortality rates of various subtypes of intra-cranial haemorrhage, as well as combined deaths from various types of intra-cranial haemorrhage with or without the sizeable group "stroke not specified as haemorrhage or infarction" were analysed (Table 2). Deaths listed as from "intra-cerebral haemorrhage" were significantly increased (SMR: 2.77; [95% CI: 1.12–5.75] $P = 0.009$) whereas all other haemorrhagic stroke groups, including conflated sub-types listed as related to haemorrhage or containing some deaths from likely intracranial haemorrhage, were not increased compared to the standard population (Table 2).

4. Discussion/conclusion

In a medical milieu of growing concerns regarding human-to-human transmissibility of non-prion neurodegenerative and related diseases, the present findings offer circumstantial support for possible CAA related to transmitted Aβ associated with cadaveric pituitary hormone treatment causing deaths from intracerebral haemorrhage. Although increased deaths from intracerebral haemorrhage plausibly aligns with recognised risks associated with premature CAA, as observed in recipients of cadaveric pituitary hormones [7–9], we found no evidence of increased deaths from other types of intra-cranial haemorrhage, including subarachnoid haemorrhage, which is somewhat surprising given the recognised risks of this type of haemorrhage related to CAA and the prominent occurrence of CAA in meningeal vessels [7–9]. Further, although the association between CAA related to transmitted Aβ and intra-cranial haemorrhage appears sequitur, the report of a significantly increased risk of haemorrhagic strokes, especially sub-arachnoid haemorrhage, in people exclusively treated with recombinant GH for short stature [20] raises the possibility of specious association and militates against premature conclusions regarding any causality between transmitted Aβ and intra-cranial haemorrhage.

In contrast to possible deaths related to CAA, we found no evidence to support increased deaths from common, non-prion neurodegenerative diseases such as AD or PD, with these findings concurring with those of a previous similar study reporting no

increased risk of such deaths [6]. This outcome was despite our conservative approach to potential neurodegenerative death certificate mis-attributions. In the study by Irwin and colleagues [6] however, they reported three deaths from Amyotrophic Lateral Sclerosis in their GH recipient cohort, with our study only finding a single listing of death from "CNS paralysis unspecified", re-emphasising uncertainties raised by these authors concerning the explanation and biological significance of their observation of three deaths from MND in US patients treated with cadaveric pituitary hormone. Also notable in our recipient cohort and similar to the findings of the study by Irwin and colleagues [6] was the young average age at death. Aware of the strong age-dependence of neurodegenerative diseases, especially AD [21], it is arguably not surprising that there would only be few deaths recorded as related to presumably neurodegenerative dementia and/or un-recognised AD. Although we were unable to determine the precise length of time from pituitary hormone treatment to death in members of our cohort, approximately 27 years had elapsed from the mid-point of the AHPHP operational period to the mean year of death for recipients with the period from treatment potentially extending up to 48 years offering the probability of sufficient time for overt neurodegenerative disease to develop in at least some persons if these diseases are truly transmissible and able to induce overt disease. Nonetheless, sporadic AD is recognised to have a long pre-symptomatic period of neuropathological evolution before first symptoms appear [22] and given this apparently very slow pathogenesis related to Aβ deposition, a longer period of disease evolution may be required, particularly in non-genetically predisposed individuals such as apolipoprotein ε4 allele non-carriers.

Unexpectedly, the SMR for overall deaths was reduced in patients treated through the AHPHP, exemplified by the significantly reduced deaths from "external causes of morbidity and mortality" and "breast cancer". The explanation for the reduced deaths in patients treated with cadaveric pituitary hormones is unclear but raises the possibility of the recipient cohort being different to the broader Australian population such that people treated with cadaveric pituitary hormones are at diminished risk of developing neurodegenerative and other serious illnesses.

The present study is acknowledged as harbouring notable limitations, including death certificate causes of death were not independently verified and that living persons potentially manifesting the diseases of interest were not ascertained. As such, our study cannot exclude the possibility of living recipients manifesting symptomatic neurodegenerative disease or cases of non-fatal CAA-related intra-cranial haemorrhage. Importantly however, death certificate recorded deaths, including those from intracranial haemorrhages and neurodegenerative diseases would be subject to analogous potential mis-attributions in both the pituitary hormone recipient cohort and the Australian population [23]. Also, while premature deaths from non-neurodegenerative causes could possibly pre-emptively camouflage development of overt neurodegenerative disease related to human-to-human transmission, this is arguably less likely to be a significant factor given the overall death SMR was reduced in pituitary hormone recipients. Nonetheless, the age-dependency of neurodegenerative diseases with its apparent implications for pathogenesis also serves to caution against undue reassurance stemming from our study, as do other methodological considerations such as the entirely retrospective nature of our study. Consequently, given the aforementioned limitations, our findings must necessarily be considered as only tentative and therefore support the need for ongoing detailed epidemiological studies assessing the risk of developing overt non-prion neurodegenerative and related diseases from human-to-human transmission.

Author contributions

	Name	Salutation	Contribution
1	Sultan H. Alnakhli	Mr.	Wrote first draft of the paper, performed statistical analyses
2	Handan Wand	Associate Professor	Performed some statistical analyses and contributed to the final version of the manuscript
3	Matthew Law	Professor	Provided guidance on statistical analysis and contributed to the final version of the manuscript
4	Shannon Sarros	Ms.	Contributed to the final version of the manuscript
5	Christiane Stehmann	Dr.	Assisted in data management and contributed to the final version of the manuscript
6	Matteo Senesi	Dr.	Contributed to the final version of the manuscript
7	Genevieve M Klug	Ms.	Performed some statistical analyses and contributed to the final version of the manuscript
8	Marion Simpson	Dr.	Contributed to the final version of the manuscript
9	Victoria Lewis	Dr.	Contributed to the final version of the manuscript
10	Colin L Masters	Professor	Contributed to the final version of the manuscript
11	Steven J Collins	Professor	Conceived the project, co-wrote the paper and assisted in data analysis

Acknowledgements

The authors thank the Commonwealth Department of Health and the Australian Institute of Health and Welfare for their support of the study and especially Ms Wendy Ho from the AIHW.

Statement of ethics

Ethical approval for the study was granted by The University of Melbourne Human Research Ethics Committee (ID#1340151.3), restricted to anonymised death certificate data only.

Disclosure statement

The authors have no conflicts of interest to declare.

Funding sources

The ANCJDR is funded by the Commonwealth Department of Health. SC is supported in part by an NHMRC Practitioner Fellowship (#APP1105784).

References

[1] Brown P, Brandel J-P, Sato T, Nakamura Y, MacKenzie J, Will RG, et al. Iatrogenic Creutzfeldt-Jakob disease, final assessment. Emerging Infect Dis 2012;18(6):901–7.
[2] Luk KC, Kehm V, Carroll J, Zhang B, O'Brien P, Trojanowski JQ, et al. Pathological α-synuclein transmission initiates Parkinson-like neurodegeneration in nontransgenic mice. Science 2012;338(6109):949–53.

[3] Eisele YS, Obermüller U, Heilbronner G, Baumann F, Kaeser SA, Wolburg H, et al. Peripherally applied Abeta-containing inoculates induce cerebral beta-amyloidosis. Science 2010;330(6006):980–2.
[4] Clavaguera F, Bolmont T, Crowther RA, Abramowski D, Frank S, Probst A, Fraser G, Stalder AK, Beibel M, Staufenbiel M, Jucker M, Goedert M, Tolnay M. Transmission and spreading of tauopathy in transgenic mouse brain. Nat Cell Biol 2009;11(7):909–13.
[5] Batlle C, Iglesias V, Navarro S, Ventura S. Prion-like proteins and their computational identification in proteomes. Expert Rev Proteom 2017;14 (4):335–50.
[6] Irwin DJ, Abrams JY, Schonberger LB, Leschek EW, Mills JL, Lee V-Y, Trojanowski JQ. Evaluation of potential infectivity of Alzheimer and parkinson disease proteins in recipients of cadaver-derived human growth hormone. JAMA Neurol 2013;70(4):462. https://doi.org/10.1001/jamaneurol.2013.1933.
[7] Jaunmuktane Z, Mead S, Ellis M, Wadsworth JDF, Nicoll AJ, Kenny J, Launchbury F, Linehan J, Richard-Loendt A, Walker AS, Rudge P, Collinge J, Brandner S. Evidence for human transmission of amyloid-β pathology and cerebral amyloid angiopathy. Nature 2015;525(7568):247–50.
[8] Ritchie DL, Adlard P, Peden AH, Lowrie S, Le Grice M, Burns K, Jackson RJ, Yull H, Keogh MJ, Wei W, Chinnery PF, Head MW, Ironside JW. Amyloid-β accumulation in the CNS in human growth hormone recipients in the UK. Acta Neuropathol 2017;134(2):221–40.
[9] Cali I, Cohen ML, Haïk S, Parchi P, Giaccone G, Collins SJ, Kofskey D, Wang H, McLean CA, Brandel J-P, Privat N, Sazdovitch V, Duyckaerts C, Kitamoto T, Belay ED, Maddox RA, Tagliavini F, Pocchiari M, Leschek E, Appleby BS, Safar JG, Schonberger LB, Gambetti P. Iatrogenic Creutzfeldt-Jakob disease with Amyloid-β pathology: an international study. Acta Neuropathol Commun 2018;6(1). https://doi.org/10.1186/s40478-017-0503-z.
[10] Jaunmuktane Z, Quaegebeur A, Taipa R, Viana-Baptista M, Barbosa R, Koriath C, Sciot R, Mead S, Brandner S. Evidence of amyloid-β cerebral amyloid angiopathy transmission through neurosurgery. Acta Neuropathol 2018;135 (5):671–9.
[11] Koch TK, Berg BO, De Armond SJ, Gravina RF. Creutzfeldt–Jakob disease in a young adult with idiopathic hypopituitarism: possible relation to the administration of cadaveric human growth hormone. N Engl J Med 1985;313 (12):731–3.
[12] Boyd A, Klug GMJA, Schonberger LB, McGlade A, Brandel J-P, Masters CL, Collins SJ. Iatrogenic Creutzfeldt–Jakob disease in Australia: time to amend infection control measures for pituitary hormone recipients?. Med J Aust 2010;193(6):366–9.
[13] Collins S, Boyd A, Lee JS, Lewis V, Fletcher A, McLean CA, Law M, Kaldor J, Smith MJ, Masters CL. Creutzfeldt-Jakob disease in Australia 1970-1999. Neurology 2002;59(9):1365–71.
[14] Australian Institute of Health and Welfare (AIHW). General Record of Incidence of Mortality (GRIM) books; 2017. Available from: URL: https://www.aihw.gov.au/reports/life-expectancy-death/grim-books/contents/grim-books.
[15] Bains N. Standardization of Rates: Association of Public Health Epidemiologists in Ontario; 2009 [cited 2018 Apr 11]. Available from: URL: http://core.apheo.ca/resources/indicators/Standardization%20report_NamBains_FINALMarch16.pdf.
[16] Australian Bureau of Statistics (ABS). 3105.0.65.001 Australian Historical Population Statistics; 2014. Available from: URL: http://www.abs.gov.au/ausstats/abs@.nsf/mf/3105.0.65.001/.
[17] HealthStats NSW. Age standardisation: General information: State of New South Wales NSW Ministry of Health; 2015 [cited 2018 Apr 11]. Available from: URL: http://www.healthstats.nsw.gov.au/Resources/Age-standardisation.pdf.
[18] Stata Statistical Software: StataCorp LLC; 2017. Available from: URL: https://www.stata.com/.
[19] Dean AG, Sullivan KM, Soe MM, Mir RA. OpenEpi: Open Source Epidemiologic Statistics for Public Health: PersonTime2–Comparing Two Person-Time Rates; 2013 [cited 2018 Jul 2]. Available from: URL: http://www.openepi.com/PersonTime2/PersonTime2.htm.
[20] Poidvin A, Touze E, Ecosse E, Landier F, Bejot Y, Giroud M, Rothwell PM, Carel J-C, Coste J. Growth hormone treatment for childhood short stature and risk of stroke in early adulthood. Neurology 2014;83(9):780–6.
[21] Brookmeyer R, Evans DA, Hebert L, Langa KM, Heeringa SG, Plassman BL, Kukull WA. National estimates of the prevalence of Alzheimer's disease in the United States. Alzheimer's Dementia 2011;7(1):61–73.
[22] Villemagne VL, Burnham S, Bourgeat P, Brown B, Ellis KA, Salvado O, Szoeke C, Macaulay SL, Martins R, Maruff P, Ames D, Rowe CC, Masters CL. Amyloid β deposition, neurodegeneration, and cognitive decline in sporadic Alzheimer's disease: a prospective cohort study. Lancet Neurol 2013;12(4):357–67.
[23] Ho W. Age-sex deaths and rates for type of haemorrhagic stroke [SEC=OFFICIAL]. Australian Institute of Health and Welfare (AIHW).
[24] Banerjee G, Adams ME, Jaunmuktane Z, Alistair Lammie G, Turner B, Wani M, Sawhney IMS, Houlden H, Mead S, Brandner S, Werring DJ. Early onset cerebral amyloid angiopathy following childhood exposure to cadaveric dura: Banerjee: Early Onset CAA. Ann Neurol. 2019;85(2):284–90.
[25] Hamaguchi T, Taniguchi Y, Sakai K, Kitamoto T, Takao M, Murayama S, et al. Significant association of cadaveric dura mater grafting with subpial Abeta deposition and meningeal amyloid angiopathy. Acta Neuropathol 2016;132 (2):313–5.

Section 8: Additional Publications Contributing to Knowledge in Prion Diseases

Section 8A: Pathogenesis Studies Emphasising the Prion Protein and Cognate Fragments

M. Jobling, C. Barrow, A. White, C. Masters, **S. Collins**, R. Cappai. The synthesis and spectroscopic analysis of the neurotoxic prion peptide 106-126: comparative use of manual Boc and Fmoc chemistry. Letters in Peptide Science 1999; 6: 129-134.

R. Cappai, L. Stewart, M. Jobling, J. Thyer, A. White, **S. Collins**, C. Masters, C. Barrow. Familial prion protein mutation alters the secondary structure of recombinant mouse prion protein: implications for the mechanism of prion formation. Biochemistry 1999; 38: 3280-3284.

M Jobling, L Stewart, A White, C McLean, A Friedhuber, F Maher, K Beyreuther, C Masters, C Barrow, **S Collins**, R Cappai. The hydrophobic core sequence modulates the neurotoxic and secondary structure properties of the prion peptide 106-126. Journal of Neurochemistry 1999; 73: 1557-1565.

A. White, **S Collins,** L. Stewart, J Thyer, F Maher**,** C Masters, R Cappai. Prion protein deficient neurons reveal lower glutathione reductase activity and increased susceptibility to hydrogen peroxide toxicity. American Journal of Pathology 1999; 155: 1723-1730.

AR White, R Guirguis, M Brazier, MF Jobling, A Hill, K Beyreuther, CJ Barrow, C Masters, **SJ Collins** and R Cappai. Sub-lethal concentrations of prion peptide PrP106-126 or the amyloid beta peptide of Alzheimer's disease activates expression of pro-apoptotic markers in primary cortical neurons. Neurobiology of Disease 2001; 8: 299-316.

Jobling MF, Huang X, Stewart LR, Barnham K, Curtain C, Volitakis I, Perugini MP, White AR, Cherny R, Masters CL, Barrow C, **Collins SJ,** Bush A, Cappai R. Copper and zinc binding modulates the aggregation and neurotoxic properties of the prion peptide PrP106-126. Biochemistry 2001; 40: 8073-8084.

Stewart LR, White AR, Jobling MF, Needham BE, Maher F, Thyer J, Beyreuther K, Masters CL, **Collins SJ,** Cappai R. The involement of arachidonic acid and 5-lipoxygenase pathways in the neurotoxicity of the prion peptide PrP106-126. Journal of Neuroscience Research 2001; 65: 565-572.

FF Yuan, S Biffin, M Brazier, M Suarez, R Cappai, AF Hill, **SJ Collins**, JS Sullivan, D Middleton, G Multhaup, AF Geczy, CL Masters. Detection of prion epitopes on PrPc and PrPsc of transmissible spongiform encephalopathies using specific monoclonal antibodies to PrP. Immunology and Cell Biology 2005; 83: 632-634.

Lawson VA, Vella L, Stewart J, Sharples R, Klemm H, Machalek DM, Masters CL, Cappai R, **Collins SJ**, Hill AF. Mouse-adapted sporadic human CJD prions propagate in cell culture. International Journal of Biochemistry and Cell Biology 2008; 40: 2793-2801.

Kralovicova S, Fontaine SN, Alderton A, Alderman J, Ragnarsdottir KV, **Collins SJ**, Brown DR. The effects of prion protein expression on metal metabolism. Cellular and Molecular Neuroscience 2009; 41: 135-147.

Lawson VA, Lumicisi B, Welton J, Machalek D, Gouramanis K, Klemm H, Stewart JD, Masters CL, Hoke D, **Collins SJ**, Hill AF. Glycosaminoglycan sulphation affects the seeded misfolding of a mutant prion protein. PLoS One 2010; 5(8): e12351. Doi:10.1371/journal.pone.0012351

Lawson VA, Haigh CL, Roberts B, Kenche VB, Klemm HM, Masters CL, **Collins SJ,** Barnham KJ, Drew SC**.** Near infra-red fluorescence imaging of apoptotic neuronal cell death in a live animal model of prion disease. ACS Chemical Neuroscience 2010; 1: 720-727.

Drew SC, Haigh CL, Klemm HM, Masters CL, **Collins SJ**, Barnham KJ, Lawson VA. Optical imaging of apoptosis in the brain and peripheral organs of prion infected mice. Journal of Neuropathology and Experimental Neurology 2011; 70: 143-150.

Klemm HMJ, Welton JM, Masters CL, Hill AF, **Collins SJ**, Lawson VA. Determining the PrPC conversion dependence of sporadic Creutzfeldt-Jakob Disease molecular subtypes. The Journal of Biological Chemistry 2012; 287: 36465-36472.

Johanssen VA, Barnham KJ, Masters CL, Hill AF, Collins SJ. Generating recombinant prion protein fragments of exact native sequence. Neurochemistry International 2012; 60: 318-326.

Ellett L, Coleman B, Shambrook M, Johanssen V, **Collins S**, Masters C, Hill A, Lawson V. Glycosaminoglycan Sulfation Determines the Biochemical Properties of Prion Protein Aggregates. Glycobiology 2015; 25: 745-755.

Collins S, Haigh CL. Simplified murine 3D neuronal cultures for investigating neuronal activity and neurodegeneration. Cell Biochemistry & Biophysics. DOI 10.1007/s12013-016-0768-z.

Wiegmans A, Saunus J, Ham S, Lobb R, Kutasovic J, Dalley A, Miranda M, Atkinson C, Foliaki S, Ferguson K, Niland C, Johnstone C, Lewis V, **Collins S**, Lakhani S, Al-Ejeh F, Möller

A. Secreted extracellular Prion protein specifically sequesters Doxorubicin/ Adriamycin via copper chelation generating therapy resistance in triple negative breast cancer. Journal of Clinical Investigation Insight 2019; 4:e124092.

Section 8B: Clinical Issues in Human Prion Disease

Duncan R, Delatycki MB, **Collins SJ**, Boyd A, Masters CL, Savulescu J. Ethical considerations in pre-symptomatic testing for vCJD. Journal of Medical Ethics 2005; 31: 625-630.

Collins SJ, Athan E, Koehler A. Letters to the Editor (reply) - Updated Creutzfeldt-Jakob Disease infection control guidelines: sifting facts from fiction. Medical Journal of Australia 2013; 199: 536.

Geevasinga N, Buckland ME, **Collins SJ**, Ng K. Sporadic Creutzfeldt-Jakob disease presenting as spastic paraparesis. European Journal of Neurology 2013: 20: e73-e74.

Ramanathan S, Fung V, Bielich A, Masters L, Russo R, Buckland M, Sarros S, Klug G, **Collins S,** Reddel S. Hyperekplexia as the initial presenting symptom of Creutzfeldt-Jakob Disease. Neurology: Clinical Practice 2015; 5: 498-501.

Section 8C: Annual National Human Prion Disease Surveillance Reports

Boyd A, Fletcher A, Lee JS, Lewis V, Masters CL, **Collins SJ**. Transmissible Spongiform Encephalopathies in Australia. Communicable Disease Intelligence 2001; 25: 248-253.

Klug GM, Lewis V, Boyd A, Lee JS, Masters CL, **Collins SJ**. Creutzfeldt-Jakob Disease Surveillance in Australia January 1970 – December 2003. Communicable Diseases Intelligence 2004; 28: 356-358.

Klug,GM, Boyd A, Lewis V, Kvasnicka M, Lee JS, Masters CL, **Collins SJ**. Creutzfeldt-Jakob disease: Australian surveillance update to 31 December 2004. Communicable Disease Intelligence 2005; 29: 269-271.

Klug,GM, Boyd A, Lewis V, Douglass S, Argent R, Lee JS, Masters CL, **Collins SJ**. Creutzfeldt-Jakob disease: Australian surveillance update to 31 December 2005. Communicable Disease Intelligence 2006; 30: 144-147.

Klug GMA, Boyd A, Lewis V, Douglass S, Roberts H, Argent R, Masters CL, **Collins SJ**. Creutzfeldt-Jakob Disease: Australian Surveillance Update to March 2007. Communicable Disease Intelligence 2007; 31: 195-198.

Klug GMA, Boyd A, Lewis V, McGlade A, Douglass S, Masters CL, **Collins SJ**. Surveillance of Creutzfeldt-Jakob Disease in Australia: 2008 update. Communicable Disease Intelligence 2008; 32: 232-236.

Klug GMA, Boyd A, Lewis V, McGlade A, Stehmann C, Masters CL, **Collins SJ**. Surveillance of Creutzfeldt-Jakob Disease in Australia: 2009 update. Communicable Disease Intelligence 2008; 32: 188-191.

Klug GM, Boyd A, McGlade A, Stehmann C, Masters CL, **Collins SJ**. Surveillance of Creutzfeldt-Jakob disease in Australia: 2010 update. Communicable Diseases Intelligence 2010; 34: 96-101.

Klug GM, Boyd A, McGlade A, Stehmann C, Masters CL, **Collins SJ**. Surveillance of Creutzfeldt-Jakob disease in Australia: update to December 2010. Communicable Diseases Intelligence 2011; 35: 149-153.

Klug GM, Boyd A, McGlade A, Stehmann C, Simpson M, Masters CL, **Collins SJ**. Surveillance of Creutzfeldt-Jakob disease in Australia: update to December 2011. Communicable Diseases Intelligence 2012; 36: E174-179.

Klug GM, Boyd A, Zhao T, Stehmann C, Simpson M, McLean C, Masters CL & **Collins SJ**. Surveillance for Creutzfeldt-Jakob Disease in Australia: update to December 2012. Communicable Diseases Intelligence 2013; 37: e115-120.

Klug G, Boyd A, Sarros S, Stehmann C, Simpson M, McLean C, Masters C, **Collins S**. Creutzfeldt-Jakob disease surveillance in Australia: update to December 2013. Communicable diseases Intelligence 2014; 38: E348–E355.

Klug G, Boyd A, Sarros S, Stehmann C, Simpson M, McLean C, Masters C, **Collins S**. Creutzfeldt-Jakob disease surveillance in Australia: update to December 2014. Communicable Diseases Intelligence 2016; 40: E207–E215.

Klug GM, Boyd A, Sarros S, Stehmann C, Simpson M, McLean C, Masters C, **Collins S**. Creutzfeldt-Jakob disease surveillance in Australia: update to December 2015. Communicable Diseases Intelligence 2016;40(3):E363–E371.

Klug G, Boyd A, Sarros S, Stehmann C, Simpson M, McLean C, Masters C, **Collins S**. Creutzfeldt-Jakob disease surveillance in Australia: update to December 2016. Communicable Diseases Intelligence 2018; 42(PII: S2209-6051(18)00023-4) Epub 17/12/2018.

Stehmann C, Sarros S, Senesi M, Lewis V, Simpson M, McLean C, Masters C, **Collins S**. Creutzfeldt-Jakob disease surveillance in Australia: update to December 2017. Communicable Diseases Intelligence 2019; 43 doi.org/10.33321/cdi.2019.43.32.

Stehmann C, Senesi M, Lewis V, Ummi M, Simpson M, Klug G, McLean C, Masters C, **Collins S**. Creutzfeldt-Jakob disease surveillance in Australia: update to 31 December 2018. Communicable Disease Intelligence 2019;43(https://doi.org/10.33321/cdi.2019.43.35) Epub 15/08/2019.

Stehmannn C, Senesi M, Sarros S, McGlade A, Simpson M, Klug G, McLean C, Masters C, **Collins S**. Creutzfedlt-Jakob disease surveillance in Australia: update to 31 December 2019. Communicable Diseases Intelligence 2020;44(https://doi.org/10.33321/cdi.2020.44.56) Epub 15/07/2020.

Section 8D: Peer-reviewed Reviews dealing with Human Prion Diseases: Clinical, Biomarkers, Treatment, Pathogenesis and Cell Biology.

Collins S, Masters C. Transmissibility of Creutzfeldt-Jakob disease and related disorders. Science Progress 1995; 78 (3): 217-227.

Collins S, Cappai R, Masters C. Recent developments in the transmissible spongiform encephalopathies: implications for clinical practice. Journal of Clinical Neurosciences 1996; 3(2): 97-101.

Collins, C. Masters. Iatrogenic and zoonotic Creutzfeldt-Jakob disease; the Australian perspective. Medical Journal of Australia 1996; 164: 598-602.

S Collins, A Boyd, A Fletcher, M Gonzales, C McLean, C Masters. Recent advances in the pre-mortem diagnosis of Creutzfeldt-Jakob disease. Journal of Clinical Neuroscience 2000; 7: 195-202.

Collins S, McLean CA, Masters CL. Gerstmann-Sträussler-Scheinker syndrome, fatal familial insomnia, and kuru: a review of these less common human transmissible spongiform encephalopathies. Journal of Clinical Neuroscience 2001; 8: 387-397.

Chan S, Collins S, Masters CL, Walker DM. Classical and new variant Creutzfeldt-Jakob diseases and their potential impact on the practice of clinical dentistry in Australia. Australian Dental Journal 2001; 46: 251-257.

Collins SJ. “Mad cows” and variant Creutzfeldt-Jakob Disease. Microbiology Australia 2001; July: 20-21.

Collins S. Variant Creutzfeldt-Jakob disease: where are we? Microbiology Australia 2002; 23: 31-32.

Brazier M, Cappai R, Collins S. Prions in skeletal muscle. Australian Veterinary Journal 2002; 80: 484-485.

Lewis V, Boyd A, Masters CL, Collins SJ. Apparently sporadic CJD and covert health care transmissions. The Lancet Neurology 2002; 1: 470-471.

Ramasamy I, Law M, Collins S, Brooke F. Organ Distribution of Prion Proteins in variant Creutzfeldt Jakob disease. Lancet, Infectious Disease 2003; 3: 214-222.

Collins S, Lawson V, Masters CL. Transmissible spongiform encephalopathies. Lancet 2004; 363: 51-61.

Lawson VA, **Collins SJ**, Masters CL, Hill AF. Prion protein glycosylation. Journal of Neurochemistry 2005; 93: 793-801.

Brazier MW, Wall VA, Brazier BW, Masters CL, **Collins SJ**. Therapeutic interventions ameliorating prion disease. Expert Reviews Anti-Infective Therapy 2009; 7: 83-105.

Haigh CL, Marom SY, **Collins SJ**. Copper, constitutive endoproteolytic processing of the prion protein and cell signalling. Frontiers in Bioscience 2010; 15: 1086-1104.

Mot A, Brown D, Wedd A, **Collins S**, Brazier M. Metal attenuating therapies in neurodegenerative disease. Expert Review of Neurotherapeutics 2011; 11: 1717-1745.

Brazier MW, Mot AI, Masters CL, White AR, **Collins SJ**. Immunotherapeutic approaches in prion disease: progress, challenges and potential directions. Therapeutic Delivery 2013; 4: 615-28. doi: 10.4155/tde.13.30..

Kenche V, Tumpach C, Barnham KJ, **Collins SJ**, Haigh CL, Drew SC. Development of a Neuroprotective Antioxidant by a “Mix-and-Match” Strategy. Oxidants and Anti-oxidants in Medical Science 2013; 2: 255-264.

Brazier M, A Wedd, **Collins SJ**. Antioxidant and metal chelation-based therapies in the treatment of prion disease. Antioxidants 2014:3(2), 288-308.

Islam A, Adlard P, Finkelstein D, Lewis V, Biggi S, Biasini E, **Collins S**. Acute Neurotoxicity Models of Prion Disease. ACS Chemical Neuroscience 2018. doi: 10.1021/acschemneuro.7b00517.

Manni G, Lewis V, Senesi M, Spagnolli G, Fallarino F, **Collins S**, Mouillet-Richard S, Biasini E. The cellular prion protein beyond prion diseases. Swiss Medical Weekly 2020;150:w20222.

Section 9: Summary and Future Directions

This thesis has presented various important, often landmark, contributions to the field of human prion disease spanning the diverse spectrum of: normal prion protein cellular biology; prion pathogenesis; human prion disease epidemiological studies; human prion disease bio-marker studies; clinical aspects of human prion disease; prion disease treatment studies; and studies of human prion-like diseases. Across this breadth of these scholastic endeavours, contributions to diagnostic bio-markers, epidemiology, normal prion protein cell biology, pathogenesis and the potential clinico-biological frequency and significance non-prion protein accumulation in the brain contentiously represent the greatest achievements. Despite the meritorious contributions described in this thesis, and the prodigious advances more generally to the field of prion diseases over the last four decades, considerable gaps in our biological understanding and clinical capacity remain to be redressed.

Pre-mortem diagnostic capabilities for human prion disease are a noteworthy success over the last approximately 25 years with this thesis containing most, if not all, seminal contributions that have prompted revision of diagnostic criteria and thereby ensured their inclusion. Starting with CSF 14-3-3 detection, moving through consolidation of MRI sequences and typical features and culminating in the unparalleled advances offered by the RT-QUIC protein amplification technology, only a small minority of human prion disease (<2-3%) will currently not display a characteristic abnormality on one of these diagnostic tests during pre-mortem evaluation of suspected prion disease. A remaining challenge, akin to the threshold being realized in AD, is to achieve validated blood tests for human prion disease that offer similar sensitivity and specificity to that currently enjoyed with CSF and imaging bio-markers. Application of technologies currently demonstrating successful deployment for blood screening in AD (eg single molecule array [SIMOA] technology; immunoprecipitation-mass spectrometry) are an avenue for further exploration, in addition to further development of protein amplification techniques such as the RT-QUIC and protein misfolding cyclic amplification assay (PMCA). Successful delivery of sensitive and specific blood tests for human prion disease will clearly simplify screening for these maladies, perhaps allowing extant bio-markers to be utilized as orthogonal diagnostic confirmation assays.

Another major achievement described in this thesis is the advancements provided epidemiologically. Through large domestic and multi-national studies our epidemiological understanding of human prion disease has improved across areas ranging from factors

influencing annual reported disease incidence, through clarifying determinants of survival and diagnostic test results across the clinical sub-types of sporadic CJD, to a better understanding of the true biological significance of sequence variations in *PRNP*. The translational benefits of this improved understanding are diverse and impact numerous clinical domains encompassing genetic counselling, better stratification of participant cohorts for treatment trials, better detection of new sub-types of human prion disease and personalization of optimal diagnostic evaluation in suspected prion disease cases. Future studies need to independently verify and elaborate these multifarious observations and additionally explore issues such as the incidence and phenotype of prion disease in other less studied Indigenous populations.

Of considerable contemporary clinical and neuro-biological interest are the frequency and consequences of transmission and propagation of non-prion proteins (such as Abeta) found in other neurodegenerative diseases (such as AD) within the CNS. The investigations provided in this thesis add weight to the burgeoning concerns that inadvertent transmission of non-prion proteins like Abeta to the brain either alone or accompanying other pathogenic proteins (such as PrP^{Sc}) leads to their sustained propagation thereafter in an uncertain percentage of exposed individuals. Based on cases of iCJD related to cadaveric pituitary hormones and dura mater grafts, and even persons treated with cadaveric pituitary hormones who did not develop iCJD, the transmission and propagation of Abeta appears potentially relatively common. Moreover, there is the likelihood that propagated Abeta may not remain sub-clinical but eventually culminate in overt disease. This of particular importance given the prevalence of non-prion neurodegenerative diseases, especially in the elderly, and the possibility that inter-individual transmission of non-prion proteins through contaminated instruments may occur, culminating in manifest serious disease decades later. Future high-quality epidemiological studies are required to better define and quantify such risks, with additional investigations required to comprehensively and unambiguously determine the efficacy of routine instrument decontamination and sterilization practices currently employed in hospitals for destroying non-prion proteins found in more common neurodegenerative diseases like AD (Abeta and tau) and PD (alpha-synuclein). Data of this type would ensure substantial disease risk mitigation through adopting validated universal best practice approaches.

Understanding the factors and cellular pathways contributing to the occurrence of sporadic CJD and the bio-physical properties of the neurotoxic form of PrP^{Sc} and its early pathophysiological effects are likely to facilitate the development of effective disease modifying treatments. Both types of contributions are described in this thesis. The largest GWAS undertaken to date has for

the first time provided unequivocal evidence implicating non-*PRNP* genetic risk factors (syntaxin-6 and galactose-3-O-sulfotransferase-1 genes) in the causation of sporadic CJD. Future *in vitro* and *in vivo* studies need to elucidate the pathogenetic mechanisms underpinning exactly how such non-prion genes lead to disease, with hopefully additional larger GWAS to define additional non-PRNP genes contributing to disease risk. These types of studies may provide the basis of therapies more specifically targeting corrupted cellular pathways directly driving pathogenesis. In addition, studies reported in this thesis have further supported enhanced oxidative stress as a key derangement in prion disease and provided mechanistic insights into cognate cellular derangements linked to PrP^{Sc} propagation; unfortunately preliminary studies untilising simple anti-oxidant treatments appear to have negligible effect on disease. Future studies are required to better define the contribution that enhanced neuronal oxidative stress plays as a driver in the overall pathogenesis of prion disease and to assess whether more potent, targeted anti-oxidant therapies may offer enhanced efficacy.

In addition, this thesis has described studies developing and thereafter utilizing a new electrophysiological disease model directly assessing the acute synaptotoxic effects of *ex vivo* PrP^{Sc} based on wild-type hippocampal slices. These experiments provided insights into the temporal occurrence, the biochemical evolution of, and the bio-physical properties of PrP^{Sc}, as well as the early deleterious pathophysiological consequences to key synaptic components. Future studies utilizing this model could be undertaken to more precisely define the bio-physical characteristics of neurotoxic PrP^{Sc} and how this contrasts with PrP^{Sc} species underscoring disease transmission. Moreover, based on the enhanced biological validity of this model, it could be employed for low throughput drug screening of promising therapeutic candidates selected based on higher throughput, less stringent techniques.

An important unresolved issue is the primary biological purpose of PrP^{C}, especially in the CNS. Studies of the normal cellular biology of PrP^{C} yielded a number of novel insights, suggesting PrP^{C} may have more than one principal role, including participation in the regulation of stem cell renewal, anti-oxidant effects via the N2 fragment and signal transduction activities. In addition, a new endogenous cleavage event denoted as “gamma” was delineated. Future studies would ideally pursue all these avenues of potential PrP^{C} function to determine those that are the most important biologically, especially whether corruption of such activities contribute to pathogenesis. Further studies are also required to more accurately define the site of gamma-cleavage, as well as determine the biological significance of this constitutive cleavage in both normal cellular homeostasis and disease.

Finally, an effective treatment for human prion disease is arguably the most important, extant unmet need. Unfortunately, the limited studies interrogating potential treatments described in this thesis were all unsuccessful, joining a vast but disappointing list of agents explored in pre-clinical assessments. Collaborative research described in this thesis however, has clarified that the rarity and unpredictability of age of onset of genetic forms of prion disease renders it unsuitable for conventional placebo-controlled human therapeutic trials and less conventional, innovative approaches are required. Based on the exciting results for other neurological diseases, especially SMA type 1, studies will hopefully commence in the very near future to assess the efficacy of ASO strategies for human prion disease. In addition, a high affinity, humanised, anti-PrP monoclonal antibody has also been developed based on promising pre-clinical studies but bureaucratic and funding hurdles have delayed transition into formal clinical trials although a very limited assessment of safety in a small number of patients has been undertaken with an outcome report not yet provided.

Bibliography

1. Prusiner SB. Novel proteinaceous infectious particles cause scrapie. Science. 1982;216(4542):136-44.
2. Prusiner SB. Prion diseases and the BSE crisis. Science. 1997;278(5336):245-51.
3. Ritchie DL, Ironside JW. Neuropathology of Human Prion Diseases. Prog Mol Biol Transl Sci. 2017;150:319-39.
4. Babelhadj B, Di Bari MA, Pirisinu L, Chiappini B, Gaouar SBS, Riccardi G, et al. Prion Disease in Dromedary Camels, Algeria. Emerg Infect Dis. 2018;24(6):1029-36.
5. Gajdusek DC, Zigas V. Degenerative disease of the central nervous system in New Guinea; the endemic occurrence of kuru in the native population. The New England journal of medicine. 1957;257(20):974-8.
6. Gajdusek DC, Gibbs CJ, Alpers M. Experimental transmission of a Kuru-like syndrome to chimpanzees. Nature. 1966;209(5025):794-6.
7. Gibbs CJ, Jr., Gajdusek DC, Asher DM, Alpers MP, Beck E, Daniel PM, et al. Creutzfeldt-Jakob disease (spongiform encephalopathy): transmission to the chimpanzee. Science. 1968;161(3839):388-9.
8. Gajdusek DC. Unconventional viruses and the origin and disappearance of kuru. Science. 1977;197(4307):943-60.
9. Masters CL, Gajdusek DC, Gibbs CJ, Jr. Creutzfeldt-Jakob disease virus isolations from the Gerstmann-Straussler syndrome with an analysis of the various forms of amyloid plaque deposition in the virus-induced spongiform encephalopathies. Brain : a journal of neurology. 1981;104(3):559-88.
10. Medori R, Tritschler HJ, LeBlanc A, Villare F, Manetto V, Chen HY, et al. Fatal familial insomnia, a prion disease with a mutation at codon 178 of the prion protein gene. The New England journal of medicine. 1992;326(7):444-9.
11. Tateishi J, Brown P, Kitamoto T, Hoque ZM, Roos R, Wollman R, et al. First experimental transmission of fatal familial insomnia. Nature. 1995;376(6539):434-5.
12. Malone TG, Marsh RF, Hanson RP, Semancik JS. Evidence for the low molecular weight nature of scrapie agent. Nature. 1979;278(5704):575-6.
13. Alper T, Cramp WA, Haig DA, Clarke MC. Does the agent of scrapie replicate without nucleic acid? Nature. 1967;214(5090):764-6.
14. Alper T, Haig DA, Clarke MC. The exceptionally small size of the scrapie agent. Biochem Biophys Res Commun. 1966;22(3):278-84.
15. Pattison IH, Jones KM. The possible nature of the transmissible agent of scrapie. Vet Rec. 1967;80(1):2-9.
16. Griffith JS. Self-replication and scrapie. Nature. 1967;215(5105):1043-4.
17. Prusiner SB, Bolton DC, Groth DF, Bowman KA, Cochran SP, McKinley MP. Further purification and characterization of scrapie prions. Biochemistry. 1982;21(26):6942-50.
18. Prusiner SB, Groth DF, Bolton DC, Kent SB, Hood LE. Purification and structural studies of a major scrapie prion protein. Cell. 1984;38(1):127-34.
19. Chesebro B, Race R, Wehrly K, Nishio J, Bloom M, Lechner D, et al. Identification of scrapie prion protein-specific mRNA in scrapie-infected and uninfected brain. Nature. 1985;315(6017):331-3.
20. Legname G, Baskakov IV, Nguyen HO, Riesner D, Cohen FE, DeArmond SJ, et al. Synthetic mammalian prions. Science. 2004;305(5684):673-6.

21. Legname G, Nguyen HO, Baskakov IV, Cohen FE, Dearmond SJ, Prusiner SB. Strain-specified characteristics of mouse synthetic prions. Proceedings of the National Academy of Sciences of the United States of America. 2005;102(6):2168-73.
22. Castilla J, Saa P, Hetz C, Soto C. In vitro generation of infectious scrapie prions. Cell. 2005;121(2):195-206.
23. Deleault NR, Harris BT, Rees JR, Supattapone S. Formation of native prions from minimal components in vitro. Proceedings of the National Academy of Sciences of the United States of America. 2007;104(23):9741-6.
24. Wang F, Wang X, Yuan CG, Ma J. Generating a prion with bacterially expressed recombinant prion protein. Science. 2010;327(5969):1132-5.
25. Makarava N, Kovacs GG, Savtchenko R, Alexeeva I, Budka H, Rohwer RG, et al. Genesis of mammalian prions: from non-infectious amyloid fibrils to a transmissible prion disease. PLoS pathogens. 2011;7(12):e1002419.
26. Lysek DA, Schorn C, Nivon LG, Esteve-Moya V, Christen B, Calzolai L, et al. Prion protein NMR structures of cats, dogs, pigs, and sheep. Proceedings of the National Academy of Sciences of the United States of America. 2005;102(3):640-5.
27. Calzolai L, Lysek DA, Perez DR, Guntert P, Wuthrich K. Prion protein NMR structures of chickens, turtles, and frogs. Proceedings of the National Academy of Sciences of the United States of America. 2005;102(3):651-5.
28. Castle AR, Gill AC. Physiological Functions of the Cellular Prion Protein. Front Mol Biosci. 2017;4:19.
29. Westergard L, Christensen HM, Harris DA. The cellular prion protein (PrP(C)): its physiological function and role in disease. Biochim Biophys Acta. 2007;1772(6):629-44.
30. Vey M, Pilkuhn S, Wille H, Nixon R, DeArmond SJ, Smart EJ, et al. Subcellular colocalization of the cellular and scrapie prion proteins in caveolae-like membranous domains. Proceedings of the National Academy of Sciences of the United States of America. 1996;93(25):14945-9.
31. Stahl N, Borchelt DR, Hsiao K, Prusiner SB. Scrapie prion protein contains a phosphatidylinositol glycolipid. Cell. 1987;51(2):229-40.
32. Brown DR, Qin K, Herms JW, Madlung A, Manson J, Strome R, et al. The cellular prion protein binds copper in vivo. Nature. 1997;390(6661):684-7.
33. Stockel J, Safar J, Wallace AC, Cohen FE, Prusiner SB. Prion protein selectively binds copper(II) ions. Biochemistry. 1998;37(20):7185-93.
34. Walter ED, Stevens DJ, Visconte MP, Millhauser GL. The prion protein is a combined zinc and copper binding protein: Zn2+ alters the distribution of Cu2+ coordination modes. J Am Chem Soc. 2007;129(50):15440-1.
35. Taylor DR, Watt NT, Perera WS, Hooper NM. Assigning functions to distinct regions of the N-terminus of the prion protein that are involved in its copper-stimulated, clathrin-dependent endocytosis. J Cell Sci. 2005;118(Pt 21):5141-53.
36. Jones CE, Klewpatinond M, Abdelraheim SR, Brown DR, Viles JH. Probing copper2+ binding to the prion protein using diamagnetic nickel2+ and 1H NMR: the unstructured N terminus facilitates the coordination of six copper2+ ions at physiological concentrations. J Mol Biol. 2005;346(5):1393-407.
37. Riek R, Hornemann S, Wider G, Glockshuber R, Wuthrich K. NMR characterization of the full-length recombinant murine prion protein, mPrP(23-231). FEBS Lett. 1997;413(2):282-8.

38. Manson J, West JD, Thomson V, McBride P, Kaufman MH, Hope J. The prion protein gene: a role in mouse embryogenesis? Development. 1992;115(1):117-22.
39. Harris DA, Lele P, Snider WD. Localization of the mRNA for a chicken prion protein by in situ hybridization. Proceedings of the National Academy of Sciences of the United States of America. 1993;90(9):4309-13.
40. Moser M, Colello RJ, Pott U, Oesch B. Developmental expression of the prion protein gene in glial cells. Neuron. 1995;14(3):509-17.
41. Ford MJ, Burton LJ, Morris RJ, Hall SM. Selective expression of prion protein in peripheral tissues of the adult mouse. Neuroscience. 2002;113(1):177-92.
42. Alperovitch A, Zerr I, Pocchiari M, Mitrova E, de Pedro Cuesta J, Hegyi I, et al. Codon 129 prion protein genotype and sporadic Creutzfeldt-Jakob disease. Lancet. 1999;353(9165):1673-4.
43. Goldfarb LG, Haltia M, Brown P, Nieto A, Kovanen J, McCombie WR, et al. New mutation in scrapie amyloid precursor gene (at codon 178) in Finnish Creutzfeldt-Jakob kindred. Lancet. 1991;337(8738):425.
44. Harris DA, Huber MT, van Dijken P, Shyng SL, Chait BT, Wang R. Processing of a cellular prion protein: identification of N- and C-terminal cleavage sites. Biochemistry. 1993;32(4):1009-16.
45. Chen SG, Teplow DB, Parchi P, Teller JK, Gambetti P, Autilio-Gambetti L. Truncated forms of the human prion protein in normal brain and in prion diseases. The Journal of biological chemistry. 1995;270(32):19173-80.
46. Lewis V, Johanssen VA, Crouch PJ, Klug GM, Hooper NM, Collins SJ. Prion protein "gamma-cleavage": characterizing a novel endoproteolytic processing event. Cell Mol Life Sci. 2016;73(3):667-83.
47. Altmeppen HC, Prox J, Puig B, Kluth MA, Bernreuther C, Thurm D, et al. Lack of a-disintegrin-and-metalloproteinase ADAM10 leads to intracellular accumulation and loss of shedding of the cellular prion protein in vivo. Molecular neurodegeneration. 2011;6:36.
48. Westergard L, Turnbaugh JA, Harris DA. A naturally occurring C-terminal fragment of the prion protein (PrP) delays disease and acts as a dominant-negative inhibitor of PrPSc formation. The Journal of biological chemistry. 2011;286(51):44234-42.
49. Lewis V, Hill AF, Haigh CL, Klug GM, Masters CL, Lawson VA, et al. Increased Proportions of C1 Truncated Prion Protein Protect Against Cellular M1000 Prion Infection. Journal of Neuropathology and Experimental Neurology. 2009;68(10):1125-35.
50. Yusa S, Oliveira-Martins JB, Sugita-Konishi Y, Kikuchi Y. Cellular prion protein: from physiology to pathology. Viruses. 2012;4(11):3109-31.
51. Bremer J, Baumann F, Tiberi C, Wessig C, Fischer H, Schwarz P, et al. Axonal prion protein is required for peripheral myelin maintenance. Nature neuroscience. 2010;13(3):310-8.
52. Cashman NR, Loertscher R, Nalbantoglu J, Shaw I, Kascsak RJ, Bolton DC, et al. Cellular isoform of the scrapie agent protein participates in lymphocyte activation. Cell. 1990;61(1):185-92.
53. Bueler H, Fischer M, Lang Y, Bluethmann H, Lipp HP, DeArmond SJ, et al. Normal development and behaviour of mice lacking the neuronal cell-surface PrP protein. Nature. 1992;356(6370):577-82.
54. Curtis J, Errington M, Bliss T, Voss K, MacLeod N. Age-dependent loss of PTP and LTP in the hippocampus of PrP-null mice. Neurobiology of disease. 2003;13(1):55-62.
55. Criado JR, Sanchez-Alavez M, Conti B, Giacchino JL, Wills DN, Henriksen SJ, et al. Mice devoid of prion protein have cognitive deficits that are rescued by reconstitution of PrP in neurons. Neurobiology of disease. 2005;19(1-2):255-65.

56. Brown DR, Clive C, Haswell SJ. Antioxidant activity related to copper binding of native prion protein. Journal of neurochemistry. 2001;76(1):69-76.
57. Mouillet-Richard S, Ermonval M, Chebassier C, Laplanche JL, Lehmann S, Launay JM, et al. Signal transduction through prion protein. Science. 2000;289(5486):1925-8.
58. Robinson SW, Nugent ML, Dinsdale D, Steinert JR. Prion protein facilitates synaptic vesicle release by enhancing release probability. Hum Mol Genet. 2014;23(17):4581-96.
59. Brown DR, Schulz-Schaeffer WJ, Schmidt B, Kretzschmar HA. Prion protein-deficient cells show altered response to oxidative stress due to decreased SOD-1 activity. Exp Neurol. 1997;146(1):104-12.
60. Wong BS, Liu T, Li R, Pan T, Petersen RB, Smith MA, et al. Increased levels of oxidative stress markers detected in the brains of mice devoid of prion protein. Journal of neurochemistry. 2001;76(2):565-72.
61. Guillot-Sestier MV, Sunyach C, Druon C, Scarzello S, Checler F. The alpha-secretase-derived N-terminal product of cellular prion, N1, displays neuroprotective function in vitro and in vivo. The Journal of biological chemistry. 2009;284(51):35973-86.
62. Black SA, Stys PK, Zamponi GW, Tsutsui S. Cellular prion protein and NMDA receptor modulation: protecting against excitotoxicity. Front Cell Dev Biol. 2014;2:45.
63. Khosravani H, Zhang Y, Tsutsui S, Hameed S, Altier C, Hamid J, et al. Prion protein attenuates excitotoxicity by inhibiting NMDA receptors. J Cell Biol. 2008;181(3):551-65.
64. Guillot-Sestier MV, Sunyach C, Druon C, Scarzello S, Checler F. The alpha-Secretase-derived N-terminal Product of Cellular Prion, N1, Displays Neuroprotective Function in Vitro and in Vivo. Journal of Biological Chemistry. 2009;284(51):35973-86.
65. Fluharty BR, Biasini E, Stravalaci M, Sclip A, Diomede L, Balducci C, et al. An N-terminal fragment of the prion protein binds to amyloid-beta oligomers and inhibits their neurotoxicity in vivo. The Journal of biological chemistry. 2013;288(11):7857-66.
66. Lauren J, Gimbel DA, Nygaard HB, Gilbert JW, Strittmatter SM. Cellular prion protein mediates impairment of synaptic plasticity by amyloid-beta oligomers. Nature. 2009;457(7233):1128-32.
67. Balducci C, Beeg M, Stravalaci M, Bastone A, Sclip A, Biasini E, et al. Synthetic amyloid-beta oligomers impair long-term memory independently of cellular prion protein. Proceedings of the National Academy of Sciences of the United States of America. 2010;107(5):2295-300.
68. Kessels HW, Nguyen LN, Nabavi S, Malinow R. The prion protein as a receptor for amyloid-beta. Nature. 2010;466(7308):E3-4; discussion E-5.
69. Schneider B, Mutel V, Pietri M, Ermonval M, Mouillet-Richard S, Kellermann O. NADPH oxidase and extracellular regulated kinases 1/2 are targets of prion protein signaling in neuronal and nonneuronal cells. Proceedings of the National Academy of Sciences of the United States of America. 2003;100(23):13326-31.
70. Collinge J, Whittington MA, Sidle KC, Smith CJ, Palmer MS, Clarke AR, et al. Prion protein is necessary for normal synaptic function. Nature. 1994;370(6487):295-7.
71. Manson JC, Hope J, Clarke AR, Johnston A, Black C, MacLeod N. PrP gene dosage and long term potentiation. Neurodegeneration. 1995;4(1):113-4.
72. Adle-Biassette H, Verney C, Peoc'h K, Dauge MC, Razavi F, Choudat L, et al. Immunohistochemical expression of prion protein (PrPC) in the human forebrain during development. J Neuropathol Exp Neurol. 2006;65(7):698-706.

73. Herms J, Tings T, Gall S, Madlung A, Giese A, Siebert H, et al. Evidence of presynaptic location and function of the prion protein. J Neurosci. 1999;19(20):8866-75.
74. Kanaani J, Prusiner SB, Diacovo J, Baekkeskov S, Legname G. Recombinant prion protein induces rapid polarization and development of synapses in embryonic rat hippocampal neurons in vitro. Journal of neurochemistry. 2005;95(5):1373-86.
75. Colling SB, Collinge J, Jefferys JG. Hippocampal slices from prion protein null mice: disrupted Ca(2+)-activated K+ currents. Neurosci Lett. 1996;209(1):49-52.
76. Herms JW, Tings T, Dunker S, Kretzschmar HA. Prion protein affects Ca2+-activated K+ currents in cerebellar purkinje cells. Neurobiology of disease. 2001;8(2):324-30.
77. Nishida N, Katamine S, Shigematsu K, Nakatani A, Sakamoto N, Hasegawa S, et al. Prion protein is necessary for latent learning and long-term memory retention. Cell Mol Neurobiol. 1997;17(5):537-45.
78. Coitinho AS, Roesler R, Martins VR, Brentani RR, Izquierdo I. Cellular prion protein ablation impairs behavior as a function of age. Neuroreport. 2003;14(10):1375-9.
79. Bueler H, Aguzzi A, Sailer A, Greiner RA, Autenried P, Aguet M, et al. Mice devoid of PrP are resistant to scrapie. Cell. 1993;73(7):1339-47.
80. Mallucci G, Dickinson A, Linehan J, Klohn PC, Brandner S, Collinge J. Depleting neuronal PrP in prion infection prevents disease and reverses spongiosis. Science. 2003;302(5646):871-4.
81. Selkoe DJ. Alzheimer's disease is a synaptic failure. Science. 2002;298(5594):789-91.
82. Shankar GM, Li S, Mehta TH, Garcia-Munoz A, Shepardson NE, Smith I, et al. Amyloid-beta protein dimers isolated directly from Alzheimer's brains impair synaptic plasticity and memory. Nature medicine. 2008;14(8):837-42.
83. Freir DB, Nicoll AJ, Klyubin I, Panico S, Mc Donald JM, Risse E, et al. Interaction between prion protein and toxic amyloid beta assemblies can be therapeutically targeted at multiple sites. Nat Commun. 2011;2:336.
84. Um JW, Nygaard HB, Heiss JK, Kostylev MA, Stagi M, Vortmeyer A, et al. Alzheimer amyloid-beta oligomer bound to postsynaptic prion protein activates Fyn to impair neurons. Nature neuroscience. 2012;15(9):1227-35.
85. Silveira JR, Raymond GJ, Hughson AG, Race RE, Sim VL, Hayes SF, et al. The most infectious prion protein particles. Nature. 2005;437(7056):257-61.
86. Tixador P, Herzog L, Reine F, Jaumain E, Chapuis J, Le Dur A, et al. The physical relationship between infectivity and prion protein aggregates is strain-dependent. PLoS pathogens. 2010;6(4):e1000859.
87. Novitskaya V, Bocharova OV, Bronstein I, Baskakov IV. Amyloid fibrils of mammalian prion protein are highly toxic to cultured cells and primary neurons. The Journal of biological chemistry. 2006;281(19):13828-36.
88. Muller WE, Ushijima H, Schroder HC, Forrest JM, Schatton WF, Rytik PG, et al. Cytoprotective effect of NMDA receptor antagonists on prion protein (PrionSc)-induced toxicity in rat cortical cell cultures. European journal of pharmacology. 1993;246(3):261-7.
89. Giese A, Brown DR, Groschup MH, Feldmann C, Haist I, Kretzschmar HA. Role of microglia in neuronal cell death in prion disease. Brain pathology. 1998;8(3):449-57.
90. Simoneau S, Rezaei H, Sales N, Kaiser-Schulz G, Lefebvre-Roque M, Vidal C, et al. In vitro and in vivo neurotoxicity of prion protein oligomers. PLoS pathogens. 2007;3(8):e125.

91. Falsig J, Sonati T, Herrmann US, Saban D, Li B, Arroyo K, et al. Prion pathogenesis is faithfully reproduced in cerebellar organotypic slice cultures. PLoS pathogens. 2012;8(11):e1002985.
92. Fang C, Imberdis T, Garza MC, Wille H, Harris DA. A Neuronal Culture System to Detect Prion Synaptotoxicity. PLoS pathogens. 2016;12(5):e1005623.
93. Sasaki K, Minaki H, Iwaki T. Development of oligomeric prion-protein aggregates in a mouse model of prion disease. J Pathol. 2009;219(1):123-30.
94. Cunningham C, Deacon R, Wells H, Boche D, Waters S, Diniz CP, et al. Synaptic changes characterize early behavioural signs in the ME7 model of murine prion disease. The European journal of neuroscience. 2003;17(10):2147-55.
95. Fuhrmann M, Mitteregger G, Kretzschmar H, Herms J. Dendritic pathology in prion disease starts at the synaptic spine. J Neurosci. 2007;27(23):6224-33.
96. Johnston AR, Fraser JR, Jeffrey M, MacLeod N. Synaptic plasticity in the CA1 area of the hippocampus of scrapie-infected mice. Neurobiology of disease. 1998;5(3):188-95.
97. Milhavet O, McMahon HE, Rachidi W, Nishida N, Katamine S, Mange A, et al. Prion infection impairs the cellular response to oxidative stress. Proceedings of the National Academy of Sciences of the United States of America. 2000;97(25):13937-42.
98. Moreno JA, Radford H, Peretti D, Steinert JR, Verity N, Martin MG, et al. Sustained translational repression by eIF2alpha-P mediates prion neurodegeneration. Nature. 2012;485(7399):507-11.
99. Hegde RS, Tremblay P, Groth D, DeArmond SJ, Prusiner SB, Lingappa VR. Transmissible and genetic prion diseases share a common pathway of neurodegeneration. Nature. 1999;402(6763):822-6.
100. Senatore A, Colleoni S, Verderio C, Restelli E, Morini R, Condliffe SB, et al. Mutant PrP suppresses glutamatergic neurotransmission in cerebellar granule neurons by impairing membrane delivery of VGCC alpha(2)delta-1 Subunit. Neuron. 2012;74(2):300-13.
101. Windl O, Dempster M, Estibeiro JP, Lathe R, de Silva R, Esmonde T, et al. Genetic basis of Creutzfeldt-Jakob disease in the United Kingdom: a systematic analysis of predisposing mutations and allelic variation in the PRNP gene. Human genetics. 1996;98(3):259-64.
102. Ladogana A, Puopolo M, Croes EA, Budka H, Jarius C, Collins S, et al. Mortality from Creutzfeldt-Jakob disease and related disorders in Europe, Australia, and Canada. Neurology. 2005;64(9):1586-91.
103. Ladogana A, Puopolo M, Poleggi A, Almonti S, Mellina V, Equestre M, et al. High incidence of genetic human transmissible spongiform encephalopathies in Italy. Neurology. 2005;64(9):1592-7.
104. Yuan J, Xiao X, McGeehan J, Dong Z, Cali I, Fujioka H, et al. Insoluble aggregates and protease-resistant conformers of prion protein in uninfected human brains. The Journal of biological chemistry. 2006;281(46):34848-58.
105. Won SY, Kim YC, Jeong BH. First Report of the Potential Bovine Spongiform Encephalopathy (BSE)-Related Somatic Mutation E211K of the Prion Protein Gene (PRNP) in Cattle. Int J Mol Sci. 2020;21(12).
106. Krasnianski A, Kaune J, Jung K, Kretzschmar HA, Zerr I. First symptom and initial diagnosis in sporadic CJD patients in Germany. J Neurol. 2014;261(9):1811-7.
107. Pocchiari M, Puopolo M, Croes EA, Budka H, Gelpi E, Collins S, et al. Predictors of survival in sporadic Creutzfeldt-Jakob disease and other human transmissible spongiform encephalopathies. Brain : a journal of neurology. 2004;127(Pt 10):2348-59.

108. Parchi P, Giese A, Capellari S, Brown P, Schulz-Schaeffer W, Windl O, et al. Classification of sporadic Creutzfeldt-Jakob disease based on molecular and phenotypic analysis of 300 subjects. Annals of neurology. 1999;46(2):224-33.
109. Wadsworth JD, Hill AF, Joiner S, Jackson GS, Clarke AR, Collinge J. Strain-specific prion-protein conformation determined by metal ions. Nat Cell Biol. 1999;1(1):55-9.
110. Cali I, Castellani R, Alshekhlee A, Cohen Y, Blevins J, Yuan J, et al. Co-existence of scrapie prion protein types 1 and 2 in sporadic Creutzfeldt-Jakob disease: its effect on the phenotype and prion-type characteristics. Brain : a journal of neurology. 2009;132(Pt 10):2643-58.
111. Gambetti P, Dong Z, Yuan J, Xiao X, Zheng M, Alshekhlee A, et al. A novel human disease with abnormal prion protein sensitive to protease. Annals of neurology. 2008;63(6):697-708.
112. Zou WQ, Puoti G, Xiao X, Yuan J, Qing L, Cali I, et al. Variably protease-sensitive prionopathy: a new sporadic disease of the prion protein. Annals of neurology. 2010;68(2):162-72.
113. Kobayashi A, Teruya K, Matsuura Y, Shirai T, Nakamura Y, Yamada M, et al. The influence of PRNP polymorphisms on human prion disease susceptibility: an update. Acta Neuropathol. 2015;130(2):159-70.
114. Collinge J, Palmer MS, Dryden AJ. Genetic predisposition to iatrogenic Creutzfeldt-Jakob disease. Lancet. 1991;337(8755):1441-2.
115. Duffy P, Wolf J, Collins G, DeVoe AG, Streeten B, Cowen D. Letter: Possible person-to-person transmission of Creutzfeldt-Jakob disease. The New England journal of medicine. 1974;290(12):692-3.
116. Gibbs CJ, Jr., Joy A, Heffner R, Franko M, Miyazaki M, Asher DM, et al. Clinical and pathological features and laboratory confirmation of Creutzfeldt-Jakob disease in a recipient of pituitary-derived human growth hormone. The New England journal of medicine. 1985;313(12):734-8.
117. Cochius JI, Burns RJ, Blumbergs PC, Mack K, Alderman CP. Creutzfeldt-Jakob disease in a recipient of human pituitary-derived gonadotrophin. Aust N Z J Med. 1990;20(4):592-3.
118. Brown P, Preece M, Brandel JP, Sato T, McShane L, Zerr I, et al. Iatrogenic Creutzfeldt-Jakob disease at the millennium. Neurology. 2000;55(8):1075-81.
119. Rudge P, Jaunmuktane Z, Adlard P, Bjurstrom N, Caine D, Lowe J, et al. Iatrogenic CJD due to pituitary-derived growth hormone with genetically determined incubation times of up to 40 years. Brain : a journal of neurology. 2015;138(Pt 11):3386-99.
120. Collinge J, Whitfield J, McKintosh E, Beck J, Mead S, Thomas DJ, et al. Kuru in the 21st century--an acquired human prion disease with very long incubation periods. Lancet. 2006;367(9528):2068-74.
121. Will RG, Ironside JW, Zeidler M, Cousens SN, Estibeiro K, Alperovitch A, et al. A new variant of Creutzfeldt-Jakob disease in the UK. Lancet. 1996;347(9006):921-5.
122. Collinge J, Sidle KC, Meads J, Ironside J, Hill AF. Molecular analysis of prion strain variation and the aetiology of 'new variant' CJD. Nature. 1996;383(6602):685-90.
123. Spencer MD, Knight RS, Will RG. First hundred cases of variant Creutzfeldt-Jakob disease: retrospective case note review of early psychiatric and neurological features. BMJ. 2002;324(7352):1479-82.
124. Hill AF, Butterworth RJ, Joiner S, Jackson G, Rossor MN, Thomas DJ, et al. Investigation of variant Creutzfeldt-Jakob disease and other human prion diseases with tonsil biopsy samples. Lancet. 1999;353(9148):183-9.

125. Wroe SJ, Pal S, Siddique D, Hyare H, Macfarlane R, Joiner S, et al. Clinical presentation and pre-mortem diagnosis of variant Creutzfeldt-Jakob disease associated with blood transfusion: a case report. Lancet. 2006;368(9552):2061-7.
126. Peden AH, Head MW, Ritchie DL, Bell JE, Ironside JW. Preclinical vCJD after blood transfusion in a PRNP codon 129 heterozygous patient. Lancet. 2004;364(9433):527-9.
127. Brandel JP, Vlaicu MB, Culeux A, Belondrade M, Bougard D, Grznarova K, et al. Variant Creutzfeldt-Jakob Disease Diagnosed 7.5 Years after Occupational Exposure. The New England journal of medicine. 2020;383(1):83-5.
128. Mok T, Jaunmuktane Z, Joiner S, Campbell T, Morgan C, Wakerley B, et al. Variant Creutzfeldt-Jakob Disease in a Patient with Heterozygosity at PRNP Codon 129. The New England journal of medicine. 2017;376(3):292-4.
129. Beck JA, Poulter M, Campbell TA, Adamson G, Uphill JB, Guerreiro R, et al. PRNP allelic series from 19 years of prion protein gene sequencing at the MRC Prion Unit. Hum Mutat. 2010;31(7):E1551-63.
130. Windl O, Giese A, Schulz-Schaeffer W, Zerr I, Skworc K, Arendt S, et al. Molecular genetics of human prion diseases in Germany. Human genetics. 1999;105(3):244-52.
131. Collinge J, Brown J, Hardy J, Mullan M, Rossor MN, Baker H, et al. Inherited prion disease with 144 base pair gene insertion. 2. Clinical and pathological features. Brain : a journal of neurology. 1992;115 (Pt 3):687-710.
132. Beck JA, Mead S, Campbell TA, Dickinson A, Wientjens DP, Croes EA, et al. Two-octapeptide repeat deletion of prion protein associated with rapidly progressive dementia. Neurology. 2001;57(2):354-6.
133. Hsiao K, Baker HF, Crow TJ, Poulter M, Owen F, Terwilliger JD, et al. Linkage of a prion protein missense variant to Gerstmann-Straussler syndrome. Nature. 1989;338(6213):342-5.
134. Goldfarb LG, Brown P, McCombie WR, Goldgaber D, Swergold GD, Wills PR, et al. Transmissible familial Creutzfeldt-Jakob disease associated with five, seven, and eight extra octapeptide coding repeats in the PRNP gene. Proceedings of the National Academy of Sciences of the United States of America. 1991;88(23):10926-30.
135. Jansen C, Parchi P, Capellari S, Vermeij AJ, Corrado P, Baas F, et al. Prion protein amyloidosis with divergent phenotype associated with two novel nonsense mutations in PRNP. Acta Neuropathol. 2010;119(2):189-97.
136. Jansen C, Voet W, Head MW, Parchi P, Yull H, Verrips A, et al. A novel seven-octapeptide repeat insertion in the prion protein gene (PRNP) in a Dutch pedigree with Gerstmann-Straussler-Scheinker disease phenotype: comparison with similar cases from the literature. Acta Neuropathol. 2011;121(1):59-68.
137. Lugaresi E, Medori R, Montagna P, Baruzzi A, Cortelli P, Lugaresi A, et al. Fatal familial insomnia and dysautonomia with selective degeneration of thalamic nuclei. The New England journal of medicine. 1986;315(16):997-1003.
138. Gambetti P, Kong Q, Zou W, Parchi P, Chen SG. Sporadic and familial CJD: classification and characterisation. Br Med Bull. 2003;66:213-39.
139. Doh-ura K, Ishikawa K, Murakami-Kubo I, Sasaki K, Mohri S, Race R, et al. Treatment of transmissible spongiform encephalopathy by intraventricular drug infusion in animal models. J Virol. 2004;78(10):4999-5006.

140. Demaimay R, Adjou K, Lasmezas C, Lazarini F, Cherifi K, Seman M, et al. Pharmacological studies of a new derivative of amphotericin B, MS-8209, in mouse and hamster scrapie. J Gen Virol. 1994;75 (Pt 9):2499-503.
141. White MD, Farmer M, Mirabile I, Brandner S, Collinge J, Mallucci GR. Single treatment with RNAi against prion protein rescues early neuronal dysfunction and prolongs survival in mice with prion disease. Proceedings of the National Academy of Sciences of the United States of America. 2008;105(29):10238-43.
142. Moreno JA, Halliday M, Molloy C, Radford H, Verity N, Axten JM, et al. Oral Treatment Targeting the Unfolded Protein Response Prevents Neurodegeneration and Clinical Disease in Prion-Infected Mice. Sci Transl Med. 2013;5(206).
143. Otto M, Cepek L, Ratzka P, Doehlinger S, Boekhoff I, Wiltfang J, et al. Efficacy of flupirtine on cognitive function in patients with CJD: A double-blind study. Neurology. 2004;62(5):714-8.
144. Geschwind MD, Kuo AL, Wong KS, Haman A, Devereux G, Raudabaugh BJ, et al. Quinacrine treatment trial for sporadic Creutzfeldt-Jakob disease. Neurology. 2013;81(23):2015-23.
145. Collinge J, Gorham M, Hudson F, Kennedy A, Keogh G, Pal S, et al. Safety and efficacy of quinacrine in human prion disease (PRION-1 study): a patient-preference trial. Lancet Neurol. 2009;8(4):334-44.
146. Haik S, Marcon G, Mallet A, Tettamanti M, Welaratne A, Giaccone G, et al. Doxycycline in Creutzfeldt-Jakob disease: a phase 2, randomised, double-blind, placebo-controlled trial. Lancet Neurol. 2014;13(2):150-8.
147. Bone I, Belton L, Walker AS, Darbyshire J. Intraventricular pentosan polysulphate in human prion diseases: an observational study in the UK. Eur J Neurol. 2008;15(5):458-64.
148. Vallabh SM, Minikel EV, Schreiber SL, Lander ES. Towards a treatment for genetic prion disease: trials and biomarkers. Lancet Neurol. 2020;19(4):361-8.
149. Baker HF, Ridley RM, Duchen LW, Crow TJ, Bruton CJ. Induction of beta (A4)-amyloid in primates by injection of Alzheimer's disease brain homogenate. Comparison with transmission of spongiform encephalopathy. Mol Neurobiol. 1994;8(1):25-39.
150. Simpson DA, Masters CL, Ohlrich G, Purdie G, Stuart G, Tannenberg AE. Iatrogenic Creutzfeldt-Jakob disease and its neurosurgical implications. Journal of clinical neuroscience : official journal of the Neurosurgical Society of Australasia. 1996;3(2):118-23.
151. Eisele YS, Obermuller U, Heilbronner G, Baumann F, Kaeser SA, Wolburg H, et al. Peripherally applied Abeta-containing inoculates induce cerebral beta-amyloidosis. Science. 2010;330(6006):980-2.
152. Eisele YS, Bolmont T, Heikenwalder M, Langer F, Jacobson LH, Yan ZX, et al. Induction of cerebral beta-amyloidosis: intracerebral versus systemic Abeta inoculation. Proceedings of the National Academy of Sciences of the United States of America. 2009;106(31):12926-31.
153. Luk KC, Kehm V, Carroll J, Zhang B, O'Brien P, Trojanowski JQ, et al. Pathological alpha-synuclein transmission initiates Parkinson-like neurodegeneration in nontransgenic mice. Science. 2012;338(6109):949-53.
154. Li JY, Englund E, Holton JL, Soulet D, Hagell P, Lees AJ, et al. Lewy bodies in grafted neurons in subjects with Parkinson's disease suggest host-to-graft disease propagation. Nature medicine. 2008;14(5):501-3.

155. Watts JC, Giles K, Oehler A, Middleton L, Dexter DT, Gentleman SM, et al. Transmission of multiple system atrophy prions to transgenic mice. Proceedings of the National Academy of Sciences of the United States of America. 2013;110(48):19555-60.
156. Woerman AL, Kazmi SA, Patel S, Aoyagi A, Oehler A, Widjaja K, et al. Familial Parkinson's point mutation abolishes multiple system atrophy prion replication. Proceedings of the National Academy of Sciences of the United States of America. 2018;115(2):409-14.
157. Clavaguera F, Bolmont T, Crowther RA, Abramowski D, Frank S, Probst A, et al. Transmission and spreading of tauopathy in transgenic mouse brain. Nat Cell Biol. 2009;11(7):909-13.
158. Jeon I, Cicchetti F, Cisbani G, Lee S, Li E, Bae J, et al. Human-to-mouse prion-like propagation of mutant huntingtin protein. Acta Neuropathol. 2016;132(4):577-92.
159. Eisele YS, Duyckaerts C. Propagation of Ass pathology: hypotheses, discoveries, and yet unresolved questions from experimental and human brain studies. Acta Neuropathol. 2016;131(1):5-25.
160. Lauwers E, Lalli G, Brandner S, Collinge J, Compernolle V, Duyckaerts C, et al. Potential human transmission of amyloid beta pathology: surveillance and risks. Lancet Neurol. 2020;19(10):872-8.
161. Jaunmuktane Z, Mead S, Ellis M, Wadsworth JD, Nicoll AJ, Kenny J, et al. Evidence for human transmission of amyloid-beta pathology and cerebral amyloid angiopathy. Nature. 2015;525(7568):247-50.
162. Hamaguchi T, Taniguchi Y, Sakai K, Kitamoto T, Takao M, Murayama S, et al. Significant association of cadaveric dura mater grafting with subpial Abeta deposition and meningeal amyloid angiopathy. Acta Neuropathol. 2016;132(2):313-5.
163. Ritchie DL, Adlard P, Peden AH, Lowrie S, Le Grice M, Burns K, et al. Amyloid-beta accumulation in the CNS in human growth hormone recipients in the UK. Acta Neuropathol. 2017;134(2):221-40.
164. Raposo N, Planton M, Siegfried A, Calviere L, Payoux P, Albucher JF, et al. Amyloid-beta transmission through cardiac surgery using cadaveric dura mater patch. J Neurol Neurosurg Psychiatry. 2020;91(4):440-1.
165. Jaunmuktane Z, Quaegebeur A, Taipa R, Viana-Baptista M, Barbosa R, Koriath C, et al. Evidence of amyloid-beta cerebral amyloid angiopathy transmission through neurosurgery. Acta Neuropathol. 2018;135(5):671-9.